

Materials Horizons: From Nature to Nanomaterials

Andrews Nirmala Grace  
Prashant Sonar  
Preetam Bhardwaj  
Arghya Chakravorty *Editors*

# Handbook of Porous Carbon Materials

 Springer

# **Materials Horizons: From Nature to Nanomaterials**

## **Series Editor**

Vijay Kumar Thakur, School of Aerospace, Transport and Manufacturing,  
Cranfield University, Cranfield, UK

Materials are an indispensable part of human civilization since the inception of life on earth. With the passage of time, innumerable new materials have been explored as well as developed and the search for new innovative materials continues briskly. Keeping in mind the immense perspectives of various classes of materials, this series aims at providing a comprehensive collection of works across the breadth of materials research at cutting-edge interface of materials science with physics, chemistry, biology and engineering.

This series covers a galaxy of materials ranging from natural materials to nanomaterials. Some of the topics include but not limited to: biological materials, biomimetic materials, ceramics, composites, coatings, functional materials, glasses, inorganic materials, inorganic-organic hybrids, metals, membranes, magnetic materials, manufacturing of materials, nanomaterials, organic materials and pigments to name a few. The series provides most timely and comprehensive information on advanced synthesis, processing, characterization, manufacturing and applications in a broad range of interdisciplinary fields in science, engineering and technology.

This series accepts both authored and edited works, including textbooks, monographs, reference works, and professional books. The books in this series will provide a deep insight into the state-of-art of Materials Horizons and serve students, academic, government and industrial scientists involved in all aspects of materials research.

### **Review Process**

The proposal for each volume is reviewed by the following:

1. Responsible (in-house) editor
2. One external subject expert
3. One of the editorial board members.

The chapters in each volume are individually reviewed single blind by expert reviewers and the volume editor.

Andrews Nirmala Grace · Prashant Sonar ·  
Preetam Bhardwaj · Arghya Chakravorty  
Editors

# Handbook of Porous Carbon Materials

 Springer

*Editors*

Andrews Nirmala Grace  
Centre for Nanotechnology Research  
Vellore Institute of Technology  
Vellore, India

Preetam Bhardwaj  
School of Electronics Engineering  
Vellore Institute of Technology  
Vellore, India

Research and Development Cell  
Battrixx  
Kabra Extrusion Technik Limited  
Pune, India

Prashant Sonar  
School of Chemistry and Physics  
Centre for Materials Science  
Queensland University of Technology  
Brisbane, QLD, Australia

Arghya Chakravorty  
School of Bio Sciences and Technology  
Centre for Nanotechnology Research  
Vellore Institute of Technology  
Vellore, India

Research and Development Action Wing  
Baranagar Baghajatin Social Welfare  
Organisation  
Kolkata, India

ISSN 2524-5384

ISSN 2524-5392 (electronic)

Materials Horizons: From Nature to Nanomaterials

ISBN 978-981-19-7187-7

ISBN 978-981-19-7188-4 (eBook)

<https://doi.org/10.1007/978-981-19-7188-4>

© The Editor(s) (if applicable) and The Author(s), under exclusive license to Springer Nature Singapore Pte Ltd. 2023

This work is subject to copyright. All rights are solely and exclusively licensed by the Publisher, whether the whole or part of the material is concerned, specifically the rights of translation, reprinting, reuse of illustrations, recitation, broadcasting, reproduction on microfilms or in any other physical way, and transmission or information storage and retrieval, electronic adaptation, computer software, or by similar or dissimilar methodology now known or hereafter developed.

The use of general descriptive names, registered names, trademarks, service marks, etc. in this publication does not imply, even in the absence of a specific statement, that such names are exempt from the relevant protective laws and regulations and therefore free for general use.

The publisher, the authors, and the editors are safe to assume that the advice and information in this book are believed to be true and accurate at the date of publication. Neither the publisher nor the authors or the editors give a warranty, expressed or implied, with respect to the material contained herein or for any errors or omissions that may have been made. The publisher remains neutral with regard to jurisdictional claims in published maps and institutional affiliations.

This Springer imprint is published by the registered company Springer Nature Singapore Pte Ltd. The registered company address is: 152 Beach Road, #21-01/04 Gateway East, Singapore 189721, Singapore

*Dedicated to the memory of  
Antoine Lavoisier*

# Foreword

The study of porous carbon materials is a comparatively adolescent discipline. It primarily gained eminence through the early eighteenth century, when the beginning of activated charcoal with well-defined structures revealed by scientists established to follow the research of this enthralling substance with a renewed vigor. In 1776, Russian Chemist Johann Lowitz revealed the preliminary discoloration properties of charcoal in liquid—a characteristic that built activated charcoal as water filters with admired preference even today. In consequence, the discovery of Graphene by Prof. Andre Geim and Prof. Kostya Novoselov in 2004 affords an enormous advance up and new measurements to materials research and nanotechnology. The multidisciplinary properties of porous carbon materials have an extensive range of applications from the medical sector to the aerospace industry. The first volume of the journal *Carbon* appeared in 1964, and 191 volumes of this journal had been published up to 2022 that is reflecting the massive growth of this field. This time period also observes the progress of a broad variety of experimental methods that are enabling the exploration of different characteristics of the porous carbon materials with respect to energetic, kinetic, structural, electronic, magnetic, and dynamic properties of porous carbon materials with enormous precision. The discovery of scanning probe techniques permitted atomic processes to be considered in unparalleled detail. The study of the porous carbon field in recent research ranges from phenomena correlated with nanotechnology and thin-film development to heterogeneous catalysis processes to industrial applications.

The current handbook comprises 41 chapters that are contributions written by numerous specialists in this carbon field globally and covers the main aspects of this fascinating branch of science and engineering. It should establish precious contributions to all those engrossed in this discipline. The editors and authors are to be eulogizing on the successful completion of this *Handbook of Porous Carbon Materials*. It will definitely be a work of enormous and lasting significance for the scientific community.



Prof. Sabu Thomas  
Vice Chancellor  
Mahatma Gandhi University  
Priyadarshini Hills  
Kottayam, Kerala, India

Director  
School of Energy Materials

Founder Director  
International and Inter University Centre for  
Nanoscience and Nanotechnology

Former Director  
Professor  
School of Chemical Sciences  
Mahatma Gandhi University  
Kottayam, Kerala, India



# Preface

Porous carbon materials such as activated carbon, carbon nanotubes, carbon nanofibers, and graphene are the novel visionary materials of this twenty-first century. These carbon materials are receiving extensive attention as novel materials to guide the prospects in the fields of electronics, biosensors, agriculture, wastewater remediation, composite materials, energy devices, hydrogen generation, secondary batteries, fuel cells, etc., not simply for nanoscaled dimensions but also due to their outstanding porosity, surface area, exceptional mechanical, chemical, physical, and electronic properties. Those who manage materials can organize technology, acknowledged by Eiji Kobayashi, Senior Scientist of Panasonic Corporation, elucidating the significance of materials science and engineering. We would interpret this quotation as researchers and scientists who control properties of materials to optimize technology and reflect on the influential growth of materials and technology on our large-scale infrastructure.

Porous carbon materials have a determinative function in the fabrication of numerous superior products around us. From the development of filter membranes to aerospace technology, none of these could be shaped devoid of these wonderful materials. The editors consider this porous materials science as the understanding of composition; characteristics of materials predicted or explained with the help of this information; experimental and theoretical tools intended and recognized for preparing, characterizing, and modifying processes. Editors also listed all-important application possibilities of these resulted materials. After defining porous carbon materials, we can simply swap this depiction for porous carbon materials discipline. Porous carbon materials are considered in all advanced applications due to their configuration, processing, characterization, and difference from the macroscopic materials. This difference is due to nanosized dimensions and porous structures.

The depiction of the porous carbon materials in this handbook pursues all fields but comprises short details of the synergy of composition, characteristics, processing, and applications. Distinctively, our aim was to point out the difference between the properties of bulk and nano-porous materials. We also discuss and explain the reasons for these differences. To accomplish these objectives, we present a reasonable description of the literature of each porous carbon materials group. The layouts pursue the

well-established configuration of the handbook with chapters as the basic units that are organized into several groups. In each chapter, authors cover materials of their proficiency; however, they centered not only on their own work, but account the remarkable and significant efforts in the society, ascertain stability between references and scientific outcomes account in tables and figures. We illustrate porous carbon materials in textbook approach for beginners in this field. We also comprise encyclopedia-like ingredients and discuss the fast space of new results. We also review and include recent research reports for the familiar readers. Ahead of scientific and ethical accuracy, we also seem for simplicity by summarizing and easy-to-follow text, well-planned and apparent figures which were all proficiently drawn by experts.

The book is divided into eight parts depicted as Parts I–VIII that cover porous carbon materials: graphene, graphene oxide, fullerenes, carbon nanotubes, activated carbon, carbon nanofibers, noble and common porous carbon-based composites, hybrid structures and solutions, and selective applications, correspondingly. This higher-level structure conforms to the porous classification of materials, and it is composed of chapters. Each chapter is self-consistent and builds up of similar parts, history, definitions, production of the given porous carbon materials, properties, and applications. All of these parts are opulently illustrated and consist of a reasonable proportion of imperative basics and recent results.

Our pleasurable commitment is to express gratitude to all authors, contributors, and colleagues who help us with the establishment of this planned and implemented handbook. Firstly, we need to recognize the conscientious work of the authors in developing the chapters which engross more attempts than a review article, and the reward is not so instantaneous and apparent. Their proficiency, energy, and time are significantly appreciated. We also would like to show gratitude for the suggestions and help of our colleagues in keeping in contact with several authors. Our book is dedicated to the memory of French Scientist Antoine Lavoisier who named the elements **carbon**, hydrogen, and oxygen and discovered oxygen's role in combustion and respiration.

The enormous workmanship of the Springer publishing team and the incessant support of the managing editors Priya Vyas and Silky Abhay Sinha are also appreciated. We also need to thank our colleagues and friends that the association with them is leaning us to understand and develop materials science aspects. Last but not least, we are thankful to our family members for their continuous support to complete this work. We wish the readers an enjoyable and advantageous time when utilizing the Handbook of Porous Carbon Materials, and we anticipate that it serves as a regularly unwrapped reference textbook.

Vellore, India  
February 2022

Andrews Nirmala Grace  
Prashant Sonar  
Preetam Bhardwaj  
Arghya Chakravorty

# Contents

## Part I Basic Sciences and Engineering

- 1 Synthesis and Fabrication of Advanced Carbon Nanostructures** ..... 3  
Anuj Kumar Tomar, Deepak Kumar, Akanksha Joshi, Gurmeet Singh, and Raj Kishore Sharma
- 2 Fabrication of Graphene, Graphene Oxide, Reduced Graphene Oxide, Fullerene (C<sub>60</sub>) and Carbon Nanotube Thin Film By Langmuir–Blodgett Method** ..... 21  
Atri Mallick, Nibedita Haldar, Suman Nandy, and Chandan Kumar Ghosh

## Part II Energy Science and Engineering

- 3 Nanoporous Carbon Materials for Energy Harvesting, Storage, and Conversion** ..... 41  
Bhawna, Janardhan Balapanuru, Varun Rai, Vinod Kumar, and Kamalakanta Behera
- 4 Lignin-Derived Carbonaceous Materials for Supercapacitor Applications** ..... 65  
Esakkiammal Sudha Esakkimuthu, Veerapandian Ponnuchamy, Tugrul Yumak, and David De Vallance
- 5 Porous Carbon Materials for Supercapacitor Applications** ..... 117  
Manas Mandal, Krishna Chattopadhyay, Amrita Jain, and Swapan Kumar Bhattacharya
- 6 Recent Advancement of Luminescent Graphene Quantum Dots for Energy-Related Applications** ..... 147  
Poonam Rani Kharangarh, Rachna Rawal, Shalu Singh, and Preetam Bhardwaj

<b>7</b>	<b>Recent Progress of Carbonaceous Materials in Third Generation Solar Cells: DSSCs</b> .....	165
	Nandhakumar Eswaramoorthy, Ravuri Syamsai, Senthilkumar Nallusamy, Selvakumar Pitchaiya, and M. R. Venkatraman	
<b>8</b>	<b>Carbon-Based Materials as Electrodes for Biofuels Electrosynthesis</b> .....	189
	Danilo Perez	
<b>Part III Catalyst Science and Engineering</b>		
<b>9</b>	<b>Photoluminescent Carbon Dots: A New Generation Nanocarbon Material</b> .....	231
	Anju Paul and Anandhu Mohan	
<b>10</b>	<b>Carbonaceous Nanostructures-Based Photocatalysts for Sustainable H<sub>2</sub> Production</b> .....	257
	E. Nandhakumar, E. Vivek, E. Vaishnavi, M. Prem Kumar, Perumal Devaraji, P. Selvakumar, and N. Senthilkumar	
<b>11</b>	<b>Design of Porous Carbon-Based Electro-Catalyst for Hydrogen Generation</b> .....	285
	Kamlesh, Satya Prakash, Deepika Tavar, Pankaj Raizda, Pradeep Singh, Manish Mudgal, A. K. Srivastava, and Archana Singh	
<b>12</b>	<b>Core–Shell Nanostructures-Based Porous Carbon Nanomaterials for Oxygen Reduction Reaction</b> .....	323
	Saravanan Nagappan, Malarkodi Duraivel, Shamim Ahmed Hira, Mohammad Yusuf, Sanjay S. Latthe, Kandasamy Prabakar, and Kang Hyun Park	
<b>13</b>	<b>Waste-Derived Activated Carbon as a Sustainable and Economical Catalyst Support</b> .....	351
	Sakshi Kabra Malpani, Renu Hada, Ajay Kumar, and Deepti Goyal	
<b>Part IV Sensor and Sensing Technology</b>		
<b>14</b>	<b>Porous Carbon-Based Sensors and Their Applications</b> .....	381
	Karunanthi Govardhan, Prabhu Ramanathan, and Mahesh Ganesapillai	
<b>15</b>	<b>Carbon Composites with Polymer Materials for Gas Sensing Application</b> .....	405
	K. Mahendraprabhu, T. Elango Balaji, Payaswini Das, and Himadri Tanaya Das	

<b>16</b>	<b>Recent Advances in Porous Carbon-Based Inorganic Flexible Sensor Journey from Material Synthesis to Sensor Prototyping</b> .....	423
	Saleem Khan, Vishal Singh, and Ajay Singh	
<b>Part V Device Engineering and Technology Sensing</b>		
<b>17</b>	<b>Biomedical Application of Porous Carbon and Its Future in Precision Medical Devices</b> .....	449
	Sabyasachi Choudhuri and Jyotirmoy Panda	
<b>18</b>	<b>Role of Graphene-Based Materials in Gas Sensing Applications: From Synthesis to Device Fabrication</b> .....	493
	R. Deji, Rahul, B. C. Choudhary, and Ramesh K. Sharma	
<b>19</b>	<b>Trends in Nanostructured Sorbent Materials for Passive Sampling Applications</b> .....	519
	Lucas A. C. Minhó, Eduard F. Valenzuela, Helvécio C. Menezesand, and Zenilda L. Cardeal	
<b>Part VI Environmental Sciences and Applications</b>		
<b>20</b>	<b>Porous Graphene-Based Materials for Enhanced Adsorption Towards Emerging Micropollutants (EMs)</b> .....	547
	Alvin Lim Teik Zheng, Supakorn Boonyuen, and Yoshito Andou	
<b>21</b>	<b>Response Surface Modelling and Optimisation of Activated Carbons Adsorption of Pollutants from Textile Wastewater</b> .....	571
	Chinenye Adaobi Igwegbe, Joshua O. Ighalo, Kingsley O. Iwuozor, Okechukwu Dominic Onukwuli, and Adewale George Adeniyi	
<b>22</b>	<b>Biochar: Porous Carbon Material, Its Role to Maintain Sustainable Environment</b> .....	595
	Debomita Dey, Debalin Sarangi, and Prithusayak Mondal	
<b>23</b>	<b>Application of Porous Carbon Material for Water Treatment and Gas Storage</b> .....	623
	Saikat Sinha Ray, Mohammed J. K. Bashir, Harshdeep Singh Bakshi, Young-Nam Kwon, and Mahesh Ganesapillai	
<b>24</b>	<b>Utilization of Aquatic Plants Dead Biomass in Adsorption of Heavy Metals from Wastewater</b> .....	655
	Asha Singh and Sunil Kumar	

<b>25 Porous Carbon Materials and Their Composites for Electromagnetic Interference (EMI) Shielding: The State-of-the-Art of Technologies</b> .....	669
Deepthi Anna David, M. J. Jabeen Fatima, Abdullah Khan, Roshny Joy, Vijay Kumar Thakur, Ramiro Rafael Ruiz-Rosas, Shemus Ozden, and Prasanth Raghavan	
<b>Part VII Food and Agriculture Applications</b>	
<b>26 Porous Carbon Materials and Their Applications in Environmental Monitoring and Food Safety</b> .....	705
Alma Mejri, Abdelmoneim Mars, and Hamza Elfil	
<b>27 Porous Carbon in Food Industry</b> .....	733
Shreyan Bardhan, Avijit Chakraborty, Sagnik Roy, Sudip Das, Dibyajit Lahiri, and Banani Ray Chowdhury	
<b>28 Chitosan-Based Porous Carbon Materials for Agriculture and Agro-waste Applications</b> .....	763
Srinivasan Latha, T. Gomathi, S. Pavithra, P. N. Sudha, Abhishek Nalluri, and Preetam Bhardwaj	
<b>Part VIII Applications in Therapeutics and Diagnostics</b>	
<b>29 Carbon-Based Porous Materials in Biomedical Applications: Concept and Recent Advancements</b> .....	815
Jnanraj Borah and Anupam Chetia	
<b>30 Fanatical Clout of Porous Carbon Materials—A Peek in Therapeutics</b> .....	841
Madhu Raina, Sonia Sharma, and Sakshi Koul	
<b>31 Porous Carbon Materials and Their Applications in Biosensing, Medical Diagnostics, and Drug Delivery</b> .....	885
Abdelmoneim Mars, Alma Mejri, and Hamza Elfil	
<b>32 Carbon Nanotubes-Based Anticancer Nanomedicine</b> .....	907
Sougata Ghosh, Ratnakar Mishra, Amrendra K. Ajay, Nanasahab Thorat, and Ebrahim Mostafavi	
<b>33 Porous Carbon Materials Enhanced the Therapeutic Efficacy of Anticancer Drugs</b> .....	939
Anuradha Duvey, Divya Chauhan, Nitin Gupta, and Vipendra Kumar Singh	
<b>34 Biocompatible Carbon-Coated Magnetic Nanoparticles for Biomedical Applications</b> .....	955
V. Vijayakanth, V. Vinodhini, and Krishnamoorthi Chintagumpala	

<b>35</b>	<b>Noscapinoids: A Family of Microtubule-Targeted Anticancer Agent</b> .....	987
	Shruti Gama Dash, Harish Chandra Joshi, and Pradeep Kumar Naik	
<b>36</b>	<b>Recent Advances in Designing Porous Carbon Nanomaterial Based for Electrochemical Biosensing Prostate Cancer</b> .....	1007
	Stephen Rathinaraj Benjamin and Eli José Miranda Ribeiro Júnior	
<b>37</b>	<b>Role of Nanosystems for Electrochemical Mapping Using Diverse Carbon-Based Nanomaterials</b> .....	1035
	Mansi Gandhi and Settu Ramki	
<b>38</b>	<b>Carbon Nanomaterial-Based Biosensors: A Forthcoming Future for Clinical Diagnostics</b> .....	1067
	Neha Saini, Prem Pandey, Shashwati Wankar, Mandar Shirolkar, Anjali A. Kulkarni, Jang Ah Kim, Taesung Kim, and Atul Kulkarni	
<b>39</b>	<b>Emerging Graphene-Based Nanomaterials for Cancer Nanotheranostics</b> .....	1091
	Arkadyuti Roy Chakraborty, R. Akshay, Subhrajeet Sahoo, Haimantika Seel, Soupam Das, Saikat Dutta, Abhishek Nalluri, Siva Sankar Sana, Karthikeyan Ramesh, and Vimala Raghavan	
<b>40</b>	<b>Synthesis of Carbon Nanotubes with Merocyanine Dyes Decorated Carbon Nanotubes for Biomedical Imaging Devices</b> .....	1127
	S. Ranjitha, R. Lavanya Dhevi, C. Sudhakar, and Rajakumar Govindasamy	
<b>41</b>	<b>Role of Carbon Nanostructures as Nano-Theranostics Against Breast and Brain Cancer</b> .....	1151
	Neha Saini, Prem Pandey, Mandar Shirolkar, Atul Kulkarni, Sang-Hyun Moh, and Anjali A. Kulkarni	



# Editors and Contributors

## About the Editors



**Andrews Nirmala Grace** is Professor and Director at the Centre for Nanotechnology Research, Vellore Institute of Technology (VIT), Vellore, India. She received her Ph.D. degree in Chemistry from the University of Madras, India, and worked as Postdoctoral/Senior Researcher Fellow at the Korea Institute of Energy Research, South Korea, on renewable energy. Her current research interests include energy materials, design and fabrication of electrodes for dye sensitized, perovskite solar cells, electrodes for supercapacitors—morphological studies of supercapacitor electrodes and study of electrochemical redox reactions at the interface of electrodes and electrolytes, engineering of inter-layer spaces in 2D materials to improve the ion accessibility, tuning the structure and porosity of electrode materials, and flexible energy devices for conversion and storage—flexible and printable supercapacitors for wearable devices such as sensors and energy conversion. She has more than 130 international peer-reviewed publications and has authored three chapters.



**Dr. Prashant Sonar** is ARC Future Fellow and Associate Professor in the School of Chemistry and Physics and leading CI at the Centre for Material Science at the Queensland University of Technology, (QUT), Australia. He was also appointed as Visiting Professor at the School of Material Science and Engineering, Indian Institute of Technology (IIT) Kanpur in 2017. He holds Adjunct Associate Professor position with Griffith University, Australia. He was awarded his Ph.D. in 2004 from Johannes-Gutenberg University in Mainz. He moved to the Swiss Federal Institute of Technology (ETH), Zurich, Switzerland, for his postdoctoral research. He received the prestigious Future Fellowship (2013) from the Australian Research Council and was appointed as Associate Professor in July 2014 at QUT, Australia. At QUT, he established the Organic and Printed Electronic Research group. Recently, he has been elected as Fellow of the Royal Chemical Society (FRSC) and Foreign Fellow of Maharashtra Academy of Sciences (FFMAS). He is interested in the design and synthesis of novel  $\pi$ -functional materials (small molecules, oligomers, dendrimers, and polymers) for printed electronics, (OFETs, OLEDs, OPVs, OLETs, OPDs, and sensors), perovskite solar cells, bioelectronics, supramolecular electronic, and wearable electronic applications. He has authored or co-authored more than 221 peer-reviewed research papers in international journals (H-index-50 according to Google Scholar with total citations 9265) and filed nine patents and patent applications at regional and international levels.



**Dr. Preetam Bhardwaj** is presently working as Research Faculty in the Centre for Nanotechnology Research and School of Electronics Engineering, Vellore Institute of Technology (VIT), India. He has research specialization in the fields of nanotechnology, energy storage devices, EMI shielding, antistatic technology, biosensors, anticorrosion coatings, anticancer materials, and radar absorbing materials for stealth technology. He received his Ph.D. degree in nanotechnology from D. C. R. University of Science and Technology, India. Presently, he is working in the areas of energy storage devices, supercapacitor electrode materials, radar absorbing materials for stealth technology, biosensors, and anticancer materials with Prof. A. N.

Grace, VIT University. He has published more than 25 research papers in peer-reviewed journals. He has also filed and published three patents in the field of energy storage devices and EMI shielding applications. He also has senior research membership of American Chemical Society, Royal Society of Chemistry, International Society of Advanced Materials, Indian Carbon Society, IEEE, and Indian Association of Chemical Engineers.



**Arghya Chakravorty** is Early Career Researcher and Member of the American Chemical Society, Solid Waste Association of North America, British Society for Antimicrobial Chemotherapy, as well as Doctoral Fellow at the Centre for Nanotechnology Research, Vellore Institute of Technology, Vellore, India. He holds five Indian patents, and his research interest lies in interdisciplinary material science and nanobiotechnology. He earned his B.Sc. Honors (Microbiology) from Midnapore College, India, and a first-class M.Sc. (Microbiology) from Hemvati Nandan Bahuguna Garhwal (Central) University, India. He has reviewed several papers for journals of national and international repute and has been awarded several recognitions.

## Contributors

**Adewale George Adeniyi** Department of Chemical Engineering, University of Ilorin, Ilorin, Nigeria

**Amrendra K. Ajay** Brigham and Women's Hospital, Harvard Center for Polycystic Kidney Disease Research and Renal Division, Harvard Medical School, Boston, MA, USA

**R. Akshay** Department of Physics, Sri Sathya Sai Institute of Higher Learning, Vidyagiri Prashanthi Nilayam, Andhra Pradesh, India

**Yoshito Andou** Graduate School of Life Science and Systems Engineering, Kyushu Institute of Technology, Fukuoka, Japan;  
Collaborative Research Centre for Green Materials On Environmental Technology, Kyushu Institute of Technology, Fukuoka, Japan

**Harshdeep Singh Bakshi** Centre for Environmental Policy, Imperial College London, South Kensington, England, United Kingdom

**Janardhan Balapanuru** Grafoid Inc., Kingston, ON, Canada

**Shreyan Bardhan** Department of Biotechnology, Bengal Institute of Technology (BIT), Kolkata, India

**Mohammed J. K. Bashir** Department of Environmental Engineering, Faculty of Engineering and Green Technology (FEGT), Universiti Tunku Abdul Rahman, Jalan Universiti, Bandar Barat, Malaysia

**Kamalakanta Behera** Department of Chemistry, Faculty of Science, University of Allahabad, Prayagraj, Uttar Pradesh, India

**Stephen Rathinaraj Benjamin** Laboratory of Neuroscience and Behavior, Department of Physiology and Pharmacology and Faculty of Medicine, Drug Research and Development Center (NPDM), Federal University of Ceará (UFC), Porangabussu, Fortaleza, Ceará, Brazil

**Preetam Bhardwaj** School of Electronics Engineering, Vellore Institute of Technology, Vellore, Tamil Nadu, India

**Swapan Kumar Bhattacharya** Physical Chemistry Section, Department of Chemistry, Jadavpur University, Kolkata, West Bengal, India

**Bhawna** Department of Chemical and Biological Engineering, University of Alabama, Tuscaloosa, USA

**Supakorn Boonyuen** Department of Chemistry, Faculty of Science and Technology, Thammasat University, Pathumthani, Thailand

**Jnanraj Borah** Department of Physics, Gauhati University, Guwahati, Assam, India

**Zenilda L. Cardeal** Departamento de Química, ICEX, Universidade Federal de Minas Gerais, Avenida Antônio Carlos, Belo Horizonte, Minas Gerais, Brazil

**Arkadyuti Roy Chakraborty** School of Bio Sciences and Technology, Vellore Institute of Technology, Vellore, India

**Avijit Chakraborty** Department of Biotechnology, Bengal Institute of Technology (BIT), Kolkata, India

**Krishna Chattopadhyay** Department of Chemistry, University of Calcutta, Kolkata, West Bengal, India

**Divya Chauhan** Department of Pharmacy, Uttarakhand Technical University, Chandanwadi, Dehradun, Uttarakhand, India

**Anupam Chetia** Department of Physics, Indian Institute of Technology, Jodhpur, Rajasthan, India

**Krishnamoorthi Chintagumpala** Center for Nanotechnology Research, Vellore Institute of Technology, Vellore, Tamil Nadu, India

**B. C. Choudhary** National Institute of Technical Teachers Training and Research (NITTTR), Chandigarh, India

**Sabyasachi Choudhuri** Department of Pharmaceutical Science and Technology, Maulana Abul Kalam Azad University of Technology, Kolkata, India

**Himadri Tanaya Das** Department of Chemical Engineering, National Taiwan University of Science and Technology, Taipei, Taiwan;  
Center of Excellence for Advance Materials and Applications, Utkal University, Vanivihar, Bhubaneswar, India

**Payaswini Das** CSIR-Institute of Minerals and Materials Technology, Bhubaneswar, Odisha, India

**Soupam Das** School of Bio Sciences and Technology, Vellore Institute of Technology, Vellore, India

**Sudip Das** Department of Biotechnology, Bengal Institute of Technology (BIT), Kolkata, India

**Shruti Ganya Dash** Centre of Excellence in Natural Products and Therapeutics, Department of Biotechnology and Bioinformatics, Sambalpur University, Burla, Sambalpur, Odisha, India

**Deepthi Anna David** Materials Science and NanoEngineering Lab (MSNE-Lab), Department of Polymer Science and Rubber Technology, Cochin University of Science and Technology, Cochin, India;  
Department of Applied Chemistry, Cochin University of Science and Technology, Cochin, India

**David De Vallance** InnoRenew CoE—Renewable Materials and Healthy Environments Research and Innovation Centre of Excellence, Izola, Slovenia;  
Faculty of Mathematics, University of Primorska, Natural Sciences and Information Technologies, Koper, Slovenia

**R. Deji** Department of Physics, Panjab University, Chandigarh, India

**Perumal Devaraji** Henan Engineering Research Center of Resource and Energy Recovery From Waste, Henan University, Kaifen, PR China

**Debomita Dey** Department of Agricultural Chemistry and Soil Science, Faculty of Agriculture, Bidhan Chandra Krishi Viswavidyalaya, Mohanpur, Nadia, West Bengal, India

**Malarkodi Duraivel** Department of Electrical Engineering, Pusan National University, Busan, Republic of Korea

**Saikat Dutta** School of Life Science, Department of Microbiology, VELS University, Chennai, India

**Anuradha Duvey** Department of Pharmacy, Uttarakhand Technical University, Chandanwadi, Dehradun, Uttarakhand, India

**T. Elango Balaji** Department of Chemistry, Utkal University, Bhubaneswar, Odisha, India

**Hamza Elfil** Desalination and Natural Water Valorization Laboratory (LaDVEN), Water Researches and Technologies Center (CERTE), Soliman, Tunisia

**Esakkiammal Sudha Esakkimuthu** InnoRenew CoE—Renewable Materials and Healthy Environments Research and Innovation Centre of Excellence, Izola, Slovenia

**Nandhakumar Eswaramoorthy** School of Mechanical Engineering, Vellore Institute of Technology, Vellore, Tamil Nadu, India

**Mansi Gandhi** Department of Chemistry, SAS, Vellore Institute of Technology, Vellore, India;  
Institute of Chemistry, Hebrew University of Jerusalem, Jerusalem, Israel

**Mahesh Ganesapillai** Mass Transfer Group, School of Chemical Engineering, Vellore Institute of Technology, Vellore, Tamil Nadu, India

**Chandan Kumar Ghosh** School of Materials Science and Nanotechnology, Jadavpur University, Jadavpur, Kolkata, India

**Sougata Ghosh** Department of Microbiology, School of Science, RK University, Rajkot, Gujarat, India

**T. Gomathi** Biomaterials Research Lab, PG and Research Department of Chemistry, D.K.M. College for Women, Vellore, Tamil Nadu, India

**Karunanthi Govardhan** Department of Micro and Nano-Electronics, School of Electronics Engineering, Vellore Institute of Technology, Vellore, Tamilnadu, India

**Rajakumar Govindasamy** Collaborative Innovation Center for Advanced Organic Chemical Materials Co-Constructed By the Province and Ministry, Ministry of Education Key Laboratory for the Synthesis and Application of Organic Functional Molecules, College of Chemistry and Chemical Engineering, Hubei University, Wuhan, China

**Deepti Goyal** Department of Applied Chemistry, School of Vocational Studies and Applied Sciences, Gautam Buddha University, Greater Noida, UP, India

**Nitin Gupta** Center for Converging Technologies, University of Rajasthan, Jaipur, Rajasthan, India

**Renu Hada** Department of Applied Chemistry and Chemical Technology, SGSITS, Indore, Madhya Pradesh, India

**Nibedita Haldar** School of Materials Science and Nanotechnology, Jadavpur University, Jadavpur, Kolkata, India

**Shamim Ahmed Hira** Department of Chemistry, Chemistry Institute for Functional Materials, Pusan National University, Busan, Republic of Korea

**Joshua O. Ighalo** Department of Chemical Engineering, Nnamdi Azikiwe University, Awka, Nigeria;  
Department of Chemical Engineering, University of Ilorin, Ilorin, Nigeria

**Chinenye Adaobi Igwegbe** Department of Chemical Engineering, Nnamdi Azikiwe University, Awka, Nigeria

**Kingsley O. Iwuozor** Department of Chemistry, University of Lagos, Lagos, Nigeria;  
Department of Pure and Industrial Chemistry, Nnamdi Azikiwe University, Awka, Nigeria

**M. J. Jabeen Fatima** Materials Science and NanoEngineering Lab (MSNE-Lab), Department of Polymer Science and Rubber Technology, Cochin University of Science and Technology, Cochin, India

**Amrita Jain** Institute of Fundamental Technological Research, Polish Academy of Sciences, Warsaw, Poland

**Akanksha Joshi** Department of Chemistry, University of Delhi, Delhi, India

**Harish Chandra Joshi** Department of Cell Biology, Emory University School of Medicine, Atlanta, GA, USA

**Roshny Joy** Materials Science and NanoEngineering Lab (MSNE-Lab), Department of Polymer Science and Rubber Technology, Cochin University of Science and Technology, Cochin, India

**Eli José Miranda Ribeiro Júnior** Department of Pharmacy, Faculty of CGESP (Centro Goiano de Ensino Superior), Goiânia, Goiás, Brazil

**Kamlesh** CSIR—Advanced Material and Processes Research Institute, Bhopal, India;  
Academy of Scientific & Innovative Research (AcSIR), Ghaziabad, India

**Abdullah Khan** Department of Materials Science and Engineering, KTH Royal Institute of Technology, Stockholm, Sweden

**Saleem Khan** Department of Nanosciences and Materials, Central University Jammu, Jammu, UT-J&K, India

**Poonam Rani Kharangarh** Department of Physics and Astrophysics, University of Delhi, Delhi, India;  
Department of Physics, New Jersey Institute of Technology, Newark, NJ, USA

**Jang Ah Kim** Department of Materials, Imperial College London, London, UK

**Taesung Kim** Nano Particles Technology Laboratory, School of Mechanical Engineering, Sungkyunkwan University, Suwon, South Korea

**Sakshi Koul** Department of Zoology, Cluster University of Jammu, Jammu, Jammu and Kashmir, India

**Anjali A. Kulkarni** Department of Botany, Savitribai Phule Pune University (Formerly University of Pune), Pune, India

**Atul Kulkarni** Symbiosis Centre for Nanoscience and Nanotechnology, Symbiosis International (Deemed University), Pune, India

**Ajay Kumar** Institute of Biomedical Sciences and Department of Mechanical and Electromechanical Engineering, National Sun Yat-Sen University, Kaohsiung City, Taiwan

**Deepak Kumar** Department of Chemistry, University of Delhi, Delhi, India

**Sunil Kumar** Department of Environmental Sciences, Maharshi Dayanand University, Rohtak, Haryana, India

**Vinod Kumar** Department of Chemistry, J. C. Bose University of Science and Technology, YMCA, Faridabad, Haryana, India

**Young-Nam Kwon** Department of Urban and Environmental Engineering (UEE), Ulsan National Institute of Science and Technology (UNIST), Ulsan, South Korea

**Dibyajit Lahiri** Department of Biotechnology, University of Engineering and Management (UEM), Kolkata, India

**Srinivasan Latha** Department of Chemistry, School of Advanced Sciences, Vellore Institute of Technology, Vellore, Tamil Nadu, India

**Sanjay S. Latthe** Self-Cleaning Research Laboratory, Department of Physics, RajeRamrao College, Affiliated to Shivaji University, Kolhapur, Maharashtra, India

**R. Lavanya Dhevi** Velalar College of Engineering and Technology, Erode, India

**K. Mahendraprabhu** Department of Chemistry, MEPCO Schlenk Engineering College (Autonomous), Sivakasi, Tamil Nadu, India

**Atri Mallick** School of Materials Science and Nanotechnology, Jadavpur University, Jadavpur, Kolkata, India

**Sakshi Kabra Malpani** Save the Water™, Plantation, Florida, USA

**Manas Mandal** Department of Chemistry, Sree Chaitanya College, Habra, West Bengal, India;

Physical Chemistry Section, Department of Chemistry, Jadavpur University, Kolkata, West Bengal, India

**Abdelmoneim Mars** Desalination and Natural Water Valorization Laboratory (LaDVEN), Water Researches and Technologies Center (CERTE), Soliman, Tunisia

**Alma Mejri** Desalination and Natural Water Valorization Laboratory (LaDVEN), Water Researches and Technologies Center (CERTE), Soliman, Tunisia

**Helvécio C. Menezesand** Departamento de Química, ICEx, Universidade Federal de Minas Gerais, Avenida Antônio Carlos, Belo Horizonte, Minas Gerais, Brazil

**Lucas A. C. Minho** Departamento de Química, ICEx, Universidade Federal de Minas Gerais, Avenida Antônio Carlos, Belo Horizonte, Minas Gerais, Brazil



**Ratnakar Mishra** Cambridge Centre for Brain Repair and MRC Mitochondrial Biology Unit, Department of Clinical Neurosciences, University of Cambridge, Cambridge, UK

**Sang-Hyun Moh** BIO-FD&C Co. Ltd., Incheon, Republic of Korea

**Anandhu Mohan** Department of Biology, Chemistry, and Environmental Sciences, American University of Sharjah, Sharjah, United Arab Emirates

**Prithusayak Mondal** Regional Research Station (Terai Zone), Uttar Banga Krishi Viswavidyalaya, Pundibari, Cooch Behar, West Bengal, India

**Ebrahim Mostafavi** Stanford Cardiovascular Institute, Stanford University School of Medicine, Stanford, CA, USA;  
Department of Medicine, Stanford University School of Medicine, Stanford, CA, USA

**Manish Mudgal** CSIR—Advanced Material and Processes Research Institute, Bhopal, India;  
Academy of Scientific & Innovative Research (AcSIR), Ghaziabad, India

**Saravanan Nagappan** Department of Chemistry, Chemistry Institute for Functional Materials, Pusan National University, Busan, Republic of Korea

**Pradeep Kumar Naik** Centre of Excellence in Natural Products and Therapeutics, Department of Biotechnology and Bioinformatics, Sambalpur University, Burla, Sambalpur, Odisha, India

**Abhishek Nalluri** Department of Materials Science and Engineering, Huazhong University of Science and Technology, Wuhan, China;  
School of Materials Science and Engineering, Huazhong University of Science and Technology, Wuhan, Hubei, China

**Senthilkumar Nallusamy** Department of Electronics and Communication Engineering, M. Kumarasamy College of Engineering, Karur, Tamil Nadu, India

**E. Nandhakumar** School of Mechanical Engineering, Vellore Institute of Technology, Vellore, India

**Suman Nandy** Department of Materials Science CENIMAT-i3N, Center for Materials Research, Faculdade de Ciências e Tecnologia da, Universidade Nova de Lisboa, Caparica, Portugal

**Okechukwu Dominic Onukwuli** Department of Chemical Engineering, Nnamdi Azikiwe University, Awka, Nigeria

**Shemus Ozden** Princeton Center for Complex Materials, Princeton University, Princeton, NJ, USA

**Jyotirmoy Panda** Department of Pharmaceutical Science and Technology, Maulana Abul Kalam Azad University of Technology, Kolkata, India

**Prem Pandey** Symbiosis Centre for Nanoscience and Nanotechnology, Symbiosis International (Deemed University), Pune, India

**Kang Hyun Park** Department of Chemistry, Chemistry Institute for Functional Materials, Pusan National University, Busan, Republic of Korea

**Anju Paul** Sree Sankara Vidyapeetom College, Valayanchirangara, Kerala, India

**S. Pavithra** Biomaterials Research Lab, PG and Research Department of Chemistry, D.K.M. College for Women, Vellore, Tamil Nadu, India

**Danilo Perez** School of Engineering, Computer and Mathematical Science, Auckland University of Technology, Auckland, New Zealand

**Selvakumar Pitchaiya** Department of Engineering and Sciences, Western Norway University of Applied Sciences, Bergen, Norway

**Veerapandian Ponnuchamy** InnoRenew CoE—Renewable Materials and Healthy Environments Research and Innovation Centre of Excellence, Izola, Slovenia; University of Primorska, Andrej Marušič Institute, Koper, Slovenia

**Kandasamy Prabakar** Department of Electrical Engineering, Pusan National University, Busan, Republic of Korea

**Satya Prakash** CSIR—Advanced Material and Processes Research Institute, Bhopal, India; Academy of Scientific & Innovative Research (AcSIR), Ghaziabad, India

**M. Prem Kumar** School of Mechanical Engineering, Vellore Institute of Technology, Vellore, India

**Prasanth Raghavan** Materials Science and NanoEngineering Lab (MSNE-Lab), Department of Polymer Science and Rubber Technology, Cochin University of Science and Technology, Cochin, India; Department of Materials Engineering and Convergence Technology, Gyeongsang National University (GNU), Jinju, Republic of Korea

**Vimala Raghavan** Centre for Nanotechnology Research, Vellore Institute of Technology, Vellore, India

**Rahul** Centre for Nanoscience and Nanotechnology, Panjab University, Chandigarh, India

**Varun Rai** School of Materials Science and Engineering, Nanyang Technological University, Singapore, Singapore; Department of Chemistry, Faculty of Science, University of Allahabad, Prayagraj, Uttar Pradesh, India

**Madhu Raina** Department of Botany, Cluster University of Jammu, Jammu, Jammu and Kashmir, India

**Pankaj Raizda** School of Chemistry, Shoolini University, Bajhol, India

**Prabhu Ramanathan** University West, Division of Production Systems, Trollhattan, Sweden

**Karthikeyan Ramesh** School of Bio Sciences and Technology, Vellore Institute of Technology, Vellore, India

**Settu Ramki** Research Center in Physics of Matter and Radiation (PMR), University of Namur, Namur, Belgium

**S. Ranjitha** Velalar College of Engineering and Technology, Erode, India

**Rachna Rawal** Department of Physics and Astrophysics, University of Delhi, Delhi, India

**Banani Ray Chowdhury** Department of Biotechnology, Bengal Institute of Technology (BIT), Kolkata, India;  
Baranagar Baghajatin Social Welfare Organization, Kolkata, India

**Saikat Sinha Ray** Department of Urban and Environmental Engineering (UEE), Ulsan National Institute of Science and Technology (UNIST), Ulsan, South Korea

**Sagnik Roy** Department of Biotechnology, Bengal Institute of Technology (BIT), Kolkata, India

**Ramiro Rafael Ruiz-Rosas** Departamento de Ingeniería Química, Andalucía Tech., Escuela de Ingenierías Industriales, Universidad de Málaga, Málaga, Spain

**Subhrajeet Sahoo** Centre for Life Sciences, Vidyasagar University, Midnapore, West Bengal, India

**Neha Saini** Symbiosis Centre for Nanoscience and Nanotechnology, Symbiosis International (Deemed University), Pune, India

**Siva Sankar Sana** School of Chemical Engineering and Technology, North University of China, Taiyuan, China

**Debalin Sarangi** Department of Agronomy and Plant Genetics, University of Minnesota, St. Paul, MN, USA

**Haimantika Seel** Department of Clinical Biochemistry and Pharmacology, Faculty of Health Science, Ben Gurion University of the Negev, Beer-Sheva, Israel

**P. Selvakumar** Department of Engineering and Sciences, Western Norway University of Applied Sciences, Bergen, Norway

**N. Senthilkumar** Department of Electronics and Communications Engineering, M. Kumarasamy College of Engineering, Karur, India

**Raj Kishore Sharma** Department of Chemistry, University of Delhi, Delhi, India

**Ramesh K. Sharma** CIL/SAIF/UCIM, Panjab University, Chandigarh, India

**Sonia Sharma** Department of Botany, Cluster University of Jammu, Jammu, Jammu and Kashmir, India

**Mandar Shirolkar** Symbiosis Centre for Nanoscience and Nanotechnology, Symbiosis International (Deemed University), Pune, India

**Ajay Singh** Department of Physics, GGM Science College, Constituent College of Cluster University of Jammu, Jammu, UT-J&K, India

**Archana Singh** CSIR—Advanced Material and Processes Research Institute, Bhopal, India;  
Academy of Scientific & Innovative Research (AcSIR), Ghaziabad, India

**Asha Singh** Department of Environmental Sciences, Maharshi Dayanand University, Rohtak, Haryana, India

**Gurmeet Singh** Department of Chemistry, University of Delhi, Delhi, India;  
Pondicherry University, Chinna Kalapet, Kalapet, Puducherry, India

**Pradeep Singh** School of Chemistry, Shoolini University, Bajhol, India

**Shalu Singh** Department of Chemistry, Bundelkhand University, Jhansi, Uttar Pradesh, India;  
Department of Chemistry, Vellore Institute of Technology, Vellore, Tamil Nadu, India

**Vipendra Kumar Singh** School of Biosciences and Bioengineering, Indian Institute of Technology, Mandi, VPO Kamand, Himachal Pradesh, India

**Vishal Singh** Department of Nanosciences and Materials, Central University Jammu, Jammu, UT-J&K, India

**A. K. Srivastava** CSIR—Advanced Material and Processes Research Institute, Bhopal, India;  
Academy of Scientific & Innovative Research (AcSIR), Ghaziabad, India

**P. N. Sudha** Biomaterials Research Lab, PG and Research Department of Chemistry, D.K.M. College for Women, Vellore, Tamil Nadu, India

**C. Sudhakar** Department of Biotechnology, Mahendra Arts & Science College, Namakkal, Tamil Nadu, India

**Ravuri Syamsai** Nanotechnology Research Center, SRM Institute of Science and Technology, Kattankulathur, Tamil Nadu, India

**Deepika Tavar** CSIR—Advanced Material and Processes Research Institute, Bhopal, India;  
Academy of Scientific & Innovative Research (AcSIR), Ghaziabad, India

**Vijay Kumar Thakur** Biorefining and Advanced Materials Research Centre, SRUC, Parkgate, Barony Campus, DGI 3NE Dumfries, Edinburgh, UK;  
School of Engineering, University of Petroleum & Energy Studies (UPES), Dehradun, India

**Nanasaheb Thorat** Nuffield Department of Women's & Reproductive Health, Division of Medical Sciences, John Radcliffe Hospital, University of Oxford, Oxford, UK

**Anuj Kumar Tomar** Department of Chemistry, University of Delhi, Delhi, India; Department of Nano Convergence Engineering, Jeonbuk National University, Jeonju, Jeonbuk, Republic of Korea

**E. Vaishnavi** Department of Chemistry, Sri GVG Visalakshi College for Women, Udumalpet, India

**Eduard F. Valenzuela** Departamento de Química, ICEx, Universidade Federal de Minas Gerais, Avenida Antônio Carlos, Belo Horizonte, Minas Gerais, Brazil

**M. R. Venkatraman** Department of Physics, Dr. NGP Arts and Science College, Coimbatore, Tamil Nadu, India

**V. Vijayakanth** Center for Nanotechnology Research, Vellore Institute of Technology, Vellore, Tamil Nadu, India

**V. Vinodhini** Center for Nanotechnology Research, Vellore Institute of Technology, Vellore, Tamil Nadu, India

**E. Vivek** Department of Physics, University College of Engineering, BIT Campus, Anna University, Tiruchirappalli, India

**Shashwati Wankar** Symbiosis Centre for Nanoscience and Nanotechnology, Symbiosis International (Deemed University), Pune, India

**Tugrul Yumak** Department of Chemistry, Sinop University, Sinop, Turkey

**Mohammad Yusuf** Department of Chemistry, Chemistry Institute for Functional Materials, Pusan National University, Busan, Republic of Korea

**Alvin Lim Teik Zheng** Department of Science and Technology, Faculty of Humanities, Management and Science, Universiti Putra Malaysia Bintulu Campus, Bintulu, Sarawak, Malaysia

**Part I**  
**Basic Sciences and Engineering**

# Chapter 1

## Synthesis and Fabrication of Advanced Carbon Nanostructures



Anuj Kumar Tomar, Deepak Kumar, Akanksha Joshi, Gurmeet Singh, and Raj Kishore Sharma

### 1 Introduction

Different methods have been adopted by researchers for synthesis of carbon nanostructures; particularly, these synthesis methods are divided into two categories: One is bottom-up and second one is top-down approaches [1–6]. In the bottom-up approach, special emphasis will be given to the use of ionic liquids owing to their low volatility and hence allowing high-yield pyrolysis and covalent organic frameworks as a new low-temperature method for high structural control [7]. With a top-down approach, more focus will be on the metal organic frameworks as sacrificial templates and carbides for nanostructured carbon [8].

#### Bottom-up

- Chemical vapor deposition
- Sol–gel nanofabrication
- Laser pyrolysis synthesis
- Ionic liquid
- Covalent organic framework.

---

A. K. Tomar · D. Kumar · A. Joshi · G. Singh (✉) · R. K. Sharma (✉)  
Department of Chemistry, University of Delhi, Delhi 110007, India  
e-mail: [gurmeet123@yahoo.com](mailto:gurmeet123@yahoo.com)

R. K. Sharma  
e-mail: [drrajksharma@yahoo.co.in](mailto:drrajksharma@yahoo.co.in)

A. K. Tomar  
Department of Nano Convergence Engineering, Jeonbuk National University, Jeonju, Jeonbuk 54896, Republic of Korea

G. Singh  
Pondicherry University, Chinna Kalapet, Kalapet, Puducherry 605014, India

## Top-down

Lithography.

- Chemical/template etching
- MOF-derived carbon
- Carbide-derived carbon and carbon onion.

During the earth civilization, carbon has occupied a significant place mainly in the energy sector and has undergone a drastic transformation from coal as an energy source to activated carbon for electrical energy (batteries, solar cells, supercapacitor, etc.) [9]. The incredible properties of carbon to form linear ( $sp^1$ ), planar ( $sp^2$ ) and tetragonal configuration ( $sp^3$ ), high abundance, and low specific weight have evoked great interest in the scientific community [10]. Over a few years, significant efforts have been made in the development of efficient carbon materials for different applications (energy storage, sensing, energy conversion, and harvesting, etc.); one of the advancements in this direction is the synthesis of carbon nanostructures. Low-dimensional materials with dimensions of structural elements (clusters, crystallites, or molecules) in the range of 1–100 nm are chiefly defined as nanostructured carbons. There is an entire range of dimensionality in the carbon nanostructures from zero-dimensional (fullerenes), one-dimensional (carbon nanotubes), two-dimensional (graphene sheets), to three-dimensional (fullerites, CNT ropes) with one another form “inverted carbons” that are basically mesoporous materials [11]. Nanodimension carbon structures comprise distinctiveness in the form of superior electrical conductivity, high surface area volume ratio, high porosity with outstanding mechanical, chemical, thermal, and optical properties [12]. In energy storage and conversion application, the role of nanostructuring is vast, and some of them are pointed here [13–16]:

- Nanostructuring provides more active sites for charge storage.
- High surface area owes to nanostructuring ensures a large contact between electrode and electrolyte.
- Stress generated during electrochemical reactions also gets reduced due to porous structure.
- Hollow and porous surfaces also provide spaces for filling other guest materials and hence can be used in multifunctional applications.
- Porous network also reduces the ionic diffusion length.

Hence, owing to these advantages, enormous research has been carried out to investigate the mechanism involved in controlling the dimension and surface chemistry of nanostructures. There are several ways in which nanostructuring can be done such as chemical vapor deposition, pyrolysis, covalent organic framework based, template oriented, and hydrothermal treatment, etc. [3]. On the basis of the process involved during synthesis, these methods are divided into two approaches: bottom-up and top-down. The bottom-up approach involves the building of structures from small atoms and molecules through covalent or other force interactions, whereas the top-down approach involves the etching of bulk structures to generate the needed



low-dimensional structures. Basically, the bottom approach is mainly focused on controlling the dimension, and a top-down approach is used to generate hollow or porous regions in the structures. However, with a top-down approach, the chances of defects generation and quantum effect increase due to the synthesis of small dimensions. The origination of defects with the nanostructuring would have an impact on the properties of carbon nanostructures. Therefore, in most cases, the combination of these approaches is carried out which is named a hybrid approach [17]. In this chapter, some of the particular bottom-up approaches and top-down approaches have been discussed that are majorly used by the researchers in pursuit of controlling the nanostructures.

Nanostructures are synthesized either by a bottom-up or top-down approach. The bottom-up approach relies on the attractive forces between the building blocks, whereas in the top-down approach, large materials are deconstructed to give nanostructures [5, 6]. Though these approaches comprise various synthesis methods, the chapter will be confined to some recent non-traditional synthesis methods.

## 2 Bottom-Up Approach

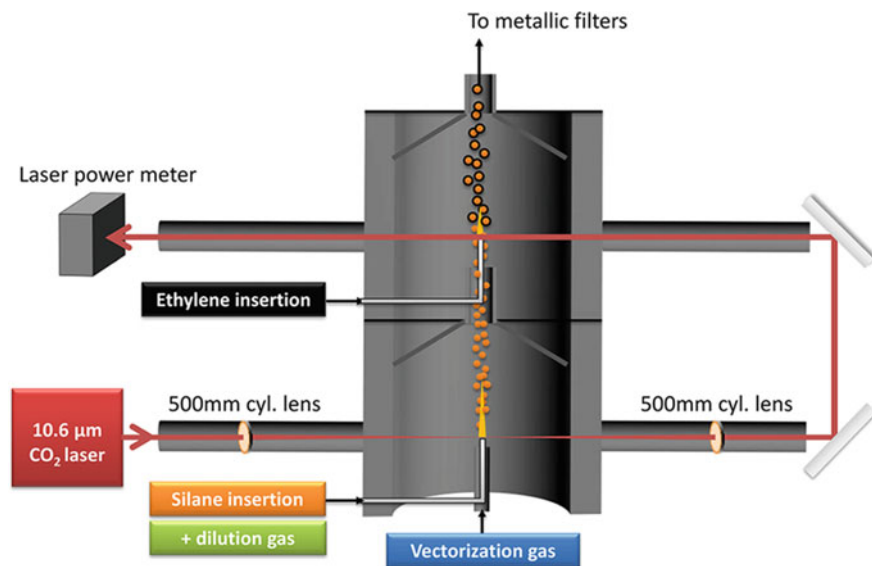
### 2.1 Chemical Vapor Deposition

In CVD, decomposition of gas-phase molecules to reactive species results in thin films with controlled stoichiometry and morphology. CVD allows for controlled deposition rates to give high-quality products having desired conformality [18]. Recently, the synthesis of carbon nanospheres via a non-catalytic chemical vapor deposition using low-rate acetylene gas with nitrogen gas was reported [19]. This strategy resulted in fluffy carbon nanospheres with spherical shape and regular size.

A new dimension to this synthesis method was added by Fischer and coworkers, where they combined CVD and template synthesis [20]. With this combined approach, graphitic carbon nanofibers were obtained. These are open-ended uniform hollow tubes and can be converted to carbon nanofibers with increasing deposition time. Although the crystallinity of CVD grown nanotubes is low, it is superior to other methods in terms of yield and purity.

### 2.2 Laser Pyrolysis

This is a recent method for the synthesis of nanoscale particles especially for carbides (Fig. 1). In laser pyrolysis, a dilute mixture of vaporized precursors is decomposed by a laser to initiate nucleation. These nuclei aggregate and transported by inert gas and depending on the amount of air different nanoparticles are formed. Owing to



**Fig. 1** Schematic representation of two-stage configuration reactor for laser pyrolysis. Reprinted with permission from Sourice et al. [21]. Copyright 2015 American Chemical Society

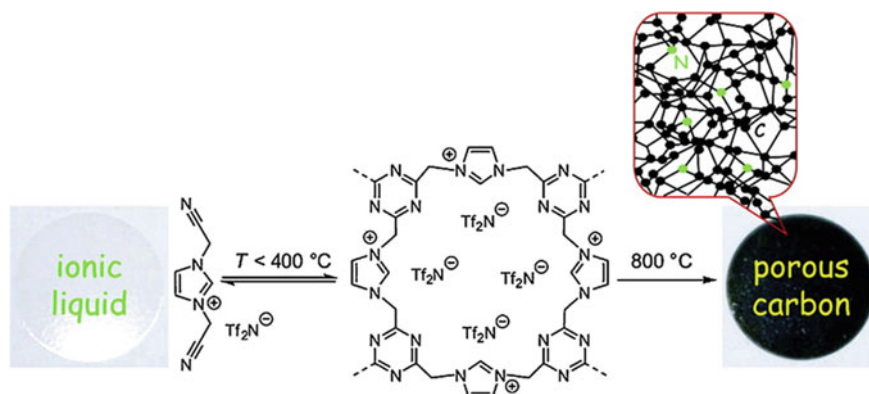
the fast nucleation and very short time in the reaction chamber, this method yields smaller nanoparticles than other vapor-phase methods.

One-step synthesis of silicon-carbon nanoparticles using laser pyrolysis was reported by Reynaud and coworkers [21]. The authors utilized a CO<sub>2</sub> laser to vaporize the reactants and beautifully utilized the working principle of laser pyrolysis. In the typical synthesis, firstly in the bottom stage, silicon cores are synthesized and transferred to the upper stage with a carrier gas where a carbon shell is deposited. This configuration prevents aerial oxidation of silicon surface. Silicon-carbon nanoparticles formed by this method were found to be very efficient for application in lithium-ion batteries with improved cycling stability.

### 2.3 Ionic Liquids

Although ionic liquids were discovered decades ago, their application to derive carbon materials is a relatively new emerging field. There are a variety of benefits that ILs offer,

- (i) most general is their negligible vapor pressure allowing much easier shaping, processing, and high yield under ambient thermal treatment,
- (ii) availability of a wide range of different cation/anion pairing enables a wide range of carbon nanostructures with varying heteroatoms,



**Fig. 2** Synthesis route for TSILs-derived N-doped porous carbon. Reprinted with permission from Lee et al. [23]. Copyright 2009 American Chemical Society

(iii) as ILs are good solvents so carbon composites with various other substances can be easily prepared by simply mixing.

Functional groups can be selectively introduced in ILs depending on the type of carbon required. Davis coined the term task-specific ionic liquids (TSILs) for ILs having specific functional groups attached for the desired property [22] as shown in Fig. 2. They selected ILs containing a nitrile group so that it can undergo cross-linking. They studied the effect of cations using 1-cyanomethyl-3-methylimidazolium [MCNIm]<sup>+</sup> and 1,3-bis(cyanomethyl)imidazolium [BCNIm]<sup>+</sup> and interestingly found that rather than cation, the surface properties of carbonaceous materials are affected to a great extent by anion. BET surface area of bis(trifluoromethylsulfoniylmide) ([Tf<sub>2</sub>N]<sup>-</sup>) and Cl<sup>-</sup> was found to be 700 m<sup>2</sup>/g and 10 m<sup>2</sup>/g, respectively [23]. Similarly, for [C(CN)<sub>3</sub>]<sup>-</sup> anion species, BET surface area was found to be 90 m<sup>2</sup>/g, whereas boron and nitrogen-doped carbon from [B(CN)<sub>4</sub>]<sup>-</sup> anion exhibits BET surface area of 500 m<sup>2</sup>/g [24].

Nowadays, ILs containing more than one type of cation/anion forming complex supramolecular structure, referred to as deep eutectic solvents (DES), were discovered. When quaternary ammonium salts in ILs complexes with hydrogen bond donors, then hydrogen bonding facilitates charge delocalization resulting in a eutectic mixture with a reduced melting point is formed.

Carbon and carbon-carbon nanotube composites can be obtained by using a choice of DES [25]. They utilized DES composed of ethylene glycol and CCl<sub>4</sub> to dissolve the reactants (resorcinol and formaldehyde). On heating monolith, resins were formed which were carbonized using thermal treatment. Results indicated high surface area for DES-based carbon monoliths than monoliths derived from aqueous media due to the structure effect of DES. Furthermore, it was found that MWCNTs form a homogeneous dispersion in DES by simple addition. This fact was observed in the SEM micrographs where MWCNTs were uniformly distributed in DES as compared to aqueous solvents.

Although ILs are gaining much importance for designing functional carbon materials, in-depth investigation of the correlation between precursor and carbon nanostructure is required to design novel need tailored materials.

## 2.4 Covalent Organic Frameworks (COFs)

Covalent organic frameworks are porous crystalline polymers composed of ordered periodic building block skeletons extended in 2/3-dimensions. They provide a low-temperature synthesis method for crystalline carbonaceous materials with a controlled structure. Based on the building blocks, different geometries and dimensions can be obtained. COFs are usually classified based on the linkage topology involved. These include (i) B–O (borates), (ii) C=N (imines), (iii) C=N<sub>aromatic</sub> (azines), (iv) C=C (alkenes), (v) C–N ( $\beta$ -ketoenamines), and (vi) B=N (borazines) [26]. Among these, C–N linkage possess high structural stability even in strong acids.

Depending on the requirement, robust materials can be designed by Schiff's base reaction of amines with aldehydes resulting in imines. Based on this strategy, Feng group reported the synthesis of the wafer-sized multifunctional conjugated polymer [27]. They carried out this synthesis of the 2D multifunctional polymer at the air–water interface by Schiff's base polycondensation. Owing to the high stability of C=N, this polymer possesses a Young's modulus comparable to graphene and conjugation lowers the band gap to 1.4 eV making it suitable for semiconductors.

## 3 Top-Down Approach

### 3.1 Lithography

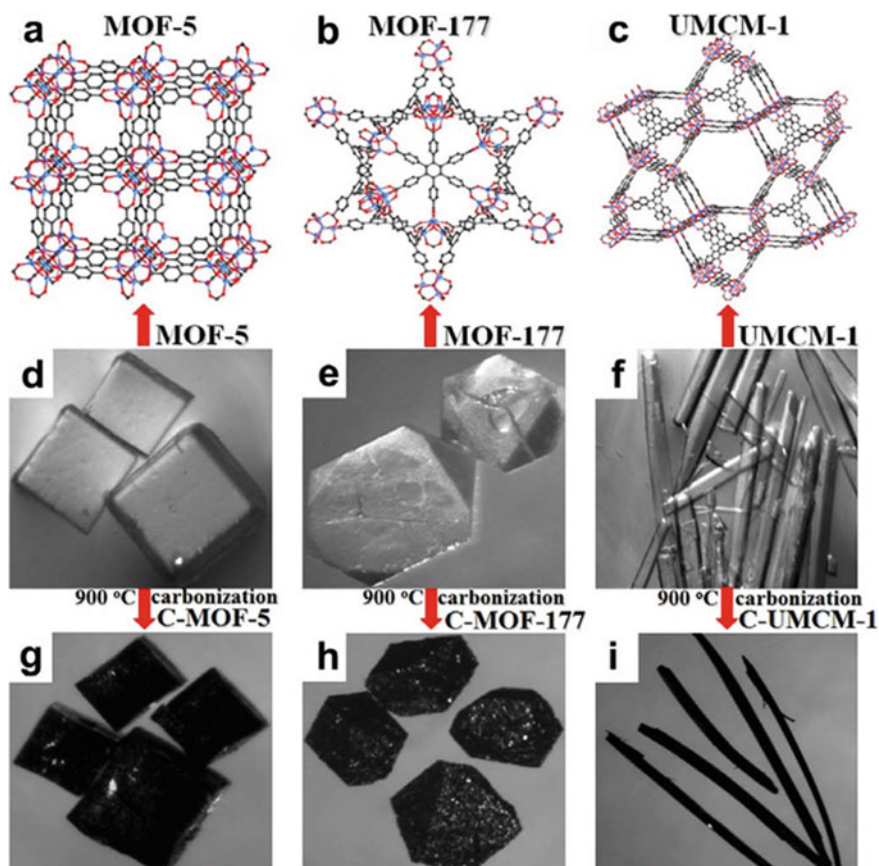
The term lithography originated from the Greek word *lithos* meaning stone and *graphein* meaning to write. Traditional lithography can generate various patterns by masking the required material and etching the exposed surface. Etching can be done by either chemicals or mechanically using high-energy electron beams. This gives rise to different types of lithography like optical lithography, soft lithography, block copolymer lithography, scanning probe, nanoimprint lithography, etc. Here, we will restrict our discussion to the recently emerged advanced technique, nanoimprint lithography (NIL) only. This is the most important lithographic technique for designing advanced nanostructures due to its ability to generate high-resolution nanopatterns with high throughput and low cost [28]. In conventional methods, the resolution is limited due to diffraction or beam scattering but in NIL, there is no such restriction. In NIL, a nanostructured mold is pressed on substrate precoated with a polymeric material. NIL is further classified as—thermoplastic, photo, and electrochemical NIL. In thermoplastic NIL, the substrate is modified with a thin layer of a

thermoplastic polymer. This is pressed with a patterned mold at the desired pressure. On heating, the polymer above glass transition temperature results in the required pattern on polymer [29]. In photo NIL, a substrate is modified with a photo-sensitive resist, and the mold is made transparent. After pressing in UV light, the resist becomes solid, and the pattern is transferred. Usually, polydimethylsiloxane (PDMS) is used for the transparent stamp as it offers a high-resolution pattern, and its low surface energy makes it easy to separate [30]. Fang group reported the use of stamps made of silver sulfide, a superionic conductor using electrochemical nanoimprint lithography (ECNIL) [31]. Henceforth pressing, when voltage is applied, it results in electrochemical etching to give the required pattern. Using ECNIL, three-dimensional micro-nanostructures (3D-MNS) were synthesized where ECNIL allowed for the synthesis of 3D-MNS with multilevel and continuously curved profiles on a crystalline GaAs wafer [32]. This suggests the high potential of ECNIL in semiconductor materials.

### 3.2 MOF-Derived Carbons

Metal organic frameworks (MOFs) consist of a regular array of metal ions and organic linkers to give crystalline porous materials [33, 34]. Uniform pore structure with tunable porosity makes them attractive candidates for various applications. To derive high surface area carbon, they can be directly carbonized or can be used as a template [35–38]. In 2008, the first synthesis of porous carbon from the MOF template was reported [35]. They carbonized furfuryl alcohol (additional carbon source) filled MOF-5 at 1000 °C. Such a high temperature helped in removing vaporized Zn metal with inert gas flow and attained metal-free carbon. The resulting carbon exhibited a high specific surface area of 2872 m<sup>2</sup> g<sup>-1</sup>, useful for charge storing applications. This process was further refined by selecting particular MOFs to reduce the need of additional carbon sources to reduce the number of steps involved. It was found that using ZIF-8 as precursor, high surface area (3148 m<sup>2</sup> g<sup>-1</sup>) carbon can be obtained without additional carbon [39].

Later on, it was realized that for some applications, bare carbon is not sufficient, and some heteroatoms may be useful for chemical functionalities and desired properties; heteroatom-doped carbon materials were searched. Here, zeolitic imidazole frameworks (ZIFs) seemed to be a suitable precursor for such materials. The same can be achieved by encapsulating the desired heteroatom rich molecule in MOF pores and then carbonizing the MOF. Using this strategy, synthesis of N, P, and S ternary-doped metal-free carbon from MOF was reported previously [40]. They selected MOF-5 as a template with dicyandiamide, with two heteroatom precursors (triarylphosphine and dimethylsulphoxide) to give high-performance carbon owing to the synergistic effect of heteroatoms (Fig. 3).



**Fig. 3** a–c Representative 3D structures, d–i optical micrographs before and after carbonization for MOF-5, MOF-177, and UMCM-1. Reprinted with permission from Li et al. [40]. Copyright 2014 Springer Nature

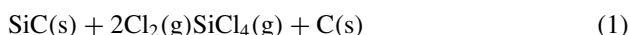
Although MOFs offer several advantages over traditional methods like tunable morphology, porosity, and heteroatom doping, there are some challenges to be considered. There is a strong need for low-cost synthesis methods for MOFs, and also, high-temperature carbonization makes it difficult to have full control over morphology. So, low temperature and cost-effective methods are required to expand the use of MOFs.

### 3.3 Carbide-Derived Carbon (CDC)

CDC is a collective term used for carbon derived from binary/ternary carbides (MAX phase) [41]. Depending on the method of metal removal and various experimental conditions, a variety of carbon nanostructures can be obtained. In this method, selective removal of metal atoms does not disturb the parent structure. The most common methods used in CDC are halogenation, hydrothermal treatment, and vacuum decomposition [42].

#### (i) Halogenation

Selective removal of metal atoms from carbide was first reported in 1918 [43]. In this method, carbon was formed as a byproduct of treating dry chlorine gas with hot silicon carbide.



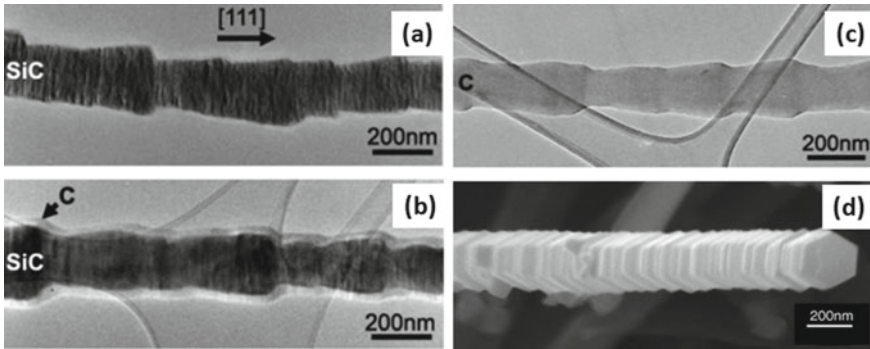
Annealing of resulting porous carbon will remove residual chlorine. Halogenation of carbides up to 1000 °C produces disordered carbon, whereas above 1000 °C graphitization predominates. Although fluorine can also be used for some metal carbides but direct fluorination is aggressive and will result in either fluorocarbon or disintegrated SiC films. Using XeF<sub>2</sub> for etching was found to produce non-fluorinated SiC that also at low temperature (120 °C) than the conventional chlorination method [44]. These equations and the choice of halogen become more complex in the case of ternary carbides due to the possibility of the formation of more than one solid reaction product.

CDC formation from carbides through halogenation is also known as conformal transformation as it maintains the shape and volume of the parent carbide precursor [45, 46]. This fact was recently confirmed that even for a carbide precursor-like β-SiC having complex morphology, it maintains it on chlorination [47] (Fig. 4). A similar conformal transformation was observed for polymer-derived carbides (PDC) also [48, 49].

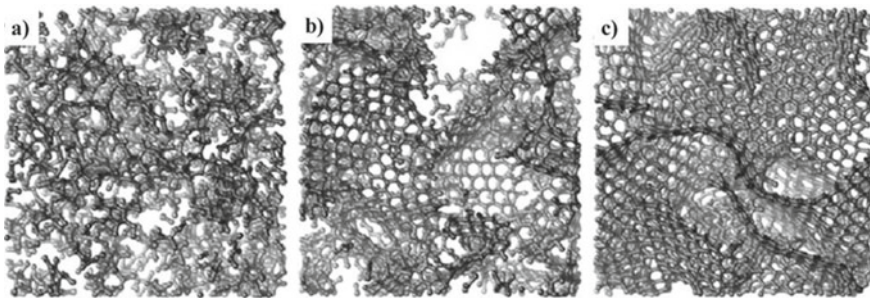
The structure of CDC mainly depends on carbide precursor and temperature. For TiC, the effect of halogenation temperature was studied and the results indicated that with increase in temperature, there is a constant increase in ordered structure (Fig. 5). Whereas at low temperatures, amorphous carbon was found. These results were further supported by quenched molecular dynamics (QMD) studies [50, 51].

#### (ii) Hydrothermal treatment

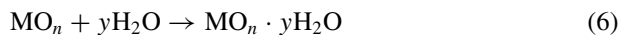
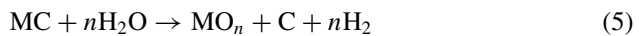
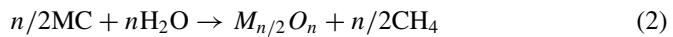
The hydrothermal method was first described for the synthesis of Tyranno (Si–Ti–C–O) fibers in the 1990s. In this method, the metal carbides area is treated with supercritical water at high pressure in the temperature range of 200–1000 °C [52, 53]. Jacobson performed Gibbs energy minimization for a large number of metal carbides at various temperatures and pressures under hydrothermal conditions [54] and found some common reaction products including carbon, MO<sub>x</sub>, CH<sub>4</sub>, CO<sub>2</sub>, CO, and H<sub>2</sub> according to the following equations:



**Fig. 4** TEM micrographs of  $\beta$ -SiC at various chlorination stages, **a** as received, **b** chlorinated at 700 °C, and **c** at 1200 °C. **d** SEM micrograph showing the conformal transformation. Reprinted with permission from Cambaz et al. [47]. Copyright 2006 John Wiley and Sons



**Fig. 5** Simulated structures of TiC-CDC quenched at different rates **a** 600 °C/fast quenching, **b** 800 °C/medium quenching, and **c** 1200 °C/slow quenching. Reprinted from Palmer et al. [51]. Copyright 2010 Elsevier



Experimental studies indicated that water/carbide (SiC) ratio is an important factor for deciding the yield. When this ratio is small, both carbon and silica are deposited



and for intermediate ratio both are formed but due to excess of water, silica gets dissolved. At a high ratio, neither carbon nor silica was formed.

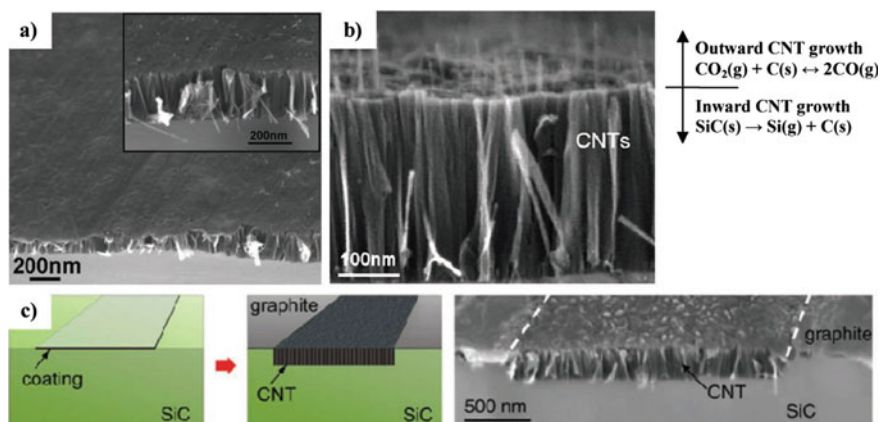
The hydrothermal method produces amorphous carbon as indicated by the appearance of D and G bands in the Raman spectra of the product. But in the case of ternary carbides, the metal oxide phase may be present. As in  $Ti_3Si_2C$ , on hydrothermal treatment rutile/anatase was reported along with carbon [55]. The use of organic compounds like polyethylene was found to produce carbon nanotubes [56].

### (iii) Thermal decomposition

Metal carbides on thermal decomposition in the vacuum will also generate CDC. It is based on the principle of incongruent decomposition. As the melting of carbon is higher than that of carbide, it remains while carbide evaporates. This method is also a conformal process like halogenation, and due to high temperatures, carbon nanostructures thus produced are more ordered. Using this method, Kusunoki group reported epitaxial carpets of self-organized carbon nanotubes (CNTs) from SiC [57]. Interestingly, this was the first time when no metal catalyst was used to obtain CNTs of the same chirality. They also presented a model to explain the mechanism of CNT formation based on residual oxygen. According to this, residual oxygen is the driving force; at low temperatures ( $< 1000\text{ }^\circ\text{C}$ ), only graphite sheets are formed no CNT were formed. At temperatures around  $1300\text{ }^\circ\text{C}$ , there is SiO gas generated which forms nanotubes (Fig. 6).

This method can also be used to produce graphene from SiC either by vacuum decomposition or heating in an inert environment. Its formation mechanism is as that for CNT assuming that prior to CNT formation, there is the formation of a thin graphene layer [58–61].

Comparisons of various properties are given in Table 1.



**Fig. 6** SEM micrographs of vacuum decomposed 6H-SiC carbon nanostructures for **a** C-face oriented in high vacuum and **b** Si-face oriented in low vacuum. **c** Effect of surface modification on CNT growth. Reprinted with permission from Cambaz et al. [50]. Copyright 2008 Elsevier

**Table 1** Comparison of various properties of carbon materials discussed

Sr. No.	Precursor	Active material	Surface are ( $\text{m}^2 \text{g}^{-1}$ )/diameter (nm)	Application	References
1	Acetylene and nitrogen	Carbon nanospheres	100–200 nm	Sensors, photo-catalysis, and opto-electronic devices	[19]
2	$\text{C}_2\text{H}_4$ and $\text{SiH}_4$	Carbon covered silicon nanoparticles	$156 \text{ m}^2 \text{ g}^{-1}$	Li-ion batteries	[21]
3	Task specific ionic liquid	N-doped carbon	$\leq 800 \text{ nm}$	Carbon coating, $\text{CO}_2$ capture	[23]
4	Ionic liquids	Boron and nitrogen rich carbon	$537 \text{ m}^2 \text{ g}^{-1}$	$\text{CO}_2$ adsorption, $\text{CO}_2/\text{N}_2$ separation	[24]
5	Resorcinol–formaldehyde	Carbon–carbon nanotube	$350 \text{ m}^2 \text{ g}^{-1}$	–	[25]
6	Covalent organic framework	2D-conjugated polymer	–	Semiconductor, electrocatalysis	[27]
7	Metal organic framework	Porous carbon	$2872 \text{ m}^2 \text{ g}^{-1}$	Supercapacitor	[35]
8	Metal organic framework	Nonporous carbon	$3405 \text{ m}^2 \text{ g}^{-1}$	Supercapacitor, hydrogen storage	[39]
9	Metal organic framework	Heteroatom-doped porous carbon	$548 \text{ m}^2 \text{ g}^{-1}$	Electrocatalysis	[40]
10	Carbide-derived carbon	Carbon fibers	$3116 \text{ m}^2 \text{ g}^{-1}$	Adsorption	[48]

Using the above methods, a variety of carbon nanostructures can be synthesized. Aggregation of atomic sheets of 2D materials like graphene hinders its applications and requires advanced methods to prevent it. Some important methods are:

(1) Shape/orientation modified growth of graphene

Synthesis of graphene directly on the substrate leads to restacking but one way to avoid this is to synthesize vertically oriented graphene. Using the CVD method, vertically oriented graphene was synthesized on Ni substrate where mostly edges are exposed and fully accessible [62]. On some substrates when this is not possible then instead of flat graphene sheets, modification of the shape of graphene to curved or crumpled sheets will also prevent aggregation. This modification provides additional surface area and pore volume essential for several applications [63].

(2) Intercalated graphene

After exfoliation, insertion of typical guest molecules in graphene interlayers is an effective strategy to prevent aggregation with a maintained flat sheets structure. To date, various spacers have been reported including metal nanoparticles, carbon nanotubes, conducting polymers, etc. Based on the type of application, the interlayer gallery height can be fine-tuned by selecting definite spacers. Recently, polyoxometalates (an emerging class of materials) have been reported as a spacer [64]. Polyoxometalates not only prevented aggregation but also provided additional redox-active sites for charge storage.

(3) 3D interconnected graphene

This strategy is utilized in certain cases when no foreign element other than graphene is required. Interconnection of a large number of 2D nanosheets results in a complex 3D network. In this complex network, each graphene sheet is supported by other sheets, resulting in a porous structure having a very low tendency to aggregate. Although there are a variety of materials reported with the 3D networks, graphene hydrogels are the important ones. In the simplest way, hydrothermal reduction of graphene oxide will induce cross-linking at multiple points leading to the hydrogel. This generates a porous structure with vast pore size distribution making it useful for a large number of applications [65].

## 4 Conclusion

The peculiar properties of carbon nanostructures require the attention of researchers to develop advanced synthesis approaches. There are many ways to synthesize carbon materials, where the structures and functions are governed by the processing conditions and precursors used. Depending on the requirement and initial conditions available, this chapter summarizes various methods for the top-down and bottom-up synthesis of carbon nanostructures. Among different approaches, some are outdated

and traditional methods that are inefficient to fulfill the present need of advanced nanostructures. This chapter discusses some of the recent methods comprising high yield and ecofriendly nature including laser pyrolysis, ionic liquids precursor, etc. Independently, both these approaches can generate different nanostructures with unique properties; however, they suffer from their limitations which demand consideration toward the generation of some new techniques comprising both top-down and bottom-up approaches for developing novel materials in various research fields.

**Acknowledgements** Authors gratefully acknowledge the financial support received from Science and Engineering Research Board Grant No. EMR/2016/002846. Financial support received from the Institute of Eminence is gratefully acknowledged. Deepak Kumar is grateful to CSIR for the financial support through SRF fellowship (09/045(1632)/2019-EMR-1). Akanksha Joshi thankfully acknowledges the financial support through SRF fellowship (09/045(1422)/2016-EMR-1).

## References

1. Casco ME, Martínez-Escandell M, Gadea-Ramos E, Kaneko K, Silvestre-Albero J, Rodríguez-Reinoso F (2015) High-pressure methane storage in porous materials: are carbon materials in the pole position? *Chem Mater* 27:959–964
2. Sahu V, Shekhar S, Sharma RK, Singh G (2015) Ultrahigh performance supercapacitor from lacey reduced graphene oxide nanoribbons. *ACS Appl Mater Interfaces* 7(5):3110–3116
3. Borchardt L, Zhu QL, Casco ME, Berger R, Zhuang X, Kaskel S, Feng X, Xu Q (2017) Toward a molecular design of porous carbon materials. *Mater Today* 20:592–610
4. Joshi A, Sahu V, Singh G, Sharma RK (2019) Performance enhancement of a supercapacitor negative electrode based on loofah sponge derived oxygen rich carbon through encapsulation of MoO<sub>3</sub> nanoflowers. *Sustainable Energy Fuels* 3:1248–1257
5. Bellah MM, Chistensen SM, Iqbal SM (2012) Nanostructures for medical diagnostics. *J Nanomater*
6. Yu HD, Regulacio MD, Ye E, Han MY (2013) Chemical routes to top-down nanofabrication. *Chem Soc Rev* 42(14):6006–6018
7. Wan MM, Sun XD, Li YY, Zhou J, Wang Y, Zhu JH (2016) Facilely fabricating multifunctional N-enriched carbon. *ACS Appl Mater Interfaces* 8:1252–1263
8. Sato H, Matsuda R, Sugimoto K, Takata M, Kitagawa S (2010) Photoactivation of a nanoporous crystal for on-demand guest trapping and conversion. *Nat Mater* 9:661–666
9. Yang Z, Ren J, Zhang Z, Chen X, Guan G, Qiu L, Zhang Y, Peng H (2015) Recent advancement of nanostructured carbon for energy applications. *Chem Rev* 115(11):5159–5223
10. Sun Q, Zhang R, Qiu J, Liu R, Xu W (2018) On-surface synthesis of carbon nanostructures. *Adv Mater* 30:1705630
11. Hoseisel TN, Schreftl S, Szilluweit R, Frauenrath H (2010) Nanostructured carbonaceous materials from molecular precursors. *Angew Chem Int Ed* 49:6496–6515
12. Kwiatkowski M, Policicchio A, Seredych M, Bandosz TJ (2016) Evaluation of CO<sub>2</sub> interactions with S-doped nanoporous carbon and its composites with a reduced GO: effect of surface features on an apparent physical adsorption mechanism. *Carbon* 98:250–258
13. Joshi A, Singh G, Sharma RK (2020) Engineering multiple defects for active sites exposure towards enhancement of Ni<sub>3</sub>S<sub>2</sub> charge storage characteristics. *Chem Eng J* 384:123364
14. Joshi A, Lalwani S, Singh G, Sharma RK (2019) Highly oxygen deficient, bimodal mesoporous silica-based supercapacitor with enhanced charge storage characteristics. *ElectrochimActa* 297:705–714

15. Tomar AK, Joshi A, Singh G, Sharma RK (2020) Triple perovskite oxide as an advanced pseudocapacitive material: multifarious element approach with an ordered structure. *J Mater Chem A* 8:24013–24023
16. Joshi A, Tomar AK, Singh G, Sharma RK (2021) Engineering oxygen defects in the boron nanosheet for stabilizing complex bonding structure: an approach for high-performance supercapacitor. *Chem Eng J* 407:127122
17. Wei Q, Xiong F, Tan S, Huang L, Lan EH, Dunn B, Mai L (2017) Porous one-dimensional nanomaterials: design, fabrication and applications in electrochemical energy storage. *Adv Mater* 29:1602300
18. Sun L, Yuan G, Gao L, Yang J, Chhowalla M, Gharahcheshmeh MH, Liu Z (2021) Chemical vapour deposition. *Nat Rev Methods Primers* 1(5)
19. Faisal AD, Aljubouri AA (2016) Synthesis and production of carbon nanospheres using noncatalytic CVD method. *Int J Adv Mater Res* 2(5):86–91
20. Che G, Lakshmi BB, Martin CR, Ruoff RS, Fisher ER (1998) Chemical vapor deposition-based synthesis of carbon nanotubes and nanofibers using a template method. *Chem Mater* 10:260–267
21. Sourice J, Quinsac A, Leconte Y, Sublemontier O, Porcher W, Haon C, Bordes A, Vito ED, Boulineau A, Larbi SJS, Herlin-Boime N, Reynaud C (2015) One-step synthesis of Si@C nanoparticles by laser pyrolysis: high-capacity anode material for lithium-ion batteries. *ACS Appl Mater Inter* 7:6637–6644
22. Davis JHJ (2004) Task-specific ionic liquids. *Chem Lett* 33(9):1072–1077
23. Lee JS, Wang X, Luo H, Baker GA, Dai S (2009) Facile ionothermal synthesis of microporous and mesoporous carbons from task specific ionic liquids. *J Am Chem Soc* 131(13):4596–4597
24. Fulvio PF, Lee JS, Mayes RT, Wang X, Mahurin SM, Dai S (2011) Boron and nitrogen-rich carbons from ionic liquid precursors with tailorable surface properties. *PhysChemChemPhys* 13:13486–13491
25. Gutierrez MC, Rubio F, del Monte F (2010) Resorcinol-formaldehyde polycondensation in deep eutectic solvents for the preparation of carbons and carbon-carbon nanotube composites. *Chem Mater* 22:2711–2719
26. Diercks CS, Yaghi OM (2017) The atom, the molecule, and the covalent organic framework. *Science* 355:eaal1585
27. Sahabudeen H, Qi H, Glatz BA, Tranca D, Dong R, Hou Y, Zhang T, Kuttner C, Lehnert T, Seifert G, Kaiser U, Fery A, Zheng Z, Feng X (2016) Wafer-sized multifunctional polyimine-based two-dimensional conjugated polymers with high mechanical stiffness. *Nat Commun* 7:13461
28. Chou SY, Krauss PR, Renstrom PJ (1996) Imprint lithography with 25-nanometer resolution. *Science* 272:85–87
29. Barcelo S, Li Z (2016) Nanoimprint lithography for nanodevice fabrication. *Nano Converg Korea Nano Technol Res Soc* 3(1):21
30. Traub MC, Longsine W, Truskett VN (2016) Advances in nanoimprint lithography. *Annu Rev Chem Biomol Eng* 7(1):583–604
31. Hsu KH, Schultz PL, Ferreira PM, Fang NX (2007) Electrochemical nanoimprinting with solid-state superionic stamps. *Nano Lett* 7(2):446–451
32. Zhang J, Zhang L, Han L, Tian ZW, Tian ZQ, Zhan D (2017) Electrochemical nanoimprint lithography: when nanoimprint lithography meets metal assisted chemical etching. *Nanoscale* 9:7476–7482
33. Furukawa H, Cordova KE, O’Keeffe M, Yaghi OM (2013) The chemistry and applications of metal-organic frameworks. *Science* 341:1230444
34. Zhu QL, Xu Q (2014) Metal-organic framework composites. *Chem Soc Rev* 43(16):5468–5512
35. Liu B, Shioyama H, Akita T, Xu Q (2008) Metal-organic framework as a template for porous carbon synthesis. *J Am Chem Soc* 130(16):5390–5391
36. Xia W, Mahmood A, Zou R, Xu Q (2015) Metal-organic frameworks and their derived nanostructures for electrochemical energy storage and conversion. *Energy Environ Sci* 8:1837–1866

37. Shen K, Chen X, Chen J, Li Y (2016) Development of MOF-derived carbon-based nanomaterials for efficient catalysis. *ACS Catal* 6(9):5887–5903
38. Wang H, Zhu QL, Zou R, Xu Q (2017) Metal-organic frameworks for energy applications. *Chem* 2(1):52–80
39. Jiang HL, Liu B, Lan YQ, Kuratani K, Akita T, Shioyama H, Zong F, Xu Q (2011) From metal-organic framework to nanoporous carbon: toward a very high surface area and hydrogen uptake. *J Am Chem Soc* 133(31):11854–11857
40. Li JS, Li SL, Tang YJ, Li K, Zhou L, Kong N, Lan YQ, Bao JC, Dai ZH (2014) Heteroatoms ternary-doped porous carbons derived from MOFs as metal-free electrocatalysts for oxygen reduction reaction. *Sci Rep* 4:5130
41. Presser V, Heon M, Gogotsi Y (2011) Carbide-derived carbons—from porous networks to nanotubes and graphene. *Adv Funct Mater* 21(5):810–833
42. Roy R, Ravichandran D, Badzian A, Brevet E (1996) Attempted hydrothermal synthesis of diamond by hydrolysis of b-SiC powder. *Diam Relat Mater* 5(9):973–976
43. Hutchins O (1918) US Patent 1271713
44. Batisse N, Guerin K, Dubois M, Hamwi A, Spinelle L, Tomasella E (2010) Fluorination of silicon carbide thin films using pure F<sub>2</sub> gas or XeF<sub>2</sub>. *Thin Solid Films* 518:6746
45. Chen L, Behlau G, Gogotsi Y, McNallan MJ (2003) Carbothermal synthesis of boron nitride coatings on silicon carbide. *J Am Ceram Soc* 86(11):1830–1837
46. Ersoy DA, McNallan MJ, Gogotsi YG (2001) Carbon coatings produced by high temperature chlorination of silicon carbide ceramics. *Mater Res Innov* 5:55–62
47. Cambaz ZG, Yushin GN, Gogotsi Y, Vyshnyakova KL, Pereselentseva LN (2006) Formation of carbide-derived carbon on  $\beta$ -silicon carbide whiskers. *J Am Ceram Soc* 89:509
48. Rose M, Kockrick E, Senkovska I, Kaskel S (2010) High surface area carbide-derived carbon fibers produced by electrospinning of polycarbosilane precursors. *Carbon* 48(2):403–407
49. Yeon SH, Reddington P, Gogotsi Y, Fischer JE, Vakifahmetoglu C, Colombo P (2010) Carbide-derived-carbons with hierarchical porosity from a preceramic polymer. *Carbon* 48:201–210
50. Cambaz ZG, Yushin G, Osswald S, Mochalin V, Gogotsi Y (2008) Noncatalytic synthesis of carbon nanotubes, graphene and graphite on SiC. *Carbon* 46:841–849
51. Palmer JC, Llobet A, Yeon SH, Fischer JE, Shi Y, Gogotsi Y, Gubbins KE (2010) Modeling the structural evolution of carbide-derived carbons using quenched molecular dynamics. *Carbon* 48:1116–1123
52. Gogotsi Y, Yoshimura M (1994) Formation of carbon films on carbides under hydrothermal conditions. *Nature* 367:628–630
53. Gogotsi Y, Yoshimura M (1994) Water effects on corrosion behavior of structural ceramics. *MRS Bull* 19(10):39–45
54. Jacobson NS, Gogotsi YG, Yoshimura M (1995) Thermodynamic and experimental study of carbon formation on carbides under hydrothermal conditions. *J Mater Chem* 5:595–601
55. Zhang H, Presser V, Berthold C, Nickel KG, Wang X, Raisch C, Chasse T, He L, Zhou Y (2010) Mechanisms and kinetics of the hydrothermal oxidation of bulk titanium silicon carbide. *J Am Ceramic Soc* 93(4):1148–1155
56. Gogotsi Y, Libera JA, Naguib N (2002) In situ chemical experiments in carbon nanotubes. *Chem Phys Lett* 365(3–4):354–360
57. Kusunoki M, Rokkaku M, Suzuki T (1997) Epitaxial carbon nanotube film self-organized by sublimation decomposition of silicon carbide. *Appl Phys Lett* 71:2620
58. Emtsev K, Bostwick A, Horn K, Jobst J, Kellogg G, Ley L, McChesney J, Ohta T, Reshanov S, Röhrl J, Rotengerg E, Schmid AK, Waldmann D, Weber HB, Seyller T (2009) Towards wafer-size graphene layers by atmospheric pressure graphitization of silicon carbide. *Nat Mater* 8:203–207
59. Van Bommel AJ, Crombeen JE, Van Tooren A (1975) LEED and Auger electron observations of the SiC(0001) surface. *Surf Sci* 48(2):463–472
60. Rollings E, Gweon GH, Zhou SY, Mun BS, Mc-Chesney JL, Hussain BS, Fedorov AV, First PN, de Heer WA, Lanzara A (2006) Synthesis and characterization of atomically thin graphite films on a silicon carbide substrate. *J Phys Chem Solids* 67(9–10):2172–2177

61. Virojanadara C, Syväjärvi M, Yakimova R, Johansson LI, Zakharov AA, Balasubramanian T (2008) Homogeneous large-area graphene layer growth on 6H-SiC(0001). *Phys Rev B* 78:245403
62. Miller JR, Outlaw RA, Holloway BC (2010) Graphene double-layer capacitor with ac line-filtering performance. *Science* 329:1637–1639
63. Liu C, Yu Z, Neff D, Zhamu A, Jang BZ (2010) Graphene-based supercapacitor with an ultrahigh energy density. *Nano Lett* 10:4863–4868
64. Kumar D, Tomar AK, Singal S, Singh S, Sharma RK (2020) Ammonium decavanadate nanodots/reduced graphene oxide nanoribbon as “inorganic-organic” hybrid electrode for high potential aqueous symmetric supercapacitors. *J Power Sources* 462:228173
65. Xu Y, Sheng K, Li C, Shi G (2010) Self-assembled graphene hydrogel via a one-step hydrothermal Process. *ACS Nano* 4:4324–4330

# Chapter 2

## Fabrication of Graphene, Graphene Oxide, Reduced Graphene Oxide, Fullerene (C<sub>60</sub>) and Carbon Nanotube Thin Film By Langmuir–Blodgett Method



Atri Mallick, Nibedita Haldar, Suman Nandy, and Chandan Kumar Ghosh

### 1 Introduction

Thin films of carbon materials those include network of graphene, graphene oxide (GO), reduced graphene oxides (RGO), fullerene (C<sub>60</sub>) carbon nanotube (CNT), etc., meet global standard in terms of flexibility, chemical stability, electrochemical tune ability as required for next-generation transparent conducting electrodes (TCEs) of various optoelectronic devices and energy storage devices. Whenever carbon-based transparent-conducting monolayer or multilayer thin films of specific application is needed to be fabricated, Langmuir–Blodgett (LB) appears to be one of the easy, cost-effective and simplest techniques ever. These carbon materials are very much stable and exist in the form of homogeneous colloidal suspensions in aqueous, as well as in organic polar solvents in spite of strong hydrophilicity. Herein, Coulombic repulsions among negatively charged sheets make them easy to collect on a substrate [1] by LB method as compared to other chemical techniques like transfer printing, electrophoretic deposition, spin or spray coating, dip coating, etc. [2–10]. As for an example, LB-deposited RGO shows high potentiality during hole injection in organic light-emitting diode. It has been identified that the recombination between electron and hole increases significantly by well-patterning and controlling thickness of these RGO films. In addition to the aspects of device application, novel properties and

---

A. Mallick · N. Haldar · C. K. Ghosh (✉)  
School of Materials Science and Nanotechnology, Jadavpur University, Jadavpur,  
Kolkata 700032, India  
e-mail: [chandan.kghosh@jadavpuruniversity.in](mailto:chandan.kghosh@jadavpuruniversity.in)

S. Nandy  
Department of Materials Science CENIMAT-i3N, Center for Materials Research, Faculdade de Ciências e Tecnologia da, Universidade Nova de Lisboa, Campus de Caparica, 2859-616 Caparica, Portugal

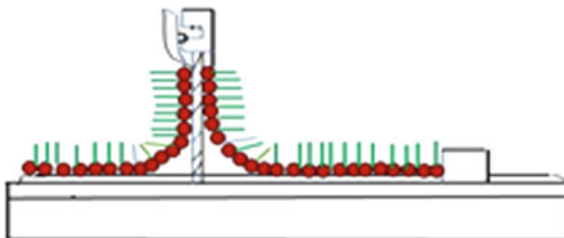


characteristic features of LB-deposited carbon network, particularly folded RGO as well GO sheets, are often noticed. As for another example, high-quality photoactive electrodes, fabricated with LB-deposited  $C_{60}$  thin films, have gained immense interest as their thickness can easily be controlled on a molecular level. In comparison with indium tin oxide (ITO), LB-deposited  $C_{60}$  photoactive electrodes are reported to have better potential; thus, it has been predicted as next-generation photoactive electrode. CNTs are quite familiar example of carbon materials since the emergence of nanotechnology globally. Its unique 1D structure and extended curved  $\pi$ -bonding configuration are extremely important for innumerable optoelectronic applications, and all these properties are significantly tuned during the synthesis using LB technique. Metallic, semi-metallic or semiconducting LB-deposited single-walled CNTs (SWCNTs) have gained wide attention. Herein, it may be stated that the bilayer SWCNTs thin films are getting transferred by employing a multilayer film of cadmiumarachidate made by LB technique onto the quartz substrate and silica-based optical fiber sensors to detect and identify volatile, organic hazardous compounds. In recent time, a quasi-LB method has also been developed to deposit pure SWCNT thin film on different substrates including fabric. Unrolled SWCNT, known as graphene, acts as the building block for different allotropes, particularly fullerenes and 3D graphite those corresponds to various important device applications. Graphene itself has monolayer of carbon atoms of  $sp^2$ -hybridization with 2D honeycomb-type lattice arrangement [11]. Owing to very high transparency in visible region as well as electrical conductivity, graphene has been adopted as another promising material for TCE. In comparison with other TCEs like ITO or F doped  $SnO_2$  (FTO), thin films of graphene possess high flexibility, mechanical strength, chemical stability and low cost. Nowadays, graphene quantum dots (GQDs), an alternative kind of graphene derivative, have been developed which are basically graphene sheets of edgewise dimension less than 100 nm and corresponds edge-related special features. In recent time, intrinsic three-dimensional structures of graphene become attractive as they have an important role in cellular interactions. Here also, LB is the most useful and potent tools to fabricate thin films based on organic compounds, the structures of which are optimized and controlled at atomic level. In general, the materials with which the films are being composed of must be amphiphilic. But, till date, only a very few molecules have been able to constitute LB-deposited thin films without long alkyl chains. In a few cases, the functional molecule does not possess an ability to make a film at the interface between air and water by itself; they may be prepared through LB technique by inserting them with film-forming materials. Likewise, films, deposited by LB method, show very good tunable conductivity after being prepared from metal complex and icosanoic acid mixture. Herein, it may be stated environment-friendly carbon-based materials have remarkable potentiality for various optoelectronic applications, where LB plays significant role in their synthesis. Therefore, in the following sections, fundamentals of the LB technique along with their advantage and disadvantages will be described in the context of carbon network-based thin film.

## 2 Fundamental Principles of Langmuir–Blodgett Technique

Langmuir–Blodgett technique is one of the cost-effective, easy, in-demand methods to prepare precise monolayer structures. It includes direct formation of nanoparticulate onto Langmuir trough, while synthesis commences after mixing metallic salts in water sub phase with subsequent exposure to gases which appears as suitable for particulate formation at the air/water interface. Commonly, nanoparticulates are produced from lipids, membranes or functionalized surfactants that injects charged ions in the subphase. Precursors are selectively attached with surfactant layer which has been spread at the air/water interface, followed by conversion into actual phase of the materials upon subsequent treatment to reagent gases. Spatial distribution of the nanoparticulate can be changed as a function of surface pressure, along with possibility exists for transfer of the nanoparticulates to substrates at any stage of their growth during monolayer formation. There are many advantages of using monolayers as templates for nanoparticulate films; specifically for 1D semiconductor nanostructures, e.g., SWCNTs, as they are essential components for various applications such as logic circuits, field-effect transistors, non-volatile memories, high-performance optoelectronic devices, biosensors. But, for all practical applications, their precise form is very much essential, possibly higher than standard lithographic limit. Unlike 0D carbon nanomaterials, alignment becomes a critical factor for 1D carbon nanostructures. Although many techniques have been developed to fabricate nanomaterials assembly into patterned arrays over large areas with prefixed spacing, while end-to-end registry becomes extremely challenging. However, LB provides an easy protocol in regard to this. It has been noticed that ordering of LB-deposited 1D carbon building blocks has been achieved by these assembled architectures; these must open opportunities to investigate the impact of size and shape on collective optical, magnetic and electronic properties, as well as to examine other scientific properties. Herein, LB also acts as a promising pathway to fabricate supra-molecular assembly in which precisely controlled and layered structure at an ultrathin scale has been achieved for different allotropes of carbon nanostructures. Most importantly, Langmuir monolayers of carbon nanostructures are getting transferred from the liquid–gas interface to solid support at the time of vertical passage through the monolayers. Herein, Langmuir monolayers are made assembled vertically which consists mainly of an amphiphilic molecule with a hydrophilic head and a hydrophobic tail within these carbon nanostructures. These LB-deposited carbon allotropic films are composed of one or more monolayers which got deposited from liquid form on a substrate by dipping. Herein, different protocols exist to transfer monolayers from water–air interface on the substrate. Among them, most conventional method is the vertical deposition that has been demonstrated first by Blodgett and then Langmuir too. In this particular case, monolayer of amphiphiles at the interface between water and air gets collected by the displacement of a vertical plate (shown in Fig. 1). While this process still has not been understood completely, it is known that there is a certain

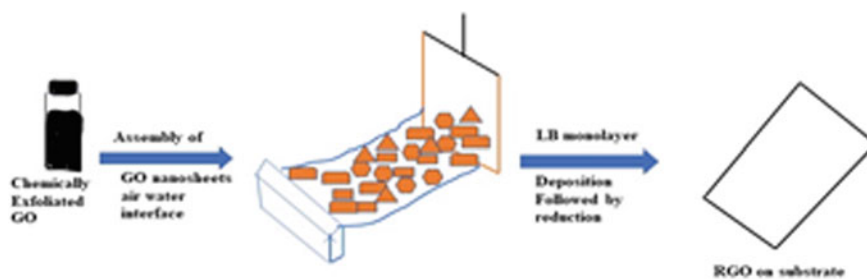
**Fig. 1** Deposition of a layer at the interface between water and air using vertical substrate



critical velocity, generally represented by  $U_m$ , above which the transfer process does not work at all.  $U_m$  is of the order of a few cm/s and usually is much smaller for viscous layers (e.g., polymeric amphiphiles).

## 2.1 *Synthesis of Thin Film and Self-Assembled Structure of Bare and Functionalized GO, RGO by LB Technique*

Graphene, i.e., monolayer sheets of  $sp^2$ -bonded carbons, has gained attention due their low weight, high tensile strength and conductivity. It exhibits very high electrochemical activity, optical properties, chemical stability; hence, it gained lots of interest in modern optoelectronic devices, specifically as transducer for biosensor, as redox active electrode material. The key success for graphene's applications is to generate a protocol to synthesis large-size uniform, aligned graphene sheets on any substrate. Currently, most of the graphene sheets are of very small size ( $\sim\mu\text{m}$ ); hence, they exhibit high contact resistance due to large number of junction between two sheets. Thus, sheets of high area ( $\sim\text{mm}$ ) are very much essential from device perspective. It has been studied that graphitization of Si-terminated SiC (0001) in the presence of Ar produces monolayer graphene sheets of several  $\mu\text{m}$ . But it appears to be very difficult to obtain graphene sheets on other substrate. Though physical processes such as plasma-enhanced chemical vapor deposition (PECVD) and chemical vapor deposition (CVD) enable graphene synthesis on Cu and Ni foils, but the process is too specific toward substrates and very costly, thus limiting industrial usage [12, 13]. Owing to scalability of production of GO or RGO or graphene, LB-based two steps synthesis protocol shows high potentiality (schematically shown in Fig. 2). Initially, thin films of GO are prepared by LB technique, later RGO or graphene thin film are being obtained by either chemical reduction or thermal annealing. In this context, it may be stated that most remarkable disadvantage of bare graphene in sensing application and catalytic activity is that due to the absence of any functional group, pristine graphene cannot be used for direct immobilization of biomolecules for sensing or redox active catalytic purposes. But, GO consists of lots of oxygen functional groups ( $-\text{COOH}$ , etc.); hence, it provides more suitable platform for immobilization and catalytic redox activity. In this context, it may be stated that electrical conductivity of GO is very poor; hence, it shows very poor



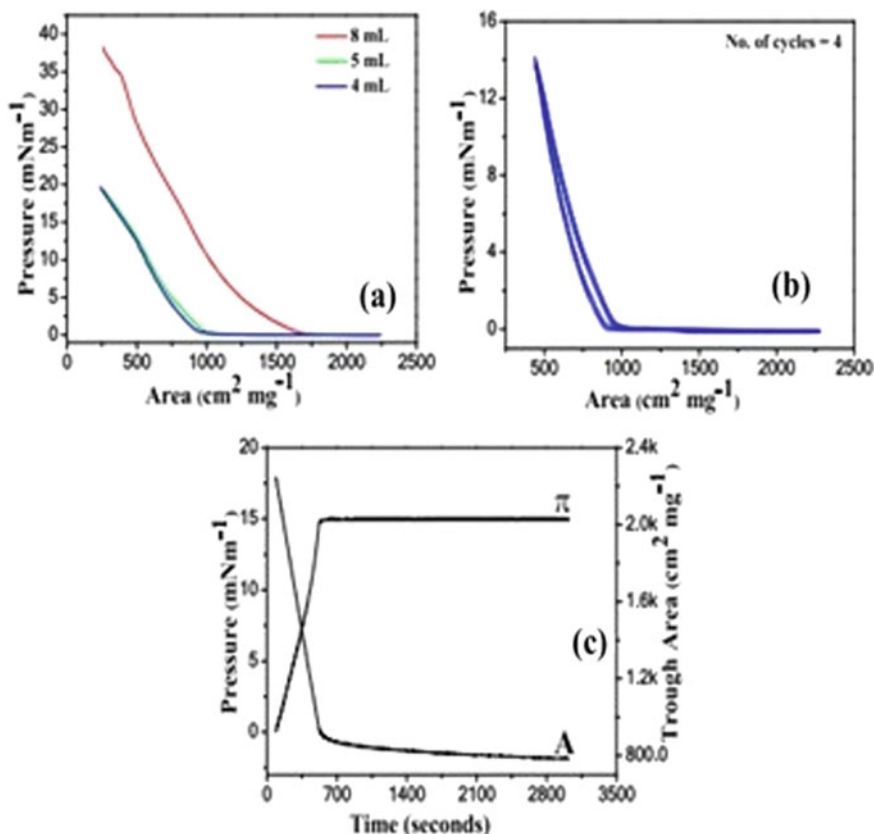
**Fig. 2** Schematic diagram of GO deposition by LB technique

electrochemical properties as well as sensitivity in biosensing. In this context, it may be stated that GO's conversion to RGO has been identified to be very essential for electrochemical or sensing applications. In addition, the presence of functional groups makes RGO more environment-friendly, water-soluble and susceptible for catalytic charge transfer processes those are essential for device fabrication including sensors, photovoltaic, photoelectronic, optical communication device, etc. Though LB provides good platform for industrial production of GO/RGO/graphene [14], it requires homogeneous suspension. In spite of hydrophilicity, colloidal solution of GO/RGO are stable, homogeneous in aqueous as well as in *N,N*-dimethylformamide (DMF), methanol, ethanol, etc., as organic solvents are obtained. Among different dispersants, methanol–water (5:1 volume) mixture is found to be most suitable with optimum ratio. Briefly, strong electrostatic repulsion between ionized carboxylic and phenolic groups, situated at basal region of GO carrying negative surface charge, leads this stability, particularly in methanol solution [15]. Thus, formed dispersed sheets get easily processed to be collected onto a substrate by this LB technique with good tunable thickness of GO/RGO/graphene films. Prior to deposition, GO powder is being synthesized by either modified Hummer method or Offeman's method [16].

In this context, it may be stated that these processes often provide GO sheets of non-uniform width; hence, they are separated by centrifugation before deposition in order obtain GO film with uniform thickness. Herein, it may be stated that Zheng et al. synthesized ultra-large GO sheets (width  $\sim 200 \mu\text{m}$ ) by exfoliating graphite powder [17]. Importantly, stability of GO monolayer is commonly evaluated from hysteresis curve. It has been examined that GO monolayer, formed at the subphase, remains unchanged during repeated compression–expansion (Fig. 3) at the optimized pressure ( $\sim 15 \text{ mN/m}$ ) confirming formation of highly stable film [16]. In addition, it is also found that surface pressure plays a crucial role in GO transfer ratio. Typical surface pressure—area isotherm exhibits variation in slope indicating transition of GO sheets from gaseous to condensed liquid, followed by solid-state phase. In the area versus pressure diagram, within high area region, surface pressure remains constant, and thus, this is referred as initial gas phase region. With decreasing area, increase of pressure is attributed to higher repulsion among GO sheets. Herein, GO sheets start to touch each other, followed by tiling over whole surface. Further increase of pressure indicates compression of the GO sheets beyond the closed-packed stage.

At this point, they start to fold at the touching regions along with their edge in spite of overlapping. In more compressed stage, partial overlapping and wrinkling are being observed and formation of monolayer from interlocked GO sheets is being noted. It has been studied that the stable 2D GO monolayers get formed only when compression/expansion of GO sheets are found to be completely reversible [18].

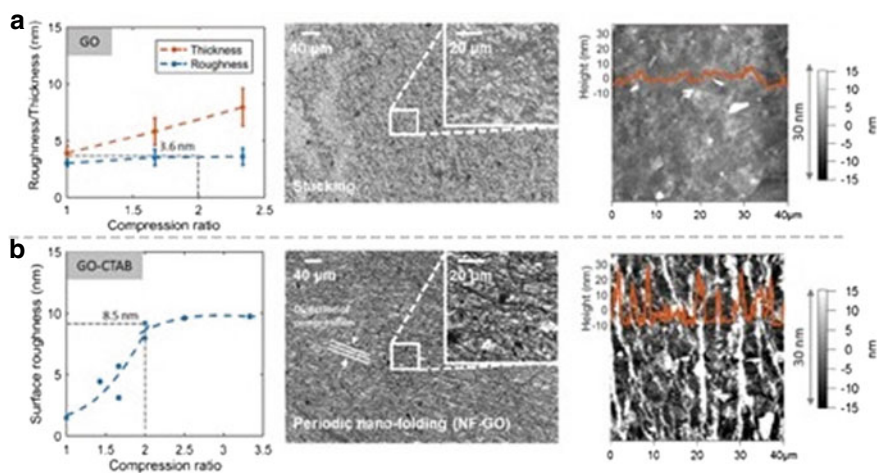
It has also been investigated that when these GO sheets get self-assembled side by side, several unique features in morphologies, namely wrinkles, folds, overlaps, etc., are being generated. The degree of wrinkling significantly depends on pulling speeds during LB transfer, and it has been noted that higher pulling rate ( $\sim 1$  mm/min) produces higher degree of wrinkling, a structure which is known as concentrated graphene oxide wrinkles. Primarily, evaporation of  $H_2O$  present between GO sheets and underlying substrate determines quality of the self-assembled GO sheets. It has been identified that large-sized GO sheets trap more water droplet producing more



**Fig. 3** a Isotherm at different GO content. b Isotherm after 4th cycle c pressure area versus time GO films [16, with permission]

wrinkled GO sheets, while water molecules get easily vaporized in case smaller-sized GO sheets, giving less wrinkling [19, 20]. Very specifically, high pulling rate does not allow larger GO sheets to be relaxed onto the substrate after evaporating water molecules and transfer onto the substrate, causing more wrinkling. Herein, it may be stated that wrinkling of GO as monolayer is crucial as many of the proposed tuneability like specific surface area, porosity, conductivity, etc., are only realized when GO is being utilized as building—blocks of 3D structures. It has been examined that low in-plane rigidity of pure GO sheets do not give good control over wrinkle, rather compression causes face-to-face sliding. This phenomenon indicates more viscous nature of GO films in comparison with elastic property. In this context, it may be stated that in-plane rigidity rather than out-of-plane rigidity plays crucial role in wrinkle formation. Herein, Silverberg et al. examined that cationic surfactant cetyltrimethylammonium bromide (CTAB) increases rigidity (in-plane) of GO; thus, it can be used to tune wrinkling and folding GO films. Briefly, interactions between CTAB's cationic head with oxygen functional group of GO with negative charge lead strong binding between them. Hydrophobic tail group of CTAB of CTAB-GO complex causes their different types of highly viscoelastic aggregation like lamellar, spherical and wormlike structures facilitating controlled wrinkle formation during LB deposition of thin film (Fig. 4).

LB is found to be most promising technique to prepare uniform, homogeneous carbon 3D thin films. The thin films of both organic [22] and inorganic [23] compounds can be deposited by this method. It produces thin films with the desired structures [24] even with range in nanometric dimension. It is capable to tune thickness of single layer effectively, uniform deposition on large surface area and the multilayers deposition with different layer compositions also [25]. A typical



**Fig. 4** Comparative studies between GO and CTAB functionalized GO films. **a** Increased thickness for composite film (three layers); roughness remains same (left). SEM (center) and AFM (right) [21, with permission]

isotherm profile from LB deposition technique incorporates the three definite regions, i.e., gaseous, liquid and solid states, which influence alignment of molecules on top of the liquid subphase [26]. The single layer can be collapsed at the breaking point or by over-compressing, forming uncontrolled multilayer which can damage the film formation [27]. Recently, Ng et al. investigated the advancement of pristine RGO electrodes for bio-photovoltaic cells [28]. In addition, RGO-containing nanofiber mats carry features of biosensor, biofuel cells, etc. [29], while 3D structure of graphene which plays a crucial role in cellular interactions. It has been studied that low surface energy and hydrophobicity of these 3D structures influence efficiency in biocatalysts during biofilm formation. Herein, several parameters like pore size, surface roughness, etc., influence the cell interaction with 3D structures [30, 31]. Like other carbon nanostructures, LB can also be adopted to prepare 3D structure of graphene as it enables effective control of the monolayer thickness, large area homogeneous deposition and the possibility to fabricate multilayer of different layer composition. Like other materials, here also typical surface-pressure isotherm profile consists of three distinguished regions ranging from gaseous, liquid and solid states correlating the molecular arrangement on top of the liquid subphase. Over-compression leads collapse of monolayer or the breaking point that giving multilayer formation in an uncontrolled manner.

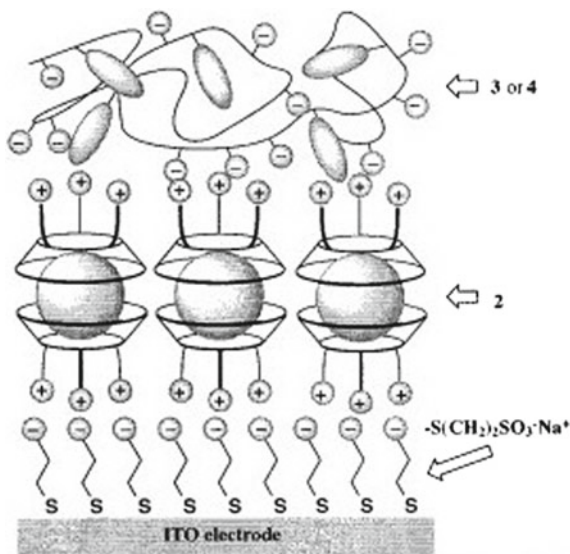
Very often, graphene, GO, RGO are made composite with other inorganic nanostructures for better application opportunity. In this context, it may be stated that the composite of 1D ZnO nanorod and 2D RGO shows remarkable memristor effect. Though these types of nanocomposites are widely being synthesized by hydrothermal technique, low temperature is rare and the research is still open in this field. Herein, Zhou et al. synthesized 1D ZnO nanorods and a 2D RGO hybrid nanocomposite adopting facile solution protocol, followed by LB technique [32]. The researchers exposed that these ZnO nanorods and 2D RGO nanocomposite show a reversible memory behavior. The narrow resistance distribution and stable behaviors of voltage switching can be assigned to the oxygen-vacancy associated conductive filaments along with ZnO nanorods. The device showed outstanding electrical reliability and mechanical robustness up to 1000 cycle of bending indicating flexibility of LB-deposited RGO thin film that was used as the bottom electrode. The literature studies suggest that low-dimensional materials based memristors extraordinary performance and stability such as excellent tolerance [33, 34]. ZnO nanorods can be used as one of the most promising candidates due to very simple chemical composition, nontoxicity and including regulated oxygen vacancies and favorable properties in the resistive memory area [35–37]. On the other hand, RGOs are utilized as most optimistic cost-effective electrode materials due to its excellent durability under tension and a facile solution-process-based large area fabrication [38, 39]. Yong et al. investigated on a light incident angle switchable memristor by using ZnO nanorods as a resistive switching medium [37]. Sun et al. discussed on development in electrical property utilizing ZnO nanorod-based memristors by surface hydrogen annealing process [37]. However, it is still challenging to evolve an acceptable structural design of memristors based on ZnO nanorods which can be used in practical flexible memory applications.

## 2.2 *Synthesis of Fullerene (C<sub>60</sub>) Thin Films By LB Technique*

One of the most important finding among all carbonaceous materials is the discovery of C<sub>60</sub> by Kroto and Smalley et al. in the year 1985 [40]. It comprises of 60 C atoms, aligned 12 pentagons linking with 20 hexagons maintaining hollow sphere geometry. It is little bit similar to soccer ball that is why it is named as buckyball. Being considered as 0D nanostructure, its diameter is found to be approximately ~7.1 Å [41]. Though fullerene is found with different carbon cages and symmetries with various number of carbon atoms, C<sub>60</sub> has gained most attention due to its stability, flexibility in different device fabrications. Herein, it may also be stated that solubility at ambient temperature varies over wide range of solvents enabling easy preparation of their allotropes [42, 43]. Though earlier researches on C<sub>60</sub> included synthesis and study of physiochemical properties of C<sub>60</sub>, but later, C<sub>60</sub> assembly and their covalent and noncovalent interaction-mediated ordered derivatives appear as upcoming topic for their remarkable impact to design and fabricate different electronic devices. In general, such assemblies form in solution, on surface, as well as at the interfaces. In this context, it may be stated that bare C<sub>60</sub> nanostructures lack of dipolar interaction, making hard to assemble them in the solid state [44]. However, it has been explored that it is very difficult to prepare pristine C<sub>60</sub> due to its low solubility, particularly in organic solvents, as well as due to high aggregation even in the presence of good solvents. To overcome this issue, chemical modification with several chemical species like crown ethers, polyhydroxylates, oligopeptides, poly(ethylene glycol), hydrophilic porphyrin, etc., have been proposed [45]. Polymers with C<sub>60</sub> at the main or side chain or dendrimers having C<sub>60</sub> as the dendrons have been reported as well. Commonly, these above-mentioned treatments with hydrophilic molecules facilitate C<sub>60</sub> to dissolve into solvents and disperse on the surface. Herein, solvents play a significant role in assembling C<sub>60</sub>. For example, C<sub>60</sub> containing ammonium amphiphile which is soluble in water leads to long fibrous which in consequence aggregates in disk-like form, while C<sub>60</sub> nanowire with high aspect ratio has been achieved using 1,2,4-trimethylbenzene as solvent [46–52]. Preparation of monolayer or multilayer C<sub>60</sub> films depends on the methodology to incorporate its unique features in bulk form, while self-assembled monolayers has attracted for this purposes. Thus, formed 2D fullerene structures serve as n-type electrode in organic field-effect transistors, fuel, photovoltaic cells, etc. [53]. Primarily, fabrication of C<sub>60</sub> assembly includes either van der Waals interaction or covalent bonding. However, physical processes like CVD, PECVD, etc., produce good quality of C<sub>60</sub> assembly, but they are too costly for industrial application. Herein, LB has been identified as an alternative easy technique to obtain C<sub>60</sub> thin film. In this process, initially Langmuir film is deposited after spreading amphiphilic molecules on surface of water. Thus, the spreaded molecules get oriented in such a way that hydrophilic parts remain contact with water, where hydrophobic part, e.g., C<sub>60</sub> edge, gets oriented out from air. Followed by Langmuir monolayer formation, thin film of fullerene is prepared by transferring as—prepared monolayer onto a solid substrate, while number of layer is being controlled by varying the dipping cycles. Carbon soot-derived C<sub>60</sub>-based thin

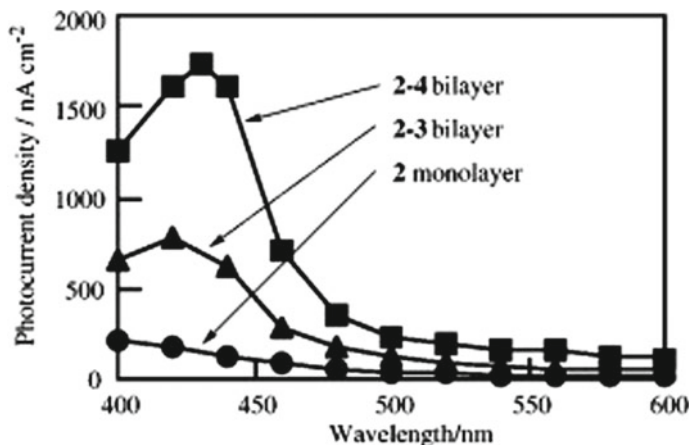


**Fig. 5** Schematic representation of sodium 3-mercaptoethanesulfonate (1st layer), 2 (2nd layer) and 3 or 4 (3rd layer) on an ITO electrode [54, with permission]



film has been synthesized by LB technique at barrier speed  $\sim 2$  cm/min at  $17^\circ\text{C}$  on quartz substrate. In this case, it is deposited at pressure  $\sim 25$  mN/m with benzene as spreading solvents. Though this process produces  $\text{C}_{60}$  film, however quality  $\text{C}_{60}$  film has been obtained in the presence of 1:1 mixture of icosanoic acid and  $\text{C}_{60}$  solution giving area per molecule  $\sim 0.07$  nm<sup>2</sup> at 25 mN/m. In this context, it may be stated that adding solution of  $\text{C}_{60}$  of benzene or  $\text{CS}_2$  to air–water interface, Langmuir films with  $\text{C}_{60}$  molecules can form after volatilization of the solvent. It has been observed that Langmuir can be deposited on various substrates like quartz, glass, silicon, etc., using this procedure. Herein, Mirkin and his co-workers have deposited covalently bonded  $\text{C}_{60}$  on  $(\text{MeO})_3\text{Si}(\text{CH}_2)_3\text{NH}_2$  functionalized ITO surface (schematically shown in Fig. 5, while pressure–area characteristics (Fig. 6) significantly depend on number of layer [54].

In addition to bare  $\text{C}_{60}$ , thin film of  $\text{C}_{60}$  nanocomposite has also gained attention in several optoelectronic devices. As an example,  $\text{C}_{60}$ –dendrimers conjugated thin films consisting of the head groups of carbohydrate-containing dendrons have been synthesized using LB technique at the air–water interface. As another example,  $\text{C}_{60}$ –dicyclohexylcarbodiimide conjugate gets formed between dicarboxylic acids and  $\text{C}_{60}$  through amide bond. The monolayers are observed to collapse at different surface pressure in comparison with bare  $\text{C}_{60}$  thin film. Repetitive compression and expansion carried out on single layer at air–water interface, indicate reversibility. When monolayer gets compressed to a certain value, the surface pressure during decompression appears very close to that of compression value. Again, recompression gives curves near to initial ones with slight reduction of deduced molecular area. Such cycles clearly indicates stability of the prepared films. Polar hydrophilic carbohydrate-dendrons gives strong amphiphilic nature among  $\text{C}_{60}$  derivatives and



**Fig. 6** Photocurrent versus wavelength curve of 2, 2-3, and 2-4 systems on ITO electrode, measured at 25 °C (irradiation  $\sim 1 \text{ Mw cm}^{-2}$ , 0.1 M  $\text{NaSO}_4$  solution containing 50 Mm ascorbic acid) [54, with permission]

bulky enough too to limit irreversible aggregation. This is the first time when lack of hysteresis, hence reversibility is noticed for  $\text{C}_{60}$  films at air–water interface.

### 2.3 Preparation of Pristine and Composite Carbon Nanotube Thin Films

CNT has gained enormous interest in recent times as an upcoming electrode material for transparent electronics, chemical sensors, transistors, etc. Though CNT thin films can be grown by several direct physical methods like CVD PECVD, etc., low temperature solution methods are most favorable due to cost, easy casting possibility on flexible substrate. LB being one of the most exquisite solution-based techniques to obtain oriented monolayer thin film is a well-accepted easy technique to prepare CNT thin film electrode. As CNT is not inherently amphiphilic, hence numbers of techniques like dispersing in organic solvents such as chloroform or chemical modification like functionalization with poly(ethylene oxide), organic molecules, surfactants, etc., have been developed to make CNT amphiphilic [55]. Sometimes, as-prepared colloidal sonication requires sonication for few hours for homogenization and after sonication colloidal mixture is allowed to settle down so that any extent of immiscible material can settle out easily. Finally, a measured volume of the solution which is to be spread dropwise on the surface of the subphase is attained from top of the above-prepared solution through a micro-syringe so that any external disturbance does not come to the sediment. For pure CNT network film deposition by LB technique, mostly ultrapure water is taken as subphase (gained by reverse osmosis, filtration, two-stage deionization and UV sterilization), while deposition is

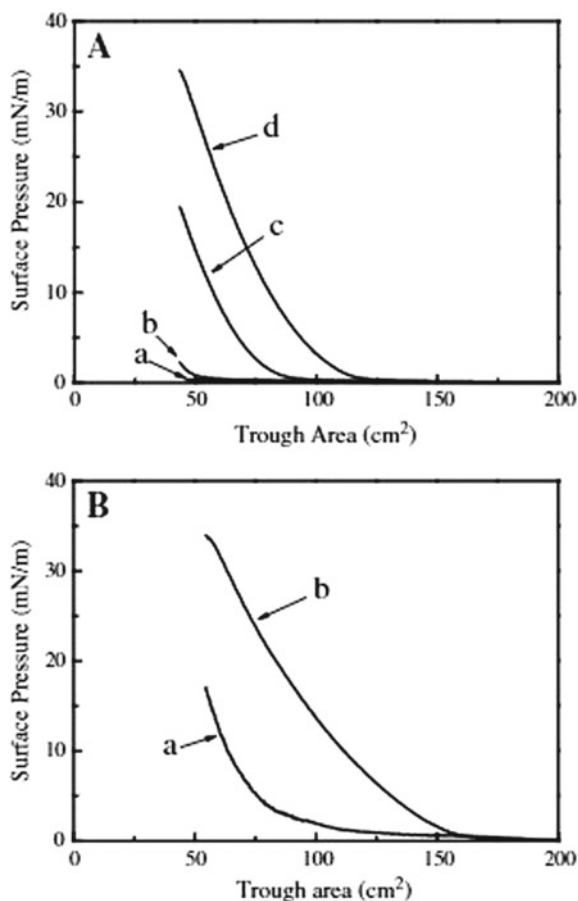
mostly carried out at pH  $\sim 6$  and temperature  $\sim 20$  °C. In the pressure-area isotherm, floating layer is commonly compressed at a barrier speed of  $1.1 \text{ cm}^2/\text{s}$  and its stability is monitored by noticing area versus surface pressure curve during compression. The generic isotherm of virgin CNT deposition using LB technique consists of an expanded up to around  $1 \text{ mN m}^{-1}$ , plateau region, followed by a significant transition region upto  $10 \text{ mN m}^{-1}$ . Such phenomenon indicates formation of organized floating layer with CNTs packing. A sharp rise of pressure up to  $14 \text{ mN m}^{-1}$  has been noted at minimum trough area  $\sim 20 \text{ cm}^2$ . At higher CNT concentration, isotherm gets right shifted, while the plateau disappears indicating formation more organized condensed phase. It has also been noted that rate of increase of surface pressure is less for low concentrated material, possibly due to aggregated CNTs on the subphase surface. Herein, increasing CNT concentration limits organization and packing of nanotubes. In addition, higher starting pressure is also observed in this case signifying coverage of water surface with CNTs. Methanol very often plays crucial role in thin film deposition as it facilitates CNT spreading. Briefly, methanol addition changes the isotherm noticeably along with overall reduction of surface pressure and shift of the transition point toward left side. Substrates on which CNTs are transferred are found to play very crucial role as adhesion of CNT on substrate mostly determines quality and stability of the film. It can be generalized that hydrophobic substrates such as polyvinyl chloride cause much better transfer of CNT in comparison with hydrophilic substrates like quartz, silicon, etc. [56]. Often, pre-treatments are avoided if structurally ordered CNT is not required for particular application. As an example, in case of sensing applications, CNT thin films with good substrate coverage rather than ordered CNT show better performance randomized CNT thin films have higher interstices and groove which are beneficial for sensing efficiency. In this context, it may be stated that CNT thin film deposition appears to be very difficult without any pre-treatment; however, Luccio et al. have prepared SWCNT thin films by depositing cadmium behenate and SWCNT alternatively [57]. Unfortunately, they have found that this sandwich-type bilayer structure is stable up to 5 number of layers due to poor adhesion of SWCNT to the substrate. Later, the same research group has found cadmium arachidate as suitable matrix where SWCNT can be easily embedded without any chemical modification [58]. Prior to LB deposition, a stable, homogeneous suspension is being prepared by mixing SWCNT into arachidic acid. Scanning electron microscopic image shows the absence of any single nanotube; thus, it suggests this mixing does not distract bundles of CNT or isolate SWCNTs. Generic isotherm features are repeated many times, indicating stability of the colloidal solution. However, it has been calculated from isotherm curve that area per molecule increases with increase of SWCNT amount to the arachidic acid, while curve shape remains unchanged up to 27% addition of SWCNTs, after that an abrupt change in slope, assigned to higher area per molecule, has been noted. This abrupt increase of area indicates that solid film gets formed at air-water interface, signifying existence of closely packed cadmium arachidate and the influence of SWCNT appears as the partial coverage of the surface. In case of 48–100% added SWCNT, isotherm gets changed significantly indicating formation of single layer. At molecular level, it is understood as SWCNT starts to interact with ordered cadmium

arachidate. This also corroborates with change in the isotherm slope in between 45 and 55 mN/m. It can be inferred that when compression of the SWCNT films reaches higher pressure then cadmium arachidate molecules appear as closely packed and leads compression of SWCNT bundles.

Though CNT plays crucial role in different applicational fields of CNT, however opportunity can be further improved by making composite of CNT with different other polymers, inorganic semiconducting materials, etc. [59–64]. Some of the composites in thin film form can be prepared by LB technique. As an example, viologens, a group of electroactive organic electrolytic materials correspond to three oxidation states (+2, +1 and 0) and are often used to make composite with CNT for electrochromic electrode [65–67]. From structural point of view, viologens have positively charged bipyridinium core, two alkylated substituents and two small counter anionic ions. During mixing with negatively charged CNT, new kinds of hybrid materials get formed. It has been studied that poly(viologen), the derivative of viologen, is highly stable at the water–air interface and facilitates layer-by-layer deposition of oxidized CNT by LB technique. Prior to deposition, the mixture of viologen and carboxylated CNT is sonicated in various polar solvents at room temperature to obtain its composite. Most importantly, viologen and CNT very poorly disperse in organic solvent-like chloroform, but their composites disperse well, enabling us to examine monolayer behavior of the functionalized CNT at the water–air interface and provide a platform to fabricate 3D multilayers as chloroform is the best solvent in this case (Fig. 7). In this context, it may be stated that Fu et al. prepared viologen–CNT composite film on quartz, Si and ITO substrates by LB technique at various surface pressure [68]. On the basis of transfer ratio, they have identified that monolayer can be deposited by down-to-up dipping only.

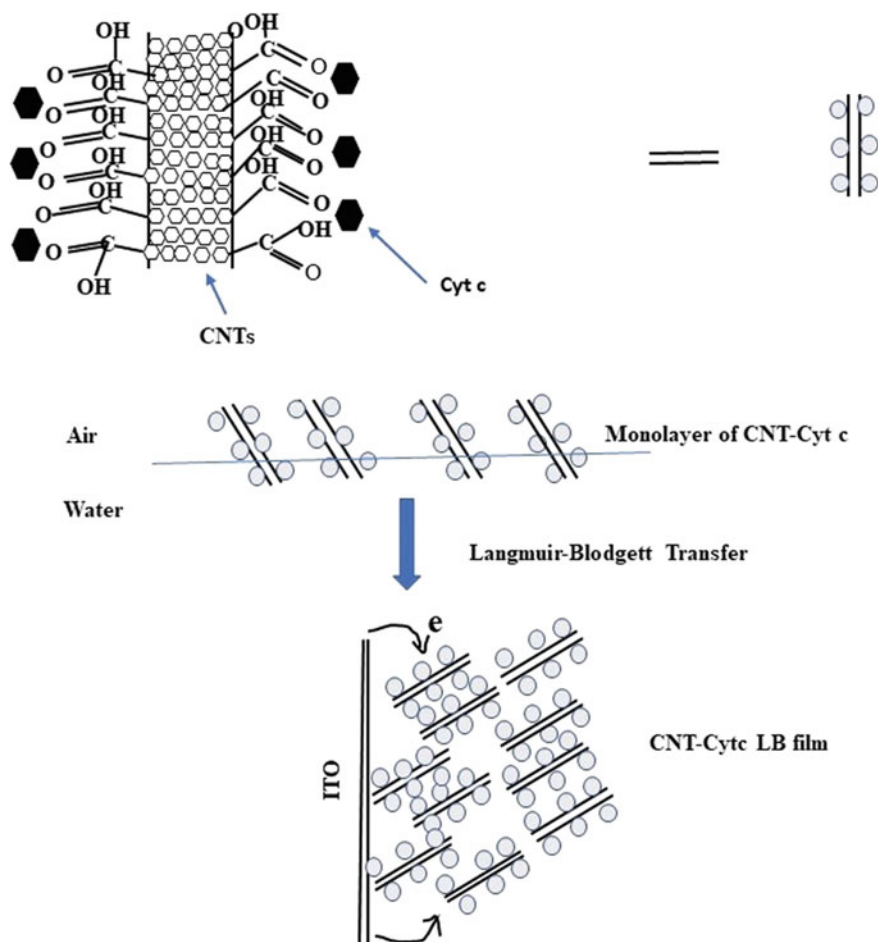
Other fields of interest of CNT include various biological and biomedical applications like nanoscale biosensors, biomolecular and biocatalytic devices where thin film of CNT composite are mostly used. In general, biocompatible oligomers, polymers are used to prepare these composites. Among them, CNT–protein conjugates have gained much attention as CNT exhibits high electrocatalytic activity as well as efficiently transfers electrons between electrode and redox active protein molecule [69, 70]. Herein, LB also provides an important easy pathway to prepare thin film of these types. As an example, CNTs (single and multi-walled)—cytochrome c conjugate thin film (schematically shown in Fig. 8) having significant electrochemical sensing property has been successfully prepared by LB technique using Tris–HCl subphase surface [71]. Prior to making composite, CNT is made water-soluble by acid oxidative method using perchloric acid (72%) and concentrated HNO<sub>3</sub> (70%). Deposition has been carried out in two barrier minitrough with barriers speed ~10 cm<sup>2</sup>/min at room temperature on quartz and ITO substrates. Best transfer of the materials has been noted at surface pressure ~10 mN/m via vertical dipping, followed by horizontal lifting. The average occupied through areas of cytochrome c has been found in the following order cytochrome c < MWCNT—cytochrome c < SWCNT—cytochrome c indicating that CNTs float on the water surface along with protein. Isotherm curves reveal the two characteristics: (1) collapsed surface is higher for CNT—cytochrome c conjugate monolayer, and (2) compressibility of monolayers obeys the following

**Fig. 7** **A** Isotherms corresponding to single layer of *a* 0.1, *b* 0.2, *c* 0.3 and *d* 0.5 mL C<sub>12</sub> – VMWCNT composites with aqueous solution, concentration ~0.19 mg/mL. **B** Isotherms *a* C<sub>8</sub> VMWCNT and *b* C<sub>16</sub> VMWCNT composites monolayer with water subphase [68, with permission]



order pure cytochrome *c*, MWCNT—cytochrome *c*, SWCNT—cytochrome *c*. Both these features suggest formation of CNT—cytochrome *c* conjugate through molecular interaction as the presence of only one collapse pressure indicates that phase remains unchanged during compression and co-existed CNT weakens interaction among proteins which is hydrophobic nature. Thus, it may be stated here, LB not only serves an important synthesis technique, but provides an indication of conjugate formation.

CNT—GO nanocomposites have also gained attention in recent time as this composite appears to be beneficial for many optoelectronic applications for tunable electrical conductivity. Intercalation of CNTs between the GO layers results in 3D conductive networks with controlled film thickness. Therefore, an environment-friendly yet optimizable synthetic route requires to increase performance and higher sized GO—CNT-hybridized TCE. Prerequisite solution is generally used to prepare thin film at an average speed ~100 mL min<sup>-1</sup> to make 5–10 mL where monolayer of GO—SWNT gets formed. Before compression, this has been kept for almost



**Fig. 8** Scheme of preparation of the CNTs-Cyt c conjugates monolayer thin film using LB method

20 min to stabilize the system. The compression is usually carried out by the movable barriers at  $10 \text{ mm min}^{-1}$ , and the corresponding pressure got noticed on tensiometer, joined with a Wilhelmy plate. After completion of the required compression, film of GO—SWNT composite having pale brown color is noticed so far. On the other hand, the monolayers of nanocarbon are transferred to a specific choiceable substrate at several phases of compression based on the common dip coating where quartz substrate is used to dip in a vertical manner and taken out at speed of  $0.1 \text{ mm min}^{-1}$ . The as-prepared composite film is then transferred as and when the meniscus is spread onto the substrate during taking it out. For this, hydrophilic surface of the substrate is needed to be controlled for required wetting to take place by the deposition of conducting layers.

### 3 Conclusion and Future Aspects

The LB offers a unique low-cost technique for large-scale synthesis of carbonaceous thin films. Primarily, they are produced in powder form, and then homogeneous colloidal solution is being prepared. Often, stability of the colloidal solution is increased by chemical modification and surface functionalization. The as-prepared solution is dropwise added to solvent where monolayer Langmuir film gets formed. Then, monolayer is transferred onto the substrate by vertical dipping and lifting process. It has been discussed that quality of thin film significantly depends on type of solvent, nature of substrate surface, etc. LB also provides a protocol to prepare patterned or oriented assembly of carbonaceous nanostructures which act as building blocks of several industrially important materials in bulk form. By varying synthesis parameters, these nanostructures can be significantly modified with porosity, surface area, surface texture, etc. In addition, LB also appears as low-cost technique to prepare carbonaceous nanocomposites for several applications, specifically for sensor and energy storage devices.

Though polymer-based and polymer-derived hybrid ultrathin films are highly demanding, but their carbonaceous material-associated composite thin film depositions by LB technique are yet to be studied a lot which could show potential applications in various domains. The idiosyncratic combinations of the properties of those LB thin films may promise revolutionary progresses as far as performance and cost-effectiveness are desired. Coatings for communications and computing applications are not studied significantly which may uncover a new sight for use of these thin films. For gas sensing applications, the conventional LB method can be modified also to study the further characterizations. Defect-free and LB films with less deformation are to be studied in detail. The amalgamation of molecular electronics and nanotubes may result in novel class of organic materials with extremely improved quality in regard to use in gas sensors. For space applications, highly stable and highly sensitive LB thin films are required which are to be optimized with further research.

**Acknowledgements** NH wants to thank UGC for her fellowship during execution of this work.

**Author Contribution** AM and NH have equal contributions in this chapter.

### References

1. Wang X, Zhi LJ, Tsao N, Tomovic Z, Li JL, Mullen K (2008) *Angew Chem, Int Ed* 47:2990–2992
2. Geim AK, Novoselov KS (2007) *Nat Mater* 6:183–191
3. Novoselov KS, Geim AK, Morozov SV, Jiang D, Zhang Y, Dubonos SV, Grigorieva IV, Firsov AA (2004) *Science* 306:666–669
4. Berger C, Song Z, Li X, Wu X, Brown N, Naud C, Mayou D, Li T, Hass J, Marchenkov AN, Conrad EH, First PN, de Heer WA (2006) *Science* 312:1191–1196

5. Reina A, Jia X, Ho J, Nezich D, Son H, Bulovic V, Dresselhaus MS, Kong J (2009) *Nano Lett* 9:30–35
6. Li D, Windl W, Padture NP (2009) *Adv Mater* 21:1243–1246
7. Kim KS, Zhao Y, Jang H, Lee SY, Kim JM, Kim KS, Ahn JH, Kim P, Choi JY, Hong BH (2009) *Nature* 457:706–710
8. Zheng QB, Ip WH, Lin XY, Yousefi N, Yeung KK, Li ZG, Kim JK (2011) *ACS Nano* 5:6039–6051
9. Zhu Y, Murali S, Cai W, Li X, Suk JW, Potts JR, Ruoff RS (2010) *Adv Mater* 22:3906–3924
10. Dreyer DR, Park S, Bielawski CW, Ruoff RS (2010) *Chem Soc Rev* 39:228–240
11. Wu ZC, Chen ZH, Du X, Logan JM, Sippel J, Nikolou M, Kamaras K, Reynolds JR, Tanner DB, Hebard AF, Rinzler AG (2004) *Science* 305:1273–1276
12. Brownson DAC, Banks CE (2012) *RSC Adv* 2(12):5385–5389
13. Huang Y, Dong X, Shi Y, Li C-M, Li L-J, Chen P (2010) *Nanoscale* 2(8):1485–1488
14. Solanki S, Soni A, Pandey MK, Biradar A, Sumana G (2018) *ACS Appl Mater Interfaces* 10(3):3020–3028
15. Aboutalebi SH, Gudarzi MM, Zheng QB, Kim J-K (2011) *Adv Funct Mater* 21:2978–2988
16. Solanki S, Soni A, Agrawal VV, Pandey MK (2021) G. Sumana. *Langmuir* 37(29):8705–8713
17. Zheng Q, Ip WH, Lin X, Yousefi N, Yeung KK, Li Z, Kim J-K (2011) *ACS Nano* 5:6039–6051
18. Cote LJ, Kim F, Huang J (2009) *J Am Chem Soc* 131:1043–1049
19. Kim J, Kim F, Huang J (2010) *Mater Today* 13:28–38
20. Kim J, Cote LJ, Kim F, Huang J (2010) *J Am Chem Soc* 132:260–267
21. Silverberg GJ, Vecitis CD (2017) *Langmuir* 33:9880–9888
22. Ahmadivand A, Semmlinger M, Dong LL, Gerislioglu B, Nordlander P, Halas NJ (2019) *Nano Lett* 19:605–611
23. Chen ZD, Wang HY, Wang YG, Lv RD, Yang XY, Wang J, Li L, Ren W (2019) *Carbon* 144:737–744
24. Kim J, Kim KS, Ryu SY, Kim S (2012) *Opt Express* 20:12966–12974
25. Lv RD, Chen ZD, Liu SC, Wang J, Li YF, Wang YG, Wang YS (2019) *Opt Express* 27:6348–6356
26. Song SJ, Shin YC, Lee HU, Kim B, Han DW, Lim D (2018) *Nanomaterials* 8:408
27. Jiang G, Miao L, Yi J, Huang B, Peng W, Zou Y, Huang H, Hu W, Zhao C, Wen S (2017) *Appl Phys Lett* 110:842
28. Jhon YI, Koo J, Anasori B, Seo M, Lee JH, Gogotsi Y, Jhon YM (2017) *Adv Mater* 29:1702496
29. Wei J, Qiu J, Li L, Ren L, Zhang X, Chaudhuri J, Wang S (2012) *Nanotechnology* 23:335707
30. Brauker JH, Carr-Brendel VE, Martinson LA, Crudele J, Johnston WD, Johnson RC (1995) *J Biomed Mater Res* 29:1517–1524
31. Flemming RG, Murphy CJ, Abrams GA, Goodman SL, Nealey PF (1999) *Biomaterials* 20:573–588
32. Li L, Lv RD, Wang J, Chen ZD, Wang HZ, Liu SC, Ren W, Liu WJ, Wang YG (2019) *Nanomaterials* 9:315
33. Wang YG, Chen HR, Wen XM, Hsieh WF, Tang J (2011) *Nanotechnol* 22:455203
34. Sirota M, Galun E, Sashchiuk A, Krupkin V, Glushko A, Lifshitz E (2003) *Proc SPIE Int Soc Opt Eng* 4970:53–60
35. Girard-Egrot AP, Morelis RM, Coulet PR (1993) *Langmuir* 9:3107–3110
36. Mirlley CL, Koberstein JT (1995) *Langmuir* 11:2837–2839
37. Periasamy V, Yieng NJ, Majid WHA (2013) *Adv Sci Lett* 19:179–182
38. Petty MC (1996) *Langmuir-Blodgett films: an introduction*. Cambridge University Press, Cambridge
39. Periasamy V (2012) *Adv Mater Res* 535–537:1119–1125
40. Kroto HW, Heath JR, O'Brien SC, Curl RF, Smalley RE (1985) *Nature* 318:162–163
41. Wilson RJ, Meijer G, Bethune DS, Johnson RD, Chambliss DD, de Vries MS, Hunziker HE, Wendt HR (1990) *Nature* 348:621–622
42. Kroto HW (1987) *Nature* 329:529–531
43. Milliken J, Dominguez DD, Nelson HH, Barger WR (1992) *Chem Mater* 4:252



44. Geng J, Zhou W, Skelton P, Yue W, Kinloch IA, Windle AH, Johnson BFG (2008) *J Am Chem Soc* 130:2527–2534
45. Amantana A, Moulton HM, Cate ML, Reddy MT, Whitehead T, Hassinger JN, Youngblood DS, Iversen PL (2007) *Bioconjugate Chem* 18:1325–1331
46. Li H, Tee BC-K, Cha JJ, Cui Y, Chung JW, Lee SY, Bao Z (2012) *J Am Chem Soc* 134:2760–2765
47. Dubois D, Kadish KM, Flanagan S, Hauffer RE, Chibante LPF, Wilson LJ (1991) *J Am Chem Soc* 113:7773
48. Allemand P-M, Koch A, Wudl F, Rubin Y, Diederich F, Alvarez MM, Anz SJ, Whetten RL (1991) *J Am Chem Soc* 113:1050
49. Ajie H, Alvarez MM, Anz SJ, Beck RD, Diederich F, Fostiropoulos K, Huffman DR, Kratochmer W, Rubin Y, Schriver KE, Senshamna D, Whetten RL (1990) *J Phys Chem* 94:8630
50. Xie Q, Perez-Cordero E, Echegoyen L (1992) *J Am Chem Soc* 114:3978
51. Zhou F, Jehoulet C, Bard AJ (1997) *J Am Chem Soc* (in press)
52. Koh W, Dubois D, Kutner W, Jones MT, Kadish KM (1992) *J Phys Chem* 96:4163
53. Avasthi S, Lee S, Loo Y-L, Sturm JC (2011) *Adv Mater* 25:5762–5766
54. Chen K, Caldwell WB, Mirkin CA (1993) *J Am Chem Soc* 115:1193–1194
55. Menon SK, Lethakumary B, Vasudevan K, Mohanan P (2002) *Phys B* 323:235–236
56. Sano M, Kamino A, Okamura J, Shinkai S (2001) *Langmuir* 17:5125
57. Kędzierski K, Rytel K, Barszcz B, Gronostaj A, Majchrzycki L, Wrobel D (2018) *Chem Phys Lett* 712:144–148
58. Luccio TD, Antolini F, Aversa P, Scalia G, Tapfer L (2004) *Carbon* 42:1119
59. Antolini F, Luccio TD, Serra E, Aversa P, Tapfer L, Sangiorgi S (2006) *Surf Interface Anal* 38:1285–1290
60. Liu Y, Kumar S (2014) *ACS Appl Mater Interfaces* 6:6069–6087
61. Dresselhaus M, Dresselhaus G, Eklund P, Saito R (1998) *Phys World* 11:33
62. Bachtold A, Hadley P, Nakanishi T, Dekker C (2001) *Science* 294:1317
63. Martel R, Schmidt T, Shea HR, Hertel T, Avouris P (1998) *Appl Phys Lett* 73:2447
64. Armitage NP, Gabriel J-CP, Gruner G (2004) *J Appl Phys* 95:3228
65. Bird CL, Kuhn AT (1981) *Chem Soc Rev* 10:49
66. Snow ES, Novak JP, Campbell PM, Park D (2003) *Appl Phys Lett* 82:2145
67. Collins PG, Bradley K, Ishigami M, Zettl A (2000) *Science* 287:1801
68. Fu Y-R, Zhang S, Chen M, Qian D-J (2012) *Thin Solid Film* 520:6994–7001
69. Karajanagi SS, Vertegel AA, Kane RS, Dordick JS (2004) *Langmuir* 20:11594
70. Wong N, Kam S, Dai H (2005) *J Am Chem Soc* 127:6021
71. Liu AR, Qian DJ, Wakayama T, Nakamura C, Miyake J (2006) *Colloids Surf A* 284–285:485–489

**Part II**  
**Energy Science and Engineering**

# Chapter 3

## Nanoporous Carbon Materials for Energy Harvesting, Storage, and Conversion



**Bhawna, Janardhan Balapanuru, Varun Rai, Vinod Kumar,  
and Kamalakanta Behera**

### 1 Introduction of Porous Carbon Materials

Design and development of advanced and sustainable carbon-based materials are most relevant now than ever before to address some of the key global challenges including global warming, energy consumption, water scarcity, air pollution, etc. [1, 2]. Toward this end, researchers are paying much attention on porous carbon materials (PCMs) due to their unique properties such as high-surface area, tunable pore size, volume, functional modifications, and high electronic conductivities associated with these materials. Some of the key areas that implemented these efficient porous carbon materials are, but not limited to water filtration, energy conversion and storage, drug delivery, catalysis, and sensing [3, 4].

---

Bhawna  
Department of Chemical and Biological Engineering, University of Alabama, Tuscaloosa AL  
35487, USA

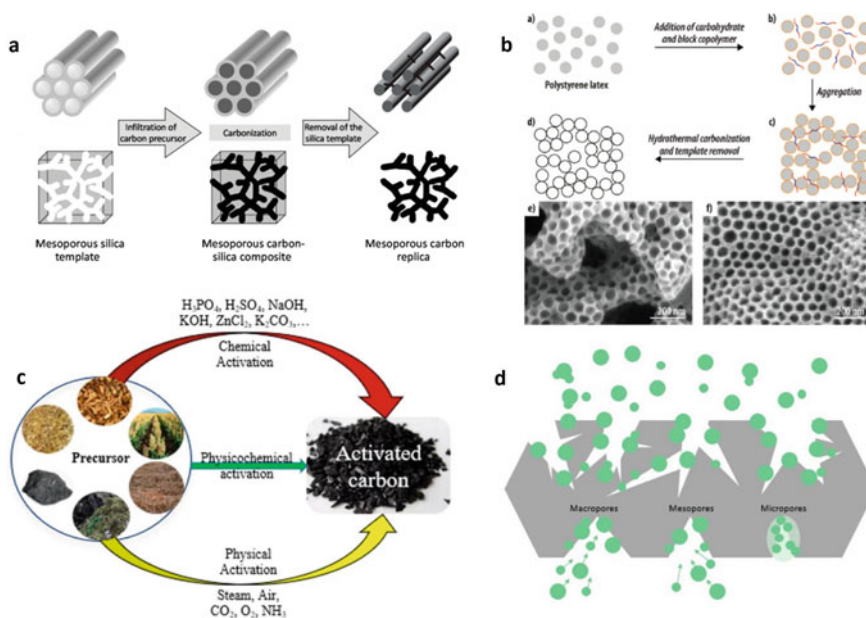
J. Balapanuru  
Grafoid Inc., 945 Princess Street, Kingston, ON K7L 0E9, Canada

V. Rai  
School of Materials Science and Engineering, Nanyang Technological University, 50 Nanyang  
Avenue, Singapore 639798, Singapore

V. Kumar  
Department of Chemistry, J. C. Bose University of Science and Technology, YMCA, Faridabad,  
Haryana 121006, India

V. Rai · K. Behera (✉)  
Department of Chemistry, Faculty of Science, University of Allahabad, Prayagraj, Uttar  
Pradesh 211002, India  
e-mail: [kkbehera@allduniv.ac.in](mailto:kkbehera@allduniv.ac.in)

PCMs are mainly classified into 3 categories such as (a) macroporous (with pore's diameter  $> 50$  nm), (b) mesoporous ( $50 \text{ nm} > \text{pore's diameter} > 2$  nm) and (c) microporous (with pore's diameter less than 2 nm) (Fig. 1d). The deep and considerable understanding of the structure–property relationship of these materials helped researchers to design the most efficient and sustainable green materials especially in the field of conversion and storage of energy [5]. Extensive research has been conducted, and there are several review articles in the literature covering the above aspects of PCMs for various applications [6, 7]. The prime objective of this chapter is to bring some of the recent work done on PCMs especially on the micro/nanoporous carbon materials and their composites for energy-related applications. In the present chapter, first, we have summarized some of the most popular methods to synthesis PCMs, then the applications of micro/nanoporous carbon materials in the field of supercapacitors, lithium-ion batteries, lithium sulfur-based batteries, solar cells, and  $\text{CO}_2$  capture.



**Fig. 1** **a** Hard-template method, reproduced with permission from [8] Copyright (2017) Creative Commons Attribution License, **b** soft-template method, reproduced with permission from [9] Copyright (2013) American Chemical Society, **c** template-free (activation) method, reproduced with permission from [10], **d** Schematic illustration comparing macro, meso, and micropores, “reprinted with permission from [10] Copyright (2019) Creative Commons Attribution License”

## 2 Synthesis Methods of Porous Carbon Materials

While there are several methods reported on how to prepare PCMs with specific pore size, volume, etc., they are mainly categorized into (a) hard-template methods, (b) soft-template methods, and (c) template-free methods.

### 2.1 *Hard-Template Method*

In this method, rigid nano or microstructured inorganic materials such as zeolites, clays, colloidal silica particles, and wires fibers are used as templates which later produces its negative replica-carbon structure [11]. It is one of the easiest and efficient methods to control the pore structures to prepare highly ordered porous carbon nanostructures. The typical process includes (i) synthesis or choosing the desired template, (ii) coat or filling the template with cross-linked precursors, (iii) chemical or thermal treatment of the processed template to convert precursors into a solid carbon network, and (iv) etching away the templates using strong acid or base [8]. For example, as shown in Fig. 1a, two types of porous mesoporous silica templates, namely SBA-15 and MCM-48, were chosen to obtain hexagonal and cubic 3D-porous structures, respectively [8]. These templates were then filled with carbon sources (typically sucrose) followed by polymerization. Later, pyrolysis/carbonization was performed by heating at elevated temperatures  $\sim 900$  °C under vacuum. The obtained silica/porous carbon composites were then washed with a strong etchant (NaOH) to remove silica templates to obtain 3D-porous mesocarbon structures called CMK-3 and CMK-1, respectively.

Even though highly ordered porous structures are produced by this method. However, the multi-step process in this method, high cost, and the usage of strong acid or base-based etchers limit its widespread industrial adaptability.

### 2.2 *Soft-Template Method*

As mentioned earlier, the disadvantages of using strong etchants drive researchers toward more sustainable methods such as the soft-template method. The typical soft-template method utilizes the inherent phase-segregation ability of the self-directing agents such as surfactants or copolymers as templates to form porous carbon networks [7]. Toward this end, ionic or non-ionic nature of self-directing agents plays an important role in deciding the pore size of the final product. For example, ionic surfactants generate PCMs with a pore size ranging from 2 to 4 nm, whereas non-ionic surfactants produce mesoporous structures in which the size is 10 nm and above [7]. Unlike hard-template methods, this method does not require any additional etching

agent since such soft-templates are either consumed or become an important part of the carbon network or decomposed during the carbonization process [12].

Even though this method has many advantages such as easy control of structure as well as pore sizes, premium quality product, easy handling, and scalability, it also suffers from a few limitations such as lower crystallinity and sensitivity to reactive conditions. Interestingly, these challenges can be easily addressed by using further chemical and thermal treatments. For example, as shown in Fig. 1b, novel porous nanostructured carbon monoliths were prepared via the self-assembled dual-block copolymer-latex template method [9]. In this method, the mixing of polystyrene latex with sugar, pluronic diblock copolymer solutions leads to the formation of inverse opal structure due to the inherent self-assembly nature of the molecules involved. The hydrothermal carbonization of sugar that was employed at the end helped in preparing the monoliths with coral-like structures with different pore sizes in the carbon network.

Along with hard and soft-template methods, researchers also used other interesting methods to generate PCMs with various pore sizes such as in situ templates, self-template, multiple templates, and salt-melt methods. Further details can be found in the recent literature reviews mentioned here [7, 9].

### 2.3 *Template-Free Method*

*Activation:* In the typical process, natural or synthetic carbon precursors are activated under an inert atmosphere by physical gaseous etchants (e.g., CO<sub>2</sub>, NH<sub>3</sub>, and steam) and/or chemical etchants (such as KOH, NaOH, or ZnCl<sub>2</sub>) to produce high-surface area porous carbon materials. Figure 1c shows the physical and chemical activation scheme of carbon precursors [10]. The most preferred carbon precursors for this process are the natural biomass-derived precursors such as wood, coconut shells, and fossil fuels. It is worth noting that chemical and physical processes can be used simultaneously. For many years, the activation methods demonstrated their capability in producing hierarchically porous structures along with very high-surface area. Recently, the usage of a few supplement activation methods such as hydrothermal and microwave-assisted carbonizations gaining importance, mainly due to their low energy consumption and ease of the process.

*Hydrothermal Carbonization:* In a typical autoclave setup, the source precursors (e.g., glucose, starch, etc.) are thermochemically converted to porous carbons in the presence of subcritical water at relatively low temperatures 180–260 °C under self-generated pressures of 2–6 MPa. The wet-char product (also known as hydro-char) further undergo activation via chemical, physical, or both processes to enhance the porosity and pore volume of the final product. In contrast to the char produced from the conventional dry pyrolysis, the hydro-char produced in this process has a significantly higher amount of oxygenated functional groups that enable an easy functionalization of these porous carbons.

*Microwave-assisted Carbonization:* It is another interesting method to perform activation at relatively low temperatures while accelerating chemical reactions with uniform heating across the substance. Compared to conventional heating, microwave activation might offer increased active surface area significantly with less energy consumption [10]. As an added advantage, microwave assistance process can be performed simultaneously with chemical or physical activation processes. Overall, even though it is still challenging to produce ordered nanostructured carbon materials through the activation processes especially for energy-related applications. However, the ease and simplicity of the processes made them widely acceptable by the industrial communities for other applications including adsorption, water treatment, etc.

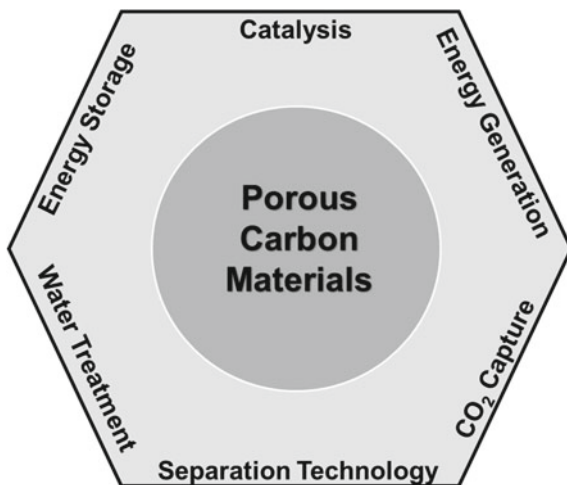
To sum-up, on the synthesis methods, it is difficult to achieve highly ordered and scalable nanoporous carbon structures through any single method. Every method has some associated advantages and disadvantages. Hence, the use of a combination of the above-mentioned methods gaining popularity recently, mainly due to the advantages and flexibility that they can offer. For example, porous carbon spheres are generated by the combination of hydrothermal activation assisted by hard-template methods. Many other reviews that highlighted the importance of using a suitable method or combination of methods to match the requirements can be found here [7, 12].

### 3 Applications of Carbon Porous Materials

Porous carbon compounds have displayed excellent performance in many applications. Numerous applications in the energy and environmental markets have used structured carbon as anode for lithium-ion batteries (LIBs) and an oxygen reduction reaction (ORR) electrocatalyst supported fuel cells, owing to the distinct properties of porous carbon compounds [13]. The design and manufacture of porous carbon nanoarchitectures have made significant progress in the past, and more work needs to be done so as to control their structure, pore sizes, and surface chemistry, when it comes to establish utilization avenues for carbon nanoarchitectures. Figure 2 shows various multidisciplinary applications of PCMs.

The high-surface area, high conductivities, chemical stability of the porous carbon-based materials including activated carbon, carbon nanotubes, and graphene enable them as stand-alone electrode materials for energy-related applications. But the low energy density of these carbon-based materials is due to their inherent low capacitance demand for a further functional modification or combination with a suitable counter material to address these issues. Many researchers have developed various synthesis strategies and also designed appropriate counter components that are suitable and compatible with carbon materials to address these challenges. For example, combining carbon materials with metal oxides such as  $\text{MnO}_2$ ,  $\text{Fe}_3\text{O}_4$ , and  $\text{TiO}_2$  tremendously improve the specific capacitance for supercapacitor applications. In a similar direction, many counterparts such as metal hydroxides, conducting polymers, perovskites, and heteroatom doping are used to enable them to advance functional carbon-based electrodes. In the next subsections, recent progress made in the

**Fig. 2** Multidisciplinary applications of porous carbon



synthesis and application of porous carbon and porous carbon-based materials as electrodes for energy conversion and energy storage is covered.

### ***3.1 Supercapacitors***

Supercapacitors offer high energy densities and capacities with excellent cyclability (capability to store and release energy) and are more powerful. The storage of energy in a supercapacitor takes place in the electrodes, or electrolyte–electrode interface, by physical charge build-up and/or faradaic charge transfer. The focus of research in supercapacitors thus far has been to try to find novel cheap materials, as well as innovative and speedy methods for creating supercapacitors with better performance. Fabrications of supercapacitor make use of some carbon-based materials, metal oxides, and conducting polymers. More specifically, researchers have been paying more attention to carbon-based materials, especially for supercapacitor applications, where activated carbon (AC) is commercially accessible [14, 15].

Electrochemical capacitors are classified as electrical double layer capacitors (EDLCs) and pseudo-capacitors. Carbon-based materials often employ the EDLC mechanism. In electrostatic ion adsorption and accumulation on the electrode surface, electrode double layer hinges form, although reversible redox processes in pseudo-capacitors store more energy in greater amounts than EDLCs. Commercial ACs employ high-surface area materials, excellent conductivity, and pore size that work with the electrolyte system. To be appropriate for EDLC capacitor design, these characteristics are critical. To study the characteristics of several present types of carbon materials, significant basic investigations have been conducted. Due to unique physicochemical properties associated with carbon-based electrodes, these materials



are commercially utilized for EDLCs as they are excellent conductors and have high-surface area ranges from 1 to 2000 m<sup>2</sup>/g [16]. Therefore, carbon-based materials are an ideal choice for EDLCs. They are also highly stable in the presence of heat, acids, and bases, as well as in the presence of large amounts of electrolytes. Carbon compounds are incredibly long-lived and provide a lot of power. These qualities together make carbon-based materials very desirable: they are abundant, inexpensive, and relatively simple to produce. Because of the advantages that carbon possesses in the field of EDLC, several carbon designs have been developed to increase energy storage capacity. Carbon materials for supercapacitor applications that have recently been investigated include carbon quantum dots, graphene, functionalized carbon, activated carbon, doped carbon, carbon aerogels, and carbon nanomaterials [17].

Porous carbon materials suited for supercapacitor applications may be synthesized using chemical activation methods such as KOH, H<sub>2</sub>SO<sub>4</sub>, AgCl, and ZnCl<sub>2</sub>. Researchers discovered that treating the cells with KOH activated AC (which has around higher specific capacitance ~ 185%) improved the specific capacitance value by 30% [18]. They speculated that the extra oomph might be attributed to a larger mesoporous surface area, i.e., 2505.6 m<sup>2</sup>/g. Similarly, comparable results were obtained by using ZnCl<sub>2</sub> as an activating agent. Presence of substantial micropores and higher specific surface area results into greater specific capacitance [19].

Yushin and coworkers reported an excellent approach that includes how to increase the surface area of activated carbon? The increased surface area consequently results into increase in the specific capacitance values [20]. One activation step was done by KOH to synthesize polypyrrole-activated carbon. Ionic liquid was observed to have an extraordinary specific capacitance of 300 F/g for the activated carbon obtained from polypyrrole. The polypyrrole-derived activated carbon has the greatest specific capacitance in an ionic liquid. The capacitance increases with an increase in temperature due to the fact that increased temperature results into a drop in viscosity and movement of ions become easy and hence an increase in conductivity of the ionic liquid. Further, using biomass sources, such as tea trash, porous activated carbon was produced and was investigated within an aqueous electrolyte [21]. The KOH electrolyte was discovered to have a remarkable specific capacitance (330 F/g), which proved to be extremely stable throughout the operation. After 20,000 cycles, the retained capacitance was extremely high, at around 92%. As previously reported, porous activated carbon was generated responsibly by composting tree seeds. Moreover, after 5000 cycles, the thermal pre-carbonization and subsequent activation with KOH resulted in a material with a capacitance value of 365 F/g, with the remaining bulk of the original value [22].

Cummings and colleagues demonstrated in theoretical research that the size of the carbon pores (mainly micropores) should be comparable with the ion size of the electrolyte liquid to offer appropriate charge accommodation [23]. On the other hand, Simon and coworkers discovered that diffusion and desolvation significantly constrain ion mobility in these sub-nanometer micropores, resulting in low to moderate charge–discharge rates. As a result, charge and discharge rates are limited to low to moderate levels, therefore limiting rate and power density performance [24]. The researchers considered this issue and developed a novel design that included

meso/macropores within the microporous carbon structure, resulting into excellent capacitance retention during process of fast charging/discharging. Additionally, they observed that by combining micro, meso, and macropores, they were able to achieve a particular capacitance, i.e., the gravimetric capacitance of  $374.7 \pm 7.7 \text{ F g}^{-1}$  at a current density of  $1 \text{ A g}^{-1}$  with a porous carbon electrode [25].

Other elements, for example, nitrogen, sulfur, boron, phosphorous, and oxygen, have been used to alter the surface chemistry of porous carbon. Bando and coworkers reported that pyridinic and pyrrolic N both could be served as faradaic sites for pseudo-capacitance in the pyridinic N oxide and graphitic N electrode, whereas positively charged pyridinic N oxide aids electrical conductivity [26]. Sun and coworkers discovered that other doped samples showed unequal charge distribution transfer, resulting in an increased charge transfer speed [27]. By employing dual doping (e.g., N, B co-doping), Kirk and coworkers claimed that this might increase the ability to accelerate electron transport and pseudo-capacitance [28]. Porous carbon materials exhibited an increase in capacitance of 30% as a result of surface oxygen functional groups. Another method for increasing pseudo-capacitance is loading transition metal oxides ( $\text{RuO}_x$  or mixed oxides;  $\text{Ru}_{1-y}\text{Cr}_y\text{O}_2/\text{TiO}_2$ ) [29] or conducting polymers like polyaniline-grafted reduced graphene oxide [30] onto the carbon surface.

Supercapacitors electrode material properties such as pore sizes and its structure and distribution mainly govern the energy storage performance for supercapacitor. The macropores ( $>50 \text{ nm}$ ) act as the ion buffering reservoirs, the mesopores ( $2\text{--}50 \text{ nm}$ ) as electrolyte ions transport, and micropores generally as the charge storage sites. Moreover, the specific capacitance and the rate capability are dependent on the volume of both micropores and mesopores, respectively. Hierarchical porous carbon electrode materials with interconnected and balanced distribution of macropores, mesopores, and micropores are very promising for high-performance supercapacitor devices. Hierarchical ordered porous carbon materials (HOPC) derived from biowaste were used to make symmetric supercapacitor [31]. The HOPC-based supercapacitor device shows high-specific capacitance of  $289 \text{ F g}^{-1}$  at a current density of  $0.5 \text{ A g}^{-1}$ , with the energy density of  $40 \text{ Wh kg}^{-1}$  at the power density of  $900 \text{ W kg}^{-1}$ . The high electrical conductivity, high-specific surface area, and pore volume of HOPC contribute to high performance of supercapacitor device.

However, overall performance and long-life cycle of supercapacitor devices highly depend on the overall assembly and electrochemical compatibility of electrodes with electrolyte interface.

### 3.2 *Lithium-Ion Batteries (LIBs)*

Batteries such as lithium-ion (LIBs, LSBs), lithium metal anode, and lithium-air are very important devices for energy storage that complement renewable energy

sources solar photovoltaic, wind energy, etc. [32]. Porous carbon electrodes are suitable electrode material utilized in these energy storage devices due to its strong electrical conductivity, great chemical stability, and readily tailored physical and chemical characteristics. Even though porous carbons have exceptional electrochemical performance when it comes to electron transport, they necessitate a design that takes into account porosity, crystal structure, morphology, electronic structure, and surface chemistry. Although three-dimensional structured nanoporous carbons are considered to be the most valuable sustainable materials, they are extensively investigated and developed as anode materials for LIBs [33].

Since Sony began marketing LIBs in 1991, many electronic gadgets, power equipment, and electric automobiles have been supported by LIBs [34]. Structure–property correlations say that in order to have a high storage capacity and stability using porous carbon as the anode material, high conductivity, appropriate surface chemistry, large specific surface areas, and porosity are necessary. Furthermore, the pores in the structure should be hierarchically organized with the goal of promoting reversible intercalation–deintercalation of  $\text{Li}^+$  to enhance  $\text{Li}^+$  storage capacity, while also supporting the rate of  $\text{Li}^+$  transfer and electrolyte mobility. Modification of the electrical and chemical structure of the carbon skeleton by adding one or two heteroatoms (B, N, S, O, and P) allows for more efficient electronic conductivity, wider interlayer spacing, and increased absorbability of Li and electrolytes. Thus, for instance, it was proven that up to 600 mAh/g of graphitic carbon frameworks contains N in the 3.9% range [35].

Graphene particle analogs, pyrolysis of zeolitic imidazolate frameworks, gave up to 17.72 wt% high N content [36]. These particles serve as the cathode in LIBs, retaining the 2132 mAh  $\text{g}^{-1}$  capacity after 50 cycles, and 785 mAh  $\text{g}^{-1}$  after 1000 cycles. The exceptional results were due to the incorporation of N into the lattice having hexagonal symmetry and carbon edges. Further, calculation findings showed that as pyridinic and pyrrolic Ns served as the active sites to adsorb Li atoms, the additional Li storage capacity (i.e., more than 395.21 mAh  $\text{g}^{-1}$ ) that emerged from doped nanopores and edges may be attributed to Li adsorption in those locations. The effect of porous carbons is also enhanced by including additional functional materials, such as silicon [37], metal oxides (Fe, Co, Ti, and Cu) [38], and metal sulfides [39]. Using the example above, the produced carbonaceous materials with pores in their bimodal mesopores (intratubular mesopores of bimodal mesoporous carbon nanotubes) include mesoporous  $\text{Co}_3\text{O}_4$ , and the material is fully surrounded by  $\text{Co}_3\text{O}_4$  in the bimodal mesopores (CMK-5) [40]. For this particular application, when the composite was used as a LIB anode, the specific capacity of 781 mAh/g was observed at 100 mA/g, very good rate capacity, and exceptional cycle behavior. The need of higher gravimetric and volumetric energy density storage devices is continually rising, which cannot be supplied by LIB technologies alone [41, 42]. New rechargeable Li-based batteries were created in order to fulfill the high energy density need of LSBs including a space for volume expansion after sulfur loading and providing a conduit for  $\text{Li}^+$  and electrolyte diffusion.

### 3.3 *Lithium-Sulfur-Based Batteries (LSBs)*

The porous carbon is used to hold sulfur, whereas the carbon framework is where the active components are held. It can both absorb lithium polysulfide (LPS) and retain lithium-sulfur batteries (LSBs) over a long period of time. Some researchers proposed that, while the sulfur level in the cathode must be  $< 70$  wt% for LSBs to have greater volumetric energy density, optimizing the pore structure to be able to achieve a high sulfur percentage is essential for practical applications [43]. The electrochemical performance may be diminished when the carbon pores are full of sulfur, but if the pores are unencumbered by sulfur, the performance improves. To keep the phenomena from occurring, it is recommended that a conductive carbon with 3D network having a very high pore volume and specific surface area might be used [44]. Carbon may improve the conductivity of sulfur having insulating features or lithium sulfides, resulting in a wide carbon/sulfur contact that facilitates charge transfer. Porous carbon with a high graphitization degree provides good electrical conductivity and a high rate of performance. During charge and discharge cycles, LPSs produced in sulfur cathodes cause battery deactivation and decreased cycling activity.

Electrochemical alteration of carbon-based hosts (e.g., heteroatom fixing, metal chalcogenides, or polymers) ameliorates these issues across three primary dimensions. Three primary dimensions, in physical interactions, or by chemical bonds, trapping LPSs. In particular, N-doping can increase the adsorption of LPSs on carbon-based surfaces, due to strong coordination or covalent bonding [45]. In porous carbon with N and P dual doping, greater chemical adsorption was observed than in carbon mono-doped with LPSs. Carbon hosts enable electron donors and acceptors to interact more easily, allowing electrons to more readily interact with them (i.e., by N atom doping).

### 3.4 *Solar Cells*

Renewable resources are on the rise in order to meet growing global energy demands as well as to address the impacts of global climate change. Solar cells are very important renewable considering the large abundance of solar energy. The development of solar cells has also been recognized as one of the most promising techniques for storing and utilizing solar energy as electricity. Currently, the vast majority of solar panels are made of crystalline silicon. One of the primary elements of solar cells (SCs) is the hole-collecting electrode (counter electrode; CE). Carbon materials are one of the interesting alternatives for platinum-carbonate conductive epoxy owing to their low cost, eco-friendly production, scalability, and surface area. Graphite-carbon black combination counter electrode was studied for the first time in 1996 by Kay and Grätzel. They obtained a promising value of photo conversion efficiency (PCE) of 6.7% [46]. Carbonous materials, such as carbon nanotubes, carbon black,

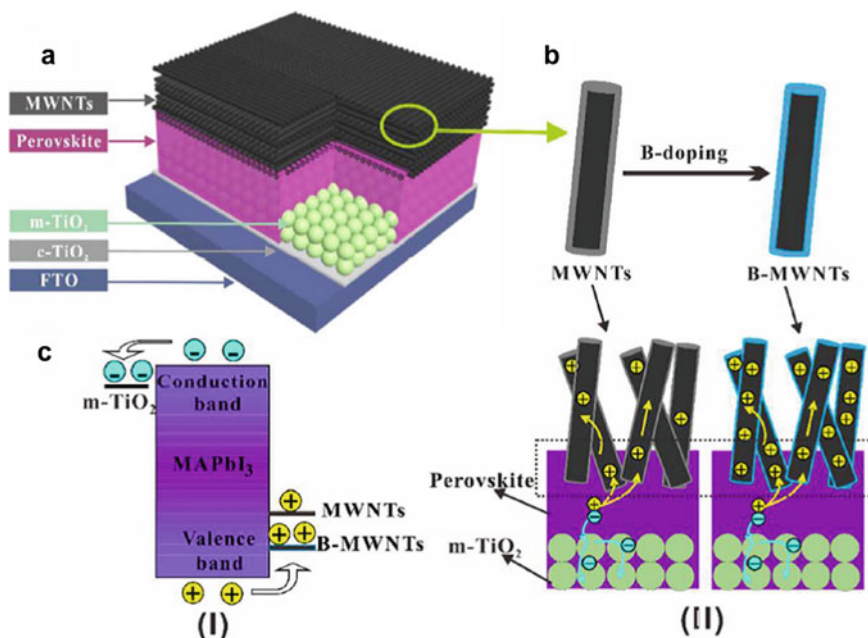
graphite, graphene, carbon nanofibers, and mesoporous carbon, have all been extensively researched, and each has been shown to be an effective counter electrode [13]. Carbon materials have been used in the CE of  $\text{CH}_3\text{NH}_3\text{PbI}_3$ -based perovskite solar cells (PSCs) for the first time. Moreover, carbon black/graphite composite was screen printed on the photoelectrode used in PSC. Further, in order to produce a photoelectrode, fluorine-doped tin oxide (FTO) glass as the substrate was used, topping with the compact layer of oxides of Ti ( $\text{TiO}_2$ ), which was followed [47] by a mesoporous  $\text{TiO}_2$  layer, and then a layer of  $\text{ZrO}_2$  (with a spacer layer of  $\text{ZrO}_2$ ). The PSC finally completed its production process by coating the  $\text{CH}_3\text{NH}_3\text{PbI}_3$  perovskite sensitizer on top of the mesoscopic carbon layer [48].

The achievement of Han's group, using different carbon compounds as CE materials in PSCs, included the goal of improving efficiency [49–51].  $\text{TiO}_2$  nanosheets on the photoelectrode resulted in a 10.6% increase in efficiency from 6.64 to 10.6%, and even more to about 11.6% when varying the thickness of the carbon counter electrodes [52, 53]. To provide a complete analysis of PSCs behavior, separate research also sought to examine the link between the thickness of the carbon black/graphite layer ranges from 3 to 15  $\mu\text{m}$  and its performance. The highest efficiency of the PSCs was attained when a carbon black/graphite counter electrode was used with an optimum thickness of 9  $\mu\text{m}$ . In addition to producing hole conductor-free and printable perovskite solar cells, Han's team also played a part in assisting Grätzel's team in manufacturing hole conductor-free and printable perovskite solar cells [54].

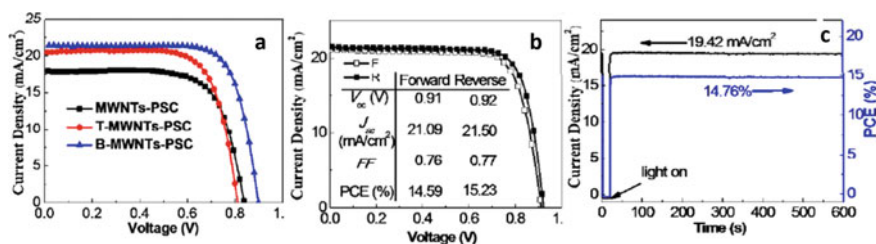
Various carbon materials such as carbon nanotubes [47, 55], viable carbon paste [56], single-layered or multi-layered graphene [57], and candle soot [57] are explored as hole extraction materials for PSCs. The collaborative efforts of perovskite and carbon material researchers have resulted in a good bond between the perovskite layer and the carbon components. One more way to look at it is that the recombination is inhibited at the interface, and the charge collection is improved. This latest research has found that when B-multiwalled nanotubes (B-MWNTs) are used, the aforementioned characteristics improve in work function, carrier concentration, and conductivity [47]. Figure 3 illustrates the MWNTs CE-based PSCs design. B atoms were used as doping atoms on the MWNTs to enhance hole extraction and transport in the PSCs.

A-MWNTs' photovoltaic performances surpass those of both the A-MWNTs and the B-MWNTs ([47], shown in Fig. 4a). Additionally, an  $\text{Al}_2\text{O}_3$  layer was formed on the m- $\text{TiO}_2$  film, functioning both as a physical barrier to considerably prevent interaction between CNTs and meso- $\text{TiO}_2$ , as well as an additional method for minimizing back electron transmission. An efficiency of 15.23% was obtained by powering the PSCs with B-MWNTs via  $\text{TiO}_2/\text{Al}_2\text{O}_3$ -B-MWNTs (14.6%). The productivity of this hole transport material (HTM)-free carbon-based PSC could be the greatest among all the PSCs that did not use HTMs ([47], Fig. 4b). Once the photocurrent density has been measured for 600 s, it became steady and offered a PCE of 14.76% ([47], Fig. 4c) offered a PCE of 14.76%.

Sun [58–60] and Ma and coworkers discovered that the commercial conductive carbon pastes could be directly applied to the layers of perovskite. 8–9% PCEs were derived from HTM-free devices [61–63]. Carbon paste was examined as a



**Fig. 3** Schematic illustration of cell configuration, B-doping of MWNTs, and charge behavior in C-PSCs. **a** Schematic illustration of the C-PSC configuration. **b** Schematic diagram of B-doping of MWNTs to B-MWNTs. **c** Schematic illustration of charge transfer enhancement by B-MWNTs through (I) lowering the *EF* of MWNTs and (II) increasing the number of conduction carriers in B-MWNTs electrode. The intimate interface between perovskite and MWNTs is marked by black dotted rectangle in (II). "Reprinted with permission from [47] Copyright 2017 American Chemical Society"



**Fig. 4** Photovoltaic device, energy level structures, and photovoltaic performances of C-PSC devices with different MWNTs. Photocurrent density–voltage curves. J–V curves measured at forward **(a)** and reverse scanning directions **(b)** (100 mV s<sup>-1</sup>). Measured photocurrent output at the maximum power point (0.76 V) and calculated PCE versus time **(c)**. "Reprinted with permission from [47] Copyright 2017 American Chemical Society"

potential HTM-free perovskite/TiO<sub>2</sub> heterojunction solar cell constituent in place of noble metallic components due to their high cost. Even in the absence of encapsulation, Ma's work revealed the unexpected capacity of heterojunction PSCs with the architecture of M-TiO<sub>2</sub>/CH<sub>3</sub>NH<sub>3</sub>PbI<sub>3</sub>/C to resist damage and remain stable for over 2000 h in air in the dark. These experiments strongly support the claim that the low-cost carbon electrodes may be processed directly on top of the perovskite layer without altering its structure, which gives exciting options for material and structural selection in the resulting device [60].

### 3.5 Oxygen Reduction Reaction (ORR)

Many conversion and storage technologies related to energies, including metal-air batteries, membrane involved proton exchange, fuel cells, make use of ORR because of its famously slow kinetics [32, 64, 65]. The limited availability, high cost, and short lifespan of the state-of-the-art ORR catalysts, their commercialization took quite large time. Discernible and heteroatom-doped porous carbons have significant potential as long-term, cheap, and active ORR electrocatalysts in alkaline environments while exhibiting less sensitivity to methanol crossover effect. One can modify morphology, concentration, electrochemical property of the surface, and electronic structure of carbon materials by using heteroatoms such as N, S, B, and P. Therefore, we can improve the performance of oxygen adsorption and activation with respect to the ORR by making suitable changes to the microstructure, composition, electrochemical property as well as electronic structure of carbon materials [66]. Consider the case of the pyridinic N-doped pyridinium doped at the edge of graphitic C. This N-doped pyridinium helps in reduction of the energy barrier for O<sub>2</sub> adsorption, and hence speed up the rate-limiting initial electron transfer. An aid to O<sub>2</sub> adsorption and desorption is provided by the tertiary ammonium quaternary which might result in C-N bonds of shorter length and unequal electron distribution. A very effective and stable ORR was accomplished in an N-doped porous carbon material because of the simultaneous adjustment of micro or mesoporous structure and surface characteristics [67]. Synergistic effects of several heteroatoms have been shown to potentiate the electrocatalytic activity [68]. Although porous carbon materials are known to serve as electrocatalysts, it is also possible to employ them as supports to aid the loading of non-noble metals. An example for the same is the investigation of a family of Fe, N-doped, and Co, N-doped porous carbon catalysts [69]. Possible applications in electrochemical conversion and storage remain uncharted territory.

Electrocatalysts are commonly used in fuel cell as ORR electrocatalyst, and both ORR as well as OER electrocatalyst in metal-air batteries that can be recharged. So far platinum when supported on carbons (Pt/C) has been widely explored and used as ORR electrocatalyst despite some limitations such as responsiveness to time dependent drift, CO poisoning, and fuel cross over. OER electrocatalysts include metal oxides such as RuO<sub>2</sub>, MnO<sub>2</sub>, and perovskite oxides. Noble metal and

metal oxides-based electrocatalysts have serious implication on large-scale production and wide spread usage due to their quite high cost and very poor durability. Therefore, nonprecious metal-based electrocatalysts such as metal free and carbon nanomaterials-based ORR electrocatalyst doped with heteroatoms are promising alternatives. 1D CNTs and 2D graphene doped with heteroatoms N, B, P, S, Br, Cl, I, etc., have been used as ORR electrocatalyst. Moreover, doping free carbon nanomaterials when adsorbed with polyelectrolytes are also promising ORR electrocatalysts. Metal free, N-doped carbon nanotubes (N-CNTs), and their graphene composites with porous structures have been used in acidic polymer electrolyte membrane fuel cells. Heteroatom doped 3D ordered porous carbon nanostructures having quite high mechanical and chemical stability, high graphitization, and surface area are of significant interest in electrocatalysts and catalyst supports for fuel cells [70]. Table 1 shows various energy harvesting, storage, and conversion devices using porous carbon materials.

**Table 1** Representative table showing various energy harvesting, storage, and conversion devices using porous carbon materials

Porous carbon materials	Devices	Performance	References
Hierarchical ordered porous carbon (HOPC) from biowaste	Supercapacitor electrodes	Specific capacitance 289 F g <sup>-1</sup> at a current density of 0.5 A g <sup>-1</sup> , Energy density 40 Wh kg <sup>-1</sup>	[31]
MesoporousSi@carbon core-shell nanowires	Lithium ion batteries	Charge capacity of 3163 mAh g <sup>-1</sup> with a high Coulombic efficiency of 86% at a rate of 0.2 C (600 mA g <sup>-1</sup> )	[71]
Honeycomb derived carbon-sulfur composite (Hierarchical porous carbon material)	Lithium-sulfur batteries	Reversible capacity of 1101 mAh g <sup>-1</sup> at 0.1 C	[72]
N-doped carbon foams decorated with heteronanostructured MoO <sub>2</sub> /Mo <sub>2</sub> C nanocrystals (MoO <sub>2</sub> /Mo <sub>2</sub> C@3D NCF) Cathode material	Lithium-oxygen batteries	Discharge capacity of 500 mA h g <sup>-1</sup> at a current density of 100 mA g <sup>-1</sup>	[73]
Porous graphitic carbon (EC-GC) as HTM/counter electrode	Perovskite solar cells	PCE of 8.52%, retention of PCE up to 94.40% after 1000 h	[74]



### **3.6 *CO<sub>2</sub> Capture***

Fossil fuel burning is a major contributor to global warming [75]. For the foreseeable future, fossil fuels will remain the primary energy source, as clean energy options (e.g., wind power, solar energy) have not been extensively embraced. In the near future, it is projected that the CO<sub>2</sub> level would grow as a result [76]. Carbon capture will probably persist, whether carried out before, during, or after combustion, as storage is a must. Post-combustion capture technology focuses on separating CO<sub>2</sub> from nitrogen after fossil fuel combustion. Reducing CO<sub>2</sub> emissions help preserve a sustainable environment. Instead of preceding techniques, pre-combustion CO<sub>2</sub> capture is typically carried out at high temperatures and pressures in order to separate CO<sub>2</sub> from H<sub>2</sub> or CO<sub>2</sub> from CH<sub>4</sub>. Additionally, the operation takes place in an oxygen-rich atmosphere that contains a fuel called oxyfuel. The last step is to enable the water vapor to condense, following which the compressed and stored gas product will be condensed to eliminate the water. A pragmatic way to implement this technique, however, the significant demand for pure oxygen adds to the cost, making it unusable for most situations.

Continuous R&D efforts have resulted in the development of some sorbents having considerable CO<sub>2</sub> capture capacity, strong regeneration ability, and outstanding CO<sub>2</sub> selectivity in post- or pre-combustion circumstances [77]. Conventional carbon capture via aqueous amine scrubbing faces some drawbacks related to their stability, toxicity, regeneration energy requirement, and their volatile nature [78]. Numerous porous solid sorbents have been developed for this purpose, including porous zeolitic imidazolate and metal-organic frameworks, organic polymers, and porous carbons, with a special emphasis on porous organic polymers and zeolitic imidazolate frameworks [79]. Use of porous carbons as sorbents is mainly due to their lightweight, great stability, structural flexibility, low cost, quite good recycling performance, and quite low regeneration energy requirement [79].

Gas adsorption can also be performed by using carbon nanomaterials having 3D ordered porous structures with controllable pore size and configuration. Hydrogen storage via adsorption over carbon materials have been reported using different forms of carbon such as activated carbon, graphite, single walled and multiwalled carbon nanotubes, and carbon nanofibers. Among all of them, carbon nanofibers with large surface area and micropore size distribution have been reported to store hydrogen up to 6.5 wt% [80]. Thermal treatments and metal doping on carbon nanomaterials have shown some degree of improvement in hydrogen storage capacities.

### **3.7 *Effect of Doping on Carbon-Based Electrodes in Energy Storage Applications***

The electrode materials that are being used as electrodes in electric double layer capacitors (EDLC) include carbon-based materials such as carbon nanotubes [81],

carbon fibers [82], graphene [83], carbide derived carbons [84], and activated carbons [85]. Electrical charge storage by EDLCs is based on similar principle like in electrostatic capacitors, however, formation of two distinct layers of electrical charges between electrolyte ions and carbon electrodes (negatively/positively charged) takes place in case of the EDLC [86]. EDLCs preserve specific capacitance to a magnitude that is six to nine times higher when compared with conventional capacitors [87, 88]. In EDLCs, charge storage is mainly a physical phenomenon that does not involve any electronic transfer making EDLCs a superior candidate for applications in which high power is required. Further, very short charging period of time and longer life cycles [89] are key factors for their potential applications. One can improve the specific capacitance by doping heteroatoms (boron, nitrogen, phosphorous, and sulfur) on the surface as well as within the structure of the aforementioned carbon-based active materials. Heteroatoms-doped carbon materials have shown superb capacitive performance due to contribution from pseudo-capacitance through a Faradic reaction which is very fast and fully reversible in nature. Furthermore, reversible Faradic reaction takes place without forfeiting the long cycle life and excellent power density [90]. So far, immense contributions related to energy storage have been made by scientists to assess the impact of these heteroatoms-doped carbon-based electrode active materials [91, 92].

It is shown that the heteroatoms doping into the carbon matrix results into improved capacitance by improving the electrodes wettability [93]. Synthesis of two B- and N-doped porous carbon electrode materials with uniform mesopores diameter has been carried out, and the performance of the synthesized electrodes in both aqueous and organic electrolyte was studied [94]. The results suggest that the pseudo-capacitance is playing the key role in improving the capacitance by B- or N-doping in both aqueous and organic electrolyte. Further, it is reported about the pseudo-capacitance effect that was induced by O-, N-doped activated carbon [95]. Researchers used polybenzoxazine to prepare nitrogen-enriched hierarchically porous carbons and observed that the largest specific capacitance (641.6 F/g at current density 1 A/g) in 6 molar aqueous KOH electrolyte. The observed specific capacitance is reported due to the large pseudo-capacitance induced by active O-III, O-II, N-5, and N-6 functionalities via O-, N-doping. Recently, scientists are working toward improving the specific capacitance via introduction of heteroatoms (O, S, B, N, and P) in the carbon matrix. Hasegawa et al. proposed that S-, P-, and N-doping in carbon matrix can be done via post-treatment route using different doping source [96]. The doping sources used are urea and  $\text{NaNH}_2/\text{NH}_4\text{Cl}$  mixture with hexamethylenetetramine (HMTA) for nitrogen source, red phosphorus for phosphorus source, and  $\text{Na}_2\text{S}_2\text{O}_5$  and  $\text{Na}_2\text{S}_2\text{O}_7$  for sulfur-doping. It is shown that S- and P-doped carbon aqueous electrolyte improves the specific capacitance as compared to that of N-doped carbon and S-doped carbon displayed the highest specific capacitance in the organic electrolyte. The energy density is observed to be linearly proportional to the operating voltage window and specific capacitance. Hence, operating voltage can also be used as an important factor to increase the specific capacitance. Deng et al. have shown that other than used electrolytes, the operating voltage window can also be extended by P-doped porous carbon [97]. The doping with the aforementioned

heteroatoms results into improved conductivity of the material due to introduction of more defects and alterations of the space charge layer density of the carbon materials due to the difference in electronegativity of the doping agent and used carbon material.

### ***3.8 Factors Affecting Performance of Carbon Materials as Electrodes***

There are so many factors that can affect the performance of carbon materials as electrodes in energy storage devices. Large surface area (implies pore surface contains vast amounts of charged ions) is one of the major requirements in achieving high capacitance of carbon-based electrodes. Micropores present in carbon electrode material perform an important function while providing a huge accumulation platform for high energy storage through controlled diffusion effects and molecular sieving [98, 99]. Activated carbons generally have predominant microporosity, and hence, these materials have been used as the most common supercapacitor electrodes. Although large surface area plays an important role for carbon-based supercapacitors (CSs), but large surface area in excess of  $1500 \text{ m}^2 \text{ g}^{-1}$  [100] may not necessarily contribute to the electrode capacitance due to limited electrochemical accessibility to the ions. In order to improve the storage capacity, one has to generate large adsorbing sites that are more exposed on the surface landscape and hence helps in relieving the barrier for surface accessibility [101]. Significant research efforts have been made so as to fabricate various carbon morphologies in which there is superior control over the surface topography as well as interior texture. A variety of synthesis methods, e.g., modified Stoeber synthesis, self-assembly, emulsion polymerization, and hydrothermal carbonization have been employed to construct spherical carbon nanoarchitectures that feature the close-packing nature and the smallest surface-to-volume ratio [102].

The pore size distribution and conductivity are very critical parameters for electrode application of porous carbon materials in different devices. In Li-air battery, the size of the of carbon materials as cathode influences the kinetics of ORR and OER processes. It is found that the smaller pore sizes assist in faster kinetics of ORR and OER. However, small pores reduce the total pore volume and in turn not suitable to accommodate the discharge products of the reactions. Therefore, one has to optimize pore size distribution to achieve maximum performance of the devices using porous carbon materials.

Advanced functionalization and structural design of progressive nanoporous carbons have produced unprecedented developments, yet many sectors remain where these advancements can still be put to use. Here, we mentioned the appealing porous carbon microstructure designs that have a significant beneficial influence on the properties of supercapacitors, LIBs, LSBs, ORR, and  $\text{CO}_2$  capture. Nanoporous carbons have a significant impact on the world, and there are several prospective avenues for

further improving their structure, manufacturing, and application in new applications. As a result, it is unsuitable for broad usage.

## References

1. Miao L, Song Z, Zhu D, Li L, Gan L, Liu M (2020) Recent advances in carbon-based supercapacitors. *Mater Adv* 1:945–966
2. Osman S, Senthil RA, Pan J, Chai L, Sun Y, Wu Y (2021) Hierarchically activated porous carbon derived from zinc-based fluorine containing metal-organic framework as extremely high specific capacitance and rate performance electrode material for advanced supercapacitors. *J Colloid Interface Sci* 591:9–19
3. Borenstein A, Hanna O, Attias R, Luski S, Brousse T, Aurbach D (2017) Carbon-based composite materials for supercapacitor electrodes: a review. *J Mater Chem A* 5:12653–12672
4. Rai V, Toh C-S (2013) Electrochemical amplification strategies in DNA nanosensors. *Nanosci Nanotechnol Lett* 5:613–623
5. Carratalá-Abril J, Rey-Martínez L, Beneito-Ruiz R, Vilaplana-Cerdá J (2016) Development of carbon-based composite materials for energy storage. *Mater Today: Proc* 3:S240–S245
6. Luo X-Y, Chen Y, Mo Y (2021) A review of charge storage in porous carbon-based supercapacitors. *New Carbon Mater* 36:49–68
7. Tian W, Zhang H, Duan X, Sun H, Shao G, Wang S (2020) Porous carbons: structure-oriented design and versatile applications. *Adv Func Mater* 30:1909265
8. Walcarius A (2017) Recent trends on electrochemical sensors based on ordered mesoporous carbon. *Sensors* 17:1863
9. Kubo S, White RJ, Tauer K, Titirici M-M (2013) Flexible coral-like carbon nanoarchitectures via a dual block copolymer-latex templating approach. *Chem Mater* 25:4781–4790
10. Pérez-Mayoral E, Matos I, Bernardo M, Fonseca IM (2019) New and advanced porous carbon materials in fine chemical synthesis. Emerging precursors of porous carbons. *Catalysts* 9:133
11. Xia Y, Yang Z, Mokaya R (2010) Templated nanoscale porous carbons. *Nanoscale* 2:639–659
12. Schrettel S, Schulte B, Frauenrath H (2016) Templating for hierarchical structure control in carbon materials. *Nanoscale* 8:18828–18848
13. Guo H, Zhu Y, Li W, Zheng H, Wu K, Ding K, Ruan B, Hagfeldt A, Ma T, Wu M (2015) Synthesis of highly effective Pt/carbon fiber composite counter electrode catalyst for dye-sensitized solar cells. *Electrochim Acta* 176:997–1000
14. Su DS, Zhang J, Frank B, Thomas A, Wang X, Paraknowitsch J, Schlögl R (2010) Metal-free heterogeneous catalysis for sustainable chemistry. *ChemSuschem* 3:169–180
15. Zhang J, Zhao XS (2012) Conducting polymers directly coated on reduced graphene oxide sheets as high-performance supercapacitor electrodes. *J Phys Chem C* 116:5420–5426
16. Faraji S, Ani FN (2015) The development supercapacitor from activated carbon by electroless plating—a review. *Renew Sustain Energy Rev* 42:823–834
17. Inagaki M, Konno H, Tanaike O (2010) Carbon materials for electrochemical capacitors. *J Power Sources* 195:7880–7903
18. Chen M, Xuan H, Zheng X, Liu J, Dong X, Xi F (2017) N-doped mesoporous carbon by a hard-template strategy associated with chemical activation and its enhanced supercapacitance performance. *Electrochim Acta* 238:269–277
19. Qin L, Xiao Z, Zhai S, Wang S, Wang H, Wang G, Cai W, Li Z, An Q (2020) Alginate-derived porous carbon obtained by Nano-ZnO hard template-induced ZnCl<sub>2</sub>-activation method for enhanced electrochemical performance. *J Electrochem Soc* 167:040505
20. Wei L, Sevilla M, Fuertes AB, Mokaya R, Yushin G (2012) Polypyrrole-derived activated carbons for high-performance electrical double-layer capacitors with ionic liquid electrolyte. *Adv Func Mater* 22:827–834

21. Peng C, Yan X-B, Wang R-T, Lang J-W, Ou Y-J, Xue Q-J (2013) Promising activated carbons derived from waste tea-leaves and their application in high performance supercapacitors electrodes. *Electrochim Acta* 87:401–408
22. Srinivasan R, Elaiyappillai E, Pandian HP, Vengudusamy R, Johnson PM, Chen S-M, Karvemu R (2019) Sustainable porous activated carbon from *Polyalthia longifolia* seeds as electrode material for supercapacitor application. *J Electroanal Chem* 849:113382
23. Feng G, Cummings PT (2011) Supercapacitor capacitance exhibits oscillatory behavior as a function of nanopore size. *J Phys Chem Lett* 2:2859–2864
24. Simon P, Gogotsi Y (2008) Materials for electrochemical capacitors. *Nat Mater* 7:845–854
25. Zhang F, Liu T, Li M, Yu M, Luo Y, Tong Y, Li Y (2017) Multiscale pore network boosts capacitance of carbon electrodes for ultrafast charging. *Nano Lett* 17:3097–3104
26. Seredych M, Hulicova-Jurcakova D, Lu GQ, Bandosz TJ (2008) Surface functional groups of carbons and the effects of their chemical character, density and accessibility to ions on electrochemical performance. *Carbon* 46:1475–1488
27. Li S, Wang Z, Jiang H, Zhang L, Ren J, Zheng M, Dong L, Sun L (2016) Plasma-induced highly efficient synthesis of boron doped reduced graphene oxide for supercapacitors. *Chem Commun* 52:10988–10991
28. Zuliani JE, Tong S, Jia CQ, Kirk DW (2018) Contribution of surface oxygen groups to the measured capacitance of porous carbon supercapacitors. *J Power Sources* 395:271–279
29. Wang G, Zhang L, Zhang J (2012) A review of electrode materials for electrochemical supercapacitors. *Chem Soc Rev* 41:797–828
30. Kumar NA, Choi H-J, Shin YR, Chang DW, Dai L, Baek J-B (2012) Polyaniline-grafted reduced graphene oxide for efficient electrochemical supercapacitors. *ACS Nano* 6:1715–1723
31. Bai X, Wang Z, Luo J, Wu W, Liang Y, Tong X, Zhao Z (2020) Hierarchical porous carbon with interconnected ordered pores from biowaste for high-performance supercapacitor electrodes. *Nanoscale Res Lett* 15:88
32. Rai V, Lee KP, Safanama D, Adams S, Blackwood DJ (2020) Oxygen reduction and evolution reaction (ORR and OER) bifunctional electrocatalyst operating in a wide pH range for cathodic application in Li–Air batteries. *ACS Appl Energy Mater* 3:9417–9427
33. Han F-D, Bai Y-J, Liu R, Yao B, Qi Y-X, Lun N, Zhang J-X (2011) Template-free synthesis of interconnected hollow carbon nanospheres for high-performance anode material in lithium-ion batteries. *Adv Energy Mater* 1:798–801
34. Tarascon JM, Armand M (2001) Issues and challenges facing rechargeable lithium batteries. *Nature* 414:359–367
35. Wang X, Weng Q, Liu X, Wang X, Tang D-M, Tian W, Zhang C, Yi W, Liu D, Bando Y et al (2014) Atomistic origins of high rate capability and capacity of N-doped graphene for lithium storage. *Nano Lett* 14:1164–1171
36. Zheng F, Yang Y, Chen Q (2014) High lithium anodic performance of highly nitrogen-doped porous carbon prepared from a metal-organic framework. *Nat Commun* 5:5261
37. Kim H-W, Lee DJ, Lee H, Song J, Kim H-T, Park J-K (2014) Glucosamine-derived encapsulation of silicon nanoparticles for high-performance lithium ion batteries. *J Mater Chem A* 2:14557–14562
38. Long W, Fang B, Ignaszak A, Wu Z, Wang Y-J, Wilkinson D (2017) Biomass-derived nanostructured carbons and their composites as anode materials for lithium ion batteries. *Chem Soc Rev* 46:7176–7190
39. Lu Y, Fong E (2016) Biomass-mediated synthesis of carbon-supported nanostructured metal sulfides for ultra-high performance lithium-ion batteries. *J Mater Chem A* 4:2738–2745
40. Gu D, Li W, Wang F, Bongard H, Spliethoff B, Schmidt W, Weidenthaler C, Xia Y, Zhao D, Schüth F (2015) Controllable synthesis of mesoporous peapod-like  $\text{Co}_3\text{O}_4$ @carbon nanotube arrays for high-performance lithium-ion batteries. *Angew Chem Int Ed Engl* 54:7060–7064
41. Ghazi ZA, Sun Z, Sun C, Qi F, An B, Li F, Cheng HM (2019) Key aspects of lithium metal anodes for lithium metal batteries. *Small* 15:e1900687

42. Bruce PG, Freunberger SA, Hardwick LJ, Tarascon J-M (2012) Li–O<sub>2</sub> and Li–S batteries with high energy storage. *Nat Mater* 11:19–29
43. Li W, Liu J, Zhao D (2016) Mesoporous materials for energy conversion and storage devices. *Nat Rev Mater* 1:16023
44. Fang R, Zhao S, Pei S, Qian X, Hou P-X, Cheng H-M, Liu C, Li F (2016) Toward more reliable lithium-sulfur batteries: an all-graphene cathode structure. *ACS Nano* 10:8676–8682
45. Zhou W, Xiao X, Cai M, Yang L (2014) Polydopamine-coated, nitrogen-doped, hollow carbon-sulfur double-layered core-shell structure for improving lithium-sulfur batteries. *Nano Lett* 14:5250–5256
46. Kay A, Grätzel M (1996) Low cost photovoltaic modules based on dye sensitized nanocrystalline titanium dioxide and carbon powder. *Sol Energy Mater Sol Cells* 44:99–117
47. Zheng X, Chen H, Li Q, Yang Y, Wei Z, Bai Y, Qiu Y, Zhou D, Wong KS, Yang S (2017) Boron doping of multiwalled carbon nanotubes significantly enhances hole extraction in carbon-based perovskite solar cells. *Nano Lett* 17:2496–2505
48. Ku Z, Rong Y, Xu M, Liu T, Han H (2013) Full printable processed mesoscopic CH<sub>3</sub>NH<sub>3</sub>PbI<sub>3</sub>/TiO<sub>2</sub> heterojunction solar cells with carbon counter electrode. *Sci Rep* 3:3132
49. Yang Y, Ri K, Mei A, Liu L, Hu M, Liu T, Li X, Han H (2015) The size effect of TiO<sub>2</sub> nanoparticles on a printable mesoscopic perovskite solar cell. *J Mater Chem A* 3:9103–9107
50. Liu L, Mei A, Liu T, Jiang P, Sheng Y, Zhang L, Han H (2015) Fully printable mesoscopic perovskite solar cells with organic silane self-assembled monolayer. *J Am Chem Soc* 137:1790–1793
51. Li X, Tschumi M, Han H, Babkair SS, Alzubaydi RA, Ansari AA, Habib SS, Nazeeruddin MK, Zakeeruddin SM, Grätzel M (2015) Outdoor performance and stability under elevated temperatures and long-term light soaking of triple-layer mesoporous perovskite photovoltaics. *Energ Technol* 3:551–555
52. Rong Y, Ku Z, Mei A, Liu T, Xu M, Ko S, Li X, Han H (2014) Hole-conductor-free mesoscopic TiO<sub>2</sub>/CH<sub>3</sub>NH<sub>3</sub>PbI<sub>3</sub> heterojunction solar cells based on anatase nanosheets and carbon counter electrodes. *J Phys Chem Lett* 5:2160–2164
53. Zhang L, Liu T, Liu L, Hu M, Yang Y, Mei A, Han H (2015) The effect of carbon counter electrodes on fully printable mesoscopic perovskite solar cells. *J Mater Chem A* 3:9165–9170
54. Mei A, Li X, Liu L, Ku Z, Liu T, Rong Y, Xu M, Hu M, Chen J, Yang Y et al (2014) A hole-conductor-free, fully printable mesoscopic perovskite solar cell with high stability. *Science* 345:295–298
55. Wei Z, Chen H, Yan K, Zheng X, Yang S (2015) Hysteresis-free multi-walled carbon nanotube-based perovskite solar cells with a high fill factor. *J Mater Chem A* 3:24226–24231
56. Chen H, Wei Z, He H, Zheng X, Wong KS, Yang S (2016) Solvent engineering boosts the efficiency of paintable carbon-based perovskite solar cells to beyond 14%. *Adv Energy Mater* 6:1502087
57. Yan K, Wei Z, Li J, Chen H, Yi Y, Zheng X, Long X, Wang Z, Wang J, Xu J et al (2015) High-performance graphene-based hole conductor-free perovskite solar cells: schottky junction enhanced hole extraction and electron blocking. *Small* 11:2269–2274
58. Zhang F, Yang X, Cheng M, Li J, Wang W, Wang H, Sun L (2015) Engineering of hole-selective contact for low temperature-processed carbon counter electrode-based perovskite solar cells. *J Mater Chem A* 3:24272–24280
59. Zhang F, Yang X, Cheng M, Wang W, Sun L (2016) Boosting the efficiency and the stability of low cost perovskite solar cells by using CuPc nanorods as hole transport material and carbon as counter electrode. *Nano Energy* 20:108–116
60. Zhang F, Yang X, Wang H, Cheng M, Zhao J, Sun L (2014) Structure engineering of hole-conductor free perovskite-based solar cells with low-temperature-processed commercial carbon paste as cathode. *ACS Appl Mater Interfaces* 6:16140–16146
61. Zhou H, Shi Y, Dong Q, Zhang H, Xing Y, Wang K, Du Y, Ma T (2014) Hole-conductor-free, metal-electrode-free TiO<sub>2</sub>/CH<sub>3</sub>NH<sub>3</sub>PbI<sub>3</sub> heterojunction solar cells based on a low-temperature carbon electrode. *J Phys Chem Lett* 5:3241–3246

62. Zhou H, Shi Y, Wang K, Dong Q, Bai X, Xing Y, Du Y, Ma T (2015) Low-temperature processed and carbon-based ZnO/CH<sub>3</sub>NH<sub>3</sub>PbI<sub>3</sub>/C planar heterojunction perovskite solar cells. *J Phys Chem C* 119:4600–4605
63. Xu T, Chen L, Guo Z, Ma T (2016) Strategic improvement of the long-term stability of perovskite materials and perovskite solar cells. *Phys Chem Chem Phys* 18:27026–27050
64. Rai V, Reddy MVV, Adams S, Blackwood DJ (2020) Comparative oxygen evolution reaction performance of cobalt oxide electrocatalyst in combination with various metal ions (MCo<sub>2</sub>O<sub>4</sub> (M = Mn<sup>2+</sup>, Cu<sup>2+</sup>, Co<sup>2+</sup>, Zn<sup>2+</sup>, Fe<sup>2+</sup>, Mg<sup>2+</sup>)). *IOP Conf Ser: Mater Sci Eng* 872:012182
65. Singh RS, Gautam A, Rai V (2019) Graphene-based bipolar plates for polymer electrolyte membrane fuel cells. *Front Mater Sci* 13:217–241
66. Ren Q, Wang H, Lu X-F, Tong Y-X, Li G-R (2018) Recent progress on MOF-derived heteroatom-doped carbon-based electrocatalysts for oxygen reduction reaction. *Adv Sci* 5:1700515
67. Liang H-W, Zhuang X, Brüller S, Feng X, Müllen K (2014) Hierarchically porous carbons with optimized nitrogen doping as highly active electrocatalysts for oxygen reduction. *Nat Commun* 5:4973
68. Zheng Y, Jiao Y, Ge L, Jaroniec M, Qiao SZ (2013) Two-step boron and nitrogen doping in graphene for enhanced synergistic catalysis. *Angew Chem Int Ed* 52:3110–3116
69. Liang H-W, Wei W, Wu Z-S, Feng X, Müllen K (2013) Mesoporous metal–nitrogen-doped carbon electrocatalysts for highly efficient oxygen reduction reaction. *J Am Chem Soc* 135:16002–16005
70. Zhang J, Xia Z, Dai L (2015) Carbon-based electrocatalysts for advanced energy conversion and storage. *Sci Adv* 1:e1500564
71. Kim H, Cho J (2008) Superior lithium electroactive mesoporous Si@carbon core-shell nanowires for lithium battery anode material. *Nano Lett* 8:3688–3691
72. Chulliyote R, Hareendrakrishnakumar H, Joseph MG (2019) Hierarchical porous carbon material with multifunctionalities derived from honeycomb as a sulfur host and laminate on the cathode for high-performance lithium-sulfur batteries. *ACS Sustain Chem Eng* 7:19344–19355
73. Lu Y, Ang H, Yan Q, Fong E (2016) Bioinspired synthesis of hierarchically porous MoO<sub>2</sub>/Mo<sub>2</sub>C nanocrystal decorated N-doped carbon foam for lithium-oxygen batteries. *Chem Mater* 28:5743–5752
74. Pitchaiya S, Eswaramoorthy N, Natarajan M, Santhanam A, Asokan V, Madurai Ramakrishnan V, Rangasamy B, Sundaram S, Ravirajan P, Velauthapillai D (2020) Perovskite solar cells: a porous graphitic carbon based hole transporter/counter electrode material extracted from an invasive plant species *Eichhornia crassipes*. *Sci Rep* 10:6835
75. Gattuso JP, Magnan A, Billé R, Cheung WW, Howes EL, Joos F, Allemand D, Bopp L, Cooley SR, Eakin CM et al (2015) Oceanography. Contrasting futures for ocean and society from different anthropogenic CO<sub>2</sub> emissions scenarios. *Science* 349:aac4722
76. Zou L, Sun Y, Che S, Yang X, Wang X, Bosch M, Wang Q, Li H, Smith M, Yuan S et al (2017) Porous organic polymers for post-combustion carbon capture. *Adv Mater* 29:1700229
77. Nugent P, Belmabkhout Y, Burd SD, Cairns AJ, Luebke R, Forrest K, Pham T, Ma S, Space B, Wojtas L et al (2013) Porous materials with optimal adsorption thermodynamics and kinetics for CO<sub>2</sub> separation. *Nature* 495:80–84
78. Rochelle GT (2009) Amine scrubbing for CO<sub>2</sub> capture. *Science* 325:1652–1654
79. Srinivas G, Krungleviciute V, Guo Z-X, Yildirim T (2014) Exceptional CO<sub>2</sub> capture in a hierarchically porous carbon with simultaneous high surface area and pore volume. *Energy Environ Sci* 7:335–342
80. Mohan M, Sharma VK, Kumar EA, Gayathri V (2019) Hydrogen storage in carbon materials— a review. *Energy Storage* 1:e35
81. Rey-Raap N, Enterría M, Martins JI, Pereira MFR, Figueiredo JL (2019) Influence of multiwalled carbon nanotubes as additives in biomass-derived carbons for supercapacitor applications. *ACS Appl Mater Interfaces* 11:6066–6077

82. Vijayakumar M, Santhosh R, Adduru J, Rao TN, Karthik M (2018) Activated carbon fibres as high performance supercapacitor electrodes with commercial level mass loading. *Carbon* 140:465–476
83. Li X, Zhi L (2018) Graphene hybridization for energy storage applications. *Chem Soc Rev* 47:3189–3216
84. Yan P, Zhang X, Hou M, Liu Y, Liu T, Liu K, Zhang R (2018) Ultrahigh-power supercapacitors based on highly conductive graphene nanosheet/nanometer-sized carbide-derived carbon frameworks. *Nanotechnology* 29:255403
85. Su X-L, Chen J-R, Zheng G-P, Yang J-H, Guan X-X, Liu P, Zheng X-C (2018) Three-dimensional porous activated carbon derived from loofah sponge biomass for supercapacitor applications. *Appl Surf Sci* 436:327–336
86. Poonam, Sharma K, Arora A, Tripathi SK (2019) Review of supercapacitors: materials and devices. *J Energy Storage* 21:801–825
87. Mandapati J, Balasubramanian K (2008) Simple capacitors to supercapacitors-an overview. *Int J Electrochem Sci* 3:1196–1217
88. Jin Z-Y, Lu A-H, Xu Y-Y, Zhang J-T, Li W-C (2014) Ionic liquid-assisted synthesis of microporous carbon nanosheets for use in high rate and long cycle life supercapacitors. *Adv Mater* 26:3700–3705
89. Abbas Q, Mirzaeian M, Ogwu AA, Mazur M, Gibson D (2020) Effect of physical activation/surface functional groups on wettability and electrochemical performance of carbon/activated carbon aerogels based electrode materials for electrochemical capacitors. *Int J Hydrogen Energy* 45:13586–13595
90. Zhou J, Hou L, Lian J, Cheng W, Wang D, Gou H, Gao F (2019) Nitrogen-doped highly dense but porous carbon microspheres with ultrahigh volumetric capacitance and rate capability for supercapacitors. *J Mater Chem A* 7:476–485
91. Wu ZS, Tan YZ, Zheng S, Wang S, Parvez K, Qin J, Shi X, Sun C, Bao X, Feng X et al (2017) Bottom-up fabrication of sulfur-doped graphene films derived from sulfur-annulated nanographene for ultrahigh volumetric capacitance micro-supercapacitors. *J Am Chem Soc* 139:4506–4512
92. Fang BZ, Binder L (2006) A novel carbon electrode material for highly improved EDLC performance. *J Phys Chem B* 110:7877–7882
93. Kwon T, Nishihara H, Itoi H, Yang QH, Kyotani T (2009) Enhancement mechanism of electrochemical capacitance in nitrogen-/boron-doped carbons with uniform straight nanochannels. *Langmuir* 25:11961–11968
94. Wan L, Wang J, Xie L, Sun Y, Li K (2014) Nitrogen-enriched hierarchically porous carbons prepared from polybenzoxazine for high-performance supercapacitors. *ACS Appl Mater Interfaces* 6:15583–15596
95. Hasegawa G, Deguchi T, Kanamori K, Kobayashi Y, Kageyama H, Abe T, Nakanishi K (2015) High-level doping of nitrogen, phosphorus, and sulfur into activated carbon monoliths and their electrochemical capacitances. *Chem Mater* 27:4703–4712
96. Deng Y, Ji Y, Wu H, Chen F (2019) Enhanced electrochemical performance and high voltage window for supercapacitor based on multi-heteroatom modified porous carbon materials. *Chem Commun* 55:1486–1489
97. Chmiola J, Yushin G, Gogotsi Y, Portet C, Simon P, Taberna PL (2006) Anomalous increase in carbon capacitance at pore sizes less than 1 nanometer. *Science* 313:1760–1763
98. Largeot C, Portet C, Chmiola J, Taberna P-L, Gogotsi Y, Simon P (2008) Relation between the ion size and pore size for an electric double-layer capacitor. *J Am Chem Soc* 130:2730–2731
99. Barbieri O, Hahn M, Herzog A, Kötz R (2005) Capacitance limits of high surface area activated carbons for double layer capacitors. *Carbon* 43:1303–1310
100. Yang B, Han K (2019) Charge-carrier dynamics of lead-free halide perovskite nanocrystals. *Acc Chem Res* 52:3188–3198
101. Liu J, Wickramaratne NP, Qiao SZ, Jaroniec M (2015) Molecular-based design and emerging applications of nanoporous carbon spheres. *Nat Mater* 14:763–774



102. Liu X, Zang W, Guan C, Zhang L, Qian Y, Elshahawy AM, Zhao D, Pennycook SJ, Wang J (2018) Ni-doped cobalt-cobalt nitride heterostructure arrays for high-power supercapacitors. *ACS Energy Lett* 3:2462–2469

# Chapter 4

## Lignin-Derived Carbonaceous Materials for Supercapacitor Applications



Esakkiammal Sudha Esakkimuthu, Veerapandian Ponnuchamy, Tugrul Yumak, and David De Vallance

### Abbreviations

AC	Activated carbon
ACN	Acetonitrile
bbACs	Biomass-based activated carbons
BET	Brunauer–Emmett–Teller
$\text{BF}_4^-$	Tetrafluoroborate
CA	Cellulose acetate
$\text{BMIM}^+$	1-Butyl-3-methylimidazolium
CNT	Carbon nanotube
CV	Cyclic voltammetry
$\text{DCA}^-$	Dicyanamide

---

E. S. Esakkimuthu (✉) · V. Ponnuchamy · D. De Vallance (✉)  
InnoRenew CoE—Renewable Materials and Healthy Environments Research and Innovation  
Centre of Excellence, Livade 6, 6310 Izola, Slovenia  
e-mail: [sudha.esakkimuthu@innorenew.eu](mailto:sudha.esakkimuthu@innorenew.eu)

D. De Vallance  
e-mail: [devallance@innorenew.eu](mailto:devallance@innorenew.eu)

V. Ponnuchamy  
e-mail: [veerapandian.ponnuchamy@innorenew.eu](mailto:veerapandian.ponnuchamy@innorenew.eu)

V. Ponnuchamy  
University of Primorska, Andrej Marušič Institute, Titov trg 4, 6000 Koper, Slovenia

T. Yumak  
Department of Chemistry, Sinop University, 57000 Sinop, Turkey  
e-mail: [tyumak@sinop.edu.tr](mailto:tyumak@sinop.edu.tr)

D. De Vallance  
Faculty of Mathematics, University of Primorska, Natural Sciences and Information  
Technologies, Glagoljaška 8, 6000 Koper, Slovenia

DFT	Density functional theory
[DIPEA][TFSI]	Diisopropyl-ethyl-ammonium bis(trifluoromethanesulfonyl)-imide
DMAC	Dimethylacetamide
DMF	Dimethylformamide
EDLC	Electrochemical double layer capacitors
EIS	Electrochemical impedance spectroscopy
ESR	Equivalent series resistance
[Et <sub>3</sub> NH][TFSI]	Triethylammonium bis(trifluoromethylsulfonyl)imide
FSI <sup>-</sup>	Bis(fluorosulfonyl)imide
GCD	Galvanostatic charge-discharge
GO	Graphene-oxide
GPE	Gel-polymer electrolyte
HOMC	Highly ordered mesoporous carbon
IL	Ionic liquids
LAC	Lignin hierarchical porous carbon
LC	Lignin-based carbon
MD	Molecular dynamics
MOF	Metal-organic framework
TEG	Thermoelectric generators
PAA	Poly(amic acid)
PAN	Polyacrylonitrile
PBI	Polybenzimidazole
PDMS	Polydimethylsiloxane
PEEK	Poly(ether ether ketone)
PEO	Poly(ethylene oxide)
PFTE	Polytetrafluoroethylene
PF <sub>6</sub> <sup>-</sup>	Hexafluorophosphate
PMMA	Polymethyl methacrylate
PVDF	Polyvinylidene fluoride
PVDF-HFP	Poly(vinylidene fluoride-hexafluoropropylene)
PVA	Polyvinyl alcohol
PVP	Polyvinylpyrrolidone
PC	Propylene carbonate
PyC	Pyrolytic carbon
PyNO <sub>3</sub>	Pyrrolidinium nitrate
[Pyr][TFSI]	Pyrrolidinium bis(trifluoromethanesulfonyl)imide
SC	Supercapacitor
SEM	Scanning electron microscopy
SFG	Surface functional group
SPE	Solid polymer electrolyte
TEM	Transmission electron microscopy
TEOS	Tetraethoxy orthosilicate
TFSI <sup>-</sup>	Bis(trifluoromethanesulfonyl)imide
T <sub>g</sub>	Glass transition temperature

THF	Tetrahydrofuran
ZDPC	Zeolite-derived porous carbon
ZIF	Zeolitic imidazolate framework

## 1 Introduction

Excessive consumption of energy from fossil fuel resources, increasing global warming, and the world's growing population demand a search for an alternative that provides a clean, efficient, and sustainable energy for modern society. There has been growing research to develop state-of-the-art technologies for harvesting electricity for various portable electronics and household appliances. In recent years, a considerable amount of energy contribution can be acquired from sustainable energy sources, such as wind, geothermal, hydroelectric, solar, and biomass. However, these energy sources are intermittent and fail to contribute consistently due to uneven distribution, geographical location, and weather dependency. Furthermore, a highly efficient energy storage device is required to collect the aforementioned sustainable energy and also to ship it to various locations for utilization. To date, two major energy storage devices—batteries and supercapacitors—have the potential to be used as power sources commercially for a wide range of electronic devices.

In addition to electrical storage applications, interest has emerged to develop energy harvesting devices for applications that vary from transportation systems (e.g., powering monitoring devices) to wearable personal items (e.g., powering watches). More recent efforts have moved toward using composite systems that generate electrical current using moisture and differences in thermal properties between materials using thermoelectric generators (TEG). In the past few years, blue energy field has shown a significant importance because of their abundant nature which can be harvested from ocean wave resource. Liu et al. [1] outlined blue energy harvesting systems based on nanostructured carbon materials that have the potential for harvesting energy derived from flowing liquid, such as rain and moisture evaporation. Research in this area is in its infancy and different technologies are being developed in small-scale systems. Currently, piezoelectric devices containing GaN, ZnO, and polyvinylidene fluoride (PVDF), as well as triboelectric devices using metals, poly-dimethylsiloxane (PDMS), polytetrafluoroethylene (PTFE), and polymethyl methacrylate (PMMA), are used for energy harvesting. However, potential opportunities exist to use lignin-derived carbon materials for these devices.

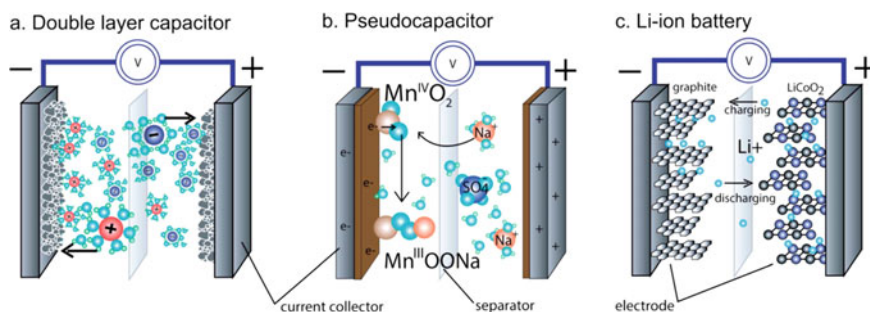
Ding et al. [2] outlined the potential for printing porous carbon films capable of producing 1 Vdc and a power density near  $8.1 \mu\text{W}/\text{cm}^3$  using water evaporation. The porous carbon films were produced using carbon nanoparticles with nanosized pores. Also, Lebrun et al. [3] and Eddia et al. [4] utilized carbon black nanopowders and carbon nanopowders, respectively, when investigating energy harvesting with polymer composites.

## 2 Supercapacitors

The electrochemical energy storage systems are divided into two most known groups such as batteries and capacitors based on the storage and release of charge. In general, a battery that converts chemical energy into electrical energy distributes energy linearly to provide higher energy density. Unlike a battery, capacitors release energy in a shorter time; therefore, they have higher power densities. A supercapacitor (ultracapacitor or electrochemical capacitors) exhibits a much higher capacitance value but with a lower voltage range to fill the gap between batteries and capacitors. The journey of supercapacitors started with a 1 F capacity, and the currently available supercapacitors can display a capacity of more than several hundred Farads and is able to give charge–discharge currents up to several tens of Amperes [5]. Supercapacitors are widely used in several fields such as consumer and portable electronics, transportation and vehicles, power backup, biomedical, military, and aerospace [6]. Depending on the requirements of the application, supercapacitors can be used in complement or instead of other energy storage devices [7].

Supercapacitors are primarily classified into two fundamental groups such as electrochemical double layer capacitors (EDLCs) and pseudocapacitors based on the charge storage mechanism involved in the device [8, 9]. The two capacitor groups, along with Li-ion batteries, are depicted in Fig. 1 [10]. In EDLCs with high surface area and carbon-based materials as electrodes, energy is stored by pure physical accumulation at the electrode/electrolyte interface [11–13]. In pseudocapacitors, however, energy is stored by the transfer of the charge produced by the reversible reduction and oxidation (redox) reactions between the electrode and electrolyte [14, 15]. Considering the electrode materials utilized in pseudocapacitors, the predominant contribution can be obtained from the transition metal-based oxides and hydroxides, and also conducting polymers [16, 17]. Among several carbon-based materials like graphene and carbon nanotubes, activated carbons are the potential and promising electrode materials due to their high surface area, low cost, environmentally benign features, and simple of processability. However, they go through inadequate energy storage capacity and low rate capability [18]. Although pseudocapacitive materials can overcome these issues, they still have some disadvantages including poor electrical conductivity of the electroactive species, low-power density, and cycling stability [19]. Recent studies have demonstrated a typical approach of combining carbon-based materials with either metal oxides/hydroxides or conducting polymers to understand the capacitive performance and cycle life by synergistic effect of pseudocapacitance and EDLC [20, 21]. In fact, some researchers suggest a new title, hybrid supercapacitors, for the energy storage systems prepared with this approach.

The specific capacitance of a supercapacitor depends on various parameters such as electrode material, composition of the electrode (additives), type of membrane, type and concentration of electrolyte, and cell architecture. However, the equivalent series resistance (ESR) and the Columbic efficiency should be considered when discussing the capacitive accomplishment of a supercapacitor. A large number of



**Fig. 1** Basic schematic comparison of **a** electrical double layer capacitor (EDLC), **b** pseudocapacitor, and **c** Li-ion battery. Reprinted with permission from Kristy et al. [10] Copyright (2014) Royal Society of Chemistry

works can be found that focus on the effect of these parameters on the capacitive performance of a supercapacitor. However, it is hard to compare the published results because of several independent variables rely on the process which may not be presented by the authors [22]. Therefore, the energy and power density calculations are generally considered when comparing the reported results.

Among the various parameters listed above, electrode material can be regarded as the most fundamental variable for determining the supercapacitor's performance. Regardless of the energy storage mechanism, recent studies put forth the importance of new electrode active materials designed with improved surface and pore characteristics, surface chemistry, and surface morphology toward designing the supercapacitors with excellent performance.

## 2.1 Precursors for Electrodes

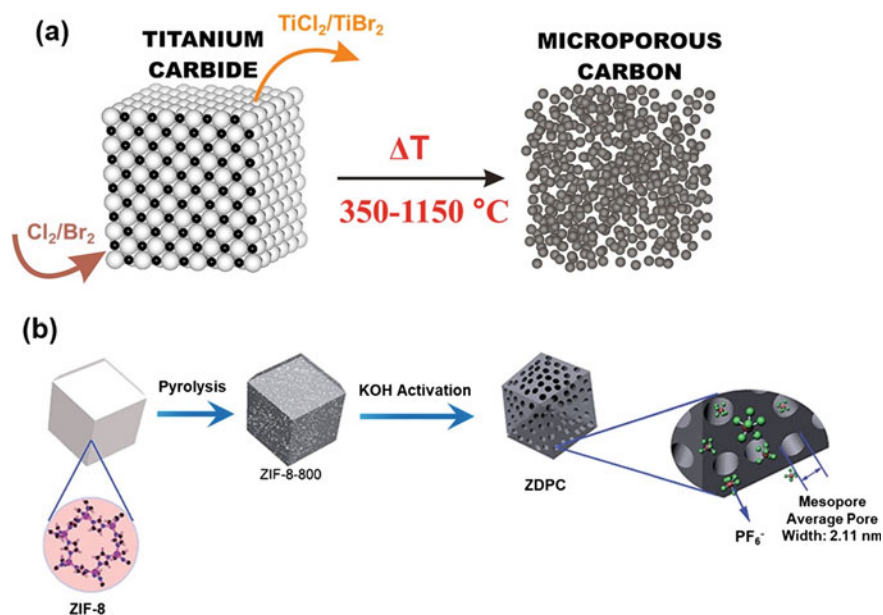
Carbon-based materials are currently the material of choice in the electronics, automotive, and aerospace industries [23] due to their excellent storage of charges electrostatically on surfaces. These carbon materials are used predominantly to fabricate the supercapacitor devices; hence, it is more imminent to choose precursors to produce activated carbon with unique properties including large surface area, good electrical conductivity, low weight, and pore distribution [24]. Several advanced materials have been used as precursors for producing carbons, and a concise overview of every precursor is reported in the following sections.

Carbide-derived carbons have been used significantly as precursors for electrodes in SC because of their large specific surface area and higher control of porosity [25]. In particular, this type of corresponding carbon materials has been obtained through chlorination of metal carbides at high temperatures (400–1200 °C) to remove non-carbon atoms and produce more uniform and disordered structures. During this process, the pore size distribution of the electrodes is largely tuned by the amount

of chlorination and the temperature employed [24]. The carbide-derived carbons can be produced with a pore size in the range of 0.6–1.1 nm, which exhibits 1000–2000 m<sup>2</sup> g<sup>-1</sup> [26]. Several types of carbon-derived precursors have been reported that include SiC, B<sub>4</sub>C, and TiC [27–32]. The authors have attempted to explore the impact of different halogenation using chlorine and bromine in TiC to synthesize carbon-derived carbon; results demonstrated that the extractive step with different halogen does not affect the final carbon structure. However, chlorination showed a noticeable improvement in the texture due to the high reactivity of chlorine, which enhances the uptake capacity of H<sub>2</sub> [33].

Similarly, precursors based on a metal–organic framework (MOF) have been demonstrated as novel materials to synthesize of porous carbon electrodes [34–36]. MOFs consist of organic and inorganic or transition metal clusters which exhibit high thermal properties because the pore size can be tuned by diverse temperature and activation process employed (Fig. 2). The pore size obtained from MOFs is more than 1 cm<sup>3</sup> g<sup>-1</sup>, and the specific surface area ranges from 800 to 3400 m<sup>2</sup> g<sup>-1</sup> [37]. Zeolite-based MOFs are the most predominant materials used to achieve the 3D porous network (shown in Fig. 2), for example, zeolitic imidazolate framework (ZIF-8), which exhibits an excellent surface area of 3680.6 m<sup>2</sup> g<sup>-1</sup> and obtained the pore size of 1 to 4 nm [36]. In addition, zeolite templated carbons (ZTC) are synthesized with non-doped and nitrogen-doped materials that have a pore size of 1.2 nm. Comparing the nitrogen-doped and non-doped ZTC, nitrogen-doped ZTC provides a maximum power that is four times higher than non-doped ZTC due to the fact of nitrogen functionality, which significantly enhances electrical conductivity and wettability [37].

Recycling waste from offices, households, and industrial sites is of interest to produce activated carbons (AC) that can eventually suppress the various issues associated with human health and the environment [38]. Significant research has been proposed for the transformation of a wide range of wastes into AC. Durairaj and the authors have demonstrated the synthesis of AC from laboratory waste and hardboard waste; the results showed that laboratory waste displays the specific capacitance rate of 260 F g<sup>-1</sup> which is higher than hardboard wastes value of 155 F g<sup>-1</sup>. They also reported that the capacitance was maintained up to 92% for laboratory waste and 71% for hardboard waste after 1000 cycles [39]. Similarly, different authors performed the efficient conversion of wastes like printed papers, filter papers, tissue papers, and waste papers into carbon materials [40–44]. Apart from paper waste, AC is also produced from industrial waste, for instance, glycerin, which is more competitive with the AC derived from wood. Glycerin is the predominant residue from biodiesel production, and Gonçalves synthesized AC from crude or unpurified glycerin. They produced AC through applying a chemical activation process with different reagents such as H<sub>3</sub>PO<sub>4</sub> and ZnCl<sub>2</sub>. The obtained AC was applied to investigate the efficiency as electrodes, and the results were indicated that a specific capacitance of up to 15.5 F g<sup>-1</sup> at the current density of 0.25 A g<sup>-1</sup> was obtained which maintained capacitance of more than 82% after 5000 cycles [45]. Similarly, Li fabricated hierarchical porous carbon nanosheets from waste engine oil that showed the specific surface area of up to 2276 m<sup>2</sup> g<sup>-1</sup> with the specific capacitance of 352 F g<sup>-1</sup> and noted that more than

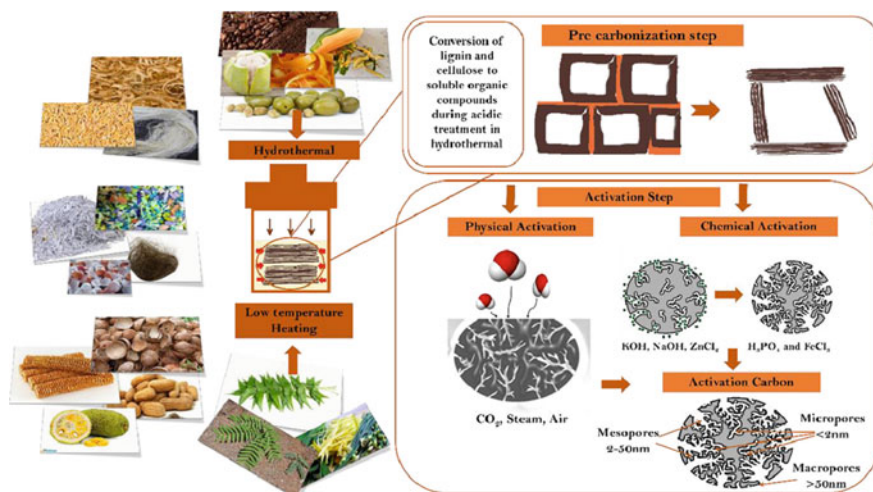


**Fig. 2** Schematic of the synthesis of the **a** carbide-derived carbons from TiC, Reprinted with permission from Stawomir et al. [33] Copyright (2019) Elsevier, **b** ZIF-8-derived porous carbon (ZDPC), Reprinted with permission from Rutao et al. [36] Copyright (2017) Royal Society of Chemistry

87.7% of capacitance was maintained even after 5000 cycles [46]. The recent review from Sundriyal discussed in detail bio-waste-derived AC for supercapacitors [38]. Figure 3 depicts the preparation of final activated carbon from various bio-based waste sources [38].

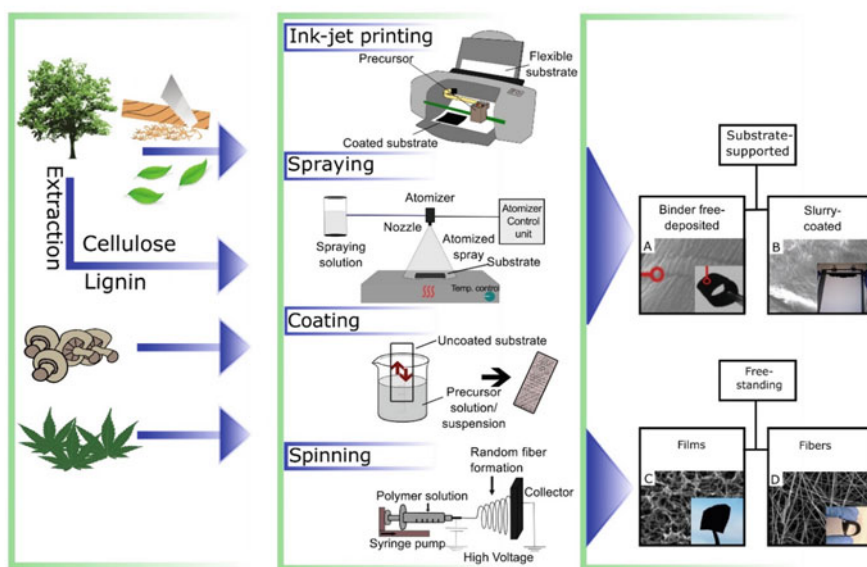
Recently, renewable-based materials have attracted significant consideration as sustainable precursors for the production of activated carbon because of their abundance and low cost. These materials possess a broad variety of functional groups including  $-OH$ ,  $-COOH$ , and  $NH_2$ , which are fundamental for achieving uniform morphologies and designing a variety of nano-functional materials [47–49]. Several types of precursors have been used from biomass, including phenols such as phloroglucinol, tannins, gallic acid, and other components, like cellulose, lignin, chitosan, and starch, are widely used to synthesize organic mesoporous carbons with a surface area of  $500\text{--}2730\text{ m}^2\text{ g}^{-1}$  [50–56]. Several methods have been considered to process biomass such as coating, spinning, spraying, and ink-jet printing that will further undergo hydrothermal treatment to prepare the carbons for electrodes; an example scheme is shown in Fig. 4.





**Fig. 3** A schematic representation of the production of activated carbons from various bio-waste materials. Reprinted with permission from Shashank et al. [38] Copyright (2021) Elsevier

### Biomass-derived Precursors    Processing/Manufacture    Sustainable Flexible Electrode



Current Opinion in Green and Sustainable Chemistry

**Fig. 4** An illustrative example of using biomass-based precursors for producing sustainable flexible electrodes through applying different processes. Reprinted with permission from Herou et al. [57] Copyright (2018) Elsevier

## 2.2 Activated Carbon Electrodes for Supercapacitors

Among various carbon-based materials, biomass-based activated carbons (bbACs) are the most used electrode materials due to their economical and environmentally friendly advantages. A unique porous structure and surface chemistry also make bbACs more attractive compared to coal-based ACs. In addition to the physical charge accumulation as a result of bbACs' porous structure, the heteroatoms such as N, O, or S present on the surface relatively contribute to the total specific capacitance by creating pseudocapacitance. Since the double layer formation is largely correlated with the interactions between the solvated ions and pores, the amount, size, and distribution of the pores as well as the size of the ions and the distortion of their solvation shell [58, 59] should be considered for constructing more efficient electrode materials. The most important problem that causes poor rate performance is mainly related to the inner-pore ion transport and diffusion distance in which its mechanism is very complex [60, 61]. A detailed study of connection between the pore size and ion size was discussed before [59, 62]. It is concluded that the capacity is normally increased when the pore size is larger than the ion size, which allows the interactions between ion and opposite pore walls without affecting the kinetics of electroadsorption and desorption [59]. In addition, the hierarchical 3D pores with interconnected micro-, meso-, and macroporous networks have the benefits of each pore through a synergistic effect [60]. The macro-sized pores (pore size > 50 nm) act as ion-buffering reservoirs to reduce the diffusion distance [63, 64], the meso-sized pores (2 nm < pore size < 50 nm) provide ion transport pathways with a minimized transport and diffuse resistance, depending on the ion size [61, 65, 66], and the micro-sized pores (< 2 nm) enhance the formation of an electrochemical double layer. It is also stressed that the pore characteristics of bbACs highly vary on the biomass type and the synthesis methods such as chemical/physical activation or hard/soft template approach, which will be discussed in the next sections.

On the other hand, the heteroatom-containing surface functional groups (SFGs) are responsible for the Faradaic reactions, which occur naturally due to the elemental composition of biomasses during thermal treatment. The important Faradaic reactions that can be summarized for oxygen-containing and nitrogen-containing SFGs are reversible quinone/hydroquinone redox reactions and negatively charged nitrogen atoms present in the pyridinic and pyrrolic-ring due to the protons attached [67, 68]. The amount and type of the oxygen-containing SFGs are not only dependent on the type of biomass but also heavily affected by the activation agent because of the different reaction mechanisms [69]. Moreover, the presence of the SFGs mainly affects electrical conductivity of the electrode, which causes an increase in the specific capacitance [70].

Due to the high number of parameters that affect the efficiency of the capacitance of the electrode material, it is very hard to put forward a formula or a direct correlation between the parameters and specific capacitance. However, the following outcomes for a high-performance electrode material property can be made from previously reported works:

- High surface area with accompanying interconnected micro-, meso-, and macro-sized pores (note that the amount and the ratio of pores are decisive);
- Heteroatom-containing SGFs with the ability of reversible Faradaic reactions; and
- Good electrical conductivity and high wettability of the electrode with the electrolyte.

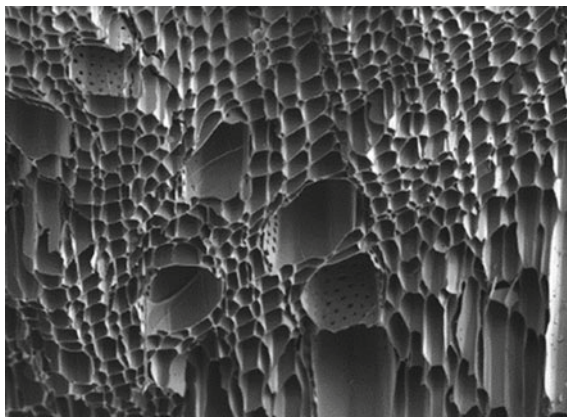
Apart from these, one should consider the fabrication process of the electrode and the supercapacitor for the determination of capacitive performance. In the electrode fabrication process, some additives are usually used, and these additives create a contradictory situation. Typically, in order to enhance the specific capacitance, carbon black or acetylene black is used as a conductive material. However, polytetrafluoroethylene (PTFE) and PVDF are generally applied as binders, which causes a decrease in the specific capacitance. Thus, it is obvious that the composition of the obtained electrode is an important factor. Moreover, the thickness of the electrode is another critical parameter that affects the specific capacitance of the device. It is reported that commercial electrode thickness extends from 10 mm to several hundred mm thick for high power and energy density, respectively [71].

### 2.2.1 Porous Carbon as an Electrode Material

There has been growing research interest in utilizing porous carbon, including biochar and biomass-based functional materials, as an electrode for electrical double layer capacitors (EDLCs). When producing carbon materials from biomass sources, the resulting porosity, chemical constituents, and surface area play key roles in the usefulness in electrical, energy storage, and supercapacitor applications (Fig. 5). In general, carbon materials obtained from biomass-based have large surface areas, desirable electrical conductivity, superior chemical stability [72], and hierarchical pore structures with wide pore ranges (micro-, meso-, and macro-pores) that are fundamental to acquire high-quality energy storage features [9, 73, 74]. These types of porous carbons can be produced at relatively low costs [75], have a low environmental impact, and are obtained from sustainable feedstock [76–78]. The key to a successful application of bio-based carbon material for energy storage and electrodes lies within their structure. For example, a carbon-based material obtained from highly ordered mesoporous carbon (HOMC) exhibits explicit nanostructures in the range of 2–50 nm which has been an essential material in many important applications such as high-performance electrochemical energy storage [79, 80] and high-efficiency enzymatic catalysts and biosensors. Mesoporous carbons are unique as they can provide both fast mass transport of molecules and possess large specific surface areas. These two properties are required for many advanced industrial applications of porous carbon involving a liquid phase (e.g., energy harvesting systems and supercapacitors using liquid electrolytes) and large organic molecules (e.g., enzyme immobilization in nano-bio-catalysis processes and biosensors).

Studies indicate that the electrical conductivity and porous structure of biochar-derived electrode materials influence the performance of supercapacitors through the

**Fig. 5** SEM image of the porous structure of the carbonized woody portion of a hemp stem



change of electrode-potential drop [81]. He et al. [82] reported that the conductivity and specific surface areas of electrodes made from activated biochar influenced the electrochemical performance of supercapacitors. They found that resistance is linked to both electron conductivity and ion mobility. High electrical conductivity of electrodes and low ionic resistance of the electrolyte within biochar pores resulted in low equivalent series resistance of the supercapacitor [78, 83]. Many studies indicated that the high surface area and porous structure of the electrode contributed to suitable electrochemical performance of activated biochar-based supercapacitors [70, 77, 84–86]. Furthermore, the specific capacitance of a supercapacitor may improve with increasing surface area and porous properties of biochar-derived electrode materials [81]. Besides, the elemental composition and functional groups of biochar-derived electrode materials can also affect the capacitive performance of the electrodes. For example, He et al. [82] also reported that hetero-atom containing functional groups (oxygen and nitrogen) improved the wetting properties of biochar-derived electrodes and committed to the Faradic redox reactions that result in an increase of the electrodes' specific capacitance. Song et al. [74] reported that the high oxygen groups (12.7–17.1 wt%) of activated corn husk carbon improved its performance in the supercapacitor.

### 2.2.2 Carbon Fibers as an Electrode Material

Carbon fibers-based electrodes provide outstanding mechanical strength and electrochemical conductivity which are normally produced from polyacrylonitrile and contribute 90% of carbon fiber production and pitch is also a primary precursor for industries [87, 88]. Acrylonitrile is a fossil-based precursor for carbon fibers that are polymerized using toxic solvents and scarce catalysts to produce polyacrylonitrile (PAN) [89]. Furthermore, numerous research activities have been exploited to

synthesize carbon materials from various sources in order to make wearable and flexible electronic devices. Although several techniques have been proposed to synthesize carbon fibers, the electrospinning technique is the widely used [90]. Table 1 illustrates the source of the carbon fiber, formation process, fiber diameter as well as the obtained specific capacitance of the prepared electrodes. It is clearly illustrated that the treatment conditions play a vital role in the production of fibers with diameters that range up to several nanometers, which greatly influence the surface area and capacitance. In addition, PAN polymer contributes more than any other polymer, including polybenzimidazole, polyvinylpyrrolidone, and poly(amic acid), as a precursor for carbon fiber synthesis. Furthermore, recent works have incorporated transition metal-based oxide and sulfide compounds such as  $\text{CoNiO}_2$  [91],  $\text{AgNO}_3$  [92],  $\text{Ni}_3\text{S}_2/\text{CoNi}_2\text{S}_4$  [93],  $\text{NiCo}_2\text{S}_4$  [94],  $\text{MoS}_2$  [95],  $\text{CoS}$  [96], and  $\text{Ni}_3\text{S}_2$  [97] to improve electrical conductivity, mechanical, and thermal stability.

Currently, PAN-based fibers are expensive and unsustainable. To improve sustainability and reduce the cost of carbon fibers, tremendous amount of work has been performed to find alternative precursor to PAN. From an economic and environmental point of view, carbon powder and carbon fibers produced from biomass for electrode applications are an attractive alternative to conventional carbon materials [88, 117]. These bio-based activated carbon fibers and carbon powder exhibit highly accessible surface area and adequate electrical conductivity, which are two key requirements for effective supercapacitors. Research on bio-based materials has been focused on producing activated carbon and carbon fibers from lignin for supercapacitor electrodes.

### 2.3 Carbonization and Activation

As mentioned above, biomass-based activated carbons (bbACs) synthesized by thermochemical conversion of biomass are widely used as an electrode material for energy storage applications due to their advantages. However, it is clear that they should be re-engineered to develop the porous texture and surface chemistry. Template and activation approaches with various experimental parameters are mainly used to produce bbACs. Although the template approach results in good surface area and manageable pore size distribution [118], the drawbacks of high cost and time-consuming or cumbersome removal of the template process make it impracticable for high-scale applications [119]. Chemical and/or physical activation of biomass-based carbon materials provides large specific surface area and the ability to form surface with heteroatom-containing functional groups. The chemical or physical activation can be applied in two different ways, direct and indirect. In direct activation, the biomass itself is subjected to the thermal treatment together with the activation agent. However, in the indirect activation, the biomass is first converted into pyrolytic carbon (PyC) via thermal treatment, then the obtained PyC is mixed with the activation agent before or during a second thermal treatment. Chemical activation agents such as  $\text{KOH}$ ,  $\text{H}_3\text{PO}_4$ , and  $\text{ZnCl}_2$  are widely used, whereas steam

**Table 1** Carbon fiber-based supercapacitor electrode materials

S. No.	Precursor	Fiber formation process	Treatment conditions	Fiber diameter (nm)	Surface area ( $\text{m}^2 \text{g}^{-1}$ )	Specific capacitance	References
1	10% PAN in dimethylformamide (DMF)	Electrospinning	Stabilized at 280 °C, performed carbonization and activation at 700–800 °C under $\text{N}_2$ and steam	200–400	1230	173 $\text{F g}^{-1}$ in 30 wt % KOH at 10 $\text{mA g}^{-1}$	[98]
2	10% PAN in DMF	Electrospinning	Stabilization at 280 °C in air, carbonized and activated at 700–1000 °C under $\text{CO}_2$ atmosphere	300	376–705	200 $\text{F g}^{-1}$ in 1 M $\text{H}_2\text{SO}_4$ 240 $\text{F g}^{-1}$ in 6 M KOH 100 $\text{F g}^{-1}$ in 1 M $\text{Et}_4\text{NBF}_4$	[99]
3	PAN and pitch mixture in DMF and tetrahydrofuran (THF)	Electrospinning	Stabilized in air at 300 °C, carbonized at 700, 800, 900 °C in $\text{N}_2$ and activated in a steam/ $\text{N}_2$	750–2000	732–1877	75.5 to 143.5 in 6 M KOH with different activation conditions	[100]
4	0.6 g of PAN in DMF + 0.8 g of cobalt nitrate + 0.75 g of polyvinylpyrrolidone in DMF	Electrospinning	Stabilized at 220 °C, further heated at 350 °C under Ar atmosphere and carbonized at 750 °C in Ar flow	~300	468.9	104.5 $\text{F g}^{-1}$ in 10 M HCl	[101]
5	Poly(amic acid) (PAA) + pyromellitic dianhydride + 4,4'-oxydianiline in THF:methanol	Electrospinning	Stabilization up to 350 °C in air, carbonized at 1000 °C and activated at 650–800 °C under 40 vol.% stream in the $\text{N}_2$	2000–3000	940–2100	175.0 $\text{F g}^{-1}$ at 1000 $\text{mA g}^{-1}$ in 30 wt% KOH	[102]

(continued)

Table 1 (continued)

S. No.	Precursor	Fiber formation process	Treatment conditions	Fiber diameter (nm)	Surface area ( $\text{m}^2 \text{g}^{-1}$ )	Specific capacitance	References
6	20 wt% of Polybenzimidazole (PBI) dissolved in dimethylacetamide (DMAc)	Electrospinning	Carbonized and activated by 40 vol.% stream in the $\text{N}_2$ at 700, 750, 800, and 850 °C	250	500–1220	125–178 $\text{F g}^{-1}$ at 1000 mA $\text{g}^{-1}$ in 30 wt% KOH	[103]
7	10 wt% of PAN + $\text{ZnCl}_2$ in DMF	Electrospinning	Stabilized at 280 °C under air, carbonized at 800 °C in Ar	200–350	310–550	140 $\text{F g}^{-1}$ in 6 M KOH	[104]
	(1) 8 wt% PAN in DMF + 0.8 wt% carbon nanotubes (CNTs) (2) 7.2 wt% PAN in DMF	Electrospinning	Stabilization at 280 °C for 2 h in air and 350 °C for 1 h in Ar, carbonization at 700 °C in Ar and activation at 650 °C under hydrogen peroxide and water	NA	(1) 810 (2) 930	(1) 310 $\text{F g}^{-1}$ at 1000 mA $\text{g}^{-1}$ in 1 M $\text{H}_2\text{SO}_4$ (2) 170 $\text{F g}^{-1}$ at 1000 mA $\text{g}^{-1}$ in 1 M $\text{H}_2\text{SO}_4$	[105]
8	Carbon black in dimethylacetamide (DMAc) and acetone + PAN	Electrospinning	Stabilized from 150 to 200 °C and carbonized at 800 °C in Ar	200	279–478	174 $\text{F g}^{-1}$ at 1000 mA $\text{g}^{-1}$ in 1 M KOH	[106]
9	PBI in DMAc	Electrospinning	Fiber webs heated up to 850 °C in $\text{N}_2$ and activated under stream and $\text{N}_2$	100–500	500–1220	36–194 $\text{F g}^{-1}$ in 1 M $\text{H}_2\text{SO}_4$	[107]
10	Polyvinylpyrrolidone (PVP) + PAN in DMF	Electrospinning	Stabilized at 280 °C for 2 h in air, carbonization from 300 to 970 °C in $\text{N}_2$ and activated at 850 °C under $\text{CO}_2$	200–500	531	221 $\text{F g}^{-1}$ in 1 M $\text{H}_2\text{SO}_4$	[108]

(continued)

Table 1 (continued)

S. No.	Precursor	Fiber formation process	Treatment conditions	Fiber diameter (nm)	Surface area ( $\text{m}^2 \text{g}^{-1}$ )	Specific capacitance	References
11	N, S doped carbon fiber synthesized by 10 wt% PAN + 20 wt% PVP in DMF	Electrospinning	Stabilized in air at 280 °C for 5 h, carbonized at 800 °C for 2.5 h in pure $\text{N}_2$	550	207.41	307.8 $\text{F g}^{-1}$ in PVA-KOH gel electrolyte	[109]
12	Tetraethoxy orthosilicate (TEOS) + PAN in DMF	Electrospinning	Stabilized in air at 280 °C and carbonized at 800, 900 and 1000 °C under $\text{N}_2$	150	980–1200	220 $\text{F g}^{-1}$ at 1000 $\text{mA g}^{-1}$ in 6 M KOH	[110]
13	PAN and $\text{AgNO}_3$ in DMF and beta-cyclodextrin	Electrospinning	Stabilized at 280 °C, performed carbonization at 800 °C and activation under $\text{N}_2$ and steam	350	1096	150 $\text{F g}^{-1}$ in 6 M KOH	[92]
14	Ag nanoparticles-containing PAN in DMF	Electrospinning	Stabilized at 250 °C and performed carbonization at 1000 °C in $\text{N}_2$	200–300	–	246 $\text{F g}^{-1}$ in 0.5 M $\text{H}_2\text{SO}_4$	[111]
15	PAN and Ru-acetylacetone in DMF	Electrospinning	Stabilized at 280 °C in air, carbonized and activated at 800 °C in steam and $\text{N}_2$	200–900	531	391 $\text{F g}^{-1}$ in 6 M KOH with 7.31 wt% of Ru content	[112]
16	PAN and cellulose acetate (CA)	Electrospinning	Stabilized at 280 °C, performed carbonization and activation at 800 °C	250–700	1160	245 $\text{F g}^{-1}$ in 6 M KOH	[113]
17	Cellulose fibers and glucose in $\text{K}_3[\text{Fe}(\text{C}_2\text{O}_4)_3] \cdot \text{H}_2\text{O}$ solution	–	Mixture was dried at 80 °C and carbonized at 750 °C under $\text{N}_2$	–	1515.6	313.0 $\text{F g}^{-1}$ at 1 A $\text{g}^{-1}$ in 6 M KOH	[114]

(continued)



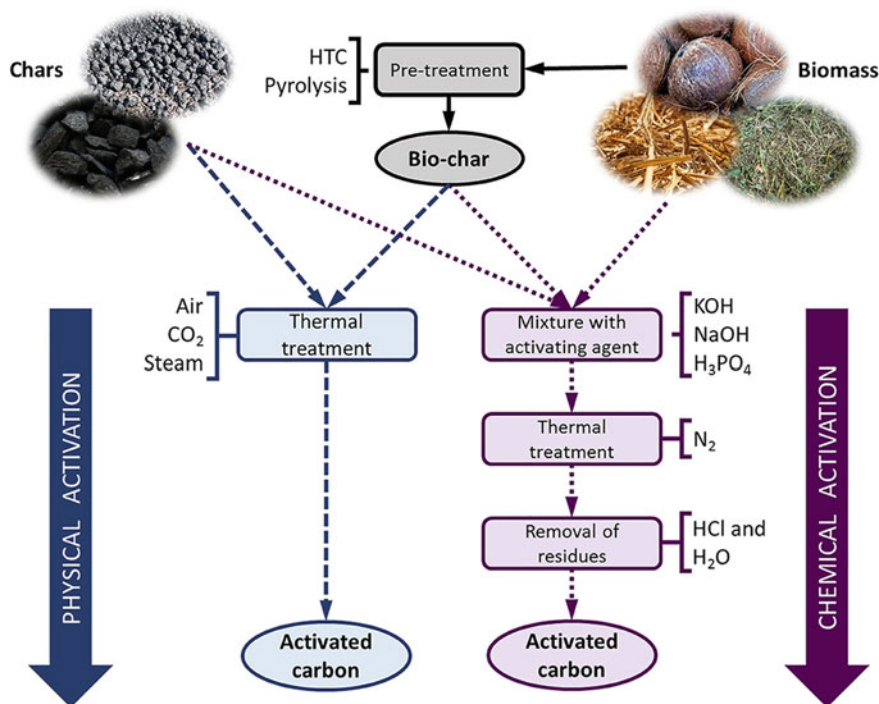
Table 1 (continued)

S. No.	Precursor	Fiber formation process	Treatment conditions	Fiber diameter (nm)	Surface area ( $\text{m}^2 \text{g}^{-1}$ )	Specific capacitance ( $\text{F g}^{-1}$ in PVA-KOH)	References
18	CoNiO <sub>2</sub> -nanowires on carbon-fibers	Hydrothermal route	Fibers were dried at 60 °C and annealed in pure Ar at 300 °C	70	106	795.4 $\text{F g}^{-1}$ at 1 A $\text{g}^{-1}$ in PVA-KOH	[91]
19	Waste wood shavings in phenol + phosphoric acid + hexamethylenetetramine	Self-made spinning apparatus	Carbonization/activation process was performed at 850 °C in N <sub>2</sub> and steam	NA	1221–2929	280 $\text{F g}^{-1}$ at 500 A $\text{g}^{-1}$ in 1 M H <sub>2</sub> SO <sub>4</sub>	[115]
20	Wood sawdust + phenol + phosphoric acid + hexamethylenetetramine	Melt-spinning	Dried at 90 °C, carbonized at 500 °C in N <sub>2</sub> flow and activated at 650–850 °C using KOH	NA	869–2294	225 $\text{F g}^{-1}$ at 0.5 A $\text{g}^{-1}$ in 6 M KOH	[116]

and  $\text{CO}_2$  are normally employed as physical activation agents. Some advantages of the chemical activation process, like lower process temperature, developed porous structure, shorter experiment time, and ease of application, make it preferable to physical activation [120]. As a consequence of different reactions during the activation process, the resulting bbAC shows different pore and surface characteristics. Prauchner compared different activation processes to understand the influence of the formation of pore size distribution. The results demonstrated that physical activation process gives narrow pores than chemical activation but later showed higher packing density and higher volumetric adsorption capacity [121]. In addition, it is reported that regardless of the type of biomass, KOH activation led to a larger amount of aromatic structure, which may enhance the specific capacitance [122]. The main reason for these differences is due to the distinct reaction pathways during activation process. The proposed reactions of the most common chemical activation agents (KOH and  $\text{H}_3\text{PO}_4$ ) were discussed in detail [123, 124]. As a summary,  $\text{K}_2\text{CO}_3$  forms via the interactions between C,  $\text{H}_2\text{O}$ , and KOH below  $400^\circ\text{C}$ . The  $\text{K}_2\text{CO}_3$  starts a decomposition process which leads to the formation of  $\text{CO}_2$  and  $\text{K}_2\text{O}$  at  $700^\circ\text{C}$  and is entirely consumed at  $\sim 800^\circ\text{C}$ . When the temperature goes higher than  $700^\circ\text{C}$ ,  $\text{K}_2\text{CO}_3$  and  $\text{K}_2\text{O}$  compounds, and  $\text{CO}_2$  are reduced by the “C” to finally produce K and CO, respectively. It is widely accepted that the reactions between K-derived compounds and C are responsible for generating the pore network; the evolved gaseous products such as  $\text{H}_2\text{O}$ , CO, and  $\text{CO}_2$  give the possibilities to contribute in the development of the porosity via the gasification of carbon; the intercalation of metallic K into the carbon leads to the expansion of the carbon lattices. In the case of  $\text{H}_3\text{PO}_4$  activation,  $\text{H}_3\text{PO}_4$  transforms into  $\text{H}_{n+2}\text{P}_n\text{O}_{3n+1}$  at  $100\text{--}400^\circ\text{C}$ ; from  $400$  to  $700^\circ\text{C}$ , it releases  $\text{H}_2\text{O}$  and turns into  $\text{P}_4\text{O}_{10}$ , which is highly oxidative; the  $\text{P}_4\text{O}_{10}$  reacts with C to produce  $\text{CO}_2$ ; from  $700$  to  $800^\circ\text{C}$ ,  $\text{P}_4\text{O}_{10}$  or  $\text{P}_4\text{O}_6$  undergo chemical reaction with C and subsequent release of  $\text{CO}_2$  and CO. The released  $\text{CO}_2$  and CO gases can be responsible for the formation of the pore network. It should be noted that the remaining K- or P-derived unreacted compounds needed to be removed from the carbon matrix after the activation process. Figure 6 elucidates the different processes such as physical treatment and chemical treatment for the production of activated carbons from char and biomass.

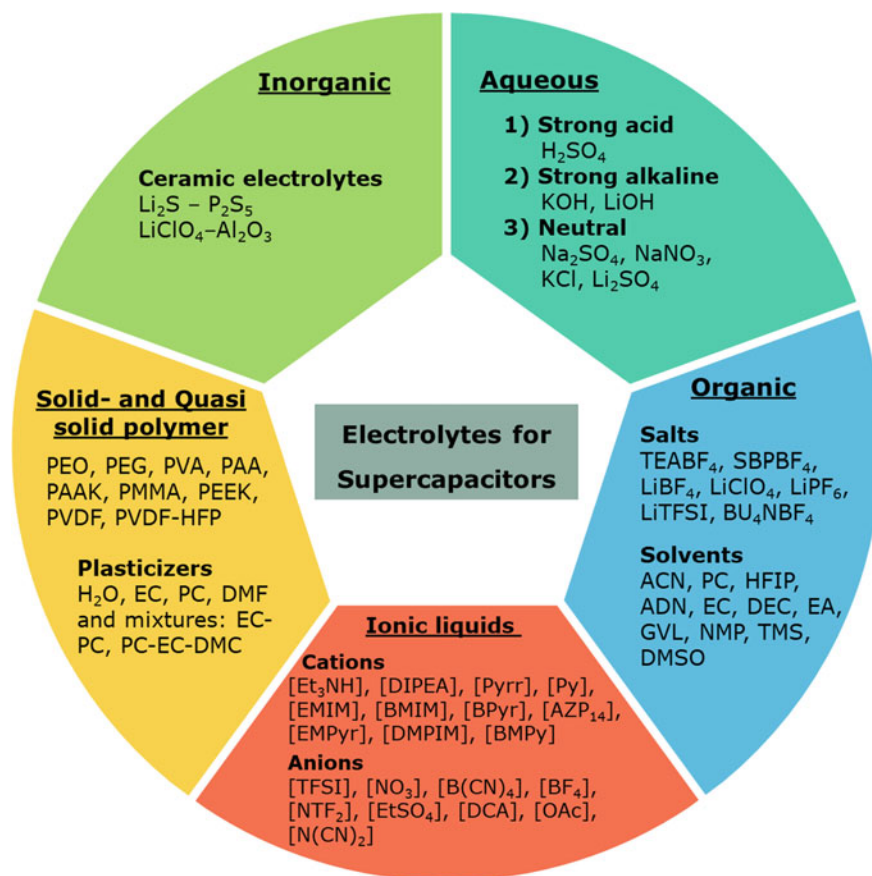
## 2.4 Electrolytes for Supercapacitors

Electrolytes are a conductive medium and play an important role in the device in order to facilitate the ion transport in the electrodes in the cell. In supercapacitors, the energy is stored in the form of an electrostatic charge at the interface between electrode and electrolyte. There have been numerous types of electrolytes exploited to optimize the device; the main types of electrolytes are aqueous electrolytes, organic electrolytes, ionic liquids (IL), solid-, and quasi-state electrolytes. An integrated representation of the different electrolytes is demonstrated in Fig. 7.



**Fig. 6** Schematic representation of different activation processes for the production of activated carbon [125]

**Aqueous electrolytes:** This type of electrolyte exhibits a narrow electrochemical window compared to other types of electrolytes, which impedes the usage of such electrolytes in supercapacitors (SCs). However, aqueous electrolytes have some advantages like easy handling in the laboratory without a cumbersome process, thus facilitating the fabricating and assembling of the cell; inexpensive and additional purification [126] is not required compared to other electrolytes such as organic and IL electrolytes. In addition, aqueous electrolytes provide high conductivity and the resulting conductivity is about one order of magnitude more than non-aqueous (organic and IL) electrolytes [127]. Considering the aqueous electrolytes, three main types of aqueous electrolytes are widely used in SCs, such as alkaline, acid, and neutral electrolytes. The most used electrolytes are KOH, H<sub>2</sub>SO<sub>4</sub>, and KCl for alkaline, acid, and neutral types, respectively. Although aqueous electrolytes exhibit high conductivity, the cell voltage is restricted to 1.0 V in the case of alkali and acid electrolytes due to the decomposition of water into H<sub>2</sub> and O<sub>2</sub>. The gas evolution causes the rupture of SC electrodes, thus influencing the cell performance and safety [127]. On the other hand, the cell voltage can go up to 2.2 V for neutral electrolytes, which is reported in Ref. [128]. As water is the main component in aqueous electrolytes,



**Fig. 7** Different types of electrolytes for electrochemical supercapacitors

the operating temperature of SCs should be controlled to circumvent any freezing or boiling issues.

**Organic electrolytes:** Organic electrolytes mainly consist of salts like  $\text{LiBF}_4$  or  $\text{LiClO}_4$  that are dissolved in any of the organic solvents, including propylene carbonate (PC) or acetonitrile (ACN). This type of electrolyte is commercially used in a wide range of energy storage devices due to its ubiquitous energy and powder density. Furthermore, it covers a large electrochemical window, ranging from 2.5 to 2.8 V, and also uses less expensive materials like Al as a current collector. Figure 7 illustrates some typical salts and mostly used organic solvents as organic electrolytes. The selection and optimization of salts with solvents are essential in order to enhance the conductivity of SCs. Recently, several studies combined more solvents with a salt to improve the conductivity and viscosity of the electrolytes [129, 130]. Compared to aqueous electrolytes, organic electrolytes exhibit some shortcomings that include flammability, lower specific capacitance, poor ionic conductivity, volatility, and

toxicity. In addition, the assembling of electrolytes should be performed under a controlled environment to avoid degradation and self-charge problems that could result from impurities like water [131]. A detailed review of electrolytes for SCs can be found in the Refs. [126, 132, 133].

**Ionic liquids:** Ionic liquids (ILs) or low melting point organic salts have demonstrated their potential as alternate electrolytes for SCs because of their ubiquitous characteristics including non-flammability, chemical and thermal stability, low vapor pressure, and environmentally benign features [134, 135]. ILs are also called room-temperature ionic liquids and are made of cations and anions. Having a wide range of available cations and anions, they are generally known as “designer solvents,” and thus, ILs can be tuned by spanning over the selection of cations and anions to improve the electrochemical window and working temperature range. The conductivity of the IL is associated with the types of cations, such as cyclic, acyclic, aromatic, or aliphatic, and anions. Based on the types of cations used in the ILs, they can be categorized into three main categories: protic, aprotic, and zwitterionic [135]. The most commonly employed ILs are imidazolium, pyrrolidinium, ammonium, sulfonium, phosphonium cations and tetrafluoroborate ( $\text{BF}_4^-$ ), hexafluorophosphate ( $\text{PF}_6^-$ ), dicyanamide ( $\text{DCA}^-$ ), bis(fluorosulfonyl)imide ( $\text{FSI}^-$ ), and bis(trifluoromethanesulfonyl)imide ( $\text{TFSI}^-$ ) anions. Comparing protic ILs such as triethylammonium bis(trifluoromethylsulfonyl)imide ( $[\text{Et}_3\text{NH}][\text{TFSI}]$ ), pyrrolidinium nitrate ( $\text{PyNO}_3$ ), diisopropyl-ethyl-ammonium bis(trifluoromethanesulfonyl)-imide ( $[\text{DIPEA}][\text{TFSI}]$ ), and pyrrolidinium bis(trifluoromethanesulfonyl)imide ( $[\text{Pyrr}][\text{TFSI}]$ ), aprotic-based ILs like imidazolium exhibit higher ionic conductivity and higher electrochemical window (3.0 V than 1.2–2.5 V for protic ILs) [130, 136–139]. Although ILs show a strong tendency as a better alternative to organic electrolytes, several issues related to high viscosity, low ionic conductivity, and high cost render its development at a commercial scale less feasible than organic electrolytes. To overcome such issues in ILs, mixtures containing ILs and organic solvents are usually considered for lowering viscosity and improving ionic conductivity. For instance, the typical mixture,  $[\text{EMIM}][\text{BF}_4]$ , and EC-PC solvents provide an ionic conductivity up to 27  $\text{mS cm}^{-1}$ , and  $[\text{EMIM}][\text{PF}_6]/\text{PC}$  shows excellent thermal stability and specific capacitance [140].

**Solid- and quasi-solid electrolytes:** These electrolytes are of great interest in recent years due to their excellent advantages such as improved conductivity, easy packaging and fabrication process, safety, and leakage-free attributes. Therefore, they have been involved in the design of flexible and wearable electronic devices, micro-electronics, and printable electronics. Considering solid-state electrolytes, polymer-based materials are the primary choice of interest rather than other solid-state electrolytes like inorganic or ceramic electrolytes [141]. Solid-state electrolytes are divided into these categories: solid polymer electrolytes (SPEs) or dry-polymer electrolytes, gel-polymer electrolytes, and polymeric electrolytes [142–146]. Typically, SPE is composed of a polymer, for example, polyethylene oxide (PEO), and a salt, LiCl without any solvents. On the other hand, GPE is composed of polymer, (e.g., polyvinylidene fluoride (PVDF)) with a salt dissolved

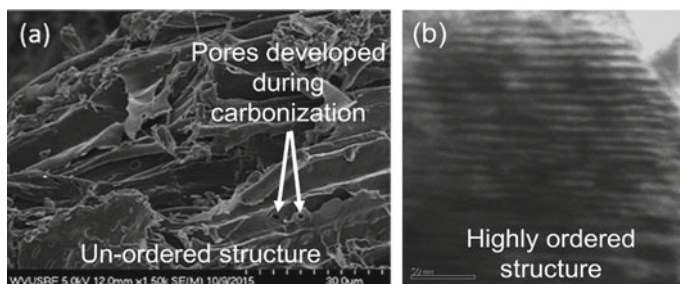
in a solvent. The most commonly used GPEs are poly(ethylene oxide) (PEO), poly(methyl methacrylate) (PMMA), polyacrylonitrile (PAN), poly(vinylidene fluoride) (PVDF) and poly(vinylidene fluoride-hexafluoropropylene) (PVDF-HFP), and poly(ether ether ketone) (PEEK) [147–149]. Among three types of solid-state electrolytes, GPEs dominate over the other two types (SPEs and polyelectrolytes) of electrolytes because of their higher ionic conductivity that can be obtained from the presence of the liquid phase. GPEs exhibit poor mechanical strength when the liquid composition is high and a narrow temperature range that causes safety problems and internal short circuits. Furthermore, it is stressed that these electrolytes provide a limited contact surface area between electrolyte and electrode, which can lead to reduced cycle rate, low performance, and low specific capacitance of SCs.

**Inorganic solid-state electrolytes:** A few studies have been exploited to design inorganic-based electrolytes for SCs despite their excellent mechanical strength and thermally stability. However, this type of electrolyte has no flexibility and no bendable nature. Some authors have demonstrated the use of inorganic electrolytes such as glass–ceramic electrolyte,  $\text{Li}_2\text{S}$ – $\text{P}_2\text{S}_5$ , a composite-solid electrolyte,  $\text{LiClO}_4$ – $\text{Al}_2\text{O}_3$ , and graphene-oxide (GO) electrolytes [141, 150–152].

Apart from the above-mentioned electrolytes, recently, a specific type of electrolyte has been proposed that is known as redox electrolytes or redox-mediated electrolytes. In this case, redox active species have been added to enhance the electrochemical performance of SCs [144, 153–159]. For instance,  $\text{Na}_2\text{MO}_4$ , KI,  $\text{Cs}_2(\text{SO}_4)_2$ , 1,4-dihydroxyanthraquinone, and hydroquinone were added into the solution of aqueous electrolytes to optimize the electrolytes and performance of SCs. A detailed review of these types of redox electrolytes can be found in the Ref. [133].

### 3 Sustainable Materials as Carbon Precursors for Supercapacitors

Kajdos et al. [160] indicated that traditional activated carbon produced from biomass by pyrolysis and subsequent physical and chemical activation, such as coal, wood, fruit shell, and stones, results in materials with high micro-porosity and irregularly curved pore structures. The limited space provided by the small pores and the tortuosity (i.e., twisted pathways) prevents fast transfer of molecules, especially in liquid states. A key factor to successfully producing bio-based conductive materials is through producing ordered structures with high porosity and activated surfaces (Fig. 8). When producing carbons from biomass sources, selection of biomass type and carbonization processes will influence the resulting porosity and development of micro-, meso-, and macro-pores. Studies indicated that the electrical conductivity and porous structure of biochar-derived electrode materials influence the performance of the supercapacitors through the change of electrode-potential drop [81, 161]. In particular, Sun indicated that specific area capacitance decreases as the percentage of microporous structure increased, suggesting that a mesoporous structure will improve



**Fig. 8** SEM and TEM images of **a** un-ordered structure from traditional carbonization [163]; **b** more ordered structure using multi-step carbonization [162]

electrodes and that ions in organic electrolytes cannot easily transfer through micropores, as compared to mesopores [81]. He also reported that the conductivity and specific surface areas of electrodes made by activated biochar influenced the electrochemical performance of supercapacitors. They found that resistance is highly related to electron conductivity and ion mobility [162].

Xie suggested that cellulose microfibrils in the lignocellulosic cell wall can be selectively removed to leave nanochannels in the material [163]. The cellulose microfibrils were selectively removed (below 500 °C) because of their poor thermal stability of cellulose carbon compared to lignin carbon [85]. This early research was limited to nanostructures in the mesopore (2–50 nm) range and without regard to pore shape. Nan [164] evaluated one-step carbonization of red oak, short rotation shrub willow, and yellow-poplar without any specific activation processes to determine the fundamental properties of carbonized wood produced between 700 and 1000 °C. Additional follow-up research determined the specific capacitance of the shrub willow treated at a pyrolysis temperature of 900 °C exhibited the highest specific capacitance (44 F g<sup>-1</sup> at 10 mA g<sup>-1</sup> current density). Conventional synthesis technologies have little control over the pore size distribution of porous carbon, producing randomly porous materials with broad pore size distributions. Traditional activated carbon produced by pyrolysis and subsequent physical and chemical activation of the organic precursor, such as coal, wood, fruit shell and stones, and polymers at high temperatures, has high microporosity and irregularly curved pore structures [160]. However, several research efforts have been attempted to develop well-structured carbons from biomass. For example, DeVallance et al. [165] detailed earlier work that followed a two-step process to improve the mesoporous structure and properties of wood-based carbon materials.

Building on these earlier works, more recent research looked at carbonizing wood and other biomass for supercapacitor applications by additional activation methodology. Yakaboyleu et al. [166] utilized slow oxidation rate, heating to 250 °C, followed by pyrolysis to various temperatures to produce hybrid willow and miscanthus activated carbon and reported the capacitance from 70–162 F g<sup>-1</sup>. They also reported that the slow oxidation rate added 25–62 F g<sup>-1</sup> of capacitance. Phiri et al. [167] performed similar work using willow carbonized at 600 °C under nitrogen, followed

by heating to 800 °C with KOH activation. Using this post-carbonization KOH activation route resulted in a specific capacitance of 394 F g<sup>-1</sup> at 100 mA g<sup>-1</sup> current density. In other studies, Yakaboğlu et al. [168] reported a capacitance of 162 F g<sup>-1</sup> at 100 mA g<sup>-1</sup> current density for miscanthus pretreated with KOH for 18 h, followed by pyrolysis to 800 °C for 1 h. Jiang [169] evaluated hybrid willow carbonization using both indirect and direct approaches. The direct approach carbonized willow under CO<sub>2</sub> conditions from 700 to 800 °C, while the indirect approach utilized pyrolysis under nitrogen conditions from 250 to 750 °C and followed by CO<sub>2</sub> activation at 800 °C. The capacitance of 80.9 (indirect) and 92.7 F g<sup>-1</sup> (direct) was at current density of 100 mA g<sup>-1</sup>. While these results are promising, more research is needed to maximize the potential and improve the capacitance of wood-based activated carbon materials for supercapacitor applications.

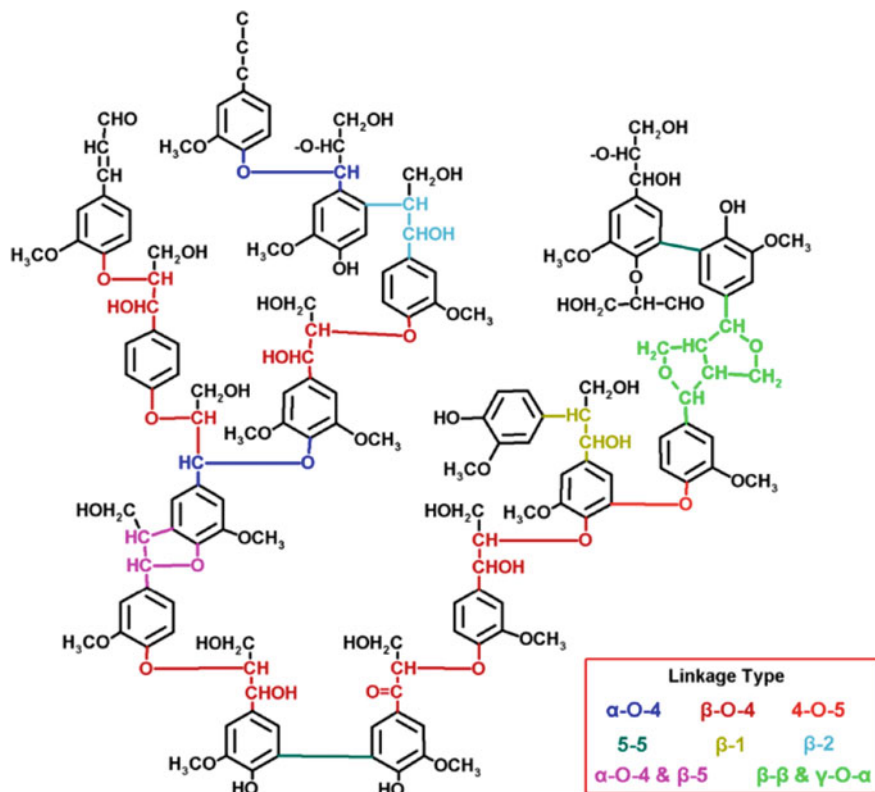
## 4 Lignin

### 4.1 Lignin Structure

Lignin is the second most abundant biopolymer after cellulose in the lignocellulosic biomass. It has an amorphous, highly branched polyphenolic macromolecular structure (shown in Fig. 9) and a high molecular weight of over 10,000 g mol<sup>-1</sup>. Lignin can be found in cell walls, and its function is to provide physical strength to plants. The chemical structure of lignin highly varies on species, geographical location, and process used for extraction [170]. It is rather hard to measure the degree of lignin polymerization; however, it can be possible after performing several depolymerization strategies [171]. Lignin structure contains various types of functional groups such as phenolic hydroxyl, aliphatic hydroxyl, methoxyl, carbonyl, and carboxyl moieties [172, 173].

Lignin's chemical structure is composed mainly of phenylpropane units (C<sub>9</sub>) originating from three aromatic alcohol precursors (monolignols, shown in Fig. 10): p-coumaryl, coniferyl, and sinapyl alcohols. However, the monolignols' ratio changes with respect to plants and cell walls [174]. The phenyl propanoic units are cross-linked through a radical polymerization during their biosynthesis to produce a lignin structure. Lignin exhibits a hydrophobic character due to the higher content of aromatic rings; therefore, it is used significantly for coating applications. Softwood lignin contains a higher amount of coniferyl alcohol (> 95%; < 5% of coumaryl alcohol); hardwood lignin is composed of sinapyl units (45–75%), coniferyl units (25–50%), and a small amount of coumaryl alcohol (0–8%). In the case of grass-based plants, all three units can be found [174, 175].

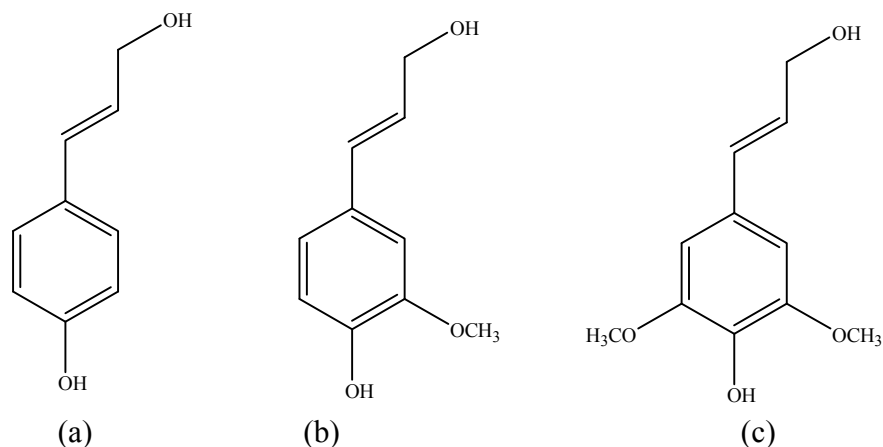




**Fig. 9** Main linkages in softwood lignin. Reprinted with permission from Tingting et al. [173] Copyright (2017) American Chemical Society

## 4.2 Different Bonds and Functional Groups

The physical and chemical properties of lignin are related to wood species, geographical region, and isolation processes employed [176]. The characterization of lignin is a cumbersome task due to its three-dimensional structure, different functional groups, various chemical links, and isolation process. The reactivity of the lignin polymer is highly dependent on the chemical structure and functional groups present. However, the hydroxyl groups and free positions in the aromatic ring determine the reactivity of lignin [177]. Lignin contains a variety of linkages; in particular, softwood lignin contains seven different linkages (Table 2) including  $\beta$ -O-4,  $\alpha$ -O-4, 5-5,  $\beta$ - $\beta$ , 4-O-5,  $\beta$ -5, and  $\beta$ -1 [178]. Among the linkages,  $\beta$ -O-4 is predominant and around 50% of linkages can be found [174, 179, 180] in both hardwood and softwood lignin. All sorts of linkages between different units are clearly shown in Fig. 10, and their availability of percentage in different wood source lignin is illustrated in Table 1 [181]. Due to the presence of various functional groups, lignin tends to be used in



**Fig. 10** Structure of C9 monomer units present in lignin: **a** p-coumaryl alcohol (4-hydroxy phenyl, H), **b** coniferyl alcohol (guaiacyl, G), **c** sinapyl alcohol (syringyl, S). Reprinted with permission from Xu et al. [171] Copyright (2014) Royal Society of Chemistry

**Table 2** Major interunit linkage types in lignin and their proportions (%) in softwood and hardwood

Linkage type	Softwood (spruce) (%)	Hardwood (birch) (%)
$\beta$ -O-4	48	60
$\alpha$ -O-4	6–8	6–8
5-5	9.5–11	4.5
$\beta$ - $\beta$	2	3
4-O-5	3.5–4	6.5
$\beta$ -5	9–12	6
$\beta$ -1	7	7
Others	13	5

bio-based products and the manufacture of industrial biomaterials and biocomposites [182, 183].

### 4.3 Extraction Processes from Lignocellulosic Biomass

Various chemical treatments have been used to fractionate the lignocellulosic biomass into its main components of cellulose, hemicellulose, and lignin and the treatments can be classified into sulfur and sulfur-free, according to the chemical used for the extraction. In the sulfur process, kraft and liginosulphonate are separated, while soda and Organosolv are obtained through the sulfur-free process. The main goal of both processes is to extract the cellulose from lignocellulosic biomass, which

can be achieved by depolymerizing the lignin fraction. The quality of the extracted components (i.e., cellulose, hemicellulose, and lignin) is greatly dependent on the chemical processes and lignin isolation techniques used. As a result of processing, the final lignin product and molecular weight are affected, along with the introduction of new functional groups. The commonly used processes—sulfur (kraft and lignosulphonate) and sulfur-free (Organosolv and alkali)—are summarized below.

Kraft process is mostly used in the pulp and paper industry to produce high-quality cellulosic fiber by employing a mixture of sodium hydroxide (NaOH) and sodium sulfide (Na<sub>2</sub>S). However, the obtained lignin fractions contain a higher sulfur content, and they are generally burnt to produce energy in pulp mills [184, 185]. During the kraft process, lignin is degraded extensively and dissolved in the cooking liquor, and the sulfide ions present in the mixtures initiate the β-O-4 ether cleavage lignin polymer which leads to several fragments with low molecular weight. Finally, the carbon–carbon bonds are formed in lignin at the end of the process and yield a lignin complex [186, 187]. The corresponding kraft lignin has a hydrophobic character and contains aliphatic thiol groups.

The extraction of lignosulphonate is carried out using an aqueous solution of sulfite (SO<sub>3</sub><sup>2-</sup>) or hydrogen sulphite (HSO<sub>3</sub><sup>-</sup>) with a wide pH range and high temperature. This process produces specialty pulp with high reactivity for chemical applications. The degradation of lignin in the sulfite process is comparatively less than the kraft process and delignification mainly occurs through sulfonation in α-O-4 linkages. Lignosulphonates are already marketed in many applications. The typical lignosulphonate biopolymer is highly cross-linked, with around 5 wt% of sulfur contents. The obtained lignin is water-soluble under most conditions, and its average molar mass is relatively larger than kraft-processed lignin with polydispersity index of about 6–8 [188]. It is specified that the chemicals used for cooking pulp cannot be recycled or reused after the process, thus leading to environmental problems.

Sulfur-free lignin is produced from two main processes, namely solvent pulping and alkaline pulping, which produce Organosolv lignin and soda lignin. Soda pulping is used to treat annual plants such as bagasse, flax, kenaf, and wheat straw because it needs a less severe cooking condition than wood biomass. The lignocellulosic raw material is cooked with sodium hydroxide (NaOH) or a mixture of soda and anthraquinone under high pressure and temperature [189]. Lignin is separated from black liquor using an acid precipitation and liquid/solid extraction; the obtained lignin is sulfur-free. The average molar mass (Mn) of soda lignin is comparatively lower than other lignin due to multiple delignifications happening during the cooking process. In particular, soda lignin is widely used as a precursor for producing value-added products by many modification reactions [186, 190].

Organic solvents such as methanol, ethanol, acetic acid, and formic acid are used to remove lignin from annual plants and hardwood, and this process is known as the Organosolv process. Organosolv lignin mostly exhibits the highest quality [191, 192] and contains a hydrophobic nature. The most common processes are all cells (ethanol, water) and acetosolv (acetic acid with a small amount of HCl or H<sub>2</sub>SO<sub>4</sub>). The cleavage of α-O-4 linkages is the dominant reaction in this process. Lignin is recovered from the solvent through precipitation by adjusting the concentration, pH,

and temperature of the black liquor. The molecular weight of Organosolv lignin is low compared to other lignin coming from different methods; it is also a sulfur-free lignin. This process has a greater environmental impact and is more expensive due to the different organic solvents used during processing [193–195].

## 5 Lignin as a Precursor for Carbonaceous Materials

High porosity and large specific surface area of the carbon materials in the electrodes are the primary factors affecting the capacitance of supercapacitors [196]. As described in Sect. 2.3, different activation methods (physical and chemical) have been employed to control the porosity of the activated carbon and the specific surface area [197]. Table 3 summarizes the synthesis of electrodes from lignin and corresponding capacitance performed in SCs.

Activated carbon from lignocellulosic biomass has been obtained from mechanical pretreatment, like milling, followed by carbonization at 600 °C and activation using KOH under argon atmosphere at 750 °C. The activated carbon was then extracted using acid hydrolysis. Similarly, activated carbon fibers were obtained from low sulphonated alkali lignin using KOH and NaOH. It has been found that KOH shows higher levels of specific capacitance and superior performance compared with NaOH [198, 199].

Carbonization temperature acts a crucial role in the development of porosity [200]. Rodríguez-Mirasol reported that inorganic minerals present in the lignin results to non-desirable ash content in the produced activated carbon. These issues can be overcome through conducting the pretreatment process as follows: pre-carbonizing process of the eucalyptus kraft lignin at 400 °C and subsequently a washing using 1% H<sub>2</sub>SO<sub>4</sub>. After carbonization, the activation was performed on the pretreated samples with a heating rate of 10 °C min<sup>-1</sup>, and the holding time for carbonization was set at 2 h. The micropore volume of the chars obtained from eucalyptus kraft lignin was analyzed by varying the temperature and reported the BET-specific area value of 496 m<sup>2</sup> g<sup>-1</sup> at 550 °C which decreases to 278 m<sup>2</sup> g<sup>-1</sup> at 900 °C [201, 202]. On the other hand, Xie tested the specific surface and pore volume at different carbonization temperatures; when the temperature increased from 500 to 700 °C, the lignin pore volume increased from 0.0087 to 0.2221 cm<sup>3</sup> g<sup>-1</sup> and BET surface area changed from 0.846 to 448.10 m<sup>2</sup> g<sup>-1</sup>. The results demonstrated that surface area increment was around 340 times higher for the lignin carbon at higher temperature as compared to the value of 80 times for cellulose [85]. The authors applied the heating rate of 2.5 °C min<sup>-1</sup>, which is contrary to the method that Rodríguez-Mirasol used, 10 °C min<sup>-1</sup>. This influence of heating rate was analyzed by Kijima for alkaline lignin that carbonized from room temperature to 900 °C. The reported results revealed that the difference in the heating rate significantly changes the specific surface area like the lower the heating rate, the higher the specific surface. For instance, a char obtained from 10 °C min<sup>-1</sup> heating rate possesses a BET surface area of 30 m<sup>2</sup> g<sup>-1</sup>, and at 1 °C min<sup>-1</sup> heating rate, it possesses 529 m<sup>2</sup> g<sup>-1</sup>, whereas it was increased to

**Table 3** Lignin-based electrodes for supercapacitors

S. No.	Carbon source	Process condition	Surface area ( $\text{m}^2 \text{g}^{-1}$ )	Specific capacitance	Capacity retention (%)	References
1	Eucalyptus kraft lignin	Precarbonization at 400 °C and 1% $\text{H}_2\text{SO}_4$ washing to remove inorganic elements and reduce the ash content followed by carbonization (450–900 °C) at the rate of $10 \text{ }^\circ\text{C min}^{-1}$ followed by activation using $\text{CO}_2$ partial gasification	213 $\text{m}^2 \text{g}^{-1}$ at 450 °C 496 $\text{m}^2 \text{g}^{-1}$ at 550 °C 463 $\text{m}^2 \text{g}^{-1}$ at 800 °C 278 $\text{m}^2 \text{g}^{-1}$ at 900 °C	NA	NA	[201, 202]
2	Organosolv lignin	Carbonized in Ar in a retort box furnace and the heating rate at $150 \text{ }^\circ\text{C h}^{-1}$ until one of the four temperatures (400, 500, 700, 1000 °C) was reached	1.321 $\text{m}^2 \text{g}^{-1}$ at 400 °C 0.846 $\text{m}^2 \text{g}^{-1}$ at 500 °C 448.10 $\text{m}^2 \text{g}^{-1}$ at 700 °C 432.33 $\text{m}^2 \text{g}^{-1}$ at 1000 °C	NA	NA	[85]
3	Alkali lignin	Room temperature to 900 °C without activation under argon gas. Heating rate of $1 \text{ }^\circ\text{C min}^{-1}$	30 $\text{m}^2 \text{g}^{-1}$ at heating rate of $10 \text{ }^\circ\text{C min}^{-1}$ 529 $\text{m}^2 \text{g}^{-1}$ at heating rate of $1 \text{ }^\circ\text{C min}^{-1}$	NA	NA	[203]
4	Steam explosion lignin	Hierarchical porous carbon from lignin derived through carbonization at 500 to 800 °C, activation with KOH, hot water wash, and sample dried at 100 °C overnight	3775 $\text{m}^2 \text{g}^{-1}$	286.7 $\text{F g}^{-1}$ at 0.2 $\text{A g}^{-1}$ In 6 mol $\text{L}^{-1}$ KOH	207.1 $\text{F g}^{-1}$ at 8 $\text{A g}^{-1}$	[204]

(continued)

**Table 3** (continued)

S. No.	Carbon source	Process condition	Surface area ( $\text{m}^2 \text{g}^{-1}$ )	Specific capacitance	Capacity retention (%)	References
5	Lignin	Lignin was converted to heteroatom-doped porous carbon using hydrothermal carbonization followed by chemical activation	1788 to 2957 $\text{m}^2 \text{g}^{-1}$	372 $\text{F g}^{-1}$	Cyclic stability over 30,000 cycles in 1 M KOH	[205]
6	Lignin	Conventional carbonization followed by bacterial activation	1831 $\text{m}^2 \text{g}^{-1}$	428 $\text{F g}^{-1}$ at 1 $\text{A g}^{-1}$	96.7% after 10,000 cycles at 5 $\text{A g}^{-1}$	[206]
7	Low sulfonated alkali lignin	Lignin and PEO (9:1 ratio) were electrospun. Carbonization and activation at 850 °C under $\text{N}_2$	NA	344.0 $\text{F g}^{-1}$	96% after 5000 cycles	[207]

740  $\text{m}^2 \text{g}^{-1}$  after washing with water. Also, well-structured lignin can produce high porous materials with a large BET surface area, 1000  $\text{m}^2 \text{g}^{-1}$  after carbonization [203]. It is clearly indicated that the porosity is associated with the temperature and the heating rate applied for thermal treatment.

W. Zhang reported hierarchical porous carbon preparation from steam-exploded lignin through carbonization at 500 to 800 °C under nitrogen atmosphere for 1 h and followed by two-step activations. First, KOH saturation on a lignin-based carbon (LC) matrix at 400 °C for 0.5 h and subsequently activation process was conducted at 700, 800, and 900 °C for 1 h in the second step. The post-treatment includes excessive alkali removal using hot water wash until neutral pH, followed by drying at 100 °C overnight. The resulting lignin hierarchical porous carbon (LAC) contains a microporous core and meso- and microporous channels. During the carbonization process, the decomposition of the oxygen-containing groups leads to a small amount of micro- and mesopores. In contrast, the activation leads to macroporous caves with several micrometers of diameters, and the authors explained that these macropores are highly beneficial to retain the electrolyte and also reduce the ion diffusion path when the charge/discharge process happens inside the supercapacitors. The capacitive performance was calculated using cyclic voltammetry and galvanostatic charge–discharge in 6 M KOH within the potential window from 0 to 1 V. The results showed that the obtained LAC specific surface area was over 3775  $\text{m}^2 \text{g}^{-1}$  and specific capacitance as high as 286.7  $\text{F g}^{-1}$  at 0.2  $\text{A g}^{-1}$  [204]. Demir prepared the heteroatom-doped porous carbon from lignin using a method called hydrothermal carbonization followed by activation. The obtained porous carbon possesses a BET surface area of 1788 to 2957  $\text{m}^2 \text{g}^{-1}$ , specific capacitance of 372  $\text{F g}^{-1}$ , and exhibits excellent cyclic stability over 30,000 cycles in 1 M KOH [205]. K. Zhang stated that the traditional

activation method to synthesis porous carbons from lignin with a higher surface area is more complex, costly, and can cause pollution. Alternatively, they proposed a lignin-derived porous carbon activation using the green bacterial activation method. The authors employed conventional carbonization and after proceeding to bacterial activation process, and reported a BET surface area of  $1831 \text{ m}^2 \text{ g}^{-1}$ , specific capacitance of  $428 \text{ F g}^{-1}$  at  $1 \text{ A g}^{-1}$ , and capacity retention of 96.7% after 10,000 cycles at  $5 \text{ A g}^{-1}$ .

## 6 Lignin-Based Composites for Electrodes

Electrospinning is a widely used, scalable, and cost-effective method to manufacture free-standing and flexible carbon fiber mats for supercapacitor electrodes. Several important parameters greatly influence the electrospinning process and characteristics of the fibers including carbon fiber precursor types, solution viscosity, molecular weight of the polymer, experimental processing and condition, and design. In particular, processing parameters including the applied voltage and feeding rate lead to different geometries and fiber diameters [208]. Liu demonstrated that the tensile strength of carbon fiber depends on the size of the fiber, wherein decreasing fiber diameter increases the molecular order and finally improves the tensile strength [209]. While the electrospinning approach can utilize low-cost precursors for the production of carbon fibers, there are few reports on the preparation of electrospun lignin fibers [200]. To obtain these high-quality carbon fibers, lignin is fractionated prior to the electrospinning process [210]. The material should be thermally stabilized, followed by carbonization, in order to produce carbon fibers from lignin.

Kadla produced carbon fiber from kraft lignin through thermal spinning and carbonization process with a 45% yield. They also reported that inorganic impurities present in the kraft lignin hinder thermal processing and the prior washing of lignin with dilute HCl is necessary to eliminate such issues. To facilitate fiber spinning, lignin was blended with polyethylene oxide (PEO), and it is noted that mechanical properties like tensile strength of 400–550 MPa and Young's modulus of 30–60 GPa were increased with decreasing fiber diameter [211]. The glass transition temperature of lignin ( $T_g$ ) is far below that of the carbonization temperature and must undergo thermal stabilization to prevent softening during the carbonization process. Braun proposed that air oxidation is a simple and cost-effective pretreatment for lignin thermal stabilization [212].

Hatakeyama has reported that softening of lignin was produced through heating, and the addition of phenolic compounds would give it melting properties for the electrospinning process [213]. In most cases, lignin combined with a high molecular weight polymers, for instance, PEO in either an alkali solution or organic solvent significantly improve the spinnability for electrospinning process and solution elasticity [214]. However, the cost of the final product is significantly increased when blending a polymer with lignin, and it is important to minimize the proportion of polymer to decrease the cost. Saha produced mesoporous carbon for electrodes from

pre-cross-linked lignin (hardwood kraft) gel combined with a surfactant which acts as a pore-forming agent, and the activated carbon exhibited a 1.5 to sixfold increase in porosity with the maximum BET surface area of  $1148 \text{ m}^2 \text{ g}^{-1}$  [215].

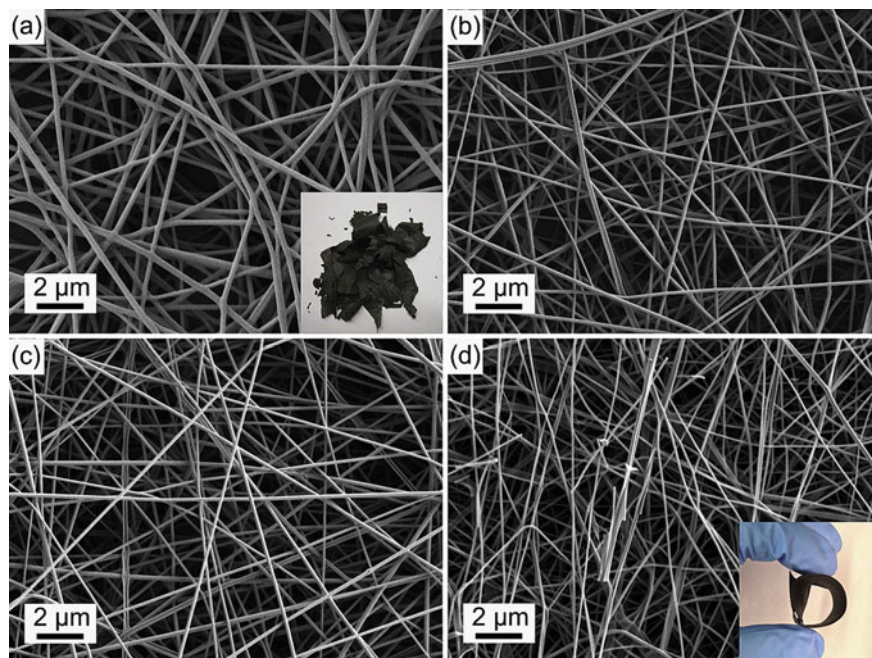
The utilization of various carbon materials (fibers and mats) from lignin as free-standing electrodes in supercapacitors is significant. Ago produced a flexible electrode from an aqueous solution of softwood alkali lignin and polyvinyl alcohol (PVA) through the electrospinning process. Electrospun mat showed a high specific capacitance ( $205 \text{ F g}^{-1}$ ) compared to the solid films ( $6.4 \text{ F g}^{-1}$ ) that were produced through the solvent casting method. The reason for the high performance of the fiber mat is related to the high surface area and well-developed mesoporous structure, with open pores available to ion/electrolyte transport [210].

Lai et al. [216] prepared a mechanically flexible binder-free electrode for supercapacitors from alkali lignin through electrospinning process followed by a stabilization and carbonization process (Fig. 11). Due to the lack of molecular entanglements in alkali lignin, it is very hard to perform electrospun process of pure lignin into nanofibers. In order to make the lignin suitable for electrospinning process, PVA polymer is incorporated and 9–2 wt% of an aqueous solution containing both lignin: PVA with different weight ratios were subjected to electrospinning. SEM results showed that the increasing lignin content results in reducing the average diameter of the composite. The composite nanofiber exhibited an average diameter of  $\sim 100 \text{ nm}$ , with a BET-specific surface area of  $\sim 583 \text{ m}^2 \text{ g}^{-1}$ . The measured gravimetric capacitance in 6 M KOH aqueous electrolyte showed  $64 \text{ F g}^{-1}$  at a current density of  $400 \text{ mA g}^{-1}$  and  $50 \text{ F g}^{-1}$  at  $2000 \text{ mA g}^{-1}$  and the capacitance was reduced  $\sim 10\%$  after 6000 cycles of charge and discharge [216].

Another flexible and free-standing electrode was produced from lignin and PVA blends and fabricated through the electrospinning process. Stabilization and carbonization, followed by  $\text{CO}_2$  activation, the activated carbon nanofibers were produced. The combined lignin and PVA with 80:20 ratio showed a surface area of  $2170 \text{ m}^2 \text{ g}^{-1}$  with a volume of  $0.365 \text{ cm}^3 \text{ g}^{-1}$ . The conductivity was measured with the electrolyte formed by ionic liquid and carbonate mixtures (ethylene carbonate and propylene carbonate) and reported  $87 \text{ F g}^{-1}$  specific capacitance and  $38 \text{ Wh kg}^{-1}$  of energy density and stated that the ionic liquid mixture showed four times higher conductivity than neat ionic liquid [217].

A 10% acrylonitrile-butadiene rubber doped lignin was prepared under solvent-free conditions and exhibited  $2120 \text{ m}^2 \text{ g}^{-1}$  surface area with a capacitance of  $215 \text{ F g}^{-1}$ , which is maintained even after 5000 cycles [218]. Sodium lignosulfonate and alkali lignin were mixed with polypyrrole separately to evaluate the electrode capacity, and it was found that alkali lignin demonstrates an increase in capacitance from 321 to  $444 \text{ F g}^{-1}$  compared to sodium lignosulfonate. Moreover, the electrochemical performance can be increased by incorporating high phenolic content into the alkali lignin via pH-driven fractionation [219]. The variation of sinapyl to guaiacyl units ratio in lignin significantly increased both the specific capacitance and charge capacity due to the formation of a quinone structure on sinapyl units, which store more charge in the electrodes [220]. Direct laser writing method is recently used to synthesis the hierarchical porous materials with large surface area, and this method





**Fig. 11** SEM images of electrospun carbon nanofiber mats prepared by combined PVA and lignin with different weight percentages: **a** PVA mat alone, brittle mat is in the inset; **b** PVA:lignin (30:70); **c** PVA:lignin (50:50); and **d** PVA:lignin (70:30), flexible mat is shown in inset. Reprinted with permission from Chuilin et al. [216] Copyright (2014) Elsevier

was successfully applied for lignin combined with PEO system to form a graphene network. The synthesized porous electrodes showed electrochemical capacitance up to  $25.44 \text{ mF cm}^{-2}$  which is superior to the materials obtained from pristine lignin [221].

Although lignin-derived nanoporous carbons are used for ESCs, the sources of lignin and certain processes employed for pretreatment significantly affect capacitance. Therefore, the optimization of lignin chemistry with other important factors such as pore distribution, surface area and higher hydrophobicity are paramount to designing electrodes for ESCs. The pore distribution plays a fundamental role toward ionic conductivity, in which the micropores with a smaller pore distribution cannot be accessed by the ions associated with electrolytes that lead to low ionic conductivity of the materials. A study has produced hydro char from enzymatic hydrolysis lignin by treating with  $\text{H}_2\text{SO}_4$  at  $180^\circ\text{C}$  for 18 h prior to mix with KOH [222]. The obtained electrode samples after carbonization process exhibit the formation both micropores and mesopores in the range between 0.5 and 3 nm, and these pores are connected internally which provide an outstanding platform for ions diffusivity. On the other hand, surface hydrophilicity of the lignin-derived carbon electrode materials

is mainly enhanced by incorporating heteroatoms in the skeleton and this process leads to improving the compatibility of electrode–electrolytes interphase [223–225].

Biomass-derived carbon exhibits poor energy density due to its distinct electronically insulating behavior, which impedes its performance. The functionality can be enhanced via chemical modification of the polymer, like lignin, and requires proper investigation. Sudo performed the modification reactions of phenolation and hydrogenation on steam-exploded lignin to optimize the lignin for the electrospinning process. They reported more than 44% carbon fiber yield with phenolated lignin, which is twice the yield compared to hydrogenolated lignin [213, 226]. Thunga employed a butyration chemical modification reaction of lignin to enhance the compatibility with PLA polymer to produce fine fiber through melt mixing with an overall concentration of 75 wt% of lignin [227]. Another approach is to derivatize the lignin through hydroxyl groups to synthesize various lignin derivatives with ester, ether, and urethane groups. In such reactions, lignin tends to copolymerize with other polymers, like phenol–formaldehyde to form the lignin–phenol–formaldehyde resins [228].

The combination of lignin with different polymers such as PVA, PEO, and PVP produced carbon materials that were exhibited a broad potential voltage window. Mechanically flexible mates were made from alkali lignin and PLA with different compositions, of which 70:30 (lignin:PVA) composite showed a potential window of 0–0.8 V in KOH electrolyte [216]. Similarly, other proposed works have demonstrated a wide potential voltage window with different electrolytes, –0.2 to 0.8 V from 75:25 (lignin:PVA in  $\text{Na}_2\text{SO}_4$ ) [210], 0 to 3.5 V from 80:20 (lignin:PVA in BMIM TFSI:PC:EC) [217], 0 to 1.6 V and 2.0 V from 90:10 (lignin:PVA in  $\text{H}_2\text{SO}_4$ , PVA: $\text{H}_2\text{SO}_4$ ) [229], 0 to 1 V from 90:10 (lignin:PEO in KOH) [207], 0 to 1.6 V from 50:50 (lignin: PAN in PVA and KOH) [230] and –0.9 to 0 V from 1:2 (lignin:PVP in KOH) [231]. These studies are clearly indicated that lignin can be applied for a wide potential window to design high-performance supercapacitors.

Various parameters affect the performance of the porous carbon electrodes derived lignin for supercapacitors which include tuning of impregnation time, activation temperature, and impregnation ratio on pore size distribution, total pore volume, and specific surface area. Activated porous carbon from Kraft lignin were produced through activation using orthophosphoric acid at different ratios (orthophosphoric acid/lignin- $P/L = 0.7$ – $1.75$ ), temperature (400–650 °C) and impregnation time (1–48 h). The results illustrated that increasing impregnation time considerably reduces the surface area and the pore volume. Activated carbon prepared at 650 °C, the surface area reduced from 1305 to 956  $\text{m}^2 \text{g}^{-1}$  when the impregnation time lasts up to 48 h.  $P/L$  ratio more than 1.4 and the impregnation time more than 1 h, the orthophosphoric acid damages the polymeric structure of the kraft lignin which leads to low porous volume and surface area [232]. Serrano reported that high surface area activated microporous carbon was obtained through chemical activation of kraft lignin using  $\text{ZnCl}_2$  in the temperature range of 400–500 °C.  $\text{ZnCl}_2$  activation method allowed to prepare the activated carbon with BET surface area upto 1800  $\text{m}^2 \text{g}^{-1}$  with 40% yield. Pore distributions were also studied by changing the impregnation ratio of

ZnCl<sub>2</sub>/lignin and reported that upto the ratio of 2.3, the mesoporous distribution remained in the low-size range below about 5 nm in diameter [233].

## 7 Supercapacitor Fabrication and Electrochemical Study

As mentioned above, the capacitive performance of a supercapacitor is controlled by various parameters such as active electrode material, electrode composition, additives, thickness of the electrode, concentration and class of the electrolyte, type of separator, and current collector. The analysis technique is also a crucial component to calculate the capacitive performance. The comparison of the analysis methods has been discussed in detail in the well-known paper by Stoller and Ruoff [71].

Cyclic voltammetry (CV) is one of the well-known techniques for determining the electrochemical behavior of the electrode material. The current on the working electrode is plotted versus the applied voltage to give information about the electrochemical changes of an analyte or of a material that is adsorbed onto the electrode [234]. CV has become the main process for evaluating the performance of capacitor devices because of the relationship between the response currents to repetitive linear voltage modulation at sweep rates [235]. In AC-based supercapacitors, a quasi-rectangular shape indicating an excellent capacitive behavior is expected. However, some deformity in the rectangular shape is usually observed. This may be from (i) the reversible or irreversible redox species or (ii) coating failures during the set-up process of a three-electrode system. To understand the pseudocapacitive effect of reversible or irreversible redox reactions, it is strongly recommended to conduct CV analysis for more than 10 cycles. To avoid coating failures, nickel foam types of current collectors are generally used for electrode-active material holders. It should be kept in mind that the capacitive contribution of Ni-foam should be subtracted from the total capacitive performance.

The galvanostatic charge–discharge (GCD) technique is employed to calculate the capacitance for ultracapacitors in industry [71]. In the GCD technique, the specific capacitance is calculated from the discharge curves after excluding the IR drop and the whole GCD curve gives charge capacity and Coulombic efficiency of the electrode material. In AC-based supercapacitors, the symmetric triangular shape of the GCD curves proving the capacitive behavior is expected. However, like in the CV technique, distortion in the symmetry with slight tailing may be observed due to the pseudocapacitance effect from the O, N surface functional groups attached to the carbon framework [236].

Electrochemical impedance spectroscopy (EIS) is also widely used to determine the resistance of a supercapacitor which consists of electronic contributions and ionic contributions [237]. The Nyquist plots obtained from the EIS data were used to determine the combined resistance of intrinsic resistance of electrode materials, ionic resistance of electrolyte and contact resistance between the electrode and current collector, and the electrode conductivity and charge-transfer resistance [238]. The semicircle that intersects the real axis at the high-frequency region and the plot that

transforms to a vertical line (Warburg line) at the intermediate-frequency region are mainly observed in AC-based supercapacitors. At the low-frequency region, a vertical line presents the domination of the capacitive behavior at the electrolyte-carbon interface due to the penetration of the electrolyte ions into pores [239].

The specific capacitance of a supercapacitor is given in different units such as gravimetric capacitance (F/g), volumetric capacitance (F/cm<sup>3</sup>), and areal capacitance (F/cm<sup>2</sup>). They are calculated based on single electrode by the following equations:

$$C(\text{F/g}) = 2 \times \frac{i \times \Delta t}{m \times \Delta V}$$

$$C(\text{F/cm}^3) = 2 \times \frac{i \times \Delta t}{v \times \Delta V}$$

$$C(\text{F/cm}^2) = 2 \times \frac{i \times \Delta t}{S \times \Delta V}$$

where  $i$ ,  $\Delta t$ ,  $m$ ,  $v$ ,  $S$ , and  $\Delta V$  are discharge current, discharge time, mass, volume and the surface area of the electrode, and the working voltage window, respectively. As it is seen, they can be converted to each other easily if the exact mass, final density and the surface area of the electrode are known. The unit in which the specific capacitance is given depends on the character of the practical application. Up to date, most of the researchers generally preferred to present their data in gravimetric capacitance value, especially for EDLCs. Nevertheless, when the development of electronics advances into more small, thriving of more technological is needed for the production of electrode materials that deliver both high areal and volumetric capacitance, without compromising the gravimetric capacitance, high rate, and cycling performances [240]. The main issue here is the intrinsic low densities of carbon nanomaterials which result in low volumetric capacitance [241]. To overcome the limitation originated from the porous structure of carbon-based materials various approaches such as heteroatom doping for additional pseudocapitance, metal-carbon composites, and tuning pore structure are still in progress [242]. The density of carbon is significantly improved due to doping of heavy hetero atoms which do not affect the number of pores and but increase the amount of electrochemically active functional groups on the surface [243, 244]. However, we still need much more research on reducing the intrinsic density of highly porous carbon-based materials.

As a result, due to the high number of parameters and differences originated from the analysis techniques, the determination of the capacitive performance of a supercapacitor may be complicated. However, those parameters are required to be reported properly in the literature [245]. Therefore, it is thought that the comparison of the obtained results with similar works and commercial ACs should be made for further development of supercapacitors.

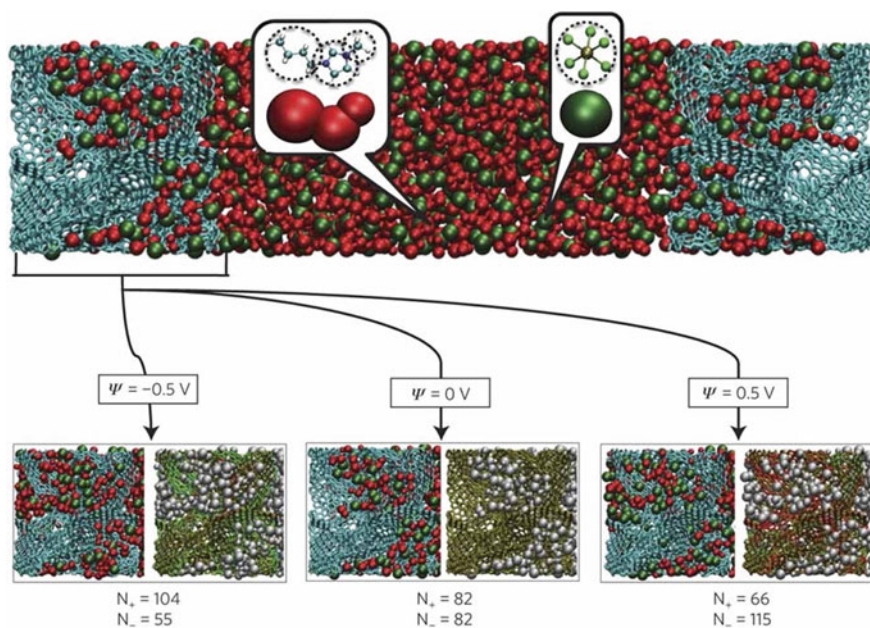
## 8 Computational Modeling Techniques for Supercapacitors

Multiscale modeling is the most powerful and efficient method that provides in-depth knowledge about the physicochemical properties of materials. By implementing a bottom-up paradigm, numerical simulations can anticipate laboratory work and optimize the system of interest for energy-related applications. Density functional theory (DFT) and molecular dynamics (MD) simulations are the fundamental methods routinely applied to compute the properties of diverse materials at the atomic and molecular levels. DFT method can be employed for systems containing a few tens of atoms to account for the properties of small molecules and analyze reactivity. Therefore, the DFT method is limited for investigating large systems, like supercapacitors (SCs), since it requires extensive computational cost to represent porous electrodes and electrodes. On other hand, MD is a successful method to illustrate the interaction between the particles or molecules and obtain their dynamical evolution behavior at the nanoscale. A comprehensive analysis of theoretical approximations, algorithms, and applications of computational modeling can be found in the reference of Frenkel and Smit [246]. Salanne group successfully applied MD simulation methods to study the separation of the positive and negative ions that occurs inside the porous disordered carbons, electrified interphases of carbide-derived carbons, and diffusivity of charges [247–252]. Several MD systems for SCs have been reported, and one of the studied MD models is presented in Fig. 12. Celene developed a realistic model for SCs with ionic liquid electrolytes, and the obtained results revealed that the increase in capacitance is not only due to the large surface of the carbons but pore size and microstructure also show a crucial role. The charging process is mainly associated with the exchange of ions in the bulk electrolyte in the electrode without affecting the total volume of liquid [247].

There has been a significant increase in applying molecular modeling techniques to understand the ion transport mechanisms involved in different types of electrodes such as carbon nanotubes [253], spherical shells [254], two-dimensional (2D) nanomaterials [255], electrical double layers [256, 257], nitrogen-doped graphene [258], oxygen-defects containing graphene [259], and MOF electrodes [260]. A detailed review of publications using MD simulation for designing SC electrodes can be found in the Refs. [261, 262].

## 9 Conclusions and Perspectives

Supercapacitors (SCs) are considered to be one of the potential power storage devices that can provide high energy density and long cycling durability. Their unique features, such as high-power density, fast charge/discharge capability, and long operating lifetimes with good safety, allow use in a broad range of electronic applications such as wearable and portable electronic devices. Porous carbon-based materials, like activated carbons (ACs), are the fundamental choice of electrodes for SCs due



**Fig. 12** MD snapshot of simulation shell containing the confined coarse-grained IL (BMIM-PF<sub>6</sub>) between two porous electrodes (top) and the structural changes of the electrodes at different voltages (bottom) (Color scheme—blue: carbon atoms, red: BMIM<sup>+</sup> ions, and green: PF<sub>6</sub><sup>-</sup> ions). Reprinted with permission from Celine et al. [247] Copyright (2012) Springer Nature

to their low cost, tunable porosity, and larger surface area. It is reported that AC pore size between 2 and 5 nm can be beneficial to obtain higher energy density and enhance the power capability of SCs. Numerous polymers have been reported as precursors to produce a broad range of porous and specific surface area ACs. Considering the depletion of fossil resources and climate change, alternate precursors for ACs are important because most polymers are synthesized from petrochemicals. Due to concerns about the environment, wood biomass-based materials have drawn much attention for SCs due to their abundance, inexpensive, and environmentally friendly characteristics; electrochemical capacitance from biomass is also more competitive for commercial ACs. Among biomass components, lignin is the second most abundant biopolymer, after cellulose, and has been considered as a vital precursor for ACs and carbon fibers due to its aromatic character and variety of functional groups. Typically, ACs can be produced using carbonization at high temperatures (500–1000 °C), followed by chemical activation using different chemical activation methods, such as potassium hydroxide, phosphoric acid, and zinc chloride, and physical activation methods, like steam and carbon dioxide. Although lignin-based materials exhibit several advantages, there are still challenges to be addressed:

- The composition of lignin in lignocellulosic biomass is highly dependent on plant type, origin, and location. The percentage of lignin content, complex structure

of lignin, and unexpected chemical reactions during activation greatly affect the final structure of lignin. Therefore, a clear understanding of lignin's functional groups and molecular weight is important before proceeding to the synthesis of porous carbon.

- Electrospinning is the predominant process to produce carbon fiber for SCs. Lignin creates compatibility issues, like spraying the solution on the collector rather than creating fiber, during the electrospinning process. Such issues impede commercial valorization of lignin for producing carbon fiber mats and ACs. To overcome this issue, current research has been carried out with the addition of polymers in the lignin solution.
- Modification of lignin can enhance the preparation of hierarchical porous lignin-derived carbons with a high specific surface area. Therefore, different modifications can be tested for creating graphitic carbon with appropriate pore structures to improve the electrochemical performance of SCs.
- The addition of metal-oxide and metal-carbide materials in lignin can advance the preparation of a broad range of porous carbons with a large electrochemical voltage window.
- Density functional theory, reactive, and classical molecular dynamics modeling methods can be employed to understand both physical and chemical properties of lignin. Pyrolysis modeling might aid in the optimization of the carbonization process of lignin toward the formation of carbon fibers and pores. The molecular dynamics simulation method can provide deep insights into electrochemical capacitance, diffusivity of charges, and electrified interfaces with different electrode pore sizes and electrolytes. These integrated modeling methods will help to scale up further research and development in the SCs research field.

**Acknowledgements** Authors acknowledge the European Commission for funding InnoRenew CoE (grant agreement #739574), under the H2020 Widespread-Teaming program, and the Republic of Slovenia (investment funding from the Republic of Slovenia and the European Union's European Regional Development Fund) and infrastructural ARRS program IO-0035. E.S.E acknowledges Marie-Curie grant MSCA-IF-101031402 (2021-2023). T.Y is grateful to the Scientific and Technological Research Council of Turkey-TUBITAK for the financial support through the project number 218M915.

## References

1. Liu G, Chen T, Xu J, Wang K (2018) Blue energy harvesting on nanostructured carbon materials. *J Mater Chem A* 6(38):18357–18377
2. Ding T, Liu K, Li J, Xue G, Chen Q, Huang L, Hu B, Zhou J (2017) All-printed porous carbon film for electricity generation from evaporation-driven water flow. *Adv Func Mater* 27(22):1700551
3. Lebrun L, Guyomar D, Guiffard B, Cottinet P-J, Putson C (2009) The Characterisation of the harvesting capabilities of an electrostrictive polymer composite. *Sens Actuators, A* 153(2):251–257

4. Eddiai A, Meddad M, Guyomar D, Hajjaji A, Boughaleb Y, Yuse K, Touhtouh S, Sahraoui B (2012) Enhancement of electrostrictive polymer efficiency for energy harvesting with cellular polypropylene electrets. *Synth Met* 162(21):1948–1953
5. Libich J, Máca J, Vondrák J, Čech O, Sedlářková M (2018) Supercapacitors: properties and applications. *J Energy Storage* 17:224–227
6. Banerjee S, De B, Sinha P, Cherusseri J, Kar KK (2020) Applications of supercapacitors. In: *Springer series in materials science*, vol 300. Springer, pp 341–350
7. Ruiz V, Blanco C, Raymundo-Piñero E, Khomenko V, Béguin F, Santamaría R (2007) Effects of thermal treatment of activated carbon on the electrochemical behaviour in supercapacitors. *Electrochim Acta* 52(15):4969–4973
8. Nandi D, Mohan VB, Bhowmick AK, Bhattacharyya D (2020) Metal/metal oxide decorated graphene synthesis and application as supercapacitor: a review. *J Mater Sci* 55(15):6375–6400
9. Li Zhang L, Zhao XS (2009) Carbon-based materials as supercapacitor electrodes. *Chem Soc Rev* 38(9):2520–2531
10. Jost K, Dion G, Gogotsi Y (2014) Textile energy storage in perspective. *J Mater Chem A* 2(28):10776–10787
11. Wang G, Zhang L, Zhang J (2012) A review of electrode materials for electrochemical supercapacitors. *Chem Soc Rev* 41(41):797–828
12. Muzaffar A, Ahamed MB, Deshmukh K, Thirumalai J (2019) A review on recent advances in hybrid supercapacitors: design, fabrication and applications. *Renew Sustain Energy Rev* 101:123–145
13. Lv H, Pan Q, Song Y, Liu X-X, Liu T (2020) A review on nano-/microstructured materials constructed by electrochemical technologies for supercapacitors. *Nano-Micro Lett* 12:118
14. Balasubramaniam S, Mohanty A, Kannan Balasingam S, Kim SJ, Ramadoss A, Saravanakumar B (2020) Comprehensive insight into the mechanism, material selection and performance evaluation of supercapacities. *Nano-Micro Lett* 12:85
15. Jiang Y, Liu J (2019) Definitions of pseudocapacitive materials: a brief review. *Energy Environ Mater* 2:30–37
16. Bryan AM, Santino LM, Lu Y, Acharya S, D’Arcy JM (2016) Conducting polymers for pseudocapacitive energy storage. *Chem Mater* 28(17):5989–5998
17. Mohd Abdah MAA, Azman NHN, Kulandaivalu S, Sulaiman Y (2020) Review of the use of transition-metal-oxide and conducting polymer-based systems for high-performance supercapacitors. *Mater Des* 186:108199
18. Bose S, Kuila T, Mishra AK, Rajasekar R, Kim NH, Lee JH (2012) Carbon-based nanostructured materials and their composites as supercapacitor electrodes. *J Mater Chem* 22(3):767–784
19. Chen T, Dai L (2013) Carbon nanomaterials for high-performance supercapacitors. *Mater Today* 16(7–8):272–280
20. Jiang J, Li Y, Liu J, Huang X, Yuan C, Lou XW (2012) Recent advances in metal oxide-based electrode architecture design for electrochemical energy storage. *Adv Mater* 24(38):5166–5180
21. Yumak T, Bragg D, Sabolsky EM (2019) Effect of synthesis methods on the surface and electrochemical characteristics of metal oxide/activated carbon composites for supercapacitor applications. *Appl Surf Sci* 469
22. Liu R, Duay J, Lee SB (2011) Heterogeneous nanostructured electrode materials for electrochemical energy storage. *Chem Commun* 47(5):1384–1404
23. Park S-J, Heo G-Y (2015) Precursors and manufacturing of carbon fibers. In: Park S-J (ed) *Carbon fibers*. Springer, Netherlands, pp 31–66
24. Wu Z, Li L, Yan J, Zhang X (2017) Materials design and system construction for conventional and new-concept supercapacitors. *Adv Sci* 4(6):1600382
25. Lee J, Kim J, Hyeon T (2006) Recent progress in the synthesis of porous carbon materials. *Adv Mater* 18(16):2073–2094
26. Zhai Y, Dou Y, Zhao D, Fulvio PF, Mayes RT, Dai S (2011) Carbon materials for chemical capacitive energy storage. *Adv Mater* 23(42):4828–4850



27. Gogotsi Y, Nikitin A, Ye H, Zhou W, Fischer JE, Yi B, Foley HC, Barsoum MW (2003) Nanoporous carbide-derived carbon with tunable pore size. *Nat Mater* 2(9):591–594
28. Pérez CR, Yeon S-H, Ségalini J, Presser V, Taberna P-L, Simon P, Gogotsi Y (2013) Structure and electrochemical performance of carbide-derived carbon nanopowders. *Adv Func Mater* 23(8):1081–1089
29. Presser V, Zhang L, Niu JJ, McDonough J, Perez C, Fong H, Gogotsi Y (2011) Flexible nano-felts of carbide-derived carbon with ultra-high power handling capability. *Adv Energy Mater* 1(3):423–430
30. Oschatz M, Borchardt L, Pinkert K, Thieme S, Lohe MR, Hoffmann C, Benusch M, Wisser FM, Ziegler C, Giebeler L, Rummeli MH, Eckert J, Eychmüller A, Kaskel S (2014) Hierarchical carbide-derived carbon foams with advanced mesostructure as a versatile electrochemical energy-storage material. *Adv Energy Mater* 4(2):1300645
31. Chmiola J, Yushin G, Gogotsi Y, Portet C, Simon P, Taberna PL (2006) Anomalous increase in carbon capacitance at pore sizes less than 1 nanometer. *Science* 313(5794):1760–1763
32. Heon M, Lofland S, Applegate J, Nolte R, Cortes E, Hettinger JD, Taberna P-L, Simon P, Huang P, Brunet M, Gogotsi Y (2010) Continuous carbide-derived carbon films with high volumetric capacitance. *Energy Environ Sci* 4(1):135–138
33. Dyjak S, Kiciński W, Norek M, Dyjak M, Cudziło S (2019) Carbide-derived carbon obtained via bromination of titanium carbide: comparative analysis with chlorination and hydrogen storage studies. *Microporous Mesoporous Mater* 273:26–34
34. Jose Amali A, Sun J-K, Xu Q (2014) From assembled metal–organic framework nanoparticles to hierarchically porous carbon for electrochemical energy storage. *Chem Commun* 50(13):1519–1522
35. Chaikittisilp W, Hu M, Wang H, Huang H-S, Fujita T, Wu C-W, Chen L-C, Yamauchi Y, Ariga K (2012) Nanoporous carbons through direct carbonization of a zeolitic imidazolate framework for supercapacitor electrodes. *Chem Commun* 48(58):7259–7261
36. Wang R, Jin D, Zhang Y, Wang S, Lang J, Yan X, Zhang L (2017) Engineering metal organic framework derived 3D nanostructures for high performance hybrid supercapacitors. *J Mater Chem A* 5(1):292–302
37. Mostazo-López MJ, Ruiz-Rosas R, Castro-Muñoz A, Nishihara H, Kyotani T, Morallón E, Cazorla-Amorós D (2018) Ultraporous nitrogen-doped zeolite-templated carbon for high power density aqueous-based supercapacitors. *Carbon* 129:510–519
38. Sundriyal S, Shrivastav V, Pham HD, Mishra S, Deep A, Dubal DP (2021) Advances in bio-waste derived activated carbon for supercapacitors: trends, challenges and prospective. *Resour Conserv Recycl* 169:105548
39. Durairaj A, Sakthivel T, Ramanathan S, Obadiah A, Vasanthkumar S (2019) Conversion of laboratory paper waste into useful activated carbon: a potential supercapacitor material and a good adsorbent for organic pollutant and heavy metals. *Cellulose* 26(5):3313–3324
40. Chang B, Guo Y, Li Y, Yang B (2015) Hierarchical porous carbon derived from recycled waste filter paper as high-performance supercapacitor electrodes. *RSC Adv* 5(88):72019–72027
41. Singu DC, Joseph B, Velmurugan V, Ravuri S, Grace AN (2018) Combustion synthesis of graphene from waste paper for high performance supercapacitor electrodes. *Int J Nanosci* 17:1760023
42. Luo Y, Luo C, Zhang S-W, Wei J, Lv W, Yang Q-H (2019) Porous carbons derived from carbonization of tissue papers for supercapacitors. *J Mater Sci: Mater Electron* 30(12):11250–11256
43. Puthusseri D, Aravindan V, Anothumakkool B, Kurungot S, Madhavi S, Ogale S (2014) From waste paper basket to solid state and Li-HEC ultracapacitor electrodes: a value added journey for shredded office paper. *Small* 10(21):4395–4402
44. Liu D, Wang Y, Qiu Z, Li Y, Wang L, Zhao Y, Zhou J (2018) Porous carbons derived from waste printing paper for high rate performance supercapacitors in alkaline, acidic and neutral electrolytes. *RSC Adv* 8(8):3974–3981
45. Gonçalves M, Castro CS, Boas IKV, Soler FC, de Pinto CE, Lavall RL, Carvalho WA (2019) Glycerin waste as sustainable precursor for activated carbon production: adsorption properties and application in supercapacitors. *J Environ Chem Eng* 7(3):103059

46. Li Y, Zhang D, He J, Wang Y, Zhang X, Zhang Y, Liu X, Wang K, Wang Y (2019) Hierarchical porous carbon nanosheet derived from waste engine oil for high-performance supercapacitor application. *Sustain Energy Fuels* 3(2):499–507
47. Lu H, Zhao XS (2017) Biomass-derived carbon electrode materials for supercapacitors. *Sustain Energy Fuels* 1(6):1265–1281
48. Wei L, Yushin G (2012) Nanostructured activated carbons from natural precursors for electrical double layer capacitors. *Nano Energy* 1(4):552–565
49. White RJ, Brun N, Budarin VL, Clark JH, Titirici M-M (2014) Always look on the “light” side of life: sustainable carbon aerogels. *Chemsuschem* 7(3):670–689
50. Sevilla M, Diez N, Ferrero GA, Fuertes AB (2019) Sustainable supercapacitor electrodes produced by the activation of biomass with sodium thiosulfate. *Energy Storage Materials* 18:356–365
51. Fuertes AB, Ferrero GA, Diez N, Sevilla M (2018) A green route to high-surface area carbons by chemical activation of biomass-based products with sodium thiosulfate. *ACS Sustain Chem Eng* 6(12):16323–16331
52. Vix-Guterl C, Frackowiak E, Jurewicz K, Friebe M, Parmentier J, Béguin F (2005) Electrochemical energy storage in ordered porous carbon materials. *Carbon* 43(6):1293–1302
53. Sanchez-Sanchez A, Izquierdo MT, Ghanbaja J, Medjahdi G, Mathieu S, Celzard A, Fierro V (2017) Excellent electrochemical performances of nanocast ordered mesoporous carbons based on tannin-related polyphenols as supercapacitor electrodes. *J Power Sources* 344:15–24
54. Moussa G, Hajjar-Garreau S, Taberna P-L, Simon P, Matei Ghimbeu C (2018) Eco-friendly synthesis of nitrogen-doped mesoporous carbon for supercapacitor application. *C* 4(2):20
55. Herou S, Crespo Ribadeneyra M, Madhu R, Araullo-Peters V, Jensen A, Schlee P, Titirici M (2019) Ordered mesoporous carbons from lignin: a new class of biobased electrodes for supercapacitors. *Green Chem* 21(3):550–559
56. Feng S, Li W, Wang J, Song Y, Elzatahry A, Xia Y, Zhao D (2014) Hydrothermal synthesis of ordered mesoporous carbons from a biomass-derived precursor for electrochemical capacitors. *Nanoscale* 6(24):14657–14661
57. Herou S, Schlee P, Jorge AB, Titirici M (2018) Biomass-derived electrodes for flexible supercapacitors. *Curr Opin Green Sustain Chem* 9:18–24
58. Seredych M, Chen R, Bandosz TJ (2012) Effects of the addition of graphite oxide to the precursor of a nanoporous carbon on the electrochemical performance of the resulting carbonaceous composites. *Carbon* 50:4144–4154
59. Eliad L, Salitra G, Soffer A, Aurbach D (2001) Ion sieving effects in the electrical double layer of porous carbon electrodes: estimating effective ion size in electrolytic solutions. *J Phys Chem B* 105(29):6880–6887
60. Huang X, Kim S, Heo MS, Kim JE, Suh H, Kim I (2013) Easy synthesis of hierarchical carbon spheres with superior capacitive performance in supercapacitors. *Langmuir* 29(39):12266–12274. <https://doi.org/10.1021/la4026969>
61. Yamada H, Moriguchi I, Kudo T (2008) Electric double layer capacitance on hierarchical porous carbons in an organic electrolyte. *J Power Sources* 175(1):651–656
62. Everett DH, Powl JC (1976) Adsorption in slit-like and cylindrical micropores in the Henry’s law region. A model for the microporosity of carbons. *J Chem Soc, Faraday Trans 1: Phys Chem Condensed Phases* 72(0):619–636
63. Xu F, Cai R, Zeng Q, Zou C, Wu D, Li F, Lu X, Liang Y, Fu R (2011) Fast ion transport and high capacitance of polystyrene-based hierarchical porous carbon electrode material for supercapacitors. *J Mater Chem* 21(6):1970–1976
64. You B, Yang J, Sun Y, Su Q (2011) Easy synthesis of hollow core, bimodal mesoporous shell carbon nanospheres and their application in supercapacitor. *Chem Commun* 47(45):12364–12366
65. Xing W, Qiao SZ, Ding RG, Li F, Lu GQ, Yan ZF, Cheng HM (2006) Superior electric double layer capacitors using ordered mesoporous carbons. *Carbon* 44(2):216–224
66. Xia K, Gao Q, Jiang J, Hu J (2008) Hierarchical porous carbons with controlled micropores and mesopores for supercapacitor electrode materials. *Carbon* 46(13):1718–1726

67. Bichat MP, Raymundo-Piñero E, Béguin F (2010) High voltage supercapacitor built with seaweed carbons in neutral aqueous electrolyte. *Carbon* 48(15):4351–4361
68. Raymundo-Piñero E, Kierzek K, Machnikowski J, Béguin F (2006) Relationship between the nanoporous texture of activated carbons and their capacitance properties in different electrolytes. *Carbon* 44(12):2498–2507
69. Yumak T, Yakaboylu GAGA, Oginni O, Singh K, Ciftiyurek E, Sabolsky EMEM (2020) Comparison of the electrochemical properties of engineered switchgrass biomass-derived activated carbon-based EDLCs. *Colloids Surf, A* 586:124150
70. Zhu Y, Murali S, Stoller MD, Ganesh KJ, Cai W, Ferreira PJ, Pirkle A, Wallace RM, Cychosz KA, Thommes M, Su D, Stach EA, Ruoff RS (2011) Carbon-based supercapacitors produced by activation of graphene. *Science* 332(6037):1537–1541
71. Stoller MD, Ruoff RS (2010) Best practice methods for determining an electrode material's performance for ultracapacitors. *Energy Environ Sci* 3:1294–1301
72. Zhao Y, Liu M, Deng X, Miao L, Tripathi PK, Ma X, Zhu D, Xu Z, Hao Z, Gan L (2015) Nitrogen-functionalized microporous carbon nanoparticles for high performance supercapacitor electrode. *Electrochim Acta* 153:448–455
73. Yang W, Yang W, Kong L, Song A, Qin X, Shao G (2018) Phosphorus-doped 3D hierarchical porous carbon for high-performance supercapacitors: a balanced strategy for pore structure and chemical composition. *Carbon* 127:557–567
74. Song S, Ma F, Wu G, Ma D, Geng W, Wan J (2015) Facile self-templating large scale preparation of biomass-derived 3D hierarchical porous carbon for advanced supercapacitors. *J Mater Chem A* 3(35):18154–18162
75. Jiang J, Zhang L, Wang X, Holm N, Rajagopalan K, Chen F, Ma S (2013) Highly ordered macroporous woody biochar with ultra-high carbon content as supercapacitor electrodes. *Electrochim Acta* 113:481–489
76. Cha JS, Park SH, Jung S-C, Ryu C, Jeon J-K, Shin M-C, Park Y-K (2016) Production and utilization of biochar: a review. *J Ind Eng Chem* 40:1–15
77. Cheng B-H, Tian K, Zeng RJ, Jiang H (2017) Preparation of high performance supercapacitor materials by fast pyrolysis of corn gluten meal waste. *Sustain Energy Fuels* 1(4):891–898
78. Qian K, Kumar A, Zhang H, Bellmer D, Huhnke R (2015) Recent advances in utilization of biochar. *Renew Sustain Energy Rev* 42:1055–1064
79. Simon P, Gogotsi Y (2009) Materials for electrochemical capacitors. In: *Nanoscience and technology*. Co-Published with Macmillan Publishers Ltd, UK., pp 320–329
80. Li W, Liu J, Zhao D (2016) Mesoporous materials for energy conversion and storage devices. *Nat Rev Mater* 1(6):1–17
81. Sun W, Lipka SM, Swartz C, Williams D, Yang F (2016) Hemp-derived activated carbons for supercapacitors. *Carbon* 103:181–192
82. He Y, Zhang Y, Li X, Lv Z, Wang X, Liu Z, Huang X (2018) Capacitive mechanism of oxygen functional groups on carbon surface in supercapacitors. *Electrochim Acta* 282:618–625
83. Kwon KY, Youn J, Kim JH, Park Y, Jeon C, Kim BC, Kwon Y, Zhao X, Wang P, Sang BI, Lee J, Park HG, Chang HN, Hyeon T, Ha S, Jung H-T, Kim J (2010) Nanoscale enzyme reactors in mesoporous carbon for improved performance and lifetime of biosensors and biofuel cells. *Biosens Bioelectron* 26(2):655–660
84. Zhang S, Pan N (2015) Supercapacitors performance evaluation. *Adv Energy Mater* 5(6):1401401. <https://doi.org/10.1002/aenm.201401401>
85. Xie X, Goodell B, Zhang D, Nagle DC, Qian Y, Peterson ML, Jellison J (2009) Characterization of carbons derived from cellulose and lignin and their oxidative behavior. *Biores Technol* 100(5):1797–1802
86. Zondlo JW, Velez MR (2007) Development of surface area and pore structure for activation of anthracite coal. *Fuel Process Technol* 88(4):369–374
87. Frank E, Stuedle LM, Ingildееv D, Spörl JM, Buchmeiser MR (2014) Carbon fibers: precursor systems, processing, structure, and properties. *Angew Chem Int Ed* 53(21):5262–5298
88. Schlee P, Herou S, Jervis R, Shearing PR, Brett DJL, Baker D, Hosseinaei O, Tomani P, Murshed MM, Li Y, Mostazo-López MJ, Cazorla-Amorós D, Sobrido ABJ, Titirici M-M

- (2019) Free-standing supercapacitors from Kraft lignin nanofibers with remarkable volumetric energy density. *Chem Sci* 10(10):2980–2988
89. Inagaki M (2000) New carbons-control of structure and functions. Elsevier
  90. Mao X, Hutton TA, Rutledge GC (2013) A review of electrospun carbon fibers as electrode materials for energy storage. *Curr Org Chem* 17(13):1390–1401
  91. Ai Y, Lou Z, Li L, Chen S, Park HS, Wang ZM, Shen G (2016) Meters-long flexible CoNiO<sub>2</sub>-nanowires@carbon-fibers based wire-supercapacitors for wearable electronics. *Adv Mater Technol* 1(8):1600142
  92. Kim B-H, Yang KS, Woo H-G (2011) Preparation and electrochemical properties of carbon nanofiber composite dispersed with silver nanoparticles using polyacrylonitrile and  $\beta$ -cyclodextrin. *J Nanosci Nanotechnol* 11(8):7193–7197
  93. He W, Wang C, Li H, Deng X, Xu X, Zhai T (2017) Ultrathin and porous Ni<sub>3</sub>S<sub>2</sub>/CoNi<sub>2</sub>S<sub>4</sub> 3D-network structure for superhigh energy density asymmetric supercapacitors. *Adv Energy Mater* 7(21):1700983
  94. Liu C, Wu X (2018) NiCo<sub>2</sub>S<sub>4</sub> nanotube arrays grown on flexible carbon fibers as battery-type electrodes for asymmetric supercapacitors. *Mater Res Bull* 103:55–62
  95. Wang J, Chao D, Liu J, Li L, Lai L, Lin J, Shen Z (2014) Ni<sub>3</sub>S<sub>2</sub>@MoS<sub>2</sub> core/shell nanorod arrays on Ni foam for high-performance electrochemical energy storage. *Nano Energy* 7:151–160
  96. Ray RS, Sarma B, Jurovitzki AL, Misra M (2015) Fabrication and characterization of titania nanotube/cobalt sulfide supercapacitor electrode in various electrolytes. *Chem Eng J* 260:671–683
  97. Zhou W, Wu X-J, Cao X, Huang X, Tan C, Tian J, Liu H, Wang J, Zhang H (2013) Ni<sub>3</sub>S<sub>2</sub> nanorods/Ni foam composite electrode with low overpotential for electrocatalytic oxygen evolution. *Energy Environ Sci* 6(10):2921–2924. <https://doi.org/10.1039/C3EE41572D>
  98. Kim C, Yang KS (2003) Electrochemical properties of carbon nanofiber web as an electrode for supercapacitor prepared by electrospinning. *Appl Phys Lett* 83(6):1216–1218.
  99. Ra EJ, Raymundo-Piñero E, Lee YH, Béguin F (2009) High power supercapacitors using polyacrylonitrile-based carbon nanofiber paper. *Carbon* 47(13):2984–2992
  100. Kim B-H, Bui N-N, Yang K-S, dela Cruz ME, Ferraris JP (2009) Electrochemical properties of activated polyacrylonitrile/pitch carbon fibers produced using electrospinning. *Bull Korean Chem Soc* 30(9):1967–1972
  101. Liu Y, Zhou J, Chen L, Zhang P, Fu W, Zhao H, Ma Y, Pan X, Zhang Z, Han W, Xie E (2015) Highly flexible freestanding porous carbon nanofibers for electrodes materials of high-performance all-carbon supercapacitors. *ACS Appl Mater Interfaces* 7(42):23515–23520
  102. Kim C, Choi Y-O, Lee W-J, Yang K-S (2004) Supercapacitor performances of activated carbon fiber webs prepared by electrospinning of PMDA-ODA poly(amic acid) solutions. *Electrochim Acta* 50(2):883–887
  103. Kim C, Park S-H, Lee W-J, Yang K-S (2004) Characteristics of supercapacitor electrodes of PBI-based carbon nanofiber web prepared by electrospinning. *Electrochim Acta* 50(2):877–881
  104. Kim C, Ngoc BTN, Yang KS, Kojima M, Kim YA, Kim YJ, Endo M, Yang SC (2007) Self-sustained thin webs consisting of porous carbon nanofibers for supercapacitors via the electrospinning of polyacrylonitrile solutions containing zinc chloride. *Adv Mater* 19(17):2341–2346
  105. Guo Q, Zhou X, Li X, Chen S, Seema A, Greiner A, Hou H (2009) Supercapacitors based on hybrid carbon nanofibers containing multiwalled carbon nanotubes. *J Mater Chem* 19(18):2810–2816
  106. Ma C, Wu L, Dirican M, Cheng H, Li J, Song Y, Shi J, Zhang X (2021) Carbon black-based porous sub-micron carbon fibers for flexible supercapacitors. *Appl Surf Sci* 537:147914
  107. Kim C (2005) Electrochemical characterization of electrospun activated carbon nanofibers as an electrode in supercapacitors. *J Power Sources* 142(1):382–388
  108. Niu H, Zhang J, Xie Z, Wang X, Lin T (2011) Preparation, structure and supercapacitance of bonded carbon nanofiber electrode materials. *Carbon* 49(7):2380–2388

109. Chen L, Wen Z, Chen L, Wang W, Ai Q, Hou G, Li Y, Lou J, Ci L (2020) Nitrogen and sulfur co-doped porous carbon fibers film for flexible symmetric all-solid-state supercapacitors. *Carbon* 158:456–464
110. Kim B-H, Yang KS, Woo H-G (2011) Thin, bendable electrodes consisting of porous carbon nanofibers via the electrospinning of polyacrylonitrile containing tetraethoxy orthosilicate for supercapacitor. *Electrochem Commun* 13(10):1042–1046
111. Park S-J, Im S-H (2008) Electrochemical behaviors of PAN/Ag-based carbon nanofibers by electrospinning. *Bull Korean Chem Soc* 29(4):777–781
112. Ju Y-W, Choi G-R, Jung H-R, Kim C, Yang K-S, Lee W-J (2007) A hydrous ruthenium oxide-carbon nanofibers composite electrodes prepared by electrospinning. *J Electrochem Soc* 154(3):A192
113. Ju Y-W, Park S-H, Jung H-R, Lee W-J (2009) Electrospun activated carbon nanofibers electrodes based on polymer blends. *J Electrochem Soc* 156(6):A489
114. Zhang X, Li H, Qin B, Wang Q, Xing X, Yang D, Jin L, Cao Q (2019) Direct synthesis of porous graphitic carbon sheets grafted on carbon fibers for high-performance supercapacitors. *J Mater Chem A* 7(7):3298–3306
115. Jin Z, Yan X, Yu Y, Zhao G (2014) Sustainable activated carbon fibers from liquefied wood with controllable porosity for high-performance supercapacitors. *J Mater Chem A* 2(30):11706–11715
116. Huang Y, Peng L, Liu Y, Zhao G, Chen JY, Yu G (2016) Biobased nano porous active carbon fibers for high-performance supercapacitors. *ACS Appl Mater Interfaces* 8(24):15205–15215
117. Mohammed AA, Chen C, Zhu Z (2019) Low-cost, high-performance supercapacitor based on activated carbon electrode materials derived from baobab fruit shells. *J Colloid Interface Sci* 538:308–319
118. Zhang L, Yang X, Zhang F, Long G, Zhang T, Leng K, Zhang Y, Huang Y, Ma Y, Zhang M, Chen Y (2013) Controlling the effective surface area and pore size distribution of sp<sup>2</sup> carbon materials and their impact on the capacitance performance of these materials. *J Am Chem Soc* 135(15):5921–5929
119. Gong Y, Wei Z, Wang J, Zhang P, Li H, Wang Y (2014) Design and fabrication of hierarchically porous carbon with a template-free method. *Sci Rep* 4:1–6
120. Le Van K, Luong Thi Thu T (2019) Preparation of pore-size controllable activated carbon from rice husk using dual activating agent and its application in supercapacitor. *J Chem*
121. Prauchner MJ, Rodríguez-Reinoso F (2012) Chemical versus physical activation of coconut shell: a comparative study. *Microporous Mesoporous Mater* 152:163–171
122. Yumak T (2021) Surface characteristics and electrochemical properties of activated carbon obtained from different parts of Pinus pinaster. *Colloids Surf, A* 625:126982
123. Wang J, Kaskel S (2012) KOH activation of carbon-based materials for energy storage. *J Mater Chem* 22(45):23710–23725
124. Li Y, Zhang X, Yang R, Li G, Hu C (2015) The role of H<sub>3</sub>PO<sub>4</sub> in the preparation of activated carbon from NaOH-treated rice husk residue. *RSC Adv* 5(41):32626–32636
125. Castro-Gutiérrez J, Celzard A, Fierro V (2020) Energy storage in supercapacitors: focus on tannin-derived carbon electrodes. *Front Mater* 7:217
126. Zhong C, Deng Y, Hu W, Qiao J, Zhang L, Zhang J (2015) A review of electrolyte materials and compositions for electrochemical supercapacitors. *Chem Soc Rev* 44(21):7484–7539
127. Galiński M, Lewandowski A, Stępnik I (2006) Ionic liquids as electrolytes. *Electrochim Acta* 51(26):5567–5580
128. Fic K, Lota G, Meller M, Frackowiak E (2012) Novel insight into neutral medium as electrolyte for high-voltage supercapacitors. *Energy Environ Sci* 5(2):5842–5850
129. Jänes A, Thomberg T, Eskusson J, Lust E (2013) Fluoroethylene carbonate as co-solvent for propylene carbonate based electrical double layer capacitors. *J Electrochem Soc* 160(8):A1025
130. Tian S, Qi L, Yoshio M, Wang H (2014) Tetramethylammonium difluoro(oxalato)borate dissolved in ethylene/propylene carbonates as electrolytes for electrochemical capacitors. *J Power Sources* 256:404–409

131. Trócoli R, Morata A, Erinmwingbovo C, La Mantia F, Tarancón A (2021) Self-discharge in Li-ion aqueous batteries: a case study on  $\text{LiMn}_2\text{O}_4$ . *Electrochim Acta* 373:137847
132. Pal B, Yang S, Ramesh S, Thangadurai V, Jose R (2019) Electrolyte selection for supercapacitive devices: a critical review. *Nanoscale Advances* 1(10):3807–3835
133. Zhang L, Yang S, Chang J, Zhao D, Wang J, Yang C, Cao B (2020) A review of redox electrolytes for supercapacitors. *Front Chem* 8:413
134. Rogers RD, Voth GA (2007) Ionic liquids. *Acc Chem Res* 40(11):1077–1078
135. Armand M, Endres F, MacFarlane DR, Ohno H, Scrosati B (2009) Ionic-liquid materials for the electrochemical challenges of the future. *Nat Mater* 8(8):621–629
136. Demarconnay L, Calvo EG, Timperman L, Anouti M, Lemordant D, Raymundo-Piñero E, Arenillas A, Menéndez JA, Béguin F (2013) Optimizing the performance of supercapacitors based on carbon electrodes and protic ionic liquids as electrolytes. *Electrochim Acta* 108:361–368
137. Timperman L, Béguin F, Frackowiak E, Anouti M (2013) Comparative study of two protic ionic liquids as electrolyte for electrical double-layer capacitors. *J Electrochem Soc* 161(3):A228
138. Lewandowski A, Galinski M (2007) Practical and theoretical limits for electrochemical double-layer capacitors. *J Power Sources* 173(2):822–828
139. Lewandowski A, Olejniczak A, Galinski M, Stepniak I (2010) Performance of carbon–carbon supercapacitors based on organic, aqueous and ionic liquid electrolytes. *J Power Sources* 195(17):5814–5819
140. Orita A, Kamijima K, Yoshida M (2010) Allyl-functionalized ionic liquids as electrolytes for electric double-layer capacitors. *J Power Sources* 195(21):7471–7479
141. Francisco BE, Jones CM, Lee S-H, Stoldt CR (2012) Nanostructured all-solid-state supercapacitor based on  $\text{Li}_2\text{S-P}_2\text{S}_5$  glass-ceramic electrolyte. *Appl Phys Lett* 100(10):103902
142. Łatoszyńska AA, Żukowska GZ, Rutkowska IA, Taberna P-L, Simon P, Kulesza PJ, Wieczorek W (2015) Non-aqueous gel polymer electrolyte with phosphoric acid ester and its application for quasi solid-state supercapacitors. *J Power Sources* 274:1147–1154
143. Verma ML, Minakshi M, Singh NK (2014) Synthesis and characterization of solid polymer electrolyte based on activated carbon for solid state capacitor. *Electrochim Acta* 137:497–503
144. Fan L-Q, Zhong J, Wu J-H, Lin J-M, Huang Y-F (2014) Improving the energy density of quasi-solid-state electric double-layer capacitors by introducing redox additives into gel polymer electrolytes. *J Mater Chem A* 2(24):9011–9014
145. Chong MY, Numan A, Liew C-W, Ng HM, Ramesh K, Ramesh S (2018) Enhancing the performance of green solid-state electric double-layer capacitor incorporated with fumed silica nanoparticles. *J Phys Chem Solids* 117:194–203
146. Thangadurai V, Weppner W (2006) Recent progress in solid oxide and lithium ion conducting electrolytes research. *Ionics* 12(1):81–92
147. Huang C-W, Wu C-A, Hou S-S, Kuo P-L, Hsieh C-T, Teng H (2012) Gel electrolyte derived from poly(ethylene glycol) blending poly(acrylonitrile) applicable to roll-to-roll assembly of electric double layer capacitors. *Adv Func Mater* 22(22):4677–4685
148. Sudhakar YN, Selvakumar M, Bhat DK (2013)  $\text{LiClO}_4$ -doped plasticized chitosan and poly(ethylene glycol) blend as biodegradable polymer electrolyte for supercapacitors. *Ionics* 19(2):277–285
149. Ramasamy C, Palma del vel J, Anderson M (2014) An activated carbon supercapacitor analysis by using a gel electrolyte of sodium salt-polyethylene oxide in an organic mixture solvent. *J Solid State Electrochem* 18(8):2217–2223
150. Ulihin AS, Mateyshina YuG, Uvarov NF (2013) All-solid-state asymmetric supercapacitors with solid composite electrolytes. *Solid State Ionics* 251:62–65
151. Zhang Q, Scrafford K, Li M, Cao Z, Xia Z, Ajayan PM, Wei B (2014) Anomalous capacitive behaviors of graphene oxide based solid-state supercapacitors. *Nano Lett* 14(4):1938–1943
152. Gao W, Singh N, Song L, Liu Z, Reddy ALM, Ci L, Vajtai R, Zhang Q, Wei B, Ajayan PM (2011) Direct laser writing of micro-supercapacitors on hydrated graphite oxide films. *Nat Nanotechnol* 6(8):496–500

153. Sankar KV, Kalai Selvan R (2015) Improved electrochemical performances of reduced graphene oxide based supercapacitor using redox additive electrolyte. *Carbon* 90:260–273
154. Sun K, Feng E, Peng H, Ma G, Wu Y, Wang H, Lei Z (2015) A simple and high-performance supercapacitor based on nitrogen-doped porous carbon in redox-mediated sodium molybdate electrolyte. *Electrochim Acta* 158:361–367
155. Wang C, Xi Y, Wang M, Zhang C, Wang X, Yang Q, Li W, Hu C, Zhang D (2016) Carbon-modified  $\text{Na}_2\text{Ti}_3\text{O}_7 \cdot 2\text{H}_2\text{O}$  nanobelts as redox active materials for high-performance supercapacitor. *Nano Energy* 28:115–123
156. Dai S, Xu W, Xi Y, Wang M, Gu X, Guo D, Hu C (2016) Charge storage in  $\text{KCu}_7\text{S}_4$  as redox active material for a flexible all-solid-state supercapacitor. *Nano Energy* 19:363–372
157. Vlad A, Singh N, Melinte S, Gohy J-F, Ajayan PM (2016) Carbon redox-polymer-gel hybrid supercapacitors. *Scien Rep* 6(1):22194
158. Mourad E, Coustan L, Lanelongue P, Zigah D, Mehdi A, Vioux A, Freunberger SA, Favier F, Fontaine O (2017) Biredox ionic liquids with solid-like redox density in the liquid state for high-energy supercapacitors. *Nat Mater* 16(4):446–453
159. Gao Z, Liu X, Chang J, Wu D, Xu F, Zhang L, Du W, Jiang K (2017) Graphene incorporated, N doped activated carbon as catalytic electrode in redox active electrolyte mediated supercapacitor. *J Power Sources* 337:25–35
160. Kajdos A, Kvit A, Jones F, Jagiello J, Yushin G (2010) Tailoring the pore alignment for rapid ion transport in microporous carbons. *J Am Chem Soc* 132(10):3252–3253
161. Wang D-W, Li F, Liu M, Lu GQ, Cheng H-M (2008) 3D aperiodic hierarchical porous graphitic carbon material for high-rate electrochemical capacitive energy storage. *Angew Chem Int Ed* 47(2):373–376
162. He N, Yoo S, Meng J, Yildiz O, Bradford PD, Park S, Gao W (2017) Engineering biorefinery residues from loblolly pine for supercapacitor applications. *Carbon* 120:304–312
163. Xie X, Goodell B, Daniel G, Qian Y, Jellison J, Peterson M (2009) Carbonization of wood and nanostructures formed from the cell wall. *Int Biodeterior Biodegradation* 63(7):933–935
164. Nan N (2016) Development of polyvinyl alcohol/wood-derived carbon thin films: influence of processing parameters on mechanical, thermal, and electrical properties. Ph.D., West Virginia University
165. DeVallance DB, Xie X, Wang T, Wang J (2020) Advancements in thermochemical modification of wood for bioenergy and biomaterial applications. In: Mitra M, Nagchaudhuri A (eds) *Practices and perspectives in sustainable bioenergy: a systems thinking approach*. Springer India, pp 207–232
166. Yakaboylu GA, Yumak T, Jiang C, Zondlo JW, Wang J, Sabolsky EM (2019) Preparation of highly porous carbon through slow oxidative torrefaction, pyrolysis, and chemical activation of lignocellulosic biomass for high-performance supercapacitors. *Energy Fuels* 33(9):9309–9329
167. Phiri J, Dou J, Vuorinen T, Gane PAC, Maloney TC (2019) Highly porous willow wood-derived activated carbon for high-performance supercapacitor electrodes. *ACS Omega* 4(19):18108–18117
168. Yakaboylu GA, Jiang C, Yumak T, Zondlo JW, Wang J, Sabolsky EM (2021) Engineered hierarchical porous carbons for supercapacitor applications through chemical pretreatment and activation of biomass precursors. *Renew Energy* 163:276–287
169. Jiang C, Yakaboylu GA, Yumak T, Zondlo JW, Sabolsky EM, Wang J (2020) Activated carbons prepared by indirect and direct  $\text{CO}_2$  activation of lignocellulosic biomass for supercapacitor electrodes. *Renew Energy* 155:38–52
170. Wardrop AB (1971) Occurrence and formation in plants. Sarkanen, KV *Lignins*
171. Xu C, Arancon RAD, Labidi J, Luque R (2014) Lignin depolymerisation strategies: towards valuable chemicals and fuels. *Chem Soc Rev* 43(22):7485–7500
172. Cateto CA, Barreiro MF, Rodrigues AE, Belgacem MN (2009) Optimization study of lignin oxypropylation in view of the preparation of polyurethane rigid foams. *Ind Eng Chem Res* 48(5):2583–2589

173. Zhang T, Li X, Guo L (2017) Initial reactivity of linkages and monomer rings in lignin pyrolysis revealed by ReaxFF molecular dynamics. *Langmuir* 33(42):11646–11657
174. Dorrestijn E, Laarhoven LJ, Arends IW, Mulder P (2000) The occurrence and reactivity of phenoxyl linkages in lignin and low rank coal. *J Anal Appl Pyrol* 54(1):153–192
175. Belgacem MN, Gandini A (2011) Monomers, polymers and composites from renewable resources. Elsevier
176. Gross GG (1977) Biosynthesis of lignin and related monomers. In: The structure, biosynthesis, and degradation of wood. Springer, pp 141–184
177. Adler E (1957) Structural elements of lignin. *Ind Eng Chem* 49(9):1377–1383
178. Windeisen E, Wegener G (2012) 10.15—Lignin as building unit for polymers. In Möller KM (ed) *Polymer science: a comprehensive reference*. Elsevier, pp 255–265
179. Chen Y, Sarkanen S (2003) Macromolecular lignin replication: a mechanistic working hypothesis. *Phytochem Rev* 2(3):235–255
180. Ralph J, Lundquist K, Brunow G, Lu F, Kim H, Schatz PF, Marita JM, Hatfield RD, Ralph SA, Christensen JH, Boerjan W (2004) Lignins: natural polymers from oxidative coupling of 4-hydroxyphenyl-propanoids. *Phytochem Rev* 3(1–2):29–60
181. Adler E (1977) Lignin chemistry—past, present and future. *Wood Sci Technol* 11(3):169–218
182. Feldman D (2002) Lignin and its polyblends—a review. In: Hu TQ (ed) *Chemical modification, properties, and usage of lignin*. Springer, US, pp 81–99
183. Wang J, Manley R, St J, Feldman D (1992) Synthetic polymer-lignin copolymers and blends. *Progr Polym Sci* 17(4):611–646
184. Doherty WO, Mousaviou P, Fellows CM (2011) Value-adding to cellulosic ethanol: lignin polymers. *Ind Crops Prod* 33(2):259–276
185. Meister JJ (2002) Modification of lignin\*. *J Macromol Sci, Part C: Polym Rev* 42(2):235–289
186. Saake B, Lehnen R (2007) Lignin. In: Ullmann's encyclopedia of industrial chemistry. [https://doi.org/10.1002/14356007.a15\\_305.pub3/full](https://doi.org/10.1002/14356007.a15_305.pub3/full)
187. Sixta H, Potthast A, Krottschek AW (2008) Chemical pulping processes: sections 4.1–4.2. In: *Handbook of pulp*, pp 109–229
188. Vishtal AG, Kraslawski A (2011) Challenges in industrial applications of technical lignins. *BioResources* 6(3):3547–3568
189. Gierer J, Lindeberg O, Noren I (1979) Alkaline delignification in the presence of anthraquinone/anthrahydroquinone. *Holzforschung* 33(6):213–214
190. Gierer J (1980) Chemical aspects of kraft pulping. *Wood Sci Technol* 14(4):241–266
191. El Hage R, Brosse N, Chrusciel L, Sanchez C, Sannigrahi P, Ragauskas A (2009) Characterization of milled wood lignin and ethanol organosolv lignin from miscanthus. *Polym Degrad Stab* 94(10):1632–1638
192. Sannigrahi P, Ragauskas AJ, Miller SJ (2009) Lignin structural modifications resulting from ethanol organosolv treatment of loblolly pine. *Energy Fuels* 24(1):683–689
193. Pye EK, Lora JH (1991) The Alcell™ process: a proven alternative to kraft pulping. *Tappi J* 74(3):113–118
194. Stockburger P (1993) An overview of near-commercial and commercial solvent-based pulping processes. Tappi J (USA)
195. Zhang M, Xu Y, Li K (2007) Removal of residual lignin of ethanol-based organosolv pulp by an alkali extraction process. *J Appl Polym Sci* 106(1):630–636
196. Pandolfo AG, Hollenkamp AF (2006) Carbon properties and their role in supercapacitors. *J Power Sources* 157(1):11–27
197. Wang L, Sun F, Gao J, Pi X, Pei T, Qie Z, Zhao G, Qin Y (2018) A novel melt infiltration method promoting porosity development of low-rank coal derived activated carbon as supercapacitor electrode materials. *J Taiwan Inst Chem Eng* 91:588–596
198. Sevilla M, Mokaya R (2014) Energy storage applications of activated carbons: supercapacitors and hydrogen storage. *Energy Environ Sci* 7(4):1250–1280
199. Mehta S, Jha S, Liang H (2020) Lignocellulose materials for supercapacitor and battery electrodes: a review. *Renew Sustain Energy Rev* 134:110345



200. Rosas JM, Berenguer R, Valero-Romero MJ, Rodríguez-Mirasol J, Cordero T (2014) Preparation of different carbon materials by thermochemical conversion of lignin. *Front Mater* 1
201. Rodríguez-Mirasol J, Cordero T, Rodríguez JJ (1993) Activated carbons from carbon dioxide partial gasification of eucalyptus kraft lignin. *Energy Fuels* 7(1):133–138
202. Rodríguez-Mirasol J, Cordero T, Rodríguez JJ (1993) Preparation and characterization of activated carbons from eucalyptus kraft lignin. *Carbon* 31(1):87–95
203. Kijima M, Hirukawa T, Hanawa F, Hata T (2011) Thermal conversion of alkaline lignin and its structured derivatives to porous carbonized materials. *Biores Technol* 102(10):6279–6285
204. Zhang W, Zhao M, Liu R, Wang X, Lin H (2015) Hierarchical porous carbon derived from lignin for high performance supercapacitor. *Colloids Surf, A* 484:518–527
205. Demir M, Tessema T-D, Farghaly AA, Nyankson E, Saraswat SK, Aksoy B, Islamoglu T, Collinson MM, El-Kaderi HM, Gupta RB (2018) Lignin-derived heteroatom-doped porous carbons for supercapacitor and CO<sub>2</sub> capture applications. *Int J Energy Res* 42(8):2686–2700
206. Zhang K, Liu M, Zhang T, Min X, Wang Z, Chai L, Shi Y (2019) High-performance supercapacitor energy storage using a carbon material derived from lignin by bacterial activation before carbonization. *J Mater Chem A* 7(47):26838–26848
207. Hu S, Zhang S, Pan N, Hsieh Y-L (2014) High energy density supercapacitors from lignin derived submicron activated carbon fibers in aqueous electrolytes. *J Power Sources* 270:106–112
208. Poursorkhabi V, Abdelwahab MA, Misra M, Khalil H, Gharabaghi B, Mohanty AK (2020) Processing, carbonization, and characterization of lignin based electrospun carbon fibers: a review. *Front Energy Res* 8(208)
209. Liu J, Wang PH, Li RY (1994) Continuous carbonization of polyacrylonitrile-based oxidized fibers: aspects on mechanical properties and morphological structure. *J Appl Polym Sci* 52(7):945–950
210. Ago M, Borghei M, Haataja JS, Rojas OJ (2016) Mesoporous carbon soft-templated from lignin nanofiber networks: microphase separation boosts supercapacitance in conductive electrodes. *RSC Adv* 6(89):85802–85810
211. Kadla JF, Kubo S, Venditti RA, Gilbert RD, Compere AL, Griffith W (2002) Lignin-based carbon fibers for composite fiber applications. *Carbon* 40(15):2913–2920
212. Braun JL, Holtman KM, Kadla JF (2005) Lignin-based carbon fibers: oxidative thermostabilization of kraft lignin. *Carbon* 43(2):385–394
213. Sudo K, Shimizu K, Nakashima N, Yokoyama A (1993) A new modification method of exploded lignin for the preparation of a carbon fiber precursor. *J Appl Polym Sci* 48(8):1485–1491
214. Kadla JF, Kubo S (2003) Miscibility and hydrogen bonding in blends of poly(ethylene oxide) and kraft lignin. *Macromolecules* 36(20):7803–7811
215. Saha D, Li Y, Bi Z, Chen J, Keum JK, Hensley DK, Grappe HA, Meyer HM, Paranthaman MP, Naskar AK (2014) Studies on supercapacitor electrode material from activated lignin-derived mesoporous carbon. *Langmuir* 30(3):900–910
216. Lai C, Zhou Z, Zhang L, Wang X, Zhou Q, Zhao Y, Wang Y, Wu X-F, Zhu Z, Fong H (2014) Free-standing and mechanically flexible mats consisting of electrospun carbon nanofibers made from a natural product of alkali lignin as binder-free electrodes for high-performance supercapacitors. *J Power Sources* 247:134–141
217. Jayawickramage RAP, Ferraris JP (2019) High performance supercapacitors using lignin based electrospun carbon nanofiber electrodes in ionic liquid electrolytes. *Nanotechnology* 30(15):155402
218. Ho HC, Nguyen NA, Meek KM, Alonso DM, Hakim SH, Naskar AK (2018) A solvent-free synthesis of lignin-derived renewable carbon with tunable porosity for supercapacitor electrodes. *Chemsuschem* 11(17):2953–2959
219. Leguizamón S, Díaz-Orellana KP, Velez J, Thies MC, Roberts ME (2015) High charge-capacity polymer electrodes comprising alkali lignin from the Kraft process. *J Mater Chem A* 3(21):11330–11339

220. Admassie S, Nilsson TY, Inganäs O (2014) Charge storage properties of biopolymer electrodes with (sub)tropical lignins. *Phys Chem Chem Phys* 16(45):24681–24684
221. Mahmood F, Zhang C, Xie Y, Stalla D, Lin J, Wan C (2019) Transforming lignin into porous graphene via direct laser writing for solid-state supercapacitors. *RSC Adv* 9(39):22713–22720
222. Guo N, Li M, Sun X, Wang F, Yang R (2017) Enzymatic hydrolysis lignin derived hierarchical porous carbon for supercapacitors in ionic liquids with high power and energy densities. *Green Chem* 19(11):2595–2602
223. Inagaki M, Konno H, Tanaike O (2010) Carbon materials for electrochemical capacitors. *J Power Sources* 195(24):7880–7903. <https://doi.org/10.1016/j.jpowsour.2010.06.036>
224. Pang J, Zhang W, Zhang J, Cao G, Han M, Yang Y (2017) Facile and sustainable synthesis of sodium lignosulfonate derived hierarchical porous carbons for supercapacitors with high volumetric energy densities. *Green Chem* 19(16):3916–3926
225. Pang J, Zhang W, Zhang H, Zhang J, Zhang H, Cao G, Han M, Yang Y (2018) Sustainable nitrogen-containing hierarchical porous carbon spheres derived from sodium lignosulfonate for high-performance supercapacitors. *Carbon* 132:280–293
226. Sudo K, Shimizu K (1992) A new carbon fiber from lignin. *J Appl Polym Sci* 44(1):127–134
227. Thunga M, Chen K, Grewell D, Kessler MR (2014) Bio-renewable precursor fibers from lignin/poly lactide blends for conversion to carbon fibers. *Carbon* 68:159–166
228. Shen Q, Zhang T, Zhang W-X, Chen S, Mezgebe M (2011) Lignin-based activated carbon fibers and controllable pore size and properties. *J Appl Polym Sci* 121(2):989–994
229. Singh M, Gupta A, Sundriyal S, Jain K, Dhakate SR (2021) Kraft lignin-derived free-standing carbon nanofibers mat for high-performance all-solid-state supercapacitor. *Mater Chem Phys* 264:124454
230. Lei D, Li X-D, Seo M-K, Khil M-S, Kim H-Y, Kim B-S (2017) NiCo<sub>2</sub>O<sub>4</sub> nanostructure-decorated PAN/lignin based carbon nanofiber electrodes with excellent cyclability for flexible hybrid supercapacitors. *Polymer* 132:31–40
231. Ma C, Li Z, Li J, Fan Q, Wu L, Shi J, Song Y (2018) Lignin-based hierarchical porous carbon nanofiber films with superior performance in supercapacitors. *Appl Surf Sci* 456:568–576
232. Fierro V, Torné-Fernández V, Celzard A (2006) Kraft lignin as a precursor for microporous activated carbons prepared by impregnation with ortho-phosphoric acid: synthesis and textural characterisation. *Microporous Mesoporous Mater* 92(1):243–250
233. Gonzalez-Serrano E, Cordero T, Rodríguez-Mirasol J, Rodríguez JJ (1997) Development of porosity upon chemical activation of kraft lignin with ZnCl<sub>2</sub>. *Ind Eng Chem Res* 36(11):4832–4838
234. Elgrishi N, Rountree KJ, McCarthy BD, Rountree ES, Eisenhart TT, Dempsey JL (2018) A practical beginner's guide to cyclic voltammetry. *J Chem Educ* 95(2):197–206
235. Pell WG, Conway BE (2001) Analysis of power limitations at porous supercapacitor electrodes under cyclic voltammetry modulation and dc charge. *J Power Sources* 96(1):57–67
236. Ye Z, Wang F, Jia C, Shao Z (2018) Biomass-based O, N-codoped activated carbon aerogels with ultramicropores for supercapacitors. *J Mater Sci* 53(17):12374–12387
237. Xiang X, Liu E, Li L, Yang Y, Shen H, Huang Z, Tian Y (2011) Activated carbon prepared from polyaniline base by K<sub>2</sub>CO<sub>3</sub> activation for application in supercapacitor electrodes. *J Solid State Electrochem* 15(3):579–585
238. Gong Y, Li D, Fu Q, Pan C (2015) Influence of graphene microstructures on electrochemical performance for supercapacitors. *Progr Nat Sci: Mater Int* 25(5):379–385
239. Liu X, Wang Y, Zhan L, Qiao W, Liang X, Ling L (2011) Effect of oxygen-containing functional groups on the impedance behavior of activated carbon-based electric double-layer capacitors. *J Solid State Electrochem* 15(2):413–419
240. Xiao K, Yang T, Liang J, Rawal A, Liu H, Fang R, Amal R, Xu H, Wang D-W (2021) Nanofluidic voidless electrode for electrochemical capacitance enhancement in gel electrolyte. *Nat Commun* 12(1):5515
241. Xu Y, Tao Y, Zheng X, Ma H, Luo J, Kang F, Yang Q-H (2015) A metal-free supercapacitor electrode material with a record high volumetric capacitance over 800 F cm<sup>-3</sup>. *Adv Mater* 27(48):8082–8087

242. Ma Y, Zhang X, Liang Z, Wang C, Sui Y, Zheng B, Ye Y, Ma W, Zhao Q, Qin C (2020) B/P/N/O co-doped hierarchical porous carbon nanofiber self-standing film with high volumetric and gravimetric capacitance performances for aqueous supercapacitors. *Electrochim Acta* 337:135800
243. Zhang TF, Xia QX, Wan Z, Yun JM, Wang QM, Kim KH (2019) Highly porous carbon nanofoams synthesized from gas-phase plasma for symmetric supercapacitors. *Chem Eng J* 360:1310–1319
244. Jin H, Feng X, Li J, Li M, Xia Y, Yuan Y, Yang C, Dai B, Lin Z, Wang J, Lu J, Wang S (2019) Heteroatom-doped porous carbon materials with unprecedented high volumetric capacitive performance. *Angew Chem* 131(8):2419–2423
245. Balducci A, Belanger D, Brousse T, Long JW, Sugimoto W (2017) Perspective—a guideline for reporting performance metrics with electrochemical capacitors: from electrode materials to full devices. *J Electrochem Soc* 164(7):A1487–A1488
246. Frenkel D, Smit B (2001) *Understanding molecular simulation: from algorithms to applications*. Elsevier
247. Merlet C, Rotenberg B, Madden PA, Taberna P-L, Simon P, Gogotsi Y, Salanne M (2012) On the molecular origin of supercapacitance in nanoporous carbon electrodes. *Nat Mater* 11(4):306–310
248. Péan C, Merlet C, Rotenberg B, Madden PA, Taberna P-L, Daffos B, Salanne M, Simon P (2014) On the dynamics of charging in nanoporous carbon-based supercapacitors. *ACS Nano* 8(2):1576–1583
249. Merlet C, Péan C, Rotenberg B, Madden PA, Simon P, Salanne M (2013) Simulating supercapacitors: can we model electrodes as constant charge surfaces? *J Phys Chem Lett* 4(2):264–268
250. Merlet C, Péan C, Rotenberg B, Madden PA, Daffos B, Taberna P-L, Simon P, Salanne M (2013) Highly confined ions store charge more efficiently in supercapacitors. *Nat Commun* 4(1):2701
251. Pean C, Daffos B, Rotenberg B, Levitz P, Haefele M, Taberna P-L, Simon P, Salanne M (2015) Confinement, desolvation, and electrosorption effects on the diffusion of ions in nanoporous carbon electrodes. *J Am Chem Soc* 137(39):12627–12632
252. Burt R, Breitsprecher K, Daffos B, Taberna P-L, Simon P, Birkett G, Zhao XS, Holm C, Salanne M (2016) Capacitance of nanoporous carbon-based supercapacitors is a trade-off between the concentration and the separability of the ions. *J Phys Chem Lett* 7(19):4015–4021
253. Shim Y, Kim HJ (2010) Nanoporous carbon supercapacitors in an ionic liquid: a computer simulation study. *ACS Nano* 4(4):2345–2355. <https://doi.org/10.1021/nn901916m>
254. Lian C, Jiang D, Liu H, Wu J (2016) A generic model for electric double layers in porous electrodes. *J Phys Chem C* 120(16):8704–8710
255. Yang H, Zhang X, Yang J, Bo Z, Hu M, Yan J, Cen K (2017) Molecular origin of electric double-layer capacitance at multilayer graphene edges. *J Phys Chem Lett* 8(1):153–160
256. Xing L, Vatamanu J, Smith GD, Bedrov D (2012) Nanopatterning of electrode surfaces as a potential route to improve the energy density of electric double-layer capacitors: insight from molecular simulations. *J Phys Chem Lett* 3(9):1124–1129
257. Noh C, Jung Y (2019) Understanding the charging dynamics of an ionic liquid electric double layer capacitor via molecular dynamics simulations. *Phys Chem Chem Phys* 21(13):6790–6800
258. Paek E, Pak AJ, Kweon KE, Hwang GS (2013) On the origin of the enhanced supercapacitor performance of nitrogen-doped graphene. *J Phys Chem C* 117(11):5610–5616
259. Kerisit S, Schwenzler B, Vijayakumar M (2014) Effects of oxygen-containing functional groups on supercapacitor performance. *J Phys Chem Lett* 5(13):2330–2334
260. Bi S, Banda H, Chen M, Niu L, Chen M, Wu T, Wang J, Wang R, Feng J, Chen T, Dincă M, Kornyshev AA, Feng G (2020) Molecular understanding of charge storage and charging dynamics in supercapacitors with MOF electrodes and ionic liquid electrolytes. *Nat Mater* 19(5):552–558

261. Bo Z, Li C, Yang H, Ostrikov K, Yan J, Cen K (2018) Design of supercapacitor electrodes using molecular dynamics simulations. *Nano-Micro Letters* 10(2):33
262. Xu K, Shao H, Lin Z, Merlet C, Feng G, Zhu J, Simon P (2020) Computational insights into charge storage mechanisms of supercapacitors. *Energy Environ Mater* 3(3):235–246

# Chapter 5

## Porous Carbon Materials for Supercapacitor Applications



Manas Mandal, Krishna Chattopadhyay, Amrita Jain,  
and Swapan Kumar Bhattacharya

### 1 Introduction

With environmental consciousness, the advancement of energy conversion and storage has been a great challenge for the fulfillment of the enormous energy demand our modern society. Day-to-day discovery of portable electronics and smart technologies needs further breakthroughs to accomplish high power and energy and definitely long-running energy storage strategies. Recently, electrochemical capacitor, or supercapacitor, or ultracapacitors got tremendous attention toward materials science researchers as it has some unique features like high-power density, moderate energy density, fast charging capacity, and extraordinary cyclic stability [1–4]. Based on their charge storage phenomena, it can be categorized into two types: electrochemical double layer capacitors (EDLCs) and pseudocapacitors [5]. The charge accumulation at the interface of electrode/electrolyte results the capacitance in EDLCs, whereas the fast Faradaic redox reaction is responsible for the capacitance in pseudocapacitor. The transition metal oxides/hydroxides/sulfides and conducting polymers are used as

---

M. Mandal (✉)

Department of Chemistry, Sree Chaitanya College, North 24 Parganas, Habra,  
West Bengal 743268, India  
e-mail: [manasmandal26@gmail.com](mailto:manasmandal26@gmail.com)

M. Mandal · S. K. Bhattacharya (✉)

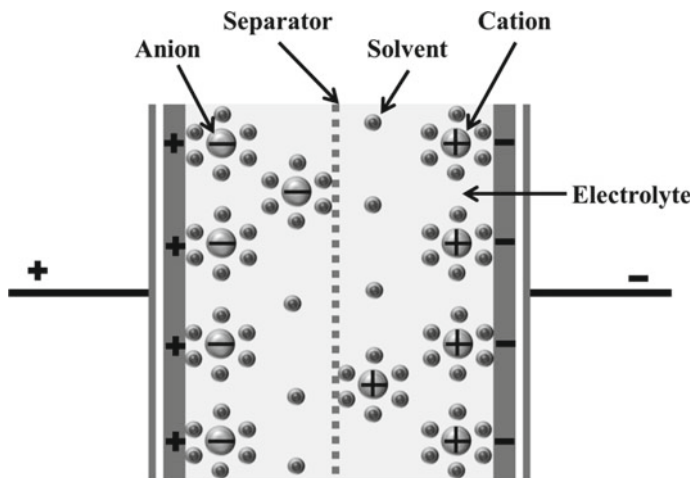
Physical Chemistry Section, Department of Chemistry, Jadavpur University, Kolkata, West  
Bengal 700032, India  
e-mail: [skbhatt7@yahoo.co.in](mailto:skbhatt7@yahoo.co.in)

K. Chattopadhyay

Department of Chemistry, University of Calcutta, 92 APC Road, Kolkata, West Bengal 700009,  
India

A. Jain

Institute of Fundamental Technological Research, Polish Academy of Sciences, Pawińskiego 5B,  
02-106 Warsaw, Poland



**Fig. 1** Schematic representation of carbon supercapacitors

pseudocapacitive materials. On the other hand, carbonaceous materials like activated carbon, graphene, carbon nanotube, aerogel etc., are used in EDLCs. Carbon supercapacitors assemble with two electrodes immersed in an aqueous or non-aqueous electrolyte and an electrolyte ion permeable porous membrane separator (Fig. 1).


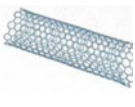
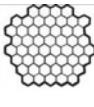
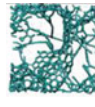
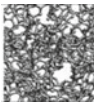
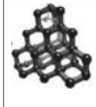
Carbon nanomaterials have been extensively developed in energy storage application because of its different architectures and tunable surface chemistry. Furthermore, it has high electrical conductivity, high electrochemical stability, excellent mechanical properties, and wide operating temperatures [6–8]. However, the most important criterion is the high specific surface area (SSA) of carbon materials for enhanced gravimetric capacitance. The different types of carbon-based materials with high SSA and high conductivity are depicted in Table 1 [9].

Every material has its unique structure and distinctive electrochemical properties. Such as zero- and one-dimensional carbon materials allow fast adsorption/desorption of the electrolyte ions on their surface, indicating high-power density. On contrary, two-dimensional graphene can deliver high charging/discharging rate and volumetric energy density. Porous 3D carbon materials acquire higher surface areas and mesoporous structure, providing higher energy densities [10].

## 2 Synthetic Strategies of Porous Carbon Materials

Porous carbon materials have been synthesized following different methods, viz., carbonization–activation methods, template methods, pyrolysis methods, etc.

**Table 1** Various types of carbon-based materials with their properties

Material	Carbon onions	Carbon nanotubes	Graphene	Activated carbon	Carbide derived carbon	Templated carbon
Dimensionality	0-D	1-D	2-D	3-D	3-D	3-D
Conductivity	High	High	High	Low	Moderate	Low
Volumetric capacitance	Low	Low	Moderate	High	High	Low
Cost	High	High	Moderate	Low	Moderate	High
Structure						

Reprinted with permission from Simon et al. [9]. Copyright 2013 American Chemical Society

## 2.1 Carbonization–Activation Methods

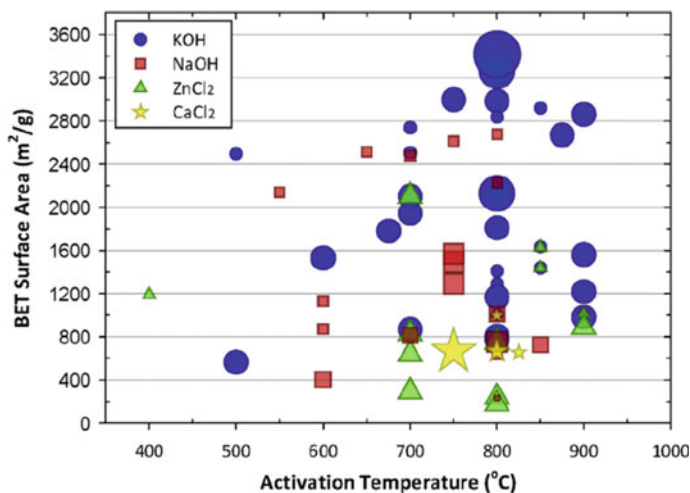
Generally, porous carbon prepared by this method is called activated carbon. The name of this process implies that it involves two different steps, viz., carbonization and activation. Carbonization produces the nonporous carbon material by pyrolysis, whereas the activation methods introduce the pores into the nonporous material chemically or physically forming activated carbon.

### 2.1.1 Carbonization

Carbonization is a method by which a carbonaceous residue is produced by thermal decomposition of organic substances (pyrolysis) under an inert atmosphere. A large number of different kinds of reactions like dehydrogenation, condensation, hydrogen transfer, crosslinking, and isomerization simultaneously occur during this process [11]. These various types of reactions help to release the volatile materials leaving behind the nonporous carbonaceous residue. This residue is also called as coal char or biochar.

### 2.1.2 Activation

In this step, the nonporous carbonaceous residue is treated with activating agents, also known as pore-forming agents or porogens. With activation agents, nonporous residue undergo oxidation reactions to create required pores into it. Based on the activating agents used in activation methods, these are categorized as either chemical or physical activation method [13]. The chemical activation process uses KOH, NaOH, Na<sub>2</sub>CO<sub>3</sub>, K<sub>2</sub>CO<sub>3</sub>, ZnCl<sub>2</sub>, or H<sub>3</sub>PO<sub>4</sub> as activating agents, whereas CO<sub>2</sub>, O<sub>2</sub>,



**Fig. 2** BET surface area vs activation temperatures of porous carbons for different chemical porogens (KOH, NaOH, ZnCl<sub>2</sub>, and CaCl<sub>2</sub>). Reprinted with permission from Gao et al. [12]. Copyright 2018 Elsevier

air, or steam in physical activation. Both the processes have several advantages and disadvantages as well. The chemical activation is comparatively low-temperature process which produces highly meso-porous carbon with high mass of yields and Brunauer–Emmett–Teller (BET) surface area (Fig. 2). On contrary, physical activation requires high activation temperatures with longer time and produces relatively lower yields with small pore sizes and low specific surface area (SSA). In spite of these advantages, physical activation process is more feasible and useful for industrial scale production than chemical activation, as it exhibits low corrosion.

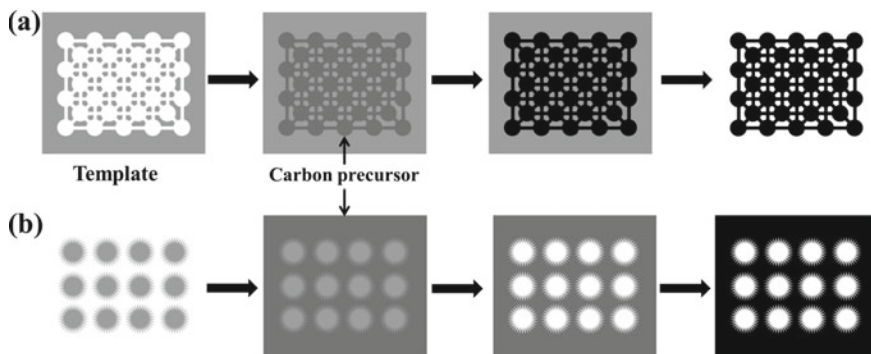
## 2.2 Template Methods

Template methods are well-known approach by which morphological information is transferred from a pre-prepared template to the derived porous carbon.

### 2.2.1 Hard Templates

The hard template method, also known as nanocasting, is an efficient route for the preparation of porous carbons with highly uniform pore structure and pore size distributions. However, this method is costly and laborious as it includes various steps. The important steps involved in this method are (i) synthesis of a hard template with specific morphology, (ii) good contact of the template with carbon sources, (iii)





**Fig. 3** Schematic diagrams of ordered meso-porous carbon preparation using **a** hard template and **b** soft template methods

heating at high temperature under inert conditions, and (iv) acid or alkali etching of the template (Fig. 3a). The extreme stability of the hard templates toward a very high-temperature facilitates the preparation of highly crystalline or sometimes single-crystal materials using this process. Templates with uniformly ordered porous structure can be easily prepared using  $\text{SiO}_2$  [14, 15],  $\text{ZnO}$  [16, 17],  $\text{MgO}$  [18, 19],  $\text{TiO}_2$  [20],  $\text{Al}_2\text{O}_3$  [21, 22] or zeolite [23], etc.

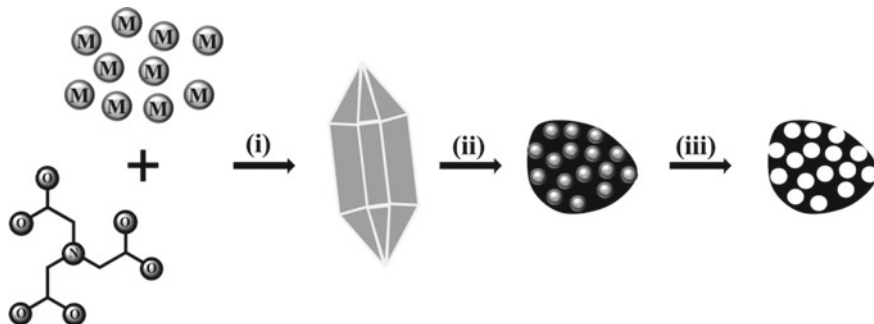
### 2.2.2 Soft Templates

Soft templates do not have solid shapes like hard template. Generally, block copolymers (BCPs) or self-assembly of amphiphilic small molecules are used to prepare soft templates under appropriate condition. In addition of proper solvent, these molecules turn into micelles due to strong interaction forces, such as hydrophilic and hydrophobic interactions [24], hydrogen bonding [25], and electrostatic interactions [26] between them. Then, the micelles blended with carbon precursor result in heterogeneous matrix which produces porous carbon materials during the carbonization (Fig. 3b). The size and architecture of the pores can be tuned by varying the ratio of solvent and micelle. Therefore, a soft template should have the capability to accumulate into nanostructures and supporting the porogens of soft template before the development of carbon skeleton. Dai and coworkers successfully synthesized the ordered meso-porous carbons (OMCs) by soft template technique using micelles of amphiphilic block copolymers for the first time [27].

### 2.2.3 Self-template Methods

In activation methods and hard/soft template methods, a pore generator chemical species, known as porogen, is required. The self-template method uses in situ

self-generated porogens to synthesize the porous carbon without addition of any external porogens. The metal–organic frameworks (MOFs), ethylenediaminetetraacetates (EDTA)-based salts, biomass-based organic salts, etc., are used as self-generated porogens in self-template methods. These materials serve as both a source and a spontaneous template for the final carbon material. Therefore, self-template synthesis of porous carbon includes following steps: (i) precipitation, (ii) pyrolysis, and (iii) washing (Fig. 4). The organic ligands are carbonized to produce the carbon matrix. During washing, the inorganic atoms or particles are washed out to form meso- and macro-pores. J ayaramulu et al. reported two-dimensional nanoporous carbon sheets (NPSs) from rod-shaped potassium-based MOF  $\{K_3[C_6H_3(CO_2)(CO_2H_{0.5})(CO_2H)]_2\}(H_2O)_2$  (denoted as K-MOF). The 2D NPSs were obtained upon two-step carbonization process at 450 °C and 800 °C where K-containing rod-shaped hollow structure and 2D NPSs were formed, respectively. Potassium was removed by etching with 5 wt% HCl followed by washing the product with a water–ethanol mixture for several times [28]. The as-prepared porous sample having a BET surface area of 1192 m<sup>2</sup> g<sup>-1</sup> showed excellent electrochemical performances. The highest specific capacitance for the sample was calculated to be 233 F g<sup>-1</sup> at scan rate of 5 mVs<sup>-1</sup> in 1 M H<sub>2</sub>SO<sub>4</sub> electrolyte with good rate capability. Yu et al. used ethylenediaminetetraacetic acid disodium zinc salt (EDTANa<sub>2</sub>Zn) for the preparation of hierarchical porous carbons (N-doped) by direct pyrolysis. The EDTANa<sub>2</sub>Zn acts as C-precursor, N-source, as well as porogen [29]. Pyrolysis generated nano-ZnO and Na<sub>2</sub>CO<sub>3</sub> act as self-template to form meso-pore in carbon matrix. The sample prepared at 700 °C, having BET surface area of 1368 m<sup>2</sup> g<sup>-1</sup> with high N-content showed a maximum specific capacitance of 275 F g<sup>-1</sup> with excellent rate capability in 6 M KOH electrolyte.



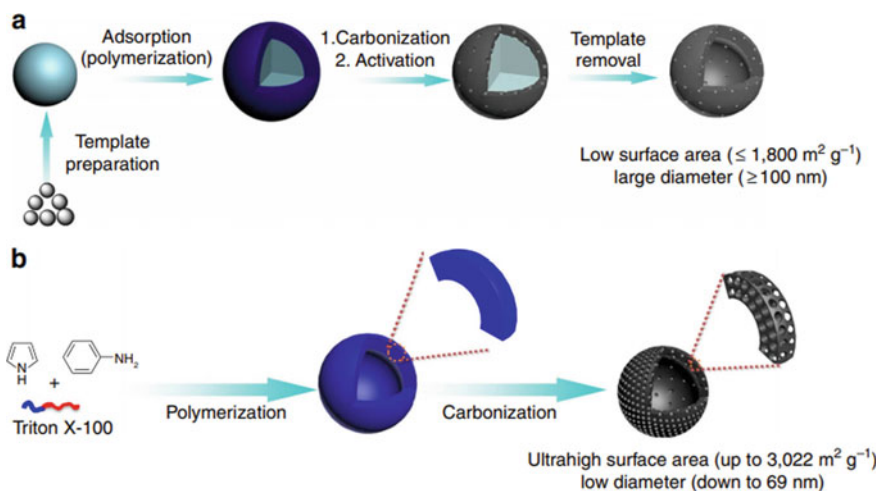
**Fig. 4** Schematic diagrams for the self-template synthesis of porous carbon including precipitation (i) pyrolysis, (ii) washing, and (iii) steps

## 2.3 Pyrolysis Methods

Although, the porous carbon with uniform pore size distribution and high specific surface area can be prepared using traditional carbonization–activation methods and templating methods, the porogens or the template need to be removed completely (Fig. 5). In that context, pyrolysis methods are more useful. During pyrolysis method, organic sources are decomposed and release gases like  $\text{CO}_2$ ,  $\text{H}_2\text{O}$ ,  $\text{NH}_2$ , and  $\text{CO}$ . These produced gases act as porogens. By optimizing the pyrolysis parameters, like heat rate, temperature, and time of carbonization, the pore size distribution and specific surface area of the porous carbon can be fine-tuned. Xu et al. prepared distinct hollow carbon nanospheres with surface area of  $3022 \text{ m}^2 \text{ g}^{-1}$  following a simple carbonization of polyaniline-co-polypyrrole (PACP) hollow spheres [30]. The as-prepared materials achieved the maximum specific capacitance of  $203 \text{ F g}^{-1}$  at specific current of  $0.1 \text{ A g}^{-1}$ .

## 3 Typical Features of Carbon Materials for Supercapacitors Electrode

The porous carbon materials are an emerging electrode of supercapacitor because of its exceptional chemical and physical properties, such as high SSA with controlled



**Fig. 5** Schematic illustration for the preparation of conventional hollow carbon nanosphere by **a** templating method and **b** by pyrolysis method. Reprinted with permission from Xu et al. [30]. Copyright 2015 Springer Nature

pore structure, high electrical conductivity, good corrosion resistance, easy processability and compatibility in composite, high-temperature stability, and relatively low cost [31].

### 3.1 Large Surface Area

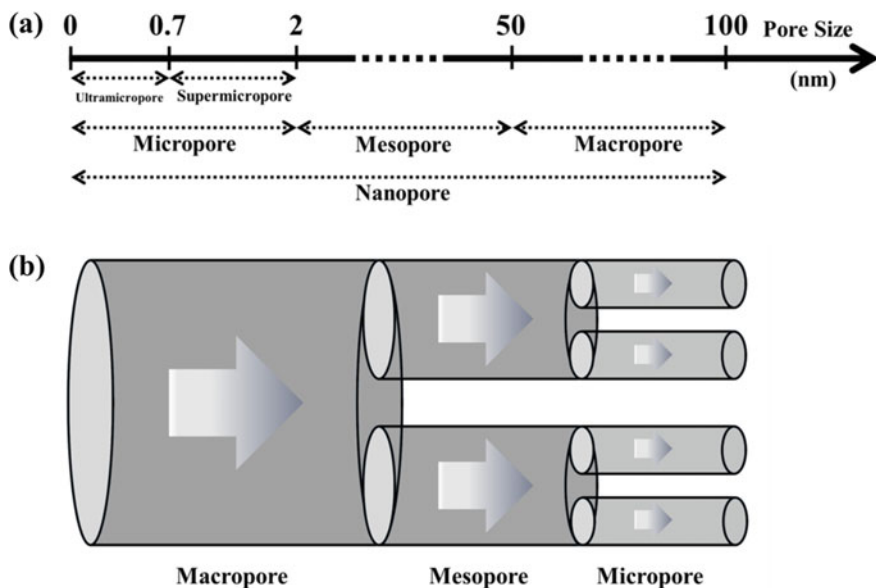
Different types of porous carbon materials have been developed as promising active materials for supercapacitor application. Ordered meso-porous carbons (OMCs) with a precise range of pore sizes have comparatively large SSA ( $\sim 1000 \text{ m}^2 \text{ g}^{-1}$ ) that provides the double layer capacitance. Carbon aerogels having surface area ranging from 500 to 800  $\text{m}^2 \text{ g}^{-1}$ , with comparatively small pore sizes is unfavorable for electrolyte ion diffusion. On contrary, macro-porous carbon materials have relatively lower surface area ( $\sim 600 \text{ m}^2 \text{ g}^{-1}$ ). Among all types of porous carbons, mixed porous carbon like activated carbon with micro-, meso-, and macro-pores show the largest SSA ( $\sim 3000 \text{ m}^2 \text{ g}^{-1}$ ) and high electrochemical activity in terms of specific capacitance, energy, and power thereof [32].

### 3.2 Hierarchical Porosity

Hierarchical porosity implies the presence of multi-scale pores having different sizes in a porous system. The pores with the diameter of smaller than 100 nm are known as nanopores. Based on the width or diameter ( $d_{\text{pore}}$ ) of pores, the International Union of Pure and Applied Chemistry (IUPAC) classified these nanopores into following (Fig. 6a) [33]:

- (i) Micro-pore: The pore having diameters less than 2 nm ( $d_{\text{pore}} < 2 \text{ nm}$ ). This type of pores is again classified into two types: ultra micro-pore ( $d_{\text{pore}} < 0.7 \text{ nm}$ ) and super micro-pore ( $0.7 \text{ nm} < d_{\text{pore}} < 2 \text{ nm}$ ).
- (ii) Meso-pore: The pore having diameters greater than 2 nm and lesser than 50 nm ( $2 \text{ nm} < d_{\text{pore}} < 50 \text{ nm}$ ).
- (iii) Macro-pore: The pore having diameters greater than 50 nm and lesser than 100 nm ( $50 \text{ nm} < d_{\text{pore}} < 100 \text{ nm}$ ).

In hierarchical porous carbons (HPCs), not only the presence of multi-scale pores but also an interconnection between them is an essential criteria to form a hierarchical network. These interconnected pores are beneficial for the infiltration of the electrolytes [34]. So that it can provide high electrochemically accessible surface area and decrease the ion diffusion path. An ion diffusion path in the hierarchical porous material is schematically represented in Fig. 6b, where the electrolyte ions enter the macro-pore first and then goes into the smaller pores which are directly interconnected. In an electrochemical capacitor, the macro-, meso- and micro-pores

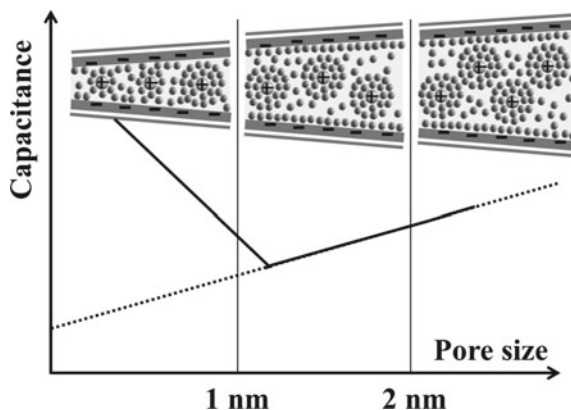


**Fig. 6** **a** Different kinds of nanopores based on IUPAC scale. **b** Schematic diagram of an ion diffusion path in a hierarchical porous material

play important roles individually and contribute to the total capacitance (Fig. 7). The micro-pores provide large surface area which acts as the main sites for the charge accumulation, whereas macro-pores and meso-pores serve as the ion-buffering reservoirs and provide channels for the rapid ion transport, respectively [34–36]. The macro-pores acting as the ion-buffering reservoirs store the electrolyte ions for meso-/micro-pores, and therefore, an easy and rapid ion transfer occur by reducing the effective diffusion pathways and enhance the electrochemical performance. Generally, the fast ion transport provides high specific power and the rate capability of the supercapacitor electrode. The time for the ion transport ( $\tau$ ) greatly depends on its diffusion coefficient ( $D$ ) and transport path ( $L$ ) according to the equation:  $\tau = L^2/D$ . Therefore, the superior ion transport kinetics can be achieved by reducing the ion transport path and enhancing the ion diffusion coefficient [37].

However, the pore size has the important role in determining the capacitance for porous carbon supercapacitor. If the size of the pore is bigger ( $\sim$ doubled) than the diameters of the hydrated electrolyte ions, also termed as solvated ions or solvation shell, is beneficial for higher capacitance. Because the high pore size allows the formation of double layer within the pore. The value of the capacitance decreases with decreasing the pore size. But when the size of the pore is much smaller ( $\sim$ 1 nm) than the solvated ions, capacitance is sharply increased. This is due to the distortion of the solvated ions in the smaller pore resulting in closer approach of the ion center to the active surface area of the electrode [38]. The research by Raymundo-Piñero et al. supports the above fact, and they showed that an ample size of pore is more significant

**Fig. 7** General trend of the capacitance value with pore size of the porous carbon



to achieve high capacitance in different types of electrolyte. They reported that the effective optimal pore size is  $\sim 0.7$  nm and  $\sim 0.8$  nm in case of aqueous (KOH) and organic (tetraethylammonium tetrafluoroborate, TEABF<sub>4</sub> in acetonitrile) electrolyte, respectively [39].

### 3.3 Electrochemical Performance in Different Electrolytes

Porous carbon electrode has excellent electrochemical stability in different types of electrolytes with wide range of operating potential. The main factor on which the operating potential window depends is electrolyte. As the decomposition potential of water is 1.23 V, the supercapacitor devices can be operated up to 1.2 V in traditional aqueous electrolyte like KOH, H<sub>2</sub>SO<sub>4</sub>. However, the neutral aqueous electrolyte such as Na<sub>2</sub>SO<sub>4</sub> provides the maximum operating voltage up to 1.9 V [40]. The common organic electrolytes such as TEABF<sub>4</sub> in acetonitrile or polycarbonate are suitable for the operating voltage as high as 3 V [41]. The different types of electrolytes affect the electrochemical performances of the porous carbon supercapacitor differently. Chen et al. investigated the electrochemical performances of biomass-derived porous carbon in different aqueous-based such as KOH, H<sub>2</sub>SO<sub>4</sub>, Na<sub>2</sub>SO<sub>4</sub>, and organic electrolyte, tetraethylammonium tetrafluoroborate in propylene carbonate (Et<sub>4</sub>NBF<sub>4</sub>/PC) [42]. Due to smaller size of solvated H<sup>+</sup> and K<sup>+</sup> ions, the porous carbon showed high capacitance in H<sub>2</sub>SO<sub>4</sub> and KOH electrolyte. Although the bigger size of Et<sub>4</sub>N<sup>+</sup> and BF<sub>4</sub><sup>-</sup> is not suitable for high capacitance, but it shows high rate capability due to shorter ion diffusion path. The higher operating potential of Et<sub>4</sub>NBF<sub>4</sub>/PC and Na<sub>2</sub>SO<sub>4</sub> helps to achieve high energy density according to the formula  $E = 1/2CV^2$ . Another class of electrolyte, i.e., ionic liquids has drawn great interest as a promising electrolyte because of their some unique properties such as high thermal stability, non-flammability, low vapor pressure, intrinsic ionic conductivity, and excellent operational voltage greater than 3 V [43]. The electrochemical

**Table 2** Electrochemical performances of the porous carbon supercapacitor in various electrolytes

Electrode	Electrolyte	Potential	Capacitance	References
Hierarchical PC	6 M KOH	1.0 V	338.5 F g <sup>-1</sup> at 1 A g <sup>-1</sup>	[44]
N, O, P-doped PC	1 M Na <sub>2</sub> SO <sub>4</sub>	1.9 V	69.8 F g <sup>-1</sup> at 0.1 A g <sup>-1</sup>	[40]
PC network	1 M Et <sub>4</sub> NBF <sub>4</sub> in acetonitrile	2.7 V	208 F g <sup>-1</sup> at 0.75 A g <sup>-1</sup>	[45]
Hierarchical PC	1 M H <sub>2</sub> SO <sub>4</sub>	1.0 V	266 F g <sup>-1</sup>	[42]
	1 M Na <sub>2</sub> SO <sub>4</sub>	1.6 V	211 F g <sup>-1</sup>	
	6 M KOH	1.0 V	309 F g <sup>-1</sup>	
	1 M Et <sub>4</sub> NBF <sub>4</sub> /PC	2.5 V	168 F g <sup>-1</sup> at 0.5 A g <sup>-1</sup>	
Meso-porous graphene	EMIMTFSI	4.0 V	244 F g <sup>-1</sup> at 5 A g <sup>-1</sup>	[46]
Micro-pore-rich activated carbon	EMIMFSI	3.5 V	120 F g <sup>-1</sup> at 0.5 A g <sup>-1</sup>	[47]
Hierarchical PC	EMIMBF <sub>4</sub>	3.8 V	217 F g <sup>-1</sup> at 0.1 A g <sup>-1</sup>	[48]

TEABF<sub>4</sub>/PC: Tetraethylammonium tetrafluoroborate in propylene carbonate; EMIMTFSI: 1-ethyl-3-methylimidazolium bis(trifluoromethylsulfonyl)imide; EMI-FSI: 1-ethyl-3-methylimidazolium bis(fluorosulfonyl)imide; EMIMBF<sub>4</sub>: 1-ethyl-3-methylimidazolium tetrafluoroborate; PC: Porous carbon

performances of different porous carbon supercapacitor in various electrolytes are depicted in Table 2.

### 3.4 Different Kinds of Morphology

High-surface area is really essential for supercapacitor electrodes, but to get maximum capacitance, whole surface area should be accessible to the electrolyte ions. But practically, it is not achievable. To increase the surface accessibility, the surface topography can be modified with abundant adsorbing sites. Therefore, significant research efforts have been devoted to engineering diverse carbon morphologies with controlled surface topography and interior texture.

#### 3.4.1 One-Dimensional Porous Carbon Electrode

Due to the unique anisotropic properties, one-dimensional (1D) porous carbon materials such as carbon nanofibers, carbon nanorods carbon nanowires, and carbon nanobelts have many advantages over the other nanostructures. These 1D nanostructures can deliver fast axial electron transport and provide short ion diffusion path, high ion-accessible specific surface area and excellent mechanical strength. The contact resistance is greatly reduced due to the more exposed edges which

behave as contact points. Furthermore, surface functionalization can be easily done chemically to improve the electrochemical performance.

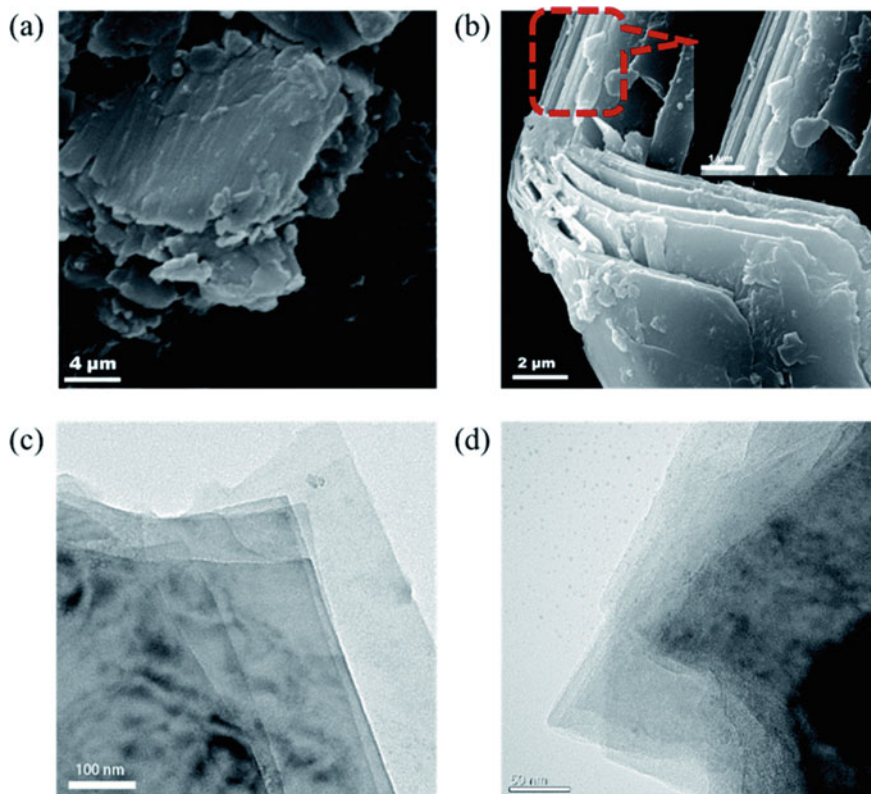
Na et al. fabricated nitrogen and fluorine doped carbon nanofibers by a simple hydrothermal treatment followed by carbonization and vacuum plasma process [49]. The as-prepared material exhibited meso-porous nature with highest BET specific surface area of  $596.1 \text{ m}^2 \text{ g}^{-1}$ . It also exhibited maximum specific capacitance of  $252.6 \text{ F g}^{-1}$  at  $0.5 \text{ A g}^{-1}$  in  $1 \text{ M H}_2\text{SO}_4$  electrolyte. Cai et al. reported inter-bonded carbon nanofibers for high-performance supercapacitor. They first prepared cellulose nanofibers by electrospinning method using cellulose acetate solution. In second step, the desired porous materials were synthesized by hydrothermal treatment followed by carbonization process. The as-prepared material exhibited maximum specific capacitance of  $241.4 \text{ F g}^{-1}$  at specific current of  $1 \text{ A g}^{-1}$  with excellent cyclic stability [50]. Using lignin as precursor, Berenguer et al. fabricated flexible interconnected porous carbon fibers with high SSA and excellent conductivity. The desired electrode material was prepared by electrospinning method followed by thermostabilization and carbonization treatments. The interconnected nature of the fibers helps to increase the charge transfer process and electrochemical performances as well [51]. Micro- and meso-porous 1D carbon nanobelts with high SSA up to  $1208 \text{ m}^2 \text{ g}^{-1}$  were synthesized by “stripping and cutting” strategy from tofu using a molten salt-assisted technique by Ouyang and coworkers. This material achieved high specific capacitance of  $262 \text{ F g}^{-1}$  at specific current of  $0.5 \text{ A g}^{-1}$  with high cyclic stability [52]. Jin et al. fabricated wood-based fibers by melt-spinning process and then finally prepared the activated carbon fibers by carbonization-activation at  $850 \text{ }^\circ\text{C}$  under steam–nitrogen mixture [53]. Comparatively, longer activation time produces highly meso-porous structure, which is easily reachable by the electrolyte ions up to the inner micropores. The as-prepared materials exhibited maximum capacitance of  $280 \text{ F g}^{-1}$  at  $0.5 \text{ A g}^{-1}$  with excellent stability.

### 3.4.2 Two-Dimensional Porous Carbon Electrode

Two-dimensional (2D) porous carbon materials are excellent in energy storage which can provide high conductivity due to their  $sp^2$  hybridized nature, high SSA with high electrochemically active sites.

Fan et al. reported 2D porous carbon nanosheets supercapacitor with superior rate performance. They prepared the porous material following a combined method of intercalation, thermal treatment, and potassium hydroxide activation using montmorillonite as nano-template and gelatin as carbon source. The porous nature of the nanosheets reduces the ion transport path and enhances the pore accessibility toward electrolyte ions and thus achieved excellent rate performance, with a high specific capacitance of  $246 \text{ F g}^{-1}$  at a ultrahigh specific current of  $100 \text{ A g}^{-1}$  [54]. Xu and coworkers synthesized layered 2D porous carbon materials (Fig. 8) by a wet-chemical synthesis method using Sonogashira–Hagihara cross-coupling polycondensation. The BET surface specific area of the as-prepared material was measured





**Fig. 8** SEM (a, b) and TEM images (c, d) of **2D porous carbon material** at different magnifications. Reprinted with permission from Xu et al. [55]. Copyright 2021 Royal Society of Chemistry

to be  $575 \text{ m}^2 \text{ g}^{-1}$  with hierarchical pore structure. The electrode material achieved high specific capacitance of  $378 \text{ F g}^{-1}$  at the specific current of  $0.1 \text{ A g}^{-1}$  [55].

### 3.4.3 Three-Dimensional Porous Carbon Electrode

Three-dimensional ordered porous carbon (3D-OPC) has shown remarkable potential in energy storage and conversion applications due to its some unique properties like large SSA with uniform pore structure, high electronic and ionic conductivity, and low cost.

Zhao et al. reported three-dimensional hierarchical ordered porous carbons (3D HOPCs) using templating technique. They used nano-array of silica ( $\text{SiO}_2$ ) sphere, triblock copolymer P123 and sucrose as hard template, soft template, and carbon source, respectively. The 3D HOPCs having SSA of  $1182 \text{ m}^2 \text{ g}^{-1}$  achieved maximum specific capacitance of  $247 \text{ F g}^{-1}$  at specific current of  $1 \text{ A g}^{-1}$  with excellent rate

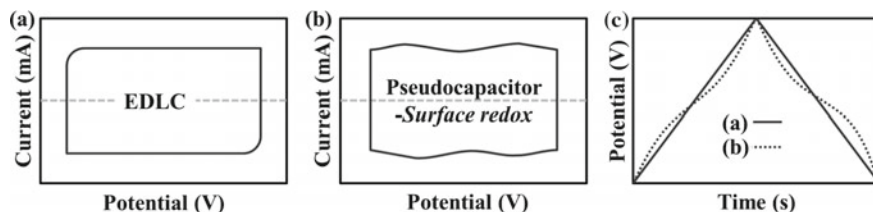
performance. Moreover, the 3D HOPCs supercapacitors showed high percentage (91%) of capacitance retentions after consecutive 10,000 cycles [56]. Li et al. prepared three-dimensional graphene-like carbon nanosheet network using a surfactant (Tween-20) as C source. The as-prepared material acquired hierarchical porous structure with a SSA of 2017.3 m<sup>2</sup> g<sup>-1</sup> [57]. It exhibited ideal capacitive behavior with maximum specific capacitance of 316.8 F g<sup>-1</sup> at a specific current of 1 A g<sup>-1</sup> in 1 M KOH electrolyte.

### 3.5 Electrochemical Characteristics of Porous Carbon Supercapacitors

Generally, supercapacitor stores charge in two ways: (i) via Faradaic fast electron transfer or/and (ii) via non-Faradaic charge storage mechanism. However, each type of supercapacitor can be identified from their electrochemical characteristics in terms of cyclic voltammograms (CVs) and galvanostatic charge/discharge (GCD) curves [58]. In general, a pure porous carbon electrode shows electrical double layer capacitive behavior giving rectangular CV curve (Fig. 9a) and a triangular-shaped GCD curve indicating linear voltage response (Fig. 9c). Usually, EDLCs exhibit the capacitance which is potential-independent and so is the obtained current in CV plot. However, surface functional groups/doping atoms on the carbon can add pseudocapacitance and therefore deviations from its ideal electrochemical signatures in terms of CV curve (Fig. 9b) and GCD curve (Fig. 9c) occur.

#### 3.5.1 Capacitance of Porous Carbon Supercapacitor

There are many ways by which capacitance of a supercapacitor can be expressed like specific or gravimetric capacitance, volumetric capacitance, and areal capacitance. The gravimetric capacitance which depends upon the mass of the active material is usually expressed in Farads per gram (F g<sup>-1</sup>), whereas the areal capacitance depends upon the foot print area, and the capacitance values are expressed in Farads per square centimeter (F cm<sup>-2</sup>). Furthermore, the volumetric capacitance is calculated



**Fig. 9** Schematic CV curve of **a** EDLC, **b** pseudocapacitor, and **c** corresponding galvanostatic charge–discharge curves

per volume, and the values are indicated in  $\text{F cm}^{-3}$ . Depending upon the application and necessity, the values are expressed differently, but gravimetric and areal capacitances are the two mostly used units to express capacitance of a device. The calculation of the capacitance also depends upon the type of working electrode used. There are certain scenarios where the calculation of areal capacitance can be difficult, for example, when metal foams are used as substrate and also for porous materials. On the other hand, gravimetric capacitance requires the exact mass of the electrode material used during the capacitance calculation. Though both the techniques are not free from errors, each technique has their own set of advantages and disadvantages when it comes to design and structure of the working electrode.

The electrochemical performance in terms of gravimetric capacitance of the porous carbon materials can be improved by increasing the SSA or the ample pore size. However, the volumetric capacitance is limited due to low bulk density of porous carbon [59]. But it is important to have the high volumetric capacitance for the practical applications. Therefore, doping with heavier heteroatoms is a highly effective method for the enhancement of the density of the porous carbon which leads to enhanced volumetric capacitance (Table 3).

## 4 Understanding of Charge Storage Mechanisms in Porous Carbon

### 4.1 *Electrochemical Double Layer Model Using 2D Electrode Materials*

The first electrochemical double layer model (EDL) was given by Helmholtz [72], and in his model, he explained the phenomenon of the charge separation which takes place at the interface of electrode–electrolyte, assuming that the surface of the electrode is planar. Helmholtz model is picturized in Fig. 10a, and from the figure, it can be seen that the charges those are accumulated at the surface of the electrode are counterbalanced by the electrostatic absorption with the ions of electrolyte which results in the formation of oppositely charged two-layers at the interface. Concept of this study was very similar to the traditional parallel plate capacitors, and therefore, the capacitance of Helmholtz layer is given by using Eq. 1:

$$\frac{C}{A} = \frac{\epsilon_r \epsilon_0}{d} \quad (1)$$

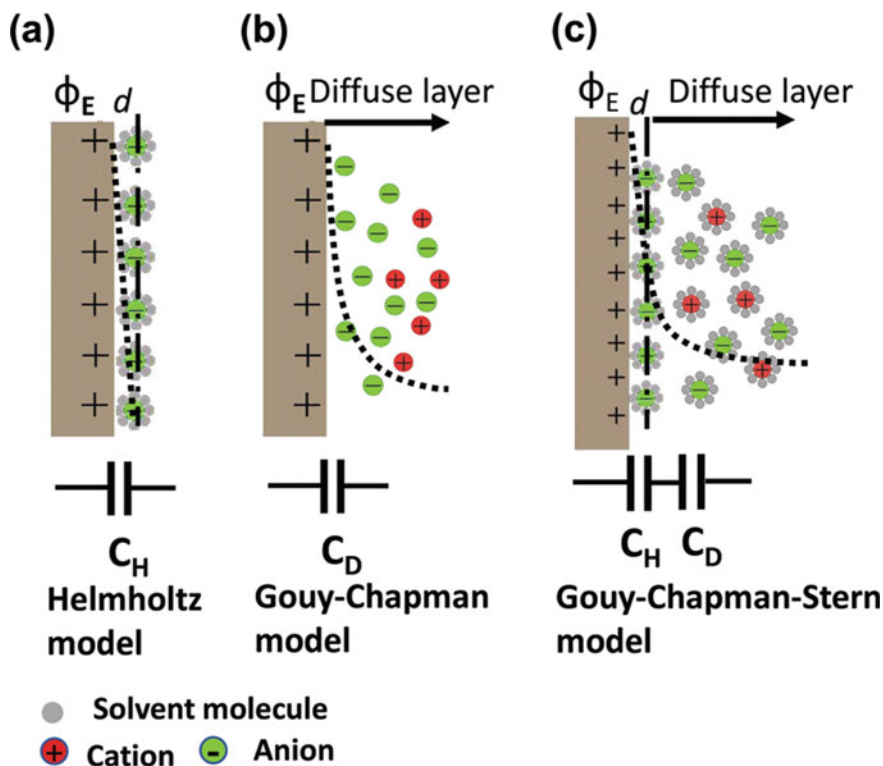
where,  $\epsilon_0$  ( $8.85 \times 10^{-12} \text{ F m}^{-1}$ ) is the vacuum permittivity,  $\epsilon_r$  is the dielectric constant of the electrolyte material which is dimensionless,  $d$  (m) is the average distance between the conductive layers, and  $A$  ( $\text{m}^2$ ) is the surface area of the electrode which is accessible.

**Table 3** Comparison between the gravimetric and volumetric capacitances of reported porous carbon materials

Electrode	Electrolyte	Gravimetric capacitance	Volumetric capacitance	Specific current/scan rate	Reference
N-doped PC nanosheets	6 M KOH	305 F g <sup>-1</sup>	287 F cm <sup>-3</sup>	2 mV s <sup>-1</sup>	[60]
P, N-doped PC	1 M H <sub>2</sub> SO <sub>4</sub>	205.7 F g <sup>-1</sup>	261 F cm <sup>-3</sup>	0.5 A g <sup>-1</sup>	[61]
PC	6 M KOH 1.5 M Et <sub>4</sub> NBF <sub>4</sub> /AN	271 F g <sup>-1</sup> 156 F g <sup>-1</sup>	252 F cm <sup>-3</sup> 145 F cm <sup>-3</sup>	2 mV s <sup>-1</sup>	[62]
Micro-porous carbon	1 M H <sub>2</sub> SO <sub>4</sub>	198 F g <sup>-1</sup>	180 F cm <sup>-3</sup>	2 mV s <sup>-1</sup>	[63]
PC	6 M KOH	262 F g <sup>-1</sup>	214 F cm <sup>-3</sup>	0.05 A g <sup>-1</sup>	[64]
High density porous graphene macroform	6 M KOH	238 F g <sup>-1</sup>	376 F cm <sup>-3</sup>	0.1 A g <sup>-1</sup>	[65]
N, P, S-doped hierarchically PC Spheres	6 M KOH	274 F g <sup>-1</sup>	219 F cm <sup>-3</sup>	0.5 A g <sup>-1</sup>	[66]
N, P, O-doped PC spheres	6 M KOH 0.5 M H <sub>2</sub> SO <sub>4</sub>	356.9 F g <sup>-1</sup> 434.7 F g <sup>-1</sup>	760 F cm <sup>-3</sup> 925 F cm <sup>-3</sup>	1 A g <sup>-1</sup> 0.1 A g <sup>-1</sup>	[67]
N, S-doped hierarchical PC	6 M KOH	358.0 F g <sup>-1</sup>	243.4 F cm <sup>-3</sup>	0.5 A g <sup>-1</sup>	[68]
N-doped hierarchical PC	1 M H <sub>2</sub> SO <sub>4</sub>	242 F g <sup>-1</sup>	306 F cm <sup>-3</sup>	0.5 A g <sup>-1</sup>	[69]
Hierarchical pomegranate-like PC	4 M H <sub>2</sub> SO <sub>4</sub>	398 F g <sup>-1</sup>	278.6 F cm <sup>-3</sup>	0.5 A g <sup>-1</sup>	[70]
F, N-doped PC nanosheets	1 M H <sub>2</sub> SO <sub>4</sub>	266 F g <sup>-1</sup>	255 F cm <sup>-3</sup>	1 A g <sup>-1</sup>	[71]

Et<sub>4</sub>NBF<sub>4</sub>/AN: Tetraethylammonium tetrafluoroborate in acetonitrile; PC: Porous carbon

Depending on the electrolyte used, the value of the dielectric constant  $\epsilon_r$  and thickness ( $d$ ) of the Helmholtz layer is used to normalize the areal capacitance (per m<sup>2</sup>) of the Helmholtz layer ( $C_H$ ). For example, the dielectric constant value of water is around 78 [73], and for most of the solvents used for EDC application, this values lies in between 1 and 100 at room temperature [73–75]. Usually, this value is not so important at sub-nanometer scale; even sometimes, it is smaller than that of bulk electrolyte [73]. In the Helmholtz model, linear potential drop taking place between Helmholtz layer is also discussed, however, the charges which are in excess at the surface of the electrode are usually not completely compensated by the Helmholtz layer, especially when the concentration of solution is not so high [74]. Moreover, it is difficult to have a single stable compact layer from counter ion layer from electrolyte as ions in the electrolyte are always in movement because of thermal



**Fig. 10** Schematic diagram of electrochemical double layer model: **a** Helmholtz model, **b** Gouy-Chapman model, and **c** Gouy-Chapman-Stern model. Reprinted with permission from Shao et al. [7]. Copyright 2020 Royal Society of Chemistry

fluctuation. Further improvement in this model was done by Gouy-Chapman [76, 77]; in their model, they have introduced a new layer called as diffused layer between the electrode and the bulk electrolyte, taking into consideration of the thermal fluctuation as per the Poisson-Boltzmann equation [1]. The Gouy-Chapman model was presented in Fig. 10b. The distribution of ions on the diffuse layer highly depends on the distance because of the electrostatic attractions which decreases from the surface of the electrode to the bulk of the electrolyte. In case of monovalent electrolytes, the average thickness of the so-called diffuse layer also called as Debye length;  $\lambda_D$  is given as

$$\lambda_D = \sqrt{\frac{\varepsilon_r \varepsilon_0 RT}{2(ZF)^2 C_0}} \quad (2)$$

where  $\varepsilon_0$  is the vacuum dielectric constant ( $F m^{-1}$ ) and  $\varepsilon_r$  is the relative permittivity of the electrolyte.  $R$  ( $J mol^{-1}$ ) is the ideal gas constant,  $T$  (K) is the absolute

temperature,  $F$  ( $\text{C mol}^{-1}$ ) is the Faraday constant, and  $C_0$  ( $\text{mol m}^{-3}$ ) is the bulk electrolyte concentration. Diffuse layer capacitance  $C_D$  can be calculated from the Poisson-Boltzmann equation which can be written as

$$C_D = \frac{\varepsilon_r \varepsilon_0}{\lambda_D} \cosh\left(\frac{zF\phi}{2RT}\right) \quad (3)$$

where  $\phi$  (V) is the electrical potential,  $F$  ( $\text{C mol}^{-1}$ ) is the Faraday's constant,  $R$  ( $\text{J mol}^{-1}$ ) is the ideal gas constant,  $T$  (K) is the temperature, and  $\varepsilon_0$  and  $\varepsilon_r$  are the vacuum and relative dielectric constant ( $\text{F m}^{-1}$ ). As per Eq. (3), differential capacitance  $C_D$  is not considered as a constant, instead, this model suggested a "U" shape of the differential capacitance with respect to the potential of the electrode, which is in-line with the experimental results, obtained using NAF solutions with Hg in low concentration [78]. Also the capacitance which was experimentally measured with liquid electrolytes was far below from the prediction from the model [79]. The main shortcoming of this model was to consider that point charges can virtually reach to the surface at zero distance which in turn leads to the infinite value of capacitance. To fix these issues, Stern improvised the model of Gouy-Chapman by taking into consideration the real size of ions as a result of which an additional compact layer called as Stern layer was created which is in series with diffuse layer, this arrangement can be seen from Fig. 10c [80]. This compact layer (Stern layer) is very much similar to Helmholtz layer from the point of physics, having thickness of  $x_H$  (m). The electrochemical double layer capacitance from this model is given by the following equation:

$$\frac{1}{C_{DL}} = \frac{1}{C_H} + \frac{1}{C_D} = \frac{X_H}{\varepsilon_0 \varepsilon_r} + \frac{\lambda_D}{\varepsilon_0 \varepsilon_r \cosh\left(\frac{zF\phi}{2RT}\right)} \quad (4)$$

where  $C_H$  is the capacitance of Stern (Helmholtz) layer and  $C_D$  is the capacitance of diffuse layer, these capacitance are measured in  $\text{F m}^{-2}$ . Overall electrochemical double layer capacitance is calculated by calculating the smallest capacitance obtained between  $C_H$  and  $C_D$ . In case of highly concentrated electrolytes, thickness of the diffuse layer drops to zero, so the Helmholtz capacitance is the only one to be considered. For sure, Gouy-Chapman-Stern model was a milestone that predicted a more realistic gross feature of the EDL, and the theoretical observations were close to experimental results. But this model also suffers from some limitations, like this model has not considered the ion-ion correlation effects, which are very important especially in solvent-free ionic liquid-based electrolyte systems [74, 81]. Similarly, considering a linear potential drop within the compact layer was inappropriate in high electrode polarization with high concentration electrolytes [74, 82]. Whatsoever, the Gouy-Chapman-Stern model has provided a constructive and well predicted interpretation of the electrochemical double layer that has certainly helped us in developing EDLC field from last few decades.

## 4.2 Capacitance in Nanoporous Carbon-Derived Electrodes

There are many factors which decide the overall electrochemical performance of nanoporous carbon-derived EDLC electrodes, like electrical conductivity, presence of the surface groups, and the most important are the BET specific surface area (SSA), pore size, and pore size distribution. Though most of the carbon materials possess high conductivity because they have high density of electronic state at Fermi level, but still there exist some carbon materials which have semiconducting properties like SWCNTs which has specific diameter and also specific helicity or bilayer graphene [83, 84]. Because of this semiconducting nature, the drop of the current near potential of zero charge is usually seen in a cyclic voltammogram curve (CV), and because of this, a CV which is closed to butterfly shape is obtained in a three-electrode system, and a trapezoid-shaped CV is seen in a two-electrode system [73]. In general, the capacitance value of carbon-based electrode in electrochemical double layer capacitor cell is strongly dependent on the surface area of material and pore size and structures of the material, and therefore, a detailed characterization of the surface and textual properties is utmost important to analyze how the specific surface area, pore size, and its structures affect the electrochemical performance of carbon-based supercapacitor cells. Although the porous carbon is usually complex materials with different kind of structures which includes local graphitized and disorder arrangements of carbon, and hence, it is impracticable and tough to predict their local structures (in real) and long-range structures [85, 86]. However, there are now various kind of experimental techniques which are well developed and sufficiently advanced to predict and analyze the materials up to great extent like gas sorption, electron microscopy, NMR, neutron scattering, X-ray scattering, and in situ techniques [87]. In addition to the experimental techniques, modeling and simulation methods like density functional theory, pair distribution function, Monte Carlo method, and gas sorption techniques are the most widely used to study the pore structures of porous carbon materials in more detail ways [87].

## 4.3 Capacitance with Respect to Specific Surface Area (SSA)

Gouy, Chapman and Stern proposed in their model that the overall double layer capacitance achieved is directly proportional to the specific surface area of the material used, and this theory triggered the race to enhance the specific surface area of the active material which will in turn increase the overall capacitance values. Several research groups had developed their interest in activated carbon and the activation techniques by which the surface area and pore volume can be increased. But, after some time, it was realized that the gravimetric capacitance of active material was limited even if the most porous samples which has very high surface area were used [88–91]. Ji et al. studied that the area-normalized capacitance was decreased by 4–5  $\mu\text{F cm}^{-2}$  when the SSA was above 1500  $\text{m}^2 \text{g}^{-1}$  [92]. This is usually because

of the presence of micro-pores, specially narrow sub-nanometer size micro-pore in porous carbon was too small to accommodate the ions of electrolyte [93, 94]. As a conclusion, still, there are no clear trends established between specific area and capacitance.

#### ***4.4 Capacitance with Respect to Pore Size***

There is a quite established proposition which states that it is always preferred to have pore size of active material (for example, carbon in case of EDLCs) larger than the solvated ion size of electrolyte, as in this scenario, pores of active materials are accessible to electrolyte ions [90]. In other words, carbon materials whose pore sizes are smaller than the solvated electrolyte ions do not contribute to capacitance, and hence, they are considered as useless. If we take into account, the most commonly used electrolytes; the size of free ions and ions with solvated shells varies in between few to tens of Å. For example, the size of free tetraethylammonium cation is around 0.68 nm, and when it is dissolved in acetonitrile, the size increased to 1.3 nm. Clearly in this situation, large micro-pore and meso-pore carbons are considered as an ideal candidate for achieving high capacitance value.

### **5 Structure–activity Relationship with Heteroatom Doped Carbon Materials**

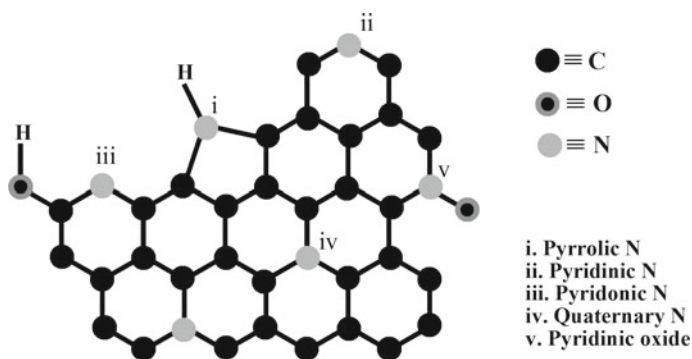
Although the prediction on acquiring capacitance is much higher, the volumetric and gravimetric capacitance of carbon nanomaterials are restricted to  $400 \text{ F cm}^{-3}$  [95] and  $300 \text{ F g}^{-1}$  [96], respectively. This is because of sole involvement of physical charge storage phenomena without any contribution of fast Faradaic redox reactions. Therefore, doping with heteroatoms could be an effective strategy for the enhancement of capacitance. The charge storage mechanism in porous carbon is discussed in Sect. 4. However, self-doped porous carbon from various biomass precursors or doping with heteroatoms like, O, N, P, B during activation process adds some more advantages like enhanced wettability due to polarized surface, improved intrinsic conductivity, and better electrochemical performances resulting from the introduction of faradaic pseudocapacitance of the redox active sites [97]. The structural distortions and electronic structure modulations generally occur due to the size and electronegativity differences between the dopant atoms and carbon. The total electrochemically active surface of the electrode material where electrolyte ions are accumulated is defined as “electrolyte infiltration” [98]. The porous hierarchical polar surface resulting from heteroatom doping facilitates a fast and adequate electrolyte infiltration which establishes multidirectional pathways for rapid ion transfer and therefore improves the



electrochemical performance. The electrolyte infiltration is directly related to the wettability of an electrolyte which is measured by contact angle meter [99].

The enhancement of electrochemical performances of oxygen doped carbon materials is mainly due to the increasing wettability of the electrode material to the electrolyte, fast Faradaic redox reactions contributing pseudocapacitance, and increased pore utilization ratio. However, oxygen functionalization can decrease the surface conductivity and prevent the electrolyte ions from entering the pore. He et al. thoroughly investigated the reasons for capacitance enhancement in oxygen containing carbon nanofibers. In acidic aqueous electrolyte,  $H_3O^+$  ion attracts the electrons on the O atom of the functional groups, and therefore charge separation occurs which facilitates the redox reaction. While the adsorption/desorption reaction of the hydrated ions of alkaline aqueous electrolyte in the pore causes the pseudocapacitance [100]. Wang et al. investigated the pseudocapacitive behavior of the O-doped carbon cloth which was prepared by annealing the carbon cloth in presence of air at low temperatures. They concluded that micro-pores having oxygen functional groups can give high pseudocapacitance than surface of pristine carbon plane, by facilitating the faradaic redox reactions due to increased ion-accessible area [101].

Nitrogen-doping in porous carbon materials distorts the structure and creates defects and available active sites. Doping with nitrogen atom can cause a shift of the Fermi level toward valence band in carbon materials, accelerating the electron transfer [102]. It can also enhance the wettability by increasing the polarity and charge density of the materials. In carbonaceous material, generally, five types of N-functionalization are encountered, such as pyrrolic nitrogen (N-5), pyridinic nitrogen (N-6), pyridonic nitrogen (N-5), quaternary or graphitic nitrogen (N-Q), and pyridinic oxide (N-X) (Fig. 11) [103]. Due to the electron donating nature, pyridinic and pyrrolic nitrogens serve as electroactive center in electrochemical capacitor. The graphitic nitrogen helps to improve the electronic conductivity and creates additional defects. However, all types of nitrogen can add pseudocapacitance to the total capacitance [104].



**Fig. 11** Schematic illustration of N atom doped porous carbons

Liu et al. prepared N-doped porous carbons from pyrrole and Na-metal using a three-step process which involves solvothermal, pyrolysis, and acid washing of metal salts. The meso-porous carbons with high specific surface areas of  $2000 \text{ m}^2 \text{ g}^{-1}$  were obtained at high-temperature pyrolysis. The as-prepared materials perform as excellent electrode materials for supercapacitor with exceptional rate performances, long lifetime, and high-power density [105]. Zhu et al. prepared high-level N-doped (up to 8.71%) micro-porous carbon materials having high specific surface areas by a facile Schiff-base reaction of 3,3'-diaminobenzidine and p-phthalaldehyde in ethanol solvent and a subsequent single-step carbonization-activation process. The as-prepared material exhibited high gravimetric capacitance with excellent rate capability and electrochemical stability [106].

The electrochemical activities of different heteroatoms doped porous carbon materials are depicted in Table 4. Although there is no linear relation between the heteroatom types/content and supercapacitive performances, the electrochemical activity is greatly enhanced by doping with heteroatoms like O, N, S, and B.

## 6 Conclusions and Prospects

Supercapacitors are getting enormous importance as these can make a bridge between a conventional capacitor and a battery. Porous carbon materials offer low-cost electrode materials having high SSA ( $1500\text{--}2000 \text{ m}^2 \text{ g}^{-1}$ ) and extraordinary electrochemical performances. For the porous carbon-based supercapacitive electrodes, the conventional synthesis strategies like carbonization-activation, templating methods, salient features to act as electrode in supercapacitors, and heteroatom functionalization have been discussed in this chapter.

Generally, physical activation methods are used to produce porous carbon electrodes for commercial purpose. The porogens like  $\text{H}_2$ ,  $\text{CO}_2$ , and air are used in physical activation to create porous carbons with high SSA. The porogens used in chemical activation methods do the same job as physical porogens do but they are highly toxic in nature and produce various pollutants during chemical activation. Therefore, the chemical activation method requires environment friendly green methods to prepare porous carbons at a reasonable cost.

Recently, the porous carbon doped with heteroatom such as O, N, S, and B have been thoroughly investigated for the supercapacitor materials. The introduction of these heteroatoms improves the electrochemical performances of the material by increasing electronic mobility, extrinsic defects, and wettability. However, the functional mechanisms of porous carbon electrodes doped with different heteroatom are largely dependent on their size and electronegativity difference. Therefore, an appropriate choice of dopants with their relative ratios is highly desirable.

The capacitance of porous carbon supercapacitor mainly comes from the fast and reversible ion adsorption-desorption at the carbon/electrolyte interfaces. For the enhancement of the electrochemical performances, the interface accessibility and

**Table 4** Supercapacitive performances of porous carbon materials doped with heteroatoms

Electrode material	Heteroatom content	Surface area ( $\text{m}^2\text{g}^{-1}$ )	Specific capacitance ( $\text{F/g}$ ) at specific current ( $\text{A g}^{-1}$ ) or scan rate ( $\text{mVs}^{-1}$ )	Electrolyte	Reference
N-rich meso-porous Carbons	N: 19.10 wt%	458	252 at $0.2 \text{ A g}^{-1}$	1 M $\text{H}_2\text{SO}_4$	[107]
N and B co-doped PC	N: 15–20%, B: 10–13%	955	188 at $0.5 \text{ A g}^{-1}$	6 M KOH	[108]
N-doped PC nanofibrous microspheres	N: 2.4 at.%, O: 6.1 at.%	1147	113 at $5 \text{ mVs}^{-1}$	EMIMTFSI	[109]
Honeycomb-like PC foam	N: 1.1 at.%, O: 11.2 at.%	1313	260 at $2 \text{ mVs}^{-1}$	1 M $\text{Na}_2\text{SO}_4$	[110]
N/S-doped PC	N: 4.5 at.%, S: 5.8 at.%	1339	464 at $0.2 \text{ A g}^{-1}$	6 M KOH	[111]
N-doped PC superstructures	N: 3.46 wt%, O: 7.99 wt%	1375	364 at $0.6 \text{ A g}^{-1}$	6 M KOH	[112]
N-doped micro-porous carbon spheres	N: 8.71 at.%, O: 7.89 at.%	1478	292 at $1 \text{ A g}^{-1}$	6 M KOH	[106]
PC nanorods	N: 1.47 at.%, O: 0.62 at.%	1559	187 at $0.05 \text{ A g}^{-1}$	1 M $\text{H}_2\text{SO}_4$	[113]
N/S-co-doped carbon nanobowls	N: 3.3 wt%, S: 1.7 wt%	1567	279 at $0.1 \text{ A g}^{-1}$	6 M KOH	[114]
3D interconnected S-doped PC	S: 5.2 wt%	1592	320 at $0.2 \text{ A g}^{-1}$	6 M KOH	[115]
N-doped PC nanosheets	N: 2.10 at.%, O: 7.11 at.%	1786.1	339 at $0.25 \text{ A g}^{-1}$	6 M KOH	[116]
N-doped multi-chamber carbon microspheres	N: 4.58 wt%, O: 2.12 wt%	1797	301 at $0.2 \text{ A g}^{-1}$	6 M KOH	[117]
2D PC nanosheets	N: 1.54 at.%, O: 6.59 at.%	1907	221 at $1 \text{ A g}^{-1}$	EMIMBF <sub>4</sub>	[118]
N and S-co-doped hierarchical PC	N: 1.88 at.%, S: 1.87 at.%	1975	333.4 at $0.1 \text{ A g}^{-1}$	6 M KOH	[119]
S-doped PC nanosheets	S: 9.6 wt%	2005	312 at $0.5 \text{ A g}^{-1}$	6 M KOH	[120]
B/N-co-doped carbon nanosheets	N: 3.1 at.%, B: 0.5 at.%	2362	235.6 at $0.5 \text{ A g}^{-1}$	1 M $\text{Na}_2\text{SO}_4$	[121]

(continued)

**Table 4** (continued)

Electrode material	Heteroatom content	Surface area ( $\text{m}^2\text{g}^{-1}$ )	Specific capacitance (F/g) at specific current ( $\text{Ag}^{-1}$ ) or scan rate ( $\text{mVs}^{-1}$ )	Electrolyte	Reference
N-rich PC nanosheets	N: 9.4 at.%, O: 4.7 at.%	2406	250 at $0.5\text{ A g}^{-1}$	EMIMBF <sub>4</sub>	[122]

EMIMTFSI: 1-ethyl-3-methylimidazolium bis(trifluoromethylsulfonyl)imide; EMIMBF<sub>4</sub>: 1-ethyl-3-methylimidazolium tetrafluoroborate; PC: Porous carbon

carbon/electrolyte compatibility should be highly improved. Therefore, the introduction of nanopores to the porous carbon material and doping pseudo-active sites improves the interfacial interactions.

**Acknowledgements** MM thanks to Sree Chaitanya College, Habra for giving permission to carry out the research work. KC acknowledges Ishaan Mandal for allowing enough time for literature survey and writing the draft during this pandemic.

## References

1. Conway BE (2013) Electrochemical supercapacitors: scientific fundamentals and technological applications. Springer Science & Business Media
2. Majumdar D, Mandal M, Bhattacharya SK (2019)  $\text{V}_2\text{O}_5$  and its carbon-based nanocomposites for supercapacitor applications. *Chem Electro Chem* 6(6):1623–1648
3. Mandal M, Ghosh D, Chattopadhyay K, Das CK (2016) A novel asymmetric supercapacitor designed with  $\text{Mn}_3\text{O}_4$ @ multi-wall carbon nanotube nanocomposite and reduced graphene oxide electrodes. *J Electron Mater* 45(7):3491–3500
4. Mandal M, Maitra A, Das T, Das CK (2015) Graphene and related two-dimensional materials. In: Graphene materials: fundamentals and emerging applications. John Wiley & Sons, Inc, pp 3–23
5. Mandal M, Ghosh D, Giri S, Shakir I, Das CK (2014) Polyaniline-wrapped 1D  $\text{CoMoO}_4 \cdot 0.75\text{H}_2\text{O}$  nanorods as electrode materials for supercapacitor energy storage applications. *RSC Adv* 4(58):30832–30839
6. Miao L, Song Z, Zhu D, Li L, Gan L, Liu M (2020) Recent advances in carbon-based supercapacitors. *Mater Adv* 1(5):945–966
7. Shao H, Wu YC, Lin Z, Taberna PL, Simon P (2020) Nanoporous carbon for electrochemical capacitive energy storage. *Chem Soc Rev* 49(10):3005–3039
8. Feng HP, Tang L, Zeng GM, Tang J, Deng YC, Yan M, Liu YN, Zhou YY, Ren XY, Chen S (2018) Carbon-based core-shell nanostructured materials for electrochemical energy storage. *J Mater Chem A* 6(17):7310–7337
9. Simon P, Gogotsi Y (2013) Capacitive energy storage in nanostructured carbon–electrolyte systems. *Acc Chem Res* 46(5):1094–1103
10. Gogotsi Y (2015) Not just graphene: the wonderful world of carbon and related nanomaterials. *MRS Bull* 40(12):1110–1121

11. Alslaibi TM, Abustan I, Ahmad MA, Foul AA (2013) A review: production of activated carbon from agricultural byproducts via conventional and microwave heating. *J Chem Technol Biotechnol* 88(7):1183–1190
12. Gao M, Pan SY, Chen WC, Chiang PC (2018) A cross-disciplinary overview of naturally derived materials for electrochemical energy storage. *Mater Today Energy* 7:58–79
13. Yin J, Zhang W, Alhebshi NA, Salah N, Alshareef HN (2020) Synthesis strategies of porous carbon for supercapacitor applications. *Small Methods* 4(3):1900853
14. Schmidt-Winkel P, Lukens WW, Zhao D, Yang P, Chmelka BF, Stucky GD (1999) Mesocellular siliceous foams with uniformly sized cells and windows. *J Am Chem Soc* 121(1):254–255
15. Liang HW, Wei W, Wu ZS, Feng X, Mullen K (2013) Mesoporous metal–nitrogen-doped carbon electrocatalysts for highly efficient oxygen reduction reaction. *J Am Chem Soc* 135(43):16002–16005
16. He S, Zhang C, Du C, Cheng C, Chen W (2019) High rate-performance supercapacitor based on nitrogen-doped hollow hexagonal carbon nanoprism arrays with ultrathin wall thickness in situ fabricated on carbon cloth. *J Power Sources* 434:226701
17. Yu S, Wang H, Hu C, Zhu Q, Qiao N, Xu B (2016) Facile synthesis of nitrogen-doped, hierarchical porous carbons with a high surface area: the activation effect of a nano-ZnO template. *J Mater Chem A* 4(42):16341–16348
18. He X, Li R, Qiu J, Xie K, Ling P, Yu M, Zhang X, Zheng M (2012) Synthesis of mesoporous carbons for supercapacitors from coal tar pitch by coupling microwave-assisted KOH activation with a MgO template. *Carbon* 50(13):4911–4921
19. Geng W, Ma F, Wu G, Song S, Wan J, Ma D (2016) MgO-templated hierarchical porous carbon sheets derived from coal tar pitch for supercapacitors. *ElectrochimActa* 191:854–863
20. de Almeida FC, Zarbin AJ (2006) Hollow porous carbon microspheres obtained by the pyrolysis of TiO<sub>2</sub>/poly (turfuryl alcohol) composite precursors. *Carbon* 44(14):2869–2876
21. Fang Y, Lv Y, Che R, Wu H, Zhang X, Gu D, Zheng G, Zhao D (2013) Two-dimensional mesoporous carbon nanosheets and their derived graphene nanosheets: synthesis and efficient lithium ion storage. *J Am Chem Soc* 135(4):1524–1530
22. Liang Y, Schwab MG, Zhi L, Mugnaioli E, Kolb U, Feng X, Müllen K (2010) Direct access to metal or metal oxide nanocrystals integrated with one-dimensional nanoporosity for electrochemical energy storage. *J Am Chem Soc* 132(42):15030–15037
23. Ania CO, Khomeiko V, Raymundo-Piñero E, Parra JB, Beguin F (2007) The large electrochemical capacitance of microporous doped carbon obtained by using a zeolite template. *Adv Funct Mater* 17(11):1828–1836
24. Zhao Y, Jiang L (2009) Hollow micro/nanomaterials with multilevel interior structures. *Adv Mater* 21(36):3621–3638
25. Chu WC, Bastakoti BP, Kaneti YV, Li JG, Alamri HR, Allothman ZA, Yamauchi Y, Kuo SW (2017) Tailored design of bicontinuous gyroid mesoporous carbon and nitrogen-doped carbon from poly (ethylene oxide-*b*-caprolactone) diblock copolymers. *Chem Eur J* 23:13734–13741
26. Wei J, Zhou D, Sun Z, Deng Y, Xia Y, Zhao D (2013) A controllable synthesis of rich nitrogen-doped ordered mesoporous carbon for CO<sub>2</sub> capture and supercapacitors. *Adv Funct Mater* 23(18):2322–2328
27. Liang C, Hong K, Guiochon GA, Mays JW, Dai S (2004) Synthesis of a large-scale highly ordered porous carbon film by self-assembly of block copolymers. *Angew Chem Int Ed* 43(43):5785–5789
28. Jayaramulu K, Dubal DP, Nagar B, Ranc V, Tomanec O, Petr M, Datta KKR, Zboril R, Gómez-Romero P, Fischer RA (2018) Ultrathin hierarchical porous carbon nanosheets for high-performance supercapacitors and redox electrolyte energy storage. *Adv Mater* 30(15):1705789
29. Yu S, Sun N, Hu L, Wang L, Zhu Q, Guan Y, Xu B (2018) Self-template and self-activation synthesis of nitrogen-doped hierarchical porous carbon for supercapacitors. *J Power Sources* 405:132–141

30. Xu F, Tang Z, Huang S, Chen L, Liang Y, Mai W, Zhong H, Fu R, Wu D (2015) Facile synthesis of ultrahigh-surface-area hollow carbon nanospheres for enhanced adsorption and energy storage. *Nat Commun* 6(1):1–12
31. Pandolfo AG, Hollenkamp AF (2006) Carbon properties and their role in supercapacitors. *J Power Sources* 157(1):11–27
32. Yang D, Ionescu MI (2017) Metal oxide–carbon hybrid materials for application in supercapacitors. In: *Metal oxides in supercapacitors*. Elsevier, pp 193–218
33. Sing KS (1985) Reporting physisorption data for gas/solid systems with special reference to the determination of surface area and porosity (Recommendations 1984). *Pure Appl Chem* 57(4):603–619
34. Yang H, Ye S, Zhou J, Liang T (2019) Biomass-derived porous carbon materials for supercapacitor. *Front Chem* 7(274):1–17
35. Sevilla M, Fuertes AB (2014) Direct synthesis of highly porous interconnected carbon nanosheets and their application as high-performance supercapacitors. *ACS Nano* 8(5):5069–5078
36. Jang M, Ko D, Choi Y, Yan B, Jin X, Kim DK, Piao Y (2021) Self-organized hierarchically porous carbon coated on carbon cloth for high-performance freestanding supercapacitor electrodes. *J Electroanal Chem* 895:115456
37. Ran F, Yang X, Xu X, Li S, Liu Y, Shao L (2021) Green activation of sustainable resources to synthesize nitrogen-doped oxygen-rich porous carbon nanosheets towards high-performance supercapacitor. *Chem Eng J* 412:128673
38. Chmiola J, Yushin G, Gogotsi Y, Portet C, Simon P, Taberna PL (2006) Anomalous increase in carbon capacitance at pore sizes less than 1 nanometer. *Science* 313(5794):1760–1763
39. Raymundo-Pinero E, Kierzek K, Machnikowski J, Béguin F (2006) Relationship between the nanoporous texture of activated carbons and their capacitance properties in different electrolytes. *Carbon* 44(12):2498–2507
40. Deng Y, Ji Y, Wu H, Chen F (2019) Enhanced electrochemical performance and high voltage window for supercapacitor based on multi-heteroatom modified porous carbon materials. *Chem Commun* 55(10):1486–1489
41. Poochai C, Srikaow A, Lohitkarn J, Kongthong T, Tuantranont S, Tuantranont S, Primpray V, Maeboonruan N, Wisitsoraat A, Sriprachuabwong C (2021) Waste coffee grounds derived nanoporous carbon incorporated with carbon nanotubes composites for electrochemical double-layer capacitors in organic electrolyte. *J Energy Storage* 43:103169
42. Chen Z, Wang X, Ding Z, Wei Q, Wang Z, Yang X, Qiu J (2019) Biomass-based hierarchical porous carbon for supercapacitors: effect of aqueous and organic electrolytes on the electrochemical performance. *ChemSusChem* 12(23):5099–5110
43. Miao L, Song Z, Zhu D, Li L, Gan L, Liu M (2021) Ionic liquids for supercapacitive energy storage: a mini-review. *Energy Fuels* 35(10):8443–8455
44. Xia M, Zhang X, Chen Y, Sun F, Wang X, Yang H, Chen H (2020) Hierarchical porous carbon derived from wood tar using crab as the template: performance on supercapacitor. *J Power Sources* 455:227982
45. Wang D, Fang G, Geng G, Ma J (2017) Unique porous carbon constructed by highly interconnected nanowalls for high-performance supercapacitor in organic electrolyte. *Mater Lett* 189:50–53
46. Li C, Zhang X, Wang K, Sun X, Liu G, Li J, Tian H, Li J, Ma Y (2017) Scalable self-propagating high-temperature synthesis of graphene for supercapacitors with superior power density and cyclic stability. *Adv Mater* 29(7):1604690
47. Nguyen QD, Patra J, Hsieh CT, Li J, Dong QF, Chang JK (2018) Supercapacitive properties of micropore- and mesopore-rich activated carbon in ionic liquid electrolytes with various constituent ions. *ChemSusChem* 12(2):449–456
48. Wu Y, Cao JP, Zhuang QQ, Zhao XY, Zhou Z, Wei YL, Zhao M, Bai HC (2021) Biomass-derived three-dimensional hierarchical porous carbon network for symmetric supercapacitors with ultra-high energy density in ionic liquid electrolyte. *ElectrochimActa* 371:137825

49. Na W, Jun J, Park JW, Lee G, Jang J (2017) Highly porous carbon nanofibers co-doped with fluorine and nitrogen for outstanding supercapacitor performance. *J Mater Chem A* 5(33):17379–17387
50. Cai J, Niu H, Wang H, Shao H, Fang J, He J, Xiong H, Ma C, Lin T (2016) High-performance supercapacitor electrode from cellulose-derived, inter-bonded carbon nanofibers. *J Power Sources* 324:302–308
51. Berenguer R, García-Mateos FJ, Ruiz-Rosas R, Cazorla-Amorós D, Morallón E, Rodríguez-Mirasol J, Cordero T (2016) Biomass-derived binderless fibrous carbon electrodes for ultrafast energy storage. *Green Chem* 18(6):1506–1515
52. Ouyang T, Cheng K, Yang F, Zhou L, Zhu K, Ye K, Wang G, Cao D (2017) From biomass with irregular structures to 1D carbon nanobelts: a stripping and cutting strategy to fabricate high performance supercapacitor materials. *J Mater Chem A* 5(28):14551–14561
53. Jin Z, Yan X, Yu Y, Zhao G (2014) Sustainable activated carbon fibers from liquefied wood with controllable porosity for high-performance supercapacitors. *J Mater Chem A* 2(30):11706–11715
54. Fan X, Yu C, Yang J, Ling Z, Hu C, Zhang M, Qiu J (2015) A layered-nanospace-confinement strategy for the synthesis of two-dimensional porous carbon nanosheets for high-rate performance supercapacitors. *Adv Energy Mater* 5(7):1401761
55. Xu Y, Sprick RS, Brownbill NJ, Blanc F, Li Q, Ward JW, Ren S, Cooper AI (2021) Bottom-up wet-chemical synthesis of a two-dimensional porous carbon material with high supercapacitance using a cascade coupling/cyclization route. *J Mater Chem A* 9(6):3303–3308
56. Zhao Q, Wang X, Liu J, Wang H, Zhang Y, Gao J, Lu Q, Zhou H (2015) Design and synthesis of three-dimensional hierarchical ordered porous carbons for supercapacitors. *ElectrochimActa* 154:110–118
57. Li Z, Zhang L, Chen X, Li B, Wang H, Li Q (2019) Three-dimensional graphene-like porous carbon nanosheets derived from molecular precursor for high-performance supercapacitor application. *ElectrochimActa* 296:8–17
58. Gogotsi Y, Penner RM (2018) Energy storage in nanomaterials—capacitive, pseudocapacitive, or battery-like? *ACS Nano* 12(3):2081–2083
59. Wang Q, Yan J, Fan Z (2016) Carbon materials for high volumetric performance supercapacitors: design, progress, challenges and opportunities. *Energy Environ Sci* 9(3):729–762
60. Wang Q, Yan J, Fan Z (2014) Nitrogen-doped sandwich-like porous carbon nanosheets for high volumetric performance supercapacitors. *ElectrochimActa* 146:548–555
61. Yan X, Yu Y, Ryu SK, Lan J, Jia X, Yang X (2014) Simple and scalable synthesis of phosphorus and nitrogen enriched porous carbons with high volumetric capacitance. *ElectrochimActa* 136:466–472
62. Hu J, Wang H, Gao Q, Guo H (2010) Porous carbons prepared by using metal–organic framework as the precursor for supercapacitors. *Carbon* 48(12):3599–3606
63. Raymundo-Piñero E, Leroux F, Béguin F (2006) A high-performance carbon for supercapacitors obtained by carbonization of a seaweed biopolymer. *Adv Mater* 18(14):1877–1882
64. Xu B, Wu F, Chen S, Zhou Z, Cao G, Yang Y (2009) High-capacitance carbon electrode prepared by PVDC carbonization for aqueous EDLCs. *ElectrochimActa* 54(8):2185–2189
65. Tao Y, Xie X, Lv W, Tang DM, Kong D, Huang Z, Nishihara H, Ishii T, Li B, Golberg D, Kang F (2013) Towards ultrahigh volumetric capacitance: graphene derived highly dense but porous carbons for supercapacitors. *Sci Rep* 3(1):1–8
66. Yan L, Li D, Yan T, Chen G, Shi L, An Z, Zhang D (2018) N, P, S-codoped hierarchically porous carbon spheres with well-balanced gravimetric/volumetric capacitance for supercapacitors. *ACS Sustainable Chem Eng* 6(4):5265–5272
67. Jin H, Feng X, Li J, Li M, Xia Y, Yuan Y, Yang C, Dai B, Lin Z, Wang J, Lu J, Wang S (2019) Heteroatom-doped porous carbon materials with unprecedented high volumetric capacitive performance. *Angew Chem Int Ed* 58(8):2397–2401
68. Liang X, Liu R, Wu X (2021) Biomass waste derived functionalized hierarchical porous carbon with high gravimetric and volumetric capacitances for supercapacitors. *Microporous and Mesoporous Mater* 310:110659

69. Xue B, Wang X, Feng Y, Chen Z, Liu X (2020) Self-template synthesis of nitrogen-doped porous carbon derived from rice husks for the fabrication of high volumetric performance supercapacitors. *J Energy Storage* 30:101405
70. Gao H, Zhang D, Zhou H, Wu J, Xu G, Huang Z, Liu M, Yang J, Chen D (2020) Boosting gravimetric and volumetric energy density of supercapacitors by 3D pomegranate-like porous carbon structure design. *Appl Surf Sci* 534:147613
71. Zhu T, Liu S, Wan K, Zhang C, Feng Y, Feng W, Liu T (2020) Fluorine and nitrogen dual-doped porous carbon nanosheet-enabled compact electrode structure for high volumetric energy storage. *ACS Appl Energy Mater* 3(5):4949–4957
72. Helmholtz HV (1853) Uebereinigtesetze der VertheilungelektrischerStröme in körperlichenLeitern, mitAnwendung auf die thierisch-elektrischenVersuche (Schluss.). *Annalen der Physik* 165(7):353–377
73. Lu M (2013) Supercapacitors: materials, systems, and applications. John Wiley & Sons
74. Fedorov MV, Kornyshev AA (2014) Ionic liquids at electrified interfaces. *Chem Rev* 114(5):2978–3036
75. Huang MM, Jiang Y, Sasisanker P, Driver GW, Weingärtner H (2011) Static relative dielectric permittivities of ionic liquids at 25 C. *J Chem Eng Data* 56(4):1494–1499
76. Gouy M (1910) Sur la constitution de la charge électrique à la surface d'un électrolyte. *J Phys Theor Appl* 9(1):457–468
77. Chapman DL (1913) LI. A contribution to the theory of electrocapillarity. *Lond Edinb Dublin Philos Mag J Sci* 25(6):475–481
78. Grahame DC (1947) The electrical double layer and the theory of electrocapillarity. *Chem Rev* 41(3):441–501
79. Bard AJ, Faulkner LR (2001) *Electrochemical methods fundamentals and applications*, 2nd edn. John Wiley & Sons Inc.
80. Stern O (1924) The theory of the electrolytic double-layer. *Z Elektrochem* 30(508):1014–1020
81. Kornyshev AA (2007) Double-layer in ionic liquids: paradigm change? *J Phys Chem B* 111(20):5545–5557
82. Fawcett WR (1979) Molecular models for solvent structure at polarizable interfaces. *Isr J Chem* 18(1–2):3–16
83. Kimizuka O, Tanaike O, Yamashita J, Hiraoka T, Futaba DN, Hata K, Machida K, Suematsu S, Tamamitsu K, Saeki S, Yamada Y (2008) Electrochemical doping of pure single-walled carbon nanotubes used as supercapacitor electrodes. *Carbon* 46(14):1999–2001
84. Geim AK, Novoselov KS (2007) The rise of graphene. *Nat Mater* 6:183–191
85. Jagiello J, Olivier JP (2013) 2D-NLDFT adsorption models for carbon slit-shaped pores with surface energetical heterogeneity and geometrical corrugation. *Carbon* 55:70–80
86. Forse AC, Merlet C, Allan PK, Humphreys EK, Griffin JM, Aslan M, Zeiger M, Presser V, Gogotsi Y, Grey CP (2015) New insights into the structure of nanoporous carbons from NMR, Raman, and pair distribution function analysis. *Chem Mater* 27(19):6848–6857
87. Cychosz KA, Guillet-Nicolas R, García-Martínez J, Thommes M (2017) Recent advances in the textural characterization of hierarchically structured nanoporous materials. *Chem Soc Rev* 46(2):389–414
88. Shi H (1996) Activated carbons and double layer capacitance. *ElectrochimActa* 41(10):1633–1639
89. Gamby J, Taberna PL, Simon P, Fauvarque JF, Chesneau M (2001) Studies and characterisations of various activated carbons used for carbon/carbon supercapacitors. *J Power Sources* 101(1):109–116
90. Endo M, Maeda T, Takeda T, Kim YJ, Koshiba K, Hara H, Dresselhaus MS (2001) Capacitance and pore-size distribution in aqueous and nonaqueous electrolytes using various activated carbon electrodes. *J Electrochem Soc* 148:A910
91. Barbieri O, Hahn M, Herzog A, Kötz R (2005) Capacitance limits of high surface area activated carbons for double layer capacitors. *Carbon* 43(6):1303–1310
92. Ji H, Zhao X, Qiao Z, Jung J, Zhu Y, Lu Y, Zhang LL, MacDonald AH, Ruoff RS (2014) Capacitance of carbon-based electrical double-layer capacitors. *Nature Commun* 5:1–7



93. Lin C, Ritter JA, Popov BN (1999) Correlation of double-layer capacitance with the pore structure of sol-gel derived carbon xerogels. *J Electrochem Soc* 146(10):3639
94. Lozano-Castello D, Cazorla-Amorós D, Linares-Solano A, Shiraishi S, Kurihara H, Oya A (2003) Influence of pore structure and surface chemistry on electric double layer capacitance in non-aqueous electrolyte. *Carbon* 41(9):1765–1775
95. Li H, Qi C, Tao Y, Liu H, Wang DW, Li F, Yang QH, Cheng HM (2019) Quantifying the volumetric performance metrics of supercapacitors. *Adv Energy Mater* 9(21):1900079
96. Liu T, Zhang F, Song Y, Li Y (2017) Revitalizing carbon supercapacitor electrodes with hierarchical porous structures. *J Mater Chem A* 5(34):17705–17733
97. Xie L, Su F, Xie L, Guo X, Wang Z, Kong Q, Sun G, Ahmad A, Li X, Yi Z, Chen C (2020) Effect of pore structure and doping species on charge storage mechanisms in porous carbon-based supercapacitors. *Mater Chem Front* 4(9):2610–2634
98. Shodiev A, Primo E, Arcelus O, Chouchane M, Osenberg M, Hilger A, Manke I, Li J, Franco AA (2021) Insight on electrolyte infiltration of lithium ion battery electrodes by means of a new three-dimensional-resolved lattice Boltzmann model. *Energy Storage Mater* 38:80–92
99. Li G, Lei W, Luo D, Deng YP, Wang D, Chen Z (2018) 3D porous carbon sheets with multidirectional ion pathways for fast and durable lithium–sulfur batteries. *Adv Energy Mater* 8(8):1702381
100. He Y, Zhang Y, Li X, Lv Z, Wang X, Liu Z, Huang X (2018) Capacitive mechanism of oxygen functional groups on carbon surface in supercapacitors. *ElectrochimActa* 282:618–625
101. Wang H, Fan R, Miao J, Deng J, Wang Y (2019) Oxygen groups immobilized on micropores for enhancing the pseudocapitance. *ACS Sustainable Chem Eng* 7(13):11407–11414
102. Veerasamy VS, Yuan J, Amaratunga GAJ, Milne WI, Gilkes KWR, Weiler M, Brown LM (1993) Nitrogen doping of highly tetrahedral amorphous carbon. *Phys Rev B* 48(24):17954
103. Kapteijn F, Moulijn JA, Matzner S, Boehm HP (1999) The development of nitrogen functionality in model chars during gasification in CO<sub>2</sub> and O<sub>2</sub>. *Carbon* 37(7):1143–1150
104. Ornelas O, Sieben JM, Ruiz-Rosas R, Morallon E, Cazorla-Amorós D, Geng J, Soïn N, Siores E, Johnson BF (2014) On the origin of the high capacitance of nitrogen-containing carbon nanotubes in acidic and alkaline electrolytes. *Chem Commun* 50(77):11343–11346
105. Liu K, Zheng X, Wang K, Wang C, Chen M (2019) Sodium metal-assisted carbonization of pyrrole to prepare N-doped porous carbons for high-rate performance supercapacitors. *Carbon* 153:265–273
106. Zhu D, Jiang J, Sun D, Qian X, Wang Y, Li L, Wang Z, Chai X, Gan L, Liu M (2018) A general strategy to synthesize high-level N-doped porous carbons via Schiff-base chemistry for supercapacitors. *J Mater Chem A* 6(26):12334–12343
107. Liu Y, Wang Z, Teng W, Zhu H, Wang J, Elzatahry AA, Al-Dahyan D, Li W, Deng Y, Zhao D (2018) A template-catalyzed in situ polymerization and co-assembly strategy for rich nitrogen-doped mesoporous carbon. *J Mater Chem A* 6(7):3162–3170
108. Luo L, Zhou Y, Yan W, Wu X, Wang S, Zhao W (2020) Two-step synthesis of B and N co-doped porous carbon composites by microwave-assisted hydrothermal and pyrolysis process for supercapacitor application. *ElectrochimActa* 360:137010
109. Duan B, Gao X, Yao X, Fang Y, Huang L, Zhou J, Zhang L (2016) Unique elastic N-doped carbon nanofibrous microspheres with hierarchical porosity derived from renewable chitin for high rate supercapacitors. *Nano Energy* 27:482–491
110. Wu X, Jiang L, Long C, Fan Z (2015) From flour to honeycomb-like carbon foam: carbon makes room for high energy density supercapacitors. *Nano Energy* 13:527–536
111. Lu Y, Liang J, Deng S, He Q, Deng S, Hu Y, Wang D (2019) Hypercrosslinked polymers enabled micropore-dominant N, S Co-Doped porous carbon for ultrafast electron/ion transport supercapacitors. *Nano Energy* 65:103993
112. Xu Z, Zhuang X, Yang C, Cao J, Yao Z, Tang Y, Jiang J, Wu D, Feng X (2016) Nitrogen-doped porous carbon superstructures derived from hierarchical assembly of polyimide nanosheets. *Adv Mater* 28(10):1981–1987
113. Pachfule P, Shinde D, Majumder M, Xu Q (2016) Fabrication of carbon nanorods and graphene nanoribbons from a metal–organic framework. *Nat Chem* 8(7):718–724

114. Wang JG, Liu H, Zhang X, Shao M, Wei B (2018) Elaborate construction of N/S-co-doped carbon nanobowls for ultrahigh-power supercapacitors. *J Mater Chem A* 6(36):17653–17661
115. Tian J, Zhang H, Liu Z, Qin G, Li Z (2018) One-step synthesis of 3D sulfur-doped porous carbon with multilevel pore structure for high-rate supercapacitors. *Int J Hydrogen Energy* 43(3):1596–1605
116. Niu Q, Gao K, Tang Q, Wang L, Han L, Fang H, Zhang Y, Wang S, Wang L (2017) Large-size graphene-like porous carbon nanosheets with controllable N-doped surface derived from sugarcane bagasse pith/chitosan for high performance supercapacitors. *Carbon* 123:290–298
117. Wang T, Sun Y, Zhang L, Li K, Yi Y, Song S, Li M, Qiao ZA, Dai S (2019) Space-confined polymerization: controlled fabrication of nitrogen-doped polymer and carbon microspheres with refined hierarchical architectures. *Adv Mater* 31(16):1807876
118. Yu J, Yu C, Guo W, Wang Z, Li S, Chang J, Tan X, Ding Y, Zhang M, Yang L, Xie Y (2019) Decoupling and correlating the ion transport by engineering 2D carbon nanosheets for enhanced charge storage. *Nano Energy* 64:103921
119. Zhang W, Cheng R, Wang Z, Ma Y, Ran S, Lv Y, Ma L (2020) A composite-hydroxide-activation strategy for the preparation of N/S dual-doped porous carbon materials as advanced supercapacitor electrodes. *J Mater Sci: Mater Electron* 31(24):22498–22511
120. Deng W, Zhang Y, Yang L, Tan Y, Ma M, Xie Q (2015) Sulfur-doped porous carbon nanosheets as an advanced electrode material for supercapacitors. *RSC Adv* 5(17):13046–13051
121. Yang L, Wu D, Wang T, Jia D (2020) B/N-codoped carbon nanosheets derived from the self-assembly of chitosan–amino acid gels for greatly improved supercapacitor performances. *ACS Appl Mater Interfaces* 12(16):18692–18704
122. Yao L, Wu Q, Zhang P, Zhang J, Wang D, Li Y, Ren X, Mi H, Deng L, Zheng Z (2018) Scalable 2D hierarchical porous carbon nanosheets for flexible supercapacitors with ultrahigh energy density. *Adv Mater* 30:1706054

# Chapter 6

## Recent Advancement of Luminescent Graphene Quantum Dots for Energy-Related Applications



Poonam Rani Kharangarh, Rachna Rawal, Shalu Singh,  
and Preetam Bhardwaj

### 1 Introduction

#### 1.1 Background of Graphene Quantum Dots from Graphene

The most abundant and fascinating element is carbon which has been attracted more attention owing to their tremendous “physical and chemical” belongings. In 1991, carbon nanotubes (CNTs), allotropy of carbon, were discovered by Iijima [1]. More than a decade, “Geim and Novoslov” [2] from “University of Manchester” conducted some experiments on graphene to develop monolayer graphene by using tool called as “scotch tape method.” After two years, “Geim and Novoslov” [2] got a “Nobel Prize” award in “physics” on behalf of the new invention on graphene. To date, nanomaterials prepared from carbon which is known as “carbon-based nanomaterials (CBNs).” Nowadays, CBNs brought a lot of attention with the recent technologies in terms of nanomaterials. The several forms of “carbon” like “amorphous carbon,” “three-dimensional graphite (3D)” and “two-dimensional (2D) diamonds,” “2D graphene oxide (GO),” [3] “one-dimensional carbon nanotubes (1D-CNTs),” [1]

---

P. R. Kharangarh (✉) · R. Rawal  
Department of Physics and Astrophysics, University of Delhi, Delhi 110007, India  
e-mail: [prk6@njit.edu](mailto:prk6@njit.edu)

P. R. Kharangarh  
Department of Physics, New Jersey Institute of Technology, Newark, NJ 07901, USA

S. Singh  
Department of Chemistry, Bundelkhand University, Jhansi, Uttar Pradesh 284128, India  
Department of Chemistry, Vellore Institute of Technology, Vellore, Tamil Nadu 632014, India

P. Bhardwaj  
School of Electronics Engineering, Vellore Institute of Technology, Vellore, Tamil Nadu 632014, India

nanodiamonds (NDs) [4], “zero-dimensional graphene quantum dots (0D-GQDs)” [5, 6] and “0D-fullerene,” “carbon quantum dots (CQDs)” [7], etc., have been discovered. Out of various forms of carbon, GQDs have gained numerous attention of researchers because of “quantum confinement,” size, and “edge effects.” These are a type of 0-D material obtained by cutting the micrometer 2-D graphene sheets into nano-sheets. The main uses of GQDs in “solar cells, light-emitting diodes (LEDs), batteries, sensors, drug carriers and photo-catalytic [8–12],” and supercapacitors [13–16] are found to be much superior in comparison with the outmoded semiconductor QDs.

## 1.2 *Outlooks of Graphene Quantum Dots (GQDs)*

Although a lot of work has been done to resolve many challenges of GQDs but still many issues of GQDs have yet to be addressed in order to come across the necessities for application purpose. Our aim is to produce low-cost GQDs in terms of mass production to meet the requirements for industrial level. To reach at industry level, we need to produce high-quality GQDs with small budget. The very low product quantum yield (QY) of GQDs has been achieved so far. It is a big task to improve the QY in case of fragments of graphene due to variation in size effects.

Moreover, the informed yields of GQDs from 7 to 44.3% [17–23] were found to be lower in comparison with traditional semiconductors. The obtained shifts with different colored such as red and blue from PL by adding impurity by using various dopants such as chlorine, sodium, potassium, boron, and nitrogen for the determination to tune the energy (emission) of GQDs [23–30]. These described approaches were inadequate because of requirement for exclusive resources and extraordinary techniques which is shown in Fig. 1. In future, GQDs will be more promising and challenging materials as they are used in various applications. Once, all the above-mentioned challenges were solved. This review addresses the existing all approaches through “top-down and bottom-up” with selecting green precursors for synthesizing GQDs in “Sect. 2” as shown in Fig. 2. “In Sect. 3,” several energy storage applications such as “supercapacitors,” “lithium cell batteries,” “photovoltaic thin film solar cells,” and “fuel cells” related with GQDs will be studied are shown in Fig. 3. At last, a summary with conclusions will be explained in brief.

## 2 *Synthesis Methods*

### 2.1 *Top-Down Method*

The “top-down” methodologies include the formation of “GQDs” via the “chemical or physical” cutting ways of reasonably microscopic structures of graphene. Green

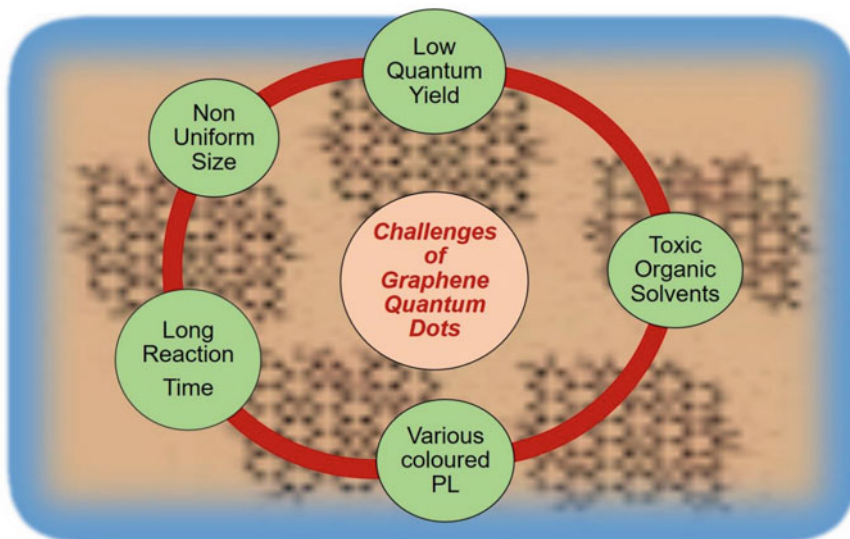


Fig. 1 Challenges of graphene quantum dots

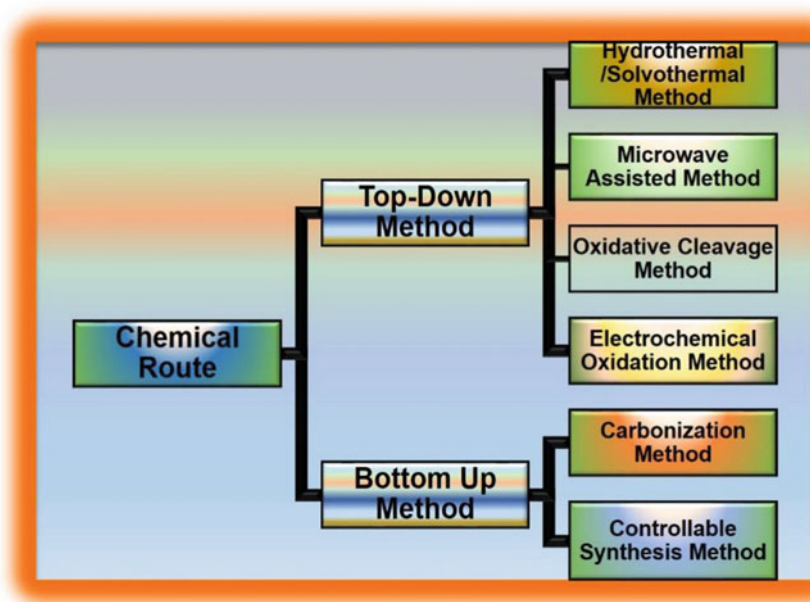
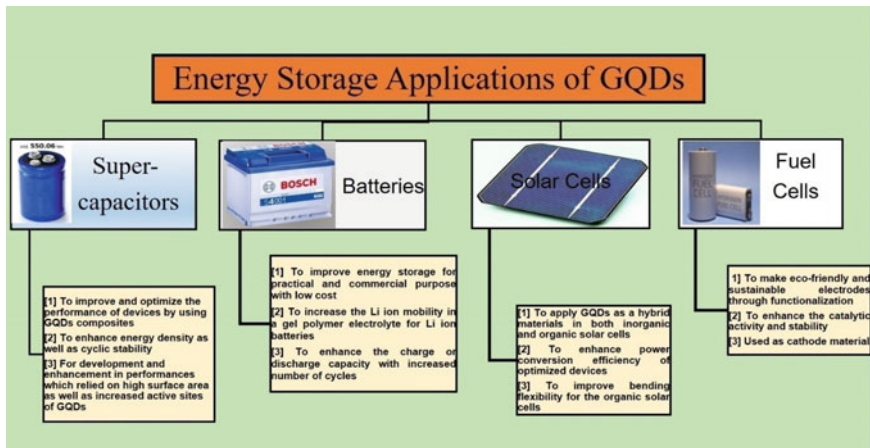


Fig. 2 Different synthesis methods of graphene quantum dots



**Fig. 3** Energy storage applications of graphene quantum dots

and low-cost raw materials were selected as the most representative sources for this method. Though, this method can be dividing up into routes of hydrothermal, solvothermal, ultrasonic and microwave-assisted, oxidative cleavage, and electrochemical oxidation by an approach with various characteristics of fabrication is provided.

### 2.1.1 Hydrothermal Method/Solvothermal Method

The “hydrothermal method” is a facile, eco-friendly, and fast process in terms of the fabrication procedures for GQDs by cutting the “carbon” sheets into small fragments below with higher pressure and higher temperature. Many researchers used hydrothermal method to produce uniform GQDs. The strongest oxidizer compounds among “conc. sulfuric acid ( $H_2SO_4$ ), nitric acid ( $HNO_3$ )” have been used for the treatment of carbon materials before the reactions happen. Firstly, the preparation of GQDs (5–13 nm) was reported from graphene oxide (GO) as a precursor material by using “hydrothermal method” under alkaline conditions for 10 h via strong oxidizing agents like  $H_2SO_4/HNO_3$  acid during the oxidation [18, 31]. Later on, modification in the fabrication process was described by giving high temperature to produce green fluorescent fine crystalline GQDs [32]. After some years, graphene-based materials and their modification by doping of nitrogen and boron elements have become so popular in many applications such as solar cells, batteries, gas sensing, and biosensors. The variation of nitrogen concentration shows a significant role to control the luminescence behavior of GQDs from violet to yellow via hydrothermal approach which effects the size and morphology for the prepared material [32]. As we know, the semiconducting properties can be improved or controlled by doping in the conventional semiconductor (SCs). Due to the presence of defects, the quality of materials

gets reduced. Although, the doping helps to increase the carrier concentration in graphene allows the production of novel material. In general, adding of impurities in graphene derivatives can be classified as either substitutional doping or chemical doping via molecule adsorption. The bandgap of graphene can be opened by substitutional doping which has been proved by the theoretical work doping elements in graphene [26–29]. The structure and variation in electronic properties were effected through doping which have been investigated through “first-principles density functional theory (DFT) and ab initio calculations” [33]. Some various dopants such as “ceria [29], fluorine [34], potassium [35], sulfur [27, 28], chlorine [36], selenium [37] as well as co-dopants like B- and N-doped GQDs [38], N-S-doped GQDs [39], and N-P-doped GQDs [40]” helped in modification of the electron density and also improve the luminescent properties at higher temperature through hydrothermal process. On the other hand, solvothermal method is a type of synthetic method in which the final product was prepared by using organic solvents instead of water. It is very highly economical, cost-effective, and non-toxic method. However, it is essential to check the nature of used chemical as well as physicochemical properties of the organic solvents which shows a very significant effect on their morphology of final products. The most common solvents such as “benzene, dimethylformamide (DMF), dimethyl sulfoxide (DMSO), methanol ( $\text{CH}_3\text{OH}$ ), dichloromethane (DCM) or methylene chloride, conc. sulfuric acid ( $\text{H}_2\text{SO}_4$ ), and nitric acid ( $\text{HNO}_3$ )” have been used to split GO into GQDs used and water. Shin et al. [41] used a unique solvothermal method based on “novel acid-free and oxone-oxidant-assisted synthesis of GQDs using various natural carbon resources, including graphite, multiwall carbon nanotubes (MWCNTs), carbon fibers (CFs), and charcoal (C)” [41]. But this method has some limitation in terms of durability and controlling the size of nanoparticles through the oxidizing agents, when the reaction takes place.

### 2.1.2 Ultrasonic and Microwave-Assisted and Ultrasonic (US) Method

Microwave-assisted method is a rapid heating, low-cost, and widely used method to produce GQDs in order to remove the limits with longer time reaction occurred by using oxidative cleavage, hydrothermal, and solvothermal methods. It not only helps to improve the quantum yield but also shorten the reaction time. The formed interaction leads to the motion (rotation and vibrational) of polar molecules and produces heat within the material. This method can be employed to prepare the nanoparticles as it is a combination of high speed reaction with homogenous heating for the selected materials. In 2012, the “electrochemiluminescent (ECL) two-color GQDs were fabricated such as greenish-yellow luminescent GQDs, i.e., gGQDs which is unreduced and bright blue luminescent GQDs, i.e., bGQDs which is further reduced with  $\text{NaBH}_4$  through the cleavage of GO in acidic medium by microwave-assisted method” [42]. By using this method, this group was able to improve the yield and reduce the time for the oxidation reaction. The nano-sheets of GO were preserved in acidic medium by using nitric acid (3.2 M) and con. sulfuric acid (0.9 M) for three hours, while for the preparation of gGQDs, they used  $\text{NaBH}_4$  as a reducing

agent resulting in reducing gGQDs within 2 h having size 2–7 nm in diameter. They demonstrate that the change in structure causes for blue shift in PL of the bGQDs after reduction instead of change in dimension. The observed PL QYs for bGQDs (22.9%) were found to be higher than gGQDs (11.7%), respectively. These ECL-active GQDs are supposed to have favorable applications to make an improvement of novel ECL biosensors due to their low cost, low cytotoxicity and excellent solubility. After four years in 2016, GQDs were synthesized by using the microwave-assisted pyrolysis method. Though, GQDs were prepared by adding aspartic acid (Asp) and  $\text{NH}_4\text{HCO}_3$  in 20 mL water and heated by microwave irradiation for 10 min [43]. The final product was obtained in the narrow range (~1.8–2.4 nm) by dialysis membrane for 7 h after purification with blue PL under the UV light ray with emission wavelength of 365 nm. The prepared GQDs keep low cellular toxicity and higher photostability which is found to be more sensitive for pH value as well as  $\text{Fe}^{3+}$  ions. Consequently, GQDs could assist as a fluorescent probe for  $\text{Fe}^{3+}$  ions detection which has been further used for live cell imaging.

On the other hand, “ultrasonic” method has been considered to be common method for synthesization of nanoparticles. The formation of small bubbles in distilled water (DI) in the ultrasonic waves produces instant higher pressure and higher energy due to breaking of C–C bond, reduction, and crumpling. But the use of ultrasound (US) method is to speed up the chemical, in degradation, and hydrolysis reactions. For instance, GQDs were reported for large-scale production through an “ultrasonic-assisted liquid phase exfoliation” tool which is eco- friendly, quick, and industrial purpose method [44]. This present work shows the preparation of GQDs by selecting various graphitic carbon where acetylene black was dispersed in “*N*-methyl-2-pyrrolidone (NMP)” solvent under mild ultrasonication conditions for completely one hour. As a result, a gray colored liquid was obtained which exhibits the dispersion of GQDs and some other residual precipitates. To get a homogeneous gray dispersion of GQDs, centrifugation was done through the frequency of 10,000 rpm for another half an hour so that these present precipitates will be removed. Finally, a very small sized somewhere between 2 and 6 nm GQDs were observed with thickness from 0.4 to 2 nm which indicates a monolayer showing strong excitation-dependent PL behavior. Interestingly, a unique method was presented by reported one [45] who combined the “merits of microwave-assisted and ultrasonic-assisted processes.” They demonstrated the “white light-emitting GQDs (WGQDs),” which have been synthesized by a “facile two-step microwave-assisted hydrothermal method.” The “white light-emitting diode (WLED)” based on WGQDs exhibits superior performance of white electroluminescence in comparison with WLED built on the GQDs or CDs. So, it exhibits that WGQDs can be used as a “single-phase white light-emitting phosphor” which is supposed to be highly expectant to make an improvement in the performance of WLED based on carbon nanomaterials (CNMs). The limitation of this method is the requirements for device so-called microwave or ultrasonic reactor is costly and exclusive for industrial outcomes.



### 2.1.3 Oxidative Cleavage or Oxidation Cutting Method

It is the extreme commonly used process to attain mass production due to its modest and real features. In this process, the C–C bonds were fragmented by using strong oxidizing agents such as “ $\text{H}_2\text{SO}_4$ ,  $\text{HNO}_3$ , or some other oxidizers” for the fabrication of GQDs. A regular procedure was shown to tune the nano-size of GO, where GO has been prepared by one of the famous methods known as modified Hummer’s method [46]. Also, the performance of GQDs for heavy metal ions with small detection limit in  $\text{Pb}^{2+}$  was determined. The reason is behind that the highly surface area concerned with GQDs can increase the interaction between “active sites” and “target ions” providing the ability of collections for metals. The final prepared product is assumed to make a progress in the development of graphene-based nanosensors as well as in biomaterial field. Also, GQDs were fabricated by selecting different precursor materials such as “fullerenes  $\text{C}_{60}$ , carbon nanotubes (CNTs), and “carbon fibers (CFs).” In 2015, an experiment was demonstrated to produce GQDs with a size of 2–3 nm by using fullerene as a precursor material [47]. This work has revealed the production of GQDs through “oxidation and cage opening of fullerene.” This method is relatively so simple to produce GQDs, which have potential uses in photodiodes and for biological purpose. In addition, the obtained fluorescent GQDs from carbon fiber were oxidized by conc. “ $\text{H}_2\text{SO}_4$  or  $\text{HNO}_3$ ” at higher temperature [23], where dimethylformamide (DMF) and dimethyl sulfoxide (DMSO) were used as polar organic solvents. As a result, the variation in size of the GQDs was observed with the reaction temperature. These obtained well-synthesized GQDs with low cytotoxicity can be used as an eco-friendly material in bio-imaging. The major limitation of this method is cause of burning or explosion due to strong oxidizing agents as well as the difficulty in post-processing route.

### 2.1.4 Electrochemical Oxidation

It demonstrates high levels of stability and the uniform size of GQDs. In this technique, “graphite, graphene, or CNTs” have been used as a “working electrode” and were cut into the fragments of graphene with maximum “redox potential” ( $\pm 1.5$  to  $\pm 3$  V). This procedure follows two methods. The first one is “C–C bonds of graphene or CNTs” which has been directly broken through “electrochemical oxidation,” while further one includes an oxidation of “water” successfully changes into a “hydroxyl free radical ( $\cdot\text{OH}$ ) or an oxygen free radical (O)” and splits them into fragments of graphene. The informed filter film of graphene was used as a working electrode, Ag/AgCl and Pt wire as a reference and counter electrodes, and the phosphate buffer solution (PBS) as an electrolyte was applied to synthesize GQDs [23]. The final prepared green luminescent GQDs were found to be stable in water for several months without any alterations. Similarly, GQDs by using MWCNTs were demonstrated which is cut by a two-step electrochemical oxidation with selecting propylene carbonate containing  $\text{LiClO}_4$  as the electrolyte [48]. The obtained GQDs with high QYs, good photostability, and their luminescent behavior are advantageous

for bio-imaging applications. Along that this method has some drawbacks that it takes longer time in prefabrication of raw ingredients as well as in purification. Moreover, it is challenging to understand for production purpose due to the low yield.

However, as top-down method has many advantages, it limited with final product yield with the necessity of costly equipments under critical fabrication environments for longer reaction time to control the size for the ultimate production. We need another strategy known as bottom-up method which will allow precisely to control the size of GQDs during synthesis. Similarly, the used organic precursors must have difficulty in procedures which have been originated for demanding.

## **2.2 Bottom-Up Method**

This method is quite simple. In “bottom-up strategy,” some organic and natural renewable raw materials are used as starting materials via temperature measurements agree to particular control of the products in terms of morphology. Though, this method can be divided up into routes of carbonization and fullerene with various characteristics of fabrication which has been carried out.

### **2.2.1 Carbonization Method**

It is an ecologically, sustainable, and superficial process where “organic molecules or polymers” were applied during carbonization for dehydration process. The obtained GQDs had been polydispersed due to difficulty in controlling the size and the structure precisely by using this method. For example, in 2017, green-colored PL with single-layer GQDs (SLGQDs) was prepared by using green precursor material glucose using this method [49]. The carbonization method was used to prepare both GQDs and GO by using “citric acid (CA)” [50]. This group used “polycyclic aromatic hydrocarbon (PAHs)” as the starting material for luminescent GQDs. This work will be more beneficial for low-cost fabrication of GQDs with biological and optoelectronic areas-related applications. Also, the produced GQDs were recorded at various pH as it shows a significant role in the development of “GQDs from CA.” The synthesized GQDs [51] from corn powder as a green precursor attain a broad application of rice husks, showing remarkable benefits in both economical as well as environmental [52]. Besides that, this method has a drawback that the synthesized GQDs with much more dispersive in nature having difficulty in controlling uniform size and structure.

### **2.2.2 Controllable Synthesis**

This scheme includes the synthesization of GQDs which have uniform size, shape, and perfect number of carbon atoms having “phenyl-containing compounds step by

step through controllable fabrication insolvent which should be organic in nature. Many researchers used this process to fabricate GQDs having 168, 132, and 170 carbon atoms [4]. The “2',4',6'-trialkyl phenyl molecules (TPM)” have been attached at edges of GQDs in order to keep them from recombining. There is a reduction in possibility for the GQDs overlapped with each other and an improvement in dispersibility in the organic phase due to difficulty caused by expansion of TPM in three-dimensional (3-D) direction.” In addition, “sulfur-doped GQDs (S-GQDs) were prepared by one-pot method with bright blue emission from 3-mercaptopropionic acid (MPA) and 1,3,6-trinitropyrene (TNP)” [54]. In brief, put the mixture of MPA and TNP for ultrasonic and kept into a bomb reactor through heating around 200 °C for 10 h. The collection of suspended S-GQDs, which is pale yellow colored, was completed after dialysis and freeze. These prepared S-GQDs can be used as a sensing probe for silver ions detection having high sensitivity. These fabricated S-GQDs have many applications in bio-imaging, sensing, optoelectronic devices, and catalysis to make this work more attractive. Besides that, this method has limitation which includes multistep complex reactions that take longer time with low yield during synthesis.

### 3 Energy-Related Applications

Nowadays, environmental pollution is increasing day by day. To reduce the pollution, our society needs some more energy storage devices for long run. This kind of critical condition is an important issue which has to be pointed out. Currently, the applications of energy storage such as “supercapacitors, (SCs),” “batteries,” “fuel cells,” and “solar cells” became more popular due to the higher necessity of our society.

A lot of metal oxides [55], conductive materials [56], polymers [57], and sulfides [58] were used for enhancement of energy-related applications till now. GQDs or fragment of graphene is considered to be promising element due to different properties such as broader area of surface, highly porous, higher intensity of PL with transparent nature. So, it has worth to bring together the energy storage applications of GQDs.

#### 3.1 *Electrochemical Capacitor/Supercapacitors*

This is based on the principal with two different mechanisms by transfer and storage for a charge which are basically central features of an electrochemical capacitor or supercapacitors (SCs). In common, the most three common categories for SCs include: (i) “electrical double-layer capacitors” (EDLCs), (ii) “pseudocapacitors,” and (iii) “hybrid” SCs. Since first one corresponds to the mechanism of “absorption and desorption” for ions with charge storage at the interface of working electrodes, while other one involves the mechanism of a “Faradaic reaction have redox

phenomenon. However, the main advantage of EDLC is that it shows high performance of fast charge storage which has low specific capacitance. For the development of SCs, a higher surface area for working electrode with low resistivity and broad potential window are essential. To date means till now.

For energy storage devices, SCs/micro-supercapacitors (MSCs) became more attractive due to their unique properties. The electrochemical double-layer capacitors (EDLC) and pseudocapacitors (PSCs) are two main types of SCs/MSCs. In most of cases, the SCs/MSCs electrode material prepared by using GQDs exist with an EDLC having “charge adsorption” mechanism on the surface of the “working electrode.” To fulfill the demands of highly flexible, lightweight, and transparent materials, SCs paid more attention. Till now, more work on highly dispersed GQDs in different solutions have been done in terms of energy storage devices as SCS due to their unique properties [59]. The simple electro-deposition method was used to investigate GQDs//GQDs symmetric micro-supercapacitors (SMSCs) in aqueous and ionic liquid (IL) electrolyte, and the obtained results were compared with GQDs//MnO<sub>2</sub> asymmetric micro-supercapacitors (ASMSCs) [60]. This group also reported GQDs//MnO<sub>2</sub> by using MnO<sub>2</sub> and ASMSCs. As a result, GQDs//MnO<sub>2</sub> AMSCs show two times higher specific capacitance (1107.4  $\mu\text{F}/\text{cm}^2$ ) and energy density (0.154  $\mu\text{Wh}/\text{cm}^2$ ) with good stability in comparison with that of GQDs//GQDs SMSCs (468.1  $\mu\text{F}/\text{cm}^2$ ) in aqueous electrolyte and GQDs//GQDs SMSCs in EMIMBF<sub>4</sub>/AN.

In addition, few layer graphene sheets (FLGs) and activated FLG powders (aFLGs) were synthesized using ultrasonication and chemical activation resulting the calculated specific capacitance of aGQD film ( $\sim 236$  F/g) on the glassy carbon electrode (GCE) was higher in comparison with aFLGs ( $C_{\text{sp}} \sim 172$  F/g), GQDs ( $C_{\text{sp}} \sim 108$  F/g), and FLGs ( $C_{\text{sp}} \sim 63$  F/g) [61]. Later on, an experiment was performed of uniform deposition onto the three-dimensional graphene (3DG) via electrochemical method in symmetrical supercapacitors. It is found that the composites prepared by “GQD–3DG” are more stabilized which displays the value of  $C_{\text{sp}}$  around 268 F/g was more than ( $\sim 90\%$ ) in comparison with pure “3DG electrodes ( $C_{\text{sp}} \sim 136$  F/g)” [62]. However, the composite of polyaniline (P) doped in GQDs (GQDP) was prepared from the GO flakes via chemical oxidation of aniline showing an excellent value for  $C_{\text{sp}}$  of 1044 F/g by selecting a particular current density ( $\sim 1$  A/g) with cyclic rate which has outstanding “retention rate” (80.1%) after 3000 cycles [63]. Furthermore, GQD-HNT nanocomposites (NCs) were fabricated of halloysite nanotubes (HNTs) combined with GQDs by the “pyrolysis of citric acid (CA),” where the functionalization of HNTs was done with “3-aminopropyl-triethoxysilane (APTES)” for increasing the storage sites of charge with fast diffusion for energy storage application [64]. They obtained the value of  $C_{\text{sp}}$  (363 F/g at 6A/g) for prepared “GQD-HNT” NCs by selecting an electrolyte of 1 M Na<sub>2</sub>SO<sub>4</sub> aqueous solution with excellent specific energy ( $E_{\text{sp}}$ ) and power densities, respectively. The obtained stability ( $\sim 88\%$ ) was found better even after 5000 cycles at a same current density. The reported cobalt (II) chloride doped graphene quantum dots (Co (II) Cl<sub>2</sub>–GQDs) can exhibit a reversible redox reaction of  $\text{Co}^{2+} \leftrightarrow \text{Co}^{4+}$  in KOH electrolyte (pH  $\sim 12$ ) with specific pseudocapacitance ( $C_{\text{s}} \sim 300$  F/g) were found to be more in comparison with GQDs [13]. Later on, different electrode materials were reported using GQDs by selecting different

metals like ceria [29], sulfur [14], Fe(II)S-GQDs [15], and NiCo<sub>2</sub>O<sub>4</sub>-GQDs [16] which exhibits higher specific capacitance with good cyclic stability in different electrolyte which are given in Table 1. These all various electrode materials have potential applications that can be drawn out for a different varieties for inorganic salt electrodes. Conducting nanofibers were prepared by using polyvinyl alcohol (PVA), GQDs, and poly(3,4-ethylenedioxythiophene) (PEDOT) can be used in symmetrical supercapacitor applications through electro-spinning and electro-polymerization tools which exhibits higher  $C_{sp}$  (~291.86 F/g), higher energy with more specific power at 2.0 A/g, superior stability with retention rate (~98%) even after 1000 cycles in comparison with PVA/PEDOT ( $C_{sp}$  ~ 220.73 F/g), and PEDOT ( $C_{sp}$  ~ 161.48 F/g) [65]. Furthermore, GOQDs@NiAl-LDH electrode material was reported [66] with  $C_{sp}$  ~ 869 F/g at 1 A/g with retention rate (~69.6%) after increment in cycles (~2000). In addition, Mn<sub>3</sub>O<sub>4</sub>-graphene QDs [67], multilayer NiO@Co<sub>3</sub>O<sub>4</sub>@graphene quantum dots hollow spheres [68], and NiCo<sub>2</sub>O<sub>4</sub>@GQDs composite [69] demonstrated supercapacitors electrode material which will be a promising energy storage and power output technologies that can be used for practical energy conversion and storage devices for enhanced high-tech supercapacitors. But still it is more challenging to get higher specific capacitance experimentally, which is far away from the theoretical calculations due to low electrical conductivity as well as blockage in migration of ions channels for thick electrodes. Table 1 explains the summary of all parameters such as electrode material, electrolyte, capacity or retention rate, and specific capacitance from cyclic voltammetry measurements.

### 3.2 Batteries

Lithium and sodium batteries have been widely developed due to their unique properties such as higher capacity, longer life cycle, and lower cost. In addition, the use of GQDs as a supporting material helps in enhancing the electrical features of the batteries. TiO<sub>2</sub> has been widely used which acts as an anode in Li-ion batteries. A lot of experiments were done by using these composites such as TiO<sub>2</sub>/GQDs [70], GQDs-Si [71], GPE-PAVM:QD [72], and VO<sub>2</sub>@GQD [73] applied on Li-ion battery have led to enhance the performance in batteries. Such kind of improvements are very cost effective. Therefore, GQDs are supposed to be suitable material which provides better energy storage in practical as well as commercial worthwhile.

### 3.3 Fuel Cell

The electricity was generated by fuel cell through a reaction of hydrogen fuel reacts with oxygen electrochemically. Fuel cells can supply of electricity with the constant flow of fuel and oxygen to carry on the reaction chemically. These energy-related tools are ecological and eco-friendly. The various kind of these cells were reported

**Table 1** Comparison table of different parameters for various electrode materials

Materials for WE	( $C_{SF}$ ) (in $\mu\text{F}/\text{cm}^2$ ) or (in F/g)	Electrolyte	$C_Y/C_R$ (%) with no of cycles	References
GQDs//MnO <sub>2</sub> AMSCs; GQDs//GQDs; GQDs//GQDs SMSCs	1107.4; 468.1	Na <sub>2</sub> SO <sub>4</sub> (0.5 M) and EMIMBF <sub>4</sub> /AN (2 M)		[60]
aQD film	236			[61]
GQD–3DG composite for 10 h	268	Conc. H <sub>2</sub> SO <sub>4</sub> Sol	>90%	[62]
GQDP	1044		80.1% after 3000	[63]
GQD-HNT NC	363	Na <sub>2</sub> SO <sub>4</sub> aq sol	88% after 5000 cycles	[64]
Co(II)Cl <sub>2</sub> -GQDs	300	KOH aq Sol	—	[13]
Fe(II)S-GQDs	476.2	K <sub>4</sub> Fe(CN) <sub>6</sub>	—	[15]
NiCo <sub>2</sub> O <sub>4</sub> /GQDs	481.4	KOH aq sol	65.88% after 300 cycles	[16]
PVA-GQD/PEDOT	291.86	H <sub>2</sub> SO <sub>4</sub> aq solution	98% after 1000 cycles	[65]
GOQDs@NiAl-LDH	869	—	69.6% after 2000 cycles	[66]
Mn <sub>3</sub> O <sub>4</sub> -GQDs	452.72	KOH aq sol	72% after 100 cycles	[67]
NiO@Co <sub>3</sub> O <sub>4</sub> @graphene quantum dots hollow spheres	1361		76.4% after 3000 cycles	[68]
NiCo <sub>2</sub> O <sub>4</sub> @ GQDs composite	1242	KOH sol	99% after 4000	[69]

WE—working electrode;  $C_{SF}$ —specific capacitance; and  $C_Y/C_R$ —capacity/capacity retention rate; NC—nanocomposites

which are essential components [74, 75]. The costly metals like palladium (Pd), platinum (Pt), silver (Ag), and gold (Au), etc., were used to prepare the electrode materials which leads to expensive fuel cells which is not easily affordable. After doing a lot of research, the functionalized GQDs can be used as efficient electrodes for fuel cells and hence as a result, there was an improvement of the catalytic activity as well as stability [76, 77]. Now onward, GQDs have been widely used as cathode materials for fuel cell.

### 3.4 Photovoltaic Thin Films Solar Cells

Solar cells are a renewable energy source, which converts sunlight to electricity exhibits clean environment. There is a development of various solar cells due to unique characteristics of GQDs to improve the power conversion efficiency. Some of the well-known solar cells have been founded such as “silicon (Si) [78], cadmium telluride (CdTe) [79–82], polymers [83–85], silicon/GQD heterojunction [86], semiconductor/GQD [87], and conductive polymer-doped GQD solar cells [78].” The almost popular solar cells are considered to be combination for “hybrid of Si and GQDs” with improved power conversion efficiency (~16.55%). Also, a “crystalline silicon with GQD heterojunction solar cell with a conversion efficiency of 6.63%” [78] was also reported. They designed energy band structure of GQDs in such way resulting more and more electron–hole pairs will be photo-generated which have been separated at the junction interface. Along that, it helps to prevent carrier recombination at the anode via electron blocking layer. The increment in “open-circuit voltage ( $V_{oc}$ )” of the device was observed, while the “short-circuit current ( $J_{sc}$ )” decreased with decrease in size. As a result, barrier in heterojunction increased due to increment in hole transportation. A dissociation and absorption improvement of “poly-3-hexyl thiophene (P3HT)” mixed with GQDs in the organic solar cell system were reported [88]. In addition, P3HT acting as a donor, phenyl-C61-butyric acid methyl ester (PCBM) as an acceptor, and polyethylene glycol (PEG) as an adhesive agent were used to make an improvement in interaction between active layers of GQDs. They did three different trials with chain lengths of PEG. The stronger electronic effect in the active layer in P3HT was observed due to shorter PEG chains. Their findings demonstrate that improved optical absorption by presence of rich functional groups in GQDs which increase  $J_s$ . Also, the fill factors and power conversion efficiency (~7.6%) were increased due to higher conductivity in GQDs. At last, GQDs have potential applications as hybrid materials which enhanced the bending flexibility of the organic solar cells. Thus, the investigation of unique features of GQDs will proceed to be a part of solar cells future technologies.

## 4 Conclusions and Future Challenges

In this section, we discussed various fabrication methods of GQDs. The main fabrication method for the preparation of GQDs was based on cleavage of carbon materials through the repetition of oxidation and reduction. The most important characteristics that are highlighted in this chapter are simple fabrication process with low cost, uniform morphology with optical properties, and high quantum yields. The various optical behaviors of GQDs have been discussed. The role of functionalized luminescent GQDs plays an important role to optimize and boost PL properties. The variation in PL colors was obtained due to lack of understanding of PL mechanism. Since after discovery in 2010, graphene material became so popular because

of their unique physical and chemical features. However, many researchers put a significant effort for the applications of GQDs which are basically fragments of graphene. We discussed how GQDs are significant material which we are likely to be useful for many applications like supercapacitors, lithium-ion batteries, electrodes, fuel cells, and photovoltaic thin films solar cells. We have been concisely introduced different fabrication methods of producing GQDs and discussed their current energy storage applications. It is necessary to some new methods for fabrication of GQDs to remove present moieties that might be reason not getting high PL QY. We require novel methods to achieve high PL QY which should not require the complete removal of graphitic impurities as a precursor material entirely for future developments. In addition, there were reproducibility issues during synthesis of photovoltaic thin films devices which effects in conversion efficiency although GQDs are supposed to perform a crucial role in specific devices. The uniform size and molecules on surface are essential to be tuned during the preparation of effective devices. All these critical issues need to be solved for further development. We expect that future researchers will investigate new methods to solve these difficulties.

**Acknowledgements** Department of Science and Technology, New Delhi, India, under “Women Scientist Scheme A” (DST WOS-A) provides the financial support for this whole research work with reference number SR/WOS-A/PM-107/2017.

## References

1. Iijima S (1991) Helical microtubules of graphitic carbon. *Nature* 354:56–58
2. Novoselov KS, Geim AK, Morozov SV, Jiang D, Zhang Y, Dubonos SV, Grigorieva IV, Firsov AA (2004) Electric field effect in atomically thin carbon films. *Science* 306:666–669
3. Hummers WS, Offeman RE (1958) Preparation of graphitic oxide. *J Am Chem Soc* 80:1339
4. Yan X, Cui X, Li LS (2010) Synthesis of large, stable colloidal graphene quantum dots with tunable size. *J Am Chem Soc* 132(17):5944–5945
5. Yan X, Cui X, Li B, Li L-S (2010) Large, Solution-Processable Graphene Quantum Dots as Light Absorbers for Photovoltaics. *Nano Lett* 10:1869–1873
6. Sandeep Kumar G, Roy R, Sen D, Ghorai UK, Thapa R, Mazumder N, Saha S, Chattopadhyay KK (2014) Amino-functionalized graphene quantum dots: origin of tunable heterogeneous photoluminescence. *Nanoscale* 6:3384–3391
7. Lim SY, Shen W, Gao Z (2015) Carbon quantum dots and their applications. *Chem Soc Rev* 44:362–381
8. Tang Q, Zhu W, He B, Yang P (2017) Rapid conversion from carbohydrates to large-scale carbon quantum dots for all-weather solar cells. *ACS Nano* 11:1540–1547
9. Song SH, Jang M-H, Chung J, Jin SH, Kim BH, Hur S-H, Yoo S, Cho Y-H, Jeon S (2014) Highly efficient light-emitting diode of graphene quantum dots fabricated from graphite intercalation compounds. *Adv Opt Mater* 11:1016–1023
10. Park J, Moon J, Kim C, Kang JH, Lim E, Park J, Lee KJ, Yu S-H, Seo J-H, Lee J, Heo J, Tanaka N, Cho S-P, Pyun J, Cabana J, Hong BH, Sung Y-E (2016) Graphene quantum dots: structural integrity and oxygen functional groups for high sulfur/sulfide utilization in lithium sulfur batteries. *NPG Asia Mater* 5:272
11. Raeyani D, Shojaei S, Ahmadi-Kandjani S (2018) Optical graphene quantum dots gas sensors: theoretical study. *Superlattice Microst* 114:321–330



12. Wang Z, Xia J, Zhou C, Via B, Xia Y, Zhang F, Li Y, Xia L, Tang J (2013) Synthesis of strongly green-photoluminescent graphene quantum dots for drug carrier. *Coll Surf B Biointerfaces* 112:192–196
13. Kharangarh PR, Umopathy S, Singh G, Sharma RK, Kumar A (2017) High performance pseudocapacitor electrode materials: Cobalt(II)chloride–GQDs electrodes. *Emerg Mater Rese (EMR)* 6(2):227–233
14. Kharangarh PR, Singh G (2019) Facile synthesis of sulfur doped graphene quantum dots for high performance supercapacitance applications. *Inte Ferroelect* 202:163–170
15. Kharangarh PR, Gupta V, Singh A, Bhardwaj P, Grace AN (2020) An efficient pseudocapacitor electrode material with co-doping of iron (II) and sulfur in luminescent graphene quantum dots. *Diam Relat Mater* 107:107913
16. Kharangarh PR, Ravindra NM, Rawal R, Singh A, Gupta V (2021) Fabrication of NiCo<sub>2</sub>O<sub>4</sub>/GQD composites as a superior supercapacitor electrode material. *J Alloys Comp*:159990
17. Tang L, Ji R, Cao X, Lin J, Jiang H, Li X, Teng KS, Luk CM, Zeng S, Hao J, Lau SP (2012) Deep ultraviolet photoluminescence of water-soluble self-passivated graphene quantum dots. *ACS Nano* 6:5102–5110
18. Pan D, Guo L, Zhang J, Xi C, Xue Q, Huang H, Li J, Zhang Z, Yu W, Chen Z, Li Z, Wu M (2012) Cutting sp<sup>2</sup> clusters in graphene sheets into colloidal graphene quantum dots with strong green fluorescence. *J Mater Chem* 22:3314–3318
19. Ain NU, Eriksson MO, Schmid S, Asghar M, Lin PC, Holtz PO, Syvajarvi M, Yazdi GR (2016) Tuning the emission energy of chemically doped graphene quantum dots. *Nanomaterials* 6:198
20. Zhou X, Zhang Y, Wang C, Wu X, Yang Y, Zheng B, Wu H, Guo S, Zhang J (2012) Photofenton reaction of graphene oxide: a new strategy to prepare graphene quantum dots for DNA cleavage. *ACS Nano* 6:6592–6599
21. Kashani HM, Madrakian T, Afkhami A (2017) Highly fluorescent nitrogen-doped graphene quantum dots as a green, economical and facile sensor for the determination of sunitinib in real samples. *New J Chem* 41:6875–6882
22. Lin Y, Chapman R, Stevens MM (2015) Integrative self-assembly of graphene quantum dots and biopolymers into a versatile biosensing toolkit. *Adv Funct Mater* 25:3183–3192
23. Li Y, Hu Y, Zhao Y, Shi G, Deng L, Hou Y, Qu L (2011) An electrochemical avenue to green-luminescent graphene quantum dots as potential electron-acceptors for photovoltaics. *Adv Mater* 23:776–780
24. Li J, Xu L, Wang T, Song J, Chen J, Xue J, Dong Y, Cai B, Shan Q, Han B, Zeng H (2017) 50-fold EQE improvement up to 6.27% of solution-processed all-inorganic perovskite CsPbBr<sub>3</sub>QLEDs via surface ligand density control. *Adv Mater* 29:1603885
25. Li X, Wu Y, Zhang S, Cai B, Gu Y, Song J, Zeng H (2016) CsPbX<sub>3</sub> quantum dots for lighting and displays: room-temperature synthesis, photoluminescence superiorities, underlying origins and white light-emitting diodes. *Adv Funct Mater* 26:2435–2445
26. Kharangarh PR, Singh V, Singh G (2019) Synthesis and optical properties of Zn (II) doped graphene quantum dots: blue to purple emission. *AIP Conf Proc* 2142:060007
27. Kharangarh PR, Umopathy S, Singh G (2018) Thermal effect of sulfur doping for luminescent graphene quantum dots. *ECS J Solid State Sci Technol* 7(3):M29–M34
28. Kharangarh PR, Umopathy S, Singh G (2018) Investigation of sulfur related defects in graphene quantum dots for tuning photoluminescence and high quantum yield. *Appl Surf Sci* 449:363–370
29. Kharangarh PR, Umopathy S, Singh G (2017) Synthesis and luminescence of ceria decorated graphene quantum dots (GQDs): evolution of band gap. *Integr Ferroelectr* 184(1):114–123
30. Kharangarh PR, Umopathy S, Singh G (2017) Effect of defects on quantum yield in blue emitting photoluminescent nitrogen doped graphene quantum dots. *J Appl Phys* 122:145107(1–7)
31. Pan D, Zhang J, Li Z, Wu M (2010) Hydrothermal route for cutting graphene sheets into blue-luminescent graphene quantum dots. *Adv Mater* 22:734–738

32. Tetsuka H (2019) Nitrogen-functionalized graphene quantum dots: a versatile platform for integrated optoelectronic devices. *20*:429–439
33. Kumar GS, Roy R, Sen D, Kumar Ghorai U, Thapa R, Mazumder N, Saha S, Chattopadhyay KK (2014) Amino-functionalized graphene quantum dots: origin of tunable heterogeneous photoluminescence. *Nanoscale* 6:3384–3391
34. Zuo W, Tang L, Xiang J, Ji R, Luo L, Rogée L, Lau S (2017) Functionalization of graphene quantum dots by fluorine: Preparation, properties, application, and their mechanisms. *Appl Phys Lett* 110:221901
35. Qian F, Li X, Tang L, Lai SK, Lu C, Lau S (2016) Potassium doping: tuning the optical properties of graphene quantum dots. *AIP Adv* 6:075116
36. Zhao J, Tang L, Xiang J, Ji R, Yuan J, Zhao J, Yu R, Tai Y, Song L (2014) Chlorine doped graphene quantum dots: preparation, properties, and photovoltaic detectors. *Appl Phys Lett* 105:111116
37. Yang S, Sun J, He P, Deng X, Wang Z, Hu C, Ding G, Xie X (2015) Selenium doped graphene quantum dots as an ultrasensitive redox fluorescent switch. *Chem Mater* 27(6):2004–2011
38. Yang P, Su J, Guo R, Yao F, Yuan C (2019) B, N-Co-doped graphene quantum dots as fluorescence sensor for detection of  $Hg^{2+}$  and  $F^{-}$  ions. *Anal Methods* 11:1879–1883
39. Ouyang Z, Lei Y, Chen Y, Zhang Z, Jiang Z, Hu J, Lin Y (2019) Preparation and specific capacitance properties of sulfur, nitrogen co-doped graphene quantum dots. *Nanoscale Res Lett* 14:219
40. Aghdam TR, Shariatnia Z, Hakkarainen M, Asl V.H (2020) Nitrogen and phosphorous doped graphene quantum dots: excellent flame retardants and smoke suppressants for polyacrylonitrile nanocomposites. *J Haz Mater* 381:121013
41. Shin Y, Park J, Hyun D, Yang J, Lee J-H, Kim J-H, Lee H (2015) Acid-free and oxone oxidant-assisted solvothermal synthesis of graphene quantum dots using various natural carbon materials as resources. *Nanoscale* 7:5633–5637
42. Li L, Ji J, Fei R (2012) A facile microwave avenue to electrochemiluminescent two-color graphene quantum dots. *Adv Funct Mater* 22:2971–2979
43. Zhang CF, Cui YY, Song L (2016) Microwave assisted one-pot synthesis of graphene quantum dots as highly sensitive fluorescent probes for detection of iron ions and pH value. *Talanta* 150:54–60
44. Lu LQ, Zhu YC, Shi C (2016) Large-scale synthesis of defect-selective graphene quantum dots by ultrasonic-assisted liquid-phase exfoliation. *Carbon* 109:373–383
45. Luo ZM (2016) Microwave-assisted preparation of white fluorescent graphene quantum dots as a novel phosphor for enhanced white-light-emitting diodes. *Adv Func Mater* 6:2739–2744
46. Zhou CF, Jiang W, Via BK (2014) Facile synthesis of soluble graphene quantum dots and its improved property in detecting heavy metal ions. *Coll Surf B Biointerfaces* 118:72–76
47. Lim CS, Hola K, Ambrosi A, Zboril R, Pumera M (2015) Graphene and carbon quantum dots electrochemistry. *Electrochem Commun* 52:75–79
48. Shinde DB, Pillai VK (2012) Electrochemical preparation of luminescent graphene quantum dots from multiwalled carbon nanotubes. *Chem Eur J* 18:12522–12528
49. Bayat A, Iranzad ES (2017) Synthesis of green-photoluminescent single layer graphene quantum dots: determination of HOMO and LUMO energy states. *J Lumin* 192:180–183
50. Dong YQ, Shao JW, Chen CQ (2012) Blue luminescent graphene quantum dots and graphene oxide prepared by tuning the carbonization degree of citric acid. *Carbon* 50:4738–4743
51. Zhou L, Geng JL, Liu B (2013) Graphene quantum dots from polycyclic aromatic hydrocarbon for bioimaging and sensing of  $Fe^{3+}$  and hydrogen peroxide. *Part Part Syst Char* 30:1086–1092
52. Teymourinia H, Niasari MS, Amiri O (2017) Synthesis of graphene quantum dots from corn powder and their application in reduce charge recombination and increase free charge carriers. *J Mol Liq* 242:447–455
53. Wang Z, Yu J, Zhang X (2016) Large scale and controllable synthesis of graphene quantum dots from rice husk biomass: a comprehensive utilization strategy. *ACS Appl Mater Interfaces* 8:1434–1439

54. Bian SY, Chao S, Qian YT (2017) Facile synthesis of sulfur-doped graphene quantum dots as fluorescent sensing probes for Ag<sup>+</sup> ions detection. *Sens Actuators B Chem* 242:231–237
55. Xia X, Tu J, Zhang Y, Wang X, Gu C, Zhao X et al (2012) High-quality metal oxide core/shell nanowire arrays on conductive substrates for electrochemical energy storage. *ACS Nano* 6:5531–5538
56. Yu G, Hu L, Liu N, Wang H, Vosgueritchian M, Yang Y (2011) Enhancing the supercapacitor performance of graphene/MnO<sub>2</sub> nanostructured electrodes by conductive wrapping. *Nano Lett* 11:4438–4442
57. Li Y, Wang Q, Wang Y, Bai M, Shao J, Ji H, Feng H, Zhang J, Ma X, Zhao W (2019) A flexible and conductive metallic paper-based current collector with energy storage capability in supercapacitor electrodes. *Dalt Trans* 48:7659–7665
58. Zhao X, Zhang Q, Chen C, Zhang B, Reiche S, Wang A et al (2012) Aromatic sulfide, sulfoxide, and sulfone mediated mesoporous carbon monolith for use in supercapacitor. *Nano Energy* 1:624–630
59. Zhang Z, Zhang J, Chen N, Qu L (2012) Graphene quantum dots: an emerging material for energy-related applications and beyond. *Energy Environ Sci* 5:8869–8890
60. Liu WW, Feng YQ, Yan XB, Chen JT, Xue QJ (2013) Superior micro-supercapacitors based on graphene quantum dots. *Adv Funct Mater* 23:4111–4122
61. Hassan M, Haque E, Raghava Reddy K, Minett AI, Chen J, Gomes VG (2014) Edge-enriched graphene quantum dots for enhanced photo-luminescence and supercapacitance. *Nanoscale* 6:11988
62. Chen Q, Hu Y, Hu C, Cheng H, Zhang Z, Shao H, Qu L (2014) Graphene quantum dots–three-dimensional graphene composites for high-performance supercapacitors. *Phys Chem Chem Phys* 16:19307
63. Mondal S, Rana U, Malik S (2015) Graphene quantum dot-doped polyaniline nanofiber as high performance supercapacitor electrode materials. *Chem Commun* 51:12365
64. Ganganboina AB, Chowdhury AD, Doong RA (2017) New avenue for appendage of graphene quantum dots on halloysite nanotubes as anode materials for high performance supercapacitors. *ACS Sustain Chem Eng* 5:4930–4940
65. Jannah Syed Zainol Abidin SN, Mamat S, Rasyid SA, Zainal Z, Sulaiman Y (2018) Fabrication of poly(vinyl alcohol)-graphene quantum dots coated with poly(3,4-ethylenedioxythiophene) for supercapacitor. *Polym Chem* 56:50–58
66. Han Y, Liu N, Wang N, He Z, Liu Q (2018) Assembly of Ni–Al layered double hydroxide and oxide graphene quantum dots for supercapacitors. *J Mater Res*:1–9
67. Ko Y, Son DI (2018) Synthesis and characterization of Mn<sub>3</sub>O<sub>4</sub>—graphene core—shell quantum dots for electrochemical pseudocapacitor applications. *J Korean Phys Soc* 72(10):1198–1202
68. Yin X, Zhi C, Sun W, Lv LP, Wang Y (2019) Multilayer NiO@Co<sub>3</sub>O<sub>4</sub>@graphene quantum dots hollow spheres for high-performance lithium-ion batteries and supercapacitors. *J Mater Chem A* 7:7800–7814
69. Luo J, Wang J, Liu S, Wu W, Jia T, Yang Z, Mu S, Huang Y (2019) Graphene quantum dots encapsulated tremella-like NiCo<sub>2</sub>O<sub>4</sub> for advanced asymmetric supercapacitors. *Carbon* 146:1–8
70. Zhang W, Xu T, Liu Z, Wu N-L, Wei M (2018) Hierarchical TiO<sub>2</sub>-x imbedded with graphene quantum dots for high-performance lithium storage. *Chem Commun* 54:1413–1416
71. Kong L, Yang Y, Li R, Li Z (2016) Phenylalanine-functionalized graphene quantum dot-silicon nanoparticle composite as an anode material for lithium ion batteries with largely enhanced electrochemical performance. *Electrochim Acta* 198:144–155
72. Chen Y-M, Hsu S-T, Tseng Y-H, Yeh T-F, Hou S-S, Jan J-S, Lee Y-L, Teng H (2018) Minimization of ion-solvent clusters in gel electrolytes containing graphene oxide quantum dots for lithium-ion batteries. *Small* 14:1703571
73. Chao D, Zhu C, Xia X, Liu J, Zhang X, Wang J, Liang P, Lin J, Zhang H, Shen ZX, Fan HJ (2015) *Nano Lett* 15:565–573
74. Bose S, Kuila T, Nguyen TXH, Kim NH, Lau K-T, Lee JH (2011) Polymer membranes for high temperature proton exchange membrane fuel cell: recent advances and challenges. *Prog Polym Sci* 36:813–843

75. Singhal SC (2000) Advances in solid oxide fuel cell technology. *Solid State Ionics* 135:305–313
76. Fei H, Ye R, Ye G, Gong Y, Peng Z, Fan X, Samuel ELG, Ajayan PM, Tour JM (2014) Boron- and nitrogen-doped graphene quantum dots/graphene hybrid nanoplatelets as efficient electrocatalysts for oxygen reduction. *ACS Nano* 8:10837–10843
77. Dhand A, Suresh S, Jain A, Varadan ON, Kerawalla MAK, Goswami P (2017) Advances in materials for fuel cell technologies-a review. *Int. J. Res. Appl. Sci. Eng. Technol.* 5(2017):1672–1682
78. Gao P, Ding K, Wang Y, Ruan K, Diao S, Zhang Q, Sun B, Jie J (2014) Crystalline Si/graphene quantum dots heterojunction solar cells. *J Phys Chem C* 118:5164–5171
79. Kharangarh P, Georgiou GE, Chin KK (2013) Impact of copper back contact in CdTe solar cells by using C-V-T measurements. *Emerg Mater Res (EMR)* 3(2):106–111
80. Kharangarh P, Misra D, Georgiou GE, Chin KK (2013) Characterization of space charge layer deep defects in n+-CdS/p-CdTe solar cells by temperature dependent capacitance spectroscopy. *J Appl Phys* 113(14):144504(1–6)
81. Kharangarh P, Misra D, Georgiou GE, Chin KK (2012) Evaluation of Cu back contact related deep defects in CdTe solar cells. *ECS J Solid State Sci Technol* 1(5):Q110–Q113
82. Kharangarh P, Misra D, Georgiou GE, Chin KK (2011) Investigation of electrically active defects in n+CdS/p-CdTe solar cells. *ECS Trans* 41(4):233–240
83. Ding Z, Hao Z, Meng B, Xie Z, Liua J, Dai L (2015) Few-layered graphene quantum dots as efficient hole-extraction layer for high-performance polymer solar cells. *Nano Energy* 15:186–192
84. Yang HB, Dong YQ, Wang X, Khoo SY, Liu B, Li CM (2013) Graphene quantum dots-incorporated cathode buffer for improvement of inverted polymer solar cells. *Sol Energy Mater Sol Cell* 117:214–218
85. Gupta V, Chaudhary N, Srivastava R, Sharma GD, Bhardwaj R, Chand S (2011) Luminescent graphene quantum dots for organic photovoltaic devices. *J Am Chem Soc* 133:9960–9963
86. Dutta M, Sarkar S, Ghosh T, Basak D (2012) ZnO/graphene quantum dot solid-state solar cell. *J Phys Chem C* 116:20127–20131
87. Chen L, Guo CX, Zhang Q, Lei Y, Xie J, Ee S (2013) Graphene quantum-dot doped polypyrrole counter electrode for high-performance dye-sensitized solar cells. *ACS Appl Mater Interfaces* 5:2047–2052
88. Novak TG, Kim J, Song SH, Jun GH, Kim H, Jeong MS (2016) Fast P3HT exciton dissociation and absorption enhancement of organic solar cells by PEG-functionalized graphene quantum dots. *Small* 12:994–999

# Chapter 7

## Recent Progress of Carbonaceous Materials in Third Generation Solar Cells: DSSCs



Nandhakumar Eswaramoorthy, Ravuri Syamsai, Senthilkumar Nallusamy, Selvakumar Pitchaiya, and M. R. Venkatraman

### 1 Introduction

Presently, environmental pollutions, especially issues with the air pollutions due to the usage of fossil fuels, have attracted increasing amounts of research efforts. Fuels, driven by solar energy, is a hypothetically approach for resolving these glitches. Since, solar energy is considered to be one of the cleanest and largest exploitable energy resources that can potentially encounters the need for world's energy elsewhere fossil fuels pollutant energy sources. In the world of photovoltaic (PV) technology, solid-state thin film-based technologies are one of the most feasible approaches to address the world's expanding energy needs by converting the abundant solar energy into electricity [1, 2]. Among various emerging third generation thin film solar cell technology (organic solar cells (OSCs) and dye-sensitized

---

N. Eswaramoorthy  
School of Mechanical Engineering, Vellore Institute of Technology, Vellore, Tamil Nadu 632014, India

R. Syamsai  
Nanotechnology Research Center, SRM Institute of Science and Technology, Kattankulathur, Tamil Nadu 603203, India

S. Nallusamy  
Department of Electronics and Communication Engineering, M. Kumarasamy College of Engineering, Karur, Tamil Nadu 639113, India

S. Pitchaiya (✉)  
Department of Engineering and Sciences, Western Norway University of Applied Sciences, Bergen, Norway  
e-mail: [sharewithselva@gmail.com](mailto:sharewithselva@gmail.com)

M. R. Venkatraman (✉)  
Department of Physics, Dr. NGP Arts and Science College, Coimbatore, Tamil Nadu 641035, India  
e-mail: [venk.phy@gmail.com](mailto:venk.phy@gmail.com)

solar cells (DSSCs)), perovskite solar cells (PSCs) have technologically advanced as an efficient solution for commercial deployment at low-cost. Nonetheless, holding facile material preparation approaches and low-cost device fabrication expenditures promises a commercialization viability [3–5]. Presently, perovskite devices are at the integral attention owing to their striking optoelectronic research application within two decades of research effort. However, one of their major hindrances of bringing these PSCs to a pilot and therefore market viability is their meager long-standing device steadiness [6]. Hence, vital measures for achieving extended device stability are; remolding the active/transporting layer interfaces by substituting suitable and exhibiting stable peer materials, or by entailing more counter balanced add-ons-based materials into the precursors.

In this context, carbonaceous materials are found to be the best candidates for the past few decades exhibiting higher durability, cost-effective, and at the ready accessible and market viable production. To begin with, carbonaceous materials was initially introduced as an electrode material. With their novel optoelectronic behaviors, were further deployed as an effective hole transporter in promising third generation solar cells. Later it was found to be an ideal material exhibiting an ideal work function (5.0 eV) equivalent to that of the high-cost back contact materials: Pt/Au/Ag/Al in third generation solar cells. Furthermore, these carbon-based materials can be facile deposal using commonly available deposition approaches as follows; spray-coating, spin deposition, doctor-blade method, inkjet/3D printing and the roll-roll fabrication method [7, 8]. Nevertheless, carbon materials known for their gleaming dual role (both as an electrode cum back contact) in HTL-free PSC devices, attracted researchers to emphasize on carbon-based materials [9]. In this regard, recent researchers have started deploying several carbonaceous materials (graphene oxide (GO), reduced graphene oxide (rGO) and CNT (single and multi-walled)) as their electrode cum transporting materials. Yang et al. [10] established at first on using the carbon material as both a hole transporter and as a back contact electrode in HTL-free PSC devices. To improve the long-standing stability and enhanced efficiency of the fabricated devices at low-cost, carbonaceous materials will be the key source in replacing unstable and high-cost organic small molecules and long polymer-based HTMs [11, 12].

This chapter rationales to offer a brief analysis on the advances in research area for the enhancement of the PV performances in third generation energy harvesting devices by utilizing various carbonaceous (0-dimensional quantum dots to 3-dimensional carbon black) and their derivative materials in an effort greatly enhance the device's efficiency as well as its long-term stability. It is concluded with the result that carbon-based materials play a crucial role in providing long-term stable and low-cost solar cells for scale-up and commercialization.

## 2 History of Solar Cells

In 1839, Alexandre Edmond Becquerel [13] reported the photovoltaic effect for the first time in a semiconductor/liquid junction-based cell. Two electrodes of platinum coated with silver halide-based materials, which were separated by a membrane when kept inside an acidic electrolyte bath under illumination produced electricity. It was also observed that there is change in current with respect to the wavelength of the illuminated light and the current generation was maximum for the blue light.

On the other hand, photovoltaic effect for the first time in solid junction-based cell was discovered in 1877 by Day and Adams [14]. Two platinum wires were connected to the opposite ends a solid selenium bar like structure, and under the illumination of light it produced detectable amount of current. Though the authors during that time reported that it is due to the crystallization process, in the later stage after a significant development in the semiconductor research it was found to be a photovoltaic phenomenon. Following this in 1883 Fritts [15] developed a selenium-based thin film PV device where selenium in molten state was introduced between gold and another metal (other than gold), in which a gold/selenium junction was able to generate current under illumination. Further several other materials such as copper/copper oxide, thallium metal-based sulfides and so forth were tried by different researchers. A major breakthrough in solid junction-based solar cells was achieved by Scaff and Ohl [16], through the invention of p–n junction in 1940, which on further improvement in 1954 [17], led to a silicon solar cell with an efficiency of 6%, now after a series of developments silicon-based solar cells have reached efficiencies over 35% using multiple junction and concentrator-based technologies.

## 3 Generation of Solar Cells

The solar cells are generally categorized into different generations, based on the technology, the preparation method and its evolution [18]. The first-generation solar cells consist of different type of wafer-based technologies predominantly based on silicon. Monocrystalline, polycrystalline and amorphous silicon-based solar cells fall under this category. These, silicon-based solar cells have been studied intensively in the last 50 years and have developed commercial modules with an efficiency of above 20% [19]. Though silicon is among the most a substantial amount of material in the earth's crust which exists in the form of silicon di oxide, these solar cells require high quality silicon which involves purification of silicon in a reactor at a temperature of 1000–1200 °C.

Polycrystalline wafers were made by melting down the silicon and the molten silicon was made into blocks and were further cut into wafers. Monocrystalline silicon solar cells were grown by crystal growth technique known as Czochralski method [20], here crystal ingot is formed by dipping the crystal nucleus in the molten silicon and it is withdrawn and rotated in a way that cylindrical ingot is formed, and the

formed ingot was found to be devoid of defects. These crystals were cut into slices in the form of wafers. As the monocrystalline silicon has less lattice imperfection, the power conversion efficiencies were found to be higher than the other two counterparts. Amorphous silicon solar cells are based on coating of thin layer of amorphous Si over a conducting substrate and are used in solar cells. Though the efficiencies were less compared to crystalline silicon solar cells, these are used in low power applications and it also has the advantage of being used in flexible solar cells.

Second generation solar cells are the thin film-based cells, which have also entered into the commercial market. As these cells require only low quantity material for coating, they have the potential for low-cost production. Gallium Arsenide (GaAs), Cadmium telluride (CdTe), Copper Indium Selenide (CIS), Copper Zinc Tin Sulfide (CZTS), Copper Indium Gallium Selenide (CIGS)-based solar cells fall under this category [21]. For selected configurations, power conversion efficiencies of about 20% have been obtained [22] at the laboratory scale and above 15% have been obtained in the commercial modules, respectively. Still the usage of toxic material such as arsenide, cadmium and selenium and scarcity of materials such as indium and tellurium are considered as a limiting factor for a longer run. Copper Zinc Tin Sulfide (CZTS) which is the latest in this category has overcome all the disadvantages stated above. But being a quaternary material, the material formation is always complex, and it requires lot of prerequisites to be satisfied for the material to be of pure phase.

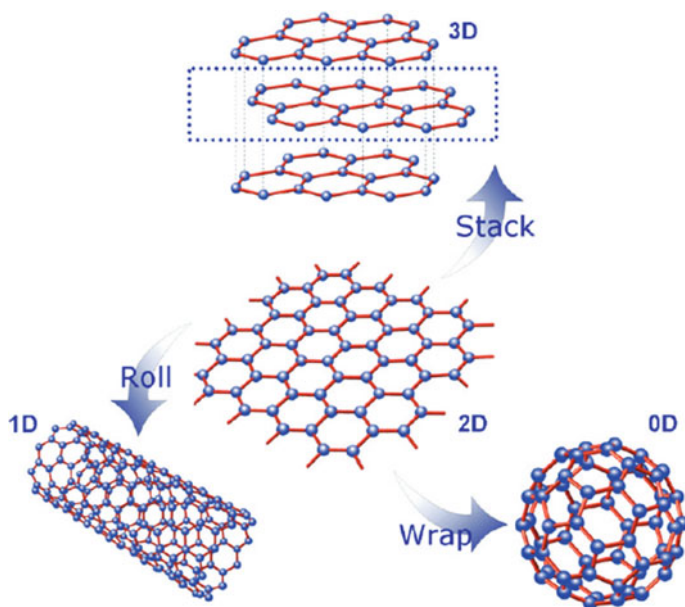
DSSC, QDSSC, perovskite solar cells and organic photovoltaics come under the category of third generation solar cells [23]. Dye-sensitized solar cells and quantum dot-sensitized solar cells which come under this category depends on the sensitizer for the light absorption and the electrons produced are transferred to the semiconductor layer, through which it reaches the outer circuit. Dye-sensitized solar cells and quantum dot-sensitized solar cells require redox electrolyte for the dye regeneration and a continuous process to occur. Whereas in perovskite solar cells a hole conductor is used, and the electrolyte leaking problem is not present here. However, dye-sensitized solar cells have the advantage of usage of low-cost material, low toxicity level and also its color can be tuned by changing the dye, this makes it a great prospect for window applications and more over they can also work under diffused light conditions. Quantum dot-based solar cells also has its advantage of tunable bandgap with respect to its size, still the efficiencies are very poor to hit the commercial market.

## 4 Classifications of Carbonaceous Materials

Carbon—the sixth element in the periodic table, which is the basis of all life forms, the most abundant among the other elements found in this universe, on earth and even in our human systems. Its ability to combine with different elements and molecules and its flexibility has attracted the interest of the scientific community. Figure 1 shows the existence of carbon in many forms is called allotropy as shown in are follows: grapheme (G), reduced graphene oxide (rGO), graphdiyne and carbon with



different structures of carbons such as nanotubes, fullerenes,  $C_{60}$ , carbon nanohorns, nanoonions, nanotori and nanowall—an advantageous property used by industrial and academic fields for a wide range of applications [24–27]. In the PV technology, carbonaceous materials—exhibiting an ideal work function (about  $-5.0$  to  $-5.1$  eV) is equivalent to that of the high-priced and high-conductivity gold electrode, which makes them a promising substitute for achieving enhanced photovoltaic performance. Due to their versatility, e.g., they exhibit different band energy orientations and their electronic properties can be tuned. Moreover, these carbon-based materials tend not to react with halides present in the perovskite structure and are therefore forgiving to ion migration, intrinsically stable and hydrophobic to moisture (and thus can act as water-repellent barriers). With these criteria, the usage of carbonaceous materials was found to be much beneficial in extending their long-term PSC device stability. Moreover, the fairly inexpensive and readily available fabrication of the carbonaceous materials on an industrial scale has promoted the commercialization of PSCs [27]. In addition, recent researchers have engrossed on fabricating PSCs with such carbon-based materials that tend to achieve superior charge transport architecture, which could be fundamental toward further increasing the performances of the constructed PSCs.



**Fig. 1** Different carbonaceous material structure. “Reproduced with reprinted with permission from Wan et al. [24]. Copyright 2009 American Chemical Society”

## 5 Dye-Sensitizer Solar Cells

Photo electrochemical cells are the basics for the dye-sensitized solar cells. The photovoltaic effect was first discovered in 1839 by Becquerel, a silver chloride dipped platinum foil was used as electrode in a bath containing electrolyte and counter electrode, this arrangement upon illumination developed a voltage between the junction and this was termed as photovoltage. But the concept behind sensitization of semiconductors was discovered around 1980s in the field of photography using silver halide coated semiconductor [28]. In both the processes the photo induced dye molecules inject an electron into the semiconductor conduction band. Further it was observed that when the same dye was chemisorbed onto the semiconductor surface the performance was enhanced and this led to the development of modern dye-sensitized solar cells.

Dye-sensitized solar cells based on zinc oxide was first published in 1972, where zinc oxide (ZnO) [29] was sensitized using chlorophyll and it showed the possibility of generation of electricity, by exciting the dye (chlorophyll) molecules using photons and the electrons were transferred to the outer circuit through the semiconductor. This work created a lot of interest among the research community working in the area of solar photovoltaics. But the efficiency was low and almost remained the same due to the poor surface area of the ZnO single crystals which were used as photo anode. As the dye being the light harvester here, the amount of dye adsorbed plays a significant role in the performance of these solar cells and the poor dye loading was identified as the reason behind the low efficiency in the ZnO-based solar cells. In 1991 Swiss scientist Professor Gratzel [30, 31] came up with a solution of using mesoporous  $\text{TiO}_2$  network to enhance the dye adsorption to a greater extent and it was considered as a breakthrough as the cell using this configuration of mesoporous  $\text{TiO}_2$  network along with the ruthenium based organic dyes exhibited an efficiency of over 7%.

The modern dye-sensitized solar cells consist of an anode, a cathode and an electrolyte. The anodes are also known as photoanodes as it holds the dye which is responsible for the absorption of light. The architecture of the dye-sensitized solar cell is given in the Fig. 2 Photoanode consists of a soda lime glass which is coated with transparent conducting oxide material such as fluorine doped tin oxide (FTO), making it to conduct electrons from the semiconductor to the outer circuit. A mesoporous wide bandgap semiconducting material is coated over the FTO and a dye is chemisorbed over the surface of the semiconductor. This whole setup is known as photoanode. The cathode consists of FTO plate typically coated with a thin layer of platinum or a carbon-based material. The cathode material should possess high catalytic property for the continuous compensation of the redox electrolyte. The redox electrolyte is used to make the oxidized dye to get back to its initial state and the electrolyte should also be able to percolate into the pores of the mesoporous semiconductor.

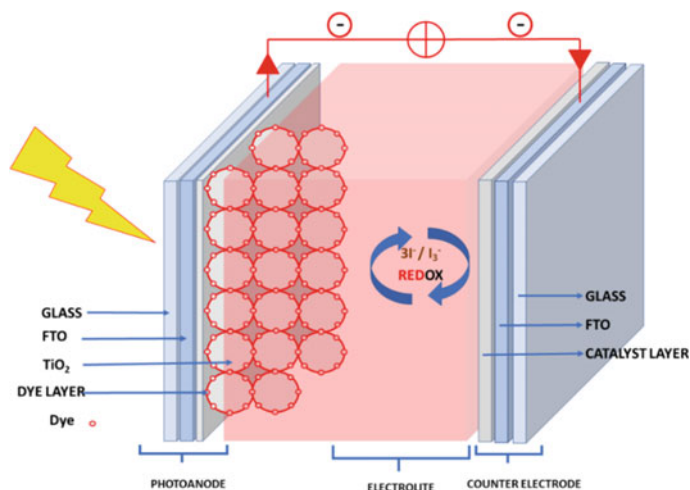


Fig. 2 Schematic diagram of dye-sensitized solar cell

### 5.1 The Factors that Play Crucial Role in the Selection of DSSC Compounds

#### Photoanode

The photoanode's purpose is to carry electrons from the chemisorbed dye to the outer circuit via the photoanode. The main requisite of a photoanode is it should be mesoporous in nature, which is essential for effective dye-loading. As a photoanode material, wide bandgap semiconductors are commonly employed because they are more stable under illumination. Narrow band gap materials, on the other hand, are not applied to avoid unwanted photo-corrosion. One strategy for improving the DSSC's energy conversion efficiency is to increase dye loading over the cross section of the photoanode [32]. To achieve a high dye loading capacity, mesoporous wide bandgap semiconductor semiconductors with a large surface area are preferred. The position of the conduction band, which must be lower than the dye's lowest unoccupied molecular orbital (LUMO) level for fast electron transfer to be feasible, is another essential consideration. Low toxicity, high chemical stability, high refractive index (which is required for light to diffuse throughout the entire mesoporous network), and high dielectric constant (which can reduce fast recombination of electrons at the semiconductor/dye interface site through electrostatic shielding) are the most commonly desired properties of a photoanode material.

#### Sensitizer

Light harvesting ability of the dye-sensitized solar cells is an important prospect, and it determines the efficiency of the dye-sensitized solar cell [33, 34]. Dye which is chemisorbed over the semiconductor surface is responsible for this. For the effective

functioning of the dye in the dye-sensitized solar cells, the following properties are desired for the dye. (I) Broader absorption spectrum to absorb most of the solar irradiation. (II) Higher molar extinction throughout the absorption spectrum. (III) Lowest unoccupied molecular orbital (LUMO) level of the dye should lie above the conduction band of the semiconductor for effective electron transfer. (IV) Potential of the highest unoccupied molecular orbital level of the dye should be positive compared to the redox electrolyte to avoid recombination of oxidized dye. (V) The lifetime of the excited state of the dye should be higher for an efficient electron transfer. (VI) The dye should have good solubility and it also should not get desorbed by the electrolyte. Organometallic dyes based on ruthenium are considered to be efficient sensitizers.

### **Redox electrolyte**

The work of the redox electrolyte in dye-sensitized solar cells is to regenerate the dye which gets oxidized after electron generation [35]. The redox in turn gets regenerated by the electron which enters from the outer circuit through the counter electrode side. For a good electrolyte to be used in DSSC, the following properties are desired. (1) Electrochemical potential of the electrolyte should be more negative compared to the dye for the reduction to take place. (2) The open circuit voltage of the cell depends on both counter electrode and electrolyte and the redox potential of it should be positive. (3) As the electrolyte regenerate the oxidized dye by providing an electron, it in turn gets oxidized and it should be reversible at the counter electrode surface for the continuous functioning of the cell and it also should not react with the photoanode. (4) The electrolyte should be able to transport up to 20 mA/cm<sup>2</sup> without any ohmic loss of significant value. (5) The long-term stability of the electrolyte is also important. Triiodide-based redox electrolytes (I<sup>-</sup>/I<sub>3</sub><sup>-</sup>) satisfy the above requirements and are used in DSSC.

### **Counter electrode**

A counter electrode's primary function is to collect and transport electrons from the outside circuit to the redox electrolyte. As a result, it should be conducting and have a minimal overvoltage for the reduction of the redox couple. If it has good optical reflection, then it may be useful for the light which gets transmitted through the photoanode to pass through the photoanode for a second time after suffering reflection from the counter electrode. Most effective counter electrodes used in dye-sensitized solar cells are the platinized FTO and carbon-based materials, respectively [36, 37].

## ***5.2 Components of Dye-Sensitized Solar Cell***

### **5.2.1 Transparent Conducting Oxide (TCO)**

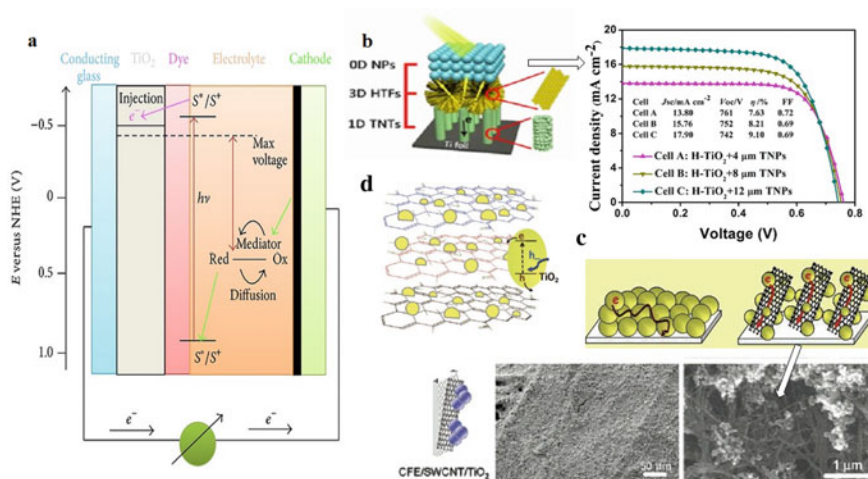
The work of a transparent conducting oxide substrate in dye-sensitized solar cell is to hold the semiconductor layer attached to it and it also acts a current collector.

Electrons produced by the dye reaches the TCO substrate through  $\text{TiO}_2$  and it further reaches the outer circuit. As most of the light enters the device through the TCO to reach the dye, the TCO should have high transparency in the visible region without any parasitic absorption and should have low electrical resistivity. Fluorine doped  $\text{SnO}_2$  (FTO) and Tin doped indium oxide (ITO) are the most used TCO. However, it has been reported that FTO is more stable than ITO at temperatures which is required for the  $\text{TiO}_2$  deposition ( $> 350\text{ }^\circ\text{C}$ ) [38]. Due to the increase in resistance of the ITO substrates at temperature above  $350\text{ }^\circ\text{C}$  it is not preferred and moreover, the corrosion resistance of FTO is also found to be higher. So, FTO substrates are generally preferred over ITO substrates as transparent conducting oxide in dye-sensitized solar cells.

### 5.2.2 Photoanodes

In general metal oxides such as  $\text{TiO}_2$  [39],  $\text{ZnO}$  [40],  $\text{SnO}_2$  [41] and  $\text{Nb}_2\text{O}_5$ , whose band gap was greater than 3 eV were employed as photoanodes [42, 43], a schematic of the typical DSSC was shown in the Fig. 3a The morphology and bandgap of these semiconducting materials greatly influence the overall efficiency of the solar cells. The photoanode performance was greatly affected by corrosion resistance, surface area, electronic conductivity, bandgap and the semiconducting material's morphology (0D, 1D, 2D and 3D) [44]. Various existing literature explains the effect of nanostructure morphology on the performance of the DSSCs [45–49]. Three crystalline forms of  $\text{TiO}_2$  were extensive studies as photoanode for DSSCs, namely, anatase, rutile and brookite, with 3.2 eV, 3.0 eV and 3.4 eV, respectively.  $\text{TiO}_2$  with 0D, 1D, 2D and 3D were also studied in detail for DSSCs [45, 50, 51].

0D  $\text{TiO}_2$  were advantageous for dye loading because of their high surface area [52, 53] On the other hand, the 1D structure of  $\text{TiO}_2$  has a better transport property with less surface area. Therefore, a hybrid of this 0D and 1D can provide high surface area and good electronic transport properties [54]. Also, 3D  $\text{TiO}_2$  hybrid morphologies can provide higher efficiency solar cells overcoming the drawback of the 0D and 1D  $\text{TiO}_2$ -based structures with good electronics, transport and surface area properties [54–56]. Qiang et al. used a  $\text{TiO}_2$ -1D/3D structure as shown in the Fig. 3b on a flexible titanium substrate and achieved an efficiency of 9.1% [56]. Mathew et al. proposed  $\text{TiO}_2$ -based nanoparticles-based film as a photoanode using a porphyrin-based sensitizer. They achieved an efficiency of 13% due to their high surface area and maximum dye loading, which can be boosted further by using single crystal  $\text{TiO}_2$  as these are extremely reactive [57]. also, the {001} of anatase  $\text{TiO}_2$  single crystal has more surface energy in comparison with {101} facets [58]. But these nanoparticles-based photoanodes are limited by lattice mismatch [12], crystallographic morphology random network and misaligned crystallites [59]. Localized surface plasmon resonance of the noble metals can be used as a strategy to improve the light scattering and total light absorption coefficient of the dye-sensitized photoanode of DSSC which in turn could be used to enhance the efficiency of the DSSC [60, 61]. It has also been reported that plasmonic metallic nanoparticles (NPs) can induce



**Fig. 3** **a** Schematic showing the construction and components of a DSSC cell (**a**) “Reprinted with permission from Yum et al. [43]. Copyright 2011 American Chemical Society”. **b** Schematic representation of  $\text{TiO}_2$  photoanodes with 0D TNPs on 1D/3D hybrid structure with J-V curves (**b**) “Reprinted with permission from Mehmood et al. [56]. Copyright 2008 American Chemical Society”. **c** Schematic explaining the importance of Nanotube support on electron transport along with SEM images of carbon fiber electrodes with dispersion of  $\text{TiO}_2$  NP on SWCNT at  $50 \mu\text{m}$  and  $1 \mu\text{m}$  (**c**) “Reprinted with permission from Kongkanand et al. [64]. Copyright 2007 American Chemical Society”. **d** Schematic of  $\text{TiO}_2$ /Graphene composite and its behavior under UV excitation, (**d**) “Reprinted with permission from Williams et al. [65]. Copyright 2008 American Chemical Society”

localized electric field which can excite dye molecules more effectively than far-field light and this can enhance the light absorption of the adsorbed dye molecules and this can increase the generation of photo-excited electrons [62]. Further, Kong et al. [63] proposed a method of an SWCNT to  $\text{TiO}_2$ -based catalyst to improve charge separation and carrier transport to electrode surface. This hybrid was successfully demonstrated with a proof change in fermi level equilibrium by 100 mV; overall efficiency was doubled [63, 64]. Whereas when SWCNT/MWCNT were employed with  $\text{TiO}_2$ , CNT's improved the roughness of the electrode and charge recombination properties and electronic transport properties as shown in Fig. 3c The maximum MWCNT was optimized to be at 0.3 wt% without compromising the cell efficiency. Graphene has better surface contact with the  $\text{TiO}_2$  than the MWCNT and SWCNT because of its phytochemical properties, charge transfer characteristics [65] as illustrated in Fig. 3d Overall, the graphene/ $\text{TiO}_2$  photoanode delivered efficiency of 6.97% with 0.6 wt% loading.

### 5.2.3 Electrolytes

The Electrolytes of DSSCs are one of the critical vital components deciding the overall efficiency. These electrolytes are responsible for regenerating dye and circuit closer by extending charge transport between photoanode and counter electrode. Extensive research and efforts are being made to engineer a stable and efficient electrolyte to match the 3rd generation solar cells to its theoretical values (Table 1).

The first DSSC prototype used an iodide/triiodide electrolyte redox couple without any additives with 7–8% efficiency. Later many formulations and additives were proposed and demonstrated with improved stability and performance and boosted the efficiency to 14% [84, 85]. Organic solvent-based electrolytes were mostly employed for DSSC because of their cost-effective, low light adsorption, non-toxicity and stability under irradiation and dark conditions with wide electrochemical potential window [61, 62, 86, 87]. ACN, one of the most preferred organic electrolytes for DSSC due to its chemical stability, low viscosity and solubility, and electrochemical potential window of > 4 V [87] with a maximum reported efficiency of 14%. But the stability and toxicity are still questionable. To solve these issues, alternatives such

**Table 1** Comparison of different electrolyte-based DSSCs

Type	Electrolyte	Jsc (mA/cm <sup>-2</sup> )	V <sub>oc</sub> (V)	FF (%)	PCE (%)	References
Liquid	Iodide/triiodide	12.71	0.667	0.53	4.50	[66]
	LiI/I <sub>2</sub> /4-tertbutyl pyridine	6.37	0.64	0.46	4.75	[67]
	TBAI/I <sub>2</sub> /EC	9.99	0.780	42.4	3.67	[68]
	NH <sub>4</sub> F/H <sub>2</sub> O	8.06	0.73	0.71	4.18	[69]
	Iodolyte AN 50	13.1	0.7	63.6	5.87	[70]
Polymer and starch	PEG/LiI/MPII	10.7	0.60	0.59	3.9	[71]
	(PAN/VA)/MPN/LiI/DMPII/TBP//I <sub>2</sub>	15.44	0.797	0.73	9.03	[72]
	PAN/PC/EC/TPAI/BMII/I <sub>2</sub>	20.1	0.694	0.702	8.44	[73]
	MPII/NaI/(PC-EC)	15.6	0.65	0.64	6.47	[74]
	(PAN-VA)/(PVdF-HFP)/ACN/LiI/I <sub>2</sub>	11.47	0.78	0.70	6.30	[75]
	PhSt/HEC/LiI/DMF	9.02	0.57	0.60	3.02	[76]
	Gel Polymer	PVA/PEO	16.41	0.63	0.61	6.26
PAN/P (VP-co-VAc)		17.77	725 mV	0.64	8.11	[78]
I <sub>2</sub> /MPII/TBP/NaI(PEO-CMC)		10.03	0.75	0.69	5.18	[79]
S-GO/PVDF-HFP and PEO		12.53	0.77	0.44	4.24	[80]
PEO:EC:PC:Pr4N <sup>+</sup> I <sup>-</sup> + KI:I <sub>2</sub>		16.93	672.3 mV	60.62	6.90	[81]
PAN-EC-(PC-I <sub>2</sub> )-TBAI		12.9	582 mV	46	3.45	[82]
HFP PGE/PVDF		24.66	587 mV	0.763	16.93	[83]

as 3-methoxy propionitrile, methoxyacetone, propylene carbonate, butyrolactone and N-methyl-2-pyrrolidone were investigated [85, 88–91].

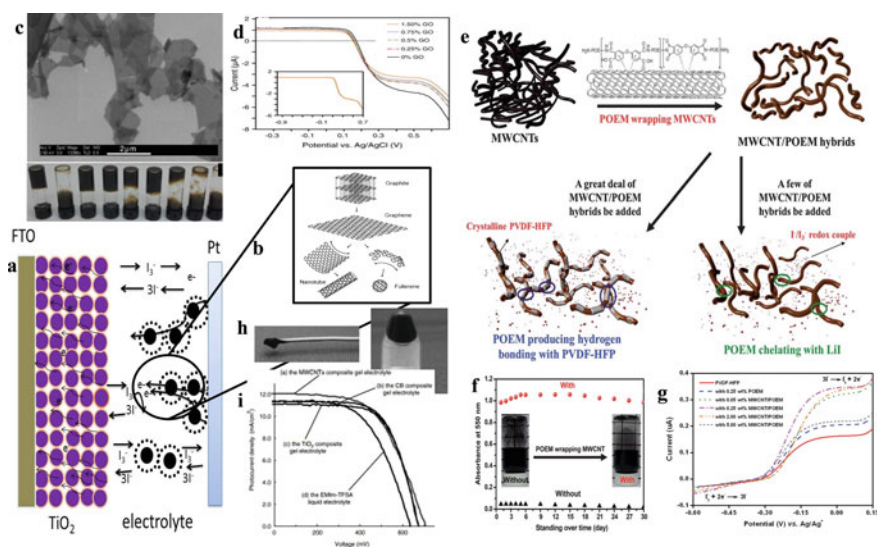
On the other hand, nonvolatile and solvent-free ionic liquids were investigated for DSSCs with advantageous properties over organic electrolytes instability and ionic conductivity [92–94]. The ionic liquids of imidazolium salts [92] were employed to improve the stability of the solar cell. Later SeCN<sup>-</sup>/(SeCN)<sup>3-</sup> redox couple was used as a solvent-free ionic electrolyte; still, the device performance of these electrolytes was poor. Bai et al. proposed ionic liquid with ruthenium sensitizer (Z907Na) and achieved 8% efficiency with 1.5G illumination [93]. With imidazolium iodides and optimized concentrations of ionic liquid-based electrolytes reported over 10% efficiency [95, 96]. At present, iodide/triiodide redox couple were commercially employed for DSSCs, which delivered efficiency of over 11.9%. However, its lower redox potential also lowers its open circuit potential because the energy mismatch between the (S<sup>+</sup>/S) results in a potential loss. To resolve this energy mismatch, one electron redox mediators such as cobalt, nickel and ferrocene-based electrolytes were developed [97, 98].

Leakage and packaging issues on device fabrication and stability have been a critical barrier to the commercialization of the DSSCs. gel electrolytes, a polymer network (PVDF, PAN, PEO, etc.) to electrolyte salts significant advancement in DSSCs packaging and development [99, 100]. These polymer gel electrolytes can deliver excellent ionic conductivity ( $10^{-3}$  to  $10^{-5}$  S/cm) and good stability with an excellent interface between photoanode and counter electrode [88, 100–102] making them compatible with printing or roll to roll fabrication processes [103–106]. Carbon and its derivatives-based composite polymer electrolytes were employed for their conductivity and electron transfer [107, 108] as illustrated in Fig. 4a, b. Gun et al. [109] experimentally proved that with lower concentrations (0.4 wt%) of graphene oxide with iodide/triiodide-based electrolyte shown in Fig. 4c along with the SEM images and anodic sweep voltammetry graphs in Fig. 4d, the efficiency was improved from 6.9% to 7.5% with 0.4 wt% GO gel electrolyte. In continuation, Venkatesan et al. [106] synthesized and employed graphene oxide sponge as a nanofiller in a PEO and PVDF based electrolyte for printable DSSCs. The influence of graphene oxide nanofillers on conductivity and diffusivity was studied with different concentrations. The addition of 1.5 wt% fillers showed improved recombination resistance at the electrolyte and lower charge transfer resistance at the counter electrode (Pt)/photoanode interface with an energy efficiency of 8.78%. The higher efficiency combines both open circuit potential and fill factor with a cell stability retention of 86% over a 500 h stability test. Chiao et al. [110] reported polymer-dispersed MWCNT gel electrolyte for DSSCs to enhance efficiency, the synthesis protocol was illustrated in Fig. 4e. Figure 4f shows the dispersion stability of the MWCNT/POEM hybrid electrolyte and its corresponding steady state voltage performance were given in Fig. 4g. The electrolyte with 0.25 wt% MWCNT/polyoxyethylene segmented oligo (amide-imide) delivered an efficiency of 6.86% in an I/3 electrolyte system. Mohan et al. [111] employed activated carbon/LiI/PAN polymer gel electrolyte. The ethylene was synthesized by mixing and hot pressing PAN with ethylene carbonate,



propylene carbonate, iodine and 4-tert butyl pyridine and 1-N-butyl-3-hexyl imidazolium iodide. The electrical conductivity of the synthesized PAN/activated carbon electrolyte is found out to be around  $8.67 \times 10^{-3}$  S/cm, an efficiency of 8.42%.

Ho et al. has incorporated polyaniline/carbon black with 1-propyl-3-methyl imidazolium iodide and used it as a DSSCs electrolyte [112, 113]. This incorporation enhanced the overall efficiency by 30% compared to the unmodified electrolyte; the higher efficiency resulted from the extended transfer surface, with a catalytic I<sub>3</sub>-ions reduction. Usui et al. has demonstrated the incorporation of CNT's, carbon black, carbon fibers with 1-ethyl-3methylimidazolium bis(trifluoromethyl sulfonyl)imide gel electrolyte [85], the photographs of the gel electrolyte were shown in Fig. 4h. It noted that the electrolytes with the carbon materials have an improved fill factor and reduced resistance, thereby improving efficiency [114]. There photocurrent densities were given in Fig. 4i.



**Fig. 4** **a** Schematic of the DSSC. **(a)** reused “Reprinted with permission from Mohan et al. [111]. Copyright 2013 Royal Society of Chemistry”. **b** A schematic showing carbon and its derivatives. **(b)** “Reprinted with permission from Badenhorst et al. [108]. Copyright 2019 Elsevier”. **c** SEM images of Graphene oxide with photographs of GO dispersed in different solvents. **d** Anodic sweep voltammetry of GO with different concentrations on Pt electrode **(c, d)** “Reprinted with permission from Gun et al. [109]. Copyright 2012 Elsevier”. **e** Schematic representation of POEM Wrapping on MWCNTs and its interaction with electrolyte. **f** Homogeneity dispersion study of MWCNT. **g** Current/Voltage curves of POEM wrapped CNT under various electrolytes. **(e, f, g)** were “Reprinted with permission from Wang et al. [110]. Copyright 2012 Royal Society of Chemistry”. **h** Photograph of MWCNT ionic gel in vial and scooped with specula. **i** Photo current density/voltage performance of MWCNT gel electrolyte

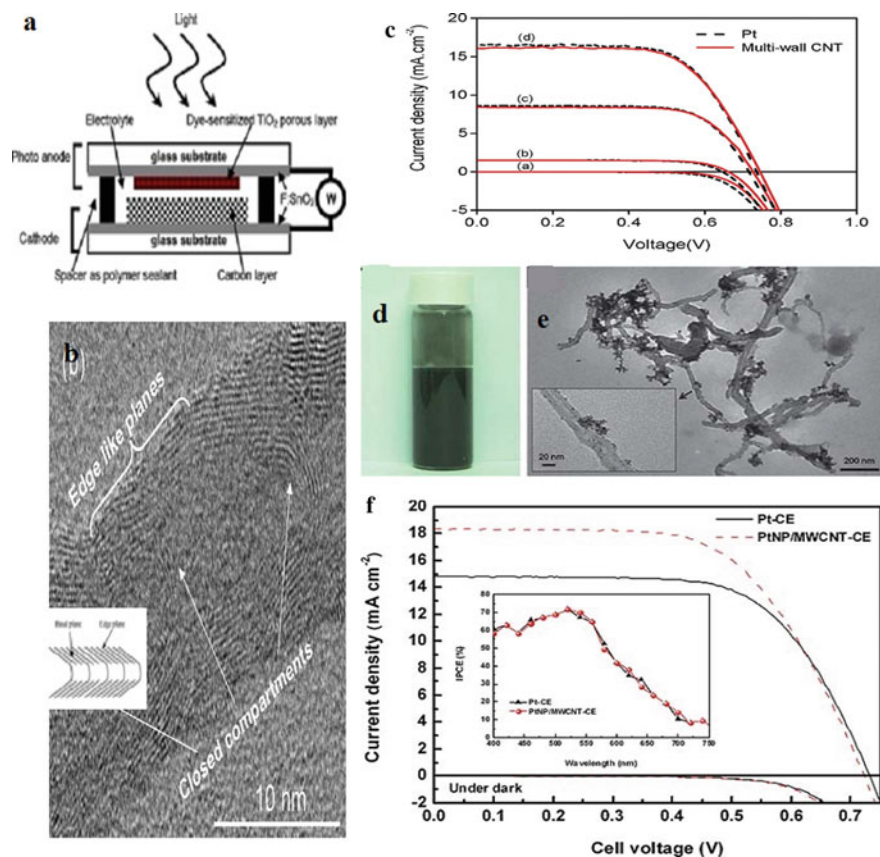
### 5.2.4 Counter Electrodes

Platinum is the most used counter electrode for DSSC applications due to its electrochemical properties and compatibility with  $I/I_3$  based redox couples. The closest match to platinum is carbon; low-cost material, highly conductive, tunable physicochemical properties and  $I/I_3$  reduction properties. Researchers employed carbon-based nanomaterials to replace platinum-based electrodes as illustrated in Fig. 5a. Murakami et al. used carbon black as a counter electrode for DSSC. They found out that the carbon layer has no influence on the short circuit potential, and the open circuit and thickness were inversely proportional [115]. The efficiency of the fabricated device using carbon black counter electrodes was around 9.1% with 14.5  $\mu\text{m}$  thick layers. Imoto et al. used a  $\text{TiO}_2$ /carbon powder hybrid as a counter electrode [116]. The employed porous carbon provided enough space for the triiodide ions to penetrate the counter electrode by reducing efficiently. Using these hybrids, they reported an efficiency of 3.8% with an electrode thickness of 153  $\mu\text{m}$ . Also, all carbon counter electrodes were proposed by Meng et al. using these all carbon electrodes can be advantageous for graphite-based substrates, thereby providing flexibility and electrical conductivity [117]. These all carbon-based DSSCs shows an efficiency of 6.46%, which was on par with Pt/FTO efficiency at 6.37%.

Lee et al. used MWCNT as a replacement for Pt in DSSCs as these CNT have a large surface area, high electrical conductivity, control over defects. These defect rich edge planes as shown in the TEM images of MWCNT (Fig. 5b) provide faster interface kinetics of electrode and electrolyte [118]. Overall the MWCNT-based counter electrode achieved an efficiency of 7.67%, which was also in line with the Pt-based solar cell at 7.83% as projected in Fig. 5c. In continuation, Ho et al. [119] used a hybrid Pt/CNT-based counter electrode as shown in Fig. 5d, e and achieved an 8% efficiency, which can be attributed to the rough electrode surface and electrocatalytic behavior of the Pt/CNT hybrid structure and suppressed the Pt/CE performance as shown in the Fig. 5f. Wang et al. investigated the performance of graphene as a counter electrode on various substrates [120]. The graphene transferred on PET substrate. The results show that the higher thickness of graphene layers showed improved results than Pt as seen in current voltage curves. But the overall efficiency was as poor as 0.51% due to the significant resistance value. In continuation, Aksay et al. reported that the oxygen functional groups in graphene and catalytic performance of the material were directly proportional. An efficiency of 4.99% was obtained with a 1/3 C/O ratio.

The surface functionalization was carried out to modify the chemistry further and to engineer the surface properties of the carbonaceous-based counter electrode. These functionalized molecules were selected based on the application requirements, such as metallic structures for plasmonic and catalysis applications.

Luminescent molecules for surface enhanced Raman substrates, etc. In the case of DSSC, the surface functionalization was mainly carried to change the wettability at the electrode/electrolyte interface [121, 122]. Roy et al. [121] had engineered the functionalized graphene-based counter electrode for DSSC by using thermolyzed ethyl cellulose. The fabricated electrode exhibits a lower charge transfer resistance



**Fig. 5** **a** Cross sectional schematic projection of DSSC with counter electrode. **(a)** “Reprinted with permission from Murakami et al. [115]. Copyright 2006 IOP Science”. **b** TEM micrograph of bamboolike MWCNT and its schematic marking basal and edge planes. **c** Current–Voltage performance MWCNT and Pt counter electrode. **(b, c)** “Reprinted with permission from Lee et al. [118]. Copyright 2009 American Chemical Society”. **d** Photograph of MWCNT with Pt nanoparticles, H<sub>2</sub>PTCL<sub>6</sub> and POEM. **e** TEM image of MWCNT in dispersion. **f** I–V performance of DSSC with Pt/CE and Pt Np/MWCNT/CE. **(d, e, f)** “Reprinted with permission from Law et al. [119]. Copyright 2010 Royal Society of Chemistry”. **g** Photograph of PET substrate with graphene film. **h** Current–Voltage curves of graphene and Pt-based DSSC. **i** CV graphs of graphene and Pt electrodes in 10 mM LiI and 1 mM I<sub>2</sub> electrolyte

of 1  $\Omega$  cm<sup>2</sup>. This performance was also stable in cobalt and sulfur-based electrolytes apart from the traditionally used triiodide-based electrolyte. The enhanced performance of the electrode was attributed to the functionalization of the carbon counter electrode as it prevented the material from restacking thereby boosting overall efficiency and stability (Table 2).

Choi et al. [122] had proposed Poly (maleic anhydride-co-p-acetoxy styrene)-block-poly(p-acetoxy styrene)/CNT as a counter electrode for DSSC. The Modified

**Table 2** Comparison of different carbon-based counter electrodes for DSSCs

Resources	Methods	Jsc (mA cm <sup>-2</sup> )	Voc (V)	FF	Surface area (S <sub>BET</sub> m <sup>2</sup> g <sup>-1</sup> )	PCE	References
Waste carbon	Two-step activation (H <sub>3</sub> PO <sub>4</sub> -NaOH)	12.62	0.67	0.62	824.16	6.76	[123]
Alkali lignin	Pyrolysis/electrospinning	13.4	0.8	0.63	583	6.75	[124]
Coffee Waste	Pyrolysis/ZnCl <sub>2</sub> activation	15.09	0.76	0.726	1200	8.32	[125]
Aloe peel	Hydrothermal/KOH activation	14.15	0.72	0.68	1286	6.92	[126]
Sunflower Stalk	Hydrothermal/KOH activation	15.20	0.67	0.64	1505	6.56	[127]
Sucrose	Template method	16.1	808 mV	68	1037	8.77	[128]
Fallen leaves	Pyrolysis/KOH activation	13.77	0.7	0.544	2196.6	5.52	[129]
Rice husk	Carbonization	14.53	680 mV	64	1094.6	6.32	[130]
Activated carbon-carbon black	Ball milling	15.50	578 mV	68	-	6.1	[131]
Soluble resoles	Hydrothermal method	14.97	745 mV	65	514	7.22	[132]
2-2'Bipyridine	Carbonization	13.10	0.65	0.61	-	5.24	[133]

CNT showed more stability in terpineol resulting in more facile CNT growth, thereby improving the overall fill factor and overall efficiency. In continuation, Alba et al. [134] has functionalized CNT via ozonolysis and employed it in DSSC applications. This functionalization via the ozonolysis method preserves “O” containing groups of C–O, O–C, COOH and C–OH on the carbon surface, which aids overall efficiency.

## 6 Remedial Measures to Be Taken on Its Challenge Perspectives

The challenge is, however, to resolve three crucial challenges in order to ensure progress in creating next generation solar cells and the development of technical applications while utilizing these carbonaceous materials in photovoltaics. First, carbon-based devices with higher recombination losses suffer from a high Schottky barrier on the interface between the carbon and metal electrodes. As a second requirement, the carbon materials require better carrier doping to decrease the series resistance losses when used as a transporting layer. Third, its transparency is crucial to enhance the photocarrier generation efficiency of carbon-based solar cells due to the management of solar light within the structure. It is believed that regardless of the fact that this is still a highly undeveloped field, continuous efforts to address the above-mentioned issues will make carbon nanomaterials stronger for photovoltaic applications.

## 7 Conclusions and Challenge

A summary of the recent progress of carbonaceous nanomaterials for photovoltaic solar cells is presented in this chapter. The development and manufacturing of solar cells using carbon-based nanomaterials has shown to be a potential application. In addition to the metal electrode (such as Ag, Al, Au and Pt) replacement, hole transport layers have been found to be effective and can be achieved using these carbon-based materials in third generation solar cells (both PSCs and DSSCs). The device without high-cost counter electrode metals which was replaced by the novel, facile and low-cost carbonaceous materials proved to exhibit an improved PV device. Thus, the carbonaceous materials can still not be made to cost a reasonable amount to fabricate solar cells that are strong, reliable, have a high production rate, and feature enhanced device performance along with the flexibility and weight advantages they offer. As a result, it has been established that utilizing carbonaceous material for increasing the performance and stability of third generation solar cells such as DSSCs, OSCs and PSC is both simple and effective. Therefore, the introduction of carbonaceous materials at various position of the components used in the third generation solar cells correspondingly found to increase the light-harvesting ability of the active layer,

boosting the charge transfer at the interface layers and most likely accelerates/extracts the charges at the transporting layers. Due to the carbonaceous material's dual impact on both optical and electrical properties, there was an associated enhancement in device performance for third generation solar cells. Chapters such as this one will not only organize this technology well, but will also provide valuable direction for future research.

## References

1. Chiticaru EA, Muraru S, Ioniță M (2021) From unidimensional carbonaceous materials to multidimensional structures through molecular modeling. Carbon related materials. Springer, Singapore, pp 1–21
2. Kuddus A, Ismail ABM, Hossain J (2021) Design of a highly efficient CdTe-based dual-heterojunction solar cell with 44% predicted efficiency. *Sol Energy* 221:488–501
3. Kokkonen M, Talebi P, Zhou J, Asgari S, Soomro SA, Elsehrawy F, Halme J, Ahmad S, Hagfeldt A, Hashmi SG (2021) Advanced research trends in dye-sensitized solar cells. *J Mater Chem A* 9:10527–10545
4. Almora O, Baran D, Bazan GC, Berger C, Cabrera CI, Catchpole KR, Erten-Ela S, Guo F, Hauch J, Ho-Baillie AW, Jacobsson TJ (2021) Device performance of emerging photovoltaic materials (version 1). *Adv Ene Mater* 11:2002774
5. Kiruthiga G, Raguram T, Rajni KS, Selvakumar P, Nandhakumar E (2021) DSSCs: a facile and low-cost MgSnO<sub>3</sub>-based transparent conductive oxides via nebulized spray pyrolysis technique. *J Mater Sci: Mater Electr* 32:22780–22791
6. Landerer D, Sprau C, Ebenhoch B, Colsmann A (2019) New directions for organic thin-film solar cells: stability and performance. In: *Advanced micro-and nanomaterials for photovoltaics*, pp 195–244
7. Wei Z, Yan K, Chen H, Yi Y, Zhang T, Long X, Li J, Zhang L, Wang J, Yang S (2014) Cost-efficient clamping solar cells using candle soot for hole extraction from ambipolar perovskites. *Energy Environ Sci* 7:3326–3333
8. Chen H, Wei Z, Yan K, Yi Y, Wang J, Yang S (2014) Liquid phase deposition of TiO<sub>2</sub> nanolayer affords CH<sub>3</sub>NH<sub>3</sub>PbI<sub>3</sub>/nanocarbon solar cells with high open-circuit voltage. *Farad Disc* 176:271–286
9. Rosas-Laverde NM, Pruna A (2021) Carbon nanomaterial-based photovoltaic solar cells. In: *Carbon related materials*, pp 187–207
10. Yang Y, Xiao J, Wei H, Zhu L, Li D, Luo Y, Wu H, Meng Q (2014) An all-carbon counter electrode for highly efficient hole-conductor-free organo-metal perovskite solar cells. *RSC Adv* 4:52825–52830
11. Rajeswari R, Mrinalini M, Prasanthkumar S, Giribabu L (2017) Emerging of inorganic hole transporting materials for perovskite solar cells. *Chem Rec* 17:681–699
12. Aitola K, Sveinbjornsson K, Correa-Baena JP, Kaskela A, Abate A, Tian Y, Johansson EMJ, Gratzel M, Kauppinen EI, Hagfeldt A, Boschloo G (2016) Carbon nanotube-based hybrid hole-transporting material and selective contact for high efficiency perovskite solar cells. *Energy Environ Sci* 9:461–466
13. Becquerel ME et al (1839) Mémoire sur les effets électriques produits sous l'influence des rayons solaires. *C R Hebd Séances Acad Sci* 9:561–567
14. Adams WG, Day RE (1877) The action of light on selenium. *Proc R Soc Lond* 25:113–117
15. Fritts CE et al (1883) On a new form of selenium cell, and some electrical discoveries made by its use. *Am J Sci* 156:465–472
16. Scaff JH, Ohl RS (1947) Development of silicon crystal rectifiers for microwave radar receivers. *Bell Syst Tech J* 26:1–30

17. Chapin DM, Fuller CS, Pearson GL (1954) A new silicon p-n junction photocell for converting solar radiation into electrical power. *J Appl Phys* 25:676–677
18. Fraas LM et al (2014) History of solar cell development. In: Fraas LM (ed) *Low-cost solar electric power*. Springer International Publishing, Cham, pp 31–42
19. Bhattacharya S, John S (2019) Beyond 30% conversion efficiency in silicon solar cells: a numerical demonstration. *Sci Rep* 9:1–15
20. Czochralski J (1918) Ein neues verfahren zur messung der kristallisationsgeschwindigkeit der metalle. *Z Phys Chem* 92:219–221
21. Ramanujam J, Singh UP (2017) Copper indium gallium selenide based solar cells—a review. *Energy Environ Sci* 10:1306–1319
22. Ravindiran M, Praveenkumar C (2018) Status review and the future prospects of CZTS based solar cell—a novel approach on the device structure and material modeling for CZTS based photovoltaic device. *Renew Sustain Energy Rev* 94:317–329
23. Yan J, Saunders BR (2014) Third-generation solar cells: a review and comparison of polymer: fullerene, hybrid polymer and perovskite solar cells. *RSC Adv* 4:43286–43314
24. Wan X, Huang Y, Chen Y (2012) Focusing on energy and optoelectronic applications: a journey for graphene and graphene oxide at large scale. *Acc Chem Res* 45:598–607
25. Milić JV, Arora N, Dar MI, Zakeeruddin SM, Grätzel M (2018) Reduced graphene oxide as a stabilizing agent in perovskite solar cells. *Adv Mater Inter* 5:1800416
26. Litvin AP, Zhang X, Berwick K, Fedorov AV, Zheng W, Baranov AV (2020) Carbon-based interlayers in perovskite solar cells. *Renew Sustain Energy Rev* 124:109774
27. Pitchaiya S, Natarajan M, Santhanam A, Asokan V, Yuvapragasam A, Ramakrishnan VM, Palanisamy SE, Sundaram S, Velauthapillai D (2020) A review on the classification of organic/inorganic/carbonaceous hole transporting materials for perovskite solar cell application. *Arab J Chem* 13:2526–2557
28. Moser J et al (1887) Notiz über Verstärkung photoelektrischer Ströme durch optische Sensibilisierung. *Monatshefte für Chemie/Chemical Monthly* 8:373–373
29. Tsubomura H, Matsumura M, Nomura Y, Amamiya T (1976) Dye sensitized zinc oxide: aqueous electrolyte: platinum photocell. *Nature* 261:402–403
30. O’regan B, Grätzel M (1991) A low-cost, high-efficiency solar cell based on dye-sensitized colloidal TiO<sub>2</sub> films. *Nature* 353(6346):737–740
31. O’Regan B, Schwartz DT (1996) Efficient dye-sensitized charge separation in a wide-band-gap p-n heterojunction. *J Appl Phys* 80(8):4749–4754
32. Ramakrishnan VM, Sandberg S, Muthukumarasamy N, Kvamme K, Balraju P, Agilan S, Velauthapillai D (2019) Microwave assisted solvothermal synthesis of worms-like TiO<sub>2</sub> nanostructures in submicron regime as light scattering layers for dye-sensitized solar cells. *Mater Lett* 236:747–751
33. Grätzel M, Kalyanasundaram K (1994) Artificial photosynthesis: efficient dye-sensitized photoelectrochemical cells for direct conversion of visible light to electricity. *Curr Sci* 66:706–714
34. Grätzel M (2000) Perspectives for dye-sensitized nanocrystalline solar cells. *Prog Photovoltaics: Res Appl* 8:171–185
35. Ito S, Murakami TN, Comte P, Liska P, Grätzel C, Nazeeruddin MK, Grätzel M (2008) Fabrication of thin film dye sensitized solar cells with solar to electric power conversion efficiency over 10%. *Thin Solids Films* 516:4613–4619
36. Yun S, Hagfeldt A, Ma T (2014) Pt-free counter electrode for dye-sensitized solar cells with high efficiency. *Adv Mater* 26:6210–6237
37. Ahmed U, Alizadeh M, Abd Rahim N, Shahabuddin S, Ahmed MS, Pandey AK (2018) A comprehensive review on counter electrodes for dye sensitized solar cells: a special focus on Pt-TCO free counter electrodes. *Sol Eng* 174:1097–1125
38. Sima C, Grigoriu C, Antohe S (2010) Comparison of the dye-sensitized solar cells performances based on transparent conductive ITO and FTO. *Thin Sol Fil* 519(2):595–597
39. Mohamad AA et al (2016) Absorbency and conductivity of quasi-solid-state polymer electrolytes for dye-sensitized solar cells: a characterization review. *J Pow Sour* 329:57–71

40. Yanagida M, Han C, Han L (2012) Surface treatment for effective dye adsorption on nanocrystalline TiO<sub>2</sub>. *Jap J Appl Phys* 51(10S):10NE16
41. Suzuki M, Hayashi N, Sekiguchi T, Sumioka K, Takata M, Hayo N, Ikeda H, Oyaizu K, Nishide H (2016) A quasi-solid state DSSC with 10.1% efficiency through molecular design of the charge-separation and-transport. *Sci Rep* 6:1–7
42. Babar F, Mehmood U, Asghar H, Mehdi MH, Khan AUH, Khalid H, ul Huda N, Fatima Z (2020) Nanostructured photoanode materials and their deposition methods for efficient and economical third generation dye-sensitized solar cells: a comprehensive review. *Renew Sustain Energy Rev* 129:109919
43. Yum JH, Baranoff E, Wenger S, Nazeeruddin MK, Grätzel M (2011) Panchromatic engineering for dye-sensitized solar cells. *Energy Environ Sci* 4:842–857
44. Shaikh JS, Shaikh NS, Mali SS, Patil JV, Pawar KK, Kanjanaboos P, Hong CK, Kim JH, Patil PS (2018) Nanoarchitectures in dye-sensitized solar cells: metal oxides, oxide perovskites and carbon-based materials. *Nanoscale* 10:4987–5034
45. Yang Y, Zhao J, Cui C, Zhang Y, Hu H, Xu L, Pan J, Li C, Tang W (2016) Hydrothermal growth of ZnO nanowires scaffolds within mesoporous TiO<sub>2</sub> photoanodes for dye-sensitized solar cells with enhanced efficiency. *Electroch Acta* 196:348–356
46. Yang L, Leung WWF (2013) Electrospun TiO<sub>2</sub> nanorods with carbon nanotubes for efficient electron collection in dye-sensitized solar cells. *Adv Mater* 25:1792–1795
47. Lan X, Voznyy O, García de Arquer FP, Liu M, Xu J, Proppe AH, Walters G, Fan F, Tan H, Liu M, Yang Z (2016) 10.6% certified colloidal quantum dot solar cells via solvent-polarity-engineered halide passivation. *Nano Lett* 16:4630–4634
48. Xia Q, Zhao H, Du Z, Wang J, Zhang T, Wang J, Lv P (2013) Synthesis and electrochemical properties of MoO<sub>3</sub>/C composite as anode material for lithium-ion batteries. *J Pow Sour* 226:107–111
49. Dong H, Wu Z, Lu F, Gao Y, El-Shafei A, Jiao B, Ning S, Hou X (2014) Optics–electrics highways: plasmonic silver nanowires@ TiO<sub>2</sub> core–shell nanocomposites for enhanced dye-sensitized solar cells performance. *Nano Energy* 10:181–191
50. Ye M, Xin X, Lin C, Lin Z (2011) High efficiency dye-sensitized solar cells based on hierarchically structured nanotubes. *Nano Lett* 11:3214–3220
51. Zhu G, Pan L, Xu T, Sun Z (2011) CdS/CdSe-cosensitized TiO<sub>2</sub> photoanode for quantum-dot-sensitized solar cells by a microwave-assisted chemical bath deposition method. *ACS Appl Mater Inter* 3:3146–3151
52. Ahmad MS, Pandey AK, Abd Rahim N (2017) Advancements in the development of TiO<sub>2</sub> photoanodes and its fabrication methods for dye sensitized solar cell (DSSC) applications. A review. *Renew Sustain Energy Rev* 77:89–108
53. Zhang X, Yao J, Li D, Chen X, Wang H, Yeo LY, Friend JR (2014) Self-assembled highly crystalline TiO<sub>2</sub> mesostructures for sunlight-driven, pH-responsive photodegradation of dyes. *Mater Res Bull* 55:13–18
54. Zhao W, Fu W, Chen J, Li H, Bala H, Wang X, Sun G, Cao J, Zhang Z (2015) Preparation of TiO<sub>2</sub>-based nanotubes/nanoparticles composite thin film electrodes for their electron transport properties. *Thin Sol Fil* 577:49–55
55. Joshi RK, Schneider JJ (2012) Assembly of one dimensional inorganic nanostructures into functional 2D and 3D architectures. synthesis, arrangement and functionality. *Chem Soc Rev* 41:5285–5312
56. Wu WQ, Xu YF, Rao HS, Su CY, Kuang DB (2014) Trilayered photoanode of TiO<sub>2</sub> nanoparticles on a 1D–3D nanostructured TiO<sub>2</sub>-grown flexible Ti substrate for high-efficiency (9.1%) dye-sensitized solar cells with unprecedentedly high photocurrent density. *J Phy Chem C* 118:16426–16432
57. Mathew S, Yella A, Gao P, Humphry-Baker R, Curchod BF, Ashari-Astani N, Tavernelli I, Rothlisberger U, Nazeeruddin MK, Grätzel M (2014) Dye-sensitized solar cells with 13% efficiency achieved through the molecular engineering of porphyrin sensitizers. *Nat Chem* 6:242–247



58. Shiu JW, Lan CM, Chang YC, Wu HP, Huang WK, Diao EWG (2012) Size-controlled anatase titania single crystals with octahedron-like morphology for dye-sensitized solar cells. *ACS Nano* 6:10862–10873
59. Zhu K, Neale NR, Miedaner A, Frank AJ (2007) Enhanced charge-collection efficiencies and light scattering in dye-sensitized solar cells using oriented TiO<sub>2</sub> nanotubes arrays. *Nano Lett* 7:69–74
60. Qin L, Liu D, Zhang Y, Zhao P, Zhou L, Liu Y (2018) Comparison of two ways using Ag nanoparticles to improve the performance of dye-sensitized solar cells. *Electrochimic Acta* 263:426–432
61. Senthilkumar N, Arulraj A, Nandhakumar E, Ganapathy M, Vimalan M, Potheher IV (2018) Green mediated synthesis of plasmonic nanoparticle (Ag) for antireflection coating in bare mono silicon solar cell. *J Mater Sci: Mater. Electron* 29:12744–12753
62. Zou M, Liu H, Feng L, Xiong F, Thomas T, Yang M (2017) Effect of nitridation on visible light photocatalytic behavior of microporous (Ag, Ag<sub>2</sub>O) co-loaded TiO<sub>2</sub>. *Micro Meso Mater* 240:137–144
63. Kong FT, Dai SY, Wang KJ (2007) Review of recent progress in dye-sensitized solar cells. *Adv OptoElectron* 1–13
64. Kongkanand A, Martínez Domínguez R, Kamat PV (2007) Single wall carbon nanotube scaffolds for photoelectrochemical solar cells. Capture and transport of photogenerated electrons. *Nano Lett* 7:676–680
65. Williams G, Seger B, Kamat PV (2008) TiO<sub>2</sub>-graphene nanocomposites. UV-assisted photocatalytic reduction of graphene oxide. *ACS Nano* 2:1487–1491
66. Francis MK, Santhosh N, Govindaraj R, Ahmed N, Balaji C (2021) Bifacial DSSC fabricated using low-temperature processed 3D flower like MoS<sub>2</sub>-high conducting carbon composite counter electrodes. *Mater Today Comm* 27:102208
67. ur Rehman S, Noman M, Khan AD, Saboor A, Ahmad MS, Khan HU (2020) Synthesis of polyvinyl acetate/graphene nanocomposite and its application as an electrolyte in dye sensitized solar cells. *Optik* 202:163591
68. Narudin N, Ekanayake P, Soon YW, Nakajima H, Lim CM (2021) Enhanced properties of low-cost carbon black-graphite counter electrode in DSSC by incorporating binders. *Sol Energy* 225:237–244
69. Wang J, Nie X, Wang W, Zhao Z, Li L, Zhang Z (2021) Single-layer graphene-TiO<sub>2</sub> nanotubes array heterojunction as photoanode to enhance the photoelectric of DSSCs. *Optik* 242:167245
70. Kim H, Choi H, Hwang S, Kim Y, Jeon M (2012) Fabrication and characterization of carbon-based counter electrodes prepared by electrophoretic deposition for dye-sensitized solar cells. *Nanosci Res Lett* 7:1–4
71. Lim SM, Moon J, Baek UC, Lee JY, Chae Y, Park JT (2021) Shape-controlled TiO<sub>2</sub> nanomaterials-based hybrid solid-state electrolytes for solar energy conversion with a mesoporous carbon electrocatalyst. *Nanomater* 11:913
72. Chen CL, Teng H, Lee YL (2011) In situ gelation of electrolytes for highly efficient gel-state dye-sensitized solar cells. *Adv Mater* 23:4199–4204
73. Jayaweera EN, Ranasinghe CSK, Kumara GRA, Wanninayake WMNMB, Senarathne KGC, Tennakone K, Rajapakse RMG, Ileperuma OA (2015) Novel method to improve performance of dye-sensitized solar cells based on quasi-solid gel-polymer electrolytes. *Electro Act* 152:360–367
74. Saidi NM, Goh ZL, Arif HM, Farhana NK, Ramesh S, Ramesh K (2021) Consolidation of ion promoters into quasi solid-state (QSS) polymer electrolytes for dye-sensitized solar cells (DSSCs). *Solid State Ionics* 363:115592
75. Venkatesan S, Obadja N, Chang TW, Chen LT, Lee YL (2014) Performance improvement of gel-and solid-state dye-sensitized solar cells by utilization the blending effect of poly (vinylidene fluoride-co-hexafluoropropylene) and poly (acrylonitrile-co-vinyl acetate) co-polymers. *J Pow Sour* 268:77–81
76. Selvanathan V, Yahya R, Alharbi HF, Alharthi NH, Alharthi YS, Ruslan MH, Amin N, Akhtaruzzaman M (2020) Organosoluble starch derivative as quasi-solid electrolytes in

- DSSC: unravelling the synergy between electrolyte rheology and photovoltaic properties. *Sol Energy* 197:144–153
77. Teo LP, Tiong TS, Buraidah MH, Arof AK (2018) Effect of lithium iodide on the performance of dye sensitized solar cells (DSSC) using poly (ethylene oxide)(PEO)/poly (vinyl alcohol)(PVA) based gel polymer electrolytes. *Opt Mater* 85:531–537
  78. Saidi NM, Farhana NK, Ramesh S, Ramesh K (2021) Influence of different concentrations of 4-tert-butyl-pyridine in a gel polymer electrolyte towards improved performance of dye-sensitized solar cells (DSSC). *Sol Energy* 216:111–119
  79. Bella F, Nair JR, Gerbaldi C (2013) Towards green, efficient and durable quasi-solid dye-sensitized solar cells integrated with a cellulose-based gel-polymer electrolyte optimized by a chemometric DoE approach. *RSC Adv* 3:15993–16001
  80. Kumar S, Manikandan VS, Panda SK, Senanayak SP, Palai AK (2020) Probing synergistic outcome of graphene derivatives in solid-state polymer electrolyte and Pt-free counter electrode on photovoltaic performances. *Sol Energy* 208:949–956
  81. Dissanayake MAKLL, Sarangika HNM, Senadeera GKR, Divarathna HKDWMNR, Ekanayake EMPC (2017) Application of a nanostructured, tri-layer TiO<sub>2</sub> photoanode for efficiency enhancement in quasi-solid electrolyte-based dye-sensitized solar cells. *J Appl Electrochem* 47:1239–1249
  82. Chowdhury FI, Buraidah MH, Arof AK, Mellander BE, Noor IM (2020) Impact of tetrabutylammonium, iodide and triiodide ions conductivity in polyacrylonitrile based electrolyte on DSSC performance. *Sol Energy* 196:379–388
  83. Venkatesan S, Liu IP, Li CW, Tseng-Shan CM, Lee YL (2019) Quasi-solid-state dye-sensitized solar cells for efficient and stable power generation under room light conditions. *ACS Sustain Chem Eng* 7:7403–7411
  84. Kakiage K, Aoyama Y, Yano T, Oya K, Fujisawa JI, Hanaya M (2015) Highly-efficient dye-sensitized solar cells with collaborative sensitization by silyl-anchor and carboxy-anchor dyes. *Chem Commun* 51:15894–15897
  85. Harikisun R, Desilvestro H (2011) Long-term stability of dye solar cells. *Sol Energy* 85:1179–1188
  86. Asghar MI, Miettunen K, Halme J, Vahermaa P, Toivola M, Aitola K, Lund P (2010) Review of stability for advanced dye solar cells. *Energy Environ Sci* 3:418–426
  87. Buzzo MC, Hardacre C, Compton RG (2006) Extended electrochemical windows made accessible by room temperature ionic liquid/organic solvent electrolyte systems. *ChemPhysChem* 7:176–180
  88. Wu J, Lan Z, Hao S, Li P, Lin J, Huang M, Fang L, Huang Y (2008) Progress on the electrolytes for dye-sensitized solar cells. *Pure Appl Chem* 80:2241–2258
  89. Kato N, Takeda Y, Higuchi K, Takeichi A, Sudo E, Tanaka H, Motohiro T, Sano T, Toyoda T (2009) Degradation analysis of dye-sensitized solar cell module after long-term stability test under outdoor working condition. *Sol Ener Mater Sol Cells* 93:893–897
  90. Wu J, Lan Z, Lin J, Huang M, Li P (2007) Effect of solvents in liquid electrolyte on the photovoltaic performance of dye-sensitized solar cells. *J Pow Sour* 173:585–591
  91. Lee HS, Bae SH, Jo Y, Kim KJ, Jun Y, Han CH (2010) A high temperature stable electrolyte system for dye-sensitized solar cells. *Electrochim acta* 55:7159–7165
  92. Gorlov M, Kloo L (2008) Ionic liquid electrolytes for dye-sensitized solar cells. *Dalton Trans* 20:2655–2666
  93. Bai Y, Cao Y, Zhang J, Wang M, Li R, Wang P, Zakeeruddin SM, Grätzel M (2008) High-performance dye-sensitized solar cells based on solvent-free electrolytes produced from eutectic melts. *Nature Mater* 7:626–630
  94. Cao Y, Zhang J, Bai Y, Li R, Zakeeruddin SM, Grätzel M, Wang P (2008) Dye-sensitized solar cells with solvent-free ionic liquid electrolytes. *J Phy Chem C* 112:13775–13781
  95. Gao F, Wang Y, Zhang J, Shi D, Wang M, Humphry-Baker R, Wang P, Zakeeruddin SM, Grätzel M (2008) A new heteroleptic ruthenium sensitizer enhances the absorptivity of mesoporous titania film for a high efficiency dye-sensitized solar cell. *Chem Comm* 23:2635–2637

96. Nazeeruddin MK, Pechy P, Renouard T, Zakeeruddin SM, Humphry-Baker R, Comte P, Liska P, Cevey L, Costa E, Shklover V, Spiccia L (2001) Engineering of efficient panchromatic sensitizers for nanocrystalline TiO<sub>2</sub>-based solar cells. *J Am Chem Soc* 123:1613–1624
97. Pradhan SC, Hagfeldt A, Soman S (2018) Resurgence of DSCs with copper electrolyte: a detailed investigation of interfacial charge dynamics with cobalt and iodine based electrolytes. *J Mater Chem A* 6:22204–22214
98. Pashaei B, Shahroosvand H, Abbasi P (2015) Transition metal complex redox shuttles for dye-sensitized solar cells. *RSC Adv* 5:94814–94848
99. Hallinan DT Jr, Balsara NP (2013) Polymer electrolytes. *Annu Rev Mater Res* 43:503–525
100. Song JY, Wang YY, Wan CC (1999) Review of gel-type polymer electrolytes for lithium-ion batteries. *J Pow Sour* 77:183–197
101. Ngai KS, Ramesh S, Ramesh K, Juan JC (2016) A review of polymer electrolytes: fundamental, approaches and applications. *Ionics* 22:1259–1279
102. Heperuma OA et al (2013) Gel polymer electrolytes for dye sensitised solar cells: a review. *Mater Tech* 28:65–70
103. Liu IP, Hung WN, Teng H, Venkatesan S, Lin JC, Lee YL (2017) High-performance printable electrolytes for dye-sensitized solar cells. *J Mater Chem A* 5:9190–9197
104. Seo SJ, Cha HJ, Kang YS, Kang MS (2014) Printable ternary component polymer-gel electrolytes for long-term stable dye-sensitized solar cells. *Electrochimica Acta* 145:217–223
105. Venkatesan S, Su SC, Hung WN, Liu IP, Teng H, Lee YL (2015) Printable electrolytes based on polyacrylonitrile and gamma-butyrolactone for dye-sensitized solar cell application. *J Pow Sour* 298:385–390
106. Venkatesan S, Surya Darlim E, Tsai MH, Teng H, Lee YL (2018) Graphene oxide sponge as nanofillers in printable electrolytes in high-performance quasi-solid-state dye-sensitized solar cells. *ACS Appl Mater Inter* 10:10955–10964
107. Brennan LJ, Byrne MT, Bari M, Gun'ko YK (2011) Carbon nanomaterials for dye-sensitized solar cell applications: a bright future. *Adv Ener Mater* 1:472–485
108. Badenhorst H (2019) A review of the application of carbon materials in solar thermal energy storage. *Sol Energy* 192:35–68
109. Gun J, Kulkarni SA, Xiu W, Batabyal SK, Sladkevich S, Prikhodchenko PV, Gutkin V, Lev O (2012) Graphene oxide organogel electrolyte for quasi solid dye sensitized solar cells. *Electrochem Comm* 19:108–110
110. Wang YC, Huang KC, Dong RX, Liu CT, Wang CC, Ho KC, Lin JJ (2012) Polymer-dispersed MWCNT gel electrolytes for high performance of dye-sensitized solar cells. *J Mater Chem* 22:6982–6989
111. Mohan VM, Murakami K, Kono A, Shimomura M (2013) Poly (acrylonitrile)/activated carbon composite polymer gel electrolyte for high efficiency dye sensitized solar cells. *J Mater Chem A* 1:7399–7407
112. Chen PY, Lee CP, Vittal R, Ho KC (2010) A quasi solid-state dye-sensitized solar cell containing binary ionic liquid and polyaniline-loaded carbon black. *J Pow Sour* 195:3933–3938
113. Lee CP, Chen PY, Vittal R, Ho KC (2010) Iodine-free high efficient quasi solid-state dye-sensitized solar cell containing ionic liquid and polyaniline-loaded carbon black. *J Mater Chem* 20:2356–2361
114. Usui H, Matsui H, Tanabe N, Yanagida S (2004) Improved dye-sensitized solar cells using ionic nanocomposite gel electrolytes. *J Photochem Photo A: Chem* 164:97–101
115. Murakami TN, Ito S, Wang Q, Nazeeruddin MK, Bessho T, Cesar I, Liska P, Humphry-Baker R, Comte P, Pechy P, Grätzel M (2006) Highly efficient dye-sensitized solar cells based on carbon black counter electrodes. *J Electrochem Soc* 153:A2255
116. Imoto K, Takahashi K, Yamaguchi T, Komura T, Nakamura JI, Murata K (2003) High-performance carbon counter electrode for dye-sensitized solar cells. *Sol Ener Mater Sol Cell* 79(4):459–469
117. Chen J, Li K, Luo Y, Guo X, Li D, Deng M, Huang S, Meng Q (2009) A flexible carbon counter electrode for dye-sensitized solar cells. *Carbon* 47:2704–2708

118. Lee WJ, Ramasamy E, Lee DY, Song JS (2009) Efficient dye-sensitized solar cells with catalytic multiwall carbon nanotube counter electrodes. *ACS Appl Mater Inter* 1(6):1145–1149
119. Huang KC, Wang YC, Dong RX, Tsai WC, Tsai KW, Wang CC, Chen YH, Vittal R, Lin JJ, Ho KC (2010) A high performance dye-sensitized solar cell with a novel nanocomposite film of PtNP/MWCNT on the counter electrode. *J Mater Chem* 20(20):4067–4073
120. Wan L, Wang S, Wang X, Dong B, Xu Z, Zhang X, Yang B, Peng S, Wang J, Xu C (2011) Room-temperature fabrication of graphene films on variable substrates and its use as counter electrodes for dye-sensitized solar cells. *Sol Sta Sci* 13:468–475
121. Roy-Mayhew JD, Boschloo G, Hagfeldt A, Aksay IA (2012) Functionalized graphene sheets as a versatile replacement for platinum in dye-sensitized solar cells. *ACS Appl Mater Interf* 4:2794–2800
122. Choi HJ, Shin JE, Lee GW, Park NG, Kim K, Hong SC (2010) Effect of surface modification of multi-walled carbon nanotubes on the fabrication and performance of carbon nanotube based counter electrodes for dye-sensitized solar cells. *Curr Appl Phys* 10:165–S167
123. Zhang Y, Yun S, Wang Z, Zhang Y, Wang C, Arshad A, Han F, Si Y, Fang W (2020) Highly efficient bio-based porous carbon hybridized with tungsten carbide as counter electrode for dye-sensitized solar cell. *Ceram Inter* 46(10):15812–15821
124. Ma X, Elbohy H, Sigdel S, Lai C, Qiao Q, Fong H (2016) Electrospun carbon nano-felt derived from alkali lignin for cost-effective counter electrodes of dye-sensitized solar cells. *RSC Adv* 6(14):11481–11487
125. Chung DY, Son YJ, Yoo JM, Kang JS, Ahn CY, Park S, Sung YE (2017) Coffee waste-derived hierarchical porous carbon as a highly active and durable electrocatalyst for electrochemical energy applications. *ACS App Mater Inter* 9(47):41303–41313
126. Wang Z, Yun S, Wang X, Wang C, Si Y, Zhang Y, Xu H (2019) Aloe peel-derived honeycomb-like bio-based carbon with controllable morphology and its superior electrochemical properties for new energy devices. *Ceram Internat* 45(4):4208–4218
127. Wang X, Yun S, Fang W, Zhang C, Liang X, Lei Z, Liu Z (2018) Layer-stacking activated carbon derived from sunflower stalk as electrode materials for high-performance supercapacitors. *ACS Sustain Chem Eng* 6(9):11397–11407
128. Younas M, Baroud TN, Gondal MA, Dastageer MA, Giannelis EP (2020) Highly efficient, cost-effective counter electrodes for dye-sensitized solar cells (DSSCs) augmented by highly mesoporous carbons. *J Pow Sour* 468:228359
129. Cha SM, Nagaraju G, Sekhar SC, Bharat LK, Yu JS (2018) Fallen leaves derived honeycomb-like porous carbon as a metal-free and low-cost counter electrode for dye-sensitized solar cells with excellent tri-iodide reduction. *J Colloid Inter Sci* 513:843–851
130. Wang G, Wang D, Kuang S, Xing W, Zhuo S (2014) Hierarchical porous carbon derived from rice husk as a low-cost counter electrode of dye-sensitized solar cells. *Renew Energy* 63:708–714
131. Li K, Luo Y, Yu Z, Deng M, Li D, Meng Q (2009) Low temperature fabrication of efficient porous carbon counter electrode for dye-sensitized solar cells. *Electrochem Comm* 11(7):1346–1349
132. Shao LL, Chen M, Yuan ZY (2014) Hierarchical porous carbons as a metal-free electrocatalyst of triiodide reduction for dye-sensitized solar cells. *J Pow Sour* 272:1091–1099
133. Kumar R, Nemala SS, Mallick S, Bhargava P (2017) Synthesis and characterization of carbon based counter electrode for dye sensitized solar cells (DSSCs) using sugar free as a carbon material. *Sol Energy* 144:215–220
134. Martínez-Muñoz A, Rana M, Vilatela JJ, Costa RD (2020) Origin of the electrocatalytic activity in carbon nanotube fiber counter-electrodes for solar-energy conversion. *Nano Adv* 2:4400–4409

# Chapter 8

## Carbon-Based Materials as Electrodes for Biofuels Electrosynthesis



Danilo Perez

### 1 Relevance of Biofuel in Low-Emission Economy

The Intergovernmental Panel on Climate Change (IPCC) concluded that global warming is one of the most serious climate change consequences, attributing a relevant role to anthropogenic greenhouse gas emissions (GHG). Among other consequences, it is expected a sea-level rise, more frequent and extreme weather events, and cyclones. All these will have an impact on human health, long-term business growth, communities, and the environment, hence, on the overall human well-being.

Due to the greenhouse effect and the long lifespan of CO<sub>2</sub> in the atmosphere, it has been pointed to as one of the key issues to work on. Reducing the CO<sub>2</sub> emission to net-zero has become the backbone of many countries' strategies to stop climate change. Therefore, low-emission economy plans are being designed to avoid surpassing the quantity of CO<sub>2</sub> that can be emitted before it starts to accumulate in the atmosphere, called carbon budget. In this context, the development of new technologies will play a pivotal role in the transition toward these new economic models.

Energy for manufacturing is an important source of CO<sub>2</sub>, particularly to produce the heat needed during production, such as drying milk powder or hot water for beer brewing and equipment cleaning.

The overall energy consumption can be reduced via improving control systems that allow adapting the process condition, or monitoring of specific equipment, although, probably the most effective action is to replace the fossil fuels with renewable sources. Important advances have been achieved by companies such as Asaleo Care that managed to reduce their greenhouse gas emissions (GHG) by 46% when started to use geothermal steam [1].

---

D. Perez (✉)

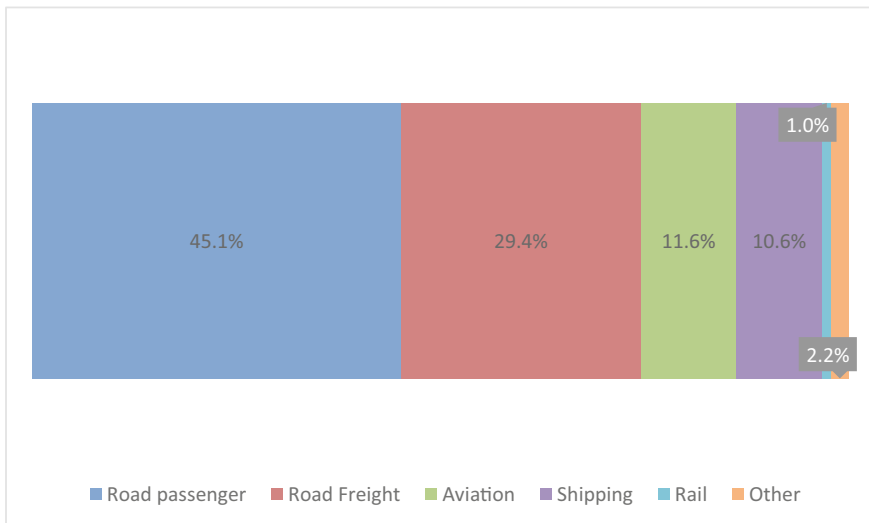
School of Engineering, Computer and Mathematical Science, Auckland University of Technology,  
55 Wellesley Street East, Auckland 1010, New Zealand  
e-mail: [danilo.perez@aut.ac.nz](mailto:danilo.perez@aut.ac.nz)

However, the use of renewable energies instead of fossil fuels has proven to be far from easy to process such as the calcination needed for cement production, as over 850 °C are needed. It can be argued then that a solution here is a strong emission pricing policy, where the inherent cost of emitting GHG will incentivize emissions reduction, decentralizing the decisions to invest, innovate, and solve technical issues [2].

Emissions pricing is indeed an effective tool to encourage a behavior change and promote investment, yet not sufficient to ensure an efficient transition toward the net-zero goal. Consequently, a range of complementary actions, regulations, and policies are needed to accelerate the development and implementation of technologies that support these behavioral changes from households to the industry [2].

According to data from the International Energy Agency, as in 2018 about 8 billion tons of CO<sub>2</sub> were emitted by the transport sector, representing 24% of the global emissions from energy. Road passenger leads the emissions with 45.1%, including cars, motorcycles, buses, and taxis, whereas trucks and lorries represent the 29.4% corresponding to the Road freight. In third and fourth place are Aviation with an 11.6% (81% passengers, 19% freighting), and shipping with a 10.6%, respectively. Interestingly, while rail and others are far below with a 1% and 2.2%, respectively, the latter relates mostly to transportation of oil and gas [3] (Fig. 1).

Given the big share of transport emission related to road passenger, it seems reasonable aiming to improve the fuel efficiency and electrification of the light fleet. To do this, some governments are introducing schemes where importers would be responsible for the fuel efficiency, via either a fee or through a rebate associated with the emission intensity. Simultaneously, governments are funding electrical vehicle



**Fig. 1** Global transport emissions by sub-sector, as percentage of the 8 billion tons of CO<sub>2</sub> emitted in 2018. Based on data from [3]

**Table 1** CO<sub>2</sub> emissions by sector of energy, in Mt CO<sub>2</sub> per year

Sub-sector	Year							% In 2018
	1990	1995	2000	2005	2010	2015	2018	
Electricity and heat producers	7622	8163	9358	10,970	12,508	13,373	13978	42
Other energy industries	975	1068	1195	1403	1643	1637	1613	5
Industry	3955	3938	3875	4928	6088	6316	6158	18
Transport	4609	5025	5770	6499	7012	7717	8258	25
Residential	1832	1849	1830	1903	1897	1864	2033	6
Commercial and public services	765	718	696	773	810	826	850	3
Agriculture	398	402	340	398	396	412	428	1
Fishing	18	18	19	24	23	20	19	0
Final consumption not elsewhere specified	342	191	159	181	205	201	177	1

Self-elaboration with data from [5]

(EV) infrastructure to push light fleet electrification forward. It is noteworthy here that an EV is as green as the fuel used to produce the electricity that charged its battery; therefore, there is much more to do beyond EV deployment. In fact, electricity and heat producers account for 42% of the total energy emissions, hence, far more significant than transport as seen in Table 1.

Even if travels are drastically reduced, mass transport modes are favored, transportation keeps improving its efficiency and vehicles shift to electricity and hydrogen, fuels are still needed for aviation, ocean shipping, and trucking. Although this demand is expected to be reduced over time, it has been estimated that by 2050 about 80% of the transportation fuel needs to be liquid fuel, and 50% by 2075.

The relevance of the energy sector and the accelerated climate change have put pressure on the R&D efforts to find low-carbon fuels. Thus, biofuels emerge as a sector with great potential. Biofuels are produced in biorefineries, where renewable raw materials are transformed into energy, energy carriers, and a broad range of valuable elements in a sustainable manner [4].

Additionally, bioprocesses are capable to produce energy carriers such as hydrogen and methane, or valuable compounds from a variety of feedstocks, including organic wastes. Thus, bioprocesses and particularly bio-electrosynthesis are changing the paradigm, considering wastes as resources, and arguably, very few processes can be more sustainable than those reclaiming energy and resources from waste streams.

**Table 2** Estimated storage capacity and timeframe for discharging for selected technologies

Technology	Discharging time				Storage capacity		
	Min		Max		Min	Max	Unit
Fly wheel	3	s	1	h	1	10	Kwh
Battery	4	min	10	h	2	90	MWh
compressed air energy storage (CAES)	8	h	4	Day	10	50,000	MWh
Pumped hydro storage (PHS)	11	h	42	Day	0.1	50	GWh
Hydrogen	1	h	50	Day	3	2000	GWh
Substitute natural gas source (SNG)	3	h	>1	Year	12	50	TWh

## 1.1 Energy Storage Requirement

In the current international scenario, where stronger climate action is demanded by society and policies are expected to become stricter, technological development beyond incremental improvements seems necessary in several aspects simultaneously.

The energy matrix is one of the topics that have drawn high attention levels during the last decade, accelerating the development of renewable energies significantly reducing its costs. In this context, an energy matrix based on renewable energies alone seems like the only sustainable path and more likely than ever. However, the transition toward a 100% renewable matrix implies a series of complexities due to the inherently fluctuant nature of renewable energy and lack of capacity to face peak demands.

On the other hand, fossil fuels are easily burnt or stored, which confers storing capacity and quick generation on demand. Several technologies have been developed to store renewable energies, such as electric batteries, flying wheels, pumping water, compressing air, and power-to-gas. As seen in Table 2, hydrogen and substitute natural gas have a better storage credentials in terms of the amount of energy and the extended discharge time, although the required investment is significantly reduced when the already available massive storing and distribution capacity of the natural gas infrastructure can be used, usually requiring storage as methane, whit the capability of working off-grid if required.<sup>1</sup>

## 2 Bio-Electrochemical Systems

At the wavefront of the technological revolution to add value to waste streams are bio-electrochemical systems (BES). Although BES is a platform that includes different types of devices and technologies, stand-out microbial electrolysis cells (MEC),

<sup>1</sup> <http://www.europeanpowertogas.com/>



microbial desalination cells, microbial electrosynthesis cells (MES), and microbial fuel cells (MFC) [6].

MFC is probably the most spread and well-known BES. As suggested by its name, an MFC aims to produce electrical energy from the chemical transformation through bio-electrochemical reactions [7]. This device requires microorganisms capable to degrade the organic matter to produce electrons and protons, although it also needs an electric system to conduct those electrons from the anode to the cathode. This simple description implies the necessity of the electric interaction between microbial cells and solid-state electrodes.

The electrical energy produced in an MFC is considered carbon neutral despite the CO<sub>2</sub> produced during the oxidation reaction, as it can be re-used for biomass growth such as animal and plant sediments that can feed later the MFC.

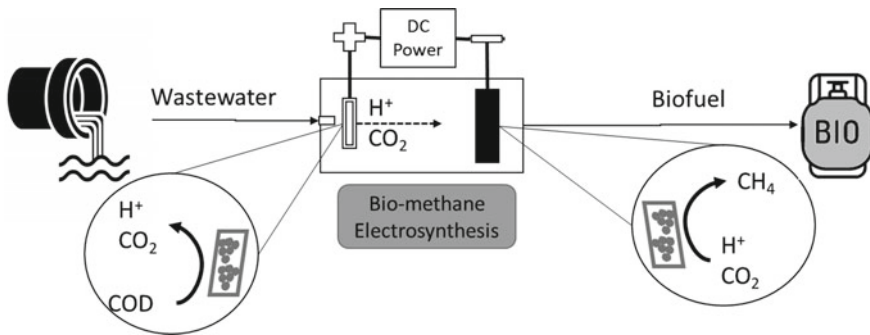
A MEC, on the other hand, needs an electrical input to produce valuable compounds and energy carriers such as methane and hydrogen. When hydrogen is targeted, the electrons are used for hydrogen evolution following the reaction  $2\text{H}^+ + 2\text{e}^- \rightarrow 2\text{H}_2$ , 0 V versus NHE or  $2\text{H}_2\text{O} + 2\text{e}^- \rightarrow \text{H}_2 + 2\text{OH}^-$ , and  $-0.828\text{ V}$  versus NHE, depending on whether the reaction occurs in an acidic or alkaline solution. Although most of the electrons come from the oxidation reactions that occur at the anode, an external supply is required to enhance hydrogen production [8].

These examples display the BES flexibility to use a variety of feedstocks as wastes to produce a variety of valuable compounds, energy, and energy carriers. A BES capacity to treat/produce a given compound depends essentially on the enzymatic arsenal of the biological component of the bio-electrodes. This highlights the importance of the electrodes colonization, to establish the bio-electrode capacity to harness the biochemical machinery, establishing an effective mechanism of electron transfer between the solid-state electric system and the biofilm and planktonic microbes present at the main reaction chamber [9].

Interestingly, the associated enzymatic machinery to a given consortium can also represent limitations and operational issues. This is the case that hydrogen-producing MECs struggle to eliminate the methanogenic activity. To achieve this, a very short hydraulic retention time and even oxygen injection has been reported necessary. Gil-Carrera et al. reported doubling the methane production of their hydrogen-producing system when the cathodic area was doubled, pointing toward a different variation of the system [10].

Thus, a variation of the described MEC targeting methane production was developed later, using hydrogen as an intermediate product. This particular application exhibits the capability for energy recovery from wastes. The methane can then act as an energy carrier suitable for long-term storage, while its production removes organic matter from waste streams. This combination makes these BES a platform that may play a pivotal role in the circular bio-economy.

In a typical methane-producing MEC, the circuit begins at the anode, where the microorganisms oxidize the organic matter (measured as chemical oxygen demand, COD), generating protons, CO<sub>2</sub>, and electrons. The latter is transferred through an external circuit to the cathode, where hydrogen is generated. Separating the two chambers is a membrane (either for anion or cation exchange), that prevents the



**Fig. 2** Single-chamber bio-methane electrosynthesis in a MEC

contact between the oxygen present at the anode and the hydrogen generated at the cathode [11]. If cathode-generated hydrogen would reach the anode, it could be re-oxidized (known as hydrogen recycling), negatively affecting the overall performance of the device [11].

In 2009, the feasibility of a single-chamber reactor was demonstrated [12]. The design (see Fig. 2) has attracted attention from researchers to evaluate different bacterial sources as well as a variety of environmental conditions such as temperature and substrate. By eliminating the requirement of a membrane, the design becomes more appealing for wastewater treatment applications, as it represents a direct capital cost, higher maintenance, and a more complex design that impedes the industrial deployment of the technology [13].

The absence of a membrane also eliminates the associated pH gradient, diminishing both potential losses and internal resistance, reducing the energy input necessary to drive the reaction [11], and hence increasing the methane production rate.

An appropriate electrode material enhances the electron transfer between the electrode and the bacterial population, achieving higher efficiency and a lower cathodic-overpotential [14]. However, as multiple factors such as cell type, design, materials, and operational parameters influence the MEC performance, an optimization for the given application is recommended.

## 2.1 Biofilm Development

Biofilm formation is a process in which microbes self-immobilize or attach to a surface, covering themselves with an extracellular polymeric matrix (EPS). Biofilms play an important role in industrial microbiology, either needing to promote or block its formation [15].

*Biofilm formation and maturation correspond to a process that implies a series of stages, including the basic stages described below:*

- (a) *Initial or reversible Attachment, commonly due to weak and reversible Van der Waals forces or hydrophobic effects.*
- (b) *Irreversible attachment, at this stage the cell would achieve a more permanent attachment by using pilla-like structures for anchoring.*
- (c) *Expansion, here new cells are included, either by cellular growing or by aggregation from motile planktonic cells.*
- (d) *Maturation, when cells can begin to actuate at a bigger organization level than individual cells (based on Quorum sensing communication). The production of extracellular polymeric substance (EPS) begins, forming slimy protection that connects all the cells as a unit.*
- (e) *Dispersion, a mature biofilm will reshape itself based on the interactions with the medium. This process includes losing parts of the biofilm that will travel downstream to colonize new sites, among other mechanisms.*

*Despite the reversible and weak nature of the initial cellular attachment to either biotic or abiotic surfaces, it is crucial for the biofilm formation of a functional bio-electrode. Some physical, architectural, and topographic features of the electrode can benefit the adhesion, including surface roughness, microbial and surface charges, hydrophobic and electrostatic interactions.*

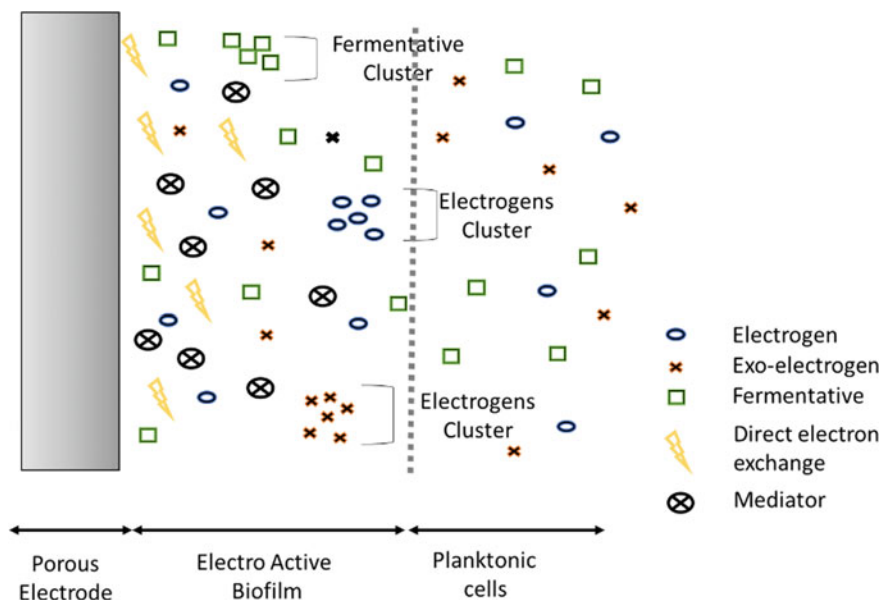
*In this sense, the initial attachment of the electroactive bacteria onto the surface of the electrode is facilitated by the ability of the bacteria to donate electrons either by direct electron transfer mechanisms as in *Geobacter* sp., *Shewanella* sp. or through mediator-assisted electron transfer as in *Pseudomonas* sp., etc.*

*It can be inferred then that biofilm formation, regardless of their nature, shares a formation process and structure, but electroactive biofilms (EAB) will exhibit particular electrochemical properties. The clearest of these differences is that EABs are formed over a surface capable to exchange electrons with the EAB, either accepting or donating them. Structurally, this capacity of extracellular electron exchange requires components such as pili (to form nanowires), c-type cytochromes, or electron mediators.*

*However, the role of the electrode in bio-electrode formation goes beyond simply electron acceptance/donation. The solid-electrode acting as the base of the bio-electrode should promote the initial attachment, as EABs are more conductive and prone to electrochemical interactions than planktonic cells.*

*The differences between planktonic cells and EABs pass the mere fact of cellular aggregation. The flocs/aggregates of cells will usually be covered by the EPS, an exopolysaccharide matrix that allows the formation of channels that benefit the nutrients flow through the matrix. However, the inherent heterogeneity of biofilms—unlike individual planktonic cells—brings the possibility of metabolic cooperation, creating microenvironments that accommodate specific metabolic capacities.*

Unlike biofilms, planktonic cells are theoretically fully available for accessing nutrients from the bulk electrolyte. As a general rule, better nutrient access translates into higher microbial performance. However, in the biofuel and BES context, the high reaction rates allow shorter hydraulic retention times that make washing out a real concern for operators [16].



**Fig. 3** Schematic of the selective enrichment of exoelectrogens in the biofilm, and cooperative association among bacterial groups

Increasing the retention time of the cells is crucial to allow the microbes to carry on their metabolism but is not the only reason to look forward to cellular immobilization. Planktonic cells are more exposed to environmental fluctuation such as temperature, feedstock, and pH, and this translates into a more robust and resilient operation when a mature biofilm is used [17, 18] (Fig. 3).

## 2.2 Overpotentials

Needing a potential much higher than the theoretical to carry on the desired reaction is commonly found in the literature. For a methane-producing MEC, over 0.5 and 0.6 V have been reported to be necessary for carrying on methane electrosynthesis by independent groups [19, 20], surpassing the  $-0.244$  V versus SHE and  $-0.410$  V via direct EET and indirect EET, respectively [14]. This is likely due to imperfect electrode materials and mass transfer-related overpotentials, which translate into more energy consumption and hence poorer energy efficiency overall.

The microbe-electrode interface plays a key role on the energy efficiency of the system, as it corresponds to physical space where the reactions take place. For this reaction to happen, a series of steps need to be carried on, mostly referred to electrochemical steps as per listed below:

1. Mass transport: This step includes the reactants transport from the bulk to the electrode surface, and this step is strongly affected by the fluid dynamic of the system; hence, it can be improved by agitation and mixing.
2. Preceding reactions: This step corresponds to the preliminary reactions or phenomena required for the reagents to be ready for reacting. For example, some molecules need to be absorbed, preliminary protonation or disassociation among other possible preliminary chemical reactions.
3. Electron transfers at the interface.
4. Surface conversions, which can include chemical reactions, desorption, etc.
5. Mass transport from the interface into the bulk of the electrolyte.

The overall reaction rate is limited by the slowest step. Each step can be a cause of overpotential, corresponding to one of the three categories: ohmic ( $\eta_o$ ), activation ( $\eta_a$ ), and transportation ( $\eta_c$ ). The overpotential can be defined as the sum of those three [21], as shown in Eq. 1.

$$\eta = \eta_o + \eta_a + \eta_c \quad (1)$$

There is a linear relationship between the ohmic potential drop and the current obtained. As the Ohmic overpotential relates to Ohm's Law, it combines the resistances of electrodes, electrolyte, membrane (when present), current collector, and the contact, and hence, it is intimately related to the materials choices. However, unless the electronic resistance is particularly high due to a poor material choice, or electrode passivation, the ohmic overpotential is predominantly controlled by the ionic resistance [21].

The material selection and electrode architecture will also directly affect steps 2 and 3 previously described, involved in the activation overpotential. Although the bioreactor operation, feeding, and lack of appropriate mixing are also involved here, a poor mix could contribute to build up electrons over the surface as consequence of the reagent concentration gradient that may be formed between the reaction site and the bulk of the electrolyte. This gradient would make difficult for new electrons to arrive, phenomena related to the steps 2 and 5 listed above (preceding reactions and mass transport).

Therefore, the difference of potential required for activation (effectively producing current) and the potential to achieve the equilibrium is considered as the "activation overpotential". However, this difference in potential can also be attributed to slow preceding/following surface reactions, as may occur when catalytic decomposition or crystallization is involved [21]. In practice, this implies a faster reaction than the mass transfer capacity of the system, which can be either a limiting number of reactants reaching the reaction site or a slow departure of products. Thus, depletion of reactants or accumulation of products will be produced over the electrode.

Here again, the material choice will be involved. In a bulk non-porous electrode, the biofilm can only develop over the surface, indirectly limiting increased currents due to the limited amount of exoelectrogens capable to effectively interact with the

electrode [9]. Contrarily, new materials such as felts offer a 3D open structure with a greater specific surface (surface per electrode volume).

The scale of the pores is also crucial for effectively provide an attachment site for the exoelectrogens. The typical exoelectrogens range between hundreds of nm to  $\mu\text{m}$ , forming biofilms that will adapt to the available topography [9]. Therefore, if the pores are too small, it will not act as a site for bacterial colonization, but even if it does and gets clogged with the biofilm, zones with very little or no mixing within the electrode thickness are unavoidable. Therefore, the pore size distribution will have an effect over the overall process, due to the combination of the direct surface are neglected of access to the reagents coming from the bulk of the solution. This could also translate into a nutrients mass transfer deficit that can limit the performance of the biofilm (when used in the BES), with the consequent further yield reduction that could drastically change the nutrient usage of the microbial consortium [22].

This effect can be counteracted by enhancing the convection via a more intense mixing/stirring. When the convection component is minimized, the mass transport depends entirely on diffusion and migration mechanisms, driven by the concentration gradient, and the electrical field, respectively [21]. Thus, due to the intrinsic relationship of fluid dynamics over mass transport, it ultimately will be key for the overpotential and overall energy consumption of the process [23].

The mass transport could control the overall reaction rate if the reaction occurs sufficiently fast over the electrode surface. This highlights the crucial role of the material selection over the system performance, as it will greatly determine the surface reaction rate, and the mass transport near the reaction interface; the balance between these two phenomena will determine whether reactants/products will increase/decrease their concentration near the electrode, affecting the obtained current [21].

When a balance is reached, and the reaction occurs instantaneously upon arrival, the concentration over the electrode is null and the obtained current is known as the critical current. The corresponding reaction rate is then the maximum achievable for the given mass transport capacity of the system. Assuming that the system relies on diffusion, the current density could be estimated with the equation below, where  $F$  is the Faraday constant,  $n$  the number of electrons involved,  $D$  the diffusion coefficient of the reactant,  $C^*$  the concentration at the bulk, and  $\delta$ , the thickness of the diffusion layer (boundary where the concentration is different to that on the bulk of the electrolyte) [21].

$$i_l = \frac{n * F * D * C^*}{\delta} \quad (2)$$

Understanding the source of the overpotential offers the implicit opportunity to reduce their impact. In this sense, different approaches have been taken to increase the overall energy efficiency by reducing the overpotentials. One approach is to tailor the electrode materials to enhance the electrode-microbe electron transfer [14]. In the context of methane production using graphite felt electrodes, an effective

overpotential reduction and improved microbial electrocatalysis activity have been reported following this last strategy.

Reducing overpotentials is a common interest among researchers, another approach to this was aiming to improve migration via imposing different voltages control strategies [23]. The authors claimed that moving from anodic control to a cathodic control strategy reduced the anodic reaction overpotential by 30%, while the cathodic overpotential remained steady. Other researchers have favored one electrode reaction surface, by modifying the relative surface area [10, 17, 24]; these experiences suggest that the best electrode to be favored depends on the targeted product. Thus, methane-producing MEC would be benefitted from a bigger cathodic surface area, whereas it would have a detrimental effect on the performance of a hydrogen-producing MEC.

Therefore, the mass transport capacity limited to diffusion and migration, combined with the chemical nature of the electrode material and architecture, are the major sources of overpotentials. Acknowledging this is crucial for the preparation of a strategy to counteract these effects; nevertheless, the best manner to address this will depend on the specific constraints and process conditions where each system operates. However, designing electrodes with a porous structure that facilitates fluid dynamics and mass transport through its thickness can be considered a good design guideline, as it would avoid reactants/product gradients, hence, including agitation would also avoid dependency on diffusion and migration, but it has a direct impact on the upfront cost, the structural design of the reaction vessel, and operational costs, so it needs to be carefully evaluated.

The importance of understanding the role of overpotentials is that it acknowledges the competence for electrons between exoelectrogens and non-exoelectrogens using CO<sub>2</sub> or sulfate as the electron acceptor, with the inherent advantage of being soluble. Therefore, it can be considered that a bio-anode is effectively competing with those dissolved and easily available in the neighborhood electron acceptors. Later, and after the electrons have traveled through the electrical component, they can reach the bio-cathode. Here again, the cathodic potential must surpass the bio-anode potential, but not the available electron acceptors nearby [9]. This inherent thermodynamic hierarchy of electron donors and acceptors works as an essential input for the material selection during the system design, as only a narrow range of energy can effectively be harvested.

### 3 Electrode Material and Bio-Electrodes

The microbes found in the consortium of BES are as varied as the operational designs; however, *Shewanella*, *Geobacter*, and *Escherichia* are genera commonly found. Species of those genera are well suited to BES as they can mediate in the electron transfer mechanism between dissolved substances and solids, so they are known as exoelectrogens that form part of electrochemically active biofilm (EAB) [9].

The presence of bio-electrodes is arguably the most essential feature of a BES. The term bio-electrode emphasizes the role of the microbial consortium and its interaction with the solid-state electrode. The achievable performance by a given feedstock is modulated by a series of factors, including operational condition, but also the electrode material, as it will contribute to the electroactive microbial communities maturation over its surface [25]. The developed microbial community formed over the electrodes, and its interaction with them will determine the biochemical pathways available for the system. Therefore, it can be understood that the overall efficiency of the system is in part controlled by the interaction between design factors such as the cathode material, structure, and operational parameters such as the metabolic diversity of the inoculum and applied potential [26]. Understanding these interactions will enable to conduct valuable chemical productions from by-products or wastes from a variety of processes. Interestingly, the interaction between these parameters is not constant; the inherent population dynamics within biofilms during its maturation will be perceived as an electrical modification of the surface of the electrode, leading the bio-electrode open circuit potential (OCP) evolution over time [26].

To improve the EET between the microbial cells forming the biofilm and the solid-state electrode that acts as physical surface is necessary to understand that this interaction is inherently a surface reaction. Thus, the electrode material will affect this interaction through its inherent biocompatibility and its topographical features. Fortunately, these factors can be selected and improved on desired to a given extent by pre-treating materials, materials combination, etc. [27]. This combination of material approach allows to use high conductivity collectors and carbon-based coatings to improve the biocompatibility, also allowing to design the topography and chemistry of the final electrode [28]. The coating would thus act as a sink for disposing of the electrons removed from the dissolved organic matter by the bio-anode [9].

The microbe-electrode interaction implies the need for an appropriate electroactive microorganism that will carry on the desired biochemical reactions. It also simultaneously suppose an appropriate design of the electrode, in terms of the configuration, location, and material to comply with the electrical conductivity and microbial compatibility necessary [29]. Thus, the solid-state electrode that will act as the base of the bio-electrode also needs to promote its colonization by the consortium, and further development of a healthy biofilm [30].

To effectively have a bio-electrode, an extracellular electron transfer is an electrical requirement [31]. To have this pathway, the appropriate electroactive biofilm needs to mature over the electrode. This mature biofilm starts with the microbial colonization of the electrode that acts as physical support for its development. Nevertheless, there are many factors influencing this process; chemotaxis (microbial movement promoted by chemical gradients) can play a significant contribution as the microbial adhesion is strongly modulated by the presence of divalent ions such as  $Mg^{2+}$  and  $Ca^{2+}$ , encouraging the biofilm formation. However, other forces such as the advective flow, preventing the attachment encouraged by shear forces, electrostatic and Van der Waals interactions will play the contrary role, so the overall balance needs to be controlled if the process is to be controlled [28].



A mature and healthy biofilm as has been referred above—usually—accounts with a series of different function that contribute to establish the extracellular electron transfer pathway between the biofilm and the solid-state electrodes. An important function, especially important during the initial stages of maturation, is the anchor that allows others to attach to this organic matrix. Other relevant function is the exoelectrogens, which account with redox-active pilus-like proteins capable of act as electrical conductive structures called nanowires [32]. This nanowires allow the extension of the interaction beyond the direct vicinity of the cell into the surrounding matrix [33]. A farther reach can be achieved when shuttles or mediators are used, and this implies the synthesis of specific molecules that will diffuse through the matrix into the wider surrounding, therefore, eliminating the need of direct physical contact. In the context of electromethanogenesis for example, hydrogen plays the role of shuttle [9] while fermentative bacteria can enhance the overall CH<sub>4</sub> production yield via producing H<sub>2</sub> and CO<sub>2</sub>, which is effectively a substrate for methanogens that originally comes from cellular lysis products.

However, and regardless of the particular metabolic capacities, composition, and maturation state of the biofilm, there is an agreement that one way of enhancing its overall production is via increasing the surface area available. On BESs, the electrode surface area will provide more reaction sites, and the roughness benefits the bacterial attachment and electrode colonization, whereas the mass transfer dynamics are partly determined by the 3-D structure as well [26]. These guidelines are important, as the ultimate purpose of including bio-electrodes is to maximize the electron transfer between the microbial cells and the power supply. The electron transfer can be monitored as the volumetric current density (A m<sup>-3</sup>) of the device, which can be either directly measured or calculated as the product of the current density (A m<sup>-2</sup>) and the specific surface area of electrodes (m<sup>2</sup><sub>electrode</sub> m<sup>-3</sup>) [9].

A very wide range of performance can be found in the literature, even for specific applications such as methane production. This range of performances relates to the biocompatibility and architectural morphology of the electrodes, and operational conditions that modulate the bacterial performance such as temperature, organic load, and the applied voltage, particularly relevant for MECs. In this regard, it is possible to find a range of values from -1200 mV [14] to 1800 mV [34]. When carbon-based electrodes are used, the values are restricted to the range between -850 and 1000 mV.

### ***3.1 Electrode Material and Architecture***

The carbon source, operational conditions, and BES design have an unquestionable role in the constitution of the microbial community growing in a BES. Some studies have shown that when it comes to the bio-cathode community, the MEC design may be the most relevant factor [35].

In addition to the compatibility, practical issues also need to be foreseen as they will reshape both the electrodes and device geometry and overall architecture.

Fouling, for instance, can alter the electrode resistance, or clog the flowing spaces if they are too small, all producing a detrimental effect on the performance [28].

Avoiding direct contact between electrodes is a basic consideration, particularly relevant in single-chamber BESs, unlike for typical two-chambered systems. At a laboratory scale, rigid supports are commonly used [34]. For instance, Yang et al. operated an H-type reactor with a 4 cm bridge, so their electrodes could only be 6 cm apart [36], whereas Guo et al. used a 9-cm-diameter cylinder, and thus, the electrodes were as close as 2 cm apart. Although avoiding contact is crucial regardless of the electrode material, the carbon-based material manageability allows more radical designs that reduce the distance and increases the surface area. Graphite granules, for instance, were used as electrodes and support for the bacteria growth, filling the whole compartment so that the electrodes were just 0.5 cm apart [37]. Other researchers work with a sandwich-like electrode [12, 13, 20] that uses a nonwoven cloth to keep the electrodes together without direct contact, minimizing ohmic overpotentials.

Table 3 offers a summary of relevant literature, where different electrodes have been used under different conditions. Besides the compatibility consideration previously commented, the literature suggests regarding the electrodes design, that specific surface area and open 3D structure show a positive correlation with the current density obtained, whereas electrode separation has the opposite trend [38]. In this sense, it has been reported that bio-electrochemical systems are benefited from porous materials with a low gravimetric density and high conductivity, although 3-D structured tends to be clogged by biofilm overgrowth [39].

As expected, due to the greater surface area available for chemical reactions, porous electrodes outperform bulk material electrodes (non-porous). Nevertheless, the use of a porous matrix for the electron transfer between the biofilm and the electrical system is necessary but not sufficient. A series of considerations such as the thermodynamic hierarchy previously mentioned need to be taken into account to allow the EAB energy requirements to be satisfied. Additionally, as the microbes are expected to form a mature biofilm, macrostructure inherently thicker than isolated cells, the scale of the porous raises as an important feature that needs to allow nutrients/products delivery/removal considering the long-term development of the biofilm without clogging [9].

In this regard, packed bed bio-electrodes such as those used by Villano et al. [31] are interesting, as the materials are cheap and every piece needs to be in direct contact with another in order to work as a conductive unit. This tight configuration will also create nooks and crannies to be colonized by the biofilm, reducing the effective porosity, thus affecting the overall volume usage. In addition, the biofilm growth in these reduced spaces can lead to dead zones where the nutrients/products flow is insufficient, with the expected detrimental effect on the obtained current density and overall performance. A practical alternative is the use of stainless steel meshes, providing superior mechanical properties, high conductivity, and low cost that will traduce in a manageable electrode design able to provide an appropriate range of porous sizes suitable for biofilm growth. However, surface modifications or coating are recommended to improve the attractiveness for bacterial colonization [9].

**Table 3** Selected BES studies using carbon-based electrodes

References	Chambers	Vol (ml)	Operation	HRT (H)	gCOD day <sup>-1</sup>	Temp (°C)	Applied mV	Control method	Anode	Cathode	MPR	MCR
[13]	1	3000	Batch versus continuous	24	0.30		1000	Cell	Carbon felt	Stainless steel	0.5	26.3
[40]	1	800	Batch	720	2.40	35	600	Cell	Reticulated vitreous carbon	Reticulated vitreous carbon	0.8	4.4
[41]	1	500	Fed-batch	120	0.50	25	950	Cell	Carbon cloth	Nickel foam	1.3	19.7
[12]	1	256	Fed-batch	5.3	1.06	22	-800	Cell	graphite granules	Graphite rod	0.1	0.5
[42]	1	10	Batch	140	0.00	65	1000	Cell	Carbon paper	Carbon paper	0.2	96.0
[43]	1	130	Batch	58	0.13	30	800	Cell	Graphite brush	Carbon cloth	3.9	61.1
[44]	1	600	Continuous	24	1.20	35	800	Cell	Graphite felt	Graphite felt	33.1	260.6
[45]	1	785	Semi-continuous	480	1.57	35	300	Cell	Graphite carbon coated with Ni	Graphite carbon coated with Cu	6.7	52.6
[43]	1	1000	Continuous	6	-		1000	Cell	Graphite	Graphite	248.5	-
[46]	1	250	Batch	72	0.83	25	1000	Cell	Carbon felt	stainless steel*	50.0	236.5
[47]	1	330	Batch	144	0.66	35	- 835	Cathode	Carbon fiber brush	Carbon fiber brush	20.0	157.9

(continued)

Table 3 (continued)

References	Chambers	Vol (ml)	Operation	HRT (H)	gcod day <sup>-1</sup>	Temp (°C)	Applied mV	Control method	Anode	Cathode	MPR	MCR
[48]	1	3000	Fed-batch	24	3.42	35	- 800	Cathodic	Graphite rod	Carbon felt	9.1	1800.0
[49]	2	560	Continuous	93	0.12	30	- 700	Cathode	Platinum	Graphite felt	0.3	18.7
[38]	2	2500	Continuous	24	2.50	30	900	Cell	Graphite fiber	Stainless steel	4.9	77.5
[50]	2	500	Continuous	6.8	3.92	23	- 800	Cathode	Graphite granules	Graphite granules	0.0	0.02
[51]	2	700	Semi-continuous	48	1.40	35	800	Cell	Carbon brush	Stainless steel	10.3	81.1
[52]	2	5	Batch	50	0.01	30	700	Cathode	Graphite plates	Graphite plates	108.0	681.2
[53]	2	500	Fed-batch	720	0.15	55	800	Cathode	Graphite felt	Carbon felt	62.5	3338.4
[36]	2	1200	Batch	100	0.23	50	- 900	Cathode	Carbon felt	Carbon felt	50.2	4044.2
[24]	2	4000	Continuous	96	-	55	- 800	Cathodic	Carbon bar	Carbon plate	148.8	-
[37]	2	867	Batch	480	0.03	25	500	Anode	Graphite plates	Graphite plates	1.8	937.7
[10]	2	150	Continuous	72	0.65	30	1200	Cell	Carbon felt	Nickel foam	6.5	23.5
[54]	2	800	Batch	72	2.40	35	800	Cell	Granular graphite	SS, Ni, Cu	25.0	131.4

(continued)

Table 3 (continued)

References	Chambers	Vol (ml)	Operation	HRT (H)	gcod day <sup>-1</sup>	Temp (°C)	Applied mV	Control method	Anode	Cathode	MPR	MCR
[14]	2	400	Batch	24	0.20	35	- 1200	Cathode	Platinum	Carbon stick coated GF	3.3	102.5
[50]	2	500	Continuous	32	1.96	55	- 800	Cathode	Carbon felt	Carbon felt	3.3	13.2
[14]	2	800	Batch	24	0.16		- 1400	Cathode	Carbon stick	Carbon stick	3.4	265.8
[23]	2	860	Continuous	8.35	0.86	25	- 200	Anode	Graphite granules	Graphite granules	9.8	154.4
[55]	2	200	Batch	200	-	35	- 700	Cathode	Graphite felt	Graphite felt	0.3	-
[56]	2	300	Fed-batch	360	0.00	30	- 1000		Graphite fiber brush	Carbon cloth	0.2	206.7
[57]	2	12,000	Continuous	12.6	16.54	25	- 2.25	Anodic	Graphite granules	Graphite granules	91.1	912.5
[58]	3	2580	Continuous	14	0.88	25	200	Anode	Graphite granules	Graphite granules	9.4	434.1
[59]	-	5000	Semi-continuous	60	0.40	55	-				59.3	21.6
[60]	NA	500 (L)	Continuous	552	650.00	35	-	-	-	-	16.3	197.1
[60]	NA	500 (L)	Continuous	552	650.00	55	-	-	-	-	40.0	485.2

Brush-like electrodes avoid biofilm-related clogging thanks to the use of a central electron collector that simultaneously works as the core of the design, spacing fibers such as graphite or other microbial-friendly material. Nevertheless, it is commonly agreed that monolithic porous electrodes such as carbon felt are more suitable for most BESs applications as they account for a high surface area per unit of volume with pores accessible for microbes, disposed of in an open 3D structure. All these features contribute to reaching a higher current density, although the cost is still a concern for important applications for as wastewater treatment [9].

### 3.2 Carbon Materials

It has been proposed in the literature that carbon-based bio-anodes can be inverted and operated as bio-cathodes when a suitable consortium is present. This capacity is based primarily on the biocompatibility and electrical conductivity of materials such as carbon and graphite felts, rods, cloths, and granules that also offer great specific surface area per unit of volume [35].

The use of carbon-based electrodes initially became popular in MFCs and later transferred to other BESs due to their chemical stability, good conductivity, and low cost [61]. It has been suggested that the similarity between felts and the natural habitat of the electrogenic bacteria allows them to use functional groups such as carboxylic acids, alcohols, and quinones to attach [27], essential for long-term operations as will assist the biofilm development.

On the other hand, carbon-based electrodes imply electric performance limitations. In the methane-producing context, current densities reported remain below  $10 \text{ A m}^{-2}$ . Additionally, the poor kinetics of hydrogen evolution of carbon-based materials requires elevated overpotentials, leading to energy losses estimated at 35% when operating at +200 mV and 62% at -200 mV [25]. Nevertheless, this electric limitation may be overcome by the superior capacity of porous carbonaceous material to interact with microbes and metallic electrodes, leading to diverse strategies of electrode designs.

The simple method of coating electrodes with materials such as graphite layer has introduced electrodes into the open three-dimensional structures, improving electron transfer efficiencies and fiber interconnectivity without affecting the inherently good electrical conductivity of metallic materials [27]. It is noteworthy that the precursor and manufacturing process of the carbon-based material will impact the properties of the final electrode. With carbon and graphite felts the most common materials to this use, the graphitization process at either 1500 or 220 °C will have a significant impact in the overall performance of the final electrode and its cost [27].

An enhanced wettability, via either plasma, thermal, or chemical treatment, will improve the overall performance of the electrodes as the electrolyte ions would access more easily the voids within the 3-D structure. Additionally, metallic nanoparticles, graphene, and carbon nanofibers have been used to enhance their conductivity [27]. Following this logic, platinum is currently considered a viable alternative due to its

low overpotential and feasibility of coating onto a wide selection of materials such as brushes, cloths, rods, and plates [44] and significantly improves the methane production of MECs as it boosts the hydrogen evolution. Promoting hydrogen evolution in the methane-producing context results beneficial as it allows the engagement of multiple metabolic pathways, particularly *Hydrogenotrophic methanogenesis* [31], a metabolic route typically considered secondary on the mesophilic production of methane, that has exhibited a production rate significantly superior to the typical *Acetoclastic methanogenesis* and became a hot topic in the field during the last decade.

It is well-known favorable hydrogen evolution of platinum electrodes, and this has led to use of this material to coat electrodes, or directly build them from it. These electrodes are technically feasible despite its sensitivity to chemicals as sulfide, commonly found in waste streams. Nevertheless, the inherently negative environmental impact and elevated prices of platinum have limited its use to laboratory scale and mostly in the foundational studies area [61]. Interestingly, even when hydrogen production is targeted and abiotic electrodes are useful, bio-electrodes seem to be preferred due to features like their self-regeneration capacity, inherent low cost, and remarkable flexibility to promote a wide range of specific reactions [37]. A good case in point are the bio-cathodes used in the wastewater treatment field, where they have been reported to resist those conditions and reduce CO<sub>2</sub> into bio-methane among other valuable molecules [37].

### 3.3 *Electrode-Microbe Interaction*

Microorganisms forming part of the biofilm exchange electrons with the solid-state electrode, to support the respiratory or anaerobic oxidation of electron donors such as organic compounds. This electron exchange is typically relying on c-type cytochromes, a heme-containing protein typically found in bacteria and archaea [35].

The c-type cytochromes are necessary for the electron transfer, but not sufficient. At the cathode, the biofilm needs specific enzymes capable to catalyze the reaction between electrons and protons, such as hydrogenases. This is an example of why bio-cathodes accounting with the capacity of enzymatic machinery outperform expensive metal electrodes [35].

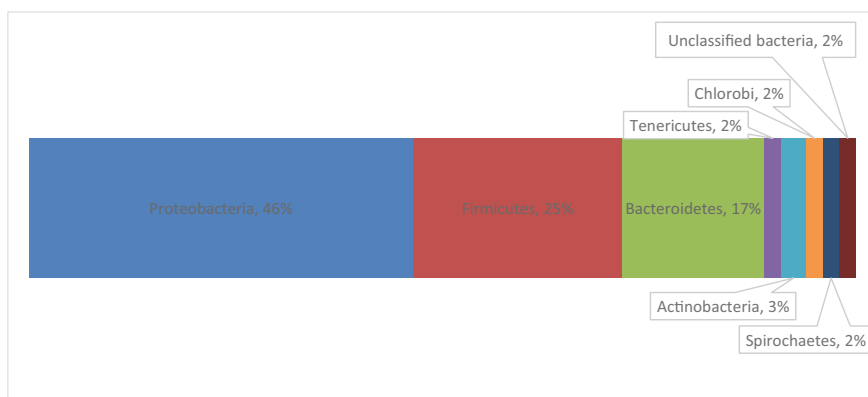
An underlying factor in these mechanisms is the portion of contact between the growing EAB and the electrode. In this regard, it has been proposed in the literature the Brunauer–Emmett–Teller (BET) method as the “one truly valid method” to determine the bio-electrochemically active surface area. This calculation would need to determine first the total BET active surface and the biofilm-covered area, requiring chronoamperometric response analysis of the porous electrodes, and the diffusion coefficient from an electroactive component [26]. This method is accurate but complex to implement, and even harder to establish as a comparison parameter as not all the parameters are commonly known, nor easily determined.

BET reports pores at the nm scale, an interesting metric for electrode roughness. However, this roughness metric is not relevant from a biofilm development point of view, as any pore under the  $\mu\text{m}$  scale is likely to be clogged and, thus, behave similarly to a non-porous bulk electrode.

A different approach to assess biofilm development is the use of SEM images. Studies following this approach commonly provide images from before and after colonization. Unfortunately, the time between them is usually short and, thus, it does not provide information regarding the long-term pores clogging associated with the biofilm growth [9].

The biofilm composition is certainly influenced by the surface roughness, electrode topography, carbon source, and overall bioreactor setup and operation [35]. Population dynamics is in fact a field that attracts important attention from researchers, probably because it will determine the potential capacity of the whole system as it provides the enzymatic machinery available, as previously mentioned. Many studies report the population composition [7, 40, 59, 62], which varies according to the conditions. In a hydrogen-producing MEC fed with acetate without methanogenic inhibitor presence, the community was dominated by Proteobacteria and Bacteroidetes as seen in Fig. 4 [35].

Among the proteobacteria, dominant on the described system is possible to find *Shewanella* and *Geobacter* previously mentioned, often used as pure culture in some studies [35, 63–66]. These two dominant genera are known metal-reducing, gram-negative bacteria that use the heme C-type cytochrome as the main extracellular electron transfer mechanism. Nevertheless, these bacteria have been proven to also be capable to establish electrical connections through filamentous conductive pili structures. This diversity of mechanism makes it hard to understand deeply the electron transfer mechanism acting in fully developed bio-electrodes, leading to the use of pure cultures. However, it is currently accepted the existence of direct and indirect electron transfer mechanisms, and the former needs direct contact between the



**Fig. 4** Microbial community composition in a hydrogen-producing MEC fed with acetate, self-elaboration with data from [35]



microbial cells and the solid-state electrode, while the indirect mechanism relies on shuttles and extracellular substrates [35].

### 3.4 *Electron Transfer Mechanisms in BES*

The existence of electrical and microbiological components is a peculiarity of BESs, combining biological and electrochemical processes over the bio-electrode surface. At the interface of these three phases (microbial cell, electrode, and bulk electrolyte), the dissolved organic matter is oxidized to free electrons that are later transferred either directly to the electrode (direct EET) or through a soluble electron acceptor (indirect EET) [63].

#### **Direct EET**

It is indispensable for this mechanism the direct microbe-electrode contact, through outer membrane proteins such as the c-type cytochrome mentioned earlier, or conductive pili forming nanowires, without any soluble redox compound taking place [63]. The commonly found *Geobacter* and *Shewanella* genera are metal-reducing bacteria and therefore need acceptors like Fe(III) oxides present in the neighborhood. Although some species have been reported to produce nanowires structures electrochemically active, connecting the cytochromes present in their membrane directly to the electrode. These electrochemically active conducts extend the reach of the direct mechanisms beyond the cell's immediate environment and hence allows biofilms to grow in 3D, and not as a monolayer over the electrode. This thicker biofilm translates into the overall higher performance of the BESs [63].

#### **The Mediated electron transfer mechanism**

Direct cellular-electrode contact is not always mandatory nor possible; in this respect, some electron shuttles can be used to communicate both surfaces. Flavins and phenazines are examples of self-produced mediators, although some gram-negative bacteria species have been reported to be capable of utilizing externally introduced molecules as mediators, such as the case of neutral red, thionine, and methyl viologen among others. When external mediators are used for enhancing the overall electron exchange, an increase of the obtained current is expected, but the selectivity and stability fall behind the performance achieved by a direct EET [63].

#### **Indirect electron transfer**

A third mechanism that has drawn attention during the last decade, especially due to the involvement of bio-methane production as a renewable energy storage mechanism, and method for energy reclaiming from wastes is the indirect EET. An indirect EET relies on reduced intermediate metabolites such as hydrogen and formate to incentivize the electron exchange. Hydrogen, for instance, can be produced by fermentative microorganisms or purely electrochemical methods, becoming anyways an electron donor for the reduction reaction.

Both direct and indirect electron transfer mechanisms have been reported to take place during the methane electrosynthesis in MECs [63]. Regardless of the electron exchange mechanism that the microbes conforming to the bio-cathode are able to use, the bio-cathode could use the electrons to reduce protons, sulfate, nitrate, or CO<sub>2</sub>, which is a key step in biofuel production.

The CO<sub>2</sub> reduction into CH<sub>4</sub> via extracellular electron transfer mechanism was reported successful in 2009, using a two-chambered MEC with a coulombic efficiency reaching 96% [56]. From this point forward, a new variant of the MECs was born, producing either hydrogen—as initially intended—or methane, embracing the methanogenic activity inherent to the MECs environment rather than trying to eliminate it from the bio-cathode.

When methane is targeted, multiple metabolic pathways should be engaged, where *acetotrophic* (starting from acetate) and *hydrogenotrophic* (starting from CO<sub>2</sub> and H<sub>2</sub>) are arguably the two most relevant pathways.

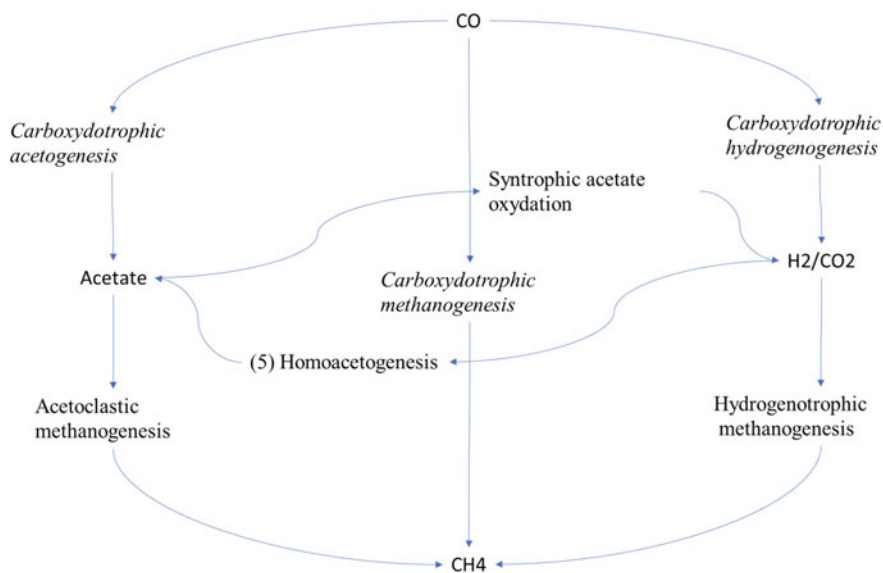
Figure 4 depicts the existing methanogenic pathways. Among the most commonly found bacteria in methane-producing bio-cathodes are *Methanobacterium*, *Methanobrevibacter*, and *Methanosaeta*, being the two first being from hydrogenotrophic and the latter acetoclastic pathways, respectively. This suggests that CO<sub>2</sub> could be reduced via using electrochemically produced hydrogen and the hydrogenotrophic capacity from bio-cathodes, becoming thus a potential biogas upgrading alternative.

This approach is possible to be carried on in a MEC. Reducing CO<sub>2</sub> into methane is possible when an external voltage is applied using the metabolic capacity of a bio-cathode [30]. Initially, anaerobic digestion (AD) was thought to produce methane mostly from acetate reduction and just a fraction from reactions involving hydrogen or other substrates [67]. Figure 4 summarizes the main metabolic pathways related to methane production. Currently, it is well accepted that the existence of two mechanisms, direct and indirect, including extracellular electron transfer (EET) as detailed above [49] (Fig. 5).

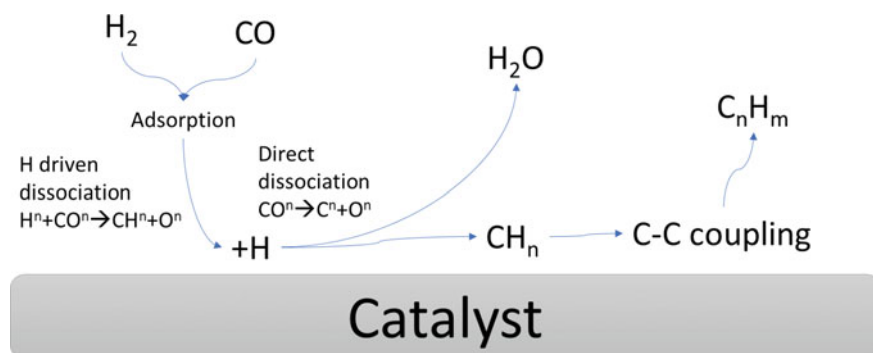
### 3.5 Catalysts for Hydrocarbon Synthesis

A promising renewable fuel for the de-fossilization of the energy matrix is the hydrocarbons synthesized from waste streams such as CO<sub>2</sub> emissions and syngas produced from inorganic waste. In this context, activation of both H<sub>2</sub> and CO is crucial and requires from catalysis such as metal sulfides, metal carbides, and nitrides, as these usually are capable to dissociate H<sub>2</sub> into H species, hence promoting the hydrogenation reaction of the CO that could be either dissociated into C and O or not over the metal surface [68].

Although the specific hydrocarbon synthesis mechanism is still a matter of discussion, Fig. 6 schematizes the simplified mechanism that has been proposed and accepted.



**Fig. 5** Main metabolic pathways involved in methane production



**Fig. 6** Schematic of the Fischer-Tropsch synthesis mechanism

Interestingly, some materials as cobalt and ruthenium have some kink sites that have been reported to help on the dissociation of CO, encouraging the adsorption of O by the H, with consequent water formation [68]. This simultaneously promotes the combination of the adsorbed C with H to form different combinations, that can go from C to CH<sub>3</sub>, resulting in an uncertain mix of molecules as the final result [69].

### 3.6 *Enzymatic Electrosynthesis*

Bio-commodities, such as hydrocarbons, are currently drawing important interest as a possible path for running the chemical industry without the carbon footprint burden. This process has taken the knowledge developed for biosensors, although these applications have significantly different requirements. A good case in point is the need for low currents and potential commonly aimed in the biosensor space to avoid the occurrence of counter-reactions, whereas in the energy and high-value molecule synthesis space the opposite tends to be true, this explains why in the biosensors enzymes are usually preferred rather than whole microorganisms [70]. Nevertheless, all processes based on biocatalysts tend to share some features that make them attractive during this re-foundational moment of the industry, such as:

- Biocatalysis processes tend to be operated at mild conditions and produce less waste than traditional methods, reducing operational expenses and simplifying specialized equipment
- Genomic information availability, and the possibility of genomic expression control, including enzymatic engineering to promote/inhibit specific functions or increase stability under industrial conditions
- Development of industrial fermentation and recombinant proteins, making available great amounts of custom enzymes, is characteristic that also leads to intellectual property generation, hence, making the research and development investments more economically attractive [71].

From this last point, it is worth mentioning that among the multiple classifications and types of enzymes existing, the oxidoreductases are capable of catalyzing the electron transfer between molecules or to electrodes, hence, of importance in the context of biofuel production in bio-electrochemical systems. Particular interest is paid to the fact that can use compounds such as hydrogen, sulfur, and heme among others [70]; this variety allows these enzymes to take part in multiple possible steps along with the reaction mechanism. However, those BES that utilize complete microbial cells as catalysts accounts for a wide enzymatic arsenal to perform either oxidation or reducing reactions with a wide range of substrates.

To emulate the enzymatic flexibility of whole microbial cells, but narrowing to the particularly interesting reactions for the desired application multiple enzymes can be immobilized over the catalyst surface, offering some benefits such as per listed below, and to some extent, these can be considered as a synthetic biology approach to select and concentrate in a single step just those desired reactions.

- Fewer unit operations
- Smaller reactor volume and shorter times cycles
- Higher volumetric yield and less waste generation.

Additionally, the development of AND recombinant technology, enzyme libraries expansions, and establishment of a well-developed vendor market of target enzymes makes it easier to think and act on the possibility of looking for the desired chemical

**Table 4** Reaction engineering versus enzyme engineering approaches for chemoenzymatic process design

Factor	Enzyme engineering	Reaction engineering
Main parameter	Volumetric productivity	Activity and operational stability
Determined by	Concentration of substrate and reaction rate	Combination of enzymes desired activity, selectivity, and stability
Key to success	Identify efficient biocatalyst, this is achieved by a thorough screening of libraries	Enzymatic stability, using whole cells, stabilized lysate, lyophilized enzymes, immobilized enzymes, etc.
Focus	Make the enzymes sufficiently active to maintain high reactions rates	Systematic alteration of reaction conditions to optimize the desire activity

Source Self-elaboration from [71]

reaction, finding the enzymes that perform that chemical transformation and design chemoenzymatic process for the specific BES application. In this sense, there are two main methods of addressing the chemoenzymatic process design, focusing on engineering either the reaction of the enzymes, as presented in Table 4. The discussion is strongly determined by factors such as the nature of the process, stage of development, number of reactions/steps involved, costs, timeframe, and regulations among others.

## 4 Electrodes Manufacturing Methods





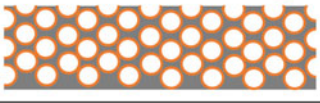
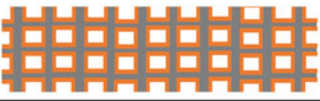

Improving the electric conductivity and catalytic activity of electrodes is key for the operation of BES. Aiming for these improvements, several methods have been developed, and material tested. Hybrid bio-cathodes with graphite felts and other materials have been used to improve microbial attachment and growth [35].

In the case of biofuels production, such as bio-methane, cathodes are more relevant. In this sense, evidence suggests that nickel-based materials reduce the ohmic overpotential, hence improving the overall efficiency of the process. On the other hand, porous carbon materials have a higher overpotential but achieve a much greater surface area that benefits microbe-electrode interaction, crucial for bio-cathode's operation. These differences have led to the development of a number of electrode types with different benefits, architectural, and topographic features [35].

In the literature can be found different strategies to improve the three-dimensional architecture design of the electrodes, a simple way of doing so is to add/subtract sheets of felts to modify the thickness of the final electrode [27]. This approach allows the indirect management of the electrode features. The total surface area is directly modified electrode, to determine the extent of this change depends on a variety of different methods can be used (physical methods, adsorption of gases, structural or electrochemical characteristics).

The second relevant architectural design feature altered directly by modifying the 3D design is the flow patterns around the electrode and through the open structure of the felt, a phenomenon that can be better understood by studying the Darcy's law that relates the differential pressure and the velocity of a fluid flowing through a control volume unit of a porous material [27]. Hence, by understanding how these phenomena relate to the architectural design of the electrode, the porosity of the felt, mass transfer limitation can be avoided, and the flowing patterns improved to achieve an overall better performance by avoiding inhibitory concentrations of metabolites or gradients.

Thirdly, as has been discussed, the electrode topography influences the biofilm formation by providing appropriate pores for its colonization. Figure 7 schematizes how the biofilm is expected to grow over selected electrode materials, exemplifying how pores too small can be clogged and will not be colonized by the exoelectrogens.

Schematic	Electrode Type
	Non Porous Bulk
	Densely Piled
	Embedded Cells
	Packed-bed
	Particle-Based Porous Electrodes
	Stainless Steel Mesh
	Carbon Brush

**Fig. 7** Schematic of the biofilm development over different types of electrodes

**Table 5** Selected works using densely piled electrodes

Reference	Coating	Current collector
[38]	Graphene powder with PTFE	Stainless steel mesh
[72]	Activated carbon/goethite powders with PTFE	Stainless steel mesh
[21]	Nano molybdenum carbide (MO <sub>2</sub> C)/CNT composite with PTFE	Carbon felt

#### 4.1 *Densely Piled Electrodes*

Piling is an electrode preparation method commonly used for electrochemical systems, as it produces 3D porous electrodes. It consists basically of using a roller press from an emulsion of the desired material. For instance, Zhang et al. used a graphite particle emulsion on polytetrafluoroethylene (PTFE), over a range from 6 to 48%. The authors recommend a 30% PTFE is optimal, stating that increases the porosity and wettability that increases the microbial attachment and electron transfer, while a higher PTFE content would diminish the electric conductivity and thickens the biofilm, hence, more easily clogging the pores [9].

Table 5 shows some researchers that used this method to produce their bio-electrodes with a variety of coating or particles that fill the pores of the current collectors made from stainless steel meshes, carbon felts, and nickel foam, although open structures were not achieved. These works effectively achieved high current densities, probably attributable to the scale of the pore comprehended between nm and  $\mu\text{m}$ . These pores are usually too small for effective colonization, as the biofilm thickness ranges between tens to hundreds of  $\mu\text{m}$ , although it could easily clog by biofilm growth but not colonized. This would lead to performance comparable to non-porous electrodes with improved electrode surface [9].

#### 4.2 *Cell Embedded Electrodes*

It seems natural to maximize an intimate microbe-electrode contact to embed the living cells within the 3D matrix. The fabrication of such an electrode requires the harvest of the consortium with the desired metabolic machinery, mix it with appropriate carbon nanoparticles, and coat the electrode collector such as carbon cloth [9].

A key element of this type of electrode is the lack of macro-scale pores. By embedding living cells into the close structure of the electrodes, the nutrients/products flow is neglected; thus, isolated cells trapped within the electrode are incapable to interact with the electrode's surroundings. Table 6 depicts some examples of works using this method for constructing electrodes [9].

**Table 6** Selected works using embedded cell electrodes

Reference	Construction	Inoculum
Typical case	Carbon nanoparticles (300 nm) and PTFE spread over carb cloth	MFC microorganisms
[73]	Cells with copper powder (<65 $\mu\text{m}$ ), soaked in $\text{CaCl}_2$ for hardening	<i>Ochrobactrum anthropi</i> SY509
[74]	MWCNT powder mixed with inoculum over carbon paper	<i>G. sulfurreducens</i>
[75]	<i>E. coli</i> on $\text{Fe}_3\text{O}_4/\text{CNT}$ nanocomposite onto carbon paper	<i>E. coli</i>

### 4.3 Packed Bed Electrode

As has been mentioned, the main issue with embedded electrodes is the lack of macroscale pores. Packed bed electrodes, on the other hand, achieve a structure where pores are both suitable for exoelectrogens colonization and allow sufficient space to avoid biofilm clogging. These macroscale pores are achieved using granules, such as activated carbon and granular graphite on the scale of mm. Given the random nature of these electrodes, they tend to be used to fill completely the compartment, and the electrolyte flows through the open 3D structure of the electrode [9].

However, using this type of electrode is no warranty of a suitable macroscale pores structure. Some authors have replaced the typical graphite granules with activated carbon granules of minor diameter, increasing the surface area. However, activated carbon granules also have pores under the  $\mu\text{m}$  scale, thus, unsuitable for exoelectrogens colonization. In addition, the typical electric conductivity of activated carbon is lower than the typical graphite granules, thus increasing the ohmic overpotential required due to the increased internal resistance.

Many researchers use packed bed electrodes [23, 25, 76], nevertheless, in the context of a bio-circular economy, seems noteworthy the case of Wang et al. and their rubber granules electrodes. As a way to recycle tires, the researchers used rubber granules of about 4–8 mm to prepare a conductive paste with graphite, and then, the resulting coated granules were used to fill the MFC chamber. Although the granules had a high specific area, the conductivity was poor, and the packing was loose. This translated into an increased internal resistance and smaller energy consumption to pump the electrolyte through the packing material.

This last example highlights how the design of the electrodes needs to balance Multiphysics effects, considering fluid dynamics, diffusion, bacterial colonization, biocompatibility, and electrical conductivity to achieve the optimal design for the particularities of the system.



#### 4.4 Coated Electrodes

It is well known that carbon-based materials have a series of features that make them “good” electrodes, such as adequate electric conductivity, relative inertly to chemical reactions, low costs, and variety of presentation as graphite rods, plates, or disks. Nevertheless, in a BES context, biocompatibility plays a crucial role in the overall performance as the substrate that will act as the template for the bio-electrode development should not just lack toxicity, and resistance to microbial degradation but also provide the structural architecture for biofilm growth. In this sense, the electrical characteristics of these materials are their weakest feature, and so researchers have tried a variety of coating to improve them:

- Multi-walled carbon nanotubes (MWCNTs)
- MWCNT/SnO<sub>2</sub> nanocomposite
- MECNT/MnO<sub>2</sub> nanocomposite
- in situ exfoliated grapheme
- Au/Pd nanoparticles
- graphite paste with Fe<sub>3</sub>O<sub>4</sub> and Ni<sup>2+</sup>
- polyaniline nanostructures
- sulfonated polyaniline/vanadate composite
- redox-active aromatic compounds.

An important factor for the deployment of BESs is the commercial availability of the materials. In this sense, carbon paper and carbon cloth are more commercially available and therefore commonly used. Carbon paper is prepared via compressing multiple layers of graphite fibers (μm thick each fiber). Carbon cloth instead is made of woven arrays of hundreds of graphite fibers. As both materials are produced from graphite fibers, the conductive of the final material is relatively high, which helps to reduce the ohmic overpotential of the BES.

Many different methods have been developed to apply the conductive coating over materials such as carbon paper working as an electron collector. Table 7 shows some examples of conductive polymers used to improve the carbon paper features, achieving higher surface roughness and hydrophilicity.

Electrochemical deposition can also be utilized as a method for coating the electrons collectors, either preparing an ink or a slurry. This method has been used by

**Table 7** Selected conductive polymers used to coat carbon papers

Reference	Conductive polymers
He et al.	Plasma-based N <sup>+</sup> ion
[77]	Mesoporous carbons
[78]	Multilayer polyethyleneimine/graphene films
[79]	Electrochemical deposits CNT network and chitosan

researchers to coat carbon cloth with ammonium bicarbonate ammonium nitrate, ammonium sulfate, nitric acid, and phosphate buffer [9].

Regardless of the method used, even when a high roughness is achieved with the previously mentioned modifications, when the pores are sub  $\mu\text{m}$  scale a significant portion of the effective surface area is not available for colonization, hence, reducing the actual bioelectrode surface. In this regard, both carbon paper and carbon cloth have been reported to achieve tens of  $\mu\text{m}$  space. Although spaces on this range may be colonizable for exoelectrogens, in long-term operation these are expected to be easily clogged.

Therefore, it is important here to bear in mind the role of the pore size discussed earlier, as some of these modifications have been reported to reduce the spacing, or even bridging the gaps. This will translate into a surface covered by the biofilm just reaching the projected geometric surface of the electrode.

#### 4.4.1 Stainless Steel

Stainless steel is a common material of choice in the electrochemical environment, especially in the industrial application context. However, the smooth surface, among other features, makes this material adequate for the food industry because microbes would not easily attach, an undesired particularity in the context of BES.

Nevertheless, due to its mechanical features, it is easily manageable to create 3D structures that guide biofilm growth. The lack of microbial affinity can be overcome using coatings, and this allows to significantly improve its biocompatibility, promoting the colonization. Lamp et al. for instance, reported using a flame synthesis method to deposit carbon nanostructures onto a stainless steel mesh, with the outcome of an improved current density and exoelectrogens affinity [9].

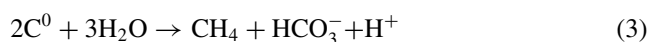
#### 4.4.2 Carbon Felt

Carbon felt is a monolithic material when carbon fibers are randomly placed, forming a porous conductive structure. The pores in the carbon felt tend to range between tens to hundreds of  $\mu\text{m}$ , which jointly with the carbon affinity/biocompatibility make these pores colonizable by exoelectrogens of both external and internal surfaces. Additionally, carbon felt is easily modifiable by either applying coatings or by simply layering up to increase the thickness of the electrode or to preserve the characteristic open structure, as shown in Table 8.

Other materials have been deposited over carbon felt electrodes, such as  $\text{MnO}_2$ ,  $\text{RuO}_2$ , polypyrrole/graphene oxide composite, and polyaniline nanowires. All these looking to improve the carbon felt electrodes' current densities. Interestingly, some authors have reported Coulombic efficiencies over 100% [14], hypothesizing that may relate with methanogenic corrosion, and hence, the cathode itself would act as the electron donor for the methane generation [52] following the reaction given below [14] and later using those protons for reducing the  $\text{CO}_2$

**Table 8** Selected modifications of carbon felt electrodes

References	Method	Improvement
[80]	Anodization	Creates micro cavities, 1 $\mu\text{m}$
[81]	Chemical vapor deposition	Grew CNTs over the fibers
[82]	Electro polymerization and Electrophoretic deposition of CNTs	Prepared electrodes with polyaniline



#### 4.4.3 Carbon Brush Electrode

As suggested by the name, carbon brush electrodes have a twisted electron collector (usually wires) that forms an axis from where the fibers trapped between the wires spread radially. Brush-like electrodes have been extensively used by a number of research groups [38, 52, 83], following the same pattern, but modifying the design to the system particularities. The lengths of the radial fibers can be determined to fit the physical space available, providing an open structure colonizable, and unlikely to be clogged by a biofilm. Nevertheless, the gaps between the individual fibers vary along the fiber's length, getting smaller near the central axis, thus reducing the microbe-electrode direct interaction.

#### 4.4.4 Carbon Nanotube Coated Textile Electrode

As discussed earlier, a variety of polymers have been used to improve the electrodes' affinity with exoelectrogens, building the electrodes around good electrically conductive materials that work as electron collectors. Most of the cases rely on the biocompatibility and conductivity of carbon-based fibers, so the construction base of the electrode acts as a substrate to organize the CNT special disposition. This logic was followed by Xie et al. although instead of using a stainless steel mesh, they used a porous textile coated with CNT layers to produce the desired open 3D structure with pores between tens to hundreds of  $\mu\text{m}$ .

This approach would allow a more relax and innovative electrode design for BES and was reported to provide a total surface area of about 10 times the projected area of the electrode, and a strong microbial attachment to the electrode.

#### 4.4.5 Carbonized Textile/Fiber Electrode

A nonwoven textile has a roughness and topography that seems adequate for electrode fabrication. However, the materials are not good electric conductive, nor are

inherently appropriate for exoelectrogens colonization. These issues were overcome by researchers as Wang et al. that carbonized textiles by applying 1000 °C for approximately 30 min in absence of oxygen, replacing the oxygen with nitrogen gas. According to the authors, about 8 A m<sup>-2</sup> was achieved with this material, thanks to the successful colonization of internal surfaces. A different group also working with carbonized textiles reported up to 30 A m<sup>-2</sup>, although just for a short-term operation.

These research groups state that the continuous fiber, inherently obtained from the solution blown fibers used to deposit the carbon fibers, is that the resulting electron pathway is continuous. Nevertheless, the overall structure is also more compact and the size of the pores tends to be smaller when compared to commercially available carbon felts [9].

A similar methodology has been used with Kenaf stems, resulting in a 3D porous material with a central channel of about 4 mm, and an external diameter of 10 mm. The walls exhibited microporous of 25 and 60 μm. According to the microscopy analysis, this network of channels that were effectively colonized by exoelectrogens, reportedly achieving up to 32 A m<sup>-2</sup>.

Interestingly, and despite the colonization of outer and inner channels, the biofilm penetration was estimated at less than 100 μm. This would probably arise from the valves present in the structure that would account for an open hole far inferior to the exoelectrogen size. A variety of materials has been tested, proving its feasibility, and avoiding the presence of valves, such as pomelo peels, mushrooms, and corn stem. Nevertheless, using these natural templates would significantly reduce the bioelectrodes costs, they may have some structural limitations such as the Kenaf stems' valves.

#### **4.5 Reticulated Vitreous Carbon (RVC) Electrode**

Textiles are not the only material becoming electrodes by carbonization. One of the most common monolithic materials used as electrodes is the reticulated vitreous carbon, which is obtained after carbonizing a sponge. Therefore, the resulting material has both the continuous conductive electron pathway expected from a monolithic material but also has the open 3D open and porous structure typical from sponges. In fact, RVC materials are usually classified based on the number of pores per unit of length, known as PPI (pores per inch). He et al. reported achieving 50 A m<sup>-2</sup> in an MFC using RVC 10PPI as electrodes, although biofilm clogging was not investigated, despite the 5 months of operation [9].

It is noteworthy here that full carbonization is not mandatory to make an electrode out of a sponge. It is also possible to apply a thin layer of conductive polymer over the natural sponge template, via either chemical vapor deposition of nickel, titanium oxide, or any other method. This would effectively produce a conductive electrode with an open 3D structure, with a roughness appropriate for delivering a surface area greater than the projected area of the electrode.

## 5 Fabrication and Modifications

The inherent characteristic of carbon-based materials have made of them the preferred materials to mediate the microbes-metallic electrode interaction. This use has led to a variety of strategies for coating of carbon-based felts, that started as a method to improve the EET but quickly developed into an improved 3D open structure and fiber interconnexion that would not affect significantly the overall electrical conduction of the system [27]. Therefore, the manufacturing procedure (felt used, and its precursor) will affect the properties of the final electrode.

### 5.1 Plasma Treatment

Wettability has been indicated to be the weakest feature of carbon-based materials. To reverse this situation, some material treatments have been developed to improve this property. Plasma treatment consists of the exposure of the carbon felt to a radiofrequency generator under variable oxygen pressure for a determined time. This treatment has been reported to induce the augmentation of functional groups with oxygen and doping nitrogen onto the surface of the carbon fibers. These modifications would translate into an enhanced reactivity.

The improved wettability comes from increased hydrophilicity provided by nitrogen doping, a consequence of the treatment. These nitrogen dopants are also highly electronically affine to the adjacent carbon atoms that act as oxidation reaction active sites. As a result of this, both the positive carbon atoms' basicity and the electrical conductivity of nitrogen-doped carbon will increase.

Researchers testing a variety of oxygen pressure, and time exposure have reported that phenolic groups could be favored rather than carboxyl groups. In either case and despite the increment on the functional group's quantity over the surface, the total surface area is not significantly increased.

Therefore, plasma treatment can induce an improved electrochemical performance by increasing the active oxygen and nitrogen functional groups in the surface of the carbon-based material, which will enhance the electrochemical interaction between the electrode surface and the electrolyte [27].

### 5.2 Thermal Treatment

As suggested by the name, thermal treatment consists of directly exposing the felt material to a high temperature, commonly on a furnace that allows for oxygen and/or nitrogen flow. As with plasma treatment, here the hydrophobicity of the material is improved.

Zhong et al. have also reported an increment on C–O groups, leading to better electrochemical performance. This improved performance relates to the increased conductivity, the number of active sites, and wettability obtained from the nitrogen groups doping on graphite felts obtained when the material is treated between 600 and 900 °C under an NH<sub>3</sub> atmosphere [27].

### 5.3 Chemical Treatment

This treatment aims to increase the number of oxygens absorbed onto the felt surface. To achieve that absorption, the felts are commonly boiled in nitric or sulfuric acid, requiring a thorough rinse and drying after the treatment before being apt to work as an electrode, but effectively improves the electrochemical performance of the material. The source of this performance improvement has been associated with the increased C–O and C=O functional groups.

Increasing these functional groups' presence can also be achieved via electrochemical oxidation, requiring the application of voltage to the material immersed in sulfuric acid. This method is expected to improve hydrophobicity and electrocatalytic activity.

Similar results have also been obtained with low-cost reagents such as ethanol and hydrazine hydrate, achieving an improvement of the hydrophilic properties and activity by including carbon nanoparticles and oxygen and nitrogen functional groups.

A further improvement can, however, be achieved by combining chemical and thermal treatments. By activating carbon felt with KOH at 800 °C has been reported to include COOH, CH=O, and OH functional groups, but also, forming micropores over the surface [27].

An enhanced wettability, via either plasma, thermal, or chemical treatment, makes it easier for electrolyte ions to access the voids within the 3-D structure. Additionally, metallic nanoparticles, graphene, and carbon nanofibers have been used to enhance their conductivity [27]. Following this logic, and due to its low overpotential and feasibility of coating onto a wide selection of materials, makes platinum an alternative [44] and significantly improves the hydrogen evolution necessary for engaging the *Hydrogenotrophic methanogenesis* [31]. Although, as previously discussed Pt and Pt-coated electrodes are limited to laboratory scale.

## 6 Final Comments

In the context of biofuel production, such as hydrogen and methane, cathodic reactions are crucial. The use of bio-cathodes brings many benefits, but at the same time requires the use of base materials that promote the development of the biofilm that will contribute to the enzymatic arsenal.

Two main approaches have been used to produce bio-electrodes with enhanced performance. The first strategy is increasing the specific surface area, which can be achieved by either use of porous materials or surface modifications. The second strategy also relies on surface modifications, aiming to improve the electron exchange between the base material and the biofilm.

When it comes to increasing the specific surface area, an open 3D structure—with pores colonizable by exoelectrogens—seems to be appropriate, and using bulk porous materials is one of the easiest ways to achieve it. Nevertheless, using an electron collector as stainless steel coated with carbon nanotubes, cell-embedded carbon fibers, or other conductive and biocompatible coatings has opened the possibility for designers to develop 3D designs that simultaneously include macro-organizational, architectural considerations, without compromising the micro-scale porosity.

The development of coating has also opened the possibility to enhance the extracellular electron transfer and catalytic activity, promoting positively charged function groups over the electrode, to induce the initial attachment of gram-negative bacteria, hence, initiating the biofilm maturation.

The diversity of methods and technological possibilities translate into the possibility to layout the size distribution of the pores to enhance the hydrogen evolution while maximizing the specific surface area coated with biocompatible materials, so the bio-electrodes are a suitable substrate for colonization, avoiding pores clogging due to the biofilm growth. All these imply somehow the involvement of carbon fibers and carbon-based bulk materials due to their known chemical resistance, low cost, and biocompatibility. Therefore, it is fair to say that carbonaceous porous material development plays a pivotal role in the future of biofuels, hence, the establishment of the low-emission economy.

## References

1. Adachi M, Okuyama K, Tohge N (1995) Particle generation and film formation in an atmospheric-pressure chemical vapour deposition process using tetraethylorthosilicate. *J Mater Sci* 30:932–937
2. Agneessens LM, Ottosen LDM, Voigt NV, Nielsen JL, de Jonge N, Fischer CH, Kofoed MVW (2017) In-situ biogas upgrading with pulse H<sub>2</sub> additions: the relevance of methanogen adaption and inorganic carbon level. *Biores Technol* 233:256–263. <https://doi.org/10.1016/j.biortech.2017.02.016>
3. Baek G, Kim J, Lee S, Lee C (2017) Development of biocathode during repeated cycles of bioelectrochemical conversion of carbon dioxide to methane. *Bioreasource Technology* 241:1201–1207
4. Bajracharya S, Srikanth S, Mohanakrishna G, Zacharia R, Strik DP, Pant D (2017) Biotransformation of carbon dioxide in bioelectrochemical systems: state of the art and future prospects. *J Power Sources* 356:256–273. <https://doi.org/10.1016/j.jpowsour.2017.04.024>
5. Cai W, Han T, Guo Z, Varrone C, Wang A, Liu W (2016) Bioresource technology methane production enhancement by an independent cathode in integrated anaerobic reactor with microbial electrolysis. *Biores Technol* 208:13–18. <https://doi.org/10.1016/j.biortech.2016.02.028>

6. Cercado-quezada B, Delia M, Bergel A (2011) Electrochemical micro-structuring of graphite felt electrodes for accelerated formation of electroactive bio films on microbial anodes. *Electrochem Commun* 13(5):440–443. <https://doi.org/10.1016/j.elecom.2011.02.015>
7. Cerrillo M, Vinas M, Bonmatí A (2017) Startup of electromethanogenic microbial electrolysis cells with two different biomass inocula for biogas upgrading. *ACS Sustain Chem Eng* 5(10):8852–8859. <https://doi.org/10.1021/acssuschemeng.7b01636>
8. Cheng K, Kang J, King DL, Subramanian V, Zhou C, Zhang Q, Wang Y (2017) Advances in catalysis for syngas conversion to hydrocarbons. *Advances in catalysis*, 1st edn, vol 60. Elsevier Inc. <https://doi.org/10.1016/bs.acat.2017.09.003>
9. Cheng S, Xing D, Call DF, Logan BE (2009) Direct biological conversion of electrical current into methane by electromethanogenesis. *Environ Sci Technol* 43(10):3953–3958. <https://doi.org/10.1021/es803531g>
10. Cho J, Park J, Yoo Y (2008) Novel 3-dimensional bioelectrode for mediatorless bioelectrochemical denitrification. *Biotech Lett* 30(9):1617–1620
11. Choi K-S, Kondaveeti S, Min B (2017) Bioelectrochemical methane (CH<sub>4</sub>) production in anaerobic digestion at different supplemental voltages. *Biores Technol* 245(July):826–832. <https://doi.org/10.1016/j.biortech.2017.09.057>
12. Clauwaert P, Verstraete W (2009) Methanogenesis in membraneless microbial electrolysis cells. *Appl Microbiol Biotechnol* 82(5):829–836. <https://doi.org/10.1007/s00253-008-1796-4>
13. Cui M, Huang J, Wang Y, Wu Y, Luo X (2015) Molecularly imprinted electrochemical sensor for propylgallate based on PtAu bimetallic nanoparticles modified graphene–carbon nanotube composite. *Biosens Bioelectron* 68:563–569
14. Deutzmann JS, Sahin M, Spormann AM (2015) Extracellular enzymes facilitate electron uptake in biocorrosion and bioelectrosynthesis. *MBio* 6(2):1–8. <https://doi.org/10.1128/mBio.00496-15.Editor>
15. Ding A, Yang Y, Sun G, Wu D (2016) Impact of applied voltage on methane generation and microbial activities in an anaerobic microbial electrolysis cell (MEC). *Chem Eng J* 283:260–265. <https://doi.org/10.1016/j.cej.2015.07.054>
16. Dou Z, Dykstra CM, Pavlostathis SG (2018) Bioelectrochemically assisted anaerobic digestion system for biogas upgrading and enhanced methane production. *Sci Total Environ* 633:1012–1021. <https://doi.org/10.1016/j.scitotenv.2018.03.255>
17. Dykstra CM, Pavlostathis SG (2017) Methanogenic biocathode microbial community development and the role of bacteria. *Environ Sci Technol* 51(9):5306–5316. <https://doi.org/10.1021/acs.est.6b04112>
18. Escapa A, Mateos R, Martínez EJ, Blanes J (2016) Microbial electrolysis cells: an emerging technology for wastewater treatment and energy recovery. From laboratory to pilot plant and beyond. *Renew Sustain Energy Rev* 55:942–956. <https://doi.org/10.1016/j.rser.2015.11.029>
19. Flores-Rodriguez C, Min B (2020) Enrichment of specific microbial communities by optimum applied voltages for enhanced methane production by microbial electrosynthesis in anaerobic digestion. *Bioresource Technology* 300(December 2019):122624. <https://doi.org/10.1016/j.biortech.2019.122624>
20. Fu Q, Kobayashi H, Kawaguchi H, Vilcaez J, Sato K (2013) Identification of new microbial mediators for electromethanogenic reduction of geologically-stored carbon dioxide. *Energy Procedia* 37(3):7006–7013. <https://doi.org/10.1016/j.egypro.2013.06.635>
21. Gajaraj S, Huang Y, Zheng P, Hu Z (2017) Methane production improvement and associated methanogenic assemblages in bioelectrochemically assisted anaerobic digestion. *Biochem Eng J* 117:105–112. <https://doi.org/10.1016/j.bej.2016.11.003>
22. Garrett TR, Bhakoo M, Zhang Z (2008) Bacterial adhesion and biofilms on surfaces. *Prog Nat Sci* 18(9):1049–1056. <https://doi.org/10.1016/j.pnsc.2008.04.001>
23. Geetha K, Raj SA (2015) Biomass-electrochemical integrated system for distillery wastewater treatment with electricity generation using anaerobic mixed consortium in microbial fuel cells. *Int J Environ Waste Manage* 15(3):217–234. <https://doi.org/10.1504/IJEW.2015.069131>
24. Geppert F, Liu D, van Eerten-Jansen M, Weidner E, Buisman C, ter Heijne A (2016) Bioelectrochemical power-to-gas: state of the art and future perspectives. *Trends Biotechnol* 34(11):879–894. <https://doi.org/10.1016/j.tibtech.2016.08.010>



25. Gil-Carrera L, Mehta P, Escapa A, Morán A, García V, Guiot SR, Tartakovsky B (2011) Optimizing the electrode size and arrangement in a microbial electrolysis cell. *Biores Technol* 102(20):9593–9598. <https://doi.org/10.1016/j.biortech.2011.08.026>
26. Gonzalez-Gutierrez L, Frontana C, Martínez E, Cardenas-Robles A (2014) Microbial bioelectrochemical reactor for wastewater treatment applications. *Procedia Chemistry* 12(442):73–79. <https://doi.org/10.1016/j.proche.2014.12.044>
27. Guo K, PrévotEAU A, Patil SA, Rabaey K (2015) Engineering electrodes for microbial electrocatalysis. *Curr Opin Biotechnol* 33:149–156. <https://doi.org/10.1016/j.copbio.2015.02.014>
28. Guo S, Chen J, Zhang Y, Liu J (2021) Graphene-based films: fabrication, interfacial modification, and applications. *Nanomaterials* 11
29. Guo X, Liu J, Xiao B (2013) Bioelectrochemical enhancement of hydrogen and methane production from the anaerobic digestion of sewage sludge in single-chamber membrane-free microbial electrolysis cells. *Int J Hydrogen Energy* 38(3):1342–1347. <https://doi.org/10.1016/j.ijhydene.2012.11.087>
30. Hara M, Onaka Y, Kobayashi H, Fu Q, Kawaguchi H, Vilcaez J, Sato K (2013) Mechanism of electromethanogenic reduction of CO<sub>2</sub> by a thermophilic methanogen. *Energy Procedia* 37:7021–7028. <https://doi.org/10.1016/j.egypro.2013.06.637>
31. Hou Y, Zhang R, Luo H, Liu G, Kim Y, Yu S, Zeng J (2015) Microbial electrolysis cell with spiral wound electrode for wastewater treatment and methane production. *Process Biochem* 50:1103–1109. <https://doi.org/10.1016/j.procbio.2015.04.001>
32. Le TXH, Bechelany M, Cretin M (2017) Carbon felt based-electrodes for energy and environmental applications: a review. *Carbon* 122:564–591. <https://doi.org/10.1016/j.carbon.2017.06.078>
33. International Energy Agency (2019) CO<sub>2</sub> emissions from fuel combustion. International Energy Agency. Retrieved from <https://iea.blob.core.windows.net/assets/474cf91a-636b-4fde-b416>
34. Jamali NS, Md Jahim J, Wan Isahak WNR (2016) Biofilm formation on granular activated carbon in xylose and glucose mixture for thermophilic biohydrogen production. *Int J Hydrogen Energy* 41(46):21617–21627. <https://doi.org/10.1016/j.ijhydene.2016.05.092>
35. Jang HM, Kim MS, Ha JH, Park JM (2015) Reactor performance and methanogenic archaea species in thermophilic anaerobic co-digestion of waste activated sludge mixed with food wastewater. *Chem Eng J* 276:20–28. <https://doi.org/10.1016/j.cej.2015.04.072>
36. Jung S, Lee J, Park YK, Kwon EE (2020) Bioelectrochemical systems for a circular bioeconomy. *Bioresource Technology* 300(November 2019). <https://doi.org/10.1016/j.biortech.2020.122748>
37. Kadier A, Simay Y, Abdeshahian P, Azman N, Chandrasekhar K, Kalil M (2016) A comprehensive review of microbial electrolysis cells (MEC) reactor design and configurations for sustainable hydrogen gas production. *Alexandria Engineering Journal* 55:427–443
38. Kalathil S, Patil SA, Pant D (2018) Microbial fuel cells: electrode materials. *Encyclopedia of interfacial chemistry: surface science and electrochemistry*. Elsevier Inc. <https://doi.org/10.1016/B978-0-12-409547-2.13459-6>
39. Kerroum D, Mossaab B, Hassen A (2014) Production of bio-energy from organic waste: effect of temperature and substrate composition. *International Journal of Energy* 38:270–276
40. Kobayashi H, Nagashima A, Kouyama M, Fu Q, Ikarashi M, Maeda H, Sato K (2017) High-pressure thermophilic electromethanogenic system producing methane at 5 MPa, 55 °C. *J Biosci Bioeng* 124(3):327–332. <https://doi.org/10.1016/j.jbiosc.2017.04.001>
41. Kumar M, Sundaram S, Gnansounou E, Larroche C, Thakur IS (2018) Carbon dioxide capture, storage and production of biofuel and biomaterials by bacteria: a review. *Bioresource Technology*, 247(July 2017):1059–1068. <https://doi.org/10.1016/j.biortech.2017.09.050>
42. Kumar R, Martinez C, Martin V, Wong J (2016) Development of chemoenzymatic processes : an industrial perspective, pp 165–178
43. Li Y, Zhang Y, Liu Y, Zhao Z, Zhao Z, Liu S, Zhao H, Quan X (2016) Enhancement of anaerobic methanogenesis at a short hydraulic retention time via bioelectrochemical enrichment of hydrogenotrophic methanogens. *Bioresource Technology* 218:505–511. <https://doi.org/10.1016/j.biortech.2016.06.112>

44. Liang P, Wang H, Xia X, Huang X, Mo Y, Cao X, Fan M (2011) Carbon nanotube powders as electrode modifier to enhance the activity of anodic biofilm in microbial fuel cells. *Biosens Bioelectron* 26(6):3000–3004. <https://doi.org/10.1016/j.bios.2010.12.002>
45. Liu H, Grot S, Logan B (2005) Electrochemically assisted microbial production of hydrogen from acetate. *Environ Sci Technol* 39(11):4317–4320
46. Liu SY, Charles W, Ho G, Cord-Ruwisch R, Cheng KY (2017) Bioelectrochemical enhancement of anaerobic digestion: comparing single- and two-chamber reactor configurations at thermophilic conditions. *Biores Technol* 245:1168–1175. <https://doi.org/10.1016/j.biortech.2017.08.095>
47. Liu W, Wang L, Gao L, Wang AJ (2018) Hydrogen and methane production in bioelectrochemical system:: biocathode structure and material upgrading. *Biomass, biofuels, biochemicals: microbial electrochemical technology: sustainable platform for fuels, chemicals and remediation*. Elsevier B.V. <https://doi.org/10.1016/B978-0-444-64052-9.00038-8>
48. Luo X, Xu J, Wang J, Chen H (2005) Electrochemically deposited nanocomposite of chitosan and carbon nanotubes for biosensor application. *Chemical Communications*
49. Moreno R, San-Martín MI, Escapa A, Morán A (2016) Domestic wastewater treatment in parallel with methane production in a microbial electrolysis cell. *Renewable Energy* 93:442–448. <https://doi.org/10.1016/j.renene.2016.02.083>
50. Nelabhotla ABT, Dinamarca C (2019) Bioelectrochemical CO<sub>2</sub> reduction to methane: MES integration in biogas production processes. *Applied Sciences (Switzerland)* 9(6):16–18. <https://doi.org/10.3390/app9061056>
51. New Zealand Productivity Commission (2017) *New Zealand low emission economy*
52. New Zealand Productivity Commission (2018) *Low-emissions economy*. Retrieved from [https://www.productivity.govt.nz/sites/default/files/ProductivityCommission\\_Low-emissions\\_economy\\_Final\\_Report\\_FINAL.pdf](https://www.productivity.govt.nz/sites/default/files/ProductivityCommission_Low-emissions_economy_Final_Report_FINAL.pdf)
53. Pachapur V, Sarma S, Brar S, Bihan Y, Soccol C, Buelna G, Verma M (2015) Co-culture strategies for increased biohydrogen production. *Int J Energy Res* 39:1479–1504
54. Pandey PK, Ndegwa PM, Soupir ML, Alldredge JR, Pitts MJ (2011) Efficacies of inocula on the startup of anaerobic reactors treating dairy manure under stirred and unstirred conditions. *Biomass Bioenerg* 35(7):2705–2720. <https://doi.org/10.1016/j.biombioe.2011.03.017>
55. Park I, Heo Y, Kim P, Nahm K (2013) Direct electron transfer in *E. coli* catalyzed MFC with a magnetite/MWCNT modified anode. *Royal Society of Chemistry Advances* (37)
56. Park JG, Lee B, Shi P, Kim Y, Jun HB (2017) Effects of electrode distance and mixing velocity on current density and methane production in an anaerobic digester equipped with a microbial methanogenesis cell. *Int J Hydrogen Energy*. <https://doi.org/10.1016/j.ijhydene.2017.07.025>
57. Peng X, Aragão R, Achu I, Liu J (2014) Impact of bioaugmentation on biochemical methane potential for wheat straw with addition of *Clostridium cellulolyticum*. *Biores Technol* 152:567–571. <https://doi.org/10.1016/j.biortech.2013.11.067>
58. Perez D, Lie TT, Weber CC (2020) Relative electrode size and organic load effects on the energy storage efficiency of microbial electrolysis cells. *Bioresource Technology Reports* 11(June):100518. <https://doi.org/10.1016/j.biteb.2020.100518>
59. Perez D, Weber C, Lie T (2021) Operationalization of a microbial electrolysis cell: the interaction of the primary factors for energy storage efficiency. *Biores Technol* 326(January):1–10. <https://doi.org/10.1016/j.biortech.2021.124788>
60. Rader GK, Logan BE (2010) Multi-electrode continuous flow microbial electrolysis cell for biogas production from acetate. *Int J Hydrogen Energy* 35(17):8848–8854. <https://doi.org/10.1016/j.ijhydene.2010.06.033>
61. Ran Z, Gefu Z, Kumar JA, Chaoliang L, Xu H, Lin L (2014) Hydrogen and methane production in a bio-electrochemical system assisted anaerobic baffled reactor. *Int J Hydrogen Energy* 39(25):13498–13504. <https://doi.org/10.1016/j.ijhydene.2014.02.086>
62. Ritchie H, Roser M (2020) CO<sub>2</sub> and greenhouse gas emissions. *Our World in Data*. Retrieved from <https://ourworldindata.org/co2-and-other-greenhouse-gas-emissions#citation>
63. Sangeetha T, Guo Z, Liu W, Cui M, Yang C, Wang L, Wang A (2016) Cathode material as an influencing factor on beer wastewater treatment and methane production in a novel

- integrated upflow microbial electrolysis cell (Upflow-MEC). *Int J Hydrogen Energy* 41:2189–2196. <https://doi.org/10.1016/j.ijhydene.2015.11.111>
64. Sasaki D, Sasaki K, Watanabe A, Morita M, Matsumoto N, Igarashi Y, Ohmura N (2013) Operation of a cylindrical bioelectrochemical reactor containing carbon fiber fabric for efficient methane fermentation from thickened sewage sludge. *Biores Technol* 129:366–373. <https://doi.org/10.1016/j.biortech.2012.11.048>
  65. Sharma M, Bajracharya S, Gildemyn S, Patil SA, Alvarez-Gallego Y, Pant D, Rabaey K, Dominguez-Benetton X (2014) A critical revisit of the key parameters used to describe microbial electrochemical systems. *Electrochimica Acta* 140:191–208. <https://doi.org/10.1016/j.electacta.2014.02.111>
  66. Siegert M, Yates MD, Call DF, Zhu X, Spormann A, Logan BE (2014) Comparison of nonprecious metal cathode materials for methane production by electromethanogenesis. *ACS Sustain Chem Eng* 2:910–917. <https://doi.org/10.1021/sc400520x>
  67. Taubner RS, Schleper C, Firneis MG, Rittmann SKMR (2015) Assessing the ecophysiology of methanogens in the context of recent astrobiological and planetological studies. *Life* 5(4):1652–1686. <https://doi.org/10.3390/life5041652>
  68. Technol JMB, Dominguez-Benetton X, Srikanth S, Satyawali Y, Vanbroekhoven K, Pant D (2013) Enzymatic electrosynthesis: an overview on the progress in enzyme-electrodes for the production of electricity, fuels and chemicals. *J Microbial Biochem Technol*. <https://doi.org/10.4172/1948-5948.S6-007>
  69. Villano M, Ralo C, Zeppell M, Aulenta F, Majone M (2016) Influence of the set anode potential on the performance and internal energy losses of a methane-producing microbial electrolysis cell. *Bioelectrochemistry* 107:1–6
  70. Villano M, Aulenta F, Ciucci C, Ferri T, Giuliano A, Majone M (2010) Bioelectrochemical reduction of CO<sub>2</sub> to CH<sub>4</sub> via direct and indirect extracellular electron transfer by a hydrogenophilic methanogenic culture. *Biores Technol* 101(9):3085–3090. <https://doi.org/10.1016/j.biortech.2009.12.077>
  71. Villano M, Monaco G, Aulenta F, Majone M (2011) Electrochemically assisted methane production in a biofilm reactor. *J Power Sources* 196(22):9467–9472. <https://doi.org/10.1016/j.jpowsour.2011.07.016>
  72. Wang W, Wei X, Choi D, Lu X, Yang G, Sun C (2015) Electrochemical cells for medium-and large-scale energy storage: Fundamentals. *Advances in batteries for medium and large-scale energy storage: types and applications*, pp 3–28. <https://doi.org/10.1016/B978-1-78242-013-2.00001-7>
  73. Wu C, Tu X (2016) Biological and fermentative conversion of syngas. In: *Handbook of biofuels production*. Elsevier Ltd. <https://doi.org/10.1016/B978-0-08-100455-5.00012-6>
  74. Xie X, Criddle C, Cui Y (2015) Design and fabrication of bioelectrodes for microbial bioelectrochemical systems. *Energy Environ Sci* 8(12):3418–3441. <https://doi.org/10.1039/c5ee01862e>
  75. Yang HY, Bao BL, Liu J, Qin Y, Wang Y-R, Su K-Z, Han JC, Mu Y (2018) Temperature dependence of bioelectrochemical CO<sub>2</sub> conversion and methane production with a mixed-culture biocathode. *Bioelectrochemistry* 119:180–188. <https://doi.org/10.1016/j.bioelechem.2017.10.002>
  76. Yin Q, Zhu X, Zhan G, Bo T, Yang Y, Tao Y, He X, Li D, Yan Z (2016) Enhanced methane production in an anaerobic digestion and microbial electrolysis cell coupled system with co-cultivation of geobacter and methanosarcina. *J Environ Sci (China)* 42(Daping Li):210–214. <https://doi.org/10.1016/j.jes.2015.07.006>
  77. Zeppilli M, Agnese L, Villano M, Majone M (2016) Anion vs cation exchange membrane strongly affect mechanisms and yield of CO<sub>2</sub> fixation in a microbial electrolysis cell. *Chem Eng J* 304:10–19. <https://doi.org/10.1016/j.cej.2016.06.020>
  78. Zeppilli M, Cristiani L, Dell'Armi E, Majone M (2020) Bioelectromethanogenesis reaction in a tubular microbial electrolysis cell (MEC) for biogas upgrading. *Renewable Energy* 158:23–31. <https://doi.org/10.1016/j.renene.2020.05.122>

79. Zeppilli M, Paiano P, Villano M, Majone M (2019) Anodic vs cathodic potentiostatic control of a methane producing microbial electrolysis cell aimed at biogas upgrading. *Biochem Eng J* 152:107393. <https://doi.org/10.1016/j.bej.2019.107393>
80. Zeppilli M, Simoni M, Paiano P, Majone M (2019) Two-side cathode microbial electrolysis cell for nutrients recovery and biogas upgrading. *Chem Eng J* 370:466–476. <https://doi.org/10.1016/j.cej.2019.03.119>
81. Zhang P, Wang L, Yang S, Schott JA, Liu X, Mahurin SM, Huang C, Zhang Y, Fulvio PF, Chisholm MF, Dai S (2017) Solid-state synthesis of ordered mesoporous carbon catalysts via a mechanochemical assembly through coordination cross-linking. *Nature Communications*. <https://doi.org/10.1038/ncomms15020>
82. Zhang Y, Angelidaki I (2014) Microbial electrolysis cells turning to be versatile technology: recent advances and future challenges. *Water Res* 56:11–25. <https://doi.org/10.1016/j.watres.2014.02.031>
83. Zhen G, Lu X, Kobayashi T, Kumar G, Xu K (2016) Promoted electromethanogenesis in a two-chamber microbial electrolysis cells (MECs) containing a hybrid biocathode covered with graphite felt (GF). *Chem Eng J* 284:1146–1155. <https://doi.org/10.1016/j.cej.2015.09.071>

**Part III**  
**Catalyst Science and Engineering**

# Chapter 9

## Photoluminescent Carbon Dots: A New Generation Nanocarbon Material



Anju Paul and Anandhu Mohan

### 1 Introduction

Carbon dots (CDs), also known as carbon quantum dots, are photoluminescent zero-dimensional carbon materials first reported in the year 2004 by Xu et al. [1, 2]. They are spherical amorphous  $sp^2$  hybridized carbon core possessing one of its dimensions less than 10 nm [3]. Since its discovery, many research groups are attracted by their multifaceted properties among which fluorescence receives the supreme attention. They have emerged as a rising star in the nanocarbon family with fascinating potentials and find applications in various fields like sensing, bioimaging, optics, drug delivery, energy harvesting, photocatalysis, and so on [4, 5]. They are characterized by tunable excitation and emission, chemical inertness, thermal stability, high quantum yield, good aqueous solubility, inexpensive synthetic methods, non-toxicity, high biocompatibility, and easy functionalization and surface passivation [6]. Size, as well as surface states, determines the physicochemical properties. Carbon dots are treated as exceptional substitutes for inorganic semiconductor dots owing to these intriguing properties as biocompatibility is considered as one among the prominent advantages in the realm of nanoscience. CDs could overcome the toxic nature and low photoluminescence of these traditional inorganic dots, and their outstanding electronic properties make them electron donors and acceptors which assist in electrochemical photoluminescence. They can be considered as a semiconductor having typical bandgap and exceptional optical characteristics.

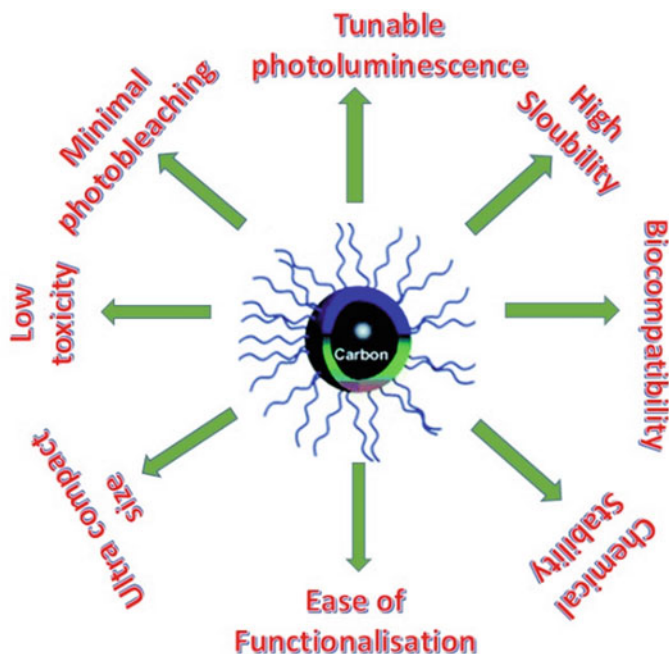
---

A. Paul (✉)

Sree Sankara Vidyapeetom College, Valayanchirangara, Kerala 683556, India  
e-mail: [anjupaul@ssvcollege.ac.in](mailto:anjupaul@ssvcollege.ac.in)

A. Mohan

Department of Biology, Chemistry, and Environmental Sciences, American University of Sharjah, Sharjah, United Arab Emirates



**Fig. 1** Different properties of CDs

Carbon dots cannot be treated as a mere carbon core, but it consists of elements such as oxygen and hydrogen. The relative proportion of these elements is decided by the method of preparation in addition to the synthetic technology [7]. It is possible to incorporate elements like sulphur, nitrogen, and potassium by choosing a precise source for the synthesis. Studies prove that doping with elements improves the properties. Tuneable photoluminescence and electron transfer properties can be considered as features of various surface functional groups [8]. Functionalized carbon dots can be synthesized in a single step. At the same time, it is possible to do surface functionalization and passivation in separate stages of preparation also [9]. These modifications can significantly improve the properties.

This chapter will describe recent advances in CDs mainly focusing upon synthetic routes among which those from green sources are given prominence, their physical, structural, and optical features, and various applications. Also, it ends with a future outlook and conclusions about the current field (Fig. 1).

## 2 Synthetic Strategies of CDs

The origin of carbon dots is an accidental discovery as a by-product during the arc discharged synthesis of carbon nanotube [10]. After the first reports of synthesis,

many advanced synthetic routes were proposed. Many reports propose readily available natural plant materials and green waste biomass as sources. Biocompatibility and high yield through cost-effective protocol are regarded as the exceptional advantage of utilizing green waste biomass as the precursors. Synthetic approaches may be categorized as top-down and bottom-up methods [11]. Fragmentation of carbonaceous materials like graphite [12], carbon fibres [13], carbon nanotube [14], and coal [15] by means of arc discharge, laser ablation, acid treatment, electrochemical oxidation, and ultrasonic methods comes under top-down methodologies. But, in the bottom-up method, precursors are carbonized by thermal pyrolysis, microwave-assisted synthesis, and hydrothermal treatments [16]. Highly efficient carbon dots of various compositions can be obtained via bottom-up methods. Many natural materials like citric acid [17], orange juice [18], lemon juice [19], egg white [20], glucose [21], and chitosan [22] were used as carbon sources in the bottom method. Altering the synthetic methods as well as precursors can change the parameters such as surface state, the extent of functionalization, quantum confinement effect, and so on [23]. These diverse techniques also offer chances in tuning the size and possibilities for the incorporation of heteroatoms as constituents in carbon dots. This section mainly consolidates the synthetic protocols utilizing various precursors, methodologies, and reaction conditions in which greener approaches are discussed in detail.

## ***2.1 Top-Down Approaches***

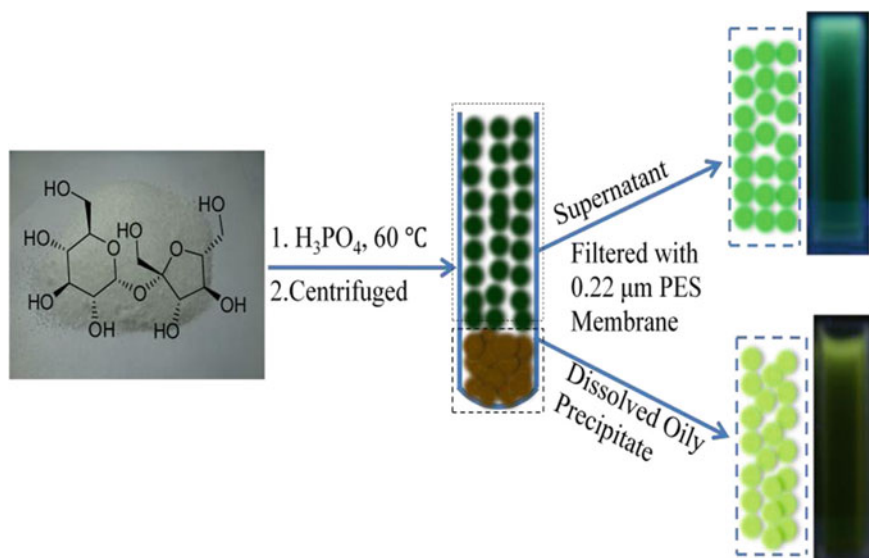
### **2.1.1 Laser Ablation**

Laser ablation is a facile technique that can prepare surface state tunable CDs in which the source is irradiated by a laser. Even though it is a rapid technology, it is limited by some disadvantages. It is an expensive method that can develop only low quantum yield dots. At the same time, it consumes a lot of energy and cannot make sure the control size of carbon dots [24]. It is carried out in three stages. High energy created by the laser pulse is absorbed by the carbon material. Electrons from atoms are stripped, and as a result, a strong repulsive force produces a high electric field fragmenting the precursor material into carbon dots [25]. Sun et al. reported the synthesis by laser ablation in which the precursors were graphite powder and cement with argon acting as the carrier gas [1]. The sample, upon surface passivation, resulted in photoluminescence which was not detectable before. Yu et al. prepared CDs from toluene via laser ablation. By using the laser furnace, they could obtain carbon dots of controlled size [26]. But, this process has a demerit that it requires extreme conditions of temperature and pressure which is not suitable in terms of energy and efficiency.



### 2.1.2 Chemical Oxidation

Chemical oxidation is considered as a convenient method to produce carbon dots in high yield and purity without the use of elaborate equipment. Here, carbon substrate is oxidized by a strong oxidant like  $\text{HNO}_3$  or  $\text{H}_2\text{SO}_4$ . Since it is an oxidation process, many oxygen comprising functional groups such as  $-\text{COOH}$ ,  $-\text{OH}$  are introduced which in turn increases the hydrophilicity and aqueous solubility of the material. A limitation of this method is the non-uniform size distribution of synthesized particles [28]. Sun et al. proposed an efficient method for the manufacture of heteroatoms-doped CDs through chemical oxidation using concentrated sulphuric acid. It was inferred that temperature has a great influence on sulphur content [29]. In another work, Bao et al. oxidized carbon fibres in nitric acid to get carbon dots. They have varied different reaction parameters like temperature, the concentration of nitric acid, and reaction time so that they could get a series of different colour emitting carbon dots. This was an innovative work to synthesize multicolour carbon dots via chemical oxidation [30]. Thus, emission wavelength can be tuned by the selection of starting material and duration of acid treatment. Both non-toxicities and multicolour emission have wide applications in bioscience. Xu and co-workers also prepared carbon dots via chemical oxidation using sucrose as the carbon substrate and phosphoric acid as the oxidant. They could also obtain carbon dots with different colour emissions. CDs could emit green and yellow colours without surface passivation [31] (Fig. 2).



**Fig. 2** Synthesis of yellow- and green-emitting CDs through chemical oxidation of sucrose. Reprinted with permission from Xu et al. [27]. Copyright 2014 Elsevier

**Table 1** Synthetic methodologies of CDs and their advantages

S. No.	Source	Synthesis method	Advantage	Disadvantage	Colour	References
1	Toluene	Laser ablation	Fast, efficient, tunable surface state	Less size control, low quantum yield	Red and blue	[26]
2	Carbohydrate	Chemical oxidation	Easily accessible, simple apparatus	Harsh conditions and numerous steps involved	Red, blue, green, yellow	[36]
3	Sodium citrate and urea	Electrochemical carbonization	Stable, high purity, size controllable	Time-consuming	Blue	[37]
4	Ascorbic acid and ammonia	Ultrasonic treatment	Ultra-small particle size, simple preparation	Long exposure time, high energy cost	Blue, green	[38]
5	Sodium citrate	Hydrothermal treatment	Easy, low cost	Poor size control	Blue	[39]
6	Citric acid	Microwave	Cost-effective, non-toxic, desired morphology	Poor size control	Blue	[40]

### 2.1.3 Electrochemical Carbonization

It is a single-step, stable synthetic route with high purity and yield. Even though it has complicated steps in the methodology and time consuming, it can produce size and morphology controllable carbon dots [32]. Both electrodes and electrolytes have a definite command over the properties. The degree of graphitization and size of carbon dots have a direct relationship with applied potential. The first synthesis in this method is demonstrated by Zhou et al. from multi-walled carbon nanotube in acetonitrile solution. The dark brown solution obtained was purified by removing acetonitrile, and it showed blue emission under UV light. These dots displayed outstanding excitation and size-dependent photoluminescent properties [33].

On the other hand, many research works were developed by altering the carbon precursors like graphite rod [34] and carbon fibres [35]. The features and sources of some synthetic methods can be summarized in Table 1.

### 2.1.4 Ultrasonic Treatment

In order to overcome the limitations of other top-down methods of using harsh chemicals and purification after synthesis, ultrasonic energy is widely used in carbon dot synthesis. It is an appropriate method in which huge carbon precursors can be

fragmented by the treatment of ultrasonic sound waves of high energy. Dang et al. prepared CDs from the oligomer-polyamide resin by this method. Less crystalline, aqueous soluble carbon dots having functional groups at the surface are obtained [41]. Similarly, ultrasonication of citric acid, urea, and poly(ethylene glycol) produced carbon dots which can be used as a lubricant. A small-sized carbon core provided a rolling effect to act as a good lubricating agent [42].

Low quantum yield values, high cost and specific complicated equipment requirements, and harsh conditions of temperature and pressure are the limitations of top-down methods [16]. Hence bottom-up syntheses are preferred which are discussed in the next section.

## 2.2 Bottom-Up Approaches

In bottom-up synthesis, carbon precursors are converted to small spherical forms via certain chemical and physical conditions like heat, pressure, and microwave which could assist in molecular transformation. It includes hydrothermal, microwave-assisted, and thermal decomposition [16, 43, 44]. Highly efficient CDs can be synthesized by this versatile method, and surface functionalization or doping can be done in the same synthesis step which is not possible in the case of top-down methods [45].

### 2.2.1 Hydrothermal/Solvothermal Treatment

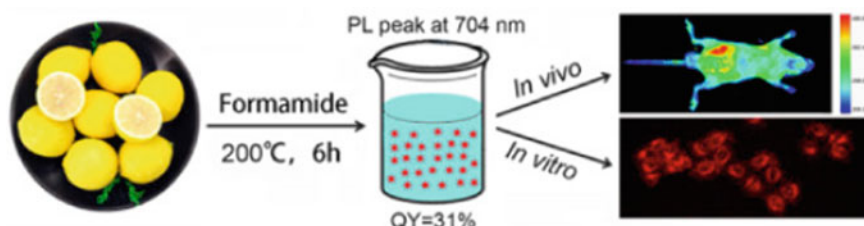
It is a cost-effective synthesis involving the carbonization of various precursors in a high-pressure hydrothermal reactor. Researchers are very much attracted to this technique because of the simplicity in procedure and eco-friendliness. It is a single-step synthesis by which we can perform inherent doping. Usually, elements such as nitrogen, sulphur, and phosphorous are used for doping. Numerous works have been reported in which organic molecules, biomolecules, and waste biomass have been taken as the precursors for the synthesis. Fluorescent CDs were first synthesized by hydrothermal treatment by Zhang et al. from L-ascorbic acid. Ascorbic acid was dispersed in water and heated at 180 °C in an autoclave for 4 h followed by membrane dialysis [46]. Other precursors include papaya [47], glucose [48], apple juice [49], orange juice [18], milk [50], egg white [20], and cornstalk [51]. Chitosan was chosen as the precursor to obtain amino functionalized CDs by Liu et al. by heating at 180 °C for 12 h [22]. These fluorescent CDs could act as excellent bioimaging agents. Schematic representation for hydrothermal synthesis of CDs is given in Fig. 3.

Similarly, solvothermal carbonization is also considered to be a popular methodology to fabricate CDs. Solvothermal treatment of carbohydrates in phosphoric acid to yield yellow- and red-emitting CDs is reported [52]. Fe<sup>3+</sup> and apoferritin detection was done by N-doped carbon dots synthesized by a cost-effective, eco-friendly single-step solvothermal treatment of ethylenediamine tetra-acetic acid and urea in ethylene



**Fig. 3** Scheme for hydrothermal synthesis

glycol at 150 °C by a 3-h process. These carbon dots were proved to be an efficient fluorescent probe, and its application can be extended in biosensing, bioimaging, and life science [53]. Figure 4 shows a scheme for the solvothermal synthesis of CDs from lemon juice in formamide by Ding et al. These CDs of average size 5.7 nm exhibited fluorescent emission at 704 nm which may be attributed to their surface states. They possess excellent photostability and high biocompatibility so that they can be used as a potential probe for bioimaging [54]. Synthesis of CDs via hydrothermal treatment from various organic molecules is given in (Table 2).



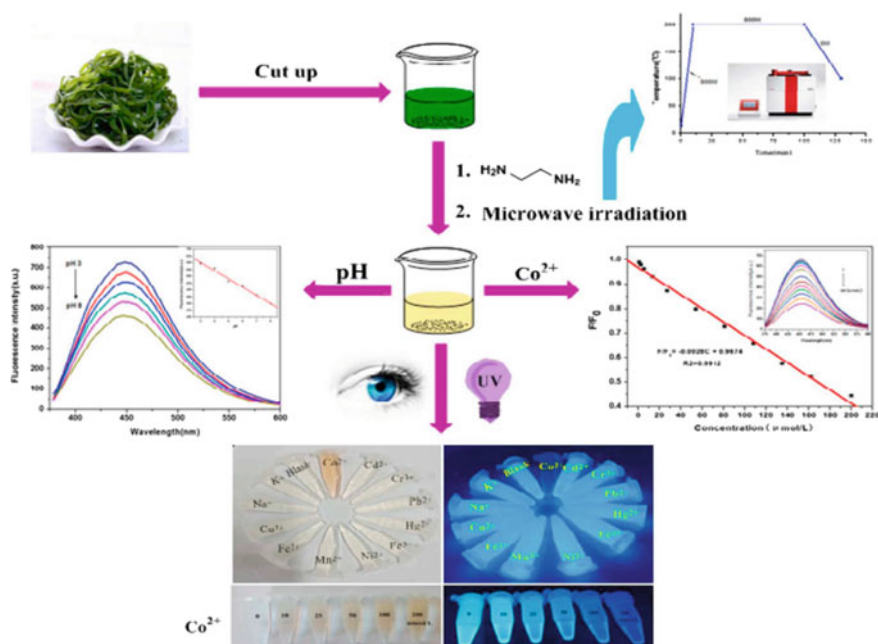
**Fig. 4** Solvothermal synthesis of CDs from lemon juice in formamide. Reprinted with permission from Ding et al. [54]. Copyright 2019 Elsevier

**Table 2** Synthesis of CDs via hydrothermal treatment from organic molecules

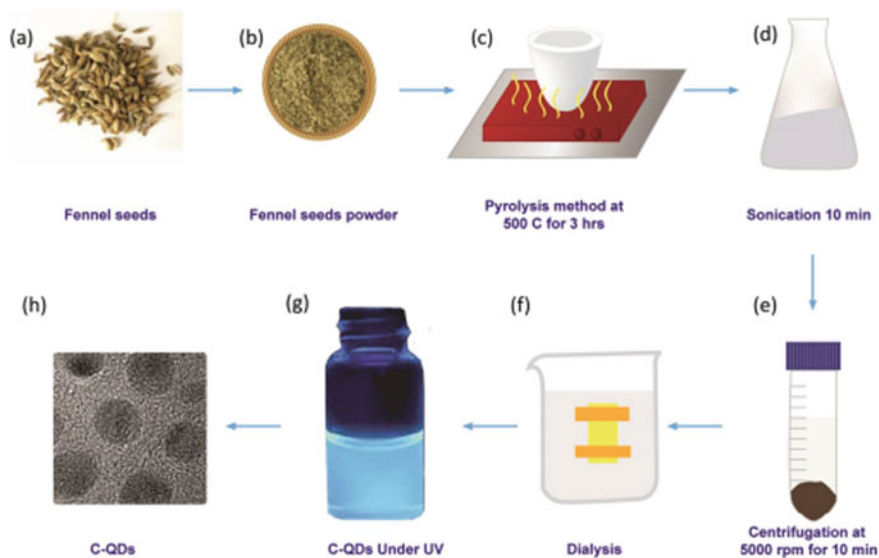
S. No.	Precursor	Colour	Size (nm)	References
1	Sodium citrate	Blue	1.59	[39]
2	Citric acid	Violet	6–15	[55]
3	Glucose	Blue	1.65	[56]
4	Folic acid, phosphoric acid	Indigo	13.2	[57]
5	Histidine	Blue	3–5	[58]
6	Dopamine	Blue, green, yellow	3.8	[59]
7	Ammonium citrate	Indigo	4.8	[60]
8	Streptomycin	Violet	2.97	[61]
9	Citric acid and ethylenediamine	Blue	2–6	[62]

## 2.2.2 Microwave-Assisted Synthesis

It is an efficient, economical, and rapid synthetic methodology for obtaining carbon dots of desired morphology by the irradiation of electromagnetic radiations through carbon precursors. This technology is rapidly developing owing to the significant interaction of carbon sources with microwaves [63]. Numerous studies have been reported to develop CDs of distinct morphology by microwave heating. Zhu et al. used saccharides to obtain CDs with controlled morphology with a size of 3.7 nm [21]. In another work, citric acid is irradiated by microwave radiations in a domestic oven by using tryptophan as the passivating agent. Water-soluble CDs of size 2.6 nm were obtained by centrifugation at 10,000 rpm [64]. Recently, Vaccinium Meridionale Sawartz extract was chosen as the source and about 80% mass fraction of thermally stable CDs were obtained only in 5 min. This method is preferred when compared to hydrothermal or electrochemical methods when the time consumption for the process is considered [65] (Fig. 5).



**Fig. 5** Microwave-assisted synthesis of CDs for the sensing of  $\text{Co}^{2+}$ . Reprinted with permission from Zhao et al. [66]. Copyright 2019 Elsevier



**Fig. 6** Thermal decomposition from fennel seeds for the synthesis of CDs. Reprinted with permission from Dager et al. [69]. Copyright 2019 Springer Nature

### 2.2.3 Thermal Decomposition

In this protocol, carbon precursors are heated at elevated temperatures. It is an irreversible decomposition involving both physical and chemical changes. Cost-effectiveness, short reaction time, solvent-free methodology, choice of numerous precursors, and simple operations are considered as the advantages of this method. Morphology, as well as optical characteristics, may be optimized by altering reaction temperature and time taken for synthesis [67]. Feng and co-workers prepared CDs from citric acid using diethylenetriamine as the passivating agent. These CDs were water-soluble fluorescent structures having size 5–8 nm [68]. Dager et al. reported the thermal decomposition of fennel seeds to obtain fluorescent CDs without any surface passivation. These highly photostable CDs exhibited excitation-independent emission. The scheme for the preparation for this reaction is given in Fig. 6.

## 3 Natural Biomass as the Source for the Fabrication of CDs

Numerous synthetic protocols were introduced utilizing natural biomass as the carbon precursors. Hazardous and toxic solvents are creating environmental issues, and expensive sources can be eliminated by the use of these green routes. Waste and biomass valorization is considered key factor when the preservation of the environment is concerned. Hence, during recent times, waste biomass has been abundantly

utilized as the green precursors for syntheses. Biomass refers to any biodegradable waste, residues from agriculture, and industrial or municipal waste [70]. In many works, fruits, vegetables, plant parts, fruit peels, etc., are used as the sources. CDs synthesized from broccoli via hydrothermal treatment were used for sensing silver ions. Water-soluble blue fluorescent CDs were obtained by the method [71]. In another work, garlic was taken as the precursor to obtain fluorescent CDs via the hydrothermal method by Zhao et al. Outstanding optical properties of the nanomaterial prove to be used in bioimaging applications [72]. Table 3 summarizes the applications of carbon dots synthesized from plants and other green sources.




Even though many synthetic protocols propose mass production of CDs, reported results are limited in number. The choice of carbon precursors was found to be one of the key factors of yield. Since acid treatment for macroscale synthesis may lead to severe environmental issues, nowadays waste biomass is replacing hazardous sources. There are works in which 120 mg CDs are produced from 1 g coffee grounds [86], 3 g CDs are obtained from 10 g bee pollens [87], and so on. Hydrothermal treatment of waste biomass like grass [88] and pomelo peel [89] could also obtain stable, photoluminescent CDs in a high yield. Through plasma-induced pyrolysis, chicken eggs were used to produce 10 g CDs [20]. In a one-pot synthesis, Yang et al. synthesized 120 g of CDs from Chinese ink [90]. From the above works, it is observed that the carbonization procedure significantly affects the yield of CDs.

## 4 Unique Properties of Carbon Dots

The remarkable features of CDs may be attributed to the surface functional groups like carboxyl group, an amino group, or hydroxyl groups [92]. The surface states as well as these functional groups greatly influence the fluorescent properties. The optical features can be optimized by varying the synthesis methods, chemical composition, and dopants. Absorption spectra generally appear between 230 and 290 nm can be assigned as  $\pi - \pi^*$  transition of C = C bond [93]. Surface functionalization and passivation can alter the absorbance to a great extent. Furthermore, carbon dots exhibit excitation-dependent photoluminescence features. Tunable emission colours are obtained by surface passivation, altering the molecular weight of precursors and surface states [94]. CDs of various colours ranging from UV to red have been fabricated, out of which blue and green are more common. Many researchers have explained the photoluminescence in terms of quantum confinement [95]. In addition to these fascinating properties, scientists have fabricated CDs with high quantum yields. Aqueous solubility and biocompatibility are the other key features providing a breakthrough for CDs to be applied in many biomedical applications, imaging, and sensing (Fig. 7).

Clinical diagnosis utilizes fluorescence imaging as a powerful tool owing to its high sensitivity and low cost. Conventional fluorophores like organic dyes and inorganic quantum dots are less preferred because of their poor fluorescence and toxicity. In such a situation, biomedicine is demanding a biocompatible nanomaterial with





**Table 3** Applications of carbon dots synthesized from plants and other green sources

Sl. No.	Source		Synthesis method	Size (nm)	Applications	References No.
1	Tamarindus indica		Hydrothermal treatment	3–3.5	Detection of Hg <sup>2+</sup> and glutathione	1. [73]
2	Watermelon peel		Ultrasonication	2 nm ± 0.5	Optical imaging	2.[74]
3	Saccharum officinarum		Hydrothermal method	3	Cellular imaging of bacteria and yeast	3.[70]

(continued)



Table 3 (continued)

Sl. No.	Source		Synthesis method	Size (nm)	Applications	References No.
4	Rose heart radish		Hydrothermal treatment	1.2–6	Fe <sup>3+</sup> sensing and cell imaging	4.[75]
5	Prawn shells		Hydrothermal treatment	4	Cu <sup>2+</sup> detection	[76]
6	Gelatin		Hydrothermal treatment	1.7	Bioimaging agent	5.[77]





(continued)

Table 3 (continued)

Sl. No.	Source	Synthesis method	Size (nm)	Applications	References No.
7	Honey	 Hydrothermal treatment	2	Detection of Fe <sup>3+</sup>	[78]
8	Ocimum sanctum	 Hydrothermal treatment	4–7	Sensing of Pb <sup>2+</sup> ions	6.[79]
9	Sugarcane bagasse waste	 Chemical oxidation and exfoliation method	4.1 ± 0.17	Bioimaging, bio-sensor, and drug delivery	7.[80]


(continued)

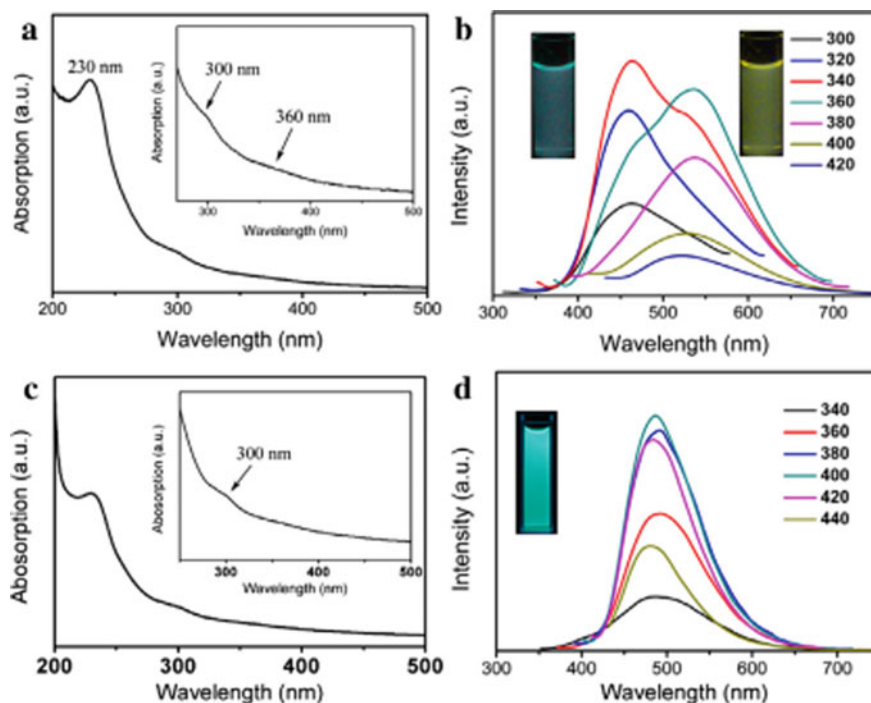
Table 3 (continued)

Sl. No.	Source		Synthesis method	Size (nm)	Applications	References No.
10	Lycii Fructus		Hydrothermal treatment	2-5	Sensing of ferric ion and cell imaging	8,[81]
11	Aloe		Hydrothermal treatment	5	Detection of tartrazine in food	9,[82]
12	Orange pericarp		Hydrothermal treatment	1.4- 3.8	Nano-biotechnology	[83]
13	Sweet potato		Hydrothermal treatment	3,39	Fe <sup>3+</sup> sensing and cell imaging	10,[84]

(continued)

**Table 3** (continued)

Sl. No.	Source		Synthesis method	Size (nm)	Applications	References No.
14	Lotus root		Microwave method	9.41	Hg(II) ions detection and cell imaging	11.[85]



**Fig. 7** **a** UV-visible absorption spectrum, **b** photoluminescence spectrum in the absence of borax, **c** UV-visible absorption spectrum, and **d** photoluminescence spectrum in the presence of borax. Reprinted with permission from Fan et al. [91]. Copyright 2014 Elsevier

flexible design via an easy synthetic route which is fulfilled by CDs. Not only blue or green fluorescence, recently CDs with deep red emission with two or multiphoton properties were synthesized by many research groups. These long-wavelength emissions can be explained by the structural features of carbon cores as well as fluorophores on the surface. The exact photoluminescence mechanism can be identified only by detailed investigation including functional groups, cross-linking, molecular weight, and so on. Overall emission is a contribution of carbon core, surface state, and molecular fluorophores. In many synthetic procedures, it is seen that the photoluminescence mechanism is dependent on organic fluorophores, but a longer reaction time leads to high carbonization which further results in loss of these fluorophores, thereby decreasing quantum yield.

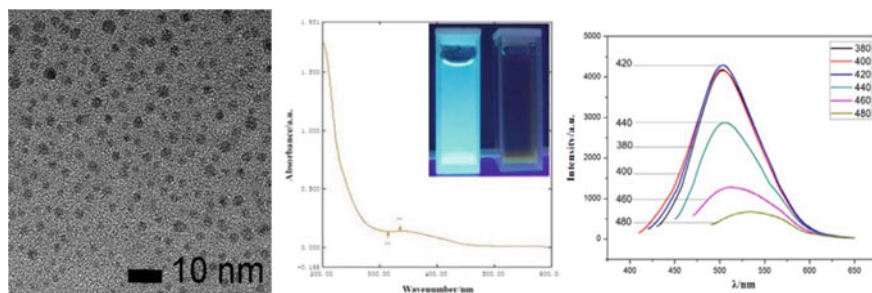
Widespread applications of CDs have been restricted as the majority of them are able to emit blue light. In this aspect, red-emitting CDs are receiving more prominence. Most of the works report that emission in the longer wavelength region is owing to CDs size, surface state, and doping elements. Red-emitting CDs can find recent applications such as imaging-dependent surgeries, drug delivery, in vitro and in vivo bioimaging, phototherapy, and so on.

The efficiency and luminescence of CDs are usually enhanced by introducing surface functional groups and surface defects. Doping with elements improves radiative recombination and creates novel energy levels which further results in excitation-independent emissions and better quantum yield. Varying colour emission can also be explained by these mechanisms. Lulu et al. reported that the application of blue fluorescence in the ultraviolet region causes high photodamage in the biological matrices [96]. Such a limitation can be nullified by achieving long-wavelength emission. They have reported the synthesis of water-soluble intense infrared emission with high quantum yield, exhibiting two-photon properties also. It is believed that red fluorescent CDs can have the advantages of high photostability, easy surface modification, and low cytotoxicity. Hence, they find applications in the biomedical field such as drug delivery, two-photon bioimaging, and tissue engineering.

## 5 Characterization of Carbon Dots

In addition to carbon atoms, CDs may also contain elements like oxygen, hydrogen, nitrogen, sulphur, and so on depending on the functional group present on the surface as well as doping. Some bottom-up synthetic methods can incorporate heteroatoms without any surface passivation or functionalization. The crystallinity of the CDs is generally studied by X-ray diffraction. Most of the CDs prepared are amorphous in nature. A broad peak at  $18^\circ$  represents the amorphous nature of the synthesized material. UV-visible absorption spectrum analyses the electronic transmissions, and it indicates the presence of carbonyl and ethylenic bonds. Photoluminescence studies are usually performed to detect the emission spectra and the dependence of excitation on emission. Fourier Transform-Infrared Spectroscopic studies and X-ray photoelectron spectroscopy help to identify the functional groups and elements in the nanostructure. Inherent doping from the precursors and hybridization of elements can be identified by these methods. Morphological studies can be carried out by transmission electron microscopy. The size, shape, and dispersion of CDs are estimated from this technique. It is a reliable technique to confirm the amorphous nature of the material (Fig. 8).

Since the source also has traces of other elements, separation and purification of CDs are one of the limitations to getting desired definite nanostructures. There are many methods utilized for the analytical separation of CDs from bulk carbon. Most of the bottom-up methods propose purification with dichloromethane; thereby, most of the unreacted moieties can be avoided. Additionally, most of the procedures separate the CDs with the desired size by means of dialysis, electrophoresis, ultracentrifugation, chromatography, and so on. Structure, size, composition, and shape are the prominent factors determining the characteristics. Hence, characterization is considered to be very important on the way to various applications. Microscopic studies also give us an idea about the dispersion and possibilities of agglomeration. Identification of phase and crystallinity is done by X-ray diffraction. Information regarding the purity of the sample may also be obtained. At the same time, amorphous CDs



**Fig. 8** **a** TEM image of CDs, **b** UV/visible absorption spectra, and **c** photoluminescence emission spectra of the CDs. Reprinted with permission from Sun et al. [97]. Copyright 2015 Springer nature

cannot be well studied by this technique. The state of carbon in the sample is analysed by Raman spectroscopy. By comparing the D band and G band intensities, it is possible to identify the purity of the sample also. Ultraviolet–visible spectroscopy and photoluminescence spectroscopy are utilized to study the optical properties as well as photoluminescence of the samples. These characterization techniques are together utilized to calculate the quantum yield of CDs.

## 6 Carbon Dot and Their Nanocomposites

Recently, many efforts have been taken for the fabrication of novel nanocomposite materials consisting of carbon dots. Different matrices for the synthesis include metal nanoparticles, metal oxides, carbon nanomaterials, ferrites, tungstates, and so on. These composites can amalgamate the physical, chemical, mechanical, and magnetic properties of the matrix and optical characteristics of CDs. Metal nanoparticles can be prepared from corresponding metal ions by using CDs as they can act as a reductant in the process [98]. In the same way, combining CDs with metal oxides extends the photoresponsive region even to visible spectra. Metal oxides such as zinc oxide and titanium oxide are well studied in this area. Hydrothermal synthesis at 200 °C for 2 h was carried out to synthesize TiO<sub>2</sub>/CDs, and this nanohybrid could obtain 9 times better results in hydrogen production from water splitting than the bare TiO<sub>2</sub> [99]. Binary metal oxides such as ZnFe<sub>2</sub>O<sub>4</sub> and CuBi<sub>2</sub>O<sub>4</sub> are also utilized as the matrix for the incorporation of CDs so that numerous reaction sites are formed by interfacial charge transfer [100]. But in the case of carbon nanomaterials like graphene and graphene oxide, in spite of good surface area and thermal conductivity, some applications are limited due to precipitation and agglomeration. These limitations can be nullified by combining them with CDs. Thus, the efficiency of materials can be significantly improved by the preparation of nanohybrids in which CDs act as nanofillers.

## 7 Catalytic Applications of Carbon Dots

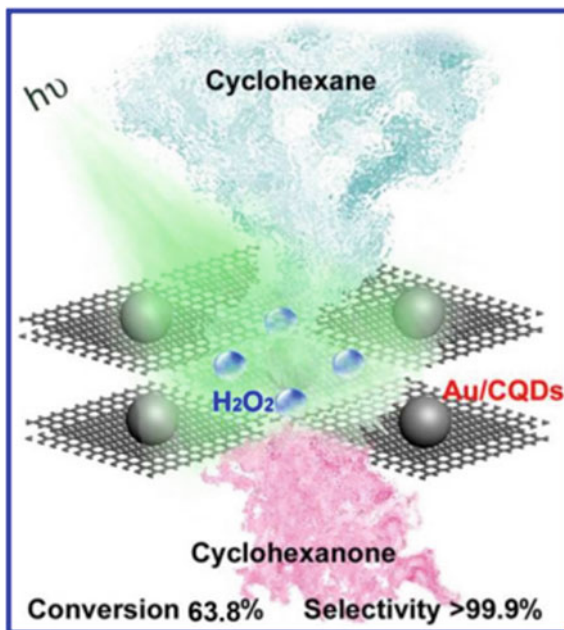
CDs act as promising heterogeneous catalysts since they satisfy many desirable properties of a good catalyst such as low cost, good yield, aqueous solubility, biocompatibility, high surface area, and diverse porous structure. These quasi-spherical nanostructures are mostly preferred for photocatalytic applications owing to their fluorescent properties. They are used for selective oxidation reactions, visible light-induced acid catalysis, photo-enhanced hydrogen bond catalytic reactions, photocatalysts for CO<sub>2</sub> conversion, water splitting, and electrocatalysis. CDs are made up of sp<sup>2</sup>-hybridized carbons and possess electron transfer properties which promote them to act as potential catalysts. Upconverted photoluminescence improves photoinduced electron transfer and drives them to be used as visible light-responsive catalysts. Additionally, CDs are capable of light-harvesting when incorporated in composites which leads to photoexcited electron transfer across their interface creating holes. This emphasizes the photoinduced electron transfer which assists them to act as photosensitizers, electron mediators, and photocatalysts [101].

Photocatalytic degradation is considered an effective tool as well as a necessity for the sustainable existence of the environment. Organic pollutants are increasing day by day with the development of industries which in turn have an adverse effect on the environment. Only active radical species from photocatalyst can degrade these organic pollutants. But, a large bandgap in conventional photocatalysts is considered to be a limitation for the purpose. Since CDs are able to absorb more light in the area, they can act as a sensitizer and transmit the photogenerated electron into the semiconductor, thereby enhancing the photocatalytic activity. Numerous works have been done to study the photodegradation of dyes and organic pollutants (Fig. 9).

Yuzhi et al. synthesized CDs by electrochemical etching methodology, and they studied the effect of CDs in aldol condensation. The irradiation with visible light resulted in improved catalytic activity with prolonged existence [103]. Xiao et al. reported the fabrication of CDs/SiO<sub>2</sub> porous nanocomposites by electrochemical synthesis. These nanocomposites have been used for selective oxidation of cis-cyclooctene [104]. Catalytic activity was shown by the carbon dots synthesized from duck blood via the hydrothermal method. Characterization techniques throw light towards the presence of the elements like nitrogen and oxygen along with carbon. These carbon dots show outstanding peroxidase-like catalytic activities and could be utilized as a sensor of glucose [105]. P-nitrophenol reduction was carried out by Cu-doped carbon dots prepared from CuCl<sub>2</sub> · 2H<sub>2</sub>O and EDTA via hydrothermal synthesis. The fluorescence property of the catalyst can be utilized for analysing the catalytic ability of the Cu-doped samples [106].



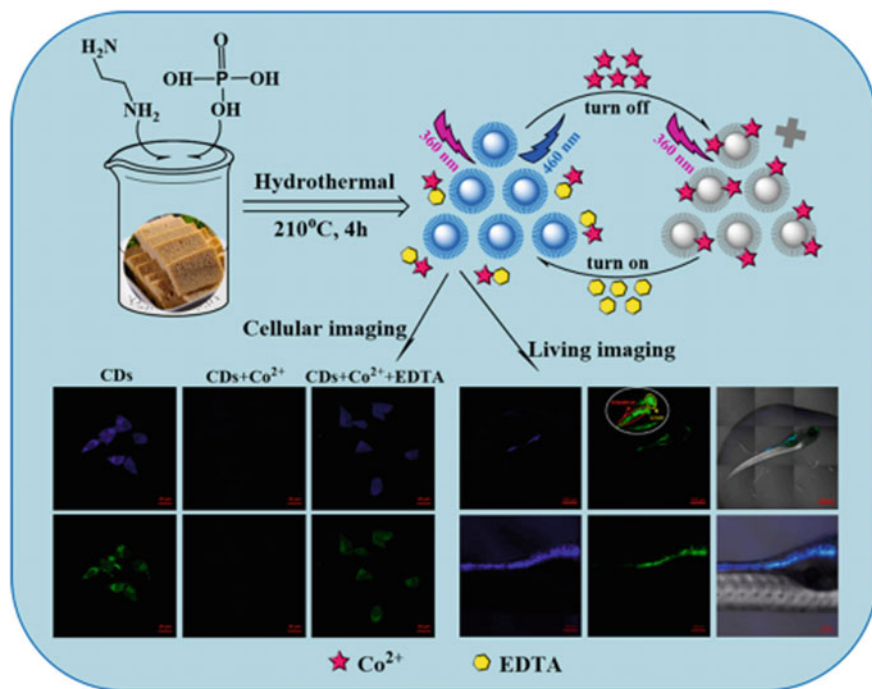
**Fig. 9** Au/CD nanocomposites acting as photocatalyst for selective oxidation of cyclohexane. Reprinted with permission from Liu et al. [102]. Copyright 2014 Americal Chemical Society



## 8 CDs for Sensor and Bioimaging Applications

A wide range of analytes such as small molecules, drugs, anions, and cations can be detected by utilizing the fluorescence of CDs. Surface functional groups can interact with metal ions like  $Hg^{2+}$ ,  $Cu^{2+}$ ,  $Ag^+$ , and  $Pb^{2+}$  and can be sensed with high selectivity and sensitivity [107]. The chelating ability of functional groups has an effect on the sensitivity of CDs. Another factor affecting the efficiency of sensing is pH (Fig. 10).

CDs are excellent candidates for biomedical applications due to their good biocompatibility, photochemical stability, and low cytotoxicity. Doping could improve the optical properties of CDs. Nitrogen- and sulphur-doped CDs are directly used for imaging of peritoneal macrophages of mice. It is found that, even after continuous excitation for 20 min, there was no reduction in photoluminescence [109]. This identifies the photostability of the nanomaterial and reveals the possibility of applications in bioimaging. Also, surface passivating agents can be used in minor concentrations for bio-labelling and it is demonstrated by using polyethylene glycol in CD synthesis. There was no prominent toxicity while conducting in vivo imaging in mice [110]. CDs as fluorescent labels for imaging in various cell lines have been investigated. There are research works in the labelling of cell lines like Ehrlich ascites carcinoma cells, HeLa cells, human lung cancer (A549), HepG2 cells, Escherichia coli (E. coli), and NIH-3T3 fibroblast cells.



**Fig. 10** Schematic illustration of the formation and cellular imaging application. Reprinted with permission from Wen et al. [108]. Copyright 2021 Elsevier

## 9 Conclusions and Future Scope

CDs have attracted recent research while considering the benefits over semiconductor quantum dots. Low cytotoxicity, high biocompatibility, water solubility, and tunable fluorescence are the key features of CDs. This chapter covers the synthetic strategies, properties, and recent advances in the applications of CDs as potential sensors and optical probes. Multicolour fluorescent emissions have been achieved by successive works by researchers. But the proper mechanism for photoluminescence is still beyond reach. Reproducibility with controlled morphology and size is still under the realm of research. Hence, there is potential interest in bringing up CDs with desirable size, shape, morphology, and functional groups. With the remarkable features, CDs could become a substitute for organic and inorganic quantum dots.

### Acknowledgements Conflicts of Interest

The authors have declared no conflicts of interest.

## References

1. Sun YP et al (2006) Quantum-sized carbon dots for bright and colorful photoluminescence. *J Am Chem Soc* 128(24):7756–7757
2. Xu X et al (2004) Electrophoretic analysis and purification of fluorescent single-walled carbon nanotube fragments. *J Am Chem Soc* 126(40):12736–12737
3. Fernando KAS et al (2015) Carbon quantum dots and applications in photocatalytic energy conversion. *ACS Appl Mater Interfaces* 7(16):8363–8376
4. Lu KQ, Quan Q, Zhang N, Xu YJ (2016) Multifarious roles of carbon quantum dots in heterogeneous photocatalysis. *J Energy Chem* 25(6):927–935
5. Shen LM, Liu J (2016) New development in carbon quantum dots technical applications. *Talanta* 156–157:245–256
6. Shen J, Zhu Y, Yang X, Li C (2012) Graphene quantum dots: emergent nanolights for bioimaging, sensors, catalysis and photovoltaic devices. *Chem Commun* 48(31):3686–3699
7. Wang D et al (2017) Facile and scalable preparation of fluorescent carbon dots for multifunctional applications. *Engineering* 3(3):402–408
8. Wang R, Wang X, Sun Y (2017) One-step synthesis of self-doped carbon dots with highly photoluminescence as multifunctional biosensors for detection of iron ions and pH. *Sensors Actuators B Chem* 241:73–79
9. Ridha AA, Pakravan P, Azandaryani AH, Zhaleh H (2020) Carbon dots; the smallest photoresponsive structure of carbon in advanced drug targeting. *J Drug Deliv Sci Technol* 55:101408
10. Hola K et al (2014) Carbon dots—emerging light emitters for bioimaging, cancer therapy and optoelectronics. *Nano Today* 9:590–603
11. Tuerhong M, Xu Y, Yin XB (2017) Review on carbon dots and their applications. *Chinese J Anal Chem* 45:139–150
12. Zheng L et al (2009) Electrochemiluminescence of water-soluble carbon nanocrystals released electrochemically from graphite. *J Am Chem Soc* 131:4564–4565
13. Peng J, Gao W, Gupta BK et al (2012) Graphene quantum dots derived from carbon fibers. *Nano Lett* 12:844–849
14. Lin L, Zhang S (2012) Creating high yield water soluble luminescent graphene quantum dots via exfoliating and disintegrating carbon nanotubes and graphite flakes. *Chem Commun* 48:10177–10179
15. Hu C et al (2014) Chemically tailoring coal to fluorescent carbon dots with tuned size and their capacity for Cu(II) detection. *Small* 10:4926–4933
16. Xie R et al (2016) Graphene quantum dots as smart probes for biosensing. *Anal Methods* 8:4001–4016
17. Dong Y et al (2012) Blue luminescent graphene quantum dots and graphene oxide prepared by tuning the carbonization degree of citric acid. *Carbon* 50(12):4738–4743
18. Sahu S, Behera B, Maiti TK, Mohapatra S (2012) Simple one-step synthesis of highly luminescent carbon dots from orange juice: Application as excellent bio-imaging agents. *Chem Commun* 48:8835–8837
19. Ding H et al (2017) Facile synthesis of red-emitting carbon dots from pulp-free lemon juice for bioimaging. *J Mater Chem B* 5:5272–5277
20. Wang J, Wang CF, Chen S (2012) Amphiphilic egg-derived carbon dots: rapid plasma fabrication, pyrolysis process, and multicolor printing patterns. *Angew Chemie Int Ed* 51:9297–9301
21. Zhu H et al (2009) Microwave synthesis of fluorescent carbon nanoparticles with electrochemiluminescence properties. *Chem Commun* 34:5118–5120. <https://doi.org/10.1039/B907612C>
22. Yang Y et al (2011) One-step synthesis of amino-functionalized fluorescent carbon nanoparticles by hydrothermal carbonization of chitosan. *Chem Commun* 48:380–382
23. Sun X, Lei Y (2017) Fluorescent carbon dots and their sensing applications. *TrAC Trends Anal Chem C* 89:163–180

24. Shuaib EP et al (2019) Carbon nanoparticles synthesized by laser ablation of coconut shell charcoal in liquids for glucose sensing applications. *Mater Res Express* (6)11:115610
25. Xiao J, Liu P, Wang CX, Yang GW (2017) External field-assisted laser ablation in liquid: an efficient strategy for nanocrystal synthesis and nanostructure assembly. *Prog Mater Sci* 87:140–222
26. Yu H, Li X, Zeng X, Lu Y (2020) Preparation of carbon dots by non-focusing pulsed laser irradiation in toluene. *Chem Commun* 56:5194–5194
27. Xu ZQ et al (2014) Low temperature synthesis of highly stable phosphate functionalized two color carbon nanodots and their application in cell imaging. *Carbon* 66:351–360
28. Ventrella A, Camisasca A, Fontana A, Giordani S (2020) Synthesis of green fluorescent carbon dots from carbon nano-onions and graphene oxide. *RSC Adv* 10:36404–36412
29. Sun D et al (2013) Hair fiber as a precursor for synthesizing of sulfur- and nitrogen-co-doped carbon dots with tunable luminescence properties. *Carbon* 64:424–434
30. Bao L, Liu C, Zhang ZL, Pang DW (2015) Photoluminescence-tunable carbon nanodots: surface-state energy-gap tuning. *Adv Mater* 27:1663–1667
31. Hu Q et al (2014) Green synthesis of fluorescent nitrogen/sulfur-doped carbon dots and investigation of their properties by HPLC coupled with mass spectrometry. *RSC Adv* 4:18065–18073
32. Devi R, Vignesh Kumar TH, Sundramoorthy AK (2018) Electrochemically exfoliated carbon quantum dots modified electrodes for detection of dopamine neurotransmitter. *J Electrochem Soc* (165)12:G3112
33. Zhou J et al (2007) An electrochemical avenue to blue luminescent nanocrystals from multiwalled carbon nanotubes (MWCNTs). *J Am Chem Soc* 129(4):744–745
34. Liu M et al (2016) Carbon quantum dots directly generated from electrochemical oxidation of graphite electrodes in alkaline alcohols and the applications for specific ferric ion detection and cell imaging. *Analyst* 141:2657–2664
35. Bao L et al (2011) Electrochemical tuning of luminescent carbon nanodots: from preparation to luminescence mechanism. *Adv Mater* 23:5801–5806
36. Peng H, Travas-Sejdic J (2009) Simple aqueous solution route to luminescent carbogenic dots from carbohydrates. *Chem Mater* 21:5563–5565
37. Hou Y et al (2015) One-pot electrochemical synthesis of functionalized fluorescent carbon dots and their selective sensing for mercury ion. *Anal Chim Acta* 866:69–74
38. Wang F, Wang S, Sun Z, Zhu H (2015) Study on ultrasonic single-step synthesis and optical properties of nitrogen-doped carbon fluorescent quantum dots. *Fuller Nanotub* 23(9):769–776
39. Guo Y, Wang Z, Shao H, Jiang X (2013) Hydrothermal synthesis of highly fluorescent carbon nanoparticles from sodium citrate and their use for the detection of mercury ions. *Carbon* 52:583–589
40. Liu H et al (2014) A multifunctional ribonuclease A-conjugated carbon dot cluster nanosystem for synchronous cancer imaging and therapy. *Nanoscale Res Lett* 9:1–11
41. Dang H et al (2016) Large-scale ultrasonic fabrication of white fluorescent carbon dots. *Ind Eng Chem Res* 55:5335–5341
42. He C, Yan H, Li X, Wang X (2019) In situ fabrication of carbon dots-based lubricants using a facile ultrasonic approach. *Green Chem* 21:2279–2285
43. Yuan F et al (2016) Shining carbon dots: synthesis and biomedical and optoelectronic applications. *Nano Today* 11:565–586
44. Namdari P, Negahdari B, Eatemadi A (2017) Synthesis, properties and biomedical applications of carbon-based quantum dots: an updated review. *Biomed Pharmacother* 87:209–222
45. Wang J, Wei J, Su S, Qiu J (2014) Novel fluorescence resonance energy transfer optical sensors for vitamin B<sub>12</sub> detection using thermally reduced carbon dots. *New J Chem* 39:501–507
46. Zhang B, Liu CY, Liu Y (2010) A novel one-step approach to synthesize fluorescent carbon nanoparticles. *Eur J Inorg Chem* 2010:4411–4414
47. Wang H et al (2016) High fluorescence S, N co-doped carbon dots as an ultra-sensitive fluorescent probe for the determination of uric acid. *Talanta* 155:62–69

48. Yang ZC et al (2011) Intrinsically fluorescent carbon dots with tunable emission derived from hydrothermal treatment of glucose in the presence of monopotassium phosphate. *Chem Commun* 47:11615–11617
49. Mehta VN et al (2015) One-step hydrothermal approach to fabricate carbon dots from apple juice for imaging of mycobacterium and fungal cells. *Sensors Actuators B Chem* 213:434–443
50. Wang L, Zhou HS (2014) Green synthesis of luminescent nitrogen-doped carbon dots from milk and its imaging application. *Anal Chem* 86:8902–8905
51. Shi J et al (2017) Green synthesis of fluorescent carbon dots for sensitive detection of Fe<sup>2+</sup> and hydrogen peroxide. *J Nanoparticle Res* 19:209
52. Bhunia SK et al (2013) Carbon nanoparticle-based fluorescent bioimaging probes. *Sci Rep* 3:1473–1479
53. Han C et al (2016) Highly fluorescent carbon dots as selective and sensitive “on-off-on” probes for iron(III) ion and apoferritin detection and imaging in living cells. *Biosens Bioelectron* 83:229–236
54. Ding H et al (2019) Highly fluorescent near-infrared emitting carbon dots derived from lemon juice and its bioimaging application. *J Lum* 211:298–304
55. Jiang Y et al (2015) A fluorescence turn-off chemosensor based on N-doped carbon quantum dots for detection of Fe<sup>3+</sup> in aqueous solution. *Mater Lett C* 141:366–368
56. Tang L et al (2012) Deep ultraviolet photoluminescence of water-soluble self-passivated graphene quantum dots. *ACS Nano* 6:5102–5110
57. Campos BB et al (2016) Carbon dots on based folic acid coated with PAMAM dendrimer as platform for Pt(IV) detection. *J Colloid Interface Sci* 465:165–173
58. Dai H et al (2014) A carbon dot based biosensor for melamine detection by fluorescence resonance energy transfer. *Sensors Actuators, B Chem* 202:201–208
59. Qu K, Wang J, Ren J, Qu X (2013) Carbon dots prepared by hydrothermal treatment of dopamine as an effective fluorescent sensing platform for the label-free detection of Iron(III) ions and dopamine. *Chem A Eur J* 19:7243–7249
60. Li Z et al (2015) Highly luminescent nitrogen-doped carbon quantum dots as effective fluorescent probes for mercuric and iodide ions. *J Mater Chem C* 3:1922–1928
61. Wang W et al (2014) Facile synthesis of water-soluble and biocompatible fluorescent nitrogen-doped carbon dots for cell imaging. *Analyst* 139:1692–1696
62. Zhu S, Meng Q et al (2013) Highly photoluminescent carbon dots for multicolor patterning, sensors, and bioimaging. *Angew Chem Int Ed Engl* 52:3953–3957
63. Li M et al (2018) Facile microwave assisted synthesis of N-rich carbon quantum dots/dual-phase TiO<sub>2</sub> heterostructured nanocomposites with high activity in CO<sub>2</sub> photoreduction. *Appl Catal B* 231:269–276
64. Wang Q et al (2014) Fluorescent carbon dots as an efficient siRNA nanocarrier for its interference therapy in gastric cancer cells. *J Nanobiotechnology* 12:1–12
65. El-Shabasy RM et al (2021) Recent developments in carbon quantum dots: properties, fabrication techniques, and bio-applications. *Process* 9:388
66. Zhao C, Li X, Cheng C, Yang Y (2019) Green and microwave-assisted synthesis of carbon dots and application for visual detection of cobalt(II) ions and pH sensing. *Microchem J* 147:183–190
67. Wang J, Qiu J (2016) A review of carbon dots in biological applications. *J Mater Sci* 51:4728–4738
68. Feng T et al (2016) Charge-convertible carbon dots for imaging-guided drug delivery with enhanced in vivo cancer therapeutic efficiency. *ACS Nano* 10:4410–4420
69. Dager A, Uchida T, Maekawa T, Tachibana M (2019) Synthesis and characterization of monodisperse carbon quantum dots from fennel seeds: Photoluminescence analysis using machine learning. *Sci Reports* 9:1–12
70. Mehta VN, Jha S, Kailasa SK (2014) One-pot green synthesis of carbon dots by using Saccharum officinarum juice for fluorescent imaging of bacteria (*Escherichia coli*) and yeast (*Saccharomyces cerevisiae*) cells. *Mater Sci Eng C Mater* 38:20–27

71. Arumugam N, Kim J (2018) Synthesis of carbon quantum dots from Broccoli and their ability to detect silver ions. *Mater Lett* 219:37–40
72. Zhao S et al (2015) Green synthesis of bifunctional fluorescent carbon dots from garlic for cellular imaging and free radical scavenging. *ACS Appl Mater Interfaces* 7:17054–17060
73. Bano D, Kumar V, Singh VK, Hasan SH (2018) Green synthesis of fluorescent carbon quantum dots for the detection of mercury(II) and glutathione. *New J Chem* 42:5814–5821
74. Zhou J et al (2012) Facile synthesis of fluorescent carbon dots using watermelon peel as a carbon source. *Mater Lett* 66:222–224
75. Liu W et al (2017) Green synthesis of carbon dots from rose-heart radish and application for Fe<sup>3+</sup> detection and cell imaging. *Sensors Actuators B Chem* 241:190–198
76. Gedda G, Lee CY, Lin YC, Wu HF (2016) Green synthesis of carbon dots from prawn shells for highly selective and sensitive detection of copper ions. *Sensors Actuators B Chem* 224:396–403
77. Liang Q et al (2013) Easy synthesis of highly fluorescent carbon quantum dots from gelatin and their luminescent properties and applications. *Carbon* 60:421–428
78. Yang X et al (2014) Novel and green synthesis of high-fluorescent carbon dots originated from honey for sensing and imaging. *Biosens Bioelectron* 60:292–298
79. Kumar A et al (2017) Green synthesis of carbon dots from *Ocimum sanctum* for effective fluorescent sensing of Pb<sup>2+</sup> ions and live cell imaging. *Sensors Actuators B Chem* 242:679–686
80. Thambiraj S, Shankaran DR (2016) Green synthesis of highly fluorescent carbon quantum dots from sugarcane bagasse pulp. *Appl Surf Sci* 390:435–443
81. Sun X et al (2017) Green synthesis of carbon dots originated from *Lycii Fructus* for effective fluorescent sensing of ferric ion and multicolor cell imaging. *J Photochem Photobiol B Biol* 175:219–225
82. Xu H et al (2015) Green synthesis of fluorescent carbon dots for selective detection of tartrazine in food samples. *J Agric Food Chem* 63:6707–6714
83. Du W et al (2015) Green synthesis of fluorescent carbon quantum dots and carbon spheres from pericarp. *Sci China Chem* 58:863–870
84. Shen J et al (2017) Facile synthesis of fluorescence carbon dots from sweet potato for Fe<sup>3+</sup> sensing and cell imaging. *Mater Sci Eng C Mater Biol Appl* 76:856–864
85. Gu D, Shang S, Yu Q, Shen J (2016) Green synthesis of nitrogen-doped carbon dots from lotus root for Hg(II) ions detection and cell imaging. *Appl Surf Sci* 390:38–42
86. Roy P et al (2015) Photoluminescent carbon nanodots: synthesis, physicochemical properties and analytical applications. *Mater Today* 18:447–458
87. Zhang J et al (2015) Scale-up synthesis of fragrant nitrogen-doped carbon dots from bee pollens for bioimaging and catalysis. *Adv Sci* (4)2:1500002
88. Liu S et al (2012) Hydrothermal treatment of grass: a low-cost, green route to nitrogen-doped, carbon-rich, photoluminescent polymer nanodots as an effective fluorescent sensing platform for label-free detection of Cu(II) ions. *Adv Mater* 24:2037–2041
89. Lu W et al (2012) Economical, green synthesis of fluorescent carbon nanoparticles and their use as probes for sensitive and selective detection of mercury(II) ions. *Anal Chem* 84:5351–5357
90. Yang S et al (2014) Large-scale fabrication of heavy doped carbon quantum dots with tunable-photoluminescence and sensitive fluorescence detection. *J Mater Chem A* 2:8660–8667
91. Fan Z et al (2014) Surrounding media sensitive photoluminescence of boron-doped graphene quantum dots for highly fluorescent dyed crystals, chemical sensing and bioimaging. *Carbon* 70:149–156
92. Tan Q et al (2019) Crystallization of zinc oxide quantum dots on graphene sheets as an anode material for lithium ion batteries. *Cryst Eng Comm* 22:320–329
93. Irvani S, Varma RS (2020) Green synthesis, biomedical and biotechnological applications of carbon and graphene quantum dots. A review. *Environ Chem Lett* 18:703–727
94. Gu C et al (2019) Bimetallic ZrHf-based metal-organic framework embedded with carbon dots: ultra-sensitive platform for early diagnosis of HER2 and HER2-overexpressed living cancer cells. *Biosens Bioelectron* 134:8–15

95. Xie Z et al (2018) Construction of carbon dots modified MoO<sub>3</sub>/g-C<sub>3</sub>N<sub>4</sub> Z-scheme photocatalyst with enhanced visible-light photocatalytic activity for the degradation of tetracycline. *Appl Catal B Environ* 229:96–104
96. Pan L et al (2016) Near-infrared emissive carbon dots for two-photon fluorescence bioimaging. *Nanoscale* 8:17350–17356
97. Sun Z, Luo Q, Ran W (2015) Preparation and characterization of amine modified carbon quantum dots from mesoporous carbon. 383–386
98. Xie YF et al (2019) Metal-mediated gold nanospheres assembled for dark-field microscopy imaging scatterometry. *Talanta* 201:280–285
99. Wang J, Gao M, Ho GW (2014) Bidentate-complex-derived TiO<sub>2</sub>/carbon dot photocatalysts: in situ synthesis, versatile heterostructures, and enhanced H<sub>2</sub> evolution. *J Mater Chem A* 2:5703–5709
100. Guo F et al (2017) Fabrication of a CuBi<sub>2</sub>O<sub>4</sub>/g-C<sub>3</sub>N<sub>4</sub> p–n heterojunction with enhanced visible light photocatalytic efficiency toward tetracycline degradation. *Inorg Chem Front* 4:1714–1720
101. Ni T et al (2020) N, Fe-doped carbon dot decorated gear-shaped W<sub>2</sub>O<sub>3</sub> for highly efficient UV-Vis-NIR-driven photocatalytic performance. *Catal* 10:416
102. Liu R et al (2014) Metal nanoparticle/carbon quantum dot composite as a photocatalyst for high-efficiency cyclohexane oxidation. *ACS Catal* 4:328–336
103. Han Y et al (2014) Carbon quantum dots with photoenhanced hydrogen-bond catalytic activity in aldol condensations. *ACS Catal* 4:781–787
104. Han X et al (2013) Synthesis of carbon quantum dots/SiO<sub>2</sub> porous nanocomposites and their catalytic ability for photo-enhanced hydrocarbon selective oxidation. *Dalt Trans* 42:10380–10383
105. Wang B et al (2018) Synthesis of catalytically active multielement-doped carbon dots and application for colorimetric detection of glucose. *Sens Actuators B Chem* 255:2601–2607
106. Du J et al (2017) Difunctional Cu-doped carbon dots: catalytic activity and fluorescence indication for the reduction reaction of p-nitrophenol. *RSC Adv* 7:33929–33936
107. Hu S et al (2016) A facile and green method towards coal-based fluorescent carbon dots with photocatalytic activity. *Appl Surf Sci* 378:402–407
108. Wen X et al (2021) Carbon dots for specific “off-on” sensing of Co<sup>2+</sup> and EDTA for in vivo bioimaging. *Mater Sci Eng C* 123:112022
109. Ding H, Yu SB, Wei JS, Xiong HM (2016) Full-color light-emitting carbon dots with a surface-state-controlled luminescence mechanism. *ACS Nano* 10:484–491
110. Cao L et al (2007) Carbon dots for multiphoton bioimaging. *J Am Chem Soc* 129:11318–11319

# Chapter 10

## Carbonaceous Nanostructures-Based Photocatalysts for Sustainable H<sub>2</sub> Production



E. Nandhakumar, E. Vivek, E. Vaishnavi, M. Prem Kumar, Perumal Devaraji, P. Selvakumar, and N. Senthilkumar

### 1 Introduction

The consumption of fossil fuels (coal, natural gas and oil) has increased as the anomalous growth of industries, power plants and automobiles, resulting in a scarcity of fossil energy resources and triggers a serious problem such as energy crisis and global warming. As a result of this, environmental pollution and energy depletion have drawn attention to the urgent need for alternative forms of clean energy production. So, the researchers are paying considerably attention to utilize hydrogen as renewable energy source and making possibilities via photocatalytic hydrogen generation [1, 2].

---

E. Nandhakumar · M. Prem Kumar  
School of Mechanical Engineering, Vellore Institute of Technology, Vellore 632014, India

E. Vivek  
Department of Physics, University College of Engineering, BIT Campus, Anna University, Tiruchirappalli 620024, India

E. Vaishnavi  
Department of Chemistry, Sri GVG Visalakshi College for Women, Udumalpet 641014, India

P. Devaraji  
Henan Engineering Research Center of Resource and Energy Recovery From Waste, Henan University, Kaifen 475007, PR China

P. Selvakumar  
Department of Engineering and Sciences, Western Norway University of Applied Sciences, Bergen, Norway

N. Senthilkumar (✉)  
Department of Electronics and Communications Engineering, M. Kumarasamy College of Engineering, Karur 639113, India  
e-mail: [senthilkumarn.ece@mkce.ac.in](mailto:senthilkumarn.ece@mkce.ac.in)



Hydrogen ( $H_2$ ) is a clean, eco-friendly and non-hazardous resource because while it combusts only water is produced during the combustion process [3, 4]. The generation of  $H_2$  using a semiconductor photocatalytic technique is a promising solution for generating energy by converting solar energy to fuel [4, 5]. At first, the photocatalysis method of hydrogen production was reported by Fujishima and Honda in 1972 using Titanium dioxide ( $TiO_2$ ) [6].  $TiO_2$  is among the most stable semiconducting material for photocatalytic hydrogen production because of its good stability and nontoxicity [7]. It has the bandgap ( $E_g$ ) of 3.2 eV which offers to absorb the solar spectrum in the range of ultraviolet region [3]. In addition, the photocatalytic efficiency of  $TiO_2$  is quietly low as of the rapid recombination occurred in the photogenerated hole pair, which hinders the practical application. Therefore, it is important to limit the charge carrier's recombination rate occurs in semiconductor photocatalyst [8]. However, the researchers are trying to improve the properties of photocatalyst through various combinations of catalyst.

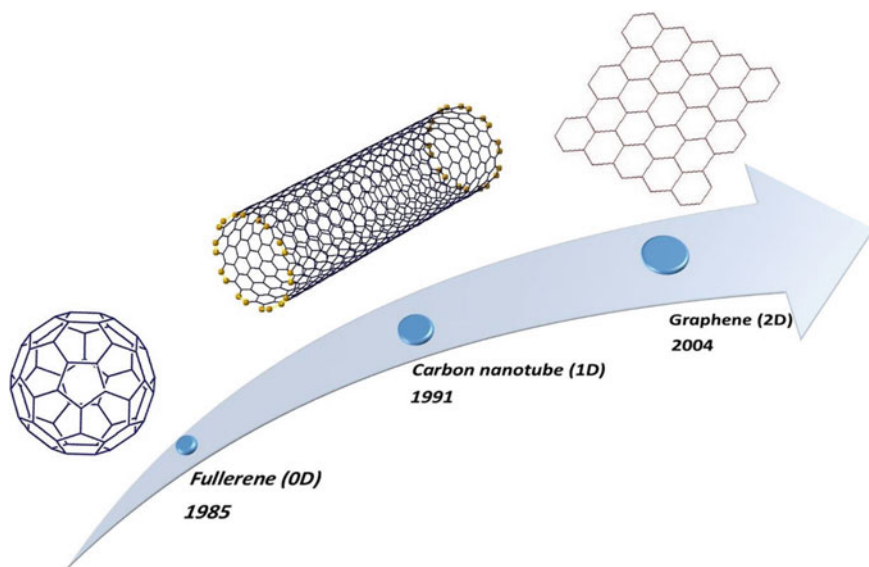
On the other hand, various carbon-based nanomaterials are attracted for its high stability, wide photo-absorbance property and high conductivity. Moreover, the discoveries of carbon nanotubes (CNTs), graphene, carbon nanofibres (CNF) and other carbon materials emerge as a building block in the arena of nanotechnology [9]. Carbon can exist in the various forms like CNT, CNFs [10], horns [11], flasks [12], carbon spheres [13, 14] and calabashes [15]. Carbon-based material has a tenable combination of  $sp$ ,  $sp^2$ ,  $sp^3$  hybridization [14]. Carbonaceous materials have been classified with their dimension which includes carbon dots, fullerenes, graphene, and graphite material as zero-dimensional (0D), one-dimensional (1D), two-dimensional (2D) and three-dimensional (3D) structures, respectively (Fig. 1). Along with that graphene is a marvel material with 2D structure of regular lattice arrangement with hexagonal pattern in  $sp^2$  hybridized form of carbon atoms [16, 17]. Therefore, the carbon-based nanomaterials have great attention in the field of semiconductor-based photocatalytic method of hydrogen production.

In this chapter, we discussed the recent advancements in carbon-based nanomaterials for photocatalytic  $H_2$  generation. We specifically discussed the different carbon materials based on their dimensions as well as the role of interface engineering between carbonaceous structures and other semiconductor nanomaterials.

## 2 Fundamentals of Hydrogen Evolution

### 2.1 Basic Principle

Three basic steps are involved in the photocatalytic process, namely (1) absorption of light and generation of photoexcited electron and holes in the valance band (VB) and conduction band (CB), respectively, and (2) separation and migration of photoexcited electron and holes to the surface of the photocatalytic materials; these two steps are deciding the efficiency of the process because the recombination of photoexcited



**Fig. 1** Different types of carbonaceous nanostructures “Reprinted with permission from Jun et al. [18]. Copy right 2018 Elsevier”

charge carriers could occur in the femtosecond in the bulk. Many semiconductor photocatalyst have been developed to enhance the charge separation efficiency which could enhance the photocatalytic activity.

For instance, noble metals such as Au, Ag and Pt [19], CdS/CdSe/Pt heterostructure, [20], Zn–Ag–In–S/Co<sub>3</sub>O<sub>4</sub> [21], Cu/TiO<sub>2</sub> [22], (Au/AgAu)@CdS [23] are greatly mitigates the recombination rate of photoexcited charge carriers. The Schottky junction between the metal and semiconductor interface increases charge transfer and reduces recombination [19]. In addition to that, introduction of carbon-based materials such as fullerene [24] g-C<sub>3</sub>N<sub>4</sub> [25] and RGO [26] to semiconductor materials predominantly increases the charge mobility and greatly reduces their recombination. The effective utilization of electron–hole pair creates for surface redox reaction. For effective reduction of proton, the conduction band potential of photocatalyst should be negative and very close to the reduction potential of proton versus normal hydrogen electrode (NHE). On the other hand, in case of oxidation of water the valance band potential of semiconductor material should be greater than the 1.23 eV versus normal hydrogen electrode. The basic process involved in photocatalyst is illustrated in Fig. 2.

The apparent quantum yield (AQY) of photocatalytic H<sub>2</sub> evolution is calculated based on the below formula:

$$\text{AQY (\%)} = \frac{\text{Number of reacted electrons}}{\text{Number of incident photons}} \times 100\% \quad (1)$$

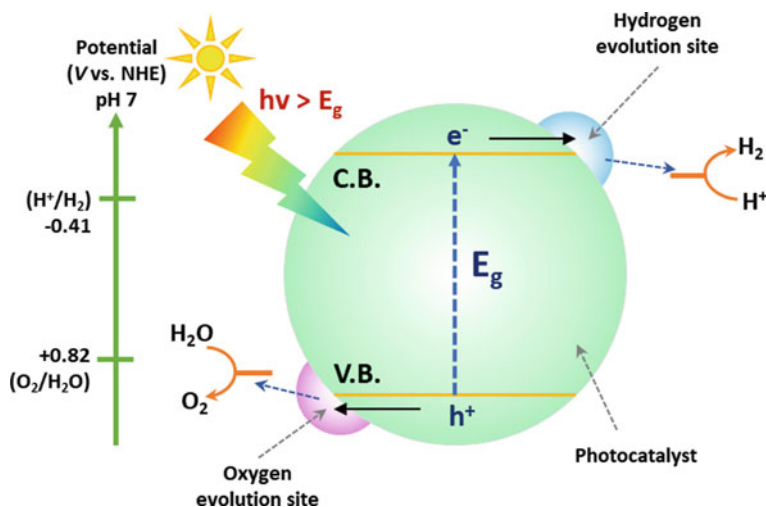


Fig. 2 Graphic representation of photocatalytic water split reaction

$$\text{AQY (\%)} = \frac{\text{Number of evolved H}_2 \text{ molecules} \times 2}{\text{Number of incident photons}} \times 100\% \quad (2)$$

## 2.2 Use of Sacrificial Agents

Efficiency of photocatalysis reaction was greatly decreased by recombinations of charge carriers. Sacrificial agents such as  $\text{CH}_3\text{OH}$ , triethylenetetramine, aqueous solution of sodium sulphide and sodium sulphate could use to hinder the recombination of electron and hole. Sacrificial agents can be utilized to scavenge indeed an electron or hole for the evolution of hydrogen or oxygen. Sacrificial agents that scavenge hole, like methanol, esoteric the hole and oxidize it to  $\text{CO}_2$ . Because of this approach, electrons excited to CB have a longer lifetime and are effectively implemented for reduction. In this context, the electron scavenging reagent like silver nitrate plays a vital role which is exactly opposite to the previously mentioned hole scavenger, as the oxidation takes place of holes. Because hole scavengers have a lower oxidation potential compared to water molecules, the thermodynamical and kinetic limitations are massively diminished. It is to be understood that water splitting is an arduous process involving a change in free energy ( $\Delta G = 237 \text{ kJ/mol}$ ). Because of the large reductions in  $\Delta G$ , it eliminates the four-electron process of molecular oxygen production. The nature of the sacrificial agents, as well as their oxidation/reduction potential, influences the decrease in  $\Delta G$ . With environmental concerns in mind, it is also implied that methanol be replaced by eco-friendly alcohols such as glycerol and carbohydrates. The use of glycerol is highly beneficial due

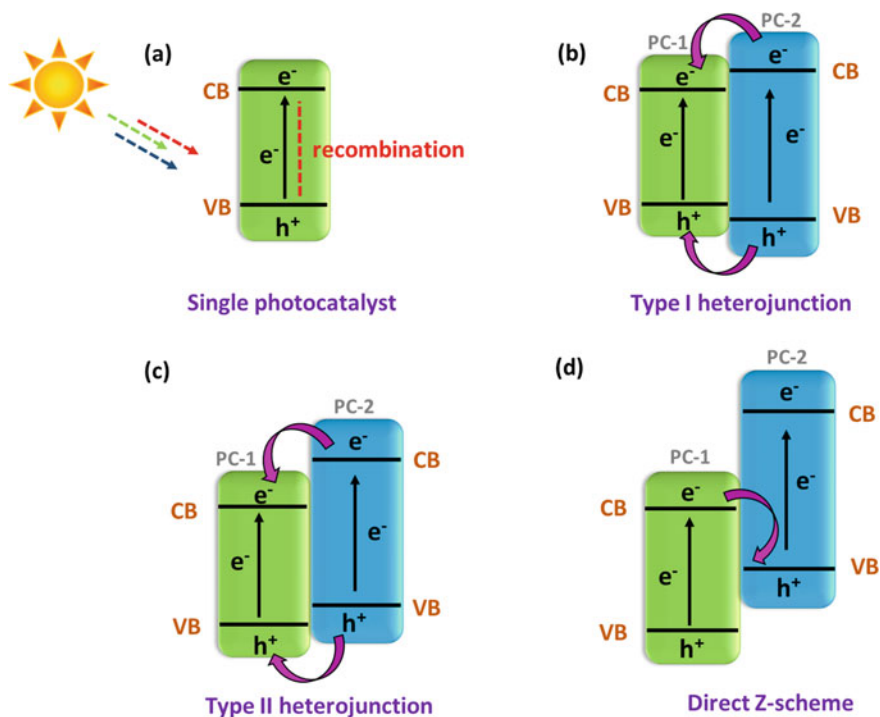
to its superior hydrogen content per molecule; however, carbon to hydrogen ratio is lower than that of methanol. Nevertheless, H<sub>2</sub> generation via water splitting reaction through a sacrificial agent, including such glycerol or methanol, could be regarded as a simple objective as it less challenging compared to overall water splitting reaction (OWSR) without the use of a sacrificial agent [27]. Considering the OWSR's rate of advancement over the past three decades, we believe it has the potential to be a big energy-conservation solution.

### 2.3 *Band Alignment*

Another interesting technique for promoting separation of photogenerated electron-hole pairs is heterojunctions fabrication. Heterojunctions are formed by joining two photocatalysts (PC-1 and PC-2) together via mechanical or electrostatic forces, as well as chemical bonds. The interface plays a major role to ensure fast transfer of charge carriers. The semiconductor heterojunctions are classified into three types: (i) Type-I (ii) Type-II and Z-scheme heterojunctions are shown in Fig. 3. In Type-I heterojunction (Fig. 3b), the two photocatalyst are activated by incident light and then the electrons from PC-2 with higher conduction band (CB) transfers to PC-1 with lower CB position beneath the force of electrostatic field. Meanwhile, photogenerated holes are transferred from lower VB to higher VB positions. As a result, the photogenerated and holes are gathered on PC-1. In Type-II heterojunction (Fig. 3c), the transfer of electron is similar to Type-1 from PC-2 to PC-1 [28]. Moreover, the holes transfer is reverse to Type-1 from PC-1 to PC-2. For this event, the reduction reaction is occurred for PC-1 when photogenerated electrons are collected on PC-1 and the holes on PC-2 for oxidation reaction. The development of a heterojunction could result in enhance of charge separation by guiding the flow of electrons and holes at the interface. And also, the charge recombination is suppressed, thus can substantially improves photocatalytic activity [29, 30].

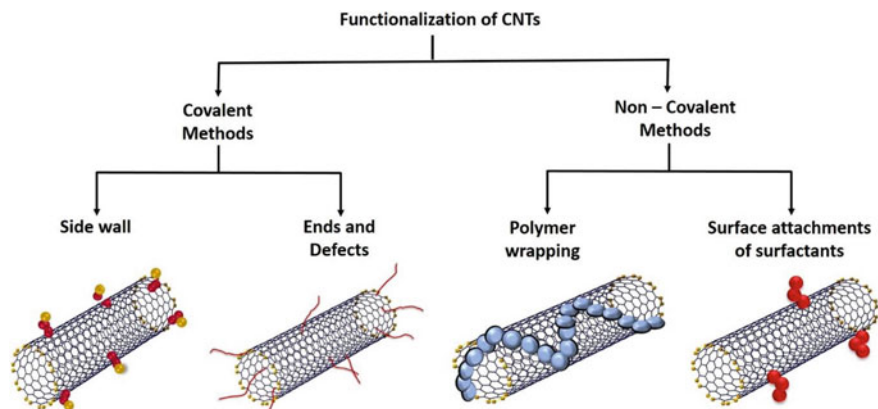
### 2.4 *Surface Functionalization*

Carbon nanomaterials have a propensity to agglomerate due to their high surface energy and high Van der Waals force between them. Weak dispersibility in solvents is a cause of these aggregation phenomena, which limits their application. So, carbon materials must be functionalized to modify their physiochemical properties to overcome this constraint [31]. The surface functionalization is a process of modifying the chemistry of the material surface to achieve a desire property. Depending on the types of interactions between active molecules and carbon atoms, functionalization techniques are broadly classified into physical functionalization and chemical functionalization (Fig. 4) [32]. The physical functionalization (non-covalent) techniques include high impact mixing, rubbing, high shear mixing, ultrasonication, etc. These



**Fig. 3** Schematic diagram of semiconductor material heterojunction formation for photocatalytic hydrogen production

procedures can keep them from aggregating, but they may break apart throughout the process and lowering the aspect ratio. As a result, it is a time-consuming and ineffective approach. Chemical functionalization (covalent) is a method of attaching functional groups using covalent bonds by means of chemical treatment. This method can improve their dispersion stability and wetting or adhesion property so covalent functionalization is the most preferred technique for changing the surface energy of the carbon materials without distressing its electrical, optical or mechanical properties. In this scenario, functionalizing the carbon nanomaterials using different chemical treatments is considered to be an effective strategy for improving the efficiency in the field of hydrogen generation via solar-mediated water splitting [33].



**Fig. 4** Functionalization methods of carbon nanotubes “Reprinted with permission from Jun et al. [18]. Copyright 2018 Elsevier”

### 3 Carbon Material Nanostructure

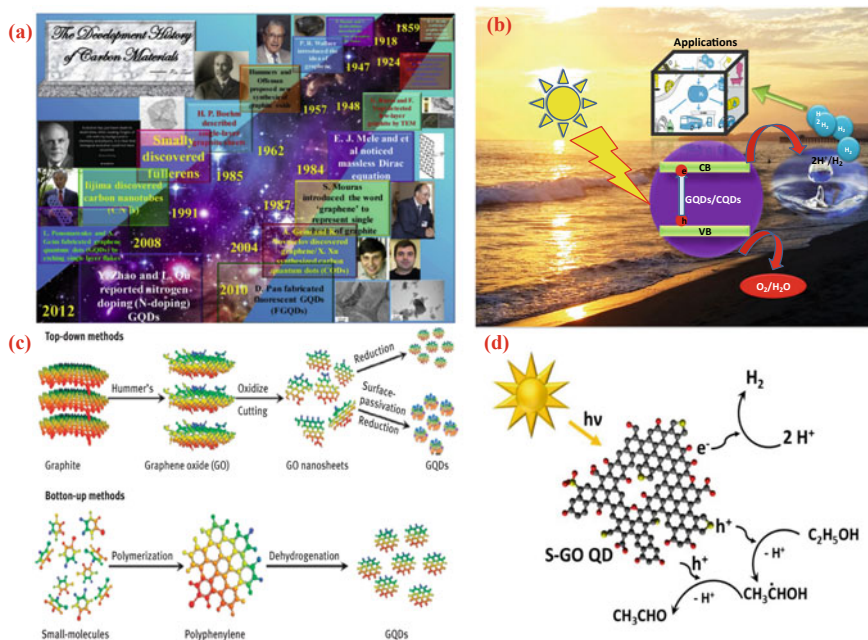
#### 3.1 0D Carbonaceous Materials

For the past two decades, chalcogenides quantum dots were appreciated for its opto-electrical properties and application in various fields ranging from biology to technology. However, the prominent toxicity is associated with such limits their industrial applications. Highest market cost of such toxic dots leads the new entrant carbon-based dots to be a promising alternative. The King of the element, namely carbon and their derivatives, can satisfy the profound quality in emerging economies [34, 35] The history of carbon materials revealing the chemistry of the quantum effects in 0D carbon material can solve the puzzle of their excellent properties (Fig. 5a) [36]. As a consequence of the quantum effect of matter at smaller atomic levels, discrete bandgap systems and edge effects are created with remarkable properties [37, 38].

##### 3.1.1 Carbon Dots

Since, after the discovery by Xu et al. carbon dot research fired up its performance in photocatalysis and sensor applications [39, 40]. These  $sp^2$  hybridized carbon materials are known for superior stability, low toxicity, and tunable optical, conducting properties, etc., [41]. Functionalizations of C-dots make them as good photon absorber and excellent electron acceptor and donor [42–44].

A blend of mixed crystal  $TiO_2$  with carbon dots (CQDs) was synthesized, characterized and revealed outstanding performance for  $H_2$  production by Tang et al. [45, 46]. The yield of  $H_2$  was  $280 \mu mol h^{-1}$ , which was higher than that using pure  $TiO_2$  alone. CQDs act as an electron storage medium which may enhance charge transfer



**Fig. 5** **a** Evolution in carbon materials from the year 1859 to 2012 was “Reprinted with permission from Tian et al. [47]. Copyright 2018 Elsevier,” **b** pictorial illustration of photocatalytic mechanism for water splitting by GQDs and CQDs, **c** GQDs different synthesis approaches reproduced with permission from “Reprinted with permission from Shen et al. [48]. Copyright 2012 Royal Society of Chemistry”, **d** S-doped GQDs hydrogen splitting mechanism in 80% of ethanol/aqueous medium at pH 8 reproduced with permission from reference “Reprinted with permission from Gliniak et al. [49]. Copyright 2017 Wiley”

and inhibit  $e^-$ - $h^+$  pair recombination. The incorporation CQDs into TiO<sub>2</sub> shifted the absorption and emission to visible region showing that electrons can be transferred from CQDs to TiO<sub>2</sub>. The inhibition of  $e^-$ - $h^+$  recombination was proved by weaker PL spectra of CQDs-TiO<sub>2</sub> system. The hydrogen treatment of CQDs-TiO<sub>2</sub> exhibited a better H<sub>2</sub> generation activity than pure TiO<sub>2</sub> due to improved optical activity of CQDs-TiO<sub>2</sub>.

The CQDs-TiO<sub>2</sub> samples showed prompt photocurrent response, while hydrogen-treated CQDs-TiO<sub>2</sub> indicated and enhanced photocurrent response. Such an observation clearly brings out the influence of CQDs in TiO<sub>2</sub> on H<sub>2</sub> yield improvement. Siu and co-workers investigated on photocatalytic hydrogen production of CQDs/TiO<sub>2</sub> nanosheets with major (001) plane. Furthermore, many previous reports on carbon quantum dots composites showed superior hydrogen gas (116.1 mol g<sup>-1</sup> h<sup>-1</sup>) production [50, 51]. C-dots can also show high performance as co-catalyst in water splitting reaction. Wang et al. [44] reported that CQDs/g-C<sub>3</sub>N<sub>4</sub> composite are well suited for enhanced hydrogen production of 2.34 mmol g<sup>-1</sup> h<sup>-1</sup> but g-C<sub>3</sub>N<sub>4</sub> alone showed only 0.51 mmol g<sup>-1</sup> h<sup>-1</sup>. The catalytic efficiency is four times that of pure material. The

interaction of CDs and  $g/C_3N_4$  hybrid improves charge transport capabilities as well as inhibits electron–hole recombination at the interface [52, 53].

Nitrogen-doped CQDs nanocomposite serves as an excellent material for photocatalytic  $H_2$  production. In addition to the early research, the superior photocatalytic activity was illuminated under visible and NIR irradiation using N-CDs/CdS nanocomposites, where lattice acid as a sacrificial reagent (consume the photogenerated holes by providing electron). The low visible light photocatalytic  $H_2$  evolution rate ( $14.8 \text{ mmol h}^{-1} \text{ g}^{-1}$ ) was achieved due to their rapid electrons (CB) and holes (VB) recombination for pure CdS. Shi et al. proved that the incorporation of N-CDs could successfully separate the charge carriers of cadmium sulphide, consequently enhancing the photocatalytic performance of N-CDs/CdS. The highest photocatalytic activity was found when 5 wt% N-CDs were loaded, with an optimum  $H_2$  evolution rate of  $58.9 \text{ mmol h}^{-1} \text{ g}^{-1}$ , which is approximately 5 times greater than cadmium sulphide alone. The  $H_2$  production rate decreased after the addition of N-CDs, which could be attributable to an excess of N-CDs covering the surface of CdS, resulting in lesser active sites for  $H_2$  production [54]. Additionally, these heterostructure carbon dots composite materials have high durability for hydrogen production.

### 3.1.2 Graphene Dots (GQDs)

Graphene dots with its incredibly smaller size, less than 30 nm, behave dually as graphene and quantum dots. GQDs derived from a 2D graphene exist mostly in elliptical or circular shapes, and even some GQDs are triangular and hexagonal [55, 56]. These ultra-small GQDs with its interesting quantum confinement and edge effect properties usually emit green or blue fluorescence (quantum yields of GQDs are mostly at a range between 2 and 22.9%). These dots have superior biocompatibility, low toxicity, good chemical stability and enhanced luminescence compared to that of inorganic semiconductor dots. GQDs possess bandgaps between 2.2 and 3.1 eV [57, 58]. Figure 5c shows the traditional Nano synthesis approach for GQDs. Eco-friendly, cheapest earth-abundant carbon materials were predominantly utilized for synthesizing GQDs [59]. Since 2008, after the discovery of GQDs, many researchers have consistently made progress in systematic tailoring and functionalization. After purification and chromatographic separation, these materials can be characterized by using material science techniques. Furthermore, the resulting GQDs function as a promising catalyst for hydrogen production and opens new prospects for carbon-based materials research Fig. 5b [60]. Figure 5d illustrates the implication of graphene dots as a photocatalytic material to split water for large-scale hydrogen generation in the near future. For example, graphene oxide (GO) has better lifetime for 200 days with photocatalytically water efficient of  $575 \mu\text{mol h}^{-1} \text{ g}^{-1}$  [61–63]. The contribution of graphene is more to improve the Water Splitting under light driven conditions [64]. N-doped graphene dots can be efficiently synthesized from carbon nano-onions using laser ablation method. Calabro et al. proved that the heteroatom-doped graphene resulted in an efficient catalytic property [65]. Theoretical work also suggested that tailoring the bond environment of carbon atoms in graphene by

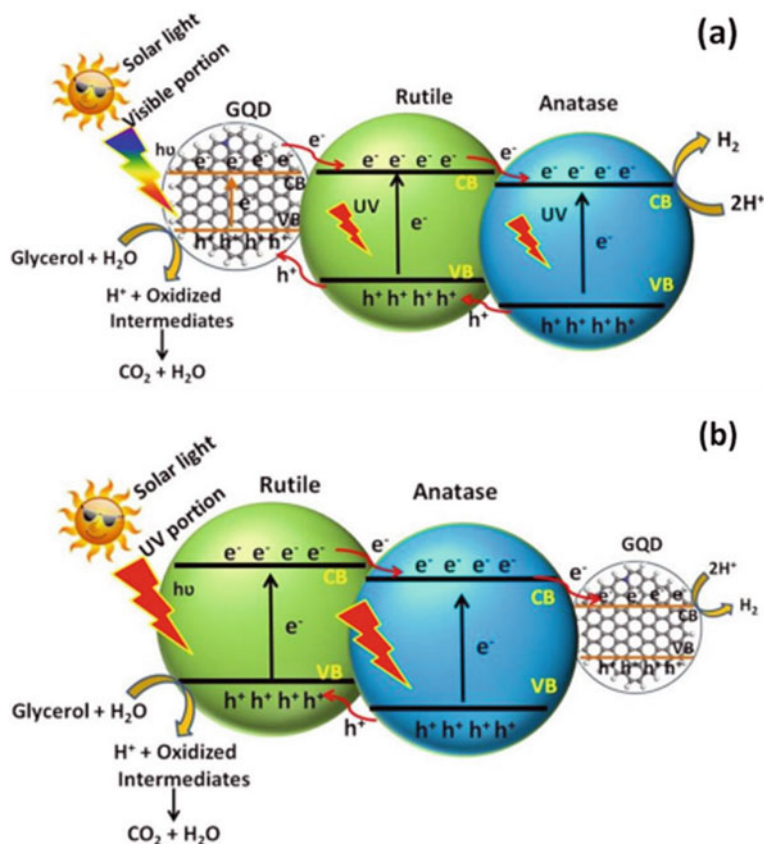


heteroatom (boron, nitrogen and sulphur) can enrich the mobility of hole and electron, respectively, henceforth enhancing the water splitting reaction [66, 67]. Table 1 illustrates hydrogen production efficiency of graphene materials. Yeh et al. employed nitrogen-graphene oxide quantum dots for water splitting application under visible light [68–70]. The rate of hydrogen generation efficiency of sulphur-doped graphene in the presence of different sacrificial electron donors was investigated by Tung et al. The results revealed that the highest performance up to 80% was detected in ethanol/aqueous medium at pH 8. Subsequently, a plausible mechanism for the improved water splitting ( $30,519 \mu\text{mol h}^{-1} \text{g}^{-1}$ ) and prolonged lifetime of the catalyst was justified by conducting the experiments in the presence of  $\text{H}_2\text{O}_2$  [68, 71, 72]. In order to achieve enhanced photocatalytic performance, it is necessary to combine the graphene dots with  $\text{TiO}_2$ . Figure 6a, b illustrates the reaction mechanism of the dual role of graphene dots as a sensitizer (for efficient light absorption) or as a co-catalyst (for enhanced charge separation) on biphasic  $\text{TiO}_2$ . Compared to single-phase  $\text{TiO}_2$ , the anatase/rutile nature of P-25  $\text{TiO}_2$  resulted in efficient charge transfer which in turn, promotes hydrogen production rate up to  $29,548 \mu\text{mol g}^{-1} \text{h}^{-1}$ . This heterojunction provides systematic separation of electron–hole pairs, in addition dots amplify the photocatalytic behaviour of  $\text{TiO}_2$  [62, 64]. Similar to this work, many researchers investigated the graphene dots modified  $\text{TiO}_2$  nanotubes, titania nanosheet [57, 73, 74] for enhancing the photocatalytic efficiency under UV light irradiation. Many worthwhile efforts have been made on the functioning of nitrogen-doped GQDs with  $\text{TiO}_2$  by Yeh et al. Also, Sudhagar et al. reported the sensitizing effect of GQDs on  $\text{TiO}_2$  nanowire and various  $\text{TiO}_2$  nanostructure [75].

To conclude, GQDs has played an eminent role in enriching the photocatalytic  $\text{H}_2$  evolution. Graphene dots' co-catalyst can also function as an efficient photo-harvester and facilitates the improving electron transfer property. As an alternative material for  $\text{TiO}_2$ , composites of ZnO nanowire and graphene dots were replaced by many scientists and the water splitting was illustrated under solar irradiation [76]. In this system, graphene dot function as aid in harnessing the visible light as well as enhance the separation of charge carriers of metal oxide by trapping the electrons and thereby delaying the recombination of charge carrier present in  $\text{TiO}_2$  which results in better photocatalytic performance. Fabrication of graphene dots onto the surface of metal sulphide nanoparticles was clearly explored by Tian et al. and Lei et al. [62, 76, 77]. Also, Dinda et al. reported on covalent linking of rhodamine dye with graphene dots to produce hydrogen efficiently under visible light without any co-catalyst [78]. Henceforth, the graphene dots can play a dual role as co catalyst as well as photosensitizer in  $\text{H}_2$  evolution. Still the reason regarding the exact role of the graphene quantum dots system in hydrogen production mechanism is unclear. With current efforts to better study the behaviour of GQDs and develop new nanomaterial functionalities, it is expected that novel applications will prosper in the near future.

**Table 1** Carbonaceous material-based nanocomposites for photocatalytic hydrogen production

Photocatalysts	Synthesis method	Sacrificial agents	Light source	H <sub>2</sub> production	References
S-graphene oxide QDs	Hydrothermal	EtOH	500 W Xe lamp	30,519 $\mu\text{mol g}^{-1} \text{h}^{-1}$	[49]
GQDs/TiO <sub>2</sub>	Hydrothermal	Na <sub>2</sub> SO <sub>4</sub>	500 W Hg lamp	79.3 $\mu\text{mol g}^{-1} \text{h}^{-1}$	[79]
Lu modified ZnO/CNTs	Sol-gel	Glycerol	300 W Xe lamp (300–1100 nm)	380 $\mu\text{mol g}^{-1} \text{h}^{-1}$	[80]
CdS/Cu <sub>7</sub> S <sub>4</sub> /g-C <sub>3</sub> N <sub>4</sub>	Ultrasoundication	Na <sub>2</sub> S + Na <sub>2</sub> SO <sub>4</sub>	300 W Xe lamp ( $\lambda > 420$ nm)	3570 $\mu\text{mol g}^{-1} \text{h}^{-1}$	[81]
Nickel-S; g-C <sub>3</sub> N <sub>4</sub>	Photodeposition	Triethanolamine	150 W Xe lamp	3628 $\mu\text{mol g}^{-1} \text{h}^{-1}$	[82]
g-C <sub>3</sub> N <sub>4</sub> /Bi <sub>4</sub> NbO <sub>8</sub> Cl	Ball milling	Na <sub>2</sub> SO <sub>4</sub>	300 W Xe lamp ( $\lambda > 420$ nm)	287.7 $\mu\text{mol g}^{-1} \text{h}^{-1}$	[83]
RGO/ZnIn <sub>2</sub> S <sub>4</sub>	Alcoholthermal method	Na <sub>2</sub> S, Na <sub>2</sub> SO <sub>4</sub>	350 W Xe lamp (420 nm)	1597 $\mu\text{mol g}^{-1} \text{h}^{-1}$	[84]
MOS <sub>2</sub> QDs/UfO-66-NH <sub>2</sub> /graphene	Ultrasoundication method	Triethanolamine	300 W Xe lamp ( $\lambda > 420$ nm)	186.37 $\mu\text{mol g}^{-1} \text{h}^{-1}$	[85]
Boron/oxygen co-doped g-C <sub>3</sub> N <sub>4</sub> nanomesh	Freeze drying method	Triethanolamine	300 W Xe lamp ( $\lambda > 420$ nm)	9751 $\mu\text{mol g}^{-1} \text{h}^{-1}$	[28]



**Fig. 6** a and b the enhanced hydrogen generation by decoration of graphene QDs onto the bi-phase TiO<sub>2</sub> nanostructures “Reprinted with permission from Raghavan et al. [64]. Copyright 2020 American Chemical Society”

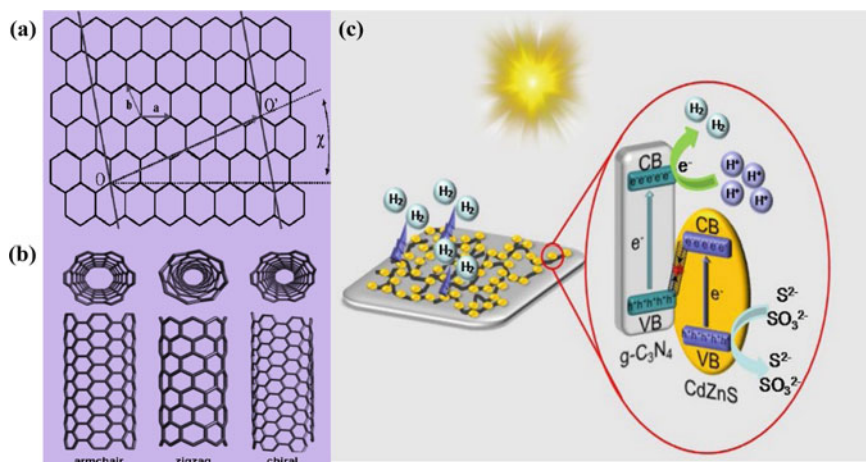
### Carbon Nanotubes (CNTs)

The carbon nanotubes (CNTs) were discovered in 1991 by Sumio Iijima; it offers large surface area, excellent thermal conductivity, high electron emission, high thermal and chemical stability [86–89]. In the recent past decade, CNTs employed in photocatalytic applications have both metallic and semiconducting capabilities due to the chiral indices of the CNTs [90, 91]. CNTs have the potential to solve the challenges that semiconductors have in photocatalysis.

CNTs are a one-dimensional structure of carbon allotropes; it is like tubular containing graphite. Also, CNTs are hollow cylinder, while rolling it formed single or multilayered graphene. The carbon nanotubes were classified into two types, (i) single-walled carbon nanotubes (SWCNTs) and (ii) multiwall carbon nanotubes (MWCNTs). The difference between SWCNTs and MWCNTs is listed in Table 2. A single-walled carbon nanotubes (SWCNTs) can be thought of as a single molecule

**Table 2** Comparative of SWCNTs and MWCNTs properties

SWCNTs	MWCNTs
Graphene arranged in single layer	Graphene arranged in multi-layer
For synthesis catalyst is required	It is possible to produce without catalyst
Difficult to do bulky synthesis required suitable growth control and environment condition	Easy to synthesis in bulk
During functionalization defect should be more	When using the arc-discharged technique, the chances of defect is reduced
SWCNTs can be easily twisted	MWCNTs cannot be easily twisted
It is easy for evaluation and characterization	It has very complex structure



**Fig. 7** **a** and **b** the formation of single-walled carbon nanotubes by rolling a graphene sheet along lattice vectors results in armchair, zigzag, and chiral tubes which are the three types of carbon nanotubes; **c** Proposed mechanism diagram of photocatalytic hydrogen production of Z-scheme g-C<sub>3</sub>N<sub>4</sub>/CNTs/CdZnS. “Reprinted with permission from Feng et al. [104]. Copyright 2021 Elsevier”

with a wide range of structural characteristics such as diameter, length, and chirality. The pure SWCNTs are visualized as tubular shell rolled of graphene sheet layered by benzene kind hexagonal rings of carbon atoms [92–94]

From these two different structures, it is possible for three different types of CNTs. They are armchair, zig-zag and chiral-type CNTs which are represented by indices of  $n$  and  $m$ . Therefore, when  $n = m$  represents armchair, when  $m = 0$  represents zig-zag and other configurations represent chiral nanotubes [95–99]. Figure 7a, b represents the types of SWCNTs. The diameter and chirality are calculated by the following equation [100]

$$D = a(n^2 + nm + m^2)^{1/2} / \pi$$

$$\theta = \tan^{-1} [3^{1/2} m / (m + 2n)]$$

The circumference of SWCNTs has 10 atoms usually and tube thickness is one-atom-thick only, this nanotube have an aspect ratio of length- diameter was about 1000, so it can be nearly considered as one-dimensional structures [95]. SWCNTs have a diameter of  $\approx 1$  nm consisting of only one atomic sheet which can be visualized by rolled graphene (i.e. honeycomb structure  $sp^2$  of carbon atom) sheet. The  $sp^2$ -bonded carbon materials give better mechanical properties [98]. The one-dimensional SWCNTs are attracted researcher to explore 1D physics in the quantum regimes and new optoelectronic devices. Moreover, the most prominent property in SWCNTs is chirality-dependent metallicity. CNTs have high thermal conductivity (3000 W/m/K, comparable to diamond), good chemical and environmental stability. Along with these properties, the lightweight of carbon nanotubes makes them extremely promising for use in industries such as aerospace [101]. MWCNTs are  $sp^2$  carbon made of elongated cylindrical nano-objects, and their diameter ranges from 3 to 30 nm, and they can grow to be several centimeters long, and therefore, their aspect ratio can range between ten and ten million. These MWCNTs can be distinguished from SWCNTs and double-wall carbon nanotubes. In MWCNTs, the wall thickness is constant along the axis; therefore, the inner channel is straight. A multi-walled carbon nanotube is made up of as many large molecules as the number of walls, and each molecule is as long as the nanotube itself. Carbon materials are mostly used as supporting materials for semiconductor photocatalysts. In addition, photocatalyst hydrogen ( $H_2$ ) production was achieved by hybrid photocatalyst of semiconductor-carbon photocatalysts. The surface chemistry of carbon materials influences the interaction between semiconductor nanoparticles and carbon materials [102]. In this aspect, Wang et al. fabricated the MWCNTs as a supporting material of  $Zn_x Cd_{1-x} S$  nanoparticles by the solvothermal process, where  $Zn(AC)_2 \cdot 2H_2O$ ,  $CdCl_2 \cdot 2/5H_2O$  and thiourea were used as the precursor material to prepare  $Zn_x Cd_{1-x} S$ . The average diameter of  $Zn_{0.83}Cd_{0.17}S$  nanoparticle was found  $\sim 100$  nm which was assembled on the surface of CNTs. Moreover, the combined  $Zn_{0.83}Cd_{0.17}S/CNTs$  nanocomposites give better dispersion and interfacial area. The excited photoelectron will move from the conduction band (CB) of  $Zn_{0.83}Cd_{0.17}S$  to the surface of CNTs, resulting in the separation of photogenerated charge carriers at the interface between  $Zn_{0.83}Cd_{0.17}S$  and CNTs. Under wavelength illumination ranging from 300 to 800 nm, the photocatalytic  $H_2$  production rate of  $Zn_{0.83}Cd_{0.17}S/CNTs$  nanocomposite was  $6.03 \text{ mmol h}^{-1} \text{ g}^{-1}$ , which was 1.5 times than that pure  $Zn_{0.83}Cd_{0.17}S$  [103].

The MWCNTs/Pd-TiO<sub>2</sub> photocatalyst was tested for  $H_2$  production under UV light which shows the production of  $H_2$  as  $25 \text{ mmol g}^{-1} \text{ h}^{-1}$ ; this can be achieved due to electronic junction supporting the charge transfer between the MWCNTs-TiO<sub>2</sub>. Moreover, the CNTs acts as a co-catalyst and excellently transfers the electron between Pd and TiO<sub>2</sub> [105]. Umer et al. investigated the montmorillonite (Mt) dispersed in single-wall carbon nanotubes (SWCNTs)/TiO<sub>2</sub> composite to produce photocatalytic  $H_2$  evolution under visible light conditions. The SWCNTs-Mt (2–10 wt%)-doped TiO<sub>2</sub> produces  $H_2$  volume of ca. 9780 ppm  $h^{-1} \text{ g}^{-1}$ . To enhance the

separation efficiency of better absorption of visible light and photogenerated charge carriers are originated through synergic effect between Mt and SWCNTs. The co-doping between Mt and  $\text{TiO}_2$  enhances the separation efficiency of electron/hole pairs [106]. As well as, CNT-Pt/ $\text{TiO}_2$  photocatalysts prepared via hydrothermal and one-pot oxidation for production of photocatalytic hydrogen from glycerol and methanol from aqueous solutions. The  $\text{H}_2$  production is increased by varying CNTs wt% in the range of 1–10 wt% loading with  $\text{TiO}_2$  reported by Naffati et al. [107]. Moreover, this synergic effect enhances the separation of charge carriers and mobility in hybrid materials promoted by CNTs. The 1 wt% of CNTs with Pt/ $\text{TiO}_2$  shows the highest photocatalytic  $\text{H}_2$  production under UV-LED of (384 nm) irradiation. Although using methanol with this reaction produce  $\text{H}_2$  of 2327 and 2091  $\mu\text{mol g}^{-1}$  was obtained using glycerol. In this aspect, Peng et al. [108] synthesized MWCNTs/CdS (cadmium sulfide) by hydrothermal method. The 10 wt% of MWCNT with CdS derived from at 160 °C shows high photocatalytic hydrogen production efficiency due to its fastest carrier separation. In MWCNTs, the presence of carboxyl leads to good chemical bonding between MWCNTs and CdS nanoparticles which result in the synergic effect of CNTs and CdS. The binary MWCNTs/CdS nanocomposite is efficient under visible light-driven photocatalysts which shows better durability due to their good chemical bonding between composites of MWCNTs/CdS, which enhanced the separation efficiency and charge separation and its potential for the developing of efficient photocatalysts for  $\text{H}_2$  production. Feng et al. [104] performed the photocatalysts hydrogen production on g- $\text{C}_3\text{N}_4$ /CNTs/CdZnS which is shown in Fig. 7c. The CdZnS nanoparticles are compounded uniformly on the surface of g- $\text{C}_3\text{N}_4$ /CNTs to form the heterojunctions which improve the photocatalytic  $\text{H}_2$  production. Moreover, the mass ratio of 1:8 (g- $\text{C}_3\text{N}_4$ /CNTs to CdZnS) displayed better performance on photocatalytic  $\text{H}_2$  production of 28.74  $\text{mmol g}^{-1} \text{h}^{-1}$ . Z-scheme heterojunctions improves the system separation efficiency and photogenerated carrier lifetime on these ternary nanocomposites, which can make better and continue to produce  $\text{H}_2$  efficiently and stably.

### 3.2 2D Materials

The material's properties are impacted not only by its chemical bonding but also by its dimensions and shape at the mesoscopic scale. This is especially true in the case of carbon-based materials. Carbon possesses four valence electrons in its ground state, two in the 2s subshell and two in the 2p subshell. While establishing bonds between neighboring atoms of carbon, the transfers of one 2s electrons into the unoccupied 2p orbital take place and then create bonds with additional atoms through the orbit of sp hybridization. Depends on the number of p orbitals (one to three) mashing up with the s orbital the sp hybridization is categorized by three types which are sp, sp<sup>2</sup>, and sp<sup>3</sup> hybridization. The hybridized carbon atoms in the form of sp<sup>2</sup> and sp<sup>3</sup> establish bonds with three and four carbon atoms, respectively. These carbon-based building blocks are known as two-dimensional (2D) materials which include graphene, graphitic

carbon nitride and graphdiyne. The arrangement of carbon atoms on a honeycomb lattice brought outstanding properties includes exceptional electronic, mechanical, and optical properties. Owing to its outstanding characteristics, two-dimensional (2D) materials have fascinated a lot of interdisciplinary research consideration in the field of energy and environmental applications. In that perspective, utilization of 2D materials for the generation of  $H_2$  from the process of photocatalytic water splitting is the most idealistic method for gaining carbon-free fuel [109].

### 3.2.1 Graphene

The wonder material “graphene” was discovered in 2004 by Geim and Novoselov [110]. The discovery of graphene ushered in a new era of the materials world and is much recognized for its exceptional properties such as large surface area ( $2630 \text{ m}^2 \text{ g}^{-1}$ ), outstanding electronic mobility ( $200,000 \text{ cm}^2 \text{ V}^{-1} \text{ s}^{-1}$ ), high thermal conductivity ( $3000 \text{ W m}^{-1} \text{ K}^{-1}$ ) and robust mechanical strength (1060 GPa). Various physical methods have been tried to isolate a single-layer defect-free graphene sheet. Chemical vapour deposition (CVD), thermal exfoliation, solvent assisted exfoliation and ultrasonication are a few examples [111]. However, commercial implementation is hampered by expensive and time-consuming methods as well as the inability to produce big quantities. So chemical oxidation method is adopted to oxidize graphite by involving strong oxidizing agents for the formation of graphite oxide, and from this procedure, graphene oxide (GO) can be obtained easily through the repulsive forces acting between negatively charged sheets [112, 113]. The GO sheets can be partially diminished via hydrothermal, chemical, or thermal exfoliation methods to obtain reduced graphene oxide (rGO) [114]. Despite the fact that these techniques generate graphene sheets with few defects, their properties are identical to graphene. When graphite is oxidized to graphene oxide (GO), it becomes a semiconductor. The addition of various oxygen-carrying functions to graphene via oxidation converts some of the  $sp^2$  carbons into  $sp^3$  carbons, owing to the breaking of the p-conjugated system [115]. The carbon skeleton of GO turns positive due to the higher electronegativity of oxygen, and GO behaves as a p-type material [116]. The presence of both  $sp^2$  (conducting) and  $sp^3$  (non-conducting) carbons results in the formation of bandgap which exclusively depends on the degree of oxidation. The bandgap of GO can be controlled by adjusting the oxidation level. At first, the splitting of water into hydrogen and oxygen using GO was reported by Yeh et al. [69]. Depending on the oxidation level, the bandgap of GO was found to be 2.4–4.3 eV, and this bandgap was capable of meeting the water splitting threshold that is 1.23 V. After 6 h of visible light irradiation, the negative conduction band produced a hydrogen ( $H_2$ ) yield of 280  $\mu\text{mol}$  and then the yield of hydrogen increased to 17,000  $\mu\text{mol}$  when methanol was used as a sacrificial donor. Furthermore, to improve the hydrogen evaluation rate, graphene oxide (GO) can be composited with other inorganic semiconducting materials. Owing to the negatively charged surface of GO, the inorganic nanomaterials were immobilized by attractive force acts between them. Additionally,

GO offers seamless nucleation sites for the growth of metal oxide semiconducting nanoparticles and also prevents them from agglomeration.

### Graphene-Based Composites

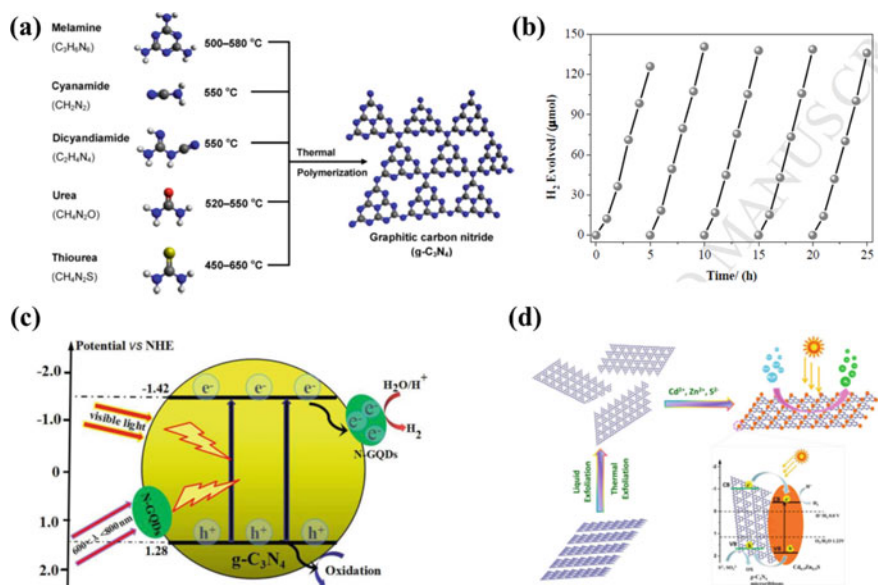
TiO<sub>2</sub> is widely utilized in photocatalytic hydrogen generation from water splitting because of its inexpensiveness, lack of toxicity and great stability [117]. Zhang et al. [118] explored photocatalytic H<sub>2</sub> evolution of TiO<sub>2</sub>/graphene sheets (GS). The results indicate the increase in H<sub>2</sub> production with increase in GS content (4.5 μmol h<sup>-1</sup>–5.4 μmol h<sup>-1</sup>), respectively. Shen et al. [119] demonstrated the superiority of TiO<sub>2</sub>/rGO synthesized via one-step hydrothermal method, and the composite displayed a H<sub>2</sub> yield of 4.0 μmol h<sup>-1</sup> under irradiation of UV–visible light. The increased activity of the composite may be due to interfacial transfer of electrons from TiO<sub>2</sub> to graphene which is assisted by the energy-level variations. Xiang et al. [120] prepared graphene-modified TiO<sub>2</sub> nanosheets through microwave-hydrothermal method and exhibits a H<sub>2</sub> yield of 736 μmol h<sup>-1</sup> g<sup>-1</sup> by an AQY of 3.1%. The high H<sub>2</sub> production may be ascribed to the composite material (TiO<sub>2</sub> modified graphene sheets) which acts as an electron acceptor and efficiently restricts the recombination rate of electron–hole pair. Lv et al. [121] demonstrated the fabrication of photocatalysts containing CdS or TiO<sub>2</sub> graphene composite by one-pot synthesis method, and hydrogen-generating ability of the photocatalysts was examined using sacrificial electron (SA) donors (Na<sub>2</sub>S and Na<sub>2</sub>SO<sub>3</sub>). Min et al. [122] investigated the MoS<sub>2</sub> confined on RGO sheets attached with Eosin Y as SA in photocatalytic systems for H<sub>2</sub> evolution, and it exhibits a AQY of 24% under visible light irradiation (≥420 nm). Tran et al. [123] studied Cu<sub>2</sub>O/rGO composite for hydrogen generation, and they tried to overcome the rapid deactivation of Cu<sub>2</sub>O via photocorrosion phenomenon, which causes due to the redox reaction of Cu<sub>2</sub>O to CuO and Cu. Khan et al. [124] investigated the significance of Al<sub>2</sub>O<sub>3</sub>/CdS/GO and ZnO/CdS/GO in H<sub>2</sub> evolution with SA (Na<sub>2</sub>SO<sub>3</sub> and Na<sub>2</sub>S) which displays an AQY of 14% and 30%. Mou et al. [125] prepared RuO<sub>2</sub>/TiSi<sub>2</sub>/graphene as photocatalyst for H<sub>2</sub> generation via water splitting. However, increasing the amount of RuO<sub>2</sub> on the surface of TiSi<sub>2</sub> resulted in charge recombination centres. Furthermore, similar action was found with addition of RGO, where 1% loading amount of RGO works as an enhanced charge transport and further increasing the loading, resulting in a decrease in H<sub>2</sub> evolution. Based on the discussion, graphene and graphene-based composites clearly act as an effective support for semiconducting photocatalysts, particularly for generating H<sub>2</sub> via water splitting. The importance of graphene and graphene-based composites in suppressing the recombination rate in single and dual semiconducting photocatalysts has received a lot of attention. Even though the performance of graphene-based photocatalysts in water splitting is critical, graphene's high production cost delays the commercialization process.



### 3.2.2 Graphitic Carbon Nitride

As another type of layered 2D material is graphitic-phase carbon nitride ( $g\text{-C}_3\text{N}_4$ ) which sparked lot of curiosity among scientists because of its unique structure and interesting characteristics. Since it discovered in 1834, carbon nitride ( $\text{C}_3\text{N}_4$ ) has been considered as one of the earliest organic conjugated polymers which has five phase classifications together with  $\alpha$ ,  $\beta$ , cubic, pseudocubic and graphitic phase. Specifically,  $g\text{-C}_3\text{N}_4$  is made up of layers of 2D conjugated structures with s-triazine or tri-s-triazine subunits linked by tertiary amines. Thermal polycondensation (Fig. 8a) is used to make  $g\text{-C}_3\text{N}_4$  from low-cost carbon-based precursors which contains nitrogen urea, cyanamide, thiourea, melamine and dicyanamide. Initially, Biureate is formed when it dimerizes and then it cyclizes to cyanuric acid, which combines with the ammonia gas to produce ammelide and melamine during pyrolysis. The graphite-like planer architecture with p-conjugated systems allows charge carriers to be transported, whereas the bandgap of 2.7 eV allows it to work in the visible region of the solar spectrum at approximately 460 nm. The benefits of  $g\text{-C}_3\text{N}_4$  consist of visible light responsive, better thermal stability in ambient conditions, good chemical resistivity and eco-friendly. Furthermore, the electronic band position of the negative conduction band (CB) is higher than  $\text{H}^+/\text{H}_2$  and the positive valence band (VB) superior than  $\text{H}_2\text{O}/\text{O}_2$  drives the  $g\text{-C}_3\text{N}_4$  specifically in the  $\text{H}_2$  production from the solar-driven water splitting process [126, 127]. Hong et al. [128] prepared  $g\text{-C}_3\text{N}_4$  nanosheets by directly thermal calcination method using an optimized hydrothermally treated melamine as precursor. The resulting nanosheets had outstanding visible light-driven photocatalytic water splitting capability of  $503 \text{ mol h}^{-1} \text{ g}^{-1}$  hydrogen evolution (Fig. 8b). One of the initial efforts by Wang et al. [129] reveals the usage of  $g\text{-C}_3\text{N}_4$  to yield  $\text{H}_2$  by water splitting process in the presence of triethanolamine which generated  $0.1\text{--}4.0 \mu\text{moles/h}$  under the irradiation source of visible light. Upon the addition of co-catalyst (3% Pt), the yield of  $\text{H}_2$  was increased by further 10–15%. However, its photocatalytic activity is limited by its lower electrical conductivity, higher recombination rate, and poor light absorption. Several approaches were indeed made to enhance the photocatalytic activity  $g\text{-C}_3\text{N}_4$  which are doping, tailoring the nanoarchitecture, incorporation of noble metal, development of heterojunctions with other photoactive materials.

The  $g\text{-C}_3\text{N}_4$  catalyst based on heterojunctions has received a lot of attention because of its synergistic behaviour. So, using the impregnation and chemical reduction method, the nanocomposites of  $g\text{-C}_3\text{N}_4$  and graphene oxide (GO) were synthesized by thermally treating melamine and GO at  $550 \text{ }^\circ\text{C}$  in inert environment [130]. In this context, graphene served as conductive pathways, allowing the charge carriers to be effectively separated. So, the graphene/ $g\text{-C}_3\text{N}_4$  nanocomposite displays a  $\text{H}_2$  production of  $451 \mu\text{mol h}^{-1}$ , which the pure  $g\text{-C}_3\text{N}_4$  possess 3.07 times lesser. Song et al. reported that their prepared rGO/ $g\text{-C}_3\text{N}_4$  via a simple hydrothermal reduction method yields a  $\text{H}_2$  production rate of around  $55.8 \mu\text{mol h}^{-1} \text{ g}^{-1}$  [131]. To increase the photoactivity of  $g\text{-C}_3\text{N}_4$ , Zou et al. [132] created a nanocomposite of N-GQDs/ $g\text{-C}_3\text{N}_4$  using a simple method. Because of the various functions served by the N-GQDs, this nanocomposite demonstrated enhanced activity in photocatalytic  $\text{H}_2$



**Fig. 8** **a** The synthesis of g-C<sub>3</sub>N<sub>4</sub> by thermal polymerization of various precursors is depicted schematically. “Reprinted with permission from Ong et al. [138]. Copyright 2016 American Chemical Society.” **b** Stability test of hydrogen production over the g-C<sub>3</sub>N<sub>4</sub> nanosheets. g-C<sub>3</sub>N<sub>4</sub>. “Reprinted with permission from Hong et al. [128]. Copyright 2017 Elsevier.” **c** Mechanism for H<sub>2</sub> evolution by using N-GQDs/CN-U. “Reprinted with permission from Zou et al. [132]. Copyright 2016 Elsevier.” **d** The synthesis of Cd<sub>0.5</sub>Zn<sub>0.5</sub>S@C<sub>3</sub>N<sub>4</sub> and visible light-driven H<sub>2</sub> production are depicted schematically. “Reprinted with permission from Yao et al. [135]. Copyright 2016 Elsevier”

evolution of around 43.6 mol h<sup>-1</sup> that would have been 2.16 times larger compared to pure g-C<sub>3</sub>N<sub>4</sub>. Figure 8c illustrates the photocatalytic H<sub>2</sub> evolution pathway in N-GQDs/g-C<sub>3</sub>N<sub>4</sub>. As per the suggested mechanism, g-C<sub>3</sub>N<sub>4</sub> absorbs in the region (420–470 nm) and results in production of charge carriers. On the contrary, absorbed light at 600–800 nm by g-C<sub>3</sub>N<sub>4</sub> generates electron and hole. As a result, electrons from the conduction band of g-C<sub>3</sub>N<sub>4</sub> migrated to the edge of N-GQDs and those electrons are having ample time to convert H<sub>2</sub>O to H<sub>2</sub> because of its effective separation of charge carrier. Another approach has been reported by utilizing ZIF-8/g-C<sub>3</sub>N<sub>4</sub> prepared by simple thermal condensation method which exhibits a H<sub>2</sub> evolution 32.6 μmol h<sup>-1</sup> that was 36.2 times higher compared to bare g-C<sub>3</sub>N<sub>4</sub> [133]. Wang et al. [134] reported the integration of silicon carbide (SiC) with g-C<sub>3</sub>N<sub>4</sub> for the first time. The composite had a high photoactivity and a rate of H<sub>2</sub> generation of 182 mol h<sup>-1</sup> that was 3.4 times higher than the pure g-C<sub>3</sub>N<sub>4</sub>. The band edges of SiC and g-C<sub>3</sub>N<sub>4</sub> matched appropriately to generate a heterojunction photocatalyst with better electron–hole separation.

Yao et al. proposed a Type-II photocatalyst with excellent efficiency composed of 2D g-C<sub>3</sub>N<sub>4</sub> micronanoribbons and Cd<sub>0.5</sub>Zn<sub>0.5</sub>S quantum dots Fig. 8d [135]. The authors integrated the virtues of nanostructure engineering based on the benefits

of Type-II structures. The composite displays the maximum  $\text{H}_2$  generation rate of  $33.41 \text{ mmol h}^{-1} \text{ g}^{-1}$  and an AQY of 46.65% at visible light irradiation (450 nm). In g- $\text{C}_3\text{N}_4$ -based Z-scheme systems, the narrow bandgap oxides have fascinating potentials throughout the evolution of  $\text{O}_2$  in water splitting process. She et al. [136] demonstrated that a 2D hybrid made up of g- $\text{C}_3\text{N}_4$  nanosheets and  $\text{Fe}_2\text{O}_3$  nanosheets coupled with a tight interface may be used to build a direct Z-scheme all-solid-state system for photocatalytic water splitting process. The composite showed an excellent hydrogen evolution rate of  $30 \text{ mmol g}^{-1} \text{ h}^{-1}$  and an AQY of 44.35% under the irradiation of visible light (420 nm). Similarly, in order to achieve optimal performance, the main factors that have a substantial impact on water splitting efficiency must be optimized are: type and concentration of redox mediator, the pH value of the reaction medium and the weight per cent between two photocatalysts. Tang et al. prepared the combination of  $\text{BiVO}_4$  and  $\text{WO}_3$  with g- $\text{C}_3\text{N}_4$  to form a Z-scheme system with taking the above factors into account. Under ideal condition, g- $\text{C}_3\text{N}_4/\text{WO}_3$  (I/ $\text{IO}_3$  as a redox mediator) exhibits a  $\text{H}_2$  and  $\text{O}_2$  evolution of 36 and  $18 \text{ mol g}^{-1} \text{ h}^{-1}$ , while for g- $\text{C}_3\text{N}_4/\text{BiVO}_4$  the corresponding evolutions are 21.2 and  $11.0 \mu\text{mol g}^{-1} \text{ h}^{-1}$  by using  $\text{Fe}^{2+/3+}$  as a redox mediator [137].

Moreover, the intriguing metal-free structure and high physicochemical stability of g- $\text{C}_3\text{N}_4$  materials offer both technical potential and mechanistic vision into the water splitting mechanism. By modifying the exterior construction of g- $\text{C}_3\text{N}_4$  built on strategies like Type-I and Z-scheme deliberately improves the efficiency and durability in mutual of hydrogen evolution half reaction and overall water splitting process.

## 4 Conclusion

The advantages of carbonaceous based (0D, 1D and 2D) nanostructures composites in photocatalytic water splitting were emphasized in this chapter. These carbonaceous nanostructure materials revealed to have strong carrier transport and electron accepting capabilities, which are the most important qualities for increasing hydrogen generation efficiency by increasing the visible light absorption. In addition, the carbonaceous nanostructured-based semiconductor photocatalytic materials enhance the hydrogen evolution efficiency and displayed outstanding stability, where the integration of semiconducting materials established the effective transfer of an electron between the heterostructures and efficient separation of charge carriers. Also, the photocatalytic semiconductors act as an efficient light adsorber and electron acceptor which enhance the overall efficiency of water splitting. In conclusion, carbon-based nanostructures have a great potential in water splitting application as photocatalytic hydrogen generation.

## References

1. Sadanandam G, Lalitha K, Kumari VD, Shankar MV, Subrahmanyam M (2013) Cobalt doped TiO<sub>2</sub>: a stable and efficient photocatalyst for continuous hydrogen production from glycerol: water mixtures under solar light irradiation. *Inter J Hydr Energy* 23:9655–9664
2. Kumar DP, Reddy NL, Srinivas B, Durgakumari V, Roddatis V, Bondarchuk O, Karthik M, Ikuma Y, Shankar MV (2016) Stable and active CuxO/TiO<sub>2</sub> nanostructured catalyst for proficient hydrogen production under solar light irradiation. *Sol Energy Mater and Sol Cells* 46:63–71
3. Asahi RY, Morikawa TA, Ohwaki T, Aoki K, Taga Y (2001) Visible-light photocatalysis in nitrogen-doped titanium oxides. *Science* 293:269–271
4. Kudo A, Miseki Y (2009) Heterogeneous photocatalyst materials for water splitting. *Chem Soc Rev* 38:253–278
5. Barber J et al (2009) Photosynthetic energy conversion: natural and artificial. *Chem Soc Rev* 38:185–196
6. Fujishima A, Honda K (1972) Electrochemical photolysis of water at a semiconductor electrode. *Nature* 238:37–38
7. Li X, Yu J, Low J, Fang Y, Xiao J, Chen X (2015) Engineering heterogeneous semiconductors for solar water splitting. *J Mat Chem A* 6:2485–2534
8. Xiang Q, Yu J, Jaroniec M (2012) Graphene-based semiconductor photocatalysts. *Chem Soc Rev* 41:782–796
9. Kang ZC, Wang ZL (1997) Chemical activities of graphitic carbon spheres. *J Mole Cat A: Chem* 118:215–222
10. Park C, Engel ES, Crowe A, Gilbert TR, Rodriguez NM (2000) Use of carbon nanofibers in the removal of organic solvents from water. *Lang* 21:8050–8056
11. Du J, Liu Z, Li Z, Han B, Sun Z, Huang Y (2005) Carbon onions synthesized via thermal reduction of glycerin with magnesium. *Mater Chem and Phy* 93:178–180
12. Rana RK, Gedanken A (2002) Carbon nanoflask: a mechanistic elucidation of its formation. *J Phy Chem B* 38:9769–9776
13. Ugrate D et al (1992) Curling and closure of graphitic networks under electron beam irradiation. *Nature* 359:707–709
14. Jin YZ, Gao C, Hsu WK, Zhu Y, Huczko A, Bystrzejewski M, Roe M, Lee CY, Acquah S, Kroto H, Walton DR (2005) Large-scale synthesis and characterization of carbon spheres prepared by direct pyrolysis of hydrocarbons. *Carbon* 43(9):1944–1953
15. Wang ZL, Yin JS (1998) Graphitic hollow carbon calabashes. *Chem Phy Lett* 289:189–192
16. Geim AK, Novoselov KS (2010) The rise of graphene. In: *Nanoscience and technology: a collection of reviews from nature journals*, pp 11–19
17. Rao CE, Sood AE, Subrahmanyam KE, Govindaraj A (2009) Graphene: the new two-dimensional nanomaterial. *Ang Chem Inter Edit* 42:7752–7777
18. Jun LY, Mubarak NM, Yee MJ, Yon LS, Bing CH, Khalid M, Abdullah EC (2018) An overview of functionalised carbon nanomaterial for organic pollutant removal. *J Ind Eng Chem* 67:175–186
19. Ma Y, Wang X, Jia Y, Chen X, Han H, Li C (2014) Titanium dioxide-based nanomaterials for photocatalytic fuel generations. *Chem Rev* 19:9987–10043
20. Bera R, Dutta A, Kundu S, Polshettiwar V, Patra A (2018) Design of a CdS/CdSe heterostructure for efficient H<sub>2</sub> generation and photovoltaic applications. *J Phy Chem C* 23:12158–12167
21. Chen H, Liu XY, Wang S, Wang X, Wei Q, Jiang X, Wang F, Xu K, Ke J, Zhang Q, Gao Q (2018) Quaternary two dimensional Zn–Ag–In–S nanosheets for highly efficient photocatalytic hydrogen generation. *J Mat Chem A* 25:11670–11675
22. Wu MC, Wu PY, Lin TH, Lin TF (2018) Photocatalytic performance of Cu-doped TiO<sub>2</sub> nanofibers treated by the hydrothermal synthesis and air-thermal treatment. *Appl Sur Sci* 430:390–398

23. Ma L, Chen YL, Yang DJ, Li HX, Ding SJ, Xiong L, Qin PL, Chen XB (2020) Multi-interfacial plasmon coupling in multigap (Au/AgAu)@ CdS core-shell hybrids for efficient photocatalytic hydrogen generation. *Nanosc* 7:4383–4392
24. Shahzad K, Tahir MB, Sagir M (2019) Engineering the performance of heterogeneous WO<sub>3</sub>/fullerene@ Ni<sub>3</sub>B/Ni (OH)<sub>2</sub> photocatalysts for hydrogen generation. *Intern J Hydro Energ* 39:21738–21745
25. Li J, Zhang L, Li J, An P, Hou Y, Zhang J (2019) Nanoconfined growth of carbon-encapsulated cobalts as cocatalysts for photocatalytic hydrogen evolution. *ACS Sustain Chem Eng* 16:14023–14030
26. Patra KK, Ghosal MK, Bajpai H, Raj S, Gopinath CS (2019) Oxidative disproportionation of MoS<sub>2</sub>/GO to MoS<sub>2</sub>/MoO<sub>3-x</sub>/RGO: integrated and plasmonic 2D-multifunctional nanocomposites for solar hydrogen generation from near-infrared and visible regions. *J Phy Chem C* 35:21685–21693
27. Rajaambal S, Sivaranjani K, Gopinath CS (2015) Recent developments in solar H<sub>2</sub> generation from water splitting. *J Chem Sci* 127(1):33–47
28. Du J, Li S, Du Z, Meng S, Li B (2021) Boron/oxygen-codoped graphitic carbon nitride nanomesh for efficient photocatalytic hydrogen evolution. *Chem Eng J* 407:127114
29. Jinbo P, Sheng S, Wei Z, Jie T, Hongzhi D, Jinbo W, Lang C, Chak-Tong A, Shuang-Feng Y (2020) Recent progress in photocatalytic hydrogen evolution. *Acta Phy-Chim Sin* 36(3):1905068
30. San Martín S, Rivero MJ, Ortiz I (2020) Unravelling the mechanisms that drive the performance of photocatalytic hydrogen production. *Catalysts* 10(8):901
31. Huang Z, Xi L, Subhani Q, Yan W, Guo W, Zhu Y (2013) Covalent functionalization of multi-walled carbon nanotubes with quaternary ammonium groups and its application in ion chromatography. *Carbon* 62:127–134
32. Mallakpour S, Soltanian S (2016) Surface functionalization of carbon nanotubes: fabrication and applications. *RSC Adv* 6:109916–109935
33. Toma FM, Sartorel A, Iurlo M, Carraro M, Rapino S, Hooper-Burkhardt L, Da Ros T, Marcaccio M, Scorrano G, Paolucci F, Bonchio M (2011) Tailored functionalization of carbon nanotubes for electrocatalytic water splitting and sustainable energy applications. *Chemsuschem* 4:1447
34. Zheng XT, Ananthanarayanan A, Luo KQ, Chen P (2015) Glowing graphene quantum dots and carbon dots: properties, syntheses, and biological applications. *Small* 14:1620–1636
35. Tian P, Tang L, Teng KS, Lau SP (2018) Graphene quantum dots from chemistry to applications. *Mater Today Chem* 10:221–258
36. Ge J, Zhang Y, Park SJ (2019) Recent advances in carbonaceous photocatalysts with enhanced photocatalytic performances: a mini review. *Materials* 12:1916
37. Gao J, Zhu M, Huang H, Liu Y, Kang Z (2017) Advances, challenges and promises of carbon dots. *Inorg Chem Front* 12:1963–1986
38. Mehta A, Mishra A, Basu S, Shetti NP, Reddy KR, Saleh TA, Aminabhavi TM (2019) Band gap tuning and surface modification of carbon dots for sustainable environmental remediation and photocatalytic hydrogen production—a review. *J Environ Manage* 250:109486
39. Xu X, Ray R, Gu Y, Ploehn HJ, Gearheart L, Raker K, Scrivens WA (2004) Electrophoretic analysis and purification of fluorescent single-walled carbon nanotube fragments. *J Am Chem Soc* 126(40):12736–12737
40. Ali H, Ghosh S, Jana NR (2020) Fluorescent carbon dots as intracellular imaging probes. *Wiley Interdisci Rev: Nanomed Nanobiotec* 4:1617
41. Reckmeier CJ, Schneider J, Susha AS, Rogach AL (2016) Luminescent colloidal carbon dots: optical properties and effects of doping. *Opt Express* 24:312–340
42. Luo H, Guo Q, Szilágyi PÁ, Jorge AB, Titirici MM (2020) Carbon dots in solar-to-hydrogen conversion. *Trends in Chemistry* 2:623–637
43. Rao VN, Reddy NL, Kumari MM, Cheralathan KK, Ravi P, Sathish M, Neppolian B, Reddy KR, Shetti NP, Prathap P, Aminabhavi TM (2019) Sustainable hydrogen production for the greener environment by quantum dots-based efficient photocatalysts: a review. *J Environ Manag* 248:109246

44. Wang Y, Zhu Y, Yu S, Jiang C (2017) Fluorescent carbon dots: rational synthesis, tunable optical properties and analytical applications. *RSC Adv* 65:40973–40989
45. Tang Y, Hao R, Fu Y, Jiang Y, Zhang X, Pan Q, Jiang B (2016) Carbon quantum dot/mixed crystal TiO<sub>2</sub> composites via a hydrogenation process: an efficient photocatalyst for the hydrogen evolution reaction. *RSC Adv* 99:96803–96808
46. Reddy NR, Bhargav U, Kumari MM, Cheralathan KK, Sakar M (2020) Review on the interface engineering in the carbonaceous titania for the improved photocatalytic hydrogen production. *Int J Hydrogen Energ* 45(13):7584–75615
47. Tian P, Tang L, Teng KS, Lau SP (2018) *Materials Today Chemistry* 10:221e258
48. Shen J, Zhu Y, Yang X, Li C (2012) Graphene quantum dots: emergent nanolights for bioimaging, sensors, catalysis and photovoltaic devices. *Chem comm* 31:3686–3699
49. Gliniak J, Lin JH, Chen YT, Li CR, Jokar E, Chang CH, Peng CS, Lin JN, Lien WH, Tsai HM, Wu TK (2017) Sulfur-doped graphene oxide quantum dots as photocatalysts for hydrogen generation in the aqueous phase. *Chemsuschem* 16:3260–3267
50. Titirici MM, White RJ, Brun N, Budarin VL, Su DS, del Monte F, Clark JH, MacLachlan MJ (2015) Sustainable carbon materials. *Chem Soc Rev* 44(1):250–290
51. Kang Z, Liu Y, Gao J, Zhu M (2017) Carbon dots for environmental and energy applications: advances, challenges and promises. *Inorg Chem Front* 4:1963–1986
52. Jiao Y, Huang Q, Wang J, He Z, Li Z (2019) A novel MoS<sub>2</sub> quantum dots (QDs) decorated Z-scheme g-C<sub>3</sub>N<sub>4</sub> nanosheet/N-doped carbon dots heterostructure photocatalyst for photocatalytic hydrogen evolution. *Appl Cat B: Environ* 247:124–132
53. Sui Y, Wu L, Zhong S, Liu Q (2019) Carbon quantum dots/TiO<sub>2</sub> nanosheets with dominant (001) facets for enhanced photocatalytic hydrogen evolution. *Appl Surf Sci* 480:810–816
54. Shi W, Guo F, Li M, Shi Y, Tang Y (2019) N-doped carbon dots/CdS hybrid photocatalyst that responds to visible/near-infrared light irradiation for enhanced photocatalytic hydrogen production. *Sep Purif Tech* 212:142–149
55. Gultom NS, Abdullah H, Kuo DH (2019) Effects of graphene oxide and sacrificial reagent for highly efficient hydrogen production with the costless Zn (O, S) photocatalyst. *Int J Hydrogen Energ* 56:29516–29528
56. Sumana K, Vijayamohan KP (2020) Synthesis and characterization of graphene quantum dots. *Phy Sci Rev* 5:20190013
57. Nguyen BS, Xiao YK, Shih CY, Nguyen VC, Chou WY, Teng H (2018) Electronic structure manipulation of graphene dots for effective hydrogen evolution from photocatalytic water decomposition. *Nanos* 22:10721–10730
58. Sk MA, Ananthanarayanan A, Huang L, Lim KH, Chen P (2014) Revealing the tunable photoluminescence properties of graphene quantum dots. *J Mater Chem C* 34:6954–6960
59. Ye R, Xiang C, Lin J, Peng Z, Huang K, Yan Z, Cook NP, Samuel EL, Hwang CC, Ruan G, Ceriotti G (2013) Coal as an abundant source of graphene quantum dots. *Nat comm* 1:1–7
60. Yan Y, Chen J, Li N, Tian J, Li K, Jiang J, Liu J, Tian Q, Chen P (2018) Systematic bandgap engineering of graphene quantum dots and applications for photocatalytic water splitting and CO<sub>2</sub> reduction. *ACS Nano* 4:3523–3532
61. Fantuzzi P, Candini A, Chen Q, Yao X, Dumsloff T, Mishra N, Coletti C, Müllen K, Narita A, Affronte M (2019) Color sensitive response of graphene/graphene quantum dot phototransistors. *J Phys Chem C* 43:26490–26497
62. Tian P, Tang L, Teng KS, Lau SP (2018) Graphene quantum dots from chemistry to applications. *Mat Today Chem* 10:221–258
63. Zhang R, Qi S, Jia J, Torre B, Zeng H, Wu H, Xu X (2015) Size and refinement edge-shape effects of graphene quantum dots on UV–visible absorption. *J Alloy Compd* 623:186–191
64. Raghavan A, Sarkar S, Nagappagari LR, Bojja S, MuthukondaVenkatakrishnan S, Ghosh S (2020) decoration of graphene quantum dots on TiO<sub>2</sub> nanostructures: photosensitizer and cocatalyst role for enhanced hydrogen generation. *Indus Eng Chem Res* 29:13060–13068
65. Calabro RL, Yang DS, Kim DY (2019) Controlled nitrogen doping of graphene quantum dots through laser ablation in aqueous solutions for photoluminescence and electrocatalytic applications. *ACS Appl Nano Mater* 11:6948–6959

66. Zhang Z, Zhang J, Chen N, Qu L (2012) Graphene quantum dots: an emerging material for energy-related applications and beyond. *Energ Environ Sci* 10:8869–8890
67. Li X, Shen R, Ma S, Chen X, Xie J (2018) Graphene-based heterojunction photocatalysts. *Appl Surf Sci* 430:53–107
68. Yeh TF, Teng CY, Chen SJ, Teng H (2014) Nitrogen-doped graphene oxide quantum dots as photocatalysts for overall water-splitting under visible light illumination. *Adv Mater* 20:3297–3303
69. Yeh TF, Syu JM, Cheng C, Chang TH, Teng H (2010) Graphite oxide as a photocatalyst for hydrogen production from water. *Adv Funct Mater* 14:2255–2262
70. Xie G, Zhang K, Guo B, Liu Q, Fang L, Gong JR (2013) Graphene-based materials for hydrogen generation from light-driven water splitting. *Adv Mater* 28:3820–3839
71. Yeh TF, Chen SJ, Teng H (2015) Synergistic effect of oxygen and nitrogen functionalities for graphene-based quantum dots used in photocatalytic H<sub>2</sub> production from water decomposition. *Nano Energy* 12:476–485
72. Chen LC, Teng CY, Lin CY, Chang HY, Chen SJ, Teng H (2016) Architecting nitrogen functionalities on graphene oxide photocatalysts for boosting hydrogen production in water decomposition process. *Adv Energ Mater* 22:1600719
73. Tian H, Shen K, Hu X, Qiao L, Zheng WN (2017) S co-doped graphene quantum dots-graphene-TiO<sub>2</sub> nanotubes composite with enhanced photocatalytic activity. *J Alloy Compd* 691:369–377
74. Qu A, Xie H, Xu X, Zhang Y, Wen S, Cui Y (2016) High quantum yield graphene quantum dots decorated TiO<sub>2</sub> nanotubes for enhancing photocatalytic activity. *Appl Surf Sci* 375:230–241
75. Sudhagar P, Herraiz-Cardona I, Park H, Song T, Noh SH, Gimenez S, Sero IM, Fabregat-Santiago F, Bisquert J, Terashima C, Paik U (2016) Exploring graphene quantum dots/TiO<sub>2</sub> interface in photoelectrochemical reactions: solar to fuel conversion. *Electro Act* 187:249–255
76. Ebrahimi M, Samadi M, Yousefzadeh S, Soltani M, Rahimi A, Chou TC, Chen LC, Chen KH, Moshfegh AZ (2017) Improved solar-driven photocatalytic activity of hybrid graphene quantum dots/ZnO nanowires: a direct Z-scheme mechanism. *ACS Sustain Chem Eng* 1:367–375
77. Lei Y, Yang C, Hou J, Wang F, Min S, Ma X, Jin Z, Xu J, Lu G, Huang KW (2017) Strongly coupled CdS/graphene quantum dots nanohybrids for highly efficient photocatalytic hydrogen evolution: unraveling the essential roles of graphene quantum dots. *Appl Cat B: Environ* 216:59–69
78. Dinda D, Park H, Lee HJ, Oh S, Park SY (2020) Graphene quantum dot with covalently linked Rhodamine dye: a high efficiency photocatalyst for hydrogen evolution. *Carbon* 167:760–769
79. Yu S, Zhong YQ, Yu BQ, Cai SY, Wu LZ, Zhou Y (2016) Graphene quantum dots to enhance the photocatalytic hydrogen evolution efficiency of anatase TiO<sub>2</sub> with exposed {001} facet. *Phy Chem Chem Phys* 30:20338–20344
80. Ahmad I, Akhtar MS, Ahmed E, Ahmad M, Naz MY (2021) Lu modified ZnO/CNTs composite: a promising photocatalyst for hydrogen evolution under visible light illumination. *J Colloid Interface Sci* 584:182–192
81. Chu J, Han X, Yu Z, Du Y, Song B, Xu P (2018) Highly efficient visible-light-driven photocatalytic hydrogen production on CdS/Cu<sub>7</sub>S<sub>4</sub>/g-C<sub>3</sub>N<sub>4</sub> ternary heterostructures. *ACS Appl Mater Interface* 10:20404–20411
82. Vu MH, Sakar M, Nguyen CC, Do TO (2018) Chemically bonded Ni cocatalyst onto the S doped g-C<sub>3</sub>N<sub>4</sub> nanosheets and their synergistic enhancement in H<sub>2</sub> production under sunlight irradiation. *ACS Sustain Chem Eng* 6:4194–4203
83. You Y, Wang S, Xiao K, Ma T, Zhang Y, Huang H (2018) Z-scheme g-C<sub>3</sub>N<sub>4</sub>/Bi<sub>4</sub>NbO<sub>8</sub>Cl heterojunction for enhanced photocatalytic hydrogen production. *ACS Sustain Chem Eng* 6:16219–16227
84. Yang R, Song K, He J, Fan Y, Zhu R (2019) Photocatalytic hydrogen production by RGO/ZnIn<sub>2</sub>S<sub>4</sub> under visible light with simultaneous organic amine degradation. *ACS Omega* 4:11135–11140

85. Hao X, Jin Z, Yang H, Lu G, Bi Y (2017) Peculiar synergetic effect of MoS<sub>2</sub> quantum dots and graphene on metal-organic frameworks for photocatalytic hydrogen evolution. *Appl Catal B: Environ* 210:45–56
86. Iijima S et al (1991) Helical microtubules of graphitic carbon. *Nature* 354:56–58
87. Liang X, Zeng M, Qi C (2010) One-step synthesis of carbon functionalized with sulfonic acid groups using hydrothermal carbonization. *Carbon* 6:1844–1848
88. Zhang WD, Xu B, Jiang L (2010) Functional hybrid materials based on carbon nanotubes and metal oxides. *J Mater Chem* 31:6383–6391
89. Liu Z, Chen K, Davis C, Sherlock S, Cao Q, Chen X, Dai H (2008) Drug delivery with carbon nanotubes for in vivo cancer treatment. *Canc Res* 16:6652–6660
90. Xiao S, Zhu W, Liu P, Liu F, Dai W, Zhang D, Chen W, Li H (2016) CNTs threaded (001) exposed TiO<sub>2</sub> with high activity in photocatalytic NO oxidation. *Nanoscale* 5:2899–2907
91. Dai K, Zhang X, Fan K, Zeng P, Peng T (2014) Multiwalled carbon nanotube-TiO<sub>2</sub> nanocomposite for visible-light-induced photocatalytic hydrogen evolution. *J Nanomat*
92. Abrahamson J, Wiles PG, Rhoades BL (1999) Structure of carbon fibres found on carbon arc anodes. *Carbon (New York, NY)*. 11:1873–1874
93. Hirlekar R, Yamagar M, Garse H, Vij M, Kadam V (2009) Carbon nanotubes and its applications: a review. *Asian J Pharma Clin Res* 4:17–27
94. Meyyappan M, Delzeit L, Cassell A, Hash D (2003) Carbon nanotube growth by PECVD: a review. *Plasma Sources Sci Technol* 2:205
95. Dresselhaus MS, Dresselhaus G, Jorio A (2004) Unusual properties and structure of carbon nanotubes. *Annu Rev Mater Res* 34:247–278
96. Terrones M et al (2003) Science and technology of the twenty-first century: synthesis, properties, and applications of carbon nanotubes. *Annual Rev Mater Res* 1:419–501
97. Zhang M, Li J (2009) Carbon nanotube in different shapes. *Materials Today* 6:12–18
98. Saifuddin N, Raziah AZ, Junizah AR (2013) Carbon nanotubes: a review on structure and their interaction with proteins. *J Chem*
99. Wang CY, Zhang YY, Wang CM, Tan VBC (2007) Buckling of carbon nanotubes: a literature survey. *J Nanosci Nanotech* 7(12):4221–4247
100. Yang Z, Ren J, Zhang Z, Chen X, Guan G, Qiu L, Zhang Y, Peng H (2015) Recent advancement of nanostructured carbon for energy applications. *Chem Rev* 11:5159–5223
101. Kim YA, Hayashi T, Endo M, Dresselhaus MS (2013) Carbon nanofibers. In: Springer handbook of nanomaterials, Springer, pp 233–262
102. Vajtai R et al (2013) Springer handbook of nanomaterials. Springer Science & Business Media
103. Wang L, Yao Z, Jia F, Chen B, Jiang Z (2013) A facile synthesis of Znx Cd1-x S/CNTs nanocomposite photocatalyst for H<sub>2</sub> production. *Dalton Trans* 27:9976–9981
104. Feng C, Chen Z, Jing J, Sun M, Tian J, Lu G, Ma L, Li X, Hou J (2021) Significantly enhanced photocatalytic hydrogen production performance of g-C<sub>3</sub>N<sub>4</sub>/CNTs/CdZnS with carbon nanotubes as the electron mediators. *J Mater Sci Tech* 80:75–83
105. Cao S, Yu J (2016) Carbon-based H<sub>2</sub>-production photocatalytic materials. *J Photochem Photob C: Photochem Rev* 1(27):72–99
106. Umer M, Tahir M, Azam MU, Tahir B, Jaffar MM, Alias H (2019) Montmorillonite dispersed single wall carbon nanotubes (SWCNTs)/TiO<sub>2</sub> heterojunction composite for enhanced dynamic photocatalytic H<sub>2</sub> production under visible light. *Appl Cla Sci* 174:110–119
107. Naffati N, Sampaio MJ, Da Silva ES, Nsib MF, Arfaoui Y, Houas A, Faria JL, Silva CG (2020) Carbon-nanotube/TiO<sub>2</sub> materials synthesized by a one-pot oxidation/hydrothermal route for the photocatalytic production of hydrogen from biomass derivatives. *Mat Sci Semic Proc* 115:105098
108. Peng T, Zeng P, Ke D, Liu X, Zhang X (2011) Hydrothermal preparation of multiwalled carbon nanotubes (MWCNTs)/CdS nanocomposite and its efficient photocatalytic hydrogen production under visible light irradiation. *Energy Fuels* 5:2203–2210
109. Kumar P, Boukherroub R, Shankar K (2018) Sunlight-driven water-splitting using two-dimensional carbon based semiconductors. *J Mater Chem A* 27:12876–12931
110. Savage N et al (2012) Materials science: super carbon. *Nature* 483:S30–S31



111. Dikin DA, Stankovich S, Zimney EJ, Piner RD, Dommett GH, Evmenenko G, Nguyen ST, Ruoff RS (2007) Preparation and characterization of graphene oxide paper. *Nature* 448:457–460
112. Hummers WS Jr, Offeman RE (1958) Preparation of graphitic oxide. *J Amer Chem Soc* 6:1339–1339
113. Marcano DC, Kosynkin DV, Berlin JM, Sinitskii A, Sun Z, Slesarev A, Alemany LB, Lu W, Tour JM (2010) Improved synthesis of graphene oxide. *ACS Nano* 8:4806–4814
114. Zhu Y, Murali S, Cai W, Li X, Suk JW, Potts JR, Ruoff RS (2010) Graphene and graphene oxide: synthesis, properties, and applications. *Adv Mater* 35:3906–3924
115. Eda G, Mattevi C, Yamaguchi H, Kim H, Chhowalla M (2009) Insulator to semimetal transition in graphene oxide. *J Phy Chem C* 35:15768–15771
116. Eda G, Fanchini G, Chhowalla M (2008) Large-area ultrathin films of reduced graphene oxide as a transparent and flexible electronic material. *Nat Nanotechnol* 5:270–274
117. Nowotny J, Bak T, Nowotny MK, Sheppard LR (2007) Titanium dioxide for solar-hydrogen I. Functional properties. *Int J Hydrogen Energ* 32(14):2609–2629
118. Zhang X, Sun Y, Cui X, Jiang Z (2012) A green and facile synthesis of TiO<sub>2</sub>/graphene nanocomposites and their photocatalytic activity for hydrogen evolution. *Int J Hydrogen Energ* 37:811–815
119. Shen J, Yan B, Shi M, Ma H, Li N, Ye M (2011) One step hydrothermal synthesis of TiO<sub>2</sub>-reduced graphene oxide sheets. *J Mater Chem* 21:3415–3421
120. Xiang Q, Yu J, Jaroniec M (2011) Enhanced photocatalytic H<sub>2</sub>-production activity of graphene-modified titania nanosheets. *Nanoscale* 9:3670–3678
121. Lv XJ, Fu WF, Chang HX, Zhang H, Cheng JS, Zhang GJ, Song Y, Hu CY, Li JH (2012) Hydrogen evolution from water using semiconductor nanoparticle/graphene composite photocatalysts without noble metals. *J Mater Chem* 22:1539–1546
122. Min S, Lu G (2012) Sites for high efficient photocatalytic hydrogen evolution on a limited-layered MoS<sub>2</sub> cocatalyst confined on graphene sheets-the role of grapheme. *J Phy Chem C* 116:25415–25424
123. Tran PD, Batabyal SK, Pramana SS, Barber J, Wong LH, Loo SCJ (2012) A cuprous oxide-reduced graphene oxide (Cu<sub>2</sub>O-rGO) composite photocatalyst for hydrogen generation: employing rGO as an electron acceptor to enhance the photocatalytic activity and stability of Cu<sub>2</sub>O. *Nanoscale* 4:3875–3878
124. Khan Z, Chetia TR, Vardhaman AK, Barpuzary D, Sastri CV, Qureshi M (2012) Visible light assisted photocatalytic hydrogen generation and organic dye degradation by CdS-metal oxide hybrids in presence of graphene oxide. *RSC Adv* 2:12122e8
125. Mou Z, Yin S, Zhu M, Du Y, Wang X, Yang P, Zheng J, Lu C (2013) RuO<sub>2</sub>/TiSi<sub>2</sub>/graphene composite for enhanced photocatalytic hydrogen generation under visible light irradiation. *Phy Chem Chem Phy* 15:2793–2799
126. Yang Z, Zhang Y, Schnepf Z (2015) Soft and hard templating of graphitic carbon nitride. *J Mater Chem A* 27:14081–14092
127. Rhimi B, Wang C, Bahnemann D (2020) Latest progress in g-C<sub>3</sub>N<sub>4</sub> based heterojunctions for hydrogen production via photocatalytic water splitting: a mini review. *J Phy: Energ* 2:042003
128. Hong Y, Li C, Fang Z, Luo B, Shi W (2017) Rational synthesis of ultrathin graphitic carbon nitride nanosheets for efficient photocatalytic hydrogen evolution. *Carbon* 121:463–471
129. Wang X, Maeda K, Thomas A, Takanabe K, Xin G, Carlsson JM, Domen K, Antonietti M (2009) A metal-free polymeric photocatalyst for hydrogen production from water under visible light. *Nat Mater* 8:76–80
130. Xiang Q, Yu J, Jaroniec M (2011) Preparation and enhanced visible-light photocatalytic H<sub>2</sub>-production activity of graphene/C<sub>3</sub>N<sub>4</sub> composites. *J Phy Chem C* 115(15):7355–7363
131. Song C, Fan M, Shi W, Wang W (2018) High-performance for hydrogen evolution and pollutant degradation of reduced graphene oxide/two-phase gC<sub>3</sub>N<sub>4</sub> heterojunction photocatalysts. *Environ Sci Pollut Res* 25:14486–14498
132. Zou JP, Wang LC, Luo J, Nie YC, Xing QJ, Luo XB, Du HM, Luo SL, Suib SL (2016) Synthesis and efficient visible light photocatalytic H<sub>2</sub> evolution of a metal-free g-C<sub>3</sub>N<sub>4</sub>/graphene quantum dots hybrid photocatalyst. *App Cat B: Environm* 15(193):103–109

133. He F, Chen G, Zhou Y, Yu Y, Li L, Hao S, Liu B (2016) ZIF-8 derived carbon (C-ZIF) as a bifunctional electron acceptor and HER cocatalyst for g-C<sub>3</sub>N<sub>4</sub>: construction of a metal-free, all carbon-based photocatalytic system for efficient hydrogen evolution. *J Mater Chem A* 4(10):3822–3827
134. Wang B, Zhang J, Huang F (2017) Enhanced visible light photocatalytic H<sub>2</sub> evolution of metal-free g-C<sub>3</sub>N<sub>4</sub>/SiC heterostructured photocatalysts. *App Sur Sci* 391:449–456
135. Yao L, Wei D, Ni Y, Yan D, Hu C (2016) Surface localization of CdZnS quantum dots onto 2D g-C<sub>3</sub>N<sub>4</sub> ultrathin microribbons: highly efficient visible light-induced H<sub>2</sub>-generation. *Nano Energ* 26:248–256
136. She X, Wu J, Xu H, Zhong J, Wang Y, Song Y, Nie K, Liu Y, Yang Y, Rodrigues MT, Vajtai R (2017) High efficiency photocatalytic water splitting using 2D  $\alpha$ -Fe<sub>2</sub>O<sub>3</sub>/g-C<sub>3</sub>N<sub>4</sub> Z-scheme catalysts. *Adv Ener Mater* 17:1700025
137. Martin DJ, Reardon PJT, Moniz SJ, Tang J (2014) Visible light-driven pure water splitting by a nature-inspired organic semiconductor-based system. *J Am Chem Soc* 36:12568–12571
138. Ong WJ, Tan LL, Ng YH, Yong ST, Chai SP (2016) Graphitic carbon nitride (g-C<sub>3</sub>N<sub>4</sub>)-based photocatalysts for artificial photosynthesis and environmental remediation: are we a step closer to achieving sustainability? *Chem Rev* 116:7159–7329
139. Bard AJ et al (1980) Photoelectrochemistry. *Science* 207:139–144
140. Xie H, Hou C, Wang H, Zhang Q, Li Y (2017) S, N co-doped graphene quantum dot/TiO<sub>2</sub> composites for efficient photocatalytic hydrogen generation. *Nano Res Lett* 1:1–8

# Chapter 11

## Design of Porous Carbon-Based Electro-Catalyst for Hydrogen Generation



Kamlesh, Satya Prakash, Deepika Tavar, Pankaj Raizda, Pradeep Singh, Manish Mudgal, A. K. Srivastava, and Archana Singh

### 1 Introduction

For the rapid growth of the nation, it is extremely required to develop sustainable and environment-friendly energy sources, which is more stable, renewable, and efficient. The electricity generated in an excess amount over the consumption, it should be important to store to be used later. Otherwise, that part will be wasted. This can be increasing the production cost per unit of electric energy. Furthermore, when electric energy is produced from primary sustainable energy sources such as the sun and wind, storage is very necessary because these renewable sources are seasonal and unstable, some time the sun doesn't shine and the wind doesn't blow. Electric energy is not easy to store on large scale. For this purpose, special devices, and methods are needed. Presently, a lot of researchers and technologists have been continuously working on the global capacity of energy storage methods and significant long-lasting device fabrication (World energy council, 2019). According to the international energy agency (IEA) report, in 2019, the energy storage capacity has risen by 100% in 2018 compared to 2017. Apart from electricity, the main necessity to store fixed energy is to meet portable forms necessary for so many widespread purposes in the present period. The first significant device was a battery such as a lithium-ion battery, which is still the most used storing device due to its greater than 90% of output.

---

Kamlesh · S. Prakash · D. Tavar · M. Mudgal · A. K. Srivastava · A. Singh (✉)  
CSIR—Advanced Material and Processes Research Institute, Bhopal 462026, India  
e-mail: [archanasingh@ampri.res.in](mailto:archanasingh@ampri.res.in)

Academy of Scientific & Innovative Research (AcSIR), Ghaziabad 201002, India

P. Raizda · P. Singh  
School of Chemistry, Shoolini University, Himachal Pradesh, Bajhol 173229, India

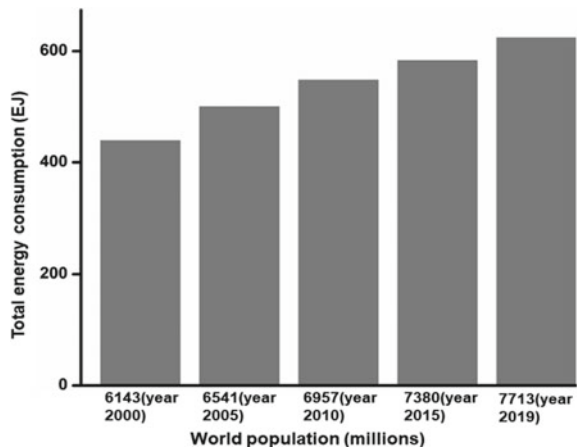
© The Author(s), under exclusive license to Springer Nature Singapore Pte Ltd. 2023  
A. N. Grace et al. (eds.), *Handbook of Porous Carbon Materials*,  
Materials Horizons: From Nature to Nanomaterials,  
[https://doi.org/10.1007/978-981-19-7188-4\\_11](https://doi.org/10.1007/978-981-19-7188-4_11)

## 2 Global Energy Perspective

The current population of the world is about 786 crore which increases annually by 1.05%. The global annual population growth rate is projected to be 81 million people [1]. Currently, the energy consumption of the world is  $624 \times 10^{18}$  J and will continue to surge as the population rises, especially as the standard of living goes up. When analyzing energy use, the way of living becomes a crucial factor to consider. Energy demand increases at the same rate as population growth as delineated in Fig. 1 [2].

In the Twenty-first-century, fossil fuel and electricity produced via coal and oil fulfilled the world's energy needs. The burning of fossils fuels singly contributes three quarters in greenhouse gases emission globally which lead to global warming. Fossil fuels are responsible for a significant amount of local air pollution, which causes at least 5 million premature deaths every year [3]. In 2018, global CO<sub>2</sub> emission from fuel combustion hit 33.5 Gt owing to vigorous growth in population and economic activity. In a similar manner to the previous year, non-OECD (organization for economic co-operation and development) countries including India was mainly responsible for emission growth in 2018. Furthermore, the United States saw a rise of over 3%, reversing a downward trend that began in 2015, while European Union and Japan continued to fall. Emission decline was observed in advanced economies like the United States, Germany, and Japan but still increases in China and became steady in India, according to provisional data for 2019. Figure 2 depicts the CO<sub>2</sub> emission in selected economies from the year 2000 to 2019 [4]. To scale down the problems related to CO<sub>2</sub> emission the world has to focus on clean and renewable sources of energy. Hydrogen is the most promising source in this regard. Here, the question arises in the mind of everyone why hydrogen and not any other element or renewable resources.

**Fig. 1** World population versus total energy consumption



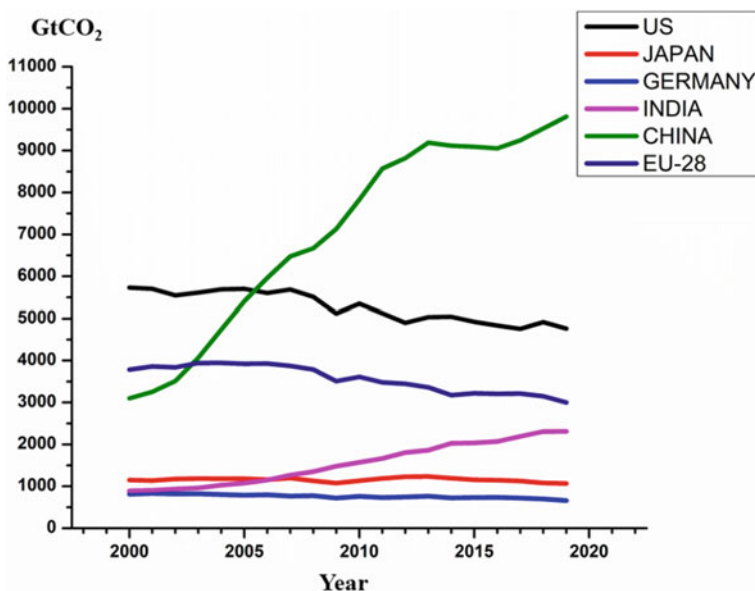


Fig. 2 CO<sub>2</sub> emission in selected economies, 2000–2019

### 3 Hydrogen Energy

To avoid these problems, there are unstable energy sources that can be alternated into stable hydrogen energy. Hydrogen energy can be used as a storage medium to supply power during these times due to its great mass-energy density (120 MJ/kg) value, with a specific energy content 2.5 times higher than hydrocarbon and zero-emission of greenhouse gases. Hydrogen as a fuel may be generated from numerous sources of fossil fuels, in which every one of these introduces a distinct amount of pollution, technological barriers, and energy inputs. For hydrogen generation, water has been the most common naturally available and cheapest raw material.

There are several reasons but the most significant is their abundance in the whole universe, accounting for approximately 75% of the universe's elemental mass and providing clean fuel. Although it is the most abundant element but does not exist as a distinct type of matter rather present in a combined form with other elements. It necessitates a significant effort and high cost to collect hydrogen molecules from its associated compounds [5]. The use of hydrogen and hydrogen-containing compounds to produce electricity for all practical purposes with high energy competence, massive environmental and social welfare, and economic competitiveness is what hydrogen energy is all about [6].

Hydrogen is referred to as an energy carrier because it is a secondary source of energy. Hydrogen is preferred as potentially green fuel because of its clean-burning properties, a higher heating value equal to 142.18 MJ/kg, domestic output capacity, development of the fuel cell vehicles besides its 2–3 times higher performance

prospects than gasoline. Because of its high energy density and low volumetric energy density as 1 kg of it produces the same amount of energy as 1 gallon of gasoline, NASA used it to propel spacecraft and rockets in the 1970s [7].

### ***3.1 Fors and Against of Hydrogen Energy***

#### **(A) Pros of Hydrogen Energy**

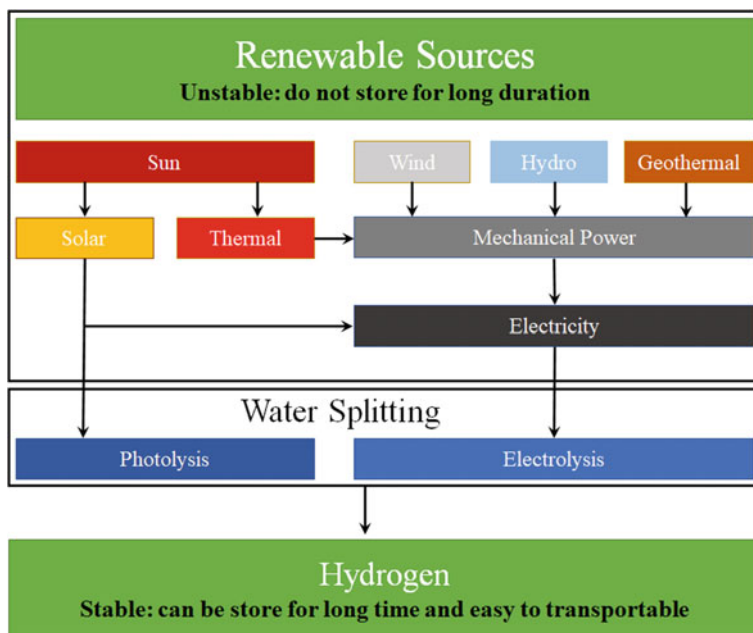
- Replenishable and ample in supply: Since hydrogen is a renewable energy source, it is a plentiful source of energy that surrounds us.
- Clean source of energy: There are no toxic byproducts emitted into the atmosphere as hydrogen is burned.
- Non-poisonous: Unlike nuclear energy or natural gas, hydrogen gas is harmless to human health. It also permits hydrogen to be used in locations where other fuels are prohibited.
- Highly efficient: Hydrogen has a high energy density and can generate a lot of electricity. Since it is three times more efficient than most fossil fuels, it needs less hydrogen to perform the same tasks. This is why hydrogen is used to power spaceships, aircraft, warships, vehicles, and fuel cells.

#### **(B) Cons of hydrogen energy.**

- Volatile: The high flammability and explosive nature of hydrogen make it a dangerous fuel to deal with.
- Expensive to produce: The two principal processes of hydrogen production, steam methane reforming, and electrolysis are very costly. Extensive research is underway to find an inexpensive, long-term process to generate hydrogen with zero CO<sub>2</sub> emissions to the atmosphere.
- Difficult to store: Hydrogen is low dense in comparison to gasoline because of which it is difficult to store and transport, so to store it must be compressed to a liquid state and kept at a low temperature.

## **4 Hydrogen Generation**

Although hydrogen is one of the highest available elements found in the universe, yet it does not find in its free form on the earth because of its low density and high reactivity with other elements. Hydrogen can be produced on this basis from other molecules. Hydrogen may be generated via different available sources including fossil fuels, biomass, water, or a combination of these. Currently, more than 95% of global hydrogen is produced from non-renewable sources, particularly steam reforming of methane from fossil fuels [8, 9]. However, using fossil fuels results



**Fig. 3** General strategy for converting unstable renewable energy sources into stable, long lasting and transportable hydrogen energy

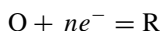
in lower hydrogen purity and the emission of higher quantities of harmful greenhouse gases [8, 10]. Nowadays, there is a lot of emphasis on ecologically sustainable energy solutions that can help to minimize existing energy sources based on fossil fuels. This is possibly achieved when renewable sources like water and primary renewable energy sources should be used for energy sources to split the water into hydrogen [8]. Figure 3 demonstrates, how the unstable renewable energy sources can be converted into a stable, long durable, and easily transportable energy source in the form of hydrogen. In such a manner, renewable energy sources like the sun can be used directly used to split water via photolysis, another way is water electrolysis, where electricity is produced from renewable energy sources. Water electrolysis is a significant approach to produce ecologically safe and high-quality hydrogen with a purity of 99.99% and oxygen gas among several types of procedures. In this chapter, we are only focusing on water electrolysis.

#### 4.1 Hydrogen by Electrolysis

Water splitting is a method where molecules of water are broken down into the separated form of hydrogen and oxygen molecules. This process is a thermodynamically non-spontaneous reaction;  $\Delta G > 0$  [11, 12], so some type of energy is required for

completion of it, which is equal to released energy during the creation of one mole of water molecules inside the fuel cell at the same condition from gaseous hydrogen and oxygen. Based on applied energy, the water-splitting process is called photolysis for photon energy, thermolysis for thermal energy, electrolysis for electric energy, and so on. Here, in this chapter, we are mainly concerned with electrolysis.

The water electrolysis is a redox process;



The electrode potential ( $E$ ) for such reaction can be calculated by the Nernst equation;

$$E = E^o - \frac{RT}{nF} \left[ \ln \left( \frac{C_R}{C_o} \right) \right] \quad (1)$$

where  $E^o$  is the standard thermodynamic equilibrium potential, it is a minimum potential value that is compulsory for water degradation reaction, and it has been calculated from the following equation;

$$\Delta G^o = -nFE^o \quad (2)$$

For the water electrolysis process, the standard change of Gibbs free energy ( $\Delta G^o$ ) is 237 kJ/mol,  $n$  represented to the number of electrons associated with the reaction, and  $F$  (96,500 C/mol) is a constant known as Faraday's constant. From Eq. (2), the standard theoretical thermodynamic required potential is 1.23 V for water electrolysis into hydrogen and oxygen.

The complete water electrolysis reaction is a combined form of two half-reactions that occur almost simultaneously, one is hydrogen evolution reaction (HER;  $4\text{H}_2\text{O} + 4e^- \rightarrow 2\text{H}_2 + 4\text{OH}^-$ ) at the cathode and the other is oxygen evolution reaction (OER;  $4\text{OH}^- \rightarrow \text{O}_2 + 2\text{H}_2\text{O} + 4\text{H}^+$ ) at the anode. The electrolysis process is more feasible in acidic or alkaline media compared to neutral because of the available free  $\text{H}^+$  ions for HER in acidic solution and  $\text{OH}^-$  ions for OER in alkaline solution. It was observed that change in pH from alkaline to acidic has a significant effect on the HER and OER kinetics, which attracted much attention in the fundamental studies based on computational modeling separately for the HER and OER half-cell. In such studies, queries arises on the importance of electrolyte used, electrolyte-electrolyte interface, pH, reaction dynamics and reaction kinetics and are currently at the forefront of the electrochemistry.

However, these reactions do not complete at thermodynamic equilibrium potential and required some extra amount of potential to overcome the energy barriers involved in the activated process correlated with specific reaction intermediates. This additional potential value is called overpotential or overvoltage and is represented by the symbol  $\eta$ . This overpotential can be calculated from Eq. (3)

$$\eta = E - E_{\text{eq}} \quad (3)$$



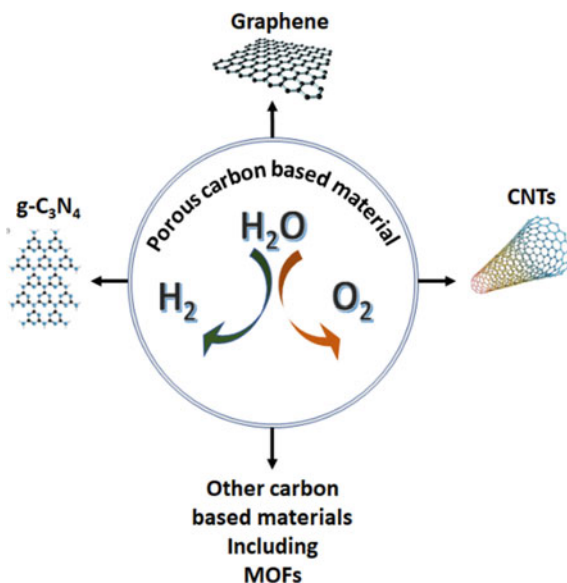
It is a difference of applied potential ( $E$ ) and the thermodynamic equilibrium potential ( $E_{eq}$ ). The  $E_{eq}$  for HER and OER are 0 and 1.23 V versus NHE, respectively. The overpotential is a specified applied potential for reaching a current density of 10 mA/cm<sup>2</sup> in water electrolysis, and a smaller value of overpotential implies the higher activity of a particular electrocatalyst [13, 14].

## 5 Electrocatalyst

As discussed above, water electrolysis is made up of two spontaneous half-cell reactions called HER on the cathode and OER on the anode. The OER is often slower than the HER in terms of kinetics, indicating that the OER has a greater overpotential at the anode due to the multi-step, and multi-electron process. The total water electrolysis efficiency depends on both HER and OER. Using a proper electrocatalyst reduced the kinetics barrier of the reactions resulting in a decrease in the overpotential value which improves the overall efficiency of the reaction.

The electrocatalysts based on expensive elements like Ir and Ru are till now reported as best for water electrolysis because of their fast kinetics, excellent stability across a broad pH range with low overpotential [13, 15]. Pt and Pd were also used despite their limited efficiency, the order of performance is Ru > Ir > Pt > Pd [16, 17]. In addition, RuO<sub>2</sub> and IrO<sub>2</sub> are higher efficient and more stable electrocatalysts in alkaline solution than their pure form because pure Ru and Ir metal electrodes are oxidized and often leach in electrolyte solution during long-term testing [18]. Generally, porous materials with large specific surface areas provide numerous advantages in electrochemical reactions. Because of their exceptional physicochemical features, huge surface area, strong electron conductivity, high abundance, and inexpensive, carbon-based materials may be widely exploited to tackle energy and environmental concerns. In the last 10 years, carbon-based materials (Fig. 4) such as graphitic carbon nitride (g-C<sub>3</sub>N<sub>4</sub>), carbon nanotubes (CNTs), and graphene, which is made up of earth-abundant non-metallic elements (C, H, N, O, and so on) have been developed as alternative water electrolysis catalyst [19–24]. Surprisingly, several of them have been discovered to have equivalent or even greater efficiency for HER and OER reaction than a pure metal-containing catalyst, in which a metal, a gaseous heteroatom, and a range of organic functional groups can be used to effectively adjust/alter the chemical properties of a carbon matrix [25]. In general, there are two types of methods for chemically doped carbon-based materials: (1) adoption-based doped materials, which is made of by adsorbing metal, heteroatoms, or organic molecules onto the carbon-based materials; (2) substitutional doped materials, which is made by replacing carbon atoms with foreign atoms. Both methods can change the physicochemical properties of the materials, resulting in catalytically active materials toward HER and OER reaction [26].

**Fig. 4** Schematic demonstration of different carbon-based materials, which can be converted into porous electrocatalyst



### 5.1 Porous Carbon-Based Materials as Water Electrocatalyst

Being a heterogeneous process, water electrolysis occurs at the interface, porous materials have attracted a lot of attention as prospective catalysts. Porous materials are distinguished from bulk materials by their unique chemical and physical properties. Porous materials are useful in water electrolysis because they provide a large surface-to-volume ratio in the form of a higher available catalytic active site and an easier path for mass diffusion. Especially carbon-based materials are stable in a large range of pH as an electrocatalyst. The surface area, pore volume, and pore size of the carbon-based materials depend on their synthesis methods and primary carbonization precursor. In such a manner, Ding et al. synthesized different porous carbon-based materials using the same parameters with silica as a template method to compare their physical and chemical properties for the electrocatalytic application. They found that the primary discharge capacity of catalysts of Li–O<sub>2</sub> batteries depends on the surface area and pore size of the electrode [27]. For water electrolysis, available active sites are the dominating factor at a limited value after that pore size plays a major role in the activity. According to Ding et al., the porous carbon material's pore size up to 60 nm exhibits no difference in OER current density after that increase in the pore size OER current density also increases [27]. This demonstrates that a bigger pore size and surface area are beneficial for an electrocatalytic process due to the diffusion of oxygen. The physiochemical properties of porous carbon materials also depend on the surface chemistry in the form of a variety of functional groups. The functional groups on the surface are mostly formed by different activation method such as thermal, microwave, and ozone treatment and post-chemical treatment of different

precursors of heteroatoms [28]. Modifying the surface chemistry of particular porous carbon materials could be a practical and attractive path to use novel uses for such materials. The hydrogen, nitrogen, oxygen, halogens, sulfur, and other heteroatoms on the surface of porous carbon bond to the edge of carbon layers and control the surface chemistry of the materials. Among all the heteroatoms, oxygen-containing functional groups also known as surface oxides were most common for sensors, electrocatalytic, energy storage, adsorption, and other catalytic application [28–30]. Except from that, porous carbon material have received a lot of interest as a potential solution for hydrogen storage because of its large surface area, light weight, faster kinetics, and totally reversible [31].

According to the International Union of pure and applied chemistry (IUPAC) based on pore size, porous materials are classified into three types: (1) having a pore size greater than 50 nm; macroporous (2) with pore size between 50 and 2 nm; mesoporous (3) with a pore size less than 2 nm microporous [32]. Furthermore, the pore size smaller than micropores known as sub-micropores can be further divided into super-microporous with pore diameter range from 2 to 0.7 nm and ultra-microporous of diameters below 0.7 nm [32]. Apart from this some of the literature used word nanopores materials which are used for the pore's diameters 100 nm or lesser. The Brunauer–Emmett–Teller (BET) and Brarrett–Joyner–Hallender (BJH) and Dubinin–Astakhov (DA) techniques have been used to calculate the specific surface area and average pore diameters of the porous carbon materials, respectively [33]. These techniques are based on gas adsorption isotherm where inert gases like nitrogen or argon molecule are adsorbed over a wide range of pressure, recently scanning tunneling microscopy has been widely used. Typically, multilayer adsorption phenomena of nitrogen molecules have been used for calculating the mesoporous range of materials. Whereas, double layer or a single layer of nitrogen or helium molecules is used for the microporous material.

## 5.2 Graphene-Based Material

Graphene is a hexagonal honeycomb-shaped 2D monolayer material, where carbon atoms are  $sp^2$  hybridized. Graphene is the fundamental building block for a wide range of graphitic materials, such as 0D fullerene, 1D CNTs, 3D graphite, and even additional for 3D carbon structure. In general, pure/ideal graphene shows very bad catalytic behavior due to its narrow bandgap [34]. However, the bulk production of graphene using a chemical process has some oxygen-related defects in the form of hydroxyl (C–OH) and acidic (C–COOH) functional groups [35]. This oxygenated graphene acts as both Lewis acid and basic sites and is strong repulsive through electrostatic forces. The force creates voids between oxygenated graphene sheets, which can help to produce the large pores which allow for easy gas transport into the electrode. As a result, such properties of graphene-based material are a good option for developing a new substrate-free catalyst material for gas-involvement reactions [36]. The main issue with such types of graphene material is that they

have a poor intrinsic activity, which can be normally improved by converting it into graphene hybrid using chemical doping of heteroatom (such as N, S, P, and B.) [26]. This might disturb the  $sp^2$  hybridized carbon network and  $sp^3$  defected carbons are generated in the graphene lattice. This type of chemical heteroatoms modified graphene are graphene oxides (GO) and reduced GO, which have lot of structural defects and variety of functional groups. Unlike graphene, GO possess larger band gap (2.4–4.3 eV) become a significant semiconductor material [26, 37]. GOs show a p-type semiconductor property due to the higher presence of electronegative oxygen atoms. This property is responsible for GOs potential application in a metal-free photocatalyst.

Zhang et al. described the N and P doped graphene catalyst for HER in which graphene oxide was chemically exfoliated into N or/and P doped graphene at 950 °C, where C and O atoms are substituted by N or/and P atoms. Every single doped graphene was greatly boosting the HER catalytic efficiency in both basic and acidic solutions, where N doping strongly affects the catalytic activity. The combined effect of N, P-graphene was highest in all and show an overpotential value of 420 mV at the current density of 10 mA/cm<sup>2</sup>, which is comparable to some bulk metallic catalysts like Au, Mo, Mo/Ni alloy, etc. [38].

In the same way, Ito et al. described the N, S doped 3D nanoporous graphene using the CVD method at different temperatures for 5 min, abbreviated NS-500. [33]. At particular temperature, it provides a large BET surface area (1320 m<sup>2</sup>/g) and pore size distribution in the 90 nm range. The higher concentration of N and S increases the lattice defects in graphene, which shows the comparable HER activity as 2D MoS<sub>2</sub> nanosheets. A significant activity of N, S-graphene toward HER catalyst in higher acidic media gives water reduction wave at 130 mV which is 160 mV lower compared previous reported N, P-doped graphene, and also from single heteroatom doped graphene (Table 1) [38]. This surprising activity was also confirmed from the Tafel slope value (= 81 mV/dec) which was also lower than another grapheme [33]. A comparative catalytic performance study of developed single N and S doped nanoporous graphene and pure nanoporous catalyst at different temperatures using the CVD method are listed in Table 1. According to Table 1, the majority of the metal-free graphene-based electrodes are just utilized for HER and only in acidic media. For broadening the area of activity, metal-graphene composite electrocatalysts have been developed.

Transition metals (TMs) such as Fe, Mn, Co, Mo, Ni, or their oxides, sulfides, carbides, and phosphides composition with graphene-based materials have been recognized as a prospective abundant and cost-effective noble metal-free catalyst. Specially metal@graphene cell structure center is one of the effective nanostructures in HER [19].

Based on this strategy, Co nanoparticle-coated on N-doped graphene and reduced graphene oxide (Co@NG/NRGO) was fabricated as HER catalyst, which was found to be highly effective and stable in large pH ranges. In near-neutral media, Co@NG/NRGO catalyst shows a lower onset potential value of 107 mV with Tafel slope of 89 mV/dec, whereas in highly basic (1 M KOH) and acidic (0.5 M H<sub>2</sub>SO<sub>4</sub>) medium current density of 10 mA/cm<sup>2</sup> obtained at 71 and 129 mV overpotential,

**Table 1** Important catalytic parameters for graphene-based catalyst in water electrolysis study

Catalyst	Structure/Carbon material specification	Electrolyte	Application	Onset overpotential (mV)	Overpotential @current density (mV@mA/cm <sup>2</sup> )	Tafel (mV/dec)	References
Graphene	2D	–	HER	–	–	206	[38]
N-doped graphene	2D sheets	0.5 M H <sub>2</sub> SO <sub>4</sub>	HER	330	490	116	
P-doped graphene	2D sheets	0.5 M H <sub>2</sub> SO <sub>4</sub>	HER	370	553	133	
N-P- doped graphene	2D sheets	0.5 M H <sub>2</sub> SO <sub>4</sub>	HER	290	420@10	91	
	2D sheets	0.1 M KOH	HER	–	585@10	145	
G-500	3D nonporous	0.5 M H <sub>2</sub> SO <sub>4</sub>	HER	–	–	237	[33]
S-500	3D nonporous	0.5 M H <sub>2</sub> SO <sub>4</sub>	HER	–	–	130	
N-500	3D nonporous	0.5 M H <sub>2</sub> SO <sub>4</sub>	HER	–	–	172	
NS-500	3D nonporous	0.5 M H <sub>2</sub> SO <sub>4</sub>	HER	130	276@10	81	
Co@NG/NRGO	N-doped graphene on N-doped rGO	1 M KOH	HER	–	70@10	64	[19]
		0.5 M H <sub>2</sub> SO <sub>4</sub>	HER	13	91@10	62	
		Neutral pH	HER	107	–	89	
NiCoP/rGO	Nanosheets	0.5 M H <sub>2</sub> SO <sub>4</sub>	HER	31	55@10	45.2	[39]
		1 M phosphate buffer solution	HER	76	124@10	91	
		1 M KOH	HER	136	209@10	124.1	
		1 M KOH	OER		270@10	65.7	
PNG-NiCo	Porous N-doped	0.1 M KOH	OER	310	373@5	156	[36]
MoS <sub>2</sub> /rGO	Reduced graphene oxide	0.5 M H <sub>2</sub> SO <sub>4</sub>	HER	100	–	41	[40]

(continued)

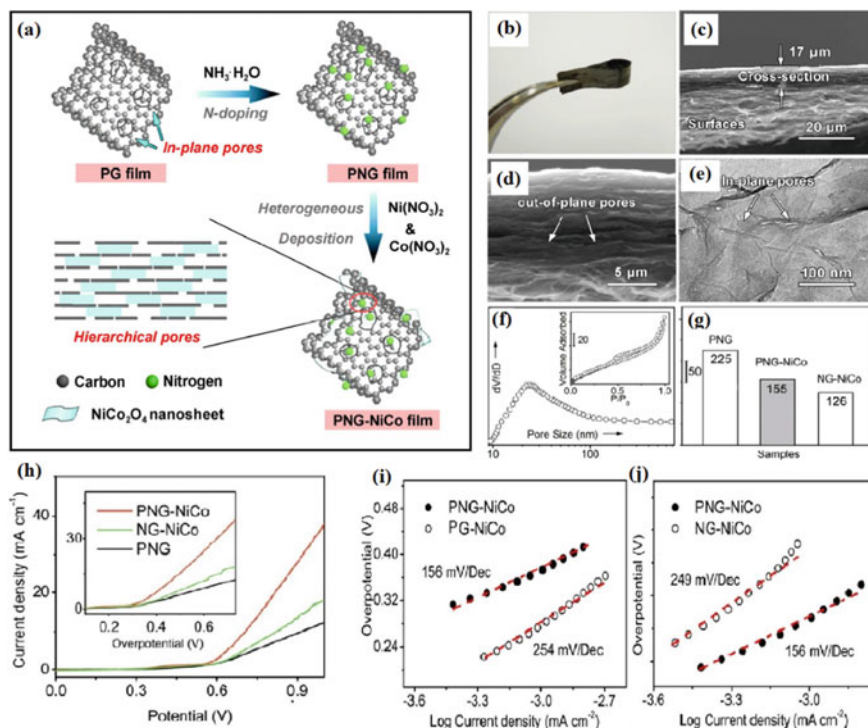
**Table 1** (continued)

Catalyst	Structure/Carbon material specification	Electrolyte	Application	Onset overpotential (mV)	Overpotential @current density (mV@mA/cm <sup>2</sup> )	Tafel (mV/dec)	References
MoS <sub>2</sub> -rGO	MoS <sub>2</sub> nanosheet perpendicular to graphene	0.5 M H <sub>2</sub> SO <sub>4</sub>	HER	–	172@10	43	[41]
Ir@VG	Nanohills	0.5 M H <sub>2</sub> SO <sub>4</sub>	HER	–	47@10	43	[42]
		1 M KOH	HER	–	17@10	29	
		0.5 M H <sub>2</sub> SO <sub>4</sub>	OER	–	300@10	59	
		1 M KOH	OER	–	320@10	52	

respectively [19]. Similarly, Ni@NG/NRGO and Mo<sub>2</sub>C@NG/NRGO catalyst were also prepared for comparative study listed in Table 1 [19, 43, 44]. Most of the noble metal-free first row TMs oxides (e.g., Mn, Fe, Co, and Ni) as a catalyst are required to achieve an onset overpotential higher than 300 mV for OER [45]. However, a good quantitative analyzed amount of more than one metal can further increase the catalytic activity. In such a manner, a bimetallic NiCoP/rGO catalyst was reported by Li et al. [39]. There was a bifunctional catalyst and stable in the 0–14 pH range. In HER, the use of rGO is necessary to decrease the overpotentials value from 59 mV for NiCoP to 42 mV for NiCoP/rGO to reach the current density of 10 mA/cm<sup>2</sup>. The NiCoP/rGO hybrid gives a Tafel slope value of 45.2 mV/dec, which is very near to Pt/C (30.4 mV/dec) in 0.5 M H<sub>2</sub>SO<sub>4</sub> solution for HER. The NiCoP/rGO was stable in all pH but with the pH increase the HER activity and Tafel slope value decrease. Furthermore, NiCoP/rGO hybrid catalyst was also shown OER activity with a minimal overpotential of 270 mV to achieve a current density of 10 mA/cm<sup>2</sup> under 1 M KOH solution.

Similar to NiCoP/rGO catalyst, a porous and 3D, N-doped graphene NiCo<sub>2</sub>O<sub>4</sub> Hybrid (PNG-NiCo) catalyst was fabricated by Chen et al. towards the OER application [36]. The synthesis process for PNG-NiCo catalyst is described in Fig. 5a. Where graphene was initially oxidized to form a porous graphene sheet (PG) followed by doping with nitrogen atoms using NH<sub>3</sub> to prepare the N-doped graphene (PNG). Finally, PNG-NiCo hybrid catalyst was developed via reaction between PNG and Ni (II), Co (II) containing solution. The PNG-NiCo was a flexible film Fig. 5b. The nitrogen adsorption isotherm and SEM images Fig. 5c–d confirm the macroporous nature out of the plane and mesoporous nature inside the plane with a surface area of 155 m<sup>2</sup>/g (Fig. 5g). The BJH method was also used to confirm the presence of mesoporous and macroporous nature with pore size distribution 10–100 nm (Fig. 5f). The PNG-NiCo showed excellent OER performance like the above reported NiCoP/rGO catalyst with a lower Tafel value 156 mV/dec with an onset potential 310 mV also smaller than NG-NiCo (340 mV) and PNG (352 mV) catalyst in slightly lower alkaline (0.1 M KOH) solution.

Bulk MoS<sub>2</sub> nanoparticle-like 2D material does not show significant activity in HER. But, a choice of a perfect substrate and resulting various structure and morphologies highly boosted the activity of nanomaterials. In such a manner, Li et al. reported the MoS<sub>2</sub> over reduced graphene oxide (MoS<sub>2</sub>/rGO) through the one-pot, one-step solvothermal method. MoS<sub>2</sub>/rGO was showing an onset overpotential at 100 mV, whereas the Tafel slope of 41 mV/dec compared to twice of bulk MoS<sub>2</sub> nanoparticle (94 mV/dec) in the highly acidic medium [40]. In the same way, the ultrathin MoS<sub>2</sub> nanosheet was perpendicularly fabricated on rGO (MoS<sub>2</sub>-rGO) using the hydrothermal method. MoS<sub>2</sub>-rGO catalyst with 15% weight ratio of MoS<sub>2</sub> to MoS<sub>2</sub>-rGO shows the highest activity of at overpotential of 172 mV for current density 10 mA/cm<sup>2</sup> and more active than MoS<sub>2</sub>/rGO, and MoS<sub>2</sub>/G and support free MoS<sub>2</sub> catalyst (Table 1). The HER activity order was MoS<sub>2</sub>-rGO > MoS<sub>2</sub>/rGO > MoS<sub>2</sub>/G > support free MoS<sub>2</sub>. The surface area of MoS<sub>2</sub>-rGO catalyst was 54.7 m<sup>2</sup>/g, which is similar to MoS<sub>2</sub> nanomaterial (50 m<sup>2</sup>/g),



**Fig. 5** a Synthesis of 3D hybrid catalyst in multi steps, b an optical photograph for representing the flexibility, c–d SEM image, e a TEM image of N-doped graphene, f pore size distribution for PNG-NiCo in  $\text{cm}^2/\text{g}$  nm, g specific surface area ( $\text{m}^2/\text{g}$ ), h LSV graph for different catalyst with scan rate 50 mV/s using 0.1 M KOH solution, i–j Tafel plots. Reprinted with permission from Chen et al. [36]. Copyright 2013 American Chemical Society

conclude that there the HER activity not affected by the surface area of the catalyst only depends on the available active sites of catalysts [41].

Roy et al., proposed the Ir on vertical graphene (Ir@VG) as a bifunctional catalyst in both acidic and alkaline mediums. They first developed vertical graphene (VG) nanohills that showed forest-like morphology on Glassy carbon (GC) substrate using the plasma-enhanced CVD method. Then crystalline Ir layers uniformly spread all over the VG using the electron beam evaporation method. The resulting hybrid structure of Ir@VG shows outstanding bifunctional catalytic performance in both media. In acidic solution, the catalyst shows HER overpotentials 147 mV to reach a current density of  $10 \text{ mA}/\text{cm}^2$  and Tafel slope 43 mV/dec, whereas in alkaline solution overpotential value only 17 mV for same current density and Tafel slope lower of 29 mV/dec was reported. Furthermore, the OER in acidic medium found an overpotential value of 300 mV and Tafel slope around 59 mV/dec, and in an alkaline medium, the overpotential value is higher than 300 mV while Tafel slope



reduced to 52 mV/dec [42]. Due to the combination of Ir metal with highly conductive graphene facilitated the electrons transfer and accelerates the reaction mechanism. The long-lasting stability of catalyst is due to forest-like morphology of VG that provides a super aerobic porous surface which reduced the size of the bubble during the desorption process and protects the Ir from corrosion.

### 5.3 Graphitic-Carbon Nitride ( $g\text{-C}_3\text{N}_4$ ) Based Porous Materials

$g\text{-C}_3\text{N}_4$  is  $sp^2$  hybridized graphite-like polymeric material where tri-s-triazine is the main component connected with planar amino group through C–N bond and functions as a p-type semiconductor material. It is one of the most well-known synthesized N-rich materials and is widely investigated in water electrolysis reactions. From the computational-based study (DFT), it was observed that the nitrogen-rich polarized carbon and nitrogen could be a favorable site for HER and OER, respectively. It was found that  $g\text{-C}_3\text{N}_4$  has a high concentration of nitrogen responsible for its thermal and chemical stability [46].

The  $g\text{-C}_3\text{N}_4$  based electrode materials may be simply synthesized via thermal condensation of a few N-rich compounds like melamine, urea, dicyandiamide, cyanamide, or a mixture of them [47]. Because of weak conductivity, whereas lower available surface area of  $g\text{-C}_3\text{N}_4$  material is usually restricted to be used in pure form for electrocatalytic applications.  $g\text{-C}_3\text{N}_4$  composite with highly conductive and large surface area material such as graphene surprisingly boosted the electrocatalytic property [48].

Tian et al. discussing the fabrication of metal-free  $g\text{-C}_3\text{N}_4$  nanosheet composites with graphene ( $g\text{-C}_3\text{N}_4/\text{G}$ ) for OER catalysis, followed by melamine pyrolysis coupled with ultrasonication.  $g\text{-C}_3\text{N}_4$  nanosheet possessed a higher specific surface area 16.2  $\text{m}^2/\text{g}$  with compared to bulk  $g\text{-C}_3\text{N}_4$  (7.97  $\text{m}^2/\text{g}$ ), resulting in an available large active site for OER [47]. The resulting  $g\text{-C}_3\text{N}_4/\text{G}$  catalyst shows a smaller OER overpotential of 539 mV at reached a current density of 10  $\text{mA}/\text{cm}^2$  than pure  $g\text{-C}_3\text{N}_4$  nanosheet (749 mV). It also confirms the Tafel slope value listed in Table 2. Similarly, Zhang et al. developed a metal-free  $g\text{-C}_3\text{N}_4$  composite with N-doped graphene ( $g\text{-C}_3\text{N}_4/\text{NG}$ ) as HER catalyst, where  $g\text{-C}_3\text{N}_4$  was synthesized by N-rich dicyandiamide [49]. The  $g\text{-C}_3\text{N}_4$  provides various surface active sites for proton adsorption whereas the N-doped graphene (NG) provide a lesser resistant surface which enhanced the electron transfer process for accelerating the kinetics of the HER mechanism [49]. The  $g\text{-C}_3\text{N}_4/\text{NG}$  catalyst shows a comparative activity concerning another developed metal-free material and shows an overpotential to reach the current density of 10  $\text{mA}/\text{cm}^2$  around 240 mV with a Tafel slope value of 51.5 mV/dec.

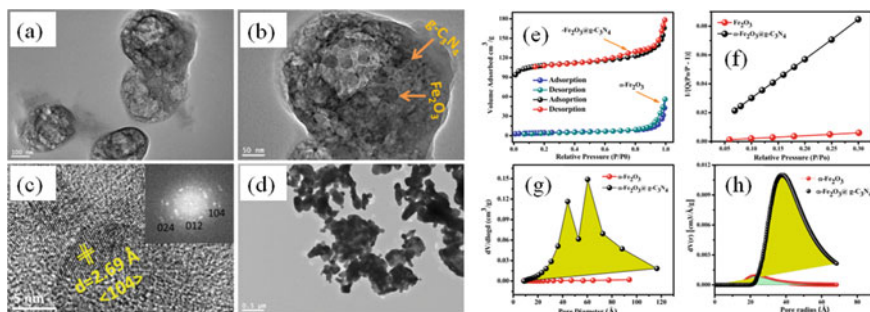
**Table 2** Important catalytic parameters for g-C<sub>3</sub>N<sub>4</sub> based catalyst in water electrolysis study

Catalyst	Structure/Carbon material specification	Electrolyte	Application	Overpotential@Current density (mV@m.A/cm <sup>2</sup> )	Tafel (mV/dec)	References
g-C <sub>3</sub> N <sub>4</sub> nanosheet	Nanosheet	0.1 M KOH	OER	749@10	120.9	[47]
g-C <sub>3</sub> N <sub>4</sub> /G	Nanosheet	0.1 M KOH	OER	539@10	68.5	
g-C <sub>3</sub> N <sub>4</sub> nanoribbon-G	Nanoribbon graphene	0.5 M H <sub>2</sub> SO <sub>4</sub>	HER	207@10	54	[48]
g-C <sub>3</sub> N <sub>4</sub> @NG	N-doped graphene	0.5 M H <sub>2</sub> SO <sub>4</sub>	HER	240@10	51.5	[49]
C <sub>3</sub> N <sub>4</sub> /NG	N-doped graphene	0.5 M H <sub>2</sub> SO <sub>4</sub>	HER	380@10	67	
SCN-MPC	Mesoporous carbon	0.5 M H <sub>2</sub> SO <sub>4</sub>	HER	145@10	51	[50]
g-C <sub>3</sub> N <sub>4</sub> @S-Se-pGr	2D multi-layered structure	0.5 M H <sub>2</sub> SO <sub>4</sub>	HER	300@10	86	[51]
		0.1 M KOH	HER	86@5	169	
C <sub>3</sub> N <sub>4</sub> -Ru-F	F more active than S	0.5 M H <sub>2</sub> SO <sub>4</sub>	HER	140@10	57	[52]
IrO <sub>2</sub> /GCN	Nanosheets	0.5 M H <sub>2</sub> SO <sub>4</sub>	OER	276@10	57	[53]
$\alpha$ -Fe <sub>2</sub> O <sub>3</sub> @g-C <sub>3</sub> N <sub>4</sub>	Mesoporous	0.5 M KOH	OER	425@10	280	[21]
Fe <sub>x</sub> Co <sub>1-x</sub> Se <sub>2</sub> /g-C <sub>3</sub> N <sub>4</sub>	-	0.5 M H <sub>2</sub> SO <sub>4</sub>	HER	83@20 209@100	83	[22]
		1 M KOH	OER	230@10 360@50	44	
TC@WO <sub>3</sub> @g-C <sub>3</sub> N <sub>4</sub> @Ni-NiO	NiWO <sub>3</sub> nanoparticles on g-C <sub>3</sub> N <sub>4</sub>	0.1 M KOH	OER	385@10	57	[54]
		0.1 M KOH	HER	535@10	246	

In the same way, S-doped  $g\text{-C}_3\text{N}_4$  incorporated into mesoporous carbon (denoted by SCN-MPC) was also shown significant HER activity with only 60 mV onset potential with Tafel slope value of 51 mV/dec and overpotential of 145 mV to achieve a current density 10 mA/cm<sup>2</sup>. The SCN-MPC is also a good oxygen reduction catalyst [50]. Another important process was reported by Zhao et al. to fabrication of 3D  $g\text{-C}_3\text{N}_4$  nanoribbon-graphene composite architecture comprising 1D  $g\text{-C}_3\text{N}_4$  nanoribbons to combined 2D graphene using a one-pot, one-step hydrothermal approach [48]. The HER onset potential for the developed  $g\text{-C}_3\text{N}_4$  nanoribbon-G was substantially lower around 80 mV than other pure carbon-based catalysts and also from noble non-noble metals or oxides.

Similar to single doped graphene, the electrocatalytic property can be further improved by coupling  $g\text{-C}_3\text{N}_4$  with double heteroatom doped nonporous graphene-like sulfur and selenium double doped hybrid  $g\text{-C}_3\text{N}_4@x\text{-pGr}$  catalyst (where  $x = \text{S, Se, S-Se}$ ) synthesized by Shinde et al. [48]. In the  $g\text{-C}_3\text{N}_4@S\text{-Se-pGr}$  synthesis process,  $\text{H}_2\text{O}_2$  oxidation is a surface area enhancement step. The pore size distribution confirmed the nonporous morphology of graphene with a specific surface area of 283 m<sup>2</sup>/g. The  $g\text{-C}_3\text{N}_4@S\text{-Se-pGr}$  hybrid shows higher catalytic properties including a small onset potential 92 mV, Tafel slope 86 mV/dec in 0.5 M  $\text{H}_2\text{SO}_4$  solution, also shows good activity and stability using 0.1 M KOH, whereas single heteroatom doped graphene catalyst follows the increasing activity order; doped free  $g\text{-C}_3\text{N}_4 < g\text{-C}_3\text{N}_4@S\text{-pGr} < g\text{-C}_3\text{N}_4@S\text{-pGr} < g\text{-C}_3\text{N}_4@S\text{-Se-pGr}$ .

Alduhaish et al. have demonstrated a mesoporous  $\alpha$ -iron oxide nanocomposite with  $g\text{-C}_3\text{N}_4$  ( $\alpha\text{-Fe}_2\text{O}_3@g\text{-C}_3\text{N}_4$ ), fabricated at 400 °C using urea–formaldehyde resins [21]. They calculated the mesoporous nature and pore size distribution of materials using electron microscopy (Fig. 6a–d) and BJH and DA model (Fig. 6g–h). The BET surface area was observed to be approximately 26 and 115 m<sup>2</sup>/g (Fig. 8e–f). The electrocatalytic behavior of the electrocatalyst was observed in 0.5 M KOH solution, demonstrating the better OER activity of  $\alpha\text{-Fe}_2\text{O}_3@g\text{-C}_3\text{N}_4$  compared to pure  $\alpha\text{-Fe}_2\text{O}_3$  nanoparticle due to mesoporous nature and higher surface area. A small onset potential and a lower Tafel plot of  $\alpha\text{-Fe}_2\text{O}_3@g\text{-C}_3\text{N}_4$  was 280 mV/dec than pure  $\alpha\text{-Fe}_2\text{O}_3$  catalyst (320 mV/dec). Another iron-based bifunctional bimetallic  $\text{Fe}_x\text{Co}_{1-x}\text{Se}_2/g\text{-C}_3\text{N}_4$  catalyst was developed by Zulqarnain et al. [22], where  $\text{FeCoSe}_2$  particles have been properly deposited on  $g\text{-C}_3\text{N}_4$ . They suggested that with the increase in the percentage of iron in catalyst composite, the electrocatalytic performance was also increased.  $\text{Fe}_{0.2}\text{Co}_{0.8}\text{Se}_2/g\text{-C}_3\text{N}_4$  with unique structure and higher available active sites showed a surprisingly HER activity with a low overpotential of 83 mV for 20 mA/cm<sup>2</sup> in 0.5 M  $\text{H}_2\text{SO}_4$  whereas OER investigated in alkaline (1 M KOH) solution, gives a very small overpotential value of 230 mV to achieve a current density of 10 mA/cm<sup>2</sup> and a Tafel slope 44 mV/dec.



**Fig. 6** a–b TEM image, c FETEM images and inserted image shows the electron diffraction for of  $\alpha\text{-Fe}_2\text{O}_3$ @ $\text{g-C}_3\text{N}_4$ , d TEM image of  $\alpha\text{-Fe}_2\text{O}_3$  nanocomposites, e–f BET specific surface area, g BJH pore size, and h DA pore size distribution. Reprinted with permission from Alduhaish et al. [21]. Copyright 2019 Nature

#### 5.4 Carbon Nanotubes Based Porous Material (CNTs)

CNT simple cylinders in geometry with either as open or closed sides, consisting of more than one layer of graphene responsible for its higher surface area and carbon atom arrangement responsible for high conductivity in nature. All such type properties including its strong corrosion resistance, are widely used as supportive material in electrocatalyst studies. It was observed that CNTs have some advantages as compared to other carbon-based materials, in which they are more durable, less expensive, and simple to activate as compared to  $\text{C}_{60}$ . Furthermore, CNTs show higher conductivity than  $\text{g-C}_3\text{N}_4$  [55, 56].

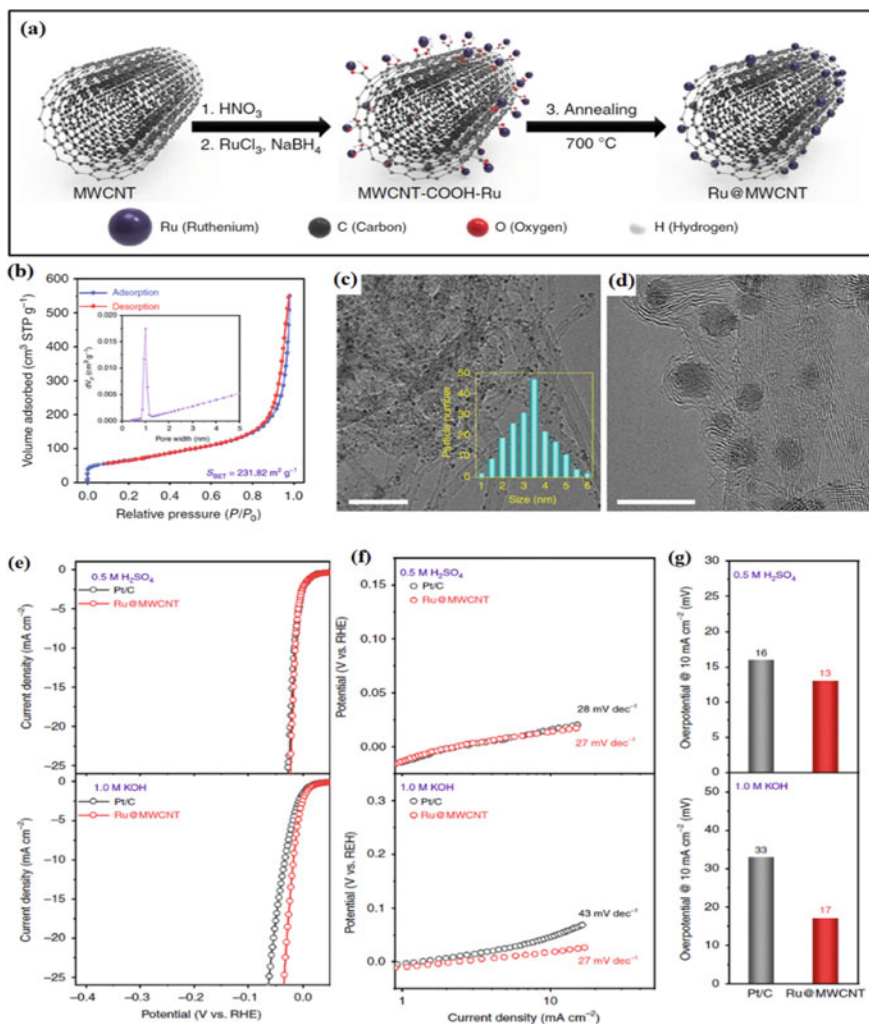
Similar to graphene, heteroatom-doped CNTs also attracted a lot of attention as cost-effective metal-free catalysts with a lot of active sites, energy-efficient, and stable. The previous section described the oxygenated graphene, strongly interacted with CNTs can be prevented CNTs from leaching from the electrode in the solution.

In such a manner, Chen et al. first time demonstrated a 3D N, O-doped graphene with CNTs (3D-NG-CNT) film as a substrate and binder-free electrocatalyst [36]. The 3D NG-CNT film was synthesized layer-over-layer through a simple filtration process of oxygenated graphene and CNTs followed by nitrogen-doped using ammonia. The nitrogen adsorption isotherm confirmed the mesoporous nature of 3D-NG-CNT material with pore size between 13 and 40 nm. The surface area of NG-CNT calculated by methylene blue adsorption was  $519 \text{ m}^2/\text{g}$  which is only  $185 \text{ m}^2/\text{g}$  for deep frizzed dry NG-CNT. The catalyst porous nature and higher surface area significantly enhanced the catalytic properties of the materials compared to nonporous materials. The 3D structure of the NG-CNT catalyst with excellent corrosion resistance and outstanding conductivity allows it directly utilized such as a binder-free substrate for OER catalysts. The 3D NG-CNT catalyst shows a lower onset potential at 315 mV compared to dry NG-CNT, G-CNT, NG, and 2D NG-CNT. The OER activity follows the same trend as the specific surface area of materials which is in decreasing order NG-CNT > NG > dry NG-CNT.

Cui et al. developed the metal-free activated CNTs for HER catalyst in acidic solution [57]. For the activation process, they first anodically oxidized to pristine multi-walled CNTs for 4 h followed by cathodic pre-treatment. The resulting activated p-MWCNT-ao-cp gives an onset overpotential of 100 mV with a Tafel slope of 71.3 mV/dec. A similar type of activation process was also observed for single-walled CNTs that gave HER wave at onset potential of 110 mV with a Tafel slope value of 81.5 mV/dec.

Development of metal incorporated carbon based-materials also one of the effective strategies for HER. In such a way, a noble metal-based Ru@MWCNTs catalyst with a higher surface area was reported by Kweon et al. [58], Ru (III) were uniformly coated on carboxylate functionalized MWCNTs followed by thermal treatment to synthesis Ru@MWCNTs (Fig. 7a). The specific surface area of developed Ru@MWCNTs is 231.82 m<sup>2</sup>/g where the size of Ru nanoparticles varied in between 2 to 5 nm (Fig. 7b–d). The Ru@MWCNTs catalyst shows excellent H<sub>2</sub> production and stability into both acidic and basic solutions as compared to commercial Pt/C catalysts. To reach a current density of 10 mA/cm<sup>2</sup> required overpotential was only 13 and 17 mV in N<sub>2</sub> saturated 0.1 M H<sub>2</sub>SO<sub>4</sub> and 1 M KOH electrolyte, respectively, which is much lower than commercial Pt/C catalyst (16 and 33 mV). The superior activity was also confirmed from the Tafel curve in Fig. 7f. The Ru@MWCNTs catalyst generates 15.4% more hydrogen per unit of electricity used than the Pt/C electrode and shows faradaic efficiency of 92.28% more than Pt/C (85.97%). Some of the TMs-based catalysts are not stable in aqueous acidic/alkaline media, such problems have been solved by unstable materials doped with CNTs (i.e., HER-inactive), which provided a significant acidity and long-term stability. In addition, noble metal-free TMs (Ni, Fe, Mn, Co, etc.) and their oxides including MnO<sub>x</sub>, CoO<sub>x</sub>, NiO<sub>x</sub>, and mixed oxides such as NiFeO<sub>x</sub> supported on CNTs as a substrate have been extensively studied for HER and OER catalyst [24, 43, 59–62], especially, Fe, Co, and Ni-doped N-rich CNTs catalyst that follows the decreasing HER activity order: Co-NRCNT > Ni-NRCNT > Fe-NRCNT [62], where highest efficient Co-NRCNT catalyst can operate into pH values from 0 to 14.

Yan et al. report the Ni@N-C NT/NRs catalyst which shows good HER activity due to their mesoporous nature with a higher BET surface area of 126 m<sup>2</sup>/g that provides easy electrode–electrolyte interaction [63]. An iron-based electrocatalyst, such as the various phase of FeOOH used for water oxidation limited from large-scale application due to lower conductivity [64–67]. However, such types of catalyst on the carbon-based substrate provides conductive surface. Zhang et al. reported the CNTs ultrathin FeOOH nanoflake on CC for OER catalyst. Where FeOOH is uniformly fabricated on the CNTs. Here, first CNTs were fabricated using the CVD technique with a radius of approximately 10 nm provides a higher surface area, which is extremely light and provides flexibility to the catalyst as compared to TMs and transition metal oxides substrate [24] (Table 3).



**Fig. 7** a Schematic illustration of forming Ru@MWCNTs, b  $\text{N}_2$  adsorption/desorption isotherm at 77 K, the inserted curve in (b) represent the pore size and surface area measured to used BET technique. c–d TEM images, the inserted in (c) representing the particles size distribution of Ru nanoparticles; scale bar (c) 50 nm, d 10 nm. e The HER polarization curve and f corresponding Tafel curve for Ru@MWCNT and Pt/C catalyst in  $\text{N}_2$ -saturated acidic and basic solution at scan rate  $5 \text{ mV/s}$ . g Overpotentials to achieved current density  $10 \text{ mA/cm}^2$ . Reprinted with permission from Kweon et al. [58]. Copyright 2020 Nature

**Table 3** Important catalytic parameters for carbon nanotubes (CNTs)-based catalyst in water electrolysis of water

Catalyst	Structure/Carbon material specification	Electrolyte	Application	Overpotential@current density (mV@mA/cm <sup>2</sup> )	Tafel (mV/dec)	References
p-MWCNT-ao-cp	Multi walled	0.5 M H <sub>2</sub> SO <sub>4</sub>	HER	–	71.3	[57]
p-SWCNT-ao-cp	Single walled	0.5 M H <sub>2</sub> SO <sub>4</sub>	HER	–	81.3	
NG-CNT	3D, Mesoporous	0.1 M KOH	OER	368@5	141	[35]
NMWNT	Multi walled CNTs	0.1 M NaOH	HER	340@10	–	[68]
		0.1 M NaOH	OER	370@10	78	
		1 M NaOH	OER	320@10	68	
echo-MWCNTs	Multi walled CNTs	0.1 M KOH	OER	450@10	72	[69]
		1 M KOH	OER	360@10	41	
N, S-CNT	Mesoporus/Dual doped CNTs	1 M KOH	HER	400@5	133	[70]
		1 M KOH	OER	360@10	56	
Ru@MWCNTs	Multi-walled CNTs	0.5 M H <sub>2</sub> SO <sub>4</sub>	HER	13@10	27	[58]
		1 M KOH	HER	17@10	27	
Co-NRCNTs	N-riched CNTs	0.5 M H <sub>2</sub> SO <sub>4</sub>	HER	260@10	69	[62]
Ni@N-CNT/NRs	N-doped CNTs	0.1 M KOH	HER	134@10	98.3	[63]
MnO <sub>x</sub> /MWCNT	Multi-walled CNTs	0.1 M potassium borate buffer	OER	190@2	–	[71]
MnO <sub>x</sub> /NCNT	Nitrogen functionalized CNTs	1 M KOH	OER	370@10	75	[72]
MnO <sub>x</sub> /NCNT	Nitrogen functionalized CNTs	1 M KOH	OER	370@10	75	[72]
MnO <sub>x</sub> /CNT/NF	–	1 M KOH	OER	330@100		[73]

(continued)

Table 3 (continued)

Catalyst	Structure/Carbon material specification	Electrolyte	Application	Overpotential@current density (mV@mA/cm <sup>2</sup> )	Tafel (mV/dec)	References
PdMn-N <sub>4</sub> /CNTs	-	1 M KOH	HER	71@10	41.7	[74]
Co/β-Mo <sub>2</sub> C@N-CNTs	N-doped CNT	1 M KOH	HER	170@10	92	[75]
		1 M KOH	OER	264@10	67	
MWCNT-PyPBF-Ni <sub>x</sub> Co <sub>3-x</sub> O <sub>4</sub>	Unoxidized multi-walled CNTs	1 M NaOH	OER	310@10	42	[76]
Co <sub>3</sub> O <sub>4</sub> /SWCNT	Single walled CNTs	1 M KOH	OER	-	104	[77]
CNT@FeOOH/CC	Ultrathin FeOOH nanoflake	1 M KOH	OER	250	36	[24]
NiFe-LDH/CNT	mildly oxidized multi-walled CNTs	1 M KOH	OER	250@5	31	[78]
		0.1 M KOH	OER	290@10	35	

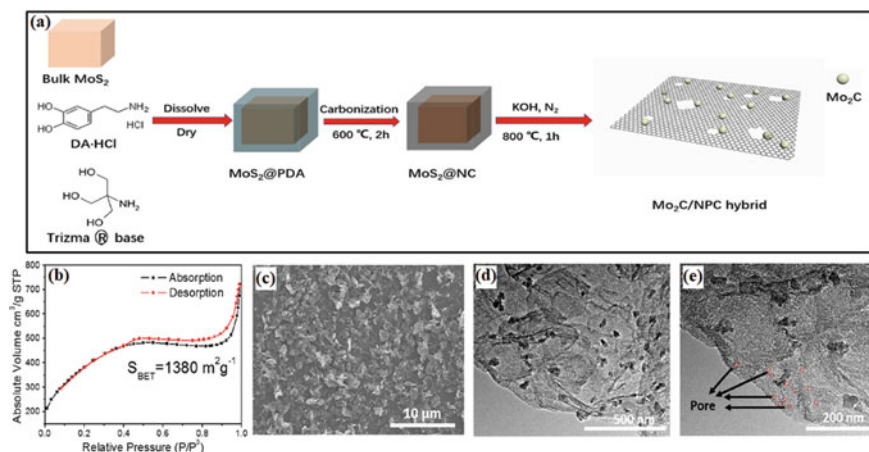


## 5.5 Other Carbon-Based Porous Material

Firstly, N-doped in carbon-based material is an effective technique to change the molecular structure, which improves the HER and OER performance. Recently, some N-doped carbon (N/C) based HER and OER electrocatalysts have been developed. In such a manner, Zhao et al. fabricated the metal-free N/C nanomaterial for OER catalyst, which shows a current density of  $10 \text{ mA/cm}^2$  at the overpotential of 380 mV, comparatively larger than N/C-NiO<sub>x</sub>, IrO<sub>2</sub>/C, and Pt/C catalyst in alkaline media. Although, the N/C-NiO<sub>x</sub> needed an overpotential of 420 mV to reach equal current density. The BET specific surface area was larger ( $560 \text{ m}^2/\text{g}$ ) at  $700^\circ\text{C}$ , which provided the highest catalytic activity. The N/C catalyst has nitrogen atom adjacent to carbon atom become negatively charged due to higher electron-withdrawing nature in N/C pi bond whereas carbon becomes positive, which easily adsorb OH<sup>-</sup> ions in alkaline water oxidation. However, the available nitrogen atom in the N/C system is responsible for the active site in the catalyst, which generated a higher OER current in the catalyst [79]. Many attempts have been tried to increase N/C functionality, including the development of a new fabrication method and the design porous structure. Nitrogen is a high-activity booster for carbon-based material in electrocatalyst application. The performance of heterogeneous catalysts depends on the available active site on the surface matrix, which increases with the concentration of doped nitrogen.

Among different TMs compounds, Mo<sub>2</sub>C attracted more attention toward HER as an efficient electrocatalyst because of its d-band electronic structure same as Pt metal. The synthesis of pure Mo<sub>2</sub>C hybrid structure requires a predominantly high temperature that causes the agglomeration of Mo<sub>2</sub>C molecules and lowers the active surface area of the materials. To reduce the agglomeration of Mo<sub>2</sub>C molecules, the conductive carbon materials can be frequently used to improve the active sites and conductivity. In such a manner, Ying lei et al. reported a nanosheet of N-doped porous carbon material coupled with molybdenum carbide (Mo<sub>2</sub>C/NPC) using MoS<sub>2</sub> as a molybdenum source [80]. The schematic synthesis steps of the Mo<sub>2</sub>C/NPC hybrid are represented in Fig. 8a, where KOH is critical in the etching of MoS<sub>2</sub> molecules to create Mo precursor, along with corroding carbon to form the high porosity and release reduced gases like CO and H<sub>2</sub>. The N<sub>2</sub>-adsorption/desorption isotherm is represented in Fig. 8b, at 77 K confirmed the BET surface area of  $1380 \text{ m}^2/\text{g}$  with BJH desorption pore size around 3.23 nm. The electron microscopy images in Fig. 8c–e, seen the porous morphology of the materials. The higher surface of the Mo<sub>2</sub>C/NPC hybrid shows superior HER performance in acidic electrolytes with a low onset potential of 93 mV and an overpotential 166 mV to achieve a current density of  $10 \text{ mA/cm}^2$ , the Tafel slope  $68 \text{ mV/dec}$ .

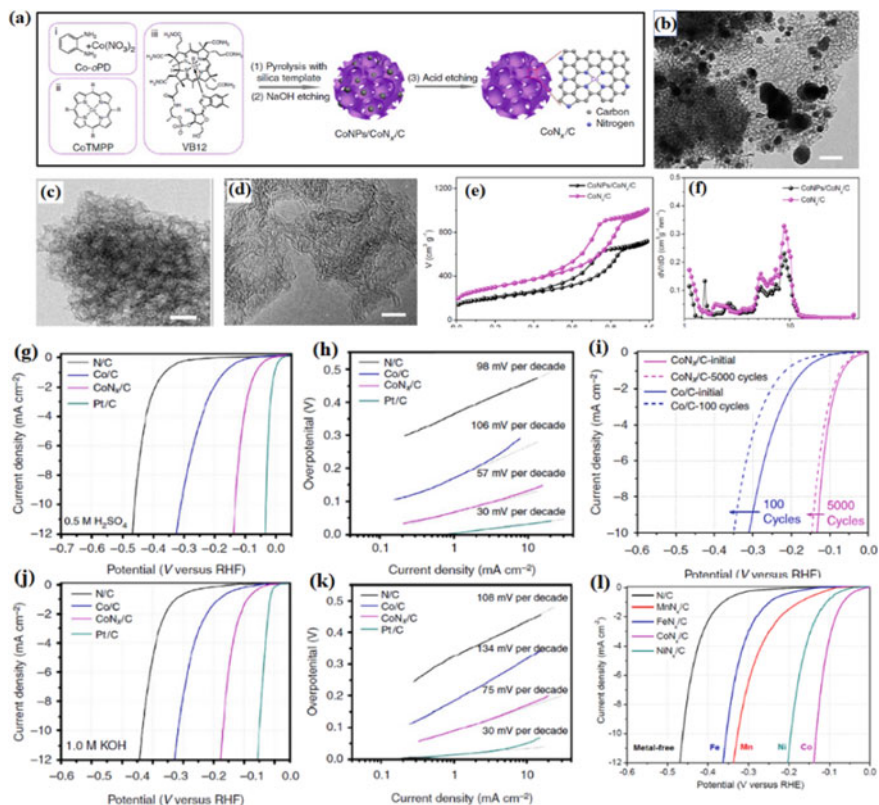
Ling et al., developed an efficient carbon based porous catalyst, fabricated with cobalt and nitrogen (CoN<sub>x</sub>/C) for the HER, under the stability of wide range of pH [81]. The schematic fabrication process of the CoN<sub>x</sub>/C catalyst is described in Fig. 9a, where Co (II)/o-phenylenediamine (Co-oPD) or porphyrin ring presented Co complexes (such as vitamin B12 etc.) are pyrolysed at a particular temperature



**Fig. 8** **a** Schematic of the synthesis of Mo<sub>2</sub>C/NPC hybrid, **b** N<sub>2</sub>-adsorption/desorption isotherm. Electron microscopic images of Mo<sub>2</sub>C/NPC hybrid, **c** SEM image, **d–e** TEM image in different magnifications. Reprinted with permission from Lei et al. [80]. Copyright 2019 Nature

using colloidal solution of silica as a template for creating the porous morphology in the catalyst. The NaOH and H<sub>2</sub>SO<sub>4</sub> were used in the etching step to remove the silica template and co-containing nanoparticles, respectively. As a consequence, a mesoporous structure of CoN<sub>x</sub>/C catalyst was formed with a large specific surface area (= 1074 m<sup>2</sup>/g) and a higher number of CoN<sub>x</sub> active sites. The CoN<sub>x</sub>/C catalyst fabricated from Co-oPD precursor gives the best performance. The HER activity (Fig. 9g–k) was tested in 0.5 M H<sub>2</sub>SO<sub>4</sub> and 1 M KOH solution gives overpotential of 133 mV for 10 mA/cm<sup>2</sup> current density having Tafel slope 57 mV/dec and overpotential 170 mV for same current density with 75 mV/dec Tafel slope value in highly acidic and alkaline solution, respectively. The CoN<sub>x</sub>/C catalyst also gives good activity in near-neutral solutions [81]. Furthermore, the CoN<sub>x</sub>/C nonporous catalyst has a substantially lower overpotential and Tafel slope value than N/C, Co/C HER catalyst in both acidic and alkaline solution (Fig. 9h, k). However, compared to benchmark Pt/C catalyst the overpotential (32 mV at 10 mA/cm<sup>2</sup>) to get a similar current density of approximately 100 mA/cm<sup>2</sup> of higher overpotential is reported in acidic media. For comparative study, different 1st-row TMs-based center MN<sub>x</sub>/C catalysts were fabricated and tested in 0.5 M H<sub>2</sub>SO<sub>4</sub> solution. The HER activity through LSV polarization curves is described in Fig. 9(l), which follows order CoN<sub>x</sub>/C > NiN<sub>x</sub>/C >> MnN<sub>x</sub>/C > FeN<sub>x</sub>/C >> metal free.

Same way, cobalt nanoparticles incorporated in porous N/C nanofibers (Co-PNCNFs) were developed by Zhao et al., using the electrospinning method followed by heat treatment [82]. The use of nitrogen-rich polyacrylonitrile (PAN) was demonstrated to be an effective strategy to form porous N/C material, which improves the catalytic performance of carbon-based material. Finally, acidic treatment is used to remove the cobalt nanoparticle from the surface of porous N/C nanofibers, which helps to improve the porosity. The Co-PNCNFs catalysts show a well-organized



**Fig. 9** a Schematic synthesis of  $\text{CoN}_x/\text{C}$  catalyst. TEM images of b  $\text{CoNPs}/\text{CoN}_x/\text{C}$ ; scale bar 100 nm, c  $\text{CoN}_x/\text{C}$ ; scale bar; 20 nm. e HRTEM image of  $\text{CoN}_x/\text{C}$ : scale bar 5 nm. d  $\text{N}_2$  adsorption-desorption isotherm, and e pore size using DFT method. Electrocatalytic performance study; g HER polarization curve and corresponding h Tafel plot in 0.5 M  $\text{H}_2\text{SO}_4$  solution, i Catalytic long-term study using CV for  $\text{CoN}_x/\text{C}$  (5000 cycles) and Co/N (100 cycles) catalyst. j HER polarization curve and k corresponding Tafel plot in 1 M KOH solution. l HER polarization curve for comparative HER activity of  $\text{MN}_x/\text{C}$  type catalyst, where  $\text{M} = \text{Co}, \text{Ni}, \text{Mn}$  and  $\text{Fe}$  in 0.5 M  $\text{H}_2\text{SO}_4$ . Reprinted with permission from Liang et al. [81]. Copyright 2015 Nature

1D structure and porous design with a large surface area that gives a wide electrode/electrolyte interface during OER. For comparative study, iron and nickel-based nanofibers catalysts (Fe-PNCNFs Ni-PNCNFs) were also synthesized in the same way, but they were less active compared to the above reported for TMs-based  $\text{MN}_x/\text{C}$  catalyst [81]. The electrocatalytic function of the Co-PNCNFs catalyst for OER and HER studied in 1 M KOH solution showed that Co-PNCNFs possess highest HER activity except for Pt/C, with overpotential 249 mV for a current density of  $10 \text{ mA}/\text{cm}^2$  and Tafel slope only 92 mV/dec comparatively better than previously reported nonporous Co-NRCNTs catalyst (overpotential 370 mV to get  $10 \text{ mA}/\text{cm}^2$  current density) under same experimental condition [62].

Another, precious metal-free Co–Fe containing OER catalyst was fabricated by Lin et al. [83], where Co-Fe nanoparticles coupled with N/C porous carbon nanosheet  $\text{Co}_y\text{Fe}_{10-y}\text{O}_x/\text{NPC}$  catalyst was developed by reduction to Schiff base network (SNW) with metals ions, followed by pyrolysis. High nitrogen-containing SNW was prepared by a one-pot solvothermal method from terephthalaldehyde and melamine. The synthesized material shows a specific surface area of  $204.82 \text{ m}^2/\text{g}$  calculated from BET adsorption isotherm. It has been observed that the activity of the  $\text{Co}_y\text{Fe}_{10-y}\text{O}_x/\text{NPC}$  catalyst towards the OER depends on the pyrolysis temperature and the concentration of Fe and Co ion. Also, Tafel slope and overpotential values depending on the ratio of Co and Fe, where 30% cobalt-containing catalyst (or CoFe ratio 3/7)  $\text{Co}_3\text{Fe}_7\text{O}_x/\text{NPC}$  was prepared at  $450 \text{ }^\circ\text{C}$  gave the highest anodic current density at a lower applied potential. The OER polarization of  $\text{Co}_3\text{Fe}_7\text{O}_x/\text{NPC}$  catalyst gave a current density of  $10 \text{ mA}/\text{cm}^2$  at only  $328 \text{ mV}$  overpotential with Tafel slope value  $31.4 \text{ mV}$  in  $1 \text{ M KOH}$ , which is slightly lower than the previous reported Co-PNCNFs catalyst due to relatively lower surface area of a material.

Nitrogen free another, carbon-coated CoP hollow microporous nano-cages (C-CoP-1/12) as a bifunctional catalyst was reported by Wanping Li et al., where calcination of Prussian blue was used as primary material followed by phosphorylation to form hollow porous CoP coated with carbon, where cobalt to phosphorus ratio was 1/12, the highest activity was reported. The nitrogen adsorption isotherm confirmed the pore size of the C-CoP-1/12 catalyst that was lower than  $2 \text{ nm}$ , whereas the surface area was  $16.91 \text{ m}^2/\text{g}$ . Impressively, the C-CoP-1/12 showed an overpotential value of  $174$  and  $33 \text{ mV}$  for HER and OER, respectively, to get the current density of  $10 \text{ mA}/\text{cm}^2$ , whereas for overall water electrolysis applied potential was  $1.65 \text{ V}$  with  $24 \text{ h}$  long-term stability at the same current density [84].

Similarly, other than cobalt, Lei and co-workers synthesized N-doped porous carbon nanosheets which when coupled with  $\text{Mo}_2\text{C}$  nanoparticles ( $\text{Mo}_2\text{C}/\text{NPC}$ ) provide a comparatively high surface area of  $1380 \text{ m}^2/\text{g}$ . The  $\text{Mo}_2\text{C}/\text{NPC}$  hybrid shows superior HER performance with the onset potential of  $93 \text{ mV}$ , overpotential value of  $166 \text{ mV}$  at a current density of  $10 \text{ mV}/\text{cm}^2$ , and Tafel slope value of  $68 \text{ mV}/\text{dec}$  [85]. The choice of suitable materials and their particular composition help to synthesis a lot of catalysts for benchmark catalyst application, among them nickel and iron for OER and molybdenum with heteroatom composition for HER, demonstrate surprisingly better performance compared to noble metal-free catalyst. Additionally, the fabrication of TMs-based materials on heteroatoms doped porous carbon is another way of enhancing the performance of TMs-based electrocatalyst [23].

Zhang and co-workers developed flexible and binder-free, TMs modified N/C porous hybrids catalyst coated on carbon fiber substrate, where particularly NiFe doped on porous N/C (NiFe-PVP) and Ni/MoC<sub>2</sub> doped on porous N/C (NiMo-PVP) used for OER and HER respectively [23]. For comparative study, the same approach was used for the fabrication of Ni-PVP, Fe-PVP, and Mo-PVP catalysts. For HER, the NiMo-PVP required approximately  $130 \text{ mV}$  overpotential to achieve a  $10 \text{ mA}/\text{cm}^2$

current density, which is substantially lower than Mo-PVP and Ni-PVP catalyst, whereas, for OER, the NiFe-PVP required only 297 mV overpotential to achieve a 10 mA/cm<sup>2</sup> current density, which is also lower than Ni-PVP and Fe-PVP catalyst described in Table 4.

## 6 Metal–Organic Frameworks (MOFs) Derived Materials as Electrocatalyst

Metal–organic frameworks (MOFs), also called porous coordination polymers, are crystalline porous materials made up of metal ions or metal clusters and organic ligands having a periodic arrangement [88–91]. Recent research has focused on developing MOF-based electrocatalysts, which is a departure from the traditional functions of MOFs, such as gas storage and purification, drug carriers, etc. The easiest customizable pore shapes and accessible metal nodes are the major benefits of employing MOFs as electrocatalysts [92, 93]. Despite these advantageous characteristics, MOFs have some drawbacks as restricted diffusion capacities because of MOFs porosity, metal centers have low reactivity owing to saturation with coordination linkers and the biggest one is poor conductivity [94, 95]. Researchers discovered that the pyrolysis of MOFs could overcome these limitations [96]. Figure 10 depicts the current developments of diverse MOFs derived carbon-based nanomaterials used in catalytic activities of HER and OER. Carbon-confined metal species produced from MOFs have lately gotten a lot of interest and have demonstrated excellent electrocatalytic efficiency [97–99]. On pyrolysis/annealing of MOFs metal ions or cluster get converted to nanoparticles, act as catalytic active sites and the organic linkers may be transformed in graphitized-amorphous carbon clusters, which acts as an electron highway and restricts metal-derivative crystal growth. In recent years, TMs-based binary and ternary compounds have been synthesized to use MOFs as a precursor/template. In such a manner, a binary molybdenum phosphide (MoP)-containing compound MoP@NPC/rGO compound was reported by Ji-Sen Li et al., which exhibits outstanding HER activity because of the synergistic contribution of rGO, NPC, and MoP, where MoP does exist noble metal Pt-like electronic structure but it suffers from a leaching problem, which can be solved to use graphene as a composite. The MoP@NPC/rGO catalyst showed an overpotential 218 mV to reach the current density of 10 mA/cm<sup>2</sup> with a Tafel slope value of 57 mV/dec. Factors that are responsible for high HER activity are a crystalline phase of MoP, introduction of rGO which enhance the electrical conductivity, increase active surface region, forming interconnecting network structure, which is advantageous for electronic transport and co-doping of heteroatoms like N, P, etc., that can also contribute in increasing the active sites [100].

As mentioned above, the catalytic activity highly depends on the porosity and surface area of the materials. Qamar et al. reported a highly efficient porous carbon-supported molybdenum carbide (Mo<sub>2</sub>C/C) catalyst with 58–168 m<sup>2</sup>/g surface area

**Table 4** Important catalytic parameters for some other carbon-based catalyst in water electrolysis study

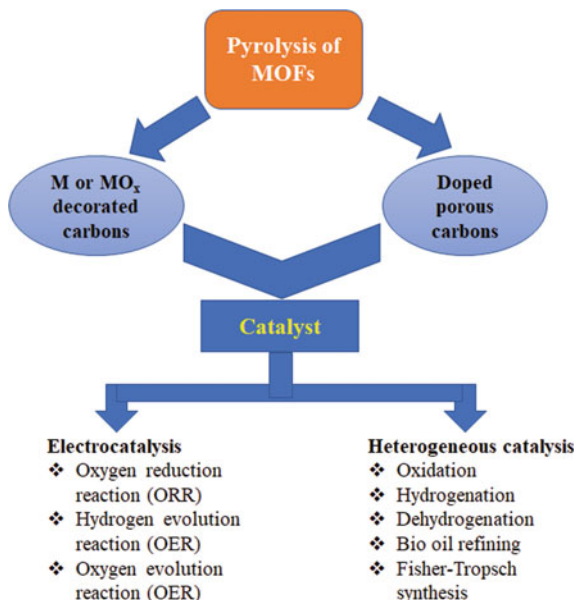
Catalyst	Structure/Carbon material specification	Application	Electrolyte	Overpotential @ current density (mV@mA/cm <sup>2</sup> )	Tafel (mV/dec)	References
N/C	N-doped carbon	OER	pH 13 (KOH)	380@10	–	[79]
ONPPGC/OCC	3D/Ti-doped porous graphite carbon	HER	1 M KOH	446@10	154	[86]
		OER	1 M KOH	410@10	83	
CoN <sub>x</sub> /C	Mesoporous	HER	0.5 M H <sub>2</sub> SO <sub>4</sub>	133@10	57	[81]
		HER	1 M KOH	170@10	75	
		HER	1 M phosphate buffer	247@10	–	
Mo <sub>2</sub> C/NPC	N-doped porous carbon nanotube	HER	0.5 M H <sub>2</sub> SO <sub>4</sub>	166@10	68	[80]
Co@N-C	N-doped carbon	HER	1 M NaClO <sub>4</sub>	200@10	100	[60]
		HER	1 M KOH	210@10	–	
		OER	1 M KOH	400@10	–	
Co-PNCNFs	Porous N/C nanofibers	HER	1 M KOH	249@10	92	[82]
		OER	1 M KOH	285@10	73	
C-CoP-1/12	C-coated CoP hollow nanocages/microporous	HER	1 M KOH	173@10	63.1	[84]
		OER	1 M KOH	333@10	71.1	
Co <sub>3</sub> Fe <sub>7</sub> O <sub>x</sub> /NPC	Porous nanosheet	OER	1 M KOH	328@10	31.4	[83]
NiMo-PVP	N-doped porous carbon	HER	1 M KOH	130@10	84	[23]
Ni-PVP	N-doped porous carbon	HER	1 M KOH	181@10	107	
Mo-PVP	N-doped porous carbon	HER	1 M KOH	208@10	70	
NiFe-PVP	N-doped porous carbon	OER	1 M KOH	297@10	48	
Ni-PVP	N-doped porous carbon	OER	1 M KOH	400@10	75	

(continued)

**Table 4** (continued)

Catalyst	Structure/Carbon material specification	Application	Electrolyte	Overpotential @ current density (mV@mA/cm <sup>2</sup> )	Tafel (mV/dec)	References
Fe-PVP	N-doped porous carbon	OER	1 M KOH	350@10	76	
Ni/Mo <sub>2</sub> C-PC	1D porous carbon support	HER	1 M KOH	179	101	[87]
		OER	1 M KOH	368	–	

**Fig. 10** Several carbon-based nanomaterials produced by the pyrolysis of MOFs and their uses in various essential reactions



which is highly dependent on temperature. The Mo<sub>2</sub>C/C gives an overpotential of 165 mV at a current density of 10 mA/cm<sup>2</sup>, lower than the upper reported MoP@NPC/rGO catalyst.

Among different methods, direct pyrolysis of MOFs may be an efficient way for manufacturing TMs-based composite [101]. In addition, bimetallic MOFs possess unique electronic structural properties which make them an efficient electrocatalysts. Among the numerous MOF materials, MOF-74-M (where M = Mg, Ni, Co, Zn, etc.) show the apparent benefit of being able to combine with multiple metal centers without affecting the MOF crystal structure (Table 5).

Using MOF-74, Feng et al. reported the porous rod-like bimetallic nitrides (Co<sub>x</sub>Ni<sub>y</sub>N) electrocatalyst as an efficient HER, which is stable in a large range of pH. The catalytic activity of Co<sub>x</sub>Ni<sub>y</sub>N varies with Co/ Ni ratio, Co<sub>2</sub>Ni<sub>1</sub>N required the lowest overpotential 102.6 mV to get a current density of 10 mA/cm<sup>2</sup> with a Tafel slope of 60.17 mV/dec [113]. Manman wang et al. also reported a binary Ni<sub>2</sub>P@C/G catalyst for OER [97]. Where first Ni-MOF supported on rGO (Ni-MOF/rGO) was fabricated using one-pot hydrothermal method followed by calcination and phosphorization formed Ni<sub>2</sub>P@C/G catalytic structure. The N<sub>2</sub>-adsorption/desorption isotherm for as prepared Ni<sub>2</sub>P@C/G confirmed a valuable surface area of 86 m<sup>2</sup>/g, much larger than without graphene Ni<sub>2</sub>P@C material (19 m<sup>2</sup>/g). The Ni<sub>2</sub>P@C/G catalyst shows a small overpotential 285 mV to achieve 10 mA/cm<sup>2</sup> current density and Tafel slope value 44 mV/dec, compared to other phosphorus-based polyhedral CoP@GC. The enhanced OER efficiency is attributed to phosphorization and the addition of graphene, that rise the active catalyst surface, exposes higher active sites, and improves charge transport [104].



**Table 5** Important catalytic parameters for metal–organic frameworks (MOFs) catalyst in water electrolysis study

Catalyst	Structure	Electrolyte	Application	Overpotential (mV) at current density 10 mA/cm <sup>2</sup>	Tafel slope (mV/dec)	References
MoP@NPC/rGO	Mesoporous	0.5 M H <sub>2</sub> SO <sub>4</sub>	HER	218	57	[100]
Mo <sub>2</sub> C/C	Mesoporous	1 M KOH	HER	165	66.41	[102]
Ni <sub>2</sub> P@C/G	Sheet-like	1 M KOH	OER	285	44	[97]
NiCo <sub>2</sub> O <sub>4</sub> /NiO-rGO	Rod-like	1 M KOH	OER	340	66	[103]
CoP@GC	Polyhedral	1 M KOH	OER	345	56	[104]
Co–N carbon	Layered	1 M KOH	HER	103	–	[66]
Co@N-CNTs@rGO	Nanotube	0.5 M H <sub>2</sub> SO <sub>4</sub>	HER	87	52	[105]
Zn – doped CoSe <sub>2</sub>	Nanosheets	1 M KOH	OER	356	88	[106]
CeO <sub>x</sub> /CoS	–	1 M KOH	OER	269	50	[107]
CeO <sub>x</sub> /CoS/CC	–	1 M KOH		232	–	
Co-Fe–P-1.7	Spindle-like	1 M KOH	OER	260	58	[108]
CNT-NC-CoP	Nanotube	1 M KOH	OER	251	82.1	[109]
CoP/Mo <sub>2</sub> C-NC	Nanorods	0.5 M H <sub>2</sub> SO <sub>4</sub>	HER	55.7	49	[110]
		1 M KOH		67.2	66	
CoPS/N–C	Polyhedral	0.5 M H <sub>2</sub> SO <sub>4</sub>	HER	80	68	[111]
		1 M KOH		148	78	
Co <sub>3</sub> O <sub>4</sub> @CoNCNT	Nanotube	0.5 M H <sub>2</sub> SO <sub>4</sub>	HER	171	121	[112]

Because of the unusual physical and chemical properties of porous carbon materials that distinguish them from bulk materials. It's widely used in electrocatalysis, where the heterogeneous phenomenon mainly occurs at the interface. The porous carbon materials are responsible for the additional surface area of the materials which facilitates the mass dispersion throughout the electrocatalysis. However, pure carbon-based materials did not show efficient water oxidation properties, but their composite with heteroatoms and metals provided effective surface-active sites for water oxidation. Table 6 represents the different heteroatom and metal-doped porous carbon composite materials with their specific surface areas and electrocatalytic performance in terms of overpotential at the current density of 10 mA/cm<sup>2</sup>. For catalytic activity, available active metal atoms are a dominating factor compared to the porosity of the materials. In such a manner, Zhang et al. reported bifunctional metal-free N, P co-doped, NPMC catalyst with the specific surface area 1663 m<sup>2</sup>/g, which is substantially greater than the porous carbon materials synthesized by the

**Table 6** Comparison between surface area and electrocatalytic activity of different porous carbon materials

Catalysts	Specification	Surface area (m <sup>2</sup> /g)	Application	Electrolyte	Overpotential@current density (mV@mA/cm <sup>2</sup> )	References
CoN <sub>x</sub> -C	Mesoporous	1074	HER	0.5 M H <sub>2</sub> SO <sub>4</sub>	133@10	[81]
				1 M KOH	170@10	
NPMCs	Mesoporous	1663	OER	0.1 M KOH	390@10	
Mo <sub>2</sub> /NPC	Micro-meso porous	1380	HER	0.5 M H <sub>2</sub> SO <sub>4</sub>	166@10	[80]
Co-PNCNFs	Micropores	356.6	HER	1 M KOH	249@10	[82]
				1 M KOH	285@10	
C-CoP-1/12	Nanocages/microporous	16.91	HER	1 M KOH	173@10	[84]
				1 M KOH	333@10	
Co <sub>3</sub> Fe <sub>7</sub> O <sub>x</sub> /NPC	Porous nanosheet	204.8	OER	1 M KOH	328@10	[83]
NG-CNT	Mesoporous	519	OER	0.1 M KOH	368@5	[35]

hard templates method [114]. Similarly, Li et al. fabricated Co-CoP-1/12 bifunctional catalyst with the lower BET surface area  $16.91 \text{ m}^2/\text{g}$  which shows higher activity with an overpotential of 333 mV at a current density of  $10 \text{ mA}/\text{cm}^2$  compared to metal-free catalyst [84].

## 7 Conclusion

Significant effort has been achieved to the development of cheaper material-based electrocatalysts as prospective replacements to noble metal catalysts over the last few decades. The major problems related to the metal oxides like low electrical conductivity, stability, and less surface area are overcome by incorporating the carbon-based materials and using MOF as a precursor/template to synthesize the MOF-derived metal oxides, phosphides, nitrides, etc. Doping of the heteroatoms such as N, P, etc., in the carbonaceous and MOF-derived materials have a great impact on their electrochemical properties. Simply developing novel materials will not suffice to meet the world's energy needs; genuine attempts to facilitate their performance and stability in sustainable energy technologies is equally important.

**Acknowledgements** Kamlesh and Satya Prakash thanks to University Grant Commission and Council of Science and Research of India for the JRF fellowship. Dr. Archana Singh thanks to Department of Science and Technology for funding.

## References

1. Current World Population (2021) Available from: <https://www.worldometers.info/world-population/>
2. Dinçer İ, Zamfirescu C (2016) Sustainable hydrogen production. Elsevier
3. IEA, Net Zero by 2050 (2021)
4. IEA (2020) CO<sub>2</sub> emissions from fuel combustion: overview
5. Johuri B (2019) The chemical element hydrogen in hydrogen energy: challenges and solutions for a cleaner future. Springer, pp 1–35
6. De Miranda PEV (2019) Hydrogen energy: sustainable and perennial, in science and engineering of hydrogen-based energy technologies. Elsevier, pp 1–38
7. Ursua A, Gandia LM, Sanchis P (2012) Hydrogen production from water electrolysis: current status and future trends. Proc IEEE 100(2):410–426
8. Shiva Kumar S, Himabindu V (2019) Hydrogen production by PEM water electrolysis—a review. Mater Sci Energy Technol 2(3):442–454
9. Borgschulte A (2016) The hydrogen grand challenge. Frontiers Energy Res 4(11)
10. Holladay JD et al (2009) An overview of hydrogen production technologies. Catal Today 139(4):244–260
11. Scott K (2020) Chapter 1 introduction to electrolysis, electrolyzers and hydrogen production. In: Electrochemical methods for hydrogen production. The Royal Society of Chemistry, pp 1–27
12. Inzelt G (2014) Crossing the bridge between thermodynamics and electrochemistry. From the potential of the cell reaction to the electrode potential. ChemTexts 1(1):2

13. Suen N-T et al (2017) Electrocatalysis for the oxygen evolution reaction: recent development and future perspectives. *Chem Soc Rev* 46(2):337–365
14. Ali A, Shen PK (2020) Recent progress in graphene-based nanostructured electrocatalysts for overall water splitting. *Electrochem Energy Rev* 3(2):370–394
15. Lee Y et al (2012) Synthesis and activities of rutile IrO<sub>2</sub> and RuO<sub>2</sub> nanoparticles for oxygen evolution in acid and alkaline solutions. *J Phys Chem Lett* 3(3):399–404
16. Li C, Baek J-B (2020) Recent advances in noble metal (Pt, Ru, and Ir)-based electrocatalysts for efficient hydrogen evolution reaction. *ACS Omega* 5(1):31–40
17. Xu Y, Zhang B (2019) Recent advances in electrochemical hydrogen production from water assisted by alternative oxidation reactions. *ChemElectroChem* 6(13):3214–3226
18. Khan MA et al (2018) Recent progresses in electrocatalysts for water electrolysis. *Electrochem Energy Rev* 1(4):483–530
19. Jiang L et al (2020) Controllable Co@N-doped graphene anchored onto the NRGO toward electrocatalytic hydrogen evolution at all pH values. *Chem Commun* 56(4):567–570
20. El-Sawy AM et al (2016) Controlling the active sites of sulfur-doped carbon nanotube-graphene nanolobes for highly efficient oxygen evolution and reduction catalysis. *Adv Energy Mater* 6(5):1501966
21. Alduhaish O et al (2019) Facile synthesis of mesoporous  $\alpha$ -Fe<sub>2</sub>O<sub>3</sub>@g-C<sub>3</sub>N<sub>4</sub>-NCs for efficient bifunctional electro-catalytic activity (OER/ORR). *Sci Rep* 9(1):14139
22. Zulfarnain M et al (2020) FeCoSe<sub>2</sub> nanoparticles embedded in g-C<sub>3</sub>N<sub>4</sub>: a highly active and stable bifunctional electrocatalyst for overall water splitting. *Sci Rep* 10(1):6328
23. Zhang Y et al (2017) Ultrafine metal nanoparticles/N-doped porous carbon hybrids coated on carbon fibers as flexible and binder-free water splitting catalysts. *Adv Energy Mater* 7(15):1700220
24. Zhang Y et al (2017) Ultrathin CNTs@FeOOH nanoflake core/shell networks as efficient electrocatalysts for the oxygen evolution reaction. *Mater Chem Frontiers* 1(4):709–715
25. Zhang H et al (2020) Ni-doped hierarchical porous carbon with a p/n-junction promotes electrochemical water splitting. *Int J Hydrogen Energy* 45(35):17493–17503
26. Li J et al (2017) Graphene and their hybrid electrocatalysts for water splitting. *ChemCatChem* 9(9):1554–1568
27. Ding N et al (2014) Influence of carbon pore size on the discharge capacity of Li–O<sub>2</sub> batteries. *J Mater Chem A* 2(31):12433–12441
28. Shen W, Li Z, Liu Y (2010) Surface chemical functional groups modification of porous carbon. *Recent Patents Chem Eng* 1:27–40
29. Feron PHM, Jansen AE (1997) The production of carbon dioxide from flue gas by membrane gas absorption. *Energy Convers Manage* 38:S93–S98
30. Li YH, Lee CW, Gullett BK (2002) The effect of activated carbon surface moisture on low temperature mercury adsorption. *Carbon* 40(1):65–72
31. Wang H, Gao Q, Hu J (2009) High hydrogen storage capacity of porous carbons prepared by using activated carbon. *J Am Chem Soc* 131(20):7016–7022
32. Seehra MS (2016) Mesoporous carbons for energy-efficient water splitting to produce pure hydrogen at room temperature. *IntechOpen*
33. Ito Y et al (2015) High catalytic activity of nitrogen and sulfur Co-doped nanoporous graphene in the hydrogen evolution reaction. *Angew Chem Int Ed* 54(7):2131–2136
34. Biswas C, Lee YH (2011) Graphene versus carbon nanotubes in electronic devices. *Adv Func Mater* 21(20):3806–3826
35. Chen S et al (2014) Nitrogen and oxygen dual-doped carbon hydrogel film as a substrate-free electrode for highly efficient oxygen evolution reaction. *Adv Mater* 26(18):2925–2930
36. Chen S, Qiao S-Z (2013) Hierarchically porous nitrogen-doped graphene–NiCo<sub>2</sub>O<sub>4</sub> hybrid paper as an advanced electrocatalytic water-splitting material. *ACS Nano* 7(11):10190–10196
37. Li T et al (2020) Metal-free photo- and electro-catalysts for hydrogen evolution reaction. *J Mater Chem A* 8(45):23674–23698
38. Zheng Y et al (2014) Toward design of synergistically active carbon-based catalysts for electrocatalytic hydrogen evolution. *ACS Nano* 8(5):5290–5296

39. Li J et al (2016) Mechanistic insights on ternary Ni<sub>2</sub>-xCoxP for hydrogen evolution and their hybrids with graphene as highly efficient and robust catalysts for overall water splitting. *Adv Func Mater* 26(37):6785–6796
40. Li Y et al (2011) MoS<sub>2</sub> nanoparticles grown on graphene: an advanced catalyst for the hydrogen evolution reaction. *J Am Chem Soc* 133(19):7296–7299
41. Deng ZH et al (2015) Synthesized ultrathin MoS<sub>2</sub> nanosheets perpendicular to graphene for catalysis of hydrogen evolution reaction. *Chem Commun* 51(10):1893–1896
42. Roy SB et al (2019) Iridium on vertical graphene as an all-round catalyst for robust water splitting reactions. *J Mater Chem A* 7(36):20590–20596
43. Ge M et al (2016) A review of one-dimensional TiO<sub>2</sub> nanostructured materials for environmental and energy applications. *J Mater Chem A* 4(18):6772–6801
44. Zhang A, Yang L, Zhang L (2020) Z-Scheme 2D/3D hierarchical MoS<sub>2</sub>@CoMoS<sub>4</sub> flower-shaped arrays with enhanced full spectrum light photoelectrocatalytic activity for H<sub>2</sub>O<sub>2</sub>/p-aminophenol production and contaminant degradation. *J Mater Chem A* 8(48):25890–25903
45. Ledendecker M et al (2015) Highly porous materials as tunable electrocatalysts for the hydrogen and oxygen evolution reaction. *Adv Func Mater* 25(3):393–399
46. Thomas A et al (2008) Graphitic carbon nitride materials: variation of structure and morphology and their use as metal-free catalysts. *J Mater Chem* 18(41):4893–4908
47. Tian J et al (2014) Ultrathin graphitic C<sub>3</sub>N<sub>4</sub> nanosheets/graphene composites: efficient organic electrocatalyst for oxygen evolution reaction. *Chemsuschem* 7(8):2125–2130
48. Zhao Y et al (2014) Graphitic carbon nitride nanoribbons: graphene-assisted formation and synergic function for highly efficient hydrogen evolution. *Angew Chem Int Ed* 53(50):13934–13939
49. Zheng Y et al (2014) Hydrogen evolution by a metal-free electrocatalyst. *Nat Commun* 5(1):3783
50. Pei Z et al (2016) Toward enhanced activity of a graphitic carbon nitride-based electrocatalyst in oxygen reduction and hydrogen evolution reactions via atomic sulfur doping. *J Mater Chem A* 4(31):12205–12211
51. Shinde SS, Sami A, Lee J-H (2015) Electrocatalytic hydrogen evolution using graphitic carbon nitride coupled with nanoporous graphene co-doped by S and Se. *J Mater Chem A* 3(24):12810–12819
52. Peng Y et al (2017) Hydrogen evolution reaction catalyzed by ruthenium ion-complexed graphitic carbon nitride nanosheets. *J Mater Chem A* 5(34):18261–18269
53. Chen J et al (2019) Low-coordinate iridium oxide confined on graphitic carbon nitride for highly efficient oxygen evolution. *Angew Chem Int Ed* 58(36):12540–12544
54. Kumar MP et al (2017) NiWO<sub>3</sub> nanoparticles grown on graphitic carbon nitride (g-C<sub>3</sub>N<sub>4</sub>) supported toray carbon as an efficient bifunctional electrocatalyst for oxygen and hydrogen evolution reactions. *Part Part Syst Charact* 34(10):1700043
55. Israr M et al (2020) Rapid conjunction of 1D carbon nanotubes and 2D graphitic carbon nitride with ZnO for improved optoelectronic properties. *Appl Nanosci* 10(10):3805–3817
56. Zheng Zx et al (2019) Palladium nanoparticles/graphitic carbon nitride nanosheets-carbon nanotubes as a catalytic amplification platform for the selective determination of 17 $\alpha$ -ethinylestradiol in feedstuffs. *Sci Rep* 9(1):14162
57. Cui W et al (2014) Activated carbon nanotubes: a highly-active metal-free electrocatalyst for hydrogen evolution reaction. *Chem Commun* 50(66):9340–9342
58. Kweon DH et al (2020) Ruthenium anchored on carbon nanotube electrocatalyst for hydrogen production with enhanced faradaic efficiency. *Nat Commun* 11(1):1278
59. Li W et al (2019) 3D hollow Co–Fe–P nanoframes immobilized on N, P-doped CNT as an efficient electrocatalyst for overall water splitting. *Nanoscale* 11(36):17031–17040
60. Wang J et al (2014) Cobalt nanoparticles encapsulated in nitrogen-doped carbon as a bifunctional catalyst for water electrolysis. *J Mater Chem A* 2(47):20067–20074
61. Liu Y et al (2019) Cobalt nanoparticles encapsulated in nitrogen-doped carbon nanotube as bifunctional-catalyst for rechargeable Zn-air batteries. *Front Mater* 6(85)

62. Zou X et al (2014) Cobalt-embedded nitrogen-rich carbon nanotubes efficiently catalyze hydrogen evolution reaction at all pH values. *Angewandte Chemie* 126
63. Yan X et al (2020) In-situ growth of Ni nanoparticle-encapsulated N-doped carbon nanotubes on carbon nanorods for efficient hydrogen evolution electrocatalysis. *Nano Res* 13(4):975–982
64. Chemelewski WD et al (2014) Amorphous FeOOH oxygen evolution reaction catalyst for photoelectrochemical water splitting. *J Am Chem Soc* 136(7):2843–2850
65. Suzuki TM et al (2017) Highly crystalline  $\beta$ -FeOOH(Cl) nanorod catalysts doped with transition metals for efficient water oxidation. *Sustain Energy Fuels* 1(3):636–643
66. Luo W et al (2017) Highly crystallized  $\alpha$ -FeOOH for a stable and efficient oxygen evolution reaction. *J Mater Chem A* 5(5):2021–2028
67. Niu S et al (2019) Se-doping activates FeOOH for cost-effective and efficient electrochemical water oxidation. *J Am Chem Soc* 141(17):7005–7013
68. Davodi F et al (2017) Straightforward synthesis of nitrogen-doped carbon nanotubes as highly active bifunctional electrocatalysts for full water splitting. *J Catal* 353:19–27
69. Lu X et al (2015) Electrocatalytic oxygen evolution at surface-oxidized multiwall carbon nanotubes. *J Am Chem Soc* 137(8):2901–2907
70. Qu K et al (2017) Polydopamine-inspired, dual heteroatom-doped carbon nanotubes for highly efficient overall water splitting. *Adv Energy Mater* 7(9):1602068
71. Mette K et al (2012) Nanostructured manganese oxide supported on carbon nanotubes for electrocatalytic water splitting. *ChemCatChem* 4(6):851–862
72. Antoni H et al (2018) Oxidative deposition of manganese oxide nanosheets on nitrogen-functionalized carbon nanotubes applied in the alkaline oxygen evolution reaction. *ACS Omega* 3(9):11216–11226
73. Melder J et al (2020) Water-oxidation electrocatalysis by manganese oxides: syntheses, electrode preparations, electrolytes and two fundamental questions. *Z Phys Chem* 234(5):925–978
74. Begum H et al (2019) Carbon nanotubes-based PdM bimetallic catalysts through  $N_4$ -system for efficient ethanol oxidation and hydrogen evolution reaction. *Sci Rep* 9(1):11051
75. Ouyang T et al (2019) Heterostructures composed of N-doped carbon nanotubes encapsulating cobalt and  $\beta$ - $Mo_2C$  nanoparticles as bifunctional electrodes for water splitting. *Angew Chem Int Ed* 58(15):4923–4928
76. Yang J, Fujigaya T, Nakashima N (2017) Decorating unoxidized-carbon nanotubes with homogeneous Ni–Co spinel nanocrystals show superior performance for oxygen evolution/reduction reactions. *Sci Rep* 7(1):45384
77. Wu J et al (2012)  $Co_3O_4$  nanocrystals on single-walled carbon nanotubes as a highly efficient oxygen-evolving catalyst. *Nano Res* 5(8):521–530
78. Gong M et al (2013) An advanced Ni–Fe layered double hydroxide electrocatalyst for water oxidation. *J Am Chem Soc* 135(23):8452–8455
79. Zhao Y et al (2013) Nitrogen-doped carbon nanomaterials as non-metal electrocatalysts for water oxidation. *Nat Commun* 4(1):2390
80. Lei Y et al (2019) Nitrogen-Doped porous carbon nanosheets strongly coupled with  $Mo_2C$  nanoparticles for efficient electrocatalytic hydrogen evolution. *Nanoscale Res Lett* 14(1):329
81. Liang H-W et al (2015) Molecular metal–Nx centres in porous carbon for electrocatalytic hydrogen evolution. *Nat Commun* 6(1):7992
82. Zhao Y et al (2016) Electrospun cobalt embedded porous nitrogen doped carbon nanofibers as an efficient catalyst for water splitting. *J Mater Chem A* 4(33):12818–12824
83. Lin X et al (2016) Precious-metal-free Co–Fe– $O_x$  coupled nitrogen-enriched porous carbon nanosheets derived from Schiff-base porous polymers as superior electrocatalysts for the oxygen evolution reaction. *J Mater Chem A* 4(17):6505–6512
84. Li W et al (2019) C–CoP hollow microporous nanocages based on phosphating regulation: a high-performance bifunctional electrocatalyst for overall water splitting. *Nanoscale* 11(36):17084–17092
85. Lv C et al (2016) The hierarchical nanowires array of iron phosphide integrated on a carbon fiber paper as an effective electrocatalyst for hydrogen generation. *J Mater Chem A* 4(4):1454–1460

86. Lai J et al (2016) Unprecedented metal-free 3D porous carbonaceous electrodes for full water splitting. *Energy Environ Sci* 9(4):1210–1214
87. Yu Z-Y et al (2017) A one-dimensional porous carbon-supported Ni/Mo<sub>2</sub>C dual catalyst for efficient water splitting. *Chem Sci* 8(2):968–973
88. Zhang M et al (2018) Novel MOF-derived Co@ N-C bifunctional catalysts for highly efficient Zn–air batteries and water splitting. *Adv Mater* 30(10):1705431
89. Xu D et al (2017) Synthesis and application of a MOF-derived Ni@ C catalyst by the guidance from an in situ hot stage in TEM. *RSC Adv* 7(42):26377–26383
90. Wang H et al (2017) Metal-organic frameworks for energy applications. *Chem* 2(1):52–80
91. Li H et al (2018) Titanium phosphonate based metal–organic frameworks with hierarchical porosity for enhanced photocatalytic hydrogen evolution. *Angew Chem* 130(12):3276–3281
92. Miner EM et al (2016) Electrochemical oxygen reduction catalysed by Ni 3 (hexaiminotriphenylene) 2. *Nat Commun* 7(1):1–7
93. Bhattacharyya S, Das C, Maji TK (2018) MOF derived carbon based nanocomposite materials as efficient electrocatalysts for oxygen reduction and oxygen and hydrogen evolution reactions. *RSC Adv* 8(47):26728–26754
94. Liu B et al (2008) Metal-organic framework as a template for porous carbon synthesis. *J Am Chem Soc* 130(16):5390–5391
95. Jahan M, Liu Z, Loh KP (2013) A Graphene oxide and copper-centered metal organic framework composite as a tri-functional catalyst for HER, OER, and ORR. *Adv Func Mater* 23(43):5363–5372
96. Abdelkader-Fernandez VK et al (2019) Noble-metal-free MOF-74-derived nanocarbons: insights on metal composition and doping effects on the electrocatalytic activity toward oxygen reactions. *ACS Appl Energy Mater* 2(3):1854–1867
97. Wang M et al (2017) Metal–organic framework derived carbon-confined Ni 2 P nanocrystals supported on graphene for an efficient oxygen evolution reaction. *Chem Commun* 53(59):8372–8375
98. Wei J et al (2015) A graphene-directed assembly route to hierarchically porous Co–N<sub>x</sub>/C catalysts for high-performance oxygen reduction. *J Mater Chem A* 3(32):16867–16873
99. Yu X, Feng Y, Guan B, David Lou XW, Paik U (2016) *Energy Environ Sci* 1246–1250
100. Li J-S et al (2017) Highly efficient hydrogen evolution electrocatalysts based on coupled molybdenum phosphide and reduced graphene oxide derived from MOFs. *Chem Commun* 53(93):12576–12579
101. Kuang M et al (2017) Electrocatalysts: Cu, Co-embedded N-enriched mesoporous carbon for efficient oxygen reduction and hydrogen evolution reactions. *Adv Energy Mater* 7(17)
102. Qamar M et al (2016) Metal–organic framework-guided growth of Mo<sub>2</sub>C embedded in mesoporous carbon as a high-performance and stable electrocatalyst for the hydrogen evolution reaction. *J Mater Chem A* 4(41):16225–16232
103. Zhang G et al (2018) Temperature effect on Co-based catalysts in oxygen evolution reaction. *Inorg Chem* 57(5):2766–2772
104. Wu R et al (2016) Porous cobalt phosphide/graphitic carbon polyhedral hybrid composites for efficient oxygen evolution reactions. *J Mater Chem A* 4(36):13742–13745
105. Chen Z et al (2018) Ultrafine Co nanoparticles encapsulated in carbon-nanotubes-grafted graphene sheets as advanced electrocatalysts for the hydrogen evolution reaction. *Adv Mater* 30(30):1802011
106. Dong Q et al (2016) MOF-derived Zn-doped CoSe<sub>2</sub> as an efficient and stable free-standing catalyst for oxygen evolution reaction. *ACS Appl Mater Interfaces* 8(40):26902–26907
107. Xu H et al (2018) MOF-derived hollow CoS decorated with CeO<sub>x</sub> nanoparticles for boosting oxygen evolution reaction electrocatalysis. *Angew Chem* 130(28):8790–8794
108. Zhang T et al (2017) Hybrids of cobalt/iron phosphides derived from bimetal–organic frameworks as highly efficient electrocatalysts for oxygen evolution reaction. *ACS Appl Mater Interfaces* 9(1):362–370
109. Wang X et al (2019) MOF derived N-doped carbon coated CoP particle/carbon nanotube composite for efficient oxygen evolution reaction. *Carbon* 141:643–651

110. Luo X et al (2018) One-dimensional porous hybrid structure of Mo<sub>2</sub>C-CoP encapsulated in N-doped carbon derived from MOF: an efficient electrocatalyst for hydrogen evolution reaction over the entire pH range. *ACS Appl Mater Interfaces* 10(49):42335–42347
111. Li Y et al (2018) Metal organic framework-derived CoPS/N-doped carbon for efficient electrocatalytic hydrogen evolution. *Nanoscale* 10(15):7291–7297
112. Singh T et al (2020) MOF derived Co<sub>3</sub>O<sub>4</sub>@ Co/NCNT nanocomposite for electrochemical hydrogen evolution, flexible zinc-air batteries, and overall water splitting. *Inorg Chem* 59(5):3160–3170
113. Feng X et al (2019) Bimetal-Organic framework-derived porous rodlike cobalt/nickel nitride for All-pH value electrochemical hydrogen evolution. *ACS Appl Mater Interfaces* 11(8):8018–8024
114. Zhang J et al (2015) A metal-free bifunctional electrocatalyst for oxygen reduction and oxygen evolution reactions. *Nat Nanotechnol* 10(5):444–452



# Chapter 12

## Core–Shell Nanostructures-Based Porous Carbon Nanomaterials for Oxygen Reduction Reaction



Saravanan Nagappan, Malarkodi Duraivel, Shamim Ahmed Hira, Mohammad Yusuf, Sanjay S. Latthe, Kandasamy Prabakar, and Kang Hyun Park

### 1 Introduction

Core–shell nanostructures (CSNs) have attracted considerable attentions in various applications such as catalysis, electrocatalysis, energy conversion and storage (ECS), optical devices, drug delivery, biomedical, sensors, actuators, environmental remediation, heavy metal adsorption due to the presence of unique structural properties [1–5]. Zhang et al. discussed the various parameters that are needed to be addressed before synthesizing the CSNs for a particular application [1]. Here, some of the points have to be considered mainly for the synthesis of various CSNs. (1) Selecting the required CSN based on the choice of mono-, di-, multi-, or porous CSNs. (2) Fix the proper shape and size requirements for constructing the CSNs with various shapes such as core–shell, yolk–shell, and hollow–shell nanostructures with controlled particles size. (3) Constructing the CSNs with proper core and shell based on the application requirement. (4) Also selecting the core centre material with one or more materials to tune the surface and morphological properties [1]. On the other hand, Gawande et al. classified the CSNs based on the presence of inorganic/inorganic,

---

S. Nagappan (✉) · S. A. Hira · M. Yusuf · K. H. Park (✉)  
Department of Chemistry, Chemistry Institute for Functional Materials, Pusan National University, Busan 46241, Republic of Korea  
e-mail: [saravananagappan@gmail.com](mailto:saravananagappan@gmail.com)

K. H. Park  
e-mail: [chemistry@pusan.ac.kr](mailto:chemistry@pusan.ac.kr)

M. Duraivel · K. Prabakar  
Department of Electrical Engineering, Pusan National University, 2 Busandaehak-ro, 63beon-gil, Geumjeong-Gu, Busan 46241, Republic of Korea

S. S. Latthe  
Self-Cleaning Research Laboratory, Department of Physics, RajeRamrao College, Affiliated to Shivaji University, Jath 416404, Kolhapur, Maharashtra, India

inorganic/organic, organic/organic, organic/inorganic materials present in the structure [2]. The core and shell chemical compositions are also tuned based on the end-use of application. Generally, the more active materials can accumulate on the shell, and core material acts as support, so that the active material can easily react with the foreign matter and exhibit better reactivity in various applications.

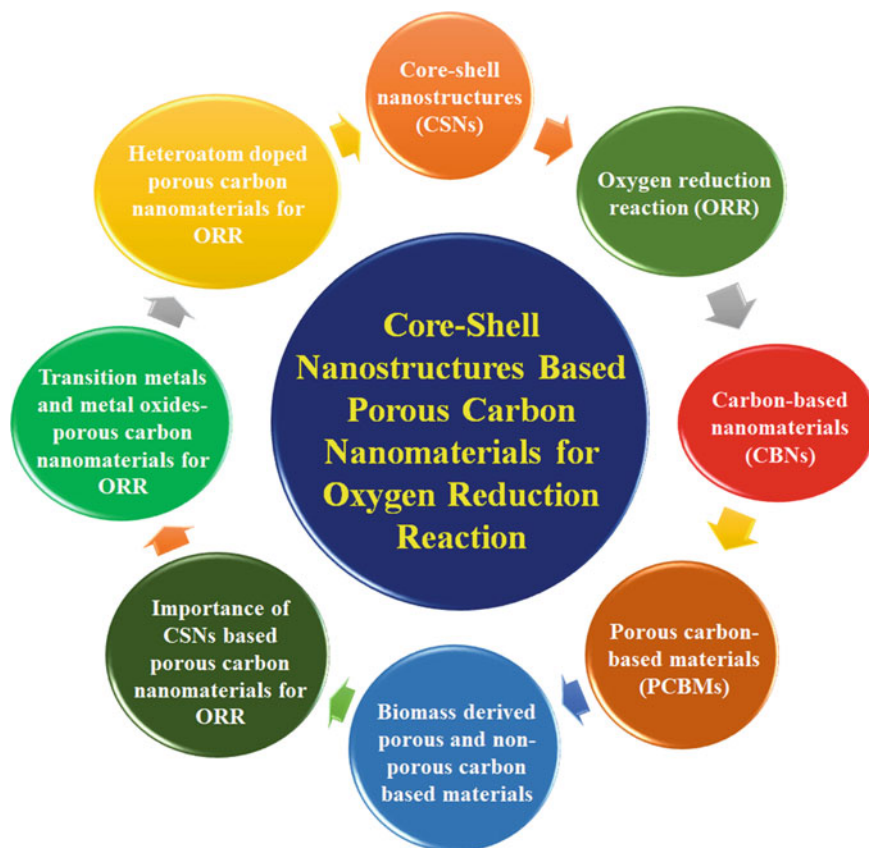
Recently, CSNs were used widely in electrocatalysis applications especially in oxygen reduction reaction (ORR), oxygen evolution reaction (OER), hydrogen evolution reaction (HER), etc., owing to the higher catalytic performance and the maintenance of excellent stability of the CSNs by the presence of active surfaces, defects, and higher pore volume and surface area, respectively for the electrocatalysis applications [6, 7]. Furthermore, CSNs also expressed considerable attentions in wide variety of fuel cells and battery applications [8–12]. One of the structural advantages of CSNs over other nanomaterials is the combinations of two or more materials in a single material with controlled size, shape, and morphology with abundant surface area and easy adjustable surface structure.

Recently, carbon-based nanomaterials were used widely for electrochemical reactions due to the ease of availability, possessing excellent stability under harsh environments and the presence of high surface area and low cost as compared with the platinum or other metal-based electrocatalysts [13–16]. Similarly, porous carbon (PC) also showed huge interest in various applications. Porous carbon materials can exhibit high pore volume and surface area, excellent porosity, better durability, and improved electrical conductivity. Various carbon-based materials like carbon materials derived from different biomasses, activated carbon (AC), carbon nanotubes (CNTs), graphene, or graphene oxide (GO) were used to design the CSNs with exceptional properties [17–21]. The synthesis of porous carbon-containing CSNs also gains significant attentions in the recent days [8, 10, 17].

In this chapter, we briefly describe the importance of porous carbon-based CSNs for electrocatalytic ORR activity. We also cover how the porous and non-porous carbon nanostructures on the CSNs playing a vital role on enhancing the ORR activity as well as stability. In addition, the effect of transition metals and metal oxide on the porous carbon-based CSNs was also analysed deeply for ORR. Finally, we summarize the various aspects of porous carbon-based CSNs and their future perspective for improving the catalytic activity, stability, and robustness from the recent literatures. Figure 1 clearly shows the possible directions of the CSNs-based porous carbons obtained at various methods with superior properties that can be used for ORR.

## 2 Oxygen Reduction Reaction (ORR)

ORR is highly important in various fuel cells and battery applications because the reaction is controlled kinetically based on the four or two-electron transfer mechanisms. In most cases, platinum (Pt)-based electrode was used in fuel cell as well as ORR activity due to the superior electrocatalytic activity of Pt-based electrode



**Fig. 1** Schematic illustration of various porous carbon nanomaterials with core-shell nanostructures for oxygen reduction reaction

[22, 23]. At the same time, this can show severe drawbacks such as low tolerance, expensive, and low durability. These parameters are widely lacking to use the Pt-based electrodes for such applications. Much efforts were devoted to overcome these drawbacks by reducing the Pt content, introducing heteroatoms as well as porous carbon-based materials, and use of highly abundant low-cost transition metals [24]. Recently, the CSNs with heteroatoms, Pt group free transition metals, and CSNs with PC nanostructures were expressed tremendous attentions in electrocatalytic ORR activity as well as for other applications [13, 25–29]. Porous carbon nanotubes (CNTs) and graphene-based carbon materials with CSNs can display improved electrical conductivity, alcohol tolerance, and electrocatalytic activity.

Dahal et al. obtained a PC nanofiber with core-shell nanostructures (CSNs) by first fabricating a zinc oxide-loaded polyacrylonitrile (PAN)-based nanofiber by in-situ mixing of PAN and zinc acetate in dimethyl formamide (DMF) and electrospun followed by annealing at 350 °C for 2 h to obtain a ZnO-PAN nanofiber

(Fig. 2a) [13]. The nanofiber is further modified with metal organic framework (MOF) using 2-methylimidazolate to form a zeolitic imadazolate framework (ZIF) structure on the ZnO-PAN nanofiber which was further modified with boron (B) and nitrogen (N) heteroatoms using 0.1 M aqueous ammonium hydrogen borate trihydrate ( $(\text{NH}_4\text{HB}_4)_7 \cdot 3\text{H}_2\text{O}$ ) and 0.1 M aqueous sodium borohydride ( $\text{NaBH}_4$ ). The modified material pyrolyzed and washed with sulphuric acid ( $\text{H}_2\text{SO}_4$ ), ethanol, and deionized water to give ZIF-8-based boron (B) and nitrogen (N)-doped PC nanofiber. The prepared nanofiber delivered an outstanding electrochemical ORR activity due to enhanced electrical conductivity as well as the presence of more active sites based on the presence of B and N heteroatoms.

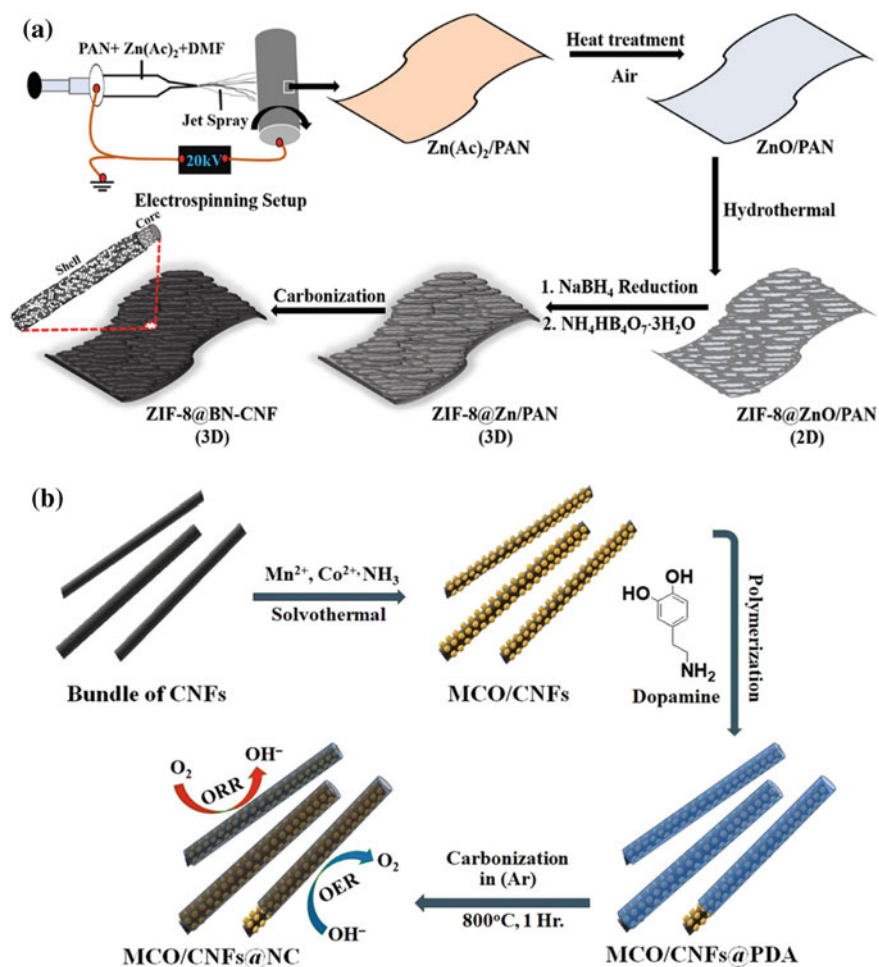
Gebremariam et al. also disclosed the preparation of manganese (Mn) and cobalt (Co) loading on the carbon nanofibers followed by the surface modification with N-doped carbon obtained from by the surface treatment of the metal-loaded nanofibers with dopamine and subsequent pyrolysis (Fig. 2b) [25]. The prepared electrocatalyst can perform excellent.

ORR behaviour and also used as a cathode electrode in Zn-air battery as well as supercapacitor applications.

The oxygen evolution reaction requires higher overpotential and demonstrated a significant interest in metal-air battery and water electrolyser applications [30]. The combinations of ORR and OER electrodes were used as cathode and anode electrodes for battery application, whereas the combination of OER and HER was used in water-splitting application. OER took place by evolving a molecular oxygen via a chemical reaction with the support of four electrons and protons. Iridium (Ir)-based catalyst has displayed benchmark OER activity and stability especially under acidic condition than various transition metals or other nanomaterials [30]. Under acidic media, most of the transition metals have exhibited lower OER activity, whereas the transition metal oxides have significant OER effect only at basic condition. To overcome these drawbacks, much efforts were drawn to develop a high-performance OER electrocatalyst having significant stability at both acidic and basic conditions with almost comparable or improved activity than the Ir-based catalyst [30].

On the other hand, Pt-based electrocatalyst has displayed outstanding electrocatalytic activity for ORR as compared with various other existing materials. Both Ir and Pt are very expensive in the commercial aspects of mass production of the electrodes for practical applications. Much attentions were paid on a new these aspects and also improve the performances significantly than the commercial electrodes by creating nanomaterial that can have the ability to solve the drawbacks. The OER activity mainly studied the overpotential value of an electrode from their specific current density. A catalyst having lower overpotential can display superior OER activity [30]. The catalysts made for ORR as well as OER both have identical features based on the end-use of applications. Recently, significant attentions were paid for the high-performance bifunctional electrocatalyst containing both OER and ORR as well as OER and HER electrocatalytic activities.

The mechanisms for OER and ORR occur in acidic and alkaline environments based on the following ways [31, 32].



**Fig. 2** **a** Schematic illustration of the synthetic process of ZIF-8-assimilated B and N co-doped core-shell 3D CNFs. Reprinted with permission from Dahal et al. [13]. Copyright 2020 Elsevier B.V. **b** Schematic illustration of synthetic route of MCO/CNFs@NC catalysts. MCO is MnCo<sub>2</sub>O<sub>4</sub>, CNFs is carbon nanofibers, and NC is nitrogen-doped carbon. Reprinted with permission from Gebremariam et al. [25]. Copyright 2018 American Chemical Society

OER	Acidic condition	$2\text{H}_2\text{O} \rightarrow \text{O}_2\uparrow + 4\text{H}^+ + 4\text{e}^-$
	Alkaline condition	$4\text{OH}^- \rightarrow \text{O}_2\uparrow + 2\text{H}_2\text{O} + 4\text{e}^-$
	Aprotic electrolyte	$\text{O}_2^{2-} \rightarrow \text{O}_2\uparrow + 2\text{e}^-$
ORR	Acidic condition	$\text{O}_2 + 4\text{e}^- + 4\text{H}^+ \rightarrow 2\text{H}_2\text{O}(4\text{e}^-)$
		$\text{O}_2 + 2\text{H}^+ + 2\text{H}_2\text{O} \rightarrow \text{H}_2\text{O}_2(2 + 2\text{e}^-)$
		$\text{H}_2\text{O}_2 + 2\text{e}^- + 2\text{H}^+ \rightarrow 2\text{H}_2\text{O}$

(continued)

(continued)

	Alkaline condition	$\text{O}_2 + 4\text{e}^- + 2\text{H}_2\text{O} \rightarrow 4\text{OH}^- (4\text{e}^-)$ $\text{O}_2 + 2\text{e}^- + \text{H}_2\text{O} \rightarrow \text{HO}_2^- (2 + 2\text{e}^-)$ $\text{HO}_2^- + 2\text{e}^- + \text{H}_2\text{O} \rightarrow 3\text{OH}^-$
	Aprotic electrolyte	$\text{O}_2 + \text{e}^- \rightarrow \text{O}_2^-$ $\text{O}_2^- + \text{e}^- \rightarrow \text{O}_2^{2-}$

OER is mostly dependent on pH, because under acidic or neutral conditions, two water molecules were oxidized and generate an oxygen molecule and four electrons, whereas hydroxyl groups were oxidized to oxygen and water under basic conditions [32]. On the other hand, ORR can occur at two possible routes such as two and four-electron pathways with partial or complete reduction. Both OER and ORR have some drawbacks such as slow kinetics, poor reversibility of oxygen, and high overpotential when using in metal-air battery [32].

### 3 Carbon-Based Nanomaterials (CBNs)

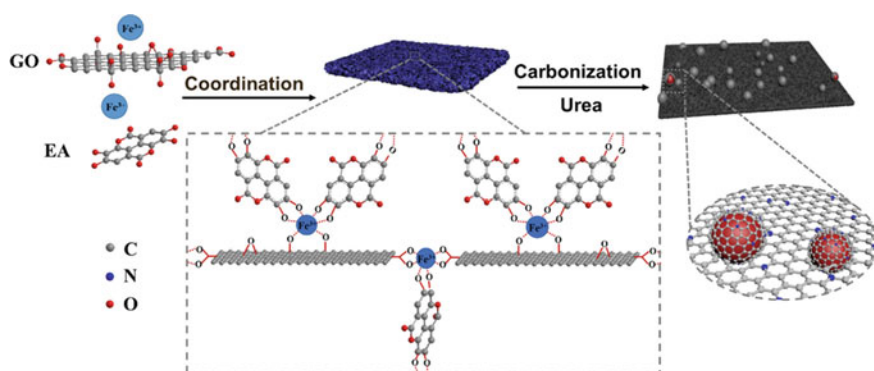
Carbon materials are mainly composed of three types of forms such as amorphous carbon, graphitic, and diamond like carbon which are varied based on the arrangement of carbon atoms [33]. In early 1985, the fullerenes-based CBNs such as C<sub>60</sub>, C<sub>70</sub>, C<sub>84</sub> were discovered and used in variety of applications due to the unique structural feature of the fullerenes [34]. Later on, CNTs with one-atom-thick tubular-shaped graphitic sheet, GO, graphene, and single-layered graphene-based CBNs were discovered via various physicochemical methods which dominate the overall research fields for the past few decades and also applied in various industrial products [34]. This is owing to the possesses of larger surface area, porosity, and superior chemical, electrical, physical, and optical properties, respectively, as compared with various other nanomaterials due to the abundant availability, flexibility, low cost, environmental-friendly, good chemical and thermal stability. CNTs have several advantages because of superior architecture obtained by the chemical vapour deposition with single or multi-layered tubular structure with uniform length and diameter, and the presence of extended SP<sup>2</sup> carbon would responsible for enhancing the electrical and optical properties [35]. In addition, due to an exceptional mechanical stability, flexibility, and rigidity of CNTs, which can be widely used as a filler for the development of various composites for high-yield applications.

In the recent days, noble metal-free materials such as platinum group metal (PGM) free transition metals, metal oxides, carbon-based nanomaterials (CBNs) were demonstrated with the wider applicability in various applications [36]. Among the transition metal-based material, CBNs were displayed with huge interest in catalysis, ECS, biological, and environmental applications [16, 32, 37–41]. The structural incorporation by doping of heteroatoms such as nitrogen, sulphur, phosphorous, boron, respectively, on the CBNs may also enhance the physicochemical properties [37], owing to the creation of surface defects and edges as well as the presence

of more active materials in the CBNs. Among the various CBNs, graphene, GO, CNTs, ACs illustrated a widespread usability in different application on account of unique physicochemical behaviours. So that these materials were used largely in several applications especially in electrocatalysis, ECS, biological, and environmental remediation. Baby et al. briefly reviewed the important aspects of CBNs for the treatment of heavy metals from the polluted water as well as other environmental applications [41]. The author discussed the role of various dimensional CBNs for their effective metal adsorption and remediation. Based on the structural and dimensional parameters, CBNs can show different behaviours in numerous applications.

The formation of CSNs on the graphite carbon surface by embedding with iron source has been achieved by two steps of processes such as first, mixing the graphene oxide (GO) with ellagic acid (EA) and iron ( $\text{Fe}^{3+}$ ) source to form a coordination complexes between these materials which further produces a well-ordered graphitic carbon which is wrapped with iron and forms CSNs on the surface under pyrolysis in the presence of urea (Fig. 3) [42]. The prepared electrocatalyst demonstrated an outstanding electrocatalytic ORR activity because of the presence of more active sites by the metal source as well as N heteroatom comes from the carbonization of urea [42]. The surface functionalization on carbon material can show a remarkable effect in the electrocatalytic ORR activity. Various methods were used to functionalize the carbon support such as strong acidic or alkali treatments, modifying the surface functionality with heteroatoms, high-temperature pyrolysis treatment, electrochemical etching, and various other methods.

Kim et al. briefly studied the important aspects of oxygen functionalization on the carbon containing Pt catalyst (Pt/C). The oxygen surface functionalization was carried out on the carbon black (CB-O) using strong acidic solutions followed by Pt loading by incipient-wetness impregnation method and subsequent hydrogen reduction [43]. The Pt/CB-O has displayed excellent ORR activity with excellent electrochemical active surface area (EASA) than the pristine Pt/CB. These results convey



**Fig. 3** Schematic illustration of the synthetic procedure for GEFs. Reprinted with permission from Zhao et al. [42]. Copyright 2018 American Chemical Society

that the oxygen functionalization on carbon could effectively improve the electrochemical ORR activity as well as stability. The main reason behind that is the partial oxidation of Pt nanoparticles in the Pt/CB-O catalyst [43]. On the other hand, doping of one or more heteroatoms such as N, B, sulphur (S), and phosphorus (P), respectively, to the carbon support can also increase the electrical conductivity and electrochemical activity for ORR due to formation of more number of active sites and defects [44–46].

## 4 Porous Carbon-Based Materials (PCBMs)

PCBMs also attracted huge interest for numerous applications than CBMs because of the controlled porosity and architecture. Porous carbon materials can be obtained by direct pyrolysis, chemical vapour deposition (CVD), templating method using hard (inorganic) or soft (organic) materials followed by calcination or pyrolysis, and electrospinning [47, 48]. Ma et al. briefly reviewed the synthesis of well-ordered mesoporous carbon nanostructures with higher surface areas and pore volumes using various kinds of hard and soft templates [49]. In particular, the authors suggested that the synthesis of mesoporous carbon is mainly based on the use of hard template by the following ways such as synthesis of mesoporous matrix followed by addition of necessary carbon precursor in order to modify the mesoporous structure by various approaches such as chemical vapour deposition, pyrolysis, calcination, hydro/solvothermal, and microwave-assisted methods, respectively. Further, polymerization of the organic precursor to develop an organic–inorganic hybrid material followed by carbonization and template removal using acidic or alcoholic wash to generate a highly PC [49]. The three-dimensional (3D) porous carbons and hollow carbon spheres derived from various sources have demonstrated the better hosting nature to S or various heteroatoms which can be used for battery, fuel cell, and other electrochemical applications [50, 51]. For example, S hosting on the PC can deliver outstanding electrochemical performance in lithium (Li)-S batteries on account of excellent loading of S atom on the PC [52]. Moreover, the presence copious amount pore structure and surface area in the PC can have better loading of S atom which boost the electron transport and Li-ion as well as stability.

The porous carbon synthesized by the use of metal organic frameworks (MOFs) also has huge impact in various electrochemical reactions owing to the presence of heteroatoms with significant amounts of pore structures which improve the electrocatalytic activity [53–55]. The ZIFs-based PC nanomaterial is also derived by the use of cobalt precursor with 2-methylimidazole (MeIM) which has abundant nitrogen atom in the PC and delivers an excellent electrochemical activity of ORR [56]. Luo et al. briefly discussed the important role of PC for supercapacitor applications with their effect of pore structure, surface area, surface heteroatoms and defects, and electrode design [57]. The materials with reasonable porosity, higher surface area, and superior physicochemical stability can deliver an excellent electrical conductivity.



Similarly, several research groups also discussed the use of various porous carbon-like materials for supercapacitor and other electrochemical ECS applications [58, 59]. Although various heteroatoms doping on the carbon-based materials are studied so far for ORR or other electrochemical reactions, the use of oxygen-rich carbon instead of heteroatoms is also playing a significant role in the recent days for ORR, because oxygen-rich carbon materials are directly responsible for the four-electron transfer reaction [60]. At the same time, this can show some drawbacks of reducing the electron-transport behaviour, possibility of de-bonding the conjugated structure, and difficult to incorporate larger quantity of oxygen atoms on the carbon network [60]. As like as the PCBNs obtained from activated carbon, CNTs, graphene, the mesoporous carbon nanospheres, nanoparticles, or hollow carbon nanomaterials obtained by the use of hard or soft template followed by pyrolysis also draw tremendous consideration in electrochemical ECS applications [47, 61].

Sun et al. synthesized a highly hierarchical PC by in-situ doping of N and S heteroatoms on the graphene like microstructures [47]. The porosity of the material was derived by the use of organic precursor by CVD followed by the impregnation with poly(vinylpyrrolidone) (PVP) and ammonium persulfate  $(\text{NH}_4)_2\text{S}_2\text{O}_8$  in aqueous solution and pyrolysed at 800 °C in an argon/hydrogen (Ar/H<sub>2</sub>) atmosphere followed by acid etching. The as-synthesized PC can express higher surface area and degree of graphitization, uniform porosity with well-controlled N and S doping as lead to superior electrochemical activity in Li-ion battery application due to the enhanced physicochemical properties [47]. A well-ordered mesoporous structure was fabricated by the mixing of polyaniline (PANI), dicyandiamide, and iron (III) nitrate nonahydrate  $(\text{Fe}_3(\text{NO})_3 \cdot 9\text{H}_2\text{O})$  in dimethyl formamide (DMF), followed by loading of silica bead (30% ethylene glycol) and continued stirring of suspension and subsequent ultrasonication to develop a well-dispersed suspension and transferred to glass petri dishes and dried at 80 °C in an oven for overnight. The sample is further pyrolysed at 900 °C under nitrogen atmosphere to yield the N-doped mesoporous carbon (Fig. 4) [62]. The as-developed materials have excellent physicochemical properties, and also the fabricated cathode electrode demonstrated an excellent ORR activity because of the presence of well-controlled PC structure with high surface area, graphitic, and pyridinic N [62].

Roberts et al. used ice as a hard template to synthesis hierarchical porous N-rich carbon monoliths [63]. They synthesized a hierarchical PC by various approaches using melamine, graphene, or the combination of melamine and graphene as an additive to synthesize the carbon monoliths. The porous N-rich carbon monoliths was prepared by dissolving polyacrylonitrile (PAN) in dimethyl sulfoxide (DMSO) and freeze-dried under liquid nitrogen which is used as an ice template followed by lyophilization in freeze drier for 48 h to remove an excess DMSO. The obtained PAN monolith immersed further in deionized water to remove the DMSO by solvent exchange method and dried at 60 °C for 3 h. The monoliths was treated under air atmosphere at 280 °C for 1 h with the heating rate of 1 °C min<sup>-1</sup>. The pyrolysis of PAN monoliths at 800 °C for 2.5 h with the heating rate of 5 °C min<sup>-1</sup> in a steel pyrolysis chamber to stable and cross-linked polymer network in order to produce a hierarchical N-rich PC. An anode electrode fabricated by the use of the N-rich PC



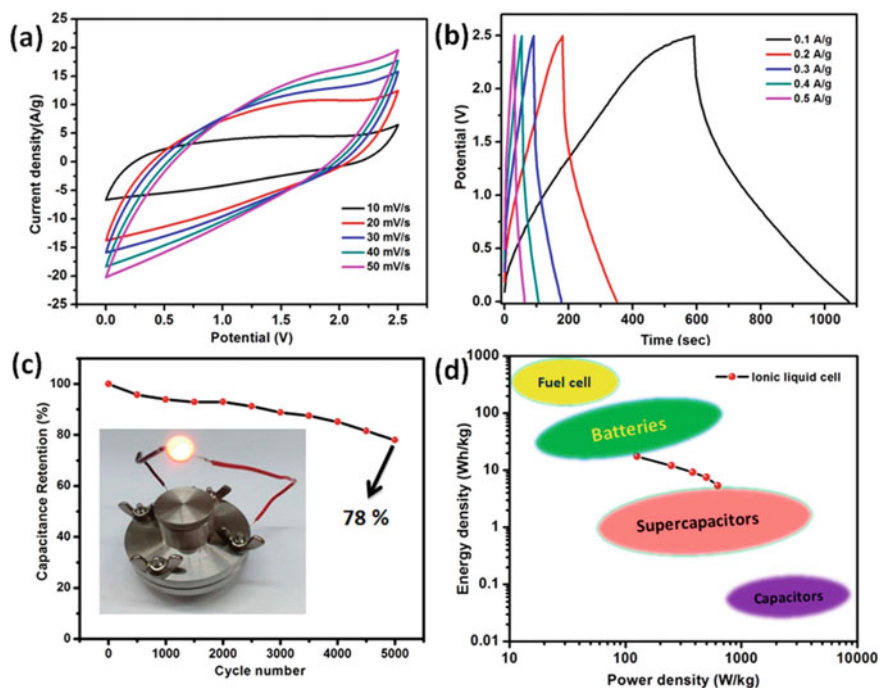
**Fig. 4** Schematic illustration of the procedure of the synthesis of porous doped carbon nanostructures. Reprinted with permission from Kwon et al. [62]. Copyright 2019 The Korean Society of Industrial and Engineering Chemistry. Published by Elsevier B.V

delivered an excellent performance in Li-ion battery due to availability of sufficient porosity and hierarchical morphology. Moreover, the presence of more nitrogen atom in the PC is also responsible to enhance the Li-ion battery performance. Furthermore, the introduction of melamine, graphene during the preparation PC also increases the N-content as well as improves the electrical conductivity due to incorporation of conductive graphene in the PC with the reversible capacity of  $300 \text{ mA h g}^{-1}$  at  $10 \text{ A g}^{-1}$  [63].

## 5 Biomass-Derived Porous and Non-Porous Carbon-Based Materials

Recently, much attentions were paid on the design and development of various porous and non-porous CBMs derived from various bio-sources because of the abundant availability of the bio-sources in the earth crust [64, 65]. Biomass are mainly differentiated based on the presence of agricultural and herbaceous sources, bacteria, fungus, plants and marine algae, animal, human, and industrial waste-based biomass which accounts for the maximum ways of developing different sources of biomass [64]. Kaur et al. briefly described the important role of biomass derived-PCBNs for electrochemical ORR activity with various ways of preparation and modification of carbon networks in the porous carbons [64]. He et al. also synthesized the bifunctional PCBNs with N and S heteroatoms for ORR and supercapacitor applications [66]. The synthesized bifunctional nanomaterials showed an excellent electrical conductivity with outstanding electrochemical performance for multiple applications.

The CBNs were derived by the direct pyrolysis of bio-sources followed by some chemical treatments, also by hydrothermal or solvothermal methods, chemical vapour deposition, and some other routes [64]. These CBNs are much useful in various applications especially in electrochemical ECS applications due to an improved electrical conductivity, abundant availability of the basic resources, development of high pore diameter, surface area, and pore volume, respectively [64–70]. Sudhan et al. used a rice straw-based biomaterial to synthesize activated PC by washing chopped, dried rice straw in water followed by drying at 80 °C for 24 h in an oven and pyrolysed at 600 °C for 4 h in argon atmosphere at the heating rate of 5 °C min<sup>-1</sup> (Fig. 5) [69]. The carbon material was activated further using KOH to yield activated PC which exhibits a superior activity for supercapacitor and showed also the improved electrocatalytic activity in fuel cell application [69], whereas the shell of pumpkin seeds was also used to get the PC by first activating the cleaned shell using potassium hydroxide (KOH) followed by heat treatment for certain temperature and further pyrolysis to yield highly PCBNs [71]. The carbon material played a vital role in the absorption of microwave.



**Fig. 5** **a** CV profile of the AA-RSC symmetric two-electrode cell in [EMIM] [BF<sub>4</sub>], **b** CD profile of the AA-RSC symmetric cell at different current densities, **c** specific capacitance of the AA-RSC symmetric cell as a function of the cycle number at 0.5 A g<sup>-1</sup> current density and the AA-RSC symmetric cell-powered LED (inset), and **d** ragone plot for the AA-RSC symmetric cell in an ionic liquid electrolyte. Reprinted with permission from Sudhan et al. [69]. Copyright 2016 American Chemical Society

Yang et al. briefly reviewed the important aspects of bio-derived carbon for the microbial fuel cell application [72]. Liu et al. studied the N heteroatom-doped PC for ORR activity by preparing the PC from the water hyacinth biomaterial [73]. The water hyacinth washed with deionized water and cut it in to small pieces and dried at 80 °C for 12 h followed by mixing with zinc chloride ( $\text{ZnCl}_2$ ) at the ratios of 1:6 and pyrolysed at 600 °C as well as 800 °C for 2 h in  $\text{N}_2$  atmosphere. The prepared carbon material was washed with 0.5 M nitric acid ( $\text{HNO}_3$ ) and 1 M hydrochloric acid (HCl) and deionized water followed by dried at 80 °C [73]. Similarly, lotus root, spinach leaves, soybean straw, and raw woods were also used to prepare the high PCBMs by activating with suitable activating agents and protocols and reported the better performance in electrochemical ORR activity [74–77]. Various other biomaterials-based PC materials were also prepared in different approaches and used an electrocatalyst with superior stability and performance for ORR activity [78–80]. More recently, Sumboja et al. prepared the iron and cobalt (FeCo) loaded with N heteroatom-doped PC using the combinations of pistachio and peanut shells which displayed an excellent performed in aluminium (Al)-air battery [81]. This finding clearly tells the important role of various biomass for the preparation of PCBMs and their wider applicability in various electrochemical energy storage and conversion as well as for other applications.

## 6 Importance of CSNs-Based Porous Carbon Nanomaterials for ORR

CSNs are highly important in various applications because the structure is controlled precisely based on the requirements with one or more atoms either in the core or shell [82]. In most cases, core is worked as a support to the shell, so that the deposition of a thin layer of Pt could have a huge impact in the electrocatalytic application. The Pt loading is also kinetically controlled by alloying with other earth-abundant Pt free transition metals or doping with heteroatoms to make more active sites or by creating defects at the edges as well as corners in shell which could make the material much suitable for superior electrocatalytic applications [83]. Likewise, the intrinsic activity of Pt-based catalyst is also controlled by the introduction of secondary transition metals by alloying with Pt such as the formation of the chemical compositions of PtCo, PtNi, PtFe, PtCu, and PtCr which also illustrated the creation of higher mass and specific activities than commercial Pt or Pt/C catalyst [84].

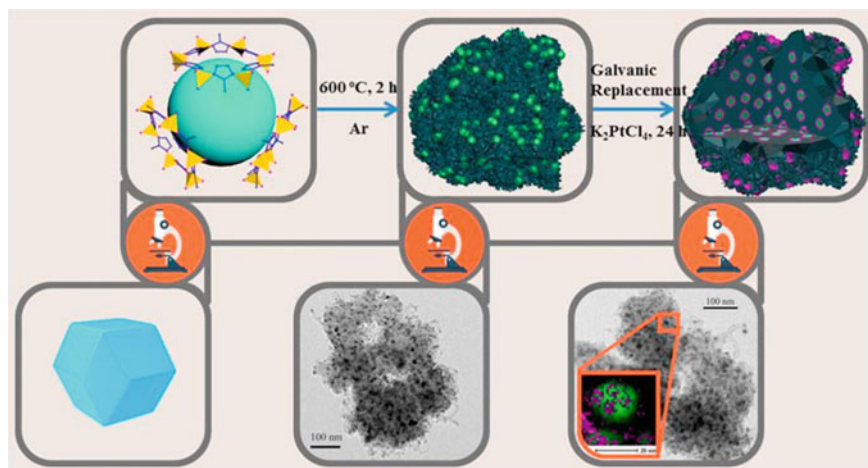
CSNs have reduced the impact of higher loading Pt by the introduction of low-cost transition metal in the core which facilitates the easier display of catalytically active sites to molecular hydrogen as well as reduces the final cost of the electrocatalyst. At the same time, the introduction of only metal sources sometimes expressed poor stability against acidic and basic conditions due to decompose or precipitation behaviour at these condition. Further, the chemical, thermal, and mechanical stability and electrical conductivity of carbon or PC materials were improved using CSNs.

In addition, the introduction of heteroatoms in the PC network structure of CSNs also eases the enhancement of electrical conductivity, specific and mass activities as well as various other properties necessary to improve the performance of the electrocatalyst for ORR and other electrochemical applications [13, 25, 84].

Wang et al. developed a N-doped ZIF-67-based PC by first synthesizing ZIF-67 and pyrolysed at 600 °C for 2 h in Ar atmosphere followed by Pt loading on the shell structure by galvanic replacement mechanism (Fig. 6) [84]. The synthesized nanostructure exhibits sufficient active sites and high specific surface area as well as better tolerance with robust property and durability in the CSNs which are practically much important to the improve ORR performance. Various MOF-based PC nanostructures also demonstrated efficient electrocatalytic applications due to the constrained architecture of MOF with interesting properties based on the presence of organic–inorganic materials used to develop the materials [54, 85]. Porous material can easily control the reaction between the electrolyte and electrode due to the easier transport of electrons and protons between the pore channels which facilitate an enhanced electrocatalytic activity as compared to the non-porous carbon-based materials. In some cases, the oxygen and N-rich porous metal-free carbons also delivered outstanding ORR activity and also used for fuel cell applications due to the presence of low overpotential, large specific capacitance, long-term stability, higher surface area and controlled porosity, uniform distribution of heteroatoms on the pore channel or carbon networks, and excellent electrical conductivity [86, 87]. Similarly, the presence transition metal with heteroatom-doped porous carbons also demonstrated a significant advancement in order to improve the electrocatalytic ORR activity [88, 89]. The structural defects are also playing a vital role in upgrading the electrocatalytic activity for ORR. Jia et al. discussed in detail the various parameters such as etching, doping, ball-milling, annealing, plasma treatment, electrochemical method, photoreduction, and hydrogenation methods, respectively, which were used to create the defects in the electrocatalyst [90]. Controlling the defects and vacancies in the CSNs containing PC frameworks would improve the catalytic activity.

## 7 Transition Metals and Metal Oxides-Embedded Porous Carbon Nanomaterials for ORR

Earth-abundant transition metals and metal oxides are playing a pivotal role in electrochemical ECS applications due to abundant availability of the transition metals as well as their low cost as compared with the noble metals such as Pt, Ru, Ir, Au, and Ag, respectively [51, 91]. The modification of these transition metals to achieve a highly porous carbon-based transition metals also considers an effective approach in electrochemical ECS because of the generation of an excellent porosity, surface area, pore volume. Moreover, the PC would facilitate an enhanced electrical conductivity and stability. Ahn et al. modified the surface of a one-dimensional nanotubes such as porous tellurium nanotubes (Te NTs) with ZIF-8 structure and embedded further by



**Fig. 6** Schematic of the preparation of Co@Pt-NC nanocomposites. Reprinted with permission from Wang et al. [84]. Copyright 2017 Elsevier B.V.

using dopamine hydrochloride as well as with ferric chloride and subsequent pyrolysis at 950 °C for 2 h with heating rate of 5 °C min<sup>-1</sup> to yield a highly PC [92]. The electrode fabricated by using these materials delivered an outstanding ORR activity under both acidic and basic media. The well-ordered FeN<sub>x</sub> active site present on the PC with large graphitic layers at the surface would be responsible for the efficient catalytic activity. In addition, the fabricated electrode also showed an outstanding result in zinc-air battery application [92].

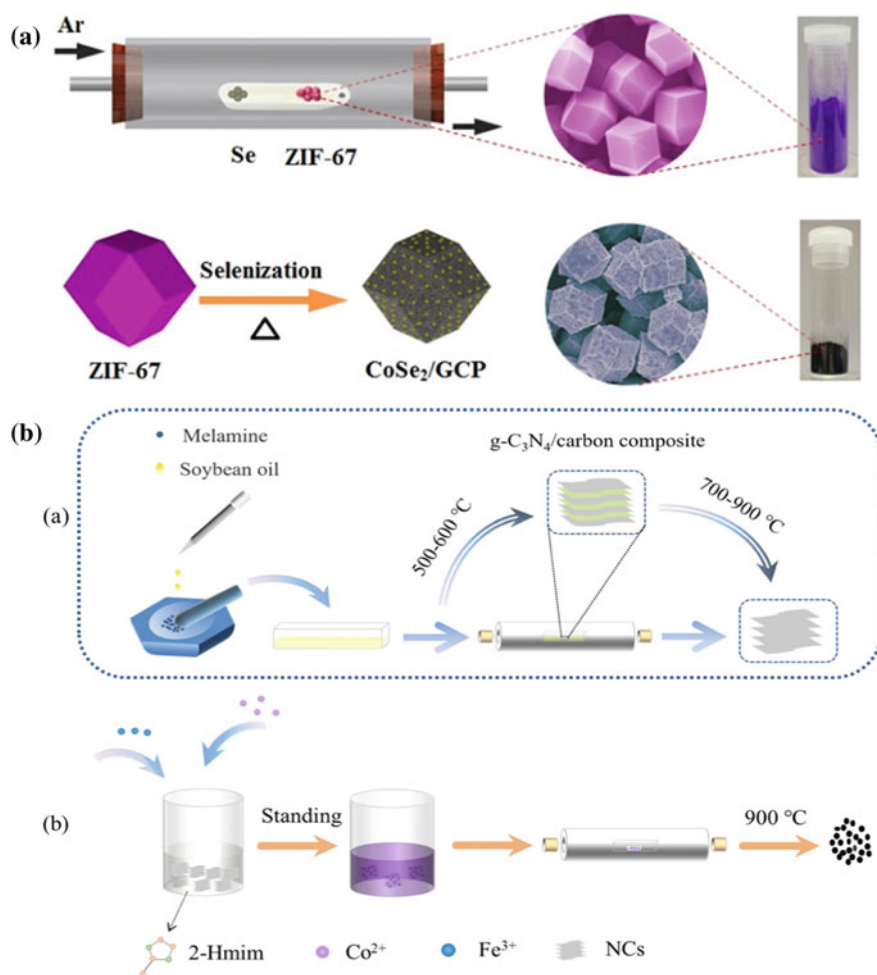
Song et al. briefly reviewed the important role of non-precious transition metal-based carbon materials with N heteroatom for the ORR as well as their future use in proton exchange membrane in fuel cell application [93]. These types of hybrid electrocatalyst with M-N<sub>x</sub>C (where M = metal source,  $x = 2$  or 4 based on metal and nitrogen bonding such as MN<sub>2</sub> or MN<sub>4</sub>) structures have acquired much observation in the recent days because of the low cost, earth abundant, excellent electrical conductivity, easier reproducibility, and existence of more active sites, respectively. The improvement in the electrocatalytic activity of ORR observed for the M-N<sub>x</sub>C-based electrode would depend up on the carbon support on the transition metals because an excellent dispersibility was encountered based on the presence of carbon atom which eases better dispersibility and enhances the electrocatalytic activity for ORR [93]. In addition, the heteroatom doping on the carbon-supported transition metals also displayed better catalytic activity as compared with the absence of heteroatom [93, 94]. This is due to the creation of more numbers of active sites on the carbon-supported transition metals by the heteroatom.

The porous carbon polyhedral (PCP) synthesized with the decoration of cobalt and diselenide by simple selenization of the as-synthesized ZIF-67 with selenium by pyrolysis technique can deliver the uniform embedding of metal sources within the PCPs and also displayed an excellent properties and also manifested an outstanding

performance in the electrocatalysis of ORR (Fig. 7a) [95]. The organic ligand in the ZIF-67 structure was converted to graphitic carbon polyhedral (GCP) during the carbonization process, and at the same time, the then diselenide also loaded uniformly throughout the cobalt (Co)/GCP [95]. These can yield a stable and strong connection between the carbon surface and metal sources which ease the formation of more active sites. Moreover, the synthesized material displayed an excellent dispersibility, electrical conductivity, and also a high surface area which are responsible to show superior durability and catalytic activity in alkaline media [95]. Similarly, a recent study of synthesizing the iron-loaded ZIF-67 structure followed by pyrolysis also yields the transition metal-embedded PC which also conveys an outstanding electrocatalytic activity to ORR (Fig. 7b) [96].

## 8 Heteroatom-Doped CSNs with Porous Carbon Nanomaterials for ORR

Heteroatoms such as N, P, B, S, and the combination of two or more heteroatoms present in the CSNs-based PC have displayed an excellent electrocatalytic activity. These heteroatoms-doped porous carbons can be applied in various ECS applications owing to the availability of abundant active sites, surface defects as well as the presence of lone pair of electrons which boost up the electron transfer and enhance the electrical conductivity for electrocatalysis applications [97–102]. The ZIF-67-based material itself having N heteroatom from the ligand and subsequent pyrolysis may indicate the appearance of more active sites and the formation graphene like carbon in their structure which is responsible for the effective ORR electrocatalytic activity as like as the commercial platinum/carbon (Pt/C) electrode [95, 96]. The synthesis of phosphorous and iron-doped PC can be easily obtained by mixing the triphenylphosphine precursor with zinc and ferric chlorides followed by carbonization at different temperatures such as 800 °C, 900 °C, and 1000 °C, respectively, and further acid washing using hydrochloric acid followed by deionized water to get the PC (Fig. 8) [103]. Various other kinds of low-cost Pt group free transition metals and metal oxide with PC were also well executed for an effectively electrocatalytic ORR reaction, because of abundant availability, low cost, compared performance as like as commercial Pt/c electrode, possessing [29, 104–107]. More studies also performed the synthesis of much effective heteroatom-doped CSNs-based porous carbons in the recent years for ORR activities because the heteroatom doping in the CSNs as well as in porous carbons not only enhances the electrochemical activities, it also enhances various physicochemical properties which are much important in various applications.

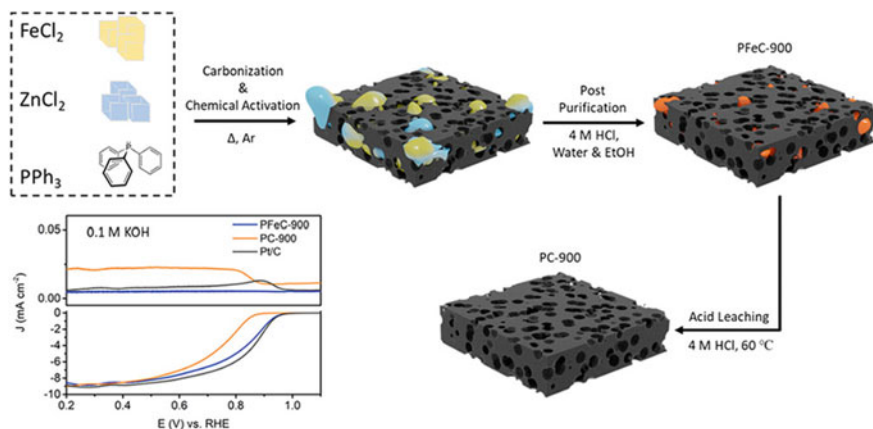


**Fig. 7** a Schematic illustration of fabrication of ZIFs-derived CoSe<sub>2</sub>/GCP hybrid composites. Reprinted with permission from Wu et al. [95]. Copyright 2016 Elsevier B.V. b Schematic illustration for the fabrication of FC@NCs. Reprinted with permission from Luo et al. [96]. Copyright 2021 Elsevier Inc.

## 9 CSNs with Carbon Nanomaterials for ORR or OER with Supercapacitor Behaviour

Supercapacitors are playing an important role for the current demand of energy storage [108]. The materials with good cyclic performance, high specific power, flexibility, fast charge–discharge rate, high surface area, and cyclic stability can be used widely for supercapacitor application [109]. A binder-free electrode fabrication method is the most desirable approach for designing an electrocatalyst for ECS





**Fig. 8** Schematic illustration of the preparation of iron phosphide-doped PC for ORR. Reprinted with permission from Norouzi et al. [103]. Copyright 2020 American Chemical Society

application due to the presence of binder would increase the contact resistance of the electrode. The electrode having an electrocatalytic ORR activity with supercapacitor behaviours attracted huge interest in fuel cell and supercapacitor applications [108, 109]. Recently, numerous works were focused on ORR as well as supercapacitive behaviours using various nanomaterials [68, 108, 109]. Gao et al. prepared the nitrogen and oxygen dual-doped carbon (NODC-800); electrocatalyst obtained from catkins was used as superior ORR catalyst in alkaline fuel cell with superior capacity of  $109 \text{ F g}^{-1}$  at  $0.5 \text{ A g}^{-1}$  and maintained the stability over 1000 cycles [108]. The author also prepared N-doped PC spheres at large scale using fermented rice-based biomass as an active material. The prepared material has high porosity ( $1.14 \text{ cm}^3 \text{ g}^{-1}$ ) with maximum surface area ( $2105.9 \text{ m}^2 \text{ g}^{-1}$ ), and outstanding electrocatalytic four-electron ORR activity [110]. In addition, the electrocatalyst also exhibits good cyclic stability and specific capacitance of  $219 \text{ F g}^{-1}$  at the discharge current density of  $15 \text{ A g}^{-1}$ . Kim et al. synthesized a nickel-mediated metal organic frameworks (MOFs)-based macroporous carbon (Ni-MOF@mC) which can deliver an outstanding electrocatalytic ORR activity and superior supercapacitive behaviour because of well-defined pore size, presence of high surface area, chemical tenability, and conductivity of the material [111]. The Ni-MOF@mC can show the specific surface area with normalized capacitance of  $26.5 \text{ mF cm}^{-2}$  as well as high capacitance performance of  $109 \text{ F g}^{-1}$ .

Likewise, a material possessing both OER and supercapacitor characteristics also displays significant interest in ECS applications [112–116]. OER took place by the oxidation of two water molecules with four electrons followed by the removal of four protons to produce a weak O–O bond [117]. The important drawbacks of OER are the need of high overpotential to reach a desirable current density as well as the use of expensive iridium- or ruthenium-based catalysts [118]. Khalid et al. have prepared highly active and low-cost electrode using natural sugar powder as a biosource by

reacting with red phosphorous to form a carbon particle [119]. The carbon-based electrode prepared from the sugar source displays the overpotential of 1.69 V versus Reversible hydrogen electrode (RHE) at  $10 \text{ mA cm}^{-2}$  current for the OER also showcases the specific capacitance of  $105.8 \text{ F g}^{-1}$  with 100% of the initial capacitance retention even after 3000 voltammogram cycles. More recently, Kale et al. fabricated a binder-free nanocrystalline cobalt sulphide (CoS) on stainless steel (SS) substrate by chemical bath deposition (CBD) that has showed a remarkable supercapacitive and OER activity [120]. The prepared electrocatalyst showcases the specific capacitance of  $252.39 \text{ F g}^{-1}$  @  $5 \text{ mV s}^{-1}$  and maintained the initial capacitance over 1000 cycles of CV. In addition, the electrode can also present the overpotential of  $300 \text{ mV}$  @  $10 \text{ mA cm}^{-2}$  and Tafel slope of  $57 \text{ mV decade}^{-1}$ . The excellent properties of the prepared electrode were due to the origination of uniform thin films of nanocrystalline hexagonal CoS on the SS substrate [120]. The surface corrosion/oxidation effects worsen the performance of most of the fabricated electrodes in both ECS [121]. This drawback can be encountered by synthesizing CSNs with conductive core and nanostructured outer shell. The core-shell FeO@CuCo<sub>2</sub>S<sub>4</sub> was fabricated on a nickel foam (NF) substrate by two-step synthesis approaches such as hydrothermal growth of CuCo<sub>2</sub>S<sub>4</sub> on NF substrate followed by FeO deposition on the substrate via magnetic sputtering technique. The fabricated electrode offers an excellent specific capacitance of  $3213 \text{ F g}^{-1}$  at  $1 \text{ A g}^{-1}$  and withholds over 99% of efficiency after 10,000 charge/discharge cycles. On the other hand, the electrode also displays low overpotential of  $\sim 240 \text{ mV}$  at  $10 \text{ mA cm}^{-2}$  and Tafel slope of  $51 \text{ mV dec}^{-1}$ . Moreover, the electrode can be usable up to the current density of  $100 \text{ mA cm}^{-2}$  for over 25 h [121]. Chu et al. fabricated phosphorous-doped NiCo<sub>2</sub>O<sub>4</sub> (P-NCO) nanowires on NF substrate by two steps such as growth of NiCo<sub>2</sub>O<sub>4</sub> on NF substrate by hydrothermal method followed by phosphatization via pyrolysis step [122]. The P-NCO electrode can have the superior specific capacitance of  $2747.8 \text{ F g}^{-1}$  at  $1 \text{ A g}^{-1}$  as well as low overpotential of  $300 \text{ mV}$  at  $10 \text{ mA cm}^{-2}$  (1 M KOH) activity during OER.

## 10 Factors that Affect the Performance of Carbon Materials in ORR

There are several factors that affect the production of carbon-based materials in ORR such as surface defects and active sites, porosity, electronic configuration, types dopants, presence of inorganic impurities, acidic and basic solutions concentration, band gap. Tian et al. discussed the important role of N-content in the transition metal carbides (TMCs) as well as kind of graphitic shells that can largely affect the performance of the carbon-based electrode during ORR [123]. Carbon-based materials like carbon nanotubes, graphene, activated carbon, carbon black, mesoporous carbon, and carbon nanofibers are considered to be inactive electrocatalyst due to unavailability of catalytic active sites for the ORR [124]. At the same time, the electrocatalytic

ORR activity was increased by the introduction of heteroatoms to the carbon material via in-situ doping during the synthesis or post-treatment of the carbon material with dopants [123, 124]. In both ways, the fabricated electrocatalyst can deliver a remarkable catalytic activity for the ORR. Likewise, the introduction of some kinds of defects to the carbon material also showed much-improved ORR activity [125].

Some studies were demonstrated that the existence of less content of N in the carbon-based material after high-temperature treatment can deliver outstanding positive onset potential and also provide almost four-electron transfer number than the presence of larger contents of N in the carbon-based material [125]. Because the introduction of N atom to the C can activate the electronic structure of the neighbouring carbon atom that facilitates the active role for ORR. So, the synthesis of defective carbon with adjustable electronic configuration can play a vital role in ORR [125]. The ORR activity of the pristine carbon can also be activated by physical intermolecular charge transfer, introducing of non-metal heteroelements to the carbon matrix, and developing structural defects [126]. The introduction of boron and nitrogen dopant to the carbon would slightly alter the energy gap, whereas increasing more dopants to the carbon would significantly increase the energy gap and reduce the conductivity [127]. So, the use of average quantity of B and N on the carbon can show outstanding ORR activity. The porosity of the carbon material with various length scales as well as the presence of dopants also showed an adverse effect in the mass transfer during ORR [126]. The availability of microporosity in the carbon material can present superior ORR activity than the mesoporosity. At the same time, some studies were suggested that the mesoporosity with larger pore size and specific surface area would facilitate the easier contact of the reactant through the pore channels [128]. On the other hand, the combination of micro and mesoporosity with wider porosity as well as hydrophilic behaviour can further enhance the electrocatalytic ORR activity [129–131]. The band gap of carbon material also plays an important role to decide the ORR activity. When the dopants are attached to the same sublattice, parts of the carbon material can deliver the maximum band gap and closed, while the dopants are placed adjust to carbon sublattice [132]. The band gap of carbon material increases with increasing doping concentrations. In general, band gap is inversely proportional to the conductivity. The outstanding ORR activity was achieved with the reduced band gap of the carbon material [133]. The B and N-doped carbon material can show smaller energy gap as compared to the pristine graphene, whereas overdoping to the carbon material can lead to increase of energy gap. The lowest energy gap of the B and N-doped carbon can demonstrate the highest chemical reactivity and catalytic performance [132, 134]. We also compared various CSNs obtained with PC nanomaterials for ORR in 0.1 M KOH (Table 1).

## 11 Future Perspectives and Outlooks

The CSNs-based PC has attracted considerable attentions in the recent days due to the maintenance of excellent properties such as high surface area, pore diameter, pore

**Table 1** Comparisons of CSNs-based porous carbon nanomaterials for ORR performance in 0.1 M KOH

Catalyst	Loading (mg cm <sup>-2</sup> )	Electrolyte	E <sub>onset</sub> vs RHE	E <sub>1/2</sub> vs RHE	References
ZIF-67-900	0.7	0.1 M KOH	0.91	0.85	[135]
NC-900 (ZIF-8)	0.11	0.1 M KOH	0.83	0.68	[136]
GNPCSs-800	0.2	0.1 M KOH	0.957	0.82	[137]
NPCS-800	–	0.1 M KOH	0.95	0.83	[138]
N-doped Fe/Fe <sub>3</sub> C@C	0.7	0.1 M KOH	0.91	0.83	[139]
CNS-800	0.28	0.1 M KOH	0.914	–	[140]
NDCN-22	0.6	0.1 M KOH	0.954	–	[141]
CoP-CMP800	0.6	0.1 M KOH	0.88	0.82	[142]
NHPC <sub>1:3</sub> -900	0.42	0.1 M KOH	–	0.87	[143]
CNM@C	–	0.1 M KOH	0.72	0.62	[144]
B <sub>1.0</sub> CNM@C <sub>1.0</sub>	–	0.1 M KOH	0.78	0.68	[144]
Co@Pt-NC	–	0.1 M KOH	0.99	0.87	[84]
CoOx/Co@GC-NC	0.464	0.1 M KOH	0.957	0.858	[145]
Co@Co <sub>3</sub> O <sub>4</sub> @C-CM	0.1	0.1 M KOH	0.93	0.81	[146]
PCN-FeCo/C	0.2	0.1 M KOH	1.0	0.85	[147]
CoS NWs@NSC-2	–	0.1 M KOH	0.93	0.84	[148]
Co-C@NWCs	0.1	0.1 M KOH	0.94	0.83	[149]

volume, good electrical and thermal conductivity. Furthermore, the introduction of heteroatoms as well as non-precious transition metals to the CSNs-based PC also facilitates the much-improved physicochemical properties and excellent usability in electrocatalytic applications. These materials would help to replace the usability of precious metal consumption by doping of small quantity of heteroatoms as well as non-precious transition metals. This obviously reduces the product cost and delivers almost identical or better electrocatalytic behaviour and also improves the stability under acidic, basic as well as alcoholic solutions as compared with the commercial high-yield products made by the use of noble metal catalysts. So, the recent studies are largely focused under this area in order to reduce the product cost and enhancing the performance of the electrocatalyst. Especially, the nitrogen heteroatom-doped porous carbons are synthesized widely using various kinds of nitrogen-containing organic compounds because the carbonization of these materials would successfully form a negatively charged pyridinic N as well as graphitic N in their structure due to the availability of lone pair of electron by the N atom. Moreover, the presence of N heteroatom in the PC would facilitate the emergence of more active sites as well as defects in the carbon nanostructures. In the addition, the presence of carbon nearer to N atom would act like Lewis basicity which helps to absorb more oxygen molecules on the carbon sites. A noticeable change in the pyridinic N was due to conversion of pyridinic N to pyridonic N which can confirm the successful ORR activity occurred

on the N-doped PC electrocatalyst. In contrast, the presence of graphitic N also exhibits some defects and active sites in the PC which are also helpful in enhancing the electrochemical oxygen adsorption and reduction activity. Based on these reasons, the N-doped porous carbons were demonstrated as an excellent electrocatalyst for ORR activity and also illustrated an outstanding stability against alcoholic solution as well as acidic and basic conditions which are much-important properties for fuel cell and battery applications. In the addition, the hierarchical porous architecture in the PC would help the easier diffusivity oxygen molecules and electrolyte in the porous networks and improve the performance of the electrocatalyst of ORR. The heteroatom doping as well as non-precious transition metal ions or oxide doping on the porous carbons also has some drawbacks due to some sensitivity against moisture or other physicochemical changes by prolonged exposure which obviously reduces the performance of the developed products. More focused studies need to be carried out in order to enhance the electrocatalytic activity and improve the stability against various stimuli.

**Acknowledgements** This research was supported by the Basic Science Research Program through a National Research Foundation of Korea (NRF) grant funded by the Korean Government (MSIP) (NRF-2020R111A3067208).

## References

1. Zhang Q, Lee I, Joo JB et al (2013) Core-shell nanostructured catalysts. *Acc Chem Res* 46(8):1816–1824
2. Gawande MB, Goswami A, Asefa T et al (2015) Core-shell nanoparticles: synthesis and applications in catalysis and electrocatalysis. *Chem Soc Rev* 44(21):7540–7590
3. Feng H, Tang L, Zeng G et al (2019) Core-shell nanomaterials: applications in energy storage and conversion. *Adv Colloid Interface Sci* 267:26–46
4. El-Toni AM, Habila MA, Labis JP et al (2016) Design, synthesis and applications of core-shell, hollow core, and nanorattle multifunctional nanostructures. *Nanoscale* 8(5):2510–2531
5. Kumar R, Mondal K, Panda PK et al (2020) Core-shell nanostructures: perspectives towards drug delivery applications. *J Mater Chem B* 8(39):8992–9027
6. Sarkar A, Manthiram A (2010) Synthesis of Pt@Cu Core-shell nanoparticles by galvanic displacement of Cu by Pt<sup>4+</sup> ions and their application as electrocatalysts for oxygen reduction reaction in fuel cells. *J Phys Chem C* 114(10):4725–4732
7. Cochell T, Li W, Manthiram A (2013) Effects of Pt coverage in Pt@PdCu<sub>5</sub>/C core-shell electrocatalysts on the oxygen reduction reaction and methanol tolerance. *J Phys Chem C* 117(8):3865–3873
8. Senthilkumar N, Gnana Kumar G, Manthiram A (2018) 3D hierarchical core-shell nanostructured arrays on carbon fibers as catalysts for direct urea fuel cells. *Adv Energy Mater* 8(6):1702207
9. Kirubakaran CJ, Kumar GG, Sha C et al (2019) Facile fabrication of Au@polyaniline core-shell nanocomposite as efficient anodic catalyst for microbial fuel cells. *Electrochim Acta* 328:135136
10. Liu J, Li W, Manthiram A (2010) Dense core-shell structured SnO<sub>2</sub>/C composites as high performance anodes for lithium ion batteries. *Chem Commun* 46(9):1437–1439

11. Fu Y, Manthiram A (2012) Core-shell structured sulfur-polypyrrole composite cathodes for lithium-sulfur batteries. *RSC Adv* 2(14):5927–5929
12. Chung SH, Chang CH, Manthiram A (2016) A core-shell electrode for dynamically and statically stable Li-S battery chemistry. *Energy Environ Sci* 9(10):3188–3200
13. Dahal B, Chae SH, Muthurasu A et al (2020) An innovative synthetic approach for core-shell multiscale hierarchically porous boron and nitrogen codoped carbon nanofibers for the oxygen reduction reaction. *J Power Sources* 453:227883
14. Laurila T, Sainio S, Caro M (2017) Hybrid carbon based nanomaterials for electrochemical detection of biomolecules. *Prog Mater Sci* 88:499–594
15. Ng YH, Ikeda S, Matsumura M, Amal R (2012) A perspective on fabricating carbon-based nanomaterials by photocatalysis and their applications. *Energy Environ Sci* 5(11):9307–9318
16. Hu C, Qu J, Xiao Y et al (2019) Carbon nanomaterials for energy and biorelated catalysis: recent advances and looking forward. *ACS Cent Sci* 5(3):389–408
17. Raj Kumar T, Gnana Kumar G, Manthiram A (2019) Biomass-derived 3d carbon aerogel with carbon shell-confined binary metallic nanoparticles in CNTS as an efficient electrocatalyst for microfluidic direct ethylene glycol fuel cells. *Adv Energy Mater* 9(16):1803238
18. He Y, Zhuang X, Lei C et al (2019) Porous carbon nanosheets: synthetic strategies and electrochemical energy related applications. *Nano Today* 24:103–119
19. Liu J, Wang S, Sun Q (2017) All-carbon-based porous topological semimetal for Li-ion battery anode material. *Proc Natl Acad Sci U S A* 114(4):651–656
20. Abbas Q, Raza R, Shabbir I, Olabi AG (2019) Heteroatom doped high porosity carbon nanomaterials as electrodes for energy storage in electrochemical capacitors: a review. *J Sci Adv Mater Devices* 4(3):341–352
21. Li X, Zhi L (2018) Graphene hybridization for energy storage applications. *Chem Soc Rev* 47:3189–3216
22. Huang L, Zaman S, Tian X et al (2021) Advanced platinum-based oxygen reduction electrocatalysts for fuel cells. *Acc Chem Res* 54(2):311–322
23. Ren X, Lv Q, Liu L et al (2019) Current progress of Pt and Pt-based electrocatalysts used for fuel cells. *Sustain Energy Fuels* 4:15–30
24. Morozan A, Josselme B, Palacin S (2011) Low-platinum and platinum-free catalysts for the oxygen reduction reaction at fuel cell cathodes. *Energy Environ Sci* 4:1238–1254
25. Gebremariam TT, Chen F, Wang Q et al (2018) Bimetallic Mn-Co oxide nanoparticles anchored on carbon nanofibers wrapped in nitrogen-doped carbon for application in Zn-air batteries and supercapacitors. *ACS Appl Energy Mater* 1(4):1612–1625
26. Ramli ZAC, Kamarudin SK (2018) Platinum-based catalysts on various carbon supports and conducting polymers for direct methanol fuel cell applications: a review. *Nanoscale Res Lett* 13:1–25
27. Ma R, Lin G, Zhou Y et al (2019) A review of oxygen reduction mechanisms for metal-free carbon-based electrocatalysts. *npj Comput Mater* 5:1–15
28. Liu D, Tao L, Yan D et al (2018) Recent advances on non-precious metal porous carbon-based electrocatalysts for oxygen reduction reaction. *ChemElectroChem* 5(14):1775–1785
29. Huang X, Shen T, Zhang T et al (2020) Efficient oxygen reduction catalysts of porous carbon nanostructures decorated with transition metal species. *Adv Energy Mater* 10(11):1900375
30. Suen N-T, Hung S-F, Quan Q et al (2017) Electrocatalysis for the oxygen evolution reaction: recent development and future perspectives. *Chem Soc Rev* 46(2):337–365
31. Priamushko T, Guillet-Nicolas R, Kleitz F (2019) Mesoporous nanocast electrocatalysts for oxygen reduction and oxygen evolution reactions. *Inorganics* 7(8):98
32. Zhang J, Xia Z, Dai L (2015) Carbon-based electrocatalysts for advanced energy conversion and storage. *Sci Adv* 1(7):e1500564
33. Dai L, Chang DW, Baek JB, Lu W (2012) Carbon nanomaterials for advanced energy conversion and storage. *Small* 8(8):1130–1166
34. Patel KD, Singh RK, Kim HW (2019) Carbon-based nanomaterials as an emerging platform for theranostics. *Mater. Horizons* 6(3):434–469

35. Cha C, Shin SR, Annabi N et al (2013) Carbon-based nanomaterials: multifunctional materials for biomedical engineering. *ACS Nano* 7(4):2891–2897
36. Sideri IK, Tagmatarchis N (2020) Noble-metal-free doped carbon nanomaterial electrocatalysts. *Chem A Eur J* 26(67):15397–15415
37. Meng Y, Huang X, Lin H et al (2019) Carbon-based nanomaterials as sustainable noble-metal-free electrocatalysts. *Front Chem* 7:759
38. Serrano-Aroca Á, Takayama K, Tuñón-Molina A et al (2021) Carbon-based nanomaterials: promising antiviral agents to combat COVID-19 in the microbial-resistant era. *ACS Nano* 15(5):8069–8086
39. Crisan L, Crisan BV, Bran S et al (2020) Carbon-based nanomaterials as scaffolds in bone regeneration. *Part Sci Technol* 38(8):912–921
40. Madima N, Mishra SB, Inamuddin I, Mishra AK (2020) Carbon-based nanomaterials for remediation of organic and inorganic pollutants from wastewater. A review. *Environ Chem Lett* 18:1169–1191
41. Baby R, Saifullah B, Hussein MZ (2019) Carbon nanomaterials for the treatment of heavy metal-contaminated water and environmental remediation. *Nanoscale Res Lett* 14:1–17
42. Zhao J, Fu N, Liu R (2018) Graphite-wrapped Fe core-shell nanoparticles anchored on graphene as pH-universal electrocatalyst for oxygen reduction reaction. *ACS Appl Mater Interfaces* 10(34):28509–28516
43. Kim JH, Cheon JY, Shin TJ et al (2016) Effect of surface oxygen functionalization of carbon support on the activity and durability of Pt/C catalysts for the oxygen reduction reaction. *Carbon N Y* 101:449–457
44. Li JC, Hou PX, Liu C (2017) Heteroatom-doped carbon nanotube and graphene-based electrocatalysts for oxygen reduction reaction. *Small* 13(45):1702002
45. Quílez-Bermejo J, Morallón E, Cazorla-Amorós D (2020) Metal-free heteroatom-doped carbon-based catalysts for ORR. A critical assessment about the role of heteroatoms. *Carbon* 165(15):434–454
46. Guo J, Niu Q, Yuan Y et al (2017) Electrospun core–shell nanofibers derived Fe–S/N doped carbon material for oxygen reduction reaction. *Appl Surf Sci* 416:118–123
47. Sun D, Yang J, Yan X (2015) Hierarchically porous and nitrogen, sulfur-codoped graphene-like microspheres as a high capacity anode for lithium ion batteries. *Chem Commun* 51:2134–2137
48. Raza A, Wang J, Yang S et al (2014) Hierarchical porous carbon nanofibers via electrospinning. *Carbon Lett* 15(1):1–14
49. Ma TY, Liu L, Yuan ZY (2013) Direct synthesis of ordered mesoporous carbons. *Chem Soc Rev* 42:3977–4003
50. Yang C, Jin H, Cui C et al (2018) Nitrogen and sulfur co-doped porous carbon sheets for energy storage and pH-universal oxygen reduction reaction. *Nano Energy* 54:192–199
51. He Z, Wei P, Chen N et al (2021) N, S-Co-doped porous carbon nanofiber films derived from fullerenes (C<sub>60</sub>) as efficient electrocatalysts for oxygen reduction and a Zn–air battery. *Chem A Eur J* 27(4):1423–1429
52. Luo S, Sun W, Ke J et al (2018) A 3D conductive network of porous carbon nanoparticles interconnected with carbon nanotubes as the sulfur host for long cycle life lithium-sulfur batteries. *Nanoscale* 10:22601–22611
53. Zhang Z, Cai Z, Wang Z et al (2021) A review on metal-organic framework-derived porous carbon-based novel microwave absorption materials. *Nano-Micro Lett.* 13:56
54. Shen K, Chen X, Chen J, Li Y (2016) Development of MOF-derived carbon-based nanomaterials for efficient catalysis. *ACS Catal* 6(9):5887–5903
55. Sen LJ, Li SL, Tang YJ et al (2014) Heteroatoms ternary-doped porous carbons derived from MOFs as metal-free electrocatalysts for oxygen reduction reaction. *Sci Rep* 4:5130
56. Li Z, Shao M, Zhou L et al (2016) Carbon-based electrocatalyst derived from bimetallic metal-organic framework arrays for high performance oxygen reduction. *Nano Energy* 25(2):100–109

57. Luo XY, Chen Y, Mo Y (2021) A review of charge storage in porous carbon-based supercapacitors. *New Carbon Mater* 36(1):49–68
58. Chen X, Paul R, Dai L (2017) Carbon-based supercapacitors for efficient energy storage. *Natl Sci Rev* 4(3):453–489
59. Zhang P, Xie S, Qiu Y et al (2018) Facile preparation of porous carbon nanomaterials for robust supercapacitors. *J Mater Res* 33:1142–1154
60. Meirinho SG, Ferraria AM, do Rego AMB et al (2020) Electrochemical properties of oxygen-enriched carbon-based nanomaterials. *J Electroanal Chem* 873:114420
61. Jain A, Jayaraman S, Ulaganathan M et al (2017) Highly mesoporous carbon from teak wood sawdust as prospective electrode for the construction of high energy Li-ion capacitors. *Electrochim Acta* 228:131–138
62. Kwon SH, Han SB, Kwak DH et al (2019) Doped porous carbon nanostructure materials as non-precious metal catalysts for oxygen reduction reaction in alkaline and acid media. *J Ind Eng Chem* 80:171–181
63. Roberts AD, Wang S, Li X, Zhang H (2014) Hierarchical porous nitrogen-rich carbon monoliths via ice-templating: high capacity and high-rate performance as lithium-ion battery anode materials. *J Mater Chem A* 2:17787–17796
64. Kaur P, Verma G, Sekhon SS (2019) Biomass derived hierarchical porous carbon materials as oxygen reduction reaction electrocatalysts in fuel cells. *Prog Mater Sci* 102:1–71
65. Zhang P, Zhu H, Dai S (2015) Porous carbon supports: recent advances with various morphologies and compositions. *ChemCatChem* 7(18):2788–2805
66. He D, Zhao W, Li P et al (2019) Bifunctional biomass-derived N, S dual-doped ladder-like porous carbon for supercapacitor and oxygen reduction reaction. *J Alloys Compd* 773:11–20
67. Yan L, Yu J, Houston J et al (2017) Biomass derived porous nitrogen doped carbon for electrochemical devices. *Green Energy Environ* 2(2):84–99
68. He G, Yan G, Song Y, Wang L (2020) Biomass juncus derived nitrogen-doped porous carbon materials for supercapacitor and oxygen reduction reaction. *Front Chem* 8:226
69. Sudhan N, Subramani K, Karnan M et al (2017) Biomass-derived activated porous carbon from rice straw for a high-energy symmetric supercapacitor in aqueous and nonaqueous electrolytes. *Energy Fuels* 31(1):977–985
70. Gao J, Chu X, He C et al (2020) Biomass-derived carbon for ORR: pine needles as a single source for efficient carbon electrocatalyst. *J Appl Electrochem* 50:1257–1267
71. Zhang Z, Zhao H, Gu W et al (2019) A biomass derived porous carbon for broadband and lightweight microwave absorption. *Sci Rep* 9:18617
72. Yang W, Chen S (2020) Biomass-derived carbon for electrode fabrication in microbial fuel cells: a review. *Ind Eng Chem Res* 59(14):6391–6404
73. Liu X, Zhou Y, Zhou W et al (2015) Biomass-derived nitrogen self-doped porous carbon as effective metal-free catalysts for oxygen reduction reaction. *Nanoscale* 7:6136–6142
74. Rajendiran R, Nallal M, Park KH et al (2019) Mechanochemical assisted synthesis of heteroatoms inherited highly porous carbon from biomass for electrochemical capacitor and oxygen reduction reaction electrocatalysis. *Electrochim Acta* 317:1–9
75. Liu X, Culhane C, Li W, Zou S (2020) Spinach-derived porous carbon nanosheets as high-performance catalysts for oxygen reduction reaction. *ACS Omega* 5(38):24367–24378
76. Liu Y, Su M, Li D et al (2020) Soybean straw biomass-derived Fe-N co-doped porous carbon as an efficient electrocatalyst for oxygen reduction in both alkaline and acidic media. *RSC Adv* 10(12):6763–6771
77. Peng X, Zhang L, Chen Z et al (2019) Hierarchically porous carbon plates derived from wood as bifunctional ORR/OER electrodes. *Adv Mater* 31(16):1900341
78. Chen Y, Xie S, Li L et al (2021) Highly accessible sites of Fe-N on biomass-derived N, P co-doped hierarchical porous carbon for oxygen reduction reaction. *J Nanoparticle Res* 23:68
79. Xiao Y, Deng S, Li M et al (2019) Immobilization of Fe-doped Ni<sub>2</sub>P particles within biomass agarose-derived porous N, P-carbon nanosheets for efficient bifunctional oxygen electrocatalysis. *Front Chem* 7:523



80. Jiang M, Yu X, Yang H, Chen S (2020) Optimization strategies of preparation of biomass-derived carbon electrocatalyst for boosting oxygen reduction reaction: a minireview. *Catalysts* 10(12):1472
81. Sumboja A, Prakoso B, Ma Y et al (2021) FeCo nanoparticle-loaded nutshell-derived porous carbon as sustainable catalyst in Al-air batteries. *Energy Mater Adv* 2021:1–12
82. Yang H, Wang K, Tang Z et al (2020) Bimetallic PdZn nanoparticles for oxygen reduction reaction in alkaline medium: the effects of surface structure. *J Catal* 382:181–191
83. Kodama K, Nagai T, Kuwaki A et al (2021) Challenges in applying highly active Pt-based nanostructured catalysts for oxygen reduction reactions to fuel cell vehicles. *Nat Nanotechnol* 16:140–147
84. Wang L, Tang Z, Yan W et al (2017) Co@Pt Core@Shell nanoparticles encapsulated in porous carbon derived from zeolitic imidazolate framework 67 for oxygen electroreduction in alkaline media. *J Power Sources* 343:458–466
85. Guo F, Yang H, Liu L et al (2019) Hollow capsules of doped carbon incorporating metal@metal sulfide and metal@metal oxide core-shell nanoparticles derived from metal-organic framework composites for efficient oxygen electrocatalysis. *J Mater Chem A* 7:3624–3631
86. Veeramani V, Raghavi G, Chen S-M et al (2020) Nitrogen and high oxygen-containing metal-free porous carbon nanosheets for supercapacitor and oxygen reduction reaction applications. *Nano Express* 1(1):010036
87. Sawant SY, Han TH, Cho MH (2017) Metal-free carbon-based materials: promising electrocatalysts for oxygen reduction reaction in microbial fuel cells. *Int J Mol Sci* 18(1):25
88. Ren G, Lu X, Li Y et al (2016) Porous core-shell Fe<sub>3</sub>C embedded N-doped carbon nanofibers as an effective electrocatalysts for oxygen reduction reaction. *ACS Appl Mater Interfaces* 8(6):4118–4125
89. Huang M, Liu S, Gong S et al (2019) Silver nanoparticles encapsulated in an N-doped porous carbon matrix as high-active catalysts toward oxygen reduction reaction via electron transfer to outer graphene shells. *ACS Sustain Chem Eng.* 7(19):16511–16519
90. Jia Y, Jiang K, Wang H, Yao X (2019) The role of defect sites in nanomaterials for electrocatalytic energy conversion. *Chem* 5(6):1371–1397
91. Wang L, Tang Z, Yan W et al (2016) Porous carbon-supported gold nanoparticles for oxygen reduction reaction: effects of nanoparticle size. *ACS Appl Mater Interfaces* 8(32):20635–20641
92. Ahn SH, Yu X, Manthiram A (2017) “Wiring” Fe-Nx-embedded porous carbon framework onto 1D nanotubes for efficient oxygen reduction reaction in alkaline and acidic media. *Adv Mater* 29(26):1606534
93. Song M, Song Y, Sha W et al (2020) Recent advances in non-precious transition metal/nitrogen-doped carbon for oxygen reduction electrocatalysts in PEMFCs. *Catalysts* 10(1):141
94. Masa J, Xia W, Muhler M, Schuhmann W (2015) On the role of metals in nitrogen-doped carbon electrocatalysts for oxygen reduction. *Angew Chemie - Int Ed* 54(35):10102–10120
95. Wu R, Xue Y, Liu B et al (2016) Cobalt diselenide nanoparticles embedded within porous carbon polyhedra as advanced electrocatalyst for oxygen reduction reaction. *J Power Sources* 330:132–139
96. Luo X, Ma H, Ren H et al (2021) Controllable synthesis of nitrogen-doped carbon containing Co and Co<sub>3</sub>Fe<sub>7</sub> nanoparticles as effective catalysts for electrochemical oxygen conversion. *J Colloid Interface Sci* 590:622–631
97. Quan L, Yu X, Wang T et al (2019) Ultrafine Co@nitrogen-doped carbon core-shell nanostructures anchored on carbon nanotubes for highly efficient oxygen reduction. *Appl Surf Sci* 494:691–699
98. Kaare K, Yu E, Volperts A et al (2020) Highly active wood-derived nitrogen-doped carbon catalyst for the oxygen reduction reaction. *ACS Omega* 5(37):23578–23587
99. Chen K, Huang X, Wan C, Liu H (2015) Hybrids based on transition metal phosphide (Mn<sub>2</sub>P, Co<sub>2</sub>P, Ni<sub>2</sub>P) nanoparticles and heteroatom-doped carbon nanotubes for efficient oxygen reduction reaction. *RSC Adv* 5:92893–92898

100. Yang W, Zhang Y, Liu X et al (2019) Polymerization-dissolution strategy to prepare Fe, N, S tri-doped carbon nanostructure for a Zn–Air battery. *Carbon* 147:83–89
101. Zhong S, Zhou L, Wu L et al (2014) Nitrogen- and boron-co-doped core-shell carbon nanoparticles as efficient metal-free catalysts for oxygen reduction reactions in microbial fuel cells. *J Power Sources* 272:344–350
102. Chen C, Zhou Z, Wang Y et al (2017) Fe, N, S-doped porous carbon as oxygen reduction reaction catalyst in acidic medium with high activity and durability synthesized using  $\text{CaCl}_2$  as template. *Chinese J Catal* 38(4):673–682
103. Norouzi N, Choudhury FA, El-Kaderi HM (2020) Iron phosphide doped, porous carbon as an efficient electrocatalyst for oxygen reduction reaction. *ACS Appl Energy Mater* 3(3):2537–2546
104. Kim S, Kato S, Ishizaki T et al (2019) Transition metal (Fe Co, Ni) nanoparticles on selective amino-N-doped carbon as high-performance oxygen reduction reaction electrocatalyst. *Nanomaterials* 9(5):742
105. Zhou R, Jaroniec M, Qiao SZ (2015) Nitrogen-doped carbon electrocatalysts decorated with transition metals for the oxygen reduction reaction. *ChemCatChem* 7(23):3808–3817
106. Yuan K, Sfaelou S, Qiu M et al (2018) Synergetic contribution of boron and Fe-Nx species in porous carbons toward efficient electrocatalysts for oxygen reduction reaction. *ACS Energy Lett* 3(1):252–260
107. Shen M, Wei C, Ai K, Lu L (2017) Transition metal–nitrogen–carbon nanostructured catalysts for the oxygen reduction reaction: from mechanistic insights to structural optimization. *Nano Res* 10:1449–1470
108. Gao S, Li X, Li L, Wei X (2017) A versatile biomass derived carbon material for oxygen reduction reaction, supercapacitors and oil/water separation. *Nano Energy* 33:334–342
109. He D, Zhao W, Li P et al (2019) Bifunctional biomass-derived 3D nitrogen-doped porous carbon for oxygen reduction reaction and solid-state supercapacitor. *Appl Surf Sci* 465:303–312
110. Gao S, Chen Y, Fan H et al (2014) Large scale production of biomass-derived N-doped porous carbon spheres for oxygen reduction and supercapacitors. *J Mater Chem A* 2(10):3317–3324
111. Kim HS, Kang MS, Yoo WC (2019) Boost-up electrochemical performance of MOFs via confined synthesis within nanoporous carbon matrices for supercapacitor and oxygen reduction reaction applications. *J Mater Chem A* 7(10):5561–5574
112. Sun Y, Li C, Jiang S et al (2021) Comparative study on supercapacitive and oxygen evolution reaction applications of hollow nanostructured cobalt sulfides. *Nanotechnology* 32(38):385401
113. Zhang Y, Zhang H, Fang L et al (2017) Facile synthesis of nickel manganese composite oxide nanomesh for efficient oxygen evolution reaction and supercapacitors. *Electrochim Acta* 245:32–40
114. Geng J, Wu H, Al-Enizi AM et al (2015) Freestanding eggshell membrane-based electrodes for high-performance supercapacitors and oxygen evolution reaction. *Nanoscale* 7(34):14378–14384
115. Zhang D, Kong X, Jiang M et al (2019) NiOOH-decorated  $\alpha$ -FeOOH nanosheet array on stainless steel for applications in oxygen evolution reactions and supercapacitors. *ACS Sustain Chem Eng* 7(4):4420–4428
116. Wang Z, Chen J, Bi R et al (2020) Supercapacitor and oxygen evolution reaction performances based on morphology-dependent Co-MOFs. *J Solid State Chem* 283:121128
117. Kanan MW, Nocera DG (2008) In situ formation of an oxygen-evolving catalyst in neutral water containing phosphate and  $\text{CO}_2$ . *Science* 321(5892):1072–1075
118. Dau H, Limberg C, Reier T et al (2010) The mechanism of water oxidation: from electrolysis via homogeneous to biological catalysis. *ChemCatChem* 2(7):724–761
119. Khalid M, Honorato AMB, Pasa AA, Varela H (2020) A sugar derived carbon-red phosphorus composite for oxygen evolution reaction and supercapacitor activities. *Mater Sci Energy Technol* 3:508–514

120. Kale SB, Lokhande AC, Pujari RB, Lokhande CD (2018) Cobalt sulfide thin films for electrocatalytic oxygen evolution reaction and supercapacitor applications. *J Colloid Interface Sci* 532:491–499
121. Ahmed ATA, Pawar SM, Inamdar AI et al (2020) Fabrication of FeO@CuCo<sub>2</sub>S<sub>4</sub> multifunctional electrode for ultrahigh-capacity supercapacitors and efficient oxygen evolution reaction. *Int J Energy Res* 44(3):1798–1811
122. Chu W, Shi Z, Hou Y et al (2020) Trifunctional of phosphorus-doped nico<sub>2</sub>o<sub>4</sub> nanowire materials for asymmetric supercapacitor, oxygen evolution reaction, and hydrogen evolution reaction. *ACS Appl Mater Interfaces* 12(2):2763–2772
123. Tian X, Lu XF, Xia BY, Lou XW (David) (2020) Advanced electrocatalysts for the oxygen reduction reaction in energy conversion technologies. *Joule* 4(1):45–68
124. Ma R, Lin G, Zhou Y et al (2019) A review of oxygen reduction mechanisms for metal-free carbon-based electrocatalysts. *npj Comput Mater* 5:78
125. Yan X, Jia Y, Yao X (2018) Defects on carbons for electrocatalytic oxygen reduction. *Chem Soc Rev* 47(20):7628–7658
126. Yang L, Shui J, Du L et al (2019) Carbon-based metal-free ORR electrocatalysts for fuel cells: past, present, and future. *Adv Mater* 31(13):1804799
127. Zheng Y, Jiao Y, Ge L et al (2013) Two-step boron and nitrogen doping in graphene for enhanced synergistic catalysis. *Angew Chemie Int Ed* 52(11):3110–3116
128. Liu YL, Shi CX, Xu XY et al (2015) Nitrogen-doped hierarchically porous carbon spheres as efficient metal-free electrocatalysts for an oxygen reduction reaction. *J Power Sources* 283:389–396
129. Gabe A, Ruiz-Rosas R, González-Gaitán C et al (2019) Modeling of oxygen reduction reaction in porous carbon materials in alkaline medium. Effect of microporosity. *J Power Sources* 412:451–464
130. Ferrero GA, Preuss K, Fuertes AB et al (2016) The influence of pore size distribution on the oxygen reduction reaction performance in nitrogen doped carbon microspheres. *J Mater Chem A* 4(7):2581–2589
131. Lee SH, Kim J, Chung DY et al (2019) Design principle of Fe-N-C electrocatalysts: how to optimize multimodal porous structures? *J Am Chem Soc* 141(5):2035–2045
132. Rani P, Jindal VK (2012) Designing band gap of graphene by B and N dopant atoms. *RSC Adv* 3(3):802–812
133. Liu H, Long W, Song W, et al (2017) Tuning the electronic bandgap: an efficient way to improve the electrocatalytic activity of carbon-supported Co<sub>3</sub>O<sub>4</sub> nanocrystals for oxygen reduction reactions. *Chem A Eur J* 23(11):2599–2609
134. Wang S, Zhang L, Xia Z et al (2012) BCN graphene as efficient metal-free electrocatalyst for the oxygen reduction reaction. *Angew Chemie Int Ed* 51(17):4209–4212
135. Wang X, Zhou J, Fu H et al (2014) MOF derived catalysts for electrochemical oxygen reduction. *J Mater Chem A* 2(34):14064–14070
136. Aijaz A, Fujiwara N, Xu Q (2014) From metal-organic framework to nitrogen-decorated nanoporous carbons: high CO<sub>2</sub> uptake and efficient catalytic oxygen reduction. *J Am Chem Soc* 136(19):6790–6793
137. Zhong H, Wang J, Zhang Y et al (2014) ZIF-8 derived graphene-based nitrogen-doped porous carbon sheets as highly efficient and durable oxygen reduction electrocatalysts. *Angew Chemie Int Ed* 53(51):14235–14239
138. Ren G, Chen S, Zhang J et al (2021) N-doped porous carbon spheres as metal-free electrocatalyst for oxygen reduction reaction. *J Mater Chem A* 9(9):5751–5758
139. Hou Y, Huang T, Wen Z et al (2014) Metal-organic framework-derived nitrogen-doped core-shell-structured porous Fe/Fe<sub>3</sub>C@C nanoboxes supported on graphene sheets for efficient oxygen reduction reactions. *Adv Energy Mater* 4(11):1400337
140. Liang J, Du X, Gibson C et al (2013) N-doped graphene natively grown on hierarchical ordered porous carbon for enhanced oxygen reduction. *Adv Mater* 25(43):6226–6231
141. Wei W, Liang H, Parvez K et al (2014) Nitrogen-doped carbon nanosheets with size-defined mesopores as highly efficient metal-free catalyst for the oxygen reduction reaction. *Angew Chemie Int Ed* 53(6):1570–1574

142. Wu Z-S, Chen L, Liu J et al (2014) High-performance electrocatalysts for oxygen reduction derived from cobalt porphyrin-based conjugated mesoporous polymers. *Adv Mater* 26(9):1450–1455
143. Xuan C, Hou B, Xia W et al (2018) From a ZIF-8 polyhedron to three-dimensional nitrogen doped hierarchical porous carbon: an efficient electrocatalyst for the oxygen reduction reaction. *J Mater Chem A* 6(23):10731–10739
144. Periasamy AP, Ravindranath R, Roy P et al (2016) Carbon–boron core–shell microspheres for the oxygen reduction reaction. *J Mater Chem A* 4(33):12987–12994
145. Yu J, Chen G, Sunarso J et al (2016) Cobalt oxide and cobalt-graphitic carbon core-shell based catalysts with remarkably high oxygen reduction reaction activity. *Adv Sci* 3(9):1600060
146. Xia W, Zou R, An L et al (2015) A metal–organic framework route to in situ encapsulation of Co@Co<sub>3</sub>O<sub>4</sub>@C core@shell nanoparticles into a highly ordered porous carbon matrix for oxygen reduction. *Energy Environ Sci* 8(2):568–576
147. Lin Q, Bu X, Kong A et al (2015) Heterometal-embedded organic conjugate frameworks from alternating monomeric iron and cobalt metalloporphyrins and their application in design of porous carbon catalysts. *Adv Mater* 27(22):3431–3436
148. Han C, Li Q, Wang D et al (2018) Cobalt sulfide nanowires core encapsulated by a N, S codoped graphitic carbon shell for efficient oxygen reduction reaction. *Small* 14(17):1703642
149. Li Y, Cheng F, Zhang J et al (2016) Cobalt–carbon core-shell nanoparticles aligned on wrinkle of N-doped carbon nanosheets with Pt-like activity for oxygen reduction. *Small* 12(21):2839–2845

# Chapter 13

## Waste-Derived Activated Carbon as a Sustainable and Economical Catalyst Support



Sakshi Kabra Malpani, Renu Hada, Ajay Kumar, and Deepti Goyal

### 1 Introduction

Porous carbon materials have reformed both materials and chemical sciences in the past decade by creating new avenues in diversified applications like adsorption, catalysis, electrical conduction, lubrication, energy storage, environmental remediation, etc. [1–4] presented in Fig. 1. Carbon, the basic element of these materials, is exceptionally versatile, abundant, allotropic, considered as ‘king of elements’ and can form numerous porous materials, viz., graphite, diamond, fullerenes, C–C composites, carbon fibers, vitreous carbon, activated carbon, etc. In recent years, activated carbon or activated charcoal (AC) has emerged as worthwhile porous carbon material. It has numerous interesting morphological features like higher internal surface area, amorphous structure, high degree of porosity, excellent compressive strength, good thermal, chemical, and mechanical stability, low ash content, easy activation, varied pore size distribution ranging from micro to macropores, high adsorption capacity, etc.

---

S. K. Malpani

Save the WaterTM, 8723 NW 11 Street, Plantation, Florida 33322, USA

R. Hada

Department of Applied Chemistry and Chemical Technology, SGSITS, Indore, Madhya Pradesh, India

A. Kumar

Institute of Biomedical Sciences and Department of Mechanical and Electromechanical Engineering, National Sun Yat-Sen University, Kaohsiung City, Taiwan

D. Goyal (✉)

Department of Applied Chemistry, School of Vocational Studies and Applied Sciences, Gautam Buddha University, Greater Noida, UP, India

e-mail: [deepti\\_skjain@yahoo.com](mailto:deepti_skjain@yahoo.com)

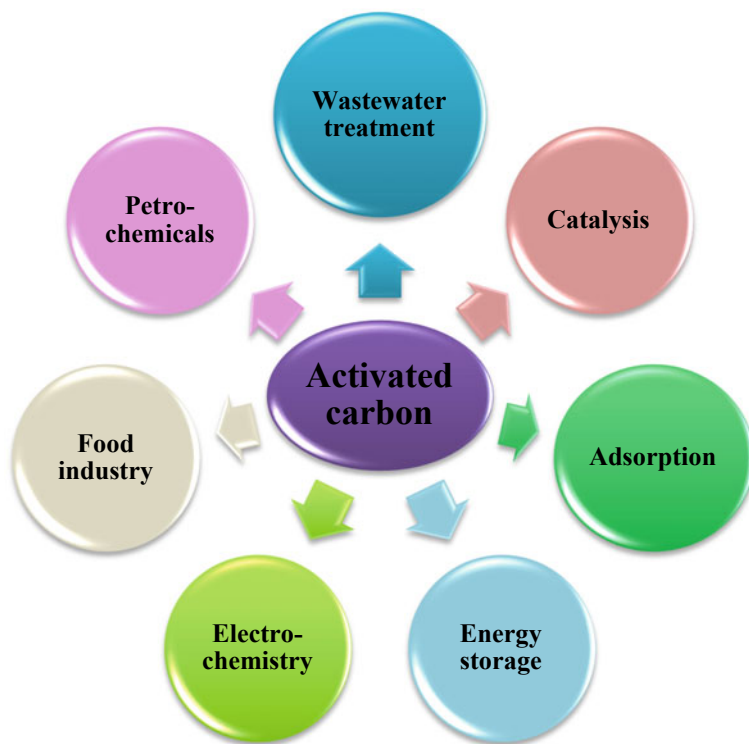
© The Author(s), under exclusive license to Springer Nature Singapore Pte Ltd. 2023

351

A. N. Grace et al. (eds.), *Handbook of Porous Carbon Materials*,

Materials Horizons: From Nature to Nanomaterials,

[https://doi.org/10.1007/978-981-19-7188-4\\_13](https://doi.org/10.1007/978-981-19-7188-4_13)



**Fig. 1** Overview of various applications of AC

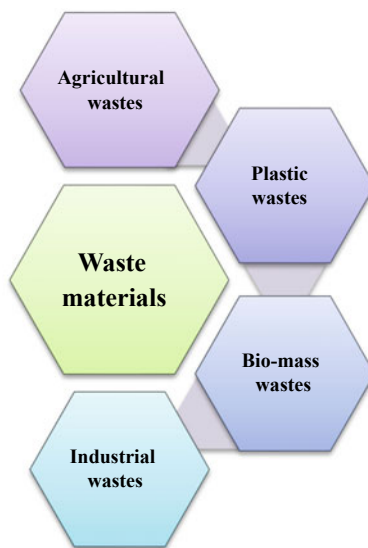
Since ancient times, AC has been consumed in the drinking water distillation, decolorization of raw sugar syrup, air filtration, etc., but its worldwide bulk-scale production was started during the middle of twentieth century. In the present scenario, AC has found wide applications in various sectors like adsorption, catalysis, gas storage and separation, electrochemistry, wastewater treatment, energy storage, refining, cosmetics and personal care, pharmaceutical and petrochemical industries, etc. [5–9]. AC is produced from a variety of carbon-rich materials which could be of mineral, plant, or animal origin. By 2027, the global market size of AC is estimated to be 14.07 billion US dollars, growing at a 9.6% compound annual growth rate. Among various conventional procedures of AC synthesis, physical and chemical activation techniques are more common. Based on the size, synthetic methodologies, nature of applications, AC can be broadly classified into—powdered, granular, extruded, bead, and impregnated AC. Commercially, AC is produced from traditional fossil fuel resources like wood, petroleum residue, coal, and its different types—peat, anthracite, lignite, etc.—which are high priced, non-renewable, and still imported from outside, in India. This dependency on natural, exhaustible resources can be alleviated by using appropriate, inexpensive, carbon-enriched, abundant, dense, slow degradable, easily activated waste precursor which has high potential to give maximum yield % of

AC. Heterogeneous catalysts act in a distinct phase from the reaction mixture. Laws of green chemistry and intensifying trepidations regarding environmental concerns have fueled the research for recyclable, heterogeneous catalysts to switch traditional, toxic, homogeneous catalysts. The catalyst support is important as it helps in better dispersion of active species and prevents their aggregation which enhances overall catalyst performance, and thus, the highest conversion and yield % of desired products are attained. As a worthwhile alternative to these expensive classical supports, activated carbon generated from different wastes has been reported to synthesize many effective heterogeneous catalysts. This review will portray the recent developments in mass production of AC from different waste raw materials (agricultural, industrial, biomass, plastic) in the past decade (2010–2020) via conventional and novel methodologies. In the sections which follow, it will also focus on the prospect of such waste-derived AC as a sustainable, economical catalyst support material. Recently, AC as catalyst support has drawn attention in the catalysis industry, due to its amicable features like inert surface, varied pore size distribution, higher surface area, but its commercial use has been hampered by its higher cost and limited availability of raw materials. Given this consideration, the proper harnessing of waste materials, which could be utilized as precursors in AC synthesis, would impart an effective resolution to few inherent glitches like the expensive nature of commercial AC, waste disposal in an appropriate manner, conservation of fossil fuel resources, issues of environmental pollution, overall higher expenses of catalytic industries, etc. Utilization of waste-derived AC as solid acid, solid base, and metal/metal oxide doped catalyst has been reported in catalyzing different classes of reactions like esterification, dehydration, hydrolysis, transesterification, deoxygenation, hydrogenation, oxidation, etc. It will assess the latent advantages of waste-derived AC over prevailing resources and methodologies and their role in the world's sustainable and economic development. In the last section, the review will briefly discuss challenges and obstructions in this path and try to find out the possible solutions to them.

## 2 Waste Precursors for the Synthesis of Activated Carbon

The properties of AC depend on the type of precursor, method of synthesis, and modifications. Due to its strong porous parameters, higher surface area, extreme stability under extreme conditions, ease of functionalization, the use of AC as either catalyst or catalyst support material has been extremely investigated in recent years. In the last decade, there has been a stimulating interest in the synthesis of low-cost, heterogeneous AC catalysts using various types of waste materials like agricultural wastes, biomass wastes, industrial and plastic wastes, etc. as precursors. In this section, different waste precursors for the synthesis of AC are outlined (Fig. 2.) and discussed. Low cost and high volatile matter content of these waste feedstocks are expedient in the production of porous AC. Different starting materials yield AC with varied ash, carbon content, surface area, porosity, etc.

**Fig. 2** Synthesis of AC from different waste materials



## 2.1 AC from Agricultural Wastes

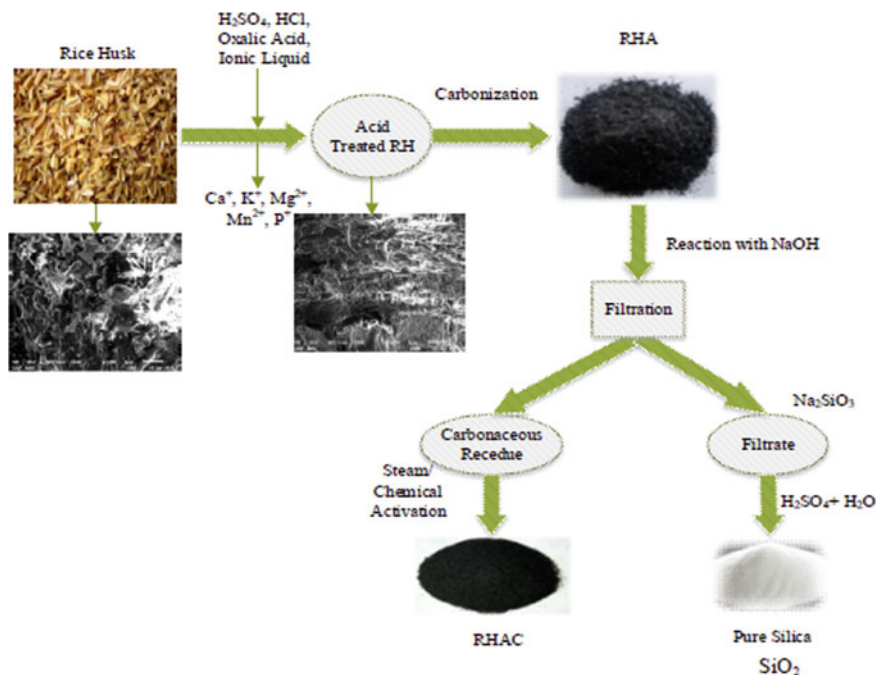
The agricultural sector plays a vital role in the social as well as economic development of a country, but a large number of wastes generated here should be managed appropriately. Agricultural wastes like rice husk, empty seed shells, straws, stalks, etc., have relatively higher carbon content and have been extensively used in the production of AC. A bunch of researchers [10] has prepared AC from rice husk ash, an abundant agricultural by-product. In this work, impregnation of hydrolysis residues of rice husk was done with different concentrations and ratios of  $\text{H}_3\text{PO}_4$  and then calcined at 300–600 °C for 0.5–2 h. In another study, palm kernel shells were physically and chemically activated to produce biochar which was then pyrolyzed by microwave vacuum method to produce AC-supported nickel catalyst. While testing in methane dry reforming reaction, it was concluded that chemically AC was better catalyst support as compared with physically AC [11]. Rajendran et al. showed that chemical activation of *Leucaena leucocephala* seed shells with 10% phosphoric acid followed by carbonization at 120–130 °C produces AC whose structural properties were studied by SEM, FT-IR, and XRD analysis [12]. Oil palm empty fruit bunch, coconut shells, and bamboo stem were pyrolyzed at 800 °C and then treated with KOH under inert atmosphere to produce AC with a higher specific surface area ( $1212 \text{ m}^2\text{g}^{-1}$ ) and microporosity percentage equivalent to the commercial ACs. In the same work, the impact of temperature and agriculture waste type on specific surface area and morphological studies were also investigated [13].

Another facile way to generate AC has been reported by using date pits. As a result of in situ carbonization of date pits under inert atmosphere and followed by sulfonation with 0.05 M  $\text{H}_2\text{SO}_4$  solution, a green, mesoporous, highly acidic, thermally



stable carbon catalyst was synthesized which was later utilized for the solvent-less tertiary butylation of phenol [14]. Koubaissy et al. derived AC from pinecone wastes by pyrolysis at 450 °C, chemically activated by using various activating agents like  $\text{ZnCl}_2$ ,  $\text{H}_2\text{SO}_4$ , and  $\text{NaOH}$ , and pyrolyzed at 600 °C. Functionalities of surface of as-obtained AC were studied in detail by FT-IR, XRD, zeta potential, BET surface area analysis [15]. Other agricultural wastes like corncob, rice husk, and wheat straw can also be employed as precursors for the formation of AC via chemical activation with  $\text{NaCl}$  in a simple, cost-effective manner [16]. Purple corn or *Zea mays L.* cob was used by Kaur et al. to make AC by using  $\text{NaOH}$  as an activating agent. SEM and TEM images revealed the highly porous, smooth surface, and rib shape of AC. More knowledge about the structural features of AC was gathered by using different characterization techniques like TGA-DTA, FT-IR, XRD, XPS, TPD,  $\text{N}_2$  adsorption–desorption isotherms, etc. [17]. In one more study done by Kaur et al., a two-step activation method was used to prepare AC from corn cob. Because of the conjugated boat structure of AC, it possesses a higher surface area ( $\sim 780 \text{ m}^2 \text{ g}^{-1}$ ) and high pore volume ( $0.428 \text{ cc/g}$ ) [18]. Gonçalves et al. demonstrated the preparation of AC by controlled pyrolysis of coconut husk, coffee grounds in a tubular furnace under nitrogen gas flow at 400 °C for 4 h [19]. Agricultural waste shells like dried brown walnut and almond shells can also form microporous AC in presence of different catalytic amounts of zinc chloride [20]. In this experiment, zinc chloride catalyst was impregnated on the powder of shells and activated by both conventional and microwave-assisted heat treatments followed by pyrolysis in an ambient and inert environment in closed and open ceramic vessels, respectively. Results showed that the microwave-assisted catalytic process is more prominent than the conventional method. Execution of optimized synthesis parameters like MW power output of 600 W, carbonization at 500 °C formed microporous AC with an average pore size of 2.4 nm. An overview of AC production is shown in Fig. 3 by taking an example of rice husk.

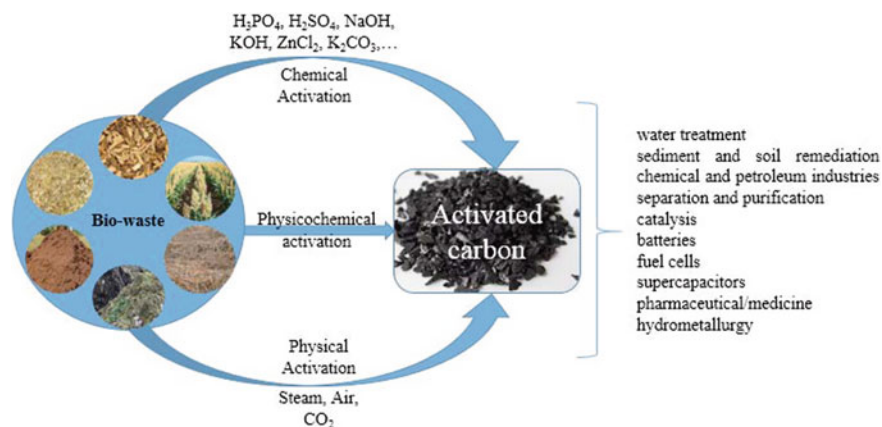
A range of other agro-wastes like strawberry seeds, pistachio shells, etc. were also utilized to develop AC by two activation processes—chemical activation by impregnation of  $\text{CH}_3\text{COOH}$  and physical activation under  $\text{CO}_2$  and water vapor atmosphere. Various factors like the type of precursors, temperature conditions, activating agents, activation time, additional activation by microwave radiations, etc. were studied by using different analytical techniques like SAXS, nitrogen adsorption–desorption, SEM, TEM, XPS, potentiometric titrations, TG-DSC, FT-IR, etc. [22]. Abdessemed et al. showed that Algerian olive-waste cakes can also produce porous AC by carbonization at 800 °C for 1 h and chemical activation by potassium hydroxide in a mass ratio of 4:1 (potassium hydroxide: pretreated carbon) [23]. A study in the mid-Anatolia region showed that chickpea husks can also produce AC by chemical activation with varying ratios of  $\text{KOH}$  and  $\text{K}_2\text{CO}_3$ . Characterization studies revealed that AC formed by activation of 50%  $\text{KOH}$  has a greater surface area ( $2082 \text{ m}^2 \text{ g}^{-1}$ ) and pore volume ( $1.07 \text{ cm}^3 \text{ g}^{-1}$ ) [5]. Apart from these wastes, tea waste or the woody part of tea obtained after harvesting tea leaves also produces highly porous AC by using chemical activation with  $\text{H}_3\text{PO}_4$  and carbonization. Temperature and time of carbonization were adjusted to obtain uniform, highly porous AC [24].



**Fig. 3** AC production from rice husk. Reprinted with permission from Alam et al. [21]. Open access, MDPI

## 2.2 AC from Biomass Wastes

Biomass wastes are lignocellulose materials often derived from agricultural products, contain higher volatile organic content, and have proven to be a useful, inexpensive resource to form AC. Mateo et al. synthesized AC-based acid catalysts by microwave-assisted carbonization of corncob chemically activated with  $H_3PO_4$  followed by sulfonation with conc.  $H_2SO_4$ . The use of microwave irradiations has reduced the time of carbonization from several hours to 30 min [25]. In another piece of work, a group of researchers has critically reviewed various synthesis procedures of solid carbon catalysts from different biomass wastes including isolated carbohydrates and plant materials like furfural, starch, oak wood, cellulose, sucrose, etc. and their catalytic applications in a variety of reactions like hydrolysis, esterification, transesterification, etc. Studies show that such biomass-derived AC catalysts, because of their tunable physical and surficial features, are comparable with other reported catalysts in respect of catalytic efficiency and product yield %. [26]. Tang et al. prepared AC-based sulfonated catalysts from different biomass waste precursors—empty fruit bunch, papaya seeds, corncob—and tested them in formation of biodiesel from esterification of methanol and palm fatty acid distillate. AC prepared in this work possesses higher porosity and surface area in the range between 639.68 and



**Fig. 4** AC production from different biomass wastes. Reprinted with permission from Bernardo et al. [29]. Open access, Boletín del Grup Español del Carbón

972.66  $m^2/g$ . AC derived from papaya seeds contained the highest carbon content, but the highest catalytic activity and reusability was shown by sulfonated AC catalyst prepared from corncob [27]. Zhou and Wang have shown contemporary growth in the transformation of biomass wastes into AC and their applications in various sectors. They have reported that AC could be derived from peanut shells, cornstalk, animal wastes through their carbonization at a temperature above 650 °C and applying chemical and physical activation methods. AC procured from these biomass wastes can be then utilized in double-layered capacitors, electrochemistry, catalysis, adsorption, etc. [28]. Figure 4 shows that a variety of biomass wastes could be used to generate AC by using different activation methods and has diversified applications in many fields.

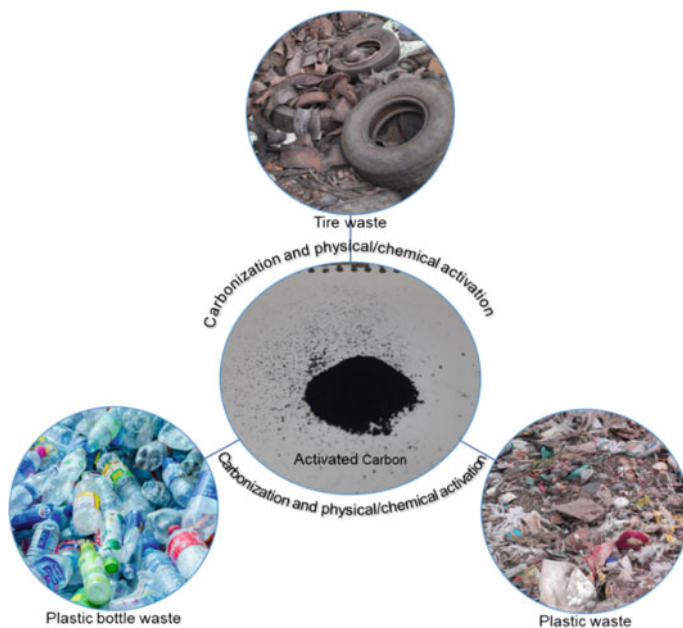
Palm shells can also be used to produce AC which was then impregnated with calcium nitrate solution to form a heterogeneous base catalyst, utilized in the transesterification reaction [30]. In a similar type of study, another waste biomass, mollusk shells (*T. striatula*) was used as a raw material for preparing AC by chemical activation with KOH, then grounded with waste shells again to form a solid base catalyst which was used in transesterification of vegetable cooking oil [31]. Dried furfural residue was utilized to prepare two types of AC-based catalysts, namely KOH and  $ZnCl_2$  AC-based catalysts. This work showed that distribution of surface functional groups, surface area, porosity, and pore structure of thus-formed AC-based catalysts are greatly affected by the type of activation technique [32]. Another work on the preparation of AC from corncob revealed that current chemical activators used in pyrolysis of biomass wastes are non-sustainable, so here, they are replaced by bio-oil and wood vinegar along with  $H_3PO_4$ . Experimental test and analytical results reveal that the adsorption potential and specific surface area of AC synthesized from wood vinegar are considerably higher and can be utilized as an activator for the sustainable conversion of biomass wastes to AC [33]. A study shows that

even low particle size rapeseed wastes can also be utilized as a biomass precursor to generate AC. Results demonstrated that chemical impregnation of rapeseed waste with  $K_2CO_3$  and activation at  $700\text{ }^\circ\text{C}$  are optimized experimental conditions to obtain AC with superior surface area (up to  $1000\text{ m}^2/\text{g}$ ) and constricted micropores advantageous in caffeine adsorption [34]. Palm empty fruit bunch, coconut coir husk wastes, coconut meal residues, etc. can be converted into AC-based sulfonated solid acid catalysts by carbonization at  $400\text{ }^\circ\text{C}$  for 5 h. Characterization study of prepared samples was done by using CHNS, EDS,  $N_2$  adsorption–desorption isotherm, SEM, FT-IR, XPS, TGA–DSC techniques [35]. Different biomass precursors like coconut shells, mango leaves, bamboo fungus, spores, fruit stones and peels, coffee husks and grounds, nutshells, corn hulls, wood, and sawdust, straw, and grasses can be utilized to produce AC. Test studies showed that catalytic hydrothermal carbonization is a better way to produce AC with desired porosity, surface area, conductivity, stability [36].

AC can be derived from castor de-oiled cake by using both physical and chemical activation methods, using a mixture of  $H_2O/CO_2$  as physical activating agent and  $K_2CO_3$  as chemical activating agent [37]. Beetroot juice can also act as a carbon source for making AC. Veerakumar et al. concentrated beetroot juice, then chemically activated with  $ZnCl_2$ , dried, and ground to form a dispersed mixture, then underwent graphitization treatment at  $600\text{--}900\text{ }^\circ\text{C}$  for 2 h. BET studies showed that pore volume, size, and surface area of AC samples increase with an increase in carbonization temperature, and porosity was created due to chemical activation with  $ZnCl_2$  [38]. Coconut shells are another biomass source that can produce AC using  $MgCl_2$  as a chemical activating agent [39]. Khan et al. have reported many lignocellulosic, carbon-abundant biomass waste precursors like corn stalk, rice husk, rubberwood fiber, hazel nutshell, pine, and white firs, kenaf fiber, etc. in the generation of AC-based products via hydrothermal carbonization method. Various parameters of this method were varied to get optimized yield %. These AC-based products have numerous applications in biofuels, catalysis, energy storage, environmental additives [40]. In another piece of work, Lu and co-workers used poplar wood, pinewood, and corn stalk as biomass wastes to produce AC with phenol as a co-product. In this process, biomass wastes were pretreated and impregnated with potassium phosphate under ultrasonic stirring for 12 h. In the course of this work, pyrolytic solid residues that remained after catalytic experiments can also be activated to generate AC with an excellent specific surface area ( $1605\text{ m}^2/\text{g}$ ) [41].

### ***2.3 AC from Plastic Wastes***

Plastics undoubtedly not only bring expediency, comfort, and color to our life but also cause interminable distresses to our environment. Plastic waste accumulation is one of the major environmental issues all over the world. Plastic bags, food wrappers and containers, bottles and container caps, COVID-19 medical equipment, and kits are the main sources of plastic waste that cause pollution in land, rivers, and oceans.



**Fig. 5** Plastic and industrial waste resources for AC production

Plastic takes many years (20–1000) to degrade, so, its disposal is a major challenge all over the globe. Many researchers are engaged to carry out more research on this threatened problem to get an effective solution. [42–44]. Reuse and recycling of plastic wastes should be promoted to reduce their accumulation. Preparation of AC from plastic waste is a smart way to utilize this non-degradable waste. So many researchers are converting plastic waste into value-added AC which can be used as an efficient catalytic support material. Figure 5 shows different plastic and industrial waste resources utilized for the formation of AC.

Recently, a group of researchers prepared AC with a surface area of  $1381.40 \text{ m}^2/\text{g}$  by chemical activation of spent char obtained by slow pyrolysis of plastic waste at  $700 \text{ }^\circ\text{C}$  in the  $\text{N}_2$  atmosphere [44]. Plastic pollution is mainly generated by the products made up of polyethylene terephthalate (PET); therefore, much concern has been taken for the degradation or utilization of PET. Many researchers have generated AC by utilizing a carbon source, PET. Oxygen-rich AC with high surface area and increased pore volume was derived from PET waste by direct carbonization at different temperature ranges from  $500$  to  $800 \text{ }^\circ\text{C}$  followed by chemical activation using KOH [45]. Carbonization of waste PET in  $\text{N}_2$  stream at  $825 \text{ }^\circ\text{C}$  and then physical activation in  $\text{CO}_2$  stream under high temperature yielded AC which showed similar microporosity to that of commercial AC. As-prepared AC has potential applications as an adsorbent for wastewater treatment, electrode materials in superconductors or fuel cells,  $\text{H}_2$  storage, etc. [46].

Regenerable and recyclable AC derived by thermochemical processes for  $\text{CF}_4$  and  $\text{CO}_2$  capture wherein waste PET bottles were used as raw material. Effect of carbonization, activation temperature, and base (KOH and NaOH) were studied in detail. These results show the significant effect of such parameters on textural properties of PET waste-derived AC [47, 48]. The autogenic pressure pyrolysis technique has been used as a modern technique to derive pyrolytic carbon. After pyrolysis, carbon was further chemically treated with KOH and  $\text{ZnCl}_2$ . AC formed after activation with KOH consists of highly ordered porous structure, high surface area, and increased surface active sites [49]. N-doped microporous carbon has been formed in one-pot and two-pot synthesis using PET waste as carbon precursor and KOH, urea as activating agents. AC obtained from one-pot synthesis at  $700^\circ\text{C}$  possesses better oxygen content and exhibited a higher  $\text{CO}_2$  uptake as compared to AC formed by two-pot procedure where base and urea treatment were carried out independently [50]. Polyurethane plastic waste has been valorized into AC using carbonization and physical activation techniques and later utilized in malachite green removal from wastewater. The comparative study was carried out between two-step simple, hydrothermal, vacuum carbonization, and one-step carbonization/activation techniques. Thus-obtained AC obtained via carbonization at high temperature in inert atmosphere has been proved an outstanding material having high surface activity [51]. Poly(vinyl chloride) (PVC) was carbonized hydrothermally in subcritical water at  $180\text{--}260^\circ\text{C}$  to generate AC in an eco-friendly manner [52]. Low-density polyethylene (LDPE) as raw material provides the opportunity to obtain AC. The process involves carbonization of transparent and black plastic at  $415^\circ\text{C}$  for 135 min and  $425^\circ\text{C}$  for 120 min, respectively. Then, it was chemically activated using KOH and acetone. The chemical activation done by using 1 M acetone produced AC possessing  $352.55\text{ m}^2/\text{g}$  surface area with 96.62% carbon composition [53]. AC with a superior surface area of  $1591.72\text{ m}^2/\text{g}$  was prepared using PET waste at lower pressure of about 34.5 bar. The carbonization was done at  $400^\circ\text{C}$  followed by physical activation using  $\text{CO}_2$  at  $975^\circ\text{C}$  [54]. N-rich AC has been synthesized by the urea–formaldehyde resin via carbonization at  $700^\circ\text{C}$  in  $\text{N}_2$  atmosphere for 2 h, and then by chemical activation using KOH as an alkali activator. As-derived AC possessed excellent surface area of  $4547\text{ m}^2/\text{g}$ , and a total pore volume of  $4.50\text{ cm}^3/\text{g}$  makes it a potential carbon material for sequestration of  $\text{CO}_2$  from flue gases of power plants [55].

## 2.4 AC from Industrial Wastes

Industrial waste generation is increasing enormously around the world, and there are no chances that it would slow down in the next few years. By 2050, it is expected that municipal solid waste generation would be approximately increased by 70% across the world and estimated to be 3.4 billion metric tons. To reduce it, a solid waste management system should be developed following 3R technologies (reduce, reuse, and recycle) by employing a variety of techniques for resource recovery, waste minimization, and proper disposal of solid waste. Many research groups all around

the world are engaging in the reuse and recycling of industrial wastes [56, 57]. Carbon-containing waste can be a good precursor for the generation of AC in this regard.

Various industrial wastes used as the precursor for the preparation of AC are summarized in Table 1.

### 3 Process of Synthesis of AC

AC can be prepared by using different methods like pretreatment, de-ashing/demineralization, salt templating and ultrasonic spray pyrolysis, physical and chemical activation, etc. Among them, activation techniques (physical and chemical) are the most frequently used methods. Usually, acids ( $\text{H}_2\text{SO}_4$ ,  $\text{H}_3\text{PO}_4$ ), bases (KOH, NaOH,  $\text{CaCl}_2$ ,  $\text{K}_2\text{CO}_3$ ), and metal salts ( $\text{ZnCl}_2$ ,  $\text{FeCl}_3$ ), etc. are used in chemical activation method. A summary of synthesis methods of AC is abridged in Table 2.

### 4 AC as Catalyst Support

AC with excellent porous parameters and greater surface area can be a suitable candidate for its use as a catalyst support material. Owing to its chemically inert nature, it does not react with the reactant which makes it an efficient catalyst support for catalyzing industrially important organic transformations [11]. In addition, the use of AC as the catalyst support material makes the process cost-effective. Some advantages of AC as compared to other commercial support materials are mentioned below:

- The inert surface of AC averts the possibility of interaction between support and the active phase.
- High surface area (200–1500  $\text{m}^2/\text{g}$ ).
- The easily adjustable pore structure.
- The tunable hydrophobicity.
- Easily regenerable active sites.
- Can be synthesized from renewable feedstocks.
- Stability in both acidic and basic medium.
- Cost-effective.

AC does not act just as a support but also sometimes takes participation in the chemical reactions and increases the catalytic efficiency of the other catalysts involved. The presence of various acidic and basic oxygen groups on the surface of AC is responsible for its efficient catalytic behavior. The most important criteria for the catalytic activity of AC as support are the presence and distribution of active sites. The interaction between these active sites and molecules of the reactants increases the overall efficiency of the catalyst support material used. Moreover, the action of active

**Table 1** Preparation of AC using different industrial wastes

Carbon precursors	Carbonization temperature (°C), time	Activator	BET (m <sup>2</sup> /g)	Applications	References
Industrial food waste	400–800	Iron salt	822	Removal of magnetic pollutants	[58]
Waste tires and tea leaves	800	KOH and ZnCl <sub>2</sub>	527.24	–	[59]
Waste paper	950 for 1 h	Orthophosphoric acid	848.5	Fluoride uptake	[60]
Wine industry waste	450 for 60 min in N <sub>2</sub>	KOH	2015	Removal of cationic dye	[61]
Distilled liquor waste	600–700 for 1 h	KOH	2434	Electrode active material used in electric double-layer capacitors	[62]
Empty fruit bunch, papaya seeds, corncob	600–1000 for 2 h	Acid	639.68–972.66	Catalyst support for biodiesel production	[27]
Date and olive seeds, wastepaper, and cotton fabrics	750–850 for 1 h	ZnCl <sub>2</sub> and CaCl <sub>2</sub>	1293.02–1496.97	Wastewater treatment	[63]
Poultry feather waste	650 for 3 h in N <sub>2</sub>	KOH	12.4–16.1	Bioanode	[64]
Carob waste	900 for 1 h in steam	–	408–762	Adsorption of pharmaceutical drugs	[65]
Papermill sludge	800 for 60 min	KOH	1389–1627	Removal of pharmaceuticals from water	[66]
Packaging waste	500 for 1 h	KOH	760–1383	CO <sub>2</sub> adsorption	[67]
Tobacco waste	800 for 5 h in N <sub>2</sub>	KOH	1297.6	Supercapacitor electrode material	[68]
Waste tire	600 for 1 h in N <sub>2</sub>	Physical activation at 900 °C for 3 h in N <sub>2</sub>	99–133	Low-temperature NO <sub>x</sub> control	[69]
Grape industrial waste	600 for 1 h in N <sub>2</sub>	ZnCl <sub>2</sub>	1455	Anionic and cationic dye removal	[70]
Waste eggshell	700 for 4 h	–	58–113	Phenol adsorption	[71]

(continued)



**Table 1** (continued)

Carbon precursors	Carbonization temperature (°C), time	Activator	BET (m <sup>2</sup> /g)	Applications	References
Oil palm fiber/biodiesel manufacturing plant	Microwave power: 90–800 W Radiation time: 2–8 min	Microwave heating	707.79	Methylene blue adsorption	[72]
Waste coconut buttons	400 for 1 h in steam	–	479	Heavy metal ion removal	[73]
Waste tire	500 for 2 h in N <sub>2</sub>	Physical activation at 950 °C under N <sub>2</sub> or CO <sub>2</sub>	1000	Adsorption of the large-sized dye molecule	[74]

sites is also influenced by the presence of heteroatoms and acidic/basic functional groups (Fig. 7) [83–86].

Due to the constricted resources of conventional carbon precursors and their high prices, the search for renewable materials is of great interest. In this direction, several researchers have put tremendous efforts into the synthesis of AC from various waste precursors that are either very economical or cost-free [87–91].

#### 4.1 Solid Acid Catalysts

Homogeneous acid catalysts like HNO<sub>3</sub>, H<sub>2</sub>SO<sub>4</sub>, H<sub>3</sub>PO<sub>4</sub>, HF, HCl, etc. have been widely used in several chemical reactions like esterification, condensation, transesterification, etc. These catalysts when used in diluted form require high temperature and time to complete the reaction, while with concentrated acids, the reaction is completed in a lesser time. Although the filtration of concentrated acid from the reaction mixture enhances, the cost of production as well as creates a huge amount of waste salts. To overcome these problems, homogeneous acids are replaced by some solid acid catalysts like zeolite, niobic acid, Amberlyst ionic resins, etc., but these catalysts are costly and less stable in the reaction medium [92, 93]. Recently, acid-functionalized AC has attracted the attention of several researchers [94–97]. The acid activation of AC can be done by using activating agents like H<sub>2</sub>SO<sub>4</sub>, HCl, and H<sub>3</sub>PO<sub>4</sub> [98–100]. Acid activation increases porosity and activity, utilization capacity, and reusability of the synthesized catalysts [101]. The acidity of AC can be generated via sulfonation using concentrated sulfuric acid in a two-step procedure that involves hydrothermal or pyrolytic carbonization followed by sulfonation at different temperatures. In addition, the use of phosphoric acid before sulfonation is also reported. This could enhance the surface area of AC and could further raise the rate of sulfonation [102]. The sulfonation process also gets affected by temperature. On increasing

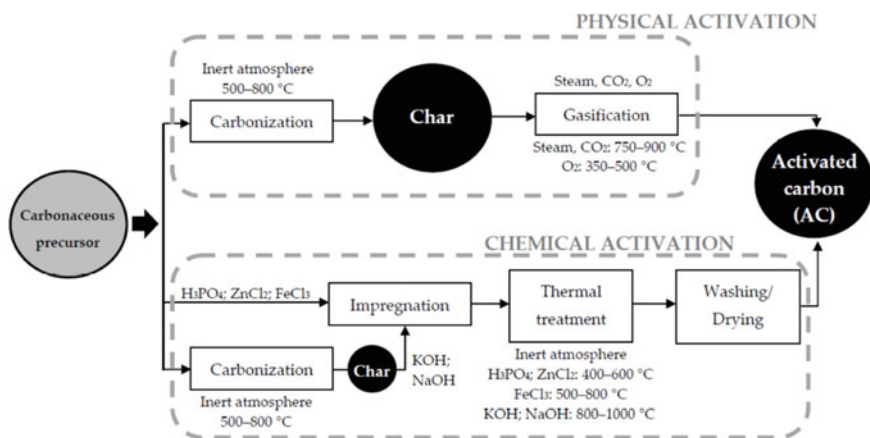
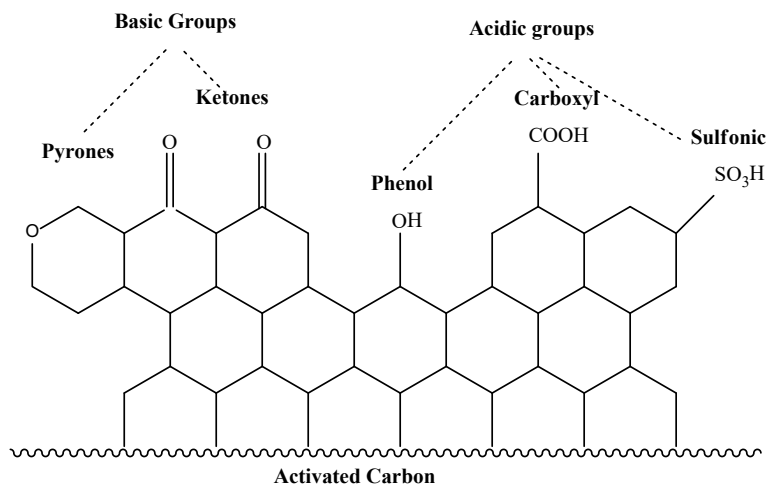
**Table 2** Conventional synthesis methods for production of AC

Pre-treatment	This method includes washing of carbon precursor, drying at 100 °C for a definite time [75] followed by crushing and sieving of dried powder [76]. This method removes impurities and moisture from the carbon material
Deashing/demineralization	This method includes leaching of carbon precursors on treatment with acidic (conc. HCl, HF, and HNO <sub>3</sub> ) or basic solutions. This results in the oxidation of the carbon precursor and the creation of some functional groups comprising of oxygen on AC surface [77]
Physical activation	This method implicates two steps: (i) The first step includes pyrolysis of carbon precursor at approximately 800 °C in an inert environment. This results in the removal of volatile impurities and thus increased carbon content (ii) The second step includes gasification of carbonized material using steam, CO <sub>2</sub> , or air. Gasification with steam and CO <sub>2</sub> occurs at high temperatures (700–900 °C), while with O <sub>2</sub> or air, it occurs at 400 °C. The low-temperature requirement for O <sub>2</sub> or air is because of superior reactivity of O <sub>2</sub> than CO <sub>2</sub> and steam. This step removes the most reactive carbon atoms, which are responsible for generating porosity in the ACs (Fig. 6). Below are the reactions that occurred during the gasification process [75, 78] $\text{C} + \text{CO}_2 \rightarrow 2\text{CO}$ $\text{C} + \text{O}_2 \rightarrow \text{CO}_2$ $\text{C} + \text{H}_2\text{O} \rightarrow \text{CO} + \text{H}_2$
Chemical activation	This method involves three basic steps: (i) first step involves the impregnation of the carbon precursor with the activating agent such as H <sub>3</sub> PO <sub>4</sub> , NaOH, or KOH (ii) Second step involves the thermal activation of chemically treated precursor in an inert environment at different temperatures, which increases the yield of carbon in the sample (iii) Third step involves the washing of the resulting material to eradicate the adhered chemical species and by-products which can block the pores present on the surface of the carbon (Fig. 6) [78, 79]
Salt templating	This method involves the mixing of carbon precursor with inorganic non-carbonizable salts at high temperatures, which helps to retain the solubility of carbon precursor and molten salt. Finally, thus-obtained material is washed to eliminate the salt impurities from the carbon material and to increase specific surface areas [80]

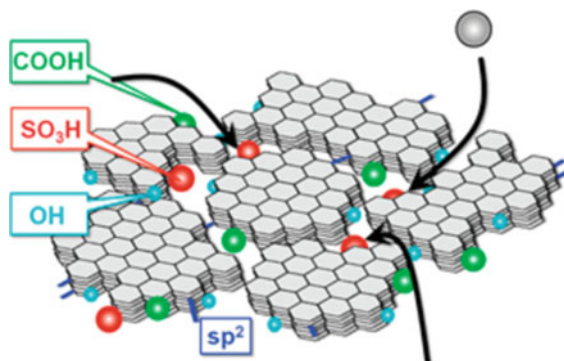
(continued)

**Table 2** (continued)

Ultrasonic spray pyrolysis (USP)	This method involves ultrasonic nebulization of a mixture of a carbon precursor and inorganic salts. Nebulization converts this mixture to steam of micro-sized droplets. This steam then passed through a furnace in an inert atmosphere, where it decomposes the carbon precursor. Thus, the obtained product is then stored in a water bubbler, where salt and by-products get dissolved and the final carbon material is obtained in the pure form [81, 82]
----------------------------------	---

**Fig. 6** Synthesis of AC via physical and chemical activation. Reprinted with permission from Bedia et al. [78]. Open access, C (Journal of Carbon Research)**Fig. 7** Acidic and basic sites on AC produced by physical/chemical activations

**Fig. 8** Schematic structure of sulfonated AC below 723 K. Reprinted with permission from Nakajima et al. [103]. Copyright 2012 American Chemical Society



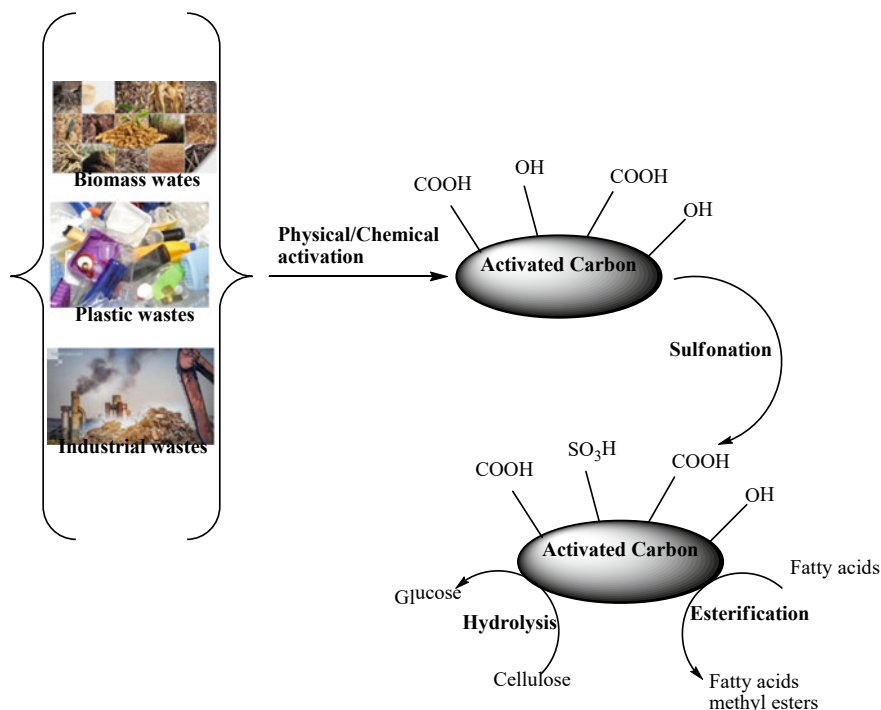
temperature, the generation of sulfonic groups decreases. Thus-prepared sulfonated carbon catalyst comprising mainly three acidic groups, namely  $-SO_3H$ ,  $-COOH$ , and phenolic  $-OH$ . These acidic functional groups are liable for the enhanced catalytic potential of acidic AC catalysts. Sulfonic and carboxylic acid groups create Bronsted acidity while phenolic hydroxyl and carboxylic groups increase the hydrophilic adsorption capacity of water and reactants during hydrolysis reaction [103]. After treating with acid, oxygen-containing functional groups increased on surface of AC as shown in Fig. 8, which are liable for their acidic properties. Furthermore, the basic groups depicted on the surface of AC becomes acidic after treatment with sulfuric acid, because of the production of new sulfonic groups over its surface.

Initially, wood-derived AC was used for acid functionalization, but its use as a catalyst is not much reported. In this sequence, researchers started the use of biomass-derived AC catalysts synthesized via sulfonation of starch, cellulose, and glucose. Thus, synthesized acid-functionalized ( $-SO_3H$  and  $-COOH$ ) AC catalysts were successfully applied in different esterification [103] and transesterification reactions [97]. Another study compared the catalytic activity of sulfonated AC and wood-derived AC catalysts in the esterification reaction. The study revealed that the sulfonated AC had higher activity and reuse capability due to greater surface area ( $1137 \text{ m}^2/\text{g}$ ) and acidic sites ( $0.81 \text{ mmol/g}$ ). A similar investigation has been done on the efficiency of a new high sulfonated AC catalyst synthesized by nitration with  $HNO_3$  in the first step and then sulfonation with  $H_2SO_4$  in the subsequent step. The thus-prepared catalyst contained whole acid density ( $4.43 \text{ mmol/g}$ ) and sulfonated acid density ( $0.93 \text{ mmol/g}$ ), owing to the high catalytic activity concerning esterification of oleic and lauric acids in methanol [104]. In another study, the efficiency of sulfonated AC catalysts was assessed in the hydrolysis of cellobiose. This research revealed that the porosity of AC catalyst is an equally significant parameter for the reaction as the type and strength of active acidic sites [105]. Furthermore, the use of functionalized carbon (sulfonated groups) is generated from rice husk and was studied to catalyze glycerol esterification reaction using acetic acid and glycerol etherification with tertiary butyl alcohol. The total acidity of the catalyst was found  $5.8 \text{ mmol g}^{-1}$ . As-prepared sulfonated carbon catalyst with sufficient Bronsted

acid sites and hydrophilicity resulted in increased conversion% of glycerol. These Bronsted acid sites increased the forward reaction rate, whereas the hydrophilicity prevented deactivating the catalyst [106]. Besides, amorphous acid AC-based catalysts have been synthesized via carbonization and sulfonation of palm kernel shells. All prepared catalysts showed high conversion of glucose with excellent selectivity to products, due to increased acid sites and good thermal stability [107]. A sulfonated AC catalyst with 6.28 mmol/g of acidity efficiently catalyzed hydrolysis of cellulose to  $\alpha$ ,  $\beta$ -methylglucoside under regulated reaction conditions. The activity of the catalyst was reported because of the presence of intense acidic sites of  $\text{SO}_3\text{H}$  functional groups and the hydrophobic planes on the AC surface [108]. Additionally, the activity of sulfonated carbon catalyst on dehydration of fructose to 5-hydroxymethylfurfural (HMF) is evaluated by a group of researchers. The catalyst was prepared by two methods: (i) hydrothermal carbonization of cellulose and subsequent sulfonation (ii) KOH-treated carbonized cellulose followed by sulfonation. The catalyst prepared by method (ii) was having higher acidity and lower surface area. Both materials were found equally efficient, but the catalyst prepared by method (ii) gave a superior yield of 83% in comparison to the catalyst prepared by method (i). This demonstrates a bigger impact of acidity of catalysts on the hydrolysis of fructose as compared with the surface area [109]. A murumuru kernel shell-derived sulfonated AC catalyst has been synthesized and utilized in the esterification reaction of different fatty acids and acid distillate. The experimental details concluded that the presence of adequate acidic sites on the catalyst surface gave high conversion (97.2%) under optimum reaction conditions. The catalyst was reused up to 4 reaction cycles and was found efficient giving 66.3% conversion [110]. An overview of the formation of acidic sites on the AC surface via physical and chemical activation by sulfonic acid is shown in Fig. 9.

## 4.2 Solid Base Catalysts

Solid base catalysts are more beneficial than traditional, liquid base catalysts as they are environmentally friendly, cost-effective, quite stable in the reaction medium, and can be synthesized by simple methods [111]. In addition, a comparatively less amount of a solid base catalyst is sufficient to catalyze the whole reaction [112]. A recent study demonstrated the use of CaO-loaded waste AC, derived from waste *T. striatula* shells. Thus, the prepared catalyst was utilized in the transesterification of waste cooking oil giving higher conversion % (96%) of methyl ester under optimized reaction variables. Besides, the catalyst displayed efficient potential till five reaction cycles [31]. In another research work, the carbonization of waste plastics into greener jet fuel and  $\text{H}_2$  is reported to be performed over AC (derived from biomass)-supported MgO catalysts. The study revealed that AC-supported MgO catalysts had an excellent catalytic efficiency toward the reaction [113]. Another solid base catalyst was synthesized by loading CaO on AC. The acidity of the catalyst was tested on the production of biodiesel from waste cooking palm oil. The CaO-loaded AC



**Fig. 9** Sulfonated AC as a solid acid catalyst

catalyst was found significant giving the highest conversion of 94% and found stable even after 4 reaction cycles [30]. A similar investigation was performed by Dhawane et al. [114] using *Jatropha curcas* seed kernel shells. The results indicated that the catalyst was quite competent giving a higher yield of biodiesel (89.81%) [114]. Similarly, transesterification of dimethyl carbonate with n-propanol by using  $K_2CO_3/AC$  showed excellent catalytic performance during 5 h of reaction duration [115]. In a similar investigation, KOH/AC catalyst was used in the production of biodiesel from palm oil. The highest conversion of palm oil was obtained at 343 K temperature using 157.04 g of the catalyst. Regeneration study demonstrated that the catalyst was effective till third reaction cycle, which was reduced on further use. The reduction in the catalytic efficiency of the used catalyst after third reaction cycle may be due to the stripping of the active phase in the reaction mixture [116]. Meanwhile, the deoxygenation reaction over  $CaO-La_2O_3/AC$  catalyst has been performed to produce green biodiesel. Results concluded that the prepared  $CaO-La_2O_3/AC$  catalyst was very efficient and gave 72% yield of straight-chain hydrocarbons (C8-C20). The catalyst was also successfully regenerated and reused up to 6 reaction cycles giving the approximately equal yield and high selectivity of hydrocarbons [117].

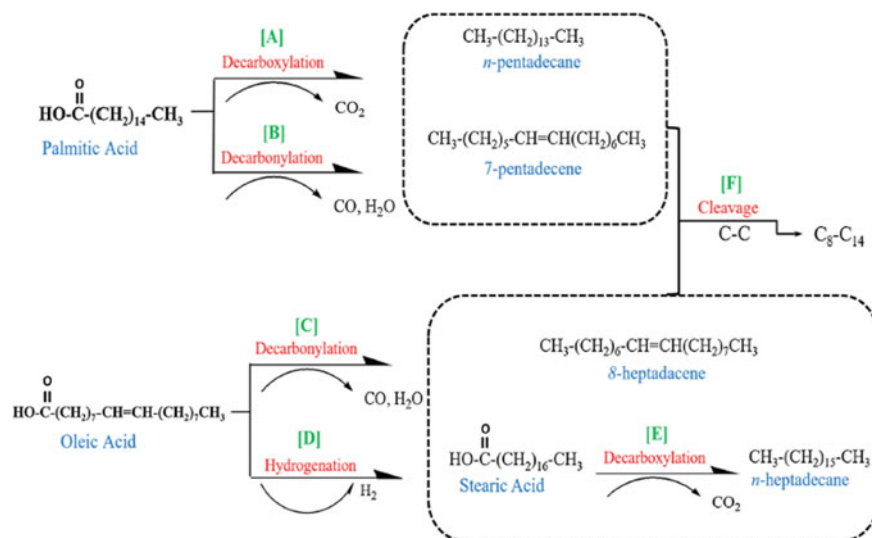
### 4.3 *Metal/metal Oxides-Doped Catalysts*

AC-supported metal/metal oxide catalysts have been employed in various organic transformations. These catalysts can be synthesized in three different ways:

- by adding metal salt to the carbon precursor,
- by exchange of ions,
- by impregnation of metal salts to carbon precursor.

The recovery of unsupported metal nanoparticles from the solution is a tedious process, while nanoparticles supported on carbon surface can easily be recovered and reused. AC support can easily be functionalized with oxygen-containing groups to enhance the interaction between metal and the support surface [118]. A study revealed the synthesis and catalytic application of AC-supported Fe catalyst. The catalytic efficiency of Fe/AC catalyst was evaluated in reforming of volatile material from palm kernel shell. The results show that the selectivity of the product is increased with the presence of Fe. The catalyst also improved the production of phenol (75.09 area%) and H<sub>2</sub> (75.12 vol.%) [119]. In another study, the catalytic activity of AC-supported metal–ligand complexes in the hydrogenation of anthracene by BaSO<sub>3</sub> was studied. The reaction was performed at different temperatures and periods. The results showed that among various metal–ligand/AC catalysts, Ni–L/AC catalysts gave maximum conversion and selectivity of the products, while BaSO<sub>3</sub>/AC gave poor results [120]. Similarly, the catalytic performance of Ru, Pd, and Ni-loaded AC catalysts in hydrogenation of 1-heptyne to 1-heptene was evaluated under mild conditions. The catalysts were prepared by mixing acidic solutions (HCl and HNO<sub>3</sub>) of Ru, Pd, and Ni and AC via the wet impregnation method. All prepared catalysts were found quite efficient and selective toward 1-heptene. The impact of the types of metals and the precursor salts on the efficiency and selectivity of 1-heptene is also evaluated. Results showed that among all metals, nickel catalyst was the most active and selective, while among precursor salts, AC-supported Pd (treated with HNO<sub>3</sub>) was more active and selective than AC-supported Pd (treated with HCl) [121]. Recently, a group of researchers has been synthesized mesoporous and high surface area AC from different wood species. Thus-produced AC was employed as support for loading AuPt nanoparticles. The catalytic efficiency of the synthesized catalyst was assessed on liquid-phase oxidation of glycerol and hydrogenation of levulinic acid (LA). The catalytic results determined that the reaction progress was affected by the structure of carbon material. The catalyst with a lesser –COOH group was found active for glycerol oxidation; on the other hand, a catalyst containing a larger aliphatic group was found active for hydrogenation of LA [122]. In addition, AC-supported bimetallic (Pd–Au/C) catalysts were found more efficient for hydrogenation of HMF to 2,5-dimethylfuran (DMF) than Pd/C and Au/C catalysts [123].

The catalytic activity of AC-supported Au catalyst has been reported on HMF oxidation to form 5-hydroxymethyl-2-furancarboxylic acid (HFCA) and 2,5-furandicarboxylic acid (FDCA). The nanosize of Au was responsible for the high yield of FDCA. On adding Pd to the Au, the catalyst reusability increased greatly. In



**Fig. 10** Proposed deoxygenation mechanism over Co/AC catalyst. Reprinted with the permission from Gamal et al. [125]. Copyright 2019 Elsevier

this study, AC was successfully utilized as a support material because of its sustainability in both acidic and basic reaction media [124]. In a recent study, palm fatty acid distillate (PFAD) was successfully converted into diesel over waste-derived Co/AC and Mn/AC catalysts. The results indicated that Co/AC catalyst was much more efficient than Mn/AC catalyst, which may be due to higher catalytic active sites on Co/AC catalyst. In addition, higher wt% loading of Co on AC is also responsible for increased selectivity and yield of products [125]. The proposed mechanism of deoxygenation over Co/AC catalyst is given in Fig. 10.

## 5 Conclusions and Future Perspectives

In conclusion, the use of wastes as renewable precursors in the production of AC which could be utilized as catalyst support, not only matches the criteria of circular economy, green chemistry principles but also satisfy the requirements for attaining UNO's Sustainable Development Goals (SDGs). In this literature review, different types of wastes that are commonly consumed for AC preparation were figured out. Some regular and emerging techniques used for AC production from such waste feedstocks prevailing in the past decade were also described. Applications of AC as catalyst support in fabricating solid acid, solid base, and metal/metal oxide dispersed catalysts have also been presented in this work. This chapter revealed that AC owing to its promising key features like high porosity, surface area, chemical, and thermal stability has proven to be a high potential aspirant for its use as catalyst support in



various catalytic applications. It also pointed out that research studies in this field are still lacking and there are abundant carbon-rich wastes like vegetable and fruit peels, food wastes, coal-based wastes, etc. which have not been utilized in AC generation. Moreover, the utilization of AC as catalyst support in the various industrially beneficial applications is also underdeveloped, and advanced efforts are required in this area to synthesize low-cost, cleaner, value-added products by upcycling of wastes. In the future, such catalysts could also play role in several other sectors like electrochemical processes involved in hydrogen and oxygen evolution reactions, wastewater treatment, air purification, antimicrobial activity, sediment remediation, etc. The work discussed in this chapter is advantageous as it paves an alternate, more economical, and environmentally safe pathway to produce AC with tunable properties comparable with commercial one by the utilization of wastes, thus solving the acute problem of waste disposal and reduce the dependence on expensive, depleted fossil fuel resources for AC production. Taking into consideration the bright future of this approach, novel waste raw materials, methods to produce AC, and its new catalytic applications will continue to be seen in industrial and academic disciplines.

## References

1. Matos I, Bernardo M, Fonseca I (2017) Porous carbon: a versatile material for catalysis. *Catal Today* 285:194–203
2. Wen Y, Kierzek K, Min J, Chen X, Gong J, Niu R, Wen X, Azadmanjiri J, Mijowska E, Tang T (2020) Porous carbon nanosheet with high surface area derived from waste poly(ethylene terephthalate) for supercapacitor applications. *J Appl Polym Sci* 137(5):1–10
3. Zhang M, Igalavithana AD, Xu L, Sarkar B, Hou D, Zhang M, Bhatnagar A, Cho WC, Ok YS (2020) Engineered/designer hierarchical porous carbon materials for organic pollutant removal from water and wastewater: a critical review. *Crit Rev Environ Sci Technol* 1–34
4. Zhang XQ, Li WC, Lu AH (2015) Designed porous carbon materials for efficient CO<sub>2</sub> adsorption and separation. *Xinxing Tan Cailiao/New Carbon Mater* 30(6):481–501
5. Özsın G, Kılıç M, Apaydın-Varol E, Pütün AE (2019) Chemically activated carbon production from agricultural waste of chickpea and its application for heavy metal adsorption: equilibrium, kinetic, and thermodynamic studies. *Appl Water Sci*. <https://doi.org/10.1007/s13201-019-0942-8>
6. Tsoncheva T, Genova I, Stoycheva I, Spassova I, Ivanova R, Tsyntsarski B, Issa G, Kovacheva D, Petrov N (2015) Activated carbon from waste biomass as catalyst support: formation of active phase in copper and cobalt catalysts for methanol decomposition. *J Porous Mater* 22(5):1127–1136
7. Vu THT, Nguyen MH, Nguyen MD (2019) Synthesis of acidic heterogeneous catalysts with high stability based on graphene oxide/activated carbon composites for the esterification of lactic acid. *J Chem*. <https://doi.org/10.1155/2019/7815697>
8. Nguyen NT, Le PA, Phung VBT (2020) Biomass-derived activated carbon electrode coupled with a redox additive electrolyte for electrical double-layer capacitors. *J Nanoparticle Res* 22(12):1–11
9. Ramón-Gonçalves M, Alcaraz L, Pérez-Ferreras S, León-González ME, Rosales-Conrado N, López FA (2019) Extraction of polyphenols and synthesis of new activated carbon from spent coffee grounds. *Sci Rep* 9(1):1–11
10. Li Y, Ding X, Guo Y, Rong C, Wang L, Qu Y, Ma X, Wang Z (2011) A new method of comprehensive utilization of rice husk. *J Hazard Mater* 186(2–3):2151–2156

11. EBSCOhost | 129703514 | Production of activated carbon as catalyst support by microwave pyrolysis of palm kernel shell: a comparative study of chemical versus physical activation.
12. Rajendran AB, Kalaiselvan S, Padmavathi R (2020) Adsorption of acid dye by activated carbon from agricultural solid waste *leucon leucocephala* seed shell waste: kinetics, equilibrium and isotherm study. *Mater Sci Res India* 17(3):251–259
13. Abdul Khalil HPS, Jawaid M, Firoozian P, Rashid U, Islam A, Akil HM (2013) Activated carbon from various agricultural wastes by chemical activation with KOH: preparation and characterization. *J Biobased Mater Bioenergy* 7(6):708–714
14. Jamil F, Al-Muhtaseb AH, Naushad M, Baawain M, Al-Mamun A, Saxena SK, Viswanadham N (2020) Evaluation of synthesized green carbon catalyst from waste date pits for tertiary butylation of phenol. *Arab J Chem* 13(1):298–307
15. Koubaissy B, Toufaily J, Cheikh S, Hassan MS, Hamieh T (2014) Valorization of agricultural waste into activated carbons and its adsorption characteristics for heavy metals. *Cent Eur J Eng* 4(1):90–99
16. Ratan JK, Kaur M, Adiraju B (2018) Synthesis of activated carbon from agricultural waste using a simple method: characterization, parametric and isotherms study. *Mater Today Proc* 5(2):3334–3345
17. Kaur J, Sarma AK, Jha MK, Gera P (2020) Rib shaped carbon catalyst derived from: *Zea mays L. cob* for ketalization of glycerol. *RSC Adv* 10(71):43334–43342
18. Kaur J, Sarma AK, Gera P, Jha MK (2021) Process optimization with acid functionalised activated carbon derived from corncob for production of 4-hydroxymethyl-2,2-dimethyl-1,3-dioxolane and 5-hydroxy-2,2-dimethyl-1,3-dioxane. *Sci Rep* 11(1):1–12
19. Goncalves M, Souza VC, Galhardo TS, Mantovani M, Figueiredo FCA, Mandelli D, Carvalho WA (2013) Glycerol conversion catalyzed by carbons prepared from agroindustrial wastes. *Ind Eng Chem Res* 52(8):2832–2839
20. Teimouri Z, Salem A, Salem S (2019) Clean and new strategy for catalytic conversion of agriculture waste shells to activated carbon via microwave-assisted impregnation: applied and eco-friendly aspect for decoloration of industrial corn syrup and process identifications. *J Environ Chem Eng* 7(3):103161
21. Alam MM, Hossain MA, Hossain MD, Johir MAH, Hossen J, Rahman MS, Zhou JL, Hasan ATMK, Karmakar AK, Ahmed MB (2020) The potentiality of rice husk-derived activated carbon: from synthesis to application. *Processes*. <https://doi.org/10.3390/pr8020203>
22. Blachnio M, Derylo-Marczewska A, Charnas B, Zienkiewicz-Strzalka M, Bogatyrov V, Galaburda M (2020) Activated carbon from agricultural wastes for adsorption of organic pollutants. *Molecules*. <https://doi.org/10.3390/molecules25215105>
23. Abdessemed A, Rasalingam S, Abdessemed S, Djebbar KEZ, Koodali R (2019) Impregnation of ZnO onto a vegetal activated carbon from algerian olive waste: a sustainable photocatalyst for degradation of ethyl violet dye. *Int J Photoenergy*. <https://doi.org/10.1155/2019/4714107>
24. Akbayrak S, Özçifçi Z, Tabak A (2020) Activated carbon derived from tea waste: A promising supporting material for metal nanoparticles used as catalysts in hydrolysis of ammonia borane. *Biomass Bioenerg*. <https://doi.org/10.1016/j.biombioe.2020.105589>
25. Mateo W, Lei H, Villota E, Qian M, Zhao Y, Huo E, Zhang Q, Lin X, Wang C, Huang Z (2020) Synthesis and characterization of sulfonated activated carbon as a catalyst for bio-jet fuel production from biomass and waste plastics. *Bioresour Technol* 297:122411
26. De S, Balu AM, Van Der Waal JC, Luque R (2015) Biomass-derived porous carbon materials: synthesis and catalytic applications. *ChemCatChem* 7(11):1608–1629
27. Tang ZE, Lim S, Pang YL, Shuit SH, Ong HC (2020) Utilisation of biomass wastes based activated carbon supported heterogeneous acid catalyst for biodiesel production. *Renew Energy* 158:91–102
28. Zhou C, Wang Y (2020) Recent progress in the conversion of biomass wastes into functional materials for value-added applications. *Sci Technol Adv Mater* 21(1):787–804
29. Bernardo M, Lapa N, Matos I, Fonseca I (2016) Critical discussion on activated carbons from bio-wastes: environmental risk assessment. *Boletín del Grup Español del Carbón* 2(40):18–21

30. Buasri A, Ksapabutr B, Panapoy M, Chaiyut N (2012) Biodiesel production from waste cooking palm oil using calcium oxide supported on activated carbon as catalyst in a fixed bed reactor. *Korean J Chem Eng* 29(12):1708–1712
31. Konwar LJ, Boro J, Deka D (2018) Activated carbon supported CaO from waste shells as a catalyst for biodiesel production. *Energy Sour, Part A Recover Util Environ Eff* 40(6):601–607
32. Lin QX, Zhang CH, Wang XH, Cheng BG, Mai N, Ren JL (2019) Impact of activation on properties of carbon-based solid acid catalysts for the hydrothermal conversion of xylose and hemicelluloses. *Catal Today* 319:31–40
33. Feng P, Li J, Wang H, Xu Z (2020) Biomass-based activated carbon and activators: preparation of activated carbon from corncob by chemical activation with biomass pyrolysis liquids. *ACS Omega* 5(37):24064–24072
34. Batista MKS, Mestre AS, Matos I, Fonseca IM, Carvalho AP (2016) Biodiesel production waste as promising biomass precursor of reusable activated carbons for caffeine removal. *RSC Adv* 6(51):45419–45427
35. Thushari I, Babel S (2018) Preparation of solid acid catalysts from waste biomass and their application for microwave-assisted biodiesel production from waste palm oil. *Waste Manag Res* 36(8):719–728
36. MacDermid-Watts K, Pradhan R, Dutta A (2021) Catalytic hydrothermal carbonization treatment of biomass for enhanced activated carbon: a review. *Waste Biomass Valorization* 12(5):2171–2186
37. Ospina V, Buitrago-Sierra R, López D (2015) HDO of guaiacol over NiMo catalyst supported on activated carbon derived from castor de-oiled cake HDO del guaiacol mediante el uso de catalizadores NiMo soportados. *Ing e Investig* 35(2):49–55
38. Veerakumar P, Panneer Muthuselvam I, Te HC, Lin KC, Chou FC, Bin LS (2016) Biomass-derived activated carbon supported Fe<sub>3</sub>O<sub>4</sub> nanoparticles as recyclable catalysts for reduction of nitroarenes. *ACS Sustain Chem Eng* 4(12):6772–6782
39. Lima SB, Borges SMS, Do Carmo Rangel M, Marchetti SG (2013) Effect of iron content on the catalytic properties of activated carbon-supported magnetite derived from biomass. *J Braz Chem Soc* 24(2):344–354
40. Khan TA, Saud AS, Jamari SS, Rahim MHA, Park JW, Kim HJ (2019) Hydrothermal carbonization of lignocellulosic biomass for carbon rich material preparation: a review. *Biomass Bioenerg* 130(September):105384
41. Lu Q, Zhang ZX, Wang X, Guo HQ, Cui MS, Yang YP (2018) Catalytic fast pyrolysis of biomass impregnated with potassium phosphate in a hydrogen atmosphere for the production of phenol and activated carbon. *Front Chem* 6(February):1–10
42. Shashank R, Raman V (2015) Preparation and characterization of activated master of technology (5 year integrated dual degree course). National Institute of Technology, Rourkela
43. Ma J, Liu J, Song J, Tang T (2018) Pressurized carbonization of mixed plastics into porous carbon sheets on magnesium oxide. *RSC Adv* 8(5):2469–2476
44. Patel H, Mangukiya H, Maiti P, Maiti S (2021) Empty cotton boll crop-residue and plastic waste valorization to bio-oil, potassic fertilizer and activated carbon—a bio-refinery model. *J Clean Prod* 290:125738
45. Kaur B, Gupta RK, Bhunia H (2019) Chemically activated nanoporous carbon adsorbents from waste plastic for CO<sub>2</sub> capture: Breakthrough adsorption study. *Microporous Mesoporous Mater* 282:146–158
46. Bratek W, Świątkowski A, Pakuła M, Biniak S, Bystrzejewski M, Szmigielski R (2013) Characteristics of activated carbon prepared from waste PET by carbon dioxide activation. *J Anal Appl Pyrolysis* 100:192–198
47. Yuan X, Cho MK, Lee JG, Choi SW, Lee KB (2020) Upcycling of waste polyethylene terephthalate plastic bottles into porous carbon for CF<sub>4</sub> adsorption. *Environ Pollut* 265:114868
48. Yuan X, Lee JG, Yun H, Deng S, Kim YJ, Lee JE, Kwak SK, Lee KB (2020) Solving two environmental issues simultaneously: waste polyethylene terephthalate plastic bottle-derived microporous carbons for capturing CO<sub>2</sub>. *Chem Eng J* 397:125350

49. Zhang H, Zhou XL, Shao LM, Lü F, He PJ (2021) Upcycling of PET waste into methane-rich gas and hierarchical porous carbon for high-performance supercapacitor by autogenic pressure pyrolysis and activation. *Sci Total Environ* 772:145309
50. Yuan X, Li S, Jeon S, Deng S, Zhao L, Lee KB (2020) Valorization of waste polyethylene terephthalate plastic into N-doped microporous carbon for CO<sub>2</sub> capture through a one-pot synthesis. *J Hazard Mater* 399:123010
51. Li Z, Chen K, Chen Z, Li W, Biney BW, Guo A, Liu D (2021) Removal of malachite green dye from aqueous solution by adsorbents derived from polyurethane plastic waste. *J Environ Chem Eng* 9(1):104704
52. Poerschmann J, Weiner B, Wozidlo S, Koehler R, Kopinke FD (2015) Hydrothermal carbonization of poly(vinyl chloride). *Chemosphere* 119:682–689
53. Yuliusman Y, Puspitasari M, Nafisah AR (2019) Preparation of activated carbon by chemical activation using KOH and acetone from low density polyethylene (LDPE) wastes. In: AIP conference proceedings. American Institute of Physics Inc., p 020027
54. Yuliusman, Nasruddin, Sanal A, Bernama A, Haris F, Ramadhan IT (2017) Preparation of activated carbon from waste plastics polyethylene terephthalate as adsorbent in natural gas storage. IOP conference series material science and engineering. Institute of Physics Publishing, p 012055
55. Tiwari D, Bhunia H, Bajpai PK (2018) Adsorption of CO<sub>2</sub> on KOH activated, N-enriched carbon derived from urea formaldehyde resin: kinetics, isotherm and thermodynamic studies. *Appl Surf Sci* 439:760–771
56. Hada R, Goyal D, Singh Yadav V, Siddiqui N, Rani A (2020) Synthesis of NiO nanoparticles loaded fly ash catalyst via microwave assisted solution combustion method and application in hydrogen peroxide decomposition. *Mater Today Proc* 119–123
57. Malpani SK, Rani A (2019) A greener route for synthesis of fly ash supported heterogeneous acid catalyst. *Mater Today Proc* 9:551–559
58. Rodríguez-Sánchez S, Ruiz B, Martínez-Blanco D, Sánchez-Arenillas M, Diez MA, Marco JF, Gorria P, Fuente E (2021) Towards advanced industrial waste-based magnetic activated carbons with tunable chemical, textural and magnetic properties. *Appl Surf Sci* 551:149407
59. Guclu C, Alper K, Erdem M, Tekin K, Karagoz S (2021) Activated carbons from co-carbonization of waste truck tires and spent tea leaves. *Sustain Chem Pharm* 21:100410
60. Mukherjee S, Kamila B, Paul S, Hazra B, Chowdhury S, Halder G (2021) Optimizing fluoride uptake influencing parameters of paper industry waste derived activated carbon. *Microchem J* 160:105643
61. Li L, Wu M, Song C, Liu L, Gong W, Ding Y, Yao J (2021) Efficient removal of cationic dyes via activated carbon with ultrahigh specific surface derived from vinasse wastes. *Bioresour Technol* 322:124540
62. Eguchi T, Tashima D, Fukuma M, Kumagai S (2020) Activated carbon derived from Japanese distilled liquor waste: application as the electrode active material of electric double-layer capacitors. *J Clean Prod* 259:120822
63. Mustafa R, Asmatulu E (2020) Preparation of activated carbon using fruit, paper and clothing wastes for wastewater treatment. *J Water Process Eng* 35:101239
64. Wang YX, Li WQ, He CS, Zhou GN, Yang HY, Han JC, Huang SQ, Mu Y (2020) Efficient bioanode from poultry feather wastes-derived N-doped activated carbon: performance and mechanisms. *J Clean Prod* 271:122012
65. Viegas RMC, Mestre AS, Mesquita E, Campinas M, Andrade MA, Carvalho AP, Rosa MJ (2020) Assessing the applicability of a new carb waste-derived powdered activated carbon to control pharmaceutical compounds in wastewater treatment. *Sci Total Environ* 743:140791
66. Jaria G, Silva CP, Oliveira JABP, Santos SM, Gil MV, Otero M, Calisto V, Esteves VI (2019) Production of highly efficient activated carbons from industrial wastes for the removal of pharmaceuticals from water—a full factorial design. *J Hazard Mater* 370:212–218
67. Idrees M, Rangari V, Jeelani S (2018) Sustainable packaging waste-derived activated carbon for carbon dioxide capture. *J CO<sub>2</sub> Util* 26(May):380–387

68. Chen H, Guo YC, Wang F, Wang G, Qi PR, Guo XH, Dai B, Yu F (2017) An activated carbon derived from tobacco waste for use as a supercapacitor electrode material. *Xinxing Tan Cailiao/New Carbon Mater* 32(6):592–599
69. Al-Rahbi AS, Williams PT (2016) Production of activated carbons from waste tyres for low temperature NO<sub>x</sub> control. *Waste Manag* 49:188–195
70. Saygılı H, Güzel F, Önal Y (2015) Conversion of grape industrial processing waste to activated carbon sorbent and its performance in cationic and anionic dyes adsorption. *J Clean Prod* 93:84–93
71. Giraldo L, Moreno-Piraján JC (2014) Study of adsorption of phenol on activated carbons obtained from eggshells. *J Anal Appl Pyrolysis* 106:41–47
72. Foo KY, Hameed BH (2011) Microwave-assisted preparation of oil palm fiber activated carbon for methylene blue adsorption. *Chem Eng J* 166(2):792–795
73. Anirudhan TS, Sreekumari SS (2011) Adsorptive removal of heavy metal ions from industrial effluents using activated carbon derived from waste coconut buttons. *J Environ Sci* 23(12):1989–1998
74. Mui ELK, Cheung WH, Valix M, McKay G (2010) Mesoporous activated carbon from waste tyre rubber for dye removal from effluents. *Microporous Mesoporous Mater* 130(1–3):287–294
75. Mazlan MAF, Uemura Y, Yusup S, Elhassan F, Uddin A, Hiwada A, Demiya M (2016) Activated carbon from rubber wood sawdust by carbon dioxide activation. *Procedia Eng*. Elsevier Ltd, pp 530–537
76. Tzvetkov G, Mihaylova S, Stoitchkova K, Tzvetkov P, Spassov T (2016) Mechanochemical and chemical activation of lignocellulosic material to prepare powdered activated carbons for adsorption applications. *Powder Technol* 299:41–50
77. Phiri Z, Everson RC, Neomagus HWJP, Wood BJ (2017) The effect of acid demineralising bituminous coals and de-ashing the respective chars on nitrogen functional forms. *J Anal Appl Pyrolysis* 125:127–135
78. Bedia J, Peñas-Garzón M, Gómez-Avilés A, Rodríguez JJ, Bolver C (2020) Review on activated carbons by chemical activation with FeCl<sub>3</sub>. *C J Carbon Res* 6(2):21
79. Samsuri AW, Sadegh-Zadeh F, Seh-Bardan BJ (2014) Characterization of biochars produced from oil palm and rice husks and their adsorption capacities for heavy metals. *Int J Environ Sci Technol* 11(4):967–976
80. Fechner N, Fellingner TP, Antonietti M (2013) “Salt templating”: a simple and sustainable pathway toward highly porous functional carbons from ionic liquids. *Adv Mater* 25(1):75–79
81. Xu H, Guo J, Suslick KS (2012) Porous carbon spheres from energetic carbon precursors using ultrasonic spray pyrolysis. *Adv Mater* 24(45):6028–6033
82. Atkinson JD, Fortunato ME, Dastgheib SA, Rostam-Abadi M, Rood MJ, Suslick KS (2011) Synthesis and characterization of iron-impregnated porous carbon spheres prepared by ultrasonic spray pyrolysis. *Carbon N Y* 49(2):587–598
83. Higai D, Lee C, Lang J, Qian EW (2021) Saccharification of cellulose using biomass-derived activated carbon-based solid acid catalysts. *Fuel Process Technol* 215:106738
84. Pezoti O, Cazetta AL, Bedin KC, Souza LS, Martins AC, Silva TL, Júnior OOS, Visentainer JV, Almeida VC (2016) NaOH-activated carbon of high surface area produced from guava seeds as a high-efficiency adsorbent for amoxicillin removal: Kinetic, isotherm and thermodynamic studies. *Chem Eng J* 288:778–788
85. Zheng C, Liu Z, Xu J, Li X, Yao Y (2017) Compressive strength and microstructure of activated carbon-fly ash cement composites. *Chem Eng Trans* 59:475–480
86. Yahya MA, Mansor MH, Zolkarnaini WAAW, Rusli NS, Aminuddin A, Mohamad K, Sabhan FAM, Atik AAA, Ozair LN (2018) A brief review on activated carbon derived from agriculture by-product. *AIP Conf Proc* 10(1063/1):5041244
87. Menya E, Olupot PW, Storz H, Lubwama M, Kiros Y (2018) Production and performance of activated carbon from rice husks for removal of natural organic matter from water: a review. *Chem Eng Res Des* 129:271–296

88. Chandane V, Singh VK (2016) Adsorption of safranin dye from aqueous solutions using a low-cost agro-waste material soybean hull. *Desalin Water Treat* 57(9):4122–4134
89. Saygılı H, Güzel F (2016) High surface area mesoporous activated carbon from tomato processing solid waste by zinc chloride activation: Process optimization, characterization and dyes adsorption. *J Clean Prod* 113:995–1004
90. Njoku VO, Islam MA, Asif M, Hameed BH (2015) Adsorption of 2,4-dichlorophenoxyacetic acid by mesoporous activated carbon prepared from H<sub>3</sub>PO<sub>4</sub>-activated langsat empty fruit bunch. *J Environ Manage* 154:138–144
91. Abbaszadeh S, Alwi SRW, Webb C, Ghasemi N, Muhamad II (2016) Treatment of lead-contaminated water using activated carbon adsorbent from locally available papaya peel biowaste. *J Clean Prod* 118:210–222
92. Sukanuma S, Nakajima K, Kitano M, Yamaguchi D, Kato H, Hayashi S, Hara M (2010) Synthesis and acid catalysis of cellulose-derived carbon-based solid acid. *Solid State Sci* 12(6):1029–1034
93. Liang X, Zeng M, Qi C (2010) One-step synthesis of carbon functionalized with sulfonic acid groups using hydrothermal carbonization. *Carbon N Y* 48(6):1844–1848
94. Liu T, Li Z, Li W, Shi C, Wang Y (2013) Preparation and characterization of biomass carbon-based solid acid catalyst for the esterification of oleic acid with methanol. *Bioresour Technol* 133:618–621
95. Lou WY, Guo Q, Chen WJ, Zong MH, Wu H, Smith TJ (2012) A highly active bagasse-derived solid acid catalyst with properties suitable for production of biodiesel. *Chemsuschem* 5(8):1533–1541
96. Zhang M, Sun A, Meng Y, Wang L, Jiang H, Li G (2015) Catalytic performance of biomass carbon-based solid acid catalyst for esterification of free fatty acids in waste cooking oil. *Catal Surv Asia* 19(2):61–67
97. Kastner JR, Miller J, Geller DP, Locklin J, Keith LH, Johnson T (2012) Catalytic esterification of fatty acids using solid acid catalysts generated from biochar and activated carbon. *Catal Today* 190(1):122–132
98. Wang J, Xu W, Ren J, Liu X, Lu G, Wang Y (2011) Efficient catalytic conversion of fructose into hydroxymethylfurfural by a novel carbon-based solid acid. *Green Chem* 13(10):2678–2681
99. Liu WJ, Jiang H, Yu HQ (2015) Development of biochar-based functional materials: toward a sustainable platform carbon material. *Chem Rev* 115(22):12251–12285
100. Wu Y, Fu Z, Yin D, Xu Q, Liu F, Lu C, Mao L (2010) Microwave-assisted hydrolysis of crystalline cellulose catalyzed by biomass char sulfonic acids. *Green Chem* 12(4):670–696
101. Kobayashi H, Komanoya T, Guha SK, Hara K, Fukuoka A (2011) Conversion of cellulose into renewable chemicals by supported metal catalysis. *Appl Catal A Gen* 409–410:13–20
102. Tao ML, Guan HY, Wang XH, Liu YC, Louh RF (2015) Fabrication of sulfonated carbon catalyst from biomass waste and its use for glycerol esterification. *Fuel Process Technol* 138:355–360
103. Nakajima K, Hara M (2012) Amorphous carbon with SO<sub>3</sub>H groups as a solid brønsted acid catalyst. *ACS Catal* 2(7):1296–1304
104. Wang C, Gui X, Yun Z (2014) Esterification of lauric and oleic acids with methanol over oxidized and sulfonated activated carbon catalyst. *React Kinet Mech Catal* 113(1):211–223
105. Foo GS, Van PAH, Krötschel D, Sauk BF, Rogers AK, Jolly CR, Yung MM, Sievers C (2015) Hydrolysis of cellobiose over selective and stable sulfonated activated carbon catalysts. *ACS Sustain Chem Eng* 3(9):1934–1942
106. Galhardo TS, Simone N, Gonçalves M, Figueiredo FCA, Mandelli D, Carvalho WA (2013) Preparation of sulfonated carbons from rice husk and their application in catalytic conversion of glycerol. *ACS Sustain Chem Eng* 1(11):1381–1389
107. Nda-Umar UI, Ramli I, Muhamad EN, Taufiq-Yap YH, Azri N (2020) Synthesis and characterization of sulfonated carbon catalysts derived from biomass waste and its evaluation in glycerol acetylation. *Biomass Convers Biorefinery*. <https://doi.org/10.1007/s13399-020-00784-0>

108. Dora S, Bhaskar T, Singh R, Naik DV, Adhikari DK (2012) Effective catalytic conversion of cellulose into high yields of methyl glucosides over sulfonated carbon based catalyst. *Bioresour Technol* 120:318–321
109. Qi X, Guo H, Li L, Smith RL (2012) Acid-catalyzed dehydration of fructose into 5-hydroxymethylfurfural by cellulose-derived amorphous carbon. *Chemsuschem* 5(11):2215–2220
110. da Luz Corrêa AP, Bastos RRC, da Rocha Filho GN, Zamian JR, da Conceição LRV (2020) Preparation of sulfonated carbon-based catalysts from murumuru kernel shell and their performance in the esterification reaction. *RSC Adv* 10(34):20245–20256
111. Negm NA, Betiha MA, Alhumaimess MS, Hassan HMA, Rabie AM (2019) Clean transesterification process for biodiesel production using heterogeneous polymer-heteropoly acid nanocatalyst. *J Clean Prod* 238:117854
112. Shokouhimehr M, Hong K, Lee TH, Moon CW, Hong SP, Zhang K, Suh JM, Choi KS, Varma RS, Jang HW (2018) Magnetically retrievable nanocomposite adorned with Pd nanocatalysts: efficient reduction of nitroaromatics in aqueous media. *Green Chem* 20(16):3809–3817
113. Huo E, Lei H, Liu C et al (2020) Jet fuel and hydrogen produced from waste plastics catalytic pyrolysis with activated carbon and MgO. *Sci Total Environ*. <https://doi.org/10.1016/j.scitotenv.2020.138411>
114. Dhawane SH, Kumar T, Halder G (2016) Biodiesel synthesis from Hevea brasiliensis oil employing carbon supported heterogeneous catalyst: optimization by Taguchi method. *Renew Energy* 89:506–514
115. Fan M, Zhang P (2007) Activated carbon supported  $K_2CO_3$  catalysts for transesterification of dimethyl carbonate with propyl alcohol. *Energy Fuels* 21(2):633–635
116. Baroutian S, Aroua MK, Raman AAA, Sulaiman NMN (2011) A packed bed membrane reactor for production of biodiesel using activated carbon supported catalyst. *Bioresour Technol* 102(2):1095–1102
117. Alsultan GA, Asikin-Mijan N, Lee HV, Albazzaz AS, Taufiq-Yap YH (2017) Deoxygenation of waste cooking to renewable diesel over walnut shell-derived nanorode activated carbon supported  $CaO-La_2O_3$  catalyst. *Energy Convers Manag* 151:311–323
118. Lam E, Luong JHT (2014) Carbon materials as catalyst supports and catalysts in the transformation of biomass to fuels and chemicals. *ACS Catal* 4(10):3393–3410
119. An Y, Tahmasebi A, Zhao X, Matamba T, Yu J (2020) Catalytic reforming of palm kernel shell microwave pyrolysis vapors over iron-loaded activated carbon: enhanced production of phenol and hydrogen. *Bioresour Technol* 306:123111
120. Giraldo L, Moreno-Piraján HJJ (2017) Metal complexes supported on activated carbon as catalysts for the hydrogenation of anthracene. *Int J Chem React Eng*. <https://doi.org/10.1515/ijcre-2017-0068>
121. Carrara N, Betti C, Coloma-Pascual F, Almansa MC, Gutierrez L, Miranda C, Quiroga ME, Lederhos CR (2018) High-Active metallic-activated carbon catalysts for selective hydrogenation. *Int J Chem Eng*. <https://doi.org/10.1155/2018/4307308>
122. Prati L, Bergna D, Villa A, Spontoni P, Bianchi CL, Hu T, Romar H, Lassi U (2018) Carbons from second generation biomass as sustainable supports for catalytic systems. *Catal Today* 301:239–243
123. Nishimura S, Ikeda N, Ebitani K (2014) Selective hydrogenation of biomass-derived 5-hydroxymethylfurfural (HMF) to 2,5-dimethylfuran (DMF) under atmospheric hydrogen pressure over carbon supported PdAu bimetallic catalyst. *Catal Today*. Elsevier, pp 89–98
124. Davis SE, Ide MS, Davis RJ (2013) Selective oxidation of alcohols and aldehydes over supported metal nanoparticles. *Green Chem* 15(1):17–45
125. Gamal MS, Asikin-Mijan N, Arumugam M, Rashid U, Taufiq-Yap YH (2019) Solvent-free catalytic deoxygenation of palm fatty acid distillate over cobalt and manganese supported on activated carbon originating from waste coconut shell. *J Anal Appl Pyrolysis* 144:104690

**Part IV**  
**Sensor and Sensing Technology**



# Chapter 14

## Porous Carbon-Based Sensors and Their Applications



Karunanthi Govardhan, Prabhu Ramanathan, and Mahesh Ganesapillai

### 1 Introduction

Carbon has been the buzzword for most chemical and material scientists towards the turn of the twenty-first century. Various allotropic nanostructures are derived from carbon. C-60 structures (O–D), famously termed Buckminster Fullerenes, were discovered by Kroto et al. in 1985 [1] paved the way in kindling interest in carbon-based materials. The discovery of 1D Carbon nanotubes by Iijima in 1991 [2] quickly followed fullerenes, field of sensors, 2D structures of carbon, the Graphene by Geim et al. lured the interest of carbon allotropes to many scientific domains. The research and developments in these materials justify two Noble Prizes awarded among these three materials. Activated carbons represent the allotropes of carbon which are either functionalized through chemical, physical, or other means to make them highly selective or reactive towards a target molecule or perform a chemical or physical function. These materials' inert or dielectric nature differs from making them selectively active or reactive with a modified parametrical response. High surface area and porosity are critical factors in this. The international union of pure and applied chemistry has categorized materials' porosity according to their pore size distribution. Macropores

---

K. Govardhan

Department of Micro and Nano-Electronics, School of Electronics Engineering, Vellore Institute of Technology, Vellore, Tamilnadu 632014, India

P. Ramanathan

University West, Division of Production Systems, Gustava Melins, Gata 2, 46132 Trollhattan, Sweden

M. Ganesapillai (✉)

Mass Transfer Group, School of Chemical Engineering, Vellore Institute of Technology, Vellore, Tamilnadu 632014, India

e-mail: [maheshgpillai@vit.ac.in](mailto:maheshgpillai@vit.ac.in)

are defined as those with a diameter higher than 50 nm, mesopores are defined as those with a diameter between 2 and 50 nm, and micropores are defined as those with a diameter less than 2 nm [3].

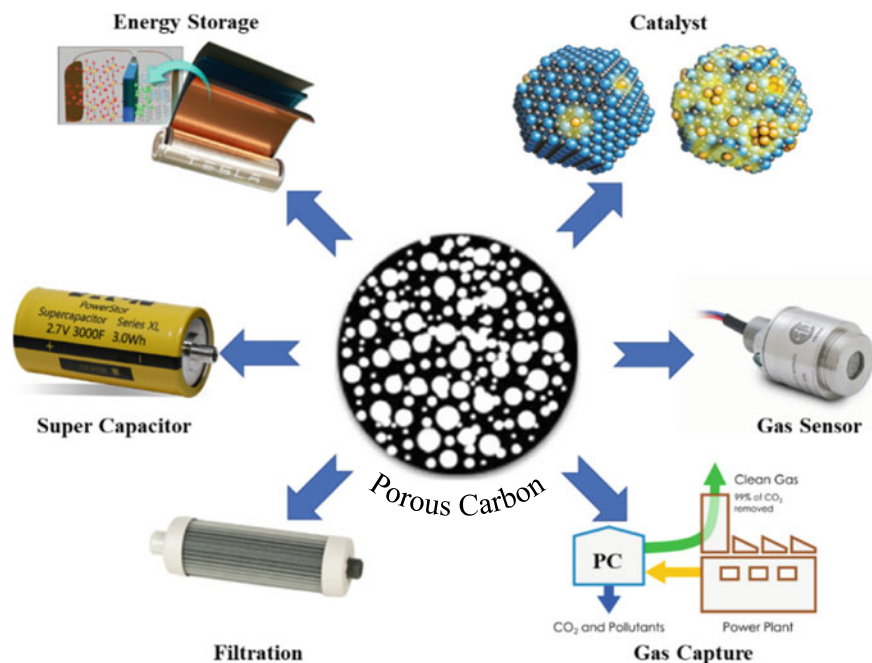
Highly porous and, in particular, tuneable porous structures were the need of the hour to enhance the performance of various catalytic and sensing reactions. Mesoporous structures synthesized since 1990 came as a boon for these domains. Mesoporous carbon, with its benefactor characteristics such as enhanced stability (chemical, mechanical, and thermal), high surface area, tuneable pore size, can be functionalized with various active elements exploited in energy storage and electrochemical sensing applications. Moreover, they exhibit variable electrical properties based on the orientation and carbon matrix ordering [4], which help better conduction of signals from the active host or sensing elements either confined or adsorbed onto the 3D mesoporous structure. Integrated formation of micropores embedded into the complex macropores enhances the selectivity towards a specific species in catalysis and sensing requirements.

Though being a newcomer to the family, porous carbon is recently gathering much momentum in various fields. Highly excellent properties exhibited by these materials such as tuneable and high porosity, synthesized with different morphological shapes and sizes, proven physical and chemical stability, functionalize with various elements to suit applications demanding highly selective and sensitive responses, the higher surface-to-volume ratio, lightweight, tuneable electrical conductivity, high mechanical strength. Prime research emphasis on porous carbon spans highly diverse domains ranging from energy storage to sensing applications (Fig. 1). Lithiated porous carbons are being viewed as an option for high-energy storage mediums. Porous carbon-mediated supercapacitors are becoming a norm, and there are products commercialized based on them. Doped or functionalized PC-based nanostructures are being used as a catalytic medium in various domains.

Along with activated carbon, PCs are also being used as effective filtration media in liquid and gas-based systems. A highly porous nature with tuneable defect sites has proven that PCs are an excellent choice for gas adsorption, which can be utilized in gas sensors or gas capturing systems. Interestingly, these materials can also be easily derived from biomass waste, thereby proving to be environmentally friendly and facilitating effective use in terms of recycling.

## ***1.1 Carbon Nano-Structured Sensors***

CNTs and graphene have become the most preferred go-to or starting material for enhancing the sensing performance of nanomaterials. This is mainly owing to their chemical, physical, electrical, mechanical properties. CNTs and graphene have been highly researched and used in various sensing applications, including gas sensors, biosensors, electrochemical, optical, pressure, and strain sensors. However, porous carbon-based systems rival them with the most significant advantage of highly tuneable porosity and simple template-based growth mechanisms. Publication data

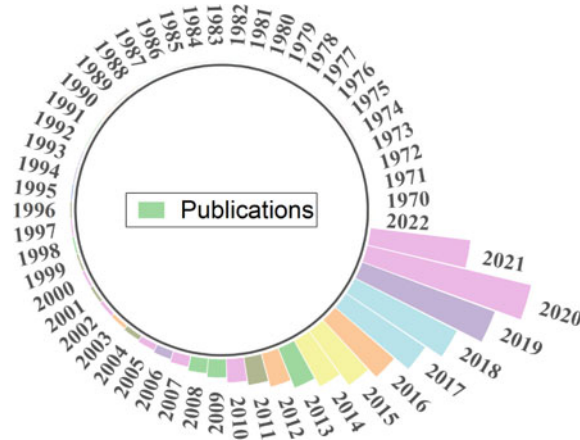


**Fig. 1** Potential applications of porous carbon-based sensors

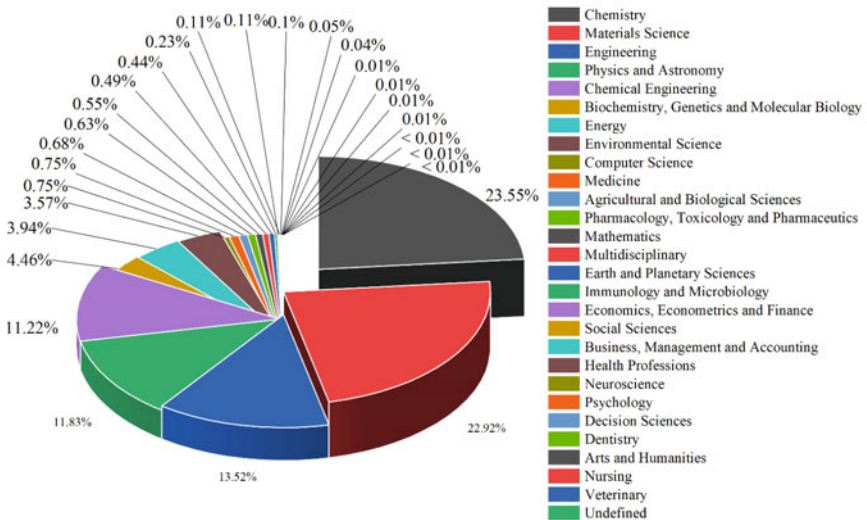
derived from scopus.com highlights the research trend in the field of porous carbon-based sensors. These materials have garnered greater interest in the past decade with a highly exponential increase in publications until 2020, only to be disturbed by the current global pandemic.

Both year-wise and domain-wise publication data analysis derived from scopus.com on porous carbon sensor derived on 4th June 2021 is depicted in Figs. 2 and 3. The publications have resulted across a wide range of domains, dominated by chemistry and materials science. PC-based materials have also created a great interest in the biomedical field with various researches reported in medicine, pharmacology, toxicology, and pharmaceuticals. The impact of PC materials has also been observed across mathematics, economics, businesses, social sciences, etc. Newer interests are being vested in neuroscience, veterinary, dentistry, etc.

Most of the applications reported on the sensing and electrochemical activity front focus on gas sensing, adsorption and storage, and energy storage and supercapacitors. All these applications involve physio-chemical or electrochemical reactions of the heteroatoms doped in the PC matrix. Various monomers, polymers, and other carbohydrates are used extensively to synthesize the 3D porous carbon structures. The PC matrix provides high specific surface area, hierarchical porous structure, greater pore accessibility, lower density, sub-micrometre edges that facilitate faster electron or molecular diffusion/transfer, availability of a large number of active sites



**Fig. 2** Year-wise publication data analysis derived from scopus.com on porous carbon sensor (data derived on 4th June 2021)



**Fig. 3** Domain-wise publication data analysis derived from scopus.com on porous carbon sensor (data derived on 4th June 2021)

to embed reactive agents, and more controllable inner pore volume enhancing the sensing and electrochemical activity which these fields demand the most [5].

### 1.1.1 Material Properties

A material chosen for sensing applications should respond to a stimulus initiated by a chemical or physical phenomenon. Suppose the response of the sensing material (stimuli) is obtained as an electrical signal. In that case, it makes the job of the instrumentation engineer to design efficient signal conditioning circuits to derive a meaningful indication of the physical or chemical changes that occurred in the process of the measurement interest. Commercial successful implementation of those sensing materials depends on the speed of the response, hysteresis, drift due to ambient condition, high sensitivity, and linear. Environment friendliness and the material's cost-effectiveness are needed for a material to be used as a sensor. PCs shall be regarded as a golden material to be used as a sensor due to its diversified forms of configurations with different characteristics properties, viz., electrical, mechanical, optical, and thermal. The high reactivity of different carbon structures allows tailor-made solutions for different applications. The use of PCs for large-scale energy storage applications, due to the stable, high yield, easy synthesis of super capacitance, is a more successful application. PCs have a large surface area, are inexpensive to manufacture, are simple to process, and have a high conductivity. This section is intended to brief the readers about the properties of the PC material, which makes them viable for sensing applications.

### 1.1.2 Mechanical Properties

Different materials have been reported for pressure measuring. If the material's mechanical properties facilitate the production of numerous sensing parameters due to the transduction mode, the same material should be utilized to measure dependent variables. For instance, simultaneous pressure and temperature measurements might be advantageous for specific industrial and medical apparatus. The material should convert applied force to electrical signals in order to monitor pressure. The force range must be sufficiently broad, ranging from a few pascals to several pascals. Additionally, the electrical signal transduction must occur within a quantifiable range, alternatively, in ohms, volts, or amps.

Additionally, the materials should have the following characteristics: sensitivity, low drift, low offset, low hysteresis, repetitive, and reproducible. Several successful researchers have reported the use of the following materials for pressure measurement; (i) active carbon [6], (ii) conductive polymers [7], (iii) graphene [8], (iv) metal nanoparticles [9], and (v) metal nanowires [10]. Following the need for multifunctional parameter measurement with the same transduction material, the following applications were reported:

- (a) Temperature and pulse pressure in artery vessels [11];
- (b) temperature and surface hardness in artificial finger development [12, 13]; and
- (c) temperature, pressure, and vibration detection in e-skin development [14].

Zhao et al. [15] successfully reported the fabrication of bi-modal sensing based on the metal–organic frameworks derived from porous carbon and polydimethylsiloxane (PDMS) composite. The article has reported simultaneous measurements of pressure and temperature. The sensitivity of the pressure measurement is about  $15.63 \text{ kPa}^{-1}$ , with a 65 ms response time. For temperature, it is about  $> 0.11 \text{ }^{\circ}\text{C}^{-1}$  with 100 ms response time.

The mechanical property of the PC/PDMS material varies the contact area inside and also between the composite films and the electrodes. When no pressure is applied to the porous structure, the resistance between the PC and the electrodes is exceptionally high. This is because the contact area between the PC and the electrodes is relatively small. External pressure compresses the PC/PDMS composite pores, lowering the resistance. Furthermore, the resistance is decreased due to the increased contact area between the substrate and the film. Similarly, removing the pressure restores the initial resistance. In the experiment, the material is exposed to different pressure loads from 60 to 2000 Pa with a constant voltage source of 3 V. The current response was recorded for varying pressure exposure. The sample has yielded a stable and linear response in the span of the varying pressure from 60 to 2000 Pa with a sensitivity of  $15.63 \text{ kPa}^{-1}$ . The pressure sensitivity is defined as  $S = (\Delta I/I_o)/\Delta P$ , where  $S$  is the sensitivity,  $\Delta P$  is the change in applied pressure,  $I_o$  is the initial current without applied pressure,  $\Delta I$  is the change in current ( $I_p - I_o$ ).

The thermal expansion characteristics of the material were experimented with from 23 to 120  $^{\circ}\text{C}$ . The material has shown a positive temperature coefficient, owing to the expansion of the polymer and eventually the breakdown of the thermal conductivity path between the fillers. The well-established relation  $\alpha$  calculated the temperature coefficient of resistance =  $(\Delta R/R_o)/\Delta T$ , where  $R_o$  is the resistance at room temperature,  $\Delta R$  is the increase or decrease of resistance ( $R - R_o$ ), and  $\Delta T$  is the change in temperature ( $T - T_o$ ). The material has exhibited a linear relationship between 23 and 50  $^{\circ}\text{C}$ . After 60  $^{\circ}\text{C}$ , the experiment has yielded an exponential increase of the response, and the sensing material responds to both pressure and temperature stimuli.

### 1.1.3 Optical Properties

Carbonaceous materials have been a well-established field of research for over a decade, owing to their ubiquitous nature and simplicity of preparation. Carbonaceous materials include porous carbon, activated carbon, carbon nanospheres, carbon aerogel, and porous graphene. These materials were also electrically conductive and structurally stable [16]. Additionally, these materials have high porosity (micropores (less than 2 nm), mesopores (2–50 nm), macropores (greater than 50 nm), or a combination thereof), which results in a more extensive specific surface area and pore volume, as well as customizable pore sizes and distributions [17].

Carbon dots (CD) are fluorescent carbon nanoparticles first observed in a study conducted by Xu et al. [18]. In a subsequent study [19], it was observed that the luminescence of CDs could be enhanced by surface passivation. Since then, research

has skewed towards CDs due to their unique properties like high water solubility, photostability, more accessible synthesis methods, and lower production costs. These nanoparticles are well-dispersed structures and could be actively stabilized in materials with nanoscale porosity—such stabilized materials exhibit desirable properties such as effective optical absorption, photo-induced electron transfer, upconverted photoluminescence, and tuneable photoluminescence. CDs are widely used in a variety of applications, including bio-imaging [20], sensing [21], catalysis [22], energy devices [23], optoelectronics [24], etc.

Porous carbonaceous materials are hence preferred as stabilizing structures because of their abundance, physical properties, and adjustable pore sizes. Furthermore, carbonaceous porous materials have been credited for generating synergistic effects with CDs. There are four prominent types of CDs—graphene quantum dots, carbon nanodots, carbon quantum dots (CQDs), and carbonized polymer dots [25]. A typical disadvantage of CDs is that they frequently exhibit the solid-state aggregation-induced luminescence quenching effect. This leads to a phenomenon of luminescence quenching and poses issues in applications based on the nanostructure's optical properties (like in optoelectronic devices). Similarly, it faces drawbacks in photocatalysis applications due to lower luminous efficiency and low photosensitization efficiency. Luminescence quenching can be actively avoided by incorporating CDs with a porous material—simultaneously, the synergistic effect of the combined structure proved to enhance the performance of the nanostructure itself [17].

The 3D porous graphene structures such as porous graphene skeleton [26, 27], graphene hydrogel [28], or aerogel have unique porous structures, higher specific surface areas, and more excellent electrical conductivity. Incorporating CDs into these porous graphene structures to construct composites can effectively enhance the performance of the resulting composite structure. Composites of CDs and porous materials combine the features of CDs with unique porous architectures, generating widespread interest in various sectors, including optics and healthcare [29], sensing, and electrochemistry [30]. CDs integrated with porous materials form viable composites with unique properties which can be used as chemical sensors. Porous materials serve as carriers of CDs and significantly improve the sensor's sensitivity owing to their porous structure. Wang et al. [31], conducted a study demonstrating the enhanced sensitivity of (a mesoporous material) MCM-41/CQD composite to acetic acid gas rather than the acetic acid solution. This was mainly credited to mesoporous MCM-41 for enriching the gas around the CDs for effective sensing. Other applications of CDs include drug delivery, imaging, and photocatalysis [32, 33].

### 1.1.4 Pore Structure and Surface Chemistry

New sensors with improved sensitivity and dependability are necessary to manufacture modern sensor devices. These sensors must also be cheap, small in size, and easy to operate [34]. Nanotechnology has enabled considerable breakthroughs in material characteristics, allowing significant advancements to transcend the boundaries of conventional materials. Compounds derived from carbon are among the

most extensively explored and widely used materials in nanotechnology world-wide. Carbonaceous structures have several advantages over other materials widely employed, including superior physical and chemical qualities [35]. Carbon-based materials could also replace currently expensive electrical chemicals because of their increased efficiency and environmental friendliness. As a result of its outstanding physical and chemical properties, carbon nanostructures have been studied for use as sensitive sensor devices. Structure defects and unsaturated chemical bonds formed by carbon atoms are responsible for the elevated surface activity of these substances [36]. Initially, sensors have relied on fullerenes, carbon nanotubes, and graphene, which have gained significant scientific attention due to their increased electron transfer rates, high specific surface area ratio, and bio-compatibility.

Tans et al. [37] identified that the carbon nanotube field-effect transistor is now considered a feasible substitute for virtually all metal oxide semiconductor field-effect transistor applications. Graphene and its variants were employed as materials for sensors in a range due to its exceptional thermal and electrical conductivity, high specific surface area, and outstanding mechanical strength. Carbon nanostructures are used as gas sensors because their porous structure allows gas adsorption and desorption, allowing gas detection and quantification. The capacity to functionalize the gas further improves selectivity. For gas sensors, carbon nanostructures can be utilized in sorption, ionization, capacitance, or resonance frequency shift sensor systems, as long as they have high specificity, rapid reaction and recovery rate, and durability [38].

Additionally, carbon-based sensors can be used when contamination is being eradicated or phased out by monitoring dangerous compounds in the surrounding environment with a response similar to gas sensors [39]. Leng et al. [40] produced a humidity sensor by mixing diamine-modified graphene oxide and Nafion polymer to create a hybrid film and carbon nanostructures as mechanical sensors for strain measurements. As a result, carbon nanostructure-based sensors are innovative systems with a wide range of applications. With comparable findings, several carbon allotropic forms can be employed in sensing applications, and thus, a variety of materials have been employed due to their superior electrical, thermal, mechanical, and chemical qualities [41].

## 2 Fabrication of Porous Carbon-Based Sensors

Porous carbon materials can be divided into three categories based on pore size: microporous 2 nm, mesoporous 50 nm, and macroporous > 50 nm, according to the International Union of Pure and Applied Chemistry. Various ways have been used to create porous carbon. Here are some traditional approaches.

- Chemical activation, physical activation, or a combination of factors [42–44];
- Utilization of metal salts or organometallic compounds to catalyse the activation of carbon precursors [45–47];

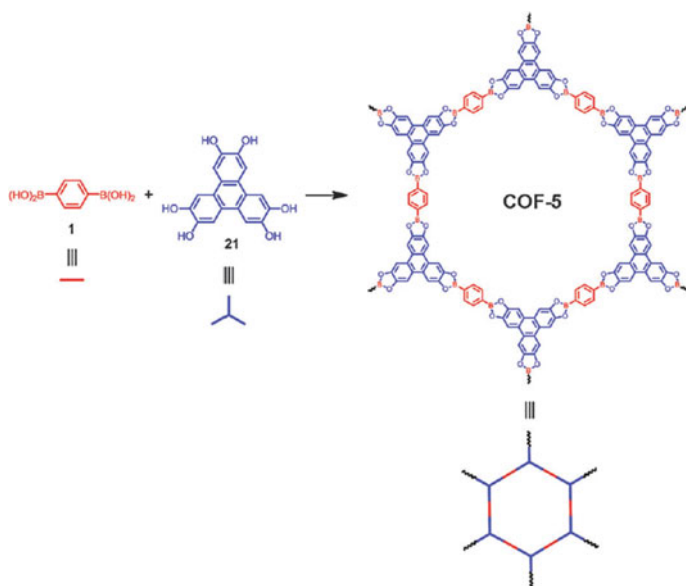


- Carbonization of polymer blends that contain both carbonizable and hydrolysable polymers [48–50]; and
- Carbonization of a polymer aerogel produced via supercritical drying [51–53].

Recent synthesis techniques have quickly and vastly improved over the traditional techniques. Pyrolysis, carbonization, and polymerization have become the standard processes, enhanced with the various additional processes including templating, hetero doping, co-polymerization, and treatment with certain dopants or functionalized molecules to increase selectivity and sensitivity of the PC-based materials towards target species.

## 2.1 Pyrolysis

Pyrolysis has been the most preferred and most straightforward technique to synthesize porous carbon structures. Organic precursors are pyrolysed at inert atmospheres. The inherent property of the organic precursor plays a dominant role in defining the characteristics of the PC nanostructures. Hence, the choice of the same is critical to tailor the PC's porosity, morphology, crystallinity, mechanical, electrical, and chemical properties. Most often, polymers have been used as precursors. Recently biomass [26, 54] and ionic liquids [55–57] are being substituted using polymers (Fig. 4).



**Fig. 4** Porous carbon structures with linkages and linkers

Porous carbon structures with heteroatom doping are preferred towards the focused application domains of sensing, catalysis, and energy storage. Porous carbon structures consist of linkages and linkers. Linkers connect different blocks of the structures. When a porous carbon structure has been doped with N, S, B, and metals, it is termed as metal-organics, and when monomer-based heteroatom has been doped, it is termed as covalent organic frameworks (COFs) [58]. Metal–organic frameworks are realized through the interconnection of organic linkers decorated by metal ions, where COFs consist of organic monomers replacing metal ions.

## 2.2 Solvothermal Carbonization

Solvothermal carbonization is the most straightforward and commonly used technique to synthesize porous carbon nanostructures. Conventional pyrolysis techniques with carbohydrate-based precursors result in hydrochar but result in reduced porosity. In order to enhance the porosity of the porous carbon nanostructures, the precursor is thermochemically converted to wet precursors by treatment with subcritical water [59]. Porous carbon materials can be synthesized at relatively lower temperatures (180–200 °C) for water treatment and dye removal [60]. To reduce the overall cost in synthesizing the porous carbon, biomass or biowaste materials have been used as the precursors [61, 62].

## 2.3 Template-Assisted Polymerization

Synthesis of PC-based nanostructures with well-defined mesoporous structures can be conveniently done using templates. This technique aims to create a mirror structure of the required PC structure using polymers and then either pyrolyse the polymers or coat conjugated polymers on the surface of the existing polymers. Highly ordered meso or nanoporous carbon structures can easily be formed through ordered silica templates. To successfully replicate the template pattern, it is critical to ensure polymerization only inside the template and not on its outer surfaces, making the template removal process more complex. In order to facilitate the internal polymerization, oxidizing agents are immobilized onto the inner surface of the templates. These agents can also be modified or embedded to act as dopants or functionalized active sites after post-synthesis treatment [63]. Santa Barbara Amorphous-15 and 16 (SBA-15, SBA-16) [63–66], Korea Advanced Institute of Science and Technology-6 (KIT-6) [67–69], Mobil Composition of Matter-41 (MCM-41) [70, 71], MCM-48 [72], and silica xerogel [73, 74] are used as templates and polypyrrole [63, 74], polyaniline [69], and thiophene [75] are used as common precursors. PPY and PANI result in nitrogen-doped PC [74, 76], and thiophene [75] results in sulphur-doped PC. Superparamagnetic nanoparticles-embedded mesoporous magnetically separable ordered carbon structures have been developed, with  $\text{FeCl}_3$  acting as an oxidizing agent. The

Fe ions left behind after polymerization stay embedded in the carbon matrix. The size of these particles is limited by the silica template and the diameter of the CNTs formed from these metal particles [77].

Exploiting the sensing and catalytic activities of the porous carbon materials requires them to be synthesized with active sites embedded with functionalized elements or molecules. The sensing nature of the material can be tailored during the synthesis process itself, making the process simpler and highly configurable as per the requirement. Newer techniques like metal–organic and covalent organic frameworks have evolved over simple carbonization techniques to meet these requirements. Both result in heteroatom-doped porous carbon structures with high dispersion. The tailored doping with interconnected meso–micropores enhances the sensing and catalytic activities owing to increased reactive surface area and greater adsorption volume of the 3D porous carbon-based materials.

## ***2.4 Metal–Organic Frameworks***

Metal–organic frameworks are a type of crystalline porous carbon-based coordination polymers with metal elements distributed among the carbon matrix. Metal–organic frameworks are characterized by permanent porosity with higher pore volumes, larger active surface area, low-density materials with uniform distribution of metal ions. They can be decorated with different metal atoms or ions to achieve a wide range of sensing or catalytic activities. They have already found their footprint well established in the field of gas sensing, adsorption and separation [78], organic pollutant degradation [79], catalysis [80], sensing of chemical [81], energy storage [82], drug delivery [83], and others.

## ***2.5 Covalent Organic Frameworks***

Covalent organic frameworks (COFs) consist only of organic molecules linked by covalent bonding with no inorganic elements or molecules in the matrix. They are characterized by higher pore volumes with controlled pore sizes and shapes through the synthesis process. COFs have been utilized towards catalysis, gas storage [24, 84–89] and separation, energy storage [90], etc. COFs are constructed through two main components, linkages, and linkers. Due to the usage of only organic monomers and polymers in the synthesis process, COFs are comparatively more ordered than metal–organic frameworks, can handle harsher environments better, and result in a variety of morphologies based on the chosen precursors [58]. Similar to metal–organic frameworks, COFs can also be doped with S, N used for oxygen reduction reaction for electrochemical sensing, co-doping of N and S for electrochemical activity [91–93]. Lanthanide-doped COF [94] have also been developed to fabricate an ultrasensitive sensor to detect perfluorooctanesulphonate in tap water. The results of this sensor

were very close to the results obtained from much costlier and complex sensing based on the liquid chromatography technique.

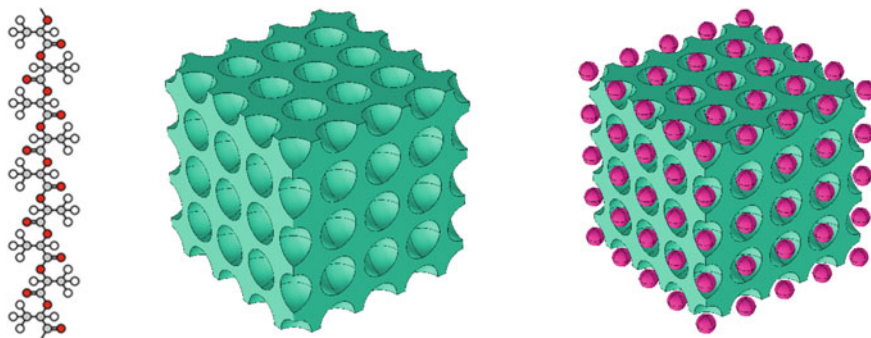
## **2.6 Dual Templating**

Superhydrophilic fabric synthesized from hierarchical porous carbon structures with enhanced conductivity has been developed to detect methanol and hydrogen peroxide. Dual templating technique with Pluronic F127 (soft template) and non-woven fabric (complex template) was employed to create mesoporous structures in macro or micropores resulting in enhanced hydrophilicity and wettability. The contact angle of hierarchical porous carbon-polyethylene terephthalate (HC-PET) was close to zero degrees with water, hydrogen peroxide, and methanol. Reduction in the carbonization temperature favoured the rise in resistivity of the HC-PET up to  $5.4 \times 10^3 \Omega\text{m}$ . HC-PET with lower carbonization temperature offered varying sensitivity depending on methanol concentrations and offered enhanced sensitivity when compared with water or hydrogen peroxide.

## **2.7 Hard Templating with Carbonization Temperature Optimization**

Sensing toxic food colourants is a complex process in conventional sensing techniques, including spectrophotometry or liquid chromatography. PC-based electrochemical sensing is a more convenient method to sense these toxic materials. PC is derived from starch carbonized at 800 °C using  $\text{CaCO}_3$  complex templates [95]. A simple differential pulse voltammetry with the 0.1 M phosphate buffer loaded with synthetic colourants such as sunset yellow, Tartrazine, Ponceau 4R, and Allura red showcased enhanced sensitivity towards them. The sensor response was linear from low concentrations of 2.5–1000  $\mu\text{g/L}$ . The PC synthesized from different ratios of starch/ $\text{CaCO}_3$  was coated on glass carbon electrodes. The sensor showed a higher electrochemical reactivity supported by more excellent signal enhancement effects due to the oxidation of the food colourants. Sunset yellow with 89.4 fold, Tartrazine with 79.3 fold, Allura red with 50.7 fold, and Ponceau 4R with 47.3 were observed with 0.7 pH 0.1 M phosphate buffer electrolyte solution.

$\text{CO}_2$  sensor based on hierarchically porous carbon derived from raw sugar has been reported to enhance the sensitivity due to the adsorption of  $\text{CO}_2$  in the interconnected meso and microporous structures. Interconnected meso and microporous structures were tuned by varying the carbonization temperature of raw sugar and nano- $\text{CaCO}_3$  mixture. The HPC carbonized at 900 °C showcased the highest adsorption capacity of 2.25 mmol/g at ambient temperature and pressure. It also possessed a higher micropore volume up to 0.215  $\text{cm}^3/\text{g}$ , which occupied nearly 56% of the entire pore



**Fig. 5** Porous carbon structures derived from polymers through pyrolysis

volume in the material. This higher micropore volume facilitated the increased  $\text{CO}_2$  adsorption.

## 2.8 Carbon-MEMS

Cost-effective and batch fabricated sensors can be derived from porous carbon materials based on Carbon-Micro Electro-Mechanical Systems (C-MEMS) technology. Highly porous structures with well-defined micropores with nanoporous edges have been utilized to develop sensitive heavy metal sensors based on electrochemical sensing techniques [96]. Polymer-based photoresists patterned with UV lithography were etched with  $\text{O}_2$  plasma etching to form micropores. These were then pyrolysed to convert polymer to porous carbon structures with nanoporous edges (Fig. 5). Hierarchical PC structures were synthesized by increasing the  $\text{O}_2$  plasma etching time. Regular tap water with elevated Cd and Pb ions concentrations was diluted with a buffer solution of 0.1 M NaAc solution which was used as the electrolyte. The electrolyte was subjected to square wave anodic stripping voltammetry.

## 3 Porous Carbon-Based Sensor Applications

### 3.1 Chemical Sensors

With uncontrollable emission rates of greenhouse gases, there is a dire requirement to control and monitor the concentration of such gases in urban and industrial areas. Studies showed that the most prominent greenhouse gas is  $\text{CO}_2$ . According to occupational safety and health administration standards, the acceptable exposure limit for  $\text{CO}_2$  in the air for an 8-h workday on a time-weighted average is 0.5%. Failure to meet

these thresholds may result in workers experiencing side effects like headaches, sore throat, nasal irritation, and severe respiratory problems [97]. Hence, a considerable amount of research was carried out in the field of CO<sub>2</sub> sensing. Initially, ceramic materials like ZnO, TiO<sub>2</sub>, CuO, NiO, Mn<sub>2</sub>O<sub>2</sub>, etc., were used to make CO<sub>2</sub> sensors. However, these sensors were only effective in specific temperature ranges and operated on high voltages. This was not a desirable trait as it hindered the functionality of the sensors and resulted in a shorter lifetime for the sensors [98]. They were also bulky and were not portable enough to be considered for compact, lightweight uses. Several investigations have reported on the fabrication of CO<sub>2</sub> sensors using graphene, carbon nanotubes, aluminium oxide, and Polyethyleneimine (PEI).

These sensor materials had enhanced flexibility, detection ranges, and comfortable operating ranges [99]. The sensor's outputs are mapped on a conductivity vs CO<sub>2</sub> concentration plot, and this data is also dependent on relative humidity. The sensors have increased detection ranges under lower relative humidity as the range for conductivity is affected by the relative humidity. Some desirable traits for CO<sub>2</sub> sensors are good repeatability and reproducibility of collected data, portability of sensors, fast response and recovery times, high selectivity and sensitivity, low operating temperatures, and lower detection limit. Most of these traits apply to any sensing system [100]. Han et al. [101] showed the effect of functionalized CNTs with polymers such as Polyethyleneimine on the sensitivity of gas sensors and their affinity to detect CO<sub>2</sub>. It was also noted that PEI-laminated devices exhibited a high increase in conductance on NO<sub>2</sub> exposure. Simultaneously, there was no discernible change due upon exposure of other common gases in the air like N<sub>2</sub>, O<sub>2</sub>, etc., proving its selective nature. Nanomaterials like CNTs and PEI are much more adaptive as sensor material due to their highly selective and customizable nature. Hence, the research trend skews towards combining nanomaterials and porous carbon mediums to attain the best possible results.

### 3.2 *Physical Sensors*

The response of a semiconductor photocatalyst to catalyse redox reactions with light as the source is known as photocatalysis. The entire photocatalyst process can be broken down into three parts: light absorption, charge separation and transfer, and the final step being surface reactions that take place on the photocatalyst selected [102]. Even if progress is being made in this area, the main difficulty that can be noted is that in order for plans to be successful using fossil fuel technologies, solar to hydrogen transformation must reach nearly 10%, but this degree of conversion is currently poor [103]. Metal oxide reactors have been widely used, but there has not been a single material that meets all of the characteristics of a photocatalyst. They are non-toxic, highly efficient, have excellent stability, cost-effective, and durable performance.

The material which has been able to replicate these properties at a certain level is TiO<sub>2</sub>, upon which various researches have been conducted, but the one place where

it falls short is the spectrum upon which it operates. It can only utilize UV radiation from the sun, which makes up only 4% of the solar spectrum [104]. Aside from that, research has been done on precious metals like palladium and platinum, but their uses are limited due to the high price and scarcity;  $g\text{-C}_3\text{N}_4$  was discovered for the first time in 2009 [105]. The photocatalyst  $g\text{-C}_3\text{N}_4$  is a two-dimensional metal-free photocatalyst [106]. A medium bandgap of around 2.7 eV is chosen due to its appealing electrical band structure. They have good chemical and thermal stability, and this special conjugated polymer offers a fantastic possibility in energy and the environment [107]. The photocatalyst itself is made up of carbon and nitrogen as the raw materials; however, several groups have been modified their composition to get better results. Zhang et al. [108] created a sheet-on-sheet structure with an accessible porous network that increased the surface area and increased the effectiveness of light-harvesting and visible light absorption while speeding up the transfer of reactant molecules to active molecules locations. Further researchers have also experimented with improving photocatalytic efficiency by reducing defects and inducing doping in the photocatalyst. This particular carbon-based photocatalyst has got vast applications, but along with it, it also fits all the essential criteria; with research still being undertaken, it could prove to be a viable photocatalyst that could help reduce the consumption of fossil fuels.

### 3.3 *Biosensors*

Glucose is a precursor of polysaccharides, one of the four major types of macromolecules (nucleic acids, proteins, carbohydrates, and lipids). It is a crucial metabolic intermediary and the primary source of energy in organisms. However, an over intake of glucose can lead to serious health consequences, as a result of which it becomes imperative to monitor the amount of glucose that is present not only inside the body of a human being but also within the various food articles which are being consumed daily. For this purpose of detection, biosensors have a considerable role to play, but there are various types of biosensors available, one of which use enzymes and some are enzyme-free.

As indicated above, glucose can be detected by several methods: a colorimetric approach. In this method, glucose is oxidized by glucose oxidase (GOx) to form gluconolactone and  $\text{H}_2\text{O}$  with the help of  $\text{H}_2\text{O}_2$ . To determine the glucose concentration, peroxidase is used to catalyse the formation of a coloured product of the peroxidase substrate. The resulting coloured product is then measured to calculate the concentration of glucose. The use of natural enzymes has some drawbacks, such as high cost and environmental factors. Yang et al. [109] developed a CFP/GWs/ $\text{Cu}_2\text{O}$  enzyme-free glucose sensor that can measure glucose concentrations at a much higher sensitivity on the surface of CFP.  $\text{CuO}$  nanoparticles create homogenous, uniformly sized spheres on the 3D framework of CFP/GWs, which have good conductivity. In contrast to previous models, which assumed that only one glucose (or 1C) could be converted into two molecules of product, the 3D framework of CFP/GWs enables a far

more significant number of catalytic sites for the glucose reaction, enabling the efficient transport of electrons. Parashuram et al. [110] prepared a non-enzymatic sensor to detect glucose in oranges; a  $\text{ZrO}_2$ -Cu(I)-modified carbon paste non-enzymatic glucose sensor was developed.

Low glucose concentrations may prevent the sensor from working. Because of the significant number of active catalytic sites and the ease with which copper can be converted into different oxidation states, the developed sensor proved to help speed up the electrocatalytic oxidation of glucose. Tam et al. [111] developed a non-enzymatic sensor based on graphene quantum dots via microwave-assisted pyrolysis. The presence of graphene quantum dots provides a porous structure that enables glucose detection at a faster rate due to the formation of an efficient diffusion pathway. The sensor as a whole shows high sensitivity and excellent selectivity against various interfering species. It is observed that both enzymatic and non-enzymatic biosensors are available; the selection of the sensor depends upon the application where it is to be employed. Along with the application, the development cost and various other factors should also be looked into while selecting a particular biosensor for glucose detection.

### 3.4 Energy Storage and Sensing

Supercapacitors are high-efficiency energy-storage devices with minimal internal resistance. Supercapacitors of today's generation are made up of two electrodes, an electrolyte and a separator, and they offer several benefits such as long cycle life and excellent adaptability. These capacitors are typically utilized in applications that require high reliability and short load cycles. Electrical double-layer capacitors, pseudo-capacitors, and hybrid capacitors (a combination of the two types) are the three main types of capacitors. One of the main issues with supercapacitors is the prevalence of low specific energy—this was addressed by altering the electrode material used. Porous carbonaceous materials are an attractive solution due to their high surface areas and pore volumes and high physical stability and enhanced conductivity [112]. They also fabricated a nitrogen-doped porous carbon ball with hyper-cross Anthracene polymer. The device formed showed a high specific capacitance and excellent rate capabilities. Furthermore, this device was capable of 96.5% capacitance retention after 5000 cycles, accounting for only a 3.5% loss of its retentive property.

Sharma et al. [113] created a material with a vast surface area and nanoporous hyper-cross-linked polyaniline. The material possessed desirable characteristics like high surface area ( $1059 \text{ m}^2 \text{ g}^{-1}$ ) and narrow pore size distribution. This resulted in it being used as a suitable electrode material for supercapacitors and a medium for gas adsorption. A study conducted by Xu et al. elaborated the synthesis of N-doped porous carbon derived from conjugated microporous polymer [58]. Their study concluded that carbonization and incorporating nitrogen in the material enhance the



material's super capacitive energy storage properties. Vinodh et al. [112] recognized this as a viable design principle for fabricating commercial-grade porous materials.

### ***3.5 Bandgap Variations in Gas Sensing Material Due to Carbon Materials***

Most gas sensing materials are metal oxides involving transition elements such as  $\text{TiO}_2$ ,  $\text{NiO}$ ,  $\text{Fe}_2\text{O}_3$  and post-transition metal oxides such as  $\text{SnO}_2$ ,  $\text{ZnO}$  owes their gas sensing property to the bandgaps [114]. The chemisorbed oxygen plays a vital role in altering the resistance or the conductance of the sensing material enabling the gas sensing property of metal oxides. Alteration of bandgaps through doping results in enhancement of the bandgap to achieve better sensing and selectivity of the gas sensors. Cations donated by doped elements and oxygen stoichiometry are the two prime factors determining the conductivity of the metal oxide-based gas sensors. The charge carriers formed due to these factors determine the semiconductivity exhibited by the metal oxide gas sensors [115].

Metal oxide-based gas sensors exhibit a lower detection limit [LOD] owing to their broader bandgap energies [116]. This wider band gap needs to be optimized to enhance the sensing characteristics of these sensors. In some cases, metal oxide or polymer-based 2D materials have replaced voluminous gas sensors as gas sensing is often a surface phenomenon. This technique tries to address the LOD, but the lower gas adsorption energy plays a spoilsport in many cases in enhancing the gas sensing properties [107]. To overcome these shortcomings, researchers have turned towards a well-known 2D material, graphene. Graphene provides an ideal substrate to adsorb the gases. Its excellent conductive property enhances the sensitivity of the gas sensors [117]. Effective charge carrier transfer across the bandgap due to adsorption of a gas on the surface of the gas sensor is a critical measure of sensitivity. Graphene oxide facilitates the charge carrier transfer by reducing or narrowing the bandgap in graphene oxide-based gas sensing nanocomposites. Park et al. [118] have synthesized graphene oxide-based narrow bandgap gas sensor to detect  $\text{NO}_2$ . The gas sensing properties have been observed to increase due to the modification of using functionalized groups.

### ***3.6 Dielectrophoresis-Based Gas Sensors***

The dielectrophoresis technique utilizes sensing based on the motion of bioparticles and or polarization when subjected to electrical fields. When an alternating field is applied to uncharged particles dispersed or suspended in a solution, they get mobilized or polarized. This mobility can be extended to the mobility of charge carriers in the gas sensing medium to sense the target gas. When DEP is coupled

with 2D structures like graphene or graphene oxide, they bring about a more significant enhancement in the sensing mechanism. DEP provides a versatile mechanism to perform non-destructive manipulation of materials at a nanometer scale.

Room temperature operating hydrogen sensor has been fabricated based on graphene oxide synthesized through ac dielectrophoresis. The dielectrophoresis process parameters such as voltage applied, frequency of excitation, and time duration were optimized to assemble nano-sized GO structures on the microgap electrode surface on the Si/SiO<sub>2</sub> substrate. The process was simulated with an electrical field increasing spatially from top to bottom, resulting in the dielectrophoresis acting from top to bottom on the substrate. The optimized parameters resulted in a 5% faster-sensing response and quicker response and recovery times while sensing hydrogen gas at a concentration of 100 ppm, operated at room temperature. Ammonia sensors operating at room temperature have been developed by formulating an rGO–CuFe<sub>2</sub>O<sub>4</sub> nanocomposite [119]. It has been observed that this sensor can sense ammonia up to 5 ppm levels even at room temperature. The hybrid rGO–CuFe<sub>2</sub>O<sub>4</sub> composite at a ratio of 10:5 was observed to provide a maximum sensitivity of 9.9% due to the enhanced electrical conductivity and increased surface area offered by rGO.

## 4 Conclusions

Carbon materials in zero, one, and two dimensions have established themselves due to their highly tuneable characteristics. The 3D carbon materials, and primarily porous carbon-based nanostructures, are in no way lesser than their low-dimensional counterparts. Porous carbon nanostructures are highly suitable and idle materials in many applications. Applications based on sensing and catalysis for a long have been dependent on surface-based reactions. Bringing in the porous carbon has changed their efficiency due to their higher surface-to-volume ratio, increased porosity with tuneable pore size, interconnect between different sized pores, and enhanced chemical and physical adsorbability tuneable defect sites, and adequate lodging of functionalized dopants or heteroatoms. Moreover, their simple synthesis processes with a wide range of precursors that can be chosen to tune the physicochemical properties of the synthesized porous carbon have made porous carbon-based materials the best choice for recent research on the sensing domain. The research trend on this material is exponentially rising, and soon they will be exploited for these applications.

## References

1. Kroto HW, Heath JR, O'Brien SC, Curl RF, Smalley RE (1985) C<sub>60</sub>: buckminsterfullerene. *Nature* 318:162–163
2. Iijima S (1991) Helical microtubules of graphitic carbon. *Nature* 354:56–58

3. Thommes M, Kaneko K, Neimark AV, Olivier JP, Rodriguez-Reinoso F, Rouquerol J, Sing KSW (2015) Physisorption of gases, with special reference to evaluating surface area and pore size distribution (IUPAC technical report). *Pure Appl Chem* 87:1051–1069
4. Jiang H, Ma J, Li C (2012) Mesoporous carbon incorporated metal oxide nanomaterials as supercapacitor electrodes. *Adv Mater* 24(30):4197–4202
5. Liu J, Wickramaratne NP, Qiao SZ, Jaroniec M (2015) Molecular-based design and emerging applications of nanoporous carbon spheres. *Nat Mater* 14(8):763–774
6. Wang F, Liu S, Shu L, Tao XM (2017) Low-dimensional carbon based sensors and sensing network for wearable health and environmental monitoring. *Carbon* 121:353–367
7. Choong CL, Shim MB, Lee BS, Jeon S, Ko DS, Kang TH, Bae J, Lee SH, Byun KE, Im J, Jeong YJ, Park CE, Park JJ, Chung UI (2014) Highly stretchable resistive pressure sensors using a conductive elastomeric composite on a micropyramid array. *Adv Mater* 26(21):3451–3458
8. Liu Q, Chen J, Li Y, Shi G (2016) High-performance strain sensors with fish-scale-like graphene-sensing layers for full-range detection of human motions. *ACS Nano* 10:7901–7906
9. Lee D, Lee H, Jeong Y, Ahn Y, Nam G, Lee Y (2016) Highly sensitive, transparent, and durable pressure sensors based on sea-urchin shaped metal nanoparticles. *Adv Mater* 28:9364–9369
10. Gong S, Zhao Y, Yap LW, Shi Q, Wang Y, Bay JAPB, Lai DTH, Uddin H, Cheng W (2016) Fabrication of highly transparent and flexible nanomesh electrode via self-assembly of ultrathin gold nanowires. *Adv Electron Mater* 2(7):1600121
11. Lou Z, Chen S, Wang L, Shi R, Li L, Jiang K, Chen D, Shen G (2017) Ultrasensitive and ultraflexible e-skins with dual functionalities for wearable electronics. *Nano Energy* 38:28–35
12. Hou C, Wang H, Zhang Q, Li Y, Zhu M (2014) Highly conductive, flexible, and compressible all-graphene passive electronic skin for sensing human touch. *Adv Mater* 26:5018–5024
13. Tien NT, Jeon S, Kim DI, Trung TQ, Jang M, Hwang BU, Byun KE, Bae J, Lee E, Tok JBH, Bao Z, Lee NE, Park JJ (2014) A Flexible bimodal sensor array for simultaneous sensing of pressure and temperature. *Adv Mater* 26(5):796–804
14. Park J, Kim M, Lee Y, Lee HS, Ko H (2015) Fingertip skin— inspired microstructured ferroelectric skins discriminate static/ dynamic pressure and temperature stimuli. *Sci Adv* 1:e1500661
15. Zhao XH, Ma SN, Long H, Yuan H, Tang CY, Cheng PK, Tsang YH (2018) Multifunctional sensor based on porous carbon derived from metal-organic frameworks for real time health monitoring. *ACS Appl Mater Interfaces* 10(4):3986–3993
16. Borchardt L, Zhu QL, Casco ME, Berger R, Zhuang Z, Kaskel S, Feng X, Xu Q (2017) Toward a molecular design of porous carbon materials. *Mater Today* 20(10):592–610
17. Chen J, Xiao G, Duan G, Wu Y, Zhao X, Gong X (2020) Structural design of carbon dots/porous materials composites and their applications. *Chem Eng J* 421:127743
18. Xu X, Ray R, Gu Y, Ploehn HJ, Gearheart L, Raker K, Scrivens WA (2004) Electrophoretic analysis and purification of fluorescent single-walled carbon nanotube fragments. *J Am Chem Soc* 126(40):12736–12737
19. Sun YP, Zhou B, Lin Y, Wang W, Fernando KAS, Pathak P, Mezziani MJ, Harruff BA, Wang X, Wang H, Luo PG, Yang H, Kose ME, Chen B, Veca LM, Xie SY (2006) Quantum-sized carbon dots for bright and colorful photoluminescence. *J Am Chem Soc* 128(24):7756–7757
20. Ma X, Tao H, Yang K, Feng L, Cheng L, Shi X, Li Y, Guo L, Liu Z (2012) A functionalized graphene oxide-iron oxide nanocomposite for magnetically targeted drug delivery, photothermal therapy, and magnetic resonance imaging. *Nano Res* 5(3):199–212
21. Mondal S, Ganguly S, Das P, Khastgir D, Das NC (2017) Low percolation threshold and electromagnetic shielding effectiveness of nano-structured carbon-based ethylene methyl acrylate nanocomposites. *Compos Part B: Eng* 119:41–56
22. Sabet M, Mahdavi K (2019) Green synthesis of high photoluminescence nitrogen-doped carbon quantum dots from grass via a simple hydrothermal method for removing organic and inorganic water pollutions. *Appl Surf Sci* 463:283–291
23. Ganguly S, Mondal S, Das P, Bhawal P, Das TK, Ghosh S, Remanan S, Das NC (2019) An insight into the physico-mechanical signatures of silylated graphene oxide in poly (ethylene methyl acrylate) copolymeric thermoplastic matrix. *Macromol Res* 27:268–281

24. Ma S, Sun D, Simmons JM, Collier CD, Yuan D, Zhou HC (2008) Metal-organic framework from an anthracene derivative containing nanoscopic cages exhibiting high methane uptake. *J Am Chem Soc* 130(3):1012–1016
25. Xia C, Zhu S, Feng T, Yang M, Yang B (2019) Evolution and synthesis of carbon dots: from carbon dots to carbonized polymer dots. *Adv Sci* 6(23):1901316
26. Cheng Y, Wu L, Fang C, Li T, Chen J, Yang M, Zhang Q (2020) Synthesis of porous carbon materials derived from *laminaria japonica* via simple carbonization and activation for supercapacitors. *J Market Res* 9(3):3261–3271
27. Shin J, Guo J, Zhao T, Guo Z (2019) Functionalized carbon dots on graphene as outstanding non-metal bifunctional oxygen electrocatalyst. *Nano-Micro Small* 15(16):1900296
28. Feng H, Xie P, Xue S, Li L, Hou X, Liu Z, Wu D, Wang L, Chu PK (2018) Synthesis of three-dimensional porous reduced graphene oxide hydrogel/carbon dots for high-performance supercapacitor. *J Electroanal Chem* 808:321–328
29. Tabatabaiean K, Simayee M, Fallah-Shojaie A, Mashayekhi F (2019) N-doped carbon nanodots at UiO-66-NH<sub>2</sub> as novel nanoparticles for releasing of the bioactive drug, rosmarinic acid and fluorescence imaging. *DARU J Pharm Sci* 27:307–315
30. Wu M, Gao Y, Hu Y, Zhao B, Zhang H (2020) Boosting sodium storage of mesoporous TiO<sub>2</sub> nanostructure regulated by carbon quantum dots. *Chin Chem Lett* 31(3):897–902
31. Wang M, Xia Y, Qiu J, Ren X (2019) Carbon quantum dots embedded mesoporous silica for rapid fluorescent detection of acidic gas. *Spectrochimica Part A* 206:170–176
32. Shen Q, You Z, Yu Y, Qin T, Su Y, Wang H, Wu C, Zhang F, Yang H (2018) A carbon quantum dots/porous InVO<sub>4</sub> microsphere composite with enhanced photocatalytic activity. *Eur J Inorg Chem* 9:1080–1086
33. Li J, Zhang C, Yin M, Zhang Z, Chen Y, Deng Q, Wang S (2019) Surfactant-sensitized covalent organic frameworks-functionalized lanthanide-doped nanocrystals: an ultrasensitive sensing platform for perfluorooctane sulfonate. *ACS Omega* 4(14):15947–15955
34. Aghaei SM, Monshi MM, Torres I, Zeidi SM, Calizo I (2018) DFT study of adsorption behavior of NO, CO, NO<sub>2</sub>, and NH<sub>3</sub> molecules on graphene-like BC<sub>3</sub>: a search for susceptible molecular sensor. *Appl Surf Sci* 427:326–333
35. Kreyling WG, Semmler-Behnke M, Chaudhry Q (2010) A complementary definition of nanomaterial. *Nano Today* 5(3):165–168
36. Peng LM, Zhang Z, Wang S (2014) Carbon nanotube electronics: recent advances. *Mater Today* 17(9):433–442
37. Tans SJ, Verschueren AR, Dekker C (1998) Room-temperature transistor based on a single carbon nanotube. *Nature* 393(6680):49–52
38. Zaporotskova IV, Boroznina NP, Parkhomenko YN, Kozhitov LV (2016) Carbon nanotubes: sensor properties. A review. *Modern Electron Mater* 2(4):95–105
39. Holland LM, Doole GJ (2014) Implications of fairness for the design of nitrate leaching policy for heterogeneous New Zealand dairy farms. *Agric Water Manag* 31(132):79–88
40. Leng X, Luo D, Xu Z, Wang F (2018) Modified graphene oxide/Nafion composite humidity sensor and its linear response to the relative humidity. *Sens Actuators, B Chem* 1(257):372–381
41. Vinícius DNB, Thaís LAM, Beatriz RC de Menezes, Renata GR, Victor ANR, Karla FR, Gilmar PT (2019) Carbon nanostructure-based sensors: a brief review on recent advances. *Adv Mater Sci Eng* 21
42. Zou Y, Han BX (2001) High-surface-area activated carbon from chinese coal. *Energy Fuels* 15(6):1383–1386
43. Yang T, Lua AC (2003) Characteristics of activated carbons prepared from pistachio-nut shells by physical activation. *J Colloid Interface Sci* 267(2):408–417
44. Zhang T, Walawender PW, Fan LT, Fan M, Daugaard D, Brown RC (2004) Preparation of activated carbon from forest and agricultural residues through CO activation. *Chem Eng J* 105(1–2):53–59
45. Marsh H, Rand B (1971) The process of activation of carbons by gasification with CO<sub>2</sub>-II The role of catalytic impurities. *Carbon* 9:63–77

46. Tamai H, Kakii T, Hirota Y, Kumamoto T, Yasuda H (1996) Synthesis of substantial mesoporous activated carbon and its unique adsorption for giant molecules. *Chem Mater* 8:454–462
47. Oya A, Yoshida S, Alcaniz-Monge J, Linares-Solano A (1995) Formation of mesopores in phenolic resin-derived carbon fiber by catalytic activation using cobalt. *Carbon* 33(8):1085–1090
48. Patel N, Okabe K, Oya A (2002) Designing carbon materials with unique shapes using polymer blending and coating techniques. *Carbon* 40(3):315–320
49. Ozaki J, Endo N, Ohizumi W, Igarashi K, Nakahara M, Oya A, Yoshida A, Iizuka T (1997) Novel preparation method for the production of mesoporous carbon fiber from a polymer blend. *Carbon* 35:1031–1033
50. Alcaniz-Monge J, Cazorla-Amores D, Linares-Solano A, Oya A, Sakamoto A, Hosm K (1997) Preparation of general purpose carbon fibers from coal tar pitches with low softening point. *Carbon* 35:1079–1087
51. Pekala RW (1989) Organic aerogels from the polycondensation of resorcinol with formaldehyde. *J Mater Sci* 24(9):3221–3227
52. Pekala RW, Alviso CT, Kong FM, Hulse SS (1992) Aerogels derived from multifunctional organic monomers. *J Non-Cryst Solids* 145:90–98
53. Pekala RW, Schaefer DW (1993) Structure of organic aerogels. 1. Morphology and scaling. *Macromolecules* 26(20):5487–5493
54. Hamouda HA, Cui S, Dai X, Xiao L, Xie X, Peng H, Ma G (2021) Synthesis of porous carbon material based on biomass derived from hibiscus sabdariffa fruits as active electrodes for high-performance symmetric supercapacitors. *RSC Adv* 11(1):354–363
55. Zhou XL, Zhang H, Shao LM, Lu FH, He PJ (2021) Preparation and application of hierarchical porous carbon materials from waste and biomass: a review. *Waste Biomass Valorisation* 12:1699–1724
56. Jeong JH, Lee JS, Roh KC, Kim KB (2017) Multimodal porous carbon derived from ionic liquids: correlation between pore sizes and ionic clusters. *Nanoscale* 9(38):14672–14681
57. Zhang L, Cai K, Zhang F, Yue Q (2015) Adsorption of CO<sub>2</sub> and H<sub>2</sub> on nitrogen-doped porous carbon from ionic liquid precursor. *Chem Res Chin Univ* 31(1):130–137
58. Xu F, Wu D, Fu R, Wei B (2017) Design and preparation of porous carbons from conjugated polymer precursors. *Mater Today* 20(10):629–656
59. Jain A, Balasubramanian R, Srinivasan MP (2016) Hydrothermal conversion of biomass waste to activated carbon with high porosity: a review. *Chem Eng J* 283:789–805
60. Alatalo SM, Sillanpää M (2020) Hydrothermal carbonization in the synthesis of sustainable porous carbon materials for water treatment. *Adv Water Treat* 445–503
61. Al Baroroh LA, Fitria D, Amal MI, Wismogroho AS, Widayatno WB (2018) Facile preparation of porous carbon from coffee bean waste using low temperature solvothermal method. *J Phys: Conf Ser* 985:012030
62. Zhou H, Wu S, Wang H, Li Y, Liu X, Zhou Y (2021) The preparation of porous carbon materials derived from bio-protic ionic liquid with application in flexible solid-state supercapacitors. *J Hazard Mater* 402:124023
63. Duraisamy V, Palanivel S, Thangamuthu R, Kumar SMS (2018) KIT-6 Three dimensional template derived mesoporous carbon for oxygen reduction reaction: effect of template removal on catalytic activity. *Chem Select* 3(42):11864–11874
64. Fulvio PF, Jaroniec M, Liang C, Dai S (2008) Polypyrrole-based nitrogen-doped carbon replicas of SBA-15 and SBA-16 containing magnetic nanoparticles. *J Phys Chem C* 112(34):13126–13133
65. Silva R, Voiry D, Chhowalla M, Asefa T (2013) Efficient metal-free electrocatalysts for oxygen reduction: polyaniline-derived N- and O-doped mesoporous carbons. *J Am Chem Soc* 135(21):7823–7826
66. Bai X, Wang Z, Luo J, Wu W, Liang Y, Tong X, Zhao Z (2020) Hierarchical porous carbon with interconnected ordered pores from biowaste for high-performance supercapacitor electrodes. *Nanoscale Res Lett* 15(1):88

67. Wang Y, Bai X, Wang F, Qin H, Yin C, Kang S, Li X, Zuo Y, Cui L (2016) Surfactant-assisted nanocasting route for synthesis of highly ordered mesoporous graphitic carbon and its application in CO<sub>2</sub> adsorption. *Sci Rep* 6:26673
68. Liu S, Wang Z, Han T, Fei T, Zhang T, Zhang H (2018) Solvent-free synthesis of mesoporous carbon employing KIT-6 as hard template for removal of aqueous rhodamine B. *J Porous Mater* 26:941–950
69. Vinu A, Anandan S, Anand C, Srinivasu P, Ariga K, Mori T (2008) Fabrication of partially graphitic three-dimensional nitrogen-doped mesoporous carbon using polyaniline nanocomposite through nanotemplating method. *Microporous Mesoporous Mater* 109(1–3):398–404
70. Wu YH, Ma YL, Sun YG, Xue K, Ma QL, Ma T, Ji WX (2020) Graded synthesis of highly ordered MCM-41 and carbon/zeolite composite from coal gasification fine residue for crystal violet removal. *J Clean Prod* 277:123186
71. Pei YR, Yang JH, Choi G, Choy JH (2020) A geopolymer route to micro and meso-porous carbon. *RSC Adv* 10(12):6814–6821
72. Costa MBG, Juárez JM, Anunziata OA (2016) Synthesis and characterization of CMK porous carbons modified with metals applied to hydrogen uptake and storage. *Microporous and Mesoporous Materials*, Chapter 3, *Microporous and Mesoporous Materials*, Intechopen 51–85
73. Fuertes AB (2004) Low-Cost synthetic route to mesoporous carbons with narrow pore size distributions and tunable porosity through silica xerogel templates. *Chem Mater* 16(3):449–455
74. Meng Y, Zou X, Huang X, Goswami A, Liu Z, Asefa T (2014) Polypyrrole-derived nitrogen and oxygen co-doped mesoporous carbons as efficient metal-free electrocatalyst for hydrazine oxidation. *Adv Mater* 26(37):6510–6516
75. Shin Y, Fryxell GE, Um W, Parker K, Mattigod SV, Skaggs R (2007) Sulfur-functionalized mesoporous carbon. *Adv Func Mater* 17(15):2897–2901
76. Yang CM, Weidenthaler C, Spliethoff B, Mayanna M, Schüth F (2005) Facile template synthesis of ordered mesoporous carbon with polypyrrole as carbon precursor. *Chem Mater* 17(2):355–358
77. Lee J, Jin S, Hwang Y, Park JG, Park HM, Hyeon T (2005) Simple synthesis of mesoporous carbon with magnetic nanoparticles embedded in carbon rods. *Carbon* 43(12):2536–2543
78. Li JR, Ma Y, McCarthy MC, Sculley J, Yu J, Jeong HK, Balbuena PB, Zhou HC (2011) Carbon dioxide capture-related gas adsorption and separation in metal-organic frameworks. *Coord Chem Rev* 255(15–16):1791–1823
79. Jiang D, Xu P, Wang H, Zeng G, Huang D, Chen M, Lai C, Zhang C, Wan J, Xue W (2018) Strategies to improve metal organic frameworks photocatalyst's performance for degradation of organic pollutants. *Coord Chem Rev* 376:449–466
80. Liu J, Chen L, Cui H, Zhang J, Zhang L, Su CY (2014) Applications of metal-organic frameworks in heterogeneous supramolecular catalysis. *Chem Soc Rev* 43(16):6011–6061
81. Yin P, Yao T, Wu Y, Zheng L, Lin Y, Liu W, Ju H, Zhu J, Hong X, Deng Z, Zhou G, Wei S, Li Y (2016) Single cobalt atoms with precise n-coordination as superior oxygen reduction reaction catalysts. *Angewandte Chemie Int Edn* 55(36):10800–10805
82. Fang Y, Ma Y, Zheng M, Yang P, Asiri AM, Wang X (2018) Metal-organic frameworks for solar energy conversion by photoredox catalysis. *Coord Chem Rev* 373:83–115
83. Khan NA, Hasan Z, Jung SH (2018) Beyond pristine metal-organic frameworks: preparation and application of nano-structured, nanosized, and analogous MOFs. *Coord Chem Rev* 376:20–45
84. Yu JT, Chen Z, Sun J, Huang ZT, Zheng QY (2012) Cyclotricatechylene based porous crystalline material: synthesis and applications in gas storage. *J Mater Chem* 22(12):5369–5373
85. Li Y, Yang RT (2007) Hydrogen storage in metal-organic and covalent-organic frameworks by spillover. *AIChE J* 54(1):269–279
86. Wu H, Gong Q, Olson DH, Li J (2012) Commensurate adsorption of hydrocarbons and alcohols in microporous metal organic frameworks. *Chem Rev* 112(2):836–868
87. Doonan CJ, Tranchemontagne DJ, Glover TG, Hunt JR, Yaghi OM (2010) Exceptional ammonia uptake by a covalent organic framework. *Nat Chem* 2(3):235–238

88. Sumida K, Rogow DL, Mason JA, McDonald TM, Bloch ED, Herm ZR, Bae TH, Long JR (2011) Carbon dioxide capture in metal–organic frameworks. *Chem Rev* 112(2):724–781
89. Phan A, Doonan CJ, Uribe-Romo FJ, Knobler CB, O’Keeffe M, Yaghi OM (2010) Synthesis, structure, and carbon dioxide capture properties of zeolitic imidazolate frameworks. *Acc Chem Res* 43(1):58–67
90. Ding SY, Wang W (2013) Covalent organic frameworks (COFs): from design to applications. *Chem Soc Rev* 42(2):548–568
91. Duan Z, Henkelman G (2020) Identification of active sites of pure and nitrogen-doped carbon materials for oxygen reduction reaction using constant-potential calculations. *J Phys Chem C* 124(22):12016–12023
92. Rodríguez-Corvera CL, Fajardo-Díaz JL, Cortés-López AJ, Jiménez-Ramírez LE, Muñoz-Sandoval E, López-Urías F (2019) Nitrogen-doped carbon fiber sponges by using different nitrogen precursors: synthesis, characterization, and electrochemical activity. *Mater Today Chem* 14:1–13
93. Tan H, Liu J, Huang G, Qian YX, Deng Y, Chen G (2018) Understanding the roles of sulfur doping for enhancing of hydrophilicity and electrochemical performance of N, S-Codoped hierarchically porous carbon. *ACS Appl Energy Mater* 1(10):5599–5608
94. Li JF, Zhong CY, Huang JR, Chen Y, Wang Z, Liu ZQ (2019) Carbon dots decorated three-dimensionally ordered macroporous bismuth-doped titanium dioxide with efficient charge separation for high performance photocatalysis. *J Colloid Interface Sci* 553:758–767
95. Cheng Q, Xia S, Tong J, Wu K (2015) Highly-sensitive electrochemical sensing platforms for food colourants based on the property-tuning of porous carbon. *Analytica Chimica Acta* 887:75–81
96. Lee J, Kim S, Shin H (2021) Hierarchical porous carbon electrodes with sponge-like edge structures for the sensitive electrochemical detection of heavy metals. *Sensors* 21:1–15
97. Erdmann CA, Apte MG (2004) Mucous membrane and lower respiratory building related symptoms in relation to indoor carbon dioxide concentrations in the 100-building BASE dataset. *Indoor Air* 14:127–134
98. Baranov A, Spirjakin D, Akbari S, Somov A (2015) Optimization of power consumption for gas sensor nodes: a survey. *Sens Actuators, A* 233:279–289
99. Molina A, Escobar-Barrios V, Oliva J (2020) A review on hybrid and flexible CO<sub>2</sub> gas sensors. *Synth Met* 270:116602
100. Kumar S, Pavelyev V, Mishra P, Tripathi N (2018) A Review on chemiresistive gas sensors based on carbon nanotubes: device and technology transformation. *Sens Actuators, A* 283:174–186
101. Han M, Jung S, Lee Y, Jung D, Kong SH (2021) PEI-functionalized carbon nanotube thin film sensor for CO<sub>2</sub> gas detection at room temperature. *Micromachines* 12(9):1053
102. Xu Q, Li W, Ding L, Yang W, Xiao H, Ong WJ (2019) Function-driven engineering of 1D Carbon nanotubes and 0D carbon dots: mechanism, properties and applications. *Nanoscale* 11:1475–1504
103. Chen S, Takata T, Domen K (2017) Particulate photocatalysts for overall water splitting. *Nat Rev Mater* 2(10):17050
104. Ong WJ, Tan LL, Chai SP, Yong ST, Mohamed AR (2014) Highly reactive (001) facets of TiO<sub>2</sub>-based composites: synthesis, formation mechanism and characterization. *Nanoscale* 6(4):1946–2008
105. Sun Z, Zheng H, Li J, Du P (2015) Extraordinarily efficient photocatalytic hydrogen evolution in water using semiconductor nanorods integrated with crystalline Ni<sub>2</sub>P cocatalysts. *Energy Environ Sci* 8(9):2668–2676
106. Wang X, Maeda K, Thomas A, Takanabe K, Xin G, Carlsson JM, Domen K, Antonietti M (2009) A metal-free polymeric photocatalyst for hydrogen production from water under visible light. *Nat Mater* 8:76–80
107. Long H, Chan L, Harley TA, Luna LE, Tang Z, Shi T, Zettl A, Carraro C, Worsley MA, Maboudian R (2017) 3D MoS<sub>2</sub> aerogel for ultrasensitive NO<sub>2</sub> detection and its tunable sensing behaviour. *Adv Mater Interfaces* 4(16)

108. Zhang Z, Liu K, Feng Z, Bao Y, Dong B (2016) Hierarchical sheet-on-sheet ZnIn<sub>2</sub>S<sub>4</sub>/g-C<sub>3</sub>N<sub>4</sub> heterostructure with highly efficient photocatalytic H<sub>2</sub> production based on photoinduced interfacial charge transfer. *Sci Rep* 6(1):19221
109. Yang H, Bao J, Qi Y, Zhao J, Hu Y, Wu W, Wu X, Zhong D, Huo D, Hou C (2020) A disposable and sensitive non-enzymatic glucose sensor based on 3D graphene/Cu<sub>2</sub>O modified carbon paper electrode. *Anal Chim Acta* 1135:12–19
110. Parashuram L, Sreenivasaa S, Akshatha S, Udayakumar V, Sandeep kumar S (2019) A non-enzymatic electrochemical sensor based on ZrO<sub>2</sub>: Cu(I) nanosphere modified carbon paste electrode for electro-catalytic oxidative detection of glucose in raw Citrus aurantium var. sinensis. *Food Chem* 300:125178
111. Tam TV, Hur SH, Chung JS, Choi WM (2021) Novel paper- and fiber optic-based fluorescent sensor for glucose detection using aniline-functionalized graphene quantum dots. *Sens Actuators, B Chem* 329:129250
112. Vinodh R, Gopi CVVM, Kummara VGR, Atchudan R, Ahamad T, Sambasivam S, Yi M, Obaidat IM, Kim HJ (2020) A review on porous carbon electrode material derived from hypercross-linked polymers for supercapacitor applications. *J Energy Storage* 32:101831
113. Sharma V, Sahoo A, Sharma Y, Mohanty P (2015) Synthesis of nanoporous hypercrosslinked polyaniline (HCPANI) for gas sorption and electrochemical supercapacitor applications. *RSC Adv* 5(57):45749–45754
114. Wang C, Yin L, Zhang L, Xiang D, Gao R (2010) Metal oxide gas sensors: sensitivity and influencing factors. *Sensors* 10:2088–2106
115. Ji H, Zeng W, Li Y (2019) Gas sensing mechanisms of metal oxide semiconductors: a focus review. *Nanoscale* 11:22664–22684
116. Geng X, Lahem D, Zhang C, Li CJ, Olivier MG, Debliquy M (2019) Visible light enhanced black NiO sensors for ppb-level NO<sub>2</sub> detection at room temperature. *Ceram Int* 45(4):4253–4261
117. Melios C, Panchal V, Edmonds K, Lartsev A, Yakimova R, Kazakova O (2018) Detection of ultralow concentration NO<sub>2</sub> in complex environment using epitaxial graphene sensors. *ACS Sensors* 3(9):1666–1674
118. Park J, Kim Y, Park SY, Sung SJ, Jang HW, Park CR (2020) Band gap engineering of graphene oxide for ultrasensitive NO<sub>2</sub> gas sensing. *Carbon*. <https://doi.org/10.1016/j.carbon.2019.11.063>
119. Achary LSK, Aniket K, Bapun B, Pratap SN, Nilakantha T, Jyoti PK, Priyabrat D (2018) Reduced graphene oxide-CuFe<sub>2</sub>O<sub>4</sub> nanocomposite: a highly sensitive room temperature NH<sub>3</sub> gas sensor. *Sens Actuators, B Chem* 272:100–109



# Chapter 15

## Carbon Composites with Polymer Materials for Gas Sensing Application



**K. Mahendraprabhu, T. Elango Balaji, Payaswini Das,  
and Himadri Tanaya Das**

### 1 Introduction

Gas sensors aimed to receive notable alerts to monitor the system for various applications. The change in physical and chemical properties is the basic driving force for getting sensor signals in sensors such as potential, current, impedance, resistance. Active and smart materials were needed to design more efficient gas sensor devices. Among various materials, peculiar properties of carbon-based materials attracted researchers because of their high surface area, different morphologies, different shapes/sizes, and porous structure, etc. [1]. Recent sustainable progress in carbon-based nanotechnology has further widened the objectives of application of carbon materials for numerous applications. Carbon-based nanocomposites attracted a great deal of interest among the research groups which can be utilized as the alternative energy sources to reduce the utilization of fossil fuels for environmental remediation. Carbon-based nanocomposites have exhibited great versatility due to the fact that they

---

K. Mahendraprabhu

Department of Chemistry, MEPCO Schlenk Engineering College (Autonomous), Sivakasi,  
Tamil Nadu, India

T. Elango Balaji

Department of Chemistry, Utkal University, Bhubaneswar, Odisha, India

P. Das

CSIR-Institute of Minerals and Materials Technology, Bhubaneswar, Odisha 751013, India

H. T. Das (✉)

Department of Chemical Engineering, National Taiwan University of Science and Technology,  
Taipei, Taiwan

e-mail: [himadridas@utkaluniversity.ac.in](mailto:himadridas@utkaluniversity.ac.in)

Center of Excellence for Advance Materials and Applications, Utkal University, Vanivihar,  
Bhubaneswar, India

© The Author(s), under exclusive license to Springer Nature Singapore Pte Ltd. 2023

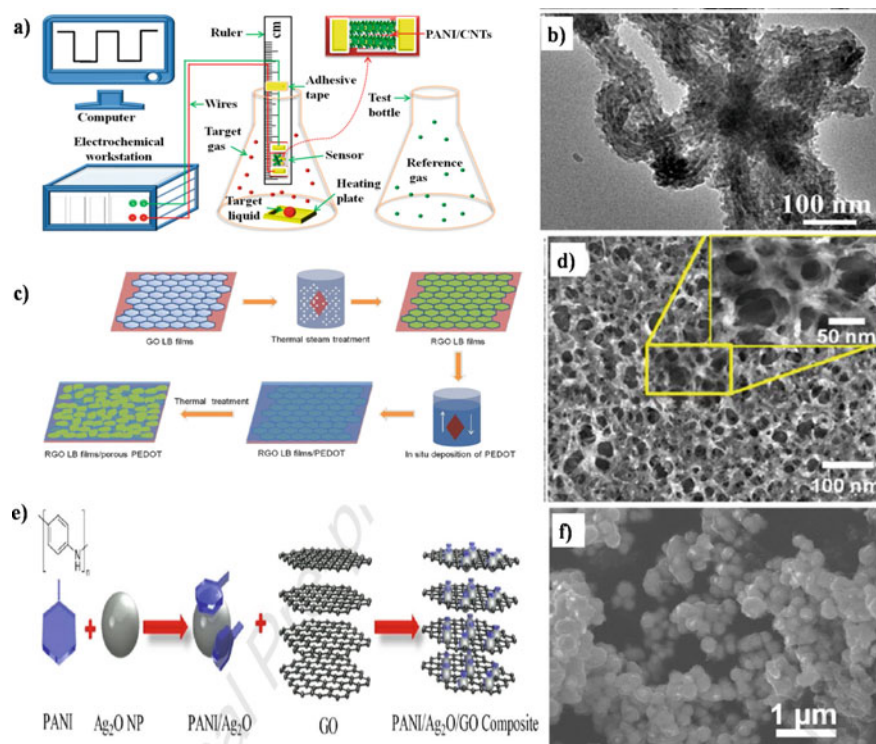
A. N. Grace et al. (eds.), *Handbook of Porous Carbon Materials*,

Materials Horizons: From Nature to Nanomaterials,

[https://doi.org/10.1007/978-981-19-7188-4\\_15](https://doi.org/10.1007/978-981-19-7188-4_15)

can be combined easily with other suitable smart materials and also with several suitable elements to create strong covalent bonds [2]. As a result, these composites show attractive characteristics like high density, strength, and hardness. Thus, carbon-based nanocomposite materials are promised to deliver highly efficient for several applications, such as the production of clean energy using the oxygen reduction reaction, the photocatalytic degradation of organic pollutants, reduction of  $\text{CO}_2$ , generation of  $\text{H}_2$ , and gas sensors, etc. [3]. This chapter mainly focuses on recently emerging trends in carbon-based nanocomposites for creating the new generation of gas sensors because of their unique properties such as mechanical, optical, and electrical properties. Smart gas sensor devices need to have adequate gas sensing characteristics such as high selectivity, sensitivity, and long-term stability with fast response and recovery rates. Operating temperature is also very essential for the practical applications of gas sensors [4]. In general, the selection of appropriate gas sensing material is the vital parameter to fabrication of gas sensor devices. Among several materials, nanostructured carbon-based polymer composite materials have been explored due to their better gas sensing performances. High-performance gas sensors attached with carbon nanostructures, especially nanocomposite materials consist of carbon and polymers, have become more convenient to monitor industrial furnaces, automobile exhausts, traffic signals, etc., to detect and quantify the range of gaseous species from small molecules such as  $\text{CO}$ ,  $\text{CH}_4$ , and also giant volatile organic compounds (VOCs) [5]. Suitable polymers can be combined with carbon materials resulting in a composite to enhance the properties and performance due to large surface area for sensing [6]. Characteristics of conducting polymers such as high environmental resistance, ductility, and lower cost are few unique properties to enhance the gas sensing performances. The carbon-polymer nanocomposite materials help in overcoming the difficulties in achieving the high performance of composites that can be used in gas sensor devices. Utilization of carbon-based nanocomposites is considered to be the robust in the gas sensor devices because of unique properties of nanocomposites which facilitate the remarkable and effective gas sensing applications. The synthesis of various nanocomposites to obtain different morphologies can determine the gas sensing ability. Thus, researchers have explored different synthesis process to develop nanocomposite and test its sensing, as given in Fig. 1.

In general, composite materials show the improved gas sensing properties of sensor devices with favorable results. Research directions are toward the development of carbon nanocomposite materials with a wide variety of structures for innovative results which are being made several smart materials for the development of gas sensor devices. This book chapter presents the fundamental and advanced developments for gas sensor devices based on nanostructured carbon-based composites with polymer materials for gas sensors with possible the commercialization of products and also discussed some recent breakthroughs in the recent years. This chapter deals with the elaborate reports and discussions on different types of gas sensors using carbon-based composites ( $\text{CO}$ , hydrocarbon,  $\text{NO}_x$ , VOCs, and  $\text{NH}_3$  sensors). At the end, an outlook and overview cover the challenges posed by various concerns and opportunities with future research perspectives and insights are discussed.



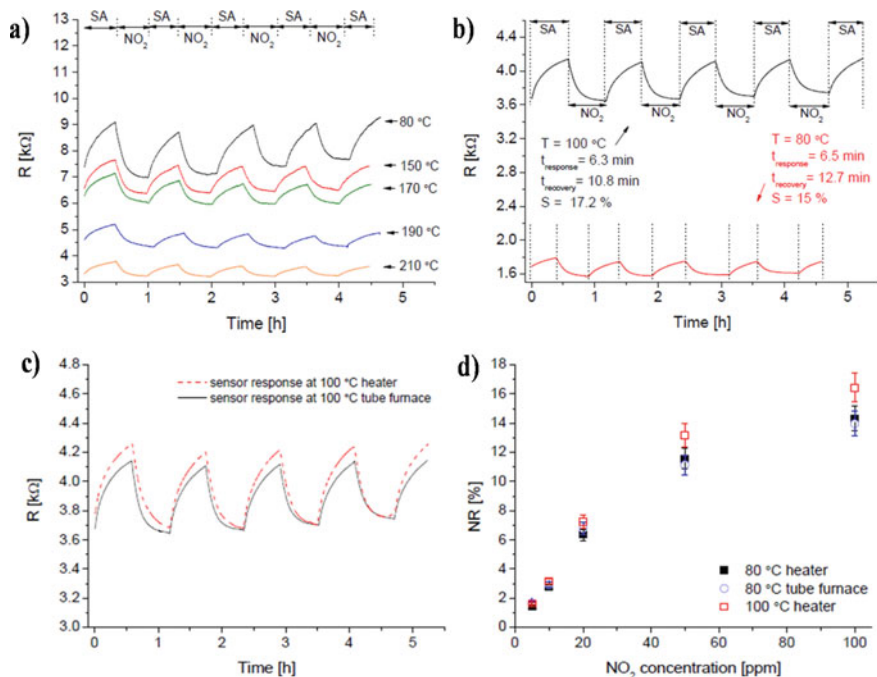
**Fig. 1** a Schematic view of sensing test for chemiresistive sensor of hierarchical PANI/CNT fibers, b TEM image of n-PANI/CNT fibers, c schematic illustration of preparing RGO/porous PEDOT nanocomposite, d SEM image of porous PEDOT layer deposited on RGO LB films, e synthesis of PANI, Ag<sub>2</sub>O nanoparticles, PANI/Ag<sub>2</sub>O nanoparticles and PANI/Ag<sub>2</sub>O/GO composite, f typical SEM images of PANI/Ag<sub>2</sub>O. Reproduced from Ref. [7–9]. Copyrights (MDPI, 2019) (Elsevier, 2021) (ACS, 2014)

## 2 Nitrogen Oxides Sensors

Nitrogen oxides are toxic pungent smelling gases which exhaust from industries, burning fossils, or vehicles emission. The gases are not only harmful for humans but also affect the plants and animals. Both nitrogen mono-oxides and dioxides are harmful for environment as causes the acid rain. Even low concentration of NO<sub>2</sub> causes discomfort in breathing and other health issues. Thus, NO<sub>x</sub> gas sensors are needed to be developed with high sensing nanomaterials such as carbon and its composites [10, 11]. The carbon-based materials have advantages in detecting the NO<sub>x</sub> gases due to the features like ecofriendly precursor, chemical/physical stability toward the pollutants, endurance of high pressure, temperature, and pH. The NO<sub>2</sub> molecules act as electron-acceptor center, where the p-type carbon derivatives usually adsorb the oxygen species of the gases and actively participate in gas sensing. So,

it is well adsorbed by carbon materials. The nanosized-CNTs based sensors are well known for room temperature sensitivity and electrical conductivity [12]. On other hand, conductive polymers are known to overcome the limitations of metal oxides, i.e., reducing the electrical resistance for more conduction [13]. However, the polymer performance gets effected by humidity, radiation or pH which limits their applications. The polymers are composite with carbon materials to obtain high sensitivity and reproducibility of the gas sensors. In this context, the CNT composite with polypyrrole (Ppy) was prepared by Lee group for NO<sub>2</sub> gas sensors [12]. Additionally, the polymers increase the surface area of the nanocomposites. Similarly, Ghada has studied nanocomposite thin film of Ppy and functionalized single-walled CNT for NO<sub>2</sub> sensors. The p-type nanocomposite Ppy/SWCNT with majority charge carriers (holes) decreases the resistance with increase of temperature and concentration of CNT. The kinetics of adsorption of oxidizing NO<sub>2</sub> gas (electron-acceptor) increases on surface of p-type Ppy/SWCNT film. The p-type polypyrrole captures electrons from the polymer matrix which resulted the decrease in resistance and holes enhanced owing to the electron accepting nature of NO<sub>2</sub> gas [14]. Quite recently, flexible NO<sub>2</sub> gas sensor was developed by nanocomposite of Ppy with nitrogen-doped multiwalled CNT (Ppy/N-MWCNT) which was synthesized by annealing method. It can be noted that the high response of 24.82% under 5 ppm of NO<sub>2</sub> gas with remarkable selectivity, greater repeatability, long-term stability, and possible flexibility [15]. Like Ppy polymer, other polymers like polytetrafluoroethylene (PTFE), polyaniline (PANI), poly(3,4-ethylenedioxythiophene) polystyrene sulfonate (PEDOT:PSS), etc., has been extensively studied [16–18]. The polymers enrich the carbon composites with enriched adsorption sites on the surface of composites. Chen et al. reported the vapors sensing by synthesizing the poly(ethylene-block-ethylene oxide) (PE-b-PEO) block into carbon black surface by using the chemical compound, N,N'-dicyclohexylcarbodiimide which is acted as a condensing agent. The electric resistance and solvent concentration were studied for the composite [19]. Along with CNT, the graphene is also highly explored for the gas sensors; its nanocomposite with different polymer provides a wide platform for gas sensing applications [20–22]. The PEDOT composite with graphene film synthesized by electropolymerisation of EDOT and reduction of graphene oxide for NO<sub>2</sub> sensor was reported by Dunst et al. [23]. The response characteristics of PEDOT/RGO are shown in Fig. 2. The material was tested for repeatability at different annealing temperatures, and also, the sensor response at 100 °C on heater and tubular furnace was compared.

The variation of sensing with temperature, humidity, concentration, and flow rate was studied. It is also found out that the reduced graphene oxide reacts actively with NO<sub>2</sub> gas and prevents over oxidation of polymer PEDOT [24]. Similarly, the rGO nanosheets were assembled with electrospun polymer nanofibers for room temperature NO<sub>2</sub> sensor which showed the high sensitivity of 1.03 ppm<sup>-1</sup> with greater selectivity, reversibility and also very good limit of detection as low as 150 ppb [20]. Interestingly, Hang et al. explored g-C<sub>3</sub>N<sub>4</sub>, similar 2D materials like graphene which is well known for its conductivity, porosity, and high surface area [22]. The g-C<sub>3</sub>N<sub>4</sub> nanosheets were exfoliated to few layers, and a heterostructure of graphene



**Fig. 2** **a** Repeatability of PEDOT/RGO-based sensor (100 ppm of NO<sub>2</sub> gas depending on the annealing temperature), **b** sensor response (with annealing the sample 20 min at 170 °C) to 100 ppm at 80 °C and 100 °C operating temperature, **c** the comparison of the sensor response in a tube furnace at 100 °C using a heater for 100 ppm of NO<sub>2</sub>/air cycles, **d** responses of the gas sensor to various concentrations of NO<sub>2</sub> at 80 °C and 100 °C. Reproduced from the Ref. [23]. Copyrights (Elsevier, 2016)

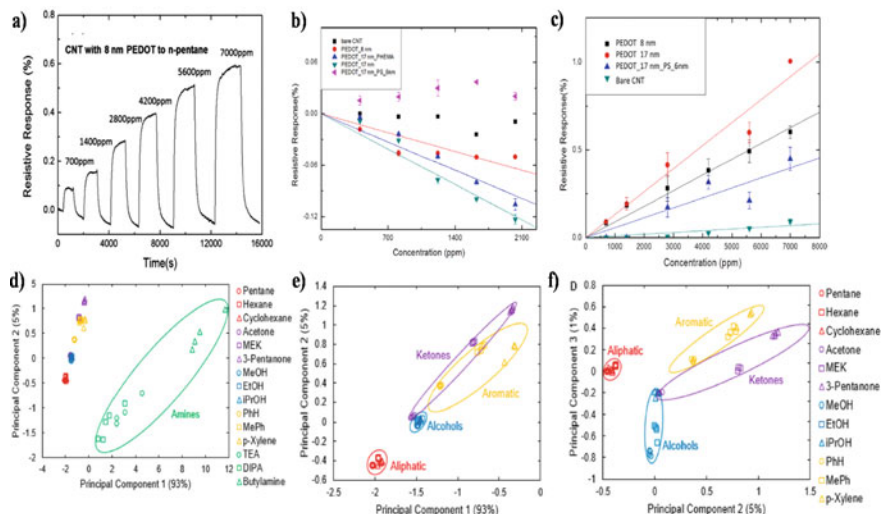
and g-C<sub>3</sub>N<sub>4</sub> was designed as NO<sub>2</sub> sensor. Such nanostructure overcomes poor electrical conductivity and instability, also performs better sensing, sensitivity, recovery as well as response time due to increase in adsorption sites. Thus, the synergistic effect confirms it as promising candidate for NO<sub>2</sub> sensor and also can be composite with different polymers to get effective performing sensor.

### 3 Volatile Organic Compound (VOCs) Sensors

Low molecular weight VOCs can evaporate even at room temperature making it most hazardous organic chemical vapors. The VOCs depend on its sources of its generation, concentration, or type of compounds. It can be hazardous for ecosystem leading to air pollution and can arise various life risk diseases in human [25]. Therefore, a low concentration selectively detector is vital for sensing of VOCs. Among several VOCs, acetone, acetylene, formaldehyde, ethanol, methanol, 2-propanol benzene,

cyclohexene, toluene, and nitrogen derivatives are commonly known VOCs [26]. The advance technologies such as mass spectroscopy and chromatographic are used to detect the VOCs, but these analyses are time consuming and high cost [27]. Alternatively, the chemical gas sensors are developed by utilizing different nanomaterials. In gas sensors, high sensitivity with selectivity can be obtained in low cost. The hybrid nanomaterials include conducting polymers, or carbonaceous materials are highly explored for VOCs sensors [28]. But, these materials face limitations like sensitivity, selectivity or poor thermal/chemical stability for long term. Both the electrochemical and electrical gas sensor depend on the volatile organic molecules diffused into working nanomaterials surface. The molecules get oxidized or reduced as per the nanomaterials used in the gas sensor [29]. The nanomaterials like conducting polymers and carbon matrix improve the electrical conductivity resulting in high current on sensing the gas. The nanomaterials are synthesized by various techniques like sol-gel, hydrothermal, electrochemical deposition, etc., to obtain different types of nanomaterials [29]. The performance of nanomaterials depends on the crystallinity, morphologies, surface area, active absorption sites, and thickness of nanomaterials [30]. Different concentrations of precursor and oxidizing agents were tested to synthesized Ppy polymer fibers for VOCs applications [31]. The electrospun polymer composite fibers blended with carbon have been reported for VOCs sensing [32]. Even personal digital portable electronics nose system for VOCs sensors were developed by Kim research group [33]. Thus, advantages of using conductive polymers, conductive carbon matrix, or nanocomposites of carbon-polymer are high sensitivity, stability, selectivity, and detection at room temperature [34]. Depending on surface free energy and chemical/physical interactions, the degree of VOCs sensitivity on nanomaterial interfaces. On the other hand, the carbon matrix like CNTs, graphene, CNFs, etc., displays a high sensing ability due to high charge mobility, porosity, and high surface area [33]. The charge transfer reactions between VOCs and carbon matrix determine the oxidation/reduction reaction during sensing [32]. When gaseous molecules act as the strong oxidizing agent (electrons receptor), they can eliminate electrons from the carbon materials which decreases its conductance, while if the gaseous molecules act as the strong reducing agent (electrons donator) they give electrons into the material which decreases the resistance. Thus, sensing depends on the nanomaterials designed and sensing activity of toward the gas. The carbon nanotubes can be combined with conducting polymers (CPs) which become a unique group of materials because some of CPs behave like semiconductors which resulted, alteration in electrical conductivity of CNT/CP composites. The charge transfer between gas molecules and CNTs which is facilitated by polymers which is believed to make the composites to be more selective and sensitive for VOC which could be the vital part of the gas sensors in the gas sensing mechanism. Compared to bare CNT, CP composited CNTs show better selectivity and sensing ability as shown in Fig. 3.

Pirsa et al. designed a polypyrrole-based sensor which is for determination of VOCs, the as-synthesized material showed a faster response of < 1 s. The sensitivity of gas sensing material follow the order for the various molecules, pyridines > acetonitrile > DMSO > ROHs > aldehydes > ketone > benzene derivatives >> alkanes



**Fig. 3** **a** Resistive response of VA-CNT coated with 8 nm PEDOT to n-pentane, **b** Response of VA-CNT and polymer-coated CNTs to methanol, **c** Response of VA-CNT and polymer-coated CNTs to n-pentane, projected detection limit for the red line is  $\sim 50$  ppm with  $S/N = 3$ , **d** PC 2 plotted against PC 1 for an array of 10 different SWCNT-based chemiresistors to 15 VOCs (3–4 trials each). **e** PC 2 plotted against PC 1 with amines excluded from the plot. **f** PC 3 plotted against PC 2 with amines excluded from the plot. Reproduced from Ref. [30, 35]. Copyrights (ACS, 2015) (ACS, 2016)

[31]. Fan et al. developed a sensor for the vapor sensing characteristics of thermo-plastic polyurethane material which is covered with carbon nanotube networks. It is observed that 0.5% of the vapor concentration was detectable with a maximum relative change (900%) for 0.8% CNT loading while sensing 7.0% chloroform [36]. Daneshkhhah et al. fabricated a PVDF-based gas sensor for the detection of VOCs. The sensor designed by PVDF-HFP/C65 showed the elevation in resistance (52.6%) in response to the acetone. Another sensor having two layers of PVDF-HFP and PVDF-HFP/C65 which were fabricated by spin coating method shows a very good response when compared to the gas sensor attached with PVDF-HFP/C65 decreased by 52% for acetone. The third sensor composited CNT with PVDF-HFP/C65 causes a decrease in resistance in response to water molecule [37].

## 4 Carbon Monoxide (CO) Sensors

It is well known that carbon monoxide is colorless, odorless, and it is also a toxic gas formed during the incomplete combustion of fossil fuels mostly in industries and automobiles. CO is one among the major air pollutants, especially in the regions of developing and developed nations across the globe [38]. It is a well-known fact that

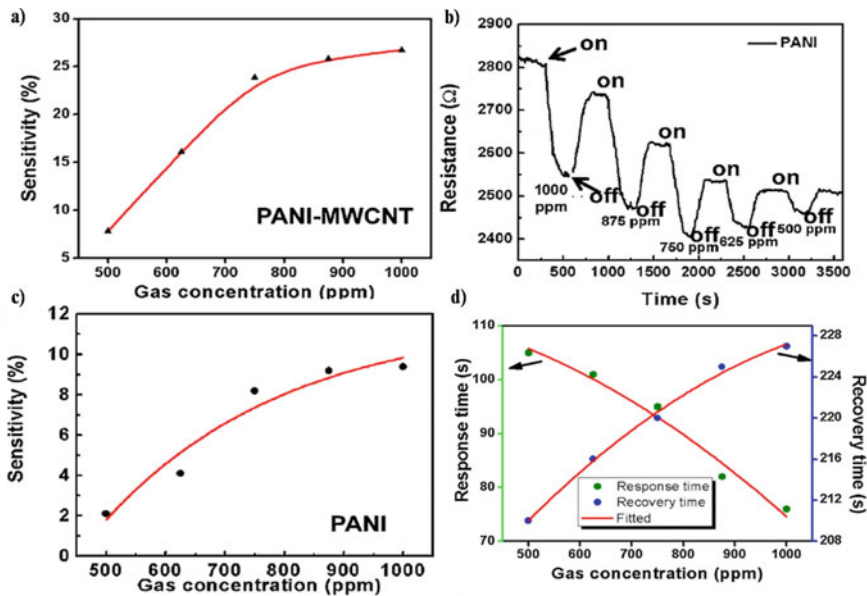
our blood has more affinity for CO than oxygen. So, the vital role of blood (oxygen-carrying capacity) is retarded abruptly by breathing the polluted air (mixed with CO) for a long time. As per the reports of WHO, 10 ppm of CO is the acceptable limit for the inhalation for about 8 h without any harmful effect [39]. So, it is very important to monitor CO in the atmosphere.

One could find several research reports on the development of CO sensors with the use of different materials. Mahajan et al. overviewed the CO sensors using different metal oxides for CO sensing applications. It analyzed various synthetic approaches for obtaining different nanostructured materials to enhance the sensing performances such as selectivity, sensitivity, stability, and response and recovery time. It is concluded that the composite materials (metal oxide and carbon materials such as CNT, graphene) can be taken to enhance the CO sensing performances [40]. Carbon-based materials received great attention which can be used in CO sensors to improve the sensing performances. For example, Basharnavaz et al. utilized the graphitic carbon nitrides (g-C<sub>3</sub>N<sub>4</sub>) as a smart adsorbing material for CO sensing applications because of the unique characteristics like electronic, structural, and textural. This study deals with the adsorption tendencies of g-C<sub>3</sub>N<sub>4</sub>-based materials in CO sensors and also studied the impact of embedding, doping, and decorating by g-C<sub>3</sub>N<sub>4</sub> added with some suitable materials on CO sensing properties of the g-C<sub>3</sub>N<sub>4</sub>-based gas sensors were explained. It is concluded with an emphasis on the shift from the laboratory research to industry scale to use the g-C<sub>3</sub>N<sub>4</sub>-based composite materials in CO sensors [41]. Roy et al. reported PANI-MWCNT composite for room temperature CO sensor, the material exhibits sensitivity of 6.8%–25.7% with a very good response and recovery time at room temperature (76 and 210 s) as seen in Fig. 4.

Metal–organic frameworks are the yet another important carbon-based composite materials that can be used along with metal oxides and other suitable additives in CO sensors to improve sensing performances. Metal–organic frameworks have different applications such as absorption of CO<sub>2</sub> gases to tackle greenhouse effect. In addition to numerous applications, Metal–organic frameworks can be utilized for CO sensors. Yang et al. used the metal–organic frameworks based nanocomposite material which consist of tin dioxide nanoparticles/molybdenum diselenide nanoflowers obtained by hydrothermal process for CO sensing applications. It is observed that the sensor was more selective to CO molecule among the various interfering gases (H<sub>2</sub>, CO<sub>2</sub>, CH<sub>4</sub>, SO<sub>2</sub>, and H<sub>2</sub>S). Development of selective CO sensors is vital for the practical applications. CO sensing characteristics especially selectivity is attributed to the fact that the availability of n–n heterojunction at the interface between SnO<sub>2</sub> nanoparticles and MoSe<sub>2</sub> nanoflowers [43].

Conducting polymers combine with metal oxides metals, and other suitable additives can be an attractive for CO sensors. For example, Nasresfahani et al., attempted for the improvement of gas sensing performances of the sensor using polyaniline in which the effect of gold (Au) nanoparticles for CO sensing properties of polyaniline is examined. It is observed that the sensor using Au/PANI (2.5%) exhibited good selectivity to CO with good response, response time (180 s), low detection limit (33 ppm), broad dynamic range (200–6000 ppm) due to the catalytic properties of Au nanoparticles [44]. Green synthesis is very important to obtain CO sensing materials. For





**Fig. 4** a Sensitivity of PANI-MWCNT with various CO concentrations, b sensing response of PANI at various CO concentrations, c sensitivity of PANI with various CO concentrations, d response and recovery time of PANI-MWCNT composite material as a function of CO concentration. Reproduced from the Ref. [42]. Copyrights (Elsevier, 2017)

example, Narayana et al. studied the transistor-based CO sensing performances of zinc oxide nanoparticles (spherical shape) prepared by the green synthesis route with a size 3–4 nm and low cost. The sensor detected CO gas at the ambient temperature. It can be noted that the sensitivity and selectivity of the sensor device showed better gas sensing performances than the other reducing gases such as ammonia, methanol vapors, and hydrogen sulfide [45].

## 5 Hydrocarbon Sensors

Hydrocarbons are made up of carbon and hydrogen atoms. Naturally, decomposed organic matters provide an abundance of hydrocarbons occur on earth in crude oil. Liquid form and gas form of hydrocarbons are called petroleum and natural gas, respectively. Some hydrocarbons exist as gases such as methane, propane. Hydrocarbon molecules like benzene and xylene affect the human health and environment. The techniques for the detection of hydrocarbon molecules need to fulfill all requirements of affordable and reliable hydrocarbons monitoring. Thus, smart hydrocarbon sensors are highly required with simple design and low cost. Methane is the major component of natural gas and also essential resource around the globe for various

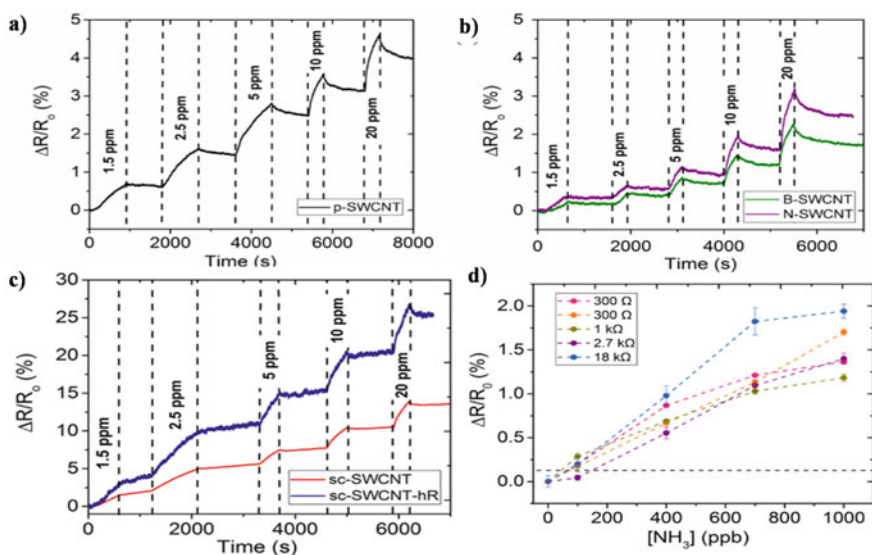
purposes such as production of electricity, heating etc. It is well known fact that methane gives environmental impact and a significant contributor for the global warming and climate change. So, it is essential to minimize the leakages in pipelines and also natural gas is considered as a cleaner alternative to fossil fuels. The detection of methane and other hydrocarbon gases in the atmosphere has become more important to minimize the greenhouse effect. Leak detection in natural gas pipeline, and automobiles requires efficient devices with low cost and also high performances for the gas sensing characteristics such as selectivity, sensitivity, and stability with quick response and recovery rates. The primary objective of hydrocarbon sensors is to detect the gases efficiently for the effective monitoring of atmosphere making pollution free. In general, hydrocarbon sensor required to monitor the hydrocarbon molecules making photochemical smog in the environment which causes respiratory problems. Sensing material plays a major role to achieve better gas sensing properties. As per the literature reports, various suitable and appropriate sensing materials such as single metal oxides, composites with carbon materials and conducting polymers utilized to study the gas sensing performances and also aimed to increase the gas sensing properties. Barriault et al. reported the use of single metal oxide semiconductors to detect the hydrocarbons such as methane and ethane in a mixture and also studied the gas sensing performances of the sensor. It is observed that sensor could able to detect methane, ethane, and binary mixtures of methane and ethane [46]. It is important that a gas sensor must detect a particular gas selectively for industries where the gas is used for various industrial processes. Seshadri et al. reported that the utilization of polymer composites to detect the hydrocarbon pollutants. Organic polymer composites based materials composed of styrene ethylene butylene styrene, ethylene vinyl acetate and isobutylene isoprene used for the fabrication of sensor device. The sensors are developed for detecting the hydrocarbon gas leak with high sensitivity and selectivity. These hydrocarbon-dissolvable polymers tested chemiresistively with the attractive gas sensing responses (+ 180% in 1 h and + 27,555% in 6 h). The development of these sensors aimed to detect hydrocarbons, especially for leakages in crude oil pipelines so it is essential to test the gas performances in presence of oil. The sensing mechanism of sensor is the measurement of resistance upon changes due to any chemical reactions [47]. Graphene-based materials can be another choice of organic materials for the detection of hydrocarbon molecules for pipeline leakage checking in industries. Toard et al. investigated the use of 3D porous graphitic carbon networks as a sensing material to sense the volatile aromatic hydrocarbon molecules. It is observed that the sensing materials with nanoporosity drastically increased sensitivity and selectivity to vaporized toxic aromatic vapors (toluene and benzene). The salient features associated with the sensing materials discussed in details. It is noted that the graphitic carbon framework as porous electrode materials for the selective detection of hazardous aromatic hydrocarbon vapors because of the high surface area and large hierarchical pore volume. As reported, carbon materials are associated with the porous nature and larger surface area as a matter of unique features which made the sensors for the enhanced gas sensing performances [48].

## 6 Ammonia Sensors

Ammonia is a colorless, strong irritant, and flammable gas which is formed during various processes such as caves, mines, chemical manufacturing and nitrogenous fertilizers. As ammonia is a toxic gas, it is required to detect in many situations such as leak-detection in air-conditioning systems, animal housing, environmental monitoring of ammonia in air, breath analysis for medical diagnosis, etc.  $\text{NH}_3$  gas is also quite corrosive in nature. Development of high-performance ammonia sensors required to monitor the systems where either ammonia gas is used or produced during the industrial processes. High sensitivity, high selectivity, quick response, and also a great tolerance to higher operating temperatures are required for the application of ammonia sensors in automobiles. Urea-SCR (selective catalytic reduction) system is used to remove the  $\text{NO}_x$  emissions in the diesel engines based automobiles. Urea solution is injected into a catalytic convertor where  $\text{NH}_3$  gas would be formed due to hydrolysis reaction and the excess ammonia is possible in SCR system so it is needed to be monitoring regularly. For example, Shimizu et al. developed the resistive-type electrochemical ammonia gas sensors using vanadium oxides and also studied the impact of dopants for the sensing characteristics of the vanadium oxides doped with aluminum and cerium. In general, a gas sensor must be selective to ammonia to be useful for the practical applications. It is found that the doped vanadium oxide selectively detected the  $\text{NH}_3$  gas in the presence of coexisting gases at high temperatures and so it is more suitable especially for monitoring the concentration of ammonia in urea-SCR system of automobiles. The selectivity of the gas sensor may be attributed due the effect of doping on vanadium oxides with aluminum and cerium [49]. Among the various materials, use of carbon-based sensing materials is believed to be more efficient to detect ammonia molecule because of the enlarged specific surface area and very sensitive to ammonia molecules adsorbed on the surface. Several materials have been utilized to develop gas sensors to detect ammonia, carbon nanomaterials like graphene and reduced graphene oxide (RGO). For example, Zhu et al. designed the ammonia gas sensor using graphene-based materials fabricated by aerosol-jet printing technology [50]. Sensors can be fabricated on a silicon substrate which exhibited its excellent sensing properties. Functionalized graphene could also be used as the carbon-based sensing materials to examine the ammonia sensing characteristics of sensor devices. Gautam et al. reported the use of functionalized graphene material with gold nanoparticles which could reach the maximum ammonia sensitivity [51]. Similarly, carbon-based hybrid sensing materials or composites could be utilized for investigating the gas sensing properties of ammonia sensors. The main objective is to study the influence of additives in gas sensing properties of hybrid materials. Huang et al. reported that the use of RGO-PANI which showed much better response. The combination of PANI and RGO sheets which made the enhancement of gas sensing characteristics of sensors. It is noteworthy that the enhancement of ammonia sensitivity in a remarkable manner by using hybrid sensing materials with polyaniline which showed the better gas sensing performances [52]. SWCNTs have attractive properties such as high surface-to-volume and ratio of length to diameter,

which enhances gas sensing abilities and SWCNT detect low concentration range of analyte molecules. Also, the conductivity and structural stability of SWCNT is high. Luis et al. reported SWCNT for  $\text{NH}_3$  gas sensor which showed very good sensing abilities as shown in Fig. 5 highest response of 3.2% at 1.5 ppm was achieved [53].

Polymer-carbon-metal oxide could be another hybrid structure to analyze the gas sensing performances of ammonia sensors. Xu et al. used the carbon-based composite material consist of graphene nanoribbon (GNR), polyaniline and indium oxide composite to detect ammonia at room temperature. Indium trioxide ( $\text{In}_2\text{O}_3$ ) nanoparticles prepared by solvothermal method were coated on GNR to act as a core component for fabricating ternary nanocomposite (PANI)/ $\text{In}_2\text{O}_3$ /GNR prepared by in situ chemical oxidative polymerization method. This sensor is highly sensitive to ammonia at room temperature with higher selectivity and repeatability and also useful for diagnosing the hepatic or kidney disease [54]. Conducting polymers explored for the fabrication of ammonia sensors due to their flexible chemical structures and attractive morphologies. Pang et al. examined the use of polyaniline-coated nanofibers for



**Fig. 5** Sensing response  $\Delta R/R_0$  under exposure to different ammonia concentrations of 1.5, 2.5, 5, 10, and 20 ppm: **a** device based on pristine SWCNTs, **b** devices based on N-SWCNTs (purple) and B-SWCNTs (green). An incomplete recovery under pure  $\text{N}_2$  flow was present in all devices. Dotted lines delimit exposure times with the corresponding concentrations, **c** sensing response  $\Delta R/R_0$  of two devices based on semiconducting SWCNTs under exposure to different ammonia concentrations of 1.5, 2.5, 5, 10, and 20 ppm. The devices had initial resistance of  $268 \Omega$  (red) and  $15 \text{ k}\Omega$  (high-resistance device, blue line), **d** Sensing response  $\Delta R/R_0$  of five devices based on sc-SWCNTs under exposure to different ammonia concentrations of 100, 400, 700, and 1000 ppb. The initial resistance values  $R_0$  for the devices are shown in legends. Colored dashed lines connecting data point are drawn to guide an eye; error bars depict signal noise at the data point. Horizontal dashed line is drawn at three times the noise averaged over all data points. Reproduced from [53]. Copyrights (ACS, 2018)

the detection of ammonia molecules. This ammonia sensor is designed by the electrospinning, and in situ polymerization process exhibited ideal gas sensing properties (50–250 ppm of ammonia at ambient temperature with good selectivity, quick sensing responses, and also very good repeatability). It can be noted that the increase in resistance and decrease in conductivity. De-doping of polyaniline molecular chains by ammonia molecules are the ammonia sensing mechanism [55].

## 7 Future Perspectives

In future, research direction would be the selection of smart materials as sensing materials to develop smart gas sensors. High-performance gas sensors are developed with the aim of monitoring the air pollutants to address the environmental issues. Researchers would prefer new or novel materials as an alternative ways for the existing various other materials with attractive properties which are helpful to increase the gas sensing characteristics to fabricate smart gas sensors. To achieve this, the utilization of carbon-based composite materials to fabricate the gas sensors has been widened among the several other sensing materials. In the book chapter, we analyzed various unique properties of carbon-based nanocomposite materials which play a vital role for the gas sensing applications. In near future, researchers may choose sensing materials with improved salient features to enhance the performances. For example, 3D nanoarchitected carbon networks would be exploited to its full potential to develop gas sensors to monitor hazardous gases such as CO, ammonia, NO<sub>x</sub>, aromatic hydrocarbons. The surface area activation, catalytic activities, pores, morphology, interaction strategy, etc., play vital roles to enhance gas sensing properties of materials used in sensor devices. We have much more scopes to develop gas sensors using ternary nanocomposites as sensing materials in the future. It is expected that ternary nanocomposite consisting of metal oxide, polymer, and carbon could be explored furthermore with different combinations to meet the demands for enhancing the gas sensing performances. It is believed that various research works on the use of different materials with low cost for gas sensors presented in the book chapter which could be utilized to focus the design or fabrication of smart and next-generation gas sensors. The key role of reliable materials with low cost for designing gas sensors is inevitable to improve the monitoring system for various applications. Sensing mechanism of gas sensors must be studied thoroughly. Some parameters must be addressed the issues in the gas sensors such as use of sensing materials, selectivity, sensitivity, response and recovery rates, operating temperatures. Gas sensors in the near future would be smarter than existing candidates in terms of sensing characteristics, economic, etc. We hope that carbon composites would promote sensor development for benefits of human health.

## References

1. Kolhe PS, Koinkar PM, Maiti N, Sonawane KM (2017) Synthesis of Ag doped SnO<sub>2</sub> thin films for the evaluation of H<sub>2</sub>S gas sensing properties. *Physica B* 524:90–96. <https://doi.org/10.1016/j.physb.2017.07.056>
2. Jang Y, Kim SM, Spinks GM, Kim SJ (2020) Carbon nanotube yarn for fiber-shaped electrical sensors, actuators, and energy storage for smart systems. *Adv Mater* 32:1902670. <https://doi.org/10.1002/ADMA.201902670>
3. Sevilla M, Mokaya R (2014) Energy storage applications of activated carbons: supercapacitors and hydrogen storage. *Energy Environ Sci* 7:1250–1280. <https://doi.org/10.1039/C3EE43525C>
4. Su PG, Yang LY (2016) NH<sub>3</sub> gas sensor based on Pd/SnO<sub>2</sub>/RGO ternary composite operated at room-temperature. *Sens Actuators B Chem* 223:202–208. <https://doi.org/10.1016/j.snb.2015.09.091>
5. Xu X, Chen Y, Zhang G, Ma S, Lu Y, Bian H, Chen Q (2017) Highly sensitive VOCs-acetone sensor based on Ag-decorated SnO<sub>2</sub> hollow nanofibers. *J Alloy Compd* 703:572–579. <https://doi.org/10.1016/j.jallcom.2017.01.348>
6. Ahuja RT, Kumar D (2009) Recent progress in the development of nano-structured conducting polymers/nanocomposites for sensor applications. *Sens Actuators B Chem* 136:275–286. <https://doi.org/10.1016/j.snb.2008.09.014>
7. Yang Y, Li S, Yang W, Yuan W, Xu J, Jiang Y (2014) In situ polymerization deposition of porous conducting polymer on reduced graphene oxide for gas sensor. *ACS Appl Mater Interfaces* 6:13807–13814. <https://doi.org/10.1021/AM5032456>
8. Umar A, Ibrahim AA, Algadi H, Albargi H, Alsairi MA, Wang Y, Akbar S (2021) Enhanced NO<sub>2</sub> gas sensor device based on supramolecularly assembled polyaniline/silver oxide/graphene oxide composites. *Ceram Int* 47:25696–25707. <https://doi.org/10.1016/J.CERAMINT.2021.05.296>
9. Zhang W, Cao S, Wu Z, Zhang M, Cao Y, Guo J, Zhong F, Duan H, Jia D (2019) High-performance gas sensor of polyaniline/carbon nanotube composites promoted by interface engineering. *Sensors* 20:149. <https://doi.org/10.3390/S20010149>
10. Lucci M, Reale A, di Carlo A, Orlanducci S, Tamburri E, Terranova ML, Davoli I, di Natale C, D'Amico A, Paolesse R (2006) Optimization of a NO<sub>x</sub> gas sensor based on single walled carbon nanotubes. *Sens Actuators B Chem* 118:226–231. <https://doi.org/10.1016/j.snb.2006.04.027>
11. Lee SW, Lee W, Lee D, Choi Y, Kim W, Park J, Lee JH, Lee G, Yoon DS (2018) A simple and disposable carbon adhesive tape-based NO<sub>2</sub> gas sensor. *Sens Actuators B Chem* 266:485–492. <https://doi.org/10.1016/j.snb.2018.03.161>
12. An KH, Jeong SY, Hwang HR, Lee YH (2004) Enhanced sensitivity of a gas sensor incorporating single-walled carbon nanotube-polypyrrole nanocomposites. *Adv Mater* 16:1005–1009. <https://doi.org/10.1002/adma.200306176>
13. Ram MK, Yavuz O, Aldissi M (2005) NO<sub>2</sub> gas sensing based on ordered ultrathin films of conducting polymer and its nanocomposite. *Synth Met* 151:77–84. <https://doi.org/10.1016/j.synthmet.2005.03.021>
14. Kadhim GA, Suhail H (2019) The nanocomposite film of polypyrrole and functionalized single walled carbon nanotubes as gas sensor of NO<sub>2</sub> oxidizing gas \*Address for Correspondence. [www.tnsroindia.org.in](http://www.tnsroindia.org.in)
15. Liu B, Liu X, Yuan Z, Jiang Y, Su Y, Ma J, Tai H (2019) A flexible NO<sub>2</sub> gas sensor based on polypyrrole/nitrogen-doped multiwall carbon nanotube operating at room temperature. *Sens Actuators B Chem* 295:86–92. <https://doi.org/10.1016/j.snb.2019.05.065>
16. Agarwal PB, Alam B, Sharma DS, Sharma S, Mandal S, Agarwal A (2018) Flexible NO<sub>2</sub> gas sensor based on single-walled carbon nanotubes on polytetrafluoroethylene substrates. *Flexible Printed Electron* 3:035001. <https://doi.org/10.1088/2058-8585/AACC8F>
17. Mangu R, Rajaputra S, Singh VP (2011) MWCNT-polymer composites as highly sensitive and selective room temperature gas sensors. *Nanotechnology* 22. <https://doi.org/10.1088/0957-4484/22/21/215502>

18. Zhang W, Cao S, Wu Z, Zhang M, Cao Y, Guo J, Zhong F, Duan H, Jia D (2020) High-performance gas sensor of polyaniline/carbon nanotube composites promoted by interface engineering. *Sensors* (Switzerland) 20. <https://doi.org/10.3390/s20010149>
19. Chen J, Tsubokawa N (200) Novel gas sensor from polymer-grafted carbon black: vapor response of electric resistance of conducting composites prepared from poly(ethylene-block-ethylene oxide)-grafted carbon black
20. Yuan W, Huang L, Zhou Q, Shi G (2014) Ultrasensitive and selective nitrogen dioxide sensor based on self-assembled graphene/polymer composite nanofibers. *ACS Appl Mater Interfaces* 6:17003–17008. <https://doi.org/10.1021/am504616c>
21. Dunst K, Jurków D, Jasiński P (2016) Laser patterned platform with PEDOT-graphene composite film for NO<sub>2</sub> sensing. *Sens Actuators B Chem* 229:155–165. <https://doi.org/10.1016/j.snb.2016.01.093>
22. Hang NT, Zhang S, Yang W (2017) Efficient exfoliation of g-C<sub>3</sub>N<sub>4</sub> and NO<sub>2</sub> sensing behavior of graphene/g-C<sub>3</sub>N<sub>4</sub> nanocomposite. *Sens Actuators B Chem* 248:940–948. <https://doi.org/10.1016/j.snb.2017.01.199>
23. Dunst K, Jurków D, Jasiński P (2016) Laser patterned platform with PEDOT-graphene composite film for NO<sub>2</sub> sensing. *Sens Actuators B Chem* 229:155–165. <https://doi.org/10.1016/J.SNB.2016.01.093>
24. Dunst KJ, Trzciński K, Scheibe B, Sawczak M, Jasiński P (2018) Study of the NO<sub>2</sub> sensing mechanism of PEDOT-RGO film using in situ Raman Spectroscopy. *Sens Actuators B Chem* 260:1025–1033. <https://doi.org/10.1016/j.snb.2018.01.089>
25. Park CH, Schroeder V, Kim BJ, Swager TM (2018) Ionic liquid-carbon nanotube sensor arrays for human breath related volatile organic compounds. *ACS Sensors* 3:2432–2437. [https://doi.org/10.1021/ACSENSORS.8B00987/SUPPL\\_FILE/SE8B00987\\_SI\\_001.PDF](https://doi.org/10.1021/ACSENSORS.8B00987/SUPPL_FILE/SE8B00987_SI_001.PDF)
26. Chatterjee S, Castro M, Feller JF (2015) Tailoring selectivity of sprayed carbon nanotube sensors (CNT) towards volatile organic compounds (VOC) with surfactants. *Sens Actuators B Chem* 220:840–849. <https://doi.org/10.1016/J.SNB.2015.06.005>
27. Chiou JC, Wu CC, Lin TM (2019) Sensitivity enhancement of acetone gas sensor using polyethylene glycol/multi-walled carbon nanotubes composite sensing film with thermal treatment. *Polymers* 11. <https://doi.org/10.3390/POLYM11030423>
28. Xie H, Yang Q, Sun X, Yang J, Huang Y (2006) Gas sensor arrays based on polymer-carbon black to detect organic vapors at low concentration. *Sens Actuators B Chem* 113:887–891. <https://doi.org/10.1016/J.SNB.2005.03.116>
29. Rattanabut C, Wongwiriyan W, Muangrat W, Bunjongpru W, Phonyiem M, Song YJ (2018) Graphene and poly(methyl methacrylate) composite laminates on flexible substrates for volatile organic compound detection. *Japanese J Appl Phys* 57:04FP10. <https://doi.org/10.7567/JJAP.57.04FP10/XML>
30. Wang X, Ugur A, Goktas H, Chen N, Wang M, Lachman N, Kalfon-Cohen E, Fang W, Wardle BL, Gleason KK (2016) Room temperature resistive volatile organic compound sensing materials based on a hybrid structure of vertically aligned carbon nanotubes and conformal oCVD/iCVD polymer coatings. *ACS Sensors* 1:374–383. [https://doi.org/10.1021/ACSENSORS.5B00208/SUPPL\\_FILE/SE5B00208\\_SI\\_001.PDF](https://doi.org/10.1021/ACSENSORS.5B00208/SUPPL_FILE/SE5B00208_SI_001.PDF)
31. Pirsá S, Alizadeh N (2010) Design and fabrication of gas sensor based on nanostructure conductive polypyrrole for determination of volatile organic solvents. *Sens Actuators, B Chem* 147:461–466. <https://doi.org/10.1016/J.SNB.2010.03.026>
32. Kessick R, Tepper G (2006) Electrospun polymer composite fiber arrays for the detection and identification of volatile organic compounds. *Sens Actuators, B Chem* 117:205–210. <https://doi.org/10.1016/J.SNB.2005.11.045>
33. Kim YS, Ha SC, Yang Y, Kim YJ, Cho SM, Yang H, Kim YT (2005) Portable electronic nose system based on the carbon black-polymer composite sensor array. *Sens Actuators, B Chem* 108:285–291. <https://doi.org/10.1016/J.SNB.2004.11.067>
34. Konwer S, Begum A, Bordoloi S, Boruah R (2017) Expanded graphene-oxide encapsulated polyaniline composites as sensing material for volatile organic compounds. *J Polym Res* 24:1–10. <https://doi.org/10.1007/S10965-017-1195-6/FIGURES/11>

35. Liu SF, Moh LCH, Swager TM (2015) Single-walled carbon nanotube-metalloporphyrin chemiresistive gas sensor arrays for volatile organic compounds. *Chem Mater* 27:3560–3563. [https://doi.org/10.1021/ACS.CHEMMATER.5B00153/SUPPL\\_FILE/CM5B00153\\_SI\\_001.PDF](https://doi.org/10.1021/ACS.CHEMMATER.5B00153/SUPPL_FILE/CM5B00153_SI_001.PDF)
36. Fan Q, Qin Z, Villmow T, Pionteck J, Pötschke P, Wu Y, Voit B, Zhu M (2011) Vapor sensing properties of thermoplastic polyurethane multifilament covered with carbon nanotube networks. *Sens Actuators, B Chem* 156:63–70. <https://doi.org/10.1016/J.SNB.2011.03.073>
37. Daneshkhan A, Shrestha S, Agarwal M, Varahramyan K (2015) Poly(vinylidene fluoride-hexafluoropropylene) composite sensors for volatile organic compounds detection in breath. *Sens Actuators, B Chem* 221:635–643. <https://doi.org/10.1016/J.SNB.2015.06.145>
38. Debatara A, Widia D, Yulianto B (2017) Investigation of nanostructured SnO<sub>2</sub> synthesized with polyol technique for CO gas sensor applications. *Procedia Eng* 170:60–64. <https://doi.org/10.1016/j.proeng.2017.03.011>
39. Moon CS, Kim HR, Auchterlonie G, Drennan J, Lee JH (2008) Highly sensitive and fast responding CO sensor using SnO<sub>2</sub> nanosheets. *Sens Actuators, B Chem* 131:556–564. <https://doi.org/10.1016/J.SNB.2007.12.040>
40. Mahajan S, Jagtap S (2020) Metal-oxide semiconductors for carbon monoxide (CO) gas sensing: a review. *Appl Mater Today* 18:100483. <https://doi.org/10.1016/J.APMT.2019.100483>
41. Basharnavaz H, Habibi-Yangjeh A, Pirhashemi M (2020) Graphitic carbon nitride as a fascinating adsorbent for toxic gases: a mini-review. *Chem Phys Lett* 754:137676. <https://doi.org/10.1016/J.CPLETT.2020.137676>
42. Roy A, Ray A, Sadhukhan P, Naskar K, Lal G, Bhar R, Sinha C, Das S (2018) Polyaniline-multiwalled carbon nanotube (PANI-MWCNT): room temperature resistive carbon monoxide (CO) sensor. *Synth Met* 245:182–189. <https://doi.org/10.1016/J.SYNTHMET.2018.08.024>
43. Yang Z, Zhang D, Wang D (2020) Carbon monoxide gas sensing properties of metal-organic frameworks-derived tin dioxide nanoparticles/molybdenum diselenide nanoflowers. *Sens Actuators, B Chem* 304:127369. <https://doi.org/10.1016/J.SNB.2019.127369>
44. Nasresfahani S, Zargarpour Z, Sheikhi MH, Nami Ana SF (2020) Improvement of the carbon monoxide gas sensing properties of polyaniline in the presence of gold nanoparticles at room temperature. *Synthetic Metals* 265:116404. <https://doi.org/10.1016/J.SYNTHMET.2020.116404>
45. Narayana A, Bhat SA, Fathima A, Lokesh SV, Surya SG, Yelamagga CV (2020) Green and low-cost synthesis of zinc oxide nanoparticles and their application in transistor-based carbon monoxide sensing. *RSC Adv* 10:13532–13542. <https://doi.org/10.1039/D0RA00478B>
46. Barriault M, Alexander I, Tasnim N, O'Brien A, Najjaran H, Hoorfar M (2021) Classification and regression of binary hydrocarbon mixtures using single metal oxide semiconductor sensor with application to natural gas detection. *Sens Actuators, B Chem* 326:129012. <https://doi.org/10.1016/J.SNB.2020.129012>
47. Seshadri A, Vedula G, Naguib HE (2020) Scalable sensing of hydrocarbon pollutants using soluble chemiresistive polymer composites. *Mater Chem Phys* 239:122119. <https://doi.org/10.1016/J.MATCHEMPHYS.2019.122119>
48. Torad NL, Ding B, El-Said WA, El-Hady DA, Alshitari W, Na J, Yamauchi Y, Zhang X (2020) MOF-derived hybrid nanoarchitected carbons for gas discrimination of volatile aromatic hydrocarbons. *Carbon* 168:55–64. <https://doi.org/10.1016/J.CARBON.2020.05.013>
49. Ichi Shimizu K, Chinzei I, Nishiyama H, Kakimoto S, Sugaya S, Matsutani W, Satsuma A (2009) Doped-vanadium oxides as sensing materials for high temperature operative selective ammonia gas sensors. *Sens Actuat B: Chem* 141:410–416. <https://doi.org/10.1016/J.SNB.2009.06.048>
50. Zhu Y, Yu L, Wu D, Lv W, Wang L (2021) A high-sensitivity graphene ammonia sensor via aerosol jet printing. *Sens Actuators, A* 318:112434. <https://doi.org/10.1016/J.SNA.2020.112434>
51. Gautam M, Jayatissa AH (2012) Ammonia gas sensing behavior of graphene surface decorated with gold nanoparticles. *Solid-State Electron* 78:159–165. <https://doi.org/10.1016/J.SSE.2012.05.059>



52. Huang X, Hu N, Gao R, Yu Y, Wang Y, Yang Z, Siu-Wai Kong E, Wei H, Zhang Y (2012) Reduced graphene oxide–polyaniline hybrid: preparation, characterization and its applications for ammonia gas sensing. *J Mater Chem* 22:22488–22495. <https://doi.org/10.1039/C2JM34340A>
53. Panes-Ruiz LA, Shaygan M, Fu Y, Liu Y, Khavrus V, Oswald S, Gemming T, Baraban L, Bezugly V, Cuniberti G (2018) Toward highly sensitive and energy efficient ammonia gas detection with modified single-walled carbon nanotubes at room temperature. *ACS Sensors* 3:79–86. [https://doi.org/10.1021/ACSSENSORS.7B00358/SUPPL\\_FILE/SE7B00358\\_SI\\_001.PDF](https://doi.org/10.1021/ACSSENSORS.7B00358/SUPPL_FILE/SE7B00358_SI_001.PDF)
54. Xu LH, Wu TM (2020) Synthesis of highly sensitive ammonia gas sensor of polyaniline/graphene nanoribbon/indium oxide composite at room temperature. *J Mater Sci: Mater Electron* 31:7276–7283. <https://doi.org/10.1007/S10854-020-03299-6>
55. Pang Z, Yildirim E, Pasquinelli MA, Wei Q (2021) Ammonia sensing performance of polyaniline-coated polyamide 6 nanofibers. *ACS Omega* 6:8950–8957. [https://doi.org/10.1021/ACSONEGA.0C06272/SUPPL\\_FILE/AO0C06272\\_SI\\_001.PDF](https://doi.org/10.1021/ACSONEGA.0C06272/SUPPL_FILE/AO0C06272_SI_001.PDF)

# Chapter 16

## Recent Advances in Porous Carbon-Based Inorganic Flexible Sensor Journey from Material Synthesis to Sensor Prototyping



Saleem Khan, Vishal Singh, and Ajay Singh

### 1 Introduction

Journey of flexible electronics started in 1900's with development of flexible electrical conductor [1] and space exploration programs paved the way for flexible electronics to meet the high quality and light weight payload demand [2]. This property of flexible electronics led to the fabrication of first thin film transistor on flexible substrate which performed efficiently under deformed conditions[3]. With advancements in flexible device fabrication technologies, researcher started integrating devices on large flexible substrate to create light weight and shape controlled thin system with apt functioning, which is future trend in electronic devices. Studies has been carried to understand the electrical properties of flexible electronic devices under external mechanical force causing bending of the substrate. The timeline development in flexible electronic devices is shown in Fig. 1 [2–25]. Future flexible electronic devices needed to have high bending and stretchable property while maintaining device functionality to meet the diversified domestic market applications. Material aspect of flexible substrate is the main challenge when developing flexible electronic devices, since the substrate should have excellent bonding with device functional material layer. The various substrate along with their properties are described in the following subsection.

---

S. Khan · V. Singh (✉)

Department of Nanosciences and Materials, Central University  
Jammu, Jammu, UT-J&K 181143, India  
e-mail: [vishal.nsm@cuammu.ac.in](mailto:vishal.nsm@cuammu.ac.in)

A. Singh

Department of Physics, GGM Science College, Constituent College of Cluster University of  
Jammu, Canal Road, Jammu, UT-J&K 180002, India

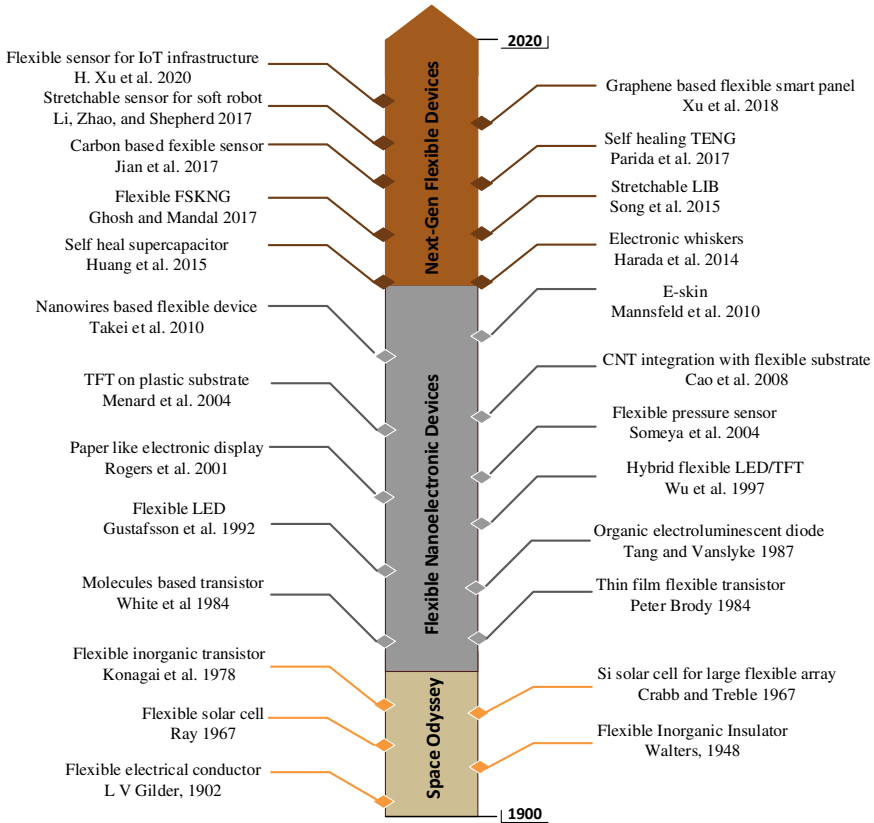


Fig. 1 Timeline development of flexible electronic devices

### 1.1 Plastic Flexible Substrate

Plastic substrates are the most commonly used for the electronic components manufacturing because of their suitability in nonvacuum semiconducting process and have cost-effective roll to roll manufacturing process [26]. Most frequently used plastic substrates are polyethylene terephthalate (PET), polydimethylsiloxane (PDMS), parylene, polyethylene naphthalate (PEN), nylon, polyvinylidene fluoride (PVDF), polyimide (PI), and polystyrene [27–29]. The physical parameters of highly used plastic substrate in electronic device fabrication are given in Table 1. The unique physical properties of plastic substrate makes them excellent candidate in sensing application [30–34].

**Table 1** Physical parameters of plastic substrates

Parameter	PET	Polyimide (PI)	PEN
Friction coefficient	0.2–0.4	0.42	0.27
Tensile modulus (GPa)	2–4	2–3	5–5.5
Tensile strength	80	70–150	200
Thermal expansion coefficient ( $10^{-6} \cdot \text{K}^{-1}$ )	20–80	30–60	20–21
Thermal conductivity at 23 °C ( $\text{W} \cdot \text{m}^{-1} \cdot \text{K}^{-1}$ )	0.15–0.4	0.1–0.35	0.15
Maximum operating temperature (°C)	115–170	400	155
Young's modulus [GPa]	2.8	2.6	3.0
Transparency [%]	91	30	87
Coefficient of expansion [ $\text{ppm} \cdot \text{°C}^{-1}$ ]	15	50	13
Dielectric constant	3	3.4	3.2
Surface resistivity ( $\Omega/\text{Sq.}$ )	$10^{13}$	$10^{16}$	$10^{14}$
Volume resistivity ( $\Omega/\text{cm}$ )	$10^{14}$	$10^{18}$	$10^{15}$

## 1.2 Paper Substrate

Paper is being actively used in fabrication of low cost flexible electronic devices because it is eco-friendly, low cost, easily accessible, and recyclable. The low thermal expansion is the main advantage of paper substrate over plastic substrate [35, 36]. Paper substrate are abundantly used in sensing and plasmonic applications [37–39]. In order to use paper as substrate in flexible electronic device it is coated with semiconducting and polymer material [40, 41] which also provide smoothness to substrate. A unique plasmonic paper substrates are obtained when the pores of the paper are filled with nanoparticles which have wide range of applications [42–44].

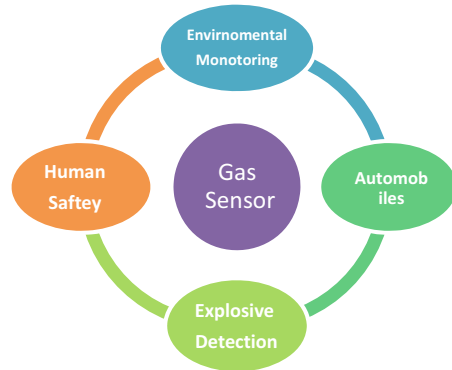
## 1.3 Textile Substrate

New generation of wearable technology requires innovative fabric which can support fabrication of electronic devices on it. Textile substrates are essential for wearable technology [29, 45–47]. A gas sensitive textile can act both as substrate and sensing layer or sensing material can be integrated with textile substrate [48–50].

## 2 Gas Sensor

Gas sensors are critical component for environment safety and life support system. The ability to detect harmful gases and volatile organic chemicals (VOCs) is the key

**Fig. 2** Gas sensor application domains



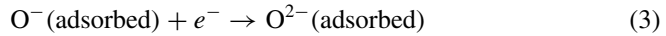
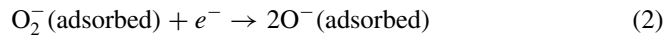
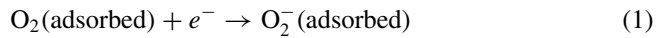
feature of these devices. Domain area where gas sensors are widely used is given in Fig. 2. Environmental gas sensor detects  $\text{H}_2\text{S}$ , VOC,  $\text{SO}_2$ ,  $\text{CO}_2$ ,  $\text{NO}_2$ , etc., toxic gas levels, human safety gas sensor are used to detect molecules of  $\text{C}_2\text{H}_5\text{OH}$  and  $\text{CH}_3\text{COCH}_3$  in breathe to avoid drunk driving and medical diagnostics respectively, gas sensors in automobiles detects the exhaust toxic gases, and explosive sensors are exclusively used to detect  $\text{C}_4\text{H}_4$ ,  $\text{H}_2$ , nitro and peroxide compounds, gasoline, etc., which threaten human life and can cause large-scale destruction [51–55]. Gas sensing mechanism are critical for selecting the sensing material for the gas sensor.

## 2.1 Theoretical Aspect of Gas Sensing Mechanism

Gas sensor analyte sensing process is established on detection of variation in electrical signal response triggered by the adsorbed gas molecules. Detection mechanism gives the insight why the analyte molecules alters the electrical characteristics of the gas sensor. Sensing mechanism can be classified into three models: adsorption/desorption, gas diffusion control, and bulk resistance control.

### 2.1.1 Adsorption/Desorption Sensing Mechanism Model

This is the most conventional and currently used gas sensing mechanism. This model can further subdivided into three models: oxygen adsorption model, chemical, and physical adsorption/desorption model. Oxygen adsorption model is mainstream mechanism suitable for metal oxide semiconductor (MOS) sensing material. When MOS chemical sensing device is exposed to oxygen molecules, these molecules are adsorbed on the active site surface of sensing material layer. MOS surface hypothetically exist in inert form, which are highly doped with oxygen vacancies in reducing environment at high temperature.



These adsorbed negative oxygen ions interact with various gas molecules causing alteration in the resistivity of the sensing material. The exposure to reducing gas molecules causes the oxidation reaction which releases the negative charge, thus increasing the conductivity and reduction in conductivity occurs if electron accepting gas molecules interact [55–58].

In chemical adsorption/desorption sensing mechanism model, gas molecules directly interact with crystal grain of sensing material which causes chemical reaction and effects the electrical signal [59]. In physical adsorption/desorption sensing model, the gas molecules interact with sensing material crystal by Coulomb forces, dipole–dipole attraction, and other intermolecular forces without causing any chemical change. Humidity sensors are most common devices with physical adsorption/desorption sensing mechanism [60, 61].

### 2.1.2 Bulk Resistance Control Sensing Mechanism Model

The fundamental idea of this mechanism model is the variation in the conductance of the sensor due to the phase transformation of the sensing material. This sensing mechanism has low scope compared to other, but it is applicable to ferroic-MOS and perovskite-MOS composite gas sensing analysis [62, 63].

### 2.1.3 Gas Diffusion Control Sensing Mechanism Model

In early 1990s, researcher proposed this sensing model in which gas molecules diffuse in sensing material [64]. Morphology of the sensing material is an important parameter affecting the diffusion process. Porous materials are highly considered for this type of sensing mechanism. At low temperature gas analytes are adsorbed at the outer surface of the material as the temperature is increased, gas diffusion probability becomes higher [65, 66].

## 2.2 Characteristics of Sensor

The static and dynamic characteristics of gas sensor are crucial to determine its working. The important characteristic parameters of gas sensor to evaluate its performance comprise of following aspects [67, 68].

### 2.2.1 Sensitivity

It represents the degree of change in response of the sensor. Sensitivity is the ratio resistance of the gas sensor in test environment to the resistance in normal air.

$$S = \frac{R_g}{R_a} \quad (4)$$

where  $R_g$  is the resistance of the target gas test environment, and  $R_a$  is the at ambient airresistance.

### 2.2.2 Selectivity

The capability of gas or chemical sensor to detectexplicit gas molecules in ambient atmosphere containing various other molecules. Selectivity characteristic of a gas sensor is of paramount importance inorder to design target specific devices.

### 2.2.3 Repeatability/Reproducibility

This parameter indicates repititive number of time a sensor can be used in test environment. An error occurs when the sensor is unable to produce same value under identical conditions. The error is maximum difference between output value of two different calibration cycle.

### 2.2.4 Reliability

It is the ability of gas sensor to accurately perform under required condition for life cycle of the sensor. Reliability is the probability of the sensor to function without faliure for specified number of times.

### 2.2.5 Receiver Operator Characteristic (ROC) Curves

The operational detection limit of a field chemical sensor is determined using a ROC-curve technique. A detection limit that is valid under realistic operating conditions is referred to as the operational detection limit. ROC-curve is robust because the detection limit is analyzed for standard that are above or below the expected detection limit [69].

### 2.3 Sensing Material

In flexible and stretchable sensor, metals are abundantly used material because of their high low resistivity and high stability. Gold (Au) thin film contacts are widely used in flexible electronics because its resistance toward oxidation. In order to increase the adhesion of Au contact to substrate, a thin layer of titanium (Ti) or chromium (Cr) is deposited underneath Au. Apart from contact pads, metals with various geometries such as nanowires, nanoparticles, and liquid conductor are used in transparent and flexible electronic [70–76].

Metal oxide semiconductor are highly used in flexible sensors because they are highly porosity and permeable shell layer which increases the effective gas diffusion phenomena, thus increases sensing performance. MOS materials also have low gas molecules detection limit and short recovery time. MOS can be synthesized in shapes like nanowires, nanotubes, nanosheets, nanoparticles, etc., to be used for sensing applications at room temperature. Table 2 summarizes MOS-based gas sensor.

Single or few-layer TMDs are used in the fabrication of bendable gas or chemical sensing devices as these materials have unique mechanical and electrical properties at nanoscale thickness. TMDs shows graphene-like properties at low dimensions. Two-dimensional structures of TMDs have superior molecular sensing capability with high surface area, sizeable bandgap, and reactive sites for redox reactions [87]. High sensing performance using TMDs is achieved with thermal and UV assistance. TMDs for gas or chemical detection at room temperature and their structures are given in Table 3.

Carbon nanomaterials inherited with nanoscale features are impeccable components for self-driven flexible sensors. Because most of the atoms in low-dimensional carbon structures are exposed to the environment, they have a large surface area, which is necessary to attain high sensitivity. Carbon-based nanomaterials like quantum dots, carbon nanotubes (CNTs), and graphene have characteristics such

**Table 2** MOS nanostructure and their gas sensing properties

Metal oxide material	Synthesized material structure	Gas detection	References
SnO <sub>2</sub>	Nanocrystalline tube	NO <sub>x</sub>	[77]
SnO <sub>2</sub>	Nanowires	CO	[78]
SnO <sub>2</sub>	Thin film	NH <sub>3</sub>	[79]
NiO	Nanowire	NH <sub>3</sub>	[80]
CuO	Nanosheets	H <sub>2</sub> S	[81]
CuO: MnO <sub>2</sub>	Nanocomposites	NH <sub>3</sub>	[82]
WO <sub>3</sub>	Nanocolumnns	Isopropanol	[83]
Na: ZnO	Nanocrystals	Acetone	[84]
In <sub>2</sub> O <sub>3</sub>	Nanocrystals	NO <sub>x</sub>	[85]
CuO/SnO <sub>2</sub>	Nanorods	Nanorods	[86]



**Table 3** Synthesized TMDs material and gas detection properties

TMDs material	Synthesized material structure	Gas detection	References
WS <sub>2</sub>	Nanosheet	NO <sub>2</sub>	[87]
WS <sub>2</sub> : Pd	Thin film	H <sub>2</sub>	[88]
WS <sub>2</sub> : TiO <sub>2</sub>	Nanohybrids	NH <sub>3</sub>	[89]
MoS <sub>2</sub>	Thin film	NH <sub>3</sub>	[90]
MoS <sub>2</sub> /ZnO	Nanocomposites	NH <sub>3</sub>	[91]
MoS <sub>2</sub> /SnO <sub>2</sub>	Nanosheet	NO <sub>2</sub>	[92]
MoS <sub>2</sub> /rGO	Hybrid	Formaldehyde	[93]
MoSe <sub>2</sub>	Thin film	NO <sub>2</sub>	[94]
SnS <sub>2</sub>	Flower shaped	NH <sub>3</sub>	[95]
Ni/MoS <sub>2</sub>	Nanoflower	SO <sub>2</sub>	[96]

as better crystal lattice quality, high mobility, and low noise which are important for transduction and surface chemistry [97]. Carbon quantum dots (CQDs) are chemically stable and conductive zero dimensional fluorescent carbon nanomaterial having size less than 10 nm. CQDs have dominance over other quantum dot materials due to dominance of edge effect and quantum confinement [98]. Synthesis of CQDs can be achieved by using bottom-up synthesis method such as electrochemical, microwave irradiation, hydrothermal/solvothermal, thermal decomposition or top-down synthesis method like electrochemical oxidation, laser ablation, chemical oxidation, arc discharge, and ultrasonication. CQDs resulting from any of the synthesis method is a combination of hydrogen, oxygen and carbon. The oxidation process enhances surface of CQDs with wide spectrum of oxygen groups like carbonyl, hydroxyl, carboxylic acid, and epoxy/ether. The heteroatom doping of CQDs with organic and inorganic materials influences their properties by altering the surface functionality. These hybrid functionalized CQDs can be explored to design novel chemical or gas sensors [99].

CNTs are member of fullerene structure group in which carbon atoms are held together in three formations, namely, spherical, tubular, or ellipsoidal. These are long hollow tubes bind together by van der Waals forces, and their ends may be capped. CNTs are composed of sp<sup>2</sup> chemical bonding which provides them unique strength and such strong bonds attributes toward low chemical reactivity. Thus, functionalization of CNTs are necessary for selective and sensitivity improvement [100]. Graphene is most promising material for flexible gas sensing device because of transparent and unique functionalities due to high electron transport property and high specific area. It also has low electrical noise which contributes toward high gas adsorption and give ultrasensitive characteristics to the material. The sensitivity and electrical properties of intrinsic graphene increases many folds with introduction of defects and doping impurities. Graphene doped with Ca, C, and Fe showed higher gas sensitivity as compared to intrinsic graphene [101]. Metal and metal oxide decorated graphene and its derivatives like graphene oxide (GO) and reduced graphene oxide (rGO)

**Table 4** Synthesized graphene nanostructures and their gas sensing properties

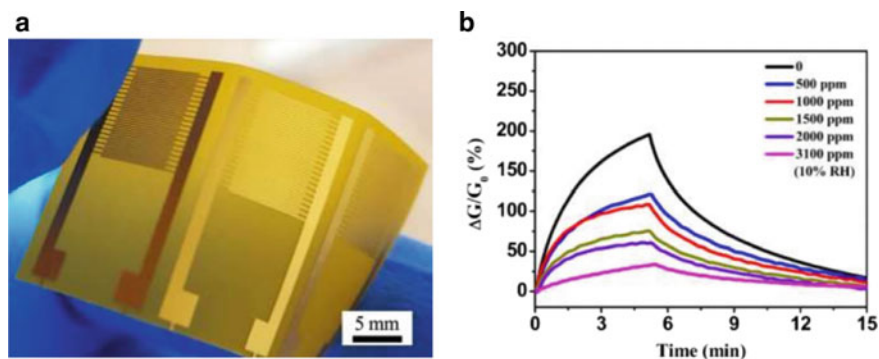
Material	Synthesized material structure	Gas detection	Lmimit of detection	References
MWCNTs	Tube	CO <sub>2</sub>	127 ppb	[104]
SnO <sub>2</sub> decorated MWCNTs	–	CH <sub>4</sub>	490 ppb	[105]
ZnO–rGO	3D	CO <sub>2</sub>	< 9 ppm	[106]
rGO–Mn <sub>3</sub> O <sub>4</sub>		CO <sub>2</sub>	4 ppm	[107]
TiO <sub>2</sub> nanotubes decorated rGO	Nanotube	CH <sub>4</sub>	10 ppm	[108]
PANI-CNT	Nanotube	NH <sub>3</sub>	< 200 ppb	[109]
CQDs	Quantum dots	NO <sub>2</sub>	2 ppm	[110]
Graphene	Sheet	CO <sub>2</sub>	10 ppm	[111]
rGO	Flakes	NH <sub>3</sub>	200 ppm	[112]
rGO	Nanosheet	SO <sub>2</sub>	5 ppm	[113]
Ag/sulfonated graphene	Film	NO <sub>2</sub>	0.5 ppm	[114]
Graphene/SnO <sub>2</sub>	Film	Acetone	10 ppm	[115]
rGO/TiO <sub>2</sub>	Hybrid	Methanol	800 ppm	[108]
rGO/CuO	Nanosheet	Formaldehyde	100 ppm	[116]
rGO/ZnO	Mesoporos	NO <sub>2</sub>	1 ppm	[117]
rGO/WO <sub>3</sub>	Nanosheet	NO <sub>2</sub>	1 ppm	[118]
NiO/rGO	Nanosheet	NO <sub>2</sub>	7 ppm	[119]
In <sub>2</sub> O <sub>3</sub> /rGO	Nanosheet	NO <sub>2</sub>	5 ppm	[120]

have high sensitivity as compared to intrinsic graphene and prove to be effective for attaining high selectivity and sensitivity [102, 103]. Table 4 shows the CQDs, CNTs, graphene, graphene derivatives, and metal oxide decorated graphene material for room temperature sensing applications.

## 2.4 Clasification of Gas Sensor Devices

### 2.4.1 Flexible Chemiresistors Sensor

Chemiresistor gas sensor operating process is based on adsorption of gas molecules over sensing material causing alteration in conductance of the sensor. The sensitivity of the device is determined by measuring the variation in resistance. Flexible chemiresistors are being investigated by many researchers because of its simple fabrication process, reusability and low power consumption. Li et al. developed high sensitive room temperature operating flexible NO<sub>2</sub> gas sensor based on silver nanoparticles

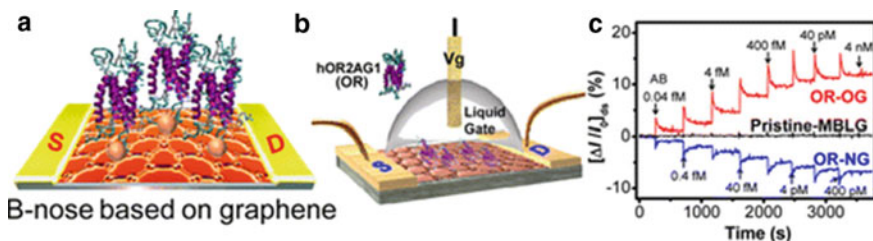


**Fig. 3** **a** Fabricated flexible chemiresistor, **b** sensing responses at 1 ppm NO<sub>2</sub> under different humidity. “Reprinted with permission from Li et al. [121]. Copyright 2019 American Chemical Society”

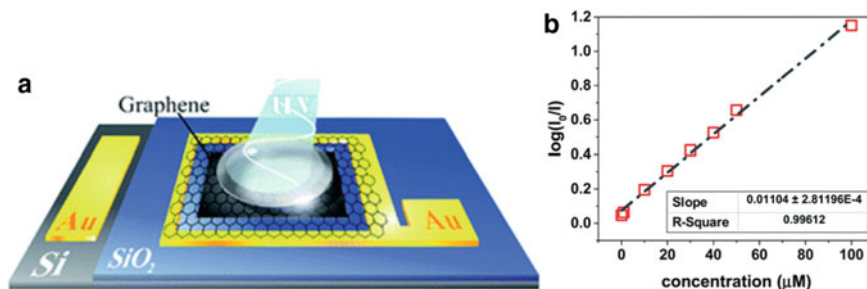
(AgNPs) decorated reduced graphene oxide (rGO) with ultralow detection limit of 0.6 ppb shown in Fig. 3 [121].

#### 2.4.2 Flexible Field-Effect Transistors (FETs) Sensor

FET-based sensors detect the presence of gas molecules by measuring the variation in drain current before and after exposing the sensing channel material to target gas. The conductivity of the sensing channel material is altered when gas molecules are adsorbed on its surface. Park et al. [122] fabricated flexible FET with double layer graphene conjugated with olfactory receptor and demonstrated it as bioelectronic nose. The detection limit is as low as 0.04 fM and has long-term stability and outstanding mechanical flexibility shown in Fig. 4.



**Fig. 4** **a** Double layer graphene-based flexible FET, **b** ionic liquid as gate contact to device, **c** detection response of olfactory receptors. “Reprinted with permission from Park et al. [122]. Copyright 2012 American Chemical Society”



**Fig. 5** **a** Designed graphene BSA sensor, and **b** sensitivity of the fabricated device with concentration. Reprinted with permission from Noroozi and Abdi [123]. Copyright 2019 Published by The Royal Society of Chemistry

### 2.4.3 Schottky Diode

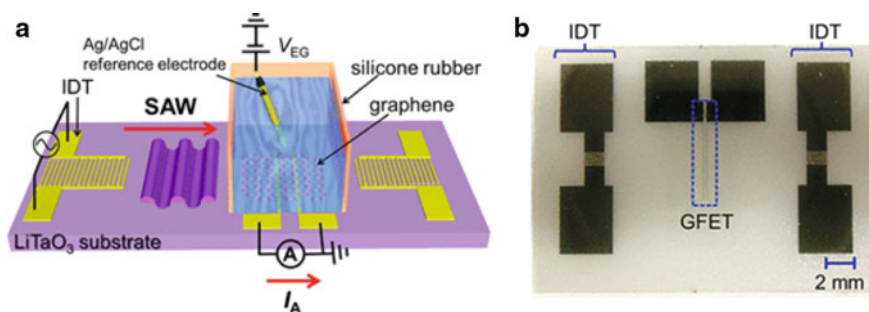
Schottky sensors are fabricated using multi-layered semiconductor heterojunction, graphene, and 2D material can be used as sensing layer. Adsorbed analyte on the surface of the gas sensing material alter the Fermi level of heterojunctions and bandgap. The reverse current varies with change in barrier height and its ease fabrication process makes Schottky diode excellently candidate for gas sensor. Noroozi and Abdi demonstrated the potential of graphene-based Schottky diode for sensing application. Figure 5 shows the fabricated device with sensitivity curve of the sensor [123].

### 2.4.4 Surface Acoustic Wave (SAW) Sensors

SAW is a promising gas sensor because of its miniaturized size, highly sensitive, ruggedness, and cost effective manufacturing process. The schematics of the device and as fabricated device is shown in Fig. 6. The physical and chemical changes in sensing material deposited in delay line area in SAW device caused by gas molecules interaction, alters the velocity of acoustic wave. The mass loading effect of acoustic wave is the sensing mechanism of the device. Okuda et al. demonstrated graphene based SAW device integrated with FET capable of detection of mass and charge changes as a multifunctional sensing device.

## 3 Synthesis and Characterization of Porous Graphene and Its Derivatives

Porous graphene can be synthesized using template-assisted and template-free approach. Based on these approaches 2D (graphene nanomesh) and 3D porous



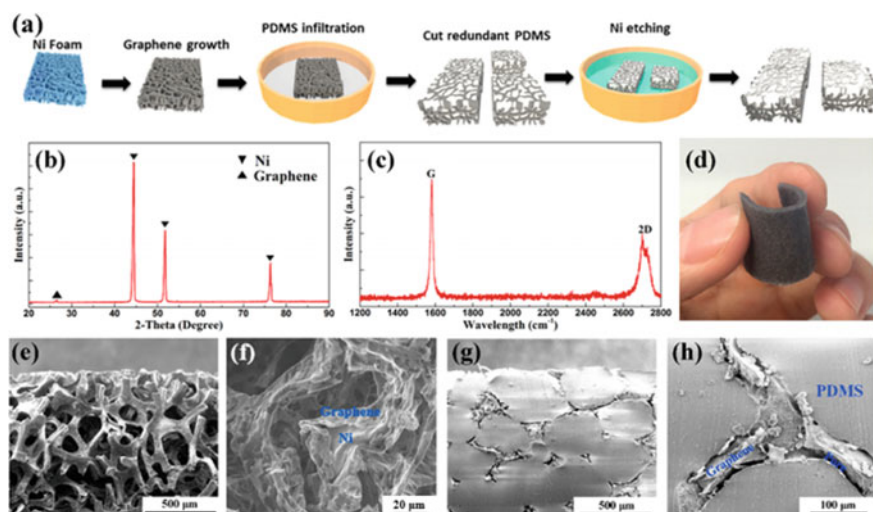
**Fig. 6** **a** Schematic SAW sensor, **b** fabricated graphene SAW sensor integrated with FET. Reprinted with permission from Okuda et al. [124]. Copyright 2018 Published by Springer Nature

(self-assembled graphene nanosheet) can be fabricated. Template-free method for synthesis of porous graphene requires chemical etching process. Graphene etching can be effectively done using hydrogen peroxide, nitric acid, potassium hydroxide, metal nanoparticles, metal oxide, and also thermal treatment can be adopted for 2D porous graphene fabrication [125–131]. Three-dimensional porous graphene can be fabricated using hydrothermal/solvothermal which is cost-effective process and have high throughput for large-scale production [132, 133]. The template-assisted give more control over the size and distribution of pores. Chemical vapor deposition (CVD), hard and soft template-assisted self-assembly are essential. Pang et al. fabricated a flexible porous graphene network structure using nickel (Ni) foam as starting material. Graphene is deposited over the using CVD. Ni deposited graphene was immersed in prepolymer of PDM. Ni was etched out resulting in the formation of graphene porous network shown in Fig. 7 with material and morphological characterization [134]. The morphology of the network have random porous structure. Table 5 shows the other methods of preparation of graphene and its derivatives.

## 4 Functionalization of Graphene

Graphene has honeycomb network of  $sp^2$ -hybridized carbon atom, which makes its excellent material for new generation gas sensor. Selectivity characteristics of graphene gas sensor can be improved by active site surface functionalization. Graphene functionalization can be done covalently (nucleophilic, cycloaddition, condensation, and electrophilic reactions) and non-covalently (electrostatic interactions) [141, 142]. Various metal NPs, metal oxide, TMDs, organic polymer, and conducting polymer decorated graphene functionalization for sensing application is presented in Table 6.

The compatibility of graphene with organic molecules is one of its features. Organic compounds, such as dye molecules, can be linked or layered with graphene. Midya et al. reported graphene with Rose Bengal organic dye molecules as functional



**Fig. 7** **a** Fabrication process flow of pressure and strain sensors with the GPN structure, **b** XRD and **c** Raman spectrum, **d** bent GPN-PDMS composite, **e** SEM image of the nickel foam coated with graphene and **f** magnified SEM image, **g** SEM image of the GPN-PDMS composite and **h** magnified SEM image of a typical connected network with three branches. Reprinted with permission from Pang et al. [134]. Copyright 2016 American Chemical Society

**Table 5** Fabrication methods of graphene over flexible substrate

Material	Substrate	Fabrication technique	References
2D porous graphene	PET	Electrochemical exfoliation	[135]
2D porous graphene	–	Partial combustion	[136]
rGO	PET	Inkjet printing	[137]
rGO	PET	Covalent anchoring	[138]
rGO	Filter paper	Vacuum filtration	[139]
Graphene	Plastic substrate	Inkjet printing	[140]
rGO	Curtain-coated recyclable paper	Spray-coating	[39]

group for binding  $\text{NH}_3$  molecules. The low detection range of 0.9 ppm is reported using Rose Bengal/rGO sensor [143].

Polymer-based functionalization of graphene: Porphyrins material added with various metals has been utilized to functionalize graphene layer as aromatic structure promotes non-covalent bonding. Mackin et al. fabricated extremely sensitive ammonia gas sensor using graphene functionalized with cobalt (Co) porphyrin functionalized, the response of sensor to ammonia increased four folds [144]. Pyo

**Table 6** Graphene and functionalized group with concentration response

Material	Functionalization group	Analyte sensing	Concentration response	References
rGO	Ag NPs	NH <sub>3</sub>	17.4%	[147]
rGO	Au, Ag, Pt NPs	NH <sub>3</sub>	6.52%/ppm	[148]
Graphene	SnO <sub>2</sub>	NH <sub>3</sub>	21% for 50 ppm	[149]
Graphene	V <sub>2</sub> O <sub>5</sub>	NH <sub>3</sub>	31% for 100 ppm	[150]
Graphene fiber	MoS <sub>2</sub>	NO <sub>2</sub> and NH <sub>3</sub>	500ppm	[151]
rGO	MoS <sub>2</sub>	NO <sub>2</sub>	59.8% toward 2 ppm	[152]
Graphene aerogel	WS <sub>2</sub>	NO <sub>2</sub>	10–15 ppb	[153]
rGO	1,8,15,22-tetra-iso-pentyloxyphthalocyanine copper	NH <sub>3</sub>	3200 ppm	[154]
rGO	tetra- $\beta$ -carboxylphenoxyphthalocyanine cobalt	NH <sub>3</sub>	100 ppm	[155]
rGO	4-aminoquinolin	NO <sub>2</sub>	10 ppm	[156]
rGO	tetra- $\alpha$ -aminophthalocyanine cobalt	NH <sub>3</sub>	100 ppm	[155]

et al. designed and fabricated flexible graphene-based sensor for VOCs detection. Graphene layer was functionalized using Co porphyrin–5,10,15,20-tetraphenyl-21H, 23H-porphyrin cobalt(II). Co porphyrin was integrated with graphene using thermal evaporation process [145]. Polymer-based functionalization of graphene is commonly used to improve gas diffusion. Polymer forms strong hydrogen bond or  $\pi$ - $\pi$  stacking with gas molecules, thus increasing the selectivity of the device. Yoon et al. reported transparent flexible ultrasensitive polypyrrole (PPy) functionalized graphene sensor. The test results showed paramount detection limit of 0.03 ppb for NO<sub>2</sub> and 0.04 ppb for NH<sub>3</sub>. This high sensitivity is achieved due to ordered structure of PPy/graphene [146].

## 5 Factors Effecting Sensing Process

Porous carbon nanomaterials possess unique properties which can be explored to design highly selective and sensitive next generation sensors. The morphological, physical, and chemical parameters of sensing material are critical to design highly sensitive gas sensor.

The morphology of the sensing material significantly impacts the sensors efficiency. Sensing material can have morphology of quantum dots (zero dimensional:

0D), nanowires or nanotubes (one dimensional: 1D), nanosheets or belts (2D), and three-dimensional (3D) structures. Large surface active site, improved gas diffusion, and better sensing rates are the key attributes provided by the different sensing material morphologies. Three-dimensional nanostructured materials have all these properties, but their synthesis process is very complex. Hence, 1D and 2D nanostructured materials are preferred for gas sensor development as they possess large surface for target gas adsorption. The surface area of these materials depends upon the synthesis process, post treatment and functionalized groups attached with them [157, 158]. The adsorption of analyte molecules on the surface also depends upon the gas molecules binding energy. Also, if the diameter of the active site is less than gas molecules, the adsorption of molecules may not occur. Conductivity of graphene is very high because of its zero bandgap, making it easier to respond toward gases. Functional groups presence on material surface enhances the adsorption process since the intrinsic material lacks in active surface sites. They also the selectivity of the sensor improves by integrating functional group with sensing material [159, 160].

## 6 Conclusion

Flexible and stretchable sensors are the emerging and essential component of wearable electronics. Continuous advancements in flexible sensors are being carried out to compete and replace traditional rigid platform based sensor. Flexible sensors can work at room temperature and consumes less power which is essential parameter for designing wearable electronics. Novel nanostructured materials can boost the progress of flexible sensor. Materials such as graphene and TMDs have exceptional morphology, electron transport properties, and tunable bandgap are leading in the area of gas sensing technology with high sensitivity and selectivity. Graphene detection limit as reached the point of parts-per-billion and even approach are being started to reach parts-per-trillion limit. Chemical modification of graphene to increase the molecule adsorption sites can help in achieving ultralow detection limit. Graphene functionalized with metal NPs, metal oxide, TMDs, and polymers based sensor array will extend the detection limit and multiple selectivity of different molecules at the same time. Next-generation flexible functionalized graphene sensor expected to play a vital role field of bio absorbable sensors and wearable electronics.

## References

1. E. M. P. L. V. Gilder (1902) US730847A—Flexible electrical conductor. Google Patents
2. Ray KA (1967) Flexible solar cell arrays for increased space power. *IEEE Trans Aerosp Electron Syst* AES-3(1):107–115. <https://doi.org/10.1109/TAES.1967.5408720>
3. Peter Brody T (1984) The thin film transistor—a late flowering bloom. *IEEE Trans Electron Devices* 31(11):1614–1628. <https://doi.org/10.1109/T-ED.1984.21762>



4. Someya T, Sekitani T, Iba S, Kato Y, Kawaguchi H, Sakurai T (2004) A large-area, flexible pressure sensor matrix with organic field-effect transistors for artificial skin applications. *Proc Natl Acad Sci USA* 101(27):9966–9970. <https://doi.org/10.1073/pnas.0401918101>
5. Menard E, Lee KJ, Khang DY, Nuzzo RG, Rogers JA (2004) A printable form of silicon for high performance thin film transistors on plastic substrates. *Appl Phys Lett* 84(26):5398–5400. <https://doi.org/10.1063/1.1767591>
6. Cao Q et al (2008) Medium-scale carbon nanotube thin-film integrated circuits on flexible plastic substrates. *Nature* 454(7203):495–500. <https://doi.org/10.1038/nature07110>
7. Takei K et al (2010) Nanowire active-matrix circuitry for low-voltage macroscale artificial skin. *Nat Mater* 9(10):821–826. <https://doi.org/10.1038/nmat2835>
8. Mannsfeld SCB et al (2010) Highly sensitive flexible pressure sensors with microstructured rubber dielectric layers. *Nat Mater* 9(10):859–864. <https://doi.org/10.1038/nmat2834>
9. Harada S, Honda W, Arie T, Akita S, Takei K (2014) Fully printed, highly sensitive multi-functional artificial electronic whisker arrays integrated with strain and temperature sensors. *ACS Nano* 8(4):3921–3927. <https://doi.org/10.1021/nn500845a>
10. Huang Y et al (2015) Magnetic-assisted, self-healable, yarn-based supercapacitor. *ACS Nano* 9(6):6242–6251. <https://doi.org/10.1021/acsnano.5b01602>
11. Song Z et al (2015) Kirigami-based stretchable lithium-ion batteries. *Sci Rep* 5. <https://doi.org/10.1038/srep10988>
12. Parida K, Kumar V, Jiangxin W, Bhavanasi V, Bendi R, Lee PS (2017) Highly transparent, stretchable, and self-healing ionic-skin triboelectric nanogenerators for energy harvesting and touch applications. *Adv Mater* 29(37):1702181. <https://doi.org/10.1002/adma.201702181>
13. Ghosh SK, Mandal D (2017) Sustainable energy generation from piezoelectric biomaterial for noninvasive physiological signal monitoring. *ACS Sustain Chem Eng* 5(10):8836–8843. <https://doi.org/10.1021/acssuschemeng.7b01617>
14. Walters TR (1948) ‘terratex’—a thin flexible inorganic insulation. *IEEE Trans Am Inst Electr Eng* 67:123–127
15. Jian M et al (2017) Advanced carbon materials for flexible and wearable sensors. *Sci China Mater* 60(11):1026–1062. <https://doi.org/10.1007/s40843-017-9077-x>
16. Li S, Zhao H, Shepherd RF (2017) Flexible and stretchable sensors for fluidic elastomer actuated soft robots. *MRS Bull* 42(2):138–142. <https://doi.org/10.1557/mrs.2017.4>
17. Xu M, Qi J, Li F, Zhang Y (2018) Transparent and flexible tactile sensors based on graphene films designed for smart panels. *J Mater Sci* 53(13):9589–9597. <https://doi.org/10.1007/s10853-018-2216-5>
18. Xu H et al (2020) Flexible waterproof piezoresistive pressure sensors with wide linear working range based on conductive fabrics. *Nano-Micro Lett* 12(1):1–13. <https://doi.org/10.1007/s40820-020-00498-y>
19. Crabb RL, Treble FC (1967) © 1967 Nature Publishing Group. *Nat Publ Gr* 216:1223–1224
20. Konagai M, Sugimoto M, Takahashi K (1978) High efficiency GaAs thin film solar cells by peeled film technology. *J Cryst Growth* 45(C):277–280. [https://doi.org/10.1016/0022-0248\(78\)90449-9](https://doi.org/10.1016/0022-0248(78)90449-9)
21. White HS, Kittlesen GP, Wrighton MS (1984) Chemical derivatization of an array of three gold microelectrodes with polypyrrole: fabrication of a molecule-based transistor. *J Am Chem Soc* 106(18):5375–5377. <https://doi.org/10.1021/ja00330a070>
22. Tang CW, Vanslyke SA (1987) Organic electroluminescent diodes. *Appl Phys Lett* 51(12):913–915. <https://doi.org/10.1063/1.98799>
23. Gustafsson G, Cao Y, Treacy GM, Klavetter F, Colaneri N, Heeger AJ (1992) Flexible light-emitting diodes made from soluble conducting polymers. *Nature* 357(6378):477–479. <https://doi.org/10.1038/357477a0>
24. Wu CC et al (1997) Integration of organic LED’s and amorphous Si TFT’s onto flexible and lightweight metal foil substrates. *IEEE Electron Device Lett* 18(12):609–612. <https://doi.org/10.1109/55.644086>
25. Rogers JA et al (2001) Paper-like electronic displays: large-area rubber-stamped plastic sheets of electronics and microencapsulated electrophoretic inks. *Proc Natl Acad Sci USA* 98(9):4835–4840. <https://doi.org/10.1073/pnas.091588098>

26. Zardetto V, Brown TM, Reale A, Di Carlo A (2011) Substrates for flexible electronics: a practical investigation on the electrical, film flexibility, optical, temperature, and solvent resistance properties. *J Polym Sci Part B Polym Phys* 49(9):638–648. <https://doi.org/10.1002/polb.22227>
27. Briand D, Oprea A, Courbat J, Bărsan N (2011) Making environmental sensors on plastic foil. *Mater Today* 14(9):416–423. [https://doi.org/10.1016/S1369-7021\(11\)70186-9](https://doi.org/10.1016/S1369-7021(11)70186-9)
28. Alrammouz R, Podlecki J, Abboud P, Sorli B, Habchi R (2018) A review on flexible gas sensors: from materials to devices. *Sens Actuators A Phys* 284:209–231. <https://doi.org/10.1016/j.sna.2018.10.036>
29. Baeg KJ, Lee J (2020) Flexible electronic systems on plastic substrates and textiles for smart wearable technologies. *Adv Mater Technol* 5(7):2000071. <https://doi.org/10.1002/admt.202000071>
30. Sapsanis C et al (2016) A nafion coated capacitive humidity sensor on a flexible PET substrate. In: *Midwest symposium on circuits and systems*, vol 0. <https://doi.org/10.1109/MWSCAS.2016.7870020>
31. Shan S et al (2014) Flexibility characteristics of a polyethylene terephthalate chemiresistor coated with a nanoparticle thin film assembly. *J Mater Chem C* 2(10):1893–1903. <https://doi.org/10.1039/c3tc32332c>
32. Yun SO et al (2017) Flexible pH sensor and system fabricated using PET film. In: *Proceedings of IEEE sensors*, vol 2017, pp 1–3. <https://doi.org/10.1109/ICSENS.2017.8233925>
33. de Araujo Andreotti IA et al (2019) Disposable and flexible electrochemical sensor made by recyclable material and low cost conductive ink. *J Electroanal Chem* 840:109–116. <https://doi.org/10.1016/j.jelechem.2019.03.059>
34. Akiyama M et al (2006) Flexible piezoelectric pressure sensors using oriented aluminum nitride thin films prepared on polyethylene terephthalate films. *J Appl Phys* 100(11):114318. <https://doi.org/10.1063/1.2401312>
35. Khan SM, Nassar JM, Hussain MM (2021) Paper as a substrate and an active material in paper electronics. *ACS Appl Electron Mater* 3(1):30–52. <https://doi.org/10.1021/acsaelm.0c00484>
36. Shafiee H et al (2015) Paper and flexible substrates as materials for biosensing platforms to detect multiple biotargets. *Sci Rep* 5(1):1–9. <https://doi.org/10.1038/srep08719>
37. Yang G, Lee C, Kim J, Ren F, Pearton SJ (2013) Flexible graphene-based chemical sensors on paper substrates. *Phys Chem Chem Phys* 15(6):1798–1801. <https://doi.org/10.1039/c2cp43717a>
38. Hassinen J et al (2013) Low-cost reduced graphene oxide-based conductometric nitrogen dioxide-sensitive sensor on paper. *Anal Bioanal Chem* 405(11):3611–3617. <https://doi.org/10.1007/s00216-013-6805-5>
39. Sarfraz J, Ihalainen P, Määttänen A, Peltonen J, Lindén M (2013) Printed hydrogen sulfide gas sensor on paper substrate based on polyaniline composite. *Thin Solid Films* 534:621–628. <https://doi.org/10.1016/j.tsf.2013.02.055>
40. Song P, Wang YH, Liu X (2017) Flexible physical sensors made from Paper substrates integrated with zinc oxide nanostructures. *Flex Print Electron* 2(3):034001. <https://doi.org/10.1088/2058-8585/aa765d>
41. Armitage BI, Murugappan K, Lefferts MJ, Cowsik A, Castell MR (2020) Conducting polymer percolation gas sensor on a flexible substrate. *J Mater Chem C* 8(36):12669–12676. <https://doi.org/10.1039/d0tc02856h>
42. Schmucker AL, Tadepalli S, Liu KK, Sullivan CJ, Singamaneni S, Naik RR (2016) Plasmonic paper: a porous and flexible substrate enabling nanoparticle-based combinatorial chemistry. *RSC Adv* 6(5):4136–4144. <https://doi.org/10.1039/c5ra21977a>
43. Jang W, Byun H, Kim JH (2020) Rapid preparation of paper-based plasmonic platforms for SERS applications. *Mater Chem Phys* 240:122124. <https://doi.org/10.1016/j.matchemphys.2019.122124>
44. Rodríguez-Sevilla E, Vázquez GV, Morales-Narváez E (2018) Simple, flexible, and ultrastable surface enhanced Raman scattering substrate based on plasmonic nanopaper decorated with graphene oxide. *Adv Opt Mater* 6(19):1800548. <https://doi.org/10.1002/adom.201800548>

45. Gimpel S, Möhring U, Müller H, Neudeck A, Scheibner W (2004) Textile-based electronic substrate technology. *J Ind Text* 33(3):179–189. <https://doi.org/10.1177/1528083704039828>
46. Oh KW, Kim SH, Kim EA (2001) Improved surface characteristics and the conductivity of polyaniline-nylon 6 fabrics by plasma treatment. *J Appl Polym Sci* 81(3):684–694. <https://doi.org/10.1002/app.1485>
47. Kim SH, Seong JH, Oh KW (2002) Effect of dopant mixture on the conductivity and thermal stability of polyaniline/nomex conductive fabric. *J Appl Polym Sci* 83(10):2245–2254. <https://doi.org/10.1002/app.10211>
48. Han JW, Kim B, Li J, Meyyappan M (2013) A carbon nanotube based ammonia sensor on cotton textile. *Appl Phys Lett* 102(19):193104. <https://doi.org/10.1063/1.4805025>
49. Mattana G et al (2013) Woven temperature and humidity sensors on flexible plastic substrates for e-textile applications. *IEEE Sens J* 13(10):3901–3909. <https://doi.org/10.1109/JSEN.2013.2257167>
50. Wicaksono I et al (2020) A tailored, electronic textile conformable suit for large-scale spatiotemporal physiological sensing in vivo. *Electron* 4(1):1–13. <https://doi.org/10.1038/s41528-020-0068-y>
51. Lü R et al (2013) Alumina decorated TiO<sub>2</sub> nanotubes with ordered mesoporous walls as high sensitivity NO<sub>x</sub> gas sensors at room temperature. *Nanoscale* 5(18):8569–8576. <https://doi.org/10.1039/c3nr01903a>
52. Liu J et al (2018) Hydrogenated TiO<sub>2</sub> nanosheet based flowerlike architectures: enhanced sensing performances and sensing mechanism. *J Alloys Compd* 749:543–555. <https://doi.org/10.1016/j.jallcom.2018.03.190>
53. Umar A, Alshahrani AA, Algarni H, Kumar R (2017) CuO nanosheets as potential scaffolds for gas sensing applications. *Sens Actuators, B Chem* 250:24–31. <https://doi.org/10.1016/j.snb.2017.04.062>
54. Kim H, Jin C, Park S, Kim S, Lee C (2012) H<sub>2</sub>S gas sensing properties of bare and Pd-functionalized CuO nanorods. *Sens Actuators B Chem* 161(1):594–599. <https://doi.org/10.1016/j.snb.2011.11.006>
55. Li T, Zeng W, Long H, Wang Z (2016) Nanosheet-assembled hierarchical SnO<sub>2</sub> nanostructures for efficient gas-sensing applications. *Sens Actuators, B Chem* 231:120–128. <https://doi.org/10.1016/j.snb.2016.03.003>
56. Zhu L, Zeng W, Li Y, Yang J (2019) Enhanced ethanol gas-sensing property based on hollow MoO<sub>3</sub> microcages. *Phys E Low-Dimen Syst Nanostruct* 106:170–175. <https://doi.org/10.1016/j.physe.2018.10.038>
57. Jiménez-Cadena G, Riu J, Rius FX (2007) Gas sensors based on nanostructured materials. *Analyst* 132(11):1083–1099. <https://doi.org/10.1039/b704562j>
58. Barsan N, Weimar U (2001) Conduction model of metal oxide gas sensors. *J Electroceramics* 7(3):143–167. <https://doi.org/10.1023/A:1014405811371>
59. Zhu L, Zeng W, Li Y (2019) A non-oxygen adsorption mechanism for hydrogen detection of nanostructured SnO<sub>2</sub> based sensors. *Mater Res Bull* 109:108–116. <https://doi.org/10.1016/j.materresbull.2018.09.033>
60. Wu M, Wu Z, Jin X, Lee JH (2020) A highly sensitive FET-type humidity sensor with inkjet-printed Pt-In<sub>2</sub>O<sub>3</sub> nanoparticles at room temperature. *Nanoscale Res Lett* 15(1):1–8. <https://doi.org/10.1186/s11671-020-03426-6>
61. Wang L et al (2015) Spontaneous formation of Cu<sub>2</sub>O-g-C<sub>3</sub>N<sub>4</sub> core-shell nanowires for photocurrent and humidity responses. *Nanoscale* 7(21):9694–9702. <https://doi.org/10.1039/c5nr01521a>
62. Wang M, Hou T, Shen Z, Zhao X, Ji H (2019) MOF-derived Fe<sub>2</sub>O<sub>3</sub>: phase control and effects of phase composition on gas sensing performance. *Sens Actuators B Chem* 292:171–179. <https://doi.org/10.1016/j.snb.2019.04.124>
63. Ming J, Wu Y, Wang L, Yu Y, Zhao F (2011) CO<sub>2</sub>-assisted template synthesis of porous hollow bi-phase  $\gamma$ -/ $\alpha$ -Fe<sub>2</sub>O<sub>3</sub> nanoparticles with high sensor property. *J Mater Chem* 21(44):17776–17782. <https://doi.org/10.1039/c1jm12879e>

64. Williams DE, Henshaw GS, Pratt KFE, Peat R (1995) Reaction-diffusion effects and systematic design of gas-sensitive resistors based on semiconducting oxides. *J Chem Soc Faraday Trans 91*(23):4299–4307. <https://doi.org/10.1039/FT9959104299>
65. Mohammad-Yousefi S, Rahbarpour S, Ghafoorifard H (2019) Describing the effect of Ag/Au modification on operating temperature and gas sensing properties of thick film SnO<sub>2</sub> gas sensors by gas diffusion theory. *Mater Chem Phys* 227:148–156. <https://doi.org/10.1016/j.matchemphys.2019.02.010>
66. Yang S et al (2017) Remarkably accelerated room-temperature hydrogen sensing of MoO<sub>3</sub> nanoribbon/graphene composites by suppressing the nanojunction effects. *Sens Actuators, B Chem* 248:160–168. <https://doi.org/10.1016/j.snb.2017.03.106>
67. Ge L, Mu X, Tian G, Huang Q, Ahmed J, Hu Z (2019) Current applications of gas sensor based on 2-D nanomaterial: a mini review. *Front Chem* 7:839. <https://doi.org/10.3389/fchem.2019.00839>
68. Wang T et al (2016) A review on graphene-based gas/vapor sensors with unique properties and potential applications. *Nano-Micro Letters* 8(2):95–119. <https://doi.org/10.1007/s40820-015-0073-1>
69. Fraga CG, Melville AM, Wright BW (2007) ROC-curve approach for determining the detection limit of a field chemical sensor. *Analyst* 132(3):230–236. <https://doi.org/10.1039/b607843e>
70. Xu H, Liu J, Zhang J, Zhou G, Luo N, Zhao N (2017) Flexible organic/inorganic hybrid near-infrared photoplethysmogram sensor for cardiovascular monitoring. *Adv Mater* 29(31):1700975. <https://doi.org/10.1002/adma.201700975>
71. Im HG et al (2014) Flexible transparent conducting hybrid film using a surface-embedded copper nanowire network: a highly oxidation-resistant copper nanowire electrode for flexible optoelectronics. *ACS Nano* 8(10):10973–10979. <https://doi.org/10.1021/nn504883m>
72. Gong S et al (2016) Fabrication of highly transparent and flexible nanomesh electrode via self-assembly of ultrathin gold nanowires. *Adv Electron Mater* 2(7):1600121. <https://doi.org/10.1002/aelm.201600121>
73. Lee W et al (2017) Transparent, conformable, active multielectrode array using organic electrochemical transistors. *Proc Natl Acad Sci USA* 114(40):10554–10559. <https://doi.org/10.1073/pnas.1703886114>
74. Chung WH, Kim SH, Kim HS (2016) Welding of silver nanowire networks via flash white light and UV-C irradiation for highly conductive and reliable transparent electrodes. *Sci Rep* 6(1):1–11. <https://doi.org/10.1038/srep32086>
75. Maurer JHM, González-García L, Reiser B, Kanelidis I, Kraus T (2016) Templated self-assembly of ultrathin gold nanowires by nanoimprinting for transparent flexible electronics. *Nano Lett* 16(5):2921–2925. <https://doi.org/10.1021/acs.nanolett.5b04319>
76. Dickey MD, Chiechi RC, Larsen RJ, Weiss EA, Weitz DA, Whitesides GM (2008) Eutectic gallium-indium (EGaIn): a liquid metal alloy for the formation of stable structures in microchannels at room temperature. *Adv Funct Mater* 18(7):1097–1104. <https://doi.org/10.1002/adfm.200701216>
77. Jiang C, Zhang G, Wu Y, Li L, Shi K (2012) Facile synthesis of SnO<sub>2</sub> nanocrystalline tubes by electrospinning and their fast response and high sensitivity to NO<sub>x</sub> at room temperature. *CrystEngComm* 14(8):2739–2747. <https://doi.org/10.1039/c2ce06405g>
78. Wang Y, Jiang X, Xia Y (2003) A solution-phase, precursor route to polycrystalline SnO<sub>2</sub> nanowires that can be used for gas sensing under ambient conditions. *J Am Chem Soc* 125(52):16176–16177. <https://doi.org/10.1021/ja037743f>
79. Khun Khun K, Mahajan A, Bedi RK (2009) SnO<sub>2</sub> thick films for room temperature gas sensing applications. *J Appl Phys* 106(12):124509. <https://doi.org/10.1063/1.3273323>
80. Wang J, Wei L, Zhang L, Jiang C, Siu-Wai Kong E, Zhang Y (2012) Preparation of high aspect ratio nickel oxide nanowires and their gas sensing devices with fast response and high sensitivity. *J Mater Chem* 22(17):8327–8335. <https://doi.org/10.1039/c2jm16934g>
81. Li Z et al (2016) Room-temperature high-performance H<sub>2</sub>S sensor based on porous CuO nanosheets prepared by hydrothermal method. *ACS Appl Mater Interfaces* 8(32):20962–20968. <https://doi.org/10.1021/acsami.6b02893>

82. Bhuvaneshwari S, Papachan S, Gopalakrishnan N (2017) Free standing CuO-MnO<sub>2</sub> nanocomposite for room temperature ammonia sensing. *AIP Conf Proc* 1832(1):050126. <https://doi.org/10.1063/1.4980359>
83. Perfecto TM, Zito CA, Volanti DP (2017) Design of nanostructured WO<sub>3</sub>-0.33H<sub>2</sub>O: via combination of ultrasonic spray nozzle and microwave-assisted hydrothermal methods for enhancing isopropanol gas sensing at room temperature. *CrystEngComm* 19(20):2733–2738. <https://doi.org/10.1039/c7ce00523g>
84. Jaisutti R et al (2017) Ultrasensitive room-temperature operable gas sensors using p-type Na:ZnO nanoflowers for diabetes detection. *ACS Appl Mater Interfaces* 9(10):8796–8804. <https://doi.org/10.1021/acsami.7b00673>
85. Gao J et al (2016) Mesoporous In<sub>2</sub>O<sub>3</sub> nanocrystals: synthesis, characterization and NO<sub>x</sub> gas sensor at room temperature. *New J Chem* 40(2):1306–1311. <https://doi.org/10.1039/c5nj02214b>
86. Xue X, Xing L, Chen Y, Shi S, Wang Y, Wang T (2008) Synthesis and H<sub>2</sub>S sensing properties of CuO-SnO<sub>2</sub> core/shell PN-junction nanorods. *J Phys Chem C* 112(32):12157–12160. <https://doi.org/10.1021/jp8037818>
87. Ko KY et al (2016) Improvement of gas-sensing performance of large-area tungsten disulfide nanosheets by surface functionalization. *ACS Nano* 10(10):9287–9296. <https://doi.org/10.1021/acsnano.6b03631>
88. Kuru C et al (2016) High-performance flexible hydrogen sensor made of WS<sub>2</sub> nanosheet-Pd nanoparticle composite film. *Nanotechnology* 27(19):195501. <https://doi.org/10.1088/0957-4484/27/19/195501>
89. Qin Z et al (2017) 2D WS<sub>2</sub> nanosheets with TiO<sub>2</sub> quantum dots decoration for high-performance ammonia gas sensing at room temperature. *Sens Actuators B Chem* 253:1034–1042. <https://doi.org/10.1016/j.snb.2017.07.052>
90. Lee K, Gatensby R, McEvoy N, Hallam T, Duesberg GS (2013) High-performance sensors based on molybdenum disulfide thin films. *Adv Mater* 25(46):6699–6702. <https://doi.org/10.1002/adma.201303230>
91. Zhang D, Jiang C, Sun Y (2017) Room-temperature high-performance ammonia gas sensor based on layer-by-layer self-assembled molybdenum disulfide/zinc oxide nanocomposite film. *J Alloys Compd* 698:476–483. <https://doi.org/10.1016/j.jallcom.2016.12.222>
92. Cui S, Wen Z, Huang X, Chang J, Chen J (2015) Stabilizing MoS<sub>2</sub> nanosheets through SnO<sub>2</sub> nanocrystal decoration for high-performance gas sensing in air. *Small* 11(19):2305–2313. <https://doi.org/10.1002/sml.201402923>
93. Li X et al (2017) Reduced graphene oxide/MoS<sub>2</sub> hybrid films for room-temperature formaldehyde detection. *Mater Lett* 189:42–45. <https://doi.org/10.1016/j.matlet.2016.11.046>
94. Baek J et al (2017) A highly sensitive chemical gas detecting transistor based on highly crystalline CVD-grown MoSe<sub>2</sub> films. *Nano Res* 10(6):1861–1871. <https://doi.org/10.1007/s12274-016-1291-7>
95. Ou JZ et al (2015) Physisorption-based charge transfer in two-dimensional SnS<sub>2</sub> for selective and reversible NO<sub>2</sub> gas sensing. *ACS Nano* 9(10):10313–10323. <https://doi.org/10.1021/acs.nano.5b04343>
96. Zhang D, Wu J, Li P, Cao Y (2017) Room-temperature SO<sub>2</sub> gas-sensing properties based on a metal-doped MoS<sub>2</sub> nanoflower: an experimental and density functional theory investigation. *J Mater Chem A* 5(39):20666–20677. <https://doi.org/10.1039/c7ta07001b>
97. Tajik S et al (2020) Carbon and graphene quantum dots: a review on syntheses, characterization, biological and sensing applications for neurotransmitter determination. *RSC Adv* 10(26):15406–15429. <https://doi.org/10.1039/D0RA00799D>
98. Llobet E (2013) Gas sensors using carbon nanomaterials: a review. *Sens Actuators B Chem* 179:32–45. <https://doi.org/10.1016/J.SNB.2012.11.014>
99. Jiao Y, Zheng Y, Davey K, Qiao SZ (2016) Activity origin and catalyst design principles for electrocatalytic hydrogen evolution on heteroatom-doped grapheme. *Nat Energy* 2016 110, 1(10):1–9. <https://doi.org/10.1038/nenergy.2016.130>

100. Peng S, Cho K (2003) Ab initio study of doped carbon nanotube sensors. *Nano Lett* 3(4):513–517. <https://doi.org/10.1021/NL034064U>
101. Li F, Zhang YH, Han LF, Xiao YH, Jia DZ, Guo ZH (2013) Understanding dopant and defect effect on H<sub>2</sub>S sensing performances of graphene: a first-principles study. *Comput Mater Sci* 69:222–228. <https://doi.org/10.1016/j.commatsci.2012.11.048>
102. Yang W, Gan L, Li H, Zhai T (2016) Two-dimensional layered nanomaterials for gas-sensing applications. *Inorg Chem Front* 3(4):433–451. <https://doi.org/10.1039/c5qi00251f>
103. Liu S, Yu B, Zhang H, Fei T, Zhang T (2014) Enhancing NO<sub>2</sub> gas sensing performances at room temperature based on reduced graphene oxide-ZnO nanoparticles hybrids. *Sens Actuators, B Chem* 202:272–278. <https://doi.org/10.1016/j.snb.2014.05.086>
104. Roy N, Sinha R, Daniel TT, Nemade HB, Mandal TK (2020) Highly sensitive room temperature CO gas sensor based on MWCNT-PDDA composite. *IEEE Sens J* 20(22):13245–13252. <https://doi.org/10.1109/JSEN.2020.3004994>
105. Navazani S, Hassanijadi M, Eskandari MM, Talaei Z (2020) Design and evaluation of SnO<sub>2</sub>-Pt/MWCNTs hybrid system as room temperature-methane sensor. *Synth Met* 260:116267. <https://doi.org/10.1016/J.SYNTHMET.2019.116267>
106. Ha NH, Thinh DD, Huong NT, Phuong NH, Thach PD, Hong HS (2018) Fast response of carbon monoxide gas sensors using a highly porous network of ZnO nanoparticles decorated on 3D reduced graphene oxide. *Appl Surf Sci* 434:1048–1054. <https://doi.org/10.1016/J.APSUSC.2017.11.047>
107. John N, Abraham KE (2020) Enhancement in carbon monoxide sensing performance by reduced graphene oxide/trimanganese tetraoxide system. *Sens Actuators B Chem* 325:128749. <https://doi.org/10.1016/J.SNB.2020.128749>
108. Acharyya D, Bhattacharyya P (2016) Highly efficient room-temperature gas sensor based on TiO<sub>2</sub> nanotube-reduced graphene-oxide hybrid device. *IEEE Electron Device Lett* 37(5):656–659. <https://doi.org/10.1109/LED.2016.2544954>
109. Xue L, Wang W, Guo Y, Liu G, Wan P (2017) Flexible polyaniline/carbon nanotube nanocomposite film-based electronic gas sensors. *Sens Actuators B Chem* 244:47–53. <https://doi.org/10.1016/J.SNB.2016.12.064>
110. Wang R, Li G, Dong Y, Chi Y, Chen G (2013) Carbon quantum dot-functionalized aerogels for NO<sub>2</sub> gas sensing. *Anal Chem* 85(17):8065–8069. [https://doi.org/10.1021/AC401880H/SUPPL\\_FILE/AC401880H\\_SI\\_001.PDF](https://doi.org/10.1021/AC401880H/SUPPL_FILE/AC401880H_SI_001.PDF)
111. Yoon HJ, Jun DH, Yang JH, Zhou Z, Yang SS, Cheng MMC (2011) Carbon dioxide gas sensor using a graphene sheet. *Sens Actuators, B Chem* 157(1):310–313. <https://doi.org/10.1016/j.snb.2011.03.035>
112. Ghosh R, Midya A, Santra S, Ray SK, Guha PK (2013) Chemically reduced graphene oxide for ammonia detection at room temperature. *ACS Appl Mater Interfaces* 5(15):7599–7603. <https://doi.org/10.1021/am4019109>
113. Kumar R, Avasthi DK, Kaur A (2017) Fabrication of chemiresistive gas sensors based on multistep reduced graphene oxide for low parts per million monitoring of sulfur dioxide at room temperature. *Sens Actuators, B Chem* 242:461–468. <https://doi.org/10.1016/j.snb.2016.11.018>
114. Huang L et al (2014) Fully printed, rapid-response sensors based on chemically modified graphene for detecting NO<sub>2</sub> at room temperature. *ACS Appl Mater Interfaces* 6(10):7426–7433. <https://doi.org/10.1021/am500843p>
115. Zhang D, Liu A, Chang H, Xia B (2015) Room-temperature high-performance acetone gas sensor based on hydrothermal synthesized SnO<sub>2</sub>-reduced graphene oxide hybrid composite. *RSC Adv* 5(4):3016–3022. <https://doi.org/10.1039/c4ra10942b>
116. Zhang D, Liu J, Jiang C, Liu A, Xia B (2017) Quantitative detection of formaldehyde and ammonia gas via metal oxide-modified graphene-based sensor array combining with neural network model. *Sens Actuators, B Chem* 240:55–65. <https://doi.org/10.1016/j.snb.2016.08.085>
117. Xia Y et al (2016) Confined formation of ultrathin ZnO nanorods/reduced graphene oxide mesoporous nanocomposites for high-performance room-temperature NO<sub>2</sub> sensors. *ACS Appl Mater Interfaces* 8(51):35454–35463. <https://doi.org/10.1021/acsami.6b12501>

118. Su PG, Peng SL (2015) Fabrication and NO<sub>2</sub> gas-sensing properties of reduced graphene oxide/WO<sub>3</sub> nanocomposite films. *Talanta* 132:398–405. <https://doi.org/10.1016/j.talanta.2014.09.034>
119. Zhang J et al (2015) Room temperature NO<sub>2</sub> sensing: What advantage does the rGO–NiO nanocomposite have over pristine NiO? *Phys Chem Chem Phys* 17(22):14903–14911. <https://doi.org/10.1039/c5cp01987g>
120. Gu F, Nie R, Han D, Wang Z (2015) In<sub>2</sub>O<sub>3</sub>-graphene nanocomposite based gas sensor for selective detection of NO<sub>2</sub> at room temperature. *Sens Actuators B Chem* 219:94–99. <https://doi.org/10.1016/j.snb.2015.04.119>
121. Li F et al (2019) Highly sensitive, selective, and flexible NO<sub>2</sub> chemiresistors based on multilevel structured three-dimensional reduced graphene oxide fiber scaffold modified with aminoanthroquinone moieties and Ag nanoparticles. *ACS Appl Mater Interfaces* 11(9):9309–9316. <https://doi.org/10.1021/acsami.8b20462>
122. Park SJ, Kwon OS, Lee SH, Song HS, Park TH, Jang J (2012) Ultrasensitive flexible graphene based field-effect transistor (FET)-type bioelectronic nose. *Nano Lett* 12(10):5082–5090. <https://doi.org/10.1021/nl301714x>
123. Noroozi AA, Abdi Y (2019) A graphene/Si Schottky diode for the highly sensitive detection of protein. *RSC Adv* 9(34):19613–19619. <https://doi.org/10.1039/c9ra03765a>
124. Okuda S et al (2018) Graphene surface acoustic wave sensor for simultaneous detection of charge and mass. *ACS Sensors* 3(1):200–204. <https://doi.org/10.1021/acssensors.7b00851>
125. Xu Y et al (2014) Holey graphene frameworks for highly efficient capacitive energy storage. *Nat Commun* 5(1):1–8. <https://doi.org/10.1038/ncomms5554>
126. Chai Y, Li Z, Wang J, Mo Z, Yang S (2019) Construction of hierarchical holey graphene/MnO<sub>2</sub> composites as potential electrode materials for supercapacitors. *J Alloys Compd* 775:1206–1212. <https://doi.org/10.1016/j.jallcom.2018.10.259>
127. Zhou H, Zhang J, Zhu J, Liu Z, Zhang C, Mu S (2016) A self-template and KOH activation co-coupling strategy to synthesize ultrahigh surface area nitrogen-doped porous graphene for oxygen reduction. *RSC Adv* 6(77):73292–73300. <https://doi.org/10.1039/c6ra16703a>
128. Wan J et al (2018) Microwave combustion for rapidly synthesizing pore-size-controllable porous graphene. *Adv Funct Mater* 28(22):1800382. <https://doi.org/10.1002/adfm.201800382>
129. Fan Z et al (2012) Easy synthesis of porous graphene nanosheets and their use in supercapacitors. *Carbon* 50(4):1699–1703. <https://doi.org/10.1016/j.carbon.2011.12.016>
130. Ma C, Zhao Y, Li Y (2017) A facile solution-free etching preparation of porous graphene nanosheets with high performances for lithium storage. *Chem Eng J* 320:283–289. <https://doi.org/10.1016/j.cej.2017.03.049>
131. Zhou L, Wang Y, Tang J, Li J, Wang S, Wang Y (2017) Facile synthesis of holey graphene-supported Pt catalysts for direct methanol electro-oxidation. *Microporous Mesoporous Mater* 247:116–123. <https://doi.org/10.1016/j.micromeso.2017.03.061>
132. Tan S, Wang J, Han Q, Liang Q, Ding M (2018) A porous graphene sorbent coated with titanium(IV)-functionalized polydopamine for selective lab-in-syringe extraction of phosphoproteins and phosphopeptides. *Microchim Acta* 185(7):1–10. <https://doi.org/10.1007/s00604-018-2846-y>
133. Xu P et al (2019) A high surface area N-doped holey graphene aerogel with low charge transfer resistance as high performance electrode of non-flammable thermostable supercapacitor. *Carbon NY* 149:452–461. <https://doi.org/10.1016/j.carbon.2019.04.070>
134. Pang Y et al (2016) Flexible, highly sensitive, and wearable pressure and strain sensors with graphene porous network structure. *ACS Appl Mater Interfaces* 8(40):26458–26462. <https://doi.org/10.1021/acsami.6b08172>
135. Lu AK, Li HY, Yu Y (2019) Holey graphene synthesized by electrochemical exfoliation for high-performance flexible microsupercapacitors. *J Mater Chem A* 7(13):7852–7858. <https://doi.org/10.1039/C9TA00792J>
136. Li Z et al (2018) Combustion fabrication of nanoporous graphene for ionic separation membranes. *Adv Funct Mater* 28(43):1805026. <https://doi.org/10.1002/adfm.201805026>

137. Dua V et al (2010) All-organic vapor sensor using inkjet-printed reduced graphene oxide. *Angew Chemie Int Ed* 49(12):2154–2157. <https://doi.org/10.1002/anie.200905089>
138. Su PG, Shieh HC (2014) Flexible NO<sub>2</sub> sensors fabricated by layer-by-layer covalent anchoring and in situ reduction of graphene oxide. *Sens Actuators B Chem* 190:865–872. <https://doi.org/10.1016/j.snb.2013.09.078>
139. Ghosh R, Singh A, Santra S, Ray SK, Chandra A, Guha PK (2014) Highly sensitive large-area multi-layered graphene-based flexible ammonia sensor. *Sens Actuators B Chem* 205:67–73. <https://doi.org/10.1016/j.snb.2014.08.044>
140. Seekaew Y, Lokavee S, Phokharatkul D, Wisitsoraat A, Kerdcharoen T, Wongchoosuk C (2014) Low-cost and flexible printed graphene-PEDOT: PSS gas sensor for ammonia detection. *Org Electron* 15(11):2971–2981. <https://doi.org/10.1016/j.orgel.2014.08.044>
141. Gupta Chatterjee S, Chatterjee S, Ray AK, Chakraborty AK (2015) Graphene-metal oxide nanohybrids for toxic gas sensor: a review. *Sens Actuators, B: Chem* 221:1170–1181. <https://doi.org/10.1016/j.snb.2015.07.070>
142. Georgakilas V et al (2012) Functionalization of graphene: covalent and non-covalent approaches, derivatives and applications. *Chem Rev* 112(11):6156–6214. <https://doi.org/10.1021/cr3000412>
143. Midya A, Ghosh R, Santra S, Ray SK, Guha PK (2016) Reduced graphene oxide-rose bengal hybrid film for improved ammonia detection with low humidity interference at room temperature. *Mater Res Express* 3(2):025101. <https://doi.org/10.1088/2053-1591/3/2/025101>
144. Mackin C et al (2018) Chemiresistive graphene sensors for ammonia detection. *ACS Appl Mater Interfaces* 10(18):16169–16176. <https://doi.org/10.1021/acsami.8b00853>
145. Pyo S, Choi J, Kim J (2019) Improved photo- and chemical-responses of graphene via porphyrin-functionalization for flexible, transparent, and sensitive sensors. *Nanotechnology* 30(21):215501. <https://doi.org/10.1088/1361-6528/ab048d>
146. Yoon T et al (2018) An ultra-sensitive, flexible and transparent gas detection film based on well-ordered flat polypyrrole on single-layered graphene. *J Mater Chem A* 6(5):2257–2263. <https://doi.org/10.1039/c7ta10019a>
147. Cui S, Mao S, Wen Z, Chang J, Zhang Y, Chen J (2013) Controllable synthesis of silver nanoparticle-decorated reduced graphene oxide hybrids for ammonia detection. *Analyst* 138(10):2877–2882. <https://doi.org/10.1039/c3an36922f>
148. Karaduman I, Er E, Çelikkhan H, Erk N, Acar S (2017) Room-temperature ammonia gas sensor based on reduced graphene oxide nanocomposites decorated by Ag, Au and Pt nanoparticles. *J Alloys Compd* 722:569–578. <https://doi.org/10.1016/j.jallcom.2017.06.152>
149. Kumar R, Kushwaha N, Mittal J (2017) Superior, rapid and reversible sensing activity of graphene-SnO hybrid film for low concentration of ammonia at room temperature. *Sens Actuators, B Chem* 244:243–251. <https://doi.org/10.1016/j.snb.2016.12.111>
150. Kodu M et al (2019) Graphene-based ammonia sensors functionalised with sub-monolayer V<sub>2</sub>O<sub>5</sub>: a comparative study of chemical vapour deposited and epitaxial graphene. *Sensors (Switzerland)* 19(4):9–12. <https://doi.org/10.3390/s19040951>
151. Niu Y et al (2015) MoS<sub>2</sub> graphene fiber based gas sensing devices. *Carbon NY* 95:34–41. <https://doi.org/10.1016/j.carbon.2015.08.002>
152. Zhou Y, Liu G, Zhu X, Guo Y (2017) Ultrasensitive NO<sub>2</sub> gas sensing based on rGO/MoS<sub>2</sub> nanocomposite film at low temperature. *Sens Actuators, B Chem* 251:280–290. <https://doi.org/10.1016/j.snb.2017.05.060>
153. Yan W, Worsley MA, Pham T, Zettl A, Carraro C, Maboudian R (2018) Effects of ambient humidity and temperature on the NO<sub>2</sub> sensing characteristics of WS<sub>2</sub>/graphene aerogel. *Appl Surf Sci* 450:372–379. <https://doi.org/10.1016/j.apsusc.2018.04.185>
154. Zhou X, Wang X, Wang B, Chen Z, He C, Wu Y (2014) Preparation, characterization and NH<sub>3</sub>-sensing properties of reduced graphene oxide/copper phthalocyanine hybrid material. *Sens Actuators, B Chem* 193:340–348. <https://doi.org/10.1016/j.snb.2013.11.090>
155. Wang B, Wang X, Li X, Guo Z, Zhou X, Wu Y (2018) The effects of amino substituents on the enhanced ammonia sensing performance of PcCo/rGO hybrids. *RSC Adv* 8(72):41280–41287. <https://doi.org/10.1039/C8RA07509C>



156. Jia R, Xie P, Feng Y, Chen Z, Umar A, Wang Y (2018) Dipole-modified graphene with ultrahigh gas sensibility. *Appl Surf Sci* 440:409–414. <https://doi.org/10.1016/j.apsusc.2018.01.166>
157. Dariyal P, Sharma S, Singh Chauhan G, Pratap Singh B, Dhakate SR (2021) Recent trends in gas sensing via carbon nanomaterials: outlook and challenges. *Nanoscale Adv*. <https://doi.org/10.1039/D1NA00707F>
158. Li W et al (2012) Low-cost synthesis of graphitic carbon nanofibers as excellent room temperature sensors for explosive gases. *J Mater Chem* 22(30):15342–15347. <https://doi.org/10.1039/C2JM32031B>
159. Wu J et al (2020) Three-Dimensional graphene hydrogel decorated with SnO<sub>2</sub> for high-performance NO<sub>2</sub> sensing with enhanced immunity to humidity. *ACS Appl Mater Interfaces* 12(2):2634–2643. [https://doi.org/10.1021/ACSAMI.9B18098/SUPPL\\_FILE/AM9B18098\\_SI\\_001.PDF](https://doi.org/10.1021/ACSAMI.9B18098/SUPPL_FILE/AM9B18098_SI_001.PDF)
160. Lin T, Lv X, Li S, Wang Q (2017) The morphologies of the semiconductor oxides and their gas-sensing properties. *Sensors* 17(12):2779. <https://doi.org/10.3390/S17122779>

**Part V**  
**Device Engineering and Technology**  
**Sensing**

# Chapter 17

## Biomedical Application of Porous Carbon and Its Future in Precision Medical Devices



Sabyasachi Choudhuri and Jyotirmoy Panda

### 1 Introduction

Carbon is one of the fascinating elements that have revolutionised science for many years. It can be found in most organic and inorganic compounds all over the planet. It is an important component in many rock formations, such as calcareous and marble. It can be found all over the world in its allotropic types of diamond, graphite, and amorphous carbon. Carbon is also present in numerous substances in the earth's atmosphere, including carbon dioxide and in oceans and in other large water bodies. Carbon-containing hydrocarbons make up multiple fuels, such as coal, gas, and oil. Carbon is present in forms of life. It accounts for much of the mass of the human body.

Carbon materials have superior properties and can be used in a wide range of manufacturing applications. It is used to produce the carbon fibres which are strongest among others, the best electric conduction materials, i.e., graphite electrodes, solid lubricants, i.e., graphite, an impermeable non-crystalline material, i.e., vitreous carbon, best porous absorbers, i.e., activated carbon, the hardest material present on earth, which is diamond and the most impressive material, the fullerenes [1]. Each of these types is produced by selecting raw materials and processing them using modern manufacturing techniques.

Porous carbon (PC) is a processed carbon type that contains tiny pores of low volume which increase the available surface area for chemical reactions or adsorption. Porous carbon materials (PCMs) are mostly classified into microporous where pores are less than 2 nm, mesoporous where pores are between 2 and 50 nm and macroporous where pores are greater than 50 nm. Porous materials are called uniform

---

S. Choudhuri (✉) · J. Panda

Department of Pharmaceutical Science and Technology, Maulana Abul Kalam Azad University of Technology, West Bengal, Kolkata, India  
e-mail: [sabya1997@gmail.com](mailto:sabya1997@gmail.com)

because they are narrow in size compared with a broad pore-size distribution. The pores may be of cylindrical, conical, or slit form. In contrast to the random network of tortuous pores, they can be well-organised with vertical orientation. PCM may be made up of either one kind of porous system, a mixture of two kinds, or all three types of pores. A combination of porous materials made up of a variety of porous systems that work together to form an integrated porous system is called hierarchically porous materials [2]. Furthermore, the form, scale and position of the current single porous system or a mixture of porous systems could be ordered or disordered. PCM can be made in one of two ways: nanocasting, which uses a hard template to make up the carbon structure, or direct synthesis, which uses a soft template. Zeolite and silica are the most common hard templates used in the nanocasting process. The carbon precursor contains such hard template materials. The porous structure is created by carbonisation followed by the elimination of the template. The zeolite template creates microporous carbon, while the silica template creates mesoporous or macroporous carbon. The resulting PCM may have all three porous systems [3]. Direct synthesis entails synthesis of the PCM with sol-gel synthesis where a soft template with a carbon precursor and a polymeriser generates a porous matrix, essentially a polymer/surfactant. PCMs are produced from naturally accessible materials, such as coconut husks, husks of paddy, tea wastage, etc., are also available as cheap materials in addition to these PCMs synthesised by the above-listed processes. Due to their high efficiency in a broad range of applications, PCMs are promising candidates in the field of material science. Their unique physicochemical and biological properties include large surfaces and large pore volumes with adjustable pores, the presence of favourable functional groups, including an easily modifiable surface and  $\pi$ - $\pi$  stacking, high thermal conversion capability, unique visual properties, very high biocompatibility and high mechanical stability and chemical inertness have given them a great deal of attention [4, 5]. PCM is used in many applications, not only for supercapacitors and electrical applications, catalytic supports and pollutant adsorbents but also in the biomedical field.

Among the inorganic nanoparticles, carbon-based nanomaterials such as fullerene, graphene, CDs and CNT have gained widespread interest for their excellent potential in biomedical fields such as the delivery of drugs, chemo-photothermal synergic treatment, gene transfection and in vivo real-time imaging [6, 7] due to their distinct physicochemical properties. For example, within the near-infrared (NIR) region, carbon nanotubes [8] and graphene [9] have ideal photothermal conversion potential and could be researched as photothermal candidates for synergistic operation. Fortunately, preclinical biodistribution, biocompatibility and hemocompatibility trials have shown that these carbon nanomaterials are non-toxic and biocompatible at appropriate doses [10].

CNT biosensors are used because they can resolve some of the drawbacks of traditional electrochemical biosensors, such as low sensitivity and durability, long reaction times and low reproducibility [11].

The high surface area of activated carbon (AC) is used in the fabrication of electrodes used in biosensors, allowing immobilisation of enzymes necessary for sensing

the compound of interest and facilitating electron transfer between the electrode and the substrate [12].

Foley et al. used fluorescence microscopy and radioactive labelling to show that a water-soluble fullerene derivative,  $C_{61}(COOH)_2$ , can cross the cell membrane and bind to mitochondria preferentially [13]. This is similar to the structural comparison between the fullerene cage and clathrin-coated vesicles, which can be used to transfer drugs to organelles.

The widespread use of biomaterials in biomedical applications is regarded as an important revolution that came in recent decades. Due to their well-known inherent characteristics such as biocompatibility, non-toxicity and biodegradability, oil-based polymer materials were eventually replaced by natural or synthetic biopolymers. The addition of porosity to a biomaterial expands the range of possible applications. Furthermore, increased porosity can be advantageous for applications that depend on their exceptional ability to load, maintain and release fluids. The biopolymer matrix must have a specific set of pore characteristics for each use.

The biomedical applications of such PCM are summarised in this chapter. The nanoporous carbon metal–organic structure and carbon quantum dots are potential contenders for biomedical applications to be improved and established in future.

## 2 Various Biomedical Applications of Porous Carbon Materials

Nanotechnology's recent advancements have provided highly efficient and versatile treatment options for many disorders in the body, resulting in improved therapeutic efficacy and fewer side effects. The development of nanomaterial-based drug delivery systems (DDSs) holds a lot of promise for bringing nanotechnology to the clinic and benefiting numerous patients.

Among the category of porous carbon nanomaterial, mesoporous carbon nanomaterial (MCN) has shown most evidently superior quality as it contains both mesopore formation and carbonaceous components, due to these characteristics features MCNs and other carbon-derived materials such as carbon nanotubes, AC, graphene, carbon dots and fullerene having advantageous position over any other inorganic nanomaterial [4].

### 2.1 Mesoporous Carbon Materials

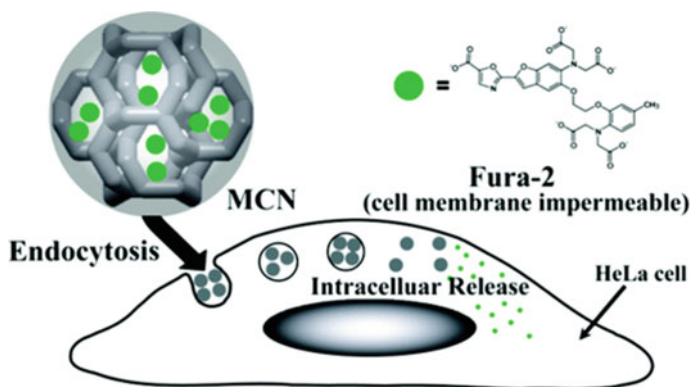
Due to the biocompatible and non-toxic nature, MCNs have attracted a large point of interest in the field of nanotechnology-based DDSs. As it is already known mesoporous nanocarbon materials have enlarged pores (2–50 nm) and surface area which makes them favourable for targeted drug delivery. Sustained release formulation can

also be achieved using MCNs as it has an adjustable porous structure on their surface which can control the release of drugs. In the cytotoxic treatment or in the treatment regimes in which highly toxic or highly potent drugs are used which can cause immense side effects if not delivered specifically in the targeted organ, this targeted drug delivery can be achieved using MCNs which make it possible by using different tools like stimuli-trigger response DDS [14], antibodies or ligand-mediated DDS [15] and endogenous enzyme-triggered DDS [16] and exert efficacious therapeutic action.

Among all the DDSs, it is widely accepted that oral DDS is the most feasible and convenient route of administration. But due to the poor bioavailability in the GI tract, the use of oral hydrophilic drugs is very limited. Recently, several works have been done by the pharmaceutical formulator to use MCN in the loading and delivery of poorly soluble hydrophobic drugs. In this context, not only MCN and mesoporous silica nanomaterial (MSN) [17] but also spherical-shaped mesoporous metal oxide [18] and hydroxyapatite mesopores [19] are significant. The work of Wang et al. [20] established the MCNs drug loading capacity and its role in targeted drug delivery of poorly soluble hydrophobic drug molecules, in the studies, they used celecoxib which is practically insoluble as a loading drug in the carrier molecule of uniform mesoporous carbon spheres to overcome the poor bioavailability of celecoxib and the studies showed that the bioavailability of celecoxib was remarkably increased in uniform mesoporous carbon spheres carrier when it compares with the conventional oral dosing.

In the field of targeted DDS, intracellular targeted drug release is one of the challenging tasks and hurdles increase tenfold when the drug is impermeable to the plasma membrane. To overcome the obstacle, MCNs are now showing a promising way for intracellular targeted formulation. Kim et al. [21] demonstrated the transmembrane drug delivery capacity of structurally ordered MCNs in HeLa cells. As per their work, it is established that MCNs are biocompatible, and they are easily taken inside the HeLa cells by the endocytosis process where they can release their cargo and make the transmembrane drug delivery possible [21]. They used Fura-2, a fluorescent dye which is plasma membrane impermeable, as their cargo package to load inside the nanocarrier of MCNs and poured the drug/guest molecule loaded MCNs into the live HeLa cells containing D-10 medium to let them cross the plasma membrane of HeLa cells and release the drug/guest molecule intracellularly [21]. This targeted drug design can be used in the delivery of cytotoxic drugs inside the cancer cells in a targeted and controlled fashion. Several other studies show that not only MCNs, but MSNs can also be used effectively as carriers for membrane drug delivery but still MCNs are considered promising and effective carriers in this regard due to their large pore volume and surface area in comparison with MSNs which give an added advantage for the drug loading. Not only that but there are several different studies also showing that the cytotoxicity of MCN is much lesser than MSNs [22–24] (Fig. 1).

Recent studies show that the MCNs not only serve as the conventional targeted DDS but also establish their importance in the field of precision medicine. In this context, mentioning the work done by Li et al. [25] is important to understand the role



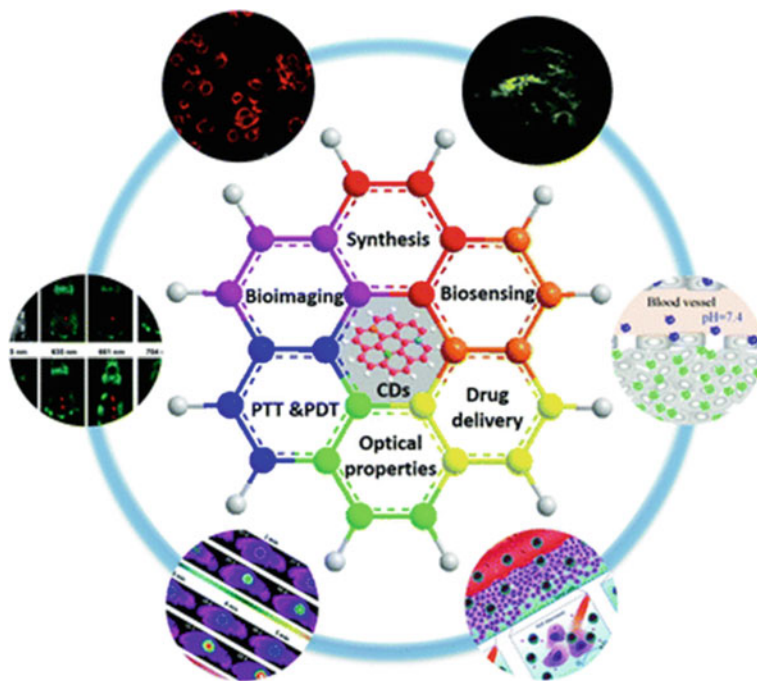
**Fig. 1** Diagrammatic illustration of intracellular migration of MCN through endocytosis and intracellular drug/guest molecule (Fura-2) release. Reprinted with permission from Kim et al. [21]. Copyright 2008 American Chemical Society

of MCNs in precision medicine. They demonstrated the dual-purpose serving application of MCNs using a single-stranded DNA, i.e.,  $P_0$  aptamers as a gated cap on the surface of the drug-loaded oxide variant of MCNs. As  $P_0$  aptamer is highly specific to cellular mucin, i.e., MUC1, so the precision in the drug delivery can be highly achieved [25]. Oxidised MCN or OMCN is highly preferable as a vehicle over MSN as it possesses photothermal therapeutics and photoacoustic imaging capabilities [26]. Not only that, but they are also the best candidate for pH-sensitive drug release [27]. In their research work, they prepared  $P_0$  aptamer capped DOX/OMCN for the fluorescence-mediated imaging of tumour cells of the transgenic nude mice and releasing chemotherapeutic agent, i.e., DOX inside the cellular mucin for on-demand pH-sensitive drug release [25].

## 2.2 Carbon Dots

CDs are zero-dimensional carbon materials that can be doped with nitrogen sulphur phosphorus and boron heteroatoms and have a size range of less than 10 nm nanometres [28]. Chemically, they may be enhanced and made with additional biomedical functional properties. CDs have a lot of potential in the bioimaging field, biosensing field and biotherapy field because it is less toxic to cells, highly soluble in water, biocompatible and has good photostable properties. Their main applications are in bioimaging [29] of cells (normal, tumour and cancer cells), in vivo imaging [30] and biosensing [31] (Fig. 2).

Scrivens et al. [33] first isolated carbon fluorescent nanoparticles in the year 2004 by purifying the mono-walled CNT. Since then, numerous synthetic processes have been devised for the manufacture of CDs with varying dimensions and using various functional molecules on its surface. The biocompatibility of CDs includes in vitro



**Fig. 2** CDs in various biomedical applications. Reprinted with permission from Su et al. [32]. Copyright 2020 Royal Society of Chemistry

and in vivo tests, the in vitro known for its cellular toxicity and the in vitro toxicity where the researchers used the whole organisms. The biosafety studies of HBCDs given through parenteral DDS in mice showed that in vivo imaging of major organs at different times after, i.e., injection of HBCDs [34]. Their results showed that HBCDs in vivo have significant biocompatibility and minimal side effects. This technique has an important role in both clinical and research fields because they allow a thorough investigation of biological systems [35, 36], which makes the morphological and physiological study of cells much easier.

Cancer cells CD-based in vitro imaging was first reported in the year 2011 [37]. Since then, there have been many attempts for imaging cancer cells with various CDs such as T47D cells [38], HeLa cells [39, 40] and MCF-7 cells [41, 42]. CDs with harmless emission are required for imaging cancer cells as that would avoid harmful UV or blue radiation and would reduce the photodamage of the biological tissues. Other than in vitro human body cell imaging, CDs are also used for in vivo imaging. The efficacy of using CDs as a fluorescent contrast agent in mice was first investigated in 2009 [43]. Later, a lot of CDs have been extracted and used for this in vivo imaging [44–46]. However, these most previous experiments on CDs emit only fluorescence of range from blue to green. In vivo imaging for CDs that emit in the red or NIR region of the spectrum is still very difficult to come by. While there



has been significant advancement in CD fluorescence imaging techniques in recent years, the spatial resolution in *in vivo* imaging is still far from showing satisfactory results. Various other imaging modalities, for example, photoacoustic imaging and magnetic resonance imaging, must be incorporated into multi-modal imaging probes [47].

The enhanced nucleus-targeted DDS depends on the successful incorporation of CDs with the parent drug. For example, Doxorubicin (DOX), a drug widely used in cancer treatment, transports through the membrane of a cell to the nucleus during cancer treatment. However, DOX does not quickly reach the nucleus of a cell and causes significant *in vivo* cardiotoxicity, limiting its use as a cancer treatment [48, 49]. Yang et al. coupled CDs to the drug DOX which enhanced the anticancer treatment, which directly implies that CDs have a significant role in nucleus-targeted drug delivery [48].

A modern *in vivo* real-time imaging technique combining MCNs and CDs has emerged. Laser excitation causes multicolour and wavelength-dependent fluorescence on CDs. Because of their nonporous nature and low drug loading capability, CDs use as a drug carrier is still constrained. Therefore, the combination of MCNs and CDs is preferred.

### 2.3 Carbon Nanotubes

Carbon nanotubes are an allotropic type of carbon discovered by Iijima in 1991 [50] and have since been widely researched and used for a variety of applications including materials reinforcement, electrode materials and/or components for nanoelectronics for biosensors, and even drug carriers in biomedicine as remote-control DDS in some cases. They can be synthesised using a variety of techniques, which includes the conventional electric-arc discharge, laser ablation and catalytic chemical vapour deposition method [51]. They are described as graphene layers with either side closed by fullerene caps. CNT is composed of one or more concentric walls which is an important factor that determines many properties of CNT. Single-walled CNT has a diameter of 1–2 nm, whereas multi-walled CNTs diameter is less than 100 nm. Double-walled CNTs are links between single-walled and multi-walled CNTs.

In the field of biosensors, CNTs have been suggested as a sensing element for detecting and monitoring a variety of diseases, including diabetes and many bacterial infections. For example, Punbusayakul et al., used electrochemical testing of immune complexes to diagnose salmonella, minimising detection time and simplifying sample preparation relative to other existing approaches [52].

In the imaging biomedical field, there are a variety of CNT-based technologies. For example, in photoluminescent imaging, the single-walled CNT gets excited to emit fluorescence in the NIR-I of wavelength range 700–900 nm and NIR-II of wavelength range 1100–1400 nm, which are nearly invisible to tissues and water, allowing for greater penetration depths [53].

In the healthcare industry, effective drug administration is a major concern. After all, poor selectivity and a short half-life cycle can lead to several administrations, which can result in undesirable side effects and even death. CNTs, due to their expected biocompatibility and basic structure, are being investigated as nanocarriers for drug delivery and gene delivery, as well as treatment of cancer.

CNT-based nanocomposites, on the other hand, have been extensively researched for the diagnosis and treatment of cancer due to the success of vesicle-based transporters such as lipid nanoparticles in reducing ailments other than cancer. A study performed by Fadel et al. [54] on f-bundled CNTs on an in vivo mouse having B16 melanoma, the MHC-I polymer caused expansion of T-cells which was boosted using a composite that served as an artificial APC.

The CNT has influenced many living cells, and nowadays, more attraction of using CNT in biomedical application is increasing day by day. CNT can change its form for 3D architecture for cellular replication improvement and bioengineering [55]. CNT also exhibits excellent capabilities for cell transfection. As a study done by Liu et al. DOX is easily quickly released in the acidic atmosphere of tumour tissues but remains bound to CNT at neutral and alkaline pH, thereby reducing toxicity in healthy body sections [56, 57]. Most of these works by various scientists mentioned above showed the toxicity of the CNT inside the cell during their usage. This may be the major drawback of CNT in biomedical application. However, this can be rectified using CNT-based hydrogel which makes water absorption possible because of its hydrophilic nature. CNT wires are also used for making precision devices which we will discuss later in this chapter.

## **2.4 Activated Carbon**

AC is a kind of carbon, i.e., known by mankind from its ancient days. The traditional medical use of AC is mostly for the cleansing purpose due to its high surface adsorbing property. In the era of the First World War [58], AC peaked high interest in war for the adsorption of poisonous gas trapped by the enemy. It is not well known for its gas cleansing property but also well known for water purification in the region of the world where proper means of water purification are not available [59]. In the medical industry, AC has a variety of applications. The ability to develop extraordinary purity in a naturally occurring substance, along with its adsorptive properties, has contributed to its introduction into medicines. These ACs are placed inside the GI tract by using nasogastric tube or oral administration. ACs are given as a water powder slurry which is administered to the victims of drug overdose toxicity. ACs have high binding affinity to many drugs, so the drug gets adsorbed and passes through the intestine without entering the blood [60].

ACs are not only used for treating endogenous poisons but also used as medication for exogenous poisons; i.e., poisons intake by mouth. But this to be effective enough it should be incorporated within a short period of time. AC antidotes cannot work with poisoning caused by lithium, malathion or cyanides [61].

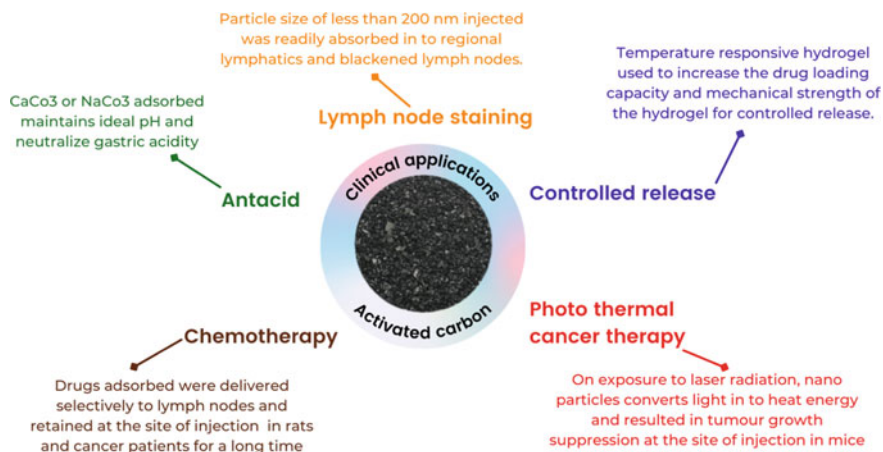
Activated charcoal, one of a kind of AC obtained from heating pulverised carbonaceous compounds of various natural sources of carbon like coconut shells [62]. The activation procedure of activated charcoal using hot air corrodes the carbon structure internally which results in increased adsorption capacity of the outer surface area [63]. This activated charcoal is known for decades as ‘Universal antidote’, and the reason is self-explanatory as it terms [64]. But later the formulation of scientifically approved ‘Universal antidote’ changed which consisted of one part of tannic acid, two parts of activated charcoal and one part of Magnesium oxide though the study demonstrated by Daly et al. [65] suggested that the effectiveness of using activated charcoal alone is much higher than the formulation, as in the formulation, some of the tannic acid adsorbed by the charcoal which leads to the reduced adsorption capacity of the activated charcoal.

Many recent studies, indicated in the research trends of activated carbon and its novel role in the DDS. In this context, a research work done by Miriyala et al. [66] is worth mentioning as it explores the possibilities of AC as a carrier molecule in amorphous DDS. Amorphous DDS is an advanced tool in the field of biopharmaceuticals to enhance solubility and bioavailability of any drug [67]. To serve as a carrier molecule in the amorphous drug delivery, several porous materials have been considered and well-researched among them porous silica materials have gathered promising interest as drug carriers, but due to its toxicity and high production cost it is not well accepted [68]. Studies showed that AC fulfilled the criteria of porous carrier in the amorphous drug delivery and as it is safe and economical, so it is a new point of interest in the search of drug carrier molecules in the amorphous DDS [66].

The role of activated carbon in magnetically guided DDS has been explored in some recent studies, in which activated carbon coating is done in the drug-loaded magnetic particles for the magnetic field-guided targeted drug delivery [69]. This kind of DDS is mainly used for the chemotherapeutic drug which demands high specificity in the drug release in the target due to its cytotoxic property [70]. Despite above all the use, some other clinical use of AC has surfaced due to several recent studies which are mentioned in Fig. 3.

## 2.5 Fullerene

This is also an allotrope of carbon with fused rings of five to seven carbon atoms joined together by single or double bonds. Fullerenes are often written as their empirical formula  $C_n$  or  $C_n$  where  $n$  is the number of carbon atoms present. One of the famous family members of fullerene is  $C_{60}$  also known as buckminsterfullerene discovered in 1985 as the shape resembles buckyballs [71]. Cylindrical fullerenes are also known as CNT or buckytubes which is previously discussed. We will discuss more about CNT and other medical devices later in this chapter. There are countless applications of fullerene in many biomedical fields such as inhibition of enzymes, DNA cleaving, and bioimaging [72]. While using these kinds of carbonaceous compounds, one of



**Fig. 3** Activated charcoal's potential therapeutic uses

the obstacles we need to think about is economically improving human health and lowering drug-induced toxicity.

From a theoretical-based calculation, in 1993 it was predicted that the fullerene C<sub>60</sub> protease hydrophobic cavity of HIV-1 virus gets fitted inside it, thereby causing inhibition of the enzyme [73]. There are many experiments done with C<sub>60</sub> derivatives against HIV-1 protease [74, 75]. C<sub>60</sub> derivatives are a much better choice of drug than any current anti-AIDS drug because in vitro conditions these current drugs show cytotoxicity which is not the case for these C<sub>60</sub> derivatives [76].

Due to the hollow structure of fullerenes, they can envelop atoms, specifically metal atoms such as alkali metal; alkaline earth metal; transitional metal; or lanthanide metals to become endohedral fullerenes. These endohedral forms of metal give rise to a new class of compounds that in activated form used for radiotherapy and in non-activated form used for imaging [77]. The major drawback of these fields of endohedral is their production yields. They are very hard to prepare; i.e., their production is almost 100 times less than normal fullerenes. Endohedrals are made up of 60–200 carbon metal atoms which are almost insoluble in water [77]. However, they possess equal chemical reactivity as normal fullerenes. Later in some studies, it was shown that C<sub>60</sub> has a unique nanocarrier-induced targeted drug delivery property that can target cancer cells for radiotherapy [72].

The C<sub>60</sub> fullerene has 30 double-bond carbons and that makes it the most efficient free radical scavenger among all known compounds present on earth [78]. This makes it a very powerful oxidising agent. This shows an action mechanism of oxidative stress. This inhibits the growth of tumour cells [79]. This also can prevent some inflammatory conditions and can recover damaged tissue [80, 81]. Recently, in a study it showed that it has an excellent anti-ageing effect. C<sub>60</sub> when taken orally with olive oil by rats has slowed down the senescence and increased the lifespan [82].

There are many more applications other than those mentioned above. Some of the unexpected properties include the preparation of anticoagulants based on nanoparticles [83], accelerating blood clot lysis [84], gene therapy using DNA vectorisation [85]. C<sub>60</sub>-based particles are also used for making minimised friction coating of various medical and dental devices [86].

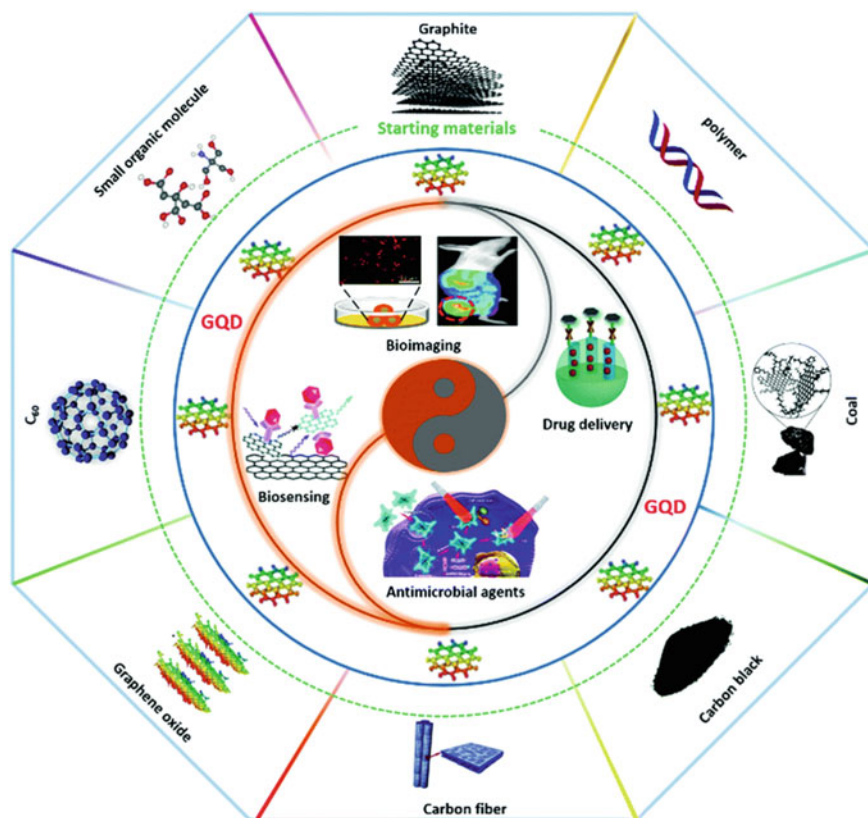
## 2.6 Graphene

Graphene is a monolayer carbon allotrope tightly bound to a 2D hexagonal honeycomb lattice with carbon–carbon single bond [87]. Graphene is the thinnest, lightest and strongest compound known to man on earth having size ranging 100 nm in every dimension [88]. Graphene is also the best conductor of electricity and heat at room temperature. It has many more surprising characteristics and is also used in a limitless number of applications [89]. Thus, it is known as ‘Wonder Material’ [90] (Fig. 4).

Its biomedical applications range from targeted DDS [92], cancer therapy [93], bioimaging [94], biosensing [95] to tissue engineering [96]. Initially, the application of graphene was limited to various electronic devices and sensors, but later its role in biomedical applications has emerged rapidly.

In the field of controlled and targeted drug delivery, nanoscale graphene oxides are proving itself as a promising nanocarrier for drug loading and targeted release. In 2008, Dai et al. first demonstrated the drug nanocarrier activity of nanoscale graphene oxide by loading various anticancer drugs with the help of polyethylene glycol and observed its uptake in the cellular level [94]. As the graphene oxide is devoided from toxicology and biocompatibility issues, it becomes a material of interest for the scientific community to explore not only its role in drug delivery but also its role in other biomedical fields such as gene delivery, intracellular and intranuclear drug delivery in cancer therapy, photothermal anticancer therapy in xenografted tumour mouse model, bioimaging and biosensor [97, 98].

In the field of bioimaging as per some recent studies, graphene oxides can contribute greatly. The bioimaging properties of graphene oxides were first discovered by Dai et al. [94], during their experiment on nanographene oxide mediated nanocarrier-loaded targeted drug delivery. As graphene oxide shows intrinsic fluorescence property in the NIR region so the GQDs can be assessed in atomic force microscopy and other spectral imaging techniques. Recent studies by Zhu et al. [37, 99] also explored the area of possibilities to use GQDs in cellular imaging as GQD possess high degree of biocompatibility and low degree of cytotoxicity so it can be a promising excellent candidate for the intracellular bioimaging in future clinical purpose. Nitrogen-doped GQDs have an oxygen-rich functional group in comparison with rGO. This GQD is produced by hydrothermal method [100] and has high electrocatalytic activity and is biocompatible with blue colour luminescence [101].



**Fig. 4** Biomedical application of graphene. Reprinted with permission from Li et al. [91]. Copyright 2017 Royal Society of Chemistry

Graphene and its derivatives have now become a point of interest for biomolecule sensing or biosensing research. Studies are going on to prepare graphene oxide-based biosensing devices to assess, detect and analyse biological molecules. We will discuss graphene-based biosensors later in detail.

The field of tissue engineering is emerging greatly in the twenty-first century as the need for artificial engineered tissues cannot be fulfilled otherwise. The biocompatibility and other unique characteristics of graphene oxides always indicated its undiscovered role in organ transplantation and artificial tissue regeneration [102]. In 2010, Ryoo et al. [103] performed a behavioural study on the NIH-3T3 Fibroblast model in which they generate mammalian tissue cells on supporting graphene oxide film which opens the gateway of unexplored regions of graphene-based tissue engineering. Several studies concluded that, in tissue engineering graphene or its derivative does not exert any detrimental effects, rather they induce the process of tissue regeneration [104]. Fan et al. [102] demonstrated the scaffolding properties of graphene–chitosan film. Their work indicated that the graphene could accelerate

human mesenchymal stem cell proliferation to a great extent. Recent studies show that graphene can not only contribute to the proliferation of human mesenchymal stem cells but also in the neuronal cells, skeletal muscle cells, bone and cartilage, and cardiac tissue regeneration [105].

Studies done by Fan et al. [102] using graphene oxide and chemically reduced graphene oxide to prove their antibacterial efficacy opens a new window of research in the search of biomedical application of graphene. Recent studies show that chemically reduced graphene oxide possesses more antibacterial properties in comparison with graphene oxides [106]. There are several studies going on to determine and standardise the antibacterial effects of graphene and its derivative against gram-positive and gram-negative bacteria.

Therapeutic efficacy is related to whether a treatment provides health advantages as compared to a placebo or other intervention in an ideal environment, such as a strictly managed clinical study. The safest medicine has the higher therapeutic index (TI). If the TI is modest, the medicine must be dosed cautiously, and the patient should be constantly watched for symptoms of drug toxicity [107]. The various therapeutic efficacies of the porous carbon nanomaterials are shown in Table 1 and inferring that we can say different materials have their respective therapeutic efficacy along with their drawbacks making them unique from one another. Due to these properties, these materials have various applications in the biomedical field.

### 3 Graphene-Based Sensors for Human Health Evaluation

Human health monitoring and human–machine interaction have increased rapidly in the last few decades and the key players behind these real-time health vitals monitoring are various kinds of biosensors. An analytical device that can sense any change, react and respond to any kind of input from the physical environment is called sensor and the first of these kinds of biosensor for glucose detection in blood was invented by Leland C. Clark who is also known as ‘Father of Biosensors’ [114]. In the twenty-first century, our population is growing rapidly and expectation of life in humans has increased, our healthcare system is currently facing inflation, and this requires the government to find a permanent solution to give interested medical care keeping in mind economical healthcare costs which force us to shift our focus from disease-oriented medicine to prevention and personalisation of the medicine, and thus, we can track health status and get an alarming ring to diagnose any abnormality in individual at its earliest stage. As the need for high precision biosensors are growing day by day which leads to the exploration of various new nanomaterials for the biosensors and graphene is one of the finest explorations in this search till date. This 2D single-layered carbon graphene has been a boon in the field of implantable devices and wearable sensors in recent years. The advantages of using graphene-based sensors are: It has some excellent physicochemical properties. These properties include high electron mobility, tenable optical properties, good mobility of electrons, high surface volume ratio and good mechanical strength [115]. All these

**Table 1** Comparative study of the therapeutic efficacy of various porous carbon materials

Porous carbon material	Therapeutic efficacy	Drawbacks	References
Mesoporous carbon materials	Drug delivery in DOX, Celecoxib; Adsorbents	Minimal toxicity found so there are no drawbacks	[108]
Carbon dots	Cancer cell inhibiting ability enhanced	Shows general cytotoxicity in higher dose administration	[48]
Carbon nanotubes	When tested on mice model with breast cancer showed dependency on time and dose administered	Causes toxicity in cells, neurons, heart and lungs based on dosage and targeted area	[109]
Activated carbon	Used as absorbents, administered depending upon the intoxicants involved	No such drawbacks	[110]
Fullerene	Photosensitisers that can be used in photodynamic therapies defend the liver from free radical damage	No toxicity	[111]
Graphene quantum dots	Magnetic hyperthermia, photothermal therapy, enhances anti-tumour efficiency	Structure and size cannot be controlled	[112]
Graphene	Gene and delivery of small drug molecules, anticancer therapy, protein biofunctionalisation	Exogenous cytotoxicity	[113]

properties make graphene an ideal nanomaterial for effective biosensor development. In this recent time, many numbers of graphene-based sensors are reported for human health monitoring system, and this includes implantable devices and real-time body vital measurements such as heart rate, rate of respiration, oxygen saturation, BP, blood sugar level, temperature, and EMG, ECG and EEG signal [116]. Graphene and its conjugated derivative are abundantly used in this biosensor, not only graphene oxide but also GQD and reduced graphene oxide (rGO) are used in the development [115]. These materials are used for their high sensitivity, i.e., detects minute quantities of target analyte, high accuracy; i.e., there is no cross-reactivity while detecting the analyte target, fast performance, low cost, prolonged storage shelf life and increased robustness and is very user-friendly. Besides all that, graphene and its derivative-based sensors are preferred due to its ultrathin thickness, mechanical flexibility and its comfortless in intimate body contact [117].

In the earliest era, silicon sensors were widely used as the options for biosensors were very limited, but its rigid pattern made it disadvantageous as the mechanical flexibility is highly demanded for both non-invasive and invasive biosensors [118]. A choice of ideal biosensors depends on various factors like it should be biocompatible,



comfortable, stable and convenient [119]. But not only that, as we are heading towards the miniaturisation of gadgets, thus miniaturisation and its suitable bio-fuelling need to be considered to provide an affordable healthcare management to the population [119]. In today's world information is a new tool to solve critical problems and as the biosensor-based gadgets demand to be upgraded with time so integration of artificial intelligence, machine learning, IoT, cloud computing, and big data management technologies are challenges for the developers [120]. In this context, privacy, security and safety of the date of an individual need to be considered very seriously.

Recent trends reveal that the porous carbon-based biosensors can be used effectively to detect various kinds of biomolecules of a physiological system such as dopamine, epinephrine, serotonin, and norepinephrine. The studies show that using the fast-scan cyclic voltammetry method, CONH<sub>2</sub>/COOH-carbon nanotube/CFME-based sensor is effectively used for detection of dopamine and serotonin; similarly using Amperometry method, reduced GO/GCE-based sensors showed effective detection of serotonin and using Differential pulse voltammetry method multi-walled CNTs-Ni(OH)<sub>2</sub> NPs/GCE-based sensors are able to detect epinephrine [121].

The growing interest in graphene-based biosensors demanded a robust toxicological and biocompatibility study of graphene and its derivatives. Though cumulative study indicates the negligible toxicity of the graphene-based nanomaterials in both invasively and non-invasively but due to the scarcity of sufficient data and lack of studies it will be very premature to conclude any concrete statement in this regard [122, 123].

### ***3.1 Non-Invasive Sensors***

Non-invasive sensors for the purpose of monitoring the individual's health are referred to those sensor-based equipment which do not invade or break into the skin or body's internal structure for the detection of its designated signals or biomarkers [116]. Usually, these sensors refer to artificial skin, patches, wearables or they can be a programmed thin layer of biosensing material. Usually, non-invasive sensors are used for real-time health monitoring to avoid alarming conditions.

In today's world, the most popular type of non-invasive graphene-based sensors is wearable sensors which can detect various biosignals and generate data for real-time monitoring [124]. Biosignals can be divided into two subtypes: one is biophysical signals and other is biochemical signals [125]. Biophysical signals are the signals which are related to physical attributes of health such as electrophysiological signals, kinematic signals and temperature signals [116]. All the live cells and the tissues of the body generate electrophysiological signals irrespective of its state. These bio-electrical currents are crucial for the development of real-time monitoring sensors as they can dictate the conditions of the cells or tissues. In cell electrophysiology, these biological currents are often referred to as resting membrane potential and action potential, and these potentials are maintained by the electrolyte ions of intracellular

fluids and extracellular fluids. In diseased conditions or in the altered body's physiological conditions, the normal distribution of the electrolyte ions of intracellular fluids and extracellular fluids are being changed which subsequently results in the significant alterations of the potential differences. Conventionally, these potentials are gathered using electrodes and processed the data for the clinical interpretation and these basic principles are followed in ECG, EEG and EMG techniques [126]. But due to their various limitations like high cost, large size, unreliable signal processing and discomfort with the skin make it disadvantageous for the real-time monitoring which paves the pathway for the search of suitable material which can overcome this limitation with the properties of mechanical flexibility and miniaturisation to produce real-time health monitoring data. As graphene-based bio-electrical electrodes provide all these ideal qualities, and thus, it is widely used for the real-time sensors [127]. As per Yun et al. [128] chemically reduced graphene oxides and porous dimethyl siloxane are ideal bioelectrodes due to its high performance. This graphene-based bioelectrodes are extremely stretchable and have a maximum stress of 150%, excellent compression life up to 5000 cycles, and a low sheet strength of approximately 1.5 k $\Omega$ /square, which demonstrate the potential for low-cost manufacturing and wide implementation for the future wearable devices [128].

The development of suitable sensors for the detection of the body movements and monitoring physical actions is crucial for any real-time non-invasive monitoring devices, as it can be able to detect individuals' movement pattern and detecting various motion-based biosignals which can help to diagnose disorders of body movement, disorder in respiration and breathing pattern and tracking muscle performance. The detection and processing of motion-based bio signals require sensitive pressure-based tactile sensors. They follow a wide diversity of mechanisms to detect signals, i.e., by changing electrical resistivity followed by charging and accumulating the charge in the nanomaterial and causing triboelectric effect on the skin-based wearables. Graphene-based materials gained popularity in the development of tactile and strain sensors due to its mechanical flexibility and piezoresistive properties. In some recent studies, it is also seen that the sensing properties of graphene-based sensors are increased greatly when used in composition with other materials. Due to the diverse way of conduction mechanism, these materials are well-suited for the pulse, breath, heartbeat and other vitals monitoring along with the detection and processing of walking pattern, body's locomotion and expression of the face. The tactile sensors are working on the pressure sensing in which mechanical pressures are converted into its complementary electrical signal which can be processed as a monitoring data for the readout.

Kou et al. [129] suggested a lightweight capacitive pressure sensor made up of a graphene/polydimethylsiloxane dielectric plate, a polydimethylsiloxane substrate, a wrinkled Au (gold) electrode, and an antenna with a sensitivity of 0.24 kPa in the low-pressure regime (0–10 kPa) and 0.0078 kPa in the high-pressure regime (10–100 kPa). This sensor also had a low sensitivity limit of 5 Pa and a reaction time of 67 ms, making it suitable for detecting subtle pressures such as facial gestures, hand bending and body movements.

The strain sensors are working on the principle of kinematic detection, and it is used to measure the deformation in the object [130]. Graphene-based strain sensors are used due to its excellent piezoresistive strain sensitivity. Recent studies show that modification of the graphene-based strain sensor structure using graphene textile glycerol–potassium chloride increased the strain sensation of the sensor effectively [131]. Despite having different composition and development, all carbon graphene-based nanoarchitecture strain sensors are popularly accepted.

The combination of 3D graphene foam and carbon nanotubes had a gauge factor of 35, high stretchability (up to 85%) and outstanding sound-to-noise ratio and could be easily placed on human skin for real-time motion control and even acoustic vibration detection [132].

The need of continuous monitoring of the body temperature is also a part of health vital monitoring. So, the need for a highly sensitive temperature sensor in real-time sensor devices was well-demanded. Graphene and its derivatives are preferred for this purpose due to their promising thermal conduction capacity [133]. Their remarkable electronic properties and mechanical flexibility make graphene-based temperature sensors widely popular in recent times.

Though several studies reported various graphene and its composite as favourable sensors for thermal conductance, cellular graphene and polydimethylsiloxane composite are mostly popular [134].

Biophysical signal-based non-invasive biosensors serve greatly in the real-time healthcare monitoring, but it has lots of disadvantages which limits its use in the critical vital monitoring for a clinical diagnosis, that's why assessing biochemical signals of the human health monitoring and evaluation is very much essential [135]. Conventionally, a body's biochemical parameters are measured and analysed using various sophisticated high-cost analytical instruments with the supervision of trained professionals [136]. This kind of analysis requires sampling of body biofluids. Though this conventional way provides accurate results, due to their high cost, time-consuming procedure and other complications it is not feasible to generate continuous real-time monitoring data. Biochemical sensors can overcome the conventional limitations by providing an economical solution for continuous real-time non-invasive monitoring data in miniaturised wearable devices which can sense biochemical signals and provide the results spontaneously for the health monitoring. The mechanism of biochemical sensors consists of signal and sensory part where sensors are specific recognition molecule, i.e., receptors, antibodies, antigens, genetic material, enzymes, etc., and biosignal refers to the physicochemical biomarkers of non-invasive biofluids, i.e., sweat, tears, saliva, etc. [137].

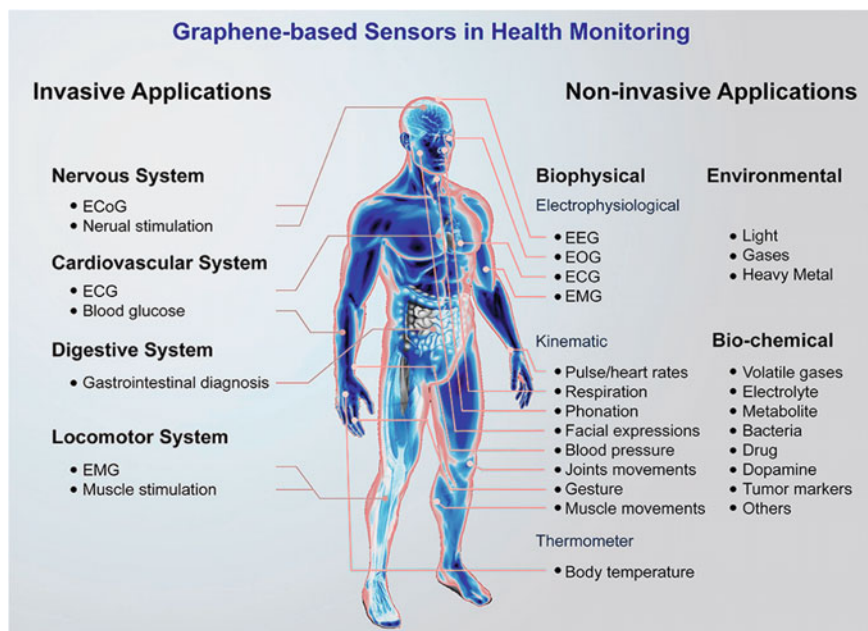
The unique characteristic of graphene in biochemical sensing makes it a material of choice in the development of biochemical sensor-based monitoring devices [138]. In comparison with other biochemical signal sensors, graphene shows high accuracy, specificity, sensitivity and quicker response time, and thus, it is used widely in the detection of various biochemical markers like electrolytes, metabolites, gaseous organic compounds and other biomarkers [139].

Biofluids are enriched with critical biochemical information which can forecast the clinical abnormalities by assessing the value of detected parameters in comparison with its normal range. Though the biochemical sensors can sense a wide range of analyte like electrolytes, blood glucose, hormones, enzymes, organic and inorganic compounds, currently most of the studies are focused into the real-time monitoring of lactate and glucose as these two contributes greatly to various clinical conditions [140]. As per the research performed by Kim et al. [141] and Park et al. [142], the presence of glucose in the tears can be a source of potential biochemical signalling to assess the glucose level in the body and they also proposed graphene and glucose oxidase-based sensing material in the contact lens platform to sense the sugar molecule. The body glucose level can also be sensed using laser-induced graphene and chitosan composite with or without platinum and gold nanoparticles from sweat, and these biosensors are gaining rocket popularity day by day [143]. Cortisol is a stress-induced hormone, the production of which shoots during fight-or-flight situations [144]. It is also a biomarker that acts as an alarming system of the body the level of which alters during stress, hypertension, and stroke [116]. The real-time monitoring of cortisol can be beneficial for the early diagnosis of disease. As per the studies by Tuteja et al. [145], cortisol antibody-loaded electro-reduced graphene oxide patch can act as excellent biosensors to sense cortisol in sweat and/or saliva.

Serum lactate level in the blood is a crucial parameter to understand the severity of tissue hypoperfusion, hypoxia and injury-mediated tissue damage [146]. This serum lactate level can be assessed continuously using biochemical signal-based real-time monitoring biosensors. Wang et al. [147] proposed  $\text{Cu}_3(\text{btc})_2$  nanocubes loaded amino functionalised graphene paper patch can be used effectively to sense the lactate in sweat. A new novel non-invasive biosensing technique has been evolved in last few years which helps in diagnosis of diseases in human breath analysis, studies show that human exhaled air contains unique biomarkers, the analysis of which can help in the diagnosis of various clinical important diseases like diabetes, thyroidism and lungs cancer. Some scientists suggested that in normal breath methanols, isoprenes and acetones are present, and during various disorders, the concentration of these compounds in exhaled air is altered significantly [148, 149]. Another scientist suggested a top-notch graphene-based gas sensor which is composed of metal nanoparticles and chemically reduced graphene oxide for the detection of various metal ions and gas based on their electrical and ionic conductivity [150] (Fig. 5).

### **3.2 Invasive Sensors**

As we have seen previously the non-invasive wearable sensors prove successful in human health tracking, they lack the capacity to collect data on the total complexities of organ processes and to consistently track real-time biological. And that's where the work of invasive sensors comes into existence. Invasive sensors are those



**Fig. 5** Summary of graphene-based sensor for human health monitoring. Reprinted with permission from Huang et al. [116]. Copyright 2019 frontiers in Chemistry

which are inserted inside our body as implants, they are placed near the tissues or organs and have more sensing capacity and restorative effect than the non-invasive sensors. As a result, it is creating a lot of interest in disease monitoring, diagnosis of diseases, care and disease management, highlighting its biomedical potential [151]. Even though there has been a lot of work done on these sensors for monitoring human health, graphene-based sensors have only been introduced very recently on a limited basis. These are neuronal monitoring and stimulation, monitoring of heart rate, blood sugar monitoring and EMG signals detection, which have mainly focused on neural implants till date. These implants are feasible in vivo in various systems in our body such as cardiovascular system, nervous system and GI system.

Neural implants are those which can record the electrical activity of the nervous system or can stimulate them. They may demonstrate the benefits for therapeutic therapies and medications for a variety of illnesses, including Parkinsonism, seizures, pigmentary retinopathy, distress and psychological disorders [152, 153]. Recently, a super advanced brain-machine interface has been demonstrated which contains neural implants that directly link the brain to the machines [154]. These graphene-based implants not only need to be inactive to the immune system but also must be highly conductive to record signals efficiently. With all these extraordinary features, these graphene-based sensors are perfect for addressing the latest challenges of neural designs than the other conductive polymers present now. To prove this, many

studies [123, 155–157] were performed in vivo with these graphene-based biosensors showing they have best in class biocompatibility and optimum optical transparency for studying the neurons and finally graphene transparent electrodes for brain simulation and neural tissue optical monitoring were developed [157–159].

The heart pumps oxygenated blood across the body through a network of blood vessels in the cardiovascular system. Damage to the heart or any difference of blood flow may lead to various cardiac diseases or may lead to death. As a result, tracking the biomarkers present in blood and heart is important. In the case of diabetic patients, monitoring blood sugar level is very important. As we have discussed previously about non-invasive biofluid-based wearable glucose sensors, who are able to provide continuous real-time data but still have low precision than direct invasive glucose monitoring. To overcome this, Lee et al. [160] developed an implantable device which can measure continuously the blood sugar level and can work as a microdialysis instrument. All these glucose biosensors have some limitations such as short lifespan, biological fouling and low biocompatibility. Cardiovascular disease is a serious public health problem, with a death rate that is greater than most cancers. Heart movements can be monitored in vitro and in vivo for the early detection and treatment of cardiac problems. Until now, cardiac implanted instruments, such as pacemakers and defibrillators, have been capable of long-term monitoring and pacing, pulse detection and treatment, and resynchronisation, all of which are challenging to do outside of the body with the same precision [161].

The digestive system is responsible for supplying nutrients to the whole body, complications with it can result in a variety of diseases. The primary component in the digestive system is the GI tract, and gastrointestinal disorders have become highly prevalent in the increasing community [162]. Invasive endoscopes were widely used for imaging and cure for treatment and diagnostics of many GI disorders. They lack spatial resolution though when it comes to identifying and treating small tumours or other anomalies. So, incorporating the miniature device on the surface of the camera which has very limited space needs to be transparent so that it does not block the visuals. Lee et al. [163] demonstrated a multifunctional hybrid graphene-based transparent endoscopy system that can detect colon cancer cells, pH and temperature. This hybrid multifunction device has radio frequency extirpation and localised chemotherapy or phototherapy with inbuilt high-resolution camera, thereby making this device remarkably compatible for in vivo colon cancer treatment with accuracy and rapid targeted treatment. Graphene-based sensors doped with acetate have remarkable sensing capacity to detect *E. coli* to a concentration of  $10^6$  cfu/ml [164].

The musculoskeletal system is solely responsible for the human body's movement capabilities. In the diagnosis of neuromuscular diseases such as Duchenne muscular dystrophy and spinal muscular atrophy, accurate and consistent tracking of EMG signals with instant feedback evaluation is crucial. Kim et al. [163, 165] proposed a hybrid shell sheet aurum doped graphene-based transparent implantable device that can record muscle signals and can simultaneously stimulate nerves and muscles. These hybrid sheets are very good conductors of electrical signals as they are doped with Au and are made extremely transparent for stimulating the tissue optically

without triggering the immune system. This multifunctional interface showed great promise in the field of soft bioelectronics.

However, while using graphene oxide as invasive sensors in in vivo animal or human body, biorecognition by the physiological system of recipient must be considered as experimental studies by Wang et al. [166] showed dose-dependent toxicity on human fibroblast cell when dose of more 50  $\mu\text{g/mL}$  was administered. Biocompatibility must be kept in mind whenever graphene oxides are used in vivo in the human or animal body.

## 4 Porous Carbon Microparticle as a Vehicle in Drug Delivery

From the last few decades as the overview of the treatment changed drastically so the need for new kinds of drug delivery has emerged greatly. Due to the various limitations of conventional drug delivery and dosage forms, their place is now replaced with a novel drug delivery system. The biocompatible nature of porous carbon forced the researchers to explore its role in DDS and various studies found the said role in most of the porous carbon materials. In DDS, a vehicle is an important part of the formulation which safeguards and carries the drug cargo and delivers the same into its destination. Among all the porous carbon material, CNT, carbon dot, graphene and AC show the most promising vehicle for targeted and controlled drug delivery. CNTs are preferred as drug delivery as it can be easily linked to different biomolecules like drug molecules, proteins and peptides, hormones and enzymes and nucleic acids [167]. But due to its solubility problem, they are used in drug delivery demands functionalisation of CNT molecules. The functional groups of the drug molecules are attached with the carbon nanotube surface either in covalent or non-covalent fashion which improves their bioavailability and target selectivity [168]. In the first-generation single-walled CNT-based drug delivery, toxicity can be a major obstacle for its role in drug delivery systems which can be countered using synthetic and natural polymer-based single-walled CNT [169]. Recent studies have shown that functional CNTs are able to invade cells through endocytosis and exocytosis, leading to the accumulation and deposition of CNTs in the target cell lysosome and endosome [170]. Endocytosis is identified as the most efficient route for cell entry of nanomaterials and relies on the molecular arrangement of the diameter and external surface. Specifically small walled CNTs enter inside the cells using clathrin coating as vehicle but multi-walled CNTs make their way inside the cell by endocytosis process or by direct penetration [171]. Single-walled CNTs need functionalisation by polyethylene glycol or DNA for intracellular drug delivery and their accumulation has been found in cell organelles like lysosomal bodies, mitochondria and endosomes [172]. Mu et al. [173] demonstrated the intranuclear drug delivery using CNTs, in that experiment he showed that multi-walled CNTs have the potential to travel through many cell organelles and make their entry inside the nucleus. To

increase the drug targeting and specificity of CNTs surface modifications is crucial, various studies show that linkage of carbohydrate binding ligands and some specific antibodies on the surface of CNTs enhance the targeting capacity of nanoparticles [174, 175]. As CNTs can induce immune responses in the body they are used as adjuvants in vaccine formulation. From some recent studies, it has been found that anticancer drugs like cisplatin, paclitaxel, DOX and cytotoxic platinum compounds can be successfully delivered intracellularly using CNTs [176, 177].

For the last few years, various studies demonstrated drug delivery capability of carbon dots synthesised from various biological molecules. Ding et al. [178] demonstrated a real-time imaging-based drug delivery using DNA synthesised carbon dots as vehicles where Rhodamine 6G was used for the real-time cellular imaging due to its fluorescent property and DOX was used as a key drug. Carbon dots are comparatively high biocompatible among other carbon-based nanomaterials, due to this property it is now widely experimented for various drug delivery studies. Studies show that carbon dots are pH sensitive thus the drug-loaded carbon dots remain intact at a neutral pH and the drug release triggers in lower pH [178]. Carbon dots are hollow in nature, they possess a hollow 2 nm pore size structure within which presents itself as an ideal drug-loading nanocarrier molecule [179]. Das et al. [180] demonstrated the drug loading capability of heteroatom-based carbon dots, where they used Capecitabine anticancer drug for the targeted tumour cell drug delivery.

Due to the  $\pi$ - $\pi$  stacking and high surface area, graphene is also considered as a promising nanocarrier molecule in DDS [181]. Their use and drug-releasing mechanism were discussed earlier. Graphene and its derivatives can successfully load-target-deliver drugs with poor solubility and various cytotoxic drugs like DOX and 5-fluorouracil effectively [182]. Currently, robust studies are going on to standardise graphene-based drug delivery and to profile its toxicity.

The role of activated carbon in drug delivery is still under research but as per various studies, it is found that ACs can be used to increase the bioavailability of crystalline drugs. Due to the amorphous nature of activated carbon, it can effectively carry the drug molecule and increase its solubility and dissolution [66].

Doping is an important strategy used in drug delivery to increase the efficiency of a given carbon nanomaterial. This makes the drug delivery process more efficient. Various studies on metals or heteroatoms doped/co-doped with these porous carbon materials are going on to prove the increase in targeted drug delivery as shown in Table 2.

The structure and morphology of various porous carbon nanomaterials influence the performances. The spatial configuration and various hybridisation of the carbon compounds build their ability to bind with almost all materials, thereby having application in drug delivery. The carbon nanomaterials have an excellent  $\pi$ - $\pi$  supramolecular stacking which makes it suitable for cancer therapy.

As we know that the drug release pattern is directly linked with the AUC in a biodistribution curve. The study performed by Liu et al. [57], where DOX-induced CNT was introduced to the tail vein of the mice. The results were inferred, and it showed in the biodistribution curve that the release was increased showing a direct



**Table 2** Effect of doping in carbon nanomaterial in drug delivery system

Carbon nanomaterial	Doped/co-doped metal or heteroatom	Benefits/Application	References
Carbon quantum dots	Duplex metal (Ag and Cu)	They have a photoluminescence property to be used as a vehicle for targeted drug delivery. These duplex metal co-doping helps in increasing the size intelligible, thereby increasing drug loading capacity.	[183]
Carbon dots	Nitrogen and sulphur	This doping is done by a method known as Herein for targeting cancer cells. These fabricated carbon dots have better photostability, water solubility and biocompatibility.	[180]
Carbon nanodots	Nitrogen	These nitrogen-doped carbon nanodots are coupled to an anticancer drug thereby inducing apoptosis in cancer cells with better efficacy as compared to the normal drug.	[184]
Graphene oxide	Zinc Oxide (ZnO)	Studies showed that graphene oxide doped ZnO has 89% higher efficiency of drug loading as compared to normal ZnO. This enhanced efficiency of drug loading paved a new trend in modern drug delivery systems.	[185]
Activated carbon	Aluminium (Al)	The efficiency of adsorption energy increased effectively by doping Al with AC for adsorption of 5-fluorouracil molecules. The study suggests Al dopant improves the adsorption capacity of Activated carbon.	[186]

proportional relationship with therapeutic efficacy. This study clearly indicated that CNT has a reasonable amount of bioavailability.

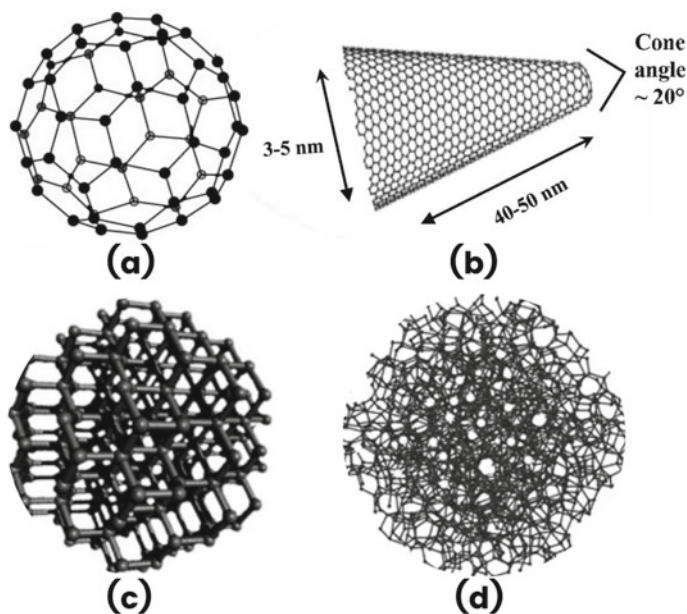
Similarly, many other studies were also performed to find the biotherapeutic efficacy parameter on various porous carbon nanomaterials such as GO [187], carbon quantum dots [188] and activated carbon nanoparticles [189]. These porous carbon materials have some extent of bioavailability, but they cannot be indicated by a single formula as they have their different pros and cons.

The role of porous carbon-based nanomaterial in drug delivery is still under research, but from the various studies it is quite clear that these nanomaterials possess immense potential to be used as vehicles which can increase the bioavailability and effectiveness of drugs greatly.

## 5 Application of Spherical Nanocarbon Materials

Spherical nanocarbon materials have gotten a lot of recognition because of their unusual shape and properties, which make them promising biomedical materials. Spherical nanocarbon material consists of fullerene, carbon NHs, nanodiamonds and porous nanosphere carbon (Fig. 6d). In this part, we are going to discuss their therapeutic applications and their toxicological effect with special emphasis on the anticancer effects of these versatile nanoparticles.

There has been considerable progress in this field in recent years, especially in the use of engineered nanomaterials in biomedical applications such as biolabelling, nanomedicine and as DDS [193–195]. These novel materials having special structures and properties have been used as diagnostic probes, nanocarriers, and



**Fig. 6** Structures of spherical nanocarbon materials—**a** Fullerene, **b** carbon NHs, **c** nanodiamonds, **d** porous nanosphere carbon. (a) Reprinted with permission from Rajesh et al. [190]. Copyright 2019 Woodhead Publishing. (b) Reprinted with permission from Fresco-Cala et al. [191]. Copyright 2018 MDPI. (c) and (d) Reprinted by permission from Wang et al. [192]. Copyright 2014 NPG Asia Mater

as biomarkers [196–198]. Nanomaterials, due to their small scale, can be used to probe, modify and monitor biological processes at the cellular and subcellular levels. For example, CNTs and carbon NHs are demonstrated to have high loading dose capacity and extended BCT, making them a potential candidate for controlled release DDS [199, 200]. Nanodiamonds emerged recently as a novel DDS, bioimaging and biosensing, thereby demonstrating improved therapeutic efficiency, photostability and increased biocompatibility [201–203].

Fullerene C<sub>60</sub> was suggested to inhibit the action of HIV protease shortly after its discovery because it has the right size to fit into the enzyme's hydrophobic cavity [73, 204]. Since then, fullerene has been reported to have various other biomedical applications such as MRI [205] and photodynamic therapy among them the most widely studied are these working as 'radical sponges' [206].

Fullerene and its derivatives are a scavenger of ROS making it a promising novel antioxidant and having various biomedical applications. Studies showed that when compared to untreated mice, fullerene-treated mice have a higher survival rate and improved memory and learning abilities [207]. There were various other studies which showed these scavenging properties of fullerene and its derivative compounds such as polyhydrates and polycarboxylate having cellular protectivity, can cross blood–brain barrier and neural cell damage prevention [208, 209]. The major cause of many acute and chronic disorders is oxidative stress, and study has shown that cancer cells have increased oxidative stress with higher ROS, thereby stimulating proliferation of cells, genetic instability and cellular mutation. As a result, fullerene, which has a scavenging property inhibiting ROS, may be highly useful as biomedicine for treatment of cancer as well as maintaining health and quality of life [192].

Many previous studies have shown that metallofullerenes were often used as radiopharmaceuticals or as contrasting agents [210–214]. It has been found out that these agents have both higher efficiency and lower toxicity. So, this becomes a novel mechanism to use these nanoparticles against the treatment of cancer. Basically, Gd@C<sub>82</sub>(OH)<sub>22</sub> metallofullerene particles have antioxidant properties with enhanced immunity, can reduce resistance caused by drugs and can efficiently suppress the spread of cancer cells [192, 214]. The most practical limitation is its yield is very low, and it is also very expensive and time-consuming making it difficult to be used practically as a novel nanomedicine.

Single-walled NHs are a potential nanomedicine having a horn-shaped tubular structure with diameter of 3 and 5 nm with length of 40–50 nm as shown in Fig. 6b [192]. They are ideal platforms for loading of drugs because of their large surface area and availability of interstitial spaces. It was shown that a very tiny water-soluble drug molecule, cisplatin, was able to deposit inside this single-walled NH molecule, and it was further shown that it released remarkably, thereby reducing cancer cells viability making it an efficient nanomedicine for controlled DDS [215]. According to a new toxicological review of single-walled NHs on mice tissues, it did not induce any apparent toxicity response after 26 weeks of administration [216]. This makes them a potential candidate for using it in a DDS due to their high drug loading capacity and minimal toxicity in treatment of cancer [199, 217].

Activated nanodiamond surfaces have been used to inject a variety of therapeutic agents into cells. Among them, cisplatin is attached and then released with pH making it a controlled release DDS for cancer treatment [218]. Several water-insoluble anti-cancer drugs were also mounted on the surface of nanodiamonds, allowing the conjugates to be used in drug delivery and illustrating improved therapeutic efficacy against cancer treatment [219].

Carbon nanoparticles which include PC nanospheres have high fluorescent properties which are used in various biomedical applications such as biological imaging, as biosensors and biolabelling [220, 221]. In the latest report, it showed that these hollow PC nanospheres are used for insulin delivery through the mouth using the biodegradable polymer coating that delays its release in a low pH as in stomach but acts as sustained release in a neutral pH [222]. In another research study, DOX is administered to the HeLa cells using a PC nanosphere of 90 nm size by pH-responsive method [223]. The drug remains inside the nanosphere at the body's normal pH and is released at a lower pH environment of tumours.

Spherical nanocarbon materials have the most promising characteristics to be used as novel nanomedicine and antitumour agents in the coming decades but still toxicological assessment and more rigidity study need to be done thoroughly before they are reinforced as nanotherapeutics.

## 6 Effect on Bacteria and Fungi by Porous Carbon Cuboid Nanoparticles

Throughout the world, deaths due to infectious diseases are increasing day by day. As per a World Health Organization study, infectious diseases share 24% in global deaths [224]. Though we can fight better and reduce the mortality rate in the post-penicillin era, still there is a large scarcity of antimicrobial agents to keep the human race as the winner in the battle against pathogenic microbes. As the advancement of nanotechnology, expanding its wings in the field of biotechnology and drug discovery, researchers are now studying extensively about the integration of nanomaterials in drug discovery to feel the void in the search for effective antimicrobial formulation.

In this lane of research, carbon-based nanoparticles have been attracting the scientific community for the last few years, nanostructures like CNT, carbon cuboid nanoparticles, graphene, fullerenes, nanodiamonds, carbon nanoscroll are mainly getting the attention [225]. Various studies found that these carbon-based nanomaterials can be used as effective antibacterial, antifungal and algacidal when they integrate with various MNP. MNP like, Ag, Cu, Au, Ti and Zn are well known for their antimicrobial properties but using them in crude forms for the treatment of infectious disease is not feasible as they show concerned toxicity and aggregation [226–228]. These problems can be solved using the immobilisation of the compound on various carbon-based nanomaterials [229].

The antibacterial efficacy of carbon nanomaterials depends on two things, functionalisation of nanomaterials with multiple oxygen and encapsulation of MNPs on the surface [227]. As per a comparative study performed by Karageorgou et al. [228] the lethal efficacy of oxygen functionalised porous carbon cuboid nanoparticles is much higher against *E. coli* cell culture in comparison with non-oxidised porous carbon cuboid nanoparticles. The reason behind the high lethal effect of oxidised form is the oxygen functional groups may produce superoxide and ROS which subsequently causes oxidative stress in the target microorganism cell [230]. Same antimicrobial efficacy is also seen in graphene-based nanocomposites and CNTs [231]. Among them multi-walled CNTs and carbon nanoscrolls encapsulated with silver nanoparticles show higher efficacy as antibacterial and antifungal [231]. Silver encapsulated carbon nanoscrolls are highly effective against *Candida albicans* and *Candida tropicalis* in comparison with silver encapsulated graphene oxide [231]. In the antifungal treatment of grey mould disease on rose petals and strawberry, CuO encapsulated fullerene shows the strongest activity in comparison with multi-walled CNT and rGO [232].

Various studies show that among the MNP, silver is the most preferred one in terms of antibacterial and antifungal as they possess comparatively higher efficacy in in vitro studies [233]. The germicidal mechanism of silver is yet not clear, but studies found that they enter the cell plasma membrane via endocytosis pathway and affect the fundamental metabolic process of the bacteria where the burst release of silver ion takes place [234]. Controlling the burst release and achieving a continuous flux of silver ions is the main challenge in the process of integration of carbon-based nanoparticles. There are some ideal properties which need to be checked before selecting any carbon-based nanoparticles for the integration such as high porosity, great stability, lightweight, surface heterogeneity, biocompatibility and minimum toxicity [235].

Carbon-based nanoparticles doped with metallic ions show antifungal activities against various organisms which can be effectively used in the formulation of fungicide for the eradication of fungal infestation of plants like *Fusarium oxysporum* and *Fusarium poae* [236, 237]. Their antibacterial efficacy is found against gram-positive *Corynebacterium glutamicum*, *Staphylococcus aureus* and gram-negative *E. coli* [228, 238].

Though the efficacy of metal ion doped carbon-based nanoparticles is well-established, still it is not well-accepted for the in vivo use due to insufficient toxicity data. Thus, it can be inferred that if the toxicological profiling can be established well, it will contribute highly to the fight against infectious diseases.

## 7 Carbon Nanotube Wire for Precision Medical Devices

Precision medical devices are a cutting-edge integrative research field that aims to achieve Richard Feynman's vision of developing tiny robots with exquisite finesse and the ability to go beyond the human body and said that one of his friends gave

an interesting idea where the surgeons are swallowed [239]. These devices will be the game changer soon where nanotechnology and electronics come together hand in hand to merge nanorobots to humans to boost intelligence and health [240]. Precision medicine entails the development of implantable miniature medical devices built on smart materials, compact sensors and actuators, as well as microscale, nanoscale and nanostructured materials. By functioning inside the body, implantable miniature medical devices can have novel medical benefits. These machines may be able to detect and track their surroundings in real time, as well as perform basic tasks like administering drugs, fluid sampling, in vivo treatment of HIV and killing cancer cells [240, 241]. Here we will be focusing only on biomedical devices made using CNT and nanowires.

A few obstacles must be overcome before CNT can be used in medical devices. The first is concerned with protection, and it entails the use of CNT of extremely high purity in order to limit the release of harmful ions during activity in any biological environment. This is a significant problem since medical-grade CNT samples are only prepared on a small scale, and a trade-off had to be made between quality and quantity [216, 242]. Recently, CNT yarns are being studied to promote the development of wounded nerves, for precision delivery of drugs, and to give power in vivo to implantable devices and biosensors. Owing to the restricted supply of CNT yarn and the fear that using CNT in the body could be dangerous, as we have been told previously, they can be toxic, research attempts are limited.

The production of implantable electronic devices and sensors has accelerated due to recent developments in electronics and biomedicine. Annually, over 1 million people around the world receive a pacemaker or an ICD [243]. The wires used here previously were made of titanium and cobalt alloy. These wires also known as leads have specific tips and are made up of a metal wire structure covered by a polymer sheath. Dislodgment, vein thrombosis, migration and acute perforation are all common complications associated with these leads, some of which are caused by the leads' bulkiness and stiffness (in comparison with tissues). Lead displacement and dislodgment are among the complications caused by the leads, occurring in 5–10% of patients, and the published rate of lead perforation ranges from 0.4 to 5.2% [244]. There is also a popular wireless ICD, Zigbee but it has electronic parts and a battery outside the sensors for optimised data transmission [245, 246]. The consumption of power is very high, and difficulties are faced while controlling it below 100  $\mu$ W [247]. All the devices later can be modified by using CNT fibres as it is ultrathin, biocompatible, electroconductive and inert so it won't corrode unlike other metals. The main reason for incorporating CNT fibres is to overcome these problems and to give it more power and optimise data transmission. There may be one limitation of CNT wire is that it is less conductive than copper, so copper-coated large diameter CNT wire can be incorporated for the use [248]. So, from all these we can say that CNT tubes can be used as cardiac implantable but still the best design for building this CNT wire for its use in vivo needs to be investigated and researched upon.

Both coated and uncoated CNT fibres were tested in vivo on a mouse and found out that there was no evidence of toxicity after two weeks [241]. Another test was also performed with copper wire. With all the three tests, the mice survived all which

proved that wire through the skin is biocompatible for a short duration, but the copper wire caused some irritation in the skin. Later, the copper wire was replaced with CNT nanowires.

Based on the recent studies by Jayasinghe et al. showed that the previous discovered CNT yarns were perfect enough for biosensors, i.e., having strength of 1-2GPa, resistivity of  $10^{-4}$ – $10^{-5}$   $\Omega$  cm, density of 1 gm/cc and electric density of  $10^5$  Acm $^{-2}$  [249, 250]. The CNT wires having tiny diameter, inert, non-toxic, high flexibility, high conductivity, will become a breakthrough technology for nanomachines and biomedical devices in recent times.

## 8 Recent Advancements

After all the discussion, we can now say that porous carbon is indeed a versatile material that can be used in many significant industries and nowadays in biomedical sciences innovations. Carbon materials and its derivatives are undergoing research by a wide range of researchers, and various changes in the structure are opening a new field of porous carbon material in biomedical applications.

Mesoporous carbons are still in a developing phase with some of its application as controlled release of drugs. These materials when compared to graphene and other carbon derivatives are rarely used in this field, although studies show that they will give good results due to their unique structure. Because of its potential combinatorial qualities, such as carbonaceous content, peculiar structure and excellent biocompatibility, mesoporous carbon is considered the next generation inorganic material for various applications, including biomedical research [251].

Carbon dots have undergone enormous development and consist of a fascinating class of nanomaterials that have various biomedical advances due to their eco-friendly and cheap methods and have high image sensing capacity. There have recently been many modifications done to the CDs [252] but these developments have tremendously improved the in vivo cell targeting capacity and shown outstanding bioimaging capacity that includes elevated efficiency and sensitivity. CDs showing strong fluorescent emissions have strong penetration ability; i.e., it can penetrate the blood–brain barrier. This opens a multifunctional designed platform for targeted cancer cell diagnosis and treatment and applications in various neuronal disorders. But CDs show some toxicity effects which need to be urgently diagnosed clinically. Meanwhile, CDs nanoprobe for cancer treatment using bioimaging need more exploration to improve the efficacy of treatment.

Similarly, CNTs which are classified into two groups, single-walled CNTs and multi-walled CNTs, show excellent biocompatibility, mechanical strength and conductivity (thermal and electrical). They are used as DDS to target drugs to specific cells for treating cancer and for targeted DNA delivery, immunotherapy and regenerative medicine. Despite all this progress, the toxicity study of CNTs, biological degradation and biosafety is a major concern and still remains a controversial topic for human clinical practice.

Fullerenes are wonders of the latest discoveries from the last century, and various new aspects have been recognised to be used in the biomedical field. Fullerenes are shown to be the lowest toxicity among all the other derivatives of carbon and that stimulates the researchers to work on this fascinating nanomaterial for finding its biomedical uses. They are used as anticancer DDS, drugs for HIV, photodynamic therapy and sometimes used in cosmetics as an anti-aging effect. The major limitation faced by fullerene was its production cost which makes it very expensive, but scientists are working on it to reduce the production cost [111].

Graphene along with its derivative has successfully paved its path since the start of its journey in 2004, to be used in biosensing, as specific targeted gene delivery, as targeted drug carrier and bioimaging and detection [253]. However, these all are still on the verge of development and face many challenges, mainly the chronic toxicity effect.

Carbon nanofiber has long been debated for having an antibacterial effect as a better choice of material for wound dressing. They are also studied to be used in bone tissue regeneration, as biosensors and as modified electrospun nanofibers [254] for targeted DDS and specific drug delivery.

Carbon NHs and nanodiamonds mostly work together as they represent the same parental structure. These two derivatives have gained tremendous attention recently for their biocompatible properties and optical properties. These features make them eligible for a platform of use as regenerative medicine with a broad range of applications such as DDS for insoluble drugs.

So, from all the recent approaches of using porous carbon materials and their derivatives in biomedical application, much more further studies are required for thorough investigation of the toxic impact of all these porous carbons and its derivatives on humans which will include teratogenic and genotoxic effects. Soon we can then use these compounds with better safety, biocompatibility and efficacy and they would change the way of using nanotechnology towards medical science.

## 9 Conclusion

Porous carbon nanomaterial is indeed a versatile material which can improve various multidisciplinary approaches of the use of nanotechnology in medical sciences. These materials and their derivatives have some super properties that can change the way we look at the future of medical sciences. They can be used for treating many fatal diseases like cancer with ease as they can be used to target drugs to the specific part inside the cell and can be made to target DNA and that can be recovered. Extensive studies are going on to explore the intracellular drug delivery of various cytotoxic and hydrophobic drugs using porous carbon as encapsulating material. Studies also found that porous carbon and its derivatives can play an important role in solving the scarcity of antibiotics. In this chapter, we discussed how the germicidal activity of various metallic nanoparticles can meet the demand for new antibiotics with the help of porous carbon-based nanomaterials.



One of the major limitations that is creating problems is about the biocompatibility of the materials and the toxic effect on the bodies. However, recent studies show some of its derivatives have low toxicity inside the body if used for a short range of time. These derivatives also showed great biocompatibility when they were doped with some non-reactive metals. So, it can be summarised that porous carbon and its derivative is a potential candidate for future DDS which have capability to solve various conventional drug delivery formulation problems. If the future studies can standardise and establish the porous carbon and its derivatives in terms of its role in DDS, it will become a game changer in the field of biomedical sciences.

In modern medicine, bioimaging-based diagnosis is the key for the determination of not only some diseases but also it helps in the researcher to understand the real-time distribution and accumulation of drugs and other molecules. For the last few years, GQD, CD and graphene oxide are changing the field of bioimaging drastically, they are now used to understand transfection-based gene delivery, cytotoxic anticancer drug delivery, intracellular imaging of xenografted tumour mouse models, etc.

As today's world relies greatly on the real-time healthcare monitoring which demands accurate, sensitive and biocompatible sensors to use invasively and non-invasively in our body. Graphene and its derivatives provide all the ideal characteristics of real-time monitoring sensors, so they are now used extensively to shape the real-time health monitoring technology.

Nanobots are also made using porous carbon derivatives that can get inside the body to treat many diseases like HIV and cancer. They have futuristic designs that can change the way of microsurgeries in future of medical sciences.

So, from the above discussion, it can be concluded that porous carbon and its derivatives are no doubt an emerging trend which will supersede the conventional technologies of biomedical sciences in near future. Though it has some limitations and issues which need to be addressed extensively, it still seems like the scientific community is confident enough about the potentiality of porous carbon-based nanomaterials in the medical field and as the studies are still going on and in the coming decades we won't be surprised if these nanomaterials up a great role in treating the untreatable diseases of human race.

## References

1. Manocha SM (2003) Porous carbons. *Sadhana* 28(1–2):335–348
2. Thambiliyagodage C (2019) Porous carbon materials in biomedical applications. *BJSTR* 22(4):1–3
3. Lee J, Kim J, Hyeon T (2006) Recent progress in the synthesis of porous carbon materials. *Adv Mater* 18(16):2073–2094
4. Zhao Q, Lin Y, Han N, Li X, Geng H, Wang X et al (2017) Mesoporous carbon nanomaterials in drug delivery and biomedical application. *Drug Deliv* 24:94–107
5. Chen Y, Shi J (2015) Mesoporous carbon biomaterials. *Sci China Mater* 58(3):241–257
6. Doane TL, Burda C (2012) The unique role of nanoparticles in nanomedicine: imaging, drug delivery and therapy. *Chem Soc Rev* 41(7):2885

7. Wei A, Mehtala JG, Patri AK (2012) Challenges and opportunities in the advancement of nanomedicines. *J Control Release* 164(2):236–246
8. Kim J, Galanzha EI, Shashkov EV, Moon H, Zharov VP (2009) Golden carbon nanotubes as multimodal photoacoustic and photothermal high-contrast molecular agents. *Nature Nanotech* 4(10):688–694
9. Akhavan O, Ghaderi E (2013) Graphene nanomesh promises extremely efficient in vivo photothermal therapy. *Small* 9(21):3593–3601
10. Li X, Wang L, Fan Y, Feng Q, Cui F (2012) Biocompatibility and toxicity of nanoparticles and nanotubes. *J Nanomater* 2012:1–19
11. Balasubramanian K, Burghard M (2006) Biosensors based on carbon nanotubes. *Anal Bioanal Chem* 385(3):452–468
12. Pinyou P, Blay V, Muresan LM, Noguier T (2019) Enzyme-modified electrodes for biosensors and biofuel cells. *Mater Horiz* 6(7):1336–1358
13. Foley S, Crowley C, Smaihl M, Bonfils C, Erlanger BF, Seta P et al (2002) Cellular localisation of a water-soluble fullerene derivative. *Biochem Biophys Res Commun* 294(1):116–119
14. Zhang Y, Han L, Zhang Y, Chang Y, Chen X, He R et al (2016) Glutathione-mediated mesoporous carbon as a drug delivery nanocarrier with carbon dots as a cap and fluorescent tracer. *Nanotechnology* 27(35):355102
15. Yuan F, Dellian M, Fukumura D, Leunig M, Berk DA, Torchilin VP et al (1995) Vascular permeability in a human tumor xenograft: molecular size dependence and cutoff size. *Cancer Res* 55(17):3752–3756
16. Wan L, Jiao J, Cui Y, Guo J, Han N, Di D et al (2016) Hyaluronic acid modified mesoporous carbon nanoparticles for targeted drug delivery to CD44-overexpressing cancer cells. *Nanotechnology* 27(13):135102
17. Zhang Y, Zhi Z, Jiang T, Zhang J, Wang Z, Wang S (2010) Spherical mesoporous silica nanoparticles for loading and release of the poorly water-soluble drug telmisartan. *J Control Release* 145(3):257–263
18. Wang T, Jiang H, Wan L, Zhao Q, Jiang T, Wang B et al (2015) Potential application of functional porous TiO<sub>2</sub> nanoparticles in light-controlled drug release and targeted drug delivery. *Acta Biomater* 13:354–363
19. Zhao Q, Wang T, Wang J, Zheng L, Jiang T, Cheng G et al (2012) Fabrication of mesoporous hydroxycarbonate apatite for oral delivery of poorly water-soluble drug carvedilol. *J Non-Cryst Solids* 358(2):229–235
20. Wang T, Zhao P, Zhao Q, Wang B, Wang S (2016) The mechanism for increasing the oral bioavailability of poorly water-soluble drugs using uniform mesoporous carbon spheres as a carrier. *Drug Delivery* 23(2):420–428
21. Kim T, Chung P, Slowing II, Tsunoda M, Yeung ES, Lin VS (2008) Structurally ordered mesoporous carbon nanoparticles as transmembrane delivery vehicle in human cancer cells. *Nano Lett* 8(11):3724–3727
22. Radu DR, Lai C, Jeftinija K, Rowe EW, Jeftinija S, Lin VS (2004) A polyamidoamine dendrimer-capped mesoporous silica nanosphere-based gene transfection reagent. *J Am Chem Soc* 126(41):13216–13217
23. Giri S, Trewyn BG, Stellmaker MP, Lin VS (2005) Stimuli-responsive controlled-release delivery system based on mesoporous silica nanorods capped with magnetic nanoparticles. *Angew Chem Int Ed* 44(32):5038–5044
24. Xu ZP, Zeng QH, Lu GQ, Yu AB (2006) Inorganic nanoparticles as carriers for efficient cellular delivery. *Chem Eng Sci* 61(3):1027–1040
25. Li C, Qian M, Wang S, Jiang H, Du Y, Wang J et al (2017) Aptavalve-gated mesoporous carbon nanospheres image cellular mucin and provide on-demand targeted drug delivery. *Theranostics* 7(13):3319–3325
26. Wang L, Sun Q, Wang X, Wen T, Yin J, Wang P et al (2015) Using hollow carbon nanospheres as a light-induced free radical generator to overcome chemotherapy resistance. *J Am Chem Soc* 137(5):1947–1955

27. Chen Y, Xu P, Wu M, Meng Q, Chen H, Shu Z et al (2014) Colloidal RBC-shaped, hydrophilic, and hollow mesoporous carbon nanocapsules for highly efficient biomedical engineering. *Adv Mater* 26(25):4294–4301
28. Wang Y, Hu A (2014) Carbon quantum dots: synthesis, properties and applications. *J Mater Chem C* 2(34):6921
29. Antaris AL, Robinson JT, Yaghi OK, Hong G, Diao S, Luong R et al (2013) Ultra-low doses of chirality sorted (6,5) carbon nanotubes for simultaneous tumor imaging and photothermal therapy. *ACS Nano* 7(4):3644–3652
30. Wang R, Lu K, Tang Z, Xu Y (2017) Recent progress in carbon quantum dots: synthesis, properties and applications in photocatalysis. *J Mater Chem A* 5(8):3717–3734
31. Zhu S, Meng Q, Wang L, Zhang J, Song Y, Jin H et al (2013) Highly photoluminescent carbon dots for multicolor patterning, sensors, and bioimaging. *Angew Chem Int Ed* 52(14):3953–3957
32. Su W, Wu H, Xu H, Zhang Y, Li Y, Li X et al (2020) Carbon dots: a booming material for biomedical applications. *Mater Chem Front.* 4(3):821–836
33. Xu X, Ray R, Gu Y, Ploehn HJ, Gearheart L, Raker K et al (2004) Electrophoretic analysis and purification of fluorescent single-walled carbon nanotube fragments. *J Am Chem Soc* 126(40):12736–12737
34. Jia Q, Zheng X, Ge J, Liu W, Ren H, Chen S et al (2018) Synthesis of carbon dots from *Hypocrella bambusae* for bimodal fluorescence/photoacoustic imaging-guided synergistic photodynamic/photothermal therapy of cancer. *J Colloid Interface Sci* 526:302–311
35. Abdullah-Al-Nahain J, Lee I, In H, Lee KD, Lee JH, Jeong SY et al (2013) Target delivery and cell imaging using hyaluronic acid-functionalized graphene quantum dots. *Mol Pharmaceutics* 10(10):3736–3744
36. Nurunnabi M, Khatun Z, Huh KM, Park SY, Lee DY, Cho KJ et al (2013) In vivo biodistribution and toxicology of carboxylated graphene quantum dots. *ACS Nano* 7(8):6858–6867
37. Zhu S, Zhang J, Qiao C, Tang S, Li Y, Yuan W et al (2011) Strongly green-photoluminescent graphene quantum dots for bioimaging applications. *Chem Commun* 47(24):6858
38. Peng J, Gao W, Gupta BK, Liu Z, Romero-Aburto R, Ge L et al (2012) Graphene quantum dots derived from carbon fibers. *Nano Lett* 12(2):844–849
39. Tan X, Li Y, Li X, Zhou S, Fan L, Yang S (2015) Electrochemical synthesis of small-sized red fluorescent graphene quantum dots as a bioimaging platform. *Chem Commun* 51(13):2544–2546
40. Fan Z, Li Y, Li X, Fan L, Zhou S, Fang D et al (2014) Surrounding media sensitive photoluminescence of boron-doped graphene quantum dots for highly fluorescent dyed crystals, chemical sensing and bioimaging. *Carbon* 70:149–156
41. Song Y, Yan X, Li Z, Qu L, Zhu C, Ye R et al (2018) Highly photoluminescent carbon dots derived from linseed and their applications in cellular imaging and sensing. *J Mater Chem B* 6(19):3181–3187
42. Dong Y, Chen C, Zheng X, Gao L, Cui Z, Yang H et al (2012) One-step and high yield simultaneous preparation of single- and multi-layer graphene quantum dots from CX-72 carbon black. *J Mater Chem* 22(18):8764
43. Yang S, Cao L, Luo PG, Lu F, Wang X, Wang H et al (2009) Carbon dots for optical imaging in vivo. *J Am Chem Soc* 131(32):11308–11309
44. Tao H, Yang K, Ma Z, Wan J, Zhang Y, Kang Z et al (2012) In vivo NIR fluorescence imaging, biodistribution, and toxicology of photoluminescent carbon dots produced from carbon nanotubes and graphite. *Small* 8(2):281–290
45. Luo PG, Sahu S, Yang S, Sonkar SK, Wang J, Wang H et al (2013) Carbon “quantum” dots for optical bioimaging. *J Mater Chem B* 1(16):2116
46. Cao L, Yang S, Wang X, Luo PG, Liu J, Sahu S et al (2012) Competitive performance of carbon “quantum” dots in optical bioimaging. *Theranostics* 2(3):295–301
47. Li Y, Lin T, Luo Y, Liu Q, Xiao W, Guo W et al (2014) A smart and versatile theranostic nanomedicine platform based on nanoporphyrin. *Nat Commun* 5(1):1–7

48. Yang L, Wang Z, Wang J, Jiang W, Jiang X, Bai Z et al (2016) Doxorubicin conjugated functionalizable carbon dots for nucleus targeted delivery and enhanced therapeutic efficacy. *Nanoscale* 8(12):6801–6809
49. Pardo J, Peng Z, Leblanc R (2018) Cancer targeting and drug delivery using carbon-based quantum dots and nanotubes. *Molecules* 23(2):378
50. Iijima S (2002) Carbon nanotubes: past, present, and future. *Physica B* 323(1–4):1–5
51. Monthieux M, Serp P, Flahaut E, Razafinimanana M, Laurent C, Peigney A et al (2010) Introduction to carbon nanotubes. *Springer Handbook of Nanotechnology*, pp 47–118
52. Punbusayakul N, Talapatra S, Ajayan PM, Surareungchai W (2013) Label-free as-grown double wall carbon nanotubes bundles for *Salmonella typhimurium* immunoassay. *Chem Cent J* 7(1):1–6
53. Yudasaka M, Yomogida Y, Zhang M, Tanaka T, Nakahara M, Kobayashi N et al (2017) Near-Infrared photoluminescent carbon nanotubes for imaging of brown fat. *Sci Rep* 7(1):1–7
54. Fadel TR, Sharp FA, Vudattu N, Ragheb R, Garyu J, Kim D et al (2014) A carbon nanotube–polymer composite for T-cell therapy. *Nature Nanotech* 9(8):639–647
55. Correa-Duarte MA, Wagner N, Rojas-Chapana J, Morszeck C, Thie M, Giersig M (2004) Fabrication and biocompatibility of carbon nanotube-based 3D networks as scaffolds for cell seeding and growth. *Nano Lett* 4(11):2233–2236
56. Liu Z, Sun X, Nakayama-Ratchford N, Dai H (2007) Supramolecular chemistry on water-soluble carbon nanotubes for drug loading and delivery. *ACS Nano* 1(1):50–56
57. Liu Z, Fan AC, Rakhra K, Sherlock S, Goodwin A, Chen X et al (2009) Supramolecular stacking of doxorubicin on carbon nanotubes for in vivo cancer therapy. *Angew Chem Int Ed* 48(41):7668–7672
58. Bubanalé S, Shivashankar M (2017) Siddaganga institute of technology. History, method of production, structure and applications of activated carbon. *Int J Eng Res Technol (Ahmedabad)* V6(06)
59. Otowa T, Nojima Y, Miyazaki T (1997) Development of KOH activated high surface area carbon and its application to drinking water purification. *Carbon* 35(9):1315–1319
60. Levy G (1982) Gastrointestinal clearance of drugs with activated charcoal. *N Engl J Med* 307(11):676–678
61. Antidotes in poisoning. *Indian J Crit Care Med* 23(S4):1–4 (2019)
62. Olson KR (2010) Activated charcoal for acute poisoning: one toxicologist’s journey. *J Med Toxicol* 6(2):190–198
63. Chin L (1980) Activated charcoal: Antidotal and other medical uses. By David O Cooney *Drugs and the pharmaceutical sciences*, vol 9. Dekker, 270 Madison Ave., New York, NY 10016. 1980, p 160. 15 × 23 cm. Price \$23.50. *J Pharmaceut Sci* 69(11):1361
64. Gaudreault P (2005) Activated charcoal revisited. *Clin Pediatr Emerg Med* 6(2):76–80
65. Daly JS, Cooney DO (1978) Interference by tannic acid with the effectiveness of activated charcoal in “universal antidote.” *Clin Toxicol* 12(5):515–522
66. Miriyala N, Ouyang D, Perrie Y, Lowry D, Kirby DJ (2017) Activated carbon as a carrier for amorphous drug delivery: effect of drug characteristics and carrier wettability. *Eur J Pharm Biopharm* 115:197–205
67. Hancock BC, Zografi G (1997) Characteristics and significance of the amorphous state in pharmaceutical systems. *J Pharm Sci* 86(1):1–12
68. Limmell T, Santos HA, Mäkilä E, Heikkilä T, Salonen J, Murzin DY et al (2011) Drug delivery formulations of ordered and nonordered mesoporous silica: comparison of three drug loading methods. *J Pharm Sci* 100(8):3294–3306
69. Ramanujan R, Purushotham S, Chia M (2007) Processing and characterization of activated carbon coated magnetic particles for biomedical applications. *Mater Sci Eng, C* 27(4):659–664
70. Kim J, Lee JE, Lee SH, Yu JH, Lee JH, Park TG et al (2008) Designed fabrication of a multifunctional polymer nanomedical platform for simultaneous cancer–targeted imaging and magnetically guided drug delivery. *Adv Mater* 20(3):478–483
71. Kroto HW, Heath JR, O’Brien SC, Curl RF, Smalley RE (1985) C<sub>60</sub>: Buckminsterfullerene. *Nature* 318(6042):162–163

72. Moussa F (2018) Fullerene and derivatives for biomedical applications. In: *Nanobiomaterials*. Elsevier, pp 113–36
73. Friedman SH, DeCamp DL, Sijbesma RP, Srdanov G, Wudl F, Kenyon GL (1993) Inhibition of the HIV-1 protease by fullerene derivatives: model building studies and experimental verification. *J Am Chem Soc* 115(15):6506–6509
74. Prato M (1999) Fullerene materials. In: *Fullerenes and related structures*. Springer Berlin Heidelberg, Berlin, Heidelberg, pp 173–87
75. Bosi S, Da Ros T, Spalluto G, Prato M (2003) Fullerene derivatives: an attractive tool for biological applications. *Eur J Med Chem* 38(11–12):913–923
76. Jensen AW, Wilson SR, Schuster DI (1996) Biological applications of fullerenes. *Bioorg Med Chem* 4(6):767–779
77. Bolskar RD (2008) Gadolinium endohedral metallofullerene-based MRI contrast agents. In: *Medicinal chemistry and pharmacological potential of fullerenes and carbon nanotubes*. Springer Netherlands, Dordrecht, pp 157–180
78. Goodarzi S, Da Ros T, Conde J, Sefat F, Mozafari M (2017) Fullerene: biomedical engineers get to revisit an old friend. *Mater Today* 20(8):460–480
79. Yin J, Lao F, Meng J, Fu PP, Zhao Y, Xing G et al (2008) Inhibition of tumor growth by endohedral metallofullerenol nanoparticles optimized as reactive oxygen species scavenger. *Mol Pharmacol* 74(4):1132–1140
80. Yudoh K, Shishido K, Murayama H, Yano M, Matsubayashi K, Takada H et al (2007) Water-soluble C60 fullerene prevents degeneration of articular cartilage in osteoarthritis via down-regulation of chondrocyte catabolic activity and inhibition of cartilage degeneration during disease development. *Arthritis Rheum* 56(10):3307–3318
81. Dellinger A, Zhou Z, Lenk R, MacFarland D, Kepley CL (2009) Fullerene nanomaterials inhibit phorbol myristate acetate-induced inflammation. *Exp Dermatol* 18(12):1079–1081
82. Baati T, Bourasset F, Gharbi N, Njim L, Abderrabba M, Kerkeni A et al (2012) The prolongation of the lifespan of rats by repeated oral administration of [60]fullerene. *Biomaterials* 33(19):4936–4946
83. Dobrovolskaia M, McNeil S, Neun BW (2008) A nanoparticle-based anticoagulant, WO/2008/063157, PCT/US2006/041838
84. Andrievsky G, Shakhnin D, Tronza A, Zhernosekov D, Tykhomyrov A (2010) The acceleration of blood plasma clot lysis in the presence of hydrated C60 fullerene nanostructures in super-small concentration. *Fullerenes, Nanotubes, Carbon Nanostruct* 18(3):303–311
85. Nakamura E, Sawamura M, Isobe H, Fullerene derivatives, a novel means for condensing DNA, WO 1999/046235, PCT/JP1999/001146
86. Klee JE, Walz U, Light-polymerizable dental composition containing an inhibitor, WO/2002/085974, PCT/US2002/011978
87. Slonczewski JC, Weiss PR (1958) Band structure of graphite. *Phys Rev* 109(2):272–279
88. Kulkarni SK (2014) *Nanotechnology: principles and practices*, 3rd edn. Springer International Publishing, Cham, Switzerland
89. Tiwari SK, Sahoo S, Wang N, Huczko A (2020) Graphene research and their outputs: status and prospect. *J Sci: Adv Mater Dev* 5(1):10–29
90. Chakraborty M, Hashmi MSJ (2018) Wonder material graphene: properties, synthesis and practical applications. *Adv Mater Process Technol* 4(4):573–602
91. Li K, Liu W, Ni Y, Li D, Lin D, Su Z et al (2017) Technical synthesis and biomedical applications of graphene quantum dots. *J Mater Chem B* 5(25):4811–4826
92. Zhang L, Xia J, Zhao Q, Liu L, Zhang Z (2010) Functional graphene oxide as a nanocarrier for controlled loading and targeted delivery of mixed anticancer drugs. *Small* 6(4):537–544
93. Yang K, Zhang S, Zhang G, Sun X, Lee S, Liu Z (2010) Graphene in mice: ultrahigh in vivo tumor uptake and efficient photothermal therapy. *Nano Lett* 10(9):3318–3323
94. Sun X, Liu Z, Welsher K, Robinson JT, Goodwin A, Zaric S et al (2008) Nano-graphene oxide for cellular imaging and drug delivery. *Nano Res* 1(3):203–212
95. Du D, Wang L, Shao Y, Wang J, Engelhard MH, Lin Y (2011) Functionalized graphene oxide as a nanocarrier in a multienzyme labeling amplification strategy for ultrasensitive electrochemical immunoassay of phosphorylated p53 (S392). *Anal Chem* 83(3):746–752

96. Chen G, Pang D, Hwang S, Tuan H, Hu Y (2012) A graphene-based platform for induced pluripotent stem cells culture and differentiation. *Biomaterials* 33(2):418–427
97. Syama S, Mohanan P (2016) Safety and biocompatibility of graphene: a new generation nanomaterial for biomedical application. *Int J Biol Macromol* 86:546–555
98. Shen H, Zhang L, Liu M, Zhang Z (2012) Biomedical applications of graphene. *Theranostics*. 2(3):283–294
99. Shen J, Zhu Y, Chen C, Yang X, Li C (2011) Facile preparation and upconversion luminescence of graphene quantum dots. *Chem Commun* 47(9):2580–2582
100. Li M, Wu W, Ren W, Cheng H, Tang N, Zhong W et al (2012) Synthesis and upconversion luminescence of N-doped graphene quantum dots. *Appl Phys Lett* 101(10):103107
101. Gajewska A, Istif A, Gul J, Chironi M, Faidiga A, Rocco M et al (2021) Chapter 1. Carbon nanostructures: drug delivery and beyond. In: *Nanoscience and nanotechnology series*. Royal Society of Chemistry, Cambridge, pp 1–38
102. Fan H, Wang L, Zhao K, Li N, Shi Z, Ge Z et al (2010) Fabrication, mechanical properties, and biocompatibility of graphene-reinforced chitosan composites. *Biomacromol* 11(9):2345–2351
103. Ryoo S, Kim Y, Kim M, Min D (2010) Behaviors of NIH-3T3 fibroblasts on graphene/carbon nanotubes: proliferation, focal adhesion, and gene transfection studies. *ACS Nano* 4(11):6587–6598
104. Nayak TR, Andersen H, Makam VS, Khaw C, Bae S, Xu X et al (2011) Graphene for controlled and accelerated osteogenic differentiation of human mesenchymal stem cells. *ACS Nano* 5(6):4670–4678
105. Shin SR, Li Y, Jang HL, Khoshkhalagh P, Akbari M, Nasajpour A et al (2016) Graphene-based materials for tissue engineering. *Adv Drug Deliv Rev* 105:255–274
106. Akhavan O, Ghaderi E (2010) Toxicity of graphene and graphene oxide nanowalls against bacteria. *ACS Nano* 4(10):5731–5736
107. Drug efficacy and safety [internet]. *Msdmanuals.com*. [cited 2021 Oct 23]. Available from: <https://www.msdmanuals.com/professional/clinical-pharmacology/concepts-in-pharmacotherapy/drug-efficacy-and-safety>
108. Rahman MM, Ara MG, Alim MA, Uddin MS, Najda A, Albadrani GM et al (2021) Mesoporous carbon: a versatile material for scientific applications. *IJMS* 22(9):4498
109. Kavosi A, Hosseini Ghale Noei S, Madani S, Khalighfard S, Khodayari S, Khodayari H, et al (2018) The toxicity and therapeutic effects of single- and multi-wall carbon nanotubes on mice breast cancer. *Sci Rep* 8(1):1–8
110. Watson WA (1987) Factors influencing the clinical efficacy of activated charcoal. *Drug Intell Clin Pharm* 21(2):160–166
111. Bakry R, Vallant RM, Najam-ul-Haq M, Rainer M, Szabo Z, Huck CW et al (2007) Medicinal applications of fullerenes. *Int J Nanomedicine* 2(4):639–649
112. Zhao C, Song X, Liu Y, Fu Y, Ye L, Wang N et al (2020) Synthesis of graphene quantum dots and their applications in drug delivery. *J Nanobiotechnol* 18(1):1–6
113. Priyadarsini S, Mohanty S, Mukherjee S, Basu S, Mishra M (2018) Graphene and graphene oxide as nanomaterials for medicine and biology application. *J Nanostruct Chem* 8(2):123–137
114. Szunerits S, Boukherroub R (2018) Graphene-based biosensors. *Interface Focus* 8(3):20160132
115. Shahdeo D, Roberts A, Abbineni N, Gandhi S (2020) Graphene based sensors. In: *Analytical applications of graphene for comprehensive analytical chemistry*. Elsevier, pp 175–199
116. Huang H, Su S, Wu N, Wan H, Wan S, Bi H et al (2019) Graphene-Based sensors for human health monitoring. *Front Chem* 11(7):1–11
117. Ameri SK, Singh PK, D'Angelo R, Stoppel W, Black L, Sonkusale SR (2016) Three dimensional graphene scaffold for cardiac tissue engineering and in-situ electrical recording. In: 2016 38th annual international conference of the IEEE engineering in medicine and biology society (EMBC). IEEE

118. Wang X, Liu Z, Zhang T (2017) Flexible sensing electronics for wearable/attachable health monitoring. *Small* 13(25):1602790
119. Pantelopoulos A, Bourbakis NG (2010) Prognosis—a wearable health-monitoring system for people at risk: methodology and modeling. *IEEE Trans Inform Technol Biomed* 14(3):613–621
120. Paulovich FV, De Oliveira MCF, Oliveira ON (2018) A future with ubiquitous sensing and intelligent systems. *ACS Sens* 3(8):1433–1438
121. Yang C, Denno ME, Pyakurel P, Venton BJ (2015) Recent trends in carbon nanomaterial-based electrochemical sensors for biomolecules: a review. *Anal Chim Acta* 887:17–37
122. Fadeel B, Bussy C, Merino S, Vázquez E, Flahaut E, Mouchet F et al (2018) Safety assessment of graphene-based materials: focus on human health and the environment. *ACS Nano* 12(11):10582–10620
123. Liu T, Chuang M, Chu C, Huang W, Lai H, Wang C et al (2016) Implantable graphene-based neural electrode interfaces for electrophysiology and neurochemistry in in vivo hyperacute stroke model. *ACS Appl Mater Interfaces* 8(1):187–196
124. Imani S, Bandodkar AJ, Mohan AMV, Kumar R, Yu S, Wang J et al (2016) A wearable chemical–electrophysiological hybrid biosensing system for real-time health and fitness monitoring. *Nat Commun* 7(1):1–4
125. Bae GY, Pak SW, Kim D, Lee G, Kim DH, Chung Y et al (2016) Linearly and highly pressure-sensitive electronic skin based on a bioinspired hierarchical structural array. *Adv Mater* 28(26):5300–5306
126. Prance H (2011) Sensor developments for electrophysiological monitoring in healthcare. In: *Applied biomedical engineering*. InTech
127. Wang T, Yang H, Qi D, Liu Z, Cai P, Zhang H et al (2018) Mechano-Based transductive sensing for wearable healthcare. *Small* 14(11):1702933
128. Yun YJ, Ju J, Lee JH, Moon S, Park S, Kim YH et al (2017) Highly elastic graphene-based electronics toward electronic skin. *Adv Funct Mater* 27(33):1701513
129. Kou H, Zhang L, Tan Q, Liu G, Lv W, Lu F et al (2018) Wireless flexible pressure sensor based on micro-patterned Graphene/PDMS composite. *Sens Actuators, A* 277:150–156
130. Wang J, Lu C, Zhang K (2020) Textile-Based strain sensor for human motion detection. *Energy Environ Mater* 3(1):80–100
131. Yu R, Zhu C, Wan J, Li Y, Hong X (2021) Review of graphene-based textile strain sensors, with emphasis on structure activity relationship. *Polymers* 13(1):151
132. Pan F, Chen S, Li Y, Tao Z, Ye J, Ni K et al (2018) 3D graphene films enable simultaneously high sensitivity and large stretchability for strain sensors. *Adv Funct Mater* 28(40):1803221
133. Fu Y, Hansson J, Liu Y, Chen S, Zehri A, Samani MK et al (2019) Graphene related materials for thermal management. *2D Mater* 7(1):012001
134. Mohan VB, Lau K, Hui D, Bhattacharyya D (2018) Graphene-based materials and their composites: a review on production, applications and product limitations. *Compos B Eng* 142:200–220
135. Sharma A, Badaea M, Tiwari S, Marty JL (2021) Wearable biosensors: an alternative and practical approach in healthcare and disease monitoring. *Molecules* 26(3):748
136. Ray TR, Choi J, Bandodkar AJ, Krishnan S, Gutruf P, Tian L et al (2019) Bio-Integrated wearable systems: a comprehensive review. *Chem Rev* 119(8):5461–5533
137. de la Guardia M (1995) Biochemical sensors: the state of the art. *Mikrochim Acta* 120(1–4):243–255
138. Cao Z, Yao B, Qin C, Yang R, Guo Y, Zhang Y et al (2019) Biochemical sensing in graphene-enhanced microfiber resonators with individual molecule sensitivity and selectivity. *Light Sci Appl* 8(1):1–6
139. Khan S, Ali S, Bermak A (2019) Recent developments in printing flexible and wearable sensing electronics for healthcare applications. *Sensors* 19(5):1230
140. Chung M, Fortunato G, Radacs N (2019) Wearable flexible sweat sensors for healthcare monitoring: a review. *J R Soc Interface* 16(159):20190217

141. Kim J, Kim M, Lee M, Kim K, Ji S, Kim Y et al (2017) Wearable smart sensor systems integrated on soft contact lenses for wireless ocular diagnostics. *Nat Commun* 8(1):1–9
142. Park J, Kim J, Kim S, Cheong WH, Jang J, Park Y et al (2018) Soft, smart contact lenses with integrations of wireless circuits, glucose sensors, and displays. *Sci Adv* 4(1):eaap9841
143. Xuan X, Kim JY, Hui X, Das PS, Yoon HS, Park J (2018) A highly stretchable and conductive 3D porous graphene metal nanocomposite based electrochemical-physiological hybrid biosensor. *Biosens Bioelectron* 120:160–167
144. Active threat solutions by defense. Fight or flee: understanding your response to stress [Internet]. *Didactivethreat.com*. [cited 2021 May 20]
145. Tuteja SK, Ormsby C, Neethirajan S (2018) Noninvasive label-free detection of cortisol and lactate using graphene embedded screen-printed electrode. *Nano-Micro Lett* 10(3):1–10
146. Andersen LW, Mackenhauer J, Roberts JC, Berg KM, Cocchi MN, Donnino MW (2013) Etiology and therapeutic approach to elevated lactate levels. *Mayo Clin Proc* 88(10):1127–1140
147. Wang Z, Gui M, Asif M, Yu Y, Dong S, Wang H et al (2018) A facile modular approach to the 2D oriented assembly MOF electrode for non-enzymatic sweat biosensors. *Nanoscale* 10(14):6629–6638
148. Bajtarevic A, Ager C, Pienz M, Klieber M, Schwarz K, Ligor M et al (2009) Noninvasive detection of lung cancer by analysis of exhaled breath. *BMC Cancer* 9(1):1–7
149. Zhou X, Xue Z, Chen X, Huang C, Bai W, Lu Z et al (2020) Nanomaterial-based gas sensors used for breath diagnosis. *J Mater Chem B* 8(16):3231–3248
150. Karaduman I, Er E, Çelikkan H, Erk N, Acar S (2017) Room-temperature ammonia gas sensor based on reduced graphene oxide nanocomposites decorated by Ag, Au and Pt nanoparticles. *J Alloy Compd* 722:569–578
151. Eckert MA, Vu PQ, Zhang K, Kang D, Ali MM, Xu C et al (2013) Novel Molecular and nanosensors for in vivo sensing. *Theranostics*. 3(8):583–594
152. Kostarelos K, Vincent M, Hebert C, Garrido JA (2017) Graphene in the design and engineering of next-generation neural interfaces. *Adv Mater* 29(42):1700909
153. Kireev D, Shokoohimehr P, Ernst M, Montes VR, Srikantharajah K, Maybeck V et al (2018) Fabrication of ultrathin and flexible graphene-based devices for in vivo neuroprosthetics. *MRS Adv* 3(29):1621–1627
154. Choi J, Kim S, Ryu R, Kim S, Sohn J (2018) Implantable neural probes for brain-machine interfaces? Current developments and future prospects. *Exp Neurobiol* 27(6):453–471
155. Park MV, Bleeker EA, Brand W, Cassee FR, van Elk M, Gosens I et al (2017) Considerations for safe innovation: the case of graphene. *ACS Nano* 11(10):9574–9593
156. Du M, Xu X, Yang L, Guo Y, Guan S, Shi J et al (2018) Simultaneous surface and depth neural activity recording with graphene transistor-based dual-modality probes. *Biosens Bioelectron* 105:109–115
157. Lu Y, Liu X, Hattori R, Ren C, Zhang X, Komiyama T et al (2018) Ultralow impedance graphene microelectrodes with high optical transparency for simultaneous deep two-photon imaging in transgenic mice. *Adv Funct Mater* 28(31):1800002
158. Liu X, Lu Y, Iseri E, Shi Y, Kuzum D (2018) A compact closed-loop optogenetics system based on artifact-free transparent graphene electrodes. *Front Neurosci* 6(12):1–9
159. Thunemann M, Lu Y, Liu X, Kılıç K, Desjardins M, Vandenberghe M et al (2018) Deep 2-photon imaging and artifact-free optogenetics through transparent graphene microelectrode arrays. *Nat Commun* 9(1):1–6
160. Lee H, Hong YJ, Baik S, Hyeon T, Kim D (2018) Enzyme-based glucose sensor: from invasive to wearable device. *Adv Healthcare Mater* 7(8):1701150
161. Freedman B, Boriani G, Glotzer TV, Healey JS, Kirchhof P, Potpara TS (2017) Management of atrial high-rate episodes detected by cardiac implanted electronic devices. *Nat Rev Cardiol* 14(12):701–714
162. Yang N, Sampathkumar K, Loo SCJ (2017) Recent advances in complementary and replacement therapy with nutraceuticals in combating gastrointestinal illnesses. *Clin Nutr* 36(4):968–979



163. Lee H, Lee Y, Song C, Cho HR, Ghaffari R, Choi TK et al (2015) An endoscope with integrated transparent bioelectronics and theranostic nanoparticles for colon cancer treatment. *Nat Commun* 6(1):1–11
164. Basu PK, Indukuri D, Keshavan S, Navratna V, Vanjari SRK, Raghavan S et al (2014) Graphene based *E. coli* sensor on flexible acetate sheet. *Sens Actuators B Chem* 190:342–347
165. Kim SJ, Cho KW, Cho HR, Wang L, Park SY, Lee SE et al (2016) Stretchable and transparent biointerface using cell-sheet-graphene hybrid for electrophysiology and therapy of skeletal muscle. *Adv Funct Mater* 26(19):3207–3217
166. Wang K, Ruan J, Song H, Zhang J, Wo Y, Guo S et al (2011) Biocompatibility of graphene oxide. *Nanoscale Res Lett* 6(1):1–6
167. Tripathi A, Saraf S, Saraf S (2015) Carbon nanotropes: a contemporary paradigm in drug delivery. *Materials* 8(6):3068–3100
168. Zhang W, Zhang Z, Zhang Y (2011) The application of carbon nanotubes in target drug delivery systems for cancer therapies. *Nanoscale Res Lett* 6(1):1–5
169. Schipper ML, Nakayama-Ratchford N, Davis CR, Kam NWS, Chu P, Liu Z et al (2008) A pilot toxicology study of single-walled carbon nanotubes in a small sample of mice. *Nature Nanotech* 3(4):216–221
170. Chakrabarti M, Kiseleva R, Vertegel A, Ray SK (2015) Carbon nanomaterials for drug delivery and cancer therapy. *J Nanosci Nanotechnol* 15(8):5501–5511
171. Kang B, Chang S, Dai Y, Yu D, Chen D (2010) Cell response to carbon nanotubes: size-dependent intracellular uptake mechanism and subcellular fate. *Small* 6(21):2362–2366
172. Wan B, Wang Z, Lv Q, Dong P, Zhao L, Yang Y et al (2013) Single-walled carbon nanotubes and graphene oxides induce autophagosome accumulation and lysosome impairment in primarily cultured murine peritoneal macrophages. *Toxicol Lett* 221(2):118–127
173. Mu Q, Broughton DL, Yan B (2009) Endosomal leakage and nuclear translocation of multi-walled carbon nanotubes: developing a model for cell uptake. *Nano Lett* 9(12):4370–4375
174. Lochner N, Pittner F, Wirth M, Gabor F (2003) Preparation, characterization and application of artificial Caco-2 cell surfaces in the silver nanoparticle enhanced fluorescence technique. *J Control Release* 89(2):249–259
175. Mehra NK, Mishra V, Jain N (2014) A review of ligand tethered surface engineered carbon nanotubes. *Biomaterials* 35(4):1267–1283
176. Liu Z, Tabakman S, Welsher K, Dai H (2009) Carbon nanotubes in biology and medicine: in vitro and in vivo detection, imaging and drug delivery. *Nano Res* 2(2):85–120
177. Hilder T, Hill J (2008) Probability of encapsulation of paclitaxel and doxorubicin into carbon nanotubes. *Micro Nano Lett* 3(2):41
178. Ding H, Du F, Liu P, Chen Z, Shen J (2015) DNA–carbon dots function as fluorescent vehicles for drug delivery. *ACS Appl Mater Interfaces* 7(12):6889–6897
179. Wang Q, Huang X, Long Y, Wang X, Zhang H, Zhu R et al (2013) Hollow luminescent carbon dots for drug delivery. *Carbon* 59:192–199
180. Das P, Ganguly S, Agarwal T, Maity P, Ghosh S, Choudhary S et al (2019) Heteroatom doped blue luminescent carbon dots as a nano-probe for targeted cell labeling and anticancer drug delivery vehicle. *Mater Chem Phys* 237:121860
181. Liu Z, Robinson JT, Sun X, Dai H (2008) PEGylated nanographene oxide for delivery of water-insoluble cancer drugs. *J Am Chem Soc* 130(33):10876–10877
182. Goenka S, Sant V, Sant S (2014) Graphene-based nanomaterials for drug delivery and tissue engineering. *J Control Release* 173:75–88
183. Han C, Zhang X, Wang F, Yu Q, Chen F, Shen D et al (2021) Duplex metal co-doped carbon quantum dots-based drug delivery system with intelligent adjustable size as adjuvant for synergistic cancer therapy. *Carbon* 183:789–808
184. Gomez JJ, Arnaiz B, Cacioppo M, Arcudi F, Prato M (2018) Nitrogen-doped carbon nanodots for bioimaging and delivery of paclitaxel. *J Mater Chem B* 6(35):5540–5548
185. Afzal H, Ikram M, Ali S, Shahzadi A, Aqeel M, Haider A et al (2020) Enhanced drug efficiency of doped ZnO–GO (graphene oxide) nanocomposites, a new gateway in drug delivery systems (DDS). *Mater Res Express*. 7(1):015405

186. Román G, Noseda Grau E, Díaz Compañy A, Brizuela G, Juan A, Simonetti S (2018) A first-principles study of pristine and Al-doped activated carbon interacting with 5-Fluorouracil anticancer drug. *Eur Phys J E* 41(9):1–8
187. Pan H, Yu Y, Li L, Liu B, Liu Y (2021) Fabrication and characterization of taurine functionalized graphene oxide with 5-fluorouracil as anticancer drug delivery systems. *Nanoscale Res Lett* 16(1):1–9
188. Yao H, Su L, Zeng M, Cao L, Zhao W, Chen C et al (2016) Construction of magnetic-carbon-quantum-dots-probe-labeled apoferritin nanocages for bioimaging and targeted therapy. *IJN* 11:4423–4438
189. Ye T, Xu W, Shi T, Yang R, Yang X, Wang S et al (2015) Targeted delivery of docetaxel to the metastatic lymph nodes: a comparison study between nanoliposomes and activated carbon nanoparticles. *Asian J Pharm Sci* 10(1):64–72
190. Mishra R, Militky J, Venkataraman M (2019) Nanotechnology in textiles. Woodhead Publishing, Duxford, UK, pp 365–385
191. Fresco-Cala B, López-Lorente Á, Cárdenas S (2018) Monolithic solid based on single-walled carbon nanohorns: preparation, characterization, and practical evaluation as a sorbent. *Nanomaterials* 8(6):370
192. Wang J, Hu Z, Xu J, Zhao Y (2014) Therapeutic applications of low-toxicity spherical nanocarbon materials. *NPG Asia Mater* 6(2):e84
193. Chen Z, Tabakman SM, Goodwin AP, Kattah MG, Daranciang D, Wang X et al (2008) Protein microarrays with carbon nanotubes as multicolor Raman labels. *Nat Biotechnol* 26(11):1285–1292
194. Valentini F, Carbone M, Palleschi G (2013) Carbon nanostructured materials for applications in nano-medicine, cultural heritage, and electrochemical biosensors. *Anal Bioanal Chem* 405(2–3):451–465
195. Kostarelos K, Bianco A, Prato M (2009) Promises, facts and challenges for carbon nanotubes in imaging and therapeutics. *Nature Nanotech* 4(10):627–633
196. Krauss TD (2009) Nanotubes light up cells. *Nature Nanotech* 4(2):85–86
197. Jiang H (2011) Chemical preparation of graphene-based nanomaterials and their applications in chemical and biological sensors. *Small* n/a
198. Swierczewska M, Choi KY, Mertz EL, Huang X, Zhang F, Zhu L et al (2012) A facile, one-step nanocarbon functionalization for biomedical applications. *Nano Lett* 12(7):3613–3620
199. Yamashita T, Yamashita K, Nabeshi H, Yoshikawa T, Yoshioka Y, Tsunoda S et al (2012) Carbon nanomaterials: efficacy and safety for nanomedicine. *Materials* 5(12):350–363
200. Shi Kam NW, Jessop TC, Wender PA, Dai H (2004) Nanotube molecular transporters: internalization of carbon nanotube–protein conjugates into mammalian cells. *J Am Chem Soc* 126(22):6850–6851
201. Chao J, Perevedentseva E, Chung P, Liu K, Cheng C, Chang C et al (2007) Nanometer-sized diamond particle as a probe for biolabeling. *Biophys J* 93(6):2199–2208
202. Krueger A (2008) New carbon materials: biological applications of functionalized nanodiamond materials. *Chem Eur J* 14(5):1382–1390
203. Man HB, Ho D (2012) Diamond as a nanomedical agent for versatile applications in drug delivery, imaging, and sensing. *Phys Status Solidi A* 209(9):1609–1618
204. Sijbesma R, Srdanov G, Wudl F, Castoro JA, Wilkins C, Friedman SH et al (1993) Synthesis of a fullerene derivative for the inhibition of HIV enzymes. *J Am Chem Soc* 115(15):6510–6512
205. Partha R, Conyers JL (2009) Biomedical applications of functionalized fullerene-based nanomaterials. *Int J Nanomedicine* 4:261–275
206. Xiao L, Takada H, Gan X, Miwa N (2006) The water-soluble fullerene derivative ‘Radical Sponge®’ exerts cytoprotective action against UVA irradiation but not visible-light-catalyzed cytotoxicity in human skin keratinocytes. *Bioorg Med Chem Lett* 16(6):1590–1595
207. Quick KL, Ali SS, Arch R, Xiong C, Wozniak D, Dugan LL (2008) A carboxyfullerene SOD mimetic improves cognition and extends the lifespan of mice. *Neurobiol Aging* 29(1):117–128
208. Isakovic A, Markovic Z, Todorovic-Markovic B, Nikolic N, Vranjes-Djuric S, Mirkovic M et al (2006) Distinct cytotoxic mechanisms of pristine versus hydroxylated fullerene. *Toxicol Sci* 91(1):173–183

209. Daroczi B, Kari G, McAleer MF, Wolf JC, Rodeck U, Dicker AP (2006) In vivo radioprotection by the fullerene nanoparticle DF-1 as assessed in a zebrafish model. *Clin Cancer Res* 12(23):7086–7091
210. Simonin J (2001) Solvent effects on osmotic second virial coefficient studied using analytic molecular models. Application to solutions of C60 fullerene. *J Phys Chem B* 105(22):5262–5270
211. Cagle DW, Kennel SJ, Mirzadeh S, Alford JM, Wilson LJ (1999) In vivo studies of fullerene-based materials using endohedral metallofullerene radiotracers. *Proc Natl Acad Sci* 96(9):5182–5187
212. Okumura M, Mikawa M, Yokawa T, Kanazawa Y, Kato H, Shinohara H (2002) Evaluation of water-soluble metallofullerenes as MRI contrast agents. *Acad Radiol* 9(2):S495–S497
213. Mikawa M, Kato H, Okumura M, Narazaki M, Kanazawa Y, Miwa N et al (2001) Paramagnetic water-soluble metallofullerenes having the highest relaxivity for MRI contrast agents. *Bioconjugate Chem* 12(4):510–514
214. Bolskar RD, Benedetto AF, Husebo LO, Price RE, Jackson EF, Wallace S et al (2003) First soluble M@C60 derivatives provide enhanced access to metallofullerenes and permit in vivo evaluation of Gd@C60[C(COOH)2]10 as a MRI contrast agent. *J Am Chem Soc* 125(18):5471–5478
215. Ajima K, Yudasaka M, Murakami T, Maigné A, Shiba K, Iijima S (2005) Carbon nanohorns as anticancer drug carriers. *Mol Pharmaceutics* 2(6):475–480
216. Tahara Y, Miyawaki J, Zhang M, Yang M, Waga I, Iijima S et al (2011) Histological assessments for toxicity and functionalization-dependent biodistribution of carbon nanohorns. *Nanotechnology* 22(26):265106
217. Tsuchida K, Murakami T (2008) Recent advances in inorganic nanoparticle-based drug delivery systems. *MRMC* 8(2):175–183
218. Guan B, Zou F, Zhi J (2010) Nanodiamond as the pH-responsive vehicle for an anticancer drug. *Small* 6(14):1514–1519
219. Chen M, Pierstorff ED, Lam R, Li S, Huang H, Osawa E et al (2009) Nanodiamond-mediated delivery of water-insoluble therapeutics. *ACS Nano* 3(7):2016–2022
220. Posthuma-Trumpie GA, Wichers JH, Koets M, Berendsen LBJM, van Amerongen A (2012) Amorphous carbon nanoparticles: a versatile label for rapid diagnostic (immuno)assays. *Anal Bioanal Chem* 402(2):593–600
221. Fang Y, Guo S, Li D, Zhu C, Ren W, Dong S et al (2012) Easy synthesis and imaging applications of cross-linked green fluorescent hollow carbon nanoparticles. *ACS Nano* 6(1):400–409
222. Ganeshkumar M, Ponrasu T, Sathishkumar M, Suguna L (2013) Preparation of amphiphilic hollow carbon nanosphere loaded insulin for oral delivery. *Colloids Surf, B* 103:238–243
223. Zhu J, Liao L, Bian X, Kong J, Yang P, Liu B (2012) pH-Controlled delivery of doxorubicin to cancer cells, based on small mesoporous carbon nanospheres. *Small* 8(17):2715–2720
224. Dyawanapelly S, Ghodke SB, Vishwanathan R, Dandekar P, Jain R (2014) RNA interference-based therapeutics: molecular platforms for infectious diseases. *J Biomed Nanotechnol* 10(9):1998–2037
225. Krolow MZ, Hartwig CA, Link GC, Raubach CW, Pereira JSF, Picoloto RS et al (2013) Synthesis and characterisation of carbon nanocomposites. In: *Carbon nanostructures*. Springer Berlin Heidelberg, Berlin, Heidelberg, pp 33–47
226. Dizaj SM, Lotfipour F, Barzegar-Jalali M, Zarrintan MH, Adibkia K (2014) Antimicrobial activity of the metals and metal oxide nanoparticles. *Mater Sci Eng, C* 44:278–284
227. Maleki Dizaj S, Mennati A, Jafari S, Khezri K, Adibkia K (2015) Antimicrobial activity of carbon-based nanoparticles. *Adv Pharm Bull* 5(1):19–23
228. Karageorgou D, Thomou E, Vourvou NT, Lyra K, Chalmpes N, Enotiadis A et al (2019) Antibacterial and algicidal effects of porous carbon cuboid nanoparticles. *ACS Omega* 4(3):4991–5001
229. Shao W, Wang S, Wu J, Huang M, Liu H, Min H (2016) Synthesis and antimicrobial activity of copper nanoparticle loaded regenerated bacterial cellulose membranes. *RSC Adv* 6(70):65879–65884

230. Gurunathan S, Woong Han J, Abdal Daye A, Eppakayala V, Kim J (2012) Oxidative stress-mediated antibacterial activity of graphene oxide and reduced graphene oxide in *Pseudomonas aeruginosa*. *IJN*, p 5901
231. Li C, Wang X, Chen F, Zhang C, Zhi X, Wang K et al (2013) The antifungal activity of graphene oxide–silver nanocomposites. *Biomaterials* 34(15):3882–3890
232. Hao Y, Cao X, Ma C, Zhang Z, Zhao N, Ali A et al (2017) Potential applications and antifungal activities of engineered nanomaterials against gray mold disease agent *botrytis cinerea* on rose petals. *Front Plant Sci* 2(8):1–6
233. Liao S, Zhang Y, Pan X, Zhu F, Jiang C, Liu Q et al (2019) Antibacterial activity and mechanism of silver nanoparticles against multidrug-resistant *Pseudomonas aeruginosa*. *IJN* 14:1469–1487
234. Holt KB, Bard AJ (2005) Interaction of silver(I) ions with the respiratory chain of *escherichia coli*: an electrochemical and scanning electrochemical microscopy study of the antimicrobial mechanism of micromolar Ag<sup>+</sup>. *Biochemistry* 44(39):13214–13223
235. Hao G, Mondin G, Zheng Z, Biemelt T, Klosz S, Schubel R et al (2015) Unusual ultra-hydrophilic, porous carbon cuboids for atmospheric-water capture. *Angew Chem Int Ed* 54(6):1941–1945
236. Lipşa F, Ursu E, Ursu C, Ulea E, Cazacu A (2020) Evaluation of the antifungal activity of gold-chitosan and carbon nanoparticles on *fusarium oxysporum*. *Agronomy* 10(8):1143
237. Wang X, Liu X, Chen J, Han H, Yuan Z (2014) Evaluation and mechanism of antifungal effects of carbon nanomaterials in controlling plant fungal pathogen. *Carbon* 68:798–806
238. Poornima Parvathi V, Umadevi M, Sasikala R, Parimaladevi R, Ragavendran V, Mayandi J et al (2020) Novel silver nanoparticles/activated carbon co-doped titania nanoparticles for enhanced antibacterial activity. *Mater Lett* 258:126775
239. Feynman RP (1960) There's plenty of room at the bottom. *Eng Sci* 23(5):22–36
240. Choudhuri S, Deb S (2020) Smart-Nanobots: the future of HIV AIDS treatment. *IJSR* 9(6):420–423
241. Yin Z, Dong Z, Cahay M, Pixley S, Haworth KJ, Rahimi M et al (2019) Carbon nanotube wire for use in precision medical devices. In: *Nanotube superfiber materials*. Elsevier, 825–849
242. Simon J, Flahaut E, Golzio M (2019) Overview of carbon nanotubes for biomedical applications. *Materials* 12(4):624
243. Neelankavil JP, Thompson A, Mahajan A (2013) Managing cardiovascular implantable electronic devices (CIEDs) during perioperative care. *Anesth Patient Saf Found NewsL* 28(2):29–35
244. Elvin E, Kayrak M (2011) Common pacemaker problems: lead and pocket complications. In: *Modern pacemakers. Present and Future*. InTech
245. Milenković A, Otto C, Jovanov E (2006) Wireless sensor networks for personal health monitoring: issues and an implementation. *Comput Commun* 29(13–14):2521–2533
246. Zheng Y, Ding X, Poon CCY, Lo BPL, Zhang H, Zhou X et al (2014) Unobtrusive sensing and wearable devices for health informatics. *IEEE Trans Biomed Eng* 61(5):1538–1554
247. Ma D, Wang JM, Somasundaram MN, Hu Z (2005) Design and optimization on dynamic power system for self-powered integrated wireless sensing nodes. In: *Proceedings of the 2005 international symposium on low power electronics and design—ISLPED '05*. ACM Press, New York, New York, USA
248. Zhao Y, Wei J, Vajtai R, Ajayan PM, Barrera EV (2011) Iodine doped carbon nanotube cables exceeding specific electrical conductivity of metals. *Sci Rep* 1(1):1–6
249. Jayasinghe C, Li W, Song Y, Abot JL, Shanov VN, Fialkova S et al (2010) Nanotube responsive materials. *MRS Bull* 35(9):682–692
250. Dong Z, Greene G, Pettaway C, Dinney CP, Eue I, Lu W et al (1999) Suppression of angiogenesis, tumorigenicity, and metastasis by human prostate cancer cells engineered to produce interferon-beta. *Cancer Res* 59(4):872–879
251. Marsh H, Reinoso FR (2006) *Activated carbon*. Elsevier
252. Li H, Yan X, Kong D, Jin R, Sun C, Du D et al (2020) Recent advances in carbon dots for bioimaging applications. *Nanoscale Horiz* 5(2):218–234

253. Yao J, Wang H, Chen M, Yang M (2019) Recent advances in graphene-based nanomaterials: properties, toxicity and applications in chemistry, biology and medicine. *Microchim Acta* 186(6):1–9
254. Yadav D, Amini F, Ehrmann A (2020) Recent advances in carbon nanofibers and their applications—a review. *Eur Polymer J* 138:109963

# Chapter 18

## Role of Graphene-Based Materials in Gas Sensing Applications: From Synthesis to Device Fabrication



R. Deji, Rahul, B. C. Choudhary, and Ramesh K. Sharma

### 1 Introduction

One of the most serious threats to human health is ambient air pollution. The World Health Organization (WHO) reported in 2012 that atmospheric pollution is responsible for approximately 3 million deaths worldwide. To combat all of these issues, the quality of indoor/outdoor air is regulated via a variety of laws and air quality standards. The “Clean Air Act” federal law governs the quality of air in the United States, intending to meet National Ambient Air Quality Standards (NAAQS) set by the EPA (the United States Environmental Protection Agency). The European Commission established a series of directives on a European scale to administer the assessment of ambient air quality. Acquiescence with these rules and regulations necessitates incessant monitoring of indoor/outdoor air quality, which can only be accomplished with the use of gas sensing systems. Because of their toxicity and associated risk, detection of various chemical contaminants present in the atmosphere caused by

---

R. Deji  
Department of Physics, Panjab University, Chandigarh 160014, India

Rahul  
Centre for Nanoscience and Nanotechnology, Panjab University, Block-II, Sector-25,  
Chandigarh 160014, India

B. C. Choudhary  
National Institute of Technical Teachers Training and Research (NITTTR), Chandigarh 160019,  
India  
e-mail: [bcc1962@nitttrchd.ac.in](mailto:bcc1962@nitttrchd.ac.in)

R. K. Sharma (✉)  
CIL/SAIF/UCIM, Panjab University, Chandigarh 160014, India  
e-mail: [ramesh@pu.ac.in](mailto:ramesh@pu.ac.in)

industrial wastes is required in a variety of human activities, particularly environmental monitoring [1]. Organic compounds, both volatile and semi-volatile; inorganic gases such as sulfur dioxide, nitric oxides, carbon monoxide, carbon dioxide, and others; and heavy metals are examples of contaminants. As a result, there is an urgent requirement to fabricate high-performance, low-cost gas sensors for testing air quality. The majority of commercial gas sensing technologies on the market are based on variations in the electrical, optical, calorimetric, gas chromatographic, and acoustic properties of materials such as metal oxide semiconductors and polymers [2]. Several indicators were used to calculate the performance of the mechanism of gas sensing such as selectivity, sensitivity, response time, reversibility, energy consumption, adsorptive capacity, and cost of fabrication. Gas sensors were primarily used to monitor air quality and detect toxic gases in the air [3, 4]. In 1923, platinum-based gas sensors become the first commercially available sensor. Naoyoshi Taguchi invented the first metal oxide gas sensor, which went on to become the most widely used gas sensor. A propane gas explosion at Lake Yamanaka prompted his investigation, and the first Taguchi gas sensor (TGS) was created using tin oxide ( $\text{SnO}_2$ ) film. Various other materials based on inorganic semiconductor, conducting polymers, solid electrolyte, metal oxide, etc., have been studied [5–8] in order to fabricate sensors with high sensitivity, long reliability, small sizes, low power consumption, etc.

Metal-oxide-based gas sensors are being investigated primarily due to their broad semiconductor tunability and type of morphology, which have properties such as high thermal stability, short response time, high sensitivity, and low operating temperature, all of which are advantageous for high-quality gas sensors [3, 9]. A variety of semiconductor metal oxide nanomaterials like tungsten oxide ( $\text{WO}_3$ ), titanium oxide ( $\text{TiO}_2$ ), zinc oxide ( $\text{ZnO}$ ), and iron oxide ( $\text{Fe}_2\text{O}_3$ ) having hierarchical structures have been lucratively synthesized via solution-based chemical routes, that are useful for production at large scale also. Metal oxide nanoparticles, carbon nanotubes (CNTs), and graphene-based nanomaterials are among them that are widely used due to their excellent responsive characteristics, mature preparation methods, and low-cost and scalable production. However, semiconducting metal oxide sensors based on silicon have attained their limits [10].

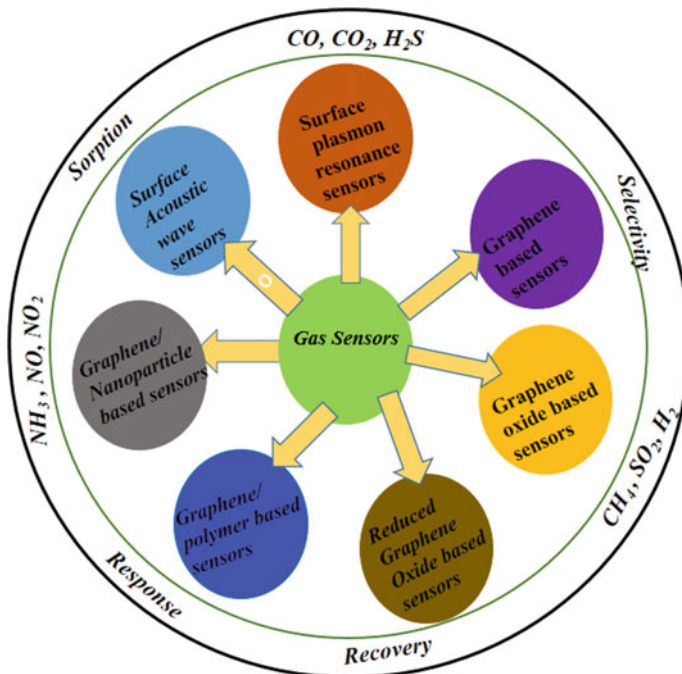
Sensing materials play critical roles in the detection and differentiation of contaminants at the molecular level in environmental processes [11]. Carbon-based nanomaterials have become the most widely studied materials for designing gas sensors in the last ten years due to their distinctive chemical and physical properties such as size, conductivity composition, magnetism, light-absorbing and emitting properties, and mechanical strength [12, 13]. The operational principle of the first gas sensor based on graphene exploits variations in its electrical conductivity owing to the adsorption of gas molecules to be sensed on the surface that acts as donors (e.g.,  $\text{CO}$ ,  $\text{NH}_3$ , ethanol) or acceptors (e.g.,  $\text{H}_2\text{O}$ ,  $\text{NO}_2$ , iodine).

Further, the properties of graphene allow it to increase its sensitivity beyond its limit. Graphene is a widely known two-dimensional (2D) material, where the entire volume is perceived by the surface adsorbates which maximizes the sensing response. It is conducting in nature, with high metallic conductivity and low Johnson noise. It

is also more advantageous owing to its easy fabrication and low power consumption in comparison to some traditional inorganic semiconducting metal oxides.

Because of its two-dimensional crystalline lattice, graphene has its low electrical noise, allowing it to screen more charge fluctuation in comparison to its one-dimensional counterpart. Thus, a very small variation in the number of electrons can bring noticeable changes in graphene conductance. Due to minute variation in resistance graphene sheet, it is possible to detect the gas adsorption even at molecular level.

Further, these sheets can be utilized to design four-point devices which are further used to eliminate contact resistances [14–18]. These RGO sheets can be further processed into ultrathin layers by using various wet techniques involving inkjet printing, layer-by-layer deposition, casting, and Langmuir–Blodgett technique; this simplifies the process of fabricating gas sensors [19, 20]. It is further possible to tune the structure of electronic level by mixing it with some sensing agent or functional groups to enhance the adsorption of gas [21]. Graphene-based materials are currently employed for sensing various toxic and volatile gases [22]. In current chapter, graphene-based sensors have been thoroughly discussed from various perspectives, including sensing mechanism, gas sensor fabrication, sensing performance, and future prospects (Fig. 1).



**Fig. 1** Graphene-based materials for gas sensing application



## 2 Gas Sensing Mechanism

A sensor is a device that operates on the principle of detecting or sensing some features of its surroundings. Gas adsorption capacity is calculated by adsorption energy. Adsorption energy ( $\Delta E_{\text{ads}}$ ) defines the chemical reactivity of foreign species on the surface. It is used to label the stability of structure of molecule's adsorption on target material. It is given by equation as under:

$$\Delta E_{\text{ads}} = E_{\text{target+gas}} - E_{\text{target}} - E_{\text{gas}}$$

where  $E_{\text{target+gas}}$  represents total energy of gas molecule adsorbed on target,  $E_{\text{target}}$  is total energy of target, and  $E_{\text{gas}}$  denotes total energy of gas molecules. For stronger molecule adsorption on target, value of  $\Delta E_{\text{ads}}$  should be more negative. Adsorption phenomenon is of two types: physisorption (physical adsorption) and chemisorption (chemical adsorption). Physical adsorption is a type of adsorption which involves the van der Waals forces of attraction between gas molecule and given substrate. Chemical adsorption is a type of adsorption which involves chemical or covalent bonding between gas molecule and substrate. Less negative or positive value of adsorption energy which corresponds to physisorption indicates less charge transfer from gas molecule to particular substrate. More negative value of adsorption energy which corresponds to chemisorption indicates more charge transfer from gas molecule to given substrate. Small value of adsorption energy and large binding distance between gas molecule and substrate indicate weak interaction as binding energy also decreases. This corresponds to a weak physisorption phenomenon [23, 24]. Gas sensors primarily identify events and record an output by identifying some physical quantities which are usually electrical or optical signals. These are classified into field-effect transistor (FET) based on silicon, surface acoustic wave (SAW) sensor, surface work function (SWF) sensor, capacitance sensor (CS), optical fiber sensor (OFS), and chemiresistor [25] based on the type of reaction with the external atmosphere. Among the above-mentioned types, chemiresistor is widely utilized as a gas/vapor sensor, as well as one of the most well-known products for a variety of practical applications, due to properties such as long-history research, simple structure, ease of implementation, operation at room temperature, and low cost [26, 27]. Currently, gas sensing plays a vital role in our society because of its ability to quickly identify toxic gases and organic vapors, which is important for human and environmental security, emission control, the industrial sector, and medical diagnosis. Graphene materials are used to detect gases using a principle based on changes in conductance caused by sensing species adsorption. Gaseous adsorbates having various structures and compositions behave differently with graphene. When they are exposed to different target gases, their electronic, optical, and electrical properties change. When the p- or n-type sensing layer of the sensor is unveiled to reducing/oxidizing gases such as CO, hydrogen, and ethanol, the device's conductivity increases.

**Table 1** Few sensor parameters and their definition

Symbols	Definition	Formula
$R_a$	Device resistance (in air)	$S (\%) = [(R_{\text{gas}} - R_{\text{air}})/R_{\text{air}}] \times 100\%$
$R_g$	Device resistance (in gas to be sensed)	
$S$	Ratio (change in resistance ( $R_a - R_g$ )/initial ( $R_a$ )) (sensor response)	
LOD	It is the least concentration of a target gas which can be sensed by a sensor	
$T_{\text{res}}$	Response time is time needed for the sensor signal to change from its pre-gas injection value to 90% of its final value during gas injection	
$T_{\text{rec}}$	Recovery time is the time taken by the sensor signal to recover 90% to its value prior to the injection of gas	
$D$	Ratio of response of target gas ( $S_c$ ) to response of disturbed gas ( $S_i$ )	

When these sorts of sensing materials are exposed to different gases, two methods can modify their conductivity. At temperatures above 100 °C, O<sub>2</sub> and O oxygen ions adsorb on the sensitive layer, and the target gas begins to react with these oxygen ions. For example, when CO interacts with the oxygen ions, it leads to the formation of CO<sub>2</sub> upon oxidation, and one electron is released which increases (decreases) the conductivity of n-type (p-type) materials. For an acceptor gas, such as NO<sub>2</sub>, the charge is accepted by the gas molecules, resulting in a drop in n-type conductivity and an increase in p-type conductivity. The adsorption of oxygen ions is unaffected by any other mechanism, and the target gas molecules are also adsorbed on the sensitive layer's surface, resulting in the direction-dependent charge transfer reaction.

There are a few critical parameters to consider when evaluating the performance of a gas or vapor sensor, such as component, measure resistance, selectivity, recovery and response time, the limit of detection, and sensitivity. Table 1 summarizes the definitions and formulas for these parameters.

### 3 Sensing Performance Parameters

Sensor performance can be demonstrated using various parameters, including sensor response, detection limit, response and recovery times, operating temperature, selectivity to a specific gas, and stability.

### ***3.1 Sensor Response***

When the target gas is released in the test chamber, the relevant changes in the signal obtained by sensor define the sensor response. As previously described for the resistive devices, relative change in electrical resistance is defined as its sensor response. It is directly related to the sensors' detection limit.

### ***3.2 Limit of Detection***

The least concentration of a target gas which can be sensed by a sensor is called the limit of detection. According to the United States Environmental Protection Agency (EPA), exposition limit for NO<sub>2</sub> is 100 ppb per hour. Thus, the detection limit of NO<sub>2</sub> sensor should be lower than 100 ppb per hour.

### ***3.3 Operating Temperature***

Another important factor in the commercialization and use of gas sensors is the operating temperature. The majority of the time, sensors based on metal oxides operate in high-temperature regions (above 100 °C). At this temperature, oxygen molecules begin to adsorb (100 °C) or chemisorbed (above 200 °C) and react with the molecules of target gas, resulting in high sensor responses. Further, the high temperatures enable quick response and recovery times. However, it enhances the power consumption and, in some particular cases, it can cause a significant change in the sensing behavior as well. As a result, in the recent years, gas sensing research has been entirely devoted toward the development of sensors operational at room temperature, in order to reduce power consumption and eliminating the need for the sensors to be heated.

### ***3.4 Response Time and Recovery Time***

Response time is time needed for the sensor signal to change from its pre-gas injection value to 90% of its final value during gas injection. Recovery time is the time taken by the sensor signal to recover 90% to its value prior to the injection of gas [28]. This can vary from one second to tens of minutes. In everyday life, it is regarded as a barrier to the use of sensors with fast response and recovery times.

### 3.5 *Selectivity and Stability*

Selectivity is defined as a sensor's ability to detect a specific gas in the existence of other gases. Under normal circumstances, the sensors are exposed to a mixture of different gases; thus, the selectivity of a sensor can be calculated by revealing it to various target gases and then recording their individual responses. Another critical parameter of gas sensors is response stability. The device's response should remain same over the months or years. These types of issues are not always addressed in scientific papers; however, this is one of the critical factors that should be tested for the engineering of these devices. The response's stability can also be influenced by changes in the chemical composition of the sensing layer, such as oxidation when exposed to air. All of these factors must be considered before deciding on the appropriate gas sensor for a particular situation or environment. After analyzing the above criteria, it is simple to differentiate between a "good" or a "bad" sensor. In the case of graphene, doped atoms and defects play a vital role in gas sensing applications because dopants and defects enhance molecule adsorption. Many experimental and theoretical investigations report that in the case of graphene the occurrence of structural defects such as pentagonal–octagon pairs, Stone–Wales defects, and vacancies increases its chemical reactivity [29]. Because graphene nanoflakes have defect sites, they are highly reactive, and their edges adsorb gas molecules and experience chemical functionalization at a quick rate. Reduced graphene oxide (RGO) is also a prominent material used for the development of gas sensors. It is much simpler to process GO in comparison to graphene, and it also provides different options for tailoring the quantity of functional groups simply by managing the degree of reduction. Reduced graphene oxide has a functionalized surface having active oxygen defects, allowing for solution chemistry decoration with metal nanoparticles.

## 4 **Classes of Gas Sensors**

### 4.1 *Chemiresistive Gas Sensors*

Gas sensors come in a variety of shapes and sizes, and they can serve a variety of purposes. The most common configurations of gas sensors are the chemiresistor. Majority of these sensors rely on measuring the variation in the resistance of sensor upon exposing to the test gas. These sensors are easy to fabricate and have a direct measurement capability. Graphene-based sensors, in general, adhere to this device configuration. The resistance is directly measured in this type of sensor by taking the current/voltage characteristics among the two contacts from the top of the sensing film. The sensor response ( $S\%$ ) is calculated as follows:

$$S(\%) = [(R_{\text{gas}} - R_{\text{air}}) / R_{\text{air}}] \times 100\%$$

here,  $R_{\text{gas}}$  ( $R_{\text{air}}$ ) are the electrical resistances of the sensor in the tested (air) gas. There are various sensing parameters of chemiresistive gas sensors such as sensitivity, selectivity, response time, and reversibility that rely upon the temperature and structure of the sensing element and molecular adsorption. The presence of low binding energy attraction with van der Waals forces causes physical adsorption. Due to the lack of chemical bonds, the electronic and chemical structure is preserved, resulting in easy and comprehensive desorption of the molecules of gas and, as a result, full and rapid sensor recovery. Physisorption, on the other hand, reduces the sensitivity and selectivity of the sensors. Chemical bonds formed between sensing and gaseous molecular elements are used to characterize chemical adsorption, allowing for the fabrication of highly selective gas sensors. Furthermore, molecular desorption for chemisorbed molecules is quite low, resulting in slow recovery.

## 4.2 *Field-Effect Transistor-Based Gas Sensors*

Physical adsorption is caused due to the presence of low binding energy attraction with van der Waals forces. The electronic and chemical structure of gas molecules is preserved due to the lack of chemical bonds, resulting in easy and complete desorption of gas molecules and, as a result, full and rapid sensor recovery. Physisorption, on the other hand, reduces the sensitivity and selectivity of the sensors. Chemical bonds formed between sensing and gaseous molecular elements are used to characterize chemical adsorption. Field-effect transistors (FETs) have also been used to detect gases [30]. In that case, the dependence of FET drain current on gate bias can be varied by exposing it to the molecules of target gas. The performance of sensor is primarily determined by the device's on/off current ratio. A higher on/off ratio usually contributes to greater sensitivity [31, 32]. The charge density in graphene sheets can be incessantly tuned by applying an electrical field due to their eccentric atomically thick 2D structure and bipolar charge carriers. These are the properties that will make graphene suitable candidate for fabricating FETs [33–36]. Gautam and Jayatissa used CVD (chemical vapor deposition) grown graphene to create a back-gated field-effect transistor for studying ammonia sensing at ppm levels [34]. The adsorption and desorption behavior of ammonia ( $\text{NH}_3$ ) on graphene in the presence of dry air was studied using a progressive shift of the Dirac peak at smaller/larger gate voltages based on different time exposures to different concentrations of  $\text{NH}_3$ . The device response dependence on concentration indicates that the graphene-based sensors exhibit two type of adsorption modes near room temperature. However, at high temperature (100 °C), it exhibits only one mode.

### 4.3 *Surface Acoustic Wave Sensors*

Surface acoustic wave (SAW) detection is another technology being researched for gas detection. SAW sensors are mass-sensitive devices that can detect changes in a sensing layer's mass down to the nanogram level. Exposure to gas molecules causes changes in the mass and/or conductance of their sensing layers, resulting in frequency change. This sensor responds to changes in mass as well as surface conductivity. In the SAW sensor construction, a delay line is coated with a thin film of sensing material that can absorb the testing gas molecules along its propagation path.

The time delay is caused by gas/vapor molecule absorption and thus the frequency of operation. The amplitude of an acoustic wave decreases exponentially as it passes through substrates as it travels along the surface of an elastic material. To generate and detect the transmission of this sonic wave, interdigital transducers are used (IDTs). Between the delay line SAW device and the IDTs, two IDTs are placed at a predetermined distance apart. The delay line connects the two IDTs and is mostly coated with chemically sensitive recognition material. The acoustic wave is damped in SAW resonators by reflection gratings spaced at intervals. As a result, the acoustic wave reflected from these gratings was detected by the IDT. Kaner reported a SAW-based sensor for the detection of CO and H<sub>2</sub>. The sensing response of 1.7 or 7.0 Hz in the presence of 1% H<sub>2</sub> or 1000 ppm CO was measured. Despite the fact that both the gases are reducing, different directions of frequency shifts were observed. Because CO has a molecular weight 14 times greater than H<sub>2</sub>. Thus, the change in mass was the most important parameter in the CO response, whereas the variation in the conductance of graphene was the most important factor in the H<sub>2</sub> response.

### 4.4 *Optical Surface Plasmon Resonance (SPR)-Based Gas Sensor*

The detection process of this sensor is also based on the idea that the SPR signal varies as the refractive indices of the analytes change. An optical SPR gas sensor fabricated by authors [37] with use of graphene oxide flakes on top of a monolayer of gold nanoparticles chemically bonded to a functionalized fused silica substrate. When flakes and nanoparticles interact with different gases, optical changes occur, including a shift in the SPR band in the presence of both (reducing and oxidizing) gases. Rifat and their group demonstrate a SPR sensor-based PCF design based on a graphene-silver coating [38]. The graphene covering is supposed to boost sensing performance by delivering a high surface-to-volume ratio, greater analyte absorption, and superior plasmonic characteristics, all while limiting silver oxidation [39].

### 4.5 *Electrochemical-Based Gas Sensor*

Analyte gas can pass through a membrane and be reduced or oxidized at an electrode in an electrochemical gas sensor [40]. It can detect a wide range of gases and quantify them in small quantities. The electrochemical gas sensor can have two or three electrodes. The three-electrode setup constitutes of a working, counter, and a reference electrode. The electrode's sensing material reacts with analytes that are also ion and electron conductors. The variation in the electronic charge density and carrier mobility is observed for semiconducting sensors [40]. The vast majority of electrochemical gas sensors are amperometric, with the rate of the electrolytic process being determined by the change in current [40]. For the time being, an electrochemical strategy is the most practical method for studying changes in graphene's chemical environment. The adsorption of different gas molecules in graphene-based gas sensors alters the interface charge layer. The electrical signal associated with the type of gas analyte used varies. When analytes containing electron donors are used, current is increased. Ion-polar analytes disrupt the charge transport and limit current flow in graphene. When analytes are detected, electrical properties such as resistance and capacitance can be measured in addition to current.

## 5 Gas Sensors Based on Pristine Graphene

Geim and colleagues used mechanical exfoliation to produce high-quality single-layer graphene in 2004 [41]. They fabricated the near to ideal crystalline structure by separating the graphene sheets into single layer. Novoselov and others [42] in 2007 exploited mechanically exfoliated graphene for gas detection. The limit of detection (LOD) of this graphene-based gas sensor was ppb, which is equivalent to the most sensitive gas sensors ever recorded. Graphene is a substance that, in theory, should have the same properties as carbon nanotubes (CNTs). Sensitivity of gas sensors is also related to pore volume and surface area of graphene-based materials. Higher surface-to-volume ratio leads to greater adsorption of gas species on them and thus increases the sensing capability with increased value of adsorption energy. More negative value of adsorption energy corresponds to short recovery time. A short recovery time enhances the adsorption of gas species on graphene's surface.

Graphene has piqued the interest of gas sensor specialists over the last decade. Graphene functionalization or reduced graphene oxide can improve graphene's chemical affinity and selectivity over other carbon materials [43, 44]. Another advantage of graphene-based sensors over conventional solid-state gas sensors is their operating temperature.

Several other groups [45–48] investigated the sensing capabilities of pristine graphene, both experimentally and conceptually, and their sensors detected a variety of gases including  $\text{NO}_2$ ,  $\text{NH}_3$ ,  $\text{CO}_2$ , and others. Temperature, target gas flow velocity,

and graphene sheet length-to-width ratio are all parameters that can affect the efficiency of these sensors. During the process of adsorption, the gas molecules can produce traps and scattering centers, causing a change in the amount of charge carriers or charge mobility. Although high-quality graphene can be produced via mechanical exfoliation, its productivity is still limited.

This disadvantage can be mitigated in part by fabricating graphene sheets of high quality using chemical vapor deposition (CVD) technique. The CVD method creates graphene sheets onto a metal substrate including Cu, Ni, and Co at moderate temperatures (1000 °C) by decomposing hydrocarbon vapors [25, 49, 50]. These sheets can then be shifted on to various substrates and used to create gas sensing devices [35, 51–53]. It has been studied that the resistance of a monolayer graphene sheets fabricated using CVD changes dramatically upon adsorption of the O<sub>2</sub> molecule [25]. These molecules act as a p-type dopant. These sensors can detect O<sub>2</sub> with a LOD of 1.25%.

For the synthesis of pure graphene (also known as defect-free graphene or intrinsic graphene IG), CVD-based methods and graphite exfoliation methods are commonly used [54]. Various researchers have used IG to detect toxic gas molecules including NO, N<sub>2</sub>O, CO<sub>2</sub>, NH<sub>3</sub>, NO<sub>2</sub>, O<sub>2</sub>, H<sub>2</sub>O, and SO<sub>2</sub> [46, 48]. The authors [42] created a few layered graphene layers using a mechanical exfoliation technique and demonstrated the first micrometer-sized sensor designed for individual single molecule NO<sub>2</sub> detection in a high vacuum environment. Graphene is an extraordinary material with low noise, and with its use, we can achieve sensitivity at the single molecule detection level [42]. For the synthesis of pure graphene (also known as defect-free graphene or intrinsic graphene IG), CVD-based methods and graphite exfoliation methods are commonly used [55]. After adsorption of gas molecule, electrical conductivity of graphene changes which leads to change in resistivity. After removing the gas flow and heating it to 150 °C in vacuum, the sensor recovered in 100–200 s. The sensitivity of the graphene sensor reported for the first time was of several orders of magnitude higher than that of existing sensors [56]. Graphene is a potential material for gas sensing at the individual molecule detection level. Later, other groups [57] experimentally studied that chemical doping of graphene increases the sensitivity of IG to various gases. They studied the sensor characteristics of IG using conventional nano-lithographic techniques and calculated the sensing response of IG by removing contamination from the graphene surface. Even in the existence of strong analytes, IG sensitivity was found to be very low. This suggests that adding dopants to graphene can increase its chemical reactivity toward various gas molecules [57]. The authors [46] demonstrated a graphene-based sensor for NO<sub>2</sub> detection where graphene layers were synthesized using mechanical exfoliation method with thicknesses ranging from 3.5 to 5 nm on a silicon substrate. They used electron-beam lithography to connect two metal contacts across this substrate. This type of graphene-based gas sensor has a very fast sensor response, as well as high reproducibility, sensitivity, selectivity, and reversibility (ratio of change in resistance upon gas exposure to resistance in air) of 0.09 after exposure to 100 ppm NO<sub>2</sub> gas at RT.

The authors [48] used cured polydimethylsiloxane (PDMS) stamps to demonstrate highly ordered pyrolytic graphite flakes (HO PGR) on SiO<sub>2</sub> substrate for CO<sub>2</sub> sensing.



This method allows for the deposition at desired locations on the substrate while leaving less residue on the substrate than the scotch-tape method. In comparison to other gas molecules, physical adsorption of  $\text{CO}_2$  on the surface of graphene results in easy desorption of  $\text{CO}_2$  due to a very short recovery time of about 10 s. As a result,  $\text{CO}_2$  gas molecule can adsorb and desorb at a much faster rate than other gas molecules [55].

The authors [58] recently demonstrated the gas sensing behavior of few-layer graphene synthesized by electrochemical exfoliation method (named FLG having 3–10 graphene layers) toward adsorption of liquefied petroleum gas (LPG) and  $\text{CO}_2$  gas at room temperature (RT). The sensitivity of an electrochemically based graphene sensor was 3.83 (0.92) for  $\text{CO}_2$  (LPG) having a response time of 11 s (5 s) and temperature of operation as 423 K (398 K), with recovery times of 14 s (8 s) [58]. The sensing behavior of a chemiresistive-based few-layer graphene sensor at low temperatures is promising for their use for detection of LPG [56].

The main disadvantage of mechanical graphene deposition is its poor selectivity, which means that we cannot distinguish between different gases. Fattah and Khatami demonstrated a graphene/n-Si Schottky junction-based  $\text{H}_2\text{S}$  gas sensor [59]. The authors used mechanical deposition to create natural graphite (high orientation) on top of an n-type Si substrate. Variations in the diode's forward bias current–voltage characteristics evaluate the sensor's sensing performance at various temperatures. When compared to previously reported  $\text{H}_2\text{S}$  sensors, the  $\text{H}_2\text{S}$  sensor based on Schottky diode had high reproducibility, easy desorption/adsorption, and good selectivity. Thus,  $\text{H}_2\text{S}$  sensor employed graphene-based Schottky diodes have potential applications in gas detection fields [55].

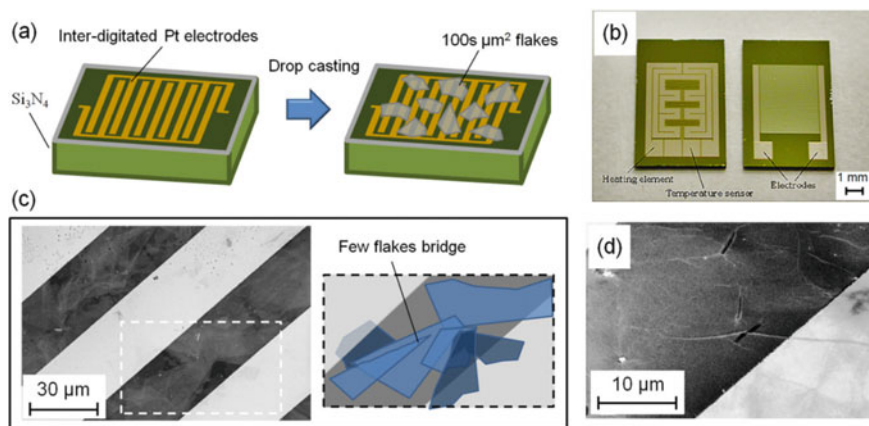
## 6 Graphene Oxide-Based Gas Sensors

It is a promising material in sensing applications because of its distinct electrical properties that involve higher electrical conductivity, lower electronic noise, and high specific surface area, which is two times greater than single-walled CNT and approximately 300 times greater than graphite. However, one of its limitations in being used as a sensitive layer in devices is its zero-energy gap. As a result, there is a need to decorate and functionalize graphene. The simplest method is to use graphene oxide (GO). GO is produced by oxidizing graphite; it is a thermally unstable compound that can be easily fabricated in large quantity and quality from graphite oxide. Graphite oxide possesses the structure similar to graphite, but it is highly enriched with functional groups such as epoxies, hydroxyls, carboxyls, and lactones attached to its surface. Among the most common approaches for graphene synthesis, chemical oxidation of graphite and reduction of graphite oxide are involved. The various functional groups present on the surface of GO increase the inter-atomic separation between layers of graphene oxide while also making these layered structures more hydrophilic or water loving [60]. Prezioso and colleagues [61] investigated various types of GO to improve efficiency of sensing as shown in Fig. 2. The authors used a drop-casting

technique to create single-layer GO flakes on Pt electrodes. The average size was found to be 27 m, with a maximum size of 500 m. It yields a typical p-type response in reducing and oxidizing environment. The sensing response to  $\text{NO}_2$  is investigated at various temperatures and gas concentrations, and a p-type response for a given sensor is observed. The detection limit (DL) for  $\text{NO}_2$  is 20 ppb, which is the lowest value given in the literature when compared to other gas sensors based on graphene. It has also been proposed that having large number of active surface sites results in higher sensitivity of GO when compared to CNTs and RGO-based sensors [55]. As a result, GO is one of the materials attributed to gas sensing that is complementary to graphene. Wang and others [62] used alternating current dielectrophoresis (ac-DEP) to utilize GO nanomaterial-based sensor for hydrogen gas detection.

By changing various parameters including processing time, frequency, and peak-to-peak voltage ( $V_{pp}$ ), the Hummers method is used to synthesize GO and GO nanostructures assembled into gold electrodes using the DEP process. The required DEP parameters for hydrogen ( $\text{H}_2$ ) gas sensing applications by utilizing GO nanostructures were found to be  $V_{pp} = 10$  V, frequency = 500 kHz, and  $t = 30$  s. For hydrogen gas concentration of 100 ppm at RT, the device made of GO nanostructures was found to be more effective, with a sensor response, response time, and recovery time of 5%, 90 s, and 60 s, respectively [62].

In order to detect low concentrations of  $\text{H}_2$  and  $\text{N}_2$  in atmospheric air, a sensing device made of GO with SAW has been developed [63]. Concentration-dependent studies of various gases at various temperatures have been conducted. GO films can also be found in humidity sensors. They [64] explored GO to create a capacitive humidity sensor at the microscale level. It was determined that the GO-based

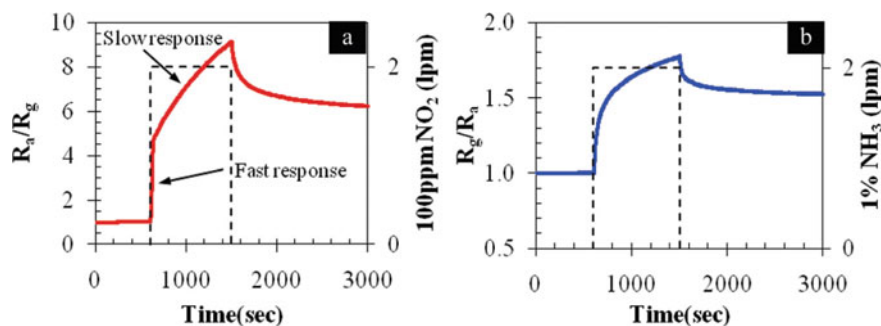


**Fig. 2** **a** Schematic depicting device fabrication. Electric contacts between pre-patterned interdigitated Pt electrodes are realized upon drop-casting deposition of large GO flakes. **b** Patterned substrate (front-size) with heating elements and temperature sensors on the backside. **c** SEM micrograph of few GO flakes linking two adjacent Pt electrodes. **d** SEM micrograph of a GO flake lying above an electrode edge. Reprinted with permission from Stefano Prezioso et al. [61]. Copyright 2013 American Chemical Society

sensor has a sensitivity that is ten times more than that of the conventional capacitive humidity sensors. The hydrophilic behavior of GO is reflected in its excellent humidity sensing ability. At lower relative humidity (RH), hydrophilic groups on the surface of GO provide active sites for physisorption of water molecules via weak double hydrogen bonding. The restriction from double hydrogen bonding allows water molecules to move freely in this interaction mechanism. Thus, the physical adsorption of water molecules requires a lot of energy, and GO films have a lot of electrical resistance. Thus, GO can be thought of as a better material for humidity sensing applications with higher sensitivity for a variety of applications. The functional groups on the surface of GO are responsible for sensing of NO<sub>2</sub> gas. At RT, a comparison of response time of NO<sub>2</sub> in terms of resistance value change has been conducted for GO, reduced GO, and graphene-based sensors [65]. It was discovered that GO has a higher response to NO<sub>2</sub> than graphene, which is not sensitive to NO<sub>2</sub>. The sensing behavior of GO is reported as p type in this study, but a few reports for n-type sensing are also available. When flakes of GO are deposited on pre-patterned substrates using the dielectrophoresis method, their n-type behavior is observed [62]. When these dielectrophoresis-assembled GO flakes are exposed to the reducing gas H<sub>2</sub>, their resistance decreases, indicating their n-type conductivity. The parameters used in dielectrophoresis are very important to have a high response value, and it was predicted that dielectrophoresis devices detect hydrogen in a dry air conditions in a range of 100–1000 ppm. Similarly, GO with SAW structure has been employed to detect low concentrations of H<sub>2</sub> and NO<sub>2</sub> in synthetic air atmosphere [63, 66].

## 7 Gas Sensors Based on Reduced Graphene Oxide

Imperfections in graphene sheets are critical for gas detection. It is easy to fabricate large quantity of RGO at low cost and is a potential material that can be used for the designing sensors for real world usage. GO which is a precursor to RGO is commonly produced by oxidizing graphite in an acidic environment with potassium permanganate. GO is oxidized form of graphene with various functional groups such as hydroxyl and epoxy groups that are present on carbon which is sp<sup>3</sup> hybridized. After functionalization, these functional groups provide reactive sites for gas adsorption. The conductivity of GO is very low due to the disruption of the conjugated electrical structure via the oxygen-containing groups, thus making them unsuitable for use in electronic devices. However, the chemical or thermal reduction is one of the appealing methods of restoring its conductivity. Incomplete reduction results in a certain number of oxygen groups remaining in the corresponding RGO. Furthermore, the reduction process may produce voids and structural flaws that can serve as sites for adsorption. Interaction of the gas molecules among the defects of high energy in graphene has been shown to differ significantly from that of conjugated carbon structures. Graphene's electrical response is dominated by defect adsorption. However, desorption from flaws was significantly slower than desorption from the pure sp<sup>2</sup> hybridized structure. Due to their high resistance, GO flakes are frequently reduced to



**Fig. 3** RGO sensor behavior for **a** 100 ppm  $\text{NO}_2$  and **b** 1%  $\text{NH}_3$  detection. Reprinted with permission from Lu et al. [74]. Copyright 2011 American Chemical Society

produce RGO flakes, which partially restore graphene conductivity. Several methods for producing graphene oxide have been revealed in recent years. The use of hydrazine is a common approach [44, 67]. Other researchers proposed using  $\text{NaBH}_4$  for three hours at  $125^\circ\text{C}$  partially reduces GO flakes [68]. Thermal annealing [69] or brief exposure to a hydrogen plasma can also be used to reduce GO flakes. In order to deoxygenate the GO, surface and selectively shaped flakes of GO, laser, Xenon lamp bursts, UV lamp, EUV laser, and synchrotron radiation have all been used [70–72]. RGO can be reduced partially to sheet-like graphene by eliminating the oxygen groups from GO and retrieving a conjugated structure. The process reducing GO has a notable impact on the nature of the produced RGO and thus on how close the RGO will be to IG. Due to similarization of the structure of graphene and functional group, RGO has been used potentially in a variety of applications, such as gas sensing [73]. RGOs outperformed IG in gas sensing due to low cost of production, structural fine-tuning and attributes like conductivity and water dispersibility, and the ability to be further modified. As a result, the sensors based on RGO have been thoroughly investigated for the identification and detection of gaseous species as shown in Fig. 3 [73, 74].

Lu and others [74] used low-temperature thermal treatments to partially reduce GO and produce high-performance gas sensors. Following a process of heating at  $200^\circ\text{C}$  (in one step) or heating at  $100$  and  $200^\circ\text{C}$  (multi-step), the gas sensor responded well to 100 ppm  $\text{NO}_2$  and 1%  $\text{NH}_3$  (for 1 h each). Non-reduced GO, on the other hand, did not react with  $\text{NO}_2$  and  $\text{NH}_3$ . The strong performance of the partially decreased GO sensor is imputed to the recovery of carbon atoms, vacancies, or microscopic holes formed while the heat treatment which intimate active sites for the adsorption of gas molecules. In comparison to  $200^\circ\text{C}$  annealed GO, which had a sensitivity of 1.41 to 100 ppm  $\text{NO}_2$ ,  $300^\circ\text{C}$  annealed GO had a higher sensitivity (1.56) and a faster reaction time (1.41). The low-power simple GO sensor demonstrated a 4.3% escalation for 1 ppm  $\text{NO}_2$  in conductance in comparison to the mechanically exfoliated graphene sensors [55]. Chemical sensors are synthesized via spin coating of chemically converted graphene dispersions on interdigitated planar electrode arrays by authors and their coworkers and result into single-layer hydrazine-reduced graphene

films [75]. Within 10 min of being exposed to 52 ppb of DNT (an explosive found in trinitrotoluene (TNT)), the sensor demonstrated accordant response with charge transfer among graphene and the analyte and a 0.028% drop in resistance. They discovered a reduction in sensitivity to 5 ppm NO<sub>2</sub> at higher temperatures using a micro-hotplate as substrate [55]. RGO films produced by reducing exfoliated GO with ascorbic acid and printing them onto flexible PET using inkjet techniques [76] warranted selective and reversible sensing of chemically threatening NO<sub>2</sub> and Cl<sub>2</sub> vapors at room temperature (RT) in an air sample containing vapor concentrations in the range of 100 ppm to 500 ppb.

Because of the high oxygen reduction level in chemically reduced GO having *C/O* ratio of 11.0, which may result in large number of sites for adsorption of gas molecules, the highest response of 100 ppm NO<sub>2</sub> was 9.15 [73]. Although the response reported for thermally reduced GO sensors was 1.3 [55], the resistance increased by 1.7 times for NH<sub>3</sub> gas. Hassinen and colleagues [77] presented a low-cost method for producing RGO-based gas sensors on paper as a substrate. They discovered that both the size and thickness, as well as the use of different reducing agents, influenced the detecting qualities of the RGO-based sensor. Nantao and colleagues [78] studied RGO sensors for the detection of NH<sub>3</sub> at room temperature by reducing GO with pyrrole as a reducing agent. The improvement in sensing is due to the combination of the intrinsic properties of the adsorbed reducing agent and graphene. The sensitivity of 2.4% to 1 ppb NH<sub>3</sub> in these low-cost and powered RGO sensors explains their practicality in practical applications.

## 8 Modified Graphene-Based Gas Sensors

The sensitivity of any sensor is an important feature to consider when designing a highly efficient gas sensor because it influences the ability of sensor to verify the target gas concentration's minimum value. Because graphene-based materials have limited sensitivity and stability, designing commercially viable gas sensing devices necessitates modified graphene systems with higher performance. In this new era, several methods are being used to optimize the interactions between graphene and gas. When graphene materials are combined with other materials such as nanoparticles (NPs), molecules, polymers, and so on, their properties frequently change, resulting in multifunctional materials that incorporate the advantages of each component. To change the physiochemical properties of graphene-based sensing applications, chemical modification is usually required. As a result, numerous chemical modification approaches, such as the insertion of metal functionalization [79, 80], polymers [81, 82], metal oxide NPs [83, 84], dopants [85, 86], and functional molecules, have been reported. These modifications enabled the physiochemical properties to be manipulated to meet the demands, and a variety of highly efficient gas sensor devices based on above strategies have been described. The following sections investigate several methods to improve the sensing effectiveness of graphene-based materials.

## 8.1 Chemically Modified Graphene-Based Gas Sensors

Graphene doping with various heteroatoms, for example, boron (B), nitrogen (N), sulfur (S), silicon (Si), and others has been studied in biosensors, supercapacitors, lithium-ion batteries, oxygen reduction reaction (ORR), high-performance FETs, water splitting, electrochemical and photocatalysts, and other applications. The bandgap is frequently used to tailor the electrical features of such heteroatoms. The presence of defects modifies the physical and chemical features, which is useful to improve the performance of gas sensors. In the lab, several graphene-based sensors with doped graphene were tested. Niu et al. fabricated ammonia gas sensor of high sensitivity by phosphorus-doped graphene nanosheets (P-GNS) with use of annealing of GO at high-temperature and tri-phenyl phosphine combination [85]. The P-GNS-based  $\text{NH}_3$  sensors demonstrated significantly better sensor responsiveness and slow response and recovery time at RT because of adsorption of  $\text{NH}_3$  onto the additional phosphorus atoms.

Liang and his coworkers [87] recently discovered that doping of graphene with sulfur atoms using hydrogen sulfide gas flow at 1000 °C was a simple and effective method for increasing graphene's  $\text{NO}_2$  adsorption capacity. Compared to adsorption study of other gases such as  $\text{NH}_3$ ,  $\text{CH}_4$ ,  $\text{SO}_2$ , and CO, sulfur-doped graphene demonstrated extremely selective  $\text{NO}_2$  detection [86]. Gas sensing behavior for gases such as NO and  $\text{NH}_3$  dramatically improved by doping of graphene with boron [88]. High-quality graphene sheets doped with boron (BG) with large surface area can detect low concentrations (e.g., ppb) with a clear signal ( $s/n = 31.5$  for 1 ppb  $\text{NO}_2$  exposure and  $s/n = 50.1$  for 1 ppm  $\text{NH}_3$  exposure). BG resulted in significant increase in sensitivity of 27 times for  $\text{NO}_2$  and 105 times for  $\text{NH}_3$ , respectively, in comparison to intrinsic graphene, and detection limits of 95 and 60 ppb were observed [88]. An effective green reducing agent such as tannic acid (TA), used in place of generally used hazardous reducing agents such as hydrazine or sodium borohydride, was used to functionalize and reduce GO, resulting in selective detection of ammonia.

As tannic acid possesses electron-donating behavior and observed response is caused by n-type doping of RGO which shows p-type behavior. Strong reducing nature of  $\text{NH}_3$  results into no change in resistance, when exposed to ethanol and acetone. This type of chemiresistive sensor demonstrated a wide detection range, operating temperature that is room temperature, better sensing efficiency, and long response and recovery times (40 and 260 s, for 1310–6550 ppm of  $\text{NH}_3$ ). Table 2 lists out the different types of graphene-based gas sensors' performance parameters.

## 8.2 Graphene/Nanoparticle Hybrid-Based Gas Sensors

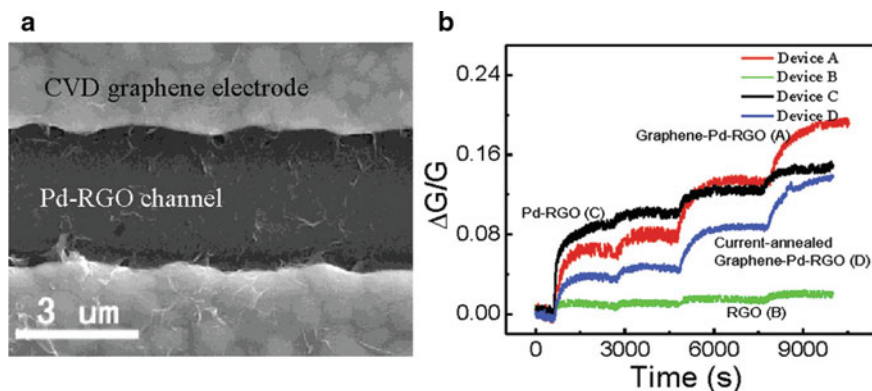
Graphene has a strong tendency for most of the gases because it changes conductance, with electron-withdrawing gases increasing conductance and with electron-donating gases decreasing conductance. Even though graphene and RGO-based sensors have

**Table 2** List of few researches about graphene-based gas sensors for sensing of several gases

Sensing device	Sensor type	Gas molecule	$T_{rec}$ (s) (recovery time)	References
RGO + Cu <sub>2</sub> O nanocrystal	Chemiresistor	H <sub>2</sub> S	120 s	[83]
PSS-doped RGO/PANI	Chemiresistor	H <sub>2</sub> S	<90 s	[89]
RGO/SnO <sub>2</sub> NFs	Chemiresistor	H <sub>2</sub> S	<198 s	[90]
RGO	SAW	H <sub>2</sub>	Nearly 1 min	[91]
G/SnO <sub>2</sub>	Chemiresistor	H <sub>2</sub> S	5 s	[92]
GR + PANI	Chemiresistor	NH <sub>3</sub>	50 s	[93]
GR/PMMA on a flexible PET substrate	Chemiresistor	NO <sub>2</sub>	1800 s	[94]
RGO/FeCl <sub>3</sub> + a-Fe <sub>2</sub> O <sub>3</sub>	Chemiresistor	NO <sub>2</sub>	44 s	[95]
Single-layered GR	FET	NO <sub>2</sub>	3000 s	[96]
RGO/WO <sub>3</sub>	Chemiresistor	NO <sub>2</sub>	1080 s	[97]
GR/SnO <sub>2</sub> NPs	FET	H <sub>2</sub>	1.6 s	[98]
GR/Al <sub>2</sub> O <sub>3</sub> QDs	Chemiresistor	CO <sub>2</sub>	22 s	[99]
GR/Sb <sub>2</sub> O <sub>3</sub> QDs	Chemiresistor	CO <sub>2</sub>	22 s	[100]

great sensitivity for sensing of wide range of toxic molecules, their performance must be improved further to fulfill the demands of practical gas sensors, like strong selectivity and a low detection limit. Gas sensing applications have showed potential for graphene-RGO hybrid nanostructures. Metal [79, 80] and metal oxide NP [83, 84] functionalization of graphene/RGO has proven to be promising methods to enhance the gas sensitivity properties of the material. Metal or metal oxide NPs show a strong synergistic effect in gas sensing when combined with graphene/RGO. These hybrids could have altered electronic properties, allowing for greater selectivity and sensitivity. Functionalization of graphene with RGO exhibits different sensor responses toward different gases. Here, in this research, selectivity of RGO-based devices is one of the main topics which can boost the sensing performance of functionalized RGO toward different gases. The potential of metal NP with graphene in sensing applications is highlighted by Gutes and colleagues [79].

For gas sensing applications, graphene coated with noble metal NPs results into graphene-NP nano-hybrids, which have been synthesized. Authors use simple drop-casting approach and synthesized Pt-decorated graphene sheets and Pt-decorated multi-walled carbon nanotubes (MWCNTs) and calculated sensing ability of H<sub>2</sub> gas sensors [101]. Comparison of sensitivity of Pt-decorated graphene and Pt-decorated MWCNT has been done at room temperature, and twofold boost in sensitivity was observed over Pt-decorated MWCNT at a detection threshold of 4% H<sub>2</sub> in air. Li et al. [102] fabricated NO gas sensor made up of graphene and ac-DEP produced graphene is used (Fig. 4a), in which sensing channel of RGO is coated with palladium (Pd) and connected across CVD-grown graphene electrodes.



**Fig. 4** **a** Pd-RGO NO sensor and **b** sensor response toward different concentrations of NO. Reprinted with permission from Li et al. [102]. Copyright 2011 American Chemical Society

These sensors, after current annealing, were capable of detecting 2 to 420 ppb with several hundred seconds response time and 1000 s recovery time for 2 ppb NO (Fig. 4b). Gravure printing Ag NP-decorated-sulfonated RGO (Ag-S-RGO) inks on a polyimide (PI) substrate with Ag pre-patterned IDEs resulted in a 74.6% of sensing response in 12 s with recovery in 20 s for 50 ppm NO<sub>2</sub> gas at RT [103]. This hybrid sensor's performance was improved by chemically modifying RGO with sulfonated groups and silver nanoparticles. Even after 100 bending cycles, this sensor demonstrated better response. Its few unique properties such as mechanical robustness, lightweight, and ease of handling make it better sensor for NO<sub>2</sub> gas [55]. Wang et al. [104] built gas sensors based on RGO which were decorated with Pt NPs using ac-DEP and mid-temperature thermal annealing, allowing for sensing of different gas molecules. At RT, RGO sensors decorated with Pt NPs had sensitivities of 14%, 8%, and 10%, respectively, for 1000 ppm H<sub>2</sub>, NH<sub>3</sub>, and NO gases. When compared to RGO sensors without Pt NP ornamentation, Pt-functionalized RGO improved performance by 25%, 60%, and 100% for NO, NH<sub>3</sub>, and H<sub>2</sub> gases, respectively. The recovery/response time for H<sub>2</sub> gas decreased with Pt ornamentation, but the opposite was reported for NH<sub>3</sub> and NO. Hybrid nanostructures made up of graphene and RGO provide increased sensitivity and selectivity. Recent papers on decoration of graphene/RGO with semiconducting metal oxide NPs such as WO<sub>3</sub> [97], SnO<sub>2</sub> [105, 106], and ZnO [84, 107] have been published, as well as their use as gas sensors.

An ideal ZnO- and RGO-based sensor (material ratio of 4:1) has been fabricated in which ZnO NPs are well dispersed on RGO, and this RGO-based sensor used for detection of acetylene gas provides sensing response of 143 at 250 °C [108]. High selectivity, long-term stability, quick responsiveness, and recovery were all obtained as well. RGO increases ZnO particle attachment and avoids particle agglomeration without creating substantial morphological or crystallographic changes, according to the physical parameters of ZnO/RGO composites made using the solvothermal process.



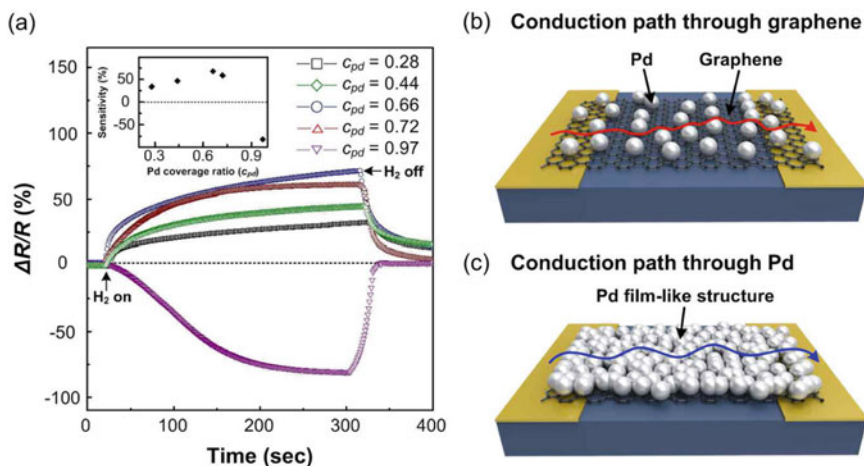
### 8.3 Graphene/Polymer Hybrid-Based Gas Sensors

Carbon nanotubes (CNTs) functionalized with polyaniline (PANI), an intrinsically conducting polymer, have been shown to improve gas sensing performance [109, 110]. In few studies, graphene and RGO are additionally functionalized with polymers. Graphene/RGO-based polymer hybrids [81, 82] improved detection properties when compared to pristine graphene and RGO. When exposed to 50 ppm  $\text{NH}_3$  gas, RGO functionalized with PANI (RGO–PANI hybrids) demonstrated a significantly faster increase in resistance of 59.2%, compared to 5.2 and 13.4% for pristine RGO and PANI nanofiber-based sensors.

The RGO–PANI hybrid sensor detects ammonia gas 3.5 times more effectively than a pristine PANI nanofiber sensor and 10.4 times more effectively than a pristine RGO sensor. Enhancement in sensitivity is caused by interaction of RGO sheets and decorated PANI NPs [81]. Despite this, authors discovered a recovery period of 4 min for devices made up of these hybrids due to more surface ratio of RGO sheets and PANI NPs. These devices demonstrated better reversibility, long-term detection stability (even after several months), and more selectivity toward ammonia gas in presence of various analytists such as DMMP, methanol, dichloromethane, cyclohexane, and chloroform. Huang et al. [111] evaluated RGO–PANI hybrids sensor's  $\text{NH}_3$  gas detection performance to that of other sensors.

T. Xie et al. synthesized sensors fabricated on organic thin film transistor (OTFT) composed of Poly(3-hexylthiophene) (P3HT) film and RGO/P3HT bilayer films for  $\text{NO}_2$  sensing, and sensing behavior of both fabricated samples was compared. It was predicted that after RGO was deposited as the bottom layer of the bilayer film in RGO/P3HT sample, the sensing response improves by about 80% [112]. Some of the RGO's distinguishing characteristics include a more surface ratio, that provides various sites for  $\text{NO}_2$  adsorption due to graphitic carbon atoms, resulting in increased sensitivity. Furthermore, the sensing response for a few gases such as  $\text{CO}_2$ ,  $\text{NH}_3$ ,  $\text{H}_2\text{S}$ ,  $\text{SO}_2$ , and  $\text{CO}$  was 2 orders lower in magnitude than that of  $\text{NO}_2$  which is because of P3HT layer that prevents the gases to come in contact with RGO.

Ye and colleagues [82] produced RGO/Poly(3-hexylthiophene) (P3HT) hybrid films for  $\text{NH}_3$  detection, and it was revealed that the sensitivity of RGO/P3HT films was higher than that of RGO film sensors. Because of shape of hybrid films and interactions between P3HT and RGO films, the RGO/Poly(3-hexylthiophene) (P3HT) sensor response was high. RGO/P3HT films have a sensitivity of 7.15, while RGO films have a sensitivity of 5.37. RGO/P3HT films have a response time of 141 s, while RGO films have a response time of 637 s. RGO/P3HT films have a recovery time of 488 s, while RGO films have a recovery time of 609 s. Based on a hybrid of PMMA membrane-coated Pd NP and SLG, J. Hong et al. synthesized a hydrogen sensor as shown in Fig. 5 with good sensitivity and selectivity (single-layer graphene). Single-layer graphene was created using the CVD process for graphene synthesis (SLG). CVD synthesized single-layer graphene is deposited with Pd nanoparticle and using spin coating technique, PMMA membrane layer coated on Pd NP/ SLG and employing a graphene-buffered galvanic displacement reaction between Cu and



**Fig. 5** a Relative resistance response of PMMA/Pd NP/SLG hybrid sensors exposed to 2%  $H_2$  with different value of  $c_{pd}$  on single-layer graphene as a function of time. The inset indicates plot of sensitivity versus  $c_{pd}$  on layer of graphene. b, c Schematic illustration of the conduction path through b graphene and c Pd. Reprinted with permission from Hong et al. [113]. Copyright 2015 American Chemical Society

Pd ions, the PMMA membrane-coated Pd NP/ SLG was formed [113]. Due to the selective filtration of  $H_2$  by the polymer membrane coating on the Pd NP/SLG hybrid, this constructed sensor did not respond to CO,  $NO_2$ , or  $CH_4$  gas. This hybrid sensor displayed a sensor response of 66.37% in 1.81 min and a recovery time period of 5.52 min after being exposed to approximately 2%  $H_2$  [113]. The low selectivity of graphene/RGO might be regained once it was functionalized with polymers, according to this research.

## 9 Conclusion

The most recent research publications linked to graphene-based materials in gas sensing applications for the detection of a wide spectrum of gases with better detection limits have been covered in this chapter. In the latest research, different new concepts are developed for achieving enhanced selectivity and sensitivity of sensors. Further, new strategies have been explored to enhance in sensitivity and response time for detection of several gases. Because of its unique physical and chemical properties, as well as its enormous surface-to-volume ratio, graphene oxide could be a possible contender for next-generation gas sensors. Functionalization of GO increases its surface activity which further helps the adsorption of gases and results

in stronger chemical adsorption with increased sensitivity for gas sensing applications. There is increasing demand for such types of sensors based on GO for future perspectives that may help in monitoring and sensing of different analytes with high sensitivity and selectivity at a low cost.

## References

1. Wagner T et al (2013) Mesoporous materials as gas sensors. *Chem Soc Rev* 42(9):4036–4053
2. Li C, Bai H, Shi G (2009) Conducting polymer nanomaterials: electro synthesis and applications. *Chem Soc Rev* 38(8):2397–2409
3. Tian W, Liu X, Wenbo Y (2018) Research progress of gas sensor based on graphene and its derivatives: a review. *Appl Sci* 8(7):1118
4. Vaseashta A et al (2007) Nanostructures in environmental pollution detection, monitoring, and remediation. *Sci Technol Adv Mater* 8(1–2):47
5. Zee F, Judy JW (2001) Micro machined polymer-based chemical gas sensor array. *Sens Actuators, B Chem* 72(2):120–128
6. Korotcenkov G (2005) Gas response control through structural and chemical modification of metal oxide films: state of the art and approaches. *Sens Actuators, B Chem* 107(1):209–232
7. Kadhim IH, Abu Hassan H, Abdullah QN (2016) Hydrogen gas sensor based on nano crystalline SnO<sub>2</sub> thin film grown on bare Si substrates. *Nano-micro Lett* 8(1):20–28
8. Mohammadi MR, Fray DJ (2009) Development of nano crystalline TiO<sub>2</sub>–Er<sub>2</sub>O<sub>3</sub> and TiO<sub>2</sub>–Ta<sub>2</sub>O<sub>5</sub> thin film gas sensors: controlling the physical and sensing properties. *Sens Actuators, B Chem* 141(1):76–84
9. Sun P et al (2011) Porous SnO<sub>2</sub> hierarchical nanosheets: hydrothermal preparation, growth mechanism, and gas sensing properties. *CrystEngComm* 13(11):3718–3724
10. Chen Z et al (2005) The role of metal–nanotube contact in the performance of carbon nanotube field-effect transistors. *Nano Lett* 5(7):1497–1502
11. Neri G (2015) First fifty years of chemo resistive gas sensors. *Chemo Sens* 3(1):1–20
12. Zhang L, Fang M (2010) Nanomaterials in pollution trace detection and environmental improvement. *Nano Today* 5(2):128–142
13. Llobet E (2013) Gas sensors using carbon nanomaterials: a review. *Sens Actuators, B Chem* 179:32–45
14. Gomez De Arco L et al (2010) Continuous, highly flexible, and transparent graphene films by chemical vapor deposition for organic photovoltaics. *ACS Nano* 4(5):2865–2873
15. Britnell L et al (2012) Electron tunneling through ultrathin boron nitride crystalline barriers. *Nano Lett* 12(3):1707–1710
16. Novoselov KS et al (2004) Electric field effect in atomically thin carbon films. *Science* 306(5696):666–669
17. Ratnac KR et al (2010) Toward ubiquitous environmental gas sensors capitalizing on the promise of graphene. *Environ Sci Technol* 44(4):1167–1176
18. Lin Y-M, Avouris P (2008) Strong suppression of electrical noise in bilayer graphene nano devices. *Nano Lett* 8(8):2119–2125
19. Wang X, Bai H, Shi G (2011) Size fractionation of graphene oxide sheets by pH-assisted selective sedimentation. *J Am Chem Soc* 133(16):6338–6342
20. Xu Y, Shi G (2011) Assembly of chemically modified graphene: methods and applications. *J Mater Chem* 21(10):3311–3323
21. Bai H, Li C, Shi G (2011) Functional composite materials based on chemically converted graphene. *Adv Mater* 23(9):1089–1115
22. Basu S, Bhattacharyya P (2012) Recent developments on graphene and graphene oxide based solid state gas sensors. *Sens Actuators, B Chem* 173:1–21

23. Calvi A et al (2016) Recognizing physisorption and chemisorption in carbon nanotubes gas sensors by double exponential fitting of the response. *Sensors* 16(5):731
24. Deji R, Choudhary BC, Sharma RK (2021) Novel hydrogen cyanide gas sensor: a simulation study of graphene nanoribbon doped with boron and phosphorus. *Phys E: Low-Dimen Syst Nanostruct* 134:114844
25. Yuan W, Shi G (2013) Graphene-based gas sensors. *J Mater Chem A* 1(35):10078–10091
26. Seiyama T et al (1962) A new detector for gaseous components using semi conductive thin films. *Anal Chem* 34(11):1502–1503
27. Shaver PJ (1967) Activated tungsten oxide gas detectors. *Appl Phys Lett* 11(8):255–257
28. Arafat MM et al (2012) Gas sensors based on one dimensional nanostructured metal-oxides: a review. *Sensors* 12(6):7207–7258
29. Omidvar A, Mohajeri A (2014) Edge-functionalized graphene nanoflakes as selective gas sensors. *Sens Actuators, B Chem* 202:622–630
30. Gisele I, Doll T, Burgmair M (2001) Low power gas detection with FET sensors. *Sens Actuators, B Chem* 78(1–3):19–25
31. Chang J et al (2013) Single-walled carbon nanotube field-effect transistors with graphene oxide passivation for fast, sensitive, and selective protein detection. *Biosens Bioelectron* 42:186–192
32. Lu Y et al (2010) High-on/off-ratio graphene nano constriction field-effect transistor. *Small* 6(23):2748–2754
33. Antonova IV et al (2011) Extremely high response of electrostatically exfoliated few layer graphene to ammonia adsorption. *Nanotechnology* 22(28):285502
34. Gautam M, Jayatissa AH (2012) Graphene based field effect transistor for the detection of ammonia. *J Appl Phys* 112(6):064304
35. Jayanthi S et al (2016) Tailored nitrogen dioxide sensing response of three-dimensional graphene foam. *Sens Actuators B: Chem* 222:21–27
36. Lu G et al (2011) Ultrafast room temperature NH<sub>3</sub> sensing with positively gated reduced graphene oxide field-effect transistors. *Chem Commun* 47(27):7761–7763
37. Cittadini M et al (2014) Graphene oxide coupled with gold nanoparticles for localized surface plasmon resonance based gas sensor. *Carbon* 69:452–459
38. Rifat AA et al (2015) Photonic crystal fiber-based surface plasmon resonance sensor with selective analyte channels and graphene-silver deposited core. *Sensors* 15(5):11499–11510
39. Iyer GRS et al (2014) Large-area, freestanding, single-layer graphene–gold: a hybrid plasmonic nanostructure. *ACS Nano* 8(6):6353–6362
40. Cretescu I, Lutic D, Manea LR (2017) Electrochemical sensors for monitoring of indoor and outdoor air pollution. In: *Electrochemical sensors technology*. Intech Open, London, UK, p 65
41. Novoselov KS et al (2005) Two-dimensional gas of massless Dirac fermions in graphene. *Nature* 438(7065):197–200
42. Schedin F et al (2007) Detection of individual gas molecules adsorbed on graphene. *Nat Mater* 6(9):652–655
43. Hummers WS, Offeman RE (1958) Preparation of graphitic oxide. *J Am Chem Soc* 80:1339
44. Stankovich S et al (2007) Synthesis of graphene-based nanosheets via chemical reduction of exfoliated graphite oxide. *Carbon* 45(7):1558–1565
45. Hwang S et al (2012) Chemical vapor sensing properties of graphene based on geometrical evaluation. *Curr Appl Phys* 12(4):1017–1022
46. Ko G et al (2010) Graphene-based nitrogen dioxide gas sensors. *Curr Appl Phys* 10(4):1002–1004
47. Romero HE et al (2009) Adsorption of ammonia on graphene. *Nanotechnology* 20(24):245501
48. Yoon HJ et al (2011) Carbon dioxide gas sensor using a graphene sheet. *Sens Actuators B: Chem* 157(1):310–313
49. Winterlin J, Bocquet M-L (2009) Graphene on metal surfaces. *Surf Sci* 603(10–12):1841–1852

50. Kalita G, Wakita K, Umeno M (2012) Low temperature growth of graphene film by microwave assisted surface wave plasma CVD for transparent electrode application. *RSC Adv* 2(7):2815–2820
51. Suk JW et al (2011) Transfer of CVD-grown monolayer graphene onto arbitrary substrates. *ACS Nano* 5(9):6916–6924
52. Levendorf MP et al (2009) Transfer-free batch fabrication of single layer graphene transistors. *Nano Lett* 9(12):4479–4483
53. Gautam M, Jayatissa AH, Sumanasekera GU (2010) Synthesis and characterization of transferable graphene by CVD method. In: 2010 IEEE nanotechnology materials and devices conference. IEEE
54. Bonaccorso F et al (2010) Graphene photonics and optoelectronics. *Nat Photon* 4(9):611–622
55. Varghese SS et al (2015) Recent advances in graphene based gas sensors. *Sens Actuators B: Chem* 218:160–183
56. Varghese SS et al (2015) Two-dimensional materials for sensing: graphene and beyond. *Electronics* 4(3):651–687
57. Dan Y et al (2009) Intrinsic response of graphene vapor sensors. *Nano Lett* 9(4):1472–1475
58. Nemade KR, Waghuley SA (2013) Chemiresistive gas sensing by few-layered graphene. *J Electron Mater* 42:2857–2866
59. Fattah A, Khatami S (2014) Selective H<sub>2</sub>S gas sensing with a graphene/n-Si schottky diode. *IEEE Sens J* 14(11):4104–4108
60. Chen D, Feng H, Li J (2012) Graphene oxide: preparation, functionalization, and electrochemical applications. *Chem Rev* 112(11):6027–6053
61. Prezioso S, Perrozzi F, Giancaterini L, Cantalini C, Treossi E, Palermo V, Nardone M, Santucci S, Ottaviano L (2013) Graphene oxide as a practical solution to high sensitivity gas sensing. *J Phys Chem C* 117:10683–10690
62. Wang J et al (2014) Dielectrophoresis of graphene oxide nanostructures for hydrogen gas sensor at room temperature. *Sens Actuators B: Chem* 194:296–302
63. Drewniak S et al (2013) Investigations of SAW structures with oxide graphene layer to detection of selected gases. *Acta Physica Polonica A* 124(3)
64. Bi H et al (2013) Ultrahigh humidity sensitivity of graphene oxide. *Sci Rep* 3(1):1–7
65. Choi YR et al (2015) Role of oxygen functional groups in graphene oxide for reversible room-temperature NO<sub>2</sub> sensing. *Carbon* 91:178–187
66. Pustelny T et al (2013) The sensitivity of sensor structures with oxide graphene exposed to selected gaseous atmospheres. *Bull Polish Acad Sci: Tech Sci*:705–710
67. Bourlinos AB et al (2003) Graphite oxide: chemical reduction to graphite and surface modification with primary aliphatic amines and amino acids. *Langmuir* 19(15):6050–6055
68. Shen J et al (2009) Fast and facile preparation of graphene oxide and reduced graphene oxide nanoplatelets. *Chem Mater* 21(15):3514–3520
69. Mattevi C et al (2009) Evolution of electrical, chemical, and structural properties of transparent and conducting chemically derived graphene thin films. *Adv Func Mater* 19(16):2577–2583
70. Matsumoto Y et al (2010) Simple photoreduction of graphene oxide nanosheet under mild conditions. *ACS Appl Mater Interfaces* 2(12):3461–3466
71. Zhou Y et al (2010) Microstructuring of graphene oxide nanosheets using direct laser writing. *Adv Mater* 22(1):67–71
72. Prezioso S et al (2012) Large area extreme-UV lithography of graphene oxide via spatially resolved photoreduction. *Langmuir* 28(12):5489–5495
73. Lu G, Ocola LE, Chen J (2009) Reduced graphene oxide for room-temperature gas sensors. *Nanotechnology* 20(44):445502
74. Lu G et al (2011) Toward practical gas sensing with highly reduced graphene oxide: a new signal processing method to circumvent run-to-run and device-to-device variations. *ACS Nano* 5(2):1154–1164
75. Fowler JD et al (2009) Practical chemical sensors from chemically derived graphene. *ACS Nano* 3(2):301–306

76. Dua V et al (2010) All-organic vapor sensor using inkjet-printed reduced graphene oxide. *Angew Chem Int Ed* 49(12):2154–2157
77. Hassinen J et al (2013) Low-cost reduced graphene oxide-based conductometric nitrogen dioxide-sensitive sensor on paper. *Anal Bioanal Chem* 405(11):3611–3617
78. Hu N et al (2013) Ultrafast and sensitive room temperature NH<sub>3</sub> gas sensors based on chemically reduced graphene oxide. *Nanotechnology* 25(2):025502
79. Gutés A et al (2012) Graphene decoration with metal nanoparticles: towards easy integration for sensing applications. *Nanoscale* 4(2):438–440
80. Chung MG et al (2012) Flexible hydrogen sensors using graphene with palladium nanoparticle decoration. *Sens Actuators B: Chem* 169:387–392
81. Parmar M, Balamurugan C, Lee D-W (2013) PANI and graphene/PANI nanocomposite films—comparative toluene gas sensing behavior. *Sensors* 13(12):16611–16624
82. Ye Z et al (2014) The investigation of reduced graphene oxide/P3HT composite films for ammonia detection. *Integr Ferroelectr* 154(1):73–81
83. Zhou L et al (2013) Stable Cu<sub>2</sub>O nanocrystals grown on functionalized graphene sheets and room temperature H<sub>2</sub>S gas sensing with ultrahigh sensitivity. *Nanoscale* 5(4):1564–1569
84. Liu S et al (2014) Enhancing NO<sub>2</sub> gas sensing performances at room temperature based on reduced graphene oxide-ZnO nanoparticles hybrids. *Sens Actuators B: Chem* 202:272–278
85. Niu F et al (2014) Phosphorus doped graphene nanosheets for room temperature NH<sub>3</sub> sensing. *New J Chem* 38(6):2269–2272
86. Niu F et al (2013) Nitrogen and silica co-doped graphene nanosheets for NO<sub>2</sub> gas sensing. *J Mater Chem A* 1(20):6130–6133
87. Liang C, Wang YL, Li T (2015) Sulfur-doping in graphene and its high selectivity gas sensing in NO<sub>2</sub>. In: 2015 Transducers-2015 18th international conference on solid-state sensors, actuators and microsystems (transducers). IEEE
88. Lv R et al (2015) Ultrasensitive gas detection of large-area boron-doped graphene. *Proc Natl Acad Sci* 112(47):14527–14532
89. Cho S et al (2014) Fabrication of water-dispersible and highly conductive PSS-doped PANI/graphene nanocomposites using a high-molecular weight PSS dopant and their application in H<sub>2</sub>S detection. *Nanoscale* 6(24):15181–15195
90. Choi S-J et al (2014) Selective detection of acetone and hydrogen sulfide for the diagnosis of diabetes and halitosis using SnO<sub>2</sub> nanofibers functionalized with reduced graphene oxide nanosheets. *ACS Appl Mater interfaces* 6(4):2588–2597
91. Arsat R et al (2009) Graphene-like nano-sheets for surface acoustic wave gas sensor applications. *Chem Phys Lett* 467(4–6):344–347
92. Zhang Z et al (2011) Highly aligned SnO<sub>2</sub> nanorods on graphene sheets for gas sensors. *J Mater Chem* 21(43):17360–17365
93. Wu Z et al (2013) Enhanced sensitivity of ammonia sensor using graphene/polyaniline nano composite. *Sens Actuators B: Chem* 178:485–493
94. Lee C et al (2012) Graphene-based flexible NO<sub>2</sub> chemical sensors. *Thin Solid Films* 520(16):5459–5462
95. Dong Y-L et al (2014) Highly selective NO<sub>2</sub> sensor at room temperature based on nanocomposites of hierarchical nanosphere-like  $\alpha$ -Fe<sub>2</sub>O<sub>3</sub> and reduced graphene oxide
96. Pearce R et al (2011) Epitaxially grown graphene based gas sensors for ultrasensitive NO<sub>2</sub> detection. *Sens Actuators B: Chem* 155(2):451–455
97. Su P-G, Peng S-L (2015) Fabrication and NO<sub>2</sub> gas-sensing properties of reduced graphene oxide/WO<sub>3</sub> nanocomposite films. *Talanta* 132:398–405
98. Zhang Z et al (2015) Hydrogen gas sensor based on metal oxide nanoparticles decorated graphene transistor. *Nanoscale* 7(22):10078–10084
99. Nemade KR, Waghuley SA (2014) Highly responsive carbon dioxide sensing by Graphene/Al<sub>2</sub>O<sub>3</sub> quantum dots composites at low operable temperature. *Indian J Phys* 88(6):577–583
100. Nemade KR, Waghuley SA (2014) Role of defects concentration on optical and carbon dioxide gas sensing properties of Sb<sub>2</sub>O<sub>3</sub>/graphene composites. *Opt Mater* 36(3):712–716

101. Kaniyoor A et al (2009) Nanostructured Pt decorated graphene and multi walled carbon nanotube based room temperature hydrogen gas sensor. *Nanoscale* 1(3):382–386
102. Li W et al (2011) Reduced graphene oxide electrically contacted graphene sensor for highly sensitive nitric oxide detection. *ACS Nano* 5(9):6955–6961
103. Huang L et al (2014) Fully printed, rapid-response sensors based on chemically modified graphene for detecting NO<sub>2</sub> at room temperature. *ACS Appl Mater Interfaces* 6(10):7426–7433
104. Wang J et al (2015) Dielectrophoretic assembly of Pt nanoparticle-reduced graphene oxide nano hybrid for highly-sensitive multiple gas sensor. *Sens Actuators B: Chem* 220:755–761
105. Mao S et al (2012) Tuning gas-sensing properties of reduced graphene oxide using tin oxide Nano crystals. *J Mater Chem* 22(22):11009–11013
106. Zhang H et al (2014) SnO<sub>2</sub> nanoparticles-reduced graphene oxide nanocomposites for NO<sub>2</sub> sensing at low operating temperature. *Sens Actuators B: Chem* 190:472–478
107. Singh G et al (2012) ZnO decorated luminescent graphene as a potential gas sensor at room temperature. *Carbon* 50(2):385–394
108. Uddin ASMI, Chung G-S (2014) Synthesis of highly dispersed ZnO Nano particles on graphene surface and their acetylene sensing properties. *Sens Actuator B: Chem* 205:338–344
109. Mangu R, Rajaputra S, Singh VP (2011) MWCNT–polymer composites as highly sensitive and selective room temperature gas sensors. *Nanotechnology* 22(21):215502
110. Srivastava S et al (2010) Study of chemiresistor type CNT doped polyaniline gas sensor. *Syn Metals* 160(5–6):529–534
111. Huang X et al (2012) Reduced graphene oxide–polyaniline hybrid: preparation, characterization and its applications for ammonia gas sensing. *J Mater Chem* 22(42):22488–22495
112. Xie T et al (2014) Thin film transistors gas sensors based on reduced graphene oxide poly (3-hexylthiophene) bilayer film for nitrogen dioxide detection. *Chem Phys Lett* 614:275–281
113. Hong J et al (2015) A highly sensitive hydrogen sensor with gas selectivity using a PMMA membrane-coated Pd nanoparticle/single-layer graphene hybrid. *ACS Appl Mater Interfaces* 7(6):3554–3561

# Chapter 19

## Trends in Nanostructured Sorbent Materials for Passive Sampling Applications



Lucas A. C. Minho, Eduard F. Valenzuela, Helvécio C. Menezesand, and Zenilda L. Cardeal

### 1 Introduction

The sampling process is a critical step in the analytical procedure. If the sampling stage is not carried out correctly, the later steps of the chemical analysis can lead to large errors that are hardly superseded. Among the environmental sampling options, the conventional sampling approach (grab sampling) is characterized by the acquisition of numerous samples, with long campaigns, covering a large area of the sampling region to generate statistically significant environmental information. On the other hand, the passive sampling modality collects pollutants over the long-term, since the pollutant uptake mechanism by passive sampling devices (PSDs) follows the laws of diffusion. Passive sampling avoids the use of pumps or more sophisticated instrumentation, making the sampling less expensive, more efficient and reliable. The calibration of PSDs provides uptake kinetics which allows the exploration not only of episodic contaminations but also provides the long-term monitoring of potential contaminants in sample bodies. PSDs allow a significant decrease in the number of samples that must be collected and analyzed in the laboratory since the process is carried out in situ involving the collection of a single sample. The aforementioned advantages of passive sampling enable more economical and sensitive monitoring; besides, contaminants can be detected in ultra-trace and trace levels, which are not available in grab sampling with low volumes collected. The correct choice and application of PSDs are mainly related to the passive sampling time and the physicochemical characteristics of the analyte. According to the exposure time and uptake mode, PSDs can report time-weighted average (TWA) concentrations in additive or kinetic mode, or equilibrium concentrations ( $C_{\text{Equil}}$ ) in equilibrium sampling mode.

---

L. A. C. Minho · E. F. Valenzuela · H. C. Menezesand · Z. L. Cardeal (✉)  
Departamento de Química, ICEx, Universidade Federal de Minas Gerais, Avenida Antônio Carlos, Belo Horizonte, Minas Gerais 662731270901, Brazil  
e-mail: [zenilda@ufmg.br](mailto:zenilda@ufmg.br)



Since the introduction of nanotechnology in the last century, great revolutionary developments have been observed in the synthesis and application of nanostructures. The diversity of these materials' physicochemical properties has facilitated revolutionary developments in areas such as electronics and medicine. In terms of environmental science, nanomaterials have been used in different applications, such as adsorbents, as enhancers of water filtration, providing antifouling, catalytic and antibacterial activity, and as catalysts, giving special attention to photoactivity and to the removal of contaminants [1]. This series of advantages of nanostructures together with the advantages of passive sampling has aroused the interest of the scientific community to merge these two tools during the manufacture of new samplers.

## 2 Principles of Passive Sampling

The diffusion laws are the core of the passive sampling theory. Considering a fluid flux,  $j_i$ , loaded with the contaminant of interest through a limiting diffusion layer, like an ideal semipermeable membrane, toward the internal environment and reaching the uptake phase (i.e., the receiving phase), the difference in concentration between the uptake and available portions is directly proportional to the solute concentration gradient between the receiving phase within the limiting membrane and the external environment (i.e., donor phase). The mathematical expression of this relationship requires the proportionality factor of the mass transfer coefficients ( $D_i$ ), as described by Fick's first law of diffusion [2]:

$$j_i = -D_i \Delta C \quad (1)$$

where mass transport expressed by  $D_i$  must be interpreted as a velocity dimension (e.g.,  $\text{cm h}^{-1}$ ). The efficiency of passive sampling devices is connected to the contaminants finity for the receiving phase, since the concentration at the interface is near zero.

On the other hand, the permeation of analytes will be affected by several physicochemical properties and external environmental conditions, such as the size or hydration sphere of the pollutant, temperature, fluid viscosity or solid compaction and turbulence [3].

More feasible description of passive sampling phenomena can be obtained by the sampler-water or air partition coefficient ( $K_{\text{sw/a}}$ ) in chemical equilibrium. The  $K_{\text{sw/a}}$  is derived from the weighted ratio of the acceptor phase-water or air partition coefficient ( $K_{L\text{w/a}}$ ) and the membrane-water or air partition coefficient ( $K_{\text{mw/a}}$ ) using the masses of the acceptor phase and membrane ( $M_L$  and  $M_m$ , respectively).

$$K_{\text{sw/a}} = \frac{M_m K_{\text{mw/a}} + M_L K_{L\text{w/a}}}{M_m + M_L} \quad (2)$$

Otherwise,  $K_{sw/a}$  can be obtained experimentally through the ratio between the contaminant final concentration in the sampler ( $C_s$ ) and in the water or air ( $C_{w/a}$ ) during chemical equilibrium (Eq. 3).

$$K_{sw/a} = \left( \frac{C_s}{C_{w/a}} \right)_{\text{eq.}} \quad (3)$$

According to the law of mass conservation, the sum of the amount of substance in the two phases must be equivalent to the initial amount of substance ( $C_0 M_{w/a}$ ):

$$C_0 M_{w/a} = C_s M_s + C_{w/a} M_{w/a} \quad (4)$$

Assembly Eq. 3 with Eq. 4 and rearranging results in the amount of solute uptake by the PSD (Eq. 5).

$$n = \frac{K_{sw/a} M_s M_{w/a}}{K_{sw/a} M_s + M_{w/a}} C_0 \quad (5)$$

It is important to note that under conventional conditions  $M_{w/a} \gg M_s$ , thus, Eq. 5 results in  $n = K_{sw/a} M_s C_0$ . Therefore, the amount of matter extracted by the device is independent of the matrix extension, which depicts a relevant property for laboratorial and in situ calibration [4].

The semipermeable membrane device (SPMD) developed by Huckins and collaborators [5] enables the improvement of passive sampling concepts, relating them to previous knowledge, mainly with regard to the pollutant uptake kinetics in aqueous matrices. In SPMDs, the increments of contaminant concentration inside the device can be described by Fick's second law adapted as a function of infinitesimal intervals of time [2]:

$$\frac{dC_s}{dt} = \frac{A\lambda}{V_s} \left( C_{w/a} - \frac{C_s}{K_{sw/a}} \right) \quad (6)$$

where  $V_s$  and  $A$  are the volume and surface area of the PSD, respectively, and  $\lambda$  is the total mass transfer coefficient, a broader term than the one presented in Eq. 1 since it is a combination of the various contributions to the restriction of mass transport and therefore describes the movement of pollutants out of the starting solution through multiple barriers to the receiving phase [6]. Devices based on diffusive gradients in thin films (DGT), which were devised and applied by Davison and Zhang [7] for trace metals in seawater, are also very efficient for the sampling of contaminants in soils and sediments, having high spatial resolution [8]. The main limiting barrier in DGT is the thickness of the diffusive gel layer ( $\delta G$ ); therefore,  $C_s$  can be easily estimated by the following equation:

$$C_s = \frac{M_a \delta G}{D_G t} \quad (7)$$

Equation 7 presents the equivalent form to the DGT uptake model in solution, where  $M_a$  is the contaminant mass that is directly measured,  $D_G$  is the effective mass transfer coefficient of the solute in the diffusive layer, and  $t$  is the total exposure time. The theoretical aspects for the use of DGT and other devices in soils and sediments are the subject of other previous reviews. Since this is not the object of this chapter, it is recommended to read the work headed by Davison et al. [8].

$\lambda$  from Eq. 6 can be described by three key components, of transport barriers of masses in water or air:

$$\lambda = D_{w/a} + D_b K_{bw/a} + D_m K_{mw/a} \quad (8)$$

In Eq. 8, the indices w/a, b, m, bw/a and mw/a refer to the water or air boundary layer (W/ABL), biofilm, membrane, biofilm-water/air and membrane-water/air, respectively. Parameters  $D$  are the specific mass transfer coefficients and  $K$ , the pollutant partition coefficients between these phases. The resistance to diffusion of contaminants through these media is called total resistance and is directly proportional to the thickness ( $\delta$ ) of each of the barriers mentioned above (Eq. 9).

$$\frac{1}{\lambda} = \frac{\delta_{w/a}}{D_{w/a}} + \frac{\delta_b}{D_b K_{bw/a}} + \frac{\delta_m}{D_m K_{mw/a}} \quad (9)$$

Based on the knowledge of the physical attributions of the above parameters, differential Eq. 6 can be solved as a function of time assuming constant  $C_{w/a}$ :

$$C_s = K_{sw/a} C_{w/a} \left( 1 - e^{-\frac{\lambda A}{K_{sw/a} V_s} t} \right) + C_0 e^{-\frac{\lambda A}{K_{sw/a} V_s} t} \quad (10)$$

where  $C_0$  is the concentration of the contaminant at time  $t = 0$ . The exponential term in Eq. 10 corresponds to the fraction of the contaminant that migrates from the interior of the sampler to the external environment, the so-called elimination factor,  $K_e$ , in which:

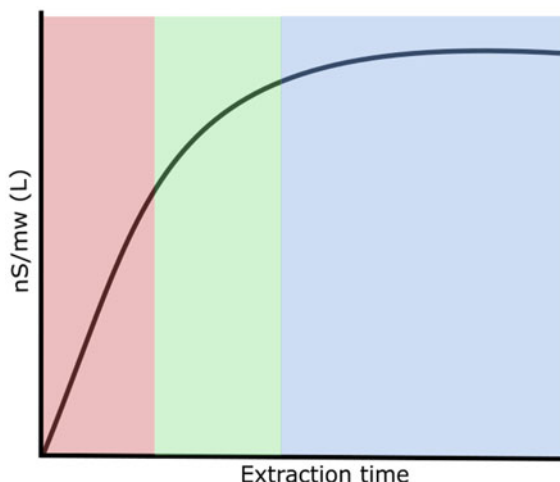
$$K_e = \frac{\lambda A}{K_{sw/a} V_s} = \frac{R_s}{K_{sw/a} V_s} \quad (11)$$

$R_s$  is the sampling rate and represents the volume of water extracted as a function of time (e.g.,  $L h^{-1}$ ) and can be interpreted as a link between passive sampling and grab sampling [9]. The graphic profile of the passive sample process is shown in Fig. 1.

The curve in Fig. 1 can be divided into three parts: linear, curvilinear and constant. For short periods of time, the contaminant concentration inside the sampler is very small when compared to the chemical equilibrium concentration ( $C_s \ll K_{w/a} C_{w/a}$ ), and therefore, Eq. 6 can be reduced to:

$$dC_s = \frac{R_s}{V_s} C_{w/a} dt \quad (12)$$

**Fig. 1** Profile of an acquisition curve in passive sampling. Red: Linear regime, green: curvilinear regime and blue: (constant) equilibrium regime



The integral solution of Eq. 12 suggests that the phenomenon is described by first-order kinetics. As the uptake rate is linearly proportional to the concentration of the analyte in the water, a sampling performed at this stage is called kinetic or additive sampling [9]. Otherwise, the curvilinear regime is the transition between the linear stage and equilibrium. The time required to reach half the equilibrium concentration,  $t_{1/2}$ , corresponds to the boundary between the kinetic uptake regime and the curvilinear, which can be estimated from the calibration data, or mathematically extrapolated through Eq. 13 [10].

$$t_{1/2} = \frac{\ln 2}{K_e} \quad (13)$$

In long-term exposure periods, with constant  $C_{w/a}$ , the pollutant concentration in the PSD does not vary with time and Eq. 6 reduces to  $C_s = C_{w/a}K_{sw/a}$ , corresponding to the last third of the sampling curve: the equilibrium regime. The samplings carried out in this uptake regime are called equilibrium sampling [9].

### 3 Passive Sampling Devices (PSDs)

Although the passive sampling technique has been implemented for decades, its application has been in yet the subject of different studies and researches. These studies have generated multiple devices, some available on the market and others with promising results to be produced on a commercial scale. Different types of passive samplers are commercially available with a variety of applications and receiving phases such as liquid absorbents (SPMDs) and sampler based on hollow fiber liquid-phase microextraction (HF-LPME), solid adsorbents (Chemcatcher and polar organic

chemical integrative sampler (POCIs)) and gels (DGT). Table 1 shows the main passive sampling devices for the analysis of environmental contaminants in water with their respective compounds extracted, passive sampling time, advantages and disadvantages.

## 4 Principles of Green Chemistry, Nanosynthesis and Miniaturized Sample Preparation Techniques

Almost 30 years ago, the United Nations Conference on Environment and Development (Earth Summit, *a.k.a.* ECO92) took place in Rio de Janeiro city (Brazil), with the participation of 179 heads of State. On the occasion, the document *Agenda 21* was prepared, in which the participating countries solemnly committed themselves to the so-called *sustainable development*, which can be succinctly defined as “development that satisfies the needs of the present without compromising the needs of the future” [17]. Thus, according to this declaration, exploration and extensive extractivism, as well as other anthropogenic activities with a high environmental impact, must be minimized and regularized, serving the progress and future of the next generations.

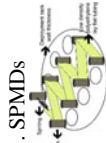
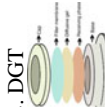
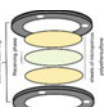
ECO92 was not only responsible for a multilateral geopolitical collision, but also fostered the establishment and strengthening of civil society representations with the decisive participation of NGOs and the implementation of public policies as well as quality standards, including the ISO 14000 which standardizes aspects of environmental management [18, 19]. Also, in Chap. 30 of *Agenda 21*, there is a proposal to adopt mass clean production together with business and industrial responsibility [18]. In line with the precepts of sustainable development, the strategic initiative known as *green chemistry* created by Anastas [20] emerged during a program launched by the US Environmental Protection Agency (EPA) a year before ECO92.

The central pillar of green chemistry is the “design of chemical products and processes to reduce or eliminate the use and generation of hazardous substances” [20, 21]. Therefore, as a guide for the development of methodologies and procedures aimed at mitigating the risks associated with chemical practices and the reduction of waste and secondary products, with subsequent treatment and intelligent management. The philosophy of green chemistry can be divided into 12 other fundamental principles [20, 22] as shown in Fig. 2.

In the synthesis of nanomaterials nowadays, certain principles of green chemistry are used; besides, the so-called *green synthesis* has become a synonym for biosynthesis. The green synthesis makes the single or combined use of natural reducing, capping and stabilizing agents through the intermediary with biological entities, without the use of high cost or toxic stoichiometric reagents and with the usual low energy consumption [23].

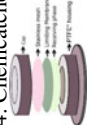
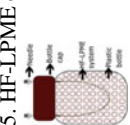
According to Duan et al. [24], the green synthesis of nanomaterials has several advantages over chemical and physical methods, such as reducing production cost, avoiding environmental pollution, improving biological compatibility and reducing

**Table 1** Some PSDs, applications, advantages and drawbacks of passive sampling devices applied for analysis in water [11]

Device	Analytes	Time	Advantages	Drawbacks	References
1. SPMDs 	Pesticides Pharmaceuticals Illicit drugs PCBS PAHs Dioxins Furans	Days to months	<ul style="list-style-type: none"> <li>• Device is marketed or commercially distributed</li> <li>• One of the most used devices (well documented—calibration data available for many pesticides)</li> <li>• TWA calculation guides available</li> <li>• Exposure times are in the range from hours to months</li> </ul>	<ul style="list-style-type: none"> <li>• Device exclusive for hydrophobic compounds. Another sampler is necessary for a wide extraction of analytes</li> <li>• Sample preparation after sampling (dialysis in organic solvents)</li> <li>• Susceptible to biofouling</li> </ul>	[12]
2. DGT 	Metals Pesticides Antibiotics Bisphenols Illicit drugs	Days to weeks	<ul style="list-style-type: none"> <li>• Versatile. It is used for metals and hydrophilic or hydrophobic organic chemicals, depending on the different sorbents employed in the configuration of the device</li> <li>• Device is marketed or commercially distributed</li> <li>• A simple, robust and low-cost sampler</li> <li>• Exposure times are in the range from hours to weeks</li> </ul>	<ul style="list-style-type: none"> <li>• Sample preparation after sampling (acid extraction (HNO<sub>3</sub>) or solvent extraction)</li> </ul>	[13]
3. POCIS 	Pesticides Pharmaceuticals Illicit drugs	Days to months	<ul style="list-style-type: none"> <li>• Device is marketed or commercially distributed</li> <li>• Exposure times are in the range from hours to months</li> <li>• One of the most used devices (well documented—calibration data available for many pesticides)</li> <li>• Low susceptibility to biofouling</li> </ul>	<ul style="list-style-type: none"> <li>• Device exclusive for hydrophilic compounds. Another sampler is necessary for a wide extraction of analytes</li> <li>• Sample preparation after sampling (solvent extraction, glass gravity-flow chromatography columns or empty solid-phase extraction cartridges)</li> </ul>	[14]

(continued)

Table 1 (continued)

Device	Analytes	Time	Advantages	Drawbacks	References
4. Chemcatcher® 	Metals Pesticides Pharmaceuticals PCBs PAHs	Days to weeks	<ul style="list-style-type: none"> <li>• Device is marketed or commercially distributed</li> <li>• One of the most used devices (well documented)</li> <li>• Exposure times are in the range from hours to weeks</li> <li>• Selectivity. It is used for hydrophilic or hydrophobic organic chemicals, depending on the combination of membrane and Empore disks</li> <li>• Low susceptibility to biofouling</li> </ul>	<ul style="list-style-type: none"> <li>• Sample preparation after sampling (solvent extraction)</li> </ul>	[15]
5. HF-LPME device 	Pesticides: Organophosphates Organochlorines Triazines Triazoles	Days to weeks	<ul style="list-style-type: none"> <li>• Easy manufactured device with parts of recyclable materials. It can be easily manufactured in the laboratory</li> <li>• Sample preparation is not necessary. Direct injection in gas chromatography (GC)</li> </ul>	<ul style="list-style-type: none"> <li>• Device is not marketed or commercially distributed</li> <li>• Fugacity or loss of the receiving phase during sampling</li> </ul>	[16]

Principles	Explanation	Principles	Explanation
▶ 1. Prevention	It is better to prevent waste than to treat or clean up waste after it is formed.	▶ 7. Use of renewable Feedstocks	A raw material or feedstock should be renewable rather than depleting whenever technically and economically practicable.
▶ 2. Atom economy	Synthetic methods should be designed to maximize the incorporation of all materials used in the process into the final product.	▶ 8. Reduce derivatives	Unnecessary derivatization should be minimized or avoided, if possible, because such steps require additional reagents and can generate waste.
▶ 3. Less hazardous chemical synthesis	Whenever practicable, synthetic methodologies should be designed to use and generate substances that pose little or no toxicity to human health and the environment.	▶ 9. Catalysis	Catalytic reagents are superior to stoichiometric reagents.
▶ 4. Designing safer chemicals	Chemical products should be designed to preserve efficacy of the function while reducing toxicity.	▶ 10. Design for degradation	Chemical products should be designed to break down into innocuous degradation products at the end of their function and do not persist in the environment.
▶ 5. Safer solvents and auxiliaries	The use of auxiliary substances should be made unnecessary whenever possible and, then used, innocuous.	▶ 11. Real-time analysis for pollution prevention	Analytical methodologies need to be further developed to allow for real-time, in-process monitoring and control prior to the formation of hazardous substances.
▶ 6. Design for energy efficiency	A raw material or feedstock should be renewable rather than depleting whenever technically and economically practicable.	▶ 12. Inherently safer chemistry for accident prevention	Substances and the form of a substance used in a chemical process should be chosen to minimize the potential for chemical accidents, including releases, explosions and fire.

**Fig. 2** Scheme of the 12 principles of green chemistry and brief explanations. Explanation taken from [20, 22]

potential physiological toxicity, in addition to be sustainable [23] and with the potential to be used for mass production of nanomaterials with strong commercial appeal [25, 26]. Thus, the green synthesis of nanomaterials is strongly aligned with several principles of green chemistry, e.g., principles 2–8 described in Fig. 2. Furthermore, in morphological, nutraceutical and bacteriological terms, many nanomaterials such as nanoparticles biosynthesized present superior characteristics than those synthesized with chemical or physical methods. Since the contact of reaction agents with biomolecules such as carbohydrates, lipids, proteins and enzymes stabilizes the structure of nanomaterials, allowing them to mold and interact with other organisms more efficiently [23, 27]

Several works using green synthesis with biological entities *in vivo* such as bacteria [28, 29], algae and cyanobacteria [30], yeasts [31], fungi [29] and other animals [32] are described in the literature. In addition, *in vitro studies* using plant extracts [33] as precursors, for example, are also described.

On the other hand, the growing demand for faster, more efficient, sustainable and environmentally friendly analytical methods is the main driver for the improvement of classical treatment and analysis techniques. In this sense, the development and progress of analytical methodologies are directed to fundamental aspects of green chemistry, such as the publications of Namieśnik [34], who coined the term *green analytical chemistry*. According to Koel and Kaljurand [35], following the 12 principles listed in Fig. 2, principles 1, 5, 6 and 12 have been the basis for the development of many modern instrumental analytical techniques and methodologies.

Also, the implementation of hyphenated instrumental techniques has led to conscious, efficient and intelligent consumption of energy, as well as helping to increase the analytical frequency and the rotation of routine analyses in laboratories, especially with regard to the development of highly automated methodologies (end to end) or with on-line sample treatment with the measurement technique or chemical speciation system. The incorporation of more efficient energy sources in

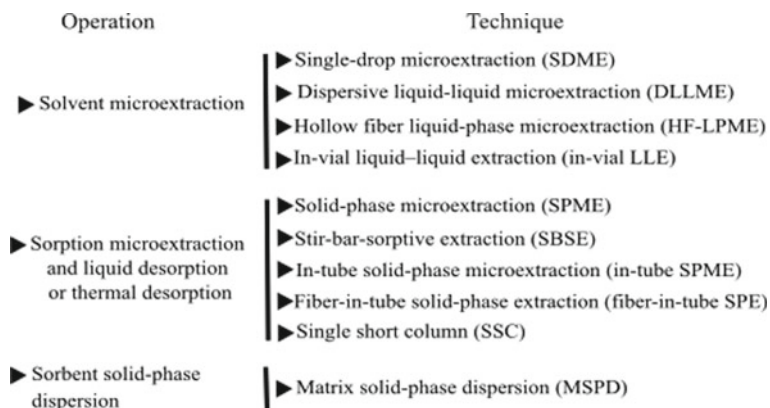


the most diverse processes such as microwave treatment [36], ultrasound [37] or, alternatively, the development of photochemical methods [38] can lead to considerable energy savings [35]. On the other hand, sample preparation procedures play a prominent role in modern chemical analyses, corresponding with the sampling, up to 90% of the total analysis time [39, 40]. Sample preparation is often introduced in order to overcome difficulties or incompatibilities with the analytical measurement system.

Until the end of the 1980s, little emphasis was given to the sample preparation, even though its importance was remarkable. Classic sample preparation techniques such as liquid–liquid extraction (LLE), solid–liquid extraction (SLE), gas extraction (GE) and solid-phase extraction (SPE) were common; however, they have been associated with a myriad of technical difficulties much due to its dependence on matrix complexity. In particular, LLE produces a large amount of waste as it demands large volumes of solvents that are harmful and/or unfriendly to the environment. In addition, the settlement and separation of phases are usually slow due to the formation of emulsions. LLE, as well as other classical extraction techniques, tends to be inefficient due to the limited concentration factor, since the ratio between the extracting phase and the sample is usually low [41].

A natural way to “greener” sample preparation techniques has been their miniaturization. Miniaturized sample preparation techniques emerged in the mid-1990s with the introduction of the solid-phase microextraction (SPME) technique [42] and the subsequent liquid-phase microextraction technique (LPME) [43]. The processes of miniaturization aimed to overcome the usual difficulties and increase reliability and efficiency, gradually supplanting classical techniques. Figure 3 presents the main miniaturized sample preparation techniques.

The miniaturization including the adoption of greener procedures led to innovations in sample preparation procedures for chemical analysis and for the synthesis of



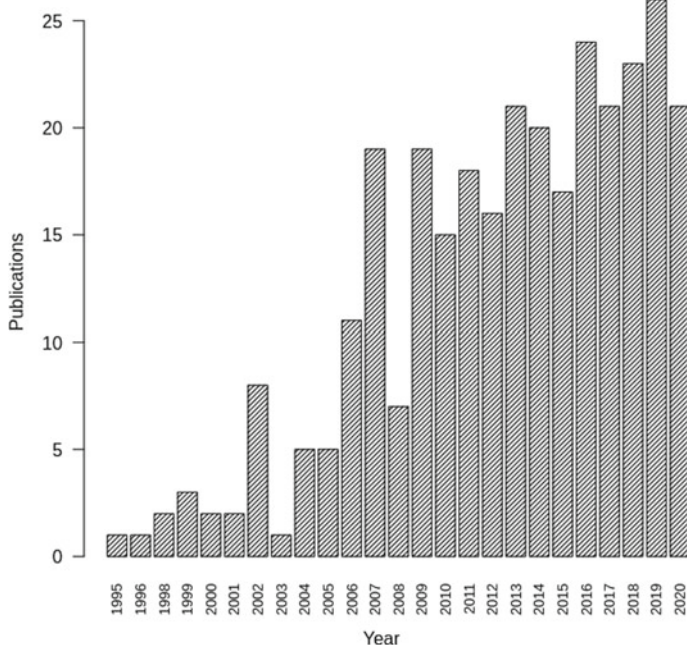
**Fig. 3** Scheme of the main representative miniaturized techniques. Adapted from Koel and Kaljurand [35]

nanomaterials. They were also the promoters for the development of more efficient and sensitive passive sampling devices and methodologies.

## 5 Trends in PSD Miniaturization

In the last 25 years, a growing trend toward the use of miniaturized passive samplers (MPSDs) (Fig. 4), which are those that use a microscale uptake phase, is noticeable, although in an incipient way, with few publications per year. The growing interest in MPSDs may be related to the development of the membrane-enclosed sorptive coating device (MESCO) by Vrana et al. [44] in 2001. The first version of MESCO was a passive sampling device adapted from the SPME technique with SBSE, which was also the approach chosen by Assoumani et al. [6, 45, 46], Zheng et al. [47] and Matsiko et al. [48] years later.

Efforts have been applied in recent research to develop more sensitive and low-costly passive samplers, adapted from miniaturized sample preparation techniques, mostly based on SPME such as those based on fibers [49–51], polydimethylsiloxane (PDMS) rods [52, 53], thin films [54, 55], silicone rubber [56–58] and even the use



**Fig. 4** Number estimate of publications related to passive sampling with MPSDs over the years. Systematic survey carried out through the Web of Science repository using the keywords “Passive sampling” and “Microextraction”.

of drones combined with SPME for monitoring volatile organic compounds in the air [59]. Although adaptation of the SPME for the purposes of passive sampling is a reality, there is still a considerable vacuum in relation to the development of devices based on LPME, largely due to the low immobilization and recovery capacity of micro-amounts of solvent in the semipermeable membrane for an extended period of time.

The natural path of passive sampling, as well as sample preparation techniques, would also be the use of miniaturized acceptor phases, but, as pointed out by Taylor et al. [60], miniaturized devices are still not able to overcome the use of typical samplers since the calibration and validation of most of these devices were carried out under restricted conditions and in short sampling times, which may be inadequate for longer exposures, or unrepresentative for the description of non-steady state.

Another limiting aspect of miniaturized passive sampling devices is the low sampling rates. According to Eq. 11, the  $R_s$  depend on the mass or volume of the acceptor phase. Large  $R_s$  do not imply greater performance or reliability of the device; nevertheless, higher  $R_s$  enhance detection sensitivities given the high concentration of substances around its useful area/volume, and at the same time, it requires tedious sample preparation processes. On the other hand, the combination of passive sampling with more efficient instruments such as gas, liquid, multidimensional chromatography and electrophoresis coupled with more selective and sensitive detectors has potential to overcome this challenge. Another alternative is the use of nanostructured materials that have an inherent high surface area as an acceptor phase.

## 6 Applications of Nanostructured Materials in Passive Sampling

### 6.1 Inorganic Nanostructures

Most passive sampling devices with acceptor phase based on nanostructured inorganic materials, surveyed in this work, are constituted in part or in whole by particulate materials, such as immobilized gold nanoparticles (AuNPs) for the capture of Hg [61–65].

Mercury is a volatile heavy metal linked to intense anthropogenic activity [66, 67]. In water, the most commonly found inorganic species is the Hg(II) ion. The ion 2+ methylation leads to its introduction into ecosystems at the trophic level and bioaccumulation at the end of the chain. Consequently, to high concentrations in fish and other animal tissues, raising concerns about the potential harmful effects of mercury residues on human health through consumption [68]. On the other hand, in the air, mercury appears in three forms: gaseous elemental mercury, Hg<sup>0</sup> (GEM), gaseous oxidized mercury, Hg(II) (GOM), and particulate bounded mercury (PBM) [63, 69]. Metallic fumes and mercury vapors are released into the atmosphere by various routes such as emissions from fossil fuels burning, from the chlor-alkali

industries, incinerations and fires, gold mining [66], in addition to industrial metallurgical processes, mineral exploration, cement factories and waste from landfills and garbage dumps [67]. According to Pirrone et al. [67], due to the unstoppable life cycle of mercury: extraction, emission and deposition, it is considered a ubiquitous pollutant, being found throughout the atmosphere and troposphere.

Mercury that is deposited in water and soil undergoes complex routes of transformation by microorganisms, forming organic complexes and other derived species. Organic mercury, such as methylmercury,  $[\text{CH}_3\text{Hg}]^+$ , due to its ability to bioaccumulate in fatty tissues such as the myelin sheaths (where it causes dysmyelination) is associated with several neurological disorders such as neuron death, memory loss and dementia, language deficit, movement abnormalities as abnormal reflexes and seizures, vision problems and also implicated in Alzheimer's disease and other chronic degenerative diseases [70]. In addition to disturbing the nervous system, mercury has the potential to affect multiple organs, leading to generalized degeneration [71].

The maximum contaminant limit (MCL) established by the US EPA is  $2 \mu\text{g L}^{-1}$  in drinking water [72] although it does not establish a quality standard for mercury in air. Gold nanoparticles that have a high surface area in addition to being highly porous are a good solution for the extraction and concentration of mercury at trace levels from sample bodies;  $\text{Hg}^0$  is trapped by gold particles by amalgamation, a factor that has been widely explored in the literature [73, 74]. Passive samplers with acceptor phase based on AuNPs have sampling rates ranging from  $0.006$  to  $0.014 \text{ m}^3 \text{ d}^{-1}$ , with linear uptake ranges ranging from a few days (1 to 2 days) to 1 year. Apparently, the association of AuNPs with other materials such as the inorganic nanocomposite  $\text{Au}@\text{TiO}_2$  [61] improves their physical–chemical properties, such as their sorption capacity.

For a more comprehensive view of the problem, the review by Huang et al. [73] covers several proposals for passive samplers for the assessment of mercury in air.

## 6.2 Carbonaceous Nanostructures

The main representatives of this category are carbon nanomaterials (CNMs). CNMs have great potential as adsorbent for organic and inorganic analytes in diverse sample matrices owing to their high surface area, three-dimensional structure, carbon large quantity, chemical stability and their negligible mass density [75]. Once the high efficiency of CNMs in remediation of different contaminants and wastewater treatment has been demonstrated, they have been introduced in passive sampling processes. Although this approach is recent, there are already different works published in environmental journals. Table 2 shows an overview of 5 passive sampling devices that use carbon nanomaterials as receiving phases. Within the allotropic forms of carbon (graphite, diamond, fullerene, graphene and carbon nanotubes), carbon nanotubes (CNTs) have the greatest use as receiving phase, with multi-walled carbon nanotubes (MWCNTs) being the most widely used. This is due to the characteristic structure

and electronic properties of CNTs allowing them to interact strongly with organic molecules, via non-covalent forces, such as hydrogen bonding,  $\pi$ - $\pi$  stacking, electrostatic forces, van der Waals forces and hydrophobic interactions [76]. These interactions improve with the oxidation of carbon which increases mainly the concentration of hydroxyl and carbonyl surface groups.

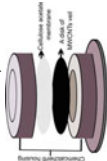
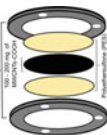
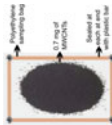
As can be seen in Table 2, some CNM samplers have been based on typical commercially available devices (1 and 2). The authors proposed to change the receiving phases of the Chemcatcher<sup>®</sup> and POCIs by phases with carbon nanotubes. These modifications can facilitate its acceptance and its subsequent commercialization by the manufacturing company. From another perspective, some works offer the possibility of building the sampler in the laboratory by the user himself in a simple and fast way such as the development of needle trap devices (NTDs) for the use of receiving phases consisting of immobilized carbon materials (devices No. 5). NTDs are miniaturized devices based on SPME; however, their choice implies some advantages compared to the direct use of solid-phase microextraction fibers in passive sampling: greater robustness, since the sorbent is protected inside a steel needle in addition to the modulation of the extraction capacity according to the exposure of the solid sorbent to the environment [85]. More details about configurations, sorbents, applications and perspectives of NTDs can be found in the study of Lord et al. [86].

### 6.3 Nanofibers

Nanofibers are recognized as elongated structures that have internal diameters lower than or equal to 500 nm and lengths ranging from a few hundred nanometers to several meters. They are materials of great interest in analytical chemistry, having as main features their large specific surface area and high aspect ratio. Thus, countless applications have been registered in the literature such as optical analysis: colorimetric, spectrophotometric, fluorescence and chemiluminescence analysis, surface-enhanced Raman scattering (SERS), ultra-thin layer chromatography, mass spectrometry ionization technologies, electrochemical analysis, gas sensors and biosensors and sample preparation techniques [87, 88]. The properties of nanofibers as sorbent materials can be modulated according to the nature of the monomers or starting particles or by the different dopants used in their synthesis and production. In addition, nanofibers show an alternative for incorporation of functionalization processes or structural modification.

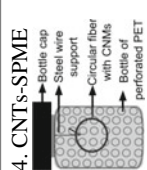

Several strategies have been applied to obtain nanofibers including mechanical drawing [89], phase separation [90, 91], molecular self-assembly [92, 93], template synthesis [94], melt blowing [95], vapor deposition [96–98] (mainly for obtaining carbon fibers), sol–gel [99, 100] and seeding [101]. The high standard techniques for the production of nanofibers nowadays are electrospun and electrospinning, since with these techniques it is possible to manufacture long and uninterrupted fibers with an internal diameter, porosity, morphology and spatial orientation, controllable

**Table 2** Main characteristics of some passive sampling devices with carbon nanomaterials as acceptor phases

Device	Analytes	Sample preparation after sampling	Advantages	Drawbacks	References
<p>1. CNTs + Chemcatcher®</p> 	Nanosilver	Acid extraction (HNO <sub>3</sub> )	<ul style="list-style-type: none"> <li>Exposure times within the average in the passive sampling area (hours to days)</li> <li>Low susceptibility to biofouling</li> <li>Sample preparation after sampling is necessary</li> </ul>	<ul style="list-style-type: none"> <li>The device is not yet marketed or distributed commercially</li> <li>One of the new devices (little documented and with little calibration data for different compounds)</li> </ul>	[77]
<p>2. CNTs + POCIS</p> 	<p>β-blockers</p> <p>Sulfonamides</p> <p>Pharmaceuticals</p> <p>Phenolic compounds</p>	Ultrasound-assisted extraction using a mixture of organic solvents	<ul style="list-style-type: none"> <li>Exposure times within the average in the passive sampling area (hours to days)</li> <li>Low susceptibility to biofouling</li> <li>Sample preparation after sampling is necessary</li> </ul>	<ul style="list-style-type: none"> <li>The device is not yet marketed or distributed commercially</li> <li>One of the new devices (little documented and with little calibration data for different compounds)</li> </ul>	[78, 79]
<p>3. CNTs + Sampling bags</p> 	PAHs	Accelerated solvent extraction (ASE), solid-liquid extraction (SLE), sonication extraction	<ul style="list-style-type: none"> <li>Easy manufactured device. It can be easily manufactured in the laboratory</li> <li>Exposure times within the average in the passive sampling area (hours to days)</li> </ul>	<ul style="list-style-type: none"> <li>The device is not yet marketed or distributed commercially</li> <li>One of the new devices (little documented and with little calibration data for different compounds)</li> <li>Susceptible to biofouling</li> </ul>	[80]

(continued)

Table 2 (continued)

Device	Analytes	Sample preparation after sampling	Advantages	Drawbacks	References
<p>4. CNTs-SPME</p> 	Pesticides: Organophosphates Organochlorines Triazines Triazoles	Thermal desorption in GC/solvent desorption with heating plate or ultrasound bath or vortex agitation using acetonitrile	<ul style="list-style-type: none"> <li>Sample preparation is not necessary for thermal desorption into GC injector</li> <li>Easy manufactured device with parts of recyclable materials. It can be easily manufactured in the laboratory</li> <li>Exposure times within the average in the passive sampling area (hours to days)</li> </ul>	<ul style="list-style-type: none"> <li>For thermal desorption in GC, a specific thermal desorption unit is required</li> <li>The device is not yet marketed or distributed commercially</li> <li>One of the new devices (little documented and with little calibration data for different compounds)</li> </ul>	[81]
<p>5. Graphene/CNTs-NTD</p> 	Perchloroethylene $CCl_4$ Organohalogenes	Thermal desorption in GC	<ul style="list-style-type: none"> <li>Fast acquisition</li> <li>Direct thermal desorption into GC injector</li> </ul>	<ul style="list-style-type: none"> <li>The setup is not yet marketed or distributed commercially</li> <li>One of the new devices (little documented and with little calibration data for different compounds)</li> </ul>	[82–84]

by the instrumental configurations; in addition, unlike wet synthesis, it has flexibility to work with various synthetic polymers such as nylon-6, polyacrylonitrile (PAN), poly( $\epsilon$ -caprolactone) (PCL), poly(ethylene oxide) (PEO), poly(lactic acid) (PLA), poly(lactic-co-glycolic acid) (PLGA), polypropylene (PP), polystyrene (PS), poly(vinyl chloride) (PVC), poly(vinylpyrrolidone) (PVP), resins, PDMS, polyaniline (PANi), poly(3,4-ethylenedioxythiophene) (PEDOT) and poly(styrenesulfonate) (PSS) and biopolymers such as cellulose, chitosan and gelatin (collagen) [102].

Although synthetic and natural nanofibers are considered new and promising sorbents, their use for passive sampling purposes is still an emerging topic. Haoran et al. [103], in a new application, proposed the use of cellulose nanofibers decorated with AuNPs as surface-enhanced Raman scattering substrates, obtaining considerable improvements in SERS. Their study also recognized the potentials of the material designed for passive sampling due to its resistance to water, acid and alkaline solutions, high surface area and potential sorption capacity.

Among the sparse publications on the application of organic nanofibers as nanostructured uptake phases, the works led by Martinez and Cwiernty [104–106] stand out. The authors developed proposals for receiving phases of equilibrium samplers and tested polymers of different natures in the manufacture of nanofibers: PAN, PMMA, PS, polyethylene terephthalate (PET), poly(vinyl acetate)) (PVAc), polyvinylidene fluoride (PVDF) and ethylene–vinyl acetate (EVA), as well as composites such as PAN@CNTs and PS@CNTs. They obtained, through the electrospun technique, fibers with controlled diameters ranging between 70 and 1000 nm depending on the treatment and the base polymer. Receiving phases were calibrated in the laboratory with hydrophilic model compounds ( $\log K_{ow} < 2$ ) such as aniline and nitrobenzene and hydrophobic ( $\log K_{ow} > 4.5$ ) such as selected PCBs and dioxins. In general, the authors assume that passive samplers equipped with nanofiber-based acceptor phases would be fast acquisition, since they would not be protected with limiting phase (such as membranes), reaching equilibrium in time lower than 7 days, with coefficients of sorbent-water partition ( $K_{ENMW}$ ) estimated between -0.07 and 2.8 log units for hydrophilic compounds and 3.2 and 6.4 for hydrophobic compounds.

A patent regarding the development of a miniaturized passive sampling device based on HF-LPME using polypropylene membranes grafted with cellulose nanofibers, as well as the methodology for obtaining this material through a simple synthetic route based on sol–gel, was recently filed [107]. This work had as main motivation the correction of stability problems from the acceptor microphase of the previous sampler [16]. Through this modification process, nanofibers with lengths ranging from 29.8 to 48.6 nm were obtained, forming a covering on the surface of the microporous extractive membrane between 1 and 100  $\mu\text{m}$ . In situ applications of these samplers include the determination of trace levels of emerging pollutants such as phthalates and pesticides (such as triazines and organochlorines) in natural waters. The device shows potential for sampling higher polarity organic compounds due to the functionalization of PP membranes with polar groups.



## 7 Outlook

Nanotechnology has covered different areas of knowledge where environmental sciences have been greatly benefited. The synthesis of nanomaterials and their respective application in the remediation of environmental pollutants has allowed the creation of new methodologies for the analysis of water, air and soil. Although initially its application was based on the emergence of microextraction techniques used in the laboratory, the introduction of passive sampling tools allowed its subsequent application in the field (in situ). Recently these nanomaterials have been proposed as receiving phases in typical samplers (Chemcatcher<sup>®</sup> and POCIs) enabling their inclusion as passive sampling alternatives. This trend in the use of conventional devices facilitates the understanding of the diffusion processes of the analytes and their subsequent adsorption on the nanoparticles since these devices are well documented and their calibration and uptake models are well known.

Although these different types of nanostructures have shown great efficiency as receiving phases in passive sampling devices, they have been limited by surface defects during exposure to the environment. Thus, the transformations on the surface of nanomaterials enable the adsorption of macromolecules and metals cations, as well as biological interactions (adsorption of viruses, bacteria and protozoa) change their colloidal stability, originating in some cases homoaggregation or heteroaggregation and biofouling, which in turn modify the surface reactivity and mobility [1]. In this sense, different investigations have focused on controlling the surface effects during nanomaterial exposure to the environment. To address this challenge, novel nanocomposite and nanoparticles have been prepared such as D-amino acid supported by polydopamine and halloysite nanotube [108], sulfonated polyelectrolyte-silver nanoparticle complexes [109] and modifications of polyvinylidene fluoride membrane by silver nanoparticles-graphene oxide hybrid nanosheet [110]. This new trend in the synthesis of nanomaterials improves the exposure times of the samplers in the different environmental compartments, allowing more efficient extractions. The properties of antimicrobial and antifouling from some carbon-based nanomaterials such as fullerene, mesoporous carbon nanoparticles (MCNs) and carbon quantum dots (CQDs) [111] make them excellent candidates as receiving phases of passive sampling, phases that should be evaluated in future studies.

Physical methods have been used successfully to produce nanoparticles. Conventional techniques like ball milling, laser ablation, evaporation/condensation and electro-spraying present the advantages of high purity, large-scale production and cost-effective, but involve high energy, long periods of time and contamination [112]. On the other hand, the chemical method approach such as the microemulsion method, sol-gel procedure, hydrothermal technique and chemical vapor deposition are able to generate high film durability, controlled surface morphology and easy operation, however, presenting some demerits such as toxic and corrosive compounds, explosive precursor gases and difficulties to material deposition [112]. In this sense, the trends associated with green chemistry have sought to diminish the disadvantages of these methods through biological methods. The green synthesis or green route

procedure to obtain nanomaterials is an efficient one-pot procedure that is generated by different biological organisms such as plants and their extracts, microorganisms (bacteria, fungi and actinomycetes), algae, enzymes, biomolecules and industrial or agricultural wastes [113]. Although these biological methods are recent, it is expected that they will be applied to the development of receiving phases for passive sampling.

## 8 Final Considerations

We are currently facing a boom in the synthesis of nanomaterials with high adsorption capacity. Besides, adsorption is today one of the most researched techniques for the elimination of pollutants which has shown equal or better results than techniques based on biotechnology, catalytic processes, membrane processes, ionizing radiation processes and magnetically assisted processes. The combination of passive sampling tools with the recent advances on nano-adsorbents offers a promising field of research in the detection and removal of pollutants which begins to take shape with the trends presented above.

Although passive sampling devices are already applied in various countries of the European Union, they are used as complementary methods in surveillance and operational monitoring. According to the water framework directive (WFD), passive sampling involves some difficulties including biofouling, back-calculating to water concentration and calibration. The passive sampling technique and its latest trends with nanomaterials show a significant advance in the analysis of environmental pollutants. These studies contribute to the introduction and acceptance of passive sampling as a monitoring method in conventional laboratories.

## References

1. Gentile GJ, de Cortalezzi MMF (2019) Nanotechnology and the environment. In: *Harnessing nanoscale surface interactions*, pp 41–76. <https://doi.org/10.1016/b978-0-12-813892-2.00002-1>
2. Tyrrell HJV (1964) The origin and present status of Fick's diffusion law. *J Chem Educ* 41(7):397. <https://doi.org/10.1021/ed041p397>
3. Kingston JK, Greenwood R, Mills GA, Morrison GM, Persson LB (2000) Development of a novel passive sampling system for the time-averaged measurement of a range of organic pollutants in aquatic environments. *J Environ Monit* 2(5):487–495
4. Chen Y, Pawliszyn J (2007) Chapter 1: Theory of solid phase microextraction and its application in passive sampling. In: *Passive sampling techniques in environmental monitoring*, pp 3–32. [https://doi.org/10.1016/s0166-526x\(06\)48001-6](https://doi.org/10.1016/s0166-526x(06)48001-6)
5. Huckins JN, Tubergen MW, Manuweera GK (1990) Semipermeable membrane devices containing model lipid: a new approach to monitoring the bioavailability of lipophilic contaminants and estimating their bioconcentration potential. *Chemosphere* 20(5):533–552. [https://doi.org/10.1016/0045-6535\(90\)90110-f](https://doi.org/10.1016/0045-6535(90)90110-f)

6. Assoumani A, Margoum C, Chataing S, Guillemain C, Coquery M (2014) Use of passive stir bar sorptive extraction as a simple integrative sampling technique of pesticides in freshwaters: determination of sampling rates and lag-phases. *J Chromatogr A* 1333:1–8
7. Davison W, Zhang H (1994) In situ speciation measurements of trace components in natural waters using thin-film gels. *Nature* 367(6463):546–548. <https://doi.org/10.1038/367546a0>
8. Davison W, Zhang H, Warnken KW (2007) Chapter 16: Theory and applications of DGT measurements in soils and sediments. In: *Passive sampling techniques in environmental monitoring*, pp 353–378. [https://doi.org/10.1016/s0166-526x\(06\)48016-8](https://doi.org/10.1016/s0166-526x(06)48016-8)
9. Booij K, Vrana B, Huckins JN (2007) Chapter 7: Theory, modelling and calibration of passive samplers used in water monitoring. In: *Passive sampling techniques in environmental monitoring*, pp 141–169. [https://doi.org/10.1016/s0166-526x\(06\)48007-7](https://doi.org/10.1016/s0166-526x(06)48007-7)
10. Morin NAO et al (2018) Kinetic accumulation processes and models for 43 micropollutants in ‘pharmaceutical’ POCIS. *Sci Total Environ* 615:197–207
11. Valenzuela EF, Menezes HC, Cardeal ZL (2020) Passive and grab sampling methods to assess pesticide residues in water. A review. *Environ Chem Lett* 18(4):1019–1048. <https://doi.org/10.1007/s10311-020-00998-8>
12. Lorimor R (2021) Environmental sampling technologies—the leader in semipermeable membrane devices (SPMDs). <http://www.est-lab.com/spmd.php>. Accessed 29 Oct 2021
13. Forbes H (2015) About DGT—DGT research, 12 Nov 2015. <https://www.dgtresearch.com/about-dgt/>. Accessed 29 Oct 2021
14. Lorimor R (2021) Environmental sampling technologies—the leader in polar organic chemical integrative samplers (POCIS). <http://www.est-lab.com/pocis.php>. Accessed 29 Oct 2021
15. How to buy Chemcatcher®. <https://chemcatcher.ie/how-to-buy-chemcatcher/>. Accessed 29 Oct 2021
16. Valenzuela EF, Menezes HC, Cardeal ZL (2019) New passive sampling device for effective monitoring of pesticides in water. *Anal Chim Acta* 1054:26–37
17. Chichilnisky G (1997) What is sustainable development? *Land Econ* 73(4):467. <https://doi.org/10.2307/3147240>
18. da Silva FM, da Silva FM, de Lacerda PSB, Junior JJ (2005) Desenvolvimento sustentável e química verde. *Quim Nova* 28(1):103–110. <https://doi.org/10.1590/s0100-40422005000100019>
19. Blazek M, Bambach B (1996) Integrating ISO 14000 environmental management systems and design for environment at AT&T. In: *Proceedings of the 1996 IEEE international symposium on electronics and the environment, ISEE-1996*. <https://doi.org/10.1109/isee.1996.501887>
20. Anastas P, Eghbali N (2010) Green chemistry: principles and practice. *Chem Soc Rev* 39(1):301–312. <https://doi.org/10.1039/b918763b>
21. Anastas PT, Warner JC (2000) *Green chemistry: theory and practice*. Oxford University Press, USA
22. Tobiszewski M, Mechlińska A, Zygmunt B, Namieśnik J (2009) Green analytical chemistry in sample preparation for determination of trace organic pollutants. *TrAC, Trends Anal Chem* 28(8):943–951. <https://doi.org/10.1016/j.trac.2009.06.001>
23. Hussain I, Singh NB, Singh A, Singh H, Singh SC (2016) Green synthesis of nanoparticles and its potential application. *Biotech Lett* 38(4):545–560. <https://doi.org/10.1007/s10529-015-2026-7>
24. Duan H, Wang D, Li Y (2015) ChemInform abstract: green chemistry for nanoparticle synthesis. *ChemInform* 46(38). <https://doi.org/10.1002/chin.201538287>
25. Iravani S (2011) Green synthesis of metal nanoparticles using plants. *Green Chem* 13(10):2638. <https://doi.org/10.1039/c1gc15386b>
26. Fan G et al (2020) Extremely facile and green synthesis of magnetic carbon composites drawn from natural bulrush for electromagnetic wave absorbing. *J Alloys Compounds* 835:155345. <https://doi.org/10.1016/j.jallcom.2020.155345>
27. Botes M, Cloete TE (2010) The potential of nanofibers and nanobiocides in water purification. *Crit Rev Microbiol* 36(1):68–81

28. Saleh GM (2020) Green synthesis concept of nanoparticles from environmental bacteria and their effects on pathogenic bacteria. *Iraqi J Sci*:1289–1297. <https://doi.org/10.24996/ijs.2020.61.6.6>
29. Vetchinkina E, Loshchinina E, Kupryashina M, Burov A, Nikitina V (2019) Shape and size diversity of gold, silver, selenium, and silica nanoparticles prepared by green synthesis using fungi and bacteria. *Ind Eng Chem Res* 58(37):17207–17218. <https://doi.org/10.1021/acs.iecr.9b03345>
30. Senthilkumar P, Surendran L, Sudhagar B, Ranjith Santhosh Kumar D (2019) Facile green synthesis of gold nanoparticles from marine algae *Gelidiellaacerosa* and evaluation of its biological potential. *SN Appl Sci* 1(4). <https://doi.org/10.1007/s42452-019-0284-z>
31. Daphne J, Francis A, Mohanty R, Ojha N, Das N (2018) Green synthesis of antibacterial silver nanoparticles using yeast isolates and its characterization. *Res J Pharm Technol* 11(1):83. <https://doi.org/10.5958/0974-360x.2018.00016.1>
32. Inbakandan D, Kumar C, Bavanilatha M, Ravindra DN, Kirubakaran R, Khan SA (2016) Ultrasonic-assisted green synthesis of flower like silver nanocolloids using marine sponge extract and its effect on oral biofilm bacteria and oral cancer cell lines. *Microb Pathog* 99:135–141
33. Ahmadian-Fard-Fini S, Salavati-Niasari M, Ghanbari D (2018) Hydrothermal green synthesis of magnetic Fe<sub>3</sub>O<sub>4</sub>-carbon dots by lemon and grape fruit extracts and as a photoluminescence sensor for detecting of *E. coli* bacteria. *Spectrochim Acta Part A Mol Biomol Spectrosc* 203:481–493. <https://doi.org/10.1016/j.saa.2018.06.021>
34. Namiesnik J (1999) Pro-ecological education. *Environ Sci Pollut Res* 6(4):243–244. <https://doi.org/10.1007/bf02987339>
35. Koel M, Kaljurand M (2006) Application of the principles of green chemistry in analytical chemistry. *Pure Appl Chem* 78(11):1993–2002. <https://doi.org/10.1351/pac200678111993>
36. Routray W, Orsat V (2012) Microwave-assisted extraction of flavonoids: a review. *Food Bioprocess Technol* 5(2):409–424. <https://doi.org/10.1007/s11947-011-0573-z>
37. Esclapez MD, García-Pérez JV, Mulet A, Cárcel JA (2011) Ultrasound-assisted extraction of natural products. *Food Eng Rev* 3(2):108–120. <https://doi.org/10.1007/s12393-011-9036-6>
38. Vieira MA, Ribeiro AS, Curtius AJ, Sturgeon RE (2007) Determination of total mercury and methylmercury in biological samples by photochemical vapor generation. *Anal Bioanal Chem* 388(4):837–847
39. Górecki T, Namieśnik J (2002) Passive sampling. *TrAC, Trends Anal Chem* 21(4):276–291. [https://doi.org/10.1016/s0165-9936\(02\)00407-7](https://doi.org/10.1016/s0165-9936(02)00407-7)
40. Płotka-Wasyłka J, Szczepańska N, de la Guardia M, Namieśnik J (2015) Miniaturized solid-phase extraction techniques. *TrAC, Trends Anal Chem* 73:19–38. <https://doi.org/10.1016/j.trac.2015.04.026>
41. Carasek E, Merib J (2015) Membrane-based microextraction techniques in analytical chemistry: a review. *Anal Chim Acta* 880:8–25
42. Arthur CL, Pawliszyn J (1990) Solid phase microextraction with thermal desorption using fused silica optical fibers. *Anal Chem* 62(19):2145–2148. <https://doi.org/10.1021/ac00218a019>
43. Liu H, Dasgupta PK (1996) Analytical chemistry in a drop. Solvent extraction in a microdrop. *Anal Chem* 68(11):1817–1821. <https://doi.org/10.1021/ac960145h>
44. Vrana B, Popp P, Paschke A, Schüürmann G (2001) Membrane-enclosed sorptive coating. An integrative passive sampler for monitoring organic contaminants in water. *Anal Chem* 73(21):5191–5200
45. Assoumani A, Lissalde S, Margoum C, Mazzella N, Coquery M (2013) In situ application of stir bar sorptive extraction as a passive sampling technique for the monitoring of agricultural pesticides in surface waters. *Sci Total Environ* 463–464:829–835
46. Assoumani A, Coquery M, Liger L, Mazzella N, Margoum C (2015) Field application of passive SBSE for the monitoring of pesticides in surface waters. *Environ Sci Pollut Res Int* 22(6):3997–4008

47. Zheng B et al (2017) Determination of phenols isomers in water by novel nanosilica/polydimethylsiloxane-coated stirring bar combined with high performance liquid chromatography-fourier transform infrared spectroscopy. *Sci Rep* 7(1):8697
48. Matsiko J et al (2018) Stir bar sorptive extraction and thermal desorption—gas chromatography/mass spectrometry for determining phosphorus flame retardants in air samples. *Anal Methods* 10(16):1918–1927. <https://doi.org/10.1039/c8ay00138c>
49. Chen Y, Pawliszyn J (2003) Time-weighted average passive sampling with a solid-phase microextraction device. *Anal Chem* 75(9):2004–2010
50. Allan IJ, Raffard V, Kringstad A, Næs K (2021) Assessment of marine sediment remediation efficiency with SPME-based passive sampling measurement. *Sci Total Environ* 756:143854
51. Lee I-S, Tsai S-W (2008) Passive sampling of ambient ozone by solid phase microextraction with on-fiber derivatization. *Anal Chim Acta* 610(2):149–155
52. Zhao W, Ouyang G, Alaei M, Pawliszyn J (2006) On-rod standardization technique for time-weighted average water sampling with a polydimethylsiloxane rod. *J Chromatogr A* 1124(1–2):112–120
53. Assoumani A et al (2013) Polydimethylsiloxane rods for the passive sampling of pesticides in surface waters. *Water* 5(3):1366–1379. <https://doi.org/10.3390/w5031366>
54. Xu C, Wang J, Richards J, Xu T, Liu W, Gan J (2018) Development of film-based passive samplers for in situ monitoring of trace levels of pyrethroids in sediment. *Environ Pollut* 242(Pt B):1684–1692
55. Ahmadi F, Sparham C, Boyacı E, Pawliszyn J (2017) Time weighted average concentration monitoring based on thin film solid phase microextraction. *Environ Sci Technol* 51(7):3929–3937
56. Mäenpää K et al (2015) Fate of polychlorinated biphenyls in a contaminated lake ecosystem: combining equilibrium passive sampling of sediment and water with total concentration measurements of biota. *Environ Toxicol Chem* 34(11):2463–2474. <https://doi.org/10.1002/etc.3099>
57. Xue J, Zhu X, Liu Z, Hua R, Wu X (2020) Using silicone rubber and polyvinylchloride as equilibrium passive samplers for rapid and sensitive monitoring of pyrethroid insecticides in aquatic environments. *Sci Total Environ* 728:138797
58. Vrana B et al (2019) Chasing equilibrium passive sampling of hydrophobic organic compounds in water. *Sci Total Environ* 664:424–435
59. Ruiz-Jimenez J, Zanca N, Lan H, Jussila M, Hartonen K, Riekkola M-L (2019) Aerial drone as a carrier for miniaturized air sampling systems. *J Chromatogr A* 1597:202–208
60. Taylor AC, Fones GR, Mills GA (2020) Trends in the use of passive sampling for monitoring polar pesticides in water. *Trends Environ Anal Chem* 27:e00096. <https://doi.org/10.1016/j.teac.2020.e00096>
61. Macagnano A et al (2018) Passive sampling of gaseous elemental mercury based on a composite TiO<sub>2</sub>NP/AuNP layer. *Nanomaterials* 8(10):798. <https://doi.org/10.3390/nano8100798>
62. Santos E, Ferlin S, Fostier A, Mazali I (2016) Using gold nanoparticles as passive sampler for indoor monitoring of gaseous elemental mercury. *J Braz Chem Soc*. <https://doi.org/10.21577/0103-5053.20160290>
63. Papa P et al (2018) Use of gold nanoparticles as substrate for diffusive monitoring of gaseous mercury. *Materials* 11(11). <https://doi.org/10.3390/ma11112119>
64. de Barros Santos E et al (2017) Proof of concept for a passive sampler for monitoring of gaseous elemental mercury in artisanal gold mining. *Sci Rep* 7(1):16513
65. Avossa J et al (2020) Characteristics and performances of a nanostructured material for passive samplers of gaseous Hg. *Sensors* 20(21). <https://doi.org/10.3390/s20216021>
66. Lisha KP, Anshup, Pradeep T (2009) Towards a practical solution for removing inorganic mercury from drinking water using gold nanoparticles. *Gold Bull* 42(2):144–152. <https://doi.org/10.1007/bf03214924>
67. Pirrone N et al (2009) Global mercury emissions to the atmosphere from natural and anthropogenic sources. In: *Mercury fate and transport in the global atmosphere*, pp 1–47. [https://doi.org/10.1007/978-0-387-93958-2\\_1](https://doi.org/10.1007/978-0-387-93958-2_1)

68. Seigneur C, Karamchandani P, Lohman K, Vijayaraghavan K, Shia R-L (2001) Multi-scale modeling of the atmospheric fate and transport of mercury. *J Geophys Res: Atmos* 106(D21):27795–27809. <https://doi.org/10.1029/2000jd000273>
69. Driscoll CT, Mason RP, Chan HM, Jacob DJ, Pirrone N (2013) Mercury as a global pollutant: sources, pathways, and effects. *Environ Sci Technol* 47(10):4967–4983
70. Nabi S (2014) Toxic effects and remedy. In: *Toxic effects of mercury*, pp 19–27. [https://doi.org/10.1007/978-81-322-1922-4\\_4](https://doi.org/10.1007/978-81-322-1922-4_4)
71. Bai L et al (2020) Association between acute severe mercury poisoning and multiple organ failure. *Am J Transl Res* 12(8):4347–4353
72. USEPA list of priority pollutants. In: *The environmental science of drinking water*, pp 243–245. <https://doi.org/10.1016/b978-075067876-6/50013-0>
73. Huang J, Lyman SN, Hartman JS, Gustin MS (2014) A review of passive sampling systems for ambient air mercury measurements. *Environ Sci Process Impacts* 16(3):374–392
74. Botasini S, Heijo G, Méndez E (2013) Toward decentralized analysis of mercury (II) in real samples. A critical review on nanotechnology-based methodologies. *Anal Chim Acta* 800:1–11. <https://doi.org/10.1016/j.aca.2013.07.067>
75. Herrero-Latorre C, Barciela-García J, García-Martín S, Peña-Crecente RM, Otárola-Jiménez J (2015) Magnetic solid-phase extraction using carbon nanotubes as sorbents: a review. *Anal Chim Acta* 892:10–26
76. Pyrzynska K (2011) Carbon nanotubes as sorbents in the analysis of pesticides. *Chemosphere* 83(11):1407–1413. <https://doi.org/10.1016/j.chemosphere.2011.01.057>
77. Shen L et al (2016) Carbon nanotube integrative sampler (CNIS) for passive sampling of nanosilver in the aquatic environment. *Sci Total Environ* 569–570:223–233
78. Godlewska K, Jakubus A, Stepnowski P, Paszkiewicz M (2021) Impact of environmental factors on the sampling rate of  $\beta$ -blockers and sulfonamides from water by a carbon nanotube-passive sampler. *J Environ Sci* 101:413–427
79. Jakubus A, Tyma M, Stepnowski P, Paszkiewicz M (2017) Application of passive sampling devices based on multi-walled carbon nanotubes for the isolation of selected pharmaceuticals and phenolic compounds in water samples—possibilities and limitations. *Talanta* 164:700–707. <https://doi.org/10.1016/j.talanta.2016.09.052>
80. Li S, Anderson TA, Maul JD, Shrestha B, Green MJ, Cañas-Carrell JE (2013) Comparative studies of multi-walled carbon nanotubes (MWNTs) and octadecyl (C18) as sorbents in passive sampling devices for biomimetic uptake of polycyclic aromatic hydrocarbons (PAHs) from soils. *Sci Total Environ* 461–462:560–567
81. Valenzuela EF, de Paula FF, Teixeira APC, Menezes HC, Cardeal ZL (2021) Assessment of pesticides in water using time-weighted average calibration of passive sampling device manufactured with carbon nanomaterial coating on stainless steel wire. *Anal Bioanal Chem* 413(12):3315–3327
82. Heidari M, Bahrami A, Ghiasvand AR, Shahna FG, Soltanian AR, Rafieiemam M (2015) Application of graphene nanoplatelets silica composite, prepared by sol-gel technology, as a novel sorbent in two microextraction techniques. *J Sep Sci* 38(24):4225–4232
83. Heidari M, Bahrami A, Ghiasvand AR, Shahna FG, Soltanian AR (2012) A novel needle trap device with single wall carbon nanotubes sol-gel sorbent packed for sampling and analysis of volatile organohalogen compounds in air. *Talanta* 101:314–321. <https://doi.org/10.1016/j.talanta.2012.09.032>
84. Heidari M, Bahrami A, Ghiasvand AR, Emam MR, Shahna FG, Soltanian AR (2015) Graphene packed needle trap device as a novel field sampler for determination of perchloroethylene in the air of dry cleaning establishments. *Talanta* 131:142–148
85. Eom I-Y, Tugulea A-M, Pawliszyn J (2008) Development and application of needle trap devices. *J Chromatogr A* 1196–1197:3–9
86. Lord HL, Zhan W, Pawliszyn J (2012) Fundamentals and applications of needle trap devices. In: *Comprehensive sampling and sample preparation*, pp 677–697. <https://doi.org/10.1016/b978-0-12-381373-2.00056-9>

87. Zhang B-T, Liu H, Liu Y, Teng Y (2020) Application trends of nanofibers in analytical chemistry. *TrAC Trends Anal Chem* 131:115992. <https://doi.org/10.1016/j.trac.2020.115992>
88. Chigome S, Torto N (2011) A review of opportunities for electrospun nanofibers in analytical chemistry. *Anal Chim Acta* 706(1):25–36
89. Jao D, Beachley VZ (2019) Continuous dual-track fabrication of polymer micro-/nanofibers based on direct drawing. *ACS Macro Lett* 8(5):588–595. <https://doi.org/10.1021/acsmacrolett.9b00167>
90. Zhao J et al (2012) Preparation and properties of biomimetic porous nanofibrous poly(L-lactide) scaffold with chitosan nanofiber network by a dual thermally induced phase separation technique. *Mater Sci Eng C Mater Biol Appl* 32(6):1496–1502
91. Qin W, Li J, Tu J, Yang H, Chen Q, Liu H (2017) Fabrication of porous chitosan membranes composed of nanofibers by low temperature thermally induced phase separation, and their adsorption behavior for Cu. *Carbohydr Polym* 178:338–346
92. Liu Z, Jiang Y, Jiang J, Zhai D, Wang D, Liu M (2020) Self-assembly of isomeric naphthalene appended glucono derivatives: nanofibers and nanotwists with circularly polarized luminescence emission. *Soft Matter* 16(17):4115–4120
93. Mendes AC, Strohmenger T, Goycoolea F, Chronakis IS (2017) Electrostatic self-assembly of polysaccharides into nanofibers. *Colloids Surf, A* 531:182–188. <https://doi.org/10.1016/j.colsurfa.2017.07.044>
94. Zhao R et al (2020) Shaddock peels as bio-templates synthesis of Cd-doped SnO<sub>2</sub> nanofibers: a high performance formaldehyde sensing material. *J Alloys Compounds* 813:152170. <https://doi.org/10.1016/j.jallcom.2019.152170>
95. Jin K, Eyer S, Dean W, Kitto D, Bates FS, Ellison CJ (2020) Bimodal nanofiber and microfiber nonwovens by melt-blowing immiscible ternary polymer blends. *Ind Eng Chem Res* 59(12):5238–5246. <https://doi.org/10.1021/acs.iecr.9b04887>
96. Singh S, Pankaj A, Mishra S, Tewari K, Singh SP (2019) Cerium oxide-catalyzed chemical vapor deposition grown carbon nanofibers for electrochemical detection of Pb(II) and Cu(II). *J Environ Chem Eng* 7(4):103250. <https://doi.org/10.1016/j.jece.2019.103250>
97. Shoukat R, Khan MI (2018) Synthesis of vertically aligned carbon nanofibers using inductively coupled plasma-enhanced chemical vapor deposition. *Electr Eng* 100(2):997–1002. <https://doi.org/10.1007/s00202-017-0561-z>
98. Wang J, Li C, Yang Z, Chen D (2017) Chemical vapor deposition-assisted fabrication of a graphene-wrapped MnO/carbon nanofibers membrane as a high-rate and long-life anode for lithium ion batteries. *RSC Adv* 7(80):50973–50980. <https://doi.org/10.1039/c7ra09942h>
99. Bukhari BS, Imran M, Bashir M, Riaz S, Naseem S (2018) Honey mediated microwave assisted sol–gel synthesis of stabilized zirconia nanofibers. *J Sol-Gel Sci Technol* 87(3):554–567. <https://doi.org/10.1007/s10971-018-4749-0>
100. Kumar NS, Kumar NS, Suvarna RP, Chandra Babu Naidu K (2019) Grain and grain boundary conduction mechanism in sol-gel synthesized and microwave heated Pb<sub>0.8-y</sub>La<sub>y</sub>Co<sub>0.2</sub>TiO<sub>3</sub> (y = 0.2–0.8) nanofibers. *Mater Chem Phys* 223:241–248. <https://doi.org/10.1016/j.matchemphys.2018.11.004>
101. Zhang X, Goux WJ, Manohar SK (2004) Synthesis of polyaniline nanofibers by ‘nanofiber seeding.’ *J Am Chem Soc* 126(14):4502–4503
102. Xue J, Wu T, Dai Y, Xia Y (2019) Electrospinning and electrospun nanofibers: methods, materials, and applications. *Chem Rev* 119(8):5298–5415. <https://doi.org/10.1021/acs.chemrev.8b00593>
103. Wei H, Rodriguez K, Renneckar S, Leng W, Vikesland PJ (2015) Preparation and evaluation of nanocellulose-gold nanoparticle nanocomposites for SERS applications. *Analyst* 140(16):5640–5649
104. Qian J, Jennings B, Cwiertny DM, Martinez A (2017) Emerging investigator series: development and application of polymeric electrospun nanofiber mats as equilibrium-passive sampler media for organic compounds. *Environ Sci Process Impacts* 19(11):1445–1456

105. Martinez A, Cwiertny D (2016) Nanofiber-enabled, multi-target passive sampling device for determination of the freely-dissolved sediment pore water concentrations of organic contaminants. US Department of Defense Strategic Environmental Research and Development Program (SERDP), 1
106. Qian J et al (2020) Polymeric nanofiber-carbon nanotube composite mats as fast-equilibrium passive samplers for polar organic contaminants. *Environ Sci Technol* 54(11):6703–6712
107. Minho LAC, de L. Cardeal Z, Menezes HC. Processo de modificação de membranas de fibra oca de polipropileno, produto, dispositivo e uso. BR1020210178957
108. Guo X, Fan S, Hu Y, Fu X, Shao H, Zhou Q (2019) A novel membrane biofouling mitigation strategy of D-amino acid supported by polydopamine and halloysite nanotube. *J Membr Sci* 579:131–140. <https://doi.org/10.1016/j.memsci.2019.02.039>
109. Yang Z, Takagi R, Zhang X, Yasui T, Zhang L, Matsuyama H (2021) Engineering a dual-functional sulfonated polyelectrolyte-silver nanoparticle complex on a polyamide reverse osmosis membrane for robust biofouling mitigation. *J Membr Sci* 618:118757. <https://doi.org/10.1016/j.memsci.2020.118757>
110. Yu Y, Yang Y, Yu L, Koh KY, Chen JP (2021) Modification of polyvinylidene fluoride membrane by silver nanoparticles-graphene oxide hybrid nanosheet for effective membrane biofouling mitigation. *Chemosphere* 268:129187
111. Wu Y et al (2020) Recent advances in mitigating membrane biofouling using carbon-based materials. *J Hazard Mater* 382:120976
112. Kumar JA et al (2021) A focus to green synthesis of metal/metal based oxide nanoparticles: various mechanisms and applications towards ecological approach. *J Clean Prod* 324:129198
113. Esa YAM, Sapawe N (2020) A short review on zinc metal nanoparticles synthesized by green chemistry via natural plant extracts. *Mater Today: Proc* 31:386–393. <https://doi.org/10.1016/j.matpr.2020.07.184>



**Part VI**  
**Environmental Sciences and Applications**

# Chapter 20

## Porous Graphene-Based Materials for Enhanced Adsorption Towards Emerging Micropollutants (EMs)



Alvin Lim Teik Zheng, Supakorn Boonyuen, and Yoshito Andou

### 1 Introduction

The contamination of emerging micropollutants (EMs) derived from various sources such as agricultural, pharmaceutical, and household has become a global issue in ensuring water security for the preservation of humankind. Emerging micropollutants can be defined as minute biological or chemical contaminants produced at trace amounts (up to microgram per litre) that enter ground or surface waters [1–3]. EMs can be categorized as a subgroup of micropollutants [4]. The risk from these micropollutants and their metabolites/side products often greatly affects the environment and human health attributed to the accumulation in water bodies that serve as drinking water reservoirs. There are significant limitations in conventional sewage treatment methods which are not adequate to remove EMs. Often, the combination of several process technologies is required to remove various EMs. In some countries, wastewater treatment plants (WWTP) treated wastewater is released to water bodies such as lakes, ponds, rivers, and ocean waters, as shown in Fig. 1. As a result, numerous

---

Y. Andou (✉)

Graduate School of Life Science and Systems Engineering, Kyushu Institute of Technology, Fukuoka 808-0196, Japan

e-mail: [yando@life.kyutech.ac.jp](mailto:yando@life.kyutech.ac.jp)

S. Boonyuen

Department of Chemistry, Faculty of Science and Technology, Thammasat University, Pathumthani 12120, Thailand

Y. Andou

Collaborative Research Centre for Green Materials On Environmental Technology, Kyushu Institute of Technology, Fukuoka 808-0196, Japan

A. L. T. Zheng

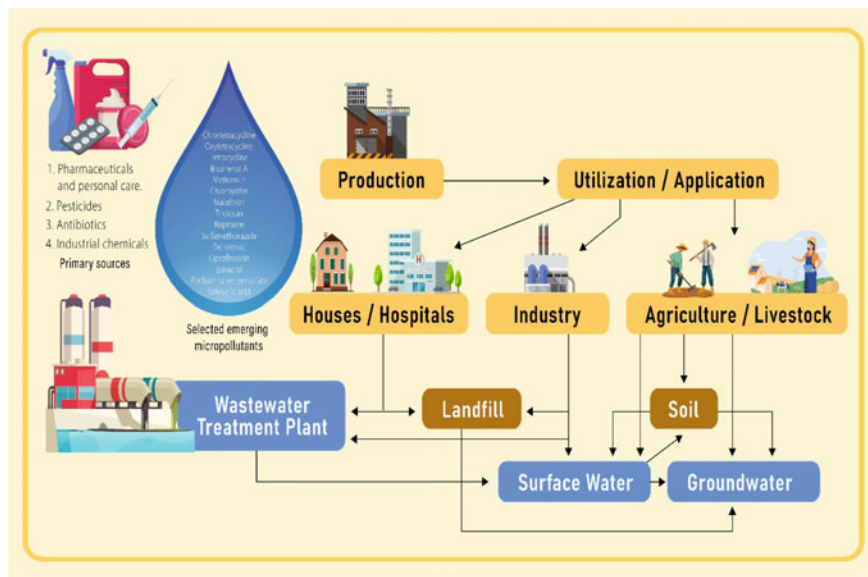
Department of Science and Technology, Faculty of Humanities, Management and Science, Universiti Putra Malaysia Bintulu Campus, Bintulu, Sarawak, Malaysia

© The Author(s), under exclusive license to Springer Nature Singapore Pte Ltd. 2023

A. N. Grace et al. (eds.), *Handbook of Porous Carbon Materials*,

Materials Horizons: From Nature to Nanomaterials,

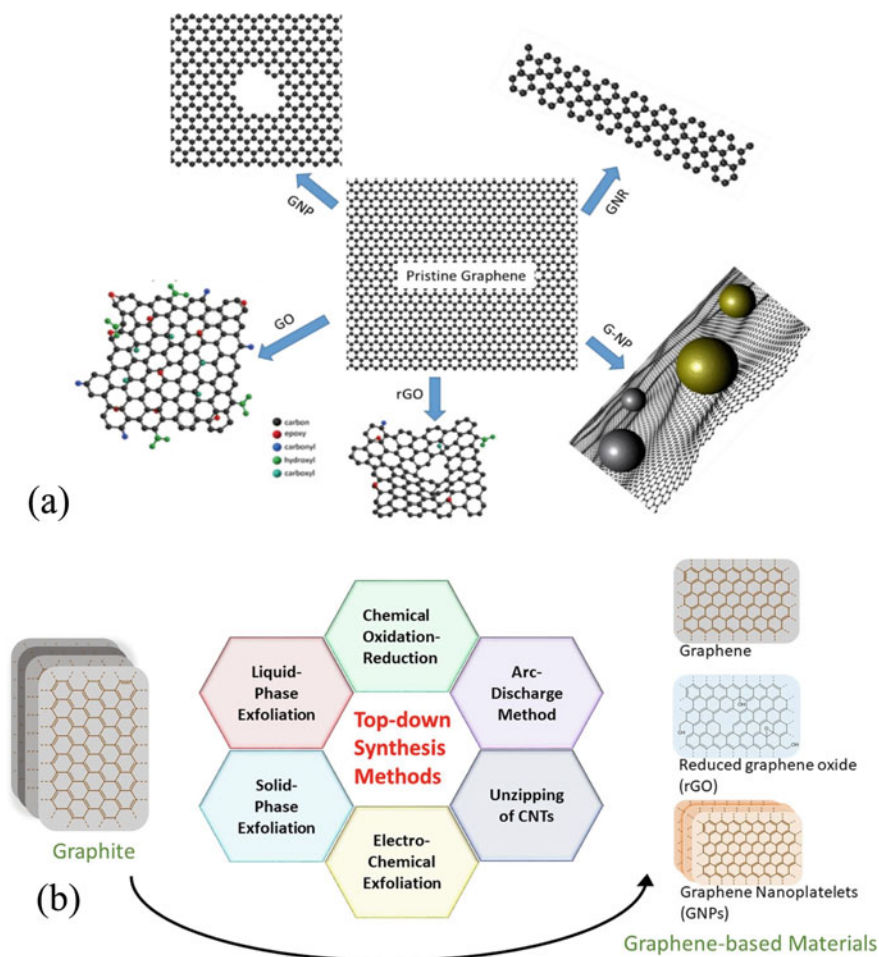
[https://doi.org/10.1007/978-981-19-7188-4\\_20](https://doi.org/10.1007/978-981-19-7188-4_20)



**Fig. 1** Emerging micropollutant (EM) sources and their destinations in the environment

EMs and their metabolites may probably end up in water bodies. Consequently, health dangers to humans may arise as EMs accumulate. There is a paucity of data on the environmental and human health implications of these chemicals. To date, many studies have reported on the harm of EMs to the living organism [5–7].

Over the past decade, there has been an increasing emphasis on leveraging nanoscience and nanotechnology to produce numerous nanostructured materials, as effective remediators for water treatment. The use of nanosized nanomaterials has been regarded as a feasible strategy in the wastewater remediation process [8–12]. Previously, it was found that various pollutants which include dyes, heavy metals ions, pesticides, and pharmaceutical compounds can be remediated using nanomaterials. In addition, they also exhibited interesting antimicrobial properties against water-borne bacteria [13]. Graphene and its derivatives have become ubiquitous in most studies spanning many applications such as energy, environment, construction, and health care [14–16]. The unique two-dimensional carbon allotrope possesses excellent electrical conductivity, unsurpassed mechanical strength, and high surface area which are sought-after [17–19]. The hype with this class of emerging material is projected to continue for at least the next few decades. However, most studies often do not use pristine graphene because of the absence of functionalities, high preparation cost, difficulty in handling, and their low yield [20]. Figure 2b depicts the derivatives of graphene which are often reported in the preparation of highly functional adsorbents.



**Fig. 2** **a** Graphene and their derivatives nanomaterials. Reprinted with permission from Wu et al. [21]. Copyright 2018 MDPI. **b** Top-down synthetic methods for graphene preparation. Reprinted with permission from Kumar et al. [22]. Copyright 2021 Elsevier

The strategy in water treatment technologies includes biological, physical, and chemical actions [23]. Among them, methods such as precipitation, photodegradation, coagulation, membrane separation, microbial assistance, and ion exchange have been reported in the wastewater remediation [24]. However, the methods mentioned above have significant setbacks, such as cost-effectiveness, the ability to selectively remove numerous contaminants, regeneration, and reusability. Of all treatment methods proposed, the adsorption process can be considered a traditional method which is relevant and appealing for eliminating micropollutants [25]. The process has numerous advantages, including ease of operation, low operational costs, robust batch process, and environmental friendliness [26]. In addition, some adsorbents

have the possibility of reuse and regeneration. Adsorption has grown in popularity due to its ability to treat dissolved pollutants after chemical oxidation or biological treatment effectively. Batch reactors that use an adsorption process, on the other hand, require secondary sludge removal, which can be improved by using hybrid systems [27]. Traditional adsorbents have a limited and non-selective adsorption capability, which is a restriction of adsorption technology. The modifications to the graphene materials can raise surface area and pore size to improve adsorption capacity. This research direction has garnered continuous attention in the preparation of highly efficient adsorbents.

Graphene materials as an adsorbent for removing EMs are still emerging compared to widely used activated carbon (AC). Compared to pollutant remediation of synthetic dyes and heavy metal, reported studies on adsorption of EMs are still developing [28]. Provided that interest in graphene's potential in EM remediation is growing steadily, collating recent studies on this subject matter is timely. Mainly, graphene-based adsorbents have gotten significant interest lately. By offering the latest trend of graphene-based composites in EM removal, this chapter intends to fill the knowledge gap in the abundance of literature present on this subject matter. The chapter begins with a brief explanation of EMs, backed up by numerous studies determining their quantity in various water sources and current methods in their analysis. The recent report on a novel yet unique graphene-based composite/membrane fabrication processes is also examined. We shared the latest study on how well graphene and composites/membranes performed in the adsorption of various EMs. Finally, the obstacles to developing graphene-based adsorbents are examined, and their potential challenges are addressed. In addition, an attempt is also made to provide suggestions for future studies on graphene-based adsorbents.

## 2 Emerging Micropollutants (EMs)—Current Status Quo

Common sources of EMs include industrial chemicals, pharmaceuticals and personal care products (PPCP), antibiotics, pesticides, and biocides [29]. However, the list of compounds listed is constantly growing with new chemical substances being registered. Most research on EMs has focused on surface waters as they are frequently found to be at high concentrations, mainly when they are linked with industrial discharges. Secondly, surface water monitoring is less complicated than monitoring groundwater [30]. Commonly applied wastewater purification involves secondary processes which include activated sludge and trickling filters that do not offer the advantage of removing a wide array of pollutants. The standard wastewater treatment processes used are inherently not able to remove EMs which led to their presence in the treated water. EM presence in the aquatic environment is associated with detrimental consequences such as prolonged toxicity and antibiotic resistance [30, 31].

The analysis to identify and quantify specific EM compounds is often carried out via chromatography methods (HPLC, LC, and GC) coupled with mass spectroscopy.

However, due to the minute quantity introduced into the environment, quantification of EMs in treated wastewater is often challenging. Many unknown substances may also be present in the wastewater. Among the micropollutants, pharmaceutical and personal care (PPCP) compounds such as tetracycline, ciprofloxacin, sulfamethoxazole, diclofenac, ibuprofen, naproxen, and triclosan are commonly found due to their complex chemical structures, multiple ionization sites, and polymorphism [32, 33]. The sources of these chemicals are often being discharged from households, hospitals, and agricultural farms, as depicted in Fig. 1. Monitoring antibiotic contamination is especially important given its link to antibiotic resistance, which is worrying [34]. As in the case of PPCPs, liquid chromatography (LC) coupled with mass spectrometry (MS) technologies was commonly used for their detection instead of gas chromatography (GC) due to their thermal instability, high solubility, and polarity.

Recent studies on the determination of various EMs in the surface waters indicated the dangers posed to living organisms. Rodriguez-Mozaz and co-workers reported antibiotic traces in final effluents of 7 European countries using an LC–MS [35]. They found at least 17 antibiotics detected in the final effluent, which posed a significant environmental risk. They proposed ciprofloxacin, azithromycin, and cefalexin to be used as markers in the determination of EMs. Antibiotic residues from at least 7–12 different compounds were found to be steadily released in freshwater and marine ecosystems. In another study, 27 PPCPs were extracted from various sources using solid-phase extraction (SPE), subsequently detected via LC–MS [36]. As for pesticide contaminants, the presence of imazalil, pyrimethanil, and thiabendazole are potential environmental risks [37]. The risk quotient (HQ) employed in the study indicated that cyprodinil, etoxazole, imazalil, and propiconazole are considered high risk for aquatic organisms.

### 3 Properties and Synthesis of Graphene Composite-Based Adsorbents

The various synthesis of graphene derivatives has been extensively covered in many literature studies in the past years [38–43]. Currently, the process to synthesize graphene materials involved top-down and bottom-up approaches. The bottom-up processes include chemical vapour deposition, pyrolysis, and epitaxial growth, which are sophisticated as they necessitate expensive equipment and controlled operating conditions [22]. Top-down approaches merely involve the conversion of graphite to various graphene derivatives, as shown in Fig. 2a. Most commercially available graphene is made top-down since it is easier to prepare and less expensive when produced on a big scale. Often, the disadvantages of this approach include large defects present on the graphene sheets and the usage of harmful reagents [44]. In most instances, graphene oxide (GO) is the starting material when preparing composite-based adsorbents ascribed to their functionalities and versatility. The preparation method of GO often follows the Hummers approach or its modified form. For

graphene composite-based adsorbents, adding graphene sheets in a composite material increases porosity, surface area, and the possibility of pollutant diffusion inside graphene pores [45].

In developing novel adsorbents with the prospects to remove environmental contaminants, graphene and its derivatives are considered to be a promising yet efficient material. Unlike EMs, the adsorption of organic pollutants such as dye molecules and heavy metals using graphene-based materials is commonly reported [46, 47]. Unmodified graphene derivatives, on the other hand, do not possess enhanced adsorption capabilities. Combining a series of modifiers with graphene materials has generated graphene composites with porous morphology and functional groups that can remediate micropollutants effectively. The various functionalization methods have yielded composites that have good adsorption capabilities and excellent regeneration capabilities. Modified hybrid composites have been shown to address the drawbacks of bare graphene materials, allowing for highly efficient micropollutant remediation. Nanoparticles (NP), polymers, and biomaterials have been used to modify graphene sheets, resulting in increased binding sites or enlarged surface area. In addition, the various functionalities of graphene-based composites may remove many types of pollutants simultaneously.

## 4 Adsorption of Micropollutants and Their Mechanism

### 4.1 2D Graphene-Based Composites

This section reports on the usage of bare graphene materials and their composites for the adsorption of various EMs. Often, adsorption behaviour on pollutants is influenced by the physical and chemical characteristics of the graphene-based materials. Among them, the surface chemistry usually determines the adsorption capacity, i.e. the presence of interaction sites and the adsorbent's surface area, which impact the removal efficiencies and mechanism.

Due to the van der Waals interactions, graphene tends to develop interconnecting pores inside the aggregates which also assisted in the adsorption of EMs. A recent study accessed the influence of the surface area and physicochemical properties of graphite and Gr-based materials towards metronidazole (MNZ) and trimethoprim (TMP) adsorption [48]. When oxygen surface group concentration is low, both antibiotics were adsorbed on graphite and rGO materials via  $\pi$ - $\pi$  interactions as the mechanism of interactions rely primarily on the surface area. However, the adsorption on bare GO corroborated the various adsorption mechanism, which is pH-dependent. In addition, they found that interlayer adsorption was not observed on GO, rGO, or N-rGO. The significant aggregation of graphene sheets due to  $\pi$ - $\pi$  interactions and strong van der Waals interactions reduces their high adsorption capacity and limits their practical applicability [49]. The influence of sheet aggregation on the adsorption of several EMs was systematically investigated [50]. The work

proved that rGO exhibited higher adsorption capacity than MWCNT and graphene, suggesting that aggregation of graphene sheets and the oxygenated functional groups played significant roles in influencing adsorption performance. Various methods have been proposed, such as adhering nanoparticles, preparing deformed graphene sheets, including spacers and conversion to a 3D network [51].

Often, chemical functionalization of the rich oxygen-based functionalities on the basal and edges of the sheet allows for more significant interactions with the pollutants. The size effect of 3D adsorbents is essential in the removal of EMs. In the first instance, the physical adsorption of contaminants adsorbed into the porous layer from the surrounding environment occurs at the liquid–solid interface. As a result, determining the diffusion rate of EMs is an essential step in accessing their removal efficiency. The high specific surface area is often contributed by the large pores present on the material, which usually stacks the finite-sized nanosheets. The control of pore size is one method in speeding up the diffusion process. The exposure of surface groups and active sites is essential in the heterogeneous interface's physicochemical process. Previously, GO prepared through the Hummers method has been accessed for the adsorption of metformin using the batch adsorption studies [52]. Compared to the modified Hummers method, adsorption of metformin is higher than GO synthesized via the modified Hummers method. Metformin was found to be adsorbed on the GO surface first in a chemisorptive pattern, followed by a physisorption trend, according to isotherm and kinetic measurements. Gao and co-workers first reported the adsorption of tetracycline and its derivatives using GO, which showed a maximum adsorption capacity of 313 mg/g, which was calculated using the Langmuir model [53]. Doxycycline adsorption capacity is greater in GO suspensions in comparison to tetracycline or oxytetracycline. They posited that the different pKa values could explain the various maximum adsorption values on GO. The adsorption mechanism is deduced to occur from the  $\pi$ – $\pi$  interaction and cation– $\pi$  bonding. The hexagonal cells of GO and the ring structure of tetracycline enable  $\pi$ – $\pi$  contact, and cation– $\pi$  bonding was anticipated to occur between the amino group on the ring C4 of tetracycline and graphene pi-electron-rich structures. In another study, Ai and co-workers compared the adsorption of GO and rGO on tetracycline (TC) antibiotics using density functional theory (DFT) and molecular dynamics (MD) simulations [54]. The less polar solvent environments and acidic medium aided TC adsorption efficiency on the graphene materials from their binding energies. Rosli and co-workers accessed the adsorption capability of commercially obtained graphene nanoplatelets (GNP) towards sulfamethoxazole (SMX) and acetaminophen (ACM) [55]. They found that the smaller surface area of commercially GNP C300 possessed more excellent adsorption capability towards SMX than GNP C750, which is ascribed to the clumping or aggregation. The molecular docking experiments led to negative binding energy indicated proving a spontaneous and exothermic adsorption. Wang and co-workers accessed the adsorption molecular mechanism of some pesticides (carbaryl, catechol, and fluridone) on GO using DFT, MD, and binding free energy calculation [56]. They discovered that  $\pi$ – $\pi$  stacking and van der Waals were mainly involved in the adsorption interactions between GO and the pesticides. The findings enabled a molecular understanding of the adsorption mechanism and also provided



easy visualization of the process. Foschi and co-workers accessed the adsorption of triazine using thermally reduced rGO films [57]. They carried out optimization using the design of experiment (DOE) and response surface methodology (RSM) to obtain the optimal adsorption parameters. The influence of epoxy and hydroxyl groups after reduction, in addition to the amine pendants on triazine rings, favoured adsorption via hydrogen bonding. Moreover, the adsorption is further enhanced via electrostatic interactions between the amino groups and oxygen-containing functionalities of the rGO. Based on the RSM analysis, the optimal GO reduction conditions were 110 °C for 24 h. The advantage of computational analysis enabled fewer preliminary tests to be conducted, saving product, cost, and time.

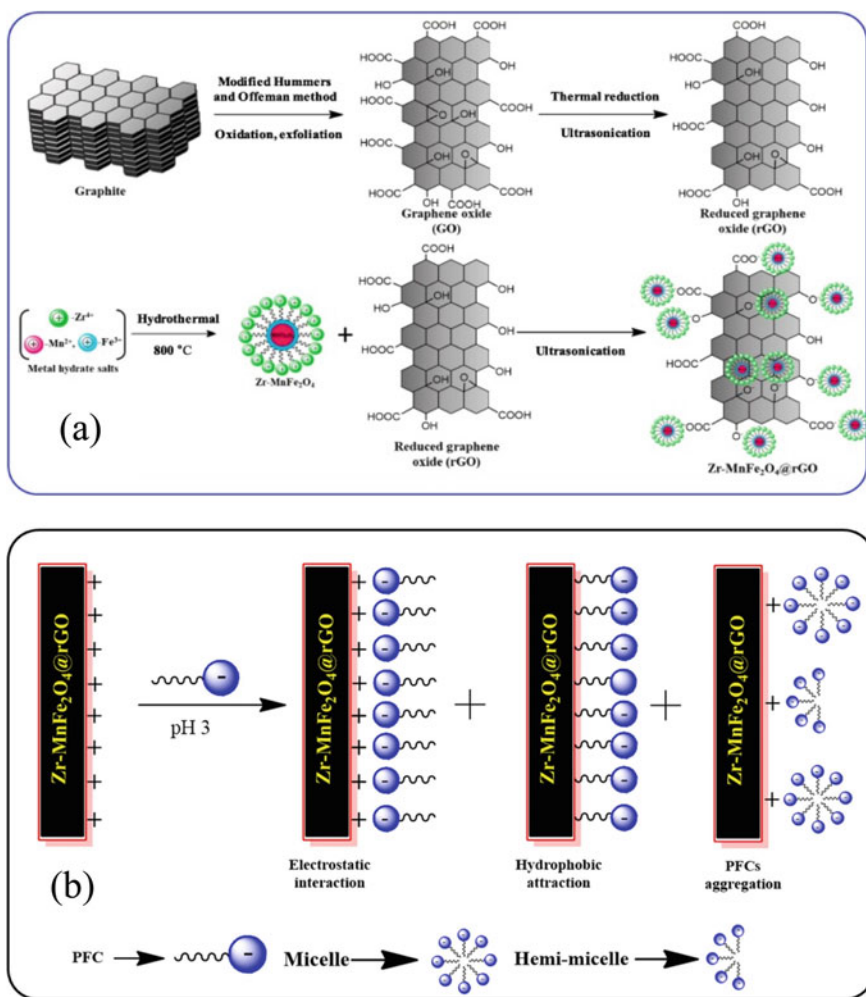
The application of pure GO as an adsorbent often results in an aggregated form that must be separated from the solution using an elaborate high-speed centrifuge [58]. Hence, the usage of polymer matrix or crosslinkers to improve mechanical stability is often attempted. Additionally, these polymers provide additional functional groups that can establish chemical interactions with the micropollutants, enhancing adsorption effectiveness for those pollutants. In one instance, GO was mixed into an alginate matrix for stabilization and to maximize the ease of recovery. When combined with divalent cations like  $\text{Ca}^{2+}$ , alginate forms a hydrogel with excellent mechanical characteristics [59]. GO/sodium alginate (SA) beads were recently studied for their adsorption of ciprofloxacin (CIP) [60]. It was found that the inclusion of GO enhanced the pore uniformity and reduced the pore sizes of the gels. Kinetic studies revealed that after incorporating GO, the adsorption capacity of SA composite gels increased approximately 7–9 times. The adsorption of TC antibiotics using GO/SA composite using Ca as the cross-linking agent prepared via freeze-drying was also recently reported [61]. The  $\pi$ – $\pi$  interaction, hydrogen bonding, and electrostatic affinity all played essential roles in enhancing the adsorption performance during the adsorption of aromatic compounds.

The typical heteroatoms for doping in graphene-based materials are S, B, P, and N [62]. The co-doping of heteroatoms can enhance reactivity in potential applications as they endow the graphitic structure with improved physicochemical and structural properties. Previously, the heteroatom-doped graphene materials have shown better adsorption performance towards dyes and oil [63]. However, in the case of EM adsorption, few studies were reported for their adsorption capability. The adsorption of bisphenol A (BPA) and bisphenol F (BPF) on N-rGO was reported to be 1.75 times in comparison to rGO due to the enhanced interaction with the lone pair electrons of the N in the graphene sheets [64]. The theoretical study in gas and aqueous phases for the adsorption of various analgesic pollutants using DFT showed that N-doped Gr nanosheets exhibited higher reactivity, adsorption, solvation, and stability [65, 66]. The theoretical findings showed that N-doped Gr showed higher stability in aqueous media which is paramount in the environmental remediation applications. Pham and co-workers found that the doping concentration of N in graphene plays a vital role in the water absorption [67]. Their DFT calculations indicated that the binding energy of water showed a linear relationship with the doping content as it enriches the occupied states at the valence band maximum.

Membrane-based technologies to remove EMs have also been regarded as another simple yet effective strategy to remediate various EMs in aqueous media. The usage of GO membrane for the rejection of various EMs has been previously reported [68, 69]. The common problem with GO-based membrane is often the swelling of membrane ascribed to the enlarged d-spacing, which hindered the formation of ordered lamellar structure. Hence, comprehensive strategies were employed to address the shortcomings of GO membrane in pollutant remediation, such as functionalization. Valizadeh and co-workers studied the interlayer spacing of GO membrane using a  $\beta$ -Alanine ( $\beta$ A) crosslinker for the rejection of antibiotics [70]. Often, the interlayer spacing increased in aqueous media due to GO hydrophilic nature which rendered the membrane unstable. The chemical bonding of the crosslinker via the carboxylic acid and amine led to less swelling and improved membrane stability.

Solid-phase extraction with magnetic separation (MSPE) allowed for ease of separation via an external magnetic field. Magnetic hybrid adsorbents offer easy removal and rapid recycling compared to conventional solid-phase extraction [71, 72]. Hence, integrating magnetic-based NPs on a graphene hybrid composite has become a plausible approach for EM removal at the trace level. However, in some instances, the adsorption performance may be reduced due to aggregation of the particles on the pores and saturated the available functionalities. The decoration of ferromagnetic  $\alpha$ - $\text{Fe}_2\text{O}_3$  on graphene sheets prepared via thermal treatment decreased the adsorption of TC compared to bare rGO under pH 7 [73]. The modification of magnetic NP modified the electrostatic interaction of the rGO layers for effective interaction with the TC, hence the regressed adsorption capacity. In a recent study, a magnetic nanohybrid composed of Zr-Mn $\text{Fe}_2\text{O}_4$ /GO has been prepared via hydrothermal and ultrasonication methods for the adsorption of perfluorinated acid (PFOA) and perfluorooctane sulfonic acid (PFOS), which is depicted in Fig. 3a [74]. The adsorption of the perfluorinated chemicals on the hybrid composite was pH-dependent, which abide by the PSO kinetic model and Langmuir isotherm. Due to protonation under acidic conditions, the prepared nanohybrid had a positive surface charge. The protonated nanohybrid can efficiently adsorb the EMs via electrostatic interaction at pH 3. The adsorption affinity towards PFOS is higher in comparison to PFOA as a result of hydrophobic interactions. In essence, perfluorinated chemical (PFC) compounds tend to form micelles and hemimicelles in water due to the C-F chain aggregations. Hence, they can be adsorbed more quickly, as shown in Fig. 3b. Bao and co-workers prepared a magnetic adsorbent based on Mn $\text{Fe}_2\text{O}_4$ /rGO nanocomposite and studied their adsorption capability towards TC [75]. The adsorption kinetics and isotherm showed good agreement with the pseudo-second-order and Freundlich models, respectively. The adsorbent was quickly removed via external magnetic energy and then simply regenerated by washing with an acid solution. A recent study also accessed the efficiency of filter based on porous graphene (PG) column to adsorb various emerging contaminants [76]. These column studies served as an efficient way to test the feasibility of the additional treatment option. They varied the column configurations and accessed their adsorption performance. The increase of PG doses and higher filter configuration increased the effectiveness of EC removal.

Herein, it can be seen that the adsorbent porosity, surface area, and functionalities played significant role in influencing the removal of various EMs.

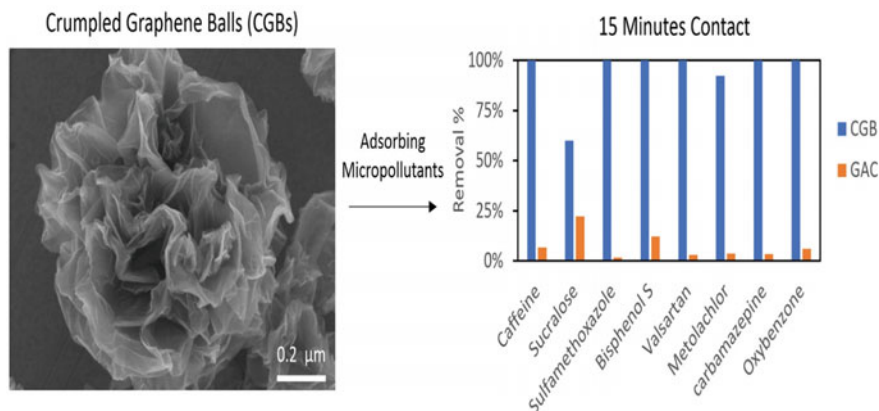


**Fig. 3** **a**  $\text{Zr-MnFe}_2\text{O}_4@\text{rGO}$  nanohybrid synthesis protocol. **b** Schematic representation of adsorption behaviours of  $\text{Zr-MnFe}_2\text{O}_4@\text{rGO}$  towards PFC. Reprinted with permission from Elanchezhyan et al. [74]. Copyright 2021 Elsevier

## 4.2 3D Graphene-Based Composites

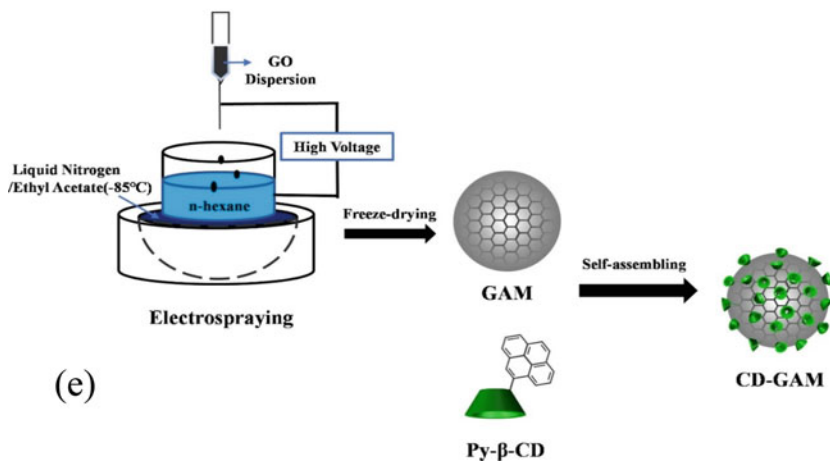
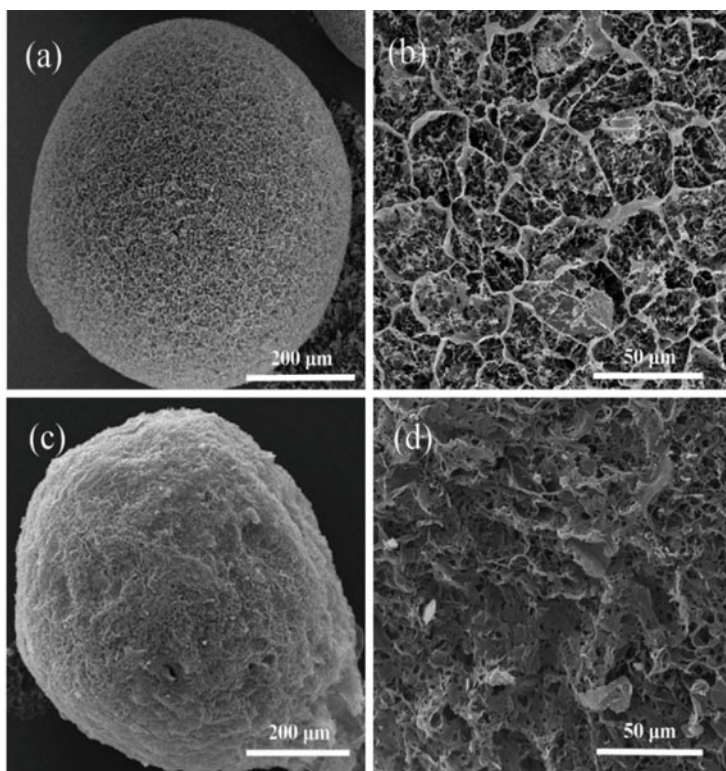
As mentioned, the strong  $\pi$ - $\pi$  stacking interaction between 2D graphene sheets often leads to aggregation, hence reducing its adsorption capability. The transformation of two-dimensional (2D) to three-dimensional (3D) graphene via hydrothermal [77–81], self-assembly using chemical reductants [82, 83], and freeze-drying [84] prevents the sheets from clumping together and makes it easier for contaminants to diffuse and adsorb. After adsorption, the 3D structure can help separate solids from liquids more easily. There are far more advantages for 3D graphene than for 2D graphene in water pollution treatment [85]. 3D graphene-based graphene materials have exhibited amazing micropollutant adsorption, attributed to their macroscopic, highly porous structures. In terms of recyclability, 3D graphene possessed a superior advantage in comparison to its 2D form. The preparation of 3D crumpled graphene oxide balls (GCBs) prepared by droplet generated method and thermal annealing was recently reported to possess up to 8 times higher adsorption capacity for various micropollutants in comparison to granular activated carbon (GAC) [86]. Figure 4 depicts the SEM image of the crumpled ball morphology and its removal percentage of selected micropollutants. The six times less specific area of GCB in comparison to GAC showed that it was still able to remove most of the micropollutants with >90% removal efficiency in 15 min. The enhanced adsorption capability of GCB is attributed to the oxygenated functional groups and improved dispersion in media and excess hydrogen bonding interactions. The GCBs have preserved many oxygen-functional groups and are amphiphilic due to the lower thermal annealing (150 °C). The hydrophilic GCB surface is less prone to aggregation and disperses more readily in water, facilitating interactions with micropollutants. In addition, the electron donor–acceptor (EDA) interactions contributed to the adsorption process. The oxygen functionalities on GCB are posited to enhance both  $\pi$ -electron depleted and rich regions, favourable for  $\pi$ -electron-donating or  $\pi$ -electron-withdrawing micropollutants.

As mentioned previously, functionalization on graphene sheets has been regarded as one of the most effective methods to improve micropollutants' adsorption performance [87]. The enhanced adsorption performance towards bisphenol A (BPA) was recently reported using a 3D N, P, and S co-doped graphene-like adsorbent material [88]. There are a variety of organic micropollutants that cyclodextrin (CDs) are good at capturing due to host–guest interactions and non-covalent interactions [89–91]. Nie and co-workers assessed the performance of 3D CD self-assembled GO aerogel microspheres (CD-GAM) for the adsorption of several organic micropollutants, namely 2,4-dichlorophenol, propranolol hydrochloride, ethynyl estradiol, and bisphenol A [92]. The self-assembly preparation of CD and GO aerogel was described in Fig. 5. The SEM micrograph showed that the aerogels were spherical with a porous framework. The inclusion of the CD is evident from the additional layer formed on the spherical structure of GAM. They found that the supramolecular activity of CD plays an essential role in improving adsorption capacity because the  $q_e$  values are higher than those of GAM and activated carbon combined.



**Fig. 4** SEM image of GCB and the removal percentage of selected micropollutants. Reprinted with permission from Fu et al. [86]. Copyright 2021 Elsevier

A critical aspect of a promising adsorbent is that it can be reused multiple times without a significant reduction in its performance [93]. Zhu and co-workers prepared a UV regenerable 3D adsorbent based on covalent triazine framework (CTF), GO, and PVA for the adsorption of various benzophenone pollutants [94]. The preparation of the 3D adsorbent with varying pore sizes is shown in Fig. 6a, while the water swelling and shape recovery test is depicted in Fig. 6b–e. The control of the pore size of the 3D adsorbent was achieved by varying the molecular weight of the PVA. The irregular pores of the 3D adsorbent prevented aggregation of GO sheets, inadvertently exposed adsorption sites via the  $\pi$ – $\pi$  EDA interactions. A seven-day adsorptive cycle of the multifunctional adsorbent in natural water shows that it is stable and universal, with an 86.0% regeneration rate. In another study, Xu and co-workers synthesized a photoregenerable 3D nanosized adsorbent (rGC) via the cyano-functionalization on the rGO surface for the adsorption of aromatic contaminants [95]. The functionalized graphene adsorbent was prepared using various amounts of 1,4-dicyanobenzene ranging from 10 to 50 mg. The covalent triazine framework between the rGO layers increased the space expansion, which enables higher adsorption capabilities towards naphthalene and benzophenone. They posited that the contained microenvironment provided for the diffusion of the pollutant in their porous surface and confined in the nanospaces. Figure 6(f) depicts the regeneration process under sunlight irradiation of the graphene composite adsorption. The excellent regeneration rate (91.24%) after four rounds of adsorption can be ascribed to the easy electron excitation, electron–hole separation, and surface reaction. The preparation of double-network (DN) hydrogel of amino-functionalized alginate/graphene was reported to enhance the adsorption of ciprofloxacin (CIP) up to 182% in comparison to ordinary single-network hydrogel [96]. The double-network hydrogel was prepared with the addition of triethylenetetramine (TETA) as the crosslinkers. The findings suggested that the adsorption of CIP inclined to a chemisorption route. The  $\text{NH}_2$ -DN surface has ample



**Fig. 5** SEM micrographs of **a, b** GAM and **c, d** CD-GAM in different magnification. **e** Preparation scheme of CD-GAM. Reprinted with permission from Nie et al. [92]. Copyright 2021 Elsevier

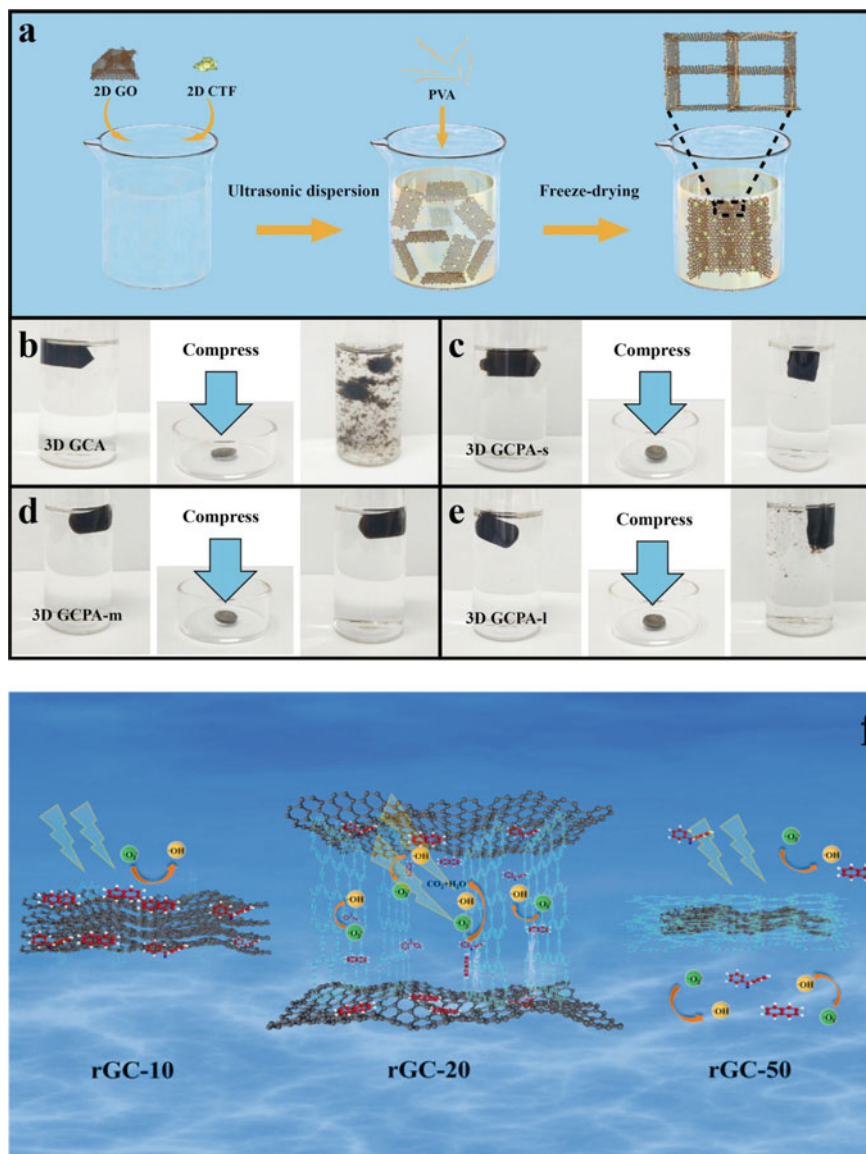
amino groups because of the TETA modification. Additionally, hydrogen donors contributed by the H atoms in CIP's hydroxy groups facilitated the easy interaction. Hydrogen bonding can occur between the amino and carboxyl groups of the adsorbent because the N atoms act as hydrogen bonding acceptors.

A hybrid microsphere composite composed of GO and cross-linked polyvinylpyrrolidone (GO/PVPP) was developed for the adsorption of 2,4,6-trichlorophenol (2,4,6-TCP) in one investigation [97]. In this study, the adsorption of micropollutants such as ofloxacin and ciprofloxacin was attempted on a GO/biopolymer aerogel prepared by embedding or coating GO in the adsorbent framework [98]. Embedding and coating are effective methods of harnessing GO adsorption capability through hydrophobic interactions (GO-organics). When it comes to enhancing antibiotic elimination efficacy, it appears that the amount of GO played the most crucial role. The adsorption performance in actual water samples often differs from laboratory experiments which can be ascribed to the presence of solid particles, metal ions, organic matter, and other pollutants which may affect adsorption. The pore-blocking by suspended particles may inherently affect the adsorption performance. Yuan and colleagues accessed the adsorption of polystyrene microplastics on 3D rGO, which exhibited a maximum adsorption capacity of 617.28 mg/g for polystyrene (PS) microplastics which was influenced by various experimental conditions [99]. The principal mechanism of adsorption is ascribed to the strong  $\pi$ - $\pi$  interactions between the aromatic rings of the rGO and the PS. The adsorption abided well to the Langmuir adsorption isotherm model and pseudo-second-order kinetic model. In addition, PS microplastic adsorption was spontaneous and endothermic process from the thermodynamic studies.

Table 1 compares the adsorption capacities of several graphene-based adsorbents for selected micropollutants based on current literature reported. The comparison between the efficiency of EMs depends mainly on the surface functionalities. It is summarized that  $\pi$ - $\pi$  interactions, cation- $\pi$ , EDA- $\pi$ , electrostatic forces, or H-bonding are among the commonly reported interactions to occur in the adsorption process. Graphene-based materials, especially in their 3D dimension, could be an effective and promising adsorbent due to their physical and surface properties in real-time analysis. All of the graphene as mentioned above and related composite for adsorption is restricted to batch adsorption experiments.

## 5 Conclusion and Future Outlook

The growing number of reports focusing on graphene-based materials and their composites shows that they are emerging as promising candidates for excellent adsorbents towards EMs. Various pollutants such as PPCP, antibiotics, industrial chemicals, and pesticides could be adsorbed on graphene-based materials and their composites efficiently. Fortunately, derivatives of Gr such as GO, rGO, and GNP offered an excellent candidate for use in the design of multifunctional adsorbents, eliminating the need to use graphene in its pure form, which had been plagued by manufacturing



**Fig. 6** a Schematic illustration of the preparation of the 3D adsorbents with different pore sizes. b–e Water swelling and shape recovery test of the adsorbent. Reprinted with permission from Zhu et al. [94]. Copyright 2021 Elsevier. f Removal mechanism and regeneration under sunlight irradiation. Reprinted with permission from Xu et al. [45]. Copyright 2021 Elsevier



**Table 1** Recent highlights of laboratory-scale adsorption performance of selected EMs using graphene-based materials/composites

Adsorbent	Selected micropollutants	Adsorption capacity	Adsorption kinetics, isotherm	Additional comments
MnFe <sub>2</sub> O <sub>4</sub> /rGO [75]	Tetracycline (TC)	41 mg/g	PSO, Freundlich	<ul style="list-style-type: none"> <li>The adsorption of TC was influenced by the molecular structure of TC and rGO</li> <li>The magnetic component of MnFe<sub>2</sub>O<sub>4</sub> enabled easy recycling of the adsorbent</li> </ul>
Magnetic/GO (MGO) [100]	Chlortetracycline (CTC) Oxytetracycline (OTC) Tetracycline (TC)	303.95 mg/g 289.86 mg/g 141.44 mg/g	PSO, Freundlich	<ul style="list-style-type: none"> <li>The adsorption followed a spontaneous and endothermic process</li> <li>MGO possessed higher adsorption efficiency for CTC under alkaline pH</li> </ul>
GO [101]	Bisphenol A (BPA)	49.26 mg/g	PSO, Freundlich /Langmuir	<ul style="list-style-type: none"> <li><math>\pi</math>-<math>\pi</math> interactions mainly drive BPA adsorption on GO</li> <li>Poor BPA adsorption is due to hydrogen bond formation with water molecules</li> </ul>
GO [102]	Metformin	49.62 mg/g	PSO, Freundlich	<ul style="list-style-type: none"> <li>Metformin adsorption increased in acidic pH values from 4.0 to 6.0 and decreased from pH 6.0 to 11.0</li> <li>The adsorption followed a spontaneous and exothermic process</li> <li><math>\pi</math>-<math>\pi</math> interactions and hydrogen bonds posited to be the main adsorption mechanism</li> </ul>
GO [103]	Chlorpyrifos Malathion	98.04 mg/g 1666.67 mg/g	PSO, Langmuir	<ul style="list-style-type: none"> <li>Interactions of EMs with adsorbents mainly through H-bonding</li> </ul>

(continued)

**Table 1** (continued)

Adsorbent	Selected micropollutants	Adsorption capacity	Adsorption kinetics, isotherm	Additional comments
Magnetic rGO (MPrGO) [104]	Triclosan (TCS)	1105.8 mg/g	PSO, Langmuir	<ul style="list-style-type: none"> <li>• Adsorption efficiency decreased with an increase in pH</li> <li>• MPrGO possessed a higher affinity than AC in WWTP effluent</li> </ul>
GO Nanopowder [105]	Naproxen (NPX)	21.93 mg/g	PSO, Freundlich	<ul style="list-style-type: none"> <li>• The adsorption followed a spontaneous and exothermic process</li> </ul>
Magnetic rGO (MPrGO) [106]	Sulfadiazine (SDZ)	6.26–6.74 $\mu\text{g/g}$	PSO, Langmuir	<ul style="list-style-type: none"> <li>• The efficient adsorption and recyclability of MrGO are ascribed to the 3D interconnected petal-like structure</li> </ul>
Gr [107]	Bisphenol A (BPA) Triclosan (TCS)	$2.0 \times 10^3 \mu\text{g/g}$ 11.60 $\mu\text{g/g}$	PSO, Langmuir PSO, Freundlich	<ul style="list-style-type: none"> <li>• Similar maximum sorption capacities (<math>q_m</math>) of BPA on Gr or AC</li> <li>• In comparison to AC, Gr has a lower adsorption capacity for TCS</li> </ul>
rGO [108]	Nimesulide (NM)	82.4 mg/g	General order, Liu	<ul style="list-style-type: none"> <li>• <math>\pi</math>-<math>\pi</math> interactions are posited to be the main adsorption mechanism</li> <li>• Functionalized rGO showed hydrogen bonding with NM (especially carboxyl)</li> </ul>
3D rGO [109]	Naproxen (NPX) Ibuprofen (IBP) Diclofenac (DFC)	357 mg/g 500 mg/g 526 mg/g	PSO, Langmuir	<ul style="list-style-type: none"> <li>• The interaction with the drugs involved EDA interactions, H-bonding, and <math>\pi</math>-hydrogen bonding</li> </ul>

(continued)

**Table 1** (continued)

Adsorbent	Selected micropollutants	Adsorption capacity	Adsorption kinetics, isotherm	Additional comments
3DGNP/BN [110]	Ciprofloxacin (CIP)	185 mg/g	PSO, Langmuir	<ul style="list-style-type: none"> <li>• BN and GNP possessed selective adsorption towards CIP. The –COO and –CO were adsorbed on the BN nanosheets and GNP</li> <li>• GNP/BNA exhibited good recyclability properties</li> </ul>
Gr wool [111]	Efavirenz (EFV) Nevirapine (NVP)	4.41 mg/g 48.31 mg/g	IPD, Sips PSO, Freundlich	<ul style="list-style-type: none"> <li>• EPV and NVP adsorptions are spontaneous exothermic and endothermic, respectively</li> </ul>
GO [112]	Carbamazepine (CBZ)	9.2 mg/g	PSO, Temkin	<ul style="list-style-type: none"> <li>• The adsorption is spontaneous and endothermic,</li> <li>• Adsorbent could be reused up to 8 times,</li> </ul>

BN—boron nitride; PSO—pseudo-second-order model kinetic model; IPD—intraparticle diffusion; Liu—Liu isotherm model

issues. In addition, the conversion to 3D graphene composite has been shown to offer the advantage of easy removal. Lately, polymeric compounds or crosslinkers have been mixed with graphene sheets to improve the stability/mechanical properties of the adsorbent. The functional adsorbents are enhanced by the inclusion of magnetic NP and supramolecular compounds such as CD. However, this research is still in its early stages, and several obstacles must be overcome before these materials can be used as adsorbents in real-world applications. Present studies have elucidated that pH inherently is vital in the adsorption process, among others, such as initial concentration of adsorbate, temperature, and contact time. The adsorbent surface characteristics and the ionization state of adsorbates are greatly affected by the solution's pH, which substantially impacts the electrostatic interactions with the EMs [113]. An assessment of the toxic properties of graphene composite is one of the more critical aspects from the standpoint of health and well-being. The leaching of materials will eventually find its way into the aquatic systems, which are possible due to the available functional groups. Previously, there was mounting evidence that the accumulation of graphene materials in the marine environment may result in bioaccumulation [114, 115]. As a result, studies to determine the release and leaching of graphene materials and their composites are critical. The understanding of micropollutant adsorption using graphene-based materials is far from perfect and continually

developing. In addition, computational simulation methods have also gained traction as an innovative tool in studying the adsorption process at an atomic level. Many previous types of research have attempted various models to access the adsorption behaviour of various pollutants [116–118]. It is possible to anticipate the adsorption affinities of different EMs on graphene nanomaterials using multiple models. To date, many research suggestions have been offered to bring added value to future research [119–122]. Future studies may delve deeper into specific areas to address some of the more complex problems. Graphene-based adsorbents have variable adsorption capacities for different EMs, in which understanding the selectivity has only been studied in a few papers. As of now, no detailed research has been done on the selectivity performance, and the physical mechanisms underlying such selectivity results are still a mystery. Adsorbed EMs must be recycled to prevent environmental damage, and photodegradation has shown to be a feasible yet cost-effective way. The future adsorbent design will benefit from knowing more about bonding behaviours and intermolecular interactions obtained using spectroscopy and microscopy. Because of this, we will have a better understanding of macroscale adsorbent system performance, such as thermodynamics and kinetics. Finally, this write-up is hoped to provide a comprehensive yet concise overview of graphene-based materials for effective adsorbent in the removal of EMs.

**Acknowledgements** Alvin Lim Teik Zheng would like to acknowledge Kyushu Institute of Technology, for the Post-Doctoral Fellowship awarded to him. The authors would also like to thank Mr. Tithiphong Sukheeket for the artwork design.

**Declaration of Competing Interest** The authors declare that they have no conflict of interest.

## References

1. Rosenfeld PE, Feng LGH (2011) Emerging contaminants. In: Risks of hazardous wastes. Elsevier, pp 215–222
2. Chavoshani A, Hashemi M, Mehdi Amin M, Ameta SC (2020) Introduction. In: Micropollutants and challenges. Elsevier, pp 1–33
3. Sauvé S, Desrosiers M (2014) A review of what is an emerging contaminant. *Chem Cent J* 8:15
4. Kümmerer K (2011) Emerging contaminants. In: Treatise on water science. Elsevier, pp 69–87
5. Lei M et al (2015) Overview of emerging contaminants and associated human health effects. *Biomed Res Int* 2015:1–12
6. Pereira LC et al (2015) A perspective on the potential risks of emerging contaminants to human and environmental health. *Environ Sci Pollut Res* 22:13800–13823
7. Sanchez W, Egea E (2018) Health and environmental risks associated with emerging pollutants and novel green processes. *Environ Sci Pollut Res* 25:6085–6086
8. Anjum M et al (2016) Remediation of wastewater using various nano-materials. *Arab J Chem*. <https://doi.org/10.1016/j.arabjc.2016.10.004>
9. Lu H et al (2016) An overview of nanomaterials for water and wastewater treatment. *Adv Mater Sci Eng* 2016:1–10
10. Yaqoob AA, Parveen T, Umar K, Mohamad Ibrahim MN (2020) Role of nanomaterials in the treatment of wastewater: a review. *Water* 12:495

11. Adeleye AS et al (2016) Engineered nanomaterials for water treatment and remediation: costs, benefits, and applicability. *Chem Eng J* 286:640–662
12. Lau GE et al (2020) Eco-friendly photocatalysts for degradation of dyes. *Catalysts* 10:1129
13. Wang L, Hu C, Shao L (2017) The antimicrobial activity of nanoparticles: present situation and prospects for the future. *Int J Nanomedicine* 12:1227–1249
14. Zhang H, Tang Y (2017) Graphene-based materials and their potential applications. In: *Hybrid polymer composite materials*. Elsevier, pp 267–287
15. Singh V et al (2011) Graphene based materials: past, present and future. *Prog Mater Sci* 56:1178–1271
16. Alvarado YEA, de la Cruz MTR, Hernández-Cocoletzi H, Cocoletzi GH (2019) Graphene structures: from preparations to applications. In: *Handbook of graphene*. Wiley, pp 323–357
17. Geim AK (2009) Graphene: status and prospects. *Science* 324(80):1530–1534
18. Allen MJ, Tung VC, Kaner RB (2010) Honeycomb carbon: a review of graphene. *Chem Rev* 110:132–145
19. Papageorgiou DG, Kinloch IA, Young RJ (2017) Mechanical properties of graphene and graphene-based nanocomposites. *Prog Mater Sci* 90:75–127
20. Mohan VB, Lau K, Hui D, Bhattacharyya D (2018) Graphene-based materials and their composites: a review on production, applications and product limitations. *Compos Part B Eng* 142:200–220
21. Wu X, Mu F, Wang Y, Zhao H (2018) Graphene and graphene-based nanomaterials for DNA detection: a review. *Molecules* 23:2050
22. Kumar N et al (2021) Top-down synthesis of graphene: a comprehensive review. *FlatChem* 27:100224
23. Singh G et al (2021) Sources, fate, and impact of pharmaceutical and personal care products in the environment and their different treatment technologies. In: *Microbe mediated remediation of environmental contaminants*. Elsevier, pp 391–407
24. Zheng ALT, Abdullah CAC, Chung ELT et al (2022) Recent progress in visible light-doped ZnO photocatalyst for pollution control. *Int. J. Environ. Sci. Technol.* <https://doi.org/10.1007/s13762-022-04354-x>
25. Nageeb M (2013) Adsorption technique for the removal of organic pollutants from water and wastewater. In: *Organic pollutants—monitoring, risk and treatment*. InTech
26. De Gisi S, Lofrano G, Grassi M, Notarnicola M (2016) Characteristics and adsorption capacities of low-cost sorbents for wastewater treatment: a review. *Sustain Mater Technol* 9:10–40
27. Sophia AC, Lima EC (2018) Removal of emerging contaminants from the environment by adsorption. *Ecotoxicol Environ Saf* 150:1–17
28. Zheng ALT, Andou Y (2021) Detection and remediation of bisphenol A (BPA) using graphene-based materials: mini-review. *Int J Environ Sci Technol.* <https://doi.org/10.1007/s13762-021-03512-x>
29. Dulio V et al (2018) Emerging pollutants in the EU: 10 years of NORMAN in support of environmental policies and regulations. *Environ Sci Eur* 30:5
30. Naidu R, Arias Espana VA, Liu Y, Jit J (2016) Emerging contaminants in the environment: risk-based analysis for better management. *Chemosphere* 154:350–357
31. Khan FSA et al (2021) A comprehensive review on micropollutants removal using carbon nanotubes-based adsorbents and membranes. *J Environ Chem Eng* 9:106647
32. Fatta-Kassinos D, Meric S, Nikolaou A (2011) Pharmaceutical residues in environmental waters and wastewater: current state of knowledge and future research. *Anal Bioanal Chem* 399:251–275
33. Patel M et al (2019) Pharmaceuticals of emerging concern in aquatic systems: chemistry, occurrence, effects, and removal methods. *Chem Rev* 119:3510–3673
34. Zheng ALT et al (2021) Accessing the anti-microbial activity of cyclic peptide immobilized on reduced graphene oxide. *Mater Lett* 304
35. Rodriguez-Mozaz S et al (2020) Antibiotic residues in final effluents of European wastewater treatment plants and their impact on the aquatic environment. *Environ Int* 140:105733

36. Fan X et al (2020) Determination of 27 pharmaceuticals and personal care products (PPCPs) in water: the benefit of isotope dilution. *Front Environ Sci Eng* 14:8
37. Campos-Mañas MC et al (2019) Determination of pesticide levels in wastewater from an agro-food industry: target, suspect and transformation product analysis. *Chemosphere* 232:152–163
38. Kyzas GZ, Deliyanni EA, Bikiaris DN, Mitropoulos AC (2018) Graphene composites as dye adsorbents: review. *Chem Eng Res Des* 129:75–88
39. Choi W, Lahiri I, Seelaboyina R, Kang YS (2010) Synthesis of graphene and its applications: a review. *Crit Rev Solid State Mater Sci* 35:52–71
40. Lee XJ et al (2019) Review on graphene and its derivatives: synthesis methods and potential industrial implementation. *J Taiwan Inst Chem Eng* 98:163–180
41. Wu Y, Wang S, Komvopoulos K (2020) A review of graphene synthesis by indirect and direct deposition methods. *J Mater Res* 35:76–89
42. Lee HC et al (2017) Review of the synthesis, transfer, characterization and growth mechanisms of single and multilayer graphene. *RSC Adv* 7:15644–15693
43. Aïssa B, Memon NK, Ali A, Khraisheh MK (2015) Recent progress in the growth and applications of graphene as a smart material: a review. *Front Mater* 2
44. Tang L et al (2012) Bottom-up synthesis of large-scale graphene oxide nanosheets. *J Mater Chem* 22:5676
45. Terzopoulou Z, Kyzas G, Bikiaris D (2015) Recent advances in nanocomposite materials of graphene derivatives with polysaccharides. *Materials (Basel)* 8:652–683
46. Abu-Nada A, McKay G, Abdala A (2020) Recent advances in applications of hybrid graphene materials for metals removal from wastewater. *Nanomaterials* 10:595
47. Yang K et al (2018) Application of graphene-based materials in water purification: from the nanoscale to specific devices. *Environ Sci Nano* 5:1264–1297
48. Carrales-Alvarado DH et al (2020) Effect of surface area and physical–chemical properties of graphite and graphene-based materials on their adsorption capacity towards metronidazole and trimethoprim antibiotics in aqueous solution. *Chem Eng J* 402:126155
49. Yang K, Chen B, Zhu L (2015) Graphene-coated materials using silica particles as a framework for highly efficient removal of aromatic pollutants in water. *Sci Rep* 5:11641
50. Liu F et al (2014) Effects of solution chemistry on adsorption of selected pharmaceuticals and personal care products (PPCPs) by graphenes and carbon nanotubes. *Environ Sci Technol* 48:13197–13206
51. Li J, Östling M (2013) Prevention of graphene restacking for performance boost of supercapacitors—a review. *Curr Comput-Aided Drug Des* 3:163–190
52. Balasubramani K, Sivarajasekar N, Naushad M (2020) Effective adsorption of antidiabetic pharmaceutical (metformin) from aqueous medium using graphene oxide nanoparticles: equilibrium and statistical modelling. *J Mol Liq* 301:112426
53. Gao Y et al (2012) Adsorption and removal of tetracycline antibiotics from aqueous solution by graphene oxide. *J Colloid Interface Sci* 368:540–546
54. Ai Y et al (2019) Insights into the adsorption mechanism and dynamic behavior of tetracycline antibiotics on reduced graphene oxide (RGO) and graphene oxide (GO) materials. *Environ Sci Nano* 6:3336–3348
55. Rosli FA et al (2021) Efficient removal of pharmaceuticals from water using graphene nanoplatelets as adsorbent. *R Soc Open Sci* 8:201076
56. Wang H et al (2021) Emerging role of graphene oxide as sorbent for pesticides adsorption: experimental observations analyzed by molecular modeling. *J Mater Sci Technol* 63:192–202
57. Foschi M et al (2021) Experimental design and response surface methodology applied to graphene oxide reduction for adsorption of triazine herbicides. *ACS Omega* 6:16943–16954
58. Liu R, Zhu X, Chen B (2017) A new insight of graphene oxide-Fe(III) complex photochemical behaviors under visible light irradiation. *Sci Rep* 7:40711
59. Gunes B et al (2021) Activated graphene oxide-calcium alginate beads for adsorption of methylene blue and pharmaceuticals. *Materials (Basel)* 14:6343
60. Fei Y, Li Y, Han S, Ma J (2016) Adsorptive removal of ciprofloxacin by sodium alginate/graphene oxide composite beads from aqueous solution. *J Colloid Interface Sci* 484:196–204

61. Zhu H, Chen T, Liu J, Li D (2018) Adsorption of tetracycline antibiotics from an aqueous solution onto graphene oxide/calcium alginate composite fibers. *RSC Adv* 8:2616–2621
62. Wang X et al (2014) Heteroatom-doped graphene materials: syntheses, properties and applications. *Chem Soc Rev* 43:7067–7098
63. Li M et al (2020) One-step generation of S and N co-doped reduced graphene oxide for high-efficiency adsorption towards methylene blue. *RSC Adv* 10:37757–37765
64. Wang X, Qin Y, Zhu L, Tang H (2015) Nitrogen-doped reduced graphene oxide as a bifunctional material for removing bisphenols: synergistic effect between adsorption and catalysis. *Environ Sci Technol* 49:6855–6864
65. Perry RH (2021) Theoretical study of the adsorption of analgesic environmental pollutants on pristine and nitrogen-doped graphene nanosheets. *Phys Chem Chem Phys* 23:1221–1233
66. Dobrota AS et al (2020) Altering the reactivity of pristine, N- and P-doped graphene by strain engineering: a DFT view on energy related aspects. *Appl Surf Sci* 514:145937
67. Pham TT et al (2021) How do the doping concentrations of N and B in graphene modify the water adsorption? *RSC Adv* 11:19560–19568
68. Yang G et al (2018) Removal of antibiotics from water with an all-carbon 3D nanofiltration membrane. *Nanoscale Res Lett* 13:146
69. El Meragawi S et al (2020) Enhanced permselective separation of per-fluorooctanoic acid in graphene oxide membranes by a simple PEI modification. *J Mater Chem A* 8:24800–24811
70. Valizadeh S, Naji L, Karimi M (2021) Controlling interlayer spacing of graphene oxide membrane in aqueous media using a biocompatible heterobifunctional crosslinker for Penicillin-G Procaine removal. *Sep Purif Technol* 263:118392
71. Ali N et al (2021) Adsorptive remediation of environmental pollutants using magnetic hybrid materials as platform adsorbents. *Chemosphere* 284:131279
72. Nawaz S et al (2021) Mitigation of environmentally hazardous pollutants by magnetically responsive composite materials. *Chemosphere* 276:130241
73. Huizar-Félix A et al (2019) Removal of tetracycline pollutants by adsorption and magnetic separation using reduced graphene oxide decorated with  $\alpha$ -Fe<sub>2</sub>O<sub>3</sub> nanoparticles. *Nanomaterials* 9:313
74. Elanchezhian SS et al (2020) Synthesis and characterization of novel magnetic Zr-MnFe<sub>2</sub>O<sub>4</sub>@rGO nanohybrid for efficient removal of PFOA and PFOS from aqueous solutions. *Appl Surf Sci* 528:146579
75. Bao J et al (2018) Adsorption of tetracycline with reduced graphene oxide decorated with MnFe<sub>2</sub>O<sub>4</sub> nanoparticles. *Nanoscale Res Lett* 13:396
76. Khalil AME et al (2021) Performance evaluation of porous graphene as filter media for the removal of pharmaceutical/emerging contaminants from water and wastewater. *Nanomaterials* 11:79
77. Zheng ALT, Boonyuen S, Ohno T, Andou Y (2021) Accessing effects of aliphatic dicarboxylic acid towards the physical and chemical changes in low temperature hydrothermally reduced graphene hydrogel. *J Porous Mater* 28:1291–1300
78. Zheng ALT, Boonyuen S, Ohno T, Andou Y (2021) Hydrothermally reduced graphene hydrogel intercalated with divalent ions for dye adsorption studies. *Processes* 9:169
79. Zheng ALT et al (2022) Cu<sub>2</sub>O/TiO<sub>2</sub> decorated on cellulose nanofiber/reduced graphene hydrogel for enhanced photocatalytic activity and its antibacterial applications. *Chemosphere* 286:131731
80. Zheng ALT et al (2021) Design of reduced graphene hydrogel with alkylamine surface functionalization through immersion/agitation method and its adsorption mechanism. *J Mol Struct*:131008
81. Zheng ALT, Phromsatit T, Boonyuen S, Andou Y (2020) Synthesis of silver nanoparticles/porphyrin/reduced graphene oxide hydrogel as dye adsorbent for wastewater treatment. *FlatChem*:100174
82. Sheng K, Xu Y, Li C, Shi G (2011) High-performance self-assembled graphene hydrogels prepared by chemical reduction of graphene oxide. *New Carbon Mater* 26:9–15

83. Lescano MI et al (2018) Development and characterisation of self-assembled graphene hydrogel-based anodes for bioelectrochemical systems. *RSC Adv* 8:26755–26763
84. Thomas T, Agarwal A (2021) A facile and scalable approach in the fabrication of tailored 3D graphene foam via freeze drying. *Materials (Basel)* 14:864
85. Zheng ALT, Ohno T, Andou Y (2022) Recent progress in photocatalytic efficiency of hybrid three-dimensional (3D) graphene architectures for pollution remediation. *Top Catal.* <https://doi.org/10.1007/s11244-022-01610-9>
86. Fu H, Huang J, Gray K (2021) Crumpled graphene balls adsorb micropollutants from water selectively and rapidly. *Carbon N Y* 183:958–969
87. Fraga TJM, Carvalho MN, Ghislandi MG, da Motta Sobrinho MA (2019) Functionalized graphene-based materials as innovative adsorbents of organic pollutants: a concise overview. *Brazilian J Chem Eng* 36:1–31
88. Wang W et al (2019) Multi-heteroatom doped graphene-like carbon nanospheres with 3D inverse opal structure: a promising bisphenol-A remediation material. *Environ Sci Nano* 6:809–819
89. Yang Z et al (2021) Preparation of  $\beta$ -cyclodextrin/graphene oxide and its adsorption properties for methylene blue. *Colloids Surfaces B Biointerfaces* 200:111605
90. Tian H et al (2020) Synthesis of graphene oxide-supported  $\beta$ -cyclodextrin adsorbent for removal of p-nitrophenol. *Water, Air, Soil Pollut* 231:495
91. Wang D et al (2015) Adsorbent for p-phenylenediamine adsorption and removal based on graphene oxide functionalized with magnetic cyclodextrin. *Appl Surf Sci* 329:197–205
92. Nie Z-J et al (2021) Cyclodextrin self-assembled graphene oxide aerogel microspheres as broad-spectrum adsorbent for removing dyes and organic micropollutants from water. *J Environ Chem Eng* 9:104749
93. Lata S, Singh PK, Samadder SR (2015) Regeneration of adsorbents and recovery of heavy metals: a review. *Int J Environ Sci Technol* 12:1461–1478
94. Zhu C et al (2021) Optimized pore configuration in solar-driven regenerable adsorbent for organic micro-pollutants removal. *Chem Eng J* 426:131244
95. Xu J et al (2022) A nanocubicle-like 3D adsorbent fabricated by in situ growth of 2D heterostructures for removal of aromatic contaminants in water. *J Hazard Mater* 423:127004
96. Sun Y et al (2020) Amino-functionalized alginate/graphene double-network hydrogel beads for emerging contaminant removal from aqueous solution. *Chemosphere* 241:125110
97. Lv X, Li S (2020) Graphene oxide-crospolyvinylpyrrolidone hybrid microspheres for the efficient adsorption of 2,4,6-Trichlorophenol. *ACS Omega* 5:18862–18871
98. Kovtun A et al (2020) Multifunctional graphene oxide/biopolymer composite aerogels for microcontaminants removal from drinking water. *Chemosphere* 259:127501
99. Yuan F, Yue L, Zhao H, Wu H (2020) Study on the adsorption of polystyrene microplastics by three-dimensional reduced graphene oxide. *Water Sci Technol* 81:2163–2175
100. Miao J et al (2019) The adsorption performance of tetracyclines on magnetic graphene oxide: a novel antibiotics adsorbent. *Appl Surf Sci* 475:549–558
101. Phatthanakittiphong T, Seo G (2016) Characteristic evaluation of graphene oxide for Bisphenol A adsorption in aqueous solution. *Nanomaterials* 6:128
102. Zhu S et al (2017) Adsorption of emerging contaminant metformin using graphene oxide. *Chemosphere* 179:20–28
103. Yadav S, Goel N, Kumar V, Singhal S (2019) Graphene oxide as proficient adsorbent for the removal of harmful pesticides: comprehensive experimental cum DFT investigations. *Anal Chem Lett* 9:291–310
104. Li Y et al (2020) Effective column adsorption of triclosan from pure water and wastewater treatment plant effluent by using magnetic porous reduced graphene oxide. *J Hazard Mater* 386:121942
105. Cığeroğlu Z, Özdemir OK, Şahin S, Haşımoğlu A (2020) Naproxen adsorption onto graphene oxide nanopowders: equilibrium, kinetic, and thermodynamic studies. *Water, Air, Soil Pollut* 231:101



106. Zhong J et al (2020) Removal of sulfadiazine using 3d interconnected petal-like magnetic reduced graphene oxide (MrGO) nanocomposites. *Water* 12:1933
107. Wang F et al (2017) Sorption behavior of bisphenol A and triclosan by graphene: comparison with activated carbon. *ACS Omega* 2:5378–5384
108. Jauris IM et al (2017) Adsorption of anti-inflammatory nimesulide by graphene materials: a combined theoretical and experimental study. *Phys Chem Chem Phys* 19:22099–22110
109. Umbreen N et al (2018) Self-assembled three-dimensional reduced graphene oxide-based hydrogel for highly efficient and facile removal of pharmaceutical compounds from aqueous solution. *J Colloid Interface Sci* 527:356–367
110. Han L et al (2022) Graphene-boron nitride composite aerogel: a high efficiency adsorbent for ciprofloxacin removal from water. *Sep Purif Technol* 278:119605
111. Adeola AO, de Lange J, Forbes PBC (2021) Adsorption of antiretroviral drugs, efavirenz and nevirapine from aqueous solution by graphene wool: Kinetic, equilibrium, thermodynamic and computational studies. *Appl Surf Sci Adv* 6:100157
112. Bhattacharya S et al (2020) Removal of aqueous carbamazepine using graphene oxide nanoplatelets: process modelling and optimization. *Sustain Environ Res* 30:17
113. da Alves DCS, Healy B, Yu T, Breslin CB (2021) Graphene-based materials immobilized within chitosan: applications as adsorbents for the removal of aquatic pollutants. *Materials (Basel)* 14:3655
114. Dong S et al (2018) Bioaccumulation of 14 C-labeled graphene in an aquatic food chain through direct uptake or trophic transfer. *Environ Sci Technol* 52:541–549
115. Lu K et al (2017) Biological uptake, distribution, and depuration of radio-labeled graphene in adult zebrafish: effects of graphene size and natural organic matter. *ACS Nano* 11:2872–2885
116. Wang Y et al (2018) Exploring adsorption of neutral aromatic pollutants onto graphene nanomaterials via molecular dynamics simulations and theoretical linear solvation energy relationships. *Environ Sci Nano* 5:2117–2128
117. Taheri Z, Nakhai Pour A (2021) Studying of the adsorption and diffusion behaviors of methane on graphene oxide by molecular dynamics simulation. *J Mol Model* 27:59
118. Tanis I, Kostarellou E, Karatasos K (2021) Molecular dynamics simulations of hyper-branched poly(ethylene imine)–graphene oxide nanocomposites as dye adsorbents for water purification. *Phys Chem Chem Phys* 23:22874–22884
119. Wang J et al (2021) Graphene-based materials for adsorptive removal of pollutants from water and underlying interaction mechanism. *Adv Colloid Interface Sci* 289:102360
120. Daud M et al (2019) A review on the recent advances, challenges and future aspect of layered double hydroxides (LDH)—containing hybrids as promising adsorbents for dyes removal. *J Mol Liq* 288:110989
121. Yusuf M et al (2015) Applications of graphene and its derivatives as an adsorbent for heavy metal and dye removal: a systematic and comprehensive overview. *RSC Adv* 5:50392–50420
122. Younas F et al (2021) Current and emerging adsorbent technologies for wastewater treatment: trends, limitations, and environmental implications. *Water* 13:215

# Chapter 21

## Response Surface Modelling and Optimisation of Activated Carbons Adsorption of Pollutants from Textile Wastewater



Chinenye Adaobi Igwegbe, Joshua O. Ighalo, Kingsley O. Iwuozor,  
Okechukwu Dominic Onukwuli, and Adewale George Adeniyi

### 1 Introduction

The textile industry is notorious for emitting massive quantities of wastewater polluted with a wide range of chemicals [1, 2]. It uses a huge amount of water and chemicals during its processes [3]. Textile dyes such as congo red, vat yellow and malachite are toxic to the aquatic entities when waters containing these dyes are discharged to the environment [4, 5]. They can also trigger unnatural-looking conditions in the receiving waters. They also obstruct the oxygen that enters the bodies of water. Also, a low dye content in water is unacceptable for agricultural, municipal, and industrial applications [6]. Dyes can damage human organs such as the brain, liver, and kidneys, as well as cause central nervous system disorder and skin irritation [3, 7].

Many methods were used by past researchers for the removal of dyes from effluents including coagulation [8–11], electrocoagulation [8, 12, 13], advanced oxidation [14–17], biological treatment [18–21], membrane filtration [22–25], bioremediation [26–29], phytoremediation [30–33] and adsorption [34–36]. However, the most popular

---

C. A. Igwegbe (✉) · J. O. Ighalo (✉) · O. D. Onukwuli  
Department of Chemical Engineering, Nnamdi Azikiwe University, P. M. B. 5025, Awka, Nigeria  
e-mail: [ca.igwegbe@unizik.edu.ng](mailto:ca.igwegbe@unizik.edu.ng)

J. O. Ighalo  
e-mail: [oshea.ighalo@yahoo.com](mailto:oshea.ighalo@yahoo.com)

J. O. Ighalo · A. G. Adeniyi  
Department of Chemical Engineering, University of Ilorin, P. M. B. 1515, Ilorin, Nigeria

K. O. Iwuozor  
Department of Chemistry, University of Lagos, P. M. B. 1029, Lagos, Nigeria

Department of Pure and Industrial Chemistry, Nnamdi Azikiwe University, P. M. B. 5025, Awka, Nigeria

and validated process is adsorption for the elimination of textile dyes in terms of cost [37, 38]. Adsorption is conveniently combined with other treatment technologies [39, 40] such as advanced oxidation [41] and membrane filtration for dyes elimination. Adsorption is low cost and does not produce sludge [39, 42, 43].

Dye sorption processes have been implemented through the use of metallic nanoparticles [44–46], nanocomposites [41, 47, 48], nanotubes [49], carbon [36, 50], raw biomass [4, 5, 51], clay [52], biochar [53–56], and polymers [57, 58]. Activated carbon (AC) is an excellent adsorbent since it is extremely porous and has a wide surface area for pollutants to be adsorbed [59]. Because of its low cost, tunable pore size, enormous high porosity, and high adsorptive capacity, activated carbon is the most commonly used adsorbent [39].

The global consumption of activated carbon is estimated to be around 275,000 tonnes per year. The efficiency of this carbon for the treatment process can be improved by activation, which can be done chemically or physically which increases the pore sizes available for faster adsorption [60]. The rapidity of pollutant uptake is favoured by larger pore sizes, and likewise [42, 61]. Kumar et al. [62] discovered that having a substantial percentage of pores in the mesoporous range boosts adsorption uptake capacity considerably. The study discovered that pores larger than 10 nm improve adsorption kinetics. Chemical modification of carbon aids in the introduction of new functional groups or the intensification of existing important groups on the material; it also aids in the removal of dwelling groups in the carbon that may interfere with its performance. Another method is to pulverise the carbon particles, which helps to enhance the surface area and accessibility to the active sites for contaminants sorption [63]. A higher adsorption capacity is associated with a larger surface area [64]. Apart from the carbon's characteristics, other factors that can improve pollutant adsorption on activated carbon include pH, adsorption duration, temperature, carbon dosage, and pollutant concentration. Amongst all these factors listed, pH is the most important process component that can directly impact the adsorption of pollutants by adsorbents because it affects the degree of pollutant ionisation as well as the surface characteristics and functional groups of the carbon [65, 66]. It also has an impact on the adsorption mechanism [65]. The contact time has a significant impact on adsorption processes and adsorption kinetics. Temperature affects the kinetics and thermodynamic properties of the process; it speeds up the mobility of the pollutants. The dose of carbon is also important; when the proper dose of carbon is used, it improves the degree of adsorption; however, when the pollutant concentration rises, the effectiveness of adsorption decreases owing to oversaturation of the employed carbon [67]. As a result, a balance between the quantity of carbon dosage and the concentration of the pollutant is needed.

Adsorption has the drawback that adsorbent recycling is expensive, time-consuming, and damages the pores of the adsorbent [39, 44]. To remove solid hazardous wastes and ensure long-term development, it is necessary to regenerate used adsorbents. This is one of the issues that the world faces when it comes to disposing of solid wastes, including wasted adsorbents [68]. Because of the cost-efficient but effective regeneration procedure, solvent desorption is the best alternative.

As per our search of the literature, no author has implemented a historical design based on data collected from textile wastewater treatment using ACs. As a result, an intriguing knowledge void exists, emphasising the study's novelty. Thus, the data on textile wastewater treatment using ACs were modelled and analysed via (response surface methodology (RSM) and historical data design (HDD) on Design expert software. Operating factors considered in the study were AC's surface area, particle size, initial pH, dosage of AC, solution temperature, adsorbate concentration and contact time. The percentage dyes elimination was the main parameter (response) investigated. The use of agro biomass aids in the reduction of waste in the environment by generating a profitable commodity, AC, by activation and carbonisation processes.

## 2 Methods

### 2.1 Development of Research Dataset

The activated carbon was developed from *Mucuna pruriens* seeds, *Hevea brasiliensis* seed shells and *Dacryodes edulis* seeds. The biomass samples were cleaned with distilled water and oven dried for 8 h at 105 °C. They were then ground, sieved (1–2 mm), and stored in a sealed container. The specific surface area of the AC was varied by using various activation techniques. And, these were by NaOH and H<sub>3</sub>PO<sub>4</sub>. The activation agent (60% or NaOH or 60% H<sub>3</sub>PO<sub>4</sub>) was used to soak the sample for 24 h at 25 ± 2 °C. They were carbonised at 300 °C for 3 h after wet impregnation in a muffle furnace (Model SX-2.5-10, Tianjin Taisete Instrument Co., Ltd., China). The carbonised sample was rinsed until there was no pH change. It was filtered and oven dried for 8 h at 105 °C. They were then cooled to room temperature, sieved to various particle sizes, and sealed in a container. The method described by Nwabanne and Igbokwe [69] was used to calculate the specific surface area.

The adsorbate for the study were Vat yellow 4 ( $\lambda_{\max} = 498$  nm, molecular mass = 332.35 g/mol, chemical formula = C<sub>24</sub>H<sub>12</sub>O<sub>2</sub>), Congo red ( $\lambda_{\max} = 419$  nm, molecular mass = 696.66 g/mol, chemical formula = C<sub>32</sub>H<sub>22</sub>N<sub>6</sub>Na<sub>2</sub>O<sub>6</sub>S<sub>2</sub>) and Malachite green ( $\lambda_{\max} = 618$  nm, molecular mass = 364.91 g/mol, formula = C<sub>23</sub>H<sub>25</sub>ClN<sub>2</sub>) manufactured by LOBA Chemie (PVT Ltd., India). All adsorbates were of high analytical quality. The investigation was conducted by batch adsorption experiments. A UV–vis spectrophotometer was used to determine the final dye concentration after uptake (Model UV–VIS 754). The dye removal efficiency was determined using Eq. 1.

$$\text{RE}\% = \frac{C_0 - C_e}{C_0} \times 100 \quad (1)$$

where  $C_0$  is the initial dye concentration (mg/L) and  $C_e$  is the final dye concentration of its solution (mg/L).

**Table 1** Designation of factors and response

S/N	Designation	Code	Data	Unit	Data band
1	Factor 1	<i>A</i>	Specific surface area	m <sup>2</sup> /g	735 < <i>x</i> < 999
2	Factor 2	<i>B</i>	Particle size (mm)	mm	0.3 < <i>x</i> < 1.5
3	Factor 3	<i>C</i>	Dosage	G	0.5 < <i>x</i> < 2.0
4	Factor 4	<i>D</i>	Initial conc	mg/L	100 < <i>x</i> < 500
5	Factor 5	<i>E</i>	Time	Min	10 < <i>x</i> < 150
6	Factor 6	<i>F</i>	Temperature	°C	30 < <i>x</i> < 50
7	Factor 7	<i>G</i>	pH	–	2 < <i>x</i> < 10
8	Response	RE%	Dye removal efficiency	%	

The factors investigated were adsorbent specific surface area (in m<sup>2</sup>/g), adsorbent particle size (in mm), adsorbent dosage (in g), initial dye concentration (in mg/L), contact time (in min), temperature (in °C) and pH. The dataset for this modelling study is shown in the supplementary material for VY4 (Table S1), CR (Table S2) and MG (Table S3). Each table consisted of 354 lines of datum.

## 2.2 Response Surface Modelling

Response surface methodology (RSM) on Design Expert v11.0 (Stat Ease Inc., Minneapolis, USA), was used to statistically analyse and model the input data. RSM is a powerful statistical optimisation tool used for numerous environmental engineering investigations [44, 70, 71]. The data was inputted based on Historical Data Design (HDD). HDD is flexible because it allows the researcher to develop the data design and specify the size of the chosen input [72, 73]. The inputted design was modelled by the software and the statistical significance was verified by ANOVA (analysis of variance) at a significance level of  $p < 0.05$ . The model was used to investigate the interaction of factors. Several factors were investigated in this study. These were summarised in Table 1.

## 2.3 Numerical Optimisation

Numerical optimisation was done using the ‘optimisation’ selection on Design Expert v11.0. The goal of the numerical optimisation was to maximise removal efficiency while maintaining all process variables within the parameters that were examined. The term ‘numerical’ indicates that the process is an iterative one [74, 75] that seeks to achieve a desirability value of unity.

### 3 Results and Discussion

#### 3.1 ANOVA and Model Accuracy

To establish the relationship between the factors and dependent variables within the domain, the ANOVA was done using the quadratic model and all its associated model terms at  $p$  less than 0.05 [76]. The  $p$ -value can be described as the probability of rejecting a null hypothesis and values [77].  $Prob > F$  greater than 0.10 indicates the model terms were insignificant while values less than 0.05 indicate the model terms were significant [77]. From the ANOVA in Tables 2, 3 and 4, the three RSM models were statistically significant. It was also observed that the independent variables were all significant except for the variables; specific surface area and pH of MG having  $p$ -values of 0.3382 and 0.5110, respectively. This implies that all factors or independent variables studied had specific impacts on the removal efficiency except for specific surface area and pH of MG. However, there were no multiple effects present. From the  $F$ -value as shown in Tables 2, 3 and 4, it is expected that the response of removal efficiency would be most affected by the variables: initial concentration, pH, and particle size, respectively, for VY4, CR and MG.

The positive sign in front of the terms indicate the presence of the synergistic effect of the independent variables rather than an antagonistic effect depicted by the negative sign in front of the terms [78, 79]. The mathematical expressions for the relationship between removal efficiency and the seven independent variables; specific surface area, particle size, dosage, initial concentration, time, temperature and pH are shown in terms of coded factors in Eqs. 2–4. The levels for the independent variables

**Table 2** ANOVA for VY4 model

S/N	Source	Sum of squares	df	Mean square	F value	$p$ -value Prob > F	
1	Model	22,731.12	7	3247.30	101.16	< 0.0001	Significant
2	A-Specific surface area	6438.18	1	6438.18	200.56	< 0.0001	
3	B-Particle size	3985.40	1	3985.40	124.15	< 0.0001	
4	C-Dosage	538.37	1	538.37	16.77	< 0.0001	
5	D-Initial conc	8116.38	1	8116.38	252.84	< 0.0001	
6	E-Time	1128.44	1	1128.44	35.15	< 0.0001	
7	F-Temperature	252.47	1	252.47	7.86	0.0053	
8	G-pH	1158.96	1	1158.96	36.10	< 0.0001	
9	Residual	11,106.75	346	32.10			
10	Lack of fit	10,296.96	294	35.02	2.25	0.0003	Significant
11	Pure error	809.79	52	15.57			
12	Cor. total	33,837.87	353				

**Table 3** ANOVA for CR model

S/N	Source	Sum of squares	df	Mean square	F value	p-value Prob > F	
1	Model	56,772.22	7	8110.32	90.75	<0.0001	Significant
2	A-Specific surface area	1061.01	1	1061.01	11.87	0.0006	
3	B-Particle size	10,244.08	1	10,244.08	114.63	<0.0001	
4	C-Dosage	7490.30	1	7490.30	83.81	<0.0001	
5	D-Initial conc	361.26	1	361.26	4.04	0.0451	
6	E-Time	973.44	1	973.44	10.89	0.0011	
7	F-Temperature	1512.01	1	1512.01	16.92	<0.0001	
8	G-pH	14,648.59	1	14,648.59	163.91	<0.0001	
9	Residual	30,921.98	346	89.37			
10	Lack of fit	23,291.40	294	79.22	0.54	0.9992	Not significant
11	Pure error	7630.58	52	146.74			
12	Cor. total	87,694.20	353				

**Table 4** ANOVA for MG model

S/N	Source	Sum of squares	df	Mean square	F value	p-value Prob > F	
1	Model	6023.56	7	860.51	70.28	<0.0001	Significant
2	A-Specific surface area	11.26	1	11.26	0.92	0.3382	
3	B-Particle size	3118.83	1	3118.83	254.72	<0.0001	
4	C-Dosage	330.60	1	330.60	27.00	<0.0001	
5	D-Initial conc	156.12	1	156.12	12.75	0.0004	
6	E-Time	1183.21	1	1183.21	96.63	<0.0001	
7	F-Temperature	203.45	1	203.45	16.62	<0.0001	
8	G-pH	5.30	1	5.30	0.43	0.5110	
9	Residual	4236.50	346	12.24			
10	Lack of fit	3576.57	292	12.25	1.00	0.5149	Not significant
11	Pure error	659.93	54	12.22			
12	Cor. total	10,260.06	353				

are  $735 < A < 999$ ,  $0.3 < B < 1.5$ ,  $0.5 < C < 2.0$ ,  $100 < D < 500$ ,  $10 < E < 150$ ,  $30 < F < 50$ , and  $2 < G < 10$ .

$$\begin{aligned} \text{VY4 RE\%} = & 140.6 - 0.0048A - 25.55B + 3.193C - 0.0438D \\ & + 0.0596E + 0.0969F - 1.417G \end{aligned} \quad (2)$$

$$\begin{aligned} \text{CR RE\%} = & 78.23 + 0.02A - 40.67B + 13.47C - 0.0092D \\ & + 0.0553E + 0.02322F - 4.959G \end{aligned} \quad (3)$$

$$\begin{aligned} \text{MG RE\%} = & 97.81 + 0.0022A - 22.21B + 2.321C - 0.006D \\ & + 0.0609E + 0.0841F - 0.0654G \end{aligned} \quad (4)$$

where  $A$  is adsorbent specific surface area (in  $\text{m}^2/\text{g}$ ),  $B$  is adsorbent particle size (in mm),  $C$  is adsorbent dosage (in g),  $D$  is dye initial concentration (in mg/L),  $E$  is contact time (in min),  $F$  is temperature (in  $^\circ\text{C}$ ) and  $G$  is pH.

Equations 2–4 were modified through the elimination of the statistically insignificant terms. The insignificant terms are variables that show no observable relationship with the responses either by increasing or decreasing the response strength. The reason for this elimination is to obtain a more accurate model that best describes the effect of the factors [80]. All factors in Eqs. 2 and 3 are statistically significant and so their equations remain unchanged, but factors  $A$  and  $G$  in Eq. 4 are statistically insignificant. Withdrawing them from the model, the final models are now given in Eq. 5–7.

$$\begin{aligned} \text{VY4 RE\%} = & 140.6 - 0.0048A - 25.55B + 3.193C - 0.0438D \\ & + 0.0596E + 0.0969F - 1.417G \end{aligned} \quad (5)$$

$$\begin{aligned} \text{CR RE\%} = & 78.23 + 0.02A - 40.67B + 13.47C - 0.0092D \\ & + 0.0553E + 0.02322F - 4.959G \end{aligned} \quad (6)$$

$$\text{MG RE\%} = 97.81 - 22.21B + 2.321C - 0.006D + 0.0609E + 0.0841F \quad (7)$$

If a model has a significant regression and a non-significant lack of fit, it is considered to be well-fitted to the experimental data [81]. The ANOVA results depicted the adequacy of the quadratic model to predict CR and MG dye removal within the various variable levels studied. This was further strengthened by the  $p$ -value of the lack of fit for both the CR and MG models which was more than 0.05 (not significant), which implies that the model fits the experimental data. Even though all the models are statistically significant, the  $p$ -value for lack of fit for the VY4 model was significant (0.0003) and depicts that the model does not fit the experimental data well. The parity plot in Fig. 1a–c reveals that there is a close match between the model predictions and actual results [82, 83].



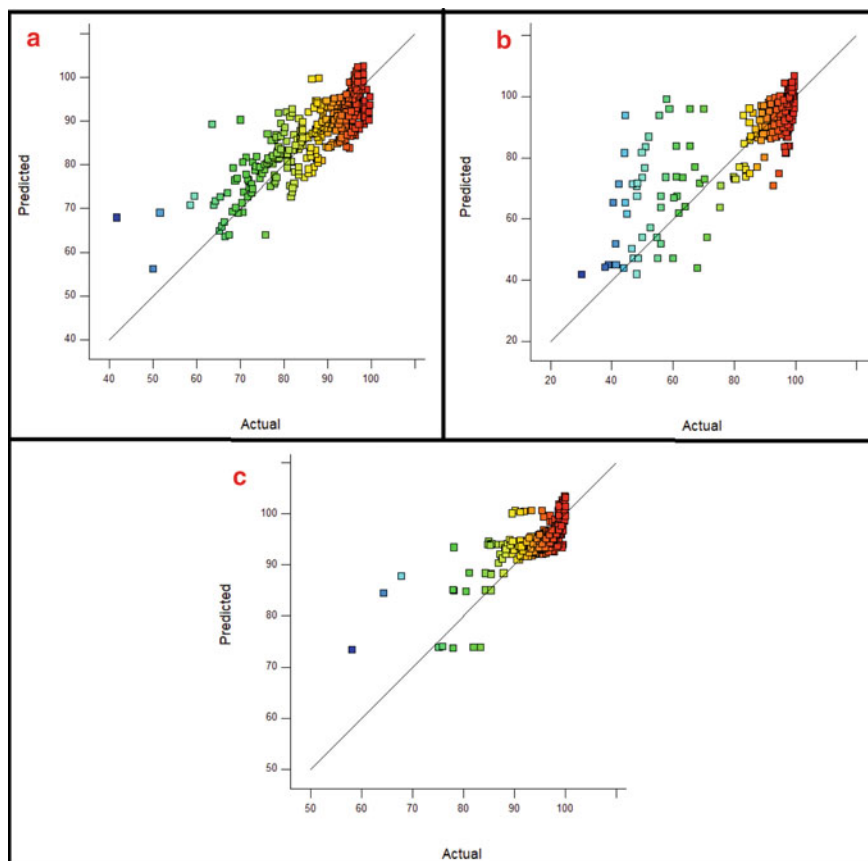


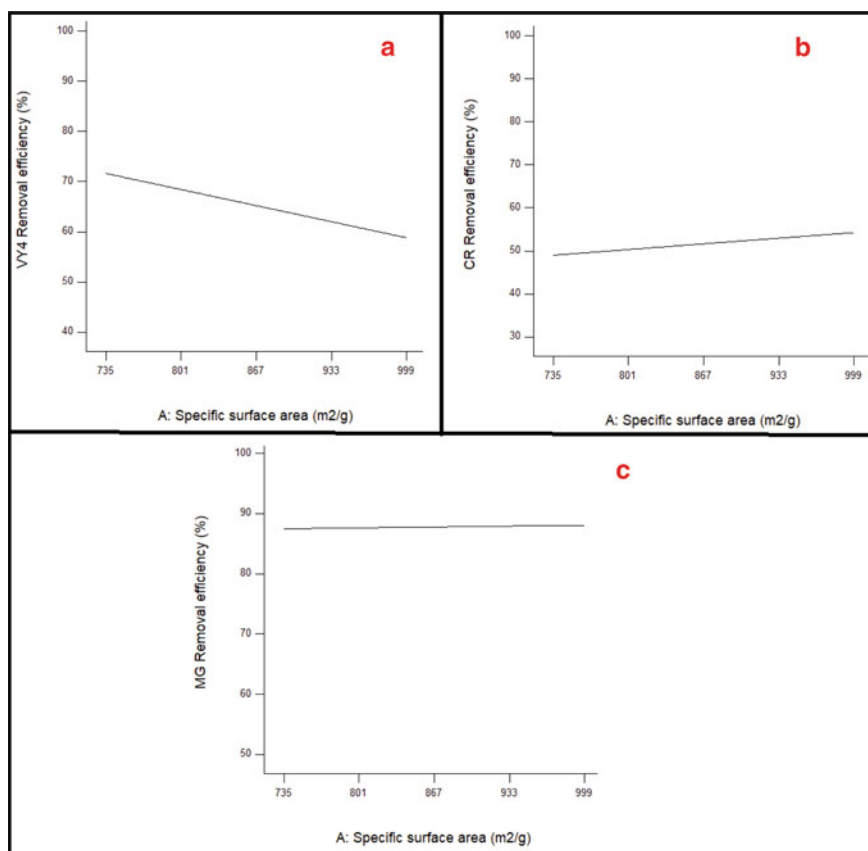
Fig. 1 Parity plots for VY4 model (a), CR model (b) and MG model (c)

### 3.2 Response Surfaces of Factor Interactions

Response surface plot for single influence of specific surface area on the elimination efficiency of the dyes is presented in Fig. 2a–c while keeping other factors constant (adsorbent size = 0.9 mm, dose = 0.85 g, initial concentration = 300 mg/L, time = 80 min, temperature = 40 °C and pH of 6). As can be seen from the plots, the dyes reacted differently to changes in the surface area of the carbon and this impacted the removal efficiency. As stated, the specific surface area had no observable impact on the removal efficiency of MG and this is also observed in Fig. 2c. It was observed that as the specific surface area of the carbon was increased, the removal efficiency of VY4 dye decreased. There is a general conception that the higher the surface area of an adsorbent, the better its adsorption properties [72, 84]. This assumption does not hold at all times because not all of the total surface area of an adsorbent is accessible for the adsorption of molecules in some applications [85, 86]. Micropores are very

much responsible for the large surface area of activated carbons as determined by nitrogen adsorption [87] and then the reduction in removal efficiency may be due to the high molecular weight of VY4 dye which requires an activated carbon with high mesoporosity as removal efficiency is also directly related to secondary micropores and mesopores of activated carbon [85, 88]. By increasing the surface area of the adsorbent, it was revealed that the removal efficiency of CR was increased. The reason for this increase may be due to the corresponding rise in the amount of active or adsorbing sites on the carbon surface [89, 90].

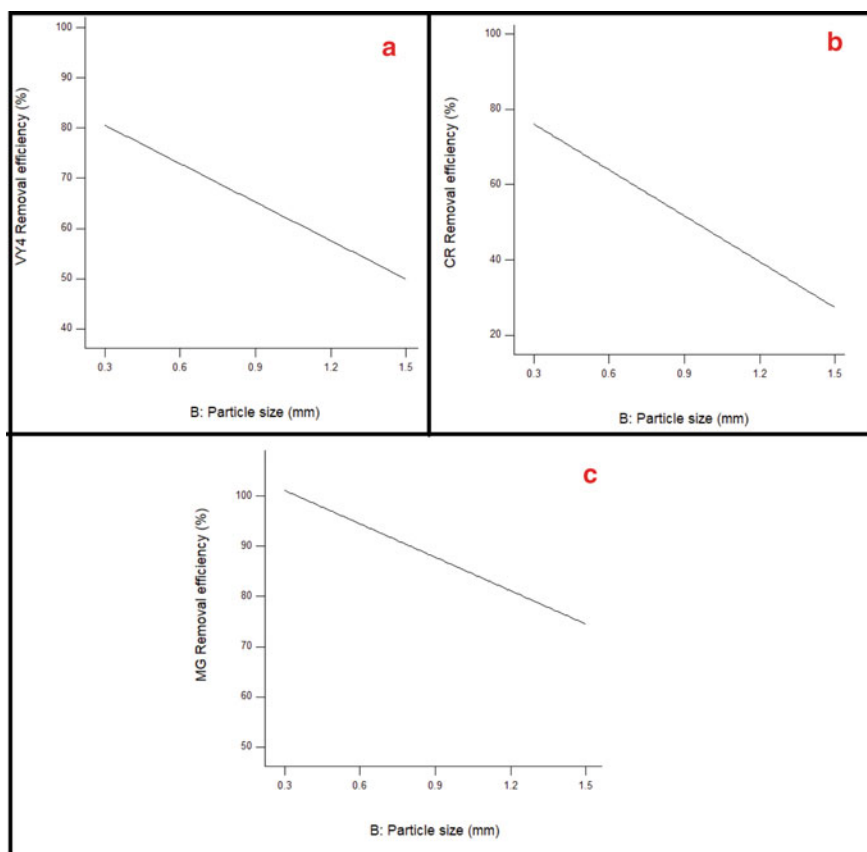
Particle size is a phenomenon related to noticeable changes in the physical as well as chemical characteristics of an adsorbent as a result of the reduction of its particles [91, 92]. The effect of activated carbon particle size on removal efficiency was also studied for the dye samples at specific surface area = 867 m<sup>2</sup>/g, dosage = 0.85 g, initial concentration = 300 mg/L, time = 80 min, temperature = 40 °C and pH = 6



**Fig. 2** Effect of specific surface area (A) on the removal of VY4 (a), CR (b) and MG (c), obtained from RSM one factor analysis at  $B = 0.9$  mm,  $C = 0.85$  g,  $D = 300$  mg/L,  $E = 80$  min,  $F = 40$  °C and  $G = 6$

as shown in Fig. 3a–c. From the plot, there is an inverse proportionality relationship between the particle size and the removal efficiency for the three dyes under study. As stated above, the removal efficiency of MG is greatly affected by the particle size and this is further buttressed in Fig. 3c. The relationship between removal efficiency to the particle size of the activated carbon is dependent on the chemistry/chemical behaviour of the dye in question as well as the intrinsic characteristics of the activated carbon [93]. The noticed increase in the removal efficiency as the particle size was decreased could be due to the rise in the activated carbon surface area in addition to the overall pore volume accessible for dye removal [94]. Also, it could be due to the increase in the adsorbent's pore diameter which permitted easier contact of the dye molecules into the activated carbon structure [95, 96].

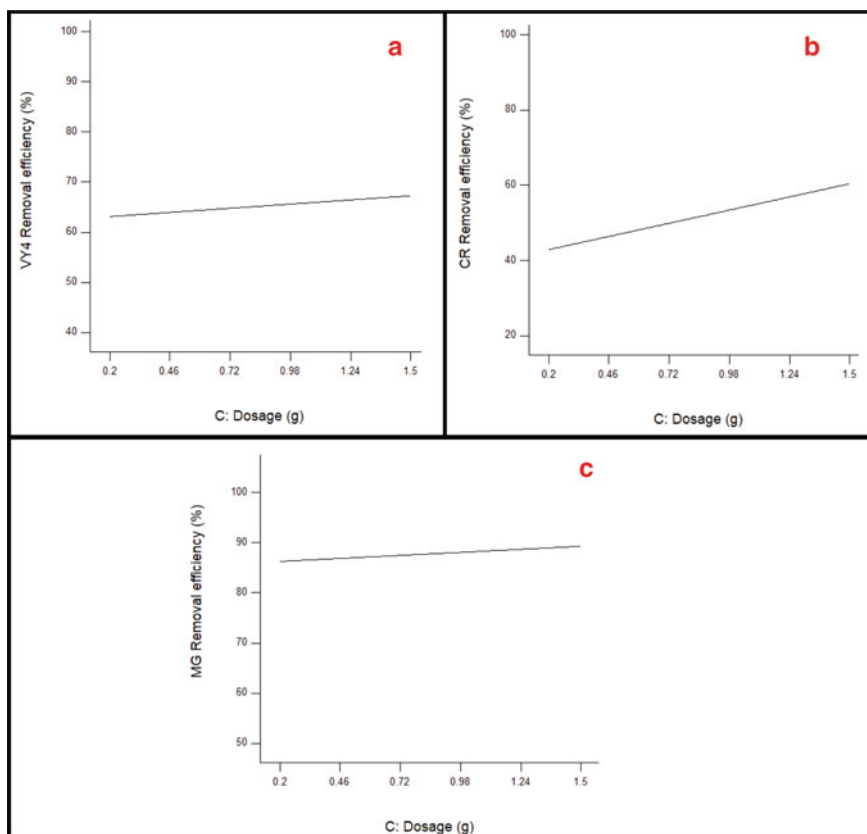
The plot of removal efficiency against adsorbent dosage as given in Fig. 4a–c shows that adsorbent dosage is one of the independent variables that can alter the dye



**Fig. 3** Influence of sorbent size ( $B$ ) on the removal of VY4 (a), CR (b) and MG (c), obtained from RSM one factor analysis at  $A = 867 \text{ m}^2/\text{g}$ ,  $C = 0.85 \text{ g}$ ,  $D = 300 \text{ mg/L}$ ,  $E = 80 \text{ min}$ ,  $F = 40 \text{ }^\circ\text{C}$  and  $G = 6$

removal efficiency. The study was performed at conditions of specific surface area =  $867 \text{ m}^2/\text{g}$ , Adsorbent particle size =  $0.9 \text{ mm}$ , initial concentration =  $300 \text{ mg/L}$ , time =  $80 \text{ min}$ , temperature =  $40 \text{ }^\circ\text{C}$  and  $\text{pH} = 6$ . The plot shows that removal efficiency increases as the adsorbent dosage is increased for the three dye samples under study. Of the three dyes, the removal efficiency of MG is greater than that of VY4 and CR as shown in the plot with changes in the activated carbon dosage. The reason for the increase in removal efficiency as the adsorbent dosage is increased may be due to the increase in surface active sites on the activated carbon for adsorption [97, 98].

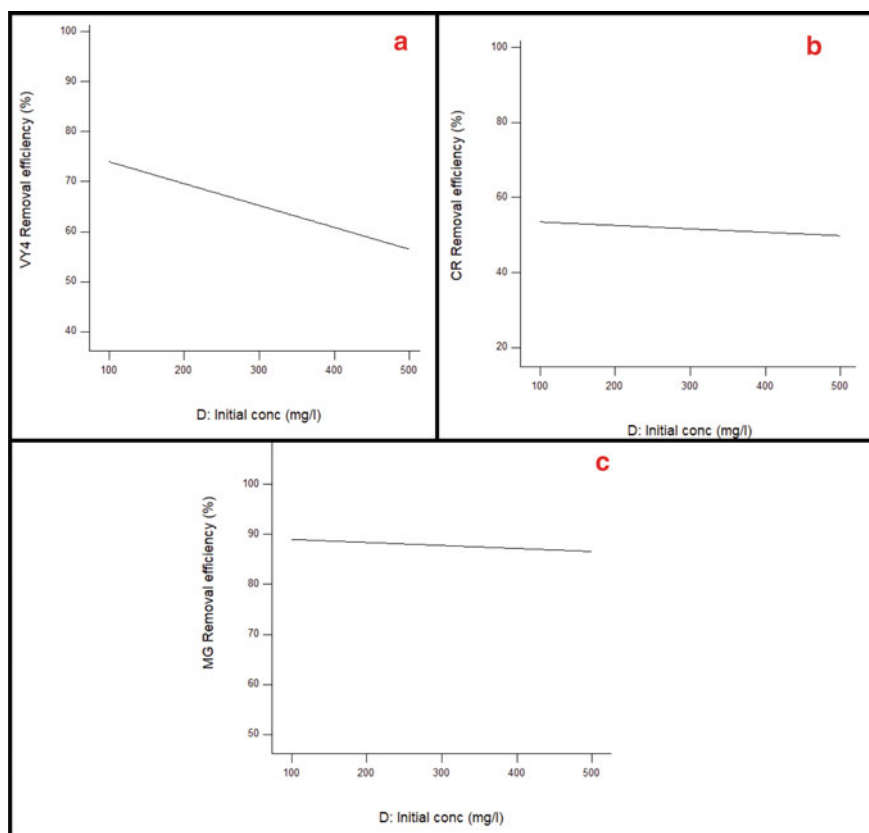
Altering the dye initial concentration can alter the mass gradient between the activated carbon and the dyes and thereby alter the removal efficiency [99]. The impact of initial dye concentration on the removal efficiency was studied at specific surface area =  $867 \text{ m}^2/\text{g}$ , Adsorbent particle size =  $0.9 \text{ mm}$ , dosage =  $0.85 \text{ g}$ , time =  $80 \text{ min}$ , temperature =  $40 \text{ }^\circ\text{C}$  and  $\text{pH} = 6$ . It was observed that the removal efficiency



**Fig. 4** Influence of sorbent dose (C) on the removal of VY4 (a), CR (b) and MG (c), obtained from RSM one factor analysis at  $A = 867 \text{ m}^2/\text{g}$ ,  $B = 0.9 \text{ mm}$ ,  $D = 300 \text{ mg/L}$ ,  $E = 80 \text{ min}$ ,  $F = 40 \text{ }^\circ\text{C}$  and  $G = 6$

reduced as the dye initial concentration was increased within the levels of initial dye concentration under study. From Fig. 5a–c, it was observed that the removal efficiency of VY4 dye was greatly affected by the change of its initial concentration than the other two dyes. This supports the claim as stated above that of all the independent factors, initial dye concentration affects the response for VY4 the most. The observed trend may be caused by the proportionate number of vacant sites on the activated number to the dye molecules at low initial dye concentration and the saturation of these active sites at a high concentration which would lead to repulsive interactions between the dye molecules on the solid and bulk phases leading to the observed decrease in the removal efficiency [67, 100].

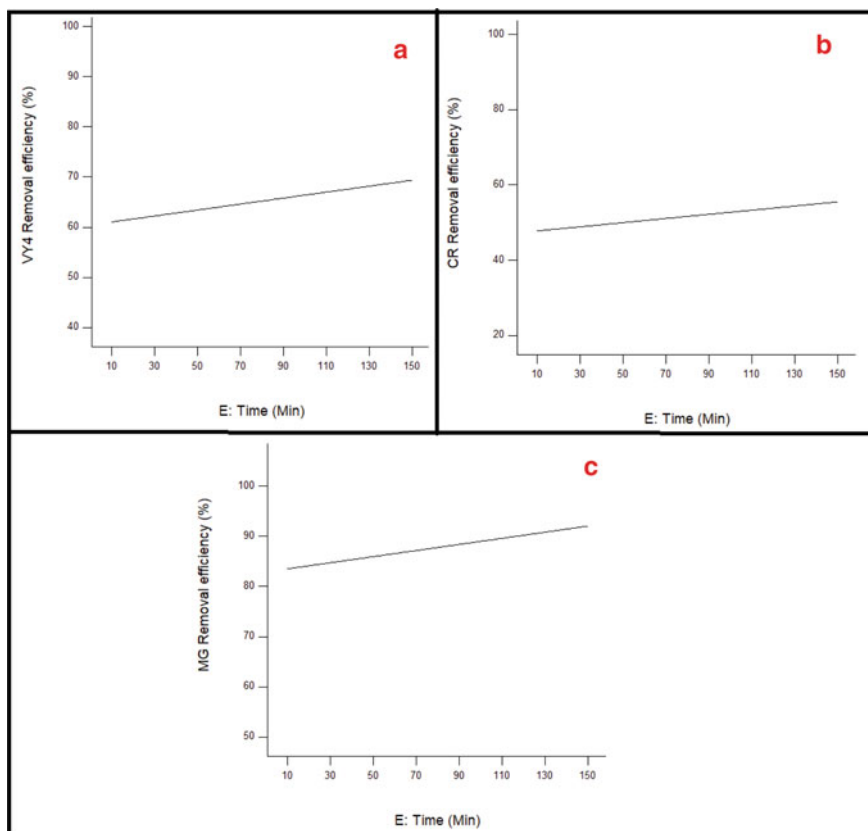
The effect of contact time on removal efficiency was studied at conditions of specific surface area = 867 m<sup>2</sup>/g, adsorbent particle size = 0.9 mm, dosage = 0.85 g, initial concentration = 300 mg/L, temperature = 40 °C and pH = 6. The removal



**Fig. 5** Effect of dye initial concentration (*D*) on the elimination of VY4 (**a**), CR (**b**) and MG (**c**), obtained from RSM one factor analysis at *A* = 867 m<sup>2</sup>/g, *B* = 0.9 mm, *C* = 0.85 g, *E* = 80 min, *F* = 40 °C and *G* = 6

efficiencies of the three dyes were affected similarly by contact time as observed from Fig. 6a–c. From the plot, it was noticed that the removal efficiency for the dyes increased with prolonging the time of contact between the activated carbon and adsorbate. This could be due to the movement of the dye molecules into the pores of the activated carbon which causes them to be adsorbed by the interior surfaces of the solid particles when the exterior surface of the activated carbon has been saturated as time progressed [93, 101].

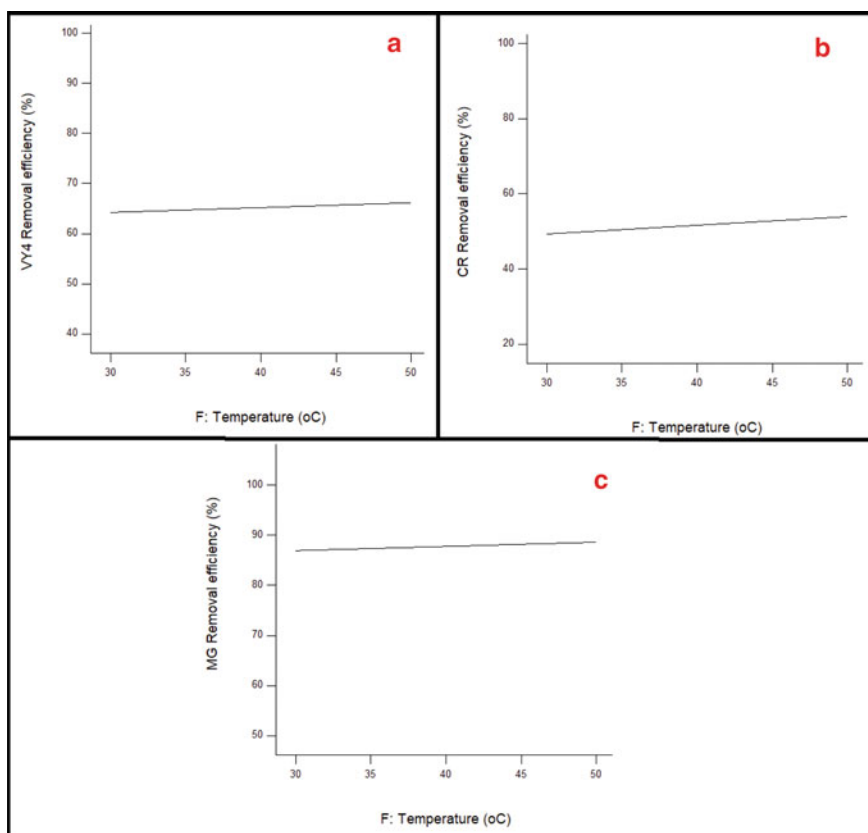
The relationship between dye removal efficiency for the three dyes with temperature at specific surface area = 867 m<sup>2</sup>/g, sorbent size = 0.9 mm, dosage = 0.85 g, initial concentration = 300 mg/L, time = 80 min and pH = 6 was studied. An important observation that can be drawn from Fig. 7a–c is that the removal efficiency of the dyes improved as the temperature was raised. This could be due to the energy which the increase in temperature provides that enables the dye molecules to



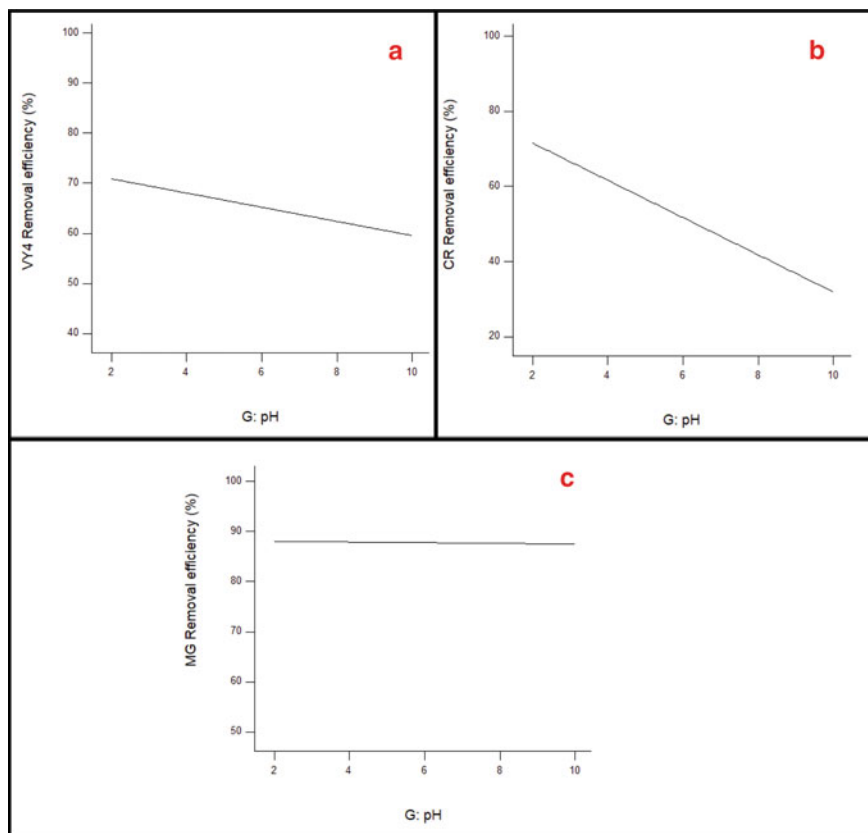
**Fig. 6** Effect of time of contact ( $E$ ) on the elimination of VY4 (a), CR (b) and MG (c), obtained from RSM one factor analysis at  $A = 867 \text{ m}^2/\text{g}$ ,  $B = 0.9 \text{ mm}$ ,  $C = 0.85 \text{ g}$ ,  $D = 300 \text{ mg/L}$ ,  $F = 40 \text{ }^\circ\text{C}$  and  $G = 6$

occupy the available active sites in the activated carbon at high concentrations amidst competition [102, 103]. The trend also relates that the adsorption of the three dyes is endothermic as it is favoured at high temperatures [104].

As stated above the removal efficiency of MG is independent of the pH of the solution, and this was also observed in Fig. 8c. The pH of the solution affects the ionization of the dye molecules as well as the activated carbon surface properties [105]. The plot of removal efficiency against pH at conditions of specific surface area = 867 m<sup>2</sup>/g, sorbent size = 0.9 mm, dosage = 0.85 g, initial concentration = 300 mg/L, time = 80 min and temperature = 40 °C as shown in Fig. 8a, b shows that the removal efficiency decreases with an increase in pH. It was also observed the removal efficiency of CR was the most affected than the other dyes with the change in pH as stated above. At low pH, there exists an abundance of hydrogen ions which leads to the protonation of the functional groups present on the activated carbon's



**Fig. 7** Temperature influence ( $F$ ) on the removal efficiency of VY4 (a), CR (b) and MG (c), obtained from RSM one factor analysis at  $A = 867 \text{ m}^2/\text{g}$ ,  $B = 0.9 \text{ mm}$ ,  $C = 0.85 \text{ g}$ ,  $D = 300 \text{ mg/L}$ ,  $E = 80 \text{ min}$  and  $G = 6$



**Fig. 8** pH impact (*G*) on the elimination of VY4 (**a**), CR (**b**) and MG (**c**), obtained from RSM one factor analysis at  $A = 867 \text{ m}^2/\text{g}$ ,  $B = 0.9 \text{ mm}$ ,  $C = 0.85 \text{ g}$ ,  $D = 300 \text{ mg/L}$ ,  $E = 80 \text{ min}$  and  $F = 40 \text{ }^\circ\text{C}$

surface and an increase in surface charge too which causes the increment of dye adsorption through electrostatic attraction [106, 107]. At high pH, the reduction in hydrogen ions promotes electrostatic repulsion between the negative charges of the activated carbon and dyes which leads to the decrease observed in the removal of VY4 and CR [108].

### 3.3 Numerical Optimisation Results

The numerical optimisation in this study seeks to find a combination of experimental variable levels that provided optimum process parameters to achieve maximum removal efficiency values for VY4, CR, and MG dyes using the activated carbon. The values of specific surface area, sorbent size, carbon dose, dye concentration,



**Table 5** Numerical optimisation results

S/N	Parameter	Unit	VY4	CR	MG
1	Specific surface area	m <sup>2</sup> /g	749.9	970.7	941.9
2	Particle size	mm	0.300	0.439	0.321
3	Dosage	g	1.127	1.464	1.063
4	Initial concentration	mg/L	123.3	214.4	311.6
5	Contact time	min	90.11	139.9	69.86
6	Temperature	°C	31.29	44.53	45.62
7	pH	–	2.457	2.407	6.203
8	Desirability	–	1.000	1.000	1.000
9	Removal	%	99.61	100.0	100.0

contact time, temperature and pH were within the study range and the conditions as stated in Table 1. Equations 2–4 were solved to obtain the best solutions such that the responses RE (%) are maximised within the experimental domain. Based on the information obtained above, all the seven independent variables under study affected the adsorption removal efficiencies of VY4 and CR dyes as they were all statistically significant while all independent variables except the specific surface area and pH contributed significantly to the adsorption removal efficiency of MG dye. Under the determined optimum process conditions as shown in Table 5, the maximum removal efficiencies were observed to be 99.61%, 100.0%, and 100.0% for VY4, CR and MG dyes, respectively. The desirability values of these parameters which is a depiction of the ideal and desired values were observed to be 1.000 (unity) for the three dyes analysed. This confirms the acceptability of the predicted adsorption removal efficiencies as well as the applicability of the model for the dyes under study [109, 110].

Table 6 shows the performance of activated carbons generated from various precursor materials used in the treatment of textile wastewater. Based on the adsorption efficiencies obtained in previous studies, it was determined that activated carbon is an effective adsorbent for textile effluent. They also have a good surface area. The greater the carbon's surface area, the more pollutant is removed.

## 4 Conclusion

Several conclusions were derived from this study. From the ANOVA, the three RSM models were statistically significant. It was also observed that the independent variables were all significant except for the variables; specific surface area and pH of MG having p-values of 0.3382 and 0.5110, respectively. This implies that all factors or independent variables studied had specific impacts on the removal efficiency except for specific surface area and pH of MG. However, there were no multiple

**Table 6** Performance of activated carbons generated from various precursor materials

S/N	Precursor	Surface area	Target pollutant	Adsorption efficiency	References
1	<i>Parthenium hysterophorus</i>	–	Methylene blue	94% (synthesised effluent) and 91% for real effluent in 100 min	[111]
2	<i>Borassus flabellifer</i> fruit husk waste	–	Reactive red 120	93.75% in 120 min	[112]
3	Vinasse wastes	2015 m <sup>2</sup> /g	Methylene blue	99% in 60 min	[113]
4	Bamboo chips	720.69 m <sup>2</sup> /g	Methylene blue	> 95% in 12.5 min	[114]
5	Corncoobs	2308.27 m <sup>2</sup> /g	Methylene blue	99.52%	[115]
6	<i>Dacryodes edulis</i> seeds	–	Congo red	99.7% in 60 min	[67]
7	Pomegranate fruit peel	845.96 m <sup>2</sup> /g	Remazol brilliant blue R	81.35%	[116]
8	Rice husks	375.02 m <sup>2</sup> /g	Methyl orange	98.5% in 30 min	[117]
9	Rice husks	375.02 m <sup>2</sup> /g	Methyl blue	82% in 30 min	[117]

effects present. The effect of process factors was also thoroughly analysed. Under the determined optimum process conditions obtained by numerical optimisation, the maximum removal efficiencies were observed to be 99.61%, 100.0%, and 100.0% for VY4, CR and MG dyes, respectively. The desirability values of these parameters which is a depiction of the ideal and desired values were observed to be 1.000 (unity) for the three dyes analysed.

**Acknowledgements** The first author wishes to acknowledge Joshua O. Ighalo and Kingsley O. Iwuozor for their support during the writing of this article.

## References

1. Shindhal T, Rakholiya P, Varjani S, Pandey A, Ngo HH, Guo W, Ng HY, Taherzadeh MJ (2021) A critical review on advances in the practices and perspectives for the treatment of dye industry wastewater. *Bioengineered* 12(1):70–87
2. Talouizte H, Merzouki M, Benlemlih M, Bendriss Amraoui M (2020) Chemical characterization of specific micropollutants from textile industry effluents in Fez city, Morocco. *J Chem* 2020
3. Ghaly A, Ananthashankar R, Alhattab M, Ramakrishnan V (2014) Production, characterization and treatment of textile effluents: a critical review. *J Chem Eng Process Technol* 5(1):1–18
4. Hevira L, Zilfa, Rahmayeni, Ighalo JO, Aziz H, Zein R (2021) *Terminalia catappa* shell as low-cost biosorbent for the removal of methylene blue from aqueous solutions. *J Ind Eng Chem*

5. Hevira L, Zilfa R, Ighalo JO, Zein R (2020) Biosorption of indigo carmine from aqueous solution by *Terminalia catappa* shell. *J Environ Chem Eng* 8(5):104290
6. Iwuozor KO, Ighalo JO, Ogunfowora LA, Adeniyi AG, Igwegbe CA (2021) An empirical literature analysis of adsorbent performance for methylene blue uptake from aqueous media. *J Environ Chem Eng* 9(4):105658
7. Igwegbe CA, Onyechi PC, Onukwuli OD, Nwokedi IC (2015) Adsorptive treatment of textile wastewater using activated carbon produced from *Mucuna pruriens* seed shells. *World J Eng Technol* 4(1):21–37
8. Merzouk B, Gourich B, Madani K, Vial C, Sekki A (2011) Removal of a disperse red dye from synthetic wastewater by chemical coagulation and continuous electrocoagulation. A comparative study. *Desalination* 272(1–3):246–253
9. Mcyotto F, Wei Q, Macharia DK, Huang M, Shen C, Chow CW (2021) Effect of dye structure on color removal efficiency by coagulation. *Chem Eng J* 405:126674
10. Obiora-Okafo I, Onukwuli O, Eli-Chukwu N (2020) Evaluation of bio-coagulants for colour removal from dye synthetic wastewater: characterization, adsorption kinetics, and modelling approach. *Water SA* 46(2):300–312
11. Obiora-Okafo I, Onukwuli O (2018) Characterization and optimization of spectrophotometric colour removal from dye containing wastewater by coagulation-flocculation. *Polish J Chem Technol* 20(4)
12. Uzoh CF (2014) Effective decolorization of eriochrome black T, Furschin basic and malachite green dyes from synthetic wastewater by electrocoag-nanofiltration. In: *Proceedings of the world congress on engineering and computer science*
13. Nandi BK, Patel S (2017) Effects of operational parameters on the removal of brilliant green dye from aqueous solutions by electrocoagulation. *Arabian J Chem* 10:S2961–S2968
14. Ahmadi S, Rahdar A, Igwegbe CA, Mortazavi-Derazkola S, Banach AM, Rahdar S, Singh AK, Rodriguez-Couto S, Kyzas GZ (2020) Praseodymium-doped cadmium tungstate ( $\text{CdWO}_4$ ) nanoparticles for dye degradation with sonocatalytic process. *Polyhedron* 190:114792
15. Ahmadi S, Igwegbe CA, Rahdar S (2019) The application of thermally activated persulfate for degradation of acid blue 92 in aqueous solution. *Int J Ind Chem* 10(3):249–260
16. Cuerda-Correa EM, Alexandre-Franco MF, Fernández-González C (2020) Advanced oxidation processes for the removal of antibiotics from water. An overview. *Water* 12(1):102
17. López Zavala MÁ, Vega DA, Álvarez Vega JM, Castillo Jerez OF, Cantú Hernández RA (2020) Electrochemical oxidation of acetaminophen and its transformation products in surface water: effect of pH and current density. *Heliyon* 6(2)
18. Hasan HA, Muhammad MH (2020) A review of biological drinking water treatment technologies for contaminants removal from polluted water resources. *J Water Process Eng* 33:101035
19. Serna-Galvis EA, Silva-Agredo J, Botero-Coy AM, Moncayo-Lasso A, Hernández F, Torres-Palma RA (2019) Effective elimination of fifteen relevant pharmaceuticals in hospital wastewater from Colombia by combination of a biological system with a sonochemical process. *Sci Total Environ* 670:623–632
20. Greenstein KE, Lew J, Dickenson ERV, Wert EC (2018) Investigation of biotransformation, sorption, and desorption of multiple chemical contaminants in pilot-scale drinking water biofilters. *Chemosphere* 200:248–256
21. Polesel F, Andersen HR, Trapp S, Plósz BG (2016) Removal of antibiotics in biological wastewater treatment systems—a critical assessment using the activated sludge modeling framework for xenobiotics (ASM-X). *Environ Sci Technol* 50(19):10316–10334
22. Xu YFMG, Guo Y, Wu B, An QF (2020) Development of antifouling nanofiltration membrane with zwitterionic functionalized monomer for efficient dye/salt selective separation. *J Membrane Sci* 601:117795
23. Ma Y, Qi P, Ju J, Wang Q, Hao L, Wang R, Sui K, Tan Y (2019) Gelatin/alginate composite nanofiber membranes for effective and even adsorption of cationic dyes. *Compos B Eng* 162:671–677

24. Li F, Huang J, Xia Q, Lou M, Yang B, Tian Q, Liu Y (2018) Direct contact membrane distillation for the treatment of industrial dyeing wastewater and characteristic pollutants. *Sep Purif Technol* 195:83–91
25. Yao L, Zhang L, Wang R, Chou S, Dong Z (2016) A new integrated approach for dye removal from wastewater by polyoxometalates functionalized membranes. *J Hazard Mater* 301:462–470
26. Lim S-L, Chu W-L, Phang S-M (2010) Use of *Chlorella vulgaris* for bioremediation of textile wastewater. *Biores Technol* 101(19):7314–7322
27. Bwapa JK, Jaiyeola AT, Chetty R (2017) Bioremediation of acid mine drainage using algae strains: a review. *South African J Chem Eng* 24:62–70
28. Andreotti V, Chindris A, Brundu G, Vallainc D, Francavilla M, García J (2017) Bioremediation of aquaculture wastewater from *Mugil cephalus* (Linnaeus, 1758) with different microalgae species. *Chem Ecol* 33(8):750–761
29. Sharma GK, Khan SA (2013) Bioremediation of sewage wastewater using selective algae for manure production. *Int J Environ Eng Manage* 4:573–580
30. Munagapati VS, Wen H-Y, Vijaya Y, Wen J-C, Wen J-H, Tian Z, Reddy GM, Raul Garcia J (2021) Removal of anionic (acid yellow 17 and amaranth) dyes using aminated avocado (*Persea americana*) seed powder: adsorption/desorption, kinetics, isotherms, thermodynamics, and recycling studies. *Int J Phytoremed*:1–13
31. Li Y, Lin J, Huang Y, Yao Y, Wang X, Liu C, Liang Y, Liu K, Yu F (2020) Bioaugmentation-assisted phytoremediation of manganese and cadmium co-contaminated soil by Polygonaceae plants (*Polygonum hydropiper* L. and *Polygonum lapathifolium* L.) and *Enterobacter* sp. FM-1. *Plant Soil*:1–15
32. Ekperusi AO, Sikoki FD, Nwachukwu EO (2018) Phytoremediation of petroleum hydrocarbons in polluted waters using *Pistia stratiotes*: gaps and future perspective. In: SPE Nigeria annual international conference and exhibition, 2018. Society of Petroleum Engineers
33. Muthusaravanan S, Sivarajasekar N, Vivek J, Paramasivan T, Naushad M, Prakashmaran J, Gayathri V, Al-Duaij OK (2018) Phytoremediation of heavy metals: mechanisms, methods and enhancements. *Environ Chem Lett* 16(4):1339–1359
34. Ahmadi S, Mohammadi L, Rahdar A, Rahdar S, Dehghani R, Igwegbe CA, Kyzas GZ (2020) Acid dye removal from aqueous solution by using neodymium (III) oxide nanoadsorbents. *Nanomaterials* 10(3):556
35. Onu CE, Nwabanne JT, Ohale PE, Asadu CO (2021) Comparative analysis of RSM, ANN and ANFIS and the mechanistic modeling in eriochrome black-T dye adsorption using modified clay. *South African J Chem Eng* 36:24–42
36. Okoye C, Onukwuli O, Okey-Onyesolu C (2019) Utilization of salt activated *Raphia hookeri* seeds as biosorbent for Erythrosine B dye removal: kinetics and thermodynamics studies. *J King Saud Univ Sci* 31(4):849–858
37. Singh K, Arora S (2011) Removal of synthetic textile dyes from wastewaters: a critical review on present treatment technologies. *Crit Rev Environ Sci Technol* 41(9):807–878
38. Aljeboree AM, Alshirifi AN, Alkaim AF (2017) Kinetics and equilibrium study for the adsorption of textile dyes on coconut shell activated carbon. *Arabian J Chem* 10:S3381–S3393
39. Oba SN, Ighalo JO, Aniagor CO, Igwegbe CA (2021) Removal of ibuprofen from aqueous media by adsorption: a comprehensive review. *Sci Tot Environ*:146608
40. Ighalo JO, Igwegbe CA, Aniagor CO, Oba SN (2021) A review of methods for the removal of penicillins from water. *J Water Process Eng* 39:101886
41. Banerjee P, Barman SR, Mukhopadhyay A, Das P (2017) Ultrasound assisted mixed azo dye adsorption by chitosan–graphene oxide nanocomposite. *Chem Eng Res Des* 117:43–56
42. Aniagor CO, Igwegbe CA, Ighalo JO, Oba SN (2021) Adsorption of doxycycline from aqueous media: a review. *J Mole Liq* 334:116124
43. Ahmadi S, Igwegbe CA (2020) Removal of methylene blue on zinc oxide nanoparticles: nonlinear and linear adsorption isotherms and kinetics study. *Sigma J Eng Nat Sci* 38(1):289–303

44. Ahmadi S, Mesbah M, Igwegbe CA, Ezeliora CD, Osagie C, Khan NA, Dotto GL, Salari M, Dehghani MH (2021) Sono electro-chemical synthesis of LaFeO<sub>3</sub> nanoparticles for the removal of fluoride: Optimization and modeling using RSM, ANN and GA tools. *J Environ Chem Eng* 9(4):105320
45. Chen J, Sheng Y, Song Y, Chang M, Zhang X, Cui L, Meng D, Zhu H, Shi Z, Zou H (2018) Multimorphology mesoporous silica nanoparticles for dye adsorption and multicolor luminescence applications. *ACS Sustain Chem Eng* 6(3):3533–3545
46. Damasceno BS, da Silva AFV, de Araújo ACV (2020) Dye adsorption onto magnetic and superparamagnetic Fe<sub>3</sub>O<sub>4</sub> nanoparticles: a detailed comparative study. *J Environ Chem Eng* 8(5):103994
47. Abou Taleb MF, Hegazy DE, Ismail SA (2012) Radiation synthesis, characterization and dye adsorption of alginate–organophilic montmorillonite nanocomposite. *Carbohydr Polym* 87(3):2263–2269
48. Agarwal S, Tyagi I, Gupta VK, Golbaz F, Golikand AN, Moradi O (2016) Synthesis and characteristics of polyaniline/zirconium oxide conductive nanocomposite for dye adsorption application. *J Mole Liq* 218:494–498
49. Balarak D, Zafariyan M, Igwegbe CA, Onyechi KK, Ighalo JO (2021) Adsorption of acid blue 92 dye from aqueous solutions by single-walled carbon nanotubes: isothermal, kinetic, and thermodynamic studies. *Environ Proc*:1–20
50. Eletta O, Mustapha S, Ajayi O, Ahmed A (2018) Optimization of dye removal from textile wastewater using activated carbon from sawdust. *Nigerian J Technol Dev* 15(1):26–32
51. Zhul-quarnain A, Ogemdi IK, Modupe I, Gold E, Chidubem EE (2018) Adsorption of malachite green dye using orange peel. *J Biomater* 2(2):31–40
52. Balarak D, Ganji F, Rajiv P, Igwegbe C, Ighalo JO (2021) Ultimate eradication of acid orange 7 from contaminated liquid via synthesised mesoporous goethite. *J Turk Chem Soc Sect B: Chem Eng* 4(1):13–26
53. Moreno-Pérez J, Pauletto PS, Cunha AM, Bonilla-Petriciolet Á, Salau NP, Dotto GL (2021) Three-dimensional mass transport modeling of pharmaceuticals adsorption inside ZnAl/biochar composite. *Colloids Surf, A* 614:126170
54. Khademi Jolgenejad A, Fekri M, Mahmoodabadi M (2021) The effect of pistachio pulp biochar on the adsorption of fluoride in aqueous solution. *Iranian J Soil Water Res*
55. Ighalo JO, Adeniyi AG, Eletta OAA, Arowoyele LT (2020) Competitive adsorption of Pb(II), Cu(II), Fe(II) and Zn(II) from aqueous media using biochar from oil palm (*Elaeis guineensis*) fibers: a kinetic and equilibrium study. *Ind Chem Eng*:1–11
56. Ighalo JO, Arowoyele LT, Ogunniyi S, Adeyanju CA, Oladipo-Emmanuel FM, Belgore RO, Omisore MO, Adeniyi AG (2020) Utilisation of biomass and hybrid biochar from elephant grass and low density polyethylene for the competitive adsorption of Pb(II), Cu(II), Fe(II) and Zn(II) from aqueous media. *Recent Inno Chem Eng* 14(2):148–159
57. Kyzas GZ, Lazaridis NK, Bikiaris DN (2013) Optimization of chitosan and β-cyclodextrin molecularly imprinted polymer synthesis for dye adsorption. *Carbohydr Polym* 91(1):198–208
58. Blanco SPD, Scheufele FB, Módenes AN, Espinoza-Quiñones FR, Marin P, Kroumov AD, Borba CE (2017) Kinetic, equilibrium and thermodynamic phenomenological modeling of reactive dye adsorption onto polymeric adsorbent. *Chem Eng J* 307:466–475
59. Saleem J, Shahid UB, Hijab M, Mackey H, McKay G (2019) Production and applications of activated carbons as adsorbents from olive stones. *Biomass Convers Biorefinery* 9(4):775–802
60. Bilal M, Ihsanullah I, Younas M, Ul Hassan Shah M (2021) Recent advances in applications of low-cost adsorbents for the removal of heavy metals from water: a critical review. *Sep Purif Technol* 278:119510
61. Ighalo JO, Iwuzor KO, Igwegbe CA, Adeniyi AG (2021) Verification of pore size effect on aqueous-phase adsorption kinetics: a case study of methylene blue. *Coll Surf A: Physicochem Eng Aspects*:127119
62. Kumar PS, Korving L, Keesman KJ, van Loosdrecht MC, Witkamp G-J (2019) Effect of pore size distribution and particle size of porous metal oxides on phosphate adsorption capacity and kinetics. *Chem Eng J* 358:160–169

63. Igwegbe CA, Ighalo JO, Onyechi KK, Onukwuli OD (2021) Adsorption of Congo red and malachite green using  $H_3PO_4$  and NaCl-modified activated carbon from rubber (*Hevea brasiliensis*) seed shells. *Sustain Water Res Manage* 7(4):1–16
64. Onyechi C (2014) Textile wastewater treatment using activated carbon from agro-wastes. M. Eng. Thesis, Department of Chemical Engineering, Nnamdi Azikiwe University, Awka
65. Iftekhhar S, Ramasamy DL, Srivastava V, Asif MB, Sillanpää M (2018) Understanding the factors affecting the adsorption of Lanthanum using different adsorbents: a critical review. *Chemosphere* 204:413–430
66. Zeng Z-w, Tan X-f, Liu Y-g, Tian S-r, Zeng G-m, Jiang L-h, Liu S-b, Li J, Liu N, Yin Z-h (2018) Comprehensive adsorption studies of doxycycline and ciprofloxacin antibiotics by biochars prepared at different temperatures. *Front Chem* 6:80
67. Igwegbe CA, Onukwuli OD, Ighalo JO, Okoye PU (2020) Adsorption of cationic dyes on *Dacryodes edulis* seeds activated carbon modified using phosphoric acid and sodium chloride. *Environ Proc* 7(4):1151–1171
68. Patel H (2021) Review on solvent desorption study from exhausted adsorbent. *J Saudi Chem Soc* 25:101302
69. Nwabanne JT, Igbokwe PK (2012) Thermodynamic and kinetic behaviors of lead (II) adsorption on activated carbon derived from palmyra palm nut. *Int J Appl Sci Technol* 2(3):245–254
70. Igwegbe CA, Mohammadi L, Ahmadi S, Rahdar A, Khadkhodaiy D, Dehghani R, Rahdar S (2019) Modeling of adsorption of methylene blue dye on Ho-CaWO<sub>4</sub> nanoparticles using response surface methodology (RSM) and artificial neural network (ANN) techniques. *MethodsX* 6:1779–1797
71. Ahmadi S, Mohammadi L, Igwegbe CA, Rahdar S, Banach AM (2018) Application of response surface methodology in the degradation of reactive blue 19 using H<sub>2</sub>O<sub>2</sub>/MgO nanoparticles advanced oxidation process. *Int J Ind Chem* 9(3):241–253
72. Ighalo JO, Adelodun AA, Adeniyi AG, Igwegbe CA (2020) Modelling the effect of sorbate-sorbent interphase on the adsorption of pesticides and herbicides by historical data design. *Iranica J Energy Environ* 11(4):253–259
73. Ekpotu WF, Ighalo JO, Nkundu KB, O. OP, Adeniyi AG (2020) Analysis of factor effects and interactions in a conventional drilling operation by response surface methodology and historical data design. *Petrol Coal* 62(4):1356–1368
74. Cui C, Chen A, Pan Z, Ma R (2019) Two-dimensional numerical model and fast estimation method for calculating crevice corrosion of cross-sea bridges. *Constr Build Mater* 206:683–693
75. Bader A, Hartwich M, Richter A, Meyer B (2018) Numerical and experimental study of heavy oil gasification in an entrained-flow reactor and the impact of the burner concept. *Fuel Process Technol* 169:58–70
76. Babatunde EO, Akolo SA, Ighalo JO, Kovo AS (2019) Response surface optimisation of the adsorption of Cu (II) from aqueous solution by crab shell chitosan. Paper presented at the 3rd international engineering conference, Minna, Nigeria
77. Ghafari S, Aziz HA, Isa MH, Zinatizadeh AA (2009) Application of response surface methodology (RSM) to optimize coagulation-flocculation treatment of leachate using poly-aluminum chloride (PAC) and alum. *J Hazard Mater* 163(2–3):650–656
78. Tan I, Ahmad A, Hameed B (2008) Optimization of preparation conditions for activated carbons from coconut husk using response surface methodology. *Chem Eng J* 137(3):462–470
79. Igwegbe CA, Onukwuli OD, Ighalo JO, Menkiti MC (2021) Bio-coagulation-flocculation (BCF) of municipal solid waste leachate using *Picralima nitida* extract: RSM and ANN modelling. *Curr Res Green Sustain Chem* 4:100078
80. Sudarjanto G, Keller-Lehmann B, Keller J (2006) Optimization of integrated chemical-biological degradation of a reactive azo dye using response surface methodology. *J Hazard Mater* 138(1):160–168
81. Bezerra MA, Santelli RE, Oliveira EP, Villar LS, Escalera LA (2008) Response surface methodology (RSM) as a tool for optimization in analytical chemistry. *Talanta* 76(5):965–977

82. Ighalo JO, Adeniyi AG (2020) Statistical modelling and optimisation of the biosorption of Cd(II) and Pb(II) onto dead biomass of *Pseudomonas aeruginosa*. Chem Prod Process Model 16(1):20190139
83. Adeniyi AG, Ighalo JO, Otoikhian KS (2019) Steam reforming of acetic acid: response surface modelling and study of factor interactions. Chem Prod Process Model 14(4):1–14
84. Adeniyi AG, Igwegbe CA, Ighalo JO (2021) ANN modelling of the adsorption of herbicides and pesticides based on sorbate-sorbent interphase. Chem Africa:1–7
85. Al-Degs YS, El-Barghouthi MI, Khraisheh MA, Ahmad MN, Allen SJ (2005) Effect of surface area, micropores, secondary micropores, and mesopores volumes of activated carbons on reactive dyes adsorption from solution. Sep Sci Technol 39(1):97–111
86. Ighalo JO, Adeniyi AG, Adelodun AA (2021) Recent advances on the adsorption of herbicides and pesticides from polluted waters: performance evaluation via physical attributes. J Ind Eng Chem 93:117–137
87. Asadullah M, Rahman MA, Motin MA, Sultan MB (2006) Preparation and adsorption studies of high specific surface area activated carbons obtained from the chemical activation of jute stick. Adsorpt Sci Technol 24(9):761–770
88. Ip A, Barford J, McKay G (2009) Reactive Black dye adsorption/desorption onto different adsorbents: effect of salt, surface chemistry, pore size and surface area. J Colloid Interface Sci 337(1):32–38
89. Lairini S, El Mahtal K, Miyah Y, Tanji K, Guissi S, Boumchita S, Zerrouq F (2017) The adsorption of crystal violet from aqueous solution by using potato peels (*Solanum tuberosum*): equilibrium and kinetic studies. J Mater Environ Sci 8(9):3252–3261
90. Loulidi I, Boukhelif F, Ouchabi M, Amar A, Jabri M, Kali A, Chraibi S, Hadey C, Aziz F (2020) Adsorption of crystal violet onto an agricultural Waste residue: Kinetics, isotherm, thermodynamics, and mechanism of adsorption. Sci World J
91. Ikenyiri P, Ukpaka C (2016) Overview on the effect of particle size on the performance of wood based adsorbent. J Chem Eng Process Technol 7(1):2
92. Igwegbe C, Umembamalu C, Osuagwu E, Oba S, Emembolu L (2021) Studies on adsorption characteristics of corn cobs activated carbon for the removal of oil and grease from oil refinery desalter effluent in a downflow fixed bed adsorption equipment. Eur J Sustain Dev Res 5(1)
93. Aljeboree AM, Alkaim AF, Al-Dujaili AH (2015) Adsorption isotherm, kinetic modeling and thermodynamics of crystal violet dye on coconut husk-based activated carbon. Desal Water Treatment 53(13):3656–3667
94. Eletta OAA, Adeniyi AG, Ighalo JO, Onifade DV, Ayandele FO (2020) Valorisation of Cocoa (*Theobroma cacao*) pod husk as precursors for the production of adsorbents for water treatment. Environ Technol Rev 9(1):20–36
95. Pimol P, Khanidtha M, Prasert P (2008) Influence of particle size and salinity on adsorption of basic dyes by agricultural waste: dried seagrape (*Caulerpa lentillifera*). J Environ Sci 20(6):760–768
96. Hossain MK, Pervez M, Uddin MJ, Tayyaba S, Mia M, Bashar M, Jewel M, Haque M, Hakim M, Khan MA (2017) Influence of natural dye adsorption on the structural, morphological and optical properties of TiO<sub>2</sub> based photoanode of dye-sensitized solar cell. Mater Sci Poland
97. Hamzezadeh A, Rashtbari Y, Afshin S, Morovati M, Vosoughi M (2020) Application of low-cost material for adsorption of dye from aqueous solution. Int J Environ Anal Chem:1–16
98. Sharma G, Sharma S, Kumar A, Naushad M, Du B, Ahamad T, Ghfar AA, Alqadami AA, Stadler FJ (2019) Honeycomb structured activated carbon synthesized from *Pinus roxburghii* cone as effective bioadsorbent for toxic malachite green dye. J Water Process Eng 32:100931
99. Arora C, Kumara P, Sonia S, Mittal J, Mittal A, Singh C (2020) Efficient removal of malachite green dye from aqueous solution using *Curcuma caesia* based activated carbon. Desal Water Treatment 195:341–352
100. Zhang X, Lin Q, Luo S, Ruan K, Peng K (2018) Preparation of novel oxidized mesoporous carbon with excellent adsorption performance for removal of malachite green and lead ion. Appl Surf Sci 442:322–331

101. Nazifa TH, Habba N, Aris A, Hadibarata T (2018) Adsorption of procion red MX-5B and crystal violet dyes from aqueous solution onto corncob activated carbon. *J Chin Chem Soc* 65(2):259–270
102. Balarak D, Zafariyan M, Igwegbe CA, Onyechi KK, Ighalo JO (2021) Adsorption of acid blue 92 dye from aqueous solutions by single-walled carbon nanotubes: isothermal, kinetic, and thermodynamic studies. *Environ Proc* 8(2):869–888
103. Ighalo JO, Eletta AAO (2020) Response surface modelling of the biosorption of Zn(II) and Pb(II) onto micropogonias undulates scales: Box-Behnken experimental approach. *Appl Water Sci* 10(8):197–209
104. Zhang J, Ou L (2013) Kinetic, isotherm and thermodynamic studies of the adsorption of crystal violet by activated carbon from peanut shells. *Water Sci Technol* 67(4):737–744
105. Hassan A, Abdel-Mohsen A, Fouda MM (2014) Comparative study of calcium alginate, activated carbon, and their composite beads on methylene blue adsorption. *Carbohydr Polym* 102:192–198
106. Azaman SH, Afandi A, Hameed B, Din AM (2018) Removal of malachite green from aqueous phase using coconut shell activated carbon: adsorption, desorption, and reusability studies. *J Appl Sci Eng* 21(3):317–330
107. Altıntig E, Onaran M, Sarı A, Altundag H, Tuzen M (2018) Preparation, characterization and evaluation of bio-based magnetic activated carbon for effective adsorption of malachite green from aqueous solution. *Mater Chem Phys* 220:313–321
108. Datta D, Kerkez Kuyumcu Ö, Bayazit ŞS, Abdel Salam M (2017) Adsorptive removal of malachite green and Rhodamine B dyes on Fe<sub>3</sub>O<sub>4</sub>/activated carbon composite. *J Dispersion Sci Technol* 38(11):1556–1562
109. Pinheiro D, Devi KS, Jose A, Bharadwaj NR, Thomas K (2020) Effect of surface charge and other critical parameters on the adsorption of dyes on SLS coated ZnO nanoparticles and optimization using response surface methodology. *J Environ Chem Eng* 8(4):103987
110. Baytar O, Şahin Ö, Horoz S, Kutluay S (2020) High-performance gas-phase adsorption of benzene and toluene on activated carbon: response surface optimization, reusability, equilibrium, kinetic, and competitive adsorption studies. *Environ Sci Poll Res* 27(21):26191–26210
111. Fito J, Abraham S, Angassa K (2020) Adsorption of methylene blue from textile industrial wastewater onto activated carbon of parthenium hysterophorus. *Int J Environ Res* 14(5):501–511
112. Selvam K, Sudhakar C, Selvankumar T (2021) Activated carbon derived from Borassus flabellifer fruit husk waste for enhanced removal of reactive red 120. *Environ Technol Innov* 23:101752
113. Li L, Wu M, Song C, Liu L, Gong W, Ding Y, Yao J (2021) Efficient removal of cationic dyes via activated carbon with ultrahigh specific surface derived from vinasse wastes. *Biores Technol* 322:124540
114. Jawad AH, Abdulhameed AS (2020) Statistical modeling of methylene blue dye adsorption by high surface area mesoporous activated carbon from bamboo chip using KOH-assisted thermal activation. *Energy, Ecol Environ* 5(6):456–469
115. Sun Z, Qu K, Cheng Y, You Y, Huang Z, Umar A, Ibrahim YS, Algadi H, Castañeda L, Colorado HA (2021) Corn-cob-derived activated carbon for efficiently adsorption dye in sewage. *ES Food & Agroforestry* 4:61–73
116. Ahmad MA, Eusoff MA, Oladoye PO, Adegoke KA, Bello OS (2020) Statistical optimization of Remazol Brilliant Blue R dye adsorption onto activated carbon prepared from pomegranate fruit peel. *Chemical Data Collections* 28:100426
117. Azam K, Raza R, Shezad N, Shabir M, Yang W, Ahmad N, Shafiq I, Akhter P, Razzaq A, Hussain M (2020) Development of recoverable magnetic mesoporous carbon adsorbent for removal of methyl blue and methyl orange from wastewater. *J Environ ChemEng* 8(5):104220



# Chapter 22

## Biochar: Porous Carbon Material, Its Role to Maintain Sustainable Environment



Debomita Dey, Debalin Sarangi, and Prithusayak Mondal

### 1 Introduction

Biochar is a fine-textured carbonization product with a considerably high amount of organic C and low susceptibility to quick deterioration. It is made by pyrolyzing biomass and biodegradable waste [1]. Adding charcoal to the soil to improve soil quality has been a practice in agriculture for thousands of years [2]. The Amazon Basin's native pre-Columbian civilizations boosted soil fertility by combining burned organic and inorganic waste remnants with the soils. These soils are called in Portuguese as "Terra Preta de Indio" (Indian black earth) due to having dark hue and origins. They are rich in organic matter and nutrients. However, at present years, the applications of biochar in agriculture are being studied extensively by the researchers worldwide. Biochar's applications are expanding all the time, mostly in industries, agricultural purposes, and activities involving the environment (Fig. 1). Biochar can be utilized as a soil amendment, often used for fodders and silages, or used in water treatment [3]. It can be used to immobilize pollutants in soil and in sewage treatment, in addition to complement composting and methane fermentation processes [4, 5].

In this chapter, different biochar manufacturing technologies, their physical characteristics, and biochemical features for attaining environmental sustainability have been explored.

---

D. Dey

Department of Agricultural Chemistry and Soil Science, Faculty of Agriculture, Bidhan Chandra Krishi Viswavidyalaya, Mohanpur, Nadia, West Bengal 741252, India

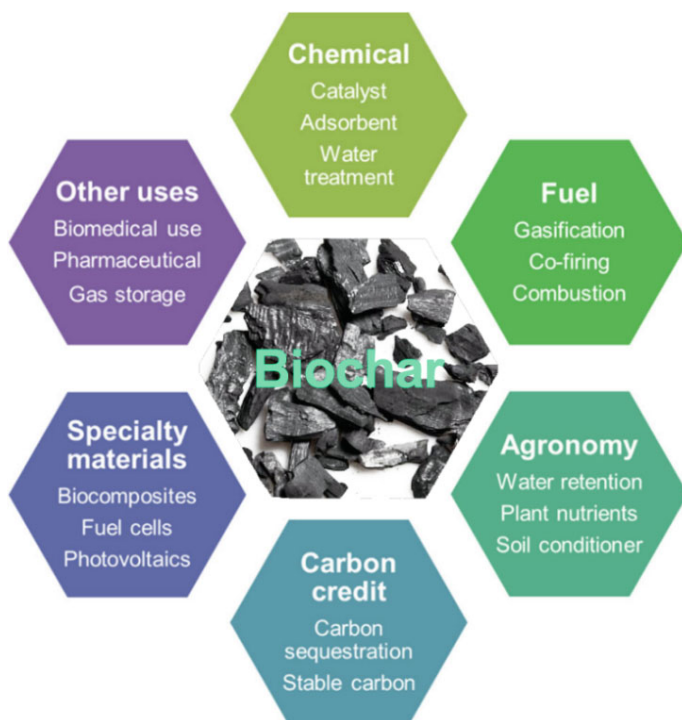
D. Sarangi

Department of Agronomy and Plant Genetics, University of Minnesota, St. Paul, MN 55108, USA

P. Mondal (✉)

Regional Research Station (Terai Zone), Uttar Banga Krishi Viswavidyalaya, Pundibari, Cooch Behar, West Bengal 736165, India

e-mail: [prithusayak@gmail.com](mailto:prithusayak@gmail.com)



**Fig. 1** Biochar and its multifarious applications (Adapted and redrawn from Nanda et al. [6]. Copyright© 2015, Springer Nature)

## 2 Biochar: Preparation and Characterization

Biochar is a C-rich, porous organic product prepared by heating carbon-rich materials or biomass such as manures, wood, leaves, or other agricultural residuals in a confined container with limited or no aeration [7]. It aids in the promotion of physical, chemical, and biological features of soil through enhancing soil carbon status [8, 9] and works as a climate change corrective tool by lowering harmful gas emissions from the ecosystem [10, 11].

Biochar can be prepared from an ample range of biomass feedstock like organic and agricultural waste (green yard waste, animal manure), bioenergy crops, forest residues, kitchen waste and sewage sludge, etc. Carbonizing biomass through pyrolysis may be done by heating those at a higher temperature (ranging between 350 and 700 °C) with little or no oxygen resulting in the fervent decomposition of lignocellulosic biomass preparing syngas, bio-oil and biochar [12]. Various methods used for biochar production are described in Fig. 2.

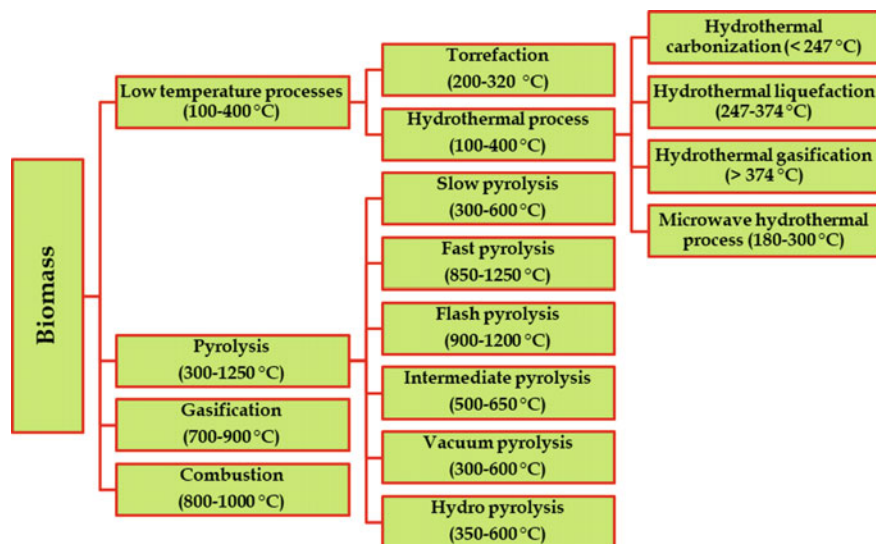
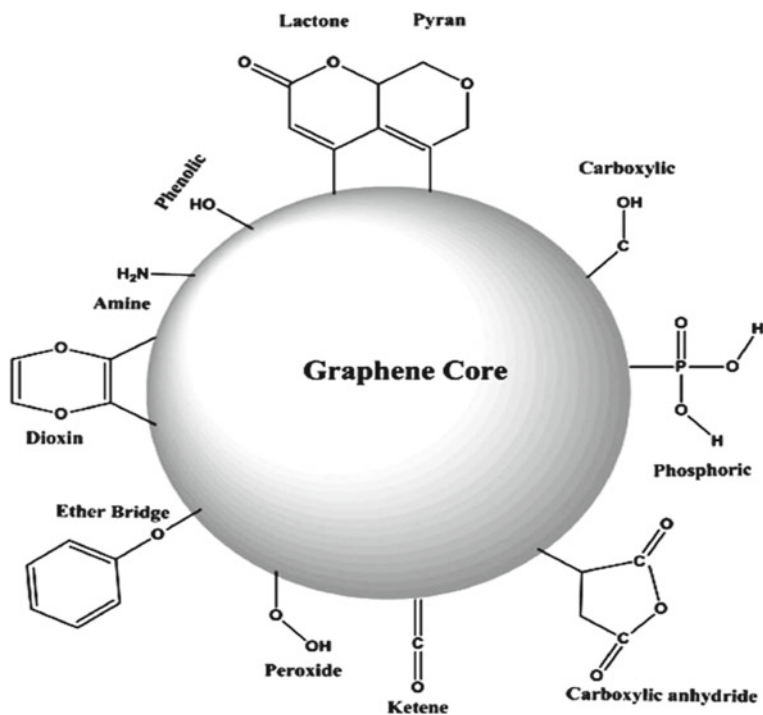


Fig. 2 Various thermochemical conversion technologies for the generation of biochar [13]

The quality and features of biochar are influenced by the feedstock materials used and the processing situations. Various morphological, spectral and physico-chemical properties of biochar are also affected by the charring temperature, residence time, and heating rate [14, 15]. The fundamental structural unit of biochar is amorphous and graphene carbon (Fig. 3). The crystalline form of biochar changes as the pyrolysis temperature changes. With rise in the pyrolysis temperature, the carbon skeleton changes from amorphous to aromatic, resulting in the amalgamation of different graphene sheets. Biochar's vesicular structure contributes to its high porosity, whereas pyrolysis induces the development of nanopores with a large surface area that can retain water and soil nutrients [16, 17].

Biochar, having porous graphene-like structure (Fig. 3), caters a good surface for pollutants to attach to, reducing their availability to other environmental components [20]. The fundamental mechanisms involved in the adsorption procedures are adsorption on surface (adhesion of contaminants on surfaces) at greater temperatures with carbonized structures and division of contaminant molecules in biochar micropores at lesser temperatures with few-carbonized structures, according to numerous studies of various isotherms and kinetics related to sorption on biochar sorption [4].

The pH ranges from neutral to alkaline when biochar is prepared at temperatures above 500 °C. While raising the pyrolysis temperature ranging between 400 and 600 °C, the volatile and nitrogen components of biochar dropped off, whereas the ash and fixed carbon content increased. The elemental ratios (H/C and O/C) are applied to ascertain the aromaticity degree of carbon structures [21]. Biochars made at 500 °C or lower temperature have H/C ratios of > 0.5, whereas those prepared at >



**Fig. 3** Biochar structure with distinct functional groups on its surface (Recreated from Brennan et al. [18] and Lehmann and Joseph [19])

500 °C temperatures have H/C ratios of 0.5, with less H/C ratios indicating a higher degree of aromaticity [22].

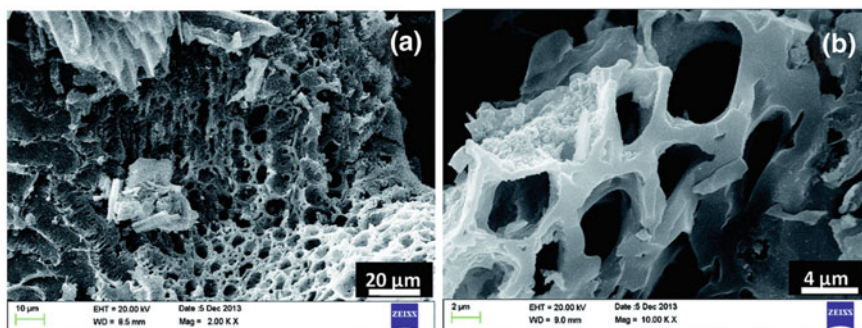
### 3 Biochar as Soil Amendment

Soil health is denoted as an ability of living soil to perform within natural or controlled ecosystem bounds, sustaining biotic communities and improving their health and productivity, maintaining or improving air and water quality. From an agricultural perspective, the receptivity of soil to maintain and boost the advancement of plants and animals along with enhancing the quality of the environment is known as soil health [23]. Depletion of soil organic matter results in severe soil deterioration including erosion, desertification, salinization, deficiency of nutrients, and most importantly reduction in soil fertility. It also hampers the soil quality, soil stability, and soil resilience. Therefore, the application of organic amendments especially stable carbon product like biochar into the soil seems to be very worthy to improve the quality of soil functions.

### 3.1 Effects on Different Physical Properties of Soil

Surface area, aggregation, porosity, water holding capacity, and aeration are all essential factors in soil fertility, which includes nutrient transformation and microbial activity [24, 25]. Biochar addition to soil helps to modify such physicochemical properties especially of degraded or nutrient-deficit soils as a soil amendment. Soil surface area has been observed to be enhanced up to 4.8 times compared to unamended soil [26]. Besides, in a long-term incubation experiment, upto 18% enhancement in surface area was recorded in clayey soil mixed with hardwood biochar @ 20 g kg<sup>-1</sup> [27]. Additionally, treatment with biochar to infertile soil helps to modify the porosity because of its porous nature [28]. The co-application of biochar, soil organic matter, and clay was reported to improve soil porosity leading to the development of higher micro-aggregates over time [29]. Thus, higher water or moisture retention occurs in biochar added soil as a function of biochars' higher porosity and surface area (Fig. 4).

Addition of biochar to barren soil has been demonstrated in several experiments to lower bulk density of soil, increase total pore volume, and increase water retention capacity [31, 32]. Gwenzi et al. [33] found that using biochar with a lower bulk density and higher stable organic carbon, they were able to reduce bulk density of soil and penetration resistance while enhancing overall soil porosity. Similarly, almost 17% and 20% decrement in bulk density of sandy and clay soil, respectively, was also observed in a column experiment designed by Barnes et al. [34]. Furthermore, in a 2-year research on rice field, biochar treatment reduced bulk density of soil in both successive rice growth cycles [35]. In a greenhouse study in Spain, Albuquerque et al. [36] found that applying biochar to sunflower at 150 and 225 Mg ha<sup>-1</sup> reduced bulk density of soil and enhanced field capacity, which had a favorable impact on plant growth and water economy. However, the influence of biochar addition to soil on soil hydrological parameters (such as moisture content, water holding capacity, hydraulic conductivity, water infiltration rate, and water retention) was significant [34, 37]. Laird et al. [27] conducted a long-term column incubation experiment and suggested



**Fig. 4** Porous structure of rice husk biochar as seen under scanning electron microscope at **a** 2 KX and **b** 10 KX magnification level (Adapted from Mohan et al. [30])

that, compared to unamended control soil, up to 15% higher water retention and soil water potentials were observed in hardwood biochar treated soil. In a field study in Finland, 11% greater water holding capacity was shown in Birch (*Betula* spp.) biochar amended silt loam soil than the control (17). In addition, adding Black locust (*Robinia pseudoacacia*) biochar to sandy soil has been observed to significantly enhance water holding capacity (97%) and saturated water content (56%), as well as decreasing hydraulic conductivity as moisture content rises [38]. In a column study, however, it was discovered that adding biochar to mesquite wood (*Prosopis* sp.) significantly reduced hydraulic conductivity in sandy soil and also reduced organic carbon significantly in organic soil, but increased hydraulic conductivity in clay-rich soil (328%) [34]. Brantley et al. [37], on the other hand, claimed that all biochars were not same in modifying soil moisture retention at varied rates of application over a wide variety of soil water conditions. Varying results in various studies were observed due to various soil types as well as different biochar production conditions and also it depends on biochar grain size, different rat of application, soil properties.

### 3.2 Effects on Soil Chemical Characteristics

Biochar has positive impacts in modifying the chemical characteristics of soils. Several soil quality indices, including soil pH, exchangeable cations, organic carbon, fertilizer usage efficiency, soil tensile strength, and others, have been shown to be significantly modified by the addition of biochar to the soil in several studies [16, 39]. In Ferro soil, the paper-mill biochar addition ( $10 \text{ t ha}^{-1}$ ) was shown to considerably improve soil pH, exchangeable Ca, CEC, and total C while reducing exchangeable Al, while in Calcarosol, the same biochar application to soil resulted in an enhancement in C and exchangeable K [40]. Enhancement in soil pH and Ca levels and reduction in Al toxicity were reported due to high-pH biochar addition to red ferralitic soils [16, 41]. A test conducted by Granatstein et al. [42] showed different impacts of various types of biochar application on soil pH. They observed that adding biochar ( $39 \text{ t ha}^{-1}$ ) made from herbaceous feedstocks to a sandy soil raised the pH from 7.1 to 8.1, whereas, application of biochars derived from woody feedstock showed a lower overall increment in soil pH when applied to silt loam soil probably due to higher initial CEC and higher buffering capacity. Contrastingly, a significant reduction in salt content by  $3.6 \text{ g kg}^{-1}$  associated with an increment of soil pH, soil bulk density, SOC, and available P by 0.3,  $0.1 \text{ g cm}^{-3}$ ,  $2.6 \text{ g kg}^{-1}$ , and  $27 \text{ mg kg}^{-1}$ , respectively, was observed owing to the joint application of biochar and poultry manure in saline soil [43]. A high negative charge is implied to aged biochar particles promoting soil aggregation as well as improves nutrient availability to plants [44]. Moreover, the use of bagasse biochar was observed to improve the soil's CEC, AEC, and nutrient retention capacity [45]. Contrastingly, no significant change in soil CEC was also documented after biochar application in soil [42]. Various functional groups (siloxane, OH, C=O, COOH, N) present on biochar surface are mainly responsible for converting the real CEC of biochar, and it largely relies on the pyrolysis temperature and the biochar

feedstock. Moreover, sorption capacity, water holding capacity (WHC), and microbial habitat are widely effected by the specific surface area of applied biochar. The composition and structure of biochar are followed by the biomass type and pyrolysis condition, resulting in significant variation in biochar characteristics correlated with the variation in the nutrient availability in soil.

### 3.3 Soil Biological Properties

Various types of microorganism such as bacteria, fungi, nematodes, virus, protozoa with their varied inhabitants live in soil. Their presence and abundance in soil depend on soil type, management factors especially related to addition of different organic amendments to soil [46]. Several researches have found that biochar application has positive impacts on soil microbial activity [47–49]. The wide surface area of biochar and capacity to absorb nutrients create a benign environment for microorganisms (bacteria, mycorrhizae, and actinomycetes) to colonize, thrive, and reproduce [50]. The improvement in bulk density, pH, nutrient and water retention owing to the addition of biochar helps to enhance and modify the composition of microbial community and their activities [49, 51]. Besides, slow pyrolysis biochars (500 °C) obtained from swine manure, fruit peels, and reed grass (*Phragmites australis*) showed a significantly positive correlation of bacteria-to-fungi ratio with soil C/N ratio, when applied to sandy loam soils [52]. Biochar addition, on the other hand, has been shown to have deleterious impacts on soil microorganisms because of the release of bio-oils and re-condensed organic molecules that are unsuitable for the microorganisms [53].

Incorporation of biochar into soil can have positive [54, 55], negative [56, 57], or no effect [58, 59] on microbial activities depending on type and rate of biochar addition, soil type, pyrolysis condition. The addition of biochar to a variety of applications from resulted in a linear enhancement in microbial activity [41]. Similarly, the incorporation of willow wood biochar (prepared at 700 °C) into sandy loam soil was reported to increase microbial biomass carbon by 29% [54]. Some other studies have also suggested that a few slow pyrolysis biochars generated at lower temperatures, from diverse feedstocks having lower lignocellulosic contents have promoted microbial biomass when applied to soil [57, 60]. On the other hand, treatment with Eucalyptus biochar (produced at 600 °C) in coarse textured sandy soil significantly reduced microbial biomass carbon by 28% [61]. Moreover, biochar addition has also positive impact on N<sub>2</sub>-fixing bacteria (diazotrophs). Various studies have reported that biochar addition showed a significant enhancement in biological nitrogen fixation by legumes [59, 62]. Increasing trend in N<sub>2</sub> fixation was observed with increasing rates (0, 30, 60, and 90 kg ha<sup>-1</sup>) of biochar application, which also enhanced yield of beans by 30–40% [63]. However, a significant reduction in the abundance of arbuscular mycorrhizal fungi (AMF) by 58% and 73% was observed due to the use of 2% (w/w) and 4% (w/w) pine biochar, respectively, also reducing soil P availability by 28% and 34%, respectively [64]. Similarly, 163% and 208% increment in P availability, while 43% and 77% decrement in AMF abundance were reported due to the

addition of mango wood biochar with 23.2 and 116.1 t C ha<sup>-1</sup> rate, respectively [64]. Therefore, the conflict nature of biochar application on soil microbial activity relies on the type and characteristics of biochar, type of soil and the production condition of biochar.

### ***3.4 Soil Nutrient Retention***

Due to its porous structure and increased surface area of biochar, it can retain and absorb nutrients while also improving soil fertility. Several studies mentioned the positive effects of biochar addition including enhanced CEC, microbial activities, liming as well as reduced nutrient leaching [47, 62, 65]. Biochars have been shown to have a brief and/or long-term impact on soil nutrient availability and recycling, particularly in soils with low fertility and exchange capabilities [66–68]. The type and quality of feedstock and rate of biochar addition largely influence the amount of nutrient uptake by crop plants and biomass production [65]. In this aspect, biochar may act as an organic fertilizer by directly attributing to soil fertility through supplying nutrients to plants or indirectly by modifying soil health and quality through enhancing fertilizer use efficiency [65, 69]. The basic chemical structure of biochars differs from other organic materials due to the presence of greater amount of aromatic carbon, especially fused aromatic C rings [47], which makes biochar highly stable in nature. High pyrolysis temperature biochars generally show greater C/N ratio that leads N deficiency in plants resulting in lower crop yields [65]. Besides, biochar application into soil can influence soil pH and electrical conductivity (EC) that also affect the availability of plant nutrients [62, 70]. The overall impacts of biochar on soil nutrient transformation and availability is discussed in Table 1.

### ***3.5 Effect on Biotic and Abiotic Stresses***

Allen [79] revealed for the first time that biochar application reduced the effects of numerous plant diseases like rust and mildew. Both soil-borne and foliar pathogens contribute to the formation of pathosystems in plants [80]. Bonanomi et al. [81] carried out an experiment for testing the impact of biochar on plant disease in 13 distinct pathosystems, and the results were reviewed and summarized. They estimated that biochar had an 85% beneficial influence in reducing the disease severity of plants, a 12% neutral impact, and a 3% negative impact by generating plant diseases. Furthermore, the influence of varying rates of biochar addition on disease suppression and severity was investigated in 30 different pathosystems with 15 pathogens to compare the impacts of various levels of biochar with the unaffected control [82]. In the case of the highest degree of biochar addition, it had no detrimental impacts on plant diseases compared to the unaffected control. Contrastingly, several other



**Table 1** Impact of different biochars on soil nutrient transformation

Source of biochar	Effect on soil nutrient transformation	References
Brazilian pepperwood biochar	Significant reduction in entire amount of $\text{NH}_4^+$ , $\text{NO}_3^-$ , and $\text{PO}_4^{3-}$ in the leachates by 34.7%, 34%, and 20.6%, respectively than the unamended control	[71]
Peanut hull biochar	Leaching reduction of $\text{NH}_4^+$ -N and $\text{NO}_3^-$ -N by 14% and 34% than control, respectively	[72]
Willow and acacia derived biochars and their co-composted mixture	Significant decrementing leaching of nitrate, nitrogen, phosphorus, potassium, calcium, magnesium, and sodium	[73]
Biochar derived from various wood species	Leaching reduction of N, P, Mg, and Ca	[74]
Eucalyptus biochar	Decreased leaching of ammonium and nitrate by 20% and 25%, respectively	[61]
Biochar derived from various tree residues	Significantly enhanced net nitrification rates, adsorption of ammonia, and promoted mineralization and immobilization of nitrogen	[75]
Biochar derived from tree residue (green waste)	Reduced application rates of N on wheat and radish biomass and enhanced uptake of nitrogen by decreasing addition of nitrogenous fertilizer up to 90%	[40]
Bamboo biochar ( <i>Bambuseae</i> spp.)	Enhanced N retention	[76]
Biochar (charcoal and smoke condensates)	Significant enhancement in retention and uptake of nitrogen by adsorbing ammonia and thus minimizing loss of nitrogen by means of volatilization	[77]
Wheat straw biochar	Significantly enhanced agronomic N use efficiency as well as maize yield with enhancing rates of biochar	[78]

reports showed the significant inhibition of diseases due to the low levels of biochar addition ( $\leq 1\%$ ) in detached growing media, while higher rates of biochar addition (3%) showed no significant effect on plant diseases [80, 83, 84].

Biochar addition has been shown in multiple studies to improve agricultural production under normal situations while also modifying crop productivity in adverse situations like drought, salinity, and sodicity [85, 86]. The permanent wilting point (PWP) of biochar enriched soil was improved, whereas the amount of water retained at field capacity (FC) was modified to a greater extent than the water retained at PWP, resulting in rise in the amount of plant accessible water [32]. Furthermore,

another *in vivo* (pot and field) experiment confirmed that application of biochar at rates of 10–20 t ha<sup>-1</sup> modified the advancement of seedling and wheat and soybean yield, most likely by reclaiming the water deficiency stress [87]. Furthermore, the use of biochar in less fertile sandy soils enhanced plant development by altering the soil–plant–water relationship under drought conditions [85].

#### 4 Impact of Biochar Addition on Yield of Different Crops

Numerous studies reported that applying biochar into soil could enhance plant growth and output by improving the availability of plant nutrients, improving soil microbial activity and fertilizer usage efficiency, and decreasing exchangeable Al<sup>3+</sup> [88–90]. Biochar has been observed to greatly boost crop growth, root biomass, and yield when applied to soil [73]. Crop output was improved by altering soil pH, CEC, and WHC, boosting nutrient availability and uptake, and directly providing nutrients to crop plants as a result of biochar addition [10, 73]. Biochar application into soil has been observed to have both beneficial [31, 91] and negative [92] effects on crop yield for a variety of crops (Table 2). Positive impacts on crop yield due to different rates of biochar addition were attributed to higher pH and greater availability of macro and micronutrients, as well as higher modification in different soil properties [32, 41], while negative effects on crop yield were attributed to the modifications in soil properties and pH initiated deficiency of micronutrients due to biochar additions [73, 93]. One of the major reasons for reducing crop yields were observed to be the nitrogen deficiency which resulted due to immobilization by microorganisms because of the application of biochars having higher C:N ratio and produced at high temperature [94]. The impact of biochar on crop output is mostly determined by parameters such as soil pH, type of soil, fertilizer rate, biochar feedstock type, rate of application, and crop species [10]. Crop yields have been reported to benefit from improved soil characteristics and water usage efficiency as a result of biochar addition. Several studies, on the other hand, have suggested that applying biochar into nutrient-rich soils has minimal effect on grain yields, if any at all [92, 95]. Most of these studies available till now are basically based on short-term experiments. Therefore, more long-term experiments are required to evaluate the effects of biochar addition on crop yield.

#### 5 Biochar and the Environment

As a soil amendment, biochar can satisfy following targets: achieving food security by enhancing crop productivity, promoting soil health and quality by modifying soil properties and avoiding land deterioration, beside of reducing the climate change by reducing greenhouse gas emission and adsorbing hazardous elements onto its surface.

**Table 2** Impact of different rates of various biochar application on crop yield

Biochar source	Biochar application rate	Crop type	Crop response	References
Wheat straw biochar	0–40 t ha <sup>-1</sup>	Maize	At 20 t ha <sup>-1</sup> and 40 t ha <sup>-1</sup> , maize yields were enhanced by 15.8% and 7.3%, respectively, without addition of N-fertilizers and by 8.8% and 12.1%, respectively, with addition of N-fertilizers	[78]
Mango wood biochar; corn stover biochar	0–16 t ha <sup>-1</sup> ; 2–91 t ha <sup>-1</sup>	Maize	Enhanced biomass (30–43%) and increased (22%) crop yield through modification in different soil physical properties and nutrient availability	[96, 97]
Acacia bark biochar	10 L m <sup>-2</sup>	Maize and peanut	Yields of maize and peanut were increased almost two-fold because of greater availability of nitrogen and bases and lower availability of Al	[98]
Teak and rose wood biochars	4–16 t ha <sup>-1</sup>	Rice and sorghum	Significant enhancement in plant growth and yield were observed	[41, 99]
Paper-mill biochar	10 t ha <sup>-1</sup>	Wheat and radish	Enhanced (around 250%) biomass modifying fertilizer use efficiency in Ferrosol, while decreased biomass in Calcarosol	[40]
Wood biochar and cow manure biochar	0–20 t ha <sup>-1</sup>	Maize	Yield increment from 14 to 150% by improving soil quality parameters and reducing exchangeable acidity	[38]

(continued)

**Table 2** (continued)

Biochar source	Biochar application rate	Crop type	Crop response	References
Green waste and poultry litter biochar	0–100 t ha <sup>-1</sup>	Radish	42–96% increment in yield because of improved soil physicochemical properties due to biochar addition	[39]
Waste water sludge biochar	10 t ha <sup>-1</sup>	Cherry and tomato	64% higher yield in biochar treated field than control because of higher NP availability	[100]
Oil palm fruit bunch biochar	0–40 t ha <sup>-1</sup>	Rice	Grain yield was enhanced by 141–472% than control	[101]
Maize straw biochar	20–40 t ha <sup>-1</sup>	Choy sum and amaranth	28–48% increment in yield	[102]

The alteration of terra-preta soil into highly fertile soil as an outcome of biochar application is a fine example of biochar's involvement in soil and environmental sustainability.

### 5.1 Biochar and Carbon Sequestration

Generally, soil has a large capacity to stock C as high as 95% of total stock of C on land. For mitigating the current higher CO<sub>2</sub> emission inducing global climate change, the long-term sequestration of terrestrial C is now considered as a beneficial way as more than 2.5 times greater carbon is held by terrestrial resources than atmosphere [103]. Different geo- and eco-engineering approaches have been suggested for enhancing terrestrial C pool such as no or zero-tillage or geological carbon sequestration, biochar sequestration, of which biochar sequestration to soil has been considered as an unique and potent way to create a long-term significant sink for conserving atmospheric CO<sub>2</sub> in terrestrial ecosystem due to its greater recalcitrance nature (fused ring aromatic structure including amorphous carbon) against microbial attacks as well as subsequent modification of soil environment [104, 105]. Almost about 50% of the initial C is sequestered due to the conversion of biomass C to biochar while only 3% and < 10–20% (after 5–10 years) of initial C is left after burning and decomposition, respectively. It suggests more C stabilizing potential of biochar production than burning or direct land application of biomass [106].

According to a report given by Woolf [107], if all the excess crop residues worldwide can be transformed into biochar, almost 1 GT of C can be sequestered into soil which can be very beneficial to mitigate the climate change. By 2050, biochar processing is expected to store around 2.2 GT C yearly over the world [1]. Different indices have been in use to determine the stability and lability of biochar, such as the recalcitrance index [108], representing the thermal stability of biochar, and the stable organic matter yield index [109], which decreases as the pyrolysis temperature rises. Biochar addition to soil can play a significant role in C sequestration due to its slow degradation and mineralization, as well as its millennial-scale residence period [90]. Biochar application into soil has also been reported to be more long-lived (> 100 years) than the application of ash and charcoal into soil (< 100 years) [110]. The stability of biochar is influenced by a number of parameters, including soil clay concentration, pyrolysis temperature, O:C ratio, H:C ratio, volatile matter content, and so on [111, 112]. Biochar with high volatile matter had lower C sequestration capacity, whereas biochar with moderate volatile matter and high O/C (> 0.2) and H/C (> 0.4) ratios had moderate sequestration potential; however, biochar with lower volatile matter (< 80%) and lower O/C and H/C ratios had greater C sequestration potential [113]. On a global scale of removal of C from atmosphere, biochar-bioenergy can play a critical role to inhibit the erratic climate change. This helps to capture and store C from atmosphere at lower prices where biochar application significantly enhances the crop yield. Biochar has been claimed to be capable of sequestering nearly 62–66% of CO<sub>2</sub> emissions [114]. The release of CO<sub>2</sub>, methane, and nitrous oxide from soil can be reduced nearly by 12%, with a total net release of 130 Pg CO<sub>2</sub>-C equivalent over a century, which could be an important sink of carbon [115].

## ***5.2 Biochar and Greenhouse Gas Emissions***

Agricultural systems are frequently regarded one of the primary sources of greenhouse gas (GHG) emissions worldwide, accounting for roughly 10–12% of global anthropogenic releases each year, with forestry and land use sectors accounting for over 24% [116, 117]. Agriculture accounts for almost a fifth of global greenhouse gas emissions, according to a report released by FAO [118]. Adaptation of modern advanced technologies is enhancing the productivity as well as the farmers' income but subsequently contributing negative effects on the climate and environment. Aside from CO<sub>2</sub>, other greenhouse gases such as methane and nitrous oxide have become a significant environmental issue. Studies showed that the agricultural soils contribute 12% in the total CH<sub>4</sub> emissions globally, mostly from paddy field whereas, N<sub>2</sub>O is produced through denitrification. Therefore, proper management of crop residues would help to slow down the emissions of GHGs. In this regard, biochar soil amelioration has been shown to be efficient in reducing GHG emissions while simultaneously enhancing agricultural productivity and generating carbon-negative biofuels based on feedstock requiring less fertilizer and water on a wide scale. However, biochar

amelioration to soil has been observed to reduce the emissions of  $\text{N}_2\text{O}$  and  $\text{CH}_4$  [119, 120]. Besides, co-composted biochar has also been reported to decrease  $\text{N}_2\text{O}$  release from soil through altering several enzyme activities (such as nosZ, nirK, and nirS) as well as effecting the activities of nitrifiers and denitrifiers in soil [121]. The mechanisms related to biochar application and GHGs emissions still cannot convincingly describe why biochar sometimes reduces GHGs emission or increases in some cases. Different methods of GHGs release like, C mineralization, denitrification, methane oxidation have been reported to show various impacts in biochar amended systems [47, 122]. Application of biochar into soil reduces the emission of  $\text{CH}_4$  by suppressing the oxidation of ambient  $\text{CH}_4$  depending upon soil type, the properties of biochar and environmental condition. On the other hand, the impact of biochar on nitrogen transformation process is still fuzzy. Compared with other fresh organic materials, biochar application helps to reduce  $\text{N}_2\text{O}$  emission as well as  $\text{NH}_4^+$  leaching from soil. Apart from that, biochar also reduces the emission of  $\text{N}_2\text{O}$  even under reduced conditions of paddy fields because of the oxidative reactions which occurs on the biochar surfaces with aging [123]. It was suggested that biochar addition at the rate 20 and 40  $\text{Mg ha}^{-1}$  could reduce the total release of  $\text{N}_2\text{O}$  by 10.7–41.8%, respectively [78]. Furthermore, soil  $\text{N}_2\text{O}$  fluxes have also been reported to be decreased up to 79% in biochar treated soil [124]. Therefore, addition of crop-residue-based biochar to soil in lieu of sole residue application into soil would be more beneficial as biochar amelioration helps to improve soil health and nutrient status simultaneously reduces the release of GHGs to a large extent especially from paddy fields [125]. However, GHGs emission from biochar treated soil depends on type of crops. Lower emission of GHGs with less intensity was observed due to addition of wheat straw biochar from wheat crop than the rice crop [125]. Now-a-days, in several studies various impacts regarding biochar application, GHGs emissions, and climatic conditions have been reported with contrasting results. To overcome such possible limits for sustainable agriculture, it is critical to investigate the inter-connections among crop-specific, biochar-origin-specific, and characteristics-specific aspects.

### **5.3 Biochar to Reduce Nutrient Pollution**

Higher and incessant application of inorganic fertilizers into soil results in higher release of readily available nutrient elements in soil that cannot be taken up by plants resulting in leaching of excess nutrients that causes nutrient pollution both in soil and water. Biochar with recalcitrant nature, higher surface area and porous structure retain nutrients like nitrate, ammonium, phosphates and reduces their leaching into groundwater. Amelioration with biochar is observed to reduce nitrogen leaching into groundwater as well as to decrease the requirement of fertilizers which are the basic source of excess readily available nitrogen [126]. The pyrolysis of animal manures can result in a significant reduction in the mobility of phosphorus in animal manures. This technique will help in converting the bulk amount of the organic wastes containing soluble inorganic phosphate into the adsorbed phosphate in biochar. It is

also evident that biochar prepared from poultry litter and pine chips through pyrolysis at 700 °C ensued reduction in *Escherichia coli* transport. Biochar and biochar-compost combination treatments were found to reduce cumulative leaching of several nutrient elements by increasing soil water conservation and reducing the volume of leachates [73].

#### 5.4 Biochar as Adsorbent Material

Biochar can stabilize many organic pollutants through adsorption, absorption, chemisorption to reduce their harmful effect on environment because of structural and surface characteristics (broader surface and presence of various functional groups [5]). Chemical adsorption, technically called as chemisorption, is a technique for determining the quantity of accessible active sites in order to expedite chemical reactions. It happens from the chemical interaction between adsorbate molecules and active sites on a material's surface. High temperature biochars are observed to be more efficient in adsorbing organic and inorganic pollutants (e.g., polyaromatic and polyaliphatic hydrocarbons, heavy metals, and toxic chemicals) from soil, sediments and water environment as compared with low temperature biochars which are more effective in removing heavy metals. As high temperature biochars are basically alkaline in nature, they approach a better way to decontaminate soil pollution. Because of its alkaline nature, biochar helps to raise soil pH, which aids in the immobilization of pollutants by precipitation, coordination by  $\pi$  electrons (C=C), or even electrostatic contact with the carboxyl group of biochar [127]. Furthermore, biochar's higher CEC and lower zeta potential aid in the reduction of toxicity of heavy metals and organic contaminants by building up negative charges on the soil surface through various means such as electrostatic interaction and precipitation for heavy metals and surface adsorption and sequestration for organic pollutants [4, 128]. Biochar's graphene-like architecture, governed by surface functional groups, is thought to help with adsorption and electron transfer from various adsorbates [129]. However, biochars cause the reduction of phytotoxicity of several organic pollutants such as herbicides (acetochlor, atrazine, fluometuron), pesticides (simazine, atrazine, pyrimethanil), fungicides, phenols. Biochar is highly able to immobilize such organic residues due to its higher sorptivity and sequestering nature. Because of having higher surface area, micro-porosity and hydrophobicity, biochars produced at high temperature can stabilize the pollutants by adsorbing and partitioning the pesticides, herbicides and fungicides on carbonized and non-carbonized fractions present in it [130]. Sorption affinity with organic residues is observed to be an unchangeable and it can enhance with reducing solid/solution ratio.

### 5.4.1 Role of Biochar in Adsorption of Heavy Metals from Soil

Materials having the capability of neutralizing the strength of contaminants through reducing their toxicity or bioavailability by lowering mobility are known as adsorbents. Biochars show higher both adsorbing and absorbing capacities due to having greater surface area and different functional groups on its surface which helps it to be a better absorbent by removing various organic and inorganic pollutants and heavy metals from soil and water. Many studies have reported about higher adsorption of heavy metals (such as Cd, Pb, Cu) by the biochar treatment [127, 131]. Besides, biochar-nacomposites (in different proportion of Fe-oxides and biochar) have been observed to effectively remove arsenic (As(V)) from contaminated soil [132]. Biochars made from dairy manure can adsorb lead, but biochar made from *Pinus radiata* has a better sorption and desorption efficiency for a pollutant called phenanthrene from the soil. However, in a Cd-contaminated rice field, application of biochar resulted in a 20–90% drop in Cd concentration in rice grain, most likely due to biochar-influenced pH changes that reduced Cd pool availability [133]. Depending on the composition of the soil, the characteristics of biochar, and the contact period between the soil and biochar, the sorption capacity of soil for hydrophobic organic molecules is increased when it is treated with biochar. Because biochar is naturally occurring, it can also absorb persistent organic pollutants (POPs) and poly aromatic hydrocarbons (PAHs), which have a high affinity for it. Immobilization of Pb, Cu, Zn was observed to be higher by oxidized biochar that is rich in carboxyl groups rather than un-oxidized ones. The enhancement in soil CEC and base saturation due to biochar amelioration helps to furnish liming effect to acidic soils polluted with Al and Fe oxides [134]. Furthermore, multiple studies have indicated a decline in extractable heavy metals such as Cu, Cd, Ni, and Pb from polluted soils when biochar and lignite fly-ash were applied together, most likely due to the increased pH caused by the combined application [20, 135, 136]. However, As biochar surface contains numerous polyaromatic hydrocarbons, it is sometimes thought as a contaminant to the soil. As a result, it must be taken into account before its administration into soil. It has been found that drying biochar before adding it to soil reduces its PAH concentration [137].

### 5.4.2 Role of Biochar in Decontaminating Heavy Metals and Organic Pollutants from Waste Water

As biochar contains several oxygen-holding functional groups such as hydroxyl, phenolic, carboxyl, it plays an important role as sorbent for purifying waste water from heavy metals and other organic contaminants. The mechanism behind this adsorption generally follows pseudo second order reaction. Such adsorption attains maximum at the pH ranging 5.0–6.0 [138]. Some metal cations (like  $Pb^{2+}$ ,  $Cd^{2+}$ ,  $Ni^{2+}$ ,  $Cu^{2+}$ ) have been reported to be removed from waste water by using digested dairy waste biochar and digested sugar beet biochar [139]. The affinity of biochar to carry



away heavy metals from solution can be enhanced by treating the biochar hydrothermally with  $H_2O_2$  as it helps to ensure the oxygen containing functional groups within biochar. Besides, by using chitosan-modified biochar as well as graphene-biochar composite which are safe economic adsorbents can be used to decontaminate waste water from heavy metals by means of surface complexation with  $C=C$ ,  $-OH$ ,  $C=O$  groups [140]. Moreover, some organic residues like salicylic acid and ibuprofen were found to be removed by using fast pyrolysis pine wood biochar. As biochar surface may contain MgO nanoparticle, phosphorus can also be removed from waste water by using it. The majority of the sorbed phosphate can be utilized as slow-release P-fertilizers (due to its bioavailability) or desorbed within 24 h [141].

### ***5.5 Biochar in Reclamation of Problem Soil***

Soil compaction, salinity, sodicity, and acidity are the major environmental factors that largely deplete the soil quality and fertility. Soils greatly affected by compaction, salinization, alkalization, acidification are known as problem soils. These have become major constraints hampering yield and productivity of crops especially in dry (arid and semi-arid) regions. According to the modern concept, application of biochar in soil helps to ameliorate problem soils by improving various physicochemical properties of soil. Co-application of biochar-manure compost along with pyroligneous solution resulted in significantly lower soil pH and salt and sodium concentrations than the unamended control in a salt affected cropland probably because of higher adsorption of  $Na^+$  from soil [43]. Besides, Lashari et al. [142] also observed that the co-application of co-composted manure with crop straw biochar along with pyroligneous solution reduced salinity stress to maize simultaneously enhanced the productivity in salt-stressed soil. However, the positive impact of biochar on physiology, growth, and yield of wheat (pot grown) was reported by Akhtar et al. [143] under salt-stressed condition. They also observed the significant decrement in  $Na^+$  concentration as well as significant increment of  $Ca^{2+}$  and  $Mg^{2+}$  in the leachates in case of biochar treated soil due to the enrichment of  $Ca^{2+}$  and  $Mg^{2+}$  on the exchangeable sites of soil surface through reducing the exchangeable  $Na^+$  in those sites which led to the modification of physical properties in salt-stressed soil. Similarly, biochar amelioration to salt affected soil was also observed to reclaim the salinity stress in potatoes due to higher sodium adsorption capacity of biochar [144]. In a glass house experiment, Thomas et al. [145] observed the reclamation of salt stress and mitigation of salts' effect on plant growth due to salt sorption by biochar derived from lignocellulosic materials. Mechanically, addition of biochar reduces transient Na ions by adsorption and also releases minerals such as K, Ca, Mg into soil solution that help in binding soil particles and improving the stability of soil structure thus ameliorating salt stress. Besides, biochar being alkaline in nature raises the soil pH that reduces the soil acidity promoting overall soil quality.

## 6 Role of Biochar in Sustaining Bioeconomy from Soil to Agricultural Production

In the context of the circular economy, biochar is used for a variety of agricultural and environmental reasons in modern society. Biochar's use as a peat substitute and in composting is promising because it decreases nitrogen losses, speeds up the process, and modifies the quality of final composts. Biochar may be tailored by choosing the suitable feedstock and optimizing the pyrolysis conditions, which improves soil characteristics and increases crop production. Biochar can also be used to partially replace peat, a nonrenewable resource, and increase the compost quality, while reducing the environmental impact [146]. Because biochar may be integrated into standard fertilization processes, particularly in organically managed food production systems, it could be crucial in building a circular economy in agriculture. For starters, biochar could be a long-term solution for managing farm pruning wastes; as for example, fruit orchards undergo severe pruning each year which may pose environmental hazard if not properly disposed of [147]. Pyrolysis is one such waste management technique that permits pruning wastes to be converted into biochar, a desirable soil supplement. The biochar produced could be incorporated into conventional fertilization approaches using manures, composts and anaerobic digestates to minimize the environmental impact, while also increasing the agronomic value of the organic amendments [148].

## 7 Constraints to Biochar Production and Application Technology

Despite the fact that various research have been undertaken with the goal of employing biochar as a possible soil ameliorant and carbon sequestration agent, three important pieces of knowledge are still missing, which is restricting the practical application of biochar as a soil supplement. The following are some of the limitations:

- (a) Higher sorption of water and nutrients on the biochar surface sometimes reduces the availability of plant nutrients causing the reduction in crop yield.
- (b) Highly recalcitrant nature of biochar produced at high temperature results in immobilization of nutrients which make them unavailable to the plants.
- (c) Uncertainty concerning the long-term nature of biochar when used in the field.
- (d) The lack of standardized application rate.
- (e) Slow pyrolysis generates Poly-aromatic hydrocarbons (PAHs) those remain attached to anionic surfaces of biochar, which could have a negative impact on the soil and microbial population, which is one of the primary limits.
- (f) In addition, during pyrolysis, condensed ring structured hazardous organic compounds having low molecular weight such as naphthalene, fluorine, furans,

and others are formed, those pose negative effects on microbial activity in the soil during the early days of application.

- (g) Pesticide and pre-emergent herbicide activity is reduced due to sorption on the surface of biochar.
- (h) Fine ash from biochar could be a source of dust, posing a danger of respiratory disease.
- (i) Mineralization of volatiles or labile fractions has a negative influence on soil microorganisms.
- (j) Increased salinity and phytotoxicity due to biochar application at a higher concentration in the soil.

## 8 Conclusion and Outlooks

Biochar is a promising bioresource for both biomaterial and energy generation, soil refinement, carbon sequestration and pharmaceuticals. Since there are many benefits and challenges associated with different biochars, some key issues must be pondered upon before their commercial adoption. The majority of the research was done in a lab setting and over a short period of time. As a result, long-term biochar field trials are required. The majority of the research was done in tropical areas, although their applications in temperate settings have not been thoroughly investigated. Due to the presence of wide variety of biochars and lack of standardization among the recently available biochars, the application of biochar can be confusing. Therefore, a firm definition and standardization of proper and good biochar, needs to be developed. Thorough trade-off analyses are required to establish the application of proper biochar into proper soil and for proper crops. Future research should be devoted on better understanding of biochar functionality and seeking novel strategies to enhance biochar performance by modifying functional groups. Application of biochar with other substances, such as compost, organic fertilizers, controlled-release fertilizers, zeolite, or beneficial microorganisms, should be explored for soil property enhancement and maximizing crop yields.

## References

1. International Biochar Initiative (IBI) (2015) Retrieved from: [https://www.biochar-international.org/wp-content/uploads/2018/04/IBI\\_Biochar\\_Standards\\_V2.1\\_Final.pdf](https://www.biochar-international.org/wp-content/uploads/2018/04/IBI_Biochar_Standards_V2.1_Final.pdf)
2. Xu G, Lv Y, Sun J, Shao H, Wei L (2012) Recent advances in biochar applications in agricultural soils: benefits and environmental implications. *CLEAN—Soil Air Water* 40:1093–1098
3. Calvelo Pereira R, Muetzel S, Camps Arbestain M, Bishop P, Hina K, Hedley M (2014) Assessment of the influence of biochar on rumen and silage fermentation: a laboratory-scale experiment. *Anim Feed Sci Technol* 196:22–31
4. Tang J, Zhu W, Kookana R, Katayama A (2013) Characteristics of biochar and its application in remediation of contaminated soil. *J Biosci Bioeng* 116:653–659

5. Mohan D, Sarswat A, Ok YS, Pittman CU Jr (2014) Organic and inorganic contaminants removal from water with biochar, a renewable, low cost and sustainable adsorbent—a critical review. *Bioresour Technol* 160:191–202
6. Nanda S, Dalai AK, Berruti F, Kozinski JA (2016) Biochar as an exceptional bioresource for energy, agronomy, carbon sequestration, activated carbon and specialty materials. *Waste Biomass Valor* 7:201–235
7. Wang B, Gao B, Fang J (2017) Recent advances in engineered biochar productions and applications. *Crit Rev Environ Sci Technol* 47:2158–2207
8. Kuzyakov Y, Subbotina I, Chen HQ, Bogomolova I, Xu XL (2009) Black carbon decomposition and incorporation into soil microbial biomass estimated by C-14 labeling. *Soil Biol Biochem* 41:210–219
9. Zimmerman AR (2010) Abiotic and microbial oxidation of laboratory-produced black carbon (biochar). *Environ Sci Technol* 44:1295–1301
10. Jeffery S, Verheijen FGA, van der Velde M, Bastos AC (2011) A quantitative review of the effects of biochar application to soils on crop productivity using meta-analysis. *Agri Ecosyst Environ* 144(1):175–187
11. Case SD, McNamara NP, Reay DS, Whitaker J (2012) The effect of biochar addition on N<sub>2</sub>O and CO<sub>2</sub> emissions from a sandy loam soil—the role of soil aeration. *Soil Biol Biochem* 51:125–134
12. Kammer DM, Lew DJ (2005) Review of technologies for the production and use of biochar. Energy and resources group and Goldman school of public policy. UC Berkeley and NREL
13. Dey D, Mondal P (2020) A comprehensive review on biochar—the black carbon: production technologies, physico-chemical properties and utilization for sustainable environment. *Chem Sci Rev Lett* 9(34):578–594
14. Abdullah H, Mediaswanti KA, Wu H (2010) Biochar as a fuel: 2. Significant differences in fuel quality and ash properties of biochars from various biomass components of Mallee trees. *Energy Fuels* 24:1972–1979
15. Novak J, Cantrell K, Watts D (2013) Compositional and thermal evaluation of lignocellulosic and poultry litter chars via high and low temperature pyrolysis. *BioEnergy Res* 6:114–130
16. Glaser B, Lehmann J, Zech W (2002) Ameliorating physical and chemical properties of highly weathered soils in the tropics with charcoal—a review. *Biol Fertil Soils* 35:219–230
17. Karhu K, Mattila T, Bergstrom I, Regina K (2011) Biochar addition to agricultural soil increased CH<sub>4</sub> uptake and water holding capacity—results from a short-term pilot field study. *Agr Ecosyst Environ* 140:309–313
18. Brennan JK, Bandosz TJ, Thomson KT, Gubbins KE (2001) Water in porous carbons. *Colloids Surf A* 187–188:539–568
19. Lehmann J, Joseph S (2009) Biochar systems. In: Lehmann J, Joseph S (eds) *Biochar for environmental management: science and technology*. Earthscan, London, pp 147–168
20. Masto RE, Ansari MA, George J, Selvi VA, Ram LC (2013) Co-application of biochar and lignite fly ash on soil nutrients and biological parameters at different crop growth stages of *Zea mays*. *Ecol Eng* 58:314–322
21. Krull ES, Baldock JA, Skjemstad JO, Smernik RJ (2009) Characteristics of biochar: organo-chemical properties. In Lehman J, Joseph S (eds) *Biochar for environmental management: science and technology*. Earthscan, London
22. Hammes K, Smernik RJ, Skjemstad JO, Herzog A, Vogt UF, Schimdt MWI (2006) Synthesis and characterization of laboratory-charred grass straw (*Oryza sativa*) and Chestnut Wood (*Castanea sativa*) as reference materials for black carbon quantification. *Org Geochem* 37:1629–1633
23. Doran JW, Zeiss MR (2000) Soil health and sustainability: managing the biotic component of soil quality. *Appl Soil Ecol* 15:3–11
24. Waters D, Van Zwieten L, Singh BP, Downie A, Cowie AL, Lehmann J (2011) Biochar in soil for climate change mitigation and adaptation. In: *Soil health and climate change*. Springer, Berlin, Heidelberg, pp 345–368

25. Batool A, Taj S, Rashid A, Khalid A, Qadeer S, Saleem AR, Ghufuran MA (2015) Potential of soil amendments (Biochar and gypsum) in increasing water use efficiency of *Abelmoschus esculentus* L. Moench. *Front Plant Sci* 6:1–13
26. Liang B, Lehmann J, Solomon D, Kinyangi J, Grossman J, O'Neill B, Skjemstad JO, Thies J, Luizao FJ, Petersen J, Neves EG (2006) Black carbon increases cation exchange capacity in soils. *Soil Sci Soc Am J* 70:1719–1730
27. Laird DA, Fleming P, Davis DD, Horton R, Wang B, Karlen DL (2010) Impact of biochar amendments on the quality of a typical Midwestern agricultural soil. *Geoderma* 158:443–449
28. Sparkes J, Stoutjesdijk P (2011) Biochar: implications for agricultural productivity. Production Canberra, Australia
29. Cheng CH, Lehmann J, Thies JE, Burton SD, Engelhard MH (2006) Oxidation of black carbon by biotic and abiotic processes. *Org Geochem* 37:1477–1488
30. Mohan D, Abhishek K, Sarswat A, Patel M, Singh P, Pittman CU (2018) Biochar production and applications in soil fertility and carbon sequestration—a sustainable solution to crop-residue burning in India. *RSC Adv* 8(1):508–520
31. Chan KY, Van Zwieten L, Meszaros I, Downie A, Joseph S (2007) Agronomic values of greenwaste biochar as a soil amendment. *Aust J Soil Res* 45:629–634
32. Abel S, Peters A, Trinks S, Schonsky H, Facklam M, Wessolek G (2013) Impact of biochar and hydrochar addition on water retention and water repellency of sandy soil. *Geoderma* 202203:183–191
33. Gwenzi W, Chaukura N, Mukome FND, Machado S, Nyamasoka B (2014) Biochar production and applications in sub-Saharan Africa: opportunities, constraints, risks and uncertainties. *J Environ Manage* 150:250–261
34. Barnes RT, Gallagher ME, Masiello CA, Liu Z, Dugan B (2014) Biochar-Induced changes in soil hydraulic conductivity and dissolved nutrient fluxes constrained by laboratory experiments. *Plos One* 9:e108340
35. Zhang A, Bian R, Pan G, Cui L, Hussain Q, Li L, Zheng J, Zheng J, Zhang X, Han X, Yu X (2012) Effects of biochar amendment on soil quality, crop yield and greenhouse gas emission in a Chinese rice paddy: a field study of 2 consecutive rice growing cycles. *Field Crop Res* 127:153–160
36. Albuquerque JA, Calero JM, Barron V, Torrent J, del Campillo MC, Gallardo A, Villar R (2014) Effects of biochars produced from different feedstocks on soil properties and sunflower growth. *J Plant Nutr Soil Sci* 177:16–25
37. Brantley KE, Brye KR, Savin MC, Longer DE (2015) Biochar source and application rate effects on soil water retention determined using wetting curves. *Open J Soil Sci* 5:1–10
38. Uzoma KC, Inoue M, Andry H, Zahoor A, Nishihara E (2011) Influence of biochar application on sandy soil hydraulic properties and nutrient retention. *J Food Agric Environ* 9:1137–1143
39. Chan KY, Van Zwieten L, Meszaros I, Downie A, Joseph S (2008) Using poultry litter biochars as soil amendments. *Aust J Soil Res* 46:437–444
40. Van Zwieten L, Kimber S, Downie A, Morris S, Petty S, Rust J, Chan KY (2010) A glasshouse study on the interaction of low mineral ash biochar with nitrogen in a sandy soil. *Aust J Soil Res* 48:569–576
41. Steiner C, De Arruda MR, Teixeira WG, Zech W (2007) Soil respiration curves as soil fertility indicators in perennial central Amazonian plantations treated with charcoal, and mineral or organic fertilisers. *Trop Sci* 47:218–230
42. Granatstein D, Kruger C, Collins H, Galinato S, Garcia-Perez M, Yoder J (2009) Use of biochar from the pyrolysis of waste organic material as a soil amendment. In: Final project report. Center for Sustaining Agriculture and Natural Resources, Washington State University, Wenatchee, WA
43. Lashari MS, Liu Y, Li L, Pan W, Fu J, Pan G, Zheng J, Zheng J, Zhang X, Yu X (2013) Effects of amendment of biochar-manure compost in conjunction with pyrolygneous solution on soil quality and wheat yield of a salt-stressed cropland from central China great plain. *Field Crop Res* 144:113–118

44. Joseph S, Peacocke C, Lehmann J, Munroe P (2009) Developing biochar classification and test methods. *Aquaculture*, pp 249–258
45. Inyang M, Gao B, Pullammanappallil P, Ding W, Zimmerman AR (2010) Biochar from anaerobically digested sugarcane bagasse. *Bioresour Technol* 101:8868–8872
46. Thies JE, Rilling MC (2009) Characteristics of biochar: biological properties. In: *Biochar for environmental management*
47. Lehmann J, Rilling MC, Thies J, Masiello CA, Hockaday WC, Crowley D (2011) Biochar effects on soil biota—a review. *Soil Biol Biochem* 43:1812–1836
48. Tong H, Hu M, Li FB, Liu CS, Chen MJ (2014) Biochar enhances the microbial and chemical transformation of pentachlorophenol in paddy soil. *Soil Biol Biochem* 70:142–150
49. Gul S, Whalen JK, Thomas BW, Sachdeva V, Deng H (2015) Physico-chemical properties and microbial responses in biochar-amended soils: mechanisms and future directions. *Agr Ecosyst Environ* 206:46–59
50. Kookana RS, Sarmah AK, Van Zwieten L, Krull E, Singh B (2011) Biochar application to soil. agronomic and environmental benefits and unintended consequences. In: *Advances in agronomy*. Academic Press, pp 103–143
51. Khodadad CLM, Zimmerman AR, Green SJ, Uthandi S, Foster JS (2011) Taxa-specific changes in soil microbial community composition induced by pyrogenic carbon amendments. *Soil Biol Biochem* 43:385–392
52. Muhammad N, Dai Z, Xiao K, Meng J, Brookes PC, Liu X, Wang H, Wu J, Xu J (2014) Changes in microbial community structure due to biochars generated from different feedstocks and their relationships with soil chemical properties. *Geoderma* 226:270–278
53. McClellan AT, Deenik JG, Antal M (2007) Effects of flash carbonized macadamia nutshell charcoal on plant growth and soil chemical properties. *American Society of Agronomy Abstracts*, New Orleans, LA 3–7 November
54. Ameloot N, De Neve S, Jegajeevagan K, Yildiz G, Buchan D, Funkuin YN, Prins W, Bouckaert L, Sleutel S (2013) Short-term CO<sub>2</sub> and N<sub>2</sub>O emissions and microbial properties of biochar amended sandy loam soils. *Soil Biol Biochem* 57:401–410
55. Hamer U, Marschner B, Brodowski S, Amelung W (2004) Interactive priming of black carbon and glucose mineralisation. *Org Geochem* 35:823–830
56. Yoshizawa S, Tanaka S, Ohata M, Mineki S, Goto S, Fujioka K, Kokubun T (2005) Composting of food garbage and livestock waste containing biomass charcoal. In: *Proceedings of the international conference and natural resources and environmental management*, Kuching, Sarawak
57. Luo Y, Durenkamp M, De Nobili M, Lin Q, Devonshire BJ, Brookes PC (2013) Microbial biomass growth, following incorporation of biochars produced at 350 °C or 700 °C, in a silty-clay loam soil of high and low pH. *Soil Biol Biochem* 57:513–523
58. Prayogo C, Jones JE, Baeyens J, Bending GD (2013) Impact of biochar on mineralisation of C and N from soil and willow litter and its relationship with microbial community biomass and structure. *Biol Fertil Soils* 50:695–702
59. Mitchell PJ, Simpson AJ, Soong R, Simpson MJ (2015) Shifts in microbial community and water-extractable organic matter composition with biochar amendment in a temperate forest soil. *Soil Biol Biochem* 81:244–254
60. Domene X, Mattana S, Hanley K, Enders A, Lehmann J (2014) Medium-term effects of corn biochar addition on soil biota activities and functions in a temperate soil cropped to corn. *Soil Biol Biochem* 72:152–162
61. Dempster DN, Gleeson DB, Solaiman ZM, Jones DL, Murphy DV (2012) Decreased soil microbial biomass and nitrogen mineralisation with eucalyptus biochar addition to a coarse textured soil. *Plant Soil* 354:311–324
62. Mia S, van Groenigen JW, van de Voorde TFJ, Oram NJ, Bezemer TM, Mommer L, Jeffery S (2014) Biochar application rate affects biological nitrogen fixation in red clover conditional on potassium availability. *Agr Ecosyst Environ* 191:83–91
63. Rondon MA, Lehmann J, Ramírez J, Hurtado M (2007) Biological nitrogen fixation by common beans (*Phaseolus vulgaris* L.) increases with biochar additions. *Biol Fertil Soils* 43:699–708

64. Warnock DD, Mummey DL, McBride B, Major J, Lehmann J, Rillig MC (2010) Influences of non-herbaceous biochar on arbuscular mycorrhizal fungal abundances in roots and soils: results from growth-chamber and field experiments. *Appl Soil Biol* 46:450–456
65. Kloss S, Zehetner F, Wimmer B, Buecker J, Rempt F, Soja G (2014) Biochar application to temperate soils: effects on soil fertility and crop growth under greenhouse conditions. *J Plant Nutr Soil Sci* 177:3–15
66. Lehmann J, Pereira da Silva J, Steiner C, Nehls T, Zech W, Glaser B (2003) Nutrient availability and leaching in an archaeological Anthrosol and a Ferralsol of the Central Amazon basin: fertilizer, manure and charcoal amendments. *Plant Soil* 249:343–357
67. Zhai L, Caiji Z, Liu J, Wang H, Ren T, Gai X, Xi B, Liu H (2014) Short-term effects of maize residue biochar on phosphorus availability in two soils with different phosphorus sorption capacities. *Biol Fertil Soils* 51:113–122
68. Dey D, Mavi MS (2021) Biochar and urea co-application regulates nitrogen availability in soil. *Environ Monit Assess* 193:326
69. Xu G, Wei LL, Sun JN, Shao HB, Chang SX (2013) What is more important for enhancing nutrient bioavailability with biochar application into a sandy soil: direct or indirect mechanism? *Ecol Eng* 52:119–124
70. Lee S, Ahmad M, Usman AARA, Awad YM, Min S, Yang JE, Oh YS (2011) Effects of biochar on soil quality and heavy metal availability in a military shooting range soil in Korea. *Korean J Soil Sci Fertilizer* 44:67–77
71. Agegnehu G, Srivastava AK, Bird MI (2017) The role of biochar and biochar-compost in improving soil quality and crop performance: a review. *Appl Soil Ecol* 119:156–170
72. Yao Y, Gao B, Zhang M, Inyang M, Zimmerman AR (2012) Effect of biochar amendment on sorption and leaching of nitrate, ammonium, and phosphate in a sandy soil. *Chemosphere* 89:1467–1471
73. Agegnehu G, Bird M, Nelson P, Bass A (2015) The ameliorating effects of biochar and compost on soil quality and plant growth on a Ferralsol. *Soil Res* 53:1–12
74. Major J, Rondon M, Molina D, Riha SJ, Lehmann J (2012) Nutrient leaching in a colombian savanna oxisol amended with biochar. *J Environ Qual* 41:1076–1086
75. Clough T, Condon L, Kammann C, Muller C (2013) A review of biochar and soil nitrogen dynamics. *Agronomy* 3:275–293
76. Hua L, Wu W, Liu Y, McBride MB, Chen Y (2009) Reduction of nitrogen loss and Cu and Zn mobility during sludge composting with bamboo charcoal amendment. *Environ Sci Pollut Res* 16:1–9
77. Steiner C, Das KC, Garcia M, Forster B, Zech W (2008) Charcoal and smoke extract stimulate the soil microbial community in a highly weathered xanthic Ferralsol. *Pedobiologia (Jena)* 51:359–366
78. Zhang A, Liu Y, Pan G, Hussain Q, Li L, Zheng J, Zhang X (2012) Effect of biochar amendment on maize yield and greenhouse gas emissions from a soil organic carbon poor calcareous loamy soil from Central China Plain. *Plant Soil* 351:263–275
79. Allen RL (1847) A brief compend of American agriculture. CM Saxton
80. Jaiswal AK, Elad Y, Graber ER, Frenkel O (2014) *Rhizoctonia solani* suppression and plant growth promotion in cucumber as affected by biochar pyrolysis temperature, feedstock and concentration. *Soil Biol Biochem* 69:110–118
81. Bonanomi G, Ippolito F, Scala F (2015) A “black” future for plant pathology? Biochar as a new soil amendment for controlling plant diseases. *J Plant Pathol* 97:223–234
82. Frenkel O, Jaiswal AK, Elad Y, Lew B, Kammann C, Graber ER (2017) The effect of biochar on plant diseases: what should we learn while designing biochar substrates? *J Environ Eng Landsc Manag* 25:105–113
83. Copley TR, Aliferis KA, Jabaji S (2015) Maple bark biochar affects *Rhizoctonia solani* metabolism and increases damping-off severity. *Phytopathology* 105:1334–1346
84. Huang WK, Ji HL, Gheysen G, Debode J, Kyndt T (2015) Biochar-amended potting medium reduces the susceptibility of rice to root-knot nematode infections. *BMC Plant Biol* 15:267

85. Haider G, Koyro HW, Azam F, Steffens D, Muller C, Kammann C (2015) Biochar but not humic acid product amendment affected maize yields via improving plant-soil moisture relations. *Plant Soil* 395:141–157
86. Pressler Y, Foster EJ, Moore JC, Cotrufo MF (2017) Coupled biochar amendment and limited irrigation strategies do not affect a degraded soil food web in a maize agroecosystem, compared to the native grassland. *GCB Bioenergy* 9:1344–1355
87. Hafeez Y, Iqbal S, Jabeen K, Shahzad S, Jahan S, Rasul F (2017) Effect of biochar application on seed germination and seedling growth of glycine max (*L.*) merr. under drought stress. *Pak J Bot* 49:7–13
88. Qian L, Chen B, Hu D (2013) Effective alleviation of aluminium phytotoxicity by manure-derived biochar. *Environ Sci Technol* 47:2737–2745
89. Agegnehu G, Bass AM, Nelson PN, Bird MI (2016) Benefits of biochar, compost and biochar-compost for soil quality, maize yield and greenhouse gas emissions in a tropical agricultural soil. *Sci Total Environ* 543:295–306
90. Wang J, Xiong Z, Kuzyakov Y (2016) Biochar stability in soil: meta-analysis of decomposition and priming effects. *GCB Bioenergy* 8:512–523
91. Blackwell P, Joseph S, Munroe P, Anawar HM, Storer P, Gilkes RJ, Solaiman ZM (2015) Influences of biochar and biochar-mineral complex on mycorrhizal colonisation and nutrition of wheat and sorghum. *Pedosphere* 25:686–695
92. Deenik JL, McClellan T, Uehara G, Antal MJ, Campbell S (2010) Charcoal volatile matter content influences plant growth and soil nitrogen transformations. *Soil Sci Soc Am J* 74:1259–1270
93. Xu C-Y, Hosseini-Bai S, Hao Y, Rachaputi RN, Wang H, Xu Z, Wallace H (2015) Effect of biochar amendment on yield and photosynthesis of peanut on two types of soils. *Environ Sci Pollut Res* 22:6112–6125
94. Sigua GC, Novak JM, Watts DW, Szögi AA, Shumaker PD (2016) Impact of switchgrass biochars with supplemental nitrogen on carbon-nitrogen mineralization in highly weathered coastal plain Ultisols. *Chemosphere* 145:135–141
95. Gaskin JW, Speir RA, Harris K, Das K, Lee RD, Morris LA, Fisher DS (2010) Effect of peanut hull and pine chip biochar on soil nutrients, corn nutrient status, and yield. *Agron J* 102:623–633
96. Rajkovich S, Enders A, Hanley K, Hyland C, Zimmerman AR, Lehmann J (2012) Corn growth and nitrogen nutrition after additions of biochars with varying properties to a temperate soil. *Biol Fertil Soils* 48:271–284
97. Rondon MA, Molina D, Hurtado M, Ramirez J, Lehmann J, Major J, Amezquita E (2006) Enhancing the productivity of crops and grasses while reducing greenhouse gas emissions through bio-char amendments to unfertile tropical soils. In: *Proceedings of the 18th world congress of soil science*, pp 138–168
98. Yamato M, Okimori Y, Wibowo IF, Anshori S, Ogawa M (2006) Effects of the application of charred bark of acacia mangium on the yield of maize, cowpea and peanut, and soil chemical properties in South Sumatra, Indonesia. *Soil Sci Plant Nutr* 52:489–495
99. Asai H, Samson BK, Stephan HM, Songyikhangsuthor K, Homma K, Kiyono Y, Inoue Y, Shiraiwa T, Horie T (2009) Biochar amendment techniques for upland rice production in Northern Laos. 1. Soil physical properties, leaf SPAD and grain yield. *Field Crop Res* 111:81–84
100. Hossain MK, Strezov V, Chan KY, Nelsona PF (2010) Agronomic properties of wastewater sludge biochar and bioavailability of metals in production of cherry tomato (*Lycopersicon esculentum*). *Chemosphere*:1167–1171
101. Bakar RA, Razak ZA, Ahmad SH, Seh-Bardan BJ, Tsong LC, Meng CP (2015) Influence of oil palm empty fruit bunch biochar on floodwater pH and yield components of rice cultivated on acid sulphate soil under rice intensification practices. *Plant Prod Sci* 18:491–500
102. Jia J, Li B, Chen Z, Xie Z, Xiong Z (2012) Effects of biochar application on vegetable production and emissions of N<sub>2</sub>O and CH<sub>4</sub>. *Soil Sci Plant Nutr* 58:503–509



103. Fowles M (2006) Black carbon sequestration as an alternative to bioenergy. *Biomass Bioenergy* 31:426–432
104. Lehmann J (2007) Bio-energy in the black. *Front Ecol Environ* 5:381–387
105. Nguyen BT, Lehmann J, Hockaday WC, Joseph S, Masiello CA (2010) Temperature sensitivity of black carbon decomposition and oxidation. *Environ Sci Technol* 44:3324–3331
106. Lehmann J, Gaunt J, Rondon M (2006) Bio-char sequestration in terrestrial ecosystems—a review. *Mitig Adapt Strat Glob Change* 11:403–427
107. Woolf D (2008) Biochar as a soil amendment: a review of the environmental implication. University of Swansea. [http://orgprints.org/13268/1/Biochar\\_as\\_a\\_soil\\_amendment\\_-\\_a\\_review.pdf](http://orgprints.org/13268/1/Biochar_as_a_soil_amendment_-_a_review.pdf)
108. Harvey OM, Kuo L, Zimmerman AR, Louchouart P, Amonette JE, Herbert BE (2012) An index-based approach to assessing recalcitrance and soil carbon sequestration potential of engineered black carbons (biochars). *Environ Sci Technol* 46:1415–1421
109. Kumar S, Masto RE, Ram LC, Sarkar P, George J, Selvi VA (2013) Biochar preparation from Parthenium hysterophorus and its potential use in soil application. *Ecol Eng* 55:67–72
110. Nguyen BT, Lehmann J, Kinyangi J, Smernik R, Riha SJ, Engelha RD (2009) Long-term black carbon dynamics in cultivated soils. *Biogeochemistry* 92:163–176
111. Wu W, Yang M, Feng Q, McGrouther K, Wang H, Lu H, Chen Y (2012) Chemical characterization of rice straw-derived biochar for soil amendment. *Biomass Bioenergy* 47:268–276
112. Bruun S, Clauson-Kaas S, Bobulka L, Thomsen IK (2014) Carbon dioxide emissions from biochar in soil: role of clay, microorganisms and carbonates. *Eur J Soil Sci* 65:52–59
113. Spokas KA (2010) Review of the stability of biochar in soils: predictability of O: C molar ratios. *Carbon Manage*. 1:289–303
114. Roberts KG, Gloy BA, Joseph S, Scott OR, Lehmann J (2010) Life cycle assessment of biochar systems: estimating the energetic economic and climate change potential. *Environ Sci Technol* 44:827–833
115. Woolf D, Amonette JE, Street-Perrott FA, Lehmann J, Joseph S (2010) Sustainable biochar to mitigate global climate change. *Nat Commun* 1:1–9. Article Number 56
116. Cheng K, Pan G, Smith P, Luo T, Li L, Zheng J, Zhang X, Han X, Yan M (2011) Carbon footprint of China's crop production—an estimation using agro-statistics data over 1993–2007. *Agric Ecosyst Environ* 142:231–237
117. IPCC (2014) Fifth assessment report. Chapter 1: introduction chapter, pp 1–65
118. FAO (2016) The state of food and agriculture: climate change, agriculture and food security. Food and Agriculture Organization of the United Nations (FAO), Rome, Italy, p 194
119. Yanai Y, Toyota K, Okazaki M (2007) Effects of charcoal addition on N<sub>2</sub>O emissions from soil resulting from rewetting air-dried soil in short-term laboratory experiments. *Soil Sci Plant Nutr* 53:181–188
120. Dalal RC, Allen DE, Livesley SJ, Richards G (2008) Magnitude and biophysical regulators of methane emission and consumption in the Australian agriculture, forest and submerged landscapes: a review. *Plant Soil* 309:43–76
121. Wang C, Lu H, Dong D, Deng H, Strong PJ, Wang H, Wu W (2013) Insight into the effects of biochar on manure composting: evidence supporting the relationship between N<sub>2</sub>O emission and denitrifying community. *Environ Sci Technol* 47:7341–7349
122. Liang B, Lehmann J, Sohi SP, Thies JE, O'Neill B, Trujillo L, Gaunt J, Solomon D, Grossman J, Neves EG, Luizão FJ (2010) Black carbon affects the cycling of non-black carbon in soil. *Org Geochem* 41:206–213
123. Singh BP, Hatton BJ, Singh B, Cowie AL, Kathuria A (2010) Influence of biochars on nitrous oxide emission and nitrogen leaching from two contrasting soils. *J Environ Qual* 39:1224–1235
124. Castaldi S, Riondino M, Baronti S, Esposito FR, Marzaioli R, Rutigliano FA, Vaccari FP, Miglietta F (2011) Impact of biochar application to a Mediterranean wheat crop on soil microbial activity and greenhouse gas fluxes. *Chemosphere* 85:1464–1471

125. Zhang A, Bian R, Hussain QB, Li L, Pan G, Zheng J, Zhang X, Zheng J (2013) Change in net global warming potential of a rice–wheat cropping system with biochar soil amendment in a rice paddy from China. *Agric Ecosyst Environ* 173:37–45
126. Zhang D, Pan G, Wu G, Kibue GW, Li L, Zhang X, Zheng J, Zheng J, Cheng K, Joseph S, Liu X (2016) Biochar helps enhance maize productivity and reduce greenhouse gas emissions under balanced fertilization in a rainfed low fertility inceptisol. *Chemosphere* 142:106–113
127. Uchimiya M, Lima IM, Klasson KT, Wartelle LH (2010) Contaminant immobilization and nutrient release by biochar soil amendment: roles of natural organic matter. *Chemosphere* 80:935–940
128. Jiang TY, Jiang J, Xu RK, Li Z (2012) Adsorption of Pb(II) on variable charge soils amended with rice-straw derived biochar. *Chemosphere* 89:249–256
129. Oh SY, Son JG, Chiu PC (2013) Biochar-mediated reductive transformation of nitro herbicides and explosives. *Environ Toxicol Chem* 32:501–508
130. Zheng W, Guo M, Chow T, Bennett DN, Rajagopalan N (2010) Sorption properties of greenwaste biochar for two triazine pesticides. *J Hazard Mater* 181:121–126
131. Cao X, Ma L, Gao B, Harris W (2009) Dairy-manure derived biochar effectively sorbs lead and atrazine. *Environ Sci Technol* 43:3285–3291
132. Zhou Y, Gao B, Zimmerman AR, Chen H, Zhang M, Cao X (2014) Biochar-supported zero valent iron for removal of various contaminants from aqueous solutions. *Bioresour Technol* 152:538–542
133. Bian R, Chen D, Liu X, Cui L, Li L, Pan G, Xie D, Zheng J, Zhang X, Zheng J, Chang A (2013) Biochar soil amendment as a solution to prevent Cd-tainted rice from China: results from a cross-site field experiment. *Ecol Eng* 58:378–383
134. Major J, Rondon M, Molina D, Riha SJ, Lehmann J (2010) Maize yield and nutrition during 4 years after biochar application to a Colombian savanna oxisol. *Plant Soil* 333:117–128
135. Mastro RE, Sunar KK, Sengupta T, Ram LC, Rout TK, Selvi VA, George J, Sinha AK (2012) Evaluation of the co-application of fly ash and sewage sludge on soil biological and biochemical quality. *Environ Technol* 33:897–905
136. Belyaeva ON, Haynes RJ (2012) Comparison of the effects of conventional organic amendments and biochar on the chemical, physical and microbial properties of coal fly ash as a plant growth medium. *Environ Earth Sci* 66:1987–1997
137. Kołtowski M, Oleszczuk P (2015) Toxicity of biochars after polycyclic aromatic hydrocarbons removal by thermal treatment. *Ecol Eng* 75:79–85
138. Kolodyńska D, Wnętrzak R, Leahy JJ, Hayes MHB, Kwapiński W, Hubicki Z (2012) Kinetic and adsorptive characterization of biochar in metal ions removal. *Chem Eng J* 197:295–305
139. Inyang M, Gao B, Yao Y, Xue Y, Zimmerman AR, Pullammanappallil P, Cao X (2012) Removal of heavy metals from aqueous solution by biochars derived from anaerobically digested biomass. *Biores Technol* 110:50–56
140. Tang J, Lv H, Gong Y, Huang Y (2015) Preparation and characterization of a novel graphene/biochar composite for aqueous phenanthrene and mercury removal. *Biores Technol* 196:355–363
141. Yao Y, Gao B, Chen J, Yang L (2013) Engineered biochar reclaiming phosphate from aqueous solutions: mechanisms and potential application as a slow-release fertilizer. *Environ Sci Technol* 47:8700–8708
142. Lashari MS, Ye Y, Ji H, Li L, Kibue GW, Lu H, Zheng J, Pan G (2014) Biochar–manure compost in conjunction with pyrolygneous solution alleviated salt stress and improved leaf bioactivity of maize in a saline soil from central China: a 2-year field experiment. *J Sci Food Agr* 95:1321–1327
143. Akhtar SS, Andersen MN, Liu F (2015) Residual effects of biochar on improving growth, physiology and yield of wheat under salt stress. *Agr Water Manage* 158:61–68
144. Akhtar SS, Andersen MN, Liu F (2015) Biochar mitigates salinity stress in potato. *J Agron Crop Sci* 201:368–378
145. Thomas SC, Frye S, Gale N, Garmon M, Launchbury R, Machado N, Melamed S, Murray J, Petroff A, Winsborough C (2013) Biochar mitigates negative effects of salt additions on two herbaceous plant species. *J Environ Manage* 129:62–68

146. Lehmann J, Joseph S (2012) Biochar for environmental management: an introduction biochar for environmental management: science and technology. In: Lehmann J, Joseph S (eds) Biochar for environmental management, 2nd edn. Routledge, Abingdon, pp 1–12
147. Di Blasi C, Tanzi V, Lanzetta M (1997) A study on the production of agricultural residues in Italy. *Biomass Bioenergy* 12(5):321–331
148. Sánchez-Monedero MA, Cayuela ML, Sánchez-García M, Vandecasteele B, Dose T, López G, Martínez-Gaitán C, Kuikman PJ, Sinicco T, Mondini C (2019) Agronomic evaluation of biochar, compost and biochar-blended compost across different cropping systems: perspective from the European project FERTIPLUS. *Agronomy* 9:5

# Chapter 23

## Application of Porous Carbon Material for Water Treatment and Gas Storage



Saikat Sinha Ray, Mohammed J. K. Bashir, Harshdeep Singh Bakshi, Young-Nam Kwon, and Mahesh Ganesapillai

### 1 Introduction

Porous materials have garnered considerable attention in recent years from materials, chemical, and energy specialists, among others. As a result, research and development of innovative porous materials are accelerated. In recent decades, greater emphasis has been placed on various fields of separation and purification technologies, catalysis, adsorption, gas storage, energy storage and conversion, etc., among others, in addition to their commercial implications [1–7]. In the twenty-first century, rapid growth in the industrial sector increased residential activities, and global population growth has resulted in an unprecedented surge in water contamination and pollution. As a result, wastewater treatment is required before discharge into the environment. The various potential strategies for the purification of micropollutants from wastewater, including adsorption and membrane technology [8, 9]. Adsorption on porous materials has typically been a promising technology due to its low cost and simplicity of disposal. Due to its structural characteristics with a higher specific

---

S. S. Ray · Y.-N. Kwon

Department of Urban and Environmental Engineering (UEE), Ulsan National Institute of Science and Technology (UNIST), Ulsan, South Korea

M. J. K. Bashir

Department of Environmental Engineering, Faculty of Engineering and Green Technology (FEGT), Universiti Tunku Abdul Rahman, Jalan Universiti, Bandar Barat, Malaysia

H. S. Bakshi

Centre for Environmental Policy, Imperial College London, South Kensington, England, United Kingdom

M. Ganesapillai (✉)

Mass Transfer Group, School of Chemical Engineering,  
Vellore Institute of Technology, Vellore 632014, Tamil Nadu, India  
e-mail: [maheshgpillai@vit.ac.in](mailto:maheshgpillai@vit.ac.in)

surface area, activated carbons have become the most extensively utilized adsorbents to remove organic contaminants. However, porous carbon materials exhibit structural heterogeneity in macro-, meso-, and micropores [1]. Several novel forms of porous carbon materials, including carbon nanotubes and carbon nanofibers, have been studied for gas storage applications in recent decades. The potential function of carbon materials in natural and hydrogen gas storage applications will be evaluated in this context. Additionally, methane ( $\text{CH}_4$ ) storage entails an adsorption mechanism utilizing porous carbon adsorbents, widely regarded as a cost-effective and environmentally friendly technology [10]. The porous carbon used for water treatment and gas storage is mostly microporous or mesoporous.

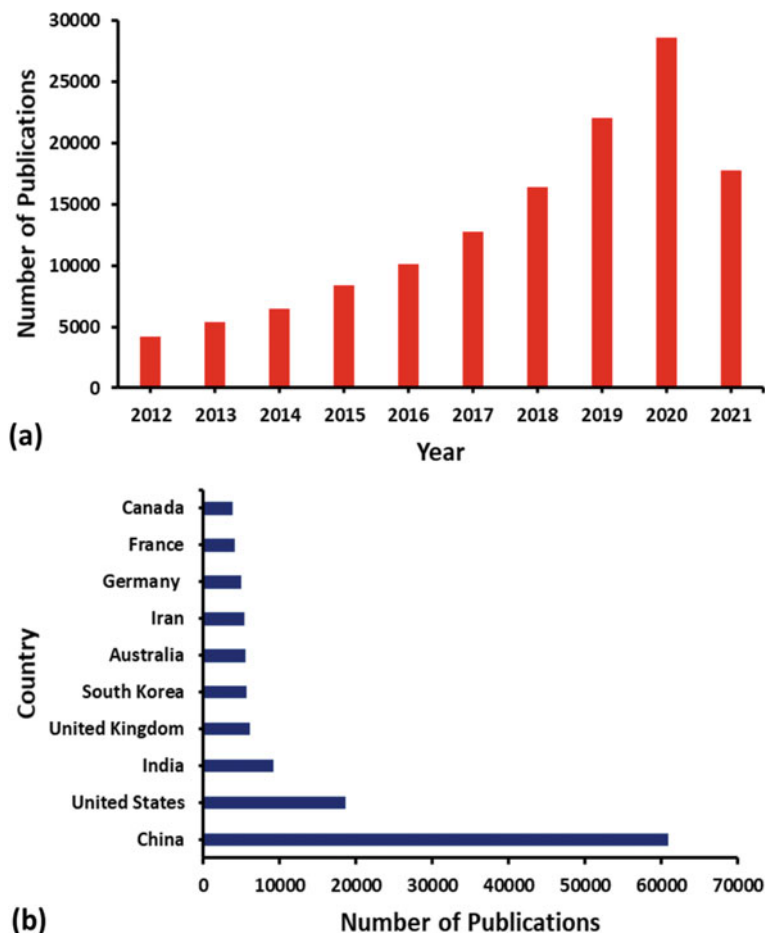
### ***1.1 Brief Insight of Carbon Materials***

Nanostructured carbon compounds exist in a wide range of shapes and sizes, and they can be employed in various applications across a wide range of industries. Carbon nanofibers, carbon nanotubes, fullerene, graphene oxide (GO), and graphene (GR) have been the most versatile research development components for the last three decades. As far as recent research is concerned, these nanostructured carbons have been successfully utilized to produce composite materials such as carbon/ceramic, carbon/metal, carbon polymer, and carbon/cement composites [11].

These nanostructured carbon compounds are strikingly distinct in terms of structure, properties, production processes, and uses. Carbon materials in various forms have recently been used in medical, biological, electrical, electromagnetic, electrochemical, and environmental applications. As a result, rigid nanostructured carbon materials have been identified as a viable research topic in the field of environmental remediation.

Environmental pollution has become a significant issue as a result of limited remedial solutions. Notably, nanostructured porous carbon materials have been effectively used for air and water purification [12]. In addition, porous carbon is successful in treating a variety of wastewater contaminants, including heavy metals, nitric acid, hydrogen sulphide, organic dyes, pharmaceutical waste, and other micropollutants, via adsorption or membrane technology. Following an extensive investigation, nanostructured porous carbon materials demonstrated an adsorption efficiency of greater than 80%. Additionally, carbon materials are typically cost-effective and ecologically sustainable [13, 14].

The relevant survey is depicted in Fig. 1a, which was analysed based on peer-reviewed articles, book chapters, and reviews, published in the last 10 years, corresponding to the phrases “porous carbon” and “environment”. Additionally, Fig. 1b illustrates the research contributions of various countries in terms of publications based on porous carbon in the environmental field. The presented database was compiled using Scopus’s advanced scholar search engine, and China was reported to be the leading in terms of numbers. The graph clearly illustrates the growing need for porous carbon materials in the field of environmental remediation. Additionally, it

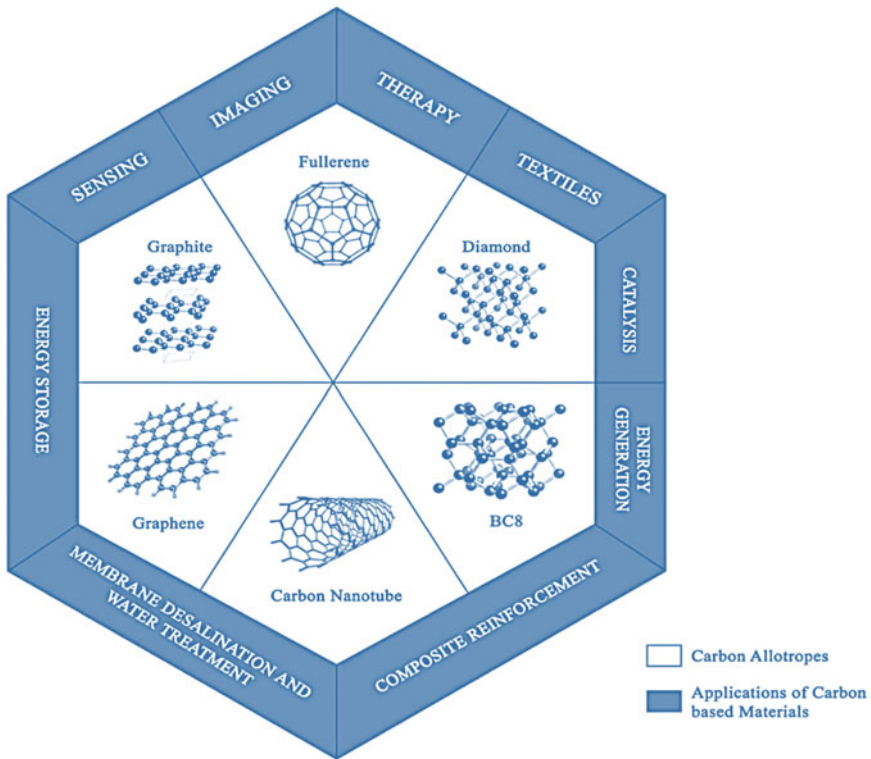


**Fig. 1** a Survey of peer-reviewed papers published since 2012; b Survey of peer-reviewed papers published since 2012 (country-wise contribution). *Note* As of May 2021, a database was obtained from Advanced Scopus Search Engine using the words “porous carbon” and “environment”

implies that various carbon-based composites have been used in water treatment and gas storage applications. Since the last decade, there has been a noticeable increase in research and development on "energy and the environment".

## 1.2 Background

Carbon-based materials are well known for their versatility, owing to their ability to create strong covalent bonds in many other materials, resulting in perfect physiochemical properties. Recently, much study has been undertaken on synthesizing



**Fig. 2** Different allotropes of carbon and their various applications

innovative carbon-based materials that meet the required characteristics for using various sectors, including membrane separation, sensor technology, energy storage and conversion, gas storage, and neurosciences. Figure 2 provides a pictorial representation of carbon allotropes and their various applications.

Carbon nanotubes have been shown to improve the strength, stability, antifouling characteristics, and flow rate of ultrafiltration (UF) membranes when composited with polymer membranes [15]. The significant improvement in membrane properties associated with carbon nanotubes incorporation can be attributed to their increased surface area, antibacterial capabilities, hydrophilicity, pore channels, and other functional features of the polymer matrix [16]. Another significant application of innovative porous carbon material such as carbon nanotubes and vapour carbon nanofibers is the storage of natural gas and hydrogen gas, facilitated by the materials' strong C–H bonds [17]. While applying carbon-based materials in the domains mentioned above presents unique problems, current research has demonstrated that these obstacles can be addressed by refining the synthesis of carbon-based materials.

## 2 Categories of Carbon Materials

Due to their highly porous surface and surface area and ease of chemical modification and regeneration, carbon materials have been employed for various applications over the last two decades, including removing organics, heavy and toxic metals, and biological contaminants. Carbon nanotubes, carbon nanofibers, graphene, graphene oxide, activated carbons, and fullerenes are all carbon materials employed in energy storage, drug delivery, water, wastewater treatment sensors, gas storage, etc. These carbon materials have been well exploited due to their superior thermal, electrical, and chemical capabilities. Carbon materials are often classified according to their dimension. Carbon materials with three sizes less than or equal to 100 nm are zero-dimensional carbon materials (fullerene and quantum dots) [18].

On the other hand, carbon materials with a single dimension greater than 100 nm and two sizes less than 100 nm are one-dimensional carbon materials (carbon nanotubes) [19, 20]. Two-dimensional carbon materials have two dimensions greater than 100 nm (graphene). Finally, three-dimensional carbon compounds have dimensions greater than 100 nm (Graphite and other nanocomposite materials) [21]. The advantages and disadvantages of various dimensional carbon compounds that are highly effective in environmental remediation are summarized in Table 1.

Graphene-based nanomaterials are thought to be toxic because of their particle size, surface functional groups, oxygen content, surface charges, and impurities. The formation of reactive oxygen species (ROS) is thought to be the most common mechanism. In some studies, the low toxicity does not seem to depend on the attached functional groups. Carbon nanodots with different amounts of nitrogen and oxygen have no effect on cell survival, but in others, the toxicity of certain functional groups is found.

ROS is one of the ways that raw GQDs can be toxic. In practice, different applications may have different needs for toxicity levels, so there are likely times when the toxicity of certain types of GQDs needs to be eased or lowered even more. So, it is also important to come up with ways to control the toxicity of GQDs. Hydroxylation was thought to make nanoparticles more biocompatible, but when it comes to GQDs, the hGQDs were the most toxic of the three GQDs that were made. If you think that surface chemistry affects the safety of nanomaterials too much, you should not generalize too much. Instead, the risk assessment of nanomaterials should be done on a case-by-case basis [28–30]. Compared to graphene sheets, GQDs are more biocompatible and less toxic. CQDs, like GQDs discovered by Pan et al. [31], are much more efficient than semiconductor QDs because they are less toxic, more biocompatible, have less chemical inertness, and can be easily absorbed by the body [31, 32]. Because of their low toxicity, great photostability, and chemical inertness, QDs are employed in many fields such as gas storage and water treatment [33, 34].



**Table 1** Characteristic features of various categories of carbon

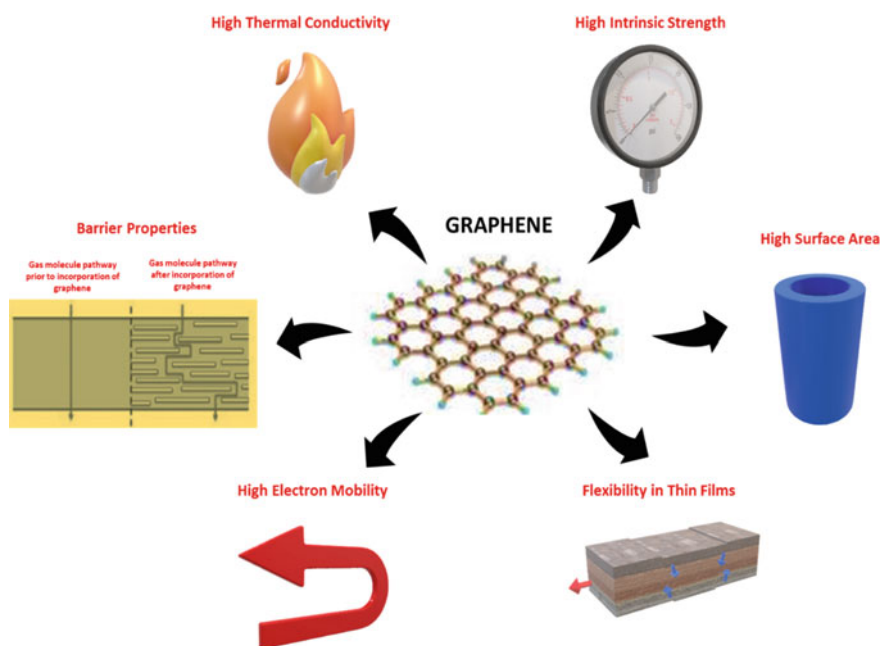
Carbon type	Dimension	Size	Advantages	Disadvantages	References
Quantum dots	0-D	2–10 nm	High optoelectrical properties High catalytic properties	Highly expensive Toxicity	[22]
Activated porous carbon	–	≤ 0.045 mm	Highly porous material Large surface area Low-cost materials Trap toxins and chemicals	Short service life Impurities may leach into liquid stream	[23]
Carbon nanodots	0-D	≤ 10 nm	Excellent photophysical and chemical characteristics Excellent biocompatibility Low cost Chemical inertness	Poor control over size Time-consuming and multi-step process	[24]
Carbon nanotubes	1-D	3–30 nm	High mechanical strength High conductivity High surface area	Oxidative stress Toxicity Additional synthesis step	[25]
Graphene	2-D	3–100 nm	High mechanical strength High conductivity Easy synthesis	Serious aggregation Toxicity	[26]
Graphene oxide	2-D	~10 μm	Interaction with organic and inorganic materials Biocompatible Hydrophilic Porous	Weak mechanical strength Low conductivity	[27]

## 2.1 Graphene

Graphene is an allotrope of carbon that shows existence as a two-dimensional planar layer. In other words, it is a single atomic graphitic layer. It is a carbon compound with extraordinary properties, as represented in Fig. 3. Due to the unique characteristics stated below, it has a wide range of applications in various fields.

- High electrical and thermal conductivity
- Maximum flexibility and elasticity
- Maximum resistance and hardness
- Lighter in weight
- Antimicrobial and antibacterial activity
- Show lesser joule effect, heating while conducting electrons
- Consume lower electricity as compared to other materials.

Graphene has the potential to increase the efficiency of solar energy significantly. Thus, solar energy efficiency and production can be increased by incorporating graphene into solar panels. Similarly, graphene exhibits potential capabilities in the same technology, specifically in water and gas separation. Due to graphene's impermeability, a single layer of atoms functions as an excellent barrier in separation and purification technologies. However, the pores in graphene may allow for the passage



**Fig. 3** Various advantageous physicochemical characteristics of graphene

**Table 2** Comparative study of various approaches for obtaining graphene

Methodologies	Expected morphology	Applications	Reference
Mechanical exfoliation	In the form of flakes	Quantum hall physics Low temperature-based physics	[35]
Chemical exfoliation	Micrometre flakes Mass production Nanosheet production	Polymer composite Gas sensing	[36]
Pyrolysis of carbon precursor(s)	Activated porous carbon in the form of molecular sieving carbons (MSC)	Gas storage Gas separation	[37]
Catalytic decomposition of carbon precursor(s)	Carbon nanofibers (CNFs)	Electrode for fuel cells Hydrogen storage Functional nanocomposites	[38]
Laser ablation and arc discharge	Carbon nanotubes (CNTs)	Energy storage Functional nanocomposites	[39]
Chemical vapour deposition (CVD)	Nanosheet Micrometre flakes	Electronic devices Gas storage Conduction films Sensing	[40]
Reduced graphene oxide (RGO)	In the form of micrometre flakes Nanosheet	Energy storage by fabricating electrodes Li-ion battery Supercapacitors	[41]
Silicon carbide (SiC) sublimation in vacuum	In the form of micrometre flakes and films Nanosheets	Compatible with Si-Tech supercapacitor	[42]

of gases and water molecules, transforming graphene into a material capable of selective gas and water permeability. Table 2 is a concise review of five typical protocols and their associated applications.

## 2.2 Nano-porous Carbon

The synthesis and study of the physicochemical characteristics of nano-porous carbon materials produced from biomass are now the focus of nanotechnology. In addition to having a large specific surface area and good electroconductivity, the carbon materials produced have a high micropore volume. The distinguishing characteristics of plant raw materials are their absence of hazardous admixtures that degrade manufactured items' quality, profitability, environmental sustainability, and ease of handling and planning for pyrolysis. The factors mentioned earlier and the promising findings of synthesizing nano-porous carbon suggest high prospects for improving

future technologies for biomass pyrolysis. Thermochemical activation is the primary approach for treating biomass that enables nano-porous carbon materials to manufacture various topologies using zinc and aluminium chlorides, alkaline metal hydroxides and carbonates, and phosphoric acid [43]. Porous carbonaceous materials are generally considered powerful adsorbents due to their high adsorptive capacity and surface area [44]. Typically, activated carbons have been widely used as an adsorbent for removing pollutants from gaseous or liquid phases, as well as catalysts and catalytic supports [45, 46].

Recent decades have seen a surge in Nano-porous carbon materials in energy conversion and energy storage applications (catalysts/additives). However, before the actual demonstration of the advantages of using nano-porous carbons as inert supports for semiconductors and electron acceptors that improve photogenerated excitons splitting, a large number of researchers have looked into the critical role of carbon matrices coupled to various types of photoactive materials. Carbon nanotubes and carbon nanofibers are two types of nano-porous carbon materials that have generated considerable interest due to their exceptional properties, including high strength and modulus, large surface area, low density, high electrical conductivity, chemical stability, thermal conductivity, and fire resistance [47].

### 2.2.1 Carbon Nanotubes

Carbon nanotubes have been lately added as adsorbents with the potential to recover heavy metals due to their ability to generate electrostatic bonds between the heavy metals and the functional groups of the nanotubes. Carbon nanotubes are a kind of molecular carbon that resemble cylinders made up of coiled graphene layers. The carbon nanotubes may be single-walled carbon nanotubes with a diameter of under one nanometre or multi-walled carbon nanotubes with more than 100 nm, depending on their size [48].

Their lengths can range from few micrometres to millimetres. Carbon nanotubes exhibit extraordinary aspect ratios (length to diameter ratios), often surpassing 1000 and occasionally reaching 2,500,000. Carbon nanotubes with multiple walls can have a wall count of tens to hundreds, with typical wall separations of 0.34 nm. Thus, every conceivable arrangement of single-walled carbon nanotube is unique due to their chiral angle. Additionally, the rolling direction, diameter, and length of a theoretical graphene layer are specified. In contrast, multi-walled carbon nanotubes each have their chiral angle [49].

Applications for these materials include field emitters, radio-wave reflectors and electrostatic discharge protectors, bio-molecular and chemical sensors, hydrogen storage media, fuel cell and catalyst support, and composites with better mechanical properties. As a result, a wide range of applications has been successfully commercialized [50, 51]. The following section discusses the applications of carbon nanotubes and their advantages and disadvantages.

Carbon nanotubes have a wide range of potential applications, which are as follows:

- Nanotubes reinforced composites
- Magnetic nanotubes
- Nano balance
- Solar energy storage
- Hydrogen energy storage
- Thermal Protection
- Space elevator
- Reinforcement polymer
- Reinforcement armour and other materials are all being researched and developed at the moment.

### **Advantages of carbon nanotubes**

Carbon nanotubes have several advantages, including the fact that they are small and lightweight, making them suitable for metallic wires. They can also improve the conductive mechanical properties of composites. The resources required to create them are in plentiful supply. Additionally, it is possible to make using a tiny amount of material. They are temperature insensitive, which means they function almost as well in severe cold as in high heat.

### **Disadvantages of carbon nanotubes**

Carbon nanotubes have several disadvantages. Regardless of how much research is done, scientists are still baffled about how carbon nanotube functions. The manufacture of nanotubes is a time-consuming and complex procedure. A thorough approach would be to use this new technology to completely replace outdated technology in all of its applications. However, because it is minimal, it is difficult to work with. Considering the rate at which technology becomes obsolete, placing a bet on this technology may be risky.

Comparing carbon nanotubes to traditional materials, they are well suited for virtually any application requiring high strength, durability, thermal conductivity, electrical conductivity, and lightweight qualities [51]. At the moment, carbon nanotubes are mainly used for and materials, such as plastics. Carbon nanotubes are available for purchase as a powder from a variety of sources. It is necessary for carbon nanotubes to be untangled and equally distributed across the substrate to unlock their properties. Another need is that the carbon nanotubes be chemically linked to the substrate, such as plastic. Carbon nanotubes are functionalized for this purpose, which means that their surface has been chemically modified to allow for optimal incorporation into diverse materials and for the specific application in question.

Carbon nanotube production reached a record high of several thousand tonnes per year in 2013, with applications in energy storage, device modelling, sporting goods, water filters, automobile parts, boat hulls, coatings, thin-film electronics, actuators, and electromagnetic shields, among other things. The number of publications on carbon nanotubes more than tripled in the previous decade, and the number of patents

issued increased substantially as well. Carbon nanotubes have indeed been suggested for a hypothetical space elevator since they enable the creation of structures such as “forests”, threads, and regular sheets in much lesser amounts [52].

Recent research has shown the possibility of utilizing carbon nanotubes as critical components in fabricating three-dimensional macroscopic all-carbon circuits for various applications, including biomedical devices. A new radical-initiated thermal crosslinking method is described in this article for the production of macroscopic, free-standing, porous, all-carbon scaffolds made of single and multi-walled carbon nanotubes as building blocks, which may be used in conjunction with other materials [53]. The porosity of these scaffolds may be adjusted to suit the requirements of specific applications, and they contain macro, micro, and nanostructured pores. Three-dimensional all-carbon scaffolds/architectures are being investigated for a variety of applications, including the creation of next-generation energy storage devices, supercapacitors, field emission transistors, high-performance catalysis, photovoltaics, and biomedical devices and implants.

### 2.2.2 Carbon Nanofibers

Carbon nanofiber has been widely studied by a large number of researchers and in a broad range of practical uses, and it has been established as the most significant member of the carbon fibre family. Carbon nanofibers are produced when a hydrocarbon feedstock reacts chemically with a metallic catalyst. Carbon nanofibers are presently one of the most reliable nanofillers accessible, and their many properties enable them to be utilized in a broad variety of applications [54]. Carbon nanofibers are potential materials for a variety of applications, including electrical and electronic devices, electrode materials for supercapacitors, and sensors. In applications where the dispersion and percolation status of the matrix materials are essential [55–57], high electrical conductivity materials are typically advantageous because they may improve dispersion and percolation. When compared to raw carbon fibre, the structural properties of carbon nanofibers are very similar. Their mechanical, electromagnetic shielding, electrical, and thermal stability, all of which are improved by their presence on the nanometre scale, make them highly versatile and well known in the field of nanotechnology.

The properties of carbon nanofibers are determined by the fibre structure, which is determined by the manufacturing technique and post-treatment processes. Typical carbon nanofibers are a sequence of long, fibrous, platelet-type carbon layers arranged in layers perpendicular to the axis of the carbon nanofibers, with each layer being perpendicular to the axis of carbon nanofibers. The catalyst used to create the carbon nanofibers has an impact on the way they are organized. It is required to use particular, complex, and microscopic techniques to evaluate the structure and content of nanofibers to research their properties. Nanofibers have an average diameter of 50–200 nm and a single atom between 0.1 and 0.5 nm [58].

Carbon nanofibers, regardless of their microscopic size, possess excellent chemical and mechanical properties. The fact that different polymers will be thermally

treated after electrospinning allows them to retain their high electrical and thermal conductivity and dimensional stability [59]. Furthermore, they are lightweight, easy to manufacture, and shape, and have excellent corrosion resistance and excellent reinforcing capabilities. Carbon nanofibers are suitable for usage in thin films because of their low density of  $1.3\text{--}2\text{ g/cm}^3$ . Depending on temperature and material, their heat transfer coefficients range from 1950 to 6000 W/m K, while their electrical resistivities range from  $1 \times 10^{-3}$  to  $1 \times 10^{-4}$ . Its tensile strengths range between 2.92 and 500 GPa and its tensile modules from 220 to 1500 GPa in this material. In some instances, the carbon nanofibers can be as long as 100  $\mu\text{m}$  in length and feature pores 0.2  $\mu\text{m}$  in diameter [58].

Carbon nanofibers with a high aspect ratio, strong adhesion, homogenous distribution, and good dispersion between the polymer matrices and the carbon nanofiber are the most important factors to consider when manufacturing multifunctional carbon nanofibers and polymer composites reinforced with exceptional mechanical properties [60–62]. A technique known as melt mixing is the most effective way for creating composites that are compounded to allow carbon nanofibers to fulfil their purpose. To help and facilitate the distribution and dispersion of carbon nanofibers and preserve the high aspect ratio of carbon nanofibers, it is essential to feed carbon nanofibers after melting polymer pellets to use a compatibilizer to prevent mixing circumstances.

### **Applications of Carbon Nanofibers**

The use of carbon nanofibers has recently been expanded to include developing lithium-ion battery electrodes that are fourfolds the total storage capacity of existing lithium-ion batteries [63]. Recently, researchers are even using carbon nanofibers to create sensors that can detect the absorption of chemical vapours by altering the colour of their appearance; accord nanofiber sensors should be used to monitor the situation in which the layer that collects and filters pollutants in a gas mask gets saturated with potentially hazardous components or compounds [64]. The remarkable and one-of-a-kind structure of carbon nanofibers is responsible for their high reversible capacity, excellent cycle stability, and excellent electrochemical performance, among other things. This property is applicable when carbon nanofibers are used as electrodes for lithium-ion batteries capable of being recharged.

The availability of raw materials at reasonable prices will determine the direction of the market's development in carbon nanofibers in the future. Using a technology combining catalytic chemical vapour deposition [65], scientists and innovators have demonstrated their ability to manufacture large quantities of highly pure carbon nanofibers at a meagre cost. Additionally, stabilizing and carbonizing carbon nanofibers after electrospinning polyacrylonitrile is a simple, appropriate, and evident method of synthesizing continuous and fibrous carbon nanofibers [62].

### 2.3 Activated Carbon

Activated carbon refers to a range of Carbon-based materials such as carbonized biomass, lignite, coal, charcoal, and peat. Activated carbons are among the most efficient adsorbents due to their high adsorption capacity, high porosity, larger surface area, thermal stability, inertness, various surface chemistry, and high surface reactivity [66]. Figure 4 illustrates the use of activated carbon as an adsorbent owing to its porous structure and other physiochemical properties. Activated carbon is employed for various applications, including wastewater, water purification, medical purposes, gas storage, and separation. Activated carbon is applied in various forms: The granulated activated carbon (GAC) consists of granules of 600–4000  $\mu\text{m}$ , and the powdered activated carbon (PAC) consists of powdered particles of size lesser than 44  $\mu\text{m}$ . Although powdered activated carbon particles allow faster adsorption owing to their small size, they are less convenient to handle in fixed adsorption beds.

On the contrary, granulated activated carbon particles are easier to handle and can be regenerated easily but are relatively costlier. On the other hand, the fibrous activated carbon materials are the most expensive but cause the least hydrodynamic resistance to their ability to easily mould according to the shape of the adsorption system [67]. Recently, a lot of research is being carried out to discover novel environmentally friendly methods of producing activated carbon and its application in various fields.

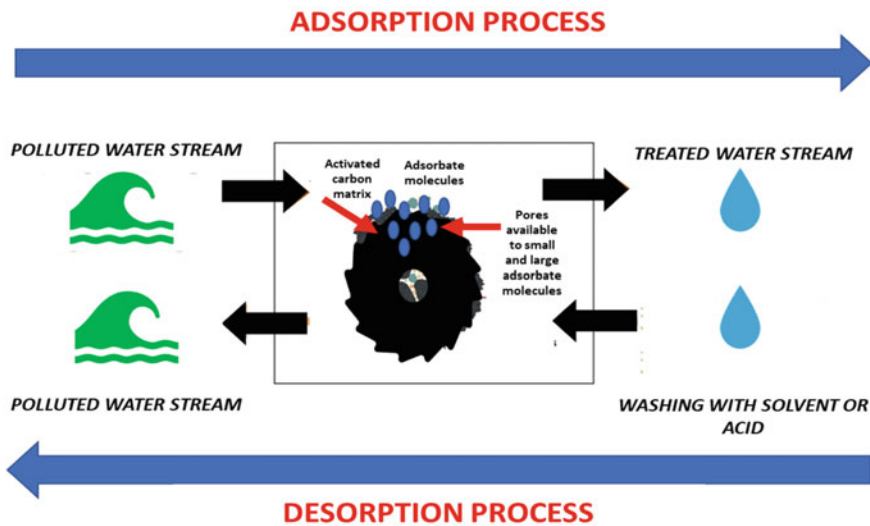


Fig. 4 Illustration of the use of activated carbon as an adsorbent for wastewater treatment



### 3 Adsorption Application

Porous carbon compounds have gotten a lot of attention due to technological advancements and the growing demand for resources. They are the most extensively used adsorbents in various environmental applications, primarily due to their microporosity and larger surface area (which substantially impacts the adsorption process). Due to their mild heat of adsorption, low energy consumption, high adsorption capacity, fast kinetics, cost-effectiveness, relatively easy regeneration, and the existence of various functional groups, they have proven to be a viable contender for adsorption. In general, the term “physisorption” is defined by the intermolecular force of interaction between adsorbents and adsorbates. The van der Waals force is a type of intermolecular force that exists. Since physisorption is also known as van der Waals adsorption, the binding force is weak with lower heat of adsorption, and the rate of adsorption and desorption rate is fast. Thus, the adsorbed gas on carbon base materials can be easily extracted without any changes. In contrast, chemical adsorption or chemisorption can be defined as the transfer, sharing, and exchange of electrons between adsorbents and adsorbates (atoms or molecules). In other words, the adsorption of adsorbates is due to the formatting of chemical bonding between them [68].

The characteristics of a carbon material are dependent on surface morphology determined by internal structure and their arrangement in the matrix. Recently, few researchers have prepared carbonic molecular sieves (CMS) and sorbents from various carbon materials. Typically, carbonic molecular sieves are microporous carbons with slit-shaped pore openings [69]. The gas adsorption of different adsorbate molecules is dependent on the size, structure, shape, and electronic interaction among the molecules with the adsorbent. Based on recent reports, adsorption of CO<sub>2</sub>, CH<sub>4</sub>, N<sub>2</sub>, and O<sub>2</sub> on carbon materials occurs in the micropores. This characteristic feature is because the carbon materials could be synthesized in fine powdered from a developed microporous structure and due to the specific nature of the interaction between gas molecules and carbon-based materials. Since carbon-based materials possess a high specific surface area and sizeable microporous volume, carbon can be considered one of the developed fast reaction adsorbents [70].

Most importantly, they are less humidity-sensitive than other CO<sub>2</sub>-philic materials currently available [8]. Based on those mentioned above, they are used in a wide range of applications such as gas adsorption and separation, decontamination of water, energy storage (supercapacitors), structural support (activated fibre), and biological applications (diagnostic materials, drug delivery). Porous carbons include activated carbon, soft and hard templated mesoporous carbons, activated carbon fibres, and porous nano-carbons, to name a few. Among all types of nano-porous materials, porous carbons are most used in numerous scientific, technological, and industrial sectors. When utilized as an adsorbent, a porous carbon material with a broad pore channel may considerably increase molecules' diffusion and diffusion properties [71].

Adsorption in porous materials is influenced by the strength of the fluid-wall and fluid-fluid interactions and the state and thermodynamic stability of fluids in narrow pores. Its absorption capacity for adsorbates is affected by the adsorbent (functional groups and pore size and structure) and the solution conditions (pH, ionic strength, and temperature). These forces influence chemical compound binding and accumulation on various adsorbents in the aqueous phase. Adsorption requires hydrogen and phosphorus bonds, covalent and electrostatic interactions, and the hydrophobic effect [72].

Physical contact (electrostatic or dispersive forces) and chemical bonding hold molecules or atoms (absorbable) to the carbon surface. As a result, CBM adsorbents must have a large specific surface area. In addition, activated carbons have micropores that are analogous to the adsorbate molecules. The ability of carbon molecular sieves to separate diverse species, particularly gas mixtures, is determined by the molecule's pore volume traversal [73]. Water vapour also affects the effectiveness of activated carbon beds in gas filters. The absorbed mixture's composition is another aspect to consider when assessing volatile chemical uptake by these carbon beds. Carbon adsorbents prefer fewer flammable chemicals. There is no clear relationship between a chemical compound's characteristics and the sorption bed's capacity [74].

Carbon aerogel, a novel form of mesoporous carbon material, is a promising adsorbent. The presence of oxygen, nitrogen, and sulphur compounds on the surface of carbon-based materials, notably carbon aerogels, can enhance the adsorbents' porosity, hydrophilicity, and selectivity [75]. Carbon nanoparticles are effective adsorbents for separating inorganic and organic contaminants due to their high selectivity and adsorption capacity. The development of carbon-based adsorbents for pollutant removal has been studied extensively. Carbon functional group interactions are critical in the elimination of contaminants from aqueous solutions. Analyses of carbon nanomaterial adsorption properties show that functionalization and decorating dominate [73]. Due to their ability to develop a large specific surface area (over 3000 m<sup>2</sup>/g.), tunable surface texture, and functionality, activated carbons have grown into a significant class of porous materials with a wide range of applications in large-scale industrial processes.

### **3.1 Gas Storage**

Typically, membrane gas separation occurs due to the differences in transport of the various species passing via the membrane itself. As far as gas separation within porous carbon materials is concerned, both porous inorganic and dense organic membranes can be used as selective gas separation films. However, mostly the gas separation membranes are made of either polymers or carbon-based materials [76], whereas the mechanism of gas storage in carbon-based materials significantly differs from the traditional gas reservoirs. The sorption capacity and amount of gas should

be analysed to evaluate the gas resources in carbon materials. The amount of gas indicates the gas content in carbon materials at starting reservoir pressure and temperature. Furthermore, the sorption capacity illustrates the maximum limit of gas content (i.e., upper limit of adsorptive capacity) as a function of pressure [77].

Carbon capture and storage technologies, which aim to reduce CO<sub>2</sub> emissions, increase attention from researchers from various backgrounds and disciplines. Most carbon capture and storage methods need an effective adsorbent to absorb CO<sub>2</sub> from sources like fossil fuels (pre-combustion) or flue gas from power production to capture CO<sub>2</sub> from sources such as these (post-combustion). Recent years have seen an increase in the series of research on the development of cost-effective adsorbents with a high capacity, strong stability, and the ability to regenerate. Because of their large surface area, superior resistance, and increased porosity, a variety of Nano-porous carbon materials, such as activated carbon, carbon nanotubes, and nanofibers, have been suggested as suitable supplies for this challenging job. These materials include activated carbon, carbon nanotubes, and nanofibers, among others. For example, the advancement of CO<sub>2</sub> capture, storage, and utilization strategies looks to be a logical solution [78].

Typically, heteroatom doping carbon materials with a tailored pore structure, surface functionality, chemical composition, and atomic architecture demonstrate exciting categories of porous carbon for various applications in the field of catalysis, energy conversion, gas storage, and water treatment. Compared to commercial carbon materials, heteroatom-doped carbon provides better electrocatalytic activity for reducing oxygen in both acidic and alkaline mediums. In addition, heteroatoms, such as nitrogen, sulphur, boron, and phosphorus with dual and ternary doped carbon materials, possess high durability in an alkaline/acidic environment. Meanwhile, heteroatoms doped with N, S, B, and P transform the surface functionality and chemical composition and impact the distribution of electrons of the carbon network, which enhances electrochemical properties and gas storage [79].

Nonetheless, one of the most pressing concerns with carbon capture and storage is that the process requires a certain level of energy consumption, resulting in extra CO<sub>2</sub> emissions [80, 81]. Hence, carbon capture and storage seek to improve CO<sub>2</sub> adsorption and adsorbent regeneration procedures to reduce offset. This has the potential to reduce CO<sub>2</sub> emissions by a significant amount. An adsorption unit packed with an adsorbent capable of high CO<sub>2</sub> absorption capacity may be included in designing a new power plant or retrofitting into an existing power plant to accomplish this objective. Depending on the technology used, CO<sub>2</sub> collected will either be transported and stored in designated CO<sub>2</sub> reservoirs or converted into other chemicals utilizing carbon capture in the early phases of development on a large commercial scale. In terms of CO<sub>2</sub> adsorption, such materials have a large surface area and pore volume, with some examples exhibiting selective adsorption to CO<sub>2</sub> from a mixture of gases. Adsorbed natural gas (ANG) technologies [82], which are currently under development, might also be beneficial to the various uses of methane as an energy vector because of its high efficiency.

When suitable adsorbents are used, the gas storage pressure within tanks may be lowered by up to 20% of the value needed for compressed natural gas (CNG). The

quantity of gas stored can be significantly increased at the same pressure [83]. It is believed that activated porous carbons are the most appealing of the different materials suggested for use in ANG applications for various reasons [84]. These characteristics include flexibility, which allows for fine-tuning of the porosity by adjusting the starting materials and reaction conditions, high mechanical and chemical stability, and the creation of low-cost and scalable performance characteristics [84]. To achieve carbon capture and sequestration at this time, several technical approaches are being pursued, including post-combustion, pre-combustion, oxy-combustion, chemical looping combustion (CLC), and even ambient air. The benefits and drawbacks of each of the routes mentioned are outlined in Table 3.

One of the most influential thermodynamic properties used to characterize the adsorption process is adsorption's differential isosteric molar heat. It yields a ratio between adsorbate/adsorbate and adsorbent/adsorbate interactions, and thus, it is deemed an essential factor for the storage of gases. The heat of adsorption plays a pivotal role in assessing the interactions between the gas species and the adsorbent

**Table 3** Advantages and disadvantages of current CO<sub>2</sub> capture technological processes [84]

Capture pathway	Advantages	Disadvantages
Post-combustion	Mature technology (e.g., aqueous monoethanolamine), commercially deployed in some industries Suitable for most existing power plants Possible for retrofit to existing plants	High parasitic power requirement Low capture efficiency due to low CO <sub>2</sub> partial pressure High capital and operating costs
Pre-combustion	High CO <sub>2</sub> concentration High partial pressure Mature physical absorption technology (e.g., Selexol and Rectisol), commercially deployed in some industries	Applicable mainly to new integrated coal gasification combined cycle (IGCC) plants H <sub>2</sub> -rich gas-induced temperature and efficiency issues
Oxyfuel combustion	Developed air separation technologies available Very high CO <sub>2</sub> concentration Possible for retrofit and repowering to existing plants	Costly and energy-intensive air separation step Retrofit unattractive due to significant plant changes
Chemical looping combustion	Very high CO <sub>2</sub> concentration Low-cost oxygen carrier materials	Immature, currently under development
Air capture	Truly and directly reduce the atmospheric CO <sub>2</sub> concentration A viable alternative for CO <sub>2</sub> captures from mobile and decentralized sources	Immature, currently under development Cost and an energy intensive due to deficient CO <sub>2</sub> concentration (–400 ppm) in air

material—both of these are positively correlated, i.e., with an increase in the heat of adsorption, the interactions between adsorbent material and gas species increase as well. This is a highly desirable trait because it increases the feasibility of the adsorption phenomenon. For hydrogen storage, an ideal adsorbent must possess small and uniform micropores at very high densities since it ensures an enhanced heat of adsorption [85]. A material like Activated Carbon with a higher heat of adsorption can perform without the requirement of excessive pressure or cooling conditions—making it an ideal candidate to be used as an adsorbent [86].

Numerous studies were conducted to successfully assess the kinetics and the thermodynamic factors associated with the process of adsorption. Both physical and chemical adsorption usually exhibit a largely endothermic nature with positive values of Enthalpy ( $\Delta H$ ). On the contrary, the Gibbs free energy ( $\Delta G$ ) calculated usually yields a negative value for both types of adsorption processes.  $\Delta G$  yielding a negative value suggests that the process is a spontaneous one and can effectively be used as an indicator to determine the feasibility of the adsorption process. The value of entropy of adsorption ( $\Delta S$ ) indicates a discernible decrease in randomness between the adsorbent and the target species (adsorbate). It also depicts a reduction in the degree of freedom for the adsorbate—this reveals that the adsorbent material has successfully entrapped the target species inside its structure. Carlos et al. conducted a study assessing a Microporous activated carbon material as adsorbent—the total entropy varied as temperature increased and ultimately declined at a steep rate indicating that molecules incurred a loss of one degree in terms of translational motion and one degree in terms of rotational movement during the adsorption process [87].

### ***3.2 Energy Storage Applications and Technology***

Large-scale gas storage for energy storage improves energy network management and integration of renewable energy sources. It also aids in the transition to a low-carbon economy by storing massive amounts of  $\text{CO}_2$ . Underground storage of  $\text{H}_2$ ,  $\text{CH}_4$ , and  $\text{CO}_2$  is proposed in porous rock formations or salt caverns, topped by impermeable rocks (cap rock) to prevent gas leakage to the surface [88]. For example, keeping natural gas (methane) at room temperature requires high density. Adsorption is utilized in bulk transportation and peak shaving in the natural gas industry. To date, the most efficient carbon adsorbents have reached the highest adsorption storage capacities. A large micropore volume per unit volume carbon is desired for methane adsorption at ambient temperatures. Commercial carbons can presently only store roughly half the compressed gas at 20 MPa (around 230 v/v methane at 298 K)[89].

Particle size selection allows for modest improvements in packing for granular carbon. Using low macropore carbon increases storage capacity. Carbides with many micropores per unit volume should be helpful for methane storage, as they adsorb more methane per unit mass than the original PVDC carbon [89]. Because of their structural stability, cyclability, and regeneration, nanopore-activated carbons are considered feasible  $\text{CO}_2$  storage materials via physisorption. Because nanopores

have a higher adsorption potential, they can condense more  $\text{CH}_4$  at lower pressures (30–40 bar). For porous materials with similar textural properties, adsorption values of 7.5 wt% are expected at 298 K [90]. Activated carbon was nitrogen doped with ammonia and then impregnated with platinum nanoparticles using ultrasonic. This is due to the lack of metal-encouraging storage mechanisms such as gas dissociation or rebuilding on platinum's surface and the negative consequences of metal pore-blocking and increased metal particle density [91].

In storing and transferring hydrogen gas, absorption (metal hydrides and complex hydrides) and adsorption are favoured (carbon materials). Adsorption of hydrogen on carbon compounds appears to be more efficient than absorption. Carbon compound pore size impacts hydrogen adsorption (50 nm). Adsorption and compression on solid surfaces combine to form physisorption capacity. The hydrogen-carbon bond is weak in any carbon material, and the low adsorption energy ruled out hydrogen adsorption in the nanotube interstitial channels. Despite its strong polarizability, graphite's interlayer distance and specific surface area (SSA) are negligible. Graphene platelets fill the gaps between the graphene sheets, providing a large surface area and more interaction sites for adsorbents [92].

### 3.3 Wastewater Treatment

For the last three decades, activated porous carbon has been widely used in water treatment or purification of wastes and gases in the industrial sector. Nevertheless, many efforts were given to produce activated porous carbon by reusing various natural resources and eventually preventing environmental pollution. Therefore, more and more innovations have been tried to optimize these carbonaceous materials in production and regeneration. Recent studies suggested that activated porous carbon comes in amorphous carbon, which can be functionalized to enhance the porous structure. Typically, these activated porous carbon are microporous, with excellent adsorption sites for the adsorption of chemical agents/species. This kind of adsorption can be attributed to the presence of van der Waals type of physical attraction. On the other hand, adsorption may cause the generation of covalent bonds between the adsorbate and active sites of porous carbon, which is also known as chemisorption [93, 94]. Table 4 demonstrates the wastewater applications of various carbonaceous material along with characteristic properties.

Recent research suggests that transforming the surface of carbon architecture improves the high adsorption performance of these carbon materials. Thus, the heteroatom-doped carbon materials with a tailored pore architecture illustrate exciting families of porous carbon materials in the area of water treatment. Many researchers have changed the surface of carbon materials by considering the reaction mechanism, permitting a higher degree of uptake of environmental contaminants by these adsorbents. Furthermore, functional chemical groups can directly interact with fused aromatic rings in hydrocarbon [68, 99]. Table 5 indicates the physicochemical

**Table 4** Characteristics features of various carbonaceous materials for wastewater treatment applications

Carbonaceous materials	Characteristic properties	Waste water treatment applications	References
Carbon nanotubes (CNTs)	Large surface area Ease of functionalization High aspect ratio Fast water transport	Brine and saline desalination Removal of heavy and toxic metals Oil water separation Removal of emerging pollutants	[95]
Graphene	High surface area Good hydrophilicity Tunable surface chemistry High mechanical strength Excellent corrosion resistance	Graphene oxide membrane filtration Water desalination Pre-treatment filtration Membrane applications	[96]
Carbon fiber	High stiffness High chemical resistance High temperature tolerance	Adsorption of organic pollutants Adsorption of inorganic pollutants Degradation of organic pollutants Microbial decontamination	[97]
Carbon black	High surface area to volume ratio Larger specific surface Ease of functionalization	Carbon-based filters for water treatment Carbon filters for removal of Biological and chemical oxygen demand and Total organic carbon Removal of Persistent organic pollutants (POPs)	[98]

surface adsorption of various activated porous carbon governed by the nature of the carbon precursor and initiating chemical reagents and activation methodologies.

#### 4 Membrane Separation by Carbon Materials

Typically, porous carbon-based membrane has become a novel approach to replace the current issues of the polymeric membrane in water and gas separation areas due to excellent sieving effect [108–110]. The pyrolysis process is one of the protocols of transforming a polymer-based membrane into a carbon-based membrane. The pyrolysis process is performed by differentiating the degree of porosity, structure, and features of separation, which are also dependent on carbonization conditions [111].

**Table 5** Experimental conditions of various activated porous carbon for removal of different chemical species

Carbon precursor	Activation process	Reagent used	Specific surface area (m <sup>2</sup> /g)	Pollutant	References
Apricot shell	Chemical	H <sub>3</sub> PO <sub>4</sub>	307	Tetracycline	[100]
Bamboo	Chemical	H <sub>3</sub> PO <sub>4</sub>	1400	Reactive black 5	[101]
Coconut husk and Shell	Chemical	KOH/NaOH	1448 and 876	Fluoride (F-), Methylene blue (MB)	[102, 103]
Durian shell	Physical	CO <sub>2</sub>	917	AMX and Tetracycline	[104]
Palm shell	Chemical	H <sub>2</sub> SO <sub>4</sub> + K <sub>2</sub> S <sub>2</sub> O <sub>8</sub>	770	Bis-A, 2,4, DNP and 4-CIP	[105]
Coffee husk and Coffee spent	Physical	H <sub>2</sub> O	383 and 464	Nickel	[106]
Acrylic fibrous waste	Physical	O <sub>2</sub>	280	Methylene blue (MB)	[107]

On the other hand, the inorganic-based membrane is usually exploited by complex fabrication methodology, problematic permeation property, and high-priced operational cost. At the same time, the simplistic approach of polymeric membranes due to simple fabrication and high mechanical strength can overpower the membrane performance compared to that of the inorganic membrane [112]. However, the operational temperature became the major limitation of the polymer membrane. Additionally, poor diffusivity and selectivity of specific gases are other drawbacks of polymeric membrane performance [54, 113, 114].

Recently, there has been an increase in the application of carbon-based membranes for water and gas separation due to the excellent sieving effect that offers better remarkable selectivity and excellent mechanical, the chemical and thermal stability of the commercially available polymeric membrane. Typically, carbon-based membranes were categorized into supported carbon membranes and unsupported carbon membranes [108]. The supported carbon membranes can be divided into two designs, namely tubular and flat. Most interestingly, supported membranes are more popular due to their excellent separation and mechanical stability in flat and tubular structures. The flat or tubular membranes are Tubular or flat supported carbon ranges attached to macro-porous substrates. At the same time, unsupported carbon-based membranes can be capillary, hollow or flat. Usually, hollow fibre membranes are used in H<sub>2</sub> separation because of cheap operational cost and excellent separation efficiency. However, the defect-free membrane layers can be produced by considering the following factors such as (a) polymer concentration; (b) percentage of



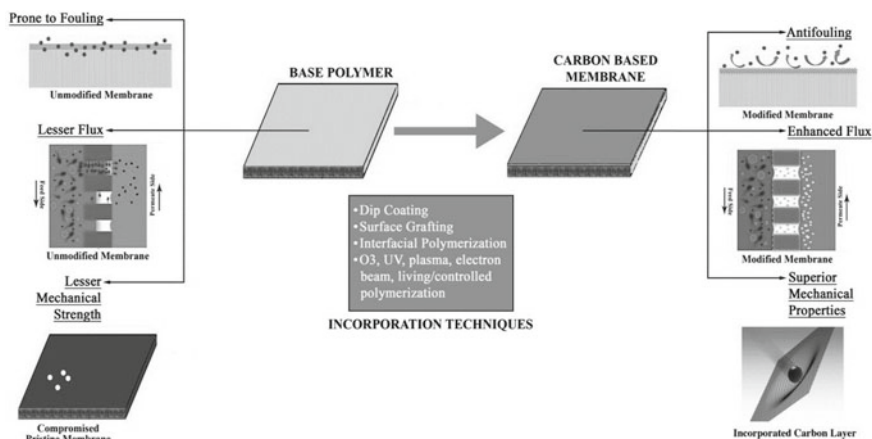
precursor solution (if needed); (b) coating methodology; (c) operational temperature; (d) operational pressure; and (e) operation time duration [115, 116].

#### **4.1 Mechanical and Chemical Stability**

Typically, carbon-based membranes were widely utilized for various purposes such as gas separation and wastewater treatment due to excellent separation efficiency, excellent mechanical stability, and lower production costs [117]. Carbon-based membranes possess remarkable mechanical stability because of their turbostratic or graphitic structure [118]. In addition, carbon-based membranes showed higher mechanical stability, which can withstand high pressure for a given membrane thickness [119]. Recent research suggested that carbon-based membranes exhibited maximum elastic modulus with lower breaking elongation points than polymeric membranes [120]. For instance, Linkov et al. has demonstrated various techniques to develop narrow pore sized distribution in carbon membranes. They fabricated carbon-based membranes by carbonizing asymmetrical polyacrylonitrile (PAN) precursors, which led to the production of a highly flexible range of porous carbon-based membranes with excellent pore size distribution along with remarkable porosity and excellent mechanical characteristics [121].

Interestingly, porous carbon-based membranes are more advantageous than polymeric membranes regarding thermal, selectivity, and chemical stability. More attention has been given to such materials (such as zeolites, silica, and carbon) having molecular sieving characteristics that seem to be emerging candidates in the field of gas separation and water treatment [122]. It was observed that carbon-based membranes exhibited remarkable absorptivity application in few specific gases, which results in better gas separation efficiency [123].

Furthermore, carbon-based membranes demonstrate good chemical stability while maintaining excellent permeate selectivity. The high permeate selectivity can be attributed to the connectivity of ultra-micropores (smaller than 0.4 nm) and micropores, leading to high porosity. Recent developments have allowed for the production of carbon-based membranes from polyimide membranes, capable of withstanding extremely high operating temperatures without deforming [113, 124, 125]. Because of their exceptional strength and extraordinary chemical and heat resistance capabilities, these carbon membranes can be manufactured with maximum carbon yields and maintain structural forms even after pyrolysis. Figure 5 illustrates the enhancement in physiochemical properties of the membrane after incorporating carbon-based material. Due to their outstanding heat and chemical tolerance, materials can be used to fabricate carbon membranes with high carbon yields and retain their structural shapes during high-temperature pyrolysis [54]. Table 6 provides an overview of carbon membranes in terms of transport method, chemical stability, and mechanical stability, as well as their mechanical properties.



**Fig. 5** Enhanced membrane characteristics after incorporation of carbon-based material

**Table 6** Insight of carbon membranes

Parameters	Impact	References
Separation mechanism	Knudson diffusion: $\geq 10 \text{ \AA}$ Solution diffusion: $\leq 50 \text{ \AA}$ Capillary condensation: $\geq 30 \text{ \AA}$ Molecular sieving: $\leq 6 \text{ \AA}$	[126]
Chemical stability	Excellent chemical stability with high permeate selectivity	[127]
Mechanical stability	Excellent mechanical strength Withstand high pressure	[128]
Advantages	Excellent thermal stability Excellent porosity It can be utilized at aggressive operation Cheap fabrication methodology	[127]
Disadvantages	Exposure to organic pollutants as well as water vapour might have a detrimental effect Brittle in nature	[129]

## 4.2 The Efficiency of Filtration Medium

New polymeric membranes are not effective enough in many separation operations, especially when dealing with emulsions with less than 20 mm droplets and usually require a follow-up treatment to separate the constituents [130]. Hence recently, a lot of research has been focussed on developing novel carbon-based materials having high separation efficiency. Out of various carbon allotropes, graphene and carbon nanotubes (CNTs) have drawn significant attention due to their one-dimensional

structure, high hydrophobicity, oleophilic nature, and large specific surface area [131]. Liu et al. used functionalized multi-walled carbon nanotubes (F-MWCNTs) for the separation process and found them highly effective for oil-water separation. The results showed that the functionalized multi-walled carbon nanotubes could remove 99.8% of oil from the oil-water emulsion [132]. In another study, Zhang et al. incorporated graphene oxide sheets on the surface of electrospun-aminated polyacrylonitrile (APAN) fibres. The modified membrane exhibited high hydrophilicity, flux over  $10,000 \text{ L}\cdot\text{m}^{-2}\cdot\text{h}^{-1}$ , very low oil adhesion, more than 98% rejection rate, and excellent antifouling properties for the separation of tested oil-water emulsion [133].

Although incorporating carbon allotropes onto a pure polymeric membrane has been shown to increase separation efficiency considerably, they are not stable enough under harsh conditions due to the base's low thermochemical stability (new polymeric membrane). To overcome this issue recently, a lot of research has been focussed on developing and using pristine carbon-based membranes having superior physicochemical properties, higher mechanical stability, and highly integrated operation. They pose high strength even in harsh conditions. However, these membranes are relatively pricey and have a higher environmental impact due to the additional chemical reagents required to clean these membranes. Hence, so far, they are not considered suitable for large-scale industrial operations.

## 5 Future Perspectives and Challenges

In today's modern world, the commercialization of carbon-based nanomaterials for environmental remediation is subjected to eco-systems [134]. Therefore, researchers are doing various studies to analyse the toxicity level, human risk assessment, life cycle assessment (LCA), and dispersion of nanomaterials in the water system. These prominent findings would result in better dispersion of nanomaterials in water systems [135, 136]. Additionally, due to extensive research and development on carbon-based nano-porous adsorbents for gas storage application, it is expected that an enhanced techno-economical process will strengthen the adsorption performance of various gas. Therefore, it can be concluded that carbon-based nanomaterials play a prominent role in advancing novel and innovative technologies for sustainable renewable energy [137].

Regardless of excellent research and development in the field of environmental remediation using gas storage, membrane fabrication, and adsorption-catalytic process using various sustainable porous carbon materials such as carbon nanofibers, carbon nanotubes, quantum dots, GO, and RGO, more attention is needed to focus on below-mentioned problems in future advancements [136, 138, 139]:

- Development of novel methodologies for fabrication of cost-effective carbon-based nanomaterials for the enhanced absorption-catalytic process.
- More emphasis on the reusability of magnetic carbon nanomaterials for water treatment.

- Research and development on cost-effective adsorbents for removal of organic dyes and pollutants.
- Reusing of biowaste-derived carbon materials of environmental remediation.
- Evaluation of life cycle assessment and toxicity of various carbon nanomaterials reduces the potential threat to human lives.
- Advancements of tunned nanomaterials with hydrogen-rich moieties to improve the hydrogen storage adaptability and performance.
- More emphasis must be given to machine learning, as it emerges as the powerful subject for improvised product designing and production of hydrogen storage materials.
- Exploring more and more 2-D carbon-based nanosheets which could improve the efficiency of hydrogen storage.

Carbon materials have attracted a great deal of scientific attention due to their wide variety of uses and exceptional characteristics. For example, porous carbon materials, such as activated carbon, have long been employed as adsorbents in water treatment, gas separation, gas purification, and storage. However, the challenges offered by these materials have maintained the researchers' attention. For example, while activated carbon has been used to treat residential and industrial water for decades, the tremendous effort of preparing them from various sources has significantly reduced adsorbent manufacturing costs [140, 141].

However, one of the most significant drawbacks of utilizing activated carbon in water treatment is that its adsorption capacity deteriorates with time, increasing foreign molecule adhesion on the active site, necessitating heat regeneration or complete medium replacement [142]. Furthermore, activated carbon treatment is insufficient since it lacks disinfection, requiring post-treatment, which raises overall expenditures and effluent discharge [143]. Therefore, other porous carbon materials, such as graphene oxide, activated carbon enhanced with nanoparticles, and Nanoporous carbon generated from metal-organic frameworks (MOF), have been developed to overcome these concerns since they have greater selectivity, permeability, and electrical conductivity.

Porous carbon compounds offer enhanced gas storage capabilities and are reversible and fast-kinetics adsorption process [144]. However, even though hydrogen is one of the cleanest fuels, storing hydrogen is challenging. Liquid hydrogen has traditionally been stored at very low temperatures and high pressures, making it difficult and dangerous. As a result, solid-state hydrogen storage based on porous carbon materials has a promising future.

Overall, it appears that porous carbon materials could be useful in water treatment and gas storage. They are affordable adsorbents with high selectivity, recyclability, and fast kinetics. However, they will need to put in more effort to expand their gas storage capacity. In addition, it is also crucial to address early activated carbon inactivation and improve long-term stability. Another area that may be looked at is the use of materials to capture harmful and hazardous gases.

## 6 Conclusion

This book chapter reviewed the progress achieved in terms of processing and applications of porous carbon nanomaterials. The low-dimensional carbon materials such as carbon nanotubes, carbon nanofibers, graphene, graphene oxides, reduced graphene oxides, and their derivatives were in the field of environmental issues, remediation, and applications. Despite the extensive use of breakthrough technologies, adsorption or integrated adsorption-catalysis can be regarded as effective in a mass production application, given porous carbon materials' feasibility, cost, and processability. Despite the extensive use of breakthrough technologies, adsorption or integrated adsorption-catalysis can be regarded as effective in a mass production application, given porous carbon materials' feasibility, cost, and processability. Thus, more research and development can be performed in the real field using collaboration among academic groups and industrial facilities.

Recently, green nanotechnology has been considered in various fields, including manufacturing, product designing, and applications development. More research and development must be explored for nanomaterials. The present book chapter presented the importance of carbon-based nanomaterials for water treatment and gas storage applications. The versatility of carbon nanomaterials was attributed to their properties, including excellent average pore size and pore size distribution, higher surface area, ease of chemical tunability, and surface modification of porous carbon nanomaterials making them promising candidates for environmental remediation and energy as well as gas storage. Tuning the surface of carbon nanomaterials provides additional opportunities to tailor desired chemical modification for the applications mentioned above. Carbon nanomaterials are highly usable for environmental remediation due to the ease of tuning surface chemistry via modification of oxidation levels, surface tailoring, and opportunities for doping. Environmentalists, scientists, engineers, and product engineers should collaborate on multidisciplinary research projects as an emerging field.

## References

1. Gupta VK, Saleh TA (2013) Sorption of pollutants by porous carbon, carbon nanotubes and fullerene-an overview. *Environ Sci Pollut Res* 20:2828–2843
2. Borchardt L, Zhu Q-L, Casco ME, Berger R, Zhuang X, Kaskel S, Feng X, Xu Q (2017) Toward a molecular design of porous carbon materials. *Mater Today* 20:592–610
3. Lee J, Kim J, Hyeon T (2006) Recent progress in the synthesis of porous carbon materials. *Adv Mater* 18:2073–2094
4. Matos I, Bernardo M, Fonseca I (2017) Porous carbon: a versatile material for catalysis. *Catal Today* 285:194–203
5. Vix-Guterl C, Frackowiak E, Jurewicz K, Friebe M, Parmentier J, Béguin F (2005) Electrochemical energy storage in ordered porous carbon materials. *Carbon* 43:1293–1302
6. Wang L, Hu X (2018) Recent advances in porous carbon materials for electrochemical energy storage. *Chem—An Asian J* 13:1518–1529

7. Xia Y, Yang Z, Zhu Y (2013) Porous carbon-based materials for hydrogen storage: advancement and challenges. *J Mater Chem A* 1:9365–9381
8. Zhang X-Q, Li W-C, Lu A-H (2015) Designed porous carbon materials for efficient CO<sub>2</sub> adsorption and separation. *New Carbon Mater* 30:481–501
9. Chen S, Wang G, Li S, Li X, Yu H, Quan X (2020) Porous carbon membrane with enhanced selectivity and antifouling capability for water treatment under electrochemical assistance. *J Colloid Interface Sci* 560:59–68
10. Akasaka H, Takahata T, Toda I, Ono H, Ohshio S, Himeno S, Kokubu T, Saitoh H (2011) Hydrogen storage ability of porous carbon material fabricated from coffee bean wastes. *Int J Hydrogen Energy* 36:580–585
11. Lu S-N, Xie N, Feng L-C, Zhong J (2015) Applications of nanostructured carbon materials in constructions: the state of the art. *J Nanomater* 2015
12. Derbyshire F, Jagtoyen M, Andrews R, Rao A, Martin-Gullon I, Grulke EA (2001) Carbon materials in environmental applications. In: *Chemistry and physics of carbon*, pp 1–66
13. Gopinath KP, Vo DVN, Prakash DG, Joseph AA, Viswanathan S, Arun J (2020) Environmental applications of carbon-based materials: a review. *Environ Chem Lett*:1–26
14. Tan CW, Tan KH, Ong YT, Mohamed AR, Zein SHS, Tan SH (2012) Energy and environmental applications of carbon nanotubes. *Environ Chem Lett* 10:265–273
15. Muqet M, Gadhi TA, Mahar RB, Bonelli B (2020) Advanced nanomaterials for ultrafiltration membranes application. In: *Nanomaterials for the detection and removal of wastewater pollutants*. Elsevier, pp 145–160
16. Shahrin S, Lau W-J, Kartohardjono S, Gohari RJ, Goh P-S, Jaafar J, Ismail AF (2019) Development of adsorptive ultrafiltration membranes for heavy metal removal. In: *Advanced nanomaterials for membrane synthesis and its applications*. Elsevier, pp 1–22
17. Nas MS, Calimli MH, Acidereli H, Karatas Y, Gulcan M, Sen F (2021) Polymer-based nanomaterials to use in hydrogen acquisition and hydrogen energy storage. In: *Nanomaterials for hydrogen storage applications*. Elsevier, pp 153–186
18. Han X, Li S, Peng Z, Al-Yuobi ARO, Bashammakh ASO, Leblanc RM (2016) Interactions between carbon nanomaterials and biomolecules. *J Oleo Sci:ess*15248
19. Lee K, Mazare A, Schmuki P (2014) One-dimensional titanium dioxide nanomaterials: nanotubes. *Chem Rev* 114:9385–9454
20. Singh RP (2011) Prospects of nanobiomaterials for biosensing. *Int J Electrochem*
21. Baby R, Saifullah B, Hussein MZ (2019) Carbon nanomaterials for the treatment of heavy metal-contaminated water and environmental remediation. *Nanoscale Res Lett* 14:1–17
22. Wang Y, Hu A (2014) Carbon quantum dots: synthesis, properties and applications. *J Mater Chem C* 2:6921–6939
23. Marsh H, Reinoso FR (2006) *Activated carbon*. Elsevier
24. Kang Z, Lee S-T (2019) Carbon dots: advances in nanocarbon applications. *Nanoscale* 11:19214–19224
25. Popov VN (2004) Carbon nanotubes: properties and application. *Mater Sci Eng R Rep* 43:61–102
26. Soldano C, Mahmood A, Dujardin E (2010) Production, properties and potential of graphene. *Carbon* 48:2127–2150
27. Zhu Y, Murali S, Cai W, Li X, Suk JW, Potts JR, Ruoff RS (2010) Graphene and graphene oxide: synthesis, properties, and applications. *Adv Mater* 22:3906–3924
28. Yao J, Wang H, Chen M, Yang M (2019) Recent advances in graphene-based nanomaterials: properties, toxicity and applications in chemistry, biology and medicine. *Microchim Acta* 186:1–25
29. Singh Z, Singh R (2017) Toxicity of graphene based nanomaterials towards different bacterial strains: a comprehensive review. *Am. J. Life Sci* 5:1–9
30. Chong Y, Ma Y, Shen H, Tu X, Zhou X, Xu J, Dai J, Fan S, Zhang Z (2014) The in vitro and in vivo toxicity of graphene quantum dots. *Biomaterials* 35:5041–5048
31. Pan D, Zhang J, Li Z, Wu M (2010) Hydrothermal route for cutting graphene sheets into blue-luminescent graphene quantum dots. *Adv Mater* 22:734–738

32. Sun Y-P, Zhou B, Lin Y, Wang W, Fernando KS, Pathak P, Mezziani MJ, Harruff BA, Wang X, Wang H (2006) Quantum-sized carbon dots for bright and colorful photoluminescence. *J Am Chem Soc* 128:7756–7757
33. Tabish TA, Scotton CJ, Ferguson DCJ, Lin L, der Veen AV, Lowry S, Ali M, Jabeen F, Ali M, Winyard PG (2018) Biocompatibility and toxicity of graphene quantum dots for potential application in photodynamic therapy. *Nanomedicine* 13:1923–1937
34. Wang S, Cole IS, Li Q (2016) The toxicity of graphene quantum dots. *RSC Adv* 6:89867–89878
35. Yi M, Shen Z (2015) A review on mechanical exfoliation for the scalable production of graphene. *J Mater Chem A* 3:11700–11715
36. Zhang L, Li X, Huang Y, Ma Y, Wan X, Chen Y (2010) Controlled synthesis of few-layered graphene sheets on a large scale using chemical exfoliation. *Carbon* 48:2367–2371
37. Lv X, Zhang T, Luo Y, Zhang Y, Wang Y, Zhang G (2020) Study on carbon nanotubes and activated carbon hybrids by pyrolysis of coal. *J Anal Appl Pyrol* 146:104717
38. Ruiz-Cornejo JC, Sebastián D, Lázaro MJ (2020) Synthesis and applications of carbon nanofibers: a review. *Rev Chem Eng* 36:493–511
39. Hynes NRJ, Sankaranarayanan R, Kathiresan M, Senthamaraikannan P, Khan A, Asiri AM, Khan I (2019) Synthesis, properties, and characterization of carbon nanotube-reinforced metal matrix composites. In: *Nanocarbon and its composites*. Elsevier, pp 805–830
40. Deokar G, Avila J, Razado-Colambo I, Codron J-L, Boyaval C, Galopin E, Asensio M-C, Vignaud D (2015) Towards high quality CVD graphene growth and transfer. *Carbon* 89:82–92
41. Huang X, Qi X, Boey F, Zhang H (2012) Graphene-based composites. *Chem Soc Rev* 41:666–686
42. Lebedev A, Lebedev S, Novikov S, Davydov VY, Smirnov A, Litvin D, Makarov YN, Levitskii V (2016) Supersensitive graphene-based gas sensor. *Tech Phys* 61:453–457
43. Bansal R, Goyal M (2005) Activated carbon adsorption and environment: adsorptive removal of organic from water, activated carbon adsorption. Taylor & Francis, Boca Raton, pp 297–372
44. Saka C (2012) BET, TG–DTG, FT-IR, SEM, iodine number analysis and preparation of activated carbon from acorn shell by chemical activation with ZnCl<sub>2</sub>. *J Anal Appl Pyrol* 95:21–24
45. Dias JM, Alvim-Ferraz MC, Almeida MF, Rivera-Utrilla J, Sánchez-Polo M (2007) Waste materials for activated carbon preparation and its use in aqueous-phase treatment: a review. *J Environ Manage* 85:833–846
46. Ruparelia J, Duttagupta S, Chatterjee A, Mukherji S (2008) Potential of carbon nanomaterials for removal of heavy metals from water. *Desalination* 232:145–156
47. Gomis-Berenguer A, Velasco LF, Velo-Gala I, Ania CO (2017) Photochemistry of nanoporous carbons: perspectives in energy conversion and environmental remediation. *J Colloid Interface Sci* 490:879–901
48. Zhang R, Zhang Y, Zhang Q, Xie H, Qian W, Wei F (2013) *ACS Nano* 7:6156
49. Bandoz TJ (2020) Nanoporous carbon materials: from char to sophisticated 3-D graphene-like structures. In: *Nanoporous materials for molecule separation and conversion*. Elsevier, pp 45–64
50. Pitroda J, Jethwa B, Dave S (2016) A critical review on carbon nanotubes. *Int J Constr Res Civ Eng* 2:36–42
51. De Volder MF, Tawfick SH, Baughman RH, Hart AJ (2013) Carbon nanotubes: present and future commercial applications. *Science* 339:535–539
52. Collins PG, Avouris P (2000) Nanotubes for electronics. *Sci Am* 283:62–69
53. Lalwani G, Kwaczala AT, Kanakia S, Patel SC, Judex S, Sitharaman B (2013) Fabrication and characterization of three-dimensional macroscopic all-carbon scaffolds. *Carbon* 53:90–100
54. Ray SS, Lee HK, Huyen DTT, Park Y-I, Park H, Nam S-E, Kim I-C, Kwon Y-N (2021) Fluorine-free anti-droplet surface modification by hexadecyltrimethoxysilane-modified silica nanoparticles-coated carbon nanofibers for self-cleaning applications. *Prog Org Coat* 153:106165

55. Guadagno L, Raimondo M, Vittoria V, Vertuccio L, Lafdi K, De Vivo B, Lamberti P, Spinelli G, Tucci V (2013) The role of carbon nanofiber defects on the electrical and mechanical properties of CNF-based resins. *Nanotechnology* 24:305704
56. Morgan P (2005) Carbon fibers and their composites. CRC Press
57. Hammel E, Tang X, Trampert M, Schmitt T, Mauthner K, Eder A, Pötschke P (2004) Carbon nanofibers for composite applications. *Carbon* 42:1153–1158
58. Yiğit A, Alma MH, Akinay Y, Mengeş N (2021) Design, synthesis and antimicrobial activities of new carbon nanotubes derivatives. *J Inst Sci Technol* 11:1420–1429
59. Ray SS, Chen S-S, Li C-W, Nguyen NC, Nguyen HT (2016) A comprehensive review: electrospinning technique for fabrication and surface modification of membranes for water treatment application. *RSC Adv* 6:85495–85514
60. Lu W, Zu M, Byun JH, Kim BS, Chou TW (2012) State of the art of carbon nanotube fibers: opportunities and challenges. *Adv Mater* 24:1805–1833
61. Chand S (2000) Review carbon fibers for composites. *J Mater Sci* 35:1303–1313
62. Wangxi Z, Jie L, Gang W (2003) Evolution of structure and properties of PAN precursors during their conversion to carbon fibers. *Carbon* 41:2805–2812
63. De las Casas C, Li W (2012) A review of application of carbon nanotubes for lithium ion battery anode material. *J Power Sour* 208:74–85
64. Ray SS, Lee HK, Huyen DTT, Chen S-S, Kwon Y-N (2022) Microplastics waste in environment: a perspective on recycling issues from PPE kits and face masks during the COVID-19 pandemic. *Environ Technol Inno*:102290
65. Yoon YJ, Baik HK (2001) Catalytic growth mechanism of carbon nanofibers through chemical vapor deposition. *Diam Relat Mater* 10:1214–1217
66. Soni R, Bhardwaj S, Shukla DP (2020) Various water-treatment technologies for inorganic contaminants: current status and future aspects, In: *Inorganic pollutants in water*. Elsevier, pp 273–295
67. Uddin MK (2017) A review on the adsorption of heavy metals by clay minerals, with special focus on the past decade. *Chem Eng J* 308:438–462
68. Rehman A, Park M, Park S-J (2019) Current progress on the surface chemical modification of carbonaceous materials. *Coatings* 9:103
69. Son S-J, Choi J-S, Choo K-Y, Song S-D, Vijayalakshmi S, Kim T-H (2005) Development of carbon dioxide adsorbents using carbon materials prepared from coconut shell. *Korean J Chem Eng* 22:291–297
70. Vasiliev L, Kanonchik L, Kulakov A, Mishkinis D, Safonova A, Luneva N (2006) Activated carbon fiber composites for ammonia, methane and hydrogen adsorption. *Int J Low-Carbon Technol* 1:95–111
71. Zhang W, Bao Y, Bao A (2020) Preparation of nitrogen-doped hierarchical porous carbon materials by a template-free method and application to CO<sub>2</sub> capture. *J Environ Chem Eng* 8:103732
72. Yang K, Xing B (2010) Adsorption of organic compounds by carbon nanomaterials in aqueous phase: Polanyi theory and its application. *Chem Rev* 110:5989–6008
73. Sabzehmeidani MM, Mahnaee S, Ghaedi M, Heidari H, Roy VA (2021) Carbon based materials: a review of adsorbents for inorganic and organic compounds. *Mater Adv* 2:598–627
74. Nelson G, Harder C (1974) Respirator cartridge efficiency studies: V Effect of solvent vapor. *Am Indus Hygiene Asso J* 35:391–410
75. Hu L, He R, Lei H, Fang D (2019) Carbon aerogel for insulation applications: a review. *Int J Thermophys* 40:1–25
76. Gugliuzza A, Basile A (2014) Membranes for clean and renewable power applications. Woodhead Publishing
77. Thakur P, Schatzel SJ, Aminian K, Rodvelt G, Mosser MH, D'Amico JS (2020) Coal bed methane: theory and applications. Elsevier 2020
78. Li L, Zhao N, Wei W, Sun Y (2013) A review of research progress on CO<sub>2</sub> capture, storage, and utilization in Chinese Academy of Sciences. *Fuel* 108:112–130



79. Gao Y, Wang Q, Ji G, Li A, Niu J (2021) Doping strategy, properties and application of heteroatom-doped ordered mesoporous carbon. *RSC Adv* 11:5361–5383
80. Williamson R (2013) Global CO<sub>2</sub> concentrations pass 400 ppm milestone. Future Sci Ltd United House, 2 Albert PL, London, N3 1QB, England
81. Yang H, Xu Z, Fan M, Gupta R, Slimane RB, Bland AE, Wright I (2008) Progress in carbon dioxide separation and capture: a review. *J Environ Sci* 20:14–27
82. Byamba-Ochir N, Shim WG, Balathanigaimani M, Moon H (2017) High density Mongolian anthracite based porous carbon monoliths for methane storage by adsorption. *Appl Energy* 190:257–265
83. Kizzie AC, Dailly A, Perry L, Lail MA, Lu W, Nelson TO, Cai M, Zhou H-C (2014) Enhanced methane sorption in densified forms of a porous polymer network. *Mater Sci Appl* 2014
84. Casco ME, Martínez-Escandell M, Kaneko K, Silvestre-Alberro J, Rodríguez-Reinoso F (2015) Very high methane uptake on activated carbons prepared from mesophase pitch: a compromise between microporosity and bulk density. *Carbon* 93:11–21
85. Schlappbach L, Züttel A (2011) Hydrogen-storage materials for mobile applications. *Mater Sustain Energy*:265–270
86. Fomkin A, Pribylov A, Men'shchikov I, Shkolin A, Aksyutin O, Ishkov A, Romanov K, Khozina E (2021) Adsorption-based hydrogen storage in activated carbons and model carbon structures. *Reactions* 2:209–226
87. Cesar-Llopiz PJ, Hotza PD, Rockwood-Sánchez TJ (2013) Thermodynamic parameters of adsorption from systems activated carbon chlordiazepoxide and activated carbon-diazepam. *Revista Cubana de Química* 25:235–249
88. Tarkowski R, Uliasz-Misiak B, Tarkowski P (2021) Storage of hydrogen, natural gas, and carbon dioxide—geological and legal conditions. *Int J Hydrogen Energy* 46:20010–20022
89. Quinn D, MacDonald J (1992) Natural gas storage. *Carbon* 30:1097–1103
90. Conte G, Stelitano S, Policicchio A, Minuto FD, Lazzaroli V, Galiano F, Agostino RG (2020) Assessment of activated carbon fibers from commercial Kevlar<sup>®</sup> as nanostructured material for gas storage: effect of activation procedure and adsorption of CO<sub>2</sub> and CH<sub>4</sub>. *J Anal Appl Pyrol* 152:104974
91. Aboud MFA, Alothman ZA, Bagabas AA (2021) Storage and separation of methane and carbon dioxide using platinum-decorated activated carbons treated with ammonia. *Mater Res Exp* 8:025503
92. Mohan M, Sharma VK, Kumar EA, Gayathri V (2019) Hydrogen storage in carbon materials—a review. *Energy Storage* 1:e35
93. Liu Y, Li X, Fan L, Li S, Maleki Kheimeh Sari H, Qin J (2019) A review of carbon-based materials for safe lithium metal anodes. *Front Chem* 7:721
94. ben Mosbah M, Mechi L, Khiari R, Moussaoui Y (2020) Current state of porous carbon for wastewater treatment. *Processes* 8:1651
95. Li Y, Zhao Y, Hu W, Ahmad I, Zhu Y, Peng X, Luan Z (2007) Carbon nanotubes—the promising adsorbent in wastewater treatment. *J Phys: Conf Ser*:140
96. Kyzas GZ, Deliyanni EA, Matis KA (2014) Graphene oxide and its application as an adsorbent for wastewater treatment. *J Chem Technol Biotechnol* 89:196–205
97. Matsumoto S, Ohtaki A, Hori K (2012) Carbon fiber as an excellent support material for wastewater treatment biofilms. *Environ Sci Technol* 46:10175–10181
98. Pollard S, Fowler G, Sollars C, Perry R (1992) Low-cost adsorbents for waste and wastewater treatment: a review. *Sci Total Environ* 116:31–52
99. Wang Y, Zhu M, Li Y, Zhang M, Xue X, Shi Y, Dai B, Guo X, Yu F (2018) Heteroatom-doped porous carbon from methyl orange dye wastewater for oxygen reduction. *Green, Energy Environ* 3:172–178
100. Marzbali MH, Esmaili M (2017) Fixed bed adsorption of tetracycline on a mesoporous activated carbon: experimental study and neuro-fuzzy modeling. *J Appl Res Technol* 15:454–463
101. AkankshaKalra HP, Hui C, Mackey H, Ansari T, Saleem J, McKay G (2019) Adsorption of dyes from water on to bamboo-based activated carbon-error analysis method for accurate isotherm parameter determination. *J Water Sci Eng* 1:1–11

102. Talat M, Mohan S, Dixit V, Singh DK, Hasan SH, Srivastava ON (2018) Effective removal of fluoride from water by coconut husk activated carbon in fixed bed column: experimental and breakthrough curves analysis. *Groundwater Sustain Dev* 7:48–55
103. Islam MA, Ahmed M, Khanday W, Asif M, Hameed B (2017) Mesoporous activated coconut shell-derived hydrochar prepared via hydrothermal carbonization-NaOH activation for methylene blue adsorption. *J Environ Manage* 203:237–244
104. Yazidi A, Atrous M, Soetaredjo FE, Sellaoui L, Ismadji S, Erto A, Bonilla-Petriciolet A, Dotto GL, Lamine AB (2020) Adsorption of amoxicillin and tetracycline on activated carbon prepared from durian shell in single and binary systems: experimental study and modeling analysis. *Chem Eng J* 379:122320
105. Pamidimukkala PS, Soni H (2018) Efficient removal of organic pollutants with activated carbon derived from palm shell: spectroscopic characterisation and experimental optimisation. *Environ Chem Eng* 6:3135–3149
106. Rodriguez MH, Yperman J, Carleer R, Maggen J, Dadi D, Gryglewicz G, Van der Bruggen B, Hernández JF, Calvis AO (2018) Adsorption of Ni (II) on spent coffee and coffee husk based activated carbon. *J Environ Chem Eng* 6:1161–1170
107. Naeem S, Baheti V, Wiener J, Marek J (2017) Removal of methylene blue from aqueous media using activated carbon web. *J Textile Inst* 108:803–811
108. Sazali N (2020) A review of the application of carbon-based membranes to hydrogen separation. *J Mater Sci* 55:11052–11070
109. Hamm JB, Ambrosi A, Griebeler JG, Marcilio NR, Tessaro IC, Pollo LD (2017) Recent advances in the development of supported carbon membranes for gas separation. *Int J Hydrogen Energy* 42:24830–24845
110. Ray SS, Dommati H, Wang J-C, Lee HK, Park Y-I, Park H, Kim I-C, Chen S-S, Kwon Y-N (2021) Facile approach for designing a novel micropatterned antiwetting membrane by utilizing 3D printed molds for improved desalination performance. *J Membr Sci* 637:119641
111. Owais C, James A, John C, Dhali R, Swathi RS (2018) Selective permeation through one-atom-thick nanoporous carbon membranes: theory reveals excellent design strategies! *J Phys Chem B* 122:5127–5146
112. Ray SS, Verma RK, Singh A, Myung S, Park Y-I, Kim I-C, Lee HK, Kwon Y-N (2022) Exploration of time series model for predictive evaluation of long-term performance of membrane distillation desalination. *Process Saf Environ Prot* 160:1–12
113. Ray SS, Lee H-K, Kwon Y-N (2020) Review on blueprint of designing anti-wetting polymeric membrane surfaces for enhanced membrane distillation performance. *Polymers* 12(2020):23
114. Ray SS, Deb CK, Chang H-M, Chen S-S, Ganesapillai M (2021) Fouling and wetting: a major challenge for membrane distillation, environmental biotechnology, vol 3. Springer, pp 161–192
115. Ma L, Lv E, Du L, Han Y, Lu J, Ding J (2017) A flow-through tubular catalytic membrane reactor using zirconium sulfate tetrahydrate-impregnated carbon membranes for acidified oil esterification. *J Energy Inst* 90:875–883
116. Salleh W, Ismail A (2013) Effect of stabilization condition on PEI/PVP-based carbon hollow fiber membranes properties. *Sep Sci Technol* 48:1030–1039
117. He X (2018) A review of material development in the field of carbon capture and the application of membrane-based processes in power plants and energy-intensive industries. *Energy, Sustain Soc* 8:1–14
118. Marsh H, Rodriguez-Reinoso F (2000) *Sciences of carbon materials*: Universidad de Alicante. Secretariado de Publicaciones, Spain
119. Koresh JE, Soffer A (1987) The carbon molecular sieve membranes. General properties and the permeability of CH<sub>4</sub>/H<sub>2</sub> mixture. *Sep Sci Technol* 22(1987):973–982
120. Ismail AF, David L (2001) A review on the latest development of carbon membranes for gas separation. *J Membr Sci* 193:1–18
121. Linkov V, Sanderson R, Jacobs E (1994) Highly asymmetrical carbon membranes. *J Membr Sci* 95:93–99

122. Chen Y, Yang R (1994) Preparation of carbon molecular sieve membrane and diffusion of binary mixtures in the membrane. *Ind Eng Chem Res* 33:3146–3153
123. Liang C, Sha G, Guo S (1999) Carbon membrane for gas separation derived from coal tar pitch. *Carbon* 37:1391–1397
124. Sinha Ray S, Singh Bakshi H, Dangayach R, Singh R, Deb CK, Ganesapillai M, Chen S-S, Purkait MK (2020) Recent developments in nanomaterials-modified membranes for improved membrane distillation performance. *Membranes* 10(2020):140
125. Ray SS, Dangayach R, Kwon Y-N (2021) Surface engineering for anti-wetting and antibacterial membrane for enhanced and fouling resistant membrane distillation performance. *Chem Eng J* 405:126702
126. Salleh WNW, Ismail AF, Matsuura T, Abdullah MS (2011) Precursor selection and process conditions in the preparation of carbon membrane for gas separation: a review. *Sep Purif Rev* 40:261–311
127. Salleh W, Ismail AF (2015) Carbon membranes for gas separation processes: recent progress and future perspective. *J Mem Sci Res* 1:2–15
128. Tománek D, Kyrilchuk A (2019) Designing an all-carbon membrane for water desalination. *Phys Rev Appl* 12:024054
129. Kluiters S (2004) Status review on membrane systems for hydrogen separation, Energy Center of the Netherlands, Petten, The Netherlands
130. Al-Anzi BS, Siang OC (2017) Recent developments of carbon based nanomaterials and membranes for oily wastewater treatment. *RSC Adv* 7:20981–20994
131. Thines R, Mubarak N, Nizamuddin S, Sahu J, Abdullah E, Ganesan P (2017) Application potential of carbon nanomaterials in water and wastewater treatment: a review. *J Taiwan Inst Chem Eng* 72:116–133
132. Klonowska-Olejnik M (2004) Redescription of *Electrogena quadrilineata* (Landa, 1969) from type material (Ephemeroptera, Heptageniidae). *Aquatic Insects* 26(2004):85–95
133. Zhang J, Xue Q, Pan X, Jin Y, Lu W, Ding D, Guo Q (2017) Graphene oxide/polyacrylonitrile fiber hierarchical-structured membrane for ultra-fast microfiltration of oil-water emulsion. *Chem Eng J* 307:643–649
134. Dwivedi AD, Dubey SP, Sillanpää M, Kwon Y-N, Lee C, Varma RS (2015) Fate of engineered nanoparticles: implications in the environment. *Coord Chem Rev* 287:64–78
135. Jackson P, Jacobsen NR, Baun A, Birkedal R, Kühnel D, Jensen KA, Vogel U, Wallin H (2013) Bioaccumulation and ecotoxicity of carbon nanotubes. *Chem Cent J* 7:1–21
136. Nasrollahzadeh M, Sajjadi M, Irvani S, Varma RS (2020) Carbon-based sustainable nanomaterials for water treatment: state-of-art and future perspectives. *Chemosphere* (2020):128005
137. Choi P-S, Jeong J-M, Choi Y-K, Kim M-S, Shin G-J, Park S-J (2016) A review: methane capture by nanoporous carbon materials for automobiles. *Carbon Lett* 17:18–28
138. Zheng J, Wang C-G, Zhou H, Ye E, Xu J, Li Z, Loh XJ (2021) Current research trends and perspectives on solid-state nanomaterials in hydrogen storage
139. Ihsanullah (2019) Carbon nanotube membranes for water purification: developments, challenges, and prospects for the future. *Sep Purification Technol* 209(2019):307–337
140. Costa LF, Ruotolo LA, Ribeiro LS, Pereira MC, Camargo ER, Nogueira FG (2021) Low-cost magnetic activated carbon with excellent capacity for organic adsorption obtained by a novel synthesis route. *J Environ Chem Eng* 9:105061
141. Serafin J, Ouzzine M, Junior OFC, Sreńscek-Nazzal J (2021) Preparation of low-cost activated carbons from amazonian nutshells for CO<sub>2</sub> storage. *Biomass Bioenerg* 144:105925
142. Simpson DR (2008) Biofilm processes in biologically active carbon water purification. *Water Res* 42:2839–2848
143. Korotta-Gamage SM, Sathasivan A (2017) A review: potential and challenges of biologically activated carbon to remove natural organic matter in drinking water purification process. *Chemosphere* 167:120–138
144. Broom D, Webb C, Hurst K, Parilla P, Gennett T, Brown CM, Zacharia R, Tylianakis E, Klontzas E, Froudakis G (2016) Outlook and challenges for hydrogen storage in nanoporous materials. *Appl Phys A* 122:151

# Chapter 24

## Utilization of Aquatic Plants Dead Biomass in Adsorption of Heavy Metals from Wastewater



Asha Singh and Sunil Kumar

### 1 Introduction

Rapid and uncensored industrialization has been seen in the past century of human society. The rapid expansion of industries outcome is the generation of metal-containing wastes which are ultimately injected into the water bodies. Water is very necessary for all life forms present on Earth, but its quality is deteriorating day by day a huge amount of waste from different sources is discharged into the fresh-water ecosystem which pollutes water. Water pollution is the undesirable change in its physical, chemical, and biological characteristics which impairs water usefulness and affects the environment and health of human beings. Various industries discharge their waste into water bodies which makes them unfit for use, but heavy metal-containing waste is of most concern area. Heavy metal is any element having an atomic weight between 63.5 and 200 and a specific gravity greater than 5.0 [1]. Heavy metals like arsenic, zinc, copper, cadmium, chromium, lead, mercury, nickel, etc., are released from metal plating industries, mining, battery and pigment manufacturing, smelting, textiles, petroleum refining, tanneries, pesticides, paint, printing, and photographic industries [2, 3]. Heavy metals are considered carcinogenic and toxic. These are non-biodegradable as they accumulate in the body through the food chain. These cause serious health threats when they entered the human body above permissible limits. Heavy metals should be eliminated from the environment as they cause lots of problems to human beings and the environment.

Various conventional methods which have been used for the elimination of heavy metals are chemical precipitation, coagulation, ultra-filtration, electro-dialysis, reverse osmosis, etc., but most of the methods are suitable for large-scale treatments

---

A. Singh · S. Kumar (✉)  
Department of Environmental Sciences, Maharshi Dayanand University, Rohtak,  
Haryana 124001, India  
e-mail: [sunilevs@yahoo.com](mailto:sunilevs@yahoo.com)

only. These methods are very expensive and economically unfavorable and technically complicated. Incomplete removal of heavy metals, production of toxic sludge, and high energy requirements are some disadvantages of conventional methods [4]. Numerous studies have been done for developing a more effective method in removing metal pollution. It was found that the adsorption process is more practicable than other conventional methods. Adsorption is an easy, most simple, economically efficient method for removing heavy metals from wastewater [5]. Adsorption is the deposition of a gas or liquid (adsorbate) at the solid's surface (adsorbent or substrate). Various substances like plant parts, plant waste, industrial by-products, agricultural waste, aquatic plants may be used as adsorbents for heavy metals adsorption. The adsorbents may be used either naturally or modified with some chemicals. Various researches show that a variety of materials have been used as adsorbents including rice husk, papaya wood, fava beans, banana and orange peels, neem bark, maize leaf, carrot residues, sugarcane bagasse, etc. The conversion of these materials as low-cost adsorbent leads to a potential and economic application for metal removal from wastewater. The adsorbent is said to be low cost as it is found in abundant amount and cost-effective as it requires less processing cost and is useful in adsorption. In this chapter, an overview of various low-cost adsorbents is shown by highlighting their capability for removing heavy metals from wastewater.

## 2 Sources of Heavy Metals

Heavy metals are found naturally on earth. Due to the staggering increase in the number of heavy metals used, a sudden increase in metallic substances in the terrestrial and aquatic environments is imminent [6]. The volcanic eruption and weathering of metal-bearing rocks are natural sources. The anthropogenic sources are mainly mining, industrial, and agricultural activities which include smelting, textile, petroleum refining, pesticides, paint, pigment manufacturing, tanneries, printing and photographic industries, agricultural chemicals, etc. The main heavy metals are copper (Cu), lead (Pb), zinc (Zn), cadmium (Cd), arsenic (As), mercury (Hg), arsenic (As), silver (Ag), chromium (Cr), iron (Fe), and cobalt (Co), and their emission sources are listed in Table 1.

## 3 Toxic Effects of Heavy Metals on Human Health

The presence of heavy metals leads to many health problems due to their accumulation in the human body. However, some heavy metals are considered essential heavy metals for their roles in biological systems. They are important to living beings and require low concentrations in the body. Some important heavy metals are Cu, Zn, Fe, and Mg. Non-essential heavy metals do not have a biological role in living organisms, and some of them are Hg, Cd, Pb [10, 11]. The health problems caused due to

**Table 1** Sources of heavy metal [7–9]

Heavy metal	Sources
Cadmium (Cd)	Alloys, pigments, metal coatings, Ni/Cd batteries, pesticides, neutron absorber in the nuclear reactor
Chromium (Cr)	Leather tanning, electroplating, paints, alloys, metal ceramics
Cobalt (Co)	Electroplating, paints, glasses, ceramics, pottery, enamels
Copper (Cu)	Electroplating, copper wires, alloys, coins, pipes, pigments
Lead (Pb)	Lead piping, lead-acid batteries, pigments, plastic, ceramic
Nickel (Ni)	Ni/Cd batteries, electroplating, arc-welding, glasses, pigments, paints, coins, jewelry, catalysts
Arsenic (As)	Pesticides, ceramics, textile and tanning, pigments, fireworks, electric components, wood preservatives, etc.
Mercury (Hg)	Barometers, thermometers, gold recovery, tooth fillings, compact fluorescent lightbulbs, insecticide, catalyst, rectifiers, electrical switches
Zinc (Zn)	Zn alloys, batteries, paints, cosmetics, pharmaceuticals, textiles, paints, and rubber industry

excess heavy metals include skin dermatitis, kidney and lung problems, dizziness, headache, irritability, anemia, weakness of muscles, gastrointestinal distress, renal damages, etc., which are summarized in the given Table 2.

**Table 2** Toxic effects of heavy metals [12]

Heavy metal	Effects on human health
Cadmium	Kidney failure, lung disease, pneumonitis, Itai-Itai disease, bone defects, osteomalacia, osteoporosis, and myocardial dysfunctions
Chromium	Necrosis, nephritis and gastrointestinal irritation, nasal and mucous membrane ulcers, and cancers
Cobalt	Asthma, allergy, respiratory failure, heart disorder, dizziness
Copper	Irritation of nose, mouth, and eyes, dizziness, diarrhea
Lead	Carcinogen, anemia, kidney problem, cause sterility
Nickel	Cancer of lungs, nasal sinus, chronic bronchitis
Arsenic	Gastrointestinal disorders, carcinogenic
Mercury	Dermatitis, anorexia, kidney damage, corrosive to skin, eyes, and muscle, Minamata disease
Zinc	Restlessness, metal fume fever (short-term illness)

## 4 Conventional Methods of Heavy Metals Removal

Various methods which have been used for the removal of heavy metals from wastewater include chemical precipitation, ultra-filtration, ion exchange, coagulation, reverse osmosis, electro-dialysis, and phytoremediation. Chemical precipitation is a method in which heavy metals are removed from inorganic effluents based on pH adjustment. Ultra-filtration uses porous membranes under pressure-driven membrane operation for the removal of heavy metals. During ion exchange, metal ions are removed from the dilute solution and replaced by the ions held in the exchange resin by electrostatic force. Reverse osmosis uses a semi-permeable membrane which is used to trap heavy metal ions at a pressure higher than the osmotic pressure which is caused by the dissolved solids in the wastewater. Phytoremediation is a method in which specific plants are used to purify metal-contaminated soil, sediments, and water. Electrochemical methods are metal selective, and pure metals are obtained in these methods. These methods are expensive, technically complicated, and there is also the release of toxic material and improper heavy metals removal [4]. Adsorption overcomes the disadvantages of conventional methods. Exploration of new and cheap methods to remove metal ions from wastewater showed that adsorption is the most economically viable method. The advantages and disadvantages of some conventional methods are summarized in Table 3.

**Table 3** Conventional methods for heavy metal removal

Methods	Advantages	Disadvantages
Chemical precipitation	Simple and inexpensive capital cost Treat high metal ion conc	Generation of toxic sludge Ineffective when metal ion conc. is low [13]
Ion exchange	Resins can be generated and widely used method for metal removal	Secondary pollution can be caused and high cost for treating at a large scale [14]
Ultra-filtration	Less chemical consumption and high efficiency	High cost and partial removal of certain ions [15]
Reverse osmosis	Recovery of metal salts	Expensive [16]
Electrochemical methods	Metal selective Less chemical consumption	Requires high amount of energy High cost [14]
Phytoremediation	To clean up soil, sediments, and water with contaminated metal	Long process and regeneration of plant for further use are not possible [17]

## 5 Adsorption: A Low-Cost Method for Heavy Metals Removal

Adsorption is the mass transfer from the liquid phase to the surface of a solid (adsorbent) to form an atomic or molecular film (adsorbate). Adsorption is practicable over other conventional methods as this is currently considered to be very suitable for removing or minimizing heavy metals from wastewater even at low concentrations. Adsorption is a simple process and cost-effective. Adsorption occurs due to the attractive forces between the surface and the adsorbate. It is of two types—physical adsorption, which is a result of the weak Van der Waals forces of attraction between the adsorbate and adsorbent, and chemisorption, which is a result of the chemical interaction between the solid and adsorbed substance. Adsorption is considered to be one of the effective methods for the removal of heavy metals from industrial effluents. This method is more suitable due to its high efficiency and low cost, no generation of sludge, less energy requirement, recovery of metal [18].

Therefore, attempts are made to use waste materials as various adsorbents, like plant waste, agricultural waste, and industrial by-products. These can be found in abundant amounts and used as an adsorbent. An adsorbent is said to be “low cost” if it is found in abundant quantity, requires less processing, or can be a byproduct or waste material from another process [19]. Conventionally activated carbon, alumina, zeolites, fly ash, and different coal forms were used as adsorbents in adsorption. Many investigators investigated the various waste material as low-cost adsorbents for heavy metal removal, namely rice husk [20], banana peel [21], tree fern [22], groundnut shells [23], maize leaf [24], neem bark [25], sawdust [26], papaya wood [27], and orange peel [28].

### 5.1 Adsorption Capacity of Adsorbents for Heavy Metals

The adsorption capacity of the adsorbent is computed as in Eq. 1:

$$q_e = \frac{(C_i - C_e)V}{x} \quad (1)$$

where  $q_e$  is the adsorption capacity of adsorbent (mg/g),  $C_i$  is initial and  $C_e$  is equilibrium concentration of the metal solution (mg/L),  $x$  is the weight of the adsorbent (g), and  $V$  is the volume of the metal solution (L).

The removal percentage of adsorbates (heavy metal) by adsorbent is calculated as removal efficiency (RE) in Eq. 2:

$$\text{Removal}(\%) = \frac{(C_i - C_e) \times 100}{C_i} \quad (2)$$

where  $C_i$  and  $C_e$  are same as in Eq. 1.



## 6 Mechanism of Adsorption

Adsorption is a mass transfer process between two phases, such as gas–solid, gas–liquid, liquid–liquid, or liquid–solid interface. The adsorbing material is adsorbent, and the substance being adsorbed is the adsorbate.

The adsorption mechanisms are complex, because no single theory fully explains the adsorption of metal ions on the adsorbent. Various studies have been reported to describe the mechanism between adsorbate and adsorbent. Langmuir’s model and Freundlich’s model are often used to describe adsorption isotherms while kinetically, pseudo-first-order kinetics, and pseudo-second-order kinetics can be used for the adsorption kinetics.

### 6.1 Adsorption Isotherm

The sorption isotherm describes the interaction mechanism of adsorption on the surface of the adsorbent. Several isotherm models are available for the analysis of experimental adsorption equilibrium parameters, but the well-known adsorption isotherm models used are the Langmuir and Freundlich isotherms.

In the Langmuir isotherm, the molecules are adsorbed on fixed and well-defined active centers that are homogeneously distributed on the adsorbent’s surface. The adsorbed molecules do not interact, and only a monolayer is formed [29].

Langmuir equation is written as

$$C_e/q_e = 1/bq_{\max} + C_e/q_{\max}$$

where  $q_e$  and  $q_{\max}$  are the metal adsorption capacity and maximum adsorption capacity of the adsorbent (in mg/g), respectively.  $C_e$  is the equilibrium solute conc., and  $b$  is Langmuir constant.

In Freundlich isotherm, adsorbate is adsorbed on heterogeneous surfaces, and there is not restricted to the formation of monolayer [30].

Freundlich equation is written as

$$\log q_e = \log K_F + 1/n \log C_e$$

where  $q_e$  is the metal adsorption capacity of adsorbent at equilibrium,  $K_f$  is the adsorption equilibrium constant while  $1/n$  is the heterogeneity coefficient related to adsorption capacity and strength, and  $C_e$  is the equilibrium concentration.

## 6.2 Adsorption Kinetics

The adsorption kinetics can be used to study the rate-limiting step in the adsorption process in terms of kinetic energy.

The pseudo-first-order kinetic equation of Lagergren model is given as [31]:

$$dq_t/dt = k_1(q_e - q_t)$$

where  $q_e$  is the amount of metal adsorbed at equilibrium and  $q_t$  is the amount of metal adsorbed (mg/g) at any instant of time  $t$  (min) and  $k_1$  is the rate constant of pseudo-first-order equation ( $\text{min}^{-1}$ ). It deals with the assumption that the rate of change of the amount of solute adsorbed over time is proportional to the difference in saturation concentrations and to the adsorption processes that determine the amount of solids adsorbed over time.

The pseudo-second-order kinetic equation is given as

$$dq_t/dt = k(q_e - q_t)^2$$

The assumption of this is based on the limiting step which may be the result of chemisorption, involving valence forces through the exchange of electrons between the adsorbate and the adsorbent [32].

## 7 Factors Affecting the Adsorption Process

Various parameters which affect the adsorption process include initial concentration, temperature, pH, contact time, adsorbent dose [33].

**pH**—pH changes the adsorbent's surface charge and adsorbate's degree of ionization. At a particular pH, metal adsorption increased with increasing pH to a certain limit but reduced when further pH increases.

**Temperature**—It influences the adsorption equilibrium which depends upon the exothermic and endothermic nature of a process, and it affects the adsorption capacity of the adsorbent.

**Contact time**—The time to achieve equilibrium interactions between adsorbate and adsorbent to ensure the completion of adsorption process is called contact time.

**Adsorbent dose**—It is the dose of adsorbent at which adsorption is maximum, and it also affects the adsorption process.

**Initial concentration**—This is an important parameter to provide a significant incentive to overcome the metal's resistance to mass transfer between the aqueous and solid phases.

## 8 Aquatic Plants Dead Biomass as Adsorbents

Aquatic plants are found to be the potential scavengers of heavy metals from wastewater as studied by various investigators in the previous years. Various aquatic plants like Lemna, Eichhornia, Hydrilla, Potamogeton, Ceratophyllum, Salvinia, Myriophyllum, Pistia, Spirodela have been used for heavy metals adsorption.

Saraswat and Rai [34] studied the adsorption of Zn(II), Cd(II), and Cr(VI) with varying different conditions of metal and biomass concentration, pH, and agitation time on *Eichhornia crassipes* dead biomass in single, bi, and tri-metal systems. The maximum adsorption capacities were observed 12.4, 9.3, and 5.6 mg/g at pH 5, pH 6, and pH 2 for Cd(II), Zn(II), and Cr(VI), respectively. Several studies were done on *Eichhornia crassipes* by different investigators for removal of heavy metals as Cr [35], arsenic removal using hyacinth roots [36], Pb, Cu, Zn, and Cd removal in the order Pb > Cd > Zn > Cu by using *Eichhornia crassipes* [37].

Keskinan et al. [38] showed that *Myriophyllum spicatum* can be used as an adsorbent for copper, lead, and zinc removal. The maximum adsorption capacities were 10.37, 46.49, and 15.59 mg/g for copper, lead, and zinc, respectively. Similar experiments were conducted by Keskinan et al. [39] with another submerged aquatic plant *Ceratophyllum demersum* for removal of copper, lead, and zinc. The maximum adsorption capacities were 6.17, 44.8, and 13.98 mg/g for Cu(II), Pb(II), and Zn(II), respectively.

Lima et al. [40] studied the adsorption of Cr<sup>3+</sup> and Pb<sup>2+</sup> ions on the aquatic macrophyte *P. stratiotes*, and the maximum removal was 0.317 and 0.225 mmol/g for Cr<sup>3+</sup> and Pb<sup>2+</sup>, respectively. Meitei and Prasad [41] examined the maximum adsorption capacities of *Spirodela polyrhiza* (L.), that is, 52.6, 35.7, and 28.5 mg/g for Cu (II), Mn (II), and Zn (II), respectively, under optimized conditions. The sequence of adsorption capacities for metals is as follows: copper > manganese > zinc.

It was noticed that the dead biomass of *Ceratophyllum demersum* can remove Cd (II) [42]. The batch study showed the fast adsorption of cadmium at pH 5 and 1.0 g of biomass in 20 min. Cadmium adsorption increases with an increasing adsorbent dose. Cadmium ions adsorbed on *Ceratophyllum demersum* were efficiently desorbed with 0.1 M EDTA (97%), 0.1 M HCl (94%), and 0.1 M HNO<sub>3</sub> (85%), indicating that the adsorbed cadmium was recovered. The equilibrium studies showed that the Freundlich isotherm model fits the sorption data, suggesting multilayer adsorption and adsorption of Cr, Cu, and Pb using non-living biomass of *Ceratophyllum demersum* [43].

The dried *Azolla filiculoides* has been used as biomass for heavy metals removal using batch experiments [44]. The maximum removal capacities of *A. filiculoides* for Ni and Cu ions were approximately 0.77 and 0.54 mmol/g, respectively. Zhao and Duncan [45, 46] investigated the adsorption of Cr(VI) and Ni on *Azolla filiculoides* from the effluent of the electroplating industry. The batch study showed that the maximum adsorption capacity of *A. filiculoides* for Cr was 20.2 mg/g at pH 2 at 32 °C. In another study done by the same researcher, the sorption capacity at pH 6.2 was observed as 31.3 mg/g. In another study, *A. filiculoides* was also used

**Table 4** Aquatic plant adsorbents used for heavy metal removal

Aquatic plant	Metals adsorbed	References
<i>Eichhornia crassipes</i>	Zn, Cd, Cr	[34]
	Pb, Cu, Zn, Cd	[37]
	Cr	[35]
	As	[36]
<i>Ceratophyllum demersum</i>	Cd	[42]
	Cr, Cu, Pb	[43]
<i>Azolla filiculoides</i>	Ni, Cu	[44]
<i>Lemna minor</i>	Fe, Cu, Zn, Pb	[48]
<i>Hydrilla verticillate</i>	Pb, Cu, Cr	[49]
<i>Spirodela polyrhiza</i>	Pb	[50]
<i>Pistia stratiotes</i>	Cr	[51]
<i>Lemna perpusila</i>	Pb	[52]
<i>Myriophyllumspicatum</i>	Zn, Pb, Cu	[38]
<i>Spirodela intermedia</i>	Cd, Cu, Zn, Ni, Pb	[53]
<i>Egeriadensa</i>	Cu	[54]
<i>Salvinia molesta</i>	Cr	[55]
<i>Typha latifolia</i>	Cr	[55]
<i>Nymphaea lotus</i>	Pb	[56]
<i>Echinodorus amazonicus</i>	Pb, Cd, Zn, Cu	[57]
<i>Ruppia maritime</i>	Pb, Cd, Zn, Cu	[57]

in zinc removal in batch systems, and the column was observed at pH 6 and pH 6.2 to be 45.2 and 30.4 mg/g, respectively [47].

Some aquatic plants which have been used for adsorption are listed below in Table 4.

## 9 Advancement in Aquatic Plant Adsorbents

Earlier aquatic plants were dried and grounded to powder for use as adsorbents in raw form for removal of heavy metals. Later on, researchers tried to increase the efficiency of adsorption. They modify or treat the adsorbents using various agents like acids (citric acid, hydrochloric acid, nitric acid, sulfuric acid, tartaric acid, thioglycollic acid), base solutions (sodium hydroxide, calcium hydroxide, sodium carbonate), organic compounds (ethylenediamine, formaldehyde, epichlorohydrin, methanol), and oxidizing agents (hydrogen peroxide). The chemical modification increases the adsorbent's active binding sites, improves ion exchange characteristics, and creates new functional groups that aid metal adsorption [58].

Ganji et al. [59] examined the adsorption of Cu, Cd, Pb, and Zn by treating *Azolla filiculoides* with H<sub>2</sub>O<sub>2</sub>/MgCl<sub>2</sub>. The *Azolla* samples (each 2 g sample) were soaked

in 2 M  $MgCl_2$  and 30 ml of 8 M  $H_2O_2$  for 12 h at 125 rpm and pH 7. The Azolla samples were washed at pH 10.5 for 6 h in NaOH solution and dried. The maximum adsorption capacities of Azolla for Cu, Cd, Pb, and Zn ions were approximately 62, 86, 228, and 48 mg/g (Azolla dry), respectively, under optimal conditions.

Elangoven et al. [60] studied the removal capacity of dried biomass of aquatic weeds like reed mat (*Cannomois vvirgata*), water lettuce (*Pistia stratiotes*), lotus flower (*Nelumbo lucifera*), water hyacinth (*Eichhornia crassipes*), arrow leaved tear thumb (*Polygonum sagittatum*), water lily flower (*Nymphaea sp.*), green taro (*Colocasia esculanta*), and mangrove leaves (*Rhizophora mangle* L) which were modified using NaOH and  $H_2SO_4$  at a concentration of 4 N. 10 g of raw adsorbent was mixed with 100 ml of NaOH and  $H_2SO_4$  solution and stirred for 24 h, washed several times until the pH was neutral, and then dried. The modification significantly increases the adsorption capacities of all adsorbents for Cr(VI) and reduces for Cr(III).

Yoonaiwong et al. [61] prepared a modified adsorbent by treating a 50 g sample of dry *Utricularia aurea* biomass with  $CaCl_2$  solution (0.2 M) at pH 5 and stirred for 24 h. The calcium-treated biomass was washed several times and dried in an oven at 103 °C for 24 h. The treated adsorbent was then passed through a 125–1000  $\mu m$  sieve to give particle sizes of 250–500  $\mu m$ . It was found that pretreated *U. aurea* for removal of Pb (II) and Cd (II) ions is inexpensive biomass due to its high abundance and has a considerably higher adsorption capacity at low concentrations.

Ferreira et al. [62] used the dried biomass of *Pistia stratiotes* and *Salvinia sp.* for adsorption of lead which was modified by treating with 0.1 M NaOH solution and stirring for 2 h. The biomass was then washed several times with distilled water and then washed with acetone and ethanol to extract soluble organic substances and dried in an oven at 70 °C for 4 h. Adsorption studies indicate modification enhances the adsorption capacity.

The nano-EC and nano-LM were synthesized using the sol-gel method by *Eichhornia crassipes* (raw EC) and *Lemna minor* (raw LM) [63]. SEM, FTIR, BET, EDX, and TGA analyzes were used to characterize the nano-adsorbents. In 120 min, the highest adsorption of Cr(VI) ions by nano-EC and nano-LM was detected at pH 2, and the maximum adsorption of Ni(II) by nano-EC and nano-LM was observed at pH 5.3. Because nano-EC is numerous and has a higher adsorption capacity than nano-LM, it was determined that it might be used as a possible nano-sorbent for the removal of Cr(VI) and Ni(II) ions.

It can be concluded that there is more need to work on the modification of the adsorbent to increase efficiency. Nano-adsorbents can be made out of this and can be prepared by green synthesis or loaded on the adsorbent.

## 10 Challenges of Aquatic Plants Adsorbents

The main problem in using aquatic plants is to collect the samples from water as they spread densely over the water surface. Also, difficulty arises in the separation of plant material from other unwanted waste like dirt, weeds found in the aquatic bodies.

They also collected in large quantities because of their lightweight. Secondly, the problem arises in the regeneration of adsorbent and disposing of. The spent adsorbent may include toxic substances which should be treated before disposal. It will require operation costs which could not be economical for use. Similarly, regeneration is also difficult for aquatic plants. Their efficiency is also low as compared to activated charcoal. They need to be modified to increase the efficiency but it also leads to add some additional costs.

## 11 Conclusions

A review of various low-cost adsorbents shows the potential and effectiveness of adsorption for the removal of heavy metals from wastewater. The study on aquatic plants for using them as adsorbents has brought the attention of many researchers for the adsorption of heavy metals. More attention should be taken to minimize metal pollution by promoting the large-scale use of non-conventional adsorbents. Adsorbents should be economically efficient and have maximum removal efficiency. Although chemical modification can also increase the adsorption of heavy metals. To make “low-cost” adsorbents, the cost of chemicals employed and techniques of modification should be considered. Further studies can be employed by using nano-adsorbents derived from aquatic plants and making the process cost-effective.

## References

1. Srivastava J, Gupta A, Chandra H (2008) Managing water quality with aquatic macrophytes. *Rev Environ Sci Biotechnol* 7(3):255–266
2. Kadirvelu K, Thamaraiselvi K, Namasivayam C (2001) Removal of heavy metals from industrial wastewaters by adsorption onto activated carbon prepared from an agricultural solid waste. *Bioresour Technol* 76(1):63–65
3. Williams CJ, Aderhold D, Edyvean RGJ (1998) Comparison between biosorbents for the removal of metal ions from aqueous solutions. *Water Res* 32(1):216–224
4. Abdel-Halim SH, Shehata AMA, El-Shahat MF (2003) Removal of lead ions from industrial waste water by different types of natural materials. *Water Res* 37(7):1678–1683
5. Shah BA, Shah AV, Singh RR (2009) Sorption isotherms and kinetics of chromium uptake from wastewater using natural sorbent material. *Int J Environ Sci Technol* 6(1):77–90
6. Gautam PK, Gautam RK, Banerjee S, Chattopadhyaya MC, Pandey JD (2016) Heavy metals in the environment: fate, transport, toxicity and remediation technologies. Nova Sci Publishers 60:101–130
7. WHO, Air Quality Guidelines for Europe, 2nd ed (2000)
8. Kaye GWC, Laby TH (1986) Tables of physical and chemical constants, 15th edn. John Wiley & Sons Ltd., United States
9. Haynes WM (ed) (2014) CRC handbook of chemistry and physics, 92nd ed. CRC press Florida 2011
10. Jović M, Onjia A, Stanković S (2012) Toxic metal health risk by mussel consumption. *Environ Chem Lett* 10(1):69–77

11. Ali H, Khan E, Ilahi I (2019) Environmental chemistry and ecotoxicology of hazardous heavy metals: environmental persistence, toxicity, and bioaccumulation. *J Chem* 1–14
12. Zwain HM, Vakili M, Dahlan I (2014) Waste material adsorbents for zinc removal from wastewater: a comprehensive review. *Int J Chem Eng* 1–13
13. Abaliwano JK, Ghebremichael KA, Amy GL (2008) Application of the purified Moringa oleifera coagulant for surface water treatment. *Water Mill Working Paper Series* 5:1–19
14. Rao KS, Mohapatra M, Anand S, Venkateswarlu P (2010) Review on cadmium removal from aqueous solutions. *Int J Eng Sci Technol* 2(7):81–103
15. Fu F, Wang Q (2011) Removal of heavy metal ions from wastewaters: a review. *J Environ Manage* 92(3):407–418
16. Joshi NC, Chhibber VK (2017) A kinetic and thermodynamic study of copper removal using Deodar (*Cedrus deodara*) leaves. *Chem J* 537–540
17. Vara Prasad MN, de Oliveira Freitas HM (2003) Metal hyperaccumulation in plants: biodiversity prospecting for phytoremediation technology. *Electron J Biotechnol* 6(3):285–321
18. Kratochvil D, Volesky B (1998) Advances in the biosorption of heavy metals. *Trends in Biotechnol* 16(7):291–300
19. Bailey SE, Olin TJ, Bricka RM, Adrian DD (1999) A review of potentially low-cost sorbents for heavy metals. *Water Res* 33(11):2469–2479
20. Ajmal M, Rao RAK, Anwar S, Ahmad J, Ahmad R (2003) Adsorption studies on rice husk: removal and recovery of Cd (II) from wastewater. *Bioresour Technol* 86(2):147–149
21. Hossain MA, Ngo HH, Guo WS, Nguyen TV (2012) Biosorption of Cu (II) from water by banana peel based biosorbent: experiments and models of adsorption and desorption. *J Water Sustain* 2(1):87–104
22. Ho YS, Chiu WT, Hsu CS, Huang CT (2004) Sorption of lead ions from aqueous solution using tree fern as a sorbent. *Hydrometallurgy* 73(1–2):55–61
23. Shukla SR, Pai RS (2005) Adsorption of Cu (II), Ni (II) and Zn (II) on dye loaded groundnut shells and sawdust. *Sep Purif Technol* 43(1):1–8
24. Babarinde NA, Babalola JO, Sanni RA (2006) Biosorption of lead ions from aqueous solution by maize leaf. *Int J Phy Sci* 1(1):23–26
25. Bhattacharya AK, Mandal SN, Das SK (2006) Adsorption of Zn (II) from aqueous solution by using different adsorbents. *Chem Engg J* 123(1–2):43–51
26. Memon SQ, Memon N, Shah SW, Khuhawar MY, Bhangar MI (2007) Sawdust—a green and economical sorbent for the removal of cadmium (II) ions. *J Hazard Mater* 139(1):116–121
27. Saeed A, Akhter MW, Iqbal M (2005) Removal and recovery of heavy metals from aqueous solution using papaya wood as a new biosorbent. *Sep Purif Technol* 45(1):25–31
28. Gönen F, Serin DS (2012) Adsorption study on orange peel: removal of Ni (II) ions from aqueous solution. *Afri J Biotechnol* 11(5):1250–1258
29. Langmuir I (1918) The adsorption of gases on plane surfaces of glass, mica and platinum. *J Am Chem Soc* 40(9):1361–1403
30. Freundlich H (1906) Adsorption in solutions. *Z Phys Chem (Germany)* 57:385–470
31. Lagergren SK (1898) About the theory of so-called adsorption of soluble substances. *Sven. Vetenskapsakad. Handlingar* 24:1–39
32. Ho YS, McKay G (1999) Pseudo-second order model for sorption processes. *Process Biochem* 34(5):451–465
33. Singh A, Kumar S, Panghal V, Arya SS, Kumar S (2019) Utilization of unwanted terrestrial weeds for removal of dyes. *Rasayan J Chem* 12:1956–1963
34. Saraswat S, Rai JPN (2010) Heavy metal adsorption from aqueous solution using *Eichhornia crassipes* dead biomass. *Int J Miner Process* 94(3–4):203–206
35. Mohanty K, Jha M, Meikap BC, Biswas MN (2006) Biosorption of Cr (VI) from aqueous solutions by *Eichhornia crassipes*. *Chem Eng J* 117(1):71–77
36. Govindaswamy S, Schupp DA, Rock SA (2011) Batch and continuous removal of arsenic using hyacinth roots. *Int J Phytoremediat* 13(6):513–527
37. Li Q, Chen B, Lin P, Zhou J, Zhan J, Shen Q, Pan X (2016) Adsorption of heavy metal from aqueous solution by dehydrated root powder of long-root *Eichhornia crassipes*. *Int J Phytoremediat* 18(2):103–109

38. Keskinan OLCAYTO GMZL, Yuceer AHMET, Basibuyuk MFCF, Forster CF (2003) Heavy metal adsorption characteristics of a submerged aquatic plant (*Myriophyllum spicatum*). *Process Biochem* 39(2):179–183
39. Keskinan OLCAYTO, Goksu MZL, Basibuyuk MESUT, Forster CF (2004) Heavy metal adsorption properties of a submerged aquatic plant (*Ceratophyllum demersum*). *Bioresour Technol* 92(2):197–200
40. Lima LK, Pelosi BT, da Silva MGC, Vieira MG (2013) Lead and chromium biosorption by *Pistia stratiotes* biomass. *Chem Eng Trans* 32:1045–1050
41. Meitei MD, Prasad MNV (2014) Adsorption of Cu (II), Mn (II) and Zn (II) by *Spirodela polyrhiza* (L.) Schleiden: equilibrium, kinetic and thermodynamic studies. *Ecol Eng* 71:308–317
42. Jayarathne DLSM, Ariharan S, Iqbal SS, Thayaparan M (2015) Isotherm study for the biosorption of Cd (II) from aqueous solution by the aquatic weed: *ceratophyllum demersum*. *J Environ Prof Sri Lanka* 4(2):10–24
43. Hassoon HA (2015) The adsorption of some trace heavy metals from aqueous solution using non living biomass of submerged aquatic plant *ceratophyllum demersum*. *Iraqi J Sci* 56(4A):2822–2828
44. Ahmady-Asbchin S, Omran AN (2012) Potential of *Azolla filiculoides* in the removal of Ni and Cu from wastewaters. *Afri J Biotechnol* 11(95):16158–16164
45. Zhao M, Duncan JR (1997) Batch removal of hexivalent chromium by *Azolla filiculoides*. *Biotechnol Appl Biochem* 26(3):179–182
46. Zhao M, Duncan JR (1998) Removal and recovery of nickel from aqueous solution and electroplating rinse effluent using *Azolla filiculoides*. *Process Biochem* 33(3):249–255
47. Zhao M, Duncan JR, Van Hille RP (1999) Removal and recovery of zinc from solution and electroplating effluent using *Azolla filiculoides*. *Water Res* 33(6):1516–1522
48. Dhabab JM (2011) Removal of Fe (II), Cu (II), Zn (II), and Pb (II) ions from aqueous solutions by duckweed. *J Oceanogr Marine Sci* 2(1):17–22
49. Bind A, Goswami L, Prakash V (2018) Comparative analysis of floating and submerged macrophytes for heavy metal (copper, chromium, arsenic and lead) removal: sorbent preparation, characterization, regeneration and cost estimation. *Geol Ecol Landscapes* 2(2):61–72
50. Tang J, Li Y, Wang X, Daroch M (2017) Effective adsorption of aqueous  $Pb^{2+}$  by dried biomass of *Landoltia punctata* and *Spirodela polyrhiza*. *J Clean Prod* 145:25–34
51. Das B, Mondal NK, Chattaraj PRS (2013) Equilibrium, kinetic and thermodynamic study on chromium (VI) removal from aqueous solution using *Pistia stratiotes* biomass. *Chem Sci Trans* 2(1):85–104
52. Tang Y, Chen L, Wei X, Yao Q, Li T (2013) Removal of lead ions from aqueous solution by the dried aquatic plant, *Lemna perpusilla* Torr. *J Hazard Mater* 244:603–612
53. Miretzky P, Saralegui A, Cirelli AF (2006) Simultaneous heavy metal removal mechanism by dead macrophytes. *Chemosphere* 62(2):247–254
54. Módenes DA, de Abreu Pietrobelli JMT, Espinoza-Quiñones FR (2009) Cadmium biosorption by non-living aquatic macrophytes *Egeria densa*. *Water Sci Technol* 60(2):293–300
55. Singh A, Kumar S, Panghal V (2021) Adsorption of chromium ( $Cr^{6+}$ ) on dead biomass of *Salvinia molesta* (Kariba weed) and *Typha latifolia* (broadleaf cattail): isotherm, kinetic, and thermodynamic study. *Appl Water Sci* 11(9):1–16
56. Galadima LG, Wasagu RSU, Lawal M, Aliero A, Magajo UF, Suleman H (2015) Biosorption activity of *Nymphaea lotus* (water lily). *Int J Eng Sci* 4(3):66–70
57. Deng PY, Liu W, Zeng BQ, Qiu YK, Li LS (2013) Sorption of heavy metals from aqueous solution by dehydrated powders of aquatic plants. *Int J Environ Sci Technol* 10(3):559–566
58. Ngah WW, Hanafiah MAKM (2008) Adsorption of copper on rubber (*Hevea brasiliensis*) leaf powder: kinetic, equilibrium and thermodynamic studies. *Biochem Eng J* 39(3):521–530
59. Ganji MT, Khosravi M, Rakhsae R (2005) Biosorption of Pb, Cd, Cu and Zn from wastewater by treated *Azolla filiculoides* with  $H_2O_2/MgCl_2$ . *Int J Environ Sci Technol* 1:265–271
60. Elangovan R, Philip L, Chandraraj K (2008) Biosorption of chromium species by aquatic weeds: kinetics and mechanism studies. *J Hazard Mater* 152(1):100–112



61. Yoonaiwong W, Kaewsarn P, Reanprayoon P (2011) Biosorption of lead and cadmium ions by non-living aquatic macrophyte. *Utricularia aurea*. *Sustain Environ Res* 21(6):369–374
62. de Moraes Ferreira R, de Souza MDP, Takase I, de Araujo Stapelfeldt DM (2016) Pb (II) adsorption by biomass from chemically modified aquatic macrophytes, *Salvinia* sp. and *Pistia stratiotes*. *Water Sci Technol* 73(11):2670–2679
63. Balasubramanian UM, Vaiyazhipalayam Murugaiyan S, Marimuthu T (2020) Enhanced adsorption of Cr (VI), Ni (II) ions from aqueous solution using modified *Eichhornia crassipes* and *Lemna minor*. *Environ Sci Pollut Res* 27(17):20648–20662

# Chapter 25

## Porous Carbon Materials and Their Composites for Electromagnetic Interference (EMI) Shielding: The State-of-the-Art of Technologies



**Deepthi Anna David, M. J. Jabeen Fatima, Abdullah Khan, Roshny Joy, Vijay Kumar Thakur, Ramiro Rafael Ruiz-Rosas, Shemus Ozden , and Prasanth Raghavan **

---

D. A. David

Department of Applied Chemistry, Cochin University of Science and Technology, Cochin 682022, India

D. A. David · M. J. Jabeen Fatima · R. Joy

Materials Science and NanoEngineering Lab (MSNE-Lab), Department of Polymer Science and Rubber Technology, Cochin University of Science and Technology, Cochin 682022, India

A. Khan

Department of Materials Science and Engineering, KTH Royal Institute of Technology, Brinellvägen 23, 11428 Stockholm, Sweden

V. K. Thakur

Biorefining and Advanced Materials Research Centre, SRUC, Parkgate, Barony Campus, DGI 3NE Dumfries, Edinburgh, UK

R. R. Ruiz-Rosas

Departamento de Ingeniería Química, Andalucía Tech., Escuela de Ingenierías Industriales, Universidad de Málaga, Campus de Teatinos s/n, 29010 Málaga, Spain

S. Ozden (✉)

Department of Chemical and Biological Engineering, Princeton University, Princeton, NJ 08540, USA

e-mail: [sozden@princeton.edu](mailto:sozden@princeton.edu)

Aramco Americas, Aramco Research Center-Houston, 16300 Park Row, Houston, TX 77084, USA

P. Raghavan (✉)

Biorefining and Advanced Materials Research Centre, Scotland's Rural College, Edinburgh EH9 3JG, UK

e-mail: [prasanth@cusat.ac.in](mailto:prasanth@cusat.ac.in)

© The Author(s), under exclusive license to Springer Nature Singapore Pte Ltd. 2023

669

A. N. Grace et al. (eds.), *Handbook of Porous Carbon Materials*,

Materials Horizons: From Nature to Nanomaterials,

[https://doi.org/10.1007/978-981-19-7188-4\\_25](https://doi.org/10.1007/978-981-19-7188-4_25)

## 1 Introduction

Today, the use of portable gadgets and smart electronic devices has become an immense need of the modern society. With the exponential growth of such electronic machines, the biggest challenge is to protect these devices from the unintentional transmission of electromagnetic radiations emitting from different sources of electromagnetic field, interfering with the electronic signals, and resulting in malfunctioning of these devices. Radio frequency electromagnetic waves are the most common cause of electronic circuit failures and known as radio frequency, or noise or electromagnetic interference (EMI). Further, synchronization and miniaturization of multi-functional electronics have brought up omnipresent electromagnetic pollution in the world which is much stronger than any natural electromagnetic field source. Due to the electrostatic discharge (ESD) from these electromagnetic field sources, EM signals are radiated and emitted which interfere with the electronic devices, degrading their performance, and resulting electronic equipment to partial or full failure [1]. For these reasons, electronic industries are seeking technology-based solutions to develop advanced materials with excellent EMI shielding capabilities over a wide temperature range which can absorb EM waves and protect the electronic devices from sudden failures [2]. EM shielding is also known as RF shielding as it is obvious from its name, blocking radio frequency electromagnetic radiations emitted from electromagnetic field sources. RF shielding helps as protective barrier by coupling of radio waves, electromagnetic fields as well as electrostatic fields. In addition, chemical composition, coating thickness of the shielding material, morphology, and geometrical design of the shield, and frequency of electromagnetic field are highly correlated to the reduction of EMI.

## 2 Electromagnetic Interference (EMI) Shielding

EMI shielding is a technique of creating a barrier that prevents leakage of strong electromagnetic fields that can interfere with sensitive devices and signals. They can be installed to isolate the electromagnetic field source or as an enclosure of the device that needs protection. Any unwanted electrical or electromagnetic energy which causes undesirable responses, degradation, or equipment failure is known as electromagnetic interference. As electronics both emit and are affected by electromagnetic (EM) waves, it is essential to shield them adequately. Some examples of the effects of EMI interference are malfunctioning flight control systems due to passengers using electronics such as mobile phones and laptops, momentary disturbance in

---

Department of Materials Engineering and Convergence Technology, Gyeongsang National University (GNU), 501 Jinju-daero, Jinju 52828, Republic of Korea

Department of Polymer Science and Rubber Technology, Cochin University of Science and Technology, Cochin 682022, India

television and radio reception due to the usage of electric shavers or coffee grinders, and failure of precision medical devices such as ventilators or ECG monitors due to EM wave interference from other electronics. EM waves from electronic source to their surroundings, or vice-versa, must be shielded according to regulations for electromagnetic compatibility (EMC). Hence, to comply with EMC regulations, it is necessary to enclose electronics with proper shielding materials so that the devices do not interfere with their own operation or the operation of other devices due to EM radiation.

### 3 Mechanism of EMI Shielding

EMI shielding depends mainly on electrical conductivity and magnetic permeability of shield material, the frequency of radiation. EM waves can be classified into near field or far field, based on the distance between the EMI source and shielding enclosure. The wavelength of EM waves divided by  $2\pi$  gives the transition point between the fields. In this dissertation, we employed an EMI setup operated in the far field, and all the equation and shielding mechanisms are explained for the far field. For the far field, EM wave is considered a plane wave with electric and magnetic fields perpendicular to each other. In the near field, the waveform is more complicated. For both, when the EM waves strike the shield material, a portion of the waves are transmitted through the shield (Fig. 1). The shielding effectiveness of the material is calculated based on the logarithmic ratio of incident power ( $P_I$ ) to transmitted power ( $P_T$ ) through the shield, as given by Eq. (1):

$$\text{EMI SE (dB)} = 10 \log(P_I/P_T) \quad (1)$$

Figure 1 Schematic of EMI shielding mechanism and EMI SE is expressed in decibels (dB). Considering Eq. 1, a shielding effectiveness of 20 dB corresponds to 99% attenuation (i.e.,  $P_T = 0.01P_I$ ) of EMI radiation; this value 20 dB is considered to be an adequate level of shielding for many commercial applications. EMI shielding mainly involves three mechanisms: reflection, absorption, and multiple reflection. The total shielding effectiveness (SET) is calculated from the summation of shielding effectiveness by reflection (SER), absorption (SEA), and multiple reflection (SEMR), as shown in Eq. (2):

$$\text{SE}_T(\text{dB}) = \text{SE}_R + \text{SE}_A + \text{SE}_{MR} \quad (2)$$

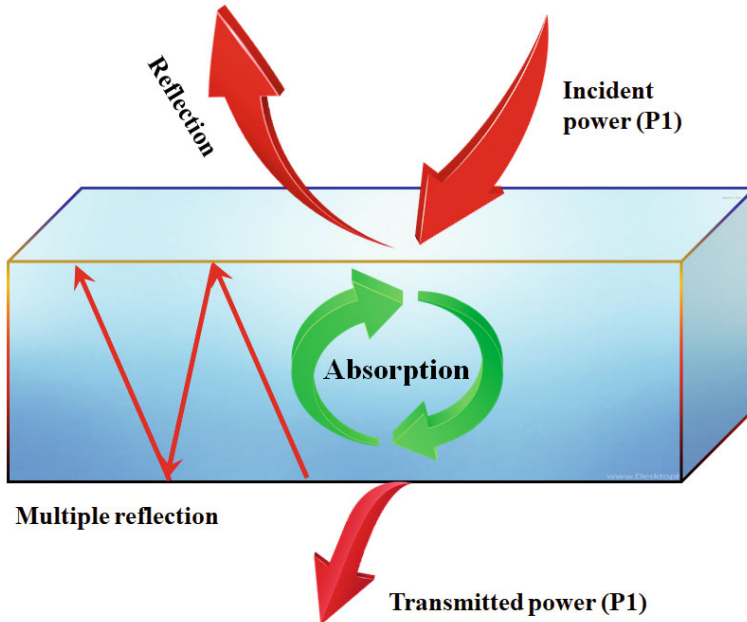


Fig. 1 Schematic illustration on EMI shielding mechanism

### 3.1 Shielding by Reflection ( $SE_R$ )

Reflection is often the primary mechanism for EMI SE for metal shields. For shielding by reflection, the shield material should possess mobile charge carriers such as electrons or holes, which interact with the EM field in the radiation. The material tends to be electrically conductive, even though high electrical conductivity is not required. For conductivity, the network of conduction path is very important, whereas for shielding, it is not. Since metals have more free electrons, they attenuate EM radiation significantly by reflection. For CPN, shielding by reflection is enhanced by increasing the surface area of the filler in the polymer material. For homogeneous materials such as bulk metals, shielding by reflection can be calculated by Eq. (3):

$$SE_R = 39.5 + 10 \log(\sigma/2\pi f\mu) \quad (3)$$

where  $\sigma$  is the volume conductivity of the shield material,  $f$  is the radiation frequency, and  $\mu$  is the magnetic permeability of the shield material. This equation can be modified for heterogeneous materials such as CPN, using the scattering parameter explained in Chap. 2.

### 3.2 *Shielding by Absorption ( $SE_A$ )*

In EMI shielding, after reflection, absorption is the second most relevant mechanism which is expected to take place. For example, polymer nanocomposites promote absorption of the EM smog which are mostly amorphous or semi-crystalline materials as compared to metals having crystalline structure favoring the reflection of EM radiations. In case of shielding by absorption, dielectric and magnetic properties of the shielding materials are important where electrical and magnetic dipoles interact with the incoming electromagnetic waves. Typical materials examples with high dielectric constant and magnetic permeability are zinc oxide or barium titanate and ferrite or nickel, respectively. Shielding mechanism by absorption generates current and magnetic fields by induced EM radiations which causes Ohmic losses and magnetic hysteresis losses. Shielding by absorption for homogeneous materials can be calculated as follows using the Eq. (4):

$$S_{EA} = 8.7d/\delta = 8.7d\sqrt{\pi}f\mu\sigma \quad (4)$$

where  $d$  represents shield material thickness,  $\delta$  is the skin depth. Based on the above equation, the incident frequency of the EM beam and shield materials thickness are directly proportional to shielding by absorption. However, in contrast, the incident EM radiation frequency is inversely proportional to the shielding by reflection.

### 3.3 *Shielding by Multiple Reflections ( $SE_{MR}$ )*

Multiple reflections help in the attenuation of EM radiation. When the incident EM waves pass through the incident surface of the shield at the adjacent surface (such as a polymer air interface) of the shield, it reflects back and forth or “multiple times”. These multiple reflections occur predominantly in materials which possess a large surface area, such as porous or foam materials and materials which possess high interfacial areas, such as multilayered shield materials. The transmitted wave increases due to multiple reflections, and this has a negative impact on the overall EMI shielding. At high frequencies, EM radiation penetrates only near the surface of the conductor, and the magnitude of the radiation exponentially decreases with thickness. The thickness at which the magnitude of the radiation drops to  $1/e$  of the incident radiation is termed “skin depth” and is calculated by Eq. (5):

$$\delta = 1/\sqrt{\pi}f\mu\sigma \quad (5)$$

Shielding due to multiple reflections can be estimated by the following equation if skin depth > material thickness,

$$SE_{MR} = 20 \log_{10}(1 - e^{-2d/\delta}) \quad (6)$$

This shielding by multiple reflections can be neglected when the shield is thicker than the skin depth ( $\delta$ ).

## 4 How the EMI Shielding Works

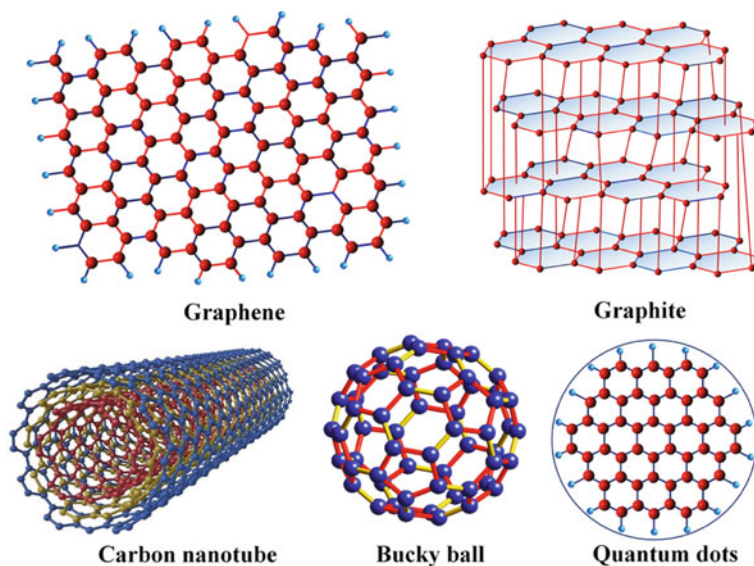
Electromagnetic radiations or waves composed of electric and magnetic components which interact with the electronic materials by inducing currents or magnetic fields and generate force fields on the static or moving charge carriers such as electrons. Example of changing magnetic field results in producing eddy current. In shielding by reflection, which is most common for conductors where applied electric field cancels the induced or generated current. Similarly, due to eddy currents generation, the applied magnetic field is canceled out. Overall, electromagnetic interference becomes null and void.

Several factors serve to limit the shielding capability of real RF shields. One is that, due to the electrical resistance of the conductor, the excited field does not completely cancel the incident field. Also, most conductors exhibit a ferromagnetic response to low-frequency magnetic fields, so that such fields are not fully attenuated by the conductor. Any holes in the shield force current to flow around them, so that fields passing through the holes do not excite opposing electromagnetic fields. These effects reduce the field-reflecting capability of the shield.

In the case of high-frequency electromagnetic radiation, the above-mentioned adjustments take a non-negligible amount of time, yet any such radiation energy, as far as it is not reflected, is absorbed by the skin (unless, it is extremely thin), so in this case, there is no electromagnetic field inside either. This is one aspect of a greater phenomenon called the skin effect. A measure of the depth to which radiation can penetrate the shield is the so-called skin depth.

## 5 Materials Used for Effective EMI Shielding

The selection of electromagnetic shielding materials plays very important role for the better shielding performance. Typical metal shields are used in the form of sheets, screens, or foams. The most common metals or alloys include copper, tin, silver, nickel, steel, and brass. Physical properties of shielding materials which have direct influence on the shielding performance include thickness, permeability, conductivity, and weight. Shield materials conductivity influences the incoming EM radiation differently such as for electrically or magnetically dominant EM waves. For instance, lower and higher conductive metals provide very effective shields to magnetically and electrically dominant waves, respectively. Homogeneity and isotropy are equally important. Presence of any defects or machined holes smaller or larger than the wavelengths of the incoming radiation have different impacts on the shielding efficiency. One should be careful while designing the effective shield. Another commonly used



**Fig. 2** Schematic illustration of the structure of different allotropes of carbon and carbon quantum dots

shielding method, especially with electronic goods housed in plastic enclosures, is to coat the inside of the enclosure with a metallic ink or similar material. The ink consists of a carrier material loaded with a suitable metal, typically copper or nickel, in the form of very small particulates. It is sprayed on to the enclosure and once dry, produces a continuous conductive layer of metal, which can be electrically connected to the chassis ground of the equipment, thus providing effective shielding. There are variety of materials employed for the fabrication of EMI shielding application including metals, polymers, carbon ceramics, and their composites materials. Among these carbon materials are the special class of materials and widely used materials including graphite, carbon nanotubes, fullerene, and graphene oxide alone or in composite with polymeric materials. Figure 2 shows the schematic illustration on the structure and morphology of the different carbon materials employed for the EMI shielding.

## 6 Porous Graphite and Amorphous Carbon for EMI Shielding

As discussed earlier, EMI shielding refers to reflection and/or absorption of electromagnetic radiations particularly at high frequencies, e.g., radio waves, which is distinguished from the magnetic shielding that represents shielding against magnetic fields at low frequencies, e.g., 60 Hz. The charge carriers (electrons or holes) mobility



in shielding materials is believed to be the primary mechanism during reflection of electromagnetic radiation, however, high conductivity is not necessarily required (an order of  $1 \Omega \text{ cm}$  volume resistivity will be sufficient for a typical shield material). The demand of carbon materials and their composites is growing for EMI shielding [2]. Exfoliated graphite or flexible graphite GraFoil® has been tested for EMI shielding application by Luo [3], which is made by compressing the exfoliated graphite flakes without using any binder. Due to honeycomb like structure and high specific surface area, shielding performance of exfoliated graphite appeared exponentially high as 130 dB, greater than that of solid copper.

Carbon materials are more attractive over metals which are by far the most common materials for this application due to their oxidation resistance, chemical and thermal stability as well as lower density, and high dielectric loss properties [4]. Since last two decades, among other 1D and 2D carbon-based materials; 3D porous graphite and amorphous carbon have been successfully developed, and their microwave absorption performance has been tested by many researchers [5–10].

Porous carbons are usually synthesized by carbonization of precursors of natural or synthetic origin, followed by activation [11]. Most of the porous carbon are micro, meso and macroporous. First time 3D mesoporous ordered carbons have been synthesized by Ryoo et al. [12] using ordered mesoporous silica templates where they obtained CMK-1 (a carbon molecular sieve) by carbonizing sucrose inside the pores of the MCM-48 mesoporous silica molecular sieve [13].

Zhou et al. [6] have successfully modified surface of ordered mesoporous carbons (OMC) CMK-3 by in situ polymerization and grafting of methyl methacrylate (MMA) without using any solvent. This new technique significantly enhanced the electric conductivity ( $0.437 \text{ Sm}^{-1}$ ) of the resulting PMMA-g-CMK-3/PMMA composite, which is almost two orders of magnitude greater than that of obtained via solvent mixing method. The maximum absorbance efficiency or minimum reflection loss increases remarkably for in situ polymerized sample ( $-27 \text{ dB}$ ) as compared to the one prepared with solvent ( $-0 \text{ dB}$ ) in an X-band frequency range (8.2–12.4 GHz), respectively. The performance data show that mesoporous carbon materials is a potential candidate for microwave absorption.

In a similar study, Guo et al. [9] reported synthesis of ordered mesoporous carbon (OMC) using a triblock copolymer F127 and soluble phenolic resin (phenol, formaldehyde, and resole) as a structure-directing agent and carbon sources, respectively. Later, this OMC was used to obtain a composite coating of Fe–Ni(0.2)/OMC by mixing metal salts with OMC in 20 ml of deionized water, followed by stirring, adding 4.6 ml of 1 M NaOH, stirring, hot water bath, and vacuum heat treatment up to  $500 \text{ }^\circ\text{C}$  for 2 h. The effective absorption bandwidth of Fe–Ni(0.2)/OMC/paraffin wax composites with 2 mm thickness was  $< -10 \text{ dB}$  at 4.8 GHz. The Fe–Ni alloy coatings on porous carbon enhanced dielectric loss and magnetic loss which played a crucial role in the EM wave-absorbing process.

Shen et al. [7] reported nitrogen-doped ordered mesoporous carbon (NOMC) decorated with ferrite nanoparticles on the surface via coprecipitation method. These composites show excellent EMI shielding performances with absorption bandwidth  $< -10 \text{ dB}$  at 5.0 GHz with 40 wt%  $\text{CoFe}_2\text{O}_4/\text{NOMC}$  composite (1.5 mm thickness).

The minimum reported reflection loss value was  $-38.3$  dB at 3.9 GHz with 30 wt%  $\text{CoFe}_2\text{O}_4/\text{NOMC}$  composite (4 mm thickness).

EMI shielding properties of multilayered carbon fiber felt (CFF)-glass fiber felt (GFF)/epoxy resin composites, with/without carbonyl iron powder, and with different layer angle were investigated in the X-band frequency range recently [5]. Study shows that at low layer angle ( $0^\circ$ ), multilayered CFF-GFF/epoxy composite with 4 mm thickness results in high shielding effectiveness, however, carbonyl iron powder improves the shielding performance beyond  $35^\circ$  of layer angle.

Carbon nanotube (CNT)-multilayered graphene edge plane (MLGEP) core-shell hybrid foams were prepared by Shen et al. [8] where CNTs were grown using a template-directed CVD approach, and then, MLGEPs were in situ grown on the CNT cores with seamless junctions using plasma enhanced CVD which forms a nanoporous shell without using metal catalyst. These hybrid porous structures exhibit ultrahigh EMI shielding performance.

Another porous carbon structure for EMI shielding reported by Xu et al. [10] where hollow graphene nano-spheres uniformly confined in porous amorphous carbon matrix by facile pyrolysis of bi-metal organic framework (bi-MOF). These bi-MOFs were fabricated by coordination reaction using cobalt and zinc ions as the metallic nodes and 2-methylimidazole as an organic linker. The amount of these hollow graphene nano-spheres can be controlled and brought to be optimum for better microwaves absorption by tuning the Co/Zn molar ratio. The minimum reflection coefficient ( $\text{RC}_{\min}$ ) reduces to  $-32.43$  dB @ 9.19 GHz (3.70 mm thickness), and with 10% of filler loading, the effective absorption bandwidth can cover the whole X-band (8.2–12.4 GHz,  $<-10$  dB, 3.50 mm).

## **6.1 Porous Graphite and Amorphous Carbon Nanoplatelets for EMI Shielding**

Carbon nanostructures and their composite species have brought great advances and contributions in EMI shielding. Among various carbon-based materials, amorphous  $sp^2$  hybridized carbon in the form of graphite and graphene and their nanocomposites have emerged excellent capability of absorbing electromagnetic radiations. Exfoliated graphite nanoplatelets (xGNP) are new forms of nanoparticles made from graphite which are produced from exfoliating the acid intercalated graphite by rapid thermal treatments. These nanoplatelets vary in size which can be obtained usually in the range of 1–10  $\mu\text{m}$  by sonication and milling. The thickness of individual platelet is in the range of 5–20 nm depending on the intercalation as well as the exfoliation processes [14].

In recent study [15], a multiphase hybrid nanocomposite of para-Toluenesulfonic acid (p-TSA) doped polyaniline (PANI)-graphene nanoplatelet (GRNP's) composite coatings (1.5 mm thickness) were successfully produced by in situ polymerization of aniline in the presence of graphene nanoplatelets. The EMI shielding performance

of these nanocomposites shows a strong correlation on GRNP's content in the PANI matrix. The nanocomposite with 10 wt% of GRNP's in PANI matrix exhibits very high shielding efficiency (>95%) in the X-band.

Synergistic effect of graphene nanoplate (GNP) and carbonized loofah fiber (CLF) with polyether-ether-ketone (PEEK) composites were reported with excellent EMI shielding properties in the X-band region [16]. With the addition of 9 wt% CLF content, the composite exhibits 27.1 dB of average total shielding effectiveness. Both additives improve the conductive network in PEEK-based composite, resulting excellent shielding performance.

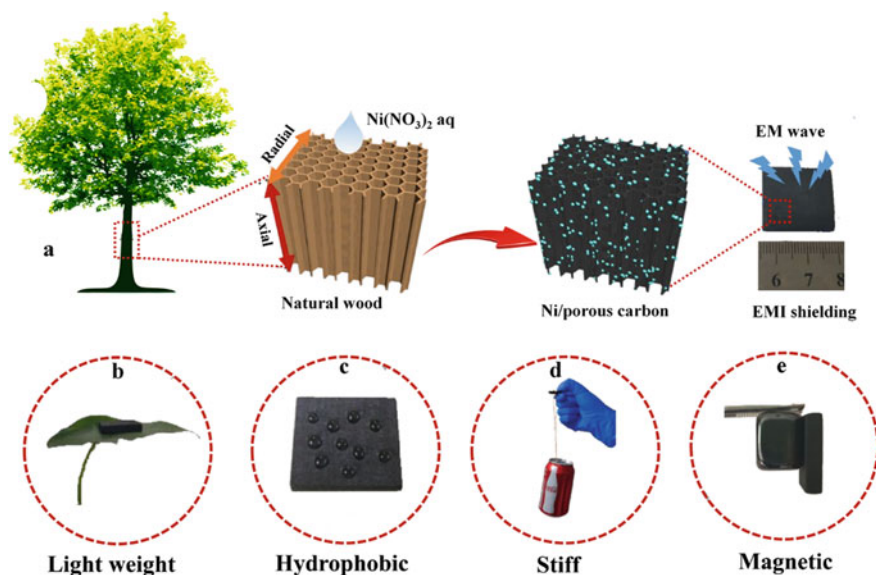
Bubble-templated rGO-graphene nanoplatelet foams encapsulated in silicon rubber have been fabricated using novel and facile foaming routes [17]. The 3D conductive GNP network in polydimethylsiloxane (PDMS) rubber composites exhibits excellent EMI shielding efficiency (~86 dB at a thickness of 2 mm).

Functionally graded polymers and graphene nanoplatelets (GnPs) composite foams have shown a great promise toward the electromagnetic shielding effectiveness, confirmed very recently [18]. These composite foams with graded microcellular structures were produced using a scalable technique of foam injection molding where supercritical fluid treatment followed by foaming via rapid depressurization in the mold cavity.

## 6.2 Porous Graphite/carbon Foams for EMI Shielding

Lightweight electrically conducting materials are considered ideal for EMI shielding capabilities. Porous graphite/carbon foams [19–23] have received a lot attention recently due to their inherent properties that are suited for EMI shielding. They are widely used in weight sensitive applications such as aircraft structures, thermal insulation [24], automobiles, and marine vessels [25, 26]. EMI capability of the material is normally enhanced by high electrical conductivity, and graphite materials are known to have better electrical conductivities. In this section, we review various graphite/carbon foams and their composites as effective EMI shielding materials.

Different techniques have been proposed to design lightweight, conducting foams mentioned above. Many have emphasized the best technique should be scalable so as to allow its wide scale adoption. We will review these techniques in the following sections. Zheng et al. [27] prepared a wood derived magnetic porous carbon composites that is a highly ordered anisotropic porous architecture (Fig. 3). The wood was obtained from natural fir and cut into different sizes along the growth direction. The wood was dried and later immersed in Ni (NO<sub>3</sub>)<sub>2</sub>·6H<sub>2</sub>O solution with varying concentrations for 30 h while being ultra-sonicated and then dried in vacuum oven at 80 °C for 12 h. The sample was later calcined under argon flow at heating rate of 5 °C/min up to 800 °C with a holding period of three hours. The resulting material is magnetic, lightweight, stiff, and hydrophobic important properties needed for EMI shielding. EMI measurement showed that addition of nickel nanoparticles has a great influence on the EMI of the porous material. When measured in the 8.2–12.4 GHz



**Fig. 3** Preparation of carbon foam for EMI shielding that is stiff, magnetic, hydrophobic, and lightweight by addition of nickel nanoparticles (reprinted from Ref. [27] with permission)

range for the radial and axial orientations at 2 mm thickness, EMI SE values of increase dramatically as the Ni nanoparticle loading is increased. The highest nickel nanoparticle content of 1.5 wt% led to the maximum value of 50.8 dB meaning the composite was able to block virtually all EM allowing only 0.001%. Also, axial direction EMI shielding is higher than radial orientation due to the aligned stacking conductive paths possessed by axial direction sample that dissipates the incident electromagnetic waves by multiple reflections.

A similar wood derived porous carbon/graphite has also been synthesized exhibiting desirable EMI shielding capability [28]. The wood used here was sapwood from poplar tree, and iron oxide nanoparticles were added and material carbonized at high temperature. The EMI absorbing reached 64.26 dB at 14.36 GHz with a thickness of 2.25 mm. The improved shielding improvement was attributed to the self-assembly morphology of iron oxide nanoparticles in the inner surfaces of the wood lumen walls permitting optimal impedance matching.

Yuan et al. [29] used a template method to synthesize a foam with an EMI shielding effectiveness of around 36–43 dB in the X-band. The graphite/carbon monolith foam consisted of honeycomb structure that was filled with a horizontal laminated reduced graphene to increase its stiffness. With its high thermal conductivity (0.057 W/(m K) and flame retardancy, this material could be used as a multifunctional one with a potential to be used in the aerospace industry. To provide EMI shielding at extreme operating temperature, a system containing graphite/graphene, carbon nanotubes, etc., were designed [30]. In this work, a core-shell 3D “nanofiller” of CNT/graphene was added into prycarbon so as to make a cellular hybrid material. The effectiveness

of shielding at the X-band was in the range of 26.6–45.3 dB. Carbon/graphite foams have also been synthesized from polymer precursors to be used as EMI shielding materials. To achieve high strength in the foam, Li et al. [31] synthesized carbon foams from thermosetting polyimide. As a result of cross-linking, the foam had excellent thermal stability and very high compressive strength (0.25 MPa at 10% strains). Foams carbonized above 1200 °C had EMI shielding effectiveness of 54 dB at 10 GHz. It was further shown that stiffness and lightweight of the foams can be adjusted by varying the properties and quantities of polyimide starting material. Another attractive material entirely made from graphite for EMI shielding is the flexible graphite. This material is made by compressing exfoliated graphite flakes and with no help of any binder. The exfoliation can be achieved using well-known graphite exfoliation species that get in-between layers and expand and exfoliate the graphite. The compression of the exfoliated graphite leads to interlocking with one another thereby forming a strong film without any binder. It is a chemically and inert materials possessing very low coefficient of thermal expansion (CTE). Effectiveness EMI shielding as high as 130 dB at 1 GHz has been reported [2].

### **6.3 Composites of Porous Graphite/carbon Foams for EMI Shielding**

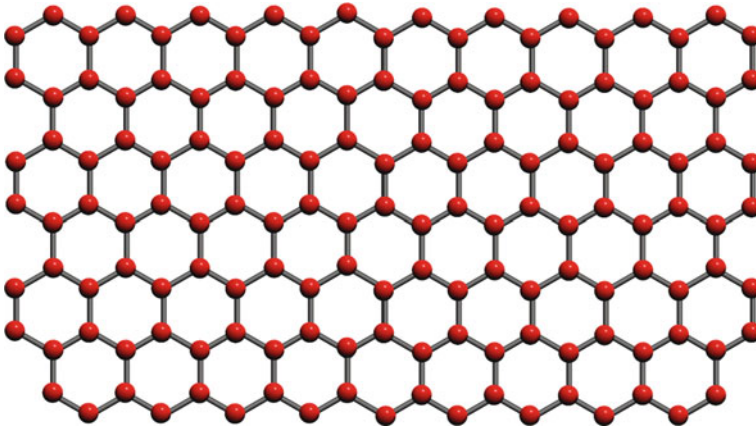
Composites of the foams or thin films mentioned in the previous section are an attractive material for EMI shielding especially in application that do not need high temperature. Several research teams have proposed methods to infiltrate polymer binders into these porous and films materials. This is mainly done to increase their toughness when the application requires it. Three-dimensional graphene/graphite foams have been widely used in this area. Scalable thin-layer graphite foam synthesized through template-directed thermal annealing process showed an EMI shielding effectiveness of 36.1 dB over a frequency range of 8.2–18 GHz [32]. The foam was synthesized by carbonizing polyacrylonitrile (PAN) polymer at high temperature and then infiltrated with polydimethylsiloxane (PDMS) polymer. Compressive strength increased by 254% compared to virgin foam. An important property of this composite was its reversible compressibility in as many as 1000 cycles without degradation in properties. And, with an improved electrical conductivity, this material is an ideal candidate for future flexible electronics. A confined foaming techniques have been used to synthesize flexible graphite/graphene films showing exceptional EMI shielding capacity [33]. This technique was thought as being more energy efficient compared to current methods. Graphite/graphene precursor was optimized by selecting flakes with few defects that led to an improved structure order thereby high mechanical strength and high electrical conductivity. The hierarchical and oriented porous structure had very low density and excellent folding capability. The EMI effectiveness (SE) was reported as 43.8 dB as a result of hierarchical structure leading to multiple reflections and dielectric loss. The specific SE/thickness of 29 178 dB cm<sup>2</sup> g<sup>-1</sup> was

the highest graphene/graphite shielding efficiency among reported graphene/graphite materials. With such improved properties, it was suggested that this could be a great material for foldable and wearable electronic devices.

An efficient method has been used to prepare lightweight, freestanding, and flexible membrane/film by cross-linking polyacrylonitrile (PAN) nanofiber and metal nanoparticles [34]. In this method, the PAN was electro-spun into nanofibers then followed by electro-less deposition of the metal nanoparticles. The composite had very high electrical conductivity and effectiveness 90 dB. This value was achieved at very thin membranes (53  $\mu\text{m}$ ) and is much higher than those synthesized from pure metals. The composite also exhibited excellent flexibility and was proposed to be used in smart portable wearable electronics. A composite of carbon and red mud has also been proposed as a lightweight EMI shielding material [35]. This material is synthesized by mixing phenolic resin (carbon source) with red mud (filler) then uses polyurethane (PU) foam as a template to infiltrate with the solution of phenolic plus red mud then carbonized above 1000  $^{\circ}\text{C}$ . Presence of red mud enhances the dielectric, thermal, and magnetic as well as EMI shielding properties of the composites. It was postulated that absorption is the main contributor to the EMI shielding effectiveness that was 51.4 dB in the frequency range of 8.2–12.4 GHz with a 20 wt% of red mud. A nanocomposite of carbon spheres and manganese dioxide has also been synthesized to be used in EMI shielding. The manganese dioxide ( $\text{MnO}_2$ ) nanoflakes are used to uniformly coat the carbon core spheres by a water-bathing method [36]. The  $\text{MnO}_2$  was estimated to be 24.7 wt% in the nanocomposite. With such a high loading, the nanocomposite had a very high dielectric loss value as well as EMI shielding effectiveness of 16–23 dB at the frequency range of 8–18 GHz attributed to enhance absorption loss.

## 7 Porous Graphene for EMI Shielding

Graphene is considered as a wonder material since the discovery of the material. The revolutionary outbreak was bought about by the accidental discovery of graphene which was honored by the prestigious Nobel Prize for Physics in 2010 shared by Kostya Novoselov and Andre Geim. The stacks of few layers of  $sp^2$  hybridized atoms hexagonally bonded together forming an extended conjugated 2D sheet structure with extra ordinary electrical conductivity, thermal conductivity as well as stability. The ballistic electron transport of graphene enables it for a wide variety of applications particularly in the electric field [37]. The structure of graphene is demonstrated in the Fig. 4. The excellent electrical property of graphene is the fundamental grounds for the shielding property. The enhanced surface area add-ons the electromagnetic shielding property of the material. The lightweight, absence of corrosion, and minimum quantity enhance the wide acceptance of the carbon allotropes for EMI shielding applications [38]. A variety of graphene products are applied for EMI applications like graphene foams, graphene films, functionalized graphene as well as graphene composites.



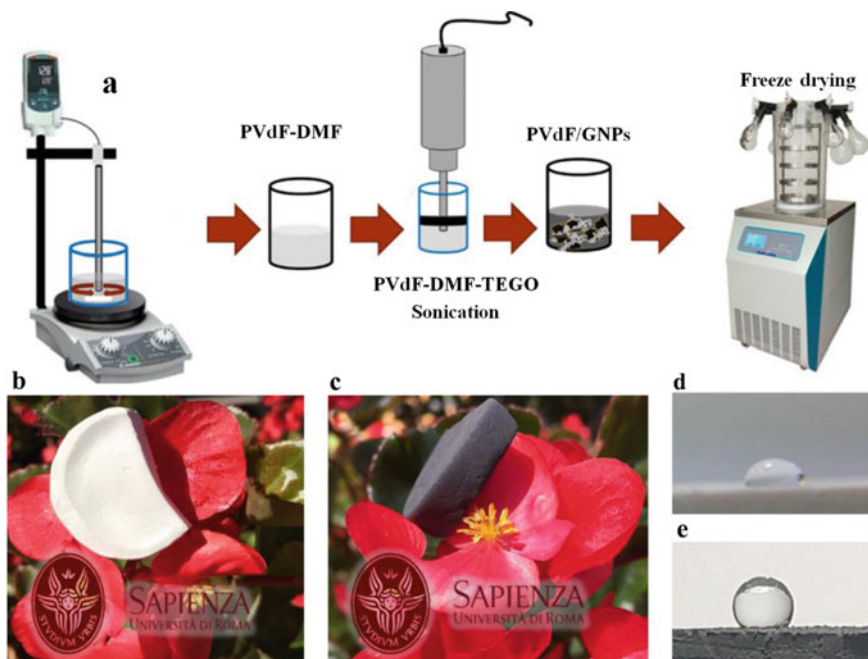
**Fig. 4** Schematic illustration of two-dimensional structure of graphene nanosheet

### ***7.1 Porous Graphene Foams for EMI Shielding***

A potential interest is enhanced for the development of lightweight, as well as multi-functional electromagnetic waves absorbing which possess extraordinary thermal and mechanical properties along with chemical stability are inevitable for EMI shielding application in for space, aerospace. A lightweight porous graphene-based aerogel for EMI shielding was synthesized compositing poly vinylidene fluoride (PVdF) polymer matrix with graphene nanoplatelets (GNPs) [39]. The synthesis procedure of PVdF/GNS composite aerogel is depicted in the Fig. 5. The varying composition of the GNS incorporated composites from 7–15 wt% was synthesized. The EMI shielding properties relied on the absorption of the EM waves. The composite aerogels containing 11 and 15 wt% of GNPs, and thickness of each absorber was confined to have a minimum reflection peak between 12 and 15 GHz as well as a maximum bandwidth with reflection coefficient below  $-20$  dB. 15 wt% samples delivered a maximum performance at a thickness of 2.2 mm absorbing panel with a reflection peak at  $\sim 13.5$  GHz and bandwidth with reflection coefficient lower than  $-20$  dB or  $-10$  dB wider than 6 GHz or 9 GHz, respectively (Table 1).

### ***7.2 Porous Graphene Films/paper for EMI Shielding***

The modification of the graphene oxide sheets to porous paper structure was achieved by appropriate chemical designing. Recently in 2020, Lai et al. [33] synthesized porous graphene films by modifying graphene oxide (GO) synthesized by modified Hummer's method by different methods (pre-oxidation modified Hummers' method (PGO), a classic modified Hummers' method (CGO), and a low-temperature modified Hummers' method (LGO)). The GO synthesized was dried at room temperature



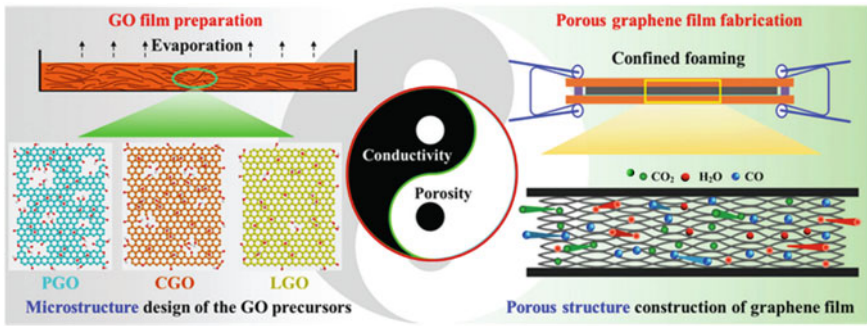
**Fig. 5** a Schematic procedure for the production of PVdF-GNP nanocomposite aerogel samples. Lightweight aerogel samples made of neat PVdF (b) and GNP-loaded PVdF (c) over flower petals. Water drop over the hydrophilic of (d) or hydrophobic (e) surfaces of aerogel samples, made of PVdF or GNP-loaded PVdF, respectively [39]

**Table 1** List of the produced graphene-based aerogel samples with their GNP concentrations, density, and porosity values

Process temperature: 65 °C				Process temperature: 85 °C			
Sample	GNP content (wt%)	Density (g/cm <sup>3</sup> )	Porosity (%)	Sample	GNP content (wt%)	Density (g/cm <sup>3</sup> )	Porosity (%)
G00A	0	0.274	78.95	G00B	0	0.289	79.97
G07A	7	0.280	65.25	G07B	7	0.265	71.58
G11A	11	0.270	80.17	G11B	11	0.190	86.61
G15A	15	0.192	70.80	G15B	15	0.187	77.00

in Petri dish. The dried samples formed a film structure which was further sandwiched between hydrazine hydrate precoated glass plates with desired thick spacers. The samples were stored in sealed containers maintained at 90 °C for approximately 2 h. The characterization of the resultant films revealed the formation of highly porous graphene sheets with variable thickness accordingly based on the spacers



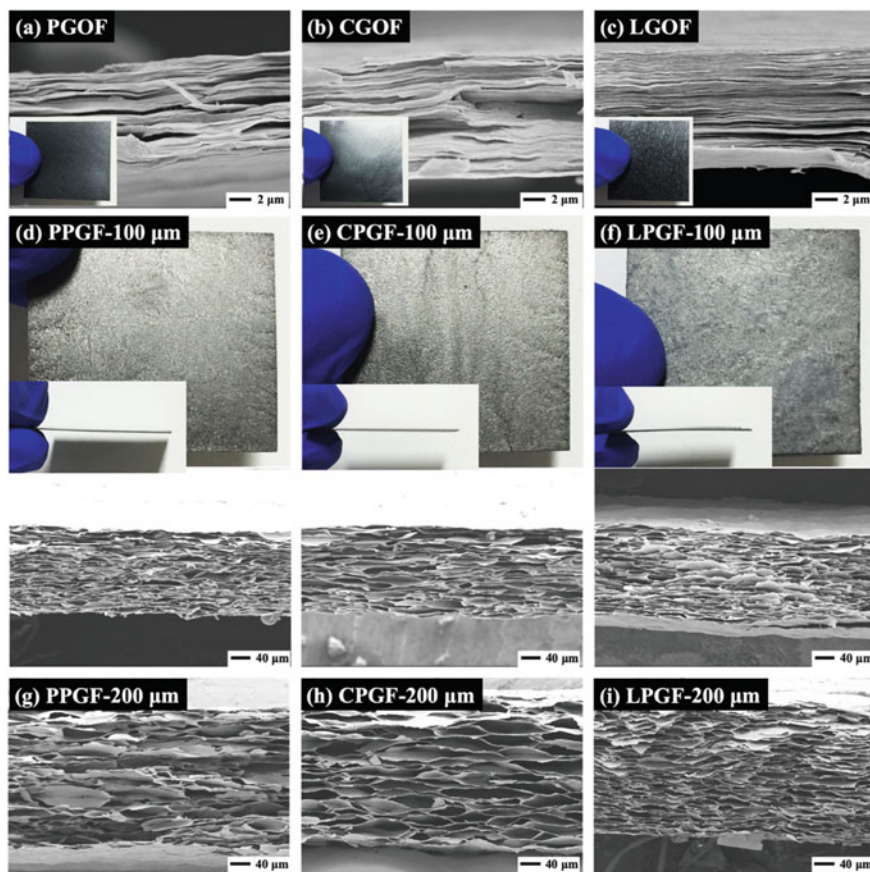


**Fig. 6** Schematic illustration of the proposed structural features of the various GO precursors and the method of confined foaming to controllably fabricate porous graphene films [33]

applied [33]. The schematic illustration of the fabricated GO films and the properties has been illustrated in the Fig. 6.

The  $I_D/I_G$  ratios of the PGO, CGO, and LGO sheets are measured to be 0.88, 0.92, and 0.98, respectively, indicating the enhanced graphitic nature of the samples synthesized at lower temperatures due to minimization in the defect states. The morphology of the films as depicted in the Fig. 7a–i reveals the presence of GO films with similar cross section despite of change in the synthesis method. The thickness of the films formed is approximately 10 mm indicating the homogeneity and interlayer binding of the samples in the proposed synthesis method. A sufficient enhancement in the performance of EMI shielding is observed for all the samples. The overall shielding effectiveness ( $SE_{Total}$ ) increases from 19.71 to 25.17 dB for PPGF, whereas  $SE_{Total}$  increases from 27.21 to 34.37 dB for CPGF sample on increase in foaming thickness from 100 to 1000 mm. The maximum performance was observed for LPGF samples which showed an increment of ~30% with an EMI SE value of 37.43–48.59 dB for 100–1000 mm thick samples, respectively.

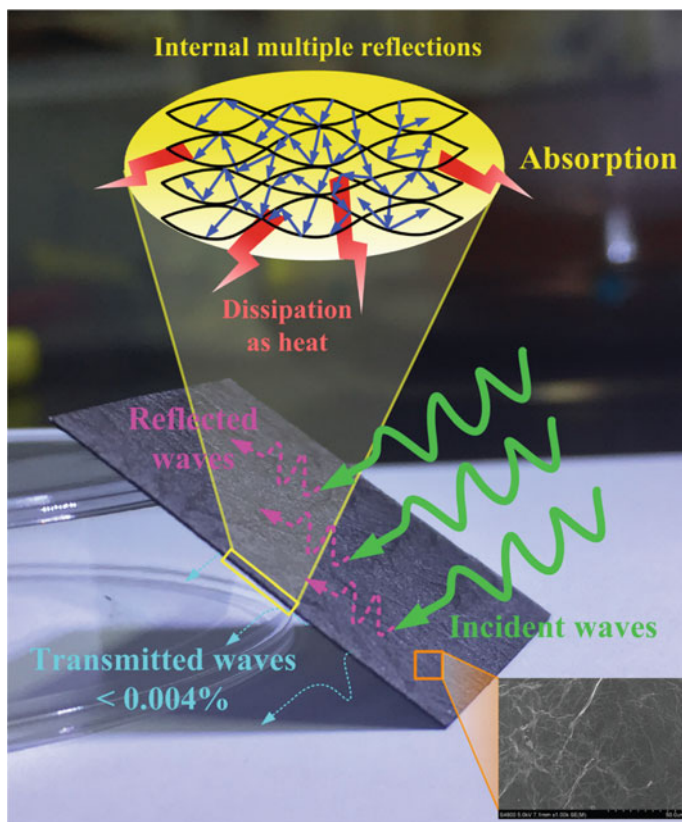
The effective performance of shielding property of the porous graphene sheets is attributed accordingly based on the proposed mechanism depicted in Fig. 8. When an electromagnetic wave is incident on the surface of the porous graphene sheets, a definite number of waves are reflected due to the enhanced impedance mismatch between the air and sample. A compact as well as conductive films always facilitates this reflection loss. A definite number of waves enter the films leading to further scattering of the electromagnetic waves due to the collision of wavelets with the sub-atomic particles to generate a counter induced field, leading to the development of polarizations and dielectric loss. The enhanced porosity and scattering of the electromagnetic waves cause a transfer of energy within the system leading to the dissipation of the excess energy as heat. Thus, a minimum number of waves are transmitted through the material leading to an effective shielding through the porous graphene sheets.



**Fig. 7** Cross-sectional SEM views and inset optical pictures of various 10 mm thick GO films of **a** PGOF, **b** CGOF, and **c** LGOF. Surface and cross-section optical pictures and cross-sectional SEM images of expanded 100 mm thick porous graphene films of **d** PPGF, **e** CPGF, and **f** LPGF. SEM images of the fracture cross sections of 200 mm thick porous graphene films of **g** PPGF, **h** CPGF, and **i** LPGF [33]

### 7.3 Functionalized Porous Graphene for EMI Shielding

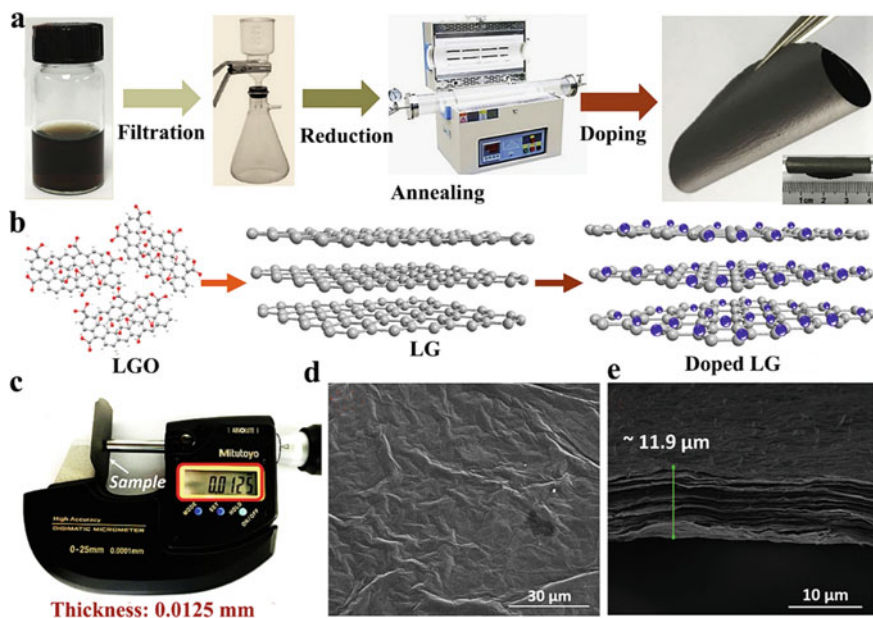
Graphene sheets form lightweight as well as flexible two-dimensional (2D) structures. The enhancement in the electronic mobility in sheet structures owing to the extended conjugation enables the elevation in the shielding property. The enhancement in the shielding property can be achieved by the functionalization of the graphene sheets by appropriate dopants. In 2017, Wan et al. [38] reported the graphene paper synthesized by reducing graphene oxide (GO) from modified Hummer's method. The GO thus prepared was doped with iodine using hydroiodic acid (HI) at a temperature of 90 °C for 12 h. The doped samples were repeatedly



**Fig. 8** Schematic illustration on the EMI shielding mechanism

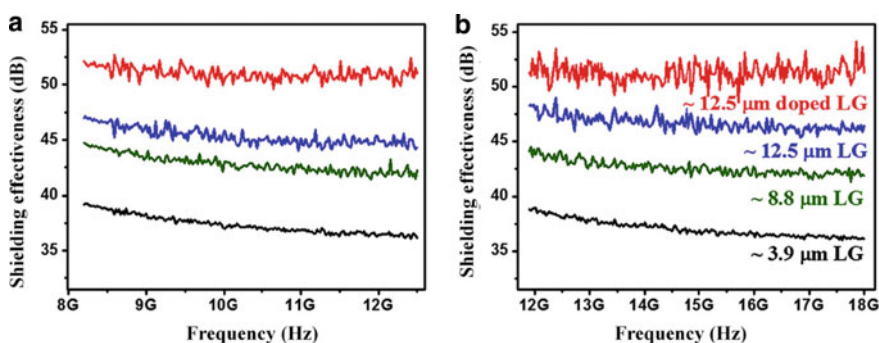
washed with water and ethanol. The samples were dried, and paper was clamped tightly between two graphite plates and annealed at 1600 °C for 60 min in inert atmosphere to prepare iodine doped graphene sheets. The schematic illustration of the synthesis and doped graphene has been depicted in Fig. 9a, b. The morphology of the shielding film is displayed in Fig. 9c. The shielding property of the paper depends on the thickness and conductivity of the graphene paper formed. The various sized graphene sheets were analyzed at a frequency range of 8.2–12.5 GHz.

The EMI shielding effect of lower sized graphene with different thickness measured at 8.2–12.5 GHz and 11.9–18 GHz is displayed in Fig. 10a, b [38]. The value of shielding effect is almost independent of all the measured frequency range, which is different from the reported carbon-based materials possessing fluctuated SE curve with frequency [38, 39]. The EMI shielding effect is increased with the thickness of LG, from 39.1 dB for 3.9 mm to 47.0 dB for 12.5 mm at 8.2 GHz. After doping process, the SE is further increased. The primary mechanism of carbon shielding materials proposed by the previous reports is the interaction between charge carriers (electrons or holes) and the electric vector of the incident electromagnetic



**Fig. 9** a Fabrication process of iodine doped LG and b its corresponding schematic illustration; c picture of thickness measurement and SEM results: d plan and e cross section of the film [38]

field, which mainly based on two ways. One is that the free carriers absorb energy from the incident wave and move in response to the EM wave. The other is that EM field caused by the moving charge carriers creates induced field, which in turn interacts with the incident EM wave [9, 40]. For the detailed information, a comparison of carbon-based EMI shielding materials is shown in Table 2.



**Fig. 10** a, b Shielding effectiveness of LG with different thickness under different frequency range and the improvement after iodine doping [38]

**Table 2** Comparison of carbon-based EMI shielding materials [38]

Sample	Conductivity ( $S\ m^{-1}$ )	Thickness ( $\mu m$ )	EMI SE (dB)	Year/reference
Electrochemically exfoliated graphene	$l$	250	17	2015 [40]
Chemically reduced GO	$2.43 \times 10^4$	15	20	2015 [41]
CVD synthesized graphene	$1.34 \times 10^4$	50	60	2015 [42]
Thermally reduced GO	$1.0 \times 10^5$	8.4	20	2014 [43]
Multilayer graphene	$1.44 \times 10^5$	18	55	2015 [44]
Graphene foam	$310 \times 10^0$	300	25.2	2016 [45]
Carbon/graphene foam	$1.5 \times 10^4$	24	24	2016 [46]
S-doped graphene	$3.1 \times 10^4$	150	38.5	2016 [47]
Graphene/WPU film <sup>a</sup>	$2.1 \times 10^3$	320	49	2016 [48]
Magnetic graphene/PVA <sup>b</sup> (6 wt%)	$3.11 \times 10^0$	360	20	2014 [49]
Iodine-doped LG paper	$1.05 \times 10^5$	12.5	52.2	2017 [38]

<sup>a</sup>WPU, waterborne polyurethane with graphene of 76.2 wt%

<sup>b</sup>PVA, poly(vinyl alcohol) with loading ~6 wt%

## 7.4 Composites Based on Porous Graphene for EMI Shielding

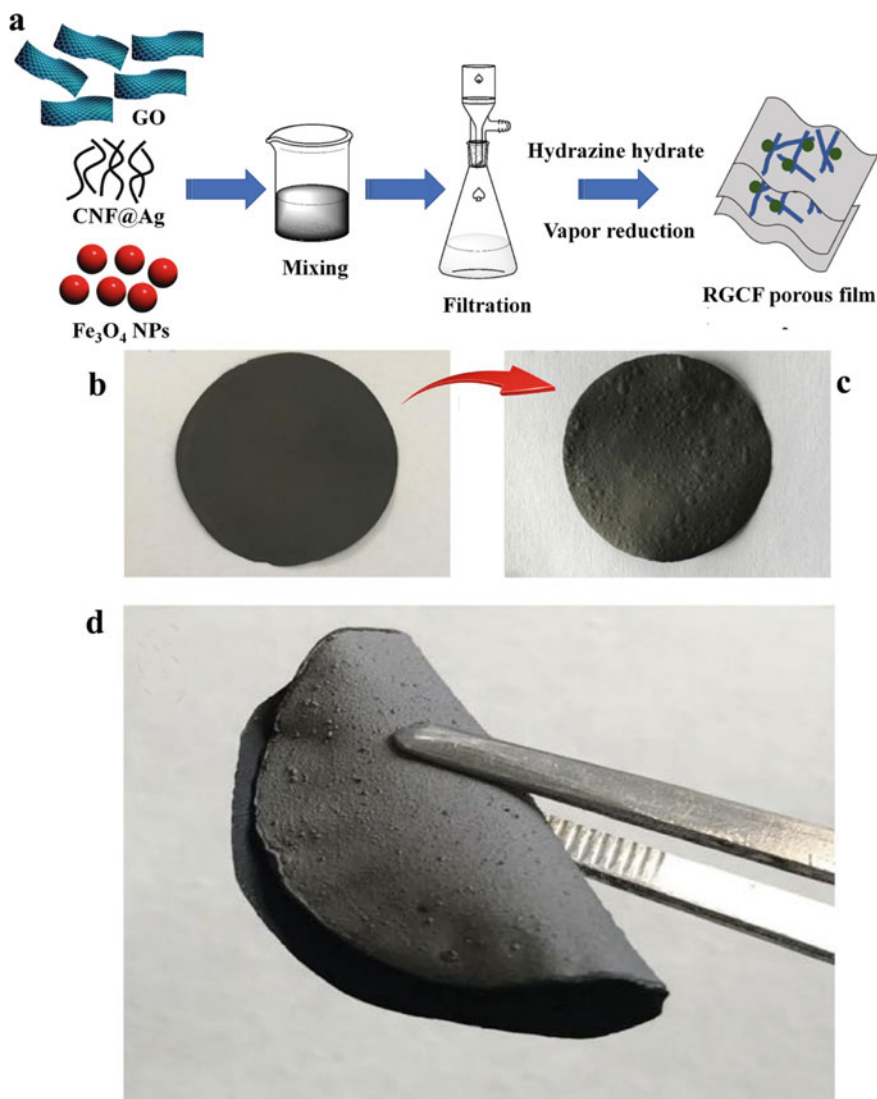
The EMI shielding effectiveness (SE) of a composite material is relied on intrinsic conductivity, dielectric constant, and aspect ratio of the material incorporated to the matrix. The synergistic effect and effective absorption/reflection of the electromagnetic waves play a crucial role in the performance efficiency. Few layers thick graphene, with large aspect ratio and high conductivity, is proven to be an effective EMI shielding material. In 2009, Liang et al. [50] reported the synthesis of graphene composites-based functionalization of graphene in epoxy matrix. The electromagnetic interference (EMI) shielding performance of the composites revealed low percolation threshold (0.52 vol.%). EMI shielding effectiveness of the composite films was analyzed in the frequency range of 8.2–12.4 GHz (X-band). The superior performance of the sample fabricated with graphene epoxy composite with 15 wt% (8.8 vol.%) loading delivering a shielding efficiency of 21 dB. Later, Yan et al. [51] reported the EMI shielding effect of graphene/polystyrene composite materials synthesized by high-pressure compression molding combined with salt leaching, fabricating the samples with specific shielding effectiveness  $64.4\ dB\ cm^3\ g^{-1}$  for a thickness of 2.5 mm. Liu et al. reported a ternary composite

with epoxy-water-inorganic filler suspended emulsion polymerization. A porous graphene nanoplatelet (GNP)/Fe<sub>3</sub>O<sub>4</sub>/epoxy nanocomposite was prepared with low density of 0.34–0.73 g cm<sup>-3</sup>. The porous nanocomposite with same ratio of graphene nanoplatelets and Fe<sub>3</sub>O<sub>4</sub> nanoparticles (7:7 wt%/wt%) exhibited enhanced performance with a specific electromagnetic interference (EMI) shielding effectiveness of ~37.03 dB/(g cm<sup>-3</sup>). The samples also delivered excellent thermal and mechanical properties. In 2020, Guo et al. [52] reported a highly flexible thin films of RGO/CNF/Ag–Fe<sub>3</sub>O<sub>4</sub> (RGCF) porous film for EMI shielding application. The graphene oxide and silver decorated carbon nanofiber along with Fe<sub>3</sub>O<sub>4</sub> nanoparticles were mixed together in the ratio 1:1:0.33, 1:1:0.666, and 1:1:1 ratio, respectively, via sonication followed by filtering the samples in an AAO membrane. The films thus obtained were subjected to autoclaving in the hydrazine hydrate atmosphere at 100 °C for about 9 h for reducing the graphene oxide to reduced graphene oxide leading to the formation of the composite membranes. A schematic illustration of the synthesis has been demonstrated in the Fig. 11. The sample with 1:1:1 ratio exhibits enhanced mechanical with EMI shielding effectiveness of 21.0 dB.

## 7.5 Graphene-CNT Hybrid Structures for EMI Shielding

The emergence of graphene has opened up innumerable opportunities in the field of materials science and nanotechnology research due to its exceptional electrical, mechanical, electronic, electrochemical, and thermal properties. Graphene has a unique band structure with band-tuning ability and extremely high carrier mobility (in excess of 1,00,000 cm<sup>2</sup>/V s) [53, 54]. Unfortunately, these properties only emerge in the 2D planar direction of the graphene structure, which limiting its scope and application. Recently, many strategies have attempted to address this weakness of graphene by developing hierarchical hybrid structures, wherein graphene acts as a platform for support, scaffold, or a 2D planar substrate for anchoring other nanomaterials. For instance, carbon nanotubes (CNTs), their properties emerge in the axial direction, can be functionalized onto the surface of 2D nanosheets of graphene, combining the properties of the two major carbon allotropes in all directions while allowing for an increased active surface area and faster electron transfer kinetics. This unique method adopted to expand the scope of its usage, graphene hybrids which combine the synergetic properties of graphene along with other nanostructured materials and is a widely emerging field of research.

The flat monolayer of *sp*<sup>2</sup> carbon atoms tightly packed in two-dimensional honeycomb-like lattice is the building block for graphene. Compared to carbon nanotubes, graphene exhibits potential advantages of high surface area, ease of processing, low cost, safety [55], and high purity (absence of transition metals, Fe, Ni, etc.) [56]. Carbon nanotubes (CNTs), consisting of cylindrical graphene sheets with nanometer diameter, have high mechanical strength and chemical stability, good electrical conductivity, rich optical properties, and high surface area. When combining these two unique nanomaterials materials result in to an intelligent and unique hybrid materials, which could overcome the shortcomings and limitations of



**Fig. 11** **a** Schematic illustration on the steps involved in the fabrication of RGCF porous film, **b** digital image of GCF film, **c** RGCF porous film, and **d** bending properties of RGCF-3

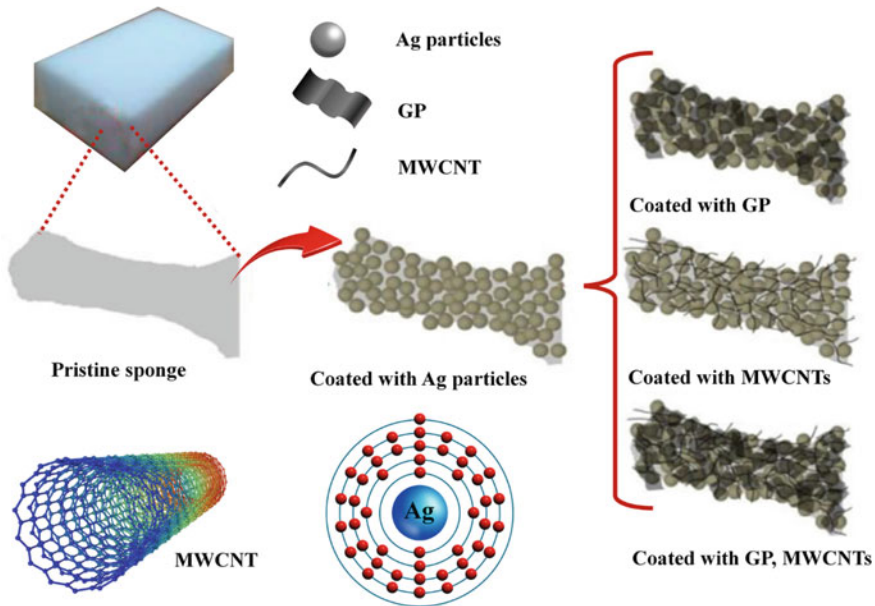
individual components. Thus, many efforts have been made so as to obtain graphene-carbon nanotube hybrids by different methods of synthesis [57–64]. Early researches on graphene-CNT are focused on the assembly of graphene and CNT to generate hybrid fillers rather than making nanostructured architectures for a specific application. The synthesis/fabrication of graphene-CNT hybrids generally categorized

into four different approaches, including solution processing/casting, [65–70] layer-by-layer deposition, [68, 71, 72] vacuum filtration, [73, 74] and chemical vapor deposition (CVD) [59, 62, 63, 75–85]. Among all the synthesis method reported for the graphene-CNY hybrids, CVD approaches are reported to build hierarchical nanostructures with reasonable structural stability and mechanical strength [75, 86]. Recently, the possibility to explore the graphene-CNT hybrids to fabricate EMI shielding materials having improved shielding efficiency than the individual components. Blending of large surface area, one-dimensional carbon nanotubes with a two-dimensional graphene matrix having high charge density, has been displays the enhanced EMI shielding properties due to the synergistic effect on magnetic, electronic, and charge transfer properties. The hybrid material also shows large specific area and catalytic properties compared with either pristine CNTs or GO/graphene [87]. Generally, when dispersing in an organic matrix, CNTs tend to agglomerate, therefore, numerous efforts were developed to disperse the CNT by using micelles, ionic liquids, surfactants, polymer wrapping, and other chemical functionalization approaches. It was demonstrated that when CNT is mixing with graphene nanosheets forms a stable dispersion of CNT, in which graphene acts as a barrier to prevent the agglomeration of seamless tubular CNT, and the resulted dispersion is called as graphene oxide-CNT hybrid filler (GO-CNT) [88]. The strong  $\pi$ - $\pi$  stacking interaction operating between graphene and CNT makes a uniform three-dimensional network similar to cross-linked structures for the hybrid material and provides exceptional stability [89].

The formation of CNT networks acts as conducting wires inside the already conducting graphene structure, thus promoting the electronic as well as thermal conductivity of the hybrid material [61]. Chen et al. [90] used graphene-MMCNTs structures to study the EMI shielding of these hybrid structures. A commercial sponge was coated with silver nanoparticles and then dip-coated with graphene (GP) ink, multi-wall carbon nanotubes (MWCNTs) ink, or hybrid GP/MWCNTs ink to form Ag/carbon nanomaterial hybrid composites and compared the EMI shielding (in the frequency range of 0.45–1.5 GHz), properties were compared with sponge without Ag coating. Figure 12 schematically depicts the coatings of Ag particles and carbon nanomaterial fillers onto the surface of inner pores within sponge and their surface morphologies. The SEM and TEM images of the samples are displayed in Fig. 13. A 50 × 50 mm size square composites sample was subjected to EMI measurements in the frequency range of 0.45–1.5 GHz. For comparison, the sponges without Ag nanoparticle coating were also prepared. The EMI SE tests using an industrial microwave oven showed that nearly 80 and 90% of the power density were shielded by the sponge composites coated with GP/MWCNTs/ink without and with the Ag nanoparticle coating, respectively. The maximum values of approximately 14.4 dB could be achieved with these sponges without Ag nanoparticles, while the hybrid composites with Ag nanoparticle coating exhibited maximum EMI shielding of 24.33 dB, predominantly by reflection due to their porous structure.

Goyal et al. [91] prepared polycarbonate (PC)/graphite nanoplatelet (GNP) nanocomposites PC/GNP by a facile solution mixing method in combination with the hot compaction method and studied effect of GNP on electrical

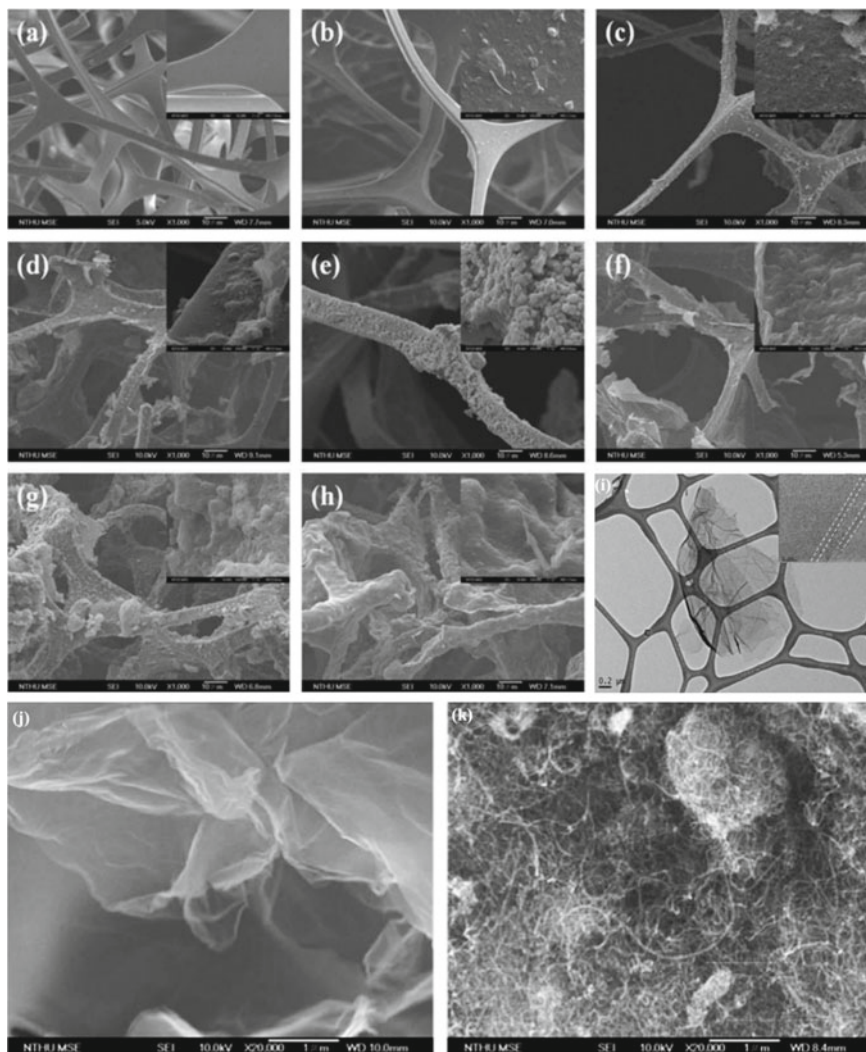




**Fig. 12** Schematic figure of the sponge composites coated with Ag nanoparticles and subsequently GP/ink, MWCNTs/ink, and GP/MWCNTs/ink

properties and electromagnetic interference shielding effectiveness (EMI SE) of the nanocomposites in X-band. A very low percolation threshold of 0.005 vol. fraction GNP was achieved for these composites. The composite having 0.037 vol. fraction GNP displayed the electrical conductivity of about 0.413 S/m. It is widely reported that an electrical conductivity of  $1.0 \text{ S m}^{-1}$  is necessary to achieve the SET of  $-20 \text{ dB}$  which is required for commercial applications. However, the 1 mm thick samples show an SET value of approximately  $-35 \text{ dB}$  for PC/GNP composite with an electrical conductivity of about 0.413 S/m. Further increase in sample thickness to 2 mm resulted in a SET value of  $-47 \text{ dB}$  (@8.2 GHz). An exponential increase in EMI SE was observed with increasing logarithm of electrical conductivity.

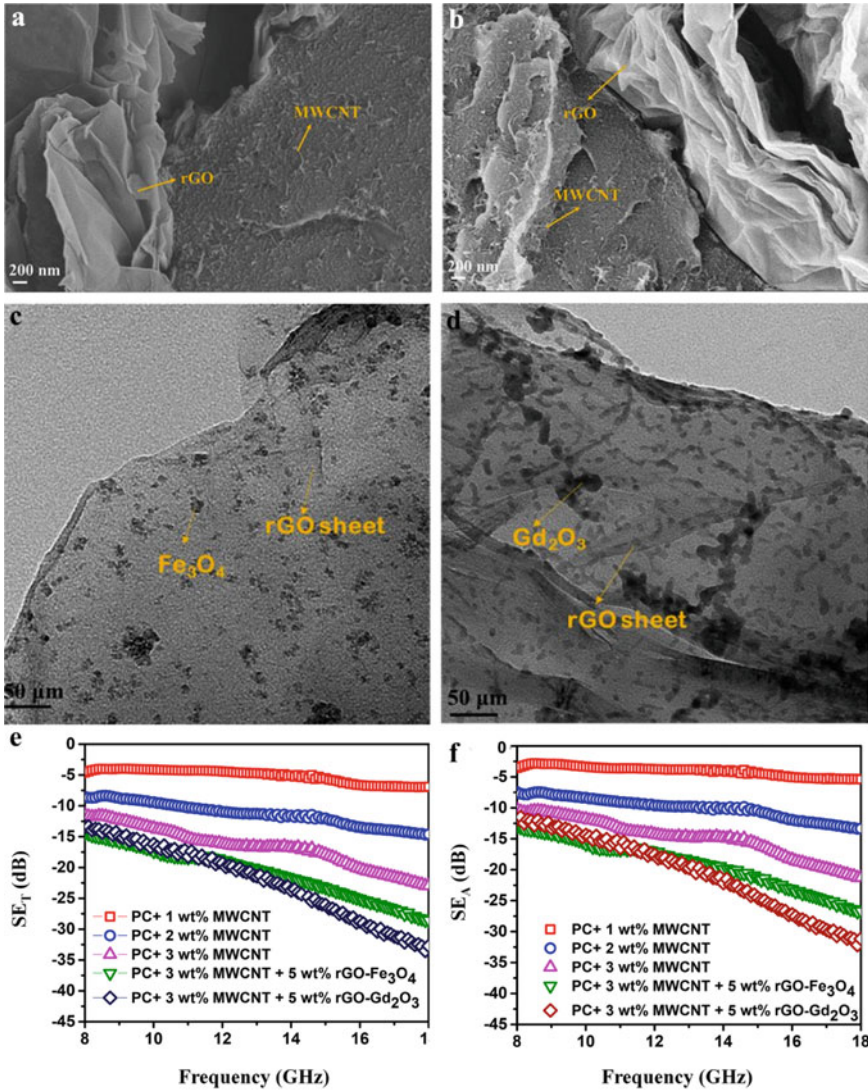
Bose et al. [92] fabricated PC-based hybrid nanocomposites with doped rGO (doped with ferromagnetic,  $\text{Fe}_3\text{O}_4$  or paramagnetic  $\text{Gd}_2\text{O}_3$ ) and CNTs as nanofillers using melt mixing, followed by a compression molding. The surface morphology (FE-SEM) and TEM images on the morphology of the composites are displayed in Fig. 14a–d. The percolation threshold of CNTs was found to be lower than 0.5 wt%. Atomic wt% of Gd (atomic mass 157.25 u) was less than Fe (atomic mass 55.845 u), and degree of GO reduction was slightly higher in rGO- $\text{Fe}_3\text{O}_4$  than rGO- $\text{Gd}_2\text{O}_3$ . It was observed that PC-based nanocomposite with 3 wt% CNT, 3 wt% CNT/5 wt% rGO- $\text{Fe}_3\text{O}_4$ , and 3 wt% CNT/5 wt% rGO- $\text{Gd}_2\text{O}_3$  resulted in the SET value of  $-23$ ,  $-28$ , and  $-33 \text{ dB}$ , respectively, for 5 mm thick samples and at 18 GHz frequency (Fig. 14e, f). Absorption was determined to be the dominant shielding mechanism in



**Fig. 13** SEM images of **a** pristine sponge; sponges coated with **b** GP/ink, **c** MWCNTs/ink, and **d** GP/MWCNTs/ink without Ag nanoparticle coating. SEM image of sponge coated with **e** Ag nanoparticles, and SEM images of the Ag-coated sponges followed by coating of **f** GP/ink, **g** MWCNTs/ink, and **h** GP/MWCNTs/ink, **i** TEM image of folded GP on grid, FE-SEM images of **j** GP and **k** MWCNTs

all the composites, with magnetic losses being the primary mechanism in the rGO-Fe<sub>3</sub>O<sub>4</sub>-based nanocomposite and dielectric losses being primary in rGO-Gd<sub>2</sub>O<sub>3</sub>-based nanocomposite.

Li et al. [93] designed a reflection-absorption compartment unit with a lossy core made up of rGO-Fe<sub>3</sub>O<sub>4</sub> (RGF) dispersed in PC and a conductive shell made up

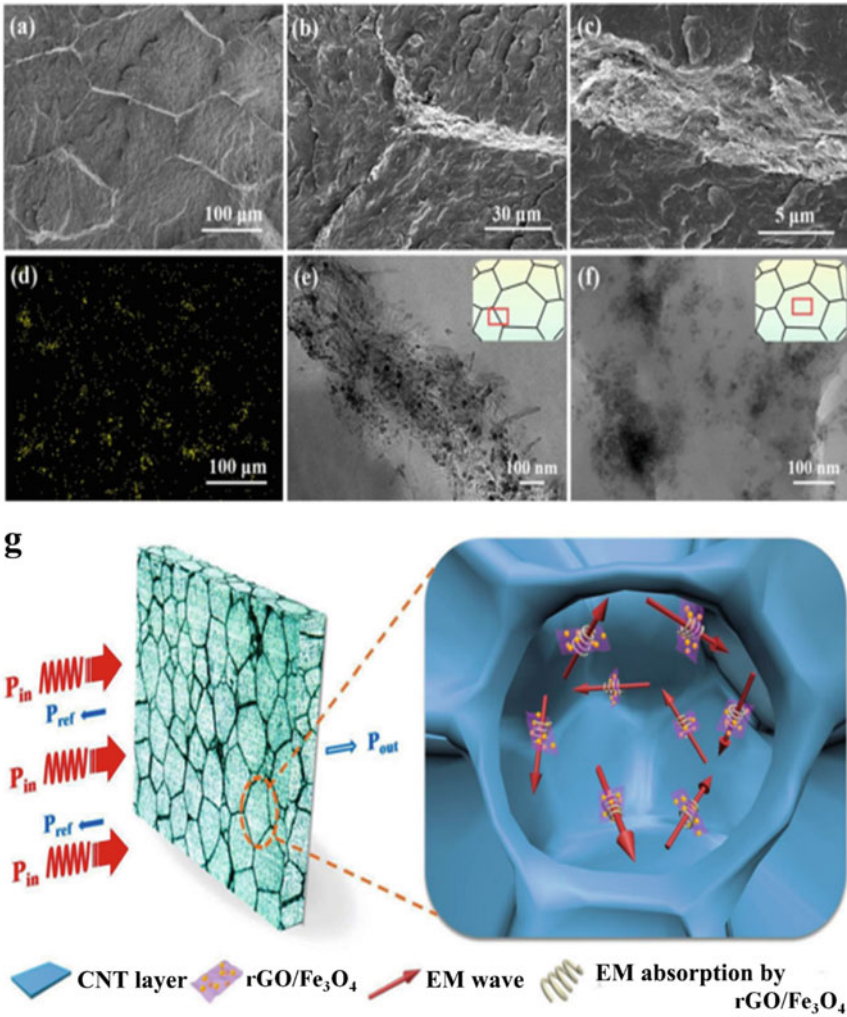


**Fig. 14** SEM micrographs of **a** PC/3 wt% MWCNT (low magnification), **b** PC/3 wt% MWCNT (high magnification), **c** PC/3 wt% MWCNT/5 wt% rGO-Fe<sub>3</sub>O<sub>4</sub> (low magnification), **d** PC/3 wt% MWCNT/5 wt% rGO-Fe<sub>3</sub>O<sub>4</sub> (high magnification), **e** PC/3 wt% MWCNT/5 wt% rGO-Gd<sub>2</sub>O<sub>3</sub> (low magnification), and **f** PC/3 wt% MWCNT/5 wt% rGO-Gd<sub>2</sub>O<sub>3</sub> (high magnification)

of CNTs wrapped onto the microspheres. CNT-wrapped microspheres of uniform size with an average diameter of  $237.9 \mu\text{m}$  were then consolidated at  $260^\circ\text{C}$  and  $100 \text{ MPa}$  to obtain a honeycomb-like architecture of CNT/RGF/PC with distinct conductive pathways formed by cementing the CNT walls between neighboring shielding compartments as shown in Fig. 15a. The average size of  $\text{Fe}_3\text{O}_4$  was around  $10 \text{ nm}$ , and the mass fraction of  $\text{Fe}_3\text{O}_4$  anchored on rGO was about  $80 \text{ wt}\%$  (saturation magnetization of RGF  $\sim 50.7 \text{ emu/g}$ ). SET value of  $-43.5 \text{ dB}$  with a SEA/SET ratio of  $\sim 90\%$  was obtained for the  $2 \text{ mm}$  thick composite shielding material prepared with  $4 \text{ wt}\%$  CNT/ $5 \text{ wt}\%$  RGF compartments in X-band. This SET value is about  $22.5\%$  higher than that of randomly dispersed filler ( $-35.5 \text{ dB}$ ). It is worthy to note that the SET value of CNT/PC compartment-based composites is inferior to that of CNT/RGF/PC compartment-based composites when adding the same CNT content due to the synergistic effect; e.g., for  $4 \text{ wt}\%$  CNT, the SET value is  $10.3 \text{ dB}$  higher in CNT/RGF/PC compartment-based composite. There was no considerable difference in electronic conductivity observed between CNT/PC and CNT/RGF/PC compartment-based composites because they have the similar three-dimensional conductive network; however, electrical conductivity for random dispersion of fillers was significantly lower than the compartment model. The shielding mechanism in these unique composites is illustrated in Fig. 15b. In this core-shell structure, the outer CNT walls act as reflectors to generate multiple reflections.

Lozano et al. [18] studied the EMI shielding effectiveness of multi-wall carbon nanotube (MWCNT) filled polypropylene composites and carbon nanofiber composite mats. The developed systems were then used to prepare interlayered composites that exhibited improved electrical conductivity and electromagnetic interference (EMI) shielding efficiency. The hybrid MWCNT-carbon nanofiber composite mats were prepared by centrifugally spinning mixtures of MWCNT suspended in aqueous poly(vinyl alcohol) solutions followed by the dehydrated under sulfuric acid vapors and then heat treated. Figure 16 shows a comparison of the SEM images of the MWCNT filled carbon nanofiber mats with different MWCNT contents, before and after the carbonization process. Interlayered samples were fabricated using a nano-reinforced polypropylene composite as a matrix and then filled with carbon fiber composite mats.

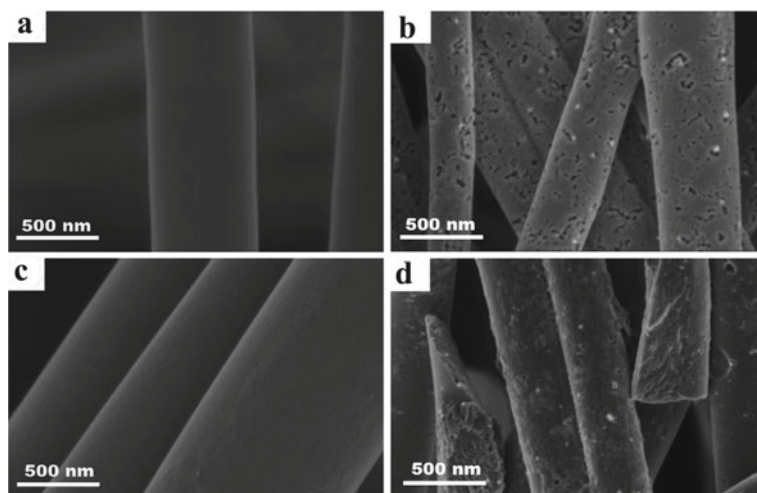
Figure 17 displays the schematics of the process used to fabricate the interlayered composites. The in-plane and through-plane electrical conductivity of an eight-layered flexible carbon composite ( $0.65 \text{ mm}$  thick) were shown to be  $6.1$  and  $3.0 \times 10^{-2} \text{ Scm}^{-1}$ , respectively. The EMI shielding effectiveness increased from  $17 \text{ dB}$  for the one-layered composite to  $52 \text{ dB}$  for the eight-layered composite at  $900 \text{ MHz}$ . It was found that the reflection of the electromagnetic waves was the dominating mechanism for EMI shielding in the developed materials. These studies utilizing the synergistic effect offered by the hybrid fillers opens up new opportunities for the fabrication of robust and novel lightweight materials that are to be used in communication systems.



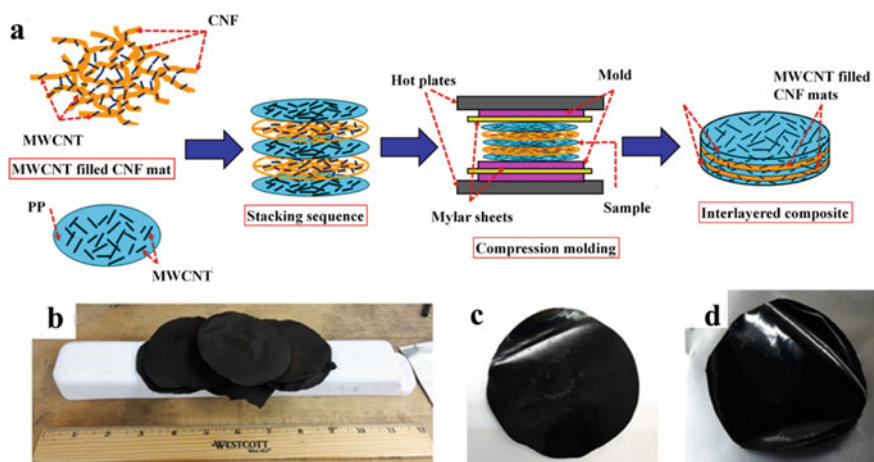
**Fig. 15** **a** Scanning electron micrograph of CNT/RGF/PC composite, **b** and **c** are the higher magnification micrographs of **(a)**, **d** energy dispersive X-ray elemental mapping of Fe and **e**, **f** transmission electron micrograph of CNT/RGF/PC composite. The inset cartoons show the composite’s observing area; **g** shielding mechanism of the reflection–absorption–integrated shielding compartment. Adapted with permission from Li et al. [81], copyright 2020 Elsevier

## 8 Conclusion

EMI shielding blocks the EM radiations (radio waves and/or microwave radiation) by acting as a radiation barrier that depends on the electrical conductivity as well as the magnetic permeability of shield material and the frequency of radiation. Unlike from the adsorption mechanism, reflection being the prominent mechanism that involves



**Fig. 16** SEM images of MWCNT filled carbon nanofiber mats with different contents of MWCNT before and after carbonization. **a, c** PVA nanofiber mats with 0.05 and 0.1 wt% MWCNT and **b, d** CNF mats filled with 0.05 and 0.1 wt% MWCNT, respectively



**Fig. 17** **a** Schematic representation of the fabrication process of interlayered composites; digital pictures of **b** MWCNT filled carbon nanofiber mats; **c** NRPCS used as starting materials; and **d** a resultant one-layer interlayered flexible composite

the interaction of EM field with the mobile charge carriers such as electrons or holes and thus attenuate the EM radiations. Materials having high dielectric constant and high magnetic permeability can be used for EMI shielding. For instance, materials like metals, polymers, carbon, ceramics, and their composite materials can be tuned for EMI shielding applications, in which carbon-based materials are found

to be more prevalent due to its oxidation resistance, chemical, and thermal stability as well as lower density and high dielectric loss properties. Carbon-based materials include porous graphite and amorphous carbon-based materials/composites, porous graphene-based materials/composites, and graphene-CNT hybrid structures. Functionalization of porous graphene can be tuned for EMI Shielding. Thus, EMI shielding can be applied in different portable gadgets and electronic devices for various applications including medical applications.

## References

1. Yousefi N, Sun X, Lin X, Shen X, Jia J, Zhang B, Tang B, Chan M, Kim JK (2014) Highly aligned graphene/polymer nanocomposites with excellent dielectric properties for high-performance electromagnetic interference shielding. *Adv Mater* 26:5480
2. Chung DDL Electromagnetic interference shielding effectiveness of carbon materials. *Carbon*
3. Luo X, Chung DDL (1997) Electromagnetic interference shielding reaching 130 DB using flexible graphite. *Mater Res Soc Symp Proc* 445:235–238
4. Qin F, Brosseau C (2012) A review and analysis of microwave absorption in polymer composites filled with carbonaceous particles. *J Appl Phys* 111:061301
5. Hu T, Wang J, Wang J (2015) Electromagnetic shielding properties of carbon fiber felt-glass fiber felt based multilayer composites with different layer angle. *Mater Lett* 153:20
6. Zhou H, Wang J, Zhuang J, Liu Q (2013) A covalent route for efficient surface modification of ordered mesoporous carbon as high performance microwave absorbers. *Nanoscale* 5:12502
7. Shen G, Mei B, Wu H, Wei H, Fang X, Xu Y (2017) Microwave electromagnetic and absorption properties of N-doped ordered mesoporous carbon decorated with ferrite nanoparticles. *J Phys Chem C* 121:3846
8. Song Q, Ye F, Yin X, Li W, Li H, Liu Y, Li K, Xie K, Li X, Fu Q, Cheng L, Zhang L, Wei B (2017) Carbon nanotube–multilayered graphene edge plane core–shell hybrid foams for ultrahigh-performance electromagnetic-interference shielding. *Adv Mater* 29
9. Guo S, Wang L, Wu H (2015) Facile synthesis and enhanced electromagnetic wave absorption of thorny-like Fe–Ni alloy/ordered mesoporous carbon composite. *Adv Powder Technol* 26:1250
10. Xu H, Yin X, Zhu M, Li M, Zhang H, Wei H, Zhang L, Cheng L (2019) Constructing hollow graphene nano-spheres confined in porous amorphous carbon particles for achieving full X band microwave absorption. *Carbon NY* 142:346
11. Biniak S (2017) Electrochemical studies of phenomena at active carbon electrolyte solution interfaces
12. Ryoo R, Joo SH, Kruk M, Jaroniec M (2001) Ordered mesoporous carbons. *Adv Mater* 13:677
13. Kresge CT, Leonowicz ME, Roth WJ, Vaturi JC, Beck JS (1992) Ordered mesoporous molecular sieves synthesized by a liquid-crystal template mechanism. *Nature* 359:710
14. Drzal LT, Xiang J (2010) Thermal conductivity of a monolayer of exfoliated graphite nanoplatelets prepared by liquid-liquid interfacial self-assembly. *J Nanomater*
15. Khasim S (2019) Polyaniline-graphene nanoplatelet composite films with improved conductivity for high performance X-band microwave shielding applications. *Results Phys* 12:1073
16. Li S, Li W, Nie J, Liu D, Sui G (2019) Synergistic effect of graphene nanoplate and carbonized loofah fiber on the electromagnetic shielding effectiveness of PEEK-based composites. *Carbon NY* 143:154
17. Li J, Zhao X, Wu W, Ji X, Lu Y, Zhang L (2021) Bubble-templated RGO-graphene nanoplatelet foams encapsulated in silicon rubber for electromagnetic interference shielding and high thermal conductivity. *Chem Eng J* 415:129054
18. Hamidinejad M, Salari M, Ma L, Moghimian N, Zhao B, Taylor HK, Filleter T, Park CB (2021) Electrically and thermally graded microcellular polymer/graphene nanoplatelet composite foams and their EMI shielding properties. *Carbon NY* 187
19. You B, Jiang J, Fan S (2014) Three-dimensional hierarchically porous all-carbon foams for supercapacitor. *ACS Appl Mater Interfaces* 6:15302

20. Vinod S, Tiwary CS, Machado LD, Ozden S, Vajtai R, Galvao DS, Ajayan PM (2016) Synthesis of ultralow density 3D graphene–CNT foams using a two-step method. *Nanoscale* 8:15857
21. Owuor PS, Park OK, Woellner CF, Jalilov AS, Susarla S, Joyner J, Ozden S, Duy L, Salvatierra RV, Vajtai R, Tour JM, Lou J, Galvão DS, Tiwary CS, Ajayan PM (2017) Lightweight hexagonal boron nitride foam for CO<sub>2</sub> absorption. *ACS Nano* 11:8944
22. Hu G, Xu C, Sun Z, Wang S, Cheng HM, Li F, Ren W (2015) 3D graphene-foam-reduced-graphene-oxide hybrid nested hierarchical networks for high-performance Li–S batteries. *Adv Mater* 1
23. Luong DX, Subramanian AK, Silva GAL, Yoon J, Cofer S, Yang K, Owuor PS, Wang T, Wang Z, Lou J, Ajayan PM, Tour JM (2018) Laminated object manufacturing of 3D-printed laser-induced graphene foams. *Adv Mater* 30:1707416
24. Owuor PS, Woellner CF, Li T, Vinod S, Ozden S, Kosolwattana S, Bhowmick S, Duy LX, Salvatierra RV, Wei B, Asif SAS, Tour JM, Vajtai R, Lou J, Galvão DS, Tiwary CS, Ajayan PM (2017) High toughness in ultralow density graphene oxide foam. *Adv Mater Interfaces* 4
25. Wu C, Huang X, Wu X, Qian R, Jiang P (2013) Mechanically flexible and multifunctional polymer-based graphene foams for elastic conductors and oil-water separators. *Adv Mater* 25:5658
26. Liu H, Wu S, Tian N, Yan F, You C, Yang Y (2020) Carbon foams: 3D porous carbon materials holding immense potential. *J Mater Chem A* 8:23699
27. Zheng Y, Song Y, Gao T, Yan S, Hu H, Cao F, Duan Y, Zhang X (2020) Lightweight and hydrophobic three-dimensional wood-derived anisotropic magnetic porous carbon for highly efficient electromagnetic interference shielding. *ACS Appl Mater Interfaces* 12:40802
28. Lou Z, Han H, Zhou M, Han J, Cai J, Huang C, Zou J, Zhou X, Zhou H, Sun Z (2018) Synthesis of magnetic wood with excellent and tunable electromagnetic wave-absorbing properties by a facile vacuum/pressure impregnation method. *ACS Sustain Chem Eng* 6:1000
29. Yuan Y, Liu L, Yang M, Zhang T, Xu F, Lin Z, Ding Y, Wang C, Li J, Yin W, Peng Q, He X, Li Y (2017) Lightweight, thermally insulating and stiff carbon honeycomb-induced graphene composite foams with a horizontal laminated structure for electromagnetic interference shielding. *Carbon NY* 123:223
30. Feng L, Zuo Y, He X, Hou X, Fu Q, Li H, Song Q (2020) Development of light cellular carbon nanotube@graphene/carbon nanocomposites with effective mechanical and EMI shielding performance. *Carbon NY* 168:719
31. Li J, Ding Y, Yu N, Gao Q, Fan X, Wei X, Zhang G, Ma Z, He X (2020) Lightweight and stiff carbon foams derived from rigid thermosetting polyimide foam with superior electromagnetic interference shielding performance. *Carbon NY* 158:45
32. Li H, Jing L, Ngoh ZL, Tay RY, Lin J, Wang H, Tsang SH, Teo EHT (2018) Engineering of high-density thin-layer graphite foam-based composite architectures with superior compressibility and excellent electromagnetic interference shielding performance. *ACS Appl Mater Interfaces* 10:41707
33. Lai D, Chen X, Wang G, Xu X, Wang Y (2020) Highly conductive porous graphene film with excellent folding resilience for exceptional electromagnetic interference shielding. *J Mater Chem C* 8:8904
34. Ji H, Zhao R, Zhang N, Jin C, Lu X, Wang C (2018) Lightweight and flexible electrospun polymer nanofiber/metal nanoparticle hybrid membrane for high-performance electromagnetic interference shielding. *NPG Asia Mater.* 10:749
35. Kumar R, Sharma A, Pandey A, Chaudhary A, Dwivedi N, Shafeeq M, Mondal MDP, Srivastava AK (2020) Lightweight carbon-red mud hybrid foam toward fire-resistant and efficient shield against electromagnetic interference. *Sci Rep* 10(1)
36. Wang H, Zhang Z, Dong C, Chen G, Wang Y, Guan H (2017) Carbon spheres@MnO<sub>2</sub> core-shell nanocomposites with enhanced dielectric properties for electromagnetic shielding. *Sci Rep* 7:1
37. Kumar RK, Bandurin DA, Pellegrino FMD, Cao Y, Principi A, Guo H, Auton GH, Ben Shalom M, Ponomarenko LA, Falkovich G, Watanabe K, Taniguchi T, Grigorieva IV, Levitov LS, Polini M, Geim AK (2017) Superballistic flow of viscous electron fluid through graphene constrictions. *Nat Phys* 13:1182



38. Wan YJ, Zhu PL, Yu SH, Sun R, Wong CP, Liao WH (2017) Graphene paper for exceptional emi shielding performance using large-sized graphene oxide sheets and doping strategy. *Carbon NY* 122:74
39. Cheraghi Bidsorkhi H, D'Aloia AG, Tamburrano A, De Bellis G, Delfini A, Ballirano P, Sarto MS (2019) 3D porous graphene based aerogel for electromagnetic applications. *Sci Rep* 9(1)
40. Tripathi P, Prakash Patel CR, Dixit A, Singh AP, Kumar P, Shaz MA, Srivastava R, Gupta G, Dhawan SK, Gupta BK, Srivastava OM (2015) High yield synthesis of electrolyte heating assisted electrochemically exfoliated graphene for electromagnetic interference shielding applications. *RSC Adv*
41. Kumar P, Shahzad F, Yu S, Hong SM, Kim YH, Koo CM (2015) Large-area reduced graphene oxide thin film with excellent thermal conductivity and electromagnetic interference shielding effectiveness. *Carbon NY*
42. Zhang L, Alvarez NT, Zhang M, Haase M, Malik R, Mast D, Shanov V (2015) Preparation and characterization of graphene paper for electromagnetic interference shielding. *Carbon NY*
43. Shen B, Zhai W, Zheng W (2014) Ultrathin flexible graphene film: an excellent thermal conducting material with efficient emi shielding. *Adv Funct Mater* 24(28):4542-4548
44. Paliotta L, De Bellis G, Tamburrano A, Marra F, Rinaldi A, Balijepalli SK, Kaciulis S, Sarto MS (2015) Highly conductive multilayer-graphene paper as a flexible lightweight electromagnetic shield. *Carbon NY*
45. Shen B, Li Y, Yi D, Zhai W, Wei X, Zheng W (2016) Microcellular graphene foam for improved broadband electromagnetic interference shielding. *Carbon NY*
46. Li Y, Shen B, Pei X, Zhang Y, Yi D, Zhai W, Zhang L, Wei X, Zheng W (2016) Ultrathin carbon foams for effective electromagnetic interference shielding. *Carbon NY*
47. Shahzad F, Kumar P, Kim YH, Hong SM, Koo CM (2016) Biomass-derived thermally annealed interconnected sulfur-doped graphene as a shield against electromagnetic interference. *ACS Appl Mater Interfaces* 8(14):9361-9369
48. Zeng Z, Chen M, Jin H, Li W, Xue X, Zhou L, Pei Y, Zhang H, Zhang Z (2016) Thin and flexible multi-walled carbon nanotube/waterborne polyurethane composites with high-performance electromagnetic interference shielding. *Carbon NY*
49. Yuan B, Bao C, Qian X, Song L, Tai Q, Liew KM, Hu Y (2014) Design of artificial nacre-like hybrid films as shielding to mitigate electromagnetic pollution. *Carbon NY*
50. Liang J, Wang Y, Huang Y, Ma Y, Liu Z, Cai J, Zhang C, Gao H, Chen Y (2009) Electromagnetic interference shielding of graphene/epoxy composites. *Carbon NY* 47:922
51. Yan DX, Ren PG, Pang H, Fu Q, Yang MB, Li ZM (2012) Efficient electromagnetic interference shielding of lightweight graphene/polystyrene composite. *J Mater Chem* 22:18772
52. Guo T, Li C, Wang Y, Wang Y, Yue J, Tang XZ (2020) A highly flexible and porous graphene-based hybrid film with superior mechanical strength for effective electromagnetic interference shielding. *Appl Phys A Mater Sci Process* 126:1
53. Novoselov KS, Geim AK, Morozov SV, Jiang D, Zhang Y, Dubonos SV, Grigorieva IV, Firsov AA (2004) Electric field in atomically thin carbon films. *Science* 306(80):666
54. Novoselov KS, Geim AK, Morozov SV, Jiang D, Katsnelson MI, Grigorieva IV, Dubonos SV, Firsov AA (2005) Two-dimensional gas of massless dirac fermions in graphene. *Nature* 438:197
55. Segal M (2009) Selling graphene by the ton. *Nat Nanotechnol* 4(410):612
56. Banks CE, Crossley A, Salter C, Wilkins SJ, Compton RG (2006) Carbon nanotubes contain metal impurities which are responsible for the "electrocatalysis" seen at some nanotube-modified electrodes. *Angew Chemie Int Ed* 45:2533
57. Yen MY, Hsiao MC, Liao SH, Liu PI, Tsai HM, Ma CCM, Pu NW, Der Ger M (2011) Preparation of graphene/multi-walled carbon nanotube hybrid and its use as photoanodes of dye-sensitized solar cells. *Carbon NY* 49:3597
58. Fan Z, Yan J, Zhi L, Zhang Q, Wei T, Feng J, Zhang M, Qian W, Wei F (2010) A three-dimensional carbon nanotube/graphene sandwich and its application as electrode in supercapacitors. *Adv Mater* 22:3723
59. Kim YS, Kumar K, Fisher FT, Yang EH (2011) Out-of-plane growth of CNTs on graphene for supercapacitor applications. *Nanotechnology* 23:015301
60. Woo S, Kim YR, Chung TD, Piao Y, Kim H (2012) Synthesis of a graphene-carbon nanotube composite and its electrochemical sensing of hydrogen peroxide. *Electrochim Acta* 59:509

61. Mani V, Devadas B, Chen SM (2013) Direct electrochemistry of glucose oxidase at electrochemically reduced graphene oxide-multiwalled carbon nanotubes hybrid material modified electrode for glucose biosensor. *Biosens Bioelectron* 41:309
62. Das S, Seelaboyina R, Verma V, Lahiri I, Hwang JY, Banerjee R, Choi W (2011) Synthesis and characterization of self-organized multilayered graphene-carbon nanotube hybrid films. *J Mater Chem* 21:7289
63. Dong X, Li B, Wei A, Cao X, Chan-Park MB, Zhang H, Li LJ, Huang W, Chen P (2011) One-step growth of graphene-carbon nanotube hybrid materials by chemical vapor deposition. *Carbon NY* 49:2944
64. Dong X, Xing G, Chan-Park MB, Shi W, Xiao N, Wang J, Yan Q, Sum TC, Huang W, Chen P (2011) The formation of a carbon nanotube-graphene oxide core-shell structure and its possible applications. *Carbon NY* 49:5071
65. Tung VC, Chen LM, Allen MJ, Wassei JK, Nelson K, Kaner RB, Yang Y (2009) Low-temperature solution processing of graphene-carbon nanotube hybrid materials for high-performance transparent conductors. *Nano Lett* 9:1949
66. Huang JH, Fang JH, Liu CC, Chu CW (2011) Effective work function modulation of graphene/carbon nanotube composite films as transparent cathodes for organic optoelectronics. *ACS Nano* 5:6262
67. King PJ, Khan U, Lotya M, De S, Coleman JN (2010) Improvement of transparent conducting nanotube films by addition of small quantities of graphene. *ACS Nano* 4:4238
68. Huang ZD, Zhang B, Oh SW, Bin Zheng Q, Lin XY, Yousefi N, Kim JK (2012) Self-assembled reduced graphene oxide/carbon nanotube thin films as electrodes for supercapacitors. *J Mater Chem* 22:3591
69. Jang WS, Chae SS, Lee SJ, Song KM, Baik HK (2012) Improved electrical conductivity of a non-covalently dispersed graphene-carbon nanotube film by chemical p-type doping. *Carbon NY* 50:943
70. Pan Y, Bao H, Li L (2011) Noncovalently functionalized multiwalled carbon nanotubes by chitosan-grafted reduced graphene oxide and their synergistic reinforcing effects in chitosan films. *ACS Appl Mater Interfaces* 3:4819
71. Kim YK, Min DH (2009) Durable large-area thin films of graphene/carbon nanotube double layers as a transparent electrode. *Langmuir* 25:11302
72. Hong TK, Lee DW, Choi HJ, Shin HS, Kim BS (2010) Transparent, flexible conducting hybrid multilayer thin films of multiwalled carbon nanotubes with graphene nanosheets. *ACS Nano* 4:3861
73. Tang Y, Gou J (2010) Synergistic effect on electrical conductivity of few-layer graphene/multiwalled carbon nanotube paper. *Mater Lett* 64:2513
74. Khan U, O'Connor I, Gun'Ko YK, Coleman JN (2010) The preparation of hybrid films of carbon nanotubes and nano-graphite/graphene with excellent mechanical and electrical properties. *Carbon NY* 48:2825
75. Tang C, Zhang Q, Zhao MQ, Tian GL, Wei F (2014) Resilient aligned carbon nanotube/graphene sandwiches for robust mechanical energy storage. *Nano Energy* 7:161
76. Su Q, Liang Y, Feng X, Müllen K (2009) Towards free-standing graphene/carbon nanotube composite films via acetylene-assisted thermolysis of organocobalt functionalized graphene sheets. *Chem Commun* 46:8279
77. Lee DH, Lee JA, Lee WJ, Kim SO (2011) Flexible field emission of nitrogen-doped carbon nanotubes/reduced graphene hybrid films. *Small* 7:95
78. Du F, Yu D, Dai L, Ganguli S, Varshney V, Roy AK (2011) Preparation of tunable 3D pillared carbon nanotube-graphene networks for high-performance capacitance. *Chem Mater* 23:4810
79. Chen S, Chen P, Wang Y (2011) Carbon nanotubes grown in situ on graphene nanosheets as superior anodes for Li-ion batteries. *Nanoscale* 3:4323
80. Li S, Luo Y, Lv W, Yu W, Wu S, Hou P, Yang Q, Meng Q, Liu C, Cheng HM (2011) Vertically aligned carbon nanotubes grown on graphene paper as electrodes in lithium-ion batteries and dye-sensitized solar cells. *Adv Energy Mater* 1:486
81. Nguyen DD, Tai NH, Chen SY, Chueh YL (2012) Controlled growth of carbon nanotube-graphene hybrid materials for flexible and transparent conductors and electron field emitters. *Nanoscale* 4:632

82. Ma Y, Sun L, Huang W, Zhang L, Zhao J, Fan Q, Huang W (2011) Three-dimensional nitrogen-doped carbon nanotubes/graphene structure used as a metal-free electrocatalyst for the oxygen reduction reaction. *J Phys Chem C* 115:24592
83. Paul RK, Ghazinejad M, Penchev M, Lin J, Ozkan M, Ozkan CS (2010) Synthesis of a pillared graphene nanostructure: a counterpart of three-dimensional carbon architectures. *Small* 6:2309
84. Kim UJ, Lee IH, Bae JJ, Lee S, Han GH, Chae SJ, Güneş F, Choi JH, Baik CW, Il Kim S, Kim JM, Lee YH (2011) Graphene/carbon nanotube hybrid-based transparent 2D optical array. *Adv Mater* 23:3809
85. Lee DH, Kim JE, Han TH, Hwang WJ, Jeon SW, Choi SY, Hong SH, Lee WJ, Ruoff RS, Kim SO (2010) Versatile carbon hybrid films composed of vertical carbon nanotubes grown on mechanically compliant graphene films. *Adv Mater* 22:1247
86. Kong HX (2013) Hybrids of carbon nanotubes and graphene/graphene oxide. *Curr Opin Solid State Mater Sci* 17:31
87. Mani V, Chen SM, Lou BS (2013) Three dimensional graphene oxide-carbon nanotubes and graphene-carbon nanotubes hybrids. *Int J Electrochem Sci* 8:11641
88. Cao MS, Wang XX, Cao WQ, Yuan J (2015) Ultrathin graphene: electrical properties and highly efficient electromagnetic interference shielding. *J Mater Chem C* 3:6589
89. Kachosangi RT, Musameh MM, Abu-Yousef I, Yousef JM, Kanan SM, Xiao L, Davies SG, Russell A, Compton RG (2008) Carbon nanotube–ionic liquid composite sensors and biosensors. *Anal Chem* 81:435
90. Chen YJ, Li Y, Chu BTT, Kuo IT, Yip M, Tai N (2015) Porous composites coated with hybrid nano carbon materials perform excellent electromagnetic interference shielding. *Compos Part B Eng* 70:231
91. Nimbalkar P, Korde A, Goyal RK (2018) Electromagnetic interference shielding of polycarbonate/GNP nanocomposites in X-Band. *Mater Chem Phys* 206:251
92. Sushmita K, Menon AV, Sharma S, Abhyankar AC, Madras G, Bose S (2019) Mechanistic insight into the nature of dopants in graphene derivatives influencing electromagnetic interference shielding properties in hybrid polymer nanocomposites. *J Phys Chem C* 123:2579
93. Yu WC, Wang T, Liu YH, Wang ZG, Xu L, Tang JH, Dai K, Duan HJ, Xu JZ, Li ZM (2020) Superior and highly absorbed electromagnetic interference shielding performance achieved by designing the reflection-absorption-integrated shielding compartment with conductive wall and lossy core. *Chem Eng J* 393:124644

**Part VII**  
**Food and Agriculture Applications**

# Chapter 26

## Porous Carbon Materials and Their Applications in Environmental Monitoring and Food Safety



Alma Mejri, Abdelmoneim Mars, and Hamza Elfil

### 1 Introduction

Considered the 5th most abundant natural element in the universe, carbon and its derivatives have aroused great interest in various fields, including materials science, electronics, biomedical sciences, nanotechnologies, etc. [1–5]. As a subclass, porous carbon materials (PCMs) exhibit interesting properties such as excellent electrical conductivity, high chemical, and thermal stability, important specific surface area, and adjustable channels and pore size [6]. Structurally, PCMs are classified into three categories based on their pore size. Microporous, mesoporous, and macroporous carbonaceous materials have pore sizes ( $d$ ) in the ranges of  $d < 2$  nm,  $2$  nm  $< d < 50$  nm, and  $d > 50$  nm, respectively [7]. Meanwhile, mesoporous carbonaceous materials have gained much of the attention devoted to PCMs due to their ease of functionalization, biocompatibility, high hydrophilicity, and good dispersibility in water [8, 9]. It is worthy to highlight that enormous attention has been paid to PCMs with designed pore architecture, and scientific publications on this subject are on the rise in recent years as presented in Fig. 1.

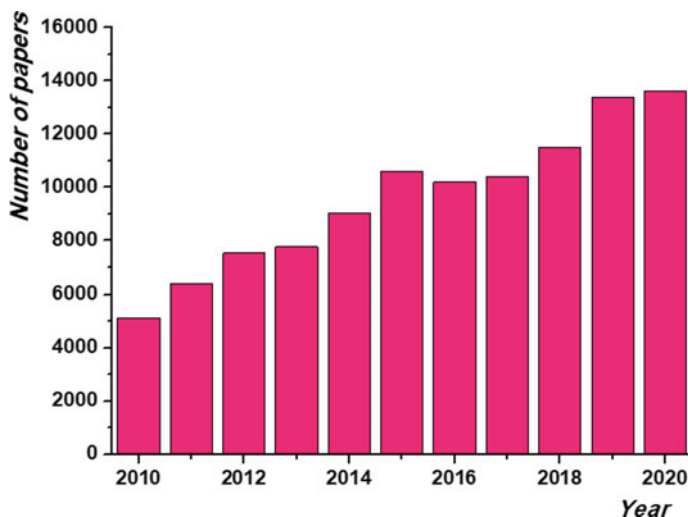
### 2 Applications of Porous Carbon in Environmental Monitoring

Currently, the rapid development of urbanization and industrialization across the world has caused the pollution of the ecosystem and water resources by various

---

A. Mejri (✉) · A. Mars · H. Elfil

Desalination and Natural Water Valorization Laboratory (LaDVEN), Water Researches and Technologies Center (CERTe), BP 273, 8020 Soliman, Tunisia  
e-mail: [almaa.mejri@gmail.com](mailto:almaa.mejri@gmail.com)



**Fig. 1** Number of publications with mentioned “porous carbon for environmental monitoring and food safety” terms

pollutants such as heavy metals, pesticides, and toxic residues from industrial activities causing a serious threat to human health [10]. To protect the environment and human life, periodic monitoring and regular control of pollution sources is an urgent necessity. For this, many international organizations, including WHO and EPA, have set up a large number of regulations to properly manage the situation. In this regard, various monitoring and remediation tools have been developed such as sensors and pollutant removal tools.

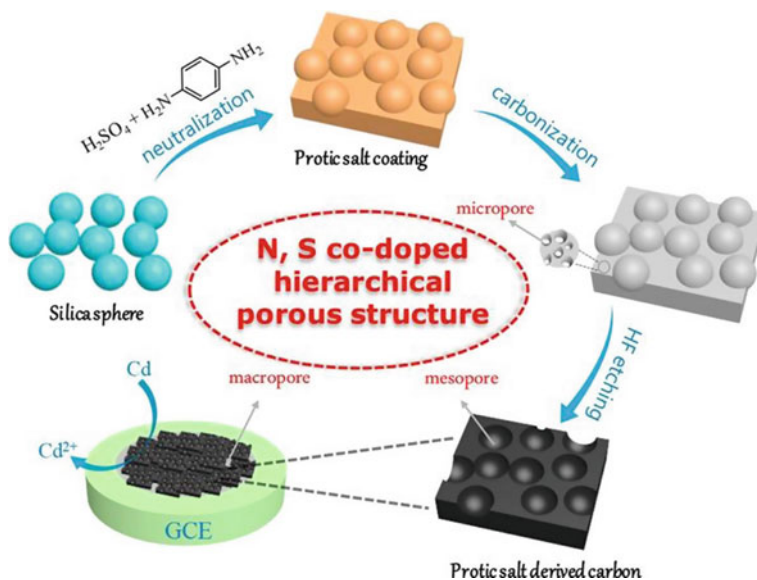
## ***2.1 Sensors Based on Porous Carbon for Environmental Contaminants***

Recently, the development of affordable, simple, and portable electrochemical sensors that enable on-site and semi-continuous monitoring of various pollutants that pose serious risks to the environment and human health has become possible thanks to PCMs. Indeed, the presence of polyvalent functional groups, high specific surface area, as well as the controllable channels and pore sizes of this nanomaterial are considered to be key parameters to achieve excellent analytic sensing parameters such as very high sensitivities and very low detection limits [11, 12]. Nowadays, numerous studies have been reported in the literature describing the use of PCMs in the development of sensitive electrochemical platforms for the quantification of traces of hazardous environmental contaminants, in particular heavy metals, and residues from industrial activities.

### 2.1.1 Sensing of Heavy Metals

Heavy metals are classified as potential environmental contaminants due to their high toxicity, persistence, and bio-accumulative nature. Thus, their presence even in trace amounts can be considered as a serious threat to human health and living organisms [13]. Therefore, the development of sensitive analytical tools for the detection of heavy metal ions in various matrices is of considerable interest to minimize risks to ecosystem and human health. In this context, electrochemical platforms based on porous carbon have been widely used for the determination of trace heavy metal ions. For instance, a selective voltammetric sensor based on nitrogen and sulfur codoped PC nanofibers for the quantification of cadmium (II) traces in water samples was developed by Gao et al. [14]. In this work, PCMs were prepared by pyrolysis of trithiocyanuric acid, polyacrylonitrile, and silica nanospheres. To design the electrochemical sensor, the authors chose N,S-codoped PC nanofibers to decorate GCE. The as-prepared platform enabled highly sensitive and selective quantification of Cd(II) ions using the differential pulse anodic sweep voltammetry method. The electrochemical results showed that porous N,S-codoped PC nanofibers can be considered as interesting candidates for monitoring cadmium (II) ions in various water samples with recovery rates of 103%. In the same context, N,S-codoped PCMs were used to sense the presence of cadmium (II) in water samples. To enhance the porosity of PCMs, Wu et al. [15] have proposed the preparation of N,S-codoped PCM by carbonization process of protic salt in the presence of a silica sphere. The latter was employed as an auxiliary template and was removed by hydrofluoric acid treatment. It has been demonstrated that the resulting nanocomposite contains rich amounts of N and S with hierarchical textural porosity. To decorate the surface of the electrode, the authors have used nafion to immobilize the as-prepared PCM (Fig. 2). The electrochemical results showed excellent sensitivity and selectivity for the presence of Cd(II) ions even in the presence of other metals. PCM-based platform was applied for the quantification of Cd(II) ions in tap water samples. The sensor was yielded promising results with good analytical performances.

Furthermore, Niu's group [16] has described the use of screen-printed porous carbon-based electrodes functionalized by bismuth nanoparticles for the simultaneous quantification of a trace of cadmium (II) and lead (II) ions in water samples. The combined process of one-step sol-gel and pyrolysis was employed for the synthesis of PC nanocomposite. The latter was used then to print the working electrode. The results demonstrated that the porosity of bismuth-based carbon material allows the sensing of Cd(II) and Pb(II) ions at very low concentrations below 4 ppb. The designed platform was applied to quantify target ions in tap water and wastewater samples. Thereafter, the same research group has reported the use of bismuth nanoparticle-PC nanocomposite for the fabrication process of screen-printed electrodes [17]. The above-mentioned nanocomposite was synthesized using a combined method between the one-step sol-gel and pyrolysis. A grinding step is necessary to obtain a specific distribution of particle size for the synthesis of screen-printing inks. Thus, this electrochemical platform was applied for the rapid and in situ quantification of lead (II) and cadmium (II) ions in various water samples with good analytical performances.



**Fig. 2** Schematic presentation of preparation process of N,S-codoped porous carbon-based platform for the detection of Cd(II) ions. Reprinted with permission from Wu et al. [15] Copyright 2021 Elsevier

More interestingly, a new method of green preparation of PCM was reported by Guan's group by exploiting an ocean resource, kelp [18]. The authors have reported that kelp, used as a carbon source, allows the amelioration of the specific surface area where a porosity-rich structure offering many active sites has been observed. The results also revealed an abundant micro/mesopore structure with an important specific surface area of 2064 m<sup>2</sup> g<sup>-1</sup>. These proprieties encourage authors to apply the prepared PCM in the sensing and the removal of lead (II) and cadmium (II) ions. The sensing process was conducted by the decoration of the GCE surface with fabricated PCM. Electrochemical results demonstrated excellent analytical sensing performances with a detection limit of 23.3 nM and 11.38 nM for Cd<sup>2+</sup> and Pb<sup>2+</sup>, respectively. To introduce the different applications of PCMs in the platform development, the authors summarize the different systems reported in the literature for the sensing of heavy metal ions in water samples (Table 1).

### 2.1.2 Sensing of Toxic Compounds

Nowadays, industry activities have resulted in the contamination of the environment and water resources by various pollutants including hydrazine and nitroaromatics. These have become one of the first on the list of priority compounds to monitor. Consequently, many scientific efforts have been devoted to develop analytical devices and improve these performances for the quantification of contaminant traces. Due to



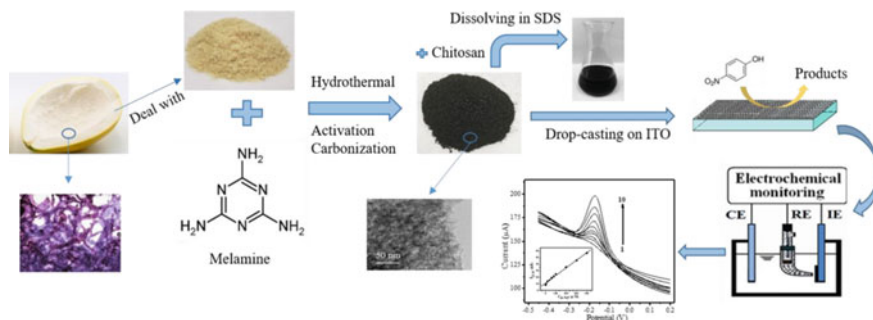
**Table 1** Selected applications of porous carbon-based sensors for heavy metal detection in water samples

Platform	Analyte	Electrochemical method	Detection limit	Linear range	References
N-PC/GCE	Cd <sup>2+</sup>	DPV	0.0022 μM	0.025–5 μM	[19]
N-PC nanofiber/GCE	Cd <sup>2+</sup>	DPASV	0.8 μg L <sup>-1</sup>	2–100 μg L <sup>-1</sup>	[20]
	Pb <sup>2+</sup>	DPASV	0.3 μg L <sup>-1</sup>	0.5–100 μg L <sup>-1</sup>	
	Hg <sup>2+</sup>	DPASV	0.35 nM	0.001–1 μM	[21]
N-PC-Au/CS/gold electrode Pd@PAC/GCE	Cd <sup>2+</sup>	SWASV	13.33 nM	25–500 nM	[22]
	Pb <sup>2+</sup>	SWASV	6.60 nM	25–500 nM	
	Cu <sup>2+</sup>	SWASV	11.92 nM	25–500 nM	
MnO <sub>2</sub> -PACs electrode	Cd <sup>2+</sup>	SWV	0.0051 μM	0.05–8 μM	[23]
Bi/HS/PC-CS/GCE	Cd <sup>2+</sup>	SWASV	1.72 pM	0.1–2 ppb 3.0–2.1 ppb	[24]
	Pb <sup>2+</sup>	SWASV	1.58 pM	0.1–2 ppb 3–2.1 ppb	
	Cd <sup>2+</sup>	SWASV	0.08 μg L <sup>-1</sup>	0.5–50 μg L <sup>-1</sup>	[25]
Bi@BAC/CPE	Pb <sup>2+</sup>	SWASV	0.13 μg L <sup>-1</sup>	0.5–50 μg L <sup>-1</sup>	
	Cd <sup>2+</sup>	DPASV	0.5 μg L <sup>-1</sup>	2–70 μg L <sup>-1</sup>	[26]
Bi/MGF-Nafion/GCE	Pb <sup>2+</sup>	DPASV	0.1 μg L <sup>-1</sup>	0.5–110 μg L <sup>-1</sup>	
	Pb <sup>2+</sup>	DPV	18 pM	50 pM–10 <sup>3</sup> nM	[27]
PtNPs@PCs-SA/bio-HP2/cDNA/MCH/HP1/AuE	Pb <sup>2+</sup>	DPASV	1.44 nM	7–7000 nM	[28]
N-HPC/GCE	Pb <sup>2+</sup>	DPASV	0.5 μg L <sup>-1</sup>	1–70 μg L <sup>-1</sup>	[29]

DPV Differential pulse voltammetry; SWVs square wave voltammetry; DPASV differential pulse anodic stripping voltammetry; DWASV square wave anodic stripping voltammetry; GCE glassy carbon electrode; Pd/NPs palladium nanoparticles; PC porous carbon; PACs porous activated carbons; HPC hierarchical porous carbon; CS chitosan; Bi bismuth; HS hollow sphere; SA streptavidin; MCH 6-Mercapto-1-hexanol; cDNA complementary DNA; HP1 Hairpin DNA 1; bio-HP2 Bio-Hairpin DNA 2; AuE gold electrode; Bi bismuth; BAC biomass derived activated carbon; CPE carbon paste electrode; MGF mesoporous graphene framework; N-PC nanoporous carbon material

its great ability to strongly concentrate target analytes in their channels and pores, PCMs have been extensively applied to build high-performance sensors. Recently, Yallappa et al. [30] have reported an eco-friendly synthesis method of mesoporous carbon nanoparticles using the Areca nut as a carbon precursor. The as-prepared PCMs were used to decorate the GCE surface. The authors have investigated this platform for the nitrite quantification in water samples. The results exhibited that the designed sensor exhibited great analytical performances such as a large linear concentration range from 0.2 to 400  $\mu\text{M}$ , a low detection limit of 0.0146  $\mu\text{M}$ , and an acceptable recovery rate. Therefore, the authors have interpreted that founded performances are attributed to the synergistic effect between the important porosity, high specific surface area, and high catalytic activity of mesoporous carbon nanoparticles. In the same context, Madhu and colleagues [31] have described a green preparation procedure for PCM using banana stems as a carbon precursor. The amounts of carbon, nitrogen, and sulfur were determined as follows: 61.12, 0.4315, and 0.349, respectively. The spectroscopic characterization revealed an important specific surface area of the order of 1465  $\text{m}^2 \text{g}^{-1}$ . In addition, the designed sensor exhibited interesting catalytic activity for nitrite oxidation with a linear concentration range of 1–127  $\mu\text{M}$ . The detection limit was found to be 0.07  $\mu\text{M}$ . Further, the platform was applied for the nitrite quantification in lake and seawater samples.

Since doping improves the hydrophilicity, the conductivity, and the reactivity of the produced PCM, many research groups have used various doped PCMs for the quantification of toxic compound traces [32, 33]. For instance, the nitrogen doping of PCMs induces the maintenance of specific porous structures and increases the charge density. In this context, N-doped porous carbon was used to construct an electrochemical sensitive sensor for hydrazine and nitrobenzene quantification by Yan's group [34]. In this work, an eco-friendly and cost-effective preparation approach using polydopamine as a precursor of carbon and nitrogen was reported. The authors have exploited the effect of nitrogen groups in enhancing the electrocatalytic activity of PCM toward the reduction and oxidation of nitrobenzene and hydrazine, respectively. Indeed, the results revealed that the electrocatalytic activity of the N-doped PCMs was improved with the larger surface area and more significant amounts of graphitic and N-pyrrolic groups. Under optimized conditions, the N-doped PC-modified GCE showed a linear dependence on the current density and target analyte concentration. The limits of detection were found to be 0.62 and 0.47  $\mu\text{M}$  for nitrobenzene and hydrazine, respectively. Moreover, Hu et al. [35] have investigated N-doped hierarchical PC-based platform for the detection of 4-nitrophenol in water samples. As shown in Fig. 3, the hierarchical N-doped PC was prepared using a cost-effective method which is based on the carbonization of pomelo peel after adsorption of melamine. The as-prepared PCMs exhibited a hierarchical porous structure, characterized by an important high surface area of the order of 1071  $\text{m}^2 \text{g}^{-1}$ . An excellent transfer rate and abundant micro, meso, and macropores were recorded. As an electrochemical application, the authors chose an indium-tin-oxide electrode to be decorated by fabricated material using chitosan as dispersing and stabilizing agent. The detection process was controlled using differential pulse voltammetry and the



**Fig. 3** Schematic presentation of preparation process and the detection process of 4-nitrophenol sensor. Reprinted with permission from Hu et al. [35] Copyright 2018 American Chemical Society

obtained results revealed a good linear correlation between the peak intensity and the 4-nitrophenol concentration. The limit of detection was found to be 5.44  $\mu\text{M}$ .

More recently, Xiao's group [36] has used the cobalt phosphide ( $\text{Co}_x\text{P}$ ) decorated N-doped porous carbon microspheres for the development of 4-nitrophenol sensor. To demonstrate the effect of N-doped PCM on enhancing the electrocatalytic activity of the sensor, the authors have developed a comparison study using various electrodes including bare GCE, N-doped PCM-modified GCE, and  $\text{Co}_x\text{P}$  decorated N-doped PC-modified GCE. The results revealed that the N-doped porous carbon-modified GCE exhibited the most remarkable electrocatalytic activity toward 4-nitrophenol. Thus, the authors have succeeded in developing a PCM-based platform for the quantification of 4-nitrophenol using an electrocatalytic sensing strategy. The limit of detection was estimated to be 2 nM.

Furthermore, several studies have investigated the effect of the functionalization of PCMs with metallic nanoparticles in order to improve the analytical performance of detection platforms. In this regard, Qin and collaborators [37] have used gold nanoparticles (AuNPs) to decorate hierarchical porous carbon. The prepared nanocomposite was applied to develop a sensitive electrocatalytic detection platform for the detection of nitroaromatic pollutants in water samples. The authors have reported that PCMs modified by AuNPs revealed high catalytic activity for the reduction of nitroaromatics. This can be explained by the abundant hierarchical pores of carbon and the synergistic effect between the carbonaceous material and the AuNPs.

More interestingly, Andy et al. [38] have proposed an electrochemical platform based on PCMs for the quantification of traces of cyanide in river water samples. To fabricate the sensor, the authors have used physical adsorption to immobilize nanocomposites on the surface of the carbon paste electrode. In this work, square wave adsorptive anodic stripping voltammetry was used as an electrochemical technique to monitor the sensing event. Under the optimized conditions, the sensor exhibited a large linear range of concentrations from  $5.9 \times 10^{-7}$  to  $9 \times 10^{-6}$  M, with a detection limit of  $7 \times 10^{-8}$  M. Table 2 regrouped various PC-based sensors which was

reported in literature and used for electrochemical detection of toxic environmental contaminants.

## 2.2 Porous Carbon-Based Systems for Environmental Monitoring

Currently, PCMs open up great prospects for applications in the fields of environmental preservation, in particular in the development of platforms for the elimination of environmental pollutants. For this reason, this section will be devoted to presenting the relevant applications of PCMs for the removal of environmental contaminants. Table 3 represents a limited overview of the use of activated PCMs for the elimination of water pollutants. In fact, the activation process of PCMs induces the improvement of the texture characteristics such as porosity, access to the internal structure, and surface functions [58]. Thus, the active PCMs allowed the removal of various toxic compounds with an important adsorption capacity. It is to highlight that the nature of carbon precursor and activating agent influences the physicochemical surface characteristics. In fact, Nowicki et al. [59] have employed various potassium carbonate materials as carbon precursors for the synthesis of PCMs which used for the elimination of methylene blue and methyl red. The results exhibited that this waste allowed the obtention of the activated PCMs with important specific surface areas reaching  $1188 \text{ m}^2/\text{g}$ . Thus, the authors have concluded that the efficiency of the removal process of methylene blue and methyl red from water samples depends on the nature of carbon precursor and that the adsorption capacity increases with the specific surface area. In the same line, Baysal et al. [60] have reported that the adsorption capacity of methylene blue enhances from 580 to 965 mg/g when the specific surface area of activated PCM increases from 2090 to 2690  $\text{m}^2/\text{g}$ . The authors have reported that the amelioration of the specific surface area can be attributed to the type of activation agent. The obtained results revealed that the most important value of adsorption capacity was recorded with sodium hydroxide.

In particular, a significant number of scientific reports have described the employ of PCMs as efficient systems for the capacitive deionization removal technology of heavy metal ions from polluted water samples to protect human health and the ecosystem. As an example, Zhang et al. [78] have synthesized a three-dimensional honeycomb-like PCM via a hydrothermal carbonization process using corncob waste as a carbon precursor. The as-prepared PCM was employed as a capacitive deionization electrode material to remove chromium (VI) from water samples. Electrochemical investigations exhibited that this electrode showed a good electrical conductivity and specific capacitance of the order of  $452 \text{ F g}^{-1}$ . Thus, the 3D-porous carbon-based electrode was applied for the elimination of chromium (VI) in water samples with

**Table 2** Selected applications of porous carbon-based sensors used for electrochemical detection of toxic compounds

Platform	Sample	Analyte	Electrochemical method	Detection limit	Linear range	References
MMPCMs/GCE	Lake water	Nitrobenzene	LSV	8 nM	0.2–40 $\mu$ M	[39]
	Tap water					
CoFe <sub>2</sub> Se <sub>4</sub> /PCF-2/GCE	Lake water	Hydroquinone	DPV	0.13 $\mu$ M	0.5–200 $\mu$ M	[40]
		Catechol	DPV	0.15 $\mu$ M	0.5–190 $\mu$ M	
		Resorcinol	DPV	1.36 $\mu$ M	5–350 $\mu$ M	
N-PCNP <sub>8</sub> -MCNTs/GCE	River water	Hydroquinone	DPV	0.03 $\mu$ M	0.2–455 $\mu$ M	[41]
		Catechol	DPV	0.11 $\mu$ M	0.7–440 $\mu$ M	
		Resorcinol	DPV	0.38 $\mu$ M	3.0–365 $\mu$ M	
		Hydroquinone	DPV	0.18 $\mu$ M	1–70 $\mu$ M	
N-PC/GCE	River water	Catechol	DPV	0.31 $\mu$ M	1–100 $\mu$ M	[42]
Alk-Ti <sub>3</sub> C <sub>2</sub> N-PC/GCE	Industrial wastewater	Hydroquinone	DPV	0.0048 $\mu$ M	0.5–150 $\mu$ M	[43]
		Catechol	DPV	0.0031 $\mu$ M	0.5–150 $\mu$ M	
PC/GCE	Tap water	Hydroquinone	CV	0.15 $\mu$ M	1–700 $\mu$ M	[44]
		Catechol	CV	0.11 $\mu$ M	1–3000 $\mu$ M	
		Nitrite	CV	0.09 $\mu$ M	$5 \times 10^{-7}$ – $4 \times 10^{-3}$ M	
N-HPCs/GCE	River water	Hydroquinone	DPV	0.32 $\mu$ M	1–360 $\mu$ M	[45]
		Catechol	DPV	0.08 $\mu$ M	0.5–320 $\mu$ M	
		Hydroquinone	DPV	0.06 $\mu$ M	0.5–340 $\mu$ M	
Fe/PC/GCE	Lake water	Hydroquinone	DPV	0.014 $\mu$ M	0.1–120 $\mu$ M	[46]
		Catechol	DPV	0.033 $\mu$ M	1–120 $\mu$ M	
CoPx/N-PC/GCE	Pond water		LSV	0.00079 $\mu$ M	0.0025–1 $\mu$ M	[47]
		Tap water			1–1000 $\mu$ M	

(continued)

Table 2 (continued)

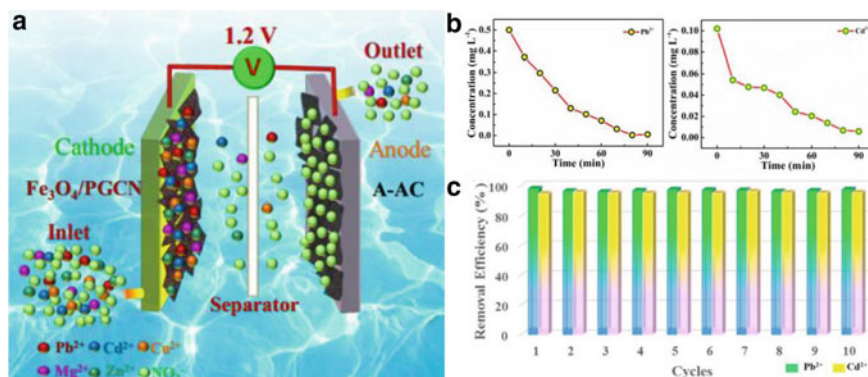
Platform	Sample	Analyte	Electrochemical method	Detection limit	Linear range	References
Pd/PC/GCE	Lake water Tap water	4-Nitrophenol	DPV	0.07 $\mu\text{M}$	0.3–1500 $\mu\text{M}$	[48]
FeOx/TiO <sub>2</sub> @mC/GCE	River water Tap water	4-Nitrophenol	CV	0.183 $\mu\text{M}$	5–310 $\mu\text{M}$	[49]
N-CMK-5/GCE	Ground water Tap water	Amitrole	DPV	0.007 mM	0.02–0.25 mM	[50]
3D-PC @MoS <sub>2</sub> /GCE	Lake water River water	Bisphenol A	DPV	0.0005 $\mu\text{M}$	0.001–10 $\mu\text{M}$	[51]
NF/ACHE/NF-Fe <sub>2</sub> O <sub>3</sub> @PC/CPE	Tap water	Paraoxon	DPV	1.210 <sup>-14</sup> M	10 <sup>-14</sup> –10 <sup>-8</sup> g mL <sup>-1</sup>	[52]
mC/GCE	Lake water	Methyl parathion	DPV	7.6 nM	0.09–61 $\mu\text{M}$	[53]
NiO /PC/GCE	Lake water Tap water	Hydrazine	DPV	1.5 $\mu\text{M}$	0.5 $\mu\text{M}$ –12 mM	[54]
3D-PC/ACHE/GCE	Moringa oleifera leaves	Trichlorfon	DPV	0.069 ng mL <sup>-1</sup>	0.2–18 ng mL <sup>-1</sup>	[55]
PC/PANI/GCE	Tap water	<b>Imidacloprid</b>	DPV	0.03 $\mu\text{g mL}^{-1}$	0.1–70 $\mu\text{g mL}^{-1}$	[56]
Fe/PC/GCE	Lake water Tap water	<b>Hydroquinone</b> <b>Catechol</b>	DPV DPV	0.014 $\mu\text{M}$ 0.033 $\mu\text{M}$	0.1–120 $\mu\text{M}$ 1–120 $\mu\text{M}$	[46]
N,P-PC/GCE	Lake water	<b>1-naphthol</b> <b>2-naphthol</b>	DPV DPV	8 nM 7.2 nM	0.025–2 $\mu\text{M}$ 0.025–2 $\mu\text{M}$	[57]

LSV Linear sweep voltammetry, DPV differential pulse voltammetry; CV cyclic voltammetry; GCE glassy carbon electrode; mC mesoporous carbon; HPCs hierarchical porous carbon; PCF porous carbon fibers; MMPCMs macro-/mesoporous carbon materials; Alk-Ti<sub>3</sub>C<sub>2</sub> alkalinization-intercalated Ti<sub>3</sub>C<sub>2</sub>; PCNPs porous carbon nanopolyhedrons; MWCNTs multi-walled carbon nanotubes (MWCNTs); N-CMK-5 N-doped carbon nanopipe-arrayed mesoporous carbon; NF nafion; AChE acetylcholinesterase; CPE carbon paste electrodes; AChE acetylcholinesterase; PANI polyaniline

**Table 3** Selected production process of activated PCMs, specific surface areas, and maximum adsorption capacities of different pollutants

Carbon precursor	Activating agent	Specific surface area (m <sup>2</sup> /g)	Pollutant	Maximum adsorption capacity (mg/g)	References
Acacia erioloba	H <sub>2</sub> SO <sub>4</sub>	10.4	Methylene blue	1.5	[61]
Acacia glauca	H <sub>3</sub> PO <sub>4</sub>	311.2	4-Nitrophenol	204.7	[62]
Bamboo	H <sub>3</sub> PO <sub>4</sub>	1400	Reactive Black 5	489.9	[63]
Banana peels	K <sub>2</sub> CO <sub>3</sub>	1188	Methylene blue	454.5	[64]
Tomato waste	ZnCl <sub>2</sub>	1093	Methylene blue	400	[65]
Corn cob	KOH	1054.2	Hg(II)	2.3	[66]
Corn cob	NaOH	2381	Pb(II)	381	[67]
Pomelo peels	K <sub>2</sub> CO <sub>3</sub>	836	Methylene blue	222.2	[59]
Potato peels	H <sub>3</sub> PO <sub>4</sub>	904.5	Bisphenol A	445.9	[68]
Potato peels	H <sub>3</sub> PO <sub>4</sub>	676	Pb(II)	8.9	[68]
Residue From biomass gasification	ZnCl <sub>2</sub>	259	Fe(II)	20.5	[69]
Sugarcane bagasse	ZnCl <sub>2</sub>	182.9	Hg(II)	11.5	[70]
Banyan tree	KOH	988	Phenol	26.9	[71]
Eucalyptus residue	H <sub>3</sub> PO <sub>4</sub>	1545	Methylene blue	977	[72]
Eucalyptus sawdust	FeCl <sub>3</sub>	645.2	Methylene blue	162.8	[73]
Black wattle bark waste	ZnCl <sub>2</sub>	414	Phenol	85.7	[74]
Waste carpets	H <sub>3</sub> PO <sub>4</sub>	953	Methylene blue	769.2	[75]
Waste tires	KOH	265	Pb(II)	49.7	[76]
			Cd(II)	10.4	
Walnut shell	ZnCl <sub>2</sub>	1626.9	Congo Red	281.4	[77]

an important removal efficiency of 91.58%. On the same line, Fe<sub>3</sub>O<sub>4</sub> nanoparticles-modified-porous graphitic carbon nanosheets (Fe<sub>3</sub>O<sub>4</sub>/PGCN) were applied as high-efficiency and low-cost electrode material for capacitive deionization removal technology. As illustrated in Fig. 4, a membrane-free hybrid capacitive deionization system was constructed using Fe<sub>3</sub>O<sub>4</sub>/PGCN and amino-functionalized commercial active carbon (A-AC) as cathode and anode, respectively. The prepared electrochemical cell was applied to remove lead (II) and cadmium (II) ions from drinking water samples. The removal capacities and removal efficiency were found to be greater than 95%. It is worthy to note that a remarkable desorption behavior assisted by the presence of magnetic nanoparticles was observed. The results revealed that



**Fig. 4** **a** Schematic presentation of the developed system. **b** The concentration variation of lead (II) and cadmium (II) ions with operation time. **c** The stability test of the developed system for the elimination process of lead (II) and cadmium (II) ions with initial concentrations of  $0.5 \text{ mg L}^{-1}$  and  $0.1 \text{ mg L}^{-1}$ , respectively. Reprinted with permission from Zhao et al. [79] Copyright 2021 Royal Society of Chemistry

the functionalization of PGCN with  $\text{Fe}_3\text{O}_4$  nanoparticles induced the amelioration of wettability, surface negative, and electrosorption capacity compared with those obtained with unmodified PGCN [79].

Furthermore, the adsorption process is considered to be an effective separation approach for wastewater treatment and water decontamination applications. Thus, high-efficiency adsorption of PCMs has been explored to reduce and remove organic contaminants. In this regard, Yan and collaborators [80] have reported the employ of hierarchical PCM for the efficient adsorption of organic contaminants from contaminated water samples. In this work, straw waste and  $\text{KHCO}_3$  were used as a carbon source and an activator agent. This porous nanocomposite presented an abundant macro, meso, and microporous structure with a large specific surface area. The obtained specific structure facilitates the adsorption process of the target pollutant and ameliorates the adsorption performance. In the presence of  $50 \text{ mg g}^{-1}$  of the amount of fluoroquinolone antibiotics, the developed system exhibited important adsorption efficiency and adsorption capacity within 30 min of 99.53% and  $199.07 \text{ mg g}^{-1}$ , respectively. Interestingly, Kundu et al. [81] have used hierarchical PC nanospheres for the elimination process of toxic organic pollutants, methylene blue and phenol, from industrial effluents. The hydrothermal method was applied to prepare PCMs using various triblock copolymers as soft templating agents. A study of the effect of different triblock copolymers on the adsorption efficiency of the resulting PCMs was developed. The results exhibited that the PC nanosphere system reached peak adsorption values of 98.9 and 100% within 10 min for phenol and methylene blue, respectively. More interestingly, the N,S-codoped PCM was used as an easy and efficacy method for adsorption and oxidation elimination of pharmaceutical contaminants by Tian et al. [82]. To synthesize the N,S-codoped PCM, a direct pyrolysis approach was utilized using glucose and thiourea as carbon and N, S elements precursors,



respectively. The PCMs showed excellent adsorption abilities and efficient catalytic activities for the oxidative degradation of the pharmaceutical pollutant, sulfachloropyridazine. The comparison study revealed that the obtained adsorption capacity is extremely important than that obtained with other carbon materials such as graphene oxide, reduced graphene oxide, and commercial single-walled carbon nanotubes. Thus, the authors have suggested that the N,S-codoped PCMs can be considered as a promising candidate for water remediation. Moreover, many reports have described the advanced oxidation process based on reactive radicals as one of the most efficient and powerful technologies for the total degradation of organic pollutants in wastewater [83]. Recently, Guo et al. [84] have applied S-doped PC as a catalyst for the persulfate activation process to degrade organic contaminants. Indeed, the activation of persulfates such as peroxymonosulfate (PMS) and peroxydisulfate (PDS) generates free radical species capable of degrading contaminants. S-doped porous carbon was synthesized using thiophene as a carbon/sulfur precursor and KOH as an activating agent. The results exhibited an interesting catalytic activity for the activation of persulfate to degrade 4-chlorophenol, chosen as an organic contaminant. Thus, doping PCMs with sulfur increases the catalytic activity of the porous carbon. Zhang and collaborators [85] have developed a porous carbon aerogel/persulfate system for efficient degradation of the phenolic contaminants. The resulting system revealed good performances on the removal process of target pollutants in a wide range of pH from 3 to 11. In the presence of persulfate, the manufactured PCM allowed the removal of p-nitrophenol, p-chlorophenol, phenol, and p-diphenol in 120 min with adsorption efficiencies of 72.7, 95.4, 99.8, and 99.9%, respectively. Therefore, PC aerogel has proven its efficiency as a green catalyst for the treatment of phenolic pollutants from wastewater. As regards the adsorption process, the negatively charged surface of carbon in the basic pH promoted the uptake of methylene blue, which is a cationic dye, via hydrogen bonding and/or electrostatic attraction. However, the phenol adsorption on PCM can be explained by different types of interaction including  $\pi - \pi$  interactions, hydrogen bonding, and electron donor-acceptor mechanism.

### 3 Applications of Porous Carbon in Food Safety

Food safety is defined as the set of methods involved in the preparation, handling, and storage of aliment to prevent the contamination and foodborne illness. There are many sources of contamination, posing a real threat to human health, present throughout the food chain such as the excessive use of veterinary drugs and pesticides, the use of illegal additives in the production process, and the formation of various toxins due to the long-time of storage [86, 87]. Therefore, it is crucial to monitor the food contaminants to keep their level within the acceptable limits for human health [88]. The scientific community devoted an important interest to the development of platforms based on PCMs for the quantification of trace pollutants in aliment matrices to protect consumers. Besides, great efforts have been dedicated to the

adsorbent material development for the food safety screening. In particular, PC was widely used as adsorbents due to its exceptional properties such as ultra-small pore size and important surface-to-volume ratios. PCMs allowed the effective elimination of contaminants from aliment matrices [89].

### ***3.1 Sensors Based on Porous Carbon for Food Safety***

PCMs is considered an essential tool for designing ultrasensitive electrochemical (bio)sensors due to its exceptional characteristics. As a result, an important number of PCM-based sensors for the quantification of various aliment contaminants such as mycotoxin, veterinary drug, and pesticide residues have been described in the literature (Table 4). Recently, Fei and collaborators [90] have developed an ultrasensitive electrochemical sensor-based ordered mesoporous carbon for the quantification of ractopamine in pork samples. In the presented work, ordered mesoporous carbon was prepared by pyrolysis process using sucrose and SBA-15 as a carbon source and template, respectively. Further, the sensor was constructed by drop-coating of prepared PCM onto a GCE. The PC-modified electrode revealed a remarkably electrocatalytic activity toward the oxidation of ractopamine with excellent analytical performances. The platform exhibited a broad linear concentration range of 0.085–8.0  $\mu\text{M}$ , with a detection limit of the order of 0.06  $\mu\text{M}$ . Thus, the reported method was applied for the ractopamine quantification in pork samples with interesting recoveries of around 104.5%. Moreover, the same sensor design was used by Yang et al. [91] for the quantification of Sudan I, a potential carcinogen aliment additive, in ketchup samples. The developed platform is a rapid and efficient method in which a large linear range of analyte concentration from  $4.03 \times 10^{-7}$  to  $6.60 \times 10^{-5}$  M was recorded. The limit of detection was estimated to be 44 nM. Additionally, it has been interpreted that the good analytical performances of the sensor were attributed to the great catalytic activity of the prepared carbon material toward the oxidation of Sudan I.

Furthermore, PCMs have aroused great interest in the development of (bio)electrochemical platforms for the quantification of mycotoxins and veterinary drugs due to their unique properties namely electrochemical signal amplification and high-capacity loading of analytes. It should be noted that these characteristics have made it possible to improve the selectivity and the analytical performance of sensors. For instance, Yin et al. [92] have employed the ordered mesoporous carbon (OMC) and multifunctional graphene-iron oxide-gold nanoparticles nanocomposite (Gr-Fe<sub>3</sub>O<sub>4</sub>-AuNPs) for the development of a highly sensitive aptasensor for the detection of the antibiotic streptomycin. In this work, OMC and Gr-Fe<sub>3</sub>O<sub>4</sub>-AuNPs were used as signal amplifiers and biosensing substrates, respectively. The prepared PCM is characterized by an important specific surface area, large pore volume, well-ordered structure of pores, and high thermal stability. In addition, the electrochemical results revealed a linear correlation between the relative intensity and the streptomycin concentration in a broad range from 0.05 to 200 ng/mL (Fig. 5). The limit of

**Table 4** Selected applications of porous carbon-based platforms used for the quantification of food contaminants

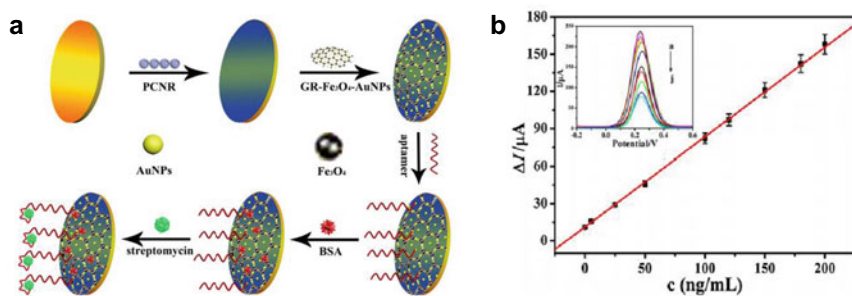
Platform	Sample	Analyte	Electrochemical method	Detection limit	Linear range	References
Pd NPs/PACs/GCE	Milk	Cd <sup>2+</sup>	DPV	41 nM	0.5–5.5 μM	[98]
		Pb <sup>2+</sup>	DPV	50 nM	0.5–8.9 μM	
		Cu <sup>2+</sup>	DPV	66 nM	0.5–5.0 Mm	
		Hg <sup>2+</sup>	DPV	54 nM	0.24–7.5 μM	
UiO-66/BMZIF-derived N-PCs/GCE	Milk	MecA gene	DPV	1.6 fM	5–1 × 10 <sup>5</sup> fM	[99]
		Nuc gene	DPV	3.7 fM	5–1 × 10 <sup>5</sup> fM	
Ni NPs/PC/GCE	Sea fish	Hg <sup>2+</sup>	DPV	2.1 nM	0–50 μM	[100]
		<b>Ochratoxin A</b>	EIS	10 <sup>-8</sup> ng mL <sup>-1</sup>	10 <sup>-8</sup> –0.1 ng mL <sup>-1</sup>	[101]
ap/Au NPs-cPC-cDNA/GCE	Soybean					
N,S,P-PC/GCE	Milk	Metronidazole	LSV	0.013 μM	0.1–45 μM 50–350 μM	[102]
CuO/3D-N-PC/GCE	ketchup and chili sauces	Sudan I	DPV	0.84 μM	2.5–100 μM	[103]
N-PC-G/CS/GCE	Soft drinks	Tartrazine	DPV	0.036 μM	0.05–15 μM	[104]
PC/GCE	Beverage (orange) Pineapple jam	3-nitroaniline	DPV	0.0551 μM	0.2–115.6 μM	[105]
		4-nitroaniline	DPV	0.0326 μM	0.5–120 μM	
PC/GCE	Drink samples	Sunset yellow	DPV	1.4 μg L <sup>-1</sup>	2.5–500 μg L <sup>-1</sup>	[106]
		Tartrazine	DPV	3.5 μg L <sup>-1</sup>	5–300 μg L <sup>-1</sup>	
		Ponceau 4R	DPV	2.1 μg L <sup>-1</sup>	2.5–1000 μg L <sup>-1</sup>	
		Allura red	DPV	1.7 μg L <sup>-1</sup>	2.5–400 μg L <sup>-1</sup>	
PtPd@N-PC/GCE	Juice	Patulin	SWV	7.5 × 10 <sup>-3</sup> μg L <sup>-1</sup>	0.01–10 μg L <sup>-1</sup>	[93]
PC/rGO/GCE	Milk Honey	Chloramphenicol	DPV	0.25 μM	1–180 μM	[107]

(continued)

Table 4 (continued)

Platform	Sample	Analyte	Electrochemical method	Detection limit	Linear range	References
MIP/Fe-PC/Au electrode	Milk	lomefloxacin	DPV	0.0002 $\mu\text{M}$	0.001–0.12 $\mu\text{M}$	[108]
RuO <sub>2</sub> @PC/ITO	Milk	Hexestrol	DPV	$2.32 \times 10^{-8}$ M	$10^{-7}$ – $2 \times 10^{-5}$ M	[109]
CuO <sub>x</sub> @mPC/GCE	Apple	Glyphosate	DPV	$7.69 \times 10^{16}$ M	$10^{-15}$ – $10^{-4}$ M	[110]

DPV Differential pulse voltammetry; SWV square wave voltammetry; GCE glassy carbon electrode; PC porous carbon; mPC mesoporous carbon; cPC carboxylic porous carbon; EIS electrochemical impedance spectroscopy; apt Ochratoxin A aptamer; CS chitosan; G graphene; NPs nanoparticles; BMZIF Co-Zn bimetallic zeolitic imidazolate framework; UiO-66-NH<sub>2</sub> metal-organic framework; ITO indium tin oxide electrode; rGO reduced graphene oxide; MIP molecularly imprinted polymer



**Fig. 5** **a** Schematic presentation of the preparation process of the streptomycin aptasensor. **b** Calibration curve of sensing response in the presence of various streptomycin concentrations (inset: DPVs recorded with different concentrations of streptomycin). Reprinted with permission from Yin et al. [92] Copyright 2021 Elsevier

detection was found to be 0.028 ng/mL. Thus, the platform was employed for the quantification of streptomycin in milk samples. The electrochemical results were in good agreement with the conventional methods.

Moreover, the molecularly imprinted technique was used for food safety applications owing its high selectivity toward the target analyte. As an example, Hu et al. [93] have developed a molecularly imprinted electrochemical platform for the patulin quantification in juice samples with a low limit of detection of  $7.5 \times 10^{-3} \mu\text{g L}^{-1}$ . The molecularly imprinted polymer produced different imprinting cavities presented on the surface of the developed platform. These sites allowed the effective recognition of patulin, the improvement of the adsorption capacity, and the selectivity of the sensor. It is to highlight that the PtPd nanoparticles decorated N-PCM was also employed for the development of patulin platform as an amplifier signal.

Nowadays, significant attention has been paid to PCM derived from metal–organic frameworks (MOFs) which are considered a promising class of hybrid porous materials. Indeed, MOFs have been extensively used as precursors of PCMs prepared due to the offered characteristics such as important porosity, diverse structures, and adjustable chemical and physical properties [2, 94]. Therefore, MOFs-derived porous carbon was widely applied in the conception of electrochemical (bio)sensors for the quantification of food contaminants, especially residues of antibiotics used for the treatment of infectious animal diseases. Recently, Du's group [95] has employed a platform based on iron oxide-mesoporous carbon (mPC) nanocomposite-modified gold electrode for the quantification of oxytetracycline. These nanocomposites were prepared by calcination of Fe(II)-based metal–organic framework (525-MOF). The electrochemical spectroscopy impedance was applied to monitor the sensing process. Further, the authors reported that the prepared mPC can easily bond with the oxytetracycline aptamer owing to its excellent bioaffinity and biocompatibility. The employ of Fe<sub>3</sub>O<sub>4</sub>@mC nanocomposites induces a high efficiency of oxytetracycline aptamer detection. Interestingly, the designed PCM-based aptasensor exhibited good analytical performances such as high selectivity, broad linear concentration range, low

detection limit, high reproducibility, and regenerability. The applicability of the designed sensing platform was investigated in milk samples and showed a good recoveries rate. Moreover, an electrochemical platform based on exfoliated PC for the quantification of chloramphenicol trace in honey samples was recently developed by Wang and collaborators [96]. This nanomaterial was synthesized by a one-step solvent exfoliation using an isoreticular-8 organometallic framework (IRMOF-8) as a carbon precursor. The as-prepared PCM was characterized by an important specific surface area of  $1854 \text{ m}^2 \text{ g}^{-1}$ . The development of the sensor was based on modifying the GCE surface with the prepared MOF-based PCM. The results demonstrated that the exfoliated PCM induced a remarkable amelioration of chloramphenicol electrochemical response compared with that obtained with its parental carbon precursor. This is due to the improved dispersibility and increasing surface area of the exfoliated PC. Besides, the electrochemical results, recorded with the square wave voltammetry technique, showed a good linear correlation between the relative current intensity and the chloramphenicol concentration.

Pesticide residues are currently considered hazardous substances in aliment products. Thus, the development of ultrasensitive platforms for the quantification of these pollutants is necessary and urgent. Interestingly, the doped PCMs were widely employed for the quantification of different pesticide residues in food samples. For instance, Wei and Feng [97] have recently developed an amperometric biosensor based on nitrogen-doped PCM for the quantification of organophosphorus pesticides, fenitrothion and dichlorvos, in vegetable samples. In this work, N-doped PCM was synthesized using silica spheres and 1-butyl-3-methylimidazolium dicyanamide ionic liquid as hard templates and precursors, respectively. The platform was constructed by the surface modification of boron-doped diamond electrodes with N-doped PCM and the immobilization of the enzyme acetylcholinesterase (AChE). Under the optimized conditions, the sensor showed good analytical performances and was applied for the trace quantification of dichlorvos and fenitrothion in lettuce.

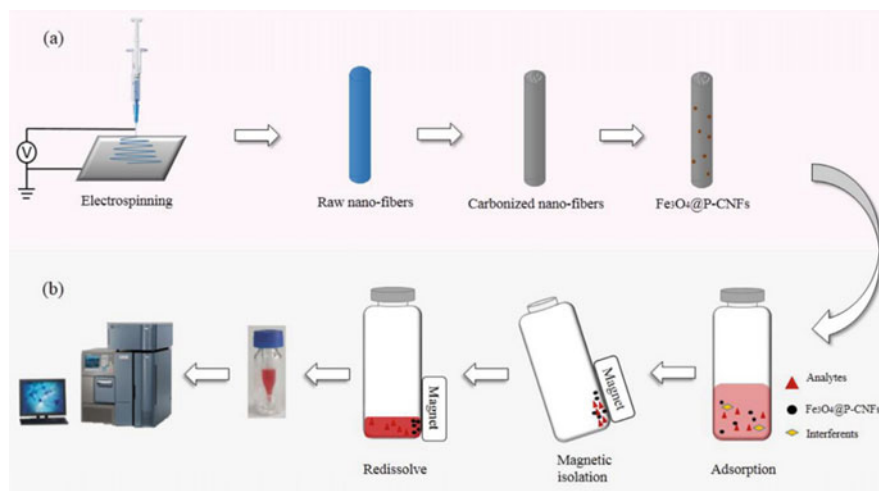
### ***3.2 Porous Carbon-Based Systems for Food Safety***

Since the number and varieties of food contaminants are enormous, the development of sanitation systems based on effective adsorbents has become an urgent matter to reduce the levels of pollutants in food samples and therefore to protect human health. In the literature, various extraction systems, in particular adsorption and magnetic solid-phase extraction, have been developed to remove food contaminants from biological matrices. The efficiency of the extraction systems generally depends on the adsorption capacity and the extraction efficiency of the used adsorbents. It has been evaluated by determining the extracted quantity of pollutants. In this regard, PCMs have been widely explored as effective adsorbents in the process of solid-phase extraction of food contaminants from biological matrices with good adsorption performance. Recently, Wang et al. [111] have used phthalocyanines-containing polymer-derived PCM as an adsorbent in the solid-phase extraction (SPE) process

to remove phenylurea herbicides. In fact, the combination of PCM-SPE and high-performance liquid chromatography technique was used for monitoring and removal of phenylurea herbicides from white turnip and cucumber samples. The obtained results exhibited that the detection limits were estimated to be in the range of 0.05–0.01 and 0.03–0.05 ng/g, with coefficients of determination of 0.9987 and 0.9998 for white turnip and cucumber, respectively.

Furthermore, magnetic solid-phase extraction (MSPE) is currently considered a promising preconcentration process used in the field of food safety. Its extraction performance depends on the properties of the adsorbents used. Characterized by an abundant porous structure, high adsorption, and separation capacities, PCMs properly played the role of adsorbent in the MSPE process [112, 113]. As an example, the magnetic PC nanofibers ( $\text{Fe}_3\text{O}_4$ @P-CNFs) were used by Meng's group [114] as an efficient adsorbent in the MSPE procedure for the extraction of Sudan dyes in foodstuffs. As shown in Fig. 6, the magnetic nanocomposite was prepared via electrospinning technique using polymethyl methacrylate and polyacrylonitrile as precursors. Then, it was decorated by  $\text{Fe}_3\text{O}_4$  nanoparticles. The developed  $\text{Fe}_3\text{O}_4$ @P-CNFs nanocomposite was employed as a magnetic adsorbent in the MSPE removal process of Sudan dye residues in complex matrices. Then, the eliminate amount was determinate using ultra-high-performance liquid chromatography-mass spectroscopy (UPLC-MS) with satisfying recoveries of 86.6–99.7%.

Besides, Zhang et al. [115] have developed three-dimensional magnetic PCM for the efficient elimination of ractopamine and clenbuterol in mutton samples. The magnetic composite exhibited significant adsorption capacities of 62.50 and 123.45  $\text{mg g}^{-1}$  for clenbuterol and ractopamine, respectively. The coupled UPLC-MS techniques were used for the quantification of target analytes in mutton samples with



**Fig. 6** a Schematic presentation of synthesis process of  $\text{Fe}_3\text{O}_4$ @P-CNFs and b MSPE procedure. Reprinted with permission from Li et al. [114] Copyright 2020 Elsevier

satisfactory recoveries ranging from 95.64 to 114.65%. The obtained results exhibited that the described magnetic PCM is an efficient adsorbent for ractopamine and clenbuterol extraction in complex matrixes. More interestingly, Wang et al. [116] have developed sensitive methods for the removal and determination of chlorophenols from peach juice and water samples. It should be highlighted those phenolic compounds are widely used in the production processes of dyes and pesticides. The magnetic PCMs were prepared using zeolite ZSM-5 and sucrose as a template and carbon sources, respectively. The as-prepared magnetic PCMs was employed as an adsorbent for removal process of chlorophenols from complex matrices. The extracted amount was quantified using the HPLC technique with recoveries in the range of 87.8–102%. Thus, the authors have demonstrated that the reported non-toxic adsorbents exhibited good adsorption capacities toward chlorophenols from peach juice and water samples.

Regardless, membrane-protected micro-solid-phase extraction ( $\mu$ -SPE) was also employed to remove and quantify food contaminants in complex matrices. This extraction procedure was based on inserting a small quantity of adequate sorbent inside a porous polypropylene bag using the heat-sealing technique [117]. In this context, Sajid et al. [118] have exploited the zinc oxide nanoparticles incorporated carbon foam as a sorbent in the  $\mu$ -SPE process for the removal of organochlorine pesticides in milk samples. The authors chose the gas chromatography–mass spectrometry technique (GC–MS) to determine the concentration of extracted pesticides. The results revealed that the developed method exhibited good analytical performances including low detection limits. Thus, zinc oxide nanoparticles incorporated carbon foam were considered as efficient and sensitive sorbent in  $\mu$ -SPE-GC–MS system for removal of organochlorine pesticides in complex biological matrices.

## 4 Conclusion

In this chapter, the authors emphasized the advanced applications of porous carbonaceous materials in the environmental monitoring and food safety fields, including the detection and removal of pollutants and toxic compounds. Regarding the metrological performances of platforms based on PCMs, the effect of the distribution and size of the pores, and the influence of functionalization or/and the doping on the improvement of the electrochemical properties, the chemical stabilities, and the adsorption efficiencies were presented and discussed. It has been shown that the doping with nitrogen and sulfur improves dramatically the electrocatalytic activities of the developed sensors toward the presence of various environmental pollutants. Furthermore, the functionalization with magnetic nanoparticles ( $\text{Fe}_3\text{O}_4$ NPs) allows the use of PCMs for the extraction of food contaminants with high extraction efficiency even in complex matrices.



**Acknowledgements** The authors are grateful to thank the Tunisian Ministry of High Education and Scientific Research and Tunisian—German **bilateral science & technique cooperation Project** (TUNGER 2 + 2 –18); “Desalination, nutrient recovery and diversified valorization techniques of nature based recycled wastewater” (WaterReTUNE)—TUNGER 18-044 for financial support of this work.

**Conflict of Interests** The authors declare the absence of conflict interest.

## References

1. Bounegru AV, Apetrei C (2020) Carbonaceous nanomaterials employed in the development of electrochemical sensors based on screen-printing technique—a review. *Catalysts* 10:680
2. Chaikittisilp W, Ariga K, Yamauchi Y (2013) A new family of carbon materials: synthesis of MOF-derived nanoporous carbons and their promising applications. *J Mater Chem A* 1:14–19
3. Yang Y, Chiang K, Burke N (2011) Porous carbon-supported catalysts for energy and environmental applications: a short review. *Catal Today* 178:197–205
4. Gu W, Yushin G (2014) Review of nanostructured carbon materials for electrochemical capacitor applications: advantages and limitations of activated carbon, carbide-derived carbon, zeolite-templated carbon, carbon aerogels, carbon nanotubes, onion-like carbon, and graphene. *Advanced Review* 3(5):424–473
5. Zhao Q, Lin Y, Han N, Li X, Geng H, Wang X, Cui Y, Wang S (2017) Mesoporous carbon nanomaterials in drug delivery and biomedical application. *Drug Delivery* 24(1):94–107
6. Fang B, Kim JH, Kim MS, Yu JS (2013) Hierarchical nanostructured carbons with meso–macroporosity: design, characterization, and applications. *Acc Chem Res* 46(7):1397–1406
7. Dutta S, Bhaumik A, Wu KCW (2014) Hierarchically porous carbon derived from polymers and biomass: effect of interconnected pores on energy applications. *Energy Environ Sci* 7:3574–3592
8. Liang C, Li Z, Dai S (2008) Mesoporous carbon materials: synthesis and modification. *Angew Chem Int Ed* 47:3696–3717
9. Zhang P, Zhang J, Dai S (2016) Mesoporous carbon materials with functional compositions. *Chem Eur J* 22:1–14
10. Ali H, Khan E (2017) Environmental chemistry in the twenty-first century. *Environ Chem Lett* 15(2):329–346
11. Yang J, Xu W, He C, Huang Y, Zhang Z, Wang Y, Hu L, Xia D, Shu D (2018) One-step synthesis of silicon carbide foams supported hierarchical porous sludge-derived activated carbon as efficient odor gas adsorbent. *J Hazard Mater* 344:33–41
12. Yuan W, Feng Y, Xie A, Zhang X, Huang F, Li S, Zhang X, Shen Y (2016) Nitrogen-doped nanoporous carbon derived from waste pomelo peel as a metal-free electrocatalyst for the oxygen reduction reaction. *Nanoscale* 8(16):8704–8711
13. Ali H, Khan E, Ilahi I (2019) Environmental chemistry and ecotoxicology of hazardous heavy metals: environmental persistence, toxicity, and bioaccumulation. *Hindawi Journal of Chemistry* 1–14
14. Gao S, Liu J, Luo J, Mamat X, Sambasivam S, Li Y, Hu X, Wågberg T, Hu G (2018) Selective voltammetric determination of Cd(II) by using N. S-codoped porous carbon nanofibers. *Microchim Acta* 185:282
15. Wu X, Wu S, Li Y, Chen H, Yuan Q, Gan W (2019) A highly sensitive electrochemical sensor for Cd(II) based on protic salt derived nitrogen and sulfur co-doped porous carbon. *Anal Chim Acta* 1046:115–122
16. Niu P, Fernández-Sánchez C, Gich M, Ayora C, Roig A (2015) Electroanalytical assessment of heavy metals in waters with bismuth nanoparticle-porous carbon paste electrodes. *Electrochim Acta* 165:155–161

17. Niu P, Fernández-Sánchez C, Gich M, Navarro-Hernández C, Fanjul-Bolado P, Roig A (2016) Screen-printed electrodes made of a bismuth nanoparticle porous carbon nanocomposite applied to the determination of heavy metal ions. *Microchim Acta* 183:617–623
18. Guan J, Fang Y, Zhang T, Wang L, Zhu H, Du M, Zhang M (2020) Kelp-derived activated porous carbon for the detection of heavy metal ions via square wave anodic stripping voltammetry. *Electrocatalysis* 11:59–67
19. Cui L, Wu J, Ju H (2014) Nitrogen-doped porous carbon derived from metal–organic gel for electrochemical analysis of heavy-metal ion. *ACS Appl Mater Interfaces* 6:16210–16216
20. Gao S, Xu C, Yalikun N, Mamat X, Li Y, Wagberg T, Hu X, Liu J, Luo J, Hu G (2017) Sensitive and selective differential pulse voltammetry detection of Cd(II) and Pb(II) using nitrogen-doped porous carbon nanofiber film electrode. *J Electrochem Soc* 164(13):H967–H974
21. Guan Q, Xiong W, Zhou L, Liu S (2016) Facile synthesis of nitrogen-doped porous carbon-gold hybrid nanocomposite for mercury(II) ion electrochemical determination. *Electroanalysis* 28:133–139
22. Zhang T, Jin H, Fang Y, Guan JB, Ma SJ, Pana Y, Zhang M, Zhu H, Liu XD, Du ML (2019) Detection of trace Cd<sup>2+</sup>, Pb<sup>2+</sup> and Cu<sup>2+</sup> ions via porous activated carbon supported palladium nanoparticles modified electrodes using SWASV. *Mater Chem Phys* 225:433–442
23. Liu H, Yu X, Chen H, Liu Y (2017) Preparation of porous carbon-manganese dioxide nanocomposite for sensitive determination of cadmium ion. *Int J Electrochem Sci* 12:9736–9746
24. Zeinu KM, Hou H, Liu B, Yuan X, Huang L, Zhu X, Hu J, Yang J, Liang S, Wu X (2016) Novel hollow sphere bismuth oxide doped mesoporous carbon nanocomposite material derived from sustainable biomass for picomolar electrochemical detection of Lead and Cadmium. *J Mater Chem A* 36:1–65
25. Zhu X, Liu B, Chen S, Wu L, Yang J, Liang S, Xiao K, Hu J, Hou H (2020) Ultrasensitive and simultaneous electrochemical determination of Pb<sup>2+</sup> and Cd<sup>2+</sup> based on biomass derived lotus root-like hierarchical porous carbon/bismuth composite. *J Electrochem Soc* 167:087505
26. Xiao L, Wang B, Ji L, Wang F, Yuan Q, Hu G, Dong A, Gan W (2016) An efficient electrochemical sensor based on three-dimensionally interconnected mesoporous graphene framework for simultaneous determination of Cd(II) and Pb(II). *Electrochim Acta* 222:1371–1377
27. Jin H, Zhang D, Liu Y, Wei M (2020) An electrochemical aptasensor for lead ion detection based on catalytic hairpin assembly and porous carbon supported platinum as signal amplification. *RSC Adv* 10:6647–6653
28. Dai R, Ma X, Xu Q, Lu L (2019) Controllable synthesis of three-dimensional nitrogen-doped hierarchical porous carbon and its application in the detection of lead. *RSC Adv* 9:18902–18908
29. Xiao L, Zhou S, Hu G, Xu H, Wang Y, Yuan Q (2015) One-step synthesis of isoreticular metal–organic framework-8 derived hierarchical porous carbon and its application in differential pulse anodic stripping voltammetric determination of Pb(II). *RSC Adv* 5:77159–77167
30. Yallappa S, Shivakumar M, Nagashree KL, Dharmaprakash MS, Vinu A, Hegde G (2018) Electrochemical determination of nitrite using catalyst free mesoporous carbon nanoparticles from bio renewable areca nut seeds. *J Electrochem Soc* 165(10):H614–H619
31. Madhu R, Veeramani V, Chen S-M (2014) Heteroatom-enriched and renewable banana-stem-derived porous carbon for the electrochemical determination of nitrite in various water samples. *Scientific Report* 4(4679):1–8
32. Tang J, Liu J, Li C, Li Y, Tade MO, Dai S (2015) Synthesis of nitrogen-doped mesoporous carbon spheres with extra-large pores through assembly of diblock copolymer micelles. *Angew Chem* 54:588
33. Liu Y, Zhang Y, Zhai C, Li X, Mao L (2016) Nitrogen-doped porous carbons supported Pt nanoparticles for methanol oxidation in alkaline medium. *Mater Lett* 166:16
34. Yan L, Bo X, Zhang Y, Guo L (2014) Facile green synthesis of nitrogen-doped porous carbon and its use for electrocatalysis towards nitrobenzene and hydrazine. *Electrochim Acta* 137:693–699

35. Hu L, Peng F, Xia D, He H, He C, Fang Z, Yang J, Tian S, Sharma VK, Shu D (2018) Carbohydrates-derived nitrogen-doped hierarchical porous carbon for ultrasensitive detection of 4-nitrophenol. *ACS Sustainable Chem Eng* 6:17391–21740
36. Xiao L, Xu R, Wang F (2018) Facile synthesis of  $\text{Co}_x\text{P}$  decorated porous carbon microspheres for ultrasensitive detection of 4-nitrophenol. *Talanta* 179:448–455
37. Qin L, Yi H, Zeng G, Lai C, Huang D, Xu P, Fu Y, He J, Li B, Zhang C, Cheng M, Wang H, Liu X (2019) Hierarchical porous carbon material restricted Au catalyst for highly catalytic reduction of nitroaromatics. *J Hazard Mater* 380:120864
38. Andy A, Riojas C, Wong A, Planes GA, Sotomayor MDPT, La Rosa-Toro A, Baena-Moncada AM (2019) Development of a new electrochemical sensor based on silver sulfide nanoparticles and hierarchical porous carbon modified carbon paste electrode for determination of cyanide in river water samples. *Sens Actuators, B Chem* 287:544–550
39. Ma J, Zhang Y, Zhang X, Zhu G, Liu B, Jinhu C (2012) Sensitive electrochemical detection of nitrobenzene based on macro-/meso-porous carbon materials modified glassy carbon electrode. *Talanta* 88:696–700
40. Yin D, Liu J, Bo X, Guo L (2020) Cobalt-iron selenides embedded in porous carbon nanofibers for simultaneous electrochemical detection of trace of hydroquinone, catechol and resorcinol. *Analytica Chim Acta* 1093:35–42
41. Liu W, Wu L, Zhang X, Chen J (2014) Simultaneous electrochemical determination of hydroquinone, catechol and resorcinol at nitrogen doped porous carbon nanopolyhedrons-multiwall carbon nanotubes hybrid materials modified glassy carbon electrode. *Bull Korean Chem Soc* 35(1):204–210
42. Zheng S, Wu D, Huang L, Zhang M, Ma X, Zhang Z, Xiang S (2019) Isomorphic MOF-derived porous carbon materials as electrochemical sensor for simultaneous determination of hydroquinone and catechol. *J Appl Electrochem* 49:563–574
43. Huang R, Liao D, Chen S, Yu J, Jiang X (2020) A strategy for effective electrochemical detection of hydroquinone and catechol: decoration of alkalization-intercalated  $\text{Ti}_3\text{C}_2$  with MOF-derived N-doped porous carbon. *Sens Actuators, B Chem* 320:128386
44. Lu Z, Wang Y, Hasebe Y, Zhang Z (2021) Electrochemical sensing platform based on lotus stem-derived porous carbon for the simultaneous determination of hydroquinone, catechol and nitrite. *Electroanalysis* 33:956–963
45. Chen D, Zhou H, Li H, Chen J, Li S, Zheng F (2017) Self-template synthesis of biomass-derived 3D hierarchical N-doped porous carbon for simultaneous determination of dihydroxybenzene isomers. *Sci Rep* 2017:7–14985
46. Huang W, Zhang T, Hu X, Wang Y, Wang J (2018) Amperometric determination of hydroquinone and catechol using a glassy carbon electrode modified with a porous carbon material doped with an iron species. *Microchim Acta* 185:37
47. Wang K, Wu C, Wang F, Jiang G (2018) MOF-derived  $\text{CoPx}$  nanoparticles embedded in nitrogen-doped porous carbon polyhedrons for nanomolar sensing of p-nitrophenol. *ACS Appl Nano Mater* 1(10):5843–5853
48. Veerakumar P, Madhu R, Chen SM, Veeramani V, Hung CT, Tang PH, Wang CB, Liu SB (2014) Highly stable and active palladium nanoparticles supported on porous carbon for practical catalytic applications. *J Mater Chem A2*:16015–16022
49. Wang M, Liu Y, Yang L, Tian K, He L, Zhang Z, Jia Q, Song Y, Fang S (2019) Bimetallic metal-organic framework derived  $\text{FeO}_x/\text{TiO}_2$  embedded in mesoporous carbon nanocomposite for the sensitive electrochemical detection of 4-nitrophenol. *Sens Actuators, B Chem* 281(15):1063–1072
50. Zhou S, Xu H, Liu J, Wei Y, Ma X, Han Z, Chen H (2021) Simplified synthesis of N-doped carbon nanotube arrayed mesoporous carbon for electrochemical detection of amitrole. *Chem Phys* 542:111074
51. Feng Y, Wang F, Wang L, Guo M, Lei Y, Feng Y, Cao Y, Yu Y (2021) In situ growth of  $\text{MoS}_2$  on three-dimensional porous carbon for sensitive electrochemical determination of bisphenol A. *J Appl Electrochem* 51:307–316

52. Wei W, Donga S, Huang G, Xie Q, Huan T (2018) MOF-derived Fe<sub>2</sub>O<sub>3</sub> nanoparticle embedded in porous carbon as electrode materials for two enzyme-based biosensors. *Sens Actuators B* 260:189–197
53. Pan D, Ma S, Bo X, Guo L (2011) Electrochemical behavior of methyl parathion and its sensitive determination at a glassy carbon electrode modified with ordered mesoporous carbon. *Microchim Acta* 173:215–221
54. Sivakumar M, Veeramani V, Chen SM, Madhu R, Liu SB (2019) Porous carbon-NiO nanocomposites for amperometric detection of hydrazine and hydrogen peroxide. *Microchim Acta* 186(59):1–8
55. Zhang J, Song Y, Ji Y, Wang R, Zhong Y, Yan J, Song Q, Chenjin CH (2021) Three-dimensional porous carbon materials from waste of botanical drugs as an efficient biosensing platform for pesticides sensing. *Int J Electrochem Sci* 16:1–16
56. Liu L, Guo J, Ding L (2021) Polyaniline nanowire arrays deposited on porous carbon derived from raffia for electrochemical detection of imidacloprid. *Electroanalysis*
57. Gao J, Zhang L, Tang Y, Qin Q, Wu C (2020) Nitrogen and phosphorus co-doped porous carbon framework with superior electrochemical activity for naphthol isomers sensing. *Analyt Chim Acta* 1138:58–167
58. Ben Mosbah M, Mechi L, Khiari R, Moussaoui Y (2020) Current state of porous carbon for wastewater treatment. *Processes* 8:1651
59. Nowicki P, Kazmierczak-Razna J, Pietrzak R (2016) Physicochemical and adsorption properties of carbonaceous sorbents prepared by activation of tropical fruit skins with potassium carbonate. *Mater Des* 90:579–585
60. Baysal M, Bilge K, Yilmaz B, Papila M, Yürüm Y (2018) Preparation of high surface area activated carbon from waste-biomass of sunflower piths: kinetics and equilibrium studies on the dye removal. *J Environ Chem Eng* 6:1702–1713
61. Rahman A, Hango HJ, Daniel LS, Uahengo V, Jaime SJ, Bhaskaruni SVHS, Jonnalagadda SB (2019) Chemical preparation of activated carbon from *Acacia erioloba* seed pods using H<sub>2</sub>SO<sub>4</sub> as impregnating agent for water treatment: an environmentally benevolent approach. *J Cleaner Prod* 237:117689
62. Dhorabe PT, Lataye DH, Ingole RS (2016) Removal of 4-nitrophenol from aqueous solution by adsorption onto activated carbon prepared from *Acacia glauca* sawdust. *Water Sci Technol* 73:955–966
63. Kalra A, Hadi P, Hui CW, Mackey H, Ansari TA, Saleem J, McKay G (2019) Adsorption of dyes from water on to bamboo-based activated carbon-error analysis method for accurate isotherm parameter determination. *J Water Sci Eng* 1:1–11
64. Liew RK, Azwar E, Yek PNY, Lim XY, Cheng CK, Ng JH, Jusoh A, Lam WH, Ibrahim MD, Ma NL (2018) Microwave pyrolysis with KOH/NaOH mixture activation: a new approach to produce micro-mesoporous activated carbon for textile dye adsorption. *Bioresour Technol* 266:1–10
65. Saygili H, Güzel F (2016) High surface area mesoporous activated carbon from tomato processing solid waste by zinc chloride activation: process optimization, characterization and dyes adsorption. *J Clean Prod* 113:995–1004
66. Liu Z, Sun Y, Xu X, Meng X, Qu J, Wang Z, Liu C, Qu B (2020) Preparation, characterization and application of activated carbon from corn cob by KOH activation for removal of Hg(II) from aqueous solution. *Bioresour Technol* 306:123154
67. Zhang Y, Song X, Zhang P, Gao H, Ou C, Kong X (2020) Production of activated carbons from four wastes via one-step activation and their applications in Pb<sup>2+</sup> adsorption: Insight of ash content. *Chemosphere* 245:125587
68. Arampatzidou AC, Deliyanni EA (2016) Comparison of activation media and pyrolysis temperature for activated carbons development by pyrolysis of potato peels for effective adsorption of endocrine disruptor bisphenol-A. *J Colloid Interface Sci* 466:101–112
69. Runtti H, Tuomikoski S, Kangas T, Lassi U, Kuokkanen T, Rämö J (2014) Chemically activated carbon residue from biomass gasification as a sorbent for iron(II), copper(II) and nickel(II) ions. *J Water Process Eng* 4:12–24

70. GiraldoS RI, Ramirez A, Florez E, Acelas N (2020) Mercury removal from wastewater using agroindustrial waste adsorbents. *SN Appl Sci* 2:1029
71. Nirmala G, Murugesan T, Rambabu K, SathiyarayananK SPL (2019) Adsorptive removal of phenol using banyan root activated carbon. *Chem Eng Commun* 208(6):831–842
72. Hassan AF, Elhadidy H (2017) Production of activated carbons from waste carpets and its application in methylene blue adsorption kinetic and thermodynamic studies. *J Environ Chem Eng* 5:955–963
73. Nieto-Márquez A, Pinedo-Flores A, Picasso G, Atanes E, Kou RS (2017) Selective adsorption of  $Pb^{2+}$ ,  $Cr^{3+}$  and  $Cd^{2+}$  mixtures on activated carbons prepared from waste tires. *J Environ Chem Eng* 5:1060–1067
74. Li Z, Hanafy H, Zhang L, SellaouiL NMS, Oliveira MLS, Seliem MK, Dotto GL, Bonilla-Petriciolet A, Li Q (2020) Adsorption of congo red and methylene blue dyes on an ashitaba waste and a walnut shell-based activated carbon from aqueous solutions: experiments, characterization and physical interpretations. *Chem Eng J* 388:124263
75. Han Q, Wang J, Goodman BA, Xie J, Liu Z (2020) High adsorption of methylene blue by activated carbon prepared from phosphoric acid treated eucalyptus residue. *Powder Technol* 366:239–248
76. Chen C, Mi S, Lao D, Shi P, Tong Z, Li Z, Hu H (2019) Single-step synthesis of eucalyptus sawdust magnetic activated carbon and its adsorption behavior for methylene blue. *RSC Adv* 9:22248–22262
77. Lütke SF, Igansi AV, Pegoraro L, Dotto GL, Pinto LAA, Cadaval TRS (2019) Preparation of activated carbon from black wattle bark waste and its application for phenol adsorption. *J Environ Chem Eng* 7:103396
78. Zhang XF, Wang B, Yu J, Wu XN, Zang YH, Gao HC, Su PC, Hao SQ (2018) Three-dimensional honeycomb-like porous carbon derived from corncob for the removal of heavy metals from water by capacitive deionization. *RSC Adv* 8:1159–1167
79. Zhao C, Wang X, Zhang S, Sun N, Zhou H, Wang G, Zhang Y, Zhang H, Zhao H (2020) Porous carbon nanosheets functionalized with  $Fe_3O_4$  nanoparticles for capacitive removal of heavy metal ions from water. *Environ Sci Water Res Technol* 6:331–340
80. Wang H, Shan L, Lv Q, Cai S, Quan G, Yan J (2020) Production of hierarchically porous carbon from natural biomass waste for efficient organic contaminants adsorption. *J Clean Prod* 263:121352
81. Kundu S, Chowdhury IH, Kanti Naskar M (2018) Hierarchical porous carbon nanospheres for efficient removal of toxic organic water contaminants of phenol and methylene blue. *J Chem Eng* 63(3):559–573
82. Tian W, Zhang H, Duan X, Sun H, Tade MO, Ang HM, Wang S (2016) Nitrogen- and sulfur-codoped hierarchically porous carbon for adsorptive and oxidative removal of pharmaceutical contaminants. *ACS Appl Mater Interfaces* 8:7184–7193
83. Pera-Titus M, Garcia-Molina V, Baños MA, Giménez J, Esplugas S (2004) Optimization of photocatalytic degradation of phenol using simple photocatalytic reactor. *Appl Catal B* 47:219–256
84. Guo Y, Zenga Z, Zhuc Y, Huang Z, Cuia Y, Yang J (2018) Catalytic oxidation of aqueous organic contaminants by persulfate activated with sulfur-doped hierarchically porous carbon derived from thiophene. *Appl Catal B* 220:635–644
85. Jiang L, Wang Q, Zhou M, Liang L, Li K, Yang W, Lu X, Zhang Y (2020) Role of adsorption and oxidation in porous carbon aerogel/persulfate system for non-radical degradation of organic contaminant. *Chemosphere* 241:125066
86. Chen H, Zhou K, Zhao G (2018) Gold nanoparticles: from synthesis, properties to their potential application as colorimetric sensors in food safety screening. *Trends Food Sci Technol* 78:83–94
87. Casado N, Pérez-Quintanilla D, Morante-Zarcero S, Sierra I (2017) Current development and applications of ordered mesoporous silicas and other sol–gel 726 silica-based materials in food sample preparation for xenobiotics analysis. *TrAC Trends Anal Chem* 88:167–184

88. Wang Y, Duncan TV (2017) Nanoscale sensors for assuring the safety of food products. *Curr Opin Biotechnol* 44:74–86
89. Azzouz A, Kailasa SK, Lee SS, Rascón AJ, Ballesteros E, Zhang M, Kim KH (2018) Review of nanomaterials as sorbents in solid-phase extraction for environmental samples. *TrAC Trends Anal Chem* 108:347–369
90. Yang X, Feng B, Yang P, Ding YL, Chen Y, Fei JJ (2014) Electrochemical determination of toxic ractopamine at an ordered mesoporous carbon modified electrode. *Food Chem* 145:619–624
91. Yang D, Zhu L, Jiang X, Guo L (2009) Sensitive determination of Sudan I at an ordered mesoporous carbon modified glassy carbon electrode. *Sens Actuators B* 141:124–129
92. Yin J, Guo W, Qin X, Zhao J, Pei M, Ding F (2017) A sensitive electrochemical aptasensor for highly specific detection of streptomycin based on the porous carbon nanorods and multifunctional graphene nanocomposites for signal amplification. *Sens Actuators B* 241:151–159
93. Hu X, Xia Y, Liu Y, Zhao F, Zeng B (2021) Determination of patulin using dual-dummy templates imprinted electrochemical sensor with PtPd decorated N-doped porous carbon for amplification. *Microchim Acta* 188:148
94. Jiang HL, Liu B, Lan YQ, Kuratani K, Akita T, Shioyama H, Zong FQ, Xu Q (2011) From metal-organic framework to nanoporous carbon: toward a very high surface area and hydrogen uptake. *J Am Chem Soc* 133:11854–11857
95. Song Y, Duan F, Zhang S, Tian J-Y, Zhang Z, Wang ZW, Liu CS, Xu WM, Du M (2017) Iron oxide@mesoporous carbon architectures derived from an Fe(II)-based metal organic framework for highly sensitive oxytetracycline determination. *J Mater Chem A* 5:19378–19389
96. Xiao L, Xu R, Yuan Q, Wang F (2017) Highly sensitive electrochemical sensor for chloramphenicol based on MOF derived exfoliated porous carbon. *Talanta* 167:39–43
97. Wei M, Feng S (2017) Amperometric determination of organophosphate pesticides using a acetylcholinesterase based biosensor made from nitrogen-doped porous carbon deposited on a boron-doped diamond electrode. *Microchim Acta* 184:3461–3468
98. Veerakumar P, Veeramani V, Chen SM, Madhu R, Liu SB (2016) Palladium nanoparticle incorporated porous activated carbon: electrochemical detection of toxic metal ions. *ACS Appl Mater Interfaces* 8:1319–1326
99. Dai G, Li Z, Luo F, Lu Y, Chu Z, Zhang J, Zhang F, Wang Q, He P (2021) Simultaneous electrochemical determination of nuc and mecA genes for identification of methicillin-resistant *Staphylococcus aureus* using N-doped porous carbon and DNA-modified MOF. *Microchim Acta* 188:39
100. Veerakumar P, Chen SM, Madhu R, Veeramani V, Hung CT, Liu SB (2015) Nickel nanoparticle-decorated porous carbons for highly active catalytic reduction of organic dyes and sensitive detection of Hg(II) ions. *ACS Appl Mater Interfaces* 7:24810–24821
101. Wei M, Zhang W (2017) A novel impedimetric aptasensor based on AuNPs–carboxylic porous carbon for the ultrasensitive detection of ochratoxin A. *RSC Adv* 7:28655–28660
102. Yalikul N, Mamat X, Li Y, Hu X, Wang P, Hu G (2019) N, S, P-triple doped porous carbon as an improved electrochemical sensor for metronidazole determination. *J Electrochem Soc* 166(13):B1131–B1137
103. Ye Q, Chen X, Yang J, Wu D, Ma J, Kong Y (2019) Fabrication of CuO nanoparticles-decorated 3D N-doped porous carbon as electrochemical sensing platform for the detection of Sudan I. *Food Chem* 287:375–381
104. An ZZ, Li Z, Guo YY, Chen XL, Zhang KN, Zhang DX, Xue ZH, Zhoua XB, Lu XQ (2017) Preparation of chitosan/N-doped graphene natively grown on hierarchical porous carbon nanocomposite as a sensor platform for determination of tartrazine. *Chin Chem Lett* 28:1492–1498
105. Manavalan S, Veerakumar P, Chen SM, Murugan K, Lin KC (2019) Binder-free modification of a glassy carbon electrode by using porous carbon for voltammetric determination of nitro isomers. *ACS Omega* 4:8907–8918

106. Cheng Q, Xia S, Tong J, Wu K (2015) Highly-sensitive electrochemical sensing platforms for food colourants based on the property-tuning of porous carbon. *Anal Chim Acta* 887:75–81
107. Yuan Y, Xu X, Xia J, Zhang F, Wang Z, Liu Q (2019) A hybrid material composed of reduced graphene oxide and porous carbon prepared by carbonization of a zeolitic imidazolate framework (type ZIF-8) for voltammetric determination of chloramphenicol. *Microchim Acta* 186:191
108. Li J, Huang X, Ma J, Wei S, Zhang H (2020) A novel electrochemical sensor based on molecularly imprinted polymer with binary functional monomers at Fe-doped porous carbon decorated Au electrode for the sensitive detection of lomefloxacin. *Ionics* 26:4183–4192
109. Chaudhary K, Mogha NK, Lalwani S, Sharma RK, Masram DT (2020) Ruthenium oxide nanoparticles immobilized over citrus limetta waste derived carbon material for electrochemical detection of hexestrol. *J Mater Chem B* 8:7956–7965
110. Gu C, Wang Q, Zhang L, Yang P, Xie Y, Fei J (2020) Ultrasensitive non-enzymatic pesticide electrochemical sensor based on HKUST-1-derived copper oxide @ mesoporous carbon composite. *Sens Actuators, B Chem* 305:127478
111. Wang Y, Xiao R, Yang E, Wu Q, Wang C, Wang Z (2018) Phthalocyanine-containing polymer derived porous carbon as a solid-phase extraction adsorbent for the enrichment of phenylurea herbicides from water and vegetable samples. *Sep Sci plus* 1:359–366
112. Amiri A, Tayebee R, Abdar A, Narenji Sani F (2019) Synthesis of a zinc-based metal-organic framework with histamine as an organic linker for the dispersive solid-phase extraction of organophosphorus pesticides in water and fruit juice samples. *J Chromatogr A* 1597:39–45
113. Alinezhad H, Amiri A, Tarahomi M, Maleki B (2018) Magnetic solid-phase extraction of non-steroidal anti-inflammatory drugs from environmental water samples using polyamidoamine dendrimer functionalized with magnetite nanoparticles as a sorbent. *Talanta* 183:149–157
114. Li P, Huang D, Huang J, Tang J, Zhang P, Meng F (2020) Development of magnetic porous carbon nano-fibers for application as adsorbents in the enrichment of trace Sudan dyes in foodstuffs. *J Chromatogr A* 1625:461305
115. Zhang X, Wen J, Lian L, Ma X, Wang X, Lou D (2020) Synthesis of 3D magnetic porous carbon derived from metalorganic framework for extraction of clenbuterol and ractopamine in mutton samples. *Analyst* 14
116. Wang C, Ma R, Wu Q, Sun M, Wang Z (2014) Magnetic porous carbon as adsorbent for the enrichment of 2 chlorophenols from water and peach juice samples. *J Chromatogr A* 1361:60–66
117. Sajid M, Basheer C, Daud M, Alsharaa A (2017) Evaluation of layered double hydroxide/graphene hybrid as a sorbent in membrane-protected stir-bar supported micro-solid-phase extraction for determination of organochlorine pesticides in urine samples. *J Chromatogr A* 1489:1–8
118. Sajid M, Basheer C, Mansh M (2016) Membrane protected micro-solid-phase extraction of organochlorine pesticides in milk samples using zinc oxide incorporated carbon foam as sorbent. *J Chromatogr A* 1475:110–115

# Chapter 27

## Porous Carbon in Food Industry



Shreyan Bardhan, Avijit Chakraborty, Sagnik Roy, Sudip Das,  
Dibyajit Lahiri, and Banani Ray Chowdhury

### 1 Introduction

Carbon materials have great qualities that may be utilized in a vast variety of industrial operations [1, 2]. Carbon is used to make the single most powerful fibers, finest solid lubricants (graphite), finest electron conducting substances like graphite, the structurally efficient substance for high temperature stress–strain applications, including some of the efficient most highly permeable gas adsorbers like activated carbon, and a primarily non impermeable material like vitreous acetate.

Every one of these morphologies are created by selecting raw ingredients and treatment conditions with care. Porous carbons are divided into two types. First are the porous carbons with enhanced active surface ligands for thermophysical applications which are being used in ceramics industry lately. Secondly, activated carbons having extra activated surface chemical groups for thermophysical applications. Active porous carbons are among the most significant kinds of industrial carbons, and they've been used for millennia.

Charcoal has been utilized in water filtration since 2000 BC, at that time when medieval the people of Egypt employed it in the filtration of water because of its use in therapeutic causes. Significant advances in the usage of porous carbons commenced

---

Shreyan Bardhan, Avijit Chakraborty, Sagnik Roy, and Sudip Das contributed equally in this chapter.

---

S. Bardhan · A. Chakraborty · S. Roy · S. Das · B. Ray Chowdhury (✉)  
Department of Biotechnology, Bengal Institute of Technology (BIT),  
Kolkata 700150, India  
e-mail: [bananiraychowdhury683@gmail.com](mailto:bananiraychowdhury683@gmail.com)

D. Lahiri  
Department of Biotechnology, University of Engineering and Management (UEM),  
Kolkata 700160, India

B. Ray Chowdhury  
Baranagar Baghajatin Social Welfare Organization, Kolkata 700036, India



around World War I, so there was no turning back thereafter. Ever since, new and much more sophisticated methods for both production and utilization of this versatile substance have emerged [3]. The most recent inclusion to the family of porous carbons is activated porous carbon fibers having big exterior area of about 2000 m<sup>2</sup>/gm [4].

The above fibrous substances have expanded the range of applications for gas preservation and power. Activated carbon is a type of substance having a significant inherent pore volume and surface area, thus a huge potential for adsorption of chemicals from liquids and gases. Porous carbons are highly adaptable industrial adsorbents that are utilized in a broad array of operations involving the elimination of unwanted species from gases or liquids by adsorption in an attempt to achieve restoration or the purification of chemical contents.

They also act as catalysts or assistance for catalysts [5–7]. The key characteristics of activated carbon adsorbents, as well as its relatively inexpensive when contrasted to other inorganic adsorbents such as zeolites, account for their prominent commercial presence. In porous carbons, wide range of shape and size of pores are typically generated, whereas pore size in zeolites is practically consistent. As a result, activated carbons are more adaptable as absorbing substances. Novel procedures for developing these substances, principles, substance characterization, and emerging applications are related with porous adsorbent carbons. The utilization of optimal sustainable energy resources has grown highly critical and crucial in recent times, as a result of rising energy necessities and the depletion of old fossil energy sources [8–11]. Academic researchers from all over the globe are working to investigate and create biomass energy as a viable alternative to fossil fuels. Due to its superior electrochemical features, namely, quick rate of charge/discharge, strong power density and great cycle stability, supercapacitors were a hot study area as electrochemical energy storage devices [12, 13]. Supercapacitors could be categorized into two classes according to their energy storage mechanisms: pseudo capacitors and electrical double-layer capacitors (EDLCs) [14]. Traditionally, the quasi-Faraday capacitance produced by redox reactions has monopolized the energy storage of pseudo capacitors [15, 16], whereas the capacitance generation of EDLCs is primarily dominated by the behavior of electrostatic charge diffusion and buildup at the electrode/electrolyte surface [17–20]. Pseudo capacitors, on the other hand, have a large capacitance, while EDLCs have a higher energy density and better cycle efficiency. Both kinds of supercapacitors have advantages. Development of resource of a thorough supercapacitor which permits the two varieties to coexist devoid of sacrificing their distinct advantages is thus a fantastic technique to obtain a higher-performance supercapacitor.

### ***1.1 What is Activated Carbon?***

Activated carbon is formed using organic substances that contain a lot of biological carbon. Most prevalent supplies are wood, peat, and coconut husk. In a reduced atmosphere, the substance is gently heated. This produces char, which is subsequently

activated using physical and/or chemical methods to greatly expand its surface region and generate a submicroscopic web of pores.

Specific compounds are drawn to the exterior molecules of activated carbon by the mechanism of adsorption, whereupon they bind to form a film. Substances can reach every possible site thanks to the large surface area and porous matrix. Activated carbons products are commonly used in the food and beverage sector to process cane sugar, cleanse edible oils, remove color from fruit juices, adjust flavor attributes in alcoholic beverages, and improve food ingredient flavors. Such activated carbons are also important in ensuring the safety of specific food items.

## ***1.2 Role of Porous Carbon in Food Industry***

Porous carbon can be used in making of various food items as follows:

### **1.2.1 Beverages**

Beverage manufacturing companies use activated carbons pulverized and dusted activated carbon materials to fulfill the needs of consumers across the globe, spanning fruit juice to liquor.

Activated carbon is employed by liquor manufacturers to eliminate off tastes and colors, and other fermentation by-products. Organic but unwanted chemicals can alter color, flavor, and odor in juices as well as other fruit-based beverages. Food chemists can have better influence over all these beverages thanks to activated carbon.

### **1.2.2 Edible Oils**

Bleaching earth is commonly used to eliminate color compounds from raw nut and vegetable oils. Activated carbons chemicals are utilized to eliminate both color and polycyclic aromatic hydrocarbons (PAH), which are a controlled substance in the European Union. This results in higher purity oils which fulfill the greatest quality and safety criteria.

### **1.2.3 Flavoring Agents**

Monosodium glutamate (MSG) and hydrolyzed vegetable proteins (HVPs) are both common flavor enhancers in the food business. The top quality dusted activated carbon from activated carbons lightens and refines the flavor of various food ingredients.

### **1.2.4 Food Chemicals**

Organic glycerin and citric acid are two of the most frequent dietary ingredients. They are employed to create unique appearances and flavors, yet they can both include substances that taint the final version. Activated carbon products are utilized to eliminate these compounds' color and odor-causing components.

### **1.2.5 Sweeteners**

Sugar as well as other sweeteners comprise organic molecules which can affect the final item's flavor, structure, and look. Activated carbons (PAC and GAC) purifies sweeteners with high grade powdered and granular activated carbon (PAC and GAC) having precise pore size distribution (PSD).

### **1.2.6 Fruit Juice**

Activated carbon is often used in the production of concentrated fruit juice. It is efficient in the removal of patulin, which is an intensely regulated organic substance frequently detected in apples and other fruit juices. It can also be utilized to modify the color and odors of food.

### **1.2.7 Lactic Acid, Gelatin, Mono Sodium Glutamate (MSG)**

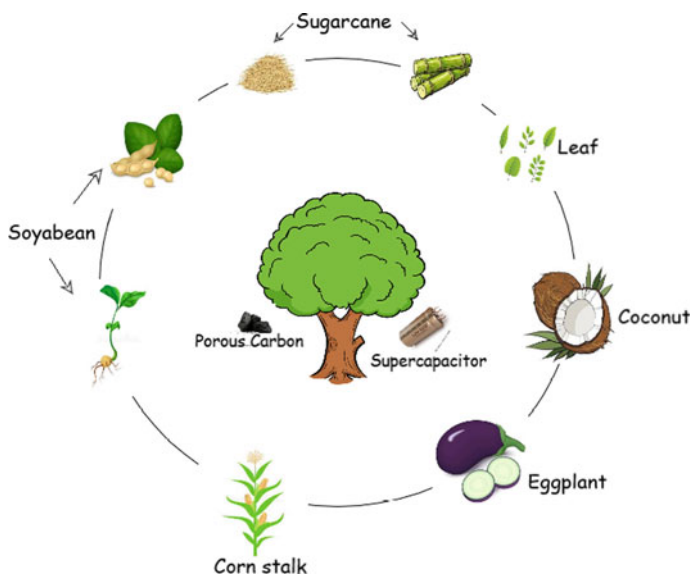
Activated carbons are widely used to produce the preservatives lactic acid, MSG (monosodium glutamate), and thickener gelatin.

### **1.2.8 Glycerin**

Activated carbon can be used for glycerin refinement, including aging control and stabilization of the ultimate product and eliminating undesired byproducts and colors.

### **1.2.9 Wine and Vinegar**

Activated carbon stocks are used in the wine and vinegar industries to eliminate undesired odors, remove contaminants, and modify color (Fig. 1).



**Fig. 1** Different sources of porous carbon

## 2 Mechanism of Porous Carbon Synthesis

Carbon is employed in a range of activities, both in dense and porous solid state. Pyrolysis and activation of carbonaceous natural and manmade precursors produce activated porous carbons. Pyrolyzed woods have the same architecture as natural wood, but have much lower surface regions and adsorption capabilities. Based on the activation circumstances, such as physical or chemical, these have enhanced adsorption capacities of 05–08 cm<sup>3</sup>/gm and exterior areas of 700–1800 m<sup>2</sup>/gm. Former carbons have a heterogeneous pore size dispersion, whereas chemically activated carbons have micropores in abundance.

As a result, these carbons can be employed to adsorb a large range of molecules, ranging from gas to liquid. Mono-layer or multi-layer molecule accumulation at pore boundaries causes molecular adsorption inside the pores, resulting in various forms of adsorption isotherms. Regulated pyrolysis and physical stimulation of unstructured carbon fibers, while on the other hand, can produce activated carbon fibers with a regulated microporous structure and surface region in the vicinity of 2500 m<sup>2</sup>/gm. Active carbon fibers with unrivalled pore architecture and surface properties are available as well as state-of-the-art porous materials for a variety of purposes ranging from pollution control to energy conservation [21].

Over the last few years, supercapacitors (SCs) have seen a considerable surge in study and marketing. Porous carbon is manufactured at an industrial level using standard carbonization-activation processes as the principal and foremost significant electrode active ingredient for commercial SCs [22].

Massive attempts have been undertaken in past years to establish innovative synthesis techniques for porous carbon substances. Whey powder, a by-product of the dairy sector, was used to create 3D porous carbon architectures at CSIC. These components can be molded with millimeter accuracy or created utilizing additional production processes with micrometric accuracy. These components can be made in desired shape or size. Filters, catalyst assistance, carbon molecular strainers, frameworks for tissue engineering, reactors, films, filtration or assistance of enzymes or biomolecules, 3D carbon electrodes are only a few of the usage. Companies of carbon materials or activated carbons are now being sought as industrial collaborators to cooperate under a patent license contract.

## ***2.1 Activated Carbon's Pore Size***

The pore width of the activated carbon is the most important component to consider prior to actually utilizing it in the adsorption procedure. The adsorption surface area is proportional to the pore size distribution of activated carbon. The larger the surface area of activated carbon, the higher the porosity. It was observed that as the porosity of the activated carbon grew, it was able to absorb more hydrogen [23]. The activated carbon's pore structure can be categorized into three categories according to the IUPAC classification: macropore (pore size greater than 50 nm), mesopore (pore size between 2 and 50 nm), and micropore (pore size less than 2 nm) [24]. Depending on the inherent structure of the starting material and the activation process, different types of activated carbon have distinct pore size distributions. The type of biomass used to make activated carbon does have a big influence on the pore diameter diversity and surface region of the finished product. Relative to biomass made of xylene and lignin, biomass dense in cellulose has the most activated carbon surface region [25].

Powder-activated carbon having a particulate width of lower than 0.2 mm have greater micropores although no macropores, whereas granular-activated carbon has a blend of various pore sizes in varying ratios. Adsorbate particles' preferential adsorption on the internal porous architecture of activated carbon is administered by pore width. Adsorbate particles should be allowed to permeate via a certain pore width of activated carbon well before the adsorption mechanism can commence. It explored the impact of activated carbon pore size dispersion on organic substance adsorption and discovered that for the greatest effective adsorption, the desired adsorbate width should be 1.3–1.8 times lower than the pore width [26]. Water and metal ions, for instance, could flow via the micropore having molecular dimensions of 2–6 Å, while bacterial cells having molecular dimensions greater than 104 Å cannot pass via the mesopore and choke at the pore wall entryway.

Moreover, based on the dimension of the adsorbed component, the aqueous phase adsorption prefers macropore, the gas phase adsorption prefers micropore, and the mesopore is appropriate for both gas and aqueous phase adsorption. Micropore's adsorption is typically a pore-filling mechanism in which pore volume governs adsorption potential. Adsorption in the mesopore is mainly caused by physical

engagement among the molecule and the pore interface; as a consequence, mono and multilayer adsorption, accompanied by pore-filling, proceeds primarily at the mesopore exterior. Owing of the macropore's wide pore size, adsorption proceeds primarily at the pore wall contact, which is viewed as inconsequential owing the adsorption region is small in contrast to the mesopore, yet the macropore serves as a pathway for compounds to enter the micropore and mesopore. As a result, utilizing the incorrect pore width in activated carbon may consequence in poor adsorption performance.

## 2.2 Surface Structure of Activated Carbon

In active regions, compounds adsorb to the activated carbon pore region. The surface chemistry of activated carbon has a well-known effect on adsorption ability. Numerous studies attempted to reconfigure the initial surface morphology of activated carbon, that consisted solely carbon atoms and had nonpolar or hydrophobic characteristics, utilizing a wide range of chemical substances, along with zinc chloride ( $ZnCl_2$ ) [27], phosphoric acid ( $H_3PO_4$ ), sodium hydroxide (NaOH) [28], potassium hydroxide (KOH), and ammonia ( $NH_3$ ) [29].

The two types of adsorptions which activated carbon frequently causes are physical and chemical adsorption. The largest prevalent form of adsorption for activated carbon is physical adsorption, wherein the adsorption energy is lower than 40 kJ/mol. It is caused by weak intermolecular interaction, like H-bonding, hydrophobic bonding, Van der Waals, or dipole bonding. This interaction proceeds fast at lower temperatures, and at higher temperatures, the homeostasis can swiftly revert.

Whenever functional groups on the surface are available, chemical adsorption involving highly covalent bonds arises. Chemical adsorption is triggered by the passage of electrons or atoms through the adsorbate units to the functional groups on the surface of activated carbon. At elevated degrees, adsorption is often permanent. A chemical activation method utilizing 10%  $H_2SO_4$  boosted the adsorption potential of organic compounds like toluene and benzene on activated carbon by 18 and 47%, accordingly [30]. In a research based on inorganic substance adsorption, it was discovered that chemical activation of activated carbon using organic acid solutions including such phosphoric acid and hydrochloric acid improved the activated carbon's adsorption potential from 3.5 to 9.8  $mg\ g^{-1}$  and 9.7  $mg\ g^{-1}$ , correspondingly [31].

The heteroatoms' existence from the surface functional groups on the microcrystalline carbon layers' periphery outcomes from chemical stimulation of activated carbon, that not just improves the permeability or contact region of the activated carbon, but as well rises the existence of heteroatoms from the surface functional groups on the periphery of the microcrystalline carbon layers, that might boost bonding to the adsorbate molecules. The hydrogen and oxygen-containing functional

groups are the most important in influencing the acidic, basic, or neutral surface characteristics. Increased carbon–oxygen groups, like carboxylic (–COOH), lactone, and phenolic groups (–OH), for instance, contribute to a rise in the polarity or hydrophilic properties of acid activated carbon (AAC). Since it includes carbon–oxygen teams such pyrone, carbonyl and benzopyranyl, or *N*-containing groups as well as pyrrolic, nitrogen oxide (NO), pyridinic, ammonia, and quaternary nitrogen groups, basic carbon is more hydrophobic than acid activated carbon [32].

The irreversible selectivity adsorption of activated carbon is centered on its functional groups on the surface that make strong interactions with the selective substances. It was discovered, for instance, that possessing oxygen-containing groups on activated carbon boosted hydrophilic properties and enhanced ion-exchange potential, meaning that activated carbon might serve a vital function in metal adsorption, such as Cd (II) ion adsorption [33]. Fundamental activated carbon, on either hand, would improve the adsorption of hydrophobic organic molecules. It was discovered, for instance, when reacting KOH activated coconut shell-based carbon using NH<sub>3</sub> increased benzene and toluene adsorption [29]. The influence of surface alteration on carbon dioxide adsorption within activated carbon that may be assisted via nitrogen functional groups like amide, imide, as well as pyridinic groups [34].

### 3 Classical and Latest Technologies in Porous Carbon Synthesis

#### 3.1 Activation

Carbons are classified into graphitic and non-graphitic based on their level of crystallographic organization. Non-graphitic carbons do not have three-dimensional symmetry like graphitic carbons [35]. As previously noted, following carbonization, the open interstices in the carbon molecules are completely or at least partially occupied by disorganized “amorphous” carbon, presumably due to material accumulation resulting in the carbonized substance having a relatively low adsorption potential. Some of the tar is likely to stay in the interspatial region of both crystallites and on their surfaces, at least for carbonization at reduced temperatures.

After eliminating waste compounds by steam-based heating or using inert gas, excavation with an appropriate solvent, or chemical reaction by carbonized substances can be partially activated. The activation procedure has resulted in the width of the holes generated through the carbonization phase are increased, and fresh porosity is generated, leading in the production of a well-formed and freely attainable pore architecture with a significant interior surface region. Activation can be accomplished in two methods, as detailed in the preceding sections (Fig. 2).

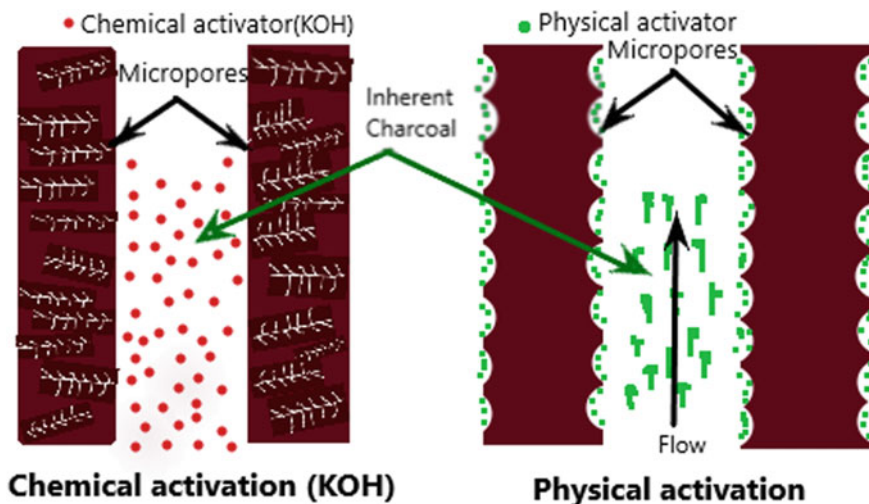


Fig. 2 Activation of porous carbon

### 3.1.1 Chemical Activation

Wood is used as the precursor material for chemical stimulation. Wood is coated with a strong solution of activating chemicals at the start. Cellulosic substance is degraded as a consequence. The chemically coated substance is therefore pyrolyzed in the lack of air at temperatures ranging from 400 to 600 °C. To eliminate the activating agent, the pyrolyzed substance is cooled and washed. Calcination causes charring and aromatization, as well as the formation of porous architecture, in coated and chemically dehydrated raw resources. Activating agents come in a variety of forms.

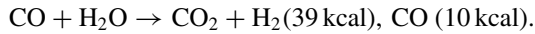
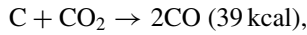
$\text{H}_3\text{PO}_4$ ,  $\text{ZnCl}_2$ ,  $\text{H}_2\text{SO}_4$ ,  $\text{K}_2\text{S}$ ,  $\text{KSNS}$ ,  $\text{KOH}$ ,  $\text{RbOH}$ ,  $\text{HCO}_3^-$ , and  $\text{Cl}^-$  of  $\text{Mg}^{+2}$ ,  $\text{Ca}^{+2}$  and  $\text{Fe}^{+3}$  are several of them [3, 36]. All activating substances are dehydrating, influencing pyrolytic breakdown and inhibiting tar accumulation. They effectively reduce the generation of acetic acid, methanol, and other hydrocarbons while increasing carbon output.

### 3.1.2 Physical Activation

It is a method wherein a carbonized substance forms a porous architecture with increased surface region and molecular dimensions after being heated to 800–1000 °C in the company of appropriate oxidizing gases like carbon dioxide, steam or air [37]. The subsequent endothermic processes result in gasification of the carbonized substance involving steam and  $\text{CO}_2$ :



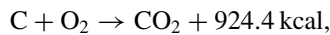




The H<sub>2</sub>O molecule is smaller than the CO<sub>2</sub> molecule, therefore, it disperses into the carbon pores more quickly. As a result, the steam process is quicker than the CO<sub>2</sub> process. When contrasted to steam stimulation, CO<sub>2</sub> stimulation accelerates external oxidation and the formation of big pores. The quantity of exterior and interior oxidation relies on how thoroughly the pores in the carbonized substance have grown. The activation of chars without the formation of significant pore architecture simply leads to a depletion in the diameter of carbon granules. Activation is linked to carbon loss and, as a result, to a reduction in the mass of the host carbon.

The rate of weight loss is proportional to the activation temperature and time. The formation of mesopores and macropores is dominated by activation at lower temperatures.

At higher activation temperatures, the efficiency of formation of pores with no capability of adsorption, known as macropores, increases, while the average pore width drops. In the instance of oxygen stimulation, the occurring reactions:



Because the pair of simultaneous reactions are exothermic, they produce a lot of heat and are difficult to manage. Furthermore, because there is constantly significant localized overheating, the final output is not uniform. Burning is unrestricted and happens on the surface of the grains as a result of the reaction's ferocity, resulting in substantial mass loss.

### 3.1.3 Mechanism of Activation

The composition of the source resources as well as the chronology of their carbonization determine the architecture of the pores and pore size dispersion [38].

Carbon atoms change in their reactivity based on how they are arranged in space. Activation removes unstructured carbon, subjecting aromatic sheets to activation chemicals and resulting in the formation of a microporous architecture. Because activation is linked to losing weight of the host carbon, the amount of carbon material burned off is used to determine the level of activation [39]. Weight loss gradually

increases with activation time at a given temperature. Usually, whenever the burn-off is around 10%, the unorganized carbon is burned primarily in the first stage. Stuck pores are opened as a consequence of all this.

As a result, the aromatic ring system's carbon begins to burn, resulting in active areas and larger pores. Severe activation reaction leads to the activated agents breaking down the walls and losing weight of more than 70% in the subsequent stage. As a consequence, the number of in transitional pores and macropores increases. There really is hardly any substantial surge in adsorption potential or inside surface region as the volume of the micropores diminishes. The variation in porosity generated by diverse activating agents becomes increasingly evident at increased burn-off.

In a classic instance, water vapor activation of a hard wood leads to the continuous formation and broadening of all size pores until the activated material has a well-developed porous architecture with a broad pore size dispersion at a burn-off of 70%. The overall adsorption volume increases from 06 to 083 cm<sup>3</sup>/gm after activation with 50–70% burn-off [40]. However, because it is mostly related with pore widening, the surface area remains nearly unchanged. Carbon dioxide activation mostly creates microporosity over the whole burn-off range. Micropores account for around 73% of total adsorption pore volume and more than 90% of total exterior area. In case of steam-activated carbon, micropores account for just 33% of overall pore volume and 63% of surface area.

As a result, carbon generated by carbon dioxide activation has overall pore volume (49 cm<sup>3</sup>/gm) than carbon generated by steam activation. Nevertheless, the effective surface region is nearly the same as in both circumstances. This is primarily owing to micropores' impact to the surface region.

Furthermore, carbon atoms along the margins and edges of aromatic sheets, as well as those near fault positions, displacements, and discontinuities, are coupled with delocalized electrons or have leftover vacancies; these have a lot of potential energy. As a result, these carbon atoms are more reactive, and during oxidative activation, they are more likely to form surface oxygen complexes [5]. Such chemical group on the material's surface promote adsorption, which is beneficial in some applications.

Conversely, these surface oxygen complexes degrade and strip away the carbon (di/mono) oxides from the surfaces, exposing fresh carbon atoms that aren't saturated for subsequent interaction with an activating agent. As a consequence, the activation process can be seen as an interaction between both the activating agent and the carbon atoms that make up the framework of the substantial carbonized product, culminating in a massive internal surface region with interlinked pores of the preferred measurements and chemical surface groups.

### 3.1.4 Activated Carbons Synthesis from Synthetic Precursors

Artificial precursors such as phenolic, poly-acrylonitrile, Poly furfuryl alcohol, and others are carbonized to produce crystal carbons with sealed porosity. As a result,

activation of these chars necessitates extremely strict temperature, timing, and environmental factors. Nevertheless, when carbonization is executed at 800–1000 °C when carbon dioxide is present, the final char has a large surface region and open pores [41]. Typical pyrolysis occurs up to 700 °C heat treatment in this situation. CO<sub>2</sub> begins an activation reaction at 700 °C before the pores seal. Pyrolysis and activation of synthetic precursors can therefore be carried out in a CO<sub>2</sub> condition.

## 3.2 *Recent Methods of Porous Carbon Synthesis*

Because of the vast range of applications, investigations on COFs and MOFs have grown tremendously in recent years.

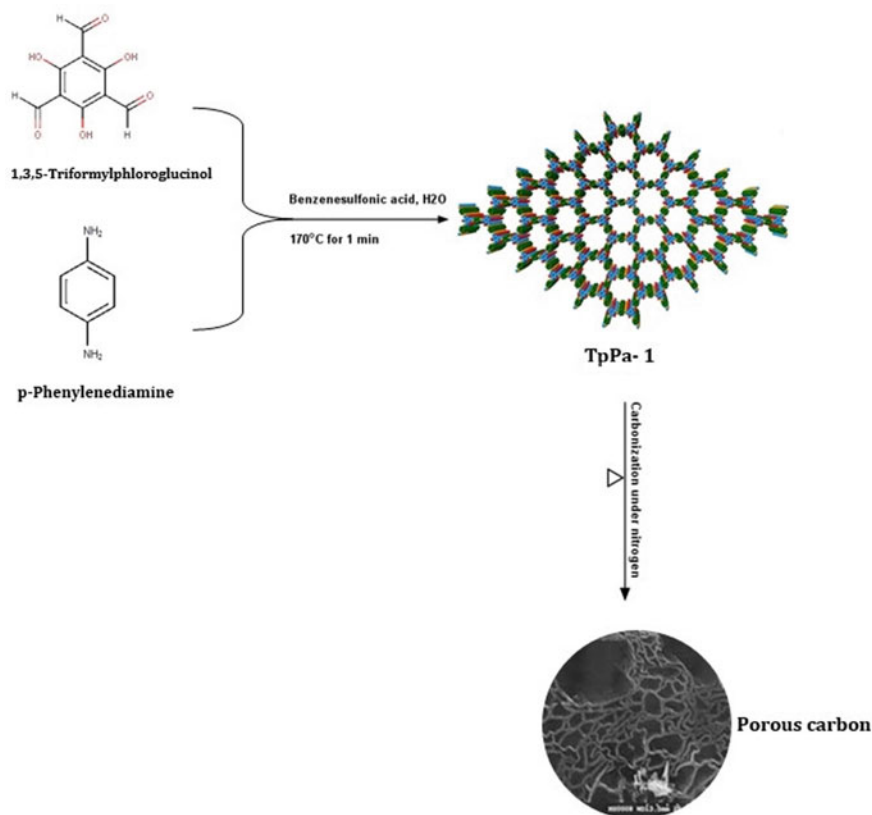
### 3.2.1 **Porous Carbon Synthesis from Covalent Organic Frameworks (COFs)**

COF substances show promise as a starting point for creating extensively customized porous carbons [42]. The linkages and linkers are the two major constituents in the creation of COFs, and numerous organic compounds have been used as these structural components. At the molecular scale, this enables for customized heteroatom species, large surface regions, and programmable shapes. A deeper structural relationship among the porous carbon produced and COFs precursors is envisaged seeing that its covalent structures are greater proof against hard conditions. COFs are excellent blueprints or precursors for fabricating porous carbons because of all of these features [43–48]. The simplest approach is to carbonize the porous organic originator without delay below regulated circumstances. The resultant carbon is usually a nano porous substance, attributable to its permeability now no longer best because of the precursor's porous structure, however additionally because of carbon burn off at some point of the carbonization. By carefully selecting the predecessors, several morphologies can be created [49–51]. In 2009, argon was used to carbonize the molded carbon-austenite fibrous and tubular polyphenylene precursors to produce one-dimensional carbon fibers and fibers. Carbon nanofibers (CNFs) and carbon nanotubes (CNTs) with exterior surface area of uptill 900 m<sup>2</sup>/g are produced and evaluated with improved electrodes in the electrochemical double-layer capacitors [52]. In 2014 *N*-doped graphitic porous carbon utilizing 2D covalent organic polymer precursors was created, allowing them to regulate the precise placement of the heteroatom [53]. The electrocatalytic activity of these substances was shown to be highly correlated with the *N*-doped carbon properties. In 2011, a thienyl-based polymer was used as a precursor to create a microporous sulfur doped carbon [54]. In 2016 the Sonogashira coupling procedure was employed to make nitrogen and sulfur linked porous polymers that can be utilized as a porous products precursor containing doped carbon. Later, coal was effectively used to reduce oxygen and store energy [55]. At catalyst-free circumstances, an imine-linked polymer produced via Schiff

base condensation yielded a microporous polymer shape with an exterior surface area of  $744 \text{ m}^2/\text{g}$  [56]. Carbons which are doped with nitrogen with narrow particle dimensions and morphology and higher nitrogen functional group density (5.58–8.74%) can be synthesized through direct pyrolysis of polymers. The carbon generated by pyrolysis at  $800 \text{ }^\circ\text{C}$  was employed for  $\text{CO}_2$  absorption, and the computed adsorption potential of  $7.41 \text{ mol of CO}_2/\text{m}^2$  at  $25 \text{ }^\circ\text{C}$  and 1 bar changed into one of the most important but recorded for porous carbon adsorbents [57]. The substances' durability and ease of renewal and reuse were also shown, with no significant degradation of  $\text{CO}_2$  adsorption capability. Directly carbonized imine-bound COF, triformylphloroglucinol and p-phenylenediamine COF (TpPaCOF) allows graphite-like N-doped carbon as the sulfur host material when preparing the cathode substrate of lithium-sulfur batteries to look for new components. You can now use it for the high efficiency lithium-sulfur batteries [58]. Spherical, hollow nitrogen-rich activated porous carbon shells were prepared by directly carbonized structured porous organic frameworks at intense temperatures [59]. This substance was created of amorphous carbon with micropores in the shell frame and a specific surface area of  $525 \text{ m}^2/\text{g}$ . Microporous N-doped carbon was effectively constructed using direct carbonization of an azine-bound 2D molecular network [60]. The carbonized COF had a large specific exterior surface area ( $1596 \text{ m}^2/\text{g}$ ), a homogeneous micropore ( $<1 \text{ nm}$ ), and a graphite-like structure of carbon, doped with nitrogen. Moreover, the creation of nitrogen gas through the thermal breakdown of the azine bond adds to the generation of nano porous structures, according to the research. The electrochemical capacitance of these substances was increased. Free-standing carbonaceous membranes of polymer structures were created [61]. The author used superacid-catalyzed copolymerization of acetyl monomers to perform thermal decomposition of the pyrrole ring containing the polymer membrane in one process. Carbonization of a triazole-functionalized-triazine framework yielded a nitrogen-doped carbonaceous free-standing porous membrane in different methods [62]. The  $\text{N}_2/\text{CO}_2$  selectivity and  $\text{CO}_2$  permeability of the carbonaceous membranes that resulted were remarkable. These approaches have demonstrated the ability to create customized carbons with specified topologies as well as the simple and effective insertion of heteroatoms into porous carbon structures. Taking advantage of the straightforward preparation procedure, vast accessibility of precursors, adaptable structure regulation, and simpler modification of the number of heteroatoms, it appears that several novel and enhanced materials are still to be produced through meticulous shortlisting of precursor frameworks and carbonization environments. However, for the ambiguous constructional relationship among the sacrificial COF and the final material, some scientists agree that the rational design of COF precursors remains a big issue [63–67] (Fig. 3).

### 3.2.2 Porous Carbons Synthesis from Metal Organic Frameworks (MOFs)

Because of its versatility and unique properties, MOFs are highly dependent on controlled thermal decomposition [68] and metal-based porous materials such as



**Fig. 3** Porous carbon synthesized from TpPa

metal carbides, oxides, sulfides, phosphides, and nitrides [69]. A suitable precursor for the formation of porous carbon. Carefully tuned temperature settings allow the production of metal-carbon hybrids and metal-free porous carbons, synthesized from MOFs. Generally, metal/carbon mixtures or metal-free porous carbon substances are formed when carbonization occurs under inert gas flow, but aerobic thermal treatments frequently result in nanostructured metal oxides. Both very porous substances are proven to be attractive substances with many uses, especially in catalysis, in this regard. It is noteworthy that organized porous carbon with high density and large surface area of catalytically active sites, wide range of heteroatoms, and adjustable porosity can be simply generated from MOFs by not using templates. This improves catalytic capacity [70, 71]. In particular, MOF-derived porous carbon can have a shape and hierarchical porosity derived from the MOF pattern, allowing for the logical engineering of porous structures with increased catalytic performance while focusing on energy conservation and the creation of important chemicals. This study outlines several key elements of the preparation and utilization of porous carbons

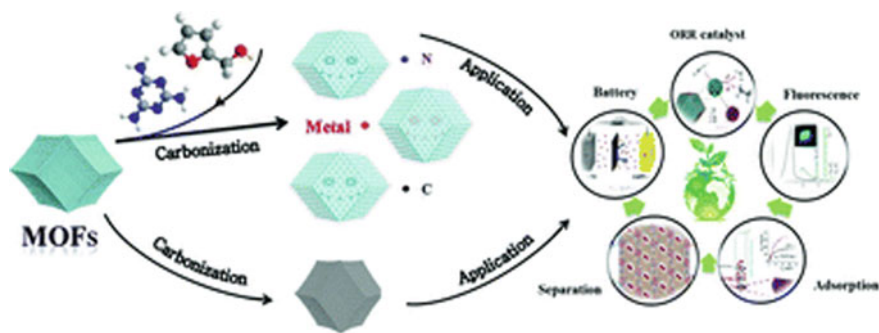


Fig. 4 Porous carbon derived from MOFs [73]

made from MOFs, both as a carbon precursor and as a sacrificial arrangement for other carbon sources that are a rapidly expanding sector [72] (Fig. 4).

#### MOFs as Precursors for Metal-Free Porous Carbon Synthesis

Recently, the ultra-porous carbon compounds production from MOFs and the future applications of them have been discussed [74]. The MOF-5 and ZIF-8 series, as well as related series, are the widely studied metal–organic networks for producing porous carbon substances. Here, we have selected and described some exemplary cases to summarize the high relevance of these highly attractive porous carbons. In this regard, a wide range of metal-free porous carbons with unique topographical features that can be used as supercapacitors have been created via direct pyrolysis of MOFs. By thermal degradation of MOF-5, it was [75] documented the production of metal-free mesoporous carbon substances with large surface regions (up to 1800 m<sup>2</sup>/g). The process, which involves the emission of CO<sub>2</sub> and benzene while creating ZnO coated by amorphous carbons, takes place at around 400 °C. The ZnO was removed in this instance after an acid treatment with HCl. It was [76] reported the direct thermolysis of MOF-5 at 900 °C to produce three forms of porous carbons, providing fascinating mechanism findings. It's worth noting that Zn cations were minimized and evaporated, preventing the need for extra washing. Researchers also used phenolic resins and carbon tetrachloride and ethylenediamine as different carbon sources to impregnate MOF5 in and around the pore structure, which affected the pore structure. All samples were treated with KOH to adjust the microstructure activation, following carbonization, changing the mechanical characteristics and pore architecture. It is generally recognized that in electric double-layer capacitors, carbons with established microporosity for mesoporous carbon have the largest capacity, and while microporous properties have a significant effect on surface expansion, faster mass transfer. Environmentally friendly and non-toxic carbon sources such as glucose [77] or glycerol [78, 79], have also been used in the carbonization of MOF-5 to produce hierarchically micro- and mesoporous carbons beneficial in the

production of electrodes. Utilizing the incipient wetness approach [68], manufacture of nano porous carbon with large pore volume and high SBET using MOF5 have been documented. However, furfuryl alcohol is also included as an additional carbon supply. Samples were pyrolyzed at various temperatures (range 530–1000 °C) and SBET was found to be temperature dependent (range 1141–3040 m<sup>2</sup>/g). Existence of Zn species on carbon is highly influenced by the temperature of carbonization. At 1000 °C, a completely metal-free sample was acquired, while at lower temperatures (800 °C), Zn was detected. These compounds outperformed carbons made from SBA-15 mesoporous silica regarding electrochemical performance as an electrode component of electric double layer capacitors. The usage of glycerol in combination with various concentrations of Bi(NO<sub>3</sub>)<sub>3</sub>·5H<sub>2</sub>O has a significant influence on the surface area and pore diameter spread of the products. CO<sub>2</sub> capture [80] and hydrogen retention [81] have also been discovered to be remarkable prospects for hierarchically porous carbons generated by direct carbonization of various MOF. Porous carbons were produced with large surface regions (up to 2734 m<sup>2</sup>/g) and increased overall pore volumes (up to 5.53 cm<sup>3</sup>/g) from three distinct MOFs (MOF-5, MOF-74, and MIL-53) [80]. Modifications in MOF precursor production settings have a significant impact on the morphology and porosity of these materials. In particular, the appearance of millimeter-sized crystals in MOFs produced in high yields can explain the increase in surface area and pore volume of these samples. ZnO and carbon with scarcely established porosity are formed through the carbonization phase at temperatures ranging from 600 to 800 °C. ZnO is diminished at higher temperatures (up to 900 °C), and Zn species evaporate and CO is released, resulting in hierarchical highly porous carbons. Using layered metal hydroxides as a template and using self-sacrificing metal sources, we have developed an ingenious synthetic approach for producing MOFs with flaky morphology. The organic ligand (2-methylimidazole) obtains a metal cation from a previously produced metal hydroxide and distributes Zn<sup>2+</sup> and Co<sup>2+</sup> in the same molar ratio. As a result, ZnCoZIF1, which is a bimetal MOF, is generated, and Zn and Co coexist and are uniformly distributed [81]. Substances with capacitive deionization include porous carbon having controllable morphological features derived from MOFs [82]. Some of the preliminary stages show excellent performance [83]. The formation of various porous carbons from Zn-containing MOFs at 1000 °C-ZIF8, [Zn (MeIM) 2], [Zn<sub>4</sub>O (bdc) 3] and Zn<sub>3</sub> (fumarate) post-pyrolysis morphology is well preserved. Some of the preliminary stages show excellent performance. In certain instances, Co species can function as catalytic species, causing graphene-like carbons to emerge. Despite the fact that most metal species were eliminated utilizing acidic HCl solution, several Zn and Co nanoparticles remained embedded in the graphitic layers [72, 84]. Note that the surface area and graphitization of carbon can be formed according to the molar ratio of the metal used to make the MOF precursor [85–87] (Fig. 5).

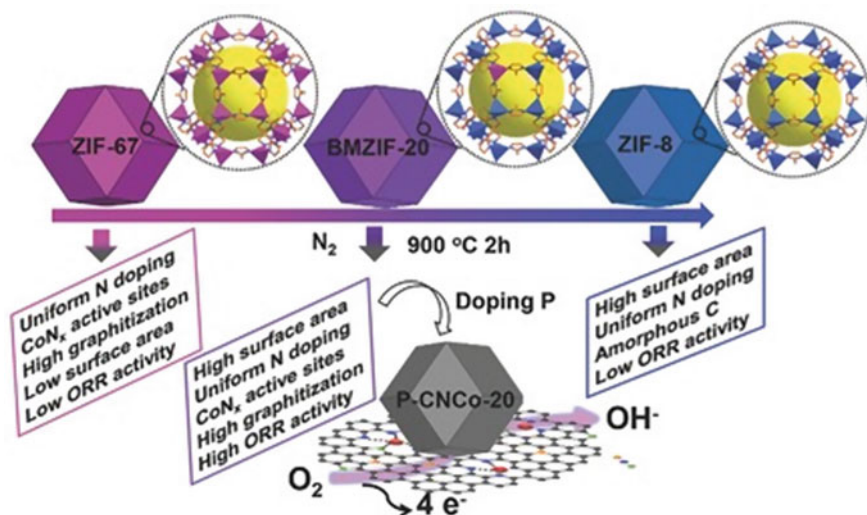


Fig. 5 Bimetallic metal–organic frameworks [88] [Under CC. By. NC. ND. 4.0]

## 4 Application of Porous Carbon in Food Industry

The existence of gaseous substances in the packing architecture like oxygen, carbon dioxide, or relative humidity, influences the integrity and hygiene of the foodstuff in the package. These factors influence the deteriorating effects of enzyme processes, chemical interactions, physical modifications, microbiological proliferation, respiration, the ripening stage, sensory attributes, and storage stability of food products, primarily fresh food that are actively respiring. The incorporation of activated carbon into packaged foods is a multipurpose way for maintaining or controlling gaseous environments in the packaging. Because activated carbon has the ability to operate as simultaneously a releaser and an absorber, it might be utilized to discharge the volatile chemical even while adsorbing the gaseous particles. As shown in the previous investigations, activated carbon can be specifically changed for specific adsorption goals, allowing it to precisely remove the dominating gas molecules that have a significant impact on the quality and safety of various meals in packaging systems. On the other hand, it can also emit antimicrobial substances like ethanol and sulfur dioxide to limit the proliferation of germs that could cause food poisoning or spoiling. The utilization of activated carbon has indeed been categorized into two ways, depending on the adsorption and release of the component, in an attempt to characterize the probable capability of activated carbon in food packaging [89] (Fig. 6).





**Fig. 6** Types of food packaging

## **5 Mechanism of Action of Porous Carbon Against Microbial Cells**

### ***5.1 The Release of Antimicrobial Compounds from Activated Carbon***

There are two forms of antibacterial agent adsorption-release on activated carbon. The primary is the adsorption of aqueous antimicrobial agents, such as ethanol and natural compounds that could be liberated from activated carbon by volatilization [90]. Before antimicrobial action occurs, the emitted antimicrobial vapor may spread through the packaging environment and settle on the surface of the food. The other is the adsorption of metal nanoparticles on the activated carbon surface, including such silver nanoparticles, that requires contact surface to transport nanoparticles from the surface of the activated carbon to the surface of the food (Table 1).

**Table 1** Antimicrobial activity of metal nanoparticle-activated carbon

Activated carbon (AC) sources	Activation agent	Metal nanoparticle	Microbes involved	References
Corncoobs	H <sub>3</sub> PO <sub>4</sub>	AC/Ag	<i>E. coli</i>	[90]
Chestnut shells	ZnCl <sub>2</sub>	Ag-AC	–	[91]
Activated carbon	–	Ag-NP	<i>E. coli</i>	[92]
Coconut shell	Physical activation	Ag/AC	<i>E. coli</i>	[93]
Palm seed	H <sub>2</sub> SO <sub>4</sub>	Pb-AC	<i>E. coli</i>	[94]

## 5.2 Release of Volatile Antimicrobial Compound by Activated Carbon

Among the numerous antibacterial substances utilized all over the globe are ethanol as well as essential oils, both of that are recognized as volatile organic compounds with antimicrobial characteristics and are utilized in a diverse array of foods, including ethanol pads, that are commonly shown in bakery packaging, as well as essential oil coatings on a wide range of fruits. Essential oil vapor has recently been acknowledged in the medical community for its potent antimicrobial properties. Nonetheless, because of its limitations in administration approach and a longevity that requires to be improved, it is unsuitable for engagement inside the food sector. Due to studies performed by the lab, the Innovation of Essential Oil for Food Safety and Packaging at Walailak University, activated carbon can be absorbed as well as generate essential oil vapor. Additionally, the vaporized essential oil has antifungal effectiveness against a number of post-harvest pathogenic molds, particularly *Penicillium*, *Aspergillus flavus*, *Aspergillus niger*, and *Rhizopus* spp. [89].

Ethanol is other volatile antibacterial chemical. It was discovered that activated carbon can adsorb ethanol as well as that 98% of the adsorbed ethanol might be readily liberated in the vapor at room temperature [95]. Physical adsorption, van der Waals force, hydrophobic-bound force, or H bonds that are readily broken at room temperature has been observed for the adsorption of polar ethanol units on activated carbon.

The notion of the adsorption energy (E) of ethanol onto activated carbon is less than 40 kJ/mol (range: 5–5.5 kJ/mol) demonstrates such. They also observed that while enhancing the amount of oxygen surface functional groups enhanced the adsorption capability of ethanol on activated carbon, the engagement among the oxygen groups as well as the ethanol on activated carbon lowered the ethanol's removing capabilities (at about 91%) [95]. It was verified that the adsorption and emission capabilities of ethanol on activated carbon via developing an adsorption model of ethanol over activated carbon [96, 97]. Considering this, hardly any research has been conducted on the antibacterial properties of the discharged ethanol.

### 5.3 Mechanism of Emission of Antimicrobial Agents Inside Food Packaging

Several mechanisms for chitosan's antimicrobial activity have already been published. Among the most widely recognized mechanisms is also that chitosan's positive charge interferes with anionic charged microbial cell membranes. The interactions among the protonated ammonium group of chitosan and the microbial cell surface, causing an osmotic imbalance, while CNT synergistically affects the membrane in situ to regulate the microbe's overall development. According to another concept, it causes the hydrolysis of intracellular peptidoglycans in microbes [98]. The presence of the outer layer of *E. coli* prevents CNT binding to introduce antibacterial activity, in all likelihood because of the robust net negative charge at the surface of *E. coli*. Direct adhesion of bacterial surface proteins with CNTs is the mechanism of active antimicrobial activity against *S. aureus*. The nanotubes are released from the hydrogel as well as target the microbes during 24 h, causing microorganism cytomembrane lysis and consequent membrane potential loss [99, 100]. *S. aureus*, a Gram-positive bacterium, was hindered by chitosan with a higher molecular weight. The major reason for this could be that chitosan's higher molecular weight inhibits nutrient absorption. Higher molecular weight chitosan, on either hand, had no effect on Gram-negative bacteria [101].

CNTs are thought to form aggregates as a result of van der Waals interactions, which can include a vast variety of pathogen cells due to the size of the aggregates. As a result, shortened CNTs self-agglomerate in a fluid system without involving a large number of microbial cells, whereas longer encapsulated CNTs affect a greater number of cells trapped within the aggregates [98].

### 5.4 Food Quality Check

The activated carbon treatment is a simple and versatile approach for enriching ACE-inhibiting peptides from a wide array of protein hydrolysates for use as ingredients in hypotensive foods with minimal side effects [102]. Polar furfural substances can be obtained from aqueous solution via p-p stacking, p-cation interaction, and hydrogen bond creation owing to the combination of the carbon skeleton and the PPDA polymer. Furthermore, the magnetic properties of MPC@PPDA enable the isolation procedure (which takes less than 18 min). Eventually, the described method has been successfully implemented to the fast separation and quantification of polar furfural substances in dry milk samples and baby food [103]. Some examples based on literature review are provided in Table 2.

**Table 2** Application of Porous carbon in food quality check

Application of porous carbon	Food type	References
Natural ACE inhibitors are selectively enriched	Functional meals that are hypotensive and have fewer adverse effects	[102]
Extraction or quantification of target compounds	Baby food and dry milk powder samples	[103]
Detecting trace PAHs	Different tea beverages	[104]
Detection of Sudan dye residues	Food stock	[105]

### 5.5 Release of Nanoparticles by Nanoporous Carbon in Activated Form

The use of nanoporous carbon in liberated metal nanoparticles restricts bacterial development and contamination. Metal nanoparticles have been shown to have antibacterial properties [91]. Numerous studies have attempted to investigate the activated carbon's antimicrobial activity covered with several forms of nanoparticles [92, 93].

Carbon nanomaterials have various functionalities in a wide range of fields. Nevertheless, their synthesis and functionalization typically necessitate complex processes or difficult experimental constraints. QCNSs with high antibacterial activity were produced by hydrothermal treatment of chitosan and hexadecyl betaine (abbreviated as BS-16). The hydrothermal process involves the direct reaction and carbonization of chitosan containing amines and BS-16 containing carboxyls. The QCNSs have a well-defined spherical shape and a homogeneous size distribution in their as-prepared state, with an average diameter of 110 nm. The QCNSs were able to kill Gram-positive bacteria at a minimum inhibitory concentration (MIC) of 2.0–5.0 g mL<sup>-1</sup>. Meanwhile, the QCNSs demonstrated high hemocompatibility with red blood cells and excellent cytocompatibility with normal human liver and lung cells [106].

### 5.6 Food Odor Adsorption Property of Activated Carbon

Foul/unpleasant odor of food is among the most important characteristics and may be employed in determining the food quality. An off-odor is unappealing to customers. This foul odor is influenced by a combination of volatile hydrophobic organic molecules which are a result of food decomposition and contamination by bacteria or biochemical processes such as lipid oxidation. The potential of activated carbon to remove odors has always been recognized. Now, it's used to get rid of odors in refrigerators at residences. It's also appropriate for its use in packaging of food. Powdered activated carbon in the packing of exposed cooked beef can reduce foul/unpleasant odors caused by the irradiation operation [107]. Furthermore, according to sensory

analysis, majority consumers favor irradiation ground beef stored with activated carbon to regular beef. Several significant volatile constituents of odors in packaging employing activated carbon are reduced both in non-irradiated and irradiated samples.

### ***5.7 Adsorption of Ethylene by Activated Carbon***

It is observed that ethylene adsorption by ethylene scavengers based on activated carbon in tomato and broccoli have delayed the depletion of chlorophyll concentration which causes loss of redness in tomatoes and yellowing of broccoli. It also improves firmness in tomato and extends the shelf-life of tomatoes and broccoli [108–111].

### ***5.8 Adsorption of Oxygen by Activated Carbon***

A multitude of methods are used to regulate the level of oxygen in preservation to maintain or enhance fruit and crop quality. Use of oxygen absorbers is a strategy for eliminating oxygen, or leftover oxygen, from preservation environments, thereby limiting grade change [112]. A wide range of compounds can be utilized for oxygen adsorption. In commercial oxygen absorbers, chemical oxidation mechanisms as iron powder bases or ascorbic acid bases, or enzyme activities including glucose oxidase/catalase bases, are utilized to absorb and decrease oxygen to lower than 0.01%. Chemical absorbers, on either hand, could be hazardous. They are not edible and can be used alongside liquids. Activated carbon, on either hand, holds a lot of potential as a low-cost, versatile, robust, non-toxic, environmentally friendly, safe, and effective adsorbent for oxygen removal in agro crop packaging. For eliminating oxygen from food packaging, activated carbon has a great promise. In contrast, activated carbon has a hydrophobic nature which attracts and physically adsorbs non-polar molecules such like oxygen [32, 33, 113]. Regardless of the unsaturated carbon atoms toward the layer edges like graphite, activated carbon could rapidly set up a strong covalent bond binding oxygen, leading in weaker interactions involving carbon–oxygen functional groups including the carbonyl and hydroxyl groups [114–117].

### ***5.9 Activated Carbon: Vapor Phase Molecule Scavenging***

Processed foods in food packaging are classified into two types depending on inherent respiration behavior: respiration food (vegetables and fresh fruits) and non-respiring food (cereals, meat, and processed foods). The gaseous circumstances which precede

the packing of food procedure affect the food's structure and hygiene in a variety of ways. Whenever it concerns respiring items, oxygen is a critical element in the operation that produces byproducts such as carbon dioxide, ethylene, as well as water vapor. Reduced oxygen levels in food packing inhibit respiration, prolonging vegetable & fruit development and resulting deterioration. Furthermore, eliminating or suppressing ethylene in preservation circumstances is crucial for maintaining freshness and extending the post-harvest life of a variety of fresh goods. It was also found that ethylene levels as minimal as 20 L/L (ppm) are sufficient to elicit unwanted maturation processes in climacteric fruits [118]. As a consequence, eliminating ethylene from fruits and vegetables may help them last longer. Many fruits and vegetables, including tomatoes and broccoli, have indeed been processed using activated carbon to reduce ethylene levels & preserve quality during preservation [108, 119, 120].

The safety and quality of non-respiring, besides that, is mostly determined by the amount of oxygen and water vapor present (moisture content). The oxidation reaction is accelerated by high oxygen levels, leading in off-odor, color alteration, and nutrition depletion. Furthermore, it creates favorable circumstances for aerobic deterioration microbes, which are responsible for food spoiling and sickness. Additionally, high moisture levels produce free molecules of water, which can be used in enzymatic operations, chemical processes, and microbiological activity, culminating in product disintegration, spoilage, and a reduction in grade. It also alters the structure of food, causing it to turn soft or shriveling. As a result, the amounts of ethylene, oxygen, and relative humidity or water vapor in food packaging must be lowered or managed in need to sustain the product's safety and quality. Furthermore, in certain items, the odor of the meal is a significant feature that is utilized to identify the product's grade and sensory attributes [27, 121].

## 6 Conclusion

The remarkable ability of adsorption of porous carbon is dependent on the surface chemistry and the size of pores of porous carbon. By modifying porous carbon's surface chemistry and pore size, we can make porous carbon capable of adsorbing several particular substances. Porous carbon can be utilized in the food industry for controlling food safety, food packaging, and food quality maintenance. Because of its antimicrobial evacuation capacity, porous carbon is useful in limiting the development of germs on foodstuff in packaged foods. The capacity of adsorption of porous carbon can reduce the agents which affect the quality of food, such as ethylene, oxygen and water vapor which results in senescence and deterioration of food. It induces the extension of the shelf-life of food products containing porous carbon in the food industry.

## References

1. Pierson HO (1993) Handbook of carbon, graphite, diamond and fullerenes properties, processing and applications. William Andrew Publishing, Noyes
2. Burchell T (ed) (1999) Carbon materials for advanced technologies. Pergamon
3. Bansal RC (1988) Active carbon. Dekker, New York
4. Suzuki M (1994) Active carbon fibre: fundamentals and applications. Carbon 32:577–586
5. Patrick JW (ed) (1995) Porosity in carbons. Characterisation and applications. Edward Arnold, London
6. Jin H et al (1996) The shape selectivity of activated carbon fibres on a palladium support. Carbon 39:421–431
7. Mochida I et al (1997) High catalytic activity of pitch based activated carbon fibres of moderate surface area for oxidation of NO and NO<sub>2</sub>. Fuel 76:543–548
8. Zhang LL, Zhao XS (2009) Carbon-based materials as supercapacitor electrodes. Chem Soc Rev 38:2520–2531
9. Jiang H, Lee PS, Li C (2013) 3D carbon based nanostructures for advanced supercapacitors. Energy Environ Sci 6:41–53
10. Lai X, Halpert JE, Wang D (2012) Recent advances in micro-/nano-structured hollow spheres for energy applications: from simple to complex systems. Energy Environ Sci 5:5604–5618
11. Dai L, Chang DW, Baek JB, Lu W (2012) Carbon nanomaterials for advanced energy conversion and storage. Small 8:1130–1166
12. Niu Z, Dong H, Zhu B, Li J, Hng HH, Zhou W, Chen X, Xie S (2013) Highly stretchable, integrated supercapacitors based on single-walled carbon nanotube films with continuous reticulate architecture. Adv Mater 25:1058–1064
13. Burke A (2000) Ultracapacitors: why, how, and where is the technology. J Power Sources 91:37–50
14. Wu Z, Li L, Yan JM, Zhang XB (2017) Materials design and system construction for conventional and new-concept supercapacitors. Adv Sci 4:1600382
15. Liu S, Kim KH, Yun JM, Kundu A, Sankar KV, Patil UM, Ray C, Chan Jun S (2017) 3D yolk-shell NiGa<sub>2</sub>S<sub>4</sub> microspheres confined with nanosheets for high performance supercapacitors. J Mater Chem A 5:6292–6298
16. Elshahawy AM, Li X, Zhang H, Hu Y, Ho KH, Guan C, Wang J (2017) Controllable MnCo<sub>2</sub>S<sub>4</sub> nanostructures for high performance hybrid supercapacitors. J Mater Chem A 5:7494–7506
17. Tan YB, Lee J-M (2013) Graphene for supercapacitor applications. J Mater Chem A 1:14814
18. Wahid M, Parte G, Phase D, Ogale S (2015) Yogurt: a novel precursor for heavily nitrogen doped supercapacitor carbon. J Mater Chem A 2015(3):1208–1215
19. Zhang W, Lin H, Lin Z, Yin J, Lu H, Liu D, Zhao M (2015) 3D hierarchical porous carbon for supercapacitors prepared from lignin through a facile template-free method. Chemsuschem 8:2114–2122
20. Islam MM, Subramaniam CM, Akhter T, Faisal SN, Minett AI, Liu HK, Konstantinov K, Dou SX (2017) Three dimensional cellular architecture of sulfur doped graphene: self-standing electrode for flexible supercapacitors, lithium ion and sodium ion batteries. J Mater Chem A 5:5290–5302
21. Manocha S (2003) Porous carbons. Sadhana 28:335–348. <https://doi.org/10.1007/BF02717142>
22. Yin J, Zhang W, Alhebshi NA, Salah N, Alshareef HN (2020) Synthesis strategies of porous carbon for supercapacitor applications. Small Methods 4:1900853
23. Sethia G, Sayari A (2016) Activated carbon with optimum pore size distribution for hydrogen storage. Carbon 99:289–294
24. The IUPAC Council (1971) Manual of symbols and terminology for physicochemical quantities and units. Washington DC, USA
25. Rodríguez Correa C, Otto T, Kruse A (2017) Influence of the biomass components on the pore formation of activated carbon. Biomass Bioenerg 97:53–64

26. Li L, Quinlivan PA, Knappe DRU (2002) Effects of activated carbon surface chemistry and pore structure on the adsorption of organic contaminants from aqueous solution. *Carbon* 40:2085–2100
27. Qian Q, Sunohara S, Kato Y, Zaini MAA, Machida M, Tatsumoto H (2008) Water vapor adsorption onto activated carbons prepared from cattle manure compost (CMC). *Appl Surf Sci* 254:4868–4874
28. Shim JW, Park SJ, Ryu SK (2001) Effect of modification with HNO<sub>3</sub> and NaOH on metal adsorption by pitch-based activated carbon fibers. *Carbon* 39:1635–1642
29. Mohammed J, Nasri NS, Ahmad Zaini MA, Hamza UD, Ani FN (2015) Adsorption of benzene and toluene onto KOH activated coconut shell based carbon treated with NH<sub>3</sub>. *Int Biodeter Biodegr* 102:245–255
30. Pak SH, Jeon MJ, Jeon YW (2016) Study of sulfuric acid treatment of activated carbon used to enhance mixed VOC removal. *Int Biodeter Biodegr* 113:195–200
31. Krishnan GR, Radhika R, Jayalatha T, Jacob S, Rajeev RK, George B, Anjali BR (2017) Removal of perchlorate from drinking water using granular activated carbon modified by acidic functional group: adsorption kinetics and equilibrium studies. *Process Saf Environ Prot* 109:158–171
32. Truong N, Alejandro M, Jorge OG, Fanor M (2002) Oxygen adsorption on nitrogen containing carbon surface. *Fuel Chem Divis. Preprints* 47:424
33. Bian Y, Bian Z, Zhang J, Ding A, Liu S, Zheng L (2015) Adsorption of cadmium ions from aqueous solutions by activated carbon with oxygen-containing functional groups. *Chin J Chem Eng* 23:1705–1711
34. Shafeeyan MS, Daud WMAW, Houshmand A, Shamiri A (2010) A review on surface modification of activated carbon for carbon dioxide adsorption. *J Anal Appl Pyrolysis* 89:143–151
35. Inagaki M (2000) New carbons: control of structure & functions. Elsevier, pp 126–146
36. Derbyshier F et al (1995) Porosity in carbons. Porosity in carbons “characterization and applications”. In: Patrick JW. Edward Arnold, London, p 227
37. ACS (1996) Active carbon symposium on production & use of carbon based materials for environmental clean up. ACS, *Fuel Chem Div* 41(1)
38. Manocha S (2002) Activated carbons from waste biomass. Project report, UGC project
39. Manocha S et al (2002) Silver uptake by modified pitches. *Carbon Sci*
40. Rodriguez R (1995) Chemistry and physics of carbon. In: Thrower PA (ed), vol 21, p 1
41. Inagaki M, Sunahara M (1998) *Tanso* 183:146
42. Ding SY, Wang W (2013) Covalent organic frameworks (COFs): from design to applications. *Chem Soc Rev* 42:548–568
43. Yao C, Li G, Wang J, Xu Y, Chang L (1867) Template-free synthesis of porous carbon from triazine based polymers and their use in iodine adsorption and CO<sub>2</sub> capture. *Sci Rep* 2018:8. <https://doi.org/10.1038/s41598-018-20003-1>
44. Kuhn P, Forget AI, Hartmann J, Thomas A, Antonietti M (2009) Template-free tuning of nanopores in carbonaceous polymers through ionothermal synthesis. *Adv Mater* 21:897–901
45. Ren S et al (2012) Porous, fluorescent, covalent triazine-based frameworks via room-temperature and microwave-assisted synthesis. *Adv Mater* 24:2357–2361
46. Bhunia A, Vasylyeva V, Jania C (2013) From a supramolecular tetranitrile to a porous covalent triazine-based framework with high gas uptake capacities. *Chem Commun* 49:3961–3963
47. Palovits R, Antonietti M, Kuhn P, Thomas A, Schuth F (2009) Solid catalysts for the selective low-temperature oxidation of methane to methanol. *Angew Chem Int Ed* 48:6909–6912
48. Rose M (2014) Nanoporous polymers: bridging the gap between molecular and solid catalysts. *ChemCatChem* 6:1166–1182
49. Xu F, Wu D, Fu R, Wei B (2017) Design and preparation of porous carbons from conjugated polymer precursors. *Mater Today* 20:629–656. <https://doi.org/10.1016/j.mattod.2017.04.026>
50. Roeser J, Kailasam K, Thomas A (2012) Covalent triazine frameworks as heterogeneous catalysts for the synthesis of cyclic and linear carbonates from carbon dioxide and epoxides. *ChemSusChem* 5:1793–1799



51. Hao L et al (2015) Bottom-up construction of triazine-based frameworks as metal-free electrocatalysts for oxygen reduction reaction. *Adv Mater* 2015(27):3190–3195
52. Feng X, Liang Y, Zhi L, Thomas A, Wu D, Lieberwirth I, Kolb U, Müllen K (2009) Synthesis of microporous carbon nanofibers and nanotubes from conjugated polymer network and evaluation in electrochemical capacitor. *Adv Funct Mater* 19:2125–2129. <https://doi.org/10.1002/adfm.200900264>
53. Xiang Z, Cao D, Huang L, Shui J, Wang M, Dai L (2014) Nitrogen-doped holey graphitic carbon from 2D covalent organic polymers for oxygen reduction. *Adv Mater* 26:3315–3320. <https://doi.org/10.1002/adma.201306328>
54. Paraknowitsch JP, Thomas A, Schmidt J (2011) Microporous sulfur-doped carbon from thienyl-based polymer network precursors. *Chem Commun* 47:8283. <https://doi.org/10.1039/c1cc12272j>
55. Bhosale ME, Illathvalappil R, Kurungot S, Krishnamoorthy K (2016) Conjugated porous polymers as precursors for electrocatalysts and storage electrode materials. *Chem Commun* 52:316–318. <https://doi.org/10.1039/C5CC08148C>
56. Wang J, Senkovska I, Oschatz M, Lohe MR, Borchardt L, Heerwig A, Liu Q, Kaskel S (2013) Imine-linked polymer-derived nitrogen-doped microporous carbons with excellent CO<sub>2</sub> capture properties. *ACS Appl Mater Interfaces* 5:3160–3167. <https://doi.org/10.1021/am400059t>
57. Férey G (2008) Hybrid porous solids: past, present, future. *Chem Soc Rev* 37:191–214
58. Shao L, Sang Y, Huang J, Liu Y-N (2018) Triazine-based hyper-cross-linked polymers with inorganic-organic hybrid framework derived porous carbons for CO<sub>2</sub> capture. *Chem Eng J* 353:1–14. <https://doi.org/10.1016/J.CEJ.2018.07.108>
59. Liu X, Zhou L, Zhao Y, Bian L, Feng X, Pu Q (2013) Hollow, spherical nitrogen-rich porous carbon shells obtained from a porous organic framework for the supercapacitor. *ACS Appl Mater Interfaces* 5:10280–10287. <https://doi.org/10.1021/am403175q>
60. Kim G, Yang J, Nakashima N, Shiraki T (2017) Highly microporous nitrogen-doped carbon synthesized from azine-linked covalent organic framework and its supercapacitor function. *Chem A Eur J* 23:17504–17510. <https://doi.org/10.1002/chem.201702805>
61. Zhu X, Tian C, Chai S, Nelson K, Han KS, Hagaman EW, Veith GM, Mahurin SM, Liu H, Dai S (2013) New tricks for old molecules: development and application of porous N-doped, carbonaceous membranes for CO<sub>2</sub> separation. *Adv Mater* 25:4152–4158. <https://doi.org/10.1002/adma.201300793>
62. Zhu X, Chai S, Tian C, Fulvio PF, Han KS, Hagaman EW, Veith GM, Mahurin SM, Brown S, Liu H et al (2013) Synthesis of porous, nitrogen-doped adsorption/diffusion carbonaceous membranes for efficient CO<sub>2</sub> separation. *Macromol Rapid Commun* 34:452–459. <https://doi.org/10.1002/marc.201200793>
63. Zhu Y, Chen X, Liu J, Zhang J, Xu DY, Peng W, Li Y, Zhang G, Zhang F, Fan X (2018) Rational design of Fe/N/S-doped nanoporous carbon catalysts from covalent triazine frameworks for efficient oxygen reduction. *Chemsuschem* 11:2402–2409. <https://doi.org/10.1002/cssc.201800855>
64. Furukawa H, Cordova KE, O’Keeffe M, Yaghi OM (2013) The chemistry and applications of metal-organic frameworks. *Science* 341:1230444
65. Bhunia A et al (2015) High adsorptive properties of covalent triazine-based frameworks (CTFs) for surfactants from aqueous solution. *Chem Commun* 51:484–486
66. Ren H et al (2010) Targeted synthesis of a 3D porous aromatic framework for selective sorption of benzene. *Chem Commun* 46:291–293
67. Chandra V et al (2012) Highly selective CO<sub>2</sub> capture on N-doped carbon produced by chemical activation of polypyrrole functionalized graphene sheets. *Chem Commun* 48:735–737
68. Liu B, Shioyama H, Akita T, Xu Q (2008) Metal-organic framework as a template for porous carbon synthesis. *J Am Chem Soc* 130:5390–5391. <https://doi.org/10.1021/ja7106146>
69. Dang S, Zhu QL, Xu Q (2017) Nanomaterials derived from metal-organic frameworks. *Nat Rev Mater* 3:17075. <https://doi.org/10.1038/natrevmats.2017.75>

70. Kuhn P, Antonietti M, Thomas A (2008) Porous, covalent triazine-based frameworks prepared by ionothermal synthesis. *Angew Chem Int Ed* 47:3450–3453
71. Kuhn P, Forget AI, Su D, Thomas A, Antonietti M (2008) From microporous regular frameworks to mesoporous materials with ultrahigh surface area: dynamic reorganization of porous polymer networks. *J Am Chem Soc* 130:13333–13337
72. Lee J, Kim J, Hyeon T (2006) Recent progress in the synthesis of porous carbon materials. *Adv Mater* 18:2073–2094
73. Wang J, Wang Y, Yang Q, Hu H, Cai J (2020) From metal-organic frameworks to nanoporous carbons: recent progress and prospect from energy and environmental perspectives. *Nanoscale* 12. <https://doi.org/10.1039/C9NR09697C>
74. Sun JK, Xu Q (2014) Functional materials derived from open framework templates/precursors: synthesis and applications. *Energy Environ Sci* 7:2071–2100
75. Zhang L, Hu YH (2010) A systematic investigation of decomposition of nano  $Zn_4O(C_8H_4O_4)_3$  metal-organic framework. *J Phys Chem C* 114:2566–2572. <https://doi.org/10.1021/jp911043r>
76. Hu J, Wang H, Gao Q, Guo H (2010) Porous carbons prepared by using metal-organic framework as the precursor for supercapacitors. *Carbon NY* 48:3599–3606. <https://doi.org/10.1016/j.carbon.2010.06.008>
77. Jin SL, Deng HG, Zhan L, Qiao WM, Ling LC (2012) Synthesis of 3D hierarchical porous carbon as an electrode material for electric double layer capacitors. *Xinxing Tan Cailiao/New Carbon Mater* 27:87–92. [https://doi.org/10.1016/S1872-5805\(12\)60005-5](https://doi.org/10.1016/S1872-5805(12)60005-5)
78. Mo S, Sun Z, Huang X, Zou W, Chen J, Yuan D (2012) Synthesis, characterization and supercapacitive properties of hierarchical porous carbons. *Synth Met* 162:85–88. <https://doi.org/10.1016/j.synthmet.2011.11.015>
79. Yuan D, Chen J, Tan S, Xia N, Liu Y (2009) Worm-like mesoporous carbon synthesized from metal-organic coordination polymers for supercapacitors. *Electrochem Commun* 11:1191–1194. <https://doi.org/10.1016/j.elecom.2009.03.045>
80. Srinivas G, Krungleviciute V, Guo ZX, Yildirim T (2014) Exceptional  $CO_2$  capture in a hierarchically porous carbon with simultaneous high surface area and pore volume. *Energy Environ Sci* 7:335–342. <https://doi.org/10.1039/c3ee42918k>
81. Yang SJ, Kim T, Im JH, Kim YS, Lee K, Jung H, Park CR (2012) MOF-derived hierarchically porous carbon with exceptional porosity and hydrogen storage capacity. *Chem Mater* 24:464–470. <https://doi.org/10.1021/cm202554j>
82. Wang M, Xu X, Liu Y, Li Y, Lu T, Pan L (2016) From metal-organic frameworks to porous carbons: a promising strategy to prepare high-performance electrode materials for capacitive deionization. *Carbon NY* 108:433–439. <https://doi.org/10.1016/j.carbon.2016.07.047>
83. Ding M, Shi W, Guo L, Leong ZY, Baji A, Yang HY (2017) Bimetallic metal-organic framework derived porous carbon nanostructures for high performance membrane capacitive desalination. *J Mater Chem A* 5:6113–6121. <https://doi.org/10.1039/c7ta00339k>
84. Bai C, Li A, Yao X, Liu H, Li Y (2016) Efficient and selective aerobic oxidation of alcohols catalysed by MOF-derived co catalysts. In: *Green chemistry*, vol 18. The Royal Society of Chemistry, London, UK, pp 1061–1069
85. Pérez-Mayoral E, Matos I, Bernardo M, Fonseca IM (2019) New and advanced porous carbon materials in fine chemical synthesis. Emerging precursors of porous carbons. *Catalysts* 9(2):133. <https://doi.org/10.3390/catal9020133>
86. Stock N, Biswas S (2012) Synthesis of metal-organic frameworks (MOFs): routes to various MOF topologies, morphologies, and composites. *Chem Rev* 112:933–969
87. Pan Y, Zhao Y, Mu S, Wang Y, Jiang C, Liu Q, Fang Q, Xue M, Qiu S (2017) Cation exchanged MOF-derived nitrogen-doped porous carbons for  $CO_2$  capture and supercapacitor electrode materials. *J Mater Chem A* 5:9544–9552
88. Chen YZ, Wang C, Wu ZY, Xiong Y, Xu Q, Yu SH, Jiang HL (2015) From bimetallic metal-organic framework to porous carbon: high surface area and multicomponent active dopants for excellent electrocatalysis. *Adv Mater (Deerfield Beach, Fla.)* 27(34):5010–5016. <https://doi.org/10.1002/adma.201502315>

89. Chaemsanit S, Matan N, Matan N (2017) Activated carbon for food packaging application: review. *Walailak J Sci Technol (WJST)* 15(4):255–271. <https://doi.org/10.48048/wjst.2018.4185>
90. Zhao Y, Wang ZQ, Zhao X, Li W, Liu SX (2013) Antibacterial action of silver-doped activated carbon prepared by vacuum impregnation. *Appl Surf Sci* 266:67–72
91. Biswas P, Bandyopadhyaya R (2016) Water disinfection using silver nanoparticle impregnated activated carbon: *Escherichia coli* cell-killing in batch and continuous packed column operation over a long duration. *Water Res* 100:105–115
92. Altintig E, Arabaci G, Altundag H (2016) Preparation and characterization of the antibacterial efficiency of silver loaded activated carbon from corncobs. *Surf Coat Tech* 304:63–67
93. Altintig E, Kirkil S (2016) Preparation and properties of Ag-coated activated carbon nanocomposites produced from wild chestnut shell by  $ZnCl_2$  activation. *J Taiwan Inst Chem Eng* 63:180–188
94. Saravanan A, Kumar PS, Karthiga Devi G, Arumugam T (2016) Synthesis and characterization of metallic nanoparticles impregnated onto activated carbon using leaf extract of *Mukia maderasapatna*: evaluation of antimicrobial activities. *Microb Pathogenesis* 97:198–203
95. Silvestre-Albero A, Silvestre-Albero J, Sepúlveda-Escribano A, Rodríguez-Reinoso F (2009) Ethanol removal using activated carbon: effect of porous structure and surface chemistry. *Microporous Mesoporous Mater* 120:62–68
96. Uddin K, El-Sharkawy II, Miyazaki T, Saha BB, Koyama S, Kil HS, Yoon SH (2014) Adsorption characteristics of ethanol onto functional activated carbons with controlled oxygen content. *Appl Therm Eng* 72:211–218
97. Bouzid M, Sellaoui L, Khalfaoui M, Belmabrouk H, Lamine AB (2016) Adsorption of ethanol onto activated carbon: modeling and consequent interpretations based on statistical physics treatment. *Phys A* 444:853–869
98. Mocanu A, Rusen E, Diacon A, Isopencu G, Mustătea G, Şomoghi R, Dinescu A (2018) Antimicrobial properties of polysulfone membranes modified with carbon nanofibers and silver nanoparticles. *Mater Chem Phys* 223. <https://doi.org/10.1016/j.matchemphys.2018.10.002>
99. Deokar A, Lin L-Y, Chang C-C, Ling Y (2013) Single-walled carbon nanotube coated antibacterial paper: preparation and mechanistic study. *J Mater Chem B* 1:2639–2646. <https://doi.org/10.1039/C3TB20188K>
100. Chen H, Wang B, Gao D, Guan M, Zheng L, Ouyang H, Chai Z, Zhao Y, Feng W (2013) Broad-spectrum antibacterial activity of carbon nanotubes to human gut bacteria. *Small* 9(16):2735–2746. <https://doi.org/10.1002/sml.201202792>
101. Venkatesan J, Jayakumar R, Mohandas A, Bhatnagar I, Kim SK (2014) Antimicrobial activity of chitosan-carbon nanotube hydrogels. *Mater (Basel, Switzerland)* 7(5):3946–3955. <https://doi.org/10.3390/ma7053946>
102. Hippauf F, Lunow D, Huettner C, Nickel W, Borchardt L, Henle T, Kaskel S (2015) Enhancing ACE-inhibition of food protein hydrolysates by selective adsorption using porous carbon materials. *Carbon* 87:309–316. <https://doi.org/10.1016/j.carbon.2015.02.023>
103. Davari S, Rabbani M, Basti A, Koohi M (2021) Synthesis and characterization of a novel magnetic porous carbon coated with poly(p-phenylenediamine) and its application for furfural preconcentration and determination in baby food and dry milk powder samples. *RSC Adv* 11:22983–22992. <https://doi.org/10.1039/D1RA00444A>
104. Feng J, Feng J, Loussala HM, Han S, Ji X, Li C, Sun H, Sun M (2021) Dendritic mesoporous silica nanospheres@porous carbon for in-tube solid-phase microextraction to detect polycyclic aromatic hydrocarbons in tea beverages. *Food Chem* 364:130379
105. Li P, Huang D, Huang J, Tang J, Zhang P, Meng F (2020) Development of magnetic porous carbon nano-fibers for application as adsorbents in the enrichment of trace Sudan dyes in foodstuffs. *J Chromatogr A* 1625:461305. <https://doi.org/10.1016/j.chroma.2020.461305>
106. Jiang Y-W, Gao G, Jia H, Wu F-G (2017) Antimicrobial carbon nanospheres. *Nanoscale* 9. <https://doi.org/10.1039/C7NR04679K>

107. Sohn SH, Jang A, Kim JK, Song HP, Kim JH, Lee M (2009) Reduction of irradiation off-odor and lipid oxidation in ground beef by  $\alpha$ -tocopherol addition and the use of a charcoal pack. *Radiat Phys Chem* 78:141–146
108. Cao J, Li X, Wu K, Jiang W, Qu G (2015) Preparation of a novel PdCl<sub>2</sub>–CuSO<sub>4</sub>-based ethylene scavenger supported by acidified activated carbon powder and its effects on quality and ethylene metabolism of broccoli during shelf-life. *Postharvest Biol* 99:50–57
109. Bailén G, Guillén F, Castillo S, Serrano M, Valero D, Martínez-Romero D (2006) Use of activated carbon inside modified atmosphere packages to maintain tomato fruit quality during cold storage. *J Agr Food Chem* 54:2229–2235
110. Hsisheng T, To HC (1998) Influence of surface characteristics on liquid-phase adsorption of phenol by activated carbons prepared from bituminous coal. *Ind Eng Chem Res* 37:3618–3624
111. Huang M, Chou C, Teng H (2002) Pore-size effects on activated-carbon capacities for volatile organic compound adsorption. *AIChE J* 48:1804–1810
112. Dastgheib SA, Karanfil T (2004) Adsorption of oxygen by heat-treated granular and fibrous activated carbons. *J Colloid Interface Sci* 274:1–8
113. Lillo-Ródenas MA, Cazorla-Amorós D, Linares-Solano Á (2005) Behaviour of activated carbons with different pore size distributions and surface oxygen groups for benzene and toluene adsorption at low concentrations. *Carbon* 43:1758–1767
114. Phillips J, Xia B, Menéndez JA (1998) Calorimetric study of oxygen adsorption on activated carbon. *Thermochim Acta* 312:87–93
115. Aroua MK, Daud WMAW, Yin CY, Adinata D (2008) Adsorption capacities of carbon dioxide, oxygen, nitrogen and methane on carbon molecular basket derived from polyethyleneimine impregnation on microporous palm shell activated carbon. *Sep Purif Tech* 62:609–613
116. Matsis VM, Grigoropoulou HP (2008) Kinetics and equilibrium of dissolved oxygen adsorption on activated carbon. *Chem Eng Sci* 63:609–621
117. Zhou Y, Wei L, Yang J, Sun Y, Zhou L (2005) Adsorption of oxygen on superactivated carbon. *J Chem Eng Data* 50:1068–1072
118. Ivanov P, Llobet E, Vergara A, Stankova M, Vilanova X, Hubalek J, Gracia I, Can C, Correig X (2005) Towards a micro-system for monitoring ethylene in warehouses. *Sens Actuat B* 111–112:63–70
119. Bailén G, Guillén F, Castillo S, Zapata PJ, Serrano M, Valero D, Romero DM (2007) Use of a palladium catalyst to improve the capacity of activated carbon to absorb ethylene, and its effect on tomato ripening. *Span J Ag Res* 5:579–586
120. Yao X, Li L, Li H, He S, Liu Z, Ma W (2014) A new model for calculating the adsorption equilibrium constant of water vapor in micropores of activated carbon. *Comp Mater Sci* 89:137–141
121. Müller EA, Rull LF, Vega LF, Gubbins KE (1996) Adsorption of water on activated carbons: a molecular simulation study. *J Phys Chem C* 100:1189–1196

# Chapter 28

## Chitosan-Based Porous Carbon Materials for Agriculture and Agro-waste Applications



Srinivasan Latha, T. Gomathi, S. Pavithra, P. N. Sudha, Abhishek Nalluri,  
and Preetam Bhardwaj

### 1 Introduction

Modern agriculture must adapt to extreme weather patterns as well as rising food requirements [1–3]. Sustainable cropping is crucial in view of limited natural resources, particularly in agricultural productions, which are more subject to climate extremes and require more agricultural inputs [4, 5]. Farmers need to manage the agricultural lands and their produce and imbibe better technologies that will be environmentally sustainable. Better soil quality, farmers supported technically for money, and expertise to raise crops under optimal conditions become crucial for food security [6]. Biostimulants, for example, are manageable, effective innovative tools or supplement to artificial components (i.e., agrochemicals) for improving nutrient usage efficiency and yield stability of agricultural and horticulture crops in ideal and sub-optimal conditions [7, 8].

The ideal impacts of biostimulants incorporate the incitement of root development, expanded supplement take-up, and the formation of phytohormones, just as

---

S. Latha

Department of Chemistry, School of Advanced Sciences, Vellore Institute of Technology, Vellore, Tamil Nadu 632014, India

e-mail: [srinivasan.latha@vit.ac.in](mailto:srinivasan.latha@vit.ac.in)

T. Gomathi · S. Pavithra · P. N. Sudha (✉)

Biomaterials Research Lab, PG and Research Department of Chemistry, D.K.M. College for Women, Vellore, Tamil Nadu, India

e-mail: [drparsu8@gmail.com](mailto:drparsu8@gmail.com)

A. Nalluri

Department of Materials Science and Engineering, Huazhong University of Science and Technology, Wuhan 430074, China

P. Bhardwaj

School of Electronics Engineering, Vellore Institute of Technology, Vellore, Tamil Nadu 632014, India

© The Author(s), under exclusive license to Springer Nature Singapore Pte Ltd. 2023

763

A. N. Grace et al. (eds.), *Handbook of Porous Carbon Materials*,

Materials Horizons: From Nature to Nanomaterials,

[https://doi.org/10.1007/978-981-19-7188-4\\_28](https://doi.org/10.1007/978-981-19-7188-4_28)

osmotic rectification through the combination of natural osmolytes. Biostimulants can likewise be used to decrease the use of mineral inorganic manures, which is viewed as an ecologically harmless method with negligible effect on organic product quality and absolute creation [9, 10].

A few specialized forward leaps have been introduced over the most recent thirty years to work on the manageability of rural creation frameworks by essentially decreasing engineered agrochemicals like pesticides and composts.

Regular plant biostimulants are promising and harmless to the ecosystem advancement that lifts blossoming, plant development, natural product improvement, crop creation, and supplement usage productivity, just as further develop resilience to a wide scope of abiotic stressors. Plant biostimulants are named humic acids, fulvic corrosive, protein hydrolysates, ocean growth removes, *N*-containing compounds, botanicals, kelp extricates, chitosan, and other related biopolymers, supportive microscopic organisms and parasites, and inorganic compounds [11, 12].

Chitosan is one of the powerful biomaterials which can animate plant development and yield, just as further developing plant resistance. Chitosan is broadly viewed as a promising and financially savvy crop assurance arrangement, harmless to the ecosystem, biocompatible, and biodegradable polymer with a wide scope of applications [13, 14]. Moreover, chitosan animates cells as well as upgrades infection and bug obstruction in the field and during storage [15].

Chitosan has been shown to trigger plant safeguard systems by improving the optional digestion, protection quality (PR 155) enactments, and collections of isoflavonoid phytoalexin and pisatin [16]. Chitin and chitosan-treated plants produce chitinase, which separates the chitin and chitosan chains into a more dissolvable structure. Indeed, even without compound compost, chitosan used in farming can support microbial populaces and convert natural supplements into inorganic supplements that are effortlessly consumed by plant roots [17]. Plants treated with chitosan may likewise be less helpless to natural burdens like the dry season, saltiness, and temperature [18–20].

The chitosan polymer has been displayed to increment photosynthetic rates, bringing about expanded dietary admission and digestion, which further develops development and advancement. It additionally shows an expansion in the level of seeds that grow and sprout [21–24]. By decreasing breath and transpirational misfortunes, the chitosan polymer shapes a semi-permeable covering that expands the postharvest life of products of the soil. When used as a covering for agricultural things, the chitosan polymer has various benefits. It has exceptional qualities like non-toxicity, biodegradability, and antibacterial and cancer prevention agent capacities. It is harmless to the ecosystem and a safe strategy for controlling pathogenic organisms and creepy crawly bothers. Accordingly, chitosan has a wide scope of uses in farming, including crop creation and insurance, stockpiling, dietary quality, etc.

## 2 Chitosan—Sources and Properties

### 2.1 Sources of Chitin/Chitosan

Chitin ( $C_8H_{13}O_5N$ )<sub>n</sub>, approach from the Greek expression “chiton,” represents a mail coat. It was at first distinguished in 1811 by scientist Henry Braconnot. The fundamental wellspring of chitin/chitosan is shellfish shell, for example, crab and shrimp [25, 26], where *N*-acetyl-D-glucosamine units are overwhelming in the polymeric chain [27]. It is the second most normal kind of polymerized carbon in nature [28, 29]. Chitin is a whitish, inflexible, inelastic, nitrogenous polymer found in the exoskeleton and in the inside life systems of spineless creatures.

Chitin exists to a great extent in three polymeric shapes:  $\alpha$ ,  $\beta$ , and  $\gamma$ . The chains are put in  $\alpha$ -chitin stacks or sheets and in an equal arrangement the adjoining c-hub sheets take a similar heading. The alpha chitin happens in scavenger exoskeletons. In the instance of  $\beta$ -chitin, adjoining sheets along the c-hub are masterminded against one another and can be found in squid pen, certain diatoms, and vestimentary creatures.  $\beta$ -chitin is available in restricting orientations [30]. Every third sheet, notwithstanding, is the other way to the past  $\gamma$ -chitin sheets. The parasite and yeast are essentially found [31].

Chitosan is a hetero-polysaccharide derived from chitin. Generally, the molecular weight of chitosan is in between 300 and 1000 k darenly upon its chitin source. Chitosan is economically possible from the crab shells produced as waste from the food sector, particularly where carotenoids are recovered. Chitin can be converted into chitosan in two methods: (1) Chemical method and (2) Biological method.

### 2.2 Physicochemical Properties

Chitin's usefulness is limited by its acetyl groups; however, it may be converted into chitosan via the deacetylation procedure. During deacetylation, the acetyl group in chitin is transformed into hydroxyl ( $-OH$ ) and amino ( $-NH$ ) groups in chitosan. By altering the reactive functional groups of chitosan, it can be used in a larger range of industries [32]. Chitosan's versatility is owing to its active amino groups, which operate as a reactive site for a range of novel group attachments under mild reaction circumstances, as well as the cationic character of chitosan materials, which is furthermore related to the amino groups in addition to so referred to as amino polysaccharide.

### 2.2.1 Color and Appearance

The nitrogenous polysaccharide chitin is monotonous to partially white and inflexible, while chitosan fine particles are moderately flaccid in nature and its color fluctuates from pastel yellow to white [33].

### 2.2.2 Molecular Weight

Chitosan's functions rely upon biological, physical, and elemental characteristics, and chitosan relies upon two factors, such as degree of deacetylation (DD) and Molecular weight [34, 35]. Chitosan is a fragile base with a pKa value of 6.5DD, and Mw of chitosan are significantly exaggerated by reaction surroundings like high temperature, reagents concentration, and reiteration of alkaline steps, time, and atmospheric surroundings of the deacetylation [36, 37]. The 500 kDa is average Mw of chitosan through 100% of DDA. The DDA enhances quickly to about 68% through the initial hour of alkali healing (50% NaOH) at 100 °C and in addition gradually augmented with time [38]. On the basis of Mw, chitosan is categorized into three diverse categories, specifically low-molecular-weight chitosan (LMWC; <50 kDa), medium-molecular-weight chitosan (MMWC; 50–250 kDa), and high-molecular-weight chitosan (HMWC) (>250 kDa) [39].

Mw is calculated using a variety of methods, including light dispersion, gel penetration chromatography (GPC), and capillary viscometry. The most basic and extensively used technique for determining the Molecular weight of chitosan is capillary viscometry.

### 2.2.3 Solubility

Chitin is a monochrome, crystalline, or nebulous fine particles that are indecipherable in aqueous and organic solvents as well as in weakened acids, and alkalis. It liquefies in strong mineral acids with instantaneous deprivation of the polymer [40]. Though chitosan is unsolvable in water, it does liquefy in aqueous organic acids, such as acetic and formic acids, in addition to inorganic acids.

In an acidic arrangement, the polymer's amino gatherings are protonated, yielding a dissolvable polysaccharide with a positive charge. Due to the various cationic locales made by acids protonating amino gatherings along the chitosan chain, its dissolvability is expanded by raising both the extremity and the level of electrostatic aversion [41]. Chitosan's solubilization is a huge quality for its numerous applications. The amino gatherings are answerable for various basic compound modifications in chitosan, which makes it a decent contender for an assortment of uses [42–44].



### 2.2.4 Viscosity

The level of polymer deacetylation, sub-atomic weight, fixation, ionic strength, pH, and temperature all affect the thickness of chitosan in arrangement. The consistency of a polymer arrangement diminishes as the temperature ascends overall. A pH adjustment in the polymer arrangement, nonetheless, may create various outcomes relying upon the kind of acids utilized. When utilizing in acidic or corrosive medium, generally chitosan viscosity will rise as pH diminishes, but when utilizing in HCl, viscosity will reduce as the pH diminishes.

Chitosan's intrinsic viscosity is a function of both ion strength and degree of ionization [45]. The intrinsic viscosity of the polymer solution would be reduced if chitosan ionization or ion strength was increased. According to their findings, chitosan acts like a non-draining worm-like molecule in dilute solution, with its molecular shape determined by electrostatic interactions between polyanion-counterions.

### 2.2.5 Degree of Deacetylation

The scale of deacetylation (DA) is described as the mole division of deacetylated component in the polymorph sequence, which has a considerable impact on the compound behavior of chitin and chitosan. The amount of deacetylation refers to the elimination of the acetyl group from the sequence and this is designed as potentiometric titration using the formula  $DD \text{ percent} = 100 - DA \text{ percent}$ , where DA stands for degree of acetylation [46]. The DDs in chitin typically vary from 5 to 15%. The low solubility of chitin in common solvents leads to higher degree of DA [33]. In nature, chitin is crystalline, and the degree of crystalline is a function of the DD [47]. Chitosan's elemental, physical, and biological characteristics, for example, adsorbent, covalent linking, and encapsulation, are all affected by DD [48].

Furthermore, due to the statistical distribution of the residues, our re-acetylated structures presented us with a wide range of DAs soluble in water, ranging from 0 to over 70%. Chitosan is an amphiphilic cationic polyelectrolyte in water-based solution. The properties of the material are then resolved through the balance of hydrophilic and hydrophobic interactions.

## 2.3 *Biocompatibility and Biodegradability*

The degree or power of unsafe consequences for living being communications is alluded to as biocompatibility [23]. Chitosan has prevalent biocompatibility with vertebrates, including human beings. In acidic to nonpartisan arrangements beneath its pKa (6.3), the amino gathering in its design goes through protonation, causing chitosan to become dissolvable and fill in as a bioadhesive, contingent upon the pH of the arrangement, its atomic weight, and level of acetylation.

Chitosan is environmentally friendly, and it is biodegradable depending on the degree of deacetylation.

According to the United States Environmental Protection Agency [49], chitosan utilization will most probably have no negative impact on the surroundings. According to Yogesh Kumar and his research colleagues, the elevated deacetylated chitosan polymers deteriorate at a slow speed [22]. Furthermore, it has been found that it can be deteriorated via microorganisms, fungi, flora, and humans, in addition to a variety of redox reactions and antioxidant reactions.

## **2.4 Antimicrobial Activity**

Chitosan has a wide range of antimicrobial activity and a higher kill rate and is less hazardous to human tissues [50]. Chitosan has been shown to have significant antibacterial action in numerous tests. However, the precise mechanism of inhibition is still unknown. The most reasonable explanation is that associations between the positively charged polysaccharide (chitosan at pH under 6.5) and the negatively charged layer cause a change in cell penetrability. The positively charged polymer on the tissue surface responds with anionic parts, for example, neuraminic acid, *N*-acetylmuramic acid, and sialic acid, resulting in bacterial growth suppression [51].

## **2.5 Antioxidant Activity**

Chitins and chitosans have a powerful biological antioxidant effect with applications in a broad variety of field. They are, however, insoluble in water, which is a limiting issue in their use in biological systems. As a result, hydrolysis of soluble chitin or chitosan derivatives is critical. To address this limitation, live cells were tested using *N*-acetyl chitoooligosaccharides of various MWs generated from crab chitin hydrolysis [52]. The oxidation of DNA and proteins was inhibited by two types of NA-COSs with MWs of 1–3 and 1 kDa.

Furthermore, their occurrence boosted intracellular glutathione levels and radical scavenging ability in mouse macrophages (RAW 264.7), which had an inhibitory influence on cellular oxidative stress. COS has also been shown to protect human embryonic hepatocytes (L02 cells) against hydrogen peroxide-induced oxidative damage [53]. Low-MW chitosans were found to limit neutrophil activation and serum albumin oxidation, both of which are frequent in hemodialysis patients, resulting in a reduction in oxidative stress associated with uremia [54].

### 3 Chitosan-Based Carbon Composites—Synthesis and Characteristics

#### 3.1 Modification of Chitosan

In chitosan, we found five functional groups such as  $C_3$ -OH,  $C_6$ -OH,  $C_2$ -NH<sub>2</sub>, and acetylamino and glycoside linkages [55]. The glycosidic bonding and acetylamino linking are equally strong, which is difficult in breaking. The vigorous chemical characteristics of  $C_2$ -NH<sub>2</sub> and  $C_6$ -OH allow additional groups to be introduced into chitosan molecules through various types of molecular design. Chitosan can be chemically modified to increase its physical and chemical characteristics, as well as to broaden its uses and study domains [56–58]. A schematic diagram of modification of chitosan is shown in Fig. 1.

Over the precedent two decades, the significance of chitosan has augmented, as it emerges to be an outstanding resolution for numerous confront facade by the business manufacturing across the world. A number of technique have been illustrated to command in fabrication of chitosan compound, and the major process of manufacturing comprises suspension inter-linking, electro-spinning, freeze drying, LBL,

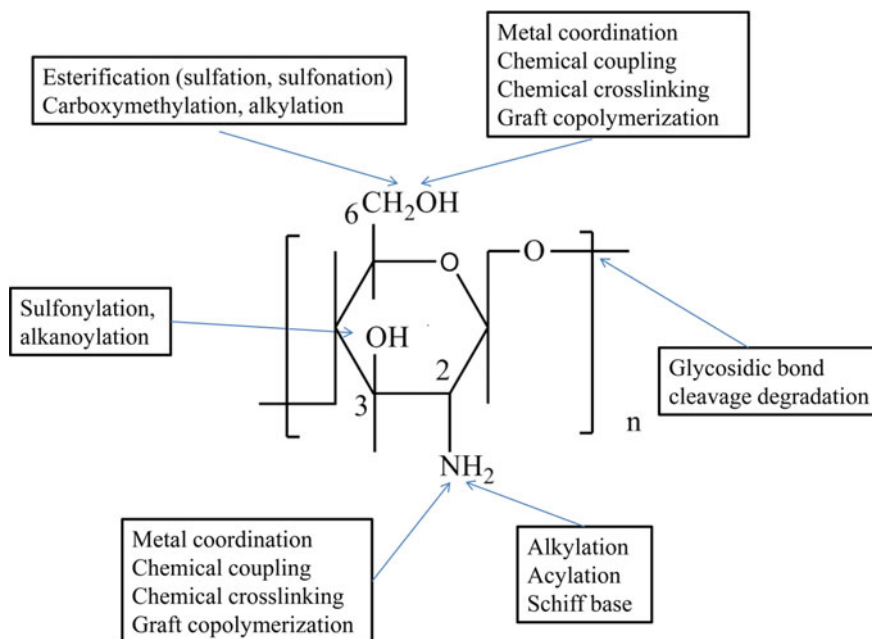


Fig. 1 Reactive functional groups of chitosan involving in chemical reaction [59]

molecular self-assembly, coacervation/precipitation, reverse micelles, template polymerization emulsion-droplet coalescence, and ionotropic gelation [60]. The preparation of any of the techniques relies on elements, for example, molecule size prerequisite, thermal and chemical constancy of the vigorous agent, replica ability of the kinetic delivery, security of the concluding item, and lingering harmfulness correlated with the concluding item.

### Emulsion Interconnection

Emulsion interconnection technique is frequently being used to yield both chitosan nano- along with micro-sized particles [61]. The emulsion cross-linking strategy uses the responsive practical gatherings of chitosan to interconnect with a cross-linking agent. The researcher [60] found a technique which employs the progress of a water-in-oil mixture by emulsifying chitosan liquid in an oily phase. An appropriate surfactant is used to stabilize the aqueous droplets. To stabilize the polysaccharide droplets, the emulsion is subsequently treated with a suitable interconnection mediator, for example, glutaraldehyde. Lastly, the particles are being washed out and dehydrated. Reference [62] Explained about the hardening agent utilized and the rate at which the mixture is stirred throughout the formation of the emulsion determines the elemental dimensions of the final product [63]. Researchers prepared the palygorskite-chitosan resins along with tannic acid (TA) as template molecules (CPRT) that were being prepared by emulsifying interconnection technique. Here, they used one type of organic one-dimensional clay, functioned as perfect part in this study to develop the property of adsorption and resistance of chitosan resin (CR).

### Electrospinning

Researchers have prepared chitosan-Zein compound in which fibrous films have been fabricated from ethanol solution by electro-spinning [64]. Composites based on chitosan, Chitin nano-scaled fibrils, and Poly(ethylene oxide) were prepared by electro-spinning[65]. Here, compound of chitosan fibers comprises 20 wt% chitin nano-scaled fibrils and 10 wt% of PEO are acquired through the electro-spinning technique. Incorporation of 0.5–25.0 wt% chitin fibrils into chitosan emulsion with proportions of 3–7.5 wt% in ethanoic acid with 75 vol.% leads to irrelevantly raise the electronic conduction, surface tension coefficient, and consistency of these mixed suspensions.

Solomon Mengistu introduces fabrication of refined and firm chitosan fibers through electro-spinning process [66]. Here, the electro spun was executed to acquire chitosan fibers from mixture of chitosan and poly(ethylene oxide). Blend of chitosan and PEO consists of 102 kg/mol of chitosan, and PEO ratio is 1000 kg/mol that was vigilantly selected to upgrade the electro-spinning procedure factors. The poly(ethylene oxide)fine particles were mixed into chitosan emulsion at various weight proportion in 0.5 M ethanoic acid.

### Freeze drying method

The blending of electronic spraying and following freeze aeration can attain chitosan fibrous 3D complex configuration from small proportion of chitosan solutions, well fiber making by different proportions. A regulated electronic praying procedure

was used to create chitosan nanoparticle suspensions, which were subsequently lyophilized to form fibrous matrix. The creation of a columnar ice stage followed by aeration resulted in chitosan fiber configuration with a radius of some microns. X-ray diffraction outcomes and fiber surface morphology designate a distinctive system of biaxial density of fiber formation [67]. This study used a freezing-lyophilization drying process to successfully manufacture novel porous chitosan microspheres, which were then used as adsorbents to remove a hazardous metallic iron, hexa-valent chromium (Cr(VI)) reported [68].

### Molecular Self-Assembly

Extensive research conducted in the agriculture, food packaging industry, and medicinal industries has focused on molecular self-assembly to generate nano-scaled structure substances, as it is considered an effective method for creating such materials [69]. As this technique is low cost, flexible, and simplistic, it unseals a route for various functions. Diffusion is followed by specialized connection of atoms by non-covalent interfaces, such as electrostatic as well as aquaphobic corporations, in the self-build procedure, which is described as the independent arrangement of elements into composition that has distinct collections. After association with a liquid environment, aquaphilic polymers instinctively form self-assembled nano-scaled particles, via intra- or intermolecular relations among the aqua phobic entities, principally to diminish the coupling free energy system. The innovative self-build chitosan and two-dimensional material composite hydrogels were efficiently fabricated by the addition of reduced graphene oxide, carbon nanotubes, and double-layered hydrotalcium converted into chitosan hydrogel with Glutaric acid dialdehyde as a cross-linking mediator [70]. The assemblage and structural dimensions of the achieved hydrogels composite were characterized by Brunauer–Emmett–Teller method, scanning electron microscope, and X-ray diffraction (XRD).

### Layer by Layer Technique (LBL)

A novel recyclable composite was attained from layer-by-layer (LBL) method by exceptionally deacetylated chitosan and cellulose nano-scaled whiskers obtained from eucalyptus timber. The layer development was pursued by UV–Visible spectroscopy during the utmost intensity of the absorption band at 195 nm and demonstrates the impeachment of  $14.5 \text{ mgm}^{-2}$  of chitosan biopolymer in every sequence. SEM graphs disclosed immense bulkiness and consistent transmission of cellulose nano-scaled whiskers that were adsorbed on every chitosan layer. Intersectional description of the composed layers expresses an average diameter of  $\sim 7 \text{ nm}$  as per reported research work [71]. Two different materials have been arranged by two different methodologies, and mixing and LBL electrostatic coatings were utilized to merge two biodegradable polymers that are gelatin and chitosan, in palatable layers or covering [72]. The enforcement of the combined and layer-by-layer complex layers along with mono-integrant gelatin and chitosan films was equated in aspects of physical, ocular, and spectroscopic characteristics. The established outcomes recommended that the LBL phrasing illustrated superior performance in

preservation of fruit quality and also slightly condensed fruit mass loss, whereas the unified formulation did not affect these factors.

## 4 Applications in Agricultural

### 4.1 Crop Production and Protection

#### 4.1.1 Crop Production

The growing requirement of food to nourish the earth growing community has led to the progress of agronomic procedures that can boost plant yield dramatically. In recent days, customers demand for more organic, harmless food, with great quality and a persistent shelf life, and without any chemical preservatives and cost-effect fertilizers [73]. Be that as it may, this has prompted an always expanding utilization of synthetic manures and pesticides and high soil utilization. To make an end to this pernicious pattern, numerous analysts explored farming uses of chitosan-dependent materials, and in a few circumstances, these materials came about ready to expand plant yield, as elucidated in Table 1. Additionally, a positive effect of chitosan has been observed as it can encapsulate it by itself and in grouping with other materials in the manufacture of slow-release fertilizers, owing to its cationic nature, biodegradability, non-toxicity, adsorption properties, and development of roots, shoots, and leaves of various plants including gerbera [74, 75].

For example, correlation of corn plants conferred with free S-nitroso-mercaptosuccinic (MSA) was found corrosive under saline conditions as compared with the plants conferred with chitosan nano-scaled particles enclosed with S-nitroso-MSA at 50–100  $\mu\text{M}$  fixation. It reveals that the dealing with S-nitroso-MSA-chitosan nano-scaled particles at the two different proportions was prevailing in alleviating the evident impressions of salt pressure in the plants contrasted with free S-nitroso-MSA. This experiment demonstrated that results are more feasible at 100  $\mu\text{M}$  fixation. Controller plants were dealt with just with refined water or salt with no handling [82]. Ram Chandra Choudhary and his co-workers reported that by Zinc-encapsulated chitosan nanoparticle to promote corn crop yield. Here, researcher synthesized Zn-chitosan nanoparticles (NPs). Zn-chitosan NPs (0.01–0.16%) displayed solid in vitro antifungal and sapling development promoted exercises. Further, Zn-chitosan NPs displayed critical infectious prevention through reinforcing of plant intrinsic invulnerability by lifting prevention agent antioxidant and guard compounds, adjusting of responsive oxygen species (ROS), and improving lignin amassing [83]. Nano chitosan-NPK fertilizer has been discovered by Heba M. M. Abdel-Aziz and his co-workers to develop the growth or production of wheat plants. Assessment of the outcomes uncovered that the life expectancy of the control and typical NPK-treated wheat plants developed on sandy soil arriving at gathering stage after 170 days from the date of planting. Then again, wheat plants developed on sandy soil and prepared

**Table 1** Chitosan effects on plant development and production

Plant varieties	Chitosan preparation and observation	Chitosan outcome	References
Rice	0.05% (plants drenching and spraying)	Expansion in plant development, higher photosynthesis rate	[76]
Maize	0.045–0.15% (seeds drenching and plant spray)	Encouragement of plant development furthermore, granule mass	[77]
Chilli	Nano-scaled chitosan, 115 kDa, 85–95%, pH 4.5	Boost in whole root and leaves weight up to 75 and 27%, correspondingly upon use of 1.1 mg/L of nano-scaled chitosan	[78]
Wheat	Chitosan-Zn nanoparticles, 60 kDa, 85%	Stomatal positioning of nano-scaled particles was witnessed. Improvement in grain zinc concentration up to 43%	[79]
Flowers, corms	Chitosan with different molecular weights	Plant development flowering and corms productivity of potted freesia	[80]
Tomato and egg	Olingo-chitosan	High yield of vegetables	[81]

with chitosan-NPK nano-fertilizers arrived at the reaping stage following 130 days from the date of planting [84].

Combination of Zinc and Copper ions along with nano chitosan has extra benefits of giving nourishment for plants and helping in their growth development of plant for additional assurance from abiotic and biotic stress. Cu/Zn-chitosan nanoparticles have been effectively tried against many plant pathogenic microbes and parasites by R. C. Choudhary and his co-researchers [85]. The enhancement of onion crop growth by chitosan and nano chitosan treatment on plants for productivity and quality has been developed by Gerjes and his co-workers. Observed results showed that the greatest upsides of development qualities (plant tallness, No. of leaves/plant, dry load of plant, explicit leaf region, leaf region list, and harvest development rate), attractive, and all out yields were gotten by soaking seedling with Nano chitosan at the pace of 75 ppm, while the base qualities were recorded under drenching with water (control), in both seasons. Showering with Nano chitosan at the pace of 50 ppm came about the most elevated upsides of all development characters, attractive and complete yields, and bulb quality boundaries (bulb width, TSS%, and DM %) as contrasted and the other showering medicines or then again, the control. From the investigation, based on the onion efficiency and the financial examination of the outcomes, it is clear the promising part of Nano chitosan as a guide to expand the productivity of conventional manures and increment the net return per took care of [86].

A pot experiment was carried out to see how different chitosan treatment methods affected tomato growth, yield, and quality by M. A. Parvin and her co-workers. The test was spread out in totally randomized plan (CRD) with four replication processes and twelve treatment blends. The investigation results reported that there were huge varieties among the treatments on number of leaves, number of blossom groups, natural product length, and production of tomato. The best return of tomato was acquired from the treatment T6 (combination of Soil application of chitosan (SAC) @80 ppm and Foliar spraying of chitosan (FSC) @60 ppm), while the most minimal was gotten from regulated treatment. Nutrient C and lycopene substance of tomato natural products differed from 2.19 to 4.09 and 2.38 to 3.58 mg 100 g<sup>-1</sup> test, individually [87].

#### 4.1.2 Crop Protection

Plant pathogens are widely regarded as economically important agricultural microbes all over the world. During the growth season, they cause deterioration in a wide range of agricultural crops and postharvest. Chitosan and chitin are natural existing compounds that have the prospective to administer plant infections in farming applications. These compounds have been discovered as non-toxic and helpful in stopping fungi expansion and growth [88]. They were accounted as vigorous compounds against infections, microscopic organisms, and other plant infections. They are employed as biocides against plant infection and manage the plant bacteria and fungi, pests and insects, plant development support, and seed coating, either alone or in combination with other products, and postharvest [89]. Chitosan has resilient outcome on farming, for example, performing as the carbon resource for microorganisms in the soil. It hastens the conversion procedure of organic material into inorganic material. Moreover, it contributes to the root structure of flora to take up additional nutritional elements from the soil.

#### 4.1.3 Antipathogen Activities of Chitosan

In pear natural plant, treatments with chitosan diminished the illness frequency and repressed the sore extension triggered by fugal microorganisms [90]. Chitosan prevented *Botrytis cinerea* development in aqueous medium and decreased gray mold infection and bunch spoil in Chardonnay and Sauvignon blanc wine grapes originated by the fungi on isolated grapevine foliage [91]. Cowpea (*Vigna unguiculata* L.) plants were protected through chitosan against *Fusarium oxysporum* disease [92]. In plants, chitosan produces several protective reactions correlated to organic and inorganic stresses. Amid of changing atmospheric circumstances and growing food requirement cause an untenable practice of artificial chemicals. The utilization of chitosan acts as an evoker that has an advanced potential for addressing stress adaptation concerns caused by abiotic and biotic pressures.



Chitosan as well as Chitin can defend plants in opposition to inorganic stress with diverse technology with reverence to divergent stresses. For example, their foliar functions bring dehydration tolerance by direct anti-transparent covering, initiation of stomatal closing, and accumulation of stress defensive enzymes and metabolites [93]. Foliar utilization of chitosan improves enlargement and adjusts appearance of protective genes in chilli pepper (*Capsicum annuum* L.), thus diminishing the rigorous losses in chilli productivity that induced by *Phytophthora capsici* disease [94].

Asgar Ali and his co-workers have developed lemongrass oil-chitosan composite and examined as possible preservative for polysaccharide-supported coverings. In this research work, the efficiency of merging of chitosan with lemongrass oil as an edible covering for bell pepper was observed. Lemongrass oil at two proportions of 0.5 and 1.0% was integrated with same ratio of chitosan solution. It was estimated that by controlling anthracnose of bell pepper in vitro and in vivo fungal growth was efficiently regulated through 0.5 and 1.0% chitosan solution. The utilization of 1.0% chitosan solution was established as an efficient proportion, and that was utilized in succeeding in vivo examination as a supported coating for preserving the protection and eminence of fresh bell peppers reserved at room temperature for 20 days [95].

Mixture of chitosan with other compounds such as alginate, starch, and gum is a suitable process to enhance its properties for premeditated discharge of pesticides. The utilization of chitosan compounds can be useful in protection of plants from 60 types of contaminations. He Liu and co-authors reported antifungal characteristics and performance of three types of chitosan in opposition to the growth of rice sheath blight infectious pathogen, called *Rhizoctonia solani*. The obtained outcomes demonstrate all chitosan types had resistance nature and have antifungal action against *R. solani* and defend rice seeds from fungal infection. By using a specific approach, two kinds of acidic soluble chitosan perform a 65–90% restrain in mycelial development, 30–85% discretion in infection occurrence, and 65–90% reduction in lesion span [96]. In a former study, chitosan inhibits the development of a broad variety of bacteria. The insignificant progressions reduce the proportions of different species that vary from 10 to 10<sup>3</sup> ppm. Chitosan-based quaternary ammonia salt, for example, *N*-propyl-*N,N*-dimethylchitosan and *N,N,N*-trimethylchitosan, was demonstrated to be an existent compound that successfully obstructed the development and progress of *Escherichia coli* [97].

## 4.2 Chitosan Seed Treatment and Micronutrients

Numerous outcomes have been given evidence for chitosan utilization in plant life. Predominantly, it can be utilizing for plant protection methods for decreasing the effect of biotic and ecological stress situations and it acts as a plant development supporter. It is also useful to escalate the stomatal conduction and decrease exhaling of water vapors or it can be useful as a covering material in seedlings. Now, chitosan is being utilized as a seedlings coat substance for fruits, nuts, cereals, and vegetables.

It varies penetrability of the seedling's plasma membrane, raising the proportions of proline and sugars; in addition to this, it improves catalase (CAT), phenylalanine ammonia-lyase (PAL), peroxidase (POD), and tyrosine ammonia lyase (TAL) actions. Chitosan was also able to regulate the seed-borne contamination of *F. graminearum* and also promote the crop productivity by 25%. Subsequently, wheat, peas, and lentil seedlings kept dealing up to 5 years of testing, plant productivity improved by 25–35%, and it also suggested the possible utilization of chitosan in postharvest conservation of vegetables and fruits [98].

Chitosan prescription of 2.5–8.5 mg/mL with wheat seedlings considerably enhanced seed sprouting that meets the seed accreditation standards that is >85%. This also provides vigor at proportions up to >4 mg/mL in two cultivars of spring wheat that are Norseman and Max by domineering seed-borne contamination by *F. graminearum*. The seed sprouting was found 85.5% in chitosan-cured seeds. The diminution of seed-borne infection was found > 50% by *F. Graminearum* and this can be improved by prominent chitosan curing that is correlated to regulating the infections [99]. Seed curing with chitosan symbiosis plant development encourageability of *Pseudomonas aeruginosa*-P17 in sorghum (*Sorghumbicolor* L.) that has been revealed by Praveen Kumar and his team [100]. Sprouting rates of seedlings enhance appreciably and seedling's growth is faster, enhanced, and vital. Seeds drenched with chitosan had improved the power of sprouting, sprouting proportion, lipase action, and gibberellic acid (GA3) and indole acetic acid (IAA) intensity in peanut. Seed priming in maize increases chilling tolerance. Blend with chitosan condensed the comparative penetrability of the plasma crust of the maize beneath lower heat conditions that cause less damage from low-temperature stress [101].

In north-eastern China, soybean seeds are attacked by a variety of pests, resulting in a lower yield. Until recently, pesticides such as insecticides were used to fulfill the purpose of pest control. Chitosan, a seed-coating compound fabricated from chitin deacetylation, which is a viable contender for controlling agrotis epsilon, soybean shell borer, and soybean aphid efficiently. An investigation of all earning of effects of different concentrations of chitosan on pest regulation and soybean productivity has been conducted in the research. Chitosan-based coatings were utilized as a feeding deterrent as well as to improve the germination and quality of soybean seedlings. In addition, seed sprouting, plant development, and soybean productivity were all improved by chitosan coating [102].

Lisbel Martínez González and his teammates studied the effect of chitosan on rice seedlings (*Oryza sativa* L.) has been developed in saline medium [103]. Here, the researcher conducted grain (*Oryza sativa* L.) seedlings type that is INCA LP-5 were cured for 24 h with different proportions of chitosan that are 0 to 500 mg L<sup>-1</sup>. The sprouted rice seedlings were placed in containers with an adulterate Hoagland nutritive solution, which were complemented with or without NaCl concentration of 100 mmol L<sup>-1</sup>, and seeds were positioned in a development cavity with regulated conditions. The progress and biochemical pointers were calculated after eleven days under stressful circumstances. Seedlings preserved with concentration of 100 mg L<sup>-1</sup> of chitosan that rouse shoot area and dried out substance in salty medium and also help in growing up saplings. It also lessens the malondialdehyde and augmented proline

intensity. Both chitosan doses increased catalase and peroxidase enzyme activity, despite the fact that a better impact becomes acquired with chitosan concentration of  $500 \text{ mg L}^{-1}$ .

Recently, in an experiment the effects of oligochitosan foliar spraying as well as oligochitosan nano-scale silica spray on the soybean seedling's productivity have been studied. Results indicated that soybean seed production was enhanced by 10–17% for oligochitosan and oligochitosan nano-scale silica spray, respectively. In this effort, oligochitosan contains an average molecular weight of  $5000 \text{ g/mol}$  that was prepared by degradation through Co-60 gamma radiations containing a 4% chitosan solution that also comprises 0.5%  $\text{H}_2\text{O}_2$  at 21 kGy. The nano-scaled silica with a size of 15–30 nm was manufactured by calcining the acidic cured rice husks at  $700^\circ\text{C}$  for 2 h. The mixture of 2.5% oligochitosan and 2.5% nano-scaled silica was synthesized by dispersing nano-scaled silica in the blend of oligochitosan and that was taken for production of soybean with enhanced seed yield [104].

The researchers evaluated the outcomes of seed priming with  $\text{GA}_3$ -containing chitosan-alginate and tripolyphosphate chitosan on the development and production of *Solanum lycopersicum* grown in the farmland. The consequence revealed that nano-carrier technology can develop great fruit yield, with the improved production by almost 5 times by utilizing  $\text{GA}_3$ -containing chitosan-alginate [105].

#### 4.2.1 Micronutrients

It is common knowledge that having enough fertilizer and irrigation, also micronutrients such as Manganese, Copper, Molybdenum, Iron, and Zinc, encourage premier development. As a result, every increase in plant output necessitates an enhanced utilization of growth-promoting micronutrients and irrigation sources. At the existing time, it is approximated that the aimed plants cannot soak up 85–95% of phosphorus, 45–75% of nitrogen, and 55–75% of potassium confined in compost. This reservoir waste is simply a money loss, but it also contaminates the environment [106].

Ngoc Minh Chau Ha and his co-workers developed KPN nano-fertilizer by filling potassium (K), phosphorous (P), and nitrogen (N) into chitosan particles. The chitosan particles were arranged through ionic gelatine of tripolyphosphate and chitosan blend. The outcomes disclosed that the nano-fertilizer boosted the acceptance of nutritious elements, photosynthesis, and development of vegetation of coffee. Utilization of the nano-fertilizer upgraded by 67% potassium, 16% phosphorous, and 17% nitrogen concentration in the leaves of cured plots correlated to the regulated; total chlorophyll concentration prominent up to 30 and 71% of photosynthesis net rate [107].

Ashwin Dapkekar and his co-researchers improvised the complex of Zinc with chitosan-TPP nano-scale particles (Zn-CNP, which have  $\sim 40 \text{ mg/L}$  of zinc) and considered its utilization in biofortification, in the durum variety of wheat. In pot experiments, they noticed 28 and 41% zinc enhancement in two genotypes of the grain [108].

Ram Chandra Choudhary and his co-workers found copper-chitosan nanoboost for maize growth. Here, Cu-chitosan nanoparticles cured plants illustrated considerable defensive reaction through the elevated actions of antioxidant (superoxide dismutase and peroxidase) and defensive enzymes (phenylalanine ammonia-lyase and polyphenol oxidase). Considerable regulation of CLS infection of maize has been observed at 0.05–0.17% of Cu-chitosan nano-scale particles cured in jar and 0.13–0.17% of NPs cured in farmland environment. NPs cured revealed development enhancer effect in provisions of plant tallness, stem width, root depthness, root quantity, and chlorophyll concentration in jar experiments [109].

Crop destruction primarily occurs due to natural causes, which consist of soil-borne phyto-pathogens, pest vermin, host-dependent organisms, and carnivore. Food rotting by different microorganisms accounts for the majority of food losses in the food sector. The usage of nanoparticles in food and agriculture can be improved because of advances in nanotechnology. So metal encapsulated chitosan composites have been used for many plant growths.

Copper-chitosan nanoparticles have been combined and utilized to investigate its effectiveness on Ragi plant (finger millet plant) as a standard plant system. The prime objective was to investigate the efficiency of CuChNputilizatin to regulate the slight ailment of Ragi. Copper-Chitosan particles were assessed to Ragi either in the form of foliar sprayer or as combined application. Here both treatment methods improved the figure millet plant's development profile and production. In the collective utilization technique, the enhanced production was about 89% [110].

Pareesh Deshpande developed a complex with Zinc and chitosan/TPP nano-scale particles for trace elements which are carrier that suits for foliar application. The main aim was to grow cereals on zinc-depleted soil; the nutritional quality of the grain suffers. They looked explored zinc complex chitosan particles as a possible “nano-carrier” for foliar fertilization in order to boost zinc density in grain. Zinc complex chitosan particles were created with tripolyphosphate as an inter-connector. Spherical diameter of Zinc complex chitosan particles is 255–302 nm which were positively charged (zeta potential, +42.34 mV) and restricted upto ~20 mg Zn/g (w/w). Plant development in zinc-deficient sand media, followed by foliar utilization of Zinc complex chitosan particles for twice-week, for 5 weeks by the following anthesis, ensures the increases in grain zinc content by 28 and 41%, respectively. This investigation demonstrates the suitability of chitosan-based nano-carriers in agronomic biofortification [111].

Copper-chitosan particles were manufactured and calculated for endorsing their development and antifungal effectiveness in tomato. In a small-scale level, the manufactured particles proved to be considerably effective in endorsing their development promotory effect on tomato seed sprouting, seedling tallness, and fresh and dry mass at 0.08–0.13% points. On the 0.13% proportions these particles originate 70 and 73% suppression of mycelia development and 61 and 83% suppression of spore sprouting in *Alternaria solani* and *F. oxysporum*, respectively, is an in vitro standard. In jar experiments, 0.13% concentration of Copper-chitosan particles was found to be of great valuable in percentage efficiency of disease regulation in tomato plants with the values of 87% in early blight and 61% in *Fusarium* wilt. The overall observed

outcomes verify the major development promotory as well as antifungal potential of Copper-chitosan particles [112].

Alternatively, chitosan can be included with plant abundant elements such as magnesium [Mg], phosphorus [P], manganese [Mn], nitrogen [N], potassium [K], manganese [Mn], and sulfur [S] and trace elements that are copper [Cu], nickel [Ni], zinc [Zn], boron [B], iron [Fe] and chlorine [Cl]. Food crop seeds frequently have vulnerability to various inorganic and organic stresses. As a result, researchers inspected the impact of Copper-chitosan particles on physiological and biochemical alterations during maize sapling growth. Improved figures show percent sprouting, shoot and root tallness, root quantity, seed size, fresh and dry mass, and seed vigor index were obtained at 0.05–0.12% proportions of Copper-chitosan particles as contrast with water, Copper sulfate, and bulk chitosan treatments. Copper-chitosan particles at 0.15% and  $\text{CuSO}_4$  (Copper sulfate) at 0.01% proportions confirmed suppressive effect on seed development [113].

### 4.3 *Biostimulant and Delivery System*

Chitosan-based products offer a variety of unique properties that make them useful in agriculture. Chitosan is used as a biostimulant to improve the plant development, raise plant tolerance to abiotic stress, and enhance the disease resistance. Chitosan actuates a few cautious qualities in plants, for example, pathogenesis-associated genes, such as glucanase and chitinase. In addition to this, it initiates numerous proteins in the responsive oxygen species scavenging method, like superoxide dismutase, catalase and peroxidase. Chitosan is usually utilized as an elicitor and biostimulant to invigorate the creation of dynamic/drug compounds both in plant and in vitro frameworks [114]. Chitosan elicitation has been likewise received as a viable procedure to upgrade auxiliary metabolite creation, such as xanthenes and other polyphenols, in *Hypericum perforatum* in vitro roots [115].

Putalun and his co-workers revealed Artemisinin formation by hairy practicalities (roots) of *Artemisia annua* L. that was augmented by 6 times to  $1.8 \text{ microg mg}^{-1}$  dry weight over 6 days via addition of 155 mg of chitosan [116]. To improve crop yield, Oscar Goni and his colleagues created chitosan oligosaccharides (CHOS) blend for plants biostimulants, it was utilized as a cost-efficient enzyme. The result of blend of CHOS establishes a considerable enhancement in the plant healthiness pointers for example improved biomass, disease control. Finally, they were conducted finest CHOS research in expressions of plant bioactivity that was extent up and authenticate by an initial field experiment with the engineering tomato cultivar H9661 [117]. The researchers used chitosan biopolymer for stimulates accumulation of antioxidants in strawberry fruit. In this report, researchers determined the outcomes of chitosan utilization in the field of plant development, fruit productivity, and antioxidant actions in strawberry plant. Here foliar utilization of chitosan on strawberry considerably improved plant expansion and fruit productivity that is up to 42% advanced as evaluate with unprocessed strawberry plants. Due to the chitosan utilization, there is

better fruit productivity that was accredited to advanced plant growth, individual fruit mass, and whole fruit mass/vegetation [118].

Chitosan utilized as a biostimulant in cucumber flora from humidity-activated diseases that are mainly originated in the presence of *Phytophthora capsica*. Here, cucumber seedlings are reacted with series of chitosan ratios, for example, 125–500 ppm, to estimate consequence on seed germination, and new root and shoot mass. Cucumber seeds from chitosan-reacted seedlings demonstrate superior opposition to humidity-activated diseases that are originated by *P. capsici* contrast to unprocessed seeds. It has been concluded that the outcomes recommend that chitosan could be utilized as an innate and surroundings protective choice to a artificial development supporter and act as insect repellent for prolong fabrication of cucumber [119]. The consequence of biostimulant in rose plants via employing chitosan in the series proportion from 0.01 to 0.02% (w/v) provides shielding against *Sphaerotheca pannosa* var. *rosae*, *Peronospora sparsa*, and *Diplocarpon rosae*. At this time, chitosan utilizes as a shower for two times in a week [120].

Chitosan diminishes fusarium head blight and mycotoxin impurity in Triticum (Wheat) plants. Commonly, *Fusarium* head blight (FHB) originated through *Fusarium graminearum* that is an infection that is responsible for production loss and mycotoxin infection in wheat crop. This particular examination discloses the consequence of a plant biostimulant fabricated from a brown macroalga *Ascophyllum nodosum* (Liquid Seaweed Extract; LSE) unaided and also prepared by blend with chitosan in controlling *Fusarium*. Wheat seeds through LSE and chitosan in mixture demonstrate a significant reduction in harshness of *F. graminearum* contamination on leaves [121].

Lesser time period that is 35 days of activities with chitosan used within soil at 0 to 0.30% (w/w), on lettuce (*Lactuca sativa*) development, chlorophyll fluorescence, and gaseous substitution were estimated in a growth chamber examination. Leaf areas were increased from 674 to 856 cm<sup>2</sup> by utilizing chitosan ratios at 0.05–0.15%, and fresh leaf mass improved from 28.7 to 39.7 g, respectively. Chitosan ratios from 0.10 to 0.30% augmented leaf chlorophyll index from 29.7 to 41.5, respectively. Chitosan at 0.20–0.30% improved leaf growth as well as improved photochemical efficacy and photochemical productivity, and chitosan at 0.10–0.30% also augmented leaf electron transportation rate [122].

Mehregan M and collaborators conducted slab creation with three replicas in the conservatory treatments that comprises chitosan spray in four stages with 0.05, 0.1, and 0.2% ratios. The regulated activity was accomplished by spraying with distilled water. Chitosan spray has been used to calculate the influence of varieties of chitosan ratios as biostimulant on floral biomass characters and act as second-class catabolite of Stevia plant. The acquired outcomes suggested that variance investigation demonstrate that chitosan sprinkling had considerable outcome on leaf dehydrated mass, shoot dried up mass, and leaf span. Here, the highest quantity of phenol was distinguished at 0.15% concentration. Also, chitosan at 0.25% proportions had the utmost result on rebaudiosides. Finally, chitosan sprinkling enhanced floral biomass characters and biochemical factors for example rebaudiosides A in stevia plants [123].

#### 4.4 Pesticide: Herbicide: Weed

Synthetic pesticides are of prime province because of their harmful influence on personal healthiness and environment. The wide ranges of synthetic pesticides are responsible for issues via focusing on helpful creatures and rehashed utilization of these manufactured pesticides prompts deficiency of biodiversity. A few pesticides are not biodegradable and industriousness in climate from not many to numerous years hence, they are answerable for soil, water, and a wide scope of natural contamination. Chitosan has been recognized globally for its prospective like a bio-control agent [124]. The studies were conducted to understand the usefulness of oligochitosan as well as chitosan on regulating plant diseases by Oliul Hassan **and his co-worker**. After the application of chitosan and oligo-chitosan, the plant can develop an increased tolerance to the stressful growth environment, as well as the method of disease protection in plants and its impact on the colonies of microbes in the rhizosphere. Beside these advantages, the stimulating outcome of chitosan on valuable microbes led to this biodegradable creation to integrate with the IPM (Integrated Pest Management) procedures.

Nano-carrier arrangement of microbicides (diuron) as a photosynthetic suppresser for the control of wild plants that were created by interconnections of carboxymethyl chitosan and 2-nitro benzyl that has 140 nm sizes as per normal HRTEM breadth dimension. The nano formulations have been created through a photograph-regulated delivery system [125]. The agricultural research system is still focused on the green revolution technology paradigm of producing short-duration high-yielding crops, irrigation, and intense fertilizer and other agrochemical use. Among the various constraints in agriculture, wild plants are always exist there and responsible for considerable constraints to crop production globally. The study found that a silver nanoparticles-chitosan encapsulated paraquat nano formulation had better herbicidal action against *Eichhornia crassipes* when tested versus controlled release. The nano-formulated herbicide was made by chemically reducing silver nitrate with sodium borohydride, then mixing the silver nanoparticles with chitosan and paraquat field concentration. Encapsulation efficacy was found to be 89.0% in this investigation. In a controlled release testing, 90.0% of the product was released after 24 h, with significantly increased herbicidal action against *E. crassipes* [126].

The microbicides imazapic and imazapyr were encapsulated in chitosan-alginate and tripolyphosphate chitosan nano-scale particles. By utilizing RT-PCR (real-time polymerase chain reactions), the impacts of microbicides and microbicides encumbered chitosan particles on soil microbes were investigated in depth. The chitosan particles had an average size of 410 nm and stayed constant in storage at room temperature for 30 days. For both types of particles, satisfactory encapsulation efficiencies of 50–70% were achieved. In cytotoxicity tests, the encapsulated herbicides were found to be less hazardous than the unbound chemicals, and genotoxicity was reduced. This research shows that encapsulating the herbicides has enhanced their type of activity and lowered their pestilential nature, indicating that they could be used in practical applications in the future [126].

#### 4.5 Soil Health Improvement and Biofertilizer

As earlier depicted, chitosan utilization can be done in a different way to lower plant illness levels what's more, improve the turn of events and spread of infections, in this manner saving harvest yield and quality. The chitosan is utilized as soil improvement to provide numerous advantages to different plant groups by sinking the pathogen assault and infectivity. Chitosan has been discovered to effectively reduce *Fusarium wilt* in a variety of plant types [127]. Similar researchers were reported against *Cylindrocladium floridanum* [128], *A. solani* [129], and subsequent to soil dealing with chitosan. The alteration of soil through chitosan is environment accommodating, while in the soil, chitosan can be debased on the significant speed, because of the plenty and diversity of microscopic organisms in variety of soils and the assumed existence of chitinases in an impressive part of the bacterial populaces.

Amena Sultana and her co-workers investigated persistent effect of chitosan (CHT) powder as a raw material on the elemental characteristics of rice-producing soils. They found that utilization of the raw material of chitosan powder in agriculture is a novel chapter and can be utilized as an another supply of raw nitrogen, increasing the effectiveness of functional inorganic nitrogen and add to expand the N content in rice-producing soils of Bangladesh. Other than this, the remaining impact of the unprocessed substance of CHT powder exaggerated morphological, conceptive, yield ascribes, and grain yield of BRRI (Bangladesh Rice Research Institute). The remaining impact of the powder additionally positively affects the enhancement in the usual nitrogen, usual carbon, usual other substances, and pH of the rice developing soils. Along with different treatments T4 is designed for outstanding consequence of the raw material of CHT powder @ 4.0 t/ha has been performed that is the best treatment in contrast with the direct dealing and other indulgences. However in this case, if there should rise in the occurrence of non-critical boundaries the behavior may be different. The examination was directed to explain the residue impact of the chitosan powder to the enhancement of the characteristics of soils. From these both the results, outcomes show that leftover impact of the crude material of CHT powder could assume an important part to improve the practical soil wellbeing [130]. Priyanka Khati and her colleagues used nano chitosan in combination for growth promotes rhizobacteria on maize growth and soil health maintenance. The results show seed germination occurs from 60 to 96.97%, plant altitude is 1.5 times enhance and leaf area is improved by two times. Other health indicators are also enhanced by this treatment [131].

Chitosan incorporation has the ability to improve the interparticle cohesiveness between the particles of soil, which leads to improvement of the mechanical qualities of sandy soil which were studied by Nader Shariatmadari and his co-workers. They found chitosan can improve soil cohesion, and its concluded form compressive strength here sample used as dried in condition [132].

Mulawarman and his colleagues investigated the plant favorable capability of chitosan, magic wet and they estimate their outcome on bacterial and nematode colony in soil.



Tomato seeds have been sown into container including a sand/soil mixture with 1:1 ratio and that have been treated with Magic Wet and chitosan at 2 hundred kg/ha. After 0, 1, 3, 7, and 14 days' time period, the soil factors are estimated for instance soil pH, microbes population density (cfu/g soil), generally extensive multiplicity of parasitic nematodes and saprophytic. Finally, samples of Fresh weight of tomato shoots and roots, as well as *Meloidogyne* infection, have been recorded. After 24 h, the bacteria in soil population densities increased after dealing with fourfold quantity of Magic Wet and 19-fold quantity of chitosan. Here, the founded bacteria species such as 32% ratio of *pseudomonas*, 42% ratio of *bacillus* for the control, and 81% ratio of *pseudomonas* for chitosan. The observed results show significant benefits of naturally harvested products like chitosan, which leads to the stimulation of soil antimicrobial action, and therefore, the antagonist probability in soils is improved in nematode infestation and finally it can improve the plant growth [133].

Chitosan fertilizer is obtained by chitin deacetylation process, which is extensively present in environment. Chitosan operates as compelling manure because of its high availability of nitrogen within it. Currently, controlled discharge fertilizers (CDF) have been chosen as majority as well as suitable technique to escalate their effectiveness, suppress the nutrient deprivation, and diminish the pestilence outcome to the atmosphere. Conversely, due to non-degradable polymer residues in the soil, many kinds of polymer-coated CDF have been fabricated that are sources of other ecological problems, including the deprivation of farming land and a diminution in soil productiveness. Hence, consequently CDF should be coated with a biodegradable material that will thrash this concern. One of the important biodegradable polymers that can be consumed as covering in CDF manufacture is chitosan biopolymer. Chitosan is accessible bounteously in environment and furthermore can frame film that does not dissolvable in water.

The study is pointed toward getting ready CRF covered by multi-facet of chitosan-polyanion as an obstruction layer that can hold the compost supplements like nitrogen, phosphorus, and potassium. The resultant polyanion-chitosan multilayer, for example, alginate chitosan, pectin chitosan, and tripolyphosphate chitosan, was proficient to create a coating as a fertilizer pellet casing that improved mechanical potency and abridged nitrogen discharge. The modified chitosan-alginate layers are also capable to suppress the nitrogen release. When altering the layer chitosan-alginate, it is founded that mechanical strength has increased and low discharge of nitrogen comparing with other layers [134].

Nano fertilizers also approach in agriculture research nowadays. To examine the deliverance of chitosan encumbered with potassium, nitrogen, and phosphorus (KNP) for wheat flora by utilizing foliar consumption. Here, chitosan-KNP compound are effortlessly pertain to leaves pedestal and goes inside the stomata during gas consumption, evade direct commencement with soil structure. The treatment with chitosan-KNP manure gives momentous enhancement in plant harvest indicator, crop yield, and mobilization indicator of the measured wheat production indicators, as evaluated with control production indicators of wheat flora extravagance with regular non fertilized crops and regularly fertilized with KNP manure crops [135].

Yang-Er Chen and his co-workers worked with chitosan and chemical fertilizer combination to the improvement of growth and disease resistant in *Begonia hiemalis* Fotsch. This work deals with chitosan as a fertilizer additive to encourage the growth of *Begonia hiemalis* Fotsch Schwabenland red development and strength for fungus *B. cinerea*. They calculated the treatment parameters with fertilizer contains in various ratios NPK with chitosan on plant growth and mainly resistant to disease. Over sixteen treatments examined, the final results founded with the ratio NPK 2:8:1:0:1.4 and chitosan 0.10 g/L had the effective plant height, crown improvement and other benefits in horticultural traits at 20, 40, and 60 days after the treatment procedure followed [136].

Chitosan can also act as plant growth regulator (PGR) that is a group of ordinary or anthropogenic complex created with plant hormone. Ethylene, jasmonic acid, auxin, cytokinins, and Gibberellins are example of low-concentration chemicals that operate at the cellular stage and work in throughout the various phases of plant growth [137]. Boonlertnium and his co-workers used chitosan for dropping the usage of chemical fertilizer in waxy corn plant. This experiment was organized by using split plot. Experiment was designed through two focal plots and four subplots and reiterated with four time periods. Chitosan was key plot and organize by non-utilization of chitosan and subplot rate is in following proportions that are 50 + 50, 50 + 25, 25 + 50 and 25 + 25 kg/rai of compound fertilizer blend with the following prescription that is 16-20-0 and 46-0-0 ratios. The outcomes showed that chitosan application fundamentally expanded ( $p < 0.05$ ) leaf region, ear size, waxy corn yield, and fiber rate. It additionally altogether held ( $p < 0.05$ ) leaf greenness at reaping time yet no critical impacts at V8 (8 genuine leaves) and R1 (silking) development stage. In any case, chitosan didn't influence leaf nitrogen content. As to substance compost rate impacts, it was tracked down that no huge distinction was found as far as waxy corn yield and agronomic qualities, aside from nitrogen substance and fiber rate. This discovery proposed that chitosan application can be utilized to improve waxy corn yield and furthermore to lessen compound compost utilizes in waxy corn developing [138].

Maize growth has been improved by utilizing sulfate based supplemented with nitrogen richer nano-fertilizer. Sulfate improved potassium, nitrogen, and phosphorus (KNP) fertilizer contents and that are nano-formulated by the ionic gelation done with tripolyphosphate and chitosan nanoparticles at pH value of 5 to bear the cost of nano-fertilizers. The chitosan nanoparticles and chitosan-based KNPS nano-fertilizers are designed by utilizing diverse portion of chitosan varying with 0.125, 0.25, 0.5, and 1% and in NPKS-based fertilizer is 25, 45, and 65 ppm. A fundamental test of these nanoparticles alongside inorganic KNP and KNPS manures is led beneath the circumstance of greenhouse by consuming maize (*Zea mays* L.) as testing crop and justify improvement conditions. Discoveries from these investigations disclosed that inorganic KNPS with ratio 20:7:3:0.5 fertilizers, chitosan nanoparticles, and planned KNPS nano-fertilizers provide better maize plant life and improved development rather than KNP manure and other regulator medicines [139] (Table 2).

**Table 2** Reported investigation on chitosan effects on the plant life

Plant and application	Chitosan formulation and observation	Functions	References
Okra (plant production)	Chitosan used as spray and pot method with different concentrations	Tallness of shrub, leaf quantity, and fruit produced	[140]
Potato (plant protection)	Plant activators Acibenzolar-S-Methyl (ASM) and chitosan in the control of potato verticillium	Elevated new weight of tuber and overall production	[141]
Chilli (antiviral)	Chitosan and Virex-H were put to the test to see how effective they were	Reduce CMV (cucumber mosaic virus) infection in chilli through biotic defense inducers	[142]
Crop (antibacterial)	Chitosan products blended with monoterpenes	Utilization of biodegradable chitosan polymeric coatings as postharvest films for unpreserved farming products, which can diminish the Lipid oxidation with less WVP rate coatings	[143]
Mango (antifungal)	Chitosan loaded with metal ions	Chitosan silver nanoparticles exhibit conidial germination was successfully inhibited of <i>C. Gloeosporioides</i> and also condensed the anthracnose incidence on mango	[144]
Chilli (biostimulant)	Oligochitosan	Plants' growth enhancement and disease infection elicitation	[145]
Soybean (pesticide)	G-Poly (acrylic acid) chitosan nanoparticles	Antifungal and insecticidal effects on fungi and insects in soybean	[146]
Soybean (seed protection)	Coating based on chitosan	Chitosan coating elevated the seed germination, plant development, and soybean production efficiently	[147]
Tomato plant (foliar spray)	Ch-derived nanoparticles	Improved plant growth and flowering	[148]
Tomato (soil addition)	Chitosan used as different concentrations 12.5 or 37 Mg/L	Decreased disease severity, controlling greenhouse diseases instigated by soil-borne pathogens	[149]

(continued)

**Table 2** (continued)

Plant and application	Chitosan formulation and observation	Functions	References
Lavender plant (micronutrient)	Combination of micronutrient Fe + Zn-chitosan	Increase the plant growth, yield components and plant pigments as well as volatile oil production of this important aromatic plant	[150]

## 5 Applications in Agro-waste Treatment

### 5.1 Wastewater Treatment

Water is the universal requirement. Sustainable Development Goal 6 targets access to clean water and sanitation by 2030. Section 6.3 addresses to get better water nature by plummeting contamination, remove dumping, and weaken discharge of harmful elements and materials, reducing the volume of unprocessed wastewater, and rising reprocessing and secure reuse worldwide.

In most areas of the earth, increase in human population, the utilization of enormous amount of industrial products in modern countries, the development and escalation of erstwhile manufacturing procedures add a huge amount of sewage and wastewater. As a result, wastewater management efforts should be attempted to eliminate substances with an elevated BOD, pestilential organisms, and injurious compounds. This has directed to enhance perceptible of procedure and handling technology and the ultimate advancement of water quality values. The figures demonstrate severe worry for the countries that countered water disaster [151].

Saran and his colleagues accounted that 41% of the worldwide people is located in serious water-worried basin, which signifies the water disaster for farming. Therefore, wastewater reutilization in cultivation is a perfect source to restore freshwater utilization in agriculture [152–154].

Subsequently, the elimination of this contaminant with high toxic content, even when currently at low concentration, has been progressively more considered in the scientific world. Numerous methods have been developed based on hybrid systems, membrane filtration, and biological degradation to diminish the concentration of contaminants in water. In adding, researchers are not very proficient when the waste matter has a less concentration of pendant colloidal elements and an elevated content of organic matter. Industrial wastewater treatment is frequently categorized as organic, chemical, and physical processes [155–160].

The generally adopted advanced techniques might be alienated into (i) pre-treatment, (ii) primary; primary processing is done to remove solids and large objects by passing the wastewater through a series of screens. Rapidly sedimentable solid particles ('grit') then settle out during flow through a grit chamber. Primary treatment removes about 60% of settle able solids and about 35% of oxygen-demanding waste.

In other words, it results in 35% reduction in BOD. (iii) secondary and tertiary; Secondary processing is required to degrade the dissolved organic compounds.

By using natural aerobic process, microorganisms degrade the organic compounds in water as secondary processing technique. The resulting sludge is either disposed of or sent to a digester. At the end of the secondary treatment the strength of the effluent is reduced to 30:20 (i.e., suspended solids 30 mg per liter and BOD 20 mg per liter), which can be discharged into water sources. However, major part of the nitrogen and phosphorus compounds still remains in the effluent. (iv) refinement and (v) purification.

Usually, industrialized wastewater is characterized into two modules: (1) organic industrialized wastewater and (2) inorganic industrialized wastewater. The major components in inorganic industrialized wastewater are present in iron and coal industry, non-metallic raw materials industry, metals built-up surface progression, and in industrial venture. Capable substitutes that deal in this process are mostly adsorption processes, because of its ease of procedure and best efficacy.

Consequently, investigators have determined solutions on the decontamination of wastewater via filtration, coagulation/flocculation, electrocoagulation, absorption, ion-exchange, advanced oxidation processes (AOPs), activated sludge processes (ASP), sequencing batch reactors (SBR). In recent times, these procedures were acknowledged extensively for elimination of contaminations from wastewater. Numerous low-cost absorbents were building up in recent times. These absorbents were extensively utilized for the healing of wastewater comprising heavy metals. These absorbents were prepared from the waste commodities created from industrial actions, waste produced from farming activities, and natural resources.

Agricultural practices have to deal a lot with nonpoint source of water pollution. Sediment runoff, nutrient runoff, and pesticides are nonpoint source of water pollution. Excessive water logging inhibits plant growth. Nutrient runoff finds its place among crop residues and irrigation water. Pesticides inhibit the water quality of the aquifer. These wastes harmed the immediate environment and necessitated the research for biopolymers for agro-industrial waste management. Literature has assessed a variety of biopolymers and their many treatment methods for their advantages and disadvantages. A huge variety of biopolymers which comprise of starch, alginate, cellulose, chitin, chitosan, etc. are aggressively implemented as nano-carriers for the managed transport of agrochemicals [158].

Adsorption can be characterized as a mass transport procedure which relocates the matter from the fluid phase to the surface of a solid and shift to extent that deals by physical and elemental exchanges. Among many methods, biosorption of pollutants using modified natural polymers and porous carbon is carving a niche now. Consequently, the investigation for novel absorbent materials to alleviate water pollutants has been encouraged. Chitin and Chitosan play a great role as they themselves are wealth from waste converters.

The biopolymer chitosan is drawing significant attention as a medium for absorbent substance progress, because this chitosan has a elevated density of hydroxyl groups ( $-OH$ ) and primary amines ( $-NH_2$ ) that perform as vigorous adsorption spots, building it a well-organized absorbent. They could be utilized as congealing and

**Table 3** Current studies about the exclusion of heavy metals and adsorption capacity of chitosan and its composites in wastewater treatment

S. no	Metal ions removed	Chitosan composites	Absorption capacity	References
1.	Cr(VI) Cu(II)	Chitosan-graphene oxide-poly-ethylenimine	90% for Cr(VI) 78% for Cu(II)	[161]
2.	Pb(II) Cu(II) As(III)	Chitosan functionalized magnetic graphene oxide and ethylene-diamine-tetra-acetic acid (EDTA)	206 mg/g 207 mg/g 42 mg/g	[162]
3.	Cr(VI)	Magnetite-chitosan composite	92	[163]
4.	Cd(II)	Chitosan-hydroxyapatite composites	122.1 mg/g	[164]
5.	Ni(II) Cu(II) Cd(II) Pb(II)	Chitosan-poly ethylene oxide (PEO)	175 mg/g 163 mg/g 143 mg/g 135 mg/g	[165]
6.	Cd(II)	Chitosan-TiO <sub>2</sub> composite	256 mg/g	[166]

gelatin agents for contaminated wastewaters, in heavy metals or metalloid absorption such as Cu(II), Cd(II), Pb(II), Fe(III), Zn(II), and Cr(III) for the elimination of dyes from industrialized wastewater (i.e., fabric wastewaters), in addition to the elimination of other organic contaminants, for example, organochloride pesticide, organic oxidized, or fatty and oil impurities [161–166]. Table 3 represents the current studies about the exclusion of heavy metals and absorption capacity of chitosan and its composites in wastewater treatment.

Chitosan is mostly utilized as an efficiently bio-sorbent in ecological engineering. The key benefit of chitosan over the ordinary activated carbon and other bio-sorbents is its cheap cost, bountiful and elevated attraction for a numeral of pollutants (because of the existence of amino and hydroxyl groups), chemical constancy, elevated reactivity and selective in relative to contaminations. Chitosan and its derivatives or composites have been productively utilized for the elimination of heavy metal ions, coloring pigments in textiles, phenols, a variety of anions, insecticides, pesticides, etc., via adsorption process.

The physicochemical characteristics of chitin and chitosan dynamically rely on molecular sequence direction and usual packing. Chitosan is more soluble and less crystalline than chitin. It is observed that by using mild acids, more cationic sites were created, thereby increasing the polarity and also the number of adsorption sites for encapsulating the pollutants. Researchers studied that the amine groups because of the presence of lone pair of electrons on the nitrogen pair had a greater affinity for metal ions. Adsorption of anionic dyes, halogens, and phenol adsorption onto chitosan hydrogel scaffold modified with carbon nanotubes was studied [167]. The presence of the amino and the hydroxyl functional groups show great affinity toward adsorbing pollutants of a spectrum nature. The simplicity was because these smart

**Table 4** Current studies about the removal of dyes and adsorption capacity of chitosan and its composites in wastewater treatment

S. No	Dyes removed	Chitosan composites	Absorption capacity	References
1.	Remazol blue	KSF montmorillonite-chitosan composite	311 mg/g	[168]
2.	Crystal violet Sunset yellow Naphthol green	sodium acrylate-co-acrylamide/nanoclay-chitosan composite	256 mg/g 208 mg/g 221 mg/g	[169]
3.	Direct blue 71 Reactive blue 19	Silicon dioxide-CNTs-chitosan composite	61 mg/g 97 mg/g	[170]
4.	Methyl orange	Chitosan-graphene oxide composites	398 mg/g	[171]
5.	Methyl orange Amido black	Porous chitosan-graphene oxide aerogels	686 mg/g 573 mg/g	[172]
6.	Acid-Red 88	Silica-chitosan Composite	25 mg/g	[173]
7.	Methylene blue	Chitosan-graphene oxide-magnetic $\beta$ -cyclodextrin composite	84 mg/g	[174]

biomaterials were low cost, easy to use, and accommodated modifications in several forms.

Researchers explored the application of chitosan-based absorbent such as chitosan with alginate and clay-tailored aerogel compound to efficiently eliminate equally cationic as well as anionic dyes and heavy metal ions from effluents and were efficient still following four cycles. The brown sea algae that originated alginate is as well accessible in abundance. Using agro-waste, chitosan derivatives mitigated agro-waste accumulation and healed the ecosystem thereby increasing environmental and economical viability. So, we see that modified chitosan has been used extensively for wastewater remediation. Table 4 represents the current studies.

## 5.2 Application of Chitosan in Air Filtration

Deep research is needed to access clean air. India trails behind China closely to top the world in infant mortality arising due to poor air quality. Immediate action by the government and the Central Pollution Control Board must be enforced to protect

infants and pregnant women from air pollution exposure. A relationship between air quality and managing COVID 19 has also been established. India needs to quickly wake up to decarbonizing its power sector and health sector policies to make the Paris agreement achievable by 2030. Farmers in the northern parts of India have understood that inefficient agro-waste management has brought down the air quality causing large losses to human lives, quality of living, and economy. Farmers in neighboring Punjab and Haryana have to set fire to their paddy stubble in their fields after harvesting the crop. Though the farmers are aware of the harm, they cannot afford the new technology due to economic viability.

New absorbents and technology that are farmer-friendly and easily adaptable to on-farm practices will help in cutting down air pollution. Agro-waste composting increases the soil microbial activity and reduces the economic load on transportation, pesticides, and fertilizers. Moreover, agro-waste can be used to improve the soil quality and sequester carbon, thereby reengineering the effects of global warming. The research community is looking for technical support to build new methods to diminish CO<sub>2</sub> emissions and to eliminate it from atmosphere. Chitosan as well as its derivatives are promising as carbon sequesters, however, their low mechanical strength is the limitation that has to be overcome.

Sundquist and his research team studied the incorporation of CO<sub>2</sub> into various carbon products like cellulose lignocellulose, chitin, hemicellulose, and lignin using autotrophic and heterotrophic organisms [175]. Another perspective is to design protective measures to prevent inhaling of air pollutants especially particulate matter and fine dust. In these lines, Nabil and his team worked on bioactive multifunctional textiles for fabricating recyclable defensive fabric materials for several applications [176]. They loaded cotton/polyester blended fabric with chitosan, various metal oxide nano-scaled particles using cross-linking agents to enhance the carboxyl group quantity. This increased the functional properties like wettability, antibacterial activity, UV protection, self-cleaning, resiliency, and durability to wash. The product sustained 15 washing cycles. This study enabled a lot of further research on protective textile materials with the onset of COVID-19. Air contamination through particulate matter (PM) has caused a remarkable hazard to human healthiness and living worth. Particulate matter, Nanoaerosols, and bacteria, for example, *E. coli* and *Staphylococcus aureus* are the major sources of air pollution. Generally, PM particles can be classified on the basis of aerodynamic corresponding dimension that is varying from nanometers to micrometers.

Liu and his colleagues have been effectively made up flexible and adaptable PMMA-chitosan and PDMS air sieve by electro-spinning process. Synergistic consequence of diminutive diameter and the polar element functional groups from the external surface of chitosan fibers has prepared the stringy membrane a perfect applicant for resourcefully detaining PM particles in addition to bacteria. The prepared nano-scaled fibrous sieve membrane is proficient of seize an exceptional detain efficacy for PM particle that is for PM<sub>2.5</sub> > 98.1%, and for PM<sub>10</sub> > 98.5%, at lower pressure fall of 20 Pa, and an elevated flow speed of 1.8 m s<sup>-1</sup> after 1 h in a soaring wetness environment. Moreover, the electrospun translucent nano-scaled fibrous membrane with 55% optical transmittance could be constantly functional in an enormously



harmful atmosphere for long 100 h with constant elimination of  $PM_{2.5}$  effectively. The filter was also capable to preserve elevated elimination efficiency subsequent to five clean-up series. In addition, the nano-scaled fibrous filters as well show outstanding antibacterial capability due to the chitosan constituent [177].

Al-Sayed A. Al-Sherbini and his team designed chitosan/Ag bionanocomposites for the removal of *E. coli* and *G. bacillus* from indoor environment and worked as air filters [178]. By utilizing nonsolvent-induced phase separation technique, Wang and his colleagues developed polyvinyl alcohol (PVA)-chitosan (CS) composite film for air micro-filtration. The depth of the film is strongly connected to the ultra-filtration execution and the undeviating capture on film surface that was the leading method for elimination of NaCl aerosol elements. M30-3 with the depth of 35  $\mu\text{m}$  display the uppermost excellence factor for air filtration and 95.59% filtration efficiency attained at pressure drop of 630 Pa. In addition, the resulting casings display elevated antibacterial capability in opposition to *E. coli* and *S. aureus* [179].

Mishra and his research colleagues prepared Lemongrass oil with chitosan-nanocellulose composite filter for bioaerosols found in indoor air that participate and have a foremost responsibility in the conduction of transferable infections to human beings. Authors evaluate restraining outcome of the composite structure on culturable bacteria in interior air done with diverse positions that is air capacity from 35 to 85  $\text{m}^3$  and in unlike dimension proportions of aerosol ( $<0.25\text{--}2.5 \mu\text{m}$ ). The composite structure had elevated encapsulation efficiency (88–91%) and citral content. A considerable diminution in cultural bacteria of aerosol was experiential in existence of cellulose-chitosan composites [180].

Mohraz and his colleagues prepared Polyurethane/chitosan nanofibers filters for Nanoaerosols and *E. coli* bacteria present in surrounding environment. They have investigated the effects in the variations in diameter and uniformity utilizing RSM statistics modeling. The prepared filter was performance evaluated against Nanoaerosols like KCl nanoparticles under optimum conditions. The researchers investigated consequence of air face speed on the filtration effectiveness and quality feature of manufactured PU/CH nanofiber filter medium. The outcomes of antibacterial action were investigated, and results confirm that chitosan is a superior option to produce an antibacterial and efficient filter medium by making blend with other materials [181].

Zhao and his co-workers studied the hazardous effects of  $PM_{2.5}$  through lung inflammation in rats. They have studied toxicity of  $PM_{2.5}$  and health issues due to excessive amount of  $PM_{2.5}$  presence in environment. They have prepared chitosan oligosaccharides and investigated the inhibition effect on toxicity of  $PM_{2.5}$ . The study demonstrates that chitosan oligosaccharides. Chitosan oligosaccharides are effective in diminishing toxicity of  $PM_{2.5}$  and stimulate lung inflammation practically. The obtained results show realistic implication of prepared chitosan oligosaccharides to stop pulmonary toxic by  $PM_{2.5}$  and 95% capture efficiency is reported [182]. Table 5 discuss the comparative study on the performance of chitosan composites in air filtration applications.

**Table 5** Comparative study on the performance of chitosan composites in air filtration applications

S. no	Materials	Targeted pollutant	Capture efficiency	Reference
1.	PDMS/PMMA-chitosan nanofiber air filters	Particulate matter (PM <sub>2.5</sub> ) Bacteria ( <i>E. coli</i> and <i>S. aureus</i> )	98.39% for PM <sub>2.5</sub> 96.5% for <i>E. coli</i> 95.2% for <i>S. aureus</i>	[177]
2.	Chitosan/Ag bionanocomposites	Bacteria ( <i>E. coli</i> ) and ( <i>G. bacillus</i> )	Anti-bactericidal	[178]
3.	Chitosan/polyvinyl alcohol blend membranes	PM <sub>2.5</sub> <i>E. coli</i> and <i>S. aureus</i>	95.59% 94.8% and 91.3%	[179]
4.	Lemongrass oil into chitosan-nanocellulose composite	<i>Pseudomonas otitidis</i> , <i>Staphylococcus</i> sp., <i>Bacillus cereus</i> , <i>Bacillus pseudomycolides</i> sp., and <i>Pseudomonas</i> sp. Cf0-3 in bioaerosols	88–91%	[180]
5.	Polyurethane/chitosan nanofibers	Nanoaerosols and <i>E. coli</i> bacteria	90%	[181]
6.	Chitosan oligosaccharides	PM <sub>2.5</sub>	95%	[182]

### 5.3 Utilization of Chitosan in Animal Fodder Supplement

Livestock rearing is a key livelihood of farmers in India. There is an increase in the livestock population in India. Limitation of animal fodder is a challenge and intensive research needs to be spearheaded to tackle the issue. The Department of Animal Husbandry & Dairying (DADH) in 2019 has recorded that only 4% of cropping area is used for animal feed cultivation. The farmers are left with no choice, but to feed the animals optimally and the animals are half starved. Fodder cooperatives are minimal in number and lack the expertise to bridge the gap. Conventional farmers have limited information on the subject to utilize agro by-products as animal feeds. Research to integrate quality control systems in feed analysis and reduction in loss of feeds is another critical area.

Xu and his colleagues evaluated the significance of chitosan nano-scaled particles on the immunity and growth performance of piglets when utilized chitosan as diet supplement. They assigned 144 piglets in four groups and were given four different amounts of chitosan nanoparticles in the base diet that are 0, 100, 200, and 400 mg/Kg and feed for four weeks. It is found that enhancement in the chitosan nanoparticle amount as supplement diet-enhanced standard daily gain and reduced the diarrhea rate. These results demonstrate that dietary supplement with chitosan nano-scaled particles also restrain the development of possible bacterial pathogens and improve the immune system of piglets [183].

Shi-bin and Hong evaluated the effect of chitosan feeding on the development and immunity factor in ducks. The ducks were fed with a control diet that having ratios of 0–4.8 g/Kg of 85% chitosan for 35 days. This was concluded that the ratios of 1.2 and 2.5 g/Kg of chitosan supplement diet were appropriate for ducks to attain an improved development and immunity index against infections [184].

Li and his research team investigated and conducted a research to examine the consequence of chitosan on immunity as well as antioxidant functions in 24 beef bulls having same body mass and age. The bulls were divided into three different groups and three different weight diets were assigned to them comprising mass ratios from 0 to 1000 mg/Kg of chitosan in the diet. The experiment conducted for 84 days. This is established that accumulation of 500 mg/Kg chitosan proportion influenced and improved immune function and also enhanced the anti-oxidative parameters of beef cattle [185].

Tiago A. Del Valle and his colleagues investigate the consequence of chitosan on the routine of milk yield and immunity system of 24 dairy cows. The study conducted on 21 days and this was concluded that chitosan inclusion in diet improved food intake, digestibility, metabolism rate, and productive performance. It also improved concentration of unsaturated fatty acids in the milk. Chitosan inhibits *in vitro* biohydrogenation [186].

Hu and his team have examined the effects of chitosan feeding as dietary supplement on pigs. They have done an evaluation on 40 piglets of same age and same weight for 28 days. The basal diet has 50 mg/Kg concentration of chitosan. The outcomes of this study clearly indicate that 50 mg/Kg concentration of chitosan enhanced the growth performance of pigs, effectively controlled the intestinal inflammation, and enhanced the intestinal barrier functions [187].

Osho and Adeola studied the performance of chitosan oligosaccharide and did experimental studies to calculate the optimized concentration to improve digestion activities, growth, intestine morphology and immunity index in chickens. The basal diet has 0–2.5 g/Kg concentration of chitosan oligosaccharide. It is found that 1.0 g/Kg concentration was the optimized concentration and results indicate that there is an enhancement in body growth as well as digestion index of chickens. The chitosan oligosaccharides also enhance the feed intake and reduce the pro-inflammatory cytokine genes. It also decreases the mortality rate of chickens [188].

Lokman and his colleagues evaluated the performance of cricket and shrimp-derived chitin and chitosan on the development routine and organ properties of chickens. In the experiment chickens were feed with 0.5 g/kg concentration of cricket chitin and cricket chitosan. The studies disclose that concentration of cricket chitin considerably enhanced growth and organ characteristics of chickens. Also, supplement diet of chitin and chitosan reduce the mortality rate of chickens [189]. Table 6 illustrate comparative study on the performance of chitosan in the animal fodder supplement application.

**Table 6** Comparative study on the performance of chitosan in the animal fodder supplement application

S. no	Materials	Targeted animal	Improving factors	Diminishing factors	Reference
1.	Chitosan nanoparticle	Pigs	Average daily gain (ADG), improved immunity factor	Decreased Feed and gain (F/G) factor and diarrhea rate ( $p < 0.05$ )	[183]
2.	Chitosan	Ducks	Average daily feed intake and feed conversion ratios Immune Index	Decrease fat digestibility	[184]
3.	Chitosan	Bulls	Immune function Anti-oxidative functions	Decrease oxidative agents	[185]
4.	Chitosan	Cows	Intake, digestibility, metabolism rate and productive performance	Inhibits in vitro bio-hydrogenation	[186]
5.	Chitosan	Pigs	Growth performance, intestinal morphology, barrier function, cytokine expression and antioxidant system	Decrease intestinal inflammation	[187]
6.	Chitosan oligosaccharides	Chickens	Growth performance, digestive functions, intestinal morphology, and immune organs	Decrease mortality rate	[188]
7.	Chitin and chitosan	Chickens	Growth performance, carcass quality, and organ characteristics	Decrease mortality rate	[189]

#### 5.4 Chitosan Agro-waste Composites

Chitosan agro-waste composites comprise of four different categories that are listed below and a comprehensive discussion has been done on the importance and use of these composites in the below sections. These composites category are:-

- (a) Chitosan-Activated carbon composite
- (b) Chitosan-biochar composite
- (c) Chitosan-lignin and
- (d) Chitosan-cellulose composite

#### 5.4.1 Chitosan-Activated Carbon Composite

Numerous absorbents, for example, metal oxides, activated carbon, clays, silica, etc., have been utilized for the elimination of heavy metals and other pollutants from aqueous environments. Though, activated carbon has been more favored absorbent for numerous time periods in the exclusion procedure of heavy pollutants because of its elevated absorption capability, high absorption speed, and excellent opposition to abrasion. Activated carbons are harmless carbonaceous creations, comprising a permeable configuration and a huge interior surface area. This material can soak up an extensive range of undesired variety of pollutants from the gaseous or fluid stage in direct to influence the consequence of decontamination of aqueous environments.

Hydari and his research team manufactured chitosan-activated carbon composite beads by sol-gel method and utilize them for the removal of cadmium. The particle size found for composite is 0.425  $\mu\text{m}$  with pH of 6. In this work, the experimental data were analyzed by Freundlich and Dubinin-Radushkevich (D-R) isotherms. Under optimum conditions 100% cadmium has been removed by chitosan-activated carbon composite beads with an adsorption capacity of 52 mg/g [190]. M. Auta and his co-workers prepared tea waste-derived activated carbon-chitosan composites for the removal of Methylene blue dye and acid blue dye from wastewater. Authors reported 495 mg/g of adsorption capacity and composite retained 50% adsorption efficiency for the removal of cationic and anionic dyes [191].

Jacques K. Fatombi and his colleagues prepared peanut shell-derived activated carbon-crab shell-derived chitosan composite by using conventional high temperature method. Authors reported the removal of indigo carmine dye with an adsorption capacity of 208 mg/g and particle size is 67 nm. Composite exhibits surface area of a 458  $\text{m}^2/\text{g}$  [192]. Fabiana Paiva de Freitas and his team synthesized plywood residue derived activated carbon-chitosan composite through carbonization method. Composite exhibits average pore diameter of 1.8 nm and surface area of a 253  $\text{m}^2/\text{g}$ . Authors reported removal of red dye from aqueous solution with an adsorption capacity of 30 mg/g [193]. A. Venault and his research team synthesized chitosan-activated carbon gels composite by using wet-casting procedure for the removal of phenol as organic pollutant in water treatment. The authors claimed a pore size of 25 nm and surface area of a 275  $\text{m}^2/\text{g}$  for the prepared composite gels.

Khalid Z. Elwakeel and his colleagues manufactured activated carbon and chitosan composite beads for the removal of copper and cadmium ions from aqueous solution. The authors reported removal of copper and cadmium ions from wastewater with maximum adsorption capacity of a 3.43 mmol/g for Cu (II) ions and a 2.38 mmol/g for cadmium ions [194].

The above studies clearly show a significant role of chitosan-activated carbon composites in the removal of heavy metals as well as dyes from the aqueous environments (Table 7).

**Table 7** Current studies on chitosan-activated carbon composites and their applications

S. no	Materials	Fabrication method	Applications	Size and surface area of composite	References
1.	Chitosan-AC composite beads	Sol gel method	Cadmium removal with adsorption capacity of 52 mg/g	0.420 nm	[190]
2.	Tea waste-derived activated carbon-chitosan composite	Sol gel method	Removal of methylene blue dye and acid blue dye, 50% adsorption efficiency and adsorption capacity of 495 mg/g	–	[191]
3.	Peanut shell-derived activated carbon-crab shell-derived chitosan composite	Conventional high temperature method	Indigo carmine dye, adsorption capacity is 208 mg/g	67 nm, surface area-458 m <sup>2</sup> /g	[192]
4.	Chitosan-activate carbon films	Carbonization and high temperature procedure	Removal of Red dye, adsorption capacity is 30 mg/g	1.8 nm and surface area of a 253 m <sup>2</sup> /g	[193]
5.	Chitosan-activate carbon gels	Wet-casting procedure	Removal of Phenol Adsorption capacity is 84 mg/g	25 nm and surface area of a 275 m <sup>2</sup> /g	[195]
6.	Sugarcane waste-derived activated carbon-chitosan composite beads	Wet chemical method	Removal of copper and cadmium ions maximum adsorption capacity is 3.439 mmol/g for copper ions and 2.38 mmol/g for cadmium ions	Specific surface area of 96 m <sup>2</sup> /g	[194]

### 5.4.2 Chitosan-Biochar Composite

On evaluation among conservative carbonaceous resources for example commercialized activated carbon, the major benefits of biochar are its cheap price and a wealth of resources of biomass to produce biochar. Due to plentiful, reusable, recyclable and non-hazardous in character biochar and its composite with chitosan biopolymer widely used in water treatment and removal of inorganic as well as organic pollutants in the aqueous environments.

Kumuduni and her team prepared iron-loaded chitosan-biochar fibrous composites utilized for removal of phosphate from aqueous solution. Biochar has been produced from paper mill sludge and composite fibers prepared by wet chemical method followed by extruder with 0.2-mm thickness plastic hub needle. The fibrous composite employed in the removal of phosphate and the adsorption capacity is 19.24 mg P/g. Authors reported a pore size of 1.8 nm and a surface area of a 12.30 cm<sup>2</sup>/g for these fibers composites [196].

Chunmiao Zhu and his co-workers synthesized chitosan-reed biochar composite through wet chemical method. The authors discover the adsorption behavior of Ofloxacin and analyzed through Langmuir model. The prepared composite shows a very promising results with an adsorption capacity of 6.64 mg/g [197]. Yang and his research team developed an innovative nano-scaled iron sulfate-biochar-chitosan composite for the adsorption of chromium heavy metals impurities from aqueous solution. Soya sauce residue is used as a biomass feedstock for the fabrication of biochar in this study. Authors revealed the removal of Chromium with an elimination capacity of 103 mg/g [198]. Liu and his colleagues productively fabricated a low-cost biochar-magnetic chitosan for the removal of arsenic from aqueous solution. XPS studies have been carried out for understanding the significant adsorption phenomenon of Arsenic ions by composite. The removal efficiency is 17.8 mg/g as per obtained results by pseudo-second order and Langmuir model [199]. Arabyarmohammadi and his research team synthesized biochar, clay, and chitosan composite for the removal of heavy metals from water. Authors synthesized biochar by using bark chips residual and embedded this with nanoclay-chitosan. This is a combination of inorganic and organic materials with chitosan utilized for removal of lead, zinc, and copper metals from aqueous solution. Correspondingly, authors revealed the highest absorption capability of the prepared composite at 25 °C for copper, lead and zinc from aqueous samples are 121, 335, and 134 mg/g. The composite exhibits pore size diameter of 1.9 nm and 252 m<sup>2</sup>/g. From the above studies, this is concluded that biochar-chitosan composites are proficient absorbents for pollutants present in atmosphere and effectively utilized for its purification. These composites expediently removed pollutants from aqueous solution by following absorption mechanism [200] (Table 8).

**Table 8** Current studies on chitosan-biochar composites and their applications

S. no	Materials	Fabrication method	Applications	Size and surface area of composite	References
1.	Iron-loaded chitosan-biochar fibrous composites	Wet chemical method followed by extruder with 0.2-mm thickness plastic hub needle	Removal of phosphate Adsorption capacity is 19.24 mg P/g	Pore size is 1.8 nm Surface area is 12.30 cm <sup>2</sup> /g	[196]
2.	Chitosan-reed biochar composite	Wet chemical method	Removal of ofloxacin Adsorption capacity is 6.64 mg/g	–	[197]
3.	Chitosan-biochar-iron sulfate composite	Wet chemical method	Removal of chromium Elimination capacity of 103 mg/g	–	[198]
4.	Rice straw-derived biochar-magnetic chitosan composite	Wet chemical method	Adsorption of arsenic ions Adsorption capacity is 17.8 mg/g	–	[199]
5.	Clay-biochar-chitosan composite	Pyrolysis method followed by wet chemical method dehydrated at 85 °C in oven	Removal of lead, zinc and copper metals from aqueous solution	Pore size is 1.9 nm Surface area is 252 m <sup>2</sup> /g	[200]

### 5.4.3 Chitosan-Lignin and Chitosan-Cellulose Composite

Lignin is an unstructured, cross-linked, and aromatic biopolymer, is clearly observed in biomasses, and is likewise a major non-sugar matter of wooden samples. Lignin is accurately revealed as a devastating spinoff from pulp and paper manufacturing companies. V. Nair and his team developed alkali lignin-chitosan composite for the exclusion of remazol Brilliant Blue R (RBBR), anthraquinonic dye, and chromium metals from aqueous environments. Authors revealed an adsorption capacity of 111–24.5 mg/g for dyes and chromium impurities in water. The dynamic adsorption locations were established through hydroxyl and functional groups of the composite, and the adsorption method was attributable to electrostatic interface of coordination bonding between amino and hydroxyl groups with anion of the dyes and



Chromium metallic ions [201]. Ajay K. Mishra and his colleagues prepared lignin, titania and chitosan composite for exclusion of black dye from aqueous solutions. Authors synthesized lignin from pulp black liquor and paper used for preparation of composite. Authors reported removal of black dye with an adsorption capacity of 15 mg/g via Langmuir model [202]. Kevin and his team prepared lignin-chitosan films by solvent casting technique and study antioxidant properties. The authors studied composite layer permeability to nitrogen as well as for oxygen calculated at 70% RH. These two gases were utilized in command to measure if lignin accumulation may change or advance the barrier property of chitosan coatings. A noteworthy variation is perceptible when lignin is integrated into the film articulation and permeability is measured for nitrogen or oxygen. There is increase in absorbent capability of films including lignin for equally in Nitrogen as well in oxygen gases. As antioxidant property is directly correlated to the surface of the films, therefore there is an enhancement in permeability that correlates with interconnected polymer arrangements [203]. Zhang and his research team prepared polyethyleneimine functionalized chitosan-lignin composite porous structures for the removal of mercury ions from aqueous environments. Porous composite shows an adsorption capacity of 663 mg/g and the adsorption kinetics learning is pre-eminently explained by a pseudo-second-order kinetic representation, and Langmuir isotherm modeling that is mainly suitable to illustrate the absorption performance of composite for Hg(II) ions. The prepared samples can eliminate 83% of the mercury ions via crucial adsorption within 1 min time period while preliminary concentration of Hg(II) ions is 665 mg/L [204]. Sohni and his team fabricated palm shell-derived nano-lignin and made chitosan composite for the removal of methylene blue dye from wastewater. Authors reported an average pore size of 150 nm. Adsorption capacity of methylene blue is 74 mg/g and removal efficiency is 83% as per analysis by Langmuir isotherms [205]. The above results also conclude that Lignin-chitosan composites diminish ecological and community health vulnerability associated with the discarding of waste matter from the paper and pulp industry (Table 9).

Cellulose is individual largely extensively dispersed natural polymer complex, with high-quality recyclability, decomposability, and environment-friendly with low cost. Specifically, cellulose-chitosan composites are extensively studied and encouraged to accomplish their applications in hemostasis, bio-waste management, water purification, and antimicrobial activities. Shan Lin and his co-workers prepared silver nanoparticles embedded chitosan-Cellulose composite films for antibacterial activities. The average size of films is 9 nm containing 7% mass loading of silver nanoparticles [206]. The prepared composite films illustrate considerably enhanced antimicrobial performance and can therefore be potentially utilized to manufacture improved bio-fouling resistant mortify membranes. Chieu D. Trana and his team fabricated chitosan-cellulose composite membranes for the elimination of microcystin from aqueous environments. Authors obtained the results that have reflected collective benefits of constituents, explicitly advanced mechanical constancy due to cellulose and admirable absorption capability. The authors revealed an adsorption capacity of 96 mg/g and 10 nm is an average size of membrane [207]. Xialian Fan and his team prepared chitosan-cellulose sponge by alkali-urea solvent method for rapid

**Table 9** Current studies on chitosan-lignin composites and their applications

S. no	Materials	Fabrication method	Applications	Size and surface area of composite	References
1.	Alkali lignin-chitosan composite	Wet chemical method	Exclusion of remazol brilliant blue R (RBBR), anthraquinonic dye and chromium metals Adsorption capacity is 111 mg/g 24.5 mg/g	30 nm pore size and surface area is 2.45 m <sup>2</sup> /g	[201]
2.	Lignin-titania-chitosan composite	Wet chemical method	Removal of brilliant black dye Adsorption capacity is 15 mg/g	15 m	[202]
3.	Chitosan-lignin composite films	Solvent casting method	Antioxidant property related to moisture	–	[203]
4.	Polyethyleneimine functionalized chitosan-lignin composite sponge	Wet chemical method	Removal of mercury ions from aqueous environments Adsorption capacity is 663 mg/g		[204]
5.	Palm shell-derived lignin-chitosan composite	Wet chemical method	Elimination of methylene blue dye Adsorption capacity is 74 mg/g	150 nm Removal efficiency is 83%	[205]

hemostasis and antibacterial activities. The fabricated combined sponge has high-quality water adsorption capability and mechanical potency, and it too has noticeable restrain consequences on *E. coli*. In vitro coalescence and entire blood cell linkage experimentation demonstrate that the combined effects on hemostatic phenomenon by sponges that have good bonding to erythrocytes and platelets, which resultant in high-quality coagulation capability [208]. Zhuang and his collaborators successfully synthesized chitosan-cellulose fibrous composite by using wet spinning technique for the removal of Cobalt from wastewater. The prepared fibrous composite exhibits an average size of 95  $\mu\text{m}$  and surface area of a 2.5 m<sup>2</sup>/g. In accordance with the Langmuir isotherm representation report, the adsorption capacity is found to be 26 mg/g for these fibrous composites. Furthermore, the production of fibrous composite through physical method is more ecological and cleaner as compared to chemical methods

[209]. Chen and his team developed an innovative oxycellulose-chitosan composite through wet chemical method for the removal of lead and chromium ions from water. Composites revealed highest adsorption capacity of 102 mg/g for lead and 126 mg/g for chromium metallic ions from water [210]. In contrast with above studies, it is anticipated that substantial variation of chitosan with cellulose significantly enhanced its adsorption capability and mechanical strength, created chitosan-based composites as a capable bio-sorbent for the removal of heavy metals, microcystin from aqueous environments as well as effectively utilized in antimicrobial activities (Table 10).

## 6 Conclusions and Future Prospects

India is an agricultural land generating economy and livelihood for many people. Agro-waste management has gained immense importance over the years. Researchers are turning toward tapping the wealth from agro-waste not only for economic viability but also for sustaining environmentally friendly practices. Waste from being a pollutant is being resourced as a useful product. Agro-waste initially was directly used as fuel in low efficiency furnaces. Later, the evolution of briquettes for hotel kitchens and the local availability attracted focus on better utilization of agro-wastes. Now, they find various applications like water treatment, drug formulation, bio-based textiles, air purifiers, and many more avenues to be explored. Chitin and particularly chitosan are organic polymers with numerous functional characteristics and are extensively utilized in a broad scope of application. Presently, the main commercial source of chitin and chitosan comprises waste streams from the marine fishery industry. The application of these biopolymers lies in the number of hydroxyl groups and free amine sites that make the wealth from waste biopolymers a potential material for versatile applications.

Though, their accessibility is restricted by natural features and season. The current enhancement in requirement of chitin and chitosan in the large-scale in market has drawn consideration to substitute resource that is independent of oceanic fishery waste. The attention has now touched insect breeding farms that generate side stream (deceased adults, exuviate, exoskeletons, frass, and remaining feed) to be optionally explored. The chitin contents availability in whole creatures is proportionally low and is characterized by function of species, their food source, and the stage they are in their life cycle stage. The challenge lies in the data excruciated from extraction, purification, deacetylation, degree of purification, and the purification processes. This is a promising evolution. In future, the knowledge gaps of this future can be investigated. Also, the limitations of low thermal and mechanical stability can be overcome by appropriate scaffolds and modifications. Chitosan can be suitably modified based on the applications, and this waste material can be put to great applications in the future.

**Table 10** Current studies on chitosan-cellulose composites and their applications

S. no	Materials	Fabrication method	Applications	Size and surface area of composite	References
1.	Silver nanoparticles-chitosan-cellulose composite films	Solvent casting method	Antimicrobial <i>E. coli</i>	Average size of film is 9 nm	[206]
2.	Chitosan-cellulose composite membranes	Solvent casting method using ionic liquid	Elimination of microcystin from aqueous environments Adsorption capacity is 96 mg/g	10 m	[207]
3.	Chitosan-cellulose composite sponge	Alkali-urea solvent method	Rapid hemostasis and antimicrobial	20 m	[208]
4.	Chitosan-cellulose fibrous composite	Wet Spinning technique	Removal of cobalt from Wastewater Adsorption capacity is 26 mg/g	95 $\mu$ m Surface area is 2.5 m <sup>2</sup> /g	[209]
5.	Chitosan-oxycellulose composite	Wet chemical method	Removal of lead and chromium metallic ions Adsorption capacity is 102 mg/g for lead and 126 mg/g for chromium	–	[210]

## References

1. Colla G, Roupshael Y (2015) Biostimulants in horticulture. *Sci Hortic* 196:1–2
2. Roupshael Y, Colla G (2018) Synergistic biostimulatory action: designing the next generation of plant biostimulants for sustainable agriculture. *Front Plant Sci* 9:9
3. Roupshael Y, Colla G (2020) Editorial: biostimulants in agriculture. *Front Plant Sci* 11:40
4. Baudoin W, Nono-Womdim R, Lutaladio N, Hodder A, Castilla N, Leonardi C, De Pascale S, Qaryouti M (2013) Good agricultural practices for greenhouse vegetable crops. Food and Agriculture Organization of the United Nations, Rome, Italy. ISBN 9789251076491
5. Calvo P, Nelson L, Kloepper JW (2014) Agricultural uses of plant biostimulants. *Plant Soil* 383:3–41
6. Jägermeyr J (2020) Agriculture's historic twin-challenge toward sustainable water use and food supply for all. *Front Sustain Food Syst* 4:35
7. Napolitano M, Colla G et al (2018) Trichoderma-based biostimulants modulate rhizosphere microbial populations and improve N uptake efficiency, yield, and nutritional quality of leafy vegetables. *Front Plant Sci* 9:9
8. Roupshael Y, Spíchal L, Panzarová K, Casa R, Colla G (2018) High-throughput plant phenotyping for developing novel biostimulants: from lab to field or from field to lab? *Front Plant Sci* 9:1197
9. Koleška I, Hasanagić D, Todorović V, Murtić S, Klokić I, Paradiković N, Kukavica B (2017) Biostimulant prevents yield loss and reduces oxidative damage in tomato plants grown on reduced NPK nutrition. *J Plant Interact* 12:209–218
10. Petropoulos SA (2020) Practical applications of plant biostimulants in greenhouse vegetable crop production. *Agronomy* 10:1569
11. Canellas LP, Olivares FL, Aguiar NO, Jones DL, Nebbioso A, Mazzei P, Piccolo A (2015) Humic and fulvic acids as biostimulants in horticulture. *Sci Hortic* 196:15–27
12. Du Jardin P (2015) Plant biostimulants: definition, concept, main categories and regulation. *Sci Hortic* 196:3–14
13. Geisberger G, Gyenge EB, Hinger D, Kach A, Maake C, Patzke GR (2013) Chitosan–thioglycolic acid as a versatile antimicrobial agent. *Biom-acromolecules* 14(4):1010–1017
14. Zhang X, Geng XD, Jiang HJ, Li JR, Huang JY (2012) Synthesis and characteristics of chitin and chitosan with the [(2-hydroxy-3-trimethylammonium) propyl] functionality, and evaluation of their antioxidant activity in vitro. *Carbohydr Polym* 89(2):486–491
15. Sultana N, Zakir HM, Parvin MA, Sharmin S, Seal HP (2019) Physiological responses and nutritional qualities of tomato fruits to chitosan coating during postharvest storage. *Asian J Adv Agric Res* 10(2):1–11
16. Hadwiger LA (2008) Pea-*Fusarium solani* interactions contributions of a system toward understanding disease resistance. *Phytopathology* 98:372–379
17. Bolto B, Dixon D, Eldridge R (2004) Ion exchange for the removal of natural organic matter. *React Funct Polym* 60:171–182
18. Lizarraga-Pauli EG, Torres-Pacheco I, Moreno Martinez E, Miranda-Castro SP (2011) Chitosan application in maize (*Zea mays*) to counteract the effects of abiotic stress at seedling level. *Afr J Biotech* 10(34):6439–6446
19. Jabeen N, Ahmad R (2013) The activity of antioxidant enzymes in response to salt stress in safflower (*Carthamus tinctorius* L.) and sunflower (*Helianthus annuus* L.) seedlings raised from seed treated with chitosan. *J Sci Food Agric* 93(7):1699–1705
20. Pongprayoon W, Roytrakul S, Pichayangkura R, Chadchawan S (2013) The role of hydrogen peroxide in chitosan-induced resistance to osmotic stress in rice (*Oryza sativa* L.). *Plant Growth Regulat* 70(2):159–173
21. Bautista-Banos S, Hernandez-Lauzardo AN, Velazquez-del Valle MG, Hernandez-Lopez M, Barka EA, Bosquez-Molina E, Wilson CL (2006) Chitosan as a potential natural compound to control pre and postharvest diseases of horticultural commodities. *Crop Prot* 25:108–118
22. Yogeshkumar GN, Atul SG, Yadav AV (2013) Chitosan and its applications: a review of literature. *Int J Res Pharma Biomed Sci* 4(1):312–331

23. Castro SPM, Paulin EGL (2012) Is chitosan a new panacea? Areas of application. <https://doi.org/10.5772/51200>
24. Hadwiger LA (2013) Plant science review: multiple effects of chitosan on plant systems: solid science or hype. *Plant Sci* 208:42–49
25. Bhardwaj N, Kundu SC (2010) Electrospinning: a fascinating fiber fabrication technique. *Biotechnol Adv* 28(3):325–347
26. Dvir T, Tsur-Gang O, Cohen S (2005) “Designer” scaffolds for tissue engineering and regeneration. *Isr J Chem* 45(4):487–494
27. Zamani A et al (2008) Determination of glucosamine and N-acetyl glucosamine in fungal cell walls. *J Agric Food Chem* 56(18):83148318
28. Hu X, Du Y, Tang Y, Wang Q, Feng T, Yang J, Kennedy JF (2007) *Carbohydr Polym* 70(4):451–458. <https://doi.org/10.1016/j.carbpol.2007.05.002>
29. Dutta PK, Ravikumar M, Dutta J (2002) *J Macromol Sci Polym Rev* 42(3):307–354. <https://doi.org/10.1081/MC-120006451>
30. Hajji S et al (2014) Structural differences between chitin and chitosan extracted from three different marine sources. *Int J Biol Macromol* 65:298306
31. Al Sagheer F et al (2009) Extraction and characterization of chitin and chitosan from marine sources in Arabian Gulf. *Carbohydr Polym* 77(2):410419
32. Lee KY, Ha WS, Park WH (1995) Blood compatibility and biodegradability of partially N-acylated chitosan derivatives. *Biomaterials* 16(16):12111216
33. Kurita K (2001) Controlled functionalization of polysaccharide chitin. *Prog Polym Sci* 26:1921–1971
34. Morganti P et al (2012) From waste material a new anti aging compound: a chitin nanofiber complex. *SÖ FW J* 138(7)
35. Ruel-Gariépy E, Leroux J (2006) Chitosan: a natural polycation with multiple applications. American Chemical Society, Washington, DC, USA, pp 243–259
36. Hwang KT et al (2002) Controlling molecular weight and degree of deacetylation of chitosan by response surface methodology. *J Agric Food Chem* 50(7):18761882
37. Tolaimate A et al (2003) Contribution to the preparation of chitins and chitosans with controlled physico-chemical properties. *Polymer* 44(26):79397952
38. Mima S et al (1983) Highly deacetylated chitosan and its properties. *J Appl Polym Sci* 28(6):19091917
39. Bough W et al (1978) Influence of manufacturing variables on the characteristics and effectiveness of chitosan products. II. Coagulation of activated sludge suspensions. *Biotechnol Bioeng* 20(12):19451955
40. Mathur NK, Narang CK (1990) Chitin and chitosan, versatile polysaccharides from marine animals. *J Chem Edu* 67(11):938
41. Mourya VK, Inamdar NN (2008) Chitosan-modifications and applications: opportunities galore. *React Funct Polym* 68:1013–1051
42. Alves V, Mano JF (2008) Chitosan derivatives obtained by chemical modifications for biomedical and environmental applications. *Int J Biol Macromol* 43:401–414
43. Clasen C, Wilhelms T, Kulicke WM (2006) Formation and characterization of chitosan membranes. *Biomacromolecules* 7:3210–3222
44. Kim IY, Seo SJ, Moon HS, Yoo MK, Park IY, Kim BC et al (2008) Chitosan and its derivatives for tissue engineering applications. *Biotechnol Adv* 26:1–21
45. Kienzle-Sterzer C, Rodriguez-Sanchez D, Rha C (1984). In: Zikakis JP (ed) Chitin, chitosan and related enzymes. Academic Press, Inc., pp 383–396
46. Zhang H, Li R, Liu W (2011) Effects of chitin and its derivative chitosan on postharvest decay of fruits: a review. *Int J Mol Sci* 12(2):917–934
47. Rathke T (1993) Determination of the degree of N-deacetylation in chitin and chitosan as well as their monomer sugar ratios by near infrared spectroscopy. *J Polym Sci Part A: Polym Chem* 31:749–753
48. Puvvada YS, Vankayalapati S, Sukhavasi S (2012) Extraction of chitin from chitosan from exoskeleton of shrimp for application in the pharmaceutical industry. *Int Curr Pharm J* 1(9):258–263

49. EPA (2008) Environmental Protection Agency review decision of chitosan EPAHQ-OPP-2007-0037 FRL-8392-6 in the Federal Register, vol 73, No 248/Wednesday, 24 Dec 2008/Notices
50. Franklin TJ, Snow GA (1981) *Biochemistry of antimicrobial action*; 3rd edn. Chapman and Hall, London, UK, p 217
51. Synowiecki J, Al-khatteb NAA (2003) Production, properties and some new applications of chitin and its derivatives. *Crit Rev Food Sci Nut* 43:144–171
52. Chen A, Taguchi T, Sakai K, Kikuchi K, Wang M, Miwa I (2003) Antioxidant activities of chitobiose and chitotriose. *Biol Pharm Bull* 26:1326–1330
53. Xu Q, Ma P, Yu W, Tan C, Liu H, Xiong C, Qiao Y, Du Y (2010) Chitooligosaccharides protect human embryonic hepatocytes against oxidative stress induced by hydrogen peroxide. *Mar Biotechnol* 12:292–298
54. Anraku M, Kabashima M, Namura H, Maruyama T, Otagiri M, Gebicki JM, Furutani N, Tomida H (2008) Antioxidant protection of human serum albumin by chitosan. *Int J Biol Macromol* 43:159–164
55. Razmi FA, Ngadi N, Wong S, Inuwa IM, Opotu LA (2019) Kinetics, thermodynamics, isotherm and regeneration analysis of chitosan modified pandan adsorbent. *J Clean Prod* 231:98–109
56. Braz EMA, Silva SCCC, Sousa Brito CAR, Brito LM, Barreto HM, Carvalho FAA, Santos LS, Lobo AO, Osajima JA, Sousa KS et al (2020) Spectroscopic, thermal characterizations and bacteria inhibition of chemically modified chitosan with phthalic anhydride. *Mater Chem Phys* 240:122053
57. Medeiros Borsagli FGL, Carvalho IC, Mansur HS (2018) Amino acid-grafted and N-acylated chitosan thiomers: construction of 3D bio-scaolds for potential cartilage repair applications. *Int J Biol Macromol* 114:270–282
58. Wang J, Wang L, Yu H, Zain ULA, Chen Y, Chen Q, Zhou,W.; Zhang, H.; Chen, X. Recent progress on synthesis, property and application of modified chitosan: an overview. *Int J Biol Macromol* 88:333–344
59. Wang W, Meng Q, Li Q, Liu J, Zhou M, Jin Z, Zhao K (2020) Review: chitosan derivatives and their application in biomedicine. *Int J Mol Sci* 21:487. <https://doi.org/10.3390/ijms21020487>
60. Shi L-E, Fang X-J, Xing L-Y, Chen M, Zhu D-S, Guo X-F, Zhao L-M, Tang Z-X (2011) Chitosan nanoparticles as drug delivery carriers for biomedical engineering. *J Chem Soc Pak* 33:929–934
61. Kunjachan S, Jose S, Lammers T (2010) Understanding the mechanism of ionic gelation for synthesis of chitosan nanoparticles using qualitative techniques. *Asian J Pharm* 4:148–153
62. Agnihotri SA, Mallikarjuna NN, Aminabhavi TM (2004) Recent advances on chitosan-based micro- and nanoparticles in drug delivery. *J Control Release* 100:5–28
63. Wu J, Zhang J, Zhang HJ, Jing Y (2011) Preparation, characterization and properties of crosslinked chitosan/palygorskite resin with tannic acid as template molecules. *Adv Mater Res* 335–336:111–115
64. Song T-Y, Yao C, Li X-s (2010) Electrospinning of zein/chitosan composite fibrous membranes. *Chin J Polym Sci* 28(2):171–179
65. Dobrovolskaya IP, Lebedeva IO, Yudin VE, Popryadukhin PV, Ivan’kova EM, Elovkovskii VY (2016) Electrospinning of composite nanofibers based on chitosan, poly(ethylene oxide), and chitin nanofibrils. *Polym Sci, Series A* 58(2):246–254
66. Lemma SM, Bossard F, Rinaudo M (2016) Preparation of pure and stable chitosan nanofibers by electrospinning in the presence of poly(ethylene oxide). *Int J Mol Sci* 17:1790
67. Kim MY, Lee J (2011) Chitosan fibrous 3D networks prepared by freeze drying. *Carbohydr Polym* 84(4):1329–1336
68. Song W, Jian X, Gao L, Zhang Q, Tong J, Ren L (2021) Preparation of freeze-dried porous chitosan microspheres for the removal of hexavalent chromium. *Appl Sci* 11:4217
69. Gonçalves C, Pereira P, Gama M (2010) Self-assembled hydrogel nanoparticles for drug delivery applications. *Materials* 3:1420–1460

70. Wang R, Zhang X, Zhu J, Bai J, Gao L, Liu S, Jiao T (2020) Facile preparation of self-assembled chitosan-based composite hydrogels with enhanced adsorption performances. *Colloids Surf* 598:124860
71. de Mesquita JP, Donnici CL, Pereira FV (2010) Biobased nanocomposites from layer-by-layer assembly of cellulose nanowhiskers with chitosan. *Biomacromolecules* 11:473–480
72. Poverenov E, Rutenberg R, Danino S, Horev B, Rodov V (2016) Gelatin-chitosan composite films and edible coatings to enhance the quality of food products: layer-by-layer vs. blended formulations. *Food Bioprocess Technol.* <https://doi.org/10.1007/s11947-014-1333-7>
73. Gol NB, Patel PR, Rao TV (2013) Improvement of quality and shelf-life of strawberries with edible coatings enriched with chitosan. *Postharvest Biol Technol* 85:185–195
74. Kashyap PL, Xiang X, Heiden P (2015) Review chitosan nanoparticle-based delivery systems for sustainable agriculture. *Int J BiolMacromol* 77:36–51
75. Wanichpongpan P, Suriyachan K, Chandkrachang S, Uragami T, Kurita K, Fukamizo T (2001) Effects of chitosan on the growth of gerbera flower plant (*Gerbera jamesonii*). In: *Chitin and chitosan in life science*, pp 198–201
76. Phothi R, Theerakarunwong CD (2017) Effect of chitosan on physiology, photosynthesis and biomass of rice (*Oryza sativa* L.) under elevated ozone. *Aust J Crop Sci* 11:624–630
77. Choudhary RC, Kumaraswamy RV, Kumari S, Pal SSS, Raliya AR, Biswas P, Saharan V (2017) Cu-chitosan nanoparticle boost defense responses and plant growth in maize (*Zea mays* L). *Sci Rep* 7:9754–9765
78. Asgari-Targhi G, Iranbakhsh A, Ardebili ZO (2018) Potential benefits and phytotoxicity of bulk and nano-chitosan on the growth, morphogenesis, physiology, and micropropagation of *Capsicum annuum*. *Plant Physiol Biochem* 127:393–402
79. Deshpande P, Dapkekar A, Oak MD, Paknikar KM, Rajwade JM (2017) Zinc complexed chitosan/TPP nanoparticles: a promising micronutrient nanocarrier suited for foliar application. *Carbohydr Polym* 165:394–401
80. Salachna P, Zawadzinska A (2014) Effect of chitosan on plant growth, flowering and corms yield of potted freesia. *J Ecol Eng* 15:97–102
81. Sultana S, Islam M, Khatun MA, Hassain M, Huque R (2017) Effect of foliar application of oligo-chitosan on growth, yield and quality of tomato and eggplant. *Asian J Agric Res* 11(2):36–42
82. Bandara S, Hongbo D, Carson L, Bradford D, Kommalapati R (2020) Agricultural and biomedical applications of chitosan-based nanomaterials, nanomaterials (basel). *Natl Libr Med* 10(10):1903
83. Choudhary RC, Kumaraswamy RV, Kumari S, Sharma SS, Pal A, Raliya R, Biswas P, Saharan V (2019) Zinc encapsulated chitosan nanoparticle to promote maize crop yield. *Int J Biol Macromol* 0141–8130
84. Abdel-Aziz HM, Hasaneen MN, Omer AM (2016) Nano chitosan-NPK fertilizer enhances the growth and productivity of wheat plants grown in sandy soil. *Span J Agric Res* 14(1):2171–9292
85. Choudhary RC, Kumaraswamy RV, Kumari S, Sharma SS, Pal A, Raliya R, Biswas P, Saharan V (2017) Cu-chitosan nanoparticle boost defense responses and plant growth in maize (*Zea mays* L.) *Natl Libr Med* 29, 7(1):9754
86. Geries LSM, Omnia HSM, Mareya RA (2020) Soaking and foliar application with chitosan and nano chitosan to enhancing growth, productivity and quality of onion crop. *Plant Archives* 20:3584–3591
87. Parvin MA, Zakir HM, Naznin Sultana, Kafi A, Seal HP (2019) Effects of different application methods of chitosan on growth, yield and quality of tomato (*Lycopersicon esculentum* Mill.). *Arch Agric Environ Sci* 4(3):261–267
88. Abdelbasset E, Hadrami LR, Adam IE, Hadrami FD (2018) Chitosan in plant protection. *Mar Drugs* 8:968–987
89. Divya K, Jisha MS (2018) Chitosan nanoparticles preparation and applications. *Environ Chem Lett* 16:101–112



90. Meng XH, Yang LY, Kennedy JF, Tian SP (2010) Effects of chitosan and oligochitosan on growth of two fungal pathogens and physiological properties in pear fruit. *Carbohydr Polym* 81:70–75
91. Reglinski T, Elmer PAG, Taylor JT, Wood PN, Hoyte SM (2010) Inhibition of *Botrytis cinerea* growth and suppression of botrytis bunch rot in grapes using chitosan. *Plant Pathol* 59:882–890
92. Berger LRR, Stamford NP, Willadino LG, Laranjeira D, de Lima MAB, Malheiros SMM, de Oliveira WJ, Stamford TCM (2016) Cowpea resistance induced against *Fusarium oxysporum* f. sp. tracheiphilum by crustacean chitosan and by biomass and chitosan obtained from *Cunninghamella elegans*. *Biol Control* 92:45–54
93. Hidangmayum A, Dwivedi P, Katiyar D, Hemantaranjan A (2019) Application of chitosan on plant responses with special reference to abiotic stress. *Physiol Mol Biol Plants* 25:313–326
94. Esyanti RR, Dwivany FM, Mahani S, Nugrahapraja H, Meitha K (2019) Foliar application of chitosan enhances growth and modulates expression of defense genes in chilli pepper (*Capsicum annuum* L.). *Aust J Crop Sci* 13:55–60
95. Ali A, Noh NM, Mustafa MA (2015) Antimicrobial activity of chitosan enriched with lemongrass oil against anthracnose of bell pepper. *Food Pack Shelf Life* 3:56–61
96. Liu H, Tian W, Li B, Wu G, Ibrahim M, Tao Z, Wang Y, GuanlinXie HL, Sun G (2012) Anti-fungal effect and mechanism of chitosan against the rice sheath blight pathogen, *Rhizoctonia solani*. *Biotechnol Lett* 34(12):2291–2298
97. Jia Z, Shen D, Xu W (2001) Synthesis and antibacterial activities of quaternary ammonium salt of chitosan. *Carbohydr Res* 333:1–6
98. Bhaskara MVJ, Arul J, Angers P, Couture L (1999) Chitosan treatment of wheat seeds induces resistance to *Fusarium graminearum* and improves seed quality. *J Agric Food Chem* 47:1208–1216
99. Li K, Xing R, Liu S, Li P (2020) Chitin and chitosan fragments responsible for plant elicitor and growth stimulator. *J Agric Food Chem* 68(44):12203–12211
100. Kumar GP, Desai S, Moerschbacher BM, Eddine-El Gueddari N (2019) Seed treatment with chitosan synergizes plant growth promoting ability of *Pseudomonas aeruginosa*-P17 in sorghum (*Sorghum bicolor* L.). *BioRxiv* 1–43
101. Guan YJ, Hu J, Wang XJ, Shao CX (2009) Seed priming with chitosan improves maize germination and seedling growth in relation to physiological changes under low temperature stress. *J Zhejiang Univ Sci* 10(6):427–433
102. Zeng D, Luo X, Tu R (2012) Application of bioactive coatings based on chitosan for soybean seed protection. *Int J Carbohydr Chem* 2012:1–5
103. Gonzalez LM, Guerrero YR, Rodríguez AF, Vázquez MN (2015) Effect of seed treatment with chitosan on the growth of rice (*Oryza sativa* L.) seedlings cv. inca lp-5 in saline medium. *CultivosTropicales* 36:136–142
104. Van Phu D, Du BD, Le Nghiem AT, Van Tam H, Hien NQ (2017) Preparation and foliar application of oligochitosan—nanosilica on the enhancement of soybean seed yield. *Int J Environ Agric Biotechnol (IJEAB)* 2:1
105. Pereira Santo AE, Oliveira HC, Fraceto LF (2019) Polymeric nanoparticles as an alternative for application of gibberellic acid in sustainable agriculture: a field study. *Sci Rep* 9(1):7135
106. Sun B, Zhang L, Yang L, Zhang F, Norse D, Zhu Z (2012) Agricultural non-point source pollution in China: causes and mitigation measures. *Ambio* 41:370–379
107. Ha NMC, Nguyen ThiHuyen, Wang S-L, Nguyen AD (2019) Preparation of NPK nanofertilizer based on chitosan nanoparticles and its effect on biophysical characteristics and growth of coffee in green house. *Res Chem Intermed* 45:51–63
108. Deshpande P, Dapkekar A, Oak MD, Paknikar KM, Rajwade JM, do Espírito Santo Pereira A, Oliveira HC, Fraceto LF (2019) Zinc complexed chitosan/TPP nanoparticle: a promising micronutrient nanocarrier suited for foliar application. *Carbohydr Polym* 9(165):394–401
109. Choudhary RC, Kumaraswamy RV, Kumari S, Sharma SS, Pal A, Raliya R, Biswas P, Saharan V (2017) Cu-chitosan nanoparticle boost defense responses and plant growth in maize (*Zea mays* L.). *Sci Rep* 7:9754

110. Sathiyabama M, Manikandan A (2018) Application of copper-chitosan nanoparticles stimulate growth and induce resistance in finger millet (*Eleusine coracana* Gaertn.) plants against blast disease. *J Agric Food Chem* 66(8):1784–1790
111. Sajid M, Basit A, Ullah Z, Shah ST, Ullah I, Mohamed HI, Ullah I (2020) Chitosan-based foliar application modulated the yield and biochemical attributes of peach (*Prunus persica* L.) cv. Early Grand. *Bull Natl Res Centre* 44:15
112. Saharan VG, Sharma M, Yadav MK, Choudhary SS, Sharma A, Pal R, Raliya P, Biswas P (2015) Synthesis and in vitro antifungal efficacy of Cu-chitosan nanoparticles against pathogenic fungi of tomato. *Int J Biol Macromol* 75:346–353
113. Saharan V, Kumaraswamy R, Choudhary RC, Kumari S, Pal A, Raliya R, Biswas P (2016) Cu-chitosan nanoparticle mediated sustainable approach to enhance seedling growth in maize by mobilizing reserved food. *J Agr Food Chem* 64:6148–6155
114. Qavami H, Badii N, Labbafi MR, Mehregan M, Tavakoli M, Mehrafarin A, Trakia (2017) Overview on chitosan as a valuable ingredient and biostimulant in pharmaceutical industries and agricultural products. *J Sci* 83–91
115. Tocci N, Auria D, Simonetti FD, Panella G, Palamara S, Debrassi AT, Debrassi A, Rodrigues A, Filho CA, Pasqua, G (2013) Bioassay-guided fractionation of extracts from *Hypericum perforatum* in vitro roots treated with carboxymethylchitosans and determination of antifungal activity against human fungal pathogens. *Plant Physiol Biochem* 70:342–347
116. Putalun W, Luealon W, De-Eknamkul W, Tanaka SH (2007) Improvement of artemisinin production by chitosan in hairy root cultures of *Artemisia annua* L. *Biotech Lett* 29:1143–1146
117. Goni O, Quille P, Shane O (2016) Connell production of chitosan oligosaccharides for inclusion in a plant biostimulant. *Pure Appl Chem* 88(9):881–889
118. Rahman M, Mukta JA, Sabir AA, Gupta DR, Mohi-Ud-Din M, Hasanuzzaman M, Miah MG, Rahman M, Islam MT (2018) Chitosan biopolymer promotes yield and stimulates accumulation of antioxidants in strawberry fruit. *Natl Libr Med* 13(9):7
119. Zohara F, Surovy MZ, Khatun A, Prince Md FRK (2019) Chitosan biostimulant controls infection of cucumber by *Phytophthora capsici* through suppression of asexual reproduction of the pathogen. *Natl Libr Med* 13(9)
120. Wojdyla AT (2004) Chitosan (biochikol 020 PC) in the control of some ornamental foliage diseases. *Commun Agric Appl Biol Sci* 69:705–715
121. Gunupuru LR, Patel JS, Sumarah MW, Renaud JB, Mantin EG, Prithiviraj B (2019) A plant biostimulant made from the marine brown algae *Ascophyllum nodosum* and chitosan reduce *Fusarium* head blight and mycotoxin contamination in wheat. *PLoS ONE* 14(9): e0220562
122. Xu E, Mou B (2018) Chitosan as soil amendment affects lettuce growth, photochemical efficiency, and gas exchange. *Am Soc Hortic Sci* 28:476–480
123. Mehregan M, Mehrafarin A, Labbafi MR, Naghdi Badi H (2017) Effect of different concentrations of chitosan biostimulant on biochemical and morphophysiological traits of stevia plant [*Stevia rebaudiana* Bertoni]. *J Med Plants* 16(62):169–181
124. Hassan O, Chang T (2017) Chitosan for eco-friendly control of plant disease. *Asian J Plant Pathol* 11:3–70. Ye Z, Guo J, Wu D, Tan M, Xiong X, Yin Y, He G (2015) Photo-responsive shell cross-linked micelles based on carboxymethyl chitosan and their application in controlled release of pesticide. *Carbohydr Polym* 132:520–528
125. Namasivayam KR, Aruna A, Gokila (2014) Evaluation of silver nanoparticles-chitosan encapsulated synthetic herbicide paraquat (AgNp-CS-PQ) preparation for the controlled release and improved herbicidal activity against *Eichhornia crassipes*. *Res J Biotechnol* 9(9)
126. Maruyama CR, Guilger M, Pascoli M, Bileshy-José N, Abhilash PC, Fraceto LF, de Lima R (2016) Nanoparticles Based on Chitosan as Carriers for the Combined Herbicides Imazapic and Imazapyr. *Sci Rep.* 6:23854
127. Rabea EI, Badawy MET, Stevens CV, Smagghe G, Steurbaut W (2003) Chitosan as antimicrobial agent: applications and mode of action. *Biomacromolecules* 4:1457–1465
128. Laflamme P, Benhamou N, Bussières G, Dessureault M (2000) Differential effect of chitosan on root rot fungal pathogens in forest nurseries. *Can J Bot* 77:1460–1468

129. Abd-El-Kareem F, Hagga WM (2014) Chitosan and citral alone or in combination for controlling early blight disease of potato plants under field conditions. *Res J Pharmaceut Biol Chem Sci* 5:941–949
130. Sultana A, Munshi MH, Kamruzzaman Md ASM, Bari F, Issak M (2020) Residual effect of raw material of chitosan powder on chemical properties of soil under rice-rice cropping system. *Res Agric Livest Fish* 7:33–42
131. Khati P, Chaudhary P, Gangola S, Bhatt P, Sharma A (2017) Nanochitosan supports growth of *Zea mays* and also maintains soil health following growth. *3 Biotech* 7(1):81
132. Shariatmadari N, Reza M, Tasuji A, Ghadir P, Javadi AA (2020) Experimental study on the effect of chitosan biopolymer on sandy soil stabilization. In: A E3S web of conferences, vol 195, p 06007
133. Mulawarman HJ, Bell D, Kopp-Holtwiesche B, Sikora RA (2001) Effects of natural products on soil organisms and plant health enhancement. *Biol Wet* 66(2b):609–617
134. Kusumastuti Y, Istiani A, Rochmadi, Purnomo CW (2019) Chitosan-based polyion multilayer coating on NPK fertilizer as controlled released fertilizer. *Adv Mater Sci Eng* 1–8
135. Heba MM, Abdel-Aziz MNA, Hasaneen AO, M, (2016) Nano chitosan-NPK fertilizer enhances the growth and productivity of wheat plants grown in sandy soil. *Span J Agric Res* 14(1):9
136. Chen YR, Yaan, Yuan S, Sichuan, Chengdu, Liu HM, Yaan, Chen ZY (2016) A combination of chitosan and chemical fertilizers improves growth and disease resistance in *Begonia x hiemalis* Fotsch. *Food and Agricultural Organization of the UN*, pp 1–10
137. Miransari M (2014) Smith DL Plant hormones and seed germination. *Environ Exp Bot* 99:110–121
138. Boonlertnirun S, Suvannasara R, Promsomboon P, Boonlertnirun K (2011) Application of chitosan for reducing chemical fertilizer uses in waxy corn growing. *Thai J Agric Sci* 44(5):22–28
139. Dhlamini B, Paumo HK, Katata-Seru L, Kutu FR (2020) Sulphate-supplemented NPK nanofertilizer and its effect on maize growth. *Mater Res Express* 7(9)
140. Mondal M, Malek M, Puteh A, Ismail M, Ashrafuzzaman M, Naher L (2012) Effect of foliar application of chitosan on growth and yield in okra. *Aust J Crop Sci* 6:918–921
141. Amini J (2015) Induced resistance in potato plants against verticillium wilt invoked by chitosan and Acibenzolar-S-methyl. *Aust J Crop Sci* 9:570–576
142. Kavyashri VV, Nagaraju N (2019) Management of cucumber mosaic virus (CMV) disease in chilli through biotic defense inducers. *Int J Curr Microbiol App Sci* 8(1):297–313
143. Badawy ME, Rabea EI, Taktak NE, El-Nouby MA (2016) the antibacterial activity of chitosan products blended with monoterpenes and their biofilms against plant pathogenic bacteria. *Hindawi Publishing Corporation Scientifica*, pp 1–10
144. Chowdappa P, Shivakumar Gowda, Chethana CS, Madhura S (2014) Antifungal activity of chitosan-silver nanoparticle composite against *Colletotrichum gloeosporioides* associated with mango anthracnose *Afr J Microbiol Res* 8(17):1803–1812
145. Dzung PD, Van Phu D, Du BD, Ngoc LS, Duy NN, Hiet HD, Nghia DH, Thang NT, Van Le B, Hien NQ (2017) Effect of foliar application of oligochitosan with different molecular weight on growth promotion and fruit yield enhancement of chili plant. *Plant Prod Sci* 20:389–395
146. Sahab AF, Waly AI, Sabbour MM, Lubna S, Nawar, (2015) Synthesis, antifungal and insecticidal potential of chitosan (CS)-g-poly (acrylic acid) (PAA) nanoparticles against some seed borne fungi and insects of soybean. *Int J Chem Tech* 8(2):589–598
147. Zeng D, Luo X, Tu R (2012) Application of bioactive coatings based on chitosan for soybean seed protection. *Int J Carbohydr Chem* 1–5
148. El Amerany F, AbdelilahMeddich SW, Porzel A, Taourirte M, Rhazi M, Hause B (2020) Foliar application of chitosan increases tomato growth and influences mycorrhization and expression of endochitinase-encoding genes. *Int J Mol Sci* 21(2):535
149. Lafontaine PF, Benhamou N (1996) Chitosan treatment: an emerging strategy for enhancing resistance of greenhouse tomato plants to infection by *Fusarium oxysporum* f. sp. *radicislycopersici*. *Biocontrol Sci Technol* 111–124

150. Asmaa Fahmy A, Nosir WS (2021) Influence of chitosan and micronutrients (Fe + Zn) concentrations on growth, yield components and volatile oil of lavender plant. *Sci J Flowers Ornamental Plants* 8(1):87–100
151. Wang P, Lombi E, Zhao F-J, Kopittke PM (2016) Nanotechnology: a new opportunity in plant sciences. *Trends Plant Sci* 21(8):699–712
152. Raliya R, Tarafdar J, Gulecha K, Choudhary K, Rameshwar R, Prakash M, Saran R (2013) Scope of nanoscience and nanotechnology in agriculture. *J Appl Biol Biotechnol* 1(3):041–044
153. Khot LR, Sankaran S, Maja JM, Ehsani R, Schuster EW (2012) Applications of nanomaterials in agricultural production and crop protection: a review. *Crop Prot* 35:64–70
154. Kumar S, Nehra M, Dilbaghi N, Marrazza G, Hassan AA, Kim K-H (2018) Nano-based smart pesticide formulations: emerging opportunities for agriculture. *J Control Release* 294:131–153
155. Arruda SCC, Silva ALD, Galazzi RM, Azevedo RA, Arruda MAZ (2015) Nanoparticles applied to plant science: a review. *Talanta* 131:693–705
156. Maghsoodi MR, Lajayer BA, Hatami M, Mirjalili MH (2019) Challenges and opportunities of nanotechnology in plant-soil mediated systems: beneficial role, phyto-toxicity and phyto-extraction. In: *Advances in phyto nanotechnology*. Elsevier, pp 379–404
157. Ghormade V, Deshpande MV, Paknikar KM (2011) Perspectives for nano-biotechnology enabled protection and nutrition of plants. *Biotechnol Adv* 29(6):792–803
158. Ghosh M, Jana A, Sinha S, Jothiramajayam M, Nag A, Chakraborty A, Mukherjee A, Mukherjee A (2016) Effects of ZnO nanoparticles in plants: cytotoxicity, genotoxicity, deregulation of antioxidant defences, and cell-cycle arrest. *Mutat Res Genet Toxicol Environ Mutagen* 807:25–32
159. Kah M, Hofmann T (2014) Nanopesticide research: current trends and future priorities. *Environ Int* 63:224–235
160. Prasad R, Kumar V, Prasad KS (2014) Nanotechnology in sustainable agriculture: present concerns and future aspects. *Afr J Biotechnol* 13(6):705–713
161. Perez JVD (2017) Response surface methodology as a powerful tool to optimize the synthesis of polymer-based graphene oxide nanocomposites for simultaneous removal of cationic and anionic heavy metal contaminants. *RSC Adv* 7:1848018490
162. Shahzad A (2017) Heavy metals removal by EDTA-functionalized chitosan graphene oxide nanocomposites. *RSC Adv* 7:97649771
163. Sureshkumar V, Kiruba Daniel SCG, Ruckmani K, Sivakumar M (2016) Fabrication of chitosan magnetite nanocomposite strip for chromium removal. *Appl Nanosci* 6:277285
164. Salah TA, Mohammad AM, Hassan MA, El-Anadouli BE (2014) Development of nano-hydroxyapatite/ chitosan composite for cadmium ions removal in wastewater treatment. *J Taiwan Inst Chem Eng* 45:15711577
165. Aliabadi MM, Irani M, Ismaeili J, Piri H, Parnian MJ (2013) Electrospun nanofiber membrane of PEO/chitosan for the adsorption of nickel, cadmium, lead and copper ions from aqueous solution. *Chem Eng J* 220:237243
166. Chen A, Zeng G, Chen G, Hu X, Yan M, Guan S, Shang C, Lu L, Zou Z, Xie G (2012) Novel thiourea-modified magnetic ion-imprinted chitosan/TiO<sub>2</sub> composite for simultaneous removal of cadmium and 2,4-dichlorophenol. *Chem Eng J* 191:8594
167. Daniele CS (2019) Alves, Adsorption of phenol onto chitosan hydrogel scaffold modified with carbon nanotubes. *J Environ Chem Eng* 7(6):103460
168. Pereira FAR, Sousa KS, Cavalcanti GGRS, França DB, Queiroga LNF, Santos IMG, Fonseca MG, Jaber M (2017) Green biosorbents based on chitosan-montmorillonite beads for anionic dye removal. *J Environ Chem Eng* 5:33093318
169. Nagarpita MV, Roy P, Shruthi SB, Sailaja RRN (2017) Synthesis and swelling characteristics of chitosan and CMC grafted sodium acrylate-co-acrylamide using modified nanoclay and examining its efficacy for removal of dyes. *Int J Biol Macromol* 102:12261240
170. Abbasi M (2017) Synthesis and characterization of magnetic nanocomposite of chitosan/SiO<sub>2</sub>/carbon nanotubes and its application for dyes removal. *J Cleaner Prod* 145:105113

171. Jiang Y, Gong J-L, Zeng G-M, Ou X-M, Chang Y-N, Deng C-H, Zhang J, Liu H-Y, Huang S-Y (2016) Magnetic chitosan/graphene oxide composite for anti-microbial and dye removal applications. *Int J Biol Macromol* 82:702–710
172. Wang Y, Xia G, Wu C, Sun J, Song R, Huang W (2015) Porous chitosan doped with graphene oxide as highly effective adsorbent for methyl orange and amido black 10B. *Carbohydr Polym* 115:686693
173. Soltani RDC, Khataee AR, Safari M, Joo SW (2013) Preparation of bio-silica/chitosan nanocomposite for adsorption of a textile dye in aqueous solutions. *Int Biodeterior Biodegrad* 85:383391
174. Fan L et al (2013) Synthesis of magnetic beta-cyclodextrin chitosan / graphene oxide as nanoadsorbent and its application in dye adsorption and removal. *Colloids Surf B* 103:601607
175. Sundquist ET, Burruss RC, Faulkner SP, Gleason RA, Harden JW, Kharaka YK, Tieszen LL, Waldrop MP (2008) Carbon sequestration to mitigate climate change: U.S. Geological Survey. *Fact Sheet* 2008–3097, 4p (1)
176. Ibrahim NA, Eid BM, Abd El-Aziz E, Abou Elmaaty TM, Ramadan SM (2017) Loading of chitosan—nano metal oxide hybrids onto cotton/polyester fabrics to impart permanent and effective multifunction. *Int J Biol Macromol* 105(1):769–776
177. Liu H, Huang J, Mao J, Chen Z, Chen G, Lai Y (2019) Transparent antibacterial nanofiber air filters with highly efficient moisture resistance for sustainable particulate matter capture. *iScience* 19:214–223
178. Al-Sherbini AA, Ghannam HEA, El-Ghanam GMA, El-Ella AA, Youssef AM (2019) Utilization of chitosan/Ag bio-nano-composites as eco-friendly photocatalytic reactor for bactericidal effect and heavy metals removal. *Heliyon* 5:e01980
179. Wang Z, Yan F, Pei H, Li J, Cui Z, He B (2018) Antibacterial and environmentally friendly chitosan/polyvinyl alcohol blend membranes for air filtration. *Carbohydr Polym* 198:241–248
180. Mishra D, Yadav R, Singh RP, Taneja A, Tiwari R, Khare P (2021) The incorporation of lemongrass oil into chitosan-nanocellulose composite for bioaerosol reduction in indoor air. *Environ Pollut* 285:117407
181. Mohraz MH, Golbabaee F, Yu JJ, Mansournia MA, Zadeh AS, Dehghan SF (2019) Preparation and optimization of multifunctional electrospun polyurethane/chitosan nanofibers for air pollution control applications. *Int J Environ Sci Technol* 16:681–694
182. Zhao Y, Xu G, Wang S, Yi X, Wu W (2018) Chitosan oligosaccharides alleviate PM<sub>2.5</sub>-induced lung inflammation in rats. *Air Filtr* 25:34221–34227
183. Xu Y, Mao H, Yang C, Du H, Wang H, Tu J (2020) Effects of chitosan nanoparticle supplementation on growth performance, humoral immunity, gut microbiota and immune responses after lipopolysaccharide challenge in weaned pigs. *J Anim Physiol Anim Nutr (Berl)* 104(2):597–605
184. Shi-bin Y, Hong C (2012) Effects of dietary supplementation of chitosan on growth performance and immune index in ducks. *Afr J Biotech* 11(14):3490–3495
185. Li T, Na R, Yu P, Shi B, Yan S, Zhao Y, Xu Y (2015) Effects of dietary supplementation of chitosan on immune and antioxidative function in beef cattle. *Czech J Anim Sci* 60(1):38–44
186. Del Valle TA, de Paiva PG, de Jesus EF, de Almeida GF, Zanferari F, Costa AGBVB, Bueno ICS, Rennó FP (2017) Dietary chitosan improves nitrogen use and feed conversion in diets for mid-lactation dairy cows. *Livestock Sci* 201:22–29
187. Hu S, Wang Y, Wen X, Wang L, Jiang Z, Zheng Z (2018) Effects of low-molecular-weight chitosan on the growth performance, intestinal morphology, and barrier function, cytokine expression and antioxidant system of weaned piglets. *BMC Vet Res* 14:215
188. Osho SO, Adeola O (2019) Impact of dietary chitosan oligosaccharide and its effects on coccidia challenge in broiler chickens. *Br Poult Sci* 60(6): 766–776
189. Lokman IH, Ibitoye EB, Hezmee MNM, Goh YM, Zuki ABZ, Jimoh AA (2019) Effects of chitin and chitosan from cricket and shrimp on growth and carcass performance of broiler chickens. *Trop Animal Health Prod* 51:2219–2225 (Animal Fodder)
190. Hydari S, Sharifard H, Nabavinia M, Parvizi Mr (2012) A comparative investigation on removal performances of commercial activated carbon, chitosan biosorbent and chitosan/activated carbon composite for cadmium. *Chem Eng J* 193–194:276–282

191. Auta M, Hameed BH (2013) Coalesced chitosan activated carbon composite for batch and fixed-bed adsorption of cationic and anionic dyes. *Colloids Surf B* 105:199–206
192. Fatombi JK, Idohou EA (2019) Adsorption of indigo carmine from aqueous solution by chitosan and chitosan/activated carbon composite: kinetics, isotherms and thermodynamics studies. *Fibers Polym* 20:1820–1832
193. de Freitas FP, Carvalho AMML, de Cassia Oliveira Carneiro A, Xisto MF, Cana WD (2021) Adsorption of neutral red dye by chitosan and activated carbon composite films. *Heliyon* 7:e07629
194. Elwakeel KZ, Aly MH, El-Howety MA, El-Fadaly E, Al-Said A (2018) Synthesis of chitosan@activated carbon beads with abundant amino groups for capture of Cu(II) and Cd(II) from aqueous solutions. *J Polym Environ* 26:3590–3602
195. Venault A, Vachoud L, Pochat C, Bouyer D, Faur C (2008) Elaboration of chitosan/activated carbon composites for the removal of organic micro-pollutants from waters. *Environ Technol* 29(12):1285–1296
196. Palansooriya KN, Kim S, Igalavithana AD, Hashimoto Y, Choi YE, Mukhopadhyay R, Sarkar B, Ok YS (2021) Fe(III) loaded chitosan-biochar composite fibers for the removal of phosphate from water. *J Hazard Mater* 415:125464
197. Zhu C, Lang Y, Liu B, Zhao H (2019) Ofloxacin adsorption on chitosan/biochar composite: kinetics, isotherms, and effects of solution chemistry. *Polycyclic Aromat Compd* 39:287–297
198. Yang Y, Zhang Y, Wang G, Yang Z, Xian J, Yang Y (2021) Adsorption and reduction of Cr(VI) by a novel nanoscale FeS/chitosan/biochar composite from aqueous solution. *J Environ Chem Eng* 9(4):105407
199. Liu S, Huang B (2017) Enhancement of As(v) adsorption from aqueous solution by a magnetic chitosan/biochar composite. *RSC Adv* 7:10891–10900
200. Arabyarmohammadi H, Darban AK (2018) Utilization of a novel chitosan/clay/biochar nanobiocomposite for immobilization of heavy metals in acid soil environment. *J Polym Environ* 26:2107–2119
201. Nair V, Panigrahy A, Vinu R (2014) Development of novel chitosan-lignin composites for adsorption of dyes and metal ions from wastewater. *Chem Eng J* 254:491–502
202. Chitosan-lignin-titania nanocomposites for the removal of brilliant black dye from aqueous solution. *Int J Biol Macromol* 120:1659–1666
203. Crouvisier-Urien K, Bodart PR (2016) Biobased composite films from chitosan and lignin: antioxidant activity related to structure and moisture. *ACS Sustain Chem Eng* 4:6371–6381
204. Zhang D, Wang L (2020) Novel polyethyleneimine functionalized chitosan-lignin composite sponge with nanowall-network structures for fast and efficient removal of Hg(II) ions from aqueous solution. *Environ Sci: Nano* 7:793–802
205. Sohni S, Hashim R (2019) Chitosan/nano-lignin based composite as a new sorbent for enhanced removal of dye pollution from aqueous solutions. *Int J Biol Macromol* 132:1304–1317
206. Lin S, Chen L, Huang L, Cao S (2015) Novel antimicrobial chitosan-cellulose composite films bioconjugated with silver nanoparticles. *Ind Crops Prod* 70:395–403
207. Trana CD, Dur S (2013) Chitosan-cellulose composite materials: preparation, characterization and application for removal of microcystin. *J Hazard Mater* 252–253:355–366
208. Fan X, Li Y (2020) Rapid hemostatic chitosan/cellulose composite sponge by alkali/urea method for massive haemorrhage. *Int J Biol Macromol* 164:2769–2778
209. Zhuang S, Zhu K (2021) Fibrous chitosan/cellulose composite as an efficient adsorbent for Co(II) removal. *J Clean Prod* 285:124911
210. Chen Y, Zhua H, Xiong J (2017) Preparation and application of novel chitosan-cellulose composite materials to adsorb Pb and Cr ions from water. *J Bioresources and Bioprod* 2(4):175–183

**Part VIII**  
**Applications in Therapeutics**  
**and Diagnostics**

# Chapter 29

## Carbon-Based Porous Materials in Biomedical Applications: Concept and Recent Advancements



Jnanraj Borah and Anupam Chetia

### 1 Introduction

Nanoscience, or the control of matter at the nanoscale scale (one billionth, or  $10^9$ th of a metre), has accelerated the development of carbon materials over the last couple of decades [1]. Even research done on one of carbon allotrope, namely graphene has been awarded Nobel Prize in Physics in the year 2010 [2]. Since the beginning of 1990, significant efforts have been made to investigate porous carbon materials [3–5]. Porous carbon materials (PCMs) are pervasive and essential in several fields due to their unique capabilities [5]. Their use in interdisciplinary fields like material science, physical chemistry, membrane science, and many more are attributed to their outstanding chemical and physical properties [1]. Porous carbon materials are utilized in many applications, including supercapacitor and electrochemical applications, catalysis supports, pollutant adsorption, etc. [6–10]. Their wide availability is also a considerable advantage for their use in diverse fields [5]. Particularly in biomedical porous carbon materials are explored extensively because of a number of their intriguing properties, for example, regular geometry, adjustable pore size, pores that are uniform and interpenetrating, abundant framework compositions and high surface area, as well as their excellent biocompatibility which are highlighted in Fig. 1 [6, 10, 11]. They can interact with different guest species (for example atoms as well as molecules or larger molecules), as compared to their bulk counterparts, not only with the external surface but also on the entire inner channels. Porous carbon materials may be a combination product for two types or the entire three types of pores or contain just one type of porous system. When such porous systems exist in

---

J. Borah (✉)

Department of Physics, Gauhati University, Guwahati, Assam 781014, India

e-mail: [jnanrajborah@gmail.com](mailto:jnanrajborah@gmail.com); [jnanrajborah@gauhati.ac.in](mailto:jnanrajborah@gauhati.ac.in)

A. Chetia

Department of Physics, Indian Institute of Technology, Jodhpur, Rajasthan 342037, India

© The Author(s), under exclusive license to Springer Nature Singapore Pte Ltd. 2023

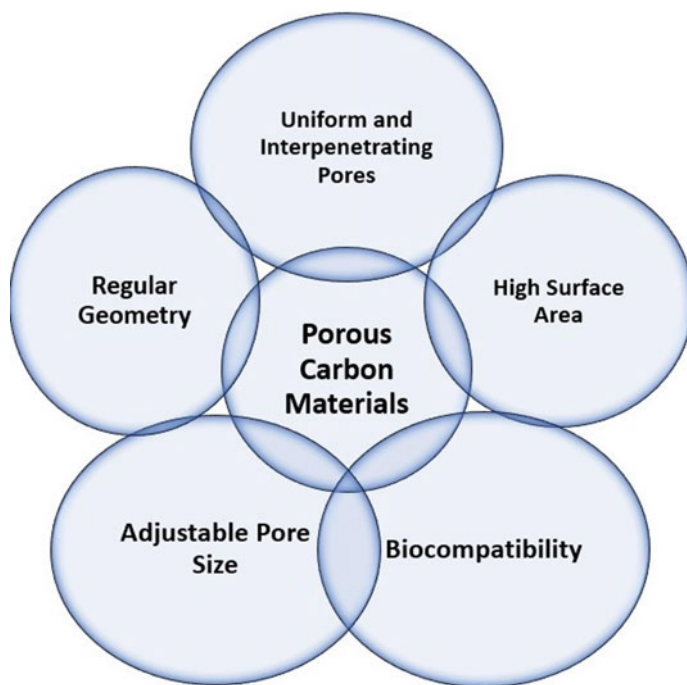
815

A. N. Grace et al. (eds.), *Handbook of Porous Carbon Materials*,

Materials Horizons: From Nature to Nanomaterials,

[https://doi.org/10.1007/978-981-19-7188-4\\_29](https://doi.org/10.1007/978-981-19-7188-4_29)





**Fig. 1** Few intriguing properties of porous carbon materials

the form of a networked or interconnected porous system, these materials are referred to be porous materials in a hierarchical way. Furthermore, the current porous system or porous systems combination can be arranged in order or disordered in terms of size, shape, and location [6].

At high temperatures, pyrolysis, as well as chemical or physical activation of organic precursors, yield traditional carbon materials with pores, such as activated carbon, carbon molecular sieves, and other porous carbon materials. Coal, wood, fruit shells, and polymers are examples of organic precursors [12–14]. These carbon compounds typically possess a wide range of pore sizes in the micropore and mesopore ranges, where micropore corresponds to the pore size  $<2$  nm and mesopore correspond to the pore range 2–50 nm [5]. Porous carbon materials can be made in one of two ways: nanocasting, which uses a hard template (HT) to construct the carbon structure, or direct synthesis, which uses a soft template (ST). Zeolite and silica are the most common HTs utilized in the nanocasting procedure [6, 15]. The synthesis of porous carbon material using sol–gel synthesis, in which a ST is employed to form the porous structure, is referred to as direct synthesis. A polymer/surfactant, as well as a carbon precursor and a polymerization agent, make up a ST. In addition to porous carbon material created using the aforementioned ways, porous carbon material created using naturally occurring resources is also accessible. Coconut husk, paddy husk, tea trash, and other naturally occurring resources are offered as low-cost materials [6].

A result of their physiochemical and biological characteristics that are unique and different, including bigger surface area and large pores with adjustable porous structure, the presence of favourable functional groups comprising  $\pi$ - $\pi$  stacking and an effectively modifiable surface, high thermal convertibility, unique optical qualities, high chemical stability, high biocompatibility, and mechanical durability, etc., these materials have gotten a lot of attention. The biological applications of such PCM are summarised in this short review.

## 2 Classification of Porous Materials

Porous materials are those that have channels or cavities termed as pores. Pores are voids in materials that occur between particles of any shape. The porosity of the materials is represented by these vacant spots, defined as the proportion of air inside the material that corresponds to the total volume filled by the material's voids divided by the total volume of the material. The zone of porous space is continuous where there is no solid substance located [16, 17].

The diameter of the pores is used to classify porous materials, in accord with the "International Union of Pure and Applied Chemistry-USA (IUPAC)". The categories are microporous, mesoporous, and microporous. The pore size of microporous materials is less than 2 nm, pore diameters in mesoporous materials vary from 2 to 50 nm, whereas pore sizes in macroporous materials are higher, exceeding 50 nm. Based on this classification porous carbon are categorized into micro, meso, and macro porous carbon and are depicted in Fig. 2 [18, 19].



**Fig. 2** Classification of porous materials based on pore diameter

### 3 Carbon-Based Porous Materials

#### 3.1 Mesoporous Carbon (MC) Materials

IUPAC's official definition of the word "**Mesoporous Carbon**" is a solid material that may be disordered or ordered and made up of networks of any number of pores with a distribution of 2–50 nm [20]. Ryoo et al. [21] published the very first complete structural composition of highly ordered MC material employing a mesoporous silica template, and since then, there has been much focus on the synthetically manufactured methodologies and their applications [22–25]. Since research had to begin quickly, for the purpose of developing mesoporous using carbon precursors and the self-assembly of copolymer molecular arrays, the rate of development was sped up [26–29]. Despite the great range of uses of microporous materials in catalysis, adsorption, and separation, there are significant drawbacks due to the processes employed to produce them. A few of the disadvantages of activated microporous carbon materials comprise: "(a) Slow mass transport of molecules due to the restriction of space that the small pore sizes introduce, (b) Low conductivity, as the huge surface functional groups and defects in the material increase, decrease conductivity, and (c) Collapse of porous structures during treatments such as high-temperature or graphitization" [5].

New synthetic techniques have been developed in order to expand upon these existing constraints. These efforts include, but are not limited to, the following: "(a) an increased degree of activation due to the use of physical or mixed physical/chemical procedures [30–32] (b) the carbonization of carbon precursors consist of one thermosetting component and one thermally unstable component, which [33, 34] explains (c). Catalytic activation of carbon precursors with metal (oxides) or organometallic compounds through a catalyst may be used [32, 35–37], (d) The carbonization of aerogels or cryogels may be used [38, 39], (e) replicative synthesis using pre-synthesized HTs, which involves impregnation, carbonization, and template removal [40, 41], and (f) self-assembly using STs, which entails co-condensation and carbonization [42–44]" [5]. Only MC compounds having wider pore-size distributions (PSD) emerge from methods (a) through (d). i.e. an extensive range of pore sizes and notable microporosity. As a result, these tactics are less alluring. With recent advances in synthesizing MC materials, methods (e) and (f) are linked to new technologies for creating MC materials with critically controlled mesopores. The use of appropriate synthetic approaches is necessary in order to develop acceptable MC materials that serve certain biological applications [5, 32, 45].

##### 3.1.1 Hard Template (HT) Method

The nanocasting technique was the first and one of the most widely used processes for producing MC materials, in which as-synthesized mesoporous silica that had been

created via the nanocasting process as the host template was used [46]. When mesoporous silica is produced, it is first used as a HT, and then an organic carbon source is added to impregnate and infuse the mesoporous structure. To get ordered MC, carbonization or polycondensation of carbon sources at high temperatures followed by chemical etching of the silica template, yields the desired product [11, 45]. Employing the nanocasting approach, Kim et al. were able to design and fabricate spherical MC nanoparticles having ordered mesoporous architectures by using MCM-48 mesoporous silica nanoparticles (SNs) as the HT [47]. Nanocasting, the conventional approach for fabricating MC nanoparticles, has many issues when it comes to manufacturing hydrophilic MC nanoparticles with uniform spherical shape and high dispersity. Organic carbon precursors included in the mesopores cannot be effectively removed during the casting process, and a washing step would remove it as well [11].

In the past, vast amounts of microporous activated carbon have been generated and employed as an adsorbent in gas or liquid adsorption. However, carbon compounds templated with mesoporous structure were not successfully synthesized until the early 1980s. Knox and associates detailed the synthesizing method of MC as a method employing spherical solid gel as a template [40, 41]. The HT deposition of MCs using precisely defined mesoporous structure typically includes the following four phases: “(a) production of a silica gel having a defined pore structure, (b) impregnation/infiltration of the silica template with monomer or polymer precursors, (c) cross-linking and carbonization of the organic precursors, and (d) silica template dissolution”[5]. After the host silica materials are eliminated, formerly occupied space by silica components is converted to carbon compounds’ pores, the carbon in the host silica pores creates a continuous carbon lattice [5].

Knox’s pioneering work continues to be the subject of extensive investigation, and this research focuses on using more ordered porous materials to provide templates for creating porous carbon materials. A study was performed by Kyotani and others, who used zeolites as template materials to create polymer materials and porous carbon. Although the exact crystalline structure of zeolites could not be reproduced in the templated porous materials, following dissolution of the zeolite frameworks [48–50]. Kyotani et al. established a dual step synthetic strategy (chemical vapour deposition after impregnation of a substrate), and a microporous carbon was successfully synthesized by the researchers [51]. In the late 1990s, there was a surge of interest in the production of ordered MC materials, after an extensive study into the development of mesoporous molecular sieves with consistent pore size and a well-ordered structure, as structural guiding agents, block copolymers, ionic surfactants, and neutral amines were used [52–56]. Wu and Bein were investigating the conductivity of carbon inside MCM-41’s hexagonally organized cylindrical mesopores, were the first to successfully produce an ordered carbon material within ordered silica pores, obtaining first ever ordered carbon substance in ordered silicon holes [57]. But, the first self-supported highly ordered MC material, which came out in 1999, was made by Ryoo et al. and their group [21], who synthesised MC materials, CMK-1, MCM-48, an ordered aluminosilicate with structural characteristics, was used as a HT. In the third month after this publication SNU-1, an ordered MC material, was synthesized

by Hyeon et al. and authors, MCM-48 was used as a template, and phenolic resin was used as a carbon precursor. Ordered MCs have also been synthesized with the use of chemical vapour deposition (CVD) [58]. As reported by Ryoo's group, this group developed a CVD method to manufacture ordered mesoporous CMK-4 at 1073 K by using acetylene as a carbon precursor and the aluminosilicate MCM-48 as a template. The structure and pore size of MC materials created utilizing hard-template synthetic techniques are significantly affected by the molecular structure of carbon precursors and carbon precursors like sucrose, sucrose, and furfuryl are frequently used with loose molecular structures like sugar, sucrose, and furfuryl and frequently produce MCs with micropores on the pore walls [21, 45]. With regard to potential applications, MC compounds with graphitic pore wall structure are gaining popularity [5, 59, 60]. For instance, the following research groups are exploring the benefits of this kind of material. Carbon materials with a well-developed pore structure have an amorphous pore-wall structure, which is distinct from graphitic crystallinity. "To make ordered MC with graphitic structure, three different synthesis techniques were utilized: the first entails the use of carbon precursors with fused aromatic structures, the second utilizes high temperature (>900 °C) CVD, and the third consists of treating carbon with amorphous pore walls at elevated temperatures (above 2000 °C) in order to promote graphitization" [5]. A number of methods for creating uniformly pored disordered MC materials have been added, rapid advancements in the formation of ordered MC compounds have been made with diverse geometries utilizing ordered silica as templates. Templating with SNs or using crystals anodic alumina, silica gel, or alumina– silica and as a template, copolymerize carbon precursors with alkoxide inorganic precursors like tetraethylorthosilicate (TEOS), are included in these procedures. The development of porous carbon materials with varying hierarchical pore architectures and/or intriguing morphologies, so progresses[5]. A group of researchers created MC material through carbon and silica nanocomposite, which was created by the copolymerization process of TEOS and furfuryl alcohol [61]. Han's team created a MC from SNs with a diameter of 12 nm that was the template for the synthesis. By partially impregnating the mesocellular aluminosilicate foam with phenol/formaldehyde, carbonising, and then removing the template, Hyeon, Sohn, and Lee created a mesocellular carbon foam with homogeneous mesopores [62].

### 3.1.2 Soft Template (ST) Method

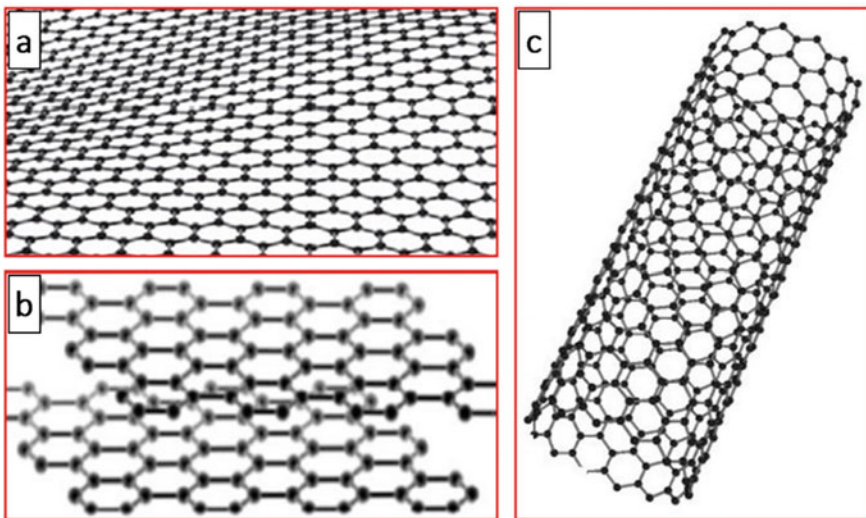
Block copolymers, for example, have been widely used as STs; surfactants and amphiphilic compounds have also been widely exploited as STs in the generation of ordered mesoporous oxides. Since researchers at the Mobil Company initially reported on the use of mesoporous silica in 1992, ordered inorganic oxides have featured regularly in the investigation of nanomaterials [5, 52]. Despite the fact that ordered polymeric mesoporous materials, which are not as popular as their inorganic siblings, have been investigated for over two decades, these materials, which first appeared in 1988, were the first ordered polymeric mesoporous materials to be discovered [63]. Porous carbon materials have distinct physicochemical features,

which may act as a technological blank canvas, ordered MC is emerging spontaneously, on which many technologies may be painted. The self-assembly method, on the other hand, makes it difficult to make organized MC compounds. It is important to note that there are four important aspects to consider while synthesizing MC materials using STs: “(1) Precursor components have the capacity to organize into nanostructures on their own. (2) At least one pore-forming component and at least one carbon-yielding component must be present. (3) the pore-forming component’s stability, which allows it to withstand the temperature necessary during carbonization for the purpose of curing the carbon-producing component while also being readily dissolved with the least amount of carbon yield and (4) the capacity of the carbon-yielding component to create a strongly cross-linked polymeric material that retains its nanostructure after the pore-forming component has been dissolved or detached” [6]. Until now, a small number of materials have proven up to these specifications. The first reported effort to synthesis ordered MC material, Moriguchi et al. did this by using micelle templates [64]. The result of their synthesis of MCM-41 inspired them to employ the surfactant cetyltrimethylammonium bromide (CTAB) as a template and lead to the successful assembly of phenolic resin and surfactant mesophases. It has also been investigated if a ST, like CTAB, may be used to synthesize MC materials. The unique phase behaviours and adjustable features of block copolymers are what interest researchers, whereas self-assembly and diverse macromolecular structures are the main reasons for their appearance. Several investigations were performed to synthesis mesoscopic carbon structures using the direct carbonization of self-assembled block copolymers [5, 65, 66]. Notable here is that the group of researchers, Matyjaszewski et al., sought to create carbon nanostructures using carbonization of a self-assembled framework [67]. Over the past two decades, there has been a considerable amount of study into the self-assembly of block copolymer thin films. It was not a happenstance that ordered MCs that were first synthesized using STs were found to be in the shape of thin films [5].

### 3.2 *Carbon Nanotubes*

Carbon nanotubes (CNTs) (Fig. 3c), the first observation of which was made in 1991 by Japanese researcher Sumio Iijima, are a different type of carbon seen for the first time in the process of synthesizing fullerenes [16]. These tubes have been referred to as graphene sheets that are twisted into themselves in the shape of microtubes, which subsequently is to be changed to the term multiwall carbon nanotubes (MWCNTs). In the early 90s, single-walled carbon nanotubes (SWCNTs) were synthesized by improving a previously known technique of synthesis in which an electric arc was used [68–70]. Carbon nanotubes form hexagonal arrays of carbon atoms on their surfaces, and other molecules or atoms interact strongly with these surface arrays. Multi sheet nanotubes are made of many stacked graphene sheets that are twisted concentrically with a space between two sheets of roughly 3.6 Å, somewhat more than the space between two sheets in graphite. The size of the nanotubes ranges

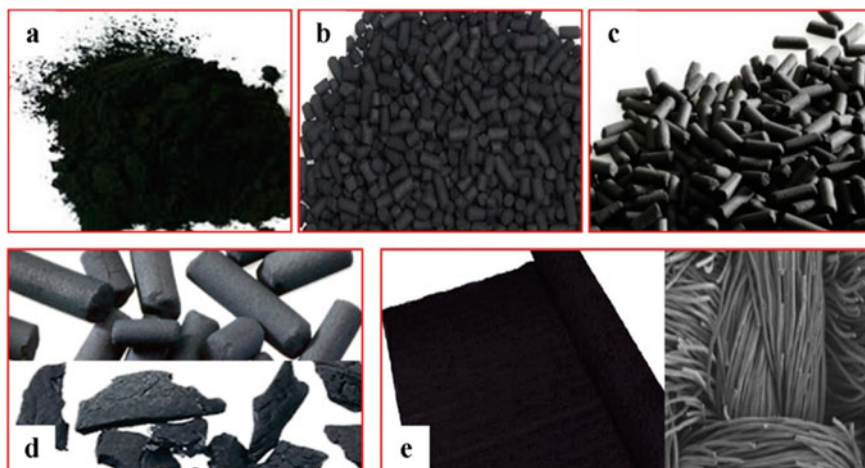
from 1 to 50 nm, and their lengths may touch 1  $\mu\text{m}$ . SWCNTs are made up of a graphene sheet that has been coiled around itself to produce a tube with a diameter ranging from 0.4 to 3 nm. CNTs are built by one or more sheets of carbon atoms, similar to graphite, which is then coiled to create a tube. CNTs are well-suited for use in both the mechanical and electrical processing, with high tensile strength, superior adhesion, and exceptional conductivity. These tubes have different electrical characteristics, some of which are metallic and others semiconductive. SWCNTs and MWCNTs are synthesized by the same general process, but there is a slight difference in how the catalyst is applied. While nickel, iron, or cobalt is usually used, generally referred to as a metal catalyst, which is necessary for the synthesis of fullerenes. These techniques generally use arcs discharge, laser ablation, and chemical vapour deposition to fabricate them. While carbon nanotubes are useful in many industries on an industrial scale, their exceptional properties in relation to the quantity of impurities are more advantageous on an individual level when it comes to being employed in reinforcement polymers and composites, nanoporous materials. Carbon nanotubes have received a lot of interest since they were discovered, thanks to their highly specific features. Their exceptional properties allow them to be used in applications like energy, biomedical, etc. [16].



**Fig. 3** a Graphene, b graphite, and c carbon nanotube is shown in a conceptual design (reprinted with permission from Ben et al. [16], copyright 2020, MDPI)

### 3.3 Activated Carbon

The porous, amorphous organic substance known as activated carbon has a complicated structure and a high carbon content. Activated carbon refers to a class of materials having a large internal surface area and porosity, and therefore a high capacity of chemical absorbing from liquids and gases. Activated carbons are highly flexible industrial adsorbents that are utilized in a broad variety of applications involving the removal of unwanted species from liquids or gases via adsorption [16, 71]. Activated carbon, which comes in a variety of forms and is produced from a variety of materials, has a long history of usage in oral medicine [72]. The unique characteristics of activated carbon adsorbents, as well as their cheap cost when compared to other inorganic adsorbents such as zeolites, account for their strong market position. Any material with a high carbon concentration may be used to make activated carbon. Activated carbon is usually made in two steps. To make a carbon surface, the first step is to carbonize the source material. This is followed by chemical oxidation or an eat treatment to improve the surface of the material produced. Activated carbon is extensively utilized in industry for a number of purposes, each of which necessitates a specific kind and form of activated carbon. Activated carbons are classified for general purpose depending on their physical characteristics, e.g. powdered, granulated, and are shown in Fig. 4 [16, 71].



**Fig. 4** Activated carbon types: **a** activated carbon powder, **b** granular activated carbon, **c** extruded activated carbon, **d** impregnated activated carbon, and **e** activated carbon fabric are all examples of activated carbon (reprinted with permission from Ben et al. [16], copyright 2020, MDPI)



### 3.4 Fullerenes

Since their discovery and mass manufacturing, the Fullerenes have played a pivotal role in science, culminating in the awarding of the 1996 Nobel Prize in Chemistry to Kroto, Curl, and Smalley for their groundbreaking discovery. Fullerene molecules are completely made of carbon and come in the shape of a hollow spherical, ellipsoid, or tube. Buckyballs are another name for spherical fullerenes. The remarkable symmetry of the C<sub>60</sub> molecule is a significant feature. Many scientists predicted numerous technological possibilities based on the unusual physical and chemical characteristics of these new forms of carbon. However, fullerenes' poor processibility has posed a significant challenge in the desperate quest for therapeutic uses. In aqueous media, C<sub>60</sub> is insoluble and readily agglomerate. Chemical reactions with high chemical activity and a wide range of adjustability are generating a lot of attention for their potential uses in developing new medicinal materials [73–75].

### 3.5 Graphene

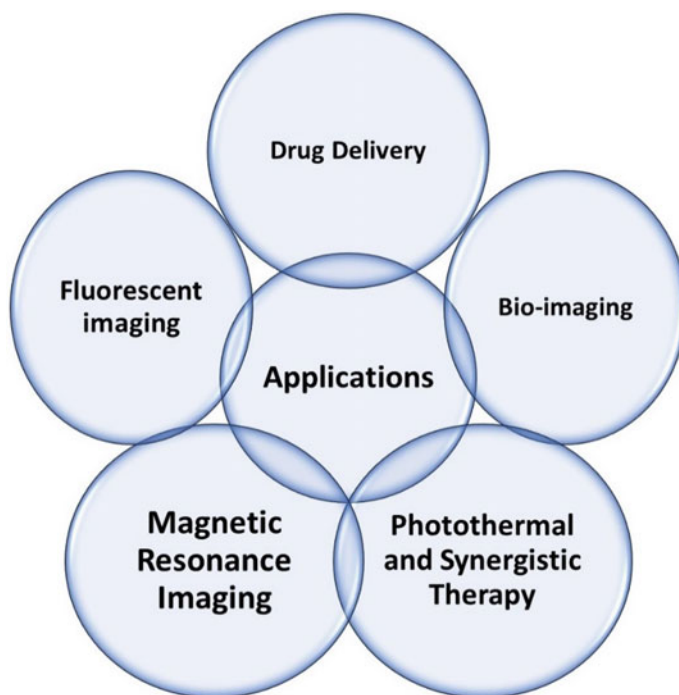
Graphene is linked to graphite, and it was first extracted experimentally from graphite in 2004. It is a hexagonal planar material (Fig. 3a) in the form of a two-dimensional crystal consisting of a simple plane of carbon atoms in *sp*<sup>2</sup> hybridization, frequently likened to a honeycomb network. It's best defined as a single layer of carbon atoms tightly packed in a structure of a benzene ring in a pure carbon monocrystalline graphitic sheet. "A top-down method from graphite (Fig. 3b), which consists of graphene layers stacked parallel to each other in a three-dimensional, crystalline, long-range arrangement", is the most common way to produce graphene [76]. Because of its strictly two-dimensional structure, graphene has unique thermal, electrical, and mechanical characteristics, and has enormous promise for technological purposes. "Graphene has a large theoretical specific surface area (2630 m<sup>2</sup> g<sup>-1</sup>), high intrinsic mobility (200,000 cm<sup>2</sup> v<sup>-1</sup> s<sup>-1</sup>), a high Young's modulus (~1.0 TPa), high thermal conductivity (~5000 Wm<sup>-1</sup> K<sup>-1</sup>), high optical transmittance (~97.7%) and good electrical conductivity" [76]. Membranes made of graphene are impervious to all liquids and gases (i.e., are vacuum-tight). The wide range of excellent biological and physicochemical characteristics mentioned above demonstrates graphene's potential for use in a wide range of scientific areas. Indeed, graphene-based materials have been used in a number of areas, including bioelectronics, tissue engineering, drug delivery, antimicrobial materials creation, biosensing, gene transfer, cancer therapy, and other biomedical applications since their introduction. Mechanical strength, electrical conductivity, biomolecule adsorption are the most responsible properties that contribute graphene based biomedical applications [16, 76].

## 4 Biomedical Application

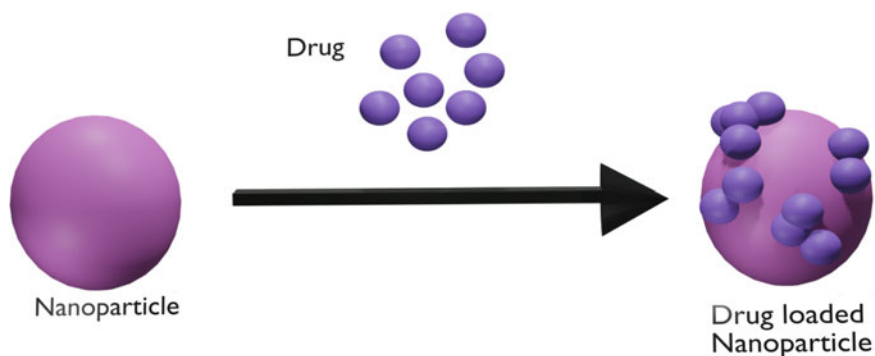
Due to the intriguing properties of porous carbon materials, a wide horizon of possibilities opens for use in biomedical applications. A few potential biomedical applications of porous carbon materials are shown in Fig. 5 and discussed in the following texts.

### 4.1 Drug Delivery

An efficient carrier or vehicle of drugs is a very challenging element in the drug delivery process. For drug delivery, a variety of carriers have been used, including polymers, nanoporous silica, nanotubes, micelles, and nanoporous carbon [77]. Porous materials are especially favourable to drug delivery matrices as the size of the pores and porous structures are controllable [78]. Nanoporous carbons, or functionalized nanoporous carbons, have recently piqued attention in the world of drug delivery [77]. A nanoparticle based targeted drug delivery system in Fig. 6. The porous carbon based drug delivery field mainly includes immediate, sustained,



**Fig. 5** Potential biomedical applications of porous carbon materials



**Fig. 6** Nanoparticle-based targeted drug delivery system

controlled and targeted drug delivery systems [10]. One of such materials is Fullerene, which is an inorganic nanoparticle that is widely available due to their tiny size (1 nm) and biological activity. The behaviours of this allotropic carbon form are based on the characteristics of the both fullerene core and its chemical change. The fullerene core is very hydrophobic, whereas functional groups linked to the core give additional intricacy to the behaviour. By adding hydrophilic components, Fullerene becomes water-soluble and can be used to transport drugs and genes [73]. A commonly used drug for the treatment of tonsillitis, pharyngitis, and sinusitis is clarithromycin, which causes adverse effects such as mucous tissue swelling. The nanoporous carbon, functionalized with amine groups, was utilized as a carrier molecule to minimize the negative impact of clarithromycin. The nanoporous carbon modified with amine was completely biocompatible [79]. Cytotoxicity assessment also studied MOF-derived nanoporous carbon and found the narrow distribution in pore size suited for the controlled release of cisplatin [80]. Zhang et al. employed porous carbon monoliths in their research with orderly macropores and uniform mesopores of around 5.2 nm as a drug carrier, also address a lack of solubility of the valsartan in water [77]. CNT can also be used in drug delivery systems. Both single and multi-walled carbon nanotubes hold exclusive mechanical, electrical, and structural properties which lends them higher forte, litheness, and electrical conductivity toward various biological entities that can be utilized for drug delivery. Functionalization reduces this bundling effect that occurs due to the van der Waals forces between the adjacent nanotube surfaces, which aids in enhancing the biocompatibility and thus helps in cellular internalization and movement. Drug entities can be attached to the functionalized CNTs sidewalls through covalent or noncovalent bonding. Saikia N and Deka RC concluded that the optimum length and chirality of the CNTs is essential to comprehend the electronic characteristics of functionalized CNTs to understand the mechanism of the delivery of drugs. Functionalized CNTs lead to PEGylation, which enhances the stability of bodily fluids. On the CNTs' terminal functional groups or on the PEG chains, hydrophilic and hydrophobic drug materials can be coupled with PEGylated CNTs [81]. Anticancer medicines such as doxorubicin, flutamide, cisplatin, methotrexate,

and paclitaxel have all been effectively conjugated with CNTs. Integrin-binding arginine-glycine-aspartic acid (iRGD)-conjugated polyethyleneimine (PEI) functionalized MWCNTs coupled with candesartan (CD) were developed by Chu et al. These components were constructed using plasmid AT (2) (pAT(2)). They used iRGD-MWCNT-CD to target tumour endothelium's avb3-integrin and AT1R, as well as lung cancer cells. A synergistic reduction in vascular endothelial growth factor (VEGF) was seen when the anticancer medicinal molecule was combined with pAT (2), suggesting that the molecule effectively inhibited angiogenesis. Curcumin, paclitaxel, docetaxel, vinca alkaloids, camptothecin, quercetin, oridonin, and other herbal anticancer medicinal substances have been successfully delivered to cancer cells when coupled with CNTs. Using a mix of chemotherapy and photothermal treatment, Zhao et al. created a drug delivery system that responds to multiple stimuli. Nanoparticles with great loading efficiency of DOX were synthesized and employed as near infrared-responsive drug carriers by the researchers [81]. Chemotherapeutic drugs [82], genes [83], peptides [84], and tissue engineering [85] have all been used to deliver these materials using graphene or its derivatives. It is possible to adsorb hydrophobic medicines, such as doxorubicin and docetaxel, onto graphene through simple physisorption via stacking and utilizing antibodies to target just cancer cells. Stacking and electrostatic or hydrophobic interactions of graphene provide a high carrying capacity of poorly soluble drugs deprived of conceding drug strength. The oxygen-rich surface of the GQDs is the key feature that makes them appropriate for drug adsorption and increasing colloidal strength in vivo, along with the features of a mono atomic layer and compact size. The fluorescent characteristics of graphene quantum dots render them traceable when targeted to e.g., cancer cells [86]. Tian et al. developed a framework of zeolite imidazolate (ZIF-8)-embedded DOX-loaded GQDs, which showed an acidic pH-responsive drug release behaviour.

## 4.2 *Photothermal and Synergistic Therapy*

Photothermal therapy (PTT) has been commonly used to control cancer as a treatment process where the absorption of near-infrared (NIR) light has been converted into cytotoxic heat by the utilization of NIR resonant nano agent to destroy malignant cells while reducing aggressive damage to normal tissues. Direct thermal ablation of cancer cells is known to usually require an elevated temperature (e.g. more than 50 °C), which may harm the other healthy cells and tissues [77]. But PTT has considerably milder photothermal effects, and the tumour ablation can be efficiently caused by raising the temperature at the tumour location to 43–45 °C and maintaining the hyperthermia for some time. NIR light with wavelengths ranging from 700 to 1100 nm can profoundly enter the tissues (up to 10 cm) while being absorbed by tissues and skin at a minimum level, allowing for efficient cancer cell ablation [87–89]. MCNs are distinguished from other photothermal agents by their significant optical absorption in the near-infrared range, indicating their possible usefulness as an NIR-resonant nanoagent for converting NIR light into heat and causing cancer

cell ablation. The MCNs were capable of achieving chemo photothermal cotherapy after being loaded with anticancer medicines [11]. MCNs updated with FA and PEI were developed by Xu et al. [10] for targeted drug delivery and chemo-photothermal treatment. HeLa cells absorption of drug-loaded MCNs which exaggerate folate receptors could be considerably improved by modifying FA. In the presence of near infrared light, the DOX filled FA/PEI/MCNs displayed increased effectiveness of treatments compared to chemotherapy alone, and the produced heat could not only lead to tumour cell demise but also expedite the release of DOX.

Carbon materials could be used as drug carriers alone or with the combination of others. Such as mesoporous silica covered carbon was produced and employed for drug delivery due to its increased biocompatibility and functionalizable surface. Wang et al. [90] developed a coreshell graphitic carbon–silica nanospheres system that had a large capacity of drug loading as well as a regulated drug releasing sequence. The semi graphitized carbon demonstrated a number of advantageous features, including: (1) enhanced drug receiving capacity due to the  $sp^2$ -hybridized structure, and (2) improved photo-thermal transfer capability due to graphitic pore wall hotspots. Furthermore, the hydrophilicity and targeted drug delivery of the mesoporous silica shell might be improved. Wang et al. [91] also coupled a novel HB5 aptamer to a MC–silica composite loaded with DOX (MSCN-PEG/DOX), which might be used to target HER2-overexpressed breast cancer cells (SK-BR-3). The combination index (CI) of MSCN-PEG-HB5/DOX chemotherapy and photothermal therapy was 0.253, showing a synergistic effect. Zhang et al. [92] published another study where MCNs with a radius of 75–100 nm were combined with copper sulphide (CuS) nanoparticles (NPs) [10].

As in many cases, conventional cancer treatment fails to entirely remove the tumour. Anti-cancer treatment may be improved by combining several therapeutic modalities in a synergistic or combination manner, which can lessen systemic toxicity and adverse effects [93, 94]. The synergistic impact of combining chemo and photothermal treatment in one system may boost cancer therapy's effectiveness [95, 96]. For chemo and photothermal therapies, Zhou and coworkers have created MWCNT loaded with DOX magneto fluorescent carbon quantum dot (CQD), a newly found nano-compost [94]. Combining photothermal PTT and photodynamic therapy (PDT) on cancer is possible using a nanohybrid of reduced nanographene oxide (rGO) with a polyethylene glycol-modified Ru(II), which is termed as the Ru-PEG nanohybrid. Through—hydrophobic interactions and  $\pi$ - $\pi$  stacking, the photosensitizer and imaging agent Ru-PEG is attached to the delivery and PTT agent rGO [95]. Facile one-step fabrication of a bimodal treatment system (Ru@SWCNTs) for PTT and two-photon PDT (TPPDT) was achieved by depositing Ru(II) complex on the surface of SWCNTs through noncovalent  $\pi$ - $\pi$  interaction and it is found that the combination of this bimodal PTT and TPPDT is more effective in fighting cancer.

### 4.3 *Bio-imaging*

The speed of developing excellent studies and tactics for efficient tumour diagnosis has accelerated as our understanding of the pathophysiology of diverse malignancies has deepened. Researchers have recently focused their focus on the following topics in order to improve treatment efficiency: (1) early detection and diagnosis; (2) tailored medication administration, and (3) real time observing *in vivo*. These procedures, known as “theranostics,” integrate cancer diagnosis and therapy technology. As a result, a slew of imaging approaches that incorporate many aspects into a multi-modal therapeutic platform and produce excellent outcomes have sprung out [46].

### 4.4 *Fluorescent Imaging*

Because of their easy functionalization, high biocompatibility, and supramolecular *p-p* stacking, MCNs have emerged as a new theranostic nanoplatform. The illumination of fluorescent compounds that have been implanted or loaded attached to MCNs can be temporarily quenched by supramolecular *p-p* stacking, but the fluorescence will rebound when the molecules are disengaged from the MCNs. Li et al. [97] created a fluorescent aptasensor by modifying a ssDNA probe (Cy3-labeled) (P0-Cy3) on the surface of oxidized MC nanospheres (OMCN). The aptasensor was able to discover the mucin1 protein in liquid and measure cancer cells in a solution with high selectivity [10]. Using an organic carbon source of citric acid solution and a precursor carbonized in hot solvent method, Kong et al. [98] produced hydrophilic MCNs with ease. The MCNs had homogenous pores and particle size distribution of around 2.7 nm and 100 nm, respectively, in the prepared state. With a quantum yield of 37%, MCNs produced using this approach have extremely steady multicolour and up conversion photoluminescence capabilities. Furthermore, the MCNs were well-tolerated by cancer cells, allowing them to be visually labelled when exposed to various wavelengths ranging from ultraviolet to near-infrared [46].

### 4.5 *Magnetic Resonance Imaging*

Magnetic resonance imaging is a strong noninvasive monitoring tool with great structural perspective. Inorganic nanoparticles, such as  $\text{Fe}_3\text{O}_4$ , gadolinium (Gd), and manganese oxide, are typically incorporated into MCNs to generate magnetic composites for MR imaging, with the mesoporous channels of the MCNs serving as room for cargo storing [99–101]. With  $\text{MnO}_x$ -decorated HMC nano capsules (HMCNs), Zhang and colleagues developed some good MCN-based stimuli responsive and diagnostic imaging nanosystem. Supramolecular *p-p* stacked between the carbon based structure of the  $\text{MnO}_x$ -HMCNs and the aromatic drug molecules was

also used to create pH/ultrasound-sensitive drug release nano platforms with an excellent anti metastasis effect and great achievement for reversing cancer cell multi drug resistance [46].

#### **4.6 Photoacoustic Imaging**

Photoacoustic (PA) imaging is a strong diagnostic imaging method that uses ultrasonic waves as the signal and a pulsed laser as the energy source. When compared to traditional optical imaging, PA overcomes the disadvantage of limited imaging depth and efficiently increases level of signal transmission into tissues, which is attributed to the ultrasonic wave's significantly longer wavelengths. Lee and colleagues developed a hollow mesoporous PEG-Si/C NP for pH responsive administration and photoacoustic imaging guided chemo thermal treatment. Wang and colleagues developed the MemHsp70 receptor-mediated multifunctional OMC nanospheres, a "four-in-one" theranostic system. PEI and a memHsp70 receptor-targeting peptide (TKD) were grafted on DOX-loaded OMCN in this system. This theranostic device was able to provide discrete PA imaging, NIR/pH sensitive drug/gene release, and synergistic targeted therapy as a result [46].

#### **4.7 Antibody-Based Biosensors for Biomedical Applications**

Antibody-based biosensors also termed as immunosensors play a crucial role in rapid diagnosis of diseases and timely diseases of such diseases. Immunosensors are being used to plenty of analytes including contaminants in food and environment, disease markers, illicit drugs, and many more. Sensors benefit greatly from the high specificity and sensitivity provided by antibodies, which are an excellent biorecognition component. Laboratories, high end equipments along with qualified personnel are required in vitro techniques, which are at the same time consumes much time. A variety of sensor devices rely on antibodies (Abs), which are among nature's most delicately built and designed molecules owing to their exceptional target selectivity and affinity [102]. A disease system's primary job is to keep the body safe from potentially hazardous infectious organisms. As part of the body's defensive mechanism, the immune system identifies and categorizes all cells and molecules inside the body as either harmful or non-harmful. Specialized immune system cells create immunoglobulins (i.e. antibodies) that selectively bind these antigens in the influx of foreign molecules (i.e. antigens). Processing and recognition of the antigen are the initial steps [103]. When an antigen is detected, the acquired immune system generates an army of immune cells that are specialized to target that antigen. As a result of their high affinity and specificity, antibodies are effective biorecognition elements. As a result, they make excellent identification components for sensors. Analytes may be detected using a variety of biosensors based on antibodies. "(i) the

ability to immobilize recognition elements (biological molecules) while maintaining their natural activity; (ii) the accessibility of the recognition element to the relevant analyte in solution; and (iii) low non-specific adsorption to the solid support” are three critical factors that determine the performance of a bio/immuno-sensor [104, 105]. An immunosensor’s most critical step is to immobilize antibodies on a sensor surface without affecting their specificity or immunological activity. The detection limit, sensitivity, and overall performance of the immunosensor are all affected by the immobilization stage. Non-covalent, covalent and affinity based immobilization are the three techniques for immobilization of antibody onto sensor surface.

Carbon nanomaterials play a crucial role in bioelectrocatalytic processes owing to their large specific surface area and greater biocompatibility. Because of its ability to incorporate large surface area, nontoxicity, and good biocompatibility, carbon nanofibers (CNFs) are particularly appealing in bioanalytics [106]. Conventional CNFs (CNFs) were shown to be excellent for mass transfer, catalyst support, and adhesion, whereas porous carbon nanofibers (PCNFs) are found to be better for electrical conductivity and adsorption. PCNF/RTIL (room temperature ionic liquid) membranes have been developed by Sheng et al. (2010) to facilitate direct electron migration of ferrous haemoglobin proteins in a suitable environment [107]. Different carbon material based immunosensors are being used for carcinoembryonic antigen detection, carbohydrate antigen detection, miRNA detection [106, 108, 109]. (Table 1).

## 5 Challenges and Need for Future Research

Carbon-based porous materials (CPMs) have great attention due to their excellent properties. Various devices based on these materials give effective techniques for therapy, diagnosis, and imaging. However, there have been several concerns about the safety of CPMs when used in biomedical scenarios. The persistence of CPMs in biological systems is thought to be a contributing factor to many of the toxicity and long-term impact issues. The pharmacokinetics, metabolism, long-term in vivo effects of CNMs, and toxicity must all be studied in detail. Studies on the toxicity of CPMs have yielded inconsistent results about their ability to be used in biological applications. Toxicity has been shown to be affected by factors such as the concentration of the substance, its lateral dimension, its surface qualities, and the kinds and presence of functional groups it contains. In addition, its manufacturing requires a significant amount of time and money, making it difficult for mass production. As a result, improvements to the problems of creating vast quantities of non-toxic carbon nanomaterials at low cost and speed are urgently needed. In the future, CPMs could be combined with new, intuitive guiding moieties to allow them to directly reach the target cells, or researchers could develop carbon nanomaterials that could be driven from the outside to the affected tissue or organ, thus avoiding the negative effects of CPMs on nearby healthy tissues. Nano-porous carbon materials deriving from a



**Table 1** Some significant studies reporting the use of porous carbon based materials in biomedical applications

Porous carbon materials	Specification	Applications	References
1. Meoporous carbon materials	Displayed high loading efficiency of DOX	Near infrared responsive carriers	[82]
	Loaded with anticancer medicines	Capable of achieving chemo photothermal cotherapy	[11]
	Updated with FA and PEI	For targeted drug delivery and chemo-photothermal treatment	[79]
	Mesoporous carbon–silica composite loaded with DOX(MSCN-PEG/DOX) with a novel HB5 aptamer	Used to target HER2-overexpressed breast cancer cells (SK-BR-3)	[93]
	Fluorescent aptasensor with a ssDNA probe (Cy3-labelled) (P0-Cy3) on the surface of oxidized MCN	The aptasensor was able to discover the mucin1 protein in liquid and measure cancer cells in solution with high selectivity	[79]
	Multifunctional OMC nanospheres (MemHsp70 receptor-mediated)	Able to provide discrete PA imaging, NIR/pH sensitive drug/gene release, and synergistic targeted therapy	[46]
2. Carbon nanotubes	Functionalized CNTs	Leads to PEGylation, which improves constancy in the body fluids	[82]
	Doxorubicin, flutamide, cisplatin, methotrexate, paclitaxel, etc., conjugated with CNTs	Anticancer therapy	[82]
	Integrin-binding arginine-glycine-aspartic acid (iRGD)-conjugated polyethyleneimine (PEI) functionalized MWCNT conjugated with candesartan (CD) assembled with plasmid AT (2) (pAT(2))	They targeted avb3-integrin, AT1R of tumor endothelium and lung cancer cells with iRGD-MWCNT-CD	[82]

(continued)

**Table 1** (continued)

Porous carbon materials	Specification	Applications	References
3. Fullerene	With the addition of hydrophilic components	Can be used to transport drugs and genes	[74]
4. Graphene	With their derivatives	Explored for the delivery of chemotherapeutic agents, genes, peptides and tissue engineering	[83–85]
	Zeolite imidazolate (ZIF-8)-embedded DOX-loaded GQDs	Showed an acidic pH-responsive drug release behaviour	[87]
5. Nano-compost	MWCNT loaded with DOX magneto fluorescent carbon quantum dot (CQD)	PTT and PTD	[97]
	Ru-PEG nanohybrid	PTT and PTD	[96]
	Ru@SWCNTs	PTT and TPPTD	[96]

metal organic framework and carbon quantum dots are also prospective options for future biological modification and development [81].

## 6 Human Health Effect of Carbon-Based Porous Materials

Though the introduction of carbon-based porous materials has paved the way for the early detection, delivery, and diagnosis of a variety of disorders but they possess some harmful effect on human health. Several research analysed the impact of carbon based porous materials on different cell types. Numerous toxic effects of carbon nanomaterials, including DNA damage, mitochondrial dysfunction, ROS generation, lysosomal damage, and eventual cell death via apoptosis or necrosis. Many cytotoxicity outcomes for carbon-based materials could be due to a variety of variables, including changes in the structures of carbon nanomaterials or physicochemical properties, target cell types, and particle dispersion methodologies [110]. These materials also have immunological effects. Some reports have demonstrated that af-SWCNTs were macrophaged and located in lysosomes, resulting in damaged mitochondrial function and phagocytic activity [111]. Acid-treated MWCNTs and taurine functionalized MWCNTs were found to cause considerable cell death and decreased cellular phagocytosis [112]. So, it is important to evaluate the materials' potential toxicity and determine the physicochemical parameters that cause toxicity.

## 7 Conclusion

Porous carbon materials are attracting the scientific global research community due to their appealing physiochemical properties, adsorption capacity and greater surface area. Some widely researched porous carbon materials such as MC, carbon nanotube, graphene, fullerene, and activated carbon are discussed in this mini review. The advancement of growth techniques of these materials with superior physical and chemical properties makes them good candidate for different applications including biomedical field. Porous carbon materials definitely have a profound impact on biomedical fields and are being employed in drug delivery, medicines, bio-imaging and many more. However, production of porous carbon materials at a rapid pace and a lower cost, and with zero toxicity is a matter of tremendous research topic.

**Declaration of Conflict of Interest** The authors declare no known conflict of interest.

## References

1. Zhang P, Zhang J, Dai S (2017) Mesoporous carbon materials with functional compositions. *Chem Eur J* 23:1986–1998
2. Geim AK, Novoselov KS (2009) The rise of graphene. *Nanoscience and technology: a collection of reviews. Nat J* 11–19
3. Huo Q, Leon R, Petroff PM, Stucky GD (1995) Mesostructure design with gemini surfactants: supercell formation in a three-dimensional hexagonal array. *Science* 268:1324–1327
4. Huo Q, Margolese DI, Ciesla U, Feng P, Gier TE, Sieger P, Leon R, Petroff PM, Schüth F, Stucky GD (1994) Generalized synthesis of periodic surfactant/inorganic composite materials. *Nature* 368(6469): 317–321
5. Liang C, Li Z, Dai S (2008) Mesoporous carbon materials: synthesis and modification. *Angew Chem Int Ed* 47:3696–3717
6. Thambiliyagodage C (2019) porous carbon materials in biomedical applications. *Biomed J Sci Tech Res* 22:16905–16907
7. Thambiliyagodage CJ, Cooray VY, Perera IN, Wijesekera RD (2020) Eco-friendly porous carbon materials for wastewater treatment. *Lecture Notes Civ Eng* 44:252–260
8. Thambiliyagodage CJ, Hakat Y, Bakker MG (2016) One pot synthesis of carbon/ni nanoparticle monolithic composites by nanocasting and their catalytic activity for 4-nitrophenol reduction. *Curr Catal* 5(2):135–146
9. Liu J, Zhao Y, Cui Y, Yue Y, Gao Y, Zhao Q, Liu J, Wang S (2016) A Eu<sup>3+</sup>/Gd<sup>3+</sup>-EDTA-doped structurally controllable hollow mesoporous carbon for improving the oral bioavailability of insoluble drugs and in vivo tracing. *Nanotechnology* 27(31):315101
10. Zhao Q, Lin Y, Han N, Li X, Geng H, Wang X, Cui Y, Wang S (2017) Mesoporous carbon nanomaterials in drug delivery and biomedical application. *Drug Delivery* 24:94–107
11. Chen Y, Shi J (2015) Mesoporous carbon biomaterials. *Sci Chin Mater* 58:241–257
12. van Oss CJ (2007) A review of: “active carbon.” R.C. Bansal, J.B. Donnet and F. Stoeckli; Marcel Dekker, New York, 1988. *J Dispersion Sci Technol* 11(3):323–323
13. Ralph TY (2003) Adsorbents: fundamentals and applications. Wiley
14. Gaffney TR (1996) Porous solids for air separation. *Curr Opin Solid State Mater Sci* 1:69–75
15. Lee J, Kim J, Hyeon T (2006) recent progress in the synthesis of porous carbon materials. *Adv Mater* 18:2073–2094

16. Mosbah M ben, Mechi L, Khiari R, Moussaoui Y (2020) Current state of porous carbon for wastewater treatment. *Processes* 8:1–24
17. Rouquerol F, Luciani L, Llewellyn P (2003) Texture of powdery or porous materials. *Techniques de l'*
18. Sing KSW, Everett DH, Haul RAW, Moscou L, Pierotti RA, Rouquerol J, Siemieniowska T (1985) Reporting physisorption data for gas/solid systems with special reference to the determination of surface area and porosity. *Pure Appl Chem* 57:603–619
19. Thommes M, Kaneko K, Neimark Av., Olivier JP, Rodriguez-Reinoso F, Rouquerol J, Sing KSW (2015) Physisorption of gases, with special reference to the evaluation of surface area and pore size distribution (IUPAC Technical Report). *Pure Appl Chem* 87:1051–1069
20. Rahman MM, Ara MG, Alim MA, Uddin MS, Najda A, Albadrani GM, Sayed AA, Mousa SA, Abdel-Daim MM (2021) Mesoporous carbon: a versatile material for scientific applications. *Int J Mol Sci* 22(9):4498
21. Ryoo R, Joo S, Jun S (1999) Synthesis of highly ordered carbon molecular sieves via template-mediated structural transformation. *ACS Publications* 103:0
22. Rouquerol J, Avnir D, Fairbridge CW, Everett DH, Haynes JM, Pernicone N, Ramsay JDF, Sing KSW, Unger KK (1994) Recommendations for the characterization of porous solids (technical report). *Pure Appl Chem* 66:1739–1758
23. Lu A, Schmidt W, Spliethoff B, Schuth F (2003) Synthesis of ordered mesoporous carbon with bimodal pore system and high pore volume. *Wiley Online Libr* 15:1602–1606
24. Kim T, Park I, Chemie RR-A (2003) A synthetic route to ordered mesoporous carbon materials with graphitic pore walls. *Wiley Online Libr* 115:4511–4515
25. Lu A, Schmidt W, Schüth F (2003) Simplified novel synthesis of ordered mesoporous carbon with a bimodal pore system. *New Carbon Mater* 18(3):181–185
26. Liang C, Hong K, Guiochon GA, Mays JW, Dai S (2004) Synthesis of a large-scale highly ordered porous carbon film by self-assembly of block copolymers. *Wiley Online Libr* 43:5785–5789
27. Zhang F, Meng Y, Gu D, Yan Y, Yu C, Tu B, Zhao D (2005) A facile aqueous route to synthesize highly ordered mesoporous polymers and carbon frameworks with Ia3d bicontinuous cubic structure. *ACS Publ* 127:13508–13509
28. Meng Y, Gu D, Zhang F, Shi Y, Yang H, Li Z, Yu C, Tu B, Zhao D (2005) Ordered mesoporous polymers and homologous carbon frameworks: amphiphilic surfactant templating and direct transformation. *Wiley Online Library* 44:7053–7059
29. Liang C, Dai S (2006) Synthesis of mesoporous carbon materials via enhanced hydrogen-bonding interaction. *J Am Chem Soc* 128:5316–5317
30. Lamond T, Carbon HM (1964) The surface properties of carbon—III the process of activation of carbons. *Carbon* 1(3):193–207
31. Hu Z, Srinivasan MP, Ni Y (2000) Preparation of mesoporous high-surface-area activated carbon. *Adv Mater* 12:62–65
32. Kyotani T (2000) Control of pore structure in carbon. *Carbon* 38:269–286
33. Ozaki J, Endo N, Ohizumi W, Igarashi K, Nakahara M, Oya A, Yoshida S, Iizuka T (1997) Novel preparation method for the production of mesoporous carbon fiber from a polymer blend. *Carbon* 35:1031–1033
34. Kowalewski T, Tsarevsky NV, Matyjaszewski K (2002) Nanostructured carbon arrays from block copolymers of polyacrylonitrile. *J Am Chem Soc* 124:10632–10633
35. Marsh H, Rand B (1971) The process of activation of carbons by gasification with CO<sub>2</sub>-II. The role of catalytic impurities. *Carbon* 9:63–77
36. Tamai H, Kaki T, Hirota Y, Kumamoto T, Yasuda H (1996) Synthesis of extremely large mesoporous activated carbon and its unique adsorption for giant molecules. *Chem Mater* 8:454–462
37. Oya A, Yoshida S, Alcaniz-Monge J, Linares-Solano A (1995) Formation of mesopores in phenolic resin-derived carbon fiber by catalytic activation using cobalt. *Carbon* 33:1085–1090
38. Tamon H, Ishizaka H, Yamamoto T, Suzuki T (1999) Preparation of mesoporous carbon by freeze drying. *Carbon* 37:2049–2055

39. Pekala RW (1989) Organic aerogels from the polycondensation of resorcinol with formaldehyde. *J Mater Sci* 24(9):3221–3227
40. Knox J, Kaur B, Millward GR (1986) Structure and performance of porous graphitic carbon in liquid chromatography. *J Chromatogr A* 325:3–25
41. Knox JH, Unqer KK, Mueller H (1983) Prospects for carbon as packing material in high-performance liquid chromatography. *J Liq Chromatogr* 6:1–36
42. Liang C, Hong K, Guiochon GA, Mays JW, Dai S (2004) Synthesis of a large-scale highly ordered porous carbon film by self-assembly of block copolymers. *Angew Chem* 116:5909–5913
43. Tanaka S, Nishiyama N, Egashira Y, Ueyama K (2005) Synthesis of ordered mesoporous carbons with channel structure from an organic–organic nanocomposite. *Chem Commun* 2125–2127
44. And CL, Dai S (2006) Synthesis of mesoporous carbon materials via enhanced hydrogen-bonding interaction. *J Am Chem Soc* 128:5316–5317
45. Ryoo R, Joo SH, Kruk M, Jaroniec M (2001) Ordered mesoporous carbons. *Adv Mater* 13(9):677–681
46. Zhang Y, Yang L, Yan L, Wang G, Liu A (2019) Recent advances in the synthesis of spherical and nanoMOF-derived multifunctional porous carbon for nanomedicine applications. *Coord Chem Rev* 391:69–89
47. Kim TW, Chung PW, Slowing II, Tsunoda M, Yeung ES, Lin VSY (2008) Structurally ordered mesoporous carbon nanoparticles as transmembrane delivery vehicle in human cancer cells. *Nano Lett* 8:3724–3727
48. Kyotani T, Nagai T, Inoue S, Tomita A (1997) Formation of new type of porous carbon by carbonization in zeolite nanochannels. *Chem Mater* 9:609–615
49. Johnson SA, Brigham ES†, Ollivier PJ, Mallouk\* TE (1997) Effect of micropore topology on the structure and properties of zeolite polymer replicas. *Chem Mater* 9:2448–2458
50. Rodriguez-Mirasol J, Cordero T†, Radovic LR, Rodriguez JJ (1998) Structural and textural properties of pyrolytic carbon formed within a microporous zeolite template. *Chem Mater* 10:550–558
51. Ma Z, Kyotani T, Liu Z, Terasaki O, Tomita A (2001) Very high surface area microporous carbon with a three-dimensional nano-array structure: synthesis and its molecular structure. *Chem Mater* 13:4413–4415
52. Beck JS, Vartuli JC, Roth WJ et al (1992) A new family of mesoporous molecular sieves prepared with liquid crystal templates. *J Am Chem Soc* 114:10834–10843
53. Zhao D, Feng J, Huo Q, Melosh N, Fredrickson GH, Chmelka BF, Stucky GD (1998) Triblock copolymer syntheses of mesoporous silica with periodic 50 to 300 angstrom pores. *Science* 279:548–552
54. Zhao D, Huo Q, Feng J, Chmelka BF, Stucky GD (1998) Nonionic triblock and star diblock copolymer and oligomeric surfactant syntheses of highly ordered, hydrothermally stable, mesoporous silica structures. *J Am Chem Soc* 120:6024–6036
55. Tanev PT, Pinnavaia TJ (1995) A neutral templating route to mesoporous molecular sieves. *Science* 267:865–867
56. Tanev PT, Pinnavaia TJ (1996) Biomimetic templating of porous lamellar silicas by vesicular surfactant assemblies. *Science* 271:1267–1269
57. Wu C-G, Bein T (1994) Conducting carbon wires in ordered, nanometer-sized channels. *Science* 266:1013–1015
58. Lee J, Yoon S, Hyeon T, Oh SM, Kim KB (1999) Synthesis of a new mesoporous carbon and its application to electrochemical double-layer capacitors. *Chem Commun* 2177–2178
59. Kim T-W, Park I-S, Ryoo R (2003) A synthetic route to ordered mesoporous carbon materials with graphitic pore walls. *Angew Chem Int Ed* 42:4375–4379
60. Kim CH, Lee D-K, Pinnavaia TJ (2004) Graphitic mesostructured carbon prepared from aromatic precursors. *Langmuir* 20:5157–5159
61. Kawashima D, Aihara T, Kobayashi Y, Kyotani T, Tomita A (2000) Preparation of mesoporous carbon from organic polymer/silica nanocomposite. *Chem Mater* 12:3397–3401

62. Han B-H, Zhou W, Sayari A (2003) Direct preparation of nanoporous carbon by nanocasting. *J Am Chem Soc* 125:3444–3445
63. Lee JS, Hirao A, Nakahama S (2002) Polymerization of monomers containing functional silyl groups. 5. Synthesis of new porous membranes with functional groups. *Macromolecules* 21:274–276
64. Moriguchi I, Ozono A, Mikuriya K, Teraoka Y, Kagawa S, Kodama M (2003) Micelle-templated mesophases of phenol-formaldehyde polymer. *Chem Lett* 1171–1172
65. Bates FS, Fredrickson GH (2008) Block copolymers—designer soft materials. *Phys Today* 52:32
66. Bockstaller MR, Thomas EL (2004) Proximity effects in self-organized binary particle–block copolymer blends. *Phys Rev Lett* 93:166106
67. Tang C (2006) Nanostructured carbon from well-defined polyacrylonitrile (co) polymers obtained by controlled/living radical polymerizations: from synthesis and characterization to device. Dissertation, Carnegie Mellon University
68. Iijima, S (1991) Helical microtubules of graphitic carbon. *Nature* 354(6348):56–58
69. Bockstaller MR, Thomas EL (2004) Proximity effects in self-organized binary particle-block copolymer blends. *Phys Rev Lett* 92(16):166103
70. Iijima SI (1993) Single-shell carbon nanotubes of 1-nm diameter. *Nature* 603–605
71. Kyotani T (2003) Porous carbon. Carbon alloys: novel concepts to develop carbon science and technology, vol 28, pp 109–127
72. Mikhailovsky Sv, Sandeman SR, Howell CA, Phillips GJ, Nikolaev VG (2012) Biomedical applications of carbon adsorbents. *Novel Carbon Adsorbents* 639–669
73. Lieber CM, Chen CC (1994) Preparation of fullerenes and fullerene-based materials. *Solid State Phys Adv Res Appl* 48:109–148
74. Fowler PW, Ceulemans A (1995) Electron deficiency of the fullerenes. *J Phys Chem* 99:508–510
75. MPrato (1997) Fullerene chemistry for materials science applications. *J Mater Chem* 7:1197–1109
76. Tadzyszak K, Wychowaniec JK, Litowczenko J (2018) Biomedical applications of graphene-based structures. *Nanomaterials* 8:1–20
77. Benzigar MR, Talapaneni SN, Joseph S, Ramadass K, Singh G, Scaranto J, Ravon U, Al-Bahily K, Vinu A (2018) Recent advances in functionalized micro and mesoporous carbon materials: synthesis and applications. *Chem Soc Rev* 47:2680–2721
78. Gunathilake TU, Ching Y, Polymers KC (2017) Biomedical and microbiological applications of bio-based porous materials: a review. *Polymers* 9:160
79. Moazzen E, Ebrahimzadeh H, Amini MM, Sadeghi O (2013) A novel biocompatible drug carrier for oral delivery and controlled release of antibiotic drug: loading and release of clarithromycin as an antibiotic drug model. *J Sol-Gel Sci Technol* 66:345–351
80. Torad NL, Li Y, Ishihara S et al (2014) MOF-derived nanoporous carbon as intracellular drug delivery carriers. *Chem Lett* 43:717–719
81. Mahor A, Singh PP, Bharadwaj P, Sharma N, Yadav S, Rosenholm JM, Bansal KK (2021) Carbon-based nanomaterials for delivery of biologicals and therapeutics: a cutting-edge technology. *C* 7:19
82. Zamani M, Rostami M, Aghajanzadeh M, Kheiri Manjili H, Rostamizadeh K, Danafar H (2018) Mesoporous titanium dioxide@ zinc oxide–graphene oxide nanocarriers for colon-specific drug delivery. *J Mater Sci* 53:1634–1645
83. Lu YJ, Lan YH, Chuang CC, Lu WT, Chan LY, Hsu PW, Chen JP (2020) Injectable thermo-sensitive chitosan hydrogel containing CPT-11-loaded EGFR-targeted graphene oxide and SLP2 shRNA for localized drug/gene delivery in glioblastoma therapy. *Int J Mol Sci* 21:1–29
84. Ren T, Wang Y, Yu Q, Li M (2019) Synthesis of antimicrobial peptide-grafted graphene oxide nanosheets with high antimicrobial efficacy. *Mater Lett* 235:42–45
85. Khalili R, Zarrintaj P, Jafari SH, Vahabi H, Saeb MR (2020) Electroactive poly (p-phenylene sulfide)/r-graphene oxide/chitosan as a novel potential candidate for tissue engineering. *Int J Biol Macromol* 154:18–24

86. Pistone A, Iannazzo D, Ansari S, Milone C, Salamò M, Galvagno S, Cirmi S, Navarra M (2016) Tunable doxorubicin release from polymer-gated multiwalled carbon nanotubes. *Int J Pharm* 515:30–36
87. Wu G, Mikhailovsky A, Khant HA, Zasadzinski JA (2009) Chapter 14 Synthesis, characterization, and optical response of gold nanoshells used to trigger release from liposomes, 1st edn. In: *Methods in enzymology*, vol 6879(09), pp 64014–3
88. Weissleder R (2001) A clearer vision for in vivo imaging: Progress continues in the development of smaller, more penetrable probes for biological imaging. *Nat Biotechnol* 19:316–317
89. Zhang Z, Wang J, Chen C (2013) Near-infrared light-mediated nanoplatforams for cancer thermo-chemotherapy and optical imaging. *Adv Mater* 25:3869–3880
90. Mesopores D, Wang Y, Wang K, Zhang R, Liu X, Yan X, Wang J, Wagner E, Huang R (2014) Synthesis of core-shell graphitic carbon @ silica nanospheres with photothermochemotherapy. *ACS Nano* 7870–7879
91. Wang K, Yao H, Meng Y, Wang Y, Yan X, Huang R (2015) Specific aptamer-conjugated mesoporous silica-carbon nanoparticles for HER2-targeted chemo-photothermal combined therapy. *Acta Biomater* 16:196–205
92. Zhang L, Li Y, Jin Z, Chan KM, Yu JC (2015) Mesoporous carbon/CuS nanocomposites for pH-dependent drug delivery and near-infrared chemo-photothermal therapy. *RSC Adv* 5:93226–93233
93. Liao L, Liu J, Dreaden EC, Morton SW, Shopsowitz KE, Hammond PT, Johnson JA (2014) A convergent synthetic platform for single-nanoparticle combination cancer therapy: ratiometric loading and controlled release of cisplatin, doxorubicin, and. *ACS Publications* 136:5
94. Zhang DY, Zheng Y, Tan CP, Sun JH, Zhang W, Ji LN, Mao ZW (2017) Graphene oxide decorated with Ru(II)-polyethylene glycol complex for lysosome-targeted imaging and photodynamic/photothermal therapy. *ACS Appl Mater Interfaces* 9:6761–6771
95. Zhang P, Huang H, Huang J, Chen H, Wang J, Qiu K, Zhao D, Ji L, Chao H (2015) Noncovalent Ruthenium(II) complexes-single-walled carbon nanotube composites for bimodal photothermal and photodynamic therapy with near-infrared irradiation. *ACS Appl Mater Interfaces* 7:23278–23290
96. Sahu A, Choi W, Lee J, Biomaterials GT (2013) Graphene oxide mediated delivery of methylene blue for combined photodynamic and photothermal therapy. *Biomaterials* 34(26):6239–6248
97. Li C, Meng Y, Wang S, Qian M, Wang J, Lu W, Huang R (2015) Mesoporous carbon nanospheres featured fluorescent aptasensor for multiple diagnosis of cancer in vitro and in vivo. *ACS Nano* 9:12096–12103
98. Kong Q, Zhang L, Liu J, Wu M, Chen Y, Feng J, Shi J (2014) Facile synthesis of hydrophilic multi-colour and upconversion photoluminescent mesoporous carbon nanoparticles for bioapplications. *Chem Commun* 50(99):155772–155775
99. Zhao L, Ge X, Yan G, Wang X, Hu P, Shi L, Wolfbeis OS, Zhang H, Sun L (2017) Double-mesoporous core-shell nanosystems based on platinum nanoparticles functionalized with lanthanide complexes for: In vivo magnetic resonance imaging and photothermal therapy. *Nanoscale* 9:16012–16023
100. Zhang Q, Wang P, Li X, Yang Y, Liu X, Zhang F, Ling Y, Zhou Y (2017) Preparation of highly dispersed  $\gamma$ -Fe<sub>2</sub>O<sub>3</sub> and GdPO<sub>4</sub> co-functionalized mesoporous carbon spheres for dual-mode MR imaging and anti-cancer drug carrying. *J Mater Chem B* 5:3765–3770
101. Deka K, Guleria A, Kumar D, Biswas J, Lodha S, Kaushik SD, Dasgupta S, Deb P (2018) Mesoporous 3D carbon framework encapsulated manganese oxide nanoparticles as biocompatible T1 MR imaging probe. *Colloids Surf A* 539:229–236
102. Sharma S, Byrne H (2016) Antibodies and antibody-derived analytical biosensors. *Essays Biochem* 60(1):9–18
103. Conroy PJ, Hearty S, Leonard P, O’Kennedy RJ (2009) Antibody production, design and use for biosensor-based applications. *Semin Cell Dev Biol* 20:10–26

104. Kim D, Herr AE (2013) Protein immobilization techniques for microfluidic assays. *Biomicrofluidics* 7(4):041501
105. Lim, Syazana A, Minhaz UA (2019) Introduction to immunosensors. In: *Immunosensors*. Royal Society of Chemistry, pp 1–20
106. Zhang Z, Peng M, Li D, Yao J, Li Y, Wu B, Wang L, Xu Z (2021) Carbon material based electrochemical immunosensor for gastric cancer markers detection. *Front Chem* 702
107. Sheng Q, Zheng J, Shang-Guan X, Lin W, Li Y (2010) Direct electrochemistry and electrocatalysis of heme-proteins immobilized in porous carbon nanofiber/room-temperature ionic liquid composite film. *Electrochim Acta* 55(9):3185–3191
108. Huang Z, Jiang Z, Zhao C, Han W (2017) Simple and effective label-free electrochemical immunoassay for carbohydrate antigen 19–9 based on polythionine-Au composites as enhanced sensing. *Int J Nanomed* 12:3049
109. Pei F, Wang P, Ma E, Yang Q, Yu H, Gao C, Li Y, Liu Q, Dong Y (2019) A sandwich-type electrochemical immunosensor based on RhPt NDs/NH<sub>2</sub>-GS and Au NPs/PPy NS for quantitative detection hepatitis B surface antigen, vol 12. Elsevier, pp 3049
110. Yuan X, Zhang X, Sun L, Wei Y, Wei X (2019) Cellular toxicity and immunological effects of carbon-based nanomaterials. *Part Fibre Toxicol* 16(1):1–27
111. Dong PX, Wan B, Wang ZX, Guo LH, Yang Y, Zhao L (2013) Exposure of single-walled carbon nanotubes impairs the functions of primarily cultured murine peritoneal macrophages. *Nanotoxicology* 7:1028–1042
112. Wang X, Guo J, Chen T, Nie H, Wang H, Zang J, Cui X, Jia G (2012) Multi-walled carbon nanotubes induce apoptosis via mitochondrial pathway and scavenger receptor. *Toxicol In Vitro Int J* (published in association with BIBRA) 26:799–806



# Chapter 30

## Fanatical Clout of Porous Carbon Materials—A Peek in Therapeutics



Madhu Raina, Sonia Sharma, and Sakshi Koul

### 1 Introduction

Porous materials are considered to be important elements for diverse maneuverings owing to their intrinsic aptitude to set up network with various atoms, molecules as well as ions. This interaction remains operational at the surface level which is maintained within the structure as well. Apparently, such interactions became prominent during the development of supercapacitors which encompassed the usage of ruthenium oxide (RuO<sub>2</sub>) electrodes [1]. The interface between these electrodes and electrolytes thereof exhibited an uncommon capacitance which was quite hefty than expected rates during redox reactions. Porous materials are, therefore, versatile resources with significant industrial applications.

Carbon, one of the most important components on this planet, is a non-metallic, tetravalent element. Its abundance and unusual ability to form polymers at varying temperatures enable it to serve as a common element of all life forms. It is the second most abundant element in human biomass (about 18.5%) exceeded only by oxygen [2]. The atomic structure of carbon imparts several inimitable bonding potential forming different structures with divergent attributes in diverse organic compounds. During the initial times, carbon was largely utilized in the form of charcoal and carbon black. While the former consists of combusted wood or coal with removed volatile substances, the latter comes when vegetable oil is moderately flamed. In the Stone Age which spans from 35,000 to 11,000 BC both the carbon forms especially charcoal was used as a black color pigment for making images in the Altamira Cave (Spain). Such special illustrations signify the apogee of Paleolithic cave art across

---

M. Raina (✉) · S. Sharma

Department of Botany, Cluster University of Jammu, Jammu, Jammu and Kashmir, India  
e-mail: [ramadhuoffshore@gmail.com](mailto:ramadhuoffshore@gmail.com)

S. Koul

Department of Zoology, Cluster University of Jammu, Jammu, Jammu and Kashmir, India

Europe [3]. Similarly, the Egyptians and Sumerians in 3750 BC utilized carbon as smokeless fuel and in the bronze manufacturing process to reduce copper, tin, and zinc minerals [4]. This exploitation continued for centuries.

The first and foremost evidence of the medicinal use of carbons dates back to 1550 BC when Egyptians used charcoal in papyrus and applied the same to adsorb stinging odors from moldering wounds. They reportedly used the same to treat intestines-related problems also [5]. However, the therapeutic use of carbon to treat various diseases was later brought into forefront by the Greeks somewhere during ca. 460–370 BC and Romans for the duration of AD 23–79. Among different diseases known to get cured using carbon that time included epilepsy, food poisoning, anthrax, and chlorosis [3, 6]. Further, Greeks were of the belief that water should be consumed only after being filtered using carbonized wood. This would facilitate the elimination of bad flavor and odor from it [7]. This did not remain limited to Greek and Rome only but during 450 BC Indian manuscripts also referred to the use of sand and charcoal filters as a means to purify water to make it amenable for drinking [5]. Carbon as a means of medical precaution gained a momentum in AD 157 when a medicine-based article from Claudius Galvanometer published the advantages of using carbon possibly to treat myriad collection of diseases. Consequently, huge information kept on adding to the medicinal values of carbon from time to time depending upon the information available at a particular time. One such information was poured from one of the earliest Sanskrit manuscripts during AD 200 which described the simple disinfection procedure of water using carbon. The document emphasized that keeping water in copper vessel and then given ample sunlight does not guarantee its disinfection but it must require coal filtration to assure degradation of contaminants from it [5]. This maneuver sustained for a pretty long time. Above and beyond thousands of years of history with heaps of medicinal and therapeutic applications, different techniques were discovered to activate the charcoal, so as to improve different properties thereof to a greater extent. And it was only twentieth century's wakeup call that presaged the most stupendous capacity of carbon-based substances: "the possibility of enclosing a huge porosity into the carbon material structure" [8]. This activation, therefore, processed the material to have small, low-volume pores roofed by the atomic carbon and produced activated carbon. Known to amplify the surface area available for adsorption of different substances and/or chemical reactions, these new materials have freshly been designated as the nanoporous carbons. Among different properties acquired by these porous materials, the most basic includes the surface area and porosity. Secondary analysis including pore shape, chemical nature and composition at the surface, exterior roughness or behavior toward electrical field is equally vital to comprehend their potential so as to unravel their other important parameters [8]. Nevertheless, hierarchical porosity certainly remains decisive. According to International Union of Pure and Applied Chemistry (IUPAC), nanopores are featured with the following pore size [9]. However, the maximum aperture does not exceed 100 nm.

- (a) pore diameter <2 nm-Micropores
- (b) diameter range from 2 to 50 nm-Mesopores
- (c) width >50 nm-Macropores.

In all probability, the structure of the porous carbons is the most imperative feature affecting its overall properties including chemical stability, electrochemical intercalation of active substances, potential of catalysis, sorption, etc. At the same time, it is quite doable to regulate the morphology of porous carbon material (PCM) both internal and external using appropriate molds [10–12]. Whereas the former include efficient or chaotic micro-, meso-, and macro-pores the latter encompass spheres, terapods, monoliths, nanowires, etc. While the system of pore classification remains to be central, more emphasis is being given on planning the pore architecture in PCMs. Accordingly based on the designed porosity significant advantages vis-a-vis distribution of pores and their access on carbon material are likely to be acquired. The following examples underline the applications of pore structure that can offer direction for future studies involving meso- and macroporous designer carbons.

## 1.1 Sensors

Selecting the accurate substrate plays an elementary role in the functionality and consistency of the assembled component. Porous carbon materials typically with large-sized pores are reasonably appropriate for sensor substrates in different applications. For instance, to avert enzyme discharge during a biological reaction, there is a possibility to fix it within the pore aperture. MSU-F-C, a carbon foam with mesopores, has been employed as a host for enzyme glucose oxidase (GOx) [13]. The carbon used is mixed with Nafion. The mixture is applied on a glassy-carbon electrode, and enzyme is made static in the process. Compared to graphitic or activated carbon material, the mesoporous MSU-F-C exhibit increased sensitivity, prompt substrate response with more loading capacity of  $39.1 \pm 0.7$  wt% for GOx. This application did not remain confined to mesoporous system but extended to porous carbon with macropores as well. 3D ordered macroporous (3DOM) carbon when used in the sensing system of solid-contact ion-selective electrode (SCISE) [14] was utilized as a solid contact. Herein the carbon and a metallic current collector were joined together and both were enveloped with a sensing membrane. This membrane typically had polyvinyl chloride (PVC) coating and sites for ionic channels including ionophores. The assembly was made discerning for  $K^+$  ions. With a detection perimeter of  $10^{-6.2}$  M, the sensor demonstrated prolonged constancy and remained defiant to meddling from  $O_2$  as well as luminosity. This is on contrary to other sensing materials including semiconducting polymers where interference by light is on record [15]. Ahead of behaving as a substitute for sorption system, porous carbons present themselves as congregation bodies for biological catalysts, for instance, enzymes.

## 1.2 Property of Sorption

A phenomenon of fixing or capturing a substance in gaseous or vapor phase by another substance in condensed state (solid or liquid) is called sorption. While the former substance is sorbate, the latter is called sorbent. Carbon-based substances particularly those with randomly or orderly arranged mesopores are frequently used as sorbents in solid–gas and solid–liquid phases. In fact porous carbon tailored to have a typical pore structure (both meso- and macropores) has a potential to house a myriad enzymes and various essential molecules. This is due to their typical surface properties including the pore architecture that sets a fine-tuning with these biomolecules. Further, due to the absence of charge, the porous carbon as sorbent remains neutral toward any functional group of the active sites of enzymes. This is in contrast to other porous materials like those of silica where acidic silanes chemically interact with the enzymes [16]. Owing to this property, PCM finds important applications in catalytic reactions, food sciences, biosensing, etc. One such application of mesoporous carbon is in water purification. The porous carbon saturated with Iron (II) Chloride and tarnished with sodium hypochlorite (NaClO) acts a sorbent to make water free from arsenic impurities [17]. Similarly, in liquid chromatographic techniques, especially the ones involving electrochemical strength, the stationary phase comprises of porous graphitic and vitreous carbon [18]. Based on the immobilization as well as neutral surface properties, it was recognized that lysozyme when interacting with such porous carbon surfaces gets adsorbed therein without losing its surface integrity and activity [16]. Two factors have been underscored and found responsible for this behavior; pore structure and pH of the solution in which enzyme mixture were prepared. It was established that with a molecular weight of approximately 14 kDa (kilo Dalton), lysozyme got adsorbed the most when its pH approached isoelectric point ( $\text{pH(I)} = 11.1$ ). At this point since enzyme carries no net charge, their packaging on the porous surface was more compact without any denaturation. This property to adsorb more enzyme molecules gained a momentum when oxidation was carried out in the presence of an inorganic, colorless, readily water-soluble ammonium persulfate  $[(\text{NH}_4)_2\text{S}_2\text{O}_8]$  [19]. This process changed interactive groups on the surface, adhesive and cohesive forces between solid and liquid phases and more importantly pore architecture got customized. This in turn assisted in making entry of proteins on adsorption surface/sites.

## 1.3 Catalysis

It is well-established that carbonaceous materials play a pivotal role in wide catalytic reactions [20] including nitrous oxide reduction, reactions involving addition or removal of hydrogen, removal of sulfur, nitrogen oxygen, and many more. In most of these reactions with bulky substrate molecules, the distribution of pores on PCM is decisive in improving the rate of reaction. In such cases, usually porous carbon with

mesopores is chosen [21]. However, after the prolonged usage of natural carbon, the impurities filtered by the pores are likely to deactivate the enzyme. To overcome this, synthetic porous carbons are usually employed [20]. Undoubtedly, despite a uniform distribution of mesopores, disparity in the scattering of the metal impurities in such enzyme-catalyzed reactions with PCM requires an urgent management. It is pertinent to mention here that not only the surface characteristics of carbon but detailed knowledge of pore architecture, its distribution, and control is also equally important to persuade the spreading of metal crystals [21]. Literature puts on record few studies of different catalyst-based reactions in a comparative mode. For instance, compared to cobalt–molybdenum catalyst system prepared on gamma-alumina, the one geared up on activated carbon based on resorcinol and formaldehyde had overall greater activity. This was due to the defined pore structure of carbon material coupled with better quality of dispersion of metal in soaring surfaces [22]. At the level of pore structure, the inherent potential was least in pores with diameter <2 nm due to blockage by metallic particles. In this case, the mesoporous carbon showed maximum activity since metal dispersion was less significant.

Based on the precursor used, a large number of methods are now available to synthesize porous carbons (PCs). While precursors include a variety of biomass derived from plants, animals, fungi, and sewage sludge materials [23], the prominent synthesis techniques encompass strategies like hard template, soft template, and template-free methods. In recent years, owing to unique physical and chemical properties of such versatile materials an implausible expansion has been seen in nano-biomedical studies, principally in exploiting engineered nanomaterials in biomedical applications [24, 25] as diagnostic probes, nano-carriers, and biomarkers [26]. Further, it is doable to explore such porous carbon materials at the cellular and subcellular levels vis-a-vis probing, adjusting, and controlling different biological processes.

In this chapter, we focus on the therapeutic applications of porous carbon (or nanocarbon) materials, primarily fullerene nanoparticles, drug delivery, carbon nanohorn, carbon nanotubes, nanodiamonds, and porous nanocarbon. In addition, the possible toxicities of these PCMs have also been highlighted. At the same moment, utmost care has been taken to juggle manifold errands, from digging up and appraising the pertinent literature to blending information from various sources via critical thought process to paraphrasing, appraise, and citation skills. It is pertinent to mention here that the probable impact of shape as well as toxicity of such PCMs on various biological traits has been described based on the reports from the literature.

## 2 Fullerenes

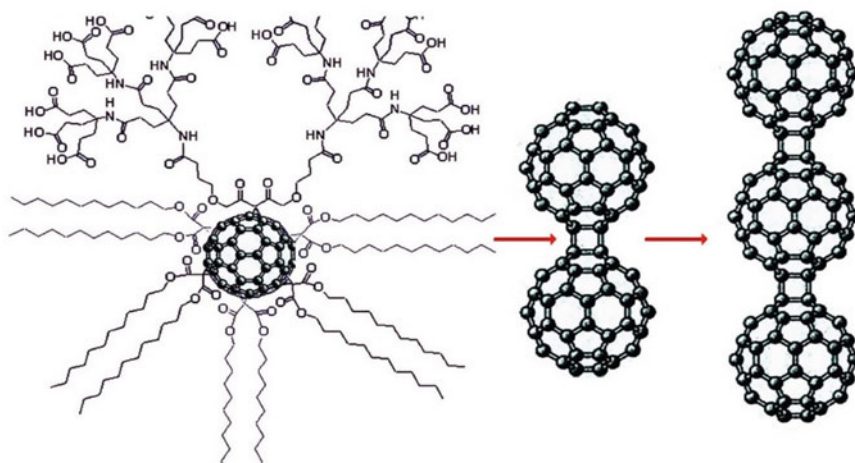
Fullerenes encompass members with pentagonal and hexagonal carbon rings structured to give them a cage-like configuration. One among such molecules is exemplified by pristine fullerene, wherein 12 five-membered carbon rings are complexed with the six-membered rings. The family takes in members such as C<sub>60</sub>, C<sub>70</sub>, C<sub>82</sub>,

and so on. The most widely accepted method to produce fullerenes includes laser technology or arc release method, wherein adulterant-free graphite is employed as main source of carbon and the synthesis takes place in the presence of inert gases, especially helium or nitrogen. During its production metal alloy is usually put inside a fullerene cage where it serves as discharge anode. Such alloys principally correspond to Lanthanoid or Scandium family. The structure so produced is known as an endohedral metallofullerene (EMFs). These include Li@C<sub>60</sub> where lithium ion is collided with C<sub>60</sub> and similarly Sc<sub>3</sub>N@C<sub>82</sub>, Gd@C<sub>82</sub>, etc. [27]. Likewise, exohedral addition of certain molecules also opens window to different such derivatives. Consequently, such endo- as well as exo-hedral amendments radically modify fullerenes both physically and chemically, augments the functionality thereof and also make them appropriate to be used in numerous applications. Fullerenes gained a momentum for having the biological effects when it was claimed that C<sub>60</sub> has an inhibitory action on protease activity of AIDS virus. This is for reason that it appropriately locks itself into the cavity of the enzyme where it shows least affinity with water [28]. Since then, there have been numerous reports on the active participation of fullerenes in the medical science, including in destruction of cancer cells by light and photosensitizer exposure, non-invasive resonance imaging technology [29]. Nevertheless, potential of fullerenes as “radical sponges” in different formats has been broadly explored and highly appreciated [30].

## ***2.1 Buckysomes as Hydrophobic Molecule Delivery System***

Paclitaxel, a potent anticancer water repellent drug (solubility ~0.3 µg/mL) [31], has been used since 1967 to treat Kaposi's sarcoma [32], ovarian, breast, and lung cancers. The drug was formerly administered through dissolution in polyoxyethylated castor oil followed by parched alcohol. On the other hand, due to the toxicity of the former [33], other alternatives for its delivery were scrutinized. Prominent among them was the use of nanoscale carrier vectors [31, 34] for example liposomes [35]. Many amphiphilic monomer fullerenes, AF-1 are self-assembled to form a spherical nanostructure with size ranging from 100 to 200 nm. This is called buckysome. Chemically, these monomers consist of C<sub>60</sub> molecules modified with dendritic unit. They contain 18 COOH (carboxylic acid) groups wherein five positions are engaged by octahedrally placed dodecyl malonates (Fig. 1). The cage-like structure so produced implants anticancer paclitaxel drug into the hydrophobic pocket to form paclitaxel-embedded buckysomes or PEBs (Fig. 1) [36]. In such buckysomes, therefore, features of both liposomes and porous nanoparticles are combined to generate a novel drug delivery system.

This exclusive fictionalization allows buckysomes to probably tender various recompenses over phospholipid liposomes as nano-vectors. This approach may perk up circulation rate in the blood, safeguards anticancer drug from degrading action of harmful enzymes, and more importantly condense absorption by phagocytic organs.



**Fig. 1** Fullerene monomer AF-1: chemical composition and formation of polymer

Further, dendritic groups present on the PEB exterior too offer furtive function to trim down clearance.

The therapeutic worth of PEBs gained an impetus when it was compared to Abraxane<sup>®</sup>, a medicine strongly recommended to treat advanced-stage breast cancers. Similar to this nab-paclitaxel, the PEBs when tested on a commonly used breast cancer cell line MCF-7 [37] facilitate the uptake of antineoplastic chemotherapy drug. This method bypassed the requirement of non-aqueous solvents, which otherwise discomfort and cause redundant reactions to the patients. Literature also puts on record the capacity of PEBs to administer increased doses of potent drug than delivered by nab-paclitaxel. These results ultimately pave a way to reduce the cocktail and increase tumor uptake for improved anticancer potency. This, in turn, opened the door to authorize the biodistribution of PEBs in animal model as possible drug carriers *in vivo*. Owing to nanoscale dimensions of fullerene-based deliverance system another attractive feature is the passive targeting. The nanoparticles enter into tumor cells via leaky blood vessels of endothelial cells and become capable to accumulate at tumor sites. Further, PEBs are also endowed with appending target assemblage to their fullerene components. With the result, they can be effortlessly made purposeful to affix active targeting.

The aptitude of fullerene to fabricate a superlative lipophilic gradual discharge arrangement offers a concrete arena for covalent bonding of drugs to craft single-bout “drug cocktails.” One such aspect can be exemplified in lung cancer therapy. A fullerene-paclitaxel conjugate, with 120–145 nm size, has been designed to facilitate gradual release of the drug paclitaxel via enzymatic hydrolysis. The formulation has 80-min shelf-life of release in bovine plasma [38]. Liposome formulation based on 1,2 dilauroylphosphatidylcholine (1,2-DLPC) conjugate reportedly has a

shared maximal inhibitory concentration (IC<sub>50</sub>) value. This is practically indistinguishable to the corresponding value for paclitaxel-DLPC expression in A549 cells, the adenocarcinomic human epithelial lung carcinoma. Thus, owing to the clinical appropriateness of hydrolytic rate and momentous cyto-lethality in *in vivo* culturing of tissues, the fullerene-paclitaxel conceptualization has proven to have aptitude for improved therapeutic efficacy of paclitaxel.

Besides playing a pivotal role in drug delivery, fullerenes have also been scrutinized as vectors in transfection process. These vectors with a potential to mediate gene transfer actively deliver exogenous DNA into cells [39, 40]. This, in turn, adds to the possible benefits in gene therapy systems. However, expertise in this field has not gained much recognition since the initially generated fullerene-based transfection vectors showed signs of high cytotoxicity as well [40]. This is understood by the fact that when different water-soluble C<sub>60</sub> derivatives were prepared, there was smooth DNA uptake, transport across cell followed by successful evocation of gene expression [41]. Notwithstanding the booming genetic expression, the efficient *in vitro* transfection has been characterized by octa- and dodeca-amino derived C<sub>60</sub> vectors. This behavior is generally reasoned for their aggregation behavior. Apparently, vector clustering of different functionalized fullerenes is liable to cause enhanced cytotoxicity. Hence, future studies based on such aggregation ought to be addressed before designing any such fullerene derivatives.

## 2.2 ROS Quenching

Reactive oxygen species or ROS refers to the miniature molecules of molecular oxygen produced as a result of their partial reduction [42]. Some commonly produced ROS by a cell include various anions like superoxide anion (O<sub>2</sub><sup>•-</sup>), hydroxyl anion (OH<sup>-</sup>); peroxides such as hydrogen peroxide (H<sub>2</sub>O<sub>2</sub>), and oxides like nitric oxide (NO). Of these, NO is generated principally by endothelial cells and acts as an effective vasodilator.

Literature is flooded with the examples of pristine fullerenes to have radical scavenging properties and produce ROS, thereby suggesting their possible role in photodynamic therapy. The benzyl radicals generated during photochemical reactions smoothly react with C<sub>60</sub> and produce various radical as well as non-radical adducts typically (C<sub>6</sub>H<sub>5</sub>CH<sub>2</sub>)<sub>n</sub> C<sub>60</sub> where  $n = 1-15$ . Those with  $n = 3$  or  $5$  stay thermally stable beyond 50 °C. Importantly, the unpaired electrons remain exceedingly confined to the C<sub>60</sub> surface and the steric fortification of these curbed radicals by benzyl substituents imparts extraordinary stability on the surface of pristine fullerenes [43]. Ever since the potential of fullerenes to scavenge ROS was documented, there has been an immense concern in using fullerenes as an antioxidant. Contrarily, in rats C<sub>60</sub> can reportedly prevent radical formation as well as damage to liver and kidney caused by carbon tetrachloride [44, 45]. For the meantime, it is acknowledged that fullerene derivatives acquire great competence to seize ROS and various radicals [46]. It is, nevertheless, pertinent to mention here that while imparting hydrophilicity to



fullerenes, elements of scavenging radicals ought to be maintained. After an innovative article on “carboxyfullerenes as neuroprotective agents” got a press in Proceedings of National Academy of Sciences USA by Dugan and co-workers [47], the versatile scavengers of ROS and free radicals especially C60 emerged as biologically unique antioxidants [48]. For instance, C60(OH)<sub>x</sub>, a polyhydroxylated fullerene are known for their cell protection properties. It reportedly averts the damage due to compounds like hydrogen peroxide and 3-morpho linosydnonimine that could be detrimental to the neurons [49, 50]. Similarly, during neuronal apoptosis and excitotoxic necrosis, carboxyfullerenes have been found to be very efficient in providing protection to the cellular system and function as neuroprotective drugs in vivo. This escorted an idea that oxidative stress, a causal factor in many persistent diseases, is a crucial impending intermediary in contrasting neuronal fatalities. In this mechanism, the water-soluble property of fullerenes imparts increase efficiency in brain and neurons. In zebrafish, the COOH groups present in C60 fullerenes scavenge radicals from ionizing radiation to safeguard the developing embryos [51]. Similar to this, *tris-malonyl group of C60*-fullerene suppresses mitochondrial damage in mice due to superoxide radicals by penetrating through the barrier between blood and brain. Compared to the untreated control mice, the given treatment of fullerenes was more superior in terms of having prolonged life with more retaining competence [52]. Fullerene nanoparticles typically C60 when modified by mechanical milling with different surfactant molecules such as cyclodextrin, sodium dodecyl sulfate (SDS), and ethylene vinyl derivatives increase ROS-scavenging aptitude. This, in turn, counterbalances the superoxide radicals from mitochondria and hence prevents apoptotic death due to nitric oxide exposure [53]. Congruent with this, colloidal derivatives of C60-polymer including poly N-vinyl pyrrolidone (NVP) exhibit antioxidant properties against ultraviolet radiations in human skin keratinocytes or superoxide radicals in CATH.a neurons produced by angiotensin II [54]. Such studies clearly indicate role of pristine fullerenes derivatives as scavengers of ROS.

In yet another study, the antioxidative property of carboxyfullerenes capable of suppressing lipid peroxidation due to iron and imparting neuroprotection against nigrostriatal dopaminergic degeneration system was demonstrated [55]. This study extended to show non-toxicity of carboxyfullerene to rat brain. Successive research confirmed its protective action against apoptosis of peripheral blood mononuclear cells and their potential in the involvement of mitochondrial membrane potential integrity [56].

Although conflicting statements on radical scavenging by pristine fullerenes are on record, there are reports on ROS interruption as well. Since scavenging ability largely depends on morphological features of fullerenes, a comparison of the same among three hydrophilic fullerenes, viz. carboxyfullerene [C60(C(COOH)2)2], fulleranol [C60(OH)22], and multihydroxylated nanoparticles [Gd@C82(OH)22] revealed greatest ROS-scavenging capacity in cells with multihydroxylated nanoparticles. Such cells were further resistant to toxicity induced by hydrogen peroxide. Of three, carboxyfullerenes were least protective and fulleranol nanoparticles showed intermediate effect [57].

Oxidative stress is a phenomenon where production and accumulation of ROS in cells do not make a tally and consequently liberate radical ions including superoxide ( $O_2^-$ ), hydroxyl radicals ( $HO^\cdot$ ), singlet oxygen ( $^1O_2$ ), hydrogen peroxide ( $H_2O_2$ ), etc. [58, 59]. Fullerenes with scavenging activity play a vital role in therapeutics. Accordingly, molecular mechanism of how fullerenes scavenge ROS needs to be understood. Interestingly, the quenching mechanism of superoxide radical anion shares similarity with superoxide dismutase [60]. The free radical approaches the fullerene cage and sets a bond with available electron-deficient area and afterward transfers electron. Binding of subsequent  $O_2^-$  to the same spot destructs  $O_2^-$ . The reaction produces  $H_2O_2$  and regenerates the fullerene. Similar mechanism is mimicked and during deactivation step, the singlet oxygen ( $^1O_2$ ) joins together with fullerene to produce a charge-transfer complex [61]. Scavenging of more radicals, like  $HO^\cdot$ , involves saturation of electron-deficit areas of fullerenes with definite proportions of radical [43]. Based on this pathway, cancer cells become susceptible to oxidative stress vis-a-vis increased ROS concentration. Consequently, cellular proliferation, mutations, and genetic instabilities get stimulated. Hence, fullerenes, with a capability to seize ROS, possibly find an application in medical science in maintaining general health during cancer therapies.

### 2.3 MRI Contrast Agents

As mentioned earlier, EMFs comprise different categories of functionalized fullerenes. With a proficiency to trap atoms within structure EMFs especially those readily soluble in water have played a pivotal role in therapeutics. Once inside the body, fullerene cage in EMFs shields the encapsulated drug-like liposomes and also assures unprovoked discharge of the metal within the body. In this framework, gadolinium-confined fullerenes are expected to enhance MRI quality [62–64]. Second attribute of such contrasting gadofullerenes is to certify the firm placement of metal atom within the cage. Such atoms usually correspond to the ones that generally require longer residency times before being utilized. Strong pH dependency of the proton requirement has made two water-soluble  $Gd@C60(OH)_x$  and  $Gd@C60[C(COOH)_2]_{10}$  fullerenes great candidates as MRI contrast agents [62]. Sitharaman and colleagues [64] proceeded this study with a success in demonstrating the promising nature of anionic gadofullerene  $\{Gd@C60[C(COOH)_2]_{10}\}$  for ex vivo labeling. This was typically achieved within 2–8 h of incubation for marrow stromal cells. Moreover, their inability to infiltrate and destroy healthy tissue under natural conditions during MRI tracing has also been brought to the forefront [64]. Non-leakage of this gadofullerene during pulse-chase experiments from the cells had similar concentrations of gadolinium irrespective of the time limit. This, in turn, is suggestive of the fact that labeling process is irreversible and gadofullerene remains reluctant to leach out post labeling. Also, cellular labeling with this fullerene derivative remains intracellular and/or there is intrusive inserting of magnetic labels deep within the cell membrane. Further assays carried out on viability and toxicity

under laboratory conditions did not result in any kind of damage to the cell due to labeling. Compared to clinically used Gd-DTPA (Magnevist™), the signal strength reportedly increases 300 folds at 0.04 mM concentration of gadofullerenes. This has been revealed from T1-weighted MRI phantoms study. Also, at similar concentration the former bestowed diminutive enrichment when balanced with distilled water. Furthermore, high relaxivity of gadofullerenes, even taken at modest concentration, testimonies for considerable reduction of T1 of labeled cells. This discrimination between labeled and unlabeled cells with respect to T1 apparently proves detrimental by MRI images at 1.5 T strength of magnet used. This in turn has proven to be a boon in medical diagnosis since it aids in detecting stem cells at resolutions prospectively accomplished in living systems under natural conditions. Studies carried out on hydrophilic metallofullerene Gd3N activated with polyethylene glycol (PEG) and [Gd3N@ C80[DiPEG5000(OH)x] have demonstrated their potential as MRI contrast agents [63]. This property is acquired due to their T1–T2 water relaxation rate constant being 40 times more than due to conservative gadolinium-containing MRI contrasting agents.

## 2.4 *Antitumor Effects*

Cancer is one among the somber menaces to human health. This multistep process encompasses alterations in tissue designing coupled with the development of preneoplastic nodules which culminates as cancer. Such changes are usually allied with the alteration in cell phenotype including epithelial to mesenchymal transition (EMT) followed by cell migration. Ultimately, local hypoxial regions are formed that uphold the endurance and expansion of tissue stem cells and encourage angiogenesis. Alternatively under unfavorable conditions like stress, autophagy also props up the endurance of preneoplastic as well as tumor cells. Whereas the escalation and continued existence of normal cells are partly controlled by hormones as well as different growth factors, occasional genetic, epigenetic and microenvironmental changes too alter the signaling pathways and make cells quite defiant and sovereign to such pathways. Understandably, the growth and proliferation of cells become independent of cell cycle checkpoints and apoptotic pathways. Owing to epigenetic modification in the gene expression of a cancerous cell, the distorted signaling pathways and altered metabolomics profile are therapeutically reversible at the outset. Contrarily, progression of tumor becomes pharmacologically more complicated to target afterward [65].

Apart from having genetic basis, growth of tumor and its spread too have a physical basis. From the biophysical perspective, metastasis is known to transpire when cells from the primary tumor separate. The process involves breaking of adhesive bonds between cells. Such loose and free cells when drift through stroma with dense matrix usually create pressure to degrade matrix composition. This takes the helm through the proteinaceous matrix fiber via pores. While doing so, the cells usually get squeezed and deformed. As the cells intravasate into vasculature, they start getting

circulated in the blood flow. To withstand the pressure of circulation, the metastatic cells adhere to the walls of the vessel. Gradually, they squeeze through the vasculature and transmigrate to colonize a secondary tissue [66].

Notwithstanding the genetic and physical backgrounds, human cancers typically stem from centrosome amplifications. These microtubule-organizing centers mainly play a pivotal role in spindle formation at two opposite poles during mitotic division. Following a synchronized pattern, the centrosome and hence the spindle account for accurate segregation of chromosomes so that each daughter cell receives equal number of genetic material [67]. In mammals, augmentation in centrosome loses control on mitosis, makes it abnormal, and thus adds to chromosomal flux and tumor formation [67, 68]. The effect of centrosome escalation gets reflected clinically since it hinders correct prophesy in various tumors like breast cancer [69]. One among various reasons for centrosome amplification is the effect of radiations which efficiently targets and damages DNA in cancerous cells. Such cells are largely devoid of p53 and chk1 activities involved in DNA damage checkpoints [67, 70]. This results in the development of spindle at multiple poles during mitosis. Conversely, division of cell at multiple poles may impart damaging effect to the cell. Thus, there is either cell arrest or progenies so derived are destined to programmed cell death [67]. However, cancer cells have developed a distinctive mechanism to restrain formation of multipolar spindles so as to break out the deleterious multipolar cell division. Known as centrosome clustering, the process encompasses clustering of numerous centrosomes to restore two typical spindle poles. Understandably, cancer cells with multiple centrosomes that do not practice centrosome clustering have death fate. Conversely, prohibition of this clustering specifically inhibits cancer cells compared to a usual cell with two functional centrosomes [71].

With short survival expectations and poor life quality, cancer patients have higher mortality rates than expected [72]. Though advanced technologies including surgery, chemotherapy, and radiotherapy have been introduced cancer treatment still requires further research. Of these, surgery in most of the cases remains incapable to completely eradicate all the cancerous cells. Similarly, the therapies usually have side effects of normal cells. These include apoptosis of normal cells in addition to the timorous ones. This is attributed to doxorubicin (DOX), a commonly used chemotherapeutic agent. However, radiotherapy has been proven to be quite effective in the treatment of nearly 50% of cancerous patients [73]. This therapy is especially recommended to the women suffering from breast cancer since it usually helps them to optimize control post-surgery [74]. Nevertheless, pneumonitis and fibrosis like several side effects due to radiation are likely to get induced to adjacent normal cells. Such drawbacks are the major impediment to the successful radiotherapy. Although several signal transduction pathways for cell survival are allied with radiation sensitivity in cancer as well as adjacent normal cells, the combined application of targeted drugs like EGFR, PI3K, and AKT and radiotherapy is still restricted by different detrimental effects [73]. Thus, there is an utmost requirement of improving the medical procedure for successful radiotherapy so that normal cells become less prone to the side effects. Recent study has shown that competence of radiotherapy in breast cancer cells can be increased when centrosome clustering is specifically targeted. The

ionized radiations provoke amplification of centrosome, and the method causes less damage to the ordinary fibroblast cells. Remarkably, when irradiated declustering of centrosome radiosensitizes such cancerous cells by multipolar spindle induction without affecting the viability of normal cells. This radiosensitizing effect of centrosome declustering is mediated by one of the centrosome clustering proteins Kinesin Family Member C1 (KIFC1) in breast cancer cells [75].

From the past few years, nanotechnology has emerged with certain noteworthy achievements, typically in application of photons in health care, assemblage of molecular complexes held together by non-covalent bonds and drug delivery systems. Apart from practical utility of EMFs in therapeutics during radioactive tracing technology or resonance imaging [76, 77], recently a holmium-containing hydrophilic MF derivative was espoused to track its distribution and biological behavior. Different studies carried out on multihydroxylated nanoparticles [Gd@C82(OH)<sub>x</sub>] have primarily focused on their involvement in MRI as contrast agents, wherein such particles have proven to be quite efficient with low toxicity. However, based on the biological impact of Gd@C82(OH)<sub>x</sub> recent research has come up with anti-proliferative properties of this popular fullerene [78, 79], wherein complementary mechanism leads to the stimulation of programmed cell death in tumorous cell lines. Compared to the clinical antineoplastic agent CTX, a Gd@C82(OH)<sub>22</sub> solution exhibits 1000 times higher tumor-inhibitory capability. While CTX, an alkylating agent, treats many types of cancer by damaging the cell's DNA and apparently kill cancer cells, the fullerene solution significantly reduces tumor density in tumor-affected mice. The mechanism of multihydroxylated nanoparticles to act in anticipation of cancer may possibly open a window of opportunity to aim and assemble novel antitumor pharmaceutical agents. Studies have shown that when Gd@C82(OH)<sub>22</sub> nanoparticles are administered into the body, only small doses reach the tumor cells [80]. Coupled with this, these nanoparticles remain non-toxic to various cells like human breast cancer cells and hepatomas. Thus, these particles do not target cancer cells directly [81] but kill the same via indirect antitumor mechanism.

As mentioned earlier, Gd@C82(OH)<sub>22</sub> fullerenes can intercept different reactive oxygen species to prevent oxidative stress owing to their stupendous antioxidant property. Co-incidentally, cancerous cells develop profuse oxidative stress too [82]. Under such conditions Gd@C82(OH)<sub>22</sub> nanoparticles regulate oxidative defense system. They do so by preventing cancer cells to proliferate, changing microenvironment of surrounding normal cells, and averting their mutation. Apart from developing the scavenging activity, Gd@C82(OH)<sub>22</sub> nanoparticles impede the pathway of tumor's involvement into normal cells and thus boost the immune system. The latter is facilitated by early maturation of dendritic cells which is typical of immune defense system to activate Th1 immune responses [83]. After administering the Gd@C82(OH)<sub>22</sub> nanoparticle, immune response was exclusively reflected by tumor tissues of affected mice while the control region/group remained unaffected [84]. This response encompassed encapsulation of neoplastic tissues, comprising particularly of capillaries, fiber tissues, and lymph nodules which inhibit the growth of tumor tissues and prevent their incursion into the surrounding healthy environment.

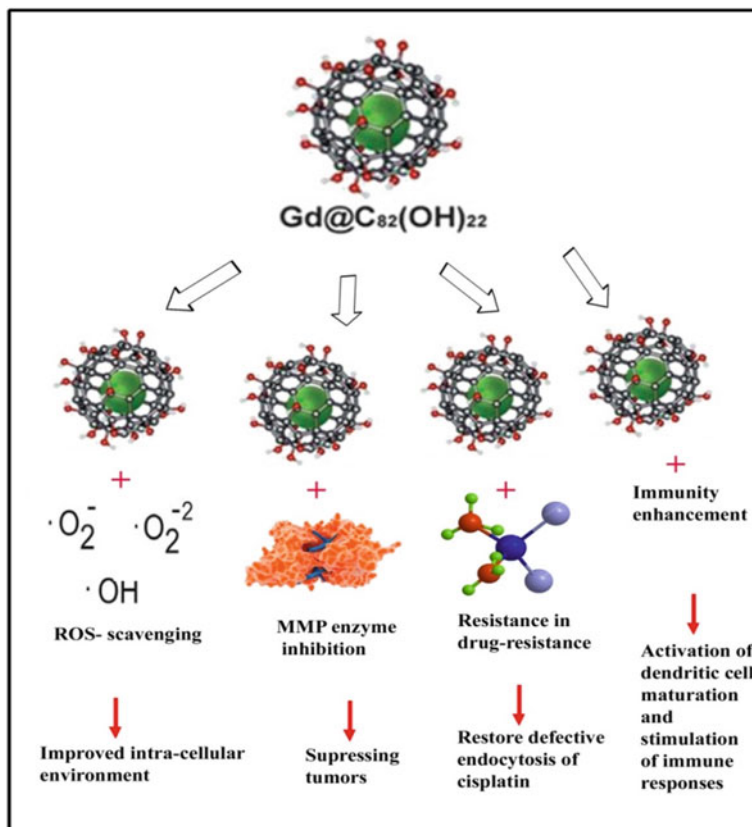
Apart from the development of envelope to restrict unwanted movement of cancerous cells, these nanoparticles put off metastasis by restraining the activity of matrix metalloproteinases (MMPs) [85]. The drug targets the enzyme and lowers down the activity of MMP-2 and MMP-9. It also extends its effect to suppress angiogenesis and hence inhibit tumor growth further. While suppressing MMP-9, Gd@C82(OH)<sub>22</sub> nanoparticles obliquely interfere with the substrate and bind to its critical regions typically to ligand specificity loop S10. This reduces the overcrowding of catalytic sites coordinated by zinc to maintain hydrophobic nature and structural integrity of protein involved [86].

Another noteworthy effect of Gd@C82(OH)<sub>22</sub> nanoparticles on biological system is their involvement in antitumor therapies. While using different chemicals as therapeutic agents, cancer cells effectively become prone to death. However, due to acute cytotoxicity and prolonged exposure to chemical agents, cancer cells sometimes become susceptible and often develop resistance to various chemicals. Consequently, serene treatment alternatives often become restricted. The multihydroxylated nanoparticles, Gd@C82(OH)<sub>22</sub> are known to bring down tumor resistance to different antineoplastic agents, typically Cisplatin [87]. In tumorous cells, the endocytic recycling compartment often becomes faulty and Cisplatin uptake gets affected. Under such conditions, nanoparticles reinstate the drug, reduce its resistance by cells, and diminish viability of Cisplatin-resistant cancerous cells. Thus, growth of tumor is effectively suppressed, thereby enhancing the antitumor effect.

Overall, porous carbon materials as fullerenes are exceedingly proficient and play a very crucial role in therapeutics. As squat toxicity antitumor agents, nanoparticles are widely accepted as antioxidants which boost immunity, curb metastasis, and trim down drug resistance (Fig. 2). They are exceedingly constructive in antitumor therapies. Nonetheless, despite these biomedical applications, their comparatively low synthetic yield poses a great challenge to develop them as unique nano-medicines on large scale. Primarily, it becomes costly and protracted to take apart identical fullerene species from unprocessed grunge. At present, researchers are working round the clock to develop certain sophisticated methods for their production at extensive scale and flippant segregation procedures for acquiring fullerenes with least impurity at economical rates so that these nanoscale particles can be exercised in drug approval [88, 89].

### 3 Drug Delivery Tools

Carbon nanomaterials (CNMs) have been comprehensively detailed out with noteworthy paradigms in technological sensors [90], medical imaging [91], catalysis [92], energy storage [93], water treatment [92], solar cells [94], etc. Emerging as an extremely adaptable cluster of nanomaterials, CNMs thus exhibit diversified and desirable properties in medical science. Owing to their frictional and chemical stabilities, carbon surfaces precisely contact blood as well as tissue systems and thus can be



**Fig. 2** An illustration showing secondary antitumor action of Gd@C<sub>82</sub>(OH)<sub>22</sub> nanoparticles

customized to meet manifold requirements [95]. Based on this, porous carbon materials actively participate in controlled drug release [96] as well as cellular delivery [97]. Graphitic-based CNMs, for instance, presently occupy a strong position in heart valve during cardiac surgery while diamond-resembling carbons find relevance in musculoskeletal system [98].

### 3.1 Targeted Delivery System Pathway

The construction of porous carbon nanomaterial-loaded drugs and their behavior toward the microenvironment of tumor cell line are crucial in attaining targeted delivery of antitumor drugs [99]. These nanomaterials are effectually studded and made functional with receptors of target cells.

However, to accomplish the successful and targeted delivery of the drug, system has to rely on certain sensitive stimuli. Some commonly used are as follows:

### 3.1.1 Endogenous Sensitive Stimulation

Such stimulations usually rely on distinctive physiological signals of tumor cells. These include:

#### (a) pH-dependent target system

The microenvironment surrounding the tumor cells has weak acidity usually ranging from 6.2 to 6.8. This is due to the fact that tumor cells require abundant energy to sustain their growth which they usually achieve by rapidly degrading sugar molecules. This results in the production of lactic acid in bulk which hoards at the tumor site. The area becomes quite distinct since pH of endosomes and lysosomes work at  $\sim 5.8$  and  $\sim 4.8$ , respectively [100]. Thus, sensitivity of drug carriers toward pH helps to construct the pathway for efficient and targeted drug delivery system. Spherical porous carbon materials with  $<100$  nm diameter reportedly have ability to act as transmembrane carriers and deliver anti-tumor drugs. However, to do so they are required to undergo certain hydrophilic surface modifications. Concurrently, owing to difference in physiological pH between normal and tumor cells, the altered porous carbon material is expected to promote the drug delivery and makes better targeting presentation. This can be exemplified by loading of pH-sensitive doxorubicin on 90-nm-sized porous carbon spheres [101]. The drug was successfully delivered to cervical cancer cells where it showed better therapeutic consequences.

#### (b) Enzyme-dependent target system

One among various important features of tumor tissues is the secretion of some marker enzymes [102]. This feature paves a way to construct targeted drug delivery systems with enzyme specificity. In this pathway, surface of porous carbon particles is modified using small stretches of oligonucleotides. These nucleotides show strong affinity toward the marker enzyme present in the tumor cells and in turn develop a concrete pathway of target recognition system. As an analogy, MUC1 (mucin) is peculiarly produced in various tumor cells. Using this transmembrane protein as a biological indicator of cancer cells, nanoparticles are coated with nucleic acid aptamer. During drug release this aptamer specifically targets and binds MUC1. The strategy thus aids in targeted tumor therapy [103].

#### (c) Redox reaction sensitive targeting

Tumor or neoplasm that arises without any obvious reason accumulates different unique things within itself. Sometimes it varies from normal cells in concentrating varying amount of different metabolites. For instance, tumor cells generally accrue more glutathione than the normal cells [104]. With a net negative charge at neutral pH, unequal distribution of glutathione develops a considerable difference in the reduction inside and outside the cell. Such an environment



establishes a reduction-sensitive targeted delivery system. Zhou et al. [105] customized hyaluronic acid on the exterior of PCM by altering few S–S bonds followed by loading doxorubicin drug. This was done to create a drug-carrying system, which can concurrently take care of glutathione and hyaluronidase in cells and release the drug in a controlled manner.

### 3.1.2 Exogenous Sensitive Targeting

These encompass certain external stimuli as discussed below;

#### (a) Light sensitivity

Researchers across globe are working round the clock to eradicate the fatal cancer disease. One such approach used by them is light sensitivity stimulation method to create antitumor drug delivery system in the tumor cells. Owing to the atypical physiological environment of tumor tissues, they are quite susceptible to heat. On the other hand, nanoporous materials are capable to take in light energy from infrared region with wavelength ranging from 700 nm to 1 mm at corresponding frequency from 430 THz (tetrahertz) to 300 GHz (Gigahertz) and release the same as heat energy. This shortly increases the surrounding temperature to  $>40$  °C. Therefore, as drug is administered via porous carbon nanospheres, tumor tissues at 37 °C undergo thermal damage due to increase in their physiological temperature [106]. One such successful attempt was made by Xu et al. [107]. These workers modified nanosphere surfaces using mixture of polyethylenimine and folic acid. Aim was to develop chemically tailored photothermal targeted deliverance system. Amalgamation of chemo- and photothermal therapies exercised enhanced therapeutic effects.

#### (b) Magnetic sensitivity

Apart from light sensitivity, another source to raise cellular temperature is the magnetic field. Carbon nanoparticles exhibiting magnetic properties are capable to produce heat [108] which translates magnetic energy into heat energy. Production of the latter raises local temperature to effectively treat the cells. Thus, during magnetic drug delivery, the magnetic field is created near the tumor cells. This strategy helps to amass maximum drug in cancer cells [109]. Porous nanoparticles containing doxorubicin drug when sequentially modified by iron oxide, ethylenediamine and hyaluronic acid exhibited better biocompatibility as well as photothermal conversion abilities. This targeted drug delivery system proved to be quite fatal to cervical cancer cells [110].

### 3.1.3 Multiple Sensitive Stimulation

It involves merging more than one stimulus to figure out a multifunctional targeting mechanism with more inductive effects. This strategy is expected to augment nanospheres to carry and deliver drugs with greater efficiency and performance and at the same time reducing the side effects [111]. These may include:

(a) **Dual-sensitivity of pH and glutathione for targeting drug delivery**

In this approach, mesopores of carbon nanospheres were specifically enveloped using polyacrylate to make them susceptible for pH and glutathione. During drug delivery, these carriers were obliterated by decreasing glutathione concentration [112].

(b) **Dual sensitivity of pH and magnetic field for targeting drug delivery**

Herein, nanospheres loaded with doxorubicin drug were sheathed with folic acid to impart dual sensitivity of pH and magnetism. During deliverance, the drug showed improved therapeutic effects, efficiently entered into tumor cells without affecting normal cells [113].

(c) **Magnetic and photothermal dual-sensitive targeting**

Chen et al. [114] prepared ordered mesoporous carbon spheres with dual functions of thermosensitivity and magnetic properties. Using doxorubicin as a model drug, the controlled release of doxorubicin was achieved, which provides a new way to construct a dual-sensitive antitumor drug delivery system. Wang et al. [115] prepared porous carbon materials modified by nano-gold and  $\text{Fe}_3\text{O}_4$  and constructed a magnetic-near-infrared dual-function sensitive drug delivery system. The release of mycin with near-infrared photothermal effect can effectively kill tumor cells while regulating the drug release rate, exerting synergistic effect of magnetocaloric and photothermal. Compared to a single sensitive stimulus, dual-sensitive stimuli can exert a better synergistic effect and have a more lethal effect on tumor cells.

(d) **Multi-sensitive targeting of pH, glutathione, and light and heat**

In this targeting strategy, hollow magnetic spheres were encapsulated with poly- $\gamma$ -glutamate to carry Adriamycin drug [116]. Thus, a triple response of pH, glutathione, and infrared light was attributed. The system develops various important therapeutic consequences and achieves outstanding capabilities of antitumor therapy. At the same time, it also prevents drug leakage from carriers before reaching to the target tissues.

Therefore, carbon furnishes inherently enduring material for amending properties so as to congregate manifold intricate demands inflicted by medical science. Three important applications of different carbon nanomaterials as drug delivery tools have been discussed as follows:

### ***3.2 Nanodiamonds as Anticancer Drug Delivery System***

Nanodiamonds also called diamond nanoparticles refer to the diamonds with  $<1 \mu\text{m}$  size [117] although they could not find a permanent place in the field of therapeutics including biolabeling and sensing, target drug delivery, etc., until recently [118]. Owing to their inertness, hardness and low toxicity, nanodiamonds have been

proven to be a better substitute for traditional nanomaterials to carry drugs, synthesize biosensors, and biomedical robots [119]. Further, due to their potential to undergo an effective alteration in surface properties nanodiamonds have been adapted to achieve potential of being used in electronic as well as quantum engineering [120]. Since this chapter aims to consolidate the therapeutic application of nanomaterials, we will focus on few such studies that lay an emphasis on the role of nanodiamonds in cellular delivery of various therapeutic agents. Diamond nanoparticles typically can be effectively produced by the process of combustion using supersonic, exothermic fronts under conditions of high temperature and high pressure. Following mechanical milling or treatment by any strong acid, the deagglomerated diamond particles with desirable size are obtained. Since its production involves the prevalence of certain abrasive conditions, different oxygenated moieties generally tag the surface of these diamond nanoparticles. Consequently, in pristine detonated nanodiamond surfaces, these oxygen-containing groups promote surface modification via interaction with polar molecules, electrostatic attraction, and covalent bonding. These modifications, in turn, make pristine diamond quite less active [121] (Krueger 2008). Further, a number of bioactive molecules, for instance, cytochrome c and *N*-acetylmuramide glycanhydrolase can be crippled on surface of nanodiamonds so as to maintain their chemical and biological activities [122, 123].

As a drug delivery agent, activated nanodiamond surfaces carry a number of therapeutic agents to be delivered into cells. This can be exemplified by the release of a hydrophilic chemotherapeutic agent Cisplatin. After being added to the carboxyl groups on surface of diamond nanoparticles, the drug was carefully released into cells [124]. Similarly, various hydrophobic anticancer drugs have also been loaded and successfully delivered to the target cells with improved therapeutic efficiency [125]. For example, with an aim of selective targeting, imaging and therapy, a multifunctional platform was constructed using diamond nanoparticles [126]. This strategy was primarily based on functionalization of nanodiamonds using sulfosuccinimidyl 6-(30-[2-pyridyldithio]propionamido)hexanoate. This acted as a cross-linker and attached thiol-containing biomolecules on the surface. To these molecules, Paclitaxel, the chemotherapeutic drug was then attached. To track their pathway inside the cell system, the assembly was coupled with fluorescently labeled oligonucleotide and a thiolated antibody. The dose administered showed a much-increased rate of cellular internalization as well as therapeutic efficiency than shown by paclitaxel alone [127]. Similar such study was carried out on wherein doxorubicin molecules were bonded to the surfaces of diamond nanoparticles. This combination of cancer-killing drug and nanoparticles created ND-DOX drug. When injected inside the body, tumor cells were unable to eject this hybrid drug, thus increasing its ability to affect tumor more appropriately without any side effect [128]. Akin to this, the large nanodiamonds exhibits potential to serve as cellular labels which owes to their high uptake efficiency [129] and increased stability and biocompatibility in solution [130]. Moreover, it is also quite possible to spawn secured and vivid fluorescent nanodiamonds by making crystal lattice vacant to introduce nitrogen atoms that aid in numerous biological processes [131].

Conclusively, a range of bioactive molecules can be administered into the cells using nanodiamond platform. However, seclusion of homogenous nanoparticles with comparable surface chemistry and electrostatic charge remains the foremost confront in applying them in drug delivery systems.

### ***3.3 Porous Nanospheres as Drug Delivery***

Amorphous or porous carbon nanospheres with large surface area and internal volumes are considered to be stupendous fluorescent nanomaterials that have been adapted to achieve diverse biological functionalities vis-a-vis biolabeling, imaging, and sensing [132]. One such application that literature puts on record pertains to their involvement in cellular delivery of therapeutic agents as during oral delivery of insulin. A biodegradable polymer is coated over nanospheres which serves the purpose of delayed insulin discharge in organs with acidic pH like stomach but facilitates the same at near neutral conditions [133].

Similarly, in case of cancer cells, mesoporous carbon nanospheres of 90 nm dimension have successfully mediated delivery of doxorubicin to HeLa cells. Again, where the drug is going to get released during its pathway is decided by the pH of the environment [101]. Since drug doxorubicin can exist in both ionized and non-ionized forms, the pH susceptibility was accredited chemically by the interactions between carbon nanospheres and state of drug existing at a particular time. Understandably, drug delivery by these mesoporous carbon nanospheres can be regulated. Usually, at physiological pH, the drug prefers to remain inside nanospheres, but gets precisely and effectively released in the acidic environment of tumor cells. Moreover, imperceptible pores present on their outer surface can be exploited to establish nanovalves with stimulus-sensitive properties. This could enhance therapeutic efficacy of the drug targeting mechanism in a controlled manner. However, despite all these advantages, some major concerns like regulating size and structure of particles need a cogent filling. Coupled with this, the biostability of porous carbon nanospheres ought to be gauged before being broadly used as carriers.

### ***3.4 Carbon Nanohorns***

Carbon nanohorns (CNHs) or carbon nanocones are one-dimensional, conical-shaped carbon nanostructures [134]. Owing to certain outstanding properties, viz. great specific surface area, exceptional catalytic properties, superior porosity, high productivity, thermodynamic stability, etc. CNHs can replace carbon nanotubes efficiently. Due to this, CNHs expanded their platform to diverse fields like quantitative detection of chemical compounds using redox currents, detection of target molecules based on immune response, biofuel cell, supercapacitors, and most importantly

biomedical application as nano-medicine [135, 136]. In addition to these advantageous properties, CNHs have an exceptional property to form, during their synthesis process, aggregate spherical clusters of diameter  $\sim 100$  nm. This is similar to that of the “dahlia” flower. These “dahlia” like CNHs correspond to the concoction of graphene and nanohorns bound securely through relatively weak electric forces [137]. This aggregation property, however, imparts certain limitation like functionalization intricacy, dispersion obscurity, severance of each nanohorn. Nevertheless, researchers in the present date are surmounting this predicament using novel approaches of synthesis and modification [138].

Under high-temperature conditions at 2500–3500 K and in the presence of collimated electron beam for  $\sim 4$  h, CNHs are known to exist in two forms. These are single (SWCNHs or SWNHs) and multi (MWCNHs)-walled CNHs. Of two, SWCNHs measure 40–50 nm in length and 2–5 nm in diameter. It encloses graphene tubes coupled with excruciating cone-shaped, horn-tipped  $sp^2$ -bonded carbon atoms [134]. Thousands of SWNHs frequently amass and form vigorous spherical aggregates of 80–100 nm diameter. Hence after, these aggregates of SWCNHs would correspond to assembled structure and only “SWNHs” to different single-carbon nanohorns.

### 3.4.1 Surface Modifications of SWNHs

SWNHs are characterized by water-repelling graphite surfaces. In order to increase their hydrophilicity and enhance biocompatibility, physical or chemical modifications of these surfaces with functional groups is central. This greatly makes them a surreptitious and also enables to execute target-specific drug delivery. To accomplish this, carboxylic acid group offers the most widely accepted and compatible functional group to be modified. Modification can also be done by making diverse oxidation reactions to take place on the surface. This encompasses the reaction between an oxidant, for instance, hydrogen peroxide, and the other on SWNHs which generates carboxylic groups and, in turn, oxidizes SWNHs [139]. Apparently, such SWNHox aggregates react with moieties like bovine serum albumin (BSA) to form BSA-modified SWNH complex. This complex becomes homogenous in phosphate buffer and is effectively assimilated by mammalian cells [139].

In order to diffuse various hydrophobic compounds in hypertonic aqueous solution, certain osmotic laxatives based on hydro- and lipophilic properties like polyethylene glycol (PEG) can be appropriately used since these efficiently avert protein engrossment to the surface. Taking this advantage, different PEG-based molecules with dispersion properties find an application to modify SWNHs surface, thus reducing imprecise binding onto SWNH aggregates [140, 141]. One such modification can be seen when PEG-doxorubicin dispersed SWNH aggregates. The conjugates so produced stimulated programmed cell death of tumor cells under the influence of anticancer pharmacokinetics of doxorubicin [142]. Another drug Cisplatin-loaded SWNH aggregate was too lucratively tailored with a dispersing agent embracing single PEG chain and a peptide aptamer [143]. The dispersibility was further improved when the hydrophobic surface of SWNH aggregates was

enveloped by increased density of PEG chains due to the introduction of comb-shaped PEG components [144].

Compared to carbon nanotubes (CNTs), SWNHs do not require any metallic catalyst during their production via laser ablation method. Consequently, SWNHs are produced with high purity and greater yield so that these could be used in practical applications. Characterized with effective surface area and volume, the same can be increased by inserting nanoholes in their side walls. Such properties with increased occupied area and abundant crystal structure make SWNHs more gifted for catalytic schemes, biosensing and other radioactive approaches, agents for drug loading and delivery of drugs [145, 146]. One such example can be given of dexamethasone. After incubation period at room temperature for 24 h, the anti-inflammatory and immune-suppressant drug is bonded to water repellent surface of oxidized SWNH or SWNHox. The reaction ensues into aggregation [147]. In other study, both vancomycin (an antibiotic agent) and prednisolone (man-made form of corticosteroid hormone) were adsorbed and absorbed by SWNH aggregates which as drug basin facilitated their systematic and precise release in a controlled manner [148]. Chopart's joint of rats affected with arthritis, for example, showed anti-provocative effects when the target was hit by SWNHs-prednisolone assembled structures. Likewise, Cisplatin effectively deposits on and inside SWNHox aggregates and when released into the cancer cells reduce their viability and kill them [136]. In gene therapy, SWNH aggregates efficiently carry polyamidoamine dendrimers and discharge genetic material skilled to moderate protein level involved in prostate cancer development [149].

Apart from having increased capacitance to load drugs, SWNHs too facilitate controlled release of drugs which can be attributed to their nano size. At the same time, there is every likelihood of diverse systems to deliver drugs to a defined target. Such systems would be advantageous in terms of cardiac output rate, elevated levels of drug accumulation under steady-state conditions and improved biocompatibility. However, there has been an equal prospective that morphological characteristics of SWNH aggregates favor penetration of drug and continue to hold it for prolonged period by exuding through the ruptured vessels of tumors and accrue at transcriptional control [150]. Another exciting asset of SWNHs is their photothermal properties that allocate them in hyperthermia treatments under low-frequency irradiation, with high tissue transmission ability. Notwithstanding the exceptional candidature in several practical biological schemes, the major limitation of these aggregates is their high withholding capacity that does not let them degrade easily [151]. Nonetheless, small-sized SWNHs could provide a way to struck these problems [152].

Above all, the absence of any metallic debasement in pristine SWNHs eliminates the possibility, if any, of their toxic nature. A recent appraisal on toxicological effects of SWNHs, carried out through histological studies on mice deduced that the endovenous presence of SWNHs barely reflect palpable pernicious response post 6 months [153]. Their marvelous aptitude to incorporate drug within the structure and squat virulence toxicity make SWNHs a hopeful contender for successful nostrum deliverance [154].

Overall, compared to myriad collection of research, only a few porous carbon material-based drugs have been put into practice clinically. To perk up the situation, additional pains need to be taken to reduce the mechanism of toxicity reduction, elucidate enhanced permeability and drug retention in human body. At the same time, mimicking in vivo environment and testing porous carbon material in models need to be considered. Therefore, advanced research is required to be elucidated on the performance of porous carbon materials. For this, defined targeting methods, tumor microenvironment drug release strategy, pooled therapies, self-assembly of nanomaterials are some of the realistic approaches to bring effectiveness as well as the bioavailability of the drug to augment the targeting specificity. These, in turn, are expected to trim down the lethality of carbon nanomaterials drugs on normal cells so as to benefit cancer patients.

#### 4 Carbon Nanohorns and Bone Marrow Formation

Owing to the idiosyncratic characteristics and favorable cyto-compatibility, nanomaterials are encouraged to be considered for applications in biomaterials [155, 156]. Of several such outstanding characteristic features, electrical conductivity [157, 158] and the typical surface structure [159] thereof correspond to their application in bone regeneration. Because of their unique network-like structure, the nanotube-coated collagen sponges, for instance, are known to assist in smooth adhesion as well as differentiation of osteoblasts [159].

Among different nanomaterials like CNHs, CNTs, graphenes, however, the presence of several impurities like amorphous carbons and metal catalysts apparently make them to scrutinize for clinical uses [160]. Contrarily, owing to less harmful effects [161] and large inner nanospaces, CNHs have gained much attention toward biomaterial and biomedical fields. These spherically assembled huge nanotubes of 100 nm diameter [137] act as a platform, wherein drugs can be loaded easily [156, 161].

Research carried out on rat skull model [162] evaluated re-construction of a new material for hard-tissue. Study shows that with slight prophlogistic effect along the membrane, CNHs promote osteoblast formation at the outset in defect made in the skull of rat after two weeks and also correlates the same with macrophages. The CNHs laminated got affixed to osseous tissue directly while those scattered entered bone matrix and managed to contact collagen fibers. Osteoblasts that emerge from phagocytic WBCs instigate from hematopoietic stem cells [163]. Therefore, macrophages involvement is apparent in the breakdown and assimilation cycle of bone growth. Thus, CNHs have been considered to be attuned with osseous tissue and effective for directing growth of new bone and gingival tissue. Undeniably, literature reveals certain evidences of negative impact of macrophages on bone marrow formation [164]. Nevertheless, majority of other studies are suggestive of their involvement in bone formation. In such studies macrophages reportedly produced osteo-inductive

factors, for instance, bone morphogenetic protein-2, GF- $\beta$  [165], and osteopontin [166] under varying conditions.

Similarly, polytetrafluoroethylene (PTFE) membrane when coated with CNH promoted bone formation within 2 weeks after surgery [162]. This property has also been allied to the macrophages [167]. When macrophages encounter CNHs, the former engulfs the latter. This hastens delineation of mesenchymal stem cells into osteoblasts through release of Oncostatin M [168]. While continuous bone remodeling was observed in the CNHs/PTFE complex, the phagocytes and macrophages were scrutinized around CNHs. Compared to SCNHs/PTFE group, the CNHs/PTFE complex specifically promoted bone marrow tissues. This was reasoned to the removal of CNHs by scrubbing. In dental implant therapy, research has shown that following anodization of CNH-coated titanium (Ti) (generating Ti oxide layer, AnTi) via electrodeposition, the complex exhibited favorable biocompatibility with bone [167]. The CNH/AnTi complex engrossed osteoblastic cells vigorously and more effectively than what AnTi alone could do. Further during bone healing the nanohorns were quite virtual since they stimulated early bone regeneration *in vivo*. Also, during the premature post-implantation phase, newly regenerated bone tissues maintained a contact with CNH/AnTi complex, suggesting their possible role in accelerating “contact osteogenesis.” Such implants where the formation of bone tissues is promoted are likely to be more efficient in aged people and diabetic patients. Thus, the CNHs/AnTi emerges as an expectation for next-generation surface implant treatments.

## 5 Carbon Nanotubes and Embryonic Development

Single-walled carbon nanotubes (SWCNTs) refer to a section of nanomaterials engineered enough to have adaptable physical and chemical properties. One among the lately developed products that exhibit a range of applications, SWCNTs have attracted much interest to serve different functions from industry to biomedicine [35]. These mainly include their role in micro-fabrication of conjugated activators of polymers, composite materials, scanning electron microscopy, etc. Although how human body responds to the exposure of CNTs is principally unraveled, detrimental effects thereof could not be ignored. In the past few years, extensive research on the toxic effects of CNTs has been carried out [169, 170] and inclusive acquaintance of their effects is yet to understand. This breach is still larger pertaining to their effects on embryonic development, for which only scrubby data are accessible and most of which refer to aquatic species [171, 172]. Owing to some advantageous characteristics, one such study has been focused on the zebrafish embryo. The embryo completes its entire development within four days in open environment. This facilitates a direct prophecy of various steps involved in morphological changes occurring. Research has demonstrated that under laboratory conditions hatching after the stimulated time indicates the presence of nickel and cobalt adulteration, and CNTs do not interfere with proper embryonic development [171].



Apart from work on zebrafish model, interaction between SWCNTs and developing embryo in mammals revealed certain contrasting facts [173]. Medication with less concentration of pristine and oxidized SWCNT when administered to expecting mice adversely targets the post-implantation embryo. The study indicated SWCNTs to have a possible role of embryotoxic agents in mammals. The teratogenic effect was observed at a dosage as high as 30  $\mu\text{g}/\text{mouse}$  and as low as of 0.1  $\mu\text{g}/\text{mouse}$ . While the former dosage of SWCNTs characterized miscarriages and gross fetal morphological abnormalities, the latter imposed fetuses with gross malformations. However, at the lowest concentration of 0.01  $\mu\text{g}$  no such results were ever observed. It is further realistic to presume that a negligible concentration of the infused drug reaches the placenta and hence the fetus. Nevertheless, the latter is highly sensitive to the drug. Also, at such a reduced dosage none of the CNTs were detected in placenta and/or fetus. Therefore, the study failed to make a proper discrimination in actual effects of SWCNTs. Of three different classes of SWCNTs used; pristine (p-SWCNTs), oxidized (o-SWCNTs) and ultra-oxidized (uo-SWCNTs), maximum malformation occurred in uo-SWCNT treated mothers followed by o-SWCNTs. This behavior has been largely ascribed to an improved scattering of the drug and its ensuing elevated availability in the medium [174]. Moreover, stringent connectivity among different stages of embryo development including retardation in placenta at any stage due to higher doses of CNTs and apparently crossing the blood-placental barrier [175] are suggestive of placenta in mediating embryotoxic effect.

Reports of crossing the placenta to have access on developing embryo by SWCNTs are obligatory. Studies suggest potential risk for occupational pregnant women when exposed to SWCNTs where the probability of inadvertent contact may become factual. Therefore, advance research is indispensable to comprehend the fundamental idea of tempting embryo toxicity by CNTs (especially oxidized CNTs) and substantiating the steadfastness of embryonic stem cell tests in speculating embryo toxicity for other ENMs.

## 6 Nanocarbon-Based Cardiovascular Applications

Cardiovascular diseases (CVDs) are one among the leading causes of mortality across globe. The basic reason of CVDs is the sudden stoppage in nutrient and oxygen supply to heart due to obstruction in blood vessels. The disease outlines as atherosclerosis. The blockage generally occurs in coronary arteries either due to fatty substances and cholesterol accumulation or by platelets and proteins. This, in turn, opens a door to the related heart diseases, viz. ischemic heart disease (IHD), cerebro-, reno- or peripheral-vascular disease, mesenteric ischemia [176, 177]. This interrupts and altogether reduces the availability of blood to the heart and eventually results in a myocardial infarction (MI), another name for heart attack. Being severe, heart attack can permanently damage cardiomyocytes. The inherent repairing thought averts cardiac shattering by a fibrotic scar, yet heart can stop pumping blood due to non-contractile nature of the scar tissue [178]. At present, accessible pharmacotherapy is based on

analgesic properties of drug [179, 180], for instance, as cholesterol-reducing agents, angiotensin-converting enzyme (ACE) inhibitors or even by surgery [181]. However, such measures often cause the random drug distribution throughout the body, reduce the competence thereof, and often become toxic to the cells. Such gaps, therefore, need a cogent filling through regenerative therapeutics and tissue engineering [182].

Introduction of CNMs has resolved this problem to a large extent. Ensuring correct design and installation as well as electric conductivity of various devices, namely cardiac patches or regenerative scaffolds used in biomedical science [183, 184] have improved progressively. This has opened new avenues to invent fresh biosensors having superior targeting properties [185]. Expectedly, this would ease scientists to prepare target specified medicine with the ability to be tailored according to patient's needs [186]. As carbon nanotechnology is emerging rapidly, surface modifications of nanocarbon with different ligands make it target-specific, especially in CVDs. This, in turn, improves its cellular interaction, reduces the toxicity thereof [187] and necessitates in different biomedical devices. Some of its applications have been discussed as follows:

## ***6.1 Drug/biomolecule Delivery***

Target drug delivery is an important aspect in cardiovascular medication. For anticipation and conduct of different CVDs, oral or intravenous drug administration is fundamental therapy [188]. Conventional drugs are dispensed to diminish fatty substances deposited on the inner walls of arteries, encourage formation of new blood vessels in ischemic tissues and enhance the affected body parts to recover [189, 190]. However, off-target effects, recurrent dosing to achieve therapeutic efficiency and poor bioavailability of the drug are some of the widespread problems embraced by these drug delivery approaches. Ultimately, such prominent parameters pose noteworthy confronts in obtaining maximum benefits from drug therapies. This ultimately calls for some advanced mechanics of drug delivery systems capable to address these concerns.

To tackle this situation, CNMs have proven to be the outstanding hauliers for transporting drugs to the target site. In fact in the budding area of nanotechnology, allotropes of carbon gained momentous attention and have been judged as one among the fundamental classes in drug delivery applications [191]. For instance, graphene derivatives due to their exorbitant surface area, soaring firmness, flippant water interacting properties bear drug heaping competence [192]. Irbesartan, a blocker of angiotensin receptor, finds application to lower down blood pressure in CVD patients. An electro-conductive hydrogel was primed by reinforcing 20% reduced graphene oxide (rGO) into three components, viz. hyaluronan, gelatin, and oxide of polyethylene hydrogel [193]. Reportedly, the hydrogel effectively regulated irbesartan availability for 10 days in the patient, giving an indication of rGO acting as well-structured drug conveyor for CVD therapy. Another example can be given of Diltiazem, a derivative of benzothiazepine with calcium channel blocking ability is

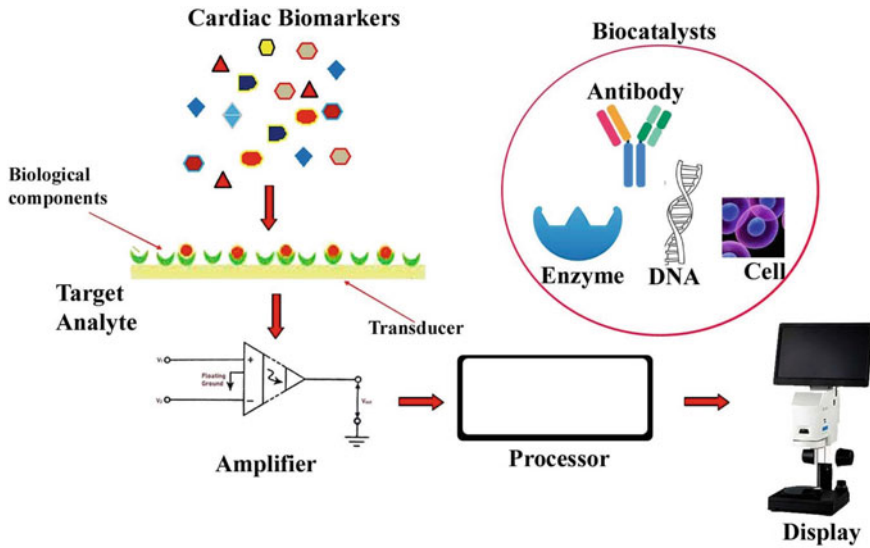
used to manage severe chest pain and treat high blood pressure. For effective and controlled release of the drug, a complex comprising of graphene oxide (GO) and methylcellulose (MC) was prepared that purportedly served the function successfully [194]. Similarly, atherosclerosis, a serious concern often causes occlusion of blood vessels. Under such conditions, therapeutic angiogenesis via introduction of vascular endothelial growth factor (VEGF) is one such treatment to develop new blood vessels from the older ones [195, 196]. This process of angiogenesis improved many fold when VEGF was functionalized with GO. Comparative analysis showed a significant increase in the density of blood vessels and availability of oxygen in the muscle with inadequate blood supply when VEGF-GO combination was used, thus demonstrating the curative interest of GO in the formulation.

## 6.2 *Biosensors*

Discovery of biosensors proved to be a boon to medical science. The promising tools facilitate CVD treatment on time and perpetuation of cardiac function by ascertaining cardiac defects at the early stage [197, 198]. An ample array of biochemical molecules, for example, proteins, nucleic acids, and even different metabolites can be easily detected using biosensors [199]. Biosensors have two components, viz. biocatalyst and transducer. While the former can be nucleic acids, antibodies or any biomolecule which detects biological component, the latter can be electrochemical and optical sensors which analyzes interaction between enzyme involved and target analyte and also quantify their concentration [200, 201]. The involvement of nanotechnology has exponentially improved sensitivity and robustness in biosensors. This is due to the fact that nanomaterials provide a larger aspect ratio for improved enzyme interaction and can have a dual function of sensing element as well as a transducer in a biosensor [202]. Akin to gold nanoparticles, CNMs serve as biosensors in various aspects in CVDs. Payable to being cost-effective, smaller size and unique optical and electrical properties, nanomaterials as sensors are used as model candidates in interpreting CVDs [203, 204]. Figure 3 explicates CNMs in diagnosis of CVD.

## 6.3 *Tissue Engineering*

During inception of necrosis of myocardium, the affected area is often characterized by colossal cell death among functional cardiomyocytes due to ischemia. Even after the recovery and restoration of regular blood circulation, cardiac muscle still lacks potential to revitalize itself completely. Consequently, ailment, yet in the latent mode, gradually makes perpetual non-conductive and inflated pockmark in the infarct site. Depending upon the extent of loss occurred, the pumping function of heart may unfavorably be affected and can even lead to heart failure [205]. The damaged

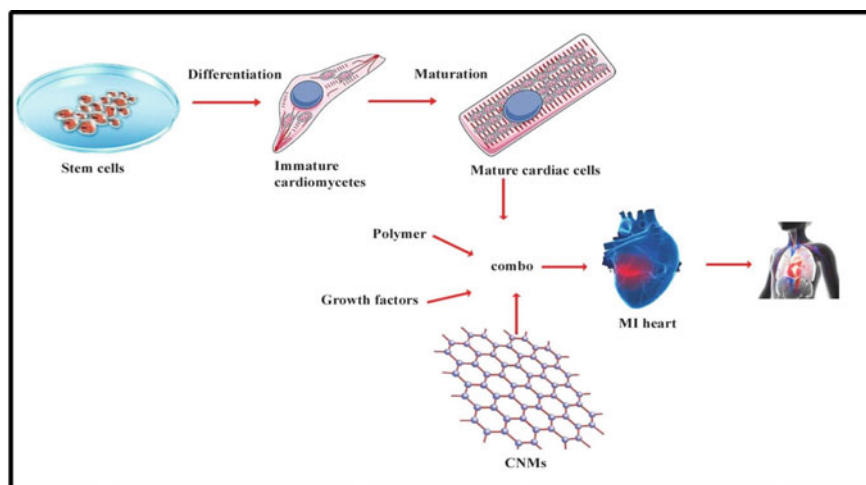


**Fig. 3** CNM application in biosensors for CVD diagnosis; note the cardiac biomarker trajectory in plasma of CVD patients and their detection by sensors carrying different biocatalysts on their surface. The value so obtained is amplified and displayed on the screen

myocardium cannot be completely repaired using conventional therapies. Alternatively, the only option left remains the heart transplantation. However, surgery is not the permanent solution since it can often lead to chronic illness. Nevertheless, these predicaments can be permanently resolved via therapies based on tissue engineering. It encompasses various cells and biomaterials to redevelop the muscular tissue lost during a myocardial infarction. Encroachments in nanotechnology have further enhanced this diagnosis by engendering advanced frameworks, boosted hydrogels, and cardiac patches. The carbon nanomaterials offer structural potency akin to collagen in the extra cellular matrix. Also, the conductive properties thereof facilitate advanced dynamism among enduring contracting cells in heart muscles and transplanted stem cell plagiarized cardiomyocytes [206]. Figure 4 demonstrates cardiac tissue engineering model based on CNM.

#### 6.4 Cardiac Patches

Porous carbon nanotubes (CNT) have been employed to generate hydrogel complex of gelatin methacrylate (CNT-GeIMA). Cardiomyocytes of neonatal rat were incorporated into this CNT complex and cardiac bioactuators were constructed [207]. This power pack combination of a caged nanomaterial with GeIMA increased the efficiency of electrophysiological functions, imparted synchronous beating rates almost



**Fig. 4** Overview of CNMs in cardiac tissue engineering. CNMs besides strengthen differentiation and maturation of stem cell-derived cardiomyocytes also participate in CNMs-based cardiac constructs. These constructs comprise of three components: cardiac cells, polymers, and growth factors which effectively treat heart-related ailments during MI

three times as compared to that from CNT-GeIMA alone. The compression modulus was also enhanced from 10- to 32-kilo pascal due to the incessant fortification round films [207]. It is of the general concern that sustained cells, if seeded on flabby tissue underlayer, are usually prone to programmed cell death [208]. Due to the nanofibrous lattice created inside the gelatin meshwork, cells consistently spread on CNT-GeIMA complex. Surprisingly, the retention rate coupled with cell viability proportion in CNT-GeIMA complex was considerably larger than those in pristine GeIMA [207].

The cardiac patches structured to have an aperture dimension ranging from 120 to 150  $\mu\text{m}$  possibly will recommend an appropriate pore aspect for dissemination and establishment of arteries, capillaries, and veins in the inner lining of endothelial heart cells. Employing CNT system as a potential biomarker in stem cell delivery greatly affected the porosity of polymeric matrix [209]. The electromotive force so produced was used to manipulate magnitude of charges within CNT construction. Consequently, it affected both the ends of dipole to align correctly so as to generate purposeful sarcomeres, thus enhancing cardiac differentiation [210].

## 6.5 *Additional Nanomaterials for Cardiovascular Therapeutics and Diagnostics*

Carbon propounds an intrinsically sustainable material to tailor and modulate surface chemistry and morphology of nanoarchitecture so as to fill a gap in the emerging requirements by medical science [211]. As mentioned earlier in this chapter, fullerene (truncated icosahedrons, 60 carbon atom compounds) together with nanodiamonds are adapted to achieve diverse functionality. Reportedly they have the potential to act as strengtheners in creating contractile tissues of heart [212]. When administered into blood vessel deficit areas of MI rats, these caged molecules significantly improved the endurance and retention of brown adipose-derived stem cells (BADSCs) in fullerene/alginate composite [213]. This proved their likelihood to be applicable in cardiovascular theranostics.

Recently, biosensors based on the amalgamation of nanodiamond and graphdiyne were structured to perceive quantitative measurement of cardiac troponin I (cTnI) in plasma and haematin extent in human serum. On comparing the CNM-based biosensors with the handy ones, for instance, black phosphorous, etc., the former was found competent enough to trace even diminutive concentration of haematin (0.01–1000 pg/ml) [214]. Nonetheless, notwithstanding these stimulating details, the relevance of nanodiamonds and fullerenes in medical science encounters different stumbling blocks, including their toxicity. It, therefore, calls for an exhaustive experimental investigation to develop advanced functional moderations for proper plan of action. This would open a window for these CNM to materialize as one of the best choices for therapeutics and diagnostics for circulatory system in the future.

## 7 **Toxicity of PCM-A Question of Safety?**

Carbon nanomaterials emerge as an awfully adaptable collection of nanomaterials. Encompassing enviable characteristics particularly those of wrangling and chemical firmness, CNMs can be customized to meet diverse requirements [95]. While carbonaceous nanomaterials have a direct bearing upon the biomedical field, a number of debates about their virulence are still underway [215, 216]. Different *in vitro* cellular studies focusing on the lethality, especially on the structure or functioning of immune system of humans or rats have made known different toxic effects of CNMs [217, 218]. And several factors such as structures, surface chemistry, impurities, method of synthesis, aspect ratio [127], critical dosage amendments, and important delivery routes have been reported to contribute to their toxic nature. For instance, SWCNTs and MWCNTs exhibit toxicity due to the presence of fibers in their structure [219]. Of two, high probability of cancer is associated with MWCNTs which owes to the presence of metal impurities in long stiff structure [160, 220]. Contrarily, spherical-shaped single-walled carbon nanohorns (SWNHs) are usually free from metal impurities [137, 221] and are not noxious [160, 219, 220] with

different surface modifications during cell viability assessments [136, 139]. Negative mutagenic and clastogenic results further authenticate their non-carcinogenic nature [153, 221]. Likewise, in various animal tests the absence of abnormal cellular degeneration, necrosis, histological abnormalities, viz. granuloma and fibrosis, undesired inflammatory responses indicate their non-damaging nature to several tissues. All of these results are, therefore, suggestive of SWNH being low toxic under natural as well as experimental conditions.

The toxicity of fullerenes, another spherical nanocarbon material promising as nano-medicine is often associated with variation in the size enclosure and surface chemistry. Pristine C60 potentially has dual functions; while it accounts for generation of reactive oxygen species, it can simultaneously scavenge free radicals. Based on this, certain combating details narrate its harmful effects. While some are of the opinion that pristine C60 is lethal and causes damage to cells others judge it to be the powerful antioxidant with no acute toxicity [44, 222]. It is quite difficult to demonstrate the toxic nature of pristine C60 since the same can be governed by the conditions applied, for instance, impurity level, light irradiations, etc. Accordingly, under certain conditions C60 becomes an effective, moderately non-toxic medication representative. On modifying the same to become water soluble, fullerenes are expected to impart acute animal toxicity. As an analogy, polyhydroxylated C60, based on surface chemistry can be second in toxicity after pristine C60 [223]. The modified compound reasoned for the meager development is hydrogen peroxide instead of superoxide. Consequently, polyhydroxylated C60 failed to persuade oxidative stress [224]. Therefore, based on various toxicological studies, fullerenes and its derivatives ordinarily show low toxicity [225].

Several studies reportedly claim toxicity of graphene and its derivatives in different cellular models which often result in complications like excessive inflammation and, if severe, can even lead to everlasting genetic disorder and even apoptosis [226]. A study carried out by Duch and co-workers [227] on lungs reported an imbalance in the production of ROS and antioxidant defense mechanism when graphene was present as an oxide. However, the same elicited no toxicity when existed as hydrophobic graphene. This study, therefore, brought into light the relevance of surface functionalization as well as dispersion that greatly enhanced the biocompatibility of graphene. Hence, size, surface chemistry, and appropriate distribution of graphene nanosheets are the key concerns that ought to be controlled to diminish harmful effects. Similar to this study was the one carried out by [228]. This group employed different sizes as well as concentrations of graphene oxide (GO) to evaluate their outcomes on embryonic development of zebrafish. The hatching time of the embryos got slower, with reduction in the body length, altered heartbeat and circulation rates and stimulated genes to promote cell death when GO was used at 100 mg/l concentration. This study, however, showed that dimensions of graphene oxide have no bearing upon the toxic nature when injection concentration exceeds 10 mg/l. Hence, selection based on the size and concentration of CNMs holds much importance not only for their safety but their unmatched efficacy for therapeutic applications as well.

Toxic nature of CNTs is reported to limit their application in biomedically important aspects, for instance in detecting biological receptors, loading and unloading of

drugs, repair and replacement tissue systems especially in heart and brain [229, 230]. Inceptive toxicity of CNTs in animals is often scrutinized using short-term exposure of lungs. The prime target of CNTs is the lungs which become brutally affected via inhalation of the nanomaterial. This effect gradually extends to the cardiac tissues [230, 231]. In order to minimize these toxic effects, the non-toxic chemical groups are either conjugated or reactive functional groups present on the surface are removed. However, a comparative study was carried out on SWCNTs and acid functionalized SWCNTs. The toxicity of both was evaluated in mice through oropharyngeal aspiration. The study revealed dose-dependent accumulation of neutrophils and increased edema formation in the lungs when exposed to acid functionalized SWCNTs. Because of their massive and outsized dimensions, such nanomaterials aggregated in aqueous solutions unlike easily dispersed smaller CNMs. This, in turn, mediates CNM toxicity inside the cells [232].

Several laboratory-based toxicological studies on carbon nanodiamonds and nanoparticles with some permanently established cell cultures have been reported to be non-pathogenic and least toxic with no detrimental effects on cellular proliferation [121, 132, 233]. Different bioassays carried out typically on nanodiamonds revealed that after being incubated these CNMs turned negative for inducing inflammation, stimulating adipokine and cytokine transmembrane proteins and even nitric oxide synthase in cells [234]. Besides this, owing to fluorescing property of nanodiamonds, their surface modifications account for non-toxic and highly biocompatible nature thereof.

Overall, it can be comprehended that the representatives of porous carbon materials are not intensely noxious up to a defined period. Even their surface functionalization demonstrates compact toxicity. It is yet obligatory to execute more meticulous and in-depth investigation to unearth the mechanics behind and evaluate persistent side effects and disintegration potential. Despite being exploited for nano-therapeutic applications, the intricate fatal side effects of nanomaterial cannot be ignored and hence need to be understood more. Nonetheless, studies based on CNMs indicate spherical shape to have taken edge over others in many biological systems.

## 8 Summary and Outlook

The present book chapter abridges promises and challenges associated with the therapeutic concerns of CNMs and their derivatives in diverse fields including targeted drug delivery, repair and replacement of tissues, physiochemical detection, and regulatory alteration of immune system. In vitro studies rated on understanding administration strategy, therapeutic dosage compensation, biological degradation, and non-hazardous performance of CNMs have opened a window of opportunity to synthesize next-generation biomaterials holding therapeutics worth. Although the clinical exercise is still premature to conclude, the biocompatibility of these materials is apparently a decisive factor for their applicability in therapeutics. Further, since CNMs own



several important properties which make them eye-catching candidates for biomedical application, numerous challenges triumph over their successful clinical applications. Hence, in-depth knowledge is crucial to comprehend the safety contour and fundamental benefits in different in vitro animal models. Understandably, this will provide an insight to the researchers for the fine-tuning of CNMs towards their pharmacokinetic and pharmacodynamic profiles. Concurrently, the presence of these products in the environment after their usage may add to the potential contamination leading to ecotoxicity problems in the near-future. Therefore, before exercising porous carbon materials in therapeutics, execution of more meticulous and exhaustive long-term toxicological studies is central. Hence, upcoming efforts should also focus on resolving these issues as well.

**Acknowledgements** We are thankful to editors of this book for giving us an opportunity to dwell upon one of the trickiest topics of medicinal biology. Acknowledgments are due to the Head of the Department of Botany, Cluster University of Jammu, for the necessary library facilities.

**Conflict of Interest Statement** The authors declare no conflict of interest.

## References

1. Alami AH (2020) Advances on porous materials. *Encycl Smart Mater*. <https://doi.org/10.1016/B978-0-12-803581-8.11756-4>
2. Reece JB, Urry LA, Cain ML, Wasserman SA, Minorsky PV, Jackson RB (2014) *Campbell biology books a la Carte edition*, 10th edn. Pearson
3. Jager H, Frohs W, Collin G, von Sturm F, Vohler O, Nutsch G (2010) *Carbon, 1. General*. Ullmann's encyclopedia of industrial chemistry. Wiley-VCH Verlag GmbH and Co. KGaA, Weinheim, Germany. <https://doi.org/10.1002/14356007.a05-095.pub2>
4. Derbyshire F, Jagtoyen M, Thwaites M (1995) *Porosity in carbons*. Edward Arnold, London
5. Cecen F (2011) Water and wastewater treatment: Historical perspective of activated carbon adsorption and its integration with biological processes. In: Çeçen F, Aktaş Ö (eds) *Activated carbon for water and wastewater treatment*. Wiley-VCH Verlag GmbH and Co. KGaA, Weinheim, Germany, pp 1–11. <https://doi.org/10.1002/9783527639441.ch1>
6. Dabrowski A (2001) Adsorption—from theory to practice. *Adv Coll Interface Sci* 93(1–3):135–224
7. Menendez-Diaz JA, Martin-Gullon I (2006) Types of carbon adsorbents and their production. In: Bandosz TJ (ed) *Activated carbon surfaces in environmental remediation*. Elsevier, New York, pp 1–48. [https://doi.org/10.1016/S1573-4285\(06\)80010-4](https://doi.org/10.1016/S1573-4285(06)80010-4)
8. Mestre AS, Carvalho AP (2018) Nanoporous carbon synthesis: an old story with exciting new chapters. In: Ghrib T (ed) *Porosity—process, technologies and applications*. <https://doi.org/10.5772/intechopen.72476>
9. Thambiliyagodage C, Mirihana S, Gunathilaka H (2019) Porous carbon materials in biomedical applications. *Biomed J Sci and Tech Res* 22(4). BJSTR. MS.ID.003798
10. Wang X, Bozhilov KN, Feng P (2006) Facile preparation of hierarchically porous carbon monoliths with well-ordered mesostructures. *Chem Mater* 18(26):6373–6381
11. Lee KT, Lytle JC, Ergang NS, Oh SM, Stein A (2007) Synthesis and rate performance of monolithic macroporous carbon electrodes for lithium-ion secondary batteries. *Adv Funct Mater* 15:547

12. Wang Z, Li F, Stein A (2007) Direct synthesis of shaped carbon nanoparticles with ordered cubic mesostructure. *Nano Lett.* 7:3223–3226
13. Lee D, Lee J, Kim J, Kim J, Na HB, Kim B et al (2005) Simple fabrication of a highly sensitive and fast glucose biosensor using enzymes immobilized in mesocellular carbon foam. *Adv Mater* 17:2828–2833
14. Lai CZ, Fierke MA, Stein A, Buhlmann P (2007) Ion-selective electrodes with three-dimensionally ordered macroporous carbon as the solid contact. *Anal Chem* 79:4621–4626
15. Stein A, Wang Z, Fierke MA (2009) Functionalization of porous carbon materials with designed pore architecture. *Adv Mater* 21:265–293
16. Vinu A, Miyahara M, Sivamurugan V, Mori T, Ariga K (2005) Large pore cage type mesoporous type, carbon nanocage: a superior adsorbent for biomaterials. *J Mater Chem* 15:5122
17. Gu Z, Deng B (2007) Use of iron-containing mesoporous carbon (IMC) for arsenic removal from drink water. *Environ Eng Sci* 24:113–121
18. Harnisch JA, Gazda DB, Anderegg JW, Porter MD (2001) Chemical modification of carbonaceous stationary phases by the reduction of diazonium salts. *Anal Chem* 73(16):3954–3959
19. Vinu A, Hossain KZ, Srinivasu P, Miyahara M, Anandan S, Gokulakrishnan N, Mori T, Ariga K, Balasubramanian VV et al (2007) Carboxy-mesoporous carbon and its excellent adsorption capability for proteins. *J Mater Chem* 17:1819–1825
20. Cameron DS, Cooper SJ, Dodgson IL, Harrison B, Jenkins JW (1990) Carbons as supports for precious metal catalysts. *Catal Today* 7:113–137
21. Radovic L, Rodriguez-Reinoso F (1997) Carbon materials in catalysis. *Chem Phys Carbon* 25:243
22. Lee JJ, Han S, Kim H, Koh JH, Hyeon T, Moon SH (2003) Performance of CoMoS catalysts supported on nanoporous carbon in the hydrodesulfurization of dibenzothiophene and 4,6-dimethyldibenzothiophene. *Catal Today* 86:141–149
23. Shrabani De, Acharya S, Sahoo S, Nayak GC (2020) Present status of biomass derived carbon-based composites for super capacitor application. In: *Nanostructured, functional, and flexible materials for energy conversion and storage systems*. Elsevier, pp 373–415. <https://doi.org/10.1016/B978-0-12-819552-9.00012-9>
24. Liu Y, Wang H (2007) Nanomedicine: nanotechnology tackles tumours. *Nat Nanotechnol* 2:20–21
25. Shim MS, Kwon YJ (2012) Stimuli-responsive polymers and nanomaterials for gene delivery and imaging applications. *Adv Drug Del Rev* 64:1046–1058
26. Jans H, Huo Q (2012) Gold nanoparticle-enabled biological and chemical detection and analysis. *Chem Soc Rev* 41:2849–2866
27. Shinohara H (2000) Endohedral metallofullerenes. *Rep Prog Phys* 63:843–892
28. Sijbesma RP, Srdanov G, Wudl F, Castoro JA, Wilkins C, Friedman SH, DeCamp DL, Kenyon GL (1993) Synthesis of a fullerene derivative for the inhibition of HIV enzymes. *J Am Chem Soc* 115:6510–6512
29. Partha R, Conyers JL (2009) Biomedical applications of functionalized fullerene-based nanomaterials. *Intl J Nanomed* 4:261–275
30. Xiao L, Takada H, Gan X, Miwa N (2006) The water-soluble fullerene derivative ‘Radical Sponge’ exerts cytoprotective action against UVA irradiation but not visible light-catalyzed cytotoxicity in human skin keratinocytes. *Bioorg Med Chem Lett* 16:1590–1595
31. Han LM, Guo J, Zhang LJ, Wang QS, Fang XL (2006) Pharmacokinetics and biodistribution of polymeric micelles of paclitaxel with Pluronic P123. *Acta Pharmacol Sin* 27:747–753
32. Spencer CM, Faulds D (1994) Paclitaxel: a review of its pharmacodynamic and pharmacokinetic properties and therapeutic potential in the treatment of cancer. *Drugs* 48:794–847
33. Weiss RB, Donehower RC, Wiernik PH et al (1990) Hypersensitivity reactions from taxol. *J Clin Oncol* 8:1263–1268
34. Ferrari M (2005) Cancer nanotechnology: opportunities and challenges. *Nat Rev Cancer* 5:161–171

35. Crosasso P, Ceruti M, Brusa P, Arpicco S, Dosio F, Cattel L (2000) Preparation, characterization and properties of sterically stabilized paclitaxel-containing liposomes. *J Control Release* 63:19–30
36. Partha R, Mitchell LR, Lyon JL, Joshi PP, Conyers JL (2008) Buckysomes: fullerene-based nanocarriers for hydrophobic molecule delivery. *ACS Nano* 2(9):1950–1958
37. Partha R, Lackey M, Hirsch A, Casscells SW, Conyers JL (2007) Self assembly of amphiphilic C60 fullerene derivatives into nanoscale supramolecular structures. *J Nanobiotech* 5:6
38. Zakharian TY, Seryshev A, Sitharaman B, Gilbert BE, Knight V, Wilson LJ (2005) A fullerene-paclitaxel chemotherapeutic: synthesis, characterization, and study of biological activity in tissue culture. *J Am Chem Soc* 127(36):12508–12509
39. Nakamura E, Isobe H, Tomita N, Sawamura M, Jinno S, Okayama H (2000) Functionalized fullerene as an artificial vector for transfection. *Angew Chem Int Ed* 39:4254–4257
40. Isobe H, Nakanishi W, Tomita N, Jinno S, Okayama H, Nakamura E (2006) Gene delivery by aminofullerenes: structural requirements for efficient transfection. *Chem Asian J* 1:167–175
41. Sitharaman B, Zakharian TY, Saraf A et al (2008) Water-soluble fullerene (C60) derivatives as nonviral gene-delivery vectors. *Mol Pharm* 5(4):567–578
42. Camargo LL, Touyz R (2019) Reactive oxygen species. In: *Textbook of vascular medicine*. [https://doi.org/10.1007/978-3-030-16481-2\\_12](https://doi.org/10.1007/978-3-030-16481-2_12)
43. Krusic PJ, Wasserman E, Keizer PN, Morton JR, Preston KF (1991) Radical reactions of C60. *Science* 254:1183–1185
44. Gharbi N, Pressac M, Hadchouel M, Szwarc H, Wilson SR, Moussa F (2005) [60]fullerene is a powerful antioxidant in vivo with no acute or subacute toxicity. *Nano Lett* 5:2578–2585
45. Sayes CM, Gobin AM, Ausman KD, Mendes J, West JL, Colvin VL (2005) Nano-C60 cytotoxicity is due to lipid peroxidation. *Biomaterial* 26:7587–7595
46. Tsai MC, Chen YH, Chiang LY (1997) Polyhydroxylated C60, fulleranol, a novel free radical trapper, prevented hydrogen peroxide- and cumene hydroperoxide-elicited changes in rat hippocampus in-vitro. *J Pharm Pharmacol* 49:438–445
47. Dugan LL, Dorothy MT, Cheng D, Doug L, Mark W, Robert CA, Clifton KFS, Tien-Yau L, Dennis WC, Tien-Sung L (1997) Carboxyfullerenes as neuroprotective agents. *PNAS* 94(17):9434–9439
48. Jain KK (2005) The role of nanobiotechnology in drug discovery. *Drug Discov Today* 10:1435–1442
49. Dugan LL, Gabrielsen JK, Yu SP, Lin TS, Choi DW (1996) Buckminster fullerene free radical scavengers reduce excitotoxic and apoptotic death of cultured cortical neurons. *Neurobiol Dis* 3:129–135
50. Isakovic A, Markovic Z, Todorovic-Markovic B, Nikolic N, Vranjes-Djuric S, Mirkovic M, Dramicanin M, Harhaji L, Raicevic N, Nikolic Z, Trajkovic V (2006) Distinct cytotoxic mechanisms of pristine versus hydroxylated fullerene. *Toxicol Sci* 91:173–183
51. Daroczi B, Kari G, McAleer MF, Wolf JC, Rodeck U, Dicker AP (2006) In vivo radioprotection by the fullerene nanoparticle DF-1 as assessed in a zebrafish model. *Clin Cancer Res* 12:7086–7091
52. Quick KL, Ali SS, Arch R, Xiong C, Wozniak D, Dugan LL (2008) A carboxyfullerene SOD mimetic improves cognition and extends the lifespan of mice. *Neurobiol Aging* 29:117–128
53. Misirkic MS, Todorovic-Markovic BM, Vucicevic LM, Janjetovic KD, Jokanovic VR, Dramicanin MD, Markovic ZM, Trajkovic VS (2009) The protection of cells from nitric oxide-mediated apoptotic death by mechano-chemically synthesized fullerene (C(60)) nanoparticles. *Biomaterial* 30:2319–2328
54. Xiao L, Takada H, Maeda K, Haramoto M, Miwa N (2005) Antioxidant effects of water-soluble fullerene derivatives against ultraviolet ray or peroxy lipid through their action of scavenging the reactive oxygen species in human skin keratinocytes. *Biomed Pharmacother* 59:351–358
55. Monti D, Moretti L, Salvioli S et al (2000) C60 carboxyfullerene exerts a protective activity against oxidative stress-induced apoptosis in human peripheral blood mononuclear cells. *Biochem Biophys Res Commun* 277(3):711–717

56. Santos SG, Santana JV, Maia FF Jr et al (2008) Adsorption of ascorbic acid on the C60 fullerene. *J Phys Chem B* 112(45):14267–14272
57. Yin JJ, Lao F, Fu PP, Wamer WG, Zhao YL, Wang PC, Qiu Y, Sun BY, Xing GM, Dong JQ, Liang XJ, Chen CY (2009) The scavenging of reactive oxygen species and the potential for cell protection by functionalized fullerene materials. *Biomaterial* 30:611–621
58. Loft S, Poulsen HE (1996) Cancer risk and oxidative DNA damage in man. *J Mol Med* 74:297–312
59. Stadtman ER, Berlett BS (1997) Reactive oxygen-mediated protein oxidation in aging and disease. *Chem Res Toxicol* 10:485–494
60. Ali SS, Hardt JI, Quick KL, Kim-Han JS, Erlanger BF, Huang TT, Epstein CJ, Dugan LL (2004) A biologically effective fullerene (C60) derivative with superoxide dismutase mimetic properties. *Free Radic Biol Med* 37:1191–1202
61. Kopylov VB, Gavronskaya YY (2001) Electronic and vibrational spectra of fullerenes in contact with oxygen. *Russian J Gen Chem* 71:1589–1592
62. Toth E, Bolskar RD, Borel A et al (2005) Water-soluble gadofullerenes: toward high-relaxivity, pH-responsive MRI contrast agents. *J Am Chem Soc* 127(2):799–805
63. Fatouros PP, Corwin FD, Chen ZJ et al (2006) In vitro and in vivo imaging studies of a new endohedral metallo-fullerene nanoparticle. *Radiology* 240(3):756–764
64. Sitharaman B, Tran LA, Pham QP et al (2007) Gadofullerenes as nanoscale magnetic labels for cellular MRI. *Contrast Media Mol Imaging* 2(3):139–146
65. Feitelson MA, Arzumanyan A, Kulathinal RJ, Blain SW, Holcombe RF, Mahajna J et al (2015) Sustained proliferation in cancer: mechanisms and novel therapeutic targets. *Semin Cancer Biol* 35(Suppl.):S25–S54
66. Reinhart-King CA (2016) Cancer cell mechanism. In: Janmey P et al (eds) Physical sciences and engineering advances in life sciences and oncology. Science policy reports. [https://doi.org/10.1007/978-3-319-17930-8\\_4](https://doi.org/10.1007/978-3-319-17930-8_4)
67. Conduit PT, Wainman A, Raff JW (2015) Centrosome function and assembly in animal cells. *Nat Rev Mol Cell Biol* 16:611–624
68. Godinho SA, Picone R, Burute M, Dagher R, Su Y, Leung CT, Polyak K, Brugge JS, Thery M, Pellman D (2014) Oncogene-like induction of cellular invasion from centrosome amplification. *Nature* 510:167–171
69. Carter SL, Eklund AC, Kohane IS, Harris LN, Szallasi Z (2006) A signature of chromosomal instability inferred from gene expression profiles predicts clinical outcome in multiple human cancers. *Nat Genet* 38:1043–1048
70. Loffler H, Fechter A, Liu FY, Poppelreuther S, Kramer A (2013) DNA damage-induced centrosome amplification occurs via excessive formation of centriolar satellites. *Oncogene* 32:2963–2972
71. Kwon M, Godinho SA, Chandhok NS, Ganem NJ, Azioune A, Thery M, Pellman D (2008) Mechanisms to suppress multipolar divisions in cancer cells with extra centrosomes. *Genes Dev* 22:2189–2203
72. Siegel RL, Miller KD, Jemal A (2016) Cancer statistics, 2016. *CA Cancer J Clin* 66:7–30
73. Begg AC, Stewart FA, Vens C (2011) Strategies to improve radiotherapy with targeted drugs. *Nat Rev Cancer* 11:239–253
74. Kim JS, Kim HA, Seong MK, Seol H, Oh JS, Kim EK, Chang JW, Hwang SG, Noh WC (2016) STAT3-survivin signalling mediates a poor response to radiotherapy in HER2-positive breast cancers. *Oncotarget* 7:7055–7065
75. Choe MH, Kim J, Ahn J, Hwang SG, Oh JS, Kim JS (2018) Centrosome clustering is a tumor-selective target for the improvement of radiotherapy in breast cancer cells. *Anticancer Res* 38:3393–3400
76. Simonin JP (2001) Solvent effects on osmotic second virial coefficient studied using analytic molecular models. Application to solutions of C60 fullerene. *J Phys Chem B* 105:5262–5270
77. Okumura M, Mikawa M, Yokawa T, Kanazawa Y, Kato H, Shinohara H (2002) Evaluation of water-soluble metallofullerenes as MRI contrast agents. *Acad Radiol* 9:S495–S497

78. Yin JJ, Lao F, Meng J, Fu PP, Zhao YL, Xing GM, Gao XY, Sun BY, Wang PC, Chen CY, Liang XJ (2008) Inhibition of tumor growth by endohedral metallofullerenol nanoparticles optimized as reactive oxygen species scavenger. *Mol Pharmacol* 74:1132–1140
79. Wang J, Gu F, Ding T, Liu XL, Xing GM, Zhao YL, Zhang N, Ma YJ (2010) [Gd@C82(OH)22]n nanoparticles inhibit the migration and adhesion of glioblastoma cells. *Oncol Lett* 1:771–775
80. Wang JX et al (2006) Antioxidative function and biodistribution of [Gd@C82(OH)22]n nanoparticles in tumor-bearing mice. *Biochem Pharmacol* 71:872–881
81. Meng J et al (2011) Epigenetic modulation of human breast cancer by metallofullerenol nanoparticles: in vivo treatment and in vitro analysis. *Nanoscale* 3:4713–4719
82. Pelicano H, Carney D, Huang P (2004) ROS stress in cancer cells and therapeutic implications. *Drug Resist Updat* 7:97–110
83. Yang D, Zhao YL, Guo H, Li YN, Tewary P, Xing GM, Hou W, Oppenheim JJ, Zhang N (2010) [Gd@C82(OH)22]n nanoparticles induce dendritic cell maturation and activate Th1 immune responses. *ACS Nano* 4:1178–1186
84. Chen CY et al (2005) Multihydroxylated [Gd@C82(OH)22]n nanoparticles: antineoplastic activity of high efficiency and low toxicity. *Nano Lett* 5:2050–2057
85. Kang S et al (2012) Molecular mechanism of pancreatic tumor metastasis inhibition by Gd@C82(OH)22 and its implication for de novo design of nanomedicine. *Proc Natl Acad Sci USA* 109:15431–15436
86. Ge CC et al (2011) Binding of blood proteins to carbon nanotubes reduces cytotoxicity. *Proc Natl Acad Sci USA* 108:16968–16973
87. Liang XJ et al (2010) Metallofullerene nanoparticles circumvent tumor resistance to cisplatin by reactivating endocytosis. *Proc Natl Acad Sci USA* 107:7449–7454
88. Li J, Zhang MY, Sun BY, Xing GM, Song Y, Guo HL, Chang Y, Ge YH, Zhao YL (2011) Separation and purification of fullerenols for improved biocompatibility. *Carbon NY* 50:460–469
89. Akiyama K, Hamano T, Nakanishi Y, Takeuchi E, Noda S, Wang ZY, Kubuki S, Shinohara H (2012) Non-HPLC rapid separation of metallo fullerenes and empty cages with TiCl4 Lewis acid. *J Am Chem Soc* 134:9762–9767
90. Baptista FR, Belhout SA, Giordani S, Quinn SJ (2015) Recent developments in carbon nanomaterial sensors. *Chem Soc Rev* 44:4433–4453. <https://doi.org/10.1039/C4CS00379A>
91. Bartelmess J, Quinn SJ, Giordani S (2015) Carbon nanomaterials: multifunctional agents for biomedical fluorescence and Raman imaging. *Chem Soc Rev* 44:4672–4698. <https://doi.org/10.1039/C4CS00306C>
92. Chen DH, Cao L, Hanley TL, Caruso RA (2012) Facile synthesis of monodisperse mesoporous zirconium titanium oxide microspheres with varying compositions and high surface areas for heavy metal ion sequestration. *Adv Funct Mater* 22:1966–1971. <https://doi.org/10.1002/adfm.201102878>
93. Liu HJ, Cui WJ, Jin LH, Wang CX, Xia YY (2009) Preparation of three-dimensional ordered mesoporous carbon sphere arrays by a two-step templating route and their application for supercapacitors. *J Mater Chem* 19:3661–3667
94. Chen DH, Huang FZ, Cheng YB, Caruso RA (2009) Mesoporous anatase TiO2 beads with high surface areas and controllable pore sizes: a superior candidate for high-performance dye-sensitized solar cells. *Adv Mater* 21:2206–2210
95. Vasconcelos JM, Zen F, Angione MD, Cullen RJ, Santos-Martinez MJ, Colavita PE (2020) Understanding the carbon-bio interface: influence of surface chemistry and buffer composition on the adsorption of phospholipid liposomes at carbon surfaces. *ACS Appl Bio Mater* 3:997–1007
96. Slowing II, Vivero-Escoto JL, Wu CW, Lin VS (2008) Mesoporous silica nanoparticles as controlled release drug delivery and gene transfection carriers. *Adv Drug Deliv Rev* 60:1278–1288
97. Liu J, Stace-Naughton A, Jiang X, Brinker CJ (2009) Porous nanoparticle supported lipid bilayers (protocells) as delivery vehicles. *J Am Chem Soc* 131:1354–1355

98. Gott VL, Alejo DE, Cameron DE (2003) Mechanical heart valves: 50 years of evolution. *Ann Thorac Surg* 76:S2230-2239
99. Singhal R et al (2011) Multifunctional carbon-nanotube cellular endoscopes. *Nat Nanotechnol* 6(1):57–64
100. Cardone RA, Casavola V, Reshkin SJ (2005) The role of disturbed pH dynamics and the Na<sup>+</sup>/H<sup>+</sup> exchanger in metastasis. *Nat Rev Cancer* 5(10):786–795
101. Zhu J, Liao L, Bian XJ, Kong JL, Yang PY, Liu BH (2012) pH-controlled delivery of doxorubicin to cancer cells, based on small mesoporous carbon nanospheres. *Small* 8:2715–2720
102. Kessenbrock K, Plaks V, Werb Z (2010) Matrix metallo proteinases: regulators of the tumor microenvironment. *Cell* 141(1):52–67
103. Schilling D et al (2017) The Hsp70 inhibiting peptide aptamer A17 potentiates radio sensitization of tumor cells by Hsp90 inhibition. *Cancer Lett* 390:146–152
104. Schafer FQ, Buettner GR (2001) Redox environment of the cell as viewed through the redox state of the glutathione disulfide/glutathione couple. *Free Radical Biol Med* 30(11):1191–1212
105. Zhou L et al (2015) Near-infrared absorbing mesoporous carbon nanoparticle as an intelligent drug carrier for dual-triggered synergistic cancer therapy. *Carbon* 82:479–488
106. Gupta N et al (2019) A Review of theranostics applications and toxicities of carbon nanomaterials. *Curr Drug Metab* 20(6):506–532
107. Xu G et al (2014) Functionalized mesoporous carbon nanoparticles for targeted chemophotothermal therapy of cancer cells under near-infrared irradiation. *RSC Advance* 4(64):33986–33997
108. Xue C et al (2017) Micro-nanomaterials for tumor microwave hyperthermia: design, preparation, and application. *Curr Drug Deliv* 14:307–322
109. Shah BP et al (2014) Core-shell nanoparticle-based peptide therapeutics and combined hyperthermia for enhanced cancer cell apoptosis. *ACS Nano* 8(9):9379–9387
110. Wu F et al (2019) Hyaluronic acid-modified porous carbon-coated Fe<sub>3</sub>O<sub>4</sub> nanoparticles for magnetic resonance imaging-guided photothermal/chemotherapy of tumors. *Langmuir* 35(40):13135–13144
111. Hai W, Yuliang Z, Guangjun N (2014) Multifunctional nanoparticle systems for combined chemoand photothermal cancer therapy. *Front Mater Sci* 7:118–128
112. Zhang Y et al (2016) Mesoporous carbon nanoparticles capped with polyacrylic acid as drug carrier for bi-trigger continuous drug release. *J Mater Chem B* 4(30):5178–5184
113. Chen L et al (2019) Folic acid-conjugated magnetic ordered mesoporous carbon nanospheres for doxorubicin targeting delivery. *Mater Sci Eng, C Mater Biol Appl* 04:109939
114. Chen L et al (2018) Thermo-sensitively and magnetically ordered mesoporous carbon nanospheres for targeted controlled drug release and hyperthermia application. *Mater Sci Eng, C Mater Biol Appl* 84:21–31
115. Wang H et al (2015) Magnetic/NIR-responsive drug carrier, multicolor cell imaging, and enhanced photothermal therapy of gold capped magnetite-fluorescent carbon hybrid nanoparticles. *Nanoscale* 7(17):7885–7895
116. Wu F et al (2018) Triple stimuli-responsive magnetic hollow porous carbon-based nanodrug delivery system for magnetic resonance imaging-guided synergistic photothermal/chemotherapy of cancer *ACS Appl. Mater Interfaces* 10(26):21939–21949
117. Chung PH, Perevedentseva E, Cheng CL (2007) The particle size-dependent photoluminescence of nanodiamonds. *Surf Sci* 601(18):3866–3870
118. Chao J, Perevedentseva E, Chung P, Liu K, Cheng C, Chang C, Cheng C (2007) Nanometer-sized diamond particle as probe for biolabeling. *Biophys J* 93:2199–2208
119. Schrand AM, Huang H, Carlson C, Schlager JJ, Osawa E, Hussain SM, Dai L (2007) Are diamond nanoparticles cytotoxic? *J Phys Chem B* 111(1):2–7
120. Mochalin VN, Shenderova O, Ho D, Gogotsi Y (2011) The properties and applications of nanodiamonds. *Nat Nanotechnol* 7(1):11–23
121. Krueger A (2008) New carbon materials: biological applications of functionalized nanodiamond materials. *Chem Eur J* 14:1382–1390

122. Bondar VS, Pozdnyakova IO, Puzyr AP (2004) Applications of nanodiamonds for separation and purification of proteins. *Phys Solid State* 46:758–760
123. Huang LL, Chang HC (2004) Adsorption and immobilization of cytochrome c on nanodiamonds. *Langmuir* 20:5879–5884
124. Guan B, Zou F, Zhi JF (2010) Nanodiamond as the pH-responsive vehicle for an anticancer drug. *Small* 6:1514–1519
125. Chen M, Pierstorff E, Lam R, Li SY, Huang H, Osawa E, Ho D (2009) Nanodiamond-mediated delivery of water-insoluble therapeutics. *ACS Nano* 3:2016–2022
126. Zhang XQ, Lam R, Xu XY, Chow EK, Kim H, Ho D (2011) Multimodal nanodiamond drug delivery carriers for selective targeting, imaging, and enhanced chemotherapeutic efficacy. *Adv Mater* 23:4770–4775
127. Wang J, Hu Z, Xu J, Zhao Y (2014) Therapeutic applications of low-toxicity spherical nanocarbon materials. *NPG Asia Mater* 6:e84–e84. <https://doi.org/10.1038/am.2013.79>
128. Feinberg A (2014) How these microscopic diamonds are going to shape the future? Gizmodo
129. Faklaris O et al (2009) Photoluminescent diamond nanoparticles for cell labeling: study of the uptake mechanism in mammalian cells. *ACS Nano* 3(12):3955–3962
130. Neugart F, Zappe A, Jelezko F, Tietz C, Boudou JP, Krueger A, Wrachtrup J (2007) Dynamics of diamond nanoparticles in solution and cells. *Nano Lett* 7(12):3588–3591
131. Chang YR et al (2008) Mass production and dynamic imaging of fluorescent nanodiamonds. *Nat Nanotechnol* 3:284–288
132. Fang YX, Guo SJ, Li D, Zhu CZ, Ren W, Dong SJ, Wang EK (2012) Easy synthesis and imaging applications of cross-linked green fluorescent hollow carbon nanoparticles. *ACS Nano* 6:400–409
133. Ganeshkumar M, Ponrasu T, Sathishkumar M, Suguna L (2013) Preparation of amphiphilic hollow carbon nanosphere loaded insulin for oral delivery. *Colloids Surf B* 103:238–243
134. Paramita K, Shrabani D, Kartick CM, Rashmi M, Prashant KS (2019) Functionalization of carbon nanostructures. In: *Comprehensive nanoscience and nanotechnology*, 2nd edn, vol 2. Elsevier, pp 123–144
135. Murata K et al (2000) Pore structure of single-wall carbon nanohorn aggregates. *Chem Phys Lett* 331(1):14–20
136. Ajima K, Yudasaka M, Murakami T, Maigne A, Shiba K, Iijima S (2005) Carbon nanohorns as anticancer drug carriers. *Mol Pharmaceut* 2:475–480
137. Iijima S et al (1999) Nano-aggregates of single-walled graphitic carbon nano-horns. *Chem Phys Lett* 309:165–170
138. Zhang M, Yudasaka M, Miyawaki J, Fan J, Iijima S (2005) Isolating single-wall carbon nanohorns as small aggregates through a dispersion method. *J Phys Chem B* 109(47):22201–22204
139. Zhang MF, Yudasaka M, Ajima K, Miyawaki A, Iijima S (2007) Light-assisted oxidation of single-wall carbon nanohorns for abundant creation of oxygenated groups that enable chemical modifications with proteins to enhance biocompatibility. *ACS Nano* 1:265–272
140. Desai N, Hubbell J (1991) Solution technique to incorporate polyethylene oxide and other water-soluble polymers into surfaces of polymeric biomaterials. *Biomaterial* 12:144–153
141. Du H, Chandaroy P, Hui S (1997) Grafted poly-(ethylene glycol) on lipid surfaces inhibits protein adsorption and cell adhesion. *Biochim Biophys Acta* 1326:236–248
142. Murakami T, Fan J, Yudasaka M, Iijima S, Shiba K (2006) Solubilization of singlewall carbon nanohorns using a PEG-doxorubicin conjugate. *Mol Pharmaceut* 3:407–414
143. Matsumura S, Ajima K, Yudasaka M, Iijima S, Shiba K (2007) Dispersion of cisplatin-loaded carbon nanohorns with a conjugate comprised of an artificial peptide aptamer and polyethylene glycol. *Mol Pharmaceut* 4:723–729
144. Matsumura S, Sato S, Yudasaka M, Tomida A, Tsururo T, Iijima S, Shiba K (2009) Prevention of carbon nanohorn agglomeration using a conjugate composed of combshaped polyethylene glycol and a peptide aptamer. *Mol Pharmaceut* 6:441–447
145. Pagona G, Mountrichas G, Rotas G, Karousis N, Pispas S, Tagmatarchis N (2009) Properties, applications and functionalization of carbon nanohorns. *Int J Nanotechnol* 6:176–195

146. Brandao L, Passreira C, Gattia DM, Mendes A (2011) Use of single wall carbon nanohorns in polymeric electrolyte fuel cells. *J Mater Sci* 46:7198–7205
147. Muralkami T, Ajima K, Miyawaki J, Yudasaka M, Iijima S, Shiba K (2004) Drug-loaded carbon nanohorns: adsorption and release of dexamethasone in vitro. *Mol Pharmaceut* 1:399–405
148. Nakamura M, Tahara Y, Ikehara Y, Murakami T, Tsuchida K, Iijima S, Waga I, Yudasaka M (2011) Single-walled carbon nanohorns as drug carriers: adsorption of prednisolone and anti-inflammatory effects on arthritis. *Nanotechnol* 22(46):465102
149. Guerra J et al (2012) Carbon nanohorns functionalized with polyamidoamine dendrimers as efficient biocarrier materials for gene therapy. *Carbon NY* 50:2832–2844
150. Maeda H (2012) Macromolecular therapeutics in cancer treatment: the EPR effect and beyond. *J Control Release* 164:138–144
151. Miyawaki J et al (2009) Biodistribution and ultrastructural localization of single-walled carbon nanohorns determined in vivo with embedded Gd<sub>2</sub>O<sub>3</sub> labels. *ACS Nano* 3:1399–1406
152. Zhang MF, Zhou X, Iijima S, Yudasaka M (2012) Small-sized carbon nanohorns enabling cellular uptake control. *Small* 8:2524–2531
153. Tahara Y, Miyawaki J, Zhang MF, Yang M, Waga I, Iijima S, Irie H, Yudasaka M (2011) Histological assessments for toxicity and functionalization-dependent biodistribution of carbon nanohorns. *Nanotechnology* 22:265106
154. Murakami T, Tsuchida K (2008) Recent advances in inorganic nanoparticle-based drug delivery systems. *Mini-Rev Med Chem* 8:175–183
155. Marangon I et al (2016) Synergic mechanisms of photothermal and photodynamic therapies mediated by photosensitizer/carbon nanotube complexes. *Carbon NY* 97:110–123
156. Miyako E et al (2012) Photothermic regulation of gene expression triggered by laser-induced carbon nanohorns. *Proc Natl Acad Sci USA* 109(19):7523–7528
157. Allahyari Z et al (2016) Optimization of electrical stimulation parameters for MG-63 cell proliferation on chitosan/functionalized multiwalled carbon nanotube films. *RSC Adv* 6(111):109902–109915
158. Nekounam H et al (2020) Simple and robust fabrication and characterization of conductive carbonized nanofibers loaded with gold nanoparticles for bone tissue engineering applications. *Mater Sci Eng C Mater Biol Appl* 117:111226
159. Hirata E et al (2011) Multiwalled carbon nanotube-coating of 3D collagen scaffolds for bone tissue engineering. *Carbon NY* 49(10):3284–3291
160. Poland CA et al (2008) Carbon nanotubes introduced into the abdominal cavity of mice show asbestos-like pathogenicity in a pilot study. *Nat Nanotechnol* 3(7):423–428
161. Murakami T et al (2008) Water-dispersed singlewall carbon nanohorns as drug carriers for local cancer chemotherapy. *Nanomedicine* 3(4):453–463
162. Kasai T, Matsumura S, Iizuka T, Shiba K, Kanamori T, Yudasaka M, Iijima S, Yokoyama A (2011) Carbon nanohorns accelerate bone regeneration in rat calvarial bone defect. *Nanotechnology* 22:065102
163. Takayanagi H (2007) Osteoimmunology: shared mechanisms and crosstalk between the immune and bone systems. *Nat Rev Immunol* 7:292–304
164. Mosser DM, Edwards JP (2008) Exploring the full spectrum of macrophage activation. *Nat Rev Immunol* 8:958–869
165. Blom AB, Van Lent PL, Holthuysen AE, Van der Kraan PM, Roth J, Van Rooijen N, den BergWB V (2004) Synovial lining macrophages mediate osteophyte formation during experimental osteoarthritis. *Osteoarthr Cartil* 12:627–635
166. Takahashi F, Takahashi K, Shimizu K, Cui R, Tada N, Takahashi H, Soma S, Yoshioka M, Fukuchi Y (2004) Osteopontin is strongly expressed by alveolar macrophages in the lungs of acute respiratory distress syndrome. *Lung* 182:173–185
167. Takada S, Hirata E, Sakairi M, Miyako E, Takano Y, Ushijima N, Yudasaka M, Iijima S, Yokoyama A (2021) Carbon nanohorn coating by electrodeposition accelerate bone formation on titanium implant. *Artif Cells Nanomed Biotechnol* 49(1):20–29



168. Hirata E et al (2016) Carbon nanohorns allow acceleration of osteoblast differentiation via macrophage activation. *Nanoscale* 8(30):14514–14522
169. Lacerda L, Bianco A, Prato M, Kostarelos K (2006) Carbon nanotubes as nanomedicines: from toxicology to pharmacology. *Adv Drug Deliv Rev* 58:1460–1470
170. Shvedova AA, Kisin ER, Porter D, Schulte P, Kagan VE, Fadeel B, Castranova V (2009) Mechanisms of pulmonary toxicity and medical applications of carbon nanotubes: two faces of janus? *Pharmacol Ther* 121:192–204
171. Cheng J, Flahaut E, Cheng SH (2007) Effect of carbon nanotubes on developing zebrafish (*Danio rerio*) embryos. *Environ Toxicol Chem* 26:708–716
172. Asharani PV, Serina NG, Nurmawati MH, Wu YL, Gong Z, Valiyaveetil S (2008) Impact of multi-walled carbon nanotubes on aquatic species. *J Nanosci Nanotechnol* 8:3603–3609
173. Pietroiusti A et al (2011) Low doses of pristine and oxidized single-wall carbon nanotubes affect mammalian embryonic development. *Am Chem Soc NANO* 5(6):4624–4633
174. Panessa-Warren BJ, Maybe MM, Warren JB, Crosson KM (2009) Single walled carbon nanotube reactivity and cytotoxicity following extended aqueous exposure. *Environ Pollut* 157:1140–1151
175. Myllynen PK, Loughran MJ, Howard CV, Sormunen R, Walsh AA, Vähäkangas KH (2008) Kinetics of gold nanoparticles in the human placenta. *Reprod Toxicol* 26:130–137
176. Barquera S et al (2015) Global Overview of the epidemiology of atherosclerotic cardiovascular disease. *Arch Med Res* 46:328–338
177. Flora GD, Nayak MK (2019) A brief review of cardiovascular diseases, associated risk factors and current treatment regimes. *Curr Pharmaceut Des* 25:4063–4084
178. Frangogiannis NG (2015) Pathophysiology of myocardial infarction. In: *Comprehensive physiology*. American Cancer Society, pp 1841–1875
179. Karwalajtys T, Kaczorowski J (2010) An integrated approach to preventing cardiovascular disease: community-based approaches, health system initiatives, and public health policy. *Risk Manag Healthc Pol* 3:39–48
180. Foex P (2017) Innovations in management of cardiac disease: drugs, treatment strategies and technology. *Br J Anaesth* 119:23–33
181. Kandaswamy E, Zuo L (2018) Recent advances in treatment of coronary artery disease: role of science and technology. *Int J Mol Sci* 19:424
182. Domenech M, Polo-Corrales L, Ramirez-Vick JE, Freytes DO (2016) Tissue engineering strategies for myocardial regeneration: acellular versus cellular scaffolds? *Tissue Eng B Rev* 22:438–458
183. Martinelli V, Cellot G, Fabbro A, Bosi S, Mestroni L, Ballerini L (2013) Improving cardiac myocytes performance by carbon nanotubes platforms. *Front Physiol* 4:239
184. Lalwani G, D'Agati M, Gopalan A, Rao M, Schneller J, Sitharaman B (2017) Three-dimensional macroporous graphene scaffolds for tissue engineering. *J Biomed Mater Res Part A* 105:73–83
185. Karimi M et al (2016) Nanotechnology in diagnosis and treatment of coronary artery disease. *Nanomedicine* 11:513–530
186. Lee Y, Veerubhotla K, Jeong MH, Lee CH (2020) Deep learning in personalization of cardiovascular stents. *J Cardiovasc Pharmacol Ther* 25:110–120
187. Swierczewska M et al (2012) A facile, one-step nanocarbon functionalization for biomedical applications. *Nano Lett* 12:3613–3620
188. Eltahir HM, Said SS, El-Khordagui LK (2018) Drug delivery for cardiac regeneration. In: *Applications of nanocomposite materials in drug delivery*. Elsevier, pp 283–321
189. Prajnamitra RP, Chen HC, Lin CJ, Chen LL, Hsieh PCH (2019) Nanotechnology approaches in tackling cardiovascular diseases. *Molecules* 24(10):2017. <https://doi.org/10.3390/molecules24102017>
190. Deng Y, Zhang X, Shen H, He Q, Wu Z, Liao W, Yuan M (2020) Application of the nano-drug delivery system in treatment of cardiovascular diseases. *Front Bioeng Biotechnol* 7:489. <https://doi.org/10.3389/fbioe.2019.00489>

191. Tripathi AC, Saraf SA, Saraf SK (2015) Carbon nanotropes: a contemporary paradigm in drug delivery. *Materials* 8:3068–3100
192. Zhang Y, Nayak TR, Hong H, Cai W (2012) Graphene: a versatile nanoplatform for biomedical applications. *Nanoscale* 4:3833–3842
193. Kaya D, Küçükada K, Alemdar N (2019) Modeling the drug release from reduced graphene oxide-reinforced hyaluronic acid/gelatin/poly(ethylene oxide) polymeric films. *Carbohydr Polym* 215:189–197
194. Sarkar G et al (2016) Cross-linked methyl cellulose/graphene oxide rate controlling membranes for in vitro and ex vivo permeation studies of diltiazem hydrochloride. *RSC Adv* 6:36136–36145
195. Deveza L, Choi J, Yang F (2012) Therapeutic angiogenesis for treating cardiovascular diseases. *Theranostics* 2:801–814
196. Rufaihah AJ, Johari NA, Vaibavi SR, Plotkin M, Di Thien DT, Kofidis T, Seliktar D (2017) Dual delivery of VEGF and ANG-1 in ischemic hearts using an injectable hydrogel. *Acta Biomater* 48:58–67
197. Bakirhan NK, Ozcelikay G, Ozkan SA (2018) Recent progress on the sensitive detection of cardiovascular disease markers by electrochemical-based biosensors. *J Pharmaceut Biomed Anal* 159:406–424
198. Gupta S, Sharma A, Verma RS (2020) Polymers in biosensor devices for cardiovascular applications. *Curr Opin Biomed Eng* 13:69–75
199. Shafiee A, Ghadiri E, Kassis J, Pourhabibi ZN, Atala A (2018) Biosensing technologies for medical applications, manufacturing, and regenerative medicine. *Curr Stem Cell Rep* 4:105–115
200. Metkar SK, Girigoswami K (2019) Diagnostic biosensors in medicine- a review. *Biocatal Agric Biotechnol* 17:271–283
201. Bhattarai P, Hameed S (2020) Basics of biosensors and nanobiosensors. In: *Nanobiosensors*. Wiley, pp 1–22. <https://doi.org/10.1002/9783527345137.ch1>
202. Shedden L (2010) 11—Biosensor technology in the treatment of cardiovascular disease. In: Gourlay T, Black RA (eds) *Biomaterials and devices for the circulatory system*. Woodhead Publishing, pp 286–308. <https://doi.org/10.1533/9780857090553.3.286>
203. Rezaee M, Behnam B, Banach M, Sahebkar A (2018) The Yin and Yang of carbon nanomaterials in atherosclerosis. *Biotechnol Adv* 36:2232–2247
204. Negahdary M (2020) Aptamers in nanostructure-based electrochemical biosensors for cardiac biomarkers and cancer biomarkers: a review. *Biosens Bioelectron* 152:112018. <https://doi.org/10.1016/j.bios.2020.112018>
205. Gabriel-Costa G (2018) The pathophysiology of myocardial infarction-induced heart failure. *Pathophysiology* 25:277–284
206. Loh KP, Ho D, Chiu GNC, Leong DT, Pastorin G, Chow EKH (2018) Clinical applications of carbon nanomaterials in diagnostics and therapy. *Adv Mater* 30(47):e1802368. <https://doi.org/10.1002/adma.201802368>
207. Shin SR et al (2013) Carbon-nanotube-embedded hydrogel sheets for engineering cardiac constructs and bioactuators. *ACS Nano* 7(3):2369–2380
208. Wang HB, Dembo M, Wang YL (2000) Substrate flexibility regulates growth and apoptosis of normal but not transformed cells. *Am J Physiol Cell Physiol* 279(5):C1345–C1350
209. Martins AM, Eng G, Caridade SG, Mano JF, Reis RL, Vunjak-Novakovic G (2014) Electrically conductive chitosan/carbon scaffolds for cardiac tissue engineering. *Biomacromol* 15(2):635–643
210. Ahadian S et al (2016) Hybrid hydrogel-aligned carbon nanotube scaffolds to enhance cardiac differentiation of embryoid bodies. *Acta Biomater* 31:134–143
211. Rehman R, Houshyar S, Wang X (2020) Nanodiamond in composite: biomedical application. *J Biomed Mater Res* 108:906–922
212. Tong H, McGee JK, Saxena RK, Kodavanti UP, Devlin RB, Gilmour MI (2009) Influence of acid functionalization on the cardiopulmonary toxicity of carbon nanotubes and carbon black particles in mice. *Toxicol Appl Pharmacol* 239:224–232

213. Hao T, Li J, Yao F, Dong D, Wang Y, Yang B, Wang C (2017) Injectable fullerene/alginate hydrogel for suppression of oxidative stress damage in Brown adipose-derived stem cells and cardiac repair. *ACS Nano* 11:5474–5488
214. Wang C, Li J, Kang M, Huang X, Liu Y, Zhou N, Zhang Z (2021) Nanodiamonds and hydrogen-substituted graphdiyne hetero nanostructure for the sensitive impedimetric aptasensing of myocardial infarction and cardiac troponin I. *Anal Chim Acta* 1141:110–119
215. Firme CP, Bandaru PR (2010) Toxicity issues in the application of carbon nanotubes to biological systems. *Nanomedicine* 6:245–256
216. Zhao X, Liu R (2012) Recent progress and perspectives on the toxicity of carbon nanotubes at organism, organ, cell, and biomacromolecule levels. *Environ Int* 40:244–255
217. Muller J, Huaux F, Moreau N, Misson P, Heiler JF, Delos M, Arras M, Fonseca A, Nagy JB, Lison D (2005) Respiratory toxicity of multi-wall carbon nanotubes. *Toxicol App Pharmacol* 207(3):221–231
218. Salvador-Morales C, Flahaut E, Sim E, Sloan J, Green MLH, Sim RB (2006) Complement activation and protein adsorption by carbon nanotubes. *Mol Immunol* 43:193–201
219. Sharifi S, Behzadi S, Laurent S, Laird Forrest M, Stroeve P, Mahmoudi M (2012) Toxicity of nanomaterials. *Chem Soc Rev* 41:2323–2343. <https://doi.org/10.1039/C1CS15188F>
220. Takagi A et al (2008) Induction of mesothelioma in p53+/- mouse by intraperitoneal application of multi-wall carbon nanotube. *J Toxicol Sci* 33:105–116
221. Miyawaki J, Yudasaka M, Azami T, Kubo Y, Iijima S (2008) Toxicity of single-walled carbon nanohorns. *ACS Nano* 2:213–226
222. Sayes CM, Marchione AA, Reed KL, Warheit DB (2007) Comparative pulmonary toxicity assessments of C60 water suspensions in rats: few differences in fullerene toxicity in vivo in contrast to in vitro profiles. *Nano Lett* 7:2399–2406
223. Sayes CM et al (2004) The differential cytotoxicity of water-soluble fullerenes. *Nano Lett* 4:1881–1887
224. Xia T et al (2006) Comparison of the abilities of ambient and manufactured nanoparticles to induce cellular toxicity according to an oxidative stress paradigm. *Nano Lett* 6:1794–1807
225. Nielsen GD, Roursgaard M, Jensen KA, Poulsen SS, Larsen ST (2008) In vivo biology and toxicology of fullerenes and their derivatives. *Basic Clin Pharmacol Toxicol* 103:197–208
226. Bostan HB, Rezaee R, Valokala MG, Tsarouhas K, Golokhvast K, Tsatsakis AM, Karimi G (2016) Cardiotoxicity of nano-particles. *Life Sci* 165:91–99
227. Duch MC et al (2011) Minimizing oxidation and stable nanoscale dispersion improves the biocompatibility of graphene in the lung. *Nano Lett* 11:5201–5207
228. Chen Z, Yu C, Khan IA, Tang Y, Liu S, Yang M (2020) Toxic effects of different-sized graphene oxide particles on zebrafish embryonic development. *Ecotoxicol Environ Saf* 197:110608. <https://doi.org/10.1016/j.ecoenv.2020.110608>
229. Madani SY, Mandel A, Seifalian AM (2013) A concise review of carbon nanotube's toxicology. *Nano Rev* 4:1. <https://doi.org/10.3402/nano.v4i0.21521>
230. Ema M, Hougaard KS, Kishimoto A, Honda K (2016) Reproductive and developmental toxicity of carbon-based nanomaterials: a literature review. *Nanotoxicology* 10:391–412
231. Snyder-Talkington BN et al (2016) Multiwalled carbon nanotube-induced pulmonary inflammatory and fibrotic responses and genomic changes following aspiration exposure in mice: a 1-year post exposure study. *J Toxicol Environ Health* 79:352–366
232. Harik VM (2017) Geometry of carbon nanotubes and mechanisms of phagocytosis and toxic effects. *Toxicol Lett* 273:69–85
233. Yan A, Lau BW, Weissman BS, Kulaots I, Yang NYC, Kane AB, Hurt RH (2006) Biocompatible, hydrophilic supramolecular carbon nanoparticles for cell delivery. *Adv Mater* 18:2373–2378
234. Huang H, Pierstorff E, Osawa E, Ho D (2007) Active nanodiamond hydrogels for chemotherapeutic delivery. *Nano Lett* 7:3305–3314

# Chapter 31

## Porous Carbon Materials and Their Applications in Biosensing, Medical Diagnostics, and Drug Delivery



Abdelmoneim Mars, Alma Mejri, and Hamza Elfil

### Abbreviations

PCMs	Porous carbon materials
UIPAC	International union of pure and applied chemistry
DNA	Deoxyribonucleic acid
MCF	Mesoporous carbon framework
Go <sub>x</sub>	Glucose oxidase
SPCE	Screen printed carbon electrode
PC	Porous carbon
Pb	Prussian blue
LIG	Laser-induced porous grapheme
TG	Triglyceride
CNFs	Porous carbon nanofibers
AgNPs	Silver nanoparticles
AuNPs	Gold nanoparticles
Lip	Lipase
PGE	Pencil graphite electrode
OMS	Ordered mesoporous carbon
rGO	Reduced graphene oxide
TPS	1.3.6.8 Pyrene tetrasulfonate
OTA	Ochratoxin A
Rct	Charge transfer resistance
MB	Methylene blue
CPE	Carbon paste electrode

---

A. Mars (✉) · A. Mejri · H. Elfil

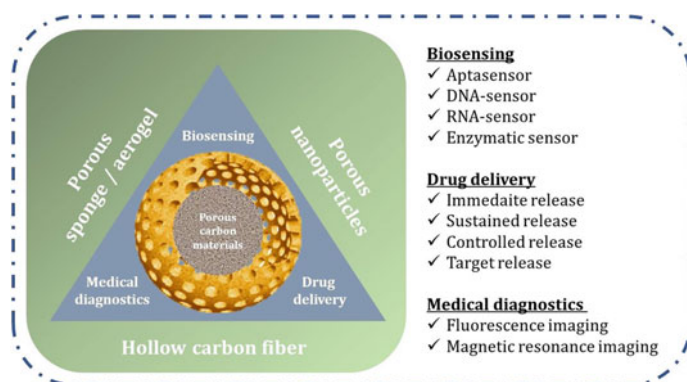
Desalination and Natural Water Valorization Laboratory (LaDVEN), Water Researches and Technologies Center (CERTe), BP 273, 8020 Soliman, Tunisia

e-mail: [abdelmoneim.mars@gmail.com](mailto:abdelmoneim.mars@gmail.com)

Fe <sub>2</sub> O <sub>3</sub> NPs	Iron oxide nanoparticles
RNA	Ribonucleic acid
NPC	Nitrogen doped porous carbon
MOF	Metal–organic framework
MCNs	Mesoporous carbon nanoparticles
MRI	Magnetic resonance imaging
MR	Magnetic resonance
PEG	Polyethylene glycol
MSN	Mesoporous silica nanoparticles
LE%	Loading efficiency %
HMC	Highly ordered mesoporous carbon
FOMC	Fibrous ordered mesoporous carbon
CEL	Celecoxib
CAR	Carvedilol
IDDSs	Immediate drug delivery systems
SDDSs	Sustained drug delivery systems
CDDSs	Controlled drug delivery systems
TDDSs	Targeted drug delivery systems
LOV	Lovastatin
HMCN	Highly mesoporous carbon nanoparticles
DOX	Doxorubicin
VER	Verapamil

## 1 Introduction

Porous carbon materials (PCMs) have emerged as promising materials in various fields, citing industrial activities, environmental monitoring, biomedicine, and biodection [1–4] due to their excellent physicochemical and electronic properties such as good chemical stability, fast electronic response, high surface area, and tightly controlled pore size [5–7]. Structurally, porous carbon materials are solid materials with three different pore sizes (micropores (< 2 nm), mesopores (2–50 nm), and macropores (> 50 nm)) [8]. Interestingly, numerous studies have revealed that the presence of the aforementioned three pore ranges in the same material is unique in that it provides a high specific surface area, good mass transfer, and numerous centers of response for guest molecules provided by macropores, micropores, and mesopores, respectively [9]. It is worth noting that various preparation methods of porous carbon materials were reported in the literature citing template, pyrolysis, hydrothermal carbonization, spray pyrolysis, chemical vapor deposition methods [10, 11]. Moreover, the functionalization of porous carbon materials with heteroatoms has generated enormous interest as it is a powerful means of dramatically improving material properties [12], thus enabling them to offer efficient solutions to global issues, including increasing energy demands, industrial pollution, and health problems. Therefore, the



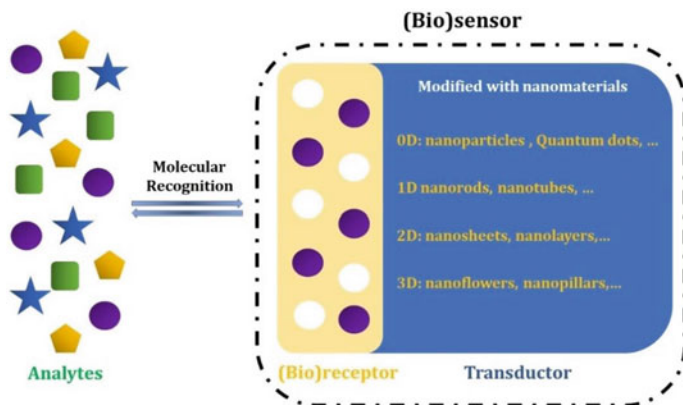
**Fig. 1** Different forms of porous carbon materials and their applications in biosensing, drug delivery, and medical diagnostics

authors emphasize the use of porous carbonaceous materials in their various forms in biosensing, drug delivery, and medical diagnostics (Fig. 1).

## 2 Porous Carbon Materials in Biosensing

The International Union of Pure and Applied Chemistry (UIPAC) has defined the biosensors as analytical sensing devices composed of the transducer and immobilized biomolecules or organisms (e.g., enzymes, DNAs, antibodies, cells, and microorganisms) as sensitive elements (bioreceptors) which can recognize selectively the target of interest [13]. The transducer is responsible for converting the molecular recognition between the bioreceptor and the target analytes into recognizable and measurable analytical signals [14] (Fig. 2).

Currently, there is a lot of interest in developing both invasive and non-invasive biosensors because of the huge promise of a plethora of applications. However, the scarcity of stable and reliable non-invasive biosensors has stymied progress in the field of invasive biosensors. Before proceeding, it is necessary to define the term “invasive biosensors”. Nowadays, numerous commercial biometrics biosensors can be found on the market, such as ACCU-CHEK (Roche Diagnostics, Inc.) and Lactate Scout (Sport Resource Group, Inc.) for glucose monitoring. It is worth highlighting that the aforementioned biosensors are non-invasive, requiring only a small volume of biological fluids, as opposed to invasive biosensors, which usually require laboratory tests of blood or other body fluids. To develop a reliable non-invasive biosensor, special attention should be paid to critical analytic parameters such as limit of detection and specificity, which are two of the most difficult challenges. As far as specificity is concerned, it is considered the most important property of a sensing system because it defines the sensor’s capacity to differentiate between target and non-target entities. Critically, the integration of nanomaterials into the structures of the biosensor



**Fig. 2** Schematic representation of biosensor structures

remarkably improves the analytical performance of the platforms, allowing them to be explored in different applications including healthcare, environmental monitoring, and military security [15]. Among these nanomaterials, porous carbon materials have widely been used to meet these requirements due to their large specific surface area, high loading capacity, controlled nanoscale structures, and high conductivity [16–18]. These unique properties endorse electron transfer reactions between the bioreceptor and the analyte, which tend to increase specific molecular recognition and enhance the detection limit. As a result, more than 13,500 scientific reports were published in 2020 using the words “porous carbon and biosensors”. A large number of them describe the application of porous carbon in the enzymatic electrochemical sensing of glucose [19–21]. In this context, Chen et al. [22] described the use of a mesoporous carbon framework (MCF) decorated with  $\text{Co}_3\text{O}_4$  nanoparticles as nanometric support for the enzyme glucose oxidase (GOx). The hydrothermally prepared  $\text{Co}_3\text{O}_4$ @MCF nanocomposite had a high porosity and a large surface area which allowed efficient immobilization of a large number of enzymes. The drop-coating construction method was adopted to develop the reported biosensor using a glassy carbon electrode as a working electrode. The electrochemical results revealed that the developed porous carbon platform exhibited excellent analytical biosensing performances toward glucose with a limit of detection of  $107.7 \mu\text{M}$ . Similarly, mesoporous carbon-chitosan nanocomposite was used to fabricate an efficient electrochemical biosensor for quantification of glucose in various biological fluids citing human saliva [23]. Indeed, S. Angaiah et al. reported that used mesoporous carbon was prepared via a combination of copolymerization and template methods. In the reported work, sucrose and melamine were used as precursors and calcium carbonate ( $\text{CaCO}_3$ ) as a template. Amperometry results showed that mesoporous carbon-based biosensor revealed good catalytic response toward glucose with a Michaelis–Menten saturation value of  $2.14 \text{ mM}$ . Chen and coworkers [24] proposed the use of porous carbon (PC) and Prussian blue (Pb) nanocomposites to fabricate a sensitive electrochemical enzymatic glucose biosensor. In this work, melamine foam was applied



**Fig. 3** LIG electrode on PI film (125  $\mu\text{m}$  in thickness). Reprinted with permission from reference Park et al. [25]. Copyright 2020 Elsevier

as a precursor synthesis of PC allowing an excellent matrix for efficient loading of the enzyme glucose oxidase (GOx). They demonstrated that the presence of Pb in the porous architecture improved the catalytic activity of the biosensor. Further, the synergistic effect between PC and Pb enhances considerably the sensitivity where it was found to be  $50.63 \mu\text{A} \cdot \text{mM}^{-1} \cdot \text{cm}^{-2}$ . The biosensor exhibits excellent analytical performance, suggesting a potential model for constructing sensing platforms that release or consume oxygen during the recognition process. More interestingly, Park and coworkers [25] have recently developed an ultrasensitive glucose biosensor based on laser-induced porous graphene (LIG) functionalized with platinum nanoparticles (PtNPs) (Fig. 3).

Indeed, they proposed the use of acetic acid treatment to alter the surface of porous graphene. This treatment reduced carbohydrate functional groups which dramatically enhanced the conductivity. Additionally, they demonstrated that this step exhibited a uniform dispersion of Pt nanoparticles on electrode surface. As result developed LIG electrode platform displayed an acceptable analytical performances (sensitivity of  $4.622 \mu\text{A} \cdot \text{mM}^{-1}$ , LOD less than 300 nM, and a wide linear range up to 2.1 mM). The practicability of the biosensor was demonstrated using sweat matrices with acceptable recovery rates. Furthermore, triglyceride (TG) ensures a key role in transporting adipose fat and blood glucose from the liver. It has been shown that a quantity above 200 mg/dL can originate serious illnesses including heart disease, diabetes, hepatic obstruction, nephrosis, and endocrine disorders [26]. So far, various analytical methods have been developed to quantify TG concentrations in biological samples, but electrochemical methods remain the fastest and most sensitive [27]. In this context, Sharma et al. [28] described the development of a highly sensitive sensing platform based on porous carbon nanofibers (CNFs) functionalized with silver nanoparticles (AgNPs) for TG sensing. They justified that the presence of AgNPs considerably increased the conductivity of the electrode and favored the graphitization of CNFs. To detect TG, the authors chose to use the lipase (Lip) and glycerol dehydrogenase bienzymatic system. The substantiated results showed that the sensitivity was four times higher for the electrode modified with Ag@CNF than for the electrode modified with only CNFs. The reported biosensor showed high



selectivity, acceptable reproducibility, and rapid response (less than 10 s). Additionally, porous carbon materials were used to fabricate sensitive DNA or aptamer-based biosensors. In this context, Karimzadeh and collaborators [29] described the fabrication of an electrochemical biosensor for the sensing of EGFR exon 21-point mutation. To develop the sensing platform, the surface of the graphite electrode pencil was modified sequentially by metallopolymetric nanoparticles (NiOTC NPs) and ordered mesoporous carbon functionalized reduced graphene oxide nanocomposite. The immobilization of the ssDNA probe was established by the formation of an amide bond between amine groups at the 5' end of ssDNA and carboxylic groups of the rGO/f-OMC/PGE surface. The results demonstrated that the prepared biosensing platform displayed great analytical performances including a great dynamic concentration range with a low limit of detection (less than 120 nM). As an aptamer-based porous carbon biosensor example, Besharati et al. [30] have recently reported the development of sensitive determination of insulin. The authors proposed the use of a serigraphic carbon electrode decorated with 1,3,6,8-pyrenetetrasulfonate (TPS) modified ordered mesoporous carbon as electrochemical support for insulin aptamer probe. By this method, insulin can be determined within the concentration range of  $10^{-15}$ – $10^{-11}$  molar, with a limit of detection less than 0.18 femtomolar. The evaluation of the applicability of the proposed biosensor was carried out in spiked human serum samples. Therefore, they described that the developed method is highly sensitive, selective, and stable. Moreover, Zhang and coworkers [31] have described the development of an impedimetric aptasensor for the highly sensitive detection of ochratoxin A which poses a serious threat to human health. The authors choose to modify the electrode surface by gold nanoparticles (AuNPs) and carboxylic porous carbon material. They reported that gold nanoparticles and porous carbon were used to amplify the impedimetric signal and improve the loading of the target analyte; respectively. The impedimetric results revealed that the developed biosensor displayed a logarithmic relationship between the concentration of OTA and the variation of charge transfer resistance DRct. The limit of detection was estimated to be 10–8 ng/mL. In another context, the combination of porous carbon materials and magnetic nanomaterials, which improve the performance of electrode materials, has been widely used to develop reliable and robust electrochemical biosensors [32]. For instance, a sensitive electrochemical thrombin aptasensor was developed by Lui's group [33]. The used porous carbonaceous material was synthesized by the carbonization of metal–organic zinc (II) -2-methylimidazole framework. Indeed, they used magnetic nanoparticles to immobilize the aptamer probe functionalized with methylene blue (MB) and to easily separate the MB released after the detection step. Consequently, the formation of the aptamer-thrombin complex induces the release of methylene blue which causes a proportional increase in the electrochemical signal MB to the concentration of thrombin detected after analysis of the supernatant solution. The authors summarized the analytical performance of the biosensor as follows: low limit of detection of 0.8 femtomolar, wide dynamic range from 10 femtomolar to 100 nM, good recovery rate from 98.1% to 99.4% with a deviation of relative type of 3.9%. More interestingly, a sensitive bienzymatic biosensor for the sensing of H<sub>2</sub>O<sub>2</sub> and paraoxon was developed by Huang and coworkers [34]. The described platform was based on

the functionalization of carbon paste electrodes (CPE) with porous carbon decorated with  $\text{Fe}_2\text{O}_3$  nanoparticles. The used porous carbon-based nanocomposite ( $\text{Fe}_2\text{O}_3@C$ ) was prepared by the annealing of Fe-1,3,5-benzenetricarboxylate metal–organic framework. In this work, the authors choose to conjugate the modified surface  $\text{Fe}_2\text{O}_3@C/CPE$  by two different probes. To sense hydrogen peroxide, the modified electrode surface was conjugated, consecutively, with ionic liquid and myohemoglobin enzyme. Concerning  $\text{H}_2\text{O}_2$  detection, the modified electrode surface was functionalized with Nafion and acetylcholinesterase enzyme. The research showed that  $\text{Fe}_2\text{O}_3@C$  was a viable material for electrode surface modification and the fabrication of several biosensors for the sensitive detection of target analytes other than  $\text{H}_2\text{O}_2$  and paraoxon. Regarding fluorometric biosensors based on porous carbon materials, enormous studies have revealed that metal–organic frameworks are one of the efficient optical quenchers for DNA/RNA sensing [35]. However, the application of these quenchers is very limited due to their weak structural stability. To overcome this issue, many groups of researchers doped the porous carbon materials with nitrogen to develop stable platforms of biosensors [36]. In this context, Duan et al. [37] reported the preparation of a stable nitrogen-doped porous carbon (NPC) using MOFs as precursors. This porous material was applied to fabricate a sensitive system for the fluorescence quantification of Zika virus RNA. Before sensing step, the presence of MOFs-based N doped porous carbon quenches the fluorescence signal by forming probe-DNA@NPC complex. Nonetheless, the DNA probe could be freed from NPC by the establishment of a double-stranded hybrid upon the addition of the complementary target Zika RNA inducing a fluorescence recovery. The report describes that the proposed method assay has a low limit of detection of 0.23 nM. Recently in 2020, Liu's group [38] has fabricated a fluorometric biosensing system using porous carbon which was prepared by the calcination of *Enteromorpha prolifera*. The authors discovered that the resulting porous carbon materials had unique enzymatic properties, such as oxidase and peroxidase-like activities. The platform was successfully applied to detect hydrogen peroxide, glucose, and acid phosphatase with limits of detection of 0.017  $\mu\text{M}$ , 30  $\mu\text{M}$ , and 0.1 U/L, respectively. Additionally, they demonstrated that bi-enzyme mimics porous carbon material induced high reproducibility and stability (Table 1).

### 3 Porous Carbon Materials in Medical Diagnosis

Nowadays, medical diagnostic techniques have rapidly developed and become one of the most important areas of modern medicine. In this regard, many researchers have relied on the use of porous materials to ensure the efficiency of the diagnostic agent [56, 57]. Among these porous materials, porous carbon nanoparticles have been widely used as theragnostic agents in early diagnosis and real-time monitoring of cancers in vivo [58]. Recently, MCNs have been integrated with fluorescence, magnetic resonance imaging, and photoacoustic imaging owing to their excellent biocompatibility, controlled pore size, and high surface-to-volume ratio.

**Table 1** Selected applications of porous carbon-based electrochemical biosensors reported in literature

Platform	Analyte	method	Detection limit ( $\mu\text{M}$ )	Linear range ( $\mu\text{M}$ )	References
3D-PC/Ni <sub>0.05</sub> NPs/GCE	Glucose	CV	4.8	15–6450	[39]
HAC/NiO nanocomposite/GCE	Glucose	CV	0.055	5–4793	[40]
GOD/3D-CVS electrode	Glucose	CV	0.19	0.58–16,000	[41]
NPC/SPCE	Glucose	CV	30	50–1500	[42]
Co <sub>7</sub> Fe <sub>3</sub> /NPC/GCE	Glucose	CV	1	1–14,000	[43]
CoS@PC/GCE	Glucose	CV	2	10–960	[44]
Cu nanospheres@PC electrode	Glucose	CV	4.8	15–5620	[45]
CoMoO <sub>4</sub> /MPC/GCE	Glucose	CV	0.13	75–725	[46]
PCMS/GCE	Dopamine	DPV	0.45 $0.10^{-3}$	$10^{-3}$ –0.1	[47]
	Uric acid	DPV	6 $0.10^{-3}$	0.01–3000	
NPCNPs/GCE	Ascorbic acid	DPV	0.74	$8.10^4$ – $2.10^6$	[48]
	Dopamine	DPV	0.011	$0.5.10^3$ – $30.10^3$	
	Uric acid	DPV	0.021	$4.10^3$ – $50.10^3$	
3D-PC electrode	Dopamine	DPV	0.1	0.8–400	[49]
3D-N,P-PC electrode	Dopamine	DPV	0.6	2–200	[50]
Fe <sub>2</sub> O <sub>3</sub> NPS/PC aerogels/GCE	Dopamine	DPV	0.109	5–500	[51]
N,Co-PC NPs/GCE	Dopamine	DPV	0.34	2–69.5	[52]
	Uric acid	DPV	0.98	5–192	
Mercapto-MP-C-CPE	Omeprazole	DPV	$4 \cdot 10^{-5}$	$0.25.10^{-3}$ –25	[53]
Nafion/OMC/GPE	Epinephrine	CV	7	20–4000	[54]
OMC/GCE	Glutathione	CV	0.09	–	[55]
	Cysteine	CV	0.5	3–130	

3D-CVS (3D) porous cane vine (wisteria) stem-derived carbon; DPV differential pulse voltammetry; CPE carbon paste electrode; GCE glassy carbon electrode; GOD glucose oxidase; HAC Heteroatom-enriched porous carbon; mercapto-MP-C-CPE mercapto-mesoporous carbon; MPC mesoporous carbon; NPs nanoparticles; OMC ordered mesoporous carbon; PC porous carbon; PCMS porous carbon nanocubes accumulated microspheres; SPCE screen-printed electrode; CV cyclic voltammetry

### 3.1 Fluorescence Imaging

Many studies have exploited the supramolecular  $\pi$ – $\pi$  stacking interactions of MCNs to develop MCNs-based fluorescence medical diagnostic agents. Indeed, this type of interaction can control the quenching of fluorescence of the MCNs based on

functionalized or loaded molecules. Recently, Li et al. [59] have reported the modulation of oxidized MCNs with Cy3-labeled ssDNA probe (P0-Cy3) to develop a fluorescence imaging agent for breast and prostate cancer tissues. They described that grafting Po-Cy3 via  $\pi$ - $\pi$  stacking supramolecular interaction on the surface of oxidized MCNs quenches the probe's fluorescence signal. Meanwhile, the formation of the complex Po-Cy3-mucin1 protein (cell-surface marker) leads to dissociation between MCNs and Po-Cy3 probe resulting in the restoration of fluorescence signal. Further, they described that the "turn-ON" feature of MCNs-based imaging agent not only can be used to sense tumor cells in fluid but also to localize cancer tumor cells with high specificity. Therefore, the authors suggested that these advanced oxidative MCNs nanocomposites could enhance cancer diagnosis by multiple detection and imaging, along with the intrinsic multifunctionality of MCNs such as drug delivery and photothermal converter for cancer photothermal therapy. More interestingly, fluorescent MCNs were developed by Kong et al. [60] for bioimaging. Indeed, they described an easy method of preparing upconverting multicolored photoluminescent mesoporous carbon nanoparticles (MCNs) using citric acid as a carbon precursor in 1-octadecane without the need of a surfactant. They reported that the developed nanocomposites are endowed with high stability of multicolor photoluminescence and upconversion with high quantum efficiency of *approx.* 37%. The results demonstrated that MCNs can effectively recognize cancerous cells when exposed to excitations ranging from ultraviolet to near-infrared.

### 3.2 Magnetic Resonance Imaging

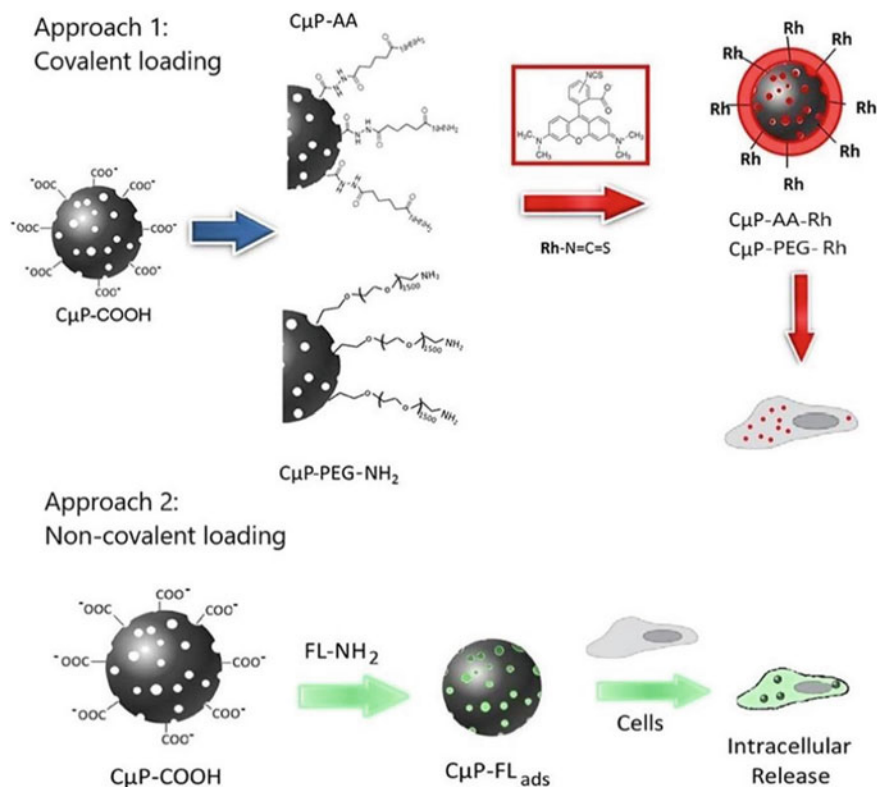
Currently, magnetic resonance imaging (MRI) is now a required tool for obtaining information with greater resolution in a non-invasive manner [57, 61]. Many groups of researchers have proposed the integration of various types of nanomaterials to improve the efficiency of the magnetic resonance imaging technique. Among these nanomaterials, porous carbonaceous nanoparticles have been largely used. Recently, Zhang and coworkers [62] have developed ordered MCNs incorporated with  $\gamma$ - $\text{Fe}_2\text{O}_3$  and  $\text{GdPO}_4$  nanoparticles. They reported that prepared nanocomposites were used for dual-mode magnetic resonance imaging *in vitro*, with relaxivity values  $r_1$  and  $r_2$  of 2.7 and  $183.7 \text{ mM}^{-1} \cdot \text{s}^{-1}$ , respectively, demonstrating a satisfying T1- and T2-weighted MR imaging effect. Furthermore, manganese oxide nanoparticles embedded in hollow MCNs were recently used as MRI agents by Zhang et al. [63]. The results showed an exceptional disease-triggered MRI performance where a 52.5-fold increase of longitudinal relaxivity ( $r_1 = 10.5 \text{ mM}^{-1} \text{ s}^{-1}$ ) and on nude mice 4T1 xenograft were observed. The authors hypothesized that developed MCNs could pave the way for new methods for developing sophisticated nanofamilies for cancer therapy.

Moreover, Wu and colleagues [64] proposed the coating of porous carbon nanomaterials modified with hyaluronic acid with  $\text{Fe}_3\text{O}_4$  nanoparticles and their simultaneous use as a guided magnetic resonance imaging agent and drug delivery system.

In this work, magnetite and hyaluronic acid were used as a fluorescent agent for IRM and as a target tumor guide, respectively.

## 4 Porous Carbon Materials in Drug Delivery

Currently, the advances in nanotechnologies and pharmaceutical researches have led to a great improvement in pharmacological and therapeutic proprieties of administered drugs notably in drug delivery systems [65]. These systems must have a nanometric size, i.e., in the range of 1–100 nm, to be able to penetrate through biological and physiological barriers. In this regard, porous materials, especially mesoporous particles with pore sizes between 2 and 50 nm, are in high demand in this application because they have a maximum surface area to volume ratio than bare particles, which makes them a good agent for loading cargo [66]. As a consequence, efforts have been made to create novel porous carbon materials (PCMs) with required properties and functions. Generally, PCMs are prepared by pyrolysis procedure using various carbon sources including bio-masses and green wastes-based cellulose and lignin. Several studies have shown that nanoarchitecture of PCMs is directly influenced by preparation methods or carbon sources, thus enhancing therapeutic effectiveness of PCMs in drug delivery systems. Recently, a new generation of mesoporous carbonaceous materials has been incorporated into drug delivery systems and generated great interest due to their exceptional active surface area, excellent biocompatibility, high drug loading capacity. Drugs, tunable pore structure, and easy functionalization improving release control and facilitating targeting of drug delivery by reducing side effects [67]. Owing to these exceptional merits, mesoporous carbon nanoparticles (MCNs) have evolved widely as effective carriers in the fields of drug delivery, including various systems (immediate, extended, controlled, and targeted drug delivery systems) [68]. Before describing these categories, it should be emphasized that the preparation of MCNs is generally carried out by hydrothermal or calcination processes at specific temperatures. The obtained MCNs are therefore hydrophobic because most of the oxygenated groups are lost during the preparation step under the effect of the very high temperature. Since the hydrophilicity of pharmaceutical vehicles is an important characteristic, MCNs must regain their hydrophilicity [69]. Thus, many studies have proposed the modification of the surface of MCNs either by oxidation or by the addition of hydrophilic groups. Oxidized MCNs could be further functionalized using a large multipurpose bio(molecule) library for a variety of uses including PEGylation, grafting, polymer coating, and stimuli-responsive [70, 71]. Moreover, Quinn et al. [72] have recently demonstrated the ability of porous carbon microparticles to carry fluorescein dye into normal (HEK 293) cell line as a low solubility material (Fig. 4).



#### 4.1 Immediate Release Drug Delivery Systems

Considered the most convenient route of drug administration, oral delivery has gained attention owing to its efficiency and reduced risk of infection. However, numerous drugs are hydrophobic compounds with limited application due to their low solubility and bioavailability in the gastrointestinal tract [73]. Nowadays, mesoporous carbon nanoparticles are presented as an effective carrier for delivering poorly soluble drugs and for meeting clinical needs [74]. Recently, Shi et al. [75] reported an important comparative study between the drug delivery performance of mesoporous carbon nanoparticles and mesoporous silica nanoparticles (MSN) which is regarded as one of the most commonly used drug delivery systems using camptothecin as drug model. The results revealed that by MCNs, the drug loading efficiency (LE%) of camptothecin was 17% higher than that achieved by MSN. They explained that the increase in the percentage of LE is related to the presence of aromatic rings of MCN which is considered a compatible environment for camptothecin. Furthermore, the response of simvastatin loading efficiency to particle sizes was studied by

Zhang et al. [76] utilizing three distinct kinds of highly ordered mesoporous carbon matrices (HMCs) with varying morphologies (including hexagonal, spherical, and fibrous) and particle sizes (700 nm, 400–900 nm, and 1–4  $\mu\text{m}$ ). The results showed that the dissolution rate of the drug simvastatin released by the spherical monodisperse HMCs was considerably faster than that obtained with the other forms. Moreover, the effect of pore size has been studied by Zhao et al. [77] using fibrous ordered mesoporous carbon (FOMC) and celecoxib (CEL) as drug delivery system and model drug, respectively. CEL is an insoluble drug and designed to be administered orally. The results showed that increasing the pore size from 4.4 nm to 7 nm accelerated the dissolution rate of CEL. Therefore, the high active surface area and high porosity of MCNs allow the encapsulation of drugs with excellent cargo rate. More interestingly, numerous studies have demonstrated that carboxylation of MCNs improves remarkably the hydrophilicity of hydrophobic drugs which improves their bioavailability after administration. For instance, Zhang et al. [78] used CAR as poorly water-soluble drug to investigate the results of the carboxylation of MCNs on the loading capacity and the bioavailability of the drug. The findings showed that a relative bioavailability of studied drug was enhanced by  $179.28 \pm 20.5\%$  in comparison with the commercial product drug. Furthermore,  $\text{Eu}^{3+}/\text{Gd}^{3+}$ -EDTA co-doped carboxylated hollow mesoporous carbon (HMC) was prepared by Liu and coworkers [79]. The studied carrier was intended to enhance the pharmacokinetic properties of poorly soluble drugs while tracing their *in vivo* administration process. The results showed that the carboxylation of hollow MCNs and the co-doping with europium and gadolinium ions enhance dramatically the bioavailability of used CAR drug in the gastrointestinal tract.

## 4.2 Sustained Release Drug Delivery Systems

Since the release of drugs from immediate drug delivery systems (IDDSs) is uncontrollable and immediate, many research groups have engaged in the fabrication of more controlled drug delivery systems such as sustained drug delivery systems (SDDSs). These can reduce the frequency of drug administration by gradually delivering the encapsulated compounds through an extended period. Generally, the release of drugs by sustained drug delivery system is controlled by three main mechanisms including pore structure and channel length, interaction force between MCNs and loaded drug, and diffusion hindrance effect.

### 4.2.1 Pore Structure and Channel Length

As demonstrated for immediate drug delivery systems (IDDSs), the morphology and pore size of the carrier directly influence the loading efficiency of the developed system. It was proven that SDDS should be produced with an interconnected porous structure and a low pore volume. Recently, Zhao and collaborators [80] have proved

the effect of the morphology of MCNs on the release rate of lovastatin (LOV) drugs. The researchers discovered that when two-dimensional nanoparticles and a longer channel length were used, the rate of LOV delivery was correspondingly slower than when three-dimensional nanoparticles and a shorter channel length were used. In this context, the hollow mesoporous carbon nanoparticles (HMCNs) have been widely used to develop SDDSs owing to their hollow cavity.

#### 4.2.2 Interaction Force

Numerous reports have investigated the influence of the strong force of interaction between MCNs and the loaded drug in delaying the rate of drug release. The MCNs-based carbonaceous framework was shown to exhibit supramolecular  $\pi$ - $\pi$  stacking interactions with aromatic drug molecules which provoked prolonged delivery [79]. Furthermore, a 90 nm diameter MCN-based carrier was used as a transmembrane delivery system for the doxorubicin drug (DOX). The authors reported that a high carrying capacity of DOX has been demonstrated, and this is due to established  $\pi$ - $\pi$  supramolecular stacking interactions between DOX and MCNs. In addition, the sustained release was observed under acidic solutions and physiological pH. As an application, Bai et al. [81] explored the dependence profile of DOX release versus pH to sustained release of DOX as a tumor-specific drug-using MCN carrier. It should be emphasized that HMCNs were also been used for the sustained release of DOX for chemo-photothermal therapy.

#### 4.2.3 Diffusion Hindrance Effect

The diffusion hindrance by grafting polymers on MCNs is considered to be a method of sustained release of the drugs most used in this profile. Indeed, grafted polymers have a direct effect on the interactions between delivered drugs and functionalized carriers by increasing the diffusion distance. In this regard, poly dimethyl diallyl ammonium (PDDA) capped mesoporous carbon nanoparticles (CMK-5) nanocomposite was used by Zhang et al. [82] to deliver nimodipine, carvedilol, and fenofibrate as water-insoluble drugs. The results showed that the release rates of the three drugs using PDDA-coated MCNs were significantly delayed compared to those achieved by carboxylated MCNs. The release using carboxylated MCNs was rapid and cumulative reaching 80% within 1 h, while it was delayed for 12 h with PDDA@MCNs. Alternatively, lipids have also been applied as a delivery delay where recently Zhang and coworkers [83] described the application of lipid bilayer modified mesoporous carbon nanocomposites as a delivery agent for nimodipine. The results showed that the presence of lipids in MCNs exhibited prolonged drug discharge into the simulated intestinal fluid. As a result, the bioavailability of nimodipine was dramatically improved, and lasting plasma drug levels were longer compared to commercial IDDS.

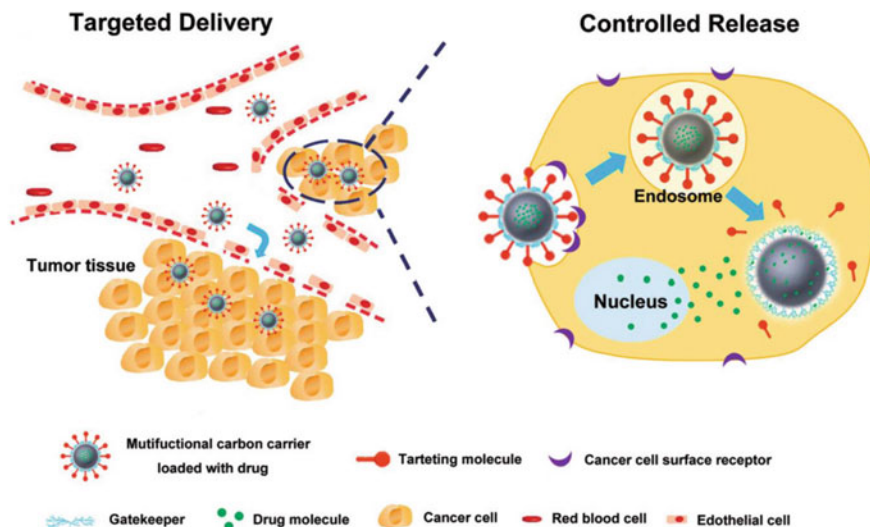


### 4.3 *Controlled Drug Delivery Systems*

Recently, controlled drug delivery systems (CDDSs) have gained the attention of several research groups because of the unique characteristics they can provide. This is because these systems prevent the premature release of the drug causing drug losses and side effects. The CDDS mechanism relies on the integration of gatekeepers or guardians at the carrier pores' entry via both covalent bonds or physical adsorptions. Essentially, the role of these gatekeepers is to restrict drug molecules from escaping carriers unless they are presented with new stimuli (pH, redox potential, enzymes, temperature, etc.). Various gatekeepers have been used to develop CDDSs patterns including carbon dots, zinc oxide quantum dots, manganese oxide, poly (N-isopropyl acrylamide), etc. [84–87]. Regarding stimuli response drug delivery systems, pH-responsive CDDSs were the most extensively employed stimuli in controlled drug delivery systems owing to presented pH variations between normal and sick tissues and between the cytoplasm and intracellular compartments [88–90]. For instance, ZnO quantum dots gated MCNs carriers were employed to achieve Rh6G drug release that was regulated by stimuli. Huang et al. [91] proposed the use of functional ZnO quantum dots (QDs) with *N*-(3-Trimethoxysilylpropyl) ethylenediamine triacetate as gatekeepers. The findings revealed that controlled drug release may be obtained by either decreasing the pH to the tumor cells' acidic microenvironment or heating. Therefore, the cumulative effects of pH and temperature may significantly increase the rate of Rh6G release from MCNs at the tumor site. Furthermore, many reports described the exploitation of temperature as a stimulus in CDDSs profile. In this context, poly(N-isopropyl acrylamide) (PNIPAM) was widely used as a thermo-responsive polymer. Recently, Zhu et al. [92] reported the use of modified ordered PNIPAM modified MCNs (CMK-3) as CDDS. They demonstrated that in aqueous media and below 25 °C, PNIPAM establishes hydrogen bonds with water leading to polymer bonding stretching and triggering of CMK-PNIPAM channels that prevents the discharge of the drug. Nonetheless, the breakage of hydrogen bonds produced between the PNIPAM and water could be induced by the monitor of the temperature of the CMK-PNIPAM environmental medium. At a temperature of 25 °C, the polymer bonds would break, which would keep the CMK-PNIPAM gates open and suitable for drug release.

### 4.4 *Targeted Drug Delivery Systems*

Generally, the administration of traditional chemotherapy medication is assisted by a loss of specificity limiting their therapeutic efficacy, inducing side effects, and causing multidrug resistance [93–96]. Recently, targeted drug delivery systems (TDDSs) have emerged as an effective solution to overcome these restrictions [97] (Fig. 5).



**Fig. 5** Illustration of difference between controlled and targeted drug delivery system based on MCNs for the in vivo process [97]

In particular, TDDSs have the potential to significantly decrease the need for significant concentrations of compounds and can harm to healthy cells and tissues. Within the last decades, mesoporous nanoparticles have been extensively applied in the development of TDDSs. Furthermore, mesoporous carbon nanoparticles are considered to be an ideal reservoir for drug delivery that could protect payload drugs from degradation during delivery. To meet the needs of TDDSs, Wan and coworkers [98] have proposed the use of uniform MCNs functionalized with fluorescein isothiocyanate (FITC) and folic acid (FA) to selectively deliver paclitaxel drug. They reported that in vivo delivery results revealed that developed carriers-based MCNs could target the FA-positive tumors. Further, they also showed that the proposed TDDSs released paclitaxel in a non-cytotoxic and regulated manner within cells. Compared with conventional paclitaxel formulations, the reported MCNs-based system showed a superior antitumor effect where the tumor growth inhibition rate was 86.53% in comparison with the control group (saline). Furthermore, folic acid functionalized uniform MCNs were used by the same group as TDDSs to enhance the oral absorption of paclitaxel medication. In fact, Wan et al. [99] described that developed carrier enhanced cellular uptake of selected drug and this because of the presence of folic acid, considered as a selective receptor to Caco-2 cells which was used as in vitro model. The results revealed that permeability across Caco-2 cell monolayers was increased by 5.37-fold compared to commercial Taxol. Moreover, in vivo results demonstrated that designed carriers decrease the gastrointestinal toxicity of paclitaxel.

More interestingly, special interest was devoted to the development of dual controlled-targeted drug delivery systems which could transport payload medicine

directly to the target region and discharge it in a controlled manner. For instance, a hyaluronic acid conjugated uniform MCNs were used by Wan et al. [100] as targeted enzyme responsive drug delivery. The presence of hyaluronic acid ensured the encapsulation of the drug into the carriers and increased the MCNs stability, biocompatibility, the ability of cell-targeting, and the control of the cargo release. The findings showed that the newly designed carrier might target cancer cells that overexpress CD44 receptors. In the tumor microenvironment, the authors revealed that developed MCNs-based delivery agent, loaded with doxorubicin (DOX) and verapamil (VER), provoked a dual pH and hyaluronidase-1 responsive release. Moreover, Zhou et al. [101] described the development of a novel multifunctional nanoplatfrom based on MCNs decorated with hyaluronic acid for dual response drug delivery and combinatorial chemo-photothermal therapy. It is worth noting that hyaluronic acid offers a drug delivery method with exceptional targeting capability for cancer cells. Thus, the MCNs-based multifunctional nanoplatfrom has an effective therapeutic efficacy vis-à-vis the target cells.

## 5 Conclusion

The present chapter summarizes the recent advances in porous carbonaceous materials (PCM) in bioscience fields citing biosensing, medical diagnosis, and drug delivery. Indeed, they have exceptional properties including a high active area and a controlled diffusion rate allowing them to be one of the most attractive materials. In biosensing, PCM is considered the key to obtaining robust, miniaturized, and portable biosensing devices due to their merits citing high robustness, high load capacities, and high electrocatalytic activities. Furthermore, due to their customizable pore size, huge channel volume, and simplicity of surface functionalization, PCM has been widely applied in drug delivery. For medical diagnostics, PCM provides an effective intervention without side effects. Despite the extensive applications of PCMs in *in vivo* applications, research on the consequences of their exposure on human health is restricted, and the human body's side effects are unknown. It is worth noting that various factors have been documented to influence MCP cytotoxicity, including size and concentration, shape, and surface modification, which is also a typical concern for MCPs in bioscience.

## References

1. Chaikittisilp W, Ariga K, Yamauchi Y (2013) A new family of carbon materials: synthesis of MOF-derived nanoporous carbons and their promising applications. *J Mater Chem A* 1:14–19
2. Sattayasamitsathit S, Mahony AMO, Xiao XY, Brozik SM, Washburn CM, Wheeler DR, Cha J, Burckel DB, Polsky R, Wang J, Wheeler DR, Cha J, Burckel DB, Polsky R, Wang J (2011) Highly dispersed Pt nanoparticle-modified 3D porous carbon: a metallized carbon electrode material. *Electrochem Commun* 13:856–860

3. Tripathi NK (2018) Porous carbon spheres: recent developments and applications. *AIMS Mater Sci* 5:1016–1052
4. Xu M, Yu Q, Liu Z, Lv J, Lian S, Hu B, Mai L, Zhou L (2018) Tailoring porous carbon spheres for supercapacitors. *Nanoscale* 10:21604–21616
5. Torad NL, Hu M, Ishihara S, Sukegawa H, Belik AA, Imura M, Ariga K, Sakka Y, Yamauchi Y (2014) Direct synthesis of MOF-Derived nanoporous carbon with magnetic Co nanoparticles toward efficient water treatment. *Small* 10:2096–2107
6. Yang SJ, Kim T, Im JH, Kim YS, Lee K, Jung H, Park CR (2012) MOF-derived hierarchically porous carbon with exceptional porosity and hydrogen storage capacity. *Chem Mater* 24:464–470
7. Xiao LL, Xu HB, Zhou SH, Song T, Wang HH, Li SZ, Gan W, Yuan QH (2014) Simultaneous detection of Cd(II) and Pb(II) by differential pulse anodic stripping voltammetry at a nitrogen-doped microporous carbon/Nafion/bismuth-film electrode. *Electrochim Acta* 143:143–151
8. Dutta S, Bhaumik A, Wu KCW (2014) Hierarchically porous carbon derived from polymers and biomass: effect of interconnected pores on energy applications. *Energy Environ Sci* 7:3574–3592
9. Fang B, Kim JH, Kim MS, Yu JS (2013) Hierarchical nanostructured carbons with meso-macroporosity: design, characterization, and applications. *Acc Chem Res* 46(7):1397–1406
10. De S, Mariana Balu A, Waal JCVD, Luque R (2015) Biomass-derived porous carbon materials: synthesis and catalytic applications. *Chem Cat Chem* 1–23
11. Lee J, Kim J, Hyeon T (2006) Recent progress in the synthesis of porous carbon materials. *Adv Mater* 18:2073–2094
12. Qie L, Chen W, Xu H, Xiong X, Jiang Y, Zou F, Hu X, Xin Y, Zhang Z, Huang Y (2013) Synthesis of functionalized 3D hierarchical porous carbon for high-performance supercapacitors. *Energy Environ Sci* 6:2497–2504
13. Thevenot DR, Tóth K, Durst RA, Wilson GS (1999) Electrochemical biosensors: recommended definitions and classification. *Pure Appl Chem* 71(12):2333–2348
14. Ronkainen NJ, Brian Halsall H, Heineman WR (2010) Electrochemical biosensors. *Chem Soc Rev* 39:1747–1763
15. Maduraiveerana G, Jin W (2017) Nanomaterials based electrochemical sensor and biosensor platforms for environmental applications. *Trends Environ Anal Chem* 13:10–23
16. Wu HL, Tang QL, Fan HN, Liu Z, Hu AP, Zhang SY, Deng WN, Chen XH (2017) Dual-confined and hierarchical-porous graphene/C/SiO<sub>2</sub> hollow microspheres through spray drying approach for lithium-sulfur batteries. *Electrochim Acta* 255:79–186
17. Yang T, Zhong Y, Liang J, Rahman MM, Lei W, Chen Y, Monteiro MJ, Shao Z, Liu J (2017) Hierarchical porous yolk-shell carbon nanosphere for highperformance lithium-sulfur batteries. *Part Part Syst Char* 34:1600281
18. Bu YK, Wu J, Zhao XT, Ding K, Liu Q, Huang YY, Lv JQ, Wang YB (2016) Sandwich-type porous carbon/sulfur/polyaniline composite as cathode material for high performance lithium-sulfur batteries. *RSC Adv* 6:104591–104596
19. Rernglit W, Teanphonkrang S, Suginta W, Schulte A (2019) Amperometric enzymatic sensing of glucose using porous carbon nanotube films soaked with glucose oxidase. *Microchim Acta* 186:616
20. Quintero-Jaime AF, Quilez-Bermejo J, Cazorla-Amoros D, Morallon E (2021) Metal free electrochemical glucose biosensor based on N-doped porous carbon material. *Electrochim Acta* 367:137434
21. Madhu R, Veeramani V, Chen SM, Manikandan A, Lo AY, Chueh YL (2015) Honeycomb-like porous carbon-cobalt oxide nanocomposite for high-performance enzymeless glucose sensor and supercapacitor applications. *ACS Appl Mater Interfaces* 7(29):15812–15820
22. Dhanjai BP, Sinha A, Wu L, Lu X, Tan D, Chen J (2019) Co<sub>3</sub>O<sub>4</sub> nanoparticles supported mesoporous carbon framework interface for glucose biosensing. *Talanta* 203:112–121
23. Barathi P, Thirumalraj B, Chen SM, Angaiah S (2019) A simple and flexible enzymatic glucose biosensor using chitosan entrapped mesoporous carbon nanocomposite. *Microchem J* 147:848–856

24. Thakur B, Guo X, Chang J, Kron M, Chen J (2017) Porous carbon and Prussian blue composite: a highly sensitive electrochemical platform for glucose biosensing. *Sens Bio-Sens Res* 14:47–53
25. Yoon H, Nah J, Kim H, Ko S, Sharifuzzaman M, Chandra Barman S, Xuan X, Kim J, Park JY (2020) A chemically modified laser-induced porous graphene based flexible and ultrasensitive electrochemical biosensor for sweat glucose detection. *Sensor Actuat B Chem* 311:127866
26. Alves-Bezerra M, Cohen DE (2017) Triglyceride metabolism in the liver. *Compr Physiol* 8(1):1–8
27. Wang J, Huang X, Tang SY, Ming Shi G, Ma X, Guo J (2019) Blood triglyceride monitoring with smartphone as electrochemical analyzer for cardiovascular disease prevention. *IEEE J Biomed Health* 23(1):66–71
28. Mondal K, Ali MA, Singh C, Sumana G, Malhotra BD, Sharma A (2017) Highly sensitive porous carbon and metal/carbon conducting nanofiber based enzymatic biosensors for triglyceride detection. *Sensor Actuator B-Chem* 246:202–214
29. Shoja Y, Kermanpur A, Karimzadeh F (2018) Diagnosis of EGFR exon21 L858R point mutation as lung cancer biomarker by electrochemical DNA biosensor based on reduced graphene oxide/functionalized ordered mesoporous carbon/Ni-oxytetracycline metal-polymer nanoparticles modified pencil graphite electrode. *Biosens Bioelectron* 113:108–115
30. Tabrizi MA, Shamsipur M, Saber R, Sarkar S, Besharati M (2018) An electrochemical aptamer-based assay for femtomolar determination of insulin using a screen printed electrode modified with mesoporous carbon and 1,3,6,8-pyrenetetrasulfonate. *Microchim Acta* 185:59
31. Wei M, Zhang W (2017) A novel impedimetric aptasensor based on AuNPs—carboxylic porous carbon for the ultrasensitive detection of ochratoxin A. *RSC Adv* 7:28655–28660
32. Li S, Wang L, Zhang X, Chai H, Huang Y (2018) A Co, N co-doped hierarchically porous carbon hybrid as a highly efficient oxidase mimetic for glutathione detection. *Sensor Actuator B-Chem* 264:312–319
33. Ren Q, Xu X, Cao G, Xia J, Wang Z, Liu Q (2019) Electrochemical thrombin aptasensor based on using magnetic nanoparticles and porous carbon prepared by carbonization of a zinc(II)-2-methylimidazole metal-organic framework. *Microchim Acta* 186:659
34. Wei W, Dong S, Huang G, Xie Q, Huang T (2018) MOF-derived Fe<sub>2</sub>O<sub>3</sub> nanoparticle embedded in porous carbon as electrode materials for two enzyme-based biosensors. *Sensor Actuator B-Chem* 260:189–197
35. Tan H, Tang G, Wang Z, Li Q, Gao J, Wu S (2016) Magnetic porous carbon nanocomposites derived from metal-organic frameworks as a sensing platform for DNA fluorescent detection. *Anal Chim Acta* 940:136–142
36. Yang R, Yan X, Li Y, Zhang X, Chen J (2017) Nitrogen-doped porous carbon-ZnO nanopolyhedra derived from ZIF-8: new materials for photoelectrochemical biosensors. *ACS Appl Mater Interfaces* 9:42482–42491
37. Li J, Yang K, Wu Z, Li X, Duan Q (2019) Nitrogen-doped porous carbon-based fluorescence sensor for the detection of ZIKV RNA sequences: fluorescence image analysis. *Talanta* 205:120091
38. Ren H, Liu X, Yan L, Cai Y, Liu C, Zeng L, Liu A (2020) Ocean green tide derived hierarchical porous carbon with bi-enzyme mimic activities and their application for sensitive colorimetric and fluorescent biosensing. *Sensor Actuator B Chem* 312:127979
39. Wang L, Zhang Y, Yu J, He J, Yang H, Ye Y, Song Y (2017) A green and simple strategy to prepare graphene foam-like three-dimensional porous carbon/Ni nanoparticles for glucose sensing. *Sensor Actuat B Chem* 239:172–179
40. Veeramani V, Madhu R, Chen SM, Veerakumar P, Hung CT, Liu SB (2015) Heteroatom-enriched porous carbon/nickel oxide nanocomposites as enzyme-free highly sensitive sensors for detection of glucose. *Sensor Actuat B Chem* 221:1384–1390
41. Shan B, Ji Y, Zhong Y, Chen L, Li S, Zhang J, Chen L, Liu X, Chen Y, Yan N, Song Y (2019) Nitrogen-containing three-dimensional biomass porous carbon materials as an efficient enzymatic biosensing platform for glucose sensing. *RSC Adv* 9:25647–25654

42. Zahmouli N, Marini S, Guediri M, Ben Mansour N, Hjiri M, El Mir L, Espro C, Neri G, Leonardis G (2018) Nanostructured nickel on porous carbon-silica matrix as an efficient electrocatalytic material for a non-enzymatic glucose sensor. *Chemosensors* 6:54
43. Li M, Yang J, Lu M, Zhang Y, Bo X (2019) Facile design of ultrafine Co<sub>7</sub>Fe<sub>3</sub> nanoparticles coupled with nitrogen-doped porous carbon nanosheets for non-enzymatic glucose detection. *J Colloid Interface Sci* 555:449–459
44. Qu P, Gong Z, Cheng H, Xiong W, Wu X, Pei P, Zhao R, Zeng Y, Zhu Z (2015) Nanoflower-like CoS-decorated 3D porous carbon skeleton derived from rose for high performance nonenzymatic glucose sensor. *RSC Adv* 5:106661–106667
45. Xie Y, Song Y, Zhang Y, Xu L, Miao L, Peng C, Wang L (2018) Cu metal-organic framework-derived Cu Nanospheres@Porous carbon/macroporous carbon for electrochemical sensing glucose. *J Alloy Compd* 757:105–111
46. Meng T, Jia H, Ye H, Zeng T, Yang X, Wang H, Zhang Y (2020) Facile preparation of CoMoO<sub>4</sub> nanorods at macroporous carbon hybrid electrocatalyst for non-enzymatic glucose detection. *J Colloid Interface Sci* 560:1–10
47. Sivasakthi S, Imran H, Karuppasamy G, Sagadevan S, Mohammad F, Dharuman V (2020) Green synthesis of porous carbon nanocubes accumulated microspheres for the simultaneous non-enzymatic sensing of uric acid and dopamine in the presence of ascorbic acid. *Synth Met* 270:116598
48. Gai P, Zhang H, Zhang Y, Liu W, Zhu G, Zhang X, Chen J (2013) Simultaneous electrochemical detection of ascorbic acid, dopamine and uric acid based on nitrogen doped porous carbon nanopolyhedra. *J Mater Chem B* 1:2742–2749
49. Wang S, Guo P, Ma G, Wei J, Wang Z, Cui L, Sun L, Wang A (2020) Three-dimensional hierarchical mesoporous carbon for regenerative electrochemical dopamine sensor. *Electrochim Acta* 360:137016
50. Zhao L, Cai Z, Yao Q, Zhao T, Chen X, Lin H, Xiao Y. Electropolymerization fabrication of three-dimensional N, P-co-doped carbon network as a flexible electrochemical dopamine sensor. *Sensor Actuat B Chem* 253:1113–1119
51. Zhang Y, Gao W, Zuo L, Zhang L, Huang Y, Lu H, Fan W, Liu T (2016) In situ growth of Fe<sub>2</sub>O<sub>3</sub> nanoparticles on highly porous graphene/polyimide-based carbon aerogel nanocomposites for effectively selective detection of dopamine. *Adv Mater Interfaces* 1600137
52. Guo H, Wang M, Zhao L, Youliwasi N, Liu C (2018) The effect of Co and N of porous carbon-based materials fabricated via sacrificial templates MOFs on improving DA and UA electrochemical detection. *Micropor Mesopor Mat* 263:21–27
53. Kalate Bojdi M, Behbahani M, Mashhadizadeh MH, Bagheri A, Hosseiny Davarani SS, Farahani A (2015) Mercapto-ordered carbohydrate-derived porous carbon electrode as a novel electrochemical sensor for simple and sensitive ultra-trace detection of omeprazole in biological samples. *Mater Sci Eng C* 48:213–219
54. Zhou M, Guo LP, Hou Y, Peng XJ (2008) Immobilization of nafion-ordered mesoporous carbon on a glassy carbon electrode: application to the detection of epinephrine. *Electrochim Acta* 53:4176–4184
55. Ndamanisha JC, Bai J, Qi B, Guo L (2009) Application of electrochemical properties of ordered mesoporous carbon to the determination of glutathione and cysteine. *Anal Biochem* 386:79–84
56. Kozitsina AN, Svalova TS, Malysheva NN, Okhokhonin AV, Vidrevich MB, Brainina KZ (2018) Sensors based on bio and biomimetic receptors in medical diagnostic, environment, and food analysis. *Biosensors* 8:34–35
57. Yang G, Gong H, Liu T, Sun X, Cheng L, Liu Z (2015) Twodimensional magnetic WS<sub>2</sub>@Fe<sub>3</sub>O<sub>4</sub> nanocomposite with mesoporous silica coating for drug delivery and imaging-guided therapy of cancer. *Biomaterials* 60:62–71
58. Xu G, Liu S, Niu H, Lv W, Wu R (2014) Functionalized mesoporous carbon nanoparticles for targeted chemo-photothermal therapy of cancer cells under near-infrared irradiation. *RSC Adv* 4:33986–33997

59. Li C, Meng Y, Wang S, Qian M, Wang J, Lu W (2015) Rongqin Huang, mesoporous carbon nanospheres featured fluorescent aptasensor for multiple diagnosis of cancer in vitro and in vivo. *ACS Nano* 9(12):12096–12103
60. Kong Q, Zhang L, Liu J, Wu M, Chen Y, Fenga J, Shi J (2014) Facile synthesis of hydrophilic multi-colour and upconversion photoluminescent mesoporous carbon nanoparticles for bioapplications. *Chem Commun* 50:15772–15775
61. Ren X, Zheng R, Fang X, Wang X, Zhang X, Yang W, Sha X (2016) Red blood cell membrane camouflaged magnetic nanoclusters for imaging-guided photothermal therapy. *Biomaterials* 92:13–24
62. Zhang Q, Wang P, Ling Y, Li X, Xia L, Yang Y, Liu X, Zhang F, Zhou Y (2017) Single molecular wells–dawson-like heterometallic cluster for the in situ functionalization of ordered mesoporous carbon: A T1- and T2-weighted dual-mode magnetic resonance imaging agent and drug delivery system. *Adv Funct Mater* 27:1605313
63. Zhang S, Qian X, Zhang L, Peng W, Chen Y (2015) Composition-property relationships in multifunctional hollow mesoporous carbon nanosystems for PH-responsive magnetic resonance imaging and on-demand drug releasing. *Nanoscale* 7:7632–7643
64. Wu F, Sun B, Chu X, Zhang Q, She Z, Song S, Zhou N, Zhang J, Yi X, Wu D, Wang J (2019) Hyaluronic acid-modified porous carbon-coated Fe<sub>3</sub>O<sub>4</sub> nanoparticles for magnetic resonance imaging-guided photothermal/chemotherapy of tumors. *Langmuir* 35:13135–13144
65. Shi J, Votruba AR, Farokhzad OC, Langer R (2010) Nanotechnology in drug delivery and tissue engineering: from discovery to applications. *Nano Lett* 10:3223–3230
66. Jafari S, Derakhshankhaha H, Alaei L, Fattahi A, Varnamkhasti BS, Saboury AA (2019) Mesoporous silica nanoparticles for therapeutic/diagnostic applications. *Biomed Pharmacother* 109:1100–1111
67. Kapri S, Maiti S, Bhattacharyya S (2016) Lemon grass derived porous carbon nanospheres functionalized for controlled and targeted drug delivery. *Carbon* 100:223–235
68. Zhao Q, Lin Y, Han N, Li X, Geng H, Wang X, Cui Y, Wang S (2017) Mesoporous carbon nanomaterials in drug delivery and biomedical application. *Drug Delivery* 24(1):94–107
69. Liang C, Li Z, Dai S (2008) Mesoporous carbon materials: synthesis and modification. *Angew Chem Int Ed* 47:3696–3717
70. Bazuła PA, Lu AH, Nitz JJ, Schuth F (2008) Surface and pore structure modification of ordered mesoporous carbons via a chemical oxidation approach. *Micropor Mesopor Mat* 108:266–275
71. Rahman MM, Gulshan Ara M, Alim MA, Uddin MS, Najda A, Albadrani GM, Sayed AA, Mousa SA, Abdel-Daim MM (2021) Mesoporous carbon: a versatile material for scientific applications. *Int J Mol Sci* 22(9):4498
72. Magno Luis M, Hinds David T, Duffy P, Yadav Rahul B, Ward Andrew D, Botchway Stan W, Colavita Paula E, Quinn Susan J (2020) Porous carbon microparticles as vehicles for the intracellular delivery of molecules. *Front Chem* 8:925
73. Homayun B, Lin X, Cho H (2019) Challenges and recent progress in oral drug delivery systems for biopharmaceuticals. *Pharmaceutics* 11:129
74. Gisbert-Garzarán M, Berkman JC, Giasafaki D, Lozano D, Spyrou K, Manzano M, Steriotis T, Duda GN, Schmidt-Bleek K, Charalambopoulou G, Vallet-Reg M (2020) Engineered pH-responsive mesoporous carbon nanoparticles for drug delivery. *ACS Appl Mater Interfaces* 12:14946–14957
75. Gu J, Su S, Li Y, Heb Q, Shi J (2011) Hydrophilic mesoporous carbon nanoparticles as carriers for sustained release of hydrophobic anti-cancer drugs. *Chem Commun* 47:2101–2103
76. Zhang Y, Wang H, Gao C, Li X, Li L (2013) Highly ordered mesoporous carbon nanomatrix as a new approach to improve the oral absorption of the water-insoluble drug, simvastatin. *Eur J Pharm Sci* 49:864–872
77. Zhao P, Jiang H, Jiang T, Zhi Z, Wu C, Sun C, Zhang J, Wang S (2012) Inclusion of celecoxib into fibrous ordered mesoporous carbon for enhanced oral bioavailability and reduced gastric irritancy. *Eur J Pharm Sci* 45:639–647
78. Zhang Y, Zhi Z, Li X, Gao J, Yaling S (2013) Carboxylated mesoporous carbon microparticles as new approach to improve the oral bioavailability of poorly water-soluble carvedilol. *Int J Pharm* 454:403–411

79. Liu J, Zhao Y, Cui Y, Yue Y, Gao Y, Zhao Q, Liu J, Wang S (2016) A  $\text{Eu}^{3+}/\text{Gd}^{3+}$ -EDTA-doped structurally controllable hollow mesoporous carbon for improving the oral bioavailability of insoluble drugs and in vivo tracing. *Nanotechnology* 27:315101
80. Zhao P, Wang L, Sun C, Jiang T, Zhang J, Zhang Q, Sun J, Deng Y, Wang S (2012) Uniform mesoporous carbon as a carrier for poorly water-soluble drug and its cytotoxicity study. *Eur J Pharm Biopharm* 80:535–543
81. Bai L, Zhao Q, Wang J et al (2015) Mechanism study on pH-responsive cyclodextrin capped mesoporous silica: effect of different stalk densities and the type of cyclodextrin. *Nanotechnology* 26:165704
82. Zhang C, Zhao Q, Wan L, Wang T, Sun J, Gao Y, Jiang T, Wang S (2014) Poly dimethyl diallyl ammonium coated CMK-5 for sustained oral drug release. *Int J Pharm* 461:171–180
83. Zhang Y, Zhao Q, Zhu W, Zhang L, Han J, Lin Q, Ai F (2015) Synthesis and evaluation of mesoporous carbon/lipid bilayer nanocomposites for improved oral delivery of the poorly water-soluble drug, nimodipine. *Pharm Res* 32(7):2372–2383
84. Dong LC, Hoffman AS (1991) A novel approach for preparation of pH-sensitive hydrogels for enteric drug delivery. *J Control Release* 15:141–152
85. Jeong B, Bae YH, Lee DS, Kim SW (1997) Biodegradable block copolymers as injectable drug-delivery systems. *Nature* 388:860
86. Qiu Y, Park K (2001) Environment-sensitive hydrogels for drug delivery. *Adv Drug Deliv Rev* 53:321–339
87. Sawant RM, Hurley J, Salmaso S, Kale A, Tolcheva E, Levchenko TS, Torchilin VP (2006) “SMART” drug delivery systems: double-targeted pH-responsive pharmaceutical nanocarriers *Bioconj. Chem* 17:943–949
88. Danhier F, Feron O, Preat V (2010) To exploit the tumor microenvironment: passive and active tumor targeting of nanocarriers for anti-cancer drug delivery. *J Control Release* 148:135–146
89. Estrella V, Chen T, Lloyd M, Wojtkowiak J, Cornnell HH, Ibrahim-Hashim A, Bailey K, Balagurunathan Y, Rothberg JM, Sloane BF, Johnson J, Gatenby RA, Gillies RJ (2013) Acidity generated by the tumor microenvironment drives local invasion. *Cancer Res* 73:1524–1535
90. Justus CR, Dong L, Yang LV (2013) Acidic tumor microenvironment and pH-sensing G protein-coupled receptors. *Front Physiol* 4:354
91. Huang X, Wu S, Du X (2016) Gated mesoporous carbon nanoparticles as drug delivery system for stimuli-responsive controlled release. *Carbon* 101:135–142
92. Zhu S, Chen C, Chen Z et al (2011) Thermo-responsive polymer-functionalized mesoporous carbon for controlled drug release. *Mater Chem Phys* 126:357–363
93. Kartner N, Riordan JR, Ling V (1983) Cell surface P-glycoprotein associated with multidrug resistance in mammalian cell lines. *Science* 221:1285–1288
94. Gottesman MM, Fojo T, Bates SE (2002) Multidrug resistance in cancer: role of ATP dependent transporters. *Nat Rev Cancer* 2:48
95. Boesch D, Gavériaux C, Jachez B, Pourtier-Manzanedo A, Bollinger P, Loo F (1991) In vivo circumvention of P-glycoprotein-mediated multidrug resistance of tumor cells with SDZ PSC 833. *Cancer Res* 51:4226–4233
96. Ganta S, Amiji M (2009) Co-administration of paclitaxel and curcumin in nanoemulsion formulations to overcome multidrug resistance in tumor cells. *Mol Pharm* 6:928–939
97. Zhao Q, Lin Y, Han N, Li X, Geng H, Wang X, Cui Y, Wang S (2017) Mesoporous carbon nanomaterials in drug delivery and biomedical application. *Drug Deliv* 24(1):94–107
98. Wan L, Zhao Q, Zhao P, He B, Jiang T, Zhan Q, Wang S (2014) Versatile hybrid polyethyleneimine–mesoporous carbon nanoparticles for targeted delivery. *Carbon* 79:123–134
99. Wan L, Wang X, Zhu W, Zhang C, Song A, Sun C, Jiang T, Wang S (2015) Folate-polyethyleneimine functionalized mesoporous carbon nanoparticles for enhancing oral bioavailability of paclitaxel. *Int J Pharm* 484:207–217



100. Wan L, Jiao J, Cui Y, Guo J, Han N, Di D, Chang D, Wang P, Jiang T, Wang S (2016) Hyaluronic acid modified mesoporous carbon nanoparticles for targeted drug delivery to CD44-overexpressing cancer cells. *Nanotechnology* 27:135102
101. Zhou L, Dong K, Chen Z, Chen Z, Ren J, Qu X (2015) Near-infrared absorbing mesoporous carbon nanoparticle as an intelligent drug carrier for dual-triggered synergistic cancer therapy. *Carbon* 82:479–488

# Chapter 32

## Carbon Nanotubes-Based Anticancer Nanomedicine



**Sougata Ghosh, Ratnakar Mishra, Amrendra K. Ajay, Nanasahb Thorat, and Ebrahim Mostafavi**

### 1 Introduction

Cancer has emerged as the key factor for global mortality that has become a significant obstacle to life expectancy. According to World Health Organization (WHO) in 2019, maximum cancer-associated death before the age of 70 years has been reported in 112 of 183 countries. An estimated 19.3 million new cancer cases and almost 10.0 million cancer deaths occurred in 2020 globally. The most common type of cancer is female breast cancer (11.7%), followed by lung (11.4%), colorectal (10.0%), prostate (7.3%), and stomach (5.6%) cancers.

Other cancer types include various organs such as lip, oral cavity, salivary glands, oropharynx, nasopharynx, hypopharynx, esophagus, stomach, colon, rectum, anus,

---

S. Ghosh (✉)

Department of Microbiology, School of Science, RK University, Rajkot 360020, Gujarat, India  
e-mail: [ghoshsibb@gmail.com](mailto:ghoshsibb@gmail.com)

R. Mishra

Cambridge Centre for Brain Repair and MRC Mitochondrial Biology Unit, Department of Clinical Neurosciences, University of Cambridge, Cambridge CB2 0PY, UK

A. K. Ajay (✉)

Brigham and Women's Hospital, Harvard Center for Polycystic Kidney Disease Research and Renal Division, Harvard Medical School, Boston, MA, USA  
e-mail: [akajay@bwh.harvard.edu](mailto:akajay@bwh.harvard.edu)

N. Thorat

Nuffield Department of Women's & Reproductive Health, Division of Medical Sciences, John Radcliffe Hospital, University of Oxford, Oxford OX3 9DU, UK

E. Mostafavi

Stanford Cardiovascular Institute, Stanford University School of Medicine, Stanford, CA, USA

Department of Medicine, Stanford University School of Medicine, Stanford, CA, USA

© The Author(s), under exclusive license to Springer Nature Singapore Pte Ltd. 2023

907

A. N. Grace et al. (eds.), *Handbook of Porous Carbon Materials*,

Materials Horizons: From Nature to Nanomaterials,

[https://doi.org/10.1007/978-981-19-7188-4\\_32](https://doi.org/10.1007/978-981-19-7188-4_32)

liver, including intrahepatic bile ducts, gallbladder, pancreas, and larynx [1]. Conventional cancer treatment includes various anticancer agents such as doxorubicin, daunorubicin, cytarabine, paclitaxel, and vincristine. However, they have potential side effects that include hypersensitivity, severe myelosuppression, nausea, neutropenia, stomatitis, rash, mucositis, vomiting, anorexia, and diarrhea [2]. Hence, it is necessary to develop innovative strategies for cancer treatment with minimum or no side effects and maximum efficacy.

Nanotechnology-driven solutions employing exotic nanostructures with notable physicochemical and opto-electronic properties have come up as an attractive alternative for cancer management [3–5]. Several metallic nanoparticles composed of gold, silver, copper, platinum, and palladium are reported to significantly inhibit the cancer cells [6–9]. Likewise, magnetic nanoparticles help in targeted delivery of drugs that avoids nonspecific drug accumulation and adverse effects [10]. The smaller dimension and the large surface area of the nanoparticles make them ideal for multifunctionalization of drugs, antibodies, peptides, nucleic acids, fluorophores, and contrast agents. Further, functionalized nanoparticles may help for tissue specific delivery of drugs, triggered release, bioimaging, and monitoring the disease progression and drug efficacy [11–13].

Carbon-based nanoparticles, particularly carbon nanotubes (CNTs) with higher penetrability, enhanced stability, and larger surface loading capacity, are considered ideal theranostic agents for their promising applications in multimodal therapy and diagnosis [14].

In this chapter, various single- and multiwalled carbon nanotubes (SWCNTs and MWCNTs)-based anticancer agents are discussed with their application in photothermal, photodynamic, chemo-photothermal, immune-photothermal, sonodynamic, and chemo-sonodynamic therapy against various cancers.

## 2 Therapeutic Modality-Based Nanomedicine

Notably, unique physicochemical and opto-electronic properties of CNTs have made them attractive nanocarriers for various drugs, targeting ligands, contrast agents for simultaneous therapy and diagnosis in cancer. Hence, CNTs-based theranostics with high capacity of binding to a wide range of biomolecules are specific to various therapeutic modalities which are discussed in detail in this section and summarized in Table 1.

### 2.1 Photothermal Therapy

The conventional cancer treatment strategies include chemotherapy, radiotherapy, or targeted therapies which have their own limitations due to severe non-specific adverse effects. Certain nanomaterials can convert near-infrared (NIR) light

**Table 1** Functionalized CNTs with various therapeutic modalities against cancer

Sr. No.	Therapy	Nanoparticles	Functionalized ligand	Type of cancer	References
1	Photothermal	SWCNTs	Imaging agent CY7, anti-IGF-IR antibody (IGF-IR Ab)	Pancreatic cancer	[17]
2	Photothermal	SWCNTs	Annexin V	Bladder cancer	[22]
3	Plasmonic photothermal	MWCNTs	AgNPs	Melanoma	[23]
4	Photothermal	MWCNTs	Polyethylene glycol (PEG)	Melanoma	[24]
5	Photothermal	MWCNTs	Polyethylene glycol <sub>5000</sub> terminated with a methoxy group (DSPE-PEG), maleimide (DSPE-PEG-Mal), and fluorescein isothiocyanate (DSPE-PEG-FITC), anti-Pgp antibody	Mouse fibroblast cell line (3T3-MDR1 cells)	[25]
6	Photodynamic	(6,4)-SWCNTs	Apolipoprotein A-I (apoA-I)	Cervical cancer cells (HeLa)	[27]
7	Photodynamic	SWCNTs	Zinc mono carboxy phenoxy phthalocyanine (ZnMCPPc) and spermine	Breast cancer cells (MCF-7)	[28]
8	Photodynamic	SWCNTs	Zinc mono carboxy phenoxy phthalocyanine (ZnMCPPc) and ascorbic acid	Breast cancer cells (MCF-7)	[29]
9	Photodynamic	SWCNTs	Hyaluronic acid (HA) and chlorin e6 (Ce6)	Colon cancer cells (Caco-2)	[30]
10	Combined phototherapy	Carbon-silica nanocomposite (CSN)	D- $\alpha$ -tocopherol polyethylene glycol	4T1 tumor model, patient-derived xenograft (PDX) tumor model	[33]

(continued)

Table 1 (continued)

Sr. No.	Therapy	Nanoparticles	Functionalized ligand	Type of cancer	References
11	Combined phototherapy	SWCNTs-PEG-Fe <sub>3</sub> O <sub>4</sub> @CQDs	sgc8c aptamer and doxorubicin	HeLa cells and HeLa tumor-bearing nude mice	[34]
12	Chemo-photothermal	SWCNTs	Phosphatidylcholine, polyvinylpyrrolidone and curcumin	Human prostate cancer PC-3 cells and S180 tumor model in mice	[35]
13	Chemo-photothermal	MWCNTs	Lentiran, tamoxifen	Breast cancer MCF-7 cells	[36]
14	Chemo-photothermal	MWCNTs	Gemcitabine, lentiran	Breast cancer MCF-7 cells, Mef-7 tumor-bearing BALB/c nude mice	[37]
15	Chemo-photothermal	MWCNTs	Metformin	HepG-2 cells	[38]
16	Immune-photothermal therapy	SWCNTs	Glycated chitosan	Mouse mammary tumor cell line EMT6, and mouse macrophage cell line RAW264.7, mouse mammary tumor model developed with EMT6 cells in BALB/c female mice	[39]
17	Immune-photothermal therapy	SWCNTs	Polyethylene glycol (PEG)-grafted amphiphilic polymer; combination with anticytotoxic T lymphocyte antigen-4 (CTLA-4) antibody therapy	BALB/c mice-derived dendritic cells, subcutaneous 4T1 murine breast tumors, murine B16 musculus skin melanoma	[40]
18	Immune-photothermal therapy	MWCNTs	Trastuzumab, diphtheria toxin	SK-BR-3 cells	[41]

(continued)

**Table 1** (continued)

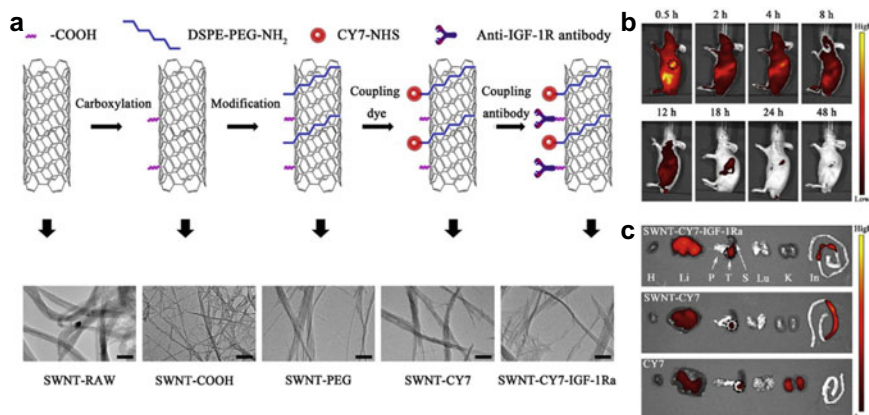
Sr. No.	Therapy	Nanoparticles	Functionalized ligand	Type of cancer	References
19	Sonodynamic therapy	MWCNTs	Polypyrrole	C540 (B16/F10) cell line and a melanoma tumor model in male BALB/c mice	[42]
20	Sonodynamic therapy	SWCNTs	Polyethylene glycol	Sarcoma 180 cells, solid tumor in CDF1 mice	[43]
21	Sonodynamic therapy	SWCNTs	Porphyrin	Human colorectal cancer cell line (HT-29)	[44]
22	Chemo-sonodynamic therapy	MWCNTs	Protohemin	HepG-2 cells, tumor in nude BALB/c mice	[45]
23	Chemo-sonodynamic therapy	MWCNTs	Folic acid, protohemin	HepG-2 cells, tumor in nude BALB/c mice	[46]

to high heat resulting in photothermal therapy (PTT) that is able to cause mitochondrial dysfunction, generation of reactive oxygen species (ROS), and eventually cytotoxicity to cells either by apoptosis or necrosis [15]. Although various nanomaterials are fabricated for cancer treatment, they have exhibited unsatisfactory performance toward ideal PTT. Hence, carbon-based nanomaterials with unique advantages for PTT have received wide attention for their applications in biomedical field, most notable being cancer therapy. The ultrahigh specific surface area, high thermal stability, photothermal conversion efficiency, photoacoustic imaging potential, and reduced toxicity make the SWCNTs candidate photothermal agents [16].

Lu et al. reported SWCNTs-based nanoprobes coupled with the sensitive imaging agent and targeting antibodies as shown in Fig. 1 [17]. Initially, the water solubility of the raw single-walled carbon nanotubes (SWNT-RAW) was enhanced by converting them into carboxylated single-walled carbon nanotubes (SWNT-COOH) after refluxing in concentrated acid. The amphiphilic molecule, 1,2-distearoyl-sn-glycerol-3-phosphoethanolamine-N-[amino(polyethylene glycol)-5000] (DSPE-PEG5000-NH<sub>2</sub>) was attached to SWNTs by non-covalent interaction. Next, the SWNTs conjugated with DSPE-PEG5000-NH<sub>2</sub> (SWNT-PEG) were reacted with Cyanine7-N-hydroxy-succinimide (CY7-NHS) to obtain SWNT-CY7 that attributed to its imaging property in the NIR region that directs PTT. It is important to note that the overexpression of insulin-like growth factor receptor (IGFR) in aggressive pancreatic cancer cells is associated with its proliferation, differentiation, survival, metastasis, and resistance to anticancer therapies. Hence, insulin-like growth factor type-1 receptor (IGF-1R) is considered as potential target for cancer therapy. Thus, SWNT-CY7 was further coupled with anti-IGF-1R antibody (IGF-1R Ab) to develop SWNT-CY7-IGF-1Ra so that the nanocomposite can reach the tumor via the enhanced permeability and retention (EPR) effect and simultaneously aggregate into the tumor region via antibody targeting. Substantial uptake of the nanotubes conjugated with IGF-1R Ab was observed in pancreatic cancer (BXPC-3 and PANC-1) cells. The accumulation of the nanoprobes (SWNT-CY7-IGF1-Ra) was highest at 18–24 h selectively in the tumor tissue of tumor-bearing mice which were later metabolized by the liver and intestine mainly. Laser irradiation (785 nm, 1 W/cm<sup>-2</sup>) for 5 min significantly elevated the tumor temperature up to  $48.53 \pm 1.38$  °C when treated with SWNT-CY7-IGF-1Ra resulting in marked cell damage associated with coagulative necrosis, pyknosis, apoptosis, and loss of adhesion.

Further, SWNT-CY7-IGF1-Ra mediated PTT effect in the orthotopic pancreatic cancer models exhibited high survival rate. This might be attributed to satisfactory pancreatic cancer ablation due to active targeting associated enhanced accumulation of nanotubes in the tumor tissue followed by laser treatment. In view of the background, SWNT-CY7-IGF-1Ra can be promising nanomedicine for imaging-guided photothermal therapy against pancreatic cancer.

In some cases, hyperthermia resistive tumors cannot be eradicated by slow heating from 39 °C–45 °C. In such cases, photothermal ablation is more effective as it uses light to increase the temperature within the biologic tissue above 60 °C within a short time. Due to high heat generation, death of cancerous tissue occurs via necrosis which can be a promising alternative for controlling chemoresistive as well as hyperthermic



**Fig. 1** Synthesis and characterization of nanotubes. **a** Schematic illustration and TEM images in the synthesis procedure of nanotubes. The bar is 100 nm; **b** Distribution of nanoprobe in vivo. In vivo continuous observations (48 h) of mice administered SWNT-CY7-IGF-1Ra via the tail vein. The black dotted circle represents the location of the pancreatic carcinoma in situ; **c** Ex vivo imaging of tumor and major organs. **Note:** *H* heart. *Li* liver. *P* pancreas. *T* tumor. *S* spleen. *Lu* lung. *K* kidney. *In* intestine. Reprinted with permission from Lu et al. [17] Copyright 2019 Elsevier Ltd

resistive tumors [18–21]. Virani et al. reported phosphatidylserine targeted SWCNTs for photothermal ablation of bladder cancer [22]. Enhancement of nanotube accumulation inside the tumor tissue specifically was achieved by conjugating the SWCNTs with annexin V (AV), which strongly binds with phosphatidylserine (PS) present on tumor cells and tumor vasculature. Interestingly, no detectable tumor after 24 h was observed in the C57BL/6J female mice with orthotopic MB49 murine bladder tumors after treatment with the SWCNT-AV conjugate and NIR light treatment at an energy and power density of  $50 \text{ J cm}^{-2}$  and  $1.67 \text{ W cm}^{-2}$ , respectively (time = 30 s). Rather it showed a 50% cure rate at 116 days after treatment.

Another innovative cancer treatment modality is plasmonic photothermal therapy (PPTT) where plasmonic nanoscale metals, such as silver nanoparticles (Ag NPs) with notable optical absorbance can be used in conjugation with CNTs with good thermal conductivity and cell penetration ability. Behnam et al. functionalized the MWCNTs with silver which could rapidly transform the photon energy into heat via a series of radiative and non-radiative phenomena, eventually ablating cancer [23]. The AgNPs had an average diameter of 20 nm, which were attached to MWCNTs were synthesized. Treatment with CNT/AgNPs against melanoma tumor induced by injection of B16/F10 cell line to the inbred mice exhibited enhanced optical absorption of CNTs mediated improved tumor destruction, which was attributed to PPTT brought about by irradiation via laser diode ( $\lambda = 670 \text{ nm}$ ,  $P = 500 \text{ mW}$ , and  $I = 3.5 \text{ W/cm}^2$ ).

Sobhani et al. improved the dispersibility of MWCNTs in water employing initial oxidation followed by surface coating with polyethylene glycol (PEG) [24]. The nanotubes with 80% PEG loading exhibited less cytotoxic activity against HeLa and



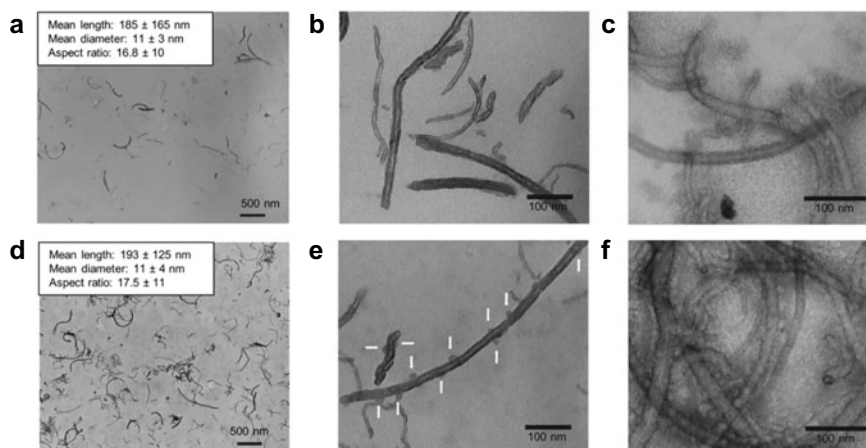
HepG-2 cell lines. On exposure to continuous-wave near-infrared laser diode ( $\lambda = 808$  nm,  $P = 2$  W and  $I = 8$  W/cm<sup>2</sup>) for 10 min, the PEG-coated oxidized MWCNTs could sharply reduce the average size of melanoma tumor from 975 to 125 mm<sup>3</sup> in mice. Hence, such coated MWCNTs can be a powerful candidate for eradicating solid tumors employing the PTT technique.

In another study, Suo et al. proposed MWCNTs-based approach to combat P-glycoprotein (Pgp)-mediated multidrug resistance (MDR), which poses a major challenge to existing cancer therapy [25]. This novel nanocomposite was designed by combination of antibody-based cancer targeting and locoregional tumor ablation with photothermal therapy. Intercellular diffusion was enhanced, and non-specific cellular interaction was reduced using a dense coating of phospholipid–poly(ethylene glycol) around the MWCNTs. The coated MWCNTs were further chemically functionalized with an anti-Pgp antibody to facilitate Pgp-specific cellular uptake. Photothermal heating efficiency determines the toxicity of MWCNTs which generally increases with the diameter. The MWCNTs with 20–30 nm diameter generated maximum heat per unit. The MWCNTs with 8–15 nm diameter were coated with a 2 w/v % solution of a mixture of polyethylene glycol<sub>5000</sub> terminated with a methoxy group (DSPE–PEG), maleimide (DSPE–PEG–Mal), and fluorescein isothiocyanate (DSPE–PEG–FITC) at a 5:4:1 mass ratio followed by conjugation with Pgp antibodies (Pab) to generate Pab–MWCNTs as illustrated in Fig. 2. Acid oxidation and coating of MWCNTs using a 2 w/v % solution of DSPE–PEG reduce nonspecific cell uptake at least sixfold compared to bare MWCNTs without any loss of heat transduction capability. Moreover, this strategy dramatically increases the diffusibility of MWCNTs through the extracellular space. Cellular uptake of FITC-labeled Pab–MWCNTs was very high in the case of 3T3-MDR1 cells. The dose-dependent phototoxicity in the presence of NIR laser irradiation was notably high in Pab–MWCNTs treated 3T3-MDR1 cells. Further, the Pab–MWCNT-mediated PTT enhanced cytotoxicity against the multicellular, NCI/ADR-RES tumor spheroids which might be attributed to high intratumor diffusion and Pgp-specific cellular uptake.

## 2.2 Photodynamic Therapy

In photodynamic therapy (PDT), oxygen-dependent cytotoxicity in cancer tissue is brought about by two individually non-toxic components, one of which is a photosensitizer. This photosensitive molecule localizes within cancer tissue. The second component activates the photosensitizer by administering a specific wavelength of light which is followed by the generation of ROS due to the transfer of energy from light to molecular oxygen. Since this reaction is associated with the light-absorbing photosensitizer, the cytotoxicity is specific and limited to only those tissues exposed to light [26]. CNTs-based nanomedicine for PDT has become an attractive alternative cancer management strategy owing to their negligible nonspecific adverse effects.

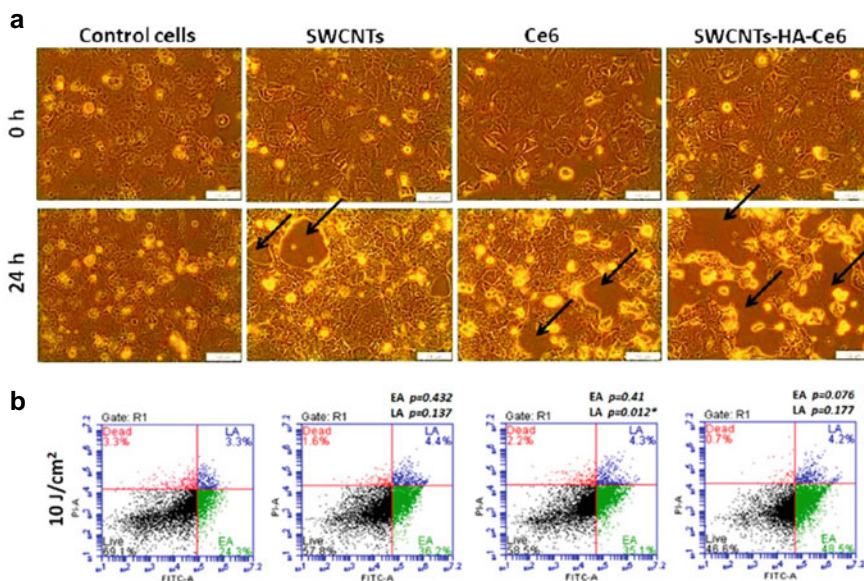
Fukuda et al. fabricated one chiral s-SWNTs, (6,4)-SWCNTs, for photogeneration of all three major ROS, i.e., singlet oxygen (<sup>1</sup>O<sub>2</sub>), superoxide anion (O<sub>2</sub><sup>•-</sup>),



**Fig. 2** Morphological features of MWCNTs and Pab-MWCNTs. **a, b** Photoelectron micrographs of unstained and **c** uranyl acetate stained MWCNTs. **d, e** Photoelectron micrographs of unstained and **f** uranyl acetate stained Pab-MWCNTs. White arrows in **e** and globular masses (approx. 10 nm diameter) in **f** indicate the location of antibody molecules on MWCNTs. Reprinted with permission from Suo et al. [25]. Copyright 2018 American Chemical Society

and hydroxyl radical ( $\bullet\text{OH}$ ) [27]. The NIR illumination at 880 nm resulted in the photogeneration of  $^1\text{O}_2$  by the (6,4)-SWCNTs while highly enriched (6,4)-SWCNTs resulted in abundant  $\bullet\text{OH}$  in the presence of NIR illumination. The photodynamic effect was attributed to the intrinsic optical function of the (6,4)-SWCNTs. Further, apolipoprotein A-I (apoA-I), a lipid-binding protein of the high-density lipoprotein type, was used for functionalization where the first truncated form conjugated with the (6,4)-SWCNTs was denoted as (6,4)-SWCNTs/apo. Labeling with fluorescent Alexa Fluor 546 (Alexa546) indicated 79% accumulation of (6,4)-SWCNTs/apo complexes specifically in the mitochondria, which is the predominant site of ROS generation and photodynamic therapy. Superior photostability and efficiency to generate significantly high level of  $\bullet\text{OH}$  attributed to the enhanced photodynamic effect in (6,4)-SWCNTs. The serum protein-coated (6,4)-SWCNTs were more stable, leading to effective cancer ablation against HeLa cells where cell viability was reduced by 40%. In an interesting study, Ogbodu et al. initially conjugated zinc mono carboxy phenoxy phthalocyanine (ZnMCPPc) to spermine via amide bond which was further functionalized onto SWCNT to develop a nanocomposite denoted as ZnMCPPc-spermine-SWCNT. The loading of ZnMCPPc-spermine on SWCNTs was 42% [28]. The complex showed superior photophysical features resulting in more than 50% increase in triplet and singlet oxygen quantum yields. Photodynamic activity indicated 95% decrease in MCF-7 cell viability at 40 mM concentration with an irradiation time of 1200 s. On a similar line, ZnMCPPc was chemically modified with ascorbic acid via an ester bond to give ZnMCPPc-AA, which was further conjugated to SWCNTs via  $\pi$ - $\pi$  interaction to give ZnMCPPc-AA-SWCNT [29]. This strategy enhanced the photophysical properties, including improved triplet lifetimes

and quantum yields and singlet oxygen quantum yields. Further, the composites showed high photodynamic activities against MCF-7 breast cancer cells with 67% decrease in cell viability. The enhanced anticancer activity might be attributed to the phthalocyanines, which are excellent photodynamic agents. Moreover, SWNTs with their photothermal properties might have enhanced the cumulative therapeutic potential. Sundaram and Abrahamse coupled SWCNTs with hyaluronic acid (HA) and chlorin e6 (Ce6) to design a nanocomposite represented as SWCNTs-HA-Ce6 [30]. The high loading efficiency of Ce6, equivalent to 70%, was attributed to the large surface area of the SWCNTs. The size and zeta potential of the nanostructure was  $203 \pm 6.6$  nm and  $-18.9 \pm 1$  mV, respectively. The  $10 \text{ J/cm}^2$  irradiated colon cancer cells (Caco-2) showed 84.9% cell death on treatment with SWCNTs-HA-Ce6, confirming the photodynamic potential of the nanocomposite against cancer as shown in Fig. 3. Among several agents, porphyrins are the major class of photosensitizers used in photodynamic therapy, and hematoporphyrin monomethyl ether (HMME) is the newer generation of photosensitizers, which has reduced toxicity and shorter skin photosensitizing ability [31]. Photodynamic therapy of HMME combined CNTs has been shown to reduce tumor growth in mouse models [32].



**Fig. 3** Photodynamic activity of SWCNTs-HA-Ce6 nanocomposite against colon cancer cells (Caco-2). **a** Microscopic images of untreated and treated cells ( $10 \text{ J/cm}^2$ ) of 0 and 24 h. Scale bar represents  $100 \mu\text{m}$ . Black arrows indicate the cellular death. **b** Flow cytometry Annexin V PI staining analysis of apoptosis. Reprinted from Sundaram et al. [30]

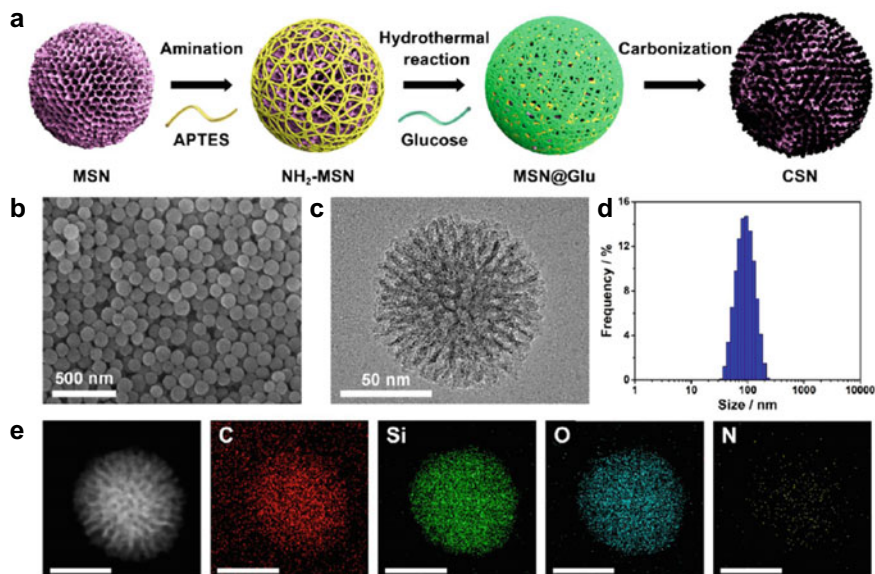
### 2.3 Combined Phototherapy

Combination of phototherapy with chemotherapy or other therapeutic modalities such as radiation, chemotherapy, pre and post-surgery treatments to enhance the cancer cell killing and achieve higher therapeutic index has gained significant interest in the past few years. The development of novel nanomaterials and their combination with phototherapy provides wide range of modulating power for designing specific and controlled therapeutic methods.

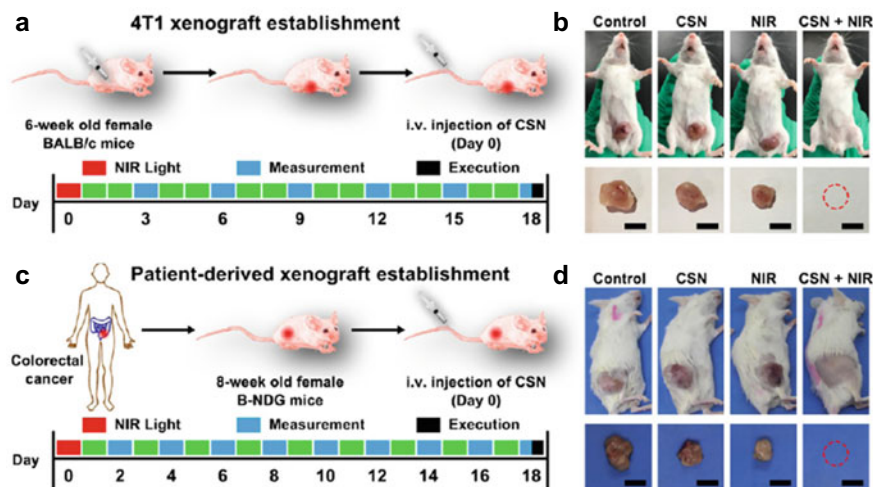
Wang et al. fabricated a degradable carbon–silica nanocomposite (CSN)-based immunoadjuvant [33]. In this process, 3D dendritic degradable mesoporous silica nanoparticle (MSN) was initially synthesized using triethanolamine (TEA), cetyltrimethylammonium chloride (CTAC), tetraethyl orthosilicate (TEOS), and cyclohexane was added at 60 °C as depicted in Fig. 4. The MSN powders were finally recovered by drying at 50 °C in a vacuum. Further, the MSNs were reacted with (3-aminopropyl)triethoxysilane (APTES) for 20 h at 80 °C in order to modify the amino group on the surface of the MSNs. The NH<sub>2</sub>-MSN was reacted with  $\alpha$ -D-glucose for 20 h at 160 °C to prepare MSN@Glu that was further dried and carbonized under a nitrogen atmosphere at 540 °C for 4 h to obtain the CSN. D- $\alpha$ -tocopherol polyethylene glycol was used for modifying the CSNs. Monodispersed CSN exhibited uniform particle size of 100 nm, which is advantageous for enhanced accumulation in the tumor region via enhanced permeability and retention (EPR) effect. The elemental composition of the CSN was contributed by carbon, silicon, oxygen, and nitrogen with mass percentages (wt%) of 36.1%, 27.6%, 35.0%, and 1.3%, respectively. The photothermal property was indicated by a sharp increase in temperatures (27.6–78.2 °C) of CSN dispersions under NIR light (808 nm, 2 W cm<sup>-2</sup>) irradiation was a function of time (10 min) and concentration (200  $\mu$ g mL<sup>-1</sup>). The photothermal conversion efficiency ( $\eta$ ) of CSN was  $\sim$ 34.5%.

Generation of singlet oxygen (<sup>1</sup>O<sub>2</sub>) by the CSN in combination with NIR increased by 124.7%, confirming its superior photodynamic property. The CSN facilitated maturation of bone marrow-derived dendritic cells (BMDCs) from BALB/c mice which was associated with higher expression of costimulatory CD80, CD86, tumor necrosis factor- $\alpha$  (TNF- $\alpha$ ) and interleukin-6 (IL-6). It was speculated that the rough surface of CSN with 100 nm size could be efficiently taken up by the DCs followed by the maturation of DCs. The superior photothermal and photodynamic properties of the CSN were exploited for antitumor efficiency in combination with NIR light in 4T1 tumor model as shown in Fig. 5a, b. Tumor in mice was inhibited up to 93.2% on treatment with CSN with NIR. Further, patient-derived xenograft (PDX) tumor model was developed by subcutaneous injection of human CRC cancer tissue fragments into B-NDG mice. Treatment with CSN in combination with NIR exhibited 92.5% suppression of the tumor growth in PDX tumor-bearing mice as shown in Fig. 5c, d. Hence, carbon–silica-nanomaterial-based therapeutic strategy can be promising next-generation anticancer nanomedicine.

Zhang et al. reported fabrication of novel magnetofluorescent Fe<sub>3</sub>O<sub>4</sub>/carbon quantum dots (CQDs)-coated SWCNTs as trimodal therapeutic agents with imaging



**Fig. 4** Synthesis and characterization of CSN. **a** Schematic illustration of CSN synthesis. **b** Scanning electron microscope (SEM) and **c** high-resolution transmission electron microscope (HR-TEM) images of CSN. **d** Size distribution of CSN. **e** High-angle annular dark field scanning TEM (HAADF-STEM) image and element mapping of CSN. Scale bar: 50 nm. Reprinted with permission from Wang et al. [33]. Copyright 2020 American Chemical Society



**Fig. 5** In vivo antitumor experiments of CSN. Schematic illustration of the establishment of **a** 4T1 and **c** PDX tumor models and therapy procedure of CSN ( $1 \text{ mg mL}^{-1}$ ,  $200 \mu\text{L}$ ) combined with NIR light ( $808 \text{ nm}$ ,  $2 \text{ W cm}^{-2}$ ,  $5 \text{ min}$ ) irradiation ( $n = 5$ ). Photographs of **b** 4T1 and **d** PDX tumor-bearing mice, as well as corresponding dissected tumors after the therapy. Scale bar: 1 cm. Reprinted with permission from Wang et al. [33] Copyright 2020 American Chemical Society

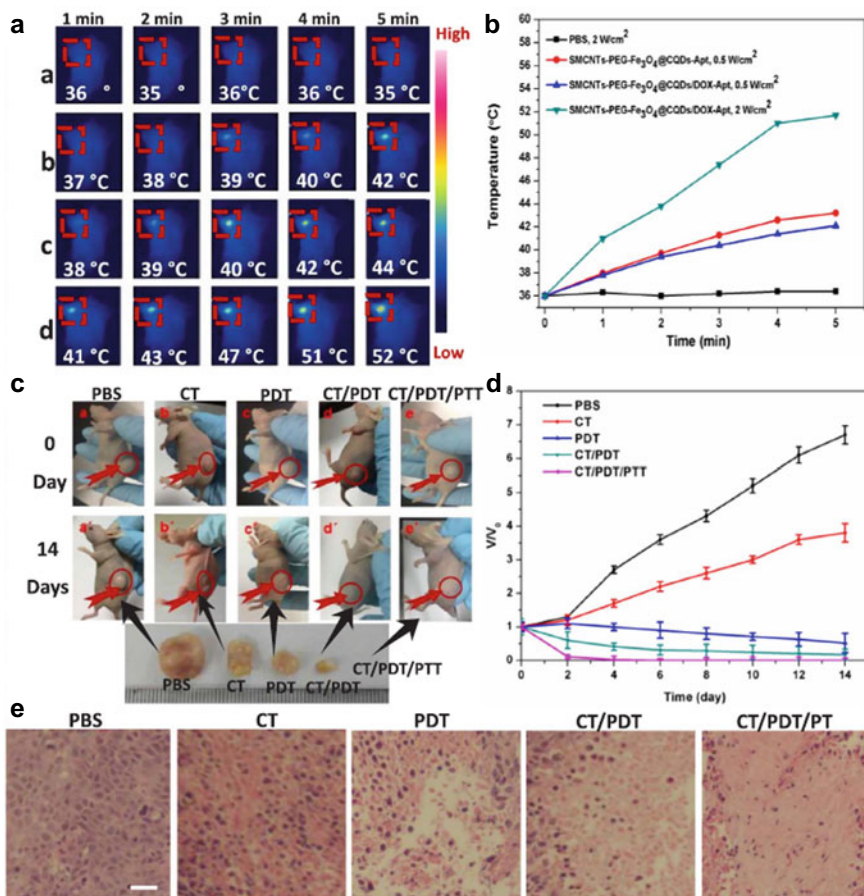
as well as chemo/photodynamic/photothermal (CT/PDT/PTT) properties [34]. Initially, the branched PEG 2000 N was grafted covalently (with 17.8% loading) on the surface of oxidized and shortened SWCNTs with more carboxylic acid group on its side walls. The polymer shell was 5–7 nm thick. Hydrothermally synthesized spherical CQDs were  $2.8 \pm 0.3$  nm in size. Further, doxorubicin (DOX), a standard anticancer drug, was loaded into the pore structure of the synthesized SWCNTs-PEG-Fe<sub>3</sub>O<sub>4</sub>@CQDs nanocarriers with high efficiency which were then conjugated with a sgc8c aptamer, denoted as SWCNTs-PEG-Fe<sub>3</sub>O<sub>4</sub>@CQDs-DOX-Apt, for targeting dual modal fluorescence/magnetic resonance (MR) imaging. It is important to note that the SWCNTs-PEG-Fe<sub>3</sub>O<sub>4</sub>@CQDs exhibited superior upconverted photoluminescence properties and can be excited by long-wavelength light ( $\lambda > 600$  nm) with the upconverted emissions located in the range of 420–520 nm. Significant reduction in viability of HeLa cells on treatment with SWCNTs-PEGFe<sub>3</sub>O<sub>4</sub>@CQDs was attributed to the simultaneous generation of OH<sup>•</sup> and <sup>•</sup>O<sub>2</sub><sup>-</sup>, DOX release and hyperthermia-associated CT, PDT, and PTT using a single NIR laser. Interestingly, Fig. 6 shows rapid increase of the temperature at the tumor site to 52 °C in the presence of SWCNTs-PEG-Fe<sub>3</sub>O<sub>4</sub>@CQDs/DOX-Apt upon NIR laser illumination (within 5 min) HeLa tumor-bearing nude mice. Due to combined therapy, the tumor volume reduced significantly.

Hence, this combined therapeutic strategy demonstrates exceptional success through irradiation to generate limited heat for cancer cell killing for more specific induction of necrosis or apoptotic cell death only in irradiated cancer cells/tissues.

## 2.4 Chemo-Photothermal Therapy

CNTs provide ideal surfaces for functionalization of chemotherapeutic agents with anticancer potential. Such nanocomposites exhibit promising chemo-photothermal properties because of their remarkable cell membrane penetrability, sustained release and noteworthy photothermal effects. In one such study, Li et al. conjugated curcumin to SWCNTs functionalized with phosphatidylcholine and polyvinylpyrrolidone to yield SWCNT-Cur [35]. Sixfold increase in the cellular uptake of SWCNTs-Cur by human prostate cancer PC-3 cells was observed. Further, the concentration of curcumin increased 18-fold in blood along with residence time on treatment with SWCNT-Cur. Synergistic tumor suppression by SWCNT-Cur in combination with 808 nm laser irradiation at 1.4 W/cm<sup>2</sup> was noticed along with reduction in tumor weight and volume in S180 mice tumor models.

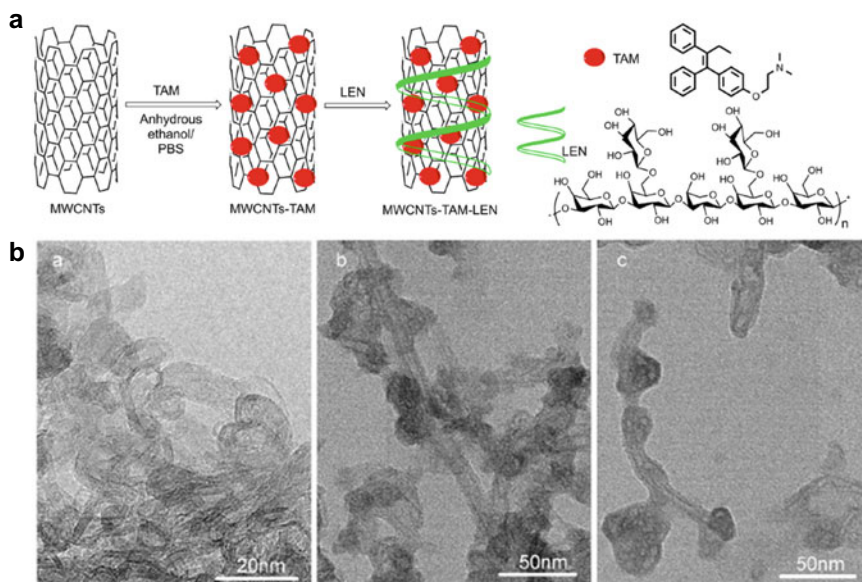
In another study, a natural biological polysaccharide, lentinan (LEN), was initially functionalized on MWCNTs for delivery of an anticancer drug, tamoxifen (TAM) which is schematically represented in Fig. 7 [36]. The loading ratio of TAM and LEN in the composite (MWCNTs-TAM-LEN) was 28.6% and 26.5%, respectively. The nanocomposite not only exhibited superior stability and water dispersibility but also demonstrated remarkable photothermal properties. The MWCNTs-TAM-LEN was further labeled with Rhodamine 123 which showed enhanced cellular uptake by



**Fig. 6** **a** IR thermal images of HeLa tumor-bearing mice incubated with various media: *a* PBS, *b* 100  $\mu\text{g/mL}$  of SWCNTs-PEG- $\text{Fe}_3\text{O}_4$ @CQDs-Apt + laser (808 nm, 0.5  $\text{W}/\text{cm}^2$ ), *c* 100  $\mu\text{g/mL}$  of SWCNTs-PEG- $\text{Fe}_3\text{O}_4$ @CQDs/DOX-Apt + laser (808 nm, 0.5  $\text{W}/\text{cm}^2$ ) and *d* 100  $\mu\text{g/mL}$  of SWCNTs-PEG- $\text{Fe}_3\text{O}_4$ @CQDs/DOX-Apt + laser (808 nm, 2  $\text{W}/\text{cm}^2$ ). **b** Heating curve of the five laser-irradiated groups. **c** Representative photographs of tumor-bearing mice after different treatments. **d** Time-dependent tumor growth curves observed after different treatments ( $n = 5$ ,  $P < 0.05$  for each group). **e** H&E staining of tumor sections gathered from various treatment groups of mice on day 2. Scale bar = 50  $\mu\text{m}$ . Reprinted with permission from Zhang et al. [34]. Copyright 2018 Elsevier B.V.

MCF-7 cells due to penetration into the cell membrane followed by accumulation in the cytoplasm. High cell growth inhibition up to  $\sim 91.7\%$  was observed when treated with MWCNTs-TAM-LEN in combination with NIR irradiation at the TAM concentration of  $5 \mu\text{g mL}^{-1}$ . Similarly, rate of apoptosis increased to 78.11% when the MCF-7 cells was treated under aforementioned condition.

Zhang et al. fabricated a drug delivering three-component composite denoted as MWCNTs-Ge-Le comprised of MWCNTs, gemcitabine (Ge) and lentinan (Le) as

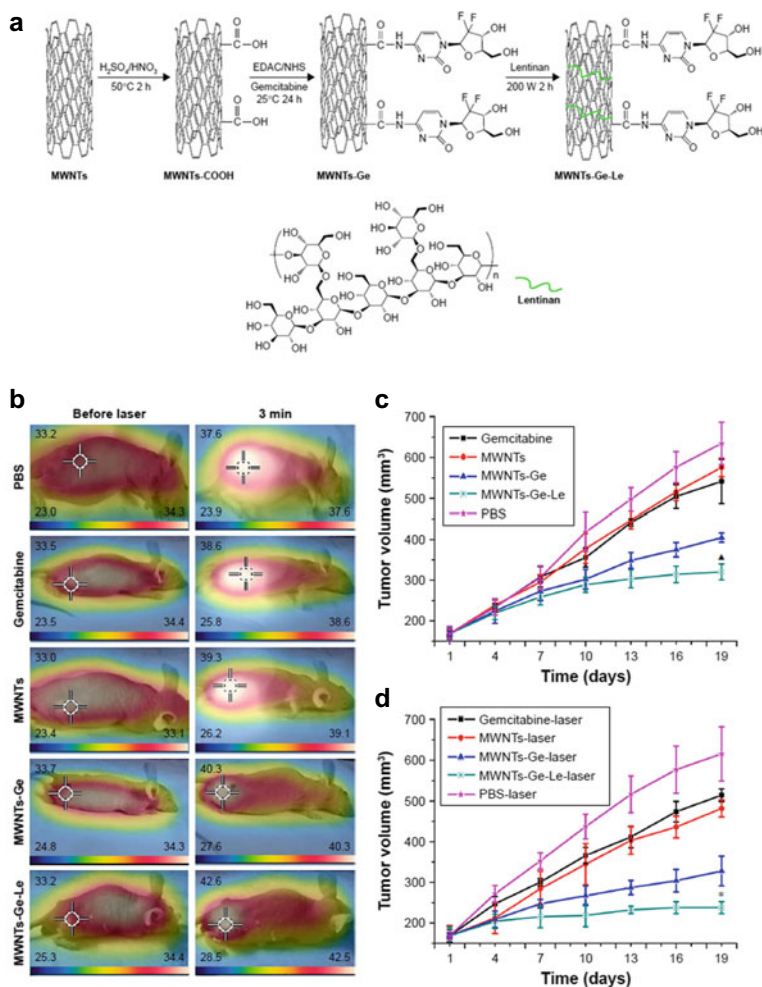


**Fig. 7** **a** Illustration diagram of MWCNTs-TAM-LEN synthesis; **b** TEM images of MWCNTs (*a*) and MWCNTs-TAM-LEN (*b* and *c*). Reprinted with permission from Yi et al. [36]. Copyright 2018 Elsevier B.V.

schematically represented in Fig. 8 [37]. The nanocomposite displayed antitumor activity which was attributed to combination of chemotherapy and photothermal therapy. Loading of gemcitabine and lentinan in MWNTs-Ge-Le was 31.8% and 10.4%, respectively. The increase in temperature from 25 to 45 °C under 2 W cm<sup>-2</sup> NIR irradiation for 10 min indicating its photothermal property of the MWCNTs-Ge-Le solution (25 μg mL<sup>-1</sup>). After tagging with rhodamine 123, the MWCNTs-Ge-Le was observed to be internalized within the MCF-7 cells within 3 h followed by dose-dependent antiproliferative effects. MWCNTs-Ge-Le combined with NIR irradiation exhibited remarkable inhibitory effects on cancer cells. The temperature of tumor site increased to 42.6 °C on treatment with MWCNTs-Ge-Le in presence of 808 nm laser NIR irradiation (1 W cm<sup>-2</sup>, 3 min). This was attributed to maximum accumulation of MWCNTs-Ge-Le nanoparticles at the tumor site through EPR effect. Hence, this synergistic strategy of combining drug therapy with near-infrared photothermal therapy can be a powerful tool for treatment and management of cancer.

In another study, Yoo et al. designed a nanocomposite (MWCNTs-Met/PEG) by functionalizing an antidiabetic drug metformin (MET) on the MWCNTs via PEGylation [38]. The nanocomposite metformin and PEG content of 22.5% and 15.7%, respectively. MWNTs-Met/PEG solution rapidly increased beyond 45 °C under 2 W cm<sup>-2</sup> NIR irradiation confirming the photothermal effect of the MWCNTs-Met/PEG toward induction of strong localized heating associated pro-apoptosis.





**Fig. 8** **a** Approach for preparing MWNTs-Ge-Le; **b** In vivo antitumor effect. Infrared thermographic images of tumor-bearing mice after treatment with PBS, gemcitabine, MWNTs, MWNTs-Ge and MWNTs-Ge-Le followed by laser irradiation. The scale bar is different for each image; **c** Average tumor volume in a MCF-7 tumor-bearing mice model of treatment without laser in vivo; **d** Average tumor volume in a MCF-7 tumor-bearing mice model of treatment with laser in vivo. The relative tumor volumes were normalized to their initial size ( $n = 4$  for each group). The bars are presented as mean  $\pm$  SEM (unpaired  $t$ -test,  $*P < 0.05$  compared with all the other experimental groups;  $\blacktriangle P < 0.05$  compared with PBS group, gemcitabine group, MWNTs group and MWNTs-Ge group). **Abbreviations:** EDAC 1-(3-dimethylaminopropyl)-3-ethylcarbodiimide; MWNTs multiwalled carbon nanotubes; MWNTs-COOH oxidized multiwalled carbon nanotubes; MWNTs-Ge multiwalled carbon nanotubes/gemcitabine; MWNTs-Ge-Le multiwalled carbon nanotubes/gemcitabine/lentinan; NHS  $N$ -hydroxysulfosuccinimide; MCF-7 Michigan cancer foundation-7; NIR near-infrared; PBS phosphate-buffered solution; SEM standard error of the mean. Reprinted with permission from Zhang et al. [37] Copyright 2018 Dove Medical Press Limited

Internalization within HepG-2 cells took place in 3 h. Cell viability in the HepG-2 cells drastically fell to  $5.7 \pm 1.2\%$  on treatment with MWNTs-Met/PEG in combination with NIR irradiation.

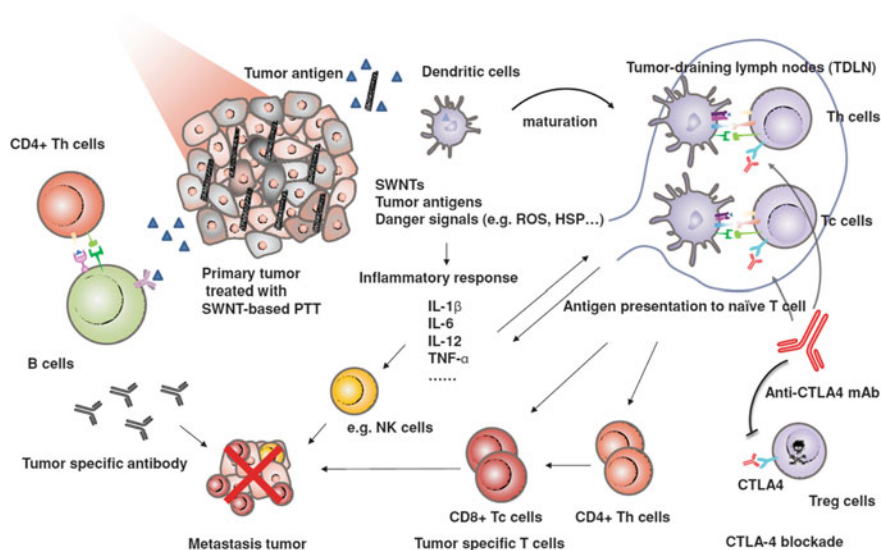
## 2.5 Immune-Photothermal Therapy

Although PTT is effective for treating cancer cells locally as they are sensitive to high temperature, weak immunogenicity of tumors is a major challenge. Hence, combination of PTT and active immunological stimulation can synergistically improve the effectiveness of the anticancer therapy. Zhou et al. designed immunologically modified SWCNTs-based system employing an immunoadjuvant, glycosylated chitosan (GC) denoted as SWCNTs-GC [39]. A concentration and laser dose-dependent rise in temperature from 30 to 60 °C was observed when the SWCNT-GC was irradiated with a 980 nm laser at 0.5–1 W/cm<sup>2</sup> for 120 s. SWNT-GC exhibited superior stimulation of NO production in macrophages along with expression of CD80 indicating the maturation of dendritic cells. The SWNT-GC tagged with FITC entered into EMT6 cells and accumulated in the cytoplasm. The nanocomposite also accumulated in the RAW264.7 cells owing to phagocytosis in macrophages and stimulated a higher level of IFN $\gamma$  secretion. Mouse mammary tumor developed by injecting EMT6 cells in the flank of Balb/c female mice was treated with SWNT-GC in combination with laser irradiation with a power density of 0.75 W/cm<sup>2</sup> for 10 min and showed drastic elevation in the temperature. Within 2 min, the tumor tissue surface temperature rose to 62 °C that began to plateau after 5 min at 72 °C which resulted in induction of 89.2% apoptosis.

In another extensive study by Wang et al., photothermal ablation of primary tumors with SWCNTs in combination with anticytotoxic T lymphocyte antigen-4 (CTLA-4) antibody therapy was demonstrated to be highly effective against tumor metastasis in mice as schematically illustrated in Fig. 9 [40]. The SWCNTs were non-covalently modified using polyethylene glycol (PEG)-grafted amphiphilic polymer. This composite not only destroyed tumor due to photothermal properties but also triggered the release of tumor-associated antigens and served as an immunological adjuvant facilitating the maturation of bone marrow-derived dendritic cells (DCs) separated from BALB/c mice. Further, the PEGylated SWCNTs up-regulated the expression of CD86 and CD80 along with enhancement of interleukin IL-1 $\beta$  and IL-12 secretion by DCs. The nanomaterial treated mice bearing subcutaneous 4T1 murine breast tumors showed high tumor ablation on irradiation with an 808-nm NIR laser at 0.5 W/cm<sup>2</sup> for 10 min due to dramatic temperature elevation to 53 °C in the tumor tissues. It is important to note that this therapeutic strategy completely eliminated all tumors in mice without showing a single case of tumor relapse at their original sites after treatment. SWCNTs-based PTT mediated enhancement in the secretion of pro-inflammatory cytokines IL-1 $\beta$ , IL-12p70, IL-6, and TNF- $\alpha$  was

speculated as the key immunomodulatory effect behind the effective tumor inhibition. Additionally, anti-CTLA-4 antibody is able to target CTLA-4, which is constitutively expressed by regulatory T cells (Tregs) and up-regulated after T cell activation. Hence, SWNT-based PTT-associated CTLA-4 blockade may favor the infiltration of effective T cells while greatly abrogate regulatory T cells at distant tumors. The study showed that primary tumor ablation employing SWNT-based PTT followed by CTLA-4 blockage significantly inhibited the development of secondary tumors. This might be attributed to the CD8<sup>+</sup> killer T cells [cytotoxic T (Tc) cells] mediated destruction of cancer cells by releasing cytotoxins perforin, granzymes, and granulysin that eventually result in apoptosis of targeted cancer cells. Moreover, a combination of SWNT-based PTT and anti-CTLA-4 therapy significantly reduced lung metastasis with less than 1 metastasis sites in lungs. Additional study in murine B16 musculus skin melanoma indicated that residues of both 4T1 cells and B16 cells after SWCNT-based PTT activated DC maturation.

In an innovative research, Kohshour et al. exploited trastuzumab (Herceptin®), a monoclonal antibody (mAb) for specific ablation of malignant breast cancer cells that over-expressed HER2 [41]. Proliferation of the cancer cells was effectively inhibited by MWCNTs-based nanoimmunoconjugate comprised of covalently immobilized trastuzumab conjugated to diphtheria toxin (DT). The cell viability of HER2-overexpressing SK-BR-3 cells was reduced to 70.42% and 80% by trastuzumab-MWCNT conjugates and trastuzumab-DT, respectively.



**Fig. 9** Hypothesized mechanism of antitumor immune responses induced by SWNT-based PTT in combination with the anti-CTLA-4 therapy. Reprinted with permission from Wang et al. [40] Copyright 2014 WILEY-VCH Verlag GmbH & Co. KGaA, Weinheim

## 2.6 Sonodynamic Therapy

Sonodynamic therapy (SDT) has come up as an innovative and effective strategy for treating solid cancers employing ultrasound irradiation of low-intensity along with a sonosensitizer. This therapeutic mode is advantageous due to its very low or negligible adverse effects and invasiveness, deep tissue penetration, and targeted uptake. Behzadpour et al. fabricated a polypyrrole-coated MWCNTs-based nanocomposite (PPy@MWCNTs) which exhibited superior sonosensitizing properties due to its efficient absorption of ultrasound irradiation by both of its components [42]. The PPy@MWCNTs were comprised nanotubes with  $36.3 \pm 5.1$  nm of diameter and several micrometer in length. Ultrasound irradiation at 1 MHz and  $1.0 \text{ W cm}^{-2}$  for 60 s resulted in rise in  $16.3 \pm 2.8$  °C increment in temperature. The nanocomposite exhibited a concentration-dependent cytotoxicity on multistep ultrasound irradiation against C540 (B16/F10) cell line and a melanoma tumor model in male balb/c mice. After ten days of SDT using PPy@MWCNTs, 75% necrosis was observed in the tumors that led to 50% decrement in tumor volume. The higher antitumorogenic properties could be attributed to the cumulative thermal effects and ROS generated during the PPy@MWCNTs-associated SDT.

In another study, Yumita et al. reported SDT using polyethylene glycol-modified carbon nanotubes (PEG-modified CNTs) [43]. Sonodynamic exposure to PEG-modified CNTs resulted in twofold cytotoxicity in sarcoma 180 cells which was attributed to the singlet oxygen generated during the treatment. Further, 100  $\mu\text{M}$  PEG-modified CNTs enhanced the nitroxide production up to threefold. Combination of ultrasound and PEG-modified CNTs synergistically inhibited the solid tumor growth in CDF1 mice with the carcinoma cells transplanted subcutaneously in the left dorsal scapula region. In a similar work, Bosca et al. fabricated a porphyrin grafted SWCNTs for SDT where three different porphyrins were covalently conjugated to SWCNTs using either Diels–Alder or 1,3-dipolar cycloadditions [44]. ROS production was enhanced and cell viability of the human colorectal cancer cell line (HT-29) significantly reduced upon ultrasound irradiation in spite of low porphyrin content indicating the efficiency of the therapy.

## 2.7 Chemo-Sonodynamic Therapy

Occasionally ultrasound-based SDT employ a sonosensitizer in combination with a chemotherapeutic agent which is referred as chemo-sonodynamic therapy. This strategy is more effective for treating cancer by induction of apoptosis and/or necrosis. Wang and Li encapsulated a sonosensitizer, protohemin (Ph) non-covalently into MWCNTs-COOH (MWCNTs-Ph) enhanced antitumor efficiency [45]. About 68.8% (w/w) Ph loading was achieved on MWCNTs-COOH carrier. In presence of ultrasound (1.0 MHz and  $0.5 \text{ W/cm}^2$  for 100 s), MWCNTs-Ph remarkably inhibited the growth of HepG-2 cells up to  $95 \pm 8.5\%$ . Tumor developed in mice

by subcutaneous injection of HepG-2 cells into the right armpit of nude BALB/c mice was inhibited more than 80% on treatment with MWCNTs-Ph and ultrasound together. Hence, MWCNTs-Ph-based cancer management can serve dual purpose of tumor inhibition and reduction of side effects. On a similar line, Wang et al. covalently attached oridonin-liposome containing microbubbles (LUMO) to folic acid-conjugated MWCNTs functionalized with protohemin (FMTP) to form a novel composite (FMTP-LUMO) [46]. Oridonin used in this composite is a chemotherapeutic drug for chemotherapy, whereas protohemin is a sonosensitizer as stated previously. In combination with ultrasound, the FMTP-LUMO inhibited the HepG-2 cells up to  $95.4 \pm 5.9\%$  which might be attributed to superior release profile (90%) of oridonin due to ultrasound exposure of 60 s. Further, FMTP-LUMO treated liver cancer induced by implantation of HepG-2 cells in BALB/c nude mice showed more than 90% tumor inhibition after ten days.

### 3 CNTs-Based Strategies Against Nervous System-Associated Cancer

Developing CNTs-based nanomedicine against cancer of the brain is one of the most challenging tasks which need thorough understanding about the physiological, biochemical, immunological, and genetic attributes of the cancer. The growing cancer cells generate a lot of pressure inside the skull and could be life-threatening. Cancer-associated uncontrolled cell growth in the brain forms a tumor-like mass in most cases and is commonly referred to as a brain tumor. A brain tumor is classified into two different classes based on its point of origin—primary and secondary type of brain tumor. Primary brain tumor originates in the brain itself while in the secondary brain, tumor metastasizes from another organ to the brain [47]. The primary brain tumor generally originates from glial cells and is referred to as glioma. There are four different grades of glioma based on size and growth (grade I–IV), grade I glioma does not infiltrate deep into the brain tissue and could be treated by surgical interventions, whereas grade IV glioma infiltrates deep into the brain tissue, called as glioblastoma are difficult for surgical interventions [48]. Stage IV glioblastoma is the most common type of brain cancer with 17,000 new diagnoses every year and is associated with a median survival rate of 14 months with poor life quality [48, 49].

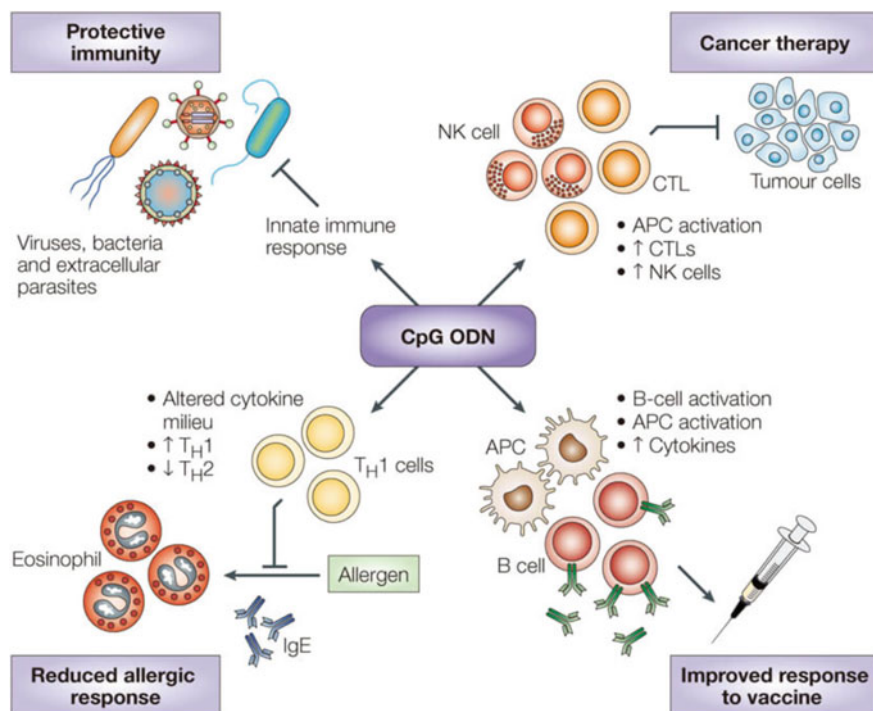
Currently, there is no complete cure for glioblastoma and the patients generally survive for less than two years [50–53]. The current treatment strategy includes the use of aggressive anticancer drugs, surgery, radiation, and chemotherapy [53–55]. Such aggressive treatment has a lot of side effects and with high chances of tumor recurrence; the patients typically die within two years of treatment. The treatment of glioblastoma is difficult even with radiation and chemotherapy due to the highly invasive nature of the brain tumor; thus, a targeted drug delivery system could be used for delivering anticancer or immunotherapeutic drugs [53].

CNTs are biocompatible, hollow, tubular nanostructures that have extensive therapeutic potential as a drug delivery system, imaging tool, and implantable devices in the nervous system as well [56]. The reason for the low success rate of brain tumor treatment lies mainly with the invasive nature of the tumor, and the penetration of the treatment molecule through the blood–brain barrier (BBB). The tumor is formed deep inside the brain tissue which is difficult to access by surgery or with radiation; therefore, a perfect drug delivery system is required to direct the therapeutic molecules to the brain tumor and cross the BBB. The latest understanding of molecular details and cellular pathways of glioblastoma is paving way for use of SWCNTs and MWCNTs for the treatment of brain gliomas due to their length/diameter ratio, electrical conductivity, biological compatibility, and easy conjugation with therapeutic or diagnostic molecules [53, 54, 57, 58].

One of the limiting factors in the treatment of glioblastoma is the migration or invasiveness of the tumor cells deep into the brain tissue. In a study, Alizadeh and colleagues demonstrated that CpG oligodeoxynucleotide (CpG ODN) bound with CNTs inhibits the migration of the glioblastoma cells via activating toll-like receptor 9 [53]. CpG ODN is a synthetic single-stranded DNA molecule that contains unmethylated cytosine and guanine motifs derived from bacterial DNA. Therapeutic mechanism of CpG ODN includes protective immunity, cancer therapy, increasing the response to the vaccine, and suppression of allergic reactions [59, 60]. Hence, the use of CpG with suitable CNTs can have multiple therapeutic potentials in cancer therapy as well as in modulating the immune response of the body as illustrated in Fig. 10.

SWCNTs conjugated with CpG (SWCNTs/CpG) showed greater immunostimulatory effects than compared to free CpG in glioma models [61, 62]. A single dose of intracranial injection of SWCNTs/CpG in a GL261 murine model eradicated the gliomas in 50–60% of the mice, suggesting the high efficacy of SWCNTs/CpG in cancer treatment [61]. Furthermore, the glioblastoma chemotherapy drug molecule temozolomide showed enhanced effect when combined with SWCNTs/CpG in the treatment of the glioma mouse model [62]. The *in vitro* glioma histology suggests that SWCNTs/CpG locally alters the invasive properties of the tumor by inhibiting the migration of glioma cells followed by decreased NF- $\kappa$ B activation and an overall reduction in intracellular ROS [53]. Thus, SWCNTs/CpG could be tested in future clinical trials for the treatment of glioblastoma due to its ability to activate the innate immune system and inhibit the migration of tumor cells to the brain tissue (migration of tumor cells is one of the most challenging aspects in treating glioblastoma).

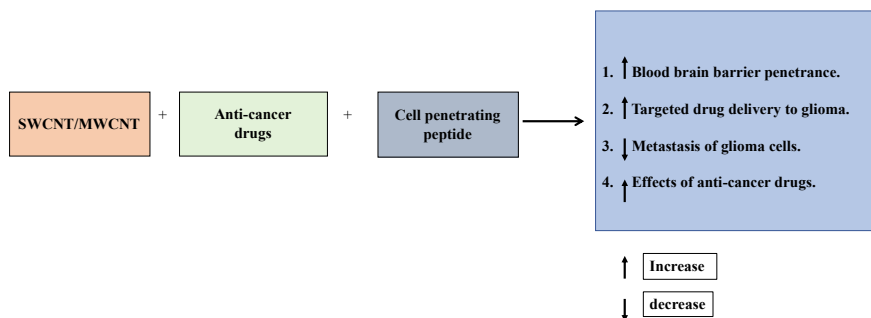
Another limiting aspect of brain tumor treatment is the delivery of therapeutic molecules across the blood–brain barrier (BBB) to the glioma [63]. BBB is a highly selective semipermeable membrane covering the central nervous system, made of tightly packed endothelial cells which prevent the passage of blood-borne pathogens and non-selective molecules from the circulating blood into the cerebrospinal fluid of the central nervous system [64]. In a study, MWCNTs conjugated with NH<sub>3</sub><sup>+</sup> were able to cross BBB in an *in vitro* model of BBB composed of porcine brain endothelial cells and rat primary astrocytes cells [65]. In cancer treatment, MWCNTs conjugated with cell-penetrating peptide (CPP) and anticancer molecule showed



**Fig. 10** Proposed therapeutic application of CpG based on the interaction of CpG with cells of the immune system. Reprinted with permission from Klinman [59]. Copyright 2004 Nature Publishing Group

enhanced BBB penetration and anticancer activity for glioma treatment [63]. CPP like trans-activating transcriptional activator (TAT) was used in the previous study to increase the permeability of BBB [66]. However, increasing the permeability also increases the chances of non-specific penetration of CPP [67]. You and colleagues have designed and synthesized MWCNTs loaded with TAT and anticancer drug oxaliplatin for the precise targeting of glioma. The results of this study suggest that the MWCNTs with TAT and oxaliplatin were more cytotoxic to the glioma cells compared to free oxaliplatin [63]. Thus, SWCNT and MWCNT could be effectively be used as drug delivery machinery which could cross the BBB and specifically target the brain tumor cells inhibiting its further migration into the deep brain tissue. However, more detailed studies are required to completely establish the molecular mechanism of CNTs interactions in brain tumor treatment before it could be tested in clinical trials. Figure 11 summarizes the key points that could be achieved by the use of CNTs in brain cancer treatment.

The brain is not the only organ of the nervous system that is affected by cancer; the cancer of the retina called retinoblastoma, is one of the most common types of intraocular cancer mostly affecting young children [68, 69]. The most common symptom of



**Fig. 11** Therapeutic potential of CNTs in brain tumor treatment

retinoblastoma is visible whiteness in the pupil of the eye called Leukocoria, noticeable in dim light [70]. Retinoblastoma is highly sensitive to chemotherapy treatment and can be treated by injecting chemotherapy drugs either directly in the ocular cavity or intravenously [68]. The use of CNTs in retinoblastoma treatment can further enhance the uptake of chemotherapy drugs during the treatment. The retinoblastoma cells have a high affinity for folic acid and biotin because of the enrichment of folate and biotin receptors on retinoblastoma cells [71–73]. Demirci and colleagues had demonstrated that CNTs conjugated with fluorescein isothiocyanate and folic acid/ biotin (CNTs-FITC-FA/Bio) injected into the vitreous humor of the transgenic retinoblastoma mice model show high penetration into the retinoblastoma cells [74]. In view of the background, CNTs-FITC-FA/Bio composite can serve as a promising drug delivery system for the delivery of chemotherapeutic agents for treatment of intraocular tumors [74]. The studies so far suggest the potential application of CNTs in the treatment of cancers of the nervous system. However, the details regarding the cytotoxicity and uptake of CNTs by the nervous system are not completely understood, which is one of the limiting factors for potential use of CNTs for treating nervous system-associated cancers.

## 4 Future Perspectives

Development of cancer drug resistance is major challenge for the existing chemotherapeutic strategy. Hence, nanotechnology-driven solutions are thought to be better candidates with multimodal therapeutic perspectives. Cancer therapy combining chemoradiation with sonodynamic therapy has been shown to decrease tumor growth in pancreatic cancer cellular models [75]. Gold nanoparticles release heat through a light-driven surface plasmonic process [76–78]. Similarly, conjugation of organic polymer particles has shown high heat transfer efficiencies [79–81]. Hence, getting synergistic efficacy by combinatorial approaches has been a topic of research to enhance cancer therapeutic efficacy. Combination of chemotherapeutic drugs with



CNTs-associated photothermal treatments can show promising for various cancer treatments that can be confirmed using cell-based *in vitro* studies and in mouse models. Photothermal treatment employing CNTs combined with daunorubicin and cytarabine may promote cell apoptosis [82]. Likewise, doxorubicin encapsulation in poly N-isopropylacrylamide-co-acrylic acid (PNA) gel in combination with CNTs mediated photothermal therapy can be an effective strategy to inhibit tumor cells [83]. Doxycycline encapsulated in photothermal agent polydopamine (PDA) has been shown to be effective in the treatment of oral squamous cell carcinoma cell lines which may further be enhanced by conjugating with SWCNTs or MWCNTs [84].

Multi drug resistance (MDR) is a major problem due to use of a single drug and combination therapy serves as a promising approach to overcome the MDR. Delivery of CNTs with doxorubicin may reduce the chemoresistance in combination of photothermal therapy against drug resistant hepatocellular carcinoma in mouse [85]. Also, ribonuclease A (RNase A) conjugated gold nanoparticles are used in combination of photothermal therapy of colon cancer cells, which in turn may be synergistically enhanced in presence of CNTs [86]. CNTs-based photothermal therapy with immune-adjuvant nanoparticles together may attribute to checkpoint blockade for effective cancer immunotherapy [81]. Quantum dots based on black phosphorus in combination with CNTs-based photothermal therapy may effectively inhibit relapse and metastasis in triple-negative breast cancer (TNBC), which is one of the aggressive cancer types to treat and causes high mortality [87]. Likewise CoFe<sub>2</sub>O<sub>4</sub>-quantum dots functionalized on SWCNTs/MWCNTs may exhibit synergistic photothermal therapy in non-small-cell lung carcinoma due to induction of apoptosis by downregulating AKT signaling pathway [88–91]. Sonosensitizers such as, adriamycin, hematoporphyrin, ATX-70, pheophorbide A, ATXS10, and porfimer sodium, may act as sonosensitizer which can be functionalized on CNTs along with anticancer drugs with effective chemo-sono-photo-dynamic properties [92, 93].

Insolubility of CNTs in water is a key obstacle for gastrointestinal absorption, blood transportation, secretion, and biocompatibility and so on. Hence, dispersion can be ensured by developing strategies for wetting the hydrophobic tube surfaces and modifying the tube surfaces to decrease tube's bundle formation. Foldvari et al. have proposed four basic approaches for ensuring the uniform dispersion of CNTs in the aqueous medium which can be summarized as follows: (1) surfactant-assisted dispersion, (2) solvent dispersion, (3) functionalization of side walls, and (4) biomolecular dispersion. Among the above mentioned strategies, functionalization with hydrophilic moieties is considered as the most effective approach [94].

Cellular uptake of CNTs is a prerequisite for the therapeutic activity. Hence, proper distribution at the target sites and selective retention at the place of delivery are of great importance in clinical pharmacology of CNTs as drug carriers. PEG chain lengths is a key determining factor of the biodistribution and circulation of CNTs. PEG-5400-modified SWCNTs have a circulation time ( $t_{1/2} = 2$  h) much longer than that of PEG-2000-modified counterpart ( $t_{1/2} = 0.5$  h). Further, functionalization of the arginine-glycine-aspartic acid (RGD) peptide with the PEGylated SWCNTs facilitates the accumulation in integrin-positive U87MG tumors.

Moreover, adsorption of the shorter chain PEG (PL-PEG-2000) to CNTs cannot protect them from macrophagocytosis. However, adsorption of longer chain PEG (PL-PEG-5000) can effectively reduce nonspecific uptake of CNTs. It is important to note that functionalization of CNTs with PEG grafted branched polymers, namely poly(maleicanhydride-alt-1-octadecene)-PEG methyl ethers (PMHC18-mPEG) and poly (g-glutamic acid)-pyrine(30%)-PEG methylethers (70%) (gPGA-Py-mPEG), can enhance circulation time in the blood after intravenous injection [95].

The morphology of CNTs plays a crucial role in determining its drug loading capacity and delivery. The wall of CNTs results from rolling up of either single or multiple layers of graphene sheets forming SWCNTs or MWCNTs, respectively. Both SWCNTs and MWCNTs are capped at both ends of the tubes in a hemispherical arrangement of carbon networks called fullerenes warped up by the graphene sheet. Although the CNTs have various lengths from several hundreds of nanometers to several micrometers, they can be rationally shortened chemically or physically for their suitability for drug carriers. Opening both ends with useful wall defects facilitates intratube drug loading and chemical functionalization. Also, appropriate chemical treatment can result in development of desired charge on the surface of the nanotube that enable ionic interactions mediated adsorption of the charged molecules like drugs, targeting ligands and contrast agents. Aromatic molecules, nucleic acids and amphiphilic peptides can be functionalized based on the  $\pi$ - $\pi$  stacking interactions between the CNT surface and aromatic bases/amino acids resulting in enhanced solubility and dispersion [95].

Another effective novel system developed by Li et al. is “dual-targeted drug nanocarrier” which was first reported by conjugating MWCNTs with iron nanoparticles and folate molecules [96]. Conjugation with targeted moieties of folate (FA) and an external magnetic field together facilitated the targeted delivery of doxorubicin into the HeLa cells. Similarly, FA-modified SWCNTs for targeted delivery of cisplatin into Ntera-2 cells, phosphatidylserine-modified SWCNTs for delivering cytochrome C into phagocytic cells, NPs-modified multiwall carbon nanotube (MWCNT) for delivering gemcitabine into lymph nodes and antibody-modified SWCNTs for delivering doxorubicin (Dox) into WiDr cells are examples for promising targeted delivery using CNTs. Such delivery systems can further be conjugated with magnetic probes for designing an effective dual targeting nanoplatform. This will ensure the delivery of anticancer drugs by guiding the nanocarriers to cancer sites efficiently using both receptor–ligand interaction and an external magnetic field.

Hence, several key factors should be considered before developing an ideal nanomedicine based on CNTs for effecting targeting and drug delivery in cancer.

## 5 Conclusions

Although, phototherapy alone has been effective against the cancer treatment since decades, Recent studies show promises for the CNTs mediated combination

therapy which can provide synergistic treatment modalities. Combination of CNTs-based phototherapy with chemotherapy may address the emerging chemoresistance among cancer cells. Similarly, combination of phototherapy with immunomodulatory inhibitors may provide great opportunities for synergistic personalized medicine. Immune checkpoint inhibitors and radiosensitizers combined with CNTs may offer novel combination to treat metastatic cancers. However, there is still a need for investigating the novel combinations of phototherapy with either chemotherapeutic agents or immunomodulatory inhibitors. Investigation of the most effective combination and performing further toxicological, pharmacokinetic and pharmacodynamic studies to confirm the efficacy and safety of CNTs-based nanomedicine for treatment and management of cancer would further help in establishing their therapeutic promises and safety.

**Conflict of Interest** The authors declare that there are no conflicts of interest.

## References

1. Sung H, Ferlay J, Siegel RL, Laversanne M, Soerjomataram I, Jemal A, Bray F (2021) Global cancer statistics 2020: GLOBOCAN estimates of incidence and mortality worldwide for 36 cancers in 185 countries. *CA Cancer J Clin* 71(3):209–249
2. Iwamoto T (2013) Clinical application of drug delivery systems in cancer chemotherapy: review of the efficacy and side effects of approved drugs. *Biol Pharm Bull* 36(5):715–718
3. Hossein Z, Ahmadi S, Ghasemi A, Ghanbari M, Rabiee N, Bagherzadeh M, Karimi M, Webster TJ, Hamblin MR, Mostafavi E (2021) Carbon nanotubes: smart drug/gene delivery carriers. *Int J Nanomedicine* 16:1681–1706
4. Zarghami Dehaghani M, Yousefi F, Sajadi SM, Tajammal Munir M, Abida O, Habibzadeh S, Mashhadzadeh AH, Rabiee N, Mostafavi E, Saeb MR (2021) Theoretical encapsulation of fluorouracil (5-FU) anti-cancer chemotherapy drug into carbon nanotubes (CNT) and boron nitride nanotubes (BNNT). *Molecules* 26(16):4920
5. Mostafavi E, Soltantabar P, Webster TJ (2019) Nanotechnology and picotechnology: a new arena for translational medicine. In: *Biomaterials in translational medicine*. Academic Press, pp 191–212
6. Ghosh S, Harke AN, Chacko MJ, Gurav SP, Joshi KA, Dhepe A, Dewle A, Tomar GB, Kitture R, Parihar VS, Banerjee K, Kamble N, Bellare J, Chopade BA (2016) *Gloriosa superba* mediated synthesis of silver and gold nanoparticles for anticancer applications. *J Nanomed Nanotechnol* 7:4
7. Rokade S, Joshi K, Mahajan K, Patil S, Tomar G, Dubal D, Parihar VS, Kitture R, Bellare JR, Ghosh S (2018) *Gloriosa superba* mediated synthesis of platinum and palladium nanoparticles for induction of apoptosis in breast cancer. *Bioinorg Chem Appl* 2018:4924186
8. Rokade SS, Joshi KA, Mahajan K, Tomar G, Dubal DS, Parihar VS, Kitture R, Bellare J, Ghosh S (2017) Novel anticancer platinum and palladium nanoparticles from *Barleria prionitis*. *Glob J Nanomedicine* 2(5):555600
9. Ghosh S, Nitnavare R, Dewle A, Tomar GB, Chippalkatti R, More P, Kitture R, Kale S, Bellare J, Chopade BA (2015) Novel platinum-palladium bimetallic nanoparticles synthesized by *Dioscorea bulbifera*: anticancer and antioxidant activities. *Int J Nanomedicine* 10(1):7477–7490

10. Ghosh S, More P, Derle A, Kitture R, Kale T, Gorain M, Avasthi A, Markad P, Kundu GC, Kale S, Dhavale DD, Bellare J, Chopade BA (2015) Diosgenin functionalized iron oxide nanoparticles as novel nanomaterial against breast cancer. *J Nanosci Nanotechnol* 15(12):9464–9472
11. Ghosh S (2019) Mesoporous silica based nano drug delivery system synthesis, characterization and applications. In: Mohapatra SS, Ranjan S, Dasgupta N, Mishra RK, Thomas S (eds) *Nanocarriers for drug delivery*. Elsevier Inc. Amsterdam, pp 285–317. ISBN: 978-0-12-814033-8
12. Kitture R, Ghosh S (2019) Hybrid nanostructures for in-vivo imaging. In: Bohara RA, Thorat N (eds) *Hybrid nanostructures for cancer theranostics*. Elsevier Inc. Amsterdam, pp 173–208, eBook ISBN: 9780128139073; Paperback ISBN:9780128139066
13. Ghosh S, Patil PD, Kitture RD (2019) Physically responsive nanostructures in breast cancer theranostics. In: Thorat ND, Bauer J (eds) *External field and radiation stimulated breast cancer nanotheranostics*. IOP Publishing Ltd, United Kingdom, pp 2-1–2-24. Online ISBN: 978-0-7503-2416-8; Print ISBN: 978-0-7503-2414-4
14. Dizaji BF, Khoshbakht S, Farboudi A, Azarbaijan MH, Irani M (2020) Far-reaching advances in the role of carbon nanotubes in cancer therapy. *Life Sci* 257:118059
15. Liang X, Shang W, Chi C, Zeng C, Wang K, Fang C, Chen Q, Liu H, Fan Y, Tian J (2016) Dye-conjugated single-walled carbon nanotubes induce photothermal therapy under the guidance of near-infrared imaging. *Cancer Lett* 383(2):243–249
16. Hernandez-Rivera M, Zaihaq NG, Wilson LJ (2016) Toward carbon nanotube-based imaging agents for the clinic. *Biomaterials* 101:229–240
17. Lu GH, Shang WT, Deng H, Han ZY, Hu M, Liang XY, Fang CH, Zhu XH, Fan YF, Tian J (2019) Targeting carbon nanotubes based on IGF-1R for photothermal therapy of orthotopic pancreatic cancer guided by optical imaging. *Biomaterials* 195:13–22
18. Nikfarjam M, Muralidharan V, Christophi C (2005) Mechanisms of focal heat destruction of liver tumors. *J Surg Res* 127:208–223
19. He X (2011) Thermostability of biological systems: fundamentals, challenges, and quantification. *Open Biomed Eng J* 5:47–73
20. Burke AR, Singh RN, Carroll DL, Wood JC, D’Agostino RB, Ajayan PM, Torti FM, Torti SV (2012) The resistance of breast cancer stem cells to conventional hyperthermia and their sensitivity to nanoparticle-mediated photothermal therapy. *Biomaterials* 33:2961–2970
21. Singh R, Torti SV (2013) Carbon nanotubes in hyperthermia therapy. *Adv Drug Deliv Rev* 65:2045–2060
22. Virani NA, Davis C, McKernan P, Hauser P, Hurst RE, Slaton J, Silvy RP, Resasco DE, Harrison RG (2018) Phosphatidylserine targeted single-walled carbon nanotubes for photothermal ablation of bladder cancer. *Nanotechnology* 29:035101
23. Behnam MA, Emami F, Sobhani Z, Koohi-Hosseinabadi O, Dehghanian AR, Zebarjad SM, Moghim MH, Oryan A (2018) Novel combination of silver nanoparticles and carbon nanotubes for plasmonic photo thermal therapy in melanoma cancer model. *Adv Pharm Bull* 8(1):49–55
24. Sobhani Z, Behnam MA, Emami F, Dehghanian A, Jamhiri I (2017) Photothermal therapy of melanoma tumor using multiwalled carbon nanotubes. *Int J Nanomedicine* 12:4509–4517
25. Suo X, Eldridge BN, Zhang H, Mao C, Min Y, Sun Y, Singh R, Ming X (2018) P-glycoprotein-targeted photothermal therapy of drug-resistant cancer cells using antibody-conjugated carbon nanotubes. *ACS Appl Mater Interfaces* 10:33464–33473
26. Dolmans DE, Fukumura D, Jain RK (2003) Photodynamic therapy for cancer. *Nat Rev Cancer* 3(5):380–387
27. Fukuda R, Umeyama T, Tsujimoto M, Ishidate F, Tanaka T, Kataura H, Imahori H, Murakami T (2020) Sustained photodynamic effect of single chirality-enriched single walled carbon nanotubes. *Carbon* 161:718–725
28. Ogbodu RO, Limson JL, Prinsloo E, Nyokong T (2015) Photophysical properties and photodynamic therapy effect of zinc phthalocyanine-spermine-single walled carbon nanotube conjugate on MCF-7 breast cancer cell line. *Synth Met* 204:122–132
29. Ogbodu RO, Nyokong T (2015) The effect of ascorbic acid on the photophysical properties and photodynamic therapy activities of zinc phthalocyanine-single walled carbon nanotube conjugate on MCF-7 cancer cells. *Spectrochim Acta A Mol Biomol Spectrosc* 151:174–183

30. Sundaram P, Abrahamse H (2020) Effective photodynamic therapy for colon cancer cells using chlorin e6 coated hyaluronic acid-based carbon nanotubes. *Int J Mol Sci* 21:4745
31. Cheng J, Liang H, Li Q, Peng C, Li Z, Shi S, Yang L, Tian Z, Tian Y, Zhang Z, Cao W (2010) Hematoporphyrin monomethyl ether-mediated photodynamic effects on THP-1 cell-derived macrophages. *J Photochem Photobiol B* 101(1):9–15
32. Shi J, Ma R, Wang L, Zhang J, Liu R, Li L, Liu Y, Hou L, Yu X, Gao J, Zhang Z (2013) The application of hyaluronic acid-derivatized carbon nanotubes in hematoporphyrin monomethyl ether-based photodynamic therapy for in vivo and in vitro cancer treatment. *Int J Nanomedicine* 8:2361–2373
33. Wang H, Pan X, Wang X, Wang W, Huang Z, Gu K, Liu S, Zhang F, Shen H, Yuan Q, Ma J, Yuan W, Liu H (2020) Degradable carbon–silica nanocomposite with immunoadjuvant property for dual-modality photothermal/photodynamic therapy. *ACS Nano* 14:2847–2859
34. Zhang M, Wang W, Cui Y, Chu X, Sun B, Zhou N, Shen J (2018) Magneto-fluorescent Fe<sub>3</sub>O<sub>4</sub>/carbon quantum dots coated single-walled carbon nanotubes as dual-modal targeted imaging and chemo/photodynamic/photothermal triple-modal therapeutic agents. *Chem Eng J* 338:526–538
35. Li H, Zhang N, Hao Y, Wang Y, Jia S, Zhang H (2019) Enhancement of curcumin antitumor efficacy and further photothermal ablation of tumor growth by single-walled carbon nanotubes delivery system in vivo. *Drug Deliv* 26(1):1017–1026
36. Yi W, Zhang P, Hou J, Chen W, Bai L, Yoo S, Khalid A, Hou X (2018) Enhanced response of tamoxifen toward the cancer cells using a combination of chemotherapy and photothermal ablation induced by lentinan-functionalized multi-walled carbon nanotubes. *Int J Biol Macromol* 120:1525–1532
37. Zhang P, Yi W, Hou J, Yoo S, Jin W, Yang Q (2018) A carbon nanotube-gemcitabine-lentinan three-component composite for chemo-photothermal synergistic therapy of cancer. *Int J Nanomedicine* 13:3069–3080
38. Yoo S, Hou J, Yi W, Li Y, Chen W, Meng L, Si J, Hou X (2017) Enhanced response of metformin towards the cancer cells due to synergism with multi-walled carbon nanotubes in photothermal therapy. *Sci Rep* 7:1071
39. Zhou F, Wu S, Song S, Chen WR, Resasco DE, Xing D (2012) Antitumor immunologically modified carbon nanotubes for photothermal therapy. *Biomaterials* 33(11):3235–3242
40. Wang C, Xu L, Liang C, Xiang J, Peng R, Liu Z (2014) Immunological responses triggered by photothermal therapy with carbon nanotubes in combination with anti-CTLA-4 therapy to inhibit cancer metastasis. *Adv Mater* 26(48):8154–8162
41. Kohshour MO, Mirzaie S, Zeinali M, Amin M, Hakhmaneshi MS, Jalili A, Mosaveri N, Jamalani M (2014) Ablation of breast cancer cells using trastuzumab-functionalized multi-walled carbon nanotubes and trastuzumab-diphtheria toxin conjugate. *Chem Biol Drug Des* 83:259–265
42. Behzadpour N, Ranjbar A, Azarpira N, Sattarahmady N (2020) Development of a composite of polypyrrole-coated carbon nanotubes as a sonosensitizer for treatment of melanoma cancer under multi-step ultrasound irradiation. *Ultrasound Med Biol* 46(9):2322–2334
43. Yumita N, Iwase Y, Umemura SI, Chen FS, Momose Y (2020) Sonodynamically-induced anti-cancer effects of polyethylene glycol-modified carbon nanotubes. *Anticancer Res* 40(5):2549–2557
44. Bosca F, Corazzari I, Foglietta F, Canaparo R, Durando G, Pastero L, Arpicco S, Dosio F, Zonari D, Cravotto G, Tagliapietra S (2020) SWCNT–porphyrin nano-hybrids selectively activated by ultrasound: an interesting model for sonodynamic applications. *RSC Adv* 10(37):21736–21744
45. Wang CJ, Li W (2016) Preparation and sonodynamic antitumor effect of protohemin-conjugated multiwalled carbon nanotubes functionalized with carboxylic group. *Drug Dev Res* 77:152–158
46. Wang CJ, Wang HZ, Li W (2019) A novel conjunction of folate-targeted carbon nanotubes containing protohemin and oridonin-liposome loaded microbubbles for cancer chemosonodynamic therapy. *J Drug Target* 27(10):1076–1083

47. Bhowmik A, Khan R, Ghosh MK (2015) Blood-brain barrier: a challenge for effectual therapy of brain tumors. *Biomed Res Int* 2015:320941. <https://doi.org/10.1155/2015/320941>
48. Omuro A, DeAngelis LM (2013) Glioblastoma and other malignant gliomas: a clinical review. *JAMA* 310(17):1842–1850
49. Salazar A, Cruz VP la, Muñoz-Sandoval E, Chavarria V, Morales M de LG, Espinosa-Bonilla A, Sotelo J, Jiménez-Anguiano A, Pineda B (2021) Potential use of nitrogen-doped carbon nanotube sponges as payload carriers against malignant glioma. *Nanomaterials*-base1 11(5):1244
50. Stupp R, Mason WP, van den Bent MJ, Weller M, Fisher B, Taphoorn MJB, Belanger K, Brandes AA, Marosi C, Bogdahn U, Curschmann J, Janzer RC, Ludwin SK, Gorlia T, Allgeier A, Lacombe D, Cairncross JG, Eisenhauer E, Mirimanoff RO (2005) Radiotherapy plus concomitant and adjuvant temozolomide for glioblastoma. *New Engl J Med* 352(10):987–996
51. Zhao D, Badie B (2007) Application of carbon nanotubes to brain tumor therapy. *Nanotechnologies for the life sciences*. Wiley-VCH Verlag GmbH & Co. KGaA, pp 381–402
52. Stupp R, Hegi ME, Mason WP, Bent MJ van den, Taphoorn MJB, Janzer RC, Ludwin SK, Allgeier A, Fisher B, Belanger K, Hau P, Brandes AA, Gijtenbeek J, Marosi C, Vecht CJ, Mokhtari K, Wesseling P, Villa S, Eisenhauer E, Gorlia T, Weller M, Lacombe D, Cairncross JG, Mirimanoff R-O, Groups EO for R and T of CBT and RO, Group NCI of CCT (2009) Effects of radiotherapy with concomitant and adjuvant temozolomide versus radiotherapy alone on survival in glioblastoma in a randomised phase III study: 5-year analysis of the EORTC-NCIC trial. *Lancet Oncol* 10(5):459–66
53. Alizadeh D, White EE, Sanchez TC, Liu S, Zhang L, Badie B, Berlin JM (2018) Immunostimulatory CpG on carbon nanotubes selectively inhibits migration of brain tumor cells. *Bioconjugate Chem* 29(5):1659–1668
54. Davis M (2016) Glioblastoma: overview of disease and treatment. *Clin J Oncol Nurs* 20(5):S2–S8
55. Wen PY, Reardon DA (2016) Progress in glioma diagnosis, classification and treatment. *Nat Rev Neurol* 12(2):69–70
56. Gheith MK, Pappas TC, Liopo AV, Sinani VA, Shim BS, Motamedi M, Wicksted JP, Kotov NA (2006) Stimulation of neural cells by lateral currents in conductive layer-by-layer films of single-walled carbon nanotubes. *Adv Mater* 18(22):2975–2979. <https://doi.org/10.1002/adma.200600878>
57. Singh R, Pantarotto D, Lacerda L, Pastorin G, Klumpp C, Prato M, Bianco A, Kostarelos K (2006) Tissue biodistribution and blood clearance rates of intravenously administered carbon nanotube radiotracers. *Proc National Acad Sci* 103(9):3357–3362
58. Kievit FM, Zhang M (2011) Cancer therapy: cancer nanotheranostics: improving imaging and therapy by targeted delivery across biological barriers. *Adv Mater* 23(36):H209–H209
59. Klinman DM (2004) Immunotherapeutic uses of CpG oligodeoxynucleotides. *Nat Rev Immunol* 4(4):249–259. <https://doi.org/10.1038/nri1329>
60. Jahrsdörfer B, Weiner GJ (2008) CpG oligodeoxynucleotides as immunotherapy in cancer. *Updat Cancer Ther* 3(1):27–32
61. Zhao D, Alizadeh D, Zhang L, Liu W, Farrukh O, Manuel E, Diamond DJ, Badie B (2010) Carbon nanotubes enhance CpG uptake and potentiate anti-glioma immunity. *Clin Cancer Res* 17(4):771–782
62. Ouyang M, White EE, Ren H, Guo Q, Zhang I, Gao H, Yanyan S, Chen X, Weng Y, Fonseca AD, Shah S, Manuel ER, Zhang L, Vonderfecht SL, Alizadeh D, Berlin JM, Badie B (2016) Metronomic doses of temozolomide enhance the efficacy of carbon nanotube CpG immunotherapy in an invasive glioma model. *PLoS ONE* 11(2):e0148139
63. You Y, Wang N, He L, Shi C, Zhang D, Liu Y, Luo L, Chen T (2018) Designing dual-functionalized carbon nanotubes with high blood-brain-barrier permeability for precise orthotopic glioma therapy. *Dalton Transactions Camb Engl* 48(5):1569–1573
64. Daneman R, Prat A (2015) The blood-brain barrier. *Csh Perspect Biol* 7(1):a020412
65. Kafa H, Wang JT-W, Rubio N, Venner K, Anderson G, Pach E, Ballesteros B, Preston JE, Abbott NJ, Al-Jamal KT (2015) The interaction of carbon nanotubes with an in vitro blood-brain barrier model and mouse brain in vivo. *Biomaterials* 53:437–452

66. Zhao X, Shang T, Zhang X, Ye T, Wang D, Rei L (2016) Passage of magnetic tat-conjugated Fe<sub>3</sub>O<sub>4</sub>@SiO<sub>2</sub> nanoparticles across in vitro blood-brain barrier. *Nanoscale Res Lett* 11(1):451
67. Gump JM, Dowdy SF (2007) TAT transduction: the molecular mechanism and therapeutic prospects. *Trends Mol Med* 13(10):443–448
68. Kaliki S, Shields CL (2015) Retinoblastoma: achieving new standards with methods of chemotherapy. *Indian J Ophthalmol* 63(2):103–109
69. Young JL, Smith MA, Roffers SD, Liff JM, Bunin GR (2012) Retinoblastoma. In: Ries LA, Smith MA, Gurney JG, Linet M, Tamra T, Young JL et al (eds) *Cancer incidence and survival among children and adolescents: United States SEER program 1975–1995*. National Cancer Institute, Maryland, SEER Program
70. Murphy D, Bishop H, Edgar A (2012) Leukocoria and retinoblastoma—pitfalls of the digital age? *Lancet Lond Engl* 379(9835):2465
71. Kansara V, Luo S, Balasubrahmanyam B, Pal D, Mitra AK (2006) Biotin uptake and cellular translocation in human derived retinoblastoma cell line (Y-79): a role of hSMVT system. *Int J Pharmaceut* 312(1–2):43–52
72. Kansara V, Paturi D, Luo S, Gaudana R, Mitra AK (2007) Folic acid transport via high affinity carrier-mediated system in human retinoblastoma cells. *Int J Pharmaceut* 355(1–2):210–219
73. Jwala J, Vadlapatla RK, Vadlapudi AD, Boddu SHS, Pal D, Mitra AK (2012) Differential expression of folate receptor-alpha, sodium-dependent multivitamin transporter, and amino acid transporter (B(0, +)) in human retinoblastoma (Y-79) and retinal pigment epithelial (ARPE-19) cell lines. *J Assoc Ocular Pharmacol Ther* 28(3):237–244
74. Demirci H, Wang Y, Li Q, Lin C-M, Kotov NA, Grisolia ABD, Guo JL (2020) Penetration of carbon nanotubes into the retinoblastoma tumor after intravitreal injection in LH<sub>BETA</sub>T<sub>AG</sub> transgenic mice reti-noblastoma model. *J Ophthalmic Vis Res* 15(4):446–452
75. Browning RJ, Able S, Ruan JL, Bau L, Allen PD, Kersemans V, Wallington S, Kinchesh P, Smart S, Kartsonaki C, Kamila S, Logan K, Taylor MA, McHale AP, Callan JF, Stride E, Vallis KA (2021) Combining sonodynamic therapy with chemoradiation for the treatment of pancreatic cancer. *J Control Release* 337:371–377
76. Yuan H, Fales AM, Vo-Dinh T (2012) TAT peptide-functionalized gold nanostars: enhanced intracellular delivery and efficient NIR photothermal therapy using ultralow irradiance. *J Am Chem Soc* 134(28):11358–11361
77. Nam J, Son S, Ochyl LJ, Kuai R, Schwendeman A, Moon JJ (2018) Chemo-photothermal therapy combination elicits anti-tumor immunity against advanced metastatic cancer. *Nat Commun* 9(1):1074
78. Lee C, Hwang HS, Lee S, Kim B, Kim JO, Oh KT, Lee ES, Choi HG, Youn YS (2017) Rabies virus-inspired silica-coated gold nanorods as a photothermal therapeutic platform for treating brain tumors. *Adv Mater* 29(13). <https://doi.org/10.1002/adma.201605563>
79. Yu G, Yang Z, Fu X, Yung BC, Yang J, Mao Z, Shao L, Hua B, Liu Y, Zhang F, Fan Q, Wang S, Jacobson O, Jin A, Gao C, Tang X, Huang F, Chen X (2018) Polyrotaxane-based supramolecular theranostics. *Nat Commun* 9:766
80. Guo B, Sheng Z, Hu D, Liu C, Zheng H, Liu B (2018) Through scalp and skull NIR-II photothermal therapy of deep orthotopic brain tumors with precise photoacoustic imaging guidance. *Adv Mater* 30(35):1802591
81. Chen Q, Xu L, Liang C, Wang C, Peng R, Liu Z (2016) Photothermal therapy with immune-adjutant nanoparticles together with checkpoint blockade for effective cancer immunotherapy. *Nature Commun* 7:13193
82. Bai H, Sun Q, Kong F, Dong H, Ma M, Liu F, Wang C, Xu H, Gu N, Zhang Y (2021) Zwitterion-functionalized hollow mesoporous Prussian blue nanoparticles for targeted and synergetic chemo-photothermal treatment of acute myeloid leukemia. *J Mater Chem B* 9:5245–5254
83. Pu XQ, Ju XJ, Zhang L, Cai QW, Liu YQ, Peng HY, Xie R, Wang W, Liu Z, Chu LY (2021) Novel multifunctional stimuli-responsive nanoparticles for synergetic chemo-photothermal therapy of tumors. *ACS Appl Mater Interfaces* 13:28802–28817
84. Gu M, Jiang L, Hao L, Lu J, Liu Z, Lei Z, Li Y, Hua C, Li W, Li X (2021) A novel theranostic nanoplatform for imaging-guided chemo-photothermal therapy in oral squamous cell carcinoma. *J Mater Chem B* 9(30):6006–6016

85. Du Z, Mao Y, Zhang P, Hu J, Fu J, You Q, Yin J (2021) TPGS-galactose-modified poly-dopamine co-delivery nanoparticles of nitric oxide donor and doxorubicin for targeted chemo-photothermal therapy against drug-resistant hepatocellular carcinoma. *ACS Appl Mater Interfaces* 13(30):35518–35532
86. Goodrich GP, Bao L, Gill-Sharp K, Sang KL, Wang J, Payne JD (2010) Photothermal therapy in a murine colon cancer model using near-infrared absorbing gold nanorods. *J Biomed Opt* 15:018001
87. Zhao P, Xu Y, Ji W, Zhou S, Li L, Qiu L, Qian Z, Wang X, Zhang H (2021) Biomimetic black phosphorus quantum dots-based photothermal therapy combined with anti-PD-L1 treatment inhibits recurrence and metastasis in triple-negative breast cancer. *J Nanobiotechnology* 19(1):181
88. Xia QH, Lu CT, Tong MQ, Yue M, Chen R, Zhuge DL, Yao Q, Xu HL, Zhao YZ (2021) *Ganoderma lucidum* polysaccharides enhance the abscopal effect of photothermal therapy in hepatoma-bearing mice through immunomodulatory, anti-proliferative, pro-apoptotic and anti-angiogenic. *Front Pharmacol* 12:648708
89. Odion RA, Liu Y, Vo-Dinh T (2021) Plasmonic gold nanostar-mediated photothermal immunotherapy. *IEEE J Sel Top Quantum Electron* 27(5):4800109
90. Liu Y, Chongsathidkiet P, Crawford BM, Odion R, Dechant CA, Kemeny HR, Cui X, Maccarini PF, Lascola CD, Fecci PE, Vo-Dinh T (2019) Plasmonic gold nanostar-mediated photothermal immunotherapy for brain tumor ablation and immunologic memory. *Immunotherapy* 11(15):1293–1302
91. Kremkau FW (1979) Cancer therapy with ultrasound: a historical review. *J Clin Ultrasound* 7:287–300
92. Umemura K, Yumita N, Nishigaki R, Umemura S (1996) Sonodynamically induced antitumor effect of pheophorbide a. *Cancer Lett* 102:151–157
93. Jin ZH, Miyoshi N, Ishiguro K, Umemura S, Kawabata K, Yumita N, Sakata I, Takaoka K, Udagawa T, Nakajima S, Tajiri H, Ueda K, Fukuda M, Kumakiri M (2000) Combination effect of photodynamic and sonodynamic therapy on experimental skin squamous cell carcinoma in C<sub>3</sub>H/HeN mice. *J Dermatol* 27:294–306
94. Foldvari M, Bagonluri M (2008) Carbon nanotubes as functional excipients for nanomedicines: I pharmaceutical properties. *Nanomedicine* 3:173–182
95. Zhang W, Zhang Z, Zhang Y (2011) The application of carbon nanotubes in target drug delivery systems for cancer therapies. *Nanoscale Res Lett* 6:555
96. Li R, Wu R, Zhao L, Hu Z, Guo S, Pan X, Zou H (2011) Folate and iron difunctionalized multiwall carbon nanotubes as dual-targeted drug nanocarrier to cancer cells. *Carbon* 49(5):1797–1805



# Chapter 33

## Porous Carbon Materials Enhanced the Therapeutic Efficacy of Anticancer Drugs



Anuradha Duvey, Divya Chauhan, Nitin Gupta, and Vipendra Kumar Singh

### Abbreviations

IUPAC	International Union of Pure and Applied Chemistry
CSCs	Cancer stem cells
CNTs	Carbon nanotubes
PCMs	Porous carbon materials
MSNs	Mesoporous silica nanoparticles
NIR	Near-infrared
SDDSs	Sustained drug delivery systems
IDDSs	Immediate drug delivery systems
CDDs	Controlled drug delivery systems
TDDs	Targeted drug delivery systems
PCNFs	Porous carbon nanofibers
HMC	Hollow mesoporous carbon
UMCS	Uniform mesoporous carbon spheres
HA	Hyaluronic acid

---

All authors contributed equally

---

A. Duvey · D. Chauhan  
Department of Pharmacy, Uttarakhand Technical University, Prem Nagar Sudhowala,  
Chandanwadi, Dehradun, Uttarakhand 248007, India

N. Gupta  
Center for Converging Technologies, University of Rajasthan, JLN Marg, Jaipur,  
Rajasthan 302004, India

V. K. Singh (✉)  
School of Biosciences and Bioengineering, Indian Institute of Technology, Mandi, VPO Kamand,  
Himachal Pradesh 175075, India  
e-mail: [vipendra\\_ksingh@projects.iitmandi.ac.in](mailto:vipendra_ksingh@projects.iitmandi.ac.in)

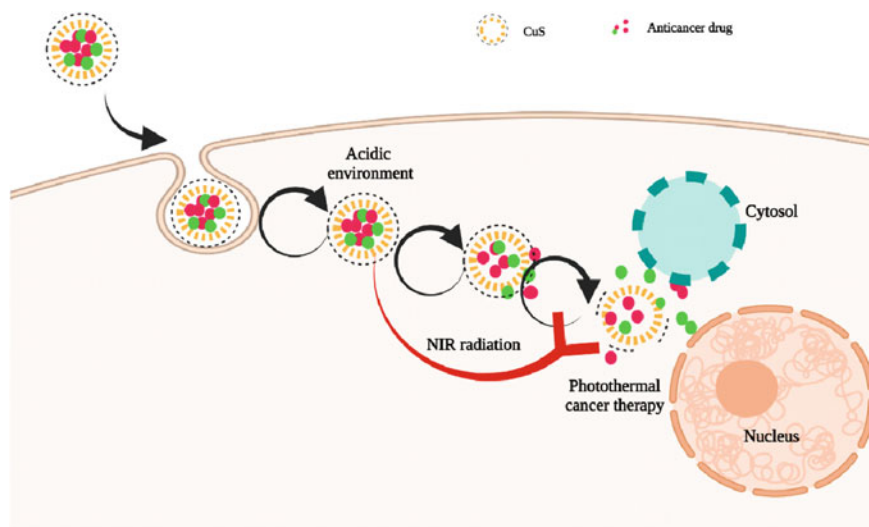
## 1 Introduction

Anticancer drugs aim to suppress cancer cell proliferation and metastasis. It is often merged with various other therapies such as surgery and radiation therapy to achieve the highest advantages [1–3]. Anticancer drugs kill cancer cells via diverse modes such as cell cycle arrest, oxidative stress, cytoskeleton damage, and DNA damage [4–6] via initiation of necroptosis, apoptosis, or necrosis that plays a crucial role in anticancer drugs induced cell death [7, 8]. At the early stages of cancer treatment, anticancer drugs play an analeptic role; however, in the progression of tumor, it has a distinct function, where it could be a neoadjuvant modality or palliative modality in different cancer [9–11]. But in the advanced stage of treatment, intrinsic and acquired chemoresistance is a major clinical challenge in treating cancer because chemoresistance induces cancer dissemination, recurrence of disease and death. Chemoresistance remains one of the major obstacles to the effective management of cancer therapy. In chemoresistance, cancer cells induce expression of various oncogene, altered mitochondrial functions, enhanced DNA repair, autophagy, and also altered epithelial to mesenchymal transition (EMT), cancer stemness, etc. Therefore, these molecular signaling pathway alterations may reduce the therapeutic efficacy of various anticancer drugs [12–14].

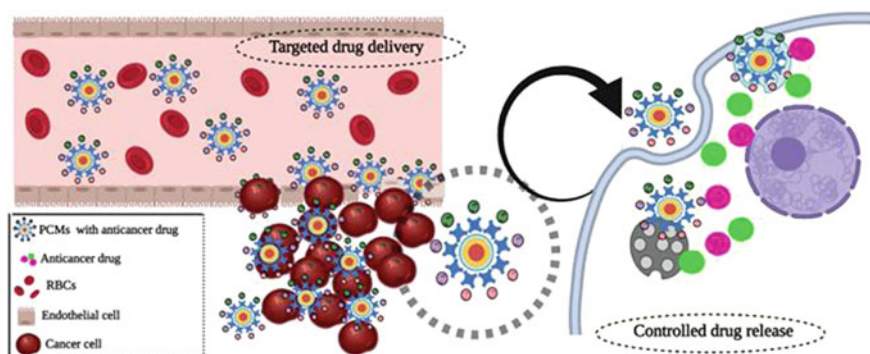
The combination of two or more chemotherapeutic agents improves the therapeutic response as compared to single therapy because it targets major signaling pathways in an especially additive or synergistic manner [5, 15–18]. This combination approach overcomes drug resistance which collectively provides better therapeutic benefits such as suppressed metastasis and reducing growth of the tumor, reducing cancer stem cells (CSCs) populations, arresting mitotically active cells and enhancing apoptosis [16, 19]. Despite the improvement of diagnostic tools and development of chemotherapy and radiotherapy in the last few decades, the overall survival rate in cancer has not increased more than 5 years [20]. These anticancer drugs serve as a promising way to manage cancer, but due to lack of selectivity, poor solubility, low stability, huge side effects, expensive and poor therapeutic benefits among patients pose a problem to determine as excellent treatment approaches [21–26]. The extensive use of traditional drugs for cancer therapy causes severe damage to fast-growing normal cells, and this is especially applied for the treatment of solid tumors, where most of the cancer cells are invaded slowly. A targeted drug delivery system (TDDS), which releases the anticancer drugs at a predetermined biosite in a regulated approach. Carbon-based drug delivery systems are building a major effect on the treatment of cancer. Some critical benefits of carbon-based drug delivery systems such as sustained half-life, better biodistribution, excellent circulation time, sustained and controlled release, the flexibility of route of administration, enhanced intracellular concentration of the anticancer drugs, etc. [27–30].

In the recent past, carbon-based materials such as carbon dots, fullerenes, graphenes, and carbon nanotubes (CNTs) seek a wide extent of attention for their assuring performance in biomedical science such as the delivery of anticancer drugs, gene transfection, and real-time imaging in animal models [31–38]. Porous carbon

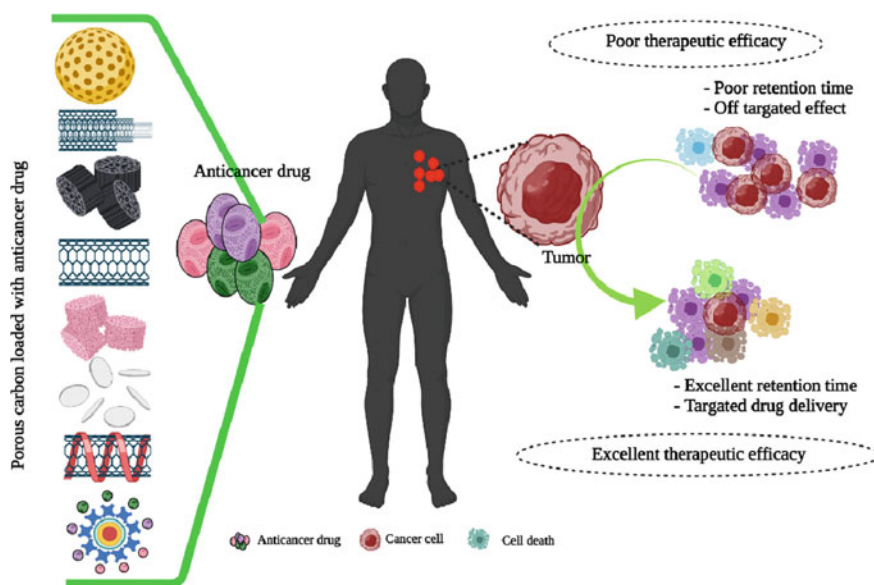
materials (PCMs) have a huge surface area, hierarchical porosity, photothermal conversion capacity, ideal compatibility, high adsorption capacity, and theranostic functions [39–41]. Over the past few decades, porous materials have acquired rapid expansion and excellent accomplishment due to their good surface area, excellent pore volume, and tunable pore size could provide better loading of anticancer drugs [42, 43]. When compared with  $sp^2$ -based carbon nanomaterials [44–47] and conventional mesoporous silica nanoparticles (MSNs) [48–50], PCMs integrate both the superiority of mesoporous silica nanoparticles (MSNs) and carbonaceous compositions including (1) extensive surface area and pore volume which are suitable for loading of anticancer drugs (2) adjustable pore structure permits better control of release of anticancer drugs (3) freely altered surface could accelerates controlled and targeted drug delivery to improve the therapeutic efficacy of anticancer drugs and minimized the side effects; (4) ideal heat conversion capacity in the region of near-infrared (NIR) could allow alternatives for photothermal therapy; (5) better biocompatibility and physicochemical stability; (6) supramolecular p-p stacking allows the huge amount of anticancer drug-loading potential and sustained anticancer drug release; (7) novel optical properties and easy fusion with various luminescent chemicals induce real-time monitoring. Due to the above merits porous carbon materials are reviewed as the next-generation platform for enhancing the therapeutic efficacy of various anticancer drugs and biomedical applications as illustrated in Figs. 1, 2, and 3.



**Fig. 1** Schematic illustration of porous carbon materials (PCMs) based drug delivery system of anticancer drugs



**Fig. 2** Schematic illustration on porous carbon materials (PCMs)-based drug delivery system for controlled and targeted drugs



**Fig. 3** Schematic illustration of advantages of using PCMs with anticancer drugs

The term immunogenicity or/and antigenicity can be defined as “the ability of a molecule or substance to provoke an immune response” or “the strength or magnitude of an immune response” [51]. The term “immune response” in the above definition ascribes “an integrated systemic response to an antigen (Ag), especially one mediated by lymphocytes and involving the recognition of Ags by specific antibodies (Abs) or previously sensitized lymphocytes” [52]. Porous carbon-like delivery systems provide the following advantages (1) improved stability both in vitro and in vivo, (2) target-specific delivery of peptides, drugs, and genes, and (3) minimized

side effects. However, porous carbon materials are often initially accumulated by phagocytic cells of the human immune network such as macrophages. There may be nonspecific interaction between various materials such as porous carbon materials and the human immune system like immunosuppression or immunostimulation. These materials may also enhance autoimmune disorders or inflammation or enhance the susceptibility of host organisms to various infections as well as cancer [53].

In the present chapter, we summarized the recent development of PCMs-based delivery of anticancer drugs including sustained drug delivery systems (SDDSs), immediate drug delivery systems (IDDSs), controlled drug delivery systems (CDDs), and targeted drug delivery systems (TDDSs). Apart from that we also highlight the current challenges and outlooks of porous carbon materials in the successful delivery of anticancer drugs.

## 2 Factors that Help PCMs to Be Effective Drug Delivery Agents

**Surface Modifications:** PCMs possess a carbonaceous framework which is generally modeled with the help of hydrothermal treatment or calcination at very high temperatures [54, 55]. As the PCMs originally possess a very high hydrophobic nature. So in order to achieve the hydrophilic surface of PCMs through surface modification, oxidation process is a commonly used strategy which is generally achieved by using strong acids such as sulfuric or hydrochloric acid which in turn improve the hydrophilic nature and generate different functional groups on the surface of PCMs [56]. Also, a simple and gentle method is also widely implemented, i.e., oxidation in the presence of ammonium persulfate in a dilute sulfuric acid ( $H_2SO_4$ ) solution which leads to the generation of a large number of functional groups generally the carboxyl groups of the surface of PCMs [57, 58]. These PCMs are further modified on the basis of the needs such as polymer coating, targeting diseases, PEGylation, diagnostic imaging, and stimuli-responsive grafting.

**Drug-loading methods:** Loading of drugs in PCMs are generally carried by mainly three methods such as solvent evaporation, physical adsorption equilibrium, and melting method. Drug-loading methods generally possess a substantial influence on the condition of the drug molecules inside the PCMs as well as in vitro dissolution. Melting methods generally achieve a higher drug-loading capacity but the drawbacks with this method are the difficulty of drug molecules to penetrate deeply into PCMs pores which results in uneven distribution of drug molecules and easily re-crystallization of drugs such as hydrophobic fenofibrate. Whereas physical adsorption method, PCMs are generally immersed in drug solution, drug molecules penetrate into the pore of PCMs until equilibrium is not achieved after which PCMs can be easily collected by centrifugation.

**Pore Size:** Rate of dissolution of drugs can also be increased by expanding the pore size which will lead to decrease in diffusion hindrance. Zhao et al. [59] have already fabricated the fibrous-ordered porous carbon material (FOPCM) for loading celecoxib which is an insoluble drug which improved its oral bioavailability and dissolution rate.

### 3 PCMs in Immediate/Sustained Drug Delivery Systems

Oral delivery of any drug is considered to be the most convenient route for administering drugs due to its safety, simplicity, and very few chances of infections. However, the clinical application and administration of hydrophobic drugs were critically restricted due to their low bioavailability and low solubility and absorption in the gastrointestinal tract. Lately, numerous kinds of porous/mesoporous, such as mesoporous metallic oxide, mesoporous carbon, mesoporous silica, have been identified and used to act as carrier molecules for the low soluble drugs [60, 61]. Out of these, PCMs have a very high surface area, high adsorption rates, high porosity, less density as well as excellent drug-loading capacity which is a crucial need for those drug molecules that require high doses to meet clinical applications needs.

Eu<sup>3+</sup>/Gd<sup>3+</sup>-EDTA-doped hollow mesoporous carbon (HMC) has been used for enhancing the oral bioavailability of carvedilol which is insoluble in nature [62]. This method increased the drug-loading efficiency of the carboxylated hollow mesoporous carbon up to 73.6%. The drug carvedilol when administered with the above HMC manifested a sustained drug release action as compared to the existing capsules of carvedilol. The oral bioavailability was also greatly improved and the pharmacokinetics results also showed that  $T_{\max}$  and area under the curve (AUC)<sub>0-48</sub> hours of carvedilol also increased 6.5 and 2.2 folds, respectively, when orally administered. It has been also found that PCMs increase the drug-loading capacity of camptothecin up to 17% due to their aromatic rings framework of mesoporous carbon nanomaterials [63, 64].

Carboxylated mesoporous carbon nanomaterials (MCNs) have been found to help in increasing the dissolution as well as solubility rate of hydrophobic carvedilol, hence enhancing the bioavailability of the drug when administered orally. When an amorphous state drug is loaded into the nanoscale pores in MCN, it enhances dissolution rates as well as the equilibrium stability of the drug in comparison to the crude drug compounds [65, 66]. It has also been found that uniform mesoporous carbon spheres (UMCS) when used as a carrier, increase the oral bioavailability of several insoluble clinical drugs such as celecoxib. It has also been found that UMCS reduces the rate of efflux and enhances the influx of celecoxib [66].

In comparison, with immediate-release PCMs which may cause the peak and valley drug concentration immediately after they are orally administered, sustained-release PCMs have been found to possess an extended ability of therapeutic effect. This extended therapeutic effect is mainly gained by slowly delivering the encapsulated drug for an extended period of time which could lead to a decrease in the

regularity of drug administration, balance the concentration of drug in the blood, decreased side effects due to immediate release of drugs, achieving preferable patient compliance.

The sustained drug delivery through PCMs can be mainly achieved by three methods: (1) Channel length and pore structure—Sustained drug delivery could be attained by modulating the morphology, constituents, and structure of mesoporous carbon structures that have a crucial role in the release rate of drug embedded. (2) Interactive forces between PCMs and drug embedded—Sustained drug delivery could be accomplished by using high interaction forces such as hydrophobic interactions, supramolecular  $\pi$ - $\pi$  stacking, and high electrostatic interaction between loaded drug and PCMs. (3) Hindrance and diffusion effect—PCMs bestow hindrance in diffusion for the loaded drug release, thus increasing the sustained drug delivery [56, 67, 68].

PCMs with a diameter (less than 90 nm) have been extensively used for transmembrane delivery of many drugs such as doxorubicin [56]. PCMs with a small diameter manifested a high loading capacity of drug molecules because of their hydrophobic interactions as well as supramolecular  $\pi$ - $\pi$  stacking as in the case of doxorubicin and PCMs. PCMs loaded with doxorubicin showed a very sustained delivery of doxorubicin under acidic conditions especially in cancer cells due to their high interactions [43, 69, 70] as shown in Fig. 1. Carbon materials such as hollow mesoporous carbon nanoparticles loaded doxorubicin have also shown a much-sustained drug delivery which helps in saving the normal cells by reducing the cytotoxicity of doxorubicin [67, 68].

Polymer poly dimethyl diallyl ammonium (PDDA) has also shown promising results in oral SDDSs for insoluble drugs (in water) such as nimodipine, fenofibrate, and carvedilol [71]. The drug release was sustained for an extended period of time more than 12 h for the PDDA-coated PCMs because of their gradual increase in pore size in an aqueous medium, which effectively hinders the actual drug release. Results effectively demonstrate that sustained drug release was obtained mainly by the blockage effect from the loading materials once they come in contact with an aqueous or release medium.

Mesoporous carbon/lipid bilayer nanocomposites (MCLN) have also shown promising results in sustained drug release for the oral delivery of insoluble drugs such as nimodipine. MCLN loaded with nimodipine manifested a sustained drug release in the gastrointestinal (GI) tract/intestinal fluid because of the diffusion hindrance bestowed by a lipid bilayer. Thus, in vivo bioavailability is increased when nimodipine was loaded into MCLN and manifested a long period of drug plasma levels in comparison with immediate-release drug formulations [72].

## 4 Porous Carbon Materials in Controlled Drug Delivery Systems (CDDSs)

Premature or early drug release is a major problem and causes severe side effects and drug loss. PCMs have been developed for CDDSs to accomplish stimuli-responsive drug delivery systems (SRDDSs). Such systems are mainly achieved by altering “gatekeepers” through physical adsorption and covalent bonds over the pore entrance, therefore preventing the loaded drug from escaping out until it comes directly in contact with particular stimuli such as redox potential, enzymes, temperature, and pH as shown in Figs. 1 and 2.

Amidst different types of SRDDSs, controlled drug delivery systems are the most popular choice due to the pH gradient between the diseased tissue and normal tissue cell [73–77]. It is a well-known fact that cancer tissues possess more acidic environments than normal tissues [19, 28, 43, 69, 70, 78–83].

CDDSs which are pH-responsive have been developed with ZnO quantum dots attached to the surface of PCMs. ZnO quantum dots act as gatekeepers through amide bonds preventing the loss of drugs [84]. Rhodamine G has been used as a drug that was loaded into the zinc oxide (ZnO) gated carbon materials with the help of electrostatic attraction. Rhodamine release profiles from the above systems manifested a strong association with the pH values of surrounding areas or mediums. As the pH values drop in the surrounding medium, i.e., less than 5.5, the “gatekeepers” start to open up leading to the release of the rhodamine. Intriguingly, as the pH decreases more percentage of drug rhodamine releases. In addition, the PCMs also generate heat under infrared radiation which will lead to an increase in temperature of the local area which further eases the release of drug rhodamine as shown in Fig. 1. Adsorptive interactions between pore cavities of PCMs and rhodamine reduce with an increase in temperature as well a drop in pH will further decrease the electrostatic repulsion between the rhodamine and PCMs. Hence, the combinatorial effect of temperature and pH could result in the controlled and rapid release of rhodamine from the PCMs when exposed to near-infrared radiation (NIR) at the tumor site [84].

Redox potential is also extensively used as a stimulus for controlled drug delivery systems with the help of glutathione concentration between the intracellular (10 mM) and extracellular matrix (2–10  $\mu$ M) [85–90]. Tumor cells have a high intracellular GSH, i.e., three times more than the normal cells GSH concentration which is mainly targeted for intracellular stimuli [91, 92]. Therefore, disulfide bonds are mainly used in designing controlled drug delivery systems dependent on redox potential as they are highly unstable in intracellular fluid due to their very high concentration of GSH in comparison with extracellular fluid where GSH level is low [93].

SRDDSs have been developed with the help of PCMs using the fluorescence carbon dots which acts as gatekeeper molecules at the pore opening site of PCMs. In high concentrations of GSH, carbon dots detach from the PCMs because of the disulfide cleavage at the pore sites leading to the swift release of the encapsulated doxorubicin as well as carbon dots release lead to the fluorescence which helps in



visualizing the whole process of drug delivery [94]. Different polymers are also used to act as a gatekeeper molecule which works as a redox-responsive gatekeeper.

Other carbon-based materials such as hollow mesoporous carbon nanomaterials (HMCN) conjugated with polyacrylic acid (PAA) have been also used as pH and redox dual-triggered controlled drug delivery systems. Disulfide bonds were used to conjugate the PAA on the pore outlet of HMCN. PAA was handpicked due to its superior biocompatibility, plenty of carboxyl groups to initiate the drug release which is pH-responsive, blood circulation time, etc. [94].

## 5 Porous Carbon Materials in Targeted Drug Delivery Systems (TDDSs)

Conventional chemotherapy anticancer drugs lack specificity causing many side effects, off-target effects, and inducing multidrug resistance which severely decreases the therapeutic efficacy [95–100]. Recently, PCMs-based drug delivery systems have made it possible to deliver drugs at the tumor site with minimal drug leakage during the drug transportation inside the body. TDDSs decrease the high drug dose demand which in turn decreases the scarring of neighboring normal cells and tissues as shown in Fig. 2.

Uniform mesoporous carbon nanomaterial sphere (UMCNS) has been also used as multifunctional TDDSs. It was used to graft branched polyethylene mine linked with folic acid (FA) and fluorescein isothiocyanate (FITC) covalently [101]. Paclitaxel was packed into the pores of UMCNS with a very high drug-loading efficiency of 51.37%. FA-functionalized nanoparticles (FA-PEI-UMCNS) loaded with paclitaxel were specifically uptaken by the cancer cells having high expression of folic acid receptor and also manifested encouraging results in terms of anti-tumor activity in comparison with other paclitaxel formulations due to increased accumulation in cancer tissue in several animal models. Besides, these PCMs also increased the oral absorption of paclitaxel which is a biopharmaceutics classification system (BCS) class IV drug having a bad oral bioavailability [102]. All results directly exhibited that FA-PEI-UMCNS manifested high cellular uptake through folic acid receptor-mediated endocytosis in human colorectal adenocarcinoma (Caco-2) cells. Moreover, FA-PEI-UMCNS remarkably enhanced the endocytosis and permeability of paclitaxel across the monolayer of Caco-2 cell as well as they also greatly improved oral bioavailability of paclitaxel and decreased the gastrointestinal toxicity of paclitaxel.

UMCNS linked with hyaluronic acid (HA) is used for TDDSs. It ensured colloidal stability, stable encapsulation, biocompatibility, controlled drug release, and cell targeting ability. It was also able to easily target the cancer cells overexpressing the CD44 receptor. When HA-UMCNS loaded with doxorubicin (DOX) and verapamil (VER) manifested hyaluronidase-1 and pH dual responsive CDDSs promoting the

drug release specifically in the tumor microenvironment. Moreover, VER/DOX/HA-UMCNS manifested an excellent therapeutic effect on xenografted BALB/c nude mice with human colon cancer HCT-116 cells [103].

## 6 Limitations of Porous Carbon Materials in Delivery of Anticancer Drugs

Porous carbon materials (PCMs) have sought attention in drug delivery in the field of biomedical sciences recently to be used as anticancer drug carriers suitable for enhancing the therapeutic efficacy of various anticancer drugs. Due to their large surface area, enhanced cellular internalization, and preferential tumor accumulation, they allow these PCMs to transport anticancer drugs to tumor sites, thereby reducing cytotoxicity of anticancer drugs by minimizing side effects. PCMs are considered as one of the novel inorganic materials for the next-generation drug delivery of anticancer drugs and other biomedical applications. Due to its appropriate combinatorial characteristics such as distinct porous structure, carbonaceous compositions, and excellent biocompatible in nature. However, in several practices like the controlled release of drugs, PCMs are still at the infant stage. Further refinements are required to strengthen the effective drug delivery of anticancer drugs by PCMs. Flexible synthesis protocols with compositional parameters and optimized structure; to date poor information of standard and controllable methodologies for the synthesis of porous carbon materials have been reported, especially for hydrophobic spherical materials and pore size-tunables. Modification of the surface of PCMs still remains difficult. Modification of the surface is critical for well-ordered catalysts development. To deliver anticancer drugs with smart drug delivery, stimuli-responsive and controlled drug release, which has been rarely applied to PCMs, while widely used in mesoporous silica and other mesoporous materials. In comparison with distinct materials, such as mesoporous silica and mesoporous metal oxides, PCMs have been hardly used in diagnostic imaging and in the biomedical field. But in the near future, it has been estimated to show excellent efficiency due to its specific structural composition and physicochemical characteristics. It is immediately needed to assess its biosafety which directly relies on the methods used in synthesis. In addition, assessment of biosafety of PCMs should be targeted on a few key parameters such as excretion, biodistribution, and biodegradation. Whether and how nanomaterials such as PCMs will influence the reproductive systems, nerve systems, and immune system have not yet been studied systematically, and therefore, more comprehensive research about the cellular-based and animal models toxicity and distribution of carbon-based materials is required. An *in vivo* quantitative assay of PCMs might be difficult owing to carbonaceous compositions of PCMs that may be influenced by the presence of carbon in the human system. In this condition, radio-labeling of PCMs may be promising for the evaluation of biosafety. Although functional modification on PCMs surface provides a better therapeutic potential for the delivery of

anticancer drugs, it is still essential to design an economically feasible approach for broad applications with excellent stability and reliability. Not only the modification of surface but also the generation of contamination-free functionalized porous materials is challenging in the future since PCMs might be contaminated with other nano-porous materials during synthesis. In the future, porous carbon materials may be considered as promising drug delivery materials in clinical settings.

## 7 Conclusions

In the present chapter, we provide a general overview of PCMs of the current literature regarding the anticancer drug delivery potential of PCMs. At present, the PCMs are in their initial stage in the field of cancer biology due to the limitation of synthesis procedure, surface modifications, oxidation, and functionalization time for enhancing the drug delivery efficiency in the tumor. In the future, for better utilization of PCMs in the delivery of anticancer drugs the role of pH, oxidation of carbon surface, reaction time uses of solvents during adsorption, functionalization parameters, and optimal time in adsorption have been denoted for a better understanding of PCMs. Among the other allotropes porous carbon materials have fascinated escalating consideration as a notably suitable vehicle for transporting different anticancer drug molecules into the cellular system because their unrefined structures and morphology promotes non-invasive insertion across the cell membranes. In the near future, researchers should focus more on the synthesis procedures, surface modification for enhancing the drug delivery efficacy of anticancer drugs in biomedical science. Various drug delivery materials designs have been developed to deliver anticancer drugs to multiple cancers. Porous carbon materials have provided the most effective results with regard to the delivery of anticancer drugs.

In conclusion, the functionalized surface characteristics or specific surface association allow PCMs a more favorable drug delivery system for drug delivery. Due to excellent drug-loading potential, adjusted release kinetics, biocompatibility and better solubility and with least cytotoxicity are essential in various target-specific drug delivery systems. Recent applications of PCMs have been investigated in target-specific cancer therapy. Numerous side effects are associated with PCMs that limit their extensive acceptance. However, each modification of the surface may check the immune response of the body that can be confirmed by *in vivo* assays. Overall, to establish PCMs in anticancer drug delivery that is compatible with clinical settings without safety concerns, more comprehensive, and additional animal studies are required for this recently and rapidly growing field of nanomedicine.

**Conflict of Interest** None.

## References

1. Arruebo M et al (2011) Assessment of the evolution of cancer treatment therapies. *Cancers* 3:3279–3330
2. Baskar R, Lee KA, Yeo R, Yeoh K-W (2012) Cancer and radiation therapy: current advances and future directions. *Int J Med Sci* 9:193–199
3. Datta NR et al (2015) Local hyperthermia combined with radiotherapy and/or chemotherapy: recent advances and promises for the future. *Cancer Treat Rev* 41:742–753
4. Dasari S, Tchounwou PB (2014) Cisplatin in cancer therapy: molecular mechanisms of action. *Eur J Pharmacol* 740:364–378
5. Singh VK et al (2017) Intracatinol synergistically enhances the anticancerous activity of cisplatin in human A549 cells via p38 MAPK/p53 signalling. *Apoptosis Int J Program Cell Death* 22:1273–1286
6. Aggarwal V et al (2019) Role of reactive oxygen species in cancer progression: molecular mechanisms and recent advancements. *Biomolecules* 9
7. Gong Y et al (2019) The role of necroptosis in cancer biology and therapy. *Mol Cancer* 18:100
8. Bertheloot D, Latz E, Franklin BS (2021) Necroptosis, pyroptosis and apoptosis: an intricate game of cell death. *Cell Mol Immunol* 18:1106–1121
9. Kang S, Nam B-H (2009) Does neoadjuvant chemotherapy increase optimal cytoreduction rate in advanced ovarian cancer? Meta-analysis of 21 studies. *Ann Surg Oncol* 16:2315–2320
10. Breugom AJ et al (2015) Adjuvant chemotherapy after preoperative (chemo)radiotherapy and surgery for patients with rectal cancer: a systematic review and meta-analysis of individual patient data. *Lancet Oncol* 16:200–207
11. Meegan MJ, O’Boyle NM (2019) Special issue ‘Anticancer drugs’. *Pharm Basel Switz* 12:E134
12. Zheng H-C (2017) The molecular mechanisms of chemoresistance in cancers. *Oncotarget* 8:59950–59964
13. Bresseur K, Gévry N, Asselin E (2017) Chemoresistance and targeted therapies in ovarian and endometrial cancers. *Oncotarget* 8:4008–4042
14. Lu C, Shervington A (2008) Chemoresistance in gliomas. *Mol Cell Biochem* 312:71–80
15. Hu Q, Sun W, Wang C, Gu Z (2016) Recent advances of cocktail chemotherapy by combination drug delivery systems. *Adv Drug Deliv Rev* 98:19–34
16. Bayat Mokhtari R et al (2017) Combination therapy in combating cancer. *Oncotarget* 8:38022–38043
17. Palmer AC, Sorger PK (2017) Combination cancer therapy can confer benefit via patient-to-patient variability without drug additivity or synergy. *Cell* 171:1678–1691.e13
18. Narayan RS et al (2020) A cancer drug atlas enables synergistic targeting of independent drug vulnerabilities. *Nat Commun* 11:2935
19. Nawara HM et al (2021) Paclitaxel-based chemotherapy targeting cancer stem cells from mono- to combination therapy. *Biomedicines* 9:500
20. Miller KD et al (2019) Cancer treatment and survivorship statistics, 2019. *CA Cancer J Clin* 69:363–385
21. Chidambaram M, Manavalan R, Kathiresan K (2011) Nanotherapeutics to overcome conventional cancer chemotherapy limitations. *J Pharm Pharm Sci* 14:67–77
22. Din FU et al (2017) Effective use of nanocarriers as drug delivery systems for the treatment of selected tumors. *Int J Nanomedicine* 12:7291–7309
23. Maeda H, Khatami M (2018) Analyses of repeated failures in cancer therapy for solid tumors: poor tumor-selective drug delivery, low therapeutic efficacy and unsustainable costs. *Clin Transl Med* 7:11
24. Senapati S, Mahanta AK, Kumar S, Maiti P (2018) Controlled drug delivery vehicles for cancer treatment and their performance. *Sig Transduct Target Ther* 3:7
25. Navya PN et al (2019) Current trends and challenges in cancer management and therapy using designer nanomaterials. *Nano Converg* 6:23

26. Singh VK, Arora D, Ansari MI, Sharma PK (2019) Phytochemicals based chemopreventive and chemotherapeutic strategies and modern technologies to overcome limitations for better clinical applications. *Phytother. Res. PTR* 33:3064–3089
27. Jain V, Jain S, Mahajan SC (2015) Nanomedicines based drug delivery systems for anti-cancer targeting and treatment. *Curr Drug Deliv* 12:177–191
28. Patra JK et al (2018) Nano based drug delivery systems: recent developments and future prospects. *J Nanobiotechnology* 16:71
29. Yao Y et al (2020) Nanoparticle-based drug delivery in cancer therapy and its role in overcoming drug resistance. *Front Mol Biosci* 7:193
30. Edis Z, Wang J, Waqas MK, Ijaz M, Ijaz M (2021) Nanocarriers-mediated drug delivery systems for anticancer agents: an overview and perspectives. *Int J Nanomedicine* 16:1313–1330
31. Doane TL, Burda C (2012) The unique role of nanoparticles in nanomedicine: imaging, drug delivery and therapy. *Chem Soc Rev* 41:2885–2911
32. Wei A, Mehtala JG, Patri AK (2012) Challenges and opportunities in the advancement of nanomedicines. *Journal of Controlled Release* 164:236–246
33. Master A, Livingston M, Sen Gupta A (2013) Photodynamic nanomedicine in the treatment of solid tumors: perspectives and challenges. *Journal of Controlled Release* 168:88–102
34. Taratula O, Kuzmov A, Shah M, Garbuzenko OB, Minko T (2013) Nanostructured lipid carriers as multifunctional nanomedicine platform for pulmonary co-delivery of anticancer drugs and siRNA. *Journal of Controlled Release* 171:349–357
35. Pardo J, Peng Z, Leblanc RM (2018) Cancer targeting and drug delivery using carbon-based quantum dots and nanotubes. *Mol Basel Switz* 23:E378
36. Zhang Y, Wu M, Wu M, Zhu J, Zhang X (2018) Multifunctional carbon-based nanomaterials: applications in biomolecular imaging and therapy. *ACS Omega* 3:9126–9145
37. Liu J, Li R, Yang B (2020) Carbon dots: a new type of carbon-based nanomaterial with wide applications. *ACS Cent Sci* 6:2179–2195
38. Riley PR, Narayan RJ (2021) Recent advances in carbon nanomaterials for biomedical applications: a review. *Curr Opin Biomed Eng* 17:100262
39. Bleda-Martínez MJ, Lozano-Castelló D, Morallón E, Cazorla-Amorós D, Linares-Solano A (2006) Chemical and electrochemical characterization of porous carbon materials. *Carbon* 44:2642–2651
40. Lee J, Kim J, Hyeon T (2006) Recent progress in the synthesis of porous carbon materials. *Adv Mater* 18:2073–2094
41. Stein A, Wang Z, Fierke MA (2009) Functionalization of porous carbon materials with designed pore architecture. *Adv Mater* 21:265–293
42. Sheng Z et al (2014) Smart human serum albumin-indocyanine green nanoparticles generated by programmed assembly for dual-modal imaging-guided cancer synergistic phototherapy. *ACS Nano* 8:12310–12322
43. Bai L et al (2015) Mechanism study on pH-responsive cyclodextrin capped mesoporous silica: effect of different stalk densities and the type of cyclodextrin. *Nanotechnology* 26:165704
44. Vijayanthimala V, Chang H-C (2009) Functionalized fluorescent nanodiamonds for biomedical applications. *Nanomed* 4:47–55
45. Ai K, Liu Y, Ruan C, Lu L, Lu GM (2013) Sp<sup>2</sup> C-dominant N-doped carbon sub-micrometer spheres with a tunable size: a versatile platform for highly efficient oxygen-reduction catalysts. *Adv Mater* 25:998–1003
46. Chung C et al (2013) Biomedical applications of graphene and graphene oxide. *Acc Chem Res* 46:2211–2224
47. Kruss S et al (2013) Carbon nanotubes as optical biomedical sensors. *Adv Drug Deliv Rev* 65:1933–1950
48. Kim T-W et al (2008) Structurally ordered mesoporous carbon nanoparticles as transmembrane delivery vehicle in human cancer cells. *Nano Lett* 8:3724–3727
49. Singh R, Lillard JW (2009) Nanoparticle-based targeted drug delivery. *Exp Mol Pathol* 86:215–223

50. Chen Y et al (2010) Core/shell structured hollow mesoporous nanocapsules: a potential platform for simultaneous cell imaging and anticancer drug delivery. *ACS Nano* 4:6001–6013
51. Jr CAJ et al (2001) *Immunobiology*. Garland Science
52. The American Heritage medical dictionary. Houghton Mifflin Co. (2007)
53. Zolnik BS, González-Fernández A, Sadrieh N, Dobrovolskaia MA (2010) Nanoparticles and the immune system. *Endocrinology* 151:458–465
54. Lee G-A, Hwang K-A, Choi K-C (2017) Inhibitory effects of 3,3'-diindolylmethane on epithelial-mesenchymal transition induced by endocrine disrupting chemicals in cellular and xenograft mouse models of breast cancer. *Food Chem Toxicol* 109:284–295
55. Liu J et al (2013) A facile soft-template synthesis of mesoporous polymeric and carbonaceous nanospheres. *Nat Commun* 4:2798
56. Zhu J et al (2012) pH-controlled delivery of doxorubicin to cancer cells, based on small mesoporous carbon nanospheres. *Small WeinH Bergstr Ger* 8:2715–2720
57. Tanaka S et al (2015) Surface modification of soft-templated ordered mesoporous carbon for electrochemical supercapacitors. *Microporous Mesoporous Mater* 217:141–149
58. Xue Z et al (2014) One-pot synthesis of silver nanoparticle catalysts supported on N-doped ordered mesoporous carbon and application in the detection of nitrobenzene. *Carbon* 69:481–489
59. Zhao P et al (2012) Inclusion of celecoxib into fibrous ordered mesoporous carbon for enhanced oral bioavailability and reduced gastric irritancy. *Eur J Pharm Sci* 45:639–647
60. Zhang X et al (2012) DNA methylation alterations in response to pesticide exposure in vitro. *Environ Mol Mutagen* 53:542–549
61. Wang K-H, Kao A-P, Chang C-C, Lin T-C, Kuo T-C (2015) Bisphenol A-induced epithelial to mesenchymal transition is mediated by cyclooxygenase-2 up-regulation in human endometrial carcinoma cells. *Reprod Toxicol Elmsford N* 58:229–233
62. Liu J et al (2016) A Eu(3+)/Gd(3+)-EDTA-doped structurally controllable hollow mesoporous carbon for improving the oral bioavailability of insoluble drugs and in vivo tracing. *Nanotechnology* 27:315101
63. Lu J, Liong M, Zink JL, Tamanoi F (2007) Mesoporous silica nanoparticles as a delivery system for hydrophobic anticancer drugs. *Small WeinH Bergstr Ger* 3:1341–1346
64. Gu J, Su S, Li Y, He Q, Shi J (2011) Hydrophilic mesoporous carbon nanoparticles as carriers for sustained release of hydrophobic anti-cancer drugs. *Chem Commun Camb Engl* 47:2101–2103
65. Zhang Y, Zhi Z, Li X, Gao J, Song Y (2013) Carboxylated mesoporous carbon microparticles as new approach to improve the oral bioavailability of poorly water-soluble carvedilol. *Int J Pharm* 454:403–411
66. Wang T, Zhao P, Zhao Q, Wang B, Wang S (2016) The mechanism for increasing the oral bioavailability of poorly water-soluble drugs using uniform mesoporous carbon spheres as a carrier. *Drug Deliv* 23:420–428
67. Chen R et al (2014) Prostate cancer in Asia: a collaborative report. *Asian J Urol* 1:15–29
68. Zhao Q et al (2017) The advantage of hollow mesoporous carbon as a near-infrared absorbing drug carrier in chemo-photothermal therapy compared with IR-820. *Eur J Pharm Sci* 99:66–74
69. Crayton SH, Tsourkas A (2011) pH-titratable superparamagnetic iron oxide for improved nanoparticle accumulation in acidic tumor microenvironments. *ACS Nano* 5:9592–9601
70. Chen Y et al (2012) Manganese oxide-based multifunctionalized mesoporous silica nanoparticles for pH-responsive MRI, ultrasonography and circumvention of MDR in cancer cells. *Biomaterials* 33:7126–7137
71. Zhang C et al (2014) Poly dimethyl diallyl ammonium coated CMK-5 for sustained oral drug release. *Int J Pharm* 461:171–180
72. Zhang Y et al (2015) Synthesis and evaluation of mesoporous carbon/lipid bilayer nanocomposites for improved oral delivery of the poorly water-soluble drug, nimodipine. *Pharm Res* 32:2372–2383
73. Dong L, Hoffman AS (1991) A novel approach for preparation of pH-sensitive hydrogels for enteric drug delivery. *Journal of Controlled Release* 15:141–152

74. Jeong B, Bae YH, Lee DS, Kim SW (1997) Biodegradable block copolymers as injectable drug-delivery systems. *Nature* 388:860–862
75. Qiu Y, Park K (2001) Environment-sensitive hydrogels for drug delivery. *Adv Drug Deliv Rev* 53:321–339
76. Gupta P, Vermani K, Garg S (2002) Hydrogels: from controlled release to pH-responsive drug delivery. *Drug Discov Today* 7:569–579
77. Sawant RM et al (2006) ‘SMART’ drug delivery systems: double-targeted pH-responsive pharmaceutical nanocarriers. *Bioconjug Chem* 17:943–949
78. Kraus M, Wolf B (1996) Implications of acidic tumor microenvironment for neoplastic growth and cancer treatment: a computer analysis. *Tumour Biol* 17:133–154
79. Trédan O, Galmarini CM, Patel K, Tannock IF (2007) Drug resistance and the solid tumor microenvironment. *J Natl Cancer Inst* 99:1441–1454
80. Frérart F et al (2008) The acidic tumor microenvironment promotes the reconversion of nitrite into nitric oxide: towards a new and safe radiosensitizing strategy. *Clin Cancer Res* 14:2768–2774
81. Danhier F, Feron O, Préat V (2010) To exploit the tumor microenvironment: passive and active tumor targeting of nanocarriers for anti-cancer drug delivery. *J Controlled Release* 148:135–146
82. Estrella V et al (2013) Acidity generated by the tumor microenvironment drives local invasion. *Cancer Res* 73:1524–1535
83. Justus CR, Dong L, Yang LV (2013) Acidic tumor microenvironment and pH-sensing G protein-coupled receptors. *Front Physiol* 4:354
84. Huang X, Wu S, Du X (2016) Gated mesoporous carbon nanoparticles as drug delivery system for stimuli-responsive controlled release. *Carbon* 101:135–142
85. Giri S, Trewyn BG, Stellmaker MP, Lin VS-Y (2005) Stimuli-responsive controlled-release delivery system based on mesoporous silica nanorods capped with magnetic nanoparticles. *Angew Chem Int Ed Engl* 44:5038–5044
86. Cheng R et al (2011) Glutathione-responsive nano-vehicles as a promising platform for targeted intracellular drug and gene delivery. *J Controlled Release* 152:2–12
87. Liu J et al (2011) Redox-responsive polyphosphate nanosized assemblies: a smart drug delivery platform for cancer therapy. *Biomacromol* 12:2407–2415
88. Wen H et al (2012) Engineered redox-responsive PEG detachment mechanism in PEGylated nano-graphene oxide for intracellular drug delivery. *Small* 8:760–769
89. Huo M, Yuan J, Tao L, Wei Y (2014) Redox-responsive polymers for drug delivery: from molecular design to applications. *Polym Chem* 5:1519–1528
90. Li Z-Y et al (2014) A redox-responsive drug delivery system based on RGD containing peptide-capped mesoporous silica nanoparticles. *J Mater Chem B* 3:39–44
91. Zhao Q et al (2014) PEGylated mesoporous silica as a redox-responsive drug delivery system for loading thiol-containing drugs. *Int J Pharm* 477:613–622
92. Zhao Q et al (2017) Hyaluronic acid and carbon dots-gated hollow mesoporous silica for redox and enzyme-triggered targeted drug delivery and bioimaging. *Mater Sci Eng C* 78:475–484
93. Saito G, Swanson JA, Lee K-D (2003) Drug delivery strategy utilizing conjugation via reversible disulfide linkages: role and site of cellular reducing activities. *Adv Drug Deliv Rev* 55:199–215
94. Zhang Y et al (2016) Mesoporous carbon nanoparticles capped with polyacrylic acid as drug carrier for bi-trigger continuous drug release. *J Mater Chem B* 4:5178–5184
95. Kartner N, Riordan JR, Ling V (1983) Cell surface P-glycoprotein associated with multidrug resistance in mammalian cell lines. *Science* 221:1285–1288
96. Thiebaut F et al (1987) Cellular localization of the multidrug-resistance gene product P-glycoprotein in normal human tissues. *Proc Natl Acad Sci U S A* 84:7735–7738
97. Boesch D et al (1991) In vivo circumvention of P-glycoprotein-mediated multidrug resistance of tumor cells with SDZ PSC 833. *Cancer Res* 51:4226–4233
98. Kane SE (1996) Multidrug resistance of cancer cells. In: Testa B, Meyer UA (eds) *Advances in drug research*, vol 28. Academic Press, pp 181–252

99. Gottesman MM, Fojo T, Bates SE (2002) Multidrug resistance in cancer: role of ATP-dependent transporters. *Nat Rev Cancer* 2:48–58
100. Ganta S, Amiji M (2009) Coadministration of paclitaxel and curcumin in nanoemulsion formulations to overcome multidrug resistance in tumor cells. *Mol Pharm* 6:928–939
101. Wan L et al (2014) Versatile hybrid polyethyleneimine–mesoporous carbon nanoparticles for targeted delivery. *Carbon* 79:123–134
102. Wan L et al (2015) Folate-polyethyleneimine functionalized mesoporous carbon nanoparticles for enhancing oral bioavailability of paclitaxel. *Int J Pharm* 484:207–217
103. Wan L et al (2016) Hyaluronic acid modified mesoporous carbon nanoparticles for targeted drug delivery to CD44-overexpressing cancer cells. *Nanotechnology* 27:135102



# Chapter 34

## Biocompatible Carbon-Coated Magnetic Nanoparticles for Biomedical Applications



V. Vijayakanth, V. Vinodhini, and Krishnamoorthi Chintagumpala

### 1 Introduction

#### 1.1 Magnetic Nanoparticles

Maghemite ( $\text{Fe}_2\text{O}_3$ ) and magnetite ( $\text{Fe}_3\text{O}_4$ ) are the most extensively used magnetic nanoparticles for diverse biomedical applications. For in vivo biomedical applications, magnetic nanoparticles should be superparamagnetic, small in size, biocompatible, and hemocompatible in order to remain in blood circulation and nontoxic. For in vitro applications, superparamagnetic nanoparticles (SPNPs) dispersed in solvents can be utilized when the size of the particle is not a major criterion [1]. Magnetic nanoparticles (MNPs) can be prepared by bottom-up and top-down techniques. The widely used bottom-up techniques for MNPs synthesis are coprecipitation, sol-gel, solvothermal, hydrothermal, spray pyrolysis, solvothermal reflux, etc. [1]. Among them, coprecipitation, sol-gel, solvothermal reflux methods are most widely used for MNPs synthesis due to controlled particle size by controlling various synthesis parameters. The solvothermal reflux method produces highly crystallized nanoparticles (NPs) due to the potent removal of crystallization exothermic energies by naturally occurring gas bubbles formed in reflux growth solvents [2]. MNPs have distinctive chemical and physical properties which play an important role in science and technology [3]. Hence, the MNPs are used in various fields such as magnetic data storage, catalysis, pigment, wastewater treatment, sensors, and biomedical fields. Among the biomedical diverse applications, magnetic resonance image (MRI)

---

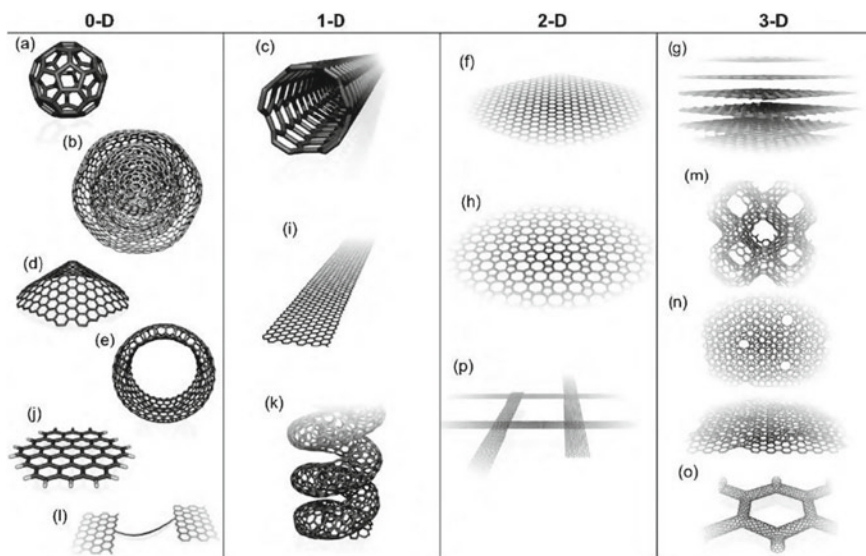
V. Vijayakanth (✉) · V. Vinodhini (✉) · K. Chintagumpala  
Center for Nanotechnology Research, Vellore Institute of Technology, Vellore,  
Tamil Nadu 632014, India  
e-mail: [vkant58@gmail.com](mailto:vkant58@gmail.com)

V. Vinodhini  
e-mail: [vinodhini.v@vit.ac.in](mailto:vinodhini.v@vit.ac.in)

agents, magnetic drug delivery, and magnetic hyperthermia (MHT) were widely researched in both in vivo and in vitro modes [4]. MNPs are further utilized in different domains including analytical, industrial, and environmental applications due to easy synthesis, size controllability, physiochemical property, and superior magnetic behavior [3, 5]. To enhance the colloidal dispersion stability and biocompatibility of MNPs, nanoparticles' surface modification with colloidal dispersants is necessary [6] due to the aggregation of nanoparticles resulting from the high surface energy and magnetic dipole interactions. The colloidal dispersant may be either polymeric dispersant or surfactant dispersant, according to the application. Further, MNPs without dispersant will undergo oxidation in the biological environment resulting in the formation of nonmagnetic or weakly magnetic particles. Colloidal stability of magnetic nanoparticles is vital for various biomedical applications and to prevent agglomeration. The optical, electrical, catalytic, and magnetic properties of nanocrystals are directly improved by dispersants (surfactants). The importance and influence of surface ligands or surface coating of NPs were thoroughly investigated by Boles and the co-workers [7]. Generally, the surface of MNPs is encapsulated or capped anchored, or ligated with various dispersants, especially with surfactants and polymers. Recently, the carbon-based materials such as fullerenes, graphene oxide (GO), carbon dots, and porous carbon shell layers were coated on core MNPs drawn a huge attention to improve biocompatibility and enhance functionalization of the surface. This chapter presents recent research progress on various biomedical applications (for cancer treatment) of different carbon materials-coated MNPs, with and without functionalization.

## ***1.2 Carbon Materials***

In biomedical applications, the following are the most extensively used carbon materials: fullerenes, carbon dots, graphene, graphene oxide (GO), reduced graphene oxide (rGO), carbon nanotubes, porous carbon, etc., compounds. Carbon materials-coated magnetic NPs are used in several applications such as MRI contrast agents, targeted drug delivery system (TDDS), magnetic hyperthermia, fluorescent biosensor, biological labeling, catalysis, and optical sensing, because the carbon materials-coated MNPs show high saturation magnetization, low toxicity, colloidal stability, good biocompatibility, and excellent fluorescent properties [3, 8]. The great advantages of carbon materials are lightweight, thermally and chemically stable, biocompatible and hemocompatible, hydrophilic, and easy to functionalize to load drugs. Graphite-coated MNPs have shown enhanced cytocompatibility and protected the surface from oxidation [9]. The first structure, synthesis, and properties of various carbon-based materials were briefly described in the following subsections. Later, biomedical applications of various carbon material-coated MNPs (MNP core and carbon shell) were presented systematically in the following sections. Targeted drug delivery, bioimaging, and magnetic hyperthermia applications of the core-shell



**Fig. 1** Various classes of carbon-based materials with structures and dimensions such as 0-dimensional structure of buckminsterfullerene, 1-dimensional structure of nanotubes, 2-dimensional structure of graphene, and 3-dimensional structure of graphite and diamond. Reprinted with permission from Terrones et al. [10]. Copyright 2010 Elsevier

nanoparticles (NPs) were discussed in detail at relevant places. Figure 1 represents various classes of carbon materials, structures, and their dimensions.

## 2 Synthesis and Biological Properties of Carbon Nanomaterials

### 2.1 Carbon Dots

Carbon dots (CDs), also called carbon quantum dots (CQDs), are nanoscopic carbon nanoparticles with high specific surface area and quantized energy states. Hence, they exhibit particle diameter-dependent optical and electrical properties. The CDs are generally prepared by both bottom-up and top-down methods. In top-down methods, macroscopic carbon materials were used as a precursor to derive nanoscopic carbon dots by laser irradiation, chemical oxidation, electrochemical, etc., techniques. In bottom-up methods, organic solvents act as a seed to grow up zero-dimensional (0D) carbon dots under certain conditions. Heat, ultrasonic waves, microwave energy-based techniques are used for molecular structure transition and energy aggregation during the synthesis. Heterogeneous carbon sources like citric acid, amino acid, sucrose, and even waste food can be taken as precursors [8]. Many researchers

have used solvothermal, hydrothermal, microwave-assisted heating methods for the making of carbon dots. CDs are used in a variety of applications due to ease in handling, eco-friendly nature, economical, homogeneity, biocompatibility, hydrophilic nature, ability to produce narrow size distributed particles by chemical methods [8, 9]. Carbon dots with surface passivation show fascinating properties such as photostability, chemical inertness, tunable excitation, and emission energies, good biocompatibility, low toxicity, and colloidal stability. In addition, carbon dots (CDs) have excellent properties such as broad optical absorption and strong photoluminescence (PL) absorption. CDs are well suitable for surface passivation or modification with diverse organic, inorganic, polymeric, and biological materials. The surface passivation enhances the physical and fluorescence characteristics and was used in biosensing, bioimaging, drug delivery, photothermal therapy, etc., applications [9, 10].

The majority of the studies have proven that carbon dots (CDs) have outstanding biocompatibility. Sun and his co-researchers evaluated the biocompatibility of CDs in both in vitro and in vivo modes using human breast cancer cells and reported that the CDs are not cytotoxic [11, 12]. Han and the co-workers have prepared multifunctional fluorescent manganese-carbon dots (Mn-CDs) hybrid nanoparticles and were paired with anti-HE4 antibody. This conjugate was effectively investigated for ovarian cancer cell targeting by bifunctional MRI and optical imaging. The novel manganese-carbon dots with anti-HE4 monoclonal antibody (mAb) exhibited great affinity to HO-8910 ovarian tumor cells. The in vivo and in vitro studies have revealed that the probes had superior cell targeting ability, extraordinary fluorescence, good biocompatibility, and efficient excretion through renal clearance [13]. Further, Chowdhuri and the research group have reported encapsulation of  $\text{Fe}_3\text{O}_4$  superparamagnetic nanoparticles (SPNPs) with O-carboxymethyl chitosan ( $\text{Fe}_3\text{O}_4@OCMC$ ). Then, a nanoscale metal organic framework (NMOF) was formed with a coating of folic acid (FA) on the surface of SPNPs ( $\text{Fe}_3\text{O}_4@OCMC@NMOF-3/FA$ ). Finally, doxorubicin (DOX) was loaded into the NMOF by physical encapsulation. The  $\text{Fe}_3\text{O}_4@OCMC@NMOF-3/FA$  nanoparticles exhibited great ability for targeted drug delivery and optical imaging [14]. Nitrogen-strengthened carbon dots (NCDs) mediated with deoxyribonucleic acid (DNA) nanoparticles were developed. The NCDs-DNA nanomaterial exhibited excellent photodynamic and photoluminescence response, high cellular uptake, and good biocompatibility. Thus, the material is highly effective for anticancer diagnosis and treatment [15].

## 2.2 Fullerenes

Fullerenes are allotropes of carbon molecules characterized by a closed or partially closed hollow structure. Carbon atoms are connected by primary and secondary bonds with fused rings of five to seven atoms in the structure. The molecular structure may be a hollow sphere, ellipsoid, and tube. The spherical fullerenes are called buckyballs,

whereas cylindrical ones are known as nanotubes. The  $C_{60}$  is known as buckminsterfullerene and is widely studied spherical fullerene. Carbon nanotubes (CNTs) are cylindrical fullerenes. Carbon-based nanomaterials have enormously contributed to the expansion of nanoscience and nanotechnology [16]. The experimental discovery of fullerenes was made in 1985, and it marked a great change in chemistry which led to a new branch: carbon chemistry [17]. Many studies were done with lower homogeneous  $C_{60}$ ,  $C_{70}$  to higher fullerenes like  $C_{240}$ ,  $C_{540}$ , and  $C_{720}$ . Fullerenes spontaneously react with free radicals, have an antibacterial property, and were used in water treatment. They were further used in therapeutics, diagnostics, hydrogen storage, supercapacitor, and drug delivery application due to their structure, biocompatibility, electronic configuration, and physiochemical properties. To carry out the synthesis of fullerenes, many methods are being used such as laser vaporization of carbon, electric arc heating of graphite, resistive arc heating of graphite, and laser irradiation of polycyclic hydrocarbons [18]. The  $C_{60}$  has a distinctive structure and is suitable for connection with the cellular environment. The fullerene NPs interact well with the biological environment and easily pass through the cell membrane, and they can also deliver therapeutic molecules [19].

Dextran-coated  $C_{70}$  fullerene has shown stable dispersion in water, and extraordinary cytocompatibility with L929 fibroblast cells, and a cell viability value of above 80% [20]. The  $C_{60}$  fullerene functionalized  $\gamma$ - $Fe_2O_3$  MNPs have shown high saturation magnetization of  $66.5 \text{ emu g}^{-1}$ , and a particle size below 10 nm was achieved by the hydrothermal synthesis method. The supreme adsorption capacity of  $C_{60}$ - $\gamma$ - $Fe_2O_3$  nanoparticles (NPs) for nonsteroidal anti-inflammatory drug (flurbiprofen), determined from Langmuir isotherm, is  $142.9 \text{ mg g}^{-1}$  [21].

### 2.3 Carbon Nanotubes (CNTs)

Sumio Iijima and his co-workers have discovered carbon nanotubes (CNTs) in 1991 [22]. CNTs are cylindrical hollow tubes with hexagon carbon rings on the wall and are a 1D material. Hence, the CNTs are categorized into two types: single-walled carbon nanotubes (SWCNTs) and multiwalled carbon nanotubes (MWCNTs). The SWCNTs are formed from a two-dimension (2D) hexagonal carbon lattice rolled up along one of the Bravais lattice vectors (BLVs) to build a hollow cylinder. MWCNTs contain nested single-walled carbon nanotubes [16]. The atoms are weakly bound by the Van der Waals interaction across the walls and are strongly bonded by  $sp^2$  orbitals electrons within the hexagon lattice. MWCNTs are sometimes referred to the double and multiwalled carbon tubes [23]. The carbon nanotubes (CNTs) exhibit several characteristic properties such as high conductivity, chemical inertness, high tensile strength, ultra-lightweight, and a protein carrier. Due to these fascinating properties, CNT has played a remarkable role in nanobiotechnology, optics, electronics, and various field of material science. They were also used in sensors, water treatment, MRI, drug delivery, anti-fungal, antibacterial, hyperthermia, etc., applications.

The CNTs are synthesized mainly by the following three methods: chemical vapor deposition (CVD), electric arc, laser deposition [24].

### 2.3.1 Single-Walled Carbon Nanotubes

In early literature, SWCNTs synthesis was mostly carried out by laser ablation and arc discharge method. SWCNTs were noticed as a byproduct of an arc discharge method for synthesizing endohedral fullerenes and metal nanoparticles. Now, researchers are preferred to prepare SWNTs by advanced chemical vapor deposition (CVD), and it is a promising route. The CVD method emerged as an efficient method to prepare SWCNTs due to its high efficiency, scalable nature, relatively low cost. An appreciable deal of progress has been made during the past two decades. Several review articles are being reported in the academic field as well as the industry [25]. SWCNTs exhibit excellent optical, mechanical as well as thermal properties. Many types of CNTs were synthesized with different electrical characteristics which play a significant role in various electronic and optoelectronic applications. The optical properties of SWCNTs are structure dependent, and they can be altered to obtain desirable properties. Low optical absorption and eminent electrical conductivity of the materials paved the way for its use in numerous applications such as liquid crystal displays (LCDs), photovoltaics, and OLEDs. SWCNTs were also fabricated as electrically conductive and optically transparent thin films. At room temperature, SWCNTs are produced with eminent thermal property with an unimaginable thermal conductivity of  $6600 \text{ Wm}^{-1} \text{ K}^{-1}$ . SWCNTs have remarkable mechanical properties such as bending strength and stiffness due to the  $sp^2$  orbital electron bonding carbon-carbon atoms in graphene hexagon rings which lead to the development of many nanocomposite materials. SWCNTs are further classified into three types based on specific chirality types and are recognized as emerging nanocomposite materials due to the growing demand for pre-established CNTs properties and structures in numerous applications [26]. The synthesized SWNTs were anchored/ligated with mesoporous silica (MS), and then, surface altered by polyethylene glycol (PEG) NPs (SWNTs@MS-PEG) exhibits a multi-functioning base tool for imaging guided adjuvant therapy of cancer. The SWNTs@MS-PEG NPs loaded with doxorubicin (DOX), a chemotherapy drug, deliver efficiently to the target resulting in synergistic cancerous tissue killing with the influence of the photothermal therapy [27]. In hyaluronic acid-coated (HA) SWCNTs and loaded with doxorubicin (DOX), DOX is associated with HA by bi-sulfide bond (-ss-) which helps the quick release of a drug under reducing conditions. The biocompatibility of gadolinium (Gd) SWCNTs-HA-ss-DOX NPs caused potent tumor cell killing efficiency with  $IC_{50}$  of  $0.61 \mu\text{g/mL}$  at 48 h. In addition, Gd-SWCNTs-HA-ss-DOX nanoparticles produced good chemophotothermal anticancer therapeutic efficiency, redox responsive releasing function, MRI imaging, and tumor targeting property [28]. The multifunctional platform-based PEG-modified  $\text{Fe}_3\text{O}_4$ @carbon quantum dots-ligated SWCNTs are synthesized and used as a collaborative treatment for cancer. Doxorubicin (DOX) drug was loaded into the SWCNTs-PEG- $\text{Fe}_3\text{O}_4$ @CDs nanoparticles to produce high efficiency. The

magnetofluorescent SWNTs-PEG-Fe<sub>3</sub>O<sub>4</sub>@CDs have shown a powerful effect on the targeted tumor cells, and these nanocarriers can be used as a potential nano-platform for adjuvant tumor photodynamic therapy (PDT), photothermal therapy (PTT), and chemotherapy (CT) under 808-nm laser radiation. These biocompatible nanocarriers are promising for drug loading and drug delivery carriers for lung and cervical cancer treatment [29].

### 2.3.2 Multiwalled Carbon Nanotubes

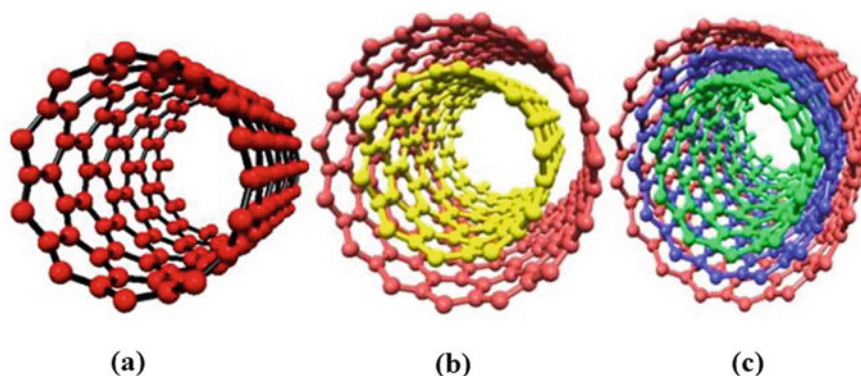
As mentioned in the previous section, multiwalled carbon nanotubes (MWCNTs) have a much concentric cylindrical structure of graphene layers (walls) or SWCNTs. The interlayer or walls separated is 3.4 Å. The inner nanotubes are shielded by the outer one. To synthesis MWCNTs, a number of synthesis routes have been tested. Among many, the following two synthesis methods are commonly used: (1) plasma-based methods: (a) arc discharge and (b) laser ablation; (2) thermal-based methods: (c) chemical vapor deposition (CVD), (d) plasma-enhanced chemical vapor deposition (PECVD).

Both SWCNTs and MWCNTs have unique thermal conductivity, mechanical strength, and electrical properties. Because of their extraordinary anisotropic properties, they showcase various attributes when analyzed under various conditions. MWCNTs are extensively studied for mechanical, thermal, and electrical applications which include heat sinks, microelectronics interconnects, and structural composites. But, SWCNTs and MWCNTs have different physical properties because of their structure and diameter. The difference between both types of carbon nanotubes was summarized in Table 1. The double-walled carbon nanotubes (DWCNTs) consist of only two concentric walls; one is nested within another, and they have similar morphology and properties of SWCNTs except for high resistance for chemicals. The three types of CNTs based on their walls are represented in Fig. 2.

CNTs produce electronic properties which are directly dependent on their helicity and diameter. Due to its small diameter and superior aspect ratio, the electrons inside CNTs cannot easily scatter during conduction. The CNTs have eminent current-carrying capacity exceeding the copper value. The thermal property of CNTs depends on the size and structure [31]. The thermal conductivity and specific heat of CNTs are greater than diamond. They are stable up to high temperatures in the atmosphere (750 °C) and vacuum (2800 °C). Due to their good thermal conductive nature, atomic bonds have been further strengthened in CNT [31, 32]. The inter-wall coupling in MWCNTs and inner wall coupling in SWCNTs leads to low temperature-specific heat that reassembles 3D graphite. Since CNT has sp<sup>2</sup> bonding between carbon atoms because of which they possess significant tensile strength compared to steel and Kevlar materials [31, 33]. Because of their significant properties, MWCNTs are used in diverse applications such as solar cells, optical antennae, ion sensors, gas sensors, nano-electrode-based sensors, hydrogen gas sensors, mechanical devices, electrical devices, TEM grids, storage devices, electromechanical devices, heat transfer applications, and also broadly used in biomedical fields [31].

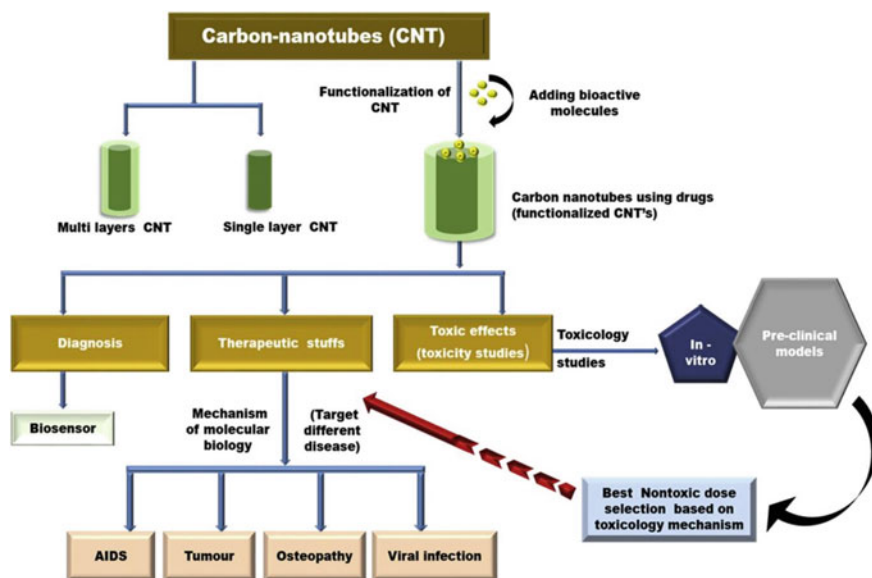
**Table 1** Differences between SWCNTs and MWCNTs properties

S. No.	SWCNTs	MWCNTs
1	SWCNTs have a single layer of graphene	MWCNTs have multiple layers of graphene
2	SWCNTs have poor mechanical strength	Remarkably stronger than SWCNTs
3	Bulk synthesis of SWCNTs is difficult	Bulk material synthesis is easy
4	The purity of the material is poor	The purity of the material is high
5	Higher loss or oxygen reduction when the catalyst is added	Lower loss or oxygen reduction when the catalyst is added than SWCNT
6	Evaluation and characterization are easy	Evaluation and characterization are a little difficult
7	The catalyst is required for the synthesis	The catalyst may or may not be essential
8	The possibility of flaws is more during functionalization	The possibility of flaws is less, but once it happens, it is difficult to improve

**Fig. 2** Classification of carbon nanotubes: **a** SWCNTs, **b** DWCNTs, and **c** MWCNTs. Reprinted with permission from Rathinavel et al. [30]. Copyright 2021 Elsevier

The most prominent applications for MWCNTs are drug delivery, cell separation, hyperthermia, gene therapy, electrochemical sensors, magnetic storage medium, catalyst, and various industrial applications [31]. There are major advantages in using MWCNTs for hyperthermia (HT) in photothermal therapy. MWCNTs limit the heating to the specific tumor zone; it has a fine ability to penetrate into cells which leads to better hyperthermia results. The MWCNTs have been played a key role in cell separation and manipulation. In addition, the greatest property of MWCNTs is their ability to assist in hydrogen-triggered (pH) drug release agents [34]. The  $\text{La}_{0.3}\text{Zn}_{0.3}\text{Co}_{0.1}\text{Fe}_{2.3}\text{O}_4$  (LZCFO) NPs in MWCNTs matrices were prepared by a wet-chemical technique. The prepared LZCFO@MWCNT nanoparticles produced effective hyperthermia values at constant alternate magnetic field and frequency





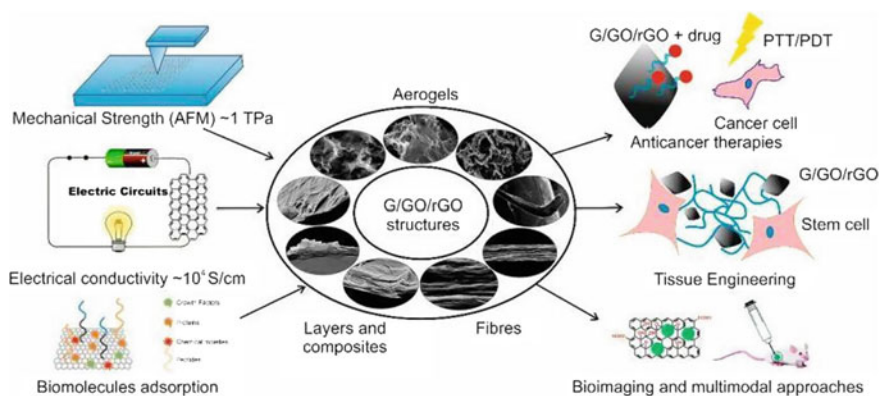
**Fig. 3** Pictorial representation of different types of carbon nanotubes and their biomedical applications. Reprinted with permission from Anzar et al. [24]. Copyright 2020 Elsevier

with less time [35]. The functionalized MWCNTs/ $\text{MnFe}_2\text{O}_4$  magnetic nanoparticles along with various functional groups were synthesized by solvothermal method, which produced notable hyperthermia values for cancer treatment [36]. Types of carbon nanotubes and diverse applications of functionalized CNTs were given in Fig. 3.

## 2.4 Graphene

Graphene is a 2D carbon material formed by  $\text{sp}^2$  carbon-carbon atomic bonding. Graphene has been studied for the past many years, due to its remarkable thermal, electric, mechanical, optical, magnetic properties, and also to its large specific surface area ( $2630 \text{ m}^2 \text{ g}^{-1}$ ). The graphene material has a great Young's modulus of 1.0 TPa, intrinsic carrier mobility ( $2,00,000 \text{ cm}^2 \text{ v}^{-1} \text{ s}^{-1}$ ), optical transmittance ( $\sim 97.9\%$ ), thermal conductivity ( $\sim 5000 \text{ Wm}^{-1} \text{ K}^{-1}$ ), and high electrical conductivity [37]. Graphene can retain stability up to  $108 \text{ A/cm}^2$  current density. Different methods were invented to prepare thin graphene film during earlier times. Later, a few layers of graphene were fabricated on a single crystal platinum surface through a chemical decomposition route. However, in recent years, the preparation of a large surface area, superior quality, and efficient graphene is achieved by top-down and bottom-up

techniques. The top-down approaches include mechanical exfoliation and chemical exfoliation of graphene from bulk graphite crystals. The bottom-up approaches include epitaxial growth, pyrolysis, and thermal and plasma-based chemical vapor deposition (CVD) methods. Among them, CVD technique is widely used due to its high efficiency and high-volume synthesis. The in-depth explanation of graphene synthesis methods and their properties were investigated in the literature [37, 38]. Chen and the co-researchers have studied that graphene-based nanoparticles such as reduced graphene oxide (rGO), graphene oxide (GO) have unique chemical and physical properties which make them eminent tools for photothermal therapy-based (PTT) hyperthermia for anticancer treatment. Due to the intrinsic absorption of near-infrared (NIR) radiation, graphene can be used in PTT and guided imaging to use as adjuvant therapy for chemotherapy, immunotherapy, and other therapeutic studies [39]. Graphene-based nanomaterials have exhibited notable promise in the area of imaging, biosensing, and biomedicine, especially in gene and drug delivery for anticancer therapy [40]. The graphene-based magnetic nanoparticles have a very strong linkage between the two compounds. Magnetic graphene hybrids have attained significant attention and were proven to improve the efficacy in the field of magnetic photothermal therapy, controlled drug delivery, imaging, cellular separation, and isolation [41]. Graphene-based materials produced unique physiochemical properties, modifiable active groups, good surface area, strong photothermal effect, and promising biocompatibility. They behave as active agents or tunable carriers for advanced cancer therapy [42]. Structure, various properties, and biomedical applications of graphene, GO, rGO were represented in Fig. 4.



**Fig. 4** Schematic image depicts various properties, scanning electron microscopy (SEM) structures, and biomedical applications of graphene, graphene oxide (GO), reduced graphene oxide (rGO) [43]

## 2.5 Graphene Oxide (GO) and Reduced Graphene Oxide (rGO)

Graphene oxide (GO) can be easily prepared by the oxidation of natural graphite powder or flake. GO is easy to synthesis, low cost, and has the ability to convert into graphene. The flake graphite (FG) is a natural forming mineral that is cleansed by eliminating heteroatomic contamination. Brodie was the first person to scrutinize the synthesis of GO by the addition of potassium chlorate ( $\text{KClO}_3$ ) to a graphite slurry in fuming nitric acid ( $\text{HNO}_3$ ) [44, 45]. Later, Staudenmaier extended this protocol by adding concentrated sulfuric acid ( $\text{H}_2\text{SO}_4$ ) and fuming nitric acid ( $\text{HNO}_3$ ) followed by slow addition of chlorate ( $\text{ClO}_3^-$ ) to the reacting mixture. These slight changes in the procedure proved to be an easy and revised method for preparing effectively oxidized GO [45, 46]. Finally, Hummers proposed an alternative route to prepare GO by using potassium permanganate ( $\text{KMnO}_4$ ), sodium nitrate ( $\text{NaNO}_3$ ) in concentrated sulfuric acid [45, 47]. The synthesis of GO involves the oxidative treatment of graphite by predominant methods invented by Brodie, Staudenmaier, and Hummers. Many recent studies have used modified Hummer's method for the initial preparation of graphene oxide.

Reduced graphene oxide (rGO) is extracted from graphene oxide by the thermal reduction of GO [45]. In other words, at high temperatures and under reducing conditions, GO will convert to rGO [48]. Till now, very few synthesis methods were investigated for reduced graphene oxide (rGO). Most of the researchers have followed the hydrazine hydrate method for the synthesis of rGO from GO. Further, some other reducing solvents are used for the synthesis of rGO. Pareds and his group have studied the effect of various reducing agents on GO. They used potassium hydroxide (KOH), ammonia ( $\text{NH}_3$ ), pyrogallol ( $\text{C}_6\text{H}_6\text{O}_3$ ), ascorbic acid (Vitamin-C) ( $\text{C}_6\text{H}_8\text{O}_6$ ), hydrazine monohydrate ( $\text{H}_6\text{N}_2\text{O}$ ), and sodium borohydride ( $\text{NaBH}_4$ ) as the reducing agent; among this, ascorbic acid (Vitamin-C) ( $\text{C}_6\text{H}_8\text{O}_6$ ) is the noble substitute for hydrazine for the synthesis of rGO [48, 49]. In general, GO and rGO exhibit smaller in size, higher density of functional group and more possibilities to interact with bacteria tissues, and also exhibits strong antibacterial property resulting in cell deposition. Their physicochemical properties such as size, conductivity, the density of functional group can be tailored and hence enhance the potential of applications or reduce risks [50]. Chwalibog and his co-workers have studied the effect of GO and rGO on glioblastoma cells in in vitro and in vivo modes. The in vitro results reveal that the graphene oxide and rGO entered glioma cells have a cytotoxic effect. Hence, both the types of platelets decreased proliferation and cell viability with rising doses, but reduced GO was more toxicity than GO. The volume and mass of the cancer cells were diminished after the injection of rGO and GO. The rGO-mediated cell death, through the apoptosis pathway, highly recommended the potential suitability of rGO in cancer therapy [51]. The well disperse and biocompatibility of folic acid (FA) conjugated with  $\text{Fe}_3\text{O}_4$  and encapsulated with nanoscale graphene oxide (nGO) and loaded with doxorubicin (DOX) NPs contributed a stable nanocarrier system. Notably, nanocomposites are highly effective in in vivo imaging. The

in vitro biocompatibility and cell viability studies of FA-Fe<sub>3</sub>O<sub>4</sub>@nGO-DOX NPs indicated their particular uptake by MGC-803 cells. The FA-Fe<sub>3</sub>O<sub>4</sub>@nGO-DOX nanoparticles-treated mice were extensively active and exhibited reduced weight loss than mice treated with Fe<sub>3</sub>O<sub>4</sub>@nGO-DOX NPs [52]. Ricci and his research group were prepared graphene oxide nanoribbons (GO-NR) for bone regeneration which caused potential cytotoxicity, bactericidal effect, and gene expression. The GO-NR nanoparticles exhibited no cytotoxicity effect up to 100 µg/mL concentration, and no gene expression was observed when used in reasonable dose [53]. Lin and his co-researchers were successfully investigated multifunctional dopamine-coated zerovalent iron (ZVI) NPs and rGO for targeted phototheragnosis in breast tumors. The ZVI/rGO@pDA nanoparticles exhibited high sensitivity in imaging compared to pure ZVI@pDA even at low concentrations. The combination of ZVI, rGO, and pDA showed potential-specific targeting capabilities, cancer phototheragnosis, outstanding biocompatibility, and tumor imaging capacity [54].

## 2.6 Porous Carbon

Porous carbon (PC) materials are classified based on the size of the pore. If the porous carbon nanoparticle diameter is <2 nm is called microporous, 2–50 nm as mesoporous, and >50 nm as macroporous carbon materials. The PC nanoparticles might have only a single type of porous system or a combination of two or all the above three types. Such a group of porous systems is present as an interconnected porous system; it could be referred to as hierarchically porous carbon material. Porous carbon nanoparticles (PCNPs) are synthesized by two important routes: (a) hard template and (b) soft template. The hard templates are used to build up the carbon nanostructures and also used for nanocasting route which mainly consists of silica and zeolite. The hard template is embedded in the carbon precursor. The zeolite template provides microporous carbon (MPC), and the silica template provides microporous or mesoporous or macroporous or all three porous systems as well [55, 56]. The soft template synthesis route involves the synthesis of PC materials by the wet-chemical approach. Generally, the sol–gel method is a soft template, and a surfactant/polymer along with carbon precursor and polymerization agent is used to produce the porous structure. In addition, we can prepare porous carbon material by naturally occurring materials such as paddy husk, tea waste, and coconut husk which are available at a low cost. The PC material has gained great attention due to their large pore volume with modification of pore structure, the suitable functional group including  $\pi$ – $\pi$  stacking and ease surface modification, large surface area (1274 m<sup>2</sup>/g), high heat conversion capacity, high biocompatibility, great mechanical stability, unique optical properties, and high chemical inertness [56, 57]. Zbair and his research group were reported a facile synthesis route of porous carbon nanoparticles (PCNPs) by microwave-assisted pyrolysis method. The prepared PCNPs are highly efficient adsorbents for antibiotic sulfamethoxazole adsorption [58]. The fluorescent carbon-coated (FC) magnetic nanoparticles (MNPs) core–shell particles were

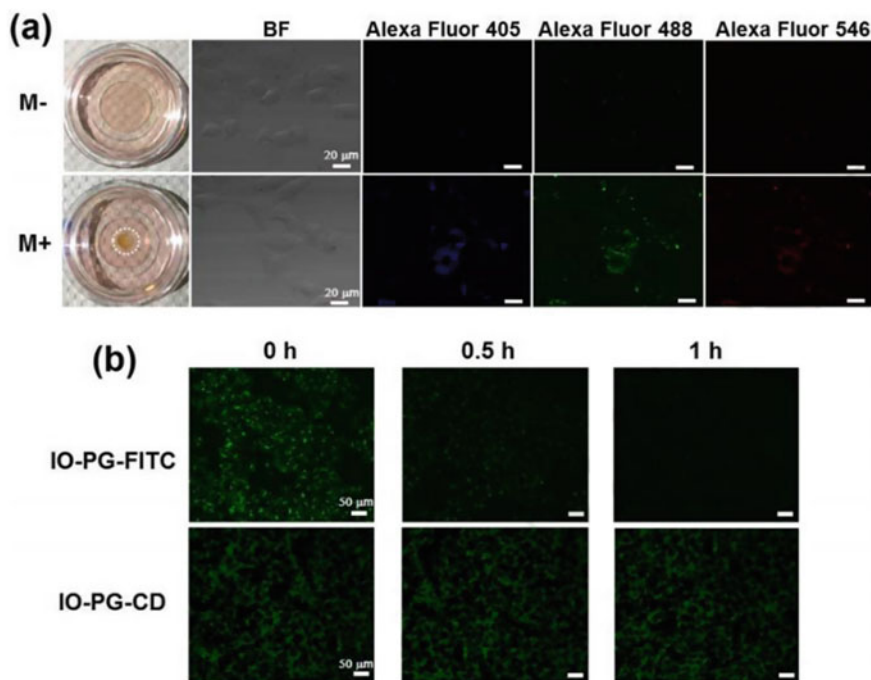
synthesized by hydrothermal one-step protocol. The FC-MNPs exhibited superior magnetic and inherent fluorescent properties and also an excellent material for neural tissue engineering applications. The FC-MNPs have shown potential due to their selective affinity toward neuronal tissues, good biocompatibility, and neuronal therapeutics in neuro-engineering applications [59]. The biocompatible porous carbon-coated magnetite ( $\text{Fe}_3\text{O}_4$ ) nanoparticles (PCCMNPs) were synthesized by a one-pot solvothermal route. To achieve targeted therapy, PCCMNPs were surface modified with hyaluronic acid (HA). The adjuvant treatment of photothermal therapy (PTT) and chemotherapy became a promising tool for cancer treatment. The biocompatible porous carbon-encapsulated MNPs had high drug loading efficacy and intelligent drug release. The *in vivo* MR imaging ( $T_2$ -weighted) confirmed the cancer cell accumulation of nanocarriers [60].

### 3 Carbon Dots-Coated Magnetic Nanoparticles for Biomedical Applications

#### 3.1 Targeted Drug Delivery

Several research studies have exploited the biocompatible, small size ( $\leq 10$  nm), and surface functionalization capabilities of carbon quantum dots for targeted drug delivery of several anticancer drugs. Carbon dots (CDs) coupled to magnetic nanoparticles (MNPs) via polyglycerol (PG) covalent bonding were researched by Wen and his co-workers for platinum-based drug delivery in cancerous cells via external magnetic attraction [61]. The *in vitro* study claimed that no cytotoxicity for CCK8 assays up to concentrations of 200  $\mu\text{g}/\text{mL}$  and increased cellular uptake in HeLa. This nanohybrid MNPs-PG-CD was explored further for fluorescence cancer cells bioimaging; these malignant cells along with nanohybrid particles showed non-bleaching, strong fluorescence of different primary colors such as red, green, and blue (RGB) under external magnetic attraction. The fluorescence phenomenon persisted in spite of irradiation under the lamp (xenon) for 1 h in comparison with dye labeled (MNPs-PG-FITC) which exhibited no fluorescence, as shown in Fig. 5 [62].

Core-shell  $\text{Fe}_3\text{O}_4$ - $\text{SiO}_2$ -CDs NPs in a study was used for magnetically targeted drug delivery for anticancer treatment. The nanohybrid had excellent high drug loading concentrations (306.7 mg/g) of gambogic acid as well as drug loading efficiency of 68% at a pH of 5.7 in contrast to 35% at neutral pH. It showed effective drug release at an acidic pH environment. The fluorescent nanohybrid had an intense toxic effect on VX2 cells (breast cancer cells) with the rate of cell survival being <20% of concentration 100  $\mu\text{g}/\text{mL}$ . The saline dispersion of gambogic acid-loaded  $\text{Fe}_3\text{O}_4$ @ $\text{SiO}_2$ -CDs core-shell NPs was injected into VX2 tumors in mice and was tested for therapeutic efficacy under external magnetic field attraction for around 2 h. 18-FDG-positron emission tomography/computed tomography imaging analysis revealed a decrease in tumor volume with time [63].



**Fig. 5** **a** Fluorescence imaging of cervical cancer cells incubated with the nanohybrid in the presence and absence of magnet. **b** Confocal imaging of HeLa cells individually treated with IO-PG-FITC and IO-PG-CD after xenon lamp irradiation for a various time duration, where iron oxide nanoparticles (IO) are MNPs. Reprinted with permission from Wen et al. [62]. Copyright 2019 Elsevier

Maghemite nanoparticles coated with carbon dots were also studied have also been used for improving anticancer drug efficacy, drug solubility at the cellular level, and biocompatibility (toxicity and drug pharmacokinetics). Borhan and his research co-workers were designed a unique lipophilic fluorescent nanocomposite synthesized by flash cooling-assisted sol-gel technique. The nanocomposite comprised of  $\text{Fe}_2\text{O}_3$ -CDs NPs was further functionalized with a cost-effective chemotherapeutic agent (NHPI) to induce instant tumor destruction. The *in vitro* cell viable cytotoxicity (MTT) test of the drug-free nanocomposite and anticancer drug (mitoxantrone) revealed cytotoxic cell death of 37% and 47%, respectively, on human osteosarcoma cells after 24 h incubation at 0.01 mg/mL concentration. The drug loading efficiency was 98% (w/w) in acidic pH of 7.4 and 97.5% in pH of 5.2. The preliminary drug content of the carbon nanoparticles was 3.2% and 3.1% (weight per weight) at pH 7.4 and 5.2, respectively [64].

Magnetic fluorescent CS nanoparticles consisting of  $\text{Fe}_3\text{O}_4$  and carbon dots as shell and chitosan as functionalized shell material were constructed for 5-fluorouracil drug delivery by a unique single-step high gravity process. The pH on drug release was estimated and observed that an acidic pH creates an ideal time for faster drug

release in contrast with physiological pH. This core–shell system created a supreme drug loading ability of 216.1 mg g<sup>-1</sup>. The presence of –NH from 5-fluorouracil and H<sup>+</sup> ions in the solution leads to the formation of amino groups (–NH<sub>2</sub>) which further causes faster drug release at low pH. The presence of chitosan, a natural biocompatible polymer, and carbon dots helps in the controlled release. The 5-fluorouracil drug release kinetics was found to be monitored by Fickian diffusion [65].

### ***3.2 Combined MRI Imaging and Drug Delivery***

Carbon quantum dots possess inherently strong fluorescence properties due to their quantum size effects, nontoxicity, and photostability because of which they have been explored and applied successfully in both MRI imaging and fluorescence imaging for cancer tumor diagnosis [66, 67]. Yao and their research group were prepared and applied nontoxic, biocompatible Fe<sub>3</sub>O<sub>4</sub>-AFn/DOX-CD nanocomposite as ideal negative T<sub>2</sub> contrast agents and also for doxorubicin drug delivery. Controlled drug release at both acidic and physiological pH was achieved, and the intracellular DOX drug uptake into breast cancer cells was proven to be time dependent from both fluorescence and bright field microscope images. The drug encapsulated within apoferritin nanocages exhibited high drug encapsulation efficiency, and the drug discharge rate was pH dependent (72% at pH 5.2 and 38% at pH 7.4) which is due to the unfolding and refolding of the apoferritin. The nanocomposite showed remarkable cell viability values of 87.17% after 48 h on MCF-7 cells. As the nanocomposite exhibited excellent results for in vitro studies and the study was further extended to in vivo mouse models as the nanocomposite showed strong magnetic properties on testing. For in vivo testing, the nanocomposite was initially injected into B16-F10 tumor-bearing C57 mice with a magnet attached to the tumor and studied for different time periods 1, 4, and 7 h by 3 T MRI scanner. After 7 h, the tumor signal intensities were found to reduce significantly in comparison with other regions of the mice [68].

## **4 Magnetic Nanoparticle-Decorated CNTs for Biomedical Applications**

### ***4.1 SWCNT for Targeted Drug Delivery and MRI Imaging***

Single-walled carbon nanotubes (SWCNTs) are being utilized for targeted drug delivery due to several fascinating features. Firstly, they bring down the aftermath of the drug applied, promote increased drug accumulation in the tumor tissues, and improve encapsulation efficiency of the therapeutic drugs because of increased aspect ratio and surface area [69]. A great asset in the use of SWCNTs is their shape,

as they can penetrate cellular components without causing any destruction. PVP-functionalized SWCNTs tagged with MNPs and further conjugated with CD105 monoclonal antibodies have been applied for MRI contrast imaging. The apoptosis cell death assays, which include TACS, TBARS, and PARP, revealed that the anti-cancer drug DOX-loaded SWCNTs-MNPs antibody complex induces apoptosis, oxidative stress, and damages DNA at a time on 4T1 breast cancer cells in contrast with PVP-functionalized SWCNTs. From the MRI imaging, the decrease in  $T_2$  values with time confirms the magnetic targeting of the SWCNT-MNPs complex using an external magnet to the tumor site. From the noninvasive bioluminescence imaging, it was observed that reduced bioluminescence from DOX-loaded composite reveals decreased tumor size. Also, the ability of the doxorubicin delivery via this magnetic targeting method prevented cancer from metastasizing further [70].

Analogous to the above research, another investigation was done by the same group on PVP-functionalized SWCNTs tagged/decorated with 40% of magnetic nanoparticles content and likewise coupled with CD105 mAb for specific active targeting to 4T1 cells. The magnetic susceptibility was enhanced which paved the way for sensitive noninvasive MRI imaging. The results reveal that high-energy magnet-based targeting was much more effective than active antibody-based targeting. When the magnet is placed over the mice, which bearing the 4T1 metastatic tumor, for a 2-h duration of post-injection of SWCNTs-based nanocarrier showed better targeting. Further, the decrease in  $T_2$  values indicates that iron-tagged SWCNTs accumulation in the tumor region and an increase in apparent diffusion coefficient (ADC) value confirmed the efficient specific magnetic targeting [71].

#### ***4.2 MWCNTs for Combined Targeted Drug Delivery and Magnetic Hyperthermia***

Multiwalled carbon nanotubes (MWCNTs) possess several important features such as superior physical and chemical stability, a high surface area, high transmission ability through cell membranes. Though its only drawback is its inherited hydrophobic surface due to which its use is limited in biomedical applications. But, in a few cases, hydrophilic polymers such as chitosan, PEG, PEI are added to compromise on its defect [72]. PEG and PEI were added to impart hydrophilicity, and folic acid (FA) was conjugated to act as a targeting ligand. Then,  $\gamma\text{-Fe}_2\text{O}_3$  was deposited on MWCNTs/PEG-PEI-FA by an atomic layer deposition method. The study concluded, the magnetic nanoparticles ( $\gamma\text{-Fe}_2\text{O}_3$ ) had no impact on drug loading capacity, release, and toxicity except in guiding the MWCNTs/PEG-PEI-FA to the targeted site [73].

Functionalized carbon nanotubes have the potential to deliver an enormous amount of drug at the targeted cancer tumor microenvironment but in a low acidic pH state. Magnetic NPs-decorated functionalized CNT is highly suitable for pH-sensitive drug release. Seyfoori and the research group were the first to report



MWCNTs decorated with manganese ferrite, containing pH-sensitive nanogel for doxorubicin delivery. The hybrid nanocomposite had 92% drug loading efficiency in comparison with 71% of the functionalized bare MWCNTs due to drug diffusion in the nanogel polymer structure also due to  $\pi$ - $\pi$  and electrostatic interaction of the carbon atoms with the drug molecules. At a pH of 5.3, hybrid nanocomposite showed greater cumulative drug release (80%) compared to f-MWCNTs (48%) and shows the pH-dependent nature of the nanogel. The report stated two main reasons for this phenomenon: (i) the role played by the  $H^+$  ions with the decrease in the hydrogen bonding between the drug and the carbon nanotubes. (ii) the Van der Waals repulsion between the  $NH_2$  groups of the hydrophilic polymer. The hybrid nanocomposite's effective drug release was further tested using Presto blue assay, and it shows increased death of U87 glioblastoma cancer cells when monitored for a period of 7 days [74]. In another report on magnetic hyperthermia performance of bare  $MnFe_2O_4$  NPs,  $MnFe_2O_4$ -decorated PEG-functionalized MWCNTs and  $MnFe_2O_4$ -decorated amine-functionalized MWCNTs were studied. Among the three, amine-functionalized nanocomposite showed the highest (SAR) value and intrinsic loss power (ILP) value. It was found to decrease with the increase of sample concentration. The amine-functionalized sample shows SAR of 28.90 W/g (ILP:  $5.18 \times 10^{-4} \text{ nHg}^{-1} \text{ m}^2$ ) at 2 mg/0.5 mL in contrast to PEG-functionalized MWCNTs sample SAR of 26.42 W/g (ILP:  $5.18 \times 10^{-4} \text{ nHg}^{-1} \text{ m}^2$ ) [75].

Some of the present study results on MWCNTs and magnetic nanoparticles composites utilized for drug delivery, and MHT applications were shown in Table 2. Tiwari and co-workers also reported amine-functionalized MWCNTs/ $MnFe_2O_4$  composites which showed superior SAR and ILP values ( $0.00109 \text{ nHg}^{-1} \text{ m}^2$ ) in comparison with PEG-based nanocomposite (ILP:  $0.00106 \text{ nHg}^{-1} \text{ m}^2$ ). The difference is attributed to the effective increase of anisotropy and diminished aggregation of the manganese ferrite nanoparticles adhered to MWCNTs [36].

In another research investigation on magnetic hyperthermia, where low Curie temperature ( $43^\circ\text{C}$ ),  $Zn_{0.54}Co_{0.46}Cr_{0.6}Fe_{1.4}O_4$  NPs were decorated on functionalized carbon nanotubes and were shown effective self-regulating temperature of  $42.7^\circ\text{C}$  under AMF. The samples were tested for self-regulating magnetic hyperthermia at a high magnetic field of 400 Oe. An enhanced SAR value of 1372 W/g was recorded for material having high dispersibility insolvent compared to standalone magnetic nanoparticles. In vitro analysis was carried out on the HaCaT cell line by CCK8 cell assay technique proving the nontoxicity of the nanocomposite from concentrations:  $6.25 \mu\text{g ml}^{-1}$  up till  $100 \mu\text{g ml}^{-1}$  [76].

MWCNTs have several roles to play in the synthesis of the magnetic luminescent nanocomposite. Functionalized MWCNTs were utilized as support materials for the growth of iron oxide nanoparticles. These MWCNTs acted as nucleation sites and were found to prevent agglomeration of the MNPs synthesized via the coprecipitation technique. They were also able to prevent the adsorption of drugs and other biological molecules and ward off the decreased fluorescence intensity caused due to changes in the biological species [77].

**Table 2** Magnetic nanoparticles-decorated functionalized MWCNTs hybrid nanocomposites applicable for various biomedical applications

S. No.	Name of hybrid nanocomposite	Drug loading efficiency (%)	Sample concentration (mg/mL), field frequency (kHz), field magnetic field strength (kA m <sup>-1</sup> )	Specific absorption rate (SAR) W/g	Type of application	References
1	Chitosan MWCNTs/MnFe <sub>2</sub> O <sub>4</sub>	80% at pH 5.3	-	-	Doxorubicin drug delivery	[74]
2	MWCNT-PEI-PEG-FA/γ-Fe <sub>2</sub> O <sub>3</sub>	55% at pH 5.5	-	-	Doxorubicin drug delivery	[73]
3	Amine-functionalized MWCNTs/MnFe <sub>2</sub> O <sub>4</sub>	-	(a) 2 mg/0.5 mL 336 kHz 12.89 kA m <sup>-1</sup> (b) 8 mg/0.5 mL 336 kHz 12.89 kA m <sup>-1</sup>	(a) 28.90 W/g (b) 6.21 W/g	Magnetic hyperthermia	[75]
4	Amine-functionalized MWCNT/MnFe <sub>2</sub> O <sub>4</sub>	-	2 mg/mL 231 kHz 20.51 kA m <sup>-1</sup>	0.10646 W/g	Magnetic hyperthermia	[36]
5	MWCNTs/Zn <sub>0.54</sub> Co <sub>0.46</sub> Ct <sub>0.6</sub> Fe <sub>1.4</sub> O <sub>4</sub>	-	112 mg/mL 100 kHz 15.95 kA m <sup>-1</sup>	1372 W/g	Magnetic hyperthermia	[76]

## 5 Graphite-Coated Magnetic Nanoparticles for Biomedical Applications

It is reported that graphite-coated magnetic nanoparticles were used for multimodal therapeutic applications such as siRNA delivery, magnetic hyperthermia, MRI contrast agents, and *in vitro* Raman analysis. The core-shell nanoparticles synthesized for this purpose had an inner core of iron-cobalt (FeCo) and an outer shell consisting of graphite carbon. This research approach had several benefits compared to other MNPs such as magnetite, iron-platinum nanoparticles, and maghemite which have great Curie temperature, high magnetization, and enhanced magnetic anisotropy-based applications. The major advantage is easy tailoring of the properties of the outer-shell carbon layer, which is ideal for improved Raman signal intensity, and the carbon shell layer makes magnetic nanoparticles chemically inert. From the MRI imaging, a high  $T_2$  relaxivity coefficient of  $392 \text{ mM}^{-1} \text{ s}^{-1}$  and  $T_2$ -weighted high contrast image were obtained compared with that of a well-known MRI contrast agent, Resovist ( $140 \text{ mM}^{-1} \text{ s}^{-1}$ ). *In vivo* MRI study showed that graphene-coated magnetic nanoparticles settled in the liver, spleen, and kidneys, and the imaging ability was retained for a period of 10 days. Graphene-coated FeCo magnetic nanoparticles did cause any cytotoxicity, from Raman imaging, as they were successfully excreted out and well absorbed by the liver and spleen. These FeCo/C magnetic nanoparticles have shown a specific absorption value of 69 W/g compared to  $\text{Fe}_3\text{O}_4$  nanoparticles (19 W/g), and the therapeutic temperature was attained much faster (10 times faster) than that of  $\text{Fe}_3\text{O}_4$  nanoparticles. For specific brain cancer cell (U87) targeting, these magnetic nanoparticles were functionalized with epidermal growth factor receptor variant III (EGFRvIII) antibodies, resulting in successful cellular uptake, and under alternate magnetic field, adequate tumor death was achieved by magnetic hyperthermia in a short duration. For combined siRNA delivery and magnetic hyperthermia, functionalized magnetic nanoparticles carrying siRNA were treated with U87 cells and subjected to hyperthermia conditions for 5 min. This technique was highly effective in the silencing of the EGFRvIII oncogene with fruitful deactivation of PI3K/AKT cell apoptosis pathway and more cancer cell death compared to control cells, evidenced from MTS assay [78].

Another study on graphitic carbon-coated (SPIONs) was carried out to assess dual-purpose MRI agents and MHT applications. Carbon-coated SPIONs diameter of 40 nm had greater fluorescence intensity, high quantum yield (8–6%), and fluorescence decay lifetime (4.7–4.2 ns) of not less than 1-grade magnitude higher than that of 10 nm carbon-coated SPIONs and carbon composite SPIONs. The MRI images indicate that the coated SPIONs have higher negative  $T_2$  contrast which increases with SPIONs concentration; the relaxivity ( $r_2$ ) was also reduced from 177 to 82 with an increase of carbon content. The SPIONs with minimum carbon coating had excellent MRI imaging capacity compared with their other counterparts. It is attributed to a high number of water molecules adsorbed onto its rough surface. The magnetic hyperthermia measurement was conducted on the three different-sized SPIONs for a

concentration of 2 mg/mL under 30 kA/m alternate magnetic field strength, among which 10 nm carbon-coated SPIONs were shown highest SAR of 430 W/g [79].

## 6 Graphene Oxide-Coated Magnetic Nanoparticles for Biomedical Applications

### 6.1 Targeted Drug Delivery

Bare magnetic nanoparticles always have very low solubility and less colloidal stability in aqueous physiological media due to nanoparticles' high surface energy and magnetic dipole interactions. On surface modification with graphene oxide (GO), they are conferred with several advantages such as improved biocompatibility, aqueous colloidal stability, and solubility for biological applications. Graphene oxide is considered a versatile host for magnetic nanoparticles (MNPs) in nanocomposites formation due to the ionizable and polar functional group's presence, ease to fabricate large scale production, and its unique optical and electronic properties. Graphene oxide is generally functionalized with various biocompatible polymers such as chitosan, pluronic acid F-127, polyethylene glycol, and its derivatives in order to minimize its toxicity for effective drug conjugation. Current reports state that the use of graphene as a surface modification or functionalization agent is widely applicable in drug delivery, MRI imaging, *in vitro*, and *in vivo* magnetic hyperthermia applications. As GO surface contains many graphene sheets, it is used effectively as a drug loading carrier, and it can also be magnetically guided with the help of magnetic materials. These sheets possess a number of organic moieties such as epoxide, hydroxide, and carboxylic acid groups. The whole GO exterior can be utilized for drug addition and surface modification due to  $\pi$ - $\pi$  interaction on the basal plane, which contains a hydroxyl group and epoxide groups (-O-), and the carboxylic group ( $\text{COO}^-$ ) which imparts a pH-sensitive (-) charge on its exterior [80][81]. Several studies have investigated the use of GO-MNPs hybrids for different biomedical applications. Mohammad and the research group have successfully prepared a multifunctional hybrid nanocomposite of chitosan-coated  $\text{Fe}_3\text{O}_4$ /rGO core-shell particles by solvothermal method for doxorubicin drug delivery and fluorescence imaging. The *in vivo* zebrafish study proved the nontoxic nature of the nanocomposite, and sufficient doxorubicin drug addition of 0.448 mg/mL was obtained. Reduced GO can interact with the drug via  $\pi$ - $\pi$  bond, while the polymeric nature of the nanocomposite backbone aids drug release in neutral pH.  $\text{Fe}_3\text{O}_4$  NPs help in guiding the drug to the targeted site with the application of an external magnetic field [82].

Several other studies report good drug loading efficacy values at the targeted site. For example, Gonzalez-Rodriguez and his research group have synthesized GO- $\text{Fe}_3\text{O}_4$  as a multifunctional biocompatible hybrid nanostructure for coupled fluorescence, MR imaging, and targeted drug delivery. As mentioned earlier, graphene possesses a high surface area and improved water solubility and aids in increasing

doxorubicin drug solubility. Doxorubicin is a therapeutic anticancer drug that is noncovalently bound to graphene oxide- $\text{Fe}_3\text{O}_4$  during the drug loading. Its drug efficacy is 2.5 times more. The noncovalent functionalization of the drug onto the nanocarrier assists in enhanced drug release at the targeted site. It does not disturb the optical and electronic properties of the nanocarrier which are required for imaging the cancerous cells. Further, the  $\text{Fe}_3\text{O}_4$ -GO-DOX nanostructure showed good cell internalization in HeLa cells in comparison with  $\text{Fe}_3\text{O}_4$ -GO for 3-h period [83].

Similarly, another research group investigated the role of PEG bis-amine (PEGA) and GO-coated MNPs for methotrexate (MTX) drug delivery. The cytotoxic nature of the MNPs-GO/PEGA/MTX hybrids was evaluated by MTT colorimetric assay on HeLa and MCF-7 cells. On HeLa cells, with an increase of MNPs-GO/PEGA/MTX concentration, around 15–40% of the cells were destroyed over a period of time, and a similar trend was observed in MCF-7 cells too. The toxic effect of the hybrid nanocomposite was proven to increase with concentration and time compared to the free MTX drug. Further, an increased MTX drug release rate (100%) was also observed at a time period of 60 h under acidic conditions as more drug release is obtained at low pH. The nanocomposite carrying the drug was also non-hemolytic (<2%) at all reported concentrations and exhibited good biological compatibility. It is confirmed from a series of tests such as complement activation, agglutination, and coagulation time assay [84]. Another study alike to this but on doxorubicin drug delivery, where pluronic F-127-coated GO-based magnetic nanocomposite, showed an overall 91% drug loading efficiency. A good hemocompatibility, pH, and temperature-sensitive drug release of around 46% at acidic pH were achieved under an alternate magnetic field for 30 min. A high intrinsic loss power (ILP) value of 2.1–2.7 nH m<sup>2</sup> kg<sup>-1</sup> was also obtained [85], which is less compared to the value reported by Sugumaran and his co-workers [86].

## 6.2 Magnetic Hyperthermia and Cancer Imaging

Graphene oxide-coated magnetic nanoparticles are also applied for dual-purpose cancer imaging and magnetic hyperthermia applications. Manganese ferrite-coupled graphene oxide nanocomposites exhibited a significant SAR value of 1588.83 W/g at 0.1 mg Fe mL<sup>-1</sup> and a high  $T_2$  ( $r_2$ ) relaxivity value of 256.2 mM<sup>-1</sup> s<sup>-1</sup> [87]. Magnetic hyperthermia is an experimental therapeutic technique for cancer treatment utilized in conjunction with chemoradiotherapy to improve cancer treatment efficacy. In MHT, local tumor temperature is elevated to around 43 °C for a short span of time resulting in programmed cell death or apoptosis of the heat susceptible cancer cells. A  $\text{Fe}_3\text{O}_4$ -rGO hybrid nanocomposite synthesized by coprecipitation method exhibited high DOX drug loading capacity because of the  $\pi$ - $\pi$  stacking and the strong H bond between the hydroxyl or epoxide group of the reduced GO with the hydrogen present in the doxorubicin structure. The combined effect of an alternate magnetic field-induced (AMF) therapy of  $\text{Fe}_3\text{O}_4$ -rGO-DOX was also investigated. At 37 °C, the nanohybrid (at 2 mg/mL) is induced 50% cell death in the absence of

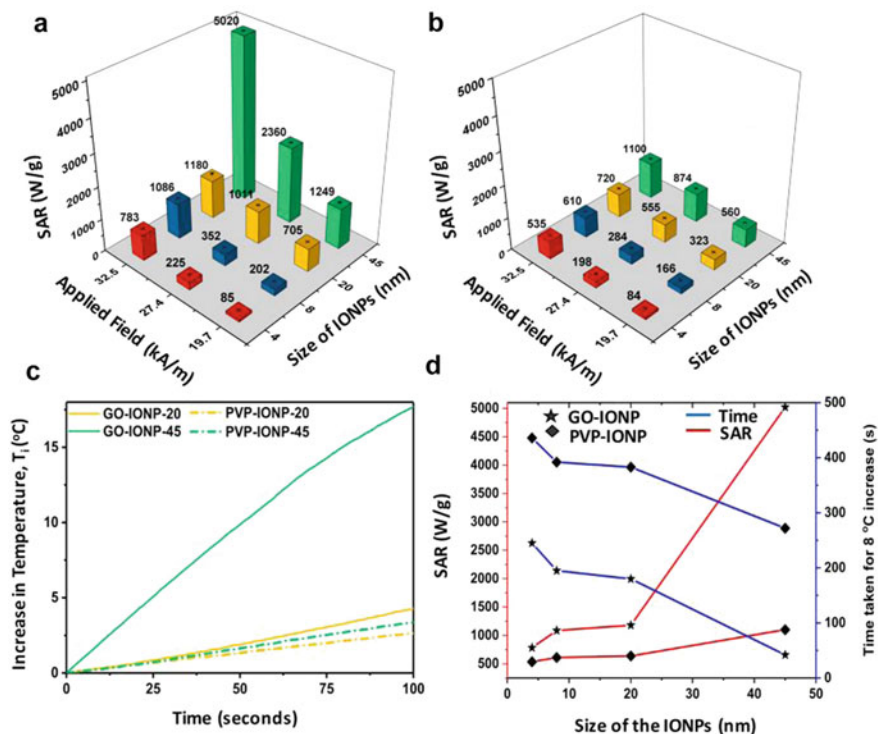
AMF due to only drug release at a low pH environment created by the cancer cells. When the same cancerous HeLa cells were subjected further to an alternate magnetic field for 35 min, around a 90% reduction in cell survival of the cancerous region was noted. It is ascribed to electrostatic interaction between the DOX molecules, which gets cleaved with the nanohybrid, and frictional force and heat generated under AMF in the tumor. The increased DOX release at the target site and diminished aftermaths of the chemotherapeutic drug are explained due to the graphene presence which is greatly sensitive at low pH [88]. Another study akin to this includes an in vivo magnetic hyperthermia effect of the MNPs-GO nanohybrids on 4T1 mouse model. Sugumaran and his group have scrutinized the performance of GO-functionalized magnetic nanoparticles of various sizes (4, 8, 20, 45, and 250 nm diameter) for magnetic hyperthermia application and its aqueous colloidal stability for use in a biological environment. Due to the amphiphilic nature of GO, it was able to maintain excellent colloidal stability in aqueous solutions even under high magnetic field strength. The GO-coated  $\text{Fe}_3\text{O}_4$  NPs of 45 nm diameter showed magnificent SAR of 5020 W/g in contrast with PVP- $\text{Fe}_3\text{O}_4$  NPs, as shown in Fig. 6, and an unprecedented intrinsic loss power value of  $12.21 \text{ nH m}^2 \text{ kg}^{-1}$ . The functionalized magnetic nanoparticles also exhibited exceptional antitumor activity in vivo mouse model and were able to achieve an  $8^\circ\text{C}$  increase in less than 50 s [86].

Some of the current research studies on GO and MNP hybrid nanocarrier used for targeted drug delivery and magnetic hyperthermia are shown in Table 3. Few magnetic nanoparticles possess inherent antibacterial activity; this nature is further enhanced in the presence of rGO. The Co/rGO/PEG nanocomposite was applied for magnetic hyperthermia and photothermal therapy. The nanocomposite at  $100 \mu\text{g/mL}$  showed 100% antibacterial activity against *E. coli* under the influence of AMF for 15 min. Bare cobalt nanoparticles which are already possessed a high antibacterial effect when combined with rGO had an accelerated deathly effect on the gram-negative bacteria because of pointed edges of the graphene sheet which could hamper the bacteria's cytomembrane [89].

## 7 Porous Carbon-Coated Magnetic Nanoparticles for Biomedical Applications

### 7.1 Drug Delivery and MRI Imaging

Like the other carbon nanomaterials, for instance, MWCNTs and graphene oxide, porous carbon is also found to have enhanced drug loading ability, biocompatibility, high specific surface area, and also adjustable porosity. A study evaluated the effectiveness of solvothermal-synthesized porous carbon-coated (PC) magnetite nanoparticles functionalized with ethylenediamine [ $(-\text{NH}_2)_2$ ] and then conjugated with hyaluronic acid (HA) (PCCMNs- $\text{NH}_2$ -HA) for magnetic resonance imaging guided chemotherapy/photothermal therapy. For cancerous cell targeting, the carboxy group



**Fig. 6** SAR values of 1 mL (3 mM Fe concentration) of **a** Graphene oxide and **b** Polyvinylpyrrolidone-modified iron oxide nanoparticles with respect to applied field. **c** Time-dependent heating outlines of 3 mM Fe of 20 and 45 nm GO- and PVP-functionalized IONPs on exposure to  $32.5 \text{ kA m}^{-1}$  alternate field strength at 400 kHz. **d** Particle diameter-dependent specific absorption rate and time duration for  $8^\circ\text{C}$  rises in temperature. Reprinted with permission from Janani et al. [86]. Copyright 2019 American Chemical Society

on the porous carbon shell was surface modified with ethylenediamine  $[(-\text{NH}_2)_2]$  and then conjugated with hyaluronic acid, which is a well-known cancer cell targeting ligand as shown in Fig. 7. The nanocomposite drug carrier possessed a high doxorubicin loading efficiency of 27.3%. This is an attribute to several interactions such as  $\pi$ - $\pi$  stacking, H bonding, and electrostatic forces between the drug DOX and porous carbon-coated magnetite. Porous carbon nanomaterial is ideal for drug encapsulation and pH-sensitive drug delivery. The porous carbon-coated magnetite also was found to be biocompatible by proving both hemocompatibility and cytocompatibility when tested on HeLa and HUVEC cells. The nanocomposite of different iron concentrations also had good  $T_2$  in vivo MRI contrasting ability and also shows good drug carrier accumulation in the targeted region with  $r_2$  value of  $81.9 \text{ mM}^{-1} \text{ s}^{-1}$ . Sufficient tumor inhibition in mice was achieved with drug-loaded nanocarrier under 808-nm laser wavelength in PTT in contrast with other materials. In the research investigation, mice which are injected with the drug-loaded PCCMNs- $\text{NH}_2$ -HA nanocarrier

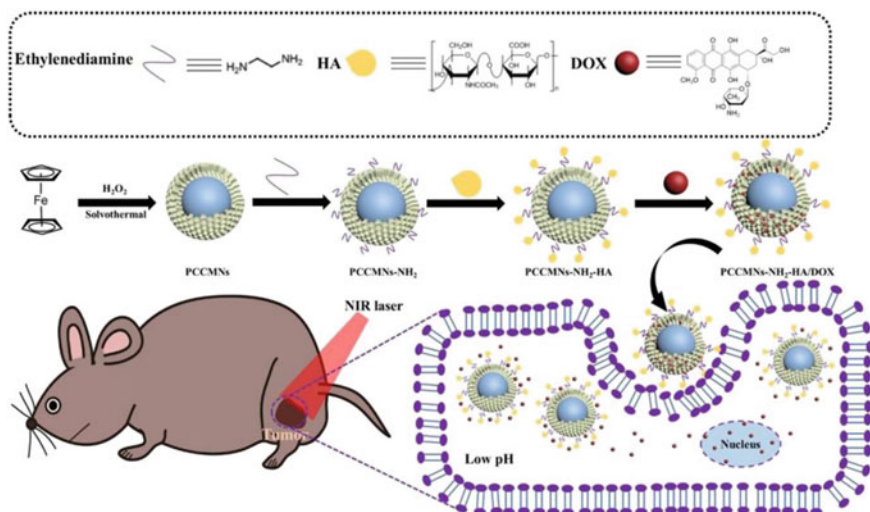
**Table 3** Recent studies on GO-magnetic nanoparticle hybrid nanocomposites used for different biomedical applications

S. No.	Type of magnetic nanoparticle functionalized with GO/rGO	Drug loading efficiency (%)	Concentration of magnetic nanocomposite (mg/mL) and frequency (kHz) and magnetic field strength ( $\text{kA m}^{-1}$ )	Specific absorption rate (SAR) W/g	Application	References
1	PEG-GO-IONPs	–	0.167-mg Fe/mL 400 kHz $32.5 \text{ kA m}^{-1}$	5020 W/g	Magnetic fluid hyperthermia	[85]
2	Graphene-based yolk–shell magnetic nanoparticles -PF-127	91%	1.5 mg/mL 340 kHz $21.0 \text{ kA m}^{-1}$	402-W/g $\text{Fe}^{-1}$	Magnetic fluid hyperthermia and drug delivery of doxorubicin	[86]
3	rGO/Co/PEG nanocomposites	–	0.005 mg/mL 400 kHz $24.8 \text{ kA m}^{-1}$	40 W/g	Magnetic fluid hyperthermia, antibacterial activity against <i>E. coli</i>	[89]
4	$\text{Fe}_3\text{O}_4$ -rGO nanohybrid	–	2 mg/mL 265 kHz $26.7 \text{ kA m}^{-1}$	20 W/g	In vitro magnetic hyperthermia	[88]
5	GO-IONPs	61.42%	–	–	Doxorubicin drug delivery and in vivo MRI imaging	[83]

exhibited tumor temperature rise when it was exposed to NIR laser radiation had excellent photothermal efficiency [60].

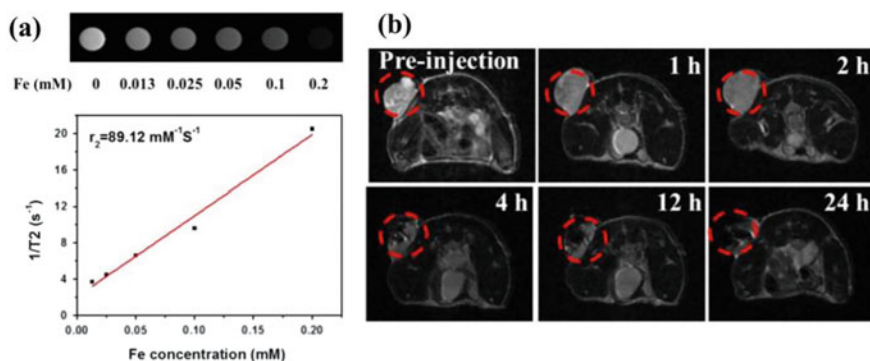
To study GSH internal stimuli response, the nanocomposite was placed in PBS (at varying pH of 5, 6.8, and 7.4) with differing GSH concentrations. At low concentrations of GSH and at pH 5, the drug release was only 18.7%, but at a moderate GSH concentration of 10 mM, 63.8% drug release was noted at the same pH due to the disulfide bond cleavage of the PGA polymer by GSH. As earlier studies showed that the drug release was much slower with the increase of pH, here, GSH concentration played a crucial role in drug release. The pH-dependent drug release occurs due to drug hydrophilicity at the acidic pH range and hydroxyl group deprotonation and weakened electrostatic interactions. Further, the nanocomposite possessed low hemolytic activity at various concentrations. The three stimuli response drug





**Fig. 7** Diagrammatic representation of the protocol for PCCMNs-NH<sub>2</sub>-HA/DOX preparation. Adjunct photothermal therapy with near-infrared (NIR) wavelength laser and chemotherapy of tumor. Reprinted with permission from Wu et al. [60]. Copyright 2019 American Chemical Society

delivery system proved to be highly effective and provided a controlled drug release rate. After treating with nanocomposites, *in vivo* tumor distribution was evaluated in HeLa tumor containing in a mouse by MRI imaging at various time periods and iron concentrations resulting inadequate tumor targeting as shown in Fig. 8 [90].



**Fig. 8** **a** T<sub>2</sub>-weighted MRI photographs and T<sub>2</sub> relaxation rates (r<sub>2</sub>) in the case MHPcNs-SS-PGA-FA/DOX at various Fe concentrations. **b** *In vivo* T<sub>2</sub>-weighted MRI photographs of a tumor-bearing mouse taken before and after injection of MHPcNs-SS-PGA-FA/DOX (14.26 mg/kg) at various time duration (1, 2, 4, 12, and 24 h). The tumor regions are pointed out in a red circle. Reprinted with permission from Wu et al. [90]. Copyright 2018 American Chemical Society

Utilization of porous carbon in multifunctional nanocomposites is also stated in earlier reports, wherein, porous carbon and carbon dots were coated on superparamagnetic iron oxide nanoparticles (core particle) by him and his co-workers for MRI imaging. The team reported a specific  $T_2$  relaxivity value of  $331.79 \text{ mM}^{-1} \text{ s}^{-1}$  making the nanomaterial highly sensitive for use in cancer tumor diagnosis by  $T_2^*$ -weighted MRI imaging. The uptake of nanomaterial was also studied in A549 cells where the increased sample concentration resulted in high cellular uptake. This is due to the reduction in  $T_2^*$  by dephasing the neighboring water spins, where finally a darker signal intensity is obtained compared to the control cells. Similarly, in vivo MRI imaging of the DOX-loaded core-shell nanoparticles showed dark  $T_2^*$  image signals in the liver in comparison to the control cells and free drug. The accumulation of CS nanoparticles in the liver as an end result indicates that the liver is the important region for nanocarrier clearance and metabolism. The average tumor inhibition efficiency was reported to be 64.5% in contrast with free DOX at 16.1% on A549 cancer tumor-bearing mice [91]. Likewise, Yang and his research co-workers have studied the flower-shaped mesoporous ZnO-capped porous carbon-magnetite composite as a suitable drug nanocarrier for pH and microwave-based drug release of doxorubicin. This nanocarrier construct consists of  $\text{Fe}_3\text{O}_4$  modified onto porous carbon nanoparticles, with the outer layer made of porous ZnO, which plays the role of sealing agent to stop untimely drug release after drug loading. The drug loading efficiency that was achieved was almost 99.1% after 24 h of drug loading. After 12 h, the drug release from the nanocomposite under various pH values (7.4, 5 and 3) at  $37^\circ\text{C}$  was found to be 8.2%, 19%, and 56.3%, respectively, due to unique attributes of the porous carbon which has a specific surface area of  $101 \text{ m}^2/\text{g}$  and the mesoporous ZnO. With temperature increased to  $42^\circ\text{C}$ , the drug release rates were 12.6%, 27.2%, and 68.9%, respectively. On irradiation with microwave, the drug release increased to 39.9% from 8.2% at pH 7.4 again after 12 h. The cell viability value of the nanocomposite, when tested on MCF-7 cells, was above 90% at a concentration below  $200 \mu\text{g}/\text{mL}$  [92].

In a study, NIR responsive fluorescent nanocomposite consisting of an innermost core of magnetite and an exterior shell of porous carbon and carbon dots was studied for image-guided photothermal therapy for cancer and doxorubicin drug delivery. The nanocomposite has the potential to transform near-infrared (NIR) light into heat energy for successful tumor heating. Under the presence of NIR light, the burst exit of the drug was observed because of the thermal effect created by the nanocomposite causing the uncoupling of the drug from the nanocarrier system. In the adjunct PTT and chemotherapy using DOX-loaded nanocarrier, the tumor size decreases to the smallest compared to the control (free doxorubicin) due to the presence of EPR effect and high anticancer efficacy. EPR effect/enhanced permeation effect is a phenomenon initially studied by Matsumura and Maeda in 1986 where nanoparticles/liposomes tend to occupy in large amounts in cancer tumor vasculature compared to normal cells. This EPR effect is a highly speculative and selective concept based on the size distribution of the nanoparticles. As the tumors have a very leaky vascular nature and a defective lymphatic drain system, nanoparticles of size  $<500$  or drugs of high molecular weight tend to accumulate in the tumor cells. The

abnormal cancerous tissue retains the nanoparticles exhibiting enhanced permeation of drug or nanoparticles [93].

Carbon-coated magnetic nanoparticles provide a large surface area for high capacity drug loading due to the presence of pores on the surface. The large surface area and the porous nature of carbon-coated magnetic nanocarrier make them highly efficient drug carriers. Porous carbon-coated  $\text{Fe}_3\text{O}_4$  exhibited good therapeutic efficiency with an increase in surface area and pore size of about 3 nm even after hyaluronic acid incorporation [94]. During drug delivery, carbon-coated magnetic nanoparticles are used as nanocarriers. When they get into our human body, our body generates an immediate immune response to these foreign entities called immune response also known as immunogenic response. Immunogenicity is an important parameter affecting the therapeutic efficiency of the drug-loaded magnetic nanocarrier. Immunogenicity, in general, refers to the evading of various foreign substances which enter our body by triggering an adaptive cellular or humoral immune response which is long-lasting. The accumulation and retention of carbon-coated magnetic nanoparticles in tissues and organs can trigger an immediate inflammatory immune response, and it can affect the therapeutic efficiency, so carbon-coated magnetic nanoparticles have to be a low immunogenic response. Carbon-coated magnetic nanoparticles have issues in controlled cancer drug delivery and in nanocarrier internalization which is either by endocytosis, receptor-mediated entry, or by cell membrane penetration. There are several other issues such as sustained and controlled drug release under certain local conditions such as acidity/GSH levels at the target location and under further external stimuli such as heat wave, X-ray signal, and light pulse. For example, in hydrophobic nanocarriers such as graphene/graphene oxide nanocarrier partially dissolve the cellular membrane interrupting its tightness [95]. All these carbon-based materials have been successfully incorporated into magnetic nanocomposites for improving various biological properties required for applications. Though a few pitfalls do exist in the design of such nanocomposites, they can be further addressed in-depth in future research reports.

## 8 Conclusion

The major goal of this chapter is to depict the immense importance of numerous carbon-encapsulated magnetic nanocomposites which are presently employed in various biomedical fields such as targeted drug delivery, in vitro and in vivo magnetic hyperthermia, and MRI imaging. Various research studies on these carbon-based materials for encapsulation or coating magnetic nanoparticles/nanocomposites have proven highly advantageous due to their tunable surface chemistry, biocompatible nature, and their extraordinary physical, optical, and electronic properties. The carbonaceous material-encapsulated/coated magnetic nanocomposites will continue to hold great prospects after considerable surface engineering and advanced intensive studies for multifaceted use in the research field and more discretely explored in several areas of nanoscience and nanotechnology.

**Conflict of Interest** The authors declare no conflicts of interest.

## References

1. Frimpong RA, Hilt JZ (2010) Magnetic nanoparticles in biomedicine: synthesis, functionalization and applications. *Nanomedicine* 5(9):1401–1414
2. Akbarzadeh A, Samiei M, Davaran S (2012) Magnetic nanoparticles: preparation, physical properties, and applications in biomedicine. *Nanoscale Research Letters* 7(1)
3. Kumar A, Chowdhuri AR, Laha D, Chandra S, Karmakar P, Sahu SK (2016) One-pot synthesis of carbon dot-entrapped chitosan-modified magnetic nanoparticles for fluorescence-based  $\text{Cu}^{2+}$  ion sensing and cell imaging. *RSC Adv* 6(64):58979–58987
4. Manohar A, Krishnamoorthi C (2017) Synthesis and magnetic hyperthermia studies on high susceptible  $\text{Fe}_{1-x}\text{Mg}_x\text{Fe}_2\text{O}_4$  superparamagnetic nanospheres. *J Magn Magn Mater* 443:267–274
5. Hedayatnasab Z, Abnisa F, Daud WMAW (2017) Review on magnetic nanoparticles for magnetic nanofluid hyperthermia application. *Mater Des* 123:174–196
6. Liu T, Bai R, Zhou H, Wang R, Liu J, Zhao Y, Chen C (2020) The effect of size and surface ligands of iron oxide nanoparticles on blood compatibility. *RSC Adv* 10(13):7559–7569
7. Boles MA, Ling D, Hyeon T, Talapin DV (2016) The surface science of nanocrystals. *Nat Mater* 15(2):141–153
8. Bordet A, Landis RF, Lee YW, Tonga GY, Asensio JM, Li CH, Fazzini PF, Soulantica K, Rotello VM, Chaudret B (2019) Water-dispersible and biocompatible iron carbide nanoparticles with high specific absorption rate. *ACS Nano* 13(3):2870–2878
9. Sarma L, Aomoa N, Sarmah T, Sarma S, Srinivasan A, Sharma G, Gupta A, Reddy VR, Satpati B, Srivastava DN, Deka S, Pandey LM, Kakati M (2018) Synthesis of finest superparamagnetic carbon-encapsulated magnetic nanoparticles by a plasma expansion method for biomedical applications. *J Alloy Compd* 749:768–775
10. Terrones M, Botello-Méndez AR, Campos-Delgado J (2010) Graphene and graphite nanoribbons: morphology, properties, synthesis, defects and applications. *Nano Today* 5(4):351–372
11. Anwar S, Ding H, Xu M (2019) Recent advances in synthesis, optical properties, and biomedical applications of carbon dots. *ACS Appl Bio Mater* 2(6):2317–2338
12. Yang ST, Wang X, Wang H (2009) Carbon dots as nontoxic and high-performance fluorescence imaging agents. *J Phys Chem C* 113(42):18110–18114
13. Han C, Xu H, Wang R, Wang K, Dai Y, Liu Q, Guo M, Li J, Xu K (2016) Synthesis of a multifunctional manganese(II)-carbon dots hybrid and its application as an efficient magnetic-fluorescent imaging probe for ovarian cancer cell imaging. *J Mater Chem B* 4(35):5798–5802
14. Chowdhuri AR, Singh T, Ghosh SK, Sahu SK (2016) Carbon dots embedded magnetic nanoparticles @Chitosan @Metal organic framework as a nanoprobe for pH sensitive targeted anticancer drug delivery. *ACS Appl Mater Interfaces* 8(26):16573–16583
15. Wu D, Li BL, Zhao Q, Liu Q, Wang D, He B, Wei Z, Leong DT, Wang G, Qian H (2020) Assembling defined DNA nanostructure with nitrogen-enriched carbon dots for theranostic cancer applications. *Small* 16(19):1906975
16. Iijima S (1991) Helical microtubules of graphitic carbon. *Nature* 354(6348):56–58
17. Kroto HW, Heath JR, O'Brien SC, Curl RF, Smalley RE (1985) C<sub>60</sub>: Buckminsterfullerene. *Nature* 318:162–163
18. Nimibofa A, Newton EA, Cyprain AY, Donbebe W (2018) Fullerenes: synthesis and applications. *J Mater Sci* 7:22–33
19. Kazemzadeh H, Mozafari M (2019) Fullerene-based delivery systems. *Drug Discovery Today* 24(3):898–905
20. Ashtami J, Anju S, Mohanan PV (2019) Conformity of dextran-coated fullerene C70 with L929 fibroblast cells. *Colloids Surf B* 184:110530

21. Kiliç E (2016) Fullerene C60 functionalized  $\gamma$ -Fe<sub>2</sub>O<sub>3</sub> magnetic nanoparticle: synthesis, characterization, and biomedical applications. *Artificial Cells, Nanomedicine and Biotechnology* 44(1):298–304
22. Sumio I, Toshinari I (1993) Single-shell carbon nanotubes of 1-nm diameter. *Nature* 363(6430):603–605
23. Oberlin M, Endo A, Koyama T (1976) Filamentous growth of carbon through benzene decomposition. *J Cryst Growth* 32(3):335–349
24. Anzar N, Hasan R, Tyagi M, Yadav N, Narang J (2020) Carbon nanotube—a review on synthesis, properties and plethora of applications in the field of biomedical science. *Sensors International* 1:100003
25. Jeon I, Xiang R, Shawky A, Matsuo Y, Maruyama S (2018) Single-walled carbon nanotubes in emerging solar cells: synthesis and electrode applications. *Adv Energy Mater* 9(23):1801312
26. Bati ASR, Yu L, Batmunkh M, Shapter JG (2018) Synthesis, purification, properties and characterization of sorted single-walled carbon nanotubes. *Nanoscale* 10(47):22087–22139
27. Liu J, Wang C, Wang X, Wang X, Cheng L, Li Y (2014) Mesoporous silica coated single-walled carbon nanotubes as a multifunctional light-responsive platform for cancer combination therapy. *Adv Func Mater* 25(3):384–392
28. Hou L, Yang X, Ren J, Wang Y, Zhang H, Feng Q, Shi Y, Shan X, Yuan Y, Zhang Z (2016) A novel redox-sensitive system based on single-walled carbon nanotubes for chemo-photothermal therapy and magnetic resonance imaging. *Int J Nanomed* 607
29. Zhang M, Wang W, Cui Y, Chu X, Sun B, Zhou N (2018) Magnetofluorescent Fe<sub>3</sub>O<sub>4</sub> carbon quantum dots coated single-walled carbon nanotubes as dual-modal targeted imaging and chemo photodynamic photothermal triple-modal therapeutic agents. *Chem Eng J* 338:526–538
30. Rathinavel S, Priyadarshini K, Panda D (2021) A review on carbon nanotube: an overview of synthesis, properties, functionalization, characterization, and the application. *Materials Science and Engineering B: Solid-State Materials for Advanced Technology* 268:115095
31. Gupta N, Gupta SM, Sharma SK (2019) Carbon nanotubes: synthesis, properties and engineering applications. *Carbon Letters* 29:419–447
32. Ibrahim KS (2013) Carbon nanotubes-properties and applications: a review. *Carbon Letters* 14(3):131–144
33. Eatemadi A, Daraee H, Karimkhanloo H, Kouhi M, Zarghami N, Akbarzadeh A, Abasi M, Hanifehpour Y, Joo SW (2014) Carbon nanotubes: properties, synthesis, purification, and medical applications. *Nanoscale Res Lett* 9(1):393
34. Samadishadlou M, Farshbaf M, Annabi N, Kavetsky T, Khalilov R, Saghi S, Akbarzadeh A, Mousavi S (2017) Magnetic carbon nanotubes: preparation, physical properties, and applications in biomedicine. *Artificial Cells, Nanomedicine and Biotechnology* 46(7):1314–1330
35. Dalal M, Greneche JM, Satpati B, Ghzaïel TB, Mazaleyrat F, Ningthoujam RS, Chakrabarti PK (2017) Microwave absorption and the magnetic hyperthermia applications of Li<sub>0.3</sub>Zn<sub>0.3</sub>Co<sub>0.1</sub>Fe<sub>2.3</sub>O<sub>4</sub> nanoparticles in multiwalled carbon nanotube matrix. *ACS Applied Materials and Interfaces* 9(46):40831–40845
36. Tiwari M, Seal P, Borah JP, Paul N (2019) Functionalization of carbon nanotubes and its nanocomposites for hyperthermia studies. *Materials Today: Proceedings* 18:1317–1323
37. Bhuyan M, Alam S, Uddin M, Islam M, Bipasha FA, Hossain SS (2016) Synthesis of graphene. *International. Nano Lett* 6(2):65–83
38. Lee HC, Liu WW, Chai SP, Mohamed AR, Aziz A, Khe CS, Hidayah NMS, Hashim U (2017) Review of the synthesis, transfer, characterization and growth mechanisms of single and multilayer graphene. *RSC Adv* 7(26):15644–15693
39. Chen YW, Su YL, Hu SH, Chen SY (2016) Functionalized graphene nanocomposites for enhancing photothermal therapy in tumor treatment. *Adv Drug Deliv Rev* 105:190–204
40. Yang K, Feng L, Liu Z (2016) Stimuli responsive drug delivery systems based on nano-graphene for cancer therapy. *Adv Drug Deliv Rev* 105:228–241
41. Alegret N, Criado A, Prato M (2017) Recent advances of graphene-based hybrids with magnetic nanoparticles for biomedical applications. *Curr Med Chem* 24(5):529–536

42. Liu J, Dong J, Zhang T, Peng Q (2018) Graphene-based nanomaterials and their potentials in advanced drug delivery and cancer therapy. *J Control Release* 286:64–73
43. Tadzyszak K, Wychowaniec JK, Litowczenko J (2018) Biomedical applications of graphene-based structures. *Nanomaterials* 8(11):944
44. Brodie BC (1859) On the atomic weight of graphite. *Philos Trans R Soc Lond* 149:249–259
45. Alam SN, Sharma N, Kumar L (2017) Synthesis of graphene oxide (GO) by modified hummers method and its thermal reduction to obtain reduced graphene oxide (rGO)\*. *Graphene* 06(01):1–18
46. Staudenmaier L (1898) Verfahren zur Darstellung der Graphitsäure. *Ber Dtsch Chem Ges* 31(2):1481–1487
47. Hummers WS, Offeman RE (1958) Preparation of graphitic oxide. *J Am Chem Soc* 80(6):1339
48. Krishanu G, Kishor S (2018) Biomedical applications of graphene nanomaterials and beyond. *ACS Biomater Sci Eng* 4(8):2653–2703
49. Fernández-Merino MJ, Guardia L, Paredes JI, Villar-Rodil S, Solís-Fernández P, Martínez-Alonso A, Tascón JMD (2010) Vitamin C is an ideal substitute for hydrazine in the reduction of graphene oxide suspensions. *J Phys Chem C* 114(14):6426–6432
50. Liu S, Zeng TH, Hofmann M, Burcombe E, Wei J, Jiang R (2011) Antibacterial activity of graphite, graphite oxide, graphene oxide, and reduced graphene oxide: membrane and oxidative stress. *ACS Nano* 5(9):6971–6980
51. Jaworski S, Grodzik M, Winnicka A (2015) In vitro and in vivo effects of graphene oxide and reduced graphene oxide on glioblastoma. *Int J Nanomed* 1585–1596
52. Li D, Deng M, Yu Z, Liu W, Zhou G, Li W, Wang X, Yang DP, Zhang W (2018) Biocompatible and stable GO-coated Fe<sub>3</sub>O<sub>4</sub> nanocomposite: a robust drug delivery carrier for simultaneous tumor MR imaging and reduced therapy. *ACS Biomater Sci Eng* 4(6):2143–2154
53. Ricci R, Leite NCS, da-Silva NS, Pacheco-Soares C, Canevari RA, Marciano FR, Webster TJ, Lobo AO (2017) Graphene oxide nanoribbons as nanomaterial for bone regeneration: effects on cytotoxicity, gene expression and bactericidal effect. *Materials Science and Engineering C* 78:341–348
54. Lin C, Chen Y, Huang P (2020) Preparation of multifunctional dopamine-coated zerovalent iron/reduced graphene oxide for targeted phototheragnosis in breast cancer. *Nanomaterials* 10(10):1957
55. Lee BJ, Kim J, Hyeon T (2006) Recent progress in the synthesis of porous carbon materials. *Adv Mater* 18(16):2073–2094
56. Thambiliyagodage C, Mirihana S, Gunathilaka H (2019) Porous carbon materials in biomedical applications. *Biomedical Journal of Scientific and Technical Research* 22(4):16905–16907
57. Zhao Q, Lin Y, Han N, Li X, Geng H, Wang X, Wang S (2017) Mesoporous carbon nanomaterials in drug delivery and biomedical application. *Drug Delivery* 24(2):94–107
58. Zbair M, Ahsaine HA, Anfar Z (2018) Porous carbon by microwave assisted pyrolysis: an effective and low-cost adsorbent for sulfamethoxazole adsorption and optimization using response surface methodology. *J Clean Prod* 202:571–581
59. Tiwari A, Kumar R, Shefi O, Randhawa JK (2020) Fluorescent mantle carbon coated core-shell SPIONs for neuroengineering applications. *ACS Appl Bio Mater* 3(7):4665–4673
60. Wu F, Sun B, Chu X (2019) Hyaluronic acid-modified porous carbon-coated Fe<sub>3</sub>O<sub>4</sub> nanoparticles for magnetic resonance imaging-guided photothermal/chemotherapy of tumors. *Langmuir* 35(40):13135–13144
61. Zhao L, Xu YH, Qin H, Abe S, Akasaka T, Chano T, Watari F, Kimura T, Komatsu N, Chen X (2014) Platinum on nanodiamond: a promising prodrug conjugated with stealth polyglycerol, targeting peptide and acid-responsive antitumor drug. *Adv Func Mater* 24:5348–5357
62. Wen Y, Xu M, Liu X, Jin X, Kang J, Xu D, Sang H, Gao P, Chen X, Zhao L (2019) Magnetofluorescent nanohybrid comprising polyglycerol grafted carbon dots and iron oxides: colloidal synthesis and applications in cellular imaging and magnetically enhanced drug delivery. *Colloids Surf B* 173:842–850
63. Guan Y, Yang Y, Wang X, Yuan H, Yang Y, Li N, Ni C (2021) Multifunctional Fe<sub>3</sub>O<sub>4</sub>@SiO<sub>2</sub>-CDs magnetic fluorescent nanoparticles as effective carrier of gambogic acid for inhibiting VX2 tumor cells. *J Mol Liq* 327:114783

64. Borhan A, Herea DD, Gherca D (2020) Flash-cooling assisted sol-gel self-ignited synthesis of magnetic carbon dots-based heterostructure with antitumor properties. *Mater Sci Eng C* 117:111288
65. Li L, Wang F, Shao Z (2018) Biomass-based magnetic fluorescent nanoparticles: one-step scalable synthesis, application as drug carriers and mechanism study. *Carbohydr Polym* 184:277–287
66. Baker SN, Baker GA (2010) Luminescent carbon nanodots: emergent nanolights. *Angew Chem Int Ed* 49(38):6726–6744
67. Ding C, Zhu A, Tian Y (2014) Functional surface engineering of C-dots for fluorescent biosensing and in vivo bioimaging. *Acc Chem Res* 47(1):20–30
68. Yao H, Long X, Cao L, Zeng M, Zhao W, Du B, Zhou J (2016) Multifunctional ferritin nanocages for bimodal imaging and targeted delivery of doxorubicin into cancer cells. *RSC Adv* 6(111):109322–109333
69. Liu Z, Tabakman SM, Chen Z, Dai H (2009) Preparation of carbon nanotube bioconjugates for biomedical applications. *Nat Protoc* 4(9):1372–1382
70. Al Faraj A, Shaik AP, Shaik AS (2014) Magnetic single-walled carbon nanotubes as efficient drug delivery nanocarriers in breast cancer murine model: noninvasive monitoring using diffusion-weighted magnetic resonance imaging as sensitive imaging biomarker. *Int J Nanomed* 10:157–168
71. Al Faraj A, Shaik AS, Al Sayed B (2015) Preferential magnetic targeting of carbon nanotubes to cancer sites: noninvasive tracking using MRI in a murine breast cancer model. *Nanomedicine* 10(6):931–948
72. Liu Z, Cai W, He L, Nakayama N, Chen K, Sun X, Chen X, Dai H (2007) In vivo biodistribution and highly efficient tumour targeting of carbon nanotubes in mice. *Nat Nanotechnol* 2:47–52
73. Ge X, Fu M, Niu X, Kong X (2020) Atomic layer deposition of  $\gamma$ -Fe<sub>2</sub>O<sub>3</sub> nanoparticles on multi-wall carbon nanotubes for magnetic drug delivery and liver cancer treatment. *Ceram Int* 46(17):26557–26563
74. Seyfoori A, Sarfarazijami S, Seyyed Ebrahimi SA (2019) pH-responsive carbon nanotube-based hybrid nanogels as the smart anticancer drug carrier. *Artificial Cells, Nanomedicine and Biotechnology* 47(1):1437–1443
75. Seal P, Paul N, Babu PD, Borah JP (2019) Hyperthermic efficacy of suitably functionalized MWCNT decorated with MnFe<sub>2</sub>O<sub>4</sub> nanocomposite. *Appl Phys A Mater Sci Process* 125(5):290
76. Zuo X, Wu C, Zhang W, Gao W (2018) Magnetic carbon nanotubes for self-regulating temperature hyperthermia. *RSC Adv* 8(22):11997–12003
77. Wan H, Li C, Gao Z, Liu Z, Dong L, Yang Q, Xiong C (2020) Facile and efficient synthesis of magnetic fluorescent nanocomposites based on carbon nanotubes. *Ceram Int* 46(7):8928–8934
78. Park JK, Jung J, Subramaniam P, Shah BP, Kim C, Lee JK, Cho JH, Lee C, Lee KB (2011) Graphite-coated magnetic nanoparticles as multimodal imaging probes and cooperative therapeutic agents for tumor cells. *Small* 7(12):1647–1652
79. Tiwari A, Verma NC, Turkkan S, Debnath A, Singh A, Draeger G, Nandi CK, Randhawa JK (2020) Graphitic carbon coated magnetite nanoparticles for dual mode imaging and hyperthermia. *ACS Applied Nano Materials* 3(1):896–904
80. Kim J, Cote LJ, Kim F, Yuan W, Shull KR, Huang J (2010) Graphene oxide sheets at interfaces. *J Am Chem Soc* 132(23):8180–8186
81. Goenka S, Sant V, Sant S (2014) Graphene-based nanomaterials for drug delivery and tissue engineering. *J Control Release* 173:75–88
82. Karthika V, AlSalhi MS, Devanesan S, Gopinath K, Arumugam A, Govindarajan M (2020) Chitosan overlaid Fe<sub>3</sub>O<sub>4</sub>/rGO nanocomposite for targeted drug delivery, imaging, and biomedical applications. *Sci Rep* 10(1):18912
83. Gonzalez-Rodriguez R, Campbell E, Naumov A (2019) Multifunctional graphene oxide/iron oxide nanoparticles for magnetic targeted drug delivery dual magnetic resonance/fluorescence imaging and cancer sensing. *PLoS ONE* 14(6):e0217072
84. Abdollahi Z, Taheri-Kafrani A, Bahrani SA, Kajani AA (2019) PEGylated graphene oxide/superparamagnetic nanocomposite as a high-efficiency loading nanocarrier for controlled delivery of methotrexate. *J Biotechnol* 298:88–97

85. Rodrigues RO, Baldi G, Doumett S (2018) Multifunctional graphene-based magnetic nanocarriers for combined hyperthermia and dual stimuli-responsive drug delivery. *Mater Sci Eng C* 93:206–217
86. Sugumaran PJ, Liu XL, Heng TS, Peng E, Ding J (2019) GO-functionalized large magnetic iron oxide nanoparticles with enhanced colloidal stability and hyperthermia performance. *ACS Appl Mater Interfaces* 11(25):22703–22713
87. Peng E, Choo ESG, Chandrasekharan P, Yang CT, Ding J, Chuang KH, Xue JM (2012) Synthesis of manganese ferrite/graphene oxide nanocomposites for biomedical applications. *Small* 8(23):3620–3630
88. Gupta J, Prakash A, Jaiswal MK, Agarrwal A, Bahadur D (2018) Superparamagnetic iron oxide-reduced graphene oxide nanohybrid-a vehicle for targeted drug delivery and hyperthermia treatment of cancer. *J Magn Magn Mater* 448:332–338
89. Hatami S, Shih PJ, Soufi Zomorod M, Heravi P, Ahadian MM, Hatami N (2020) Hyperthermia response of PEGylated magnetic graphene nanocomposites for heating applications and accelerate antibacterial activity using magnetic fluid hyperthermia. *Appl Phys A Mater Sci Process* 126(4):1–10
90. Wu F, Zhang M, Lu H (2018) Triple stimuli-responsive magnetic hollow porous carbon-based nanodrug delivery system for magnetic resonance imaging-guided synergistic photothermal/chemotherapy of cancer. *ACS Appl Mater Interfaces* 10(26):21939–21949
91. He M, Zhou J, Chen J, Zheng F, Wang D, Shi R, Guo Z, Wang H, Chen Q (2015) Fe<sub>3</sub>O<sub>4</sub>@carbon@zeolitic imidazolate framework-8 nanoparticles as multifunctional pH-responsive drug delivery vehicles for tumor therapy in vivo. *J Mater Chem B* 3(46):9033–9042
92. Yang Z, Wang L, Liu Y, Liu S, Tang D, Meng L, Cui B (2020) ZnO capped flower-like porous carbon-Fe<sub>3</sub>O<sub>4</sub> composite as carrier for bi-triggered drug delivery. *Mater Sci Eng, C* 107:110256
93. Bommana MM, Raut S (2018) Brain targeting of payload using mild magnetic field: site specific delivery. *Nanostructures for the Engineering of Cells, Tissues and Organs: From Design to Applications* 167–185
94. Wu F, Sun B, Chu X, Zhang Q, She Z, Song S, Zhou N, Zhang J, Yi X, Wu D, Wang J (2019) Hyaluronic acid-modified porous carbon-coated Fe<sub>3</sub>O<sub>4</sub> nanoparticles for magnetic resonance imaging-guided photothermal/chemotherapy of tumors. *Langmuir* 35(40):13135–13144
95. Hepel M (2020) Magnetic nanoparticles for nanomedicine. *Magnetochemistry* 6(1):3



# Chapter 35

## Noscapinoids: A Family of Microtubule-Targeted Anticancer Agent



Shruti Gamy Dash, Harish Chandra Joshi, and Pradeep Kumar Naik

### 1 Introduction

Cancer is generally an unusual and uncontrolled population cell, which at a later stage can invade tissues and metastasize to distant sites within the body. The normal cells convert into cancerous cells due to some mutations and the resultant changes in protein structure/function or the altered gene expression patterns that perturb cell proliferation or cell death. Although more prevalent at advanced ages, cancer can affect people of any age including the fetus and is currently one of the major causes of death. Moreover, the incidence of different types of cancer increases with increasing age worldwide according to the latest GLOBOCAN database. Although substantial advances in the treatment have successfully managed the severity and the advancement of this devastating disease, the complete cure is still largely elusive.

Cancer is the world's second most prevalent disease with the highest mortality rate of around 0.3 million deaths per year. According to a 2020 Indian report [1], tobacco-related cancers are estimated to account for 3.7 lakhs (27.1%) of the total cancer burden [2]. Breast cancers are anticipated to reach 2.0 lakhs (14.8%) among women, and cervix cancer is reported to make a significant contribution of 0.75 lakhs (5.4%), whereas gastrointestinal tract cancers are estimated to contribute 2.7 lakhs (19.7%) of the total cancer incidence both for men and women (The national cancer registry program, India, 2020). Based on the cancer data compiled by ICMR from 2004 to 2010, the number of males, females, and total cancer patients were 390,809,

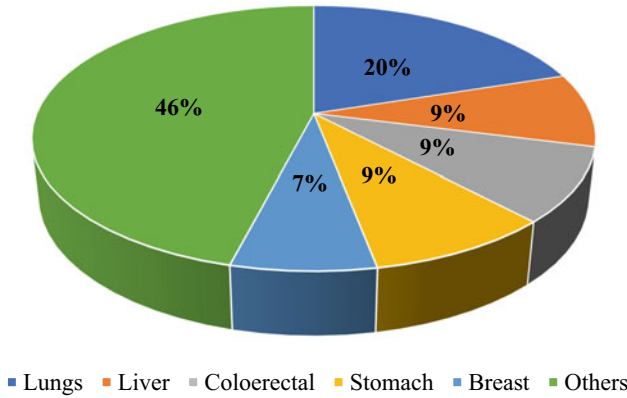
---

S. G. Dash · P. K. Naik (✉)

Centre of Excellence in Natural Products and Therapeutics, Department of Biotechnology and Bioinformatics, Sambalpur University, Jyoti Vihar, Burla, Sambalpur, Odisha 768 019, India  
e-mail: [pknai1973@suniv.ac.in](mailto:pknai1973@suniv.ac.in)

H. C. Joshi

Department of Cell Biology, Emory University School of Medicine, 615 Michael Street, Atlanta, GA 30322, USA



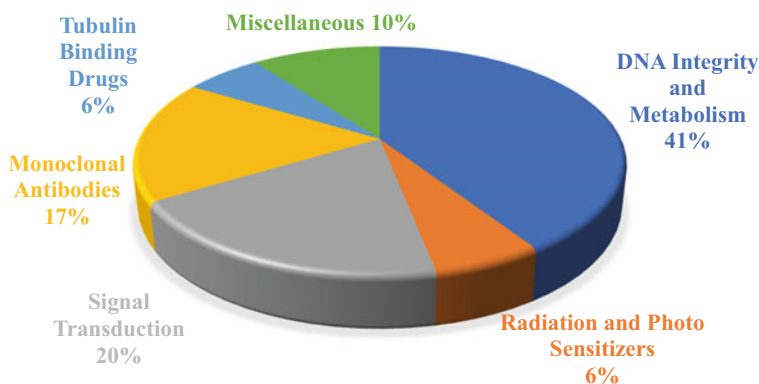
**Fig. 1** Worldwide percentage distribution of cancer types. The incidence of lung cancer was found to be highest in number (20%)

428,545, and 819,354, respectively. It was depicted that the number of most cases of cancers has gradually improved over time. Among these, the cancers of the lung, the esophagus, belly, and mouth are the most common in men, whereas in women, these were mostly of the cervix and breast in India (Fig. 1).

## 2 Modalities of Treatment for Cancer

The modalities of treatment of cancer depend on their advancement, location and progression stage. Surgery, radiation-based therapy, chemotherapy, and combinations thereof are some of the most traditional and widely used therapeutic interventions. The modalities of treatment include hormone-based therapy, immunotherapy, anti-angiogenic modalities, DNA integrity/metabolism, tubulin-binding drugs, combination therapy, and even stem cell therapy in some blood cancers (Fig. 2) [3–6].

Traditionally chemotherapy, the use of chemicals to kill cancer cells is considered to be the most common in clinics. The chemical agents execute this through different mechanisms such as interference with the metabolism of DNA, the division of the cell, signal transduction, and cytotoxicity [7]. However, most of the chemotherapeutics also target normally growing blood cells in the bone marrow, lining of the gastrointestinal tract, hair cells within the hair follicles, thereby resulting in adverse effects such as leukocytopenia, immunocompromise, nausea, vomiting, diarrhea, hair loss, etc. [8]. These immunocompromised patients may thus acquire secondary complications due to sometimes lethal infections. A total of 132 cytotoxic chemotherapeutic drugs have been approved by the FDA. These drugs through a variety of their cytotoxic mechanisms often induce cell death (apoptosis or necrosis) in tumor cells [8, 9].



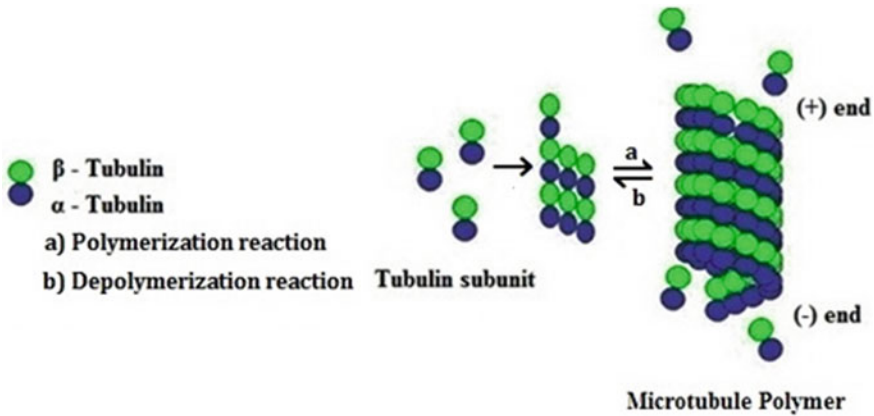
**Fig. 2** Distributions of various mechanisms/drugs available currently in the management of cancer therapy

Among the microtubule-targeting chemotherapeutics in clinics, the most common are taxanes and several vinca alkaloids for the treatment of a wide range of human cancers. Taxanes are the most important class of anticancer agents. Paclitaxel (Taxol), derived from bark extracts of the pacific yew tree, *Taxus brevifolia*, or its derivative, is administered to patients with breast, ovarian, lung, head and neck, oesophageal, prostate, and bladder cancers [9]. Similarly, vinca alkaloids are probably the most frequently utilized microtubule agents in the clinic. These alkaloids have been isolated from *Catharanthus roseus*. Two major vinca alkaloids, vincristine and vinblastine, and a few structural variants such as vinorelbine, vindesine, and vinflunine, are commonly used in the clinic to diagnose various forms of cancer [10].

### 3 Microtubules: A Robust Target for Chemotherapy

#### 3.1 Biology of Microtubule

Microtubules (MTs) are intracellular tubular structures that, together with actin and microfilaments, comprise the dynamic cytoskeleton of nearly all cell types. They continually arrange to form certain specialized super assemblies such as the mitotic apparatus for partitioning duplicated chromosomes during the cell division and then rearrange into normal interphase arrangements [9–12]. Thus, they are not only critical for cell proliferation, but also are required for subcellular trafficking, signaling, and migration. Microtubules assemble from tubulin, which itself is a dimer of  $\alpha$ - and  $\beta$ -tubulin subunits each of a molecular weight  $\sim 50,000$  Da. Both tubulin subunits comprise a chain of approximately 450 amino acids compacted into complex structures: a center of two  $\beta$ -sheets enveloped by  $\alpha$ -helices and a bound guanine nucleotide



**Fig. 3** Organization of microtubules

that is non-exchangeable when attached to the  $\alpha$ -subunit and is freely exchangeable with the externally added guanine nucleotide when bound to the  $\beta$ -subunit (E-site) [13].

The unique functions of microtubules, as well as the mode of action of antimicrotubule agents, depend upon the dynamic equilibrium between  $\alpha$ - and  $\beta$ -tubulin subunits and the microtubule polymer. Every monomer is asymmetric with approximate dimensions of  $46 \times 40 \times 65 \text{ \AA}$  (width, height, and depth, respectively). Each tubulin subunit is split into three domains: the amino-terminal domain containing the nucleotide-binding region, the intermediate domain, and the carboxyl-terminal domain that coordinates drug interactions such as vinblastine and colchicine. The tightly bound  $\alpha$ - and  $\beta$ -subunits form a single tubulin heterodimer. Tubulin dimers assemble head to tail to initiate assembly of a tubulin protofilament, 13 of which then associate sideways to form a microtubule cylinder that can elongate or shorten at the ends (Fig. 3).

The rates of polymerization/depolymerization and the threshold concentration of tubulin required for polymerization at either end of a microtubule varies. One end, called the "plus end," has faster kinetics and a lower critical concentration than the other "minus end." Thus, under some conditions, the plus end can elongate by adding new tubulin dimers, and at the same time, the minus end can shorten by losing tubulin dimers. If the rate of the growth and shortening is the same, the tubulin subunits can simply flux (or "treadmill") from the plus end toward the minus end of a fixed length microtubule lattice). This type of dynamic behavior of a microtubule is referred to as treadmilling. Also, within a population of slowly growing microtubules with a particular "growth rate," certain individual microtubules can transition catastrophically to depolymerization at a certain "catastrophe frequency" to a "shortening rate" until they disappear, or be "rescued" at a certain "rescue frequency" and "pause" before resuming growth. This type of dynamic behavior is termed "dynamic instability." All

these parameters of the dynamic instability, i.e., growth rate, catastrophe-frequency, rescue frequency, pause, and shortening rate can be measured.

Both types of microtubule dynamics described above require the hydrolysis of GTP at the exchangeable E-site of the beta-tubulin subunit [14, 15]. Magnesium ions ( $Mg^{2+}$ ) are also required for assembly because GTP binds as an Mg-GTP complex [16].

The heterodimers of  $\alpha$ - and  $\beta$ - tubulin arrange one above the other to form a polymer of protofilament and 13 of these protofilaments arranged sidewise to form a microtubule. The heterodimers polymerize at one end called (+) end and at the same time depolymerizes from another end, called as (-) end. The process of polymerization and depolymerization takes place simultaneously that gives dynamic structure to microtubule (a behavior called “treadmilling”).

Within the cellular interior, these intrinsic dynamic behaviors of microtubules also depend upon the expression of many other microtubule stabilizing and destabilizing proteins. There are many microtubule-linked proteins (MAPs: tau, MAP1, MAP2, MAP4, XMAP215), regulatory proteins responsible for microtubule destabilization (stathmin, XKCM1, XKIF2, katanin) [17, 18]. The composition of cellular tubulin itself varies among different cell types due to the variable expression patterns of different tubulin isoforms and their post-translational modifications. Thus, the distinct tubulin pool of different cell types also differs in microtubule dynamics both directly due to the intrinsic assembly property of unique tubulin composition as well as indirectly via its differential interactions with various microtubule interacting proteins. This relevance of tubulin assembly and disassembly can also be hindered by different chemical agents that bind to a particular site in the  $\beta$ -tubulin subunit of the alpha-tubulin subunit or at their binding interfaces. Because cell division requires the most exquisite control of microtubule dynamics, these tubulin-binding agents often arrest cells in mitosis, ultimately resulting in cell death, through apoptosis and necroptosis.

### ***3.2 Tubulin-Interacting Antimitotic Agents***

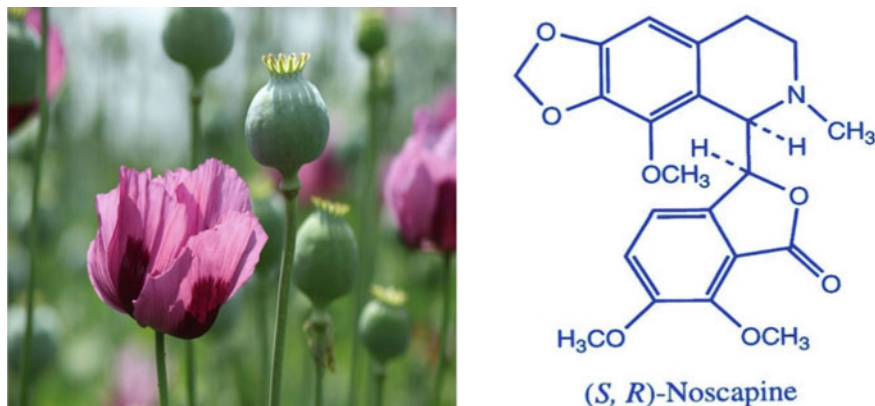
The antimitotic agents act by binding specific sites on various structural domains of the tubulin heterodimer either on its unassembled or assembled forms. Three drug-binding sites have been outlined, the colchicine-binding site, the binding site of vinca alkaloids ( $\alpha$ -tubulin) and that of the taxanes ( $\beta$ -tubulin) [19]. Colchicine primarily binds to  $\beta$ -tubulin near its  $\alpha/\beta$  tubulin interface and modulates the peripheral protofilament interaction by inhibiting microtubule polymerization [20]. Vinca alkaloids prevent microtubule assembly by cross-linking the interdimer interactions, thereby sterically deforming the protofilament and inducing the formation of alternative polymers of tubulin [14, 21].

Although the microtubule-targeted drugs are successfully used in the treatment of a large spectrum of different cancers, some of these drugs sometimes also cause peripheral neuropathy, myeloid toxicity and neutropenia. Moreover, patients often develop drug resistance to a limited number of available and effective microtubule

drugs. Therefore, there is still an urgent need for expanding this series of effective drugs with the discovery of new bioavailable microtubule agents with minimal side effects that can overcome drug resistance. In a quest of finding such compounds, we explored naturally available alkaloids, in particular the opium alkaloids family. Opium alkaloids are widely used in clinics as analgesics, antimalarials, antispasmodics, etc. There are at least 25 active chemicals that can be derived from opium, called opiates. One of the alkaloids, noscapine, is being used as a safe antitussive drug [22] in the clinic for several decades and has recently been screened to have anticancer activity through tubulin binding [23].

### 3.3 *Noscapine and Its Analogs: A Microtubule Modulating Agent*

Noscapine ( $C_{22}H_{23}NO_7$ ), (413.43 Da), a benzyloisoquinoline alkaloid consisting of carbon, was initially described by Professor Pierre-Jean Robiquet in the year 1817 [24] from the opium plant (*Papaver somniferum*) (Fig. 4). From opium (*P. somniferum*), he identified two major compounds: codeine and noscapine [24, 25]. One of the most predominant opium alkaloids is noscapine (21%); other notable alkaloids include morphine (42%), codeine (12%), papaverine (18%), and thebaine (6.5%) tubocurarine, berberine, and sanguinarine. Since then, substantial progress has been accomplished in the development of complete synthetic methods. Nevertheless, the existence of noscapine's availability from natural sources is may be more cost-effective than synthetic alternatives. It was found that noscapine binds stoichiometrically to tubulin (one noscapine molecule for each  $\alpha\beta$ -tubulin dimer), modifies tubulin compliance, and arrests mammalian cells at the mitosis phase [23, 26]. Unlike vinca alkaloids and taxols, however, it does not induce over-polymerization, depolymerization, or any change in the general interphase MT organization. Because of its relatively low impact on the kinetic properties of dynamic instability of MTs, noscapine inhibits mitosis at prometaphase and arrests dividing cancer cells and normal cells in mitosis. Cancer cells, perhaps due to their mutations that compromise cell cycle checkpoints, often do not sustain arrested mitoses for a long time and undergo apoptosis while the arrested normal cells can resume mitosis after drug removal due to metabolic clearance [27]. It is reported previously that different diverse mechanisms were discovered to emerge the pathways of apoptosis in cancerous cells administered with noscapine and its congeners. These pathways involve the induction of stress-activated jun N-terminal kinase, mitochondrial depolarization, downward regulation of cell survival cascades, and upward regulation of pro-apoptotic signals, and eventually, all converging into caspase 3/7 activation. In comparison to the other MT interacting agents such as taxanes and vinca alkaloids, in treatment of cancer, noscapine has a number of advantages: (a) Noscapine induces apoptosis in a range of mammalian cancer cells, including drug-resistant varieties, by arresting them in mitosis [22, 28, 29]; (b) it is an insufficient



**Fig. 4** Structure of *opium poppy* and the lead molecule, noscapine

target for drug efflux (poly glycoproteins and MDR-related proteins), which are a primary source of drug resistance [22]; (c) it suppresses the development of murine melanoma, lymphoma, glioblastoma, and human breast tumors transplanted in nude mice without causing harm to the rapidly proliferating cells of post-mitotic cells such as neurons; (d) noscapine does not hinder primary humoral and cellular responses in mice [30]; (e) noscapine does not cause measurable immunological and neurological toxicity in mice, (f) noscapine is orally administered as opposed to other anti-MT drugs that require peritoneal injections or intravenous infusions with a risk of anaphylactic reactions and infection at the site of injection causing pain, blood vessel thrombosis or embolism; (g) noscapine has a mean bioavailability of ~30–32% over a dose range of 10–300 mg/kg in mice [29].

To further improve its efficacy, efforts were based on rational drug design and synthesis of new generations of noscapine derivatives for better therapeutic outcomes. Nevertheless, noscapine faces some difficulty as its two ring systems, i.e., the isoquinoline and the isobenzo-furanone are connected by a single rotating c–c bond between two chiral centers. Thus, ordinary chemical reactions necessarily lead to a racemic mixture of 4-stereoisomers of noscapine. Out of these, only one stereoisomer, the RS form, is biologically active [23, 27]. The antimetastatic anti-cancer effect of noscapine was discovered back in 1998 [23, 27]. This was achieved through a structurally based justification for screening a modest library of naturally obtained molecules that shared structural similarities with highly cytotoxic MT depolymerizing drugs such as podophyllotoxin, MTC [2-methoxy-5-(2,3,4-trimethoxyphenyl)-2,4,6-cycloheptatrien-1-one] TKB [2,3,4-trimethoxy-4'-acetyl-1,1'-biphenyl], and colchicine. However, noscapine (6) has two chiral centers and four possible stereoisomers.

### ***3.4 Noscapine is a Safe Cough Suppressant***

The antitussive property of noscapine was suggested initially in the year 1930, and it was further comprehensively studied in 1954 [31]. Many researchers have already proven its antitussive activity and the relief it gives to bronchial asthma patients [32–35]. Noscapine has been commonly used as an antitussive drug in Europe, Japan, North and South America, and South Africa since the early 1960s. It is documented in several countries' pharmacopeias, including Europe, Japan, and the USA. It is administered orally in the form of tablets, lozenges, or syrup, or a rectal suppository form.

### ***3.5 Noscapine's Potential Against Cancer***

Antimicrotubule drugs interfere with the formation and proper function of microtubule assemblies such as the mitotic spindle, thereby preventing cell division. Exquisite regulation of coordinated microtubule growth, shortening, and treadmilling are all required for the mitotic function. Therefore, antimicrotubule drugs that either alter assembly or disassembly both interfere with cell division.

Noscapine has shown tremendous potential effectivity *in vitro* and *in vivo* against breast cancerous cells. By inducing apoptosis, it was demonstrated to suppress the development of murine and human breast tumors injected in mice. Noscapine's ability to prevent the growth of human MCF-7 breast cancerous cells, which are estrogen-positive receptors, was analyzed using *in vitro* proliferation assays. Noscapine brings about an 80% regression of human breast tumors grafted in athymic mice *in vivo*. Noscapine is also effective against hormone-insensitive, triple-negative breast cancer cells and in MDAMB-231 xenografts in nude mice. Noscapine-loaded estrone-conjugated gelatin nanoparticles (Nos-ES-GN) were designed to target estrogen receptor-positive breast cancer MCF-7 cells to overcome noscapine's short biological half-life, poor absorption, low aqueous solubility, and significant first-pass metabolism. The  $IC_{50}$  value of Nos-ES-GN seemed to be approximately 50% lower than that of the free drug. The same study found that estrogen receptor-positive (MCF-7) cells accumulated more estrone-conjugated noscapine-loaded gelatin nanoparticles than estrogen receptor-negative MDAMB-231 cells, indicating that estrone-conjugated nanoparticles have the potential to target estrogen receptor-positive breast cancer cells.

Consequently, experiments were carried out to assess the efficacy of noscapine against other cancer types. It includes ovarian cancer [36], malignant melanoma [37], bladder cancer [23], and glioblastoma [38]. Besides interfering with mitosis, it turns out that noscapine has several other metabolic effects that may explain its full repertoire of anticancer mechanisms. To determine the exact mechanisms by which noscapine prevents cancer growth, comprehensive experiments were performed by Dr. Joshi and his team and published in numerous medical journals [36, 39].



### 3.6 *Anti-Angiogenic Effects of Noscapine*

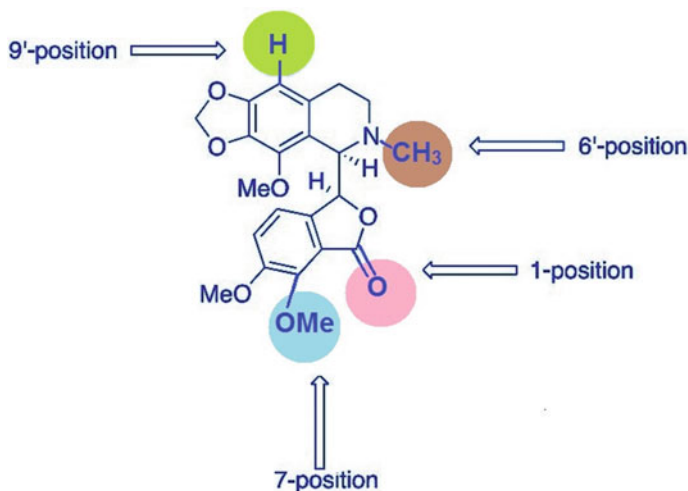
According to Newcomb et al. [40] noscapine inhibited the hypoxia-inducible factor-1 $\alpha$  (HIF-1 $\alpha$ ) pathway in hypoxic human glioma cells and human umbilical vein endothelial cells. HIF-1 $\alpha$  is a transcription factor that promotes the formulation of vascular endothelial growth factor (VEGF), a potent angiogenesis promoter. As a result of its inhibition of HIF-1 $\alpha$ , noscapine has been shown to inhibit VEGF production, thereby identifying its anti-angiogenic properties, another possible mechanism for the anticancer effect. Also, noscapine increased the radiation sensitivity of GL261 glioma tumors delaying tumor growth via an anti-angiogenic mechanism.

### 3.7 *Advancement of Noscapine Analogs as a Promising Drug Candidate*

To improve noscapine's cytotoxicity activity, various analogs have been formulated and chemically synthesized (known as noscapinoids). A series of noscapinoid were synthesized by functionalizing the natural  $\alpha$ -noscapine units of both isoquinoline and isobenzofuranone ring systems. Some of these derivatives have far better lists of treatments and better pharmacological profiles than the parent compound. Currently, more than three generations of noscapinoid have been developed, chemically synthesized, and their activities have been studied against cancer cells and normal cells [38, 41–44]. The first-generation noscapinoids include nitro, azido, amino, and halogenated (fluoro, chloro, bromo, and iodine) as analogs of  $\alpha$ -noscapine by chemical functionalization of the 9th position of noscapine structural system, which is most widely explored by multiple groups [45]. The other two positions of modifications include the 6th and the 1st position of noscapine (Fig. 5). These three generations of noscapinoids [43, 44] represent chemical modifications of the functional groups of noscapine that have been demonstrated to drastically reduce its biological activity [46, 47] (Fig. 5).

### 3.8 *9'-Halogenated Noscapine Analogs*

These first-generation noscapine analogs developed by substitution of halogen groups at 9th position demonstrated better therapeutic effect compared to noscapine. For example, 9'-bromonoscapine (9'-Br-Nosc) and reduced 9'-bromonoscapine (Rd 9'-Br-Nosc) were able to bind more effectively to tubulin and were able to prevent mitosis at a much lower effective dose (ED50) than the parent compound noscapine. In certain cell lines, they showed as high as 20 to 40 times more potency than noscapine [42, 43].



**Fig. 5** Noscapine scaffold and sites of modification

A large spectrum of biological activity was also demonstrated by these compounds. Among the groups of noscapinoids, halogenated noscapinoids are implemented for their impact on the proliferation of cancer cells, antitumor potency, and associated risks [41]. The halogenated noscapine compounds, which are synthesized by chemical modifications, are outlined in Fig. 6. These compounds arrested mitosis at G2 and M phase much more efficiently than noscapine, leading to selective cancer cell apoptosis [48]. The computational blind docking approaches revealed a binding site at the interdimer region of the alpha ( $\alpha$ ) and beta ( $\beta$ ) tubulin, overlapping with the colchicine-binding site for the noscapine and its derivatives with tubulin [43]. A cyclic ether derivative of 9'-fluronoscapine (Fig. 7) was found to be an even more promising antibreast cancer agent [49]. This cyclic ether derivative of noscapine was chemically synthesized by the reduction of noscapine in the presence of boron trifluoride dietherate, and subsequent dropwise addition of a solution of sodium borohydride in dry THF at 0 °C.

### 3.9 Nitro-noscapine

The nitro-derivative (Fig. 8) of noscapine was developed by adding a nitro-group at the diversity point of the 9th position to the noscapine scaffold. It inhibits the growth of ovarian cancer cells of paclitaxel-resistant mutant cells, human lymphoblastoid cells, and their vinblastine- and teniposide-resistant variants [41]. Further, it also inhibits the cell cycle kinetics and induces apoptosis in cancerous cells. Surprisingly, there was no substantial inhibition of the growth of normal human fibroblast cells, demonstrating a specific effect for cancer cells [41, 50].

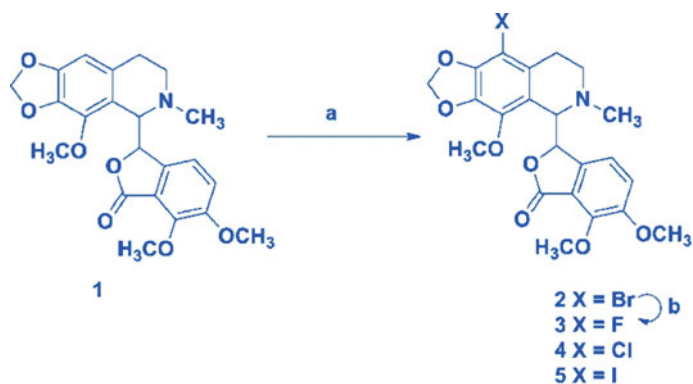


Fig. 6 Halogenated derivatives noscapine

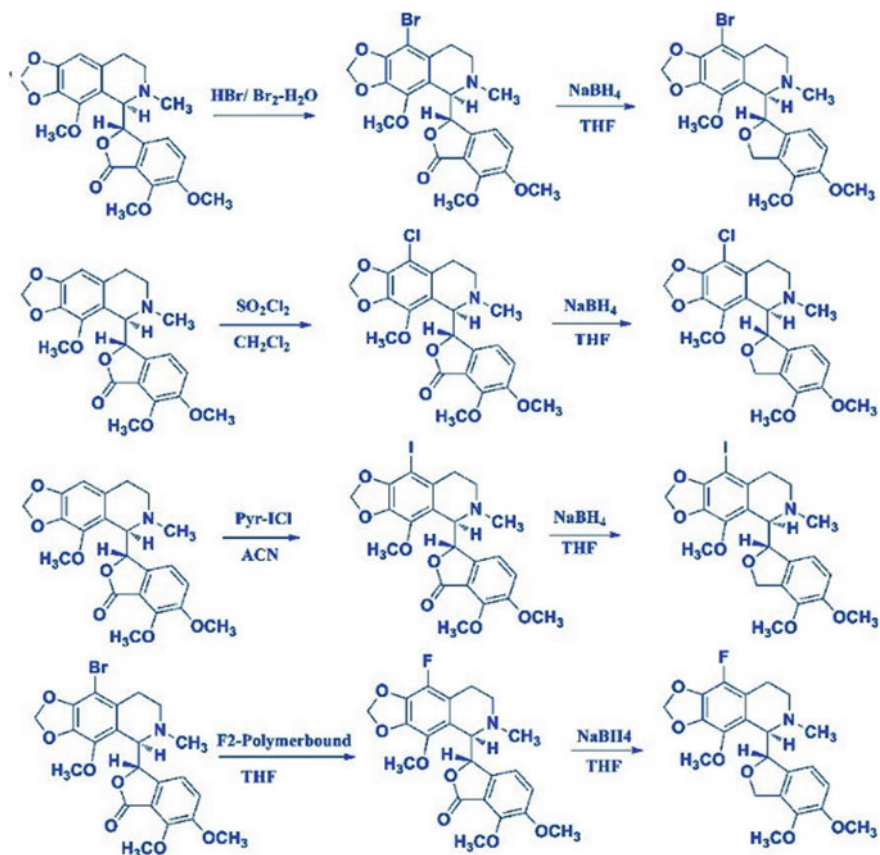


Fig. 7 Cyclic ether halogenated derivatives of noscapine (viz. Rd-9-F-nos; Rd-9-Cl-nos; Rd-9-Br-nos; Rd-9-I-nos)



### 3.11 Amino Derivative of Noscapine

The amino derivatives of noscapine were developed depending on the binding free energies of several noscapinoid, estimated in combination with a surface generalized Born (SGB) continuum solvation model using the linear interaction energy (LIE) method [43]. The assessment of the binding free energy revealed that the amino derivative of noscapine binds tubulin more strongly than the lead molecule. It inhibited the proliferation of cancer cells of different types more effectively compared to noscapine [43]. However, it did not directly influence the extent of polymerization/depolymerization of tubulin subunits [51, 52]. The amino derivatives of noscapine show promising anticancer activity in combination with docetaxel.

## 4 N-Substituted Derivatives of Noscapine

We proposed to add modifications as part of our efforts to design new noscapine derivatives at diversity point of 6' position (Fig. 5) by functionalization of "N" in isoquinoline unit of natural noscapine (named them as third-generation-noscapine analogs) which are anticipated to enhance biological activity. According to the earlier reports on functionalization at "N" mostly through urea-type linkages, and very few of these noscapinoids have been analyzed for their biological efficacy. We believe that urea-type linkage is not the right approach because it will cause delocalization of the electron density at isoquinoline N (Fig. 10).

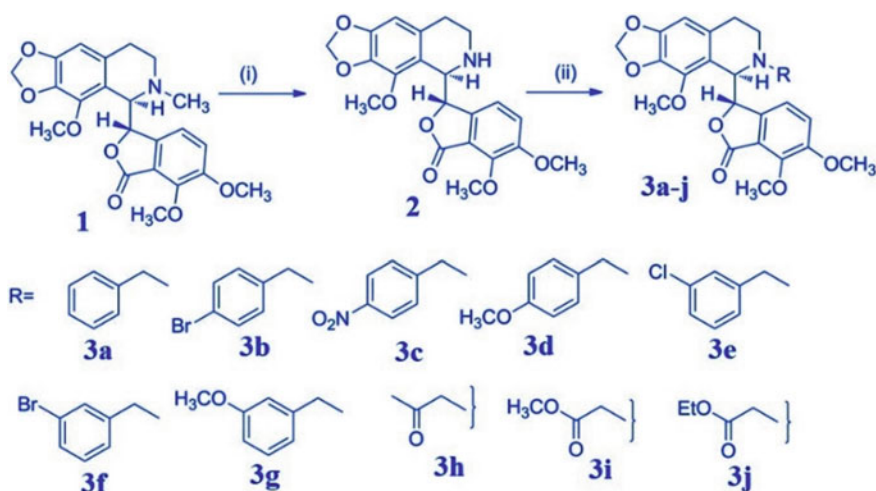


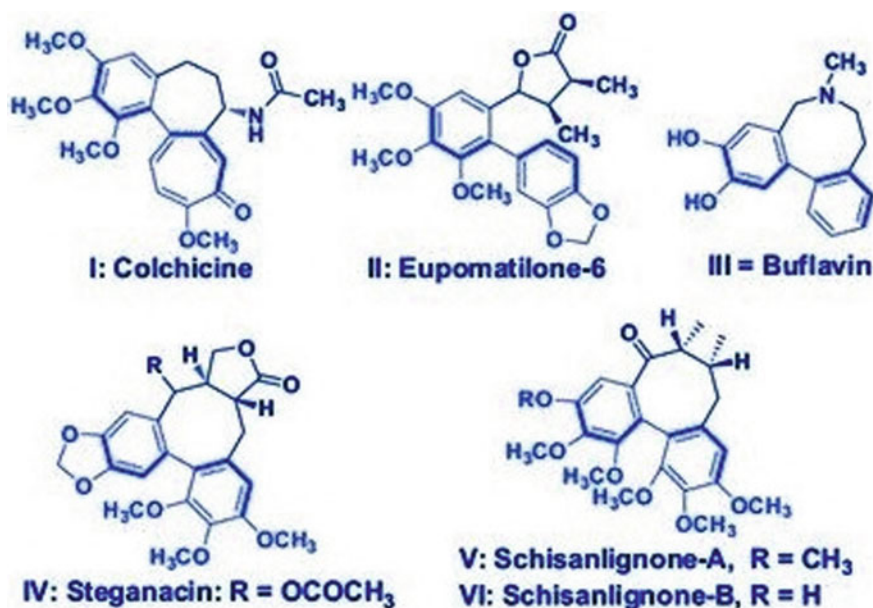
Fig. 10 N-substituted derivatives of noscapine

The third-generation noscapine congeners 3a-j, which vary in the side chain attached to isoquinoline "N" of natural  $\alpha$ -noscapine, are described here as well. Depending upon the reasonable predictive mode, in silico molecular modeling, studies of these derivatives with tubulin complex have been used to evaluate their binding affinity as well as show prominent results in the cellular study.

#### 4.1 Biaryl-Type Derivatives of Noscapine

As per the earlier literature, natural  $\alpha$ -noscapine has biaryl-binding sites, which shows close similarity to colchicine. Colchicine's use as an anticancer agent is strictly limited because of its toxic side effects. Only a few natural products with biaryl architectural design are potent antimetabolic agents that affect the tubulin-microtubule steady state [53] (Fig. 11).

Inspired by this, we propose to formulate novel biaryl type  $\alpha$ -noscapine congeners by implementing a biaryl ring structure into the natural  $\alpha$ -noscapine skeleton and testing them as chemotherapeutic agents. It is revealed that all of the newly developed biaryl noscapine derivatives (Fig. 12) bind tubulin with a higher affinity than that of the parent molecule and that the modification tends to affect their therapeutic efficacy for a variety of cancer types [46].



**Fig. 11** Biaryl pharmacophore is a major defining component of natural and synthesized microtubule-targeting agents

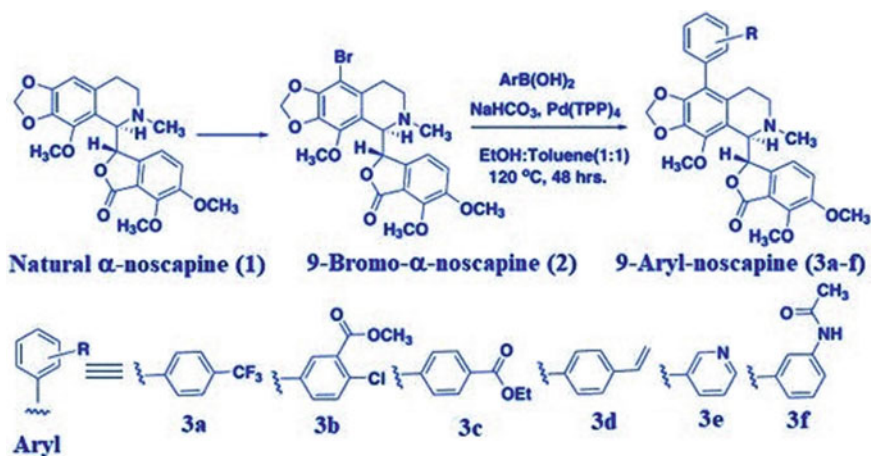


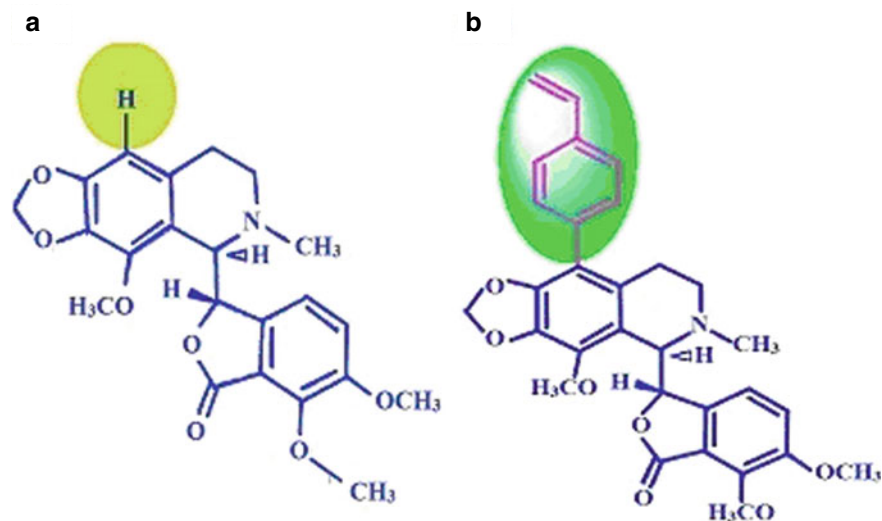
Fig. 12 Biaryl derivatives of noscapine

## 4.2 9-(4-vinylphenyl) Noscapine

Efforts have been focused on rational designing and synthesis of the new generation of noscapine derivatives. Noscapine docks onto  $\beta$ -tubulin near the interface between its dimerization partner,  $\alpha$ -tubulin [54]. This is supported by the earlier finding of 1:1 stoichiometry of tubulin binding [23]. A closer look at the binding site revealed side chains surrounding the predicted binding pocket and the presence of empty space around position 9 of noscapine. In response to the *in-silico* findings, we have rationally coupled a bulky 4-vinyl phenyl functional group at the C-9 position of the noscapine scaffold in the context of improving a more potent derivative of noscapine (Fig. 13) [55, 56]. The inhibition of proliferative activity was significantly enhanced when the VPN, used for treatment in comparison to the parent noscapine. Also, this derivative of noscapine shows much efficacy in combinations with other cytotoxins and targeted agents to design preclinical studies [56].

## 4.3 Bromo-Trimethoxy Benzyl Noscapine

The C–C bond between isoquinoline and isobenzofuranone ring components of noscapine is labile to treatments with strong acids and bases. Therefore, it is often difficult and time-consuming to synthesize the novel TMB-Nos possessing 3,4,5-trimethoxybenzyl group appended at the 7th position on the lower isobenzofuran unit of noscapine. However, for the amalgamation of Br-OH-Nos and N-methyl pyrrolidone as starting material, we have optimized the reaction conditions without affecting



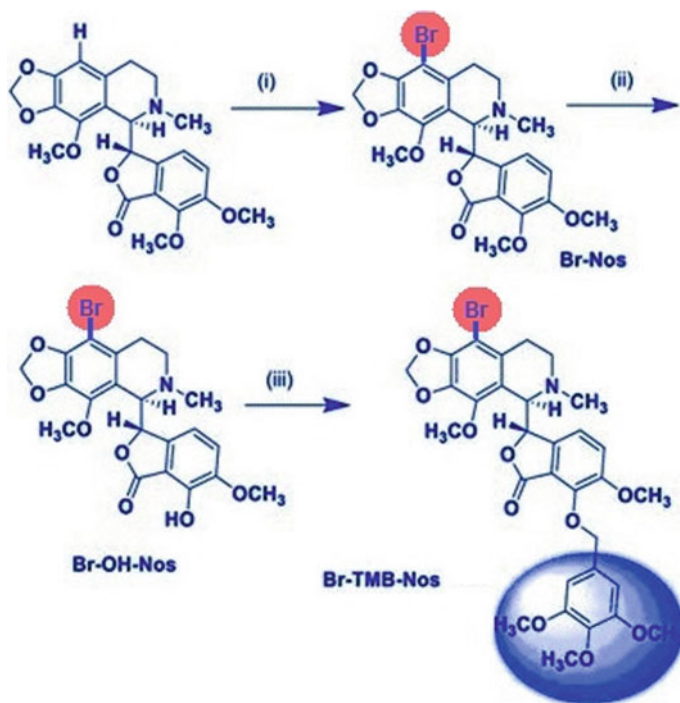
**Fig. 13** Molecular structures of **a** noscopine **b** rationally designed derivative, 9-(4-vinylphenyl)-noscopine (VPN)

the sensitive C–C bond. These derivatives display superior anticancer efficiency than noscopine (Fig. 14) [57]. Furthermore, the newly synthesized TMB noscopine also found to have much potent and promising anticancer activity in combination with docetaxel [58, 59].

## 5 Current Status, Challenges, and Future Prospects

Since the discovery of noscopine's antimitotic and anticancer effects in 1998, much progress has been made in the development of its derivatives as effective anticancer drugs. It has always been widely recognized that, in addition to treating cough, noscopine has a wide range of other potential applications that can effectively help a wide spectrum of patients, particularly those with cancer. Despite its high tumor suppressive dose (300 mg/kg), noscopine seems still safer than other antimitotic therapeutic agents. Noscopine also has another powerful property of synergizing with other anticancer treatments. The ability to synthesize novel derivatives with improved efficacy against numerous cancer cell lines demonstrates noscopine's adaptability to further enhance the potential armory of anticancer drugs. Noscopine and its derivatives subtly modulate microtubule dynamicity, making them gentler than other microtubule-targeting anticancer drugs currently on the market [60–62]. Thus, a combination of sophisticated new methods in computational biology, bioinformatics, pharmacogenomics, engineering, and/or nanotechnology will continue to inspire the synthesis of new more effective analogs.





**Fig. 14** Synthetic scheme of Br-TMB-noscaine

**Conflicts of Interest** The authors declare that they have no conflicts of interest that are relevant to the content of this manuscript.

## References

1. Global initiative for cancer registry development (2020) International Agency for Research on Cancer, Lyon. <https://gicr.iarc.fr/about-the-gicr/the-value-of-cancer-data/>. Accessed February 2021
2. Mathur P, Sathishkumar K, Chaturvedi M, Das P, Sudarshan KL, Santhappan S, Nallasamy V, John A, Narasimhan S (2020) Roselind FS and ICMR-NCDIR-NCRP investigator group cancer statistics: report from national cancer registry programme, India. *JCO Glob Oncol* 6:1063–1075. <https://doi.org/10.1200/GO2000122>
3. Zorn KC, Gofrit ON, Steinberg GD, Arieh L, Shalhav MD (2007) Evolution of robotic surgery in the treatment of localized prostate cancer. *Curr Treat Options Oncol* 8:197–210. <https://doi.org/10.1007/s11864-007-0028-y>
4. Medeiros LR, Rosa DD, Bozzetti MC, Fachel JM, Furness S, Garry R, Rosa MI, Stein AT (2009) Laparoscopy versus laparotomy for benign ovarian tumour. *The Cochrane Database of Syst Rev* 2:CD004751. <https://doi.org/10.1002/14651858CD004751pub3>
5. Luh SP, Liu HP (2006) Video-assisted thoracic surgery—the past present status and the future. *J Zhejiang Univ Sci B* 7(2):118–128. <https://doi.org/10.1631/jzus2006B0118>

6. Gerber DE, Chan TA (2008) Recent advances in radiation therapy. *Am Fam Physician* 78:1254–1262
7. DeVita VT Jr, Chu E (2008) A history of cancer chemotherapy. *Can Res* 68(21):8643–8653. <https://doi.org/10.1158/0008-5472.CAN-07-6611>
8. Rodgers GM 3rd, Becker PS, Blinder M, Cella D, Chanan-Khan A, Cleeland C, Coccia PF, Djulbegovic B, Gilreath JA, Kraut EH, Matulonis UA, Millenson MM, Reinke D, Rosenthal J, Schwartz RN, Soff G, Stein RS, Vlahovic G, Weir AB 3rd (2012) Cancer and chemotherapy induced anemia. *J Natl Comprehensive Cancer Netw: JNCCN* 10(5):628–653. <https://doi.org/10.6004/jnccn20120064>
9. Naidu MU, Ramana GV, Rani PU, Mohan IK, Suman A, Roy P (2004) Chemotherapy induced and/or radiation therapy induced oral mucositis complicating the treatment of cancer. *Neoplasia* (New York NY) 6(5):423–431. <https://doi.org/10.1593/neo04169>
10. Kuruppu AI, Paranagama P, Goonasekara CL (2019) Medicinal plants commonly used against cancer in traditional medicine formulae in Sri Lanka. *Saudi Pharm J: SPJ: Off Publ Saudi Pharm Soc* 27(4):565–573. <https://doi.org/10.1016/j.jsps.201902004>
11. Manfredi JJ, Horwitz SB (1984) Taxol: an antimetabolic agent with a new mechanism of action. *Pharmacol Ther* 25(1):83–125. [https://doi.org/10.1016/0163-7258\(84\)90025-1](https://doi.org/10.1016/0163-7258(84)90025-1)
12. Desai A, Mitchison TJ (1997) Microtubule polymerization dynamics. *Annu Rev Cell Dev Biol* 13:83–117. <https://doi.org/10.1146/annurevcellbio.13.183>
13. Howard J, Hyman AA (2003) Dynamics and mechanics of the microtubule plus end. *Nature* 422(6933):753–758. <https://doi.org/10.1038/nature01600>
14. Jordan MA, Wilson L (2004) Microtubules as a target for anticancer drugs. *Nat Rev Cancer* 4(4):253–265. <https://doi.org/10.1038/nrc1317>
15. Downing KH, Nogales E (1998) Tubulin structure: insights into microtubule properties and functions. *Curr Opin Struct Biol* 8(6):785–791. [https://doi.org/10.1016/s0959-440x\(98\)80099-7](https://doi.org/10.1016/s0959-440x(98)80099-7)
16. Rowinsky EK, Calvo E (2006) Novel agents that target tubulin and related elements. *Semin Oncol* 33(4):421–435. <https://doi.org/10.1053/jseminoncol.2006.04006>
17. Nogales EA (1999) Structural view of microtubule dynamics. *CMLS Cell Mol Life Sci* 56:133–142. <https://doi.org/10.1007/s000180050012>
18. Dehmelt L, Halpain S (2005) The MAP2/Tau family of microtubule-associated proteins. *Genome Biol* 6(1):204. <https://doi.org/10.1186/gb-2004-6-1-204>
19. Correia JJ, Beth AH, Williams RC Jr (1988) Tubulin exchanges divalent cations at both guanine nucleotide-binding sites. *J Biol Chem* 263(22):10681–10686
20. Correia JJ, Lobert S (2001) Physicochemical aspects of tubulin-interacting antimetabolic drugs. *Curr Pharm Des* 7(13):1213–1228. <https://doi.org/10.2174/1381612013397438>
21. Jordan MA, Wilson L (1999) The use and action of drugs in analyzing mitosis. *Methods Cell Biol* 61:267–295. [https://doi.org/10.1016/s0091-679x\(08\)61986-x](https://doi.org/10.1016/s0091-679x(08)61986-x)
22. Altinoz MA, Topcu G, Hacimuftuoglu A, Ozpinar A, Hacker E, Elmaci İ (2019) Noscaphine a non-addictive opioid and microtubule-inhibitor in potential treatment of glioblastoma. *Neurochem Res* 44(8):1796–1806. <https://doi.org/10.1007/s11064-019-02837-x>
23. Karlsson MO, Dahlstrom B, Eckernas SA, Johansson M, Alm AT (1990) Pharmacokinetics of oral noscaphine. *Eur J Clin Pharmacol* 39(3):275–279. <https://doi.org/10.1007/BF00315110>
24. Ye K, Ke Y, Keshava N, Shanks J, Kapp JA, Tekmal RR, Petros J, Joshi HC (1998) Opium alkaloid noscaphine is an antitumor agent that arrests metaphase and induces apoptosis in dividing cells. *Proc Natl Acad Sci USA* 95(4):1601–1606. <https://doi.org/10.1073/pnas9541601>
25. Wells WA (1996) The spindle-assembly checkpoint: aiming for a perfect mitosis every time. *Trends Cell Biol* 6(6):228–234. [https://doi.org/10.1016/0962-8924\(96\)10018-0](https://doi.org/10.1016/0962-8924(96)10018-0)
26. Alisaraie L, Tuszynski JA (2011) Determination of noscaphine's localization and interaction with the tubulin- $\alpha/\beta$  heterodimer. *Chem Biol Drug Des* 78(4):535–546. <https://doi.org/10.1111/j1747-0285201101189x>
27. Lettre H (1954) Synergists and antagonists of mitotic poisons. *Ann N Y Acad Sci* 58(7):1264–1275. <https://doi.org/10.1111/j1749-66321954tb45907x>

28. Warolin C (1999) Pierre-Jean Robiquet: (Rennes 14 janvier 1780—Paris 29 avril 1840) [Pierre-Jean Robiquet]. *Revue d'histoire de la Pharmacie* 47(321):97–110
29. Jordan MA, Toso RJ, Thrower D, Wilson L (1993) Mechanism of mitotic block and inhibition of cell proliferation by taxol at low concentrations. *Proc Natl Acad Sci USA* 90(20):9552–9556. <https://doi.org/10.1073/pnas90209552>
30. Wang Y, O'Brate A, Zhou W, Giannakakou P (2005) Resistance to microtubule-stabilizing drugs involves two events: beta-tubulin mutation in one allele followed by loss of the second allele. *Cell Cycle (Georgetown Tex)* 4(12):1847–1853. <https://doi.org/10.4161/cc4122264>
31. Drukman S, Kavallaris M (2002) Microtubule alterations and resistance to tubulin binding agents (review). *Int J Oncol* 21(3):621–628
32. Konzett H, Rothlin E (1954) Zur Wirkung von Narkotin auf den Hustenreflex und auf die Bronchialmuskulatur [The effect of narcotine on cough reflex and on bronchial musculature]. *Experientia* 10(11):472–473. <https://doi.org/10.1007/BF02170409>
33. Bolser DC (2006) Cough suppressant and pharmacologic protussive therapy: ACCP evidence-based clinical practice guidelines. *Chest* 129(1 Suppl):238S–249S. [https://doi.org/10.1378/chest1291\\_suppl238S](https://doi.org/10.1378/chest1291_suppl238S)
34. Bateman ED, Hurd SS, Barnes PJ, Bousquet J, Drazen JM, FitzGerald JM, Gibson P, Ohta K, O'Byrne P, Pedersen SE, Pizzichini E, Sullivan SD, Wenzel SE, Zar HJ (2008) Global strategy for asthma management and prevention: GINA executive summary. *Eur Respir J* 31(1):143–178. <https://doi.org/10.1183/0903193600138707>
35. Mahmoudian M, Rahimi-Moghaddam P (2009) The anti-cancer activity of noscapiroid: a review. *Recent Pat Anti-Cancer Drug Discov* 4(1):92–97. <https://doi.org/10.2174/157489209787002524>
36. Ukena D, Fishman L, Niebling WB (2008) Bronchial asthma: diagnosis and long term treatment in adults. *Deutsches Arzteblatt Int* 105(21):385–394. <https://doi.org/10.3238/arztebl20080385>
37. Zhou J, Gupta K, Yao J, Ye K, Panda D, Giannakakou P, Joshi HC (2002) Paclitaxel resistant human ovarian cancer cells undergo c-Jun NH2-terminal kinase mediated apoptosis in response to noscapiroid. *J Biol Chem* 277(42):39777–39785. <https://doi.org/10.1074/jbcM203927200>
38. Landen JW, Lang R, McMahon SJ, Rusan NM, Yvon AM, Adams AW, Sorcinelli MD, Campbell R, Bonaccorsi P, Ansel JC, Archer DR, Wadsworth P, Armstrong CA, Joshi HC (2002) Noscapiroid alters microtubule dynamics in living cells and inhibits the progression of melanoma. *Can Res* 62(14):4109–4114
39. Landen JW, Hau V, Wang M, Davis T, Ciliax B, Wainer BH, Van Meir EG, Glass JD, Joshi HC, Archer DR (2004) Noscapiroid crosses the blood-brain barrier and inhibits glioblastoma growth. *Clin Cancer Res: An Off J Am Asso Cancer Res* 10(15):5187–5201. <https://doi.org/10.1158/1078-0432.CCR-04-0360>
40. Newcomb EW, Lukyanov Y, Schnee T, Ali MA, Lan L, Zagzag D (2006) Noscapiroid inhibits hypoxia mediated HIF-1 alpha expression and angiogenesis in vitro: a novel function for an old drug. *Int J Oncol* 28(5):1121–1130
41. Ye K, Zhou J, Landen JW, Bradbury EM, Joshi HC (2001) Sustained activation of p34 (cdc2) is required for noscapiroid induced apoptosis. *J Biol Chem* 276(50):46697–46700. <https://doi.org/10.1074/jbcC100550200>
42. Aneja R, Vangapandu SN, Joshi HC (2006) Synthesis and biological evaluation of a cyclic ether fluorinated noscapiroid analog. *Bioorg Med Chem* 14(24):8352–8358. <https://doi.org/10.1016/j.bmc.2006.09.012>
43. Santoshi S, Naik PK, Joshi HC (2011) Rational design of novel anti-microtubule agent (9-azido-noscapiroid) from quantitative structure activity relationship (QSAR) evaluation of noscapiroids. *J Biomol Screen* 16(9):1047–1058. <https://doi.org/10.1177/1087057111418654>
44. Naik PK, Chatterji BP, Vangapandu SN, Aneja R, Chandra R, Kanteveri S, Joshi HC (2011) Rational design synthesis and biological evaluations of amino-noscapiroid: a high affinity tubulin-binding noscapiroid. *J Comp Aided Mole Des* 25(5):443–454. <https://doi.org/10.1007/s10822-011-9430-4>
45. Mishra RC, Karna P, Gundala SR, Pannu V, Stanton RA, Gupta KK, Robinson MH, Lopus M, Wilson L, Henary M, Aneja R (2011) Second generation benzofuranone ring substituted

- noscapine analogs: synthesis and biological evaluation. *Biochem Pharmacol* 82(2):110–121. <https://doi.org/10.1016/j.bcp.201103029>
46. Manchukonda NK, Naik PK, Santoshi S, Lopus M, Joseph S, Sridhar B, Kantevari S (2013) Rational design synthesis and biological evaluation of third generation  $\alpha$ -noscapine analogues as potent tubulin binding anti-cancer agents. *PLoS ONE* 8(10):e77970. <https://doi.org/10.1371/journal.pone0077970>
  47. DeBono A, Capuano B, Scammells PJ (2015) Progress toward the development of noscapine and derivatives as anticancer agents. *J Med Chem* 58(15):5699–5727. <https://doi.org/10.1021/jm501180v>
  48. Rida PC, LiVecche D, Ogden A, Zhou J, Aneja R (2015) The noscapine chronicle: a pharmacohistoric biography of the opiate alkaloid family and its clinical applications. *Med Res Rev* 35(5):1072–1096. <https://doi.org/10.1002/med21357>
  49. Aneja R, Dhiman N, Idnani J, Awasthi A, Arora SK, Chandra R, Joshi HC (2007) Preclinical pharmacokinetics and bioavailability of noscapine a tubulin-binding anticancer agent. *Cancer Chemother Pharmacol* 60(6):831–839. <https://doi.org/10.1007/s00280-007-0430-y>
  50. Mukhtar E, Adhami VM, Mukhtar H (2014) Targeting microtubules by natural agents for cancer therapy. *Mol Cancer Ther* 13(2):275–284. <https://doi.org/10.1158/1535-7163.MCT-13-0791>
  51. Horio T, Murata T (2014) The role of dynamic instability in microtubule organization. *Front Plant Sci* 5:511. <https://doi.org/10.3389/fpls.201400511>
  52. Dash SG, Kantevari S, Naik PK (2021) Combination regimen of amino-noscapine and docetaxel for evaluation of anticancer activity. *Anal Chemistry Lett* 11(2):215–229. <https://doi.org/10.1080/22297928.2021.1896380>
  53. Otto T, Sicinski P (2017) Cell cycle proteins as promising targets in cancer therapy. *Nat Rev Cancer* 17(2):93–115. <https://doi.org/10.1038/nrc2016138>
  54. Manchukonda NK, Naik PK, Sridhar B, Kantevari S (2014) Synthesis and biological evaluation of novel biaryl type  $\alpha$ -noscapine congeners. *Bioorg Med Chem Lett* 24(24):5752–5759
  55. Checchi PM, Nettles JH, Zhou J, Snyder JP, Joshi HC (2003) Microtubule interacting drugs for cancer treatment. *Trends Pharmacol Sci* 24:361–365
  56. Dash SG, Kantevari S, Suri C, Naik PK (2021) Rational design of 9-vinyl-phenyl noscapine as potent tubulin binding anticancer agent and evaluation of the effects of its combination on Docetaxel. *J Biomol Struct Dyn* 39(14):5276–5289. <https://doi.org/10.1080/07391102.2020.1785945>
  57. Mahaddalkar T, Manchukonda N, Choudhary S, Cheriyaundath S, Mohanpuria N, Kantevari S, Lopus M (2016) Subtle alterations in microtubule assembly dynamics by Br-TMB-noscapine strongly suppress triple-negative breast cancer cell viability without mitotic arrest. *Chemistry Select* 1(14):4313–4319. <https://doi.org/10.1002/slct201600959>
  58. Dash SG, Dash SG, Kantevari S, Guru SK, Naik PK (2021) Combination of docetaxel and newly synthesized 9-Br-trimethoxybenzyl-noscapine improve tubulin binding and enhances antitumor activity in breast cancer cells. *Comput Biol Med*. <https://doi.org/10.1016/j.compb.2021.104996>
  59. Dash SG, Kantevari S, Pandey SK, Naik PK (2021) Synergistic interaction of N-3-Br-benzyl-noscapine and docetaxel abrogates oncogenic potential of breast cancer cells. *Chem Biol Drug Des* 98(3):466–479. <https://doi.org/10.1111/cbdd.13902>
  60. Mahaddalkar T, Naik PK, Choudhary S, Manchukonda N, Kantevari S, Lopus M (2017) Structural investigations into the binding mode of a novel noscapine analogue 9-(4-vinylphenyl) noscapine with tubulin by biochemical analyses and molecular dynamic simulations. *J Biomol Struct Dyn* 35(11):2475–2484. <https://doi.org/10.1080/0739110220161222969>
  61. Stanton RA, Gernert KM, Nettles JH, Aneja R (2011) Drugs that target dynamic microtubules: a new molecular perspective. *Med Res Rev* 31(3):443–481. <https://doi.org/10.1002/med20242>
  62. Zhang D, Kanakkanthara A (2020) Beyond the paclitaxel and vinca alkaloids: next generation of plant-derived microtubule-targeting agents with potential anticancer activity. *Cancers* 12(7):1721. <https://doi.org/10.3390/cancers12071721>

# Chapter 36

## Recent Advances in Designing Porous Carbon Nanomaterial Based for Electrochemical Biosensing Prostate Cancer



Stephen Rathinaraj Benjamin and Eli José Miranda Ribeiro Júnior

### 1 Introduction

Over the last several decades, non-communicable chronic disorders have surpassed infectious diseases as the leading cause of mortality and disability in the global population. According to the results of epidemiological research, the second biggest cause of death is cancer, behind only cardiovascular disorders insignificance. A large rise in the number of individuals diagnosed with cancer has been recorded in both developed and developing nations, with developed countries seeing the greatest increase. Cancer risk is gradually growing as a consequence of population aging and globalization of unhealthy lifestyles, and it does not cease even during a pandemic. Prostate cancer (PCa) is a malignant tumor that most often originates in the outermost region of the prostate. It is produced by a number of epigenetic changes that result in proliferation and migration, differentiation, and invasion of adjacent tissues. Prostate cancer is a silent assailant due to the presence of asymptomatic tumor development. According to the International Agency for Research on Cancer (IARC), PCa will be the second most often diagnosed and fifth most fatal disease in men by 2020 [1]. The capacity to diagnose cancer in its early stage is essential to the survival of cancer patients. It involves implementing effective screening systems that deliver important information with little discomfort and danger. Prostate-specific antigen (PSA), a serine protease, is the biomarker of choice for early detection of prostate cancer

---

S. R. Benjamin (✉)

Laboratory of Neuroscience and Behavior, Department of Physiology and Pharmacology and Faculty of Medicine, Drug Research and Development Center (NPDM), Federal University of Ceará (UFC), Rua Cel. Nunes de Melo 1127, Porangabussu, Fortaleza, Ceará 60430-270, Brazil  
e-mail: [steaje@gmail.com](mailto:steaje@gmail.com)

E. J. M. R. Júnior

Department of Pharmacy, Faculty of CGESP (Centro Goiano de Ensino Superior), Rua A, Nº 490 - Setor Oeste, Goiânia, Goiás 74110-020, Brazil

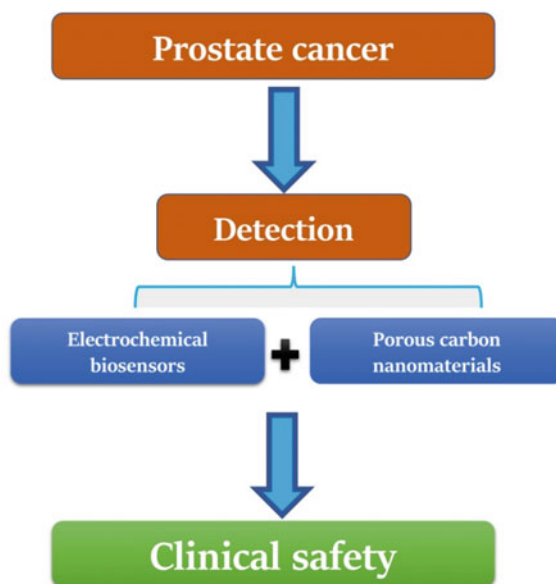
[2]. Furthermore, a serological test detecting PSA in tandem with a digital rectal examination (DRE) of the prostate is utilized as a risk indication for PCa. However, further tissue biopsy is performed if the results indicate a high risk. Despite its adequate clinical sensitivity, the screening test has a low level of clinical specificity.

Several antibody-based approaches have been used to detect this biomarker in the past [3], including radioimmunoassay [4], surface plasmon resonance (SPR) immunoassay [5], enzyme-linked immunosorbent assay (ELISA) [6], and fluorescence immunoassay [7]. The main drawbacks of these approaches are their high cost, sophisticated technology, laboratory test limits, absence of portable equipment, and the influence of interfering variables. Although biosensors are less costly to design and manufacture, they can identify analytes with high specificity and sensitivity [8].

However, the majority of antigen–antibody interactions are inadequate to produce a very sensitive signal for direct impedance measurement. For the purpose of enhancing the generated signal, two ways may be utilized. One strategy is the use of an effective immobilization technique that maximizes the loading of functional antibodies or antigens. The second possibility is to modify the electrodes with conductive materials to induce signal amplification.

Porous carbon is a porous separation material having a well-developed high porosity, higher specific surface area, good biocompatibility, rapid regeneration, and several other characteristics. Furthermore, it has the potential to be used for energy storage and conversion in addition to environmental restoration and catalytic applications [9, 10]. Due to the abundance of electric double-layer capacitors, porous carbon materials may be employed as a significant component of the electrode materials for supercapacitors [11, 12]. On this account, the rational procurement and exploitation of porous carbon material is critical for the improvement of electrodes materials in the future. Porous carbon materials include heteroatoms of nitrogen and sulfur, which may provide increased pseudo capacitance, compared to carbon materials with fewer heteroatoms. The growing need for improved electrochemical performances from porous carbon materials has increased interest in heteroatom doping carbon materials [13]. The emergence of mesoporous or macroporous carbon materials may also give various applications such as massive organic molecule adsorption and electrochemical double-layer capacitor [13, 14]. Porous carbon nanoparticles (PCN) are a suitable alternative for fabrications for sensors, due to their great features such as structural stability, porosity, and readily modifiable surface [15]. This review focuses on recent breakthroughs in the early detection of PCa using porous carbon nanomaterials of distinctive types. We propose to present a detailed review of the challenges in establishing high sensitivity, selectivity, and repeatability for PCa biomarker identification, particularly prostate-specific antigen. This study focuses on recent developments in the early diagnosis of PCa using porous carbon nanomaterials of various types. Even though porous carbon nanomaterials are widely employed in electrochemical detection, we have focused on the use of metal–organic frameworks (MOFs) and covalent organic frameworks (COFs) for electrochemical biosensors (Fig. 1).

**Fig. 1** Schematic representation of porous carbon materials in clinical safety applications



## 2 Cancer Biomarkers

Biomarkers are biological chemicals found in excretory products such as urine, feces, or body fluids including blood, serum, or tissues that may be used to examine normal biological and pathogenic processes, as well as pharmacological response to any therapy. Antibodies, proteins, peptides, and nucleic acids are only a few types of biomarkers. A major biomarker is proteins, which may show diagnosis through varying levels of their concentration in different physiological fluids (blood, serum, saliva, and tissue). Biomarkers of cancer may be detected using electrochemical biosensors because of their sensitivity, selectivity, and low cost [16]. In analytic techniques, the precise and reasonable correlation between the concentrations of the analyte (for example, the biomarker) and the intensity of the analyte signals allows us to make an effective assessment of the analyte concentration. Furthermore, the ability of a method to accurately and selectively record (and develop) strong and effective analytical signals are determined by its record (and construct) of precise and effective analytical signals [17].

## 3 Prostate Cancer (PCa)

Prostate cancer is expected to be the second most prevalent cancer in men and the fifth major diagnosed cancer globally by 2020, with 1.4 million cases with 375,000 mortality [1]. The most sensitive blood test for PCa is a prostate-specific antigen, a

serine protease. PSA is a 33–34 kDa single-chain glycoprotein that is secreted by the prostate gland [18]. In recent years, researchers have identified that it may be a potential identification of prostate cancer biomarkers. PSA values greater than or equal to  $10 \text{ ng mL}^{-1}$  indicate significant chances of obtaining prostate cancer [19]. The PSA reading above  $4 \text{ ng mL}^{-1}$  is generally regarded as positive. A PSA level between 4 and  $10 \text{ ng mL}^{-1}$  indicates the necessity for a biopsy in 30% of men who have already been diagnosed with prostate cancer [20]. Men with prostate cancer had higher total PSA levels and lower free PSA levels (fPSA).

Apart from prostate cancer, a range of benign (non-cancerous) disorders can induce an increase in PSA levels. On the other hand, PSA is not cancer-specific, and numerous non-malignant conditions, including benign prostatic hyperplasia and prostatitis, can produce an increase in PSA levels [21]. Both prostatitis (a prostate inflammatory condition) and benign prostate hyperplasia (enlarged prostate position) are the two most frequent benign prostate disorders that are associated with a rise in PSA values. Other disorders, such as prostatic hyperplasia -BPH or cystitis, may induce a rise in PSA levels. Due to PSA poor diagnostic capabilities, researchers are searching for new biomarkers that may accurately diagnose PCa. This type II transmembrane glycoprotein, PSMA prostate-specific membrane antigen, is a potential for prostate cancer biomarker diagnosis and a viable alternative to PSA [22]. Biomarkers for prostate cancer include PCA3, Engrailed-2 protein, sarcosine, alpha-methyl acyl-CoA racemase (AMACR), micro-RNA, microsemipoprotein-beta (MSMB), and TMPRSS2: ERG transcripts. Prostate cancer is currently diagnosed by biopsy and medical imaging; however, it has spread to many other regions of the body. Many techniques, including electrochemiluminescence-ECL [23], surface plasmon resonance, SPR biosensors [24], microfluidic ELISA [25], and electrochemical biosensors [26, 27], have been implemented to enhance the PSA detection sensitivity. In general, ELISA has traditionally served as the gold conventional method for PSA detection; nevertheless, this method inherited several drawbacks, including a time-consuming process, high cost, and labor-intensive nature, which restricts its full usage.

Diagnostic imaging studies (CT or MRI) are required in the case of an increased PSA level [28]. It is commonly accepted that tissue biopsy is the only treatment that can accurately diagnose and treat cancer. Currently, PSA has a false-positive rate of 75%. Unnecessary biopsies and over-the-top therapy are the results of this high risk of error. A novel diagnostic biomarker for prostate cancer is therefore urgently required [29]. Additionally, it necessitates the development of a complex and compact biological diagnostic system that provides high sensitivity, selectivity, and stability. Recently, biosensors have gained acquired popularity because of their excellent sensitivity and selectivity in detecting a wide range of biomarkers. Nevertheless, a biosensor for prostate cancer detection may present a tremendous potential to build low-cost, ultrasensitive POCT for prostate cancer at the point of care. Additionally, this would considerably minimize the requirement for sample transportation to central labs that would contribute to the establishment of a new healthcare economic model. Electrochemical sensors have a number of advantages over other technologies, such as a fast reaction and inexpensive cost. In clinical



diagnostics and biochemical testing, an electrochemical immunosensor based on precise correlations between antigen and antibody has shown excellent sensitivity and selectivity [30, 31]. Various techniques like voltammetry, impedimetric, and potentiometry may be used to explain electrochemical biosensors. Voltammetric assays for prostate-specific antigen include the development of cyclic voltammetry-CV, differential pulse voltammetry-DPV, square wave voltammetry-SWV, electrical impedance spectroscopy-EIS, and chronoamperometry-CA. The extensive review of electrochemical biosensors developed for prostate cancer biomarkers detection in real samples will be provided in the next section. Each biomarker's potential will be discussed in detail before functionalization and subsequent analytical performance of produced biosensors are discussed. Recent and future issues in the use of electrochemical sensors in point-of-care diagnostics (POC) are discussed.

## 4 Electrochemical Biosensors: Basic Principles

Electrochemical (EC) biosensors have several advantages from a point-of-care standpoint, including portability, simplicity, ease of use, cost-effectiveness, and the fact that they are typically disposable [32, 33]. Electrochemical biosensors depend on electrochemical reactions on the electrode surface to work effectively, resulting in changes in electrical signals. In most cases, the electrochemical signal is the consequence of an electrode being applied with potential, current, or frequency.

The design of a biosensor requires three integrated components: (a) connection exists between the sample and the bio-recognition component; (b) by interacting with specific proteins, the transducer produces a detectable signal, and (c) a computerized system for collecting and organizing biosensor data [34]. The function of the biosensor device is influenced in part by the detection molecules high specificity and sensitivity. The detection of biomarkers has made use of a variety of molecular recognition elements [35]. The antibody, enzyme, and synthesized specific molecular elements, including DNA molecules, peptides, and aptamers, are most typically used for recognizing a molecule. Affinity materials for analyte interaction and particular detection have been utilized in their development. There are four kinds of immunosensors: aptasensors, enzymatic, and geosensors. Aptasensors use biorecognition molecules that are designed specifically for them (nucleic acid biosensors). Additionally, electrochemical biosensors include a transducer, which turns the binding interactions that occur involving biomarkers and other molecules into detectable electrochemical signals. Amperometric, potentiometric, conductometric, and impedimetric transducers are examples of electrochemical transducers [36, 37]. However, amperometric and potentiometric transducers are also often utilized for the rapid identification of electrochemical biomarkers.

## 5 Electrochemical Biosensors Based on Immunoassays

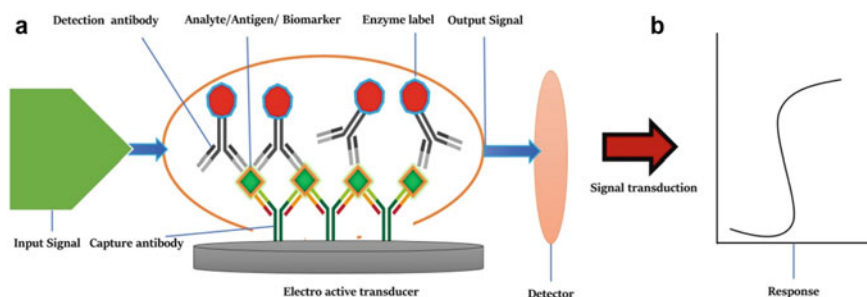
Antibody contact with antigen causes an electrochemical response on the electrode surface in an electrochemical immunoassay [38]. As illustrated in Fig. 2, the electrochemical immunoassay may be designed using two distinct strategies: (a) a simple (label-free) antibody–antigen (Ab–Ag) interaction; and (b) a sandwich-type antibody–antigen interaction [39].

### 5.1 Simple Antibody–Antigen Interaction (Label-Free)

The (label-free) approach starts with the application of an immobilized antibody (Ab), the surface of the electrode, followed by incorporation of antigen (Ag) and completion of the immunoassay. The concentration of Ag is determined using this method in a solution containing one redox pair, including, Ferric-Ferro cyanide ( $[\text{Fe}(\text{CN})_6]^{3-/4-}$ ) solution. This electrochemical reaction is induced by the existence of redox pairs in the occurrence of different concentrations of Ag. The biosensor surface's electrical characteristics are altered as a consequence of the coupling of Ab and Ag. Consequently, the surface conductivity of the biosensor impacts the Ag concentrations on the surface of the electrodes [40]. Figure 2 depicts the basic Ab–Ag contact and electrochemical reaction.

### 5.2 Sandwich Antigen–Antibody Interaction

Furthermore, the response signals could not be amplified by the initial forms of label-free electrochemical biosensors. Consequently, the sensitivity and detection limit of these immunosensors were unsuitable for analytical purposes, and a better design approach was required. The sandwich-type of  $\text{Ab}_1\text{-Ag-Ab}_2$  interactions was



**Fig. 2** Schematic representations of **a** a simple (label-free) antibody–antigen (Ab–Ag) interaction; and **b** a sandwich-type antibody–antigen interaction

made in order to maximize the selectivity and sensitivity in the detection of different biomarkers. The secondary antibody amplifies the electrochemical signal provided by sandwich-type immunosensors ( $Ab_2$ ). Consequently, as the result of this design, the target Ag is first incubated with the electrode, which has the primary Ab ( $Ab_1$ ) adsorbed on its surface. The electrode surface is exposed to labeled  $Ab_2$ , which has been placed there after the immunoassay has been created. Selective interaction of labeled Abs with Ag results in an electrochemical signal being enhanced by the label applied [41].

## 6 The Role of Porous Carbon Nanomaterials on Electrochemical Sensing

Porous carbon nanomaterials (PCNs) relate to carbon nanomaterials with distinct pore structures. They can be classified into three types according to the dimension of the pores: microporous (pores  $< 2$  nm), mesoporous (2–50 nm), and macroporous ( $> 50$  nm). In order to fulfill the needs of a certain practical application, its pore size can be adjusted. In general, materials featuring lower pore sizes have a greater surface area than those with larger pore sizes. The capacity of most porous carbon materials will vary depending on the pore structure of the substance. PCNs have been constantly developed during the last several decades. PCNs have been synthesized or generated from a variety of various materials, including MOFs [42], COFs [43], and biomasses [44], to provide a diverse range of properties. PCNs are utilized in a variety of diverse applications, including sample preparation, catalysis [45], electrochemistry [46], and biology [47], since the presence of large surface and porous structure nature, adjustable porous morphology, increased number of active areas, high electrical conductivity, and chemical resistance.

## 7 Porous Carbon Nanomaterials Fabrication

PCNs can be fabricated in a number of various techniques, including via the use of a template, activation, or calcination technique. In order to fabricate porous carbon materials, a number of approaches were developed, including activation of the chemical/physical method, the wet-chemical method, template replication method, and chemical vapor deposition (CVD) [48, 49]. CVD is a popular technique for depositing carbon consisting of carbon nanowalls, carbon nanotubes, and other carbon-based nanostructured materials, among others [50, 51]. However, most carbon nanostructured materials need high temperatures for processing and catalysis for production, restricting their application on low-melting-temperature materials like polymers or paper.

The hard-template technique and the soft-template technique are both common preparation methods for porous carbon compounds. The nanocasting technology's hard-template path includes the following steps: Construction of the adjustable mesoporous matrix (i) an appropriate precursor is incorporated via solution impregnation or CVD into the aforementioned matrix template; (ii) polymerization of the carbon precursor results in the formation of an organic–inorganic composite; (iii) carbonization occurs as a result of the organic–inorganic combination; (iv) to make porous carbon materials, an appropriate removal reagent removes the template; (v) as a consequence, the porous carbon materials are designed to replicate the characteristics of the design; a wide range of materials, including zeolite,  $\text{Al}_2\text{O}_3$ ,  $\text{MgO}$ , ice, salt, and others, have been quickly developing as templates for the “hard template” approach in recent years [52].

Since porous carbon materials can be synthesized directly using the “soft-template” procedure rather than the “hard template” method, this method is frequently employed for designing and fabricating porous carbon materials. The processes of the soft-template method are typically depicted as follows: (i) preparation of a supramolecular alignment of appropriate molecules, (ii) high-temperature polymerization produces a highly crosslinked composite, (iii) removal of the carbonization of the composite template, (iv) “soft-template” approach must depend on supramolecular self-assembly for template generation rather than template aggregation like the “hard-template” approach. In another crucial aspect, calcination in an inert gas can be used to easily remove the template [53]. Many porous carbon materials with large pore distributions, such as micropores, mesopores, and macropores, have been synthesized by supramolecular self-assembly.

Porous carbon materials derived from biomass typically contain heteroatoms of nitrogen and sulfur that provide additional pseudo capacitance and show a greater capacitance than carbon materials with a restricted number of heteroatoms. Recently, heteroatom-doped carbon materials have raised the interest of attention due to the increased need for porous carbon materials with superior electrochemical performance. Porous carbon nanomaterials may also be doped with heteroatoms including nitrogen and boron, oxygen, sulfur, phosphorus, among other components [54]. Recently, porous carbon materials enriched with the atom N were produced using hard or soft-template techniques [55]. In recent years, carbon-based materials including such coating of amorphous carbon materials, type of graphene foams, graphene sponges, graphene nanotubes, fibers, and walls made of carbon have been recognized as potential prospects for surfaces of superhydrophobic owing to minimal surface charge and adjustable topological nanostructured materials [56, 57]. This study discussed the categorization of porous carbon nanomaterials and their application in the implementation of the effective electrochemical method for prostate cancer detection. Table 1 summarizes electrochemical biosensors and their performance in detecting prostate cancer biomarkers.

**Table 1** List of porous carbon nanomaterials for prostate cancer biomarkers detection

Prostate cancer biomarker type	Type of electrode	Recognition matrix/electrode (modification)	Linear range/linearity	Detection limit (LOD)	Detection time	Sample	Capture probe	References
PSA	Conductometric immunosensor, current voltage	TCNO <sub>2</sub> -Cu <sub>3</sub> (BTC) <sub>2</sub> Gold screen printed electrodes (GSPPE)	0.1–100 ng/mL	0.06 ng/mL	2 min	Human serum	PSA antibody	[56]
PSA	Electrochemical immuno sensors CV, Amperometry	Cu <sub>3</sub> (BTC) <sub>2</sub> Gold (Au) electrodes	0.1–10 ng/mL	0.025 ng/mL	–	Human serum	PSA antibody	[57]
PSA	Sandwich-electrochemical immuno sensors CV, DPV, EIS Amperometry	ZIF-67- Pd/GCE	0.0001–50 ng/mL	0.03 pg/mL	–	Human serum	PSA antibody	[58]
PSA	Amperometric immunosensor CV, EIS, SWV (H <sub>2</sub> O <sub>2</sub> )	Au/Fe-MOF (Fe-MIL-88B-NH <sub>2</sub> ) Catalytic labels	0.001–100 ng/mL	0.13 pg/mL	–	Human serum	PSA antigen	[59]
PSA	Electrochemical immunosensor, SWV	Cu(1,4-NDC)/MOF nanowire arrays/Cu foam	0.1–20 pg/mL	4.4 pg/mL	–	Human serum	PSA antibody	[60]
PSA	Sandwich electrochemical biosensor, DPV	Au@PDA@BCN/AuPt@MnO <sub>2</sub> @COF/GCE	0.00005–10 ng/mL	0.0167 pg/mL	–	Artificial Serum	peptide-PSA-antibody	[61]
PSA	Label-free electrochemical immunosensor CV, DPV, EIS	BSA/Anti-PSA/AuNPs/MoS <sub>2</sub> -GAs/GCE	0.00001–50 ng/mL	0.003 pg/mL	–	Human serum	PSA antibody	[62]
PSA	Electrochemical DNA Aptamer CV, DPV, EIS	AuNPs@GMCs PGE	0.25–200 ng/mL	0.25 ng/mL	–	Human serum	PSA target	[63]
PSA	Label-free electrochemical immunosensor DPV	Ap/MSTf/Au	1–300 ng/mL	0.28 ng/mL	20 min	Serum and artificial urine	tPSA-Ab <sub>1</sub>	[64]

(continued)

Table 1 (continued)

Prostate cancer biomarker type	Type of electrode	Recognition matrix/electrode (modification)	Linear range/linearity	Detection limit (LOD)	Detection time	Sample	Capture probe	References
PSA	Dual optoplasmonic-impedimetric biosensor EIS	Au NPs-porous silicon Ni/Cr interdigitated electrode	1–500 ng/mL	1 ng/ml	greater than 1 h	Standard solutions (tPSA)	tPSA-Ab1	[65]
PSA	Label electrochemical immunosensor Amperometry, EIS	GCE/NH <sub>2</sub> -graphene@ferrocene-carboxaldehyde/c-Ab/PSA/Ag NPs@NH <sub>2</sub> -MCM48 labeled s-A	0.01–10 ng/mL	2 pg/ml	2 h	Human serum	tPSA-Ab1	[66]
PSA	Label-free electrochemical immunosensor, CV	Ag@MSN/GCE	0.05–50 ng/ml	15 pg/ml	1 h	Human serum	tPSA-Ab1	[67]
PSA	Sandwich-type electrochemical immunosensor CV, Amperometry	Mesoporous core-shell Pd@Pt nanoparticle/amino group functionalized graphene nanocomposite-GCE	10 fg/ml to 50 ng/ml	3.3 fg/ml	–	Human serum	tPSA-Ab1	[68]
PSA	Electrochemical immunosensor DPV, EIS	Au/Pd@flower-like SnO <sub>2</sub> /GCE	0.01–100 ng/ml	3 pg/mL	2 h	Human serum	tPSA-Ab1	[69]
PSA	Electrochemical sensor DPV	Porous-hollowed-Ag-Au core-shell nanoparticles (PHSGNPs) anti-PSA/GP-P3A/BA/SPCE	0.01–80 ng/ml	0.13 pg/mL	–	Human serum	tPSA-Ab1	[70]
PSA	Electrochemical immunosensor DPV, CV, EIS	MOF-235/MB	0.01–1.2 ng/mL	3 pg/mL	–	Human serum	tPSA-Ab1	[71]
PSA	Electrochemical immunosensor DPV	AuNPs/BPene/Fe <sub>3</sub> O <sub>4</sub> -COF/GCE	0.0001–10 ng/mL	30 fg/mL	–	Human serum	tPSA-Ab1	[72]

(continued)

**Table 1** (continued)

Prostate cancer biomarker type	Type of electrode	Recognition matrix/electrode (modification)	Linear range/linearity	Detection limit (LOD)	Detection time	Sample	Capture probe	References
Creatinine	Electrochemical sensor CV, EIS, Amperometry	Sb/NPC-GCE	0.5–200 M	0.083 M	–	Human serum	tPSA-Ab1	[73]
Sarcosine	Electrochemical sensor CV	Fe <sub>3</sub> O <sub>4</sub> @ZIF-8@MIP/AuE	1–100 pM	0.4 pM	–	Urine	SAR	[74]

Cu<sub>3</sub>(BTC)<sub>2</sub> (BTC = benzene-1,3,5-tricarboxylic acid); TCNQ-tetracyano quinodimethane; Au/Fe-MOF-Gold nanocomposite/Fenton-AuPt@MnO<sub>2</sub>@COF; Gold Platinum-manganese dioxide (MnO<sub>2</sub>)-functionalized covalent organic frameworks (COF); Au@PDA@BCN; Au@PDA@BCN; polydopamine-coated boron-doped carbon nitride, AuNPs/MoS<sub>2</sub>-Gas-Au nanoparticles/MoS<sub>2</sub>-graphene aerogels nanocomposite; AuNPs@GMCs; Graphitized mesoporous carbon nanoparticles; N-doped porous carbon antimony (Sb/NPC) nanoparticles, Fe<sub>3</sub>O<sub>4</sub>@ZIF-8@MIP/AuE; Iron(II, III) oxide-zelolitic imidazolate framework-8-molecularly imprinted polymer; SAR-Sarcosine, IP-SA—Free PSA, PEI; polyethyleneimine, GS-Graphene sheets, GMCs; Graphitized mesoporous carbons; BPene: black phosphorene

## 8 Covalent Organic Frameworks

Covalent organic frameworks (COFs), a novel form of crystalline organic polymers, have considerable potential for applications in adsorption, electrochemistry, and other fields [77–80]. They feature a higher surface area, orderly channels, high degree of porosity, adjustable structure via pre-selection of building blocks, simple functionalization, and excellent thermal and chemical stability. COFs have found widespread use in electrochemical sensing due to their special properties, which have the potential to increase the sensitivities of the electrochemical sensors. In addition, certain magnetic covalent organic framework-based biosensors for the detection of prostate-specific antigens were developed. Liang's team has designed a comparable electrochemical sensor that uses magnetic COFs to measure prostate-specific antigens in both buffer and blood samples. The sandwich immunosensor was designed to immobilize primary antibodies on the gold nanoparticles-phosphorene nanocomposite substrate. Methylene blue (MB) and secondary antibody-functionalized AuNP-loaded magnetic COFs generated the electrochemical signal. The study developed an assay for the detection of PSA in the concentration range of 100 fg/mL to 10 ng/mL, by using DPV an optimal combination of black phosphorene (BPene) improved electron transfer, MB efficient enrichment in the COF, and  $\text{Fe}_3\text{O}_4$  molecules outstanding catalytic activity [74].

In recent years, cyclodextrin (CDs)-derived MOFs increased significant attention with various unique structures and capabilities as a distinctive kind of porous material. In theory, CDs may have a significant number of coordination active sites for metal chelation because of the many glycosidic oxygens in the structure. Hongmin and colleagues prepared  $\text{Ag@Pb(II)-CD}$  was used as a substrate material in the construction of a new type of ECL immunosensor for the label-free approach of PSA detection. The specificity of antibodies toward antigens was exploited in the detection approach. One step of the approach was to use  $\text{Ag@Pb(II)-CD}$ 's adsorption capacity toward proteins to bind PSA's antibody on its surface. In the presence of silver nanoparticles, it is easy to immobilize the PSA-capturing PSA antibody. The reduction in ECL signals is caused by the specific attachment of PSA to the surface of the electrode. After optimizing the experimental conditions, a linear range between 0.001 and 50 ng/mL was found LOD value of 0.34 pg/mL [81].

## 9 Porous Graphitic Carbon Nitride ( $\text{C}_3\text{N}_4$ )

Mesoporous graphite (MPG)-like carbon nitride ( $\text{C}_3\text{N}_4$ ) exhibited multiple active sites for incorporating gold nanoparticles and luminol, in addition to its higher surface area and large porosity. Recently, Ma and coworkers designed a luminol- $\text{H}_2\text{O}_2$ -based ECL immunosensor for PSA detection using MPG- $\text{C}_3\text{N}_4$ , and AuNPs. In this case, the Au- $\text{NH}_2$  link between the nanocomposite and the  $\text{Ab}_1$  (main Ab) would increase sensitivity and improve the catalytic effect. The ECL immunosensor developed had



demonstrated sensitivity to detect PSA in a wide range of 0.001 and 15 ng/mL, LOD was determined as 0.927 pg/mL [82]. Moreover, the immunosensor developed had outstanding stability as well as reproducibility. The sandwich-type immunosensor for the detection of prostate-specific antigen was developed by Feng et al. using AuNPs and thionine-functionalized GO. Additionally, rGO/graphitic carbon nitride was loaded with bimetallic PtCu NPs and used as labels for the combination of Ab<sub>2</sub> and signal amplification. Antibody-based immunosensor for detection of PSA has a wide range of 50–40 ng/mL and LOD value of 16.6 fg/mL [83].

PSA immunosensors have been accomplished by utilizing SnS<sub>2</sub>@mesoporous composed of graphite-like materials with carbon nitride nanocomposite on the surface of indium tin oxide. It was found that the nanocomposite had a greater photocurrent output than either SnS<sub>2</sub> or mpg-C<sub>3</sub>N<sub>4</sub> alone, because of the lower charge recombination of photoexcited electron–hole pairs. The reduction in photocurrent caused by an increase in steric hindrance on the nanocomposite surface indicated the existence of PSA [84].

## 10 Aptamer-Based Electrochemical Biosensors

In the past few decades, antibodies have been found as biorecognition molecules employed in biosensing assay development. In recent studies, researchers have revealed that aptamers, which are nucleotide sequences with specific binding capabilities, have high-affinity sites toward their targets. SELEX technique, which uses systematic evolution of ligands to enrich aptamers, may be used to find new aptamers. Additionally, aptamers, like synthetic antibodies, offer a number of benefits over antibodies.

Aptamers are single-strand DNA or RNA molecules that may efficiently and robust connection with a wide range of receptors in molecular levels, from smaller molecules to proteins and whole cells. Antibodies are slower to synthesize and more difficult to regulate chemically. There are several advantages to using aptamers instead of peptides, including speed and ease of manipulation in the lab; long durability; and their capacity to tolerate denaturation. This research used a single-strand DNA aptamer (ssDNA1, 5'-HS-(CH<sub>2</sub>)<sub>6</sub>-ATTAAAGCTCGCCATCAAATAGC-3') since it was specific to PSA.

Furthermore, Liu et al. developed aptamers based on the electrochemical nanobiosensor method employing graphite mesoporous NPs covered with AuNPs to enhance prostate cancer detection with the LOD value of 0.25 ng/mL. DPV was utilized to detect PSA in blood samples using an affinity approach using biotin-conjugated aptamers on AuNPs embedded in graphitized mesoporous carbon [65].

Argoubi et al. produced the label-free electrochemical aptasensor by coating gold electrodes with silica thin films to enhance the sensor's surface area. Interfacial or electrical modifications induced by the development of aptamer antigen compounds may be utilized to demonstrate the influence of these modifications on label-free

tumor marker detection techniques. The development of a label-free electrochemical aptasensor system contributes to the prevention of diffusion of the  $\text{Fe}(\text{CN})_6^{3/4}$  reactive site through the nanostructure of the mesoporous material. The researchers observed that using the aptasensor for PSA concentrations between 1 and 300 ng/mL could be detected down to 280 pg/mL. Electrochemical biosensors were used in their studies because they are low cost and provide an analytical response in a shorter amount of time with high sensitivity [66]. Mesoporous silica thin films (MSFs), commonly used as transducing materials and catalyst support in electrochemical biosensors, were also used. Additionally, MSF is widely used in DNA-based electrochemical sensors because of the regular pores' structure, uniform size, and ease of modification. According to Wu et al., an innovative sandwich-type immunoassay was generated by using nanoporous gold (NPG) material with primary anti-PSA antibody to immobilize through an amine-Au binding process, followed by the attachment of a secondary anti-PSA antibody. In order to designate the secondary anti-PSA antibody ( $\text{Ab}_2$ ), hollowed mesoporous silica microspheres (HSMs) were conjugated to the antibody. The researchers observed a linearity range of 0.01–10 ng/ml and LOD obtained 6.0 pg/ml, with high stability and reproducibility respectively [85].

Porous graphene is employed to address the issue of excessively permeable detecting surface areas for high antibody loadings, resulting in an exceptionally sensitive immunoassay. Due to the PDA-PG (polydopamine functionalized—porous graphene) abundance of functional groups, particularly the catechol groups, it was shown to be potential targets for potent antibody linkers. The PDA polymer coating exhibited outstanding biocompatibility and adhesive characters, and it dynamically polymerized on graphene, demonstrating its potential as a biomaterial.  $\text{Cu}_3(\text{BTC})_2$  (BTC = benzene-1,3,5-tricarboxylic acid) is a very interesting copper-based metal–organic framework due to its vast surface area, great chemical durability, and electrical characteristics. Remarkably,  $\text{Cu}_3(\text{BTC})_2$  has unoccupied coordination and catalytic sites on the Cu(II) centers.  $\text{Cu}_3(\text{BTC})_2$  may be a potential electrocatalytic label for immunosensors because of these properties.  $\text{Cu}_3(\text{BTC})_2$  strong electrocatalytic activity toward  $\text{H}_2\text{O}_2$  as a label generates and amplifies electrochemical signals with great sensitivity. The PSA biomarker has recently been detected using a very sensitive electrochemical immunosensor based on  $\text{Cu}_3(\text{BTC})_2$  linked  $\text{Ab}_2$  on a PDA-porous graphene sensing substrate. It is clear that the PDA layer has strong adhesion, which makes it possible to load a significant quantity of  $\text{Ab}_1$  onto the  $\text{Ab}_2$  labeled with  $\text{Cu}_3(\text{BTC})_2$  and excellent ability to perform electrocatalysis on  $\text{H}_2\text{O}_2$ . The PSA immunosensing assay has a linear response range of 0.1–10 ng/mL, a LOD value of 0.025 ng/mL, sufficient recovery for the assessment of specific biological real blood samples that have great reproducibility and selectivity. There are a number of non-enzymatic MOF-based labels that might be used in point-of-care (POC) diagnostic techniques due to the obvious large variety of MOF materials [59].

Fluorescent nanoparticles are highly valued in imaging and sensing. Organic fluorophores have weak photo-stability, limiting their use in long-term bioimaging. In this sense, semiconductor quantum dots (semi-QDs) are a prospective alternative to organic fluorophores due to their size-dependent emission color variation. However, QDs limited water solubility and toxicity restrict their use in bioimaging.

Carbon quantum dots (CQDs) are a novel type of luminous nanomaterials from the nanocarbon group. Carbon dots-based fluorescence detection methods have attracted gained prominence in bioanalytical applications owing to their remarkable optical properties, strong photostability, improved water absorption, high biocompatibility, and low toxicity. These characteristics make compounds ideal donors for FRET systems used to detect a broad variety of biomolecules in biomedical and bioimaging applications [86].

He et al. [87] designed a simple fluorescence-based technique for sensitive PSA detection using CDs/GO FRET and the CHA circuit. On the detecting platform, three hairpin DNA sequences were engineered to self-assemble (Y-shaped dsDN product). This method improved sensitivity and specificity. This confirmed its universal detection technique potential for clinical diagnostics and biological research investigations. CQD/g-C<sub>3</sub>N<sub>4</sub> heterostructures were used to construct a photoelectrochemical immunoassay for PSA detection with great sensitivity. The combination of CQDs and g-C<sub>3</sub>N<sub>4</sub> (graphitic carbon nitride) was shown to be beneficial for photogenerated electrons, and the photocurrents of the nanoheterostructures were significantly increased. The proposed nanoheterostructures showed strong photocurrent responses for PSA detection with a wide range from 0.02–100 ng/mL and a LOD value of 5.0 pg/mL [88].

The use of fluorescence-based techniques in bioanalytical research has opened the door to new quantitative methods for identifying biological processes. Fluorescent resonance energy transfer (FRET) has generated a lot of interest in sectors like biology and biomedical research [89, 90]. The key characteristics of FRET are its high sensitivity, specificity, distance dependence, rapid response, simplicity, and the fact that it is a homogenous assay [91]. FRET benefits include spatial and temporal dispersion of fluorescent compounds and real-time signals [92]. FRET has been proven to be a non-abundant fluorescent subsiding mechanism in that the energy transfer from an excited source to a fluorescence receptor proceeds in a functionally acceptable manner despite the fact that the donor is excited. The FRET depressurization method was used to develop the PSA biosensor. Recently, Kavosi and colleagues have developed the accurate and simple aptasensor PSA detection premised on FRET technique from CdTe QDs modified to AuNps with poly amido amine (PAMAM) composite. The developed system used Ab-modified CdTe QDs as a donated donor and aptamer-adorned PAMAM-AuNPs as contributed the acceptor. The antigen detection was accomplished by measuring the immunocomplex formed by PSA and an aptamer. This simple, quick and highly selective aptasensor had a linear range of 0.01–100 ng/mL, and the LOD value was determined as 1 pg/mL. Lastly, PAMAM dendrimers are adsorbed onto the surface in order to maximize their effectiveness. Dendrimers with different functional groups, including QDs, can be used to increase the sensitivity of PSA measurements and can also be used in FRET-based biosensors to detect a variety of other analyses, such as PSA detection. Furthermore, due to its very high specificity and sensitivity, the presented approach has the prospective can be used in the identification of many cancer diagnoses [93].

## 11 Metal–Organic Frameworks (MOFs)

MOFs have lately developed as a novel type of porous, crystalline inorganic–organic composite materials [94]. MOFs are porous coordination polymers with a three-dimensional (3D) structure generated by the coupling of organic and inorganic compounds with ligands [95]. The wide range of applications, which include gas storage [96], chemical sensing [97, 98], catalysis [99], and drug delivery [100, 101]. MOFs are supramolecular complexes that exhibit a number of distinguishing characteristics, including porous structure, a large surface to volume area ratio (500–8000 m<sup>2</sup>/g), and outstanding mechanical (thermal) durability. Furthermore, most MOFs with a high crystalline structure can be synthesized at ambient temperature or using a solvothermal synthesis method [102]. MOFs have been suggested as labels in electrochemical sensing because of their electrochemical efficiency and larger availability of surface-active areas with better enzyme-like functional capabilities [103]. Taking these benefits into account, an abundance of MOF-based sensing applications using intrinsic MOF characteristics and composites has been described recently, with multiple extensive evaluations [104]. Metal–organic frames (MOFs) have the advantage over standard porous materials in that the coordination number of metal centers may be adjusted to change the geometry of crystal pores and hence the size of organic ligands. Moreover, due to various high electrical conductivity and catalytic activity, MOFs are often used in electrochemically oriented immunosensors [105].

Recently, the electrochemical-based immunosensor for PSA detection was constructed including a new redox mediator, Pd/NH<sub>2</sub>-ZIF-67. Additionally, the electroactive lamellar frameworks of ZIF-67 were shown to be an effective vehicle for PdNPs and a synergistically mediator for H<sub>2</sub>O<sub>2</sub> degradation, while the PdNPs demonstrated great biocompatibility and enhanced catalytic activity. A low LOD of 0.03 pg mL<sup>-1</sup> was exhibited broad linearity of 100 fg mL<sup>-1</sup> to 50 ng mL<sup>-1</sup> using the amperometric technique, and the immunosensor was utilized to quantify PSA [60]. Cu-MOF doped with tetracyano quinodimethane (TCNQ) was synthesized to improve the sensor electronic conductivity in the conductometric immunosensing method. For the first time, MOFs with a conducting thin film were proposed for the physical adsorption of antibodies as a novel aspect of this work. The introduction of TCNQ as a dopant has also improved the MOF platform's electrical conductivity. However, it has developed a hydrophobic surface that can be used to attach anti-PSA antibodies. The composite provided as a new building block for the biosensor used for PSA detection from spiked in serum samples. The presence of TCNQ-Cu<sub>3</sub>(BTC)<sub>2</sub>-constructed aptasensor for PSA detection achieved a LOD of 0.06 ng mL<sup>-1</sup> in the stable linearity of 0.1–100 ng mL<sup>-1</sup> and showed acceptable specificity with a rapid response time (2 min) for PSA in the existence of other proteins; accordingly, this sensor demonstrated effectiveness with spiked serum samples [58].

## 12 DPV-Based Prostate Cancer Biomarker Detection

A number of studies have demonstrated experience in developing sensitive biosensors for prostate cancer biomarkers using the DPV approach. Zheng et al. designed sandwich antibody electrochemical assays employing PDA-coated BCN substrates, MnO<sub>2</sub>-COF enrichment of MB, and probe material as signal amplification platforms and amplification. In this technique, synergistic effects between the nanoparticles of manganese dioxide and COF have been found to effectively prevent COF from aggregating during use and hence boost the composite's long-term stability. MnO<sub>2</sub> has been demonstrated to be highly catalytic in the reduction of MB. COF pores contain benzene ring ligands that may be coupled with MB. Moreover, the combination of COF and MnO<sub>2</sub> can be used in MB signal amplification. Additionally, the probe material contains Au@Pt metallic nanoparticles (Au@Pt NPs) that have the potential to enhance electrochemical signals. The biosensor exhibiting demonstrated a low LOD value (16.7 fg/mL), linear range (0.00005–10 ng/mL), by using DPV technique with high specificity, great stability, and may be utilized to detect PSA in the diagnosis and analysis of PCa [63]. Yang et al. employed gold mesoporous carbon (CMK-3) nanocomposites to detect PSA electrochemically and reached a detection value of 3 pg/mL in buffer solutions. PSA detection using nanocomposite nanocarriers to immobilize MB and secondary antibody (Ab<sub>2</sub>) for detection of PSA [71].

The use of porous materials used in the manufacturing of labels/carriers is effective in increasing the number of signal molecules since porous materials possess a high specific surface area ratio. Also, nanocomposite materials have gained popularity for their ability to combine the benefits of individual components with the enhanced attributes of the final nanocomposite. Graphene's strong electrical conductivity makes it a great choice for reducing electrode impedance and as a sensing material in clinical diagnostics. According to recent research, Pothipor and colleagues have designed a detection of biosensor for prostate cancer that uses electrodes modified with graphene poly(3, 3-aminobenzoic acid) and porous hollow silver-gold nanoparticle labeling to detect the presence of disease. In addition, the modified biosensor detection limit (0.13 pg/mL) is larger than the clinically significant level in serum samples. This sensor has shown promise in detecting prostate cancer and other medical purposes [72].

Mesoporous silica nanoparticles (MSNs) recently attracted the attention of researchers worldwide since their synthesis utilizes cationic quaternary ammonium surfactants as templates [106]. The use of MSNs in adsorption and drug administration and enzyme immobilization has become more popular because of their large surface area, variable average pore range, and homogenous structure. MSNs have also been proposed as a potential material for electrochemical sensors, particularly as a sensing component [69, 107]. Electrochemical immunosensors for the PSA detection method based on AuNps and PdPtCu nanospheres were developed by Li et al. Bimetallic nanoparticles have shown several benefits over single nanoparticles due to their synergistic impact. The sulfonic acid group-functionalized carbon nanotubes

(SWCNTs-SO<sub>3</sub>H) were employed as a supporting layer to expand the surface area and increase the conductance of glassy carbon electrodes. The amperometric response approach detected prostate-specific antigens from 10 fg/mL to 50 ng/mL, and gold nanoparticles were used to boost the loading efficiency of the capture antibody as well as electron transfer velocity. Graphene-based immunosensor with mesoporous core-shell Pd@Pt nanoparticles has demonstrated a LOD of 3.3 fg/mL and excellent stability for measuring PSA. The immunosensor's catalytic activity in reducing H<sub>2</sub>O<sub>2</sub> is improved by M-Pd@Pt/NH<sub>2</sub>-GS which is used as the signal labels, and this amplifies the current signal efficiently [17].

Electroactive material leakage and signal instability are common problems with conventional electrochemical immunosensors. The electrochemical immunosensors for PSA sensitive detection were proposed in this work to address the issue [65]. It utilizes on MOF-235 adsorption aggregation signal amplification approach. Cationic dye MB exhibits redox characteristics. It possesses excellent electron transfer rates, electrochemical reversibility, and strong biocompatibility. Consequently, it is often used in electrochemical immunosensors as an electroactive agent. However, due to MB's lack of specificity and instability, diagnostic findings will be distorted, and its usefulness would be restricted as a consequence. These studies employed MOF-235, a fluffy metal porous MOF with higher specific surface area and biocompatibility due to its two carboxyl groups. MOF-235, a MOF material with excellent adsorption characteristics, was synthesized and its surface area exceeds 835 m<sup>2</sup>/g. Methyl blue signal leakage during testing might be successfully prevented with this technology MOF-235 has the ability to regulate the reunification of MB after it has been adsorbed, which is advantageous for electron transmission. MB's amino groups are connected to the MOF material by electrostatic attraction, which helps to avoid signal leaks. It can also hold methylene blue securely in place on the MOF material, ensuring that MB does not leak its signal throughout the test. Methyl bromide is adsorbed and then re-adsorbed, which accelerates electron transport. There is high reproducibility and stability in the electrochemical immunosensor developed. The analyte concentration determines the electrical signal. The suggested immunosensor has a wide range value of 10–1200 pg/mL with a LOD of 3 pg/mL under optimal circumstances.

The combination of MOFs with DNA has been extensively explored since it enables novel modes of interaction with the environment or among the MOF crystals, as well as applications such as gene transfer and biosensing [108]. The photoelectrochemical (PEC) test, a novel, and promising analytical approach has attracted researchers attention owing to its ideal qualities of low signal background, excellent sensitivity, and exceptional stability. The PEC immunoassay devoid of enzymes was created for ultrasensitive prostate cancer detection using DNA-mediated nanoscale zirconium-porphyrin MOFs. In this research, a DNA-tagged anti-PSA antibody was used as a PSA signaling probe in conjunction with the Zr6 nodes of a nanoscale Zr-porphyrin- MOF. The presence of porphyrin MOF produced a cathodic photocurrent in the presence of PSA by a photoelectrochemical process in which the PSA concentrations were proportional to the photocurrent obtained. The immunosensor recognized PSA in specimens linear range of 1 pg/mL to 10 ng/mL, LOD value of (0.2 ng/mL) with sensitivity and selectivity.

## 13 SWV-Based Prostate Cancer Biomarker Detection

According to, Feng et al. created the sandwich electrochemical immunosensor premised on Fe-MOF, an immunoprobe with high catalytic activity. The amperometric immunosensor can be constructed using  $H_2O_2$  as well as Fe-MOF, which can degrade the Au-rGO-coated MB on the substrate and the amperometric response of 0.18 V (vs. Ag/AgCl) was generated using a redox-active component, modified on a glass carbon electrode. Fe-MOF may represent the reaction of Fenton, which reduces MB coated with Au-rGO on a surface. The oxidation of the electrode surface residual MB results in the generation of a current signal. SWV was used to study the electrochemical measurements of PSA. The sensor has a wide linearity value of (0.001–100 ng/mL) and a LOD of (0.13 pg/mL) [61].

A family of porous materials known as MOFs or porous coordination polymers (PCPs) is produced by the easy hydrothermal or solvothermal interactions of metal ions with bridging organic ligands, both of which occur at very low temperatures. Chen and coworkers reported the electrochemical immunosensor for PSA the Cu-MOF nanowire arrays were employed as a redox signal transducer. Antibody binding to PSA antigen results in decreased current signal due to antigen's electrical insulating properties. The increase in PSA concentration is inversely related to the decrease in current. This work highlighted the attachment of the antibody from the amino group through the carboxyl functional group exposed in Cu(1,4-NDC). The immunosensor has a LOD of (4.39 fg/mL) and a wider linear range of 0.1 pg/mL to 20 ng/mL by using the SWV method, respectively [62].

### 13.1 Creatinine

Creatinine is a marker of renal failure and obstruction to urine. Late-stage prostate cancer is identified by elevated levels of creatinine. Prostate cancer fatalities may be reduced by early and effective creatinine diagnosis [109]. Prostate cancer biomarkers include changes in serum creatinine levels, which may be used to predict the prognosis of the disease. Estimating PSA levels is a better way to diagnose prostate cancer than using a specialized and sensitive test. Apart from PSA, other indicators are examined in a subgroup of prostate cancer patients with normal PSA levels. The ratio of sarcosine to creatinine, as well as the phase of metastatic prostate cancer or tumor, may be utilized to determine diagnostic features. Prostate cancer in the advanced stages may be identified by elevated levels of creatinine [110].

Recently, Jamil and colleagues have developed nitrogen-doped porous carbon antimony nanomaterials for use in the fabrication of a non-enzymatic biosensor. Owing to its high electrical conductivity, potential redox action, and ease of synthesis, Sb/NPC is an ideal research topic for this study. In addition, the rod-like structure offers additional active areas on the surface. The electrodes are coated with a Sb/NPC nanocomposites to allow non-enzymatic detection of creatinine in phosphate buffer

and prostate cancer patients' blood samples. The biosensor has a linearity of 0.5–200 M, LOD value of 0.083 M [75].

### 13.2 Sarcosine

Sarcosine (SAR), also termed as N-methylglycine, or N-methyl derivative of glycine, an amino acid, is produced by glycine-N-methyltransferase (GNMT). Researchers hypothesize that GNMT may have a function in the methylation process and the development of prostate cancer. Sarcosine's role as a prostate cancer biomarker has been revived as a result of this discovery [111]. Previous research on sarcosine as a prostate cancer biomarker has shown inconsistent findings, with some studies showing an increased risk and others a lower risk [112].

SAR detection was accomplished by the development of the electrochemical sensor based on  $\text{Fe}_3\text{O}_4$  included MOFs with molecularly imprinted polymer-MIP in this research. The magnetic  $\text{Fe}_3\text{O}_4$  nanoparticles implanted in the zeolitic imidazolate framework-8 (ZIF-8) were employed as the support for the MIP. The authors Tang et al. explored the electrochemical sensor sensing unit made of super-magnetic  $\text{Fe}_3\text{O}_4$ @ZIF-8@MIP produced in a magnetic field. Electrochemical behavior was monitored using cyclic voltammetry, and the interaction of SAR led to a decline in the current that was observed. The present study demonstrated a dynamic range for residual SAR measurement of 1–100 pM and an exceptionally LOD of 0.4 pM, and it showed high selectivity, sensitivity, repeatability, and robustness respectively [76].

Ren et al. proposed a homogenous electrochemical immunoassay technique for simple PSA biomarker detection. A mesoporous silica nanoprobe (MSN) was used in conjunction with target-induced proximity hybridization to develop an electrochemical "DNA biogate" for use in the very sensitive homogenous electrochemical immunoassay. This technique allows recently designed proximity hybridization controlled "DNA-biogate" in conjunction with using an in situ enzymatic recycling coupling of the proximal complexes; this technique allows for the attainment of the highest possible sensitivity and selectivity with using a low volume of DNA sample. The proposed result demonstrates a dynamic linear range between 0.002 and 100 ng/mL, LOD value obtained 1.3 pg/mL [113].

Xu and colleagues developed a gold nanoparticles/molybdenum disulfide ( $\text{MoS}_2$ )/graphene aerogels (Gas) nanocomposite-based electrochemical immunosensor (label-free) for the detection of PSA biomarkers. The porous nature of  $\text{MoS}_2$ -graphene aerogels nanocomposite allows for a large surface area immobilized with AuNPs, increasing PSA antibody (PSA-Ab) loading. The conductivity and biocompatibility of AuNPs/ $\text{MoS}_2$ -GAs increased the rate of electron transport at the interface of the electrode, further proving their utility as an electrode. Additionally, its signal-amplification capabilities have increased the assay sensitivity. The electrochemical immunosensor had linearity of 0.00001–50 ng/mL, LOD of 0.003 pg/mL. The novel immunosensor was evaluated to analyze real blood samples; the results showed that it had high recovery rates for prostate-specific antigen [64].



## 14 Conclusion and Future Perspectives

Analytical techniques for prostate cancer early diagnosis should benefit significantly from the high probe loading capacity and resistance to probe degradation of EC biosensors constructed on MOF or MOF nanostructured composite materials. These characteristics have the potential to dramatically improve the detection for biosensors sensitivity. miRNAs, cancer markers, and cancer cells may be detected with great specificity using MOFs-based EC biosensors using a variety of sensing approaches. Furthermore, the distinctive structural characteristics of MOFs, such as homogeneous pores, varied composition, permeability, and extremely large surface area, make them particularly attractive as EC biosensors for the detection of PCa. The porous structure and vast surface area enable the anchoring of additional electroactive species, aptamers, enzymes, and metal nanoparticles, considerably magnifying the electrochemical impulses and enhancing the detection limit of targets. Additionally, the MOFs connected pore structure and the surface can facilitate efficient mass transfer and other functional materials to improve sensing properties. These new structures enable the fabrication of MOF-based composite materials with enhanced sensing capabilities.

The development of MOF-based hybrid materials, in addition to providing novel active sites for reaction and other functional materials, is enabled by these innovative concepts. Due to their remarkable EC biosensing properties, the new MOF structures will be employed in cancer diagnostics in conjunction with EC sensors. Consequently, pure MOFs are difficult to use in electrochemical sensors due to their inability to conduct electrons efficiently. Since monometallic MOFs have very low EC activities and monotonous characteristics, they have been difficult to include in biosensors used to detect biomarkers or live cells. Researchers have shown that combining noble/metal nanostructures with carbon-based conductors and conductive polymers, fabricating two-dimensional (2D) MOFs, and pyrolyzing MOF oxides into metallic oxides may overcome these barriers and improve the performance of their instruments for analyzing live cells or biomarkers. Due to their superior conductivity and nanoscale thickness, 2D MOFs, in particular, may make excellent catalysts. MOF ligands may also be modified to include additional materials, including COFs, MOFs, and enzymes. ECL biosensors are used to detect a wide range of analytes utilizing fluorescent materials like cyclodextrin and other fluorescent materials that enhance the ECL signals of MOFs with high conductivity and intrinsic EC luminescence.

In addition, the EC MOF biosensors, MOF composites, and heterostructures of distinct MOFs can both detect and identify the presence or absence of cancer biomarkers and cancer cells. These MOF-based nanomaterials exhibit excellent electrochemical activity, excellent fluorescence performance, compact size, and great biocompatibility. High sensing, cell endocytosis, and spectacular imaging are all made possible by these inherent features of the linked materials. Consequently, it is extremely desired to produce more MOF materials for constructing enhanced tumor tissue detection biosensors. However, MOFs mixed with other EC-active components

are a viable technique to increase the EC efficiency of MOF-based sensors; nevertheless, the composites' manufacturing processes, high cost, and convoluted structure prevent their widespread usage in biosensing and medical applications. Furthermore, the utilization of heterostructures as a suitable platform for EC biosensors can be a useful technique for MOFs-based biosensor manufacturing. The “dual-potential” ratiometric ECL immunosensor is capable of significantly reducing the likelihood of false positives in biomolecule detection while simultaneously increasing the exactitude of assessment. The sensor's performance characterization and real sample analysis demonstrate that it has exceptional performance and has a great deal of promise in clinical detection in the future.

**Acknowledgements** The authors express their gratitude to the Coordination for the Improvement of Higher Education Personnel (CAPES)-Brazil and the Drug Research and Development Center (NPDM) of the Federal University of Ceará (UFC) in Fortaleza, Brazil, for their assistance.

## References

1. Sung H, Ferlay J, Siegel RL et al (2021) Global cancer statistics 2020: GLOBOCAN estimates of incidence and mortality worldwide for 36 cancers in 185 countries. *CA Cancer J Clin* 71:209–249. <https://doi.org/10.3322/caac.21660>
2. Ilic D, Djulbegovic M, Jung JH et al (2018) Prostate cancer screening with prostate-specific antigen (PSA) test: a systematic review and meta-analysis. *BMJ* k3519. <https://doi.org/10.1136/bmj.k3519>
3. Benjamin SR et al (2022) Zero-dimensional carbon nanomaterials for cancer diagnosis. In: *Zero-dimensional carbon nanomaterials*, pp 7–14, IOP Publishing. <https://doi.org/10.1088/978-0-7503-4048-9ch7>
4. Graves HC, Wehner N, Stamey TA (1992) Ultrasensitive radioimmunoassay of prostate-specific antigen. *Clin Chem* 38:735–742. <https://doi.org/10.1093/clinchem/38.5.735>
5. Cao C, Kim JP, Kim BW et al (2006) A strategy for sensitivity and specificity enhancements in prostate specific antigen- $\alpha$ 1-antichymotrypsin detection based on surface plasmon resonance. *Biosens Bioelectron* 21:2106–2113. <https://doi.org/10.1016/j.bios.2005.10.014>
6. Johnson ED, Kotowski TM (1993) Detection of prostate specific antigen by ELISA. *J Forensic Sci* 38:13403J. <https://doi.org/10.1520/JFS13403J>
7. Yu F, Persson B, Löfås S, Knoll W (2004) Surface plasmon fluorescence immunoassay of free prostate-specific antigen in human plasma at the femtomolar level. *Anal Chem* 76:6765–6770. <https://doi.org/10.1021/ac048937w>
8. Tamayo J, Kosaka PM, Ruz JJ et al (2013) Biosensors based on nanomechanical systems. *Chem Soc Rev* 42:1287–1311. <https://doi.org/10.1039/C2CS35293A>
9. Singh G, Lakhi KS, Sil S et al (2019) Biomass derived porous carbon for CO<sub>2</sub> capture. *Carbon N Y* 148:164–186. <https://doi.org/10.1016/j.carbon.2019.03.050>
10. Xia H, Zhang J, Yang Z et al (2017) 2D MOF nanoflake-assembled spherical microstructures for enhanced supercapacitor and electrocatalysis performances. *Nano-Micro Lett* 9:43. <https://doi.org/10.1007/s40820-017-0144-6>
11. Abioye AM, Noorden ZA, Ani FN (2017) Synthesis and characterizations of electroless oil palm shell based-activated carbon/nickel oxide nanocomposite electrodes for supercapacitor applications. *Electrochim Acta* 225:493–502. <https://doi.org/10.1016/j.electacta.2016.12.101>
12. Zhang W, Xu J, Hou D et al (2018) Hierarchical porous carbon prepared from biomass through a facile method for supercapacitor applications. *J Colloid Interface Sci* 530:338–344. <https://doi.org/10.1016/j.jcis.2018.06.076>

13. Wang L, Zhang Q, Chen S et al (2014) Electrochemical sensing and biosensing platform based on biomass-derived macroporous carbon materials. *Anal Chem* 86. <https://doi.org/10.1021/ac401563m>
14. Teng W, Wu Z, Fan J et al (2013) Ordered mesoporous carbons and their corresponding column for highly efficient removal of microcystin-LR. *Energy Environ Sci* 6:2765. <https://doi.org/10.1039/c3ee41775a>
15. Amiripour F, Ghasemi S, Azizi SN (2021) A novel non-enzymatic glucose sensor based on gold-nickel bimetallic nanoparticles doped aluminosilicate framework prepared from agro-waste material. *Appl Surf Sci* 537. <https://doi.org/10.1016/j.apsusc.2020.147827>
16. Rathinaraj Benjamin S, de Lima F (2021) Current and prospective of breast cancer biomarkers. In: *Molecular biotechnology* pp 1–21 IntechOpen. <https://doi.org/10.5772/intechopen.91151>
17. Li M, Wang P, Pei F et al (2018) A novel signal amplification system fabricated immunosensor based on Au nanoparticles and mesoporous trimetallic PdPtCu nanospheres for sensitive detection of prostate specific antigen. *Sens Actuators B Chem* 261:22–30. <https://doi.org/10.1016/j.snb.2018.01.136>
18. Ibaou C, Md Arshad MK, Gopinath SCB (2017) Current advances and future visions on bioelectronic immunosensing for prostate-specific antigen. *Biosens Bioelectron* 98:267–284. <https://doi.org/10.1016/j.bios.2017.06.049>
19. Siegel RL, Miller KD, Jemal A (2019) Cancer statistics, 2019. *CA Cancer J Clin* 69:7–34. <https://doi.org/10.3322/caac.21551>
20. Arya SK, Bhansali S (2012) Anti-prostate specific antigen (Anti-PSA) modified interdigitated microelectrode-based impedimetric biosensor for PSA detection. *Biosens J* 1:1–7. <https://doi.org/10.4303/BJ/H110601>
21. Stephan C, Cammann H, Meyer H-A et al (2007) PSA and new biomarkers within multivariate models to improve early detection of prostate cancer. *Cancer Lett* 249:18–29. <https://doi.org/10.1016/j.canlet.2006.12.031>
22. Lawhn-Heath C, Salavati A, Behr SC et al (2021) Prostate-specific membrane antigen PET in prostate cancer. *Radiology* 299:248–260. <https://doi.org/10.1148/radiol.2021202771>
23. Wu D, Liu Y, Wang Y et al (2016) Label-free electrochemiluminescent immunosensor for detection of prostate specific antigen based on aminated graphene quantum dots and carboxyl graphene quantum dots. *Sci Rep* 6. <https://doi.org/10.1038/srep20511>
24. Ertürk G, Özen H, Tümer MA et al (2016) Microcontact imprinting based surface plasmon resonance (SPR) biosensor for real-time and ultrasensitive detection of prostate specific antigen (PSA) from clinical samples. *Sens Actuators B Chem* 224:823–832. <https://doi.org/10.1016/j.snb.2015.10.093>
25. Chikkaveeraiah BV, Mani V, Patel V et al (2011) Microfluidic electrochemical immunoarray for ultrasensitive detection of two cancer biomarker proteins in serum. *Biosens Bioelectron* 26. <https://doi.org/10.1016/j.bios.2011.05.005>
26. Srivastava M, Nirala NR, Srivastava SK, Prakash R (2018) A comparative study of aptasensor vs immunosensor for label-free PSA cancer detection on GQDs-AuNRs modified screen-printed electrodes. *Sci Rep* 8. <https://doi.org/10.1038/s41598-018-19733-z>
27. Çevik E, Bahar Ö, Şenel M, Abasıyanık MF (2016) Construction of novel electrochemical immunosensor for detection of prostate specific antigen using ferrocene-PAMAM dendrimers. *Biosens Bioelectron* 86. <https://doi.org/10.1016/j.bios.2016.07.064>
28. Carter HB (2013) American Urological Association (AUA) guideline on prostate cancer detection: process and rationale. *BJU Int* 112:543–547. <https://doi.org/10.1111/bju.12318>
29. Lo ST, Martins AF, Jordan VC, Sherry AD (2017) Zinc as an imaging biomarker of prostate cancer. *Isr J Chem* 57
30. Kokkinos C, Economou A, Prodromidis MI (2016) Electrochemical immunosensors: critical survey of different architectures and transduction strategies. *TrAC—Trends Anal Chem* 79
31. Felix FS, Angnes L (2018) Electrochemical immunosensors—a powerful tool for analytical applications. *Biosens Bioelectron* 102:470–478. <https://doi.org/10.1016/J.BIOS.2017.11.029>
32. Arduini F, Micheli L, Moscone D et al (2016) Electrochemical biosensors based on nanomodified screen-printed electrodes: recent applications in clinical analysis. *TrAC Trends Anal Chem* 79:114–126. <https://doi.org/10.1016/J.TRAC.2016.01.032>

33. Rotariu L, Lagarde F, Jaffrezic-Renault N, Bala C (2016) Electrochemical biosensors for fast detection of food contaminants—trends and perspective. *TrAC Trends Anal Chem* 79:80–87. <https://doi.org/10.1016/J.TRAC.2015.12.017>
34. Bandodkar AJ, Wang J (2014) Non-invasive wearable electrochemical sensors: a review. *Trends Biotechnol* 32:363–371. <https://doi.org/10.1016/J.TIBTECH.2014.04.005>
35. Justino CIL, Freitas AC, Pereira R et al (2015) Recent developments in recognition elements for chemical sensors and biosensors. *TrAC—Trends Anal Chem* 68
36. Zhu X, Wu G, Lu N et al (2017) A miniaturized electrochemical toxicity biosensor based on graphene oxide quantum dots/carboxylated carbon nanotubes for assessment of priority pollutants. *J Hazard Mater* 324:272–280. <https://doi.org/10.1016/J.JHAZMAT.2016.10.057>
37. Marquitan M, Bobrowski T, Ernst A et al (2018) Miniaturized amperometric glucose sensors based on polymer/enzyme modified carbon electrodes in the sub-micrometer scale. *J Electrochem Soc* 165. <https://doi.org/10.1149/2.0021812jes>
38. Akter R, Kyun Rhee C, Rahman MA (2013) A stable and sensitive voltammetric immunosensor based on a new non-enzymatic label. *Biosens Bioelectron* 50:118–124. <https://doi.org/10.1016/J.BIOS.2013.06.016>
39. Shan J, Ma Z (2017) A review on amperometric immunoassays for tumor markers based on the use of hybrid materials consisting of conducting polymers and noble metal nanomaterials. *Microchim Acta* 184
40. Yang P, Li X, Wang L et al (2014) Sandwich-type amperometric immunosensor for cancer biomarker based on signal amplification strategy of multiple enzyme-linked antibodies as probes modified with carbon nanotubes and concanavalin A. *J Electroanal Chem* 732. <https://doi.org/10.1016/j.jelechem.2014.08.030>
41. Proença CA, Freitas TA, Baldo TA et al (2019) Use of data processing for rapid detection of the prostate-specific antigen biomarker using immunomagnetic sandwich-type sensors. *Beilstein J Nanotechnol* 10. <https://doi.org/10.3762/bjnano.10.210>
42. Wei F, He Y, Qu X et al (2019) In situ fabricated porous carbon coating derived from metal-organic frameworks for highly selective solid-phase microextraction. *Anal Chim Acta* 1078. <https://doi.org/10.1016/j.aca.2019.05.061>
43. Xu Q, Qian J, Luo D et al (2020) Ni/Fe clusters and nanoparticles confined by covalent organic framework derived carbon as highly active catalysts toward oxygen reduction reaction and oxygen evolution reaction. *Adv Sustain Syst* 4. <https://doi.org/10.1002/adsu.202000115>
44. Sun Y, Ouyang Y, Luo J et al (2021) Biomass-derived nitrogen self-doped porous activation carbon as an effective bifunctional electrocatalysts. *Chinese Chem Lett* 32. <https://doi.org/10.1016/j.ccllet.2020.09.027>
45. Zhao H, Zhang Y, Li L et al (2021) Synthesis of an ordered porous carbon with the dual nitrogen-doped interfaces and its ORR catalysis performance. *Chinese Chem Lett* 32. <https://doi.org/10.1016/j.ccllet.2020.11.035>
46. Xue B, Wang X, Feng Y et al (2020) Self-template synthesis of nitrogen-doped porous carbon derived from rice husks for the fabrication of high volumetric performance supercapacitors. *J Energy Storage* 30:101405. <https://doi.org/10.1016/J.EST.2020.101405>
47. Mao X, Cao Z, Yin Y et al (2018) Direct synthesis of nitrogen and phosphorus co-doped hierarchical porous carbon networks with biological materials as efficient electrocatalysts for oxygen reduction reaction. *Int J Hydrogen Energy* 43:10341–10350. <https://doi.org/10.1016/J.IJHYDENE.2018.04.100>
48. Lee J, Kim J, Hyeon T (2006) Recent progress in the synthesis of porous carbon materials. *Adv Mater* 18
49. Chuenchom L, Kraehnert R, Smarsly BM (2012) Recent progress in soft-templating of porous carbon materials. *Soft Matt* 8
50. Jung YH, Kang H, Choi WS et al (2016) Effects of plasma treatment on carbon nanowalls grown by microwave plasma enhanced chemical vapor deposition. *J Nanosci Nanotechnol* 16. <https://doi.org/10.1166/jnn.2016.12211>
51. Li J, Su S, Zhou L et al (2013) Carbon nanowalls grown by microwave plasma enhanced chemical vapor deposition during the carbonization of polyacrylonitrile fibers. *J Appl Phys* 113. <https://doi.org/10.1063/1.4774218>

52. Xue T, Sun ZP, Wei L et al (2013) One-step dual template synthesis of platinum on mesoporous carbon nanowires for electrocatalysts. *Int J Hydrogen Energy* 38:2754–2759. <https://doi.org/10.1016/j.ijhydene.2012.12.034>
53. Noyce SG, Vanfleet RR, Craighead HG, Davis RC (2019) High surface-area carbon microcantilevers. *Nanoscale Adv* 1. <https://doi.org/10.1039/c8na00101d>
54. Liu T, Zhang F, Song Y, Li Y (2017) Revitalizing carbon supercapacitor electrodes with hierarchical porous structures. *J Mater Chem A* 5
55. Liang J-Y, Wang C-C, Lu S-Y (2015) Glucose-derived nitrogen-doped hierarchical hollow nest-like carbon nanostructures from a novel template-free method as an outstanding electrode material for supercapacitors. *J Mater Chem A* 3:24453–24462. <https://doi.org/10.1039/C5TA08007J>
56. Banerjee D, Mukherjee S, Chattopadhyay KK (2010) Controlling the surface topology and hence the hydrophobicity of amorphous carbon thin films. *Carbon N Y* 48. <https://doi.org/10.1016/j.carbon.2009.11.021>
57. Ko TJ, Her EK, Shin B et al (2012) Water condensation behavior on the surface of a network of superhydrophobic carbon fibers with high-aspect-ratio nanostructures. *Carbon N Y* 50. <https://doi.org/10.1016/j.carbon.2012.06.048>
58. Bhardwaj SK, Sharma AL, Bhardwaj N et al (2017) TCNQ-doped Cu-metal organic framework as a novel conductometric immunosensing platform for the quantification of prostate cancer antigen. *Sens Actuators B Chem* 240:10–17. <https://doi.org/10.1016/J.SNB.2016.08.138>
59. Liu X, Yue T, Qi K et al (2020) Porous graphene based electrochemical immunosensor using Cu<sub>3</sub>(BTC)<sub>2</sub> metal-organic framework as nonenzymatic label. *Talanta* 217:121042. <https://doi.org/10.1016/j.talanta.2020.121042>
60. Dai L, Li Y, Wang Y et al (2019) A prostate-specific antigen electrochemical immunosensor based on Pd NPs functionalized electroactive Co-MOF signal amplification strategy. *Biosens Bioelectron* 132:97–104. <https://doi.org/10.1016/j.bios.2019.02.055>
61. Feng J, Wang H, Ma Z (2020) Ultrasensitive amperometric immunosensor for the prostate specific antigen by exploiting a Fenton reaction induced by the metal-organic framework nanocomposite of type Au/Fe-MOF with peroxidase mimicking activity. *Microchim Acta* 187:95. <https://doi.org/10.1007/s00604-019-4075-4>
62. Chen Z-A, Lu W, Bao C et al (2019) Copper(II) 1,4-naphthalenedicarboxylate on copper foam nanowire arrays for electrochemical immunosensing of the prostate specific antigen. *Microchim Acta* 186:758. <https://doi.org/10.1007/s00604-019-3891-x>
63. Zheng J, Zhao H, Ning G et al (2021) A novel affinity peptide–antibody sandwich electrochemical biosensor for PSA based on the signal amplification of MnO<sub>2</sub>-functionalized covalent organic framework. *Talanta* 233:122520. <https://doi.org/10.1016/j.talanta.2021.122520>
64. Xu Q, Jia H, Duan X et al (2020) Label-free electrochemical immunosensor for the detection of prostate specific antigen based three-dimensional Au nanoparticles/MoS<sub>2</sub>-graphene aerogels composite. *Inorg Chem Commun* 119. <https://doi.org/10.1016/j.inoche.2020.108122>
65. Liu B, Lu L, Hua E et al (2012) Detection of the human prostate-specific antigen using an aptasensor with gold nanoparticles encapsulated by graphitized mesoporous carbon. *Microchim Acta* 178:163–170. <https://doi.org/10.1007/s00604-012-0822-5>
66. Argoubi W, Sánchez A, Parrado C et al (2018) Label-free electrochemical aptasensing platform based on mesoporous silica thin film for the detection of prostate specific antigen. *Sens Actuators B Chem* 255:309–315. <https://doi.org/10.1016/j.snb.2017.08.045>
67. Rodríguez C, Torres-Costa V, Ahumada O et al (2018) Gold nanoparticle triggered dual optoplasmonic-impedimetric sensing of prostate-specific antigen on interdigitated porous silicon platforms. *Sens Actuators, B Chem* 267. <https://doi.org/10.1016/j.snb.2018.03.179>
68. Li Y, Han J, Chen R et al (2015) Label electrochemical immunosensor for prostate-specific antigen based on graphene and silver hybridized mesoporous silica. *Anal Biochem* 469. <https://doi.org/10.1016/j.ab.2014.09.022>
69. Wang H, Zhang Y, Yu H et al (2013) Label-free electrochemical immunosensor for prostate-specific antigen based on silver hybridized mesoporous silica nanoparticles. *Anal Biochem* 434:123–127. <https://doi.org/10.1016/j.ab.2012.11.012>

70. Li M, Wang P, Li F et al (2017) An ultrasensitive sandwich-type electrochemical immunosensor based on the signal amplification strategy of mesoporous core-shell Pd@Pt nanoparticles/amino group functionalized graphene nanocomposite. *Biosens Bioelectron* 87:752–759. <https://doi.org/10.1016/j.bios.2016.08.076>
71. Yang L, Zhao H, Deng G et al (2015) Immunosensor for prostate-specific antigen using Au/Pd@flower-like SnO<sub>2</sub> as platform and Au@mesoporous carbon as signal amplification. *RSC Adv* 5:74046–74053. <https://doi.org/10.1039/C5RA15046A>
72. Pothipor C, Wiriyakun N, Putnin T et al (2019) Highly sensitive biosensor based on graphenepoly (3-aminobenzoic acid) modified electrodes and porous-hollowed-silver-gold nanoparticle labelling for prostate cancer detection. *Sens Actuators B Chem* 296:126657. <https://doi.org/10.1016/j.snb.2019.126657>
73. Zhang M, Hu X, Mei L et al (2021) PSA detection electrochemical immunosensor based on MOF-235 nanomaterial adsorption aggregation signal amplification strategy. *Microchem J* 171:106870. <https://doi.org/10.1016/j.microc.2021.106870>
74. Liang H, Xu H, Zhao Y et al (2019) Ultrasensitive electrochemical sensor for prostate specific antigen detection with a phosphorene platform and magnetic covalent organic framework signal amplifier. *Biosens Bioelectron* 144:111691. <https://doi.org/10.1016/j.bios.2019.111691>
75. Jamil M, Fatima B, Hussain D et al (2021) Quantitative determination of creatinine from serum of prostate cancer patients by N-doped porous carbon antimony (Sb/NPC) nanoparticles. *Bioelectrochemistry* 140:107815. <https://doi.org/10.1016/j.bioelechem.2021.107815>
76. Tang P, Wang Y, He F (2020) Electrochemical sensor based on super-magnetic metal-organic framework@molecularly imprinted polymer for Sarcosine detection in urine. *J Saudi Chem Soc* 24. <https://doi.org/10.1016/j.jscs.2020.06.004>
77. Lohse MS, Bein T (2018) Covalent organic frameworks: structures, synthesis, and applications. *Adv Funct Mater* 28. <https://doi.org/10.1002/adfm.201705553>
78. Medina DD, Sick T, Bein T (2017) Photoactive and conducting covalent organic frameworks. *Adv Energy Mater* 7. <https://doi.org/10.1002/aenm.201700387>
79. Song Y, Sun Q, Aguila B, Ma S (2019) Opportunities of covalent organic frameworks for advanced applications. *Adv Sci* 6
80. Jarju JJ, Lavender AM, Espiña B et al (2020) Covalent organic framework composites: synthesis and analytical applications. *Molecules* 25
81. Ma H, Li X, Yan T et al (2016) Electrochemiluminescent immunosensing of prostate-specific antigen based on silver nanoparticles-doped Pb (II) metal-organic framework. *Biosens Bioelectron* 79:379–385. <https://doi.org/10.1016/j.bios.2015.12.080>
82. Ma H, Zhao Y, Li L et al (2018) Label-free electrochemiluminescent immunosensor for detection of prostate specific antigen based on mesoporous graphite-like carbon nitride. *Talanta* 188. <https://doi.org/10.1016/j.talanta.2018.06.029>
83. Feng J, Li Y, Li M et al (2017) A novel sandwich-type electrochemical immunosensor for PSA detection based on PtCu bimetallic hybrid (2D/2D) rGO/g-C<sub>3</sub>N<sub>4</sub>. *Biosens Bioelectron* 91:441–448. <https://doi.org/10.1016/j.bios.2016.12.070>
84. Zhang Y, Liu Y, Li R et al (2017) Visible-light driven photoelectrochemical immunosensor based on SnS<sub>2</sub>@mpg-C<sub>3</sub>N<sub>4</sub> for detection of prostate specific antigen. *Sci Rep* 7:4629. <https://doi.org/10.1038/s41598-017-04924-x>
85. Wu D, Li R, Wang H et al (2012) Hollow mesoporous silica microspheres as sensitive labels for immunoassay of prostate-specific antigen. *Analyst* 137:608–613. <https://doi.org/10.1039/C2AN16033A>
86. Hassan M, Gomes VG, Dehghani A, Ardekani SM (2018) Engineering carbon quantum dots for photomediated theranostics. *Nano Res* 11. <https://doi.org/10.1007/s12274-017-1616-1>
87. He JH, Cheng YY, Zhang QQ et al (2020) Carbon dots-based fluorescence resonance energy transfer for the prostate specific antigen (PSA) with high sensitivity. *Talanta* 219:121276. <https://doi.org/10.1016/j.talanta.2020.121276>
88. Lv S, Li Y, Zhang K et al (2017) Carbon dots/g-C<sub>3</sub>N<sub>4</sub> nanoheterostructures-based signal-generation tags for photoelectrochemical immunoassay of cancer biomarkers coupling with

- copper nanoclusters. *ACS Appl Mater Interfaces* 9:38336–38343. <https://doi.org/10.1021/acsami.7b13272>
89. Bunt G, Wouters FS (2017) FRET from single to multiplexed signaling events. *Biophys Rev* 9:119–129. <https://doi.org/10.1007/s12551-017-0252-z>
  90. Yao H, Wang L, Guo J et al (2020) Genetically encoded FRET biosensor detects the enzymatic activity of prostate-specific antigen. *Mol Cell Biomech* 17:101–111. <https://doi.org/10.32604/mcb.2020.09595>
  91. Zhang X, Hu Y, Yang X et al (2019) Förster resonance energy transfer (FRET)-based biosensors for biological applications. *Biosens Bioelectron* 138:111314. <https://doi.org/10.1016/j.bios.2019.05.019>
  92. Charron DM, Zheng G (2018) Nanomedicine development guided by FRET imaging. *Nano Today* 18:124–136. <https://doi.org/10.1016/j.nantod.2017.12.006>
  93. Kavosi B, Navae A, Salimi A (2018) Amplified fluorescence resonance energy transfer sensing of prostate specific antigen based on aggregation of CdTe QDs/antibody and aptamer decorated of AuNPs-PAMAM dendrimer. *J Lumin* 204. <https://doi.org/10.1016/j.jlumin.2018.08.012>
  94. Zhong L, Ding J, Qian J, Hong M (2021) Unconventional inorganic precursors determine the growth of metal-organic frameworks. *Coord Chem Rev* 434:213804. <https://doi.org/10.1016/j.ccr.2021.213804>
  95. Yaghi OM, O’Keeffe M, Ockwig NW et al (2003) Reticular synthesis and the design of new materials. *Nature* 423
  96. Yu B, Wang F, Dong W et al (2015) Self-template synthesis of core-shell ZnO@ZIF-8 nanospheres and the photocatalysis under UV irradiation. *Mater Lett* 156:50–53. <https://doi.org/10.1016/j.matlet.2015.04.142>
  97. Wu Y-P, Wu X-Q, Wang J-F et al (2016) Assembly of two novel Cd<sub>3</sub>(Cd<sub>3</sub> + Cd<sub>5</sub>)-cluster-based metal-organic frameworks: structures, luminescence, and photocatalytic degradation of organic dyes. *Cryst Growth Des* 16:2309–2316. <https://doi.org/10.1021/acs.cgd.6b00093>
  98. Wang L, Xu H, Gao J et al (2019) Recent progress in metal-organic frameworks-based hydrogels and aerogels and their applications. *Coord Chem Rev* 398:213016. <https://doi.org/10.1016/j.ccr.2019.213016>
  99. Guo W, Zhang K, Liang Z et al (2019) Electrochemical nitrogen fixation and utilization: theories, advanced catalytic materials and system design. *Chem Soc Rev* 48:5658–5716. <https://doi.org/10.1039/C9CS00159J>
  100. Al-Kutubi H, Gascon J, Sudhölter EJR, Rassaei L (2015) Electrosynthesis of metal-organic frameworks: challenges and opportunities. *ChemElectroChem* 2:462–474. <https://doi.org/10.1002/celec.201402429>
  101. Wang S, McGuirk CM, D’Aquino A et al (2018) Metal-organic framework nanoparticles. *Adv Mater* 30:1800202. <https://doi.org/10.1002/adma.201800202>
  102. Stock N, Biswas S (2012) Synthesis of metal-organic frameworks (MOFs): routes to various MOF topologies, morphologies, and composites. *Chem Rev* 112:933–969. <https://doi.org/10.1021/cr200304e>
  103. Zhao F, Sun T, Geng F et al (2016) Metal-organic frameworks-based electrochemical sensors and biosensors. *Int J Electrochem Sci* 14
  104. Doherty CM, Buso D, Hill AJ et al (2014) Using functional nano- and microparticles for the preparation of metal-organic framework composites with novel properties. *Acc Chem Res* 47. <https://doi.org/10.1021/ar400130a>
  105. Zhao S, Zhang Y, Ding S et al (2019) A highly sensitive label-free electrochemical immunosensor based on AuNPs-PtNPs-MOFs for nuclear matrix protein 22 analysis in urine sample. *J Electroanal Chem* 834:33–42. <https://doi.org/10.1016/j.jelechem.2018.12.044>
  106. Beck JS, Vartuli JC, Roth WJ et al (1992) A new family of mesoporous molecular sieves prepared with liquid crystal templates. *J Am Chem Soc* 114. <https://doi.org/10.1021/ja00053a020>
  107. Narayan R, Nayak UY, Raichur AM, Garg S (2018) Mesoporous silica nanoparticles: a comprehensive review on synthesis and recent advances. *Pharmaceutics* 10

108. Zhang G, Shan D, Dong H et al (2018) DNA-mediated nanoscale metal-organic frameworks for ultrasensitive photoelectrochemical enzyme-free immunoassay. *Anal Chem* 90. <https://doi.org/10.1021/acs.analchem.8b03762>
109. Weinstein SJ, Mackrain K, Stolzenberg-Solomon RZ et al (2009) Serum creatinine and prostate cancer risk in a prospective study. *Cancer Epidemiol Biomarkers Prev* 18:2643–2649. <https://doi.org/10.1158/1055-9965.EPI-09-0322>
110. Wang M, Zou L, Liang J et al (2018) The urinary sarcosine/creatinine ratio is a potential diagnostic and prognostic marker in prostate cancer. *Med Sci Monit* 24:3034–3041. <https://doi.org/10.12659/MSM.909949>
111. Cernei N, Heger Z, Gumulec J et al (2013) Sarcosine as a potential prostate cancer biomarker—a review. *Int J Mol Sci* 14
112. De Vogel S, Ulvik A, Meyer K et al (2014) Sarcosine and other metabolites along the choline oxidation pathway in relation to prostate cancer—a large nested case-control study within the JANUS cohort in Norway. *Int J Cancer* 134. <https://doi.org/10.1002/ijc.28347>
113. Ren K, Wu J, Zhang Y et al (2014) Proximity hybridization regulated DNA biogate for sensitive electrochemical immunoassay. *Anal Chem* 86:7494–7499. <https://doi.org/10.1021/ac5012377>



# Chapter 37

## Role of Nanosystems for Electrochemical Mapping Using Diverse Carbon-Based Nanomaterials



Mansi Gandhi and Settu Ramki

### 1 Introduction and Background

The escalating world populace of growing demands has led to a state where the topic of environmental protection and safety is quite a vital aspect for forthcoming advancement of industrial and agricultural processes that helps in meeting the sustainable development goals. Nanotechnology has become the most exciting forefront fields which is described as “creation of functional materials, devise and systems through control of matter in the scale of 1–100 nm.” Nanotechnology offers a lot of promise in areas of pollution, sensing and prevention via exploitation of novel properties of nanosized objects. Because of size, nanosensors, nanoprobes and nanosystems are revolutionizing the field of environment and life of humans, particularly designing novel mapping systems with enhancing performance of sensors. As Clarke quoted “Any sufficiently advanced technology is indistinguishable for magic.” This concept has become true making the detection limits lower and lower reaching zeptomolar scale. The synthesis, characterization and utilization have become an emerging and rapidly growing field owing to the magic of it.

Electrochemistry is a multidisciplinary science applied to a variety of applications. As quoted by *Bard and Murray*, “The introduction of flexible electrochemical equipment based on non-ubiquitous amplifier, unleashed an accelerated evolution of different ways to manipulate currents and potential” [1]. This led to evolution/development of various different techniques evoked from stationary electrode

---

M. Gandhi (✉)

Department of Chemistry, SAS, Vellore Institute of Technology, Vellore 632014, India

e-mail: [mansigandhi.mg@gmail.com](mailto:mansigandhi.mg@gmail.com); [mansi.gandhi@mail.huji.ac.il](mailto:mansi.gandhi@mail.huji.ac.il)

Institute of Chemistry, Hebrew University of Jerusalem, 9190401 Jerusalem, Israel

S. Ramki

Research Center in Physics of Matter and Radiation (PMR), University of Namur, Namur, Belgium

© The Author(s), under exclusive license to Springer Nature Singapore Pte Ltd. 2023

1035

A. N. Grace et al. (eds.), *Handbook of Porous Carbon Materials*,

Materials Horizons: From Nature to Nanomaterials,

[https://doi.org/10.1007/978-981-19-7188-4\\_37](https://doi.org/10.1007/978-981-19-7188-4_37)

polarography to single triangular wave potential scan to cyclic voltammetry and so on and so forth. This enchanting bonanza of information provoked the wide research circle for the present and future with multitude set of objectives. With the time, encountered mathematical equations, serious impediment from two-electrode to three-electrode set-up, digital simulation and commercial programs became available to tune/boost the scope of study.

The analysis via electrochemistry is a simple and profitable technique that helps in quantitative and qualitative levels of determination for electro-active species in a solution. Innumerable advantages of electro-analytical systems are offered over other classical/routine detection methods such as; chromatography, luminescence, spectroscopy, low-cost/economical set-up, ease of usage by semi-skilled workers, reliability of data, accuracy without pre-concentration steps involved and so on. Variety of techniques are available in the field of electro-analytical branch to understand the process incurred.

With arrival of nanotechnology, came the capability of manipulation of atomic level with benefit of synthesizing uniquely organized molecular structures. Nanomaterials (NMs) have become the focal point of inquisitive research mainly due to noteworthy mechanical and electronic attributes coupled to their chemical inertness and heat conduction characteristics. Carbon is an element with atomic number 6 and belonging to group 14 of periodic table. It has various forms, one of them is the hardest and an insulator, i.e., diamond, while the other is the softest, i.e., graphite and is conducting. The electronic characteristics for carbon lineage are quite exceptional, because of their occasional atomic structure with mechanical deformations for progress of miniaturized sensors, sensitive to various environments (chemical, mechanical and physical) [2–7].

Nanotechnologic advancement has unlocked arenas for human understanding of world [8, 9]. This innovative and high-tech domain wherein the atoms are controlled at nanoscale level, in order to attain detailed product manufacturing cum refining with optimized tailoring of their characteristics for studying of specific material. The world of nanomaterials (NMs) is the understanding of materials that at least 1D of their 3D space lies within the range nanosize. These exhibit various exclusive mechanical, catalytic, optical and electrical qualities due to their cumulative surface effects, macroscopic quantum tunneling and small size effects. These NMs offer broad scenarios for the development of the most “promising materials” for the twenty-first century [10]. Their rise has opened the doors for expansion of bio-electro-analytical chemistry, particularly for the basis of mapping platforms [11, 12]. Noteworthy, their special characteristics (especially compatibility, structural, strong adsorption, orientation patterns, their novel approach) can effectively help in immobilizing the biomolecules and labeling systems that promote the electron transfer abilities to facilitate their electrochemical signals such as amplification of bio-electrochemical sensors [13]. In particular, the above-mentioned ability has led to remarkable approach in the field of electrochemistry [14, 15].




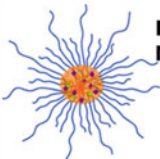
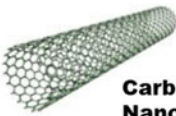
## 2 Role of Nanomaterials in Electrochemistry

Numerable techniques in electrochemistry can be accounted via cyclic voltammetry, chronoamperometry, linear sweep voltammetry, rotating disk electrode techniques, etc. Procedure in electro-analysis depends upon the material aspects (chemical and physical attributes of the electrode matrix and transducer with adsorption, effects of potential, number of layers coated on electrode, etc.). Basically, the nanomaterials as projected in Fig. 1 and Table 1 are extensively employed in the fabrication setups due to their chemical inertness, suitability, adhesion features, low background current, electron transfer characteristics, wider potential windows and compatibility. This particular review target to showcase the light on use of carbon nanoforms in the field of electro-analytical domain with encouraging their implications in multiple fields of sensors [16–19], catalyst scaffolds, energy storage and conversion [19–21], electronic devices [16, 22, 23], pollutant analysis [24] and gas-based sensors [25]. As suggested by *Ndamanisha and Guo*, reduced potential bars and lifetimes are crucial for efficient mapping of bioanalytes [26].

## 3 Amalgamation of Electrochemistry with Choice of Carbon Nanoparticles

An electrochemical sensor is a set-up of an electrolytic cell consisting of minimum two electrodes with a closed electrical circuit and a transducer wherein charge transport is established. The transportation/movement of charges in the analyte is either electronic in nature or ionic or a mixture of both. The electronic features exist as a compilation of charge transportation in an analyte, consequently of nanomaterials particularly involving carbon or metal-based systems. The rich  $\pi$ -cloud is due to electron cloud distortion of carbon nanoforms helping it to be electrochemically active [48–50]. While initiating the doping (e.g.,  $\text{NH}_3$ ,  $\text{NO}_2$ ,  $\text{O}_2$ ) in the carbon nanotubes with electron withdrawing and donating properties that can in turn boost the charge carriers or holes, further expanding and condensing their conductance, respectively [51].

Bio-electrochemical sensor systems are a special kind of device consisting of a superior recognition ability employing use of target biological macromolecules (enzymes, receptors, antibodies, recognition elements) [52, 53]. Owing with specific recognition and rapid catalysis, that can meet the of modern analysis process with their characteristics of specificity, rapidity, instantaneous and readily accessible detection methods to complete the void of research and development lacuna. The subbranches of sensors functions based on the specific recognition between the transducer and analyte [54]. This inbuilt feature of specific recognition and further amplification of signal output led to remarkable achievements in respective domains [55, 56]. These sensors can be described as electrochemical, optical, calorimetric, piezoelectric, etc. among which the most extensive class is electrochemical-based

 <b>Liposomes</b>	100-200 nm	Lipid bilayer membrane vesicles with an aqueous core.	They are inert systems.
 <b>Dendrimer</b>	25-100 nm	Simple DNA molecules	Self-assembly attributes
 <b>Gold</b>	20-30 nm	Significantly different properties than bulk	Various geometrical forms with no cytotoxic effects and has different size ranges.
 <b>Polymeric Micelles</b>	10-100 nm	Self-assembly with ability to entrap hydrophobic systems. Amphiphilic block copolymers	Approved for human use.
 <b>Carbon Nanotubes</b>	>1 nm	Chemically stable, cell penetration ability, customizable properties with pore size and functionality	Enhanced surface area and electronic properties

**Fig. 1** Pictorial representation of few nanomaterials with their characteristics

integrated devices. Thus, development and popularization of sensors are based on signals varying due to current, potential, conductance and impedance. Redox-based sensors are used to amplify and detect the mismatches and complementary target systems. These can be applied in diverse systems of clinical inspection [57], food and environmental monitoring [58, 59], health point-of-care systems [60], energy generation, diodes and storage systems [61, 62], capacitors [51], etc. wherein their irreplaceable roles are highly significant. This has directed to the production of several commercialized products and pipeline innovations [63]. Table 2 constitutes few carbons modified sensing platforms in the fields of various application spheres.

In this review, the principle behind use of nanomaterials after suitable tailoring, expansion and new fabrications for the progress of electro-analytical platforms based on various types of indicators is explained/explored in detail. The source/mindset behind the significance of different nanosystems for refining electrochemical performance is the prima facie of this article. Thus, this review helps in summarizing past literature studies of nanosystem-based electro-biochemical sensor which support

**Table 1** Widely used NMs highlighting their role with the use of techniques involved for applications

S. No.	NMs	Application field	Role of molecule	Electrochemical technique involved	References
1	Pd	Electrochemical ORR	Pd gave ORR with enhanced kinetics > 1 V with higher catalytic properties	In situ photo electro spectroscopy and ring rotating disk electrode	[27]
2	Graphene-PEDOT NPs	Electrochemical immunosensing of prostate specific antigen	An aerogel composite; PEDOT hollow microflower	Electrochemical; DPV	[28]
3	Ferrite NPs	MEMS (micro-electro-mechanical systems)	Ferrite as magnetic thin films for fabrication of cost-effective, high-yield arrays	Magnetization curve study; non-electrochemical	[29]
4	Different nanocomposite polymer (PEDOT, PDMS, etc.)	Polymer-based microfluidics	Microsensors, actuators and packing	Non-electrochemical; Young's modulus variation, conductivity studies	[30]
5	Ag NPs	Bio-MEMS construction	As a stamping material onto surface of fabrics	Non-electrochemical; AFM studies, resistivity studies	[31]
6	rGO-Nafion	Pesticide determination	Biocompatible matrix for adsorption of acetylcholinesterase	CV; EIS	[32]
7	Au-Alcohol dehydrogenase	Disease biomarker	Visible using naked eye due to change in colors	Non-electrochemical	[33]
8	4-Mercaptobenzoic acid Au-NPs	Dengue virus serotypes	It is water soluble, label free, and high selectivity	CV; EIS	[34]
9	Au-nanorod	Bio-detection	No labeling required; eliminating of CTAB is quite	Localized surface plasmon resonance	[35]

(continued)

Table 1 (continued)

S. No.	NMs	Application field	Role of molecule	Electrochemical technique involved	References
10	Ferrocene tagged peptide (phenylalanine) nanowire	Serum biomarker	Ultrasensitive detection; no extra signal tags required	SWV	[36]
11	Probe of magnetic Nickel-Fe core	Detection of carcino-embroygenic cancer detection	Magnetic system allows the enrichment of hotspots and further towards targeted antigen	SERS	[37]
12	AuNPs/CNT	Detection of alpha-fetoprotein	Enzyme-free catalysis	DPV	[38]
13	3D-Au nanoclusters	Herbicide detection	Detecting efficient carcinogenic from raw samples diluted using PBS	CV, current-time curve	[39]
14	Multifullerene encapsulated Pd nanocage	<i>Streptococcus suis</i> strain	High SA with efficient photocatalytic activity	EIS; $V$ versus ECL intensity	[40]
15	Cu monolayered using under deposition technique	Pollutant	Ultradeposition allows stronger self-deposition monolayers	CV, Chrono-amperograms	[41]
16	Pt nanodendrite	Alpha fetoprotein tumor marker	Multiple signal enhancement due to dendrimer pattern	CV, Amp $i-t$	[42]
17	DNA-wrapped CNT	<i>E. coli</i>	Alteration in base pairs could be easily accounted	DPV	[43]
18	Fe <sub>3</sub> O <sub>4</sub> NPs	DNA hybridizing	Label-free sensing; excellent electron transfer abilities and easy mismatched	EIS	[44]
19	Nanocrystalline diamond surface	Neurons growth affinity	Antibacterial and non-corrosive; excellent biocompatibility	Non-electrochemical	[45]
20	<i>f</i> -MWCNT-Pt	H <sub>2</sub> gas sensor	Self-recovery film, high sensitivity at room temperature	$I-V$ measurements	[46]

(continued)

**Table 1** (continued)

S. No.	NMs	Application field	Role of molecule	Electrochemical technique involved	References
21	SnO <sub>2</sub> nanocrystals	CH <sub>4</sub> sensor	Chemoresistive sensor; resistance modulator	Resistivity studies	[47]

*CNTs*—carbon nanotubes; *AuNPs*—gold nanoparticles; *rGO*—reduced graphene oxide; *PBS*—phosphate buffer solution; *EIS*—Electrochemical Impedance Spectroscopy; *DPV*—Differential Pulse Voltammetry; *CV*—Cyclic Voltammetry; *AFM*—Atomic Force Microscopy

**Table 2** Accounts various carbon modified electrochemical platforms in the field of different applications

S. No.	Element	Morphologies	Use in field	References
1	Carbon nanodots/quantum dots	Spherical	Metal ion sensing	[64]
2	Polypyrrole film	Thin film	Pesticide detection	[65]
3	Carbon nanofiber + Polyaniline	Fibers of nanometer thickness	Supercapacitor application	[66]
4	MWCNT + Pt NPs	Nanotubes	Methanol fuel cells	[67]
5	Carbon felt + boron doped diamond + carbon nanotubes	BDD coated felt seed for CNT growth	Field emission applications	[68]

their coordinated expansion across distinct research and technological fields that in turn helps in expanding their realistic applications.

#### 4 Role of Electrodeposition, Nanopatterning and Its Relevance

Another lookout for the combined field of nano cum electrochemical discipline wherein rapid development of nanotechnology involving use of nanoscaled systems portraying excellent performance is having a broader display place for creation of high-performance analytical sensors. Few of the electrodeposited materials are gold, metal oxides, layered double hydroxides (LDHs), polymers, etc. Technique of electrochemical deposition allows synthesis of nanostructures with defined and optimized morphologies, even without involvement of add ons (such as template) and flexible size options simply by controlling the experimental synthesis conditions. Various constraints especially current density, time duration and applied potential (constant, pulsed, ramped) play a significant part in defining shape and size of resulting nanostructures. The realization of modified electrodes has been a pivotal point/interface which is quite essential for the growth of new generation electro-analytical devices with improved responsiveness since the modifiers confer stimulating features, thereby leading to the precise recognition and pre-concentration of the bio-systems. The vital/ultimate studies on these chemically modified platforms are being studied inside the films for accomplishment of a relatively better command on characteristics for the nature of charge transfer with charge transport. The critical and appealing properties of nanomaterials depend on the synthetic procedure, growth and morphology. Electrochemical deposition is an efficient procedure for the preparation of nanoparticles (NPs) which is less utilized compared to wet chemical methods. This approach includes equal limitations as their dimensions in addition to allowed

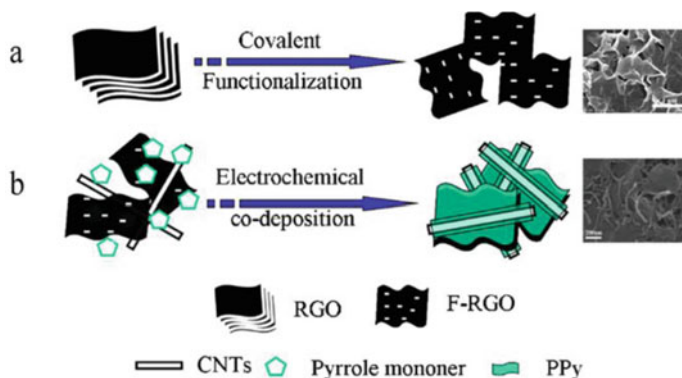


morphologies. In continuation, the procedure of electrochemical deposition provides advantages for rapid synthesis without need of chemical oxidants and undesired by products [69]. Example, the modifier films are deposited on the electrode for better adhesion. The technique of electrodeposition is being extensively explored via cyclic voltammetry, potential step and double pulse deposition [70]. Table 3 accounts the electrodeposition via various methodologies. This helps in enabling the control of particle size by regulating of current density, applied potential, time duration, electrolysis time, number of cycles scanning potential bar, etc. In addition, templates can be employed to achieve distinct three-dimensional structures like honeycomb-mesoporous silica. Later, introduction of colloidal silica, geometrical shapes like star, rhombus, square, triangle, etc. star silica, sponge and core shell-type morphologies has been synthesized via altering dimensions and shapes of silica additives. Thus, this paper accounts for recent applications of nanomaterials for the electrochemical supports being obtained via electrosynthesis, inorganics and organic modifications.

Nanopatterning incorporates peculiar chemical and physical properties that are extremely suitable as electrochemical sensors that display reduced over-potentials towards electro-active response reactions and further helps to enrout into reversible systems that are irreversible at classic electrodes. Nanopatterning is important for nanostructuration which further creates a choice for alteration of oxide layer via square wave perturbing potential (SWV) via anodizing the gold platform versus saturated hydrogen electrode at 2.44 V potential. In continuation, the formed oxide layer is let for electroreduction under a slow potential sweep in the 0.5 M H<sub>2</sub>SO<sub>4</sub>

**Table 3** Electrodeposition of various different morphologies obtained via electrochemical technique

S. No.	Element	Morphologies	Electrochemical technique	References
1	Au nanocrystals	Crystals	LSW	[71]
2	Ni, Al LDH	LDH	CV	[72]
3	Au microstructure	Flower-like	Amp <i>i-t</i>	[73]
4	NiS/Acetylene Black, NiS/Vulcan Carbon, NiS/MWCNT	Spherical and film	CV	[74]
5	Ionic liquids	Star, snow-flake, nanothorn	AC/DC/pulse parameters	[75]
6	CNT	Quasi-spherical and nanotubular carbon	CV	[76]
7	Au	Star	Applied potential	[77]
8	Silicon-carbon films	Compact grains	–	[78]
9	Ag–Au nanoalloy	Grain	Anodic polarization	[79]
10	Co–Al LDH	LDH	Cathodic reduction	[80]



**Fig. 2 a and b** Chemically modified electrochemical system fabricated after nanopatterning, Reprinted with permission Punetha et al. [7], Copyright 2013 Progress in Polymer Science

solution [81]. The mapping of arsenic (III) and selenium (IV) has been reported on GCE modified with Au nanoparticles by potential cycling via anodic stripping voltammetry technique in the window of  $-0.4$  V to  $+1.1$  V [82]. Similarly, different carbon systems can be modified with various carbon nanomaterial nanopatterning as in Fig. 2 which is the reprint [7] with copyright permission.

## 5 Versatility of Nanoparticles

The use of nanoparticles is termed as “labeled systems” that helps in establishing better signal amplification compared to other nanomaterials with probability of secondary amplification for detection response improving its cofactors significantly. Thus, nanomaterial composites were used in combination to these systems for better platform fabrication. Simple example being  $\text{MoS}_2$ -Au composite film which displayed well-catalytic activity for  $\text{H}_2\text{O}_2$  and later glucose oxidase and secondary antibody integration modified AgNPs to obtain AgNPs-Ab<sub>2</sub>-GO<sub>x</sub> composite. Other nanoalternative metals include copper, nickel, palladium, platinum and other metals, etc. have been incorporated for fabrication of other platforms that enhance the detection sensitivity [40–42]. This encourages enhanced sensitivity, good reproducibility and defined stability for both detection modes suitable for use. Carbon is the most abundant element in living species; carbon nanosystems have effectively promoted the rapid expansion of nanoscience. Carbon-based nanosized systems have good electrical conductivity, biocompatibility thereby improving active sites of electrochemical reactions. They account for large specific surface area that allows enhancement in immobilization of transducers and enzymes. The attribute of surface-to-volume ratio increases with decreasing feature size, and for nearly meagre sizes, characteristics are no longer dominated by the bulk of the system by rather by surface atoms.

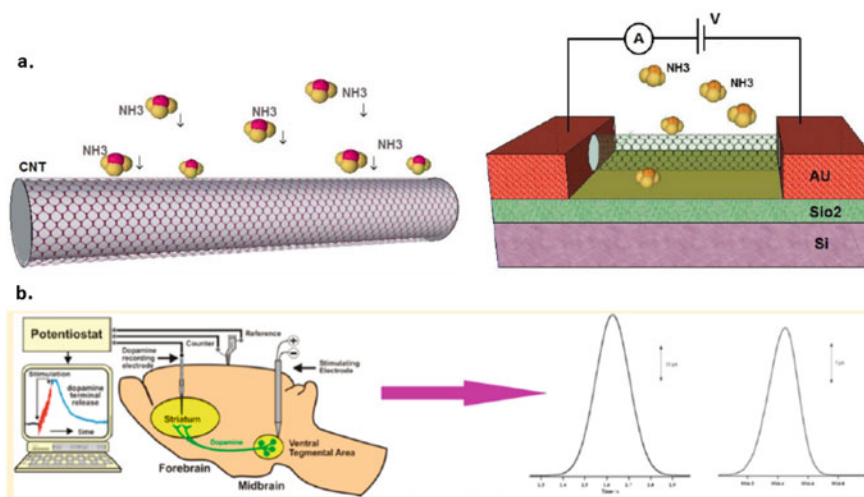
Based on coordination, one can differentiate between three types of surface atoms which, in the order of decreasing coordination, are terrace atoms, step edge atoms and kink sites. Simple geometrical reflections disclose that in case of curved surfaces, having high surface area is controlled by undercoordinated step edge and kink site surface atoms. It is indeed the undercoordination which gives rise to new properties such as stability, surface stress, tensile strain, physical and chemical detailing based on its electronic charge transfer. In addition to above, surface engineering is one such complete topic in this approach for tuning of surface-to-volume ratios. They are further subdivided as follows.

### 5.1 Carbon-Based Allotropic Forms

Carbon nanoforms, such as graphene, CNTs, diamond-like carbon, graphite nanoforms, fullerenes, diamond, portray extraordinary characteristics with wider scope of applications (Fig. 3a is the reprint from [16] with copyright permission). The potential range is unquestionable in sensing applications due to their larger surface-to-volume ratio, high conductivity and mobility at room temperature that has led to new arenas of exploration. The 1D carbon-based nanosized materials, i.e., CNTs, have special structures (radius 2–20 nm) with high surface area. These account for an extensive series of delocalized bonds having substantial conjugation properties leading to substantial conductivity. Due to its exceptional and excellent characteristics, CNTs have a wide range of usages in the domain of electrochemical sensing especially for the stability issues, labeling of markers and for modification of substrates, etc. *Rustling and his coworkers* studied the in-depth properties and found that intermolecular electron transfer properties are enhanced when linked to horse radish peroxidase enzyme (HRP) [83]. They are a perfect system for adsorption with specific surface area (enhanced many folds) and reflect the synergetic effects. CNTs have significant potential for various applications as protein immobilization, maintaining their inherent activity, ability to facilitate electron transfer at the interface and with species in solution [19–21]. They have demonstrated a better behavior than traditional electrode interfaces with good conductivity and better stability. The transducing element exploits CNTs as substrate materials offering better performance and improved signal-to-noise ratio counterparts. Different types of carbon nanotubes and their derivative-based transducers amplify the bio-electro-catalytic reactions providing an alternative option for multiple enzyme tags. These carbon alignments as “forests” acts corresponding to molecular wires, establishing the required electron transfer between the redox probes. As resistivity is directly proportional to the electron carriers, probable accessibility of electron holes in the carbon-graphite can lead to free movement of  $\pi$  bonding between graphitic molecules and quasi-1D shapes. The defined circumference of carbon tubes restricts the potential electron states but helps in establishing a uniformity of transitions, as a consequence of which, opening of band gap at Fermi energy level. And this potential bandgap decreases as the spacing between the graphene layers decreases. Therefore, the electron transfer

can occur without scattering over relatively large distances of several micrometers depending on mechanical quality of nanotubes [84–86]. The transfer of electron in a CNT is chiefly due to variable conducting states that provides a quantum conduction through transportation of 1 spin up and 1 down electron/hole. Though substantial reflections at carbon nanotube contact interface occurs, resultants of bottlenecks for retrieving various electronic states due to their condensed numbers and particular conformations are a major constraint. The transmitted  $e^-$ (s) or holes vary based on the existing states that leads to fall in voltage conducted through CNTs but not sideways the tube itself [86, 87]. Furthermore, when conjugated with non-scattering “ballistic” electron transfer, the CNTs mechanical robustness lets them to survive current density up to 3–4 times higher than most metals [88–90]. In continuation, a potent substitute for silicon-based circuits is quite a promising system in the domain of nano-electro-mechanical system [3, 91–95]. Separate tubes have exceptional characteristic (being metallic and semiconducting) of being utilized to construct transistors and necessary contacts between integrated circuits [96, 97]. It is quite a valuable and fast approaching pathway for miniaturization of traditional MOx (metal oxide) semiconductors and silicon transistors [97]. *Vishnu and Annamalai Senthil Kumar* has reported MWCNT modified system for the interconversion of electro-inactive benzene to respective electro-active quinones in pH 2 HCl-KCl solution with added  $H_2O_2$  [98] while *Mansi and her colleagues* reported an electro-inactive benzene derivative as a redox-active chemically modified hydroquinone on a multiwalled carbon nanotube [24]. Another such report in which *Michael and his coworkers* reported Flavin group at GCE/SWCNT/glucose oxidase/Nafion modified sensor pH 7 [99].

CNT modified systems have showcased the ability of alleviating the surface-fouling features that arise due to high overpotential during analyte oxidations. The involvement of surfactants to disrupt the strong van der Waal forces between the CNTs helps in improving their stability while preserving their structure and providing better alternative for covalent modification [101]. CNT-based tips (Fig. 3b is the reprint from [100], copyright permission) account for small intrinsic diameters, with high aspect ratios allowing them to probe deep cervices and trench with profound capability to fasten elasticity and reduces deformation to samples, while creating functional probes [102, 103]. The functionalized CNTs (*f*-MWCNT) in the field of atomic force microscope (AFM) have led to gateways for studying of chemical and biological subjects in domains of molecular recognition and chemically sensitive imaging. Their capabilities can be investigated using optimization for more challenging samples with smaller tips to enhance peak force. An interesting example is the use of SWCNT-based tips which enhance the current voltage maps for multiple measurements with high bias atomic force microscopic applications. The functionalization of CNTs can help in improvement of performance and sensitivity along with utility of nanomaterials for various applications. These include (1) the activation of the carbon nanotubes by generating reactive species such as hydroxyl groups, amine groups, and carboxylic groups; and (2) the direct covalent attachment of the desired functionalities using radical addition, cycloaddition, and electrophilic and nucleophilic addition reactions. Moreover, via the sidewalls and ends/defects are two



**Fig. 3** **a** Cartoonist illustration for the gas adsorption mechanism where NH<sub>3</sub> molecules act as electron donors, Reprinted with permission Akbari et al. [16], Copyright 2014 Sensors. **b** Dopamine detection using hydrogenated carbon tip conical electrode, Reprinted with permission Chandra et al. [100], Copyright 2014 Analytical Chemistry

subcategories for covalent functionalization of CNTs. In addition to above, heating of CNTs under strongly acidic and oxidative conditions results could enhance the oxygen-containing functionalities.

## 5.2 Diamond

Carbon can crystalline in either form of hybridization ( $sp^2$ , i.e., graphite and  $sp^3$ , i.e., diamond) that are chemically inert. They can interact with liquids and gases due to influence of sliding contacts, especially due to influence of interfacial terminating bonds. Amorphous diamond-like carbon films are a non-crystalline carbon having characteristics and desirable properties of enhanced modulus, semi-conducting properties, inertness, mechanical hardness, low surface roughness, and band gap of 1–4 eV [104]. These sensors improved the signal response by 100-fold. When working in conjugation with target and its derivative, the detection of bioanalyte has been attained by monitoring the variation of impedance/conductance owing to the displacement reaction.

The potential of diamond as an electrochemical transducer has remarkable interest due to its chemical stability, wider potential window, low background current and biocompatibility compared to silicon, silicon dioxide, tin dioxide, gold and glassy carbon [105–110]. The diamond interface has distinct properties with optimized termination by either oxygen, hydrogen and hydroxide groups making it hydrophilic

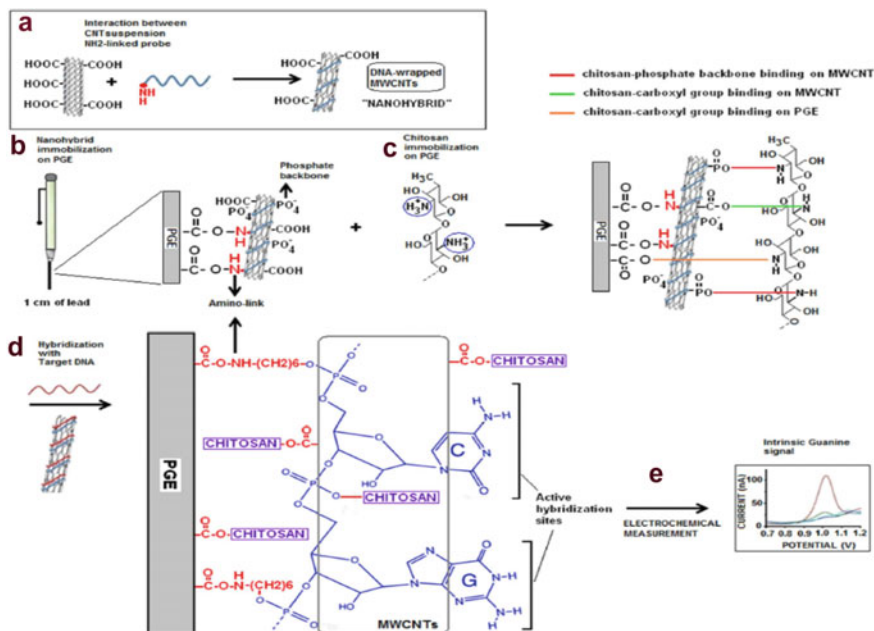
and hydrophobic [100, 111, 112]. Diamond has other attributes of DNA binding stability, biocompatibility, chemical inertness and their applications for chemical and electronic sensors. A nontoxic nanoscale diamond carrier for simultaneous transfection of cells and spatiotemporal imaging of DNA with any labeling technique has been reported which is established on fluorescent nanodiamond particles coated polyethylenimine to form reversible complexes with DNA via electrostatic interaction [113].

### ***5.3 Graphene and Its Oxide***

Graphene displays exclusive properties, a monolithic structure with enhanced conductivity, no toxicity complications and high specific area with good electron mobility, hence widely extended in the fields of sensing and biosensing. Graphene-based systems consist of high-density defects on its surface and establishes predominantly constructive electrochemical properties. Extension of graphene has been illustrated by combining them with a diverse section of inorganic and organic electroactive composites, as a promising new carbon substrate in the field of electrochemical analysis. The advancement of graphene materials had led many researchers to introduce functional groups on their surface as graphene derivatives (especially GO and rGO) [32]. The 3D interfaces have defined reaction sites for redox-systems, strengthening electron transfer ability between transducer element and the electrode, thereby amplifying the detection limit and sensitivity. Pencil graphite electrodes are another broader area of research interest with prominent exploitation of a cheap electrode without any complications. A pencil-based graphite electrode was used for the determination of fish freshness using differential pulse voltammetry in pH 7 buffer in a small potential window via analysis of the three important protein metabolites [114]. Further, a 6B-pencil-based system has been a prominent platform for the efficient sensing of tea quality via a simplistic approach within a time span of 45 s [115]. A simple schematic illustration is provided in Fig. 4 which is the reprint from [43], copyright permission portraying PGE for guanine oxidation.

### ***5.4 Metal Nanoparticles***

Semiconductor nanomaterials principally involve silica and quantum dots, exhibiting impressive characteristics especially high surface area, adhesion, reaction, and adsorption capacity providing a new route for biomedical research. The surface coordination characteristic especially for nano-SiO<sub>2</sub> particles present with large number of unsaturated residues and different bonds with hydroxyl groups allows materials to be readily surface functionalized. Furthermore, researchers have explored a pathway of incorporating the ionic liquid for the modification of sensors onto a porous sphere

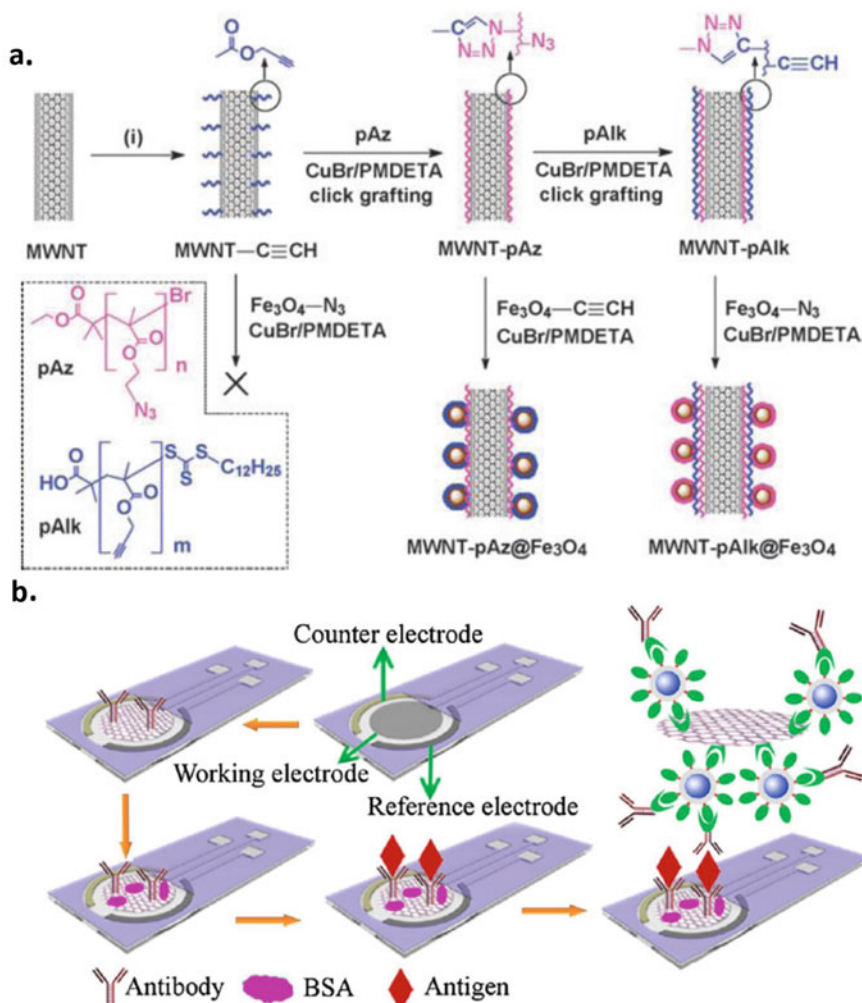


**Fig. 4** a–e Cartoonist illustration of DNA wrapped CNT modified PGE for guanine oxidation, Reprinted with permission Ozkan et al. [43], Copyright 2017 Talanta

for biomolecular immobilization. Another report involved different semiconductor nanomaterials (namely zinc sulfide, cadmium sulfide, lead sulfide, and copper sulfide) is employed for labeling of various proteins (namely microalbumin, IgG, C-reactive protein, bovine serum albumin) which have been used with carbon-based matrices. The positioning of the redox/electro-active peak and its current using stripping voltammetry, immobilization of enzymes were incorporated for mapping of proteins.

Metal nanoparticles have expanded wide consideration for expansion of non-enzymatic H<sub>2</sub>O<sub>2</sub> sensors due to their high stability on comparison of enzymatic sensors [116]. A major drawback is assemblage of Au-NP which bounds their performance in terms of detection limit. To overcome such problems, electrochemical sensor of electrodeposited gold nanoparticles on an ITO support with cobalt and manganese-based layer double hydroxide is quite sensitive for H<sub>2</sub>O<sub>2</sub> detection at –0.55 V versus Ag/AgCl [117]. An illustration using MWCNT with click magnetic nanohybrids is supported in Fig. 5 reprint from [7, 118] with copyright permission.

Porous noble nanostructures are essential alternates for sensing which are equally appealing with enhanced surface area having porous structures that facilitates both electron and mass transfers allowing fabrication of sensors with high sensitivities using carbon integrated electrodes [119]. The three-dimensional nanoporous gold films comprising of interlinked filaments and pores which can be easily obtained via de-alloying method.



**Fig. 5** **a** Synthetic procedure for click magnetic nanohybrids, Reprinted with permission Punetha et al. [7], Copyright 2017 Progress in Polymer Science. **b** Fabrication of disposable electrochemical sensor of cancer antigen 153 detection, Reprinted with permission Ge et al. [7, 118], Copyright 2014 Sensors and Actuators B

Layered double hydroxides or LDHs were first reported by *Indira* and *Kamath* in early 1994 for containing Co(II) and Ni(II) with Al(III) via cathodic reduction of nitrate ions and water for their preparation using polarization techniques [80, 120]. These films provide controlled thickness, homogeneously coating the surface. Ni LDH are quite popular for alcohol oxidation, polyhydric compound and amine oxidation wherein the modified electrodes exploit the electrocatalytic oxidation process occurring in the anodic potential range [72, 121].



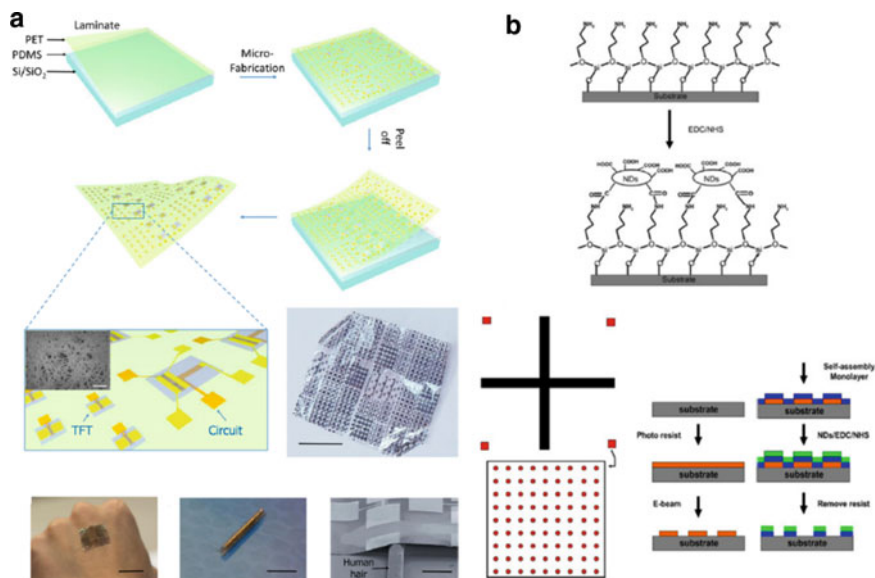
Transition metal nanoparticles such as Fe, Cu, Co, Ni, Mg make a prominent mark in the sensor domain, and a special comprehensive review has been published recently [122]. Extensively Cu-based metal oxide nanostructures with different morphologies on various electrodes enhance the charge transfer and device performance for oxidation of glucose in alkaline solution that helps to explore Cu as a redox mediator [123–125]. The size control can be achieved via electrolytic bath in presence of ethylene diamine from size range of 50–1000 nm [126].

## 5.5 Polymeric Films

Electrosynthesis of conductive polymers are also carried out via oxidation of a suitable monomer and can be referred to as “nanopolymers.” Especially, polythiophenes, polypyrroles and polyanilines belong to this approach. The induction of polymerization starts with anodic potential to form a radical cation followed by coupling of cations and proton elimination. The important/essential point is that higher the repetitive units, lower the oxidation potential will be. Further the soluble oligomers are generated in the diffusion layer owing to dimerization reactions. They precipitate on surface of electrode via nucleation and growth process. Later, the polymerization process can be performed via manipulating the potentiostatic and potentiodynamic approach. Characteristic cauliflower-like morphology is linked to electrosynthesis of conductive polymers [127].

Nanocauliflowers, nanovesicles, nanorods, and nanotubes are achieved by controlling the finely stated electrochemical constraints. Intriguing approach of using conducting polymer nanotubes in electronic circuits was stated in a report for template-free electrodeposition of Si with of L-camphosulfonic acid via template-free technique [128]. Their interface was exploited in terms of Schottky junction to detect m-hydroxybenzene due to variation in electrical conductivity. The nanonet-works can be achieved by manipulating natural oxygen evolution at anodic potentials. A report for the fabrication of methanol gas sensor using nanopolypyrrole film on the interdigital electrodes, in presence of perchlorate dopant has been published by Babaei and Alizadeh [129].

Molecularly imprinted polymers are another class that outperform biological receptors in terms of economic value, robustness and chemical inertness. They involve signal transduction through surface plasmon resonance with conjugation to quartz microbalance. A successful example is SnO<sub>2</sub> nanocrystal functionalized NM chemoresistive sensor for sensing of CH<sub>4</sub> gas with a least limit of 10 ppm with sensitivity of trace analytes. The reversible relative resistance was linked to extend of SiO<sub>2</sub> functionalization as no response was observed in case of unfunctionalized NM on multiwalled carbon nanotube platform [47]. A carbon nanotube-based electronic and nanodiamond SAM has been portrayed in Fig. 6 reprint from [43, 108] copyright permission.



**Fig. 6** **a** Imperceptible carbon nanotube macroelectronics, Reprinted with permission Cao et al. [96], Copyright 2016 ACS Nano. **b** Systematic functionalization of nanodiamonds to the SAM substrate and its template fabrication, Reprinted with permission Liu et al. [108], Copyright 2010 Nanoscale Research Letters

## 6 Domains of Application

Nanotechnology is one of the fundamentals of twenty-first century offering numerous benefits in development of various diagnostics and therapeutic systems that helps in welfare of mankind, including use of nanomaterials sized complying with many biological mechanisms in human body enabling nanoparticles to cross the biological barriers and enter the organs, tissues, and cells. Significant contributions of nanotechnology to clinic therapeutics are possible with nanoscale drug carriers. They offer efficient and safer delivery of drugs, providing longer circulation half-life, improved pharmacokinetics, increased drug exposure to target cells and reduced undesired side effects. Nanotechnology has offered preparation of nanomaterials especially trace minerals improving digestive efficiency, immunity, and performance for livestock and poultry [130, 131]. Due to brevity of the topic with reference to electrochemical nanomaterials applications, detailed information is tabulated to make it concise and crisp. The versatilities of few carbon nanomaterials with their arenas of exploration have been tabulated in Table 4.

**Table 4** Accounts various nanoparticles with their domain and use in accordance to its specificities

S. No.	Electrochemical nanomaterial platform	Domain application	Properties exhibited	Relevance of their system	References
1	PANI@GO	Food additive sensing (Clenbuterol hydrochloride)	Label-free sensing	Portable strip testing of food safety	[132]
2	MWCNT@PhOCH <sub>3</sub> -Redox	Environmental sensor (water testing)	Safe, speedy	Environmental toxic chromium (VI) sensing	[12]
3	MWCNT@H <sub>2</sub> Q	Energy based (ascorbic acid)	Green, efficient	Fuel cell applications	[11]
4	CB@Ses-Qn	Immunosensor	Label free, no false positive response	Disposable immunosensor (Penaacid Shrimp-Aquaculture Industry)	[133]
5	Pencil graphite electrode	Food quality testing	Microfluidic and multiplexed analysis	Tea quality testing, nanoquantity of sample	[115]

## 6.1 Protein Biomarker Detection

The development of nanotechnology for scaling up of novel nanostructured systems having exceptional presentation has been advanced, thereby provided that inclusive stage for expansion of enhanced performance output of biosensor with durability and obtaining reliable and reproducible signals [134]. They are preferably involved as: (i) a device suitable for direct attachment/bonding of biological moiety to accelerate the load concentration, thereby promoting its reactivity; (ii) as a protein or antibody/antigen biomarker deprived of impairing biomolecule activity. The target analyte concentration is based on the electro-analytical sensing of nanoscale systems and later employ amplification markers which can significantly enhance/increase the output signal to yield for redox-based immunosensor especially for ultrasensitive processes [135].

Use of nanoparticles has been a prominent approach in fields of biomedical and environmental research for recognition of pollutants, microorganisms (virus and bacteria), genetic diseases, etc. Potential applications for micro and nanotextured crystalline diamond surfaces for cochlear implant array electrodes have been reported by Cai [45]. They concluded that exclusive properties, i.e., antibacterial and electrical properties of nanocrystalline diamond, patterned surfaces are produced for generation of independent electrical stimulation signals in cochlear implants for neural population [45]. Bulk gold is good conductor while the nanogold exhibits strong adsorption and prominent biocompatibility that can be extended for immobilization of biomolecules that helps in supplying a defined atmosphere that effectively maintains activity of enzyme and other biological proteins. The carbon nanomaterials

are used in conjugation with other nanometals (AuNPs [33, 34], Au nanorods [35, 136], Au nanowires [36]) and so on portraying fascinating characteristics, owed to their advantage of simplicity, rapidity and defined stability [37, 137]. A low noise immunosensor is one of the important aspects targeted by medical technicians and one such system has been attempted involving indirect determination for reduction of p-nitrophenol to subsequent electro-active p-aminophenol using AuNPs-labeled 2° antibodies [138]. Another interesting report for AuNPs-MWCNT was used for antibody labeling for fabrication of a sandwich immunoassay. The report involved the cycling reaction phenomena for 4-nitrophenol, NaBH<sub>4</sub> and later thionine catalyzed system thereby allowing better detection limit and sensitivity with enhanced stability of electrode [38]. In continuation, p-methylmercaptobenzene (cross-linking agent) in conjugation of nanoporous gold was reported having high conductivity with larger surface area prepared by layer-by-layer self-assembly of gold and silver NPs on GCE surface. The base was well suitable for adsorption of thio-based molecules as Au-S is a strong bond due to electrostatic interaction that further enhances sensitivity of fabricated sensor on carbon electrode [139]. *Chen and his group* has worked on the storage stability of the fabricated sensor using a 3D-ordered Au nanoclusters using electrodeposition technique with spatial obstruction/direction of polycarbonate membrane as a sensor for detecting picloram [39]. Carbon NPs have interesting size and shape dependent physiological properties (inert material, vivid chemical reactivity which increases as a function of physical parameters like crystallinity, shape, size, dispersion, composition and morphology). Different chemical methods have been proposed for controlled size and shape of AuNPs. The electrochemical approach for nanometer scale preparation has some limitations and morphologies that can be realized and concerned. Electrochemical depositions are anchored to surface quite swiftly, without any expensive protocol involving chemical and binding agents, and are environmentally sustainable compared to ones produced via chemicals. Therefore, effective electrochemical methods are preferable for their deposition. Studies involved mechanisms of nucleation and crystal growth mechanisms of metal phase on conductive matrix such as GCE.

CNTs having conjugated systems and nucleobases are ideal for ribonucleic acid (RNA) and deoxyribonucleic acid (DNA) detection. They amplify the DNA/RNA ensuring signals due to their inherent conductivity and methods of amplification via addition of NPs and enzymes to strengthen the signal platform. *Li and Lee* reported improved detection limit value i.e., twice the D<sub>L</sub> limits for DNA mapping with reduction in fabrication times after incorporating *f*-MWNT [43] and reducing the use of mediator and extra experimental steps/layers. While *Zhang* described a simplistic and methodological construction using CNT-Fe<sub>3</sub>O<sub>4</sub> as a supporting probe for substrate for label-free impedimetric genosensor [44]. The need of gas sensing in industrial, environmental, and medical analysis both quantitatively and qualitatively is achieved by bulky instrumentation. But with the advent of CNTs, small-scale sensors which are less expensive have been accepted with established analytical instrumentations offering an interface with distinct advantages of sensitivity and reproducibility. *Dhall and Jaggi* established a CNT-hybrid composite for H<sub>2</sub> gas detection. They compared NiO<sub>2</sub>-Pt decorated MWCNTs to be more sensitive compared to Cu<sub>2</sub>O-Pt decorated

MWCNT hybrid composite systems [46]. Another report in the field of fuel cells for methanol generation has reported non-enzymatic graphitized mesoporous carbon-based system in pH 7 PBS for efficient incorporation of transducer complexes [13]. In addition to above, Yang and his colleagues equated the electrochemical properties to their biosensing performance for nanodiamond derived carbon nano-onions with three different carbon-based systems, i.e., MWCNT, graphene, and GCE. Overall, the nanodiamond derived nano-onions displayed interesting electrocatalytic activities including facile electron transfer kinetics and large oxidant current densities thus accommodating a set of potential for mapping redox-active molecules for preferable sensitivity at the material level [140].

Biosensors are an important research field with metal NP being largely used particularly when assisted on conductive materials [141]. These nanoconstituents behave as electrical wires display to establish a direct communication among the biocatalyst or the transducing element and the electrode via a thick insulating protein shell surrounding enzyme active sites. The major advancement can be accounted due to direct electron transfer or DET that have been initiated a wild fire among the research community. An example is cholesterol biosensor wherein AuNP was deposited on carbon electrodes (nanosystems) by tailoring its variables. Cholesterol oxidase was immobilized on the electrode for determination of cholesterol via use of efficient redox transducers, contributing high sensitivity and selectivity [119]. 3D macroporous Au was developed as an innovative tag-free biosensor using electrochemical impedance spectroscopy for mapping of C-reactive protein. The interconnected NPs exhibited 15 times larger surface compared to Au bulk electrodes and parallelly attributing linear increase in impedance values with C-protein concentration. Square wave voltammetric-based sensor was reported for the sensing of promyelocytic leukemia/retinoic acid receptor fusion genes using methylene blue as a probe [142].

## 7 Downside of Using These Carbon Systems

The choice of nanoparticles depends on the physicochemical characteristics, stability, labeling, study duration, analysis type, sample type, detailing, etc. All these attributes need careful planning and controls. Any misread information or assumptions can lead to wrong detailing or conclusion. Despite all the glaring prospects, they have a few bottlenecks and downside. Even this shortcoming has been conceived in their industrial scale production. The most common nanomaterial is graphene oxide which was initiated back in 1898 and has been considered as the most common resource itself and further its derivatives for numerous applications prospects. But its commercialization has been a challenge for scale-up processing.

Many different carbon nanomaterials are being processed together with other materials due to open demand. The other aspects of accessibility, costs, accuracy, resolution, complexity, toxicity, and procedure duration need special attention during the course of experimentation. The major constraint is the portability, reliability, reproducibility, and duplicability for nanodevices, as the sensing systems

are affected by the orientation, chirality, and minute properties. Hence, more appropriate estimates are required before potential commercialization. One of the significant concerns relating to NMs that cannot be overlooked is its pathogenicity and toxicity constraints, which is still poorly understood, and is a vital concern for environment, domestic, and industrial usage. The exact degree of cellular pathogenicity is unclear. There is a complete lacuna of knowledge in regard to this topic and hence needs efforts from the scientific community to bridge the gap between rapid development and in-vivo aftereffects. A proper and systematic understanding for the complete interaction with cells, tissues, and proteins is critical for the safe design and commercialization of nanotechnology.

Yet the positive points far exceed its downside, making it one of the ideal materials. Nevertheless, the exact potentials and its role could be further harnessed in the near future. New arenas for studying of electron transfer in biological systems, interfacial biology, and circuit technology can help in development of advanced portable devices for both mankind and environmental holistically.

## 8 Conclusion

This review gives a complete compilation of strategies based on electrochemical involvement of carbon-based nanosystems. The preceding sections account the special attention provided to nanomaterials, specifically carbon nanomaterials and its derivatives that can be justified by the enormous magnitude of publications describing their indistinct properties that could be tailored for precise applications. Carbon nanoparticles have undoubted uniqueness which is unmatched over conventional nanosystems. The impact of their usage is coupled with their electrochemical ability with enhanced surface area and antifouling capability. Adding to above, tunable methodologies for synthesis and functionalization that authors envision will consequence in increasing the count of electro-analytical implications uplifting multiple fields of interest especially for rapidity and sensitivity in medical and environmental analysis. Carbon nanomaterials give add on advantages such as wider potential window, exclusiveness, minimally invasive options, reversible redox systems and help in continuous monitoring of molecules without periodical cleaning.

Many advanced applications of using carbon nanomaterials in point-of-care systems have come up especially for improved HIV drug therapies, self-heatable devices, DNA-based single-electron fabricated set-ups, light-seeking synthetic nanorobots, brain-inspired artificial intelligence devices, super-powered bionic plant and many more. These support the futuristic vision of global scientific community. This review is a gist of the role of carbon nanoparticles that has attracted the attention of scientific domain from different walks of life. They have drawn remarkable attention of engineering, medical, science, condensed matter physics, drug discovery including both from academia and industry. Thus, emphasizing the focus on carbon nanomaterials including graphene, nanotubes, carbon black, nanopowder, mesoporous carbon, activated charcoal, nanofibers, etc., thereby undoubtedly promoting

the science of nanotechnology in an inestimable variety from domains of electronics, media, energy storage, optics, and health care. Their uniqueness is unrivalled by any other known material as compared in this review. Both innovative and improved carbon probes have displayed improved analytical performance over non-nanostructured point-of-care-based electrochemical counterparts. Electro-analytical biosensing materials as a promising platform to real-life analytical detection using CNTs and diamonds for a myriad of analytes. Many authors have anticipated that huge proportion of future will emphasize on discovery of bio-inspired novel hybrid chemical sensors that can be processed on flexible substrates.

**Acknowledgements** Mansi Gandhi thanks the Indian Council of Medical Research (ICMR) for the award of her SRF (2019-4952).

**Declaration of Competing Interest** We wish to confirm that there are no known conflicts of interest associated with this publication and there has been no significant.

## References

1. Bard AJ, Murray RW (2012) Electrochemistry. *Proc Natl Acad Sci USA* 109:11484–11486. <https://doi.org/10.1073/pnas.1209943109>
2. Campuzano S, Wang J (2011) Nanobioelectroanalysis based on carbon/inorganic hybrid nanoarchitectures. *Electroanalysis* 23:1289–1300. <https://doi.org/10.1002/elan.201100186>
3. Jiang S, Shi T, Zhan X et al (2015) Scalable fabrication of carbon-based MEMS/NEMS and their applications: a review. *J Micromech Microeng* 25:113001. <https://doi.org/10.1088/0960-1317/25/11/113001>
4. Llobet E (2013) Gas sensors using carbon nanomaterials: a review. *Sens Actuators, B Chem* 179:32–45. <https://doi.org/10.1016/j.snb.2012.11.014>
5. Dang VT, Nguyen DD, Cao TT et al (2016) Recent trends in preparation and application of carbon nanotube-graphene hybrid thin films. *Adv Nat Sci Nanosci Nanotechnol* 7. <https://doi.org/10.1088/2043-6262/7/3/033002>
6. Nardecchia S, Carriazo D, Ferrer ML et al (2013) Three dimensional macroporous architectures and aerogels built of carbon nanotubes and/or graphene: synthesis and applications. *Chem Soc Rev* 42:794–830. <https://doi.org/10.1039/c2cs35353a>
7. Punetha VD, Rana S, Yoo HJ et al (2017) Functionalization of carbon nanomaterials for advanced polymer nanocomposites: a comparison study between CNT and graphene. *Prog Polym Sci* 67:1–47. <https://doi.org/10.1016/j.progpolymsci.2016.12.010>
8. Bayda S, Adeel M, Tuccinardi T et al (2020) The history of nanoscience and nanotechnology: from chemical-physical applications to nanomedicine. *Molecules* 25:1–15. <https://doi.org/10.3390/molecules25010112>
9. Shrivastava S, Dash D (2009) Applying nanotechnology to human health: revolution in biomedical sciences. *J Nanotechnol* 2009:1–14. <https://doi.org/10.1155/2009/184702>
10. Gehrke I, Geiser A, Somborn-Schulz A (2015) Innovations in nanotechnology for water treatment. *Nanotechnol Sci Appl* 8. <https://doi.org/10.2147/NSA.S43773>
11. Gandhi M, Rajagopal D, Senthil Kumar A (2021) In-situ electro-organic conversion of lignocellulosic-biomass product-syringaldehyde to a MWCNT surface-confined hydroquinone electrocatalyst for biofuel cell and sensing of ascorbic acid applications. *Appl Surf Sci* 562:150158. <https://doi.org/10.1016/j.apsusc.2021.150158>

12. Gandhi M (2021) RSC Advances In situ electro-organic synthesis of hydroquinone using anisole on MWCNT/Na fi on modified electrode surface and its heterogeneous. 4062–4076. <https://doi.org/10.1039/d0ra10370e>
13. Saravanan N, Gandhi M, Senthil Kumar A (2020) High-valent ruthenium(IV)-oxo complex stabilized mesoporous carbon (graphitized)/nafion modified electrocatalyst for methanol oxidation reaction in neutral pH. *J Electroanal Chem* 874:114457. <https://doi.org/10.1016/j.jelechem.2020.114457>
14. Gandhi M, Amreen K (2022) ‘Electrochemical Profiling of Plants.’, *Electrochem* 3:434–450. <https://doi.org/10.3390/electrochem3030030>
15. Tite T, Chiticaru EA, Burns JS, Ioniță M (2019) Impact of nano-morphology, lattice defects and conductivity on the performance of graphene based electrochemical biosensors. *J Nanobiotechnology* 17:1–22. <https://doi.org/10.1186/s12951-019-0535-6>
16. Akbari E, Buntat Z, Ahmad MH et al (2014) Analytical calculation of sensing parameters on carbon nanotube based gas sensors. *Sensors (Switzerland)* 14:5502–5515. <https://doi.org/10.3390/s140305502>
17. Ali K, Hafez M (2013) Growth and structure of carbon nanotubes based novel catalyst for ultrafast nano-temperature sensor application. *Superlatt Microstruct* 54:1–6. <https://doi.org/10.1016/j.spmi.2012.10.007>
18. Lorestani F, Shahnavaz Z, Mn P et al (2015) One-step hydrothermal green synthesis of silver nanoparticle-carbon nanotube reduced-graphene oxide composite and its application as hydrogen peroxide sensor. *Sens Actuators, B Chem* 208:389–398. <https://doi.org/10.1016/j.snb.2014.11.074>
19. Lu HL, Lu CJ, Tian WC, Sheen HJ (2015) A vapor response mechanism study of surface-modified single-walled carbon nanotubes coated chemiresistors and quartz crystal microbalance sensor arrays. *Talanta* 131:467–474. <https://doi.org/10.1016/j.talanta.2014.08.027>
20. Zhang Q, Uchaker E, Candelaria SL, Cao G (2013) Nanomaterials for energy conversion and storage. *Chem Soc Rev* 42:3127–3171. <https://doi.org/10.1039/c3cs00009e>
21. Wang DW, Su D (2014) Heterogeneous nanocarbon materials for oxygen reduction reaction. *Energy Environ Sci* 7:576–591. <https://doi.org/10.1039/c3ee43463j>
22. Jariwala D, Sangwan VK, Lauhon LJ et al (2013) Carbon nanomaterials for electronics, optoelectronics, photovoltaics, and sensing. *Chem Soc Rev* 42:2824–2860. <https://doi.org/10.1039/c2cs35335k>
23. Park S, Vosguerichian M, Bao Z (2013) A review of fabrication and applications of carbon nanotube film-based flexible electronics. *Nanoscale* 5:1727–1752. <https://doi.org/10.1039/c3nr33560g>
24. Gandhi M, Rajagopal D, Senthil Kumar A (2021) In situ electro-organic synthesis of hydroquinone using anisole on MWCNT/Nafion modified electrode surface and its heterogeneous electrocatalytic reduction of toxic Cr(vi) species. *RSC Adv* 11:4062–4076. <https://doi.org/10.1039/d0ra10370e>
25. Zuo P, Wang R, Li F et al (2021) A trace ppb-level electrochemical H<sub>2</sub>S sensor based on ultrathin Pt nanotubes. *Talanta* 233:122539. <https://doi.org/10.1016/j.talanta.2021.122539>
26. Ndamaniha JC, Guo L (2012) Ordered mesoporous carbon for electrochemical sensing: a review. *Anal Chim Acta* 747:19–28. <https://doi.org/10.1016/j.aca.2012.08.032>
27. Holade Y, Canaff C, Poulin S et al (2016) High impact of the reducing agent on palladium nanomaterials: new insights from X-ray photoelectron spectroscopy and oxygen reduction reaction. *RSC Adv* 6:12627–12637. <https://doi.org/10.1039/c5ra24829a>
28. Jia H, Xu J, Lu L et al (2018) Three-dimensional Au nanoparticles/nano-poly(3,4-ethylene dioxythiophene)-graphene aerogel nanocomposite: a high-performance electrochemical immunosensing platform for prostate specific antigen detection. *Sens Actuators, B Chem* 260:990–997. <https://doi.org/10.1016/j.snb.2018.01.006>
29. Lyshevski SE, Martirosyan KS (2011) Ferrite nanoparticles for MEMS technology sensors and actuators. In: *Proceedings of IEEE conference on nanotechnology*, pp 1252–1256. <https://doi.org/10.1109/NANO.2011.6144379>



30. Gray BL (2014) New opportunities for polymer nanocomposites in microfluidics and biomedical MEMS: an introduction to cutting-edge composite polymer materials for use in microfluidics and biomedical MEMS. *IEEE Nanotechnol Mag* 8:6–16. <https://doi.org/10.1109/MNANO.2014.2309495>
31. Rajdi NNZM, Salleh SM, Bakir AA, et al (2013) Silver nanoparticles stamping for the production of fabrics-based bio-MEMS. In: *Proceedings 2013 international conference on robotics, biomimetics, and intelligent computational systems, ROBIONETICS 2013*, pp 10–14. <https://doi.org/10.1109/ROBIONETICS.2013.6743569>
32. Wu S, Huang F, Lan X et al (2013) Electrochemically reduced graphene oxide and Nafion nanocomposite for ultralow potential detection of organophosphate pesticide. *Sens Actuators, B Chem* 177:724–729. <https://doi.org/10.1016/j.snb.2012.11.069>
33. Peng MP, Ma W, Long YT (2015) Alcohol dehydrogenase-catalyzed gold nanoparticle seed-mediated growth allows reliable detection of disease biomarkers with the naked eye. *Anal Chem* 87:5891–5896. <https://doi.org/10.1021/acs.analchem.5b00287>
34. Luna DMN, Avelino KYPS, Cordeiro MT et al (2015) Electrochemical immunosensor for dengue virus serotypes based on 4-mercaptobenzoic acid modified gold nanoparticles on self-assembled cysteine monolayers. *Sens Actuators, B Chem* 220:565–572. <https://doi.org/10.1016/j.snb.2015.05.067>
35. Truong PL, Cao C, Park S et al (2011) A new method for non-labeling attomolar detection of diseases based on an individual gold nanorod immunosensor. *Lab Chip* 11:2591–2597. <https://doi.org/10.1039/c1lc20085b>
36. Ding Y, Li D, Li B et al (2013) A water-dispersible, ferrocene-tagged peptide nanowire for amplified electrochemical immunosensing. *Biosens Bioelectron* 48:281–286. <https://doi.org/10.1016/j.bios.2013.04.030>
37. Li J, Skeete Z, Shan S et al (2015) Surface enhanced Raman scattering detection of cancer biomarkers with bifunctional nanocomposite probes. *Anal Chem* 87:10698–10702. <https://doi.org/10.1021/acs.analchem.5b03456>
38. Tang J, Tang D, Su B et al (2011) Enzyme-free electrochemical immunoassay with catalytic reduction of p-nitrophenol and recycling of p-aminophenol using gold nanoparticles-coated carbon nanotubes as nanocatalysts. *Biosens Bioelectron* 26:3219–3226. <https://doi.org/10.1016/j.bios.2010.12.029>
39. Chen L, Zeng G, Zhang Y et al (2010) Trace detection of picloram using an electrochemical immunosensor based on three-dimensional gold nanoclusters. *Anal Biochem* 407:172–179. <https://doi.org/10.1016/j.ab.2010.08.001>
40. Wang H, Bai L, Chai Y, Yuan R (2014) Synthesis of multi-fullerenes encapsulated palladium nanocage, and its application in electrochemiluminescence immunosensors for the detection of streptococcus suis serotype 2. *Small* 10:1857–1865. <https://doi.org/10.1002/sml.201303594>
41. Liu X, Wang X, Zhang J et al (2012) Detection of estradiol at an electrochemical immunosensor with a Cu UPD/DTBP-Protein G scaffold. *Biosens Bioelectron* 35:56–62. <https://doi.org/10.1016/j.bios.2012.02.002>
42. Jiao L, Mu Z, Zhu C et al (2016) Graphene loaded bimetallic Au@Pt nanodendrites enhancing ultrasensitive electrochemical immunoassay of AFP. *Sens Actuators, B Chem* 231:513–519. <https://doi.org/10.1016/j.snb.2016.03.034>
43. Ozkan-Ariksoysal D, Kayran YU, Yilmaz FF et al (2017) DNA-wrapped multi-walled carbon nanotube modified electrochemical biosensor for the detection of *Escherichia coli* from real samples. *Talanta* 166:27–35. <https://doi.org/10.1016/j.talanta.2017.01.005>
44. Zhang W (2016) Application of Fe<sub>3</sub>O<sub>4</sub> nanoparticles functionalized carbon nanotubes for electrochemical sensing of DNA hybridization. *J Appl Electrochem* 46:559–566. <https://doi.org/10.1007/s10800-016-0952-2>
45. Cai Y, Edin F, Jin Z et al (2016) Strategy towards independent electrical stimulation from cochlear implants: guided auditory neuron growth on topographically modified nanocrystalline diamond. *Acta Biomater* 31:211–220. <https://doi.org/10.1016/j.actbio.2015.11.021>
46. Dhall S, Jaggi N (2016) Hydrogen gas sensing characteristics of multiwalled carbon nanotubes based hybrid composites. *J Electron Mater* 45:695–702. <https://doi.org/10.1007/s11664-015-4176-8>

47. Humayun MT, Divan R, Liu Y et al (2016) Novel chemoresistive CH<sub>4</sub> sensor with 10 ppm sensitivity based on multiwalled carbon nanotubes functionalized with SnO<sub>2</sub> nanocrystals. *J Vac Sci Technol A Vacuum, Surfaces, Film* 34:01A131. <https://doi.org/10.1116/1.4936384>
48. Power A., B. Gorey, S. Chandra JC (2011) Carbon nanomaterials and their application to electrochemical sensors
49. Paquin F, Rivnay J, Salleo A et al (2015) Multi-phase semicrystalline microstructures drive exciton dissociation in neat plastic semiconductors. *J Mater Chem C* 3:10715–10722. <https://doi.org/10.1039/b000000x>
50. Wang Z, Dai Z (2015) Carbon nanomaterial-based electrochemical biosensors: an overview. *Nanoscale* 7:6420–6431. <https://doi.org/10.1039/c5nr00585j>
51. Itkis ME, Pekker A, Tian X et al (2015) Networks of semiconducting SWNTs: contribution of midgap electronic states to the electrical transport. *Acc Chem Res* 48:2270–2279. <https://doi.org/10.1021/acs.accounts.5b00107>
52. Amreen K, Shukla VK, Shukla S et al (2017) Redox behaviour and surface-confinement of electro active species of ginger extract on graphitized mesoporous carbon surface and its copper complex for H<sub>2</sub>O<sub>2</sub> sensing. *Nano-Struct Nano-Objects* 11:56–64. <https://doi.org/10.1016/j.nanoso.2017.06.004>
53. Ogata AF, Edgar JM, Majumdar S et al (2017) Virus-enabled biosensor for human serum albumin. *Anal Chem* 89:1373–1381. <https://doi.org/10.1021/acs.analchem.6b04840>
54. Stanković V, Đurđić S, Ognjanović M et al (2020) Anti-human albumin monoclonal antibody immobilized on EDC-NHS functionalized carboxylic graphene/AuNPs composite as promising electrochemical HSA immunosensor. *J Electroanal Chem* 860:113928. <https://doi.org/10.1016/j.jelechem.2020.113928>
55. Omidfar K, Dehdast A, Zarei H et al (2011) Development of urinary albumin immunosensor based on colloidal AuNP and PVA. *Biosens Bioelectron* 26:4177–4183. <https://doi.org/10.1016/j.bios.2011.04.022>
56. Chuang YH, Chang YT, Liu KL et al (2011) Electrical impedimetric biosensors for liver function detection. *Biosens Bioelectron* 28:368–372. <https://doi.org/10.1016/j.bios.2011.07.049>
57. Shaikh MO, Chang LY, Chen CH et al (2018) Paper-based immunosensor utilizing dielectrophoretic trapping of microprobes for quantitative and label free detection using electrochemical impedance spectroscopy. *Biomicrofluidics* 12. <https://doi.org/10.1063/1.5057731>
58. Sadeghi S, Garmroodi A (2013) A highly sensitive and selective electrochemical sensor for determination of Cr(VI) in the presence of Cr(III) using modified multi-walled carbon nanotubes/querctetin screen-printed electrode. *Mater Sci Eng C* 33:4972–4977. <https://doi.org/10.1016/j.msec.2013.08.020>
59. Saladino R, Neri V, Mincione E, Filippone P (2002) Selective oxidation of phenol and anisole derivatives to quinones with hydrogen peroxide and polymer-supported methylrhenium trioxide systems. *Tetrahedron* 58:8493–8500. [https://doi.org/10.1016/S0040-4020\(02\)01025-6](https://doi.org/10.1016/S0040-4020(02)01025-6)
60. Caballero D, Martinez E, Bausells J et al (2012) Impedimetric immunosensor for human serum albumin detection on a direct aldehyde-functionalized silicon nitride surface. *Anal Chim Acta* 720:43–48. <https://doi.org/10.1016/j.aca.2012.01.031>
61. Tekoglu S (2018) Sustainable materials and process techniques for engineering solution-based organic light-emitting devices, 96–103
62. Lange A, Schindler W, Wegener M et al (2013) Inkjet printed solar cell active layers based on a novel, amorphous polymer. *J Nanosci Nanotechnol* 13:5209–5214. <https://doi.org/10.1166/jnn.2013.7500>
63. Das R, Chatterjee B, Kapil A, Sharma TK (2020) Aptamer-NanoZyme mediated sensing platform for the rapid detection of *Escherichia coli* in fruit juice. *Sens Bio-Sensing Res* 27:100313. <https://doi.org/10.1016/j.sbsr.2019.100313>
64. Gao X, Du C, Zhuang Z, Chen W (2016) Carbon quantum dot-based nanoprobe for metal ion detection. *J Mater Chem C* 4:6927–6945. <https://doi.org/10.1039/c6tc02055k>

65. Dutta R, Puzari P (2014) Amperometric biosensing of organophosphate and organocarbamate pesticides utilizing polypyrrole entrapped acetylcholinesterase electrode. *Biosens Bioelectron* 52:166–172. <https://doi.org/10.1016/j.bios.2013.08.050>
66. Jang J, Bae J, Choi M, Yoon SH (2005) Fabrication and characterization of polyaniline coated carbon nanofiber for supercapacitor. *Carbon NY* 43:2730–2736. <https://doi.org/10.1016/j.carbon.2005.05.039>
67. Li W, Liang C, Zhou W et al (2003) Preparation and characterization of multiwalled carbon nanotube-supported platinum for cathode catalysts of direct methanol fuel cells, pp 6292–6299
68. Rosolen JM, Tronto S, Marchesin MS et al (2006) Electron field emission from composite electrodes of carbon nanotubes-boron-doped diamond and carbon felts. *Appl Phys Lett* 88:50–53. <https://doi.org/10.1063/1.2178247>
69. Cioffi N, Colaianni L, Ieva E et al (2011) Electrosynthesis and characterization of gold nanoparticles for electronic capacitance sensing of pollutants. *Electrochim Acta* 56:3713–3720. <https://doi.org/10.1016/j.electacta.2010.12.105>
70. Domínguez-Domínguez S, Arias-Pardilla J, Berenguer-Murcia Á et al (2008) Electrochemical deposition of platinum nanoparticles on different carbon supports and conducting polymers. *J Appl Electrochem* 38:259–268. <https://doi.org/10.1007/s10800-007-9435-9>
71. Finot MO, Braybrook GD, McDermott MT (1999) Characterization of electrochemically deposited gold nanocrystals on glassy carbon electrodes. *J Electroanal Chem* 466:234–241. [https://doi.org/10.1016/S0022-0728\(99\)00154-0](https://doi.org/10.1016/S0022-0728(99)00154-0)
72. Scavetta E, Mignani A, Prandstraller D, Tonelli D (2007) Electrosynthesis of thin films of Ni, Al hydrotalcite like compounds. *Chem Mater* 19:4523–4529. <https://doi.org/10.1021/cm071132v>
73. Guo S, Wang L, Wang E (2007) Templateless, surfactantless, simple electrochemical route to rapid synthesis of diameter-controlled 3D flowerlike gold microstructure with “clean” surface. *Chem Commun* 3:3163–3165. <https://doi.org/10.1039/b705630c>
74. Theerthagiri J, Senthil RA, Arunachalam P et al (2017) Electrochemical deposition of carbon materials incorporated nickel sulfide composite as counter electrode for dye-sensitized solar cells. *Ionics (Kiel)* 23:1017–1025. <https://doi.org/10.1007/s11581-016-1885-9>
75. Murdoch HA, Limmer KR, Labukas JP (2017) Nanoarchitecture control enabled by ionic liquids. *Jom* 69:1034–1040. <https://doi.org/10.1007/s11837-017-2354-2>
76. Hu L, Song Y, Ge J et al (2017) Electrochemical deposition of carbon nanotubes from CO<sub>2</sub> in CaCl<sub>2</sub>-NaCl-based melts. *J Mater Chem A* 5:6219–6225. <https://doi.org/10.1039/c7ta00258k>
77. Liao HG, Jiang YX, Zhou ZY et al (2008) Shape-controlled synthesis of gold nanoparticles in deep eutectic solvents for studies of structure-functionality relationships in electrocatalysis. *Angew Chemie—Int Ed* 47:9100–9103. <https://doi.org/10.1002/anie.200803202>
78. Plugotarenko NK, Myasoedova TN, Grigoryev MN, Mikhailova TS (2019) Electrochemical deposition of silicon-carbon films: a study on the nucleation and growth mechanism. *Nanomaterials* 9:1–12. <https://doi.org/10.3390/nano9121754>
79. Senior NA, Newman RC (2006) Synthesis of tough nanoporous metals by controlled electrolytic dealloying. *Nanotechnology* 17:2311–2316. <https://doi.org/10.1088/0957-4484/17/9/040>
80. Dixit M, Vishnu Kamath P (1995) Electrosynthesis and stabilization of  $\alpha$ -cobalt hydroxide in the presence of trivalent cations. *J Power Sources* 56:97–100. [https://doi.org/10.1016/0378-7753\(95\)80015-9](https://doi.org/10.1016/0378-7753(95)80015-9)
81. Rahman TS, Abello L, Genet F, Nigretto JM (1988) A290 surface enhanced Raman spectra on a silver electrode of Methionini combination study on the electrochemical growth mechanism and structure of gold overlayers. In: A quantitative approach to electrochemical metal surface roughening and direct measurements, pp 290–291
82. Idris AO, Mabuba N, Arotiba OA (2017) Electrochemical co-detection of arsenic and selenium on a glassy carbon electrode modified with gold nanoparticles. *Int J Electrochem Sci* 12:10–21. <https://doi.org/10.20964/2017.01.30>

83. Schneider JR, Chadee DD, Mori A, Jeanne Romero-Severson DWS (2008) 基因的改变 NIH public access. *Bone* 23:1–7
84. Kong L, Chen W (2014) Carbon nanotube and graphene-based bioinspired electrochemical actuators. *Adv Mater* 26:1025–1043. <https://doi.org/10.1002/adma.201303432>
85. Michardière AS, Mateo-Mateo C, Derré A et al (2016) Carbon nanotube microfiber actuators with reduced stress relaxation. *J Phys Chem C* 120:6851–6858. <https://doi.org/10.1021/acs.jpcc.5b12673>
86. Palmre V, Torop J, Arulepp M et al (2012) Impact of carbon nanotube additives on carbide-derived carbon-based electroactive polymer actuators. *Carbon NY* 50:4351–4358. <https://doi.org/10.1016/j.carbon.2012.04.071>
87. Xie X, Qu L, Zhou C et al (2010) An asymmetrically surface-modified graphene film electrochemical actuator. *ACS Nano* 4:6050–6054. <https://doi.org/10.1021/nn101563x>
88. Marega R, De Leo F, Pineux F et al (2013) Functionalized Fe-filled multiwalled carbon nanotubes as multifunctional scaffolds for magnetization of cancer cells. *Adv Funct Mater* 23:3173–3184. <https://doi.org/10.1002/adfm.201202898>
89. Göbel G, Dietz T, Lisdat F (2010) Bienzyme sensor based on an oxygen reducing bilirubin oxidase electrode. *Electroanalysis* 22:1581–1585. <https://doi.org/10.1002/elan.200900540>
90. Guinovart T, Parrilla M, Crespo GA et al (2013) Potentiometric sensors using cotton yarns, carbon nanotubes and polymeric membranes. *Analyst* 138:5208–5215. <https://doi.org/10.1039/c3an00710c>
91. Kumar VR, Majumder MK, Alam A et al (2015) Stability and delay analysis of multi-layered GNR and multi-walled CNT interconnects. *J Comput Electron* 14:611–618. <https://doi.org/10.1007/s10825-015-0691-3>
92. Mustonen K, Laiho P, Kaskela A et al (2015) Uncovering the ultimate performance of single-walled carbon nanotube films as transparent conductors. *Appl Phys Lett* 107:1–6. <https://doi.org/10.1063/1.4932942>
93. Stan F, Sandu L, Fetecau C (2015) Investigation on the effect of carbon nanotubes concentration on the electrical and rheological properties of PP/MWCNTs composites. In: ASME 2015 international manufacturing science and engineering conference, MSEC 2015, vol 1, pp 1–10. <https://doi.org/10.1115/MSEC20159411>
94. Garel J, Zhao C, Popovitz-Biro R et al (2014) BCN nanotubes as highly sensitive torsional electromechanical transducers. *Nano Lett* 14:6132–6137. <https://doi.org/10.1021/nl502161h>
95. Zang X, Zhou Q, Chang J et al (2015) Graphene and carbon nanotube (CNT) in MEMS/NEMS applications. *Microelectron Eng* 132:192–206. <https://doi.org/10.1016/j.mee.2014.10.023>
96. Cao X, Cao Y, Zhou C (2016) Imperceptible and ultraflexible p-type transistors and macro-electronics based on carbon nanotubes. *ACS Nano* 10:199–206. <https://doi.org/10.1021/acs.nano.5b02847>
97. Chen K, Gao W, Emaminejad S et al (2016) Printed carbon nanotube electronics and sensor systems. *Adv Mater* 28:4397–4414. <https://doi.org/10.1002/adma.201504958>
98. Vishnu N, Kumar AS (2016) Intrinsic iron-containing multiwalled carbon nanotubes as electro-fenton catalyst for the conversion of benzene to redox-active surface-confined quinones. *ChemElectroChem* 3:986–992. <https://doi.org/10.1002/celec.201600052>
99. Lyons MEG, Keeley GP (2008) Carbon nanotube based modified electrode biosensors. Part 1. Electrochemical studies of the flavin group redox kinetics at SWCNT/glucose oxidase composite modified electrodes. *Int J Electrochem Sci* 3:819–853
100. Chandra S, Miller AD, Bendavid A et al (2014) Minimizing fouling at hydrogenated conical-tip carbon electrodes during dopamine detection in vivo. *Anal Chem* 86:2443–2450. <https://doi.org/10.1021/ac403283t>
101. Ata S, Yamada T, Hata K (2017) Relationship between primary structure and hansen solubility parameter of carbon nanotubes. *J Nanosci Nanotechnol* 17:3310–3315. <https://doi.org/10.1166/jnn.2017.13080>
102. TermehYousefi A, Bagheri S, Shahnazari S et al (2016) Computational local stiffness analysis of biological cell: high aspect ratio single wall carbon nanotube tip. *Mater Sci Eng C* 59:636–642. <https://doi.org/10.1016/j.msec.2015.10.041>

103. Choi J, Park BC, Ahn SJ et al (2016) Evaluation of carbon nanotube probes in critical dimension atomic force microscopes. *J Micro/Nanolithography, MEMS, MOEMS* 15:34005. <https://doi.org/10.1117/1.jmm.15.3.034005>
104. Silva TA, Zanin H, May PW et al (2014) Electrochemical performance of porous diamond-like carbon electrodes for sensing hormones, neurotransmitters, and endocrine disruptors. *ACS Appl Mater Interfaces* 6:21086–21092. <https://doi.org/10.1021/am505928j>
105. Bai L, Wen D, Yin J et al (2012) Carbon nanotubes-ionic liquid nanocomposites sensing platform for NADH oxidation and oxygen, glucose detection in blood. *Talanta* 91:110–115. <https://doi.org/10.1016/j.talanta.2012.01.027>
106. Domonkos M, Izak T, Stolcova L et al (2014) Fabrication of periodically ordered diamond nanostructures by microsphere lithography. *Phys Status Solidi Basic Res* 251:2587–2592. <https://doi.org/10.1002/pssb.201451172>
107. Kromka A, Izak T, Davydova BRM (2016) Nanocrystalline diamond films for electronic monitoring of gas and organic molecules. In: *ASDAM 2016 International conference on advanced semiconductor devices and microsystems*, pp 193–199
108. Liu YL, Sun KW (2010) Protein functionalized nanodiamond arrays. *Nanoscale Res Lett* 5:1045–1050. <https://doi.org/10.1007/s11671-010-9600-7>
109. Cimen D, Caykara T (2015) Micro-patterned polymer brushes by a combination of photolithography and interface-mediated RAFT polymerization for DNA hybridization. *Polym Chem* 6:6812–6818. <https://doi.org/10.1039/c5py00923e>
110. Lokhande CD, Dubal DP, Joo OS (2011) Metal oxide thin film based supercapacitors. *Curr Appl Phys* 11:255–270. <https://doi.org/10.1016/j.cap.2010.12.001>
111. Nemanich RJ, Carlisle JA, Hirata A, Haenen K (2014) CVD diamond—research, applications, and challenges. *MRS Bull* 39:490–494. <https://doi.org/10.1557/mrs.2014.97>
112. Roeser J, Alting NFA, Permentier HP et al (2013) Boron-doped diamond electrodes for the electrochemical oxidation and cleavage of peptides. *Anal Chem* 85:6626–6632. <https://doi.org/10.1021/ac303795c>
113. Petrakova V, Benson V, Buncek M et al (2016) Imaging of transfection and intracellular release of intact, non-labeled DNA using fluorescent nanodiamonds. *Nanoscale* 8:12002–12012. <https://doi.org/10.1039/c6nr00610h>
114. Vishnu N, Gandhi M, Rajagopal D, Kumar AS (2017) Pencil graphite as an elegant electrochemical sensor for separation-free and simultaneous sensing of hypoxanthine, xanthine and uric acid in fish samples. *Anal Methods* 9:2265–2274. <https://doi.org/10.1039/c7ay00445a>
115. Vishnu N, Gandhi M, Badhulika S, Kumar AS (2018) Tea quality testing using 6B pencil lead as an electrochemical sensor. *Anal Methods* 10:2327–2336. <https://doi.org/10.1039/c8ay00557e>
116. Guadagnini L, Ballarin B, Tonelli D (2013) Dendritic silver nanostructures obtained via one-step electro-synthesis: effect of nonanesulfonic acid and polyvinylpyrrolidone as additives on the analytical performance for hydrogen peroxide sensing. *J Nanoparticle Res* 15. <https://doi.org/10.1007/s11051-013-1971-0>
117. Xu L, Lian M, Chen X et al (2017) Amperometric sensing of hydrogen peroxide via an ITO electrode modified with gold nanoparticles electrodeposited on a CoMn-layered double hydroxide. *Microchim Acta* 184:3989–3996. <https://doi.org/10.1007/s00604-017-2428-4>
118. Ge S, Sun M, Liu W et al (2014) Disposable electrochemical immunosensor based on peroxidase-like magnetic silica-graphene oxide composites for detection of cancer antigen 153. *Sens Actuators, B Chem* 192:317–326. <https://doi.org/10.1016/j.snb.2013.10.127>
119. Sharma D, Lee J, Seo J, Shin H (2017) Development of a sensitive electrochemical enzymatic reaction-based cholesterol biosensor using nano-sized carbon interdigitated electrodes decorated with gold nanoparticles. *Sensors (Switzerland)* 17. <https://doi.org/10.3390/s17092128>
120. Indira L, Vishnu Kamath P (1994) Electrogeneration of base by cathodic reduction of anions: novel one-step route to unary and layered double hydroxides (LDHs). *J Mater Chem* 4:1487–1490. <https://doi.org/10.1039/jm9940401487>

121. Carpani I, Tonelli D (2006) Electrooxidation of aliphatic and aromatic amines at a Ni, Al based hydrotalcite modified electrode. *Electroanalysis* 18:2421–2425. <https://doi.org/10.1002/elan.200603696>
122. George JM, Antony A, Mathew B (2018) Metal oxide nanoparticles in electrochemical sensing and biosensing: a review. *Microchim Acta* 185. <https://doi.org/10.1007/s00604-018-2894-3>
123. Yang J, Jiang LC, De ZW, Gunasekaran S (2010) A highly sensitive non-enzymatic glucose sensor based on a simple two-step electrodeposition of cupric oxide (CuO) nanoparticles onto multi-walled carbon nanotube arrays. *Talanta* 82:25–33. <https://doi.org/10.1016/j.talanta.2010.03.047>
124. Quoc Dung N, Patil D, Jung H, Kim D (2013) A high-performance nonenzymatic glucose sensor made of CuO-SWCNT nanocomposites. *Biosens Bioelectron* 42:280–286. <https://doi.org/10.1016/j.bios.2012.10.044>
125. Yang Q, Long M, Tan L et al (2015) Helical TiO<sub>2</sub> nanotube arrays modified by Cu-Cu<sub>2</sub>O with ultrahigh sensitivity for the nonenzymatic electro-oxidation of glucose. *ACS Appl Mater Interfaces* 7:12719–12730. <https://doi.org/10.1021/acsami.5b03401>
126. Lan T, Fallatah A, Suiter E, Padalkar S (2017) Size controlled copper (I) oxide nanoparticles influence sensitivity of glucose biosensor. *Sensors (Switzerland)* 17. <https://doi.org/10.3390/s17091944>
127. Ma M, Qu L, Shi G (2005) Glucose oxidase electrodes based on microstructured polypyrrole films. *J Appl Polym Sci* 98:2550–2554. <https://doi.org/10.1002/app.22455>
128. Ameen S, Akhtar MS, Seo HK, Shin HS (2015) High sensitivity Schottky junction diode based on monolithically grown aligned polypyrrole nanofibers: broad range detection of m-dihydroxybenzene. *Anal Chim Acta* 886:165–174. <https://doi.org/10.1016/j.aca.2015.05.038>
129. Babaei M, Alizadeh N (2013) Methanol selective gas sensor based on nano-structured conducting polypyrrole prepared by electrochemically on interdigital electrodes for biodiesel analysis. *Sens Actuators, B Chem* 183:617–626. <https://doi.org/10.1016/j.snb.2013.04.045>
130. Hao Y, Wang Y, Ma C et al (2019) Carbon nanomaterials induce residue degradation and increase methane production from livestock manure in an anaerobic digestion system. *J Clean Prod* 240:118257. <https://doi.org/10.1016/j.jclepro.2019.118257>
131. Sarathi Swain P, Prusty S, Bala Nageswara Rao S et al (2021) Essential nanominerals and other nanomaterials in poultry nutrition and production. *Adv Poult Nutr Res*. <https://doi.org/10.5772/intechopen.96013>
132. Shi Z, Tian Y, Wu X et al (2015) A one-piece lateral flow impedimetric test strip for label-free clenbuterol detection. *Anal Methods* 7:4957–4964. <https://doi.org/10.1039/c5ay00706b>
133. Gandhi M, Rajagopal D, Parthasarathy S et al (2018) In situ immobilized sesamol-quinone/carbon nanoblack-based electrochemical redox platform for efficient bioelectrocatalytic and immunosensor applications. *ACS Omega* 3:10823–10835. <https://doi.org/10.1021/acsomega.8b01296>
134. Guo S, Dong S (2009) Biomolecule-nanoparticle hybrids for electrochemical biosensors. *TrAC—Trends Anal Chem* 28:96–109. <https://doi.org/10.1016/j.trac.2008.10.014>
135. Wang F, Hu S (2009) Electrochemical sensors based on metal and semiconductor nanoparticles. *Microchim Acta* 165:1–22. <https://doi.org/10.1007/s00604-009-0136-4>
136. Cao J, Sun T, Grattan KTV (2014) Gold nanorod-based localized surface plasmon resonance biosensors: a review. *Sens Actuators, B Chem* 195:332–351. <https://doi.org/10.1016/j.snb.2014.01.056>
137. AHIRWAL GK, MITRA CK (2010) Gold nanoparticles based sandwich electrochemical immunosensor. *Biosens Bioelectron* 25:2016–2020. <https://doi.org/10.1016/j.bios.2010.01.029>
138. Das J, Aziz MA, Yang H (2006) A nanocatalyst-based assay for proteins: DNA-free ultrasensitive electrochemical detection using catalytic reduction of p-nitrophenol by gold-nanoparticle labels. *J Am Chem Soc* 128:16022–16023. <https://doi.org/10.1021/ja0672167>
139. Sun X, Ma Z (2013) Electrochemical immunosensor based on nanoporous gold loading thionine for carcinoembryonic antigen. *Anal Chim Acta* 780:95–100. <https://doi.org/10.1016/j.aca.2013.04.023>

140. Dai W, Li M, Gao S et al (2016) Fabrication of nickel/nanodiamond/boron-doped diamond electrode for non-enzymatic glucose biosensor. *Electrochim Acta* 187:413–421. <https://doi.org/10.1016/j.electacta.2015.11.085>
141. White RJ, Luque R, Budarin VL et al (2009) Supported metal nanoparticles on porous materials. Methods and applications. *Chem Soc Rev* 38:481–494. <https://doi.org/10.1039/b802654h>
142. Zhong G, Liu A, Chen X et al (2011) Electrochemical biosensor based on nanoporous gold electrode for detection of PML/RAR $\alpha$  fusion gene. *Biosens Bioelectron* 26:3812–3817. <https://doi.org/10.1016/j.bios.2011.02.039>

# Chapter 38

## Carbon Nanomaterial-Based Biosensors: A Forthcoming Future for Clinical Diagnostics



Neha Saini, Prem Pandey, Shashwati Wankar, Mandar Shirolkar,  
Anjali A. Kulkarni, Jang Ah Kim, Taesung Kim, and Atul Kulkarni

### 1 Introduction

Biosensors are becoming ubiquitous in today's rapidly growing concept of non-invasive, early, ultrasensitive diagnosis, and evolution of robust sensing platforms [10, 89]. Sensors are the analytical devices which converts the physical, chemical, or biological fluctuations into a measurable signal [65]. Assisted with the specific recognition element (it responds for the respective analytes in any given samples, reducing the hindrance from unwanted components), transducer/detector for signal production and occasionally, a signal processor to collect and amplify displays the readable signals [65]. Biosensors are the sensors with a combination of bioreceptor component (biorecognition element; BRE) and transducer element to detect and quantify target analytes. The enhanced sensitivity of biosensors is furnished by selective binding of BRE such as bio-enzymes, tissues, cells, immunoglobulins, deoxy ribonucleic acid (DNA) and ribonucleic acid (RNA), aptamers. Signals are generated in the form

---

N. Saini · P. Pandey · S. Wankar · M. Shirolkar · A. Kulkarni (✉)  
Symbiosis Centre for Nanoscience and Nanotechnology, Symbiosis International (Deemed  
University), Pune, India  
e-mail: [atul.kulkarni@snn.edu.in](mailto:atul.kulkarni@snn.edu.in)

A. A. Kulkarni  
Department of Botany, Savitribai Phule Pune University (Formerly University of Pune), Pune,  
India

J. A. Kim  
Department of Materials, Imperial College London, London, UK

T. Kim (✉)  
Nano Particles Technology Laboratory, School of Mechanical Engineering, Sungkyunkwan  
University, Suwon, South Korea  
e-mail: [tkim@skku.edu](mailto:tkim@skku.edu)



of change in heat, light, mass change, pH change, after interaction between bioreceptor and target analyte and are termed as biorecognition. The growing reliability, repeatability, specificity, and sensitivity of biosensors can be exploited in a substantial capacity to provide direct, minimally invasive, and precise detection of various diseases [10, 89]. Although the biosensors is quite naïve domain, the genesis of biosensors dates back to “1906 by Max Cremer”. Cremer was the first to establish the direct proportionality between acid concentration in a liquid and electric potential arising between parts of the fluid located on opposite sides of a glass membrane. However, “Leland L. Clark Jr.” was the first to invent a “biosensor” to gauge oxygen levels in blood by combining the enzyme glucose oxidase with an amperometric oxygen electrode [29] in 1956. The original “Clark’s Electrode” is still the most effective and widely used electrode for glucose monitoring even in contemporary times.

Nanotechnology has been extensively applied in sensor development and diversification. Reduction in size of biosensors (miniaturization) to micro- or nanoscale leads to better signal-to-noise ratio, increases active sensing area ratio, requires less sample volume, thereby reducing assay cost considerably. Incorporation of nanomaterials also reduces non-specific binding and increases binding efficiency towards target biomarkers, making possible detection of single-molecules, thus acting as molecular enrichers [80]. The development of nanoprobables has perhaps revolutionized the field of biosensors in the last few decades [80]. The emergence of carbon nanomaterials (CNMs) such as graphene, graphene oxide, quantum dots (QDs), single-walled carbon nanotubes (SWCNTs) and multi-walled carbon nanotubes (MWCNTs), carbon nanowires, fullerene has opened new frontiers in the field of biosensors. Carbon-based nanoprobables exhibit exceptional opto-electric and optical properties, making them extremely suitable and effectual in biosensor [54]. In this chapter, we will review the sensing properties of different forms of CNMs-based electrochemical (EC) and optical biosensors. We will also summarize the applications, limitations, and advantages of CNMs in various hybridization and dimensional forms and their emerging applicability in the clinical diagnostics, biosensor innovations, and future prospects.

## 2 Fundamentals of Biosensors

Quantification of biochemical and physiological fluctuations is the foremost step for early diagnosis of human ailments. Analysis of these changes requires some type of sensors either chemical or biological. Thus, biosensors are the analytical devices which convert these changes into digital or readable signals [29]. Various analysis methods are utilized for detection of the analytes; however, in this chapter, our main emphasis will be on two main transduction methods, i.e. electrochemical and optical. Electrochemical (EC) biosensors are the chemical sensors which combine the high sensitivity of EC transducers or electro-analytical methods and inherently high specificity of biological recognition elements (BRE). Binding of BRE with the analytes

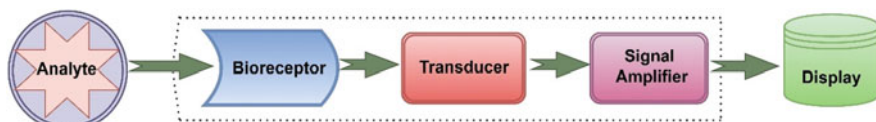
produces the signal that in turn is recognized by transducer. These electric signals produced are directly proportional to the amount/concentration of analyte present in the sample [65], while the optical biosensors provide the benefit of non-contact diagnosis and are non-invasive. The need of hour is to develop reliable, economic, and sensitive biosensors for early diagnosis of various deadly diseases such as cancer, cardiovascular disease. These tools should be effective at ultra-low concentration detection of disease biomarker/analyte [53].

## 2.1 Components of Biosensors

The biosensor devices have four elements which are essential for quantification, analysis, and conversion of signals to readable form. However, two principal components of biosensors are bioreceptor and transducers [43]. It includes: bioreceptor/BRE, transducer, amplifier/electric element, and display. A typical biosensors' structural components are illustrated in Fig. 1. These components are individually described in the following sub-sections.

### 2.1.1 Bioreceptor/Biorecognition Elements (BRE)

Specific sequestration of target analyte is the main focus of biosensors. Biomolecules which specifically recognize the target analytes are frequently used as bioreceptors. Till date, enzymes and antibodies are the most substantially used bioreceptor molecules. However, other natural and synthetic bioreceptors are also available. Synthetic receptors mimic the functionality of natural bioreceptors and provide improved affinity. The biorecognition element (BRE) is the core of a biosensor for exclusively targeting the capture of the analyte. The inherent complementarity between functional groups of the bioreceptor and analyte is the key attribute to consider when selecting a BRE [52]. Being an integral part of the biosensor devices, BRE and its types will be discussed in a separate upcoming section of this chapter.



**Fig. 1** Components of a typical biosensor

### **2.1.2 Transducer**

A transducer is the second most important component of a biosensor. The conversion of energy and unreadable signals to readable signal is the main function of the transducer. The biochemical signal generated upon reaction between the analyte and BRE is converted into quantifiable optical, electrochemical, or piezo-electrical signal by a transducer [10]. Optical transducers convert biochemical signals into visible readouts, while EC transducers are based on detection of electrochemical changes such as redox conc. of ions. The signals generated can be easily correlated to the analyte concentration in the system. The key factors for choosing a transducer are its range of detection and reaction time.

### **2.1.3 Amplifier**

The electronic component of the biosensor that interprets the transduced signal and prepares it for display is called an amplifier. It captures the signal generated by the transducer, amplifies it, and transmits it to the display unit.

### **2.1.4 Display**

It is a combination of hardware and software, user-friendly interface that generates the results of the biosensor and displays them over a screen, e.g. Computer monitor, smart-phone, etc.

## ***2.2 Bioreceptor/Biorecognition Elements (BRE)***

BRE is an integral part of biosensors for exclusively capturing the analyte. The inherent complementarity between functional groups of the bioreceptor and analyte is the key attribute to consider when selecting a BRE [52]. Several classes of BREs exist, such as natural, pseudo-natural, and synthetic [52]. This diversified classification of BREs provides a plethora of different structures and complementary functional group assortment while selecting a BRE specific for the analyte. BRE can be classified in the following categories [9, 52].

### **2.2.1 Natural BREs**

It includes enzymes, antibodies, nucleic acids, etc.

Enzymes are bio-catalysts that accelerate biological and biochemical reactions, mostly protein molecules with 3D structures that bind to substrate molecules and convert them into smaller molecules called products. Enzymes bind their substrates

by a typical “lock and key” binding mechanism using hydrogen bonding, electrostatic binding, and other non-covalent interactions [90]. Enzymes exhibit structural as well as chemical specificity towards their target analyte, and this makes them very popular BRE. Nanoenzymes or nanozymes are often embedded within the surface structures of the biosensors, allowing the formation of short diffusion pathways for target recognition and transduction [27]. Enzymatic sensors are thus simple, sensitive, low LOD, and cost-effective.

Antibodies or immunoglobulins are protein molecules that bind to the target antigens and are an integral part of the immune system. It has a Y-shaped 3D conformation with heavy and light chains responsible for the recognition and capture of pathogens. Antibody BREs are typically affinity based, and the event of biorecognition is triggered by antigen–antibody binding and formation of Ag-Ab immunocomplex [17]. Although antibodies show specificity, they may still experience cross-reactivity with antigens of the same class, exhibiting similar surface functionalities [50]. To overcome this hitch, monoclonal antibodies may be used. Monoclonal Abs are yet another class of antibodies that are synthesized to recognize a single epitope or a very specific biomarker of the target. Their storage is expensive limiting its use. However, due to their ultrasensitive recognition capabilities, they are still a very popular choice as a BRE.

Another natural BRE is nucleic acid (NA), and the sensor having NA as BRE is called as genosensors. The complementary binding motifs of DNA recognize target analytes and can be bio-engineered for specific targets [44]. Nucleic acid BREs also include locked nucleic acids (LNAs) and peptide nucleic acids (PNAs) [25]. LNA and PNA are synthetic oligonucleotides, which recognize highly charged target molecules. The signal responses generated by their binding are free of noise and are greatly used in spectroscopic analysis, making them ideal as BRE [76].

### 2.2.2 Pseudo-Natural or Semi-Synthetic BREs: Aptamers

Aptamers are small, single-stranded oligonucleotides (< 100 bases), non-traditional, pseudo-natural BRE famous for its wide target selection range such as metal ions, environmental pollutants, pathogens, small targets, proteins, and even whole cells [89]. Aptamers may be classified as oligonucleotide (ssDNA and RNA) aptamers and peptide aptamers [19]. Aptamers have great potential for use as novel antibodies in cancer theranostics, bioimaging, and biomedical research.

### 2.2.3 Synthetic BREs: Molecularly Imprinted Polymers

BRE with high selectivity and long-term stability is highly desirable for sensor developments. These sensory materials are able to enrich and rapidly detect pathogens by using a synthetic recognition element. Molecularly imprinted polymers (MIPs) are frequently used as alternative to natural receptors in sensors due to their low cost, robustness, and reproducibility [59].

### 2.3 Optical Techniques

In this chapter, we are focusing on two major optical techniques for biosensor applications. These are.

#### 2.3.1 Surface Plasmon Resonance (SPR)

SPR is the electromagnetic property due to collective oscillations of the free electrons in metal-dielectric interfaces under the electromagnetic field. The changes in refractive indices are monitored in SPR optical spectroscopy [26]. These changes are either in form of a shift in the resonant wavelength or in resonance angle of the incident light [10, 40]. SPR-based sensors work on the detection of this change in either the angle or the shift in the resonant wavelength. Both these principles are widely applied because of the ease of detection and their cost-effectivity [58]. The graphical representation of SPR as a surface sensing tool is illustrated in Fig. 2.

Most metals exhibit SPR in the visible region [58]. Although the sensing profile of metals is quite impressive, a major limitation to metal nanolayers is not being able to provide the desired sensitivity and optical enhancement properties [66]. In recent years, carbon nanostructures are emerging as the most extensively used class of nanoparticles in optical biosensing technique [30]. The variable nature of carbon structures bestows them unique electrical and thermal conductivities and exceptional optical properties, making them very attractive as biosensing materials [31].

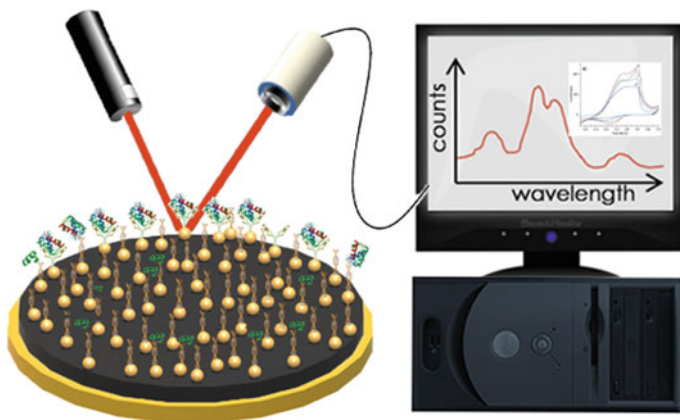


Fig. 2 Graphical illustration of surface plasmon resonance (SPR) technique

### 2.3.2 Surface-Enhanced Raman Spectroscopy/scattering (SERS)

SERS is a derivative of the Raman scattering effect. When light hits certain materials, some photon packets get transmitted, some reflected, and some get scattered. When there is change in energy and direction of scattered photons, it is called Raman scattering. Raman spectroscopy is based on the measurement of Raman scattering [68]. It is a powerful tool in chemistry and solid-state physics and plays an important role in the surface characterization of novel nanoparticles [87]. SERS is a surface-sensitive phenomenon that enhances Raman scattering effect of the molecular adsorption on rough metal surfaces or nanomaterials, such as magnetic nanomaterials, CNTs [85]. CNMs have garnered significant interest as highly active SERS materials. The 2D and 3D CNMs have been in conjugation with noble metal nanoparticles such as gold nanoparticles to be used as enhanced nanoprobe to detect certain bio-analyte. Shape and size of the nanoparticles have a substantial effect on the signal strength, absorption ratio, and enhancement factor in SERS [60]. Such techniques have tremendous application potential in the fields of biosensors, theranostics, point-of-care (POC) device development, etc. [5, 39].

## 2.4 Electrochemical Analysis

Electrochemical analysis includes the techniques in which analysis of the chemical reactivity of the solution/compound, i.e. rate of oxidation and reduction and is performed under the applied electrical stimulation via electrodes in a standard electrolyte. Alongside, being a surface technology electrochemistry has many advantages in biosensor field. Numerous electrochemical analyses methods are used for the biosensor's application. Electrochemical analysis is usually done on the basis of three main measurement methods (current/I, potential/V, impedance/Z). Our primary focus is based on the mode of transduction/measurement technique of I and V because it is the most commonly used techniques; such methods are [65] described as follows.

### 2.4.1 Amperometry

In this method, a constant V is applied to working electrode (WE) and the I produced due to electrolysis is measured, similar to voltammetry [29, 77]. The only difference from voltammetry is absence of scanning potential range, and V is directly stepped (or kept constant) to desired value. The current measured is proportional to the concentration of electroactive analyte in the solution. Amperometric analysis is done with bio-catalytic and affinity sensors, due to its uncomplex nature and low LOD [65].

### 2.4.2 Voltammetry

In this method, a potential range (V) is applied to WE and the current produced due to electrolysis/redox of electrolyte is measured [29] which in turn is limited by mass transport rate of the ions to WE. The current height is usually a peak which is directly proportional to the concentration of the analyte in the solution, but is temperature-dependent. Voltammetry is of multiple types varying from wide dynamic ranges and used for quantification of low concentrations [65]. Certain commonly used voltammetric techniques are: linear sweep voltammetry (LSV), cyclic voltammetry (CV), differential pulse voltammetry (DPV), square-wave voltammetry (SWV), stripping voltammetry, etc.

### 2.4.3 Potentiometry

In this method, V of EC cell is measured at negligible current [77]. It uses EC cell with two reference electrodes, to measure potential difference [65].

### 2.4.4 Impedimetry

In 1975, Lorenz and Schulze described EIS, where they measured the resistance (R) and capacitance current of the sample material upon fluctuations by potential of usually 2–10 mV and varied frequency range to get impedance spectrum. (in-phase current for resistance and out-phase for capacitance). The electron transfer R changes when the analyte binds the BRE and directly observable in label-free detection of Ag–Ab response [65]. EIS is a strong analysis as it measures electron transfer at high mass transfer and at low frequency. Thus, EIS-based sensors are good as affinity biosensors and are stable with environmental fluctuations. However, non-specific binding must be avoided using CNMs especially CNTs in EIS-based sensors as it has high surface area, electric conductivity, etc. [65].

### 2.4.5 Conductometry

It measures changes in electrical conductivity of the sample during the course of chemical reactions [77]. It uses enzymes which increase the conductivity by making ionic products in the solution [65].

## 3 Biosensors in Clinical Diagnostics: Overview

Biosensors are the advanced analytical tool for quantification of bio-analytes/biomarkers. These are quick, economic, easy to handle, and could detect

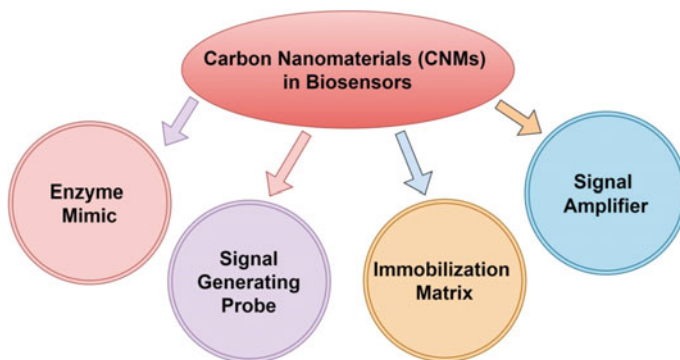
multianalyte at a time, i.e. multi-array biosensors [23] for cancer and certain other diseases; Alzheimer disease, diabetes are few examples [28]. Considering the World Health Organization (WHO) report, to reduce premature mortality from non-communicable diseases (NCDs) and to achieve target no. 3.4 of UN-SDGs 2030, the comprehensive control of NCDs must be implemented and executed in an efficient manner, by improving accessibility to prompt early diagnosis and effective treatments for cancer. Various evidences have also shown that timely diagnosis holds the key for effective treatment [1, 2, 23, 61]. Patients receiving therapy in the early stages of cancer have more and longer survival chance and better quality of life in comparison to those receiving late treatment [32]. As conventional tools are bulky, time-consuming, expensive, and complex, thus, more simple tools, POC settings, economic devices are needed, for resource limited areas. A lot of research is going on in this area; however, new molecular tools having high specificity and non-invasive nature would be a path-breaking achievement in oncology [23].

WHO characterized the features of a diagnostic tool calling it ASSURED. Electrochemical biosensors basically unite the advantages of various electro-analytical processes; like high accuracy, sensitivity and precise selectivity, ease of handling and miniaturized form [65]. The EC biosensors have been promoted as one of the most promising next-generation of biosensors due to their excellent performance, very low and precise LOD [28], and quick diagnosis as POC device [23]. Alongside, multiplexing improves the accuracy of diagnosis; thus, multiplexed analytes/biomarkers show new paths towards personalized early detection and prognosis [65]. Multiplexed sensors are effective at ultra-low concentration detection [53]. Multiplexing of biomarkers for molecular screening and for simultaneous analysis will be a great advancement in biosensing field [47 53]. The quantitative and qualitative detection of cancer biomarkers could be of great help in clinical analysis as it leads to detection of cancer at primary stages, cancer classifications, prognosis, and therapeutic guidelines [65]. An ideal screening test must have 100% specificity and 100% sensitivity, with no false negative diagnosis, but there is no ideal screening test yet present [53]. Thus, biosensors are in high demand and an urgent need in clinical routine practice. The combination of immunotherapeutic-based on biomarkers will lead to better management of cancer and enhanced survival [71]. One of the conductometric EC biosensor, e.g. tyrosinase biosensor to measure level of food herbicides, atrazine, etc., food pathogen like Enterohemorrhagic (*Escherichia coli*), Salmonella, etc., an immunosensors, and potentiometric sensor, e.g. pH electrode coated with penicillinase to detect penicillin indirectly by pH changes due to H<sup>+</sup> ion concentration have been experimented to develop for clinical purposes [65].

## 4 Carbon Nanomaterials (CNMs) in Biosensors

In the last few decades, nanotechnology is no longer just a buzzword, but a rather tangible and attractive reality in the field of material sciences. Since Norio Taniguchi coined the term “nano” in 1974, the field has rapidly achieved a lot of attention





**Fig. 3** Multi-factorial role of CNMs in clinical applications

from the research community [75]. CNMs are the most widely explored NPs in the field of nanotechnology due to its cost-effectiveness as a result of economy of scale (i.e. mass production), multi-functional surface functionalization and low intrinsic toxicity [38]. Due to the contributions by material engineers, physicists, and chemists, a large number of complex carbon nanostructures can be grouped under the term “carbon-based nanomaterials”. In this section, we will take into account the different CNMs and their general applications in biosensors. Various applications of CNMs have been illustrated in Fig. 3 indicating its multi-factorial role in clinical applications. CNMs have been classified into three classes based on the dimensions in nanoscale and are described below.

#### **4.1 Carbon Nanomaterials (0-D)**

All dimensions are within nanoscale (dimensionless): graphene quantum dots, carbon quantum dots, quantum dots, fullerenes.

##### **4.1.1 Carbon Quantum Dots (CQDs) and Carbon Nanodots (CNDs)**

CQDs or CNDs are quasi-spherical to spherical nanoparticles (NPs) of carbon having a size < 10 nm. They were first discovered accidentally during the gel electrophoretic purification of SWCNTs. Surface functionality of CDs (carbon dots) is highly dependent on the synthesis process used and functional moieties attached on the surface [85]. Due to its huge surface to volume ratio and good biocompatibility, CDs are used as novel nanocarriers and nanoprobe. CDs are used to monitor Cu ions in rat brain microdialysate and to measure dopamine [78]. Easily tuneable properties of fluorescent CQDs make it easier to control their physicochemical properties based on the application [21, 46]. Properties such as high stability, low toxicity, environmentally

friendly make them highly operational in the fields of biomedicine, imaging, and DDS [64].

#### 4.1.2 Graphene Quantum Dots (GQDs)

GQDs are CNMs with 1 atom-thick graphite sheets ( $< 2$  nm in thickness) and extremely minute transverse dimensions ( $< 10$  nm in general) [4]. The photoluminescence (PL) property of GQDs can be easily tuned by adjusting their dimensions, morphology, and dopant [20] and allow it to be used extensively in bioimaging and biosensing [15]. The GQDs possess oxygen-rich moieties at the edges that contribute highly to their water solubility and biocompatibility. This facilitates the detection of various ions and charged biomarkers and diagnosis of various diseases [35]. In a study conducted by Xi et al. [81], a pH-responsive fluorescent sulphur-nitrogen-doped GQD probe (pRF-GQDs) was fabricated and clinically tested to distinguish tumour tissues from normal tissues [81]. This biosensor is based on the difference in pH of healthy tissues from tumour tissues [8]. GQDs are also soluble in aqueous medium and biocompatible with minimum cytotoxicity. All these properties make them excellent biosensing molecules [11].

#### 4.1.3 Fullerene

Fullerene (C<sub>60</sub>) is a synthetic carbon allotrope having 60-sp<sup>2</sup>-hybridized carbon atoms linked in a hollow sphere with 0D assembly [20] and are commonly known as the buckyball. Fullerenes display fascinating levels of heat resistance, superconductivity, and superaromaticity (no delocalization of electrons over the surface) [82]. Their variable structural conformations enable them to act as elastic meshes with substitutable sites available for binding of other elements making them versatile nanoparticles. These attributes make fullerene a good candidate for drug delivery systems (DDSs), high contrast bioimaging, tumour treatment, and highly sensitive biosensing molecules [85]. Fullerene (C<sub>60</sub>) has been used as a mediator for electron transfer in amperometric glucose sensor, with higher sensitivity and selectivity for glucose [78].

### 4.2 Carbon Nanomaterials (1D)

These CNMs have one dimension in the nanoscale. It includes CNTs and graphene nanoribbons.

### 4.2.1 Carbon Nanotubes

CNTs can be defined as cylindrical tubes with undetermined carbon walls in which  $sp^2$  carbon is linked in a honeycomb like structures and diameters  $> 100$  nm, i.e. basically a rolled up graphene (GR) sheet. CNTs have outstanding mechanical, electrical, thermal, and optical properties and are proving to be excellent semi-conductors in biosensing applications [24]. It was discovered by Sumo Iijima in 1991. Two main types of CNTs are used in clinical applications because of its composition and structural heterogeneity. These are single-walled carbon nanotubes (SWCNTs) and multi-walled carbon nanotubes (MWCNTs) [78].

Their photo-physical properties (capacity to emit in near-IR region), photostability, fluorescence, and easily tuneable surface properties make them promising nanoprobe in biosensing and as high contract optical probes for non-invasive bioimaging. CNTs show the capacity to promote electron transfer between heterologous phases, which render the presence of ion-to-electron transfer promoter unnecessary [16]. Just like GR, CNTs are also used as nanoprobe and nanocarriers [78]. DNA biosensor based on electrocatalysis of MWCNTs for G/A bases of ssDNA was made [37]. Also, chitosan-grafted MWCNTs have been used for  $H_2O_2$  amperometric sensors and also in EC immunosensors as CNTs resist unspecific antibody (Ab) binding, thus are highly specific [78]. Another CNT-based EC biosensor is a glucose sensor which is made of "Rubianes and Rivas-modified CNT Paste Electrode (CNTPE)" coated with glucose oxidase and no mediator [43]. A protease biosensor with peptide/SWCNT/gold nanoparticle-modified electrode which was made had higher sensitivity due to SWCNT [78].

## 4.3 Carbon Nanomaterials (2-D)

These CNMs have two dimensions in the nanoscale. It includes: graphene.

### 4.3.1 Graphene (GR)

GR is single-atom thick sheet of  $sp^2$  hybridized carbons arranged in honeycomb structure. However, due to its small size and hydrophobicity, GR is usually functionalized as graphene oxide (GO) to increase hydrophilicity but reduced conductivity. Thus, GO is again reduced to enhance the conductivity, and reduced GO (rGO) is made. GO is used as a label in thrombin EC sensor. GR is also used as a nanocarrier and nanoprobe [78]. Graphene was first isolated by A. K. Geim and K. S. Novoselov at the University of Manchester in 2004 [74]. The lattice structure of graphene is comparable to that of CNTs and partially to that of fullerenes and glassy carbon [30]. The versatile surface charge and electronic properties due to presence of the  $\pi$ -electrons facilitates the binding of aromatic compounds via  $\pi$ - $\pi$  stacking [70] and incites its usage in various field. GR exhibits unique optical property of absorbing

light from visible to infrared region (IR) because of the low energy, stable monolayer structure with monodispersed electrons [11]. In glucose biosensor, reduced carboxyl GR is used. Alongside, it provides larger surface to immobilize double enzymes (Oxidase and catalase) in cholesterol sensors and help to detect multiple analytes in glucose and urea-combined sensor [78].

## 5 Optical Biosensors

The field of biosensor development has witnessed great strides since the amalgamation of nanotechnology with sensing techniques [18]. Optical biosensors are a highly recommended for biomedical applications, especially in no-contact and non-invasive detection.

### 5.1 CNMs-Based SPR Biosensors

SPR is a well-established technology within the field of optical biosensing and has been validated as a powerful and accurate tool due to their wide range of sample analytes, ease of handling, portability, and fast detection [48]. The first practical sensing application of SPR sensors for biomolecular detection was reported by Liedberg and Nylander in 1983 for the gas detection and biosensing applications [56]. Since then, SPR biosensors have been utilized for qualitative as well as quantitative analysis. Noble metal NPs (Ag and Au) have been used for plasmon support because of its desired surface characteristics for SPR [41, 66]. However, they show poor biomolecular absorptivity and high thermal conductivity, which may prove to be detrimental to biological analytes causing protein denaturation. To overcome this issue, hybrid biosensors were made, combining CNMs with metal NMs, to provide optimum study conditions [86]. Kulkarni et al. developed a simple graphene-deposited fibre optic SPR sensor for detection of biotinylated double crossover DNA (DXB) lattice and Streptavidin (SA) proteins. Thus, graphene can be a better material for biomolecular detection by SPR sensors due to its highly tuneable surface properties, low heat transfer, and extremely low toxicity [41].

Localized SPR (LSPR) is a phenomenon in which the electron charge oscillations induced by light excitation are confined to the surface of metal nanoparticles (Au, Ag). Each NP is acting as a nanoscale plasmonic resonator and creating sharp LSPR bands, in the visible region, facilitating naked eye detection [49]. Thus has potential for application in biosensing and bioimaging and targeted drug delivery [72]. To prevent high thermal emission properties and low stability of metal NPs, several transition metal oxides (TMOs) have been explored [45]. SPR spectroscopy is a versatile tool that can be used for the micro to nanolevel detection of trace elemental pollutants from environmental matrices [66]. A novel chitosan-graphene oxide/cadmium sulphide quantum dots (CdS QDs) decorated gold coupled with cobalt ion ( $\text{Co}^{2+}$ ) detection

has been effectively formulated and monitored. This type of sensors can also be used for the detection of metal ion toxicity from serum and blood samples [35].

GO and rGO are highly stable, biocompatible, and can be functionalized easily. The functionalization provides attachment sites to various biomolecules. Thus are good candidate for bioimaging, phototherapy, drug delivery, etc. [83]. The high surface area of GO and rGO films contributes highly to the SPR phenomenon and provides effective signal enhancement [33]. GR-based CNMs have the ability to detect even slight changes in temperature (thermo-resistance). The recent concept of wearable, flexible temperature and pressure sensors is largely based on thermo-sensitive properties of CNMs [13].

## 5.2 CNMs-Based SERS Biosensors

SERS is an effective tool for vibrational spectroscopy by virtue of its higher sensitivity than spontaneous Raman scattering. Metal NPs cause heat-induced protein denaturation. However, biosensors should be durable, sensitive, and reproducible [9, 69]. Reliability of SERS substrate is the key to extracting useful data from the substrate, interpretation of the data, and reaching a plausible conclusion while undertaking biomedical studies [38]. The current trend in SERS substrate development is use of non-conventional, semiconducting NMs such as graphene, GO, rGO, CQDs, nanodiamonds, CNTs and carbon nanowires, fullerenes [42]. Signal enhancement in CNMs originates from structural and charge transfer resonance [85].

SERS could be a good platform as POC diagnostics because of its quick and sensitive nature [62]. The CNMs have higher stability and reusability, thus better suitable for SERS biosensors. Ju et al. in 2017, used silver NPs decorated with nitrogen-doped GQD for fabrication of real-time evaluation of glucose in mouse blood samples [36]. The Ag NP@N-GQD was much more stable for more than 30 days than pure Ag NP substrate that lost stability after 10 days. Thus, GQD is highly cost-effective substrate for SERS biosensor [3].

## 6 Electrochemical Biosensors

As per the definition of International Union of Pure and Applied Chemistry (IUPAC), an EC biosensor is a self-contained quantitative/semi-quantitative device, which provides information using BRE which is in direct spatial contact with a transducer [77]. EC biosensors are classified in two major classes as described in the sub-sections below.

## **6.1 CNMs-Based EC Biosensors**

CNMs on nanoscale comprise of amazing properties like electric conductivity and high surface area, ease of functionalization which enhances the specificity and sensitivity of sensors, thus are suitable fabrication materials for EC biosensors. Nowadays, different CNMs from 0 to 3D are being utilized in EC biosensors for clinical diagnostics due to its chemical inertness and economic price [78]. Various EC biosensors based on the nature of BRE with CNMs are classified into various categories which are described below in brief.

### **6.1.1 Bio-Catalytic Sensors**

It has enzymes, cells, or tissue as the BRE to detect the analytes [34]. Due to high bio-catalytic activity and specificity, it is used for clinical or industrial purposes, e.g. enzymatic electrodes for glucose, xanthine, and lactose detection [65].

### **6.1.2 Affinity Sensors**

It selectively and strongly binds the analytes using BRE made of Ab, nucleic acid, or receptors, etc., e.g. immunosensors and DNA hybridization biosensors. The recognition and binding is based on the complementary size and shape of the binding site to the analyte. Most famous commercially available immunosensors based on affinity binding are pregnancy test kits [65].

Immunosensors are highly sensitive and require small sample, e.g. detection of methamphetamine in human urine via conductometry [65]. GR-based voltammetric immunosensors are used for measuring okadaic acid (OA) in shellfish by carboxy-phenyl-modified GR electrode, and another EC immunosensor that has been used was vascular endothelial growth factor receptor 2 (VEGFR2) [78].

Another major type of affinity sensor is aptasensors; aptamers (single-stranded bio-engineered oligonucleotide) are quite conventional BRE providing synergistic detection of various biomarkers. Thus, aptasensors are excellent diagnostics for cancer biomarkers due to its quick, economic, POC, and highly sensitive nature. But various conditions need to be optimized like pH, temperature, ionic concentration, etc. However, till now no such biosensor is available that can be used in clinical practices.

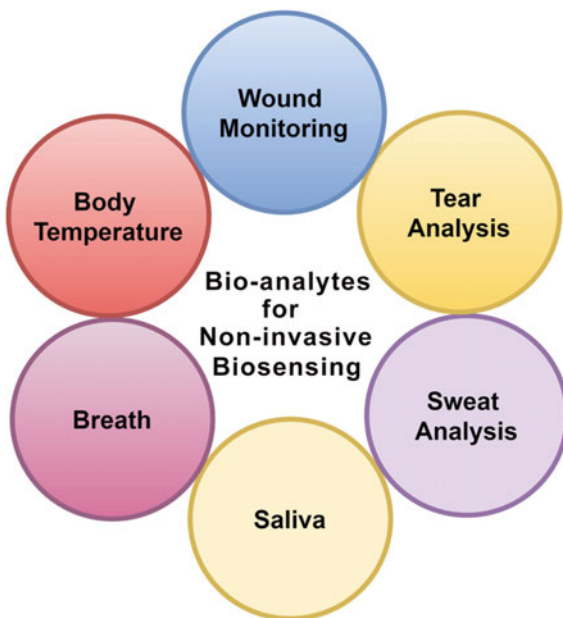
## **6.2 Pre-Clinically Assessed EC Biosensors**

Based on transducer, the wearable sensors are mainly EC or optical. However, EC biosensors have additional advantage of miniaturized, high sensitivity, etc. The use

of body fluids other than blood such as saliva, tears, urine provides a non-invasive diagnosis, necessary for continuous health monitoring [84]. These analytes which are derived from a living organism are called as “bio-analytes” and are listed in Fig. 4; as they do not require any invasive tool for extraction. Thus cause no pain to the patient. Amperometric sensors are used for detection of glucose and norepinephrine in tear. These sensors had shown good sensitivity and quick response. However, on-body real-time monitoring/sensing has still not established [7]. CNT-based amperometric EC sensors have been used for non-enzymatic glucose sensing [6, 12].

For non-enzymatic oxidation and detection of glucose, SWCNTs have shown high sensitivity. Alongside, GR and carbon nanofibre (CNF) also possess great sensitivity for glucose [67]. A non-invasive, wearable EC sensor for continuous monitoring of body homeostasis [55] via calcium ion and pH detection has also been reported. Also, CNT coated with gold nanosheets were reported to have sensitivity for calcium ions and pH changes [57]. Some pre-clinically tested EC biosensors are listed in Table 1; with their dynamic response range, LOD, and transduction analysis method.

**Fig. 4** Biological samples as a source of bio-analyte for non-invasive diagnosis



**Table 1** List of electrochemical biosensors and their transduction analysis

Biosensor	Method	LOD	Dynamic response range	References
Aptasensors	Voltammetry	50 nM	1.5 $\mu$ M	Zhao et al. [88]
Immunoassay	–	0.13 nM and 2.75 ng/ml	104–107 cells/ml	
Sandwich aptasensors	DPV	0.62 ppb	1–12 ppb	Taleat et al. [73]
Nano-aptasensors	DPV	0.95 ng/ml	–	
Nanogold-based aptasensing	–	2.2 nM	8.8–353.3 nM	
Nanobiosensor	Amperometric	8 cells/ml	15 to $1 \times 10^6$ cells/ml	Mir et al. [51]

## 7 Advantages and Limitations of CNMs-Based Biosensors

### 7.1 Advantages

In the contemporary times, the non-invasive diagnostic and therapy options are in demand. Multiple commercial options are although available in the market in the form of flexible and wearable device. Most of these devices are based on electrochemical and optical biosensing tools, due to their intrinsic property of being miniaturized. Alongside, the CNMs add the additional advantage of making them more sensitive and on chips. The biosensors are highly miniaturized, LOC and provide the POC diagnosis without the need of patient visiting the clinical set ups.

Biosensors are highly efficient to diagnose cellular changes at very early stage and in ultra-low amount within broad ranges fg/ml to ng/ml. Thus can detect cancer biomarkers which are secreted even before the onset of disease but in ultra-low amount and require no sample preparations/pre-treatment. This early detection can provide timely treatment, better management, and high survival chance of cancer patients [23, 53]. LOC can improve analysis tools with integration of more economic, portable, miniature, and disposable device, using samples like blood, urine, and saliva, etc. [22]. Current techniques like ELISA and advanced multiplex assays integrating with label-free optical sensors could provide an economic and simple LOC detection platform [22]. Alongside, high sensitivity, selectivity, response time (i.e. the time between addition of the analyte and sensor response to reach 95% of its final value), ease of use, and portability make the biosensors a better future candidate in the field of clinical diagnosis and therapeutics [65]. And due to dynamic nature, biosensors are also useful in multi-step analysis and on-line/filed monitoring. EC biosensors when combined with NMs provide a good cancer diagnostic. NMs provide high surface area, higher signal-to-noise ratio and thus accelerates electron transfer, leading to signal amplification. Thus, use of NMs in biosensors would further enhance their sensitivity [23] and lead to its ultra-low LOD. However, no



cancer biosensor is commercially fully developed [23]. Attributes such as minimal or no sample pre-treatment, high stability, ultrasensitivity, and label-free detection make biosensors ideal for diverse applications in fields of diagnostics, POC monitoring [10, 89]. In recent times, EC biosensors are one of the most sensitive devices to detect biomarkers for cancer and other diseases [14, 63, 79]. Consequently, early diagnosis provides better therapy options and prognosis.

## 7.2 *Limitations*

Biosensors are quite expensive sometimes, due to high extraction and isolation costs of disease biomarkers, and its time-consuming nature [23, 53]. Even after being the trendsetter in the current field of diagnostics, EC biosensors do have certain limitations like cross-reactivity, electrode fouling issues, and EC hindrance, etc. [22]. These limitations of EC biosensors could be overpass using optical transducer. Optical biosensors based on fluorescence, Raman effect, SPR effect, etc. could be used to integrate in LOC, while some optical biosensors needs no label and are called label-free biosensors. However, to enhance the sensitivity, the interaction between light beam and surface target molecules should be maximum in optical biosensors. Despite its advantages, many challenges need to be overcome before its clinical implementation of optical sensors, such as bio-compatibility, reproducibility, detection limit, sensitivity. If all these drawbacks are tackled, label-free optical biosensors might be a reality of near future [22]. Binding with the transducer needs to follow stringent conditions in biosensing, making it ideal for one time use [23]. Thus, it is non-regenerable and does not provide continuous monitoring, etc. Alongside, sensitivity of BREs is subject to conditions such as pH, temperature, and stirring which also limits the potential of biosensors. However, implementation of stable NMs might improve their sensitivity and stability.

## 8 **Conclusion and Future Prospects**

Rapid and timely diagnosis of human ailments brings out the best clinical outcomes and effective disease management. Conventional diagnostics requires technical experts, proper laboratories, time-taking and are quite expensive. However, being POC and LOC technology biosensors does not require any special training and is quite simple to use. In the past few years, multiple biosensors were developed and proposed for early diagnosis of human ailments based on biomarkers. The primary results indicated their good sensitivity, specificity, rapid and quick nature in low cost, requiring no manpower. Alongside, with the growth in nanotechnology, CNMs have gained peculiar attention in the field of biosensors especially for clinical diagnostics. Carbon atoms have chemically inert, stable nature and shows an exclusive property of self-catenation, which allows it to form various stable allotropic forms,

with the major breakthroughs from the past two years. Due to its biocompatibility, conductivity, optical and electrical properties, and higher surface-to-volume ratio, CNMs have been frequently used in the biosensor developments. Application of CNMs provides high sensitivity, specificity, and diversifies interface for analytes, thus, helping in efficient signal transduction and amplification. However, the laboratory working sensors, when applied to the real fields faces multiple challenges such as interferences due to unwanted analytes, environmental fluctuations, physiological changes (in living samples). Since full-fledged sensor devices must be able to produce repeatable results and need to be stable. To achieve this target and successful development of real-time sensor on field, various combinations of CNMs and biological elements need to be tested. Thus, biosensors could be of great importance in socially backward and resource limited area for cancer and other clinical diagnosis with the help of biomarkers, as these are secreted at very early stage of disease progression. In this chapter, we have reviewed and stated few examples of CNMs-based EC and optical biosensors for clinical diagnosis. These NMs have been used for multiple applications in biosensors developments and fabrications and contributed to the higher sensitivity and specificity of sensor devices. Alongside, the advantage and limitations of these fabricated biosensor and their future scope in sensing technology have also been discussed.

**Acknowledgements** The authors would like to express the gratitude to the Symbiosis International (Deemed University) for the encouragement to carry out this work. Alongside, we would like to thank Symbiosis Centre for Nanoscience and Nanotechnology (SCNN) for its constructive feedback and providing opportunity for this work.

## References

1. Abbott SB, Stornetta RL, Socolovsky CS, West GH, Guyenet PG (2009) Photostimulation of channelrhodopsin-2 expressing ventrolateral medullary neurons increases sympathetic nerve activity and blood pressure in rats. *J Physiol* 587:5613–5631
2. Al-Zwaini YKH, Al-Mugdadi SFH, Abbas WAK (2020) Detection of Novel apyrimidinic endonuclease 1 (APE1) in a sample of Iraqi cervical cancer patients using immunohistochemistry technique. *Res J Pharm Technol* 13:3193–3198
3. Ayas S, Cinar G, Ozkan AD, Soran Z, Ekiz O, Kocaay D, Tomak A, Toren P, Kaya Y, Tunc I (2013) Label-free nanometer-resolution imaging of biological architectures through surface enhanced Raman scattering. *Sci Rep* 3:1–8
4. Bacon M, Bradley SJ, Nann T (2014) Graphene quantum dots. *Part Part Syst Charact* 31:415–428
5. Bahadir EB, Sezgintürk MK (2015) Applications of commercial biosensors in clinical, food, environmental, and biothreat/biowarfare analyses. *Anal Biochem* 478:107–120
6. Bandothkar AJ, Jeerapan I, You J-M, Nuñez-Flores R, Wang J (2016) Highly stretchable fully-printed CNT-based electrochemical sensors and biofuel cells: combining intrinsic and design-induced stretchability. *Nano Lett* 16:721–727
7. Bandothkar AJ, Wang J (2014) Non-invasive wearable electrochemical sensors: a review. *Trends Biotech* 32:363–371

8. Bettegowda C, Sausen M, Leary RJ, Kinde I, Wang Y, Agrawal N, Bartlett BR, Wang H, Lubner B, Alani RM, Antonarakis ES (2014) Detection of circulating tumor DNA in early- and late-stage human malignancies. *Sci Transl Med* 6:224ra24–224ra24
9. Bhalla N, Jolly P, Formisano N, Estrela P (2016) Introduction to biosensors. *Essays Biochem* 60:1–8
10. Bojorge Ramirez N, Salgado A, Valdman B (2009) The evolution and developments of immunosensors for health and environmental monitoring: problems and perspectives. *J Chem Eng* 26:227–249
11. Caballero-Díaz E, Benítez-Martínez S, Valcárcel M (2017) Rapid and simple nanosensor by combination of graphene quantum dots and enzymatic inhibition mechanisms. *Sens Actuators, B Chem* 240:90–99
12. Chen J, Zhang W-D, Ye J-S (2008) Nonenzymatic electrochemical glucose sensor based on MnO<sub>2</sub>/MWNTs nanocomposite. *Electrochem Commun* 10:1268–1271
13. Chen Z, Zhao D, Ma R, Zhang X, Rao J, Yin Y, Wang X, Yi F (2021) Flexible temperature sensors based on carbon nanomaterials. *J Mater Chem* 9:1941–1964
14. Chikkaveeriah BV, Bhirde AA, Morgan NY, Eden HS, Chen X (2012) Electrochemical immunosensors for detection of cancer protein biomarkers. *ACS Nano* 6:6546–6561
15. Chung S, Revia RA, Zhang M (2021) Graphene quantum dots and their applications in bioimaging, biosensing, and therapy. *Adv Mater* 33:1904362
16. Crespo GA, Macho S, Rius FX (2008) Ion-selective electrodes using carbon nanotubes as ion-to-electron transducers. *Anal Chem* 80:1316–1322
17. Crivianu-Gaita V, Thompson M (2016) Aptamers, antibody scFv, and antibody Fab' fragments: an overview and comparison of three of the most versatile biosensor biorecognition elements. *Biosens Bioelectron* 85:32–45
18. Damborský P, Švitel J, Katrlík J (2016) Optical biosensors. *Essays Biochem* 60:91–100
19. Darmostuk M, Rimpelova S, Gbelcova H, Ruml T (2015) Current approaches in SELEX: an update to aptamer selection technology. *Biotech Adv* 33:1141–1161
20. Diana N, Yamada Y, Gohda S, Ono H, Kubo S, Sato S (2021) Carbon materials with high pentagon density. *J Mater Sci* 56:2912–2943
21. Dong Y, Zhou N, Lin X, Lin J, Chi Y, Chen G (2010) Extraction of electrochemiluminescent oxidized carbon quantum dots from activated carbon. *Chem Mater* 22:5895–5899
22. Donzella V, Crea F (2011) Optical biosensors to analyze novel biomarkers in oncology. *J Biophoton* 4:442–452
23. Eshghi MG, Fruhdeh Z, Alviri VM, Asem MM (2019) Electrochemical biosensors for cancer detection using different biomarkers. In: 2019 IEEE 9th annual computing and communication workshop and conference (CCWC). IEEE, pp 0989–0996
24. Farrera C, Torres Andon F, Feliu N (2017) Carbon nanotubes as optical sensors in biomedicine. *ACS Nano* 11:10637–10643
25. Ferapontova EE (2018) DNA Electrochemistry And Electrochemical Sensors For Nucleic Acids. *Ann Rev Anal Chem* 11:197–218
26. Fu X, Chen L, Choo J (2017) Optical nanoprobe for ultrasensitive immunoassay. *Anal Chem* 89:124–137
27. Gaudin V (2017) Advances in biosensor development for the screening of antibiotic residues in food products of animal origin—a comprehensive review. *Biosens Bioelectron* 90:363–377
28. Gorodetskaya I, Gorodetsky A (2015) Analytical chemistry: clamping down on cancer detection. *Chem Nat*
29. Grieshaber D, Mackenzie R, Vörös J, Reimhult E (2008) Electrochemical biosensors—sensor principles and architectures. *Sensors* 8:1400–1458
30. Harris PJ (2018a) Transmission electron microscopy of carbon: a brief history. *C* 4:4
31. Heydari-Bafrooei E, Ensafi AA (2019) Typically used carbon-based nanomaterials in the fabrication of biosensors. *Electrochem Biosens*
32. Higgins MJ, Ettinger DS (2009) Chemotherapy for lung cancer: the state of the art in 2009. *Expert Rev Anticancer Therapy* 9:1365–1378

33. Huang C-F, Yao G-H, Liang R-P, Qiu J-D (2013) Graphene oxide and dextran capped gold nanoparticles based surface plasmon resonance sensor for sensitive detection of concanavalin A. *Biosensors Bioelectron* 50:305–310
34. Huang Y, Xu J, Liu J, Wang X, Chen B (2017) Disease-related detection with electrochemical biosensors: a review. *Sensors* 17:2375
35. Hwang HS, Jeong JW, Kim YA, Chang M (2020) Carbon nanomaterials as versatile platforms for biosensing applications. *Micromachines (Basel)* 11:814
36. Ju J, Liu W, Perlaki CM, Chen K, Feng C, Liu Q (2017) Sustained and cost effective silver substrate for surface enhanced Raman spectroscopy based biosensing. *Sci Rep* 7:1–11
37. Kałuża D, Jaworska E, Mazur M, Maksymiuk K, Michalska A (2019) Multiwalled carbon nanotubes–poly (3-octylthiophene-2, 5-diyl) nanocomposite transducer for ion-selective electrodes: Raman spectroscopy insight into the transducer/membrane interface. *Anal Chem* 91:9010–9017
38. Kasinathan B, Zawawi RM (2014) Carbon-based nanomaterials for drugs sensing: a review. *Mater Sci Forum* 807:13–39
39. Keshavarz M, Chowdhury AKMRH, Kassanos P, Tan B, Venkatakrishnan K (2020) Self-assembled N-doped Q-dot carbon nanostructures as a SERS-active biosensor with selective therapeutic functionality. *Sens Actuators B Chem* 323
40. Kim H-M, Jeong DH, Lee H-Y, Park J-H, Lee S-K (2021) Design and validation of fiber optic localized surface plasmon resonance sensor for thyroglobulin immunoassay with high sensitivity and rapid detection. *Sci Rep* 11:1–9
41. Kim JA, Hwang T, Dugasani SR, Amin R, Kulkarni A, Park SH, Kim T (2013) Graphene based fiber optic surface plasmon resonance for bio-chemical sensor applications. *Sens Actuators, B Chem* 187:426–433
42. Kim N, Thomas MR, Bergholt MS, Pence IJ, Seong H, Charchar P, Todorova N, Nagelkerke A, Belessiotis-Richards A, Payne DJ, Gelmi A, Yarovsky I, Stevens MM (2020) Surface enhanced Raman scattering artificial nose for high dimensionality fingerprinting. *Nat Commun* 11:207
43. Koyun A, Ahlatcolu E, Koca Y, Kara S (2012) Biosensors and their principles. *Roadmap Biomed Eng Milstones* 117–142
44. Li C-Z, Karadeniz H, Canavar E, Erdem A (2012) Electrochemical sensing of label free DNA hybridization related to breast cancer 1 gene at disposable sensor platforms modified with single walled carbon nanotubes. *Electrochim Acta* 82:137–142
45. Li R, An H, Huang W, He Y (2018) Molybdenum oxide nanosheets meet ascorbic acid: tunable surface plasmon resonance and visual colorimetric detection at room temperature. *Sens Actuators, B Chem* 259:59–63
46. Lim SY, Shen W, Gao Z (2015) Carbon quantum dots and their applications. *Chem Soc Rev* 44:362–381
47. Maruvada P, Wang W, Wagner PD, Srivastava S (2005) Biomarkers in molecular medicine: cancer detection and diagnosis. *Biotech* 38:S9–S15
48. Masson JF (2020) Portable and field-deployed surface plasmon resonance and plasmonic sensors. *Analyst* 145:3776–3800
49. Mayer KM, Hafner JH (2011) Localized surface plasmon resonance sensors. *Chem Rev* 111:3828–3857
50. Miller E, Sikes HD (2015) Addressing barriers to the development and adoption of rapid diagnostic tests in global health. *Nanobiomed* 2:2–6
51. Mir TA, Akhtar MH, Gurudatt N, Kim J-I, Choi CS, Shim Y-B (2015) An amperometric nanobiosensor for the selective detection of K<sup>+</sup>-induced dopamine released from living cells. *Biosens Bioelectron* 68:421–428
52. Morales MA, Halpern JM (2018) Guide to selecting a biorecognition element for biosensors. *Bioconjug Chem* 29:3231–3239
53. Nimse SB, Sonawane MD, Song K-S, Kim T (2016) Biomarker detection technologies and future directions. *Analyst* 141:740–755
54. Novoselov KS, Fal'Ko VI, Colombo L, Gellert PR, Schwab MG, Kim K (2012) A roadmap for graphene. *Nature* 490:192–200

55. Nyein HYY, Gao W, Shahpar Z, Emaminejad S, Challa S, Chen K, Fahad HM, Tai L-C, Ota H, Davis RW (2016) A wearable electrochemical platform for noninvasive simultaneous monitoring of  $\text{Ca}^{2+}$  and pH. *ACS Nano* 10:7216–7224
56. Nylander C, Liedberg B, Lind T (1982) Gas detection by means of surface plasmon resonance. *Sens Actuators* 3:79–88
57. Oh SY, Hong SY, Jeong YR, Yun J, Park H, Jin SW, Lee G, Oh JH, Lee H, Lee S-S (2018) Skin-attachable, stretchable electrochemical sweat sensor for glucose and pH detection. *ACS Appl Mater Interface* 10:13729–13740
58. Omar NAS, Fen YW (2018) Recent development of SPR spectroscopy as potential method for diagnosis of dengue virus E-protein. *Sens Rev*
59. Pan J, Chen W, Ma Y, Pan G (2018) Molecularly imprinted polymers as receptor mimics for selective cell recognition. *Chem Soc Rev* 47:5574–5587
60. Pan J, Li F, Choi JH (2017) Single-walled carbon nanotubes as optical probes for bio-sensing and imaging. *J Mater Chem B* 5:6511–6522
61. Pardridge WM (2007) Blood–brain barrier delivery. *Drug Discovery Today* 12:54–61
62. Qazi S, Raza K (2020) Smart biosensors for an efficient point of care (PoC) health management. *Smart Biosens Med Care*
63. Qureshi A, Gurbuz Y, Niazi J (2012) Biosensors for cardiac biomarkers detection: a review. *Rev Sensor Actuators B, Chem* 171:62–76
64. Raja IS, Song S-J, Kang MS, Lee YB, Kim B, Hong SW, Jeong SJ, Lee J-C, Han D-W (2019) Toxicity of zero- and one-dimensional carbon nanomaterials. *Nanomaterial* 9:1214
65. Ronkainen NJ, Halsall HB, Heineman WR (2010) Electrochemical biosensors *Chem Soc Rev* 39:1747–1763
66. Saleviter S, Wing Fen Y, Daniyal WEMEMM, Abdullah J, Sadrolhosseini AR, Omar NAS (2019) Design and analysis of surface plasmon resonance optical sensor for determining cobalt ion based on chitosan-graphene oxide decorated quantum dots-modified gold active layer. *Optics Express* 27:32294–32307
67. Si P, Huang Y, Wang T, Ma J (2013) Nanomaterials for electrochemical non-enzymatic glucose biosensors. *RSC Adv* 3:3487–3502
68. Singh MK, Ryu S, Jang HM (2005) Polarized Raman scattering of multiferroic  $\text{BiFeO}_3$  thin films with pseudo-tetragonal symmetry. *Phys Rev* 72:132101
69. Smith E, Dent G (2019) *Modern Raman spectroscopy: a practical approach*. John Wiley & Sons
70. Su S, Sun Q, Gu X, Xu Y, Shen J, Zhu D, Chao J, Fan C, Wang L (2019) Two-dimensional nanomaterials for biosensing applications. *TrAC Trends Anal Chem* 119
71. Szopa W, Burley TA, Kramer-Marek G, Kaspera W (2017) Diagnostic and therapeutic biomarkers in glioblastoma: current status and future perspectives. *BioMed Res Int* 2017
72. Tabassum R, Kant R (2020) Recent trends in surface plasmon resonance based fiber–optic gas sensors utilizing metal oxides and carbon nanomaterials as functional entities. *Sens Actuators B: Chem* 310
73. Taleat Z, Cristea C, Marrazza G, Mazloum-Ardakani M, Săndulescu R (2014) Electrochemical immunoassay based on aptamer–protein interaction and functionalized polymer for cancer biomarker detection. *J Electroanal Chem* 717:119–124
74. Tang Q, Zhou Z, Chen Z (2015) Innovation and discovery of graphene-like materials via density-functional theory computations. *Rev Comput Mol Sci* 5:360–379
75. Taniguchi N (1974) On the basic concept of nanotechnology. *Proc ICPE*
76. Teengam P, Siangproh W, Tuantranont A, Henry CS, Vilaivan T, Chailapakul O (2017) Electrochemical paper-based peptide nucleic acid biosensor for detecting human papillomavirus. *Anal Chimica Acta* 952:32–40
77. Thévenot DR, Toth K, Durst RA, Wilson GS (2001) Electrochemical biosensors: recommended definitions and classification. *Biosens ans Bioelectron* 16:121–131
78. Wang Z, Dai Z (2015) Carbon nanomaterial-based electrochemical biosensors: an overview. *Nanoscale* 7:6420–6431

79. Wang ZL, Song J (2006) Piezoelectric nanogenerators based on zinc oxide nanowire arrays. *Science* 312:242–246
80. Wu X, Sun S, Wang Y, Zhu J, Jiang K, Leng Y, Shu Q, Lin H (2017) A fluorescent carbon-dots-based mitochondria-targetable nanoprobe for peroxynitrite sensing in living cells. *Biosens Bioelectron* 90:501–507
81. Xi J, Xie C, Zhang Y, Wang L, Xiao J, Duan X, Ren J, Xiao F, Wang S (2016) Pd nanoparticles decorated N-doped graphene quantum dots@ N-doped carbon hollow nanospheres with high electrochemical sensing performance in cancer detection. *ACS Appl Mater Interfaces* 8:22563–22573
82. Yadav B, Kumar R (2008) Structure, properties and applications of fullerenes. *Int J Nanotech Appl* 2:15–24
83. Yang H-W, Lu Y-J, Lin K-J, Hsu S-C, Huang C-Y, She S-H, Liu H-L, Lin C-W, Xiao M-C, Wey S-P (2013) EGRF conjugated PEGylated nanographene oxide for targeted chemotherapy and photothermal therapy. *Biomaterials* 34:7204–7214
84. Yang Y, Gao W (2019) Wearable and flexible electronics for continuous molecular monitoring. *Chem Soc Rev* 48:1465–s1491
85. Yap SHK, Chan KK, Tjin SC, Yong K-TJS (2020) Carbon allotrope-based optical fibers for environmental and biological sensing: a review. *Sensors (Basel)* 20:2046
86. Yin PT, Kim TH, Choi JW, Lee KB (2013) Prospects for graphene-nanoparticle-based hybrid sensors. *Phys Chem Chem Phys* 15:12785–12799
87. Zhang JXJ, Hoshino K (2014) Optical Transducers. *Mol Sens Nanodevices*
88. Zhao J, He X, Bo B, Liu X, Yin Y, Li G (2012) A “signal-on” electrochemical aptasensor for simultaneous detection of two tumor markers. *Biosens Bioelectron* 34:249–252
89. Zhou J (2014) An emerging role for Hippo-YAP signaling in cardiovascular development. *J Biomed Res* 28:251
90. Zhou Y, Liu B, Yang R, Liu J (2017) Filling in the gaps between nanozymes and enzymes: challenges and opportunities. *Bioconjugate Chem* 28:2903–2909

# Chapter 39

## Emerging Graphene-Based Nanomaterials for Cancer Nanotheranostics



**Arkadyuti Roy Chakraborty, R. Akshay, Subhrajeet Sahoo, Haimantika Seel, Soupam Das, Saikat Dutta, Abhishek Nalluri, Siva Sankar Sana, Karthikeyan Ramesh, and Vimala Raghavan**

### 1 Introduction

Cancer is the leading cause of death in most first-world countries with expected number of cases of up to 29.5 million, of which there may be 16.4 million deaths to

---

Authors 'Arkadyuti Roy Chakraborty, R Akshay, Subhrajeet Sahoo, Karthikeyan Ramesh' have the same contribution in this chapter

---

A. R. Chakraborty · S. Das · K. Ramesh  
School of Bio Sciences and Technology, Vellore Institute of Technology, Vellore 632014, India

R. Akshay  
Department of Physics, Sri Sathya Sai Institute of Higher Learning, Vidyagiri Prashanthi Nilayam, Andhra Pradesh 515134, India

S. Sahoo  
Centre for Life Sciences, Vidyasagar University, Midnapore, West Bengal 721102, India

H. Seel  
Department of Clinical Biochemistry and Pharmacology, Faculty of Health Science, Ben Gurion University of the Negev, P.O.B. 653, 8410501 Beer-Sheva, Israel

S. Dutta  
School of Life Science, Department of Microbiology, VELS University, Chennai 600117, India

A. Nalluri  
School of Materials Science and Engineering, Huazhong University of Science and Technology, Wuhan 430074, Hubei, China

S. S. Sana  
School of Chemical Engineering and Technology, North University of China, Taiyuan 030051, China

V. Raghavan (✉)  
Centre for Nanotechnology Research, Vellore Institute of Technology, Vellore 632014, India  
e-mail: [vimararagu@gmail.com](mailto:vimararagu@gmail.com)

be expected by the year 2040. The WHO reports the most common cancers being that of lung (2.09 million), breast (2.09 million), colorectal (1.80 million), prostate (1.28 million), skin non-melanoma (1.04 million), and lastly stomach (1.03 million) worldwide. In each case, there may be deaths in the range of 0.5–1.8 million deaths worldwide. Cancer emerges from the transformation of a benign cell into a tumorous one which comprises of a multi-stage mechanism of a pre-cancerous lesion developing into a malignant tumor. Population aging and growth as well as an increased adherence to cancer-inducing lifestyle choices like smoking, drinking, physical inactivity, and fast-food-centric diets are the primary reasons for the burden of cancer in developed countries [1, 2]. The biggest challenge is in translating the preventive measures from the confines of a safety chart to being implemented in our daily lives. The added burden is to find more long-term cures with minimal time needed to return to normalcy as an alternative to chemotherapy, radiotherapy, tumor surgery, and hormonal therapy that are used in the present narrative. The priorities of health and palliative care are paramount but we also must have a more streamlined health-care with emphasis on people-centric measures. The current COVID-19 pandemic raises issues like the vulnerability of cancer-treated patients with suppressed immune systems to COVID. Does that mean the patient must risk COVID infection in order to treat his/her cancer?

Oncologists would have to continue balancing the chances of mortality and morbidity from COVID-19 against the advantages of cancer therapy during the pandemic [3, 4]. Doctors face the herculean task of extending immediate and effective care to COVID patients while balancing the usual care given to non-COVID patients [5]. The patients with weakened immune systems are particularly susceptible [6], with an elevated risk to COVID-19 in cases of patients undergoing chemo or radiotherapy or suffering from blood or bone marrow tumors [3]. The absence of selectivity for tumor cells is the primary downside to these therapies and necessitates the advent of more effective approaches [7].

**Theranostics** is a recently proposed concept combining therapeutics and diagnostics aimed at personalizing medicine and real-time monitoring of the therapeutic process. The word “theranostics” was coined to create precise and individualized therapies for different pathologies and to bring about a union of diagnostic and therapeutic applications into a single agent. This forms a model involving diagnosis, drug delivery, and therapy response tracking. Use of nanotechnology-based solutions leads to targeted killing of tumor cells with minimal collateral damage. This can also be utilized as a preventive measure to kill cancerous cells before they turn into tumors. Furthermore, nanotechnology serves to improve accuracy in the surgical excision of tumors. This technology provides the opportunity to manipulate macromolecules in real time and at the earlier stages of cancer progression. Owing to their unique physicochemical properties [8, 9], nanomaterials have been used as medical agents that can be engineered to acquire highly integrated multiple functions in a single system and also to give the control of drug release which is promising for the next generation cancer theranostics [7, 10].

Graphene has attracted a significant interest in the area of biomedicine in recent years [11–13]. Graphene is composed of single-layered carbon atoms packed into a



two-dimensional (2D) honeycomb lattice [14]. It can be enriched in functional groups like carboxyl and hydroxyl groups which facilitate its surface modifications [15–17]. Graphene and graphene oxide (GO) have an ultra-high surface area enabling a greater amount of interaction with biomolecules in a variety of applications like biosensors, drug delivery, and gene transfection [17, 18]. Biocompatibility is a primary concern in this case [18]. High NIR absorbance range of graphene and associated materials enable their use as a photothermal agent for in vivo cancer treatment [11–13]. The toxic effects of graphene can be a positive point with respect to cancer cells and find use as inhibitors of cancer cell metastasis [19, 20]. So, the purpose of this chapter is to broaden the knowledge of graphene and derived materials as biomedicine for cancer treatment and diagnosis.

## 2 Surface Chemistry of Graphene to Formulate Biomedicine

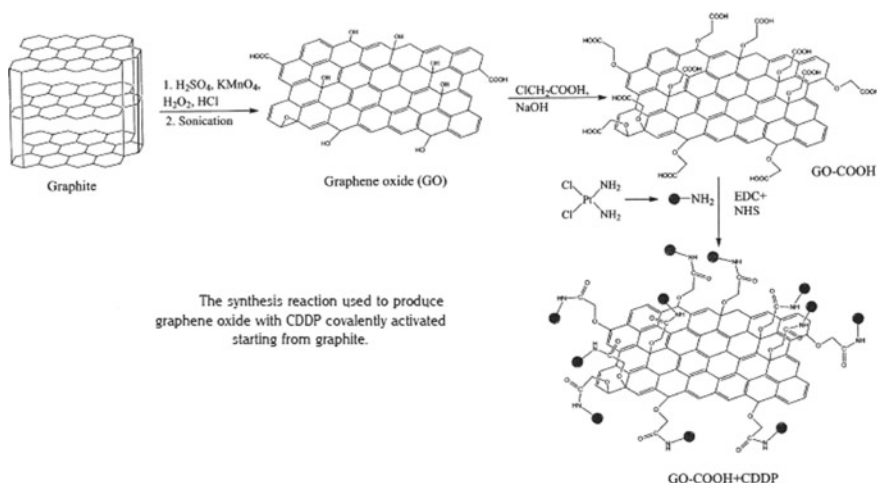
Graphene-based materials have piqued interest in biological applications for some time, owing to its large surface area, chemical stability, conductivity, and, most critically, biocompatibility [21–23]. Graphene has a 2D planar structure composed of single layer of carbon atoms with  $sp^2$ -hybridization, arranged in a hexagonal crystal lattice [24]. Its structure opens up new avenues of application such as a new generation of nanocarriers, biosensors, bioimaging, cell culture, tissue engineering, theranostics [25, 26]. An important point of note that cripples such applications is their limited solubility in aqueous solutions. Graphene oxide (GO) on the other hand has abundant oxygen-containing functional groups (hydroxyl, carboxyl, and epoxide) which impart improved water solubility and  $\pi$ – $\pi$  interactions, hydrophobic or hydrogen bonds which endow a greater drug loading potential [27–29]. Hence, it is quite evident that these materials need a variety of surface modifications in order to have any utility. Additionally, the chosen method of synthesis can also lead to impurities like sulfates, peroxides, residues from permanganate, hydrazine, borohydrate surfactants which may enhance toxicity levels [30]. The surface modifications impart a number of properties which are more suitable towards the development of successful theranostic tools.

## 2.1 Functionalization of Graphene (Covalent and Non-Covalent)

### 2.1.1 Covalent Modifications

A strong and irreversible bonding was observed between GO nanosheets and histidine-proline-rich glycoprotein peptides to form a hybrid structure [31]. It caricaturist the anti-angiogenic domain of HPRG protein and serves to induce toxicity in prostate cancer cells as well as blocks cell migration and prostaglandin arbitrated inflammatory process in **PC-3** (prostate cancer cell line) and **human retinal endothelial cells** (HREC). Cisplatin is a broad-spectrum anti-cancerous remedy but persuades chemoresistance in a lot of cancer cells. GO as a nanomaterial which aggravates autophagy in CT26 colon cancer cells as well as confers antitumor effects. Lin et al. attempted to evaluate the combinatorial effect of these two in order to overcome chemoresistance in cancer cells [32] (Fig. 1).

Chitosan functionalized magnetic graphene (CMG) nanoparticle was used as a platform for parallel gene–drug (doxorubicin) and superparamagnetic iron oxide SPIO (contrast agent) delivery to tumor cells [34]. Most polymers like chitosan directly functionalize GO via COOH groups but these groups are limited on the edge of GO. So, GO is chemically reduced with chloroacetic acid, thereby preventing aggregation of graphene sheets. The chitosan further increases the solubility without affecting cell viability [35, 36]. Gold nanoparticles (AuNPs), quantum dots, silica nanoparticles, and metal nanomaterials have all been used extensively as delivery vehicles as well as for cancer diagnostics and treatment [37]. Functionalized GO with folic acid (FA)/polyethylene glycol (PEG) to synchronously deliver histone deacetylase (HDAC1) and K-Ras siRNA specifically targeted for anti-pancreatic



**Fig. 1** Synthesis of graphene oxide-CDDP conjugate [33] [CC. BY. 4.0]

cancer therapy. RNAi has gathered affection due to its specificity in knocking down targeted genes. However; it suffers from natural instability and low uptake efficiency of siRNA in vivo [38, 39]. Using the solvothermal technique, Wang et al. [40] created hydrophilic GO sheets with covalent attachment to allyl-amines. The advantage here is that allyl-amines and their derivatives like poly-allyl amine hydrochloride (PAH) give an overall positive character to the polymer which enhances the electrostatic interaction and thereby increases the possibility of penetrating the nucleus.

Graphene oxide–iron oxide nanocomposites (GFNCs) have been synthesized by an electrochemical, sonochemical–ultrasonication, and lastly co-precipitation method [41]. Co-precipitating iron salts onto graphene oxide nanosheets lead to variety of structures where intercalation of GO within iron oxide nanoparticles helps in its biocompatibility and stability [42]. A supermagnetic nanoparticle may be used for magnetic hyperthermia therapy [43, 44] where magnetic material proves to be a heating source while being injected into tissue. After absorbing radio frequency power through an oscillating magnetic field, heat is produced [45]. The heat produced destroys tumor cells without affecting neighboring cells [46, 47].

Polyethylene glycol (PEG) is hydrophilic polymer that makes graphene or other such nanoparticles more palatable to the biological system. It improves biotolerance, reduces non-specific adsorption, and thereby results in better targeting of tumor components. Dai and coworkers [48] have bonded PEG to GO for drug delivery applications. The produced composites demonstrated high aqua-stability, as previously demonstrated [48]. Wang et al. [49] successfully prepared a polyamidoamine (PAMAM) and PEG functionalized nanographene oxide (NGO) conjugate (NGO-PEG-dendrimer) to act as a gene carrier to deliver exogenous antimir-21 oligonucleotides into cells to inhibit miR against cancer.

### 2.1.2 Non-Covalent Modifications

Addition of PEG enhances the solubility and loading potential for drugs like doxorubicin (DOX) and camptothecin. This can be attributed to  $\pi$ – $\pi$  stacking [15, 50]. GO nanosheets can be coated with polyethylimine (PEI), thereby improving the electrostatic interactions with DNA and allowing effective gene delivery for acting against HeLa cells with minimum cytotoxicity [51, 52]. Positively charged  $\text{Fe}_3\text{O}_4$  can be integrated to negatively charged GO sheets via electrostatic interaction. This serves as an alternative cure in the form of magnetic hypothermia therapy [53–55]. Sol–gel techniques used in this method of synthesis lead to increased degree of defects in GO sheets due to thermal annealing. The preference of non-covalent functionalization of graphene-based particles is due to the fact that such modification doesn't alter the structure. The addition of new chemical groups can elaborate the number of potential ligands but it doesn't alter the electrically conductive properties of the material [56]. Several laboratories [57–59] exhibited a chain of pyrene-ended polymers to functionalize R-GO via  $\pi$ – $\pi$  stacking interaction. Repeated aromatic polymer can strongly bind graphene monolayers as a complete unit resulting in increased thermal, mechanical, and conductive properties [60, 61]. Conversely, non-aromatic polymers

have also been reinforced with graphene oxide (GO) or reduced graphene oxide (rGO) nanosheets. A prime example would be the use of cetyltrimethylammonium bromide (cTAB) surfactant to disperse off GO or rGO into natural rubber. It results in a polymer composite with enhanced properties [62]. Similarly, surfactant functionalized rGO has also been used to disperse into aqua-soluble polyurethane. The ionic forces between sulfonate of polyurethane and tertiary amine groups of surfactants are the primary force behind homogenized dispersion [63].

Some biomolecules like heparin are favored by rGO due to hydrophobic backbone of the former and the rGO surface. The repulsion between charged surfaces of this nanomaterial keeps it stable in a hydrophilic environment [64]. Hydrophobic interactions are also crucial in fixing of horseradish peroxidase onto rGO surface [65]. Aromatic biomolecules can interact with graphene through  $\pi$ - $\pi$  interactions with a classic example being that of glucose oxidase on graphene [66]. Electrodes covered in graphene have been shown to display the ability to differentiate between dopamine and ascorbic acid displaying a characteristic use in bioimaging in the absence of direct interaction with graphene surface [67]. Graphene-based materials have piqued interest in biological applications for some time, owing to its large surface area, chemical stability, conductivity, and, most critically, biocompatibility. These may be put to use as biosensors against characteristic nucleotides of a variety of diseases and genetic disorders [68, 69].

## ***2.2 Incorporation of Nanoparticles onto the Graphene Surface***

Fe nanoparticles were restricted to an interlamination of graphite employed as a catalyst, and graphene was synthesized into an interconnected 3D carbon nanotubule (CNT) web using in-situ chemical vapor deposition (CVD). This web may be seeded with dissociated cortical cells which can grow across the carbon nanotubule web and henceforth simulate the 3D trajectory and velocity distribution of cancer cell invasion [70]. Hong et al. used nanographene to target tumor cells in animal cancer model. Nano-GO sheets with covalently linked PEG chains were conjugated to NOTA (1,4,7-triazacyclononane-1,4,7-triacetic acid for Ga<sup>66</sup>-labeling) and TRC105 (antibody specific to CD105) to target tumor cells in mice. This was done to elucidate the pharmacokinetics and targeting efficacy via positron emission tomography (PET) [71]. Similar experiment was performed with rGO instead of GO to study vasculature in breast cancer tissue with Cu<sup>64</sup> as the imaging agent [72].

Gadolinium (Gd) nanoparticles were incorporated onto graphene oxide and then functionalized by polyethylene glycol (PEG); with further attachment to folic acid (FA), a tumor-targeting molecule. Doxorubicin was loaded onto this conjugate to form a targeted drug delivery system [73]. A novel phototheranostic nano-agent with enhanced photoacoustic (PA) and photothermal treatment (PTT) effects for cancer theranostics was created using indocyanine green-loaded polydopamine-reduced

graphene oxide nanocomposites (ICG-PDA-rGO). According to the data, the combination exhibits bigger PTT effects and higher PA contrast patterns than pure GO and PDA-rGO [74].

Chen et al. [75] demonstrated a novel theranostic platform for SERS imaging and chemo-photothermal therapy based on GO and AuNP (gold nanoparticle) core polyaniline shell (GO-Au@PANI) nanocomposites. PANI is a novel PTT agent with significant NIR absorption that is dispersed onto AuNPs using one-pot oxidative polymerization followed by stacking and electrostatic forces to connect AU@PANI core-shell NPs to GO sheet. MUC1 aptamer-NAS-24 aptamer-graphene oxide and MUC1 aptamer-Cytochrome C aptamer-GO were designed by Bahreyni et al. to trigger apoptosis in MDA-MB-231 and MCF-7 cells (breast cancer cell lines) [4]. Another study reports an approach to fabricate Tamoxifen citrate modified rGO with increased stability with lower toxicity. The composite was used to ablate breast cancer cells in vivo by way of stimulation of nano-rGO to produce the photothermal effect [76]. A nanocomposite was developed containing chemically formed rGO combined with manganese-doped zinc sulfide quantum dots and functionalized with folic acid (FA-rGO/ZnS:Mn). This was used as a drug delivery system for doxorubicin as a treatment for cancer [77]. Aqueous soluble graphene quantum dots (GQDs) made from cow milk were utilized to image and administer medication to cancer cells. The GQDs@Cys-BHC combination was created by using Cysteamine hydrochloride (Cys) to bind an anti-cancer medicine, berberine hydrochloride (BHC), to the N-doped and oxygen-rich GQDs. On a range of cancer cell lines, including HeLa cells and MDA-MB-231 breast cancer cells, the combination was found to have a potent cytotoxic effect [78].

### 3 Aspect of Drug and Gene Delivery of Graphene

Graphene oxide is constituted of a number of oxygen-containing functional groups, namely hydroxyl, carboxyl, epoxide group, etc., which enables GO to exhibit excellent hydrophilic properties and makes it a highly functional substrate with abundant anchoring sites. There has been a spike in the development of nanotechnology-based drug and gene delivery systems [79]. The graphene-derived family of nanomaterials had first been isolated through the process of exfoliation. But ever since then it has shown its potential towards biomedical application and therapeutics delivery such as drugs, genetic material, and biopharmaceutical. The significance of graphene relies on the high surface-to-volume ratio and polyaromatic structure that makes it effective and flexible enough for cargo loading, transport, and earmarking tissues [80]. This material binds to drugs by a combination of  $\pi$ - $\pi$  stacking interaction, hydrogen bond, and hydrophobic interactions [81]. Gene therapy is a much more attractive solution by the use of gene to protect DNA from nuclease degradation along with high transfection efficiency [82, 83]. Graphene derivatives should be modified into polymers such as chitosan, polyethylimine (Table 1) on account of the cationic surface charge

**Table 1** Gene delivery through different types of nano-composite

Components	Applications	References
PEI-conjugated GO	Low toxicity along with high transfection efficacy	[16, 84]
Lactosylated chitosan oligosaccharide (LCO)-functionalized graphene oxides	Gene sequences delivery to hepatic carcinoma cells	[85]
Folate-conjugated trimethyl chitosan (FTMC)/GO nanocomplexes (FG NCs)	Through electrostatic interaction, delivery of plasmid DNA	[86]

properties which enable binding with anionic oligonucleotide through electrostatic interaction. This helps us in decreasing the cytotoxicity of graphene within system.

### 3.1 Anticancer

Cancer can be summarized as a sequential progression of events starting with uncontrolled cell division, aberrant gene function and results in altered patterns of gene expression. It silently spreads across neighboring junctions and creeps into surrounding tissue which themselves are trying to prevent malignancy [103, 104]. The current health care does place chemotherapy as an important solution but in essence it is inadequate. The primary reason is the intolerable toxicity in conjunction with acquired drug resistance. The complex of multi-therapeutic agents and their molecular targets show up to impede the process of cancer adaptation and activate immunity for higher therapeutic efficacy and target selectivity [34]. A newer approach is to integrate gene delivery with chemotherapy. An entire new set of challenges arise in safe and efficient delivery of this nanomaterial inside the body [30, 105]. Graphene is much more palatable to the human physiology owing to the binding affinity to a number of functional groups [106]. Graphene is more bioactive in its interaction with the cell membranes and on approaching cell it undergoes endocytosis [27, 107]. The drug carrier must depart the endosomal compartment and release medicines into the cytosolic compartments for targeted drug delivery to the cell nucleus. This method involves a scheme to overcome drug resistance to cancer in DOX-sensitive MCF-7/ADR cells by filling DOX through physical mixing on the graphene oxide surface. In vitro, high pH-dependent relaxation was observed for drug content with DOX. In MCF-7/ADR cells, GO improved DOX sediments, leading to increased cytotoxicity compared to free DOX [108]. The cancer micro-environment like the intracellular lysosomes and endosomes has been established to be acidic in nature. In targeted drug delivery, regulated activation of DOX and CPT led to significant sensitivity in MCF-7 conditions treated to GO-loaded DOX or CPT exclusively. Therefore, in the development of drugs, MRI, and bioimaging, graphene and GO-modified magnetic nanoparticles lead to different biomedical applications [109] (Table 2).

Iron oxide along with graphene and its derivatives are considered superparamagnetic amongst biomaterials and significant for drug delivery. The resulting magnetic

**Table 2** Case studies treating cancers using variety of nano-drug conjugates

Therapy	Cancer	Cell line	Tumor cell type	Nano-drug component	Cell viability	References
Drug therapy	Breast cell	L929 and MDA-MB-231	Human	GO-PE-GQDS	–	[87]
Gene and drug therapy	Colon cancer and ovarian cancer	CT26 and SKOV-3	Human	GO-CDPP	36.5% and 37.7%, respectively	[32]
Drug therapy	Multi-drug-resistant breast cancer	MCF-7/ADR cell	Human	Hematin-conjugated dextran-functionalized GO hybrids-doxorubicin		[88]
Photothermal therapy	Cervical cancer	HeLa	Human	GO-Fe <sub>3</sub> O <sub>4</sub> nanocomposite	23.7% with IC-50 value 100 µg/mL	[89]
Drug therapy and imaging therapy	Breast cancer	MDA-MB-231	Murine Model	NOTA-GO-FSHR		[90]
Drug therapy	Colon cancer	HT-29 and SW-948, cells	Human	rGO-curcumin (CUR)-capped gold (CAG) nanoparticle	IC 50 Value–100 µg/ml	[91]
Gene therapy	Human melanoma cell line	SK28	Human	Bovine serum albumin—functionalized graphene oxide thin film		[92]
Drug delivery therapy	Breast cancer and fibroblast cancer cell line	MCF 7 and L929	Human	Hyperbranched polyglycerol functionalized graphene oxide along with quercetin drug	60% (IC 50 = 100 µg/ml at 72 h)	[93]
Drug delivery and imaging	Colon cancer	HCT 115	Human	NGs quantum dot-curcumin	–	[94]
Anticancer therapy	Glioma cells	U87 and U118	Human	Graphene platelet	Mortality rate = 54% and 58% (100 µg/mL)	19

(continued)

Table 2 (continued)

Therapy	Cancer	Cell line	Tumor cell type	Nano-drug component	Cell viability	References
Drug delivery	Renal cancer	786-0	Human	GO/BSA-Gd <sub>2</sub> O <sub>3</sub> /AS1411-DOX and Apt and DOX	-	[95]
Drug delivery	Bone cancer	MG-63		NGO-PEG-ICG	-	[96]
Drug delivery	Cervical cancer	HeLa	Human	Fe <sub>3</sub> O <sub>4</sub> @SiO <sub>2</sub> @GQD-FA/DOX	-	[97]
Drug and gene delivery	Lung, prostate cancer	A549, LLC1, PC3, C42b	Human	DOX-CMG-GFP-DNA	-	[34]
Drug delivery	Burkitt's Lymphoma	Raji B-cell	Human	NGO-PEG/DOX + Rituxan	-	[81]
Photochemical and drug therapy	Tumor cell	-	Mice	DOX-loaded rGO-PEG	-	[98]
Drug therapy and imaging therapy	Carcinoma cells	SGC-7901 and NCI-N87	Human	SN38-rGO	Cell viability 5% and 16%, respectively	[99]
Drug delivery and photodynamic therapy	Lung cancer	A549	Human	rGO and hypocrellin A and camptothecin	-	[100]
Photothermal therapy and imaging	Pancreatic cancer	PANC-1, HuP-T3	Human	GO-ION	-	[101]
Photothermal and gene therapy	Pancreatic cancer	MIA PaCa-2	Human	SIRNA delivery with PEGylated graphene oxide nanosheets	> 80% inhibition of pancreatic cancer	[102]



hybrids are distributed evenly before and after DOX loading in aqueous phase. Depending on the pH and magnetic hybrid property of nanomaterials, GO-Fe<sub>3</sub>O<sub>4</sub> plays a role in drug delivery [15, 27, 110, 111].

Bone morphogenic protein-2(BMP-2) being enclosed by the layers of positive and negative charged graphene oxide nanosheets alternatively, maintain bioactivity. Ti-coated GO surfaces transporting BMP-2 are supplemented with proliferation and differentiation of MSCs in comparison with Ti surfaces coated with BMP-2 alone. In vivo mouse tests often showed robust new bone formation with Ti-GO-BMP2 implants, thereby introducing the composite as a very successful transporter of anticancer drugs [112].

Cisplatin (CDDP) is a cancer-fighting medication; however, chemoresistance prevents it from being widely used in cancer treatment. Autophagy is a physiological process in which damaged organelles and misfolded proteins are removed from the cytoplasm during biogenesis. In CT26 colon cancer cells, graphene oxide (GO) is a nanomaterial that promotes autophagy and has anticancer characteristics. Chemoresistance in cancer cells is eliminated by the GO/CDDP complex, which also elucidates the mechanism behind it. GO/CDDP kills not only CT26 cells, but also ovarian, cervical, and prostate cancer cells [113, 114]. CT26 and Skov-3 cells had 71.5% and 66.4% vitality in the MTT experiment, respectively, after which both cell lines developed gradual chemoresistance to CDPP. GO/CDDP, on the other hand, reduced viability to 36.5 and 37.7%, indicating that GO chemo-sensitized CT26 and Skov-3 cells to CDDP. Though CDDP alone is unable of killing HeLa and Tramp-C11in, the combination of GO and CDDP enhances the deadly effect. After treatment with GO, CDDP, and GO/CDDP, only A549 cells show high vitality [32].

Genetically inherited disorders like cystic fibrosis, sickle cell anemia, cancer, Parkinson and Huntington diseases are caused by mutation of one or more gene. For critical disorders, an effective gene vector is used as a protection for DNA against nuclease degradation and high transfection efficiency of DNA uptake [13]. Since 2012, graphene and its composites along with other components such as chitosan-GO complex and polyethylene imine have spread out into gene and drug-gene delivery. As a non-viral gene vector, polyethylene imine has exhibited strong electrostatic interactions with negatively charged RNA and DNA, resulting in less cytotoxicity, increased transfection efficiency, and increased cell sensitivity [115]. Chitosan-graphene oxide transforms into a stable nano-sized complex using parental plasmid DNA in gene and drug delivery [35].

### 3.2 *Anti-Tumor*

Angio arising from the Greek word “angeion” implies vessel and genesis refers to synthesis or creation. Hence, angiogenesis is the physiological process of the formation of new blood vessels for the delivery of oxygen and nutrients to tissues. It is one of the fundamental needs for tumor growth and further metastasis, in the absence of

which cells have to face a hypoxic environment and thereby cellular death. Therefore, it is important to target angiogenic markers using the delivery of nanomaterials without invasive options. Nanotechnology has been previously cited for therapy and diagnosis of cancer [90, 116]. Case in point is when nano-graphene oxide along with monoclonal antibody is introduced against follicle stimulating receptor (FSH) while treating breast cancer in murine model. The FSH receptor is a highly specific tumor vasculature marker found in both primary and metastasized cancers [117, 118]. FSHR is a G protein-coupled receptor and acts as a standard marker for the detection of various cancers and conjugates safely with nanomaterials with enhanced specificity and stability. One of the classical drug carriers in case of breast cancer is NOTA-GO-FSHR-mAB [90]. In leukemia patients, monocytes are malignant and primarily responsible for necrosis. Mononuclear cells from peripheral blood of the patient were treated with few-layered graphene using CD4+ biomarker and its cytotoxicity was analyzed. The viability of the monocytes was found to be decreased but T, B, natural killer and dendritic cells remained unchanged. Graphene has showcased potential in control and improvement of necrosis in monocytoid cancer cells of patients suffering from symptomatic myeloid and chronic myelomonocytic leukemia [119]. Melanoma is a well-established skin disorder which involves secretion of excess melanin from melanocytes and change in skin pigmentation. Non-covalently conjugated graphene oxide and functionalized protein bio-coating are prepared by matrix-assisted pulsed laser evaporation (MAPLE) and used as a chassis in targeting carcinomas. Another example is when Dabrafenib (DAB) and Trichostatin A (TSA) inhibitors are integrated with hybrid GON-BSA nanocoatings. This is done for cells carrying a BRAFV600E pathway-triggering mutation and is mounted on adherent cells using the MAPLE technique. We can configure the GON-BSA systems by checking the inhibition of cellular BRAF expression and suppressed activity of histone deacetylases, respectively [92]. The diminishing ERK phosphorylation in primary melanoma cells (SKmelBRAFV600E cell line) proved DAB involvement. The TSA effect is established by the accumulation of acetylated histones in nuclei (SKmel23 BRAF WT cell line). It must be noted that the overall viability of melanoma cells has not been decreased but laser immobilization of anti-cancer drugs onto GON-BSA plays a role in inhibition of the mutation causing genes BRAF and HDAC. The dose-dependent effect on target expression and activity lies in conjunction with exposure to GON-BSA materials with a compositional gradient of inhibitors [92]. The aforementioned bio-platforms serve as better examples of cell-biomaterial interaction engineering to be practiced.

#### **4 Graphene as Phototherapeutic Agent Against Cancer**

An approach to cancer treatment with minimal side effects is the need of the hour. Graphene is a multifunctional carbon nanomaterial that has the potential to be exploited to build cancer-treatment technologies. The physiochemical properties of

## Cancer cell

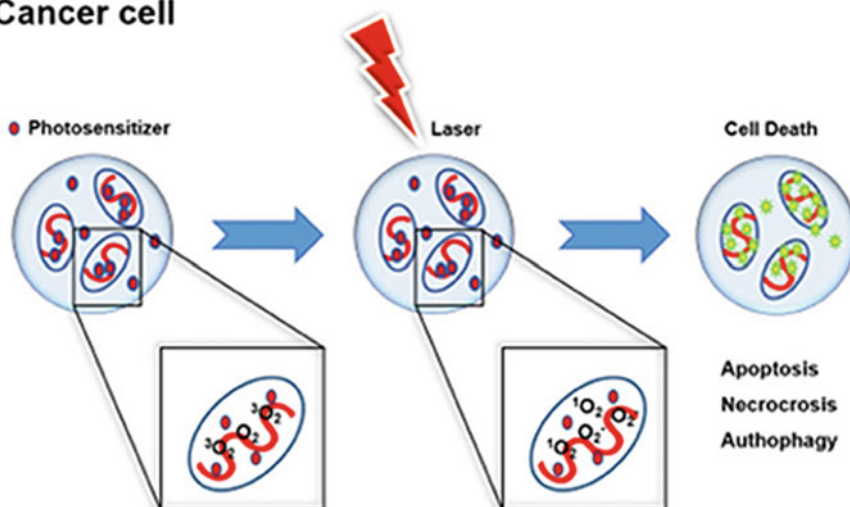


Fig. 2 Action of PDT mechanism [121] [CC. BY. 4.0]

graphene can be used to promote photodynamic and photothermal therapy for the treatment of superficial or deep tissue cancers [120].

**Photodynamic therapy (PDT):** This is a treatment intended for the breakdown of cancerous cell and pre-cancerous cell triggered by activation of light. It is a two-step process which integrates the energy of light with the drug (photosensitizer) for the cancer treatments. Photosensitizers are triggered using distinct wavelength of light, and more commonly lasers are being used for this purpose [121]. In recent years, photosensitizers are widely used to treat varied diseases, which include skin, lung, bladder, acne, head, and neck. In addition, PDT is used to treat viral, fungal, and bacterial infections too. Technological improvements have allowed PDT to integrate with anti-cancer treatment (Fig. 2).

**Photothermal therapy (PTT):** Photothermal effect is characterized by material photoexcitation, resulting in the production of thermal energy. In medical terms, this process is called **hyperthermia**. Photothermal effect is used for treatment in cases of laser hair removal, laser surgery, blood vessel lesions. PTT is minimally invasive while not sacrificing its therapeutic potential. PTT uses **near-infrared (NIR)** spectrum to generate heat by thermal ablation for further use [121] (Fig. 3).

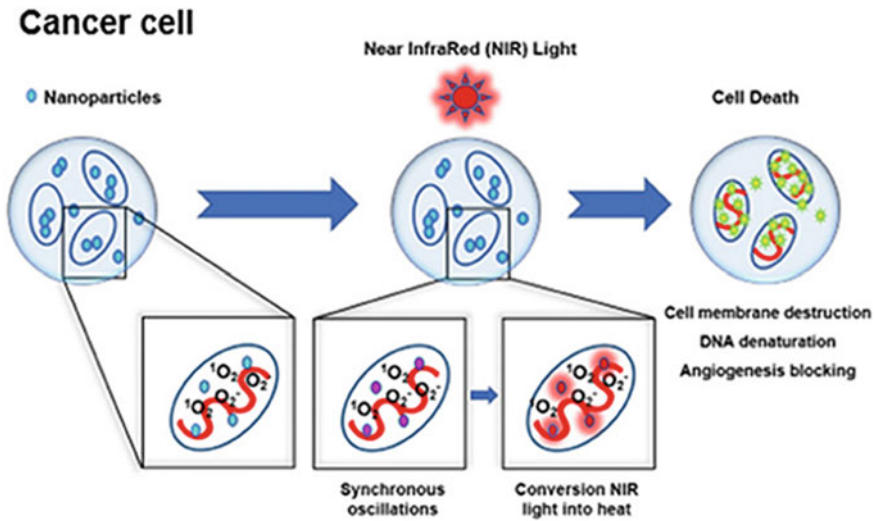


Fig. 3 Action of PTT mechanism [121] [CC. BY. 4.0]

## 4.1 Photodynamic Therapy by Graphene

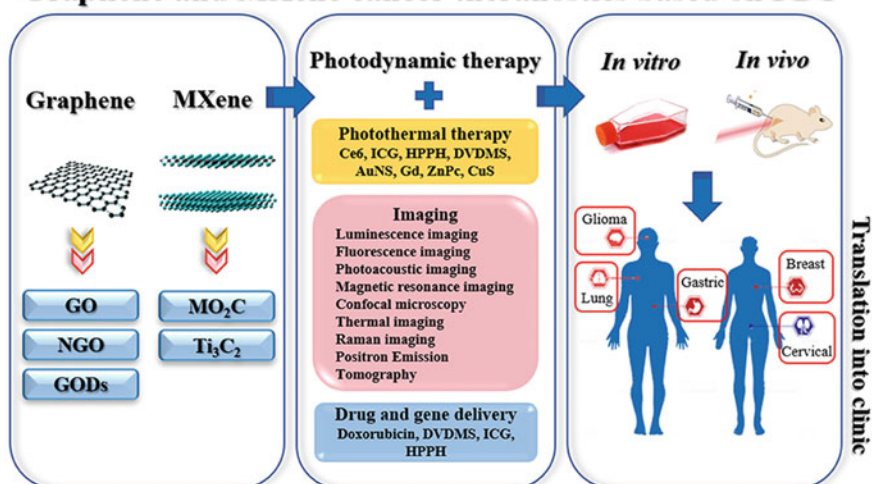
### 4.1.1 Breast Cancer

Breast cancer is the most common disease in the USA, with an estimated 333,000 diagnoses and 41,000 deaths in 2018 [122]. The field of nanotechnology has now become a promising instrument via the synthesis and development of nanomaterials used in the treatment, diagnosis, and the identification of cancer. Clinics have approved PDT as a minimally invasive treatment with provisions for selective toxicity. The potential uses of carbon nanomaterials as therapeutic agents, judiciously handled drug release systems and contrast agents for tumor diagnosis and location are demonstrated by recent scientific evidence [123]. Due to the presence of carbon nanomaterials in the PDT, cancer cells accumulate photosensitive molecules which absorb infrared radiation and turn it into heat in the presence of oxygen. There are many reported cases of the use of PDT carbon nanomaterials, and these are therefore used as a standard method for the treatment of breast cancer [123] (Figs. 4 and 5).

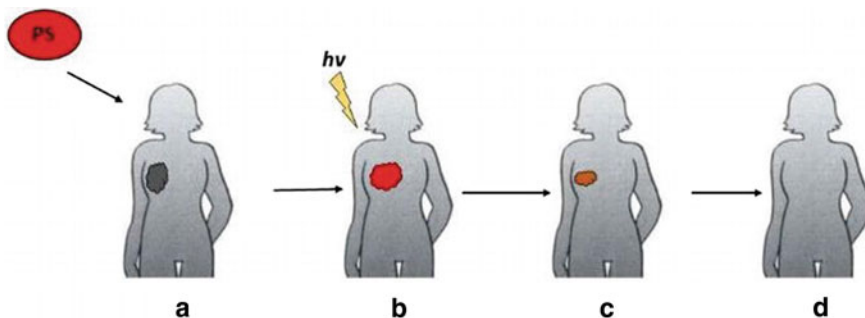
### 4.1.2 Cervical Cancer

Cervical cancer is the eighth most common cancer worldwide, and the fourth most in case of women, according to the World Health Organization (WHO). The in vitro phototoxicity research (laser radiation 670 nm, 1.8 J/square cm) of HA-GO/Ce<sub>6</sub> nanohybrids towards human cervical carcinoma HeLa cells revealed a photodynamic efficacy 10 times more than free Ce<sub>6</sub> (IC<sub>50</sub> changed from 1 to 0.1 gm/ml) [125]. The

## Graphene and MXene cancer theranostics based on PDT

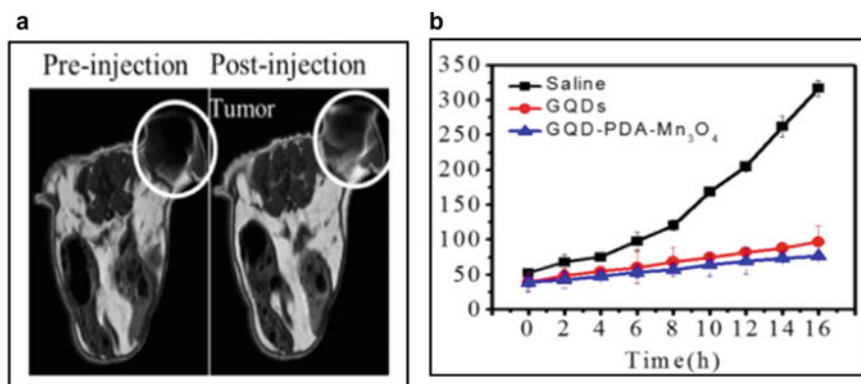


**Fig. 4** Schematic representation of the current PDT applications for graphene and MXene-based cancer theranostics. Panel on the left: representation of graphene and MXene. Middle panel: combined PDT applications, types of conjugated molecules (for PTT), types of imaging, and examples of conjugated medications (for drug delivery). Right panel: cancer types were that were examined in vitro and in vivo [121] [CC. BY. 4.0]



**Fig. 5** During photodynamic diagnosis, elementary chronological events. **a** Patients with cancer receive intravenous photosensitizer (PS) administration. **b** Irradiation and activation of photosensitizer, located at the site of cancer [124] [CC. BY. 4.0]

results demonstrated that in the presence of an external magnetic field, magnetic GO-Fe<sub>3</sub>O<sub>4</sub> nanocomposites can be used as a tumor-targeted PS delivery technique, as well as a photosensitive PDT agent capable of creating <sup>1</sup>O<sub>2</sub> at 671 nm in the presence of laser irradiation.



**Fig. 6** **a** In vivo real-time MRI images at 1 h after injection of GQD-PDA-Mn<sub>3</sub>O<sub>4</sub> nanoparticles (2.5 mg/kg) in nude mice, **b** tumor volume in mice treated with saline, GQD (2.5 mg/kg) and GQD-PDA-Mn<sub>3</sub>O<sub>4</sub> nanoparticles (2.5 mg/kg) for 16 days [126] [CC. BY. 4.0]

### 4.1.3 Lung Cancer

Image-guided therapy is a critical component in addressing the inadequacies of traditional cancer treatments. A multipurpose probe was devised to serve as a therapeutic and imaging agent, respectively, in order to correctly pinpoint tumor cells and prevent side effects. In a human lung cancer xenograft model, these nanoparticles also allowed for good T1-weighted MRI and were effectively used for combined visible red-imaging guided PDT and T1-weighted MRI [125]. A549 tumor-bearing mice were exposed to graphene quantum dots, saline, and graphene quantum dot-polydopamine-manganese oxide (GQD-PDA-Mn<sub>3</sub>O<sub>4</sub>) for two days, with a two-hour interval between each exposure. The tumor cells in the GQD-PDA-Mn<sub>3</sub>O<sub>4</sub>-treated mice were significantly smaller. As a result, GQD-PDA-Mn<sub>3</sub>O<sub>4</sub> nanoparticles could be useful for imaging as well as increasing the therapeutic potency of PDT in cancer therapy [125].

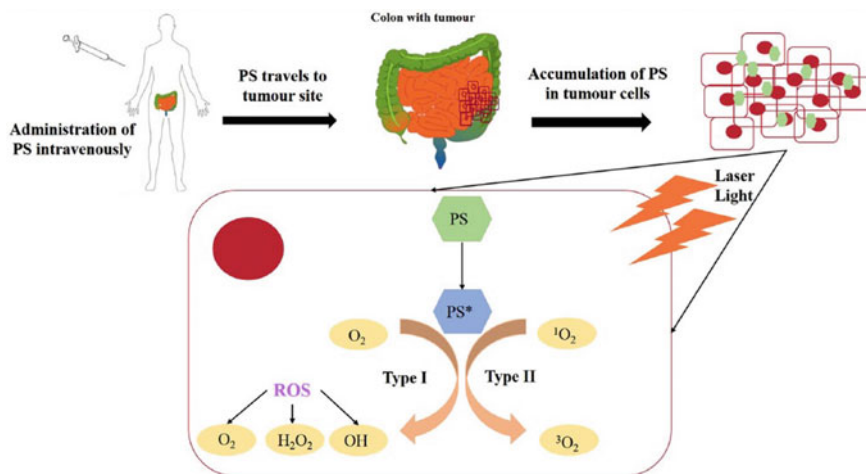
### 4.1.4 Colon Cancer

See the Fig. 6.

As a method of treatment for colon treatment, PDT is being explored. It has been shown that PDT becomes excited when exposed to light source of some specific wavelength and releases a type of oxygen that harms the cancer cell [127] (Fig. 7).

### 4.1.5 Skin Cancer

Melanoma with its increased prevalence along with its poor prognosis in its advanced stages is the most dangerous form of skin cancer [128]. The biocompatibility, in vivo



**Fig. 7** Cancer treatment using photodynamic therapy. PDT begins with the injection of a photosensitizer into a patient, followed by bloodstream transport of the photosensitizer to the tumor site and uptake of the PS by tumor cells. After the PS has been located in the tumor cells, laser light is administered to the area, penetrating the skin and exciting the PS. The PS then undergoes a type I or type II photoreaction, which produces reactive oxygen species or singlet oxygen, both of which can cause cell death [127] [CC. BY. 4.0]

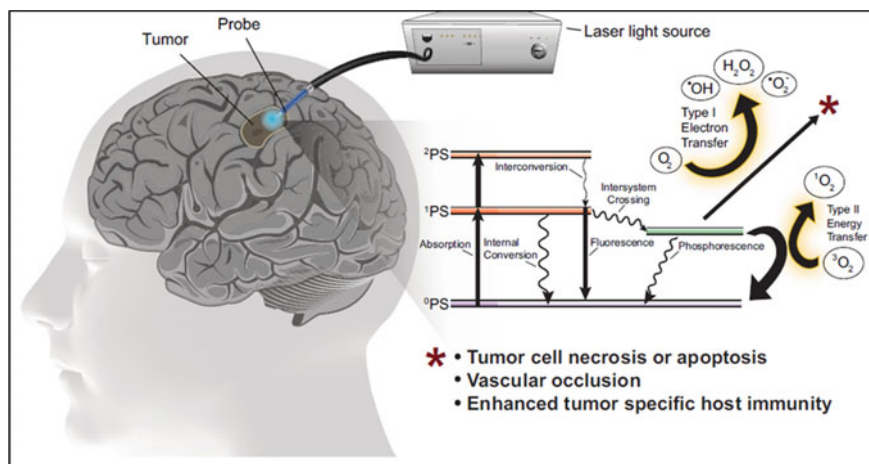
biodistribution, and PDT performance of TAG were investigated using B16F1 tumor xenograft-bearing mice. The above study showed excellent PDT potency under simulated solar irradiation. Compared to TA, TG, and Tt, TAG displayed the most significant *in vivo* PDT effect. TAG is an effective SSR-mediated PDT agent which has excellent biocompatibility.

#### 4.1.6 Prostate Cancer

Ge et al. presented a PDT agent focused on graphene quantum dots (GQDs) which can generate <sup>1</sup>O<sub>2</sub> through multistate sensitization process. GQD has a wide absorbing range which spans from UV, visible up to far red emission. The findings have ushered in a new era of carbon-based nanomaterial PDT agents that outperform traditional agents in terms of pH stability, water dispersibility, and <sup>1</sup>O<sub>2</sub> quantum yield for pancreatic tumors [129].

#### 4.1.7 Brain Cancer

Glioblastoma is a particularly aggressive type of brain cancer. The cytotoxic action of PDT requires the influx of oxygen, and hence, we need multisession treatment. The figure below shows the schematic for PDT of glioblastoma [130]. PDT uses



**Fig. 8** A simplified energy diagram of the oxygen-dependent photodynamic response is shown in this diagram of PDT for the treatment of glioblastoma. The photosensitizer in the ground state (0PS) is stimulated to one of two states, the first excited singlet state (1PS) or the second excited singlet state (2PS), by light stimulation at the proper wavelength and power (2PS). Intersystem crossover can then transform the 1PS to the excited triplet state (3PS). The 3PS may perform Type I or Type II redox reactions in the presence of molecular oxygen, resulting in reactive oxygen species that cause tumor cell death [130] [CC. BY. 4.0]

the wavelength window of 600–800 nm and excitation wavelength can be applied continuously or in pulsed mode, taking into account that pulsed delivery can facilitate the reoxygenation of the tumor among pulses [130] (Fig. 8).

## 4.2 Photothermal Therapy by Graphene

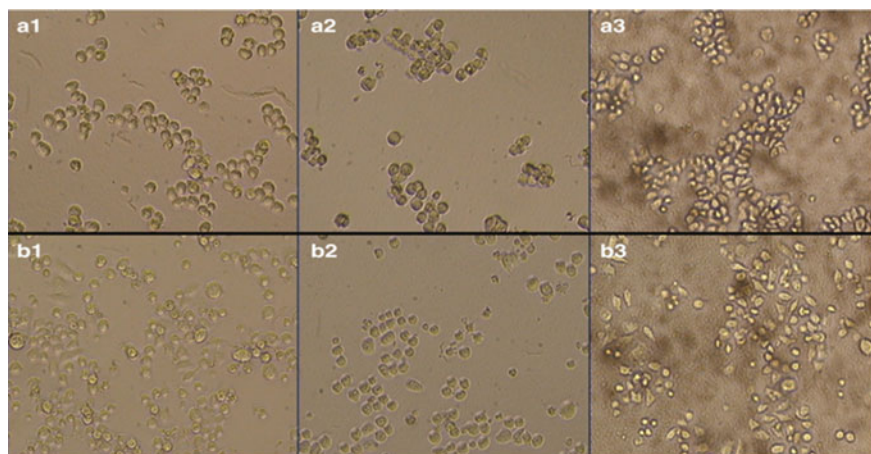
### 4.2.1 Graphene Photothermal Therapy Breast Cancer

The launch of nanosystems as contrast agents actually improves the quality of “magnetic resonance imaging” (MRI) resolution and imaging, “X-ray computed tomography” (X-CT), “positron emission computed tomography” (PET), “fluorescent imaging” (FI) [131].

### 4.2.2 Graphene Photothermal Therapy Lung Cancer

A novel class of reduced photothermal therapeutics based on graphene oxide for the ablation of lung cancer cells (A549) has been shown by Wang et al. [132]. The prepared reduced graphene oxide (RGO) was studied as a photothermal therapeutic agent for ablation of lung cancer (A549). Further, the generated results could show





**Fig. 9** Optical microscopy images of **a** HT29 and **b** SW48. a-1 and b-1: control samples. a-2 and b-2: after 15 min NIR ablation. a-3 and b-3: after 10 min NIR ablation to rGO [134] [CC. BY. 4.0]

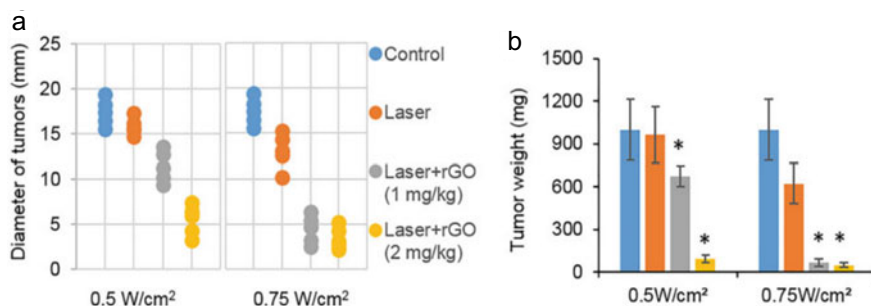
a path for the design of PTT agents, which would respond to the stimulus from the environment.

### 4.2.3 Graphene Photothermal Therapy Colon Cancer

For the treatment of HT29 and SW48 colon cancer, green tea-reduced graphene oxide (GT-rGO) sheet has been used for its high absorption at or near-infrared spectrum. New investigations have shown positive results in destroying cancer cells using polyethylene glycol (PEG) layered graphene. In recent times, [133] used nano-sized PEG layered rGO for cancer PTT using a very low concentration of graphene compared to previous reports for the destruction of cancer cell. Abdolahad et al. in his work involving biocompatible reduction of GO and used GT-rGO applied GT for cancer cell PTT. The attachment of GT-rGO sheets to the surface of cancer cells was illustrated by granularity research of the cells in flow cytometry tests [134]. It was observed that there was an improvement in the efficiency of the photothermal cancer cell therapy by the order of two by magnitude (Fig. 9).

### 4.2.4 Graphene Photothermal Therapy Pancreatic Cancer

In a recent study, researchers looked into the therapeutic effects of reduced graphene oxide combined with a near-infrared laser in animals with pancreatic cancer. The rGO showed a strong absorption of wavelength between 600 and 1100 nm. The experimental results indicated that the improvement in the photothermal conversion effect of rGO relies on two factors, namely light dosage and GO concentration.



**Fig. 10** Therapeutic effects of rGO on tumors under laser irradiation by a 980-nm laser. Diameter (A) and weight (B) of tumors 10 days after indicated treatment ( $n = 5$ ;  $*p < 0.05$ ) [135] [CC. BY. 4.0]

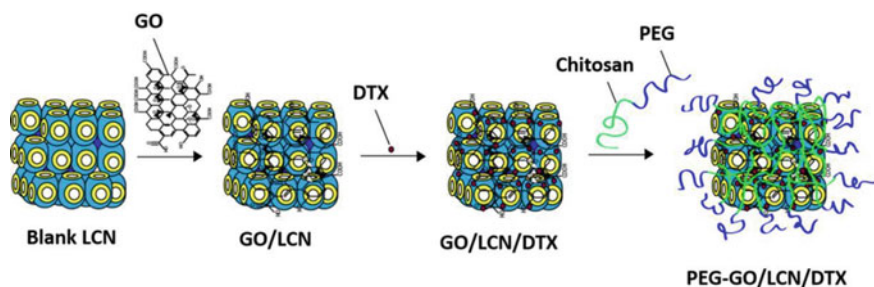
Combining the GO with 980 nm laser irradiation against mice pancreatic cancer cells achieves an ideal quantum of lethality [135] (Fig. 10).

#### 4.2.5 Graphene Photothermal Therapy Skin Cancer

Non-melanoma skin cancer (NMSC) is characterized by its high lethality. In recent years, PTT has become a very powerful technique to treat cancer. The goal of research was to develop a graphene-based PTT agent that could be used to treat NMSC using low-power NIR-induced laser hyperthermia therapy [136]. A lethal impact was seen when NIR radiation was combined with reduced graphene oxide nanoparticle-polyethylene glycol (rGON-PEG) in concentrations greater than  $100 \text{ g} \bullet \text{mL}^{-1}$ . The findings also support the adoption of a straightforward approach to generate functionalized rGON as a promising photo absorption agent for use in non-melanoma skin care therapy using PTT [136].

#### 4.2.6 Graphene Photothermal Therapy Prostate Cancer

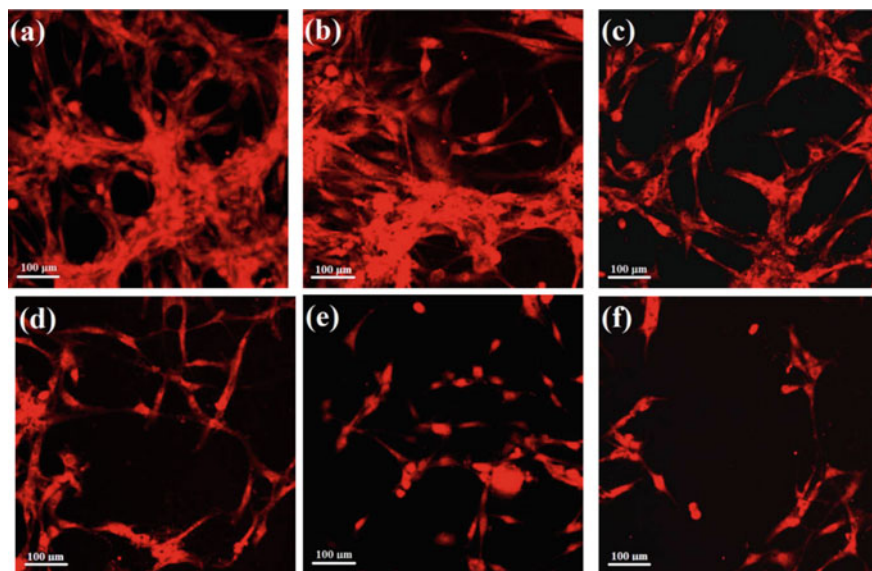
In Western European men, prostate cancer is the second largest cause of death. Thapa et al. describe the development of a PEGylated liquid crystalline nanoparticle (LCN) wrapped in GO and loaded with docetaxel (DTX) for chemo-photothermal treatment of metastatic prostate cancer cells [137]. For in vitro cell research, the DU145 prostate cancer cell line was used, but this cell line is highly metastatic and could develop DTX resistance. The findings of Thapa et al. investigation's suggested that the PEG-GO/LCN/DTX complex could be used to treat prostate cancer [137]. The augmentation of nanoparticles in combination with PTT generated by GO suggests that it could be employed to prevent DTX resistance as well as prostate cancer spread (Fig. 11).



**Fig. 11** PEG-GO/LCN/DTX stands for graphene oxide-wrapped PEGylated liquid crystalline nanoparticles loaded with docetaxel (PEG-GO/LCN/DTX); PEG stands for polyethylene glycol; GO stands for graphene oxide; LCN stands for liquid crystalline nanoparticle; DTX is for docetaxel [137] [CC. BY. 4.0]

#### 4.2.7 Graphene Photothermal Therapy Brain Cancer

Biocompatible porphyrin functionalized graphene oxide (PGO) was synthesized as a photothermal platform which has an absorbance at 800 nm for the brain cancer therapy. “Most importantly, the efficiency of photothermal conversion of PGO is increased by 89% and 33% compared to GO and rGO with 808 nm laser irradiation, causing large number of brain cancer cells ablation *in vitro*” [127] (Fig. 12).



**Fig. 12** Fluorescence microscope images (20 ×) of U87-MG after irradiation by 808 nm NIR **a** without PGO, and with PGO for **b** 0 min, **c** 4 min, **d** 6 min, **e** 8 min, and **f** 10 min [127] [CC. BY. 4.0]

#### **4.2.8 Graphene Photothermal Therapy Gastric Cancer**

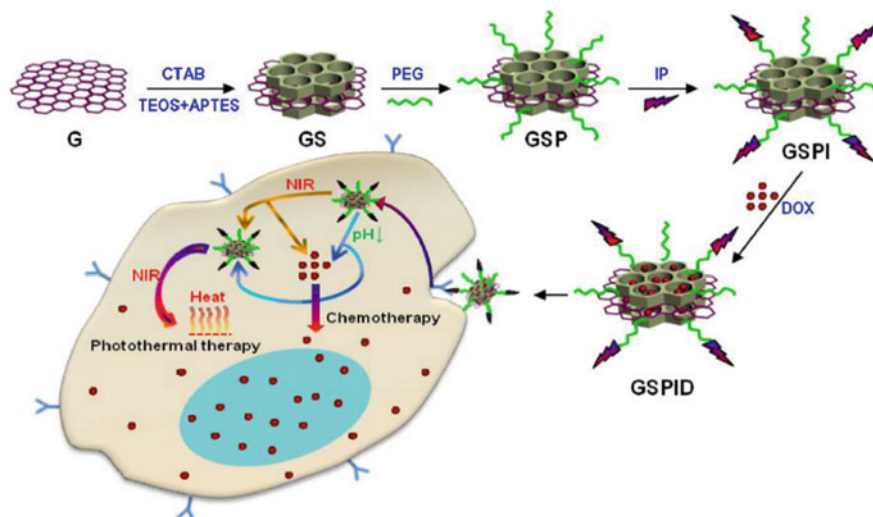
Gastric cancer is the second highest cause of malignant growth-related death in China with 5-year stability of less than 24%. Hence, it is important to perceive, monitor, or execute early gastric disease cells [127]. SN38 has been used as a graphene oxide coating agent in recent investigations (GO). When compared to earlier data, SN38-rGO NPs showed a significant improvement. The MTT assay was used to assess the photothermal efficiency and cytotoxicity of the SN38-rGO. The findings suggested that reduced graphene oxide coated with SN-38 could be employed in gastric cancer PTT [127].

#### **4.2.9 Graphene Photothermal Therapy Glioma Cancer**

Glioma is a deep-seated brain tumor that demands the delivery of a photothermal agent through the skull into the diseased tissue using near-infrared (NIR) radiation. The effectiveness of this approach has been demonstrated in studies using orthotopic mouse glioma models and 808 nm NIR lasers to accomplish successful photothermal excision of cancer cells. One of the standard ways of treatment to glioma is through Chemotherapy, on its own or combined with radiotherapy. This approach comes with a number of problems like insufficient dosage to affected regions and sustained damage or side effects to the neighboring tissues. The results of cytotoxicity tests and IP modification resulted in an excellent drug delivery system. Because of its advanced chemo-photothermal (synergistic) targeted therapy and strong drug release characteristics, GSPID was found to be useful in glioma combination therapy, reducing frequent and intrusive dosing and improving patient compliance [131] (Fig. 13).

#### **4.2.10 Graphene Combinational Therapy Breast Cancer**

PDT and PTT in combination have been thoroughly researched. It includes a historical investigation that demonstrates the anticancer and biosafety of graphene oxide-polyethylene glycol (GO-PEG). Under the 980 nm wavelength, a PEGylated graphene oxide of nanosize is co-loaded with photosensitizer and two photon chemicals for cascading TP-PDT and PTT against breast cancer [138]. The combined therapy dramatically slowed tumor growth. This combinational therapy has a lot of potential as a new cancer theranostics technique (Fig. 14).



**Fig. 13** GSPID is developed as a multifunctional drug delivery system for chemo-photothermal targeted therapy [131] [CC. BY. 4.0]

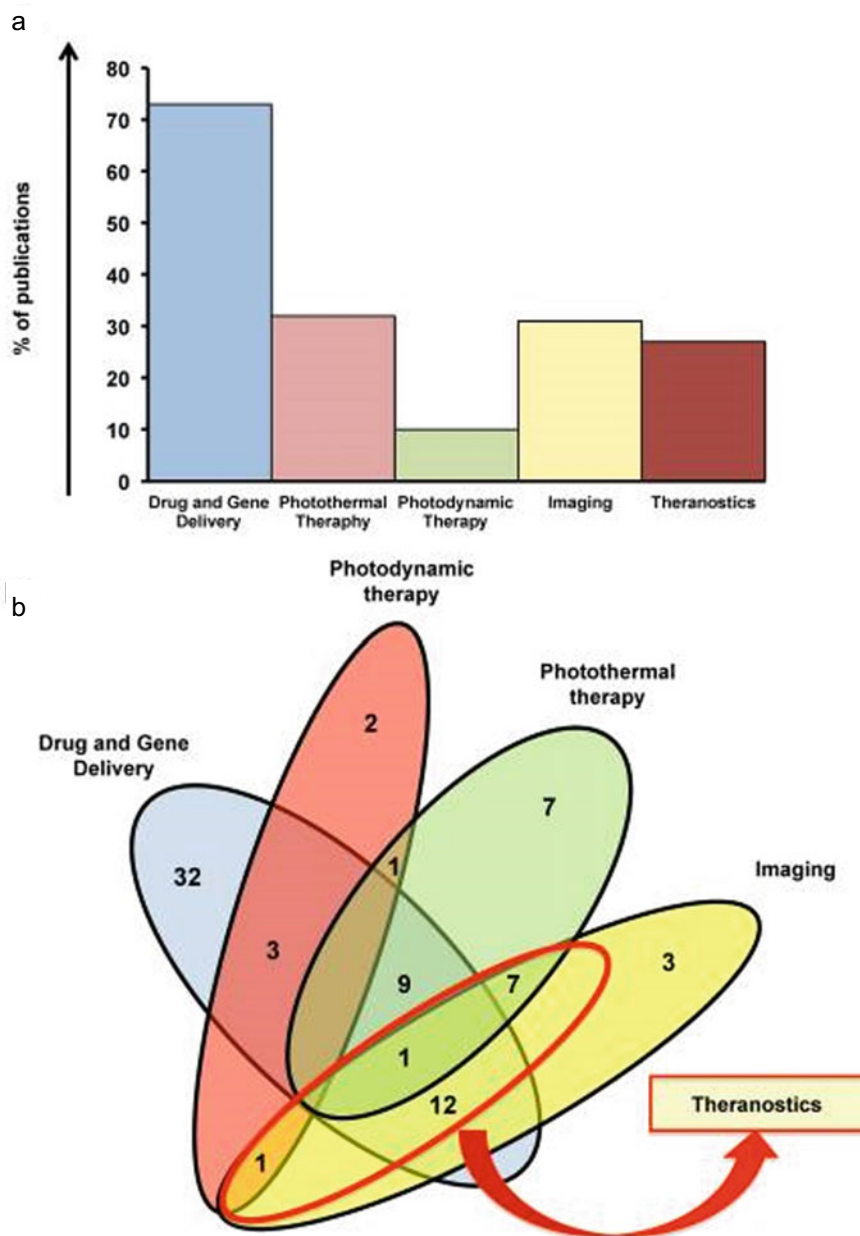
### 4.3 Graphene Combinatorial Therapy

#### 4.3.1 Cervical Cancer

Cervical cancer is a type of gynaecological cancer that has shown significant impacts on cell proliferation, cytotoxicity, and apoptosis when Cis and rGO-AgNPs were combined. The study's major goal was to see how Cis and a reduced graphene oxide–silver nanoparticle nanocomposite worked together in human cervical carcinoma (HeLa) (rGO-AgNPs) [125]. The researchers discovered that combining Cis and rGO-AgNPs had a greater direct impact on apoptotic and autophagy gene expression, as well as a significant increase in the accumulation of autophagosomes and autophagolysosomes associated with reactive oxygen species formation [125].

#### 4.3.2 Lung Cancer

GO toxicity encompasses cytotoxicity, genotoxicity, and in vivo toxicity. The studies have demonstrated that GO can cause lung cancer and apoptosis. Because it is a non-invasive treatment with several major benefits such as spatiotemporal selectivity, remote controllability, and repeatability without cumulative toxicity, phototherapy (PT) is considered a potential cancer therapy as a non-operative medical treatment, including PDT and PTT [129]. One of the effective and safe methods for selective eradication of cancer cells while avoiding side effects on healthy tissues are PTT and PDT.



**Fig. 14** **a** Percentage of manuscripts based on the applications against cancer, **b** Venn diagram based on the main applications (drug delivery, photothermal therapy, photodynamic therapy, imaging). In the red round the theranostics studies [138] [CC. BY. 4.0]

### 4.3.3 Colon Cancer

During comparison to irinotecan, the results demonstrated a 2–3 order of magnitude increase in chemotherapeutic drug feasibility in colon cancer HCT-116 cell line. The use of graphene-based formulations as a multifunctional platform for colon cancer therapies has a lot of promise [120].

### 4.3.4 Pancreatic Cancer

Pancreatic cancer incidence increased in China from 12.80/100000 in 2004 to 15.66/100000 in 2009. The median duration to survival was only 3.9 months, and the 5-year survival rate was only 4.1%. The researchers used a strong laser dose ( $0.75 \text{ W/cm}^2$ ) in their research [139]. Under varied light intensities, a same volume of rGO solution (50 g/mL) was able to achieve fluctuating degrees of temperature development.

### 4.3.5 Skin Cancer

With an ultralow-intensity near-infrared (NIR) light source, a synchronously activated “Chemo/PTT/PDT” nanoplatfrom has been constructed [140]. The nanoplatfrom is constituted of three parts, namely upconversion core (UC) which is highly emissive, doxorubicin hydrochloride which is an anticancer drug and chlorine e6 ( $\text{Ce}_6$ ) photosensitizer. On the one hand, the 808 nm wavelength with ultralow intensity ( $0.25 \text{ W cm}^2$ ) seems to be the max permeable exposure for the skin. The modest PGO hyperpyrexia caused irreversible cancer cell death for PTT and significantly increased medication release for improved treatment. The upconverted 660 nm light from UC, on the other hand, was utilized to activate  $\text{Ce}_6$  and form reactive oxygen species for PDT, while the upconverted 540 nm light from UC could be used to visualize the treatment process [140]. In vivo and in vitro anticancer investigations revealed that ultralow-intensity Near-infrared light synchronously activated “PDT/chemo/PTT” nanoplatforms had a remarkable therapeutic effectiveness while causing very little photo-damage.

### 4.3.6 Prostate Cancer

Prostate cancer is a well-known cancer which has been known for a thousand years [141]. For the targeted capture of accurate diagnosis, combined therapeutic action of prostate cancer and prostate CTCs, theranostics graphene oxide (GO) with magnetic nanoparticles was evolved. The data resulted from the Chaya et al. showed that the indocyanine green (ICG)-bound A9-aptamer-attached GO is very capable to drive

photodynamic and photothermal treatment at 785 nm for prostate cancer. The experimental result also showed that theranostics GO can also have extensive potential for its real-life applications [141].

### 4.3.7 Brain Cancer

Due to side effects and limited transport through the blood–brain barrier, current medications for malignant glioma treatment have a low therapeutic efficiency (BBB). On combining the photothermal and chemotherapy resulted in overcoming this issue (Table 3), it was found that transferrin-conjugated PEGylated nanoscale graphene oxide (TPGD) performs dual function in photothermal therapy and chemotherapy. It was observed that combinational TPGD therapy resulted in higher rates of glioma cell death. For combination glioma therapy, a possible nanoscale drug delivery system has been designed that can effectively reduce side effects and improve treatment outcomes [142] (Fig. 15).

### Future Prospectives

Research in the field of nanomaterials is exponentially increasing following the discovery of graphene and derived materials. Nanosystems made using bioactive nanomaterials have displayed capability in tumor diagnosis and therapy. Nanographene and its derivatives have outperformed other formulations as carriers due to their high loading capacity for therapeutic agents, genes, and siRNAs. This also makes economic sense due to ease of manufacture and replicability. Nonetheless, these properties can further be improved by surface functionalization which may lead to their band (atomic energy) alignment and additional functions to their property. This also increases biocompatibility and decreases toxicity. Further grafting with stress-responsive organic/inorganic materials imparts another use of detection/monitoring along with treatment. But we must be careful in the aforementioned applications as is evident in the following observations. Covalent functionalization may influence the electrical and structural properties of these materials by affecting the binding strength between transition metal and chalcogen atoms. Similarly, non-covalent functionalization can cause functionalized molecules to desorb and degrade during operations. As a result, we must encourage a proper understanding and analysis of the impact of such functionalization on the structure and electrical characteristics of graphene-based materials. When it comes to clinical contexts, the impact of surface charge, size/shape, functionalization on biocompatibility, safety, and stability must be considered. It is also necessary to investigate the nature of the interfacial contact between graphene-associated systems and functionalized molecules. Insufficient charge transfer may come from a weak contact, resulting in reduced performance. The adsorption of organic molecules in media is limited by the surface charge and hydrophilic character of most graphene-related materials. So, it is important to layer such surface in order to make them hydrophobic and thereby facilitate maximal



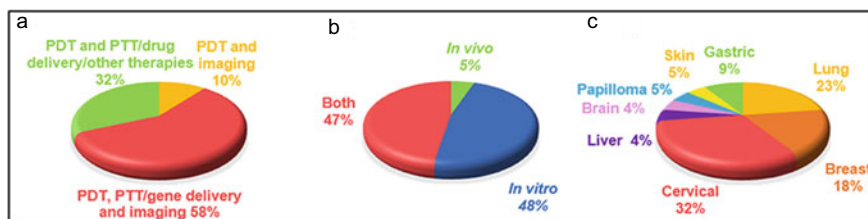
**Table 3** Table regarding different kinds of studies using GBMs for PDT and PTT theragnostic applications [2] [CC. BY. 4.0]

Place of cancer	Type of applications	Model	Drug/PS	Imaging	Material
Cervix	PDT and drug delivery	In vitro	Chlorine e6	-	GO-PEG
Gastric	PDT and drug delivery	In vitro	Chlorine e6	-	FA-GO-Ce6
Lung	PDT and drug delivery	In vitro	Hypocrellin A and Camptothecin	-	rGO
Papilloma cervix	Imaging, PDT, and PTT	In vitro and in vivo	Doxorubicin	CLSM and MRI	UCNPs-NGO/ZnPc
Cervix	PDT and PTT	In vitro and in vivo	Methylene blue	-	GO
Lungs	Imaging, PDT, and PTT	In vitro	Chlorine e6	NIR fluorescence imaging	GO-HA-Ce6
Breast	Imaging and PDT	In vitro, In vivo, and ex vivo	HPPH	PET imaging, (NIR) fluorescence imaging	GO-PEG-HPPH
Lungs	PDT and drug delivery	In vitro	Hypocrellin A and Camptothecin	-	HA/SN-38/GO
Cervix	Imaging, PDT, and PTT	In vitro	-	Fluorescence imaging and MRI	MFG (magnetic and fluorescent graphene)
Cervix, Breast	Imaging and PDT	In vitro and in vivo	-	Fluorescence imaging	NGs-QDs
Lungs	Imaging, PDT, and PTT	In vitro and in vivo	DVDMS	Fluorescence imaging and PAI	GO-PEG-DVDMS
Breast	Imaging, PDT, PTT, and drug delivery	In vitro	Indocyanine green	NIR fluorescence imaging	pGO-CuS/ICG
Brian	Imaging, PDT and drug delivery	In vitro, In vivo, and ex vivo	DVDMS	Fluorescence imaging	GO-PEG-DVDMS
Cervix	Imaging, PDT, and PTT	In vitro	Au	Raman bioimaging	PEG-Au@GON NPs

(continued)

**Table 3** (continued)

Place of cancer	Type of applications	Model	Drug/PS	Imaging	Material
Lungs	Imaging, PDT, and PTT	In vitro and in vivo	–	Fluorescence confocal microscope NIR fluorescence and thermal imaging	NGO-808
Melanoma	Imaging, PDT, and PTT	In vitro	–	Fluorescence imaging	GO-PEG-folate
Esophagus	PDT, PTT, drug delivery, and magneto-mechanical therapy	In vitro	Doxorubicin	–	HMNS/SiO <sub>2</sub> /GQDs-DOX
Breast	Imaging, PDT, and PTT	In vitro and in vivo	Chlorine e6	CLSM, thermal/PT imaging	GO/AuNS-PEG and GO/AuNS-PEG/Ce <sub>6</sub>
Liver, Cervix	Imaging, PDT, and PTT	In vitro, In vivo, and ex vivo	Chlorine e6	UCL imaging	NGO-UCNP-Ce <sub>6</sub> (NUC)



**Fig. 15** Overview of graphene-based PDT theranostics. Percentages of manuscripts (19 papers) on the basis of **a** type of applications combined with PDT, **b** model used for the study (in vivo or in vitro), **c** type of cancer studied [121] [CC. BY. 4.0]

adsorption. Finally, the cooperative effects of nanomaterials and its conjugates should be scrutinized thoroughly to fully exploit their potential, which can widen their applicability in the future.

## References

- Bray F, Ferlay J, Soerjomataram I, Siegel RL, Torre LA, Jemal A (2018) Global cancer statistics 2018: GLOBOCAN estimates of incidence and mortality worldwide for 36 cancers in 185 countries. *CA A Cancer J Clin* 68:394–424
- Madeddu R, Solinas G, Forte G, Bocca B, Asara Y, Tolu P, Delogu LG, Muresu E, Montella A, Castiglia P (2011) Diet and nutrients are contributing factors that influence blood cadmium levels. *Nutr Res* 31:691–697
- Hanna TP, Evans GA, Booth CM (2020) Cancer, COVID-19 and the precautionary principle: prioritizing treatment during a global pandemic. *Nat Rev Clin Oncol* 17:268–270
- Bahreyni A, Yazdian-Robati R, Hashemitabar S, Ramezani M, Ramezani P, Abnous K, Taghdisi SM (2017) A new chemotherapy agent-free theranostic system composed of graphene oxide nano-complex and aptamers for treatment of cancer cells. *Int J Pharm* 526:391–399
- Rubin GA, Wan EY, Saluja D et al (2020) Restructuring electrophysiology during the COVID-19 pandemic: a practical guide from a New York City hospital network. *Crit Pathways Cardiol J Evid-Based Med* 19:105–111
- van de Haar J, Hoes LR, Coles CE et al (2020) Caring for patients with cancer in the COVID-19 era. *Nat Med* 26:665–671
- Kim J, Piao Y, Hyeon T (2009) Multifunctional nanostructured materials for multimodal imaging, and simultaneous imaging and therapy. *Chem Soc Rev* 38:372–390
- Liu Z, Robinson JT, Tabakman SM, Yang K, Dai H (2011) Carbon materials for drug delivery and cancer therapy. *Mater Today* 14:316–323
- Hare JI, Lammers T, Ashford MB, Puri S, Storm G, Barry ST (2017) Challenges and strategies in anti-cancer nanomedicine development: an industry perspective. *Adv Drug Deliv Rev* 108:25–38
- Barreto JA, O'Malley W, Kubeil M, Graham B, Stephan H, Spiccia L (2011) Nanomaterials: applications in cancer imaging and therapy. *Adv Mater* 23:H18–H40
- Feng L, Liu Z (2011) Graphene in biomedicine: opportunities and challenges. *Nanomedicine* 6:317–324
- Yang K, Wan J, Zhang S, Tian B, Zhang Y, Liu Z (2012) The influence of surface chemistry and size of nanoscale graphene oxide on photothermal therapy of cancer using ultra-low laser power. *Biomaterials* 33:2206–2214

13. Shen H, Zhang L, Liu M, Zhang Z (2012) Biomedical applications of graphene. *Theranostics* 2:283–294
14. Novoselov KS, Geim AK, Morozov SV, Jiang D, Zhang Y, Dubonos SV, Grigorieva IV, Firsov AA (2004) Electric field effect in atomically thin carbon films. *Science* 306:666–669
15. Zhang L, Xia J, Zhao Q, Liu L, Zhang Z (2010) Functional graphene oxide as a nanocarrier for controlled loading and targeted delivery of mixed anticancer drugs. *Small* 6:537–544
16. Feng L, Zhang S, Liu Z (2011) Graphene based gene transfection. *Nanoscale* 3:1252–1257
17. Dinescu S, Ionita M, Pandele AM, Galateanu B, Iovu H, Ardelean A, Costache M, Hermenean A (2014) In vitro cytocompatibility evaluation of chitosan/graphene oxide 3D scaffold composites designed for bone tissue engineering. *Bio-Med Mater Eng* 24:2249–2256
18. Russier J, Treossi E, Scarsi A, Perrozzi F, Dumortier H, Ottaviano L, Meneghetti M, Palermo V, Bianco A (2013) Evidencing the mask effect of graphene oxide: a comparative study on primary human and murine phagocytic cells. *Nanoscale* 5:11234–11247
19. Chwalibog A, Jaworski S, Sawosz E, Grodzik M, Winnicka A, Prasek M, Wierzbicki M (2013) In vitro evaluation of the effects of graphene platelets on glioblastoma multiforme cells. *Int J nanomed* 8:413–420
20. Gurunathan S, Han JW, Park JH, Kim J-H (2014) An in vitro evaluation of graphene oxide reduced by *Ganoderma* spp. in human breast cancer cells (MDA-MB-231). *Int J Nanomed* 9:1783–1797
21. Geim AK (2009) Graphene: status and prospects. *Science* 324:1530–1534
22. Kakran M, Li L (2012) Carbon nanomaterials for drug delivery. *Key Eng Matter* 508:76–80
23. Akinwande D, Brennan CJ, Bunch JS et al (2017) A review on mechanics and mechanical properties of 2D materials—graphene and beyond. *Extreme Mech Lett* 13:42–77
24. Geim AK, Novoselov KS (2007) The rise of graphene. *Nature Mater* 6:183–191
25. Yang K, Feng L, Shi X, Liu Z (2013) Nano-graphene in biomedicine: theranostic applications. *Chem Soc Rev* 42:530–547
26. Dhand V, Rhee KY, Ju Kim H, Ho Jung D (2013) A comprehensive review of graphene nanocomposites: research status and trends. *J Nanomater* 2013:1–14
27. Yang X, Zhang X, Liu Z, Ma Y, Huang Y, Chen Y (2008) High-efficiency loading and controlled release of doxorubicin hydrochloride on graphene oxide. *J Phys Chem C* 112:17554–17558
28. Yoon S, In I (2010) Role of poly(N-vinyl-2-pyrrolidone) as stabilizer for dispersion of graphene via hydrophobic interaction. *J Mater Sci* 46:1316–1321
29. Trapani G, Caruso VCL, Cucci LM, Attanasio F, Tabbi G, Forte G, La Mendola D, Satriano C (2020) Graphene oxide nanosheets tailored with aromatic dipeptide nanoassemblies for a tuneable interaction with cell membranes. *Front Bioeng Biotechnol* 8:427. <https://doi.org/10.3389/fbioe.2020.00427>
30. Ali-Boucetta H, Bitounis D, Raveendran-Nair R, Servant A, Van den Bossche J, Kostarelos K (2012) Purified graphene oxide dispersions lack in vitro cytotoxicity and in vivo pathogenicity. *Adv Healthcare Mater* 2:433–441
31. Verde V, Longo A, Cucci LM, Sanfilippo V, Magrì A, Satriano C, Anfuso CD, Lupo G, La Mendola D (2020) Anti-Angiogenic and anti-proliferative graphene oxide nanosheets for tumor cell therapy. *IJMS* 21:5571
32. Lin KC, Lin MW, Hsu MN, Yu-Chen G, Chao YC, Tuan HY, Chiang CS, Hu YC (2018) Graphene oxide sensitizes cancer cells to chemotherapeutics by inducing early autophagy events, promoting nuclear trafficking and necrosis. *Theranostics* 8:2477–2487
33. Ciobotaru CC, Damian CM, Matei E, Ionu H (2014) Covalent functionalization of graphene oxide with cisplatin. *Mater Plast* 51:75–80
34. Wang C, Ravi S, Garapati US, Das M, Howell M, Mallela J, Alwarappan S, Mohapatra SS, Mohapatra S (2013) Multifunctional chitosan magnetic-graphene (CMG) nanoparticles: a theranostic platform for tumor-targeted co-delivery of drugs, genes and MRI contrast agents. *J Mater Chem B* 1:4396–4405
35. Bao H, Pan Y, Ping Y, Sahoo NG, Wu T, Li L, Li J, Gan LH (2011) Chitosan-functionalized graphene oxide as a nanocarrier for drug and gene delivery. *Small* 7:1569–1578

36. Rana VK, Choi M-C, Kong J-Y, Kim GY, Kim MJ, Kim S-H, Mishra S, Singh RP, Ha C-S (2010) Synthesis and drug-delivery behavior of chitosan-functionalized graphene oxide hybrid nanosheets. *Macromol Mater Eng* 296:131–140
37. Pan Y, Wang L, Kang S, Lu Y, Yang Z, Huynh T, Chen C, Zhou R, Guo M, Zhao Y (2015) Gd–Metallofullerenol nanomaterial suppresses pancreatic cancer metastasis by inhibiting the interaction of histone deacetylase 1 and metastasis-associated protein 1. *ACS Nano* 9:6826–6836
38. Whitehead KA, Langer R, Anderson DG (2009) Knocking down barriers: advances in siRNA delivery. *Nat Rev Drug Discov* 8:129–138
39. Shim MS, Kwon YJ (2010) Efficient and targeted delivery of siRNA in vivo. *FEBS J* 277:4814–4827
40. Wang G, Wang B, Park J, Yang J, Shen X, Yao J (2009) Synthesis of enhanced hydrophilic and hydrophobic graphene oxide nanosheets by a solvothermal method. *Carbon* 47:68–72
41. Sebastian N, Yu W-C, Hu Y-C, Balram D, Yu Y-H (2019) Sonochemical synthesis of iron-graphene oxide/honeycomb-like ZnO ternary nanohybrids for sensitive electrochemical detection of antipsychotic drug chlorpromazine. *Ultrason Sonochem* 59:104696
42. Zubir NA, Yacou C, Motuzas J, Zhang X, Diniz da Costa JC (2014) Structural and functional investigation of graphene oxide–Fe<sub>3</sub>O<sub>4</sub> nanocomposites for the heterogeneous Fenton-like reaction. *Sci Rep*. <https://doi.org/10.1038/srep04594>
43. Pandey B, Shetake N, Balla Murali MS, Kumar A (2016) Magnetic hyperthermia therapy: an emerging modality of cancer treatment in combination with radiotherapy. *J Radiat Cancer Res* 7:13–17
44. Xie J, Yan C, Yan Y, Chen L, Song L, Zang F, An Y, Teng G, Gu N, Zhang Y (2016) Multimodal Mn–Zn ferrite nanocrystals for magnetically-induced cancer targeted hyperthermia: a comparison of passive and active targeting effects. *Nanoscale* 8:16902–16915
45. Oh Y, Lee N, Kang HW, Oh J (2016) In vitro study on apoptotic cell death by effective magnetic hyperthermia with chitosan-coated MnFe<sub>2</sub>O<sub>4</sub>. *Nanotechnology* 27:115101
46. Dudar TE, Jain RK (1984) Differential response of normal and tumor microcirculation to hyperthermia. *Can Res* 44(2):605–612
47. van der Zee J (2002) Heating the patient: a promising approach? *Ann Oncol* 13:1173–1184
48. Debnath SK, Srivastava R (2021) Drug delivery with carbon-based nanomaterials as versatile nanocarriers: progress and prospects. *Front Nanotechnol*. <https://doi.org/10.3389/fnano.2021.644564>
49. Wang F, Zhang B, Zhou L, Shi Y, Li Z, Xia Y, Tian J (2016) Imaging dendrimer-grafted graphene oxide mediated anti-miR-21 delivery with an activatable luciferase reporter. *ACS Appl Mater Interfaces* 8:9014–9021
50. Lu C-H, Zhu C-L, Li J, Liu J-J, Chen X, Yang H-H (2010) Using graphene to protect DNA from cleavage during cellular delivery. *Chem Commun* 46:3116–3118
51. Guo X, Mei N (2014) Assessment of the toxic potential of graphene family nanomaterials. *J Food Drug Anal* 22:105–115
52. Ren T, Li L, Cai X, Dong H, Liu S, Li Y (2012) Engineered polyethylenimine/graphene oxide nanocomposite for nuclear localized gene delivery. *Polym Chem* 3:2561–2569
53. Kumar R, Chauhan A, Jha SK, Kuanr BK (2018) Localized cancer treatment by radio-frequency hyperthermia using magnetic nanoparticles immobilized on graphene oxide: from novel synthesis to in vitro studies. *J Mater Chem B* 6:5385–5399
54. Cheng G, Liu Y-L, Wang Z-G, Zhang J-L, Sun D-H, Ni J-Z (2012) The GO/rGO–Fe<sub>3</sub>O<sub>4</sub> composites with good water-dispersibility and fast magnetic response for effective immobilization and enrichment of biomolecules. *J Mater Chem* 22:21998–22004
55. Cheng G, Yu X, Zhou M-D, Zheng S-Y (2014) Preparation of magnetic graphene composites with hierarchical structure for selective capture of phosphopeptides. *J Mater Chem B* 2:4711–4719
56. Georgakilas V, Tiwari JN, Kemp KC, Perman JA, Bourlinos AB, Kim KS, Zboril R (2016) Noncovalent functionalization of graphene and graphene oxide for energy materials, biosensing, catalytic, and biomedical applications. *Chem Rev* 116:5464–5519

57. Liu J, Tao L, Yang W, Li D, Boyer C, Wuhrer R, Braet F, Davis TP (2010) Synthesis, characterization, and multilayer assembly of pH sensitive graphene–polymer nanocomposites. *Langmuir* 26:10068–10075
58. Liu J, Yang W, Tao L, Li D, Boyer C, Davis TP (2009) Thermosensitive graphene nanocomposites formed using pyrene-terminal polymers made by RAFT polymerization. *J Polym Sci A Polym Chem* 48:425–433
59. Lian M, Fan J, Shi Z, Li H, Yin J (2014) Kevlar®-functionalized graphene nanoribbon for polymer reinforcement. *Polymer* 55:2578–2587
60. Zhang J, Xu Y, Cui L, Fu A, Yang W, Barrow C, Liu J (2015) Mechanical properties of graphene films enhanced by homo-telechelic functionalized polymer fillers via  $\pi$ – $\pi$  stacking interactions. *Compos A Appl Sci Manuf* 71:1–8
61. Chandra V, Kim KS (2011) Highly selective adsorption of  $Hg^{2+}$  by a polypyrrole–reduced graphene oxide composite. *Chem Commun* 47:3942
62. Matos CF, Galembeck F, Zarbin AJG (2014) Multifunctional and environmentally friendly nanocomposites between natural rubber and graphene or graphene oxide. *Carbon* 78:469–479
63. Hsiao S-T, Ma C-CM, Tien H-W, Liao W-H, Wang Y-S, Li S-M, Huang Y-C (2013) Using a non-covalent modification to prepare a high electromagnetic interference shielding performance graphene nanosheet/water-borne polyurethane composite. *Carbon* 60:57–66
64. Lee DY, Khatun Z, Lee J-H, Lee Y, In I (2011) Blood compatible graphene/heparin conjugate through noncovalent chemistry. *Biomacromol* 12:336–341
65. Zhang Y, Zhang J, Huang X, Zhou X, Wu H, Guo S (2011) Assembly of graphene oxide-enzyme conjugates through hydrophobic interaction. *Small* 8:154–159
66. Alwarappan S, Liu C, Kumar A, Li C-Z (2010) Enzyme-doped graphene nanosheets for enhanced glucose biosensing. *J Phys Chem C* 114:12920–12924
67. Wang Y, Li Y, Tang L, Lu J, Li J (2009) Application of graphene-modified electrode for selective detection of dopamine. *Electrochem Commun* 11:889–892
68. Zhu C, Du D, Lin Y (2015) Graphene and graphene-like 2D materials for optical biosensing and bioimaging: a review. *2D Mater* 2:032004
69. Liu Y, Dong X, Chen P (2012) Biological and chemical sensors based on graphene materials. *Chem Soc Rev* 41:2283–2307
70. Xiao M, Li X, Song Q, Zhang Q, Lazzarino M, Cheng G, Ulloa Severino FP, Torre V (2018) A fully 3D interconnected graphene-carbon nanotube web allows the study of glioma infiltration in bioengineered 3D cortex-like networks. *Adv Mater* 30:1806132
71. Hong H, Zhang Y, Engle JW, Nayak TR, Theuer CP, Nickles RJ, Barnhart TE, Cai W (2012) In vivo targeting and positron emission tomography imaging of tumor vasculature with  $^{66}Ga$ -labeled nano-graphene. *Biomaterials* 33:4147–4156
72. Shi S, Yang K, Hong H, Valdivinos HF, Nayak TR, Zhang Y, Theuer CP, Barnhart TE, Liu Z, Cai W (2013) Tumor vasculature targeting and imaging in living mice with reduced graphene oxide. *Biomaterials* 34:3002–3009
73. Shi J, Wang B, Chen Z, Liu W, Pan J, Hou L, Zhang Z (2016) A multi-functional tumor theranostic nanoplatfrom for MRI guided photothermal-chemotherapy. *Pharm Res* 33:1472–1485
74. Hu D, Zhang J, Gao G, Sheng Z, Cui H, Cai L (2016) Indocyanine green-loaded polydopamine-reduced graphene oxide nanocomposites with amplifying photoacoustic and photothermal effects for cancer theranostics. *Theranostics* 6:1043–1052
75. Chen H, Liu Z, Li S, Su C, Qiu X, Zhong H, Guo Z (2016) Fabrication of graphene and AuNP core polyaniline shell nanocomposites as multifunctional theranostic platforms for SERS real-time monitoring and chemo-photothermal therapy. *Theranostics* 6:1096–1104
76. Zhang Y, Li B, Li Z, Xia N, Yu H, Zhang Y (2018) Synthesis and characterization of Tamoxifen citrate modified reduced graphene oxide nano sheets for breast cancer therapy. *J Photochem Photobiol, B* 180:68–71
77. Diaz-Diestra D, Thapa B, Badillo-Diaz D, Beltran-Huarac J, Morell G, Weiner B (2018) Graphene oxide/ZnS: Mn nanocomposite functionalized with folic acid as a nontoxic and effective theranostic platform for breast cancer treatment. *Nanomaterials* 8:484

78. Thakur M, Mewada A, Pandey S, Bhoori M, Singh K, Sharon M, Sharon M (2016) Milk-derived multi-fluorescent graphene quantum dot-based cancer theranostic system. *Mater Sci Eng, C* 67:468–477
79. Moghimi SM, Hunter AC, Murray JC (2001) Long-circulating and target-specific nanoparticles: theory to practice. *Pharmacol Rev* 53(2):283–318
80. McCallion C, Burthem J, Rees-Unwin K, Golovanov A, Pluen A (2016) Graphene in therapeutics delivery: problems, solutions and future opportunities. *Eur J Pharm Biopharm* 104:235–250
81. Sun X, Liu Z, Welsler K, Robinson JT, Goodwin A, Zaric S, Dai H (2008) Nano-graphene oxide for cellular imaging and drug delivery. *Nano Res* 1:203–212
82. Goenka S, Sant V, Sant S (2014) Graphene-based nanomaterials for drug delivery and tissue engineering. *J Control Release* 173:75–88
83. Das B, Eswar Prasad K, Ramamurty U, Rao CNR (2009) Nano-indentation studies on polymer matrix composites reinforced by few-layer graphene. *Nanotechnology* 20:125705
84. Burdanova MG, Kharlamova MV, Kramberger C, Nikitin MP (2021) Applications of pristine and functionalized carbon nanotubes, graphene, and graphene nanoribbons in biomedicine. *Nanomaterials* 11:3020
85. Cao X, Zheng S, Zhang S, Wang Y, Yang X, Duan H, Huang Y, Chen Y (2015) Functionalized graphene oxide with hepatocyte targeting as anti-tumor drug and gene intracellular transporters. *J Nanosci Nanotechnol* 15:2052–2059
86. Hu H, Tang C, Yin C (2014) Folate conjugated trimethyl chitosan/graphene oxide nanocomplexes as potential carriers for drug and gene delivery. *Mater Lett* 125:82–85
87. Orecchioni M, Cabizza R, Bianco A, Delogu LG (2015) Graphene as cancer theranostic tool: progress and future challenges. *Theranostics* 5:710–723
88. Jin Y, Wang J, Ke H, Wang S, Dai Z (2013) Graphene oxide modified PLA microcapsules containing gold nanoparticles for ultrasonic/CT bimodal imaging guided photothermal tumor therapy. *Biomaterials* 34:4794–4802
89. Barrera CC, Groot H, Vargas WL, Narváez DM (2020) Efficacy and molecular effects of a reduced graphene oxide/Fe<sub>3</sub>O<sub>4</sub> nanocomposite in photothermal therapy against cancer. *IJN* 15:6421–6432
90. Yang D, Feng L, Dougherty CA et al (2016) In vivo targeting of metastatic breast cancer via tumor vasculature-specific nano-graphene oxide. *Biomaterials* 104:361–371
91. Sharma H, Mondal S (2020) Functionalized graphene oxide for chemotherapeutic drug delivery and cancer treatment: a promising material in nanomedicine. *IJMS* 21:6280
92. Sima LE, Chiritoiu G, Negut I, Grumezescu V, Orobeti S, Munteanu CVA, Sima F, Axente E (2020) Functionalized graphene oxide thin films for anti-tumor drug delivery to melanoma cells. *Front Chem*. <https://doi.org/10.3389/fchem.2020.00184>
93. Islami M, Zarrabi A, Tada S, Kawamoto M, Isoshima T, Ito Y (2018) Controlled quercetin release from high-capacity-loading hyperbranched polyglycerol-functionalized graphene oxide. *IJN* 13:6059–6071
94. Some S, Gwon A-R, Hwang E et al (2014) Cancer therapy using ultrahigh hydrophobic drug-loaded graphene derivatives. *Sci Rep*. <https://doi.org/10.1038/srep06314>
95. Li Y, Boraschi D (2016) Endotoxin contamination: a key element in the interpretation of nano safety studies. *Nanomedicine* 11:269–287
96. Zhang C, Lu T, Tao J, Wan G, Zhao H (2016) Co-delivery of paclitaxel and indocyanine green by PEGylated graphene oxide: a potential integrated nanoplatform for tumor theranostics. *RSC Adv* 6:15460–15468
97. Su X, Chan C, Shi J, Tsang M-K, Pan Y, Cheng C, Gerile O, Yang M (2017) A graphene quantum dot@Fe<sub>3</sub>O<sub>4</sub>@SiO<sub>2</sub> based nanoprobe for drug delivery sensing and dual-modal fluorescence and MRI imaging in cancer cells. *Biosens Bioelectron* 92:489–495
98. Mousavi SM, Low FW, Hashemi SA et al (2020) Development of hydrophobic reduced graphene oxide as a new efficient approach for photochemotherapy. *RSC Adv* 10:12851–12863

99. Chen J, He G-M, Xian G-Y, Su X-Q, Yu L-L, Yao F (2020) Mechanistic biosynthesis of SN-38 coated reduced graphene oxide sheets for photothermal treatment and care of patients with gastric cancer. *J Photochem Photobiol, B* 204:111736
100. Zhou L, Zhou L, Wei S, Ge X, Zhou J, Jiang H, Li F, Shen J (2014) Combination of chemotherapy and photodynamic therapy using graphene oxide as drug delivery system. *J Photochem Photobiol, B* 135:7–16
101. Wang S, Wang X, Draenert FG, Albert O, Schröder HC, Mailänder V, Mitov G, Müller WEG (2014) Bioactive and biodegradable silica biomaterial for bone regeneration. *Bone* 67:292–304
102. Yin F, Hu K, Chen Y, Yu M, Wang D, Wang Q, Yong K-T, Lu F, Liang Y, Li Z (2017) SiRNA delivery with PEGylated graphene oxide nanosheets for combined photothermal and gene therapy for pancreatic cancer. *Theranostics* 7:1133–1148
103. Kerr JFR, Winterford CM, Harmon BV (1994) Apoptosis. Its significance in cancer and cancer therapy. *Cancer* 73:2013–2026
104. Kaur M, Agarwal C, Agarwal R (2009) Anticancer and cancer chemopreventive potential of grape seed extract and other grape-based products. *J Nutr* 139:1806S–1812S
105. Brown DM, Kinloch IA, Bangert U, Windle AH, Walter DM, Walker GS, Scotchford CA, Donaldson K, Stone V (2007) An in vitro study of the potential of carbon nanotubes and nanofibres to induce inflammatory mediators and frustrated phagocytosis. *Carbon* 45:1743–1756
106. Yang X, Niu G, Cao X, Wen Y, Xiang R, Duan H, Chen Y (2012) The preparation of functionalized graphene oxide for targeted intracellular delivery of siRNA. *J Mater Chem* 22:6649
107. Liu Z, Robinson JT, Sun X, Dai H (2008) PEGylated nanographene oxide for delivery of water-insoluble cancer drugs. *J Am Chem Soc* 130:10876–10877
108. Yang K, Wan J, Zhang S, Zhang Y, Lee S-T, Liu Z (2010) In vivo pharmacokinetics, long-term biodistribution, and toxicology of PEGylated graphene in mice. *ACS Nano* 5:516–522
109. Depan D, Shah J, Misra RDK (2011) Controlled release of drug from folate-decorated and graphene mediated drug delivery system: synthesis, loading efficiency, and drug release response. *Mater Sci Eng, C* 31:1305–1312
110. Yang X, Zhang X, Ma Y, Huang Y, Wang Y, Chen Y (2009) Superparamagnetic graphene oxide-Fe<sub>3</sub>O<sub>4</sub> nanoparticles hybrid for controlled targeted drug carriers. *J Mater Chem* 19:2710–2714
111. Fan X, Jiao G, Gao L, Jin P, Li X (2013) The preparation and drug delivery of a graphene-carbon nanotube-Fe<sub>3</sub>O<sub>4</sub> nanoparticle hybrid. *J Mater Chem B* 1:2658–2664
112. La W-G, Park S, Yoon H-H, Jeong G-J, Lee T-J, Bhang SH, Han JY, Char K, Kim B-S (2013) Delivery of a therapeutic protein for bone regeneration from a substrate coated with graphene oxide. *Small* 9:4051–4060
113. Shen D-W, Pouliot LM, Hall MD, Gottesman MM (2012) Cisplatin resistance: a cellular self-defense mechanism resulting from multiple epigenetic and genetic changes. *Pharmacol Rev* 64:706–721
114. Chen G-Y, Meng C-L, Lin K-C, Tuan H-Y, Yang H-J, Chen C-L, Li K-C, Chiang C-S, Hu Y-C (2015) Graphene oxide as a chemosensitizer: diverted autophagic flux, enhanced nuclear import, elevated necrosis and improved antitumor effects. *Biomaterials* 40:12–22
115. Jäger M, Schubert S, Ochrimenko S, Fischer D, Schubert US (2012) Branched and linear poly(ethylene imine)-based conjugates: synthetic modification, characterization, and application. *Chem Soc Rev* 41:4755–4767
116. Folkman J (2002) Role of angiogenesis in tumor growth and metastasis. *Semin Oncol* 29:15–18
117. Radu A, Pichon C, Camparo P, Antoine M, Allory Y, Couvelard A, Fromont G, Hai MTV, Ghinea N (2010) Expression of follicle-stimulating hormone receptor in tumor blood vessels. *N Engl J Med* 363:1621–1630
118. Siraj A, Desestret V, Antoine M et al (2013) Expression of follicle-stimulating hormone receptor by the vascular endothelium in tumor metastases. *BMC Cancer* 13(1):246. <https://doi.org/10.1186/1471-2407-13-246>



119. Russier J, León V, Orecchioni M et al (2017) Few-layer graphene kills selectively tumor cells from myelomonocytic leukemia patients. *Angew Chem Int Ed* 56:3014–3019
120. Patel SC, Lee S, Lalwani G, Suhrland C, Chowdhury SM, Sitharaman B (2016) Graphene-based platforms for cancer therapeutics. *Ther Deliv* 7:101–116
121. Gazzi A, Fusco L, Khan A, Bedognetti D, Zavan B, Vitale F, Yilmazer A, Delogu LG (2019) Photodynamic therapy based on graphene and MXene in cancer theranostics. *Front Bioeng Biotechnol*. 10.3389/fbioe.2019.00295
122. Monroe JD, Belevkov E, Er AO, Smith ME (2019) Anticancer photodynamic therapy properties of sulfur-doped graphene quantum dot and methylene blue preparations in MCF-7 breast cancer cell culture. *Photochem Photobiol* 95:1473–1481
123. Casais-Molina ML, Cab C, Canto G, Medina J, Tapia A (2018) Carbon nanomaterials for breast cancer treatment. *J Nanomater* 2018:1–9
124. Abrahamse H, Sosthene Mfouo Tynga I (2018) Photodynamic therapy, a potential therapy for improve cancer management. *Breast Cancer Surgery*. <https://doi.org/10.5772/intechopen.74697>
125. Youssef Z, Vanderesse R, Colombeau L et al (2017) The application of titanium dioxide, zinc oxide, fullerene, and graphene nanoparticles in photodynamic therapy. *Cancer Nano*. <https://doi.org/10.1186/s12645-017-0032-2>
126. Nafujjaman M, Nurunnabi M, Kang S, Reeck GR, Khan HA, Lee Y (2015) Ternary graphene quantum dot–polydopamine–Mn<sub>3</sub>O<sub>4</sub> nanoparticles for optical imaging guided photodynamic therapy and T1-weighted magnetic resonance imaging. *J Mater Chem B* 3:5815–5823
127. Paquin F, Rivnay J, Salleo A, Stingelin N, Silva-Acuña C (2015) Multi-phase microstructures drive exciton dissociation in neat semicrystalline polymeric semiconductors. *J Mater Chem C* 3:10715–10722
128. Cheng Y, Chang Y, Feng Y, Liu N, Sun X, Feng Y, Li X, Zhang H (2017) Simulated sunlight-mediated photodynamic therapy for melanoma skin cancer by titanium-dioxide-nanoparticle-gold-nanocluster-graphene heterogeneous nanocomposites. *Small* 13:1603935
129. Ge J, Lan M, Zhou B et al (2014) A graphene quantum dot photodynamic therapy agent with high singlet oxygen generation. *Nat Commun*. <https://doi.org/10.1038/ncomms5596>
130. Cramer SW, Chen CC (2020) Photodynamic Therapy for the Treatment of Glioblastoma. *Front Surg*. <https://doi.org/10.3389/fsurg.2019.00081>
131. Wang Y, Wang K, Zhao J, Liu X, Bu J, Yan X, Huang R (2013) Multifunctional mesoporous silica-coated graphene nanosheet used for chemo-photothermal synergistic targeted therapy of glioma. *J Am Chem Soc* 135:4799–4804
132. Wang C, Wang X, Chen Y, Fang Z (2020) In-vitro photothermal therapy using plant extract polyphenols functionalized graphene sheets for treatment of lung cancer. *J Photochem Photobiol, B* 204:111587
133. Robinson JT, Tabakman SM, Liang Y, Wang H, Sanchez Casalongue H, Vinh D, Dai H (2011) Ultrasmall reduced graphene oxide with high near-infrared absorbance for photothermal therapy. *J Am Chem Soc* 133:6825–6831
134. Abdolahad M, Janmaleki M, Mohajerzadeh S, Akhavan O, Abbasi S (2013) Polyphenols attached graphene nanosheets for high efficiency NIR mediated photodestruction of cancer cells. *Mater Sci Eng, C* 33:1498–1505
135. Wu J, Li Z, Li Y, Pettitt A, Zhou F (2018) Photothermal effects of reduced graphene oxide on pancreatic cancer. *Technol Cancer Res Treat* 17:153303461876863
136. Costa-Almeida R, Bogas D, Fernandes JR, Timochenko L, Silva FALS, Meneses J, Gonçalves IC, Magalhães FD, Pinto AM (2020) Near-Infrared radiation-based mild photohyperthermia therapy of non-melanoma skin cancer with PEGylated reduced nanographene oxide. *Polymers* 12:1840
137. Thapa RK, Youn YS, Jeong J-H, Choi H-G, Yong CS, Kim JO (2016) Graphene oxide-wrapped PEGylated liquid crystalline nanoparticles for effective chemo-photothermal therapy of metastatic prostate cancer cells. *Colloids Surf, B* 143:271–277
138. Liu J, Yuan X, Deng L, Yin Z, Tian X, Bhattacharyya S, Liu H, Luo Y, Luo L (2020) Graphene oxide activated by 980 nm laser for cascading two-photon photodynamic therapy and photothermal therapy against breast cancer. *Appl Mater Today* 20:100665

139. Stepanov EA, Lanin AA, Voronin AA, Fedotov AB, Zheltikov AM (2016) Solid-State source of subcycle pulses in the midinfrared. *Phys Rev Lett.* <https://doi.org/10.1103/physrevlett.117.043901>
140. Han R, Tang K, Hou Y, Yu J, Wang C, Wang Y (2020) Ultralow-intensity near infrared light synchronously activated collaborative chemo/photothermal/photodynamic therapy. *Biomater Sci* 8:607–618
141. Chavva SR, Pramanik A, Nellore BPV et al (2014) Theranostic graphene oxide for prostate cancer detection and treatment. *Part Part Syst Charact* 31:1252–1259
142. Dong H, Jin M, Liu Z, Xiong H, Qiu X, Zhang W, Guo Z (2016) In vitro and in vivo brain-targeting chemo-photothermal therapy using graphene oxide conjugated with transferrin for Gliomas. *Lasers Med Sci* 31:1123–1131

# Chapter 40

## Synthesis of Carbon Nanotubes with Merocyanine Dyes Decorated Carbon Nanotubes for Biomedical Imaging Devices



S. Ranjitha, R. Lavanya Dhevi, C. Sudhakar, and Rajakumar Govindasamy

### 1 Introduction

Carbon nanotubes (CNTs) have become a primary source of industry applications since its first discovery in 1990 [1]. The main demand of CNTs was used as nanocomposite materials, optoelectronics, waste conversion management, biomedical industry in addition as well as in the area of medicine and nanotechnology. A different kind of CNT-based bio-imaging technology with different optical conversion process has been discussed by various groups for identification of various biological molecules and their properties like drug delivery mechanism with CNTs. In recent decades, several research articles and review papers have been reported based on the growth of using SWCNTs in biomedical applications. Tasis et al. [2] published an outstanding study on the structure of CNT, in which they discussed the three alternative ways to molecular chemical structural variation of CNT. Wu and his colleagues discovered that multiple surface modification procedures of functionalised SWCNTs could be obtained for biomedical use, and their findings assessed the benefits and obstacles of employing CNTs in biomedicine [3, 4]. 1D diffusion-ordered spectroscopy, DOSY, was used for the first time in the analysis of CNT

---

S. Ranjitha (✉) · R. Lavanya Dhevi  
Velalar College of Engineering and Technology, Erode 638012, India  
e-mail: [ranjilotus31@gmail.com](mailto:ranjilotus31@gmail.com)

C. Sudhakar  
Department of Biotechnology, Mahendra Arts & Science College, Kalippatti, Namakkal,  
Tamil Nadu 637501, India

R. Govindasamy  
Collaborative Innovation Center for Advanced Organic Chemical Materials Co-Constructed By  
the Province and Ministry, Ministry of Education Key Laboratory for the Synthesis and  
Application of Organic Functional Molecules, College of Chemistry and Chemical Engineering,  
Hubei University, Wuhan 430062, China

derivatives by Marega et al. They synthesised selected CNT derivatives and investigated them using a 1D DOSY experiment with high magnetic field gradients up to  $42.6 \text{ G cm}^{-1}$ . TGA-DTA, TEM, SEM and AFM techniques were also used to characterise and functionalise carbon nanotubes. The identification covalently modified CNT derivatives which was easily found by effective method of diffusion-based NMR spectroscopy. The authors also mentioned that NMR-DOSY can be used to distinguish linking PEG functional groups conjugated and non-conjugated generated by precipitation with oxidised SWCNT. This potential NMR-DOSY analytical approach can be used to analyse biopolymer conjugated ox-SWCNTs [5, 6]

Marega et al. described dispersed form of CNT by condensation of COOH functional groups attached to the network of carbon with primary amine moieties bound in the simply developing self-associating biopolymer hyaluronan in another study. Various model pharmaceuticals such as ibuprofen and methotrexate can be covalently modified using the produced hyaluronic acid-CNT derivatives [7]. Hua Gong et al. noted that this model has made tremendous progress in recent times in utilisation of CNT as multifunctional nano-probes for biological imaging.

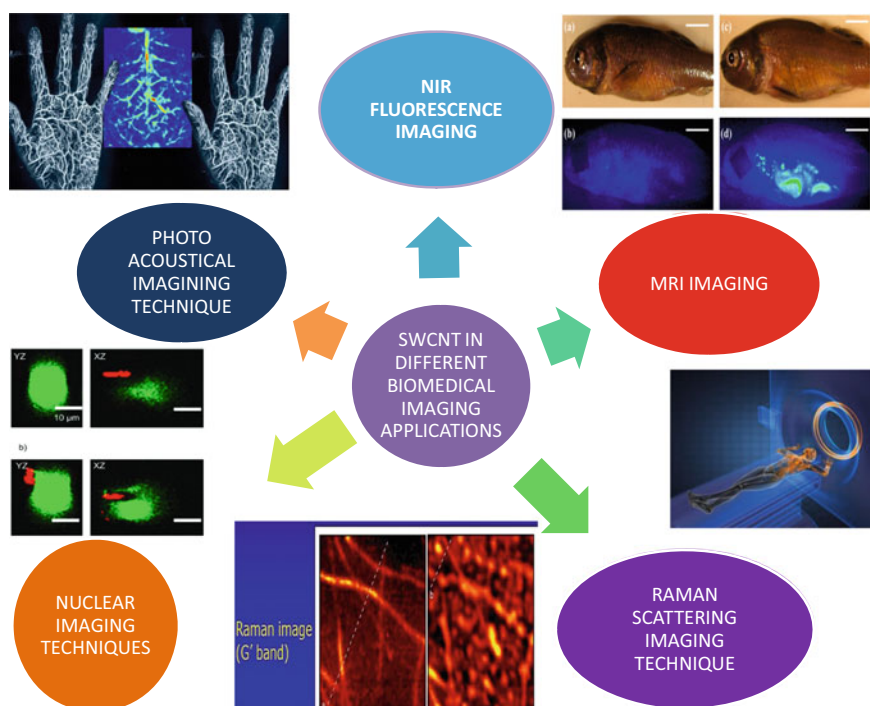
CNTs can be employed in photoacoustic imaging techniques because of their great NIR absorbance, and their photoacoustic wave pattern can be amplified by adding cyanine and organic dyes or covering with nanostructured gold shells. As a result, CNTs were examined as novel bio-imaging probes with tremendous potential in molecular imaging terminology [8–10].

The current chapter may provide a relevant update in biomedical imaging. Because of the photon scattering in the NIR-II region examined with the visible ( $4000\text{--}7000 \text{ \AA}$ ) and traditional NIR-I region ( $7000\text{--}9000 \text{ \AA}$ ), fluorescence medical imaging in the NIR-II biological transparent opening with SWCNTs opens the door to in vivo optical imaging with deep tissue penetration and high spatial resolution [6, 10–12]. There is huge possibility of chemical alterations of carbon nanotubes with photo and electro-active chemicals or polymers [13–15].

Although SWCNT with NIR dyes-based biomedical imaging research has shown considerable promise in biomedical tools device applications diagnosis, there are still substantial obstacles in using such nanomaterials for true in vivo clinical applications. Velocity can vary the networks' electrical and optical properties. Furthermore, researchers have demonstrated that surface coatings, such as CTA film and PEG, have no evident toxicity in vitro and in vivo and can be excretion pathways, resulting in linear growth of the networks. Dip-coating CTA film with dye/SWCNT is a simple, repeatable process that can be scaled up for mass manufacturing [16–18]. As an outcome of its growing popularity, several applications that employ SWCNT networks are likely to rise. In the future, dip-coating method of constructing SWCNT networks with dye-coating technique was applied widely by resolving challenges around SWCNT networks, such as corrosion resistance and adhesion nature of substrate on SWCNT.

## 2 Role of Carbon Nanotubes in Bio-Imaging Technique

Individual tubes or short bundles of functionalised SWCNTs with size of one to two nm and lengths of above 50 nm are commonly employed in biomedicine (Fig. 1a). SWCNTs are being one variety of optical characteristics that are relevant in biological scanning technique. The variety of darkest materials SWCNT had significant optical absorption over the ultraviolet to NIR wavelength range (Fig. 1b). Photothermal therapy and photoacoustic imaging can both benefit from the light. SWCNTs' nature of high peak SERS enables tracking, detection and picturing in vitro and in vivo. SWCNTs with semiconducting oxides with energy gaps of the range of 1.1 eV exhibit fluorescence in the near IR to normal IR which spans the substance transparent window and is thus appropriate for tomography in biological systems (Fig. 1d). Positron emission tomography (PET) imaging is using the SWCNT due to their intrinsic physicochemical features. SWCNT within the nanowires samples or gadolinium attached CNT is being used in MRI. The materials analysis shows the uniqueness, potential and limitations of SWCNT-based bio-imaging in this paper, which summarises recent achievements in employing SWCNTs in various biomedical imaging applications.



**Fig. 1** CNTs in different biomedical imaging techniques

## 2.1 *Fluorescence Imaging*

Fluorescence imaging with near-infrared dyes is an important part of scientific study in the medical sector of diagnosis applications. The depth of light penetration in fluorescence imaging will become a critical issue in the development of future applications. The scientists and industrial researchers have been creating and applying fluorescent probes with high-energy transfer and emission of wavelengths that fall within the biologically crystalline nature of NIR window to overcome complication [19–22]. In the biomedical imaging application, nature of the low quantum yield is a major barrier for further approach. Several recent studies focused on developing a simple sol–gel separation process to enhance intrinsic semiconducting and SCWNTs with unique resonance absorption and emission at 800 and 1200 nm. To generate even ‘brighter’ fluorescence, further advancement in this approach requires improved SWCNT specimens with high quantum yield [24–27]. The research is needed for imaging with various and emission wavelengths. Williams first described cyanine dyes in 1856, when he used olefinic bonds to join two nitrogen-contained heterocycles, resulting in a complicated conjugated system with region. Until now, cyanine derivatives have been widely used in laser dyes, photographic sensitisers and fluorescent probes. The fluorescence emission of the majority of the observed cyanine dyes was in the long-wavelength region 550–767 nm with CY3 to CY7. Those dyes were great platforms for fluorescent probes design due to low damage to biosamples from deep penetration on tissues. Furthermore, the water solubility of the ammonium salt moiety was adequate for bio-studies. Fluorescein dyes (FITC or FLUO) and cyanine dyes (Cy3 (indocarbocyanine) and Cy5 (indodicarbocyanine)) are often employed. Cy3 (excited at 550 nm and emitting at 570 nm) absorbs green light and emits red light, whereas Cy5 (excited at 650 nm and emitting at 670 nm) absorbs red light and emits infrared light. Although fluorescent microscope filters for detecting Cy5-labelled probes are available, cells hybridised with such probes are difficult to spot. As a result, Cy5-labelled probes should only be used if the hybridised biomass is inspected using a confocal laser scanning microscope (CLSM) with suitable lasers. Fluorescent probes generating green light (exciting at 592 nm, emitting at 520 nm) are frequently employed in conjunction with Cy3-labelled probes because they are easy to identify using fluorescence microscopy. Bioproteins, anti-agents, peptides, RNA probes and other polysaccharides are labelled with cyanine dyes and employed in different detection techniques of fluorescence imaging [28, 29].

## 2.2 *Raman Imaging Analysis*

The inelastic scattering of photons is a phenomenon that involves the ejection of photons with shifting of wavelength under light radiation. Without the use of an amplification mechanism like SERS, the natural Raman effect signals of molecules are quite weak in normal conditions. In resonance Raman scattering, the scattering

efficiency increases were matched with the energy required for the free electron shift from the ground state to excited bands, Raman spectra of SWCNT are examined, and those with excitation resonance exhibit strong resonant. Heller et al. used SWCNTs' intrinsic Raman characteristics for live cell imaging for the first time in 2005 [30, 31]. For live cell tracking research, DNA oligonucleotide wrapped with CNT was used as markers. SWCNTs exhibit a small G-band peak with FWHM of 2 nm, permitting higher multiple wavelength and excitation wavelength of 785 nm, and scattered photons within range of 8920–8970 Å are both in the NIR transparent opening in Raman imaging, which has minimum space tissue absorption and background of spontaneous fluorescence emission. For single peak intensity mapping, scan wavelength of five was captured at once by only one laser stimulation for analysis of five separate objects. SWCNT Raman peak intensity tags outperform frequently applied cyanine organic dyes and rhodamine derivatives extensively. As a sequence of the Stokes shift of SWCNT, photoluminescence and Raman scattering spectra enable for mapping the biological sample auto-fluorescence, which fluctuates in spot over biological samples [32, 33]. Furthermore, under imaging conditions, the Raman signals of SWCNTs are highly robust without quenching or washout. Using chirality/diameter-separated SWCNTs could potentially yield even more Raman hues. SWCNTs SERS techniques were boosting the Raman signals even more, boosting sensitivity detection and cutting imaging time [34, 35].

### ***2.3 Photoacoustic (PA) Imaging***

The laser beam can be absorbed by biological sample due to molecules, causing transitory thermal expansion and ultrasonic emission, which was captured by an ultrasound microphone and used to create two- and three-dimensional images. By removing the phenomenon of absorption and emission of light by fluorescence imaging, PA imaging identifies the sound alternatively by light, demonstrates better tissue penetration and enhances resolutions in a better way. In PA imaging, several nanomaterials with significant absorbance in the NIR range are suitable brightening agents [36–38]. Because of their significant NIR absorbance, both MWNTs and SWCNTs have been used as photothermal agents. Nanotubes, on the other hand, are good contrast agents for photoacoustic imaging due to their great NIR absorption. A thin gold layer and few organic molecules with absorbance of NIR were connected with SWCNTs to boost their absorbance in the NIR region, further increasing the light sensitivity of the SWCNTs photoacoustic signal. To improve the intrinsic PA signals of SWCNTs, Zharov and colleagues generated a new methodology [36, 37, 39, 40]. The researchers used a small layer of gold encapsulated on the surface of SWCNTs to boost their optical density in the near-infrared range and then coupled the GNTs with antibodies that precisely target the endothelium of murine lymphatic arteries. Using extremely low laser fluency levels of a few mJ/cm<sup>2</sup>, the obtained GNTs

are provided. The lymphatic endothelia receptor was also mapped using antibody-conjugated GNTs. In both cases, the photoacoustic and photothermal signals in the antibody-conjugated group outperformed the endogenous background and were preferentially located in the wall of lymphatic vessels, whereas the GNTs without antibody conjugation produced only random signals and no signals in the lymphatic wall of vessels. GNTs were later used to detect circulating tumour cells (CTCs) under PA imaging in a later study by the same group. Folate conjugated CNTs were employed as the PA contrast agent to photograph CTCs in vivo after being collected by an external magnetic field, taking advantage of GNTs' high PA signals. Loaded indocyanine green (ICG) molecules on PEGylated SWCNTs using indocyanine green (SWCNT-ICG) in particular demonstrated robust and distinct absorbance spectra, allowing and enabling sensitive multicolour PA imaging in vivo. As a result, CNTs with high NIR merocyanine dye absorption are attractive photoacoustic imaging reagents. In addition to their intrinsic optical absorbance, CNTs could be used as a versatile nano-platform for improved or multiplexed photoacoustic imaging by linking them with other light-absorbing nanostructures or molecules, although SWCNTs are used in the majority of already published CNT-based photoacoustic imaging probes.

## ***2.4 Magnetic Resonance Imaging Technology***

Magnetic resonance imaging (MR imaging) is clinically relevant than optical-based imaging techniques because it allows for complete body imaging including depth limit. T1 (positive) and T2 (negative) contrast agents are used in MRI (negative). During the synthesis of CNTs, metal catalysts (e.g. Fe, Co) are frequently utilised. Faraj et al. examined the biodistribution of SWCNTs by detecting MR signals in vivo, taking use of the iron impurities included in SWCNT [42, 43]. Faraj et al. used in vivo MR imaging to analyse the biodistribution of SWCNTs in animals using the ferromagnetic properties of metal impurity containing SWCNT samples. The presence of SWCNTs was shown to be closely related to the MR contrasts introduced by metal nanoparticle contaminants in numerous organs. Another recent investigation by other groups found that increased iron oxide nanoparticle concentrations in SWCNT samples did not always result in a better T2-shortening impact. T1 contrast agents made of carbon nanotubes can also be employed in MR imaging [41]. In magnetic resonance (MR) imaging of SWCNT-labelled merocyanine, metallic catalyst nanoparticles connected to nanotubes can be used as a T2 contrast agent [44]. SWCNTs with proper surface functionalisation could be used as multifunctional nano-probes for stem cell labelling and multi-modal in vivo tracking, according to this research [45–47].



## 2.5 Nuclear Imaging

The same group also developed an alternative method for tracking the long-term biodistribution of MWNTs that used  $^{14}\text{C}$  instead of  $^{125}\text{I}$  [48]. Several groups have also reported *in vivo* tumour imaging in mice models using radionuclide labelled SWCNTs [49, 50]. This was possible due to the particular anti-CD20 antibody was conjugated with  $^{111}\text{In}$  in labelled SWCNTs and applied to focus on human Burkitt lymphoma in addition to RGD peptide. Radioisotopes could be introduced into nanotubes for radiolabelling instead of using standard chelation chemistry to create radiolabelled CNTs [51, 52]. They can be efficiently triggered by light and cause target cell death. Cyanine dyes trigger cell death predominantly therapy since it minimises an overabundance of inflammation. The dyes can be further changed, for example, by introducing organic or other groups, to alleviate the difficulty of low water solubility. Sensitisation of cyanine dyes by increasing their toxicity in an acidic environment, which is typical of cancer fluid, can improve cancer tissue. Merocyanines are also noteworthy for their unique immunological regulatory features, particularly their capacity to interact with lymphocytes. Merocyanines are now being tested in preclinical research for the treatment of leukaemia. Current research involving a variety of cyanine dyes suggests that they may help to replenish the permanently used pool of agents in PDT.

## 3 Merocyanine Dye in Biomedical Imaging

Merocyanine dyes have a bright future in optical devices, dye sensitised solar cell and hydrogen fuel energy, dye laser technology and quantum dots [53]. They have been used in a variety of scientific and technological fields. Their potential to be used as light sensitisers in PDT and as photoradiation sensitisers in different tumour treatment has been investigated completely. Merocyanine dyes show promising activity in cancer photodynamic medical treatment (PDT) sensitisers. In particular, it can inactivate neoplastic cells in leukaemia, lymphoma and harmful viruses in bone marrow and blood fractions. Merocyanines (I) are naturally unsymmetrical polymethine dyes that are made up of two fragments: a  $\text{N}_2$  donor and an  $\text{O}_2$  acceptor linked together by an ethylene or polyethylene chain. The deep colour is caused by the transfer of energy from donor to acceptor along the polyethylene chain, which is dependent on chain length as well as the type of the donor and acceptor groups, which are commonly carbo- or heterocycles (II) [52, 54].

Merocyanines, also known as photomerocyanines, are produced when spiropyran are exposed to UV light or heated. They have been proposed for memory devices and optical switches, extraction of metal ions, photo-controlled ferromagnetics, and biological things due to their photo- and thermochromic characteristics [55–57].

Several dyes have been reported for use in cancer treatment. Merocyanines showed remarkable selectivity for cancer cells, giving hope for low-invasive lymphoma and

leukaemia [58–60]. The chemicals are currently being tested in preclinical research as a leukaemia therapy. The MC540 dye's extraordinary permeability to leukemic leukocytes and immature haemopoietic precursors prompted substantial research. There are two disadvantages of the group due to maximum light absorbance beyond NIR (556 nm) limit and particularly oxidation of phospholipids in the plasma membrane [61].

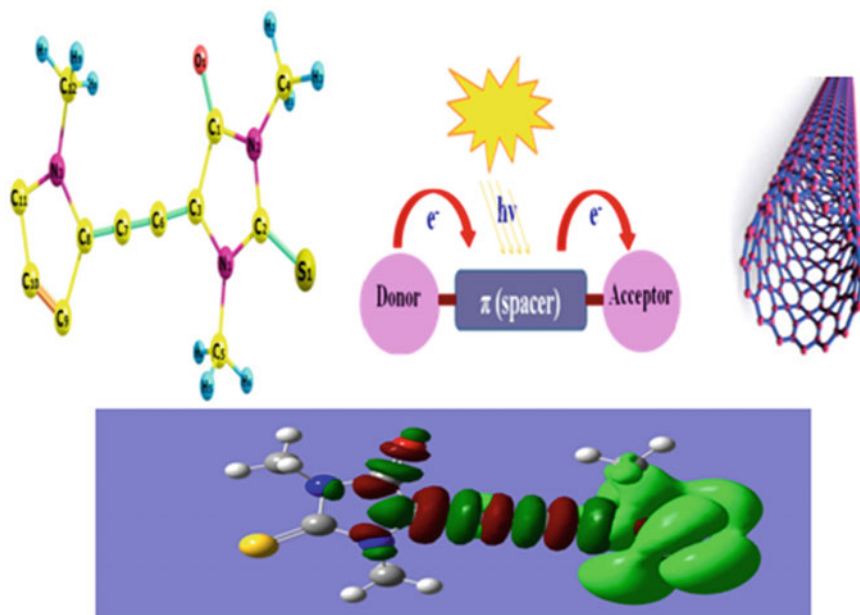
Merocyanines are still being studied as a possible treatment for haematological cancers. In vitro testing of a merocyanine rhodamine complex on K562 leukaemia cells demonstrated a decrease in cancer cell viability. Merocyanines are being tested as an antibacterial therapy against *Staphylococcus aureus* in addition to cancer treatment.

Despite their importance, the current research is limited to traditional dyes of general structure II. Brooker and colleagues created merocyanines with a variety of terminal groups, resulting in dyes with intrinsic polarities ranging from low polar molecules to strongly polar molecules. As the solvent polarity increased, the solvent effect can be utilised to create a dye solution with a specific wavelength and strength of absorption. Merocyanines' solvatochromic characteristics have been extensively researched.

Merocyanines are ideal model compounds for developing notions on the electronic structure of conjugated systems and evaluating the potentials of contemporary quantum chemical computations as donor–acceptor polyenes. The donor (D)–spacer (S)–acceptor (A) design of an organic sensitizer allows intramolecular charge transfer (ICT) following light excitation. To collect photons primarily in the UV–visible and NIR ranges, approaches to high efficiency organic dyes made by double bonds were added to key chromophores to increase the  $\pi$  conjugation length and to extend the absorption zone in the red shift region. The one with anthraquinone backbone has gained greater attention among the examined sensitizers since it has a remarkable solar-to-energy conversion efficiency because it has conjugation to red shift the absorption spectra [62]

Wüthner and Yao produced and investigated the effects of imide functional groups on hydrogen bonding to melamine receptors in various merocyanine colours. They showed that the ditopic melamine's triple hydrogen-bonding coordination helps dissolve the extremely dipolar dye even in nonpolar solvents like methylcyclohexane. Colloidal assemblies are generated via supramolecular polymerisation via hydrogen bonding to melamines and dipolar aggregation between the dyes, according to the optical characteristics of the resultant solutions. The temperature dependency of the electronic spectra of merocyanines has also been discovered in practical applications. In thermal printing and other thermographic procedures, certain thermochromes were utilised to safeguard securities (Fig. 2).

In this study, researchers used merocyanine dyes doped with SWCNT, each with a distinct combination of donor and acceptor functional groups, to investigate the orbital structure–performance relationship and identification of the colours that perform best for various biomedical imaging applications. The formation of different synthetic dye agents and dye chemistry breakthroughs has substantially increased the possibility for the manufacture of innovative pharmaceuticals based



**Fig. 2** Donor–acceptor transformation of CNT with merocyanine

on dyes and dye-containing substances with medical applications. The controlling system multi-neuronal activity in central nervous system has been analysed by using a number of high-voltage-sensitive cyanine dyes and merocyanines with various techniques [131]. It must be proposed to employ a simple *in vitro* approach to screen photoelectric dyes for use in retinal prosthetics.

#### 4 Cellulose Acetate Films Properties

The most important cellulose ester is cellulose acetate (CA). It is a durable, simple-to-work-with thermoplastic with outstanding clarity and gloss. It has a low haze rating, a high moisture vapour transmission rating, but a low water permeability rating, and is easy to cut and tear. It can also withstand organic and inorganic weak acids, hydrocarbons, vegetable oils and other chemicals. Cellulose esters are mixed more to promote elasticity such as butyrate–acetate and propionate–acetate that are generated, which have improved flexibility, hardness and corrosion resistance. Cotton linters are the most prevalent source of cellulose. The fibres are combined and treated with glacial. The hydroxyl groups of cellulose are converted to acetyl groups during acetylation, resulting in a far more soluble product. Water is introduced in the next stage to stop the reaction and partially hydrolyse the triacetate [63]

With a degree of acetylation (degree of replacement of hydroxyl groups) of roughly 2.4 and 2.9, cellulose acetate can be divided into two types: cellulose diacetate (CDA) and cellulose triacetate (CTA). The physical and mechanical properties of the two forms of CA differ. The permeability to gas and moisture reduces as the acetyl concentration rises, whereas chemical resistance, glass transition temperature and modulus rise. The most common cellulose mixed ester is cellulose acetate–butyrate (CAB). This resin improves the flexibility, toughness and moisture resistance of films. CAB films feature excellent clarity, scratch resistance and UV resistance, as well as strong dimensional stability.

## 5 Materials and Methods

Merocyanine dye of CY 334 (C<sub>12</sub>H<sub>17</sub>N<sub>3</sub>O<sub>5</sub>) and CTA film were purchased from sigma Aldrich chemical [check correct or not] with purity of 100%, and methanol was used as solvent for the cellulose triacetate (CTA) film preparation. SWCNT was purchased from Shilpent chemicals with purity 100%, with diameter 5–20 nm and length of the tube 10 μm.

### 5.1 Preparation of Carbon Nanotubes

It is required to prepare a well-distributed SWCNT colloidal solution in order to manufacture consistent SWCNT networks. For purification and dispersion, we used the following procedure. SWCNTs (Iljin Nanotech's ASP-100F) were sonicated in nitric acid at 50 °C for 30 min to purify and exfoliate from bundles [10, 11]. The SWCNTs were then neutralised with deionised (DI) water and captured using a vacuum filtration process on a membrane filter (millipore, 0.2 mm pore size, 47 mm diameter). The prepared SWCNTs were sonicated in ethanol for 10 h to solubilise them.

### 5.2 Preparation of Cellulose Triacetate Film (CTA)

Hundred grams of cellulose triacetate in a one litre wide mouth glass stopper bottle is added [slowly?] with a 500 ml of solvent mixture (methylene chloride and methanol by 9:1 ratio). In a one litre wide mouth glass stopper bottle, weigh 100 g of cellulose triacetate and add 500 ml of solvent combination (methylene chloride and methanol in a 9:1 ratio). A stopper is used to close the bottle's mouth. When the material has thickened, place the bottle on a tumbling style shaker and shake until the solution is complete. The obtained viscous solution was then cast on an Au-coated glass plate and dried at room temperature, yielding clear cellulose triacetate (CTA) films.

Merocyanine dye solution was dip-coated onto cellulose triacetate (CTA) films. The obtained films will be referred to as merocyanine dye films from now on.

### 5.3 Film Coating on CTA Film

The following processes were utilised to make CTA film using. The glass substrate is dropped in the SWCNT gel solution in the beaker at a particular space, be pulled out of the solution at a constant withdrawal velocity. As illustrated in Fig. 3, a motor was added on the spin coater to allow movement of the platform different direction and control its pace. During the process, SWCNT molecular nanostructures were generated on the plate. To create asymmetrical cyanine dyes/CNT nano hybrids, estimated amounts of dyes and CNTs were sonicated in an ice bucket, followed by ultracentrifugation at high speed to remove undispersed CNTs.

CNT/asymmetrical cyanine dye nano hybrids are fabricated by the following ideal parameters: a dispersal solution of 0.5 mL was made with 0.1 mg/mL CNTs and 30 M asymmetrical cyanine dyes. The solution was sonicated for 30 min with a microprobe (Q Sonica, Q700), with 2 s of on and 5 s of in ice pulses. The supernatant, which is the dark CNT-coloured dispersion, was removed into a clean tube, and it was labelled as CNT/dye dispersion after being ultra-centrifuged at 14,000 rpm for 10 min. The sample was put into a Microcon centrifugal filter device and spun at 14,000 rpm until the filtrate volume was decreased to roughly 50 mL in order to eliminate the unbound dye molecules. The solution that remained in the filter device was extracted and diluted with water to 400 mL.

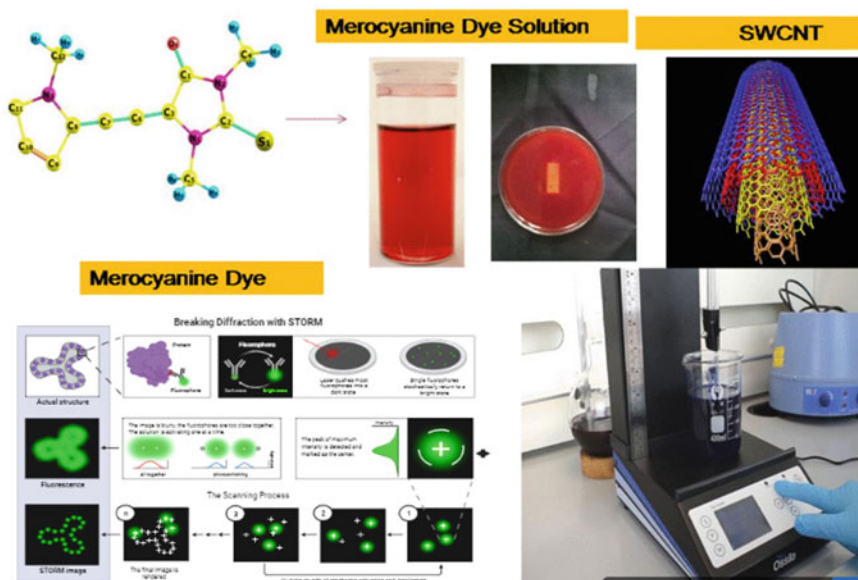


Fig. 3 Preparation of SWCNT/merocyanine film in dip-coating technology

## 6 Results and Discussion

### 6.1 Optical Analysis of UV–Visible and Fluorescence Spectral Analysis

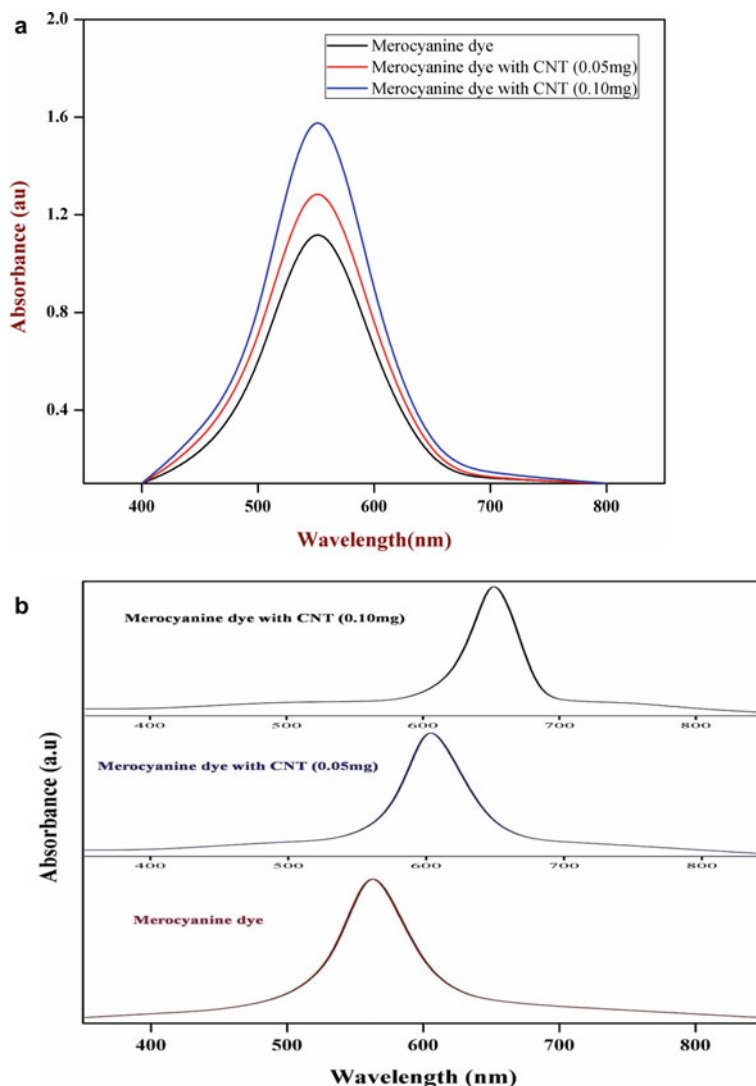
Figure 2 shows the change in the electronic structure of dye molecules after attaching to CNTs using UV–visible spectroscopy. In this wavelength range, are there any merocyanine dye/SWCNT \* 0.05 M dye/SWCNT (0.010 M) dispersions that are compensated for CNT absorbance? While the unbound dye has the highest intensity, when the dye is bound to SWCNTs, the intensity of the absorbance drops. The molar extinction coefficient was modified due to covalent interaction between CNTs and merocyanine dye because the dye concentrations were equal. The interactions between dye and SWCNT are thought to be stronger because the dye/SWCNT has the biggest modification in molar extinction coefficient of dye [64, 65].

Figure 4a shows the UV–visible and fluorescence spectra of merocyanine dye-coated carbon nanotube surface in 400–700 nm. It is observed that the bands were shifted hypsochromic which corresponds to the first electron transition. The absorption spectra for merocyanine dye-coated carbon nanotube surface show that the absorption takes place at the range of 500–600 nm corresponding to  $\pi$ – $\pi^*$  electron transition from lower state ( $s_0$ ) to the first singlet high excited ( $s_1$ ) state [23].

The optical transition from the ground state to lower one excitation states gives rise to a stronger absorption band for higher concentration of merocyanine dye-coated carbon nanotube surface compared to lower concentration [3]. The transition is allowed only between the ground state and the lowest one-exciton states, resulting a sharp, intense absorption band with broadening of dye molecules. The increase in the amplitude of the peak in the absorbance spectrum formed by increase in the concentration of the dye which is the requirement for optical device applications is observed [66].

As the concentration grew, the absorbance increased; however, values over 0.10 M [results precipitation] resulted in precipitation in the aqueous dispersion. The creation of H-aggregates or sandwich-like configurations of the dye molecules within SWCNT nanorods was linked to the hypsochromic shift in the absorption spectra of merocyanine. The emergence of a new strong red-shifted band at 590 nm was observed in the film. This new red-shifted peak indicated the production of J-aggregates within the needle-like nanostructures. The absorption spectra's broadness over the visible spectrum and into the near-infrared might be considered particularly crucial for their use as photosensitisers in biomedical imaging systems [67, 68].

Because of intermolecular quenching or surplus molecules that act as filters, aggregation of dyes utilised as sensitisers in DSSCs might result in lower conversion efficiency. To improve resolution, the ability to reduce or manage aggregation is critical [20, 69–75].



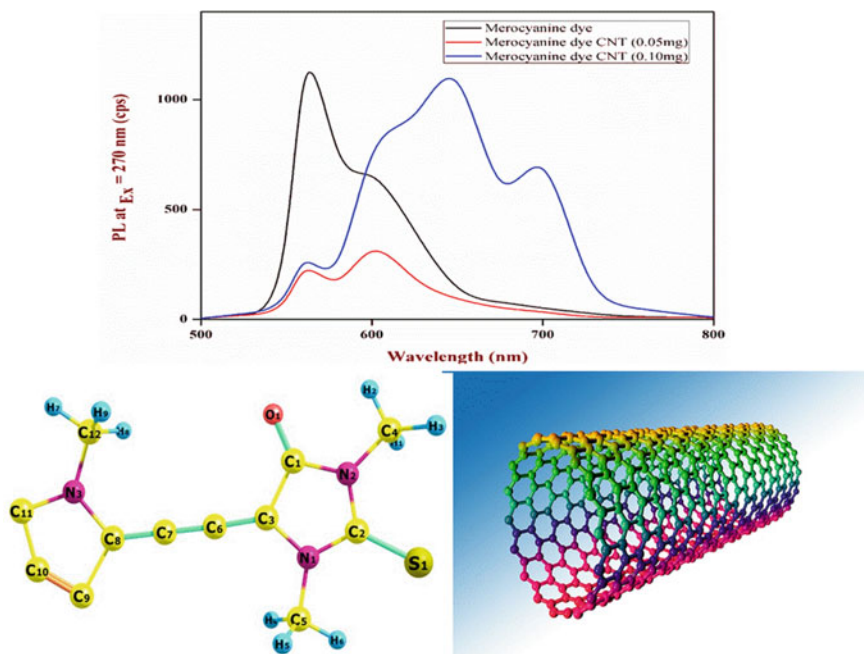
**Fig. 4** **a** Absorption spectra for merocyanine dye coated on carbon nanotube surface, **b** fluorescence emission wavelength spectra of peak intensity for merocyanine dye coated on carbon nanotube surface

## 6.2 Photoluminescence Spectrum (PL)

The PL spectral analysis of the interaction of merocyanine dye with carbon nanotube is shown in Fig. 5. The results show that the excitation–emission with x-axis represents the emission wavelength and y-axis of wavelength for merocyanine dye and merocyanine dye-coated carbon nanotube surface [76–78]. The PL emission peaks

are measured from within range of 500–800 nm. The new emission band is centred at 550 nm. The intensities of the emission band increase because of the formation of a nanostructured complex of the dye. The intensity of the peaks is used to monitor the amount of dye associated with carbon nanotubes.

At greater concentrations of the dye in the mixes, the merocyanine showed prominent peaks of aggregates with PL at EM = 595 and 635 nm (bands) in the range of EM = 670,770 nm. The strength of the bands is extremely low in the wide range of EX in the PLE maps, falling below the limit for signal restoration, and the peaks begin to fade several hours after mixing. The peaks may be distinguished adequately at short-wavelength excitation due to the modest contribution of the dye merocyanine PL in the spectra, as illustrated above for the PL peak at EM = 595 and 635 nm with merocyanine with SWCNT (0.05 M and 0.10 M) [79–81]. Low-intensity long-wavelength PL features could represent the entire contribution of unstable particles. We found non-permanent short-lived PL shoulders (bands) in the range of EM = 670–770 nm (Fig. 5) at greater concentrations of the dye in the mixtures, in addition to prominent peaks of aggregates with PL at EM = 595 and 635 nm (from Fig. 5). Due to the modest contribution of the merocyanine, the peaks may be identified properly at shorter wavelength excitation. The more the quantity of nanotubes, the higher the concentration of CNT with merocyanine in the mixture. Nanotubes in the shape of needles have small bended components. The first is at  $E_{\max} = 595$  nm, with a minor



**Fig. 5** a Photoluminescence spectra of peak intensity for merocyanine dye coated on carbon nanotube surface



red shift in comparison with monomer emission forms right after mixing. Furthermore, the SWCNT's PL peaks are quenched in the presence of cyanine chirality at EX = 650 nm and EM = 690 nm in Fig. 5, implying that the dye molecules alter the SWCNT's intrinsic qualities. The inclusion of surfactant at the premicellar concentration caused the aggregates to generate red-shifted wavelength photoluminescence peaks at 596, 636 and 695 nm. The aggregation of dye cyanine molecules has no effect on the energy transfer from the dye to the nanotubes, which amplifies near-infrared photoluminescence from the nanotubes [82, 83].

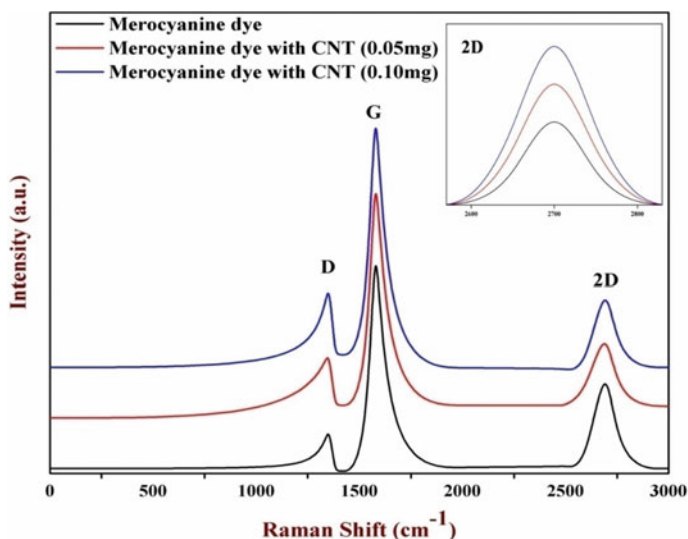
### 6.3 Raman Spectroscopy Analysis on Film

Among the different optical spectroscopic measurement, the most impressive strategy to acquire data about essential properties of the carbon nanotubes and dyes is Raman spectroscopy. Raman estimations were performed utilising a helium–neon laser working at a frequency of 632.8 nm (1.96 eV) and info force of  $\sim 300 \mu\text{W}$  at surface of merocyanine with SWCNT between the forces. The proportion between the D and G groups is normally utilised for assessing the defectivity of the carbon organisation. The sharp bands at 1300, 1592 and  $2600 \text{ cm}^{-1}$  compare to the D-band (imperfection), G-band and G'-band, separately. The D-band is an after-effect of a photon-imperfection cooperation. The G-band is expected to be the longitudinal and less significantly the circumferential. The G'-band originates from a photon–second photon association [84–86].

The band around  $3392.79 \text{ cm}^{-1}$  is recruited to N–H extending vibrations [6, 11], while the solid groups at  $1548.84$  and  $1224.8 \text{ cm}^{-1}$  are endowed to C = N extending vibrations and C–N symmetric twisting. The groups at  $1668.43$  and  $1099.43 \text{ cm}^{-1}$  are chosen for C = C stretching and C–N stretching vibrations [87–89]. The C–N symmetric extending vibrations are engaged to the groups at  $1384.89 \text{ cm}^{-1}$ . The band at  $929.69 \text{ cm}^{-1}$  is assigned to N–C–H symmetric bending vibrations. The presence of cyanine vibrational peak intensity at  $2231 \text{ cm}^{-1}$  for Fig. 6 and at  $2216 \text{ cm}^{-1}$  due to the formation of the nanoconjugate-shaped structure. Besides, the presence of another trademark groups in merocyanine at  $1200$ – $1096 \text{ cm}^{-1}$  confirms the appearance of merocyanine atoms in nanotubes [90].

### 6.4 AFM Analysis of Morphology

The thin-film surface morphologies were studied using AFM measurements. The top texture of dye/SWCNT on CTA thin films made using dip-coating method is examined using an AFM instrument. Figure 7 shows the following images: the surface morphology of the thin films was roughest, and the pattern of particle alignment became compact as the MWCNT concentration in the MWCNT/TiO<sub>2</sub>

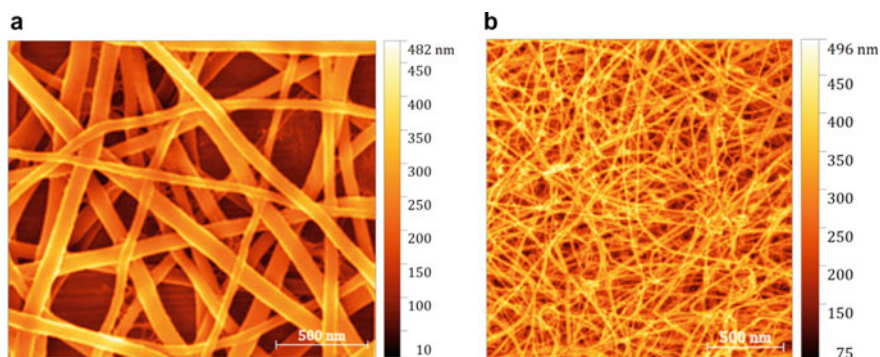


**Fig. 6** Raman spectra of peak intensity for merocyanine dye coated on carbon nanotube surface

sample increased. (a) Merocyanine dye, (b) 0.05 g, (c) 0.10 mg (7a, 7b), demonstrates that the texture of the thin films became rougher, and the particle arrangement became compact as the MWCNT aggregation in the MWCNT/TiO<sub>2</sub> sample increased. Figure 3c depicts an AFM image of a dye-SWCNT network after transfer to the CTA film, where the dye clumps dominate the larger-scale surface morphology. CNTs are graphite tubes with a tubular form. The tubes were at least two layers thick, and typically many more, with an outside diameter of 35–25 nm. The roughness rises as more MWCNT is applied, with wavelengths of 17 nm for 0.05 mg, 23 nm for 0.05 mg and 26 nm for 0.10 mg. The AFM topography reveals an extremely compact and rough surface; all films have rms values in the 10–25 nm range. AFM was used to examine the topography and upper surface of the CNT/dye thin film. The dye dispersed tubes are more isolated and exhibit signs of a considerable surface coating than the raw tubes, which are grouped together [91].

## 7 Analysis of Surface Morphology Using SEM and TEM

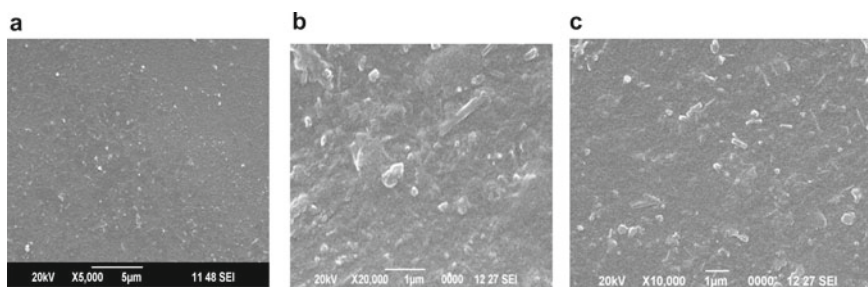
Surface morphologies of nanoporous CNT/merocyanine films are seen by SEM and TEM [6]. The films were made with a diluted ethanol solution that served as both a solvent and a soft template. The CNT/merocyanine nanoparticles interact well thanks to this method of production. Pore development within the nanocomposite thin films is also improved by the diluted ethanol. Furthermore, owing to the significant chemical



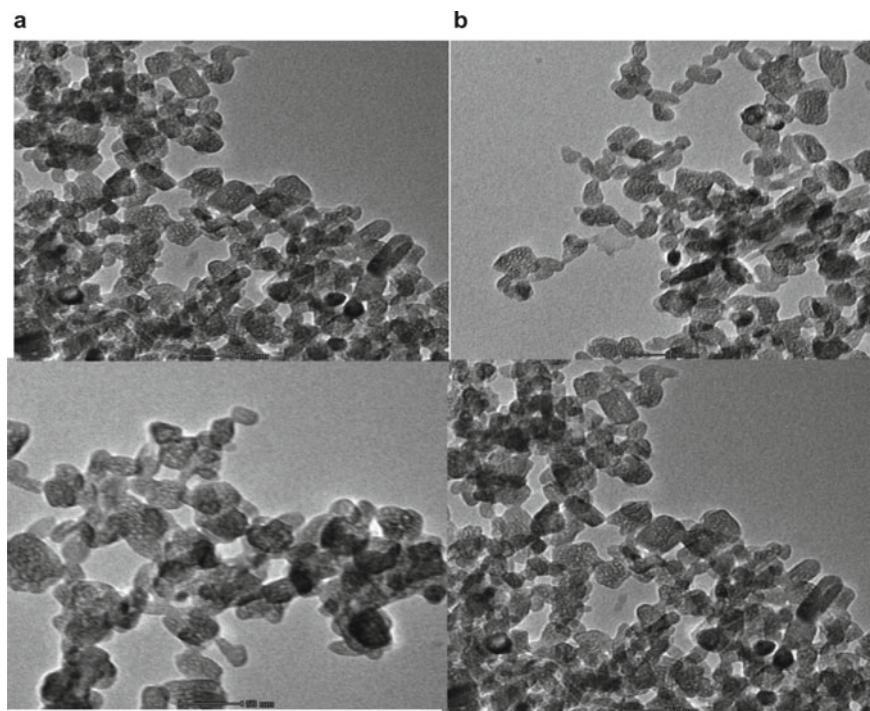
**Fig. 7** a and b AFM morphology of merocyanine dye coated on carbon nanotube surface

absorption, the acid-catalysed modification approach aids in the creation of contacts between CNT and dye nanoparticles [92] (Fig. 8).

Although this method of production reduces the nanocomposite's crystalline development, it nonetheless improves dye absorption for biomedical imaging applications. The dye and CNT nanoparticles in all of the annealed samples were irregularly organised and shaped. The thin-film nanoparticles were attached to a non-crack surface at random. We also discovered that the morphological structures of the films were altered by temperature changes. The dispersion of the CNT/merocyanine nanoparticles was aided by the addition of diluted ethanol figure title. In turn, highly dispersed films aided electron transit within the films. Huge particles of roughly 10 nm to 20 nm were produced by annealing the films at high temperatures, resulting in large surface areas with high porosities inside the films for dye absorption (Fig. 9).



**Fig. 8** SEM morphology of a merocyanine dye, b SWCNT with dye 0.05 M and c SWCNT with dye 0.10 M



**Fig. 9** TEM morphology of **a** merocyanine dye, **b** SWCNT with dye 0.05 M and **c** SWCNT with dye 0.10 M

### **7.1 Nonlinear Optical Property**

Many organic compounds have recently been created, and their nonlinear optical (NLO) properties have been explored for future optical signal processing and optical computer applications. A collection of compounds having interfacial molecular electro-optical transfer (CT) interactions, which include donor on one side of a molecule and acceptor on the other, has been found to have significant molecular hyperpolarisabilities [93, 94]. We should explore two alternative chemical designs to achieve strong charge transfer interactions in atoms to utilise materials with major changes NLO: strong electron donor–acceptor pairs and efficient molecular  $\pi$ -conjugated chain structures. Since many compounds with aromatic rings as conjugated chains were produced due to their chemical stability, method of synthesis at room temperature acts as NLO compounds with ethylenic double bonds. The ICT nature of two kinds of molecular structures acts as a key impact in the peak shifts in absorption spectrum and the HOMO–LUMO energy levels, according to both electrochemical and UV–visible spectra studies. The novel cyanine dyes were discovered to have high water solubility, and these new functional compounds surprisingly maintained the features of the natural cyanine dye extending their wavelength by

absorption at NIR range. In recent years, many organic dyes (NLO) materials have sparked a lot of attention by absorbing nature in near-infrared (NIR) range because of their promise in critical applications such as optical power limitation, two-photon microscopic imaging, optical data storage and photodynamic therapy. Porphyrins, fullerenes and organometallic compounds are examples of oil-soluble materials that have been studied previously. The limited water solubility of these organic nonlinear conjugate compounds, however, limits their biological applicability. Merocyanine dyes have attracted a lot of attention because of its prospective advantages, such as high molar extinction coefficients, higher-order polarisabilities, superior solubility in water and tunable optical properties. The C–C and C–N double bonds are similarly effective as conjugated chains for NLO materials; however, the C–C triple molecular hyperpolarisabilities are higher. Sheng et al. demonstrated that one of the beneficial ways for improving the NLO characteristics of porphyrins is to develop good p-electronic complexes [38]. It was discovered that changing the relative acceptor monomers of these dimers can improve their NLO characteristics. Based on the aforementioned phenomenon, these experimental results and prior papers have led us to believe that strong electron-removal phenomenon and  $\pi$  conjugation length can alter NLO characteristics. The optical characteristics of related compounds were clearly varied, implying that various NLO properties will be reported. However, there are many issues with NIR absorbing range functional cyanine dyes, such as limited fabricated products, difficulty in synthesising process and so on. As a result, today's research in this subject is focused on how to broaden the scope of cyanine dyes maximum and improve their application performance. For biological detection reporters, the ionised cyanine dye gave high water solubility. This enables the dye molecules to function as effective nonlinear optical molecules in the near-infrared range, which are predicted to be utilised in biological applications in the future. The effect of cyanine dyes on the electro-optical waveguides, phase modulation and photorefractive index properties of a composite composed of CTA and closed single-walled carbon nanotubes was investigated in this article (SWCNTs). This allows for charge carrier photogeneration, and photosensitivity in the NIR range up to 2000 nm and made changes inherent property of SWCNT acts as third-order nonlinear optical chromophores.

## 8 Conclusion

The synthesis of a new type of NIR absorbing nanomaterials, anionic merocyanine-based SWCNTs nanostructure prepared by dip-coating method and analysed by UV–visible analyses (TGA), FT-Raman spectroscopy, fluorescence spectrum analysis, atomic force microscopy (AFM) and scanning electron microscopy (SEM) confirmed the covalent attachment of the merocyanine moiety to the carbon nanotubes. Furthermore, using Raman and UV–visible NIR spectroscopes, the electronic properties of the nanoconjugates were examined, confirming the covalent bond between the electrochemical active species. The new hybrid conjugated nanomaterials have a pleasing

absorbance in the near-infrared region, paving the path for future optoelectronic and biological imaging applications. Fluorescence imaging technology is being used in more research to assess early stages of cancer. As a result, a promising novel method for detecting the initial stages of different cancer and other diseases using the chemical presented has been established.

## References

1. Iijima S (1991) Helical microtubules of graphitic carbon. *Nature* 354:56–58
2. DimitriosTasis NT (2006) Alberto Bianco, and maurizio prato, chemistry of carbon nanotubes. *Chem Rev* 106:1105–1136
3. Wang X, Wang C, Cheng L, Lee S-T, Liu Z (2012) Noble metal coated single-walled carbon nanotubes for applications in surface enhanced Raman scattering imaging and photothermal therapy. *J Am Chem Soc* 134:7414–7422
4. Wu HC et al (2010) Chemistry of carbon nanotubes in biomedical applications. *J Mater Chem* 20(6):1036–1052
5. Marega R, Bergamin M, Aroulmoji V, Dinon F, Prato M, Murano E (2011) Hyaluronan–carbon nanotube derivatives: synthesis, conjugation with model drugs, and DOSY NMR Characterization. *Eur J Org Chem* 5617–5625
6. Viel S, Mannina L, Segre A (2002) Detection of a complex by diffusion-ordered spectroscopy (DOSY). *Tetrahedron Lett* 43:2515–2519
7. Marega R, Aroulmoji V, Bergamin M, Feruglio L, Dinon F. Two-Dimensional diffusion-ordered NMR spectroscopy as a tool for monitoring functionalized carbon nanotube purification and composition
8. Dai HJ (2002) Carbon nanotubes: synthesis, integration, and properties. *Acc Chem Res* 35:1035–1044
9. Dresselhaus MS, Dai H (2004) Carbon nanotubes: continued innovations and challenges. *MRS Bull* 29:237–239
10. Bekyarova E, Ni Y, Malarkey EB, Montana V, McWilliams JL, Haddon RC, Parpura V (2005) Applications of carbon nanotubes in biotechnology and biomedicine. *J Biomed Nanotechnol* 1:3–17
11. Kostarelos K, Bianco A, Prato M (2009) Promises, facts, and challenges for carbon nanotubes in imaging and therapeutics. *Nat Nanotechnol* 4:627–633
12. Liu Z, Yang K, Lee S-T (2011) Single-walled carbon nanotubes in biomedical imaging. *J Mater Chem* 21:586–598
13. Diao S, Hong G, Robinson JT, Jiao L, Antaris AL, Wu JZ, Choi CL, Dai H (2012) Chirality-enriched (12,1) and (11,3) single-walled carbon nanotubes for biological imaging. *J Am Chem Soc* 134:16971–16974
14. Setaro A, Adeli M, Glaeske M, Przyrembel D, Bisswanger T, Gordeev G, Maschietto F, Faghani A, Paulus B, Weinelt M, Arenal R, Haag R, Reich S (2017) Preserving  $\pi$ -conjugation in covalently functionalized carbon nanotubes for optoelectronic applications. *Nat Comm* 8:14281
15. Guo XF, Small JP, Klare JE, Wang YL, Purewal MS, Tam IW et al (2006) Covalently bridging gaps in single-walled carbon nanotubes with conducting molecules. *Science* 311(5759):356–359
16. Tournus F, Latil S, Heggie MI, Charlier JC (2005)  $\pi$ -stacking interaction between carbon nanotubes and organic molecules. *Phys Rev B* 72:075431
17. Heller DA, Jin H, Martinez BM, Patel D, Miller BM, Yeung TK et al (2009) Multimodal optical sensing and analyte specificity using single-walled carbon nanotubes. *Nat Nanotechnol* 4:114–120

18. Welsher K, Sherlock SP, Dai H (2011) Deep-tissue anatomical imaging of mice using carbon nanotube fluorophores in the second near-infrared window. *Proc Natl AcadSci USA* 108:8943
19. O'Connell MJ, Bachilo SM, Huffman CB, Moore VC, Strano MS, Haroz EH et al (2002) Band gap fluorescence from individual single-walled carbon nanotubes. *Science* 297:593
20. Ju S-Y, Kopcha WP, Papadimitrakopoulos F (2009) Brightly fluorescent single-walled carbon nanotubes via an oxygen excluding surfactant organization. *Science* 323:1319
21. Welsher K, Liu Z, Sherlock SP, Robinson JT, Chen Z, Daranciang D et al (2009) A route to brightly fluorescent carbon nanotubes for near-infrared imaging in mice. *Nat Nanotechnol* 4:773
22. Kim J-H, Heller DA, Hong Jin, Barone PW, Song C, Zhang J et al (2009) The rational design of nitric oxide selectivity in single-walled carbon nanotube near-infrared fluorescence sensors for biological detection. *Nat Chem* 1:473
23. James NS, Cheruku RR, Missert JR, Sunar U, Pandey RK (1842) Measurement of cyanine dye photobleaching in photosensitizer cyanine dye conjugates could help in optimizing light dosimetry for improved photodynamic therapy of cancer. *Molecules* 2018:23
24. Velapoldi RA, Tonnesen HH (2004) Corrected emission spectra and quantum yields for a series of fluorescent compounds in the visible spectra region. *J Fluoresc* 14:465-472
25. Touthkine A, Han W, Ullmann M, Liu T, Bashford D, Noodleman L, Hahn KM (2007) Experimental and DFT studies: novel structural modifications greatly enhance the solvent sensitivity of live cell imaging dyes. *J Phys Chem A* 111:10849-10860
26. Ishizawa T, Fukushima N, Shibahara J, Masuda K, Tamura S, Aoki T, Hasegawa K, Beck Y, Fukayama M, Kokudo N (2009) Real-time identification of liver cancers by using indocyanine green fluorescent imaging. *Cancer* 115:2491-2504
27. Sekijima M, Tojimbara T, Sato S, Nakamura M, Kawase T, Kai K, Urashima Y, Nakajima I, Fuchinoue S, Teraoka S (2004) An intraoperative fluorescent imaging system in organ transplantation. *Transplant Proc* 36:2188-2190
28. Morimoto S (2007) In-vivo imaging of tumors with protease activated near-infrared fluorescent probes. *Tanpakushitsukakusankoso, Protein, Nucleic Acid Enzyme* 52:1774-1775
29. Zavaleta CL, Smith BR, Walton I, Doering W, Davis G, Shojaei B, Natan MJ, Gambhir SS (2009) Multiplexed imaging of surface enhanced Raman scattering nanotags in living mice using noninvasive Raman spectroscopy. *Proc Natl Acad Sci U S A* 106:13511-13516
30. Lamprecht C, Gierlinger N, Heister E, Unterauer B, Plochberger B, Brameshuber M, Hinterdorfer P, Hild S, Ebner A (2012) Mapping the intracellular distribution of carbon nanotubes after targeted delivery to carcinoma cells using confocal Raman imaging as a label-free technique. *J Phys Condens Matter* 24:164206-164216
31. Wagnieres GA, Star WM, Wilson BC (1998) In vivo fluorescence spectroscopy and Raman imaging for oncological applications. *Photochem Photobiol* 68:603-632
32. Beqa L, Fan Z, Singh AK, Senapati D, Ray PC (2011) Gold nano-porcorn attached SWCNT hybrid nanomaterial for targeted diagnosis and photothermal therapy of human breast cancer cells. *ACS Appl Mater Interfaces* 3:3316-3324
33. Liu Z, Tabakman S, Sherlock S, Li X, Chen Z, Jiang K, Fan S, Dai H (2010) Multiplexed five-color molecular imaging of cancer cells and tumor tissues with carbon nanotube Raman tags in the near-infrared. *Nano Res* 3:222-233
34. Yang K, Hu L, Ma X, Ye S, Cheng L, Shi X, Li C, Li Y, Liu Z (2012) Multimodal imaging guided photothermal therapy using functionalized graphene nanosheets anchored with magnetic nanoparticles. *Adv Mater* 24:1868-1872
35. Ku G, Zhou M, Song S, Huang Q, Hazle J, Li C (2012) Copper sulfide nanoparticles as a new class of photoacoustic contrast agent for deep tissue imaging at 1064 nm. *ACS Nano* 6:7489-7496
36. Agarwal A, Huang S, O'Donnell M, Day K, Day M, Kotov N, Ashkenazi S (2007) Targeted gold nanorod contrast agent for prostate cancer detection by photoacoustic imaging. *J Appl Phys* 102:064701-064704
37. Robinson JT, Welsher K, Tabakman SM, Sherlock SP, Wang H, Luong R, Dai H (2010) High performance in vivo near-IR (N1  $\mu\text{m}$ ) imaging and photothermal cancer therapy with carbon nanotubes. *Nano Res* 3:779-793

38. Liu X, Tao H, Yang K, Zhang S, Lee S-T, Liu Z (2011) Optimization of surface chemistry on single-walled carbon nanotubes for in vivo photothermal ablation of tumors. *Biomaterials* 32:144–151
39. Moon HK, Lee SH, Choi HC (2009) In vivo near-infrared-mediated tumor destruction by photothermal effect of carbon nanotubes. *ACS Nano* 3:3707–3713
40. MacNevin CJ, Gremyachinskiy D, Hsu CW, Li L, Rougie M, Davis TT, Hahn KM (2013) Environment-sensing merocyanine dyes for live cell imaging, applications. *Bioconjugate Chem* 24:215–223
41. Al Faraj A, Cieslar K, Lacroix G, Gaillard S, Canet-Soulas E, Cremillieux Y (2009) In vivo imaging of carbon nanotube bio distribution using magnetic resonance imaging. *Nano Lett* 9:1023–1027
42. Miyawaki J, Yudasaka M, Imai H, Yorimitsu H, Isobe H, Nakamura E, Iijima S (2006) Synthesis of ultrafine Gd<sub>2</sub>O<sub>3</sub> nanoparticles inside single-wall carbon nanohorns. *J Phys Chem B* 110:5179–5181
43. Richard C, Doan B-T, Beloeil J-C, Bessodes M, Tóth É, Scherman D (2008) Noncovalent functionalization of carbon nanotubes with amphiphilic Gd<sup>3+</sup> chelates: toward powerful T<sub>1</sub> and T<sub>2</sub> MRI contrast agents. *Nano Lett* 8:232–236
44. Wu H, Liu G, Wang X, Zhang J, Chen Y, Shi J, Yang H, Hu H, Yang S (2011) Solvothermal synthesis of cobalt ferrite nanoparticles loaded on multiwalled carbon nanotubes for magnetic resonance imaging and drug delivery. *Acta Biomater* 7:3496–3504
45. Ananta JS, Matsun ML, Tang AM, Mandal T, Lin S, Wong K, Wong ST, Wilson LJ (2009) Single-walled carbon nanotube materials as T<sub>2</sub>-weighted MRI contrast agents. *J Phys Chem C* 113:19369–19372
46. Wang H, Wang J, Deng X, Sun H, Shi Z, Gu Z, Liu Y, Zhao Y (2004) Biodistribution of carbon single-wall carbon nanotubes in mice. *J Nanosci Nanotechnol* 4:1019–1024
47. Deng X, Yang S, Nie H, Wang H, Liu Y (2008) A generally adoptable radiotracing method for tracking carbon nanotubes in animals. *Nanotechnology* 19:075101
48. McDevitt MR, Chattopadhyay D, Jaggi JS, Finn RD, Zanzonico PB, Villa C, Rey D, Mendenhall J, Batt CA, Njardarson JT (2007) PET imaging of soluble yttrium-86-labeled carbon nanotubes in mice. *PLoS ONE* 2:e907
49. Hong SY, Tobias G, Al-Jamal KT, Ballesteros B, Ali-Boucetta H, Lozano-Perez S, Nellist PD, Sim RB, Finucane C, Mather SJ (2010) Filled and glycosylated carbon nanotubes for in vivo radio emitter localization and imaging. *Nat Mater* 9:485–490
50. Brooker LGS, White FL, Sprague RH (1951) Color and constitution. IX. Absorption of cyanines derived from 3-methylisoquinoline, a rule relating basicity and absorption in symmetrical cyanines. *J Am Chem Soc* 73:1087–1093
51. Brooker LGS, Keyes GH, Sprague RH, VanDyke RH, VanLare E, VanZandt G, White FL, Cressman HWJ, Dent SG Jr (1951) Color and constitution. X. Absorption of the merocyanines. *J Am Chem Soc* 73:5332–5350
52. Kulnich AV, Ishchenko AA (2009) Merocyanine dyes: synthesis, structure, properties and applications. *Russ Chem Rev* 78(2):141–164
53. Shirinian VZ, Shimkin AA (2008) Merocyanines: synthesis and application. *Top Heterocycl Chem* 14:75–105. [https://doi.org/10.1007/7081\\_2007\\_110](https://doi.org/10.1007/7081_2007_110)
54. Toutchkine A, Nguyen D-V, Hahn KM (2007) Merocyanine dyes with improved photostability. *Org Lett* 9(15):2775–2777
55. Bouit PA, Rauh D, Neugebauer S, Delgado JL, Piazza ED, Rigaut S, Maury O, Andraud C, Dyakonov V, Martín N (2009) A “cyanine–cyanine” salt exhibiting photovoltaic properties. *Org Lett* 11:4806–4809
56. Brooker LGS, Keyes GH, Sprague RH, VanDyke RH, VanLare E, VanZandt G, White FL (1951) The cyanine dye series. XI The merocyanines. *J Am Chem Soc* 73:5326–5332
57. Lavanya Dhevi R, Vijayalakshmi KA, Ranjitha S. A review-DFT, UV, FT-Raman, FT-IR, homolumo and hyper polarizability of 1, 3-dimethyl-5-[(1-methyl-2pyrrolidinylidene) Ethylidene]. *Int J Chem Sci Res* 08–21



58. Steiger R, Pugin R, Heier J (2009) J-aggregation of cyanine dyes by self-assembly. *Colloids Surf B* 74:484–491
59. Behera GB, Behera PK, Mishra BK (2007) Cyanine Dyes: self aggregation and behaviour in surfactants. A review. *J Surface Sci Technol* 23:1–31
60. Lutsyk P, Piryatinski Y, AlAraini M, Arif R, Shandura M, Kachkovsky O, Verbitsky A, Rozhin A (2016) Emergence of Additional visible-range photoluminescence due to aggregation of cyanine dye: astraphloxin on carbon nanotubes dispersed with anionic surfactant. *J Phys Chem C* 120(36):20378–20386
61. Del Canto E, Flavin K, Natali M, Perova T, Giordan S (2010) Functionalization of single-walled carbon nanotubes with optically switchable spiropyrans. *Carbon* 48(10):2815–2824
62. Edge M, Allen NS, Jewitt TS, Horie CV (1989) Fundamental aspects of the degradation of cellulose triacetate base cinematograph FLM. *Polym Degrad Stabil* 25:345–362
63. Carter EA, Swarbrick B, Harrison TM et al (2020) Rapid identification of cellulose nitrate and cellulose acetate film in historic photograph collections. *HeritSci* 8:51. <https://doi.org/10.1186/s40494-020-00395-y>
64. Bürckstümmer NM, Kronenberg K, Meerholz F (2010) Würthner near-infrared absorbing merocyanine dyes for bulk heterojunction solar cells. *H. Org Lett* 12:3666
65. Zhao X, Yang Y, Yu Y, Guo S, Wang W, Zhu S (2019) A cyanine-derivative photosensitizer with enhanced photostability for mitochondria-targeted photodynamic therapy. *Chem Commun* 55:13542–13545
66. Delaey E, van Laar F, De Vos D, Kamuhabwa A, Jacobs P, de Witte P (2000) A comparative study of the photosensitizing characteristics of some cyanine dyes. *J Photochem Photobiol B Biol* 55:27–36
67. Hogley J, Malatesta V, Millini R, Parker WO (2000) Merocyanine and photomerocyanine dyes. *Mol Cryst Liq Cryst Sci Technol. Sect A. Mol Cryst Liq Cryst* 345(1):329–334
68. Takayanagi M, Nakata M, Ozaki Y, Iriyama K, Tasumi M (1997) Intermolecular interactions of merocyanine dyes studied by visible absorption, resonance Raman and infrared spectroscopies. *J Molecul Struct* 407(2–3):85–92
69. Carlson LJ, Maccagnano SE, Zheng M, Silcox J, Krauss TD (2007) Fluorescence efficiency of individual carbon nanotubes. *Nano Lett* 7:3698
70. Hong G et al (2012) Multifunctional in vivo vascular imaging using near-infrared II fluorescence. *Nat Med* 18:1841
71. Hoebeke M, Piette J, Van de Vorst A (1990) Viscosity dependent isomerization and fluorescence yields of Merocyanine 540. *J Photochem Photobiol B* 4:273–282
72. Shandura MP, Kovtun YuP, Yakubovskiy VP, Piryatinski YuP, Lutsyk PM, Perminov RJ, Arif RN, Verbitsky AB, Rozhin A (2014) Dioxaborine dyes as fluorescent probes for amines and carbon nanotubes. *Sens Lett* 12:1361–1367
73. Macuil RD, Lopez MR, Díaz AO, Camacho Pernas V (2009) Spectroscopy analysis of spiropyran-merocyanine molecular transformation. *J Phys: Conf Series* 167: 012038; Delgado R, Published Under Licence Byiop publishing Ltd.; Delgado Macuil R et al, Latin American symposium on solid state physics, 5–10, October 2008, Puerto Iguazú, Argentina
74. Hong G, Tabakman SM, Welscher K, Wang H, Wang X, Dai H, Matsuda K, Kanemitsu Y, Irie K, Saiki T, Someya T, Miyauchi Y, Maruyama S (2010) Metal-enhanced fluorescence of carbon nanotubes. *J Am Chem Soc* 132:15920
75. Gauffrès E, Tang NY-W, Lapointe F, Cabana J, Nadon M-A, Cottenye N, Raymond F, Szkopek T, Martel R (2014) Giant Raman scattering from J-aggregated dyes inside carbon nanotubes for multispectral imaging. *Nat Photonics* 8:72
76. Liu Z, Davis C, Cai W, He L, Chen X, Dai H (2008) Circulation and long-term fate of functionalized, biocompatible single-walled carbon nanotubes in mice probed by Raman spectroscopy. *Proc Natl AcadSci USA* 105:1410
77. Cronin SB, Swan AK, Uuml nl, SM, Goldberg BB, Dresselhaus MS, Tinkham M (2004) Measuring the uniaxial strain of individual single-wall carbon nanotubes: resonance Raman spectra of atomic-force-microscope modified single-wall nanotubes. *Phys Rev Lett* 93(16):167401

78. Cronin SB, Swan AK, Uuml nl, SM, Goldberg BB, Dresselhaus MS, Tinkham M (2005) Resonant Raman spectroscopy of individual metallic and semiconducting single-wall carbon nanotubes under uniaxial strain. *Phys Rev B* 72(3):035425
79. Gao B, Jiang L, Ling X, Zhang J, Liu Z (2008) Chirality-dependent Raman frequency variation of single-walled carbon nanotubes under uniaxial strain. *J Phys Chem C* 112(51):20123–20125
80. Liu Z, Zhang J, Gao B (2009) Raman spectroscopy of strained single-walled carbon nanotubes. *Chem Commun* (45):6902–6918
81. Onai Y, Mamiya M, Kobayashi M, Shinohara H, Sato H (1992) Raman spectroscopic studies of long-lived colored merocyanine conformers in the aggregates: a poor-man's time-resolved study. In: Takahashi H (eds) *Time-resolved vibrational spectroscopy V. Springer proceedings in physics*, vol 68. Springer, Berlin, Heidelberg Pl
82. Sayama K, Hara K, Ohga Y, Shinpou A, Suga S, Arakawa H (2001) Significant effects of the distance between the cyanine dye skeleton and the semiconductor surface on the photo electrochemical properties of dye-sensitized porous semiconductor electrodes. *New J Chem* 25:200–206
83. Bluemmel P, Setaro A, Maity C, Hecht S, Reich S (2012) Tuning the interaction between carbon nanotubes and dipole switches: the influence of the change of the nanotube–spiropyran distance. *J. Phys. Condensed Matt* 24:394005
84. Lefebvre J, Homma Y, Finnie P (2003) Bright band gap photoluminescence from unprocessed single-walled carbon nanotubes. *Phys Rev Lett* 90, 17401
85. Oyama Y, Saito R, Sato K, Jiang J, Samsonidze GG, Grüneis A, Miyauchi Y, Maruyama S, Jorio A, Dresselhaus G, Dresselhaus M (2006) Photoluminescence intensity of single-wall carbon nanotubes. *Carbon* 44:873
86. Sakashita T, Miyauchi Y, Matsuda K, Kanemitsu Y (2010) Plasmon-assisted photoluminescence enhancement of single walled carbon nanotubes on metal surfaces. *Appl Phys Lett* 97:063110
87. Bachilo SM, Strano MS, Kittrell C, Hauge RH, Smalley RE, Weisman RB (2002) *Science* 298:2361–2366. <https://doi.org/10.1126/science.1078727>
88. Bachilo SM, Balzano L, Herrera JE, Pompeo F, Resasco DE, Weisman RB (2003) *J Am Chem Soc* 125:11186–11187. [https://doi.org/10.1021/ja036622cControllingDye\(Merocyanine-540\)AggregationonNanostructuredTiO2Films](https://doi.org/10.1021/ja036622cControllingDye(Merocyanine-540)AggregationonNanostructuredTiO2Films)
89. Chami Khazraji A, Hotchandani S, Das S, Kamat PV (1999) An organized assembly approach for enhancing the efficiency of photosensitization. *J Phys Chem B* 103:4693–4700
90. Mei X, Cho SJ, Fan B, Ouyang J (2010) High-performance dye-sensitized solar cells with gel-coated binder-free carbon nanotube films as counter electrode. *Nanotechnology* 21, 395202
91. Ikeda H, Sakai T, Kawasaki K (1991) Nonlinear optical properties of cyanine dyes. *Chem Phys Lett* 179(5,6)
92. Pan F, Wong MS, Gramlich V, Bosshard C, Gunther P (1996) *J Am Chem Soc* 118:6315
93. Tsuboi K, Seki K, Ouchi Y, Fujita K, Kajikawa K (2003) *Jpn J Appl Phys* 42:607
94. Cambré S, Campo J, Beirnaert C, Verlactt C, Cool P, Wenseleers W (2015) Asymmetric dyes align inside carbon nanotubes to yield a large nonlinear optical response. *Nat Nanotechnol* 10:248

# Chapter 41

## Role of Carbon Nanostructures as Nano-Theranostics Against Breast and Brain Cancer



Neha Saini, Prem Pandey, Mandar Shirolkar, Atul Kulkarni, Sang-Hyun Moh, and Anjali A. Kulkarni

### 1 Introduction

Cancer is caused due to agglomeration of genetic and epigenetic mutations that result in altered translation (protein synthesis) or post-translational modifications. Consequently, the number of proteins synthesized will increase, decrease, or perform faulty functions. It leads to the secretion of certain molecules which are either varying in amount or not present in normal individuals. These molecules which indicate the fluctuated bodily metabolism, biochemical reactions, and physiology are the molecular biomarkers. These include cDNA, mRNA, altered proteins, and other metabolites [25, 70, 77]. Hypothesis-driven as well as technology-driven approaches can be utilized for biomarkers discovery [70]. Nanomaterial-based biosensors could be of great help in cancer biology as these are highly accurate and quick in cancer detection, even before the appearance of symptoms and will not only save many lives but also greatly reduce the financial burden of cancer treatment. Cancer is one of the major drivers of deaths in developed countries and is fast becoming a cause of concern in developing countries as well. The contemporary therapies carry multiple side effects and higher chances of cancer recurrence. Therefore, oncologists are focusing on developing procedures with bare minimum side effects. Utilizing

---

N. Saini · P. Pandey · M. Shirolkar · A. Kulkarni (✉)  
Symbiosis Centre for Nanoscience and Nanotechnology, Symbiosis International (Deemed University), Pune 412115, India  
e-mail: [atulkin@gmail.com](mailto:atulkin@gmail.com)

S.-H. Moh (✉)  
BIO-FD&C Co. Ltd., Incheon 21990, Republic of Korea  
e-mail: [biofdnc@gmail.com](mailto:biofdnc@gmail.com)

A. A. Kulkarni (✉)  
Department of Botany, Savitribai Phule  
Pune University (Formerly University of Pune), Pune 411 007, India  
e-mail: [anjali.uop@gmail.com](mailto:anjali.uop@gmail.com)

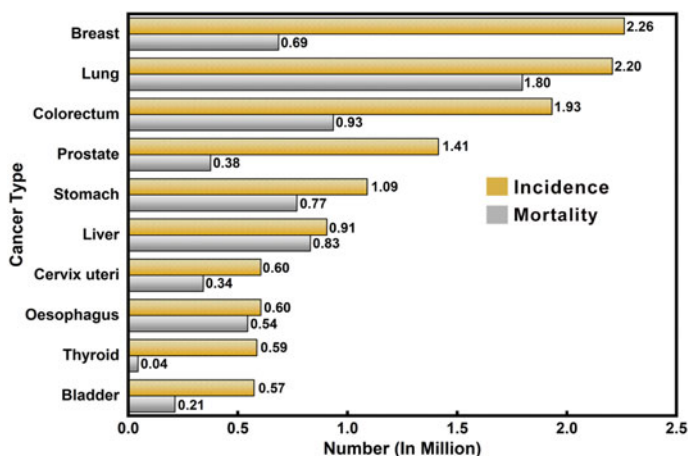
nanomaterial-based systems can be a step in that direction. In the present review, we would like to concentrate on the high potential of nanomaterials in biomedical applications, especially carbon nanomaterials (CNMs) with special reference to drug delivery.

## 1.1 Breast Cancer

Breast cancer continues to haunt the women across the globe. Year 2020 alone contributed 2.3 million new cancer cases with 6,85,000 deaths globally (Fig. 1) [82]. It attained the status of the most prevalent cancer by December 2020 with 7.8 million existing breast cancer patients' during the last 5 years [101]. Broadly, breast cancer is clinically divided into two groups [48, 59]:

- (a) Hormone-Responsive (HR+) phenotypes- Luminal A: ER/PR (HR+) & ERBB2 (-), Luminal B: ER/PR (HR+) & ERBB2 (+)
- (b) Hormone Irresponsive (HR-) phenotypes- ERBB2 enriched: ER/PR (HR-) & ERBB2 (+) and triple-negative breast cancer (TNBC): ER/PR (HR-) & ERBB2 (-)

Hormones are biochemical messengers in human body. Female hormones estrogen and progesterone are required for development of female sexual characteristics, regulation of female menstrual cycle and pregnancy. These hormones also promote growth of hormone-sensitive breast cancer [67]. About 65–75% of breast



**Fig. 1** Estimated number of incident cancer cases and deaths globally for both the sexes and all age groups in 2020. Breast cancer continues to be the most prevalent one followed by lung, colorectum, and prostate cancers. The yellow bar represents number of incident cancer cases while the gray bar represents number of deaths (Data Source GLOBOCAN 2020, Global Cancer Observatory: <http://gco.iarc.fr/>)

cancer patients are estrogen/progesterone receptors (ER/PR) positive at diagnosis [37, 48]. The hormone-responsive breast cancer cells contain hormone receptor proteins. These receptors get activated upon binding with hormones and lead to specific gene expression that promotes cancer cell growth [50]. The second most prevalent breast cancer cases are ERBB2 (+) type, that was previously known as HER2 (+) breast cancer. ERBB2 (avian erythroblastic leukemia viral oncogene homolog 2) gene translates a receptor tyrosine protein kinase ERB-2 from epidermal growth receptor family and is found to be amplified in approximately 20% of the breast cancer cases [92]. Different from this league, triple-negative breast cancer lacks receptors which are found in other breast cancer types. It is found in approximately 15% of the patients, has been poorly understood, and is associated with destitute prognosis [21]. It carries a very high risk of relapse during first 5 years from diagnosis [28]. Four stages have been defined for breast cancer. Stage I has been characterized with solid tumor lesser than 2 cm while stage IV with metastasis. Stage I HR (+) and ERBB2 (+) breast cancer patients have approximately 99% and 94% 5-year survival rates, respectively, while triple-negative breast cancer patients have approximately 85% 5-year survival rate. Notably stage IV HR (+), ERBB2 (+) breast cancer patients have overall median survival rate of 5 years while TNBC patients have approximately 1 year [9, 83].

## 1.2 Brain Cancer

Nervous system (NS) cancers account for just 3% of all cancers worldwide, but still impose a greater risk on the life of patients, being the most dangerous form; due to drug delivery challenges posed by the presence of blood–brain barrier (BBB), cerebrospinal fluid (CSF) barrier, different morphological subgroups with different behavioral patterns and are the toughest to treat [13, 16].

According to WHO report, to achieve the comprehensive control of cancer, accessibility to prompt early diagnosis and effective treatments for cancer need to be improved [80].

Glioblastoma (GBM) is the most prevalent malignant brain cancer in adults and 12–15% of all intracranial tumors and approximately 50% of the astrocytic tumors belong to this class. Despite the most advanced present therapeutic regimens, significant number of patients suffer relapse due to the GBM tumor heterogeneity [84]. The incidence of brain cancer is rising drastically in India. According to a Globocan 2020 report, presented by ‘International Association of Cancer Registries’ (IARC) associated with WHO, around 28,142 new cases of brain tumor are reported annually in India and the death toll is approximately around 24,003 per annum. It affects almost all age ranges between 7 and 78 years (~ 42.38 year’s average). Worldwide, out of all cancer cases, 1% cases are of brain cancer, i.e., approximately 3 lakhs [82]. In India, brain tumors were the 10th most common tumors in 2018, making up ~ 10% of all cancer cases [15]. Brain tumor could be cancerous (malignant/metastatic) or non-cancerous (Benign) [25, 104]. Benign can become malignant in some cases.

If brain tumor starts from the brain and does not move to other organs, it is called as primary brain tumor (BT, while if it starts from other organs and then migrates to brain, it is called as secondary brain tumor. Secondary BT is more common and may originate from cancers of breast, lung, kidney, colon, and skin. ([www.webmd.com](http://www.webmd.com)).

According to a Globocon 2018 report, incidences of brain and NS cancers in high Human Development Index (HDI) countries were 4% (females) and 5% (males) while for low HDI countries, it was 1.7% (females) and 2.4% (males). The mortality rate for high HDI countries was 2.8% (females) and 2.4% (males) while for low HDI countries, it was 1.4% (females) and 2.2% (males). Thus, higher incidences of brain cancers were seen in males than in females, in both low and high HDI countries [15].

Gene profiling was the first high-end technological tool applied for human cancers [40]. Recent genomic advancements led to more precise GBM classifications, consequently enhancing patient's stratification, targeted therapeutics, etc. It also became clear that isocitrate dehydrogenase (IDH) mutated GBM is distinct from non-IDH mutated GBM [2, 40]. IDH 1/2 mutations at early-stage indicate grades 2 and 3 glioma while GBM grade 4 (the deadliest form) originates without IDH mutation. Thus, genetic tools proved useful to classify various subtypes of brain cancers [40]. In 2016, central nervous system (CNS) tumors classification got an update, where for the first time, molecular biomarkers along with histology were used as classification criteria, indicating huge differences in glioma and medulloblastoma classes [4].

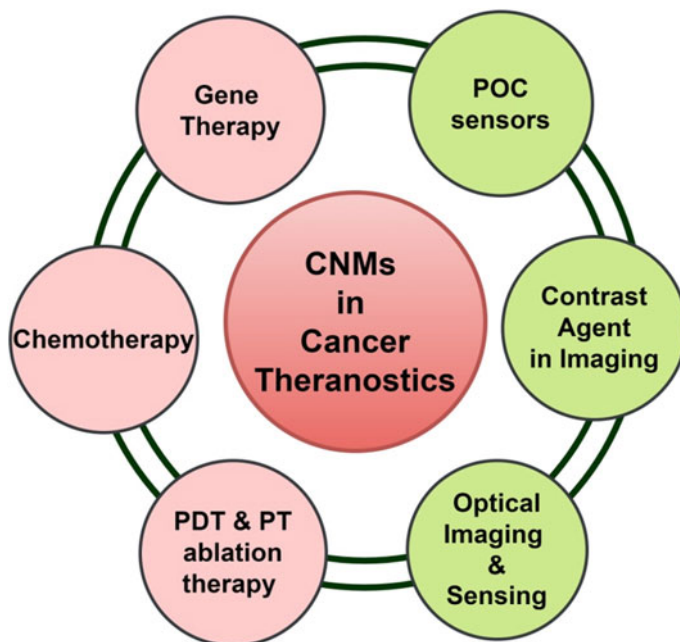
GBMs which develop from preexisting gliomas are less common and are known as secondary GBMs. The primary GBMs affect elderly (TERT, PTEN, EGFR mutations) while the secondary GBMs are more common among younger people (IDH 1/2, TP53, ATRX, PDGFRA, EGFR and EGFRvIII, NF1, MGMT, hTERT and BRAF mutations) [2].

### ***1.3 Nano-Theranostics***

The major hurdle for commercial use of nanomedicine is the receptor-mediated, targeted, and sustained delivery of nanoparticles and the cargo drug inside the cells. Owing to their unique physical and biochemical properties, nanoscale materials have immense potential in cancer 'theranostics', improving both treatment specificity (therapy) and diagnosis accuracy. Such theranostic nanomaterials can be porous, hollow, or solid structures [79, 94] (Fig. 2).

As compared to other metal or non-metal derived nanomaterials, nanomaterials derived from carbon have gained immense popularity in recent years; the major reason being, the presence of carbon in a large number of biomolecules and hence the implicit biocompatibility. Additionally, they have demonstrated improved and prolonged blood circulation time, enhanced drug solubility as well as therapeutic efficacy and reduced side effects. On the diagnosis side, CNMs can be a potential fluorescence imaging agent for vital cells [94].

These CNMs can be functionalized as per the target site to enhance their specificity, thus making them a suitable drug delivery vehicle [78]. Targeted



**Fig. 2** An illustration of role of CNMs in cancer theranostics with 2nd and 3rd quadrants representing therapy and 1st and 4th quadrants representing diagnostics

delivery is required as the most effective treatment of metastatic cancer. In general, chemotherapy is untargeted and causes huge impact on surrounding tissues [61] and many cancer types are resistant to many drugs resulting into multidrug-resistant (MDR) cancers [30]. Considering huge potential of nanomedicines, oncologists are utilizing them to reduce the side effects on surrounding cells [7]. These nanostructures have the ability to concentrate in the tumor targets because of enhanced permeability and retention (EPR) effect of cancer cells as the capillaries draining the cancer cells are more permeable than healthy cells. This provides high drug concentration and more drug efficacy specifically in the tumors [34].

## 2 Contemporary Therapy and Diagnostics Tools

### 2.1 Therapy

#### 2.1.1 Chemotherapy

Chemotherapy is the conventional cancer drug treatment that uses a single anti-cancer drug or a combination of anticancer drugs to kill or prohibit fast-growing

cancer cells in the human body. These drugs belong to specific classes, for example alkylating agents, biological response modifiers, antimetabolites, histone deacetylase inhibitors, monoclonal antibodies, hormonal agents, topoisomerase inhibitors, alkaloids, taxanes, and other miscellaneous drugs [22]. Although numerous side effects have been reported due to chemotherapy drugs [3], researchers across the globe have been consistently making efforts to develop tumor-specific targeted drugs [6, 29].

### **2.1.2 Radiotherapy**

Radiotherapy or radiation therapy is a part of cancer treatment that uses ionizing radiation [63]. One of the first reports of effective radiotherapy treatment was reported by Thor Stenbeck when he cured a skin cancer patient with radiotherapy in 1900 [12]. Since then, radiotherapy has seen many advancements. Between 1950 and 1960s, radiotherapy was done with the help of cobalt therapy machines that could kill deeper tumor cells [12] with subsequent use of linear accelerator, computerized tomography (2-D and 3-D), integrated computerized image therapy (IMRT & IGRT). Normally, radiotherapy can be classified into teletherapy (radiation through external therapy), brachytherapy (radiation through internal therapy), and radioisotopes-assisted systemic therapy [63].

### **2.1.3 Surgery**

Cancer surgery is the oldest form of cancer treatment and is done by the removal of solid tumors and nearby cancerous cells. These solid tumors are often localized. There are multiple types of cancer surgeries which include debulking (removal of a portion of the cancerous tumor), curative surgery (localized tumor removal, considered as primary treatment), preventive surgery (removal of susceptible tissues which are likely to be cancerous), diagnostic surgery (removal of a tissue sample for testing and evaluation), staging surgery (removal or viewing of tissue sample to ascertain the extent of cancer), palliative surgery (performed in advanced stages of cancer to relieve discomfort), and reconstructive surgery (the surgery performed to repair the damage due to cancer, e.g., breast reconstruction surgery) [17, 69].

## **2.2 Diagnostic Tools**

Imaging tools recognize disease at a very advanced stage and ignore smaller details, thus failing the early diagnosis and timely treatment in most of the cases [70]. In current times, biomarkers are in great demand, either as diagnostic tools or to complement imaging tools.



### 2.2.1 Genomics Tools

They help in analysis and monitoring of genetic level alterations which are caused by environmental issues and include high throughput assay methods, which can amplify DNA, RNA with suboptimal/negligible secretion in sample.

- *DNA Microarrays* (or Oligonucleotide-based/Gene Chip): These are based on the principle of binding of complementary sequences [1]. The technique compares DNA, RNA from normal cells with the affected cells, simultaneously in thousands, thus providing gene expression comparisons under various biological conditions [70]. But they give only relative information of nucleotide levels and not quantitative information of mRNA levels.
- *PCR-Based Assays*: Real-Time Polymerase Chain Reaction (RT-PCR) provides quantitative analysis of mRNA levels and its amplification [1]. It can study multiple samples simultaneously. Multiple reports suggest RT-PCR as a strong multiplexing assay and are useful in screening genetic disorders associated with cancer [70].
- *Fluorescence In-situ Hybridization (FISH)*: It determines content of nucleic acids (DNA, RNA) in circulating cells. With the help of cDNA and RNA probes, genetic mutations such as amplifications, deletions, fusions, translocations of nucleic acids/chromosomes in the cancer cells can be understood, e.g., used for EGFR and ERBB2 genes to check amplification of copies [1].
- *Sanger Sequencing Method*: It examines DNA and RNA and checks mutations, by the method of selective incorporation of dideoxynucleotides (ddNA) which act as terminators in an in vitro DNA synthesis process [1].

### 2.2.2 Proteomics Tools

Proteomics of cancer cells include study of altered protein levels as well as post-translational fluctuations in body fluids. It provides separation and identification of proteins and peptides, along with structural and functional analysis of proteins, and may also include immune-based assays [68]. Most clinical cancer biomarkers are antibody (Ab)-based tests in serum. e.g., CA-125 (cancer antigen) of ovarian cancer.

- *Two-Dimensional Electrophoresis (2-DE) and Liquid Chromatography*: Proteins from healthy control and cancerous cells are separated on polyacrylamide gels in two perpendicular dimensions and then compared. But the technique is not highly reproducible, has low resolution, and needs large volumes of samples [70].
- *Mass Spectrometry (MS)*: Cellular proteins separated by electrophoresis are identified by MS. Isotope-labeled proteins are used for comparative analysis of the number of peptides. It is low throughput and quite expensive [70].
- *Protein Arrays*: These are made up of recombinant proteins or immunoglobulins and are akin to DNA microarrays. They are based on immunoassay principles and detect multiple cancer antigens (Ag) in a single assay. Specific Ag-Ab interaction

helps in accurate diagnosis of cancer. This is a portable and good screening tool [70].

- *Surface-Enhanced Laser Desorption/Ionization Time-of-Flight MS (SELDI-TOF MS)*: It is one of the most widely used proteomic tools and can be a useful clinical device. Samples are spotted on chromatographic paper which binds selectively to proteins (protein chip arrays). Sample loaded chips are further ionized and analyzed by TOF MS, e.g., the identification of  $\alpha$ -haptoglobin (HP) in case of ovarian cancer. The data can also be used for making patterns in pattern recognition algorithms. Other techniques like matrix-associated (MALDI) TOF MS could also be used [70]. However, interfering proteins in sample, diet changes, inflammation, sample quality, etc., affect intensity of protein levels and pose some limitations to proteomics as an effective diagnostic tool.
- *Enzyme-linked Immunosorbent Assay (ELISA)*: It measures proteins, antigens, and antibodies in the sample. It produces highly reproducible and quantitative results. But antibody quality and detection of single molecule at a time are some of the limitations [23].

### 2.2.3 Metabolomics Tools

These analyze various metabolites present in the body fluids. Smaller number of signature metabolites is an advantage as it reduces the interference in detection. Molecular level changes are identified at various stages like transcription, translation, and post-translation. Some of the techniques are:

- Nuclear Magnetic Resonance Spectroscopy (NMR).
- High-Performance Liquid Chromatography (HPLC).
- Gas-Liquid Chromatography (GLC).
- Mass Spectrometry (MS).

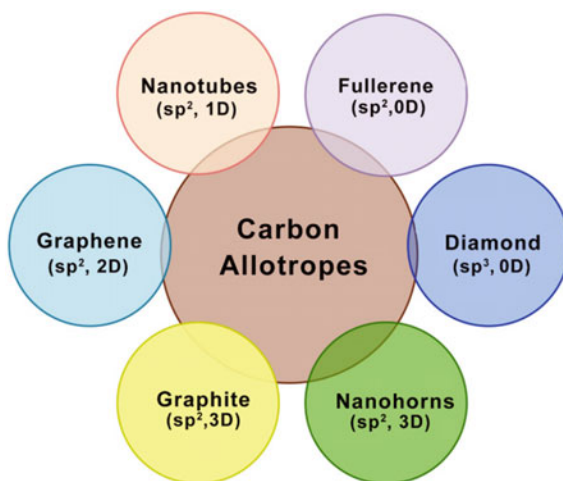
### 2.2.4 Multiplex Approaches

These consist of more than one pair of primers to amplify multiple genes in a single PCR reaction [20]. Technologies like quantitative multiplex-methylation-specific PCR (QM-MSP), invader assays, lab-on-chip technology with 2100 Bioanalyzer can analyze DNA, RNA, proteins, and metabolites in a single sample, thus reducing the preparation and the analysis time [70]. But the main issue arises out of dynamic ranges for various molecules in a particular sample [23].

## 3 Carbon Nanomaterials (CNMs)

Carbon is one of the multifaceted elements and can exist in various dimensions (from 0-D to 3-D, Fig. 3) with different hybridization states of  $sp^2$  and/or  $sp^3$  [87].

**Fig. 3** Types of carbon allotropes (from 0-D to 3-D)



CNMs are used for advanced tumor therapy as therapeutics, carriers, and diagnostic or theranostic systems such as carbon nanotubes (CNTs). CNT is utilized in gene therapy or chemotherapies [97] and in tumor photothermal ablation, producing thermal cytotoxicity in tumors [81].

Porous carbon nanomaterials (PCNMs) have attracted attention of material scientists owing to properties such as flexible pore structure, high porosity, and surface area, better stability and surface modification ability, e.g., carbon black, glassy carbon, activated carbon, graphite, graphene, diamonds, onions, fullerenes, carbon nanotubes, carbon nanofibers, carbon dots, carbon-based hybrids, and other porous carbon-based materials [94].

### **3.1 Zero-Dimensional (0-D) CNMs**

**Zero-dimensional** nanomaterials are the materials having all the dimensions in nanoscale range (all dimensions  $< 100$  nm). These materials have radically small sizes, substantial surface-to-volume ratio and demonstrate improved novel properties such as photoluminescence and chemiluminescence [99]. They include fullerenes, nanodiamonds, graphene quantum dots, and carbon quantum dots.

#### **3.1.1 Quantum Dots (QDs)**

QDs are ultra-small particles in 2–10 nm diameter range with unique optical, electrical, and fluorescence properties such as high photochemical stability, improved

quantum yield, narrow emission spectra [111]. These properties along with ultra-small size and high surface-to-volume ratio shape them to be an ideal candidate as biosensors [43, 44], drug delivery [65], and cancer therapeutic agent [53, 103].

### 3.1.2 Carbon Nanoparticles (CNPs)

CNPs have huge potential because of greater solubility in water, biocompatibility, good cellular permeability, smaller size, and high photostability [8]. CNPs are good theranostic molecules for safe drug delivery and biomedical imaging. Carbon nanodots (CNDs), graphene quantum dots (GQDs), single-walled carbon nanohorns (SWNHs) have structures akin to SWCNTs, where a single graphene sheet is rolled into a cone-like structure [112]. The 80–100 nm size range of SWNH clusters is suitable for EPR effect and favors their accumulation into the tumor site with reduced cytotoxicity and easily gets endocytosed [18]. Reduced graphene oxide nanomesh (RGONM) with 55–65 nm diameter range and an average thickness of 0.9 nm, and with pore size of approximately 8 nm is highly suitable for photothermal therapy [100].

### 3.1.3 Fullerenes

Fullerenes have a cage-like structure and are electron deficient. This leads to fascinating properties and had attracted the attention of researchers across the globe. The most known fullerene, C<sub>60</sub>, is well within the realm of nanotechnology [89]. It has relatively inert cage interior and facilitates the binding of ionic, atomic, and small molecules [73].

### 3.1.4 Nanodiamonds (NDs)

NDs seem to have substantial potential because of their shape and small size, large surface area and a satisfactory proportion of sp<sup>2</sup>/sp<sup>3</sup> hybridized bonds. As drug delivery systems (DDSs), NDs demonstrate better capability for oncological applications [109]. The advantage is that the NDs have the highest biocompatibility, highly targeted delivery with maximal drug bioavailability.

## 3.2 *One-Dimensional (1-D) CNMs*

One-dimensional (1-D) nanomaterial has two dimensions in nanoscale range and one dimension outside the nanoscale range. It includes nanotubes (CNTs), nanowires, nanorods, nanofibers, and nanofilaments [10].

### 3.2.1 Carbon Nanotubes (CNTs)

CNTs discovered by Sumo Iijima in 1991 are novel materials with significant hollow and cylindrical structures. Graphene layer arrangements could be classified as single-walled carbon nanotubes (SWCNTs), double-walled carbon nanotubes (DWCNTs), triple-walled carbon nanotubes (TWCNTs), or multiple-walled carbon nanotubes (MWCNTs) [39] with multiple layers of cylinders having an interlayer spacing range between 0.30 and 0.40 nm [76]. Functionally modified SWCNTs have been utilized in mice for tumor-targeted accumulation with high biocompatibility, and minute toxicity [55].

## 3.3 Two-Dimensional (2-D) CNMs

In general, 2-D nanomaterials (e.g., graphene) have sheet-like structures with length greater than 100 nm and thickness less than 5 nm [36].

### 3.3.1 Graphene

Graphene is highly conductive, has large surface area, and is biocompatible [95], thus having high potential for biomedical applications, e.g., biosensors [93], DDSs [109], and NIR fluorescence imaging techniques [18]. However, graphene oxide (GO), a 0-D nanomaterial, is used in biomedical imaging, biomarkers detection in biosensors [60], as it is water-soluble and is cheaper as compared to CNTs.

## 3.4 Functionalization of CNMs

For providing the specific targeting property, enhancing the non-toxicity, and pharmacokinetics profile, the CNMs or graphene are functionalized via chemical modifications [34]. Additionally, graphene is made soluble and dispersible to enhance its biomedical potentials by functionalization. For example, PEGylation is a common technique [14] used to enhance biological properties such as stability, biocompatibility, high drug storage capacity, high photothermal conversion [27], colloidal stability in water and for better circulation and lower accumulation into reticuloendothelial system (RES) [41]. Also, immune stimulation via activation of cytokines can be enhanced [14]. These immunologically modified functionalized CNMs are synthesized by using the immune-adjuvant glycosylated chitosan (GC) [14]. The synergistically combined immune stimulation with the thermal laser irradiation produces anti-tumor effect at metastatic tumors. Stabilization of magnetic nanoparticles via carbon encapsulation is done via functionalization using polyvinyl-alcohol (PVA) [34]. Nitrogen-doped gold quantum dots (N-GQDs) carrying anticancer drug

methotrexate (MTX), appeared to be an excellent drug delivery vehicle [45]. To resolve the issues of insolubility of CNTs in various organic solvents, supramolecular complexes are fabricated via chemical modifications. Functionalization of CNTs at their conjugated  $sp^2$  hybridized carbon enables their biomedical applications, such as better bio-absorption and ease of dispersion [33].

## 4 Role of CNMs

Carbon has the ability to exist in various dimensionalities (from zero to three dimensions). It demonstrates NIR photoluminescence [55, 62], great flexibility in surface chemical modification [58, 90], excellent biocompatibility [56], transportability in biological fluids, water solubility and permeability to cell membrane [56]. With so many unique properties, CNMs are excellent candidates for biomedical applications.

### 4.1 For Targeted Drug Delivery

CNT-based nano-vectors, particularly functionalized CNTs, demonstrate better performance as therapeutic drug delivery system. Functionalized CNTs are good nanocarriers for anticancer drugs [34], such as doxorubicin (DOX), methotrexate (MTX), betulinic acid (BA), paclitaxel (PTX), camptothecin (CPT). Scientists formulated BA drug composite with MWCNTs with more dispersibility, lesser cytotoxicity, and enhanced cytotoxicity against lung cancer cell line. The studies showed that the composite was more efficient than the free drug [86]. The PLGA [poly (lactic-co-glycolic)]-coated CNTs had higher loading percentage for PTX and better cytotoxicity against prostate cancer cell line. A targeted delivery vehicle with SWCNTs and DOX displayed enhanced therapeutic efficacy of nanodrug delivery systems for in vivo mice models than free drugs alone [61]. Various other CNMs also exhibited great potential for anticancer therapy. Green synthesized CNPs have multiple biomedical applications such as DOX delivery. They also delivered fluorescence dye Fura-2 in human cervical cancer cell line efficiently across a cell membrane. Thus, mesoporous carbon nanoparticles have huge potential of becoming new generation of nanodevices as targeted delivery applications [31].

Functionalization of MWCNTs or GO by polyvinyl alcohol (PVA) was reported for drug loading and delivery of CPT [75]. These composites showed higher cytotoxicity than free CPT. Thus, GO is a promising CNM for drug delivery due to the enormity of available surfaces for drugs on all sides. CNT drug delivery shows high efficacy in cancer treatment, that too with lesser drug dose. In another study, in vivo drug delivery with SWCNT for tumor inhibition in mice was done. PTX with polyethylene glycol (PEG) was conjugated with SWCNTs. This hydrophilic conjugate had improved efficacy in tumor inhibition than Taxol alone in a breast cancer mice model, owing to enhanced PTX uptake in tumor by SWCNT [55].

Nanoparticles have higher retention times in tumors as compared to healthy cells providing EPR effect of tumors [42]. EPR effect is an exclusive property of solid tumors, showing hypervascularity (high vascular density) due to angiogenesis. Tumor tissue angiogenic blood vessels have spaces unlike normal tissues (600–800 nm). Such defective vascularization induces the EPR effect, [24] leading to the preferential nanocarrier accumulation in tumors [42]. Physical characteristics such as size, surface features, and degree of angiogenesis affect the degree of nanoparticles' accumulation in tumors [42]. Such CNMs have also been used for targeted delivery of biomacromolecules, e.g., cancer-specific proteins and peptides [32]. Villa et al. [91] delivered peptide antigen in vivo with SWCNTs for improved immune responses to tumor-linked antigen. These nanostructures were also internalized into antigen-presenting cells rapidly [91]. Also, there are numerous reports available about delivery of genes and nucleic acids by carbon nanomaterials. [108] modified SWCNTs with siRNA to silence tumor proteins and mRNA in vivo [108]. Branched polyethyleneimine (BPEI)-GO composite had an improved nucleic acid binding and transfection efficiency [46]. Another research group reported folate-conjugated trimethyl chitosan-GO (FTMC-GO) conjugate for plasmid DNA delivery to cancer cell line with no cytotoxicity due to FTMC-GO conjugate [35]. These reports suggest that CNMs are an efficient drug delivery system.

## 4.2 For Imaging

Owing to unique optical, fluorescent, and electrical properties, their dynamic interaction with the probes and signal transduction toward the target molecules, CNMs are perfect bioimaging candidates [62]. Due to large surface-to-volume ratio, graphene conductivity changes with a fractional concentration change in the target molecule [66, 85]. Liu et al. [57] reported the use of graphene oxide silver nitrate composite as an extremely sensitive optical probe for faster SERS imaging in vitro [57]. Lee et al. [52] used graphene-based hybrid electronic device in a multifunctional endoscope system to detect colon cancer [52]. Another research group used bio-conjugated graphene oxide to probe breast cancer cells in vitro and provided a window for label-free Raman assay for improved diagnostic sensitivity of cancer cell lines [5]. Many early-stage cancer biomarkers have been identified using CNT-based electrochemical biosensors [98].

## 4.3 As Immunogens/Immunomodulatory

Studies in the past also suggest immunomodulatory effect of CNMs. Kinaret et al. [47] reported macrophage polarization as a result of 48 h exposure to graphene nanofibers (GNFs) and CNTs. They further reported that acute phase

pro-inflammatory tumor necrosis factor (TNF) and cytokine Interleukin 1 beta (IL-1 $\beta$ ) were expressed in GNF exposed cells along with anti-inflammatory cytokine: Interleukin 10 (IL-10) [47]. CNTs have been used as physical adsorption platforms for anti-CD3 molecules which stimulate T-cell proliferation [11]. Fadel et al. [26] reported that engineered CNTs can efficiently present major histocompatibility complex class-1 (MHC-1) for T-cell stimulation [26]. Yue et al. [107] reported that graphene induces release of cytokines and manages inflammatory response [107]. Chen et al. [19] reported that GO induces toll-like receptors and subsequent inflammatory response [19, 49]. Meng et al. [64] reported that CNTs can enhance host immune activity in mice with solid tumors [64].

## 5 Interaction of CNMs with Cancer Cells

### 5.1 *In Vitro Studies*

In order to demonstrate enhanced drug loading and drug release ability of CNTs, Lay et al. [51] grafted poly (ethylene glycol) (PEG) over single and multi-walled CNTs (PEG-CNTs) and physically loaded them with anticancer drug paclitaxel (PTX). The faster release of PTX was observed but in a sustained manner, where considerably less PTX was released over 40 days at neutral pH [51]. Another group demonstrated successful loading of doxorubicin on CNTs in vitro [38]. Wang et al [96] also loaded anticancer drug doxorubicin over graphene coated with phospholipid monolayer [62, 96]. Zheng et al. reported anticancer drug doxorubicin delivery to cancer cells overexpressing ERBB2 by reduced graphene oxide (rGO) functionalized with antibodies or receptors [110]. Another group reported the ability of Fe<sub>3</sub>O<sub>4</sub>-PEG-GO nanocomposite for magnetic imaging as well as for anticancer drug delivery [95]. With strong NIR absorption capability, these materials also act as near-perfect contrast agents for photoacoustic imaging. Photoacoustic imaging technique offers improved spatial resolution and deep tissue imaging as compared to other optical imaging methods. The enhancement during real time photoacoustic imaging invitro [102]. Another class of carbon nanomaterials, i.e., zero-dimensional carbon dots, demonstrated promising biosensing and imaging capability due to tunable photoluminescence (PL) and electrochemiluminescence (ECL) activity, biocompatibility and safety to healthy cells.

### 5.2 *In Vivo Studies*

Liu et al. functionalized biocompatible CNTs with PEG and used them as vehicle to deliver anticancer drug doxorubicin to the mice tumor [56]. Another group fabricated graphene oxide/chitosan oligosaccharide/ $\gamma$ -polyglutamic acid composite and used it



for doxorubicin delivery to the tumor site in a controlled fashion [54]. Pei et al. [71] reported the development of dual drug (cisplatin and doxorubicin) delivery system with PEGylated nano-graphene oxide (pGO). The group reported effective delivery of the drugs to the tumor cells, and the dual drug system's tumor inhibition efficacy was substantially higher than the individual free drugs. The spectroscopic features of CNTs provide a unique feature to track the real-time status of drug delivery, pharmacodynamics behavior, and disease status [88]. Photostability, fluorescence and at tunable emission spectra allow CNMs to demonstrate remarkable optical features in vivo [74, 105, 106]. Pramanik et al. reported sixfold signal enhancement with CNTs as compared to control during photoacoustic tomography (PAT) [72]. Similarly, carbon dots demonstrated strong fluorescence in vivo [105].

## 6 Advantages and Limitations of CNMs

### 6.1 Advantages

Unique properties such as NIR photoluminescence, optical tunability, high surface-to-volume ratio, ease of surface modification provides CNMs an edge over others in biomedical application. CNTs, particularly SWNTs hold a great promise in biomedicine. CNTs have only carbon as a component, while metal nanomaterials (e.g., quantum dots) contain more precarious elements including heavy metals. The tunable length and distinguishable 1-D structure of CNTs provide a lot of opportunity to explore size and shape effects in mice models. Moreover, SWCNTs properties such as NIR absorption, Raman scattering, photo and chemiluminescence provide unique detection and imaging ability unlike organic drug carriers [62]. Overall CNTs hold a lot of biomedical potential particularly in cancer therapy and imaging [56].

### 6.2 Limitations

Chemical inertness of CNMs poses a big hurdle for their smooth bio-clearance (even if they are exposed for extended period in vivo) despite good biocompatibility. The bio-clearance becomes further difficult for amorphous and bigger-sized CNMs (greater than 8 nm). These materials are expelled from the body with liver and spleen playing an important role in their excretion instead of biodegradation [56]. Also, a majority of mesoporous CNMs-based drug delivery systems suffer due to substantial synthesis costs, bigger particles, shape irregularity, and difficulty in scalability. Multiple reports suggest that functionalized CNMs are safe in vitro and in vivo at various concentrations of selected tested doses. But further regulatory authorities approved preclinical as well as clinical trials will be required on a larger scale.

## 7 Conclusion and Future Prospects

The cancer cases are on the rise globally. Even with the advancement of contemporary treatment and diagnostic methods, the unwanted side effects of the drugs are also on the rise. Focusing on the reduction of these side effects, new methods of theranostics and targeted drug delivery are in demand, promising more efficacy and lesser invasive therapy. In this regard, CNMs, due to their prolonged stay in blood circulation, are being extensively used in oncology for targeted and controlled drug release, early diagnosis, etc. Functionalizations of CNMs can help to enhance their biocompatibility, dispersity, hydrophilicity and can reduce their toxicity. CNMs have an added advantage of passive movements across the cell membrane over other nanomaterials, targeted delivery, and higher efficacy with EPR effect at tumor sites. Thus, CNMs would be the most potent tool in upcoming decade for cancer theranostics. Functionalization of CNMs for crossing across plasma-membrane (PM) and blood–brain barrier (BBB) has been achieved. It is done via opening of the tight junctions, leading to the treatment of difficult ailments such as brain tumors.

Numerous anticancer functionalized nanomedicines have been clinically approved by regulatory authorities. Most of these nanomedicines are based upon PEGylation and entrapment technique to enhance the efficacy of the anticancer drugs. Thus, combination of advanced techniques such as drug entrapment, specific targeting, and surface functionalization leads to a triple targeting approach and has the potential to reach the patients. This, combined with improved manufacture level scale-up of NPs production as a commercially viable system would truly lead to the delivery of next-generation nanomedicines into the clinic.

**Acknowledgements** The authors would like to express the gratitude to the Symbiosis International (Deemed University), and Savitribai Phule Pune University (SPPU), for the encouragement to carry out this work. Alongside, we would like to thank Symbiosis Centre for Nanoscience and Nanotechnology (SCNN) and Department of Botany, SPPU, for its constructive feedback and providing opportunity for this work.

## References

1. Al-Mugdadi SFH, Shakur DA, Al-Saedi F (2020) Important diagnostic methods of cancer biomarkers related diagnosis and treatment: a review. *J Crit Rev* 7:675–677
2. Aldape K, Zadeh G, Mansouri S, Reifenberger G, von Deimling A (2015) Glioblastoma: pathology, molecular mechanisms and markers. *Acta Neuropathol* 129:829–848
3. Altun İ, Sonkaya A (2018) The most common side effects experienced by patients were receiving first cycle of chemotherapy. *Iran J Public Health* 47:1218–1219
4. Anshu Gupta TD (2017) A simplified overview of WHO classification update. *Neuroscience* 8:4103–4103
5. Antwi-Boasiako AA, Dunn D, Dasary SSR, Jones YK, Barnes SL, Singh AK (2017) Bioconjugated graphene oxide-based Raman probe for selective identification of SKBR3 breast cancer cells. *J Raman Spectrosc* 48:1056–1064

6. Aronson MR, Medina SH, Mitchell MJ (2021) Peptide functionalized liposomes for receptor targeted cancer therapy. *APL Bioeng* 5:011501
7. Arruebo M, Vilaboa N, Sáez-Gutierrez B, Lambea J, Tres A, Valladares M, González-Fernández A (2011) Assessment of the evolution of cancer treatment therapies. *Cancers (Basel)* 3:3279–3330
8. Baker SN, Baker GA (2010) Luminescent carbon nanodots: emergent nanolights. *Angew Chem Int Ed Engl* 49:6726–6744
9. Bardia A, Mayer IA, Diamond JR, Moroosse RL, Isakoff SJ, Starodub AN, Shah NC, O'Shaughnessy J, Kalinsky K, Guarino M, Abramson V, Juric D, Tolane SM, Berlin J, Messersmith WA, Ocean AJ, Wegener WA, Maliakal P, Sharkey RM, Govindan SV, Goldenberg DM, Vahdat LT (2017) Efficacy and safety of anti-trop-2 antibody drug conjugate sacituzumab govitecan (IMMU-132) in heavily pretreated patients with metastatic triple-negative breast cancer. *J Clin Oncol* 35:2141–2148
10. Bashir S, Liu J (2015) Chapter 1—nanomaterials and their application. In: Liu JL, Bashir S (eds) *Advanced nanomaterials and their applications in renewable energy*. Elsevier, Amsterdam
11. Battigelli A, Ménard-Moyon C, Bianco A (2014) Carbon nanomaterials as new tools for immunotherapeutic applications. *J Mater Chem B* 2:6144–6156
12. Berg HM (1962) Swedish contributions to radiology. *Radiology* 78:471–473
13. Bhowmik A, Khan R, Ghosh MK (2015) Blood brain barrier: a challenge for effectual therapy of brain tumors. *Biomed Res Int* 2015:320941
14. Bottini M, Rosato N, Bottini N (2011) PEG-modified carbon nanotubes in biomedicine: current status and challenges ahead. *Biomacromol* 12:3381–3393
15. Bray F, Ferlay J, Soerjomataram I, Siegel RL, Torre LA, Jemal A (2018) Global cancer statistics 2018: GLOBOCAN estimates of incidence and mortality worldwide for 36 cancers in 185 countries. *CA Cancer J Clin* 68:394–424
16. Calimeri T, Marcucci F, Corti AJAOL (2021) Overcoming the blood-brain barrier in primary central nervous system lymphoma: a review on new strategies to solve an old problem 5
17. Care SH (2021) Types of surgery for cancer treatment [Online]. Stanford Health Care, USA. Available: <https://stanfordhealthcare.org/medical-treatments/c/cancer-surgery/types.html>. Accessed on 28 Nov 2021
18. Chen D, Wang C, Nie X, Li S, Li R, Guan M, Liu Z, Chen C, Wang C, Shu C, Wan L (2014) Photoacoustic imaging guided near-infrared photothermal therapy using highly water-dispersible single-walled carbon nanohorns as theranostic agents. *Adv Func Mater* 24:6621–6628
19. Chen GY, Yang HJ, Lu CH, Chao YC, Hwang SM, Chen CL, Lo KW, Sung LY, Luo WY, Tuan HY, Hu YC (2012) Simultaneous induction of autophagy and toll-like receptor signaling pathways by graphene oxide. *Biomaterials* 33:6559–6569
20. Chifiriuc MC, Gheorghe I, Czobor I, Florea DA, Mateescu L, Caplan ME, Caplan DM, Lazar V (2017) 18—Advances in molecular biology based assays for the rapid detection of food microbial contaminants. In: Grumezescu AM (ed) *Food preservation*. Academic Press
21. Denkert C, Liedtke C, Tutt A, von Minckwitz G (2017) Molecular alterations in triple-negative breast cancer—the road to new treatment strategies. *Lancet* 389:2430–2442
22. Diseases BMNIODADAK (2012) Antineoplastic agents [Online]. National Institute of Diabetes and Digestive and Kidney Diseases, Bethesda, USA. Available: <https://www.ncbi.nlm.nih.gov/books/NBK548022/>. Accessed on 28 Nov 2021
23. Donzella V, Crea F (2011) Optical biosensors to analyze novel biomarkers in oncology 452:442–452
24. Edens HA, Levi BP, Jaye DL, Walsh S, Reaves TA, Turner JR, Nusrat A, Parkos CA (2002) Neutrophil transepithelial migration: evidence for sequential, contact-dependent signaling events and enhanced paracellular permeability independent of transjunctional migration. *J Immunol* 169:476
25. Eshghi MG, Fruhdeh Z, Alviri VM, Modarresi Asem M (2019) Electrochemical biosensors for cancer detection using different biomarkers. In: 2019 IEEE 9th annual computing and communication workshop and conference, CCWC 2019, pp 989–996

26. Fadel TR, Li N, Shah S, Look M, Pfefferle LD, Haller GL, Justesen S, Wilson CJ, Fahmy TM (2013) Adsorption of multimeric T cell antigens on carbon nanotubes: effect on protein structure and antigen-specific T cell stimulation. *Small* 9:666–672
27. Fernandez-Fernandez A, Manchanda R, McGoron AJ (2011) Theranostic applications of nanomaterials in cancer: drug delivery, image-guided therapy, and multifunctional platforms. *Appl Biochem Biotechnol* 165:1628–1651
28. Foulkes WD, Smith IE, Reis-Filho JS (2010) Triple-negative breast cancer. *N Engl J Med* 363:1938–1948
29. Ghaemi A, Bagheri E, Abnous K, Taghdisi SM, Ramezani M, Alibolandi M (2021) CRISPR-cas9 genome editing delivery systems for targeted cancer therapy. *Life Sci* 267:118969
30. Gottesman MM, Fojo T, Bates SE (2002) Multidrug resistance in cancer: role of ATP-dependent transporters. *Nat Rev Cancer* 2:48–58
31. Gu J, Su S, Li Y, He Q, Shi J (2011) Hydrophilic mesoporous carbon nanoparticles as carriers for sustained release of hydrophobic anti-cancer drugs. *Chem Commun* 47:2101–2103
32. Hassan HAFM, Smyth L, Rubio N, Ratnasothy K, Wang JTW, Bansal SS, Summers HD, Diebold SS, Lombardi G, Al-Jamal KT (2016) Carbon nanotubes' surface chemistry determines their potency as vaccine nanocarriers in vitro and in vivo. *J Control Release* 225:205–216
33. Hirsch A, Vostrowsky O (2005) Functionalization of carbon nanotubes. In: Schlüter AD (ed) *Functional molecular nanostructures*. Springer Berlin Heidelberg, Berlin, Heidelberg
34. Hosnedlova B, Kepinska M, Fernandez C, Peng Q, Ruttkay-Nedecky B, Milnerowicz H, Kizek R (2019) Carbon nanomaterials for targeted cancer therapy drugs: a critical review. *Chem Rec* 19:502–522
35. Hu H, Tang C, Yin C (2014) Folate conjugated trimethyl chitosan/graphene oxide nanocomplexes as potential carriers for drug and gene delivery. *Mater Lett* 125:82–85
36. Hu T, Mei X, Wang Y, Weng X, Liang R, Wei M (2019) Two-dimensional nanomaterials: fascinating materials in biomedical field. *Sci Bull* 64:1707–1727
37. Hua H, Zhang H, Kong Q, Jiang Y (2018) Mechanisms for estrogen receptor expression in human cancer. *Exp Hematol Oncol* 7:24
38. Huang H, Yuan Q, Shah JS, Misra RD (2011) A new family of folate-decorated and carbon nanotube-mediated drug delivery system: synthesis and drug delivery response. *Adv Drug Deliv Rev* 63:1332–1339
39. Huang JY, Chen S, Wang ZQ, Kempa K, Wang YM, Jo SH, Chen G, Dresselhaus MS, Ren ZF (2006) Superplastic carbon nanotubes. *Nature* 439:281–281
40. Huse JT, Aldape KD (2014) The evolving role of molecular markers in the diagnosis and management of diffuse glioma. *Clin Cancer Res* 20:5601–5611
41. Jasim DA, Ménard-Moyon C, Bégin D, Bianco A, Kostarelos K (2015) Tissue distribution and urinary excretion of intravenously administered chemically functionalized graphene oxide sheets. *Chem Sci* 6:3952–3964
42. Jiang S, Gnanasammandhan MK, Zhang Y (2010) Optical imaging-guided cancer therapy with fluorescent nanoparticles. *J R Soc Interface* 7:3–18
43. Kalkal A, Kadian S, Pradhan R, Manik G, Packirisamy G (2021) Recent advances in graphene quantum dot-based optical and electrochemical (bio)analytical sensors. *Mater Adv* 2:5513–5541
44. Kalkal A, Pradhan R, Kadian S, Manik G, Packirisamy G (2020) Biofunctionalized graphene quantum dots based fluorescent biosensor toward efficient detection of small cell lung cancer. *ACS Appl Bio Mater* 3:4922–4932
45. Khodadadei F, Safarian S, Ghanbari N (2017) Methotrexate-loaded nitrogen-doped graphene quantum dots nanocarriers as an efficient anticancer drug delivery system. *Mater Sci Eng C Mater Biol Appl* 79:280–285
46. Kim H, Namgung R, Singha K, Oh I-K, Kim WJ (2011) Graphene oxide-polyethylenimine nanoconstruct as a gene delivery vector and bioimaging tool. *Bioconjug Chem* 22:2558–2567
47. Kinaret PAS, Scala G, Federico A, Sund J, Greco D (2020) Carbon nanomaterials promote M1/M2 macrophage activation. *Small* 16:e1907609

48. Kohler BA, Sherman RL, Howlander N, Jemal A, Ryerson AB, Henry KA, Boscoe FP, Cronin KA, Lake A, Noone AM, Henley SJ, Ehemann CR, Anderson RN, Penberthy L (2015) Annual report to the nation on the status of cancer, 1975–2011, featuring incidence of breast cancer subtypes by race/ethnicity, poverty, and state. *J Natl Cancer Inst* 107:djv048
49. Lalwani G, D'Agati M, Khan AM, Sitharaman B (2016) Toxicology of graphene-based nanomaterials. *Adv Drug Deliv Rev* 105:109–144
50. Lange CA, Yee D (2008) Progesterone and breast cancer. *Womens Health (Lond Engl)* 4:151–162
51. Lay CL, Liu HQ, Tan HR, Liu Y (2010) Delivery of paclitaxel by physically loading onto poly(ethylene glycol) (PEG)-graft-carbon nanotubes for potent cancer therapeutics. *Nanotechnology* 21:065101
52. Lee H, Lee Y, Song C, Cho HR, Ghaffari R, Choi TK, Kim KH, Lee YB, Ling D, Lee H, Yu SJ, Choi SH, Hyeon T, Kim DH (2015) An endoscope with integrated transparent bioelectronics and theranostic nanoparticles for colon cancer treatment. *Nat Commun* 6:10059
53. Li S, Su W, Wu H, Yuan T, Yuan C, Liu J, Deng G, Gao X, Chen Z, Bao Y, Yuan F, Zhou S, Tan H, Li Y, Li X, Fan L, Zhu J, Chen AT, Liu F, Zhou Y, Li M, Zhai X, Zhou J (2020) Targeted tumour theranostics in mice via carbon quantum dots structurally mimicking large amino acids. *Nature Biomedical Engineering* 4:704–716
54. Liu B, Che C, Liu J, Si M, Gong Z, Li Y, Zhang J, Yang G (2019) Fabrication and antitumor mechanism of a nanoparticle drug delivery system: graphene oxide/chitosan oligosaccharide/ $\gamma$ -polyglutamic acid composites for anticancer drug delivery 4:12491–12502
55. Liu Z, Chen K, Davis C, Sherlock S, Cao Q, Chen X, Dai H (2008) Drug delivery with carbon nanotubes for in vivo cancer treatment. *Cancer Res* 68:6652–6660
56. Liu Z, Fan AC, Rakhra K, Sherlock S, Goodwin A, Chen X, Yang Q, Felsher DW, Dai H (2009) Supramolecular stacking of doxorubicin on carbon nanotubes for in vivo cancer therapy. *Angew Chem Int Ed* 48:7668–7672
57. Liu Z, Guo Z, Zhong H, Qin X, Wan M, Yang B (2013) Graphene oxide based surface-enhanced Raman scattering probes for cancer cell imaging. *Phys Chem Chem Phys* 15:2961–2966
58. Liu Z, Robinson JT, Tabakman SM, Yang K, Dai HJMT (2011) Carbon materials for drug delivery & cancer therapy 14:316–323
59. Loibl S, Poortmans P, Morrow M, Denkert C, Curigliano G (2021) Breast cancer. *Lancet* 397:1750–1769
60. Lu CH, Yang HH, Zhu CL, Chen X, Chen GN (2009) A graphene platform for sensing biomolecules
61. Madani SY, Naderi N, Dissanayake O, Tan A, Seifalian AM (2011) A new era of cancer treatment: carbon nanotubes as drug delivery tools. *Int J Nanomed* 6:2963–2979
62. Maiti D, Tong X, Mou X, Yang K (2019) Carbon-based nanomaterials for biomedical applications: a recent study 9
63. Martins P (2018) A brief history about radiotherapy 4:8–11
64. Meng J, Yang M, Jia F, Kong H, Zhang W, Wang C, Xing J, Xie S, Xu H (2010) Subcutaneous injection of water-soluble multi-walled carbon nanotubes in tumor-bearing mice boosts the host immune activity. *Nanotechnology* 21:145104
65. Nair A, Haponiuk JT, Thomas S, Gopi S (2020) Natural carbon-based quantum dots and their applications in drug delivery: a review. *Biomed Pharmacother* 132:110834
66. Nangare SN, Patil PO (2021) Affinity-based nanoarchitected biotransducer for sensitivity enhancement of surface plasmon resonance sensors for in vitro diagnosis: a review. *ACS Biomater Sci Eng* 7:2–30
67. NIH (2021) Hormone therapy for breast cancer [Online]. National Institute of Health, National Cancer Institute, USA. Available: <https://www.cancer.gov/types/breast/breast-hormone-therapy-fact-sheet#what-are-hormones-and-hormone-receptors>. Accessed on 7 July 2021
68. Nimse SB, Sonawane MD, Song KS, Kim T (2016) Biomarker detection technologies and future directions. *Analyst* 141:740–755

69. Oncology TASOC (2020) Reconstructive surgery [Online]. The American society of Clinical Oncology, USA. Available: <https://www.cancer.net/navigating-cancer-care/how-cancer-treated/surgery/reconstructive-surgery>. Accessed on 28 Nov 2021
70. Padma Maruvada WWPDW, Sudhir S (2006) FM as a business enabler solutions for managing the built environment 15:4–4
71. Pei X, Zhu Z, Gan Z, Chen J, Zhang X, Cheng X, Wang J et al (2020) PEGylated nanographene oxide as a nanocarrier for delivering mixed anticancer drugs to improve anticancer activity. *Sci Rep* 10(1):1–15
72. Pramanik M, Swierczewska M, Green D, Sitharaman B, Wang LV (2009) Single-walled carbon nanotubes as a multimodal-thermoacoustic and photoacoustic-contrast agent. *J Biomed Opt* 14:034018
73. Rašović I (2017) Water-soluble fullerenes for medical applications. *Mater Sci Technol* 33:777–794
74. Rauti R, Musto M, Bosi S, Prato M, Ballerini L (2019) Properties and behavior of carbon nanomaterials when interfacing neuronal cells: How far have we come? *Carbon* 143:430–446
75. Sahoo NG, Bao H, Pan Y, Pal M, Kakran M, Cheng HKF, Li L, Tan LP (2011) Functionalized carbon nanomaterials as nanocarriers for loading and delivery of a poorly water-soluble anticancer drug: a comparative study. *Chem Commun* 47:5235–5237
76. Saito R, Fujita M, Dresselhaus G, Dresselhaus MS (1992) Electronic structure of chiral graphene tubules 60:2204–2206
77. Sanjay ST, Fu G, Dou M, Xu F, Liu R, Qi H, Li X (2015) Biomarker detection for disease diagnosis using cost-effective microfluidic platforms. *Analyst* 140:7062–7081
78. Sawdon A, Weydemeyer E, Peng CA (2014) Antitumor therapy using nanomaterial-mediated thermolysis. *J Biomed Nanotechnol* 10:1894–1917
79. Setua S, Jaggi M, Yallapu MM, Chauhan SC, Danilushkina A, Lee H, Choi IS, Fakhruddin R, Esposti LD, Tampieri A, Iafisco M, Shevtsov M, Multhoff G (2018) Chapter 6—targeted and theranostic applications for nanotechnologies in medicine. In: Uskoković V, Uskoković DP (eds) *Nanotechnologies in preventive and regenerative medicine*. Elsevier
80. Shah SC, Kayamba V, Peek RM, Heimburger D (2019) Cancer control in low- and middle-income countries: Is it time to consider screening? *J Glob Oncol* 5:1–8
81. Singh R, Torti SV (2013) Carbon nanotubes in hyperthermia therapy. *Adv Drug Deliv Rev* 65:2045–2060
82. Sung H, Ferlay J, Siegel RL, Laversanne M, Soerjomataram I, Jemal A, Bray F (2021) Global cancer statistics 2020: GLOBOCAN estimates of incidence and mortality worldwide for 36 cancers in 185 countries. *CA Cancer J Clin* 71:209–249
83. Swain SM, Baselga J, Kim SB, Ro J, Semiglazov V, Campone M, Ciruelos E, Ferrero JM, Schneeweiss A, Heeson S, Clark E, Ross G, Benyunes MC, Cortés J (2015) Pertuzumab, trastuzumab, and docetaxel in HER2-positive metastatic breast cancer. *N Engl J Med* 372:724–734
84. Szopa W, Burley TA, Kramer-Marek G, Kaspera W (2017) Diagnostic and therapeutic biomarkers in glioblastoma: current status and future perspectives. *BioMed Res Int*
85. Tade RS, Nangare SN, Patil PO (2021) Fundamental aspects of graphene and its biosensing applications. *Funct Compos Struct* 3:012001
86. Tan JM, Karthivashan G, Arulselvan P, Fakurazi S, Hussein MZ (2014) Characterization and in vitro studies of the anticancer effect of oxidized carbon nanotubes functionalized with betulinic acid. *Drug Des Devel Ther* 8:2333–2343
87. Tang L, Wang Y, Li Y, Feng H, Lu J, Li J (2009) Preparation, structure, and electrochemical properties of reduced graphene sheet films. *Adv Func Mater* 19:2782–2789
88. Tasis D, Tagmatarchis N, Bianco A, Prato M (2006) Chemistry of Carbon nanotubes. *Chem Rev* 106:1105–1136
89. Taylor R, Walton DRM (1993) The chemistry of fullerenes. *Nature* 363:685–693
90. Teradal NL, Jelinek R (2017) Carbon nanomaterials in biological studies and biomedicine. *Adv Healthcare Mater* 6:1700574

91. Villa CH, Dao T, Ahearn I, Fehrenbacher N, Casey E, Rey DA, Korontsvit T, Zakhaleva V, Batt CA, Philips MR, Scheinberg DA (2011) Single-walled carbon nanotubes deliver peptide antigen into dendritic cells and enhance IgG responses to tumor-associated antigens. *ACS Nano* 5:5300–5311
92. Waks AG, Winer EP (2019) Breast cancer treatment: a review. *JAMA J Am Med Assoc* 321:288–300
93. Wang J, Musameh M, Lin Y (2003) Solubilization of carbon nanotubes by nafion toward the preparation of amperometric biosensors. *J Am Chem Soc* 125:2408–2409
94. Wang J, Zhang B, Sun J, Hu W, Wang H (2021) Recent advances in porous nanostructures for cancer theranostics. *Nano Today* 38
95. Wang J, Zhang Z, Zha S, Zhu Y, Wu P, Ehrenberg B, Chen JY (2014) Carbon nanodots featuring efficient FRET for two-photon photodynamic cancer therapy with a low fs laser power density. *Biomaterials* 35:9372–9381
96. Wang X, Wang C, Cheng L, Lee S-T, Liu Z (2012) Noble metal coated single-walled carbon nanotubes for applications in surface enhanced raman scattering imaging and photothermal therapy. *J Am Chem Soc* 134:7414–7422
97. Wang Y, Santos A, Evdokiou A, Losic D (2015) An overview of nanotoxicity and nanomedicine research: principles, progress and implications for cancer therapy. *J Mater Chem B* 3:7153–7172
98. Wang Z, Dai Z (2015) Carbon nanomaterial-based electrochemical biosensors: an overview. *Nanoscale* 7:6420–6431
99. Wang Z, Hu T, Liang R, Wei M (2020) Application of zero-dimensional nanomaterials in biosensing 8
100. Watanabe H, Kondo H, Okamoto Y, Hiramatsu M, Sekine M, Baba Y, Hori M (2014) Carbon nanowall scaffold to control culturing of cervical cancer cells. *Appl Phys Lett* 105:244105
101. WHO (2021) Breast cancer [Online]. United Nations, WHO. Available: <https://www.who.int/news-room/fact-sheets/detail/breast-cancer>. Accessed on 26 March 2021
102. Wu L, Cai X, Nelson K, Xing W, Xia J, Zhang R, Stacy AJ, Luderer M, Lanza GM, Wang LV, Shen B, Pan D (2013) A green synthesis of carbon nanoparticles from honey and their use in real-time photoacoustic imaging. *Nano Res* 6:312–325
103. Wu Y-F, Wu H-C, Kuan C-H, Lin C-J, Wang L-W, Chang C-W, Wang T-W (2016) Multi-functionalized carbon dots as theranostic nanoagent for gene delivery in lung cancer therapy. *Sci Rep* 6:21170
104. Xiao F, Lv S, Zong Z, Wu L, Tang X, Kuang W, Zhang P, Li X, Fu J, Xiao M, Wu M, Wu L, Zhu X, Huang K, Guo H (2020) Cerebrospinal fluid biomarkers for brain tumor detection: clinical roles and current progress. *Am J Trans Res* 12:1379–1396
105. Yang S-T, Cao L, Luo PG, Lu F, Wang X, Wang H, Mezziani MJ, Liu Y, Qi G, Sun Y-P (2009) Carbon dots for optical imaging in vivo. *J Am Chem Soc* 131:11308–11309
106. Yang Y, Wang L, Wan B, Gu Y, Li X (2019) Optically active nanomaterials for bioimaging and targeted therapy 7
107. Yue H, Wei W, Yue Z, Wang B, Luo N, Gao Y, Ma D, Ma G, Su Z (2012) The role of the lateral dimension of graphene oxide in the regulation of cellular responses. *Biomaterials* 33:4013–4021
108. Zhang Z, Yang X, Zhang Y, Zeng B, Wang S, Zhu T, Roden RB, Chen Y, Yang R (2006) Delivery of telomerase reverse transcriptase small interfering RNA in complex with positively charged single-walled carbon nanotubes suppresses tumor growth. *Clin Cancer Res* 12:4933–4939
109. Zhao X, Liu L, Li X, Zeng J, Jia X, Liu P (2014) Biocompatible graphene oxide nanoparticle-based drug delivery platform for tumor microenvironment-responsive triggered release of doxorubicin. *Langmuir* 30:10419–10429
110. Zheng XT, Ma XQ, Li CM (2016) Highly efficient nuclear delivery of anti-cancer drugs using a bio-functionalized reduced graphene oxide. *J Colloid Interface Sci* 467:35–42

111. Zia-Ur-Rehman M, Qayyum MF, Akmal F, Maqsood MA, Rizwan M, Waqar M, Azhar M (2018) Chapter 7—recent progress of nanotoxicology in plants. In: Tripathi DK, Ahmad P, Sharma S, Chauhan DK, Dubey NK (eds) *Nanomaterials in plants, algae, and microorganisms*. Academic Press
112. Zimmermann KA, Inglefield DL, Zhang J, Dorn HC, Long TE, Rylander CG, Rylander MN (2014) Single-walled carbon nanohorns decorated with semiconductor quantum dots to evaluate intracellular transport. *J Nanopart Res* 16:2078